

1 Elements of the IVth group and IV-IV compounds

1.0 Crystal structure and electronic structure

1.0.1 Crystal structure

The semiconductors C (Diamond), Si, Ge, Sn (grey tin) crystallize in the diamond lattice.

In this lattice each atom is surrounded by four nearest neighbors which lie with equal distances at the corner of a tetrahedron (Fig. 1.0.1). The lattice can be seen as two interpenetrating face-centered cubic lattices (Fig. 1.0.2).

The *space group* of the diamond lattice is $O_h^7 - Fd3m$.

Carbon also occurs in a hexagonal modification (graphite, Fig. 1.0.3); *tin* crystallizes at room temperature normally in a tetragonal modification (white tin, β -Sn, Fig. 1.0.4), whereas the diamond-like grey tin (α -Sn) is stable only below 13.20°C.

Semiconducting phases also occur in *silicon carbide*. In this binary compound the energy differences between cubic, hexagonal and rhombohedral structures are so small, that a large number of polymorphic modifications occur. More than hundred different *polytypes* exist. In all polytypes every atom is surrounded by four atoms of the other species.

The polytypes of SiC can be described in terms of a hexagonal system, the stacking order along the *c*-axis differing from polytype to polytype; the cubic form fits into this system by taking the [111] direction as "*c*-axis". Fig. 1.0.5 shows the elementary cells of the 3C (cubic, zincblende, β -SiC), 2H (hexagonal, wurtzite, α -SiC), 4H and 6H polytypes. Other hexagonal (H) and rhombohedral (R) polytypes occur.

1.0.2 Electronic structure

General remarks on the band structure of elements with diamond structure

The *Brillouin zone* of the diamond structure is the Brillouin zone of the face-centered lattice, Fig. 1.0.6. Symmetry lines and points within the Brillouin zone are designed by letters (Γ , X, L, Δ ...).

The qualitative *band structure* is shown in Fig. 1.0.7 along the Δ and Λ axes in the Brillouin zone. Subscripts to the letters defining the location of a given energy state in the Brillouin zone designate the irreducible representation of the respective state (1, 1', 2, 12, 25'...).

Conduction band edge: Fig 1.0.7 shows only the topological connection of the subbands of the conduction band. Two possibilities are to be considered in connection with the band structure of group IV elements:

Lowest band state at Γ : In this case the energy $E(\mathbf{k})$ can be approximated near the band edge by a scalar quadratic \mathbf{k} -dependence: $E(k) = E(\Gamma) + \hbar^2 k^2 / 2m_n$.

Lowest band state along a symmetry axis (Δ or Λ): In the case that the lowest band state lies at a point \mathbf{k}_0 at a symmetry axis the band edge can be approximated by $E(\mathbf{k}) = E(\mathbf{k}_0) + \hbar^2 \kappa_x^2 / 2m_{\parallel} + \hbar^2 (\kappa_y^2 + \kappa_z^2) / 2m_{\perp}$ where $\boldsymbol{\kappa} = \mathbf{k} - \mathbf{k}_0$ and $\kappa_x \parallel k_0$, $\kappa_y, \kappa_z \perp k_0$ (*ellipsoidal energy surfaces*).

Valence band edge: In all group IV elements the top of the valence band is situated at the center Γ of the Brillouin zone (Γ_{25}'). According to Fig. 1.0.7 this state is triply degenerated if the spin-orbit coupling can be neglected. Taking spin into account the (now sixfold degenerated) state splits into the fourfold degenerated Γ_8^+ state and a lower lying Γ_7^+ state, separated by the spin-orbit splitting Δ . At $\mathbf{k} \neq 0$ two subbands (degenerated at Γ) build the band edge. Their energy can be approximated by

$$E(\mathbf{k}) = E(\Gamma) + (\hbar^2 k^2 / 2m_0)(A \pm (B^2 + sC^2)^{1/2}), \quad s = (k_x^2 k_y^2 + k_y^2 k_z^2 + k_z^2 k_x^2) / k^4$$

The \pm -sign refers to the two bands into which $E(\Gamma_8^+)$ splits (*warped surfaces*).

Special band structures

According to Figs. 1.0.8 ... 1.0.13 the semiconducting group IV elements and IV-IV compounds show the following band structures:

Diamond and *silicon* are indirect semiconductor, the lowest minima of the conduction band being located on the Δ -axis.

Germanium is an indirect semiconductor too, but in contrast to C and Si the lowest minima of the conduction band are located at the endpoints L of the Λ -axis.

Grey tin is a zero gap semiconductor, where the top of the valence band and the bottom of the conduction band are degenerated..

Silicon carbide is an indirect semiconductor, the lowest minima of the conduction band being located at the end points X of the cubic axes (X in the cubic polytype, K in the hexagonal 2H polytype).

The valence bands of all five semiconductors are identical as shown in Fig. 1.0.7 (warped surfaces).

For details of the band structure, see the respective sections.

Figures to 1.0

Fig. 1.0.1

Orientation of tetrahedra in the diamond structure.

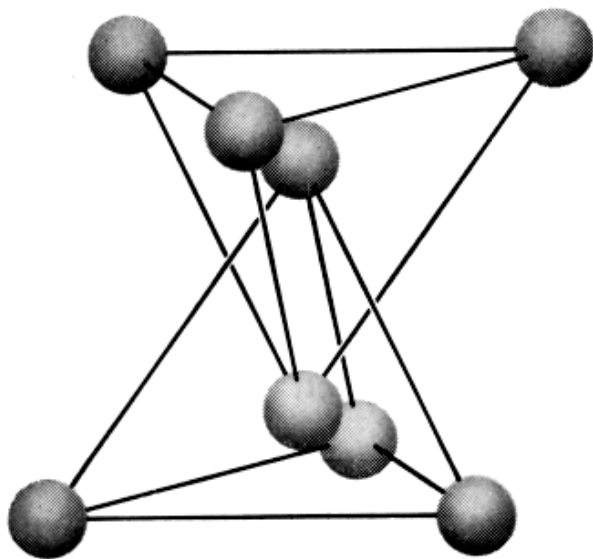


Fig. 1.0.2

The diamond lattice. The elementary cubes of the two face-centered cubic lattices are shown.

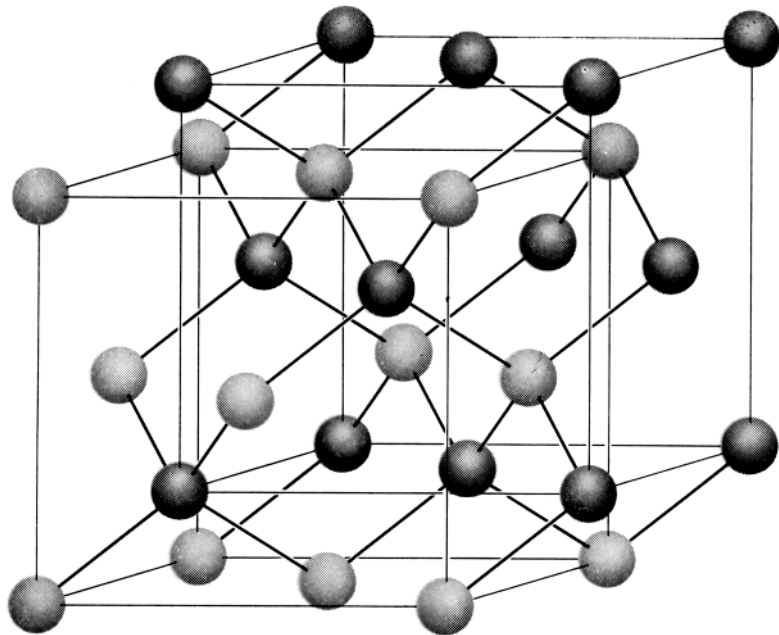


Fig. 1.0.3

The graphite lattice

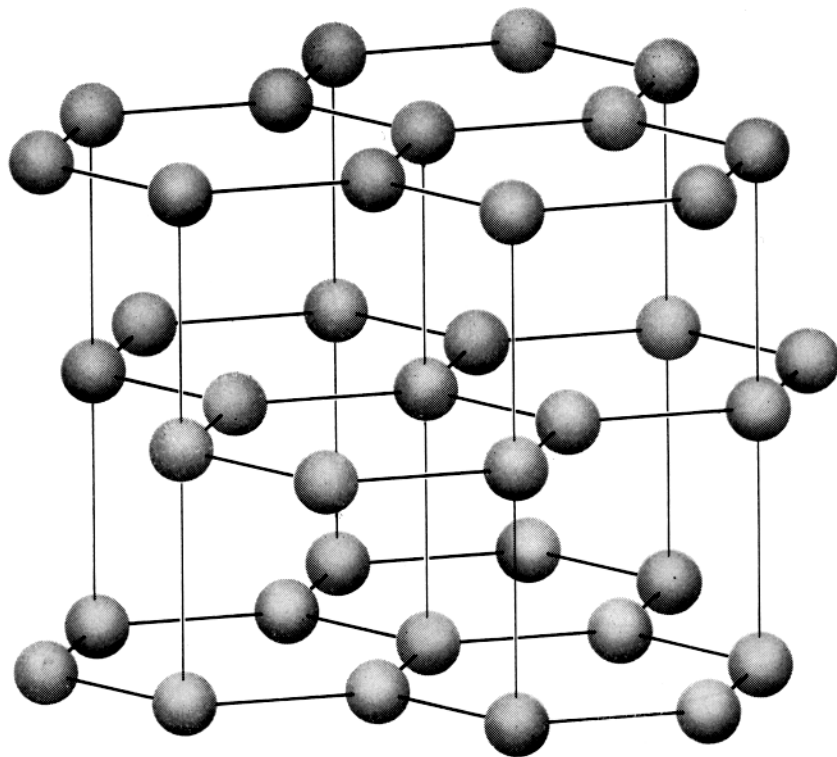


Fig. 1.0.4

Unit cell of the white tin lattice

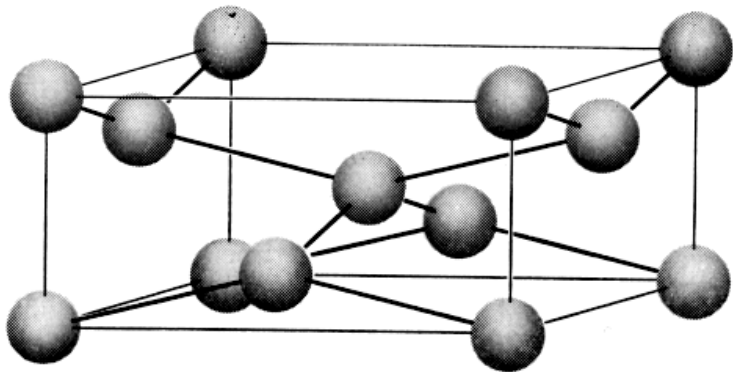


Fig. 1.0.5

Elementary cells of 3C, 2H, 4H, 6H structures. The 3C structure is also drawn in the hexagonal cell. Stacking sequences are indicated.

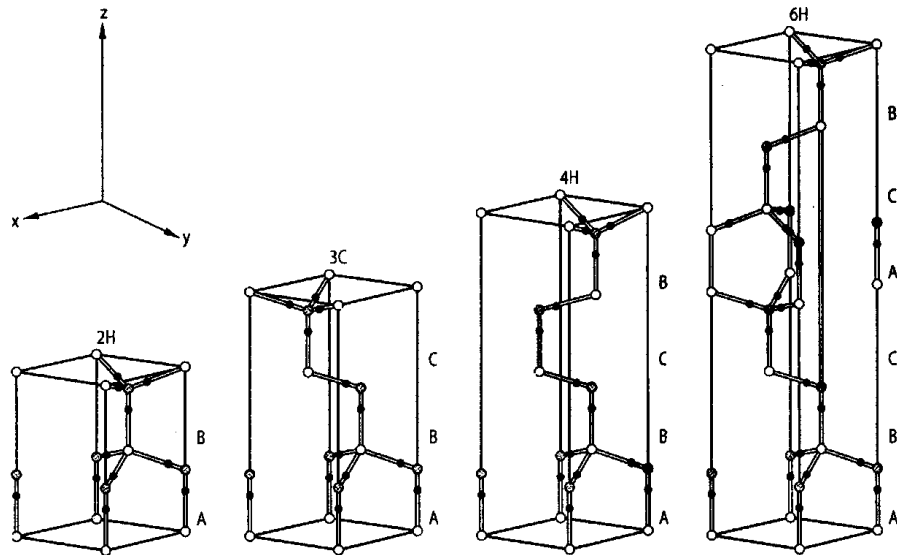


Fig. 1.0.6

Brillouin zone of the diamond lattice.

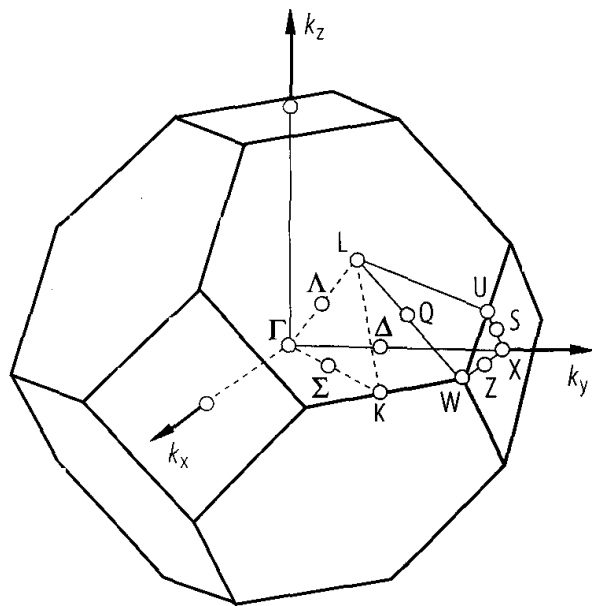


Fig. 1.0.7

Qualitative picture of the band structure of a semiconductor with diamond structure (a) without inclusion of spin, (b) with spin taken into account. This qualitative shape applies both to the valence and the conduction bands. The symmetry symbols are the same for the two cases except where valence band symbols differing from those for the conduction band are shown in brackets. Where a point or line is labeled with two symbols without brackets, it means that symmetry arguments alone cannot distinguish between the two possibilities. Degeneracies of the band are given in brackets.

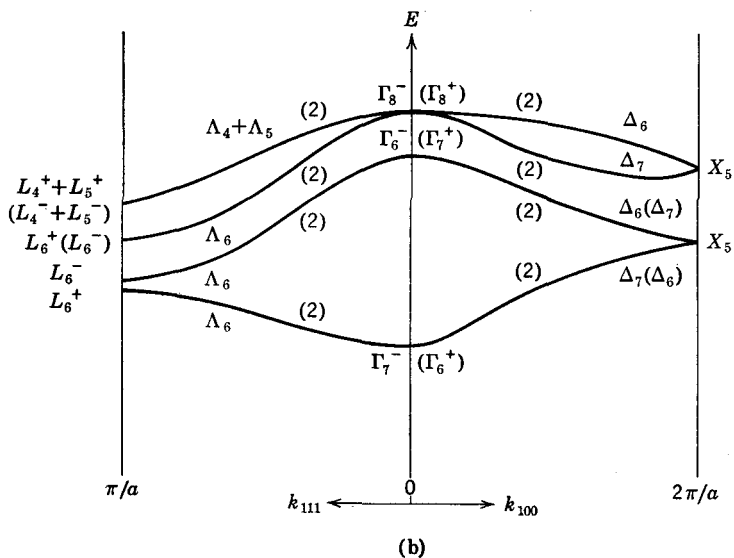
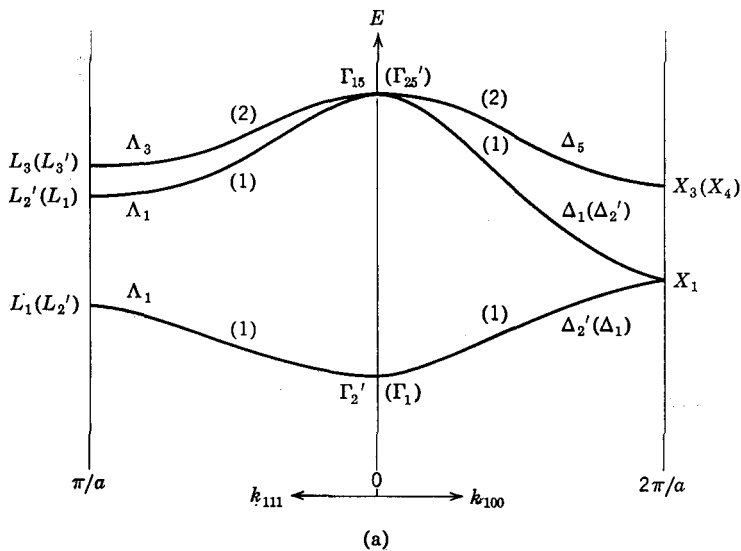


Fig. 1.0.8

Band structure of diamond.

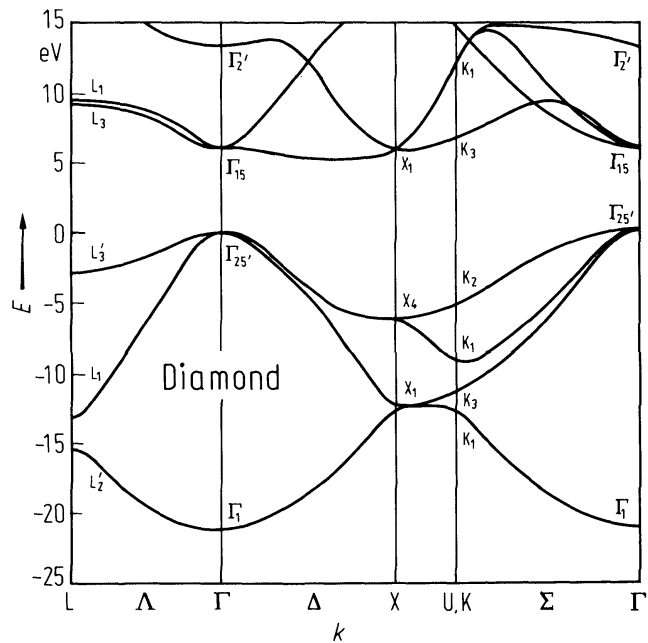


Fig. 1.0.9

Band structure of silicon.

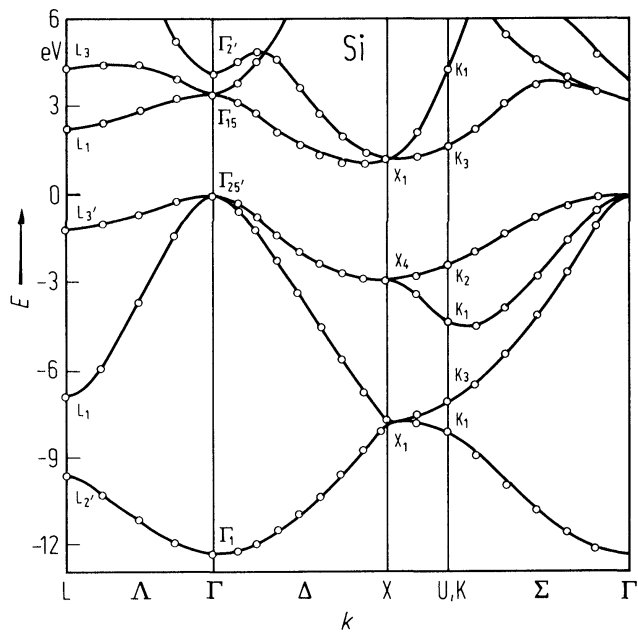


Fig. 1.0.10

Band structure of germanium.

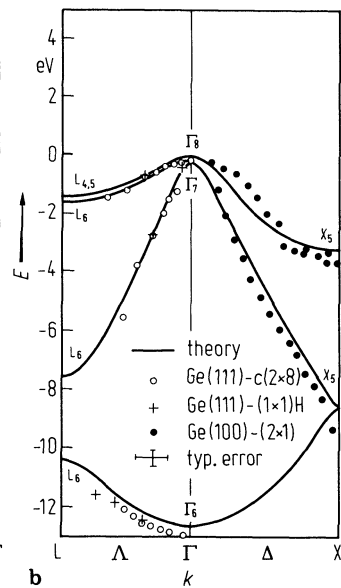
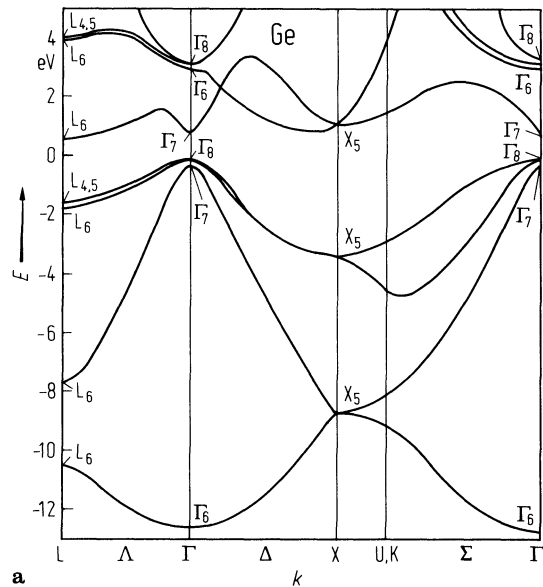


Fig. 1.0.11

Band structure of grey tin

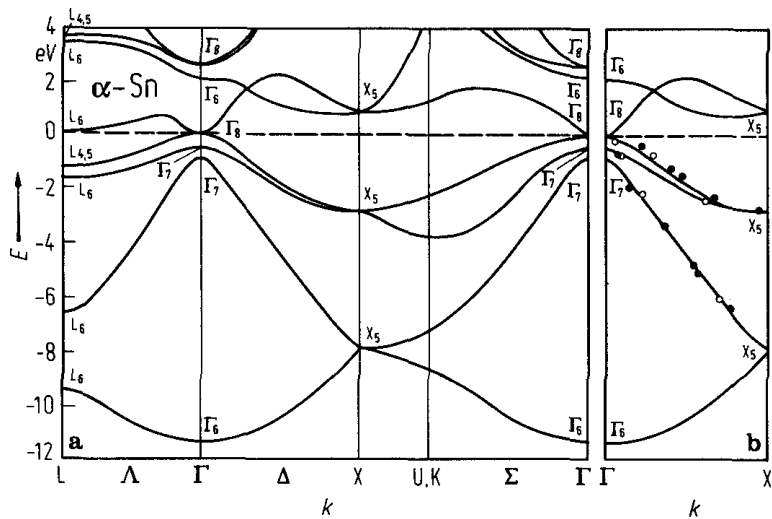


Fig. 1.0.12

Band structure of 3C silicon carbide

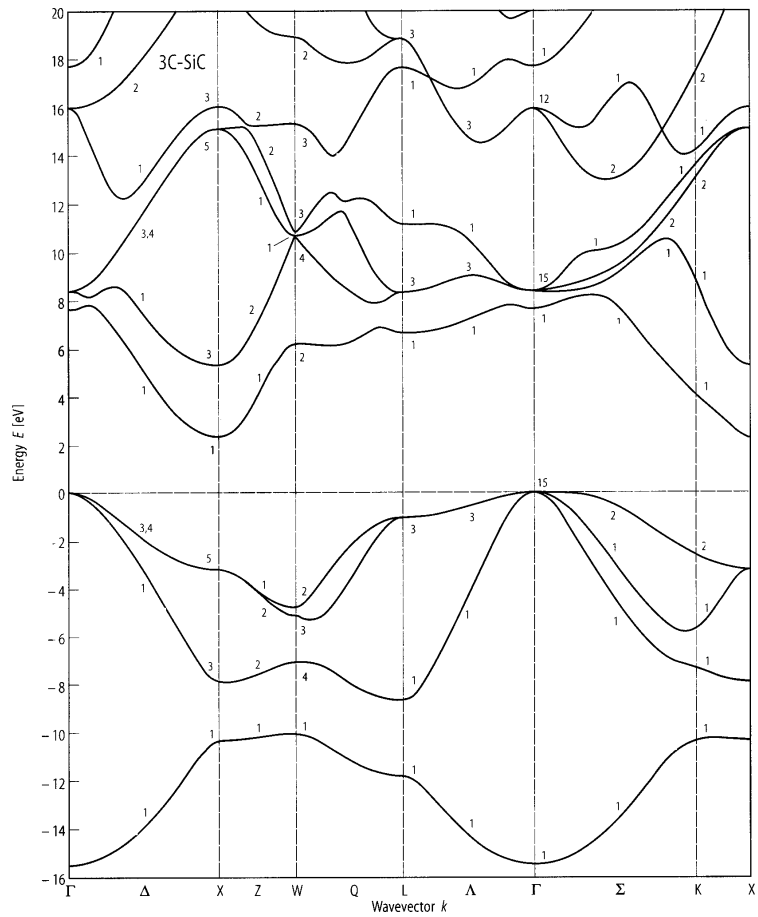
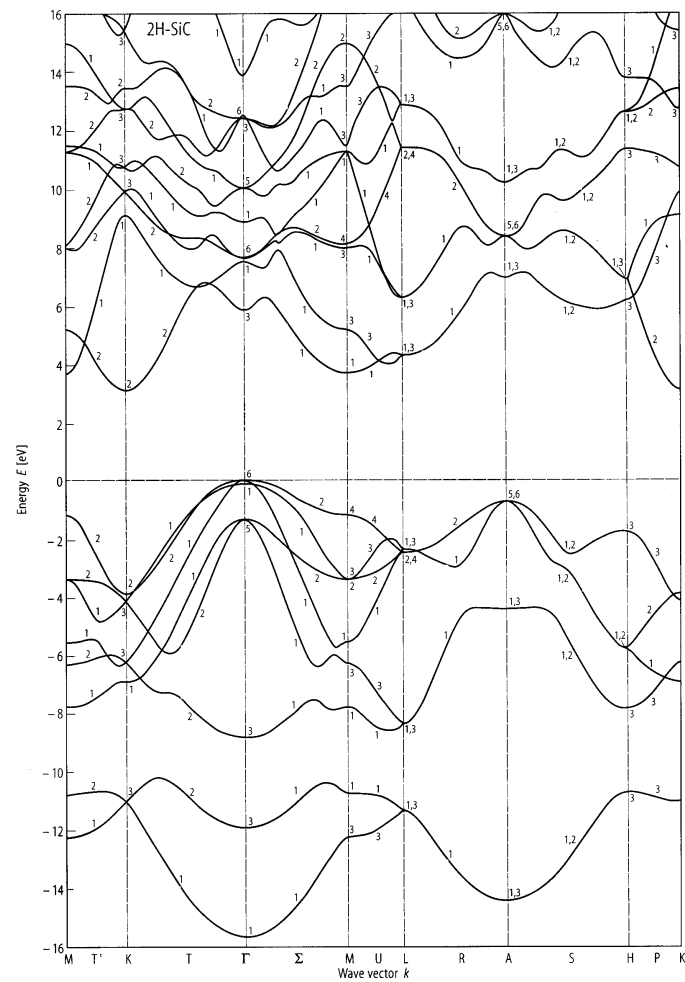


Fig. 1.0.13

Band structure of 2H silicon carbide



1.1 Diamond, C

Crystal structure

The crystallization of the element carbon usually takes place in two modifications: diamond (cubic) and graphite (hexagonal). Under ambient conditions graphite is stable, diamond is metastable. Diamond occurs naturally (mineral name: sphalerite) and can be synthesized under high pressure.

The diamond lattice (space group: cubic $O_h^7 - Fd3m$) is shown in Fig. 1.0.2.

high pressure phases

Diamond can be formed under compression to 14 to 20 GPa at 800 to 1200 °C; for the transition from graphite to diamond under shock compression, see [91E]; from ultradisperse diamond to graphite, see [97A]. Another form, n-diamond (structure not determined yet, but similar to an fcc structure) is formed at 40 GPa, RT, and at 14 GPa, 1200 °C or under shock compression [91H]. A modification with crystal structure Im3 has been reported in [79M]. A variety of polytypes is formed under vapour deposition [84P, 89F]; for a review of vapour-grown carbon, see [88A, 90Y].

Electronic properties

band structure : Figs. 1.0.8, Brillouin zone: Fig. 1.0.6.

Diamond is an indirect gap semiconductor. The lowest minima of the conduction band are located at [0.75, 0, 0]. The valence band has the structure common to all group IV semiconductors: three at Γ degenerate bands (spin neglected, symmetry $\Gamma_{25'}$). The spin orbit splitting of these bands is negligible. Only few further transitions have been positively identified.

energies of symmetry points of the band structure (relative to the top of the valence band $E(\Gamma_{25'v})$)

$E(\Gamma_{1v})$	- 21.03 eV (-21(1) eV)	theoretical data:
$E(\Gamma_{15c})$	6.02 eV (6.0(2) eV)	ab initio LCAO calculations [84C],
$E(\Gamma_{2'c})$	13.41 eV (15.3(5) eV)	see Fig. 1.0.8
$E(X_{1v})$	- 12.43 eV	in brackets: experimental data [80H]
$E(X_{4v})$	- 6.27 eV	
$E(X_{1c})$	5.91 eV	
$E(X_{4c})$	16.77 eV	
$E(L_{2'v})$	- 15.29 eV (-15.3(3) eV)	
$E(L_{1v})$	- 13.09 eV (-12.8(3) eV)	
$E(L_{3'v})$	- 2.82 eV	
$E(L_{3c})$	9.23 eV	
$E(L_{1c})$	9.58 eV	

Position of the minima of the conduction band along the Δ -axis: $k = (0.76(1), 0, 0)$ [65D].

energy gaps

$E_{g,ind}(\Gamma_{25'v} - \Delta_{1c})$	5.50(5) eV	RT	quantum photoyield	79H
$E_{gx,ind}$	5.416(2) eV	natural diamond,	indirect exciton gap with	65D
	5.409(2) eV	$T = 100$ K	lower valence band	
			indirect exciton gap with	
			upper valence band	
$dE_{g,ind}/dT$	- $5 \cdot 10^{-5}$ eV/K	$T = 135...300$ K	see Fig. 1.1.1	64C

exciton binding energy

$E_b(1S)$	0.19(15) eV	binding energy of the 1S core exciton	85M
E_b	0.07 eV	indirect exciton binding energy,	64C
		optical absorption	
	0.080(5) eV	recombination radiation	65D

spin-orbit splitting energy

$\Delta(\Gamma_{25'}\nu)$	0.006(1) eV		cyclotron resonance	62R
---------------------------	-------------	--	---------------------	-----

effective masses

$m_{n\parallel}$	1.4 m_0		field dependence of electron drift velocity	80N
$m_{n\perp}$	0.36 m_0			
$m_{p,h}$	1.08 m_0		calculated density of states from best set of valence band parameters (see below)	83R
$m_{p,l}$	0.36 m_0			
m_{so}	0.15 m_0			
$m_{p,ds}$	0.75 m_0	$T = 300$ K	Hall effect	79F

g-factor

g	2.0030(3)	$T = 140...298$ K	type IIb; electron spin resonance	67B2
-----	-----------	-------------------	-----------------------------------	------

valence band parameters

$ A $	3.61		most probable set of parameters out of six sets published by various authors, from fitting Hall data to theory	83R
$ B $	0.18			
$ C $	3.67			

Lattice properties

lattice parameter

a	3.56685 Å	$T = 298$ K	X-ray diffraction; for temperature dependence, see Fig. 1.1.2	57S
-----	-----------	-------------	---	-----

linear thermal expansion coefficient

α	0.0·10 ⁻⁶ K ⁻¹	$T = 100$ K	X-ray diffraction ("best" values from several authors);	75S
	1.0·10 ⁻⁶ K ⁻¹	$T = 300$ K	for temperature dependence, see Fig. 1.1.2	
	4.4·10 ⁻⁶ K ⁻¹	$T = 1000$ K		

density

d	3.51537(5) g cm ⁻³	$T = 298$ K	type Ia, flotation	64M
	3.51506(5) g cm ⁻³	$T = 298$ K	type IIb, flotation	

melting point

T_m	4100 K	$p = 125$ kbar	diamond-graphite-liquid eutectic	63B
-------	--------	----------------	----------------------------------	-----

phonon dispersion relations : Fig. 1.1.4

phonon frequencies

$\nu_{TO/LO}(\Gamma_{25'})$	39.9 THz	$T = 300$ K	Raman spectra	70S
$\nu_{TA}(L_3)$	16.9 THz			
$\nu_{LA}(L_1)$	30.2 THz			
$\nu_{LO}(L_2')$	37.5 THz			
$\nu_{TO}(L_3')$	36.2 THz			
$\nu_{TA}(X_3)$	24.2 THz			
$\nu_{LA/LO}(X_1)$	35.5 THz			
$\nu_{TO}(X_4)$	32.0 THz			

sound velocity

v_{LA}	1.833·10 ⁶ cm s ⁻¹	$T = 298$ K, $f = 1$ GHz (extra-polated)	type II, resonance method, direction of particle motion: [110]	72M
v_{TA}	1.283·10 ⁶ cm s ⁻¹		direction of particle motion: [100]	
	1.166·10 ⁶ cm s ⁻¹		direction of particle motion: [110]	

second order elastic moduli

c_{11}	$10.764(2) \cdot 10^{12} \text{ dyn cm}^{-2}$	$T = 296 \text{ K}$	Brillouin scattering	75G
c_{12}	$1.252(23) \cdot 10^{12} \text{ dyn cm}^{-2}$		temperature dependence: Fig. 1.1.4	
c_{44}	$5.774(14) \cdot 10^{12} \text{ dyn cm}^{-2}$			

third order elastic moduli

c_{111}	$-62.6 \cdot 10^{12} \text{ dyn cm}^{-2}$	$T = 300 \text{ K},$	Raman scattering	78G
c_{112}	$-22.6 \cdot 10^{12} \text{ dyn cm}^{-2}$	$p = 0 \dots 10 \text{ kbar}$		
c_{123}	$+1.12 \cdot 10^{12} \text{ dyn cm}^{-2}$			
c_{144}	$-6.74 \cdot 10^{12} \text{ dyn cm}^{-2}$			
c_{166}	$-28.6 \cdot 10^{12} \text{ dyn cm}^{-2}$			
c_{456}	$-8.23 \cdot 10^{12} \text{ dyn cm}^{-2}$			

Poisson's ratio

ν	0.104		calculated from elastic moduli	75G
-------	-------	--	--------------------------------	-----

bulk modulus

$B(T) [\text{GPa}]$	$444.8 - 0.000012 (T^2 - 3002)$	$T = 300 \dots 1600 \text{ K}$		98Z
---------------------	---------------------------------	--------------------------------	--	-----

Debye temperature

Θ_D	$2220(20) \text{ K}$	$T = 0 \text{ K}$	evaluation of heat capacitance and	62V
	$1860(10) \text{ K}$	$T = 273 \dots 1100 \text{ K}$	thermal expansion data	

heat capacity

C_p	$6.195 \text{ J mol}^{-1} \text{ K}^{-1}$	$T = 300 \text{ K}$	for temperature dependence,	62V
C_v	$6.186 \text{ J mol}^{-1} \text{ K}^{-1}$		see Fig. 1.1.5	

Transport properties

Due to the large band gap (5.48 eV) and the high ionization energy of donors, most diamonds are insulators at room temperature. The electron mobility, therefore, can only be derived from photoconductivity experiments.

Natural (type IIb) and synthetic semiconducting diamonds are always p-type. Typical $\rho(T)$ -curves are shown in Fig. 1.1.6.

electron mobility

μ_n	$2000 \text{ cm}^2/\text{Vs}$	RT	for temperature dependence of Hall and drift mobility, see Fig. 1.1.7	80N
---------	-------------------------------	----	---	-----

hole mobility

μ_p	$2100 \text{ cm}^2/\text{Vs}$	RT	for temperature dependence of Hall and drift mobility, see Fig. 1.1.8	81R
---------	-------------------------------	----	---	-----

thermal conductivity

κ	$6 \dots 10 \text{ W cm}^{-1} \text{ K}^{-1}$	$T = 293 \text{ K}$	type Ia; steady-state heat flow; for dependence on temperature and impurity concentration, see Fig. 1.1.9	76B
----------	---	---------------------	---	-----

Optical properties

refractive index

n	3.5	$\lambda = 177.0 \text{ nm}$		62P
-----	-----	------------------------------	--	-----

n fits the empirical formula

$$n^2 - 1 = a\lambda^2/(\lambda^2 - \lambda_1^2) + b\lambda^2/(\lambda^2 - \lambda_2^2): \quad a = 0.3306, \quad b = 4.3356, \quad \lambda_1 = 175.0 \text{ nm}, \quad \lambda_2 = 106.0 \text{ nm}$$

high frequency dielectric constant

$\epsilon(\infty)$	5.70(5)	$T = 300\text{ K},$ $f = 10^3 \dots 10^4\text{ Hz}$	capacitance measurement	77F
	$5.70 - 5.35 \cdot 10^{-5}T + 1.66 \cdot 10^{-7}T^2$		T in °C ($T = 5.5 \dots 340\text{ K}$)	77F

elastooptic constants

p_{11}	- 0.244	for dispersion, see Fig. 1.1.10		57D,
p_{12}	+ 0.042			75G
p_{44}	- 0.172			

Details of the i.r. absorption spectrum of a type IaA diamond can be seen from Fig. 1.1.11. Reflectivity data in the 4...28 eV region are given in Fig. 1.1.12.

Impurities and defects

Most electrical, optical and thermal properties of diamond are extrinsic, i.e. strongly dependent on the impurity content, the most important impurities being nitrogen and boron.

binding energies of impurity levels

donors

	$E_c - E_d$			
N	1.7 eV	$T = 300\text{ K}$	substitutional nitrogen; combined photoconduction, optical absorption, and resistance vs. temperature measurement	69F
	4 eV (1.45 eV above valence band)	$T = 300\text{ K}$	nitrogen aggregates (A centers, "platelets"), later identified with pairs of adjacent substitutional N atoms	67D 74C 94W
Li	0.103(15) eV	$T = 300 \dots 600\text{ K}$	ion implantation; conductivity measurements	79V

acceptors

	$E_a - E_v$			
B	370 (10) meV	$T = 200 \dots 400\text{ K}$	$n_a = 2 \cdot 10^{16}\text{ cm}^{-3}$; conductivity measurements	78M
	368.5 (15) meV	$T = 150 \dots 1250\text{ K}$	$n_a \approx 5 \cdot 10^{16}\text{ cm}^{-3}$; Hall measurements	79C
	370 meV	$T = 300 \dots 1000\text{ K}$	synthetic diamond; $n_a = 2 \cdot 10^{16}\text{ cm}^{-3}$; conductivity measurements	79B 95B

defects

Important vacancy-related absorption peaks are summarized in the following table.

Designation	Type of defect	Zero phonon line (77 K)		
GR1	neutral vacancy	741.1 nm	1.673 eV	81C
ND1	negative vacancy	393.6 nm	3.150 eV	84L
—	vacancy plus single nitrogen atom	637.3 nm	1.945 eV	81C 82C
H3	vacancy plus two neighboring nitrogen atoms	503.2 nm	2.463 eV	81C 85C
H4	vacancy plus nitrogen cluster (probably four nitrogen atoms)	496.0 nm	2.499 eV	81C 82C
N3	vacancy plus three nitrogen atoms in (111) plane	415.3 nm	2.985 eV	84L

Hydrogen is contained in natural diamonds (concentration 100 ... 1100 ppm) but also plays an important role in the CVD-growth of synthetic diamond films. It serves as a carrier gas for hydrocarbons dissociated near the growth surface, and is itself dissociated to satisfy sp^3 bonds needed for tetrahedral carbon growth [90A]. Ion implantation of diamond with hydrogen creates several specific optical spectra [82G]. This is important when compared to silicon: Here hydrogen not only passivates deep level states associated with the presence of impurities and defects [92P] but is also incorporated in optical defects created by radiation damage.

References to 1.1

- 54R Redfield, A. G.: Phys. Rev. 94 (1954) 526.
- 57D Denning, R. M., Giardini, A. A., Poindexter, E., Slawson, C. B.: Am. Mineral. 42 (1957) 556.
- 57S Skinner, B. J.: Am. Mineral. 42 (1957) 39.
- 62P Philipp, H. R., Taft, E. A.: Phys. Rev. 127 (1962) 159.
- 62R Rauch, C. J.: Proc. Int. Conf. on the Physics of Semiconductors, Exeter 1962 (ed. A. C. Strickland), The Inst. of Phys. and the Phys. Soc., London, p. 276.
- 62V Victor, A. C.: J. Chem. Phys. 36 (1962) 1903.
- 63A Aust, R. B., Drickamer, H. G.: Science 140 (1963) 817.
- 63B Bundy, F. P.: J. Chem. Phys. 38 (1963) 631.
- 63J Jamieson, J. C.: Science 139 (1963) 845.
- 64C Clark, C. D., Dean, P. J., Harns, P. V.: Proc. Roy. Soc. London A 277 (1964) 312.
- 64M Mykolajewycz, R., Kalnajs, J., Smakula, A.: J. Appl. Phys. 35 (1964) 1773.
- 65D Dean, P. J., Lightowers, E. C., Wright, D. R.: Phys. Rev. A 140 (1965) 352.
- 67B1 Bundy, F. P., Kasper, J. S.: J. Chem. Phys. 46 (1967) 3437.
- 67B2 Beil, M. D., Leivo, W. J.: J. Appl. Phys. 38 (1967) 337.
- 67D Denham, P., Lightowers, E. C., Dean, P. J.: Phys. Rev. 161 (1967) 762.
- 67H Hanneman, R. E., Strong, H. M., Bundy, F. P.: Science 155 (1967) 995.
- 67K Konorova, E. A., Shevchenko, S. A.: Sov. Phys. Semicond. (English Transl.) 1 (1967) 299, Fiz. Tekh. Poluprovodn. 1 (1967) 364.
- 67W Warren, J. L., Yarnell, J. L., Dolling, G., Cowley, R. A.: Phys. Rev. 158 (1967) 805.
- 69F Farrer, R.G.: Solid State Commun. 7 (1969) 685
- 70S Solin, S. A., Ramdas, A. K.: Phys. Rev. B1 (1970) 1687.
- 71C Collins, A. T., Williams, A. W. S.: J. Phys. C (Solid State Phys.) 4 (1971) 1789.
- 72M McSkimin, H. J., Andreatch, P., Glynn, P.: J. Appl. Phys. 43 (1972) 985.
- 74C Collins, A. T.: Ind. Diamond Rev. 34 (1974) 131.
- 74D Donahue, J.: The structure of the elements, J. Wiley & Sons, New York 1974.
- 75G Grimsditch, M. H., Ramdas, A. K.: Phys. Rev. B 11 (1975) 3139.
- 75S Slack, G. A., Bartram, S. F.: J. Appl. Phys. 46 (1975) 89.
- 76B Berman, R., Martinez, M.: Diamond Research 1976 (Suppl. Ind. Diamond, Rev.) 7.
- 77D Davies, G.: Chemistry and Physics of Carbon 13 (1977) 1.
- 77F Fontanella, J., Johnston, R. L., Colwell, J. H., Andeen, C.: Appl. Opt. 16 (1977) 2949.
- 78G Grimsditch, M. H., Anastassakis, E., Cardona, M.: Phys. Rev. B 18 (1978) 901.
- 78M Massarani, B., Bourgoin, J. C., Chrenko, R. M.: Phys. Rev. B17 (1978) 1764.
- 79B Bourgoin, J. C., Krynicki, J., Blanchard, B.: Phys. Status Solidi (a) 52 (1979) 293.
- 79C Collins, A. T., Lightowers, E. C.: The Properties of Diamond, Field, J. E. (ed.), London, New York, San Francisco: Academic Press 1979, p. 79.
- 79F Field, J. E. (ed.): The Properties of Diamond, Academic Press, London, New York, San Francisco 1979.
- 79G Grimsditch, M. H., Anastassakis, E., Cardona, M.: Phys. Rev. B 19 (1979) 3240.
- 79H Hanke, W.: Festkörperprobleme (Advances in Solid State Phys.) XIX (ed. J. Treusch), Vieweg, Braunschweig 1979, p. 43.
- 79M Matyoshenko, N. N., Strel'nitskii, V. E., Gusev, V. A.: Pisma Zh. Eksp. Teor. Fiz. 30 (1979) 218; JETP Letters 30 (1979) 199 (Engl. Transl.).
- 79V Vavilov, V. S., Konorova, E. A., Stepanova, E. B., Trukhan, E. M.: Sov. Phys.-Semicond. 13 (1979) 635.
- 80H Himpsel, F. J., van der Veen, J. F., Eastman, D. E.: Phys. Rev. B 22 (1980) 1967.
- 80N Nava, F., Canali, C., Jacoboni, C., Reggiani, L.: Solid State Commun. 33 (1980) 475.
- 81C Collins, A. T.: Inst. Phys. Conf. Ser. (1981) 247.
- 81R Reggiani, L., Bosi, S., Canali, C., Nava, F.: Phys. Rev. B 23 (1981) 3050.
- 82C Collins, A. T.: J. Phys. D18 (1982) 1431.
- 82G Gippius, A.A., Vavilov, V.S., Zaitsev, A.M., Zhakupbekov, B.S.: Physica 116B (1983) 187
- 83R Reggiani, L., Waechter, D., Zukotynski, S.: Phys. Rev. B 28 (1983) 3550.
- 83T Takeda, K., Sakui, K., Taguchi, A., Sakata, M.: J. Phys. C 16 (1983) 729.
- 84C Chelikowsky, J. R., Louie, S. G.: Phys. Rev. B 29 (1984) 3470.
- 84L Lowther, J. E.: J. Phys. Chem. Solids 45 (1984) 127.

- 84P Palatnik, L. S., Guseva, M. B., Babaev, V. G., Savchenko, N. F., Fal'ko, I. I.: Zh. Eksp. Teor. Fiz. 87 (1984) 914; Sov. Phys. JETP 60 (1984) 520 (Engl. Transl.).
- 85C Collins, A. T., Stanley, M.: J. Phys. D18 (1985) 2537.
- 85M Morar, J. F., Himpsel, F. J., Hollinger, G., Hughes, G., Jordan, J. L.: Phys. Rev. Lett. 54 (1985) 1960.
- 88A Angus, J. C., Hayman, C. C.: Science 241 (1988) 913.
- 89F Frenklach, M., Kematick, R., Huang, D., Howard, W., Spear, K. E., Phelps, A. W., Koba, R.: J. Appl. Phys. 66 (1989) 395.
- 90A Anthony, T.R.: Vacuum 41 (1990) 1356
- 90Y Yarbrough, W. A., Messier, R.: Science 247 (1990) 688.
- 91E Erskine, D. J., Nellis, W. J.: Nature 349 (1991) 317.
- 91H Hirai, H., Kondo, K. I.: Science 253 (1991) 772.
- 92P Pearton, S.J., Corbett, J.W., Stavola, M.: *Hydrogen in Crystalline Semiconductors*, Springer, Berlin/Heidelberg (1992)
- 94W Woods, G.S.: "The A aggregate of nitrogen in diamond", in Ref. [94D1], p. 88
- 95B Borst, T.H., Weis, O.: Diam. Rel. Mater. 4 (1995) 948
- 97A Aleksei, A. E., Baidakova, M. V., Vul', A. Yu., Davydov, V. Yu., Pevtsova, Yu. A.: Fiz. Tverd.
- 97R Ristein, J., Stein, W., Ley, L.: Phys. Rev. Lett. 78 (1997) 1803.
- 98Z Zouboulis, E. S., Grimsditch, M., Ramdas, A. K., Rodriguez, S.: Phys. Rev. B57 (1998) 2889.

Figures to 1.1

Fig. 1.0.2

The diamond lattice. The elementary cubes of the two face-centered cubic lattices are shown.

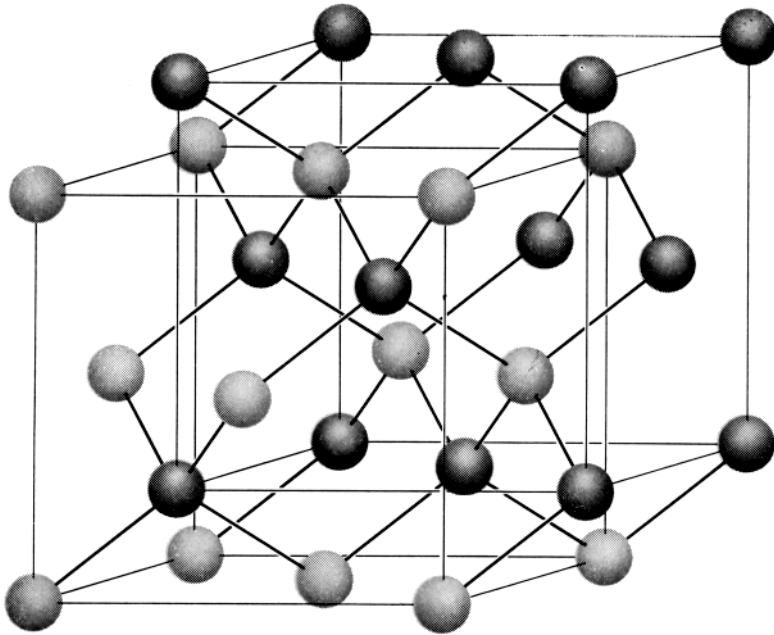


Fig. 1.0.6

Brillouin zone of the diamond lattice

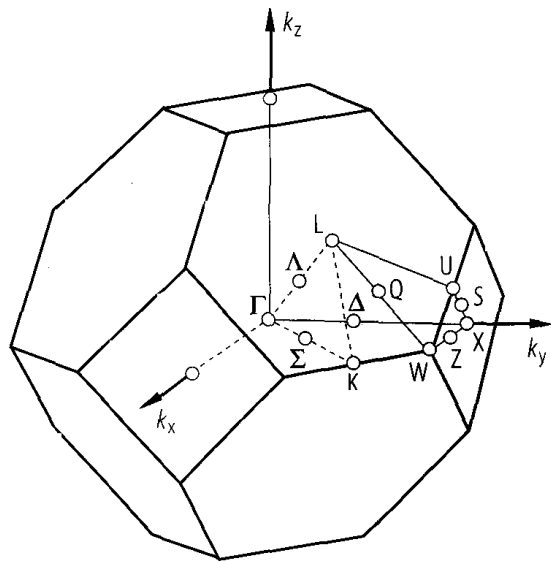


Fig. 1.0.8

Diamond. Band structure calculated by an ab initio LCAO method [84C].

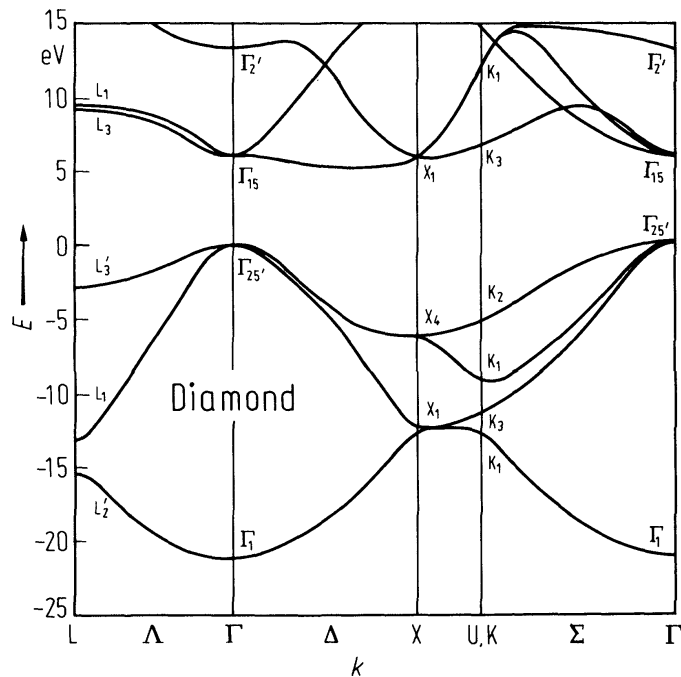


Fig. 1.1.1

Diamond. Indirect gap vs. temperature [64C].

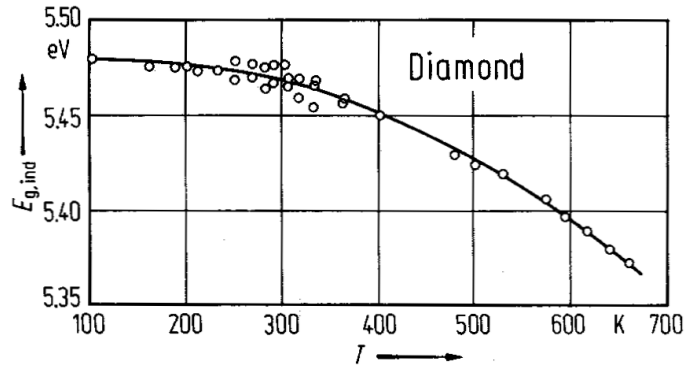


Fig. 1.1.2

Diamond. (a) Lattice parameter vs. temperature [57S], (b) linear thermal expansion coefficient vs. temperature [75S].

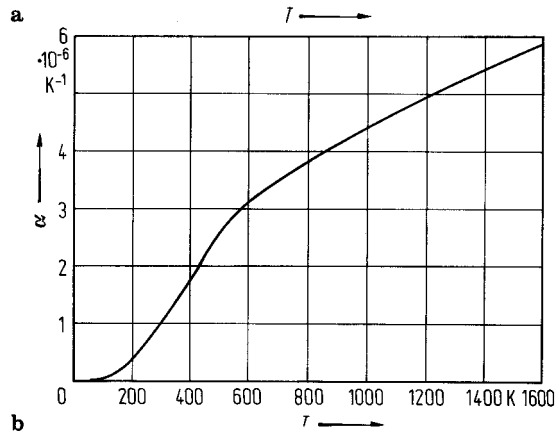
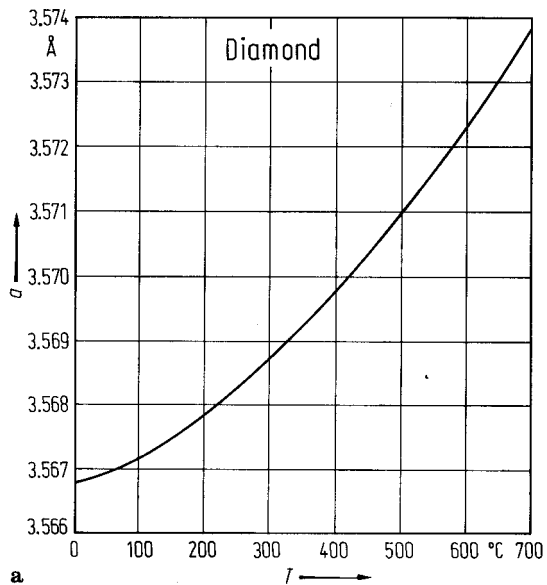


Fig. 1.1.3

Diamond. Phonon dispersion curves. Experimental data from neutron scattering, full curves: shell model calculation [67W].

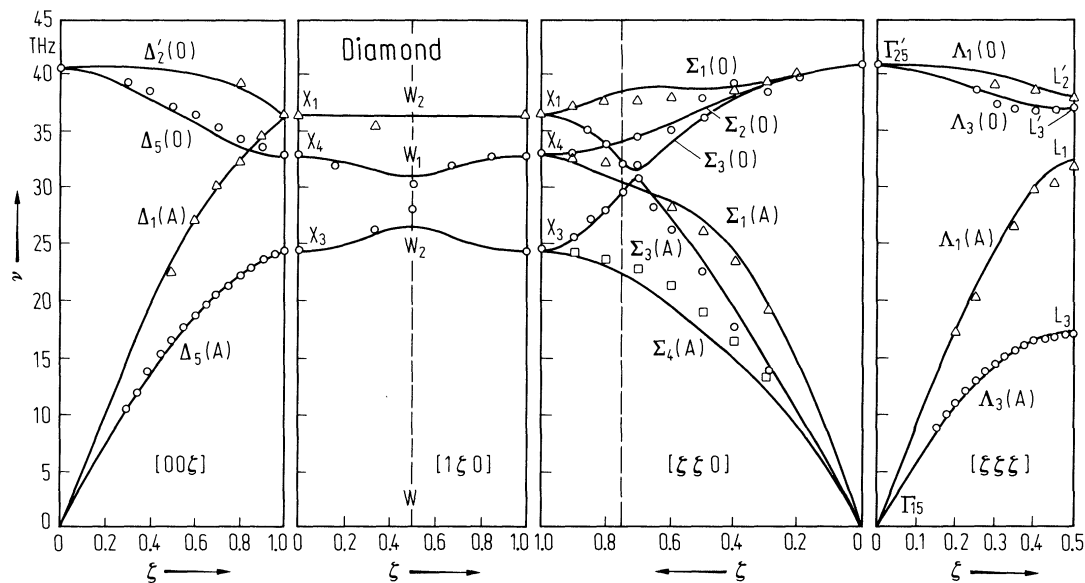


Fig. 1.1.4

Diamond. Reduced elastic moduli ($c_{lm}(T)/c_{lm}(25^{\circ}\text{C})$) vs. temperature [72M].

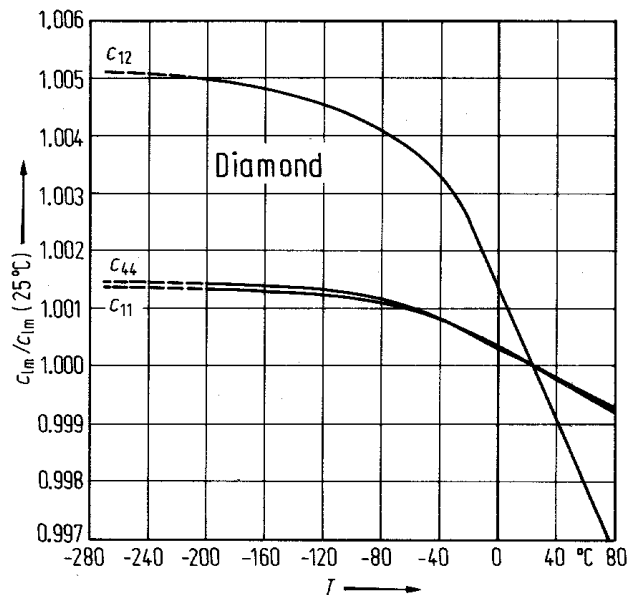


Fig. 1.1.5

Diamond. Molar heat capacity vs. temperature [62V].

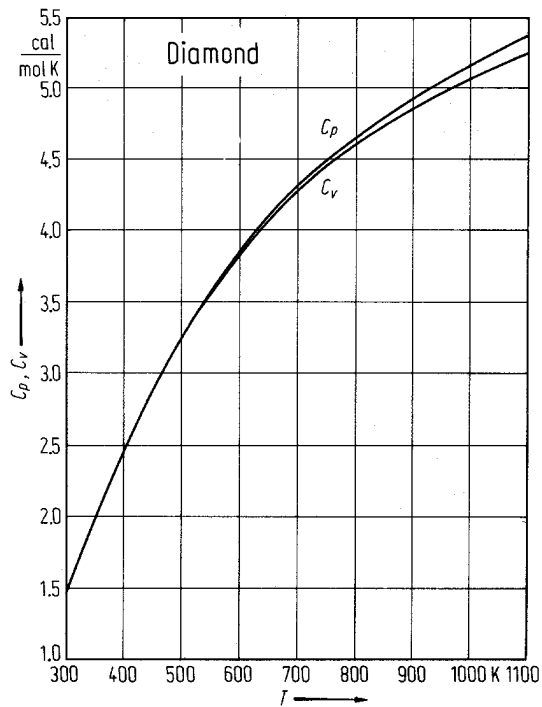


Fig. 1.1.6

Diamond. Resistivity vs. reciprocal temperature for a type IIb diamond [71C].

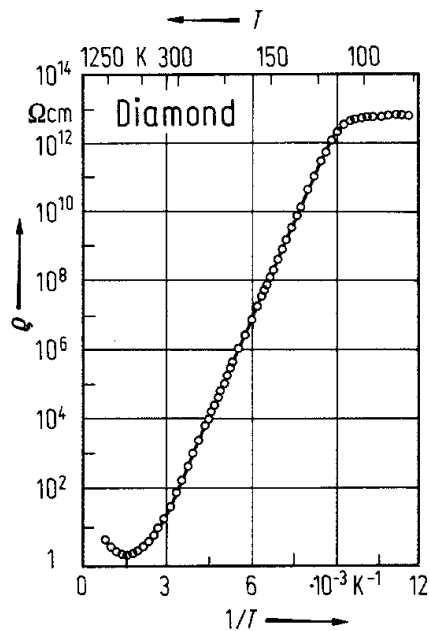


Fig. 1.1.7

Diamond. Electron mobility vs. temperature. Open circles: drift mobility data of [80N], full triangles and circles: Hall mobility data of [54R] and [67K], respectively. Continuous curve: theoretical drift mobility [80N].

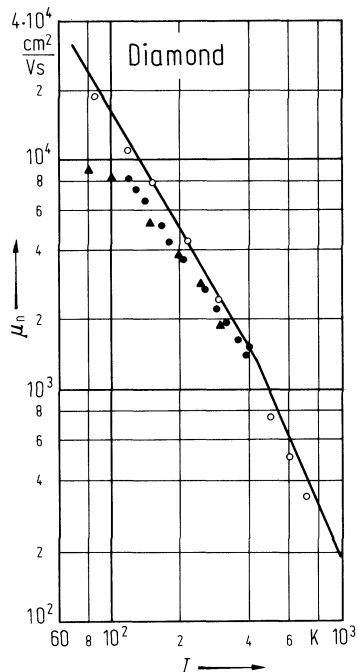


Fig. 1.1.8

Diamond. Hole mobility vs. temperature. Open circles: drift mobility data from [81R], full circles and triangles: Hall mobility data of [67K] and [65D], respectively. Solid and dashed curves: calculated drift and Hall mobilities, respectively [83R].

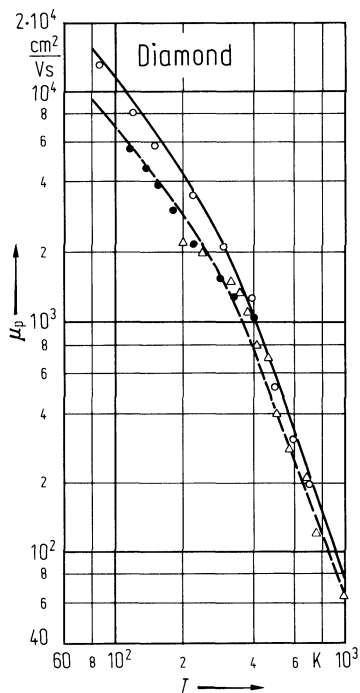


Fig. 1.1.9

Diamond. Thermal conductivity vs. temperature for three type Ia diamonds [76B].

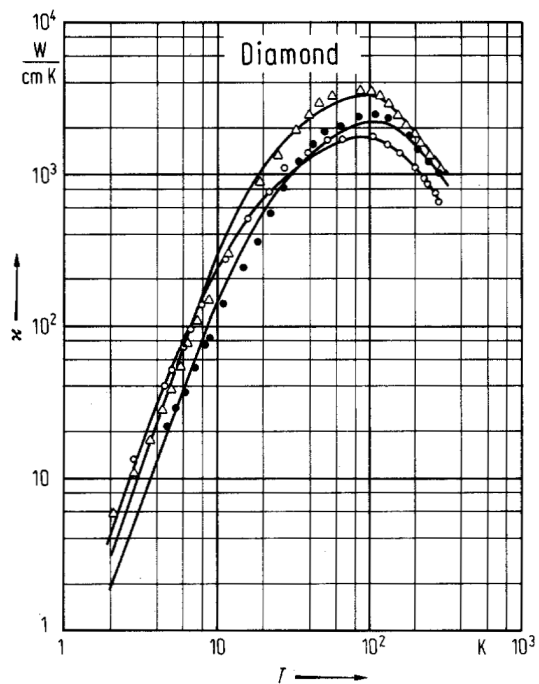


Fig. 1.1.10

Diamond. Elastooptical constants vs. wavelength [79G].

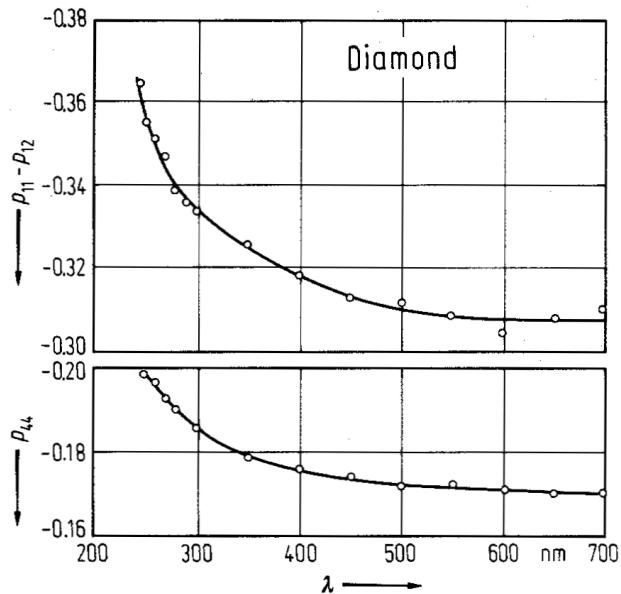


Fig. 1.1.11

Diamond. Absorption coefficient vs. photon energy and wavenumber for a type IaA diamond [77D].

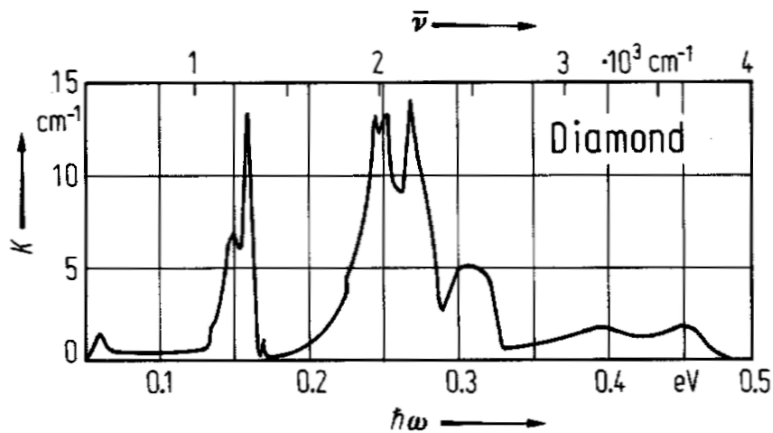
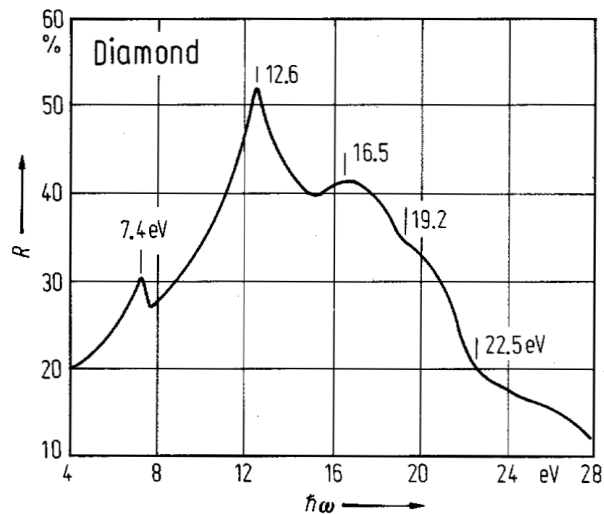


Fig. 1.1.12

Diamond. Ultraviolet reflectivity vs. photon energy for a type IIa diamond [64W].



1.2 Silicon, Si

Crystal structure

The element silicon crystallizes under ambient conditions in the diamond lattice (space group: cubic $O_h^7 - Fd3m$, Fig. 1.0.2).

high pressure phases

The phase sequence under pressure is presently believed to be Si-I (diamond structure) \rightarrow Si-II (β -tin structure, at about 10 GPa) \rightarrow Imma (Si-XI according to [93M, 94M, 96M]), previously thought to be a mixed Si-II and Si-V phase [84H, 94M] \rightarrow Si-V (simple hexagonal structure, at about 15 GPa [84O2, 84H] \rightarrow Si-VI (at 38 GPa, space group Cmca) \rightarrow Si-VII (hexagonal close-packed, at about 40 GPa [84O2, 86H, 87D, 90D]) \rightarrow face-centered cubic Si-X (at about 80 GPa, notation according to [93M]) [87D, 90D]. A rhombohedral phase (R8) was observed at 8.2 GPa and a mixture of R8 and BC8 phases at 3.2 GPa [94C].

The diamond and β -tin phases coexist between 8 and 16 GPa [78D1], between 11.2(2) and 12.5(2) GPa [84H], between 11.7 GPa and 13.4 GPa [94M]. The Si-II and Si-V phases coexist between 13.2(3) and 16.4(5) GPa upon pressurising and between 14.5 and 11 GPa upon depressurising; phase Si-V is stable up to at least 25 GPa [84H, 84S1]. The Si-VI phase persists up to at least 43 GPa [90D]; the Si-V (sh) and Si-VI (Cmca) phases coexist between 38 and 40 GPa [99H], and the Si-VI (Cmca) and Si-VII (hcp) modifications coexist between 40 and 49 GPa [99H].

Electronic properties

band structure : Fig. 1.0.9, Brillouin zone: Fig. 1.0.6, density of states in valence and conduction band: Fig. 1.2.1.

The conduction band is characterized by six equivalent minima along the $[100]$ axes of the Brillouin zone located at about $k_0 = 0.85$ ($2\pi/a$) (symmetry Δ_1). The surfaces of constant energy are ellipsoids of revolution with major axes along $[100]$. Higher minima are located at Γ and along the $[111]$ axes about 1 eV above the $[100]$ minima. The valence band maximum is situated at Γ (symmetry type Γ_8^+), the light and heavy hole bands being degenerate at this point. Both bands show warping. The third (spin-orbit split off) band has Γ_7^+ symmetry. The spin-orbit splitting energy at Γ is small compared to most interband energy differences. Thus, spin-orbit interaction is mostly neglected in band structure calculations (as in Fig. 1.0.9) and the notation of the single group is used to denote the symmetry of a band state.

energies of symmetry points of the band structure (relative to the top of the valence band $E(\Gamma_{25'v})$)

$E(\Gamma_{1v})$	– 12.34 eV (– 12.5(6) eV)	theoretical data:
$E(\Gamma_{15c})$	3.50 eV (3.34 ... 3.36 eV)	localized atomic orbital calculation
$E(\Gamma_{2'c})$	4.09 eV (4.15(5) eV)	[85S], Fig. 1.0.9
$E(X_{1v})$	– 7.75 eV	experimental data (in brackets):
$E(X_{4v})$	– 2.89 eV (– 2.9 eV)	from a compilation in [83M], mostly
$E(X_{1c})$	1.12 eV (1.13 eV)	photoemission data
$E(L_{2'v})$	– 9.62 eV (– 9.3(4) eV)	
$E(L_{1v})$	– 7.01 eV (– 6.8(2) eV)	
$E(L_{3'v})$	– 1.25 eV (– 1.2(2) eV)	
$E(L_{1c})$	2.29 eV (2.04(6) eV)	
$E(L_{3c})$	4.34 eV (3.9(1) eV)	
$E(K_{1v})$	– 8.15 eV	
$E(K_{3v})$	– 7.16 eV	
$E(K_{1v})$	– 4.41 eV	
$E(K_{2v})$	– 2.47 eV	
$E(K_{3c})$	1.70 eV	
$E(K_{1c})$	4.79 eV	

indirect energy gap

$E_{g,ind}(\Gamma_{25'v}-\Delta_{1c})$	1.1700 eV	$T = 0$ K, extrapol.	wavelength modulated transmission	74B
	1.1242 eV	$T = 300$ K		
$E_{g,th}$	1.205 eV	$T = 0$ K, extrapol.	linear extrapolation from temperature dependence above 200 K	67B

Temperature dependence: $E_{g,ind} = A + BT + CT^2$ with $A = 1.170$ eV, $B = 1.059 \cdot 10^{-5}$ eV/K, $C = -6.05 \cdot 10^{-7}$ eV/K² up to 300 K [74B], see also Fig. 1.2.2.

exciton ground state

$E(1S)$	1.1552(3) eV	$T = 1.8$ K	wavelength modulated absorption	70S
$E(1S, \Delta_6)$	0.29(5) meV	$T = 77$ K	valley-anisotropy splitting from wavelength modulated absorption with uniaxial stress, extrapolated to zero stress	77C
$E(1S, \Delta_7)$	0.31(3) meV	$T = 4.2$ K	free exciton luminescence	78H
$E(1S_{1/2}^{3/2}(\Delta_6))$	14.12 meV		calculated binding energy of the	77L1
$E(1S_{3/2}^{3/2}(\Delta_7))$	14.66 meV		ground state components (valley-anisotropy splitting) including valence band degeneracy and conduction band anisotropy	

excited exciton states (from $1S_{3/2}^{3/2}$)

$E(2S)$	10.7(3) meV	$T = 1.8$ K	wavelength modulated absorption, valley-anisotropy and exchange splitting not resolved	70S
$E(2P)$	10.2 meV	$T \leq 13$ K	$2P_{3/2}^{3/2}, (2P_{1/2}^{3/2}, 2P_{1/2}^{5/2})$	78T
	11.4 meV		$(2P_{1/2}^{3/2}, 2P_{1/2}^{5/2}), 2P_{5/2}^{5/2}$	
	12.0 meV		$2P_{3/2}^{5/2}, 2P_{1/2}^{1/2}$	

direct gap

$E_{g,dir}$	4.185(10) eV	$T = 4.2$ K	electroreflection	72A
$(\Gamma_{25'v} - \Gamma_{2'c})$	4.135 eV	$T = 190$ K		

At higher temperatures $E_{g,dir} (= E_0)$ cannot be optically resolved from the dominating E_2 critical point. Temperature dependence, see Fig. 1.2.3.

spin-orbit splitting energies

$\Delta_0(\Gamma_{25'v})$	0.0441(3) eV	$T = 1.8$ K	wavelength modulated absorption	74N
$\Delta(\Gamma_{15c})$	0.03...0.04 eV		calculated	71W
$\Delta(L_{3'v})$	0.03 eV			
$\Delta(L_{3c})$	0...0.2 eV			

second indirect gap

$E_{g,ind}$	1.650(10) eV		optical absorption	74F
$(\Gamma_{25'v} - L_{1c})$				

higher band-band transitions (critical point energies)

E'_0	3.378 eV	$T = 10$ K	ellipsometry	83J
--------	----------	------------	--------------	-----

Direct transitions at Γ to higher conduction band. Nearly degenerate with the E_1 critical point, but different temperature shift. E'_0 and E_1 cannot clearly be resolved by experiment.

E_1	3.46(15) eV	$T = 10$ K	electroreflectance	78D2
-------	-------------	------------	--------------------	------

Contributions mainly from transitions along the Λ -axes and at L.

$E_1(\Lambda_{3v}-\Lambda_{1c}),$ ($L_{3v}-L_{1c}$)	3.495 eV	$T = 77$ K	electroreflectance	77K
--	----------	------------	--------------------	-----

$E'_1(\Lambda_{3v}-\Lambda_{3c})$	5.50 eV	$T = 5$ K	wavelength modulated reflectance,	70Z
	5.45 eV	$T = 10$ K	electroreflectance	78D2

$E_2(1)(\Sigma_{2v}-\Sigma_{3c})$	4.336 eV	$T = 90$ K	electroreflectance, M_1 critical point	77K
-----------------------------------	----------	------------	--	-----

$E_2(2)$	4.459 eV			
----------	----------	--	--	--

$E_2(3)(\Delta_{5v}-\Delta_{1c})$	4.598 eV			
-----------------------------------	----------	--	--	--

E_2	4.330 eV	$T = 10$ K	ellipsometry	83J
-------	----------	------------	--------------	-----

Contributions to E_2 from various transitions along the Σ and Δ axes.

conduction band, effective masses

$m_{n\perp}$	0.1905(1) m_0	$T = 1.26$ K	cyclotron resonance with uniaxial stress;	65H
$m_{n\parallel}$	0.9163(4) m_0		temperature dependence of the	
			transverse mass, Fig. 1.2.4	
$m_{n,ds}$	1.062 m_0	$T = 4.2$ K	calculated from cyclotron resonance	67B
$m_{n,opt}$	0.43 m_0	$T = 297$ K;	infrared reflectance	60C
		$n = 6.5 \cdot 10^{19} \text{ cm}^{-3}$		

position of conduction band minima

k_{\min}/k_0	0.85(3)		electron spin resonance	59F1
----------------	---------	--	-------------------------	------

g-factor of electrons

g_c	1.99893(28)		electron spin resonance	66K
-------	-------------	--	-------------------------	-----

valence band, effective masses

$m_{p,h}$	0.537 m_0	$T = 4.2$ K	calculated from cyclotron resonance	67B
$m_{p,l}$	0.153 m_0		results	
m_{so}	0.234 m_0			
$m_{p,ds}$	0.591 m_0			

In non-parabolic bands the density of states mass obtained through a calculation of the carrier concentration becomes temperature dependent, whereas the mass obtained directly from a calculation of the density of states becomes energy dependent. The former is the weighted thermal average of the latter: $m_p^{3/2}(T) = \langle m_{p,ds}^{3/2}(E) \rangle$. For the temperature and energy dependences of both masses, see Fig. 1.2.5.

valence band parameters

A	-4.27(2)		cyclotron resonance	65B
B	-0.63(8)			
$ C $	4.93(15)			

Lattice properties

lattice parameter

a	0.543102018(34) nm	$T = 295.7$ K	high purity single crystal measured in vacuum temperature dependence, see Fig. 1.2.6	82B
-----	--------------------	---------------	--	-----

temperature dependence of the lattice parameter: $a(T)$ in high-purity material can be approximated in the range 20...800°C by $a(T) = 5.4304 + 1.8138 \cdot 10^{-5}(T - 298.15 \text{ K}) + 1.542 \cdot 10^{-9}(T - 298.15 \text{ K})^2$ [73Y].

linear thermal expansion coefficient

α	$2.92(6) \cdot 10^{-6} \text{ K}^{-1}$	$T = 293$ K	recommended	88K
----------	--	-------------	-------------	-----

Temperature dependence: see Fig. 1.2.7. The data of Fig. 1.2.7 can be approximated in the temperature range 120...1500 K by the formula:

$$\alpha(T) = (3.725 [1 - \exp(-5.88 \cdot 10^{-3} [T - 124])] + 5.548 \cdot 10^{-4} T) \cdot 10^{-6} \text{ K}^{-1} \text{ (} T \text{ in K)}.$$

density

d	2.329002 g cm ⁻³	$T = 25^\circ\text{C}$, high-purity crystal	hydrostatic weighing	64H
-----	-----------------------------	---	----------------------	-----

melting point

T_m	1687 K		recommended	86D
	1685(2) K			73H
dT_m/dp	$-0.0038 \text{ K atm}^{-1}$			67K

phonon dispersion curves : Fig. 1.2.8, Brillouin zone: Fig. 1.0.6.

one-phonon density of states : Fig. 1.2.9

phonon frequencies

$\nu_{\text{LTO}}(\Gamma_{25'})$	15.53(23) THz	$T = 296$ K	inelastic neutron scattering	63D
$\nu_{\text{TA}}(\text{X}_3)$	4.49(6) THz			
$\nu_{\text{LAO}}(\text{X}_1)$	12.32(20) THz			
$\nu_{\text{TO}}(\text{X}_4)$	13.90(30) THz			
$\nu_{\text{TA}}(\text{L}'_3)$	3.43(5) THz			
$\nu_{\text{LA}}(\text{L}_2)$	11.35(30) THz			
$\nu_{\text{LO}}(\text{L}_1)$	12.60(32) THz			
$\nu_{\text{TO}}(\text{L}_3)$	14.68(30) THz			

sound velocities

v_1	$8.4796 \cdot 10^5 \text{ cm s}^{-1}$	$T = 77$ K	v_1 : long./[001]/[001],	64M
v_2	$5.8694 \cdot 10^5 \text{ cm s}^{-1}$	$\rho = 410 \text{ } \Omega\text{cm}$	v_2 : shear/[001]/[110],	
v_3	$9.1828 \cdot 10^5 \text{ cm s}^{-1}$		v_3 : long./[110]/[110],	
v_4	$5.8693 \cdot 10^5 \text{ cm s}^{-1}$		v_4 : shear/[110]/[001],	
v_5	$4.6929 \cdot 10^5 \text{ cm s}^{-1}$		v_5 : shear/[110]/[1 $\bar{1}$ 0]	
v_3	$9.117 \cdot 10^5 \text{ cm s}^{-1}$	$T = 298$ K	from ultrasound	68E
v_4	$5.825 \cdot 10^5 \text{ cm s}^{-1}$	$\rho = 0.22 \text{ } \Omega\text{cm}$	measurements (30 MHz)	
v_5	$4.665 \cdot 10^5 \text{ cm s}^{-1}$			

For the temperature dependence of v_3 , v_4 , and v_5 , see also Figs. 1.2.10a...c.

second order elastic moduli

c_{11}	$16.577 \cdot 10^{11} \text{ dyn cm}^{-2}$	$T = 298$ K	p-type sample, from ultrasound	64M
c_{12}	$6.393 \cdot 10^{11} \text{ dyn cm}^{-2}$	$\rho = 410 \text{ } \Omega\text{cm}$	measurements (20/40 MHz),	
c_{44}	$7.962 \cdot 10^{11} \text{ dyn cm}^{-2}$			

Temperature dependence: Figs. 1.2.11a...c.

third order elastic moduli

c_{111}	$-8.34(11) \cdot 10^{12} \text{ dyn cm}^{-2}$	$T = 298 \text{ K}$	ultrasonic harmonic generation	81P
c_{112}	$-5.31(32) \cdot 10^{12} \text{ dyn cm}^{-2}$		combined with pressure derivative	
c_{144}	$-0.95(24) \cdot 10^{12} \text{ dyn cm}^{-2}$		of elastic constants	
c_{123}	$-0.02(18) \cdot 10^{12} \text{ dyn cm}^{-2}$		temperature dependence: Fig. 1.2.12	
c_{166}	$-2.96(12) \cdot 10^{12} \text{ dyn cm}^{-2}$			
c_{456}	$-0.074(22) \cdot 10^{12} \text{ dyn cm}^{-2}$			

internal strain parameter (bond bending parameter, describing relative movement of sublattices under strain)

ζ	0.74(4)	X-ray diffraction under uniaxial stress	82A
---------	---------	---	-----

Young's modulus, torsion modulus : see Fig. 1.2.13

bulk modulus

B_S	$0.9788 \cdot 10^{12} \text{ dyn cm}^{-2}$	$T = 298 \text{ K}$		
		$\rho = 410 \text{ } \Omega \text{ cm}$	p-type, calculated from	64M
	$0.9783 \cdot 10^{12} \text{ dyn cm}^{-2}$	$\rho = 159 \text{ } \Omega \text{ cm}$	n-type, ultrasound measurements	67H

For temperature dependence below 300 K, see Fig. 1.2.14

Debye temperature

$\Theta_D(0)$	636 K	heat capacity, for $\Theta_D(T)$, see Fig. 1.2.15	59K
---------------	-------	--	-----

heat capacity

C_p	0.1650 cal/g deg	$T = 273 \text{ K}$	calorimetric measurements;	63S
	0.2345 cal/g deg	$T = 1373 \text{ K}$	temperature dependence: Fig. 1.2.16	

Transport properties

Contributions to the electric transport are exclusively made by electrons in the [100]-conduction band minima, and holes in the two uppermost (heavy and light hole) valence bands. The impurity content of the specimen determines which scattering process dominates the mobility. Only samples with impurity concentrations below 10^{12} cm^{-3} are governed by pure lattice scattering down to temperatures of about 10 K (n-type) or 50 K (p-type), respectively. Higher impurity concentrations lead to deviations from the lattice mobility at appropriately higher temperatures. For electrons the lattice mobility below 50 K is dominated by deformation potential coupling to acoustic phonons. At higher temperatures, intervalley scattering between the six equivalent minima of the conduction band through mixed LA + TO phonons and LO phonons is added to the intravalley process, modifying the familiar $T^{-1.5}$ dependence of the acoustic mode dominated mobility to $T^{-2.42}$. At $T < 100 \text{ K}$, the lattice mobility of holes is dominated by acoustic scattering, but does not follow the $T^{-1.5}$ law due to the non-parabolicity of the valence bands. The proportionality of μ_p to $T^{-2.2}$ around room temperature is a consequence of optical phonon scattering.

intrinsic electrical conductivity

σ_i	$3.16 \cdot 10^{-2} \text{ } \Omega^{-1} \text{ cm}^{-1}$	$T = 300 \text{ K}$	temperature dependence, see Fig. 1.2.17	54M
------------	---	---------------------	---	-----

The intrinsic conductivity up to 1273 K is given by the phenomenological expression

$$\log_{10} \sigma_i = 4.247 - 2.924 \cdot 10^3 T^{-1} \quad (\sigma_i \text{ in } \Omega^{-1} \text{ cm}^{-1}, T \text{ in K, agreement to Fig. 1.2.17 better than } \pm 5 \% [68F])$$

intrinsic carrier concentration

n_i	$1.02 \cdot 10^{10} \text{ cm}^{-3}$	$T = 300 \text{ K}$		77W
-------	--------------------------------------	---------------------	--	-----

Phenomenological expression for n_i :

$$200 \text{ K} < T < 500 \text{ K:} \quad n_i(T) = 5.71 \cdot 10^{19} (T/300)^{2.365} \exp(-6733/T) \quad (n_i \text{ in } \text{cm}^{-3}, T \text{ in K})$$

electron mobility

μ_n	1450 cm ² /Vs	$T = 300$ K, $n_d =$ $2.6 \cdot 10^{15}$ cm ⁻³	lattice scattering mobility determined by subtracting computed ionized impurity scattering rate from measured overall scattering rate.	54M
---------	--------------------------	---	---	-----

Around RT μ_n can be expressed by $\mu_n = 1.43 \cdot 10^9 T^{-2.42}$ cm²/Vs (T in K) [54M], see also Fig. 1.2.18.

electron drift velocity

The expression $v_{dr,n} = v_m(E/E_c)/(1+(E/E_c)^{\beta'})^{1/\beta'}$ cm/s fits experimental results if the field is applied along a $[111]$ -direction and $T \geq 250$ K [77J]. $v_m = 1.53 \cdot 10^9 T^{-0.87}$ cm/s, $E_c = 1.01 \cdot T^{1.55}$ V/cm, $\beta' = 2.57 \cdot 10^{-2} T^{0.66}$ (T in K).

electron diffusion coefficient

$D_{n\parallel}(E)$	≈ 35 cm ² /s	$T = 300$ K, $E < 10^3$ V/cm	at higher fields, $D_{n\parallel}$ begins to show anisotropic properties and the Einstein relation loses its validity	77J
---------------------	---------------------------------	---------------------------------	---	-----

hole mobility

$\mu_{H,p}$	370 cm ² /Vs $2 \cdot 10^5$ cm ² /Vs	$T = 300$ K $T = 20$ K	ultrapure sample see Fig. 1.2.19(b)	82H, 83S1, 83S2, 83S3
$\mu_{c,p}$	505 cm ² /Vs $1.6 \cdot 10^5$ cm ² /Vs	$T = 300$ K $T = 20$ K	see Fig. 1.2.19(a)	

hole drift velocity

Above 250 K experimental results can be fitted by the same expression as for the electron drift mobility with the following parameters: $v_m = 1.62 \cdot 10^8 T^{-0.52}$ cm/s, $E_c = 1.24 T^{1.68}$ V/cm, $\beta' = 0.46 \cdot T^{0.17}$ (T in K) [77J].

piezoresistance coefficients

n-type material				
π_{11}	$-102.2 \cdot 10^{-12}$ cm ² /dyn	$T = 300$ K	resistivity measurements with n-type Si under uniaxial tensile stress of $10^7 \dots 10^8$ dyn/cm ²	54S
$(\pi_{11} + \pi_{12} + \pi_{44})/2$	$-31.2 \cdot 10^{-12}$ cm ² /dyn	$\rho = 11.7 \Omega\text{cm}$		
π_{44}	$-13.6 \cdot 10^{-12}$ cm ² /dyn			
p-type material				
π_{11}	$6.6 \cdot 10^{-12}$ cm ² /dyn	$T = 300$ K		
π_{12}	$-1.1 \cdot 10^{-12}$ cm ² /dyn	$\rho = 7.8 \Omega\text{cm}$		
$(\pi_{11} + \pi_{12} + \pi_{44})/2$	$71.8 \cdot 10^{-12}$ cm ² /dyn			

elastoresistance coefficients

n-type material				
m_{44}	- 10.8	$T = 300$ K,	Calculated from the piezoresistance coefficients with the aid of the elastic constant tensor. For $(m_{11}+2m_{12})/3$ adiabatic values are cited here; isothermal quantities differ slightly	54S
$(m_{11}-m_{12})/2$	- 79.5	$\rho = 11.7 \Omega\text{cm}$		
$(m_{11}+2m_{12})/3$	4.6			
p-type material				
m_{44}	110.0	$T=300$ K,		
$(m_{11}-m_{12})/2$	3.9	$\rho = 7.8 \Omega \text{ cm}$		
$(m_{11}+2m_{12})/3$	4.4			

Seebeck coefficient (thermoelectric power) (absolute values)

S_n	$0.3...1.6 \cdot 10^{-3}$ V/K	$T = 300$ K, $n_d = 2.7 \cdot 10^{19}...$ $2.75 \cdot 10^{14}$ cm $^{-3}$	For dependence of S on impurity concentration and temperature in n-type Si, see Fig. 1.2.20, in p-type Si, Fig. 1.2.21	55G
S_p	$0.5...1.5 \cdot 10^{-3}$ V/K	$T = 300$ K, $n_a = 1.5 \cdot 10^{19}$ $... 9.2 \cdot 10^{14}$ cm $^{-3}$		55G

thermal conductivity

κ_L	1.56 W cm $^{-1}$ K $^{-1}$	$T = 300$ K	lattice contribution, for temperature dependence, see Fig. 1.2.22	64G
------------	-------------------------------	-------------	--	-----

κ_L^{-1} can be represented by a temperature dependence $a + bT + cT^2$ with
 $a = 0.03$ cm KW $^{-1}$, $b = 1.56 \cdot 10^{-3}$ cm W $^{-1}$, $c = 1.65 \cdot 10^{-6}$ cm K $^{-1}$ W $^{-1}$ 64G

Optical properties

optical constants

real and imaginary parts of the dielectric constant measured by spectroscopical ellipsometry, n , k , R , K calculated from these data [83A]. See also Figs. 1.2.23 and 1.2.25.

$h\nu$ [eV]	ϵ_1	ϵ_2	n	k	R	K [10^3 cm $^{-1}$]
1.5	13.488	0.038	3.673	0.005	0.327	0.78
2.0	15.254	0.172	3.906	0.022	0.351	4.47
2.5	18.661	0.630	4.320	0.073	0.390	18.48
3.0	27.197	2.807	5.222	0.269	0.461	81.73
3.5	22.394	33.818	5.610	3.014	0.575	1069.19
4.0	12.240	35.939	5.010	3.586	0.591	1454.11
4.5	− 19.815	24.919	2.452	5.082	0.740	2317.99
5.0	− 10.24 2	11.195	1.570	3.565	0.675	1806.67
5.5	− 9.106	8.846	1.340	3.302	0.673	1840.59
6.0	− 7.443	5.877	1.010	2.909	0.677	1769.27

refractive index

The refractive index in the range 2.4...25 μ m can be approximated by the dispersion formula $n = A + BL + CL^2 + D\lambda^2 + E\lambda^4$ (λ in μ m) with $L = (\lambda - 0.028)^{-1}$ μ m $^{-1}$, $A = 3.41983$, $B = 0.159906$ μ m, $C = - 0.123109$ μ m 2 , $D = 1.26878 \cdot 10^{-6}$ μ m $^{-2}$, $E = - 1.95104 \cdot 10^{-9}$ μ m $^{-4}$ [80E]. See also Fig. 1.2.24.

absorption coefficient

(fitting parameters K_0 and T_0 in the formula $K = K_0 \exp(T/T_0)$, data for eleven commonly used laser wavelengths), from [82J]. See also Fig. 1.2.29.

K_0 [10^3 cm $^{-1}$]	T_0 [K]	λ [nm]	laser-type
1.34(29)	427(82)	694	Ruby
2.08 (32)	447(62)	633	HeNe
5.02(49)	430(39)	532	Nd:YAG doubled
6.28 (55)	433(39)	514	Argon ion
9.07 (66)	438(33)	488	Argon ion
9.31(67)	434(31)	485	Nitrogen pumped dye
14.5 (8)	429(34)	458	Argon pumped
55.1(15)	420(69)	405	Nitrogen pumped dye
1090(1)	8700(5320)	355	Nd:YAG triple
1130(1)	25200(25100)	337	Excimer
1430(1)	4680(1330)	308	Excimer

reflectance

In the temperature range 1100...1400°C *R* the reflectance can be approximated by $R = 30.37 + 1 \cdot 10^{-2}T - 1.3 \cdot 10^{-5}T^2 + 9.19 \cdot 10^{-10}T^3 + 5.65 \cdot 10^{-12}T^4$ (*R* in %, *T* in °C) [81L].

dielectric constant

$\epsilon(\infty)$	11.97	$T = 300$ K	capacitance measurement	83S4
ϵ	12.1	$T = 4.2$ K	$\nu = 750$ MHz, capacitance bridge	66R
	11.9	$T = 300$ K		
$(1/\epsilon_1)(d\epsilon_1/dT)$	$7.8 \cdot 10^{-5}$ K ⁻¹	$T = 77 \dots 400$ K	$\lambda = 3$ μm, optical interference	59C

piezooptic constants

$(\pi_{11}-\pi_{12})_r$	$11.1(7) \cdot 10^{-14}$ dyn ⁻¹ cm ²	$T = 300$ K, $h\nu = 1.92$ eV	Raman scattering	78C
$(\pi_{44})_r$	$7.2(4) \cdot 10^{-14}$ dyn ⁻¹ cm ²	$h\nu = 1.64$ eV		

third order susceptibilities

The second order susceptibilities are zero as a result of inversion symmetry. The third order susceptibility has two independent components

$ \chi_{1111} $	$6(3) \cdot 10^{-12}$ esu	CO ₂ -laser,	optical third order mixing	69W
	$5 \cdot 10^{-12}$ esu	$T = 300$ K	calculated	70V
$ \chi_{1122} $	$3(1) \cdot 10^{-12}$ esu	CO ₂ -laser,	optical third order mixing	69W
		$T = 300$ K		

Further properties

thermodynamic functions

<i>T</i> [K]	C_p^0 [J mol ⁻¹ K ⁻¹]	$H^0_T - H^0_{298.15}$ [J mol ⁻¹]	S^0 [J mol ⁻¹ K ⁻¹]	$-(G^0 - H^0_{298.15})/T$ [J mol ⁻¹ K ⁻¹]	86D
298.15	20.007	0	0.000	18.806	
300	20.006	37	0.124	18.806	
400	22.258	2164	6.228	19.624	
500	23.588	4462	11.349	21.232	
600	24.420	6865	15.728	23.093	
700	25.050	9339	19.541	25.006	
800	25.608	11872	22.923	26.889	
900	26.110	14459	25.969	28.710	
1000	26.569	17093	28.744	30.457	
1100	26.988	19771	31.296	32.128	
1200	27.360	22489	33.661	33.726	
1300	27.707	25242	35.864	35.253	
1400	28.045	28030	37.930	36.715	
1500	28.372	30851	39.876	38.115	
1600	28.674	33703	41.717	39.458	
1687	28.930	36210	43.245	40.587	
1687	27.200	86460	73.032	40.587	
1700	27.200	86814	73.241	40.980	
1800	27.200	89534	74.796	43.861	
1900	27.200	92254	76.266	46.518	
2000	27.200	94974	77.661	48.981	
2200	27.200	100414	80.254	53.417	
2400	27.200	105854	82.620	57.321	
2600	27.200	111294	84.798	60.798	
2800	27.200	116734	86.813	63.929	
3000	27.200	122174	88.960	66.771	
3200	27.200	127614	90.445	69.372	
3400	27.200	133054	92.094	71.767	
3500	27.200	135774	92.883	72.896	
3600	27.200	138494	93.649	73.985	

vapor pressure

(p in Pa)

$$\ln p = 25.9374 - 4.7556 \cdot 10^4 T^{-1} + 78 \cdot 10^{-7} T - 0.0857 \ln T, \quad T = 1700 \dots 2500 \text{ K}$$

84S2

see also Fig. 1.2.26.

Impurities and defects

binding energies and structural information on impurities

Negative energy refers to conduction band edge, positive energy refers to valence band edge.

A-center	- 0.18		see O-Vac complex	
Ag			many different levels reported, recently most authors attribute the following donor and acceptor level to substitutional Ag: C-V, DLTS, photoionization	88P, 86L1, 87B1, 81G1
	+ 0.37	d	optical transition at the neutral donor at 0.826 eV: PTIS, FTIR absorption photoluminescence	88O1 89N
	- 0.57	a	C-V, DLTS, TSCAP, photoionization	88P, 86L1, 87B1, 71Y
Ag related	- 0.28		Ag _{sub} -Ag _i ? anneals out at 600 °C	95L, 96L
Ag-H			generated by hydrogen plasma treatment, wet chemical etching; annealing at 400...500 °C destroys all Ag-H complexes	
	+ 0.28	d	Ag-H ₁ complex ?, DLTS	97Y
	- 0.45	a		97Y
	- 0.09	aa		97Y
	+ 0.38		Ag-H ₂ complex ?, DLTS	97Y
	neutral		passivated defect, Ag-H ₃ ?	87P, 97Y
Al	+ 0.06903	a	IR-spectroscopy of excited states, T _d -symmetry, substitutional uniaxial stress	83F2, 82S2, 59H, 83S4 67O
	+ 0.067	a	electrical measurements, photoconductivity	76S, 84S1
	+ 0.43		DLTS, solar material, grown-in	83R, 80C2
	+ 0.47		Al-related defect	
	+ 0.17	d	interstitial Al after irradiation, DLTS, recombination enhanced annealing	79T1
Al-C	+ 0.0563	a	aluminum-carbon pair, (X-center), IR-spectroscopy, Hall effect, DLTS	83S4, 82S1, 81J2, 78S1, 78S2
Al-Co			Co (interstitial)-Al (substitutional) Moessbauer spectroscopy, anneals out at 100...250 °C	83B1
Al-Cr	+ 0.45	d	Cr(interstitial)-Al(substitutional) donor-acceptor pair, DLTS Hall effect, ESR formation at 380 K binding energy 0.8 eV	86G 85F3 83L4 83L1
Al-Cu			see Cu-Al	
Al-Fe	+ 0.19	d	Fe(interstitial)-Al(substitutional) donor-acceptor pair, T ₂ -symmetry, uniaxial stress, Hall effect, DLTS, ESR (binding energy 0.7 eV)	89W2, 82W1, 81G1, 80G, 86G, 83L4, 86C1, 83S5, 86N, 83W1, 85C1, 85F3

Al-Fe (cont.)	+ 0.13	d	configuration bistability, transition at $T = 180$ K, DLTS, transient anneals	89W2, 86C1, 86N, 85C1, 82W1, 84K2, 80G
Al-H			passivation by atomic hydrogen dissociation energy 1.44 eV review of properties	87S, 85P2, 84P1, 89Z2, 91P1, 91Z2 87P, 92P1
Al-Li			Li(interstitial)–Al(substitutional) donor–acceptor pair	65W1
Al-Mn	– 0.45	d	Mn(interstitial)–Al(substitutional) donor–acceptor pair, Hall effect, ESR, DLTS, TSCAP binding energy 1.2 eV	85F3, 83L1 83L1
Al-O	+ 0.214 + 0.312 + 0.393		high- T annealing, pn-junction measurements	77M1, 77M2
Al-Se	– 0.2	d	Hall effect, ESR, ENDOR	79V, 88O4
Al-V			V(interstitial)–Al(substitutional) donor–acceptor pair, DLTS, no level found	86G
Al-Vac	+ 0.52	d	DLTS, quenched-in after laser irradiation, ESR $T \leq 230$ °C	85C1, 67W, 84D2
Al-X	+ 0.0563	a	see Al–C, X-center	
Al-Zn	+ 0.2...0.4		several Al and Zn related levels	77M1, 57F
As	– 0.05377	d	substitutional, $1s(A_1)$ ground state, IR-absorption at 10 K	82G2, 65A, 79P, 56P
	– 0.054	d	isothermal transient capacitance, Hall effect	83J, 87N 85N2, 84S1
As-C			DLTS, e-irradiation	90G1
As-Se	– 0.15	d	DLTS, radioactive decay	95A2
As-Vac	– 0.47	d	E-center, irradiation, anneals out at $T > 450$ K, DLTS	79T2, 77E
As ₄ -Vac			EXAFS, theory	88P
Au	+0.345	d	substitutional Au donor (Au(0/+)) Hall effect, DLTS	96D, 80L2, 95L, 86S2, 81G1, 74P, 87M1, 57C, 85F2, 74B
			photoionization noise measurements absorption from neutral donor ground state to excited EM electron states at 793 meV, photoluminescence	89J1 91W, 84T
	+ 0.267	dd?	Noise measurements	89J1
	– 0.555	a	substitutional Au acceptor (Au(–/0)) DLTS	96D, 81G1, 80L2, 95L, 85F2, 86S2, 74P, 57C, 87M1 74B
			photoionization absorption from neutral acceptor ground state to excited EM hole states at 611 meV, photoluminescence	91W, 87K1, 85A1
			no EPR of Au ⁰ ($g_- \approx 0$) EPR of Au ⁰ in Ag diffused samples (questionable) pressure coefficient for donor and acceptor state, see document below	91W, 91A, 97H 92S2 93P1
			Au acceptor and donor level belong to the same center:	85F1

Au (cont.)			Zeeman splitting of donor and acceptor absorption lines	91W
			radioactive isotopes	90P1
			photocapacitance	83L2
			DLTS profiling	84U
Au related defects:				
	– 0.560	d	produced by rapid thermal annealing,	74Y, 87M1
Au–Au pairs ?			Au(substitutional)–Au(substitutional), IR-absorption at 5700 cm ^{–1} , trigonal symmetry, dissociation energy 1.7 eV	94T
			IR-absorption at 6120 cm ^{–1} , trigonal symmetry, possibly Au–Au–Fe?	91K2
			ESR, C _{2v} symmetry, two equivalent Au	96W
Au–C	– 0.49	a	optical nuclear polarization, 700 °C anneals, elastic field fluctuation	85B3
Au–Cr	+ 0.35	d	Au(substitutional)–Cr(interstitial), DLTS, Photo-ESR	83L1
			binding energy 1.1 eV	88R
Au–Fe	+ 0.434	d	Au(substitutional)–Fe(interstitial)	84B1, 83L1, 81K,
	– 0.354	a	DLTS, ESR , theory dissociation $T > 200$ °C , formation below $T = 350$ °C binding energy 1.22 eV	85A2, 84B1 85B1
Au–Gd			cluster formation	80B1
Au–H	neutral		passivation by hydrogen plasma, possibly Au–H ₃ , Au reactivation $T > 200$ °C	95S1, 87P, 97R
	+ 0.21(G2)	d	DLTS, MCTS; G2, G4, G1 belong to the	95S2, 96D
	– 0.56 (G4)	a	same Au–H complex, created by wet chemical	96P
	– 0.19 (G1) aa + 0.47(G3)		etching or hydrogen plasma, anneal at $T > 150$ °C into the passive complex , possibly Au–H ₁	97R
Au–Li	neutral		passivation, bound exciton at 1122 meV ESR, orthorhombic	95S1, 95G 94A
	– 0.41	a	DLTS, photoluminescence at 765 meV from excited EM states to neutral acceptor	95S1, 95G
Au–Li ₃	– 0.4	d	ESR, trigonal	94A
Au–Mn	+ 0.57	a	Au(substitutional)–Mn(interstitial)	83L1
	– 0.24	d	binding energy 0.9 eV, theory	86A3
Au–Pt			no complex formed, replacement on substitutional site at $T > 800$ °C, DLTS	85S3
Au–V	+ 0.42	d	Au(substitutional)–V(substitutional)	83L1
	– 0.20	a	binding energy 1.6 eV	
Au–Vac	– 0.55	a	possible identification of Au acceptor?	76V
B	+ 0.04439	a	substitutional acceptor, IR-spectroscopy, excited states	83F2, 83S5, 81A1, 82S1, 67O
	+ 0.044	a	electrical measurements	75A, 54M
			B(interstitial): generated after low temperature electron irradiation, negative U system, anneals out at $T = 240$ K	80T, 80W 82H
	– 0.45	a	DLTS, ESR , acceptor state,	
	– 0.13	d	donor state	

B–B	+ 0.30	d	interstitial–substitutional pair after electron–irradiation, high B-concentration, stable up to 400 °C	85D2, 89K
B–C	+ 0.0371	a	boron-carbon pair, X-center, Hall effect, DLTS, IR-spectroscopy, thermal annealing	83S5, 82S1, 81J2
	+ 0.29		B(i)–C(s), irradiation	89K
B–Co	– 0.48 – 0.26		DLTS Moessbauer spectroscopy stable at 100 ... 250 °C	89M3, 83B1
B–Cr	+ 0.27	d	B(substitutional)–Cr(interstitial) Hall effect, ESR, NAA, DLTS, photo- luminescence, formation at 380 K pair binding energy 0.4...0.65 eV trigonal symmetry	86K2, 85F3, 86G 83W2, 83L3, 94N1, 81G1, 83L2, 96A1 83C1 83C2
B–Cu			see Cu–B	
B–D			passivation by atomic deuterium, reactivation at $T > 200$ °C	85M, 85J3, 90Z, 91P1
B–Fe	+ 0.100 – 0.23	d a	B(substitutional)–Fe(interstitial) first-nearest neighbor pairs DLTS, Hall effect, photoconductivity, optical absorption at the donor and acceptor states ODLTS, recombination-enhanced dissociation, binding energy 0.6 eV, stable at 20 ... 150 °C pressure dependence several metastable B-Fe complexes corresponding to different B–Fe separations, only observed after minority-carrier injection	92N, 86G, 81L3, 82W1, 83W1, 81L2, 83K2 94G1 85B2 83L2 83G, 81G2 82W1 94N2, 94N1
B–H			passivation by atomic hydrogen, dissociation energy 1.28 eV	87S, 87P, 5P2, 85P1, 85J1, 85J2, 85A3, 85J3, 84P1, 84H3, 83S5, 89Z2, 91Z2
B–In			dissociation at $T > 240$ °C pairing observed in exciton luminescence	80F, 80M2
B–Li			Li(interstitial)–B(substitutional) donor–acceptor pair	65W2
B–Mn	– 0.55	d	B(substitutional)–Mn(interstitial), Hall effect, ESR, DLTS, TSCAP binding energy 1.1 eV	86G, 83W2, 83L2, 82K, 83C1, 81L2, 81L1, 91N, 4N1 83L4
B–O	+ 0.26		B (interstitial)–O (interstitial) after e–irradiation, stable up to 200 °C	85D2, 89K
B–Se	– 0.2	d	Hall effect	79V
B–V			B(substitutional)–V(interstitial) Donor-acceptor pair, DLTS, no level found	86G

B–Vac	+ 0.36	d	DLTS, after quenching irradiation, metastability ion implantation, 3 levels, 550 °C annealing	85C2 85B4 80M1
	+ 0.5	d		
	+ 0.31			
	+ 0.27			
	...+0.43			
B–X	+ 0.0371	d	see B–C	82S1
B–Zn	+ 0.092	a	electrical measurements	57F, 72H
	+ 0.126	a		
	...+0.167			
Be			double acceptor on substitutional site and Be-related complexes, the level identification is not yet certain	
	+ 0.192	a	substitutional Be, IR-spectroscopy at 20 K, effective mass-like spectrum	72C, 68R, 86K1
	+ 0.43		substitutional Be, second charge state? unstable incorporation	80C2, 75H, 72F
	+ 0.145	a	Be-related complex, IR-spectroscopy at 20 K	72C, 68R
			Be(substitutional)–Be(substitutional)? or Be–C (X-center)?	85G1 86K1
	+ 0.093	a	Be-related	86K1
	+ 0.200	a		
	– 0.36	d	interstitial Be?, photoluminescence, ion implantation, 400...600 °C annealing	85G1
	+ 0.17	a	Hall effect, DLTS	82T1, 80C2, 72C, 70T, 77S
Be–Be			Be(substitutional)–Be(interstitial) isoelectronic complex, photoluminescence	85G1, 82T2, 81H
Be–D,H	+ 0.073	a	H, D implant, 1000 °C annealing, quenching, analogon to Be–Li pair, IR-spectroscopy dynamical tunneling, isotope shift of D	74C, 86M, 90P1 86M
	+ 0.091	a		
Be–Li	+ 0.081	a	IR-spectroscopy at $T < 20$ K, or Be–C (X center)	72G, 72C, 86K1
	+ 0.106	a		
Bi	– 0.0710	d	substitutional, $1s(A_1)$ ground state, IR-absorption, excited states spectrum at 4 K Hall effect, TSCAP	85H3, 82G2, 79P, 59H 74S1, 76S, 84S1
	– 0.069	d		
	...–0.074			
C			(substitutional) isoelectronic, no level, lattice contraction $\Delta d/d = -6.5 \cdot 10^{-24}$ [C]	94D 68B
	+ 0.28	d	(interstitial), e-irradiation, stable up to 100 °C, ESR, DLTS photoluminescence T-line at 0.9351 eV	85D2, 85B2, 89K, 80L1, 90S, 94D 87T
	– 0.12	a		
C–C	– 0.17,	a	C(substitutional)–C(interstitial), e-irradiation, DLTS, EPR, bistability, optical transition at 969 meV configuration diagram	89W2, 88S1, 94D 89W2
	– 0.11			
	+ 0.09	d		
C–Al	+ 0.0563	a	aluminum–carbon pair, (X-center), IR-spectroscopy, Hall effect, DLTS	83S4, 82S1, 81J2, 78S1, 78S2
C–As			DLTS, e-irradiation	90G1
C–Au	– 0.49	a	optical nuclear polarization, 700 °C anneals, elastic field fluctuation	85B3

C–B	+ 0.0371	a	boron-carbon pair, X-center, Hall effect, DLTS, IR-spectroscopy, thermal annealing	83S4, 82S1, 81J2
	+ 0.29		B(i)–C(s), irradiation	89K
C–Fe			no pairing	85B4
C–Ga	+ 0.0572	a	Ga(substitutional)–C(substitutional) pair (X-center), IR-spectroscopy, Hall effect, DLTS, enhanced by irradiation, annealing at $T = 600\text{ }^{\circ}\text{C}$	85F5, 85F4, 83S4, 82S1, 81J2, 78S1
C–H	– 0.16	d	C(substitutional) – H only stable in + charge state	89E, 91E
	– 0.2	d	C(interstitial) – H photoluminescence T-line at 0.9351 eV	96S
C–In	+ 0.1128		In(substitutional)–C(substitutional) (X-center) Hall effect. DLTS. IR-absorption photoluminescence binding energy 0.7 eV	82S1, 83S4 81A2, 81J2, 78L, 81J1, 79S2, 80L2, 77B1, 78T, 78S1 81Z 79B
C–O	+ 0.35		C(interstitial)– O(interstitial), e-irradiation optical transition at 789 meV, absorption, photoluminescence, PTIS	77K, 87M2 94D, 85T, 88K1
C–P	– 0.38	a	e–beam irradiation, annealing, pn-junction measurements, DLTS, instability, sequence of metastable configurations	86C1, 90G1, 91Z1, 86S1, 92G1, 92Z
C–Sb	– 0.27		C(interstitial)–Sb(substitutional), e–irradiation, anneals at $T > 350\text{ K}$, bistability	89B, 90G1
C–Si	+ 0.30		e–irradiation, anneals out at RT	77L
C–Tl	+ 0.1800	a	X-center, IR-spectroscopy, DLTS, thermal annealing	83S4, 82S1, 81J2
Ca	– 0.55	d	implantation, DLTS, ODLTS, passivated by hydrogen	94H2
	– 0.065	d	Ca–H complex	94H2
Cd	+ 0.485	a	DLTS, Hall, photoconductivity substitutional acceptor Cd(–/0) single charge state	91L, 81D, 71G
	– 0.45	aa	Cd(– –/–) double charge state	91L, 81D, 71G
Co			four levels are associated with Co, not clear if they all belong to one center, DLTS, TSCAP, recently questioned by DLTS on radioactive samples double donor level of substitutional Co ?	96A1 95g 96L, 90N, 86G, 85L2, 85K 96L, 86G, 85L2 90N, 85L2
	+ 0.23	d		
	+ 0.40	d		
	– 0.41	a		
	– 0.21	a		
Co–Al			Co (interstitial)–Al (substitutional) donor–acceptor pair, Moessbauer spectroscopy, anneals out at 100...250 $^{\circ}\text{C}$	83B2

Co–B	– 0. 48 – 0. 26		DLTS Moessbauer spectroscopy stable at 100 . . . 250 °C	89M3, 83B1
Co–Ga			Co(interstitial)–Ga(substitutional) donor–acceptor pair, Moessbauer spectroscopy, anneals out at 100...250 °C	83B2
Co–H	+ 0.09 + 0.17 + 0.22		CoH ₂ complex? CoH ₁ complex?, bistable, has a neutral configuration	96J1 96J1 96J1
	– 0.40 – 0.39 – 0.26 – 0.22 – 0.17 – 0.06			96J2 96J2 96J2 96J2 96J2 96J2
Cr	– 0.23	d	interstitial Cr Cr(0/+) 3d ⁶ /3d ⁵ DLTS, Hall effect, ESR, NAA, photoconductivity Hall effect,	96A1, 94S2, 94N, 86G 83C1, 83W2 83K2, 81F 81G 92D, 81K
	+ 0.11	dd?		
Cr–Al	+ 0.45	d	Cr(interstitial)–Al(substitutional) donor–acceptor pair, DLTS Hall effect, ESR formation at 380 K binding energy 0.8 eV	86G 85F 83L3 83L2
Cr–Au	+ 0. 35	d	Au(substitutional)–Cr(interstitial), DLTS, Photo-ESR binding energy 1. 1 eV	83L1 88R
Cr–B	+ 0.27	d	B(substitutional)–Cr(interstitial) Hall effect, ESR, NAA, DLTS, photo- luminescence, formation at 380 K pair binding energy 0.4...0.65 eV trigonal symmetry	86K2, 85F, 86G 83W2, 83L3, 94N, 81G, 83L2, 96A1 83C1 83C2
Cr–Cu	+ 0.40		Photo-ESR	88R
Cr–Ga	+ 0.48	d	Cr(interstitial)–Ga(substitutional) donor–acceptor pair Hall effect, ESR DLTS, TSCAP, binding energy 0.35 eV	86G 85F 83L2
Cr–H	– 0.54 – 0.45 – 0.28		several hydrogen complexes generated by wet chemical etching, anneals out at 200 °C	94S1, 94S2
Cr–In			Cr (interstitial)–In (substitutional) donor–acceptor pair, DLTS, no level	86G
Cr–Pt			Cr(interstitial)–Pt(substitutional), DLTS, no level found	86G
Cr–Vac	– 0.32 – 0.52		DLTS, quenching from $T = 1200$ °C	85A

Cr–Zn	– 0.10	a	Cr(substitutional)–Zn(substitutional) donor–acceptor pair, DLTS, TSCAP	86G, 82L
Cu	+ 0.23 + 0.46 – 0.16 no level	d a aa	Cu(substitutional), DLTS, Cu(interstitial) ⁺ , fast diffusor	87B2, 86L2 82B2 83W2, 96M1
Cu–Cu	+ 0.09	d	DLTS, photoluminescence at 1.014 eV, anneals out at $T > 450$ K	81G1, 87B2, 95E1
neutral Cu-complexes: Cu–B Cu–Al Cu–Ga Cu–In			CV-profiling, resistivity, PACS, LVM generated by electrochemical polishing (X-defect), Cu diffusion and quench, not stable at $T > 300$ K, dissociation energies: $E_d(\text{Cu–B}) = 0.61$ eV, $E_d(\text{Cu–Al}) = 0.70$ eV, $E_d(\text{Cu–Ga}) = 0.71$ eV, $E_d(\text{Cu–In}) = 0.69$ eV	88Z, 89P2, 90K, 90W1
	+ 0.210		theory M-center, Cu complex with unknown defect, possibly electrically active cluster of Cu atoms, DLTS, only detected after cooling under reverse bias, dissociation energy 0.96 eV, several levels of unknown origin introduced by electron irradiation in Cu doped Si	90E 92M 86K2, 95A1
Cu–H			passivation by atomic H	87P
Cu–H?	– 0.31		after proton implantation, Cu Schottky contacts	92T
Cu–Mn			ESR	86D2
Cu–Pt	+ 0.560		DLTS, dissociation energy 0.85 eV	92P2
D			deuterium, interstitial, similar to hydrogen	78P2, 78P1, 87P, 92P1
D–B			passivation by atomic deuterium, reactivation at $T > 200$ °C	85M, 85J3, 90Z, 91P1, 92P1
D,H–Be	+ 0.073 + 0.091	a a	H, D implant, 1000 °C annealing, quenching, analogon to Be–Li pair, IR-spectroscopy dynamical tunneling, isotope shift of D	74C, 86M, 90P1 86M
e ⁺			positronium, deep donor localized in A-center	77A3
E-center			see P–Vac, As–Vac, Sb–Vac	
Er	– 0.09, – 0.06, – 0.14, – 0.18, – 0.27, – 0.31, – 0.32, – 0.48 + 0.145	d a	several donor states in Er implanted n-type Si, possibly Er–O or Er–C complexes, DLTS, spreading resistance, differential Hall-effect 4f-internal optical transition at $\lambda = 1.54$ μm electroluminescence at RT	89W1, 91B, 93P2 93N 83E 94Z
Eu			internal luminescence, implantation damage	83E, 80C2
F	shallow – 0.15	d d	F implantation and anneal, CV profiling DLTS	96H

Fe	+ 0.385	d	interstitial after quenching DLTS, EPR, single charge (+ 0.43 in uncorrected DLTS) EPR, ENDOR, Fe ⁰ (3d ⁸), Fe ⁺ (3d ⁷) Hall effect, photocapacitance pressure dependence T _d -symmetry optical absorption from neutral Fe(interstitial) state to excited EM electron states at 790 meV several Fe related levels produced by quenching or processing	86G, 83W2 86B2, 85B2, 94N1, 83F1, 85A5, 84P2 81L3, 84G2 83W1 87N, 82W2, 83J 78F 88O5 81G1, 95E2
Fe–Al	+ 0.19	d	Fe(interstitial)–Al(substitutional) donor–acceptor pair, T ₂ –symmetry, uniaxial stress, Hall effect, DLTS, ESR (binding energy 0.7 eV)	89W2, 82W1, 81G1, 80G, 86G, 83L2, 86C1, 83S3, 86N, 83W1, 85C1, 85F3
	+ 0.13	d	configuration bistability, transition at <i>T</i> = 180 K, DLTS, transient anneals pressure dependence	89W2, 86C1, 86N, 85C1, 82W1, 84K2, 80G 86N, 82W2
Fe–Au	+ 0.434 – 0.354	d a	Au(substitutional)–Fe(interstitial) DLTS, ESR, theory dissociation <i>T</i> > 200 °C, formation below <i>T</i> = 350 °C binding energy 1.22 eV	84B1, 83L4, 81K1 85A3 84B1 85B1
Fe–B	+ 0.100 – 0.23	d a	B(substitutional)–Fe(interstitial) first-nearest neighbor pairs DLTS, Hall effect, photoconductivity, optical absorption at the donor and acceptor states ODLTS, recombination-enhanced dissociation, binding energy 0.6 eV, stable at 20 . . . 150 °C pressure dependence several metastable B–Fe complexes corresponding to different B–Fe separations, only observed after minority-carrier injection	92N, 86G, 81L3, 82W1, 83W1, 81L2, 83K1 94G1 85B2 83L2 83G, 81G2 82W2 94N2, 94N1
Fe–C			no pairing	85B2
Fe–Ga	+ 0.14 + 0.23	d d	Fe(interstitial)–Ga(substitutional) donor–acceptor pair, configuration bistability, DLTS, <i>T</i> = 170 K transition Hall effect, ESR, photocapacitance, photoconductivity, TSCAP, binding energy 0.47 eV	86G, 86C1 85F3, 83W1, 83L2, 83S3 83L2
Fe–H			passivation of Fe (i) by atomic H	87P, 84P2
Fe–In	+ 0.160 + 0.27	d d	Fe(interstitial)–In(substitutional) donor–acceptor pair bistability DLTS at <i>T</i> = 180 K ESR, luminescence optical excitation within the acceptor states:	86G1 86C1, 89W2 84W3, 81W2, 83S3 96T
	– 0.39 – 0.32	a a	orthorhombic configuration trigonal configuration	

Fe–O	+ 0.33		no level, no pairing DLTS after moderate quenching	85B2 84P2, 81W1
Fe–Pt			no levels found, DLTS Fe(interstitial)–Pt(substitutional)	86G
Fe–S			ESR identification	83S2
Fe–Zn	– 0.47	a	Fe(substitutional)–Zn(substitutional) donor–acceptor pair, DLTS, TSCAP	86G, 82L
Ga	+ 0.07273	a	IR-spectroscopy substitutional acceptor	83S4, 83F2 82S1
	+ 0.072	a	electrical measurements, photoconductivity	82G1, 76S, 67G, 64S, 57S
Ga–Ga	+ 0.0404	a	pair formation, IR-spectroscopy, annealing at $T = 600\text{ }^{\circ}\text{C}$, Ga–Vac?	84F, 85F4 85F4
Ga–C	+ 0.0572	a	Ga(substitutional)–C(substitutional) pair (X-center), IR-spectroscopy, Hall effect, DLTS, enhanced by irradiation, annealing at $T = 600\text{ }^{\circ}\text{C}$	85F5, 85F4, 83S4, 82S1, 81J2, 78S1
Ga–Co			Co(interstitial)–Ga(substitutional) donor–acceptor pair, Moessbauer spectroscopy, anneals out at 100...250 $^{\circ}\text{C}$	83B2
Ga–Cr	+ 0.48	d	Cr(interstitial)–Ga(substitutional) donor–acceptor pair, DLTS, Hall effect, ESR, TSCAP binding energy 0.35 eV	86G, 85F3 83L2
Ga–Fe	+ 0.14	d	Fe(interstitial)–Ga(substitutional) donor–acceptor pair, configuration bistability, DLTS, $T = 170\text{ K}$ transition	86G, 86C1
	+ 0.23	d	Hall effect, ESR, photocapacitance, photoconductivity, TSCAP, binding energy 0.47 eV	85F3, 83W1, 83L2, 83S3 83L2
Ga–H			passivation by atomic hydrogen dissociation energy 1.40 eV	87S, 87P, 85P2, 89Z2, 84P1, 91P1, 92P2
Ga–Li			Ga(substitutional)–Li(interstitial) donor–acceptor pair, IR–spectroscopy	82Z, 65W1, 82E
Ga–Mn	– 0.42	d	Mn(interstitial)–Ga(substitutional) donor–acceptor pair, Hall effect, ESR DLTS, TSCAP, binding energy 1.1 eV	86G, 85F3 85F3 83L2
Ga–Se	– 0.2	d	Hall effect	79V
Ga–V			V(interstitial)–Ga(substitutional) donor–acceptor pair, DLTS, no level found	86G
Ga–X	+ 0.0570	a	see Ga–C	
Ga–Zn	+ 0.083		electrical measurements	57F
Gd			causes elastical strain life time reduction	85B5 80C2, 81N
	+ 0.55		DLTS, quenched at 1000 $^{\circ}\text{C}$ clusters, radiation hardening	80C2 78A2, 77A1, 77A2

Gd–Au			cluster formation	80B1
Ge			substitutional, isoelectronic, damage levels after implants	73S, 72F
H	– 0.16	d	interstitial hydrogen (bond center), bistable, DLTS IR absorption at 1990 cm^{-1} EPR	92P1, 91H2, 87P 91H1 79S1 87G
	– 0.5	a	interstitial hydrogen (T_d site) negative U -center?	94J
H–H			stable incorporation, not electrically active: H_2 - molecule H_2^* -defect	96M2 93H2
H–Ag			generated by hydrogen plasma treatment, wet chemical etching; annealing at $400 - 500\text{ }^\circ\text{C}$ destroys all AgH complexes	
	+ 0.28	d	Ag– H_1 complex ?, DLTS	97Y
	– 0.45	a		97Y
	– 0.09	aa		97Y
	+ .38		Ag– H_2 complex ?, DLTS	97Y
	neutral		passivated defect, Ag– H_3 ?	87P, 97Y
H–Al			passivation by atomic hydrogen dissociation energy 1.44 eV review of properties	87S, 85P2, 84P1, 89Z2, 91P1, 91Z2 87P, 92P1
H–Au	neutral		passivation by hydrogen plasma, possibly Au– H_3 , Au reactivation $T > 200\text{ }^\circ\text{C}$	95S2, 87P, 97R
	+ 0.21 (G2)	d	DLTS, MCTS; G2, G4, G1 belong to the	95S2, 96D
	– 0.56 (G4)	a	same Au–H complex, created by wet chemical	96P
	– 0.19 (G1)	aa	etching or hydrogen plasma, anneal at	
	+ 0.47 (G3)		$T > 150\text{ }^\circ\text{C}$ into the passive complex , possibly Au– H_1	97R
H–B			passivation by atomic hydrogen dissociation energy 1.28 eV	87S, 87P, 85P2, 85P1, 85J3, 85J1, 85A3, 85J2, 84P1, 84H3, 83S5, 89Z2, 92P1
			dissociation at $T > 240\text{ }^\circ\text{C}$	91Z2
D,H–Be	+ 0.073	a	H, D implant,	74C, 86M, 90P1
	+ 0.091	a	1000 $^\circ\text{C}$ annealing, quenching, analogon to Be–Li pair, IR-spectroscopy dynamical tunneling, isotope shift of D	86M
H–Cu			passivation by atomic H	87P
H–Fe			passivation of Fe (i) by atomic H	87P, 84P2
H–Ga			passivation by atomic hydrogen	87S, 87P, 85P2, 89Z2
			dissociation energy 1.40 eV	84P1, 91P1, 92P1
H–In			passivation by atomic H, dissociation energy 1.24 eV	87P, 87S, 85T, 84P1, 85P2, 89Z2, 91P1, 92P1

H-Pd			passivation by atomic hydrogen plasma and wet chemical etching	87P, 83P1 97S3
	+ 0. 07		several electrically active hydrogen complexes generated by wet chemical etching, anneals out at 500 - 700 K	97S3
	+ 0. 08			
	+ 0. 23			
	+ 0. 55			
	- 0. 43			
	- 0. 29			
	- 0. 10			
H-Pt			neutralization by hydrogen plasma	87P, 83P1
			several electrically active levels generated by wet chemical etching, anneal out at $T > 530$ K	97S1
			electrically inactive Pt-H complexes	
	+ 0. 40			
	+ 0. 30			
	- 0. 50		so called midgap level, dominant recombination center?	97S2
	- 0. 18	d	correlation with Pt-H ₂ complex, ESR, IR absorption	93W, 95U
	- 0. 53	d	Pt-O?, identical to Pt-H?	86S2, 87K2, 90G2
H-Tl			passivation by atomic H	87P, 85T, 85P2
He-Vac			EPR, implantation, stable up to 180 °C	85G2
Hf	+ 0. 32	dd	DLTS	90L
	- 0. 39	d		
	- 0. 10	a		
			several Hf related levels close to the surface	90L
Hg	+ 0.25	d	photoconductivity 77 K, identifications uncertain	85Z1, 68S, 64Z
	...+0.33			
	- 0.3	a	photoluminescence at 1067.9 meV, Hg-C complex?	93H1
Ho			two acceptor levels	75V1
In	+ 0.15558	a	substitutional acceptor, IR-spectroscopy	83S4, 81P, 83F2, 82S3, 82S1, 78S3
	+ 0.157	a	electrical measurements	85H2, 80B2, 82G1, 85H1, 77G1, 78L, 84S1, 72M
			photo-Hall effect	80H, 83P2, 72M
			photoconductivity	81J1
			DLTS	79F
			IR-MOSFET	79E
			ground level splitting 4.1 meV, dynamic Jahn-Teller effect	
	+ 0.018	a	supershallow In-level, low-concentration Hall effect	85C3
In-B			pairing observed in exciton luminescence	80F, 80M2
In-C	+ 0.1128		In(substitutional)-C(substitutional) (X-center) Hall effect. DLTS. IR-absorption	82S1, 83S4 81A2, 81J2, 78L, 81J1, 79S2, 80L2, 77B1, 78T, 78S1
			photoluminescence	81Z
			binding energy 0.7 eV	79B
In-Cr			Cr(interstitial)-In(substitutional) donor-acceptor pair, DLTS, no levels found	86G

In–Fe	+ 0.160	d	Fe(interstitial)–In(substitutional) donor–acceptor pair bistability DLTS at $T = 180$ K ESR, luminescence optical excitation within the acceptor states: orthorhombic configuration trigonal configuration	86G 86C1, 89W2 84W3, 81W2, 83S2 96T
	+ 0.27	d		
	– 0.39	a		
	– 0.32	a		
In–H			passivation by atomic H, dissociation energy 1.42 eV	87P, 87S, 85T, 84P1, 85P2, 89Z2, 91P1, 92P1
In–Li			Li(interstitial)–In(substitutional)	82Z, 81Z
In–Mn			donor–acceptor pair, luminescence	86G
			Mn(interstitial)–In(substitutional) donor–acceptor pair, DLTS, no level found	
In–Se	– 0.2	d	Hall effect	79V
In–V			V(interstitial)–In(substitutional)	86G
			donor–acceptor pair, DLTS, no level found	
In–X	+ 0.1128	a	see In–C	
Ir	– 0.24	a	amphoteric center	85L2, 96L
	– 0.62	d	transient capacitance	
	– 0.17...– 0.18		Ir-related	
Li	– 0.03381	d	interstitial, IR-spectroscopy,	81S3, 65A, 77G2, 75L 78H 84L2
			electrical measurements	
			rhombic strain field, EPR	
			Li–complex, luminescence	
Li–Al			Li(interstitial)–Al(substitutional) donor–acceptor pair	65W1
Li–B			Li(interstitial)–B(substitutional) donor–acceptor pair	65W2
Li–Be	+ 0.081	a	IR-spectroscopy at $T < 20$ K, or Be–C(X) center	72G, 72C 86K1
	+ 0.106	a		
Li–Ga			Li(interstitial)–Ga(substitutional) donor–acceptor pair, IR-spectroscopy	82Z, 82E, 65W1
Li–In			Li(interstitial)–In(substitutional) donor–acceptor pair, luminescence	82Z, 81Z
Li–O	– 0.039	d	optical measurement, IR-spectroscopy uniaxial stress	65A 80J1
Mg	– 0.055	d	Mg(interstitial) shallow donor states, PTIS, Hall passivation by hydrogen	86K2, 82L
	– 0.093	dd		
	+ 0.34	a	substitutional Mg, DLTS, photoionization	88B1
	– 0.115	a	Mg-related complexes	79O, 94H2
	– 0.40	d,a	Hall effect, DLTS, absorption	
	– 0.227	d	passivation by hydrogen	
Mn	+ 0.26	d	Mn ^{+/++} 3d ⁵ interstitial, EPR,	86G, 81G1, 85W, 85A6, 83C1, 83W2, 83L1, 81L1, 91N 86G, 85C4, 84L1, 87H 83C, 88K2 87C2
	– 0.42	d	Mn ^{0/+} 3d ⁶ DLTS, Hall effect,	
	– 0.12	a	Mn ^{–/0} 3d ⁷ quenching	
	+ 0.34	d	Mn ^{0/+} 3d ² substitutional,	
	– 0.43	a	Mn ^{–/0} 3d ⁵ EPR, DLTS	
	– 0.28	d	Mn ₄ -cluster, EPR, Hall effect	
			photoluminescence	

Mn–Al	– 0.45	d	Mn(interstitial)–Al(substitutional) donor–acceptor pair, Hall effect, ESR, DLTS, TSCAP binding energy 1.2 eV	85F3, 83L2 83L2
Mn–Au	+ 0.57 – 0.24	a d	Au(substitutional)–Mn(interstitial) binding energy 0.9 eV theory	83L1 86A3
Mn–B	– 0.55	d	B(substitutional)–Mn(interstitial) Hall effect, ESR, DLTS, TSCAP binding energy 1.1 eV	86G, 83W2, 83L2, 82K, 83C1, 81L2, 81L1, 91N, 94M1 83L5
Mn–Cu			ESR	86D2
Mn–Ga	– 0.42	d	Mn(interstitial)–Ga(substitutional) donor–acceptor pair, Hall effect, ESR DLTS, TSCAP, binding energy 1.1 eV	86G, 85F3 85F3 83L2
Mn–In			Mn(interstitial)–In(substitutional) donor–acceptor pair, DLTS, no level found	86G
Mn–O			electrically inactive, passivation of O, Mn	85A7
Mn–Pt			Mn(substitutional)–Pt(substitutional) DLTS, no levels found	86G
Mn–Zn	+ 0.18	d	Mn(substitutional)–Zn(substitutional)– donor–acceptor pair, DLTS, TSCAP	86G, 82L
Mo	+ 0.30	d	DLTS	96L, 94L1, 89J2, 91P2, 83R, 83L5, 80D
N	– 0.19	d	N–N pairs main incorporation off-center substitutional partial incorporation 0.1% electrical activity	86S3 86S3 82T3, 85H4
			N-complex, 0.01% activity, DLTS, stable up to $T = 700\text{ }^{\circ}\text{C}$	85N1, 82T3
	– 0.28	d	N-complex, DLTS, stable above $T \geq 900\text{ }^{\circ}\text{C}$	85N1, 82B3
	– 0.58		ESR, distorted site	80B3
	– 0.045	d	low activity after implantation	76P
Na			no level after indiffusion levels after implantation, Hall effect, irradiation	69P 85Z2, 83Z, 79Z1, 69D, 74S2
Nb	+ 0.163 – 0.583 – 0.293		all levels are Nb related, same defect? DLTS, photocapacitance	93P3
Nd	+ 0.12		DLTS, metallurgical grade levels after implantation or irradiation	83R 80C2, 65G2, 65G1

Ni			more than 15 Ni related complexes reported, most of them only close to the surface frequently reported bulk levels which belong to one Ni (substitutional?) center:	87L2
	+ 0.16	d	DLTS, TSCAP, Hall effect	94N1, 91K1, 87L2, 87K3, 81G1
	− 0.38	a	DLTS, TSCAP, Hall effect	94N1, 91K1, 87L2, 77S, 87K3, 87L2, 96L
	− 0.06	aa	DLTS	
			other frequently reported Ni-related levels, which belong to different centers:	
	+ 0.21 ...			
	+ 0.24	a	DLTS, TSCAP, Hall effect, photoconductivity	87L2, 86G, 77S 77C1
	+ 0.33	a	DLTS, Ni-Vac?	87I, 83P3
	− 0.34...0.36	a	DLTS, Hall effect, TSCAP, admittance	87L2, 86G, 74A, 77B2, 85J4 91K1, 87L2, 77C1
	− 0.45	a	TSCAP, Hall effect, DLTS	
O			Si–O–Si bridging, displaced [111]–axis, electrically inactive "thermal donor" TD, double donor Hall-effect, DLTS,	94M1
	− 0.06	d	single donor state (0/+)	94M1, 89W3 84W1
	− 0.13	dd	double donor state (++/+)	83O, 85S1 84H2
			formation at 350 ...500 °C structure uncertain, C _{2v} symmetry metastability correlation TD with EPR NL8 centers IR-spectroscopy reveals at least 16 different TD species with different binding energies, uniaxial stress, local modes several differing series of thermal donors with shallow donor levels, possible association with N, H, Al	87C1
	− 0.05... −0.2	d	"new donor" ND, continuous level spectrum, SiO _x precipitation	85L1 94M1, 92G2
O–Al	+ 0.214 + 0.312 + 0.393		high- <i>T</i> annealing, pn-junction measurements	94L2, 87W 89G, 88S2, 94H1, 94M2, 94K 89P1, 86H, 84H1, 84B3, 83Y
O–B	+ 0.26		B (interstitial)–O (interstitial) after e–irradiation, stable up to 200 °C	77M1, 77M2
O–Fe	+ 0.33		no level, no pairing DLTS after moderate quenching	85D2, 89K
O–Li	− 0.039	d	optical measurement, IR-spectroscopy uniaxial stress	85B2 84P2, 81W1
O–Mn			electrically inactive, passivation of O, Mn	65A 80J2
O–Pt	− 0.53	d	O(interstitial)–Pt(substitutional), DLTS, Pt indiffusion at <i>T</i> = 850...1000 °C identical to Pt–H?	85A7
O–Vac	− 0.18	a	A-center, after irradiation, DLTS, Hall effect, ESR, ENDOR, C _{2v} -symmetry, (100)-orientation	87K2 86S2, 90G1
				85A8, 83M, 83B4, 83B3, 86K3, 76L, 85S2, 85J5

Os	+ 0.30 – 0.22		DLTS	94L1
P	– 0.04558 d		substitutional, single donor IR-spectroscopy, $1s(A_1)$, $T = 4...10$ K	82G2, 79P 84S1, 83B5, 81J3, 79J
	– 0.045 d		electrical measurements, Hall effect, DLTS, MOS measurements	65A, 84R, 84D1, 73N, 80Y, 80L3, 79S3
	– 0.0037 a		D [–] -center, binding of a second electron at 4 K	82N, 77N, 76N, 73N
P–C	– 0.38 a		e–beam irradiation, annealing, pn-junction measurements, DLTS, instability, sequence of metastable configurations	86C2, 90G2, 91Z1, 86S1, 92G1, 92Z
P–Vac	– 0.45 a		E-center, irradiation damage, DLTS, anneals out at $T \geq 150$ °C enhanced annealing under bias configurational instability	77K, 86C1, 86B1, 81G3, 85J4, 83C3, 71K, 82B2, 75K 86B1 86C1
Pb			no grown-in levels ion implantation	83R 77C2, 72F
Pd	+ 0.11 dd		substitutional Pd double donor (Pd(+/+)) DLTS	97S4, 84L2
	+ 0.31 d		substitutional Pd donor (Pd(0/+)) DLTS, TSCAP, optical admittance photoluminescence at 1.0084 eV	97S4, 91R, 84L2 88T
	– 0.22 a		substitutional Pd acceptor (Pd(–/0)) DLTS, TSCAP, optical admittance uniaxial stress several other Pd related levels	97S4, 86S2, 93G, 91R, 84L2, 89Z1 86S2 93G, 86S2, 89J2
Pd–H			passivation by atomic hydrogen plasma and wet chemical etching	87P, 83P1, 97S3
	+ 0.07 + 0.08 + 0.23 + 0.55 – 0.43 – 0.29 – 0.10		several electrically active hydrogen complexes generated by wet chemical etching, anneal out at 500...700 K	97S2
Pt	+ 0.067 dd		substitutional Pt double donor (Pt(+/+)) bound-to-bound optical transitions at 990 meV	91Z3 89O
	+ 0.32 d		substitutional Pt donor (Pt(0/+)) Pt donor bound-to-bound optical transitions at 805 meV, T _d -symmetry (interstitial Pt?) at 811 meV, C _{2v} -symmetry (substitutional Pt)	86S2, 90P1, 79B 86A1, 86A2
	– 0.24 a		substitutional Pt acceptor (Pt(–/0)) Pt acceptor bound-bound optical transitions at 920 meV correlation of substitutional Pt EPR signal and DLTS by photoionization and uniaxial stress measurements pressure dependence, similarity to A center vacancy-like model for substitutional Pt	86S2, 90P1, 88O2 85A9, 88K3 77B3, 86S2, 87O 86S4 92A

Pt–Au			no complex formed, replacement on substitutional site at $T > 800\text{ }^{\circ}\text{C}$, DLTS	85S3
Pt–Cr			Cr(interstitial)–Pt(substitutional), DLTS, no level found	86G
Pt–Fe			no levels found, DLTS Fe(interstitial)–Pt(substitutional)	86G
Pt–H			neutralization by hydrogen plasma several electrically active levels generated by wet chemical etching, anneal out at $T > 530\text{ K}$ electrically inactive Pt–H complexes	87P, 83P1 97S1
	+ 0.40			
	+ 0.30			
	– 0.50		so called midgap level, dominant recombination center?	97S2
	– 0.18	d	correlation with Pt–H ₂ complex, ESR, IR absorption	93W, 95U
	– 0.53	d	Pt–O?, identical to Pt–H?	86S2, 87K1, 90G1
Pt–Li			ESR	89H
Pt–Mn			Mn(substitutional)–Pt(substitutional) DLTS, no levels found	86G
Pt–O	– 0.53	d	O(interstitial)–Pt(substitutional), DLTS, Pt indiffusion at $T = 850\ldots 1000\text{ }^{\circ}\text{C}$ identical to Pt–H?	87K2 86S2, 90G1
Pt–Pt	+ 0.50	a	ESR, two equivalent Pt ions, ESR	88B2
Re	– 0.35		DLTS	94L
	– 0.07			
Rh	– 0.33		Rh(substitutional) -donor?	85L2
	– 0.57		-acceptor?	89C, 89J2
Ru	+ 0.34...+ 0.26		DLTS	89J2, 94L
	– 0.45		photocapacitance	79Y, 74Y
	– 0.24...– 0.14		DLTS, photocapacitance	94L, 79Y
S	– 0.3182	d	substitutional S(0/+) double donor, IR-absorption, Hall effect, DLTS	86P, 85K, 84W1, 84Q, 85J6, 83J, 94G2, 84J
			pressure dependence	82J, 87N, 84K1, 83J
			T _d -symmetry	65L, 86K1, 84G1
	– 0.6132	d	substitutional S(+/++)double donor. IR-absorption, Hall effect, DLTS	86P, 86K1, 85K 84W1, 83J, 84J, 85J6
			T _d -symmetry	86K1, 84G1
			pressure dependence	83J, 82J
S–S	– 0.1875	d	sulfur pair S ₂ (0/+), DLTS, IR-spectroscopy, Hall effect transient annealing, C _{1v} symmetry dissociation 0.58 eV C _{3v} -symmetry	86P, 84W1, 86K1, 84J, 85J6 76Z, 88O1 86K1
	– 0.3700	d	sulfur pair S ₂ (+/++), DLTS, IR-spectroscopy, Hall effect transient annealing, dissociation 0.58 eV C _{3v} -symmetry	86P, 84W1, 79B, 86K1 86K1, 88O3
S–complexes			series of complex levels, IR-spectroscopy	84W1

S-Fe			ESR identification	83S1
S-H	- 0.0824 d - 0.0826 d - 0.092 d - 0.13507 d		absorption, five hydrogen related donors	90P2
S-Se	- 0.1919 d		double donor S-Se(0/+), C _{3v} -symmetry, IR-spectroscopy	84W1
S-Te	- 0.1562 d		double donor S-Te(0/+), IR-spectroscopy, C _{3v} -symmetry	84W1
S-Vac	- 0.184 d - 0.25 d		DLTS, S indiffusion, groups of levels	83L6
Sb	- 0.04277 d		substitutional single donor IR-spectroscopy, 1s(A1), T = 4...10 K	84S1, 82G2 79P, 65A, 56P
Sb-C	- 0.27		C(interstitial)-Sb(substitutional), e-irradiation, anneals at T > 350 K, bistability	89B, 90G2
Sb-Vac	- 0.44	a	E-center, irradiation, anneals out at T = 460 K	79T2
Sc	+ 0.20 - 0.50 - 0.21 + 0.34		triple donor levels of interstitial Sc? DLTS radioactive decay identifies levels -0.21, -0.47, -0.50 as Sc related uncertain assignment, DLTS	96L, 96A2 86G
Se	- 0.3065 d - 0.5932 d		substitutional double donor Se(0/+), IR-spectroscopy, DLTS, Hall effect, T _d -symmetry, 1s(A1) pressure dependence substitutional double donor Se(+/+), IR-spectroscopy, DLTS, Hall effect, T _d -symmetry, 1s(A1) pressure dependence	86P, 85K, 84W1, 82G2, 81G4, 80S, 84G1, 84G2, 84J, 85J6, 89P3, 94G2 83J, 82J 86P, 85K, 84W1, 82G2, 81G4, 80S, 84J, 85J6 84W1 83J, 82J
Se-complexes		d	series of complexes	84W1, 84J
Se-Al	- 0.2	d	Hall effect, ESR, ENDOR	79V, 88O
Se-As	- 0.15	d	DLTS, radioactive decay	95A2
Se-B	- 0.2	d	Hall effect	79V
Se-Ga	- 0.2	d	Hall effect	79V
Se-In	- 0.2	d	Hall effect	79V
Se-S	- 0.1919 d		double donor S-Se(0/+), C _{3v} -symmetry, IR-spectroscopy	84W1
Se-Se	- 0.2064 d - 0.3892 dd		Se-pair, Se ₂ (0/+) D _{3d} -symmetry, DLTS, Hall effect, IR-spectroscopy, radioactive decay Se-pair, Se ₂ (+/+) D _{3d} -symmetry, DLTS, Hall effect, IR-spectroscopy, radioactive decay	94G2, 86P, 84J 84W1, 85A1, 95A2 94G2, 86P 84W1, 85A1, 95A2

Se–Te	– 0.1706	d	double donor Se–Te (0/+), C _{3v} -symmetry, IR-spectroscopy	84W1
Si			isolated interstitial, not visible amphoteric, estimate from diffusion	85H5, 80L4 81F, 70C
Si–C	+ 0.30		e-irradiation, anneals out at RT	77L
Sm			cluster formation, electrically inactive	77G3, 75V2
Sn			no levels, grown-in and after implantation and annealing, SIMS, luminescence, DLTS substitutional, Moessbauer effect	83R, 86D1, 75S, 84S2 81B
Sn–Vac	+ 0.07 + 0.13	d d	double donor Sn–Vac(+/+), double donor Sn–Vac(0/+), anneal at 500 K, DLTS, Hall effect	84W2, 79T2, 84S2
Ta	– 0.19 – 0.23 – 0.47	d d d	DLTS, TSCAP, pn-junction measurements	77B2, 76M, 96L
Te	– 0.1987	d	substitutional double donor Te(0/+), IR-spectroscopy, Hall effect, DLTS, T _d -symmetry, 1s(Al)	86P, 85K, 84W1, 82G2, 81L, 81G4, 85J6, 94G2, 83N2
	– 0.4112	d	pressure dependence substitutional double donor Te(+/+), IR-spectroscopy, Hall effect, DLTS, T _d -symmetry	83J, 82J 86P, 85K, 84W1, 84H4, 82G2, 81L, 81G4, 85J6
	– 0.14	d	pressure dependence other frequently reported level, DLTS, Hall effect, implantation, T _d -symmetry	83J, 82J 83K3, 84H4
Te–Te	– 0.1580	d	double donor pair Te ₂ (0/+), IR-spectroscopy, D _{3d} -symmetry	84W1, 85J6
Te-complexes			series of levels, IR-spectroscopy	84W1
Te–S	– 0.1562	d	double donor S–Te(0/+), IR-spectroscopy, C _{3v} -symmetry	84W1
Te–Se	– 0.1706	d	double donor Se–Te (0/+), C _{3v} -symmetry, IR-spectroscopy	84W1
Th			ion bombardment, no level found	65G1
Ti			DLTS, photocapacitance, MCTS, radioactive decay	96J3, 91T1, 95A3
	+ 0.26	dd	interstitial double donor Ti	89M2, 86C2, 81G1, 83M
	– 0.27	d	recombination center interstitial donor Ti	84W5, 93B 96J3, 91T1, 89M2, 86C2, 84W4, 81G1, 83M
	– 0.08	a	interstitial acceptor Ti	96J3, 91T1, 89M2, 81G1, 81R, 83M
Ti–H	– 0.57 – 0.31		reactivation of Ti at T>570 K, 3h passivated defect, electrically neutral	96J3

Tl	+ 0.2460	a	substitutional acceptor, IR-spectroscopy	83S4, 82S1, 78S2
	0.23...+ 0.26		electrical measurements, photoconductivity	85A10, 84S1, 4B4, 83P2, 83K4, 78B, 81S1, 77S, 75N
Tl–C	+ 0.1800	a	X-center, IR-spectroscopy, DLTS, thermal annealing	83S4, 82S1, 81J2
Tl–H			passivation by atomic H	87P, 85T, 85P2
Tl–X			see Tl–C	
Tm	– 0.49		photoconductivity	77S
V	+ 0.36	d	double donor V(+/+) interstitial 3d ⁴ –3d ³ , EPR, DLTS, CV, photocapacitance radioactive decay	86G, 83W2, 81L2, 81L1, 91T2, 92S1, 81G1, 80O 95A3
	– 0.48	d	single donor V(0/+), interstitial 3d ⁵ –3d ⁴ , DLTS, photocapacitance, CV	86G, 83W2, 85D1, 84O, 83R, 92S1, 91T2, 81L2, 81L1, 81G1, 80O 95A3
	– 0.21	a	radioactive decay single acceptor V(–/0), interstitial 3d ⁶ –3d ⁵ , DLTS, CV	86G, 83W2, 81L2, 81L1, 81G1, 80O, 91T2, 92S1 95A3
			radioactive decay pressure dependence	83J, 82W2
V–Al			V(interstitial)–Al(substitutional) donor–acceptor pair, DLTS, no level found	86G
V–Au	+ 0.42	d	Au(substitutional)–V(substitutional) binding energy 1.6 eV	83L1
	– 0.20	a		
V–B			B(substitutional)–V(interstitial) donor–acceptor pair, DLTS, no level found	86G
V–Ga			V(interstitial)–Ga(substitutional) donor–acceptor pair, DLTS, no level found	86G
V–H	– 0.49	d	after wet chemical etching, anneal out at 200 °C, 30 min	94S1, 92S1
V–In			V(interstitial)–In(substitutional) donor–acceptor pair, DLTS, no level found	86G
V–Pt			V(interstitial)–Pt(substitutional), DLTS, no levels found	86G
V–Zn	+ 0.29	d	V(interstitial)–Zn(substitutional) donor–acceptor pair, DLTS, TSCAP	86G, 82L
Vac			isolated vacancy	85B4
	+ 0.05	d	metastable center, single charge, negative Hubbard <i>U</i> , EPR, Hall effect, DLTS	84W2, 83N1, 80W, 80M3
Vac–Vac	+ 0.25	d	divacancy (0/+)	91S, 87S, 88S3, 83B1, 83B4
	– 0.42	a	divacancy (–/0)	82K, 82B2,
	– 0.23	aa	divacancy (– –/–) generated by irradiation, DLTS, IR-absorption at 0.34 eV, photoconductivity stable at <i>T</i> ≤ 300 °C	82B1, 81S2, 78K, 75W 76E

W	+ 0.38	d	DLTS, photoconductivity	94L3, 91P2, 83L5
Yb	+ 0.38 + 0.49		indiffusion at $T = 1050\text{ }^{\circ}\text{C}$, low active concentration, cluster formation	85F6, 85L3, 82A, 80C1, 77S
Zn	+0.28	a	substitutional acceptor Zn(−/0) IR spectroscopy, transient capacitance, DLTS	86G, 84W4, 81L2, 72H, 70Z, 84S1, 81S2, 89M1, 87L1, 90W2
	− 0.55 (+ 0.60)	aa	acceptor Zn(− −/−)	86G, 84W4, 84S1, 81S2, 72H, 70Z, 90W2, 87L1
Zn–Al	+ 0.2...0.4		several Al and Zn related levels	77M1, 57F
Zn–B	+ 0.09 + 0.092 + 0.126 ...+0.167	a a a	DLTS TSCAP, transient capacitance	90W2, 90L, 72H
Zn–Cr	− 0.10	a	Cr(substitutional)–Zn(substitutional) donor–acceptor pair, DLTS, TSCAP	86G, 82L
Zn–Fe	− 0.47	a	Fe(substitutional)–Zn(substitutional) donor–acceptor pair, DLTS, TSCAP	86G, 82L
Zn–Ga	+ 0.083		electrical measurements	57F
Zn–Mn	+ 0.18	d	Mn(substitutional)–Zn(substitutional)– donor–acceptor pair, DLTS, TSCAP	86G, 82L
Zn–V	+ 0.29	d	V(interstitial)–Zn(substitutional) donor–acceptor pair, DLTS, TSCAP	86G, 82L
Zr	+ 0.32 − 0.41 − 0.14	dd d a	DLTS	90L
			several Zr related levels close to the surface	90L

References to 1.2

A. References to "Physical properties"

(For references to "Impurities and defects", see below)

- 53M McSkimin, H. J.: J. Appl. Phys. 24 (1953) 988.
54M Morin, F. J., Maita, J. P.: Phys. Rev. 96 (1954) 28.
54S Smith, C. S.: Phys. Rev. 94 (1954) 42.
55G Geballe, T. H., Hull, G. W.: Phys. Rev. 98 (1955) 940.
56L Ludwig, G. H., Watters, R. L.: Phys. Rev. 101 (1956) 1699.
57C Carlson, R. O.: Phys. Rev. 108 (1957) 1390.
59C Cardona, M., Paul, W., Brooks, H.: J. Phys. Chem. Solids 8 (1959) 204.
59F1 Feher, G.: Phys. Rev. 114 (1959) 1219.
59F2 Flubacher, P., Leadbetter, A. J., Morrison, J. A.: Philos. Mag. 4 (1959) 273.
59K Keesom, P. H., Seidel, G.: Phys. Rev. 113 (1959) 33.
60C Cardona, M., Paul, W., Brooks, H.: Helv. Phys. Acta 33 (1960) 329.
60P Philipp, H. R., Taft, E. A.: Phys. Rev. 120 (1960) 37.
61H Hall, R. O. A.: Acta Crystallogr. 14 (1961) 1004.
63D Dolling, G.: in "Inelastic Scattering of Neutrons in Solids and Liquids" IAEA, Vienna 1963, Vol. 11, p. 37.
63P Philipp, H. R., Ehrenreich, H.: Phys. Rev. 129 (1963) 1550.
63S Shanks, H. R., Maycock, P. D., Sidles, P. H., Danielson, G. C.: Phys. Rev. 130 (1963) 1743.
64G Glassbrenner, C. J., Slack, G. A.: Phys. Rev. 134 (1964) A1058.
64H Henins, J.: J. Res. Nat. Bur. Std. 68A (1964) 529.
64M McSkimin, H. J., Andreatch, P., Jr.: J. Appl. Phys. 35 (1964) 2161.
65B Balslev, I., Lawaetz, P.: Phys. Lett. 19 (1965) 6.
65H Hensel, J. C., Hasegawa, H., Nakayama, M.: Phys. Rev. 138 (1965) A225.
66K Koder, H.: J. Phys. Soc. Jpn. 21, Suppl. (1966) 578.
66R Rao, K. V., Smakula, A.: J. Appl. Phys. 37 (1966) 2840.
67B Barber, M. D.: Solid State Electron. 10 (1967) 1039.
67H Hall, J. J.: Phys. Rev. 161 (1967) 756.
67K Krestovnikov, A. N., Evgenyev, S. B., Glazov, V. M.: Dokl. Akad. Nauk SSSR 174 (1967) 634.
68E Ezz-El-Arab, M., Galperin, B., Brielles, J., Vodar, B.: Solid State Commun. 6 (1968) 387.
68F Fulkerson, W., Moore, J. P., Williams, R. K., Graves, R. S., McElroy, D. L.: Phys. Rev. 167 (1968) 765.
69W Wynne, J. J.: Phys. Rev. 178 (1969) 1295.
70J Joshi, Y. P., Verma, G. S.: Phys. Rev. B 1 (1970) 750.
70S Shaklee, K. L., Nahory, R. E.: Phys. Rev. Lett. 24 (1970) 942.
70V van Vechten, J. A., Cardona, M., Aspnes, D. E., Martin, R. M.: Proc. Int. Conf. Phys. Semicond. 1970, U. S. At. Energy Comm. 1970, p. 82.
70Z Zucca, R. R. L., Shen, Y. R.: Phys. Rev. B 1 (1970) 2668.
71W Wepfer, G. G., Collins, T. C., Euwema, R. N.: Phys. Rev. B 4 (1971) 1296.
72A Aspnes, D. E., Studna, A. A.: Solid State Commun. 11 (1972) 1375.
72N1 Nikanorov, S. P., Burenkov, Yu. A., Stepanov, A. V.: Sov. Phys. Solid State (English Transl.) 13 (1972) 2516; Fiz. Tverd. Tela 13 (1971) 3001.
72N2 Nilsson, G., Nelin, G.: Phys. Rev. B 6 (1972) 3777.
72T Tubino, R., Piseri, L., Zerbi, G.: J. Chem. Phys. 6 (1972) 1022.
73C Chelikowski, J., Chadi, D. J., Cohen, M. L.: Phys. Rev. B 8 (1973) 2786.
73H Hultgren, R., Desai, P. D., Hawkins, D. T., Gleiser, M., Kelley, K. K., Wagman, D. D.: The Thermodynamic Properties of the Elements, Am. Soc. for Metals, Metals Park, Ohio 1973.
73N Norton, P., Braggins, T., Levinstein, H.: Phys. Rev. B 8 (1973) 5632.
73Y Yin, W. M., Paff, R. J.: J. Appl. Phys. 45 (1973) 1456.
74B Bludau, W., Onton, A., Heinke, W. J. Appl. Phys. 45 (1974) 1846.
74F Foreman, R. A., Aspnes, D. E.: Solid State Commun. 14 (1974) 100.
74N Nishino, T., Takeda, M., Hamakawa, Y.: Solid State Commun. 14 (1974) 627.
75C Canali, C., Jacoboni, C., Nava, F., Ottaviani, G., Alberigi Quaranta, A.: Phys. Rev. B 12 (1975) 2265.
76O Ousset, J. C., Leotin, J., Askenazy, S., Skolnick, M. S., Stradling, R. A.: J. Phys. C 9 (1976) 2802.
77C Capizzi, M., Merle, J. C., Fiorini, P.: Solid State Commun. 24 (1977) 451.
77J Jacoboni, C., Canali, C., Ottaviani, G., Alberigi Quaranta, A.: Solid State Electron. 20 (1977) 77.
77K Kondo, K., Moretani, A.: Nuovo Cimento 39B (1977) 387.

- 77L1 Lipari, N. O., Altarelli, M.: Phys. Rev. B 15 (1977) 4883.
77L2 Lyon, K. G., Salinger, G. L., Swenson, C. A., White, G. K.: J. Appl. Phys. 48 (1977) 865.
77W Weber, W.: Phys. Rev. B 15 (1977) 4789.
78C Chandrasekhar, M., Grimsditch, M. H., Cardona, M.: Phys. Rev. B 18 (1978) 4301.
78D1 Dyuzheva, T. I., Kabalkina, S. S., Novichkov, V. P.: Zh. Eksp. Teor. Fiz. 74 (1978) 1784; Sov. Phys. JETP 47 (1978) 931 (Engl. Transl.).
78D2 Daunois, A., Aspnes, D. E.: Phys. Rev. B 18 (1978) 1824.
78H Hammond, R. B., Silver, R. N.: Solid State Commun. 28 (1978) 993.
78T Timusk, T., Navarro, H., Lipari, N. O., Altarelli, M.: Solid State Commun. 25 (1978) 217.
80E Edwards, D. F., Ochoa, E.: Appl. Opt. 19 (1980) 4130.
81L Lampert, M. O., Koebel, J. M., Siffert, P.: J. Appl. Phys. 52 (1981) 4975.
81P Philip, J., Breazeale, M. A.: J. Appl. Phys. 52 (1981) 3383.
82A d'Amour, H., Denner, W., Schulz, H., Cardona, M.: J. Appl. Cryst. 15 (1982) 148.
82B Becker, P., Seyfried, P., Siegert, H.: Z. Physik B 48 (1982) 17.
82H Haug, A., Schmid, W.: Solid State Electron. 25 (1982) 665.
82J Jellison, G. E., Modine, F. A.: Appl. Phys. Lett. 41 (1982) 180.
82M Mitchel, W. C., Hemenger, P. M.: J. Appl. Phys. 53 (1982) 6880.
83A Aspnes, D. E., Studna, A. A.: Phys. Rev. B 27 (1983) 985.
83J Jellison, G. E., Modine, F. A.: Phys. Rev. B 27 (1983) 7466.
83L Lang, J. E., Madarasz, F. L., Hemenger, P. M.: J. Appl. Phys. 54 (1983) 3612.
83M Mascovic, D.R., Vukajlovic, F. R., Zekovic, S.: J. Phys. C 16 (1983) 6731.
83P Philip, J., Breazeale, M. A.: J. Appl. Phys. 54 (1983) 752.
83S1 Szmulowicz, F.: Appl. Phys. Lett. 43 (1983) 485.
83S2 Szmulowicz, F.: Phys. Rev. B 28 (1983) 5943.
83S3 Szmulowicz, F., Madarasz, F. L.: Phys. Rev. B 27 (1983) 2605.
83S4 Samara, G. A.: Phys. Rev. B 27 (1983) 3494.
84H Hu, J. Z., Spain, I. L.: Solid State Commun. 51 (1984) 263.
84O1 Okada, Y., Tokumaru, Y.: J. Appl. Phys. 56 (1984) 314.
84O2 Olijnyk, H., Sikka, S. K., Holzapfel, W. B.: Phys. Lett. 103A (1984) 137.
84S1 Spain, I. L., Hu, J. Z., Menoni, C. S., Black, D.: J. Phys. (Paris) 45 Suppl., Colloq. C8 (1984) C8-407.
84S2 Stevanovic, M. M.: Thermochim. Acta 77 (1984) 167.
85K Kagaya, H.-M., Soma, T.: Phys. Status Solidi (b) 127 (1985) K5.
85L Lee, S., Sanchez-Dehesa, J., Dow, J. D.: Phys. Rev. B 32 (1985) 1152.
85S Sieh, K. S., Smith, P. V.: Phys. Status Solidi (b) 129 (1985) 259.
86D Desai, P. D.: J. Phys. Chem. Ref. Data 15 (1986) 967.
86H Hu, J. Z., Merkle, L. D., Menoni, C. S., Spain, I. L.: Phys. Rev. B 34 (1986) 4679.
87D Duclos, S. J., Vohra, Y. K., Ruoff, A. L.: Phys. Rev. Lett. 58 (1987) 775.
88K Keppler, U.: Z. Metallkd. 79 (1988) 157.
90D Duclos, S. J., Vohra, Y. K., Ruoff, A. L.: Phys. Rev. B 41 (1990) 12021.
91G Giannozzi, P., de Gironcoli, S., Pavone, P., Baroni, S.: Phys. Rev. B 43 (1991) 7231.
93M McMahon, M. I., Nelves, R. J.: Phys. Rev. B 47 (1993) 8337; see also [95N2].
94C Crain, J., Ackland, G. J., Maclean, J. R., Piltz, R. O., Hatton, P. D., Pawley, G. S.: Phys. Rev. B 50 (1994) 13043.
94M McMahon, M. I., Nelves R. J., Wright, N. G., Allan, D. R.: Phys. Rev. B 50 (1994) 739; see also [95N2].
96M McMahon, M. I., Nelves, R. J.: Phys. Status Solidi (b) 198 (1996) 389.
99H Hanfland, M., Schwarz, U., Syassen, K., Takemura, K.: Phys. Rev. Lett. 82 (1999) 1197.

B. References to "Impurities and defects"

- 54M Morin, F. J., Maita, J. P.: Phys. Rev. 96 (1954) 975.
56B Burstein, E., Picus, G., Hennis, G., Wallis, R.: J. Phys. Chem. Solids 1 (1956) 65.
56P Picus, G., Burstein, E., Hennis, B.: J. Phys. Chem. Solids 1 (1956) 75.
57C Collins, C. B., Carlson, R. O., Gallagher, C. J.: Phys. Rev. 105 (1957) 1168.
57F Fuller, C. S., Morin, F. J.: Phys. Rev. 105 (1957) 379.
57S Shulman, R. G.: J. Phys. Chem. Solids 2 (1957) 115.
59H Hrostowski, H. J.: Infrared Absorption in Semiconductors, Hannay, N. B. (ed.), New York: Reinhold Publ. 1959.
61W Watkins, G.-D., Corbett, J. W.: Phys. Rev. 121 (1961) 1001.

- 64S Schultz, M. L.: *Infrared Phys.* 4 (1964) 93.
- 64Z Zibuts, A. Y., Paritskii, L. G., Ryvkin, S. M.: *Sov. Phys. Solid State* 5 (1964) 2416.
- 65A Aggarwal, R. L., Ramdas, A. K.: *Phys. Rev. A* 140 (1965) 1246.
- 65G1 Gibbons, F. F., Moll, J. L.: *Nucl. Instrum. Methods.* 38 (1965) 165.
- 65G2 Gilmer, T. E., Franks, R. E., Bell, R. J.: *J. Phys. Chem. Solids* 26 (1965) 1195.
- 65L Ludwig, G. W.: *Phys. Rev.* 137 (1965) A 1520.
- 65W1 Weltzin, R. D., Swalin, R. A., Hutchinson, T. E.: *Acta Metall.* 13 (1965) 115.
- 65W2 Waldner, M., Hiller, M. A., Spitzer, W. G.: *Phys. Rev. A* 140 (1965) 172.
- 67G Godik, E. E., Pokrovskii, Y. E.: *Sov. Phys. Semicond.* 1 (1967) 333.
- 67O Onton, A., Fisher, P., Ramdas, A. K.: *Phys. Rev.* 163 (1967) 686.
- 67W Watkins, G. D.: *Phys. Rev.* 155 (1967) 802.
- 68B Baker, J. A., Tucker, T. N., Moyer, N. E., Buschert, R. C.: *J. Appl. Phys.* 39 (1968) 4365.
- 68R Robertson, J. B., Franks, R. K.: *Solid State Commun.* 6 (1968) 825.
- 68S Sze, S. M., Irvin, J. C.: *Solid State Electron.* 11 (1968) 599.
- 69D Donbrava, P.: *Phys. Status Solidi* 34 (1969) K2.
- 69P Parry, E. P., Porter, M. S., McCaldin, J. O.: *Solid State Electron.* 12 (1969) 500
- 70C Chik, K. P.: *Radiat. Eff.* 4 (1970) 33.
- 70T Taft, E. A., Carlson, R. O.: *J. Electrochem. Soc.* 117 (1970) 711.
- 70Z Zavadskii, Yu. I., Kornilov, B. V.: *Phys. Status Solidi* 42 (1970) 617.
- 71G Gulamova, M. A., Karimova, I. Z., Knigin, P. I.: *Sov. Phys. Semicond.* 5 (1971) 687.
- 71K Kimerling, L. C., De Angelis, H. M., Carnes, C. P.: *Phys. Rev. B* 3 (1971) 427.
- 71Y Yau, L. D., Sah, C. T.: *Phys. Status Solidi A6* (1971) 561.
- 72C Crouch, R. K., Robertson, J. B., Gilmer, T. E.: *Phys. Rev. B* 5 (1972) 3111.
- 72F Fahrner, W., Goetzberger, A.: *Appl. Phys. Lett.* 21 (1972) 329.
- 72G Grinberg, I. S., Knigin, P. I., Korolev, Y. S.: *Fiz. Tekh. Poluprovodn.* 6 (1972) 410; *Sov. Phys. Semicond.* 6 (1972) 354.
- 72H Herman, J. M., Sah, C. T.: *Phys. Status Solidi* 14 (1972) 405.
- 72M Mason jr., AG., Blakemore, A. S.: *J. Appl. Phys.* 43 (1972) 2810.
- 73N Norton, P., Braggins, T., Levinstein, H.: *Phys. Rev. Lett.* 30 (1973) 488.
- 73S Schulz, M.: *Appl. Phys. Lett* 23 (1973) 31.
- 74A Azimov, S. A., Sultanov, N. A., Islamov, L. I., Nagmatov, R. N.: *Sov. Phys. Semicond.* 7 (1974) 1227.
- 74B Braun, S., Grimmeiss, H. G.: *J. Appl. Phys.* 45 (1974) 2658.
- 74C Crouch, R. K., Robertson, J. B., Morgan, H. T., Gilmer jr., T. E., Franks, R. K.: *J. Phys. Chem. Solids* 35 (1974) 833.
- 74P Penchina, C. M., Moore, J. S.: *Phys. Rev. B* 9 (1974) 5217.
- 74S1 Sah, C. T., Wang, C. T., Lee, S. H.: *Appl. Phys. Lett.* 25 (1974) 523.
- 74S2 Schulz, M.: *Appl. Phys.* 4 (1974) 225.
- 74Y Yau, L. D., and Sah, C. T.: *Solid State Electron.* 17 (1974) 193.
- 75A Anderson, W. W.: *Solid State Electron.* 18 (1975) 3108.
- 75H Hurrel, A., Schulz, M.: *Lattice, Defects in Semiconductors 1974, Inst. Phys. Conf. Ser.* 23 (1975) 474.
- 75K Kimerling, L. C., DeAngelis, H. M., Diebold, J. W.: *Solid State Commun.* 16 (1975) 171.
- 75L Lyubchik, B. G.: *Sov. Phys. Semicond.* 9 (1975) 686.
- 75N Nevin, J. H., Henderson, H. J.: *J. Appl. Phys.* 46 (1975) 2130.
- 75S Seregin, P. P., Nisturyuk, P. V., Nasredinov, F. S.: *Fiz. Tverd. Tela* 17 (1975) 2330
- 75V1 Voronkova, G. I., Iglitsyn, M. I., Salmanov, A. R.: *Sov. Phys. Semicond.* 8 (1975) 1043.
- 75V2 Voronkova, G. I., Iglitsyn, M. I., Salmanov, A. R.: *Sov. Phys. Semicond.* 9 (1975) 328.
- 75W Watkins, G. D.: *Lattice Defects in Semiconductors, in: Inst. Phys. Conf. Ser.* 23 (1975) 1.
- 76E Evwaraye, A. O., Sun, E.: *J. Appl. Phys.* 47 (1976) 3172.
- 76L Lee, Y. H., Corbett, J. W.: *Phys. Rev. B* 13 (1976) 2653.
- 76M Miyata, K., and Sah, C. T.: *Solid-State Electron.* 19 (1976) 611.
- 76N Norton, P.: *J. Appl. Phys.* 47 (1976) 308.
- 76P Pavlov, P. V., Zorin, E. I., Tetelbaum, D. I., Khokhlov, A. F.: *Phys. Status Solidi (a)* 35 (1976) 11.
- 76S Sclar, N.: *Infrared. Phys.* 16 (1976) 435.
- 76V van Vechten, J. A., Thurmond, C. D.: *Phys. Rev. B* 14 (1976) 3539.
- 76Z Zhdaonovich, N. S., Kozlov, Y. I.: *Fiz. Tekh. Poluprovodn.* 10 (1976) 1846; *Sov. Phys. Semicond.* 10 (1976) 1102.
- 77A1 Antonenko, R. S., Korniyushin, S. I., Shakhovtsov, V. I., Shindich, V. L., Yaskovets, I. I.: *Sov. Phys. Semicond.* 10 (1977) 942.
- 77A2 Akhmetov, V. D., Bolotov, V. V., Vasileev, A. V., Karpov, Y. A., Shakhovtsov, V. I., Shindich, V. L.: *Fiz. Tekh. Poluprovodn.* 11 (1977) 2243.

- 77A3 Areev, K. P., Vorobeev, S. A., Prokopeev, E. P., Tsoi, A. A.: Sov. Phys. Solid State 11 (1977) 1320.
- 77B1 Baron, R., Young, M. H., Neeland, J. K., Marsh, O. J.: Appl. Phys. Lett. 30 (1977) 594.
- 77B2 Busta, H. H., Waggener, H. A.: J. Electrochem. Soc. 124 (1977) 1424.
- 77B3 Braun, S., Grimmeiss, H. G., Spann, K.: J. Appl. Phys. 48 (1977) 3883.
- 77C1 Chiavarotti, G., Conti, M., Messina, A.: Solid State Electron. 20 (1977) 907.
- 77C2 Christodoulides, C. E., Grant, W. A., Williams, J. S.: Appl. Phys. 13 (1977) 391.
- 77E Evwaraye, A. O.: J. Appl. Phys. 48 (1977) 1840.
- 77G1 Godik, E. E., Sinis, V. P.: Sov. Phys. Semicond. 11 (1977) 347.
- 77G2 Grinshtein, P. M., Orlova, E. V., Fistul', V. I.: Sov. Phys. Semicond. 11 (1977) 977.
- 77G3 Grishin, V. P., Korpov, Y. A., Korniyushin, S. I., Stas, V. F., Shakovtsov, V. I., Shindich, V. L.: Ukr. Fiz. Zh. 22 (1977) 1037.
- 77K Kimerling, L. C.: Inst. Phys. Conf. Ser. 31 (1977) 221.
- 77L Lee, Y. H., Cheng, L. J., Gerson, J. D., Mooney, P. M., Corbett, J. W.: Solid State Commun. 21 (1977) 109.
- 77M1 Marchand, R. L., Stivers, A. R., Sah, C. T.: J. Appl. Phys. 48 (1977) 2576.
- 77M2 Marchand, R. L., Sah, C.-T.: J. Appl. Phys. 48 (1977) 336.
- 77N Norton, P., Slusher, R. E., Sturge, M. O.: Appl. Phys. Lett. 30 (1977) 446.
- 77S Sclar, N.: Infrared Phys. 17 (1977) 71.
- 78A1 Abakumov, V. N., Perel', V. I., Yassievich, I. N.: Soc. Phys. Semicond. 12 (1978) 1.
- 78A2 Adrianov, D. G., Bochkarev, E. P., Grishin, V. P., Karpov, Y. G., Savelev, A. S.: Fiz. Tekh. Poluprovodn. 12 (1978) 511.
- 78B Brotherton, S. D., Gill, A.: Appl. Phys. Lett. 33 (1978) 953.
- 78F Feichtinger, H., Waltl, J., Gschwandtner, A.: Solid State Commun. 27 (1978) 867.
- 78H Höhne, M.: Phys. Status Solidi (b) 85 (1978) 525.
- 78K Kimerling, L. C., Blood, P., Gibson, W. M.: Radiation Defects in Semiconductors, in: Inst. Phys. Conf. Ser. 46 (1978) 276.
- 78L Larrabee, R. D.: Semiconductor Characterization Techniques, Barnes, R. A., Rozgonyi, G. A. (eds.), The Electrochem. Soc. 1978, p. 71.
- 78P1 Picraux, S. T., Vook, F. L.: Phys. Rev. B 18 (1978) 2066.
- 78P2 Picraux, S. T., Vook, F. L.: Phys. Rev. B 18 (1978) 957.
- 78S1 Scott, W.: Appl. Phys. Lett. 32 (1978) 540.
- 78S2 Scott, W., Schmit, J. L.: Appl. Phys. Lett. 33 (1978) 294.
- 78S3 Sundström, B. O., Huldt, I., Nilsson, N. G.: Phys. Scr. 18 (1978) 413.
- 78T Thomas, R. N., Braggins, T. T., Hobgood, H. M., Takei, W. J.: J. Appl. Phys. 49 (1978) 2811.
- 79B Baron, R., Baukus, J. P., Allen, S. D., McGill, T. C., Young, M. H., Kimura, H., Winston, H. V., Marsh, O. J.: Appl. Phys. Lett. 34 (1979) 257.
- 79E Elliott, K. R., Lyon, S. A., Smith, D. L., McGill, T. C.: Phys. Lett. 70A (1979) 52.
- 79F Forbes, L., Brown, R., Sheikholeslam, M., Current, W.: Solid State Electron. 22 (1979) 391.
- 79J Jaganath, C., Grabowski, Z. W., Ramdas, A. K.: Solid State Commun. 29 (1979) 355.
- 79O Ohta, F., Sakata, M.: Solid State Electron. 22 (1979) 677.
- 79P Pajot, B., Kauppinen, J., Anttila, R.: Solid State Commun. 31 (1979) 759.
- 79S1 Stein, H.J.: Phys. Rev. Lett. 43 (1979) 1030.
- 79S2 Swaminathan, V., Lang, J. E., Hemenger, P. M., Smith, S. R.: Appl. Phys. Lett. 35 (1979) 184.
- 79S3 Saks, N. S., Nordbryhn, A.: J. Appl. Phys. 50 (1979) 6962.
- 79T1 Troxel, J. R., Chatterjee, A. P., Watkins, G. D.: Phys. Rev. B 19 (1979) 5336.
- 79T2 Troxel, J. R.: Ph. D. Thesis, Lehigh University, U. S. A. 1979.
- 79V Vydianath, H. R., Helm, W. J., Lorenzo, J. S., Hoelke, S. T.: Infrared Phys. 19 (1979) 93.
- 79Y Yunusov, M. S., Tursunov, N. A.: Sov. Phys. Semicond. 13 (1979) 204.
- 79Z1 Zastavnyi, A. V., Korol, V. M., Mikhaleva, A. N., Prozorovskii, V. D.: Sov. Phys. Semicond. 13 (1979) 580.
- 79Z2 Zeile, H., Mathussi, O., Lassmann, K.: Phys. Lett. 40 (1979) L53.
- 80B1 Bagraev, N. T., Vlasenko, L. S., Karpov, Y. A.: J. Cryst. Growth 50 (1980) 764.
- 80B2 Braggins, T. T., Hobgood, H. M., Swartz, J. C., Thomas, R. N.: IEEE Trans. Electron Devices ED-27 (1980) 2.
- 80B3 Brower, K. L.: Phys. Rev. Lett. 44 (1980) 1627.
- 80C1 Campisano, S. U., Grimaldi, M. G.: Lett. Nuovo Cimento 29 (1980) 413.
- 80C2 Chen, J.-W., Milnes, A. G.: Annu. Rev. Mater. Sci. 10 (1980) 157.
- 80D Davis jr., J. R., Rohatgi, A., Hopkins, R. H., Blais, P. D., Rai-Chaudhuri, P., McCormick, J., Mollenkopf, H.: IEEE Trans. Electron Devices ED-27 (1980) 677.
- 80F Feenstra, R. M., McGill, T. C.: Solid State Commun. 36 (1980) 1039.
- 80G Graff, K.: J. Electrochem. Soc. 128 (1980) 669.

- 80H Hell, W., Helbig, R., Schulz, M.: IEEE Trans. Electron. Devices ED-27 (1980) 10.
- 80J1 Jagannath, C., Ramdas, A. K.: J. Phys. Soc. Jpn. 49, Suppl. A (1980) 201.
- 80J2 Jagannath, C., Ramdas, A. K.: J. Phys. Soc. Jpn. 49, Suppl. A (1980) 201.
- 80L1 Litvinko, A. G., Makarenko, L. F., Murin, L. I.: Fiz. Tekh. Poluprovodn. 14 (1980) 776; Sov. Phys. Semicond. 14 (1980) 455.
- 80L2 Larrabee, R. D.: J. Electrochem. Soc. 127 (1980) 1640.
- 80L3 Lawaetz, P., Proctor, W. G.: J. Phys. Jpn. Soc. 49 Suppl. A (1980) 333.
- 80L4 Lefevre, H.: Appl. Phys. 22 (1980) 15.
- 80M1 Mitic, A., Sato, T., Nishi, H., Hashimoto, H.: Appl. Phys. Lett. 37 (1980) 727.
- 80M2 Mitchard, G. S., McGill, T. C.: Appl. Phys. Lett. 37 (1980) 959.
- 80M3 Mukashev, B. N., Kolodin, L. G., Nussupov, K. H., Spitsyn, A. V., Vavilov, V. S.: Radiat. Eff. 46 (1980) 79.
- 80O Ohta, E., Sakata, M.: Solid State Electron. 23 (1980) 759.
- 80S Schwartz, J. C., Lemmon, P. H., Thomas, R. N.: Solid State Commun. 36 (1980) 331.
- 80T Troxel, J. R., Watkins, G. D.: Phys. Rev. B 22 (1980) 921.
- 80W Watkins, G. D., Troxell, J. R.: Phys. Rev. Lett. 44 (1980) 1484.
- 80Y Yoshida, M.: Jpn. J. Appl. Phys. 19 (1980) 2427.
- 81A1 Altukhov, P. D., Eltsov, K. N., Rogachev, A. A.: Fiz. Tverd. Tela 23 (1981) 643; Sov. Phys. Solid State (English Transl.) 23 (1981) 367.
- 81A2 Arch, D. K., Schafer, D. E.: Proc. Soc. Photo Opt. Instrum. Eng. 285 (1981) 175.
- 81B Bakhieva, S. R., Kehna, M. G., Seregin, P. P.: Phys. Status Solidi (a) 63 (1981) 23.
- 81D Dyunaidov, S. S., Urmanov, N. A., Gafurova, M. V.: Phys. Status Solidi (a) 66 (1981) K79.
- 81F Frank, W.: Festkörperprobleme XXI, Treusch, J. (ed.), Braunschweig: Vieweg 1981, p. 221.
- 81G1 Graff, K., Pieper, H.: Proc. Electrochem. Soc. 81-5 (1981) 331.
- 81G2 Graff, K., Pieper, H.: J. Electrochem. Soc. 128 (1981) 669.
- 81G3 Garrido, J., Calleja, E., Piqueras, J.: Solid State Electron. 24 (1981) 1121.
- 81G4 Grimmeiss, H. G., Janzen, E., Ennen, H., Schirmer, O., Wörner, R., Holm, C., Sirtl, E., Wagner, P.: Phys. Rev. B 24 (1981) 4571.
- 81H Henry, M. O., Lightowers, E. C., Killoran, N., Dunstan, D. J., Cavenett, B. C.: J. Phys. C 14 (1981) L255.
- 81J1 Jones, C. E., Johnson, G. E.: J. Appl. Phys. 52 (1981) 5159.
- 81J2 Jones, C. E., Schafer, D., Scott, W., Hager, R. J.: J. Appl. Phys. 52 (1981) 5148.
- 81J3 Jagannath, C., Grabowski, Z. W., Ramdas, A. K.: Phys. Rev. B 23 (1981) 2082.
- 81K1 Kleinhenz, R. L., Lee, Y. H., Corbett, J. W., Sieverts, E. G., Muller, S. H., Ammerlaan, C. A. J.: Phys. Status Solidi (a) 108 (1981) 363.
- 81K2 Kunio, T., Nishino, T., Ohta, E., Sakata, M.: Solid State Electron. 24 (1981) 1087.
- 81L Lin, A. L., Crouse, A. G., Wendt, J., Campbell, A. G., Newman, R.: Appl. Phys. Lett. 38 (1981) 683.
- 81L1 Lemke, H.: Phys. Status Solidi (a) 64 (1981) 549.
- 81L2 Lemke, H.: Phys. Status Solidi (a) 66 (1981) 541.
- 81L3 Lemke, H.: Phys. Status Solidi (a) 64 (1981) 215.
- 81N Neimash, V. B., Sosnin, M. G., Shakhovtsov, V. I., Shindick, V. L.: Fiz. Tekh. Poluprovodn. 15 (1981) 786.
- 81P Pajot, B., Debarre, D., Roche, D.: J. Appl. Phys. 52 (1981) 5774.
- 81R Rohatgi, A., Hopkins, R. H., Davis jr., JR.: IEEE Trans. Electron Devices ED-28 (1981) 103.
- 81S1 Schafer, D. E.: Proc. Soc. Photo Opt. Instrum. Eng. 285 (1981) 183.
- 81S2 Sclar, N.: Solid State Electron. 24 (1981) 1133.
- 81S3 Szablak, B., Altarelli, M.: Solid State Commun. 37 (1981) 341.
- 81W1 Wünnstel, K., Wagner, P.: Solid State Commun. 40 (1981) 797.
- 81W2 Weber, J., Sauer, R., Wagner, P.: J. Lumin. 24/25 (1981) 155.
- 81Z Ziemelis, U. O., Thewalt, M. L. W., Parsons, R. R.: Appl. Phys. Lett. 39 (1981) 972.
- 82A Antonenko, R. S., Nejman, V. B., Shakhovtsov, V. I., Shindich, V. L.: Fiz. Rad. Povrezh. I. Rad. Mat. 4 (1982) 38.
- 82B1 Brotherton, S. D., Bradley, P.: J. Appl. Phys. 53 (1982) 5720.
- 82B2 Benton, J. L., Kimerling, L. C.: J. Electrochem. Soc. 129 (1982) 2098.
- 82B3 Brower, K. L.: Phys. Rev. B 26 (1982) 6040.
- 82E Elliot, K. R.: Phys. Rev. B 25 (1982) 1460.
- 82G1 Geim, K., Pensl, G., Schulz, M.: Appl. Phys. A 27 (1982) 71.
- 82G2 Grimmeiss, H. G., Janzen, E., Larsson, K.: Phys. Rev. B 25 (1982) 2627.
- 82H Harris, R. D., Newton, J. L., Watkins, G. D.: Phys. Rev. Lett. 48 (1982) 1271.
- 82J Jantsch, W., Wünnstel, K., Kumagai, O., Vogl, P.: Phys. Rev. B 25 (1982) 251.
- 82K Kreissl, J., Gehlhoff, W.: Phys. Status Solidi (b) 112 (1982) 695.

- 82L Lemke, H.: Phys. Status Solidi (a) 72 (1982) 177.
- 82N Narita, S., Shinbashi, T., Kobayashi, M.: J. Phys. Soc. Jpn. 51 (1982) 2186.
- 82S1 Searle, C. W., Ohmer, M. C., Hemenger, P. M.: Solid State Commun. 44 (1982) 1597.
- 82S2 Schirmer, O. F.: J. Phys. C 15 (1982) L645.
- 82S3 Schelter, W., Hell, W., Helbig, R., Schulz, M.: J. Phys. C 15 (1982) 5839.
- 82T1 Tomokage, H., Hagiwara, M., Hashimoto, K.: Jpn. J. Appl. Phys. 21 (1982) 402.
- 82T2 Thewalt, M. L. W., Watkins, S. P., Ziemelis, U. O., Lightowlers, E. C., Henry, M. O.: Solid State Commun. 44 (1982) 573.
- 82T3 Tokumaru, Y., Okushi, H.: Jpn. J. Appl. Phys. 21 (1982) L443.
- 82W1 Wünnel, K., Wagner, P.: Appl. Phys. A 27 (1982) 207.
- 82W2 Wünnel, K., Kumagai, O., Wagner, P., Jantsch, W.: Appl. Phys. A 27 (1982) 251.
- 82Z Ziemelis, U. O., Thewalt, M. L. W., Parsons, R. R.: Can. J. Phys. 60 (1982) 1041.
- 83B1 Baliga, B. J., Ewvaraye, A. O.: J. Electrochem. Soc. 30 (1983) 1916.
- 83B2 Bergholz, W.: Physica B 116 (1983) 312.
- 83B3 Benton, J. L., Kimerling, L. C., Stavola, M.: in [83a1], p. 271; Physica B 116 (1983) 271.
- 83B4 Brotherton, S. D., Parker, G. J., Gill, A.: J. Appl. Phys. 54 (1983) 5112.
- 83B5 Barrie, R., Parent, L. G., Parsons, R. R.: Can. J. Phys. 61 (1983) 67.
- 83C1 Czaputa, R., Feichtinger, H., Oswald, J.: Solid State Commun. 47 (1983) 223.
- 83C2 Conzelmann, H., Weber, J.: Physica B 116 (1983) 291.
- 83C3 Chantre, A., Kechouane, M., Bois, D.: Physica B 116 (1983) 547; also in [83a1], p. 547.
- 83E Ennen, H., Schneider, G., Pomrenke, G., Axman, A.: Appl. Phys. Lett. 43 (1983) 943.
- 83F1 Feichtinger, H., Czaputa, R.: Phys. Status Solidi (a) 79 (1983) K143.
- 83F2 Fischer, D. W., Rome, J. J.: Phys. Rev. B 27 (1983) 4826.
- 83G Gösele, U., Tan, T. Y.: Aggregation Phenomena of Point Defects in Si, Sirtl, F. (ed.), The Electrochem. Soc. 1983, p. 17.
- 83J Jantsch, W., Wünnel, K., Kumagai, D., Vogl, P.: Physica B/C 117/118 (1983) 188.
- 83K1 Kimerling, L. C., Benton, J. L.: Physica B 116 (1983) 297.
- 83K2 Kunio, T., Yamasaki, T., Ohta, E., Sakata, M.: Solid State Electron. 26 (1983) 155.
- 83K3 Kalyanaraman, V.: J. Appl. Phys. 54 (1983) 6417.
- 83K4 Keller, W., Pensl, G., Schulz, M.: Physica B 116 (1983) 244.
- 83L1 Lemke, H.: Phys. Status Solidi (a) 75 (1983) 473.
- 83L2 Lemke, H.: Phys. Status Solidi (a) 76 (1983) 223.
- 83L3 Lemke, H.: Phys. Status Solidi (a) 75 (1983) K49.
- 83L4 Ledebø, L.-Å., Wang, Z. -G.: Appl. Phys. Lett. 42 (1983) 680.
- 83L5 Lemke, H.: Phys. Status Solidi (a) 76 (1983) K193.
- 83L6 Lebedev, A. A.: Sov. Phys. Semicond. 17 (1983) 1376.
- 83M Meese, J. M., Farmer, J. W., Lamp, C. D.: Phys. Rev. Lett. 51 (1983) 1286.
- 83N1 Newton, J. L., Chatterjee, A. P., Harris, R. D., Watkins, G. D.: in [83a1], p. 219; Physica B 116 (1983) 219.
- 83N2 Niklas, J. R., Spaeth, J. M.: Solid State Commun. 46 (1983) 121.
- 83O Oeder, R., Wagner, P.: Mater. Res. Soc. Symp. Proc. 14 (1983) 171.
- 83P1 Pearton, S. J., Haller, E. E.: J. Appl. Phys. 54 (1983) 3613.
- 83P2 Peschel, W., Kuhnert, R., Schulz, M.: Appl. Phys. A 30 (1983) 59.
- 83P3 Pearton, S. J., Tavendale, J.: J. Appl. Phys. 54 (1983) 1375.
- 83R Rohatgi, A., Davis, J. R., Hopkins, R. H., McMullin, P. G.: Solid State Electron. 26 (1983) 1039.
- 83S1 Schirmer, O. F.: Physica B 116 (1983) 306.
- 83S2 Sauer, R., Weber, J.: Physica B 116 (1983) 195.
- 83S3 Sirtl, F.: Defects in Silicon; Bullis, W. M., Kimerling, L. C. (eds.), The Electrochem. Soc. 1983, p. 45.
- 83S4 Searle, C. W., Hemenger, P. M., Ohmer, M. C.: Solid State Commun. 48 (1983) 995.
- 83S5 Sah, C. T., Sun, J. Y., Tzou, J. J.: Appl. Phys. Lett. 43 (1983) 204.
- 83W1 Wünnel, K., Fröhner, K.-H., Wagner, P.: Physica B 116 (1983) 301.
- 83W2 Weber, E. R.: Appl. Phys. A 30 (1983) 1.
- 83Y Yamamoto, N.: J. Appl. Phys. 54 (1983) 3475.
- 83Z Zastavnyi, A. V., Korol', V. M., Ustinova, E. L.: Sov. Phys. Semicond. 17 (1983) 1081.
- 84B1 Brotherton, S. D., Bradley, P., Gill, A., Weber, F.: J. Appl. Phys. 55 (1984) 952.
- 84B2 Burger, W., Lassmann, K.: Phys. Rev. Lett. 53 (1984) 2035.
- 84B3 Bourret, A., Thibault-Desseaux, J., Seidman, D. N.: J. Appl. Phys. 55 (1984) 825.
- 84B4 Bobrova, E. A., Vavilov, V. S., Vulis, Yu. D., Galkin, G. N., Pospelov, V. V.: Sov. Phys. Semicond. 18 (1984) 432.

- 84D1 Dargis, A. Yu., Zhuravskas, S. V.: Sov. Phys. Semicond. 18 (1984) 371.
- 84D2 Dvurechenskii, A. V., Kashnikov, B. P., Suprunchik, V. V.: Phys. Status Solidi (a) 86 (1984) 155.
- 84F Fischer, D. W., Mitchel, W. C.: Appl. Phys. Lett. 45 (1984) 167.
- 84G1 Greulich-Weber, S., Niklas, J. R., Spaeth, J.-M.: J. Phys. C 17 (1984) L911.
- 84G2 Greulich-Weber, S., Niklas, J. R., Weber, E. R., Spaeth, J. M.: Phys. Rev. B 30 (1984) 6292.
- 84H1 Hölzlein, K. H., Pensl, G., Schulz, M.: Appl. Phys. A 34 (1984) 155.
- 84H2 Henry, P. M., Farmer, J. W., Meese, J. M.: Appl. Phys. Lett. 45 (1984) 454.
- 84H3 Hansen, W. L.: Appl. Phys. Lett. 44 (1984) 606.
- 84H4 Hofmann, K., Schulz, M.: Appl. Phys. A 33 (1984) 19.
- 84J Janzen, E., Stedman, R., Grossmann, G., Grimmeiss, H. G.: Phys. Rev. B 29 (1984) 1907.
- 84K1 Keller, W.: J. Appl. Phys. 55 (1984) 3471.
- 84K2 van Kooten, J. J., Weller, G. A., Ammerlaan, C. A. J.: Phys. Rev. B 30 (1984) 4564.
- 84L1 Lemke, H.: Phys. Status Solidi (a) 83 (1984) 637.
- 84L2 Lightowers, E. C., Canham, L. T., Davies, G., Thewalt, M. L. W., Watkins, S. P.: Phys. Rev. B 29 (1984) 4517.
- 84O Ohta, E., Kunio jr., T., Sato, T., Sakata, M.: J. Appl. Phys. 56 (1984) 2890.
- 84P1 Pankove, J. I., Wance, R. O., Berkeyheiser, J. E.: Appl. Phys. Lett. 45 (1984) 1100.
- 84P2 Pearton, S. J., Tavendale, A. J.: J. Phys. C 17 (1984) 6701.
- 84Q Queisser, H.-J., Theodorou, D. E.: Solid State Commun. 51 (1984) 875.
- 84R Rosencher, E., Mosser, V., Vincent, G.: Phys. Rev. B 29 (1984) 1135.
- 84S1 Sclar, N.: Appl. Phys. 55 (1984) 2972.
- 84S2 Solov'eva, E. V., Lazareva, G. V., Leiverov, B. M., Lototskii, A. G., Milvidskii, M., Rytova, N., Tvirova, E.: Sov. Phys. Semicond. 18 (1984) 985.
- 84T Thebault, D., Barrau, J., Armelles, G., Laurent, N., Noguier, J. P.: Phys. Status Solidi (a) 125 (1984) 357.
- 84U Utzig, J., and Schröter, W.: Appl. Phys. Lett. 45 (1984) 761.
- 84W1 Wagner, P., Holm, C., Sirtl, E., Oeder, R., Zulehner, W.: Festkörperprobleme XXIV, Grosse, P. (ed.), Braunschweig: Vieweg 1984, p. 191.
- 84W2 Watkins, G. D.: Festkörperprobleme XXIV, Grosse, P. (ed.), Braunschweig: Vieweg 1984, p. 163.
- 84W3 Watkins, S. P., Thewalt, M. L. W., Steiner, T.: Phys. Rev. B 29 (1984) 5727.
- 84W4 Wang, A. C., Lu, L. S., Sah, C. T.: Phys. Rev. B 30 (1984) 5896.
- 84W5 Wang, A. C., Sah, C. T.: J. Appl. Phys. 56 (1984) 1021.
- 85A1 Astrova, E. V., Bolshakov, I. B., Lebedev, A. A., Mikhno, O. A.: Sov. Phys. Semicond. 19 (1985) 371.
- 85A2 Assali, L. V. C., Leite, J. R., Fazzio, A.: Phys. Rev. B 32 (1985) 8085.
- 85A3 Assali, L. V. C., Leite, J. R.: Phys. Rev. Lett. 55 (1985) 980.
- 85A4 Astrova, E. V., Lebedev, A. A., Sultanov, N. A.: Sov. Phys. Semicond. 19 (1985) 563.
- 85A5 Abdurakhmanov, K. P., Umarov, T. A., Teshabaev, A. T., Khodzhaev, M. D.: Sov. Phys. Semicond. 19 (1985) 719.
- 85A6 Abdurakhmanov, K. P., Lebedev, A. A., Kreissl, J., Utamuradova, Sh. B.: Sov. Phys. Semicond. 19 (1985) 133.
- 85A7 Abdurakhmanov, K. P., Vitman, R. F., Daliev, Kh. S., Lebedev, A. A., Utamuradova, Sh. B.: Sov. Phys. Semicond. 19 (1985) 711.
- 85A8 Abdurakhmanov, K. P., Daliev, Kh. S., Lebedev, A. A., Utamuradova, Sh. B.: Sov. Phys. Semicond. 19 (1985) 995.
- 85A9 Armellas, G., Barrau, J., Brosseau, M., Pajot, B., Naud, C.: Solid State Commun. 56 (1985) 303.
- 85A10 Astrova, E. V., Gontar, V. M., Lebedev, A. A.: Sov. Phys. Semicond. 19 (1985) 778.
- 85B1 Brotherton, S. D., Bradley, P., Gill, A.: J. Appl. Phys. 57 (1985) 1783.
- 85B2 Brotherton, S. D., Bradley, P., Gill, A.: J. Appl. Phys. 57 (1985) 1941.
- 85B3 Bagraev, N. T., Vlasenko, L. S., Lebedev, A. A.: Phys. Status Solidi (a) 91 (1985) 165.
- 85B4 Bains, S. K., Banbury, P. C.: J. Phys. C 18 (1985) L109.
- 85B5 Bugai, A. A., Kustov, V. E., Semenov, Y. G., Shakhovtsov, V. I., Shindich, V. L.: Sov. Phys. Solid State 27 (1985) 1093.
- 85C1 Chantre, A.: Appl. Phys. Lett. 46 (1985) 263.
- 85C2 Chantre, A.: Phys. Rev. B 32 (1985) 3687.
- 85C3 Cerofolini, G. F., Pignatelli, G. U., Mazzega, E., Ottaviani, G.: J. Appl. Phys. 58 (1985) 2204.
- 85C4 Czaputa, R., Feichtinger, H., Oswald, J., Sitter, H., Haider, M.: Phys. Rev. Lett. 55 (1985) 758.
- 85D1 Daliev, Kh. S., Lebedev, A. A., Sultanov, N. A., Ecke, W.: Sov. Phys. Semicond. 19 (1985) 211.
- 85D2 Drevinsky, P. J., DeAngelis, H. M.: Proc. Defect Conf., Coronado, Kimmerling, L. C. (ed.), The Met. Soc. of AIME 1985, p. 807.

- 85F1 Feenstra, R. M., Pantelides, S. T.: Phys. Rev. B 31 (1985) 4083.
- 85F2 Fazzio, A., Caldas, M. J., Zunger, A.: Phys. Rev. B 32 (1985) 934.
- 85F3 Feichtinger, H., Oswald, J., Czaputa, R., Vogl, P., Wünstel, K.: Proc. Defect Conf. Coronado, Kimerling, L. C. (ed.), The Met. Soc. of AIME 1985, p. 855.
- 85F4 Fischer, D. W., Mitchel, W. C.: Appl. Phys. Lett. 47 (1985) 281.
- 85F5 Fischer, D. W., Mitchel, W. C.: J. Appl. Phys. 58 (1985) 3118.
- 85F6 Fu, C.-Y., Lu, Y.-L.: Chin. Phys. 5 (1985) 527.
- 85G1 Gerasimenko, N. N., Zaitsev, B. A., Safronov, L. N., Smirnov, L. S.: Sov. Phys. Semicond. 19 (1985) 762.
- 85G2 Gorelinskii, Y. V., Nevinnyi, N. N., Ajazbaev, S. S.: Phys. Lett. A 110 (1985) 157.
- 85H1 Helbig, R.: Festkörperprobleme XXV, Grosse, P. (ed.), Braunschweig: Vieweg 1985, p. 573.
- 85H2 Hurm, V., Hornung, J. C. R., Manek, O.: J. Appl. Phys. 58 (1985) 588.
- 85H3 Hertel, N., Materlik, O., Zegenhagen, J.: Z. Phys. B 58 (1985) 199.
- 85H4 Hjalmarsen, H. P., Jennison, D. R.: Phys. Rev. B 31 (1985) 1208.
- 85H5 Harris, R. D., Watkins, G. D.: Proc. Defect. Conf. Coronado, Kimerling, L. C., (ed.), The Met. Soc. of AIME 1985, p. 799.
- 85J1 Johnson, N. M., Moyer, M. D.: Appl. Phys. Lett. 46 (1985) 787.
- 85J2 Johnson, N. M.: Phys. Rev. B 31 (1985) 5525.
- 85J3 Johnson, N. M.: Appl. Phys. Lett. 47 (1985) 874.
- 85J4 Jaraiz, M., Duenas, S., Vicente, J., Bailon, L., Barbolla, J.: Solid State Electron. 29 (1985) 883.
- 85J5 Jackson, D. B., Sah, C. T.: J. Appl. Phys. 58 (1985) 2225.
- 85J6 Janzén, E., Grossmann, G., Stedman, R., Grimmeiss, H. G.: Phys. Rev. B 31 (1985) 8000.
- 85K Kleverman, M., Grimmeiss, H. G., Litwin, A., Janzen, E.: Phys. Rev. B 31 (1985) 3659.
- 85L1 Lee, K. M., Trombetta, J. M., Watkins, G. D.: Mater. Res. Symp. Proc. 46 (1985) 263.
- 85L2 Lemke, H.: Phys. Status Solidi (a) 91 (1985) 649.
- 85L3 Lu, Y., Fu, C., Zeng, S.: Chin. J. Semicond. 6 (1985) 128.
- 85M Mikkelsen jr., J. C.: Appl. Phys. Lett. 46 (1985) 882.
- 85N1 Nauka, K., Goorsky, M. S., Gatos, H. C., Lagowski, J.: Appl. Phys. Lett. 47 (1985) 1341.
- 85N2 Newman, P. F., Hirsch, M. J., Holcomb, D. F.: J. Appl. Phys. 58 (1985) 3779.
- 85P1 Pankove, J. I., Zanzucchi, P. J., Magee, C. W.: Appl. Phys. Lett. 46 (1985) 421.
- 85P2 Pankove, J. I., Magee, C. W., Wance, R. O.: Appl. Phys. Lett. 47 (1985) 748.
- 85S1 Stavola, M., Lee, K. M., Nabity, J. C., Freeland, P. E., Kimerling, L. C.: Phys. Rev. Lett. 54 (1985) 2639.
- 85S2 Sememyuk, A. K., Nazarchuk, P. F.: Sov. Phys. Semicond. 19 (1985) 816.
- 85S3 Saito, R., Momma, N., Naito, M.: J. Electrochem. Soc. 132 (1985) 225.
- 85T Thewalt, M. L. W., Lightowlers, E. C., Pankove, J. I.: Appl. Phys. Lett. 46 (1985) 689.
- 85W Weber, E. R.: Proc. Soc. Photo-Opt. Instrum. Eng. 524 (1985) 160.
- 85Z1 Zakirov, A. S., Igamberdiev, Kh. T., Kakharov, S. S., Mamadalimov, A. T., Khabibulaev, P. K.: Sov. Phys. Semicond. 19 (1985) 1043.
- 85Z2 Zastavnyi, A. V., Korol', V. M.: Sov. Phys. Semicond. 19 (1985) 785.
- 86A1 Armelles, G., Barrau, J., Brousseau, M., Nougier, J. P.: Phys. Rev. B 33 (1986) 1243.
- 86A2 Armelles, G., Barrau, J., Thomas, V., and Brousseau, M.: J. Phys. C: Solid State Phys. 19 (1986) 2593.
- 86A3 Assali, L. V. C., Leite, J. R.: Solid State Commun. 58 (1986) 577.
- 86B1 Barnes, C. E., Samara, G. A.: Appl. Phys. Lett. 48 (1986) 934.
- 86B2 Borenstein, J. T., Jones, J. T., Corbett, J. W., Oehrlein, G. S., Kleinhenz, R. L.: Appl. Phys. Lett. 49 (1986) 199.
- 86C1 Chantre, A., Kimerling, L. C.: Appl. Phys. Lett. 48 (1986) 1000.
- 86C2 Chantre, A., Benton, J. L., Asom, M. T., Kimerling, L. C.: Proc. 14th. Int. Conf. on Defects in Semiconductors, Paris 1986.
- 86D1 Delfino, M., Sadana, D. K., Morgan, A. E.: Appl. Phys. Lett. 49 (1986) 575.
- 86D2 Dietrich, H., Vollmer, H., Labusch, R.: Solid State Commun. 58 (1986) 811.
- 86G Graff, K.: Semiconductor Silicon 1986, Huff, H. R., Abe, T., Kolbesen, B. (eds.), The Electrochem. Soc. 1986, p. 751.
- 86H Hölzlein, K., Pensl, G., Schulz, M., Johnson, N. M.: Appl. Phys. Lett. 48 (1986) 916.
- 86K1 Klevermann, M., Grimmeis, H. G.: Semicond. Sci. Techn. 1 (1986) 45.
- 86K1 Krag, W. F., Kierner, W. H., Zeiger, H. J.: Phys. Rev. B 33 (1986) 8304.
- 86K2 Kai-Mao, C., and Guo-Gang, Q.: Materials Science Forum Vol. 10-12 (1986) 1093.
- 86K2 van Kemp, R., Sieverts, E. G., Ammerlaan, C. A. J.: Proc. 14th. Int. Conf. on Defects in Semiconductors, Paris 1986, Trans. Tech. Publ. 1986.

- 86L1 Lemke, H.: Phys. Status Solidi (a) 94 (1986) K 55.
- 86L2 Lemke, H.: Phys. Status Solidi (a) 95 (1986) 665.
- 86M Muro, K., Sieverts, A. J.: Phys. Rev. Lett. 57 (1986) 897.
- 86N Nolte, D. D., Haller, E. E., Omling, P.: Proc. 14th. Int. Conf. on Defects in Semiconductors, Paris 1986.
- 86P Pensl, G., Roos, G., Holm, C., Wagner, P.: Mater. Sci. Forum 10-12 (1986) 911.
- 86S1 Song, L. W., Benson, B. W., Watkins G. D.: Phys. Rev. 33 (1986) 1452.
- 86S2 Stöffler, W., Weber, J.: Mater. Sci. Forum 10-12 (1986) 705.
- 86S3 Stein, H. J.: Proc. MRS Meeting Boston 1986, Mikkelsen, J. (ed.), MRS Pittsburgh, Pa. 1986, p. 523.
- 86S4 Stöffler, W., Weber, J.: Phys. Rev. B 33 (1986) 8892.
- 87B1 Barber, H., Grimmeiss, H. G., Kleverman, M., Omling, P., Zafar Iqbal, M.: J. Appl. Phys. 62 (1987) 2853.
- 87B2 Brotherton, S. D., Ayres, J. R., Gill, A., van Kesteren, H. W., Greidanus, F. J. A. M.: J. Appl. Phys. 62 (1987) 1826.
- 87C1 Chantre, A.: Appl. Phys. Lett. 50 (1987) 1500.
- 87C2 Conzelmann, H.: Appl. Phys. A 42 (1987) 1.
- 87G Gorelinskii, Yu. V., and Nevinnii, N. N.: Sov. Tech. Phys. Lett. 13 (1987) 45.
- 87H Haider, M., Sitter, H., Czaputa, R., Feichtinger, H., Oswald, J.: J. Appl. Phys. 62 (1987) 3785.
- 87I Indusekhar, H., Kumar, V.: J. Appl. Phys. 61 (1987) 1449.
- 87K1 Kleverman, M., Oljaos, J., Grimmeiss, H. G.: Phys. Rev. B 35 (1987) 4093.
- 87K2 Kwon, Y. K., Ishikawa, T., Kuwano, H.: J. Appl. Phys. 61 (1987) 1055.
- 87K3 Kitagawa, H., Nakashima, H.: Phys. Status Solidi (a) 99 (1987) K49.
- 87L1 Lemke, H.: Phys. Status Solidi (a) 101 (1987) 193.
- 87L2 Lemke, H.: Phys. Status Solidi (a) 99 (1987) 205.
- 87M1 Mesli, A., Courcelle, E., Zundel, T., Siffert, P.: Phys. Rev. B 36 (1987) 8049.
- 87M2 Murin, L. I., Phys. Status Solidi (a) 101 (1987) K107.
- 87N Nolte, D. D., Walukiewicz, W., Haller, E. E.: Phys. Rev. B 36 (1987) 9392.
- 87O Omling, P., Emanuelsson, P., Grimmeiss, H. G.: Phys. Rev. B 36 (1987) 6202.
- 87P Pearton, S. J., Corbett, J. W., Shi, T. S.: Appl. Phys. A 43 (1987) 153.
- 87S Stavola, M., Pearton, S. J., Lopata, J., Dautremont-Smith, W. C.: Appl. Phys. Lett. 50 (1987) 1086.
- 87T Thonke, K., Teschner, A., Sauer, R.: Solid State Commun. 61 (1987) 241.
- 87W Wagner, P., Gottschalk, H., Trombetta, J., Watkins, G. D.: J. Appl. Phys. 61 (1987) 346.
- 88B1 Barber, N., Montelius, L., Kleverman, M., Bergman, K., Grimmeiss, H. G.: Phys. Rev. B 38 (1988) 10483.
- 88B2 von Bardeleben, H. J., Stievenard, D., Brousseau, M., Barrau, J.: Phys. Rev. B 38 (1988) 6308.
- 88K1 Kleverman, M., Fornell, J. -O., Olajos, J., Grimmeiss, H. G., Lindström, J. L.: Phys. Rev. B 37 (1988) 10199.
- 88K2 Kreissel, J., Gehlhoff, W.: Phys. Status Solidi (a) 145 (1988) 609.
- 88K3 Kleverman, M., Olajos, J., and Grimmeiss, H. G.: Phys. Rev. B 37 (1988) 2613.
- 88O van Oosten, A. B., Ammerlaan, C. A. J.: Solid State Commun. 65 (1988) 1039.
- 88O1 Oljaos, J., Kleverman, M., Grimmeiss, H. G.: Phys. Rev. B 38 (1988) 10633.
- 88O2 Omling, P., Kleverman, M., Emanuelsson, P., Olajos, J., Grimmeiss, H. G.: Solid State Commun. 65 (1988) 557.
- 88O3 van Oosten, A. B., Ammerlaan, C. A. J.: Phys. Rev. B 38 (1988) 13291.
- 88O4 van Oosten, A. B., Ammerlaan, C. A. J.: Solid State Commun. 65 (1988) 1039.
- 88O5 Olajos, J., Bech Nielsen, B., Kleverman, M., Omling, P., Emanuelsson, P., Grimmeiss, H. G.: Appl. Phys. Lett. 53 (1988) 2507.
- 88P Pandey, K. C., Erbil, A., Cargil, G. S., Boehme, R. F.: Phys. Rev. Lett. 61 (1988) 1282.
- 88R Rodewald, D., Severitt, S., Vollmer, H., Labusch, R.: Solid State Commun. 67 (1988) 573.
- 88S1 Song, L. W., Zhan, X. D., Benson, B. W., Watkins, G. D.: Phys. Rev. Lett. 60 (1988) 460.
- 88S2 Suezawa, M., Sumino, K., Harada, H., Abe, T.: Jpn. J. Appl. Phys. 27 (1988) 62.
- 88S3 Svensson, J. H., Svensson, B. G., Monemar, B.: Phys. Rev. B 38 (1988) 4192.
- 88T Thomas, V., Barrau, J., Brousseau, M., Kirouni, K., Couloumiers, G.: Phys. Status Solidi (a) 148 (1988) 723.
- 88Z Zundel, T., Weber, J., Benson, B., Hahn, P. O., Schnegg, A., Prigge, H.: Appl. Phys. Lett. 53 (1988) 1426.
- 89B Benson, B. W., Güler, E., Watkins, G. D.: Mater. Sci. Forum 38-41 (1989) 391.
- 89C Czaputa, R.: Appl. Phys. A 49 (1989) 431.
- 89E Endrös, A.: Phys. Rev. Lett. 63 (1989) 70.
- 89G Griffin, J. A., Hartung, J., Weber, J., Navarro, H., Genzel, L.: Appl. Phys. A 48 (1989) 41.
- 89H Höhne, M.: Phys. Status Solidi (b) 156 (1989) 325.
- 89J1 Jang, S. -L., Bosman, G.: J. Appl. Phys. 65 (1989) 201.
- 89J2 Jie, Z., Xiujiang, J., Shuying, L., Jian, W., Jilin, G., Zhiyoung, H.: Mater. Sci. Forum 38-41 (1989) 457.

- 89K Kimerling, L. C., Asom, M. T., Benton, J. L., Drevinsky, P. J., Cafer, C. E.: Mater. Sci. Forum 38-41 (1989) 391.
- 89M1 Merk, E., Heyman, J., Haller, E. E.: Solid State Commun. 72 (1989) 851.
- 89M2 Mathiot, D., Hocine, S.: J. Appl. Phys. 66 (1989) 5862.
- 89M3 Mathiot, D.: J. Appl. Phys. 65 (1989) 1554.
- 89N Nazare, M. H., Carmo, M. C. Duarte, A. J.: Mater. Sci. Engin. B 4 (1989) 273.
- 89O Olajos, J., Kleverman, M., Grimmeiss, H. G.: Phys. Rev. B 40 (1989) 6196.
- 89P1 Pensl, G., Schulz, M., Hölzlein, K., Bergholz, W., Hutchison, J. L.: Appl. Phys. A 48 (1989) 49.
- 89P2 Prescha, T., Zundel, T., Weber, J.: Mater. Sci. Engin. B4 (1989) 79.
- 89P3 Pavelka, T., Hemm, B.: Mater. Sci. Forum 38-41 (1989) 469.
- 89W1 Widdershoven, F. P., Naus, J. P. M.: Mater. Sci. Engin. B4 (1989) 71.
- 89W2 Watkins, G. D.: Mater. Sci. Forum 38-41 (1989) 39.
- 89W3 Wagner, P., Hage, J.: Appl. Phys. A 49 (1989) 123.
- 89Z1 Zhou, J., Wang, X. C., Yao, X. C., Qin, G. G.: Mater. Sci. Forum 38-41 (1989) 403.
- 89Z2 Zundel, T., Weber, J.: Phys. Rev. B 39 (1989) 13 549.
- 90E Estreicher, S. K.: Phys. Rev. B 41 (1990) 5447.
- 90G1 Gill, A. A., Barber, N., Iqbal, M. Z.: J. Appl. Phys. 67 (1990) 1130.
- 90G2 Güter, E., Benson, B. W.: Mater. Res. Soc. Symp. Proc. 163 (1990) 295.
- 90K Keller, R., Deicher, M., Pfeiffer, W., Skudlik, H., Steiner, D., Wichert, Th.: Phys. Rev. Lett. 65 (1990) 2023.
- 90L Lemke, H.: Phys. Status Solidi (a) 122 (1990) 617.
- 90N Nakashima, H., Tsumori, Y., Miyagawa, T., Hashimoto, K.: Jpn. J. Appl. Phys. 29 (1990) 1395.
- 90P Peale, R. E., Muro, K., Sievers, A. J.: Phys. Rev. B 41 (1990) 5881.
- 90P1 Peterson, J. W., Nielson, J.: Appl. Phys. Lett. 56 (1990) 1122.
- 90P2 Peale, R. E., Muro, K., Sievers, A. J.: Mater. Sci. Forum 65-66 (1990) 151.
- 90S Song, L. W., Watkins, G. D.: Phys. Rev. B 42 (1990) 5759.
- 90W1 Wagner, P., Hage, H., Prigge, H., Prescha, Th., Weber, J.: Semiconductor Silicon 1990, Proc. 6th Int. Symp. Silicon Mater. Technol., Huff, H. R., Barraclough, K. G., Chikawa, J. (eds.), The Electrochem. Soc. (1990) Pennington, p. 675.
- 90W2 Weiss, S., Beckmann, R., Kassing, R.: Appl. Phys. A 50 (1990) 151.
- 90Z Zundel, T., and Weber, J.: Mater. Res. Soc. Symp. Proc. 163 (1990) 443.
- 91A Anderson, F. G.: J. Phys.: Condens. Matter 3 (1991) 4421.
- 91B Benton, J. L., Michel, J., Kimerling, L. C., Jacobson, D. C., Xie, Y. -H., Eaglesham, D. J., Fitzgerald, E. A., Poate, J. M.: J. Appl. Phys. 70 (1991) 2667.
- 91E Endrös, A. L., Krühler, W., Grabmaier, J.: Physica B 170 (1991) 365.
- 91H1 Holm, B., Bonde Nielson, K., Bech Nielsen, B.: Phys. Rev. Lett. 66 (1991) 2360.
- 91H2 Herring, C., Johnson, N. M.: Semicond. Semimet. 34 (1991) 225.
- 91K1 Kitakawa, H., Tanaka, S., Nakashima, H., Yoshida, M.: J. Electron. Mater. 20 (1991) 441.
- 91K2 Kleverman, M., Ghatnekar, S., and Grimmeiss, H. G.: Phys. Rev. Lett. 67 (1991) 1146.
- 91L Lang, L., Pensl, G., Gebhard, M., Achtziger, N., Uhrmacher, M.: Appl. Phys. A 53 (1991) 95.
- 91N Nakashima, H., Hashimoto, K.: J. Appl. Phys. 69 (1991) 1440.
- 91P1 Pankove, J. I.: Semicond. Semimet. 34 (1991) 65.
- 91P2 Pettersson, H., Grimmeiss, H. G., Tilly, L., Schmalz, K., Tittelbach, K., Kerkow, H.: Semicond. Sci. Technol. 6 (1991) 237.
- 91R Rubio, E., Vicente, J., Jaraiz, J., Bailon, L., Barbolla, J.: J. Appl. Phys. 69 (1991) 298.
- 91S Svensson, B. G., Mohadjeri, B., Hallen, A., Svensson, J. H., Corbett, J. W.: Phys. Rev. B 43 (1991) 2292.
- 91T1 Tilly, L., Grimmeiss, H. G., Pettersson, H., Schmalz, K., Tittelbach, K., Kerkow, H.: Phys. Rev. B 43 (1991) 9171.
- 91T2 Tilly, L., Grimmeiss, H. G., Pettersson, H., Schmalz, K., Tittelbach, K., Kerkow, H.: Phys. Rev. B 44 (1991) 12 809.
- 91W Watkins, G. D., Kleverman, M., Thilderkvist, A., Grimmeiss, H. G.: Phys. Rev. Lett. 67 (1991) 1149.
- 91Z1 Zhan, X. D., Watkins, G. D.: Appl. Phys. Lett. 58 (1991) 2144.
- 91Z2 Zundel, T., Weber, J.: Phys. Rev. 43 (1991) 4361.
- 91Z3 Zimmermann, H., Ryssel, H.: Appl. Phys. Lett. 58 (1991) 499.
- 92A Anderson, F. G., Milligan, R. F., Watkins, G. D.: Phys. Rev. B 45 (1992) 3279.
- 92D Demidov, E. S., Karzanov, V. V.: Sov. Phys. Semicond. 26 (1992) 930.
- 92G1 Güter, E., Benson, B. W., Watkins, G. D.: Mater. Sci. Forum. 83-87 (1992) 339.
- 92G2 Götz, W., Pensl, G., Zulehner, W.: Phys. Rev. B 46 (1992) 4312.
- 92M Mesli, A. Heiser, T.: Phys. Rev. B 45 (1992) 11632.
- 92N Nakashima, H., Sadoh, T.: Mater. Res. Soc. Proc. Vol. 262 (1992) 555.

- 92P1 Pearton, S. J., Corbett, J. W., Stavola, M.: Hydrogen in Crystalline Semiconductors, Springer Ser. Mater. Sci. 16, Berlin: Springer 1992.
- 92P2 Prescha, T., Weber, J.: Mater. Sci. Forum Vol 83-87 (1992) 167.
- 92S1 Sadoh, T., Nakshima, H., Tsurushima, T.: J. Appl. Phys. 72 (1992) 520.
- 92S2 Son, N. T., Grekorkiewicz, T., Ammerlaan, C. A. J.: Phys. Rev. Lett. 69 (1992) 3185.
- 92T Tamulevicius, S., Svennsson, B. G., Aboelfotoh, M. O., Hallen, A.: J. Appl. Phys. 71 (1992) 4212.
- 92Z Zhan, X. D., Watkins, G. D.: Mater. Sci. Forum. 83-87 (1992) 345.
- 93B Borenstein, J. T., Hanoka, J. I., Bathey, B. R., Kalejs, J. P., Mil'shtein, S.: Appl. Phys. Lett. 62 (1993) 1615.
- 93G Gill, A. A., Iqbal, M. Z., and Zafar N.: Semicond. Sci. Technol. 8 (1993) 675.
- 93H1 Henry, A., Monemar, B., Bergman, J. P., Lindström, J. L., Holtz, P. O.: Phys. Rev. B 47 (1993) 13309.
- 93H2 Holbech, J. D., Bech Nielsen, B., Jones, R., Sitch, P., Öberg, S.: Phys. Rev. Lett. 71 (1993) 875.
- 93N Nakayama, H., Matsuura, A., Kohono, M., Nishino, T.: Mater. Sci. Forum 117-118 (1993) 279.
- 93P1 Pfeiffer, G., Prescha, Th., Weber, J.: Jpn. J. Appl. Phys. 32 - 1 (1993) 239.
- 93P2 Priolo, F., Coffa, S., Franzo, G., Spinella, C., Carena, A., Bellani, V.: J. Appl. Phys. 74 (1993) 4936.
- 93P3 Petterson, H., Grimmeiss, H. G., Tilly, L., Schmalz, K., Kerkov, H.: Semicond. Sci. Technol. 8 (1993) 1247.
- 93W Williams, P. M., Watkins, G. D., Uftring, S., Stavola, M.: Phys. Rev. Lett. 70 (1993) 3816.
- 94A Altheld, P., Greulich-Weber, S., Spaeth, J. M., Overhof, H., Höhne, M.: Mater. Sci. Forum 143-147 (1994) 1173.
- 94D Davies, G., Newman, R. C.: in Handbook on Semiconductors, ed. by T.S. Moss, Amsterdam: North Holland, vol. 3 (1994) 1557.
- 94G1 Ghatnekar-Nilsson, S., Kleverman, M., Emanuelsson, P., Grimmeiss, H. G.: Mater. Sci. Forum 143-147 (1994) 171.
- 94G2 Grimmeiss, H. G., Janzen, E.: in Handbook on Semiconductors, ed. by T.S. Moss, Amsterdam: North Holland, vol. 3 (1994) 1755.
- 94H1 Hara, A., Masaki, A., Koizuka, M., Fukuda, T.: J. Appl. Phys. 75 (1994) 2929.
- 94H2 Häßler, C., Pensl, G.: Mater. Sci. Forum 143-147 (1994) 123.
- 94J Johnson, N. M., Herring, C., Van de Walle, C. G.: Phys. Rev. Lett. 73 (1994) 130.
- 94K Kaczor, P., Godlewski, M., Gregorkiewicz, T.: Mater. Sci. Forum 143-147 (1994) 1185.
- 94L1 Lemke, H.: Semiconductor Silicon 1994, Huff, H. R., Bergholz, W., Sumino, K. (eds.), The Electrochem. Soc., Pennington, NJ., Vol. PV94-10 (1994), p. 695
- 94L2 Lindström, J. L., Hallberg, T.: Phys. Rev. Lett. 72 (1994) 2729.
- 94L3 Lemke, H.: Semiconductor Silicon 1994, Huff, H. R., Bergholz, W., Sumino, K. (eds.), The Electrochem. Soc., Pennington, NJ., Vol. PV94-10 (1994), p. 695
- 94M1 Michel, J., Kimmerling, L. C.: Semicond. Semimet. 42 (1994) 251.
- 94M2 McQuaid, S. A., Newman, R. C., Lightowlers, E. C.: Semicond. Sci. Technol. 9 (1994) 1736.
- 94N1 Nakashima, H., Sadoh, T., Kitagawa, H., Hashimoto, K.: Mater. Sci. Forum 143-147 (1994) 761.
- 94N2 Nakashima, H., Sadoh, T., Tsurushima, T.: Phys. Rev. B 49 (1994) 16 983.
- 94S1 Sadoh, T., Watanabe, M., Nakashima, H., Tsurushima, T.: Mater. Sci. Forum 143-147 (1994) 939.
- 94S2 Sadoh, T., Watanabe, M., Nakashima, H., Tsurushima, T.: J. Appl. Phys. 75 (1994) 3978.
- 94T Thilderkvist, A., Nilsson, S. G., Kleverman, M., Grimmeiss, H. G.: Phys. Rev. B 49 (1994) 16926.
- 94Z Zheng, B., Michel, J., Ren, F. Y. G., Kimerling, L. C., Jacobson, D. C., Poate, J. M.: Appl. Phys. Lett. 64 (1994) 2842.
- 95A1 Aboelfotoh, M. O., Svensson, B. G.: Phys. Rev. B 52 (1992) 2522.
- 95A2 Achtziger, N., Witthuhn, W.: Phys. Rev. Lett. 75 (1995) 4484.
- 95A3 Achtziger, N., Gottschalk, H., Licht, T., Meier, J., Rüb, M.: Appl. Phys. Lett. 66 (1995) 2370.
- 95E1 Erzgräber, H. B., Schmalz, K.: J. Appl. Phys. 78 (1995) 4066.
- 95E2 Erlesand, U., Östling, M.: Semicond. Sci. Technol. 10 (1995) 1645.
- 95G1 Gislason, H. P., Kristjansson, S., Sveinbjörnsson, E. Ö.: Mater. Sci. Forum 196-201 (1995) 695.
- 95G2 Graff, K.: Metal Impurities in Silicon-Device Fabrication, Berlin: Springer 1995.
- 95L Lemke, H.: Mater. Sci. Forum 196-201 (1995) 683.
- 95S1 Sveinbjörnsson, E. Ö., Kristjansson, S., Gislason, H. P.: J. Appl. Phys. 77 (1995) 3146.
- 95S2 Sveinbjörnsson, E. Ö., Engström, O.: Phys. Rev. B 52 (1995) 4884.
- 95U Uftring, S. J., Stavola, M., Williams, P. M., Watkins, G. D.: Phys. Rev. B 51 (1995) 9612.
- 96A1 Achtziger, N., Licht, T., Reislöhner, U., Rüb, M., Witthuhn, W.: Proc. ICPS Berlin (1996) 2717, Singapore: World Scientific.
- 96A2 Achtziger, N.: J. Appl. Phys. 80 (1996) 6286.
- 96D Davidson, J. A., Evans, J. H.: Semicond. Sci. Technol. 11 (1996) 1704.
- 96H Holm, B., Nielsen, B. K.: J. Appl. Phys. 79 (1996) 1807.
- 96J1 Jost, W., Weber, J., Lemke, H.: Semicond. Sci. Technol. 11 (1996) 525.

- 96J2 Jost, W., Weber, J., Lemke, H.: *Semicond. Sci. Technol.* 11 (1996) 22.
- 96J3 Jost, W., Weber, J.: *Phys. Rev. B* 54, (1996) R11038.
- 96L Lemke, H.: in "High Purity Silicon IV", Claeys, C.L., Rai-Choudhury, P., Stallhofer, P., Manrits, J.E. (eds.), *The Electrochem. Soc., Pennington, NJ. Proc.* vol. 96-13, (1996) 272.
- 96M1 Mesli, A., Heiser, T.: *Defect Diffus. Forum* 131-132 (1996) 89.
- 96M2 Murakami, K., Fukata, N., Sasaki, S., Ishioka, K., Kitajima, M., Fujimura, S., Kikuchi, J., Haneda, H.: *Phys. Rev. Lett.* 77 (1996) 3161.
- 96P Parakhonskii, A. L., Feklisova, O. V., Karelin, S. S., Yarykin, N. A.: *Semicond.* 30 (1996) 362.
- 96S Safonov A. N., Lightowers, E. C., Davies, G., Leary, P., Jones, R., Öberg, S.: *Phys. Rev. Lett.* 23 (1996) 4812.
- 96T Tidlund, P., Kleverman, M., Grimmeiss, H. G.: *Semicond. Sci. Technol.* 11 (1996) 748.
- 96W Williams, P. M., Mason, P. W., Watkins, G. D.: *Phys. Rev. B* 53 (1996) 12570.
- 97H Hoffmann, K., Vollmer, H., Labusch, R.: *J. Phys.: Condens. Matter* 9 (1977) 4909.
- 97R Resende, A., Goss, J., Briddon, P. R., Öberg, S., Jones, R.: *Mater. Sci. Forum* 258-263 (1997) 295.
- 97S1 Sachse, J. -U., Jost, W., Weber, J., Lemke: *Appl. Phys. Lett.* 71 (1997) 1379.
- 97S1 Sachse, J. -U., Sveinbjörnsson, E. Ö., Jost, W., Weber, J., Lemke, H.: *Phys. Rev. B* 55 (1997) 16176
- 97S2 Sachse, J. -U., Sveinbjörnsson, E. Ö., Jost, W., Weber, J., Lemke, H.: *Appl. Phys. Lett.* 70 (1997) 1584.
- 97S2 Sachse, J. -U., Weber, J., Lemke, H.: *Mater. Sci. Forum* 258-263 (1997) 307.
- 97S3 Sachse, J. -U., Weber, J., Lemke, H.: *Mater. Sci. Forum* 258-263 (1997) 307.
- 97Y Yarykin, N., Sachse, J. -U., Weber, J., Lemke, H.: *Mater. Sci. Forum* 258-263 (1997) 301.

Figures to 1.2

Fig. 1.0.2

The diamond lattice. The elementary cubes of the two face-centered cubic lattices are shown.

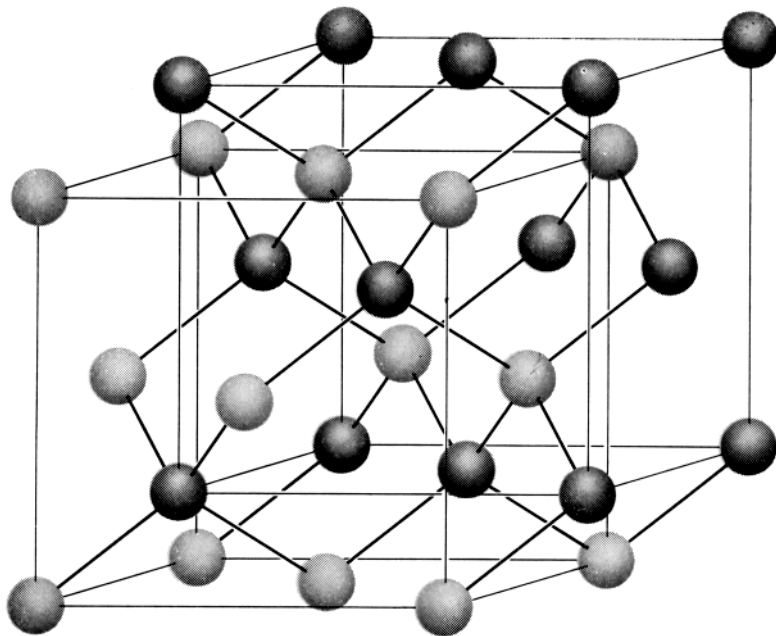


Fig. 1.0.6

Brillouin zone of the diamond lattice

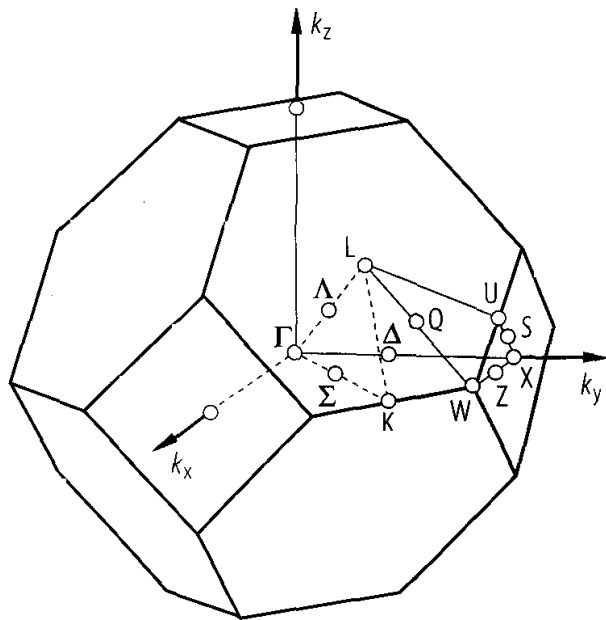


Fig. 1.0.9

Si. Band structure. Solid line: nonlocal, energy-dependent pseudopotential calculation, circles: localized atomic orbital method [85S].

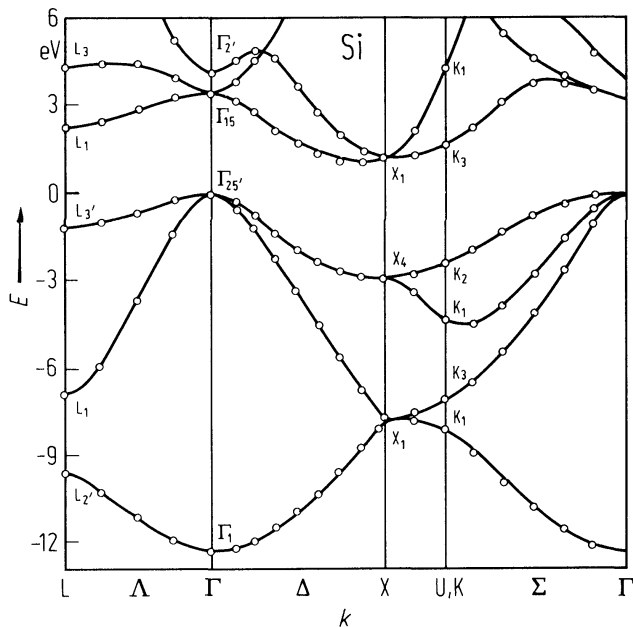


Fig. 1.2.1

Si. Density of states on the valence and conduction band obtained by an empirical pseudopotential calculation [73C].

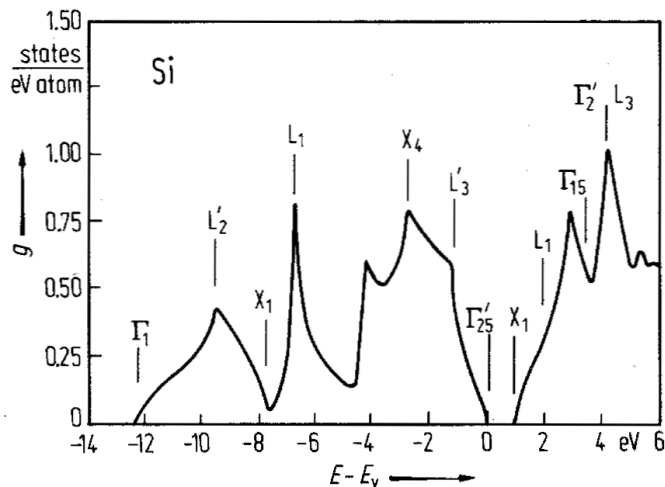


Fig. 1.2.2

Si. Temperature dependence of the indirect energy gap. Solid line: calculated, circles: experimental [85L];

$$\Delta E_{g,\text{ind}} = E_{g,\text{ind}}(T) - E_{g,\text{ind}}(0).$$

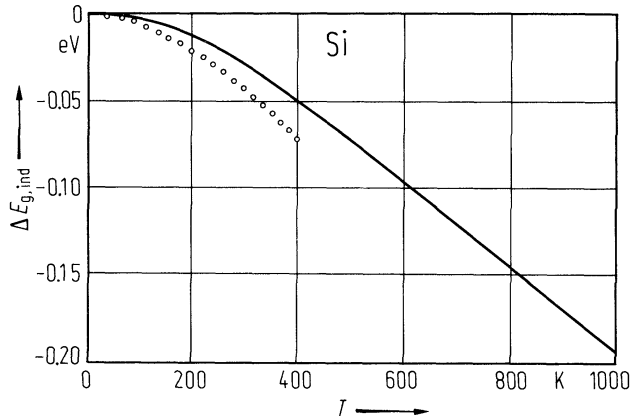


Fig. 1.2.3

Si. Temperature dependence of the direct band gap ($\Delta E_{g,\text{dir}} = E_{g,\text{dir}}(T) - E_{g,\text{dir}}(0)$). Solid line: calculated [85L], circles: experimental [72A].

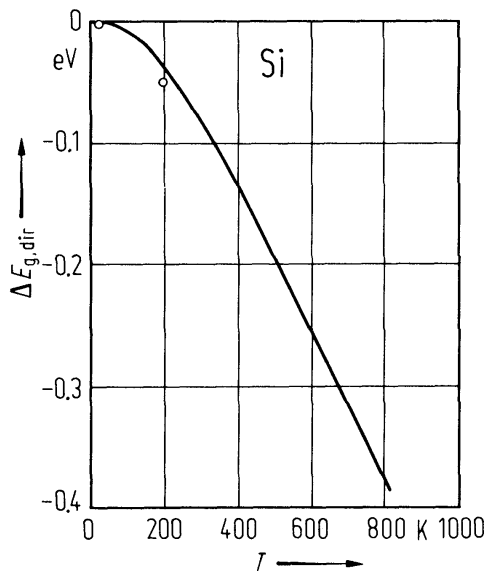


Fig. 1.2.4

Si. Transverse electron mass determined by cyclotron resonance vs. temperature [76O].

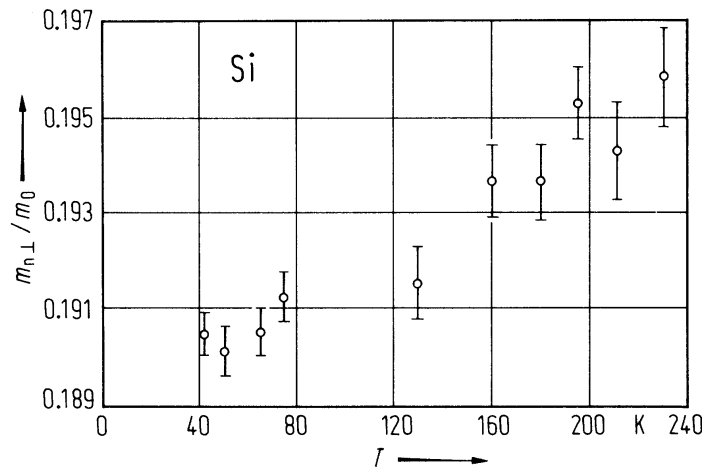


Fig. 1.2.5

Si. (a) Density of states mass obtained from carrier concentration vs. temperature for the three valence bands, (b) density of states mass obtained from the calculated density of states vs. energy measured from the top of the valence band. Both masses are related to each other by $m_p^{3/2}(T) = \langle m_{ds}^{3/2}(E) \rangle$, where $\langle \dots \rangle$ means a weighted thermal average [83L].

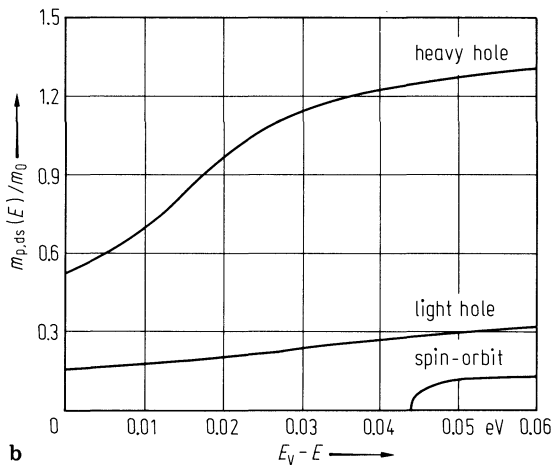
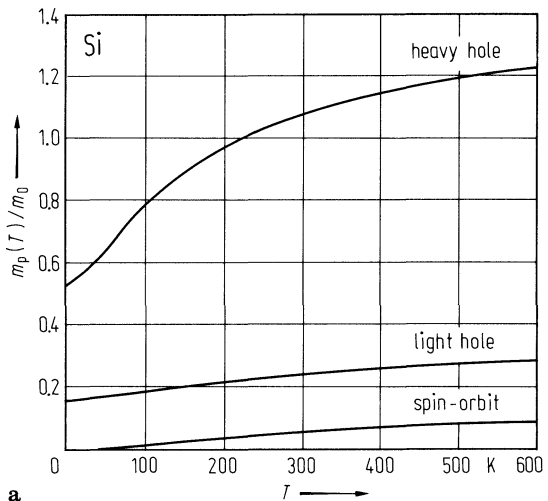


Fig. 1.2.6

Si. Lattice parameter vs. temperature in the range 20...740°C, measurements on various samples [61H].

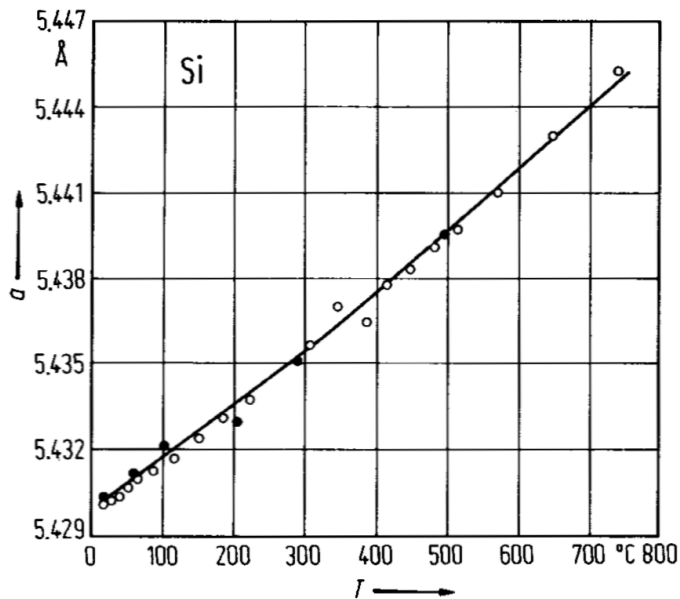


Fig. 1.2.7

Si. Linear thermal expansion coefficient vs. temperature. Experimental data from [77L2] (full circles) and [84O1] (open circles).

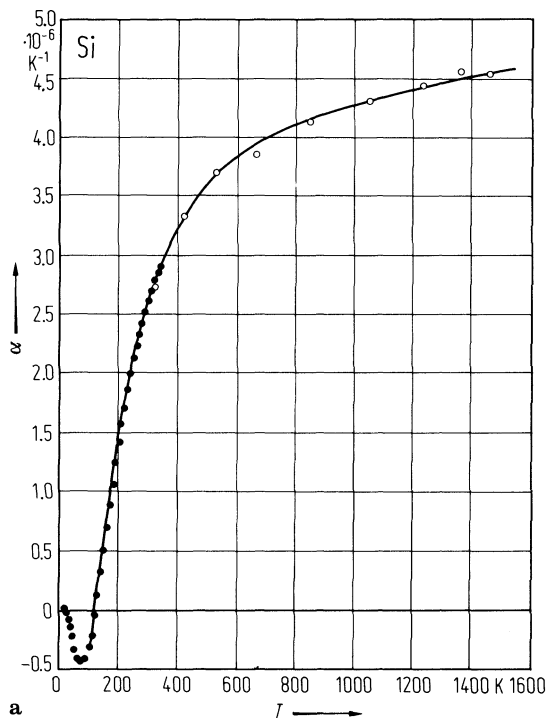


Fig. 1.2.8

Si. Phonon dispersion curves (left panel) and phonon density of states (right panel) [91G]. Experimental data points [63D], [72N2] and ab-initio calculations [91G].

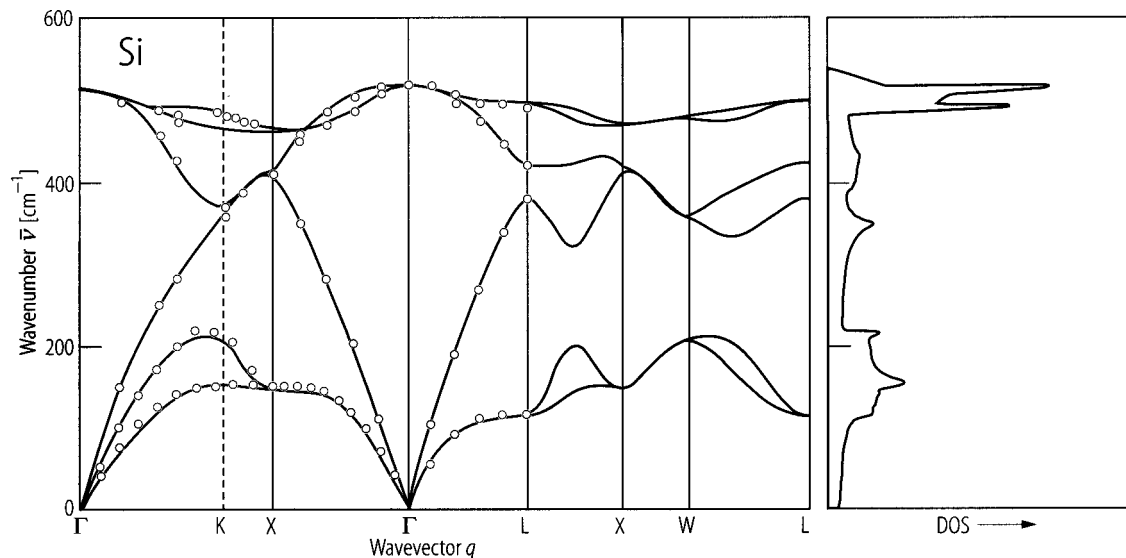


Fig. 1.2.9

Si. One-phonon density of states at 300 K obtained from bond charge model calculations [77W].

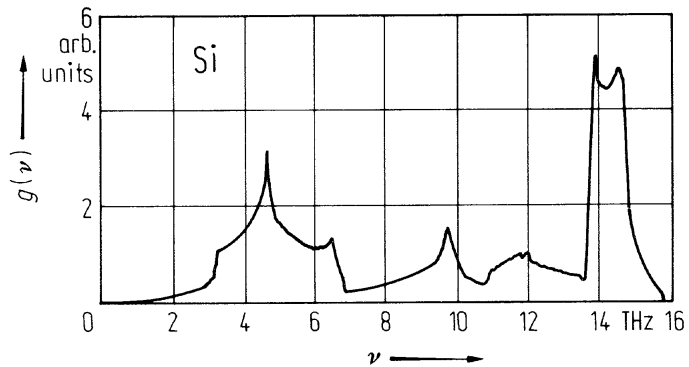


Fig. 1.2.10a Si. Velocity v_3 of longitudinal waves vs. temperature. Propagation along $[110]$ direction $[53M]$.

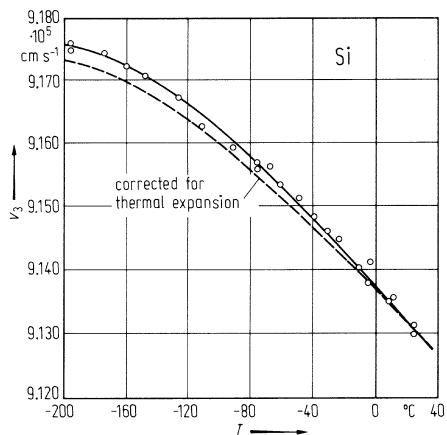


Fig. 1.2.10b Si. Velocity v_4 of shear waves vs. temperature. Propagation along $[110]$ direction, particle motion parallel to $[001]$ direction $[53M]$.

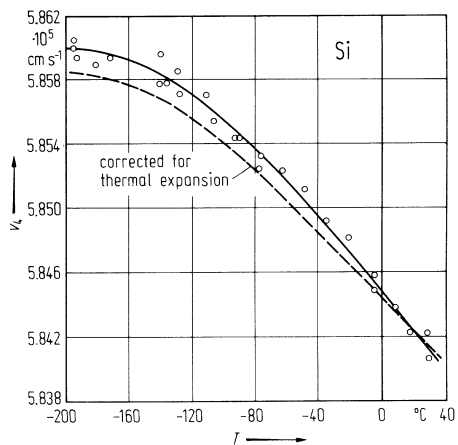


Fig. 1.2.10c Si. Velocity v_5 of shear waves vs. temperature. Propagation along $[110]$ direction, particle motion parallel to $[1(-1)0]$ direction $[53M]$.

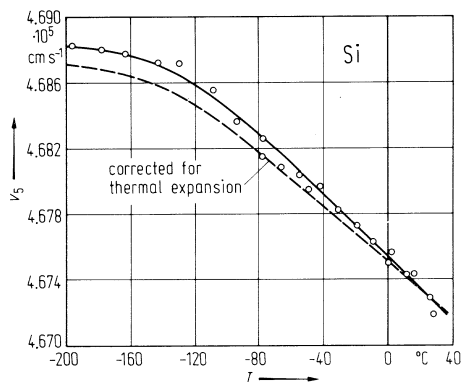


Fig. 1.2.11a Si. Elastic constant c_{11} vs. temperature [53M].

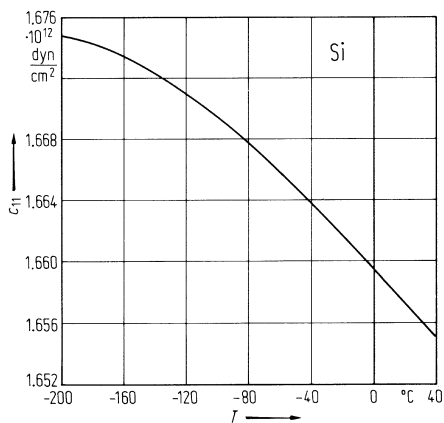


Fig. 1.2.11b Si. Elastic constant c_{12} vs. temperature [53M].

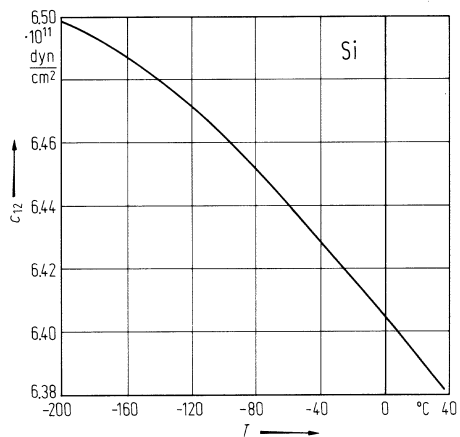


Fig. 1.2.11c Si. Elastic constant c_{44} vs. temperature [53M].

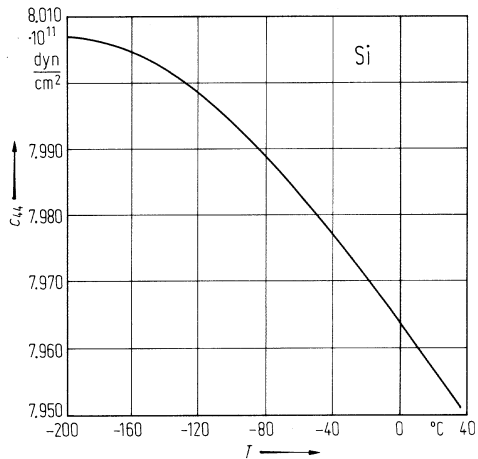


Fig. 1.2.12

Si. Third-order elastic moduli vs. temperature. Solid lines: fit to the data [83P].

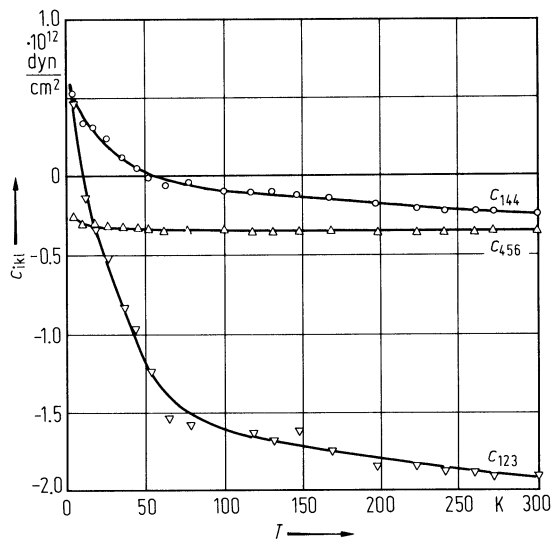
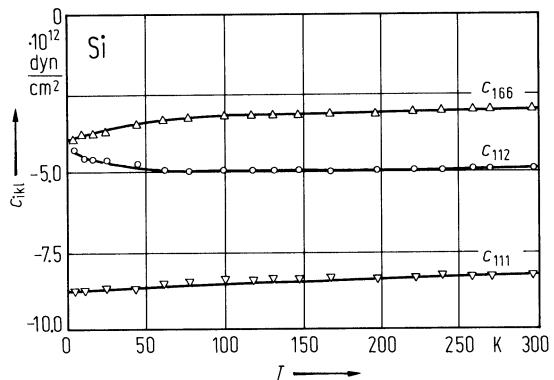


Fig. 1.2.13

Si. Young's moduli and torsion modulus vs. temperature according to [72N1] (1) and [53M] (2).

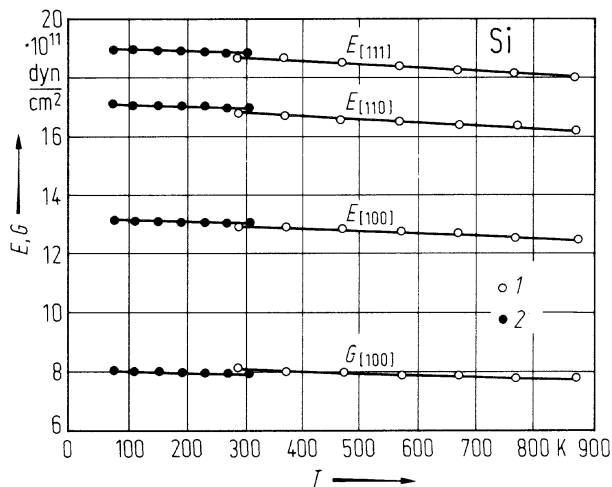


Fig. 1.2.14

Si. Bulk modulus B_S vs. temperature [67H].

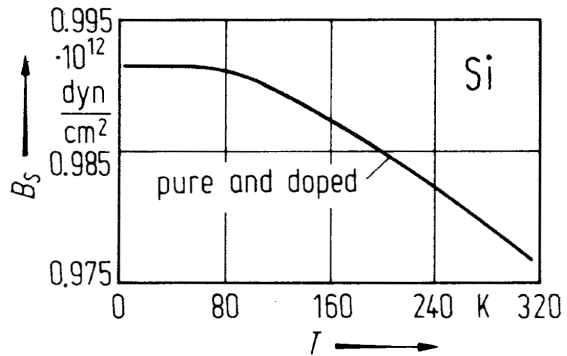


Fig. 1.2.15

Si. Debye temperature vs. temperature below 300 K [59F2].

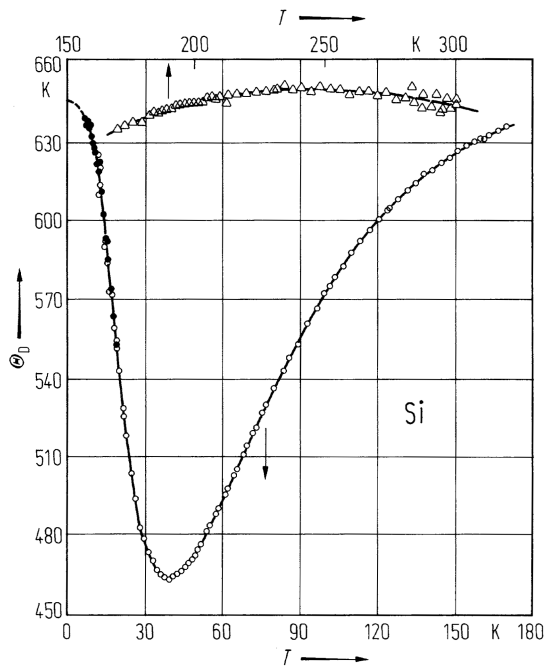


Fig. 1.2.16

Si. Heat capacity at constant volume vs. temperature. Fig. from [85K].

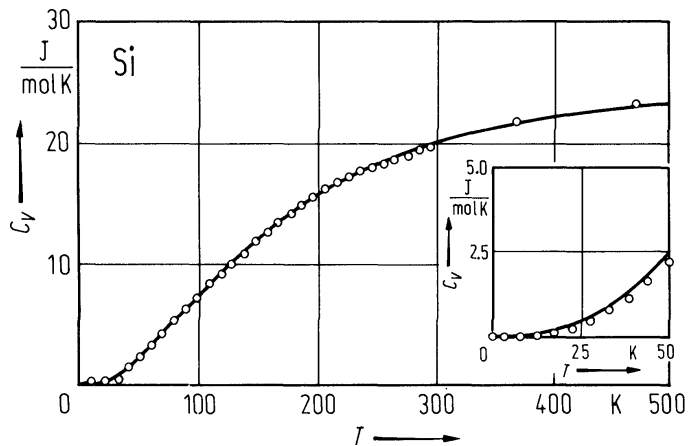


Fig. 1.2.17

Si. Conductivity and Hall coefficient vs. reciprocal temperature in the range of intrinsic conduction. n- and p-type samples with doping concentrations of $1.7 \cdot 10^{14} \text{ cm}^{-3}$ and above [54M]. Different symbols from different samples.

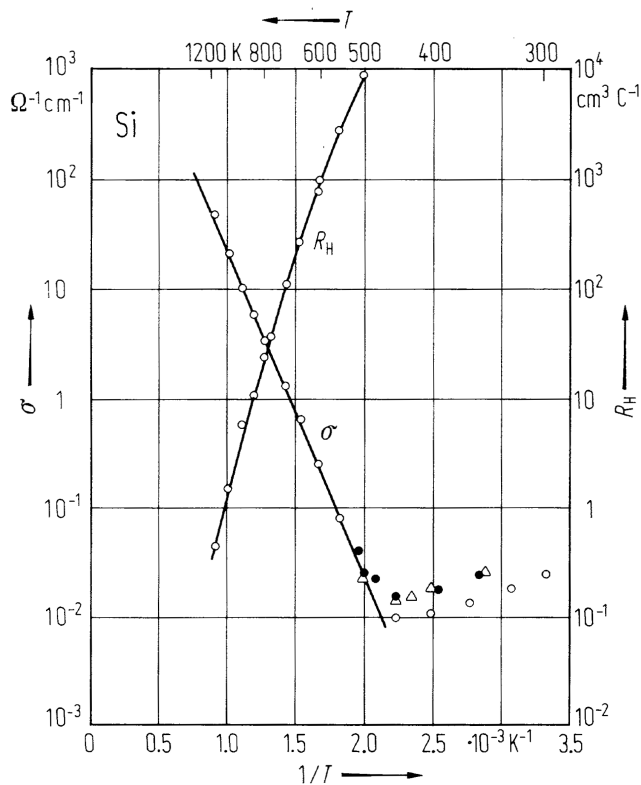


Fig. 1.2.18

Si. Electron mobility vs. temperature [77J]. Data points with $n_d \leq 10^{12} \text{ cm}^{-3}$ obtained by time-of-flight technique [75C]. Other experimental values taken from [73N] ($4 \cdot 10^{13} \text{ cm}^{-3}$) and [54M] ($1.3 \cdot 10^{17} \text{ cm}^{-3}$). Continuous line indicates theoretical lattice mobility after [75C]. Dash-dotted line: $T^{-2.42}$ dependence of μ_p around room temperature.

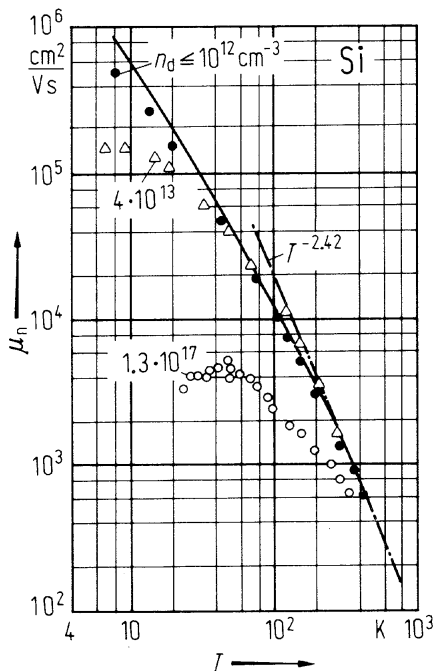


Fig. 1.2.19

Si. (a) Conductivity hole mobility vs. temperature (circles from [82M], triangles from [56L]). Solid lines: calculated contributions from the three valence bands. (b) Hall hole mobility vs. temperature (circles from [82M]). Solid lines as in (a). Experimental points from two samples [82M], solid line: theoretical curve. Figs. (a) and (b) from [83S1, 83S2].

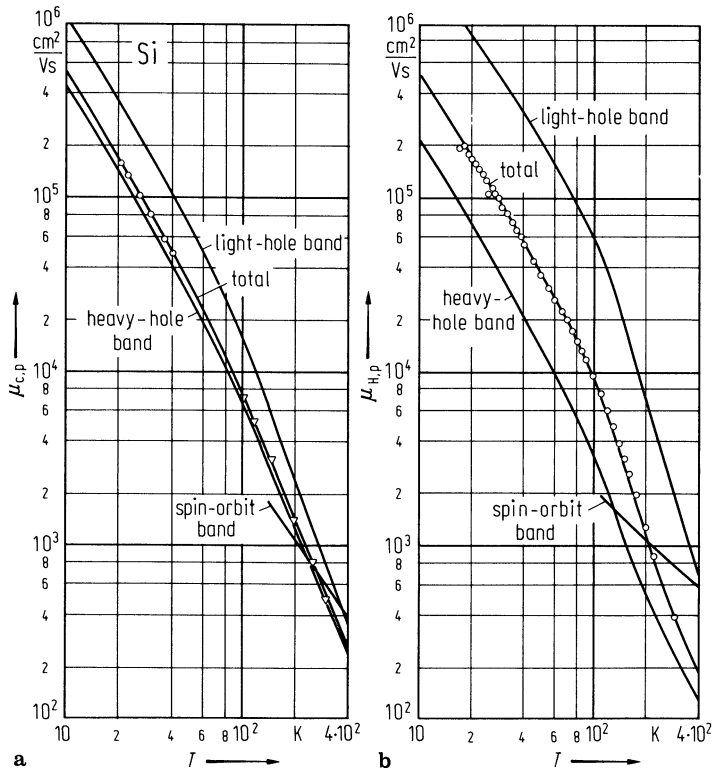


Fig. 1.2.20

Si. Seebeck coefficient (thermoelectric power) times temperature (absolute value) vs. temperature for n-type. Si. Sample no. 1: $n_d = 2.75 \cdot 10^{14} \text{ cm}^{-3}$; 2: $3.7 \cdot 10^{14} \text{ cm}^{-3}$; 3: $2.6 \cdot 10^{15} \text{ cm}^{-3}$; 4: $2.2 \cdot 10^{16} \text{ cm}^{-3}$; 5: $1.3 \cdot 10^{17} \text{ cm}^{-3}$; 6: $1.1 \cdot 10^{18} \text{ cm}^{-3}$ (counterdoped with $n_a = 1.0 \cdot 10^{18} \text{ cm}^{-3}$); 7: $2.2 \cdot 10^{18} \text{ cm}^{-3}$; 8: $2.7 \cdot 10^{19} \text{ cm}^{-3}$ [55G].

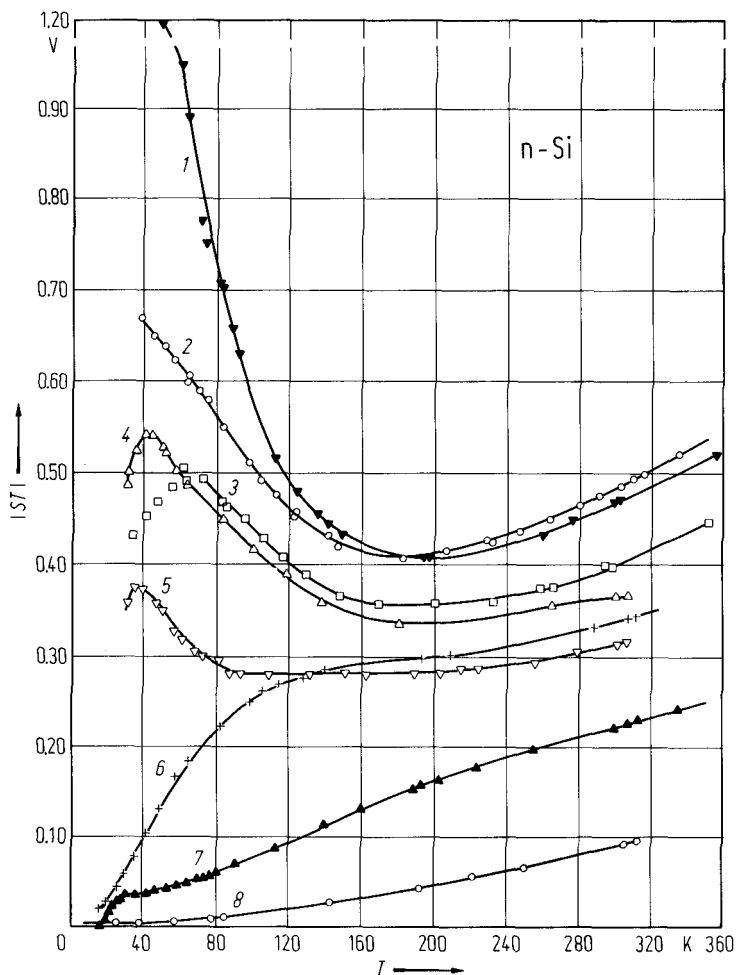


Fig. 1.2.21

Si. Seebeck coefficient (thermoelectric power) times temperature (absolute value) vs. temperature for p-type. Si. Sample no. 1: $n_a = 1.0 \cdot 10^{15} \text{ cm}^{-3}$; 2: $9.2 \cdot 10^{14} \text{ cm}^{-3}$; 3: $2.6 \cdot 10^{16} \text{ cm}^{-3}$; 4: $2.0 \cdot 10^{17} \text{ cm}^{-3}$; 5: $1.0 \cdot 10^{18} \text{ cm}^{-3}$; 6: $1.5 \cdot 10^{19} \text{ cm}^{-3}$ [55G].

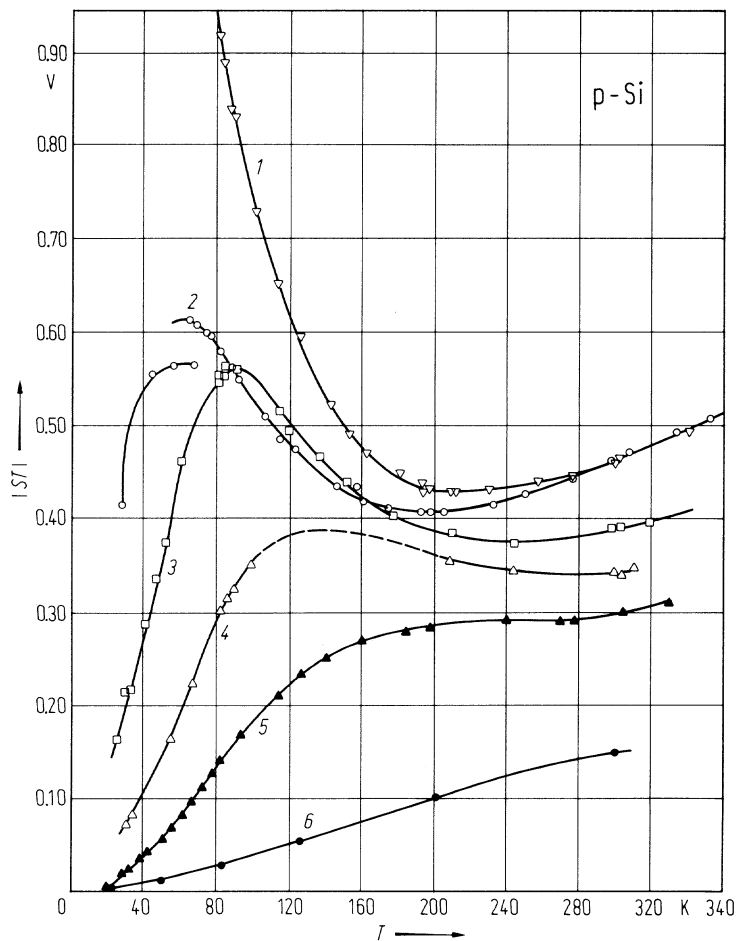


Fig. 1.2.22

Si. Lattice thermal conductivity vs. temperature according to [64G] (full circles), [68F] (open circles) and [63S] (triangles). Curves marked with κ_L and $2\kappa_T$ represent the contribution of the longitudinal and transverse phonons, respectively [70J].

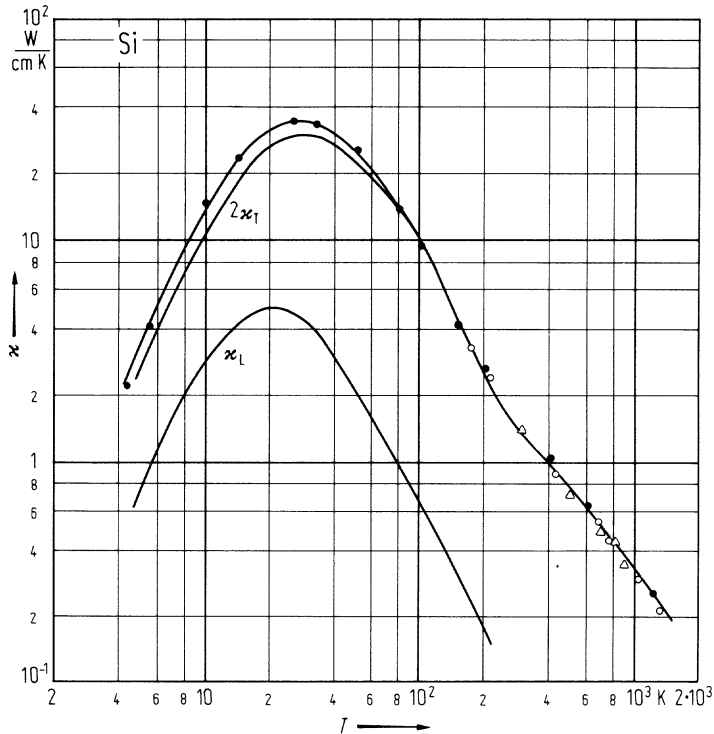


Fig. 1.2.23

Si. Real and imaginary parts of the dielectric constant vs. photon energy [83A].

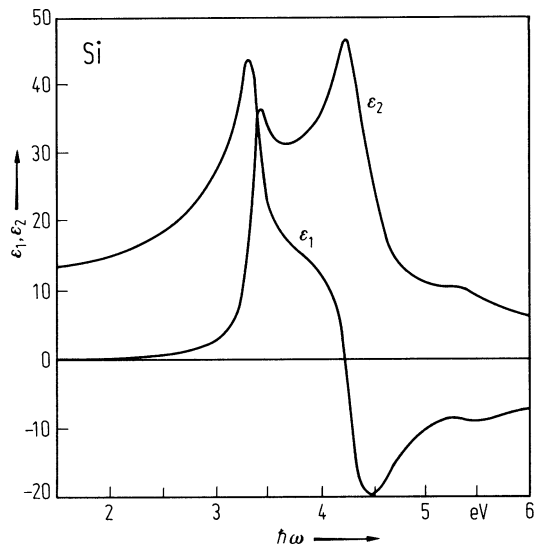


Fig. 1.2.24

Si. Optical constants below 10 eV vs. photon energy. (a) Absorption coefficient, (b) extinction coefficient, (c) refractive index [57C, 60P].

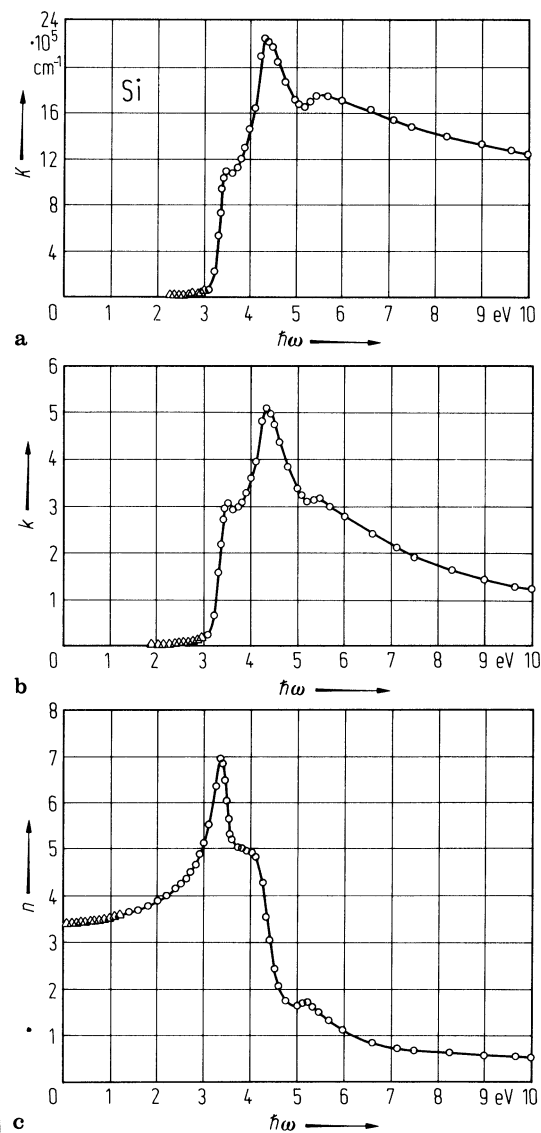


Fig. 1.2.25

Si. Real (ϵ_1) and imaginary (ϵ_2) part of the dielectric constant and energy loss function $-\text{Im}(\epsilon^{-1})$ vs. photon energy [63P].

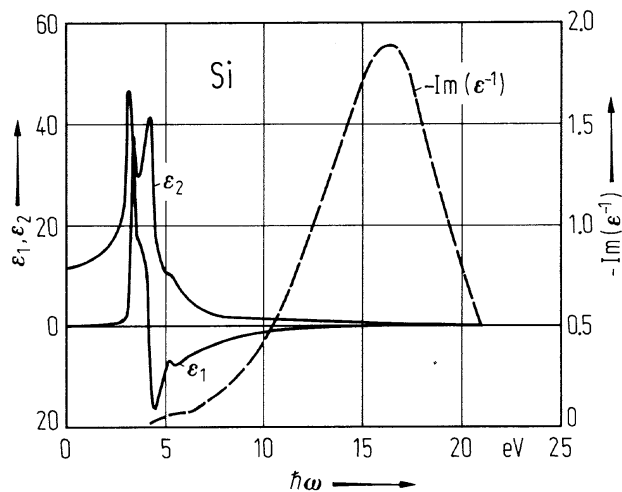
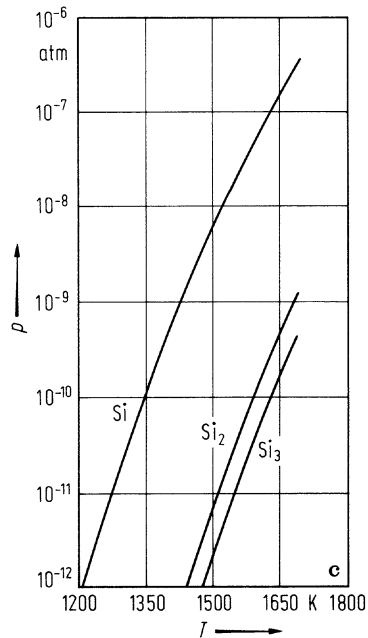
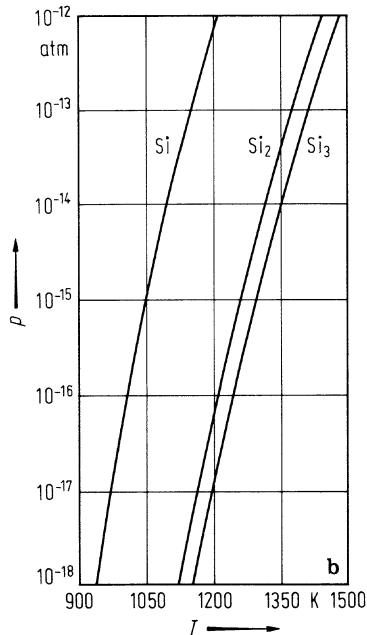
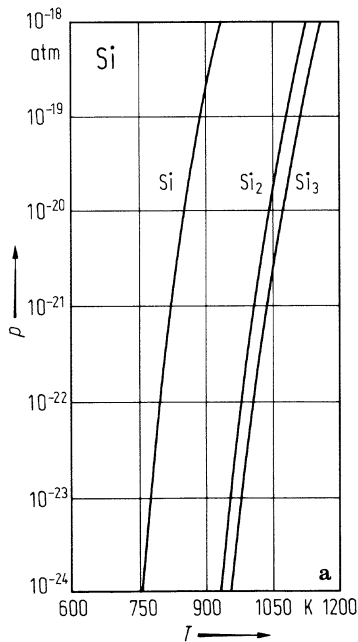


Fig. 1.2.26

Si. Vapor pressure vs. temperature in different temperature ranges a)...c) [73H]. The total pressure is nearly identical with the curve for monoatomic. Si.



1.3 Germanium, Ge

Crystal structure

The element germanium crystallizes under normal conditions in the diamond lattice (space group: cubic O_h^{7-} – $Fd3m$), see Fig. 1.0.2.

high pressure phases

Under pressure there is a transition from the diamond structure (Ge-I) to the tetragonal β -tin structure (Ge-II) around 10 GPa [63J, 78A, 84O, 86M]. Around 75 GPa there is a transformation from the β -Sn structure (Ge-II) to the simple hexagonal (sh) structure [86V], and around 100 GPa to an intermediate structure, and to the hexagonal close-packed structure [86V]. Recently it has been found that the β -tin transforms continuously to the hexagonal phase via an intermediate phase with $Imma$ structure, as previously found in Si, predicted by [94L] and experimentally found by [96N]; this phase is not a mixture of the β -tin and hexagonal phases [96N]; a high-pressure double-hexagonal close-packed (dhcp) structure has been found above 100 GPa [86V].

Upon depressurising the Ge-II modification, Ge-III (ST12 structure, simple tetragonal with 12 nearest neighbours, space group $P4_32_12$, D_4^8) is obtained at RT [63B, 64K, 65B, 83Q, 86M2], a mixture of Ge-III and Ge-IV at 170 ... 200 K, nearly pure Ge-IV (BC8 structure, body centred cubic with 8 nearest neighbours, space group $Ia3$, T_h^7) at 160 ... 170 K, a mixture of Ge-IV and a glassy phase at 130 ... 160 K, and mostly glassy Ge at 90 ... 130 K [92B].

Electronic properties

band structure : Fig. 1.0.10, Brillouin zone: Fig. 1.0.6

density of states in valence and conduction bands: Fig. 1.3.1.

The conduction band is characterized by eight equivalent minima at the end points L of the $[111]$ -axes of the Brillouin zone (symmetry: L_6^-). The surfaces of constant energy are ellipsoids of revolution with their major axes along $[111]$. Higher energy minima of the conduction band are located at Γ and (above these) on the $[100]$ -axes. The valence band is of the general structure shown in Fig. 1.0.7 with its maximum at Γ (symmetry: Γ_8^+), the light and heavy hole bands being degenerate at this point. Both bands are warped. The third spin-orbit split-off band has Γ_7^+ symmetry. In contrast to silicon the spin-orbit splitting energies are considerable. Thus, the symmetry notation of the double group of the diamond lattice is mostly used for Ge.

energies of symmetry points of the band structure (E relative to the top of the valence band)

$E(\Gamma_{6v})$	– 12.66 eV	theoretical data, Fig. 1.0.10a	76C
$E(\Gamma_{7v})$	– 0.29 eV		
$E(\Gamma_{8v})$	0.00 eV		
$E(\Gamma_{7c})$	0.90 eV		
$E(\Gamma_{6c})$	3.01 eV		
$E(\Gamma_{8c})$	3.22 eV		
$E(X_{5v})$	– 8.65 eV		
$E(X_{5v})$	– 3.29 eV	for experimental data from angular	
$E(X_{5c})$	1.16 eV	resolved photoemission, see Fig. 1.0.10b	
$E(L_{6v})$	– 10.39 eV	[85W] and [84H, 85N]	
$E(L_{6v})$	– 7.61 eV		
$E(L_{6v})$	– 1.63 eV		
$E(L_{4,5v})$	– 1.43 eV		
$E(L_{6c})$	0.76 eV		

indirect energy gap

$E_{g,ind}(\Gamma_{8v}^+ - L_{6c}^-)$	0.744(1) eV	$T = 1.5$ K	magnetotransmission	59Z
	0.664 eV	$T = 291$ K		
$E_{g,th}$	0.785 eV	$T = 0$ K (extrapol.)	temperature dependence of the intrinsic conductivity	54M1

For $E_{g,ind}(T)$ below 425 K, see Fig. 1.3.2.

direct energy gap

$E_{g,dir}$	0.898(1) eV	$T = 1.5$ K
$(\Gamma_{8v}^{+}-\Gamma_{7c}^{-})$	0.805(1) eV	$T = 293$ K

temperature dependence of $E_{g,dir}$, see Fig. 1.3.2

exciton ground state

$E(1S_{3/2}^{3/2}(L_4^{+}+L_5^{+}))$	740.46(3) meV		absorption (at 2.1 K) and luminescence	79M
$E(1S_{1/2}^{3/2}(L_6^{+}))$	741.58 (3) meV		(at 5.1 K), the energy of the assisting LA(L)-phonon is subtracted, the exchange splitting has not been resolved so far	
E_b	4.18 meV		$1S_{3/2}^{3/2}(L_4^{+}+L_5^{+})$	76A
	3.17 meV		$1S_{1/2}^{3/2}(L_6^{+})$	
$E(2S_{3/2}^{3/2})$	1.32 meV		theory including valence band degeneracy and conduction band anisotropy	76A
$E(2S_{1/2}^{3/2})$	0.87 meV			
$E(2P)$	2.35(5) meV	$T = 5$ K	$(2P_{3/2}^{3/2}, 2P_{3/2}^{5/2})$	76B2,
	3.13 (5) meV		$2P_{1/2}^{3/2}$	76L
	3.35(5) meV		$(2P_{3/2}^{5/2}, 2P_{-5/2}^{5/2})$	
	3.42(5) meV		$(2P_{3/2}^{5/2}, 2P_{3/2}^{3/2}), (2P_{-5/2}^{5/2}, 2P_{1/2}^{5/2})$	
			far-infrared absorption	

critical point energies

E_1	2.111(3) eV	RT	from ellipsometric data by a two- dimensional critical point analysis (2D CP)	84V
$E_1 + \Delta_1$	2.298(3) eV	RT	2D CP	
Δ_1	0.187(3) eV	RT	2D CP	
E'_0	3.123(19) eV	$T = 100$ K	3D CP	
$E'_0 + \Delta'_0$	3.309(19) eV	$T = 100$ K	3D CP	
$E'_{0,av}$	3.110 eV	RT	2D CP; mean value of E'_0 and $E'_0 + \Delta'_0$	
E_2	4.368 (4) eV	RT	2D CP	
	4.346(3) eV	RT	1D CP	

spin-orbit splitting energies

$\Delta_0(\Gamma_{7v}^{+}-\Gamma_{8v}^{+})$	0.297 eV	$T = 10$ K	electroreflectance	75A
$\Delta'_0(\Gamma_{6c}^{-}-\Gamma_{8c}^{-})$	0.200 eV			
$\Delta_1(\Lambda_{4,5v}-\Lambda_{6v})$	0.184 eV			
$\Delta'_1(L_{4,5c}^{-}-L_{6c}^{-})$	0.266 eV			
$\Delta''_1(L_{4,5v}^{-}-L_{6v}^{-})$	0.228 eV			

conduction band, effective masses

$m_{n\perp}(L_6)$	0.0823 m_0	$T = 120$ K	magnetophonon resonance	82H
	0.0807(8) m_0	$T = 30...100$ K	cyclotron resonance at 891 GHz	76F
$m_{n\parallel}(L_6)$	1.59 m_0	$T = 120$ K	magnetophonon resonance	82H
	1.57 (3) m_0	$T = 30...100$ K	cyclotron resonance at 891 GHz	76F
$m_n(\Gamma_7)$	0.0380(5) m_0	$T = 30$ K	piezomagnetorefectance	70A

For the dependence of the transverse electron mass in the L_6 -minima on the energy above the bottom of the band, see Fig. 1.3.3a.

g-factor of electrons

g_c	$-3.0(2)$	$T = 30\text{ K}$	piezomagnetoabsorption	70A
-------	-----------	-------------------	------------------------	-----

valence band, effective masses

$m_{p,l}$	$0.0438(3) m_0$	$T = 4\text{ K}, B \parallel [100]$	cyclotron resonance	56D
	$0.0426(2) m_0$	$T = 4\text{ K}, B \parallel [111]$		
	$0.0430(3) m_0$	$T = 4\text{ K}, B \parallel [110]$		
$m_{p,h}$	$0.284(1) m_0$	$T = 4\text{ K}, B \parallel [100]$		
	$0.376(1) m_0$	$T = 4\text{ K}, B \parallel [111]$		
	$0.352(4) m_0$	$T = 4\text{ K}, B \parallel [110]$		
m_{so}	$0.095 (7) m_0$	$T = 30\text{ K}$	piezomagnetoabsorption	70A

For the dependence of the light hole mass on the energy below the top of the band, see Fig. 1.3.3b.

valence band parameters

A	-13.3	extrapolated using a five level $k\cdot p$ scheme	75W2
B	-8.57		
$ C $	12.78		

Lattice properties

lattice parameter

a	5.6579060 \AA	$T = 298.15\text{ K}$	single crystal	75B
-----	------------------------	-----------------------	----------------	-----

For the temperature dependence of a in the range 20...812°C, see Fig. 1.3.4.

linear thermal expansion coefficient

For temperature dependence, see Fig. 1.3.5.

α	$0.00 \cdot 10^{-6}\text{ K}^{-1}$	$T = 0\text{ K}$	recommended values from different measurements	75S2
	$5.90 \cdot 10^{-6}\text{ K}^{-1}$	$T = 300\text{ K}$		
	$7.20 \cdot 10^{-6}\text{ K}^{-1}$	$T = 600\text{ K}$		
	$8.51 \cdot 10^{-6}\text{ K}^{-1}$	$T = 1000\text{ K}$		

density

d	5.3234 g/cm^3	$T = 25^\circ\text{C}$	hydrostatic weighing	52S
-----	------------------------	------------------------	----------------------	-----

melting point

T_m	1210.4 K			73H
dT_m/dp	$-2.04 \cdot 10^{-3}\text{ K atm}^{-1}$			67K

phonon dispersion curve, one phonon density of states : Fig. 1.3.6.

phonon frequencies

$\nu_{LTO}(\Gamma_{25'})$	$9.02(2)\text{ THz}$	$T = 300\text{ K}$	coherent inelastic neutron scattering	72N
$\nu_{TA}(X_3)$	$2.38(2)\text{ THz}$			
$\nu_{LAO}(X_1)$	$7.14(2)\text{ THz}$			
$\nu_{TO}(X_4)$	$8.17(3)\text{ THz}$			
$\nu_{TA}(L_3')$	$1.87(2)\text{ THz}$			
$\nu_{LA}(L_2)$	$6.63(4)\text{ THz}$			
$\nu_{TO}(L_3)$	$8.55(3)\text{ THz}$			
$\nu_{LO}(L_1)$	$7.27(2)\text{ THz}$			

sound velocities

v_1	$4.9138 \cdot 10^5 \text{ cm s}^{-1}$	$T = 298 \text{ K},$	ultrasound measurement (20 MHz),	63M
v_2	$3.5424 \cdot 10^5 \text{ cm s}^{-1}$	$\rho = 45 \text{ } \Omega \text{ cm}$	n-type samples	
v_3	$5.3996 \cdot 10^5 \text{ cm s}^{-1}$		designation: mode/direction of propaga-	
v_4	$3.5425 \cdot 10^5 \text{ cm s}^{-1}$		tion/direction of particle displacement	
v_5	$2.7458 \cdot 10^5 \text{ cm s}^{-1}$		v_1 : long./[001]/[001], v_2 : shear/[001]/[1 $\bar{1}$ 0]	
			v_3 : long./[110]/[110], v_4 : shear/[110]/[001]	
			v_5 : shear/[110]/[1 $\bar{1}$ 0]	

elastic moduli

c_{11}	$12.40 \cdot 10^{11} \text{ dyn cm}^{-2}$	$T = 298 \text{ K},$	ultrasound measurement	71B2
c_{12}	$4.13 \cdot 10^{11} \text{ dyn cm}^{-2}$	$\rho = 37 \text{ } \Omega \text{ cm}$	temperature dependence: Figs. 1.3.7a...c	
c_{44}	$6.83 \cdot 10^{11} \text{ dyn cm}^{-2}$			

third order elastic moduli

c_{111}	$-7.10(6) \cdot 10^{12} \text{ dyn cm}^{-2}$	$T = 298 \text{ K},$	from ultrasound measurements,	64M
c_{112}	$-3.89(3) \cdot 10^{12} \text{ dyn cm}^{-2}$	$\rho = 45 \text{ } \Omega \text{ cm}$	temperature dependence: Fig. 1.3.8	
c_{123}	$-0.18(6) \cdot 10^{12} \text{ dyn cm}^{-2}$			
c_{144}	$-0.23(16) \cdot 10^{12} \text{ dyn cm}^{-2}$			
c_{166}	$-2.92(8) \cdot 10^{12} \text{ dyn cm}^{-2}$			
c_{456}	$-0.53(7) \cdot 10^{12} \text{ dyn cm}^{-2}$			

Young's modulus, torsion modulus : see Fig. 1.3.9.

bulk modulus

B_S	$7.502 \cdot 10^{11} \text{ dyn cm}^{-2}$	$T = 298 \text{ K},$	from ultrasound measurements	63M
		$\rho = 45 \text{ } \Omega \text{ cm}$		

internal-strain parameter

0.76(4)	X-ray diffraction	64S
---------	-------------------	-----

Debye temperature

$\Theta_D(0)$	374 K	for $\Theta_D(T)$, see Fig. 1.3.10	59F
---------------	-------	-------------------------------------	-----

heat capacity : Fig. 1.3.11.

Transport properties

Low field transport is maintained by electrons in the L_6^+ minima of the conduction band and holes near the point Γ_8^+ in the valence bands. At room temperature, the mobility of samples with impurity concentrations below 10^{15} cm^{-3} is limited essentially by lattice scattering; higher donor or acceptor concentrations result in an increasing influence of impurity scattering. At 77 K, even for doping concentrations below 10^{13} cm^{-3} the mobilities depend on the impurity concentration. Low temperatures and high concentrations lead to the replacement of free carrier conduction by impurity conduction.

intrinsic conductivity

σ_i	$2.1 \cdot 10^{-2} \text{ } \Omega^{-1} \text{ cm}^{-1}$	$T = 300 \text{ K}$	for temperature dependence, see Fig. 1.3.12	54M1
------------	--	---------------------	---	------

intrinsic carrier concentration

n_i	$2.33 \cdot 10^{13} \text{ cm}^{-3}$	$T = 300 \text{ K}$	for temperature dependence, see Fig. 1.3.13	54M1
-------	--------------------------------------	---------------------	---	------

The best fit to the curve in Fig. 1.3.13 is given by the empirical expression

$$n_i^2 = 3.10 \cdot 10^{32} T^3 \exp(-0.785/kT) \text{ cm}^{-6} \quad (kT \text{ in eV}, T \text{ in K})$$

electron mobility

μ_n	3800 cm ² /Vs	$T = 300$ K	lattice mobility determined by conductivity measurements of high purity samples.	54M1
---------	--------------------------	-------------	--	------

Temperature dependence in the range 77...300 K given by $\mu_n = 4.90 \cdot 10^7 T^{-1.66}$ cm²/Vs (T in K); see also Fig. 1.3.14 and 1.3.15.

hole mobility

μ_p	1800 cm ² /Vs	$T = 300$ K	lattice mobility in high purity samples.	54M2
---------	--------------------------	-------------	--	------

Temperature dependence in the range 100...300 K given by $\mu_p = 1.05 \cdot 10^9 T^{-2.33}$ cm²/Vs (T in K); see also Fig. 1.3.15.

piezoresistance coefficients

n-type material

π_{11}	$-2.7 \cdot 10^{-12}$ cm ² /dyn	$T = 300$ K	uniaxial tensile stress	54S
π_{12}	$-3.9 \cdot 10^{-12}$ cm ² /dyn	$\rho = 5.7 \Omega$ cm		
$(1/2)(\pi_{11} + \pi_{12} + \pi_{44})$	$-71.7 \cdot 10^{-12}$ cm ² /dyn			
$(1/2)(\pi_{11} + \pi_{12} - \pi_{44})$	$62.0 \cdot 10^{-12}$ cm ² /dyn			

p-type material

π_{11}	$-3.7 \cdot 10^{-12}$ cm ² /dyn	$T = 300$ K	resistivity measurements	
π_{12}	$3.2 \cdot 10^{-12}$ cm ² /dyn	$\rho = 1.1 \Omega$ cm		
$(1/2)(\pi_{11} + \pi_{12} + \pi_{44})$	$48.1 \cdot 10^{-12}$ cm ² /dyn			

elastoresistance coefficients

n-type material

m_{44}	-93.0	$T = 300$ K,	calculated from measured	54S
$(m_{11} - m_{12})/2$	0.4	$\rho = 1.5 \Omega$ cm	piezoresistance coefficients with the	
$(m_{11} + 2m_{12})/3$	-6.6		aid of elastic constants tensor c_{ij}	

p-type material

m_{44}	65.1	$T = 300$ K		
$(m_{11} - m_{12})/2$	-2.8	$\rho = 1.1 \Omega$ cm		
$(m_{11} + 2m_{12})/3$	2.0			

Seebeck coefficient (thermoelectric power) (absolute values)

S_n	$1.07 \cdot 10^{-3}$ V/K	$T = 300$ K,	temperature difference used: 1.5...4 K	65F
		$\rho = 17.0 \Omega$ cm		
S_p	$1.06 \cdot 10^{-3}$ V/K	$T = 280$ K	temperature dependence: Fig. 1.3.16	
		$\rho = 10.5 \Omega$ cm		

thermal conductivity

Temperature dependence: Fig. 1.3.17.

Optical properties

optical constants

real and imaginary parts of the dielectric constant measured by spectroscopical ellipsometry, n , k , R , K calculated from these data [83A2]. See also Fig. 1.3.18.

$h\nu$ [eV]	ϵ_1	ϵ_2	n	k	R	K [10^3 cm^{-1}]
1.5	21.560	2.772	4.653	0.298	0.419	45.30
2.0	30.361	10.427	5.588	0.933	0.495	189.12
2.5	13.153	20.695	4.340	2.384	0.492	604.15
3.0	12.065	17.514	4.082	2.145	0.463	652.25
3.5	9.052	21.442	4.020	2.677	0.502	946.01
4.0	4.123	26.056	3.90	3.336	0.556	1352.55
4.5	− 14.655	16.782	1.953	4.297	0.713	1960.14
5.0	− 8.277	8.911	1.394	3.197	0.650	1620.15
5.5	− 6.176	7.842	1.380	2.842	0.598	1584.57
6.0	− 6.648	5.672	1.023	2.774	0.653	1686.84

refractive index , spectral dependence at RT

n	4.00541(11)	$\lambda = 8 \mu\text{m}$	mean values for ten samples from	82E1
	4.00412(12)	$9 \mu\text{m}$	various suppliers measured at	
	4.00319(11)	$10 \mu\text{m}$	20.0°C	
	4.00248(10)	$11 \mu\text{m}$		
	4.00194(11)	$12 \mu\text{m}$	temperature coefficient between	
	4.00151(10)	$13 \mu\text{m}$	20°C and 25°C : $4.0 \cdot 10^{-4} \text{ }^\circ\text{C}^{-1}$	

The spectral dependence of n , k , and K below 10 eV is shown in Fig. 1.3.19. For spectral dependence of n and k , see also Fig. 1.3.20. Temperature dependence: Fig. 1.3.21.

dielectric constant

$\epsilon(\infty)$	16.00	$T = 300 \text{ K}$	capacitance measurement	83S
$d \ln \epsilon(\infty)/dT$	$13.8(8) \cdot 10^{-5} \text{ K}^{-1}$	$T = 77 \dots 400 \text{ K}$	optical interference	59C
		$T [\text{K}]$ $\nu [\text{MHz}]$		
ϵ	16.5	4.2 750	capacitance bridge	66R
	16.0	4.2 9200	microwave measurement	56A
	16.2	300 9200		
	15.8	77 1	capacitance bridge	53D

For spectra of the real and imaginary parts of the dielectric constant, see Fig. 1.3.22. Temperature dependence of $\epsilon(\infty)$: Fig. 1.3.23.

elastooptic constants

p_{11}	− 0.154	$T = 300 \text{ K},$	interferometric technique	78F
p_{12}	− 0.126	$\lambda = 10.6 \mu\text{m}$		
p_{44}	− 0.073		polarimetric technique	

third order susceptibilities

The second order susceptibilities are zero as a result of inversion symmetry. The third order susceptibility has two independent components.

$ \chi_{1111} $	$1.0(5) \cdot 10^{-10} \text{ esu}$	$\text{CO}_2 \text{ laser},$	optical third order mixing	69W
$ \chi_{1122} $	$0.6(3) \cdot 10^{-10} \text{ esu}$	$\lambda = 10.6 \mu\text{m},$		
$ \chi_{1111} $	$1 \cdot 10^{-10} \text{ esu}$	$T = 300 \text{ K}$	calculated	70V

Impurities and defects

shallow donors binding energies

binding energies of group V substitutional donors

Impurity	E_b [meV]	T [K]	Experimental method, remarks	Ref.
Theory	9.81		donor effective mass calculation	69F
Sb	10.29	10, 4	optical absorption (photothermal ionization)	75S1, 64R
Bi	12.81	10	optical absorption	64R
P	12.89	10	photoconductivity, absorption	74S
As	14.17	10	absorption	64R

other shallow single donor binding energies

Impurity	E_b [meV]	T [K]	Remarks	Ref.
Li	10.02	4	photoconductivity, absorption	72S, 78H2
O–Li	10.47	6	piezophotoconductivity	78H2
O–H	12.46	4	photoconductivity	78H1, 80J
D ₁	9.38		photoconductivity, observed in oxygen doped crystals	78C
D ₂	10.75		photoconductivity, observed in oxygen doped crystals	78C
Ia	17.25		photoconductivity, "thermal donor"-related	82C, 84C
Ib	17.6		photoconductivity, "thermal donor"-related	82C, 84C
Ic	18.1		photoconductivity, "thermal donor"-related	82C, 84C

ground state energies of group VI substitutional donors

Impurity	E [meV]	T [K]	Remarks	Ref.
Se ⁰	$E_c - 268.2$	20...160	Hall effect, photoconductivity	59T, 85G 88G, 98O
Se [−]	$E_c - 512.4$	140	DLTS	
Te ⁰	$E_c - 93$		Hall effect, photoconductivity,	57A, 59N, 59T, 88G
Te [−]	$E_c - 330$		DLTS	
S ⁰	$E_c - 280$		Hall effect, DLTS	88G
S [−]	$E_c - 590$			
O	$E_c - 17$		Hall effect, photoconductivity	61F, 62K, 63W, 82C
	$E_c - 40$			
	$E_c - 200$			
	$E_c - 60...80$			78E
	$E_c - 160...180$			
	$E_c - 16...17.3$	7...40	Absorption, D ⁰ state of oxygen-related thermal double donor.	84C, 82C
	$E_c - 34...37$	7...40	Singly ionized D ⁺ state of thermal donor	84C

shallow acceptors binding energies

binding energy of group III substitutional acceptors

Impurity	E_b [meV]	T [K]	Remarks	Ref.
Theory	11.2		acceptor EMT calculation	76B1
B	10.82	4, 8	photoconductivity, optical absorption	74H
Al	11.15		full series of EMT	65J
Ga	11.32		like excited states	
In	11.99			
Tl	13.45		optical absorption	65J

binding energy of other shallow singly charged acceptors

Impurity	E_b [meV]	Remarks	Ref.
H, Si(A ₂ /A ₁)	11.66, 10.59	hydrogen-silicon associated quenched-in defect. 1.07 meV ground state splitting due to strain dipole acting on central cell. + 21 μ eV isotope shift on deuteration.	78H1, 85H1, 87K, 89D
H, C(A ₆)	12.28, 11.30	1.98 meV ground state tunnel splitting	78H1, 87K
CN	11.32	crystals grown in nitrogen atmosphere in	78H2, 85M, 85H1
substitutional (A ₃ , A ₅)		graphite coated crucible. 1.1 meV ground state splitting	
CN	10.77		
interstitial (A ₄)			
A ₇	11.01	no correlation with chemical impurity reported	78H1
SA ₁	8.69, 9.48	crystals quenched from 900°C. Detailed	81K, 81B, 82B
SA ₂	8.86, 9.59	identifications uncertain. SA _{1,2} hole	
SA ₁ (Ni)	9.02, 9.21, 9.37, 9.62	repulsive cores since binding energy less than effective mass value	
SA ₁ (Cu)	9.73, 10.5		
SA ₂	13.89		
SA ₂	14.42		
SA ₃	17.89		
Be, H	11.29, 10.79	Be-doped crystal grown in hydrogen atmosphere, 0.50 meV ground state splitting	85M, 87K
Zn, H	12.53, 9.87	Zn-doped crystal grown in hydrogen atmosphere, 2.66 meV ground state splitting	85M, 87K
A ₈	10.34		
A ₉	10.90		
A ₁₀	11.45, 12.03	0.58 meV ground state splitting	82D

group II substitutional double acceptors

neutral double acceptor binding energies

Impurity	E_b [meV]	T [K]	Remarks	Ref.
Be ⁰	24.80	2, 8	optical absorption and/or photoconductivity	67S, 71M, 74H, 83C
Zn ⁰	32.98	2, 8	optical absorption and/or photoconductivity	60F, 71M
Mg ⁰	35.85		optical absorption and/or photoconductivity	85M
Cd ⁰	54.96		optical absorption and/or photoconductivity	71M
Hg ⁰	91.65	6...20	optical absorption and/or photoconductivity	67C, 71M
Mn ⁰	55		optical absorption and/or photoconductivity	85M

singly ionized double acceptor binding energies

Impurity	E_b [meV]	T [K]	Remarks	Ref.
Be ⁻	58.02		optical absorption	83C
Zn ⁻	86.51	8...10	optical absorption, excited states observed	83C, 73B
Cd ⁻	160	20	Hall effect, photoconductivity	59T
Hg ⁻	230	10	optical absorption	67C
Mn ⁻	100			85M

positively charged multiple acceptor binding energies

Impurity	E_b [meV]	T [K]	Remarks	Ref.
Be ⁺	5.1	1.2	photoconductivity	85M, 85L,
Zn ⁺	2.0	1.2	photoconductivity	83H
Mg ⁺	2.9	1.2	photoconductivity	
Mn ⁺	3.2	1.2	photoconductivity	
Hg ⁺	12.2	1.2	photoconductivity	
Cu ⁺	2.0	1.2	photoconductivity	
Ag ⁺	35	10	DLTS	89H

energy levels of group I substitutional triple acceptors and related complexes

energy levels of group I impurities

Impurity	E [meV]	T [K]	Remarks	Ref.
Cu ⁰	$E_v + 43.25$	20...300	Hall effect, photo conductivity	54D, 57W, 85S1
Cu ⁻	$E_v + 330$	20...300		57W, 84P1
Cu ²⁻	$E_c - 260, E_v + 410$	20...300		57W, 84P1
Cu donor			Cu interstitial	64H
CuH ₂	$E_v + 16.42, 16.81, 16.92, 10$ 16.96, 17.03, 17.08, 17.14, 17.21, 17.29, 17.70, 17.81		photoconductivity (photothermal ionization) produced by Cu diffusion in hydrogen atmosphere grown crystals	77H1, 86K
CuH	$E_v + 175$			77H1
Cu, (D,H)	$E_v + 18.10$			86K
Cu,(H,T)	$E_v + 18.12$			86K
Cu, D ₂	$E_v + 18.20$			86K
Cu, T ₂	$E_v + 18.24$			86K
Cu, Li ₂	$E_v + 20.41$		assignments of Cu, Li ₂ and Cu, (Li, H) may be reversed	85H2
Cu, (Li,H)	$E_v + 25.30$			85H2
Cu, As	$E_v + 10.05/9.15$		split ground state, complex with C _{3v} symmetry, found in Cu and As doped,vacuum grown crystals	96S
Au donor	$E_v + 44$		Hall effect, photoconductivity	55D, 57W,
Au ⁰	$E_v + 135$		and DLTS, the DLTS data given	59N, 65O,
Au ⁻	$E_c - 215$		here have not been corrected for	87S
Au ²⁻	$E_c - 56$		the capture cross section activation energy. All levels are assigned to substitutional Au.	
Ag ⁰	$E_v + 116$		Hall effect, DLTS	59N, 89H
Ag ⁻	$E_c - 261$			
Ag ²⁻	$E_c - 113$			

energy levels of transition metal impurities

Unless otherwise stated, transition metals give rise to acceptor levels. Ground state energy levels for the two ionization states (where relevant) are given.

Impurity	E [meV]	T [K]	Remarks	Ref.
Cr	$E_v + 70, E_v + 120$		resistivity	59N
Mn	$E_v + 160, E_c - 370$	30...400	resistivity, photoconductivity	55W, 59T
Fe	$E_v + 350, E_c - 270$	30...400	resistivity, photoconductivity	54T, 59T
Co	$E_v + 250, E_c - 300$	77...300	resistivity, Hall effect and photoconductivity	55T, 59T
Co-donor	$E_v + 83$			71B3
Ni ⁰	$E_v + 207$		only level found with DLTS in hydrogen free, pure germanium	55T, 59T, 92H, 92Z
Ni - H	$E_v + 159/E_v + 299$		the two levels correlate with the presence of both nickel and hydrogen	92Z
Pt	$E_v + 40$		resistivity, three acceptor levels. interpretation not clear	59N, 54D
Pd	$E_v + 0.03, E_c - 0.18$		resistivity, Hall effect	80G

energy levels of defect centers

Defect	E [meV]	Generation	Remarks	Ref.
Di-vacancy (V ₂)-donor			$E_v + 100, 120, 160$ meV levels are interpreted as di-vacancy-donor complexes and are double acceptors	75M, 77M
	$E_v + 100$	1 MeV	P, As doped Ge	
	$E_v + 120$	γ -irr. at 280 K	Sb doped Ge	
	$E_v + 160$		Bi doped Ge	
Group V interstitial	$E_c - 200$	1 MeV γ -irr. at 280 K	n-Ge, interpreted as structural modification of group V interstitial (D _i). Anneals at 100.. 160°C. This level can also be introduced by fast neutrons and electron irradiation.	64P, 77M
Acceptors labeled by annealing		γ -irr. at 42 K	(a) double acceptors, anneal at 65 K, interpreted as vacancy-interstitial (Frenkel) pair "65 K" defects. (b) acceptors, anneal at 160...200 K, arise from interstitial defects observed in dislocation free, high purity Ge	77M
Di-vacancy (V ₂)-H	$E_v + 80$ $E_v + 200$		grown in H-atmosphere; also produced by γ -irr. of dislocated material. Attributed to di-vacancyhydrogen complexes (c.f. di-vacancy-donor complexes above). $E_v + 71$ meV obtained if degeneracy factor of 4 assumed.	77H1, 77H2 82E2
Di-vacancy (V ₂)-Li	$E_v + 100$	γ -irr. at 280 K	Li doped, high purity Ge; resistivity, Hall effect	77H1
γ -irr. Ge	$E_v + 270$	γ -irr. at 280 K	acceptor, oxygen related defect	72C
γ -irr. Ge	$E_v + 340$	γ -irr. at 280 K	acceptor, silicon-self interstitial interaction	77M
γ -irr. Ge	$E_c - 80$	γ -irr. at 280 K	Hall effect, Ge:Li	81V
γ -irr. Ge	$E_v + 230, 380$	γ -irr. at 280 K	DLTS	82P1
γ -irr. Ge	$E_c - 420$			84P2

γ -irr. Ge	$E_c - 200$	γ -irr. at 280 K	Sb doped Ge	81T
e^- -irr. Ge	$E_c - 200, 400$	e^- -irr.	1.5 MeV irradiation, n-type Ge, DLTS studies	81F, 82F
e^- -irr. Ge	$E_v + 210, 240, 310$	e^- -irr.	10 MeV irradiation, p-type Ge, DLTS	83F1
e^- -irr. Ge	$E_v + 240, 290$	e^- -irr.	n-type Ge (As doped)	
e^- -irr. Ge	$E_c - 260, 370, 380, 410$	e^- -irr.		82P2
		e^- -irr.	3.5 MeV irradiation, DLTS studies	83A1
	$E_c - 190, 260, 310, 430$	e^- -irr.	n-type Ge, 430meV trap dominant	83A1
	$E_v + 160, 229, 350$	e^- -irr.	p-type Ge, 350 meV trap dominant	83A1
	2.4 μ m infrared absorption band	3...5 MeV e^- irr. 400 keV proton bombardment	vibrational levels of a complex defect. Attributed to di-vacancies in [75S1]. Anneals at 200 K. The electron irradiation gives rise to acceptor levels at $E_v + 80$ meV, $E_v + 160$ meV.	77G
			<110> axis from polarization experiments. Di-vacancy suggested.	82G
	2.72 μ m infrared absorption band	fast irr.	IR absorption	75N
Oxygen related defect	$E_c - 0.13, 0.25, 0.29$	1.5 MeV e^- -irr.	DLTS studies. Correlations with local mode spectra in [65W] for electron irradiated Ge:O suggested.	83F2
	$E_v + 0.27$ eV (donor)	4 MeV e^- -irr.	Resistivity	84L
	$E_v + 0.14, 0.20$ (acceptor)			
	$E_c - 200, 220, 270, 400$	thermal n	DLTS studies As, Sb doped Ge $E_c - 220$ suggested to contain interstitial As	84F
Multi-vacancy complexes	$E_v + 16$ $E_v + 20$ $E_v + 14$ $E_v + 60...80$ $E_v + 160...180$	fast n irr.	acceptor levels obtained from Hall effect and resistivity measurements 17...300 K. Observed in Sb-, As-, Ga-doped Ge. Attributed to multivacancy complexes – independent of impurity content	77D, 55C, 70T
Edge dislocation (?)	$E_v + 90$	plastically deformed Ge	Hall effect, resistivity	74O, 75L, 79S
	$E_v + 75, 190, 270, 390$	plastically deformed Ge	DLTS	83B
Screw dislocation	$E_v + 35, 590$	twisted Ge	Hall effect, resistivity	75W1
Grownin dislocations			DLTS	85S2
	$E_v + 25, 100$		p-type Ge	
	$E_c - 90$		n-type Ge	
"E _T I"	$E_v + 0.17, 0.36$	Laser irr. Ge	DLTS	83P1
	$E_c - 40...100$		DLTS on ultrapure Ge.	85H2

References to 1.3

- 52S Straumanis, M. E., Aka, A. Z.: J. Appl. Phys. 23 (1952) 330.
- 53D Dunlap, W. C., Watters, R. L.: Phys. Rev. 92 (1953) 1396.
- 53F Fine, E. M.: J. Appl. Phys. 24 (1953) 338.
- 53M McSkimin, H. J.: J. Appl. Phys. 24 (1953) 988.
- 54D Dunlap, W. C.: Phys. Rev. 96 (1954) 40.
- 54G Geballe, T. H., Hull, G. W.: Phys. Rev. 94 (1954) 1134.
- 54M1 Morin, F. J., Maita, J. P.: Phys. Rev. 94 (1954) 1525.
- 54M2 Morin, F. J.: Phys. Rev. 93 (1954) 62.
- 54S Smith, C. S.: Phys. Rev. 94 (1954) 42.
- 54T Tyler, W. W., Woodbury, H. H.: Phys. Rev. 96 (1954) 874.
- 55C Cleland, J. W., Crawford, J. H., Pigg, J. G.: Phys. Rev. 99 (1955) 1170.
- 55D Dunlap, W. C.: Phys. Rev. 97 (1955) 664.
- 55F Fine, M. E.: J. Appl. Phys. 26 (1955) 862.
- 55T Tyler, W. W., Newman, R., Woodbury, H. H.: Phys. Rev. 97 (1955) 669.
- 55W Woodbury, H. H., Tyler, W. W.: Phys. Rev. 100 (1955) 659.
- 56A D'Altroy, F. A., Fan, H. Y.: Phys. Rev. 103 (1956) 1671.
- 56D Dexter, R. N., Zeiger, H. J., Lax, B.: Phys. Rev. 104 (1956) 637.
- 57A Armstrong, J. A., Tyler, W. W., Woodbury, H. H.: Bull. Am. Phys. Soc. 2 (1957) 265.
- 57W Woodbury, H. H., Tyler, W. W.: Phys. Rev. 105 (1957) 84.
- 59C Cardona, M., Paul, W., Brooks, H.: J. Phys. Chem. Solids 8 (1959) 204.
- 59F Flubacher, P., Leadbetter, A. J., Morrison, J. A.: Philos. Mag. 4 (1959) 273.
- 59M McSkimin, H. J.: J. Acoust. Soc. Am. 31 (1959) 287.
- 59N Newman, R., Tyler, W. W.: Solid State Physics, Vol. 8, Seitz, F., Turnbull, D. (eds.) New York: Academic Press 1959, p. 49.
- 59P Philipp, H. P., Taft, E. A.: Phys. Rev. 113 (1959) 1002.
- 59T Tyler, W. W.: J. Phys. Chem. Solids 8 (1959) 59.
- 59Z Zwerdling, S., Lax, B., Roth, L. M., Button, K. J.: Phys. Rev. 114 (1959) 80.
- 60F Fisher, P., Fan, H. Y.: Phys. Rev. Lett. 5 (1960) 195.
- 60L Lukeš, F.: Czech. J. Phys. B 10 (1960) 742.
- 60M McLean, T. P.: in Progress in Semiconductors, Vol. 5, A. F. Gibson ed., Heywood, London 1960.
- 61F Fuller, C. S., Doleiden, F. H.: J. Phys. Chem. Solids 19 (1961) 251.
- 62K Kaiser, W.: J. Phys. Chem. Solids 23 (1962) 255.
- 63B Bundy, F. P., Kasper, J. S.: Science 139 (1963) 340.
- 63J Jamieson, J. C.: Science 139 (1963) 762.
- 63M McSkimin, H. J., Andreatch, Jr., P.: J. Appl. Phys. 34 (1963) 651.
- 63P Philipp, H. P., Ehrenreich, H.: Phys. Rev. 129 (1963) 1550.
- 63W Whan, R. A., Stein, H. J.: Appl. Phys. Lett. 3 (1963) 187.
- 64H Hall, R. N., Racette, J. H.: J. Appl. Phys. 35 (1964) 379.
- 64K Kasper, J. S., Richards, S. M.: Acta Crystallogr. 17 (1964) 752.
- 64M McSkimin, H. J., Andreatch, Jr., P.: J. Appl. Phys. 35 (1964) 3312.
- 64P Pigg, J. C., Crawford, J. H.: Phys. Rev. 135 (1964) A1 141.
- 64R Reuszer, J. H., Fisher, P.: Phys. Rev. 135 (1964) A1 125.
- 64S Segmüller, A.: Phys. Kond. Mater. 3 (1964) 18.
- 65B Bates, C. H., Dacheille, F., Roy, R.: Science 147 (1965) 860.
- 65F Freud, P. J., Rothberg, G. M.: Phys. Rev. 140 (1965) A1007.
- 65J Jones, R. L., Fisher, P.: J. Phys. Chem. Solids 26 (1965) 1125.
- 65O Ostroborodova, V. V.: Fiz. Tverd. Tela 7 (1965) 610; Sov. Phys.-Solid State (English Transl.) 7 (1965) 484.
- 65W Whan, R. E.: Phys. Rev. 140 (1965) A690.
- 66P Potter, R. F.: Phys. Rev. 150 (1966) 562.
- 66R Rao, K. V., Smakula, A.: J. Appl. Phys. 37 (1966) 2840.
- 67C Chapman, R. A., Hutchinson, W. G.: Phys. Rev. 157 (1967) 615.
- 67K Krestronikov, A. N., Ev'genev, S. B., Ulazov, V. M.: Dokl. Akad. Nauk SSSR 174 (1967) 634.
- 67S Shenker, H., Swiggard, E. M., Moore, W. J.: Trans. Metall. Soc. AIME 239 (1967) 347.
- 68S Singh, H. P.: Acta Crystallogr. 24a (1968) 469.
- 69A Aggarwal, R. L., Zuteck, M. D., Lax, B.: Phys. Rev. 180 (1969) 800.
- 69F Faulkner, R. A.: Phys. Rev. 184 (1969) 713.
- 69W Wynne, J. J.: Phys. Rev. B 1978 (1969) 1295.
- 70A Aggarwal, R. L.: Phys. Rev. B 2 (1970) 446.

- 70T Tkachev, V. D., Urenev, V. I.: Fiz. Tekh. Poluprovodn. 4 (1970) 2405; Sov. Phys. Semicond. (English Transl.) 4 (1970) 2075.
- 70V Van Vechten, J. A., Cardona, M., Aspnes, D. E., Martin, R. M. Proc. Int. Conf. Phys. Semicond. 1970, U. S. At. Energy Com., 1970, p. 82.
- 71B1 Buchenauer, C. J., Cerdeira, F., Cardona, M.: in Proc. 2nd Int. Conf. Light Scattering in Solids. Balkanski, M. ed., Flammarion, Paris 1971, p. 280.
- 71B2 Burenkov, Yu. A., Nikanorov, S. P., Stepanov, A. V.: Sov. Phys. Solid State (English Transl.) 12 (1971)1940; Fiz. Tverd. Tela 12 (1970) 2428.
- 71B3 Barnik, M. I., Beglov, D. I., Romanychev, D. A., Kharionovskii, Y. S.: Fiz. Tekh. Poluprovodn. 5 (1971) 106; Sov. Phys. Semicond. (English Transl.) 5 (1971) 87.
- 71M Moore, W. J.: J. Phys. Chem. Solids 32 (1971) 93.
- 71N Nilsson, G., Nelin, G.: Phys. Rev. B 3 (1971) 364.
- 72C Cleland, J. W.: IEEE Trans. Nucl. Sci. N519 (1972) 224.
- 72N Nilsson, G., Nelin, G.: Phys. Rev. B 6 (1972) 3777.
- 72S Seccombe, S. D., Korn, D.: Solid State Commun. 11 (1972) 1539.
- 73H Hultgren, R., Desai, P. D., Hawkins, D. T., Gleiser, M., Kelly, K. K., Wagram, D.: Selected values of the thermodynamic properties of the elements. American Society for Metals, Metals Park, Ohio 1973.
- 74H Haller, E. E., Hansen, W. L.: Solid State Commun. 15 (1974) 687.
- 74L Ley, L., Pollak, R. S., McFeely, F. R., Kowalezyk, S. P., Shirley, D. A.: Phys. Rev. B9 (1974) 600.
- 74O Osipyan, Y. A., Shevchenko, S. A.: Zh. Exp. Teor. Fiz. 65 (1973) 698; Sov. Phys. JETP (English Transl.) 38 (1974) 345.
- 74S Skolnick, M. S., Eaves, L., Stradling, R. A., Portal, J. C., Askenazy, S.: Solid State Commun. 125 (1974) 1403.
- 75A Aspnes, D. E.: Phys. Rev. B12 (1975) 2297.
- 75B Baker, J. F. C., Hart, M.: Acta Crystallogr. 31a (1975) 364.
- 75L Labusch, R., Schroter, W.: Int. Conf. on Defects in Semicond., Freiburg 1974, London and Bristol: Institute of Physics 1975, p. 103.
- 75M Mashovets, T. M., Emstev, V. V.: Int. Conf. on Defects on Semicond., Freiburg 1974, London and Bristol: Institute of Physics 1975, p. 103.
- 75N Newman, R. C., Totterdell, D. H. J.: Int. Conf on Lattice Defects in Semiconductors, Freiburg 1974, Huntley, F. A. (ed.), London and Bristol: Institute of Physics 1975, p. 172.
- 75S1 Skolnick, M. S., Eaves, L., unpublished.
- 75S2 Slack, G. A., Bartram, S. F.: J. Appl. Phys. 46 (1975) 89.
- 75W1 Wagner, R., Hansen, P.: Int. Conf. on Defects in Semicond., Freiburg 1974, London and Bristol: Institute of Physics 1975, p. 387.
- 75W2 Wiley, J. D.: in "Semiconductors and Semimetals", Vol. 10, R. K. Willardson, A. C. Beer eds., Academic Press, New York 1975.
- 76A Altarelli, M., Lipari, N. O.: Phys. Rev Lett. 36 (1976) 619.
- 76B1 Baldereschi, A., Lipari, N. O.: Proc. 13th Int. Conf. on the Physics of Semicond. . Rome 1976, Fumi, F. G. (ed.), Marves 1976, p. 595.
- 76B2 Buchanan, M., Timusk, T.: Proc. 13th Int. Conf. Physics Semiconductors, Rome 1976, ed. by F. G. Fumi, Marves, p. 821.
- 76C Chelikowski, J. R., Cohen, M. L.: Phys. Rev. B 14 (1976) 556.
- 76F Fink, D., Braunstein, R.: Phys. Status Solidi (b) 73 (1976) 361.
- 76I Icenogle, H. W., Platt, B. C., Wolfe, W. L.: Appl. Opt. 15 (1976) 2348.
- 76L Lipari, N. O., Altarelli, M., Tosatti, E.: Solid State Commun. 21 (1976) 979.
- 77D Dobrego, V. P., Ermdaev, O. P., Tkachev, V. F.: Phys. Status Solidi (a) 44 (1977) 435.
- 77G Gerasimov, A. B., Dolidze, N. D., Konovalenko, B. M.: Fiz. Tekh. Poluprovodn. 11 (1977) 1349; Sov. Phys. Semicond. (English T~tsl.) 11 (1977) 793.
- 77H1 Haller, E. E., Hubbard, G. S., Hansen, W. L.: IEEE Trans. Nucl. Sci. N524 (1977) 48.
- 77H2 Haller, E. E., Hubbard, G. S., Hansen, W. L., Seeger, A.: Int. Conf. on Radiation Effects in Semiconductors, Dubrovnik 1976, Institute of Physics Conf. Ser. No. 31 1977, p. 309.
- 77M Mashovets, T. M.: Int. Conf. on Radiation Effects in Semiconductors, Dubrovnik 1976. Institute of Physics Couf. Ser. No. 31 1977, p. 30.
- 78A Asaumi, K. A., Minomura, S.: J. Phys. Soc. Jpn. 45 (1978) 1061.
- 78C Clauws, P., van der Steen, K., Broeckx, J., Schoenmaekers, W.: Int. Conf. on Defects and Radiation Effects in Semiconductors, Nice 1978, Institute of Physics Conf. Ser. No. 46, p. 218.

- 78E Emtsev, V. V., Goncharev, L. A., Dostkhodzhoev, T. N.: Fiz. Tekh. Poluprovodn. 12 (1978) 139; Sov. Phys. Semicond. (English Transl.) 12 (1978) 78.
- 78F Feldmann, A., Waxler, R. M., Horowitz, D.: J. Appl. Phys. 49 (1978) 2589.
- 78H1 Haller, E. E.: Phys. Rev. Lett. 40 (1978) 584.
- 78H2 Haller, E. E., Falicov, L. M.: Phys. Rev. Lett. 41 (1978) 1192.
- 79M Martin, T. P., Schaber, H.: Z. Physik B 35 (1979) 61.
- 79S Schroter, W.: Int. Conf. on Defects and Radiation Effects in Semiconductors, Nice 1978, Institute of Physics Conf. Ser. No. 46 1979, p. 114.
- 80G Golubev, N. F., Latyshev, A. V.: Sov. Phys. Semicond. (English Transl.) 14 (1980) 1074.
- 80J Joos, B., Haller, E. E., Falicov, L. M.: Phys. Rev. B22 (1980) 832.
- 80Z Zverev, V. N.: Sov. Phys. Solid State (English Transl.) 22 (1980) 1921; Fiz. Tverd. Tela 22 (1980) 3282.
- 81B Broeckx, J., Kamiura, Y., Clauws, P., Vennik, J.: Solid State Commun. 40 (1981) 149.
- 81F Fukuoka, N., Saito, H.: Jpn. J. Appl. Phys. 20 (1981) L519.
- 81J Jacoboni, C., Nava, F., Canali, C., Ottaviani, G.: Phys. Rev. B 24 (1981) 1014.
- 81K Kamiura, Y., Broeckx, J., Clauws, P., Vennik, J.: Solid State Commun. 38 (1981) 883.
- 81T Tarasik, M. I., Tkachev, V. D., Yavid, V. U., Yanchenko, A. M.: Phys. Status Solidi (0) 104 (1981) K117.
- 81V Vasileva, E. D., Daluda, Y. N., Emstev, V. V., Kervalishvili, P. D., Mashovets, T. V.: Sov. Phys. Semicond. (English Transl.) 15 (1981) 55.
- 82B Broeckx, J., Kamiura, Y., Clauws, P., Vennik, J.: Solid State Commun. 43 (1982) 499
- 82C Clauws, P., Broeckx, J., Simeon, E., Vennik, J.: Solid State Commun. 44 (1982) 1011.
- 82D Darken, L. S.: J. Appl. Phys. 53 (1982) 3754.
- 82E1 Edwin, R. P., Dudermeil, M. T., Lamare, M.: Appl. Optics 21 (1982) 878.
- 82E2 Emstev, V. V., Mashovets, T. V., Nazaryan, E. K., Haller, E. E.: Sov. Phys. Semicond. (English Transl.) 16 (1982) 182.
- 82F Fukuoka, N., Saito, H.: Jpn. J. Appl. Phys. 21 (1982) 930.
- 82G Gerasimov, A. B., Dolidze, N. D., Donina, R. M., Konovalenko, B. M., Ofengein, G. L., Tsertsvadze, A. A.: Phys. Status Solidi (a) 70 (1982) 23.
- 82H Hirose, Y., Shimomac, K., Hamaguchi, C.: J. Phys. Soc. Jpn. 51 (1982) 2226.
- 82P1 Pearton, S. J., Tavendale, A. J., Williams, A. A.: Radiat. Eff. 60 (1982) 129.
- 82P2 Poulin, F., Bourgoin, J. C.: Phys. Rev. B26 (1982) 6788.
- 83A1 Aeshin, A. I., Smirnov, L. S., Stas, V. F.: Sov. Phys. Semicond. (English Transl.) 17 (1983) 977.
- 83A2 Aspnes, D. E., Studna, A. A.: Phys. Rev. B 27 (1983) 985.
- 83B Baumann, F. H., Schroter, W.: Phys. Status Solidi (a) 79 (1983) K123.
- 83C Cross, J. W., Holt, L. T., Ramdas, A. K., Sauer, R., Haller, E. E.: Phys. Rev. B28 (1983) 6953.
- 83F1 Fukuoka, N., Saito, H.: Physica 116B (1983) 343.
- 83F2 Fukuoka, N., Saito, H.: Jpn. J. Appl. Phys. 22 (1983) L353.
- 83H Haller, E. E., McMurray, R. E., Falicov, L. M., Haegel, N. M., Hansen, W. L.: Phys. Rev. Lett. 51 (1983) 1089.
- 83P1 Pearton, S. J., Tavendale, A. J.: J. Appl. Phys. 54 (1983) 440.
- 83P2 Philip, J., Breazeale, M. A.: J. Appl. Phys. 54 (1983) 752.
- 83Q Qadri, S. B., Skelton, E. F., Webb, A. W.: J. Appl. Phys. 54 (1983) 3609; see also Spain, I. L., Qadri, S. B., Menoni, C. S., Webb, A. W., Skelton, E. F.: in "Physics of Solids under High Pressure", Schilling, J. S., Shelton, R. N. (eds.), North-Holland, Amsterdam, 1982, p. 73.
- 83S Samara, G. A.: Phys. Rev. B 27 (1983) 3494.
- 84B Bakhchieva, S. R., Kekelidse, N. P., Kekua, M. G.: Phys. Status Solidi (a) 83 (1984) 139
- 84C Clauws, P., Vennik, J.: Phys. Rev. B30 (1984) 4837.
- 84F Fukuoka, N., Saito, H.: Jpn. J. Appl. Phys. 23 (1984) 203.
- 84H Hsieh, T. C., Miller, T., Chiang, T. C.: Phys. Rev. B 30 (1984) 7005.
- 84L Litvinov, V. V., Urenev, V. I., Shershel, V. A.: Sov. Phys. Semicond. (English Transl.) 18 (1984) 707.
- 84O Olijnyk, H., Sikka, S. K., Holzapfel, W. B.: Phys. Lett. 103A (1984) 137; Olijnyk, H., Holzapfel, W. B.: J. Phys. (Paris) 45 Suppl., Colloq. C8 (1984) C8-153.
- 84P1 Pearton, S. J., Haller, E. E., Kahn, J. M.: J. Phys. C17 (1984) 2375.
- 84P2 Pearton, S. J., Tavendale, A. J., Kahn, J. M., Haller, E. E.: Radiat. Eff. 81 (1984) 293.
- 84V Vina, L., Logothetidis, S., Cardona, M.: Phys. Rev. B 30 (1984) 1979.
- 85G Grimmeiss, H. G., Larsson, K., Montelius, L.: Solid State Commun. 54 (1985) 863.
- 85H1 Haller, E. E. in: Microscopic identification of electronic defects in semiconductors, MRS Symposia Proceedings, Vol. 46, Johnson, N. M., Bishop, S. G., Watkins, G. D. (eds.), 1985, p. 495.
- 85H2 Hubbard, G. S., Haller, E. E., Pearton, S. J.: IEEE Trans. Nucl. Sci. N532 (1985) 549.
- 85K Kagaya, H.-M., Soma, T.: Phys. Status Solidi (b) 127 (1985) K5.

- 85L Labrie, D., Thewalt, M. L. W., Clayman, B. P., Timusk, T.: Phys. Rev. B32 (1985) 5514
- 85M McMurray, R. E.: Solid State Commun. 53 (1985) 1127.
- 85N Nichols, J. M., Hansson, G. V., Karlsson, U. O., Persson, P. E. S., Uhrberg, R. I. G., Engelhard, R., Flodström, S. A., Koch, E. E.: Phys. Rev. B 32 (1985) 6663.
- 85S1 Salib, E. H., Fisher, P., Simmonds, P. E.: Phys. Rev. B32 (1985) 2424.
- 85S2 Simeon, E., Clauws, P., Vennik, J.: Solid State Commun. 54 (1985) 1025.
- 85W Wachs, A. L., Miller, T., Hsieh, T. C., Shapiro, A. P., Chiang, T. C.: Phys. Rev. B 32 (1985) 2326.
- 86K Kahn, J. M., Falicov, L. M., Haller, E. E.: Phys. Rev. Lett. 57 (1986) 2077.
- 86M Menoni, C. S., Hu, J. Z., Spain, I. L.: Phys. Rev. B 34 (1986) 362.
- 86V Vohra, Y. K., Brister, K. E., Desgreniers, S., Ruoff, A. L., Chang, K. J., Cohen, M. L.: Phys. Rev. Lett. 56 (1986) 1944.
- 87K Kahn, J.M., McMurray, Jr., R.E., Haller, E.E., Falicov, L.M., Phys. Rev. B 36 (1987) 8001.
- 87S Simoen, E., Clauws, P., Huylebroeck, G., Vennik, J., Semicond. Sci. Technol. 2 (1987) 507.
- 88G Grimmeis, H., Montelius, L., Larsson, K.: Phys. Rev. B37 (1988) 6916.
- 89D Denteneer, P. J. H., Van de Walle, C. G., Pantelides, S. T., Phys. Rev. Lett. 62 (1989) 1884.
- 89H Huylebroeck, G., Clauws, P., Simoen, E., Rotsaert, E., Vennik, J., Semicond. Sci. Technol. 4 (1989) 529.
- 91G Giannozzi, P., de Gironcoli, S., Pavone, P., Baroni, S.: Phys. Rev. B 41 (1991) 7231.
- 92B Brazhkin, V. V., Lyapin, A. G., Popova, S. V., Voloshin, R. N.: Pisma Zh. Eksper. Teor. Fiz. 56 (1992) 156; JETP Letters 56 (1992) 152 (Engl. Transl.); Brazhkin, V. V., Lyapin, A. G., Popova, S. V.: in: *"High Pressure in Materials Science and Geoscience"* (XXXII. Annual Meeting EHPRG), Kamarad, J. et al. (eds.) (1994) 65.
- 92H Huylebroeck, G., Clauws, P., Simoen, E., Vennik, J. Solid State Commun. 82 (1992) 367.
- 92Z Zach, F.X., Grimmeiss, H., Haller, E.E., Materials Science Forum 83-87 (1992) 245.
- 94L Lewis, S. P., Cohen, M. L.: Solid State Commun. 89 (1994) 483.
- 96K Klotz, S., Besson, J. M., Braden, M., Karch, K., Bechstedt, F., Strauch, D., Pavone, P.: Phys. Status Solidi (b) 198 (1996) 105.
- 96N Nelmes, R. J., Liu, H., Belmonte, S. A., Loveday, J. S., McMahon, M. I., Allan, D. R., Häusermann, D., Hanfland, M.: Phys. Rev. B 53 (1996) R2907.
- 96S Sirmain, G., Dubon, O.D., Hansen, W.L., Olsen, C.S., Haller, E.E., J. Appl. Phys. 79 (1996) 209.
- 98O Olsen, C.S., Beeman, J.W., Itoh, K.M., Farmer, J., Ozhogin, V.I., Haller, E.E.: Solid State Commun. 108 (1998) 895.

Figures to 1.3

Fig. 1.0.2

The diamond lattice. The elementary cubes of the two face-centered cubic lattices are shown.

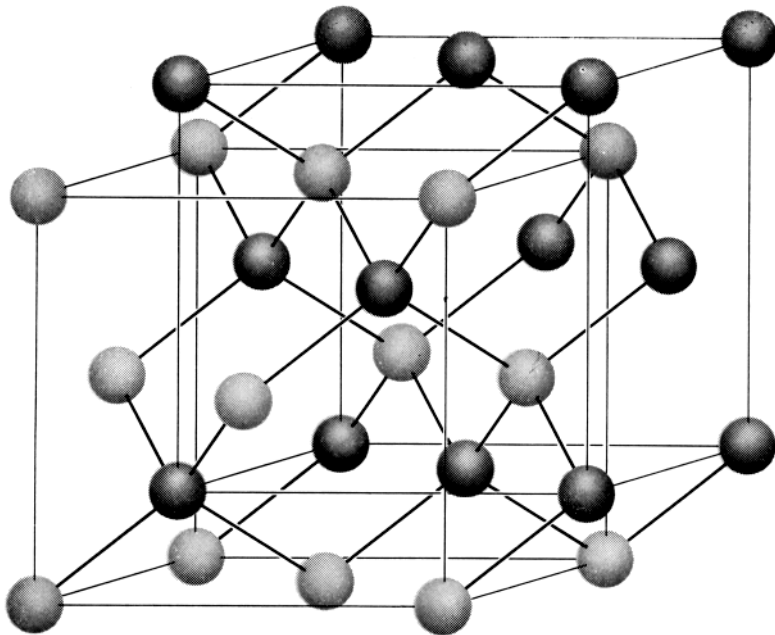


Fig. 1.0.6

Brillouin zone of the diamond lattice

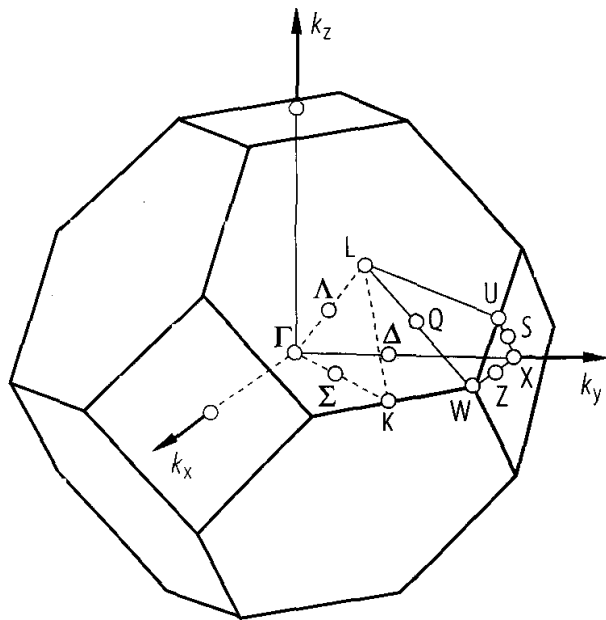


Fig. 1.0.10

Ge. (a) Band structure obtained by a non-local pseudopotential calculation including spin-orbit interaction [76C], (b) comparison of the calculated valence bands along the Δ - and Λ -axes with angular resolved photoemission data [85W].

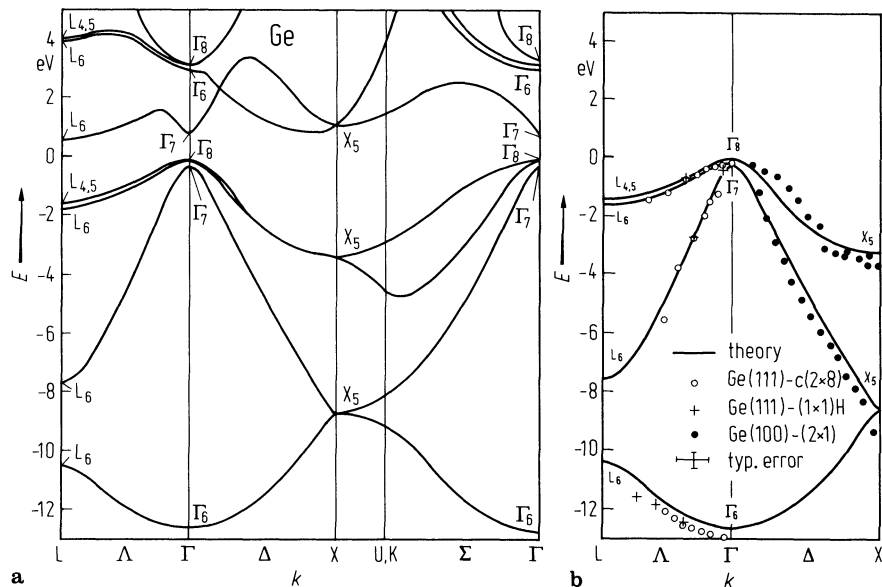


Fig. 1.3.1

Ge. Density of states of valence and conduction bands (solid line: obtained by a non-local pseudopotential calculation [76C], dashed line: XPS spectra showing the valence band density of states [74L]). $E - E_v$ in eV.

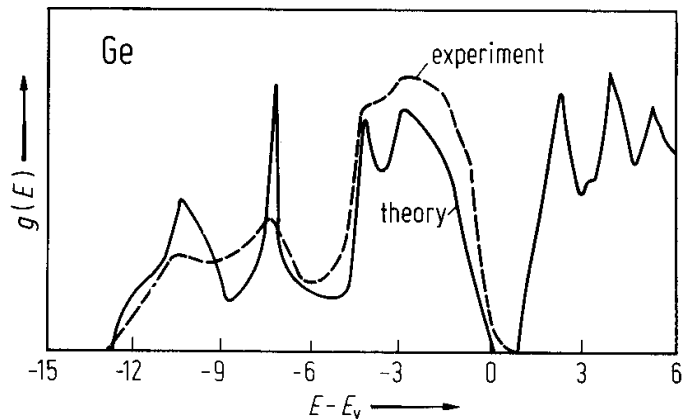


Fig. 1.3.2

Ge. Indirect and direct energy gaps vs. temperature [60M].

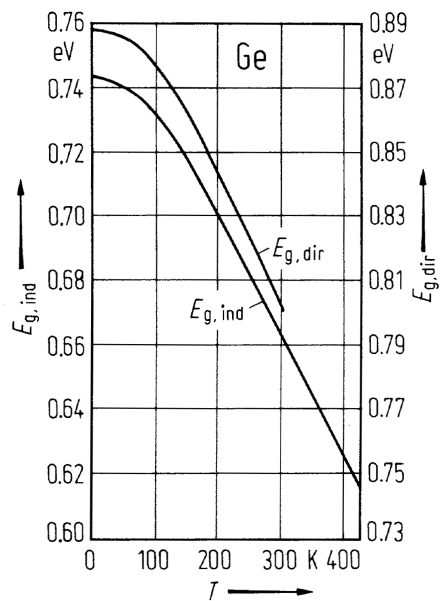


Fig. 1.3.3

Ge. (a) Dependence of the transverse electron mass in the L_6 minima on energy above the bottom of the conduction band measured by magnetopiezotransmission [69A], (b) cyclotron mass of light holes vs. energy below the top of the valence band ($B \parallel [111]$, $[110]$ and $[100]$) [80Z].

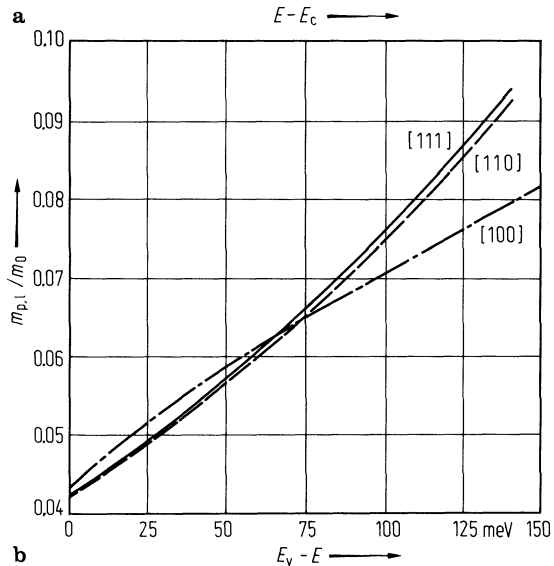
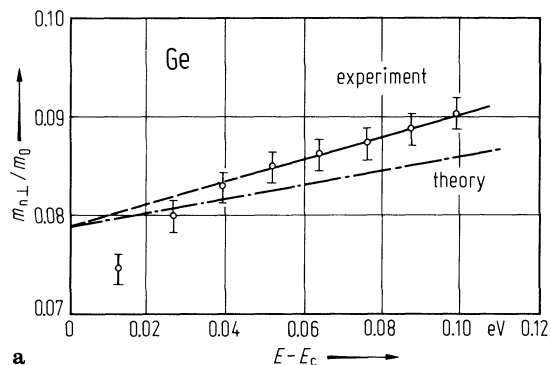


Fig. 1.3.4

Ge. Lattice parameter vs. temperature [68S].

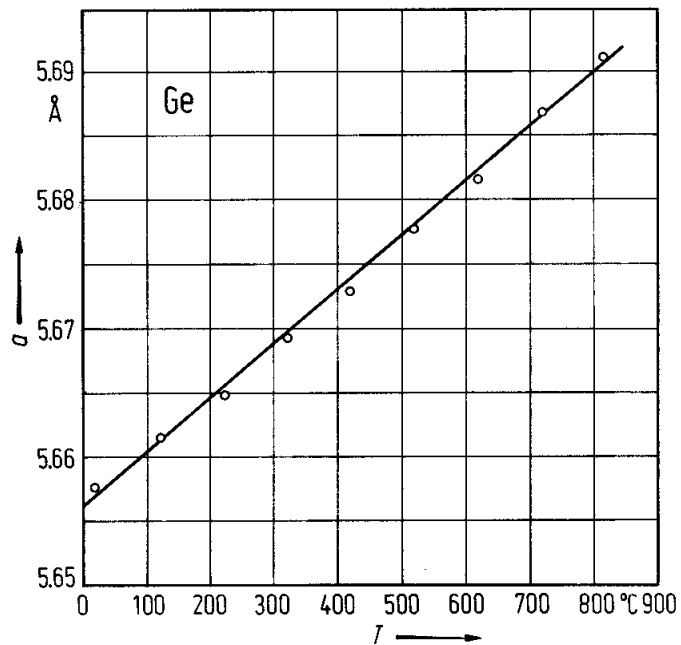


Fig. 1.3.5

Ge. Linear thermal expansion coefficient vs. temperature. Experimental data from various authors and theoretical results (solid line) [85K].

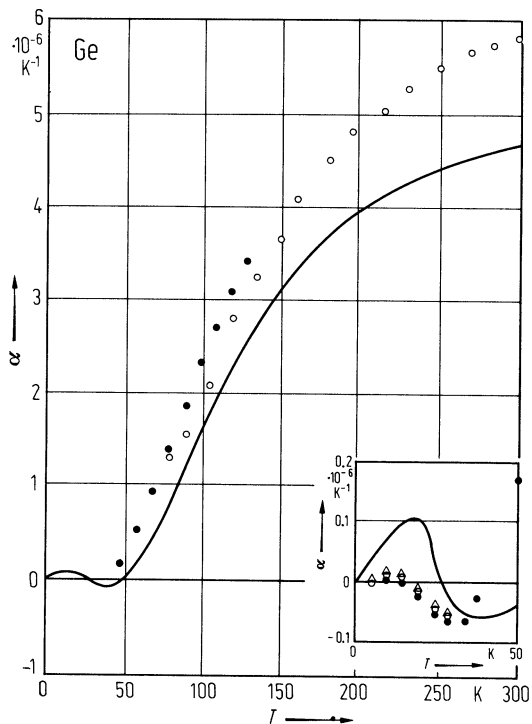


Fig. 1.3.6

Ge. Phonon dispersion curves (left panel) and phonon density of states (right panel) [91G]. Experimental data [71N] and ab-initio calculations [91G].

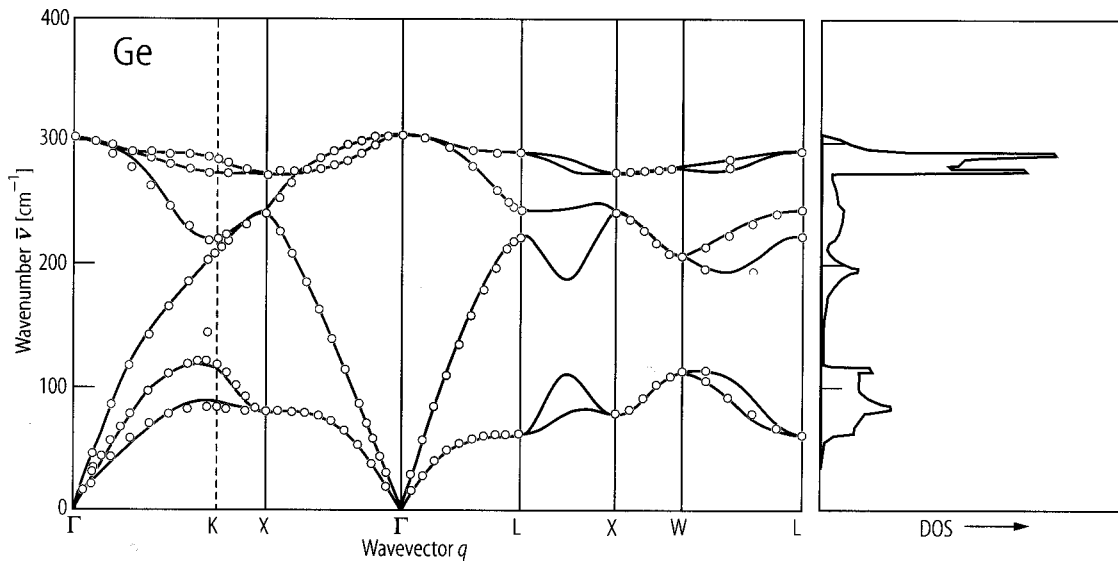


Fig. 1.3.7a Ge. Elastic modulus c_{11} vs. temperature [53M].

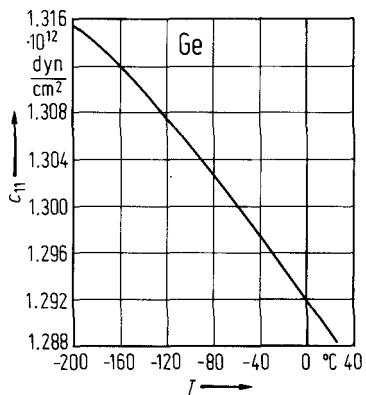


Fig. 1.3.7b Ge. Elastic modulus c_{12} vs. temperature [53M].

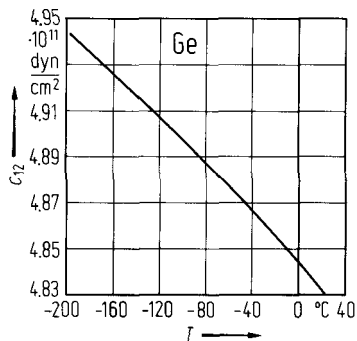


Fig. 1.3.7c Ge. Elastic modulus c_{44} vs. temperature [53M].

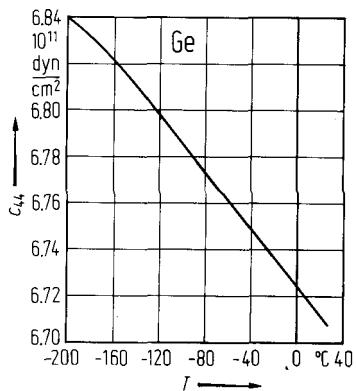


Fig. 1.3.8

Ge. Third-order elastic moduli vs. temperature. Solid lines: best fit to the data [83P2].

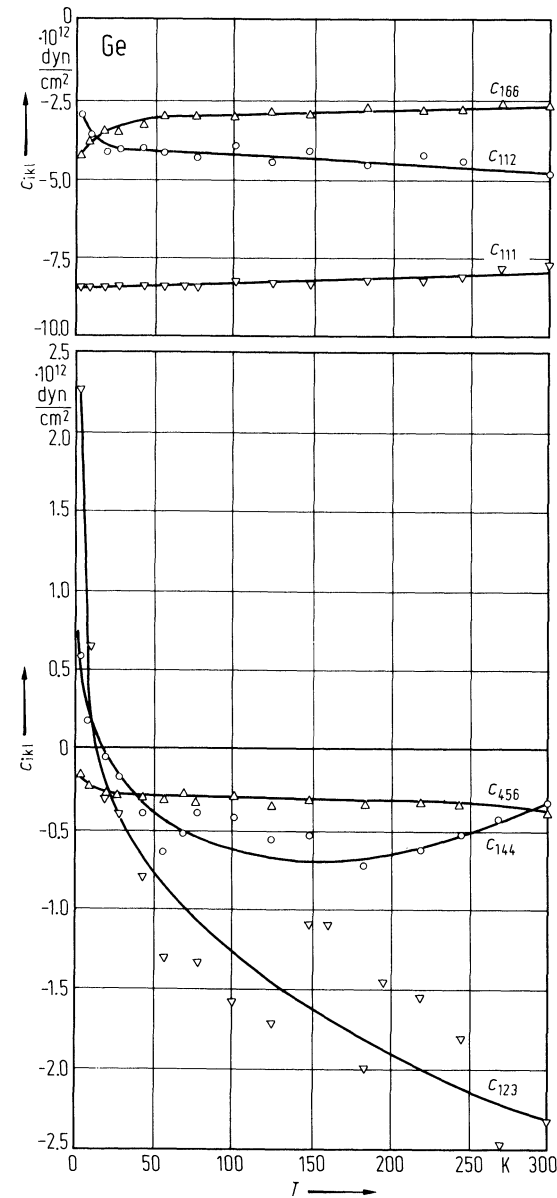


Fig. 1.3.9

Ge. Young's moduli E and torsion modulus G vs. temperature according to [71B1] (1); [53F, 55F] (2); [53M, 59M] (3).

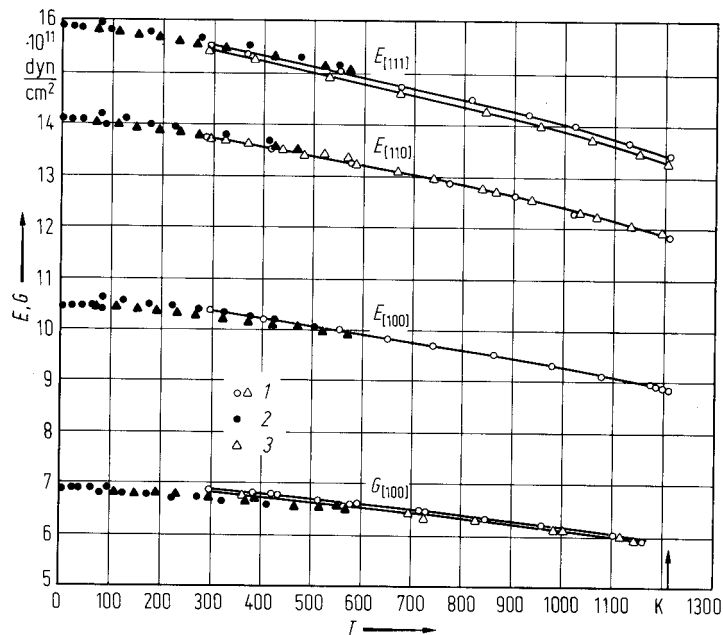


Fig. 1.3.10

Ge. Debye temperature $\Theta_D(T)$ vs. temperature [59F].

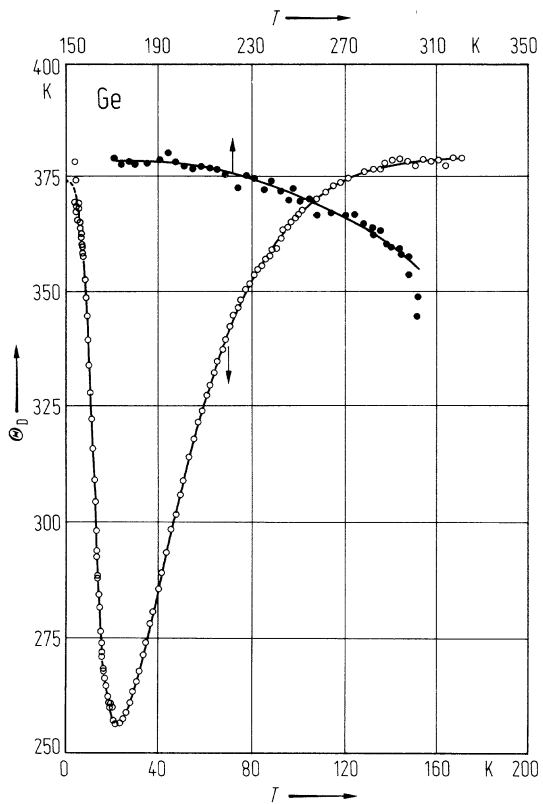


Fig. 1.3.11

Ge. Heat capacity at constant volume vs. temperature. Experimental points from [70T], solid line: theoretical [85K].

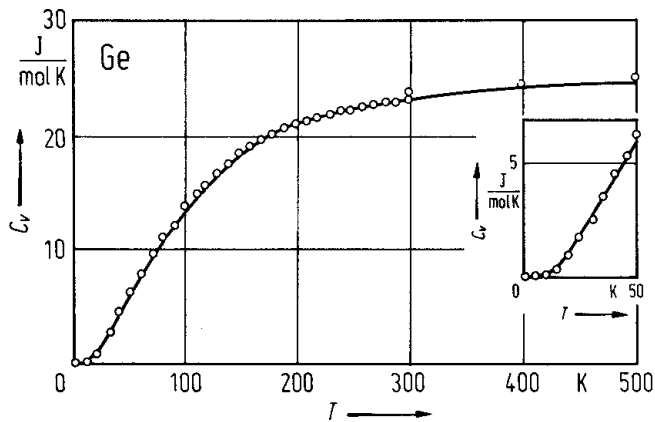


Fig. 1.3.12

Ge. Conductivity vs. reciprocal temperature in the range of intrinsic conduction [54M1].

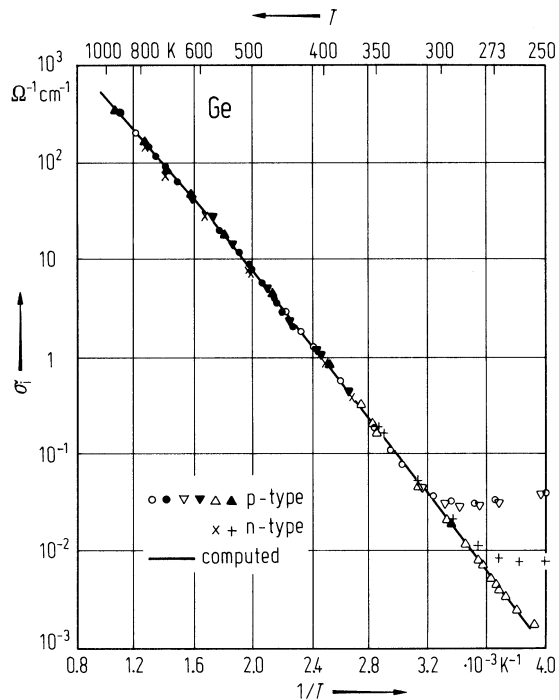


Fig. 1.3.13

Ge. Intrinsic carrier concentration vs. reciprocal temperature [54M1].

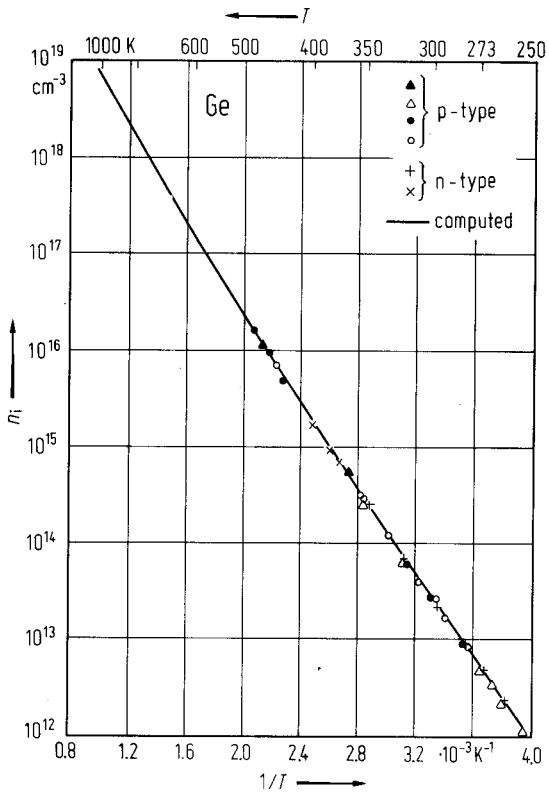


Fig. 1.3.14

Ge. (Ohmic) drift mobility of electrons vs. temperature obtained with a time-of-flight technique in hyperpure material (open circles); other symbols: data from five references; solid line: theory [81J].

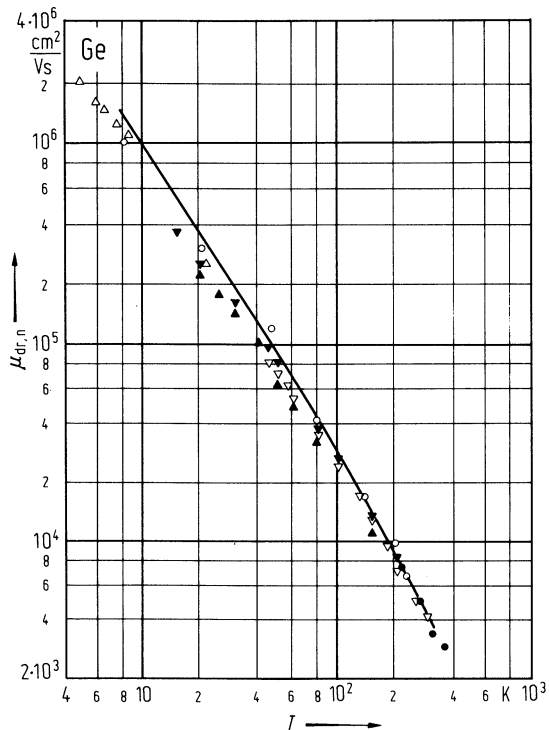


Fig. 1.3.15

Ge. Electron and hole mobilities vs. temperature for constant carrier concentration (high purity samples) [54M2].

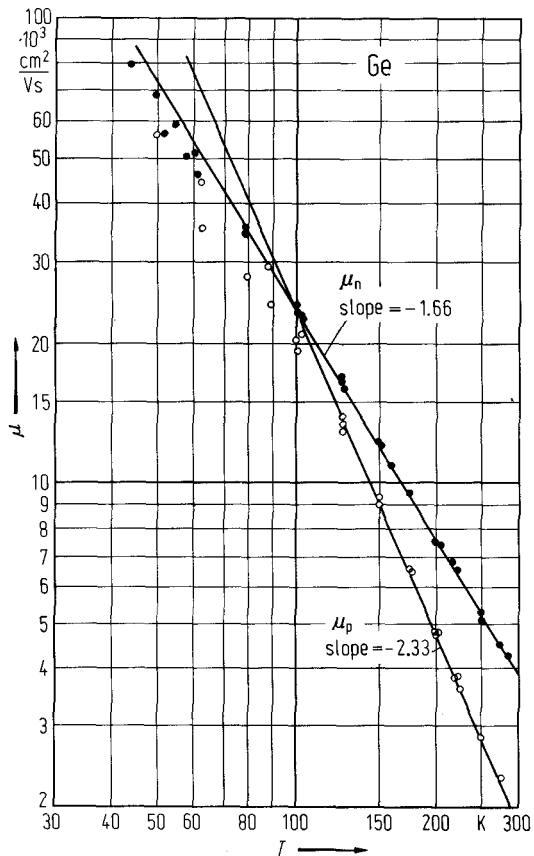


Fig. 1.3.16

Ge. Thermoelectric power times temperature vs. temperature. Full triangles: $n_a = 1.6 \cdot 10^{14} \text{ cm}^{-3}$; open circles: $n_a = 8.0 \cdot 10^{13} \text{ cm}^{-3}$; open triangles: $n_d = 8 \cdot 10^{12} \text{ cm}^{-3}$; full circles: $n_d = 8.9 \cdot 10^{13} \text{ cm}^{-3}$ [54G].

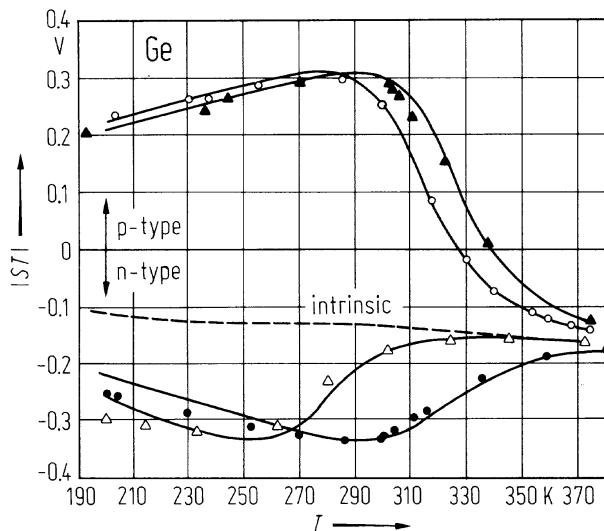


Fig. 1.3.17

Ge. Thermal conductivity vs. temperature. (a) 3...400 K, (b) 400...1200 K. Solid curve in (a) and data in (b) from [64G], experimental data in (a) from [84B]. Dashed line in (b): extrapolated lattice component.

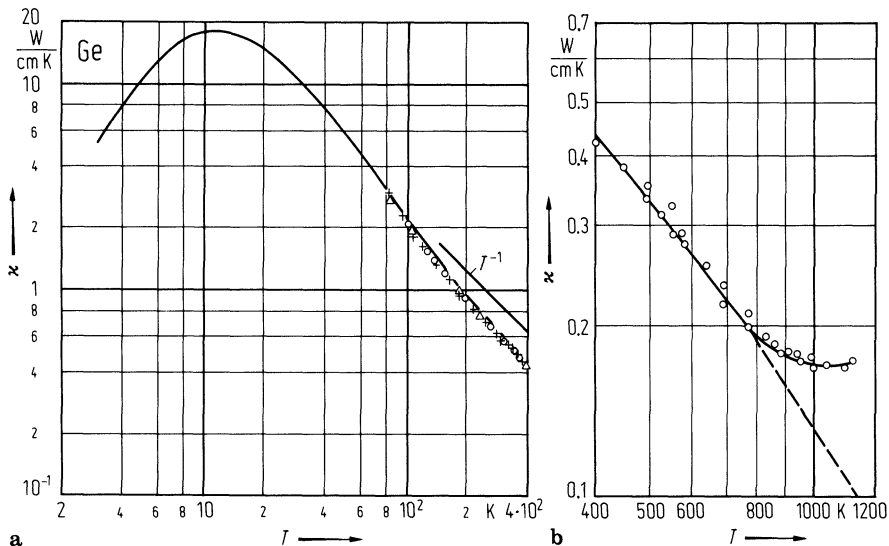


Fig. 1.3.18

Ge. Real and imaginary parts of the dielectric constant vs. photon energy [83A2].

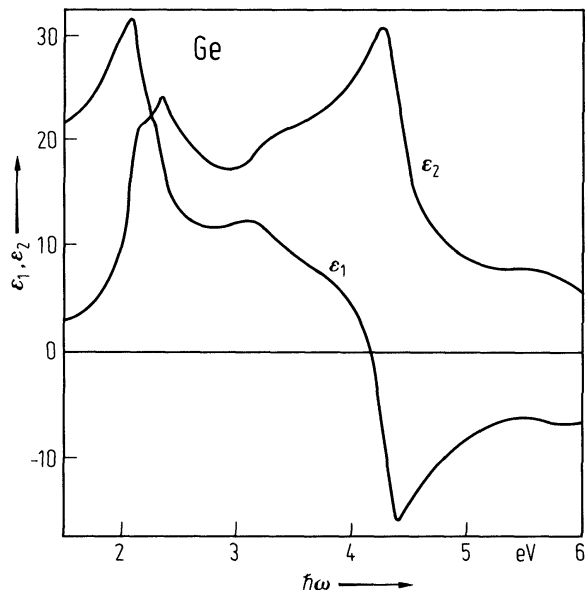


Fig. 1.3.19

Ge. Spectral dependence of (a) the refractive index, (b) the extinction coefficient and (c) the absorption coefficient [59P].

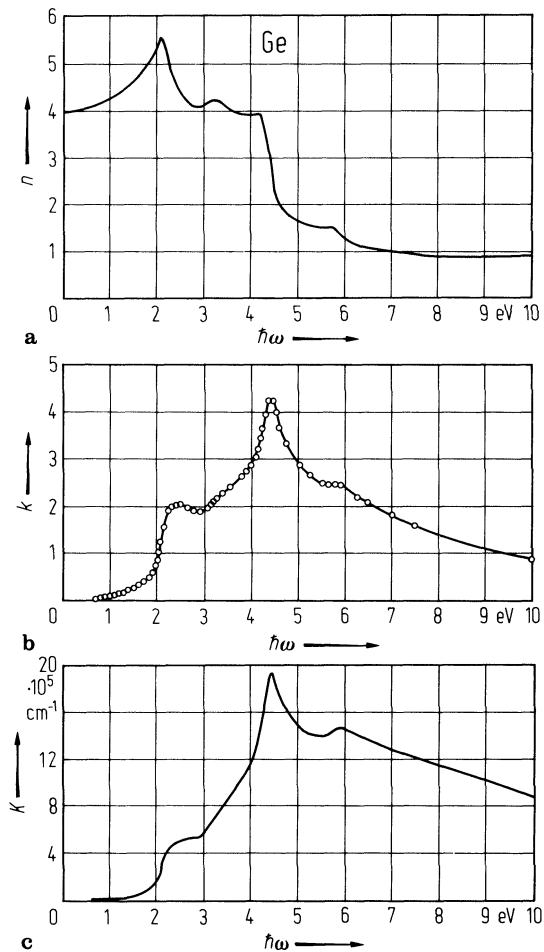


Fig. 1.3.20

Ge. Refractive index and extinction coefficient vs. photon energy in the region of the E_1 critical point at 120K [66P].

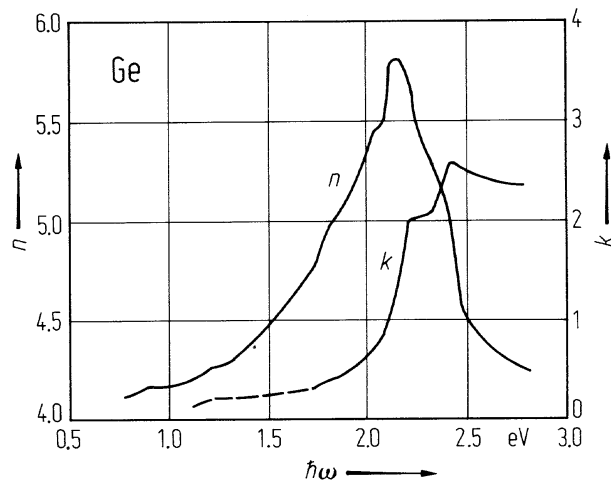


Fig. 1.3.21

Ge. Temperature and wavelength dependence of the refractive index. Open circles Curve 1: $\lambda = 1.970 \mu\text{m}$; 2: $\lambda = 2.190 \mu\text{m}$; 3: $\lambda = 2.409 \mu\text{m}$; 4: $\lambda = 3.826 \mu\text{m}$; 5: $\lambda = 5.156 \mu\text{m}$ [60L].

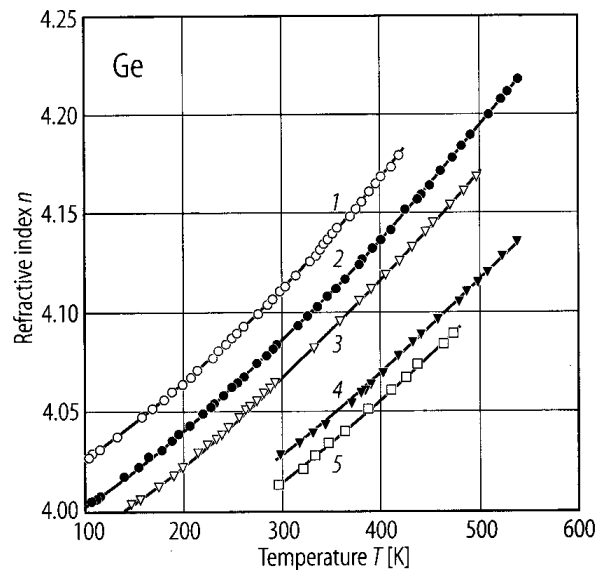


Fig. 1.3.22

Ge. Real and imaginary parts of the dielectric constant and energy loss function vs. photon energy [63P].

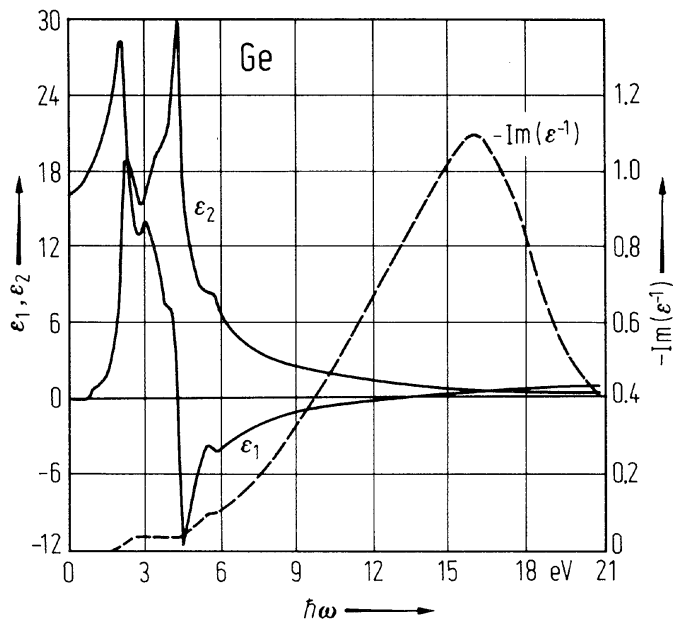
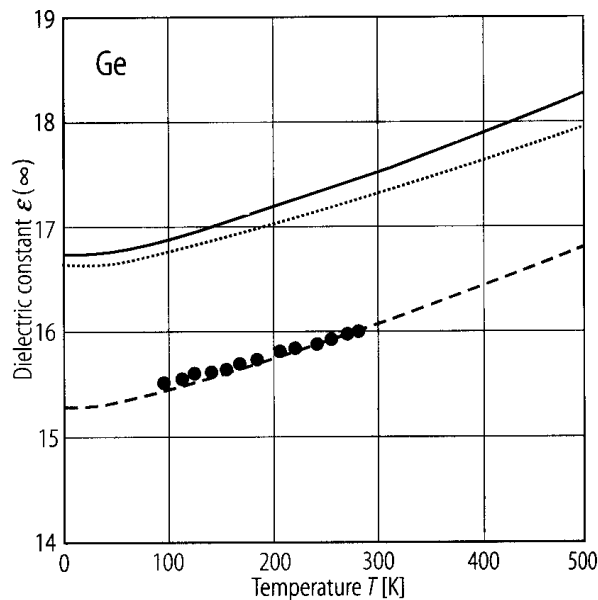


Fig. 1.3.23

Ge. Temperature dependence of the high-frequency dielectric constant [96K]. Experimental data points [76I] and ab-initio calculations (full line); dotted line is the theoretical result without the effect of thermal expansion, and dashed line is the full line shifted to match the experimental data.



1.4 Grey tin, α -Sn

Crystal structure

Grey tin (α -Sn) crystallizes in the diamond structure, space group $O_h^7 - Fd3m$ (Fig. 1.0.2). Slightly below RT it transforms into the metallic high-temperature β -modification (Fig. 1.0.4). This transformation can be inhibited by alloying Ge or Si or by stabilizing grey tin as a heteroepitaxial layer on a substrate with a nearly equal lattice constant. Upon alloying with In or Hg, a simple hexagonal γ -Sn structure is observed.

high pressure phases

Under pressure the diamond structure transforms to the β -tin structure (Sn-I) [65M]. The back transformation is sluggish [72N]; with decreasing temperature the transition pressure increases [72N]. The β -tin phase persists up to 25 GPa [65M], up to 9.5 GPa [84O]. In the pressure range 9.5 to 40 GPa Sn-III (bct structure, sometimes called Sn-II) is formed. Above 40 GPa one obtains Sn-IV with body-centred cubic (bcc) structure. The co-existence regime of the bct and bcc phases has been reported to be between 40.5 and 56 GPa [84O], between 46.5 and 53.4 GPa [86L], the upper limit of coexistence is lower than 52.1(2) GPa [89D]. The bcc structure is stable up to at least 120 GPa [89D].

Electronic properties

band structure : Fig. 1.0.11, Brillouin zone: Fig. 1.0.6

The band structure of α -Sn is qualitatively different to those of the other group IV elements. The s-like Γ_7^- -conduction band edge – decreasing drastically with atomic number in the sequence C – Si – Ge – is situated in α -Sn below the p-like Γ_8^+ -valence band edge. This causes an inversion of the curvature of the Γ_8^+ -light-hole band. Consequently, α -Sn is a zero-gap semiconductor with its lowest conduction band and its highest valence band being degenerated at Γ (symmetry Γ_8^+). A second conduction band with L_6^+ -minima follows at a slightly higher energy. It determines the properties of n-type samples for $n > 10^{17} \text{ cm}^{-3}$ ($T > 77 \text{ K}$ in intrinsic samples).

Two further valence bands with Γ_7^- - and Γ_7^+ -symmetry, respectively, are situated below the Γ_8^+ -valence band.

energies of symmetry points of the band structure (relative to the top of the valence band $E(\Gamma_{8v,c})$)

$E(\Gamma_{6v})$	- 11.34 eV	non-local pseudopotential calculation	76C
$E(\Gamma_{7v})$	- 0.80 eV	(see Fig. 1.4.1)	
$E(\Gamma_{7c})$	- 0.42 eV	note that the Γ_7 conduction band has	
$E(\Gamma_{6c})$	2.08 eV	shifted below the Γ_{8v} band! Thus $E(\Gamma_{7c})$	
$E(\Gamma_{8c})$	2.66 eV	is negative.	
$E(X_{5v})$	- 7.88 eV		
$E(X_{5v})$	- 2.75 eV		
$E(X_{5c})$	0.90 eV		
$E(L_{6v})$	- 9.44 eV		
$E(L_{6v})$	- 6.60 eV		
$E(L_{6v})$	- 1.68 eV		
$E(L_{4,5v})$	- 1.20 eV		
$E(L_{6c})$	0.14 eV		
$E(L_{6c})$	3.48 eV		
$E(L_{4,5c})$	3.77 eV		

energy differences within the conduction band

$E(L_{6c}^+ - \Gamma_{8c}^+)$	0.094 eV	$T = 0 \text{ K}$	conductivity and Hall coefficient in the	56K
	0.12 eV	(extrapolated)	range 70...270 K	
			"optical band gap"	81F

energy differences within the valence band

$E(\Gamma_{8v}^+ - \Gamma_{7v}^-)$	0.413 eV	$T = 1.5...85 \text{ K}$	interband magnetoreflexion	70G
$\Delta_0(\Gamma_{8v}^+ - \Gamma_{7v}^+)$	0.8 eV			

critical point energies (measured by ellipsometry on InSb substrate stabilized layers)

E_1	1.316(5) eV	$T = 200$ K	$\Lambda_{4,5v}-\Lambda_{6c}$	85V
$E_1+\Delta_1$	1.798(6) eV		$\Lambda_{6v}-\Lambda_{6c}$	
E'_0	2.42(3) eV		at or near $\Gamma_{8v}-\Gamma_{6c}$	
$E'_0+\Delta'_0$	2.72(3) eV		$\Gamma_{8v}-\Gamma_{8c}$	
E	2.94(3) eV		$\Delta_{7v}-\Delta_{6c}$ (?)	
E_2	3.681(4) eV		$X_{5v}-X_{5c}$ and other contributions	
E'_1	4.28(4) eV		$L_{4,5v}-L_{6c}$	
$E'_1+\Delta'_1$	4.51(4) eV		$L_{4,5v}-L_{4,5c}$	

Temperature dependence of critical point energies: Fig. 1.4.1.

effective masses

$m_{n,l}(\Gamma_8^+)$	0.0236(2) m_0	$T = 1.3$ K	density of states mass,	68B
$m_{n,h}(L_6^+)$	0.21 m_0	$T = 4.2$ K		71L
$m_p(\Gamma_8^+)$	0.195 m_0		interband magnetoreflexion	70G
$m_p(\Gamma_7^-)$	0.058 m_0		interband magnetoreflexion	70G
$m_p(\Gamma_7^+)$	0.041 m_0		(estimate from Kane's theory)	

Luttinger parameters

γ_1	15.24		used in [79A] for a discussion	
γ_2	11.40		of stress-induced band gap	
γ_3	8.02			

Lattice properties

lattice parameter

a	6.4892(1) Å	$T = 20^\circ\text{C}$	X-ray	59T
da/dT	$3.1 \cdot 10^{-5}$ Å K ⁻¹	$T = -130 \dots 25^\circ\text{C}$		

linear thermal expansion coefficient

α	$4.7 \cdot 10^{-6}$ K ⁻¹	$T = 20^\circ\text{C}$	for temperature dependence, see Fig. 1.4.2	59T
----------	-------------------------------------	------------------------	--	-----

density

d	7.285 g cm ⁻³	$T = 18^\circ\text{C}$		60B
-----	--------------------------	------------------------	--	-----

phonon dispersion relations : Fig. 1.4.3.

No peculiarities in the phonon dispersion compared to the other group IV semiconductors occur. Due to the degeneracy of the conduction and valence bands at Γ_8^+ the dielectric constant depends strongly on carrier concentration in very pure samples.

phonon frequencies

$\nu_{\text{TO/LO}}(\Gamma_{25'})$	6.00(6) THz	$T = 90$ K	inelastic thermal neutron scattering,	71P
$\nu_{\text{TA}}(L_3)$	1.00(4) THz			
$\nu_{\text{LA}}(L_1)$	4.15(4) THz			
$\nu_{\text{LO}}(L_2')$	4.89(8) THz			
$\nu_{\text{TO}}(L_3')$	5.74(12) THz			
$\nu_{\text{TA}}(X_3)$	1.25(6) THz			
$\nu_{\text{LA/LO}}(X_1)$	4.67(6) THz			
$\nu_{\text{TO}}(X_4)$	5.51(8) THz			

second order elastic moduli

c_{11}	$0.690 \cdot 10^{12} \text{ dyn cm}^{-2}$			71P
c_{12}	$0.293 \cdot 10^{12} \text{ dyn cm}^{-2}$			
c_{44}	$0.362 \cdot 10^{12} \text{ dyn cm}^{-2}$			

bulk modulus

B	$5.3(1) \cdot 10^{11} \text{ dyn cm}^{-3}$		from neutron diffraction data for acoustic phonons	71B
-----	--	--	---	-----

Debye temperature

Θ_D	220 K	$T = 50 \text{ K}$	see Fig. 1.4.4 for temperature dependence	52H
------------	-------	--------------------	---	-----

heat capacity

C_v	4.65 cal/K g-atom	$T = 100 \text{ K}$	for temperature dependence	52H
C_p	4.56 cal/K g-atom		below 100 K, see Fig. 1.4.5	

Transport properties

In intrinsic samples light electrons and holes in the Γ_8^+ -bands determine the transport properties. The hole mobility is limited by acoustic phonon scattering. The important scattering processes limiting the light electron mobility are screened impurity scattering at 4.2 K and electron-hole scattering at elevated temperatures. When the Fermi level crosses the energy of the L_6^+ -minima heavy electrons will become of influence. This leads e.g. to a screening enhancement of the light electron mobility (Fig. 1.4.6) and in heavily doped n-type samples to a dominating role of the L-electrons: heavily doped n-type samples behave as indirect gap semiconductors with E_g of about 0.09 eV.

electron concentration vs. donor concentration : Fig. 1.4.7.

temperature dependence of electrical conductivity : Fig. 1.4.8.

carrier mobilities

$\mu_n(\Gamma_8^+)$	$1.2 \cdot 10^5 \text{ cm}^2/\text{Vs}$	100 K	from Hall data	71L
$\mu_n(L_6^+)$	$1.6 \cdot 10^3 \text{ cm}^2/\text{Vs}$		conductivity and Hall coefficient using the n_I/n_{tot} -ratio of Fig. 1.4.8	
μ_p	$1 \cdot 10^4 \text{ cm}^2/\text{Vs}$		for temperature dependence, see Fig. 1.4.9	

Optical properties

Refractive index, extinction coefficient and absorption coefficient: Fig. 1.4.10.

dielectric constant

ϵ	24	$T = 300 \text{ K}$	background dielectric constant in the free carrier absorption region (from infrared reflectance measurements)	64L
------------	----	---------------------	---	-----

Real and imaginary parts of the dielectric constants: Fig. 1.4.11.

References to 1.4

- 52H Hill, R. W., Parkinson, D. H.: *Philos. Mag.* 43 (1952) 309.
- 55E Ewald, A. W., Kohnke, E. E.: *Phys. Rev.* 97 (1955) 607.
- 56K Kohnke, E. E., Ewald, A. W.: *Phys. Rev.* 102 (1956) 1481.
- 59T Thewlis, J., Davey, A.R.: *Nature (London)* 174 (1959) 1011.
- 60B Busch, G. A., Kern, R.: *Solid State Physics* (ed. F. Seitz, D. Turnbull), Vol. 11, p. 1, Academic Press, N. Y. 1960 (review article).
- 61N Novikova, S. I.: *Sov. Phys. Solid State (English Transl.)* 2 (1961) 2087; *Fiz. Tverd. Tela* 2 (1960)
- 61T Tufte, O. N., Ewald, A. E.: *Phys. Rev.* 122 (1961) 1431.
- 63G Groves, S. H., Paul, W.: *Phys. Rev. Lett.* 11(1963) 194.
- 64H Hinkley, E. D., Ewald, A. W.: *Phys. Rev.* 134 (1964) A1261.
- 64L Lindquist, R. E., Ewald, A. W.: *Phys. Rev.* 135 (1964) A1 91.
- 65M Martin, J. E., Smith, P. L.: *Brit. J. Appl. Phys.* 16 (1965) 495.
- 68B Booth, B. L., Ewald, A. W.: *Phys. Rev.* 168 (1968) 805.
- 70G Groves, S. H., Pidgeon, C. R., Ewald, A. W., Wagner, R. J.: *J. Phys. Chem. Solids* 31 (1970) 2031.
- 71B Buchenauer, C. J., Cardona, M., Pollak, F. H.: *Phys. Rev. B* 3 (1971) 1243.
- 71H Hanyu, T.: *J. Phys. Soc. Jpn.* 31 (1971) 1738.
- 71L Lavine, C. F., Ewald, A. W.: *J. Phys. Chem. Solids* 32 (1971) 1121.
- 71P Price, D. L., Rowe, J. M., Nicklow, R. M.: *Phys. Rev. B* 3 (1971) 1268.
- 72N Nikolaev, I. N., Mar'in, V. P., Panyushkin, V. N., Pavlyukov, L. S.: *Fiz. Tverd. Tela* 14 (1972) 2337; *Sov. Phys. Solid State* 14 (1973) 2022 (Engl. Transl.).
- 76C Chelikowski, J. R., Cohen, M. L.: *Phys. Rev. B* 14 (1976) 556.
- 77Z Zdetsis, A. D.: *J. Phys. Chem. Solids* 38 (1977) 1113.
- 79A Averous, M.: *Phys. Status Solidi (b)* 95 (1979) 9.
- 81F Farrow, R. F. C., Robertson, D. S., Williams, G. M., Cullis, A. G., Jones, G. R., Young, I. M., Dennis, P. N. J.: *J. Crystal Growth* 54 (1981) 507.
- 83H Höchst, H., Hernandez-Calderon, I.: *Surf. Sci.* 126 (1983) 25.
- 84O Olijnyk, H., Holzapfel, W. B.: *J. Phys. (Paris)* 45 Suppl., Colloq. C8 (1984) C8-153.
- 85V Vina, L., Höchst, H., Cardona, M.: *Phys. Rev. B* 31 (1985) 958
- 86L Liu, M., Liu, L. G.: *High Temp. High Pressures* 18 (1986) 79.
- 89D Desgrenier, S., Vohra, Y. K., Ruoff, A. L.: *Phys. Rev. B* 39 (1989) 10359.
- 96P Pavone, P., Bauer, R., Karch, K., Schütt, O., Vent, S., Windl, W., Strauch, D., Baroni, S., de Gironcoli, S.: *Physica B* 219 & 220 (1996) 439.

Figures to 1.4

Fig. 1.0.2

The diamond lattice. The elementary cubes of the two face-centered cubic lattices are shown.

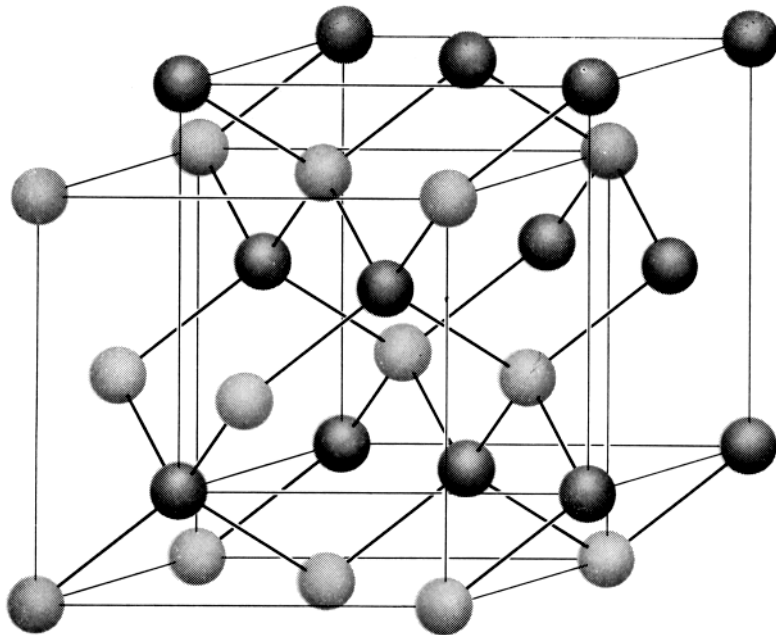


Fig. 1.0.4

Unit cell of the white tin lattice.

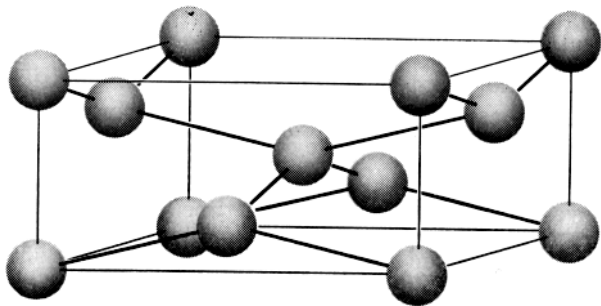


Fig. 1.0.6

Brillouin zone of the diamond lattice

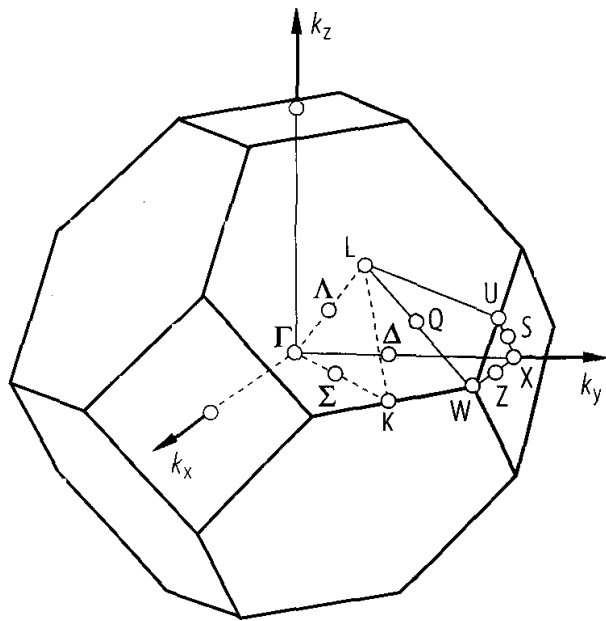


Fig. 1.0.11

α -Sn. (a) Band structure calculated by a non-local pseudopotential method [76C], (b) comparison with data from angular resolved photoemission along the $\Gamma - X$ axis [83H].

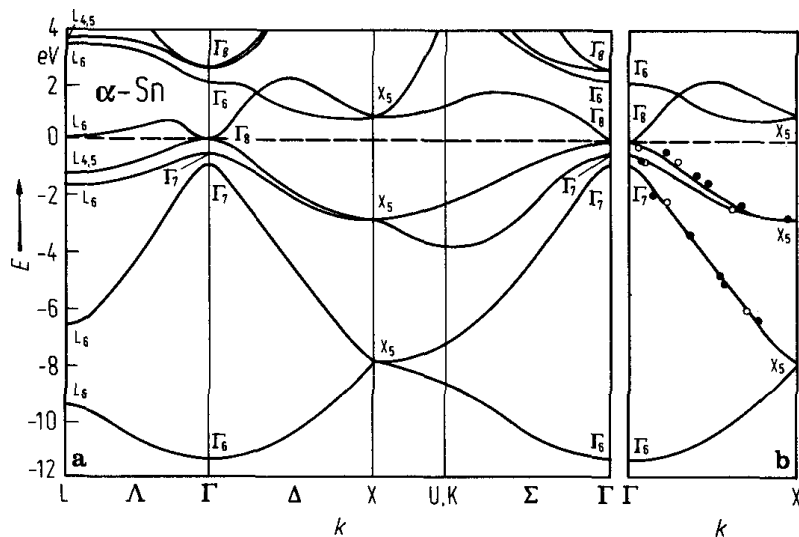


Fig. 1.4.1

α -Sn. Critical point energies vs. temperature. The lines are the best fit to a linear temperature dependence (see the tables) [85V].

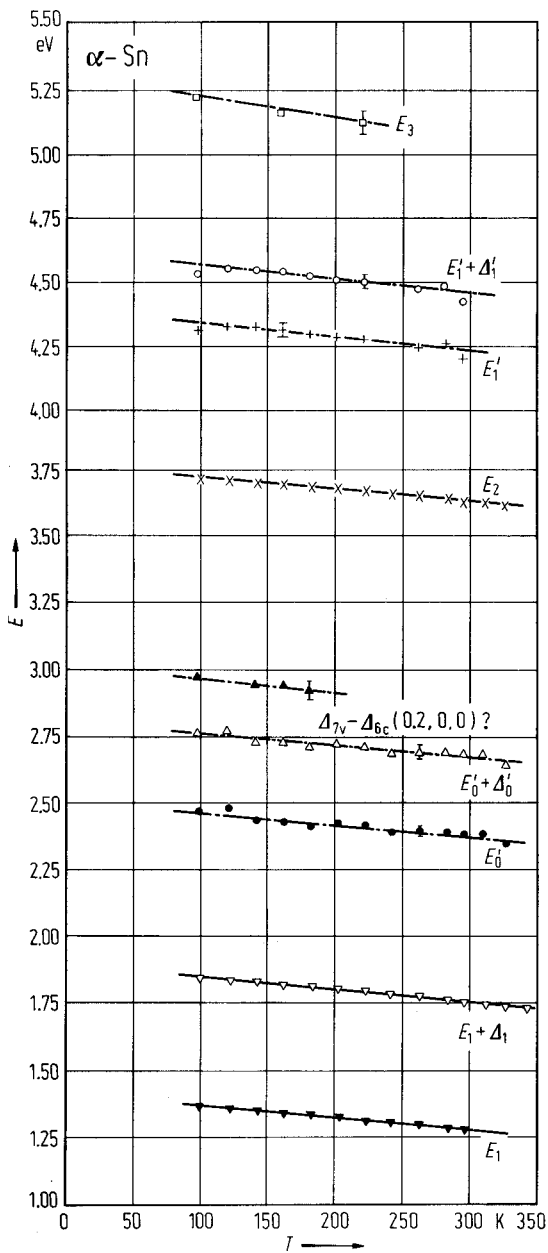


Fig. 1.4.2

α -Sn. Coefficient of linear thermal expansion vs. temperature [61N].

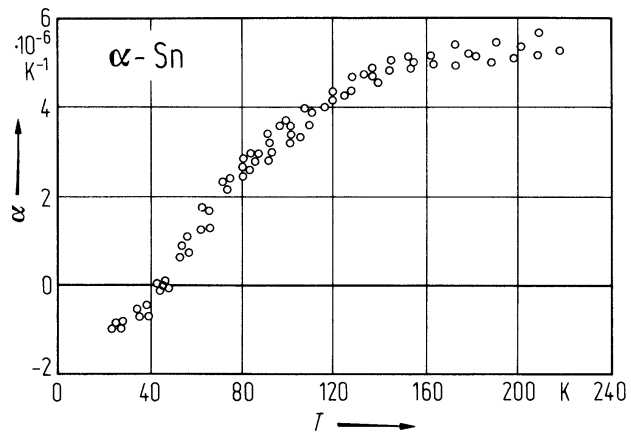


Fig. 1.4.3

α -Sn. Phonon dispersion curves (left panel) and phonon density of states (right panel) [96P]. Experimental data points from inelastic neutron scattering at 90 K [71P]. Solid lines: ab-initio pseudopotential calculation [96P].

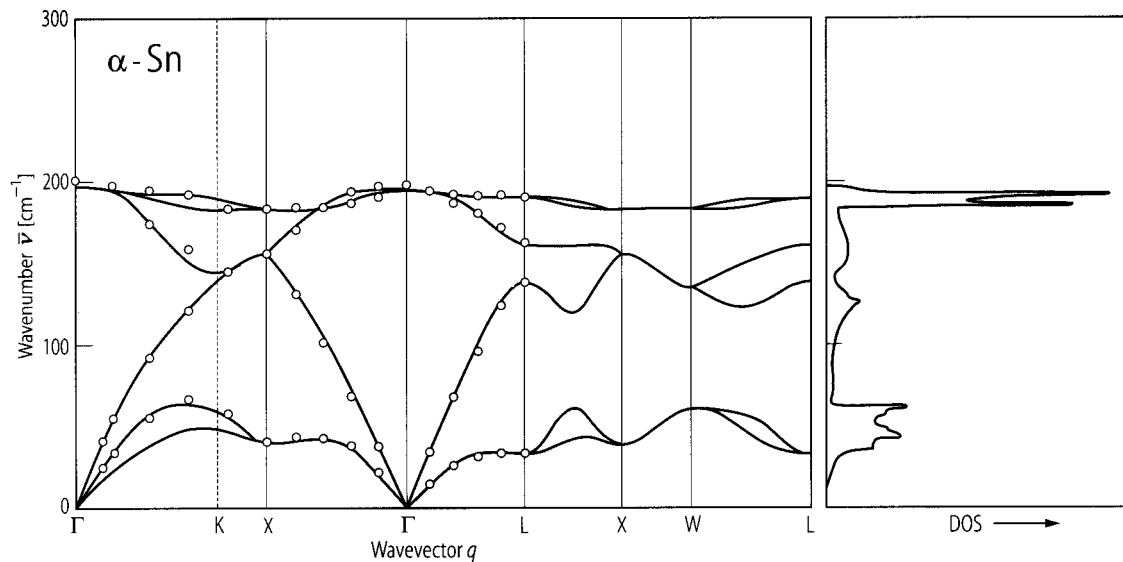


Fig. 1.4.4

α -Sn. Debye temperature $\Theta_D(T)$ vs. temperature. Experimental points from [52H], theoretical curve from a shell model fitted to experimental data [77Z].

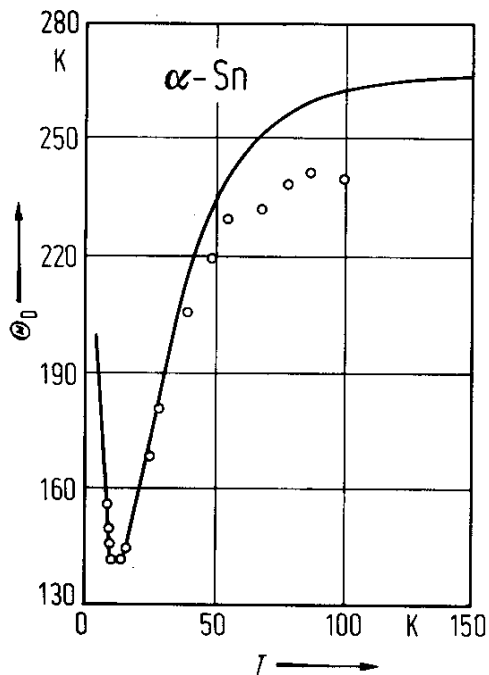


Fig. 1.4.5

α -Sn. Heat capacity C_V vs. temperature. Lower curve: temperature range 0...20 K, upper curve: temperature range 0...105 K [52H].

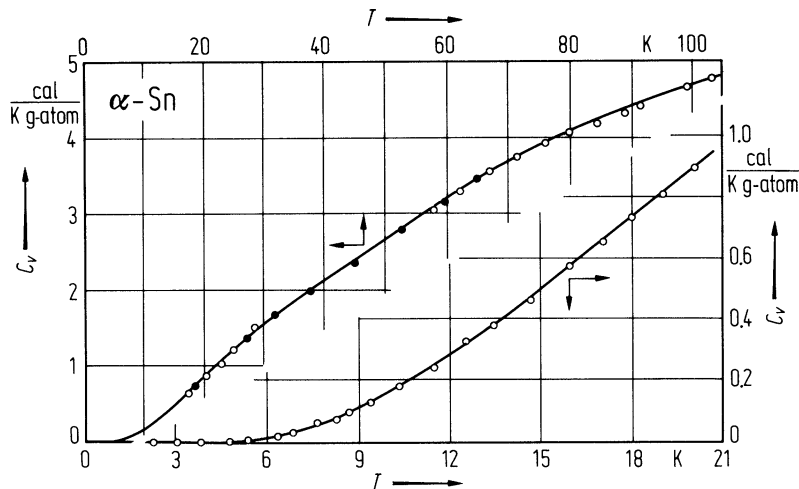


Fig. 1.4.6

α -Sn. Light electron mobility $\mu_{n,l}$ at 4.2 K vs. donor concentration n_d . The solid line represents calculated values using a screened-ionized impurity scattering theory. The dashed line results from a similar calculation using the dielectric constant values given in [71L]. The mobility increase due to screening enhancement by heavy electrons may be seen for concentrations greater than $5 \cdot 10^{17} \text{ cm}^{-3}$. Experimental points are from [63G], [61T], [64H] and [71L].

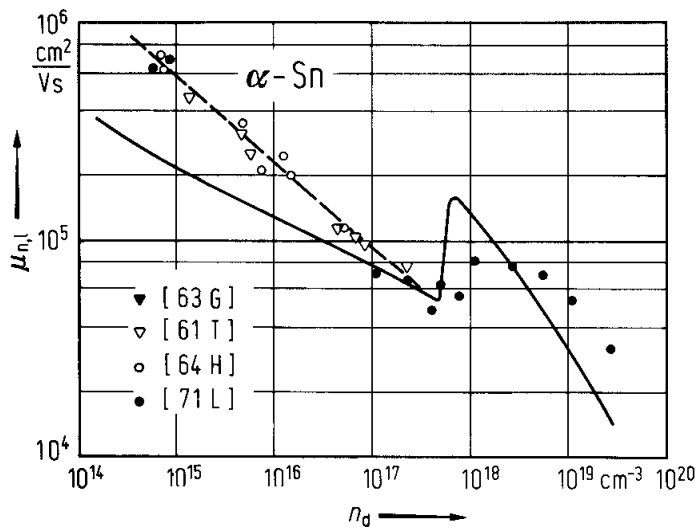


Fig. 1.4.7

α -Sn. Electron concentration at 4.2 K vs. donor concentration; n_l (light electron concentration) from oscillatory magnetoresistance, n_{tot} (total electron concentration) from Hall coefficient [71L].

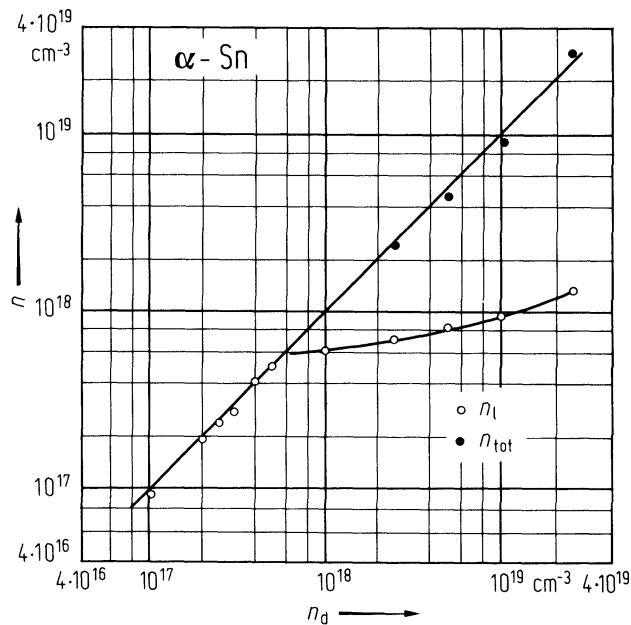


Fig. 1.4.8

α -Sn. Electrical conductivity of n-type samples vs. temperature. Donor concentrations: curve 1: $3.1 \cdot 10^{17} \text{ cm}^{-3}$, 2: $1.3 \cdot 10^{18} \text{ cm}^{-3}$, 3: $7.7 \cdot 10^{18} \text{ cm}^{-3}$. The broken line refers to a "pure" sample [55E].

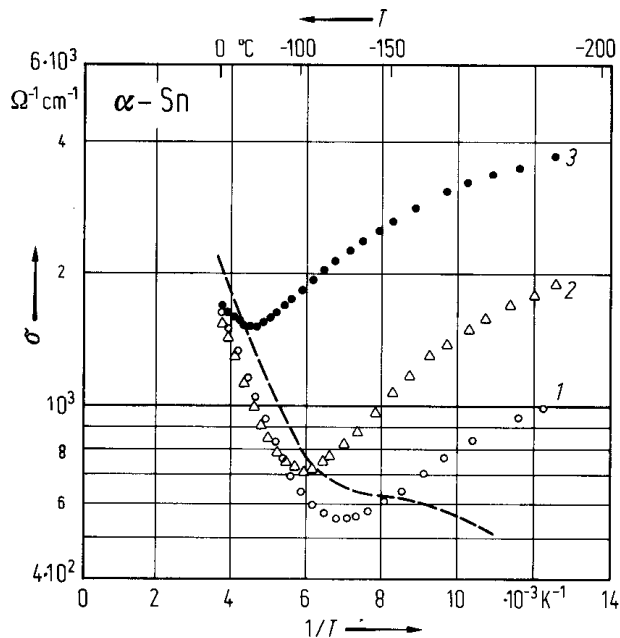


Fig. 1.4.9

α -Sn. Temperature dependence of the light electron and hole mobilities. The electron mobility $\mu_{n,l}$ agrees well with theory if a carrier concentration dependent dielectric constant is introduced. The hole mobility μ_p obeys a $T^{-3/2}$ -power law that strongly suggests acoustic phonon scattering as the dominant mechanism [71L].

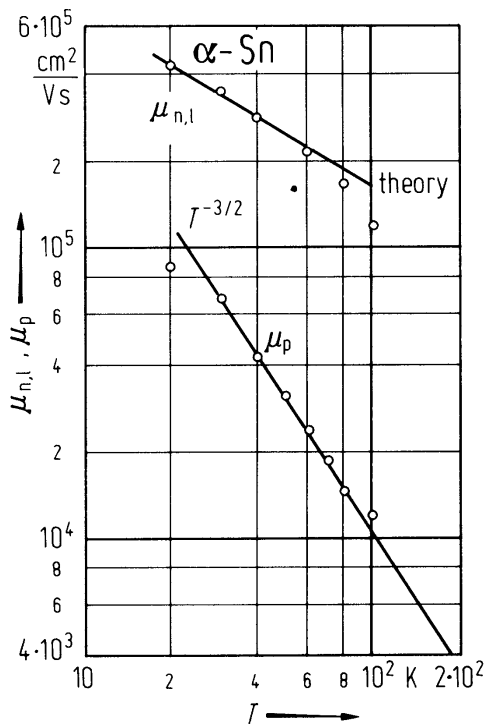


Fig. 1.4.10

α -Sn. Index of refraction n , extinction coefficient k and absorption coefficient K vs. photon energy [71H].

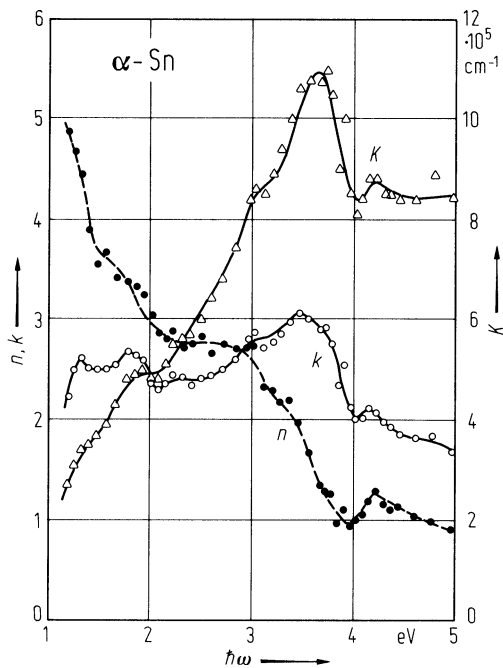
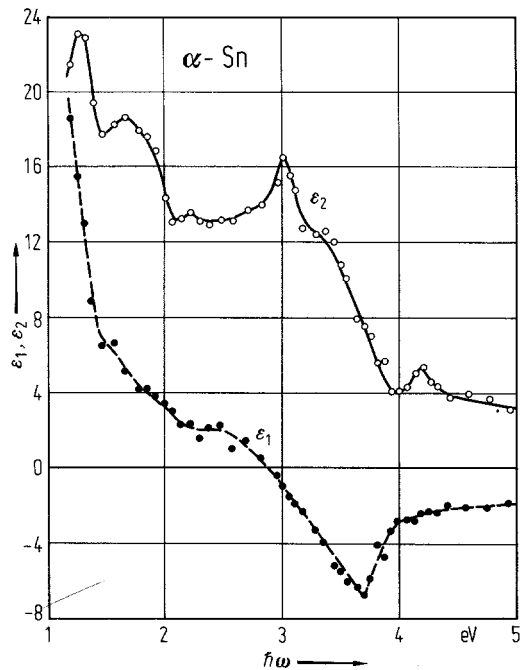


Fig. 1.4.11

α -Sn. Real part ϵ_1 and imaginary part ϵ_2 of the dielectric constant vs. photon energy [71H].



1.5 Silicon carbide, SiC

Crystal structure

Silicon carbide (SiC) crystallizes in numerous (more than hundred) different modifications, called polytypes. The number of polytypes is very large due to small energy differences between the different structures. See Fig. 1.0.5 for elementary cells of the 3C (cubic zincblende, β -SiC), 2H (hexagonal wurtzite, α -SiC), 4H, and 6H structures.

The most important are:

cubic unit cell:

3C-SiC	space group: $T_d^2 - F\bar{4}3m$	lattice: zincblende
--------	--------------------------------------	---------------------

hexagonal unit cell:

2H-SiC	space group: $C_{6v}^4 - P6_3mc$	lattice: wurtzite
--------	-------------------------------------	-------------------

Other polytypes with hexagonal unit cell: 4H-SiC, 6H-SiC, 8H-SiC etc.

rhombohedral unit cell:

15R-SiC	space group: $C_{3v}^5 - R3m$
---------	----------------------------------

Other polytypes with rhombohedral unit cell: 21 R-SiC, 24R-SiC, 27R-SiC etc.

In all polytypes except 3C- and 2H-SiC atomic layers with cubic (c) and hexagonal (h) symmetry follow in a regular alternation in the direction of the c axis. This can be thought of as a natural one-dimensional superlattice imposed on the "pure" – i.e. h-layer free – 3C-SiC [77D1], the period of the superlattice being different for different modifications.

SiC(4H)	$a = 3.08051(6) \text{ \AA}$ $c = 10.08480(4) \text{ \AA}$	98B
SiC(6H)	$a = 3.08129(4) \text{ \AA}$ $c = 15.11976(6) \text{ \AA}$	98B
SiC(15R)	$a = 3.08043 \text{ \AA}$ $c = 37.8014 \text{ \AA}$	83T
SiC(21R)	$a = 3.08111 \text{ \AA}$ $c = 52.9034 \text{ \AA}$	83T
SiC(27R)	$a = 3.08028 \text{ \AA}$ $c = 68.0495 \text{ \AA}$	83T

Electronic properties

3C-SiC

band structure : Fig. 1.0.12

energy gaps

$E_{g,ind}(\Gamma_{15v}-X_{1c})$	2.417(1) eV	$T = 2 \text{ K}$	wavelength modulated absorption	80H, 81H
	2.2 eV	$T = 300 \text{ K}$	optical absorption	60P
$E_{g,dir}$	6.0 eV	$T = 300 \text{ K}$	optical absorption	69C

exciton energy gap

E_{gx}	2.390 eV	$T = 2 \text{ K}$	80H, 81H
----------	----------	-------------------	----------

For temperature dependence of excitonic energy gap E_{gx} see Figs. 1.5.1.

2H-SiC and 4H-SiC

band structure

2H-SiC: Fig. 1.0.13.

exciton energy gaps

E_{gx}	3.330 eV	$T = 4 \text{ K}$	2H, optical absorption	66P
E_{gx}	3.265 eV	$T = 4 \text{ K}$	4H, optical absorption;	64C2

For temperature dependence of excitonic gap for 2H-SiC and 4H-SiC, see Fig. 1.5.1.

6H-SiC

$E_{\text{g,ind}}$	3.02 eV	$T = 300 \text{ K}$	exciton gap plus exciton binding energy for 3C-SiC	89C
$E_{\text{g,ind}}$	2.86 eV	$T = 300 \text{ K}$	optical absorption;	60P
E_{gx}	3.023 eV	$T = 4 \text{ K}$	optical absorption	65C, 81H

According to [79R] the temperature dependence of E_{gx} can be described by the empirical formula:

$E_{\text{gx}} = 3.024 - 0.3055 \cdot 10^{-4} T^2 / (311 \text{ K} - T) \text{ eV}$ (T in K). See also Fig. 1.5.1.

8H-SiC

E_{gx}	2.80 eV	$T = 4 \text{ K}$	luminescence	64C1
-----------------	---------	-------------------	--------------	------

For temperature dependence of the excitonic gap of 8H-SiC, see Fig. 1.5.1.

15R-SiC

E_{gx}	2.9863 eV	$T = 2 \text{ K}$		81H
Δ_{so}	7.0 meV	$T = 2 \text{ K}$		81H
	7.15(25) meV		wavelength modulated absorption spectroscopy	01D

For temperature dependence of the excitonic gap, see Fig. 1.5.1.

21R-SiC

E_{gx}	2.853 eV	$T = 4 \text{ K}$	21R, optical absorption	65H
-----------------	----------	-------------------	-------------------------	-----

For temperature dependence of the excitonic gap, see Fig. 1.5.1.

24R-SiC

E_{gx}	2.728 eV	$T = 8 \text{ K}$	24R, optical absorption;	64Z
-----------------	----------	-------------------	--------------------------	-----

For temperature dependence of the excitonic gap see Fig. 1.5.1.

33R-SiC

E_{gx}	3.003 eV	$T = 4 \text{ K}$	optical absorption	65C
-----------------	----------	-------------------	--------------------	-----

For temperature dependence of the excitonic gap, see Fig. 1.5.1.

further electronic properties**3C-SiC**

E_b	27 meV	$T = 2$ K	wavelength modulated absorption	80H
$E_b(1S,3/2)$	26.7 meV		calculated from valence band	81B
$E_b(1S,1/2)$	25.9 meV		parameters	
$E_b(2S,1/2)$	16.7 meV			
Δ_0	10 meV	$T = 2$ K	wavelength modulated absorption	80H
$E(\Gamma_{15v}-\Gamma_{1c})$	7.4 eV	$T = 300$ K	reflectivity, band structure calculations	97L
$E(L_{3v}-L_{1c})$	7.5 eV			
$E(X_{5v}-X_{1c})$	5.8 eV			
$E(X_{5v}-X_{3c})$	8.3(1) eV			
$E(\Gamma_{15v}-\Gamma_{15c})$	9.0(2) eV			
$E(L_{3v}-L_{3c})$	9.4 eV			
$m_{n\parallel}$	0.677(15) m_0	$T = 45$ K	cyclotron resonance	85K1
$m_{n\perp}$	0.247(11) m_0			
m_p	0.45 m_0		high field cyclotron resonance	93K
A	- 1.98		from fit to ab-initio band structure	97W
B	- 0.28			
$ C $	2.38			

4H-SiC

E_{gx}	3.20 eV			77D2
$m_n(ML)$	0.33(1) m_0	$T = 1.6$ K	optical detection of cyclotron resonance	96V
$m_n(M\Gamma)$	0.58(1) m_0			
$m_n(MK)$	0.31(1) m_0			
$m_{p\parallel}$	1.75(2) m_0		optical detection of cyclotron resonance	00S
$m_{p\perp}$	0.66(2) m_0			

6H-SiC

Δ_{so}	7.1 meV		wavelength modulated absorption	81H
E	4.3 eV		electroreflectance, direct gap (?)	78G
	4.98(1) eV		critical point, for further critical points, see [78G]	
$m_{n\parallel}$	3-6 m_0		optical detection of cyclotron resonance	02S
$m_{n\perp}$	0.48(2) m_0			
$m_{p\parallel}$	1.85(3) m_0			
$m_{p\perp}$	0.66(2) m_0			

8H-SiC

E_{gx}	2.86 eV			77D2
----------	---------	--	--	------

15R-SiC

E_{gx}	3.05 eV			77D2
Δ_{so}	7.0 meV			81H
	4.8 meV			63P
E	4.20 eV	$T = 300$ K, $E \perp c$	critical point energies	84G
	4.62 eV		in electroreflectance	
	5.21 eV			
	5.14 eV	$E \parallel c$		
$m_{n\parallel}$	0.53 m_0		Faraday rotation	67E
$m_{n\perp}$	0.28(2) m_0			

21R-SiC

E_{gx}	2.92 eV			77D2
E	4.68 eV	$T = 300 \text{ K}, E \perp c$	critical point energies in electroreflectance	84G
	5.20 eV			
	5.20 eV	$E \parallel c$		

24R-SiC

E_{gx}	2.80 eV			77D2
-----------------	---------	--	--	------

27R-SiC

E	4.30 eV	$T = 300 \text{ K}, E \perp c$	critical point energies in electroreflectance	84G
	5.08 eV			
	4.32 eV	$E \parallel c$		
	4.42 eV			

Lattice properties

lattice parameters

a	4.3596 Å	$T = 297 \text{ K}$	3C, Debye-Scherrer, for temperature dependence, see Fig. 1.5.2	60T
a	3.0763(10) Å	$T = 300 \text{ K}$	2H, Laue and Weissenberg patterns	59A
c	5.0480(10) Å			
a	3.0806 Å	$T = 297 \text{ K}$	6H, Debye-Scherrer, for temperature dependence, see Fig. 1.5.3	60T
c	15.1173 Å			

For lattice constants of other modifications, see the beginning of this chapter.

linear thermal expansion coefficients

$\alpha(3\text{C})$	$2.77(42) \cdot 10^{-6} \text{ K}^{-1}$	$T = 300 \text{ K}$	3C, recommended value; for temperature dependence, see Fig. 1.5.4	75S
---------------------	---	---------------------	---	-----

$$\alpha(3\text{C}) = 3.19 \cdot 10^{-6} + 3.60 \cdot 10^{-9} T - 1.68 \cdot 10^{-12} T^2 [\text{K}^{-1}] \quad 87\text{L}$$

$$\alpha_{33}(6\text{H}) = 3.18 \cdot 10^{-6} + 2.48 \cdot 10^{-9} T - 8.51 \cdot 10^{-13} T^2 [\text{K}^{-1}] \quad 87\text{L}$$

commercial SiC-4H powder (< 15% 6H, < 5% 15R):

$$\alpha_{11}(4\text{H}) = 3.21 \cdot 10^{-6} + 3.56 \cdot 10^{-9} T - 1.62 \cdot 10^{-13} T^2 [\text{K}^{-1}] \quad 86\text{L}$$

$$\alpha_{33}(4\text{H}) = 3.09 \cdot 10^{-6} + 2.63 \cdot 10^{-9} T - 1.08 \cdot 10^{-12} T^2 [\text{K}^{-1}] \quad 86\text{L}$$

density

d	3.166 g cm ⁻³	$T = 293 \text{ K}$	3C, polycrystalline; may contain slight excess (less than 1 %) of free silicon and/or free carbon. For temperature dependence, see Fig. 1.5.5	69K
	3.211 g cm ⁻³	$T = 300 \text{ K}$		

melting temperature (peritectic temperature)

T_{m}	3103(40) K	$p = 35 \text{ bar}$	decomposes	60S
----------------	------------	----------------------	------------	-----

transformation temperature

T_{tr}	> 215 °C		3C → 6H	91Y2
-----------------	----------	--	---------	------

phonon dispersion relations (3C-, 2H-, 4H-, 6H-SiC): Fig. 1.5.6.

phonon wavenumbers

$\bar{\nu}_{TA}(L)$	266 cm ⁻¹	RT	3C, discussion of Raman spectra including data from previous publications	82O
$\bar{\nu}_{LA}(L)$	610 cm ⁻¹			
$\bar{\nu}_{TO}(L)$	766 cm ⁻¹			
$\bar{\nu}_{LO}(L)$	838 cm ⁻¹			
$\bar{\nu}_{TA}(X)$	373 cm ⁻¹			
$\bar{\nu}_{LA}(X)$	640 cm ⁻¹			
$\bar{\nu}_{TO}(X)$	761 cm ⁻¹			
$\bar{\nu}_{LO}(X)$	829 cm ⁻¹			

phonon frequencies (in THz) for the polytypes 2H [66P], 6H [63P], 15R [63P] and 21R [65H]. Derived from photoluminescence data.

ν_{TA}	
2H:	12.7, 15.0
6H:	8.1, 8.8, 9.5, 9.8, 10.6, 11.2, 12.9
15R:	8.3, 8.5, 9.5, 9.6, 10.5, 11.2, 12.6
21R:	11.3, 12.8
ν_{LA}	
2H:	15.0
6H:	12.2, 12.9, 16.2, 16.7, 18.6
15R:	12.4, 12.6, 16.7, 17.0, 18.9
21R:	18.8
ν_{TO}	
2H:	22.1, 25.0
6H:	22.9, 23.1, 23.7
15R:	22.9, 23.1, 23.2, 23.5
21R:	22.7
ν_{LO}	
2H:	24.2
6H:	25.2, 25.5, 25.9
15R:	29.1, 25.7, 25.9
21R:	25.2

sound velocity

v_l	12210 m s ⁻¹		sound wave propagation, sintered 3C-SiC	66S
v_s	7690 m s ⁻¹			
v	13.3·10 ⁵ cm/s	$T = 300$ K	6H, direction of c -axis	65A

second order elastic moduli

c_{11}	289 GPa	$T = 300$ K	3C, experimental	74M
c_{12}	234 GPa			
c_{44}	55.4 GPa			
c_{11}	507(6) GPa	RT	4H, Brillouin scattering	97K
c_{33}	547(6) GPa			
c_{44}	159(7) GPa			
c_{12}	108(8) GPa			
c_{11}	504(20) GPa	$T = 300$ K	6H, double-pulse echo	65A
c_{33}	566(11) GPa			
c_{44}	170(3) GPa			
c_{66}	203(1) GPa			
c_{12}	98(21) GPa			

bulk modulus

B (3C)	248(9) GPa	at 25 GPa		87S
B (15R)	224(3) GPa	at 45 GPa	15R	91Y1

Debye temperature

Θ_D	1270(20) K	$T = 800$...1300 K	3C, polycrystalline; evaluation of heat capacity data	69K
	1200 K	$T = 300$ K	6H, single crystal; evaluation of heat conductivity data	64S

heat capacity

C_p	28.5 J mol ⁻¹ K ⁻¹	$T = 293$ K	3C, polycrystalline	69K
	36.9 J mol ⁻¹ K ⁻¹	$T = 473$ K		
	47.0 J mol ⁻¹ K ⁻¹	$T = 1273$ K		
	50.4 J mol ⁻¹ K ⁻¹	$T = 2273$ K		

Transport properties**carrier concentrations**

For the temperature dependence of the carrier concentration in 3C-SiC films, see Fig. 1.5.7; in 4H-SiC: Fig. 1.5.8; in 6H-SiC: Fig. 1.5.9.

electron mobility

μ_n	510 cm ² /Vs	$T = 296$ K	3C, epitaxial film grown on Si(100); for temperature dependence, see Fig. 1.5.10	86S
	948 cm ² /Vs	$T = 300$ K	4H, basal plane, van der Pauw technique; CVD epilayer grown on p-type substrate; $N_d = 3 \cdot 10^{15}$ cm ⁻³	97C
	480 cm ² /Vs	$T = 300$ K	6H, basal plane, van der Pauw technique CVD homoepitaxial film for temperature dependence of N-doped 6H-SiC see Fig. 1.5.11	93S
	380 cm ² /Vs	$T = 300$ K	15R, $n = 1.6 \cdot 10^{17}$ cm ⁻³ , van der Pauw technique; for temperature dependence, see Fig. 1.5.11	

hole mobility

μ_p	15...21 cm ² /Vs		3C	83N
	98.5 cm ² /Vs	$T = 305$ K	4H bulk, probably B doped; $p(305K) = 5 \cdot 10^{14}$ cm ⁻³ ; for temperature dependence, see Fig. 1.5.12	97R
	50 cm ² /Vs	$T = 300$ K	6H, $p = 10^{17}$ cm ⁻³ ; for temperature dependence, see Fig. 1.5.13	63V

thermal conductivity

κ	4.9 Wcm ⁻¹ K ⁻¹	$T = 300$ K	6H, single crystal, steady-state heat flow ($\perp c$ -axis); for temperature dependence, see Fig. 1.5.14	64S
----------	---------------------------------------	-------------	--	-----

Optical properties

refractive index

3C-SiC:			
n follows the empirical relation:	$n(\lambda) = 2.55378 + 3.417 \cdot 10^4 / \lambda^2$	$(\lambda = 467 \dots 691 \text{ nm})$	69S
2H:			
$n_o(\lambda)$	$= 2.5513 + 2.585 \cdot 10^4 / \lambda^2 + 8.928 \cdot 10^8 / \lambda^4$		70P
$n_e(\lambda)$	$= 2.6161 + 2.823 \cdot 10^4 / \lambda^2 + 11.490 \cdot 10^8 / \lambda^4$		
6H:			
n_o	$= 2.5531 + 3.34 \cdot 10^4 / \lambda^2$		71S
n_e	$= 2.5852 + 3.68 \cdot 10^4 / \lambda^2$		
15R:			
n_o	$= 2.5558 + 3.31 \cdot 10^4 / \lambda^2$		71S
n_e	$= 2.5889 + 3.74 \cdot 10^4 / \lambda^2$		
See also Fig. 1.5.15.			

absorption : absorption edges of several polytypes, see Fig. 1.5.16.

dielectric constants

$\varepsilon(0)$	9.52	$T = 300 \text{ K}$	3C, infrared transmission	95M
$\varepsilon(\infty)$	6.38	$T = 300 \text{ K}$		
$\varepsilon(0)$	10.0		2H, infrared spectroscopy	59S
$\varepsilon(\infty)$	6.7			
$\varepsilon_{\perp}(\infty)$	6.50		4H, experimental	97H
$\varepsilon_{\parallel}(\infty)$	6.7			
$\varepsilon(0)$	9.66	$T = 300 \text{ K}$	6H ($\perp c$ -axis)	70P
	10.03	$T = 300 \text{ K}$	6H ($\parallel c$ -axis)	
$\varepsilon(\infty)$	6.52	$T = 300 \text{ K}$	6H ($\perp c$ -axis)	
	6.70	$T = 300 \text{ K}$	6H ($\parallel c$ -axis)	
$\varepsilon_{\perp}(\infty)$	6.520	$T = 297 \text{ K}$	15R, infrared reflectivity	77P
$\varepsilon_{\parallel}(\infty)$	6.742			

second order nonlinear optical coefficients

$\chi_{zzz}^{(2)}$	$\pm 1.2 \cdot 10^{-7} \text{ esu}$	6H-SiC; 1.064 μm excitation wavelength	95L1
$\chi_{zxx}^{(2)}$	$-/+1.2 \cdot 10^{-8} \text{ esu}$		
r_{zzz}	2.2 pm/V	6H-SiC; Pockel's coefficient; 1.064 μm fundamental wavelength	95L2

Impurities and defects

binding energies of impurities and identified defect centers

(for donors $E_b = E_C - E_d$, for acceptors $E_b = E_a - E_V$)

Impurity/ Defect	Binding energy [eV]	Type d/a	Polytype	Remarks	Ref.
Al	0.230	a	3C	PL	68Z
	0.168	a	4H	PL, SiC crystals grown from Si melt	77S
	0.239	a	6H	PL, SiC crystals grown from Si melt	80I
	0.213	a	15R	PL, SiC crystals grown from Si melt	80I
B	0.210	a	3C	Hall effect, B-doped during CVD growth, $[B] = 4.8 \times 10^{18} \text{ cm}^{-3}$	
	0.285	a	4H	Hall effect, B-doped by implantation, $[B] = (5-20) \times 10^{18} \text{ cm}^{-3}$	96P
	0.300	a	6H	PL, B-doped during Lely growth	63A
	0.279	a	15R	Hall effect, B-doped during epitaxial growth, $[B] = 2.5 \times 10^{18} \text{ cm}^{-3}$	
D-center	0.740	a	3C	PL, B-doped during LPE growth	73Y
(B _{Si} -V _C)	0.730	a	3C	PL, B-doped during LPE growth	75K
(B _C -V _{Si})	0.502...0.552	a	3C	DLTS, evaluated with PFC, $[B] = 4.8 \times 10^{18} \text{ cm}^{-3}$	
Be	0.420	a	6H	Hall effect, Be-doped by diffusion	68M
Cr	0.150		4H	DLTS, impl. of radioactive isotopes	97A1
	0.540	a	6H		97A2
Ga	0.343	a	3C	PL, crystals grown from Si melt	76K
	0.267	a	4H	PL, crystals grown from Si melt	80I
	0.317	a	6H	PL, crystals grown from Si melt	80I
	0.282	a	15R	PL, crystals grown from Si melt	80I
N	0.056	d	3C	PL, Lely platelet	76K
	0.055	d	4H	PL, Lely platelet	77S
	0.095	d	6H	Hall effect, $[N] = 5 \times 10^{16} \text{ cm}^{-3}$	70H
	0.052	d	15R	Hall effect, $[N] = 3 \times 10^{16} \text{ cm}^{-3}$	70H
O-related	0.180	d	3C	Hall effect, O-doped during growth	86P
	0.280...0.312	d	4H	AS, O-doped by implantation, termed O _I	
	0.425...0.464	d	4H	termed O _{II}	
	0.720...0.785	a	4H	DLTS, termed O _{III}	
	0.880...0.945	a	4H	termed O _{IV}	
	0.925...0.990	a	4H	termed O _V	
	0.270...0.129	d	6H	Hall effect, O-doped by implantation $[O] = 5 \times 10^{17} \text{ cm}^{-3}$ to $5 \times 10^{18} \text{ cm}^{-3}$	99D
				termed O _I	
	0.360...0.191	d		termed O _{II}	
	0.455...0.498	a	6H	DLTS, O-doped by implantation $[O] = 3 \times 10^{15} \text{ cm}^{-3}$ to $1 \times 10^{17} \text{ cm}^{-3}$	
				termed O _{III}	
	0.500...0.543			termed O _{IV}	
	0.532...0.576	a	6H	termed O _V	
	0.582...0.596	a	6H	termed O _V	
P	0.100	d	6H	Hall effect, P-doped by neutron transmutation, $[P] = 4 \times 10^{16} \text{ cm}^{-3}$	86V
Sc	0.52	a	6H	DLTS, evaluated with PFC	91B
Ti	0.130		4H	DLTS, implantation of radioactive	97A1

Ti–N	0.600	d	6H	photo-ESR, (Ti _{Si} –N _C)-complex	92M
V	1.700	d	3C	photo-ESR,	94D
	1.730		4H	optical AS, as-grown	95E
	1.310	d	6H	absorption	92D
V _{Si}	0.50	a	3C	estimated from PL and ESR (Si vacancy)	

References to 1.5

- 44T Thibault, N. W.: Am. Mineral. 29 (1944)327.
- 55D Dresselhaus, G.: Phys. Rev. 100 (1955) 580-586.
- 59A Adamski, R. F., Merz, K. M.: Z. Kristallogr. 111(1959)350.
- 59R Rashba, E. I.: Fiz. Tverd. Tela (Leningrad) 1 (1959) 407; Sov. Phys. Solid State (English Transl.) 1 (1959) 368-380.
- 59S Spitzer, W. G., Kleinman, D.A., Walsh, D.: Phys. Rev. 113 (1959) 127.
- 60P Philipp, H. R., Taft, E. A.: Silicon Carbide – A High Temperature Semiconductor (eds. J. R. O'Connor and J. Smiltens), Pergamon Press, Oxford, London, New York, Paris 1960, 366.
- 60S Scace, R. I., Slack, G. A.: Silicon Carbide – A High Temperature Semiconductor (eds. J. R. O'Connor and J. Smiltens), Pergamon Press, Oxford, London, New York, Paris 1960, 24.
- 60T Taylor, A., Jones, R. M.: Silicon Carbide – A High Temperature Semiconductor (eds. J. R. O'Connor and J. Smiltens), Pergamon Press, Oxford, London, New York, Paris 1960. 147.
- 63A Addamiano, A., Potter, R.M., Ozarow, V.: J Electrochem. Soc. 110 (1963) 517.
- 63P Patrick, L., Hamilton, D. R., Choyke, W. J.: Phys. Rev. 132 (1963) 2023.
- 63V Van Daal, H. J., Knippenberg, W. F., Wasscher, J. D.: J. Phys. Chem. Solids 24 (1963)109.
- 63W Wyckoff, R. W. G.: Crystal Structures, Vol. 1, J. Wiley & Sons, New York, London, Sydney 1963, p. 113.
- 64C1 Choyke, W. J., Hamilton, D. R., Patrick, L.: Phys. Rev. 133 (1964) A 1163.
- 64C2 Choyke, W. J., Patrick, L., Hamilton, D. R.: Proc. Int. Conf. on Semiconductor Phys., Paris (ed. M. Hulin), Friedr. Vieweg & Sohn, Braunschweig 1964, 751.
- 64S Slack, G. A.: J. Appl. Phys. 35 (1964) 3460.
- 64Z Zanmarchi, G.: Proc. Int. Conf. on Semiconductor Phys., Paris (ed. M. Hulin), Friedr. Vieweg & Sohn, Braunschweig 1964, p. 57.
- 65A Arlt, G., Schodder, G. R.: J. Acoust. Soc. Am. 37 (1965) 384.
- 65C Choyke, W. J., Hamilton, D. R., Patrick, L.: Phys. Rev. 139 (1965) A1262.
- 65H Hamilton, D. R., Patrick, L., Choyke, W. J.: Phys. Rev. 138(1965) A1472.
- 66P Patrick, L., Hamilton, D. R., Choyke, W. J.: Phys. Rev. 143 (1966) 526.
- 66S Schreiber, E., Soga, N.: J. Am. Ceram. Soc. 49 (1966) 342.
- 67B Barrett, D. L., Campbell, R. B.: J. Appl. Phys. 38 (1967) 53.
- 67E Ellis, B., Moss, T. S.: Proc. Royal Soc. (London) A 299 (1967) 383, 393.
- 68F Feldman, D. W., Parker, J. H., Choyke, W. J., Patrick, L.: Phys. Rev. 173 (1968) 787.
- 68M Maslakovets, Yu.P., Mokhov, E.N., Vodakov, Yu.A., Lomakina, G.A.: Sov. Phys. Solid State 10 (1968) 634.
- 68Z Zanmarchi, G.: J. Phys. Chem. Solids 29 (1968) 1727.
- 69C Choyke, W. J., Patrick, L.: Phys. Rev. 187 (1969)1041.
- 69K Kern, E. L., Hamill, D. W., Deem, H. W., Sheets, H. D.: Mater. Res. Bull. 4 (1969) 25.
- 69S Shaffer, P. T. B., Naum, R. G.: J. Opt. Soc. Am. 59 (1969)1498.
- 70H Hagen, S.H., Kapteyns, C.J.: Philips Res. Repts. 25 (1970) 1.
- 70P Patrick, L., Choyke, W. J.: Phys. Rev. B 2 (1970) 2255.
- 71S Shaffer, P. T. B.: Appl. Opt. 10 (1971)1034.
- 72P Powell, J. A.: J. Opt. Soc. Am. 62 (1972) 341.
- 73Y Yamada, S., Kuwabara, H.: Silicon Carbide, 1973, Proceedings of the Third International Conference on Silicon Carbide, p.305, Marshall, R.C., Faust, J.W., Ryan, C.E. (eds.), Columbia, South Carolina: University of South Carolina Press.
- 74M Marshall, R. C., Faust, J. W., Ryan, C. E. (eds.), "Silicon Carbide 1973", University of South Carolina Press, Columbia, South Carolina, 1974, Appendix II.
- 75K Kuwabara, H., Yamada, S.: Phys. Status Solidi (a) 30 (1975) 739.
- 75S Slack, G. A., Bartram, S. F.: J. Appl. Phys. 46 (1975) 89.
- 76K Kuwabara, H., Yamanaka, K., Yamada, S.: Phys. Status Solidi (a) 37 (1976) K 157.
- 77D1 Dean, P. J., Choyke, W. J., Patrick, L.: J. Lumin. 15 (1977) 299.
- 77D2 Dubrovskii, G. B., Lepneva, A. A.: Sov. Phys. Solid State (English Transl.) 19 (1977) 729; Fiz. Tverd. Tela 19 (1977) 1252.
- 77P Pikhtin, A. N., Prokopenko, V. T., Rondarev, V. S., Yaskov, A. D.: Opt. Spektrosk. 43 (1977) 711; Optic. Spectrosc. 43 (1977) 420 (Engl. Transl.).
- 77S Suzuki, A., Matsunami, H., Tanaka, T.: J. Electrochem. Soc. 124 (1977) 241.
- 78G Gavrilenko, V. I., Zuev, V. A., Katrich, G. A., Tarashchenko, D. T.: Sov. Phys. Semicond. (English Transl.) 12 (1978) 959; Fiz. Tekh. Poluprovodn. 12 (1978) 1621.
- 79R Ravindra, N. M., Srivastava, V. K.: J. Phys. Chem. Solids 40 (1979) 791.
- 80H Humphreys, R. G., Bimberg, D., Choyke, W. J.: J. Phys. Soc. Jpn. 49 Suppl. A (1980) 519.

- 80I Ikeda, M., Matsunami, H., Tanaka, T.: Phys. Rev. B 22 (1980) 2842.
- 81B Bimberg, D., Altarelli, M., Lipari, N. O.: Solid State Commun. (1981).
- 81H Humphreys, R. G., Bimberg, D., Choyke, W. J.: Solid State Commun. 39 (1981) 163.
- 82O Olego, D., Cardona, M.: Phys. Rev. B 25 (1982) 1151.
- 83N Nishino, S., Powell, J. A., Will, H. A.: Appl. Phys. Lett. 42 (1983) 460.
- 83T Tairov, Y. M., Tsvetkov, V. F.: Prog. Cryst. Growth Charact. 7 (1983) 111.
- 84G Gorban', I. S., Gubanov, V. A., Lysenko, V. G., Pletyushkin, A. A., Timofeev, V. B.: Sov. Phys. Solid State (English Transl.) 26 (1984) 1385; Fiz. Tverd. Tela 26 (1984) 2282.
- 85K1 Kaplan, R., Wagner, R. J., Kim, H. J., Davis, R. F.: Solid State Commun. 55 (1985) 67.
- 85K2 Koshenko, V. I.: Inorg. Mater. 21 (1985) 197.
- 86L Li, Z., Bradt, R. C.: J. Am. Ceram. Soc. 69 (1986) 612.
- 86P Podlasov, S.A., Sidiyagin, V.G.: Sov. Phys. Semicond. 20 (1986) 462.
- 86S Suzuki, A., Uemoto, A., Shigeta, M., Furukawa, K., Nakajima, S.: Appl. Phys. Lett. 49 (1986) 450.
- 86V Veinger, A.I., Zbradskii, A.G., Lomakina, G.A., Mokhov, E.N.: Sov. Phys. Solid State 28 (1986) 917.
- 87L Li, Z., Bradt, R. C.: J. Am. Ceram. Soc. 70 (1987) 445.
- 87S Strössner, K., Cardona, M., Choyke, W. J.: Solid State Commun. 63 (1987) 113.
- 89C Choyke, W. J.: The Physics and Chemistry of Carbides, Nitrides and Borides (ed. R. Freer), NATO ASI Series Vol. 185, Kluwer, Dordrecht, 1990, p. 563.
- 91B Ballandovich, V.S.: Sov. Phys. Semicond. 25 (1991) 174.
- 91Y1 Yakovenko, E. V., Goncharov, A. F., Stishov, S. M.: High Press. Res. 8 (1991) 433.
- 91Y2 Yoo, W. S., Matsunami, H.: Jpn. J. Appl. Phys. 30 (1991) 545.
- 92D Dörnen, A., Latushko, Y., Suttrop, W., Pensl, G., Leibenzeder, S., Stein, R.: Mater. Sci. Forum 83-87 (1992) 1213.
- 92M Maier, K., Schneider, J., Wilkening, W., Leibenzeder, S., Stein, R.: Mater. Sci. Eng. B 11 (1992) 27.
- 93K Kono, J., Takeyama, S., Yokoi, H., Miura, N., Yamanaka, M., Shinohara, M., Ikoma, K.: Phys. Rev. B 45 (1993) 10909.
- 93P Pensl, G., Choyke, W. J.: Physica B185 (1993) 264.
- 93S Schaffer, W. J., Kong, H. S., Negley, G. H., Palmour, J. W.: Inst. Phys. Conf. Ser. No 137 (1993) 155.
- 94D Dombrowski, K.F., Kaufmann, U., Kunzer, M., Maier, K., Schneider, J., Shields, V.B., Spencer, M.G.: Appl. Phys. Lett. 65 (1994) 1811.
- 94H Hofmann, M., Zywiets, A., Karch, K., Bechstedt, F.: Phys. Rev. B 50 (1994) 13401.
- 95C Choyke, W. J.: Materials for High Temperature Semiconductor Devices, National Academy of Sciences, Washington, D. C., 1995, p.17.
- 95E Evwaraye, A.O., Smith, S.R., Mitchel, W.C.: Appl. Phys. Lett. 67 (1995) 3319.
- 95L1 Lundquist, P. M., Lin, W. P., Wong, G. K., Razeghi, M., Ketterson, J. B.: Appl. Phys. Lett. 66 (1995) 1883.
- 95L2 Lundquist, P. M., Lin, W. P., Wong, G. K., Razeghi, M., Ketterson, J. B.: Appl. Phys. Lett. 67 (1995) 2887.
- 95M Moore, W. J., Holm, R. T., Yang, M. J., Freitas, Jr., J. A.: J. Appl. Phys. 78 (1995) 7255.
- 96P Pensl, G., Afanas'ev, V.V., Bassler, M., Schadt, M., Troffer, T., Heindl, J., Strunk, H.P., Maier, M., Choyke, W.J.: Inst. Phys. Conf. Ser. No. 142 (1996) 275.
- 96V Volm, D., Meyer, B. K., Hofmann, D. M., Chen, W. M., Son, N. T., Persson, C., Lindefelt, U., Kordina, O., Sörman, E., Konstantinov, A. O., Monemar, B., Janzén, E.: Phys. Rev. B 53 (1996) 15409.
- 97A1 Achtziger, N., Grillenberger, J., Witthuhn, W.: Appl. Phys. Lett. 71 (1997) 110.
- 97A2 Achtziger, N., Grillenberger, J., Witthuhn, W.: Appl. Phys. A 65 (1997) 329.
- 97C Choyke, W. J., Pensl, G.: MRS Bulletin, March (1997) 25.
- 97H Hobert, H., Dunken, H.: private communication to [97A].
- 97K Kamitani, K., Grimsditch, M., Nipko, J. C., Loong, C. K., Okada, M., Kimura, I.: J. Appl. Phys. 82 (1997) 3152 (with incomplete and wrong references).
- 97L Lambrecht, W. R. L., Limpijumnong, S., Rashkeev, S., Segall, B.: Phys. Status Solidi (b) 202 (1997) 5.
- 97R Rutsch, G., Devaty, R. P., Choyke, W. J., for a Northrop-Grumman sample; unpublished results.
- 97W Wellenhofer, G., Rössler, U.: Phys. Status Solidi (b) 202 (1997) 107.
- 98B Bauer, A., Kräußlich, J., Dressler, L., Kuschnerus, P., Wolf, J., Goetz, K., Käckell, P., Furthmüller, J., Beckstedt, F.: Phys. Rev. B57 (1998) 2647.
- 99D Dalibor, T., Trageser, H., Pensl, G., Kimoto, T., Matsunami, H., Nizhner, D., Shigiltchoff, O., Choyke, W.J.: Mater. Sci. Eng. B 61-62 (1999) 454.
- 00S Son, N. T., Hai, P. N., Chen, W. M., Hallin, C., Monemar, B., Janzén, E.: Phys. Rev. B 61 (2000) R10544.
- 01D Devaty, R. P., Bai, S., Choyke, W. J., Hobgood, D., Larkin, D. J.: Mater. Sci. Forum 353-356 (2001) 357.
- 02S Son, N. T., Hallin, C., Janzén, E.: Mater. Sci. Forum 289-393 (2002) 525.

Figures to 1.5

Fig. 1.0.5

Elementary cells of 3C, 2H, 4H, 6H structures. The 3C structure is also drawn in the hexagonal cell. Stacking sequences are indicated.

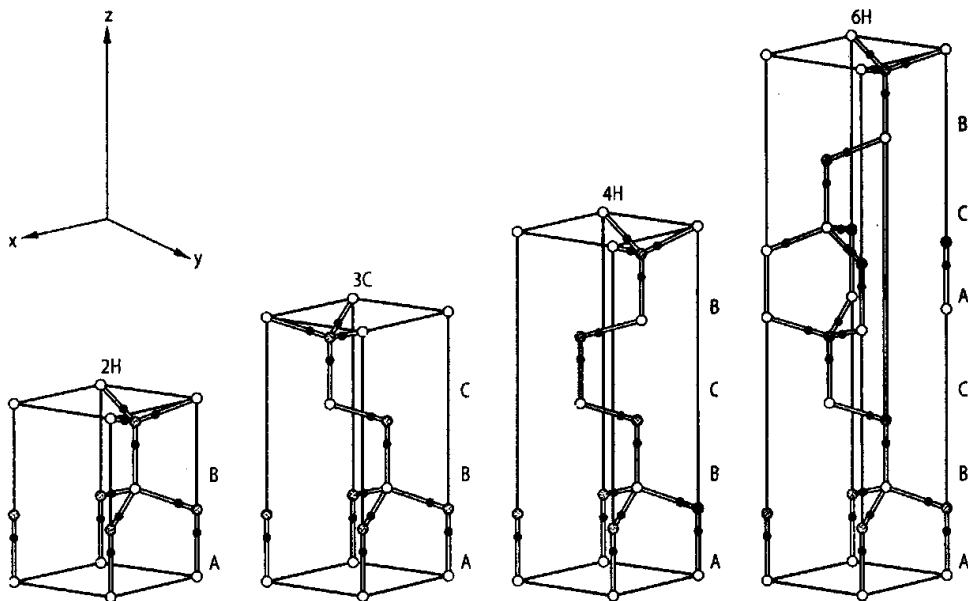


Fig. 1.0.12

SiC. Band structure of 3C-SiC calculated using the full-potential linear muffin-tin orbital method within the local density approximation and including a 1.00 eV upward shift of the conduction bands to account approximately for quasiparticle self-energy corrections [97L]. The symmetry labeling follows the notation of G. Dresselhaus [55D].

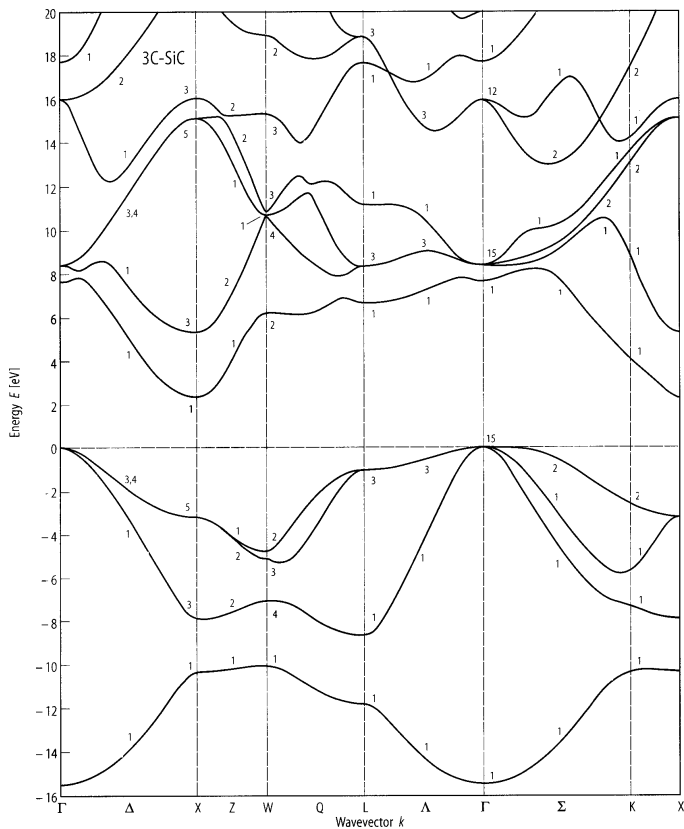


Fig. 1.0.13

SiC. Band structure of 2H-SiC calculated using the full-potential linear muffin-tin orbital method within the local density approximation and including a 1.00 eV upward shift of the conduction bands to account approximately for quasiparticle self-energy corrections [97L]. The symmetry labeling follows the notation and character tables of É. I. Rashba [59R].

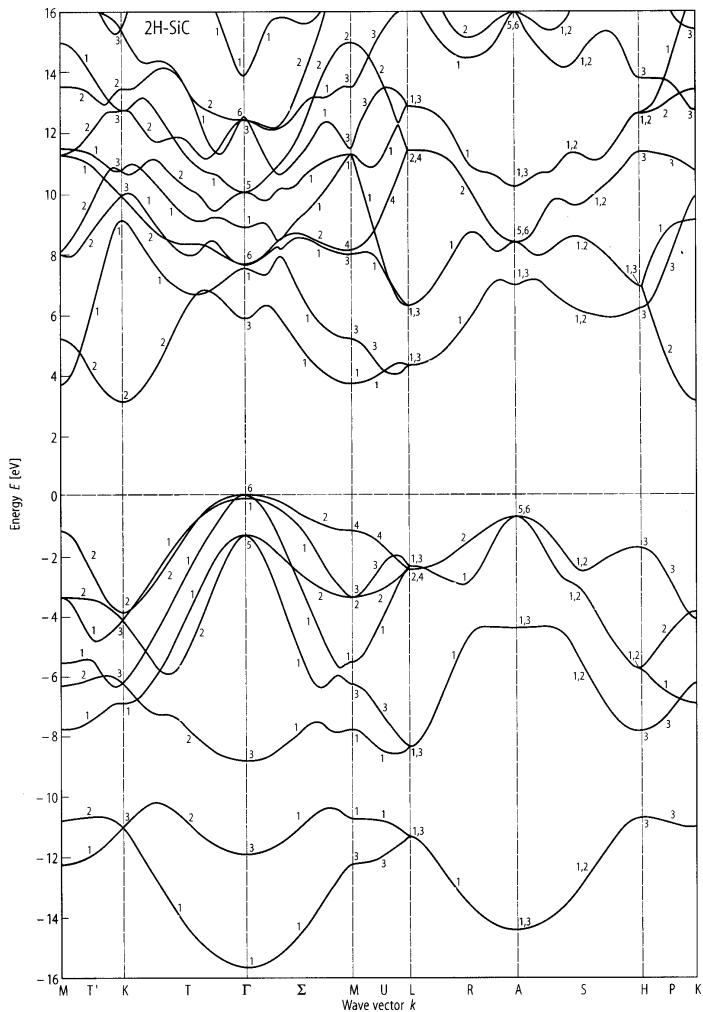


Fig. 1.5.1

SiC. Temperature dependence of exciton energy gaps in SiC polytypes [95C]. Exciton energy gaps for various polytypes: $E_{gx} = E_g - E_b$ (E_b : exciton binding energy for 3C-SiC ≈ 0.027 eV); at 4.2 K, E_{gx} [eV] = 3.330 (2H), 3.265 (4H), 3.023 (6H), 3.003 (33R), 2.986 (15R), 2.853 (21R), 2.80 (8H), 2.73 (24R), 2.390 (3C); at RT, E_{gx} [eV] = 3.300 (2H), 3.235 (4H), 2.995 (6H), 2.972 (33R), 2.957 (15R), 2.82 (21R), 2.77 (8H), 2.71 (24R), 2.360 (3C).

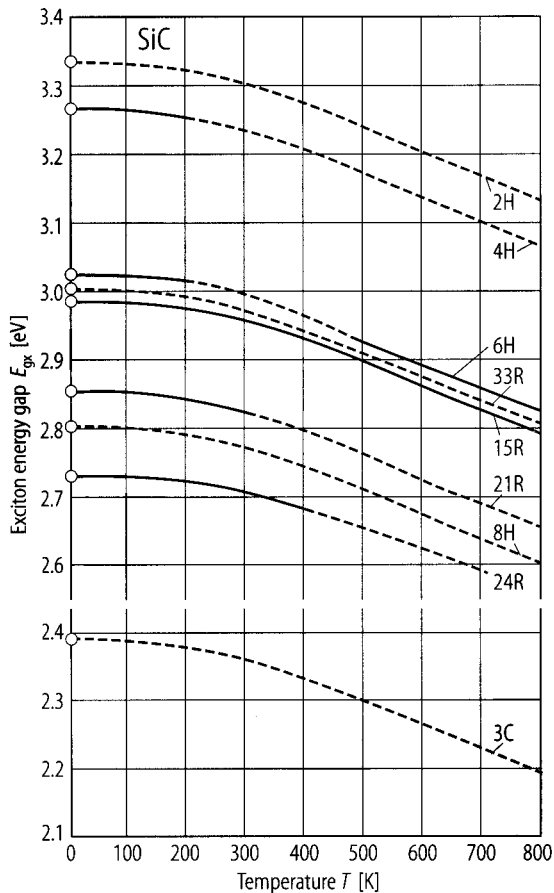


Fig. 1.5.2

SiC (3C). Lattice constant vs. temperature [60T].

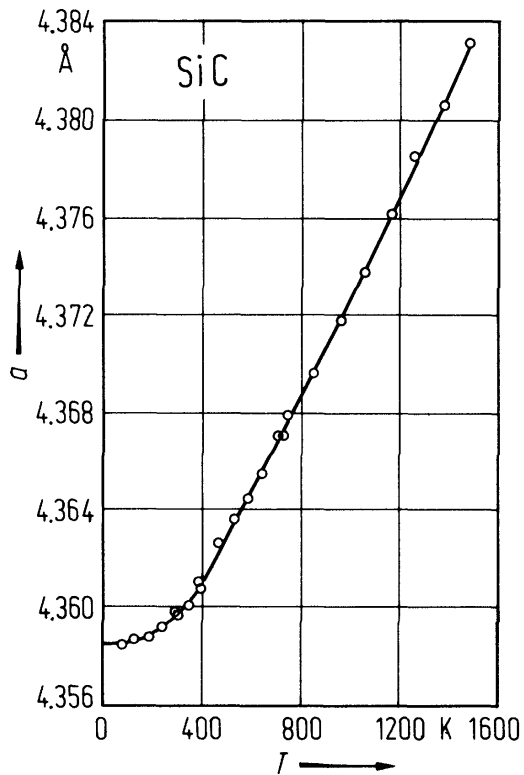


Fig. 1.5.3

SiC (6H). Lattice constants vs. temperature [60T].

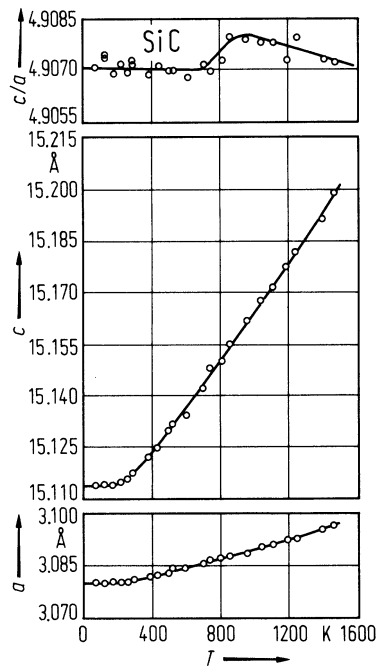


Fig. 1.5.4

3C-SiC. Recommended linear thermal expansion coefficient vs. temperature according to an analysis of data from nine references [75S].

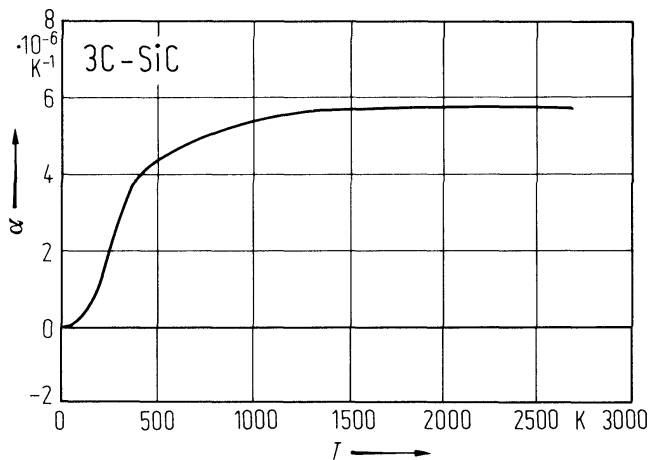


Fig. 1.5.5

SiC (3C). Density vs. temperature [69K].

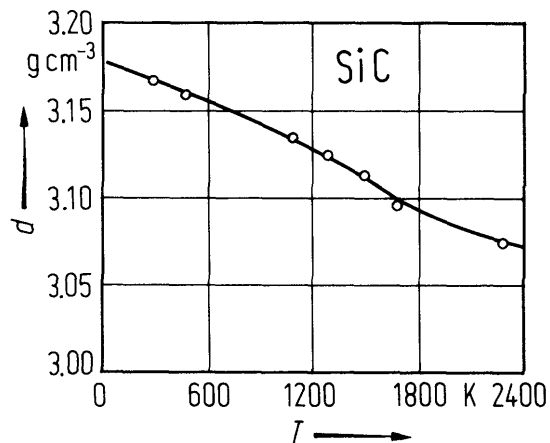


Fig. 1.5.6

SiC. Phonon dispersion curves for the 3C, 2H, 4H, and 6H modifications from a bond-charge model calculation [94H]. Symbols represent experimental data. Different lines indicate different polarization states.

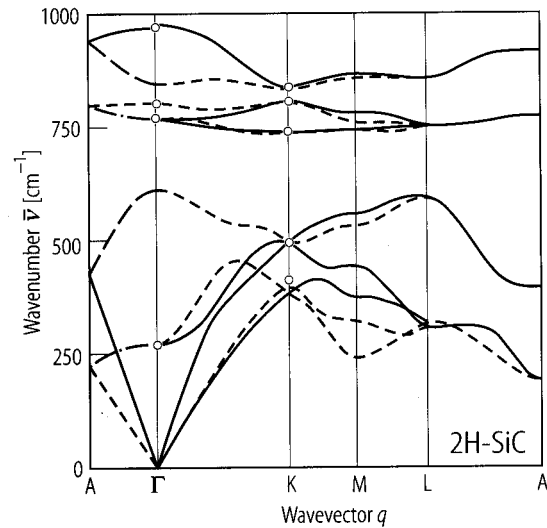
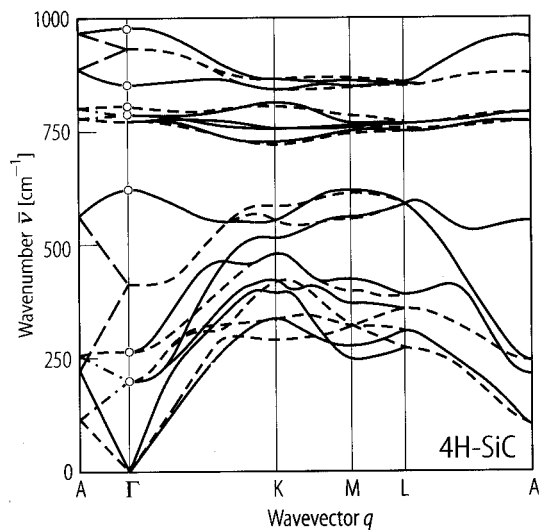
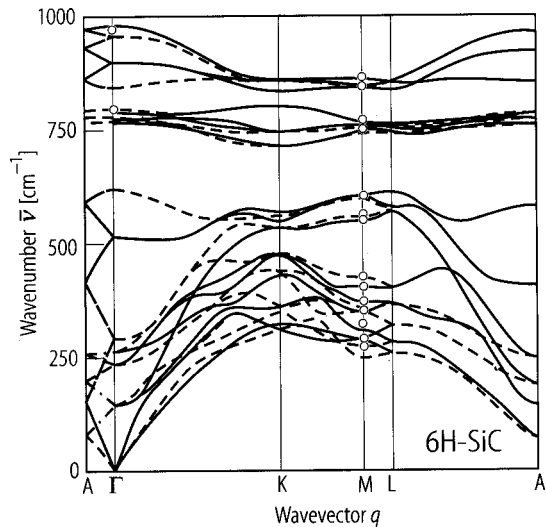
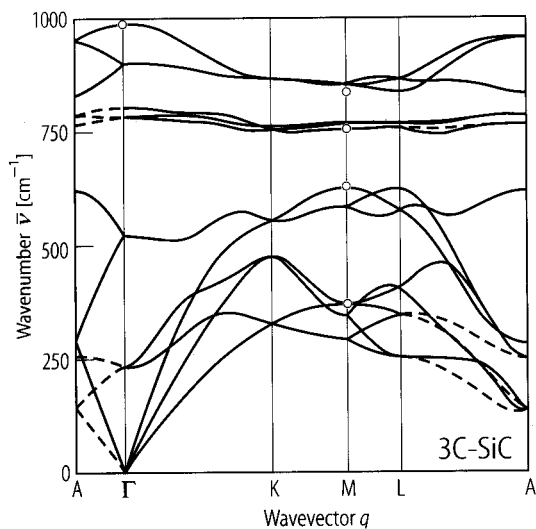


Fig. 1.5.7

SiC (3C). Temperature dependence of carrier concentration for n-type films grown by CVD on Si(100) substrates [86S]. Solid lines are calculated. Si/C: ratio of source gases.

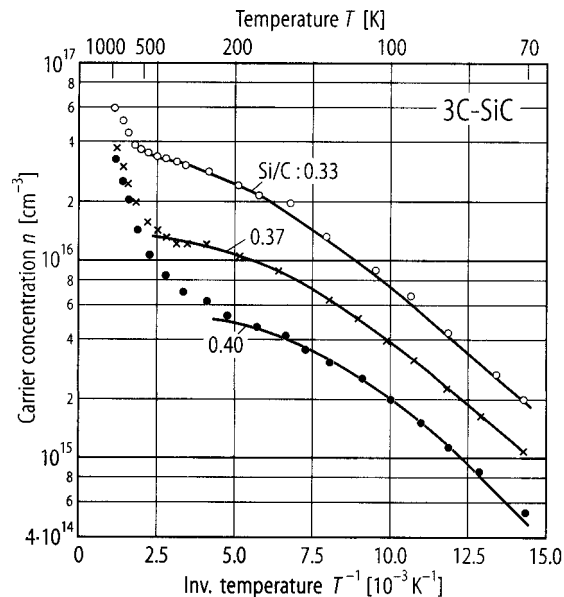


Fig. 1.5.8

SiC (4H). Temperature dependence of the free electron concentration, resistivity (a) and Hall mobility (b) for an undoped epitaxial layer [97C].

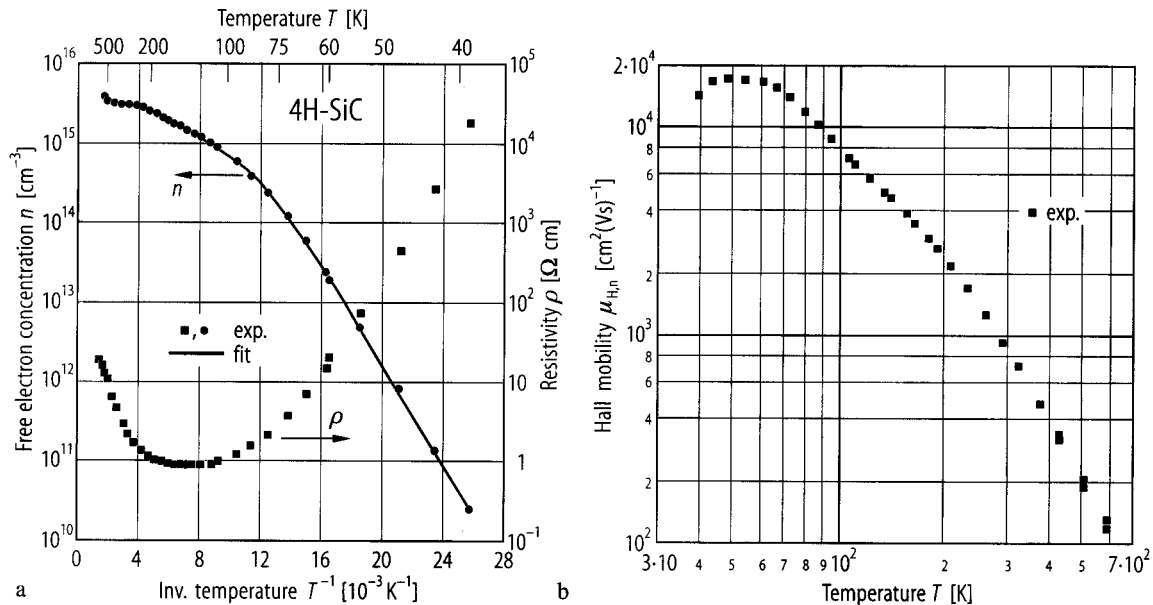


Fig. 1.5.9

SiC (6H). Temperature dependence of the carrier concentration and Hall mobility for N-doped n-type samples grown by three different techniques [93P].

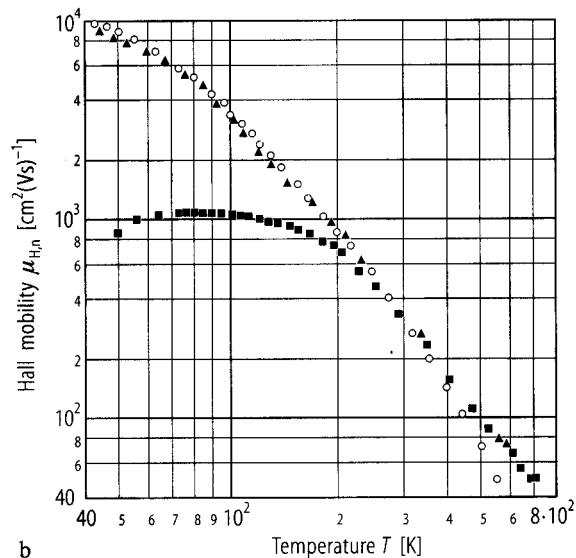
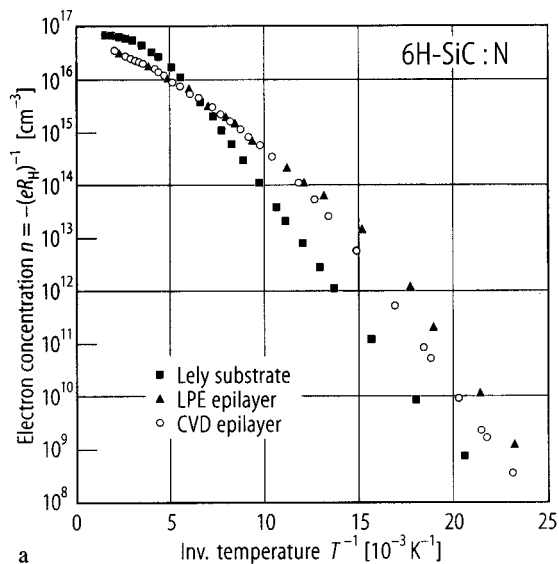


Fig. 1.5.10

SiC (3C). Temperature dependence of electron Hall mobility for n-type films grown by CVD [86S]. Solid and broken lines are calculated. Si/C is the ratio of source gases. μ_{ac} : calculated contribution of acoustic phonon scattering to the electron Hall mobility; μ_{pol} : calculated contribution of polar optical phonon scattering to the electron Hall mobility; μ_{ac+pol} : total calculated electron Hall mobility.

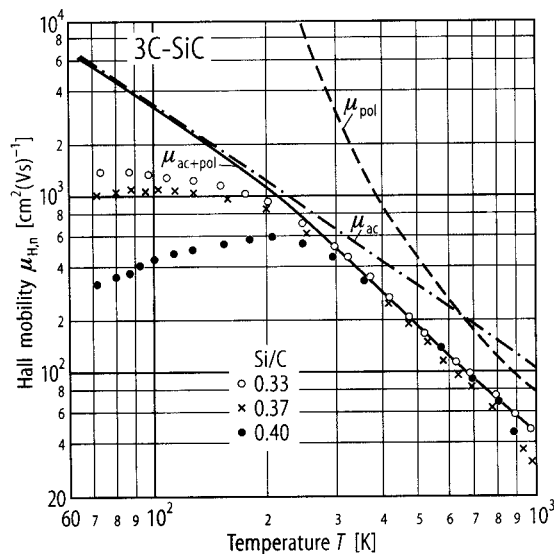


Fig. 1.5.11

SiC (6H, 15R). Electron mobility vs. temperature in 6H and 15R samples [67B].

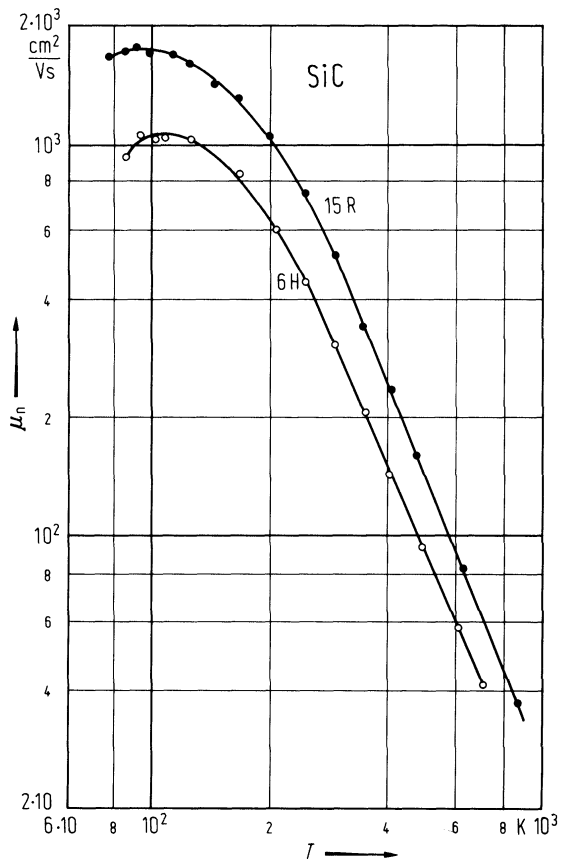


Fig. 1.5.12

SiC (4H). Temperature dependence of the Hall mobility for a p-type bulk sample [97R]. The dashed vertical line corresponds approximately to room temperature.

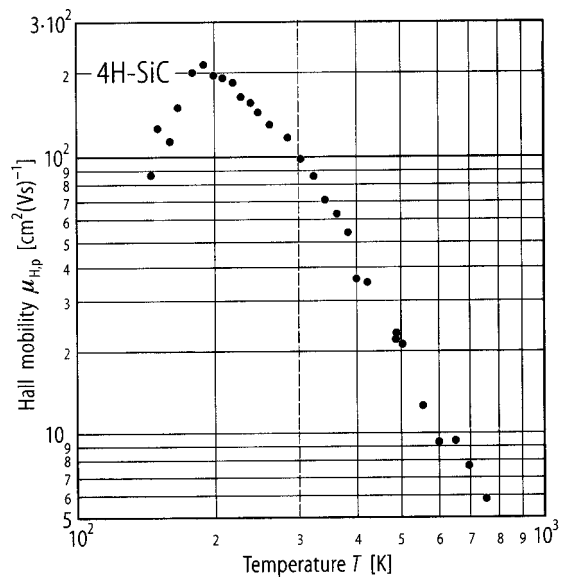


Fig. 1.5.13

SiC (6H). Hole mobility of different samples vs. temperature [63V].

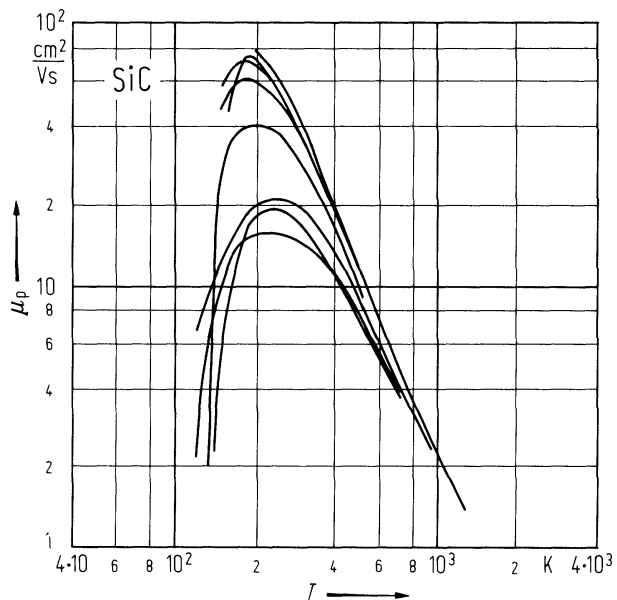


Fig. 1.5.14

SiC (6H). Thermal conductivity ($\perp c$ -axis) vs. temperature for two different samples [64S].

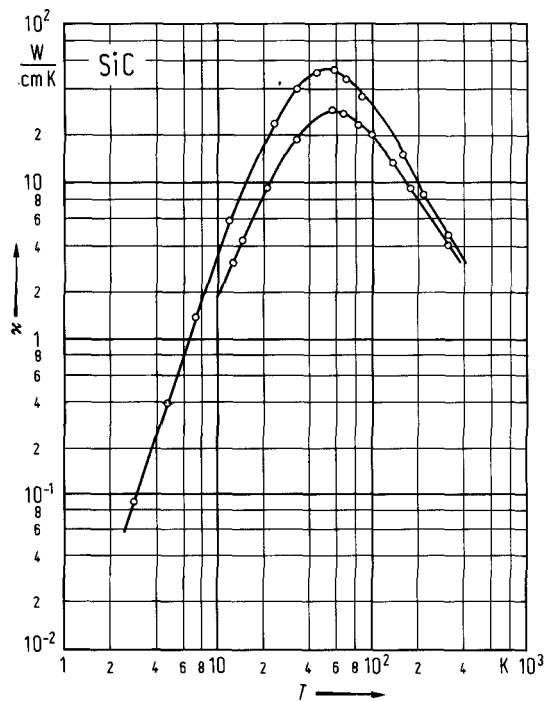


Fig. 1.5.15

SiC. Dispersion of refractive indices of several polytypes [72P].

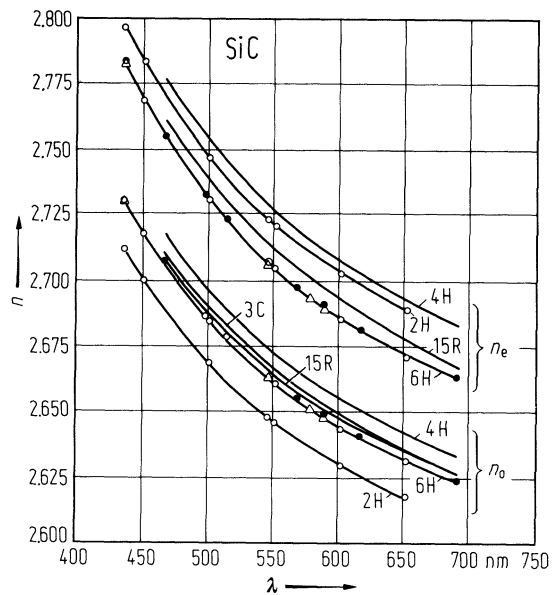
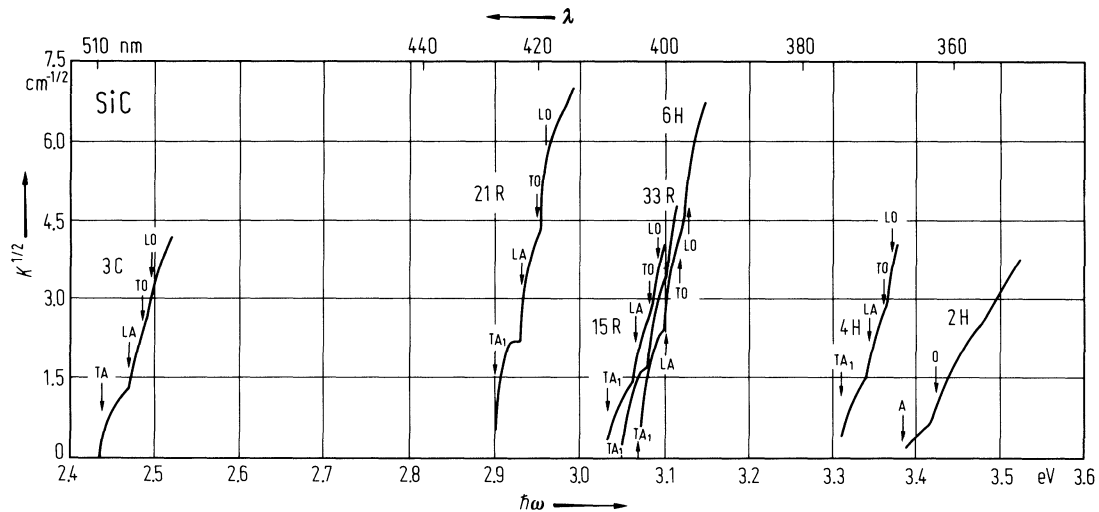


Fig. 1.5.16

SiC. Absorption edge of several polytypes at 4.2 K; light polarized, $E \perp c$ [69C].



1.6 Silicon-germanium mixed crystals, $\text{Si}_x\text{Ge}_{1-x}$

Silicon and germanium form a continuous series of solid solutions with gradually varying properties.

Physical properties

band structure

The band structure is characterized by a crossover in the lowest conduction band edge from Ge-like [111]-symmetry to Si-like [100]-symmetry at $x \approx 0.15$. According to [83K] this value should lie a little bit higher ($x \approx 0.25$). Figs. 1.6.1 and 1.6.2 show the composition dependence of indirect and direct transitions between valence and conduction bands. The shape of the band edge, i.e. the effective masses varies only slightly as a function of x .

$E_g(\Gamma-X)$	$0.8941 + 0.0421x + 0.1691x^2$	calculated	85K
$E_g(\Gamma-L)$	$0.7596 + 1.0860x + 0.3306x^2$		

lattice parameter : The lattice parameter shows a small deviation from Vegard's law: Fig. 1.6.3

transport properties have been mostly investigated on single crystals. The mobility is influenced by alloy scattering which contributes according to $\mu_{\text{alloy}} \propto T^{0.8} x^{-1} (1-x)^{-1}$. Near the band crossover ($x \approx 0.15$) intervalley scattering has to be taken into account.

Figures: composition dependence of the intrinsic conductivity: Fig. 1.6.4, of electron and hole mobility: Figs. 1.6.5 and 1.6.6.

References to 1.6

- 54J Johnson, E. R., Christian, S. M.: Phys. Rev. 95 (1954) 560.
- 58B Braunstein, R., Moore, A. R., Herman, F.: Phys. Rev. 109 (1958) 695.
- 60B Busch, G., Vogt, O.: Helv. Phys. Acta 33 (1960) 437.
- 83K Kustov, E. F., Mel'nikov, E. A., Sutchonkov, A. A., Levadnii, A. I., Filikov, V. A.: Sov. Phys. Semicond. (English Transl.) 17 (1983) 481; Fiz. Tekh. Poluprovodn. 17 (1983) 769.

Figures to 1.6

Fig. 1.6.1

$\text{Si}_x\text{Ge}_{1-x}$. Composition dependence of the (indirect) energy gap at 296 K based on a one-phonon analysis of the absorption edge. At about $x = 0.15$ a crossover occurs of the Ge-like $[111]$ conduction band minima and the Si-like $[100]$ conduction band minima [58B].

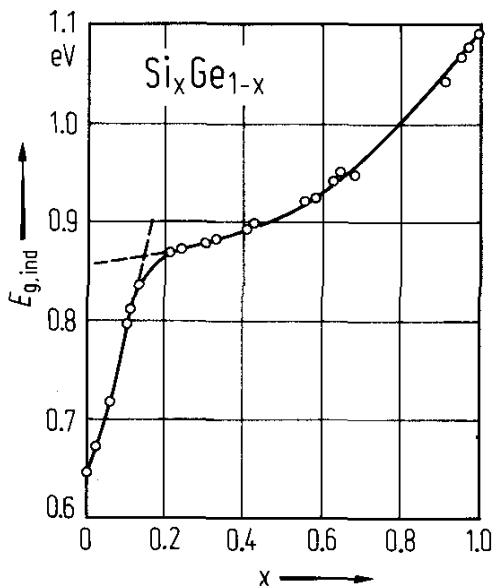


Fig. 1.6.2

$\text{Si}_x\text{Ge}_{1-x}$. Temperature dependence of the indirect energy gap for a series of samples with different composition x [58B].

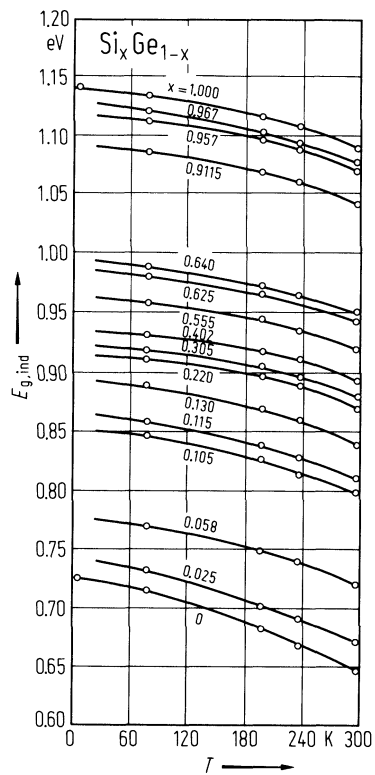


Fig. 1.6.3

$\text{Si}_x\text{Ge}_{1-x}$. Compositional dependence of the lattice parameter. Circles: experimental, from X-ray diffraction; dashed curve: calculated by Vegard's law with the values of pure Ge and Si; solid curve: experimental results from [54J].

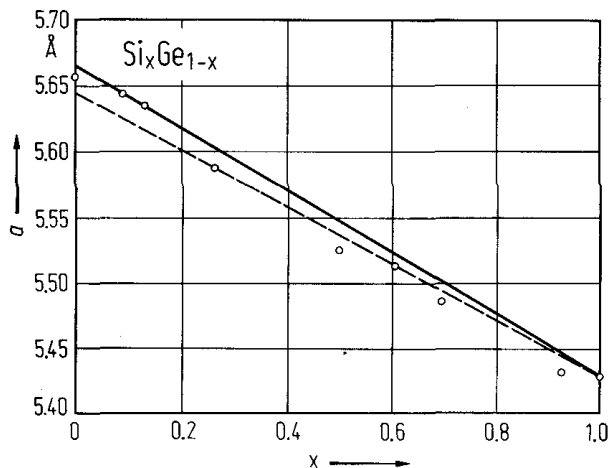


Fig. 1.6.4

$\text{Si}_x\text{Ge}_{1-x}$. Composition dependence of the intrinsic conductivity at room temperature [60B].

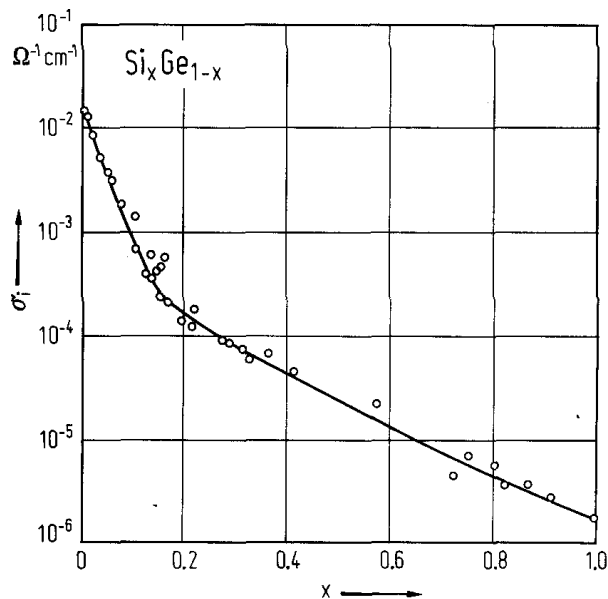


Fig. 1.6.5

$\text{Si}_x\text{Ge}_{1-x}$. Composition dependence of the electron Hall mobility at room temperature [60B].

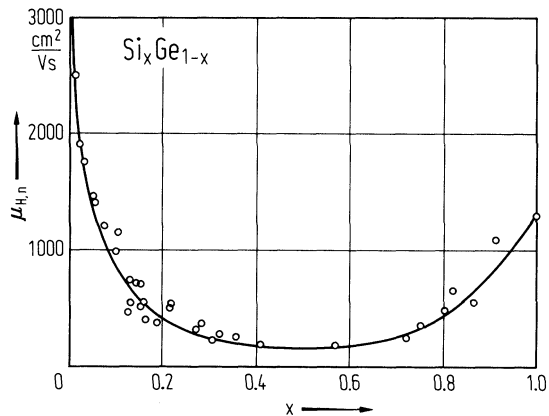
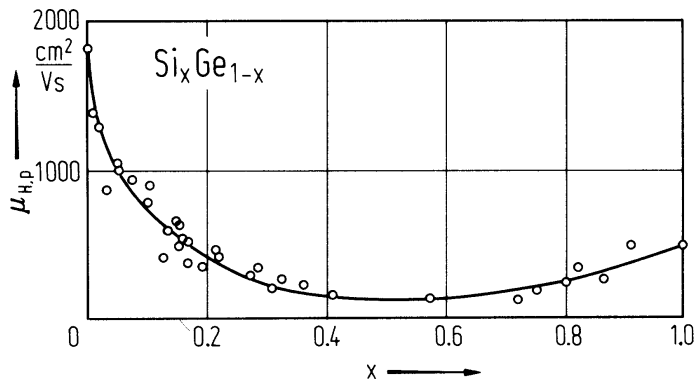


Fig. 1.6.6

$\text{Si}_x\text{Ge}_{1-x}$. Composition dependence of the hole Hall mobility at room temperature [60B].



2. III-V compounds

2.0 Crystal structure and electronic structure

2.0.1. Crystal structure

All *phosphides, arsenides and antimonides of boron, aluminum, gallium and antimony* (BP, BAs, BSb, AlP, AlAs, AlSb, GaP, GaAs, GaSb, InP, InAs, InSb) crystallize under normal conditions in the (cubic) zincblende lattice (space group $T_d^2 - F\bar{4}3m$).

Gallium nitride and *indium nitride* crystallize under normal conditions in the (hexagonal) wurtzite lattice (space group $C_{6v}^4 - P6_3mc$). Besides the wurtzite form (α -GaN) a metastable cubic modification (β -GaN) can be stabilized in thin layers.

Boron nitride crystallizes under normal conditions in two modifications: hexagonal BN (h-BN, space group $P6_3/mmc$) and cubic BN (c-BN).

Both, the zincblende and the wurtzite lattices, are tetrahedrally bonded. They differ only by the orientation of nearest-neighbor tetrahedrons (Fig. 2.0.1). From the diamond lattice the zincblende lattice differs only in the fact, that the two interpenetrating face-centered lattices are occupied by different atoms.

Figs. 2.0.2 ... 2.0.4 show the zincblende lattice, the wurtzite lattice, and the hexagonal lattice of h-BN.

2.0.2 Electronic structure

a. Compounds with zincblende structure

The *Brillouin zone* of the zincblende structure is the Brillouin zone of the face-centered lattice, Fig. 2.0.5. Symmetry lines and point within the Brillouin zone are designed by letters (Γ , X, L, Δ ...).

The qualitative *band structure* is shown in Fig. 2.0.6 along the Δ and Λ axes in the Brillouin zone. Subscripts to the letters defining the location of a given energy state in the Brillouin zone designate the irreducible representation of the respective state (1, 1', 2, 12, 25'...). A comparison with the qualitative band structure of elements with diamond structure shows that the main features are identical, besides of a peculiarity in the conduction band resulting from the lack of inversion symmetry in the zincblende lattice:

conduction band edge: As in the diamond lattice two possibilities are to be considered in connection with the band structure of III-V compounds elements:

lowest band state at Γ : The energy $E(\mathbf{k})$ can be approximated near the band edge by a scalar quadratic \mathbf{k} -dependence: $E(\mathbf{k}) = E(\Gamma) + \hbar^2 k^2 / 2m_n$.

lowest band state along a symmetry axis: In the case that the lowest band state lies at a point \mathbf{k}_0 at a symmetry axis (Δ or Λ) the band edge can be approximated by $E(\mathbf{k}) = E(\mathbf{k}_0) + \hbar^2 \kappa_x^2 / 2m_{\parallel} + \hbar^2 (\kappa_y^2 + \kappa_z^2) / 2m_{\perp}$ where $\mathbf{\kappa} = \mathbf{k} - \mathbf{k}_0$ and $\kappa_x \parallel k_0$, $\kappa_y, \kappa_z \perp k_0$ (*ellipsoidal energy surfaces*).

camel's back structure: By the lack of inversion symmetry a third case has to be considered: the splitting of the degenerate bands at the point X at the boundary of the Brillouin zone (compare Fig. 1.0.7 with Fig. 2.0.6).

This splitting can be described by the equation

$$E(\mathbf{k}) = \hbar^2 k_{\parallel}^2 / 2m_{\parallel} + \hbar^2 k_{\perp}^2 / 2m_{\perp} - ((\Delta/2)^2 + \Delta_0 \hbar^2 k^2 / 2m_{\parallel})^{1/2}$$

perpendicular to the $[100]$ -direction, respectively, m_{\perp} : effective mass perpendicular to the $[100]$ -direction; Δ_0 : parameter describing the non-parabolicity; all other parameters are explained in the figure.

nonparabolicity: In several III-V compounds the parabolic approximation at a Γ -minimum fails because of a low effective electron mass. Low m_n means a strong curvature of the band and, thus, a electron population up to higher band states. The quadratic $E(k)$ -dependence has to be supplied by terms of the 4th order:

$$E(\mathbf{k}) = E(\Gamma) + \hbar^2 k^2 / 2m_n + \alpha k^4 + \beta (k_x^2 + k_y^2 + k_z^2) \pm \gamma (k_x^2 k_y^2 + k_y^2 k_z^2 + k_z^2 k_x^2) - 9 k_x^2 k_y^2 k_z^2)^{1/2}.$$

α and β are the (isotropic and anisotropic) parabolicity parameters, γ the spin-splittig parameter, which vanishes for semiconductors with diamond structure.

valence band edge: In all compounds with zincblende structure the top of the valence band is situated at the center Γ of the Brillouin zone (Γ_{25}'). According to Fig. 2.0.6 this state is triply degenerated if the spin-orbit coupling can be neglected. Taking spin into account the (now sixfold degenerated) state splits into the fourfold degenerated Γ_8^+ state and a lower lying twofold degenerated Γ_7^+ state, separated by the spin-orbit splitting energy Δ . At $\mathbf{k} \neq 0$ two subbands (degenerated at Γ) build the band edge. Their energy can be approximated by

$$E(\mathbf{k}) = E(\Gamma) + (\hbar^2 k^2 / 2m_0)(A \pm (B^2 + sC^2)^{1/2}), \quad s = (k_x^2 k_y^2 + k_y^2 k_z^2 + k_z^2 k_x^2)k^4$$

The \pm -sign refers to the two bands into which $E(\Gamma_8^+)$ splits at $\mathbf{k} \neq 0$. (*warped surfaces*).

b. Compounds with wurtzite structure

The point group of the wurtzite lattice is the hexagonal lattice. The corresponding reciprocal lattice is hexagonal as well (Brillouin zone: Fig. 2.0.8).

Band structures are given usually along the paths $A - R - L - U - M - \Sigma - \Gamma - A$ and $A - S - H - P - K - T - \Gamma - \Delta - A$.

At Γ all bands can be represented in first order approximation by

$$E(\mathbf{k}) = E(\Gamma) + \hbar^2 k_{\parallel}^2 / 2m_{\parallel} + \hbar^2 k_{\perp}^2 / m_{\perp}.$$

The top of the wurtzite-type valence bands often consists of narrow situated Γ_6^- and Γ_1 bands. Taking interaction between both bands into account leads to

$$E_1(\mathbf{k}) = E(\Gamma_6) + ak_{\parallel}^2 + bk_{\perp}^2, \quad E_{2,3}(\mathbf{k}) = E(\Gamma_6) \pm \Delta/2 + ck^2 + dk_{\perp}^2 \pm ((\Delta/2 + c'k_{\parallel}^2 + d'k_{\perp}^2)^2 + (c''k_{\parallel}^2 + d''k_{\perp}^2)^2)^{1/2}.$$

$E_1(0)$ and $E_{2,3}(0)$ are separated by the crystal-field splitting energy Δ (Δ_{cf}).

c. Special band structures

According to Figs. 2.0.9 ... 2.0.24 the semiconducting III-V compounds show the following band structures:

Nitrides:

Boron nitride seems to have an indirect gap in both, cubic and hexagonal modifications. *Aluminum, gallium and indium nitride* (hexagonal lattice) have direct gaps.

Phosphides, arsenides and antimonides:

The *phosphides, arsenides and antimonides of aluminum* as well as *gallium phosphide* have indirect gaps. For AlAs, AlSb and GaP a camel's back structure of the conduction band edge is proved.

Gallium arsenide and antimonide and *indium phosphide, arsenide and antimonide* have a direct gap. In GaAs and GaSb conduction bands with minima along the Δ - or Λ -axes are also of importance for their physical properties. InAs and InSb have low effective electron masses, so that the nonparabolicity of the conduction band has to be taken into account.

For details see the respective sections.

Figures to 2.0

Fig. 2.0.1

The two possible orientations of nearest-neighbor tetrahedrons surrounding one of the atoms in the tetrahedral phase: (a) base triangles are rotated 60 degrees with respect to each other (zincblende lattice); (b) all base triangles are oriented parallel to each other (wurtzite lattice).

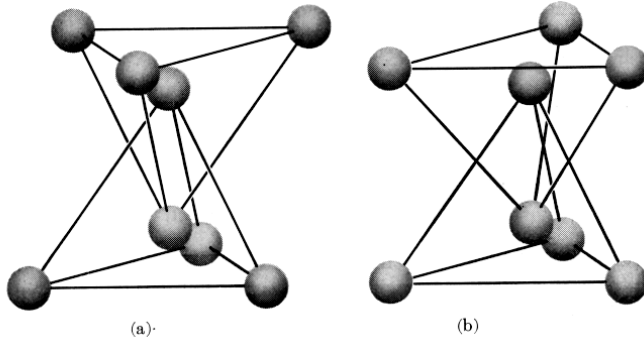


Fig. 2.0.2

The zincblende lattice.

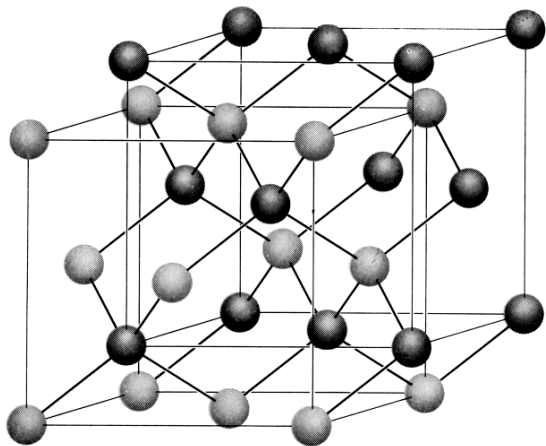


Fig. 2.0.3

The wurtzite lattice.

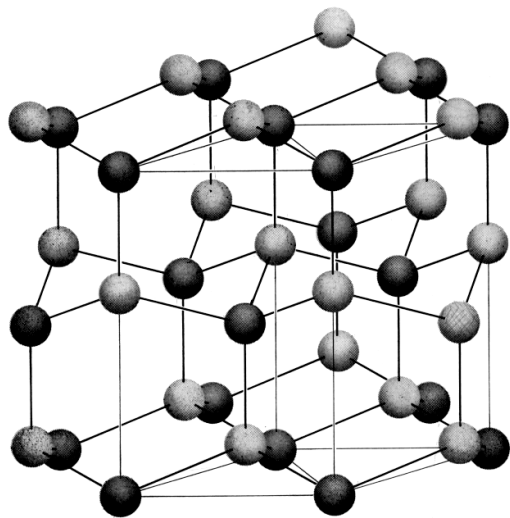


Fig. 2.0.4

The hexagonal lattice of h-BN.

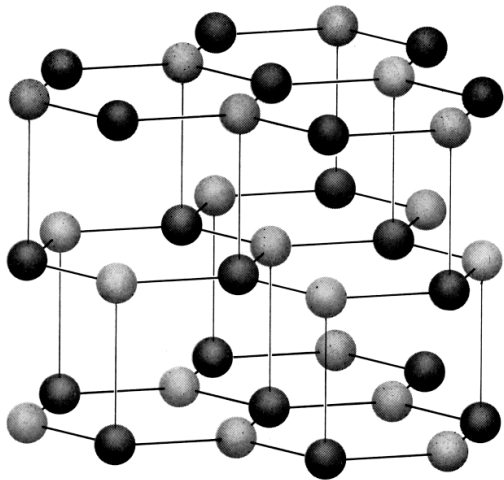


Fig. 2.0.5

Brillouin zone of the zincblende lattice.

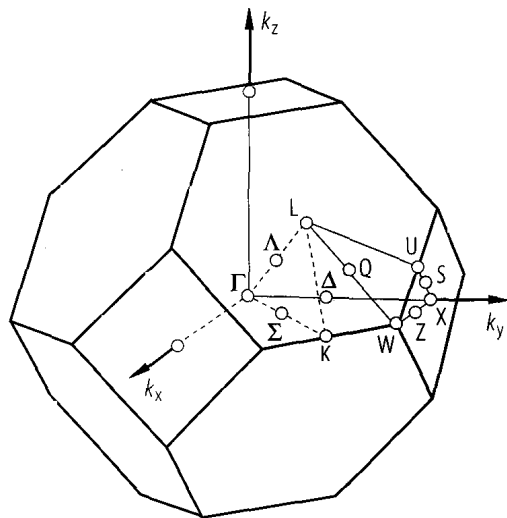
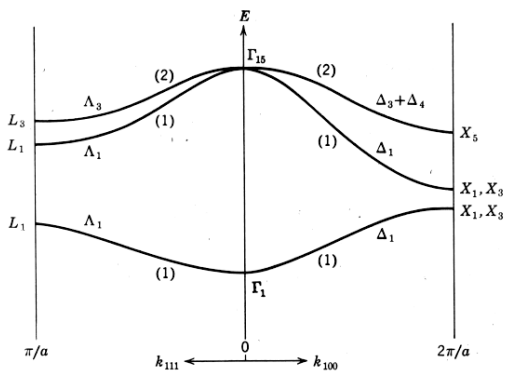
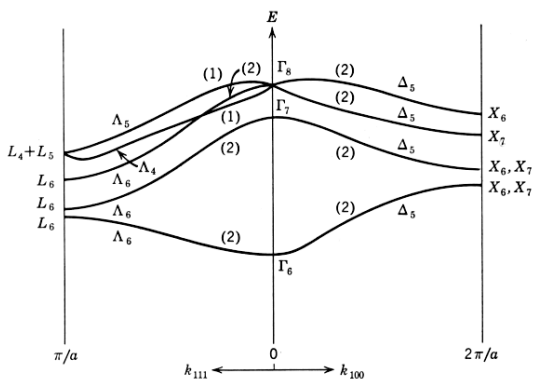


Fig. 2.0.6

Qualitative picture of the band structure of a semiconductor with zincblende structure (a) without inclusion of spin, (b) with spin taken into account. This qualitative shape applies both to the valence and the conduction bands. The symmetry symbols are the same for the two cases except where valence band symbols differing from those for the conduction band are shown in brackets. Where a point or line is labeled with two symbols without brackets, it means that symmetry arguments alone cannot distinguish between the two possibilities. Degeneracies of the band are given in brackets.



(a)



(b)

Fig. 2.0.7

The camel's back structure.

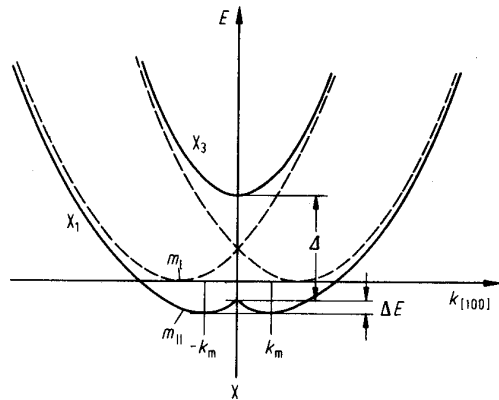


Fig. 2.0.8

The hexagonal Brillouin zone.

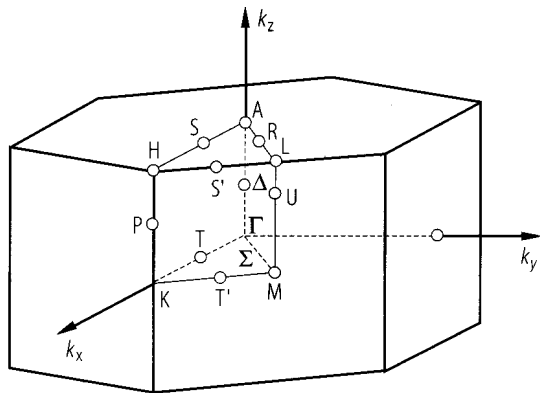


Fig. 2.0.9

Band structures of cubic boron nitride (left) and hexagonal boron nitride (right).

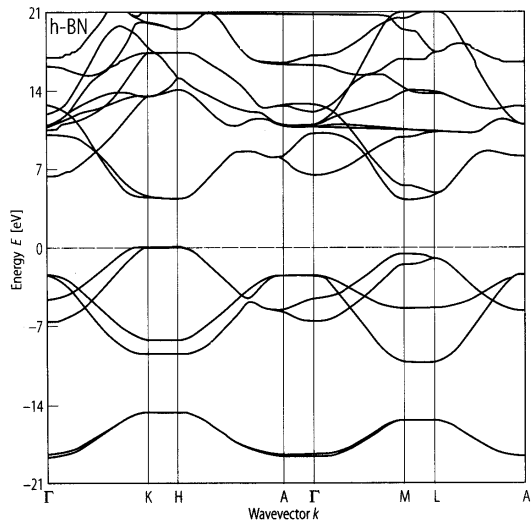
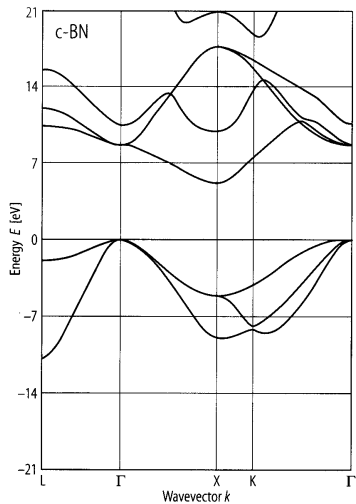


Fig. 2.0.10

Band structure of boron phosphide.

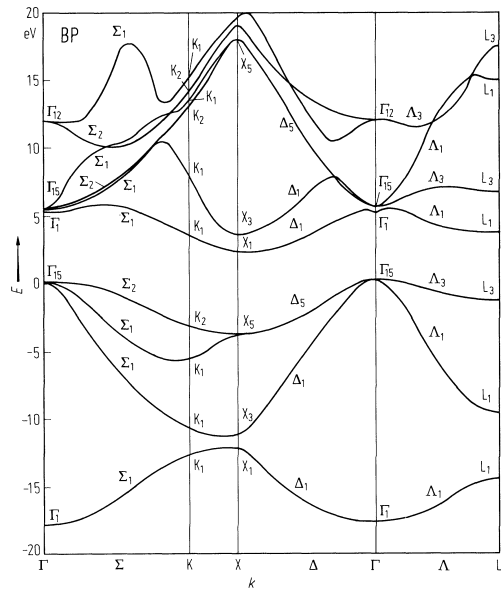


Fig. 2.0.11

Band structure of boron arsenide.

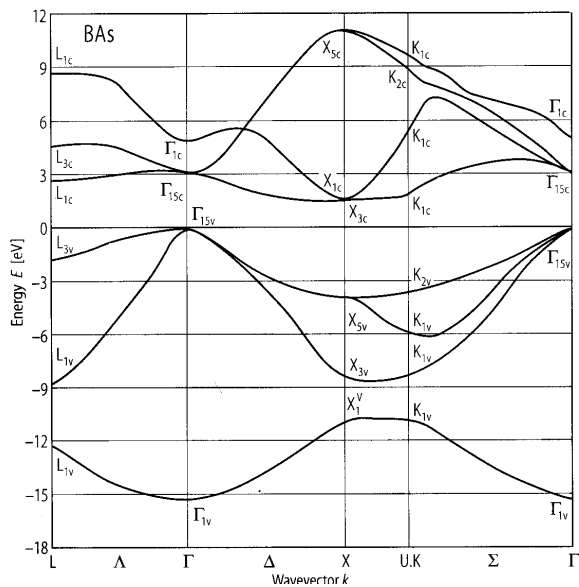


Fig. 2.0.12

Band structure of boron antimonide.

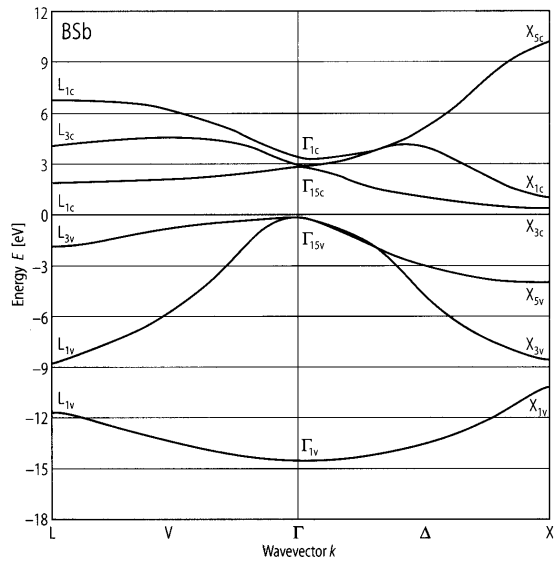


Fig. 2.0.13

Band structure of aluminum nitride

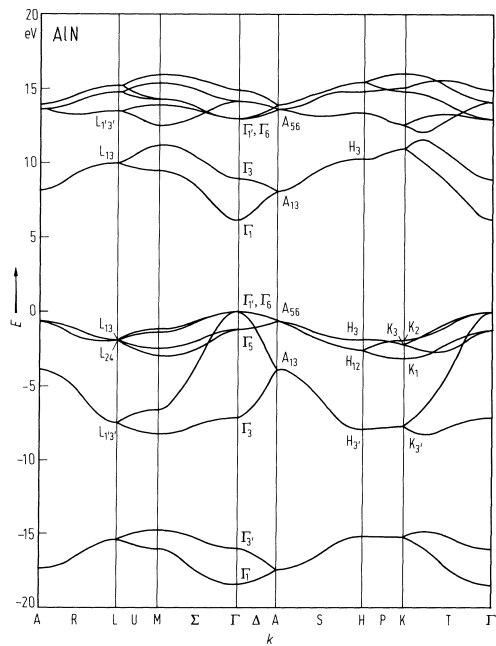


Fig. 2.0.14

Band structure of aluminum phosphide.

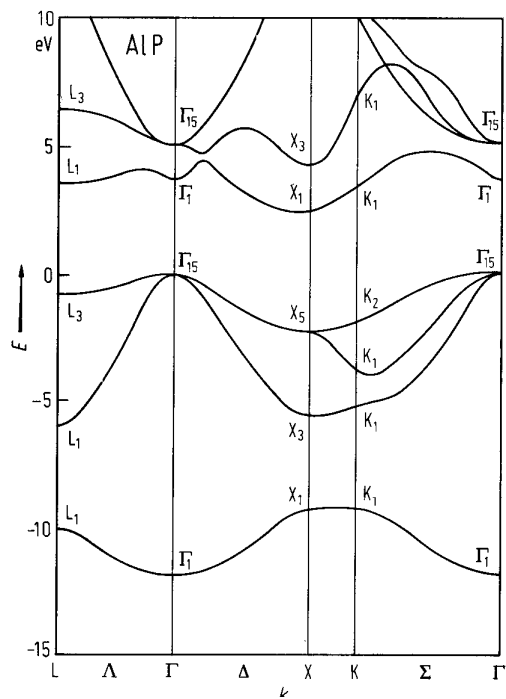


Fig. 2.0.15

Band structure of aluminum arsenide.

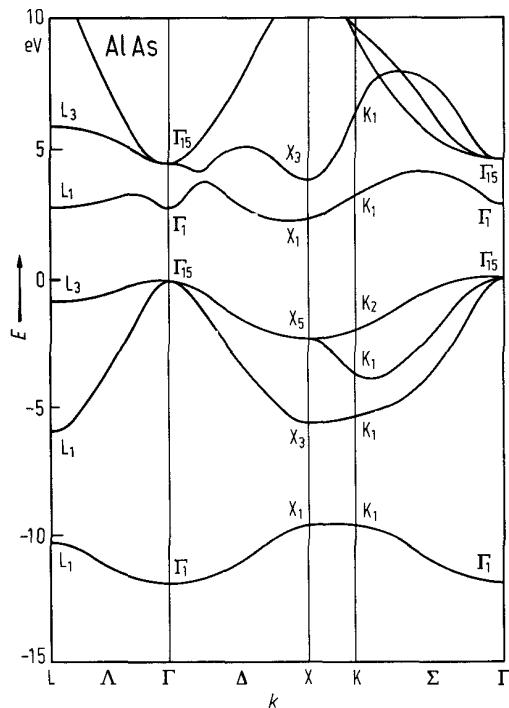


Fig. 2.0.16

Band structure of aluminum antimonide.

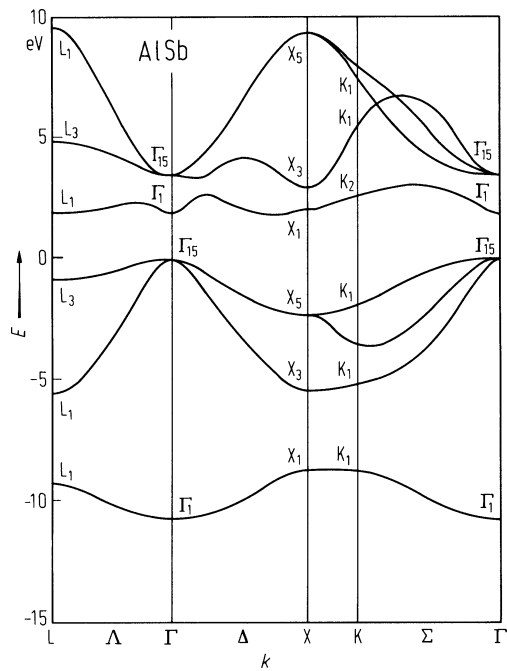


Fig. 2.0.17

Band structure of gallium nitride.

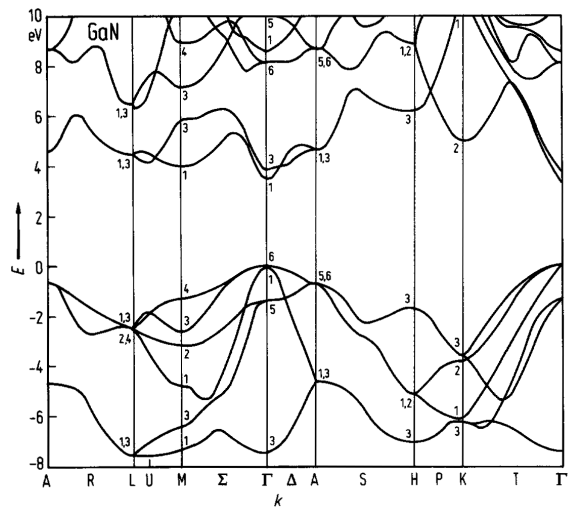


Fig. 2.0.18

Band structure of gallium phosphide.

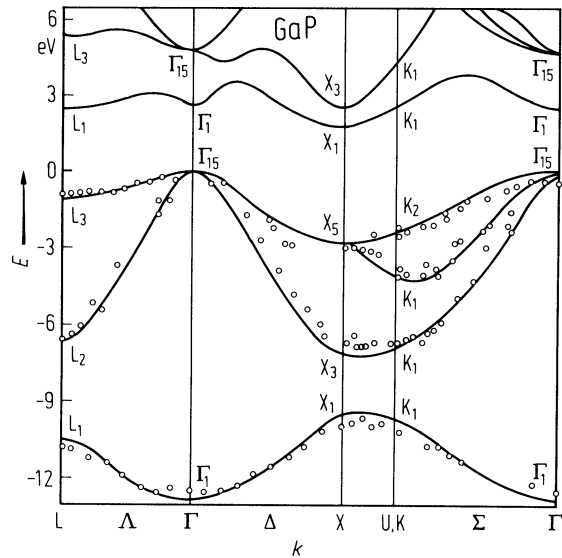


Fig. 2.0.19

Band structure of gallium arsenide.

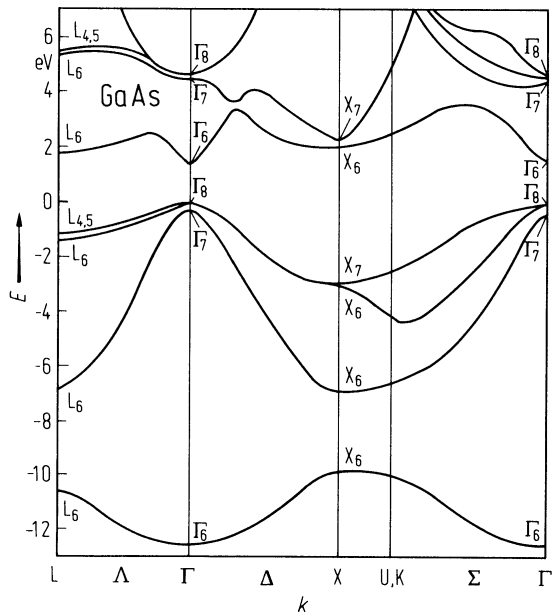
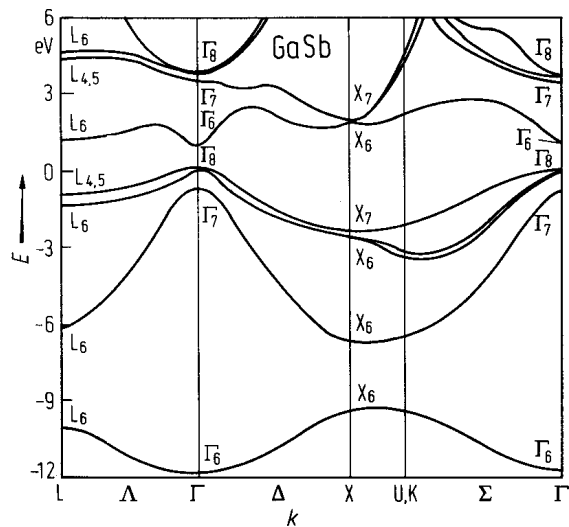
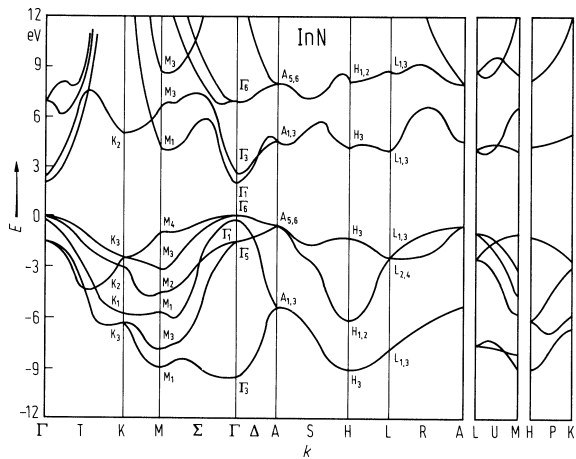


Fig. 2.0.20

Band structure of gallium antimonide.



Band structure of indium nitride.



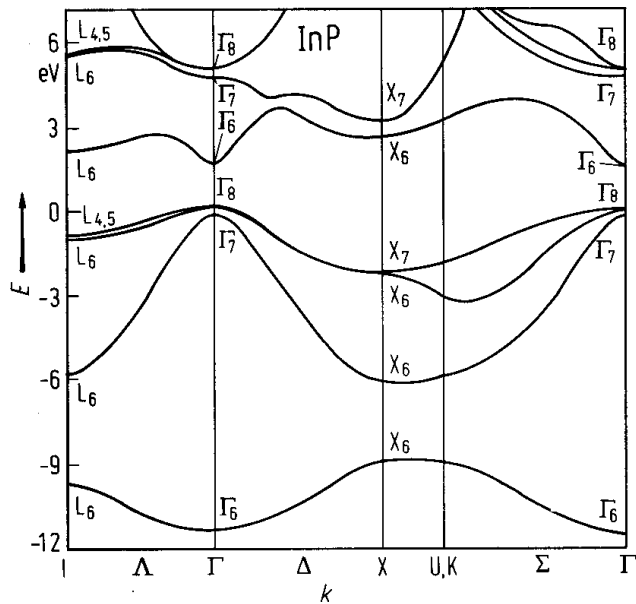


Fig. 2.0.22

Band structure of indium phosphide.

Fig. 2.0.23

Band structure of indium arsenide.

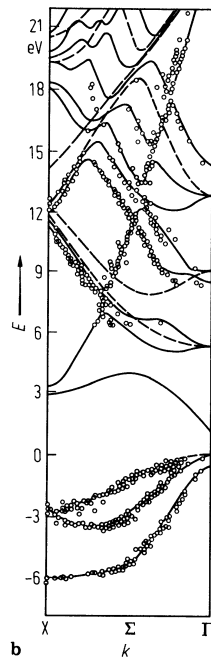
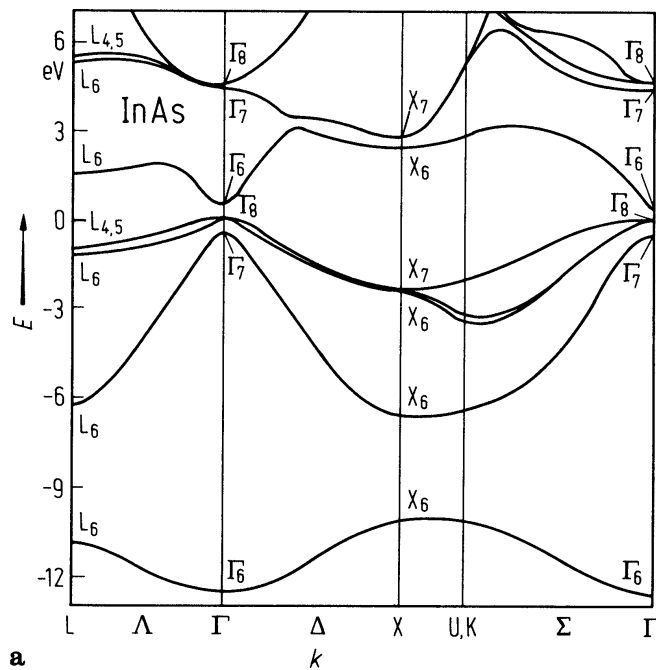
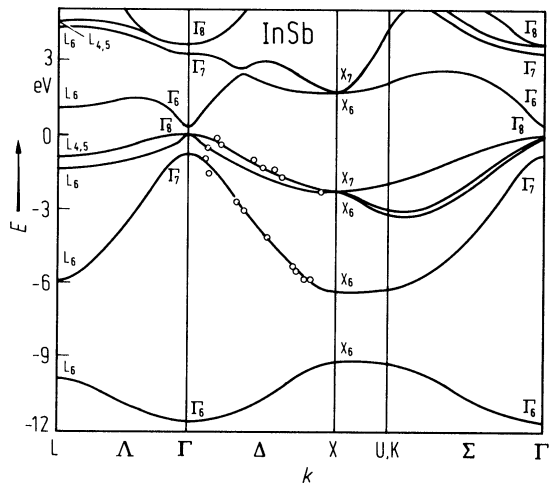


Fig. 2.0.24

Band structure of indium antimonide.



2.1 Boron nitride (BN)

Crystal structure

Boron nitride crystallizes in two modifications: c-BN (cubic BN, zincblende structure, Fig. 2.0.2) and h-BN (hexagonal BN, Fig. 2.0.4). c-BN is stable and h-BN metastable under normal conditions, but the phase diagram is still controversially discussed. Other phases are not stable below a pressure of 10 GPa.

The structure of h-BN is built from hexagonal BN rings, which are stacked strictly above each other so that B and N atoms alternate along the threefold axis (Fig. 2.0.4). The crystal structure of ordered h-BN is represented by the stacking sequence AA', AA' [94G1].

h-BN: space group: P6₃/mmc, *c-BN*: space group: F4̄3m . 97A

No change of phase has been observed at temperatures between 4 and 1433 K [75S].

high pressure phases

Under pressure, hexagonal BN can be transformed into the zincblende form between 2500 and 4000 K and to the wurtzite structure at lower temperature [63B, 72W]. The transition from hexagonal to wurtzite-structure BN occurs at 10.4 GPa (298 K), 9.8 GPa (597 K), 8.5 GPa (873 K) [86W]. No transition to another structure has been observed for pressures below 106 GPa in X-ray diffraction experiments [93U]. But from theory there is a transformation from the wurtzite structure to the rocksalt structure under very high pressure.

A. Cubic modification

Electronic properties

band structure : Fig. 2.0.9a. Brillouin zone: Fig. 2.0.5.

All recent calculations yield indirect band gaps.

energy gap

$E_{g,ind}(\Gamma_{15v}-X_{1c})$	6.2 eV	soft X-ray emission spectroscopy	96A
$E_{g,dir}(\Gamma_{15v}-\Gamma_{1c})$	14.5 eV	reflectivity	62P

effective masses

m_n	0.752 m_0	calculated from band structure data	85H
$m_{p,h}$	0.375 m_0		
	0.926 m_0		
$m_{p,l}$	0.150 m_0		
	0.108 m_0		

Lattice properties

lattice constant

a	0.36160(3) nm	standard conditions	X-ray diffraction	98S
-----	---------------	---------------------	-------------------	-----

Temperature dependence of lattice constant, see Fig. 2.1.1

linear thermal expansion coefficient

α	1.15·10 ⁻⁶ K ⁻¹	$T = 300$ K	X-ray measurements	75S
----------	---------------------------------------	-------------	--------------------	-----

Linear thermal expansion coefficient, see Fig. 2.1.2.

elastic constants

c_{11}	820 GPa	Brillouin scattering	94G2
c_{12}	190 GPa		
c_{44}	480 GPa		

phonon wavenumbers

$\bar{\nu}_{\text{LO}}$	1305(1) cm^{-1}	RT	Raman scattering	83S
$\bar{\nu}_{\text{TO}}$	1054.7(6) cm^{-1}			

melting temperature

T_{m}	> 2973 $^{\circ}\text{C}$			57W
----------------	---------------------------	--	--	-----

density

d	3.4863 g cm^{-3}	standard conditions	X-ray diffraction	98S
-----	---------------------------	---------------------	-------------------	-----

phonon dispersion relation : see Fig. 2.1.3.

bulk modulus

B	372.3(3.7) GPa	normal conditions	ultrasonic measurements	98M
-----	----------------	-------------------	-------------------------	-----

Temperature dependence of B_0 see Fig. 2.1.4.

shear modulus

G	377.8 GPa	normal conditions	ultrasonic measurements	98M
-----	-----------	-------------------	-------------------------	-----

Temperature dependence of G see Fig. 2.1.4.

Young's modulus

E	846.9 GPa	normal conditions	ultrasonic measurements	98M
-----	-----------	-------------------	-------------------------	-----

Poisson's ratio

ν	0.121	normal conditions	ultrasonic measurements	98M
-------	-------	-------------------	-------------------------	-----

Debye temperature

Θ_{D}	1730(70) K	RT...1000 $^{\circ}\text{C}$		86K
---------------------	------------	------------------------------	--	-----

For temperature dependence see Fig. 2.1.5.

heat capacity : temperature dependence see Fig. 2.1.6.

Transport properties

Data on electrical properties of c-BN crystals and films are extremely scarce and, if existing, incomplete.

electrical conductivity and activation energy

E_{A}	0.23(2) eV	$T = 20 \dots 1000$ $^{\circ}\text{C}$	p-type crystal, Be doped	87M
σ	$\approx 10^{-2}$ $\Omega^{-1}\text{cm}^{-1}$			90M
E_{A}	0.24(3) eV	$T = 20 \dots 1000$ $^{\circ}\text{C}$	n-type crystal, Si doped	87M
σ	$\approx 10^{-3}$ $\Omega^{-1}\text{cm}^{-1}$			90M

For Be doped polycrystals, the activation energy depends on dopant concentration (see Fig. 2.1.7).

For the temperature dependence of dark conductivity, see Fig. 2.1.8.

carrier mobility

μ	500 $\text{cm}^2 \text{V}^{-1}\text{s}^{-1}$	thin film, p-type ($5 \cdot 10^{18} \text{ cm}^{-3}$)	nominally undoped, Hall measurements	98L
-------	--	--	---	-----

thermal conductivity : see Fig. 2.1.9.

Optical properties

refractive index

n	2.097	$\lambda = 712.5 \text{ nm}$	95E
-----	-------	------------------------------	-----

dielectric constants

$\varepsilon(0)$	7.1	$T = 300 \text{ K}$	infrared reflectivity, Fig. 2.1.10	67G
$\varepsilon(\infty)$	4.5			

B. Hexagonal modification

Electronic properties

band structure : Fig. 2.0.9b. Brillouin zone: Fig. 2.0.8.

All recent calculations yield indirect band gaps.

According to [76Z] the valence band consists of a triplet of overlapping bands (topmost: π -band with maximum at P, two overlapping σ -bands) and one lower subband built from the 2s states of N and B. The conduction band minimum is situated at P. In [76Z] an extensive comparison has been made with several other calculations and experimental results.

energy gap

E_g	5.9(1) eV	inelastic electron scattering	89T
$E_{g,th}$	7.1(1) eV	temperature dependence of resistivity	82C

Lattice properties

lattice parameters

a	0.25072(1) nm	prepared from amorphous BN in 100% N ₂ atmosphere	94A
c	0.687(1) nm	at room temperature	

temperature dependence of lattice parameters

$c = 6.6516 \text{ \AA} + 2.74 \cdot 10^{-4} T \text{ \AA } ^\circ\text{C}^{-1}$	X-ray diffraction	52P
$a = 2.50424 \text{ \AA} - 7.42 \cdot 10^{-6} T \text{ \AA } ^\circ\text{C}^{-1} + 4.79 \cdot 10^{-9} T^2 \text{ \AA } ^\circ\text{C}^{-2}$		

See Fig. 2.1.11.

linear thermal expansion coefficient

α_{vol}	$40.6(4) \cdot 10^{-6} \text{ K}^{-1}$	standard conditions	X-ray measurements	97S
----------------	--	---------------------	--------------------	-----

density

d	2.279 g cm^{-3}	X-ray density	94G1
-----	---------------------------	---------------	------

decomposition temperature

T_{dec}	2600(100) K		65J
-----------	-------------	--	-----

melting temperature

T_m	3200...3400 K	N ₂ ambient [1...50 MPa]	pyrometric measurements	91V
-------	---------------	--	-------------------------	-----

phonon dispersion curves : Fig. 2.1.12.

phonon wavenumber				
$\bar{\nu}_{\text{TO1}}$	783 cm^{-1}	$E\parallel c$	IR reflectivity	66G
$\bar{\nu}_{\text{LO1}}$	828 cm^{-1}			
$\bar{\nu}_{\text{TO2}}$	1510 cm^{-1}			
$\bar{\nu}_{\text{LO2}}$	1595 cm^{-1}			
$\bar{\nu}_{\text{TO1}}$	767 cm^{-1}	$E\perp c$		
$\bar{\nu}_{\text{LO1}}$	778 cm^{-1}			
$\bar{\nu}_{\text{TO2}}$	1367 cm^{-1}			
$\bar{\nu}_{\text{LO2}}$	1610 cm^{-1}			
second order elastic moduli				
c_{11}	750 GPa		pyrolytic BN	77J
c_{12}	150 GPa			
c_{33}	18.7 – 67.28 ($d - 3.33$) GPa		(d is interlayer spacing in Å)	
c_{44}	2.52 (154) GPa		pyrolytic BN (with defects)	92D
compressibility				
$\Delta a/a\Delta p$	1.4·10 ⁻¹² m ² /N	$p = 0 \dots 6.3$ GPa	X-ray diffraction	95F
$\Delta c/c\Delta p$	18·10 ⁻¹² m ² /N			
Young's modulus				
E	18.6 GPa	t-BN films	nanindentation	96C
Poisson's ratio				
ν	0.306	t-BN films	calculated from data in [92D]	96C
Debye temperature				
Θ_{D}	598(7) K		calorimetry	54D
Transport properties				
electrical resistivity				
ρ	2·10 ¹¹ Ωcm		undoped nanocrystalline film	98S
	1.3·10 ² Ωcm		S-doped n-type nanocrystalline film	
Fig. 2.1.13 shows the temperature dependence of the resistivity at high temperatures and a comparison with earlier literature data.				
thermal conductivity				
κ	150...220 W m ⁻¹ K ⁻¹	$T = 300$ K	p-BN	92D
	30 W m ⁻¹ K ⁻¹	$T = 300$ K	t-BN	
For the temperature dependence of κ for pyrolytic BN in the range from 1 to 500 K see Fig. 2.1.14.				
Optical properties				
refractive index				
n	1.65	perpendicular to c axis		
	2.13	parallel to c axis		83I
dielectric constants				
$\epsilon(0)_{\parallel}$	5.09	parallel to c -axis	IR reflectivity	66G
$\epsilon(0)_{\perp}$	7.04	perpendicular to c -axis		
$\epsilon(\infty)_{\parallel}$	4.10	parallel to c -axis	IR reflectivity,	66G
$\epsilon(\infty)_{\perp}$	4.95	perpendicular to c -axis		

Impurities and defects

(cubic boron nitride)

Only limited information is available on impurities in c-BN. Experimental data on energy levels etc. are completely missing.

energy levels

$E-E_v$	1.76 eV	a1 band	Vac _[N] (relaxed)	97P
$E-E_v$	4.90 eV	a1 band	Vac _[N] (relaxed)	
$E-E_v$	4.81 eV	a1 band	B _[N] (relaxed)	97P

intrinsic or unidentified electron traps

apparent thermal activation energies of electrons E_{na}

E_{na}	0.05... 0.12 eV	S, Si, KNC doped	electrical conductivity	57W, 61W, 62W
	0.2 eV	$T = 80...150$ K	electrical conductivity	75H
	0.3 eV	$T = 150... 300$ K	electrical conductivity	75H
	0.4 eV	$T > 300$ K	electrical conductivity	75H

intrinsic or unidentified hole traps

apparent thermal activation energies of holes E_{pa}

E_{pa}	0.2 eV	Be-doped	electrical conductivity	57W, 61W, 62W
----------	--------	----------	-------------------------	---------------

intrinsic or unidentified electron traps

apparent optical activation energies of electrons E_b

E_b	$E_c - 0.15...0.4$ eV		thermoluminescence	75H
	$E_c - 0.1$ eV	$T = 77$ K	photoconductivity	75H
	$E_c - 2.5$ eV	$T = 77$ K	photoconductivity and thermoluminescence	75H

References to 2.1

- 52P Pease, R. S.: *Acta Crystallogr.* 5 (1952) 536.
- 54D Dworkin, A. S., Sasmor, D. J., van Artsdalen, E. R.: *J. Chem. Phys.* 22 (1954) 837.
- 57W Wentorf, R. H.: *J. Chem. Phys.* 26 (1957) 956.
- 61W Wentorf, R. H.: *J. Chem. Phys.* 34 (1961) 809.
- 62P Philipp, H. R., Taft, E. A.: *Phys. Rev.* 127 (1962) 159
- 62W Wentorf, R. H.: *J. Chem. Phys.* 36 (1962) 1990.
- 63B Bundy, F. P., Wentorf, R. H.: *J. Chem. Phys.* 38 (1963) 1144.
- 65J Janaf Thermochemical Tables, US Dept. of Commerce NBS PB16384 (1965) .
- 66G Geick, R., Perry, C. H., Rupprecht, G.: *Phys. Rev.* 146 (1966) 543.
- 67G Giellisse, P. J., Mitra, S. S., Plendl, J. N., Griffis, R. D., Mansur, L. C., Marshall, R., Pascoe, E. A.: *Phys. Rev.* 155 (1967) 1039.
- 72W Wakatsuki, M., Ichinose, K., Aoki, T.: *Mater. Res. Bull.* 7 (1972) 999.
- 73S Slack, G. A.: *J. Phys. Chem. Solids* 34 (1973) 321
- 75H Halperin, A., Katzir, A.: *J. Phys. Chem. Solids* 36 (1975) 89.
- 75S Slack, G. A., Bartram, S. F.: *J. Appl. Phys.* 46 (1975) 89.
- 76S Sichel, E. K., Miller, R. E., Abrahams, M. S., Buiocchi, C. J.: *Phys. Rev. B* 13 (1976) 4607.
- 76B Ham, I. S., Davidenko, V. M., Sidorov, V. G., Fel'dgun, L. I., Skagalov, M. D., Shalabutov, Y. K.: *Sov. Phys. Semicond. (English Transl.)* 10 (1976) 331; *Fiz. Tekh. Poluprov.* 10 (1976) 554.
- 76Z Zunger, A., Katzir, A., Halperin, A.: *Phys. Rev. B* 13 (1976) 5560.
- 77J Jager, B.: PhD thesis, Grenoble 1977; as cited in [92D]. 82C Carpenter, L. G., Kirby, P. J.: *J. Phys. D* 15 (1982) 1143.
- 82C Carpenter, L. G., Kirby, P. J.: *J. Phys. D* 15 (1982) 1143.
- 83I Ishii, T., Sato, T.: *J. Cryst. Growth* 61 (1983) 689.
- 83S Sanjurjo, J. A., López-Cruz, E., Vogl, P., Cardona, M.: *Phys. Rev. B* 28 (1983) 4579.
- 85H Huang, M., Ching, W. Y.: *J. Phys. Chem. Solids* 46 (1985) 977.
- 86K Kolupayeva, Z. I., Fuks, M. Ya., Gladkikh, Z. I., Arinkin, A. V., Malikhin, S. V.: *J. Less-Common Met.* 117 (1986) 259.
- 86W Wakatsuki, M., Takano, K. J., Fujita, G.: *Physica B* 139 & 140 (1986) 256.
- 87M Mishima, O., Tanaka, J., Yamaoka, S., Fukunaga, O.: *Science* 338 (1987) 181.
- 89T Tarrio, C., Schnatterly, S. E.: *Phys. Rev. B* 40 (1989) 7852.
- 90A Akate, T., Honda, A., Sato, Y., Saito, K.: *Jpn. J. Appl. Phys.* 29 (1990) L1869.
- 90M Mishima, O.: *Mater. Sci. Forum.* 54/55 (1990) 313.
- 91V Vinogradov, V. L., Kostanovskii, A. V.: *High Temperature* 29 (1991) 901.
- 92D Duclaux, L., Nysten, B., Issi, J.-P., Moore, A. W.: *Phys. Rev. B* 46 (1992) 3362.
- 93T Taniguchi, T., Tanaka, J., Mishima, O., Ohsawa, T., Yamaoka, S.: *Appl. Phys. Lett.* 62 (1993) 576.
- 93U Ueno, M., Yoshida, M., Onodera, A., Shimomura, O., Takemura, K.: *Jpn. J. Appl. Phys. Suppl.* 32 (1993) 42.
- 94A Andreev, Yu. G., Lundström, T.: *J. Alloys Compounds* 216 (1994) L5.
- 94F Furthmüller, J., Hafner, J., Kresse, G.: *Phys. Rev. B* 50 (1994) 15606.
- 94G1 Gavrichev, K. S., Solozhenko, V. L., Lazarev, V. B.: *Inorg. Mater.* 30 (1994) 1025.
- 94G2 Grimsditch, M., Zouboulis, E. S., Polian, A.: *J. Appl. Phys.* 76 (1994) 832.
- 94S Solozhenko, V. L.: in Edgar, J. H. (ed.), *Properties of Group III Nitrides*, ch. 2.1, p.43, INSPEC, London 1994.
- 95E Eremets, M. I., Gauthier, M., Polian, A., Chervin, J. C., Besson, J. M., Dubitskii, D. A., Semenova, Ye. Ye.: *Phys. Rev. B* 52 (1995) 8854.
- 95F Fujinaga, Y., Syono, Y.: *J. Japan. Inst. Metals* 59 (1995) 519.
- 96A Agui, A., Shin, S., Fujisawa, M., Tezuka, Y., Ishii, T., Mishima, O., Era, K., Shigemasa, E., Yagashita, A.: *J. Electron Spect. Relat. Phenom.* 79 (1996), 194.
- 96C Cardinale, G. F., Howitt, D. G., McCarthy, K. F., Medlin, D. L., Mirkarimi, P. B., Moody, N. R.: *Diamond Relat. Mater.* 5 (1996) 1295.
- 96K Karch, K., Bechstedt, F., Pavone, P., Strauch, D.: *Physica B* 219 & 220 (1996) 445.
- 97A Albe, K.: *Phys. Rev. B* 55 (1997) 6203.
- 97K Karch, K., Bechstedt, F.: *Phys. Rev. B* 56 (1997) 7404.
- 97P Piquini, P., Mota, R., Schmidt, T.M., Fazzio, A.: *Phys. Rev. B* 56 (1997) 3556.

- 97S Solozhenko, V. L., Peun, T.: J. Phys. Chem. Solids 58 (1997) 1321.
- 98L Litvinov, D., Taylor II, C. A., Clarke, R.: Diamond Relat. Mater 7 (1998) 360.
- 98M Manghnani, M. H.: Advanced Materials 98, NIRIM, Tsukuba, 1998, p.73.
- 98S Solozhenko, V. L., Hausermann, D., Mezouar, M., Kunz, M.: Appl. Phys. Lett. 72 (1998) 1691.
- 99K Kern, G., Kresse, G., Hafner, J.: Phys. Rev. B 59 (1999) 8551.

Figures to 2.1

Fig. 2.0.2

The zincblende lattice

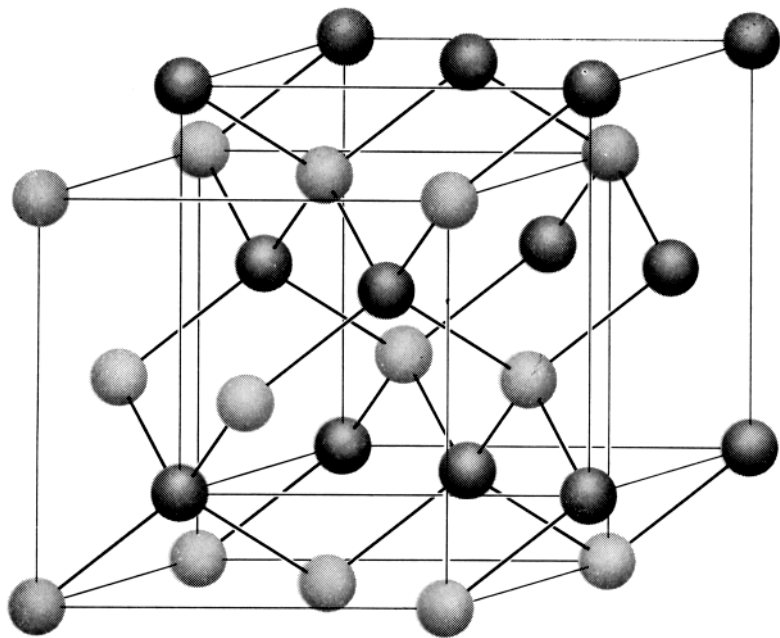


Fig. 2.0.4

The hexagonal lattice of h-BN

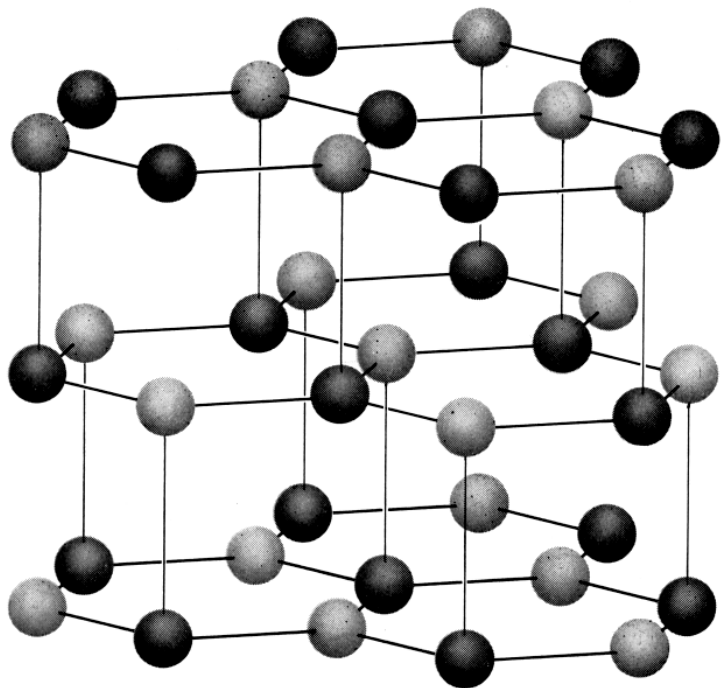


Fig. 2.0.5

Brillouin zone of the zincblende lattice.

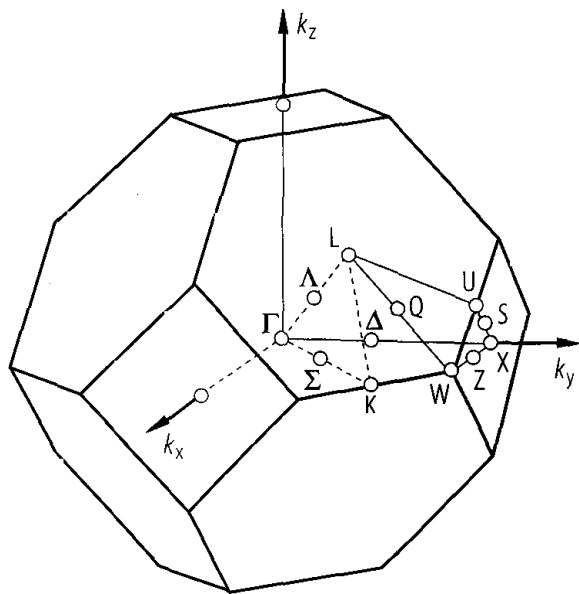


Fig. 2.0.9

c-BN. Band structure, calculation with ultrasoft pseudopotentials [94F].

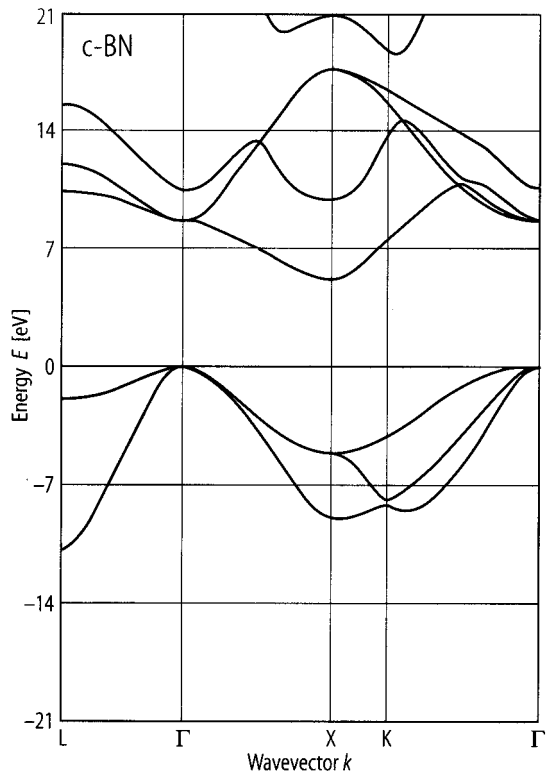


Fig. 2.0.10

h-BN. Band structure, calculation with ultrasoft pseudopotentials [94F].

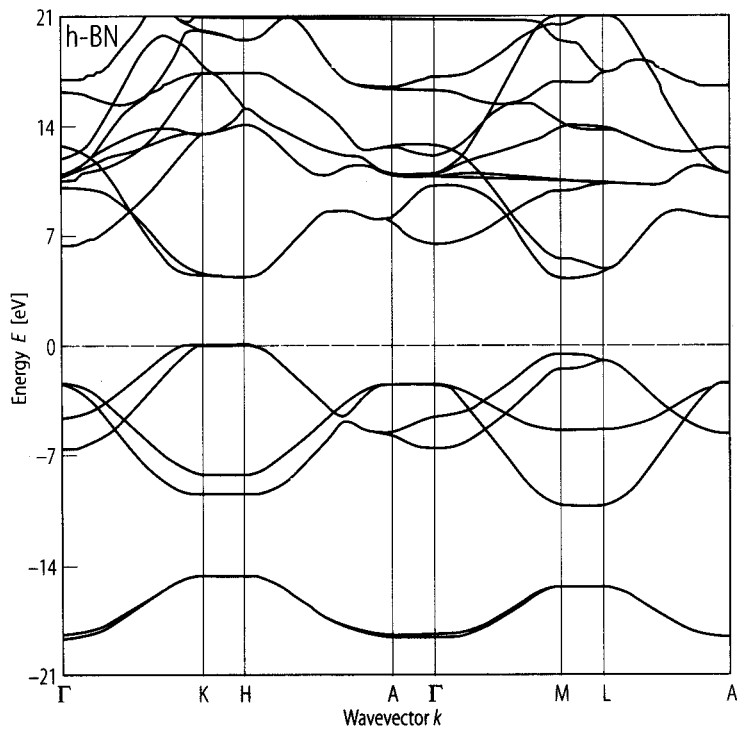


Fig. 2.1.1

c-BN. Temperature dependence of the lattice parameter a from X-ray diffraction [86K].

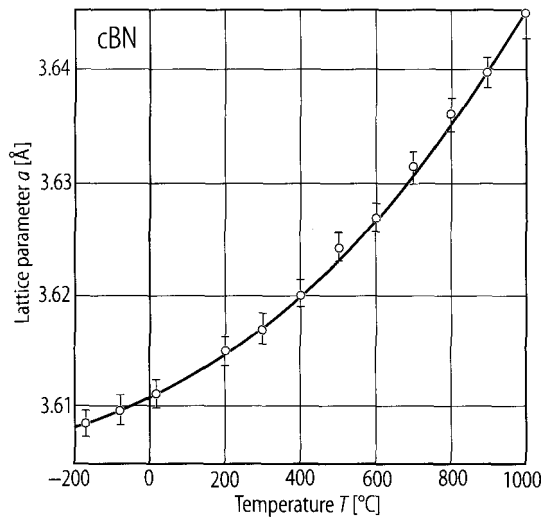


Fig. 2.1.2

c-BN. Linear thermal expansion coefficient temperature measured by an X-ray technique [75S].

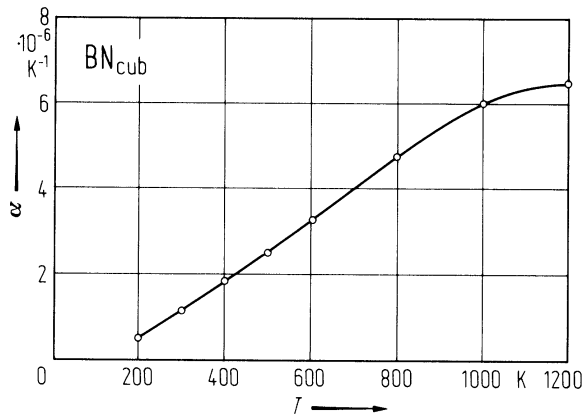


Fig. 2.1.3

c-BN. Phonon dispersion curves (left panel) and phonon density of states (right panel). Experimental data points from [83S] and curves from ab-initio calculations [96K]. From [96K]; see also [97K].

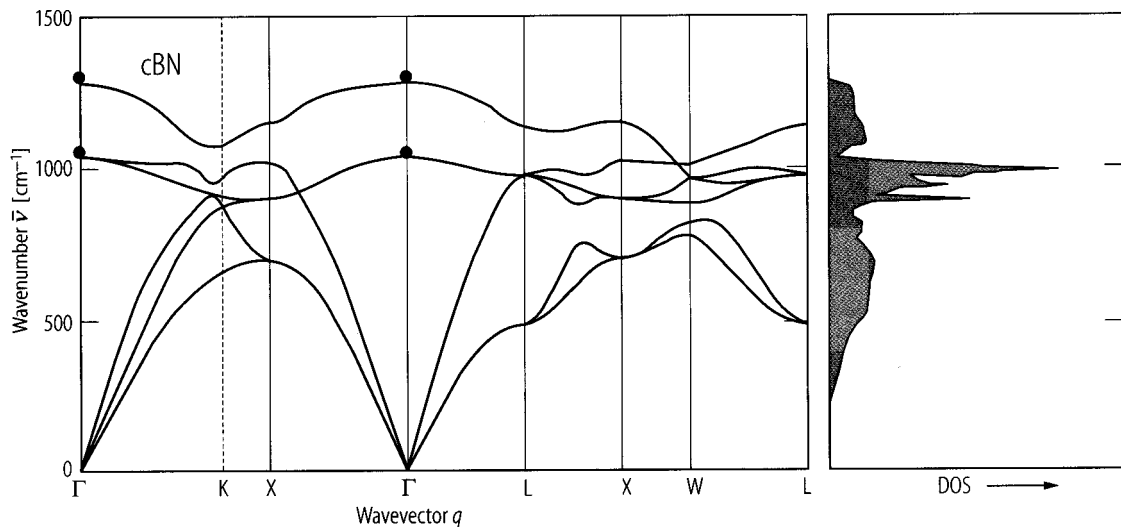


Fig. 2.1.4

c-BN. Temperature dependence of bulk modulus (B) and shear modulus (G). The derivatives at 200°C and 600°C are dB_0/dT (200°C) = -0.057 GPa/K, dG/dT (200°C) = -0.181 GPa/K, dB_0/dT (600°C) = -0.146 GPa/K, dG/dT (600°C) = -0.205 GPa/K [98M].

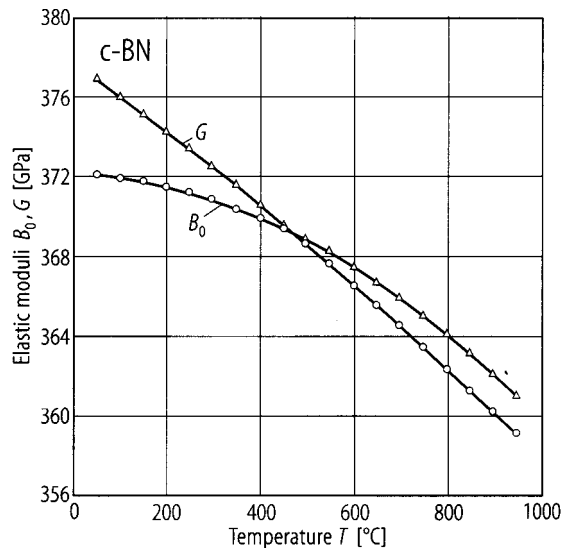


Fig. 2.1.5

c-BN. Temperature dependence of Debye temperature [90A].

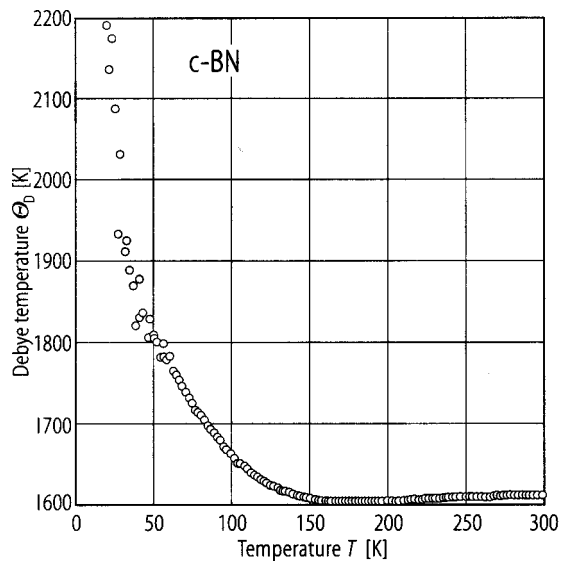


Fig. 2.1.6

BN. Heat capacities for four polymorphic boron nitride modifications. Data taken from [94S].

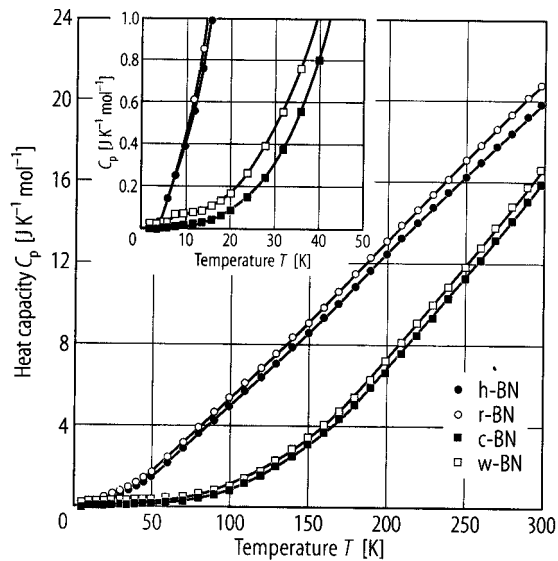


Fig. 2.1.7

c-BN. Temperature dependence of resistance of Be-doped polycrystals [93T]. $R_0 = 1 \Omega$. Activation energies are indicated. Be doped single crystal from other literature.

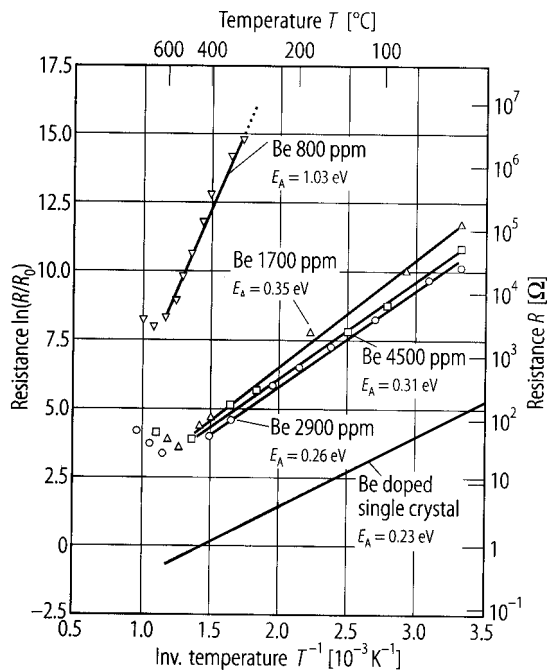


Fig. 2.1.8

c-BN. Electrical conductivity vs. reciprocal temperature for different polycrystalline samples above RT [76B].

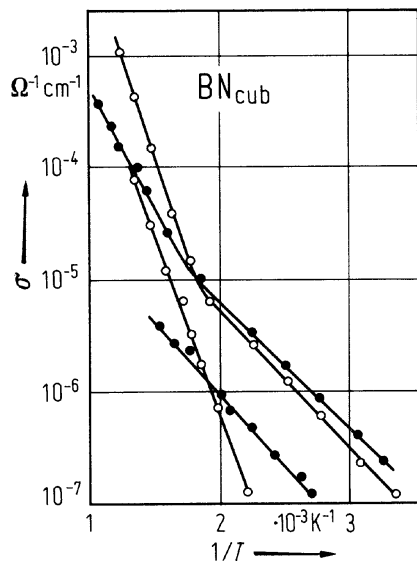


Fig. 2.1.9

c-BN. Thermal conductivity vs temperature of ceramic compact samples [73S].

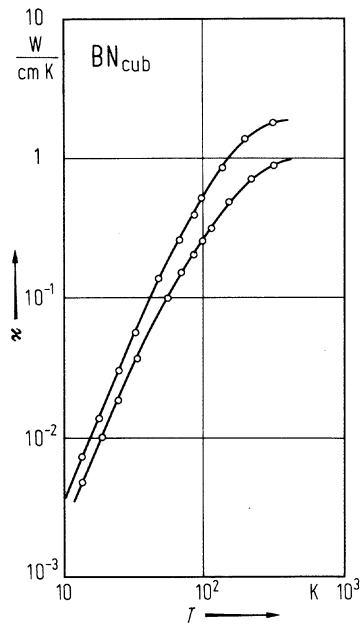


Fig. 2.1.10

c-BN. Reflectivity, refractive index and extinction coefficient vs. wavenumber in the infrared region [67G].

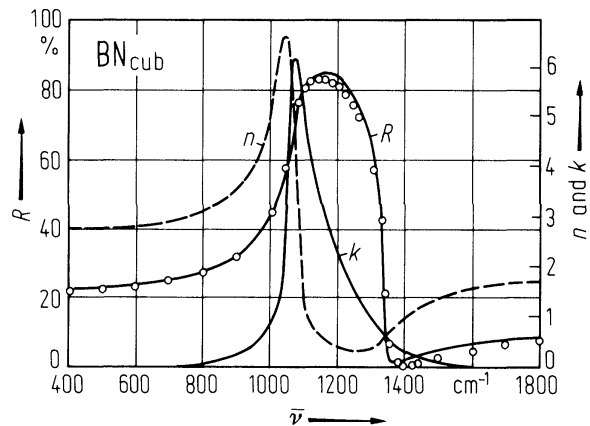


Fig. 2.1.11

h-BN. Temperature dependence of the lattice parameters a and c from X-ray diffraction [86K].

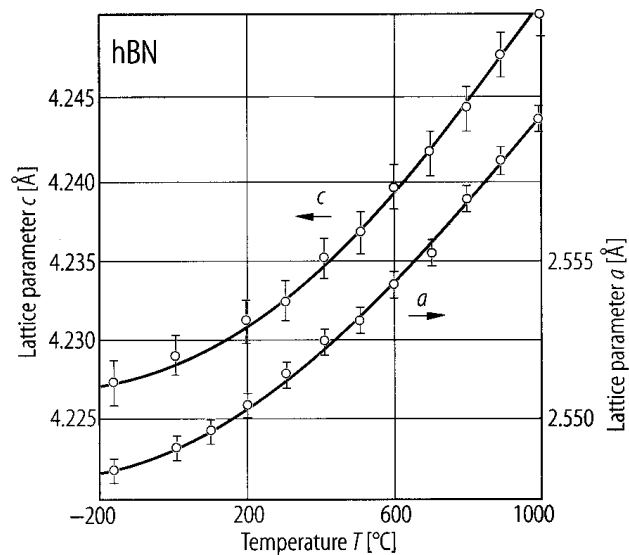


Fig. 2.1.12

h-BN. Phonon-dispersion relations (ab initio calculations. Crosses at Γ indicate experimental Raman and infrared data, open circles HREELS data.) [99K].

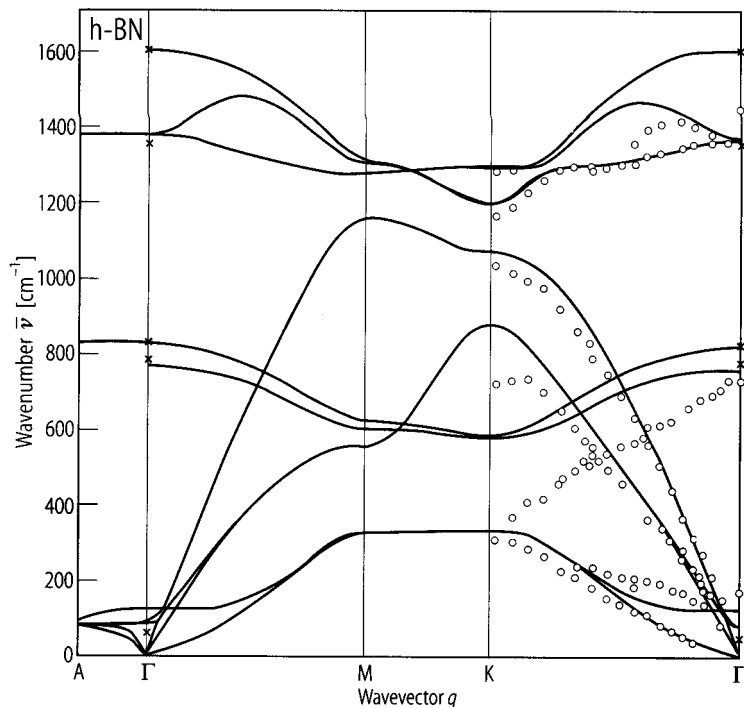


Fig. 2.1.13

h-BN. Resistivity vs. temperature above 700°C. A: from bulk resistance of a disk measured in c direction. B...E: earlier literature data for comparison [82C].

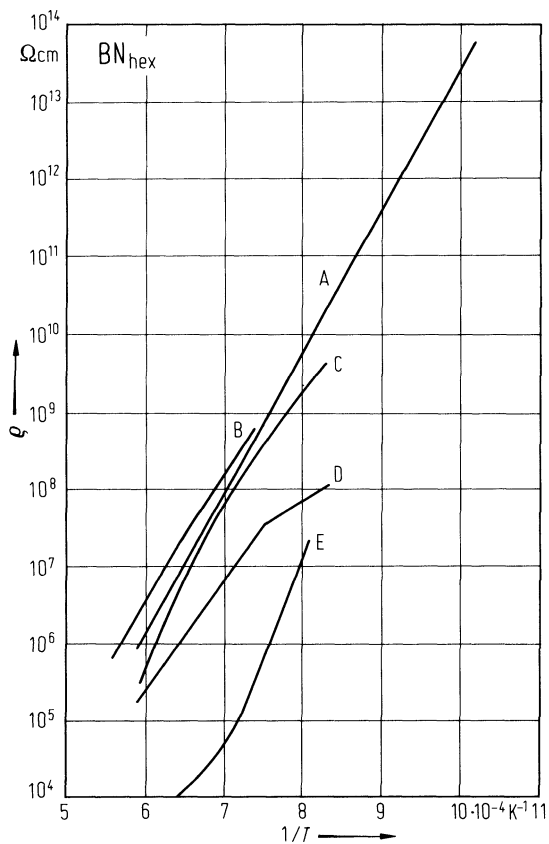
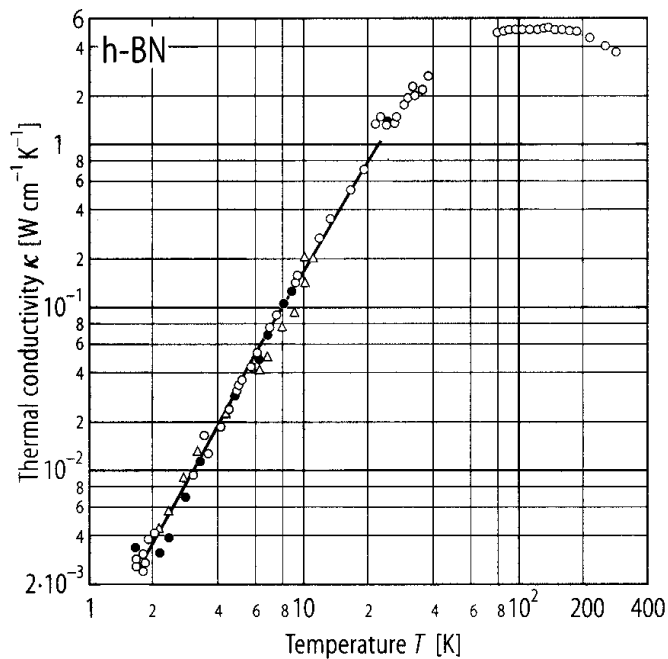


Fig. 2.1.14

h-BN. Thermal conductivity of pyrolytic h-BN as a function of temperature [76S]. Open circles: steady state technique, full circles: from diffusivity, triangles: moments method.



2.2 Boron phosphide (BP)

Crystal structure

Under ambient conditions boron phosphide crystallizes in the zincblende structure (space group $T_d^2 - F\bar{4}3m$, Fig. 2.0.2). There seems to be a continuous transition to a metallic state upon pressuring. In energy-dependent X-ray diffraction experiments the zincblende phase has been found to be stable up to a pressure of 110 GPa.

Electronic properties

band structure : Fig. 2.0.10, Brillouin zone: Fig. 2.0.5.

BP is an indirect gap semiconductor. The direct band gaps are 4.4, 6.5 and 6.5 eV at Γ , X and L, respectively.

energy gap

$E_{g,ind}$	2.1 eV	RT	measurement of soft-Xray emission and absorption spectra using synchrotron radiation	99A
-------------	--------	----	--	-----

Lattice properties

lattice parameter

a	4.5383(4) Å	$T = 297\text{ K}$	temperature dependence of lattice parameter of Si-grown epitaxial layers: Fig. 2.2.1	75S
-----	-------------	--------------------	--	-----

linear thermal expansion coefficient

α	$3.65 \cdot 10^{-6}\text{ K}^{-1}$ $5.17 \cdot 10^{-6}\text{ K}^{-1}$	$T = 400\text{ K}$ $T = 800\text{ K}$	crystals grown from liquid Pd, Fig. 2.2.2	75S
----------	--	--	---	-----

melting temperature : BP decomposes at 1400 K 60W

phonon dispersion curves, phonon density of states : Fig. 2.2.3.

phonon wavenumbers and frequencies

$\nu_{TO}(\Gamma)$	24.25 THz	ab-initio pseudopotential calculation	92L
$\nu_{LO}(X)$	24.00 THz		
$\nu_{LA}(X)$	15.81 THz		
$\nu_{TO}(X)$	21.04 THz		
$\nu_{TA}(X)$	9.20 THz		
$\nu_{LO}(L)$	22.91 THz		
$\nu_{LA}(L)$	15.18 THz		

phonon energies

$h\nu_{LO}(\Gamma)$	102.8 meV	$T = 300\text{ K}$	Raman spectroscopy	68B
$h\nu_{TO}(\Gamma)$	101.7 meV		ir-spectroscopy	67G

zone center phonon wavenumbers

$\bar{\nu}$	828.9(6) cm^{-1}	RT	Raman scattering	83S
-------------	---------------------------	----	------------------	-----

second order elastic moduli

c_{11}	$5.15(1) \cdot 10^{12}\text{ dyn cm}^{-2}$	RT	Brillouin scattering	84W
c_{12}	$1.0(1) \cdot 10^{12}\text{ dyn cm}^{-2}$			
c_{44}	$1.60(5) \cdot 10^{12}\text{ dyn cm}^{-2}$			

bulk modulus

B	152(5) GPa			94X
-----	------------	--	--	-----

shear modulus

G	139 GPa	calculated	95R
-----	---------	------------	-----

Debye temperature

Θ_D	985 K	Fig. 2.2.4	63S
------------	-------	------------	-----

For heat capacity see also Fig. 2.2.4 [90K].

Transport properties

BP is extrinsic at RT, the transport limited by impurity scattering. Fig. 2.2.5 and Fig. 2.2.6 show temperature dependencies of the conductivities σ_i , the carrier concentration n and p , and Hall mobility $\mu_{H,n}$ and $\mu_{H,p}$ for single crystalline wafers.

electrical conductivity

σ	$4...20 \Omega^{-1} \text{ cm}^{-1}$	$T = 300 \text{ K}$	typical single p-type crystals, $p = 1...5 \cdot 10^{18} \text{ cm}^{-3}$	60S
	$3...6 \Omega^{-1} \text{ cm}^{-1}$		typical single n-type crystals, $n = 10^{18} \text{ cm}^{-3}$	77K

thermal conductivity : Fig. 2.2.7.

carrier concentrations

n	$7 \cdot 10^{16} ... 4 \cdot 10^{19} \text{ cm}^{-3}$	$T = 300 \text{ K}$	single crystals	77K
	$8 \cdot 10^{17} ... 2 \cdot 10^{21} \text{ cm}^{-3}$		thin films	75T
p	$2 \cdot 10^{16} ... 5 \cdot 10^{18} \text{ cm}^{-3}$	$T = 300 \text{ K}$	single crystals	71I
	$10^{19} ... 10^{20} \text{ cm}^{-3}$		thin films	74S

carrier mobilities

μ_n	$30...40 \text{ cm}^2/\text{Vs}$	$T = 300 \text{ K}$	single crystals, $n = 10^{18} \text{ cm}^{-3}$	75I
	$5...80 \text{ cm}^2/\text{Vs}$		thin films, $n = 8 \cdot 10^{17} ... 10^{20} \text{ cm}^{-3}$	74S
μ_p	$500 \text{ cm}^2/\text{Vs}$	$T = 300 \text{ K}$	single crystal, $p = 10^{18} \text{ cm}^{-3}$	64W
	$10...20 \text{ cm}^2/\text{Vs}$		thin films, $p = 10^{19} \text{ cm}^{-3}$	74S

Optical properties

absorption index

k	$0.74 \cdot 10^{-4}$	$T = 300 \text{ K}, \lambda = 0.71 \mu\text{m}$	transmission	64A
	$1.0 \cdot 10^{-4}$		$0.57 \mu\text{m}$	64W
	$4.3 \cdot 10^{-4}$		$0.48 \mu\text{m}$	
	$6.5 \cdot 10^{-4}$		$0.422 \mu\text{m}$	

refractive index

n	3.34(5)	$\lambda = 454.5 \text{ nm}, \text{ RT}$	Brewster angle method	84W
	3.34(5)	458 nm		
	3.32 (5)	488 nm		
	3.30(5)	496 nm		
	3.26(5)	514.5 nm		
	3.00(5)	632.8 nm		

dielectric constant

$\varepsilon(0)$	11	$\lambda = 589.3 \text{ nm}$	Schottky barrier reflectance	
$\varepsilon(\infty)$	7.8		semi-ab-initio tight-binding calculation	91M

References to 2.2

- 60W Williams, F. V., Ruehrwein, R. A.: J. Am. Chem. Soc. 82 (1960) 1330.
- 60S Stone, B., Hill, D.: Phys. Rev. Lett. 4 (1960) 282.
- 63S Steigmeier, E. F.: Appl. Phys. Lett. 3 (1963) 6.
- 64A Archer, R. J., Koyama, R. Y., Loebner, E. E., Lucas, R. C.: Phys. Rev. Lett. 12 (1964) 538.
- 64W Wang, C. C., Cardona, M., Fischer, A. G.: RCA Rev. 25 (1964) 159
- 67G Gielisse, P. J., Mitra, S. S., Plendl, J. N., Griffis, R. D., Mansur, L. C., Marshall, R., Pascoe, E. A.: Phys. Rev. 155 (1967) 1039.
- 68B Brafman, O., Lengyel, G., Mitra, S. S., Gielisse, P. J., Plendl, J. N., Mansur, L. C.: Solid State Commun. 6 (1968) 523.
- 71I Iwami, M., Fujita, N., Kawabe, K.: Jpn. J. Appl. Phys. 10 (1971) 1746.
- 72H Hemstreet, L. A., Fong, C. Y.: Phys. Rev. B 6 (1972) 1464.
- 73S Slack, G. A.: J. Phys. Chem. Solids 34 (1973) 321
- 74S Shohno, K., Takenaka, T., Takigawa, M.: Proc. 12th Int. Conf. Phys. Semicond., Stuttgart 1974, B. G. Teubner, Stuttgart 1974, p. 286.
- 75I Iwami, M., Tohda, T., Kawabe, K.: Electron. Eng. Jpn. 95 (1975) 19.
- 75S Slack, G. A., Bartram, S. F.: J. Appl. Phys. 46 (1975) 89.
- 75T Takenaka, T., Takigawa, M., Shohno, K.: Jpn. J. Appl. Phys. 14 (1975) 579.
- 76M Mizutani, T., Ohsawa, J., Nishinaga, T., Uchiyama, S.: Jpn. J. Appl. Phys. 15 (1976) 1305.
- 77K Kato, N., Kamura, W., Iwami, M., Kawabe, K.: Jpn. J. Appl. Phys. 16 (1977) 1623.
- 83S Sanjurjo, J. A., López-Cruz, E., Vogl, P., Cardona, M.: Phys. Rev. B 28 (1983) 4579.
- 84W Wettling, W., Windschleif, J.: Solid State Commun. 50 (1984) 33.
- 85H Huang, M., Ching, W. Y.: J. Phys. Chem. Solids 46 (1985) 977.
- 88K Kumashiro, Y., Hirabayashi, M., Kosiuro, T.: J. Less-Common Metals 143 (1988) 159.
- 90K Kumashiro, Y.: J. Mater. Res. 5 (1990) 2933.
- 91M Moss, D. J., Ghahramani, E., Sipe, J. E.: Phys. Status Solidi (b) 164 (1991) 578.
- 92L Leite Alves, H. W., Kunc, K.: J. Phys. Condens. Matter 4 (1992) 6603.
- 94X Xia, H., Xia, Q., Ruoff, A. L.: AIP Conf. Proc. No. 309, part 1 (1994) 97.
- 95R R-Hernandez, P., G-Diag, M., Munoz, A.: Phys. Rev. B 51 (1995) 14705.
- 99A Agui, A., Shin, S., Kumashiro, Y.: J. Phys. Soc. Jpn. 68 (1999) 166.
- 99P Pletl, T., Pavone, P., Engel, U., Strauch, D.: Physics B 263/264 (1999) 392.

Figures to 2.2

Fig. 2.0.2

The zincblende lattice

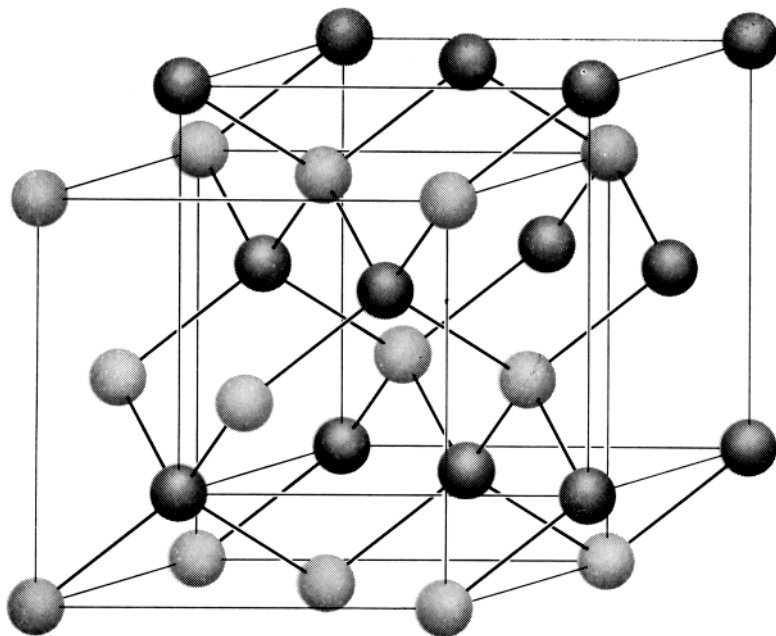


Fig. 2.0.5

Brillouin zone of the zincblende lattice.

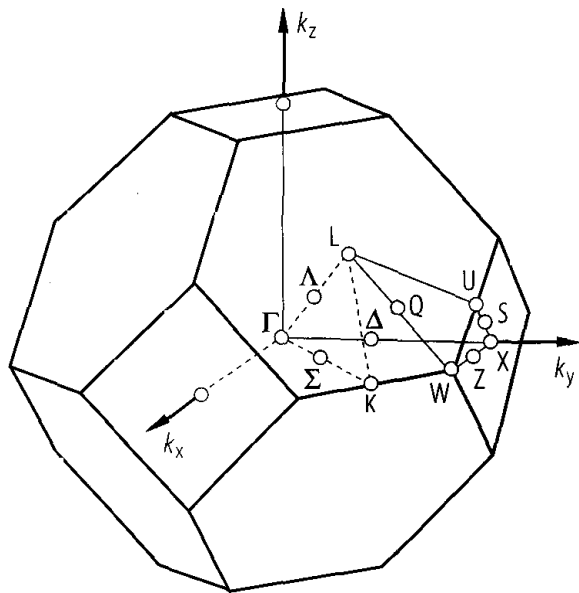


Fig. 2.0.10

BP. Band structure (a) calculated by a non-local empirical pseudopotential method [72H], (b) calculated by an ab initio LCAO method [85H].

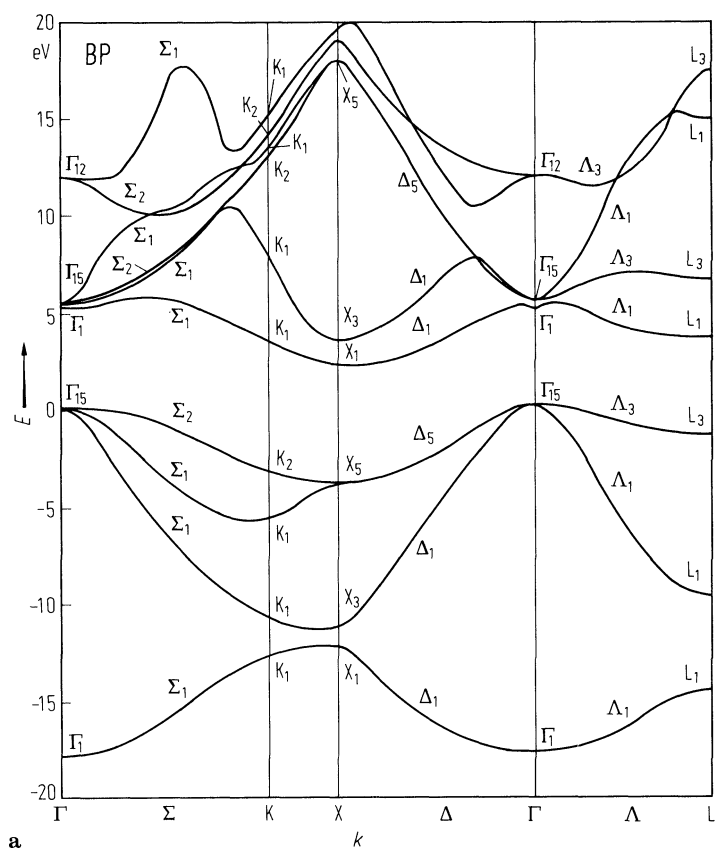


Fig. 2.2.1

BP. Lattice constants of epitaxially grown samples vs. temperature; (curve 1) grown on Si (100), (curve 2) grown on Si (111) [76M].

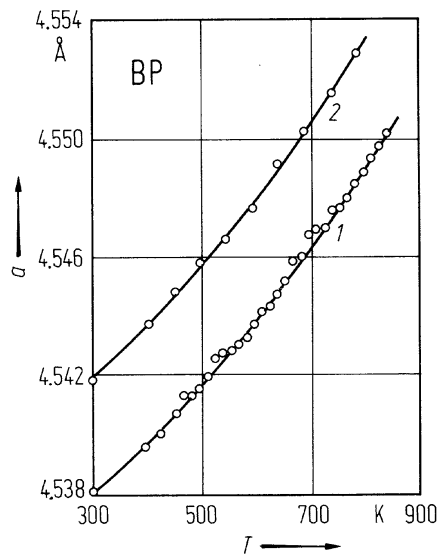


Fig. 2.2.2

BP. Linear thermal expansion coefficient vs. temperature (a) acc. to [76M], (b) acc. to [75S].

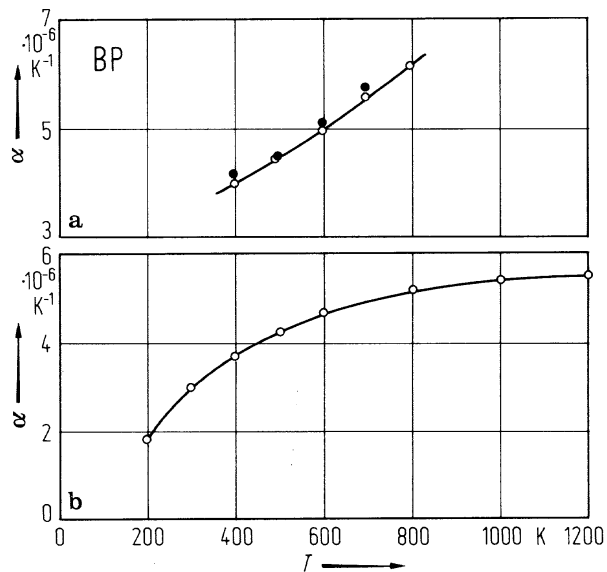


Fig. 2.2.3

BP. Phonon dispersion curves (left panel) and phonon density of states (right panel) from ab-initio calculations [99P].

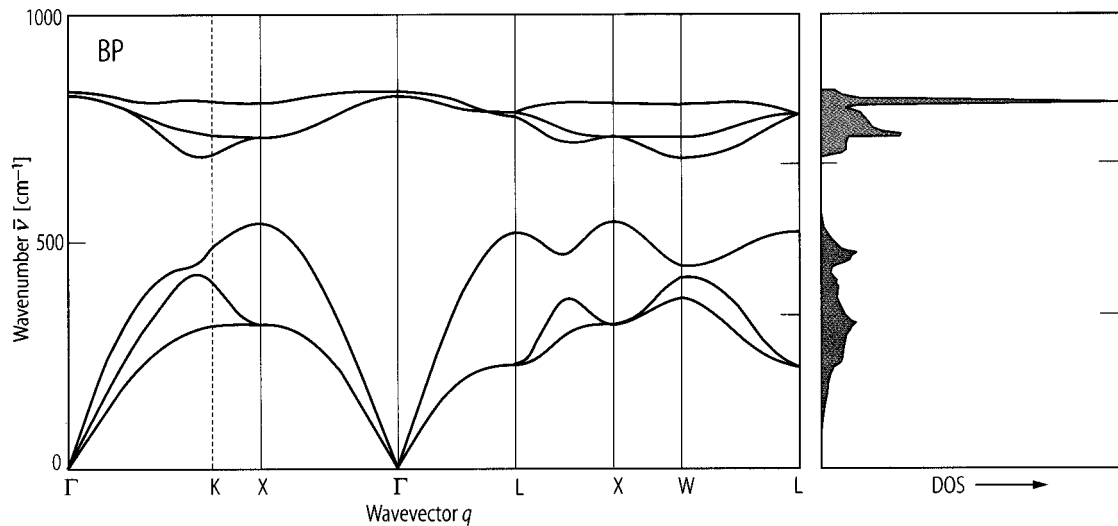


Fig. 2.2.4

BP. Temperature dependence of specific heat capacity and Debye temperature [90K].

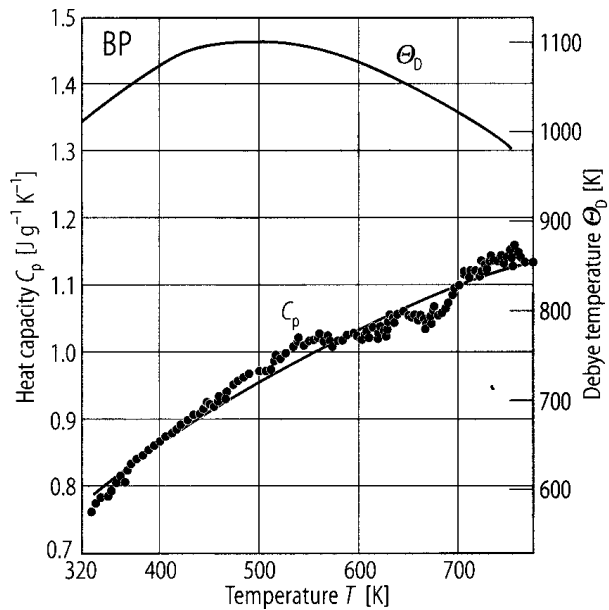


Fig. 2.2.5

Temperature dependencies of the conductivity σ_1 , the carrier concentration n and mobility $\mu_{H,n}$ of n-BP(100) wafers [88K]. No.1 contains autodoped Si with the concentration of $5 \cdot 10^{18}$ atoms/cm³ while in case of No.3 the concentration is $5 \cdot 10^{19}$ atoms/cm³.

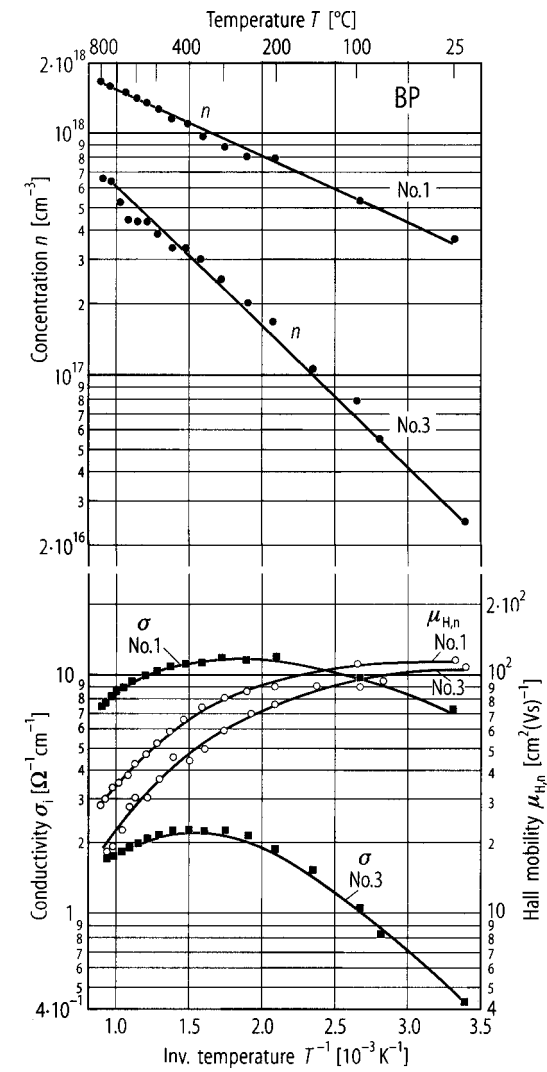


Fig. 2.2.6

BP. Temperature dependencies of the conductivity σ_i , the carrier concentration p and the mobility $\mu_{H,p}$ of p-BP wafers [88K]. No.2 contains autodoped Si with the concentration of $5 \cdot 10^{18}$ atoms/cm³ while in case of No.4 the concentration is 10^{20} atoms/cm³.

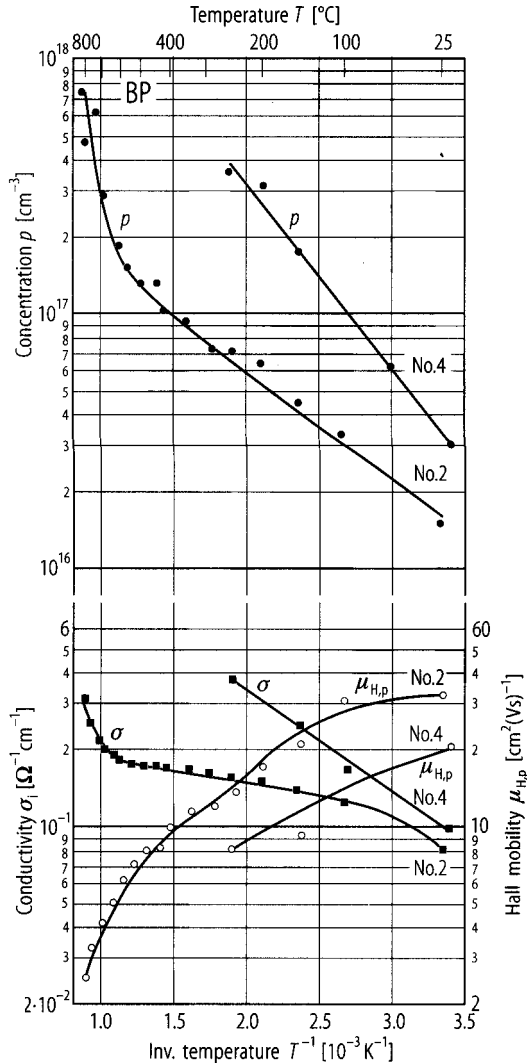
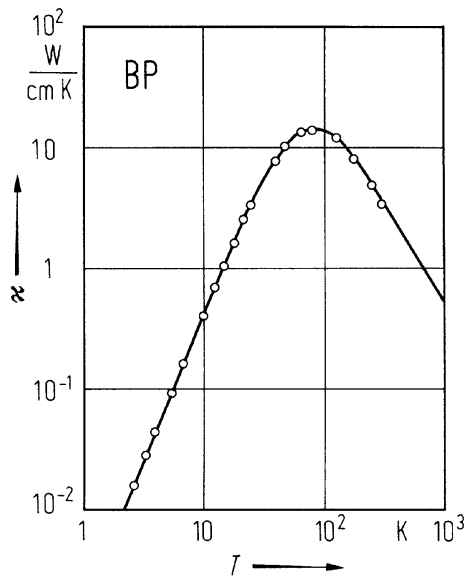


Fig. 2.2.7

BP. Thermal conductivity vs. temperature for sample with less than 10^{19} impurities/cm³ [73S].



2.3 Boron arsenide (BAs)

Crystal structure

Boron arsenide crystallizes under normal conditions in the zincblende structure (space group $T_d^2 - F\bar{4}3m$, Fig. 2.0.2).

Under pressure, the zincblende structure is transformed to an amorphous state. Upon pressure release, the amorphous state persists down to zero pressure with no trace of zincblende material. Theoretically a transition to the rocksalt structure is predicted.

Electronic properties

band structure : Fig. 2.0.11, Brillouin zone: Fig. 2.0.5.

The calculated band structure shows an indirect ($\Gamma - X$) gap of a few eV. The conduction band minimum is on the Δ axis close to the X point, where the X_{3c} level is below the X_{1c} level. As in Si the Γ_{15c} level is below the Γ_{1c} level.

energy gap

$E_{g,ind}$	0.67 eV	absorption	74C
or $E_{g,dir}$	1.46 eV		

Lattice properties

lattice parameter

a	4.777 Å		77M
-----	---------	--	-----

temperature dependence of lattice parameter (a in Å, T in K)

$a = 4.777 + 2.306 \cdot 10^{-5} T - 5.555 \cdot 10^{-9} T^2$	Tersoff model potential MD simulation	99B
---	---------------------------------------	-----

linear thermal expansion coefficient

α	$4.1 \cdot 10^{-6} K^{-1}$	Tersoff model potential MD simulation	99B
----------	----------------------------	---------------------------------------	-----

density

d	$5.22 g cm^{-3}$		77M
-----	------------------	--	-----

bulk modulus

B	138 GPa		85C
-----	---------	--	-----

Debye temperature

Θ_D	800 K		75D
------------	-------	--	-----

phonon dispersion relation and density of states : Fig. 2.3.1.

zone center phonon wavenumbers

$\bar{\nu}_{LO}(\Gamma)$	$714 cm^{-1}$	RT	Raman scattering	94G
$\bar{\nu}_{TO}(\Gamma)$	$695 cm^{-1}$			

References to 2.3

- 70S Stuckel, D. J.: Phys. Rev. B 1 (1970) 3458.
- 74C Chu, T. L., Hyslop, A. E.: J. Electrochem. Soc. 121 (1974) 412.
- 75D Demidenko, A. F., Koshchenko, V. J., Medvedeva, Z. S., Radchenko, S. F.: Inorg. Mater. (English Transl.) 11 (1975) 1817; Izv. Akad. Nauk SSSR, Neorg. Mater. 11 (1975) 2117.
- 77M Merrill, L.: J. Phys. Chem. Ref. Data 6 (1977) 1205.
- 85C Cohen, M. L.: Phys. Rev B32 (1985) 7988.
- 94G Greene, R. G., Luo, H., Ruoff, A. L., Trail, S. S., DiSalvo, F. J.: Phys. Rev. Lett. 73 (1994) 2476.
- 99B Benkabou, F., Chelahi Chikr. Z, Aourag, H., Becker, P. J., Certier, M.: Phys. Lett A 252 (1999) 71.
- 99P Pletl, T., Pavone, P., Engel, U., Strauch, D.: Physics B 263/264 (1999) 392.

Figures to 2.3

Fig. 2.0.2

The zincblende lattice

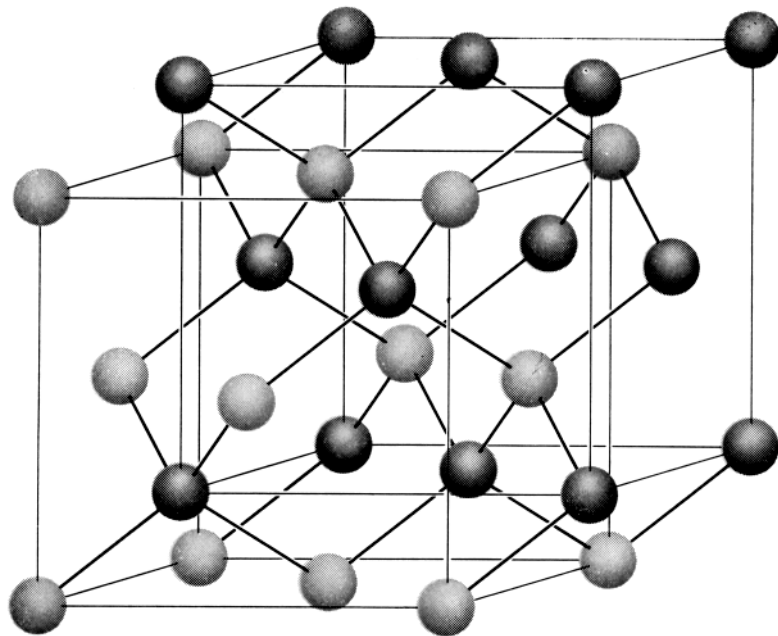


Fig. 2.0.5

Brillouin zone of the zincblende lattice.

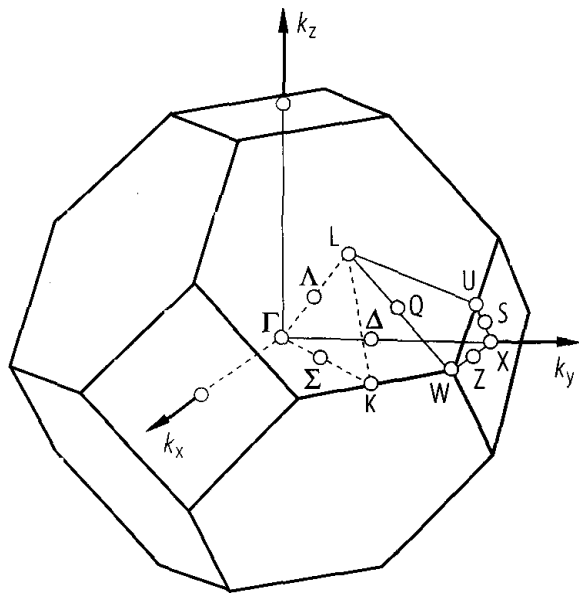


Fig. 2.0.11

BAs. Band structure calculated with a combined self-consistent OPW and pseudopotential method [70S].

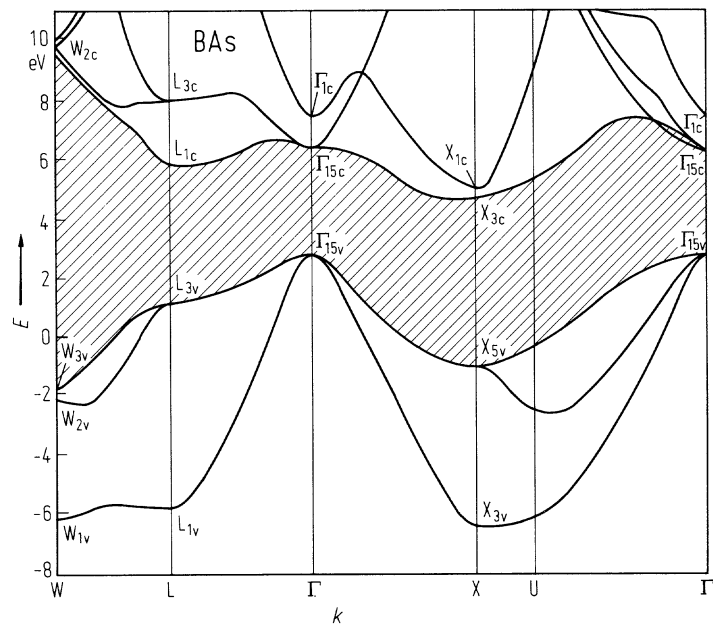
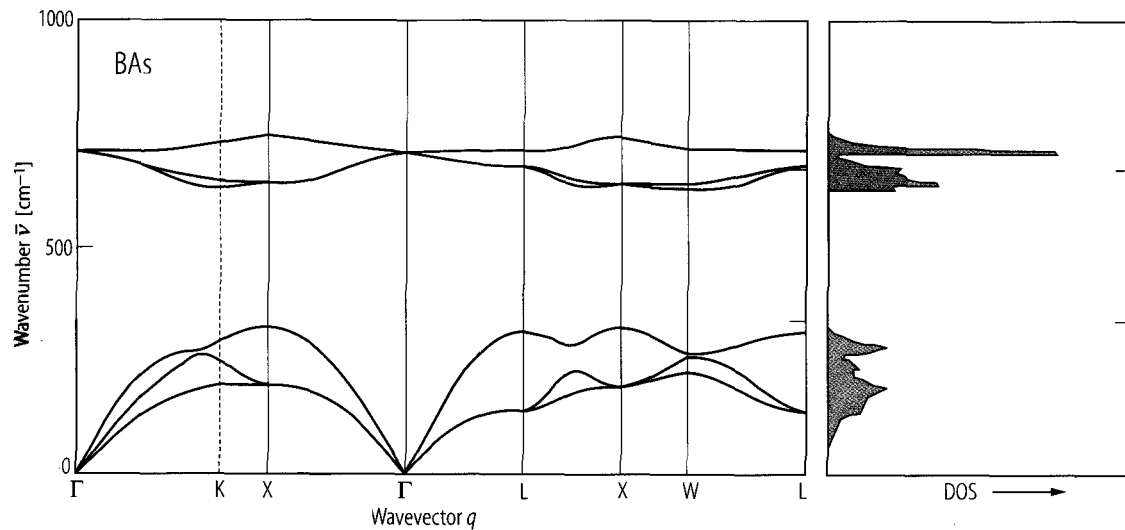


Fig. 2.3.1

BAs. Phonon dispersion curves (left panel) and phonon density of states (right panel) from ab-initio calculations [99P].



2.4 Boron antimonide (BSb)

Crystal structure

Boron antimonide crystallizes under normal conditions in the zincblende structure (space group $T_d^2 - F\bar{4}3m$, Fig. 2.0.2).

Electronic properties

The conduction band minimum is on the Δ axis close to the X point, where the X_{3c} level is below the X_{1c} level. As in Si the Γ_{15c} level is below the Γ_{1c} level.

band structure : Fig. 2.0.12, Brillouin zone: Fig. 2.0.5.

energy gap

E_g	0.527 eV	$\Gamma - \Delta$	calculated	98F
-------	----------	-------------------	------------	-----

Lattice properties

lattice parameter (zincblende structure)

a	5.12 Å	ab-initio pseudopotential calculation	98F
-----	--------	---------------------------------------	-----

phonon dispersion relation and phonon density of states : Fig. 2.4.1.

References to 2.4

- | | |
|-----|--|
| 98F | Ferhat, M., Bouhafs, B., Zaoui, A., Aourag, H.: J. Phys. Condens. Matter 10 (1998) 7995. |
| 99P | Pletl, T., Pavone, P., Engel, U., Strauch, D.: Physics B 263/264 (1999) 392. |

Figures to 2.4

Fig. 2.0.2

The zincblende lattice

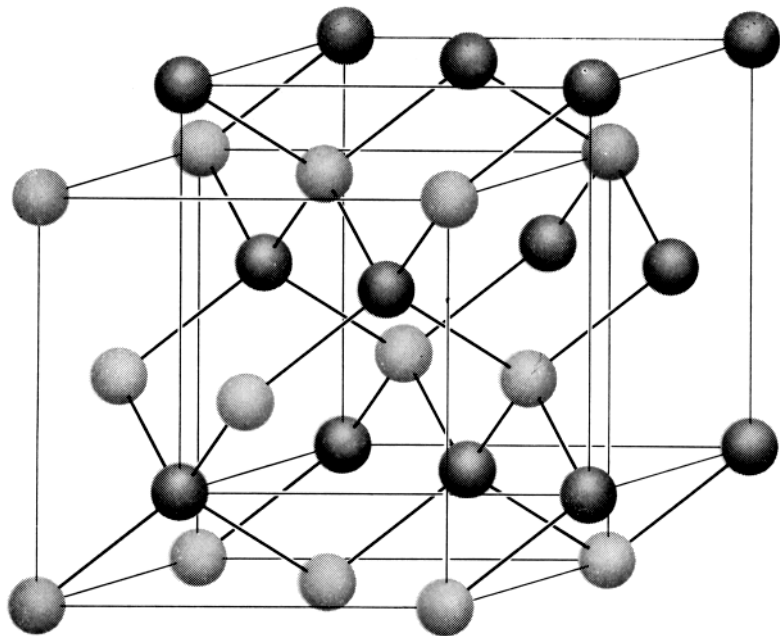


Fig. 2.0.5

Brillouin zone of the zincblende lattice.

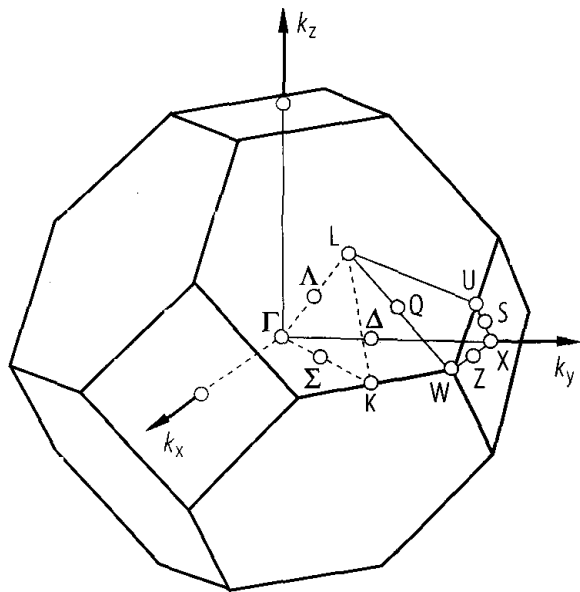


Fig. 2.0.12

BSb. Electronic band structure of zincblende BSb at the calculated volume [98F].

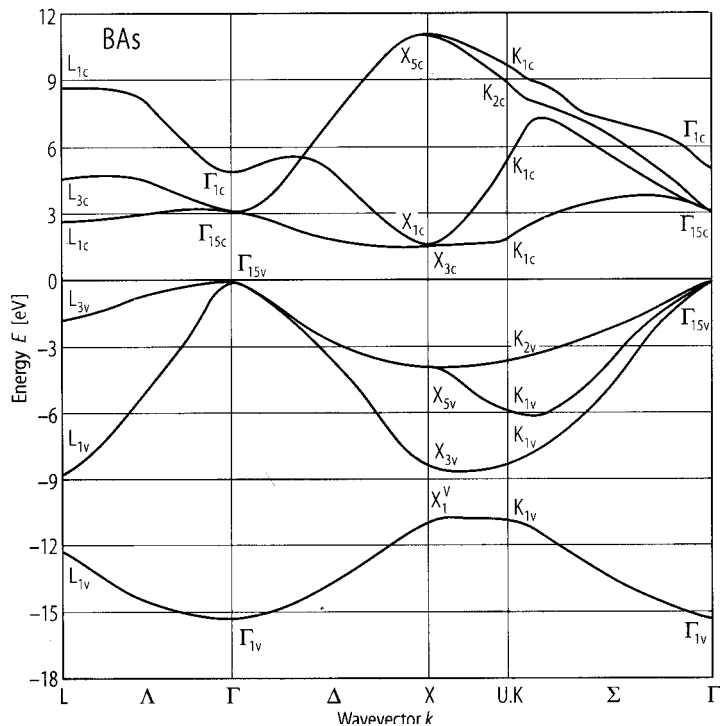
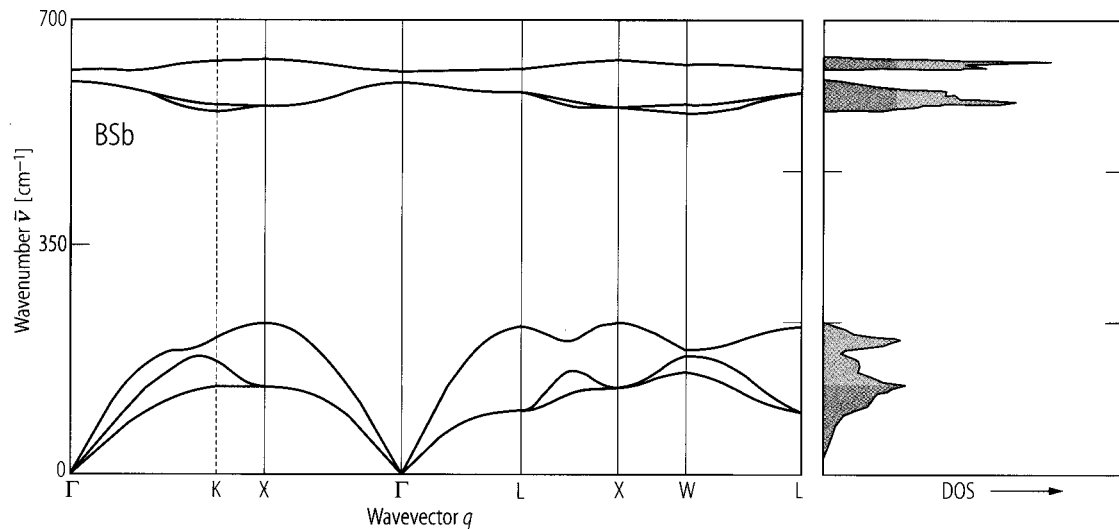


Fig. 2.4.1

BSb. Phonon dispersion curves (left panel) and phonon density of states (right panel) from ab-initio calculations [99P].



2.5 Aluminum nitride (AlN)

Crystal structure

AlN crystallizes at normal pressure in the wurtzite structure (space group P6₃mc, Fig. 2.0.3).

high pressure phases

A phase transition at 21(1) GPa (tentatively to a NaCl phase) has been measured by shock compression [81K]. From the visual appearance, a phase transition occurs at a pressure of around 15 GPa (increasing pressure) [91G, 92U]. From X-ray diffraction, this phase transition seems to be connected with the onset of a transition to the rocksalt structure, with coexistence of the wurtzite and zincblende phases up to a pressure of around 20 GPa [93X]; the rocksalt phase appears at 20 GPa and persists up to at least 132 GPa [97U]; the wurtzite and rocksalt phases coexist between 20 and 31.4 GPa [97U]. With decreasing pressure, both phases coexist down to zero pressure [91G].

Electronic properties

band structure : Fig. 2.0.13; Brillouin zone: Fig. 2.0.8.

energies of symmetry points of the band structure (relative to the top of the valence band $E(\Gamma_{6v}, \Gamma_{1'v})$)

$E(\Gamma_{1v})$	– 18.40 eV	calculated, see Fig. 2.0.13	83K
$E(\Gamma_{3v})$	– 7.10 eV		
$E(\Gamma_{5v})$	– 1.22 eV		
$E(\Gamma_{1c})$	6.2 eV		
$E(\Gamma_{3c})$	8.92 eV		
$E(\Gamma_{6c}, \Gamma_{1'c})$	13.0 eV		
$E(L_{1'3'v})$	– 7.52 eV		
$E(L_{24v})$	– 1.97 eV		
$E(L_{13v})$	– 1.87 eV		
$E(L_{13c})$	9.99 eV		
$E(L_{1'3'c})$	13.53 eV		

energy gap

$E_{g,dir}$	6.19 eV	$T = 7\text{ K}$	optical absorption	97B
	6.13 eV	$T = 300\text{ K}$		

conduction band effective masses

$m_{n }$	0.33 m_0	calculated value	96C
$m_{n\perp}$	0.25 m_0		

valence band effective masses (excluding spin-orbit effects)

$m_{A }$	3.53 m_0	calculated value	97K
$m_{A\perp}$	11.14 m_0		
$m_{B }$	3.53 m_0		
$m_{B\perp}$	0.33 m_0		
$m_{C }$	0.26 m_0		
$m_{C\perp}$	4.05 m_0		

Lattice properties

lattice parameters

a	3.1111 Å	$T = 300\text{ K}$	powder X-ray diffraction	00I
c	4.9788 Å			
c/a	1.600			

linear thermal expansion coefficient

α_{\perp}	$4.35 \cdot 10^{-6} \text{K}^{-1}$	$T = 300 \text{ K}$	powder X-ray diffraction	00I
α_{\parallel}	$3.48 \cdot 10^{-6} \text{K}^{-1}$		T -dependence: Fig. 2.5.1	
$\alpha_{\perp}/\alpha_{\parallel}$	1.25			

temperature dependence of the lattice parameters (a and c in Å)

$a = 3.1071 + 1.211 \cdot 10^{-5} T + 2.36 \cdot 10^{-9} T^2$, powder X-ray scattering, $T = 293 \dots 1373 \text{ K}$	00I
$c = 4.9739 + 1.455 \cdot 10^{-5} T + 4.65 \cdot 10^{-9} T^2$	
$c/a = 1.6009 - 0.162 \cdot 10^{-5} T + 0.34 \cdot 10^{-9} T^2$	

density

d	3.255 g cm^{-3}	X-ray	73S
-----	---------------------------	-------	-----

melting temperature

T_{m}	3025 K		96K
----------------	--------	--	-----

phonon dispersion curves, phonon density of states : Fig. 2.5.2.

The phonon dispersion spectrum of AlN possesses nine optical branches. Only TO_1 , TO'_1 , LO_1 -modes are infrared active (symmetry $E_1(\Gamma_5)$, $A_1(\Gamma_1)$). The same modes as well as $E_2(\Gamma_6)$ -modes are Raman active. The remaining B_1 -modes are inactive.

zone center optical phonon wavenumbers

$(\nu/c)(E_2^{(1)})$	248.6 cm^{-1}	$T = 300 \text{ K}$	Raman scattering	96D
$(\nu/c)_{\text{TO}}(A_1)$	611.0 cm^{-1}			
$(\nu/c)(E_2^{(2)})$	657.4 cm^{-1}			
$(\nu/c)_{\text{TO}}(E_1)$	670.8 cm^{-1}			
$(\nu/c)_{\text{LO}}(A_1)$	890.0 cm^{-1}			
$(\nu/c)_{\text{LO}}(E_1)$	912.0 cm^{-1}			

sound velocities

v_{L}	10127 m s^{-1}	experimental, polycrystal	86G
v_{T}	6333 m s^{-1}		

second order elastic moduli

c_{11}	411 GPa	Brillouin scattering	93M
c_{12}	149 GPa		
c_{13}	99 GPa		
c_{33}	389 GPa		
c_{44}	125 GPa		

bulk modulus

B	201.7 GPa	ultrasound	81T
-----	-----------	------------	-----

Young's modulus

E	294.5 GPa	ultrasound	81T
-----	-----------	------------	-----

Debye temperature

Θ_{D}	950 K	estimate	87S
---------------------	-------	----------	-----

specific heat : Fig. 2.5.3.

Transport properties

AlN is an extrinsic semiconductor.

electrical conductivity

σ [$\Omega^{-1} \text{ cm}^{-1}$]	$10^{-3} \dots 10^{-5}$	$T = 290 \text{ K}$	doped (Al_2OC) single p-type crystals (blue)	65E
	$10^{-11} \dots 10^{-13}$	$T = 300 \text{ K}$	undoped single crystals (colorless or pale yellow)	65E, 67C2

activation energy of electrical conductivity

E_A	0.17(1) eV	$T = 400 \dots 700 \text{ K}$	hot pressed material, dc and ac (1592 Hz), measurements, see Fig. 2.5.4	76F
	1.82(6) eV	$T = 950 \dots 1300 \text{ K}$	undoped single crystals	67C2

thermal conductivity

κ	$3.19 \text{ W cm}^{-1} \text{ K}^{-1}$	$T = 300 \text{ K}$	measured	87S
----------	---	---------------------	----------	-----

see also Fig. 2.5.5

hole mobility

μ_p	$14 \text{ cm}^2/\text{Vs}$	$T = 290 \text{ K}$	doped single crystal	65E
---------	-----------------------------	---------------------	----------------------	-----

Optical properties

dielectric constants

$\varepsilon(0)$	9.14	$T = 300 \text{ K}$	reflectivity	67C1
$\varepsilon_{\perp}(\infty)$	4.71(22)		optical interferometry ($\lambda = 589.0 \text{ nm}$)	66P
$\varepsilon_{\parallel}(\infty)$	4.93(22)			

refractive index

n	2.17...2.34		CVD films at 250 nm	77B
	2.04...2.18		CVD films at 300 nm	

Spectral dependence, see Fig. 2.5.6.

reflectance vs. photon energy, Fig. 2.5.7.

References to 2.5

- 65E Edwards, J., Kawabe, K., Stevens, G. Tredgold, R. H.: Solid State Commun. 3 (1965) 99.
- 66P Pastrnak, J., Roskocova, L.: Phys. Status Solidi 14 (1966) K5.
- 67C1 Collins, A. T., Lightowlers, E. C., Dean, P. J.: Phys. Rev. 158 (1967) 833.
- 67C2 Cox, G. A., Cummins, D. O., Kawabe, K., Tredgold, R. H.: J. Phys. Chem. Solids 28 (1967) 543.
- 73S Slack, G. A.: J. Phys. Chem. Solids 34 (1973) 321.
- 75S Slack, G. A., Bartram, S. F.: J. Appl. Phys. 46 (1975) 89.
- 76F Francis, R. W., Worrell, W. L.: J. Electrochem. Soc. 123 (1976) 430.
- 77B Bauer, J., Biste, L., Bolze, D.: Phys. Status Solidi 39 (1977) 173.
- 78S Sobolev, V. V., Kroitoru, S. G., Sokolev, E. B., Chegnov, V. P.: Sov. Phys. Solid State (English Transl.) 20 (1978) 2167; Fiz. Tverd. Tela 20 (1978) 3743.
- 81K Kondo, K., Sawaoka, A., Sato, K., Ando, M.: AIP Conf. Proc. 78 (1981) 325.
- 81T Tsubouchi, K., Sugai, K., Mikoshiba, N.: in: Proc. 1981 IEEE Ultrasonics Symposium, McAvoy, B. R., (ed.), IEEE, New York (1981), p. 375.
- 83K Kobayashi, A., Sankey, O. F., Volz, S. M., Dow, J. D.: Phys. Rev. B 28 (1983) 935.
- 85K Koshchendo, V. I., Grinberg, Y. K., Demidenko, A. F.: Inorg. Mater. 20 (1985) 1550.
- 86G Gerlich, D., Dole, S. L., Slack, G. A.: J. Phys. Chem. Solids 47 (1986) 437.
- 87S Slack, G. A. Tanzill, R. A., Pohl, R. O., Vandersande, J. W.: J. Phys. Chem Solids 48 (1987) 641.
- 91G Gorczyca, I., Christensen, N. E., Perlin, P., Grzegory, I., Jun, J., Bockowski, M.: Solid State Commun. 79 (1991) 1033.
- 92U Ueno, M., Onodera, A., Shimomura, O., Takemura, K.: Phys. Rev. B 45 (1992) 10123.
- 93M McNeil, L. E., Grimsditch, M., French, R. H.: J. Am. Ceram. Soc. 76 (1993) 1132.
- 93X Xia, Q., Xia, H., Ruoff, A. L.: J. Appl. Phys. 73 (1993) 8198.
- 96C Chuang, S. L., Chang, C. S.: Phys. Rev. B 54 (1996) 2491.
- 96D Davydov, S. Yu., Tikhonov, S. K.: Fiz. Tekh. Poluprovodn. 30 (1996) 834; Semicond. 30 (1996) 447 (English Transl.).
- 96K Konstanovskii, A. V., Kirrillin, A. V.: Int. J. Thermophys. 17 (1996) 507.
- 97B Brunner, D., Angerer, H., Bustarret, E., Freudenberg, F., Höpler, R., Dimitrov, R., Ambacher, O., Stutzmann, M.: J. Appl. Phys. 82 (1997) 5090.
- 97K Kim, K. K., Lambrecht, W. R. L., Segall, B., Van Schilfgaarde, M.: Phys. Rev. B 56 (1997) 7363.
- 97U Uehara, S., Masamoto, T., Onodera, A., Ueno, M., Shimomura, O., Takemura, K.: J. Phys. Chem. Solids 58 (1997) 2093.
- 98N Nipko, J. C., Loong, C. K.: Phys. Rev. B 57 (1998) 10550; Loong, C. K.: in "*Gallium Nitride and Related Materials*", Ponce, F. A., Dupuis, R. D., Nakamura, S., Edmond, J. A. (eds.), MRS Symposia Proceedings No. 395, Materials Research Society, Pittsburgh (1996), p. 423.
- 00I Iwanaga, H., Kunishige, A., Takeuchi, S.: J. Mater. Sci. 35 (2000) 2451.

Figures to 2.5

Fig. 2.0.3

The wurtzite lattice

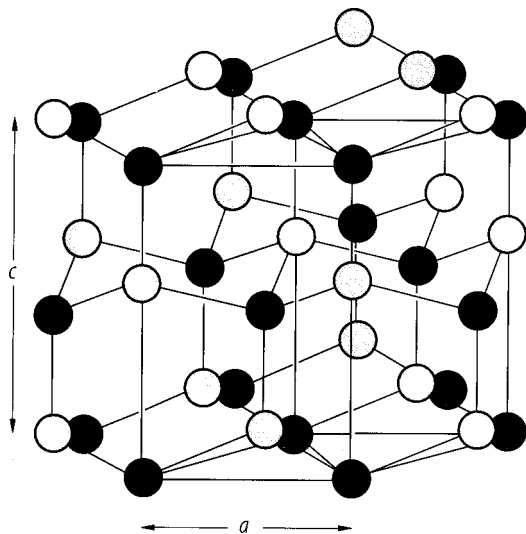


Fig. 2.0.8

The hexagonal Brillouin zone.

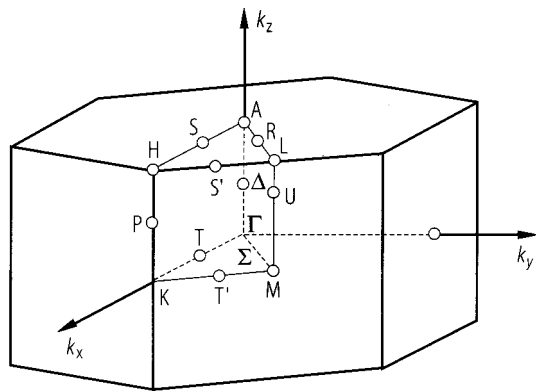


Fig. 2.0.13

AlN. Band structure calculated with a semi-empirical tight binding method [83K].

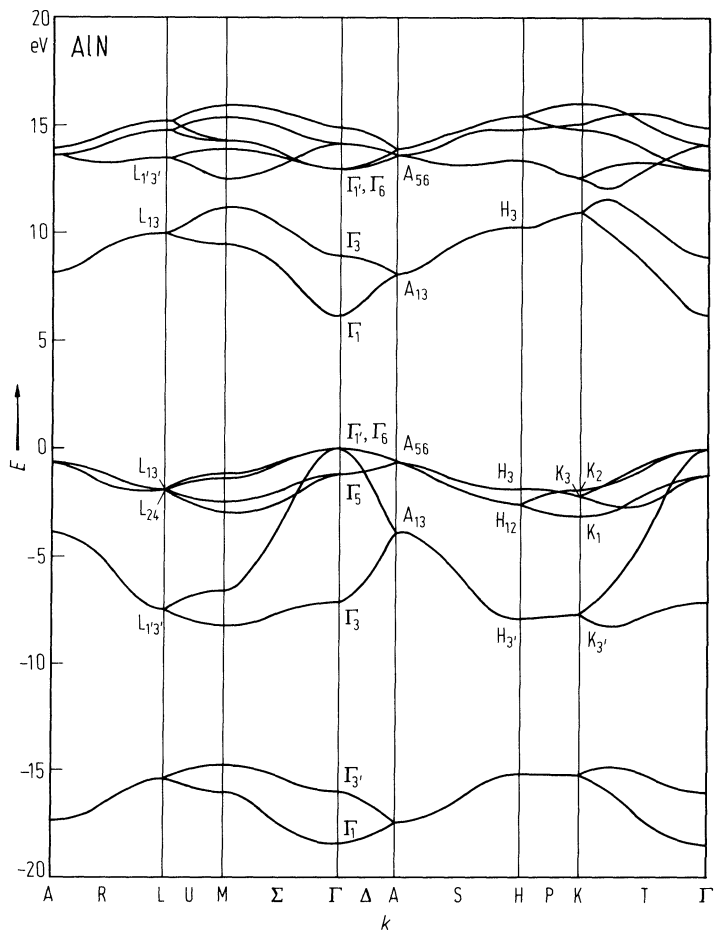


Fig. 2.5.1

AlN. Averaged linear thermal expansion coefficient $(a_{\parallel} + a_{\perp})/3$ vs. temperature measured by an X-ray technique [75S].

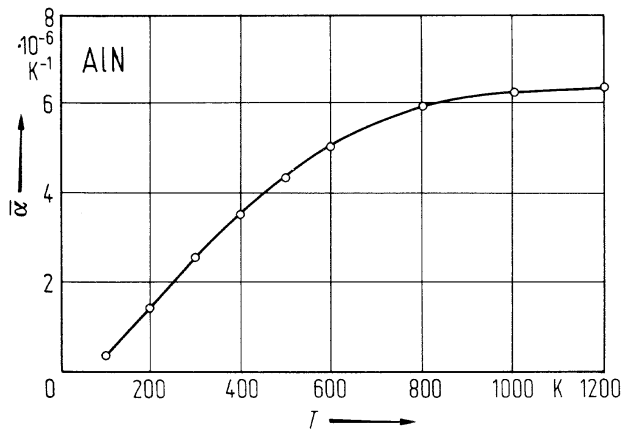


Fig. 2.5.2

AlN (wurtzite structure). Phonon dispersion curves (left panel) and phonon density of states (right panel) from a rigid-ion model calculation [98N].

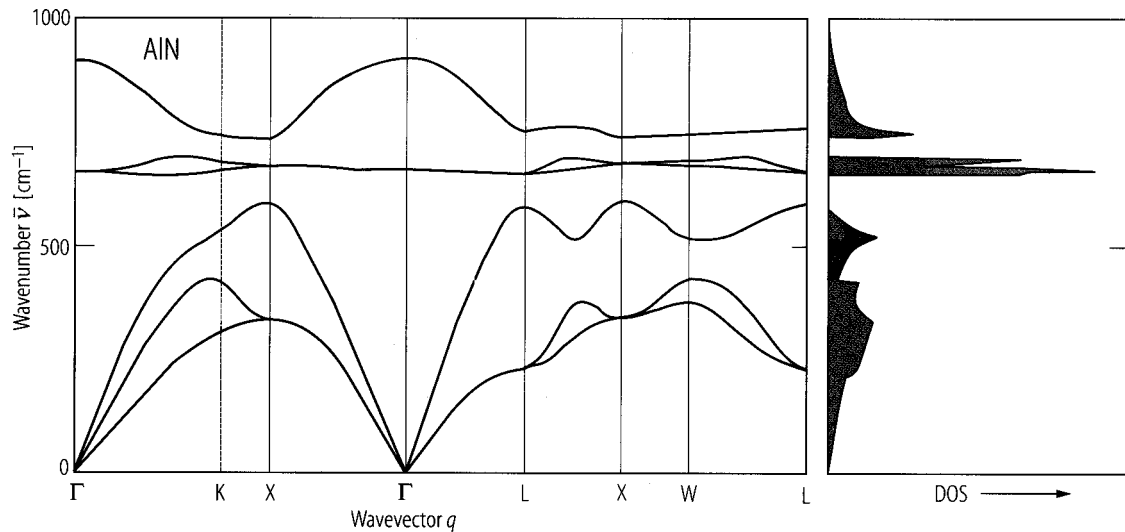


Fig. 2.5.3

AlN (wurtzite structure). Temperature dependence of the specific heat at constant volume. The circles are the experimental results by [85K], and the full line is the theoretical result by [98N] using the rigid-ion model. The inset shows the calculated temperature dependence of the Debye temperature [98N].

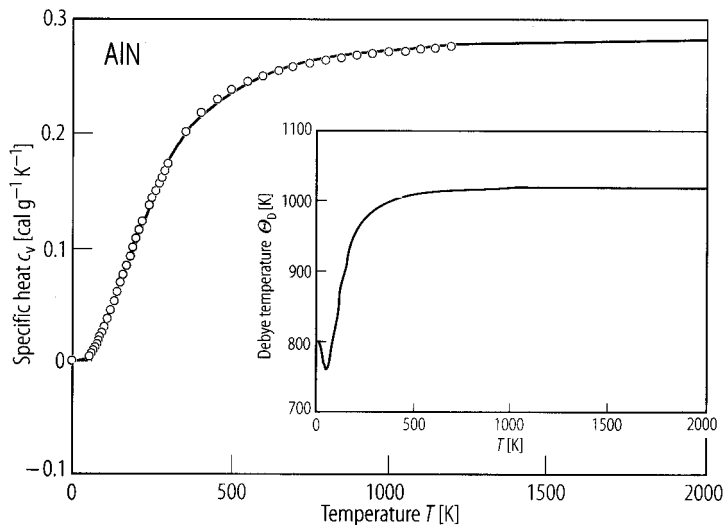


Fig. 2.5.4

AlN. Electrical conductivity vs. reciprocal temperature for hot-pressed material [76F]. E_A : activation energy for conductivity.

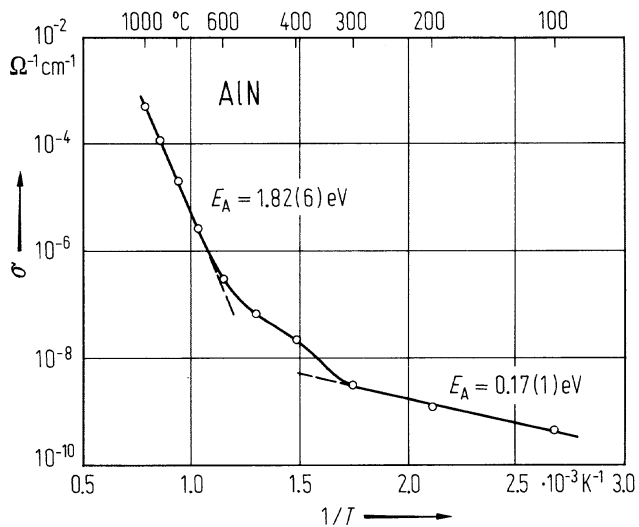


Fig. 2.5.5

AlN. Temperature dependence of the thermal conductivity for two single crystals (curves 1, 2) and several ceramic samples (curves 3...6). Other published results are included (curves 7...10) as well as a theoretical estimate of the upper limit [73S].

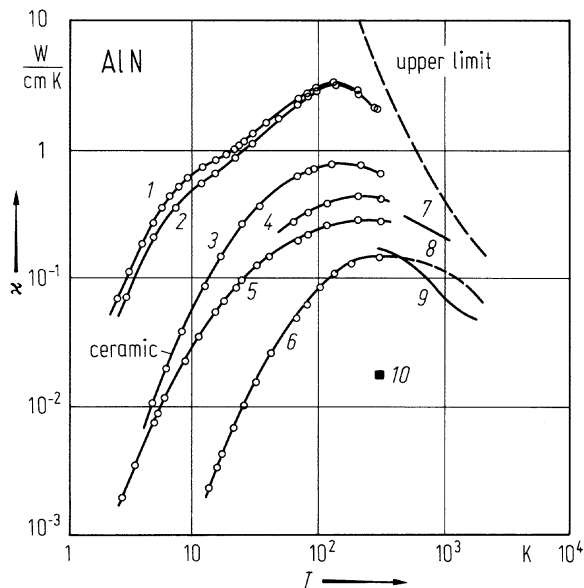


Fig. 2.5.6

AlN. Spectral dependence of the refractive index (symbols 1: ordinary ray, symbols 2: extraordinary ray) [66P].

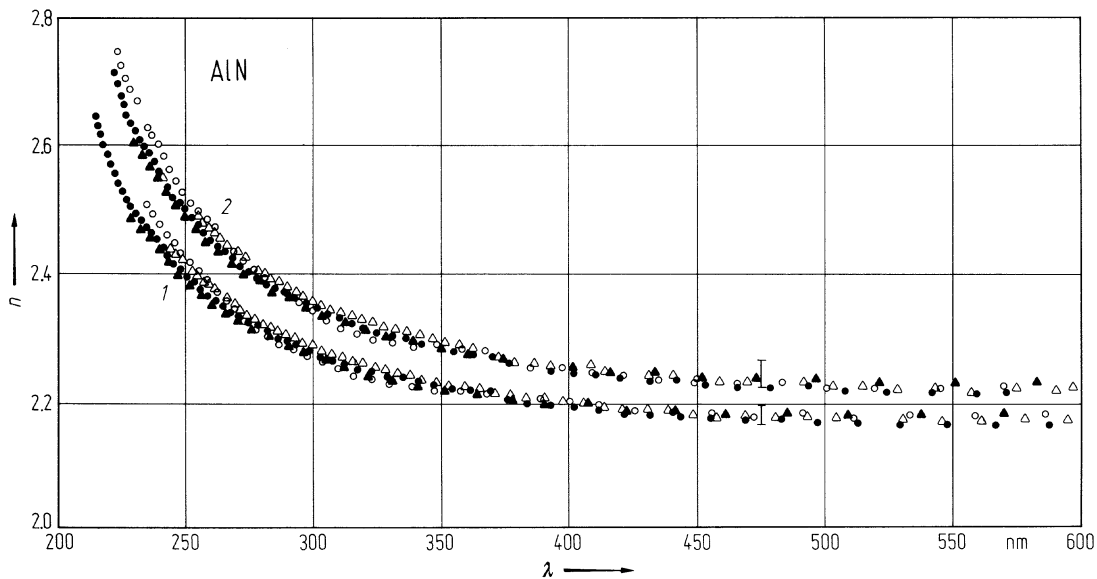
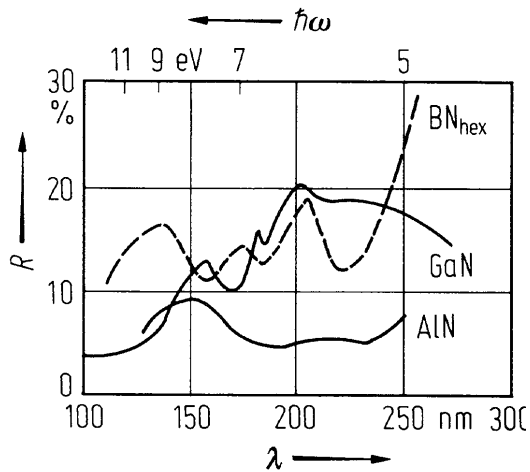


Fig. 2.4.7

BN_{hex} , AlN , GaN . Reflectance vs. photon energy (wavelength) for BN_{hex} , GaN , and AlN [78S].



2.6 Aluminum phosphide (AlP)

Crystal structure

Aluminum phosphide crystallizes under normal conditions in the zincblende structure (space group $T_d^2 - F\bar{4}3m$, Fig. 2.0.2). AlP can also be grown in the wurtzite structure. AlP is not stable in air.

high pressure phases

Under pressure, AlP undergoes a transition from the zincblende structure to the rocksalt structure, but according to [94G] from the semiconducting zincblende structure to the metallic NiAs structure; this phase is stable up to a pressure of at least 44 GPa [94G].

Electronic properties

band structure : Fig. 2.0.14, Brillouin zone: Fig. 2.0.5.

AlP is an indirect wide gap semiconductor, the minima of the conduction bands are situated at the X points of the Brillouin zone. The top of the valence band has the structure common to all zincblende semiconductors.

energies of symmetry points of the band structure (relative to the top of the valence band $E(\Gamma_{15v})$)

$E(\Gamma_{1v})$	- 11.82 eV	calculated, see Fig. 2.0.14	85H
$E(\Gamma_{1c})$	3.74 eV		
$E(\Gamma_{15c})$	5.09 eV		
$E(X_{1v})$	- 9.20 eV		
$E(X_{3v})$	- 5.58 eV		
$E(X_{5v})$	- 2.27 eV		
$E(X_{1c})$	2.51 eV		
$E(X_{3c})$	4.30 eV		
$E(L_{1v})$	- 9.94 eV		
$E(L_{1v})$	- 5.92 eV		
$E(L_{3v})$	- 0.80 eV		
$E(L_{1c})$	3.57 eV		
$E(L_{3c})$	6.41 eV		

band gaps

$E_{g, \text{ind}}(\Gamma_{15v}-X_{1c})$	2.5(1) eV	$T = 2 \text{ K}$	absorption, excitonic gap $E_{gx, \text{ind}}(1S)!$	70L
	2.45 eV	$T = 300 \text{ K}$	for temperature dependence, see Fig. 2.6.1	
$E_{g, \text{dir}}(\Gamma_{15v}-\Gamma_{1c})$	3.63(2) eV	$T = 4 \text{ K}$	photoluminescence, excitonic gap!	73M
	3.62(2) eV	$T = 77 \text{ K}$		

effective masses

$m_{n\parallel}$	$3.67 m_0$		calculated from band structure of	85H
$m_{n\perp}$	$0.212 m_0$		Fig. 2.0.15	
$m_{p,h}$	$0.513 m_0$	$\parallel [100]$		
	$1.372 m_0$	$\parallel [111]$		
$m_{p,l}$	$0.211 m_0$	$\parallel [100]$		
	$0.145 m_0$	$\parallel [111]$		

parameters of valence band

A	- 3.47	calculated using $k \cdot p$ theory	75W
B	- 0.130		
$ C $	3.96		

Lattice properties

lattice parameter

a	5.4635(4) Å	$T = 25^{\circ}\text{C}$	epitaxial film on GaP	82B
-----	-------------	--------------------------	-----------------------	-----

For temperature dependence of the coefficient of linear thermal expansion, see Fig. 2.6.2

density

d	2.40(1) g cm ⁻³			68C
-----	----------------------------	--	--	-----

melting temperature

T_{m}	2823 K			75O
----------------	--------	--	--	-----

phonon dispersion relations : Fig. 2.6.3.

phonon wavenumbers

$\bar{\nu}_{\text{LO}}(\Gamma)$	504.5(4) cm ⁻¹	$T = 5 \text{ K}$	Raman spectroscopy	70O
	501.0(2) cm ⁻¹	$T = 300 \text{ K}$		
$\bar{\nu}_{\text{TO}}(\Gamma)$	442.5(2) cm ⁻¹	$T = 5 \text{ K}$		
	439.4(2) cm ⁻¹	$T = 300 \text{ K}$		

second order elastic moduli

c_{11}	18.83...14.59·10 ¹¹ dyn cm ⁻²		theoretical estimates	85K
c_{12}	6.71...8.44·10 ¹¹ dyn cm ⁻²			
c_{44}	3.69...4.24·10 ¹¹ dyn cm ⁻²			

bulk modulus

B	185(5) GPa	$T = 298.15 \text{ K}$	for wurtzite type	93X
-----	------------	------------------------	-------------------	-----

Debye temperature

Θ_{D}	588 K		temperature dependence, see Fig. 2.6.4	63S
---------------------	-------	--	--	-----

Transport and optical properties

electrical conductivity

σ	5·10 ⁴ Ω ⁻¹ cm ⁻¹	$T = 300 \text{ K}$	p-type crystals	60G
	0.4...300 Ω ⁻¹ cm ⁻¹	$T = 298 \text{ K}$	n-type crystals and layers, epitaxially grown, main impurity Si.	67R

For temperature dependence of electrical conductivity see Fig. 2.6.5.

activation energy for electrical conductivity

E_{A}	0.15eV	$T = 450...520 \text{ K}$	p-type crystals	60G
	< 0.02 eV	$T = 120...520 \text{ K}$	n-type crystals	60G

electron mobility

μ_{n}	10...80 cm ² /Vs	$T = 298 \text{ K}$	single crystals, $n = 1.3 \cdot 10^{18}...5.5 \cdot 10^{19} \text{ cm}^{-3}$	67R
------------------	-----------------------------	---------------------	--	-----

thermal conductivity

κ	0.9 Wcm ⁻¹ K ⁻¹	$T = 300 \text{ K}$		63S
----------	---------------------------------------	---------------------	--	-----

refractive index : energy and temperature dependence: Figs. 2.6.6 and 2.6.7.

dielectric constants

$\epsilon(0)$	9.8		refractive index	70M
$\epsilon(\infty)$	7.5		experimental	96D

References to 2.6

- 60G Grimmeiss, H. G., Kischio, W., Rabenau, A.: J. Phys. Chem. Solids 16 (1960) 302.
- 63S Steigmeier, E. F.: Appl. Phys. Lett. 3 (1963) 6.
- 67R Reid, F. J.: Batelle Memorial. Inst. Ohio, High-Temperature Material Study, NASA CR-86021, June 1967, Contract No. NAS 12-107 N68-14557.
- 68C Caveney, R. J.: Philos. Mag. 17 (1968) 943.
- 70L Lorenz, M. R., Chikotka, R., Pettit, G. D., Dean, P. J.: Solid State Commun. 8 (1970) 693.
- 70M Monemar, B.: Solid State Commun. 8 (1970) 1295.
- 70O Onton, A.: Proc. of the 10th Int. Conf. on Physics of Semiconductors, Cambridge/Mass. 1970, USAC, Oak Ridge 1970.
- 71G Grimmeiss, H. G., Monemar, B.: Phys. Status Solidi. (a) 5 (1971) 109.
- 73M Monemar, B.: Phys. Rev. BS (1973) 5711.
- 75O Osamura, K., Murakami, Y.: J. Phys. Chem. Solids 36 (1975) 931.
- 75W Wiley, J. D.: Semiconductors and Semimetals, Vol. 10, Willardson, R. K., Beer, A. C. eds, Academic Press, New York 1975.
- 82B Bessolov, V. N., Konnikov, S. G., Umanskii, V. I. Yakovlev, Yu. P.: Sov. Phys. Solid State (English Transl.) 24 (1982) 875; Fiz. Tverd. Tela 24 (1982) 1528.
- 85H Huang, M., Ching, W. Y. J. Phys. Chem. Solids 46 (1985) 977.
- 85K Kagaya, H.-M., Soma, T.: Phys. Status Solidi (b) 127 (1985) 89.
- 93X Xia, H., Xia, Q., Ruoff, A. L.: J. Appl. Phys. 73 (1993) 8198.
- 94G Greene, R. G., Luo, H., Ruoff, A. L.: J. Appl. Phys. 76 (1994) 7296.
- 96D Dal Corso, A., Mauri, F., Rubio, A.: Phys. Rev. B 53 (1996) 15638.
- 99P Pletl, T., Pavone, P., Engel, U., Strauch, D.: Physics B 263/264 (1999) 392.

Figures to 2.6

Fig. 2.0.2

The zincblende lattice

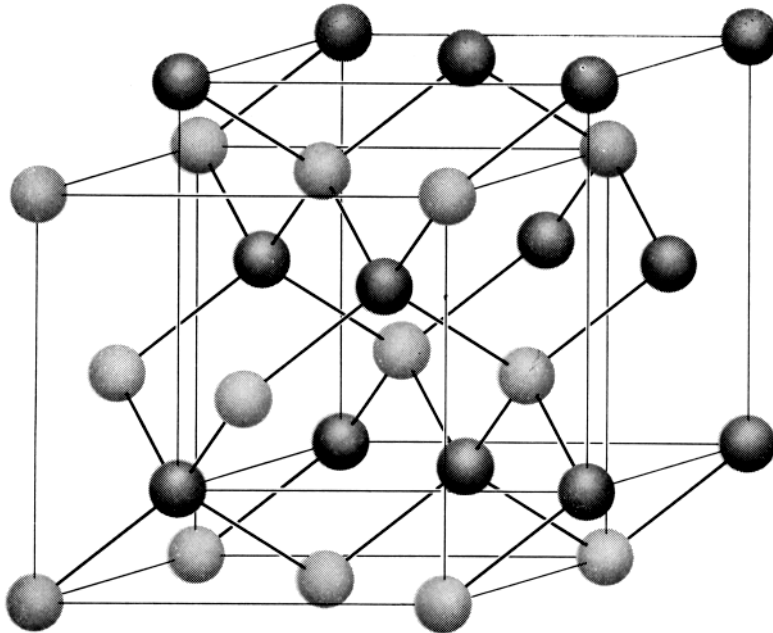


Fig. 2.0.5

Brillouin zone of the zincblende lattice.

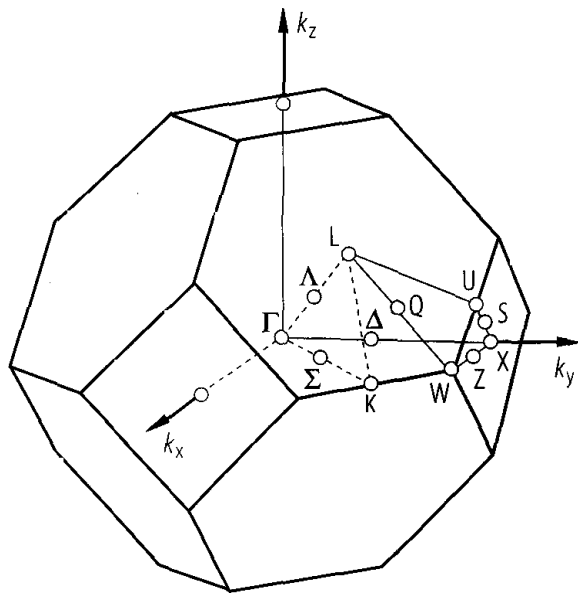


Fig. 2.0.14

AlP. Band structure calculated with an orthogonalized LCAO method [85H].

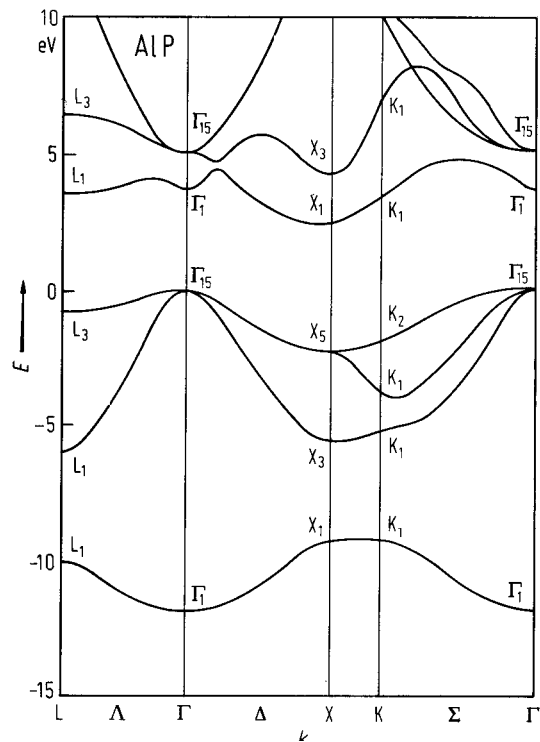


Fig. 2.6.1

AIP. Indirect gap vs. temperature (extrapolation of the linear parts of the curves of Fig. 4 to zero absorption) [70M].

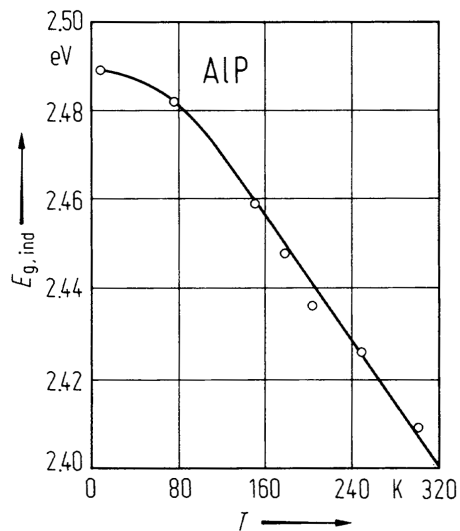


Fig. 2.6.2

AlP, AlAs. Estimated temperature dependence of the coefficient of linear thermal expansion below room temperature [71G].

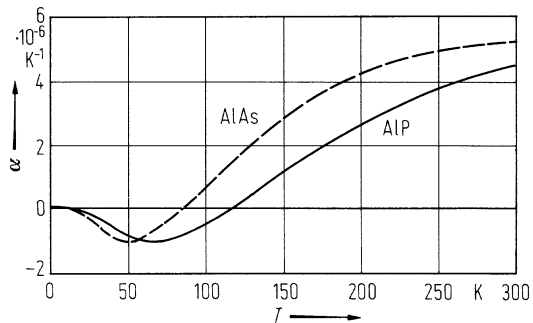


Fig. 2.6.3

AIP. Phonon dispersion curves (left panel) and phonon density of states (right panel) from ab-initio calculations [99P]. The data points are from Raman scattering [70O].

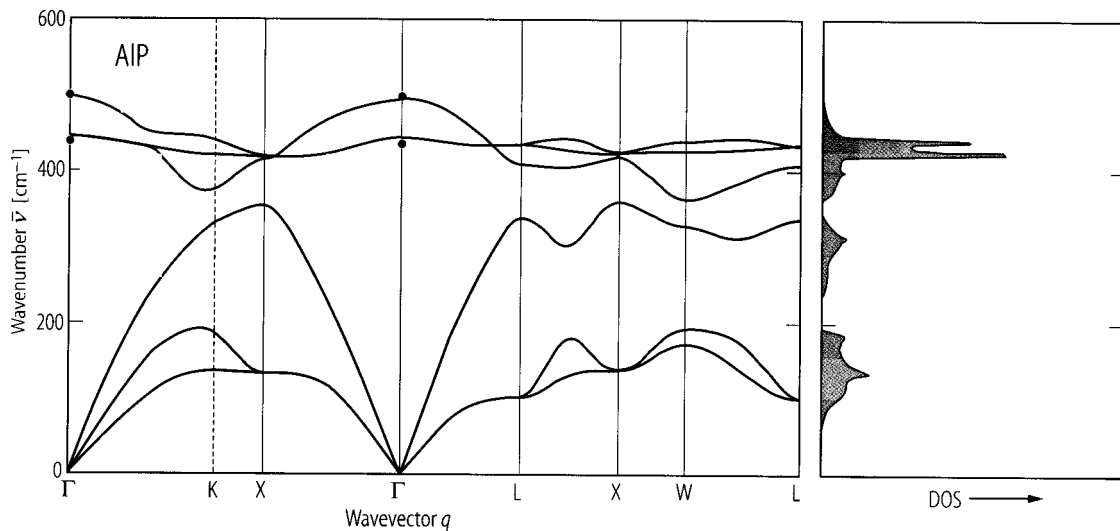


Fig. 2.6.4

AlP, AlAs. Debye temperature $\Theta_D(T)$ vs. temperature estimated from experimental results using the dielectric theory of semiconductors (Penn's model) [71G].

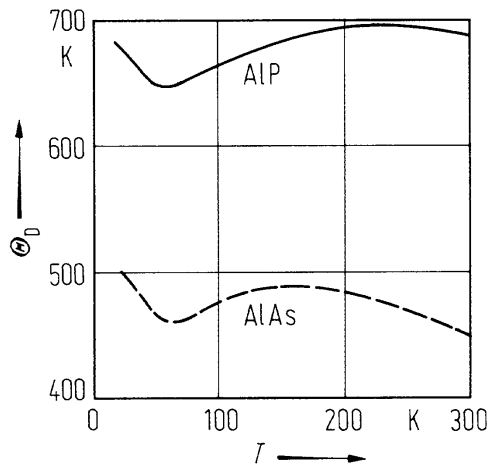


Fig. 2.6.5

AIP. Natural logarithm of electrical conductivity vs. reciprocal temperature in an undoped sample [60G]. σ in $\Omega^{-1} \text{ cm}^{-1}$. Activation energies are also shown.

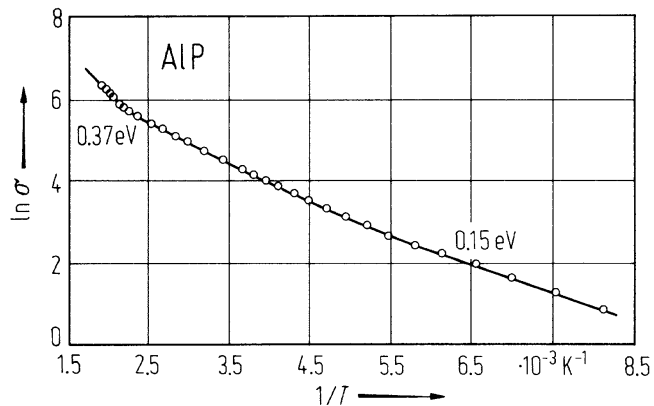


Fig. 2.6.6

AlP. Refractive index vs. photon energy at 300K [70M].

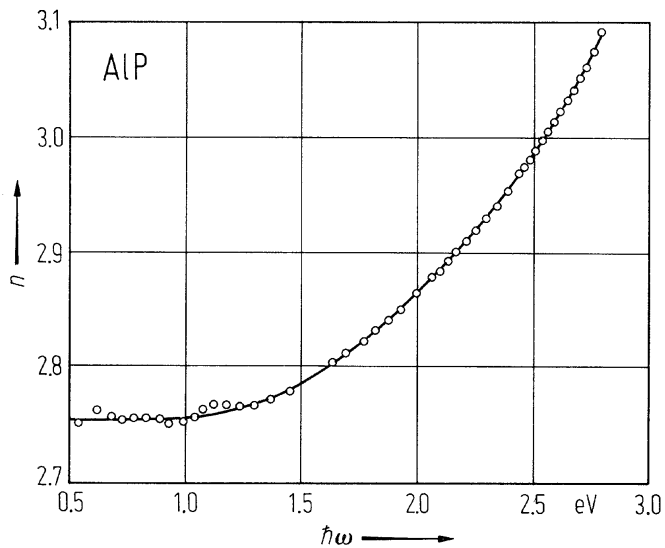
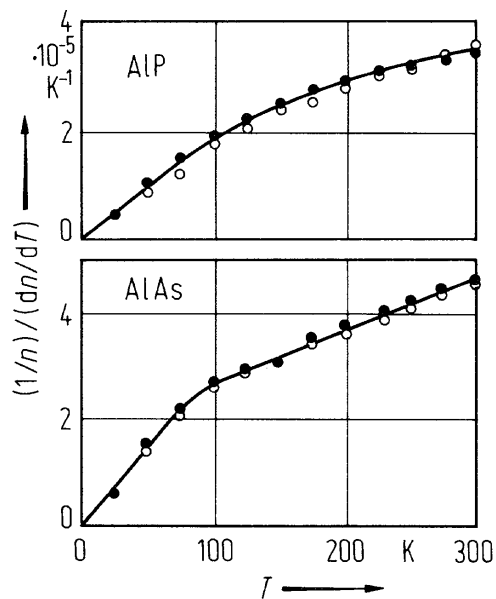


Fig. 2.6.7

AIP, AlAs. Temperature dependence of the refractive index corrected for thermal expansion. Different symbols refer to measurements on two different crystals [71G].



2.7 Aluminum arsenide (AlAs)

Crystal structure

AlAs crystallizes under normal conditions in the zincblende structure (space group $T_d^2 - F\bar{4}3m$, Fig. 2.0.2).

high pressure phases

From X-ray scattering experiments under pressure, AlAs has been found to undergo a phase transition from the zincblende (α phase, B3 phase) to the NiAs structure (β phase, B8 phase); the transformation is very sluggish [92V]; the back transformation occurs at much lower pressures (between 4 and 2 GPa) than the upstroke transformation (around 12 GPa) [94G]; the hysteresis is about 6 GPa [92V]. A phase transition to a phase with unknown structure has been observed at 12.3 GPa [87W].

Electronic properties

band structure : Fig. 2.0.15, Brillouin zone: Fig. 2.0.5

AlAs is a wide gap semiconductor with a band structure similar to those of AlP and AlSb. Measurements revealed a camel's back structure near X (band minimum at $k = (0.903, 0, 0)$ on the Δ -axes) [81B].

energies of symmetry points of the band structure (relative to the top of the valence band $E(\Gamma_{15v})$)

$E(\Gamma_{1v})$	- 11.95 eV	calculated, see Fig. 2.0.15	85H
$E(\Gamma_{1c})$	2.79 eV		
$E(\Gamma_{15c})$	4.48 eV		
$E(X_{1v})$	- 9.63 eV		
$E(X_{3v})$	- 5.69 eV		
$E(X_{5v})$	- 2.38 eV		
$E(X_{1c})$	2.37 eV		
$E(X_{3c})$	3.84 eV		
$E(L_{1v})$	- 10.28 eV		
$E(L_{1v})$	- 5.95 eV		
$E(L_{3v})$	- 0.88 eV		
$E(L_{1c})$	2.81 eV		
$E(L_{3c})$	5.86 eV		

energy gaps

$E_{g, ind}(\Gamma_{15v}-X_{1c})$	2.229(1) eV	$T = 4$ K	excitonic gap, photoluminescence	73M
	2.223(1) eV	$T = 77$ K		
	2.153(2) eV	$T = 300$ K		
$E_{g, ind}(\Gamma_{15v}-L_{1c})$	2.363 eV	$T = 295$ K	transport	80L
$E_{g, dir}(\Gamma_{15v}-\Gamma_{1c})$	3.13(1) eV	$T = 4$ K	photoluminescence, excitonic gap	73M
	3.03(1) eV	$T = 300$ K		
	3.14(1) eV	$T = 300$ K	transmission	71Y

For temperature dependence of indirect and direct gap, see Fig. 2.7.1.

E_b	0.0176 eV	estimate, lowest indirect gap	94A
	0.0128 eV	estimate, lowest direct gap	

spin-orbit splitting energies

$\Delta_0(\Gamma_{15v})$	0.275 eV	$T = 300$ K	electroreflectance	70O
$\Delta_1(L_{15v})$	0.20 eV			
$\Delta_0'(\Gamma_{15c})$	0.15 eV			

higher band-band transitions (critical point energies)

E_0	3.02 eV	$T = 300$ K	direct gap, data from [70O], assignment corrected by [71B] (from a compilation in [85A])
$E_0 + \Delta_0$	3.32 eV		$L_{3v}-L_{1c}$ (and $\Lambda_{3v}-\Lambda_{1c}$)
$E_1(1)$	3.83 eV		
$E_1(2)$	3.96 eV		
E'_0	4.34 eV		$\Gamma_{15v}-\Gamma_{15c}$ ($\Delta_{5v}-\Delta_{1c}$)
E_2	4.54 eV		$X_{5v}-X_{1c}$ ($\Sigma_{2v}-\Sigma_{1c}$ and others)
$E_{2+\delta}$	4.89 eV		$X_{5v}-X_{3c}$

camel's back structure of the conduction band at X

A camel's back structure of the bottom of the conduction band near X has been proved experimentally.

Δ	350 meV	from luminescence spectra of an electron-hole liquid in $\text{Ga}_{0.08}\text{Al}_{0.92}\text{As}$	81B
ΔE	2.5 meV		
k_m	0.097 ($2\pi/a$)		
m_l	1.56 m_0	longitudinal mass far above the band minimum (polaron correction included)	

effective masses, conduction band

$m_{n\perp}(X)$	0.19 m_0	effective masses at X and L	94A
$m_{n\parallel}(X)$	1.1 m_0	neglecting camel's back structure;	
$m_{n,ds}(X)$	0.71 m_0	density of states masses	
$m_{n,c}(X)$	0.26 m_0	obtained from	
$m_{n\perp}(L)$	0.15 m_0	$m_{ds} = N^{2/3} m_{\perp}^{2/3} m_{\parallel}^{1/3}$	
$m_{n\parallel}(L)$	1.32 m_0	with N = number of equivalent minima;	
$m_{n,ds}(L)$	0.78 m_0	conductivity effective mass obtained from $m_c = 3(2/m_{\perp} + 1/m_{\parallel})^{-1}$	
$m_{n,c}(L)$	0.21 m_0		

effective masses, valence band

$m_{p,h}$	0.409 m_0	$\parallel [100]$	calculated from band structure data	85H
	1.022 m_0	$\parallel [111]$		
$m_{p,l}$	0.153 m_0	$\parallel [100]$		
	0.109 m_0	$\parallel [111]$		

band structure parameters

A	- 4.03			75W
B	- 2.09			
$ C $	4.63			

Lattice properties

lattice parameter

a	5.66139(5) Å	high-resolution X-ray diffraction	98D
-----	--------------	-----------------------------------	-----

For temperature dependence, see Fig. 2.7.2 [67P].

coefficient of linear thermal expansion

α	5.20(5)·10 ⁻⁶ K ⁻¹	$T = 15 \dots 840$ °C	X-ray diffraction	70E
----------	--	-----------------------	-------------------	-----

See also Fig. 2.7.3.

density

d	3.760 g cm ⁻³	calculated from lattice parameter	85A
-----	--------------------------	-----------------------------------	-----

melting temperature

T_m	2013(20) K	$p = 1 \text{ atm}$		64K
-------	------------	---------------------	--	-----

phonon dispersion curves : Fig. 2.7.4.

phonon wavenumbers

$\bar{\nu}_{LO}(\Gamma)$	404(1) cm^{-1}	$T = 36 \text{ K}$	1 st order Raman scattering,	94S
$\bar{\nu}_{TO}(\Gamma)$	361(1) cm^{-1}		0.5 μm layer AlAs, on GaAs, 40 Å GaAs cap	
$\bar{\nu}_{LO}(X)$	403(8) cm^{-1}		from 2 nd order spectrum	
$\bar{\nu}_{TO}(X)$	335(8) cm^{-1}			
$\bar{\nu}_{TA}(X)$	109(8) cm^{-1}			
$\bar{\nu}_{LA}(X)$	222(12) cm^{-1}			

sound velocities

v_{LA}	$5.7 \cdot 10^5 \text{ cm s}^{-1}$	$[100]/[001]$	from the c_{ik} (table below)	85A
$v_{T1} (v_{T2})$	$3.9 \cdot 10^5 \text{ cm s}^{-1}$		designation: direction of propagation/	
v_{LA}	$6.2 \cdot 10^5 \text{ cm s}^{-1}$	$[110]/[001]$	direction of particle movement	
v_{T1}	$4.0 \cdot 10^5 \text{ cm s}^{-1}$			
v_{T2}	$2.9 \cdot 10^5 \text{ cm s}^{-1}$			

second order elastic moduli

c_{11}	119.9(12) GPa		Brillouin scattering,	95K
c_{12}	57.5(13) GPa		AlAs layer on GaAs,	
c_{44}	56.6(7) GPa			

bulk modulus

B	74(4) GPa		from X-ray diffraction data	94G
-----	-----------	--	-----------------------------	-----

Debye temperature

Θ_D	414 K	$T = 0 \text{ K}$	estimated	85A
	446 K	$T = 300 \text{ K}$		

Temperature dependence of $\Theta_D(T)$, see Fig. 2.7.5.

Transport properties

Only few reliable data exist on the transport and optical properties of AlAs. Most results are extrapolations from data obtained on the technologically more important solid solutions of the type $\text{Al}_x\text{Ga}_{1-x}\text{As}$.

electrical conductivity

σ	$9.5 \Omega^{-1}\text{cm}^{-1}$	$T = 300 \text{ K}$	p-type crystal grown by MBE	84C
	$0.29 \Omega^{-1}\text{cm}^{-1}$	$T = 77 \text{ K}$	(at dark)	
	$9.4...80 \Omega^{-1}\text{cm}^{-1}$		n-type single crystal layers on GaAs	72S

thermal conductivity

κ	$0.91 \text{ W cm}^{-1} \text{ K}^{-1}$	$T = 300 \text{ K}$		73A
----------	---	---------------------	--	-----

carrier mobilities

μ_n	$294...75 \text{ cm}^2/\text{Vs}$	$T = 300 \text{ K}$	single crystal layers	72S
μ_p	$105 \text{ cm}^2/\text{Vs}$	$T = 300 \text{ K}$	MBE-grown, Be-doped crystal	92L

For temperature dependence of the Hall mobility, see Fig. 2.7.6.

Optical properties

Although AlAs is one endpoint of the heavily studied $\text{Al}_x\text{Ga}_{1-x}\text{As}$ ternary system, its optical properties have not been investigated nearly as much because of its hygroscopic nature.

dielectric constants

$\epsilon(0)$	10.1	from infrared reflectivity	87P
$\epsilon(\infty)$	8.2		

Spectral variation of the dielectric function and the complex refractive index, see Figs. 2.7.7 and 2.7.8. For the temperature dependence of the refractive index, see Fig. 2.6.7.

References to 2.7

- 64K Kischio, W.: Z. Anorg. Allg. Chem. 328 (1964) 187
- 65W Whitaker, J.: Solid State Electron. 8 (1965) 649.
- 67P Pearson, W. B.: A Handbook of Lattice Spacings and Structure of Metals and Alloys, Pergamon Press, Oxford-London 1967.
- 70E Ettenberg, M., Paff, R. J.: J. Appl. Phys. 41 (1970) 3926.
- 70O Onton, A.: Proc. 10th Int. Conf. Phys. Semicond., Cambridge/Mass. 1970, USAEC, New York 1970, p. 107.
- 71B Berninger, W. H., Rediker, R. H.: Bull. Am. Phys. Soc. 16 (1971) 305.
- 71G Grimmeiss, H. G., Monemar, B.: Phys. Status Solidi. (a) 5 (1971) 109.
- 71Y Yim, W. M.: J. Appl. Phys. 42 (1971) 2854.
- 72S Sigai, A. G., Abrahams, M. S., Blanc, J.: J. Electrochem. Soc. 119 (1972) 952.
- 73A Afromowitz, M. A.: J. Appl. Phys. 44 (1973) 1292.
- 73M Monemar, B.: Phys. Rev. B 8 (1973) 5711.
- 75W Wiley, J. D.: Semiconductors and Semimetals, vol. 10, Willardson, R. K., Beer, A. C. eds., Academic Press, New York 1975.
- 80L Lee, H. J., Juravel, L. Y., Woolley, J. C., SpringThorpe, A. J.: Phys. Rev. B 21 (1980) 659.
- 81B Bimberg, D., Bludau, W., Linnenbach, R., Bauser, E.: Solid State Commun.
- 84C Chand, N., Henderson, T., Klem, J., Masselink, W. T., Fischer, R., Chang, Y.-C., Morkoç, H.: Phys. Rev. B 30 (1984) 4481.
- 85A Adachi, S.: J. Appl. Phys. 58 (1985) 81.
- 85H Huang, M., Ching, W. Y.: J. Phys. Chem. li'olids 46 (1985) 977.
- 87G Garriga, M., Lautenschlager, P., Cardona, M., Ploog, K.: Solid State Commun. 61 (1987) 157.
- 87K Kagaya, H. M., Soma, T.: Solid State Commun. 62 (1987) 707; Phys. Status Solidi (b) 142 (1987) 411.
- 87P Perkowitz, S., Sudharsanan, R., Yom, S. S., Drummond, T. J.: Solid State Commun. 62 (1987) 645.
- 87W Weinstein, B. A., Hark, S. K., Burnham, R. D., Martin, R. M.: Phys. Rev. Lett. 58 (1987) 781.
- 91G Giannozzi, P., de Gironcoli, S., Pavone, P., Baroni, S.: Phys. Rev. B 43 (1991) 7231.
- 92L Look, D. C., Lorange, D. K., Sizelove, J. R., Stutz, C. E., Evans, K. R., Whitson, D. W.: J. Appl. Phys. 71 (1992) 260.
- 92V Venkateswaran, U. D., Cui, L. J., Weinstein, B. A., Chambers, F. A.: Phys. Rev. B 45 (1992) 9237.
- 94A Adachi, S.: GaAs and Related Materials: Bulk semiconducting and superlattice properties, World Scientific, Singapore, 1994.
- 94G Greene, R. G., Luo, H., Ruoff, A. L.: J. Appl. Phys. 76 (1994) 7296.
- 94S Spencer, G. S., Grant, J., Gray, R., Zolman, J., Menéndez, J., Droopad, R., Maracas, G. N.: Phys. Rev. B 49 (1994) 5761.
- 95K Krieger, M., Sigg, H., Herres, N., Bachem, K., Köhler, K.: Appl. Phys. Lett. 66 (1995) 682.
- 98D De Caro, L., Giannini, C., Tapfer, L., Schönherr, H. P., Däweritz, L., Ploog, K. H.: Solid State Commun. 108 (1998) 599.

Figures to 2.7

Fig. 2.0.2

The zincblende lattice

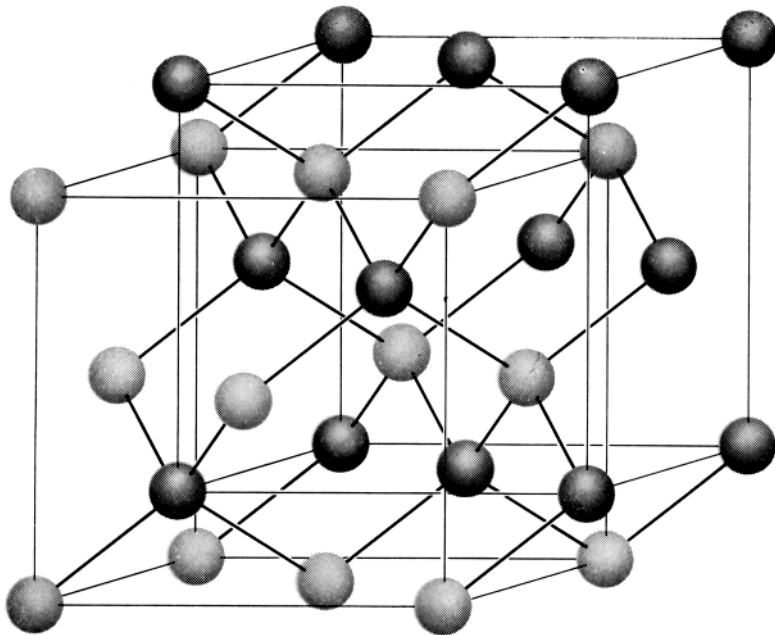


Fig. 2.0.5

Brillouin zone of the zincblende lattice.

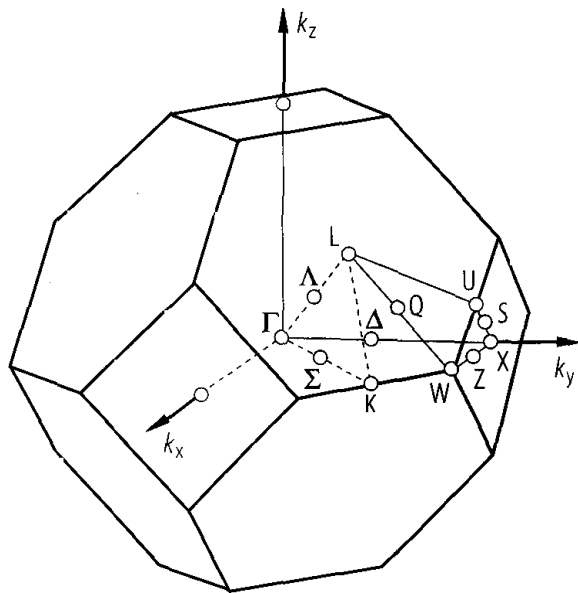


Fig. 2.0.15

AlAs. Band structure calculated with an orthogonalized LCAO method [85H].

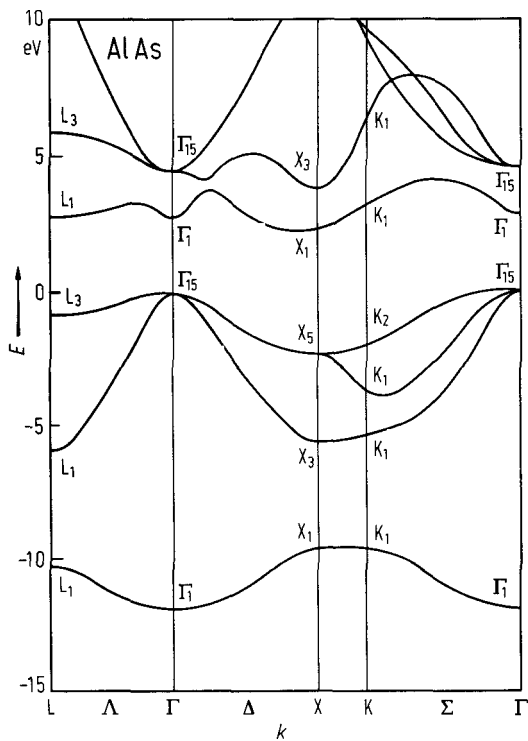


Fig. 2.7.1

AlAs. (a) Indirect excitonic gap and (b) direct gap vs. temperature. Due to a high impurity content the curve in (b) is believed to represent an energy a few meV above the exciton edge in pure AlAs [73M].

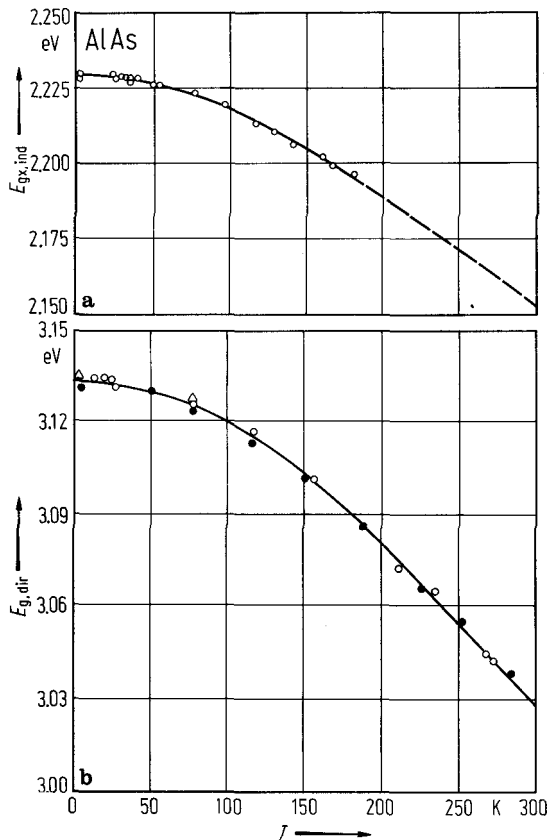


Fig. 2.7.2

AlAs. Lattice parameter vs. temperature [70E]. The lattice parameter of GaAs is shown for comparison.

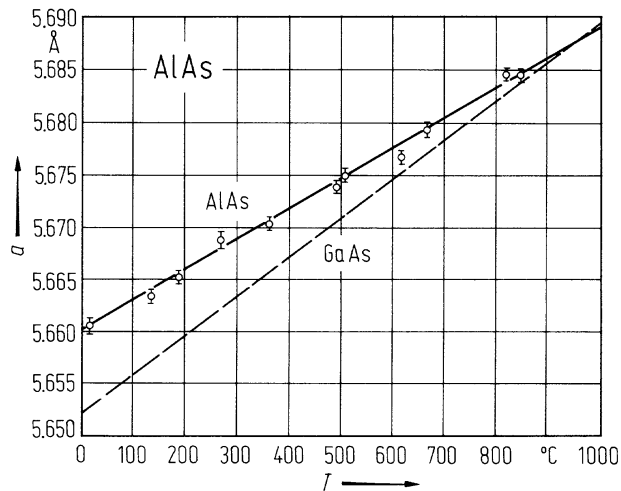


Fig. 2.7.3

AlAs. Coefficient of linear thermal expansion calculated from model pseudopotential mode-Grüneisen parameters. From [87K].

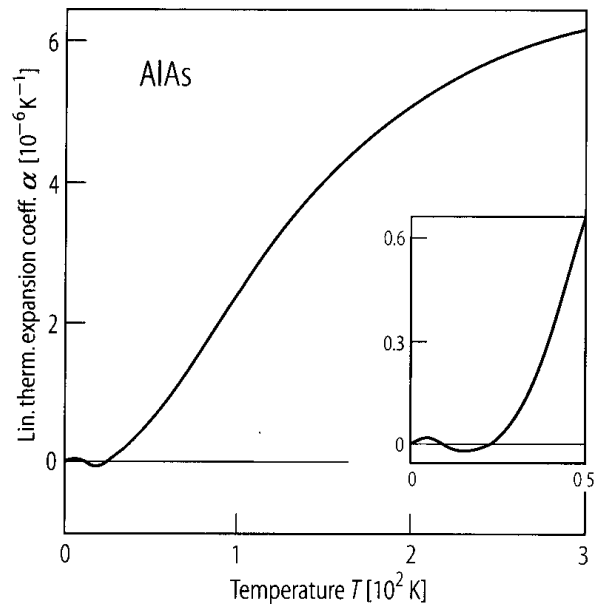


Fig. 2.7.4

AIAs. Phonon dispersion curves (left panel) and phonon density of states (right panel). Experimental data points [70O], [73M] and ab-initio calculations [91G]. From [91G].

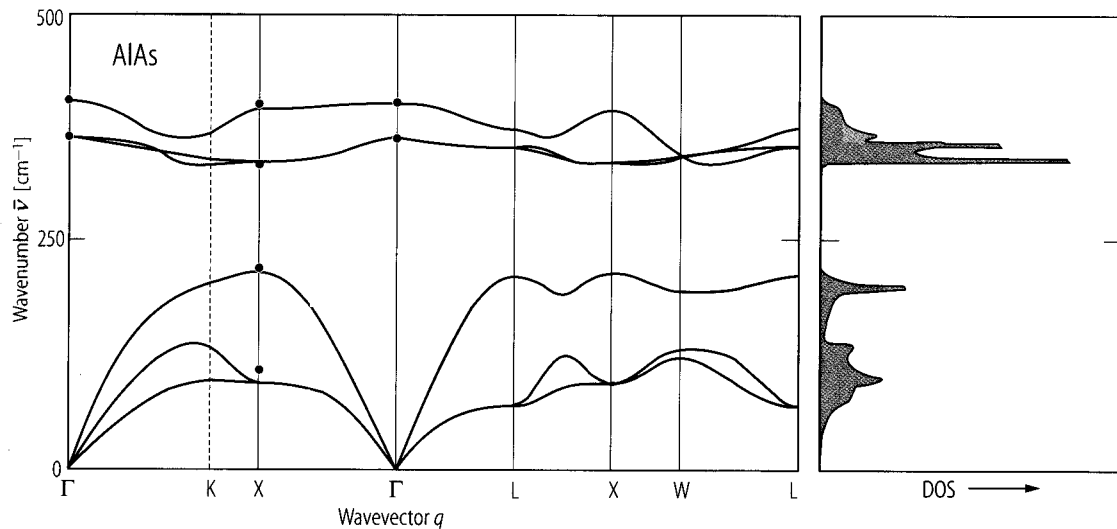


Fig. 2.7.5

AlP, AlAs. Debye temperature $\Theta_D(T)$ vs. temperature estimated from experimental results using the dielectric theory of semiconductors (Penn's model) [71G].

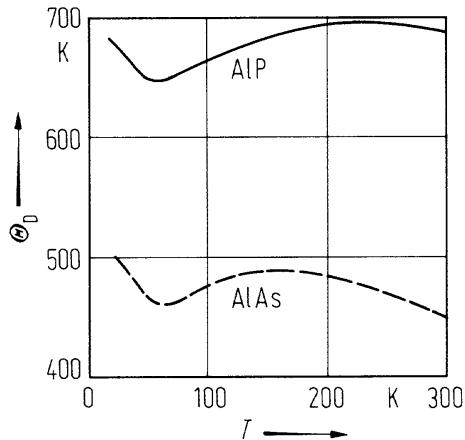


Fig. 2.7.6

AlAs. Electron Hall mobilities vs. temperature [65W].

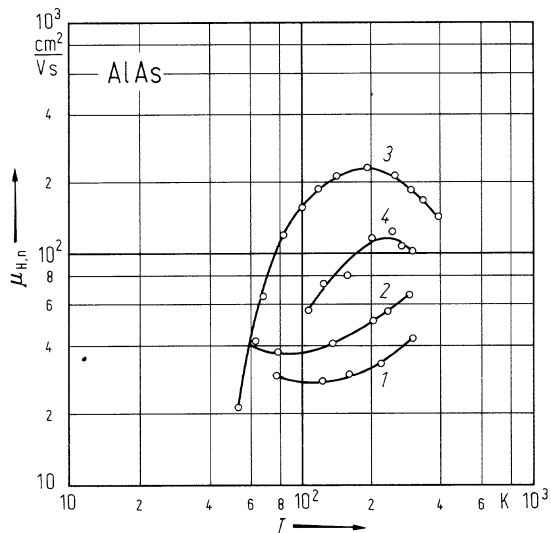


Fig. 2.7.7

AlAs. Spectral variation of the dielectric function at 300 K [87G].

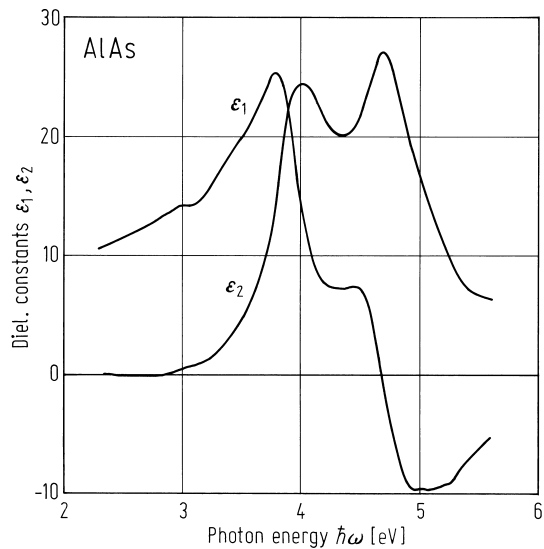
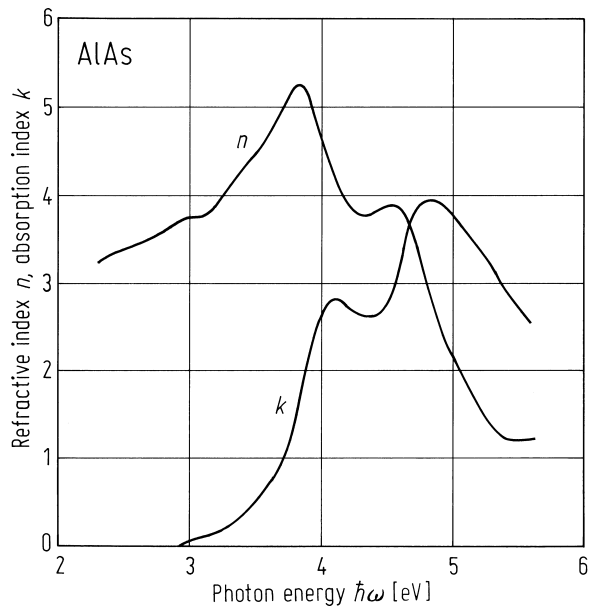


Fig. 2.7.8

AlAs. Spectral variation of the complex refractive index calculated from the dielectric function [94A].



2.8 Aluminum antimonide (AlSb)

Crystal structure

Aluminum antimonide crystallizes under normal conditions in the zincblende structure (space group $T_d^2 - F\bar{4}3m$, Fig. 2.0.2).

AlSb is the semiconductor with the largest band gap among the antimony-containing III-V compounds. Since the material is highly reactive with atmospheric oxygen and water only few work on bulk crystals is available. Most of the recent work has been performed on epitaxially grown ternary and quaternary layers.

high pressure phases

Under pressure, AlSb transforms to what was assumed the β -tin structure, see e.g., [63J, 95G], coexisting with the zincblende phase between about 7 and 10 GPa [95G], but the (220) and (301) Bragg reflections missing [83B, 95G]; the rocksalt structure has been found instead [78Y]; more recent studies assign orthorhombic Cmc symmetry [97N]. A transition to an unknown structure (AlSb-III) occurs near 40 GPa; this structure persists up to at least 59 GPa [95G].

Electronic properties

band structure : Fig. 2.0.16, Brillouin zone: Fig. 2.0.5.

AlSb has an indirect band gap with conduction band minima near X.

energies of symmetry points of the band structure (relative to the top of the valence band $E(\Gamma_{15v})$)

$E(\Gamma_{1v})$	- 10.77 eV	calculated, see Fig. 2.0.17	85H
$E(\Gamma_{1c})$	2.05 eV		
$E(\Gamma_{15c})$	3.50 eV		
$E(X_{1v})$	- 8.72 eV		
$E(X_{3v})$	- 5.44 eV		
$E(X_{5v})$	- 2.31 eV		
$E(X_{1c})$	2.08 eV		
$E(X_{3c})$	3.02 eV		
$E(L_{1v})$	- 9.30 eV		
$E(L_{1v})$	- 5.58 eV		
$E(L_{3v})$	- 0.90 eV		
$E(L_{1c})$	1.94 eV		
$E(L_{3c})$	4.84 eV		

energy gaps

$E_{g,ind}$	1.615(3) eV	$T = 300$ K	excitonic gap (see Fig. 2.8.1),	83A
$(\Gamma_{15v}-\Delta_{1c})$	1.686(1) eV	$T = 27$ K	modulation spectroscopy	75M
$E_{g,ind}$	2.211 eV	$T = 295$ K	electroreflectance	82J
$(\Gamma_{15v}-L_{1c})$	2.327 eV	$T = 35$ K		
$E_{g,dir}$	2.300 eV	$T = 295$ K	electroreflectance	82J
$(\Gamma_{15v}-\Gamma_{1c})$	2.384 eV	$T = 25$ K		
$E(1S_{3/2})$	- 19.1 meV		preliminary calculation from	79G
$E(1S_{1/2})$	- 17.2 meV		several data	

conduction band, camel's back structure and effective masses

Δ	261 meV	estimates using $k \cdot p$ theory	85K
ΔE	7.4 meV	and GaP data	
k_m	$0.101(2\pi/a)$		
m_{\perp}	$0.259 m_0$		
m_{\parallel}	$1.8 m_0$		

spin-orbit splitting energies

$\Delta_0(\Gamma_{8v}-\Gamma_{7v})$	0.673 eV	$T = 295$ K	splitting of Γ_{15v}	82J
$\Delta_1(L_{4,5v}-L_{6v})$	0.426 eV	$T = 295$ K	splitting of L_{3v}	

critical point energies

E_0	2.27(1) eV	$T = 300$ K	ellipsometric measurements	89Z
E_1	2.838(2) eV			
$E_1 + \Delta_1$	3.23(1) eV			
E_0'	3.76(1) eV			
$E_0' + \Delta_0'$	3.97(3) eV			
E_2	4.23(1) eV			
E_1'	5.30(1) eV			

conduction band, effective masses

$m_{n\perp}(\Delta_1)$	0.26 m_0		estimate in calculating camel's back structure	79G
$m_{n\parallel}(\Delta_1)$	1 m_0			
m_n	1.2(4) m_0	$T = 600...900$ K	density of states mass from thermo-electric power measurements, acoustic mode scattering assumed	59N

valence band, effective masses

$m_{p,h}$	0.336 m_0	$\parallel [100]$	theoretical estimates	85H
	0.872 m_0	$\parallel [111]$		
$m_{p,l}$	0.123 m_0	$\parallel [100]$		
	0.091 m_0	$\parallel [111]$		

valence band parameter

A	- 4.12			75W
B	- 2.09			
$ C $	4.71			

Lattice properties

lattice parameter

a	6.1355(1) Å	$T = 291.15$ K	powder, X-ray measurements	58G
-----	-------------	----------------	----------------------------	-----

linear thermal expansion coefficient : Fig. 2.8.2

density

d	4.26 g cm ⁻³	$T = 293.15$ K	for temperature dependence,	69G
	4.34 g cm ⁻³		see Fig. 2.8.3	67P

melting temperature

T_m	1327(1) K			89Y
-------	-----------	--	--	-----

phonon dispersion relations : Fig. 2.8.4. Brillouin zone: Fig. 2.0.5.

phonon wavenumbers

$\bar{\nu}_{\text{TO}}(\Gamma)$	316 cm^{-1}	ab-initio pseudopotential calculation	91G
$\bar{\nu}_{\text{LO}}(\Gamma)$	334 cm^{-1}		
$\bar{\nu}_{\text{TA}}(\text{X})$	64 cm^{-1}		
$\bar{\nu}_{\text{LA}}(\text{X})$	153 cm^{-1}		
$\bar{\nu}_{\text{TO}}(\text{X})$	290 cm^{-1}		
$\bar{\nu}_{\text{LO}}(\text{X})$	343 cm^{-1}		
$\bar{\nu}_{\text{TA}}(\text{L})$	49 cm^{-1}		
$\bar{\nu}_{\text{LA}}(\text{L})$	149 cm^{-1}		
$\bar{\nu}_{\text{TO}}(\text{L})$	306 cm^{-1}		
$\bar{\nu}_{\text{LO}}(\text{L})$	327 cm^{-1}		
$\bar{\nu}_{\text{LO}}(\Gamma)$	340.0(7) cm^{-1}	first order Raman scattering	86V
$\bar{\nu}_{\text{TO}}(\Gamma)$	318.7(7) cm^{-1}		

sound velocities

v_1	$4.528(4) \cdot 10^5 \text{ cm s}^{-1}$	$T = 300 \text{ K}$	ultrasound (10 MHz) designation: mode/direction of pro- propagation/direction of particle displacement v_1 : long./001/001, v_2 : shear/001/110, v_3 : long/110/110, v_4 : shear/110/001, v_5 : shear/110/110	60B
v_2	$3.087(3) \cdot 10^5 \text{ cm s}^{-1}$			
v_3	$4.977(4) \cdot 10^5 \text{ cm s}^{-1}$			
v_4	$3.085(3) \cdot 10^5 \text{ cm s}^{-1}$			
v_5	$2.276(2) \cdot 10^5 \text{ cm s}^{-1}$			

second order elastic moduli

c_{11}	$8.769(20) \cdot 10^{11} \text{ dyn cm}^{-2}$	$T = 300 \text{ K}$	ultrasound (10 MHz), values reevaluated by [72W] using the correct density	60B
c_{12}	$4.341(20) \cdot 10^{11} \text{ dyn cm}^{-2}$			
c_{44}	$4.076(8) \cdot 10^{11} \text{ dyn cm}^{-2}$			

bulk modulus

B	55.1 GPa	energy dispersive X-ray	86V
-----	----------	-------------------------	-----

Debye temperature

Θ_D	292 K	from elastic moduli using interpolated value from other III–V compounds	63S
------------	-------	--	-----

For temperature dependence of $\Theta_D(T)$, see Fig. 2.8.5

Transport properties

AlSb grown without intentional doping is p-type, and it becomes intrinsic at about 1000 K. Below room temperature the transport is limited by ionized impurity scattering and at higher temperatures acoustic-mode scattering dominates for the holes and polar optical-mode scattering for the electrons.

For temperature dependence of electrical conductivity, see Fig. 2.8.6

intrinsic conductivity

$\sigma_i = \sigma_0 \exp(-E_g/2kT):$	$T > 1000 \text{ K}$	$p = 4 \dots 8 \cdot 10^7 \text{ cm}^{-3}$	58N
σ_0	$1.12 \cdot 10^4 \Omega^{-1} \text{ cm}^{-1}$		
E_g	1.57 eV		

thermal conductivity : Fig. 2.8.7.

carrier concentration

p	10^{16} cm^{-3}	$T = 300 \text{ K}$	purest material	60A
n_i	10^{17} cm^{-3}	$T = 1000 \text{ K}$		

electron mobility

μ_n	$200 \text{ cm}^2/\text{Vs}$	$T = 295 \text{ K}$	single crystal, Te-doped, $n = 4.7 \cdot 10^{16} \text{ cm}^{-3}$	66S2
	$700 \text{ cm}^2/\text{Vs}$	$T = 77 \text{ K}$		

See Fig. 2.8.8a for temperature dependence ($T^{-1.8}$ -dependence above 200 K).

hole mobility

μ_p	$400 \text{ cm}^2/\text{Vs}$	$T = 300 \text{ K}$	single crystal, $p \approx 10^{16} \text{ cm}^{-3}$	60A, 58R
	$2000 \text{ cm}^2/\text{Vs}$	$T = 77 \text{ K}$	single crystal, $p \approx 3 \cdot 10^{16} \text{ cm}^{-3}$ (at 300 K)	66S1

For temperature dependence of hole mobility, see Fig. 2.8.8b.

light holes

p_l/p_h	0.075	$T = 50 \dots 100 \text{ K}$	calculated from the magneto-resistance field dependence	66S1
μ_{pl}/μ_{ph}	2.6			

piezoelectric coefficients

e_{14}	$6.8 \cdot 10^{-6} \text{ C/cm}^2$ $\pm 20\%$	$T = 300 \text{ K}$	piezoelectric Hall effect measurements. Polarity: negative, if the crystal is expanded in the $[111]$ direction, the A-faces (metal atoms) become negatively charged. Three different mechanisms contribute to the piezoelectric effect, ionic polarization, change in ionicity, electronic polarization	68A2
d_{14}	$1.64 \cdot 10^{-10} \text{ cm/V}$			
g_{14}	$1.61 \cdot 10^2 \text{ cm}^2/\text{C}$			
h_{14}	$6.7 \cdot 10^6 \text{ V/cm}$			

Optical properties

refractive index and extinction coefficient : Fig. 2.8.9.

complex dielectric function : real and imaginary part vs. photon energy, see Fig. 2.8.10.

refractive index

		$T [\text{K}]$,	$\lambda [\mu\text{m}]$		
n	3.652	300,	40	transmission and reflectance	62T
	2.995		20		
	3.080		15		
	3.100		10	transmission and reflectance	54O
	3.182		4		
	3.300		2		
	3.445		1.1		

dielectric constants

$\varepsilon(0)$	12.04	$T = 300 \text{ K}$	ir reflectance, oscillator fit	62H
$\varepsilon(\infty)$	10.24			

Impurities and defects

Undoped AlSb is generally p-type. Low- T photoexcitation spectroscopy shows several lines that are attributed to excited states of donor [68A1] or acceptor [69A] levels.

binding or activation energy of shallow donors

Te and Se donors exhibit DX-like metastability. The following data refer to the hydrogenic donor level.

Impurity	E_a [meV]	E_b [meV]	T [K]	Remarks	Ref.
Theory		E_c -140		effective-mass theory	95B
Te	68	77-500		Hall, extrapolated at 0K	66S2
Te		E_c -71.3	4.2	photoexcitation spectroscopy	68A1
Se	160			Hall	66S1
Se		E_c -146.5	4.2	photoexcitation spectroscopy	68A1
Se		E_c -110	77	optical absorption, resistivity	95B
S?		E_c -151	4.2	photoluminescence	90H

binding or activation energy of shallow acceptors

Impurity	E_a [meV]	E_b [meV]	T [K]	Remarks	Ref.
unknown	33	77-500		Hall, extrapolated at 0K	66S1
C?		E_v +37	4.2	photoluminescence	90H

binding or activation energy of deep levels

Impurity	E_a [eV]	E_b [eV]	T [K]	Type	σ_n [cm ²]	Remarks	Ref.
Te	0.1			DX		DLTS, Hall, CV on MBE samples	90N
Te	0.26			elec. trap	$2.9 \cdot 10^{-15}$	DLTS, Hall, CV on MBE samples	90N
Se		E_c -0.18	77	DX		optical absorption, resistivity	95B
		E_v +0.41		deep donor		magnetoresistance, NPPC	96W

References to 2.8

- 53W Welker, H.: Z. Naturforsch. 5a (1953) 248.
- 54O Oswald, F., Schade, R.: Z. Naturforsch. 9a (1954) 611.
- 58G Giesecke, G., Pfister, H.: Acta Crystallogr. 11 (1958) 369.
- 58N Nasledov, D. N., Slobodchikov, S. V.: Sov. Phys. Tech. Phys. 3 (1958) 669.
- 58R Reid, F. J., Willardson, R. K.: J. Electron. Control 5 (1958) 54.
- 59F Flubacher, P., Leadbetter, A. J., Morrison, J. A.: Philos. Mag. 4 (1959) 273.
- 59N Nasledov, D. N., Slobotchikov, S. V.: Sov. Phys. Solid State (English Transl.) 1 (1959) 681 Fiz. Tverd. Tela 1 (1959) 748.
- 60A Allred, W. P., Meffert, W. L., Willardson, R. K.: J. Electrochem. Soc. 107 (1960) 117
- 60B Bolef, D. T., Menes, M.: J. Appl. Phys. 31 (1960) 1426.
- 62H Hass, M., Hennis, B. W.: J. Phys. Chem. Solids 23 (1962) 1099.
- 62T Turner, W. J., Reese, W. E.: Phys. Rev. 127 (1962) 126.
- 63J Jamieson, J. C.: Science 139 (1963) 845.
- 63N Novikova, S. I., Abrikosov, N. Kh.: Sov. Phys. Solid State (English Transl.) 5 (1963) 1558, Fiz. Tverd. Tela 5 (1963) 2138.
- 63S Steigmeier, F. F.: Appl. Phys. Lett. 3 (1963) 6.
- 66S1 Stirn, R. J., Becker, W. M.: Phys. Rev. 148 (1966) 907.
- 66S2 Stirn, R. J., Becker, W. M.: Phys. Rev. 141 (1966) 621.
- 67P Pearson, W. B.: A Handbook of Lattice Spacings and Structures of Metals and Alloys, Pergamon Press, Oxford-London 1967.
- 67S Seraphin, B. O., Bennett, H. E., in: Semiconductors and Semimetals, Willardson, R. K., Beer, A. C., (eds.), Academic Press, New York, 1967, vol. 3, p. 499.
- 68A1 Ahlburn, B. T., Ramdas, A. K.: Phys. Rev. 167 (1968) 717.
- 68A2 Ant, G., Quadflieg, P.: Phys. Status Solidi 25 (1968) 323.
- 69A Ahlburn, B. T., Ramdas, A. K.: Phys. Rev. 187 (1969) 932.
- 69G Glazov, V. M., Chizhevskaya, S. N., Evgen'ev, S. B.: Zh. Fiz. Khim. 43 (1969) 373.
- 69M Muzhdaba, V. M., Nashel'skii, A. Ya., Tamarin, P. V., Shalyt, S. S.: Sov. Phys. Solid State (English Transl.) 10 (1969) 2265; Fiz. Tverd. Tela 10 (1968) 2866.
- 72W Weil, R.: J. Appl. Phys. 43 (1972) 4271.
- 73S Sirota, N. N., Lukomskii, A. I.: Sov. Phys. Semicond. (English Transl.) 7 (1973) 140; Fiz. Tekh. Poluprov. 7 (1973) 196.
- 75M Mathieu, H., Auvergne, D., Merle, P., Rustagi, K. C.: Phys. Rev. B 12 (1975) 5846
- 75W Wiley, D. J.: in Semiconductors and Semimetals", vol. 10 Willardson, R. K., Beer, A. C. eds., Academic Press, New York 1975.
- 79G Glinskii, O. F., Kopylov, A. A., Pikhtin, A. N.: Solid State Commun. 30 (1979) 631.
- 82J Joullié, A., Girault, B., Joullié, A. M., Zien-Eddine, A.: Phys. Rev. B 25 (1982) 7830.
- 83A Alibert, C., Joullié, A., Joullié, A. M., Ance, C.: Phys. Rev. B 27 (1983) 4946.
- 83B Baublitz, M., Ruoff, A. L.: J. Appl. Phys. 54 (1983) 2109.
- 85H Huang, M., Ching, W. Y.: J. Phys. Chem. Solids 46 (1985) 977.
- 85K Kopylov, A. A.: Solid State Commun. 56 (1985) 1.
- 86V Ves, S., Strössner, K., Cardona, M.: Solid State Commun. 57 (1986) 483.
- 89Y Yamagushi, K.: J. Jpn. Inst. Met. 53 (1989) 764.
- 89Z Zollner, S., Chengtian, L., Schönherr, E., Böhringer, A., Cardona, M.: J. Appl. Phys. 66 (1989) 383.
- 90H Hofmann, G., Lin, C. T., Schönherr, E., Weber, J.: J. Appl. Phys. 67 (1990) 1478.
- 90N Nakagawa, A., Pekarik, J. J., Kremer, H., English, J. H.: Appl. Phys. Lett. 57 (1990) 1551.
- 90S Strauch, D., Dorner, B., Karch, K.: in: "Phonons 89" Hunklinger, S., Ludwig, W., Weiss, G. (eds.), Singapore: World Scientific, 1990, p. 82.
- 91G Giannozzi, P., deGironcoli, S., Pavone, P., Baroni, S.: Phys. Rev. B 43 (1991) 7231.
- 95B Becla, P., Witt, A., Lagowski, J., Walukiewicz, W.: Appl. Phys. Lett. 67 (1995) 395.
- 95G Greene, R. G., Luo, H., Ghandehari, K., Ruoff, A. L.: J. Phys. Chem. Solids 56 (1995) 517.
- 96W Wang, F. -C., Zhan, W. E., Yang, C. H., Yang, M. J., Bennett, B. R.: Appl. Phys. Lett. 69 (1996) 1417.
- 97N Nelmes, R. J., McMahon, M. I., Belmonte, S. A.: Phys. Rev. Lett. 79 (1997) 3668.

Figures to 2.8

Fig. 2.0.2

The zincblende lattice

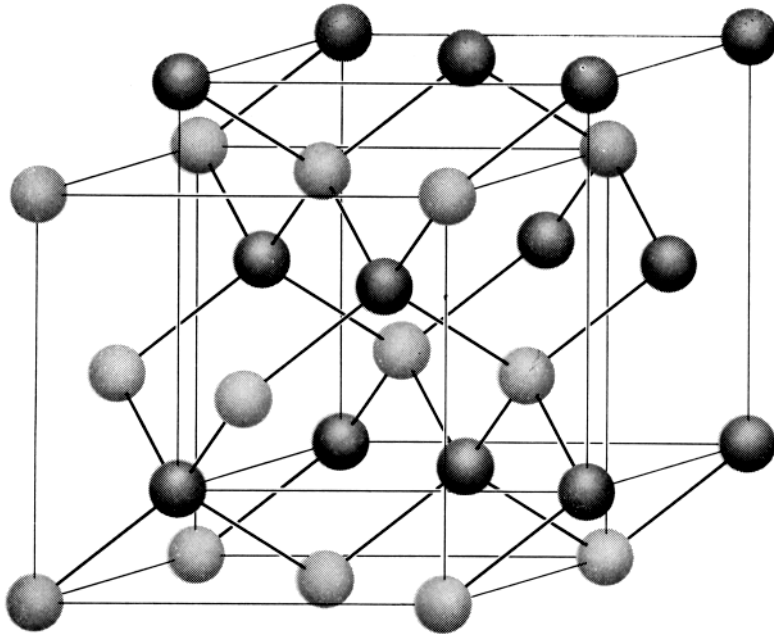


Fig. 2.0.5

Brillouin zone of the zincblende lattice.

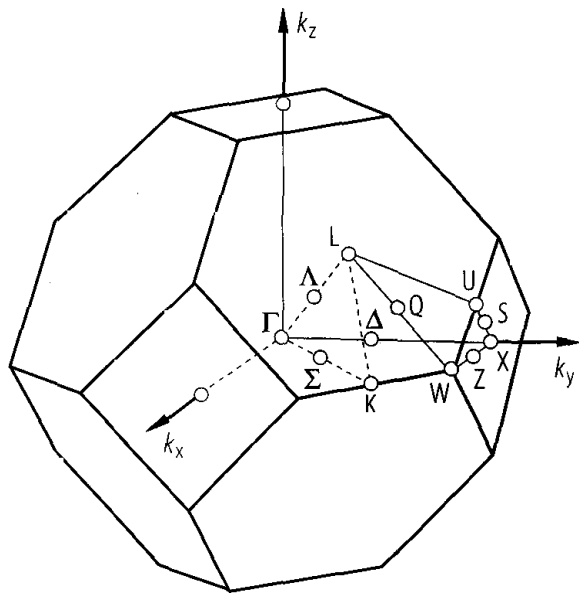


Fig. 2.0.16

AlSb. Band structure calculated with an orthogonalized LCAO method [85H].

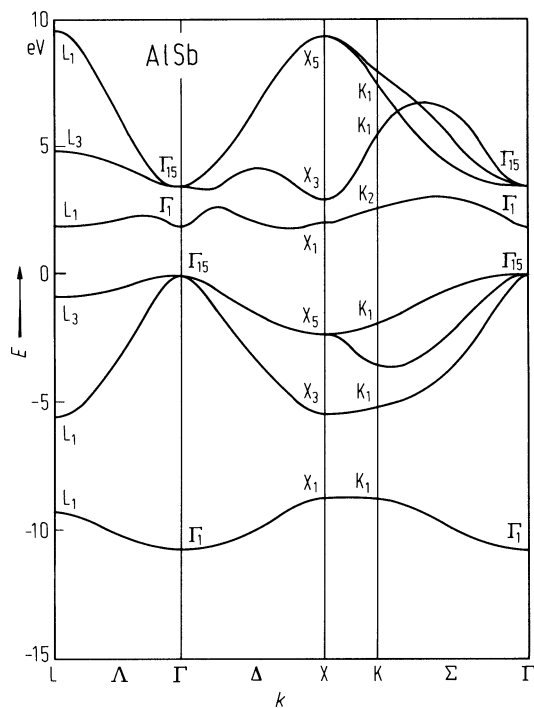


Fig. 2.8.1

AlSb. Indirect energy gap vs. temperature assuming an exciton binding energy of 10 meV [73S]. According to [79G] the binding energy is about 20 meV; thus $E_{g,\text{ind}}$ is about 0.01 eV higher than shown in the figure.

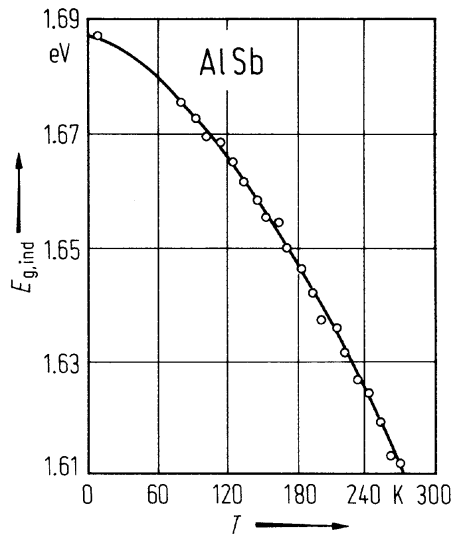


Fig. 2.8.2

AlSb. Coefficient of linear thermal expansion vs. temperature [63N].

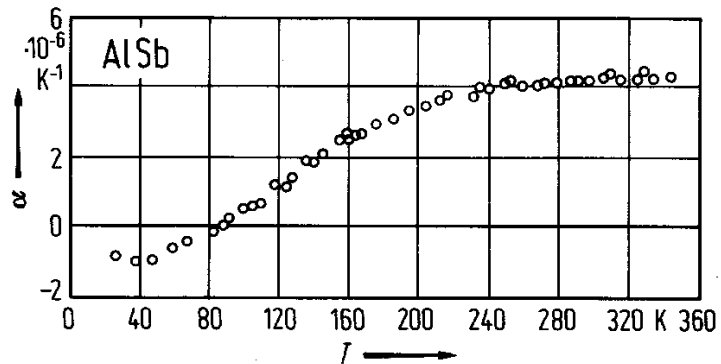


Fig. 2.8.3

AlSb. Density vs. temperature [69G].

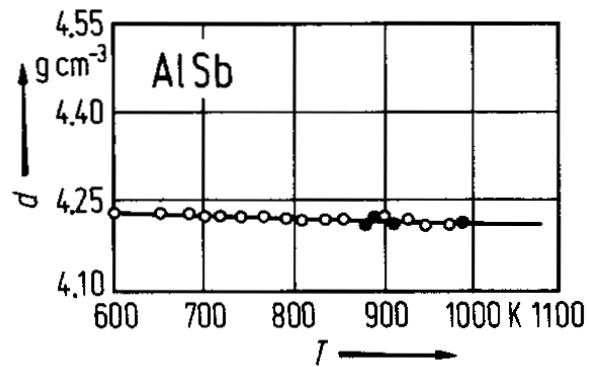


Fig. 2.8.4

AlSb. Phonon dispersion curves (left panel) and phonon density of states (right panel). Experimental data points [90S] and ab-initio calculations [91G]. From [91G].

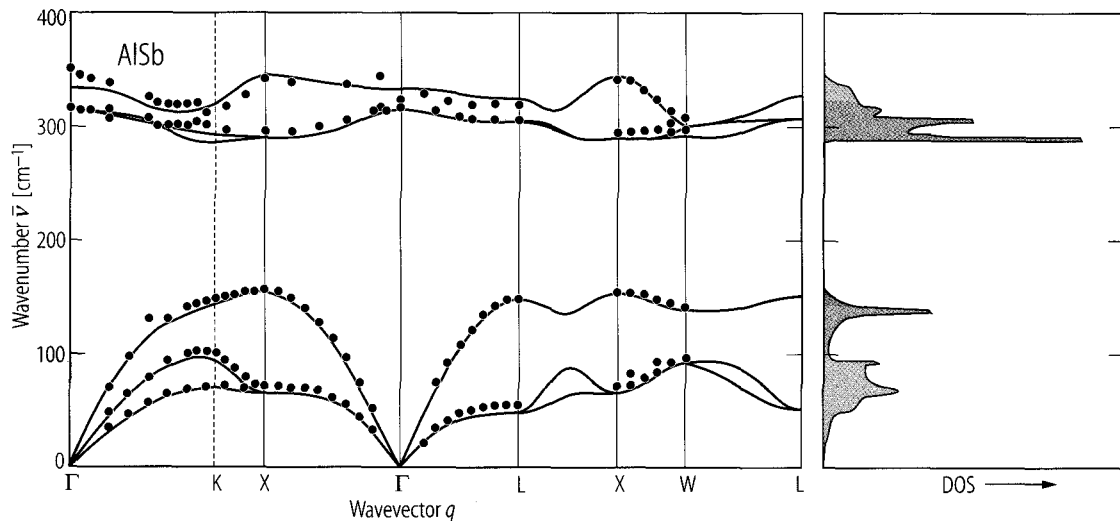


Fig. 2.8.5

AlSb. Debye temperature vs. temperature [59F].

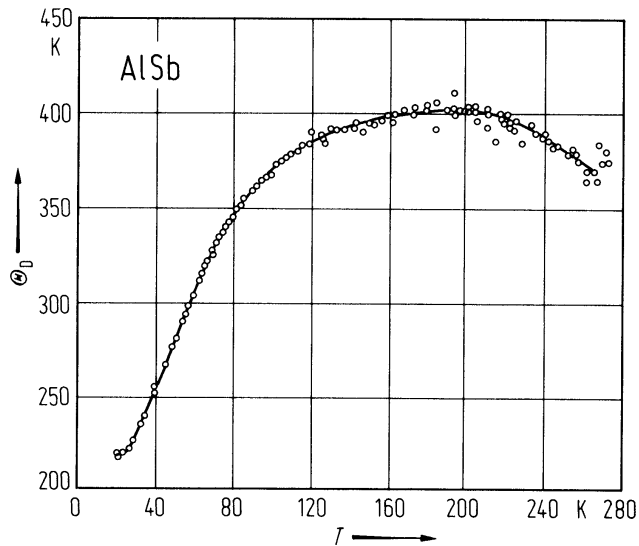


Fig. 2.8.6

AlSb. Electrical conductivity vs. reciprocal temperature for three different polycrystalline p-type samples [53W].

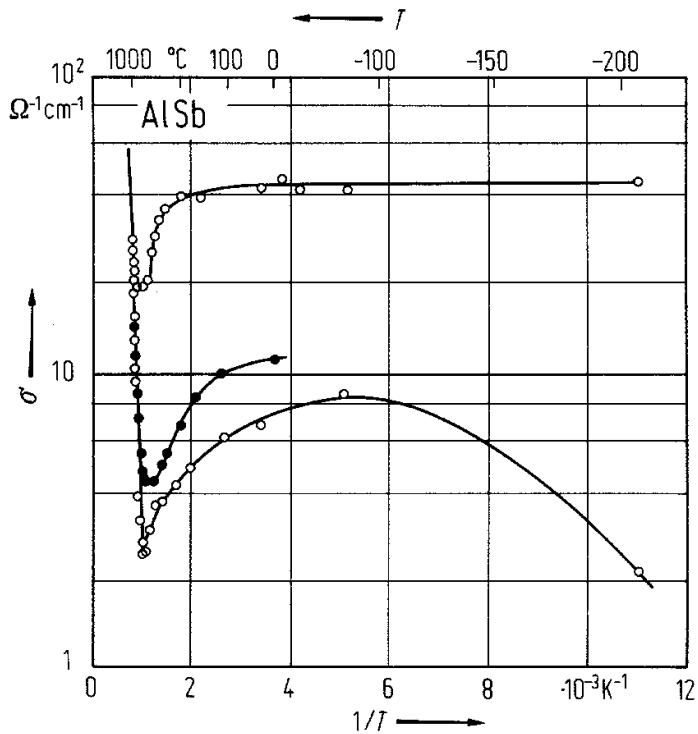


Fig. 2.8.7

AlSb. Thermal conductivity vs. temperature for an n-type and a p-type sample, low temperature range [69M].

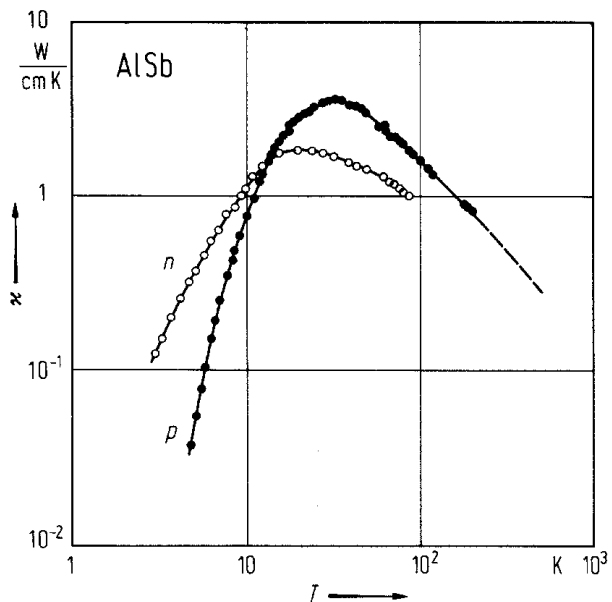


Fig. 2.8.8

AlSb. (a) Electron Hall mobility vs. temperature [66S1, 66S2], (b) hole Hall mobility vs. temperature [58R].

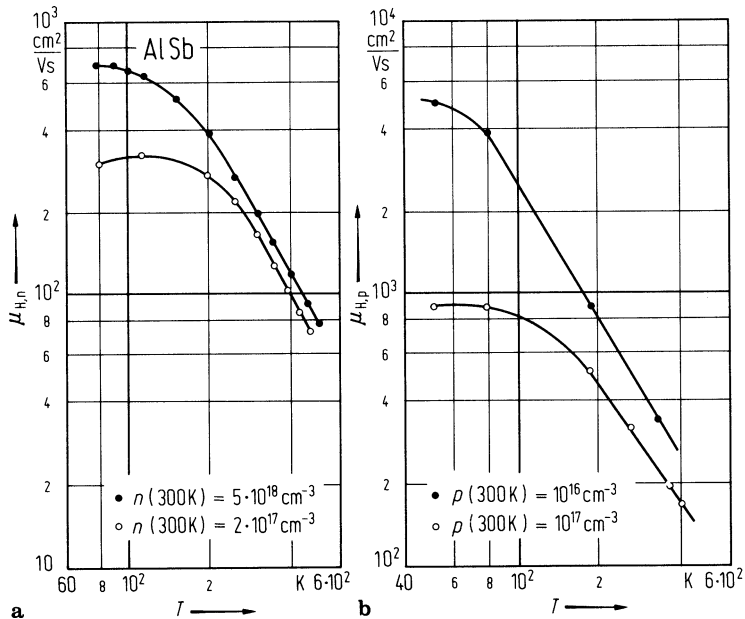


Fig. 2.8.9

AlSb. Refractive index n and extinction coefficient k vs. wavelength in the region of lattice absorption [62T].

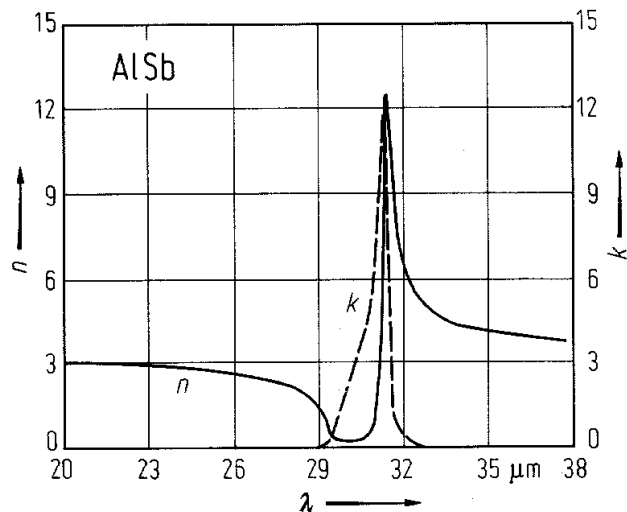
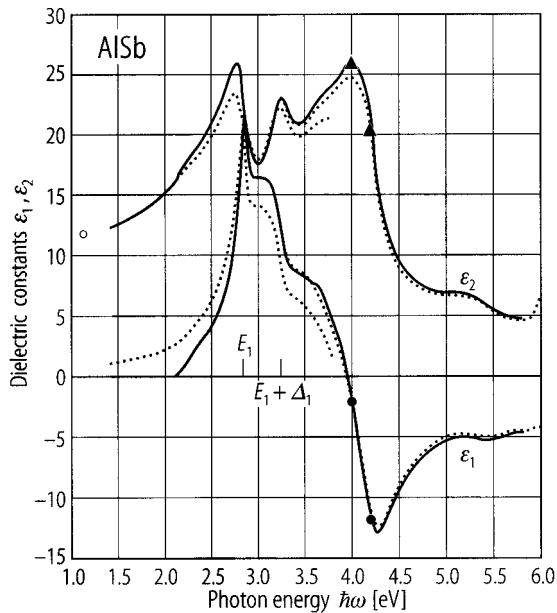


Fig. 2.8.10

AlSb. Real and imaginary part of the dielectric function at 300 K as measured (dotted lines) and after correction for a 0.3 nm thick oxide layer (solid lines) to reproduce the values obtained while etching (closed circles and triangles). A value at 1.13 eV from [67S] is shown for comparison. From [89Z].



2.9 Gallium nitride (GaN)

Crystal structure

The wurtzite structure (α -GaN, space group $P6_3mc$, Fig. 2.0.3) is the stable phase of GaN at ambient pressure. A zincblende phase (β -GaN, Fig. 2.0.2) is very close in energy and can be stabilized by epitaxial growth on cubic substrates.

high pressure phases

GaN undergoes a transition from the wurtzite structure to the rocksalt structure under pressure. The rocksalt structure is stable up to at least 70 GPa [93X]], up to at least 91 GPa [97U].

Electronic properties

band structure (α -GaN)

Fig. 2.0.17 Brillouin zone: Fig. 2.0.8.

Due to spin-orbit interaction the two top valence bands (Γ_6 and Γ_1) split into three spin-degenerate bands with quantum numbers $J_z = 3/2$ (Γ_9), $J_z = 1/2$ (Γ_7), and $J_z = 1/2$ (Γ_7). For convenience the denotation A, B, C is used for the bands.

energy gap

$E_{g,dir}$	3.503(2) eV	$T = 1.6$ K	α -GaN, photoluminescence, from excitonic gap adding the exciton binding energy	74M
	3.4751(5) eV		A-exciton (transition from Γ_{9v})	
	3.4815(10) eV		B-exciton (transition from upper Γ_{7v})	
	3.493(5) eV		C-exciton (transition from lower Γ_{7v})	
	3.44 eV	$T = 300$ K	temperature dependence below 295 K given by $E_g(T)-E_g(0) = -5.08 \cdot 10^{-4} T^2 / (996 - T)$ eV	74M
$E_{g,dir}$	3.17 eV	$T = 300$ K	β -GaN, ellipsometry	95P

exciton ground state

In correspondence with the three valence bands A, B, C one observes a series of A-, B-, C-exciton transitions to the conduction band.

exciton transition energies (α -GaN)

E_{gx}^A	3.4876 eV	$T = 10$ K	photoreflectance,	97C
E_{gx}^B	3.4962 eV		4 μ m thick epitaxial film on sapphire	
E_{gx}^C	3.5320 eV			

See also Fig. 2.9.1.

binding energy of excitons (α -GaN)

The binding energies of the A-, B-, C-excitons are calculated from the energetic difference between the ($n = 1$) ground and ($n = 2$) first excited state transitions, which in a simple hydrogenic effective mass approximation is 3/4 of the binding energy.

A-exciton

E_b^A	20 meV	A-exciton, photoreflectance	96T
E_b^B	18.5 meV	B-exciton, photoreflectance	96T
E_b^C	22.4 meV	C-exciton, photoluminescence	98S

β -GaN:

E_b	26 meV	$T = 2$ K	photoluminescence	97A
-------	--------	-----------	-------------------	-----

higher interband transition energies

α -GaN:

$E_{1A}(\Gamma_{5v}-\Gamma_{3c})$	5.30(5) eV	$\Lambda_{3v} - \Lambda_{3c}$	74B
$E_{1B}(U_{4v}-U_{3c})$	6.25(5) eV	$\Lambda_{3v} - \Lambda_{3c}$	

$E_1(M_{2v}-M_{1c},$ $M_{4v}-M_{3c})$	7.05(5) eV		
$E_2(K_{3v}-K_{2c})$	7.65(5) eV	$X_{5v} - X_{1c}$	
$E'_0(\Gamma_{6v}-\Gamma_{6c})$	8.5(2) eV	$\Gamma_{15v} - \Gamma_{15c}$	
$E'_1(\Gamma_{5v}-\Gamma_{6c})$	9.4(1) eV	$\Lambda_{3v} - \Lambda_{3c}$	

β -GaN:

$E(\Gamma_v-\Gamma_c)$	1.8 eV	$T = 300$ K	LDA-based calculation	95P
$E_0(\Gamma_{15v}-\Gamma_{1c})$	3.25 eV	$T = 300$ K	ellipsometry	94L
$E_1(L_{3v}-L_{1c})$	7.0 eV	$T = 300$ K	ellipsometry	94L
$E_2(X_{3v}-X_{1c})$	7.0 eV	$T = 300$ K	ellipsometry	94L

crystal field splitting and spin-orbit splitting parameters

α -GaN:

$\Delta_1 = \Delta_{cf},$	$3\Delta_3 = 3\Delta_2 = \Delta_{so}$			
Δ_1	9.8 meV		reflectance measurements, epitaxial films	97E
Δ_2	5.6 meV			
Δ_3	5.6 meV			

β -GaN:

Δ_{cf}	17 meV	$T = 10$ K	photoreflectance	96R2
---------------	--------	------------	------------------	------

conduction band, effective masses

α -GaN:

Values are given for polaron mass. Taking the Fröhlich coupling constant $\alpha = 0.49$ the difference between the polaronic and bare electron mass is 10%.

m_n	$0.22 m_0$	$T = 6$ K	cyclotron resonance no anisotropy resolvable	95D
-------	------------	-----------	---	-----

for dependence on electron concentration, see Fig. 2.9.2

$m_{n\perp}$	$0.20(2) m_0$		fit of reflectance spectrum	73B
$m_{n\parallel}$	$0.20(6) m_0$			

β -GaN:

m_n	$0.19 m_0$		calculated	97K
m_{hh}	$0.74 m_0$		calculated	96F
m_{lh}	$0.21 m_0$			
m_{so}	$0.33 m_0$			

valence band, effective masses

α -GaN:

m_A	$1.01\ m_0$	$T = 7\ \text{K}$	estimate from binding energy of A-exciton	97S2
m_B	$1.1\ m_0$	$T = 7\ \text{K}$	estimate from the binding energy of B-exciton	97S2
m_C	$1.6\ m_0$	$T = 7\ \text{K}$	estimate from the binding energy of B-exciton	97S2

Lattice properties

lattice parameters

a	$3.190(1)\ \text{\AA}$	α -GaN, X-ray diffraction, monocrystal		77S1
c	$5.189(1)\ \text{\AA}$			

temperature dependence (a, c in \AA):

$a = 3.1840 + 0.739 \cdot 10^{-5} T + 5.92 \cdot 10^{-9} T^2$, powder X-ray scattering,			$T = 293...1173\ \text{K}$	00I
$c = 5.1812 + 1.455 \cdot 10^{-5} T + 4.62 \cdot 10^{-9} T^2$				
$c/a = 1.6274 + 0.051 \cdot 10^{-5} - 1.5 \cdot 10^{-9} T^2$			see also Fig. 2.9.3	

a	$4.531(5)$	$T = 300\ \text{K}$	β -GaN, X-ray diffraction	93P
-----	------------	---------------------	---------------------------------	-----

thermal expansion coefficients

α_{\parallel}	$5.59 \cdot 10^{-6}\ \text{K}^{-1}$	$T = 300...900\ \text{K}$	X-ray measurements, below 340K $\alpha_{\parallel} > \alpha_{\perp}$,	69M
α_{\perp}	$3.17 \cdot 10^{-6}\ \text{K}^{-1}$	$T = 300...700\ \text{K}$	above 340K $\alpha_{\parallel} < \alpha_{\perp}$, see Fig. 2.9.4	

melting point

T_m	$2791\ \text{K}$			96A3
	$> 2000\ \text{K}$	GaN sublimes without decomposition around 800°C [65M]		74K

density

d	$6.07\ \text{g cm}^{-3}$	α -GaN		96A3
-----	--------------------------	---------------	--	------

phonon dispersion curves : α -GaN: Fig. 2.9.5, β -GaN: Fig. 2.9.6

phonon wavenumbers

$\bar{\nu}_{\text{low}}(E_2)$	$145\ \text{cm}^{-1}$	$T = 300\ \text{K}$	α -GaN, Raman spectroscopy	98S
$\bar{\nu}_{\text{TO}}(A_1)$	$533\ \text{cm}^{-1}$			
$\bar{\nu}_{\text{TO}}(E_1)$	$560\ \text{cm}^{-1}$			
$\bar{\nu}_{\text{high}}(E_2)$	$567\ \text{cm}^{-1}$			
$\bar{\nu}_{\text{LO}}(A_1)$	$735\ \text{cm}^{-1}$			
$\bar{\nu}_{\text{LO}}(E_1)$	$742\ \text{cm}^{-1}$			
$\bar{\nu}_{\text{TO}}$	$554\ \text{cm}^{-1}$	$T = 80\ \text{K}$	β -GaN, Raman	95G
$\bar{\nu}_{\text{LO}}$	$740\ \text{cm}^{-1}$			

sound velocities

v_{11}	7744 m s ⁻¹		α -GaN, Brillouin scattering	97Y1
v_{12}	4702 m s ⁻¹			
v_{13}	4336 m s ⁻¹			
v_{33}	7914 m s ⁻¹			
v_{44}	4240 m s ⁻¹			
v_{66}	4351 m s ⁻¹			

second order elastic moduli

c_{11}	377 GPa	$T = 300$ K	α -GaN, ultrasound resonance technique, 0.29 mm film, 0.2 % accuracy	97S1
c_{12}	160 GPa			
c_{13}	114 GPa			
c_{33}	209 GPa			
c_{44}	81.4 GPa			
c_{11}	264 GPa		β -GaN, estimated from elastic moduli of the wurtzite structure using Martin's formula	91S
c_{12}	153 GPa			
c_{44}	68 GPa			

bulk modulus

B	195 GPa	RT	α -GaN, from powder X-ray diffraction data	78S
-----	---------	----	---	-----

Young's modulus

E	324 GPa		α -GaN, Brillouin scattering	96A2
-----	---------	--	-------------------------------------	------

Debye temperature

Θ_D	608 K		β -GaN (zincblende)	95P
	600 K		α -GaN, estimate from refractive index	71E

Transport properties

Undoped GaN is normally n-type conducting. Carrier concentrations in undoped films might vary from $5 \cdot 10^{19} \text{ cm}^{-3}$ to $5 \cdot 10^{16} \text{ cm}^{-3}$ by unintentional incorporation of extrinsic impurities, mainly silicon and oxygen.

All following data refer to α -GaN.

electrical conductivity

σ	6...12 $\Omega^{-1} \text{ cm}^{-1}$	$T = 300$ K	purest material, $n \approx 10^{17} \text{ cm}^{-3}$, undoped layers grown by vapor phase technique on sapphire	72I, 73I1, 78C
----------	--------------------------------------	-------------	--	----------------

For temperature dependence of resistivity, see Fig. 2.9.7.

thermal conductivity

κ	1.3 W/cm K	$T = 300$ K	$n = 3 \cdot 10^{17} \text{ cm}^{-3}$; see Fig. 2.9.8	77S2
----------	------------	-------------	--	------

carrier mobilities

The mobility depends on different standard scattering mechanisms: piezoelectric acoustic phonon scattering, acoustic deformation potential scattering, ionized impurity scattering, polar mode optical phonon scattering, and additional scattering arising from short range potential of native defects at very high electron concentrations.

electron Hall mobility

in nominally undoped α -GaN films

$\mu_{H,n}$	900 cm ² /Vs	$T = 300$ K, $n = 3 \cdot 10^{16}$ cm ⁻³	α -GaN, Hall effect, see Fig. 2.9.9	92N
-------------	-------------------------	--	--	-----

For temperature dependence, see Fig. 2.9.11

$\mu_{H,n}$	760 cm ² /Vs	$T = 300$ K, $n = 6 \cdot 10^{17}$ cm ⁻³	β -GaN. Hall-measurements	94K
-------------	-------------------------	--	---------------------------------	-----

hole Hall mobility

$\mu_{H,p}$	350 cm ² /Vs	$T = 300$ K, $p = 5 \cdot 10^{13}$ cm ⁻³	β -GaN Hall-measurements	96A4
-------------	-------------------------	--	--------------------------------	------

piezoelectric coefficients

d_{33}	2.0(1) pm/V	$\nu = 1 \dots 100$ kHz	α -GaN, optical interferometry	98M
e_{14}	0.375 C m ⁻²		β -GaN, estimated from mobility	96B

Optical properties

The physical properties are mostly extrinsic (energy gap about 3.5 eV). Thus investigations on luminescence centers etc. are predominant.

Reflection and absorption spectra: Figs. 2.9.10 and 2.9.11.

index of refraction

n	2.29(5)	$T = 300$ K (extra- polated to 0 eV), $E \parallel c$	α -GaN, interference method (the value for $E \parallel c$ is 1.5(2)% lower at 500 nm); for energy dependence, see Fig. 2.9.12	71E
n	2.25		β -GaN, optical transmission at 0.8 eV	96V
	2.50		optical transmission at 3.1 eV	96V

dielectric constants

α -GaN:

$\varepsilon_{\perp}(0)$	10.4(3)		$\varepsilon(\infty)$ assumed to be isotropic	73B
$\varepsilon_{\parallel}(0)$	9.5(3)			
$\varepsilon_{\perp}(\infty)$	5.2(1)	$T = 300$ K	infrared reflectivity	92S
$\varepsilon_{\parallel}(\infty)$	5.2(1)			

β -GaN:

$\varepsilon(0)$	8.9		calculated	98M
$\varepsilon(\infty)$	4.86	$T = 300$ K	optical absorption	96V

Impurities and defects

shallow donors

Undoped GaN is n-type with electron concentrations $n_i \geq 10^{17}$ cm⁻³. The dominant donor is believed to be the nitrogen vacancy [75P]. The binding energy of this donor is subject to large controversy. Values given range from 42(1) meV [71D1] over 29(6) meV [74L] to 17meV [79V]. A deep donor level with $E_d = 110$ meV is also postulated [74V]. No detailed information exists about the identity of these donors.

donor binding energies

Impurity	E_b [meV]	T [K]	Remarks	Ref.
cubic GaN:				
E_D	32 meV	$T = 10 \dots 100$ K	electronic Raman scattering	96R1
	75 meV	$T = 5$ K	cathodoluminescence,	96M2
	25 meV	$T = 2$ K	photoluminescence	97A2
hexagonal GaN:				
residual	29 meV	$T = 1.7$ K	two electron replica of the neutral donor bound exciton of undoped GaN in magnetic field	97S3
residual	31.1 meV	$T = 4.2$ K	1s→2p transition in magnetic field	97M2
residual	33.8 meV	$T = 4.2$ K	1s→2p transition in magnetic field	97M2
residual	34.5 meV	$T = 10$ K	1s→2p transition	95M, 97M1
residual	54 meV	$T = 2$ K	distant donor-acceptor pair recombination	96K1
	57 meV			
Si	29 meV	$T = 5$ K	infrared transmission in magnetic field,	96W
		Si-doped GaN		
Si	34 meV	$T = 9$ K	free hole - neutral donor recombination	97L
		Si-doped GaN		

shallow acceptors

The most shallow residual acceptor has a binding energy of 220 meV and is tentatively identified with C [95F] or V_{Ga} [80M2]. Only by Mg doping efficient p-type conduction is achievable.

acceptor binding energies

Impurity	E_b [meV]	T [K]	Remarks	Ref.
cubic GaN:				
E_A	100	5	cathodoluminescence	96M2
	130	2	photoluminescence	97A
	160	12	photoluminescence	98G
	90	6	photoluminescence,	97W
		acceptor A ₁		
	212	6	photoluminescence,	97W
		acceptor A ₂		
hexagonal GaN:				
C or V _{Ga}	225	4.2	photoluminescence	80M
	225	4.2	photoluminescence	95F
	220	9	photoluminescence	97L
Mg	260	4.2	photoluminescence	89A
	265	9	photoluminescence	97L
	224	60	photoluminescence	97J
			band - acceptor transition	
V _{Ga}	225	4.2	photoluminescence	80M1
Hg	410	78	infrared quenching of luminescence	74E
Li	750			
Zn _{Ga} (A-band)	480	4.2		
	370(40)	4.2	photoluminescence	80M1
Zn _N (B-band)	650(80)			
Zn _N ⁻ (C-band)	1020(50)			
Zn _N ²⁻ (D-band)	1420(80)			

References to 2.9

- 65M Munir, Z. A., Searcy, A. W.: J. Chem. Phys. 42 (1965) 4223.
- 69M Maruska, H. P., Tietjen, J. J.: Appl. Phys. Lett. 15 (1969) 327.
- 71D1 Dingle, R., Ilegems, M.: Solid State Commun. 9 (1971) 175.
- 71D2 Dingle, R., Sell, D. D., Stokowski, S. F., Ilegems, M.: Phys. Rev. B 4 (1971) 1211.
- 71E Ejder, E.: Phys. Status Solidi (a) 6 (1971) K39.
- 72I Ilegems, M.: J. Cryst. Growth 13/14 (1972) 360.
- 73B Barker, A. S., Ilegems, M.: Phys. Rev. B 7 (1973) 743.
- 73I1 Ilegems, M., Dingle, R.: J. Appl. Phys. 44 (1973) 4234.
- 73I2 Ilegems, M., Montgomery, H. C.: J. Phys. Chem. Solids 34 (1972) 885.
- 73P Pankove, J. I.: J. Lumin. 7 (1973) 114.
- 74B Bloom, S., Harbeke, G., Meier, E., Ortenburger, J. B.: Phys. Status Solidi (b) 66 (1974) 161.
- 74E Ejder, E., Grimmeiss, H.G.: Appl. Phys. 5 (1974) 275.
- 74K Kesamanly, F. P.: Sov. Phys. Semicond. (English Transl.) 8 (1974) 147; Fiz. Tekh. Poluprov. 8 (1974) 225.
- 74L Lagerstedt, O., Monemar, B.: J. Appl. Phys. 45 (1974) 2266.
- 74M Monemar, B.: Phys. Rev. B 10 (1974) 676.
- 74V Vavilov, V.S., Makarov, S.I., Chukichev, M.V., Chetverikova, I.F.: Sov. Phys. Semicond. (English Transl.) 13 (1979) 1259; Fiz. Tekh. Poluprovodn. 13 (1979) 2153.
- 75P Pankove, J.I., Bloom, S., Harbeke, G.: RCA Rev. 36 (1975) 163.
- 76S1 Sheleg, A. U., Savastenko, V. A.: Vesti Akad. Nauk BSSR, Ser. Fiz. Mat. Nauk 3 (1976) 126.
- 76S2 Sidorov, V. G., Sveshkova, L. S., Shagalov, M. D., Shalabutov, Yu. K.: Sov. Phys. Semicond. (English Transl.) 10 (1976) 1309; Fiz. Tekh. Poluprov. 10 (1976) 2200
- 77S1 Schulz, H., Thiemann, K. H.: Solid State Commun. 23 (1977) 815.
- 77S2 Sichel, E. K., Pankove, J. I.: J. Phys. Chem. Solids 38 (1977) 330.
- 78C Crouch, R. K., Debnam, W. J., Fripp, A. L.: J. Mater. Sci. 13 (1978) 2358.
- 78S Savastenko, V. A., Sheleg, A. U.: Phys. Status Solidi (a) 48 (1978) K135.
- 79V Vavilov, V.S., Makarov, S.I., Chukichev, M.V., Chetverikova, I.F.: Sov. Phys. Semicond. 13 (1979) 1259.
- 80M1 Monemar, B., Lagerstedt, O., Gislason, H.P.: J. Appl. Phys. 51 (1980) 625.
- 80M2 Monemar, B., Gislason, H.P., Lagerstedt, O.: J. Appl. Phys. 51 (1980) 640.
- 89A Amano, H., Kito, M., Hiramatsu, K., Akasaki, I.: Jpn. J. Appl. Phys. 28 (1989) L2112.
- 91S Sherwin, M. E., Drummond, T. J.: J. Appl. Phys. 69 (1991) 8423.
- 92N Nakamura, S., Mukai, T., Senoh, M.: J. Appl. Phys. 71 (1992) 5543.
- 92S Sobotta, H., Neumann, H., Franzheld, R., Seifert, W.: Phys. Status Solidi (b) (1992) K57.
- 93P Powell, R. C., Lee, N.-E., Kim, Y.-W., Greene, J. E.: J. Appl. Phys. 73 (1993) 189.
- 93X Xia, H., Xia, Q., Ruoff, A. L.: Phys. Rev. B 47 (1993) 12925.
- 94K Kim, J. G., Frenkel, A. C., Liu, H., Park, R. M.: Appl. Phys. Lett. 65 (1994) 91.
- 94L Logothetidis, S., Petalas, J., Cardona, M., Moustakas, T. D.: Phys. Rev. B 50 (1994) 18017.
- 95D Drechsler, M., Hofmann, D. M., Meyer, B. K., Detchprohm, T., Amano, H., Akasaki, I.: Jpn. J. Appl. Phys. 34 (1995) 1178.
- 95F Fischer, S., Wetzel, C., Haller, E.E., Meyer, B.K.: Appl. Phys. Lett. 67 (1995) 1298.
- 95G Giehler, M., Ramsteiner, M., Brandt, O., Yang, H., Ploog, K. H.: Appl. Phys. Lett. 67 (1995) 733.
- 95M Meyer, B.K., Volm, D., Graber, A., Alt, H.C., Detchprohm, T., Amano, H., Akasaki, I.: Solid State Commun. 95 (1995) 597.
- 95P Petalas, J., Logothetidis, S., Boultaakis, S., Alouani, M., Wills, J. M.: Phys. Rev. B 52 (1995) 8082.
- 95S Shan, W., Schmidt, T. J., Yang, X. H., Hwang, S. J., Song, J. J., Goldenberg, B.: Appl. Phys. Lett. 66 (1995) 985.
- 96A1 Azuhata, T., Matsunaga, T., Shimada, K., Yoshida, K., Sota, T., Suzuki, K., Nakamura, S.: Physica B 219 & 220 (1996) 493;
- 96A2 Azuhata, T., Sota, T., Suzuki, K.: J. Phys. Condens. Matter 8 (1996) 3111.
- 96A3 Ambacher, O., Bergmaier, A., Brandt, M. S., Dimitrov, R., Dollinger, G., Fischer, R. A., Miehr, A., Metzger, T., Stutzmann, M.: J. Vac. Sci. Technol. 14 (1996) 3532.
- 96A4 As, D. J., Schikora, D., Greiner, A., Lübbers, M., Mimkes, J., Lischka, K.: Phys. Rev. B 54 (1996) R11118.
- 96B Bykhovski, A. D., Kaminski, V. V., Shur, M. S., Chen, Q. C., Khan, M. A.: Appl. Phys. Lett. 68 (1996) 818.
- 96F Fan, W. J., Li, M. F., Chong, T. C., Xia, J. B.: J. Appl. Phys. 79 (1996) 188.

- 96K1 Kaufmann, B., Dörnen, A., Härle, V., Bolay, H., Scholz, F., Pensl, G.: Appl. Phys. Lett. 68 (1996) 203.
- 96K2 Kaufmann, U., Kunzer, M., Merz, C., Akasaki, I., Amano, H.: Mater. Res. Soc. Symp. Proc. 395 (1996) 633.
- 96M1 Mohammad, S.N., Morkoc, H.: Prog. Quant. Electr. 20 (1996) 361.
- 96M2 Menninger, J., Jahn, U., Brandt, O., Yang, H., Ploog, K.: Phys. Rev. B 53 (1996) 1881.
- 96R1 Ramsteiner, M., Menninger, J., Brandt, O., Yang, H., Ploog, K.H.: Appl. Phys. Lett. 69 (1996) 1276.
- 96R2 Reynolds, D. C., Look, D. C., Kim, W., Aktas, O., Botchkarev, A., Salvador, A., Morkoc, H., Talwar, D. N.: J. Appl. Phys. 80 (1996) 594.
- 96T Tchounkeu, M., Briot, O., Gil, B. Alexis, J.P., Aulombard, R.L.: J. Appl. Phys. 80 (1996) 5352.
- 96V Vidal, M. A., Ramirez-Flores, G., Navarro-Contreras, H., Lastras-Martinez, A., Powell, R. C., Greene, J. E.: Appl. Phys. Lett. 68 (1996) 441.
- 96W Wang, Y.J., Ng, H.K., Doverspike, K., Gaskill, D.K., Ikeda, T., Akasaki, I., Amano, H.: J. Appl. Phys. 79 (1996) 8007.
- 97A As, D. J., Schmilgus, F., Wang, C., Schöttker, B., Schikora, D., Lischka, K.: Appl. Phys. Lett. 70 (1997) 1311.
- 97C Chichibu, S., Okumura, H., Nakamura, S., Feuillet, G., Azuhata, T.: Jpn. J. Appl. Phys. 36 (1997) 1976.
- 97E Edwards, N. V., Yoo, S. D., Bremser, M. D., Weeks Jr., T. W., Nam, O. H., Liu, H., Stall, R. A., Horton, M. N., Perkins, N. R., Kuech, T. F., Aspnes, D. E.: Appl. Phys. Lett. 70 (1997) 2001.
- 97J Johnson, M.A.L., Yu, Z., Boney, C., Hughes, W.C., Cook jr., J.W., Schetzina, J.F., Zhao, H., Skromme, B.J., Edmond, J.A.: Mater. Res. Soc. Symp. Proc. 449 (1997) 215.
- 97K Kim, K., Lambrecht, W. R. L., Segall, B., van Schilgaarde, M.: Phys. Rev. B 56 (1997) 7363.
- 97L Leroux, M., Beaumont, B., Grandjean, N., Massies, J., Gibart, P.: Mater. Res. Soc. Symp. Proc. 449 (1997) 695.
- 97M1 Meyer, B.K.: Mater. Res. Symp. Proc. 449 (1997) 497.
- 97M2 Moore, W.J., Freitas, J.A., Molnar, R.J.: Phys. Rev. B 56 (1997) 12073.
- 97S1 Schwarz, R. B., Khachatryan, K., Weber, E. R.: Appl. Phys. Lett. 70 (1997) 1122.
- 97S2 Steube, M., Reimann, K., Fröhlich, D., Clarke, S. J.: Appl. Phys. Lett. 71 (1997) 948.
- 97S3 Skromme, B.J., Zhao, H., Goldenberg, B., Kong, H.S., Leonard, M.T., Bulman, G.E., Abernathy, C.R., Pearton, S.J.: Mater. Res. Soc. Symp. Proc. 449 (1997) 713.
- 97U Uehara, S., Masamoto, T., Onodera, A., Ueno, M., Shimomura, O., Takemura, K.: J. Phys. Chem. Solids 58 (1997) 2093.
- 97W Wu, J., Yaguchi, H., Onabe, K., Ito, R.: Appl. Phys. Lett. 71 (1997) 2067.
- 97Y1 Yamaguchi, M., Yagi, T., Azuhata, T., Sota, T., Suzuki, K., Chichibu, S., Nakamura, S.: J. Phys. Condens. Matter 9 (1997) 241.
- 98D1 Davydov, V. Yu., Kitaev, Yu. E., Goncharuk, I. N., Smirnov, A. N., Graul, J., Semchinova, O., Uffmann, D., Smirnov, M. B., Mirgorodsky, A. P., Evarestov, R. A.: Phys. Rev. B 58 (1998) 12899.
- 98G Godlewski, M., Yu Ivanov, V., Bergman, J.P., Monemar, B., Barski A., Langer, R.: Mater. Sci. Forum 264-268 (1998) 1343.
- 98K1 Karch, K., Wagner, J. M., Bechstedt, F.: Phys. Rev. B 57 (1998) 7043.
- 98M1 McGill, S. A., Cao, K., Fowler, W. B., DeLeo, G. G.: Phys. Rev. B 57 (1998) 8951.
- 98M2 Muensit, S., Guy, I. L.: Appl. Phys. Lett. 72 (1998) 1896.
- 98S Siegle, H.: Thesis, Berlin (1998).
- 98S Skromme, B.: Mater. Sci. Eng. B 50 (1998) 117.
- 00I Iwanaga, H., Kunishige, A., Takeuchi, S.: J. Mater. Sci. 35 (2000) 2451.

Figures to 2.9

Fig. 2.0.2

The zincblende lattice

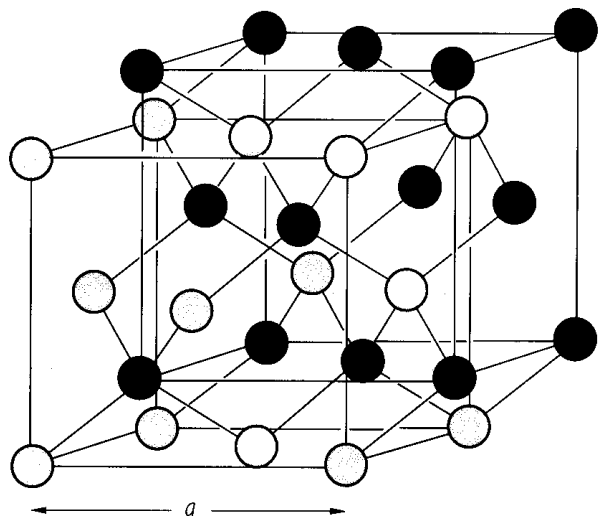


Fig. 2.0.3

The wurtzite lattice

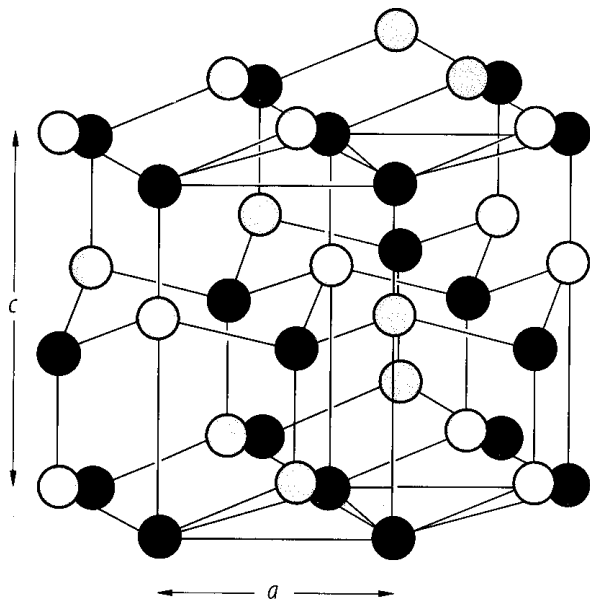


Fig. 2.0.8

The hexagonal Brillouin zone.

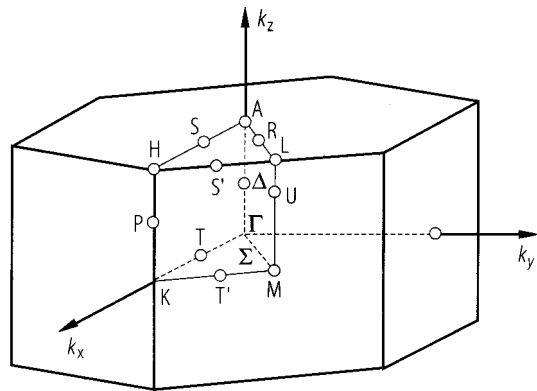


Fig. 2.0.17

GaN. Band structure calculated with an empirical pseudopotential method [74B].

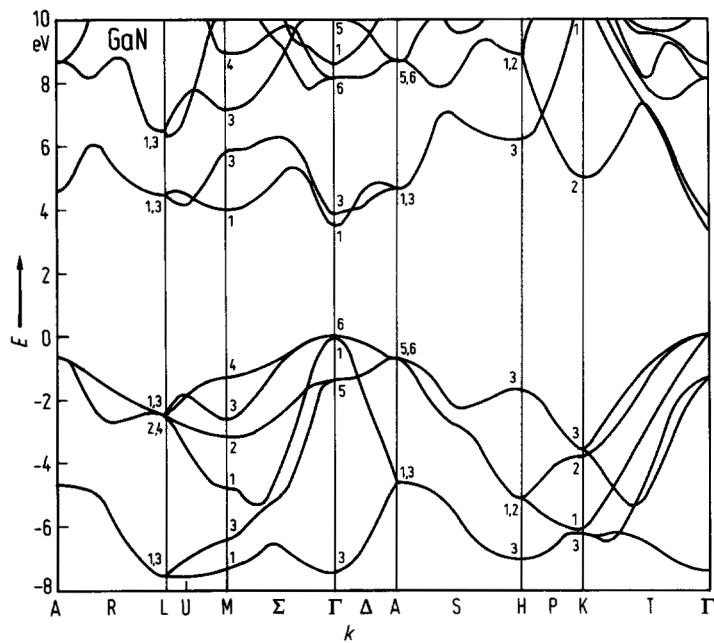


Fig. 2.9.1

α -GaN. Interband transition energies of excitons vs. temperature [95S].

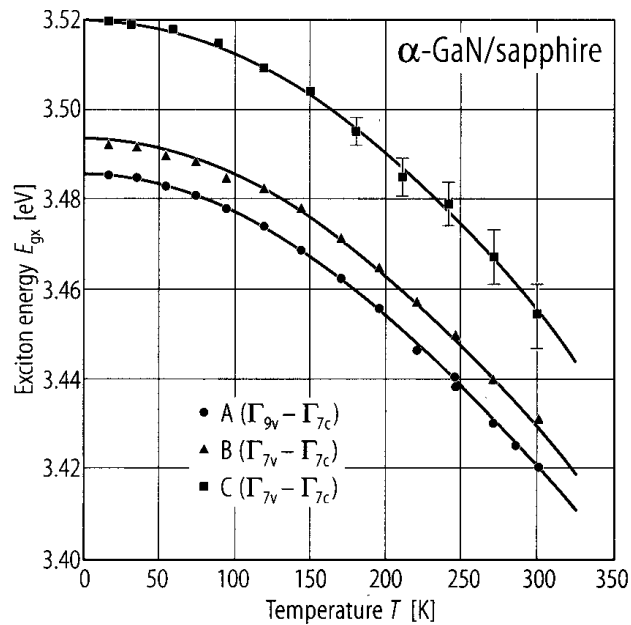


Fig. 2.9.2

GaN. Effective electron mass vs. electron concentration determined from Seebeck effect. Curve 1: acoustic-phonon scattering assumed, curve 2: impurity scattering assumed [76S2].

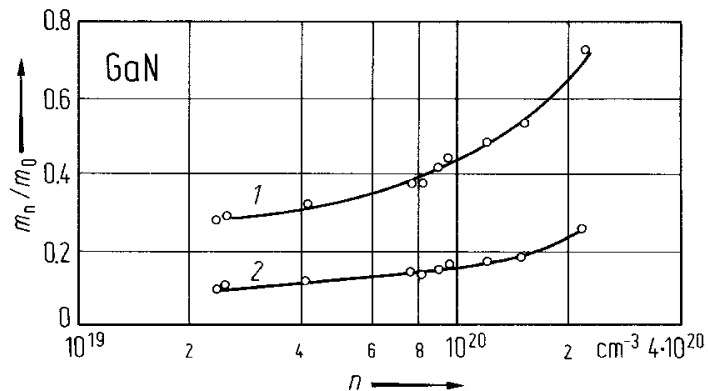


Fig. 2.9.3

GaN. Lattice parameters a and c vs. temperature for a single crystal layer [69M].

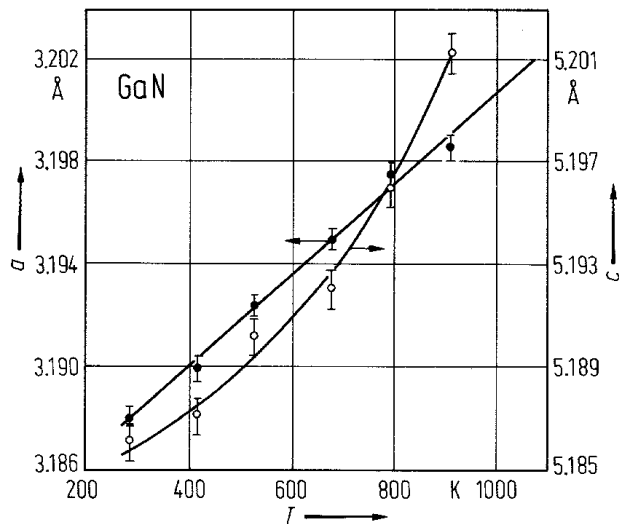


Fig. 2.9.4

GaN. Coefficient of linear thermal expansion vs. temperature; curve 1: α_{\perp} , 2: α_{\parallel} [76S1].

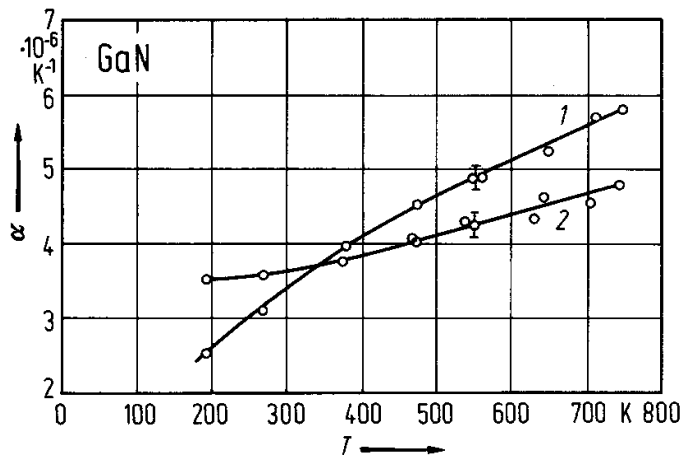


Fig. 2.9.5

GaN (wurtzite structure). Phonon dispersion curves (decomposed according to different irreducible representations along the main symmetry directions) and density of states from a model-potential calculation. The solid squares are Raman data from [96A1]. From [98D1].

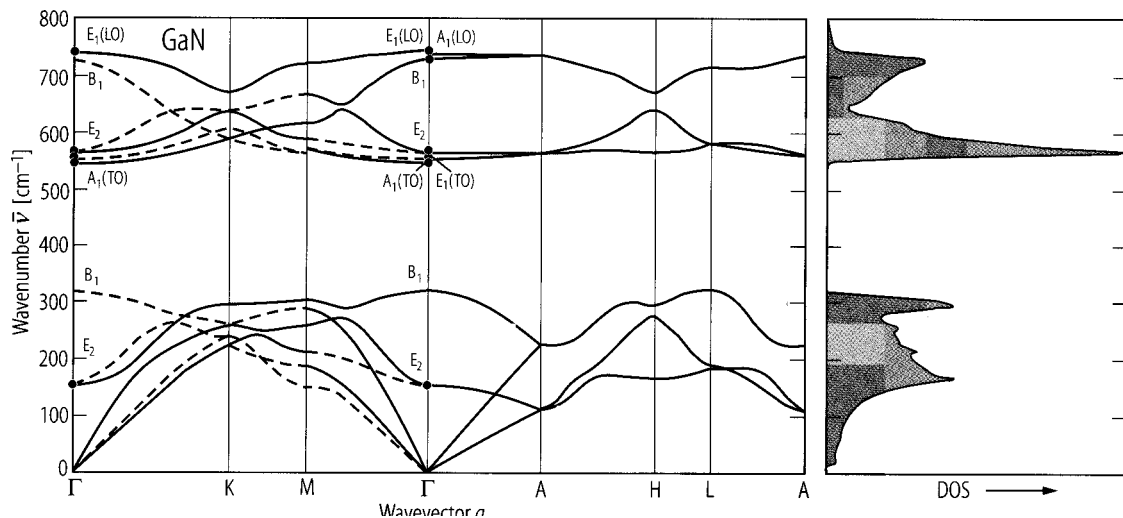


Fig. 2.9.6

GaN (cubic). Phonon dispersion curves (left) and phonon density of states (right) from an ab-initio pseudopotential calculation [97K, 98K1, 98S].

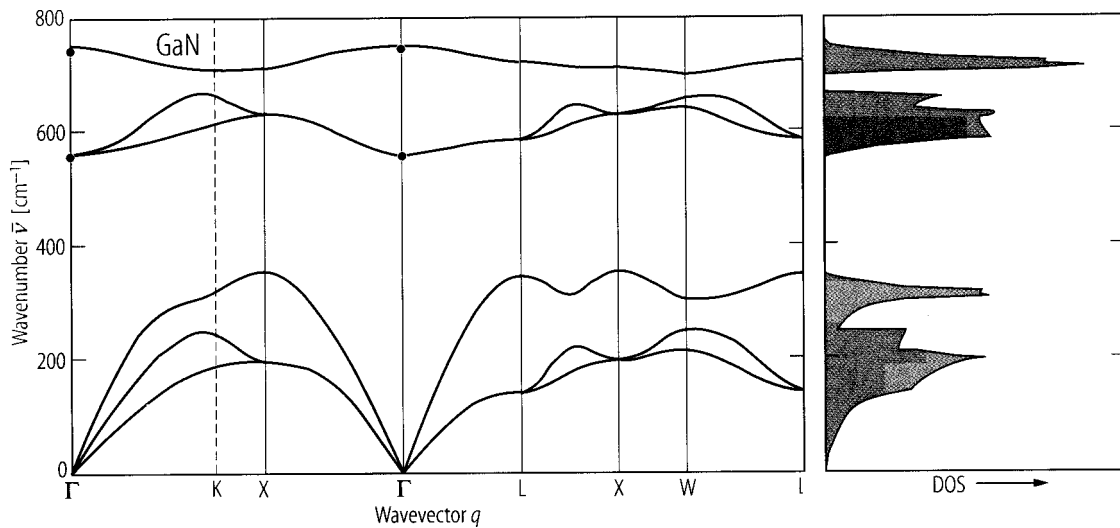


Fig. 2.9.7

GaN. Resistivity of several undoped (1...7) and a Zn-doped (8) sample vs. reciprocal temperature [7312].

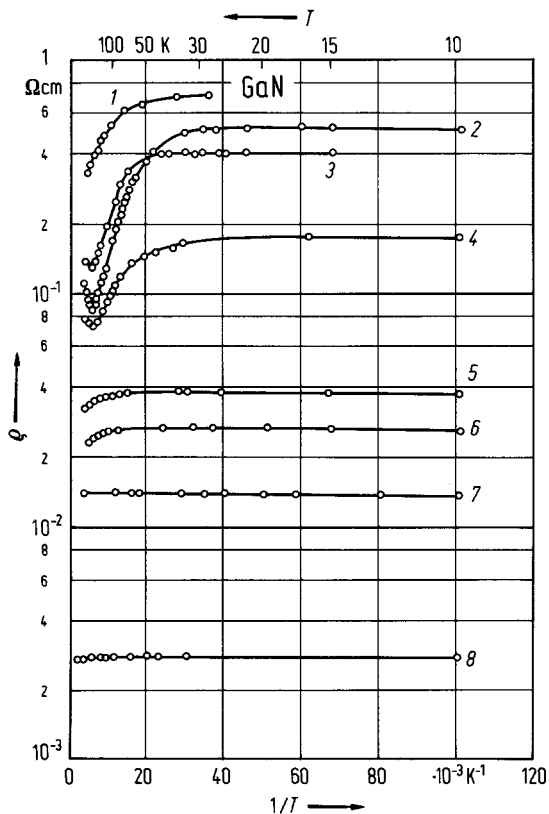


Fig. 2.9.8

GaN. Thermal conductivity along the c -axis vs. temperature [77S2].

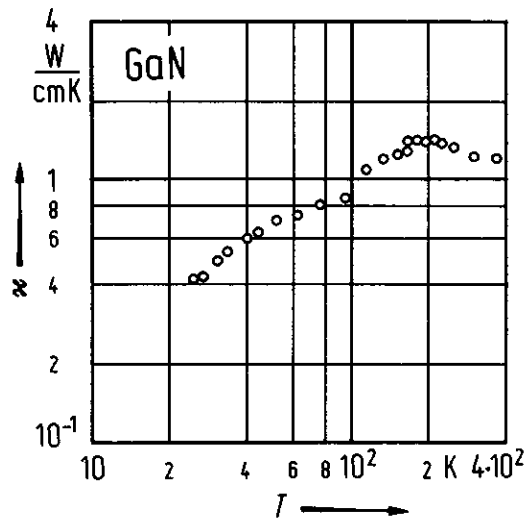


Fig. 2.9.9

GaN. Electron Hall mobility vs. temperature for 2 samples [73I2].

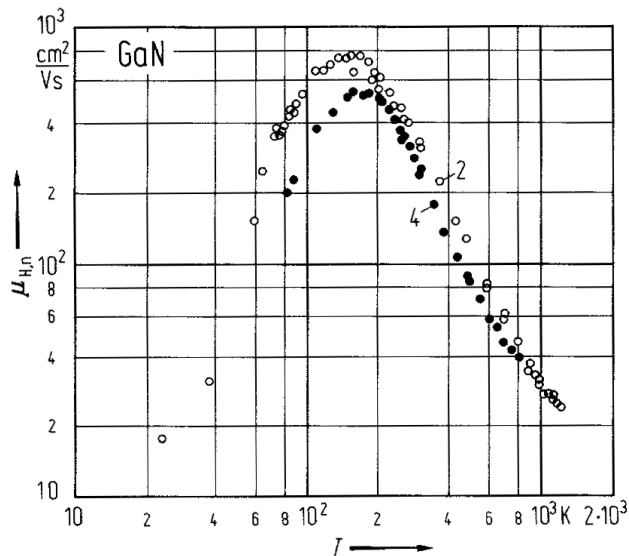


Fig. 2.9.10

GaN. Reflection coefficient vs. photon energy at 2 K [71D2]. The three polarizations are $\pi(E \parallel c, k \perp c)$, $\sigma(E \perp c, k \perp c)$, $\alpha(E \parallel c, k \parallel c)$.

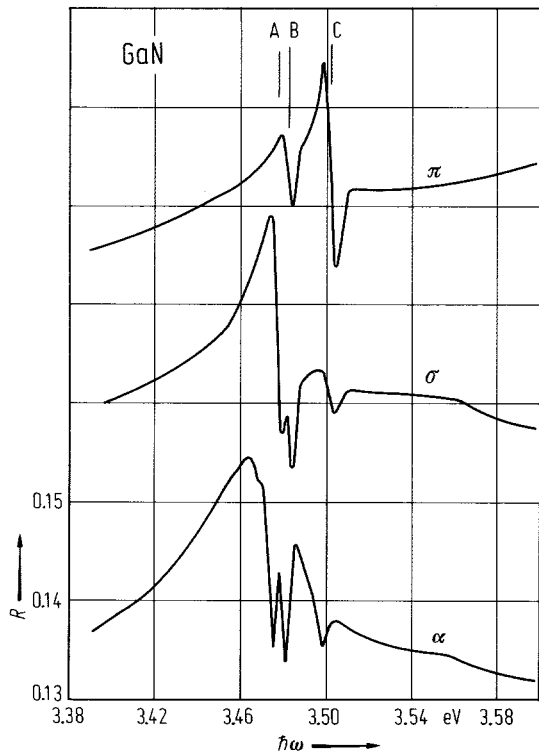


Fig. 2.9.11

GaN. Absorption coefficient vs. wavelength in the region of free electron absorption. The solid line has a slope of 3.4 [73P].

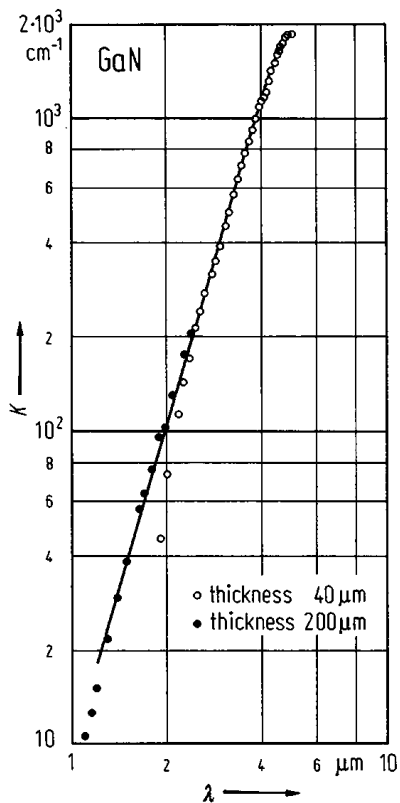
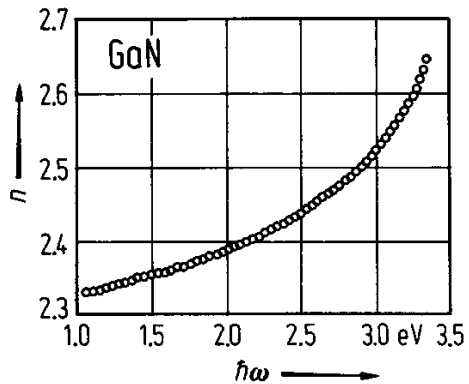


Fig. 2.9.12

GaN. Refractive index vs. photon energy at 300 K; $E \perp c$ [71E].



2.10 Gallium phosphide (GaP)

Crystal structure

Under normal conditions gallium phosphide crystallizes in the zincblende structure ($T_d^2 - F\bar{4}3m$, Fig. 2.0.2). GaP can also be grown in the wurtzite structure.

high pressure phases

Under pressure, the zincblende structure is transformed to the β -tin structure (GaP-II) above a pressure which depends on the (non)hydrostatic conditions (21 GPa [82B2]; 30 GPa [84H]; 26 GPa [89I]); GaP-I and GaP-II coexist above 15 GPa [84H]. The β -tin structure was questioned in favour of a face-centred tetragonal structure [78Y, 82B2, 90P] and was recently identified as having Cmc m symmetry [96M, 97N].

Electronic properties

band structure : Fig. 2.0.18, Brillouin zone: Fig. 2.0.5.

GaP is an indirect gap semiconductor. The lowest set of conduction bands shows a camel's back structure: the band minima are situated at the Δ -axes near the zone boundary. A higher band minimum at Γ is responsible for direct transitions in optical absorption. The valence bands show the usual structure characteristic for all zincblende semiconductors.

The band structure shown in Fig. 2.10.1 has been calculated without inclusion of spin-orbit splitting; therefore the symmetry symbols of the high symmetry band states are symbols of the single group of the zincblende structure.

energies of symmetry points of the band structure (relative to the top of the valence band $E(\Gamma_{15v})$)

$E(\Gamma_{1v})$	- 12.99 eV	- 12.3 eV	- 13.2 eV	symmetry symbols in single group notation first row: theoretical data according to [76C1] second row: experimental data from angle resolved photoemission [84S1] third row: XPS data [74L]
$E(\Gamma_{1c})$	2.88 eV			
$E(\Gamma_{15c})$	5.24 eV			
$E(X_{1v})$	- 9.46 eV		- 9.6 eV	
$E(X_{3v})$	- 7.07 eV	- 6.8 eV		
$E(X_{5v})$	- 2.73 eV	- 3.0 eV	- 2.7 eV	
$E(X_{1c})$	2.16 eV			
$E(X_{3c})$	2.71 eV			
$E(L_{1v})$	- 10.60 eV	- 10.8 eV	- 10.6 eV	
$E(L_{2v})$	- 6.84 eV	- 6.8 eV	- 6.9 eV	
$E(L_{3v})$	- 1.10 eV	- 0.9 eV	- 1.2 eV	
$E(L_{1c})$	2.79 eV			
$E(L_{3c})$	5.74 eV			
$E(\Sigma_1^{\min})$	- 4.3 eV	- 3.8 eV	- 4.0 eV	

indirect energy gap

$E_{g, \text{ind}}(\Gamma_{8v}-\Delta_{5c})$	2.350(1) eV	$T = 0 \text{ K}$, extrapol.	from exciton data and X_7 binding energy	78H
	2.272 eV	$T = 300 \text{ K}$	from [78H] using temperature dependence of excitonic gap	

For temperature dependence of excitonic gap, see Fig. 2.10.1. For $E_g(T)$, see also Fig. 2.10.2.

second indirect energy gap

$E_{g, \text{ind}}$ ($\Gamma_{15v}-L_{1c}$)	2.637(10) eV	$T = 78 \text{ K}$	electroabsorption	78K
--	--------------	--------------------	-------------------	-----

camel's back structure near conduction band minimum, effective masses

Δ	355 meV (295(10) meV)		fitting of cyclotron resonance data obtained	83M1 83M2
Δ_0	433 meV		in very high magnetic fields	
m_t	$0.25 m_0$			
m_l	$0.91 m_0$			
ΔE	3.5 meV		from $\Delta E = (\Delta_0/4)(1 - \Delta/\Delta_0)^2$	83M1
$m_{ }$	$10.9 m_0$		from $m_{ } = m_l (1 - (\Delta/\Delta_0)^2)^{-1}$	83M2
k_m	$0.025(2\pi/a)$		from $k_m = (2m_l\Delta E/(h/2\pi)^2)^{1/2}$	

location of conduction band minimum

k_0	$0.07\dots 0.1(2\pi/a)$	$T = 4.2$ K	wavelength modulated spectroscopy with uniaxial stress	78H
-------	-------------------------	-------------	---	-----

exciton ground state

$E_{gx}(1S, X_7)$	2.3284 eV	$T = 4.2$ K	excitonic gap from wavelength modulated transmission; this value corresponds to the dip of the camel's back	78H
$E(1S, X_6-X_7)$	1.9 meV 2.3 meV	$T = 4.2$ K	valley-anisotropy splitting of the exciton ground state at the dip (1.9 meV) and the hump (2.3 meV) of the camel's back [78G]	78H
$\Delta_{cb}(X_7)$	2.4 meV		height of the camel's back of the X_7	78H
$\Delta_{cb}(X_6)$	2.8 meV		and of the X_6 exciton	

direct energy gap

$E_{g, dir}(\Gamma_{8v}-\Gamma_{6c})$	2.895(4) eV	$T = 0$ K (extra- polated)	photoconductivity temperature dependence $E_0(\text{eV}) = 2.895(4) - 1.17(1) \cdot 10^{-6} T^2$ eV, ($T < 300$ K)	64N
---------------------------------------	-------------	-------------------------------	--	-----

For temperature dependence of the direct excitonic gap, see Fig. 2.10.2.

spin-orbit splitting energy at the top of the valence band

(splitting of Γ_{15v} into Γ_{8v} (upper level) and Γ_{7v} (lower level))

$\Delta_0(\Gamma_{8v}-\Gamma_{7v})$	0.080(3) eV	$T = 100\dots 200$ K	wavelength modulated reflectivity	83T
-------------------------------------	-------------	----------------------	--------------------------------------	-----

higher band-band transitions (critical point energies)

$E_0+\Delta_0(\Gamma_{7v}-\Gamma_{6c})$	2.949(1) eV	$T = 2$ K	energy-derivative reflectance (transition from split-off valence band to lowest conduction band in Γ)	72S1
$E'_0(\Gamma_{8v}-\Gamma_{7c})$	4.77(1) eV	$T = 2$ K		72S1
$E'_0(\Gamma_{8v}-\Gamma_{8c})$	4.85(1) eV		same transition with spin-orbit splitting resolved	
$E''_0(\Gamma_{15v}-\Gamma_{1c})$	9.38(1) eV	$T = 80$ K	electroreflectance	75A1
$E'''_0(\Gamma_{15v}-\Gamma_{15c})$	10.27(1) eV	$T = 80$ K		
$E_1(L_{3v}-L_{1c})$	3.91(1) eV	$T = 80$ K		
$E_1(\Lambda_{4,5}-\Lambda_{6c})$	3.785(5) eV	$T = 2$ K	energy-derivative reflectance	72S1
$E_1+\Delta_1(\Lambda_{6v}-\Lambda_{6c})$	3.835(5) eV	$T = 2$ K		
$E'_1(\Lambda_{4,5v}-\Lambda_{3c})$	6.80(5) eV	$T = 80$ K	electroreflectance	75A1
$E''_1(L_{3v}-L_{2c})$	10.7(2) eV	$T = 80$ K		
$E_2(\Sigma)$	5.21(1) eV	$T = 2$ K	energy-derivative reflectance	72S1

conduction band, effective masses

The longitudinal electron mass at the Δ -minimum is strongly energy dependent because of the camel's back structure.

m_{\perp} (near Δ_{\min})	0.21 m_0	$T = 1...20$ K	luminescence ($m_{\parallel}/m_{\perp} \approx 5.5$)	68K
m_{\parallel} (near Δ_{\min})	7.25 m_0		effective mass at bottom of camel's back	79B1
m_{\parallel} (away of Δ_{\min})	2.2 m_0		effective mass high above the bottom of camel's back	79B1

valence band, effective masses

$m_{p,h}$	0.67(4) m_0	$\parallel [111]$	cyclotron resonance at 1.6K	72S2
$m_{p,l}$	0.17(1) m_0	$\parallel [111]$	cyclotron resonance at 1.6K	72S2
$m_{p,so}$	0.4649 m_0	$T = 0$ K	calculated from $k\cdot p$ model	83S1

valence band parameters

A	-4.20		calculated using $k\cdot p$ theory	75W
B	-1.97			
$ C $	4.60			

Lattice properties

lattice parameter

a	5.4506(4) Å	RT	single crystal temperature dependence: Fig. 2.10.3	73K
-----	-------------	----	---	-----

linear thermal expansion coefficient

α	$4.65 \cdot 10^{-6}$ K ⁻¹	$T = 300$ K	recommended value (accuracy 10%) temperature dependence: Fig. 2.10.4	75S
----------	--------------------------------------	-------------	---	-----

density

d	4.138 g cm ⁻³	$T = 300$ K		77M
-----	--------------------------	-------------	--	-----

melting temperature

T_m	1749 K			94A
-------	--------	--	--	-----

phonon dispersion curves : Fig. 2.10.5, Brillouin zone: Fig. 2.0.5

phonon frequencies

$\nu(\Gamma)$	10.95(1) THz 12.06(1) THz	TO, RT LO	from an analysis of Raman, neutron, luminescence and absorption data	83P
$\nu(X)$	3.13(3) THz 7.46(6) THz	TA LA		
$\nu(L)$	10.58(3) THz	TO		
	11.09(6) THz	LO		
	2.58 (3) THz	TA		
	6.45 (3) THz	LA		
	10.64(3) THz	TO		
	11.24(3) THz	LO		

sound velocities

v_1	$5.847 \cdot 10^5 \text{ cm s}^{-1}$	$T = 300 \text{ K}$	n-type, $n \approx 5 \cdot 10^{16} \text{ cm}^{-3}$ ultrasound	68W
v_2	$4.131 \cdot 10^5 \text{ cm s}^{-1}$		($f = 12 \text{ MHz}$)	
v_6	$6.648 \cdot 10^5 \text{ cm s}^{-1}$		designation: mode/direction of propaga- tion/direction of particle displacement	
v_7	$3.466 \cdot 10^5 \text{ cm s}^{-1}$		v_1 : long./001/001, v_2 : shear/001/110, v_6 : long/111/111, v_7 : shear/111/1 $\bar{1}$ 0	

second order elastic moduli

c_{11}	$14.050(28) \cdot 10^{11} \text{ dyn cm}^{-2}$	$T = 300 \text{ K}$	ultrasound ($f = 10/30 \text{ MHz}$)	81Y
c_{12}	$6.203(24) \cdot 10^{11} \text{ dyn cm}^{-2}$		temperature dependence: Fig. 2.10.6	
c_{44}	$7.033(7) \cdot 10^{11} \text{ dyn cm}^{-2}$			

third order elastic moduli

c_{111}	$-7.37 \cdot 10^{12} \text{ dyn cm}^{-2}$	$T = 300 \text{ K}$	ultrasound ($f = 10/30 \text{ MHz}$);	81Y
c_{112}	$-4.74 \cdot 10^{12} \text{ dyn cm}^{-2}$		hydrostatic pressure up	
c_{123}	$-1.31 \cdot 10^{12} \text{ dyn cm}^{-2}$		to 1.5 kbar, uniaxial	
c_{144}	$-1.07 \cdot 10^{12} \text{ dyn cm}^{-2}$		pressure up to 30 bar	
c_{155}	$-2.34 \cdot 10^{12} \text{ dyn cm}^{-2}$			
c_{456}	$-0.62 \cdot 10^{12} \text{ dyn cm}^{-2}$			

Young's moduli and torsional modulus

E_{100}	$10.173 \cdot 10^{11} \text{ dyn cm}^{-2}$	$T = 300 \text{ K}$	$n = 2 \cdot 10^{17} \text{ cm}^{-3}$, ultrasound	78G
G_{100}	$7.034 \cdot 10^{11} \text{ dyn cm}^{-2}$	$T = 300 \text{ K}$		

bulk modulus

B	87.4 GPa			89I
-----	----------	--	--	-----

Debye temperature

Θ_D	445 K		for temperature dependence, see Fig. 2.10.7	68W
------------	-------	--	--	-----

heat capacity

C_p	$49.4 + 1.34 \cdot 10^{-3} T - 5.26 \cdot 10^5 T^{-2}$	$\text{J mol}^{-1} \text{ K}^{-1}$	$T = 800 \dots 1510 \text{ K}$	90I
-------	--	------------------------------------	--------------------------------	-----

Transport properties

Intrinsic conductivity in GaP occurs even in high purity samples only above 500°C. GaP therefore is an extrinsic semiconductor. In n-type material above 100 K the transport is limited by intervalley and acoustic-mode scattering [75R, 75K] and in p-type material above room temperature by acoustic-mode and nonpolar optical-mode scattering [75W, 76S].

As in GaAs semi-insulating GaP can be obtained by doping with shallow donors and acceptors as well as deep centers. Resistivities at RT are of the order of $10^8 \dots 10^{11} \Omega \text{ cm}$. Typical data at high temperatures are shown in Fig. 2.10.8

electrical conductivity

σ	$0.15 \dots 0.9 \Omega^{-1} \text{ cm}^{-1}$	$T = 300 \text{ K}$	pure n-type material	67M
	$10^{-9} \dots 10^{-14} \Omega^{-1} \text{ cm}^{-1}$	$T = 300 \text{ K}$	semi-insulating material (compensated n- and p-type material)	76A3

thermal conductivity

κ	$0.77 \text{ W K}^{-1} \text{ cm}^{-1}$	$T = 300 \text{ K}$	for temperature dependence, see Fig. 2.10.9	63S
----------	---	---------------------	--	-----

piezoelectric coefficients

e_{14}	$-1 \cdot 10^{-5} \text{ C/cm}^2$	$T = 300 \text{ K}$	$\sigma = 10^{-7} (\Omega \text{ cm})^{-1}$, approximate value only	68N
----------	-----------------------------------	---------------------	---	-----

electron mobility

$\mu_{H,n}$	$160 \text{ cm}^2/\text{Vs}$	RT, LPE grown layers	maximum mobility, temperature dependence $\propto T^{-1.7}$	83K
-------------	------------------------------	-------------------------	--	-----

Temperature dependence of electron mobility (LPE grown layers): Fig. 2.10.10.

hole mobility

$\mu_{H,p}$	$135 \text{ cm}^2/\text{Vs}$		maximum mobility, temper- ature dependence $\propto T^{-2.3}$	83K
-------------	------------------------------	--	--	-----

For temperature dependence of hole mobility, see Fig. 2.10.10.

Optical properties

optical constants

real and imaginary parts of the dielectric constant measured by spectroscopical ellipsometry, n , k , R , K calculated from these data [83A]. See also Fig. 2.10.11.

$h\nu [\text{eV}]$	ϵ_1	ϵ_2	n	k	R	$K [10^3 \text{ cm}^{-1}]$
1.5	10.102	0.000	3.178	0.000	9.272	0.00
2.0	11.114	0.000	3.334	0.000	0.290	0.00
2.5	12.996	0.046	3.605	0.006	0.320	1.63
3.0	18.601	1.832	4.081	0.224	0.369	68.26
3.5	24.833	8.268	5.050	0.819	0.458	290.40
4.0	9.652	16.454	3.790	2.171	0.452	880.10
4.5	11.073	17.343	3.978	2.180	0.461	994.27
5.0	0.218	26.580	3.661	3.631	0.580	1839.99
5.5	-10.266	10.974	1.543	3.556	0.677	1982.53
6.0	-5.521	7.041	1.309	2.690	0.583	1635.71

refractive index

range 1.5...2.7 eV: Fig. 2.10.12.

n		$T =$	λ [μm]		
	2.529		20	reflectance	60K
	2.90	300 K	10	reflectance and transmission	55W
	2.94		5		
	3.02		2		
	3.17		1		

absorption index

k		$T =$	λ [μm]		
	$3.44 \cdot 10^{-5}$		0.553	transmission	59S
	$2.47 \cdot 10^{-3}$	300 K	0.5		
	$3.12 \cdot 10^{-2}$		0.452		

dielectric constants

$\varepsilon(0)$	11.11	$T = 300 \text{ K}$	$\varepsilon(0)$: low-frequency capacitance measurements	83S2
	10.86	$T = 75.7 \text{ K}$		
$\varepsilon(\infty)$	9.11	$T = 300 \text{ K}$	$\varepsilon(\infty)$: derived from refractive index data	

temperature dependence: Fig. 2.10.13.

absorption spectrum : Fig. 2.10.14.

second order nonlinear dielectric susceptibilities

$d(\text{SHG})$	$1.09 \cdot 10^{-10} \text{ mV}^{-1}$	$T = 300 \text{ K}$, CO ₂ laser $\lambda = 10.6 \mu\text{m}$	second harmonic generation, should contain only $\chi_e^{(2)}$	69W
	$0.77(17) \cdot 10^{-10} \text{ mV}^{-1}$	$T = 300 \text{ K}$, CO ₂ laser $\lambda = 2.12 \mu\text{m}$	wedge second harmonic generation, should contain only $\chi_e^{(2)}$	76C2
	$0.82(15) \cdot 10^{-10} \text{ mV}^{-1}$	$T = 300 \text{ K}$, CO ₂ laser $\lambda = 1.318 \mu\text{m}$		

elasto-optical constants

p_{11}	-0.156	from Brillouin scattering	82C
	-0.166	first value: at 2.41 eV	
p_{12}	-0.119	second value: at 2.54 eV	
	-0.144		
p_{44}	-0.077		
	-0.064		

Impurities and defects

shallow impurities

The effect of deviations from the ellipsoidal form of the conduction band (camel's back structure) on the donor states becomes serious since $E_{\min}(\Delta) - E(X)$ is comparable to the binding energies of the donor excited states. Each state splits into two subcomponents involving a symmetric and antisymmetric contribution from the individual sub-minima [77K]

binding energies of donors
relative to the lowest conduction band minimum

Impurity	E_b [meV]	T [K]	Remarks	Ref
Theory	59(2)		effective mass theory	77K
Op	897(1)	2	infrared photoluminescence	68D
Sp	107(1)	20	infrared absorption	78K
Sep	105(1)	2	donor-acceptor pair spectra	73D2
Te _p	92.6(1.0)	20	infrared absorption	78K
Si _{Ga}	85(1)	20	infrared absorption	78K
Ge _{Ga}	204(1)	2	donor-acceptor spectra	73D2
Sn _{Ga}	72(1)		donor-acceptor spectra	73D2
Li _p	91(1)	2	bound exciton 'two-electron' replicas	73D1
Li _{Ga}	61(2)	2	unresolved donor acceptor pair spectra	

binding energies of acceptors
relative to the valence band maximum

Impurity	E_b [meV]	T [K]	Remarks	Ref.
Theory	45.3 or 56.3		effective mass theory according to [74B], re-evaluated for ϵ =11.02	78K
C _p	54.3(5)	2	donor-acceptor pair spectra (all data from [73D2] revised upward by 7.9meV because of the increase in E_g discussed in [78K] and [78R], see also [78S] where an increase of 8.3 meV is preferred)	73D2
Si _p	210(1)			
Ge _p	265(1)			
Cu _p	530(30) 580 650	4 77	photoconductivity, absorption (the complex and ill-understood behavior of GaP:Cu in thermally stimulated current measurements has been noted by [78R])	72M, 73G 62A, 71O, 74K
Be _{Ga}	56.6(5)	2	photoconductivity, absorption	73D2
Mg _{Ga}	59.9(5)			
Zn _{Ga}	69.7(5)	20	infrared absorption	78K
Cd _{Ga}	102.2(5)			
X	52(1)	2	donor-acceptor pair spectra	73D2

energy levels related to isolated, substitutional transition metal impurities

"+" above valence band edge, "-" below conduction band edge

Impurity	E [eV]I	Type	Remarks	T [K]	Ref.
Ti	- 0.50(2)	a	DLTS and DLOS	77...350	87R
	+ 1.0(2)	d			
	- 0. 56	a	Optical absorption, PL		
V	- 0.58	a	Temperature dependent Hall effect		86U
	- 0.8	a	Coexistence of Ni ⁺ , Ni ²⁺ , V ²⁺ and V ³⁺		85C2
	+ 0.20(5)	d	Electrical + optical measurements		89U
Cr	- 1.2	1st a	Reinterpretation of		81C
	- 0.5	2nd a	photo-ESR data and photoconductivity data plus two step excitation of luminescence		
		d	A donor level exists in the band gap, its energy is not known		
Mn	+ (0.4...0.43)	a	Temperature dependent Hall effect.		76E
			σ_p^0 absorption photoionization process		
	+ 0.41(2)	a	σ_p^0 absorption photoionization process		
Co	+ 0.43	a	DLTS: hole trap in n-type samples	4. 2	81B
	+0. 455	1st a	Photoionization		94W

Fe	+ 0.70(2)	1st a	Temperature dependent resistivity and Hall measurements		76A1
	+ 0.75	1st a	σ_p^0 absorption photoionization process		76A1
	− 1.5	1st a	Photoinduced rise of ESR	100...300	79M
	+ 0.86	1st a	Excitation of luminescence		83S3
	+ 0.82	1st a	DLTS and single shot dark capacitance transients		83Y
	+ 0.78	1st a	σ_p^0 photoionization from optical capacitance transients 2nd threshold corresponding to the 5T_2 excited state of Fe^{2+} at $E_v + 1.2$ eV		83Y
Co	+ 0.82	1st a	DLTS, σ_p^0 and σ_n^0 photoionization from optical DLTS		85B
	− 0.26	2nd a	DLTS		85B
	+ 0.41	1st a	Temperature dependent Hall and resistivity measurements		66L
	− 0.33	2nd a	The Co^{2+} profile does not correspond to the compensated donor profile [83J] which suggests that cobalt acts as a double acceptor [83J]. The level observed in DLTS at -0.33 eV [81B] is a candidate for the double acceptor level.		83J
Ni	+ (0.47...0.52)	1st a	Temperature dependent Hall measurements		76A2
	+ 0.50(3)	1st a	σ_p^0 absorption photoionization process		76A2
	+ 0.51	1st a	DLTS, σ_p^0 photocapacitance and photo-ESR		84P
	− 0.82	2nd a	DLTS and transient capacitance		84Y
	− 0.88	2nd a	Photocapacitance	300	84S3
Ag _{Ga}	+0. 66	a	Capacitance spectroscopy, PL		81K
Au _{Ga}	+0. 56	a	Capacitance spectroscopy, PL		81K

energy levels related to transition metal complex impurities

Impurity	E [eV])	Type	Remarks	T [K]	Ref.
Mn	− 0.15	a	DLTS	2	81B
	− 0.36	a	DLTS	2	81B
Fe	− 0.64	a	DLTS	2	81B
Ni	+ 0.92	d	Photocapacitance		77D
	+ 0.95	d	Optical DLTS		79P
	+ 0.92	d	DLTS	2	81B

Reference to 2.10

- 55W Welker, H.: J. Electron. 1 (1955) 181.
- 59S Spitzer, W. G., Gershenson, M., Frosch, C. J., Gibbs, D. F.: J. Phys. Chem. Solids 11 (1959) 339.
- 60K Kleinman, D. A., Spitzer, W. G.: Phys. Rev. 118 (1960) 110.
- 62A Allen, J.W., Cherry, R.J.: J. Phys. Chem Solids 23 (1962) 509.
- 63P Philipp, H. R., Ehrenreich, H.: Phys. Rev. 129 (1963) 1550.
- 63S Steigmeier, E. F., Kudman, J.: Phys. Rev. 132 (1963) 508.
- 64N Nelson, D. F., Johnson, L. F., Gershenson, M.: Phys. Rev. 135 (1964) A1399.
- 66D Dean, P. J., Thomas, D. G.: Phys. Rev. 150 (1966) 690
- 66L Loescher, D.H., Allen, J.W., Pearson, G.L.: J. Phys. Soc. Jpn. 21 Suppl. (1966) 239.
- 67D Dean, P. J., Kaminsky, G., Zetterstrom, R. B.: J. Appl. Phys. 38 (1967) 3551.
- 67M Miyauchi, T., Sonomura, H., Yamamoto, N.: Japan. J. Appl. Phys. 6 (1967) 1409.
- 68D Dean, P.J., Henry, C.H.: Phys. Rev. 176 (1968) 928.
- 68K Kasami, A.: J. Phys. Soc. Jpn. 24 (1968) 551.
- 68N Nelson, D. F., Turner, F. H.: J. Appl. Phys. 39 (1968) 3337.
- 68W Weil, R., Groves, W. O.: J. Appl. Phys. 39 (1968) 4049.
- 68Y Yarnell, J. L., Warren, J. L., Wenzel, R. G., Dean, P. J.: in "*Neutron Inelastic Scattering*", International Atomic Energy Agency, Vienna (1968), p. 301.
- 69M Muzhdaba, V. M., Nashel'skii, A. Ya., Tamarin, P. V., Shalyt, S. S.: Sov. Phys. Solid State (English Transl.) 10 (1969) 2265; Fiz. Tverd. Tela 10 (1968) 2866
- 69W Wynne, J. J., Bloembergen, N.: Phys. Rev. 188 (1969) 1211.
- 71O Olsson, R.: Phys. Status Solidi (b) 46 (1971) 299.
- 72M Monemar, B.: J. Lumin. 5 (1972) 472.
- 72S1 Stokowski, S. F., Sell, D. D.: Phys. Rev. B 5 (1972) 1636.
- 72S2 Suto, K., Nishizawa, J.: J. Appl. Phys. 43 (1972) 2247.
- 73D1 Dean, P.J.: Luminescence of Crystals, Molecules and Solutions, Williams, F.E. (ed.), New York: Plenum Press, 1973, p. 535.
- 73D2 Dean, P. J.: Progress in Solid State Chemistry, Vol. 8, McCaldin, J.O., Somorjai, G. (eds.), New York: Pergamon Press, 1973, p. 1.
- 73G Grimmeiss, H.G., Monemar, B.: Phys. Status Solidi (a) 19 (1973) 505.
- 73K Kishino, S.: Adv. X-Ray Anal. 16 (1973) 367.
- 74B Baldereschi, A., Lipari, N.O.: Phys. Rev. B 9 (1974) 1525.
- 74K Kopylov, A.A., Pikhtin, A.N.: Sov. Phys. Solid State (English Transl.) 16 (1974) 1837; Fiz. Tverd. Tela 16 (1974) 1837.
- 74L Ley, L., Pollak, R. A., McFeely, F. R., Kowalczyk, S. P., Shirley, D. A.: Phys. Rev. B 9 (1974) 600.
- 75A1 Aspnes, D. F., Olson, C. G., Lynch, D. W.: Phys. Rev. B 12 (1975) 2527.
- 75A2 Auvergne, D., Merle, P., Mathieu, H.: Phys. Rev. B 12 (1975) 1371.
- 75A3 Abagyan, S.A., Ivanov, G.A., Koroleva, G.A., Kuznetsov, Yu.N., Okunev, Yu.A.: Fiz. Tekh. Poluprovodn. 9 (1975) 369; Sov. Phys. Semicond. (English Transl.) 9 (1975) 243.
- 75B Boyle, W. F., Sladek, R. J.: Phys. Rev. B 11 (1975) 2933.
- 75K Kocsis, S.: Phys. Status Solidi (a) 28 (1975) 133.
- 75R Rode, D. L.: in "*Semiconductors and Semimetals*", vol. 10, R. K. Willardson, A. C. Beer eds., Academic Press, New York 1975.
- 75S Slack, G. A., Bartram, S. F. J. Appl. Phys. 46 (1975) 89.
- 75W Wiley, J. D.: in "*Semiconductors and Semimetals*", Vol. 10, R. K. Willardson, A. C. Beer eds., Academic Press, New York 1975.
- 76A1 Andrianov, D.G., Grinshtein, P.M., Ippolitova, G.K., Omel'yanovskii, E.M., Suchkova, N.I., Fistul', V.I.: Fiz. Tekh. Poluprovodn. 10 (1976) 1173; Sov. Phys. Semicond. (English Transl.) 10 (1976) 696.
- 76A2 Abagyan, S.A., Ivanov, G.A., Koroleva, G.A.: Fiz. Tekh. Poluprovodn. 10 (1976) 1773; Sov. Phys. Semicond. (English Transl.) 10 (1976) 1056.
- 76A3 Andrianov, D. G., Grinshtein, P. M., Ippolitova, G. K., Omel'yanovskii, F. M., Suchkova, N. I., Fistul', V. J.: Sov. Phys. Semicond. (English Transl.) 10 (1976) 696; Fiz. Tekh. Poluprov. 10 (1976) 1173.
- 76C1 Chelikowski, J. R., Cohen, M. L.: Phys. Rev. B 14 (1976) 556.
- 76C2 Choy, M. M., Byer, R. L.: Phys. Rev. B 14 (1976) 1693.
- 76E Evwaraye, A.O., Woodbury, H.H.: J. Appl. Phys. 47 (1976) 1595.
- 76S Somogyi, K.: Phys. Status Solidi (a) 37 (1976) 653.
- 77D Dean, P.J., White, A.M., Hamilton, B., Peaker, A.R., Gibb, R.M.: J. Phys. D 10 (1977) 2545.
- 77K Kopylov, A.A., Pikhtin A.N.: Sov. Phys. Semicond. (English Transl.) 11 (1977) 510; Fiz. Tekh. Poluprovodn. 11 (1977) 867.
- 77M Merrill, L.: J. Phys. Chem. Ref. Data 6 (1977) 1205
- 78G Gyrbu, I. N.: Sov. Phys. Solid State (English Transl.) 20 (1978) 2006; Fiz. Tverd. Tela 20 (1978) 3470.

- 78H Humphreys, R. G., Rössler, U., Cardona, M.: Phys. Rev. B 18 (1978) 5590.
- 78K Kopylov, A. A., Pikhtin, A. N.: Solid State Commun. 26 (1978) 735.
- 78R Richter, G.: Acta Phys. Acad. Sci. Hung. 44 (1978) 111.
- 78S Sturge, M.D., Vink, A.T., Kuijpers: Appl. Phys. Lett. 32 (1978) 49.
- 78Y Yu, S. C., Spain, I. L., Skelton, E. F.: Solid State Commun. 25 (1978) 49.
- 79B1 Bimberg, D., Skolnick, M. S., Sander, L. M.: Phys. Rev. B 19 (1979) 2231.
- 79B2 Borchers, P. H., Kunc, K., Alfrey, G. F., Hall, R. L.: J. Phys. C Solid State Phys. 12 (1979) 4699.
- 79M Masterov, V.F., Sobolevskii, V.K.: Fiz. Tekh. Poluprovodn. 13 (1979) 1655; Sov. Phys. Semicond. (English Transl.) 13 (1979) 965.
- 79P Peaker, A.R., Brunwin, R.F., Jordan, P., Hamilton, B.: Electron. Lett. 15 (1979) 663.
- 80G Goswami, N.K., Newman, R.C., Whitehouse, J.E.: Solid State Commun. 36 (1980) 897.
- 80K Kaufmann, U., Schneider, J.: Appl. Phys. Lett. 36 (1980) 747.
- 80S Soma, T.: Solid State Commun. 34 (1980) 375.
- 81B Brunwin, R.F., Hamilton, B., Hodgkinson, J., Peaker, A.R., Dean, P.J.: Solid State Electron. 24 (1981) 249.
- 81C Clerjaud, B., Gendron, F., Porte, C.: Appl. Phys. Lett. 38 (1981) 212.
- 81K Khudyakov, S.V.: Sov. Phys. Semicond. 15 (1981) 4.
- 81Y Yogurtcu, Y. K., Miller, A. J., Saunders, G. A.: J. Phys. Chem. Solids 42 (1981) 49.
- 82B1 Burkhard, H., Dinges, H. W., Kuphal, E.: J. Appl. Phys. 53 (1982) 655.
- 82B2 Baublitz, M., Ruoff, A. L.: J. Appl. Phys. 53 (1982) 6179.
- 82C Calleja, J. M., Vogl, H., Cardona, M.: Philos. Mag. A 45 (1982) 239.
- 83A Aspnes, D. E., Studna, A. A.: Phys. Rev. B 27 (1983) 985.
- 83J Jezewski, M., Baranowski, J.M.: 4th "Lund" Int. Conf. on Deep Level Impurities in Semicond., Eger: Hungary, 1983, unpublished.
- 83K Kao, Y. C., Eknayan, O.: J. Appl. Phys. 54 (1983) 2468.
- 83M1 Miura, N., Kido, G., Suekane, M., Chikazumi, S.: J. Phys. Soc. Jpn. 52 (1983) 2838.
- 83M2 Miura, N., Kido, G., Suekane, M., Chikazumi, S.: Physica 117B&118B (1983) 66.
- 83P Pödaar, B.: Phys. Status Solidi (b) 120 (1983) 207.
- 83S1 Sharma, A. C., Ravindra, N. M., Auluck, S., Stivastava, V. K.: Phys. Status Solidi (b) 120 (1983) 715.
- 83S2 Samara, G. A.: Phys. Rev. B 27 (1983) 3494.
- 83S3 Shanabrook, B.V., Klein, P.B., Bishop, S.G.: Physica B116 (1983) 444.
- 83T Takizawa, T.: J. Phys. Soc. Jpn. 52 (1983) 1057.
- 83Y Yang, X.Z., Grimmeiss, H.G., Samuelson, L.: Solid State Commun. 48 (1983) 427.
- 84H Hu, J. Z., Black, D. R., Spain, I. L.: Solid State Commun. 51 (1984) 285.
- 84P Peaker, A.R., Kaufmann, U., Zhan-Guo Wang, Wörner, R., Hamilton, B., Grimmeiss, H.G.: J. Phys. C 17 (1984) 6161.
- 84S1 Solal, F., Jezequel, G., Houzay, F., Barski, A., Pinchaux, R.: Solid State Commun. 52 (1984) 37 and private communication from G. Jezequel.
- 84S2 Sirota, N. N., Antyukhov, A. M., Sidorov, A. A.: Dokl. Akad. Nauk SSSR 277 (1984) 1379; Sov. Phys. Dokl. 29 (1984) 662 (English Transl.).
- 84S3 Szawelska, H.R., Mudhar, P.S., Allen, J.W.: J. Phys. C 17 (1984) 2981.
- 84Y Yang, X.Z., Samuelson, L., Grimmeiss, H.G.: J. Phys. C 17 (1984) 6521.
- 85B Brehme, S.: J. Phys. C 18 (1985) L319.
- 85C1 Campi, D., Papuzza, C.: J. Appl. Phys. 57 (1985) 1305.
- 85C2 Clerjaud, B., Naud, C., Deveaud, B., Lambert, B., Plot, B., Bremond, C., Benjeddou, C., Guillot, G., Nouailhat, A.: J. Appl. Phys. 58 (1985) 4207.
- 86K Kagaya, H.-M., Soma T.: Phys. Status Solidi (b)134 (1986) K101.
- 86U Ulrici, W., Eaves, L., Friedland, K., Halliday, D.P., Kreissl, J.: Defects in Semiconductors, Proc. 14th Internat. Conf. Defects in Semicond., Paris (1986), von Bardeleben, H.J. (ed.), Materials Science Forum, Vol. 10...12, Trans. Tech. Publications, Switzerland, 1986, p. 639.
- 87R Roura, P., Bremond, G., Nouailhat, A., Guillot, G., Ulrici, W.: Appl. Phys. Lett. 51 (1987) 1696.
- 88U Ulrici, W., Friedland, K., Eaves, L., Halliday, D.P.: Phys. Status Solidi (b) 150 (1988) 177.
- 89I Itie, J. P., Polian, A., Jaubertie-Carillon, C., Dartyge, E., Fontaine, A., Polentino, H., Tourillon, G., Phys. Rev. B 40 (1989) 9709.
- 89R Roura, P., Benyatton, T., Guillot, G., Moncorge, R., Ulrici, W.: Semicond. Sci. Technol. 4 (1989) 943.
- 90I Itagaki, K., Yamagushi, K.: Thermochim. Acta 163 (1990) 1.
- 90P Polian, A., Itié, J. P., Jaubertie-Carillon, C., Dartyge, A., Fontaine, A., Tolentino, H.: High Pressure Res. 4 (1990) 309.
- 94A Ansara, I., Chatillon, C., Lukas, H. L., Nishizawa, T., Ohtani, H., Ishida, K., Hillert, M., Sundman, B., Argent, B. B., Watson, A., Chart, T. G., Anderson, T.: CALPHAD: Comput. Coupling Phase Diagrams Thermochem. 18 (1994) 177.
- 94W Wolf, T., Ulrici, W., Côte, D., Clerjaud, B., Bimberg, D.: Mater. Sci. Forum 143-147 (1994) 317.

- 96E Eckl, Ch., Pavone, P., Fritsch, J., Schröder, U.: in "*The Physics of Semiconductors*" Scheffler, M., Zimmermann, R., (eds.), Singapore: World Scientific, 1996, Vol. 1, p. 229.
- 97M Mujica, A., Needs, R. J.: Phys. Rev. B 55 (1997) 9659; B 56 (1977) 12653(E).
- 97N Nelmes, R. J., McMahon, M. I., Belmonte, S. A.: Phys. Rev. Lett. 79 (1997) 3668.

Figures to 2.10

Fig. 2.0.2

The zincblende lattice

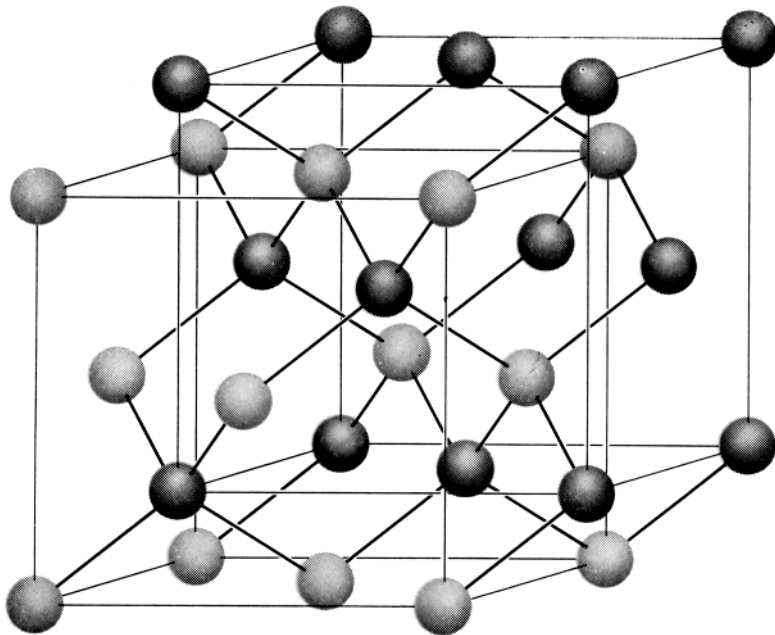


Fig. 2.0.5

Brillouin zone of the zincblende lattice.

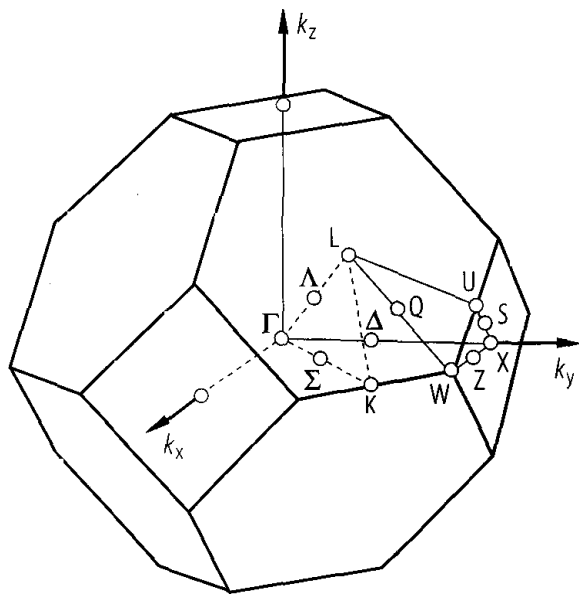


Fig. 2.0.18

GaP. Band structure calculated by a pseudopotential method neglecting spin-orbit interaction [76C1]; circles: data from angle resolved photoemission [84S1].

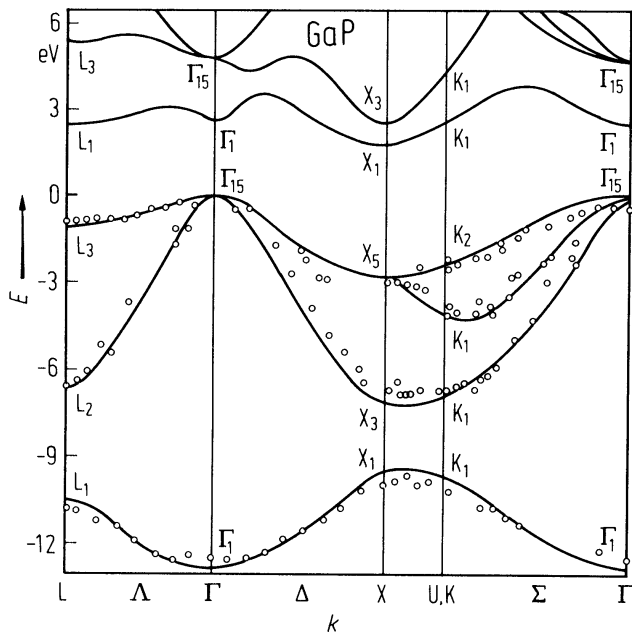


Fig. 2.10.1

GaP. Indirect transition thresholds vs. temperature below room temperature. The dashed line gives the energy of the indirect excitonic gap E_{gx} , the energy of the indirect gap $E_{g,ind}$ is thought to be 13(1) meV higher. The solid lines give the threshold energies for transitions involving absorption or emission of phonons (indices A, E) [75A2].

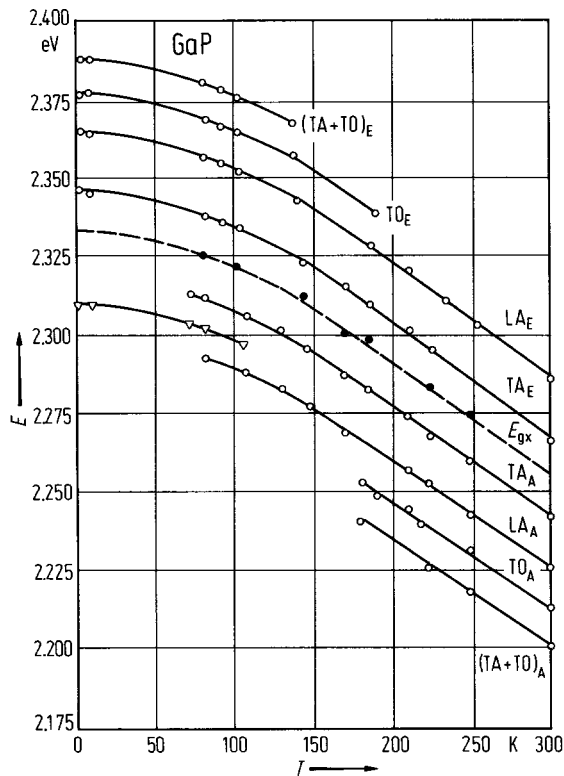


Fig. 2.10.2

GaP. Direct and indirect excitonic gap vs. temperature [67D].

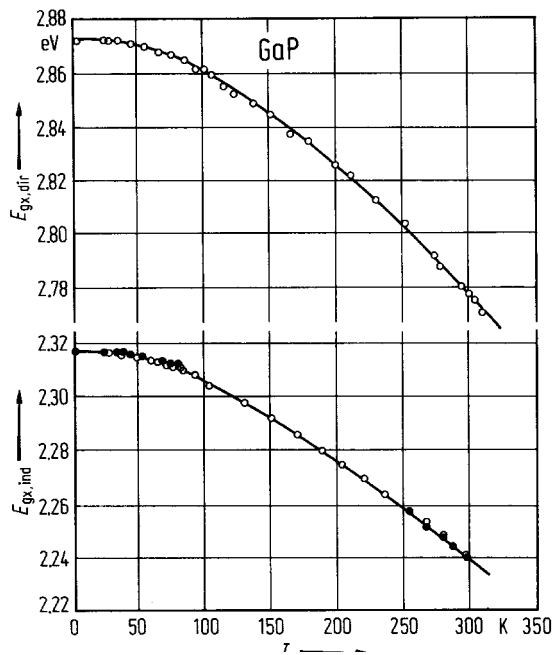


Fig. 2.10.3

GaP, GaAs, InP, InAs. Lattice parameter as a function of temperature from X-ray diffraction [84S2].

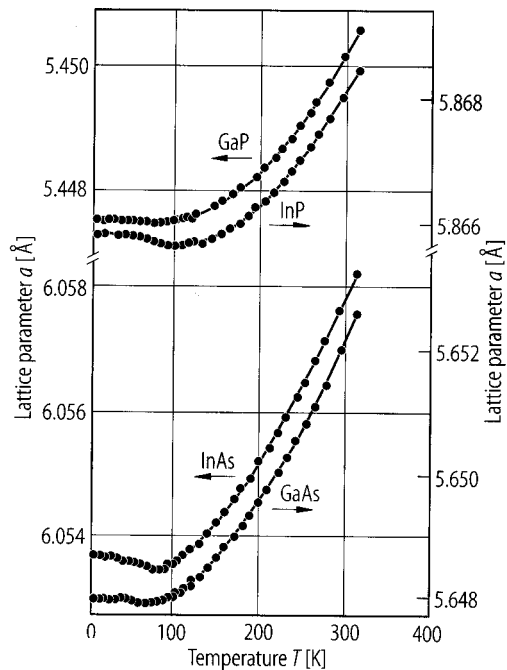


Fig. 2.10.4

GaP. Linear thermal expansion coefficient vs. temperature between 0 K and 300 K [80S].

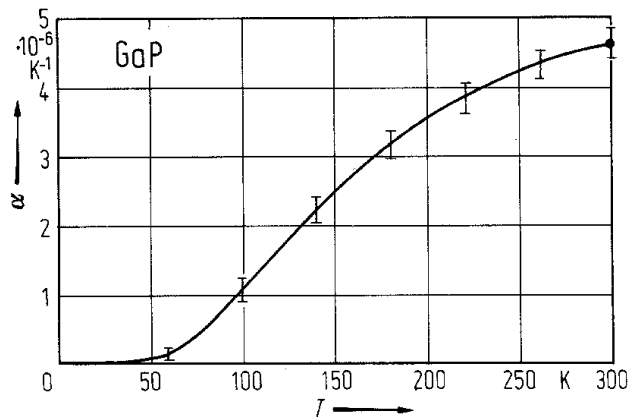


Fig. 2.10.5

GaP. Phonon dispersion curves (left panel) and density of states (right panel). Experimental data points from [68Y] (open symbols) and from [79B2] (full symbols) and theoretical curves from ab-initio calculations [96E]. From [96E].

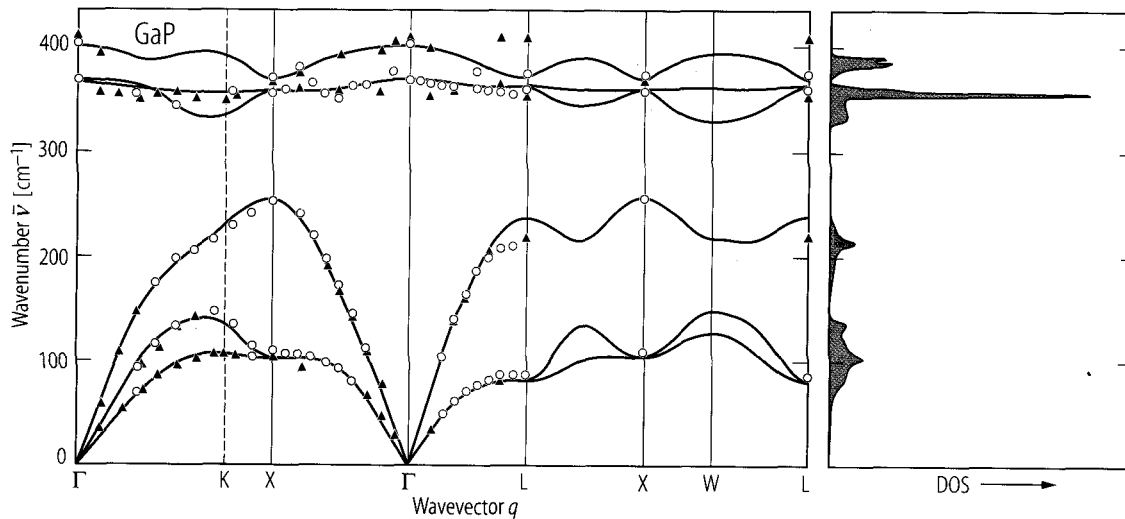


Fig. 2.10.6

GaP. Second order elastic moduli vs. temperature [75B].

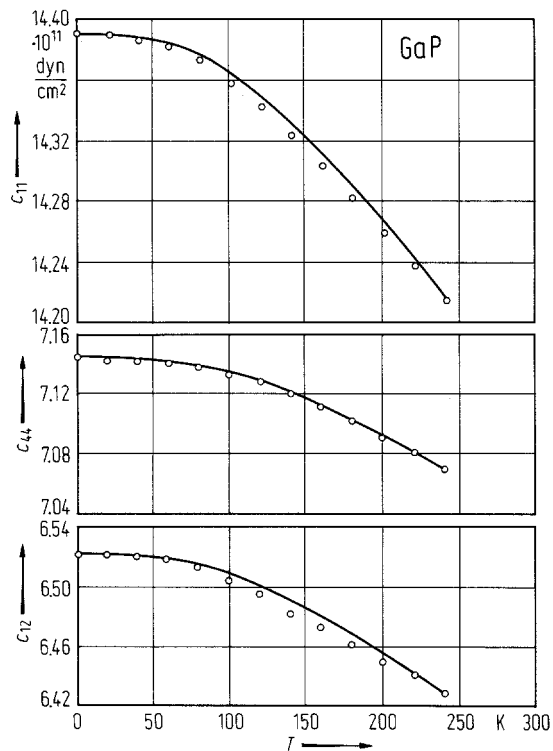


Fig. 2.10.7

GaP. Debye temperature of GaP and InP, Θ_D vs. T [86K].

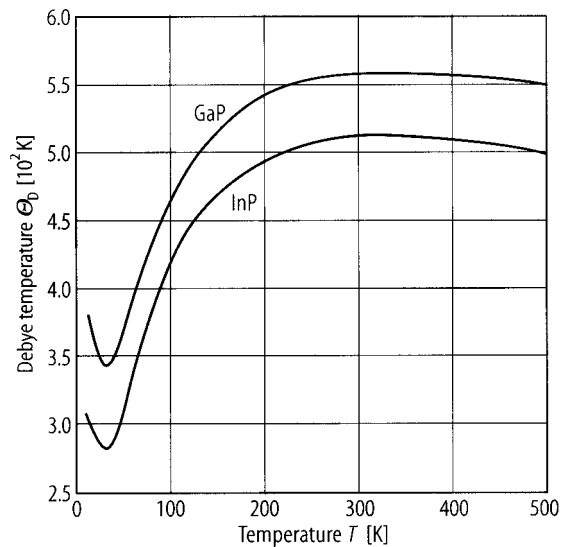


Fig. 2.10.8

GaP. Resistivity, Hall mobility and electron concentration (over $T^{-3/2}$) vs. temperature for a semiinsulating sample [83K].

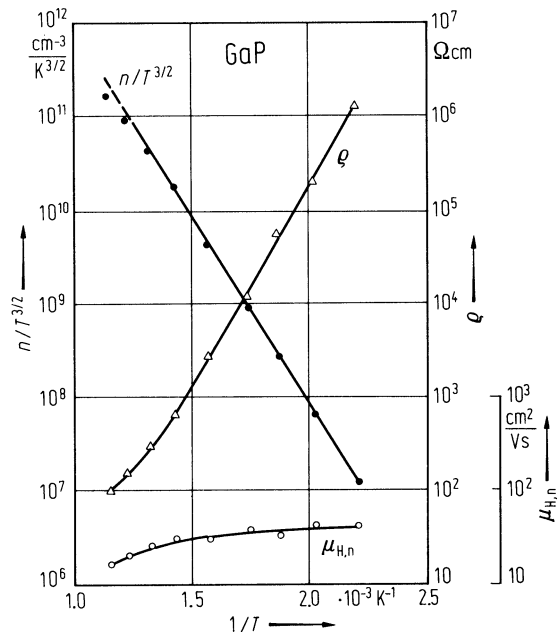


Fig. 2.10.9

GaP. Thermal conductivity vs. temperature for a p-type sample [69M].

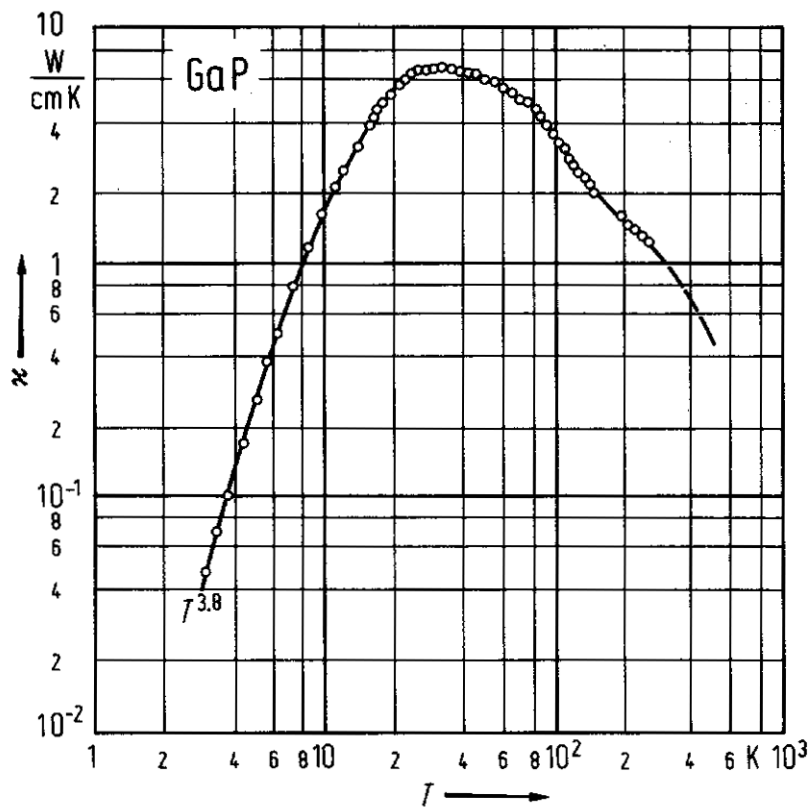


Fig. 2.10.10

GaP. Hall mobility in n-type (a) and p-type (b) LPE-grown layers vs. temperature [83K].

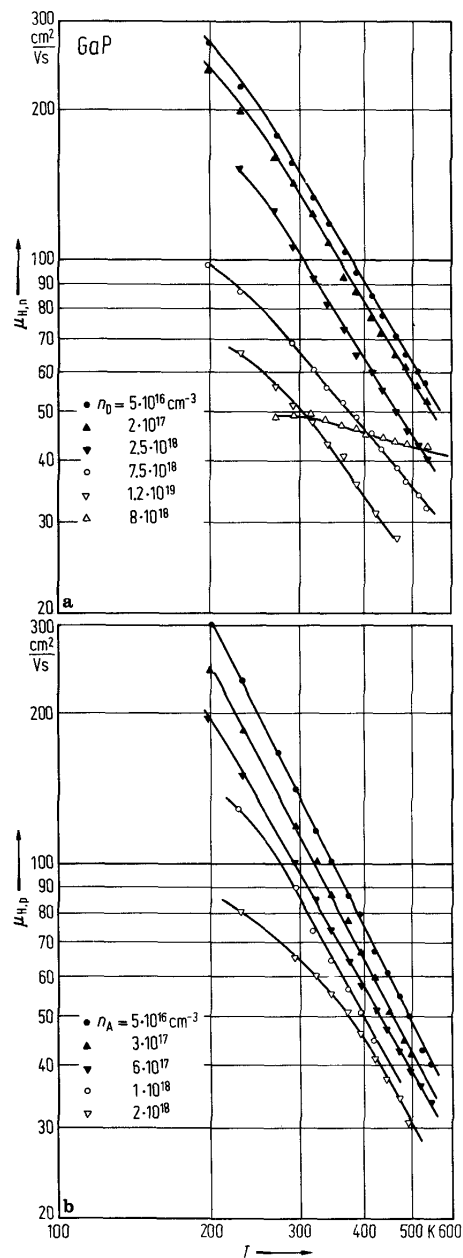


Fig. 2.10.11

GaP. Real and imaginary parts of the dielectric constant vs. photon energy [83A].

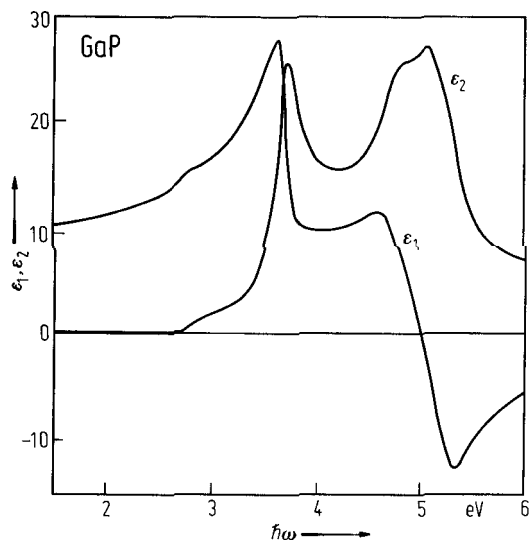


Fig. 2.10.12

GaP. Refractive index vs. photon energy in the range 1.5...2.7 eV. Circles and solid curve: calculated, triangles from [82B1], [85C1].

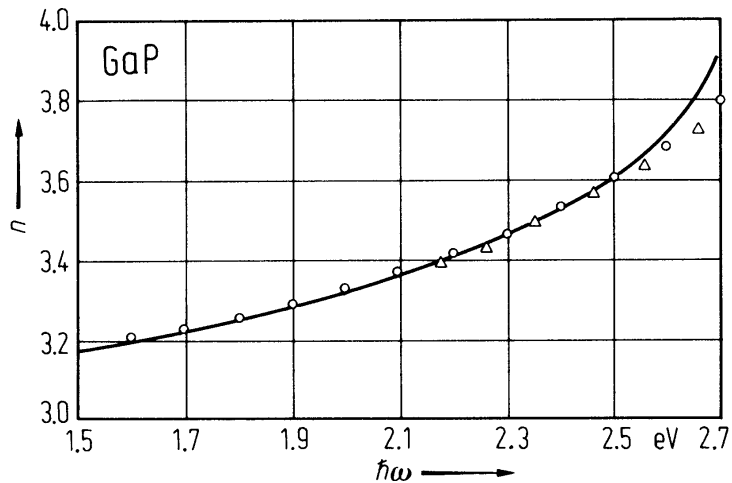


Fig. 2.10.13

GaP. (a) Static dielectric constant $\epsilon(0)$ and dielectric loss ($\tan \delta$ vs. temperature obtained from low-frequency capacitance measurements. For clarity, the actual data points at only one frequency (100 kHz) are shown. The data have been corrected for dimensional change due to thermal expansion. (b) Change in static dielectric constant vs. pressure at two temperatures [83S2].

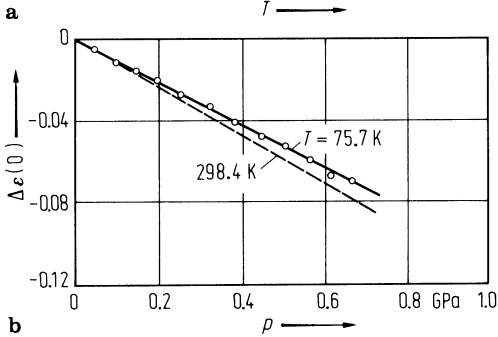
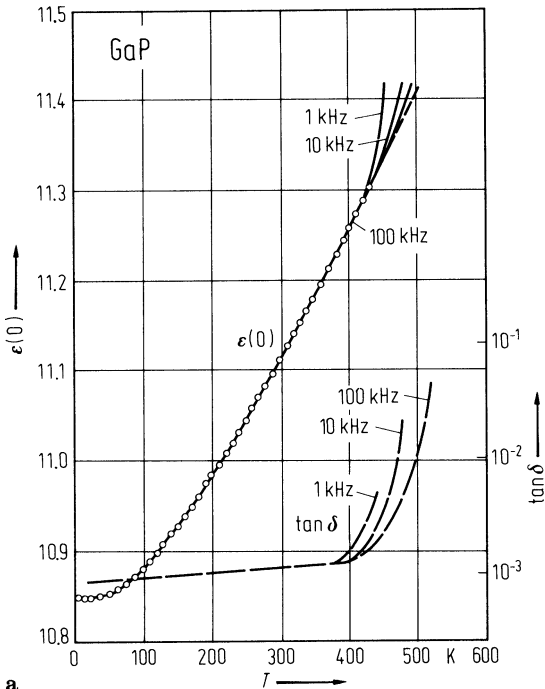


Fig. 2.10.14

GaP. Real (ϵ_1) and imaginary (ϵ_2) part of the dielectric constant and energy loss function $-\text{Im}(\epsilon^{-1})$ vs. photon energy in the range 0...25 eV [63P].

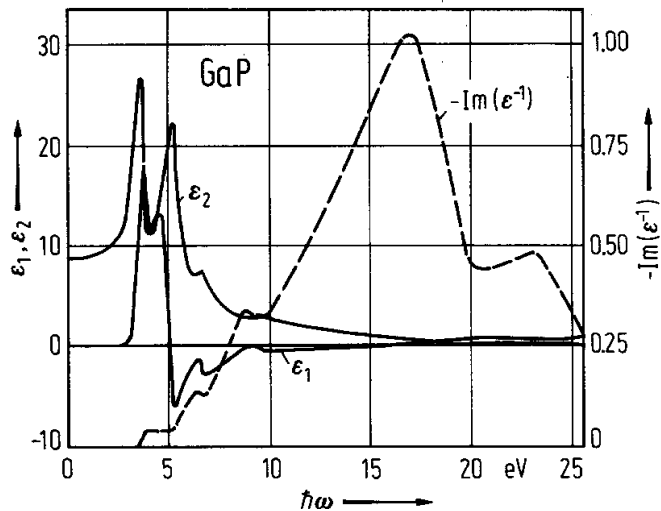
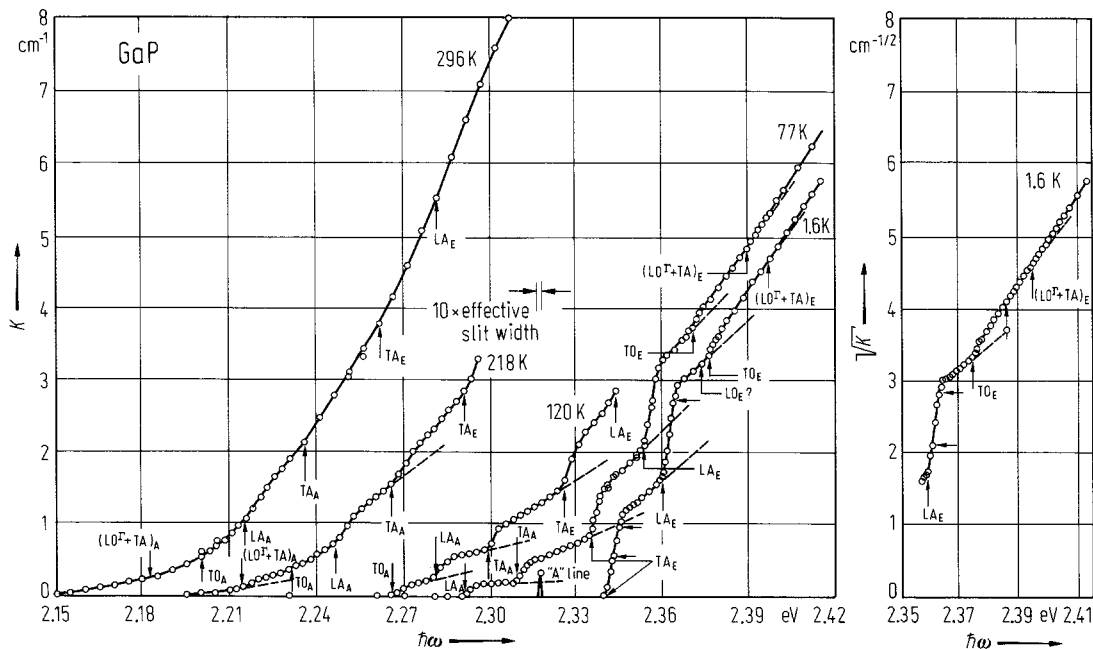


Fig. 2.10.15

GaP. Fine structure of the absorption edge (absorption coefficient vs. photon energy) at different temperatures [66D]. The assisting phonons are indicated. $TA_{A,E}$: transition involving absorption or emission of TA phonons.



2.11 Gallium arsenide (GaAs)

Crystal structure

Under normal conditions gallium arsenide crystallizes in the zincblende structure ($T_d^2 - F\bar{4}3m$, Fig. 2.0.2).

high pressure phases

Under pressure, there is a transformation from the zincblende structure with four-fold coordination (GaAs-I) at about 17 GPa to a structure with sixfold coordination (GaAs-II), namely either orthorhombic structure [78Y] (possibly Fmmm) [82B4], or primitive orthorhombic (space group Pmm2) [89W, 90V], later identified as having Cmc symmetry [96M1]. At higher pressures there is a transition from the orthorhombic phase to a body-centered orthorhombic structure (GaAs-III, space group Imm2) [89W]; but the II-III transition is disputed since X-ray reflections of the Cmc rather than Pmm2 symmetry persist up to pressures of 32 GPa [96M1]). With increasing pressure the structure gradually changes into the simple hexagonal structure (GaAs-IV) which persists up to at least 108 GPa [89W].

Electronic properties

band structure : Fig. 2.0.19, Brillouin zone: Fig. 2.0.5.

GaAs is a direct gap semiconductor. The minimum of the lowest conduction band is situated at Γ , higher sets of minima at L and near X (about 10% away from zone boundary [78P]) are important for optical as well as transport properties. The X-minimum has most probably a camel's back like structure similar to GaP, AlAs and AlSb [81B]. The valence bands have the usual structure characteristic for all zincblende crystals

energies of symmetry points of the band structure (relative to the top of the valence band $E(\Gamma_{8v})$, $E(\Gamma_{15v})$)

$E(\Gamma_{6v})$	– 12.55 eV	$E(\Gamma_{1v})$	– 13.1 eV	first row: designation of symmetry	76C,
$E(\Gamma_{7v})$	– 0.35 eV	$E(\Gamma_{15v})$	–	point in double group notation,	80C
$E(\Gamma_{6c})$	1.51 eV	$E(\Gamma_{1c})$	1.632 eV	data according to a nonlocal pseudopotential calculation [76C], (see Fig. 2.0.20)	
$E(\Gamma_{7c})$	4.55 eV	$E(\Gamma_{15c})$	4.716 eV		
$E(\Gamma_{8c})$	4.71 eV	$E(\Gamma_{15c})$	4.716 eV		
$E(X_{6v})$	– 9.83 eV	$E(\Gamma_{1c})$	8.33 eV	third row: designation of symmetry	
$E(X_{6v})$	– 6.88 eV	$E(X_{1v})$	– 10.75 eV	point in single group notation, data	
$E(X_{6v})$	– 2.99 eV	$E(X_{3v})$	– 6.70 eV	from angle resolved photoemission	
$E(X_{7v})$	– 2.89 eV	$E(X_{5v})$	– 2.80 eV	emission [80C] and photoelectron	
$E(X_{6c})$	2.03 eV	$E(X_{5v})$	– 2.80 eV	spectroscopy [85S]	
$E(X_{7c})$	2.38 eV	$E(X_{1c})$	2.18 eV		
$E(L_{6v})$	– 10.60 eV	$E(X_{3c})$	2.58 eV		
$E(L_{6v})$	– 6.83 eV	$E(L_{1v})$	– 11.24 eV		
$E(L_{6v})$	– 1.42 eV	$E(L_{1v})$	– 6.70 eV		
$E(L_{4,5v})$	– 1.20 eV	$E(L_{3v})$	– 1.30 eV		
$E(L_{6c})$	1.82 eV	$E(L_{3v})$	– 1.30 eV		
$E(L_{6c})$	5.47 eV	$E(L_{1c})$	1.85 eV		
$E(L_{4,5c})$	5.52 eV				

direct energy gap

$E_{g,dir}$	1.5194 eV	$T = 0$ K (extrapol.)	fitting of photoluminescence data	84S
$(\Gamma_{8v}-\Gamma_{6c})$	1.424(1) eV	$T = 300$ K	differentiated reflectivity	74S2
$E_{g,th}$	1.604 eV	$T = 0$ K, extrapol.	intrinsic carrier concentration	82B2

temperature dependence of direct energy gap

Empirical relation: $E_{g,dir}(T) = 1.515 - 5.5 \cdot 10^{-4} T^2 / (T + 255)$ eV ($T = 77 \dots 600$ K) (see also Fig. 2.11.1) 96K

exciton ground state energies

$E(1S, \Gamma_{5T})$	1.515 eV	$T = 2$ K	reflectance	87S2
$E(1S, \Gamma_{5L})$	1.51508 eV	$T = 2$ K	reflectance	87S2
$E_b(1S)$	4.0(1) meV	$T = 200$ K	transmission	90G
Δ_{LT}	0.13 meV			83S1
$E(2S)$	3.15 meV	$T = 2$ K	transmission	70S2
$E(3S)$	3.21 meV			

indirect energy gaps

$E_{g,ind}(\Gamma_{8v}-L_{6c})$	1.81 eV	$T = 100$ K	electroreflectance	76A
$E_{g,ind}(\Gamma_{8v}-X_{6c})$	1.98 eV			

higher conduction band minima (energy above Γ_{6c} minimum)

$\Delta E_{\Gamma L}(\Gamma_{6c}-L_{6c})$	0.300(20) eV	$T = 120$ K	photoemission	85D
$\Delta E_{\Gamma X}(\Gamma_{6c}-X_{6c})$	0.460(20) eV			

spin-orbit splitting energies

$\Delta_0(\Gamma_{15v})$	0.3464(5) eV	$T = 1.7$ K	splitting of Γ_{15} valence band state into Γ_{7v} and Γ_{8v} , magnetoabsorption	96A
$\Delta'_0(\Gamma_{15c})$	0.171(15) eV	$T = 4.2$ K	splitting of Γ_{15} conduction band state into Γ_{7c} and Γ_{8c} , electroreflectance	73A

critical point energies

$E_0 + \Delta_0(\Gamma_{7v}-\Gamma_{6c})$	1.850(2) eV	$T = 22$ K	spectroscopic ellipsometry	87L
$E_1(\Lambda_{4,5v}-\Lambda_{6c})$	3.038(1) eV	$T = 22$ K		
$E_1 + \Delta_1(\Lambda_{6v}-\Lambda_{6c})$	3.262(2) eV			
E_2 (at Σ)	5.118(3) eV			
$E_2(X_{7v}-X_{6c})$	4.898(16) eV			

lowest conduction band minimum

General structure according to $k \cdot p$ theory:

E (near Γ_{6c}) = $\hbar^2 k^2 / 2m_n + (\alpha + s\beta)k^4 \pm \gamma(s-9t)^{1/2}k^3$, with $s = (k_x^2 k_y^2 + k_y^2 k_z^2 + k_z^2 k_x^2) / k^4$, $t = k_x^2 k_y^2 k_z^2 / k^6$; the first term describes the parabolic band, the second the non-parabolicity, the third the band warping.

α	-1969 eV \AA^4	calculated	84R,
β	-2306 eV \AA^4	value for small k ; for larger k terms proportional to k^2 have to be added	85B2
γ	28 eV \AA^3		

conduction bands, effective masses

$m_n(\Gamma)$	0.0662(2) m_0	$T = 1.6$ K	cyclotron resonance	95K1
---------------	-----------------	-------------	---------------------	------

Temperature dependence: Fig. 2.11.2.

camel's back structure of conduction band minimum (at X_6)

ΔE	9.3 meV			85K
Δ	304 meV			
k_m	0.102(2 π/a)		values extrapolated from GaP	
m_l	1.8 m_0		using a $k \cdot p$ model	
m_t	0.257 m_0			

valence bands, effective masses

m_{hh}	0.34 m_0	[100]	electronic Raman scattering, quantum-well structure ($T = 10$ K)	89S
	0.75 m_0	[111]		
m_{lh}	0.094 m_0	[100]		
	0.082 m_0	[111]		

valence band parameters

A	-7.15	cited in [89G], A, B, C in units of $\hbar^2/(2m_0)$
B	-4.06	
C	7.46	

Lattice properties

lattice parameter

a	5.65359 Å	RT	95K1
-----	-----------	----	------

Temperature dependence of lattice parameters see Fig. 2.11.3.

linear thermal expansion coefficient

Empirical relations recommended in [82B1] from a discussion of various published data:

α [10^{-6} K $^{-1}$]	$-1.12 + 4.1 \cdot 10^{-2} T$	$120 < T < 350$ K
	$-5.9 \cdot 10^{-5} T^2$	
	$4.24 + 5.82 \cdot 10^{-3} T$	$200 < T < 1000$ K
	$-2.82 \cdot 10^{-6} T^2$	

Temperature dependence: 2.11.4

density

d	5.3161(2) g cm $^{-3}$	$T = 298.15$ K, single crystal	for temperature dependence. see Fig. 2.11.5	63W
-----	------------------------	-----------------------------------	--	-----

melting temperature

T_m	1511 K	optimized	90C
-------	--------	-----------	-----

phonon dispersion curves, phonon density of states : Fig. 2.11.6, Brillouin zone: Fig. 2.0.5.

phonon frequencies

$\nu_{LO}(\Gamma_{15})$	8.55(20) THz	$T = 296$ K	coherent inelastic neutron scattering,	65D
$\nu_{TO}(\Gamma_{15})$	8.02(8) THz			
$\nu_{TA}(X_1)$	2.36(2) THz			
$\nu_{LA}(X_3)$	6.80(6) THz			
$\nu_{LO}(X_1)$	7.22(15) THz			
$\nu_{TO}(X_5)$	7.56(8) THz			
$\nu_{TA}(L_3)$	1.86(2) THz			
$\nu_{LA}(L_1)$	6.26(10) THz			
$\nu_{LO}(L_1)$	7.15(7) THz			
$\nu_{TO}(L_3)$	7.84(12) THz			

sound velocities

v_1^L	$4.731(5) \cdot 10^5 \text{ cm s}^{-1}$	$[100]/[100]$	recommended values	82B1
v_2^T	$3.345(3) \cdot 10^5 \text{ cm s}^{-1}$	$[100]/[011]$	$(T = 300 \text{ K})$	
v_3^L	$3.350(3) \cdot 10^5 \text{ cm s}^{-1}$	$[110]/[110]$		
v_4^T	$3.345(3) \cdot 10^5 \text{ cm s}^{-1}$	$[110]/[001]$		
v_5^T	$2.476(5) \cdot 10^5 \text{ cm s}^{-1}$	$[1\bar{1}0]/[110]$		
v_6^L	$5.397(8) \cdot 10^5 \text{ cm s}^{-1}$	$[111]/[111]$		
v_7^T	$2.796(7) \cdot 10^5 \text{ cm s}^{-1}$	$[111]/[1\bar{1}0]$		

second order elastic moduli

c_{11}	$11.9(1) \cdot 10^{11} \text{ dyn cm}^{-2}$	$T = 300 \text{ K}$	recommended values from a discussion	82B1
	$11.26 \cdot 10^{11} \text{ dyn cm}^{-2}$	$T = 0 \text{ K}$	of several published data	
c_{12}	$5.38(1) \cdot 10^{11} \text{ dyn cm}^{-2}$	$T = 300 \text{ K}$	$T = 0 \text{ K}$ data: extrapolated	
	$5.71 \cdot 10^{11} \text{ dyn cm}^{-2}$	$T = 0 \text{ K}$		
c_{44}	$5.95(1) \cdot 10^{11} \text{ dyn cm}^{-2}$	$T = 300 \text{ K}$	temperature dependence: Fig. 2.11.7	
	$6.00 \cdot 10^{11} \text{ dyn cm}^{-2}$	$T = 0 \text{ K}$		

third order elastic moduli

c_{111}	$-6.75(20) \cdot 10^{12} \text{ dyn cm}^{-2}$	RT,	ultrasound	66D
c_{112}	$-4.02(10) \cdot 10^{12} \text{ dyn cm}^{-2}$	$n < 10^{17} \text{ cm}^{-3}$		
c_{123}	$-0.04(10) \cdot 10^{12} \text{ dyn cm}^{-2}$			
c_{144}	$-0.70(10) \cdot 10^{12} \text{ dyn cm}^{-2}$			
c_{166}	$-3.20(20) \cdot 10^{12} \text{ dyn cm}^{-2}$			
c_{456}	$-0.69(3) \cdot 10^{12} \text{ dyn cm}^{-2}$			

bulk modulus

B	$7.54 \cdot 10^{11} \text{ dyn cm}^{-2}$			89W
-----	--	--	--	-----

Young's and torsional moduli : temperature dependence, see Fig. 2.11.8

Debye temperature

$\Theta_D(0)$	344 K	for temperature dependence, see Fig. 2.11.9	63P2
---------------	-------	--	------

heat capacity

C_p	$24.34062 + 1.1158 \cdot 10^{-3}T + 2.1413 \cdot 10^{-6}T^2 - 1.27671 \cdot 10^{-5}T^{-2} \text{ J mol}^{-1} \text{ K}^{-1}$	$T = 298 \dots 1211 \text{ K}$	90C
	(mol $\text{Ga}_{0.5}\text{As}_{0.5}$)		

Transport properties

At low fields, the electrons are in the Γ_6 minima at the zone center. The dominating scattering process at room temperature is polar optical scattering, while below 60 K the most important contribution to the lattice mobility is made by piezoelectric potential scattering. At 300 K, the hole mobility of samples with $p < 5 \cdot 10^{15} \text{ cm}^{-3}$ is governed by lattice scattering alone.

intrinsic carrier concentration

n_i	$2.1 \cdot 10^6 \text{ cm}^{-3}$	$T = 300 \text{ K}$	82B1
-------	----------------------------------	---------------------	------

The temperature dependence can be expressed by $n_i(T) = 1.05 \cdot 10^{16} T^{3/2} \exp(-1.604/2kT)$ (T in K; kT in eV) for the range $33 \text{ K} < T < 475 \text{ K}$. For the range $250 \text{ K} < T < 1500 \text{ K}$ and for comparison of various literature data, see Fig. 2.11.10.

thermal conductivity (lattice contribution)

κ	0.455 W/deg cm	$T = 300$ K	for temperature and doping dependence, see Fig. 2.11.11	63S
	0.44 W/deg cm			66S

typical data for semi-insulating GaAs

(see also Fig. 2.11.12)

σ	$2.38 \cdot 10^{-9} \Omega^{-1} \text{cm}^{-1}$	RT, undoped sample	n and $\mu_{H,n}$ obtained from R_H and σ , by a mixed conduction analysis	83W
n	$3.73 \cdot 10^6 \text{cm}^{-3}$			
$\mu_{H,n}$	$3970 \text{cm}^2/\text{Vs}$			

electron mobility

For temperature dependence of $\mu_{H,n}$ see Fig. 2.11.13.

$\mu_{H,n}$	2400...3300 cm^2/Vs	$T = 300$ K	bulk GaAs, Bridgman	96L
	7200 cm^2/Vs		LPE-grown GaAs, liquid-phase electroepitaxy	
	6230...8865 cm^2/Vs		VPE-grown GaAs, AsCl_3 -Ga-Ar system	
	9000 cm^2/Vs		MOCVD-grown GaAs, AsH_3 -triethylgallium source	

hole mobility

Note that the hole mobilities in p-GaAs are considerably less than the mobilities measured for n-type samples, predominantly due to the effective hole masses being much greater than the electron effective mass. For temperature dependence of $\mu_{H,p}$, see Fig. 2.11.14.

$\mu_{H,p}$	$400(300/T)^{2.3} \text{cm}^2/\text{Vs}$	near $T = 300$ K	(T in K)	75W
$\mu_{dr,p}$	$320(300/T)^{2.3} \text{cm}^2/\text{Vs}$			

piezoresistance tensor coefficients

π_{11}	$-3.2 \cdot 10^{-12} \text{cm}^2/\text{dyn}$	$T = 300$ K, $n_d \approx 10^{19} \text{cm}^{-3}$	accuracy $\pm 10\%$. Piezoresistance of [110]-oriented n-type GaAs as a function of temperature (78.400 K) in [74D], [111]-oriented p-type (80...450 K) in [78K].	62Z
π_{12}	$-5.4 \cdot 10^{-12} \text{cm}^2/\text{dyn}$	$T = 300$ K, $n_d \approx 10^{19} \text{cm}^{-3}$		
π_{44}	$-2.5 \cdot 10^{-12} \text{cm}^2/\text{dyn}$	$T = 300$ K, $n_d \approx 10^{19} \text{cm}^{-3}$	Superlinear piezoresistance at high	

elastoresistance coefficients

$(1/2)(m_{11}-m_{12})$	0.5	$T = 300$ K, $n_d = 8 \cdot 10^{16} \text{cm}^{-3}$	calculated from measured piezo-resistance coefficients	58S
$(1/3)(m_{11}+2m_{12})$	-7.4	$T = 300$ K, $n_d = 8 \cdot 10^{16} \text{cm}^{-3}$		
m_{44}	-1.4	$T = 300$ K, $n_d = 8 \cdot 10^{16} \text{cm}^{-3}$		

piezoelectric constants

e_{14}	$1.6 \cdot 10^{-5} \text{C}/\text{cm}^2$	$T = 300$ K	piezoelectric Hall effect measurements. Polarity: negative, if the crystal is expanded in the [111] direction (the A-faces (metal atoms) become negatively charged).	68A
	$\pm 10\%$			
d_{14}	$2.7 \cdot 10^{-10} \text{cm}/\text{V}$			
g_{14}	$2.4 \cdot 10^2 \text{cm}^2/\text{C}$			
h_{14}	$1.45 \cdot 10^7 \text{V}/\text{cm}$			

Seebeck coefficient (thermoelectric power)

S_n	$-520 \mu\text{V/K}$	$T = 300 \text{ K},$ $n = 9.5 \cdot 10^{15} \text{ cm}^{-3}$	for temperature dependence, see Fig. 2.11.15.	62C
S_p	$\approx +220 \mu\text{V/K}$	$T = 300 \text{ K},$ $p = 2.7 \cdot 10^{19} \text{ cm}^{-3}$	for temperature dependence, see Fig. 2.11.15	73E

Optical properties

optical constants

real and imaginary parts of the dielectric constant measured by spectroscopical ellipsometry, n , k , R , K calculated from these data [83A]. See also Fig. 2.11.16

$h\nu [\text{eV}]$	ϵ_1	ϵ_2	n	k	R	$K [10^3 \text{ cm}^{-1}]$
1.5	13.435	0.589	3.666	0.080	0.327	12.21
2.0	14.991	1.637	3.878	0.211	0.349	42.79
2.5	18.579	3.821	4.333	0.441	0.395	111.74
3.0	16.536	17.571	4.509	1.948	0.472	592.48
3.5	8.413	14.216	3.531	2.013	0.425	714.20
4.0	9.279	13.832	3.601	1.920	0.421	778.65
4.5	6.797	22.845	3.913	2.919	0.521	1331.28
5.0	-11.515	18.563	2.273	4.084	0.558	2069.81
5.5	-6.705	8.123	1.383	2.936	0.613	1636.68
6.0	-4.511	6.250	1.264	2.472	0.550	1503.20

refractive index

n	$3.255 \cdot (1 + 4.5 \cdot 10^{-5} T)$	$(T \text{ in K})$	82B1
-----	---	--------------------	------

Dependence on photon energy: range 1...1.7 eV: Fig. 2.11.17. In the range 0.3...1.4 eV various published data can be fitted by

$$n^2 = 7.10 + 3.78 / (1 - 0.18(h\nu)^2) \quad (h\nu \text{ in eV})$$

82B1

absorption coefficient

K	$4 \cdot 10^4 \text{ cm}^{-1}$	$T = 21 \text{ K},$ $h\nu = 2 \text{ eV}$	transmission, Fig. 2.11.18	62S
-----	--------------------------------	--	----------------------------	-----

dielectric constants

$\epsilon(0)$	12.80(5)	$T = 300 \text{ K}$	microwave technique	88S
$\epsilon(\infty)$	10.86	$T = 300 \text{ K}$	optical transmission interference	96M2
$d(\ln \epsilon(0))/dT$	$20.4(3) \cdot 10^{-5} \text{ K}^{-1}$	$T = 300 \text{ K}$		88S
$d(\ln \epsilon(\infty))/dT$	$11.4 \cdot 10^{-5} \text{ K}^{-1}$	$T = 300 \text{ K}$		

reflectance : Fig. 2.11.19.

linear electrooptic constant

r_{41}	$-1.86(20) \cdot 10^{-12} \text{ m/V}$	$\lambda = 0.877 \mu\text{m}$	94A
	$-1.74(20) \cdot 10^{-12} \text{ m/V}$	$\lambda = 0.888 \mu\text{m}$	
	$-1.3 \cdot 10^{-12} \text{ m/V}$	$\lambda = 1.00 \mu\text{m}$	
	$-1.68(9) \cdot 10^{-12} \text{ m/V}$	$\lambda = 1.15 \mu\text{m}$	
	$-1.54(8) \cdot 10^{-12} \text{ m/V}$	$\lambda = 1.32 \mu\text{m}$	
	$-1.50(8) \cdot 10^{-12} \text{ m/V}$	$\lambda = 1.52 \mu\text{m}$	
	$-1.8 \cdot 10^{-12} \text{ m/V}$	$\lambda = 3.0 \mu\text{m}$	
	$-1.5 \cdot 10^{-12} \text{ m/V}$	$\lambda = 10.6 \mu\text{m}$	

quadratic electrooptic constant

R_{11}	$-29(7) \cdot 10^{-21} \text{ m}^2/\text{V}^2$	$\lambda = 1.09 \text{ }\mu\text{m}$	90F
R_{12}	$-24(6) \cdot 10^{-21} \text{ m}^2/\text{V}^2$		

second order nonlinear dielectric susceptibilities

$d(\text{SHG})$	$1.89 \cdot 10^{-10} \text{ mV}^{-1}$	$T = 300 \text{ K,}$ $\text{CO}_2 \text{ laser,}$ $\lambda = 10.6 \text{ }\mu\text{m}$	second harmonic generation	69W
-----------------	---------------------------------------	--	----------------------------	-----

third order susceptibility

$\chi_{1111}^{(3)}$	$0.97 \cdot 10^{-11} \text{ esu}$	$T = 300 \text{ K,}$	$\chi^{(3)}(\omega_1, \omega_1, -\omega_2)$	72Y
$\chi_{1212}^{(3)}$	$0.51 \cdot 10^{11} \text{ esu}$	$\lambda = 10.6 \text{ }\mu\text{m}$		

piezooptic constants, piezobirefringence

The piezobirefringence is strongly dispersive as the lowest absorption edge is approached.

$d_{11} - d_{12}$	$111 \cdot 10^{-8} \text{ cm}^2/\text{N}$	$\lambda = 3.5 \text{ }\mu\text{m}$	tables in intervals of	82F
	$101 \cdot 10^{-8} \text{ cm}^2/\text{N}$	$10.59 \text{ }\mu\text{m}$	$0.5 \text{ }\mu\text{m}$ in [82F]	
d_{44}	$140 \cdot 10^{-8} \text{ cm}^2/\text{N}$	$3.5 \text{ }\mu\text{m}$	d_{ik} : piezodielectric tensor	
	$133 \cdot 10^{-8} \text{ cm}^2/\text{N}$	$10.59 \text{ }\mu\text{m}$	$(\Delta \epsilon_i - X_k)$	
$q_{11} - q_{12}$	$-0.91 \cdot 10^{-8} \text{ cm}^2/\text{N}$	$3.5 \text{ }\mu\text{m}$	q_{jk} : piezooptic tensor	
	$-0.86 \cdot 10^{-8} \text{ cm}^2/\text{N}$	$10.59 \text{ }\mu\text{m}$	$(\Delta(\epsilon^{-1})_i - X_k)$	
q_{44}	$-1.15 \cdot 10^{-8} \text{ cm}^2/\text{N}$	$3.5 \text{ }\mu\text{m}$		
	$-1.14 \cdot 10^{-8} \text{ cm}^2/\text{N}$	$10.59 \text{ }\mu\text{m}$		
$k_{11} - k_{12}$	7.2	$3.5 \text{ }\mu\text{m}$	k_{ik} : photoelastic tensor	
	6.5	$10.59 \text{ }\mu\text{m}$	$(\Delta \epsilon_i - e_k)$	
k_{44}	8.3	$3.5 \text{ }\mu\text{m}$		
	7.9	$10.59 \text{ }\mu\text{m}$		
$p_{11} - p_{12}$	-0.059	$3.5 \text{ }\mu\text{m}$	p_{ik} : elastooptic tensor	
	-0.056	$10.59 \text{ }\mu\text{m}$	$(\Delta(\epsilon^{-1})_i - e_k)$	
p_{44}	-0.068	$3.5 \text{ }\mu\text{m}$		
	-0.067	$10.59 \text{ }\mu\text{m}$		

Impurities and defects

shallow donors

Shallow donors mix states from the conduction band producing a bound state in the gap. Such states are well described by effective mass theory. The small electron effective mass and the large dielectric constant result in small binding energies which are typically less than 10 meV. Central cell shifts for different donor species are similar, with a spread of around 0.1 meV, because of the strong delocalisation of the bound electron wave function. Internal stress and random electric fields result in a significant broadening of donor-related signatures. These factors make donor discrimination and spectroscopic characterisation a difficult task requiring high-quality, lightly doped crystals.

binding energy of residual donors

(Possible assignments to impurities are shown in brackets).

Impurity	E_b [meV]	Experimental conditions	Experimental method	Ref.
X_1 (Si)	5.804	Zero magnetic field	High resolution photo-luminescence (0.007 meV)	81A
X_2 (S)	5.870	1.2...2.1 K		
X_3 (C, Ge)	5.978			

acceptor ground state binding energies

(F-B: free to bound transition, DAP: donor-acceptor-pair)

Impurity	E_b [meV]	T [K]	Remarks	Ref.
1S _{3/2} calculation	25.82		Effective mass theory using valence band parameters of [76S] for the calculation [75L, 77B]	74B 78K
Be	28.0	5	F-B Photoluminescence	75A
C	26.9	20	Far infrared photoconductivity	78K
	26.0	5	F-B Photoluminescence	75A
Cd	34.7	5	F-B Photoluminescence	75A
Ge	40.4	5	F-B Photoluminescence	75A
Mg	28.7	20	Far infrared photoconductivity	78K
	28.4	5	F-B Photoluminescence	75A
Mn	113.1	28	F-B Photoluminescence	74S1
Si	34.8	20	Far infrared photoconductivity	78K
	34.5	5	F-B Photoluminescence	75A
	35.2	5	F-B Photoluminescence	80K
Ca	28.4	2	F-B Photoluminescence	94S1
Hg	52.5	2	temperature dependence F-B photoluminescence	95K2
Sn	170.5	5	F-B Photoluminescence	75A
	167.2	1.8	DAP Photoluminescence	76S
Zn	30.6	20	Far infrared photoconductivity	78K
	30.7	5	F-B Photoluminescence	75A
Ga _{As} (neutral)	78	5	Photoluminescence	86S
Ga _{As} (negative)	204	5		

copper :

Copper is a potentially important contaminant in GaAs.

properties of Cu-related complexes

Defect characterization	E [eV]	Remarks	Ref.
Cu associated acceptors: hole binding energies	0.156	Measured from valence band by Hall effect	64H2
	0.45	0.156eV acceptor: possible assignment single to doubly ionized transition of the Cu ^{Ga} acceptor	85W
Bound exciton line C ₀ (C-center)	1.5026	Photoluminescence, $T = 2$ K	67G 85W
C ₀ exciton binding energy	0.017		85W
		C ₀ exciton shows magnetic splitting of the ground state $g_{\text{eff}} = 2.44$	85G1
C-center possible assignment		Acceptor with trigonal <111> symmetry involving a compressional local crystal field. Possibly <111> oriented Cu _{Ga} Cu _i .	85W
		Survey of previous assignments.	85W 85W
Bound exciton line F ₀ (F-center)	1.4832		
F ₀ exciton binding energy	0.036		85W
		F ₀ exciton shows magnetic splitting of the ground state $g_{\text{eff}} = 2.30$	85G2

F-center possible assignment	Acceptor with orthorhombic symmetry.		85W
	Suggested complexes include:		69G2
	$V_{As}Cu_{Ga}V_{As}$		69G2
	$V_{As}Cu_{Ga}$		78G
	$Cu_{Ga}Ga_i$		85W
1.36 eV photoluminescence	Recombination between conduction band (or donors) and the 0.156 eV acceptor		85W
1.36 eV band	Orthorhombic symmetry		82A
	Cu_{Ga} with $\langle 100 \rangle$ Jahn Teller distortion (see [85W1] for previous assignments)		82A
complex defect T_1	0.25	ionisation energy from TSC measurements this T_1 trap compensates EL2 and T_2 .	94K
complex defect T_2	0.52	ionisation energy from TSC measurements associated to a $Cu_{Ga}-V_{As}$ complex, rules the p-type doping	94K

oxygen :

Oxygen is used to produce semi-insulating epitaxial GaAs. Two oxygen related defects have been observed in GaAs: interstitial O and off-centre substitutional defect. O_i is electrically inactive, while off-centre O, in the form of $O-V_{As}$ complex, introduces two defect levels in the band gap at 0. 15 (0/-) and 0. 58 eV (-/-) below the conduction band [90S]. Other reports quote the following energy for electron traps induced by O: 0. 75 and 0. 95 eV below the conduction band [94H].

hydrogen :

Passivation of electrically active impurities and native defect by atomic hydrogen is a well known phenomenon. Post-passivation annealing experiments done on Schottky diodes show that the reactivation of shallow donors and acceptors, through the debonding of hydrogen, is strongly enhanced by the electric field present in the depletion region of reverse biased diodes. This is explained by assuming that H has two levels in the gap at the energy of eV. This conclusion is revisited by [93M] who postulates the existence of a deep donor level at $E_c-0. 75$ eV.

energy levels associated to hydrogen

level	energy [eV]	method	Ref.
(-/0)		Bridgman, n-type, dopant reactivation	91Y
(-/0)	$E_v + 1.4$	Bridgman, n-type different composition, diffusion	92C
(0/+)	$E_v + 0.5$	LEC, p-type, IR measurements	91C
(0/+)	$E_c - 0.75$	modelling diffusion data, p-type	93M

energy levels related to isolated, substitutional transition metal impurities

Impurity	E [eV]	Type	Remarks	T [K]	Ref.
Ti	- 0.23(1)	a	DLT and capacitance, transient measurements		86H
	- 0.20(2)	a	DLTS + DLOS		86G
	- 1.00(3)	d	DLTS and capacitance, transient measurements		86B
	+ 0.60(2)	d	DLTS		86G
V	- 0.14	a	DLTS		80M1
	- 0.15(1)	a	DLTS and capacitance, transient measurements		85B1
	- 0.14	a	DLTS + σ_p^0 photoionization absorption process		85C1
	- 0.14	a	Temperature dependent Hall effect + σ_p^0 photoionization absorption process		85U1
Cr	+ 0.79	a	Temperature-dependent Hall effect		64H1
	+ 0.750(20)	a	DLTS (capture cross-section)	320	80M2
	+ 0.660(20)	a	DLTS	390	80M2
	+ 0.685(20)	a	DLTS	400	80M2
	+ 0.655(20)	a	DLTS	408	80M2

Cr (cont.)	+ 0.654(20)	a	DLTS	425	80M2
	+ 0.645(20)	a	DLTS	437	80M2
	+ 0.736(7)	a	σ_p^0 absorption photoionization process	4	81M
	$E_c + 0.06(2)$	Cr^{2+}/Cr^+	Resistivity as a function of pressure	77	81H
	$E_c + 0.115(2)$	Cr^{2+}/Cr^+	Hall effect as a function of pressure	300	82H
	$E_c + 0.055(2)$	Cr^{2+}/Cr^+	Hall effect as a function of presure	77	82H
	$E_c + 0.045(5)$	$Cr2 +/Crt$	de Haas-Shubnikov measurementw	4	85G2
	+ (0.324–1..4 ·10 ⁻⁴ T)	d	Temperature-dependent Hall effect		82L1
	+ 0.40(3)	d	σ_p^0 absorption photoionization		82U
		d	σ_n^0 absorbtion photoionization		85U2
	+ 0.45	d	σ_p^0 photoconductivity threshold		82B3
	+ 0.42(1)	d	σ_p^0 photo-Hall photoionization threshold	100...160	82R
Mn	+ 0.094	a	Temperature-dependent Hall effect		64H1
	+ 0.111(2)	a	σ_p^0 absorption photoionization	10	67C
	+ 0.1130	a	Reinterpretation of [67C]		87S1
	+ 0.1130(5)	a	Luminescence	4	74S1
Fe	+ 0.11243	a	absorption and photoconductivity experiments		97L
	+ 0.52	a	Temperature-dependent Hall effect		64H1
	+ 0.52	a	DLTS		
	+ 0.59	a	DLTS		77M
	+ 0.50	a	σ_p^0 photoconductivity, 2nd threshold corres- ponding to the 5T_2 excited state of Fe^{2+} is observed		76K
	+ 0.49	a	Excitation of luminescence	4.2	83S2
	+ 0.6	a	σ_p^0 obtained from DLOS	218	82L2
	– 0.85	a	σ_n^0 obtained from DLOS	218	82L2
	+ 0.54	a	DLTS and capacitance measurementw		83K
	+ 0.46	a	Photocapacitance transients	50	83K
			2nd threshold corresponding to the 5T_2 excited state of Fe^{2+} is observed		
Co	+ 0.16	a	Temperature-dependent Hall effect		64H1
	+ 0.14	a	σ_p^0 absorption photoionization	18	72B1
	+ 0.156	a	Temperature-dependent Hall effect and or σ_p^0 absorption photoionization	77	72B2
	+0.14	a	σ_p^0 photoluminescence excitation photoionization	4.2	86D
	$E_v + 0.140(5)$	Co^{2+}/CO^+	Resistivity and Hall effect measurementw under pressure	300	86W
	$E_v + 0.110(5)$	Co^{2+}/Co^+	Resistivity and Hall effect measurements under pressure	77	86W
Ni	+ 0.21	1st a	Temperature-dependent Hall effect		64H1
	+ 0.20	1st a	Temperature-dependent Hall effect		72B2
	– 0.40(4)	2nd a	DLTS	0	86B
	+ 1.03(3)	2nd a	σ_p^0 photoionization from ODLTS	202	86B
Ag	+ 0.238	a	σ_n^0 photoluminescence	4	70B
	+ 0.235(4)	a	Temperature-dependent Hall effect		76H
	+ 0.230	a	DLTS		82Y
Au	+ 0.405(2)	a	Temperature-dependent Hall effect		76H
	+ 0.397	a	DLTS		82Y
Rh	– 0. 88	a	estimate from DLTS measurements in GaInAs		94S2
Ir	– 0. 90	a	estimate from DLTS measurements in GaInAs		94S2

References to 2.11

- 58S Sagar, A.: Phys. Rev. 112 (1958) 1533.
- 62C Carlson, R. O., Silverman, S. J., Ehrenreich, H.: J. Phys. Chem. Solids 23 (1962) 422.
- 62G Garland, C. W., Park, K. C.: J. Appl. Phys. 33 (1962) 759.
- 62S Sturge, M. D.: Phys. Rev. 127 (1962) 768.
- 62Z Zerbst, M.: Z. Naturforsch. 17a (1962) 649.
- 63P1 Philipp, H. R., Ehrenreich, H.: Phys. Rev. 129 (1963) 1550.
- 63P2 Piesbergen, U.: Z. Naturforsch. 18a (1963) 141.
- 63S Steigmeier, E. F., Kudman, J.: Phys. Rev. 132 (1963) 508.
- 63W Weisberg, L. R., Blanc, J.: J. Appl. Phys. 34 (1963) 1002.
- 64H1 Haisty, R.W., Cronin, G.R.: Physics of Semiconductors, Hulin, M., (ed.), Paris: Dunod, 1964, p. 1161.
- 64H2 Hall, R.N., Racette, J.H.: J. Appl. Phys. 35 (1964) 379.
- 64H3 Holland, M. G.: in: Proc. 7th Int. Conf. Phys. Semiconductors, Paris 1964, Dunod, Paris 1964, p.1161.
- 65D Dolling, G., Waugh, J. L. T.: in Lattice Dynamics, R. F. Wallis ed., Pergamon Press, Oxford 1965, p. 19.
- 66D Drabble, J. R., Brammer, A. J.: Solid State Commun. 4 (1966) 467.
- 66P Pierron, E. D., Parker, D. L., McNeely, J. B.: Acta Crystallogr. 21 (1966) 290.
- 66S Steigmeier, E. F., Kudman, I.: Phys. Rev. 141 (1966) 767.
- 67C Chapman, R.A., Hutchinson, W.G.: Phys. Rev. Lett. 18 (1967) 443; Errata p. 822.
- 67G Gross, E.F., Safarov, V.I.: Sov. Phys. Semicond. 1 (1967) 241.
- 68A Arlt, G., Quadflieg, P.: Phys. Status Solidi 25 (1968) 323.
- 68K Kendall, D.L.: Semiconductors and Semimetals, Vol. 4, Willardson, R.K., Beer, A.C. (eds.), New York, London: Academic Press 1968, p. 163.
- 69B Beilin, V. M., Vekilov, Yu. Kh., Krasil'nikov, O. M.: Sov. Phys. Solid State (English Transl.) 10 (1969) 2443; Fiz. Tekh. Poluprov. 10 (1968) 3103.
- 69G1 Glazov, V. M., Chizhevskaya, S. N., Evgen'ev, S. B.: Zh. Fiz. Khim. 43 (1969) 373.
- 69G2 Gross, E.F., Safarov, V.I., Sedov, V.E., Marushchak, V.A.: Sov. Phys. Solid State 11 (1969) 277.
- 69P Panish, M. B., Casey, H. C.: J. Appl. Phys. 40 (1969) 163.
- 69W Wynne, J. J., Bloembergen, N.: Phys. Rev. 188 (1969) 1211.
- 70B Blätte, M., Schairer, W., Willmann, F.: Solid State Commun. 8 (1970) 1265.
- 70S1 Stradling, R. A., Wood, R. A.: J. Phys. C3 (1970) L94.
- 70S2 Stulman, G. E., Wolfe, C. M., Dimmock, J. O.: J. Phys. Chem. Solids 31 (1970) 1199.
- 72B1 Baranowski, J.M., Grynberg, M., Magerramov, E.M.: Phys. Status Solidi (b) 50 (1972) 433.
- 72B2 Brown, W.J., Blakemore, J.S.: J. Appl. Phys. 43 (1972) 2242.
- 72Y Yablonovitch, E., Flytzanis, C., Bloembergen, N.: Phys. Rev. Lett. 29 (1972) 865.
- 73A Aspnes, D. E., Studna, A. A.: Phys. Rev. B7 (1973) 4605.
- 73B Burenkov, Yu. A., Burdukov, Yu. M., Davydov, S. Yu: Sov. Phys. Solid State (English Transl.) 15 (1973) 1175; Fiz. Tekh. Poluprov. 15 (1973) 1757.
- 73C Casey, H.C.: Atomic Diffusion in Semiconductors, Shaw, D. (ed.), New York: Plenum Press 1973, p. 351.
- 73E Emel'yanenko, O. V., Skripkin, V. A., Popova, V. A.: Sov. Phys. Semicond. (English Transl.) 7 (1973) 667; Fiz. Tekh. Poluprov. 7 (1973) 981.
- 74B Baldereschi, A., Lipari, N.O.: Phys. Rev. B 9 (1974) 1525.
- 74D Dragunov, V. P., Kozeev, E. V., Kravchenko, A. F., Kholyavko, V. N.: Sov. Phys. Semicond. (English Transl.) 7 (1974) 983; Fiz. Tekh. Poluprov. 7 (1973) 1466.
- 74S1 Schairer, W., Schmidt, M.: Phys. Rev. B 10 (1974) 2501.
- 74S2 Sell, D. D., Casey, H. C., Wecht, K. W.: J. Appl. Phys. 45 (1974) 2650.
- 75A Ashen, D.J., Dean, P.J., Hurle, D.T.J., Mullin, J.B., White, A.M.: J. Phys. Chem. Solids 36 (1975) 1041.
- 75L Lin-Chung, P.J., Wallis, R.F.: Phys. Rev. B 12 (1975) 630.
- 75W Wiley, J. D.: in "Semiconductors and Semimetals", Vol. 10, R. K. Willardson, A. C. Beer eds., Academic Press, New York 1975.
- 76A Aspnes, D. E., Olson, C. G., Lynch, D. W.: Phys. Rev. Lett. 37 (1976) 766.
- 76C Chelikowski, J. R., Cohen, M. L.: Phys. Rev. B14 (1976) 556.
- 76H Hiesinger, P.: Phys. Status Solidi (a) 33 (1976) K39.
- 76K Kitahara, K., Nakai, K., Ozeki, M., Shibatomi, A., Dazai, K.: Jpn. J. Appl. Phys. 15 (1976) 2275.
- 76S Skolnick, M.S., Jam, A.K., Stradling, R.A., Leotin, J., Ousset, J.C., Askenazy, S.: J. Phys. C 9 (1976) 2809.

- 77B Bernolc, J., Pantelides, S.T.: Phys. Rev. B 15 (1977) 4935.
- 77M Mitonneau, A., Martin, G.M., Mircea, A.: Electron. Lett. 13 (1977) 666.
- 78G Guislain, H.J., De Wolf, L., Clauws, P.: Electron. Mater. 7 (1978) 83.
- 78K Kirkman, R.F., Stradling, R.A., Lin-Chung, P.J.: J. Phys. C 11 (1978) 419.
- 78P Pinczuk, A., Lovie, S. G., Welber, B., Tsang, J. C., Bradley, J. A.: Proc. 14th Int. Conf. Phys. Semiconductors, Edinburgh 1978, The Institute of Physics, London 1978, p. 1191.
- 78Y Yu, S. C., Spain, I. L., Skelton, E. F.: Solid State Commun. 25 (1978) 49.
- 80C Chiang, T. C., Knapp, J. A., Aono, M., Eastman, D. E.: Phys. Rev. B21 (1980) 3513.
- 80K Kasahara, J., Watanabe, N.: Jpn. J. Appl. Phys. 19 (1980) LiS1.
- 80M1 Martin, G.M.: Thesis Univ. P. et M. Curie, 1980, unpublished.
- 80M2 Martin, G.M., Mitonneau, A., Pons, D., Mircea, A., Woodard, D.W.: J. Phys. C 13 (1980) 3855.
- 81A Almasy, R.J., Reynolds, D.C., Litton, C.W., Bajaj, K.K., McCoy, G.L.: Solid State Commun. 38 (1981) 1053.
- 81B Bimberg, D., Bludau, W., Linnebach, R., Bauser, E.: Solid State Commun., in press.
- 81H Hennel, A.M., Szuszkiewicz, W., Balkanski, M., Martinez, G., Clerjaud, B.: Phys. Rev. B 23 (1981) 3933.
- 81M Martinez, G., Hennel, A.M., Szuszkiewicz, W., Balkanski, M., Clerjaud, B.: Phys. Rev. B 23 (1981) 3920.
- 82A Averikiev, N.S., Ashirov, T.K., Gutkin, A.A.: Sov. Phys. Solid State 24 (1982) 1168.
- 82B1 Blakemore, J. S.: J. Appl. Phys. 53 (1982) R123.
- 82B2 Blakemore, J. S.: J. Appl. Phys. 53 (1982) 520.
- 82B3 Blakemore, J.S., Johnson, S.G., Rahimi, S.: Semi-Insulating III-V Materials, Evian 1982, Makram-Ebeid, S., Tuck, B. (eds.), Nantwich: Shiva Publishing, 1982, p. 172.
- 82B4 Baublitz, M., Ruoff, A. L.: J. Appl. Phys. 53 (1982) 6179.
- 82F Feldman, A., Waxier, R. M.: J. Appl. Phys. 53 (1982) 1477.
- 82H Hennel, A.M., Martinez, G.: Phys. Rev. B 25 (1982) 1039.
- 82L1 Look, D.C., Chaudhuri, S., Eaves, L.: Phys. Rev. Lett. 49 (1982) 1728.
- 82L2 Leyral, P., Litty, F., Bremond, G., Nouailhat, A., Guillot, G.: Semi-Insulating III-V Materials, Evian 1982, Makram-Ebeid, S., Tuck, B. (eds.), Nantwich: Shiva Publishing, 1982, p. 192.
- 82R Ridley, B.K., Arian, M.C., Bishop, P.J., Hassan, M.F.M., Machado, W.V.: J. Phys. C 15 (1982) 6865.
- 82U Ulrici, W.: Phys. Status Solidi (b) 114 (1982) K87.
- 82Y Yan, Z.X., Milnes, A.G.: J. Electrochem. Soc. 129 (1982) 1353.
- 83A Aspnes, D. E., Studna, A. A.: Phys. Rev. B 27 (1983) 985.
- 83K Kleverman, M., Omling, P., Ledebro, L.-A., Grimmeiss, H.G.: J. Appl. Phys. 54 (1983) 814.
- 83L Lindemann, G., Lassnig, R., Seidenbusch, W., Gornik, E.: Phys. Rev. B 28 (1983) 4693.
- 83S1 Sharma, A. C., Ravindra, N. M., Auluck, S., Srivastava, V. K.: Phys. Status Solidi (b) 120 (1983) 715.
- 83S2 Shanabrook, B.V., Klein, P.B., Bishop, S.O.: Physica 116B (1983) 444.
- 83W Winter, J. J., Leupold, H. A., Ross, R. L., Ballato, A.: J. Appl. Phys. 54 (1983) 5176.
- 84R Rössler, U.: Solid State Commun. 49 (1984) 943.
- 84S Shantharama, L. G., Adams, A. R., Ahmad, C. N., Nicholas, R. J.: J. Phys. C 17 (1984) 4429.
- 85B1 Brandt, C.D., Hennel, A.M., Pawlowicz, L.M., Dabkowski, F.P., Lagowski, J., Gatos, H.C.: Appl. Phys. Lett. 47 (1985) 607.
- 85B2 Braun, M., Rössler, U.: J. Phys. C 18 (1985) 3365.
- 85C1 Campi, D., Papuzza, C.: J. Appl. Phys. 57 (1985) 1305.
- 85C2 Clerjaud, B., Naud, C., Deveaud, B., Lambert, B., Plot, B., Bremond, C., Benjeddou, C., Guillot, G., Nouailhat, A.: J. Appl. Phys. 58 (1985) 4207.
- 85D Drouhin, H.-J., Hermann, C., Lampel, G.: Phys. Rev. B 31 (1985) 3859.
- 85G1 Gislason, H.P., Monemar, B., Wang, Z.G.: Phys. Rev. B 32 (1985) 3723.
- 85G2 Guimaraes, P.S.S., Duncan, K.R., Eaves, L., Stevens, K.W.H., Bowley, R.M., Cisowski, J., Skolnick, M.S., Stirland, D.J.: J. Phys. C 18 (1985) 1431.
- 85K Kopylov, A. A.: Solid State Commun. 56 (1985) 1.
- 85S Straub, D., Skibowski, M., Himpsel, F. J.: Phys. Rev. B 32 (1985) 5237.
- 85U1 Ulrici, W., Friedland, K., Eaves, L., Halliday, D.P.: Phys. Status Solidi (b) 131 (1985) 719.
- 85U2 Ulrici, W., Kiemert, P.: Phys. Status Solidi (b) 129 (1985) 339.
- 85W Wang, Z.G., Gislason, H.P., Monemar, B.: J. Appl. Phys. 58 (1985) 230.
- 86B Brandt, C.D., Rennel, A.M., Pawlowicz, L.M., Wu, Y.T., Bryskiewicz, T., Lagowski, J., Gatos, H.C.: Appl. Phys. Lett. 48 (1986) 1162.

- 86D Deveaud, B., Lambert, B., Auvray, P., Hennel, A.M., Clerjaud, B., Naud, C.: J. Phys. C 19 (1986) 1251.
- 86G Guillot, G., Bremond, G., Bencherifa, A., Nouailhat, A., Ulrici, W.: Semi-Insulating III-V Materials, Hakone 1986, Kukimoto, H., Miyazawa, S. (eds.), Ohmsha, Tokyo, 1986, p. 483.
- 86H Hennel, A.M., Brandt, C.D., Wu, Y.T., Bryskiewicz, T., Ko, K., Lagowski, J., Gatos, H.C.: Phys. Rev. B 33 (1986) 7353.
- 86S Shanabrook, B.U., More, W.J., Bishop, S.G.: J. Appl. Phys. 59 (1986) 2535.
- 86W Wasik, D., Baj, M., Hennel, A.M.: Phys. Rev. B (1986) 4099.
- 87L Lautenschlager, P., Garriga, M., Logothetidis, S., Cardona, M.: Phys. Rev. B 35 (1987) 9174.
- 87S1 Schneider, J., Kaufmann, U., Wilkening, W., Baumler, M., Köhl, F.: Phys. Rev. Lett. 59 (1987) 240.
- 87S2 Schultheis, L., Köhler, K., Tu, C. W.: Phys. Rev. B 36 (1987) 6609.
- 88S Seeger, K.: J. Appl. Phys. 63 (1988) 5439.
- 89G Guzzi, M., Staehli, J. L.: Solid State Phenom. 10 (1989) 25.
- 89S Shanabrook, B. V., Glembocki, O. J., Broido, D. A.: Phys. Rev. B 39 (1989) 3411.
- 89W Weir, S. T., Vohra, Y. K., Vanderborgh, C. A., Ruoff, A. L.: Phys. Rev. B 39 (1989) 1280.
- 90C Chatillon, C., Ansara, I., Watson, A., Argent, B. B.: CALPHAD: Comput. Coupling Phase Diagrams Thermochem. 14 (1990) 203.
- 90F Faist, J., Reihart, F.-K.: J. Appl. Phys. 67 (1990) 7006.
- 90G Goñi, A. R., Cantarero, A., Syassen, K., Cardona, M.: Phys. Rev. B 41 (1990) 10111.
- 90S Strauch, D., Dorner, B.: J. Phys. Condens. Matter 2 (1990) 1457.
- 90V Vohra, Y. K., Xia, H., Ruoff, A. L.: Appl. Phys. Lett. 57 (1990) 2666.
- 91C Clerjaud, B., Gendron, F., Krause, M.: Mod. Phys. Lett. 5 (1991) 877.
- 91G Giannozzi, P., deGironcoli, S., Pavone, P., Baroni, S.: Phys. Rev. B 43 (1991) 7231.
- 91K Kim, M. H., Bose, S. S., Skromme, B. J., Lee, B., Stillman, G. E.: J. Electron. Mater. 20 (1991) 671.
- 91Y Yuan, M.H., Wang, L.P., Jin, S.X., Chen, J.J., Qin, G.G., Appl. Phys. Lett. 58 (1991) 925.
- 92C Chevallier, J., Matchayekhi, B., Grattapain, C.M., Rahbi, R., Theys, B., Phys. Rev. B 45 (1992) 8803.
- 93M Morrow, R.A.: J. Appl. Phys. 74 (1993) 6174.
- 94A Adachi, S.: GaAs and Related Materials: Bulk semiconducting and superlattice properties, World Scientific, Singapore, 1994.
- 94H Hannak, R. M., Rühle, W. W.: Phys. Rev. B 50 (1994) 15445.
- 94K Kuriyama, K., Tomizawa, K., Uematsu, S., Takahashi, H.: Appl. Phys. Lett. 65 (1994) 746.
- 94S1 Shen, H.-L., Makita, Y., Kimura, S., Tanoue, H., Yamada, A., Shibata, H., Obara, A., Sakuragi, S.: Appl. Phys. Lett. 65 (1994) 1427.
- 94S2 Srocka, B., Scheffler, H., Bimberg, D.: Appl. Phys. Lett. 64 (1994) 2679.
- 95K1 Kozhevnikov, M., Ashkinadze, B. M., Cohen, E., Ron, A.: Phys. Rev. B 52 (1995) 17165.
- 95K2 Ka, O., Fons, P.J.: Appl. Phys. Lett. 67 (1995) 1465.
- 96A Aliev, G. N., Luk'yanova, N. V., Seisyan, R. P.: Phys. Solid State (English Transl.) 38 (1996) 590; Fiz. Tverd. Tela 38 (1996) 1067.
- 96D Debernardi, A., Cardona, M.: Phys. Rev. B 54 (1996) 11305.
- 96K Kraisingdecha, P., Gal, M.: Appl. Phys. Lett. 69 (1996) 1355.
- 96L Lancefield, D.: in: Properties of Gallium Arsenide, Brozel, M. R., Stillman, G. E., (eds.), INSPEC/IEE, London, 1996, pp. 46–53.
- 96M1 McMahon, M. I., Nemes, R. J.: Phys. Status Solidi (b) 198 (1996) 389.
- 96M2 Moore, W. J., Holm, R. T.: J. Appl. Phys. 80 (1996) 6939; erratum, *ibid.* 81 (1997) 3732.
- 97L Linnarsson, L., Janzen, E. Monemar, B., Leverman, M., Thilderkvist, A.: Phys. Rev. B 55 (1997) 6938.

Figures to 2.11

Fig. 2.0.2

The zincblende lattice

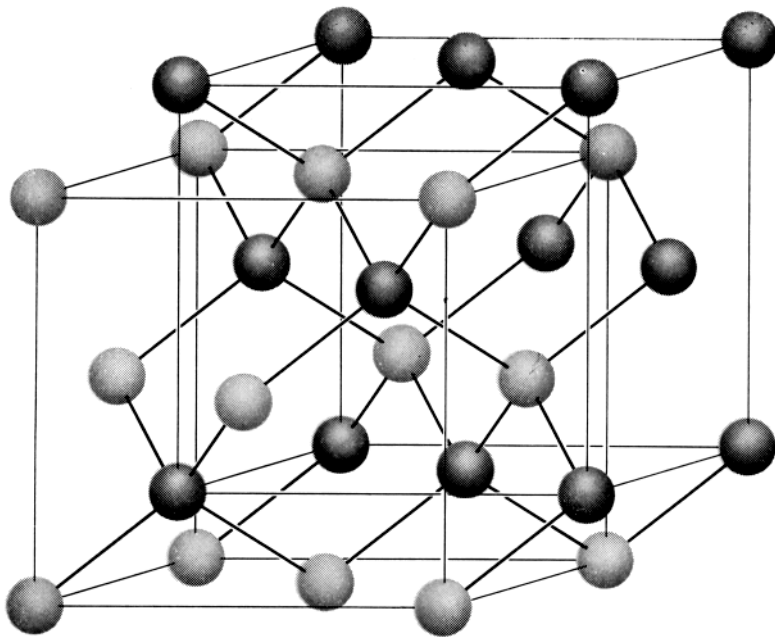


Fig. 2.0.5

Brillouin zone of the zincblende lattice.

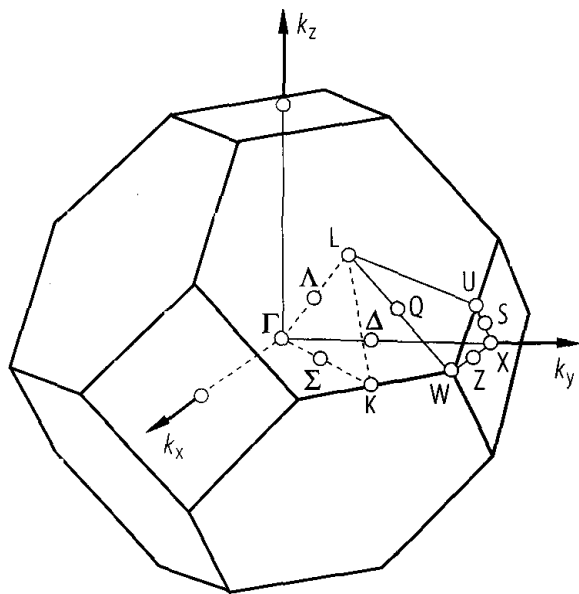


Fig. 2.0.19

GaAs. Band structure obtained by a non-local pseudopotential calculation the subbands are designated by double group notation [76C].

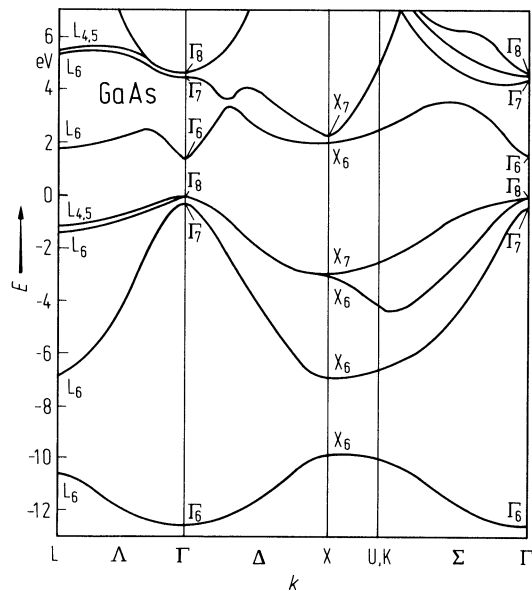


Fig. 2.11.1

GaAs. Direct energy gap vs. temperature. Data from two authors. The solid curve was calculated from the formula given in the tables [69P].

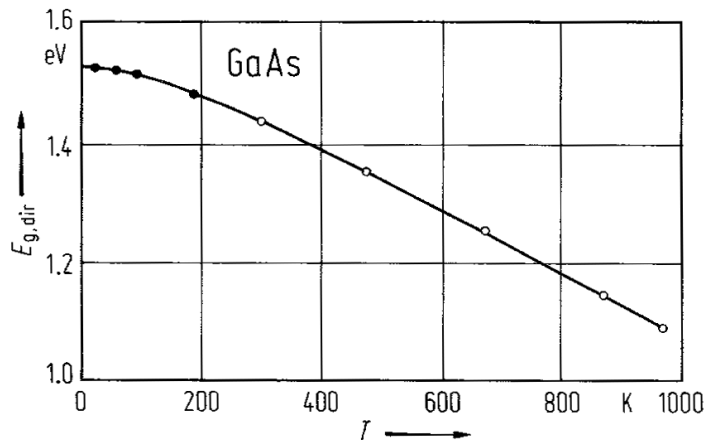


Fig. 2.11.2

GaAs. Electron effective mass vs. temperature as measured by the magnetophonon magnetoresistance [70S]. The solid line represents the result of the three-level $k \cdot p$ calculation [94A].

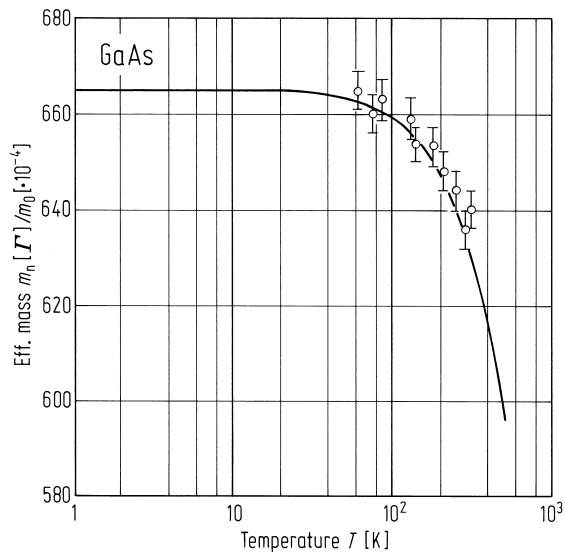


Fig. 2.11.3

GaAs. Lattice parameter vs. temperature [66P]. Different symbols according to various authors.

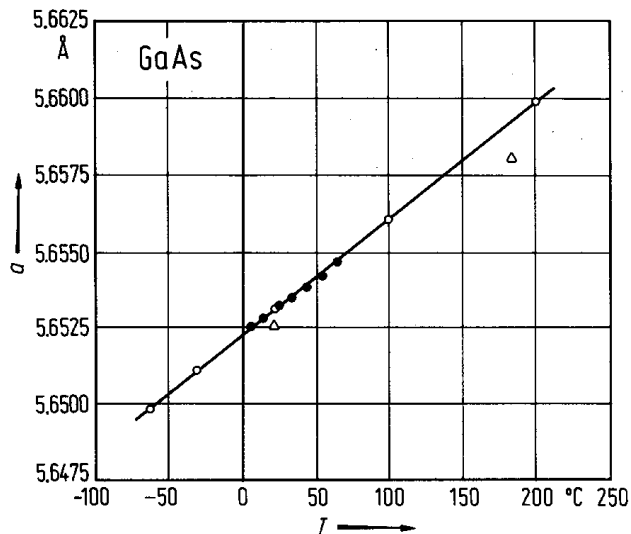


Fig. 2.11.4

GaAs. Coefficient of linear thermal expansion. Experimental data points and curves from an ab-initio pseudopotential calculation [96D].

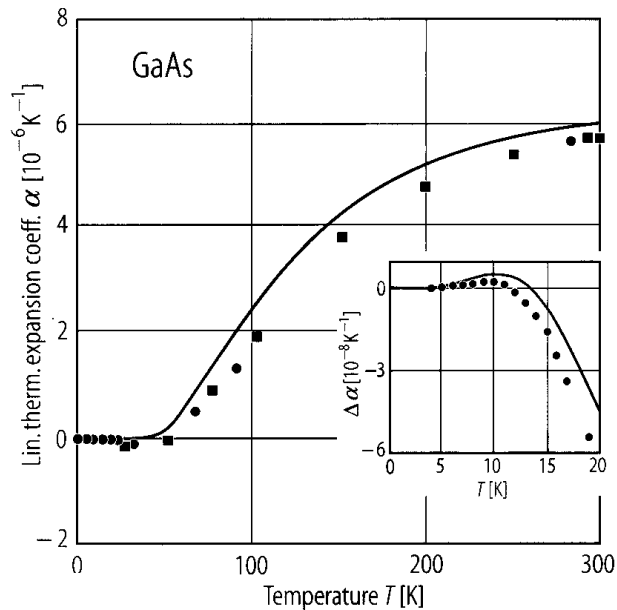


Fig. 2.11.5

GaAs. Density vs. temperature [69G1].

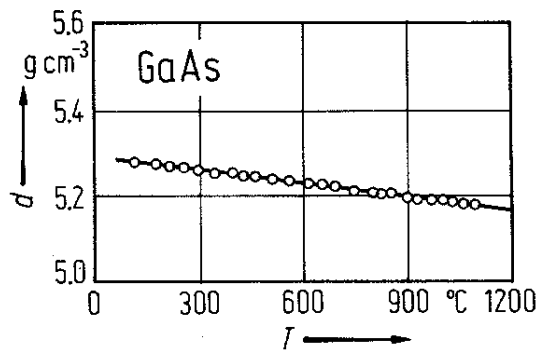


Fig. 2.11.6

GaAs. Phonon dispersion curves (left panel) and phonon density of states (right panel) [91G]. Experimental data points [90S] and ab-initio calculations [91G].

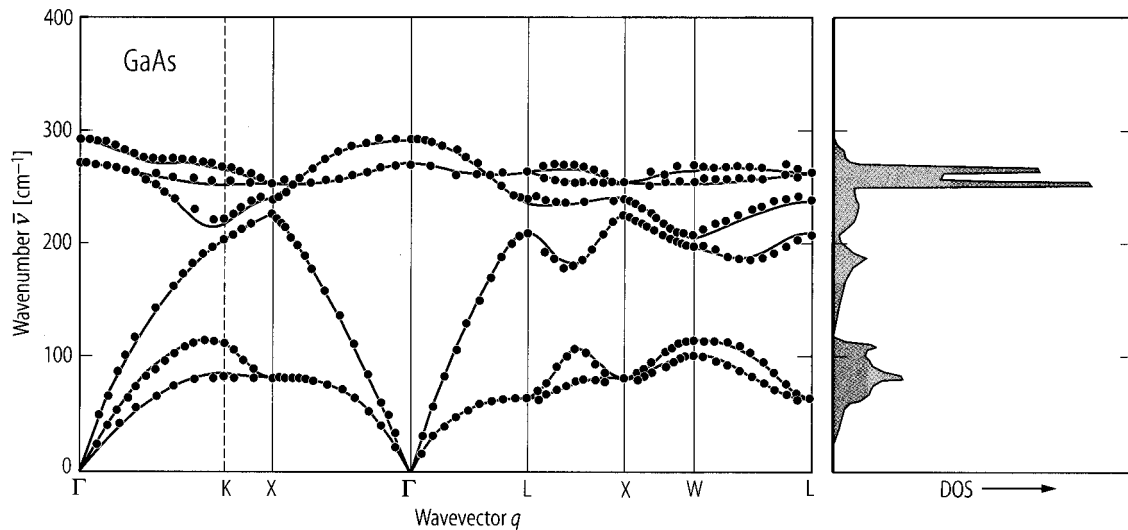


Fig. 2.11.7

GaAs. Temperature dependence of the elastic moduli. Full circles, data of [62G]; triangles, data of [69B]; open circles, data of [73B]; lines, interpolating and extrapolating the data of [73B]. From [73B]. $c_s = (c_{11} - c_{12})/2$.

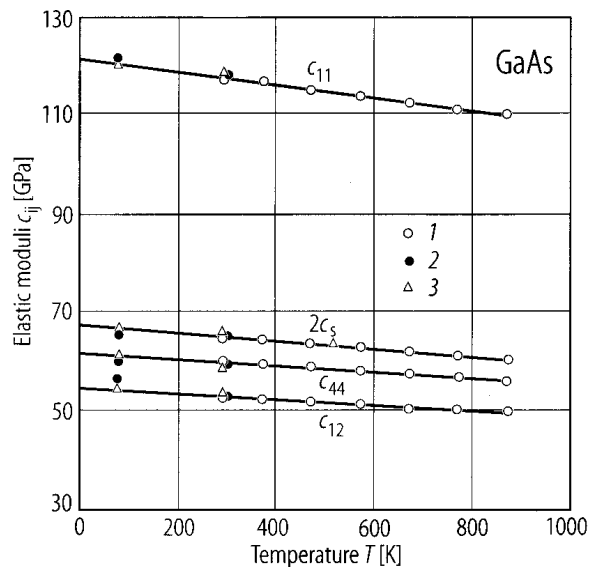


Fig. 2.11.8

GaAs. Young's modulus and torsional moduli vs. temperature (curve 1: [73B], 2: [62G], 3: [69B]).

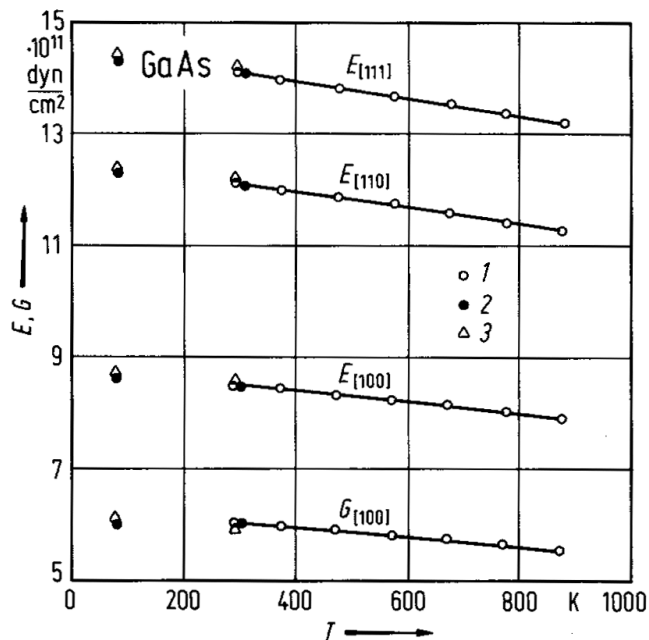


Fig. 2.11.9

GaAs. Debye temperature vs. temperature [63P1].

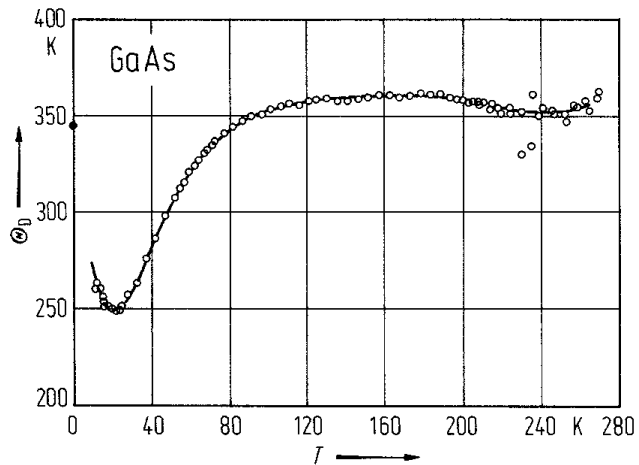


Fig. 2.11.10

GaAs. Intrinsic carrier concentration vs. reciprocal temperature for the range 250...1000 K (a) and vs. temperature for the range 800...1500 K (b). The solid curves (A) are the result of a critical discussion of the literature data. Curves (B)...(G) represent data from other sources [82B1].

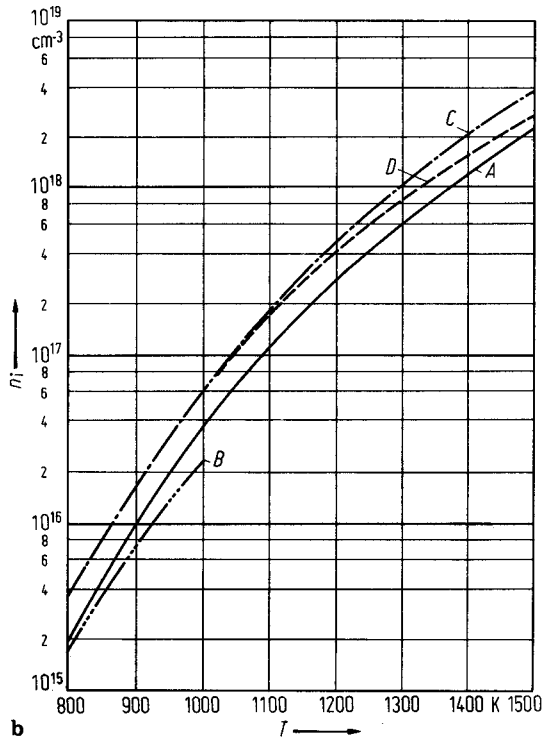
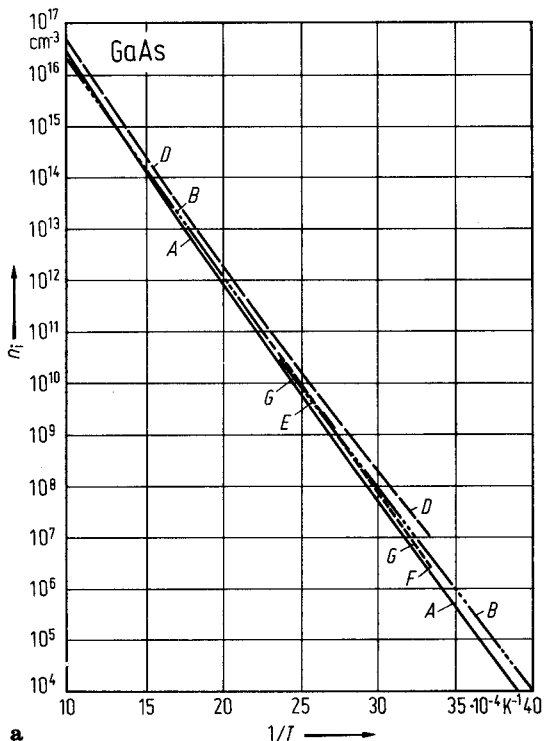


Fig. 2.11.11

GaAs. Thermal conductivity vs. temperature for seven samples with impurity concentrations between $7 \cdot 10^{15} \text{ cm}^{-3}$ and $2.6 \cdot 10^{18} \text{ cm}^{-3}$ [64H3].

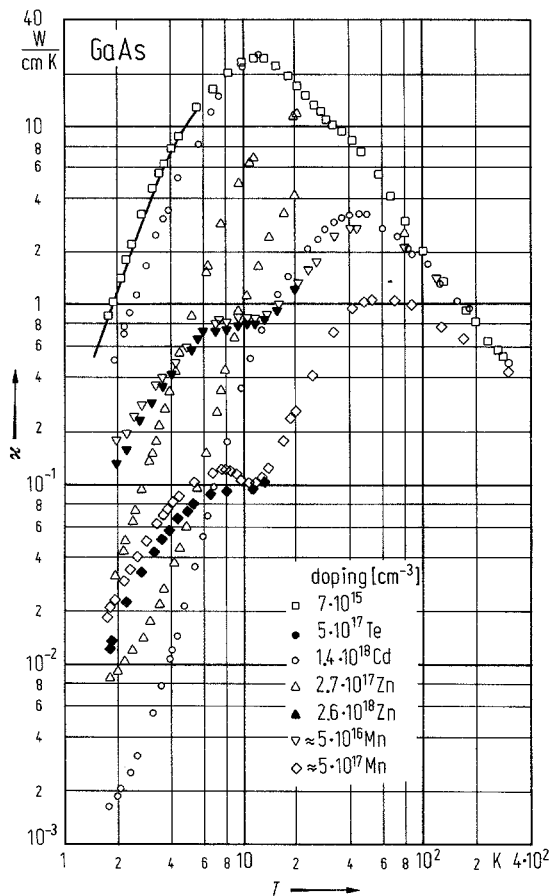


Fig. 2.11.12

GaAs. Typical temperature dependence of the electrical conductivity and the Hall coefficient of a vacuum annealed (A) and a Cr-doped (B) sample. Solid curves: theoretical fit [83L].

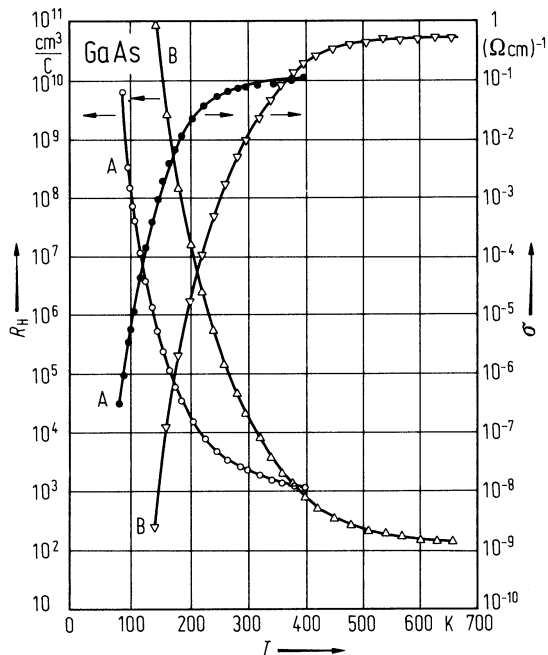


Fig. 2.11.13

GaAs. Temperature variation of Hall mobility at 5 kG for three n-GaAs samples. In the temperature range from 300 K to 77 K, the electron mobility of sample *a* is dominated by polar optical scattering. Samples *b* and *c* show increased effects of ionized impurity scattering [70S1].

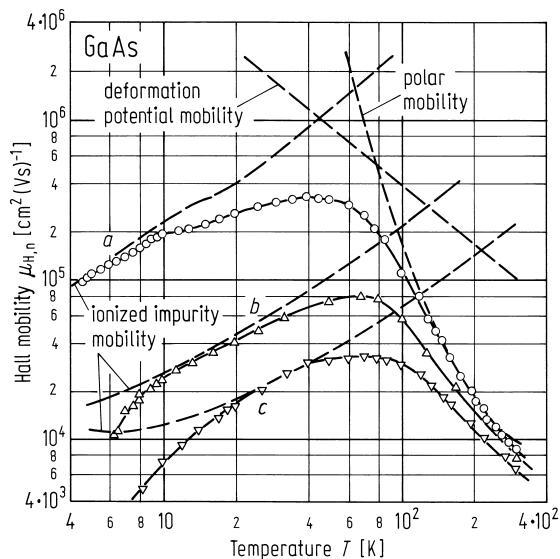


Fig. 2.11.14

GaAs. Hall mobilities of holes vs. temperature for MBE- and MOCVD-grown samples. The solid line represents the empirical relation, $\mu_{H,n} = 450 \cdot (300/T)^{2.3}$ [91K].

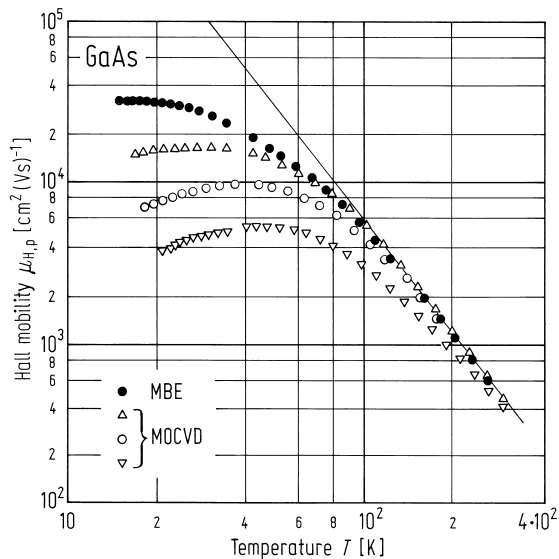


Fig. 2.11.15

GaAs. Seebeck coefficient (thermoelectric power, absolute value) vs. temperature for n- and p-type material. Curve 1: $p = 1.4 \cdot 10^{20} \text{ cm}^{-3}$; 2: $p = 1.0 \cdot 10^{20} \text{ cm}^{-3}$; 3: $p = 2.7 \cdot 10^{19} \text{ cm}^{-3}$; 4: $n = 9.0 \cdot 10^{18} \text{ cm}^{-3}$; 5: $n = 2.5 \cdot 10^{18} \text{ cm}^{-3}$ [73E].

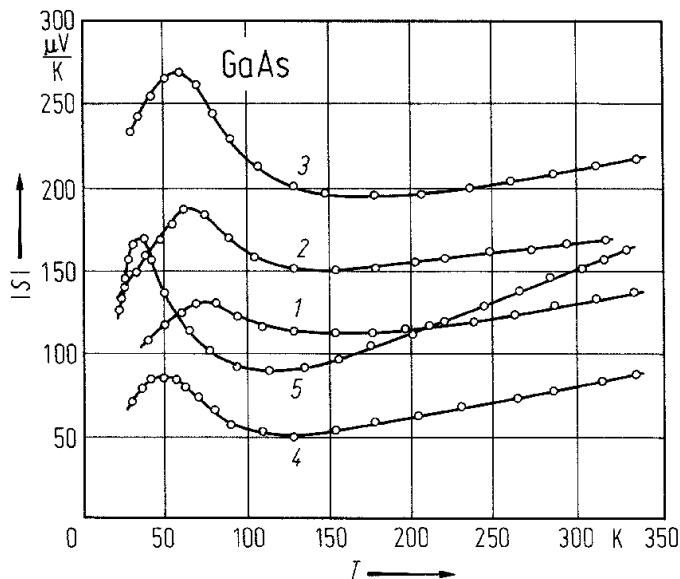


Fig. 2.11.16

GaAs. Real and imaginary parts of the dielectric constant vs. photon energy [83A].

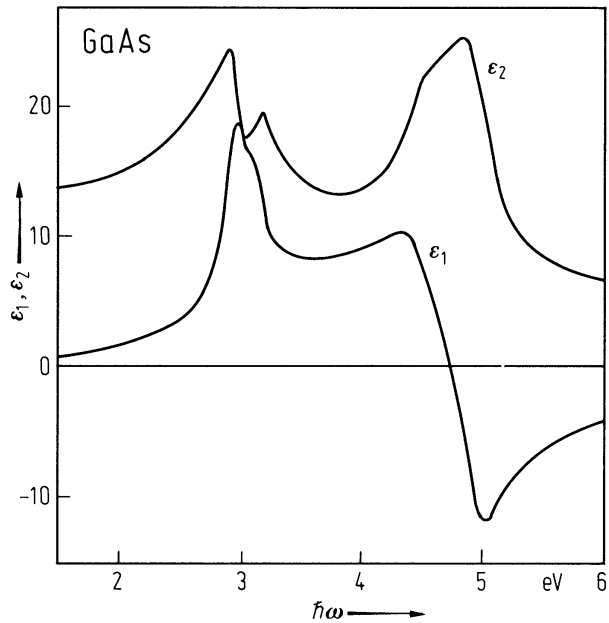


Fig. 2.11.17

GaAs. Refractive index vs. photon energy in the range 1.0...1.7 eV [85C2], solid line: calculated, symbols: experimental data from three sources.

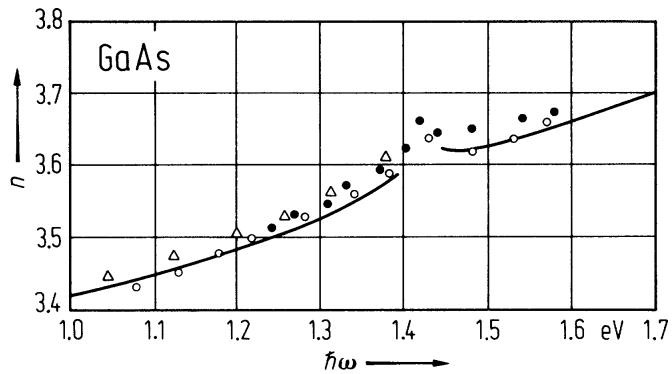


Fig. 2.11.18

GaAs. Absorption coefficient vs. photon energy from 1.5 eV to 2.8 eV at 21 K [62S].

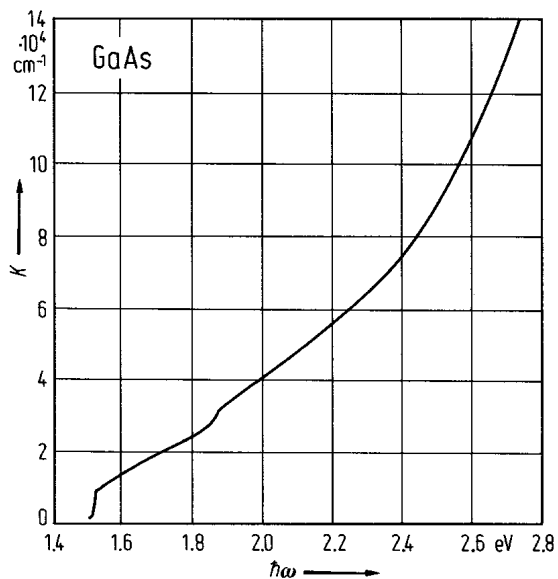
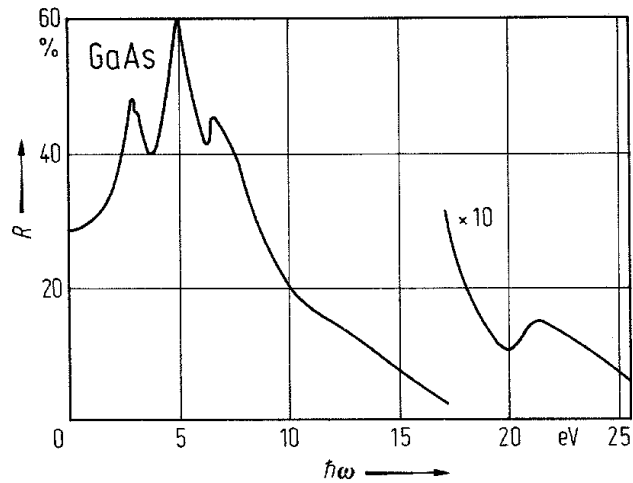


Fig. 2.11.19

GaAs. Reflectance vs. photon energy at 300 K in the range 0...25eV [63P1].



2.12 Gallium antimonide (GaSb)

Crystal structure

Gallium antimonide crystallizes under normal conditions in the zincblende structure (space group $T_d^2 - \bar{F}43m$, Fig. 2.0.2).

high-pressure phases

From resistivity experiments under a pressure, GaSb undergoes a transition from the cubic zincblende phase (GaSb-I) to the metallic phase (GaSb-II, β -Sn structure) [87W] at 8 to 10 GPa with a large hysteresis at room temperature. Samples, when quenched at 9 GPa from room temperature, contained the β -Sn (white tin) structure. The GaSb-II phase was reported to have an orthorhombic structure [94M]; the structure is site-disordered and thus has Imma rather than Imm2 symmetry; the phase is stable from 7 to at least 61 GPa [95N] and does not transform to the hexagonal structure; but it is also claimed that the Imma phase is stable only under non-hydrostatic conditions and that the high-pressure structure is a disordered β -tin structure [99M].

Electronic properties

band structure : Fig. 2.0.20, Brillouin zone: Fig. 2.0.5.

The conduction band of GaSb is characterized by two types of minima, the lowest minimum at Γ and slightly higher minima at the L points at the surface of the Brillouin zone. A third set of minima at the X points has been detected in optical experiments. The valence band shows the usual structure common to all zincblende semiconductors.

energies of symmetry points of the band structure (relative to the top of the valence band $E(\Gamma_{8v})$)

$E(\Gamma_{6v})$	- 12.00 eV	symmetry symbols in double notation	76C
$E(\Gamma_{7v})$	- 0.76 eV		
$E(\Gamma_{6c})$	0.86 eV		
$E(\Gamma_{7c})$	3.44 eV		
$E(\Gamma_{7c})$	3.77 eV		
$E(L_{6v})$	- 10.17 eV		
$E(L_{6v})$	- 6.25 eV		
$E(L_{6v})$	- 1.45 eV		
$E(L_{4,5v})$	- 1.00 eV		
$E(L_{6c})$	1.22 eV		
$E(L_{4,5c})$	4.43 eV		
$E(L_{6c})$	4.59 eV		
$E(X_{6v})$	- 9.3 eV		
$E(X_{6v})$	- 6.76 eV		
$E(X_{6v})$	- 2.61 eV		
$E(X_{7v})$	- 2.37 eV		
$E(X_{6c})$	1.72 eV		
$E(X_{7c})$	1.79 eV		

direct energy gap

$E_{g, \text{dir}}(\Gamma_{8v}-\Gamma_{6c})$	0.822 eV	$T = 0 \text{ K}$, extrapol.	electroreflectance	81J
	0.75 eV	$T = 300 \text{ K}$		

exciton ground state

$E(1S)$	0.8102 eV	$T = 4.2 \text{ K}$	magnetoabsorption	76V
E_b	1.6 meV		calculated binding energy of exciton ground state including valence band degeneracy	76V

energies of valence band critical points (all energies referred to the valence band maximum, critical points given in double group notation)

$E(\Gamma_{8v})$	0 eV	$T = 4.2$ K	angle resolved photoelectron spectroscopy	80C
$E(\Gamma_{7v})$	− 0.82(7) eV			
$E(\Gamma_{6v})$	− 11.64(10) eV			
$E(L_{4,5v})$	− 1.10(7) eV			
$E(L_{6v})$	− 1.55(10) eV			
$E(L_{6v})$	− 6.60(10) eV			
$E(L_{6v})$	− 10.06(10) eV			
$E(X_{7v})$	− 2.86 eV			
$E(X_{6v})$	− 3.10(7) eV			
$E(X_{6v})$	− 6.90(10) eV			
$E(X_{6v})$	− 9.62(10) eV			
$E(\Sigma_{3,4v}^{\min})$	− 3.64(15) eV			

energies of conduction band critical points

derived from the valence band critical point energies (table above) by addition of transition energies of [76A]

$E(\Gamma_{8c})$	7.9(1) eV	E''_0 transition	80C
$E(\Gamma_{8c})$	3.404(10) eV	$E'_0 + \Delta'_0$ transition	
	3.34(7) eV	$E'_0 + \Delta'_0 + \Delta''_0$ transition	
$E(\Gamma_{7c})$	3.191(5) eV	E'_0 transition	
$E(\Gamma_{6c})$	0.8102 eV	E_0 transition (direct gap)	
$E(L_{6c})$	4.49(8) eV	E'_1 transition	
	4.49(10) eV	E''_1 transition	
$E(L_{4,5c})$	4.36(7) eV	E'_1 transition	
	4.35(12) eV	E''_1 transition	
$E(L_{6c})$	1.10(7) eV	E_1 transition	

all values referred to the valence band maximum.

higher conduction band minima

energy difference to lowest minimum

$E(L_{6c} - \Gamma_{6c})$	0.0845 eV	$T = 0$ K, extrapol.	magnetoresistance, Hall effect, Fig. 2.12.1	66H
$E(X_{6c} - \Gamma_{6c})$	0.43(2) eV	$T = 10$ K	electroreflectance	76A

spin-orbit splitting energies

$\Delta_0(\Gamma_{8v} - \Gamma_{7v})$	0.756(15) eV	$T = 10$ K	electroreflectance	76A
$\Delta'_0(\Gamma_{7c} - \Gamma_{8c})$	0.213(10) eV			
$\Delta_1(L_{4,5v} - L_{6v})$	0.430(10) eV			
$\Delta'_1(L_{4,5c} - L_{6c})$	0.13 eV			

camel's back structure at the X conduction band minimum

Δ	178 meV	estimate from $k \cdot p$ theory	85K
ΔE	25.1 meV	using GaP data	
k_m	0.127($2\pi/a$)		
m_t	0.250 m_0		
$m_{ }$	1.2 m_0		

structure of top of valence band

By the linear $E(k)$ -term in the structure of the valence band of semiconductors with zincblende lattice the spin-degeneracy is lifted. The maxima of the heavy hole bands are shifted in $[111]$ -direction, that of the light hole bands in $[100]$ -direction. From an analysis of transport data the following values for the difference of energies at the top of the bands and at $k = 0$ have been found:

$\Delta E[111]$	20 meV	see also Fig. 2.12.2	79M
$\Delta E[100]$	5 meV		
$\Delta E[111] - \Delta E[100]$	7.5 meV		85H

conduction band, effective masses

$m_n(\Gamma)$	0.039(5) m_0	$T = 2$ K	optically detected cyclotron resonance	88J
$m_n(L_{6c})$	0.11 m_0		transverse	81L
	0.95 m_0		longitudinal	
	0.226 m_0		density of states analysis	
$m_n(L): m_{\perp}$	0.14 m_0	$T = 77$ K	Faraday rotation	64P
m_{\parallel}	1.2 m_0			
m_{ds}	0.729 m_0			

electron g-factor

g_c	-9.1(2)	$T = 4.2 \dots 50$ K	magnetoluminescence	74B
-------	---------	----------------------	---------------------	-----

valence band, effective masses

$m_{p,h}$	0.29(9) m_0	$T = 30$ K,	stress modulated magnetorefectance	72R
	0.36(13) m_0	$B \parallel [100]$		
	0.40(16) m_0	$[110]$		
		$[111]$		
$m_{p,l}$	0.042(2) m_0	$T = 30$ K	stress modulated magnetorefectance	72R

spin-orbit split valence band

m_{so}	0.15(3) m_0	$T = 30$ K	stress modulated magnetorefectance	70R
----------	---------------	------------	------------------------------------	-----

valence band parameters

A	-11.0(6)	$T = 12 \dots 20$ K	cyclotron resonance	66S
B	-6.0(1.5)			
$ C $	11(4)			

Lattice properties

lattice parameter

a	6.09593(4) Å	$T = 298.15$ K	powder, X-ray, Fig. 2.12.3	65S
temperature dependence: $a = a_0 + a_1 T + a_2 T^2 + a_3 T^3 + a_4 T^4$ with				82B
a_0	6.095882 Å	T in °C	up to 680°C	
a_1	$3.4963 \cdot 10^{-5}$ Å °C ⁻¹			
a_2	$3.3456 \cdot 10^{-8}$ Å °C ⁻²			
a_3	$4.6309 \cdot 10^{-11}$ Å °C ⁻³			
a_4	$2.6369 \cdot 10^{-14}$ Å °C ⁻⁴			

linear thermal expansion coefficient

α	7.75(50) $\cdot 10^{-6}$ K ⁻¹	$T = 283 \dots 343$ K	X-ray, for temperature dependence, see Fig. 2.12.4	65S
----------	--	-----------------------	--	-----

density

d	5.6137(4) g cm ⁻³	$T = 300$ K	for temperature dependence in the range 670...970 K, see Fig. 2.12.5	65S
-----	------------------------------	-------------	--	-----

melting temperature

T_m	991(1) K			89Y
-------	----------	--	--	-----

phonon dispersion curves : Fig. 2.12.6, Brillouin zone: Fig. 2.0.5.

phonon wavenumbers

$\bar{\nu}_{TA}(L)$	46 cm ⁻¹	$T = 300$ K	second order Raman effect	76K1
$\bar{\nu}_{TA}(X)$	56 cm ⁻¹			
$\bar{\nu}_{TA}(W)$	75 cm ⁻¹			
$\bar{\nu}_{LA}(L)$	155 cm ⁻¹			
$\bar{\nu}_{LO}(L)$	204 cm ⁻¹			
$\bar{\nu}_{LO}(X)$	210 cm ⁻¹			
$\bar{\nu}_{TO}(L,X,\Sigma)$	218 cm ⁻¹			

sound velocities

v_l	4240(30) m/s	$T = 290$ K	pulse-echo overlap method	97B
v_t	2460(20) m/s			

second order elastic moduli (from ultrasound measurements)

c_{11}	$8.834 \cdot 10^{11}$ dyn cm ⁻²	$T = 296$ K,	n-type, ($f = 30$ MHz),	75B
c_{12}	$4.023 \cdot 10^{11}$ dyn cm ⁻²	$\rho = 0.1 \dots 0.07$ Ω cm		
c_{44}	$4.322 \cdot 10^{11}$ dyn cm ⁻²		see also Fig. 2.12.7	

third order elastic moduli

c_{111}	$-4.75(6) \cdot 10^{12}$ dyn cm ⁻²	$T = 300$ K	ultrasound ($f = 10$ MHz), uniaxial	76R
c_{112}	$-3.08(2) \cdot 10^{12}$ dyn cm ⁻²		stress up to 0.108 kbar	
c_{123}	$-0.44(29) \cdot 10^{12}$ dyn cm ⁻²			
c_{144}	$+0.50(25) \cdot 10^{12}$ dyn cm ⁻²			
c_{166}	$-2.16(13) \cdot 10^{12}$ dyn cm ⁻²			
c_{416}	$-0.25(15) \cdot 10^{12}$ dyn cm ⁻²			

bulk modulus

B	56.1 GPa	room temperature		87W
-----	----------	------------------	--	-----

shear modulus

G	34.0(5) GPa	$T = 290$ K	pulse-echo overlap method	97B
-----	-------------	-------------	---------------------------	-----

Young's modulus

E	85.0(15) GPa	$T = 290$ K	pulse-echo overlap method	97B
-----	--------------	-------------	---------------------------	-----

Debye temperature

Θ_D	266 K		for temperature dependence, see Fig. 2.12.8	63P
------------	-------	--	---	-----

Transport properties

Transport in n-type GaSb is complicated by the contribution of three sets of conduction bands with minima situated at Γ , L and X. Data on transport coefficients can be consistently explained by a three band model (Fig. 2.12.9), the X-bands contributing to transport above 180°C.

In p-type GaSb a multiellipsoidal model has to be used at low temperatures taking into account the shift of the heavy and light hole band away from $k = 0$. At high temperatures a warped sphere model (as in Si and Ge) is adequate.

intrinsic carrier concentration

n_i	10^{14} cm^{-3}	$T = 365 \text{ K}$	calculated with $m_p = 0.34 m_0$,	73C
	10^{15} cm^{-3}	$T = 435 \text{ K}$	$m(\Gamma_6) = 0.042 m_0$, $m(L_6) = 0.57 m_0$	
	10^{16} cm^{-3}	$T = 525 \text{ K}$	and $E_g = 0.813 - 6.0 \cdot 10^{-4} T^2 / (T + 265)$	
	10^{17} cm^{-3}	$T = 645 \text{ K}$	eV (T in K)	
	10^{18} cm^{-3}	$T = 825 \text{ K}$		

electron mobility

$\mu_{H,n}$	$7620 \text{ cm}^2/\text{Vs}$	$T = 300 \text{ K}$,	material grown with MBE	93T
		$n = 1.2 \cdot 10^{16} \text{ cm}^{-3}$	on GaSb substrates	

electron mobility in the Γ_6 minima:

$\mu_n(\Gamma_6)$	$3760 \text{ cm}^2/\text{Vs}$	$T = 298 \text{ K}$,	calculated from magnetoresistance	72B
		$n(\Gamma_6) = 3.76 \cdot 10^{17} \text{ cm}^{-3}$	resistance measurements	

electron mobility in the L_6 minima:

$\mu_n(L_6)$	$> 3100 \text{ cm}^2/\text{Vs}$	$T = 298 \text{ K}$,	calculated from magnetoresistance	72B
		$n(\Gamma_6) = 3.76 \cdot 10^{17} \text{ cm}^{-3}$	resistance measurements	

hole mobility

$\mu_{H,p}$	$680 \text{ cm}^2/\text{Vs}$	$T = 300 \text{ K}$	typical value for Hall mobility	85H
-------------	------------------------------	---------------------	---------------------------------	-----

mobilities of heavy holes ($\mu_{p,h}$) and light holes ($\mu_{p,l}$):

$T = 77 \text{ K}$				
$\mu_{p,l}$	$10800 \text{ cm}^2/\text{Vs}$	$p_l = 4.74$	two band analysis of Hall coefficient.	73M
		$\cdot 10^{14} \text{ cm}^{-3}$,		
$\mu_{p,h}$	$1600 \text{ cm}^2/\text{Vs}$	$p_h = 3.09$		
		$\cdot 10^{16} \text{ cm}^{-3}$		

piezoresistance tensor coefficients

n-type material				
$\pi_{11} + 2\pi_{12}$	$-140 \cdot 10^{-12} \text{ cm}^2/\text{dyn}$	$T = 300 \text{ K}$	Te-doped, conduction bands not degenerate, applied pressure of the order 3000 kg/cm ² .	70A
π_{44}	$-80 \cdot 10^{-12} \text{ cm}^2/\text{dyn}$			

p-type material

π_{11}	$5.0 \cdot 10^{-12} \text{ cm}^2/\text{dyn}$	$T = 300 \text{ K}$	π_{11} down to 4.2 K	64T
π_{12}	$-2.4 \cdot 10^{-12} \text{ cm}^2/\text{dyn}$			
π_{44}	$87.0 \cdot 10^{-12} \text{ cm}^2/\text{dyn}$			

elastoresistance coefficients

m_{11}	2.4	$T = 300 \text{ K}$,	calculated from piezoresistance coefficients with the aid of elastic constants tensor c_{lm}	64T
m_{12}	-1.2	$p \approx 10^{17} \text{ cm}^{-3}$		
m_{44}	37			

piezoelectric constants

e_{14}	$1.26 \cdot 10^{-5} \text{ C/cm}^2$	$T = 300 \text{ K}$	piezoelectric Hall effect measurements.	68A
	$\pm 20\%$			
d_{14}	$2.9 \cdot 10^{-10} \text{ cm/V}$		Polarity: negative (if the crystal is expanded along the [111] direction,	
g_{14}	$2.2 \cdot 10^2 \text{ cm}^2/\text{C}$		the A-faces (metal atoms) become	
h_{14}	$9.5 \cdot 10^6 \text{ V/cm}$		negatively charged)	

Seebeck coefficient (thermoelectric power)

S_n	$-250 \text{ }\mu\text{V/K}$	$T = 300 \text{ K}$	Te-doped, n-type sample with $\sigma(77 \text{ K}) = 1930 \text{ }\Omega^{-1}\text{cm}^{-1}$ (corresponding to $n \approx 1.7 \cdot 10^{18} \text{ cm}^{-3}$).	70P
-------	------------------------------	---------------------	--	-----

Temperature dependence: Fig. 2.12.10.

thermal conductivity

Fig. 2.12.11.

Optical properties

optical constants

real and imaginary parts of the dielectric constant measured by spectroscopical ellipsometry, n , k , R , K calculated from these data [83A]. See also Fig. 2.12.12.

$h\nu \text{ [eV]}$	ϵ_1	ϵ_2	n	k	R	$K \text{ [} 10^3 \text{ cm}^{-1}\text{]}$
1.5	19.135	3.023	4.388	0.344	0.398	52.37
2.0	25.545	14.442	5.239	1.378	0.487	279.43
2.5	13.367	19.705	4.312	2.285	0.484	579.07
3.0	9.479	15.838	3.832	2.109	0.444	641.20
3.5	7.852	19.267	3.785	2.545	0.485	902.86
4.0	-1.374	25.138	3.450	3.643	0.583	1477.21
4.5	-8.989	10.763	1.586	3.392	0.561	1547.17
5.0	-5.693	7.529	1.369	2.751	0.585	1394.02
5.5	-5.527	5.410	1.212	2.645	0.592	1474.51
6.0	-4.962	4.520	0.935	2.416	0.610	1469.28

refractive index

n		$T \text{ [K]},$	$\lambda \text{ [}\mu\text{m]}$		
		300,	14.9		
	3.880		10	reflectance and transmission	54O
	3.843		4		
	3.833		2	prism method	59E
	3.789	300,	1.9		
	3.802		1.8		
	3.820				

absorption index

k		$\lambda \text{ [}\mu\text{m]}$		
	$1.08 \cdot 10^{-4}$	300 K,	2	transmission
	$1.83 \cdot 10^{-3}$		1.75	
	$4.06 \cdot 10^{-2}$		1.7	
	$7.39 \cdot 10^{-2}$		1.6	

absorption coefficient

K	$4 \cdot 10^3 \text{ cm}^{-1}$	$T = 1.7 \text{ K},$ $h\nu = 0.815 \text{ eV}$	transmission	62J
-----	--------------------------------	---	--------------	-----

dielectric constants

$\epsilon(0)$	15.7	$T = 300\text{ K}$	reflectance and oscillator fit	97P
$\epsilon(\infty)$	14.5			

second order nonlinear dielectric susceptibilities

$d(\text{SHG})$	$6.3 \cdot 10^{-10} \text{ mV}^{-1}$	$T = 300\text{ K}$, CO_2 laser $10.6\text{ }\mu\text{m}$	second harmonic generation, should only contain $\chi_e^{(2)}$	69W
-----------------	--------------------------------------	--	---	-----

Impurities and defects

shallow impurities and defects

Undoped, relatively pure GaSb is usually p-type. Thus, neutral donor states are not populated in equilibrium.

binding energies of donors

Impurity	E_b [meV]	T [K]	Remarks	Ref.
Te(L)	20(5)	230	pressure dependence of Hall coefficient	69P
Te(X)	< 80			71V
Se(L)	85	77	pressure dependence of conductivity	66K
Se(L)(?)	30	4.2	Shubnikov-de Haas effect	76H
Se(X)	200	290		71V
S(L)	140...150			69P, 71V
S(X)	300			71V

binding energies of acceptors

The dominant acceptor of undoped GaSb seems to be a native defect. Hall measurements show that this acceptor is doubly ionizable.

PL = Photoluminescence, MOCVD = Metalorganic Chemical Vapour Deposition, LPE = Liquid Phase Epitaxy.

Impurity or Label	E_b [meV]	T [K]	Remarks	Ref.
Li	10		PL	73B, 76K2
Si	9.4(5)	1.8	PL	76J
	13...15	4.2	PL	71B
Ge	9.5(5)	1.8	PL	76J
Mn	18	2	PL	91G1
Fe	22(3)		PL, Hall	78K
	3	10	PL, Hall, undoped MOCVD samples	93S
A	32	10	PL, Hall, undoped MOCVD samples	93S
B	52	10	PL, Hall, undoped MOCVD samples	93S
	58	10	PL, Hall, undoped MOCVD samples	93S
	80	10	PL, Hall, undoped MOCVD samples	93S
A ⁻	102	10	PL, Hall, undoped MOCVD samples	93S
	130	10	PL, Hall, undoped MOCVD samples	93S
A	32	16	PL on LPE samples	92W
B	52	16	PL on LPE samples	92W
A	34	4.5	PL on LPE samples - shallow level	95I
B	54	4.5	PL on LPE samples	95I
Te	68	4.5	PL on LPE samples	95I

Te	83	4.5	PL on LPE samples	95I
A ⁻	97	4.5	PL on LPE samples - deep level	95I
A	~35	77	Cathodoluminescence	95M
B	~54	77	Cathodoluminescence	95M

deep states introduced by donors

Doping GaSb with shallow donors is known to induce deep traps. The table contains emission (E_e) and capture (E_b) activation energies for the Te, Se, S induced traps that have been measured by DLTS [90P, 92P, 94D] and by TSCAP (thermally stimulated capacitance) [94D].

(N_T/N_d is the ratio between the number of traps and the number of dopants.)

Impurity	E_e [meV]	E_b [meV]	σ_n at T	N_T/N_d	Ref.
Te	312	174	$2 \cdot 10^{-20}$ 133K	0.010	94D
Te	310	190	$6 \cdot 10^{-19}$ 150K	0.015	90P
Se	320	180	$9 \cdot 10^{-21}$ 133K	0.030	94D
Se	315	195	$2 \cdot 10^{-20}$ 150K	0.045	90P
S	287	220	$7 \cdot 10^{-19}$ 133K	1	94D
S	280	200	$6 \cdot 10^{-18}$ 150K	1	90P

References to 2.12

- 54O Oswald, R., Schade, R.: Z. Naturforsch. 9a (1954) 611.
- 59E Edwards, D. F., Hayne, G. S.: J. Opt. Soc. Am. 49 (1959) 414.
- 61B Becker, W. M., Ramdas, A. K., Fan, H. Y.: J. Appl. Phys. Suppl. 32 (1961) 2094.
- 62J Johnson, E. J., Filinski, I., Fan, H. Y.: Proc. Int. Conf. Phys. Semicond., Exeter 1962, Institute of Physics and Physical Society, London 1962, p. 375.
- 63N Novikova, S. I., Abrikosov, N. Kh.: Sov. Phys. Solid State (English Transl.) 5 (1963) 1558; Fiz. Tverd. Tela 5 (1963) 2138.
- 63P Piesbergen, U.: Z. Naturforsch. 15a (1963) 141.
- 64H Holland, M. G.: Proc. Int. Conf. Phys. Semicond., Paris 1964, Dunod, Paris 1964 p. 713.
- 64P Piller, H.: Proc. 7th Int. Conf. Phys. Semiconductors, Paris 1964, Dunod, Paris 1964, p. 297.
- 64T Tufte, O. N., Stelzer, E. L.: Phys. Rev. 133 (1964) A1450.
- 65S Straumanis, M. E., Kim, C. D.: J. Appl. Phys. 36 (1965) 3822.
- 66H Harland, H. B., Woolley, J. C.: Can. J. Phys. 44 (1966) 2715.
- 66K Kosicki, B.B., Paul, W.: Phys. Rev. Lett. 17 (1966) 246.
- 66S Stradling, R. A.: Phys. Lett. 20 (1966) 217.
- 68A Arlt, G., Quadflieg, P.: Phys. Status Solidi 25 (1968) 323.
- 69G Glazov, V. M., Chizhevskaya, S. N., Evgen'ev, S. B.: Zh. Fiz. Khim. 43 (1969) 373
- 69P Pitt, G.D.: High Temp. High Pressures 7 (1969) 111.
- 69W Wynne, J. J., Bloembergen, N.: Phys. Rev. 188 (1969) 1211.
- 70A Averous, M., Bougnot, G., Calas, J., Chevrier, J.: Phys. Status Solidi 37 (1970) 807.
- 70P Parfen'ev, R. V., Matveenko, A. V., Vekshina, V. S., Lang, I. G., Pavlov, S. T.: Sov. Phys. Solid State (English Transl.) 11 (1970) 2663; Fiz. Tverd. Tela 11 (1969) 3287.
- 70R Reine, M., Aggarwal, R. L., Lax, B.: Solid State Commun. 8 (1970) 35.
- 71B Burdiyan, I.I., Mal'tsev, S.B., Mironov, I.F., Shreter, Yu.G.: Sov. Phys. Semicond. (English Transl.) 5 (1972) 1734; Fiz. Tekh. Poluprovodn. 5 (1971) 1996.
- 71V Vul, A.Ya., Bir, G.L., Shmartsev, Y.V.: Sov. Phys. Semicond. (English Transl.) 4 (1971) 2005; Fiz. Tekh. Poluprovodn. 4 (1970) 2331.
- 72B Basinski, J., Kwan, C. C. Y., Wooley, J. C.: Can. J. Phys. 50 (1972) 1068.
- 72R Reine, M., Aggarwal, R. L., Lax, B.: Phys. Rev. B 5 (1972) 3033.
- 73B Burdiyan, I.I.: Sov. Phys. Semicond. 7 (1973) 449.
- 73C Casey, H. C. Jr.: in "Atomic Diffusion in Semiconductors", D. Shaw ed., Plenum Press, London-New York 1973, p. 422.
- 73M Metzler, R. A., Becker, W. M.: Phys. Rev. B 12 (1973) 5604.
- 74B Bimberg, D., Rühle, W.: Proc. 12th Int. Conf. on Physics of Semiconductors, Stuttgart 1974, ed. M. H. Pilkuhn, Teubner, Stuttgart 1974, p. 561.
- 75B Boyle, W. F., Sladek, R. J.: Phys. Rev. B 11 (1975) 2933.
- 75F Farr, M. K., Traylor, J. G., Sinha, S. K.: Phys. Rev. B 11 (1975) 1587.
- 76A Aspnes, D. E., Olson, C. G., Lynch, D. W.: Phys. Rev. B 14 (1976) 4450.
- 76C Chelikowski, J. R., Cohen, M. L.: Phys. Rev. B 14 (1976) 556.
- 76H Hoo, K., Becker, W.M., Sun, R.-Y.: Solid State Commun. 18 (1976) 313.
- 76J Jakowetz, W., Barthruff, D., Benz, K.W.: Proc. 6th Int. Symp. on GaAs and related compounds, Hilsum, C. (ed.), London: Inst. Phys. 1976, p. 41.
- 76K1 Klein, P. B., Chang, R. K.: Phys. Rev. B 14 (1976) 2498.
- 76K2 Kukukadze, G.V., Vashakisze, D.Z., Chikhladze, M.N., Bakradze, Sh.R.: Izv. Akad. Nauk SSSR Neorg. Mater. 12 (1976) 1480.
- 76R Raja, V. S., Reddy, P. J.: Phys. Lett. A 56 (1976) 215.
- 76V Varfolomeev, A. V., Ryskin, A. A., Seisyan, R. P.: Sov. Phys. Semicond. (English Transl.) 10 (1976) 1234; Fiz. Tekh. Poluprov. 10 (1976) 2072.
- 78K Krukovskaya, L.P., Mironov, I.F., Titkov, A.N.: Sov. Phys. Semicond. 12 (1978) 401.
- 79M Mathur, P. C., Jam, S.: Phys. Rev. B 19 (1979) 3152.
- 80C Chiang, T. C., Eastman, D. E.: Phys. Rev. B 22 (1980) 2940.
- 81J Joullie, A., Zein Eddine, A., Girault, B.: Phys. Rev. B 23 (1981) 928.
- 81L Lee, H. J., Woolley, J. C.: Can. J. Phys. 59 (1981) 1844.
- 82B Bublik, V. T., Wilke, J., Pereversev, A. T.: Phys. Status Solidi (a) 73 (1982) K271.
- 83A Aspnes, D. E., Studna, A. A.: Phys. Rev. B 27 (1983) 985.
- 85H Heller, M. W., Hamerly, R. G.: J. Appl. Phys. 57 (1985) 4626.

- 85K Kopylov, A. A.: Solid State Commun. 56 (1985) 1.
- 87W Weir, S. T., Vohra, Y. K., Ruoff, A. L.: Phys. Rev. B 36 (1987) 4543.
- 88J Johnson, G. R., Cavanett, B. C., Kerr, T. M., Kiby, P. B., Wood, C. E. C.: Semicond. Sci. Technol. 3 (1988) 1157.
- 89Y Yamaguchi, K.: J. Jpn. Inst. Met. 53 (1989) 764.
- 90P Poole, I., Lee, M.E., Cleverley, I.R., Peaker, A.R., Singer, K.E.: Appl. Phys. Lett. 57 (1990) 1645.
- 91G1 Georgitse, E.I., Gutsulyak, L.M., Ivanov-Omskii, V.I., Smirnov, V.A., Yuldashev, Sh.U.: Sov. Phys. Semicond. 25 (1991) 1180.
- 91G2 Giannozzi, P., deGironcoli, S., Pavone, P., Baroni, S.: Phys. Rev. B 43 (1991) 7231.
- 92P Polyakov, A., Stam, M., Milnes, A.G., Schlesinger, T.E.: Mater. Sci. Eng. 12 (1992) 337.
- 92W Wu, M.-C., Chen, C.-C.: J. Appl. Phys. 72 (1992) 4275.
- 93S Su, Y.K., Chen, S.M. : J. Appl. Phys. 73 (1993) 8349.
- 93T Turner, G. W., Eglash, S. J., Strauss, A. J.: J. Vac. Sci. Technol. B 11 (1993) 864.
- 94D Dutta, P.S., Koteswara Rao, K.S.R., Sangunni, K.S., Bhat, H.L., Kumar, V.: Appl. Phys. Lett. 65 (1994) 1412.
- 94M McMahon, M. I., Nemes, R. J., Wright, N. G., Allan, D. R.: Phys. Rev. B 50 (1994) 13047; see also [95N].
- 95I Iyer, S., Small, L., Hedge, S.M., Bajaj, K.K., Abul-Fadl, A.: J. Appl. Phys. 77 (1995) 5902.
- 95M Méndez, B., Dutta, P.S., Piqueras, J., Dieguez, E.: Appl. Phys. Lett. 67 (1995) 2648.
- 95N Nemes, R. J., McMahon, M. I., Wright, N. G., Allan, D. R., Liu, H., Loveday, J. S.: J. Phys. Chem. Solids 56 (1995) 539.
- 97B Brazhkin, V. V., Lyapin, A. G., Goncharova, V. A., Stal'gorova, O. V., Popova, S. V.: Phys. Rev. B 56 (1997) 990.
- 97P Patrini, M., Guizzetti, G., Galli, M., Ferrini, R., Bosacchi, A., Franchi, S., Magnanini, R.: Solid State Commun. 101 (1997) 93.
- 99M Mezouar, M., Libotte, H., Députier, S., Le Bihan, T., Häusermann, D.: Phys. Status Solidi (b) 211 (1999) 395.

Figures to 2.12

Fig. 2.0.2

The zincblende lattice

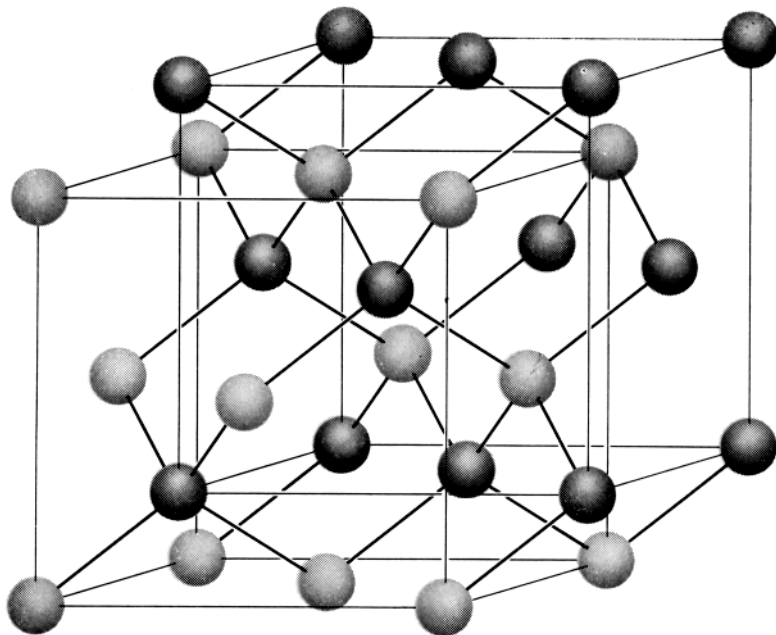


Fig. 2.0.5

Brillouin zone of the zincblende lattice.

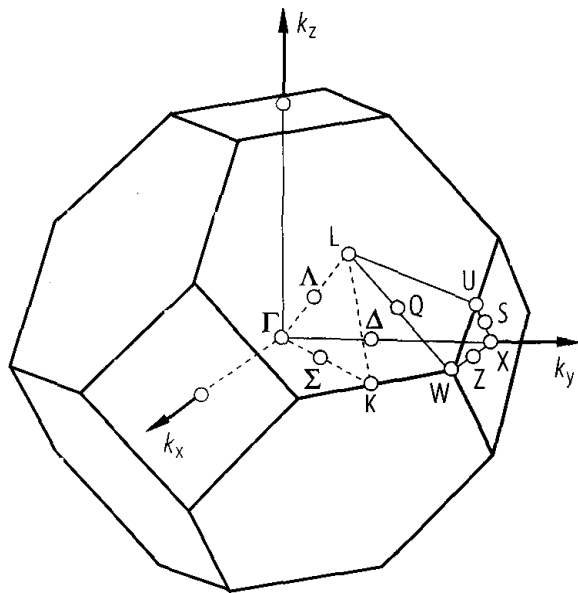


Fig. 2.0.20

GaSb. Band structure obtained with a non-local pseudopotential calculation [76C].

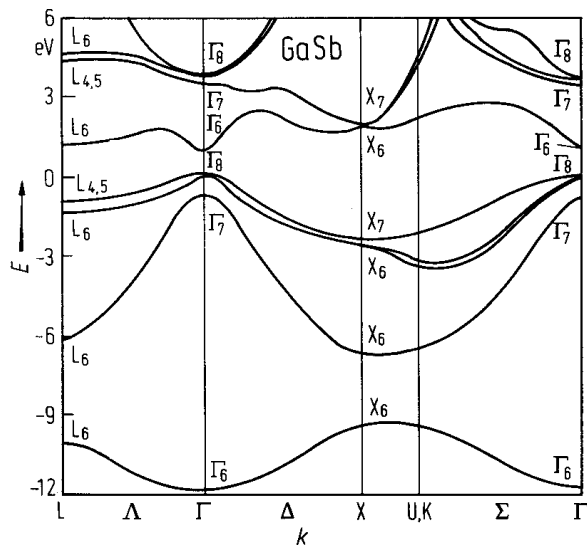


Fig. 2.12.1

GaSb. Energy of L-conduction band minima above the Γ -minimum. Measurements on different samples [66H].

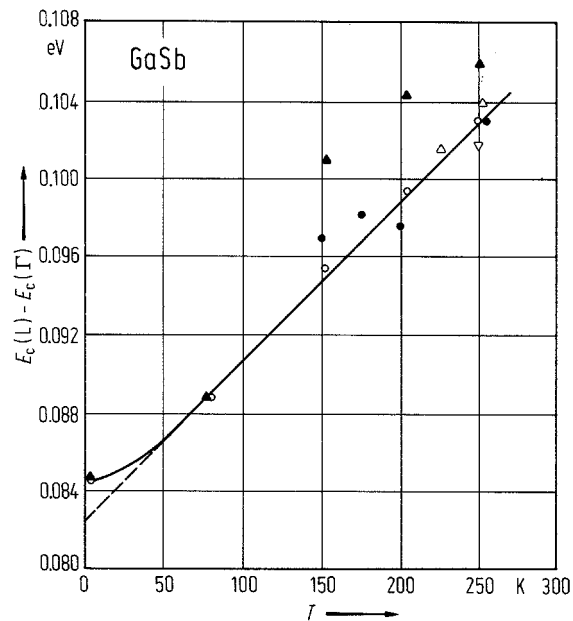


Fig. 2.12.2

GaSb. Energies of electroreflectance peaks vs. temperature. $E_{g,dir}$: direct $\Gamma_{8v}-\Gamma_{6c}$ transition, L: indirect $\Gamma_{8v}-L_{6c}$ transition, dotted line: $\Gamma_{8v}-L_{6c}$ gap obtained from L by subtracting the LA phonon energy of 17 meV [81J].

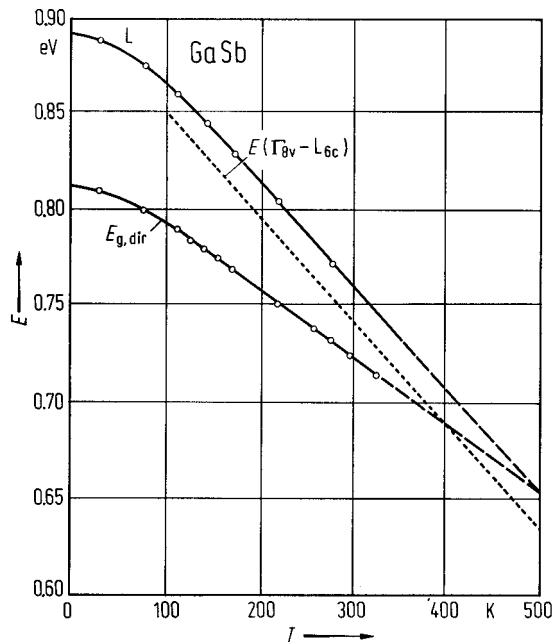


Fig. 2.12.3

GaSb. Lattice parameter vs. temperature [65S].

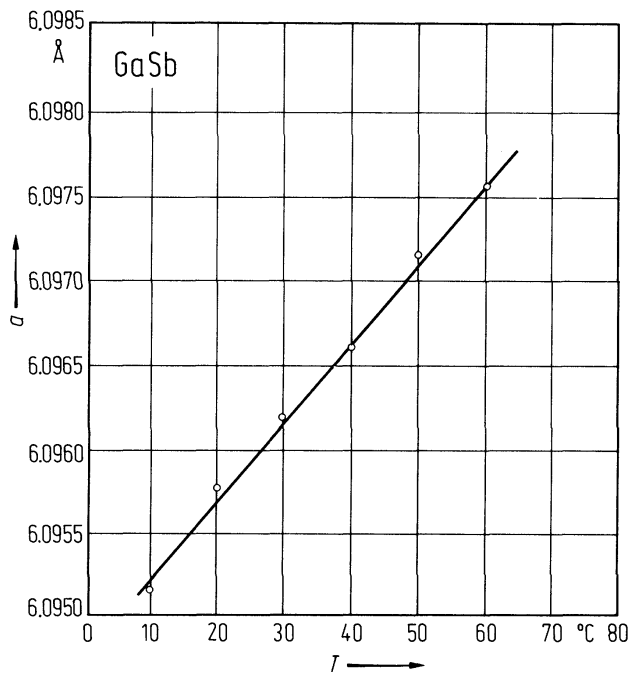


Fig. 2.12.4

GaSb. Linear thermal expansion coefficient vs. temperature measured with a quartz dilatometer. High temperature range [63N].

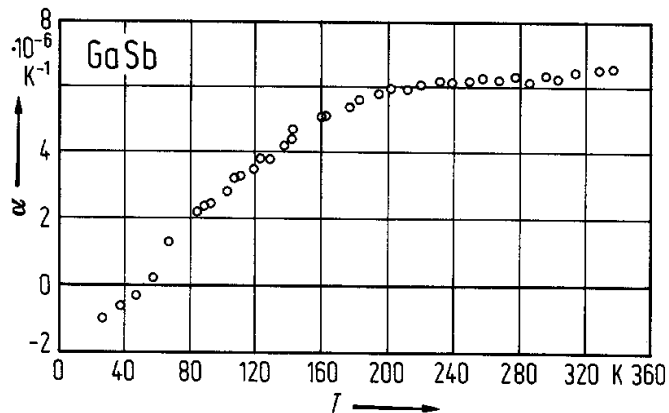


Fig. 2.12.5

GaSb. Density vs. temperature [69G].

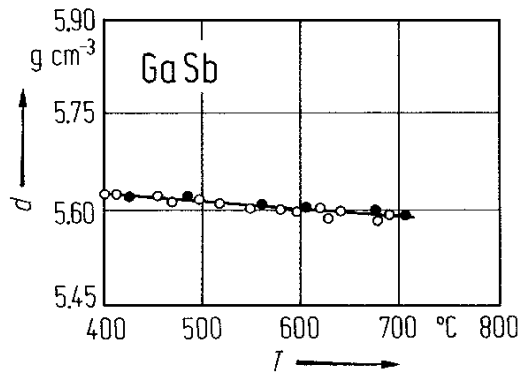


Fig. 2.12.6

GaSb. Phonon dispersion curves (left panel) and phonon density of states (right panel) [91G2]. Experimental data points [75F] and ab-initio calculations [91G2].

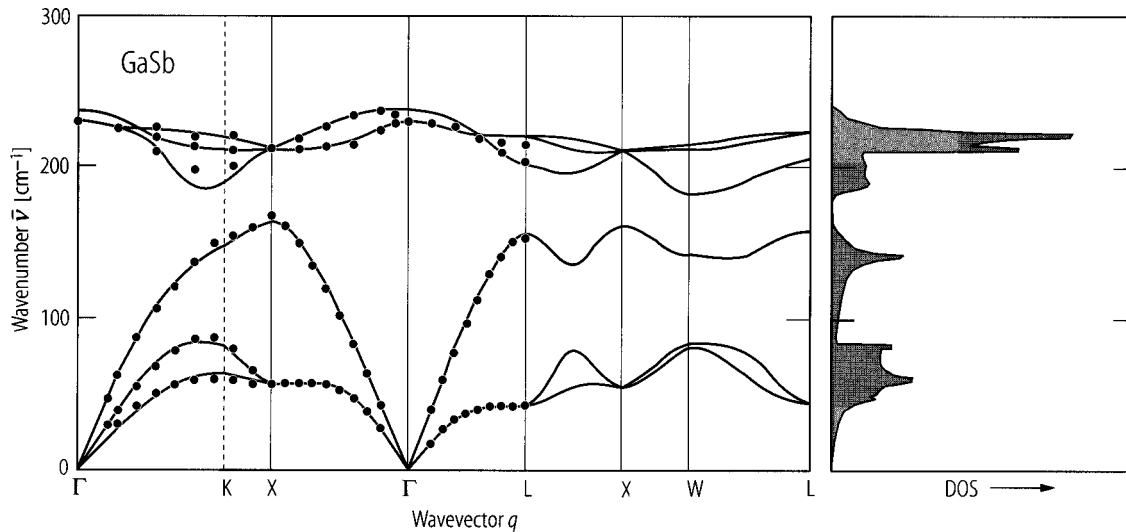


Fig. 2.12.7

GaSb. Second order elastic moduli vs. temperature [75B].

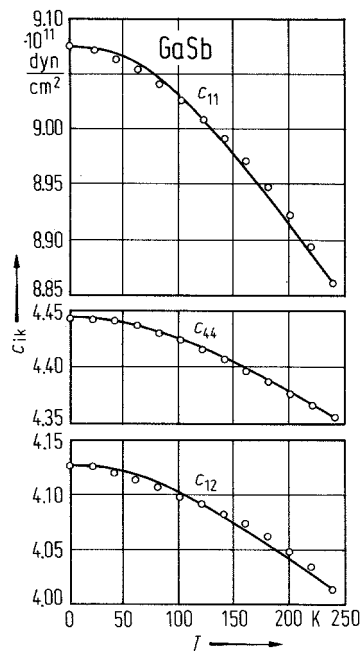


Fig. 2.12.8

GaSb. Debye temperature Θ_D vs. temperature [63P].

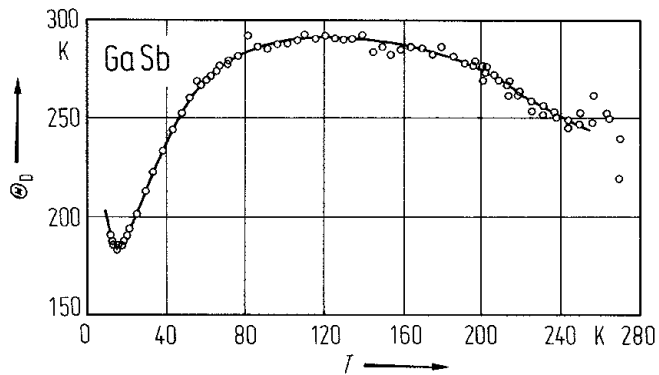


Fig. 2.12.9

GaSb. (a) Hall coefficient and electrical conductivity vs. temperature for a sample with $n = 1.49 \cdot 10^{18} \text{ cm}^{-3}$, (b) reciprocal magnetoresistance vs. magnetic field for the same sample, (c) longitudinal and transverse Nernst-Ettingshausen coefficients vs. magnetic field for the same sample, (d) pressure dependence of resistivity and Hall coefficient at RT for a sample with $n = 1.87 \cdot 10^{18} \text{ cm}^{-3}$. Symbols: experimental, lines: theoretical fit [81L].

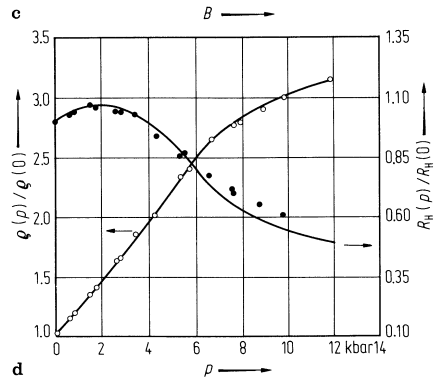
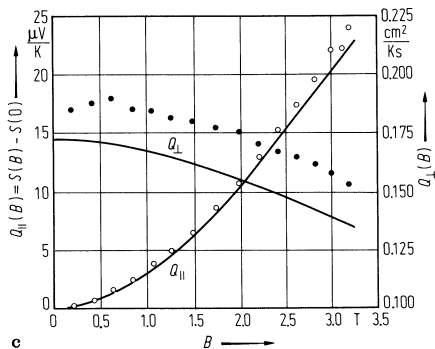
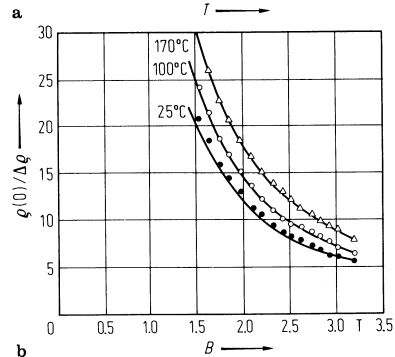
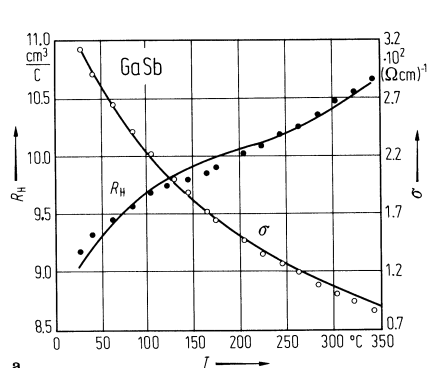


Fig. 2.12.10

GaSb. Seebeck coefficient (thermoelectric power) vs. temperature for n-type material (Te-doped, $\sigma(77\text{ K}) = 1930\ \Omega^{-1}\text{ cm}^{-1}$) [70P].

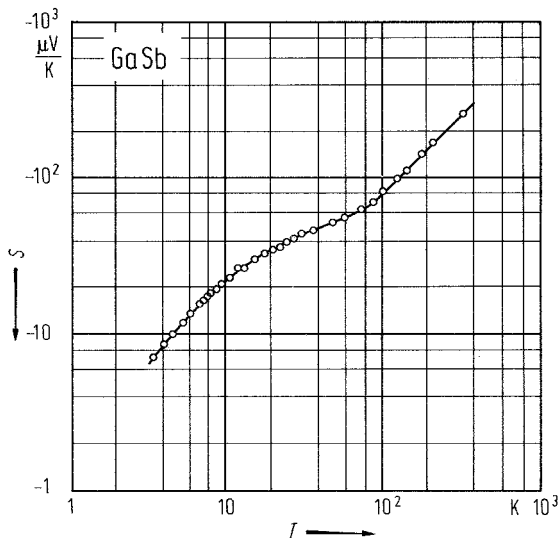


Fig. 2.12.11

GaSb. Thermal conductivity of two n-type samples with impurity content of $4 \cdot 10^{18} \text{ cm}^{-3}$ (1) and $1.4 \cdot 10^{18} \text{ cm}^{-3}$ (2) and of two p-type samples with $1 \cdot 10^{17} \text{ cm}^{-3}$ (3) and $2 \cdot 10^{17} \text{ cm}^{-3}$ (4) [64H].

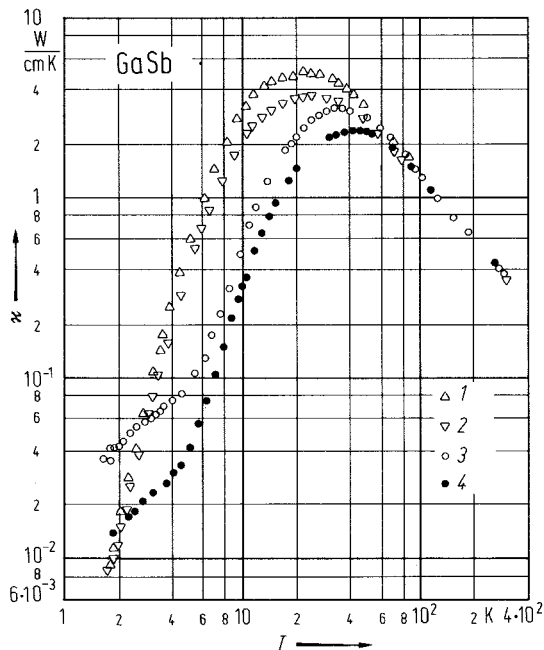
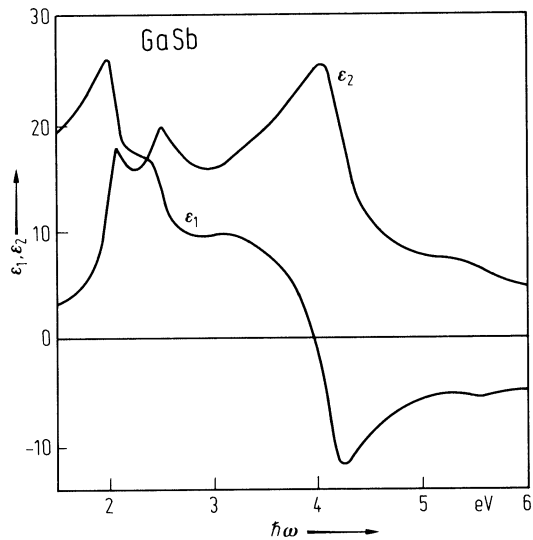


Fig. 2.12.12

GaSb. Real and imaginary parts of the dielectric constants vs. photon energy [83A].



2.13 Indium nitride (InN)

Crystal structure

Indium nitride crystallizes under normal conditions in the wurtzite structure (space group P6₃mc, Fig. 2.0.3). Under pressure one observes a phase transition to the rocksalt structure [93U, 94U].

Electronic properties

band structure : Fig. 2.0.21, Brillouin zone: Fig. 2.0.8

The band structure shows a direct gap at Γ , closely similar to that of GaN. A low lying many-valley conduction band leading to an indirect gap has been suggested by [77T].

energy gap

$E_{\text{g, dir}}$	1.95 eV	$T = 300 \text{ K}$	polycrystalline film, absorption edge	72O
---------------------	---------	---------------------	---------------------------------------	-----

Lattice properties

lattice parameter

a	3.5446 Å	epitaxial layers, X-ray	78P
c	5.7034 Å		

temperature dependence of lattice parameters (a and c in Å, T in K)

$a(T) = 3.5341(3) + 1.27(7) \cdot 10^{-5} T$	$100 \text{ K} < T < 673 \text{ K}$	X-ray diffraction	99P
$c(T) = 5.7016(7) + 1.46(18) \cdot 10^{-5} T$			

linear thermal expansion coefficient

α_a	$3.6(2) \cdot 10^{-6} \text{ K}^{-1}$	$100 \text{ K} < T < 673 \text{ K}$	X-ray diffraction	99P
α_c	$2.6(3) \cdot 10^{-6} \text{ K}^{-1}$		temperature dependence: see Fig. 2.13.1	

density

d	6.78(5) g cm ⁻³		pycnometric	98K
-----	----------------------------	--	-------------	-----

melting temperature

T_{m}	1900 K	at 60 kbar N ₂	estimated	98K
----------------	--------	---------------------------	-----------	-----

phonon wavenumbers

$\bar{\nu}_{\text{TO}}(\Gamma)$	478 cm ⁻¹	$T = 300 \text{ K}$	reflectivity, Kramers-Kronig analysis	75O
$\bar{\nu}_{\text{LO}}(\Gamma)$	694 cm ⁻¹			
$\bar{\nu}_{\text{TO}}(\text{A}_1)$	400 cm ⁻¹		experimental	95I
$\bar{\nu}_{\text{TO}}(\text{E}_1)$	484 cm ⁻¹			
$\bar{\nu}_{\text{LO}}(\text{E}_1)$	570 cm ⁻¹			
$\bar{\nu}_{\text{TO}}(\text{E}_2^{(1)})$	190 cm ⁻¹			
$\bar{\nu}_{\text{TO}}(\text{E}_2^{(2)})$	590 cm ⁻¹			

second order elastic moduli

c_{11}	190(7) GPa	calculated from the mean square displacements of the lattice atoms measured by X-ray diffraction	79S
c_{12}	104(3) GPa		
c_{13}	121(7) GPa		
c_{33}	182(6) GPa		
c_{44}	9.9(11) GPa		

bulk modulus

B	147 GPa	calculated	96K
-----	---------	------------	-----

Debye temperature

Θ_D	660 K			98K
------------	-------	--	--	-----

heat capacity

C_p	$9.1 + 2.9 \cdot 10^{-3} T$ (T in K)	cal·mol ⁻¹ K ⁻¹	calorimetry	87S, 77B
-------	--	---------------------------------------	-------------	-------------

Transport properties

electrical conductivity

σ	2...3 ·10 ² Ω ⁻¹ cm ⁻¹	$T = 300$ K	temperature coefficient of resistivity 3.7·10 ⁻³ K at 200...300 K for pressed powder	56J, 72H, 74T
----------	--	-------------	---	---------------------

electron mobility

μ_n	250(50) cm ² /Vs	$T = 300$ K		72H
	20 cm ² /Vs	$T = 300$ K		74T
	35...50 cm ² /Vs	$T = 300$ K		77M

The temperature dependence of the electron mobility is shown in Fig. 2.13.2.

thermal conductivity

κ	38.4 W m ⁻¹ K ⁻¹			98K
----------	--	--	--	-----

Optical properties

refractive index

n	2.56	$T = 300$ K, $n = 3 \cdot 10^{20}$ cm ⁻³ $\lambda = 1.0$ μm	interference method	77T
	2.93	0.82 μm		
	3.12	0.66 μm		

dielectric constants

$\varepsilon(0)$	9.3	heavily doped film	infrared reflectivity	77T
$\varepsilon_{33}(0) \equiv \varepsilon_{ }(0)$	15.3		optical reflectivity	95I
$\varepsilon(\infty)$	8.4		experimental	79M

References to 2.13

- 56J Juza, R., Rabenau, A.: Z. Anorg. Allg. Chem. 285 (1956) 212.
- 72H Hovel, H. J., Cuomo, J. J.: Appl. Phys. Lett. 20 (1972) 71.
- 72O Osamura, K., Makajima, K., Murakami, Y., Shingu, P. H., Ohtsuki, A.: Solid State Commun. 11 (1972) 617.
- 74T Trainor, J. W., Rose, K.: J. Electron. Mater. 3 (1974) 821.
- 75O Osamura, K., Naka, S., Murakami, Y.: J. Appl. Phys. 46 (1975) 3432.
- 76S Sheleg, A. U., Savastenko, V. A.: Vestsi Akad. Nauk BSSR, Ser. Fiz. Mat. Nauk 3 (1976) 126.
- 77B Barin, I., Knacke, O., Kubaschewski, O.: Thermodynamical properties of inorganic substances, Springer Verlag, Berlin-Heidelberg-New York 1977.
- 77M Marasina, L. A., Pichugin, E. G., Tlaczala, M.: Krist. Techn. 12 (1977) 541.
- 77T Tyagai, V. A., Evstigneev, A. M., Krasiko, A. N., Adreeva, A. F., Malakhov, V. Ya.: Sov. Phys. Semicond. (English Transl.) 11 (1977) 1257; Fiz. Tekh. Poluprovodn. 11 (1977) 2142.
- 78P Pichugin, I. G., Tlachala, M.: Izv. Akad. Nauk SSSR, Neorg. Mater. 14 (1978) 175.
- 79M Misek, J., Srobar, F.: Elektrotech. Cas. 30 (1979) 690; as cited in [94C].
- 79S Sheleg, A. U., Savastenko, V. A.: Izv. Akad. Nauk SSSR, Ser. Neorg. Mater. 15 (1979) 1598. (as cited in [97W]); Inorg. Mater. 15 (1979) 1257 (English Transl.).
- 84T Tansley, T. L., Foley, C. P.: Electron. Lett. 20 (1984) 1087.
- 86F Foley, C. P., Tansley, T. L.: Phys. Rev. B 33 (1986) 1430.
- 87S Slack, G. A., Tanzili, R. A., Pohl, R. O., Vandersande, J. W.: J. Phys. Chem. Solids 48 (1987) 641.
- 93U Ueno, M., Yoshida, M., Onodera, A., Shimomura, O., Takemura, K.: Jpn. J. Appl. Phys. Suppl. 32 (1993) 42.
- 94U Ueno, M., Yoshida, M., Onodera, A., Shimomura, O., Takemura, K.: Phys. Rev. B 49 (1994) 14.
- 95I Inushima, T., Yaguchi, T., Nagase, A., Iso, A., Shiraishi, T., Ooya, S.: Proc. 7th Int. Conf. on InP and Related Materials, 1995, IEEE Cat. #95CH35720, p. 187; Inushima, T., Yaguchi, T., Nagase, A., Iso, A., Shiraishi, T.: J. in "*Silicon Carbide and Related Materials*", Nakashima, S., Matsunami, H., Yoshida, S., Harima, H. (eds.), Conference Series No. 142, Bristol: Institute of Physics, 1996, p. 971.
- 98K Krukowski, S., Witek, A., Adamczyk, J., Jun, J., Bockowski, M., Grzegory, I., Lucznik, B., Nowak, G., Wroblewski, M., Presz, A., Gierlotka, S., Stelmach, S., Palosz, B., Porowski, S., Zinn, P.: J. Phys. Chem. Solids 59 (1998) 289.
- 99P Paszkowicz, W., Adamczyk, J., Krukowski, S., Leszczynski, M., Porowski, S., Sokolowski, J. A., Michalec, M., Lasocha, W.: Phil. Mag. A 79 (1999) 1145.

Figures to 2.13

Fig. 2.0.3

The wurtzite lattice

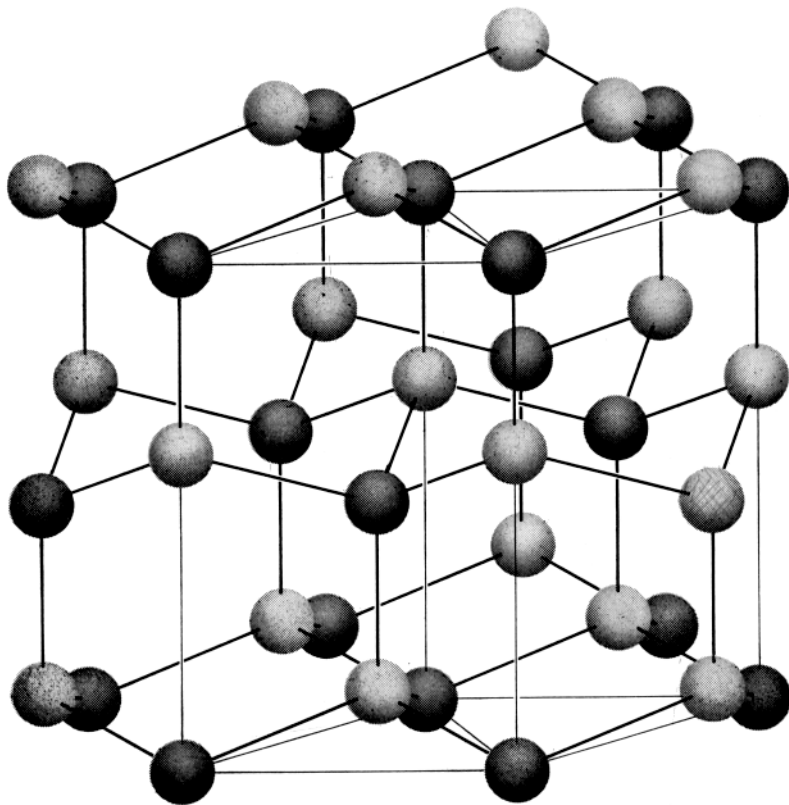


Fig. 2.0.8

The hexagonal Brillouin zone.

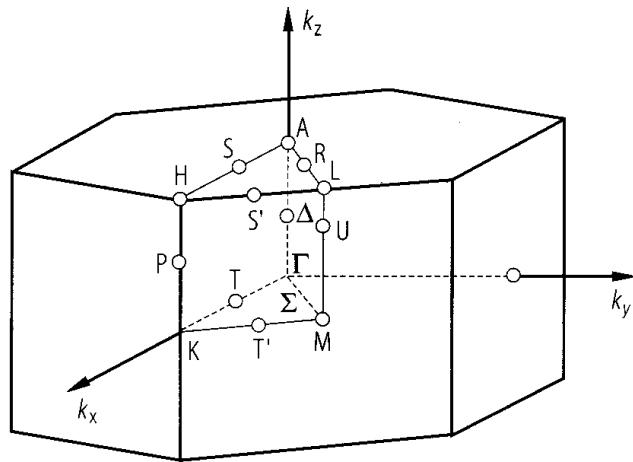


Fig. 2.0.21

InN. Band structure calculated by a pseudopotential method [86F].

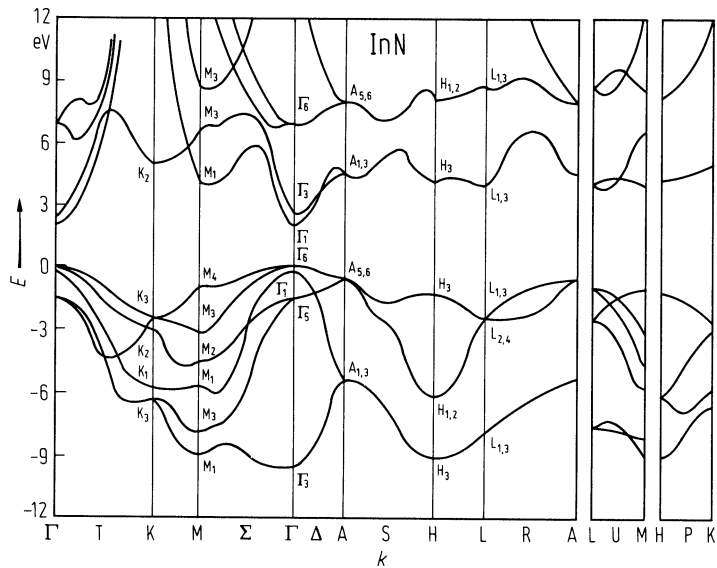


Fig. 2.13.1

InN. Coefficient of linear thermal expansion vs. temperature [76S].

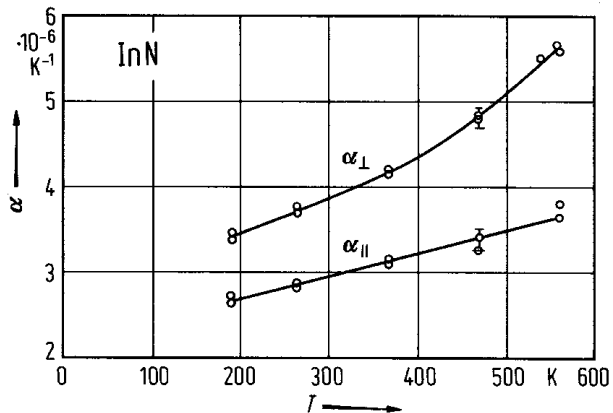
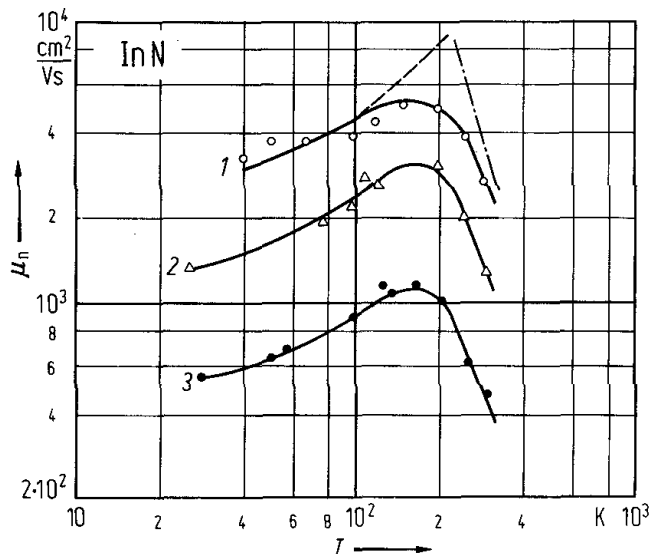


Fig. 2.13.2

InN. Electron mobility vs. temperature for three samples with RT carrier concentrations of $5.3 \cdot 10^{16}$ (1), $7.5 \cdot 10^{16}$ (2) and $1.8 \cdot 10^{17} \text{cm}^{-3}$ (3). Broken line: calculated ionized impurity scattering mobility, dot-dashed line: empirical high-temperature mobility ($\mu \propto T^{-3}$) for sample 1. Solid lines: total mobility calculated for each sample [84T].



2.14 Indium phosphide (InP)

Crystal structure

Indium phosphide crystallizes under normal conditions in the zincblende structure (space group $T_d^2 - F\bar{4}3m$, Fig. 2.0.2).

high-pressure phases

Under pressure the zincblende structure (InP-I) transforms first to the rocksalt structure (InP-II) and then to the β -tin structure (InP-III). InP-I and InP-II coexist up to about 12.00(5) GPa [87M]. In more recent experiments the transition at 19 GPa has not been confirmed, the rocksalt phase seems to appear at 34 GPa, and InP-III was identified as having actually Cmc symmetry [95N, 96M, 97N2].

Electronic properties

band structure : Fig. 2.0.22, Brillouin zone: Fig. 2.0.5.

InP is a direct semiconductor. The conduction band minimum is situated at Γ . Higher conduction band minima at L and X have been detected in optical experiments. The X band minima show no camel's back structure, in contrast to most other III–V compounds with zincblende structure [82K, 85K]. The valence band has the structure common to all zincblende type semiconductors.

structure of top of valence band

By the linear term in $\Gamma(k)$ the maxima of the heavy hole valence band are shifted on the $[111]$ axes, the energy of the band maximum relative to the energy at $k = 0$ being:

$\Delta E[111]$	6 meV	$T = 78\text{ K}$	electroabsorption	77V
	38 meV	$T = 298\text{ K}$		

energies of symmetry points of the band structure (relative to the top of the valence band $E(\Gamma_{8v})$)

$E(\Gamma_{6v})$	– 11.42 eV		symmetry symbols in double
$E(\Gamma_{7v})$	– 0.21 eV	– 0.108 eV	group notation
$E(\Gamma_{6c})$	1.50 eV	1.42 eV	first row: calculated data from
$E(\Gamma_{7c})$	4.64 eV	4.8 eV	[76C], see Fig. 2.0.23
$E(\Gamma_{8c})$	4.92 eV	4.87 eV	second row:
$E(X_{6v})$	– 8.91 eV		comparison with experiment
$E(X_{6v})$	– 6.01 eV	– 5.9 eV	
$E(X_{6v})$	– 2.09 eV		
$E(X_{7v})$	– 2.06 eV	– 2.2 eV	
$E(X_{6c})$	2.44 eV	2.38 eV	
$E(X_{7c})$	2.97 eV		
$E(L_{6v})$	– 9.67 eV		
$E(L_{6v})$	– 5.84 eV		
$E(L_{6v})$	– 1.09 eV	– 1.23 eV	
$E(L_{4,5v})$	– 0.94 eV	– 1.12 eV	
$E(L_{6c})$	2.19 eV	2.03 eV	
$E(L_{6c})$	5.58 eV		
$E(L_{4,5c})$	5.70 eV		

energy gap

$E_{g,dir}(\Gamma_{8v} - \Gamma_{6c})$	1.4236(1) eV	$T = 1.6\text{ K}$	from excitonic gap	85M
	1.344 eV	$T = 300\text{ K}$	absorption, photoluminescence	85B

temperature dependence, Fig. 2.14.1.

exciton states and parameters

(obtained from fitting of exciton fine structure in reflectivity at $T = 1.6$ K [85M] and photoconductivity at $T = 4.2$ K [82S]):

$E(1S,T)$	1.41850(5) eV	$T = 1.6$ K	transverse exciton, ground state	85M
$E(1S,L)$	1.41867(7) eV		longitudinal exciton, ground state	
$E(2S,T)$	1.42230(5) eV		transverse exciton, 2S state	
$E(2S,L)$	1.42232(7) eV		longitudinal exciton, 2S state	

higher conduction band minima

$\Delta E_{\Gamma L}$	0.86(2) eV		analysis of published optical data	90Z
$\Delta E_{\Gamma X}$	0.96(2) eV			

interband transition energies (critical point energies)

E_0	1.336 eV	$T = 300$ K	ellipsometry	95H
$E_0 + \Delta_0$	1.422 eV			
E_1	3.149 eV			
$E_1 + \Delta_1$	3.275 eV			
E_0'	4.704 eV			
$E_0' + \Delta_0'$	4.937 eV			

spin-orbit splitting energies

$\Delta_0(\Gamma_{8v}-\Gamma_{7v})$	0.108(8) eV	$T = 4.2$ K	wavelength modulated photovoltaic effect	75R
$\Delta_1(\Lambda_{4,5v}-\Lambda_{6c})$	0.13 eV	$T = 77$ K	thermoreflectance	68M
	0.15(5) eV	$T = 300$ K	electroreflectance	67C
$\Delta_0'(\Gamma_{8c}-\Gamma_{7c})$	0.07 eV	$T = 300$ K	electroreflectance	66S

valence band splitting due to linear $E(k)$ term

δE_v	0.006 eV	$T = 78$ K	electroabsorption; splitting of	77V
	0.038 eV	$T = 298$ K	Γ_8 states at top of valence band near Γ	

conduction band, effective mass

m_n	0.0808(10) m_0	$T = 0$ K	magnetophonon resonance	96S
	0.073 m_0	$T = 300$ K	Faraday rotation	59M

concentration dependence of effective electron mass

m_n/m_0	$0.077 \cdot (1 - 5.845 \cdot 10^{-14} n^{2/3})$ (n in cm^{-3})		from Kane's theory using the $E_{g,\text{dir}}(n)$ data , see Fig. 2.14.2	85B
-----------	---	--	--	-----

electron g-factor

g_c	1.48(5)	$T = 4.2$ K	modulated photovoltaic effect	75R
-------	---------	-------------	-------------------------------	-----

valence band, effective masses

$m_{p,h}$	0.45(5) m_0	$T = 4.2$ K	piezomodulated photovoltaic effect	75R
$m_{p,l}$	0.12(1) m_0	$T = 4.2$ K		
m_{so}	0.121(1) m_0	$T = 110$ K, $B \parallel [111]$, $B \parallel [100]$		

valence band parameters

A	- 6.28		calculated using $k \cdot p$ theory	75W1
B	- 4.17			
$ C $	6.24			

Lattice properties

lattice parameter

a	5.8687(10) Å	$T = 291.15$ K	powder, X-ray	58G
-----	--------------	----------------	---------------	-----

For the temperature dependence of the lattice constant, see Fig. 2.14.3.

linear thermal expansion coefficient

α	$4.75(10) \cdot 10^{-6}$ K ⁻¹	$T = 298.15$ K	see also Fig. 2.14.4	72K
----------	--	----------------	----------------------	-----

density

d	4.81 g cm ⁻³			63P, 77M
-----	-------------------------	--	--	-------------

melting temperature

T_m	1327 K		optimized	94A
-------	--------	--	-----------	-----

phonon dispersion curves : Fig. 2.14.5.

phonon density of states : Fig. 2.14.6.

phonon frequencies

$\nu_{LO}(111)(0.05)$	10.3(3) THz	RT,	coherent inelastic neutron scattering	75B1
$\nu_{TO}(\Gamma_{15})$	9.2(2) THz	$n = 10^{12}$ cm ⁻³		
$\nu_{TA}(X_5)$	2.05(10) THz			
$\nu_{LA}(X_3)$	5.8(3) THz			
$\nu_{TO}(X_5)$	9.70(10) THz			
$\nu_{LO}(X_1)$	9.95(20) THz			
$\nu_{TA}(L_3)$	1.65(2) THz			
$\nu_{LA}(L_1)$	5.00(10) THz			
$\nu_{TO}(L_3)$	9.50(15) THz			
$\nu_{LO}(L_1)$	10.2(3) THz			

sound velocities

v_3	$5.130(10) \cdot 10^5$ cm s ⁻¹	RT,	n-type, ultrasound ($f = 30$ MHz)	66H
v_4	$3.103(4) \cdot 10^5$ cm s ⁻¹	$\rho = 0.03$ Ω cm	designation: mode/direction of propagation/direction of particle displacement	
v_5	$2.160(3) \cdot 10^5$ cm s ⁻¹		v_3 : long/110/110, v_4 : shear/110/001,	
v_6	$5.271(5) \cdot 10^5$ cm s ⁻¹		v_5 : shear/110/1 $\bar{1}$ 0, v_6 : long./111/111,	
v_7	$2.524(5) \cdot 10^5$ cm s ⁻¹		v_7 : shear/111/1 $\bar{1}$ 0.	

second order elastic moduli

c_{11}	$10.11 \cdot 10^{11}$ dyn cm ⁻²	RT	ultrasonic wave transit times	80N
c_{12}	$5.61 \cdot 10^{11}$ dyn cm ⁻²			
c_{44}	$4.56 \cdot 10^{11}$ dyn cm ⁻²			

temperature dependence of second order elastic moduli

$d \ln c_{11}^S/dT$	$-1.351 \cdot 10^{-4}$ K ⁻¹	RT,	ultrasound, pulse echo	80G
$d \ln c_{12}^S/dT$	$-1.431 \cdot 10^{-4}$ K ⁻¹	$p = \text{const.}$		
$d \ln c_{44}^S/dT$	$-0.981 \cdot 10^{-4}$ K ⁻¹			

third order elastic moduli

c_{111}	$-8.6 \cdot 10^{12} \text{ dyn cm}^{-2}$	calculated from elastic moduli, their pressure dependence and other literature parameters	80N
c_{112}	$-1.85 \cdot 10^{12} \text{ dyn cm}^{-2}$		
c_{123}	$-5.1 \cdot 10^{12} \text{ dyn cm}^{-2}$		
c_{144}	$-6.5 \cdot 10^{12} \text{ dyn cm}^{-2}$		
c_{166}	$+1.6 \cdot 10^{12} \text{ dyn cm}^{-2}$		
c_{456}	$-0.042 \cdot 10^{12} \text{ dyn cm}^{-2}$		

bulk modulus

B	$7.1 \cdot 10^{11} \text{ dyn cm}^{-2}$		80N
-----	---	--	-----

shear moduli

G_L	$13.19 \cdot 10^{11} \text{ dyn cm}^{-2}$	for longitudinal waves propagating along [111]	80N
G_T	$3.02 \cdot 10^{11} \text{ dyn cm}^{-2}$	for shear waves propagating along [111]	

Debye temperature

Θ_D	321 K	for temperature dependence, see Fig. 2.14.7	63P
------------	-------	--	-----

Transport properties

The transport properties are mainly determined by the electrons in the Γ_{1c} minimum. Above 800 K multi-valley conduction (L_{1c}) becomes important. At room temperature polar scattering is dominant. Below 200 K ionized-impurity and neutral-impurity scattering, and below 60 K piezoelectric scattering are important [71R, 70G2].

electrical conductivity

σ	$4...5 (\Omega\text{cm})^{-1}$	$T = 300 \text{ K}$	pure material, n-type, $n = 6.3 \cdot 10^{15} \text{ cm}^{-3}$	62R
	$25 (\Omega\text{cm})^{-1}$	$T = 77 \text{ K}$	pure material	
	$< 10^{17} (\Omega\text{cm})^{-1}$	$T = 300 \text{ K}$	for temperature dependence, see Fig. 2.14.8 semi-insulating material, prepared by Fe-doping, $n = 10^9 \text{ cm}^{-3}$	75M

intrinsic concentration

n_i	$3.3 \cdot 10^7 \text{ cm}^{-3}$	$T = 300 \text{ K}$	magnetoresistance in semiinsulating InP	93B
-------	----------------------------------	---------------------	---	-----

thermal conductivity : Fig. 2.14.9.

electron mobility (typical data from the literature)

$\mu_{H,n}$	$130000 \text{ cm}^2/\text{Vs}$	$T = 77 \text{ K}$	VPE layer, $n = 6 \cdot 10^{13} \text{ cm}^{-3}$	83T
	$4.2...5.4 \cdot 10^3 \text{ cm}^2/\text{Vs}$	$T = 300 \text{ K}$	pure material, $n = 0.5...1 \cdot 10^{16} \text{ cm}^{-3}$	75R, 70G1

Temperature dependence of electron mobility: Fig. 2.14.10.

hole mobility

$\mu_{H,p}$	$190 \text{ cm}^2/\text{Vs}$	$T = 300 \text{ K}$	Hall effect	90B
	$14800 \text{ cm}^2/\text{Vs}$	$T = 77 \text{ K}$		
	$150(T/300)^{-2.2} \text{ cm}^2/\text{Vs}$	above 200 K (T in K)	see Fig. 2.14.11	75W2

piezoresistance tensor coefficient

$\pi_{11} + 2\pi_{12}$	$8.2(3) \cdot 10^{-3} \text{ kbar}^{-1}$	$T = 300 \text{ K}$	$n = 2.5 \cdot 10^{16} \text{ cm}^{-3}$ at 300 K, resistance is proportional to pressure, maximum pressure used 7 kbar	60S
$(1/2)(\pi_{11} + \pi_{12} + \pi_{44})$	$1.3(5) \cdot 10^{-3} \text{ kbar}^{-1}$	$T = 77 \text{ K}, 300 \text{ K}$	stress $\approx 50 \text{ bar}$	60S

Seebeck coefficient (for a review see [72U])

S	$-400 \dots 600 \text{ } \mu\text{V K}^{-1}$	$T = 300 \text{ K}$	pure material, $n = 10^{16} \dots 10^{17} \text{ cm}^{-3}$
-----	--	---------------------	--

For dependence of Seebeck coefficient on temperature, see Fig. 2.14.12.

piezoelectric constants

$ e_{14} $	0.040 C m^{-2}		ultrasound attenuation	75B2
d_{14}	$-1.89 \cdot 10^{-12} \text{ V}^{-1}\text{m}$	RT	piezo resonance	93R

Optical properties

optical constants

real and imaginary parts of the dielectric constant measured by spectroscopical ellipsometry, n , k , R , K calculated from these data [83A]. See also Fig. 2.14.13

$h\nu [\text{eV}]$	ϵ_1	ϵ_2	n	k	R	$K [10^3 \text{ cm}^{-1}]$
1.5	11.904	1.400	3.456	0.203	0.395	30.79
2.0	12.493	2.252	3.549	0.317	0.317	64.32
2.5	14.313	3.062	3.818	0.511	0.349	129.56
3.0	17.759	10.962	4.395	1.247	0.427	379.23
3.5	5.400	12.443	3.193	1.948	0.403	691.21
4.0	6.874	10.871	3.141	1.730	0.376	701.54
4.5	8.891	16.161	3.697	2.186	0.449	996.95
5.0	-7.678	14.896	2.131	3.495	0.613	1771.52
5.5	-4.528	7.308	1.426	2.562	0.542	1428.14
6.0	-2.681	5.644	1.336	2.113	0.461	1285.10

refractive index : see Fig. 2.14.14 for the range 1.0...1.6 eV.

n	3.03	$T = 300 \text{ K},$			
		$\lambda [\mu\text{m}]$	14.85	transmission and reflectance	54O
	3.08		5		
	3.134		2	prism method	65P
	3.327		1		
	3.410		0.652	reflectance and dispersion relations	65C
	4.100		0.399		
	1.525		0.200		
	0.793		0.062		

dielectric constants

$\epsilon(0)$	12.56(20)	$T = 300 \text{ K}$	capacitance measurements	86M
	11.93(20)	$T = 77 \text{ K}$		
$\epsilon(\infty)$	10.9(10)	$T = 297 \text{ K}$	film interference	61C

second order nonlinear dielectric susceptibilities

$d(\text{SHG})$	$4.2 \cdot 10^{-10} \text{ mV}^{-1}$	$T = 300 \text{ K},$ CO ₂ laser, 10.6 μm	second harmonic generation should only contain	69W
-----------------	--------------------------------------	--	--	-----

Impurities and defects

shallow impurities and defects : general remarks

Discrimination of donor chemical species is made difficult because of the small electron effective mass ($m_n < 0.1 m_0$) and large dielectric constant ($\epsilon_s \approx 12$). This leads to small values of electron binding energy at donor states. The effective mass donor Rydberg for InP is 7.31 meV [74H1]. The large extend of the electron wave function makes the central cell corrections small ($\psi^2(r=0)$), typically ≈ 0.1 meV. Random electric fields, strain and other effects can produce line widths for donor-related optical transitions which are larger than the central cell corrections, especially at zero magnetic field.

properties of acceptor impurities

Zinc, magnesium, beryllium and carbon are often common residual acceptors in InP. The group IV elements, except for C and Ge, do not substitute for P, and so show no amphoteric behavior.

Since m_h^* is much greater than m_e^* , acceptor-hole binding energies are correspondingly deeper [40...50 meV], however the difference in binding energy between different chemical species is small, typically 0.1 meV. Material of high purity is required for shallow defect analysis showing $\mu_{77K} > 10^5$ cm²/Vs.

binding energy of acceptors

Element	E_b [meV]	T [K]	Remarks	Ref.
Zn	48	4.2	Free-bound photoluminescence.	79D
	46.4(10)	10		76H
Cd	57.0(10)	1.8	No lineshape fits of emission lines were attempted introducing some uncertainty for the binding energies thus determined.	72W
Hg	98(2)	6		73W
Cp	41.3(5)	1.8		74H2
Ge _p	41.5	4.2		79D
	210(20)	2		76W
Cp	44.6±0.3	1.7...20	PL on low-dose implanted samples	84S
	44.3±0.3	2	PL, see Fig. 2	88C
Be	41.3±0.3	1.7...20	PL on low-dose implanted samples	84S
Mg	41.0±0.3	1.7...20	PL on low-dose implanted samples	84S
	40.9±0.3	2	PL, see Fig. 2	88C
Zn	46.1±0.3	1.7...20	PL on low-dose implanted samples	84S
unknown	41.2±0.3	1.7...20	PL on low-dose implanted samples	84S

deep impurities, general

A number of states in InP have been characterized by measurements of the thermal emission rate of electrons e_n to the conduction band together with a determination of the cross sections for electron capture σ_n using a direct measurement technique. This enables a calculation of the change in thermal Gibbs free energy ΔG_n . In a few cases, the electron capture cross section σ_n has also been determined as a function of temperature T so allowing the calculation of the change in enthalpy ΔH_n . In general $\Delta G_n = \Delta H_n - T\Delta S$ where ΔS is the change in entropy at the temperature T . If the majority capture cross section σ_n is temperature independent, the slope E_{na} of an Arrhenius plot of the corrected thermal emission rate e_n gives the change in enthalpy of the state. It is necessary to divide the emission rate by T^2 because of the temperature dependence of the density of states-thermal velocity product in the detailed balance equation. All other centers are characterized only by the apparent activation energies E_{na} for thermal emission which due to an unknown temperature dependence of the capture cross section may be different from the true thermal trap depth. All data available on deep states in InP have been obtained by deep level transient spectroscopy (DLTS).

energy levels related to isolated, substitutional transition metal impurities

"+" above valence band, "-" below conduction band. DDLTS stands for Double Correlation DLTS.

Impurity	E [eV]	Type	Remarks	T [K]	Ref.
Ti	-0.59±0.02	d	DDLTS, zero-field extrapolation		92B
	-0.63(3)	d	DLTS		86B1
	-0.64	d	Temperature dependent Hall effect (Ti + Zn doped samples)		86I
	-0.61	d	Temperature dependent Hall effect (Ti + Cd doped samples)		86I

Ti (cont.)	-0.56	d	DLTS (Ti + Hg doped samples)		86B2
	-0.53(1)	d	Temperature dependent Hall effect (Ti + Hg doped samples)		87L
V	+0.21	d	DLTS + σ_p^0 photoluminescence excitation photoionization	4	86D
Cr	-0.39(1)	a	Temperature dependent resistivity and Hall effect measurements		79I
	-0.40	a	Photoconductivity	300	81F
	-0.45	a	Photoconductivity	77	81F
	-0.47	a	Photoconductivity	6	81F
	+0.96(1)	a	PICTS		82R
	-0.4	a	DLTS and DLOS (σ_p^0 and σ_n^0 photoioniz.)		86B3
	+0.56	d	Temperature dependent Hall measurements		86L
Mn	+0.25	a	Hall, DLTS		90H
	+0.21	a	Temperature dependent resistivity and Hall measurements		84K
Fe	+0.220	a	σ_p^0 absorption photoionization	4	85L
	-0.49	a	DLTS at $T = 300$ K		94Z
	-0.62±0.01	a	DLTS, DDLTS		97D
	-0.65	a	Temp. dependent resistivity and Hall meas.		79I
	-0.63(2)	a	DLTS		81B
	-0.59	a	DLTS and photocapacitance		81T
	-0.65	a	Photoconductivity		81E
	+0.7850	a	σ_p^0 absorption photoionization; 5T_2 excited state located at + 1.1379	1.3	86J
Co	+0.32	a	Temperature dependent Hall measurements and DLTS		83S
	+0.24	a	DLTS and ODLTS		84R
Ni	+0.48(4)	1st a	DLTS		89K
	-0.27(2)	2nd a	DLTS		89K
Au	-0.55	d	DLTS		87P
Rh(A)	+0.71±0.01	a	DLTS, DDLTS on MOCVD samples Rh ³⁺ /Rh ²⁺ acceptor of Rh _{In}		96D1
Hf(A)	-0.51	d	DLTS on MOCVD samples		95S
Zr(1)	-0.53	d	DLTS on MOCVD samples		95S
Ru	0.53±0.03	a	thermal activation energy, DLTS, DDLTS		96D2
Os	0.31±0.03	a	thermal activation energy, DLTS, DDLTS		96D2

binding energy of rare earths levels

("+" above valence band, "-" below conduction band).

Impurity	E_b [meV]	Remarks	Ref.
Yb	~ - 30	acceptor-like el. trap, $s_n = 4 \times 10^{-16} \text{cm}^2$	88W
Yb	~ - 30	DLTS, Hall on MOCVD samples	
Yb	~ - 30	Yb ³⁺ /Yb ²⁺ acceptor state of Yb _{In}	92S
Yb	~ + 30	Time-resolved photoluminescence	
Yb	- 29±3	donor-like state	90T
Yb	- 29±3	Admittance spectroscopy, p-type samples	92S
Yb	+ 50±5	Admittance spectroscopy, n-type samples	92S
Er	~ - 60	acceptor-like electron trap	
Er	~ - 60	Hall, DLTS, n-type samples	90L
Er	~-40	Room-Temperature Photoreflectance	97N1

References to 2.14

- 54O Oswald, F.: Z. Naturforsch. 9a (1954) 181.
- 55F Folberth, O. G., Weiss, H.: Z. Naturforsch. 10a (1955) 615.
- 58G Giesecke, G., Pfister, H.: Acta Crystallogr. 11 (1958) 369.
- 59M Moss, T. S., Walton, A. K.: Physica 25 (1959) 1142.
- 60S Sagar, A.: Phys. Rev. 117 (1960) 101.
- 61C Cardona, M.: J. Appl. Phys. 32 Suppl. (1961) 2151.
- 62R Richman, D.: in: Compound Semiconductors, ed. by R. K. Willardson and H. L. Goering, Reinhold, New York, 1962.
- 63P Piesbergen, U.: Z. Naturforsch. 18a (1963) 141.
- 64T Turner, W. J., Reese, W. E., Pettit, G. D.: Phys. Rev. 136 (1964) A1467.
- 65A Aliev, S. A., Nashelskii, A. Ya., Shalyt, S. S.: Sov. Phys. Solid State (English Transl.) 7 (1965) 1287; Fiz. Tverd. Tela 7 (1965) 1590.
- 65C Cardona, M.: J. Appl. Phys. 36 (1965) 2181.
- 65P Petit, G. D., Turner, W. J.: J. Appl. Phys. 36 (1965) 2081.
- 66H Hickernell, F. S., Gayton, W. R.: J. Appl. Phys. 37 (1966) 462.
- 66M Mooradian, A., Wright, G. B.: Solid State Commun. 4 (1966) 431.
- 66S Shaklee, K. L., Cardona, M., Pollak, F. H.: Phys. Rev. Lett. 16 (1966) 48.
- 67C Cardona, M., Shaklee, K. L., Pollak, F. H.: Phys. Rev. 154 (1967) 696.
- 68M Matatagui, E., Thompson, A. E., Cardona, M.: Phys. Rev. 176 (1968) 950.
- 69W Wynne, J. J., Bloembergen, N.: Phys. Rev. 188 (1969) 1211
- 70G1 Galavanov, V. V., Siukaev, N. V.: Phys. Status Solidi 38 (1970) 523.
- 70G2 Galavanov, V. V., Metreveli, S. G., Staroseltseva, S. P.: Sov. Phys. Semicond. (English Transl.) 3 (1970) 1159; Fiz. Tekh. Poluprovodn. 3 (1969) 1391.
- 71R Rode, D. L.: Phys. Rev. B 3 (1971) 3287.
- 72K Kudman, I., Paff, R. J.: J. Appl. Phys. 43 (1972) 3760.
- 72U Ure, R. W., Jr.: in "Semiconductom and Semimetals ", vol. 8, R. K. Willardson, A. C. Beer, eds., Academic Press, New York 1972.
- 72W White, A.M., Dean, P.J., Taylor, L.L., Clarke, R.C., Ashen, D.J., Mullin, J.B.: J. Phys. C 5 (1972) 1727.
- 73W Williams, E.W., Elder, W., Astles, M.G., Webb, M., Mullin, J.B., Straughan, B., Tulton, P.J.: J. Electrochem. Soc. 120 (1973) 1741.
- 74H1 Hoult, R.A., Stradling, R.A., Bradley, C.C.: J. Phys. C 7 (1974) 1164.
- 74H2 Hess, K., Stath, N., Benz, K.W.: J. Electrochem. Soc. 121 (1974) 1208.
- 75B1 Borchers, P. H., Alfrey, G. F., Saunderson, D. H., Woods, A. D. B.: J. Phys. C 8 (1975) 2022.
- 75B2 Boyle, W. F., Sladek, R. J.: Solid State Commun. 16 (1975) 323.
- 75M Mizuno, O., Watanabe, H.: Electronic Lett. 11 (1975) 118.
- 75R Rochon, P., Fortin, F.: Phys. Rev. B 12 (1975) 5803.
- 75W1 Wiley, J. D.: in "Semiconductors and Semimetals", Vol. 10, R. K. Willardson, A. C. Beer eds., Academic Press, New York 1975.
- 75W2 Weisbuch, C., Herrmann, C.: Solid State Commun. 16 (1975) 659.
- 76C Chelikowski, J. R., Cohen, M. L.: Phys. Rev. B 14 (1976) 556.
- 76H Hess, K.: Dissertation, Stuttgart 1976.
- 76W White, A.M., Dean, P.J., Day, B.: Proc. XIIIth Int. Conf. on Physics of Semiconductors, Fumi, F.G. (ed.), Rome: Tipografia Marves 1976, p. 1037.
- 77M Merrill, L.: J. Phys. Chem. Ref. Data 6 (1977) 1205.
- 77V Vorob'ev, L. E., Shturbin, A. V., Osokin, F. I.: Sov. Phys. Semicond. (English Transl.) 11 (1977) 879; Fiz. Tekh. Poluprovodn. 11 (1977) 1497.
- 79D Dean, P.J., Robbins, D.J., Bishop, S.G.: J. Phys. C 12 (1979) 5567.
- 79I Iseler, G.W.: Inst. Phys. Conf. Ser. 45 (1979) 144.
- 80G Gerlich, D., Wolf, M.: in "High Pressure Science and Technology", Vodar, B., Marteau, Ph. (eds.), Pergamon, Oxford etc. (1980) p. 506 (Vol. 1).
- 80N Nichols, D. N., Rimai, D. S., Sladek, R. J.: Solid State Commun. 36 (1980) 667.
- 80W Walukiewicz, W., Lagowski, J., Jastrzebski, L., Rava, P., Lichtensteiger, M., Gatos. C. H. . Gatos. H. C.: J. Appl. Phys. 51 (1980) 2659.
- 81B Bremond, G., Nouailhat, A., Guillot, G., Cockayne, B.: Electron. Lett. 17 (1981) 55.
- 81E Eaves, L., Smith, A.W., Williams, P.J., Cockayne, B., MacEwan, W.R.: J. Phys. C 14 (1981) 5063.
- 81F Fung, S., Nicholas, R.J.: J. Phys. C 14 (1981) 2135.
- 81T Tapster, P.R., Skolnick, M.S., Humphreys, R.G., Dean, P.J., Cockayne, B., MacEwan, W.R.: J. Phys. C 14 (1981) 5069.
- 82B Burkhard, H., Dinges, H. W., Kuphal, E.: J. Appl. Phys. 53 (1982) 655.

- 82K Kopylov, A. A.: Sov. Phys. Semicond. (English Transl.) 16 (1982) 1380; Fiz. Tekh. Poluprovodn. 16 (1982) 2141.
- 82R Rhee, J.K., Battacharya, P.K.: J. Appl. Phys. 53 (1982) 4247.
- 82S Skolnick, M. S., Dean, P. J.: J. Phys. C 15 (1982) 5863.
- 83A Aspnes, D. E., Studna, A. A.: Phys. Rev. B 27 (1983) 985.
- 83S Skolnick, M.S., Humphreys, R.G., Tapster, P.R., Cockayne, B., MacEwan, W.R.: J. Phys. C 16 (1983) 7003.
- 83T Taylor, L. L., Anderson, D. A.: J. Cryst. Growth 64 (1983) 55.
- 84K Kuznetsov, V.P., Messerer, M.A., Omel'yanovskii, E.M.: Fiz. Tekh. Poluprovodn. 18 (1984) 446; Sov. Phys. Semicond. (English Transl.) 18 (1984) 278.
- 84R Rojo, P., Leyral, P., Nouailhat, A., Guillot, G., Lambert, B., Deveaud, B., Coquille, R.: J. Appl. Phys. 55 (1984) 395.
- 84S Skromme, B.J., Stillman, G.E., Oberstar, J.D., Chan, S.S.: Appl. Phys. Lett. 44 (1984) 319.
- 85B Bugajski, M., Lewandowski, W.: J. Appl. Phys. 57 (1985) 521.
- 85C Campi, D., Papuzza, C.: J. Appl. Phys. 57 (1985) 1305.
- 85K Kopylov, A. A.: Solid State Commun. 56 (1985) 1.
- 85L Lambert, B., Clerjaud, B., Naud, C., Deveaud, B., Picoli, G., Toudic, Y.: J. Electron. Mater. 14a (1985) 1141.
- 85M Mathieu, H., Chen, Y., Camassel, J., Allegre, J., Robertson, D. S.: Phys. Rev. B 32 (1985) 4042.
- 86B1 Brandt, C.D., Hennel, A.M., Pawlowicz, L.M., Wu Y.T., Bryskiewicz, T., Lagowski, J., Gatos, H.C.: Appl. Phys. Lett. 48 (1986) 1162.
- 86B2 Bremond, G., Guillot, G., Nouailhat, A., Lambert, B., Toudic, Y., Gauneau, M., Deveaud, B.: J. Phys. C 19 (1986) 4723.
- 86B3 Bremond, G., Guillot, G., Nouailhat, A., Picoli, G.: J. Appl. Phys. 59 (1986) 2038.
- 86D Deveaud, B., Plot, B., Lambert, B., Bremond, G., Guillot, G., Nouailhat, A., Clerjaud, B., Naud, C.: J. Appl. Phys. 59 (1986) 3126.
- 86I Iseler, G.W., Ahern, B.S.: Appl. Phys. Lett. 48 (1986) 1656.
- 86J Juhi, A., Bimberg, D.: Semi-Insulating III-V Materials, Hakone 1986, Kukimoto, H., Miyazawa, S. (eds.), OHM, North-Holland, 1986, p. 477.
- 86L Lambert, B., Toudic, Y., Coquille, R., Grandpierre, G., Gauneau, M.: Defects in Semiconductors, Proc. 14th Internat. Conf. Defects in Semicond., Paris (1986), von Bardeleben, H.J. (ed.), Materials Science Forum 10...12, Trans. Tech. Publications, Switzerland, 1986, p. 651.
- 86M Meiners, L. G.: J. Appl. Phys. 59 (1986) 1611.
- 87H Haruna, K., Maeta, H., Ohashi, K., Koike, T.: J. Phys. C: Solid State Phys. 20 (1987) 5275.
- 87L Lambert, B., Toudic, Y., Grandpierre, G., Gauneau, M., Deveaud, B.: Semicond. Sci. Technol. 2 (1987) 78.
- 87M Menoni, C. S., Spain, I. L.: Phys. Rev. B 35 (1987) 7520.
- 87P Parguel, V., Favennec, P.N., Gauneau, M., Rihet, Y., Chaplain, R., L'Haridon, H., Vaudry, C.: J. Appl. Phys. 62 (1987) 824.
- 88C Cheng, T.S., Airaksinen, V.M., Stanley, C.R.: J. Appl. Phys. 64 (1988) 6662.
- 88W Whitney, P.S., Uwai, K., Nakagome, H., Takahei, K.: Appl. Phys. Lett. 53 (1988) 2074.
- 89K Korona, K., Hennel, A.M.: Appl. Phys. Lett. 55 (1989) 1085.
- 90B Benzaquen, M., Belache, B., Blaauw, C., Bruce, R. A.: J. Appl. Phys. 68 (1990) 1694.
- 90H Huang, K., Wessel, B.W.: J. Appl. Phys. 67 (1990) 6882.
- 90L Lambert, B., Le Corre, A., Toudic, Y., Grandpierre, C., Gauneau, M.: J. Phys. Condens. Matter 2 (1990) 479.
- 90T Thonke, K., Pressel, K., Bohnert, G., Stapor, A., Weber, J., Moser, M., Molassioti, A., Hangleiter, A., Scholz, F.: Semicond. Sci. Technol. 5 (1990) 1124.
- 90Z Zollner, S., Schmid, U., Christensen, N. E., Cardona, M.: Appl. Phys. Lett. 57 (1990) 2339.
- 92B Baber, N., Scheffler, H., Ostmann, A., Wolf, T., Bimberg, D.: Phys. Rev. B 45 (1992) 4043.
- 92S Seghier, D., Benyattou, T., Bremond, G., Ducroquet, F., Gregoire, J., Guillot, G., Lhomer, C., Lambert, B., Toudic, Y., Le Corre, A.: Appl. Phys. Lett. 60 (1992) 983.
- 93B Betko, J., Merinsky, K.: Phys. Status Solidi (a) 135 (1993) K67.
- 93R Rottner, K., Helbig, R., Müller, G.: Appl. Phys. Lett. 62 (1993) 352.
- 94A Ansara, I., Chatillon, C., Lukas, H. L., Nishizawa, T., Ohtani, H., Ishida, K., Hillert, M., Sundman, B., Argent, B. B., Watson, A., Chart, T. G., Anderson, T.: CALPHAD: Comput. Coupling Phase Diagrams Thermochem. 18 (1994) 177.
- 94Z Zach, F.S.: J. Appl. Phys. 75 (1994) 7894.
- 95F Fritsch, J., Pavone, P., Schröder, U.: Phys. Rev. B 52 (1995) 11326.
- 95H Herzinger, C. M., Snyder, P. G., Johs, B., Woollam, J. A.: J. Appl. Phys. 77 (1995) 1715.
- 95N Nelmes, R. J., McMahon, M. I., Wright, N. G., Allan, D. R., Liu, H., Loveday, J. S.: J. Phys. Chem. Solids 56 (1995) 539.

- 95S Scheffler, H., Baber, N., Dadgar, A., Bimberg, D., Winterfeld, J., Schumann, H.: Phys. Rev. B 51 (1995) 14142.
- 96D1 Dadgar, A., Ammerlahn, D., Näser, A., Heitz, R., Kuttler, M., Bimberg, D., Baber, N., Hyeon, J.Y., Schumann, H.: Phys. Rev. B 53 (1996) 7190.
- 96D2 Dadgar, A., Köhne, L., Bimberg, D., Zafar Iqbal, M.: Proc. 23rd Int. Conf. on the Physics of Semiconductors, Scheffler, M., Zimmermann, R. (eds.), p. 2837 (World Scientific, Singapore, 1996).
- 96M McMahon, M. I., Nemes, R. J.: Phys. Status Solidi (b) 198 (1996) 389.
- 96S Schneider, D., Ruerup, D., Schoenfelder, B., Schlachetzki, A.: Z. Phys. B 100 (1996) 33.
- 97D Dadgar, A., Engelhardt, R., Kuttler, M., Bimberg, D.: Phys. Rev. B 56 (1997) 10241.
- 97N1 Nukeaw, J., Yanagisawa, J., Matsubara, N., Fujiwara, Y., Takeda, Y.: Appl. Phys. Lett. 70 (1997) 84.
- 97N2 Nemes, R. J., McMahon, M. I., Belmonte, S. A.: Phys. Rev. Lett. 79 (1997) 3668.

Figures to 2.14

Fig. 2.0.2

The zincblende lattice

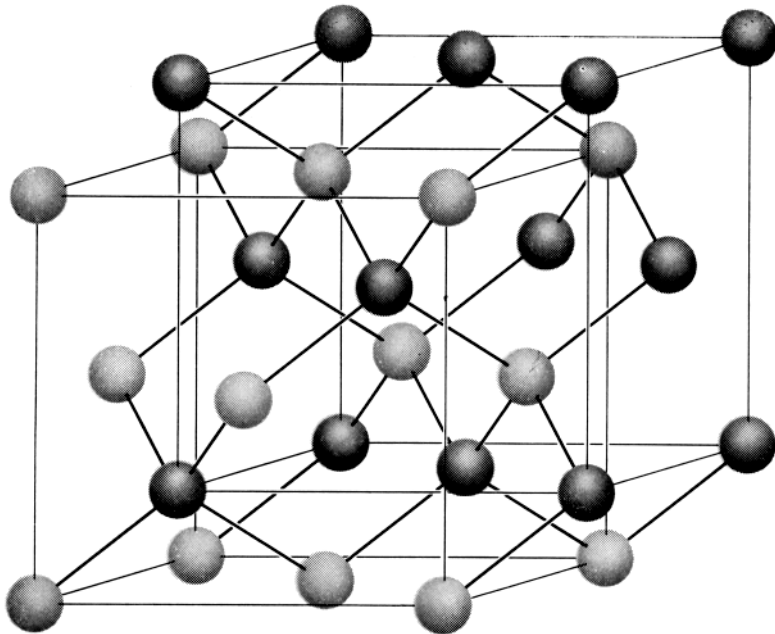


Fig. 2.0.5

Brillouin zone of the zincblende lattice.

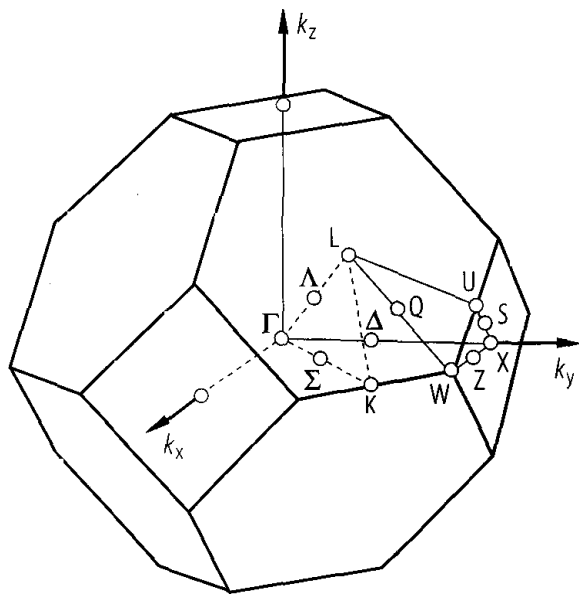


Fig. 2.0.22

InP. Band structure obtained with a non-local pseudopotential method [76C].

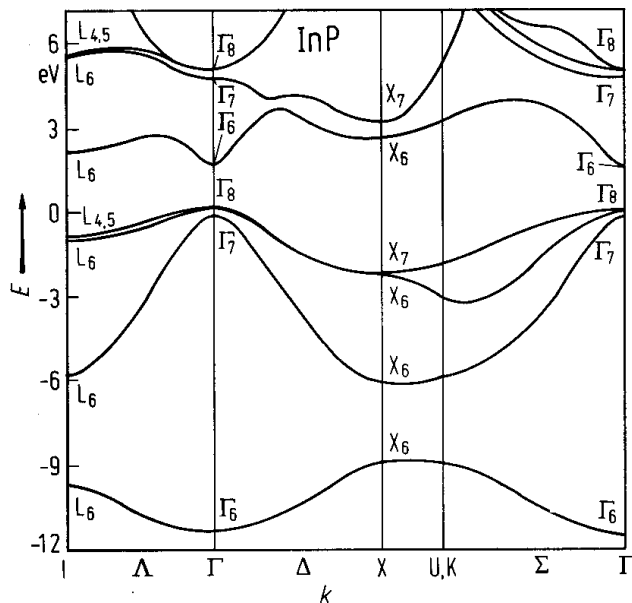


Fig. 2.14.1

InP. Energy gap and exciton peak energy vs. temperature from absorption and emission data [64T].

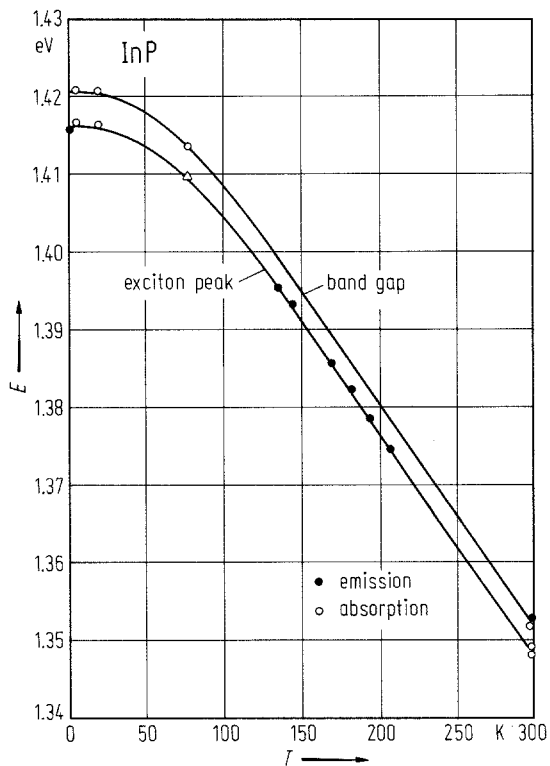


Fig. 2.14.2

InP. Electron effective mass vs. electron concentration calculated using experimental data [85B].

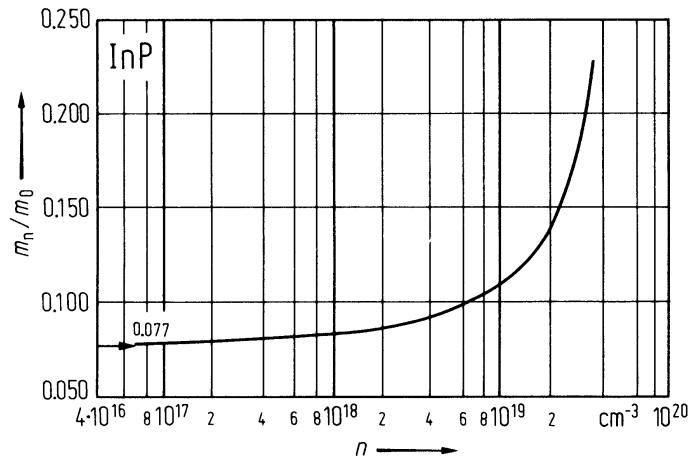


Fig. 2.14.3

InP. Temperature dependence of the lattice constant from the Bond method [87H].

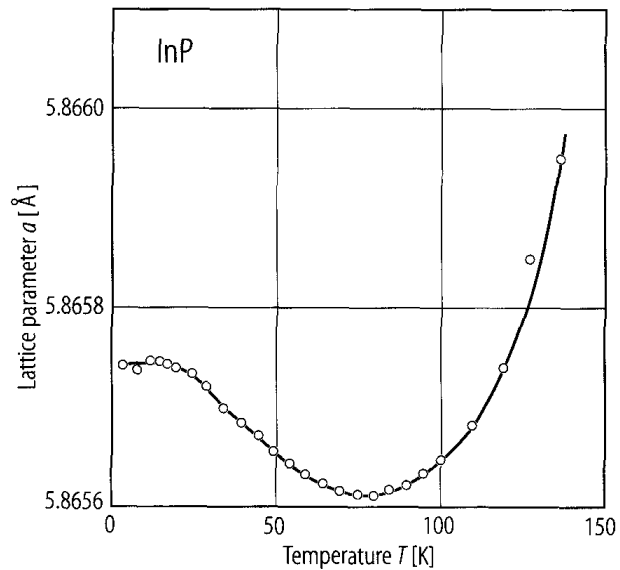


Fig. 2.14.4

InP. Temperature dependence of the coefficient of linear thermal expansion from the Bond method [87H].

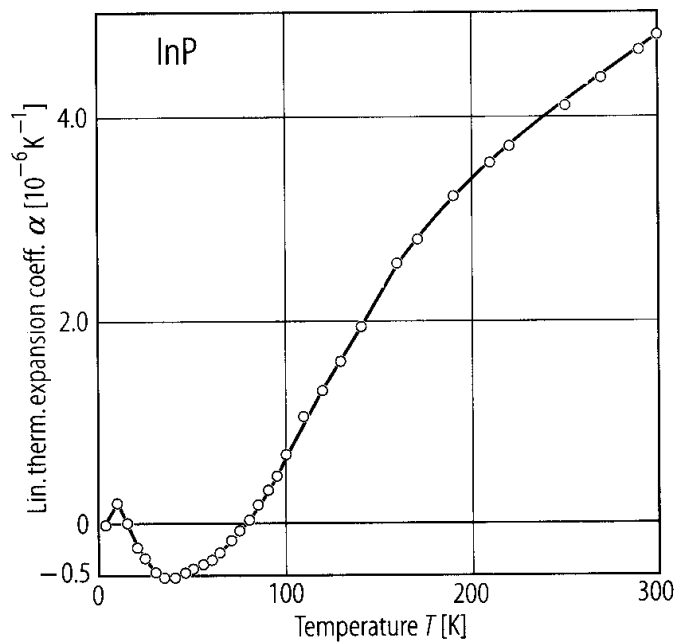


Fig. 2.14.5

InP. Phonon dispersion curves. Experimental neutron data (diamonds [75B1]) and Raman data (triangles [66M]) and ab-initio pseudopotential calculations (full curves [95F]). From [95F].

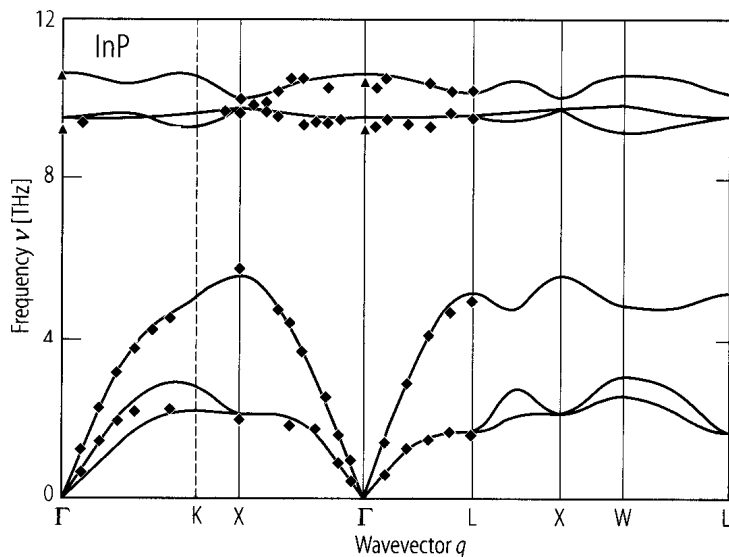


Fig. 2.14.6

InP. Phonon density of states from ab-initio pseudopotential calculations. From [95F].

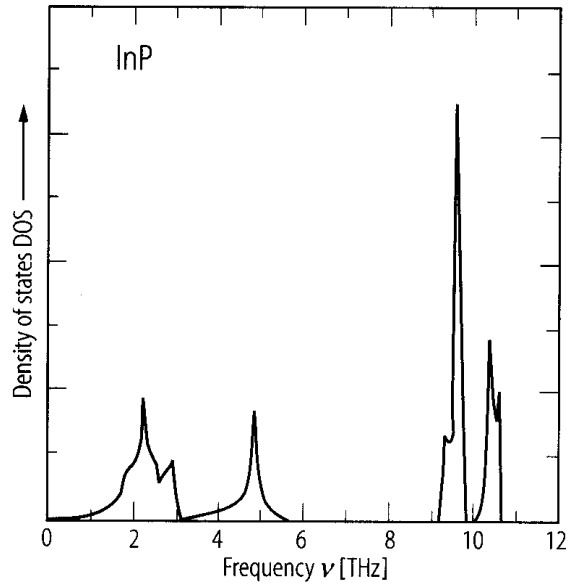


Fig. 2.14.7

InP. Debye temperature Θ_D vs. temperature [63P].

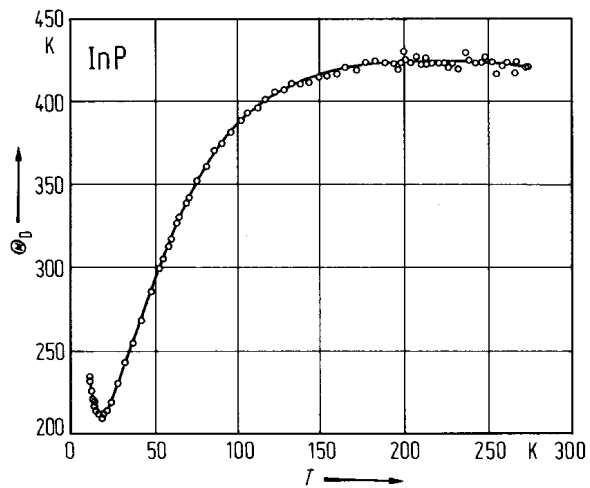


Fig. 2.14.8

InP. Electrical conductivity and Hall coefficient vs. reciprocal temperature for two n-type samples (curves A, B) and one p-type sample (curve 1) [55F].

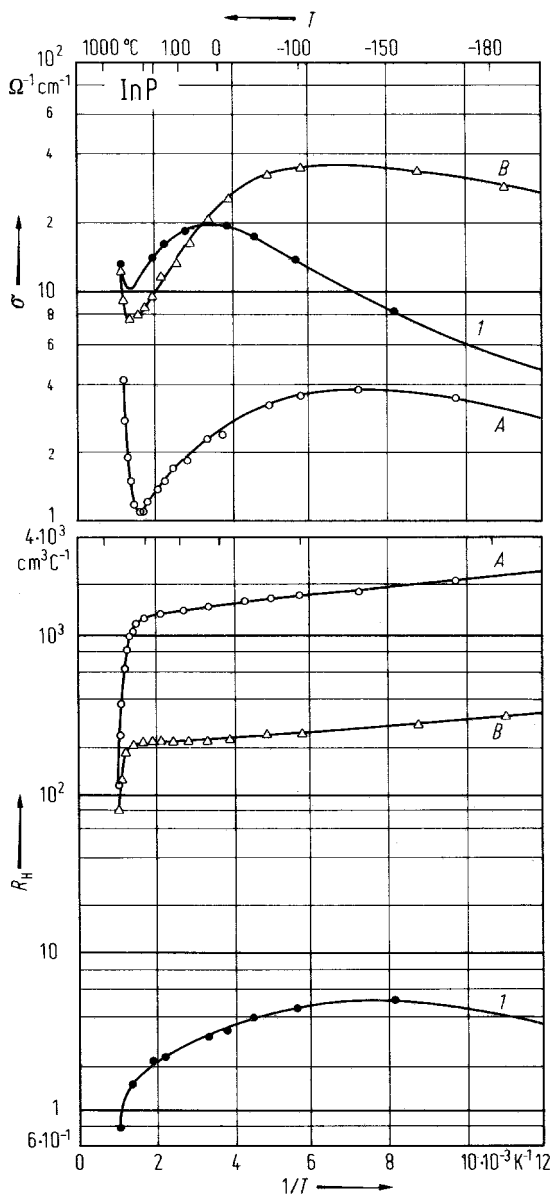


Fig. 2.14.9

InP. Thermal conductivity vs. temperature [65A].

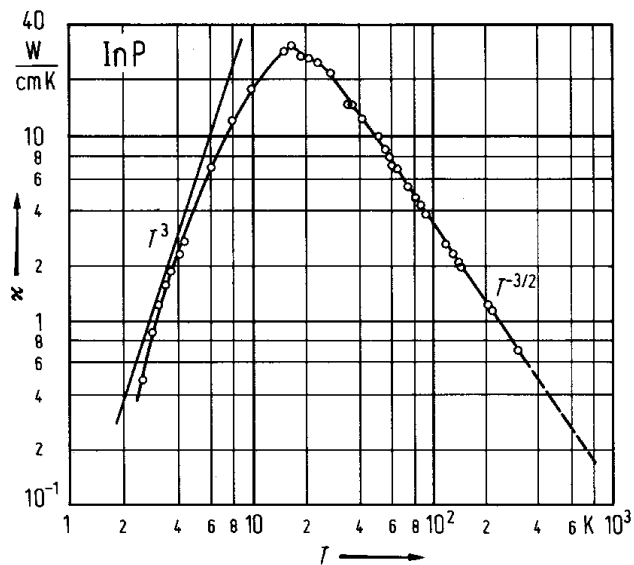


Fig. 2.14.10

InP. Electron mobility vs. temperature calculated for two concentrations of ionized impurities. Contributions from scattering mechanisms are indicated (dashed lines) [80W].

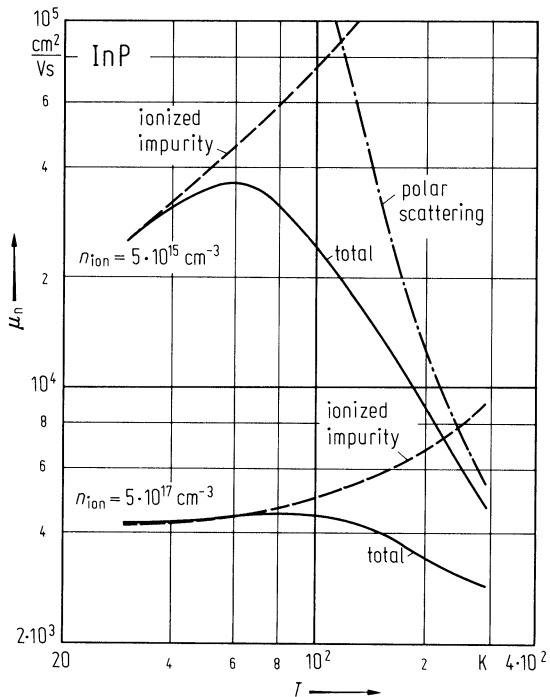


Fig. 2.14.11

InP. Hole Hall mobility vs. temperature for pure p-type samples, after [75W1].

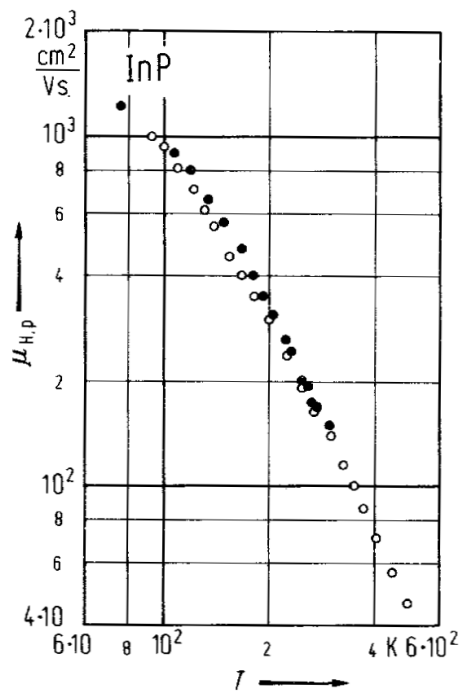


Fig. 2.14.12

InP. Seebeck coefficient (thermoelectric power) vs. temperature for low temperatures, polycrystalline material, $n = 2 \cdot 10^{16} \text{ cm}^{-3}$, compensated, at 77K [65A].

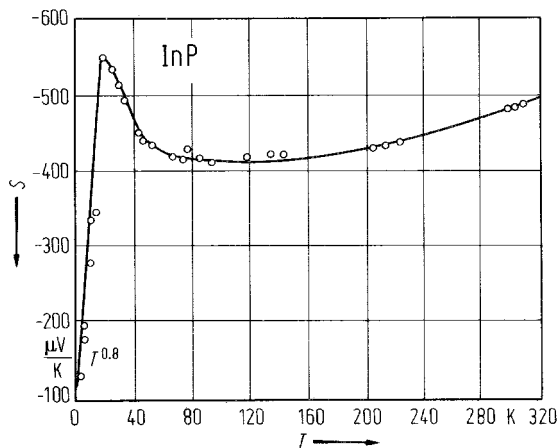


Fig. 2.14.13

InP. Real and imaginary parts of the dielectric constant vs. photon energy [83A].

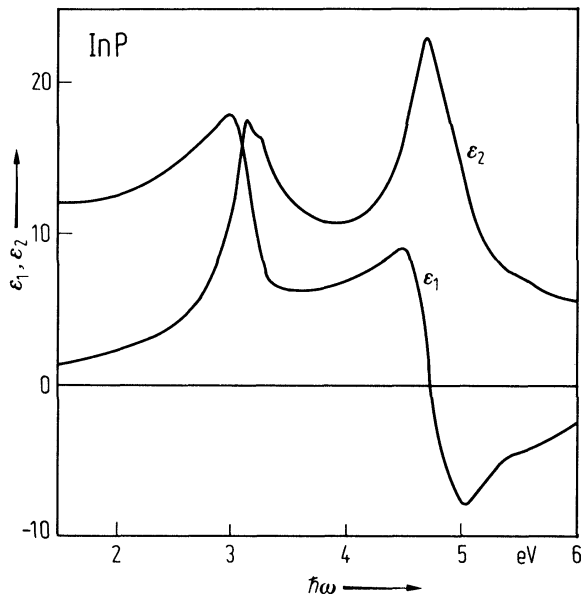
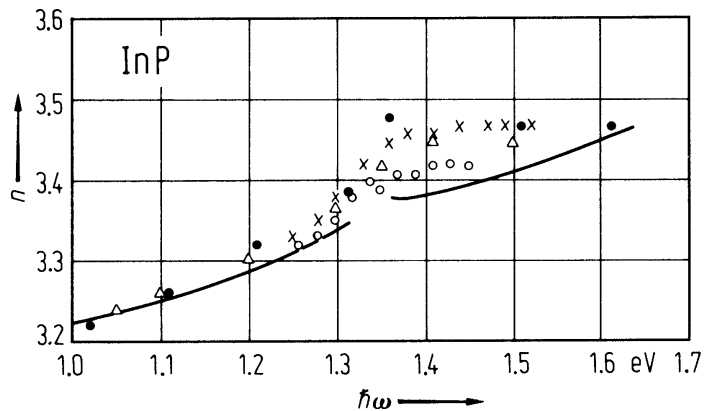


Fig. 2.14.14

InP. Refractive index vs. photon energy in the range 1...1.6 eV. Theoretical curve and experimental points from [82B] (triangles), [82S1] (full circles) and [85C] (open circles: p-type, crosses: n-type samples).



2.15 Indium arsenide (InAs)

Crystal structure

Indium arsenide crystallizes under normal conditions in the zincblende structure (space group $T_d^2 - F\bar{4}3m$, Fig. 2.0.2).

high-pressure phases

Under pressure there is a transition to the rocksalt structure (InAs-II) at around 4 GPa and then to a site-disordered β -tin structure (InAs-III) at 17 GPa [85V], while the predicted pressure for the transition to a site-ordered β -tin structure is at variance [86C, 87C, 97M]. Missing reflection intensities in the angle-dispersive diffraction experiments [95N1] have cast some doubt about the rocksalt structure, and an additional reflection suggests the existence of an intermediate phase, later proposed as having Cmcm (distorted rocksalt) symmetry [95N1, 96M].

Electronic properties

band structure : Fig. 2.0.23, Brillouin zone: Fig. 2.0.5.

InAs resembles in its band structure InSb, having only a slightly larger energy gap and a smaller spin-orbit splitting of the top of the valence band. The conduction band minimum (Γ_6) is situated in the center of the Brillouin zone. Near the minimum, $E(k)$ is isotropic but non-parabolic. The valence band shows the usual structure common to all zincblende-type III–V compounds.

energies of symmetry points of the band structure (relative to the top of the valence band $E(\Gamma_{8v})$)

$E(\Gamma_{6v})$	– 12.69 eV	symmetry symbols in double group notation	76C
$E(\Gamma_{7v})$	– 0.43 eV		
$E(\Gamma_{6c})$	0.37 eV		
$E(\Gamma_{7c})$	4.39 eV		
$E(\Gamma_{8c})$	4.63 eV		
$E(X_{6v})$	– 10.20 eV		
$E(X_{6v})$	– 6.64 eV		
$E(X_{6v})$	– 2.47 eV		
$E(X_{7v})$	– 2.37 eV		
$E(X_{6c})$	2.28 eV		
$E(X_{7c})$	2.66 eV		
$E(L_{6v})$	– 10.92 eV		
$E(L_{6v})$	– 6.23 eV		
$E(L_{6v})$	– 1.26 eV		
$E(L_{4,5v})$	– 1.00 eV		
$E(L_{6c})$	1.53 eV		
$E(L_{6c})$	5.42 eV		
$E(L_{4,5c})$	5.55 eV		

energy gap

$E_{g, \text{ dir}}(\Gamma_{8v}-\Gamma_{6c})$	0.4180(5) eV	$T = 4.2 \text{ K}$	magnetotransmission	75V
	0.354(3) eV	$T = 295 \text{ K}$	electroreflectance	77L
$E_{g, \text{ th}}$	0.42...0.47 eV		from transport data	54F

temperature and pressure dependence of energy gap

$E_g(T)$ (in meV, T in K))	$415 - [0.276 T^2/(T + 83)]$	photoluminescence	90F
---------------------------------	------------------------------	-------------------	-----

For temperature dependence of energy gap, see Fig. 2.15.1

free exciton binding energy

E_b	1.0 meV	$T = 4.2$ K	magnetoabsorption	97T
-------	---------	-------------	-------------------	-----

excitonic band gap

E_{gx}	415.65(1) meV	$T = 1.4$ K	photoluminescence	96L
----------	---------------	-------------	-------------------	-----

spin-orbit splitting energies

$\Delta_0(\Gamma_{8v}-\Gamma_{7v})$	0.38(1) eV	$T = 1.5$ K	magneto-electroreflectance	67P
$\Delta_1(L_4, 5v-L_{6v})$ or $(\Lambda_4, 5-\Lambda_{6v})$	0.267 eV	$T = 5$ K	wavelength modulated reflectance	70Z

higher band-band transitions (critical point energies)

$E'_0(\Gamma_{8v}-\Gamma_{7c})$	4.39 eV	$T = 5$ K	wavelength modulated reflectance	70Z
$E_1(L_4, 5v-L_{6c})$ or $(\Lambda_4, 5v-\Lambda_{6c})$	2.612 eV			
$E_1+\Delta_1(L_{6v}-L_{6c})$ or $(\Lambda_{6v}-\Lambda_{6c})$	2.879 eV			
$E_2(X_{5v}-X_{1c})$	4.74 eV			

conduction band, effective masses

m_n	0.0265 m_0	$T = 4.2$ K	analysis of various published data	95N2
	0.023 m_0	$T = 300$ K		

For dependence on carrier concentration, see Fig. 2.15.2.

electron g-factor

g_c	-15.3(2)	$T = 1.4$ K	magnetoluminescence	96L
-------	----------	-------------	---------------------	-----

valence band, effective masses

$m_{p,h}$	0.57 m_0	$T = 300$ K	analysis of various published data	95N2
m_{100}	0.35 m_0			
m_{111}	0.85 m_0			

valence band parameters

A	-19.7		calculated using $k \cdot p$ theory	75W
B	-16.8			
$ C $	13.66			

Lattice properties

lattice parameter

a	6.0583 Å	$T = 298.15$ K	temperature dependence, see Fig. 2.15.3	63O
-----	----------	----------------	---	-----

linear thermal expansion coefficient

α	$4.52 \cdot 10^{-6}$ K ⁻¹	$T = 20...250$ K	average value, X-ray; for temperature dependence in other temperature ranges, see Fig. 2.15.3	58S
----------	--------------------------------------	------------------	---	-----

density

d	5.667 g cm ⁻³	$T = 300$ K	X-ray	69R
-----	--------------------------	-------------	-------	-----

temperature dependence of density: Fig. 2.15.4

melting temperature

T_m	1221(1) K			89Y
-------	-----------	--	--	-----

phonon dispersion curves, phonon density of states : Fig. 2.15.5, Brillouin zone: Fig. 2.0.5.

phonon wavenumbers

$\bar{\nu}_{\text{TO}}(\Gamma)$	217.3 cm ⁻¹	$T = 300 \text{ K}$	Raman scattering,	80C
$\bar{\nu}_{\text{LO}}(\Gamma)$	238.6 cm ⁻¹			
$\bar{\nu}_{\text{TA}}(\text{X})$	53 cm ⁻¹			
$\bar{\nu}_{\text{LA}}(\text{X})$	160 cm ⁻¹			
$\bar{\nu}_{\text{TO}}(\text{X})$	216 cm ⁻¹			
$\bar{\nu}_{\text{LO}}(\text{X})$	203 cm ⁻¹	$T = 100 \text{ K}$		
$\bar{\nu}_{\text{TA}}(\text{L})$	44 cm ⁻¹	$T = 300 \text{ K}$		
$\bar{\nu}_{\text{LA}}(\text{L})$	139.5 cm ⁻¹			
$\bar{\nu}_{\text{TO}}(\text{L})$	216 cm ⁻¹			
$\bar{\nu}_{\text{LO}}(\text{L})$	203 cm ⁻¹	$T = 100 \text{ K}$		

sound velocities

v_3	$4.282 \cdot 10^5 \text{ cm}^{-1}$	RT,	n-type, ultrasound ($f=15 \text{ MHz}$), designation: mode/direction of propagation/	63G
v_4	$2.646 \cdot 10^5 \text{ cm}^{-1}$	$n = 3 \cdot 10^{17} \text{ cm}^{-3}$	direction of particle displacement	
v_5	$1.830 \cdot 10^5 \text{ cm}^{-1}$		v_3 : long/110/110, v_4 : shear/110/001,	
v_6	$4.420 \cdot 10^5 \text{ cm}^{-1}$		v_5 : shear/110/110, v_6 : long./111/111	

second order elastic moduli

c_{11}	$8.329 \cdot 10^{11} \text{ dyn cm}^{-2}$	RT	n-type, ultrasound ($f=15 \text{ MHz}$)	63G
c_{12}	$4.526 \cdot 10^{11} \text{ dyn cm}^{-2}$	$n = 3 \cdot 10^{17} \text{ cm}^{-3}$		
c_{44}	$3.959 \cdot 10^{11} \text{ dyn cm}^{-2}$		temperature dependence, Fig. 2.15.6	

third-order elastic moduli

c_{111}	- 518 GPa	$T = 293 \dots 873 \text{ K}$	ultrasound resonance	75B
c_{112}	- 225 GPa			
c_{123}	- 239 GPa			
c_{144}	- 190 GPa			
c_{166}	- 18 GPa			
c_{456}	- 68 GPa			

bulk modulus

B	58 GPa		ultrasound	73K
-----	--------	--	------------	-----

Debye temperature

$\Theta_D(0)$	247 K, 262 K		cited after different authors [63P1] For temperature dependence, see Fig. 2.15.7	
---------------	--------------	--	---	--

Transport properties

The transport properties are mainly determined by the electrons in the Γ_6 minimum. Pure material with intrinsic conduction down to 450 K is available. Above room temperature the electron mobility is determined by polar scattering, below 150 K impurity scattering dominates and below 80K piezoelectric and deformation-potential scattering become important [71R, 75R].

electrical conductivity

σ	$50 (\Omega\text{cm})^{-1}$	$T = 300 \text{ K}$	pure material, for temperature dependence, see Fig. 2.15.8	
----------	-----------------------------	---------------------	--	--

thermal conductivity : see Fig. 2.15.9.

intrinsic carrier concentration

n_i	$2.14 \cdot 10^{15} T^{3/2} \exp(0.47/2kT) \text{ cm}^{-3}$ (T in K)	$T = 350 \dots 900 \text{ K}$	n- and p-material, see also Fig. 2.15.10	54F
-------	--	-------------------------------	--	-----

electron mobility

μ_n	$0.8 \dots 1 \cdot 10^5 \text{ cm}^2/\text{Vs}$ $2 \dots 3.3 \cdot 10^4 \text{ cm}^2/\text{Vs}$	$T = 77 \text{ K}$ $T = 300 \text{ K}$	pure material, $n = 10^{16} \text{ cm}^{-3}$	75R
---------	--	---	--	-----

For temperature dependence, see Fig. 2.15.11.

hole mobility

μ_p	$100 \dots 450 \text{ cm}^2/\text{Vs}$ $\propto T^{-m}$	$T = 300 \text{ K}$ $T = 80 \dots 300 \text{ K}$	$m \approx 1$, low temperatures; $m > 2$, high temperatures	54F 63M
---------	--	---	---	------------

piezoresistance tensor coefficients

π_{11}	$-3(3) \cdot 10^{-6} \text{ bar}^{-1}$ $-5(3) \cdot 10^{-6} \text{ bar}^{-1}$	$T = 77 \text{ K}$ $T = 300 \text{ K}$	$n = 1.1 \cdot 10^{17} \text{ cm}^{-3}$ at 77 K, single crystal	58T
π_{12}	$-8(3) \cdot 10^{-6} \text{ bar}^{-1}$ $-5(3) \cdot 10^{-6} \text{ bar}^{-1}$	$T = 77 \text{ K}$ $T = 300 \text{ K}$		
π_{44}	$-1(3) \cdot 10^{-6} \text{ bar}^{-1}$ $0(3) \cdot 10^{-6} \text{ bar}^{-1}$	$T = 77 \text{ K}$ $T = 300 \text{ K}$		

piezoelectric constants

e_{14}	$4.5(9) \cdot 10^{-6} \text{ C/cm}^2$	$T = 300 \text{ K}$	piezoelectric Hall effect measurements Polarity: negative, if the crystal is expanded in the $[111]$ direction, the A-faces (metal atoms) become negatively charged.	68A
d_{14}	$1.14 \cdot 10^{-10} \text{ cm/V}$			
g_{14}	$0.89 \cdot 10^2 \text{ cm}^2/\text{V}$			
h_{14}	$3.5 \cdot 10^6 \text{ V/cm}$			

Seebeck coefficient

S	$-400 \mu\text{V/K}$ $300 \dots 600 \mu\text{V/K}$	$T = 300 \text{ K}$ $T = 300 \text{ K}$	pure material p-material	56W
-----	---	--	-----------------------------	-----

The Seebeck coefficient for p-type material changes sign in the temperature range between 400 K and 700 K, depending on impurity concentration.

Optical properties

optical constants

real and imaginary parts of the dielectric constant measured by spectroscopical ellipsometry, n , k , R , K calculated from these data [83A]. See also Fig. 2.15.12.

$h\nu [\text{eV}]$	ϵ_1	ϵ_2	n	k	R	$K [10^3 \text{ cm}^{-1}]$
1.5	13.605	3.209	3.714	0.432	0.337	65.69
2.0	15.558	5.062	3.995	0.634	0.370	128.43
2.5	15.856	15.592	4.364	1.786	0.454	452.64
3.0	6.083	13.003	3.197	2.034	0.412	618.46
3.5	5.973	10.550	3.008	1.754	0.371	622.13
4.0	7.744	11.919	3.313	1.799	0.393	729.23
4.5	-1.663	22.006	3.194	3.445	0.566	1571.19
5.0	-5.923	8.752	1.524	2.871	0.583	1455.26
5.5	-3.851	6.008	1.282	2.344	0.521	1305.62
6.0	-2.403	6.005	1.434	2.112	0.448	1284.15

refractive index

<i>n</i>		<i>T</i> =	λ [μm]		
			λ [μm]		
	3.26	300 K	25	interference	65L
	3.42		10		
	3.52		3.74	reflectance and dispersion relations	63P2
	3.516		1.38		
	4.558		0.517		
	3.800		0.282		
	1.139		0.049		

absorption index

<i>k</i>		<i>T</i> =	λ [μm]		
			λ [μm]		
	0.002	300 K	3.65	transmission	61D
	0.2		1.68		
	0.047		1.38	reflectance and dispersion relations	63P2
	1.954		0.443		
	3.264		0.264		
	0.168		0.049		

reflectance

<i>R</i>		<i>T</i> =	λ [μm]		
			λ [μm]		
	0.3	300 K	6.198		63P2
	0.437		0.451		
	0.559		0.264		
	0.015		0.062		

dielectric constants

$\varepsilon(0)$	15.15	300 K	infrared reflectance and oscillator fit	62H
$\varepsilon(\infty)$	12.37		fitting of transport parameters	82Y

second order nonlinear dielectric susceptibility

<i>d</i> (SHG)	10.0(30)·10 ⁻⁷ esu (= 4.2(13)·10 ⁻¹⁰ mV ⁻¹)	<i>T</i> = 300 K	second harmonic generation	66P
----------------	--	------------------	----------------------------	-----

Impurities and defects

shallow impurities

Little is known about impurities in this material. The binding energies of some acceptors and donors are determined from photoluminescence experiments. It is, however, not known whether these impurities are point defects or complexes.

energy of main luminescence bands [96L]

energy [meV]	attribution
415.31	DX
413.624	A ₁ X
413.665	A ₂ X
410.9	A ₃ X
397.1	DA ₂
396.5	DA ₁
391.3	DA ₃
374	B ₂

acceptor binding energies

Impurity	E_b [meV]	T [K]	Remarks	Ref.
Sn	10	77	photoluminescence of implanted material	75G
Ge	14		photoluminescence	74G
Si	20			
(?)	20		photoluminescence of Sn-doped material	76Z
structure defect	35	4.2		

intrinsic or unidentified electron traps

E_{na} [eV]	Defect type	Experimental method	Ref.
0.11	complexes based on In vacancies	DLTS	84F
0.15		DLTS	84F
0.002	shallow donor	PC and Hall	92B
0.01...0.02	clusters of donors		
0.1...0.2	associate to As vacancy		

intrinsic or unidentified hole traps

E_{pa} [eV]	Defect type	Experimental method	Ref.
0.035	deep acceptor level	photoluminescence, $T = 77$ K. 4.2 K	71A, 75Z
0.05		PC and Hall	92B

energy levels of isolated substitutional transition metal impurities

(" +" above valence band).

Impurity	E [eV]	Type	Remarks	Ref.
Mn	+ 0.028	a	Temperature dependent resistivity measurements	77A

References to 2.15

- 54F Folberth, O. G., Madelung, O., Weiss, H.: Z. Naturforsch. 9a (1954) 954.
- 56W Weiss, H.: Z. Naturforsch. 11a (1956) 131.
- 58S Sirota, N. N., Pashintsev, Yu. I.: Inzh. Fiz. Zh., Akad. Nauk BSSR 1 (1958) 38.
- 58T Tuzzolino, A. J.: Phys. Rev. 112 (1958) 30.
- 61D Dixon, J. R., Ellis, J. M.: Phys. Rev. 123 (1961) 1560.
- 62H Hass, M., Hennis, B. W.: J. Phys. Chem. Solids 23 (1962) 1099.
- 63G Gerlich, D.: J. Appl. Phys. 34 (1963) 2915.
- 63M Mikhailova, M. P., Nasledov, D. N., Slobodchikov, S. V.: Sov. Phys. Solid State (English Transl.) 5 (1964) 1685; Fiz. Tverd. Tela 5 (1963) 2317.
- 63O Ozolin'sh, J. V., Averkieva, G. K., Ilvin'sh, A. F., Goryunova, N. A.: Sov. Phys. Cryst. (English Transl.) 7 (1963) 691.
- 63P1 Piesbergen, U.: Z. Naturforsch 15a (1963) 141.
- 63P2 Philipp, H. R., Ehrenreich, H.: Phys. Rev. 129 (1963) 1550.
- 64G Gerlich, D.: J. Appl. Phys. 34 (1964) 3062.
- 65L Lorimor, O. G., Spitzer, W. G.: J. Appl. Phys. 36 (1965) 1841.
- 66P Patel, C. K. N.: Phys. Rev. Lett. 16 (1966) 613.
- 67P Pidgeon, C. R., Groves, S. H., Feinleib, J.: Solid State Commun. 5 (1967) 677.
- 67S Sparks, P. W., Swenson, C. A.: Phys. Rev. 163 (1967) 779.
- 68A Arlt, G., Quadflieg, P.: Phys. Status Solidi 25 (1968) 323.
- 69G Glazov, V. M., Chizhevskaya, S. N., Evgen'ev, S. B.: Zh. Fiz. Khim. 43 (1969) 373.
- 69R Reifenberger, B., Keck, M. J., Trivisonno, J.: J. Appl. Phys. 40 (1969) 5403.
- 70Z Zucca, R. R. L., Shen, Y. R.: Phys. Rev. 155 (1970) 2668.
- 71A Allaberenov, O. A., Zotova, N. V., Nasledov, D. N., Neumina, L. D.: Sov. Phys. Semicond. 4 (1971) 1662.
- 71L LeGuillou, G., Albany, H. J.: Phys. Rev. B5 (1971) 2301.
- 71R Rode, D. L.: Phys. Rev. B3 (1971) 3287.
- 73K Kunc, K.: Ann. Phys. (Leipzig) 8 (1973) 319; cited in [85V].
- 74G Guseva, M. I., Zotova, N. V., Koval, A. V., Nasledov, D. N.: Sov. Phys. Semicond. (English Transl.) 8 (1974) 34; Fiz. Tekh. Poluprovodn. 8 (1974) 59.
- 75B Burenkov, Yu. A., Davydov, S. Yu., Nikanorov, S. P.: Fiz. Tverd. Tela 17 (1975) 2183; Sov. Phys. Solid State 17 (1976) 1446 (English Transl.).
- 75G Guseva, M. I., Zotova, N. V., Koval, A. V., Nasledov, D. N.: Sov. Phys. Semicond. (English Transl.) 8 (1975) 1323; Fiz. Tekh. Poluprovodn. 8 (1974) 2034.
- 75R Rode, D. L.: in: Semiconductors and Semimetals. Vol. 10, ed. by R. K. Willardson and A. C. Beer, Academic Press, New York 1975.
- 75V Varfolomeev, A. V., Seisyan, R. P., Yakimova, R. N.: Sov. Phys. Semicond. (English Transl.) 9 (1975) 530; Fiz. Tekh. Poluprovodn. 9 (1975) 804.
- 75W Wiley, J. D.: in "Semiconductors and Semimetals", Vol. 10, R. K. Willardson, A. C. Beer eds., Academic Press, New York 1975.
- 75Z Zotova, N. V., Karataev, V. V., Koval, A. V.: Sov. Phys. Semicond. 9 (1975) 1275.
- 76C Chelikowski, J. R., Cohen, M. L.: Phys. Rev. B14 (1976) 556.
- 76Z Zotova, N. V., Karataev, V. V., Koval, A. V.: Sov. Phys. Semicond. (English Transl.) 9 (1976) 1275; Fiz. Tekh. Poluprovodn. 9 (1975) 1944.
- 77A Andrianow, D.G., Karataev, V.V., Lazareva, G.V., Muravlev, Yu.B., Saval'ev, A.S.: Fiz. Tekh. Poluprovodn. 11 (1977) 1252; Sov. Phys. Semicond. (English Transl.) 11 (1977) 738.
- 77L Lukes, F.: Phys. Status Solidi (b) 84 (1977) K113.
- 78S Semikolenova, N. A., Nesmelova, I. M., Khabarov, E. N.: Sov. Phys. Semicond. (English Transl.) 12 (1978) 1139; Fiz. Tekh. Poluprovodn. 12 (1978) 1915.
- 80C Carles, R., Saint-Cricq, N., Renucci, J. B., Renucci, M. A., Zwick, A.: Phys. Rev. B22 (1980) 4804.
- 82Y Yang June Jung, Byung Ho Kim, Hyung Jae Lee, Wolley, J. C.: Phys. Rev. 26 (1982) 3151.
- 83A Aspnes, D. E., Studna, A. A.: Phys. Rev. B 27 (1983) 985.
- 83O Orlova, N. S.: Phys. Status Solidi (b) 119 (1983) 541.
- 84F Fomin, I. A., Lebedeva, L. V., Annenko, N. M.: Sov. Phys. Semicond. 18 (1984) 457.
- 85O Orlova, N. S.: Cryst. Res. Technol. 20 (1985) 233.
- 85V Vohra, Y. K., Weir, S. T., Ruoff, A. L.: Phys. Rev. B 31 (1985) 7344.
- 86C Christensen, N. E.: Phys. Rev. B 33 (1986) 5096.

- 87C Chelikowsky, J. R.: Phys. Rev. B 35 (1987) 1174.
- 89Y Yamaguchi, K.: J. Jpn. Inst. Met. 53 (1989) 764.
- 90F Fang, Z. M., Ma, K. Y., Jaw, D. H., Cohen, R. M., Stringfellow, G. B.: J. Appl. Phys. 67 (1990) 7034.
- 92B Baranov, A.N., Voronina, T.I., Gorelenok, A.A., Lagunova, T.S., Litvak, A.M., Sipovskaya, M.A., Starosel'tseva, S.P., Tikhomirova, V.A., Sherstnev, V.V.: Sov. Phys. Semicond. 26 (1992) 905.
- 95N1 Nemes, R. J., McMahon, M. I., Wright, N. G., Allan, D. R., Liu, H., Loveday, J. S.: J. Phys. Chem. Solids 56 (1995) 539.
- 95N2 Nakwaski, W.: Physica B 210 (1995) 1.
- 96E Eckl, Ch., Pavone, P., Fritsch, J., Schröder, U.: in "*The Physics of Semiconductors*", Scheffler, M., Zimmermann, R., (eds.), Singapore: World Scientific, 1996, p. 229 (Vol. 1).
- 96L Lacroix, Y., Tran, C. A., Watkins, S. P., Thewalt, M. L. W.: J. Appl. Phys. 80 (1996) 6416.
- 96M McMahon, M. I., Nemes, R. J.: Phys. Status Solidi (b) 198 (1996) 389.
- 97M Mujica, A., Needs, R. J.: Phys. Rev. B 55 (1997) 9659; B 56 (1997) 12653(E).
- 97T Tang, P. J. P., Pullin, M. J., Phillips, C. C.: Phys. Rev. B 55 (1997) 4376.

Figures to 2.15

Fig. 2.0.2

The zincblende lattice

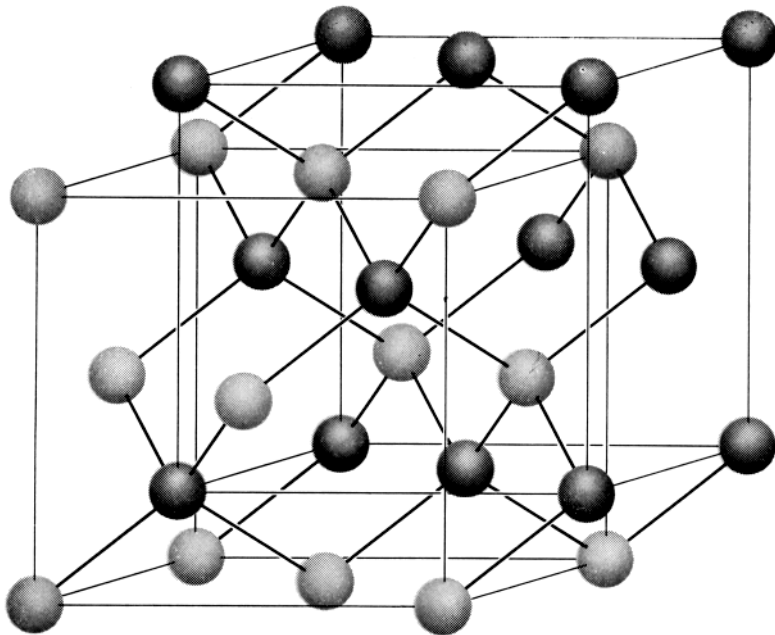


Fig. 2.0.5

Brillouin zone of the zincblende lattice.

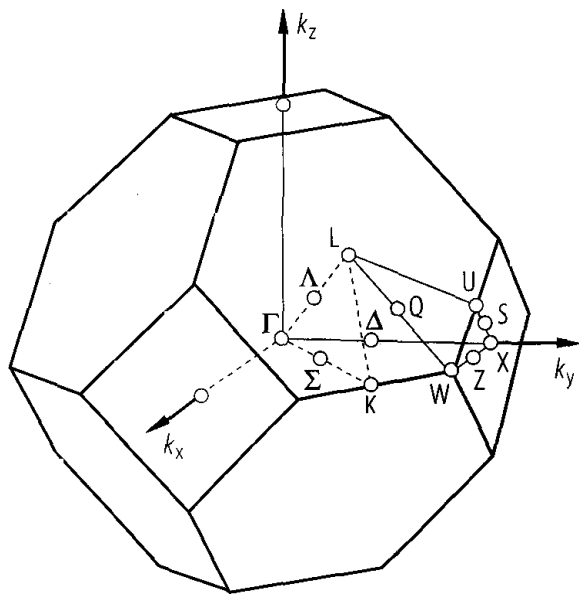


Fig. 2.0.23

InAs. Band structure obtained with a non-local pseudopotential calculation [76C]

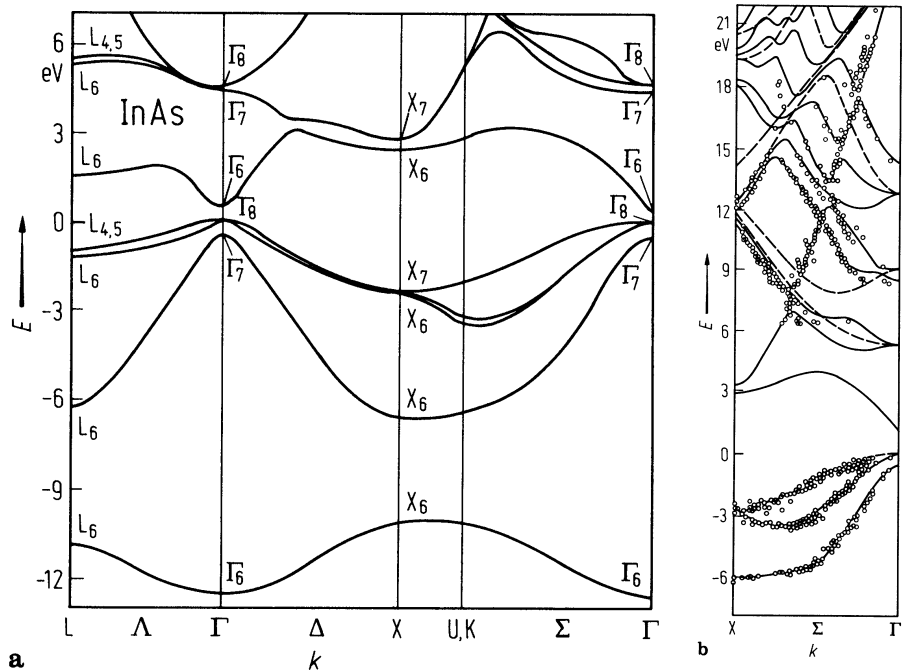


Fig. 2.15.1

InAs. Band gap vs. temperature. Solid line: optical band gap calculated from parameters used for fitting various transport data; symbols: thermal band gap of six samples obtained from conductivity and Hall coefficient [82Y].

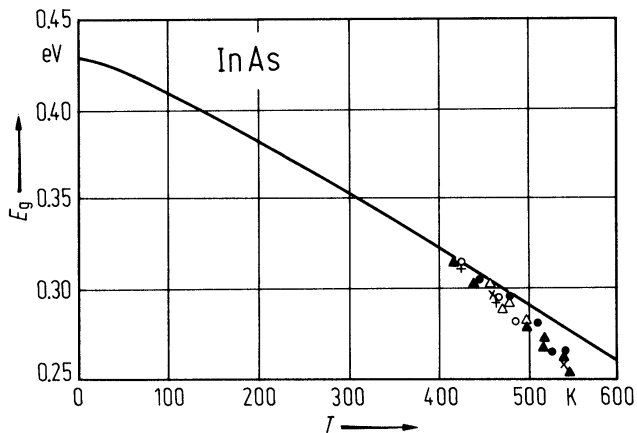


Fig. 2.15.2

InAs. Electron effective mass vs. electron concentration. Experimental data obtained by (1) Seebeck effect, (2) infrared reflectivity, (3) magnetic susceptibility, (4) Faraday effect, (5) recombination radiation, (6) cyclotron resonance [78S].

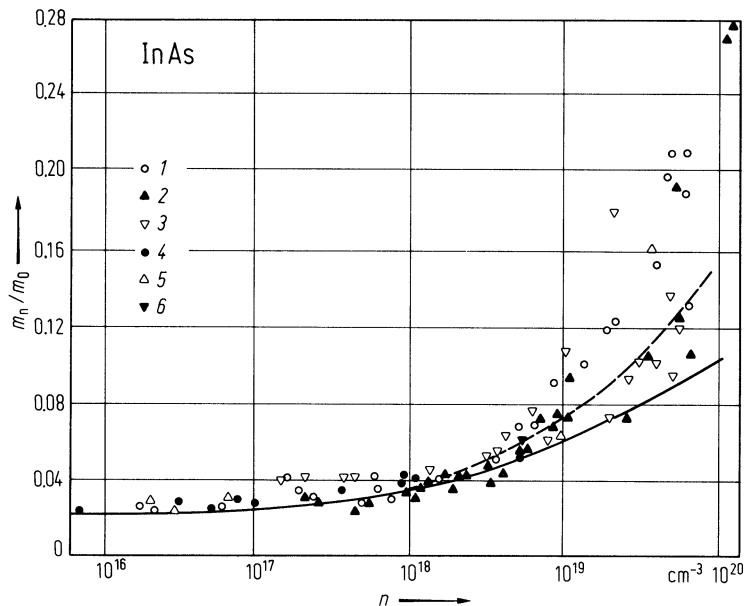


Fig. 2.15.3

InAs, InSb. Linear thermal expansion coefficient vs. temperature measured with a variable transformer dilatometer [67S].

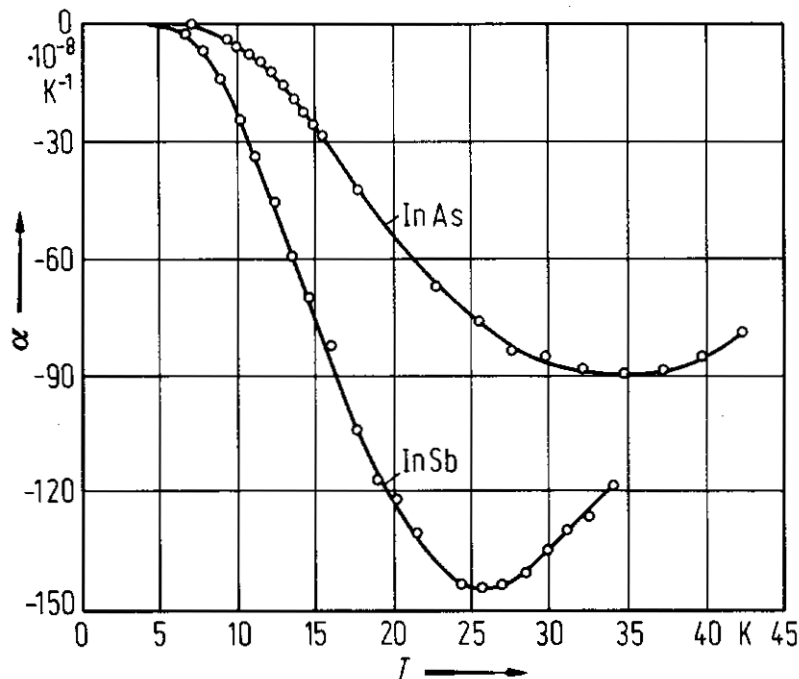


Fig. 2.15.4

InAs. Density vs. temperature [69G].

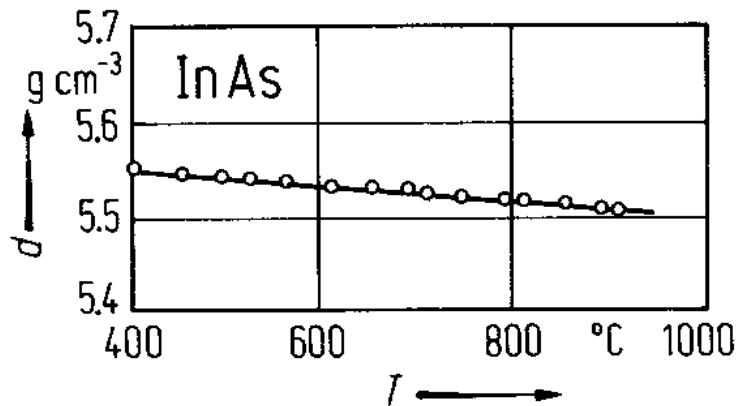


Fig. 2.15.5

InAs. Phonon dispersion curves (left panel) and density of states (right panel) [96E]. Experimental neutron data (full circles, $T = 300$ K [83O]), thermal-diffuse X-ray data (open diamonds, $T = 80$ K [83O]), and Raman data (full squares, $T = 330$ K [80C]) and ab-initio calculations (solid curves [96E]). From [96E].

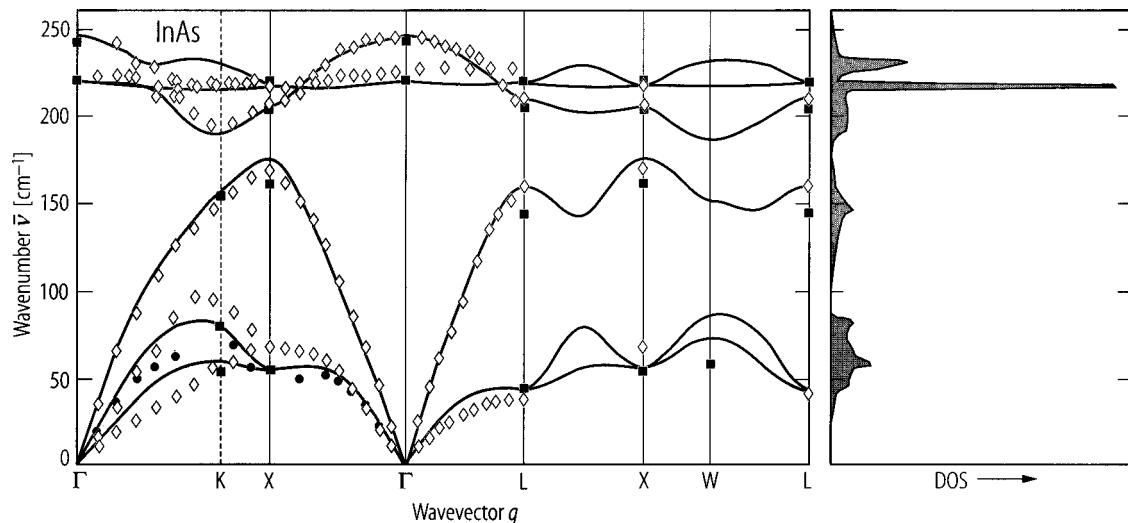


Fig. 2.15.6

InAs. Temperature dependence of the elastic moduli. Triangles, data of [64G]; open circles, data of [75B]; full circles, data from thermal-diffuse X-ray scattering [85O]. From [85O].

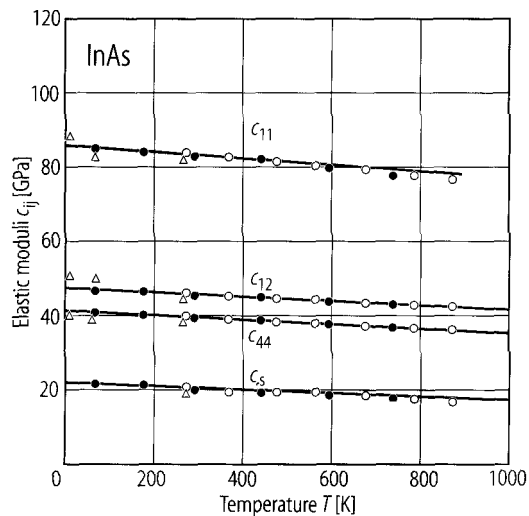


Fig. 2.15.7

InAs. Debye temperature vs. temperature [63P1].

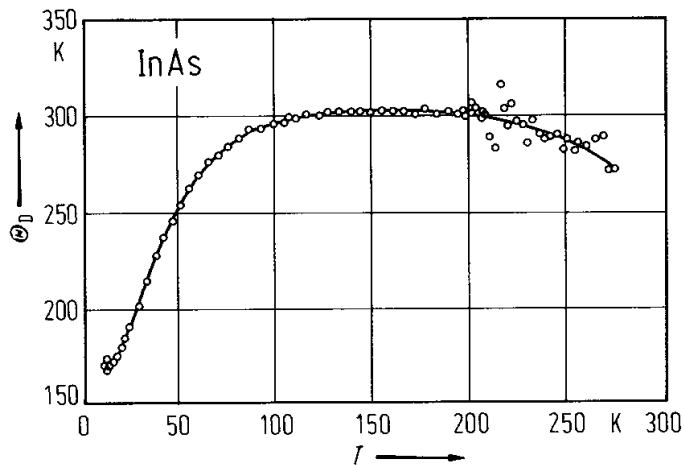


Fig. 2.15.8

InAs. Electrical conductivity vs. reciprocal temperature [54F]. *A*: $n = 1.2 \cdot 10^{15} \text{ cm}^{-3}$, *B*: $n = 1.7 \cdot 10^{16} \text{ cm}^{-3}$, *C*: $n = 4 \cdot 10^{16} \text{ cm}^{-3}$, *D*: $n = 7 \cdot 10^{16} \text{ cm}^{-3}$, *E*: $n = 2 \cdot 10^{18} \text{ cm}^{-3}$, *1*: $p = 2 \cdot 10^{17} \text{ cm}^{-3}$, *2*: $p = 7 \cdot 10^{18} \text{ cm}^{-3}$.

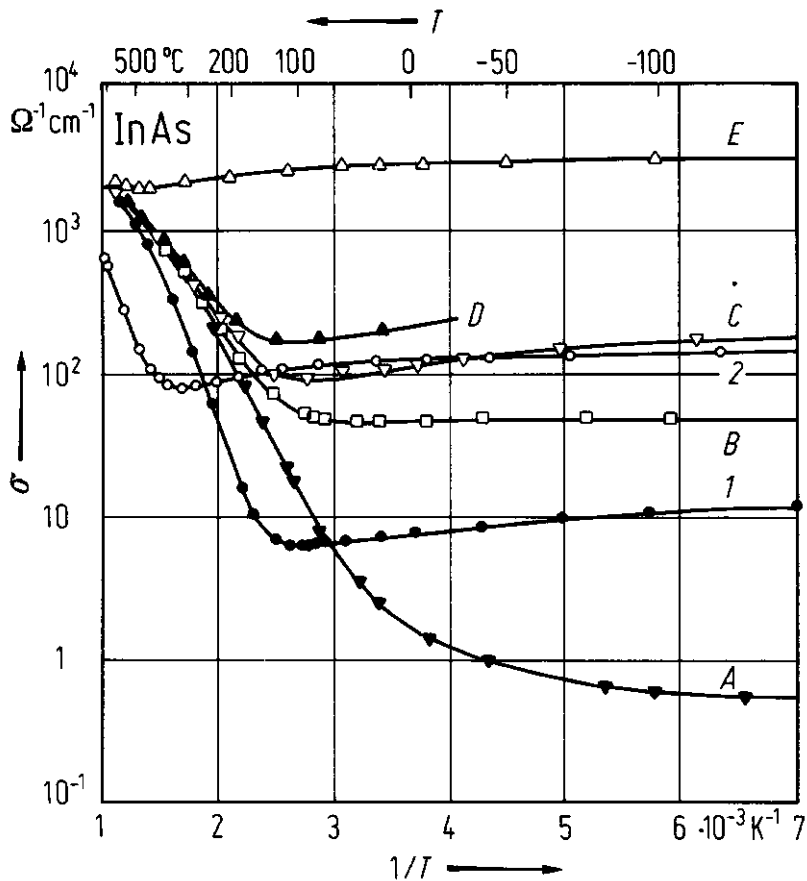


Fig. 2.15.9

InAs. Thermal conductivity vs. temperature below room temperature and theoretical curves showing the contributions of transverse and longitudinal phonons [71L].

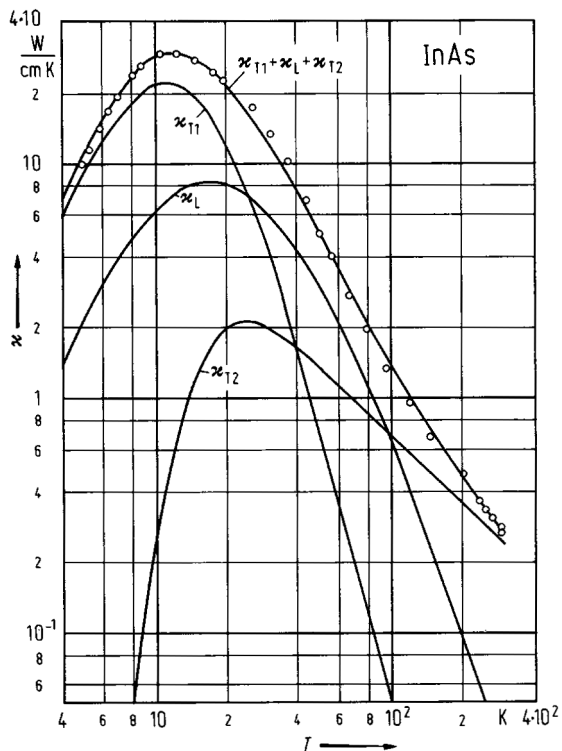


Fig. 2.15.10

InAs. Square of the intrinsic carrier concentration over T^3 vs. reciprocal temperature for different samples [54F].

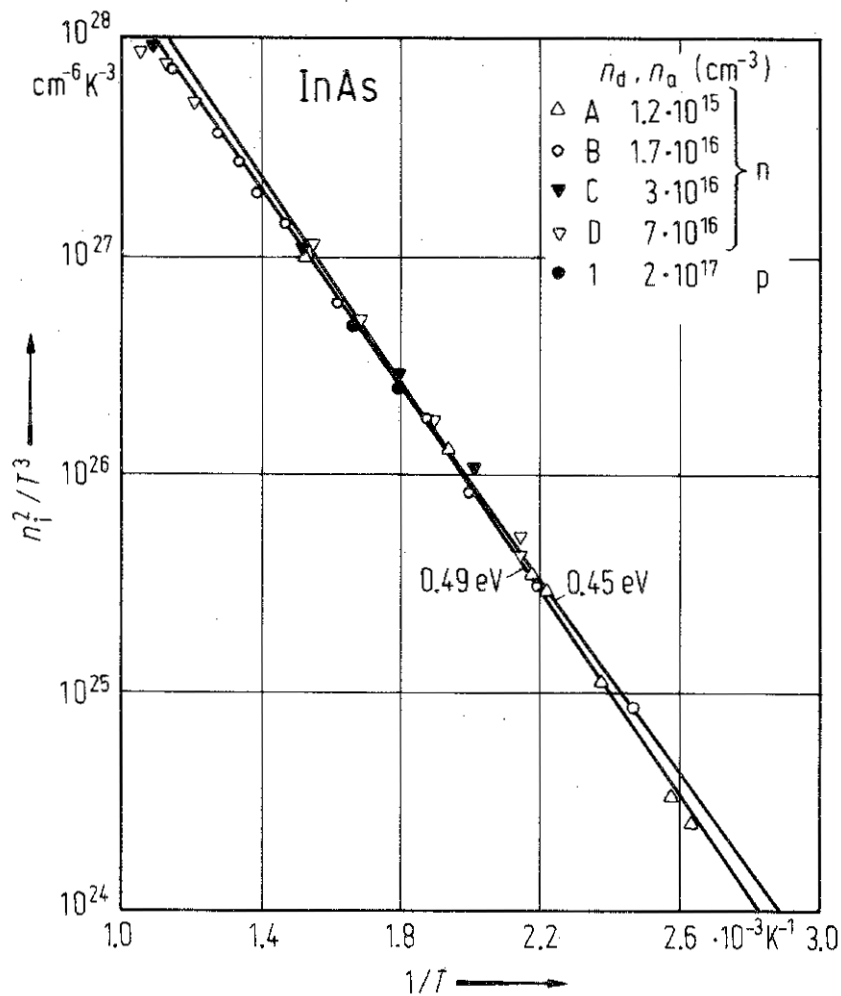


Fig. 2.15.11

InAs. Electron Hall mobility of pure material vs. temperature [75R]. Open triangles: $n = 1.7 \cdot 10^{16} \text{ cm}^{-3}$, circles: $n = 4 \cdot 10^{16} \text{ cm}^{-3}$, full triangles: $n = 4 \cdot 10^{15} \text{ cm}^{-3}$, theoretical curve after [75R].

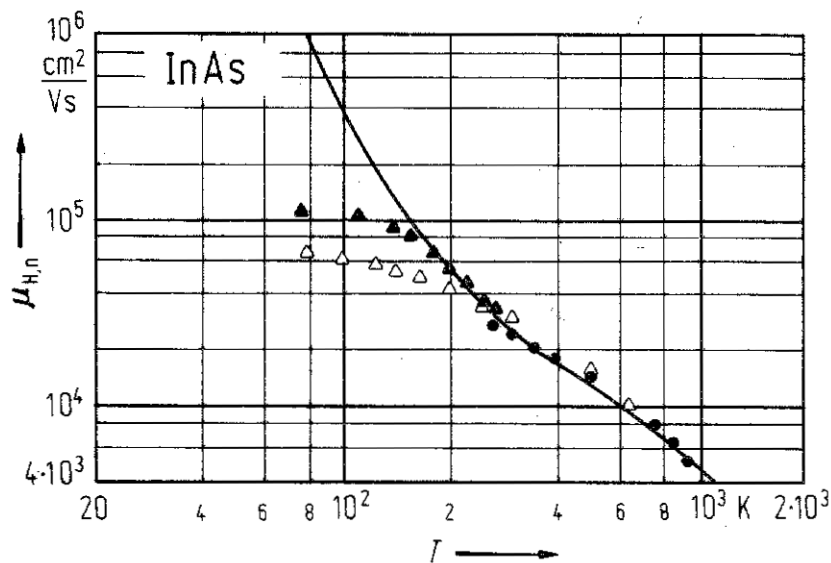
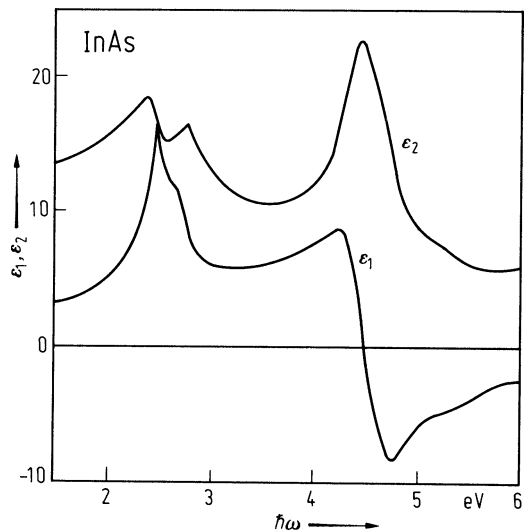


Fig. 2.15.12

InAs. Real and imaginary parts of the dielectric constant vs. photon energy [83A].



2.16 Indium antimonide (InSb)

Crystal structure

Indium antimonide crystallizes under normal conditions in the zincblende structure (space group $T_d^2 - F\bar{4}3m$, Fig. 2.0.2).

high-pressure phases

Angle-dispersive powder diffraction studies has led to a scenario of pressure-induced phase transitions from the zincblende structure InSb-I (at ambient pressure) to high-pressure phases [93N, 96M]: At about 2.1 GPa the cubic phase (InSb-I) transforms via a mixture of metastable tetragonal (P2, β -tin structure, but not identical to InSb-II) and orthorhombic (P3, body centred, Immm, InSb-II) phases to another stable orthorhombic high-pressure P4 phase (InSb-IV). At about 3 GPa there is often a direct transition from the P1 phase to the P4 phase, in particular at elevated temperature (100 °C). The P2 phase exists over a very small pressure range. The transition from InSb-IV to InSb-III (Immm structure) is via an intermediate P5 phase (Imma, without long-range site order). It is also concluded [96N, 96M] that InSb-II and InSb-III is the same phase (Immm structure).

Electronic properties

band structure : Fig. 2.0.24, Brillouin zone: Fig. 2.0.5.

InSb is a direct gap semiconductor. The minimum of the conduction band (Γ_6) is situated in the center of the Brillouin zone. Near the minimum, $E(k)$ is isotropic but non-parabolic. Thus the effective mass of the electrons is scalar and depends strongly on the electron concentration. Higher band minima (about 0.63 eV above the lowest minimum Γ_6) seem to be established by transport measurements in heavy doped n-InSb [75F]. The valence band shows the structure common to all zincblende semiconductors i.e. two subbands degenerate at Γ_8 and one spin-orbit split band (Γ_7).

energies of symmetry points of the band structure (relative to the top of the valence band $E(\Gamma_{8v})$)

$E(\Gamma_{6v})$	- 11.71 eV	- 11.7 eV	symmetry symbols in double group notation
$E(\Gamma_{7v})$	- 0.82 eV	- 0.850 eV	first row: theoretical data of [76C, 84C],
$E(\Gamma_{6c})$	0.25 eV	0.235 eV	see Fig. 2.0.25
$E(\Gamma_{7c})$	3.16 eV	3.141 eV	second row: experimental data deduced from
$E(\Gamma_{8c})$	3.59 eV	3.533 eV	data given in [74L1], [85L], [83L] and [81M]
$E(X_{6v})$	- 9.20 eV	- 9.5 eV	
$E(X_{6v})$	- 6.43 eV	- 6.4 eV	
$E(X_{6v})$	- 2.45 eV	- 2.4 eV	
$E(X_{7v})$	- 2.24 eV		
$E(X_{6c})$	1.71 eV	1.79 eV	
$E(X_{7c})$	1.83 eV		
$E(L_{6v})$	- 9.95 eV	- 10.5 eV	
$E(L_{6v})$	- 5.92 eV		
$E(L_{6v})$	- 1.44 eV	- 1.4 eV	
$E(L_{4,5v})$	- 0.96 eV	- 0.9 eV	
$E(L_{6c})$	1.03 eV		
$E(L_{6c})$	4.30 eV	4.32 eV	
$E(L_{4,5c})$	4.53 eV	4.47 eV	

energy gap

$E_{g, \text{dir}}(\Gamma_{8v}-\Gamma_{6c})$	0.2352 eV	$T = 1.7 \text{ K}$	emission spectra, from exciton data	79K
	0.180 eV	$T = 300 \text{ K}$	reflectance	62L
			magnetoabsorption	57Z
E_{th}	0.258 eV	$T = 0 \text{ K}$, linear extrapolated	Hall effect measurements between	70C
			150...300 K	

temperature dependence of energy gap

$E_g(T)$	$E_g(0) - aT^2/(b+T)$ with $a = 0.6 \text{ meV K}^{-1}$, $b = 500 \text{ K}$,	Fig. 2.16.1	85L
----------	---	-------------	-----

exciton ground state

$E(1S)$	0.2363(2) eV	$T = 2 \text{ K}$, $n_{77\text{K}} = 6 \cdot 10^{13} \text{ cm}^{-3}$	exciton ground state, from luminescence and absorption, theory including valence band degeneracy, using band parameter from [69P] E_b : binding energy of ground state	79K
E_b	0.52 meV			71B

spin-orbit splitting energies

$\Delta_0(\Gamma_{8v}-\Gamma_{7v})$	0.81(1) eV	$T = 1.5 \text{ K}$	magneto-electroreflectance	67P
$\Delta'_0(\Gamma_{7v}-\Gamma_{8c})$	0.39 eV	$T = 5 \text{ K}$	wavelength modulated reflectance	70Z
$\Delta_1(\Lambda_{4,5v}-\Lambda_{6v})$	0.495 eV			
$\Delta'_0(\Delta)$	0.369(16) eV		splitting of the upper valence band along Δ at (0.3, 0, 0)	81M
	0.250(40) eV		the same at (0.5, 0, 0)	
$\Delta'_1(L_{4,5c}-L_{6c})$	0.154(28) eV			81M

higher band-band transitions (critical point energies)

$E'_0(\Gamma_{8v}-\Gamma_{7c})$	3.39 eV	$T = 5 \text{ K}$	wavelength modulated reflectance	70Z
$E'_0(\Delta)$	3.348(9) eV		at (0.3, 0, 0) from uppermost valence band to lower conduction band	85L
	4.56(3) eV		at (0.5, 0, 0) from uppermost valence band to higher conduction band	
$E_1(\Lambda_{4,5v}-\Lambda_{6c})$	1.983 eV	$T = 5 \text{ K}$	wavelength modulated reflectance	70Z
$E'_1(L_{3v}-L_{3c})$	5.33 eV			
$E(\Gamma_{8v}-X_{6c})$	2.6 eV		angular resolved photoemission	83W
$E(\Gamma_{8v}-\Sigma_c^{\min})$	3.7 eV			
$E(\Gamma_{8v}-X_{6c})$	6.7 eV			
$E_2(X_{5v}-X_{1c})$	4.23 eV	$T = 5 \text{ K}$	several critical points in the E_2 range of wavelength modulated reflectance (largest c.p. at 4.23 eV)	70Z
	4.56 eV			
	4.75 eV			
	4.92 eV			

conduction band, effective masses

(no polaronic corrections are necessary. With a value of 0.022 for Fröhlich's coupling constant the difference between polaron and bare electron mass is 0.3% [72K])

$m_n(\Gamma_{6c})$	0.01359(3) m_0	$T = 4.2 \text{ K}$, $n = 4.6 \cdot 10^{13} \text{ cm}^{-3}$	Faraday effect	83Z
	0.0118 m_0	$T = 300 \text{ K}$	cyclotron resonance	93L

Dependence of electron effective mass on carrier concentration: see Fig. 2.16.2; for temperature dependence, see Fig. 2.16.3.

m_n (higher conduction band)	0.5 m_0		analysis of reflectance spectra in heavily doped samples	74L2
--------------------------------	-----------	--	--	------

g-factor of electrons

g_c	- 51.31(1)	$T = 1.4 \text{ K}$	esr	68I
-------	------------	---------------------	-----	-----

valence band, effective masses

$m_{p,h}$	0.44 m_0	$T = 20\text{ K}, k \parallel [111]$	magnetoabsorption, Faraday rotation	66P1
	0.42 m_0			
	0.32 m_0			
$m_{p,l}$	0.016 m_0	$T = 20\text{ K}$	magnetoabsorption, Faraday rotation	66P2
$m_{p,ds}$	0.430 m_0	$T = 0\text{ K}$ (extrapol.)	Hall effect	70C

For temperature dependence of the light-hole effective mass, see Fig. 2.16.4.

valence band parameters

A	-35	calculated using $k \cdot p$ theory	75W
B	-31.4		
$ C $	20.92		

Lattice properties

lattice parameter

a	6.47937(3) Å	$T = 298.15\text{ K}$	X-ray, powder; for temperature dependence, see Fig. 2.16.5	65S2
-----	--------------	-----------------------	--	------

linear thermal expansion coefficient

α	$5.37(50) \cdot 10^{-6}\text{ K}^{-1}$	$T = 283...343\text{ K}$	X-ray; for temperature dependence, see Fig. 2.16.6	65S2
----------	--	--------------------------	--	------

density

d	5.7747(4) g cm ⁻³		X-ray	65S2
-----	------------------------------	--	-------	------

melting temperature

T_m	800(1) K		drop calorimetry	89Y
-------	----------	--	------------------	-----

phonon dispersion curves, density of states : Fig. 2.16.7.

phonon frequencies

$\nu_{LO}(\Gamma_{15})$	5.90(25) THz	$T = 300\text{ K},$ $n = 8 \cdot 10^{13}\text{ cm}^{-3}$	coherent inelastic neutron scattering	71P
$\nu_{TO}(\Gamma_{15})$	5.54(5) THz			
$\nu_{TA}(X_5)$	1.12(5) THz			
$\nu_{LA}(X_3)$	4.30(10) THz			
$\nu_{LO}(X_1)$	4.75(20) THz			
$\nu_{TO}(X_5)$	5.38(17) THz			
$\nu_{TA}(L_3)$	0.98(5) THz			
$\nu_{LA}(L_1)$	3.81(6) THz			
$\nu_{LO}(L_1)$	4.82(10) THz			
$\nu_{TO}(L_3)$	5.31(6) THz			

temperature dependence, see Fig. 2.16.8

sound velocities

v_1	$3.4068(3) \cdot 10^5\text{ cm s}^{-1}$	RT	ultrasound ($f = 10\text{ MHz}$)	67D
v_2	$2.2864(2) \cdot 10^5\text{ cm s}^{-1}$	pure,	designation: mode/direction of propaga-	
v_3	$3.7664(3) \cdot 10^5\text{ cm s}^{-1}$	$n_{ion} = 2 \cdot 10^{14}\text{ cm}^{-3}$	tion/direction of particle displacement	
v_4	$2.2862(2) \cdot 10^5\text{ cm s}^{-1}$	v_1 : long./100/100,	v_2 : shear/100/011,	
v_5	$1.6251(1) \cdot 10^5\text{ cm s}^{-1}$	v_3 : long/110/110,	v_4 : shear/110/001, v_5 : shear/110/110	

electromechanical coupling coefficient

K^2	$5.15 \cdot 10^{-4}$	$q/e: [111]/[111]$	q : direction of propagation, e : direction of particle displacement	82C
-------	----------------------	--------------------	--	-----

second order elastic moduli

c_{11}	$6.918 \cdot 10^{11}$ dyn cm $^{-2}$	$T = 0$ K, extrapol.	$(f = 10$ MHz), see Fig. 2.16.9	59S
c_{12}	$3.788 \cdot 10^{11}$ dyn cm $^{-2}$	from 4.2 K		
c_{44}	$3.132 \cdot 10^{11}$ dyn cm $^{-2}$			

third order elastic moduli

c_{111}	$-3.56(36) \cdot 10^{12}$ dyn cm $^{-2}$	$T = 300$ K,	ultrasound ($f = 10$ MHz), uniaxial stress	77S2
c_{112}	$-2.66(15) \cdot 10^{12}$ dyn cm $^{-2}$	$n = 1.5 \cdot 10^{16}$ cm $^{-3}$		
c_{123}	$-1.00(11) \cdot 10^{12}$ dyn cm $^{-2}$			
c_{144}	$+0.16(12) \cdot 10^{12}$ dyn cm $^{-2}$			
c_{166}	$-1.39(8) \cdot 10^{12}$ dyn cm $^{-2}$			
c_{456}	$-0.004(70) \cdot 10^{12}$ dyn cm $^{-2}$			

bulk modulus

B	46.50(5) GPa			90V
-----	--------------	--	--	-----

Debye temperature

$\Theta_D(0)$	203 K	data for Θ_D cited in [66P] from two different sources for temperature dependence see Fig. 2.16.10	
	208 K		

Transport properties

The transport properties are mainly determined by an extremely high mobility of the electrons in the Γ_6 minimum of the conduction band. Pure material with intrinsic conduction down to 200 K is available. Low-temperature transport properties are determined by impurity scattering and – in heavily doped and compensated samples at temperatures as high as 140 K – by impurity band conduction.

electrical conductivity

σ	$220 \Omega^{-1}$ cm $^{-1}$	$T = 300$ K	pure material; for temperature dependence, see Fig. 2.16.11
----------	------------------------------	-------------	---

thermal conductivity : see Fig. 2.16.12

intrinsic carrier concentration

n_i	$1.89(35) \cdot 10^{16}$ cm $^{-3}$	$T = 300$ K	Helicon-interferometry with polycrystalline n-InSb	73B
	$5.76 \cdot 10^{14} T^{3/2} \exp(-0.26/2kT)$ cm $^{-3}$	$(T$ in K, kT in eV)		70C

electron mobility

$\mu_{H,n}$	$7.7 \cdot 10^4 (T/300)^{-1.66}$ cm 2 /Vs			64M
	70000 cm 2 /Vs	$T = 300$ K		90T
$\mu_{dr,n}$	$5.25 \cdot 10^5$ cm 2 /Vs			

For temperature dependence, see Fig. 2.16.13. For dependence on electron concentration, see Fig. 2.16.14.

hole mobility

μ_p	$850(T/300)^{-\beta}$ cm 2 /Vs		see also Fig. 2.16.15	75W
	$\beta = 2.1$	$T = 60 \dots 125$ K	Hall measurement	55H
	$\beta = 2.0$	$T = 200 \dots 500$ K	Nernst-Ettinghausen-effect	67A

piezoelectric constants

e_{14}	$7.1(7) \cdot 10^{-6} \text{ C/cm}^2$	$T = 300 \text{ K}$	piezoelectric Hall effect measurements	68A
d_{14}	$2.35 \cdot 10^{-10} \text{ cm/V}$		polarity: negative, if the crystal is	
g_{14}	$1.57 \cdot 10^2 \text{ cm}^2/\text{C}$		expanded in the [111] direction, the	
h_{14}	$4.7 \cdot 10^6 \text{ V/cm}$		A-faces (metal atoms) become negatively	
			charged.	

Seebeck coefficient

S	$-300 \mu\text{V/K}$	$T = 300 \text{ K}$	pure intrinsic material	71T
	$-500 \mu\text{V/K}$	$T = 77 \text{ K}$	pure n-type material	

The Seebeck coefficient for p-type material changes sign in the temperature region between 150 and 210 K, depending on impurity concentration [74A].

Temperature dependence, see Fig. 2.16.16.

Optical properties

optical constants

real and imaginary parts of the dielectric constant measured by spectroscopical ellipsometry, n , k , R , K calculated from these data [83A]. See also Fig. 2.16.17

$h\nu [\text{eV}]$	ϵ_1	ϵ_2	n	k	R	$K [10^3 \text{ cm}^{-1}]$
1.5	19.105	5.683	4.418	0.643	0.406	97.79
2.0	14.448	14.875	4.194	1.773	0.443	359.46
2.5	7.811	15.856	3.570	2.221	0.447	562.77
3.0	7.354	13.421	3.366	1.994	0.416	606.27
3.5	5.995	17.673	3.511	2.517	0.474	892.82
4.0	-6.722	19.443	2.632	3.694	0.608	1497.79
4.5	-6.297	8.351	1.443	2.894	0.598	1320.24
5.0	-4.250	6.378	1.307	2.441	0.537	1237.01
5.5	-4.325	4.931	1.057	2.333	0.563	1300.55
6.0	-3.835	3.681	0.861	2.139	0.572	1300.85

refractive index

n	2.57	$T = 300 \text{ K}$	$\lambda [\mu\text{m}]$ 45	reflectance and transmission. $n = 6 \cdot 10^{15} \text{ cm}^{-3}$	56Y
	3.814		21.15		
	3.826		19.98	interference technique, $n = 2 \cdot 10^{16} \text{ cm}^{-3}$	57M
	3.953		10.06		
	4.001	$T = 100 \dots 400 \text{ K}$ $\lambda = 5 \dots 20 \mu\text{m}$	7.87		
	4.03		2.07	reflectance and dispersion relations	63P
	5.13		0.689		
	1.17		0.062		
$(1/n)dn/dT$	$1.19(2) \cdot 10^{-4} \text{ K}^{-1}$			interference method, see Fig. 2.16.18	60C

absorption index

			λ [μm]		
k	$5.4 \cdot 10^{-2}$	$T =$ 300 K	45	reflectance and transmission $n = 6 \cdot 10^{15} \text{ cm}^{-3}$	56Y
	$2 \cdot 10^{-3}$		20		
	$1.9 \cdot 10^{-3}$		9.50	transmission $p = 2.75 \cdot 10^{16} \text{ cm}^{-3}$	59K
	0.037		6.90	transmission $n = 2 \cdot 10^{16} \text{ cm}^{-3}$	57M
	0.18		1.60		
	0.20		1.55	reflectance and dispersion relations	63P
	1.88		0.656		
	0.21		0.062		

reflectance

			λ [μm]	
R	0.93	$T =$ 300 K	500	65S1
	0.83		200	
	0.19		50	
	0.35		20	
	0.488		0.677	
	0.016		0.062	

dielectric constants

$\varepsilon(0)$	16.8(2)		gyroscopic sphere resonance	80D
	17.3.. 18.0		range of results obtained by infrared reflectivity (from a compilation of data obtained by several methods in [80D])	
$\varepsilon(\infty)$	15.68		infrared reflectance and oscillator fit For dependence of real and imaginary parts of dielectric constant on photon energy, see Fig. 2.16.19	62H, 65S1

Impurities and defects

binding energies of shallow impurities

donors

Shallow, effective-mass like donors are always present in concentrations of at least 10^{13} cm^{-3} . Their influence on the semiconductor properties is strong due to their small binding energy of 0.7 meV. In Te-doped samples the Te donor level is found in the conduction band [92P].

acceptor binding energies

Energy values are relative to the valence band maximum.

Impurity	E_b [meV]	T [K]	Remarks	Ref.
Theory	8.5		$1S_{3/2}$, acceptor effective mass calculation	73L
Cd	9.86	4.5	Fourier transform spectroscopy	73K
	10.24	10.3	Fourier transform spectroscopy	83M
	8.1 ± 0.3	4.2	magneto-optical	83L
	7	4.2	photoluminescence	92I
Zn	9.86			
	9.1	1.5	infrared absorption	72M
Ge	9.25			
	7	1.1-4.2	resistivity	88O
X	120	77	generation-recombination noise and	73G,
			lifetime measurements, origin unknown	74V

binding energy of intrinsic or unidentified electron traps

Defect label	E_b [eV]	Defect type	Experimental method	Ref.
E1	$E_c - (0.045-0.050)$	electron trap	DLTS	89D
E1	$E_c - 0.050$	donor, intrinsic	DLTS, n-type sample	89V
E2	$E_c - 0.010$	electron trap	DLTS, n-type sample	89V
E	$E_c - 0.015$	Ge donor	DLTS, p-type sample	89V
E3	$E_c - 0.175$	electron trap	DLTS, thin n-type film	89V
E4	$E_c - 0.085$	electron trap	DLTS, thin n-type film	89V

Defect label	E_b [eV]	T [K]	Experimental method, remarks	Ref.
E ₁	$E_c - 0.116$	230	magnetic circular dichroism, donor	85G
E ₂	$E_c - 0.12$	4.2...77	lifetime measurements, lattice defect	82S
E ₃	$E_c - 0.074$	4.2	magneto-optical	82S
E ₁	$E_c - 0.17$	4.2	magneto-optical	82S
Au	$E_v + 0.0425$	4.2	magneto-optical, double acceptor	82L1
E ₁	$E_v + 0.048$	0	optical absorption, donor, T extrapolated to 0 K	73V
	$E_v + 0.059$	78	photoconductivity	82E
E ₂	$E_v + 0.067$	0	optical absorption, donor, T extrapolated to 0 K	73V
	$E_v + 0.071$	78	photoconductivity	82E
	$E_v + 0.074$	78	photoconductivity	82E
E ₁	$E_v + 0.103$	0	optical absorption, photoconductivity, donor, T extrapolated to 0 K	73V, 82E
	$E_v + 0.107$	78	photoconductivity	82E
	$E_v + 0.109$	78	photoconductivity	82E
	$E_v + 0.115$	78	photoconductivity	82E

binding energy or apparent thermal activation energy of intrinsic or unidentified hole traps

Defect label	E_b [eV]	E_{pa} [eV]	Defect type	Experimental method	Ref.
A		0.095	Hole trap	DLTS	82T
H1	$E_v + (0.10 - 0.11)$		Hole trap	DLTS	89D
H2	$E_v + (0.055 - 0.060)$		Hole trap	DLTS	89D
H3	$E_v + (0.030 - 0.035)$		Hole trap	DLTS	89D
Cu or Ag?		0.028	Acceptors	electrical conductivity	79K
Cu or Ag?		0.056	Acceptors	electrical conductivity	79K
E1		0.065		noise spectra	73G
E2		0.120		noise spectra	73G
H1	$E_v + 0.050$		Hole trap	DLTS, n-type sample	89V
H2	$E_v + 0.010$		Hole trap	DLTS, n-type sample	89V
H3	$E_v + 0.100$		Hole trap	DLTS, p-type Ge-doped	89V
H4	$E_v + 0.108$		Ge acceptor	DLTS, p-type Ge-doped	89V
Ge	$E_v + 0.106$		Ge defect		89V
H5	$E_v + 0.120$		Hole trap	DLTS, p-type Ge-doped	89V
H6	$E_v + 0.047$		Hole trap	DLTS, p-type Ge-doped	89V
H7	$E_v + 0.020$		Hole trap	DLTS, p-type Ge-doped	89V
H8	$E_v + 0.055$		Hole trap	DLTS, thin n-type film	89V
H9	$E_v + 0.044$		Hole trap	DLTS, thin n-type file	89V

References to 2.16

- 54M Madelung, O., Weiss, H.: Z. Naturforsch. 9a (1954) 527.
- 55H Hrostowski, H. J., Morin, F. J., Geballe, T. H., Wheatley, G. H.: Phys. Rev. 100 (1955) 1672.
- 56P Potter, R. F.: Phys. Rev. 103 (1956) 47.
- 56W Weiss, H.: Z. Naturforsch. 11 (1956) 131.
- 56Y Yoshinaga, H., Oetjen, R. A.: Phys. Rev. 101 (1956) 526.
- 57M Moss, T. S., Smith, S. D., Hawkins, T. D. F.: Proc. Phys. Soc. B70 (1957) 776.
- 57Z Zwerdling, S., Lax, B., Roth, L.: Phys. Rev. 108 (1957) 1402.
- 58G Gibbons, D. F.: Phys. Rev. 112 (1958) 779.
- 59B Blum, A. I., Ryabtjova, G. P.: Sov. Phys. Solid State (English Transl.) 1 (1959) 692; Fiz. Tverd. Tela 1 (1959) 766.
- 59K Kurnick, S. W., Powell, J. M.: Phys. Rev. 116 (1959) 597.
- 59S Slutsky, L. J., Garland, C. W.: Phys. Rev. 113 (1959) 167.
- 59V Volokobinskaya, N. I., Galavanov, V. V., Nasledov, D. N.: Sov. Phys. Solid State (English Transl.) 1 (1959) 687; Fiz. Tverd. Tela 1 (1959) 756.
- 60C Cardona, M.: Proc. Int. Conf. Phys. Semicond., Prague 1960, Publ. House of the Acad. of Sci., Prague 1960, p. 388.
- 61B Busch, U., Steigmeier, E.: Helv. Phys. Acta 34 (1961) 1.
- 62H Hass, M., Hennis, B. W.: J. Phys. Chem. Solids 23 (1962) 1099.
- 62L Lukes, F., Schmidt, E.: Proc. 6th Int. Conf. Physics of Semicond., Exeter 1962, The Institute of Physics and the Physical Society, London 1962, p. 389.
- 63P Philipp, H. R., Ehrenreich, H.: Phys. Rev. 129 (1963) 1550.
- 64M Madelung, O.: Physics of III-V Compounds, J. Wiley & Sons, New York 1964.
- 65S1 Sanderson, R. B.: J. Phys. Chem. Solids 26 (1965) 803.
- 65S2 Straumanis, M. E., Kim, C. D.: J. Appl. Phys. 36 (1965) 3822.
- 66P1 Piesbergen, U.: in "Semiconductors and Semimetals", vol. 2, R. K. Willardson, A. C. Beer eds., Academic Press, New York 1966.
- 66P2 Pidgeon, C. R., Brown, R. N.: Phys. Rev. 146 (1966) 575.
- 67A Agaev, Ya., Mosanov, O., Ismailov, O.: Sov. Phys. Semicond. (English Transl.) 1 (1967) 711; Fiz. Tekh. Poluprovodn. 1 (1967) 855.
- 67D Drabble, J. R., Brammer, A. J.: Proc. Phys. Soc. 91 (1967) 959.
- 67P Pidgeon, C. R., Groves, S. H., Feinleib, J.: Solid State Commun. 5 (1967) 677.
- 67S Sparks, P. W., Swenson, C. A.: Phys. Rev. 163 (1967) 779.
- 68A Arlt, G., Quadflieg, P.: Phys. Status Solidi 25 (1968) 323.
- 68I Isaacson, R. A.: Phys. Rev. 169 (1968) 312.
- 69P Pidgeon, C. R., Groves, S. H.: Phys. Rev. 186 (1969) 824.
- 70C Cunningham, R. W., Gruber, J. B.: J. Appl. Phys. 41 (1970) 1804.
- 70S Stradling, R. A., Wood, R. A.: J. Phys. C3 (1970) L94.
- 70Z Zucca, R. R. L., Shen, Y. R.: Phys. Rev. 155 (1970) 2668.
- 71B Baldereschi, A., Lipari, N. O.: Phys. Rev. B3 (1971) 439.
- 71K Katzman, H., Moss, J., Libby, W. F.: J. Phys. Chem. Solids 32 (1971) 2786.
- 71P Price, D. L., Rowe, J. M., Nicklow, R. M.: Phys. Rev. B3 (1971) 1268.
- 71R Rode, D. L.: Phys. Rev. 3 (1971) 3287.
- 71T Tamarin, P. V., Shalyt, S. S.: Sov. Phys. Solid State (English Transl.) 13 (1971) 1186; Fiz. Tverd. Tela 13 (1971) 1420.
- 72K Kartheuser, E.: in "Polarons in Ionic Crystals and Polar Semiconductors", J. T. Devreese ed., North Holland Publ. Comp., Amsterdam 1972.
- 72M Murzjn, V. N., Demishina, A. I., Umarov, L. M.: Sov. Phys. Semicond. (English Transl.) 6 (1972) 419; Fiz. Tekh. Poluprovodn. 6 (1972) 488.
- 73B Bernot, H., Hinsch, H.: Appl. Phys. 1 (1973) 147.
- 73G Galavanov, V. V., Ivchenko, E. L., Oding, V. G.: Sov. Phys. Semicond. (English Transl.) 7 (1973) 547; Fiz. Tekh. Poluprovodn. 7 (1973) 798.
- 73K Kaplan, R.: Solid State Commun. 12 (1973) 191.
- 73L Lipari, N. O.: Ref. 6 in[73K].
- 73V Valyashko, E. G., Pleskacheva, T. B.: Sov. Phys. Semicond. 7 (1973) 573.
- 74A Abrikosov, N. Kh., Laptev, A. V., Mirgalovskays, M. S.: Sov. Phys. Semicond. (English Transl.) 7 (1974) 1502; Fiz. Tekh. Poluprovodn. 7 (1973) 2253.

- 74L1 Lang, I. G., Nasledov, D. N., Pavlov, S. Z., Radaikina, L. N., Filipchenko, A. S.: Sov. Phys. Solid State (English Transl.) 16 (1974) 54; Fiz. Tverd. Tela 16 (1974) 92.
- 74L2 Ley, L., Pollak, R. A., McFeely, F. R., Kowalczyk, S. P., Shirley, D. A.: Phys. Rev. B9 (1974) 600.
- 75F Filipchenko, A. S., Nasledov, D. N.: Phys. Status Solidi (a) 27 (1975) 11.
- 75W Wiley, J. D.: in: Semiconductors and Semimetals, Vol. 10, ed. by R. K. Willardson and A. C. Beer, Academic Press, New York and London, 1975.
- 76C Chelikowski, J. R., Cohen, M. L.: Phys. Rev. B 14 (1976) 556.
- 77S1 Stillman, G. E., Wolfe, C. M., Dimmock, J. O.: in "Semiconductors and Semimetals", Vol. 12, R. K. Willardson, A. C. Beer eds., Academic Press 1977, p. 169.
- 77S2 Sundara, V., Jayarama Reddy, P.: Solid State Commun. 21 (1977) 701.
- 79K Kurilenko, I. N., Litvak-Gorskaya, L. B., Lugovaya, G. E.: Sov. Phys. Semicond. (English Transl.) 13 (1979) 906; Fiz. Tekh. Poluprovodn. 13 (1979) 1556.
- 80D Dixon, J. R., Furdyna, J. K.: Solid State Commun. 35 (1980) 195.
- 81L Litwin-Staszewska, E., Szymanska, W., Piotrkowski, R.: Phys. Status Solidi (b) 106 (1981) 551.
- 81M Mattausch, H. J., Aspnes, D. E.: Phys. Rev. B 23 (1981) 1896.
- 82C Ceeke, J. D. N., Madore, G.: Solid State Commun. 41 (1982) 899.
- 82E Egembardieva, S. Sh., Luchinin, S. D., Seisenbaev, T., Feoktistov, A. I., Filipchenko, A. S.: Sov. Phys. Semicond. 16 (1982) 347.
- 82K Kolchanova, N. M., Sipovskaya, M. A., Smetannikova, Yu. S.: Sov. Phys. Semicond. 16 (1982) 1418.
- 82L Littler, C. L., Seiler, D. G., Kaplan, R., Wagner, R. J.: Appl. Phys. Lett. 41 (1982) 880.
- 82S Seiler, D. G., Goodwin, M. W.: J Appl. Phys. 53 (1982) 7505.
- 82T Tsukioka, K., Miyazawa, H.: Jpn. J. Appl. Phys. 21 (1982) L526.
- 83A Aspnes, D. E., Studna, A. A.: Phys. Rev. B 27 (1983) 985.
- 83H Höchst, H., Hernandez-Calderon, I.: Surf. Sci. 126 (1983) 25.
- 83L Littler, C. L., Seiler, D. G., Kaplan, R., Wagner, R. J.: Phys. Rev. B 27 (1983) 7473.
- 83L Littler, C. L., Seiler, D. G., Kaplan, R., Wagner, R. J.: Phys. Rev. B 27 (1983) 7473.
- 83M Meisel, R., Kuchar, F.: Phys. Status Solidi B 116 (1983) 557.
- 83W Williams, G. P., Cerrina, F., Anderson, J., Lapeyre, G. J., Smith, R. J., Hermanson, J., Knapp, J. A.: Physica 117B & 118B (1983) 350.
- 83Z Zengin, D. M.: J. Phys. D 16 (1983) 653.
- 84C Chelikowski, J. R., Cohen, M. L.: Phys. Rev. B 30 (1984) 4828.
- 84L Liarokapis, W., Anastassakis, E.: Phys. Rev. 30 (1984) 2270.
- 85G Galanov, E. K., Potikhonov, G. N., Petukhov, I. P.: Sov. Phys. Semicond. 19 (1985) 926.
- 85L Logothetidis, S., Vina, L., Cardona, M.: Phys. Rev. B 31 (1985) 947.
- 88O Obukhov, S. A.: Sov. Phys. Semicond. 22 (1988) 19.
- 89D Druzhinina, L. V., Molodtsova, E. V., Kozhukhova, E. A., Polyakov, A. Ya., Popkov, A. N., Tishkin, M. V., Shlenskii, A. L.: Sov. Phys. Semicond. 23 (1989) 1292.
- 89V Volkov, V. V., Padalko, A. G., Belotelov, S. V., Bozhko, V. V., Lazarev, V. B.: Sov. Phys. Semicond. 23 (1989) 871.
- 89Y Yamaguchi, K.: J. Jpn. Inst. Met. 53 (1989) 764.
- 90T Tsukamoto, S., Bhattacharya, P., Chen, Y. C., Kim, J. H.: J. Appl. Phys. 67 (1990) 6819.
- 90V Vanderborgh, C. A., Vohra, Y. K., Ruoff, A. L.: Phys. Rev. B 40 (1990) 12450.
- 91U Ugrin, Y. O., Sheregii, E. M.: Phys. Status Solidi (b) 166 (1991) 249.
- 92I Ivanov-Omskii, V. I., Smirnov, V. A., Yuldashev, Sh. U., Gadaev, O. A., Stradling, R. A., Ferguson, I.: Partin, D. L., Heremans, J., Thrush, C. M., Morelli, D. T.: J. Appl. Phys. 71 (1992) 2328.
- 92P Partin, D. L., Heremans, J., Thrush, C. M., Morelli, D. T.: J. Appl. Phys. 71 (1992) 2328.
- 93L Liu, P. Y., Maan, J. C.: Phys. Rev. B 47 (1993) 16279.
- 93N Nelmes, R. J., McMahon, M. I., Hatton, P. D., Crain, J., Piltz, R. O.: Phys. Rev. B 47 (1993) 35; Phys. Rev. B 48 (1993) 9949 (E); Nelmes, R. J., McMahon, M. I., Hatton, P. D., Piltz, R. O., Crain, J.: Jpn. J. Appl. Phys. Suppl. 32 (1993) 1.
- 96M McMahon, M. I., Nelmes, R. J.: Phys. Status Solidi (b) 198 (1996) 389.
- 96N Nelmes, R. J., McMahon, M. I.: Phys. Rev. Lett. 77 (1996) 663.
- 99P Pletl, T., Pavone, P., Engel, U., Strauch, D.: Physics B 263/264 (1999) 392.

Figures to 2.16

Fig. 2.0.2

The zincblende lattice

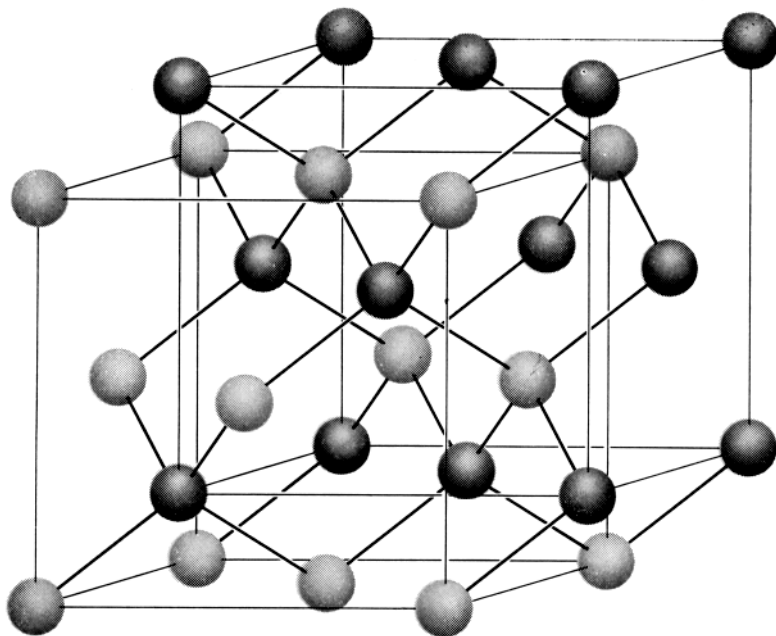


Fig. 2.0.5

Brillouin zone of the zincblende lattice.

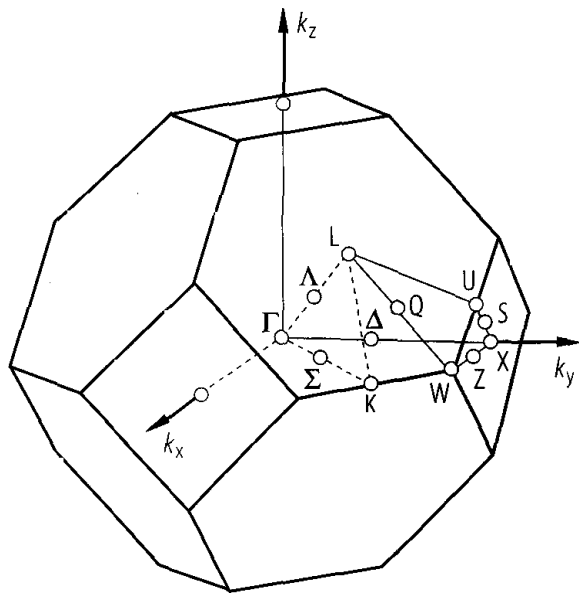


Fig. 2.0.24

InSb. Band structure obtained with a non-local pseudopotential calculation [76C], corrected in [84C] (Fig. from [84C]). Experimental data from angular resolved photo-emission from a InSb (001) surface [83H] have been included (circles).

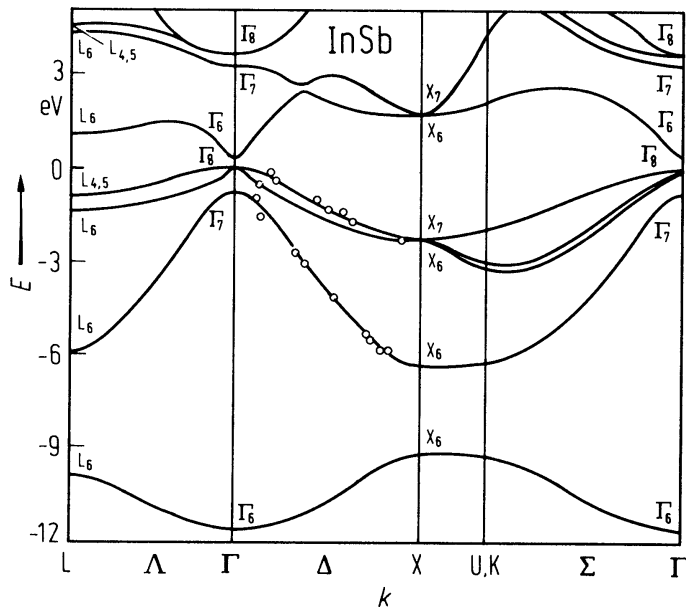


Fig. 2.16.1

InSb. Energy gap vs. temperature below RT measured by resonant two-photon photo-Hall effect (full circles); open circles and triangles: earlier literature data for comparison. Solid curve: fit by Varshni's formula as given in the tables [85L].

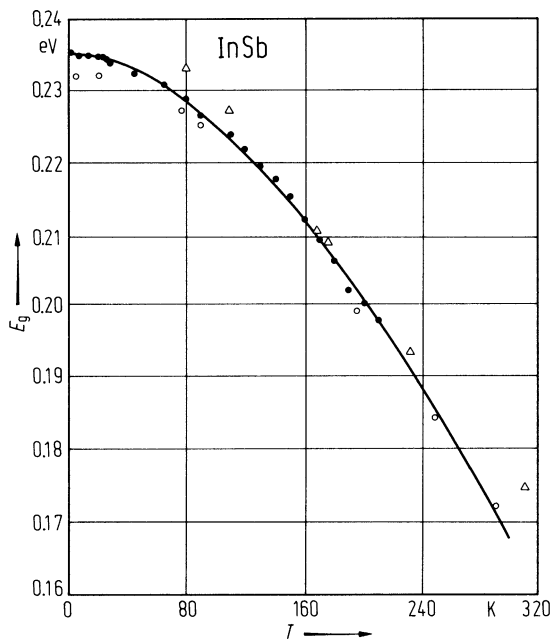


Fig. 2.16.2

InSb. Electron effective mass vs. carrier concentration. Comparison of results of several experimental measurements. Solid line: Kane's theory [77S1].

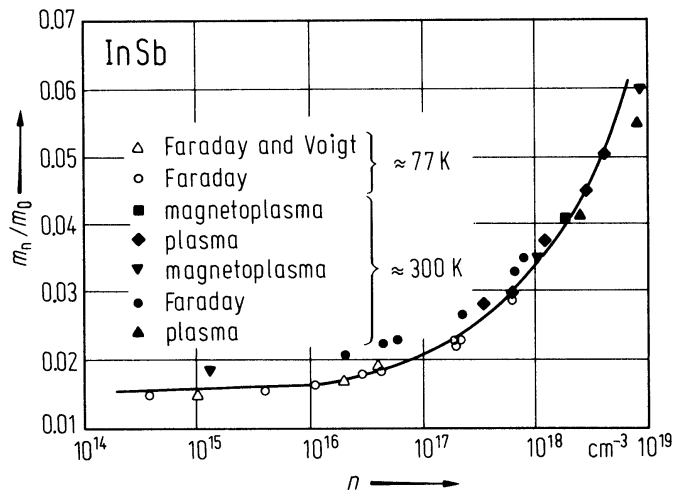


Fig. 2.16.3

InSb. Effective electron mass vs. temperature determined by magnetophonon magnetoresistance measurements [70S].

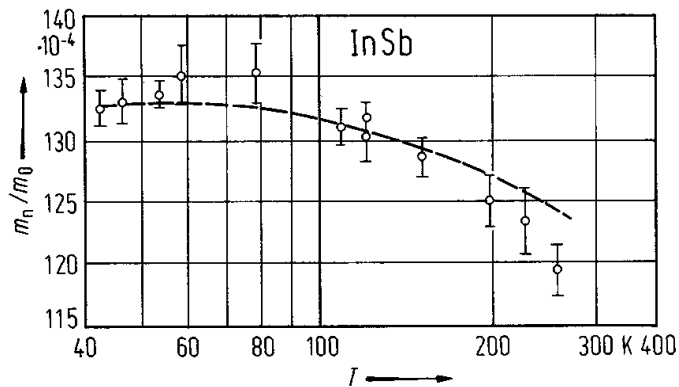


Fig. 2.16.4

InSb. Temperature dependence of the light-hole effective mass as derived from magnetophonon resonance measurements [91U]. I and II stand for two different interpretations of the data.

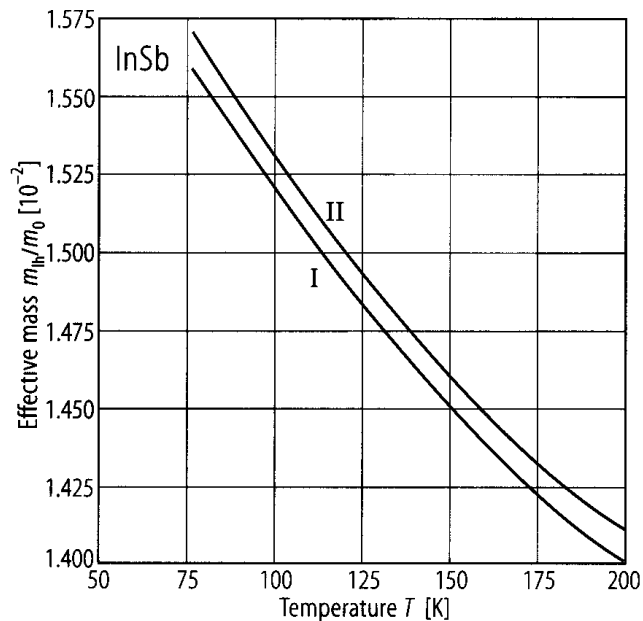


Fig. 2.16.5

GaSb, InSb. Lattice parameter vs. temperature [65S1].

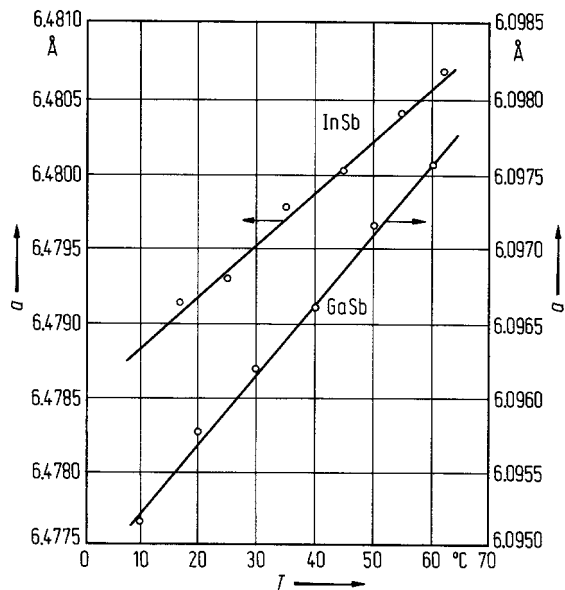


Fig. 2.16.6

InSb. Linear thermal expansion coefficient vs. temperature; (a) low temperature region [67S], (b) high temperature region [58G].

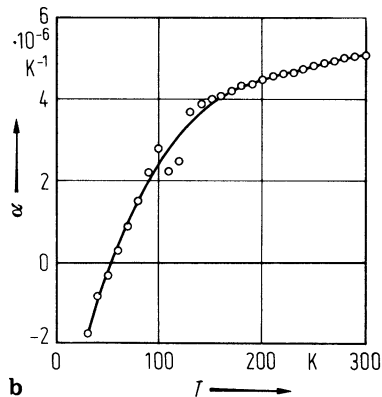
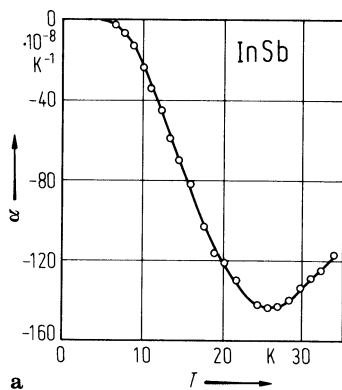


Fig. 2.16.7

InSb. Phonon dispersion curves. Experimental neutron data (circles [71P]) and ab-initio pseudopotential calculations (full curves [99P]). For the corresponding phonon density of states see right panel. From [99P].

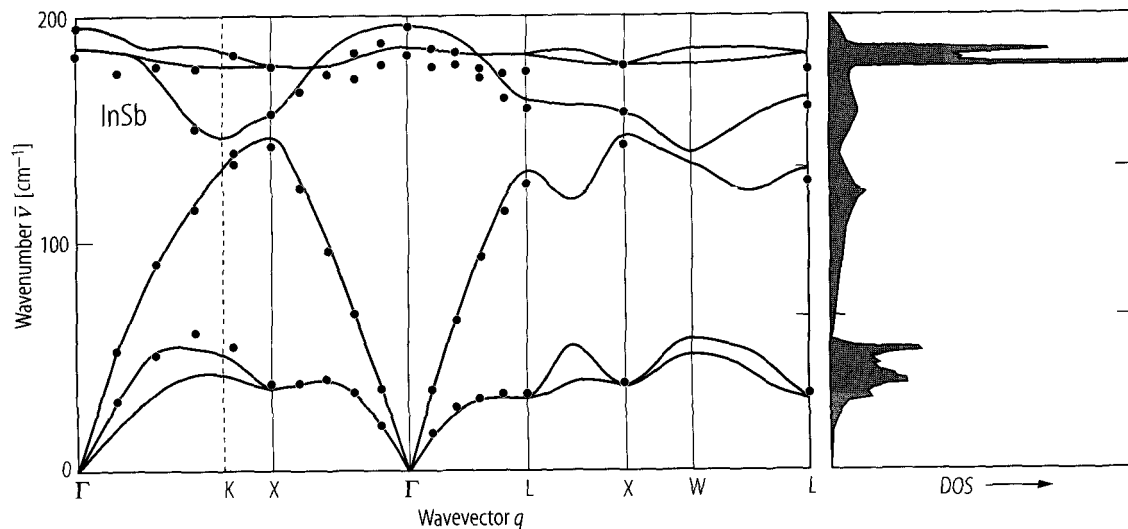


Fig. 2.16.8

InSb. Zone center optical phonon wavenumbers vs. temperature. Solid lines are best fits to theory [84L].

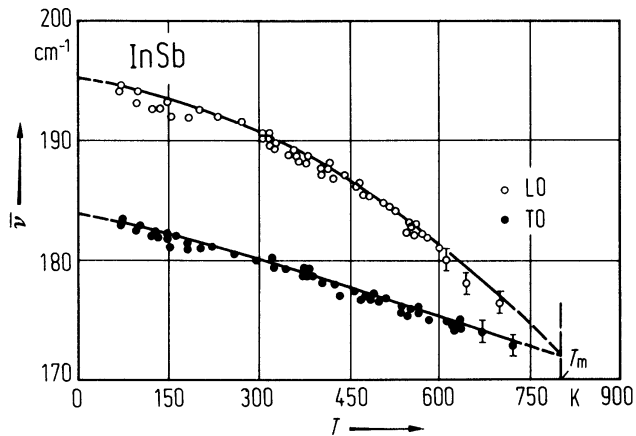


Fig. 2.16.9

InSb. Second order elastic moduli vs. temperature [59S], full circles: [56P].

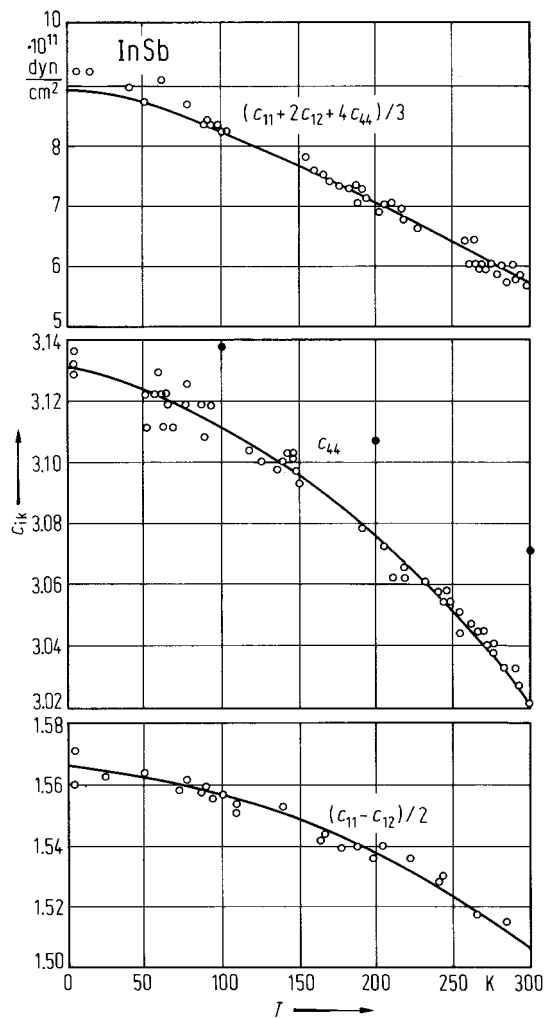


Fig. 2.16.10

InSb. Debye temperature vs. temperature [66P1].

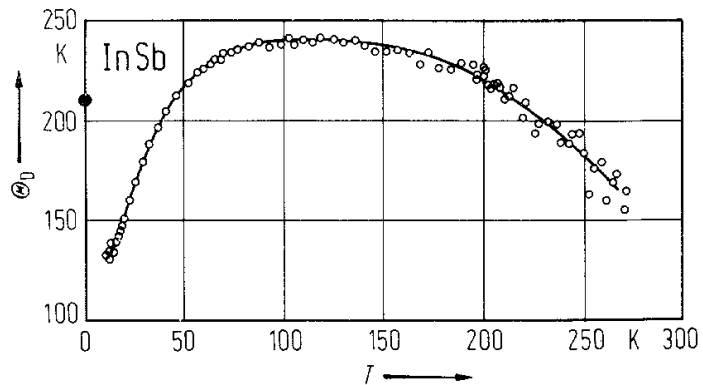


Fig. 2.16.11

InSb. Electrical conductivity vs. reciprocal temperature. Curve *V*: $n \approx 10^{13} \text{ cm}^{-3}$, *A*: $n = 1.3 \cdot 10^{16} \text{ cm}^{-3}$, *B*: $n = 1 \cdot 10^{16} \text{ cm}^{-3}$, *1*: $p = 4 \cdot 10^{15} \text{ cm}^{-3}$, *2*: $p = 2.2 \cdot 10^{16} \text{ cm}^{-3}$, *3*: $p = 6 \cdot 10^{16} \text{ cm}^{-3}$, *4*: $p = 2 \cdot 10^{17} \text{ cm}^{-3}$ [54M].

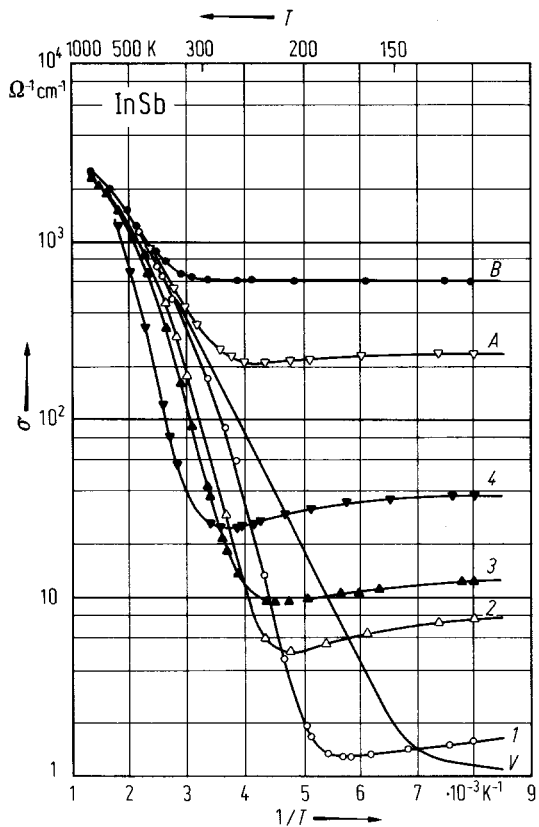


Fig. 2.16.12

InSb. Thermal conductivity vs. temperature of an n-type sample and theoretical curve showing the contribution of the longitudinal and transverse phonons [71K].

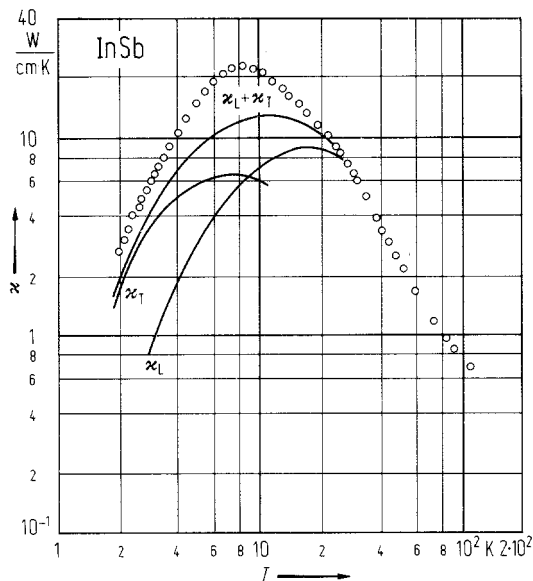


Fig. 2.16.13

InSb. Electron mobility vs. temperature. Experimental data are Hall mobilities. Triangles: [61B], full circles: [55H], open circles: [59V], solid line: calculated drift mobility [71R].

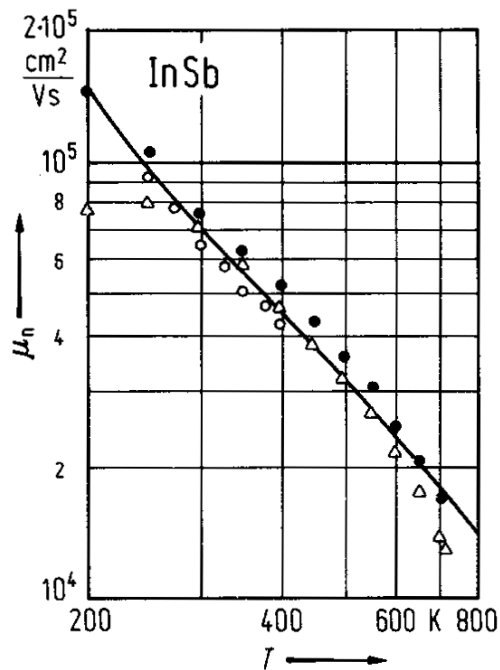


Fig. 2.16.14

InSb. Electron mobility vs. electron concentration (a) at RT, (b) at 77 K. Experimental data taken from various publications, solid line: theoretical [81L].

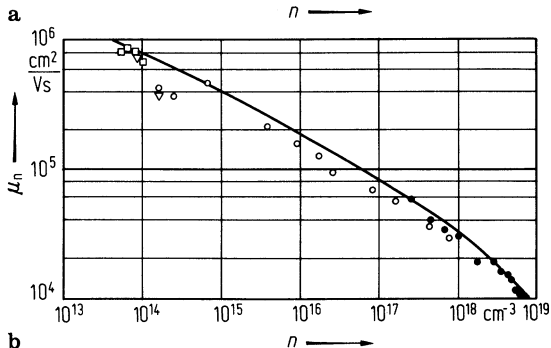
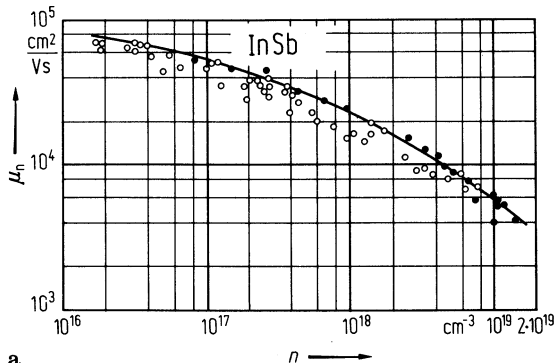


Fig. 2.16.15

InSb. Hole Hall mobility vs. temperature [75W]. The vertical bars indicate the ranges for the experimental values. The solid line has the slope -1.8 .

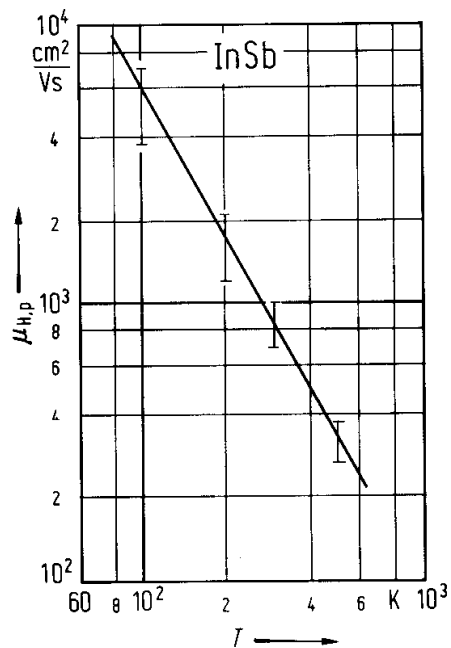


Fig. 2.16.16

InSb. Seebeck coefficient (thermoelectric power) vs. temperature for intrinsic InSb [71R]. Full circles: [61B], open circles: [59B], triangles: [56W], theoretical curve [71R].

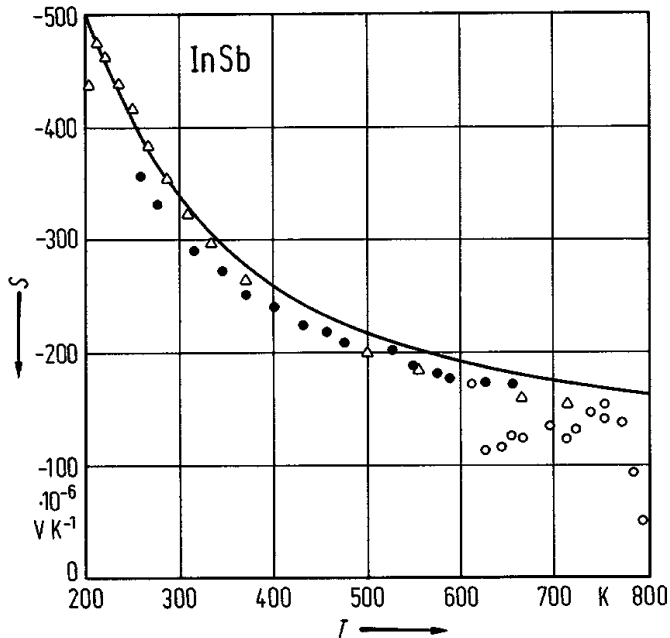


Fig. 2.16.17

InSb. Real and imaginary parts of the dielectric constant vs. photon energy [83A].

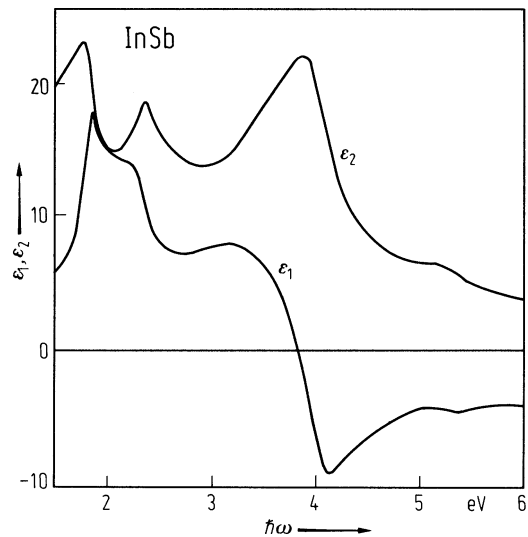


Fig. 2.16.18

InP, InSb. Refractive index vs. temperature [60C].

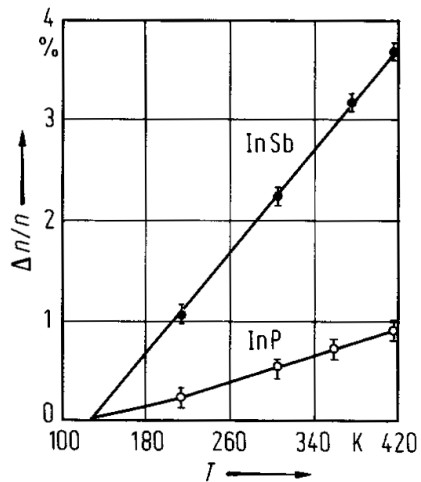
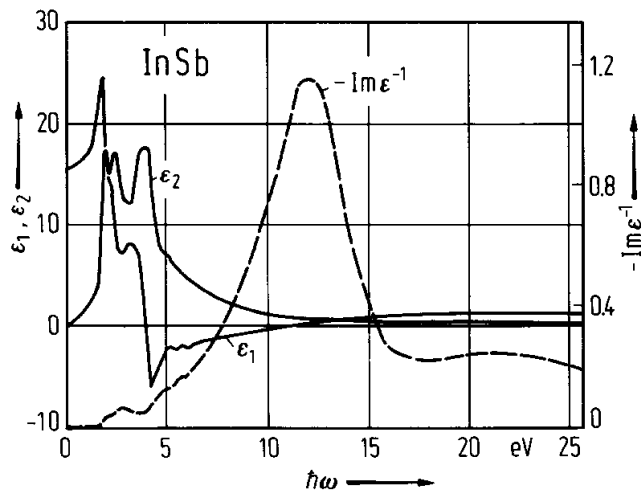


Fig. 2.16.19

InSb. Real part (ϵ_1), imaginary part (ϵ_2) of the dielectric constant and energy loss function (ϵ^{-1}) vs. photon energy from 0 to 25 eV [63P].



2.17 Ternary alloys lattice matched to binary III-V compounds

Solid solutions between III–V compounds have become increasingly important for microelectronic applications, giving the possibility to choose the energy range e.g. for optoelectronic or laser applications more appropriate than with the binary compounds. The more recent progress has mostly been achieved for epitaxial layers on substrates of III–V binary compounds. Fig. 2.17.1 shows the lattice parameter vs. the energy gap of various III–V compounds and their ternary and quaternary alloys. The alloys appropriate for lattice matching on GaSb, InP and GaAs and the energy gaps available with such alloys can easily be found.

There exists a tremendous amount of investigations on solid solutions between III–V compounds. We restrict the information given in the following to alloys lattice matched to III-V compounds.

According to Fig. 2.17.1 these are the ternary alloys:

- 2.17.1 $\text{Al}_{0.49}\text{In}_{0.51}\text{P}$
- 2.17.2 $\text{Al}_{0.48}\text{In}_{0.52}\text{As}$
- 2.17.3 $\text{Ga}_{0.51}\text{In}_{0.49}\text{P}$
- 2.17.4 $\text{Ga}_{0.47}\text{In}_{0.53}\text{As}$
- 2.17.5 $\text{AlAs}_{0.96}\text{P}_{0.04}$
- 2.17.6 $\text{GaAs}_{0.5}\text{Sb}_{0.5}$

For quaternary alloys lattice matched to binary III-V compounds, see the section 2.18.

2.17.1 $\text{Al}_{0.49}\text{In}_{0.51}\text{P}$ (lattice matched to GaAs)

lowest energy gap

$E_g(X_c)$	2.347(2) eV	$T = 12 \text{ K}$	photoluminescence excitation spectra	97I
------------	-------------	--------------------	--------------------------------------	-----

direct energy gap

$E_g(\Gamma)$	2.685 eV	$T = 5 \text{ K}$	photoluminescence	94D
	2.54(1) eV	$T = 300 \text{ K}$	dark-field spectroscopy	96S

spin-orbit splitting

Δ_{so}	0.085 eV	$T = 300 \text{ K}$	dark-field spectroscopy	96S
----------------------	----------	---------------------	-------------------------	-----

2.17.2 $\text{Al}_{0.48}\text{In}_{0.52}\text{As}$ (lattice matched to InP)

For $x = 0.48$ $\text{Al}_x\text{In}_{1-x}\text{As}$ is lattice matched to InP. For possible applications for microwave and optoelectronic devices lattice matched layers on InP substrate have been grown by MBE (see e.g. [81O2, 82C2]), VPE [83F] and LPE [83T]. Most more recent publications concentrate on such layers.

energy gap (linear approximation in the range $x = 0.44 \dots 0.54$, Fig. 2.17.2, in eV):

$E_g(\Gamma)$	$0.357 + 2.29x$	$T = 300 \text{ K}$	position of cathodoluminescence peak, exact lattice match at $x = 0.477$; data not corrected for mismatch strain	84D
	$0.447 + 2.22x$	$T = 4 \text{ K}$		
$E_g(\Gamma)(x=0.48)$	1.439(5) eV	$T = 300 \text{ K}$	photoluminescence	89O
	1.541(2) eV	$T = 0$		

conduction band, effective mass

m_n	$0.10(1) m_0$	$T = 4.2 \text{ K}$	cyclotron resonance	89W
-------	---------------	---------------------	---------------------	-----

deformation potential, valence band

a_v	-0.8 eV	$T = 300 \text{ K}$	high pressure photoluminescence	95Y
-------	-------------------	---------------------	---------------------------------	-----

transport properties

The transport properties of lattice matched layers have been investigated in [81C1,81O1, 82C1, 83M, 84D]. Fig. 2.17.3 shows the dependence of the electron mobility on carrier concentration. Higher RT mobilities have been reported in [83T] ($4600 \text{ cm}^2/\text{Vs}$, $n = 4.7 \cdot 10^{15} \text{ cm}^{-3}$) and [81O1] ($8800 \text{ cm}^2/\text{Vs}$, $n = 1 \cdot 10^{16} \text{ cm}^{-3}$).

electron mobility : see Fig. 2.17.4 for dependence on carrier concentration

electron drift velocity : see Fig. 2.17.5 for dependence on electric field.

2.17.3 $\text{Ga}_{0.51}\text{In}_{0.49}\text{P}$ (lattice matched to GaAs)

energy gap

$E_g(\Gamma_{6c})$	1.970(2) eV	$x = 0.51$, $T = 25 \text{ K}$	photoluminescence	91C
	1.905 eV	$T = 400 \text{ K}$	pressure-dependent photoluminescence	94U
$E_g(\Gamma)$	1.903 eV	$x = 0.56$, RT	photoluminescence	85Z
		VPE-layer		
	$1.295 + 1.151x$	$0.50 < x < 0.53$	photoluminescence	81R
		MBE-layer		78O
	$1.469 + 0.511x$ $+ 0.6043x^2$	$0.49 < x < 0.55$		
	1.902 eV	$x = 0.515$, OMVPE layer	photoluminescence	85K

The compositional variation of the energy gap near the lattice match depends on the strain in the layer.

temperature dependence of energy gap (in eV)

$$E_g(\Gamma) = 2.0536 - E_v - 0.129 \{1/[\exp(515/T) - 1] + 1/2\} - 0.0086 \{1/[\exp(55/T) - 1] + 1/2\} \quad 94I$$

For temperature and pressure dependence of the energy gap, see Figs. 2.17.6 and 2.17.7.

energy difference between conduction bands

$E(L_{6c}) - E(\Gamma_{6c})$	0.10(2) eV	$T = 50 \text{ K}$	high pressure photoluminescence	96P
	0.12 eV	$T = 2 \text{ K}$	photoluminescence	95P
$E(X_{6c}) - E(\Gamma_{6c})$	0.18(4) eV	$T = 50 \text{ K}$	high pressure photoluminescence	96P

higher energy transitions

E_0	1.87(2) eV	$T = 300 \text{ K}$	ellipsometry	95S
E_1	3.21(2) eV			

electron effective mass

m_n	0.092(3) m_0	$T = 6 \text{ K}$	optically detected cyclotron resonance	94E
-------	----------------	-------------------	--	-----

Values for the compositional parameter at lattice match lie in the range 0.51 to 0.56.

electron mobility

$\mu_{H,n}$	$3000 \text{ cm}^2/\text{Vs}$	$T = 300 \text{ K}$	Hall effect	86O
-------------	-------------------------------	---------------------	-------------	-----

For carrier density dependence of the electron mobility, see Fig. 2.17.8; for temperature dependence of electron mobility, see Fig. 2.17.9.

hole mobility

$\mu_{H,p}$	$45 \text{ cm}^2/\text{Vs}$	$T = 300 \text{ K}$	Hall effect	86O
-------------	-----------------------------	---------------------	-------------	-----

electron drift velocity : see Fig. 2.17.10.

electron saturation velocity

v_{sat}	$4.4 \cdot 10^6$ cm/s	$T = 300$ K	analysis of hetero-bipolar transistors	93L
------------------	-----------------------	-------------	--	-----

hole drift velocity : see Fig. 2.17.11.

dielectric constant

$\epsilon(\infty)$	9.43(2)	$T = 300$ K, $x = 0.51$	ellipsometry	95S
--------------------	---------	-------------------------	--------------	-----

refractive index

wavelength dependence for nearly lattice matched material ($x = 0.51$):

$n(\lambda) = 9.236 + 0.795\lambda^2/(\lambda^2 - 0.370)$, λ in nm, range $700\text{nm} < \lambda < 1700$ nm	81R
---	-----

2.17.4 Ga_{0.47}In_{0.53}As (lattice matched material to InP)

As a member of the InP lattice matched quaternary Ga_xIn_{1-x}As_yP_{1-y} alloys, Ga_{0.47}In_{0.53}As has been investigated very intensively.

energy gap

$E_g(\Gamma)$	0.8215(2) eV	$T = 0$	optical absorption	86Z
	0.728(2) eV	$T = 300$ K	photoreflectance	90G

temperature dependence of energy gap

$E_g(\Gamma) = 0.814 - 4.906 \cdot 10^{-4} T^2/(T + 301)$	photoluminescence, T in K	84Y
---	-----------------------------	-----

For temperature dependence of the energy gap, see also Fig. 2.17.13.

compositional dependence of energy gap

Fig. 2.17.12 shows the dependence near $x = 0.47$ for unstrained layers. Strain causes a shrinking of the energy gap by breaking the degeneracy of the light and heavy hole bands at $k = 0$ [85K].

energy difference between Γ and L conduction bands

$E(L_{6c}) - E(\Gamma_{6c})$	0.55 (5) eV	$T = 300$ K	photoemission	82C2
------------------------------	-------------	-------------	---------------	------

higher transition energies

E_0	0.739 eV	$T = 300$ K	transmittance and reflectance	90N
Δ_0	0.345 eV			
E_1	2.552 eV			
$E_1 + \Delta_1$	2.883 eV			

exciton binding energy

E_b	2.5(3) meV	$T = 1.5$ K	optical absorption	86Z
	2.8(6) meV	$T = 300$ K	photoreflectance	90G

effective electron mass

m_n	0.0411(3) m_0	$T = 2$ K	magnetoabsorption	91K
-------	-----------------	-----------	-------------------	-----

For carrier density dependence of effective mass, see Fig. 2.17.14.

valence band, effective mass

m_p	$0.463(5) m_0$	$T = 4.2 \text{ K}$	magnetoluminescence	93Z
$m_{p,h} (100)$	$0.435(35) m_0$	$T = 2 \text{ K}$	magnetoabsorption	91K
$m_{p,l}$	$0.064 m_0$			
$m_{p,h}$	$0.465 m_0$	$\parallel [001]$		80A
	$0.56 m_0$	$\parallel [110]$		
	$0.60 m_0$	$\parallel [111]$		
$m_{p,l}$	$0.0503 m_0$			

electron g-factor

g_c	-4.50			80A
-------	---------	--	--	-----

phonon wavenumbers

$\bar{\nu}$	226 cm^{-1}	TO	Raman active modes	83P
	270.5 cm^{-1}	LO		
	235 cm^{-1}	LO, GaAs-type	magnetophononresonance	85S
	271 cm^{-1}	LO, GaAs-type		
	258 cm^{-1}	LO	replica of exciton line	83G
	274 cm^{-1}	LO	hot electron spectra	80S

hole drift velocity

$v_{dr,p}$	$4.8(2) \cdot 10^6 \text{ cm s}^{-1}$	$T = 300 \text{ K}$	photodiode frequency response	87H
------------	---------------------------------------	---------------------	-------------------------------	-----

ambipolar diffusion constant

D_a	$4.0(8) \text{ cm}^2 \text{ s}^{-1}$	$T = 300 \text{ K}$	light-induced grating	93J
-------	--------------------------------------	---------------------	-----------------------	-----

radiative recombination coefficient

B	$0.96 \cdot 10^{-10} \text{ cm}^3 \text{ s}^{-1}$	$T = 300 \text{ K}$	analysis of optical absorption data	86Z
-----	---	---------------------	-------------------------------------	-----

Auger recombination coefficient

C	$3.0 \cdot 10^{-28} \text{ cm}^6 \text{ s}^{-1}$	$T = 300 \text{ K}$	time-resolved luminescence	90H
-----	--	---------------------	----------------------------	-----

electron mobilities

See Figs. 2.17.15 and 2.17.16 for dependence on temperature and carrier concentrations. Further typical values from papers on characterization of layers:

μ_n	$13800 \text{ cm}^2/\text{Vs}$	$T = 300 \text{ K}$	$n = 2 \cdot 10^{15} \text{ cm}^{-3}$, LPE-layer	81O3
	$70000 \text{ cm}^2/\text{Vs}$	$T = 77 \text{ K}$		
	$11200 \text{ cm}^2/\text{Vs}$	$T = 300 \text{ K}$	$n \approx 10^{15} \text{ cm}^{-3}$, MOCVD-layer	85C1
	$64000 \text{ cm}^2/\text{Vs}$	$T = 77 \text{ K}$		
	$80000 \text{ cm}^2/\text{Vs}$	$T = 4.2 \text{ K}$	the high 4.2 K-value seems to be connected with a 2-dimensional electron gas in the layer	

By doping with Fe semiinsulating $\text{Ga}_{0.47}\text{In}_{0.53}\text{As}$ can be produced. Typical data: $\rho = 650 \text{ } \Omega \text{ cm}$, $\mu_n = 6890 \text{ cm}^2/\text{Vs}$ [85C2], $\rho = 2420 \text{ } \Omega \text{ cm}$, $\mu_n = 7070 \text{ cm}^2/\text{Vs}$ [85B].

2.17.5 AlAs_{0.96}P_{0.04}

The only interest in this system has been an improvement of the lattice match of AlAs on GaAs by adding a small amount of phosphorus. AlAs_{0.96}P_{0.04} layers made by MOCVD lattice-match exactly on GaAs at RT (see Fig. 2.17.17).

2.17.6 GaAs_{0.5}Sb_{0.5}

Both components are direct gap semiconductors. The system has a miscibility gap with a peritectic temperature of 751°C limiting the range of composition which can be obtained by near equilibrium growth techniques at ordinary temperatures. Good quality InP-matched layers ($x = 0.5$) have been obtained by OMVPE [84C] (see also e.g. [83S]). For InAs-matched layers. see [81D].

References to 2.17

- 78O Olsen, G. H., Nuese, C. J., Smith, R. T.: J. Appl. Phys. 49 (1978) 5523.
- 80A Alavi, K., Aggarwal, R. L., Groves, S. H.: Phys. Rev. B 21 (1980) 1311.
- 80C Chandrasekhar, H. R., Ramdas, A. K.: Phys. Rev. B. 21 (1980) 1511.
- 80S Shah, A. J., Leheny, R. F., Nahory, R. E., Pollak, M. A.: Appl. Phys. Lett. 37 (1980) 475.
- 81C1 Chen, A., Sher, A.: Phys. Rev. 13 23 (1981) 5360.
- 81C2 Cheng, K. Y., Cho, A. Y., Wagner, W. R.: J. Appl. Phys. 52 (1981) 6328.
- 81D Dvoryankin, V. F., Kokovibhin, S. V., Telegin, A. A., Ormont, A. B.: Inorg. Mater. (USSR) 17 (1981) 538.
- 81O1 Ohno, H., Wood, C. E. C., Rathburn, L., Morgan, D. V., Wicks, G. W., Eastman, L. F.: J. Appl. Phys. 52 (1981) 4033.
- 81O2 Oliver, J. D.: J. Cryst. Growth 54 (1981) 64.
- 81O3 Oliver, J. D.: J. Cryst. Growth 54 (1981) 64.
- 81P Pearsall, T. P., Hirtz, J. P.: J. Cryst. Growth 54 (1981) 127.
- 81R Roberts, J. S., Scott, G. H., Gowers, J. P.: J. Appl. Phys. 52 (1981) 4018.
- 82C1 Cheng, K. Y., Cho, A. Y.: J. Appl. Phys. 53 (1982) 4411.
- 82C2 Cheng, K. Y., Cho, A. Y., Christman, S. B., Pearsall, T. P., Rowe, J. E.: Appl. Phys. Lett. 40 (1982) 423.
- 83F di Forte-Poisson, M. A., Razheghi, M., Duchemin, J. P.: J. Appl. Phys. 54 (1983) 7187.
- 83G Goetz, K.-H., Bimberg, D., Jurgensen, H., Selders, J., Solomonov, A. V., Glinskii, G. F., Razhegi, M.: J. Appl. Phys. 54 (1983) 4543.
- 83M Massies, J., Rochette, J. F., Etienne, P., Delesciuse, P., Huber, A. M., Chevrier, J.: J. Cryst. Growth 64 (1983) 101.
- 83P Pearsall, T. P., Caries, R., Portal, J. C.: Appl. Phys. Lett. 42 (1983) 436.
- 83S Stringfellow, G. H., Cherng, M. J.: J. Cryst. Growth 64 (1983) 413.
- 83T Tanahashi, T., Nakajima, K., Yarnaguchi, A., Umebu, I.: Appl. Phys. Lett. 43 (1983) 1030.
- 84C Cherng, M. J., Stringfellow, G. H., Cohen, R. M.: Appl. Phys. Lett. 44 (1984) 677.
- 84D Davies, G. J., Kerr, T., Tuppen, C. G., Wakefield, B., Andrews, D. A.: J. Vac. Sci. Technol. 132 (1984) 219.
- 84K Kobayashi, N., Fukui, T.: J. Cryst. Growth 67 (1984) 513.
- 84Y Yu, P. W., Kuphal, E.: Solid State Commun. 49 (1984) 907.
- 85B Bhattacharya, A., Chattopadhyay, D., Ghosal, A.: Phys. Rev. B 31 (1985) 2524.
- 85C1 Chan, K. T., Zhu, L. D., Ballantyne, J. M.: Appl. Phys. Lett. 47 (1985) 44.
- 85C2 Carey, K. W.: Appl. Phys. Lett. 46 (1985) 89.
- 85K Kuo, C. P., Vong, S. K., Cohen, R. M., Stringfellow, G. H.: J. Appl. Phys. 57 (1985) 5428.
- 85S Sarkar, C. K., Nicholas, R. J., Portal, J. C., Razhegi, M., Chevrier, J., Massies, J.: J. Phys. C 18 (1985) 2667.
- 85Z Zarrahi, H. J., Alfano, R. R.: Phys. Rev. B 32 (1985) 3947.
- 86O Ohba, Y., Ishikawa, M., Sugawara, H., Yamamoto, M., Nakanisi, T.: J. Cryst. Growth 77 (1986) 374.
- 86Z Zielinski, E., Schweizer, H., Streubel, K., Eisele, H., Weimann, G.: J. Appl. Phys. 59 (1986) 2196.
- 87H Hill, P., Schlafer, J., Powazinik, W., Urban, M., Eichen, E., Olshansky, R.: Appl. Phys. Lett. 50 (1987) 1260.
- 88A Aina, L., Mattingly, M.: J. Appl. Phys. 64 (1988) 5253.
- 89O Oertel, D., Bimberg, D., Bauer, R. K., Carey, K. W.: Appl. Phys. Lett. 55 (1989) 140.
- 89P Patel, D., Chen, J., Kurtz, S. R., Olson, J. M., Quigley, J. H., Hafich, M. J., Robinson, G. Y.: Phys. Rev. B 39 (1989) 10978.
- 89W Wright, M. G., Kana'ah, A., Cavenett, B. C., Johnson, G. R., Davey, S. T.: Semicond. Sci. Technol. 4 (1989) 590.
- 90G Gaskill, D. K., Bottka, N., Aina, L., Mattingly, M.: Appl. Phys. Lett. 56 (1990) 1269.
- 90H Haußer, S., Fuchs, G., Hangleiter, A., Streubel, K., Tsang, W.: Appl. Phys. Lett. 56 (1990) 913.
- 90N Nee, T. W., Green, A. K.: J. Appl. Phys. 68 (1990) 5314.
- 91C Chen, J., Sites, J. R., Spain, I. L., Hafich, M. J., Robinson, G. Y.: Appl. Phys. Lett. 58 (1991) 744.
- 91K Kokhanovskii, S. I., Makushenko, Y. M., Seisyan, R. P., Efros, A. L., Yazeva, T. V., Abdullaev, M. A.: Sov. Phys. Semicond. 25 (1991) 298.
- 91S Syrbu, N. N., Snigur, A. P., Chumak, V. A., Khachaturova, S. B.: Sov. Phys. Semicond. 25 (1991) 693.
- 92B Brennan, K. F., Chiang, P.-K.: J. Appl. Phys. 71 (1992) 1055.
- 92K Kim, H. S., Tian, H., Kim, K. W., Littlejohn, M. A.: Appl. Phys. Lett. 61 (1992) 1202.
- 93J Juodkakis, S., Petrauskas, M., Quacha, A., Willander, M.: Phys. Status Solidi (a) 140 (1993) 439.
- 93L Liu, W., Henderson, T., E., I. B., Fan, S. K.: Electron. Lett. 29 (1993) 1885.
- 93Z Zhao, Q. X., Holtz, P. O., Monemar, B., Lundstrom, T., Wallin, J., Landgren, G.: Phys. Rev. B 48 (1993) 11890.

- 94D Dawson, M. D., Najda, S. P., Kean, A. H., Duggan, G., Mowbray, D. J., Kowalski, O. P., Skolnick, M. S., Hopkinson, M.: Phys. Rev. B 50 (1994) 11190.
- 94E Emanuelsson, P., Drechsler, M., Hofmann, D. M., Meyer, B. K., Moser, M., Scholz, F.: Appl. Phys. Lett. 64 (1994) 2849.
- 94I Ishitani, Y., Minagawa, S., Tanaka, T.: J. Appl. Phys. 75 (1994) 5326.
- 94U Uchida, K., Yu, P. Y., Noto, N., Weber, E. R.: Appl. Phys. Lett. 64 (1994) 2858.
- 94Z Zhang, B., Lan, S., Li, L.-Q., Xu, W.-J., Yang, C.-Q., Liu, H.-D.: Solid State Commun. 92 (1994) 419.
- 95S Schubert, M., Gottschalch, V., Herzinger, C. M., Yao, H., Snyder, P. G., Woollam, J. A.: J. Appl. Phys. 77 (1995) 3416.
- 95Y Yeh, C. N., McNeil, L. E., Nahory, R. E., Bhat, R.: Phys. Rev. B 52 (1995) 14682.
- 96P Patel, D., Interholzinger, K., Thiagarajan, P., Robinson, G. Y., Menoni, C. S.: Phys. Status Solidi (b) 198 (1996) 337.
- 96S Schubert, M., Rheinländer, B., Franke, E., Pietzonka, I., Skrinarova, J., Gottschalch, V.: Phys. Rev. B 54 (1996) 17616.
- 97I Ishitani, Y., Nomoto, E., Tanaka, T., Minagawa, S.: J. Appl. Phys. 81 (1997) 1763.

Figures to 2.17

Fig. 2.17.1

Lattice parameter vs. energy gap (RT values) for various III–V compounds and their alloys.

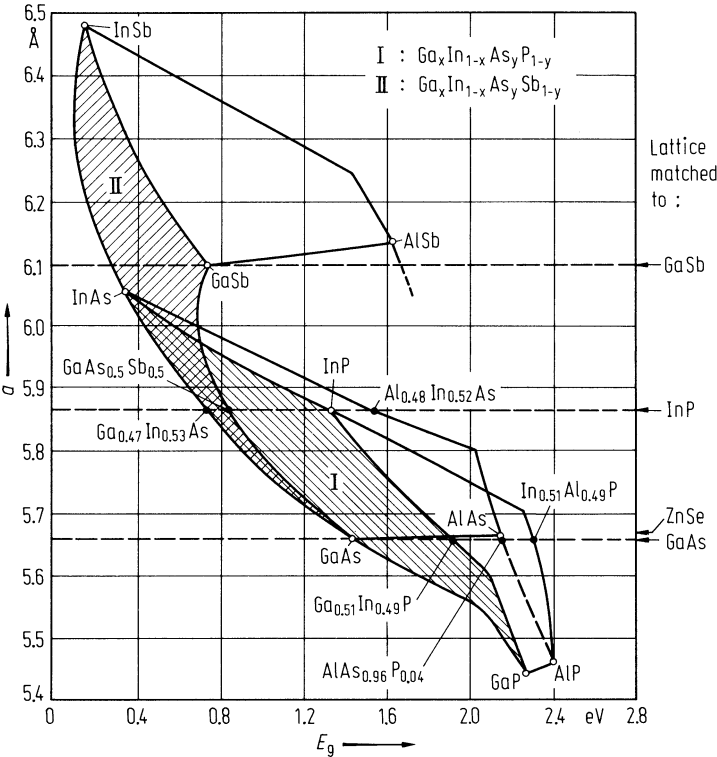


Fig. 2.17.2

$\text{Al}_x\text{In}_{1-x}\text{As}$. Energy gap (peaks in the cathodoluminescence spectrum) vs. composition in the range $x = 0.44\ldots 0.54$ (open circles: 4 K, full circles: 300 K). Solid lines: linear approximation, dashed line: relation expected at RT in the absence of mismatch strain [84D].

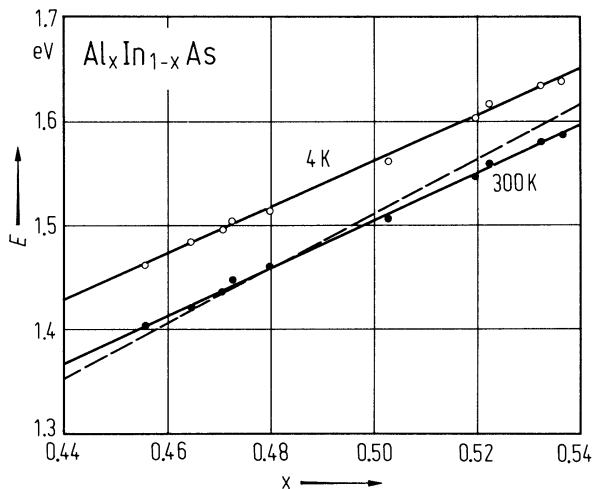


Fig. 2.17.3

$\text{Al}_x\text{In}_{1-x}\text{As}$, $x = 0.48$. Electron Hall mobility vs. carrier concentration at RT. Full circles from [84D], open circles from [81C2]. Solid line: interpolated.

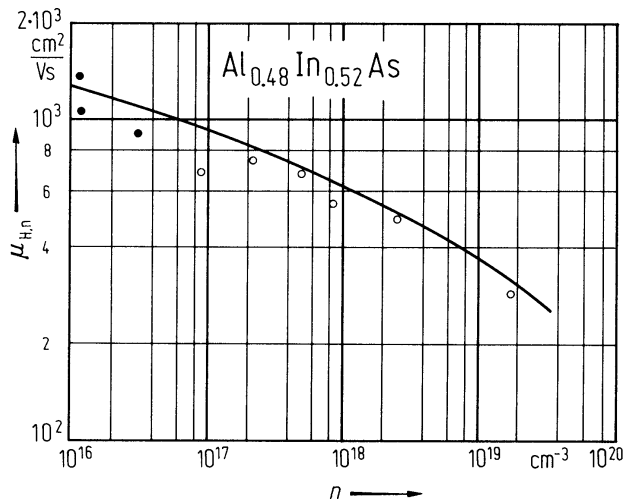


Fig. 2.17.4

$\text{Al}_{0.48}\text{In}_{0.52}\text{As}$. Electron mobility vs. electron concentration at $T = 300$ K (experimental data: diamonds). The lines are theoretical calculations using an alloy scattering potential of 1.44 eV (full line) and of 0.42 eV (dotted line) [88A].

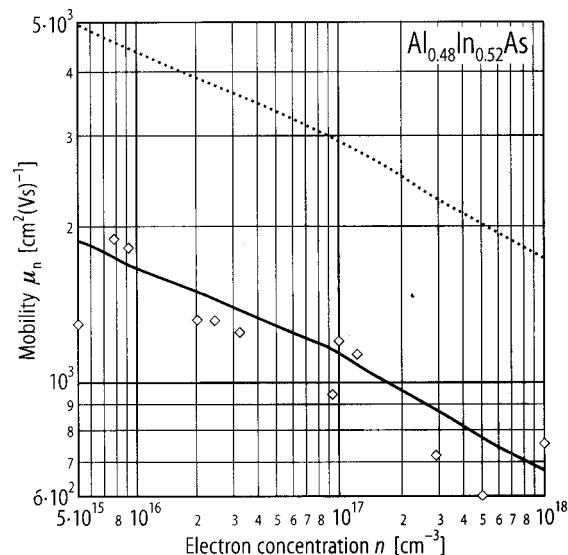


Fig. 2.17.5

$\text{Al}_{0.48}\text{In}_{0.52}\text{As}$. Electron drift velocity as a function of electric field for uncompensated n-type material at 300 K with doping concentrations ranging from $1 \cdot 10^{16}$ to $1 \cdot 10^{18} \text{ cm}^{-3}$ [92K]. The data with $S = 0$ do not include alloy scattering.

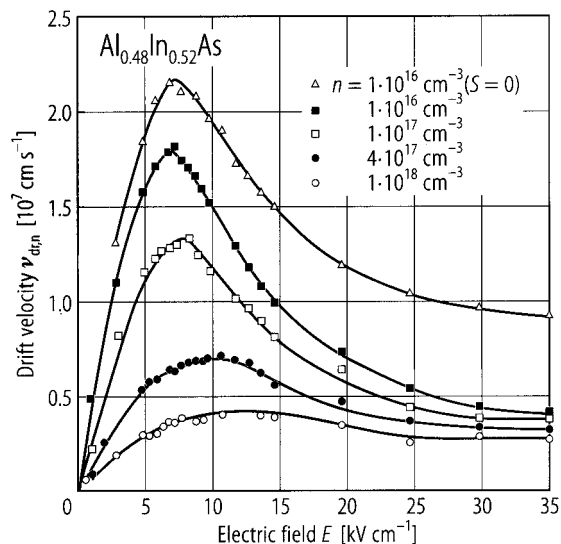


Fig. 2.17.6

$\text{Ga}_{0.5}\text{In}_{0.5}\text{P}$. Temperature dependence of the band-gap energy. The full line represents a fit including thermal expansion and both optical phonon and acoustic phonon contributions [94I]. The dashed line gives the dependence due to volume change only.

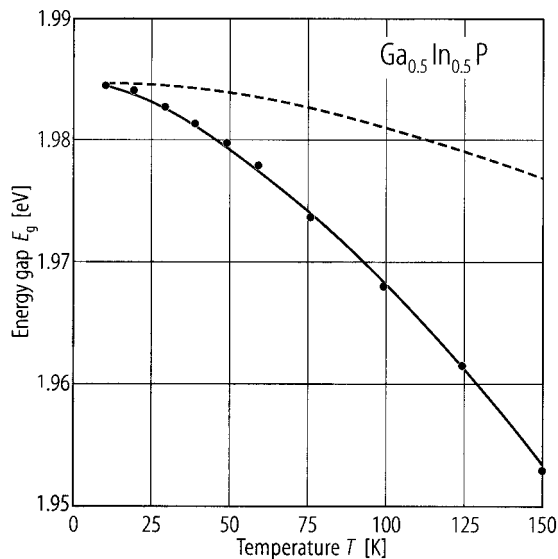


Fig. 2.17.7

$\text{Ga}_{0.49}\text{In}_{0.51}\text{P}$ (a) and $\text{Ga}_{0.52}\text{In}_{0.48}\text{P}$ (b). Pressure dependence of the energy gap at room temperature [89P]. The open symbols are for decreasing pressure measurements, the full line represents a second-order least-squares fit.

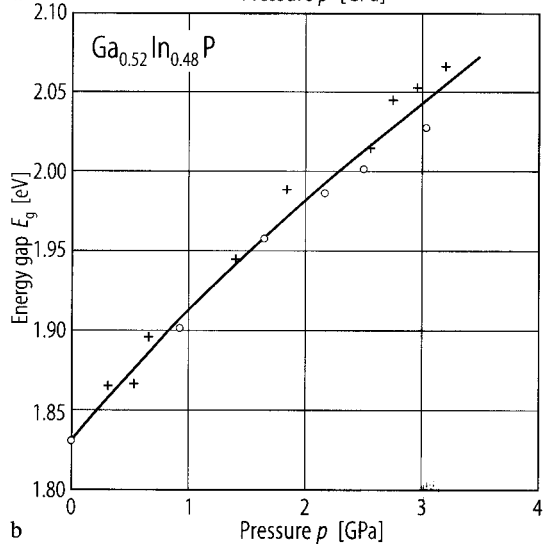
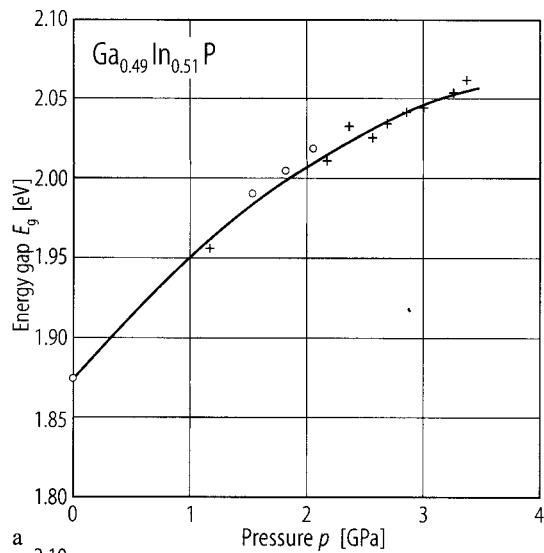


Fig. 2.17.8

$\text{Ga}_{0.52}\text{In}_{0.48}\text{P}$. Room temperature electron and hole mobilities versus carrier concentration [86O].

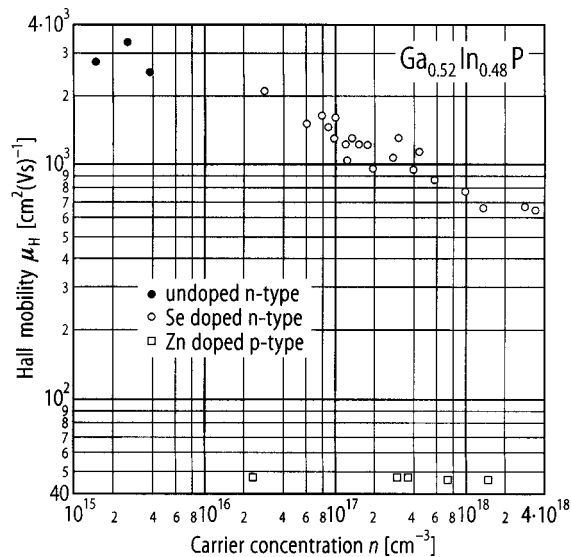


Fig. 2.17.9

$\text{Ga}_{0.52}\text{In}_{0.48}\text{P}$. Temperature dependence of the electron mobility. At low temperature, electron transport is dominated by ionized impurity scattering (μ_i), whereas at high temperature alloy scattering (μ_a) and polar optical phonon scattering (μ_l) become most important [94Z].

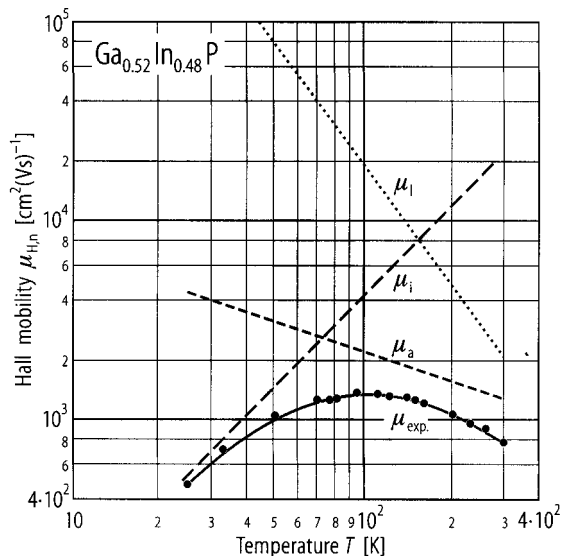


Fig. 2.17.10

$\text{Ga}_{0.52}\text{In}_{0.48}\text{P}$ and $\text{Al}_{0.26}\text{Ga}_{0.26}\text{In}_{0.48}\text{P}$. Calculated steady-state electron drift velocity at 300 K in bulk material as a function of applied electric field [92B].

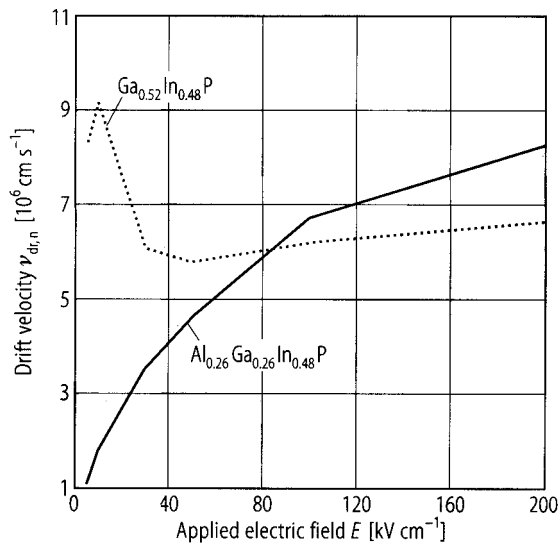


Fig. 2.17.11

$\text{Ga}_{0.52}\text{In}_{0.48}\text{P}$ and $\text{Al}_{0.26}\text{Ga}_{0.26}\text{In}_{0.48}\text{P}$. Calculated steady-state hole drift velocity at 300 K in bulk material as a function of applied electric field [92B].

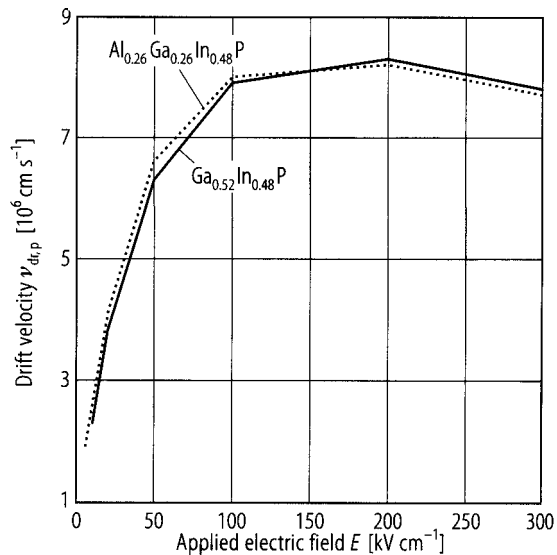


Fig. 2.17.12

$\text{Ga}_x\text{In}_{1-x}\text{As}$. Energy gap vs. composition at 2 K near the lattice match on InP. Full circles: LPE layers, open circles: VPE layers. Solid line: $E_g = 0.4105 + 0.6337x + 0.475x^2$ [83G].

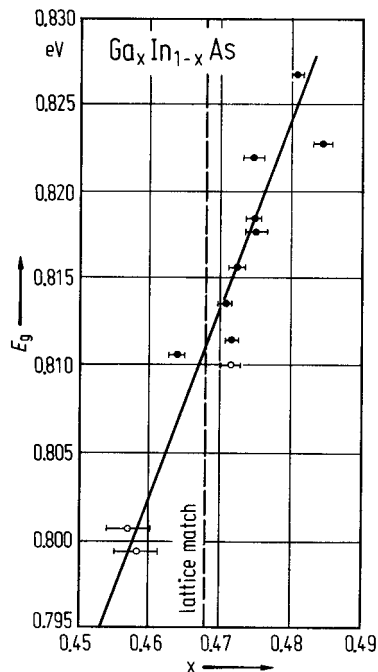


Fig. 2.17.13

$\text{Ga}_{0.47}\text{In}_{0.53}\text{As}$. Temperature dependence of the energy gap as determined from optical absorption (circles) [86Z]. The curved solid line represents a fit based on a model considering both phonon-phonon and electron-phonon interactions, the dashed and dotted lines include corrections due to the biaxial stress arising from different thermal expansion coefficients of the substrate and the epitaxial layer.

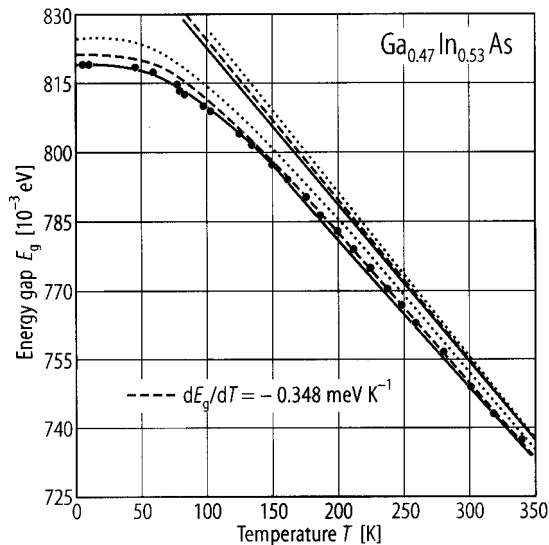


Fig. 2.17.14

$\text{Ga}_{0.47}\text{In}_{0.53}\text{As}$. Conduction band effective mass in dependence on carrier concentration (+) determined from cyclotron resonance [91S]. For comparison, the values for GaAs (circles) from [80C] are also shown.

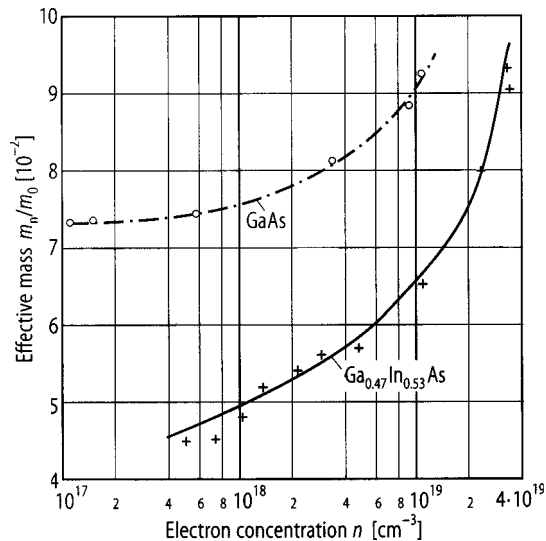


Fig. 2.17.15

$\text{Ga}_x\text{In}_{1-x}\text{As}$, $x = 0.47$. Electron Hall mobility vs. temperature and decomposition into contributions of three scattering mechanisms [81O].

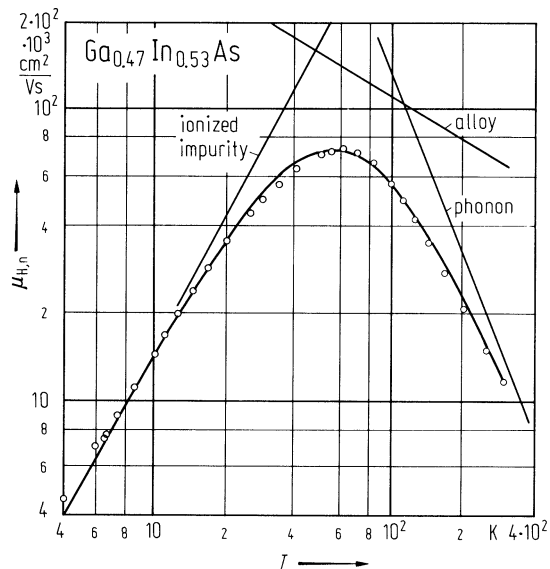


Fig. 2.17.16

$\text{Ga}_x\text{In}_{1-x}\text{As}$, $x = 0.47$. Hall mobilities of n- and p-type films at 300 K (a) and 77 K (b) vs. total impurity concentration $n_{\text{imp}} = n_{\text{d}} + n_{\text{a}}$. Calculated electron mobilities with (solid lines) and without (dashed lines) alloy scattering are also shown [81P].

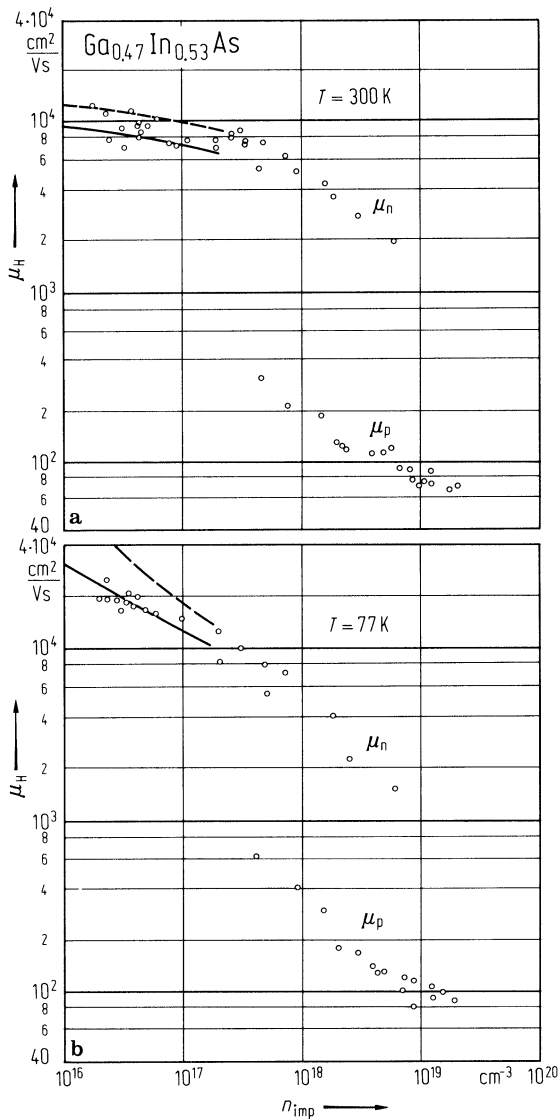
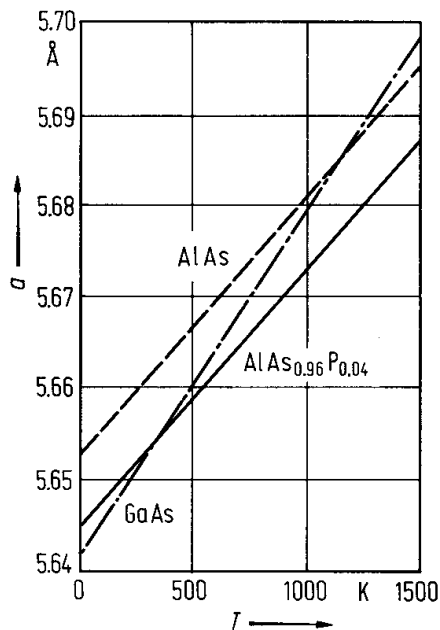


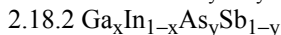
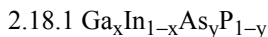
Fig. 2.17.17

$\text{AlAs}_{1-x}\text{P}_x$. Lattice parameters of AlAs, GaAs and $\text{AlAs}_{0.96}\text{P}_{0.04}$ vs. temperature [84K].



2.18 Quaternary alloys lattice matched to binary III-V and II-VI compounds

According to Fig. 2.17.1 (shaded areas I and II) two *quaternary systems of the type* $III_xIII_{1-x}V_yV_{1-y}$ can be lattice matched to binary III-V compounds:



The condition for lattice matching can easily be derived from the interpolation scheme for the determination of a material parameter $P(x,y)$ for an alloy $A_xB_{1-x}C_yD_{1-y}$ from the same parameters of the four constituents:

$$P(x,y) = (1-x)yP(BC) + (1-x)(1-y)P(BD) + xyP(AC) + x(1-y)P(AD).$$

For lattice matching on substrate BD ($x = y = 0$) the condition $a(x,y) = a(BD)$ leads to

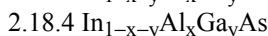
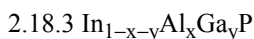
$$x = [a(BC) - a(BD)]y / ([a(BD) - a(AD)] - [a(BC) + a(AD) - a(BD) - a(AC)]y)$$

or, in a linear approximation to this formula exact at $y = 0$ and $y = 1$:

$$x/y = [a(BC) - a(BD)] / (a(BC) - a(AC)).$$

The main interest in quaternary III-V alloys stems from the possible applications in micro- and optoelectronic devices. Thus most of the data on quaternary alloys of the type $III_xIII_{1-x}V_yV_{1-y}$ refer to quaternary alloys lattice matched to GaSb, InP and GaAs (see Fig. 2.17.1).

Furtheron two *quaternary systems of the type* $III_{1-x-y}III_xIII_yV$ can be lattice matched to binary III-V compounds:



2.18.1 $Ga_xIn_{1-x}As_yP_{1-y}$

The quaternary alloy GaInAsP is commonly used for optoelectronic devices like semiconductor lasers and photodiodes for the 1.3 μm and 1.55 μm windows of optical fibers. For such applications, the substrate material of choice is InP, i.e. the relevant compositions of GaInAsP are those lattice matched to InP.

As shown in Fig. 2.17.1 alloys of this system can be lattice matched on InP (E_g range: 73...1.35 eV), GaAs (E_g range: 1.42...1.90 eV) and ZnSe (slightly lower range). The matching conditions according to the formula above are ($0 \leq y \leq 1$):

x	$0.1894y / (0.4184 - 0.013y) \approx 0.47y$	on InP substrate
	$(1.00 + y) / 2.08$	on GaAs substrate
	$(1.06 + y) / 2.06$	on ZnSe substrate.

Most data have been obtained for InP lattice matched samples. All data in the following tables and figures refer – if not stated otherwise – to InP lattice matched material.

direct energy gap (in eV)

$E_{g,dir}(y)$	$1.35 - 0.775y + 0.149y^2$	$T = 298 \text{ K}$	calculated, fitting photo-luminescence and electroluminescence measurements, Fig. 2.18.1a	82P
	$1.425 - 0.7668y + 0.149y^2$	$T = 4.2 \text{ K}$	calculated, fitting absorption and transmission measurements, Fig. 2.18.1b	

The compositional variation of $E_{g,dir}$ for GaAs and ZnSe lattice matched material is shown in Fig. 2.18.2.

bowing parameters for band gaps at L and X (in eV)

$c(\Gamma-L)$	0.10(5)	L-conduction band	84K
$c(\Gamma-X)$	0.21(7)	X-conduction band	
		from synchrotron radiation reflection spectroscopy	

higher interband transition energies (in eV)

$E_1(y)$	$3.136 - 0.788y + 0.222y^2$	RT		80P
$E_2(y)$	$5.04 - 0.309y + 0.149y^2$			
$E'_0(y)$	$4.72(1) - 0.31(2)y - 0.01(5)y^2$	RT	ellipsometry	82K

spin-orbit splitting energies (in eV)

$\Delta_0(y)$	$0.119 + 0.300y - 0.107y^2$	RT	electroreflectance,	80P
$\Delta_1(y)$	$0.145 + 0.173y - 0.064y^2$			

electron effective mass (in units of m_0)

$m_n(y)$	$0.077 - 0.050y + 0.014y^2$	RT	Shubnikov - de Haas effect see also Fig. 2.18.3	80P
----------	-----------------------------	----	--	-----

electron g-factor

g_c	$1.35 - 2.47y - 2.26y^2$	RT	electroreflectance	80P
-------	--------------------------	----	--------------------	-----

lattice properties

The system of InP lattice matched alloys shows a miscibility gap.

lattice parameter (in Å)

$a(x,y)$	$5.8688 - 0.4176x + 0.1896y + 0.0125xy$		linear interpolation from lattice parameters of four constituents	82A1
----------	---	--	--	------

thermal expansion : Fig. 2.18.4.**density (in g cm⁻³):**

d	$5.477 - 0.712y$			82A1
-----	------------------	--	--	------

phonon wavenumbers

for InP lattice matched material: Fig. 2.18.5, for GaAs lattice matched material: Fig. 2.18.6 [84I]. See also [86S] for Raman scattering data.

transport properties

Mobility data have been reported in many papers on the characterization of epitaxial layers. We only show two typical diagrams: Fig.2.18.7 for the electron mobility and Fig. 2.18.8 for the hole mobility.

dielectric constant

$\varepsilon = 1 + A_1/[1 - (E/(E_p + E_1)^2)] + A_2/[1 - (E/(E_p + E_2)^2)]$		E_p : photoluminescence peak energy	
A_1	$13.3510 - 5.4554 E_p + 1.2332 E_p^2$	$T = 300$ K; E_p is the energy of the	85H
A_2	$0.7140 - 0.3606 E_p$	luminescence peak under low excitation	
E_1	2.5048 eV	conditions, which depends on composition	
E_2	0.1638 eV		
$\varepsilon(0)$	$12.40 + 1.5y$		82A2
$\varepsilon(\infty)$	$9.55 + 2.2y$		

2.18.2 Ga_xIn_{1-x}As_ySb_{1-y}

This system is shown as shaded area (II) in Fig. 2.17.1. It is the only system applicable for the growth of low band gap epitaxial layers on GaSb substrate. In spite of interesting applications for optical sources and detectors in the 2...4 μm range only few reliable data on intrinsic properties have been published.

MBE layers ($x = 0.75$, $y = 0.21$) with an energy gap of about 0.69 eV have been investigated in [85T]. Various other compositions have been studied in [86C]. LPE growth is possible but meets difficulties by the existence of a miscibility gap (see [85T] and literature cited therein).

2.18.3 In_{1-x-y}Al_xGa_yP

AlGaInP is an important material for optoelectronic devices in the visible spectral range, i.e. from 630 to 700 nm wavelength. Whereas the longer-wavelength Ga_{0.51}In_{0.49}P is a direct-gap material, the short-wavelength limiting compound Al_{0.51}In_{0.49}P exhibits an indirect gap (X minimum).

(Al_zGa_{1-z})_{0.49}In_{0.51}P (lattice-matched on GaAs)

The boundary alloys of the GaAs lattice matched series are In_{0.49}Ga_{0.51}P and In_{0.49}Al_{0.51}P (see Fig. 2.17.1). Introducing the compositional parameter z by $x = 0.51z$ and the lattice matching condition $x + y = 0.51$ the series can be written as In_{0.49}(Al_zGa_{1-z})_{0.51}P.

The system exhibits a crossover between direct gap (Γ) and indirect gap (X minimum) at $z = 0.52(2)$ [96N].

direct energy gap

(in eV)

$E_{g,dir}(z)$	$1.962 + 0.629z$	$T = 4 \text{ K}$	photoluminescence	96N
	$1.958 + 0.673z$	$T = 76 \text{ K}$	$z \leq 0.52$	
	$1.861 + 0.706z$	$T = 300 \text{ K}$		
$E_{\Gamma}(z)$	$1.985 + 0.610z$	$T = 2 \text{ K}$	high-pressure photoluminescence	95M
$E_{\Gamma}(z)$	$1.900 + 0.610z$	$T = 300 \text{ K}$	see also Fig. 2.18.9	
$dE_{g,dir}/dp$	$9.1(3) \text{ meV/kbar}$	$T = 76 \text{ K};$ $z = 0.2...0.5$	photoluminescence	96N

energies of conduction band minima (in eV, with respect to the valence band)

$E_X(z)$	$2.26 + 0.085z$	$T = 2 \text{ K}$	high-pressure photoluminescence	95P2
	$2.282 + 0.085z$	$T = 2 \text{ K}$	high-pressure photoluminescence	95M
	$2.204 + 0.085z$	$T = 300 \text{ K}$		
	$2.20 + 0.16z$	$T = 300 \text{ K}$	ellipsometry, thermorefectance	96O
$E_L(z)$	$2.25 + 0.47z$	$T = 300 \text{ K}$	ellipsometry, thermorefectance	96O

higher energy transitions (in eV)

$E_0 + \Delta_0$	$1.97 + 0.65z + 0.07z^2$	$T = 300 \text{ K},$	electroreflectance	96A
E_1	$3.22 + 0.48z + 0.06z^2$			
$E_1 + \Delta_1$	$3.430 + 0.106z + 0.257z^2$			
E_2	$4.77 + 0.02z$			
$E_2 + \delta$	$5.07 + 0.03z$			

electron effective mass

m_n	$0.14(1) m_0$	$T = 6 \text{ K}$	cyclotron resonance, $z = 0.15$	94E
-------	---------------	-------------------	---------------------------------	-----

electron and hole mobility : see Fig. 2.18.10.

refractive index

n	3.00 3.50	$\hbar\omega = 1 \text{ eV}$ 2 eV	optical transmission, $z = 0.66$	94M
$n^2(E) - 1 = G_{\text{TO}}/(E_{\text{TO}}^2 - E^2) + (A/\pi)\ln[(E_1^2 - E^2)/(E_g^2 - E^2)] + G_1/(E_1^2 - E^2) + G_2/(E_2^2 - E^2)$				
A	$0.72 + 0.35z$	$T = 300 \text{ K}$	ellipsometry	94M
G_{TO}	$4.4 \cdot 10^{-3} \text{ eV}^2$			
G_1	34.7 eV^2			
G_2	140 eV^2			
E_{TO}	40 meV			
E_1	$(3.35 + 0.38z) \text{ eV}$			
E_2	$(5.20 + 0.35z) \text{ eV}$			
E_g	$(1.90 + 0.48z) \text{ eV}$			

2.18.4 $\text{In}_{1-x-y}\text{Al}_x\text{Ga}_y\text{As}$

The boundary alloys of the InP lattice matched series are $\text{In}_{0.53}\text{Ga}_{0.47}\text{As}$ and $\text{In}_{0.52}\text{Al}_{0.48}\text{As}$ (see Fig. 2.17.1). Introducing the compositional parameter z by $x = 0.48z$ and the lattice matching condition $0.98x + y = 0.47$ the series can be written as $(\text{In}_{0.52}\text{Al}_{0.48})_z(\text{In}_{0.53}\text{Ga}_{0.47})_{1-z}\text{As}$.

An often used approximation is $\text{In}_{0.53}(\text{Al}_z\text{Ga}_{1-z})_{0.47}\text{As}$ with $x = 0.47z$, $x + y = 0.47$.

Like GaInAsP, AlGaInAs is frequently used for optoelectronic devices related to optical fiber communications based on InP substrates. Thus, the lattice-matched compound on InP is most important in practice.

energy gap (in eV):

$E_g(x,y)$	$0.36 + 2.093x + 0.629y + 0.577x^2 + 0.436y^2 + 1.013xy - 2.0xy(1-x-y)$	82O
------------	---	-----

For the lattice matching condition (given in [82O] more exactly as $0.983x + y = 0.468$) using $z = x/0.48$ the experimental data obtained from photoluminescence at RT give:

$E_g(z)$	$0.76(4) + 0.49(5)z + 0.20(3)z^2$	see Fig. 2.18.11	82O
----------	-----------------------------------	------------------	-----

higher band-band transitions (in eV):

coefficients in the formula $E = a + bz + cz^2$ obtained from electroreflectance at RT [83P]

	a [eV]	b [eV]	c [eV]
E_0	0.73 (3)	0.54(4)	0.28 (4)
$E_0 + \Delta_0$	1.10(3)	0.64(4)	0.18(4)
E_1	2.55(3)	0.36(4)	0.11(4)
$E_1 + \Delta_1$	2.83(3)	0.39(4)	0.08(4)
$E'_0 + \Delta'_0$ (?)	4.74(4)	0.25(5)	-0.13(5)
Δ_0	0.37(2)	0.10(2)	-0.10(3)
Δ_1	0.28(2)	0.03(2)	-0.03(3)

electron effective mass (in units of m_0):

m_n	$0.0427(15) + 0.0328(7)z$	see Fig. 2.18.12	82O
-------	---------------------------	------------------	-----

electron mobility : Fig. 2.18.13..

refractive index

<i>n</i>	$3.6 - 0.51z + 0.12z^2$	$\lambda = 1.55 \text{ }\mu\text{m}, T = 300 \text{ K}$	95P1, 96H
	$3.60 - 0.55z + 0.18z^2$	$\lambda = 1.55 \text{ }\mu\text{m}, T = 300 \text{ K}$	
	$3.61 - 0.22z + 0.14z^2$	$\lambda = 1.30 \text{ }\mu\text{m}, T = 300 \text{ K}$	
	$3.92 - 0.32z$	$\lambda = 0.65 \text{ }\mu\text{m}, T = 300 \text{ K}$	

References to 2.18

- 78P Pinczuk, A., Worlock, J. M., Nahory, R. F., Pollack, M.A.: Appl. Phys. Lett. 33 (1978) 461.
- 80A Amirtharaj, P. M., Holah, G. D., Perkowitz, S.: Phys. Rev. B 21 (1980) 5656.
- 80P Perea, E. H., Mendez, E. E., Fonstad, C. G.: Appl. Phys. Lett. 36 (1980) 978.
- 81P Pickering, C.: J. Electron. Mater. 10 (1981) 901.
- 82A1 Adachi, S.: J. Appl. Phys. 53 (1982) 8775.
- 82A2 Adachi, S.: J. Appl. Phys. 53 (1982) 5863.
- 82H Hayes, J. R., Adams, A. R., Greene, P. D.: "GaInAsP Alloy Semiconductors", T. P. Pearsall ed., J. Wiley & Sons, New York 1982, p. 275.
- 82K Kelso, S. M., Aspnes, D. E., Pollack, M. A., Nahory, R. E.: Phys. Rev. B 26 (1982) 6669.
- 82L Leheny, R. F.: "GaInAsP Alloy Semiconductors", T. P. Pearsall ed., J. Wiley & Sons, New York 1982, p. 275.
- 82O Olego, D., Chang, D. Y., Silberg, E., Caridi, E. A., Pinczuk, A.: Int. Phys. Ser. No.65, Int. Symp. GaAs and related Compounds, Albuquerque, 1982, p.195
- 82P Pearsall, T. P.: "GaInAsP Alloy Semiconductors", T. P. Pearsall ed., J. Wiley & Sons, New York 1982, p. 295.
- 82S Stanley, C. R., Welch, D., Wicks, G. W., Wood, C. E. C., Palmstrom, C.: Inst. Phys. Conf. Ser. No. 65, Int. Symp. GaAs and Related Compounds, Albuquerque 1982, p. 173.
- 83P Parayanthal, P., Pollak, f. H.: Phys. Rev. B 28 (1983) 3632.
- 84I Inoshita, T.: J. Appl. Phys. 56 (1984) 2056.
- 84K Kelso, S. M., Aspnes, D. E., Olson, C. G., Lynch D. W., Bachmann, K. J.: Proc. SPIE Int. Soc. Opt Eng. 452 (1984) 200.
- 85H Henry, C. H., Johnson, L. F., Logan, R. A., Clarke, D. P.: IEEE J. Quantum Electron. QE-21 (1985) 1887.
- 85T Tsang, W. T., Chiu, T. H., Kisker, D. W., Ditzcnberger, J. A.: Appl. Phys. Lett. 46 (1985) 283.
- 86C Cherng, M. J., Stringfellow, G. B., Kisker, D. W., Srivastava, A. K., Zyskind, J. L.: Appl. Phys. Lett. 48 (1986) 419.
- 86O Ohba, Y., Ishikawa, M., Sugawara, H., Yamamoto, M., Nakanisi, T.: J. Cryst. Growth 77 (1986) 374.
- 86S Soni, R. K., Abbi, S. C., Jam, K. P., Balkanski, M., Slemkes, S., Benchimol, J. L.: Appl. Phys. 59 (1986) 2184.
- 94E Emanuelsson, P., Drechsler, M., Hofmann, D. M., Meyer, B. K., Moser, M., Scholz, F.: Appl. Phys. Lett. 64 (1994) 2849.
- 94M Moser, M., Winterhoff, R., Geng, C., Queisser, I., Scholz, F., Dörnen, A.: Appl. Phys. Lett. 64 (1994) 235.
- 95M Meney, A. T., Prins, A. D., Phillips, A. F., Sly, J. L., O'Reilly, E. P., Dunstan, J. D., Adams, A. R., Valster, A.: J. Sel. Topics Quantum Electron. 1 (1995) 697.
- 95P1 Pan, J.-W., Shieh, J.-L., Gau, J.-H., Chyi, J.-I., Lee, J.-C., Ling, K.-J.: J. Appl. Phys. 78 (1995) 442.
- 95P2 Prins, A. D., Sly, J. L., Meney, A. T., Dunstan, D. J., O'Reilly, E. P., Adams, A. R., Valster, A.: J. Phys. Chem. Solids 56 (1995) 349.
- 96A Adachi, S., Ozaki, S., Sato, M., Ohtsuka, K.: Jpn. J. Appl. Phys. 35 (1996) 537.
- 96H Hillmer, H.: in: Optische Telekommunikationssysteme, Chap. Materialien für die optische Nachrichtentechnik und deren Eigenschaften, Hultsch, H. (ed.), Damm Verlag, Gelsenkirchen, 1996.
- 96N Nelson, J. S., Jones, E. D., Myers, S. M., Follstaedt, D. M., Hjalmarson, H. P., Schirber, J. E., Schneider, R. P., Fouquet, J. E., Robbins, V. M., Carey, K. W.: Phys. Rev. B 53 (1996) 15893.
- 96O Ozaki, S., Adachi, S., Sato, M., Ohtsuka, K.: J. Appl. Phys. 79 (1996) 439.

Figures to 2.18

Fig. 2.17.1

Lattice parameter vs. energy gap (RT values) for various III–V compounds and their alloys.

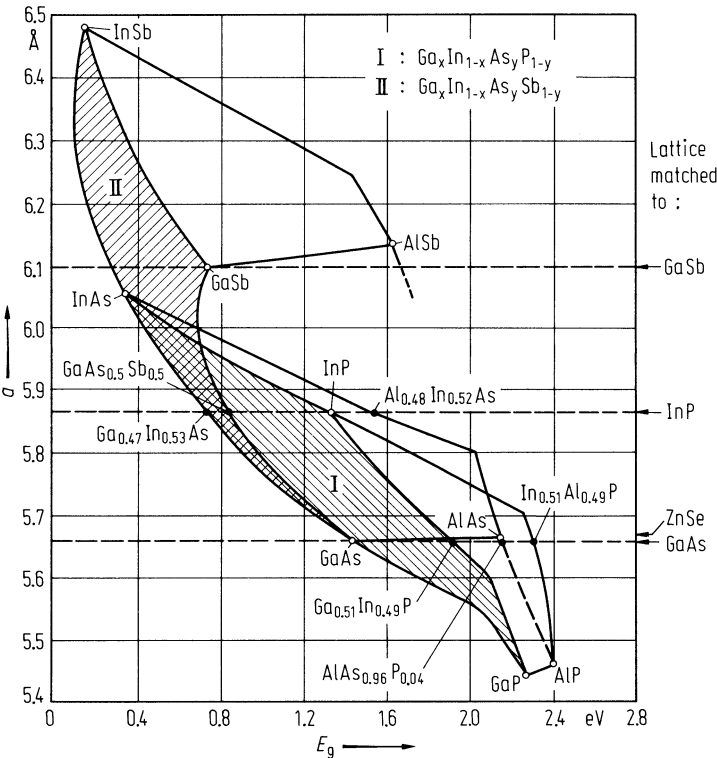


Fig. 2.18.1

$\text{Ga}_x\text{In}_{1-x}\text{As}_y\text{P}_{1-y}$. Direct energy gap and spin orbit splitting at Γ vs. composition (a) at 298 K, (b) at 4.2 K for InP lattice matched material. Solid curves calculated (see tables), experimental data from five (a) and three (b) sources, respectively [82P].

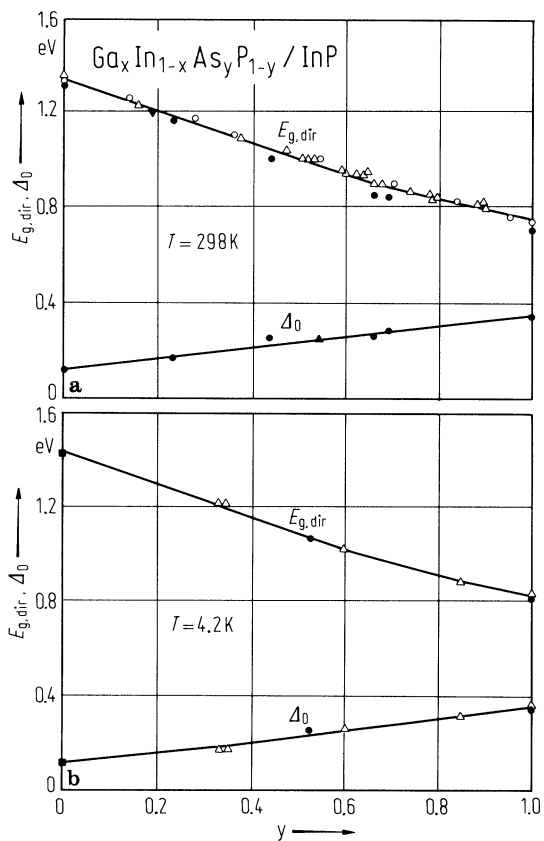


Fig. 2.18.2

$\text{Ga}_x\text{In}_{1-x}\text{As}_y\text{P}_{1-y}$. Compositional variation of the energy gap of GaAs and ZnSe lattice matched layers; calculated from the data of the four constituents [82A1].

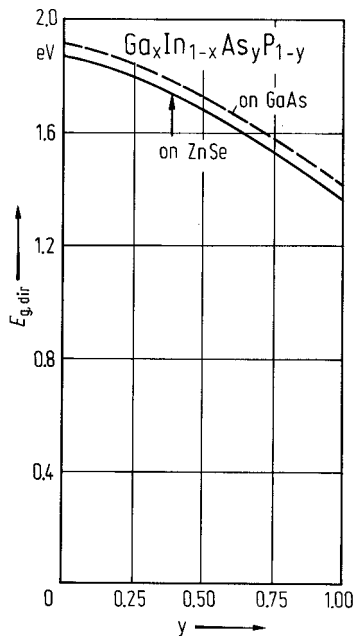


Fig. 2.18.3

$\text{Ga}_x\text{In}_{1-x}\text{As}_y\text{P}_{1-y}$. Conduction band edge effective mass vs. composition for InP lattice matched material. Solid curve calculated from $k\cdot p$ theory, experimental data from six sources [82P].

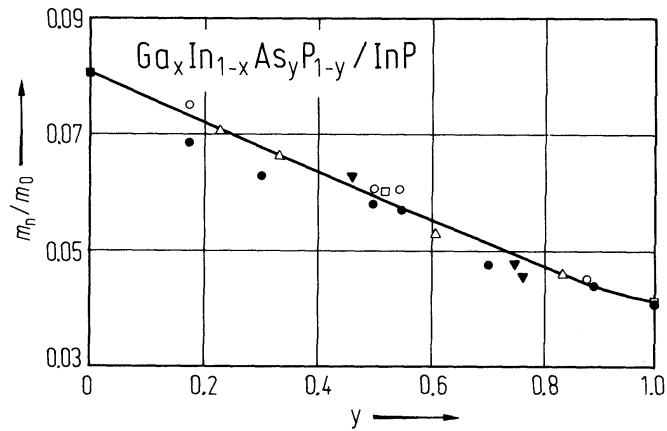


Fig. 2.18.4

$\text{Ga}_x\text{In}_{1-x}\text{As}_y\text{P}_{1-y}$. Thermal expansion coefficient for material lattice matched to InP, ZnSe and GaAs; curves calculated, open circles experimental [82A1].

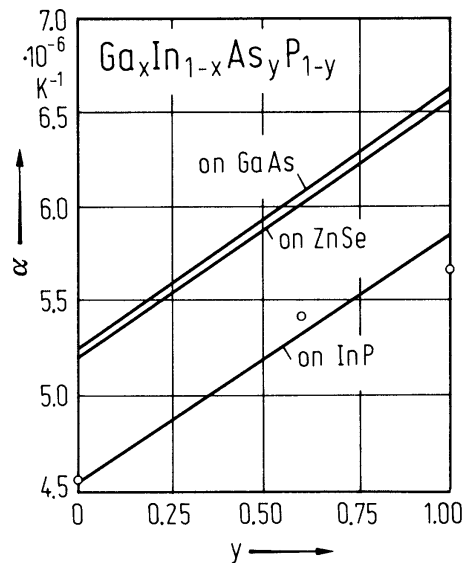


Fig. 2.18.5

$\text{Ga}_x\text{In}_{1-x}\text{As}_y\text{P}_{1-y}$. Optical phonon wavenumbers vs. composition for InP lattice matched material. (a) according to [84I], solid curves calculated, experimental data from [78P] (open symbols and crosses) and [81P] (full symbols), (b) from [82L], reflectivity data from [80A], Raman data from [78P] (broken lines).

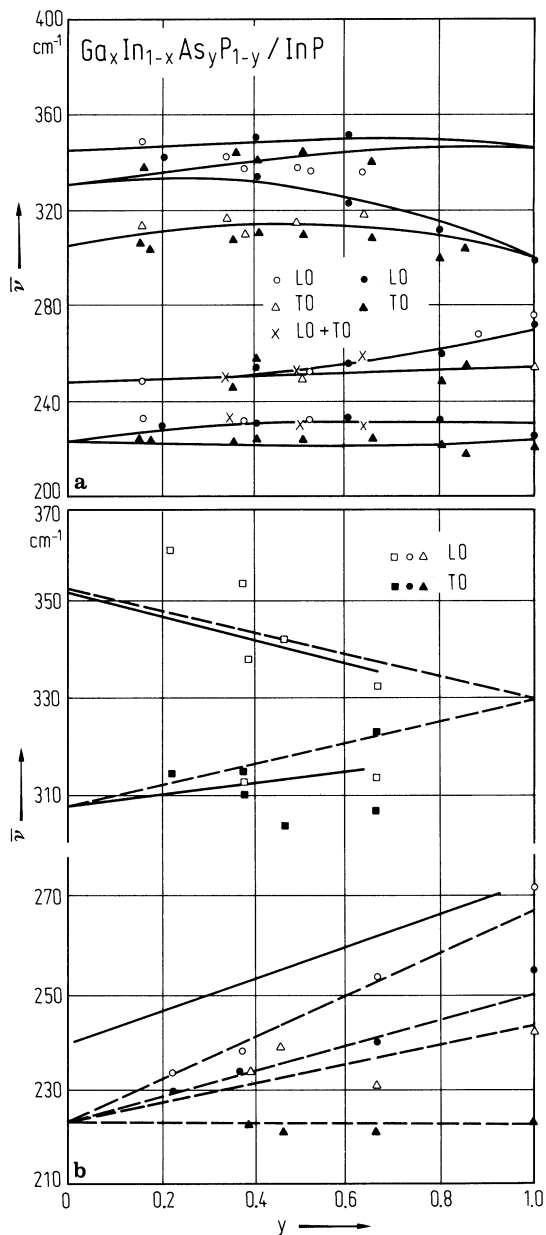


Fig. 2.18.6

$\text{Ga}_x\text{In}_{1-x}\text{As}_y\text{P}_{1-y}$. Phonon wavenumbers vs. composition for GaAs lattice matched material; solid curves: calculated, open circles and full circles: identified and unidentified Raman peaks [84I].

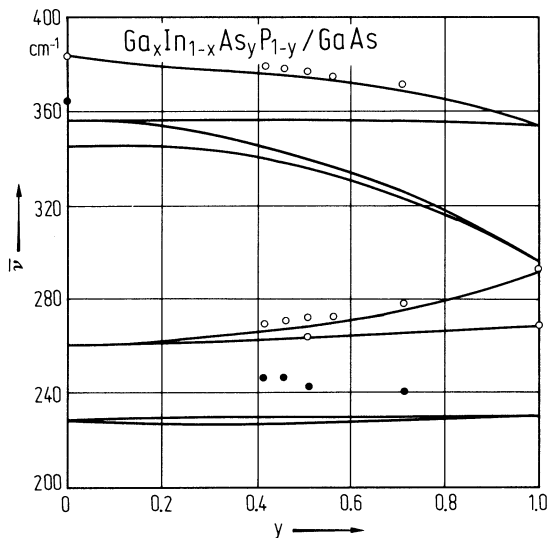


Fig. 2.18.7

$\text{Ga}_x\text{In}_{1-x}\text{As}_y\text{P}_{1-y}$. Electron mobility vs. composition for InP lattice matched material at RT. Experimental data from literature for samples with electron concentration in the range $10^{15} \dots 5 \cdot 10^{15} \text{ cm}^{-3}$, calculated curve for $n_d = 10^{15} \text{ cm}^{-3}$ [82H].

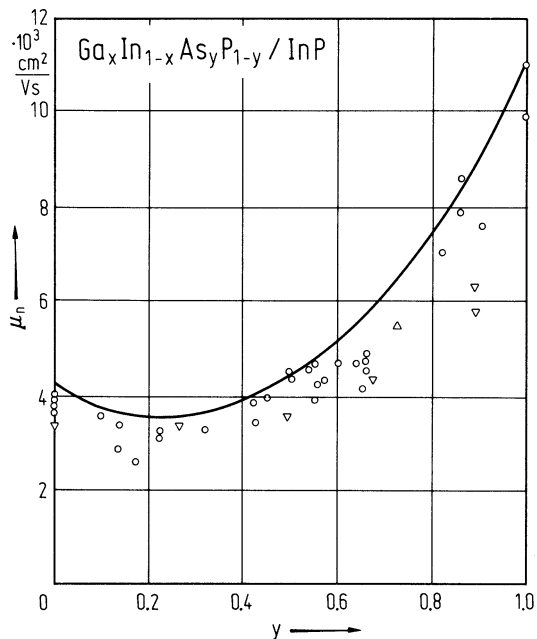


Fig. 2.18.8

$\text{Ga}_x\text{In}_{1-x}\text{As}_y\text{P}_{1-y}$. Hole mobility vs. composition for InP lattice matched material at RT. Experimental data for hole concentrations around $4 \cdot 10^{16} \text{ cm}^{-3}$ and $2 \cdot 10^{18} \text{ cm}^{-3}$, calculated curves for the same concentrations [82H].

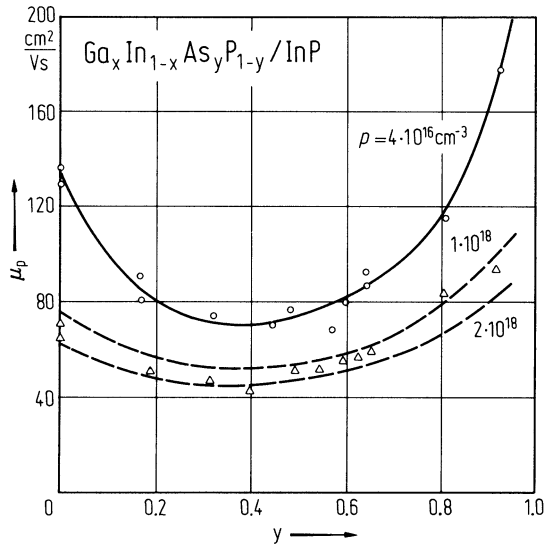


Fig. 2.18.9

$(\text{Al}_z\text{Ga}_{1-z})_{0.5}\text{In}_{0.5}\text{P}$. Composition dependence of X and Γ band gap energies at $T = 2$ K. The data points were determined from high-pressure photoluminescence measurements [95P]. Solid lines are least squares fits to these data.

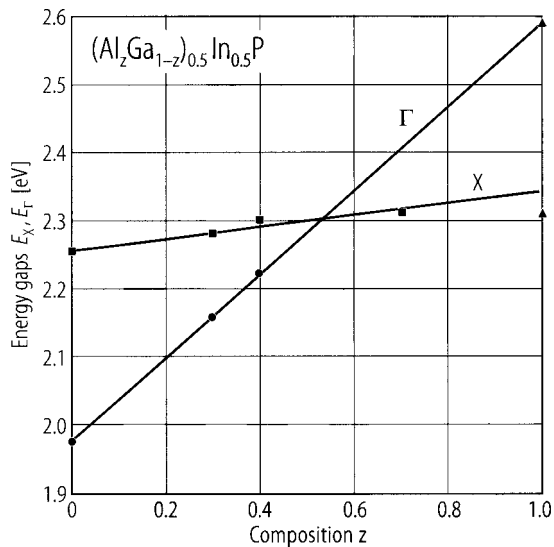


Fig. 2.18.10

$(\text{Al}_z\text{Ga}_{1-z})_{0.5}\text{In}_{0.5}\text{P}$. Room temperature carrier concentration and mobility versus Al composition for (a) Se-doped and (b) Zn-doped material [86O].

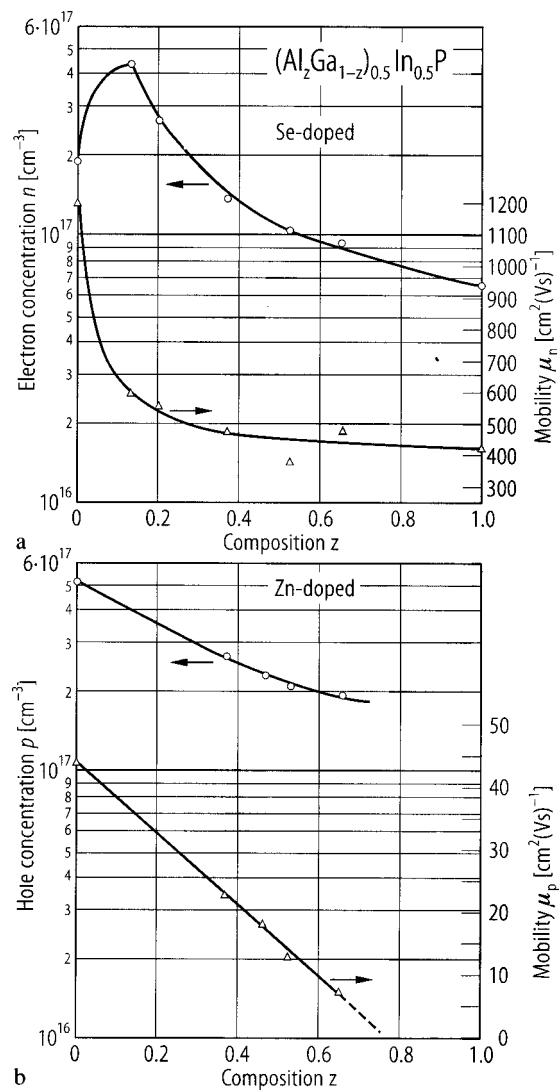


Fig. 2.18.11

$\text{In}_{1-x-y}\text{Al}_x\text{Ga}_y\text{As}$. Compositional dependence of the energy gap for InP lattice matched layers at RT ($x = 0.48z$, $y = 0.47(1-z)$). Solid line: according to the formula given in the tables [82O].

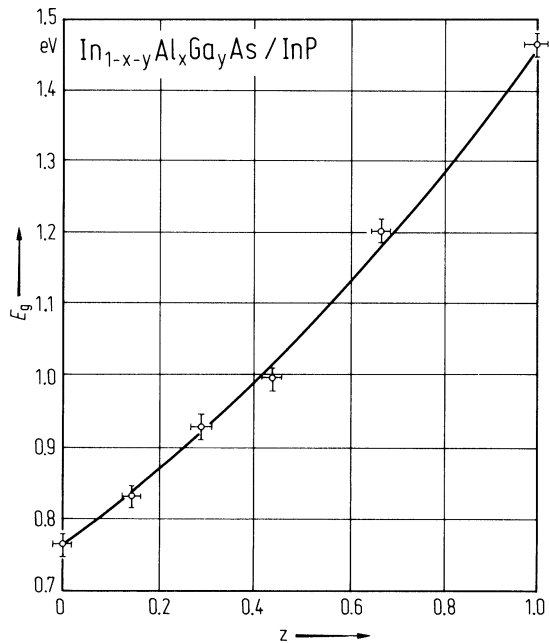


Fig. 2.18.12

$\text{In}_{1-x-y}\text{Al}_x\text{Ga}_y\text{As}$. Compositional dependence of the electron effective mass for InP lattice matched layers ($x = 0.48z$, $y = 0.47(1-z)$) [82O].

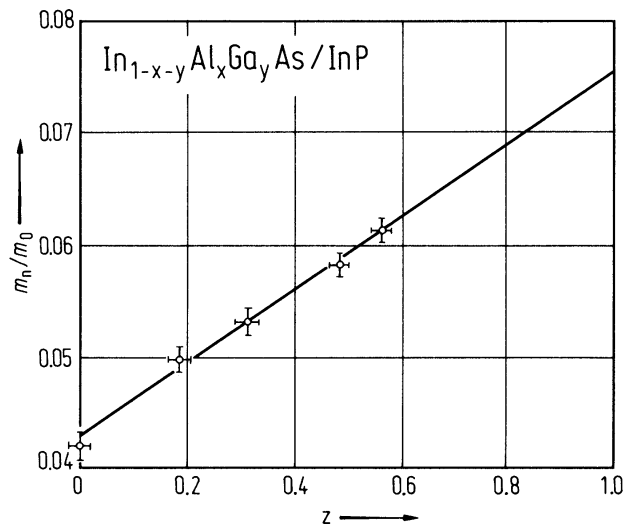
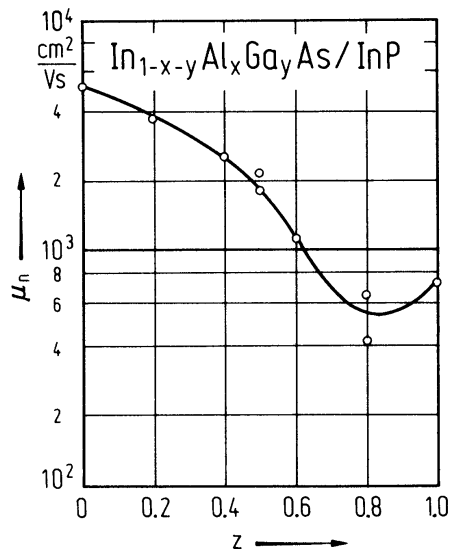


Fig. 2.18.13

$\text{In}_{1-x-y}\text{Al}_x\text{Ga}_y\text{As}$. Compositional dependence of the electron mobility at RT for InP lattice matched layers ($x = 0.47z$, $x + y = 0.47$); Sn-doped sample with $n_d - n_a \approx 10^{17} \text{ cm}^{-3}$ [82S].



3 II-VII compounds

3.0 Crystal structure and electronic structure

3.0.1 Crystal structure

Three crystal structures dominate in II-VI compounds: the zincblende and wurtzite structures already mentioned for III-V compounds in chapter 2, and the NaCl (rocksalt) structure. A fourth structure occurring in II-VI compounds is the cinnabar lattice.

The *beryllium compound* BeO crystallizes under normal conditions in the wurtzite structure, whereas BeS, BeSe and BeTe crystallize in the zincblende structure.

The *magnesium compounds* MgO, MgS and MgSe show the rocksalt structure and MgTe the wurtzite structure.

The *oxides of Ca, Sr, and Ba* crystallize in the rocksalt structure. For the *Zn, Cd and Hg compounds* the following sequences are found:

ZnO: wurtzite, ZnS: wurtzite / zincblende, ZnSe and ZnTe: zincblende.

CdO: rocksalt, CdS: wurtzite, CdSe: (wurtzite) / zincblende, CdTe: zincblende.

HgO: rhombohedral, orthorhombic, HgS: trigonal / zincblende, HgSe and HgTe: zincblende.

Figs. 3.0.1 ...3.0.3 show the crystal lattices of the zincblende, wurtzite, and rocksalt structures.

3.0.2 Electronic structure

General remarks on the band structure of II-VI compounds

The Brillouin zones of the zincblende and the rocksalt structures is the Brillouin zone of the face-centered lattice (Fig. 3.0.4); the Brillouin zone of the wurtzite structure the Brillouin zone of the hexagonal lattice (Fig. 3.0.5).

Figs. 3.0.6 ... 3.0.24 show the band structures of the semiconducting II-VI compounds. For an interpretation of these structures see the respective sections.

For the qualitative shape of energy bands in cubic and hexagonal structures see the remarks in section 2.0.2.

Figures to 3.0

Fig. 3.0.1

The zincblende lattice.

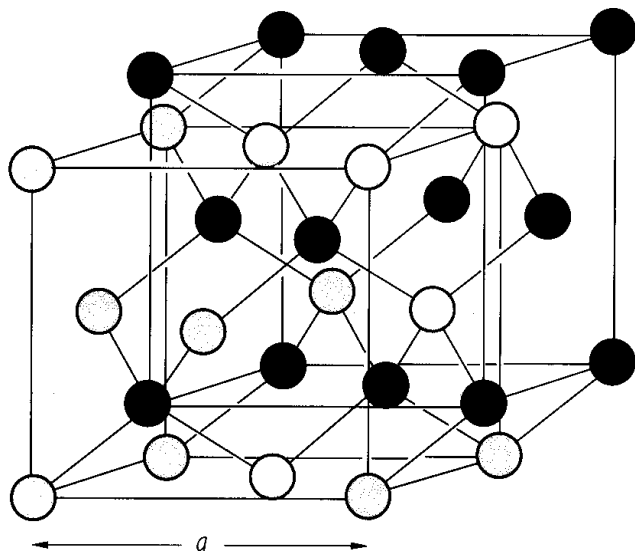


Fig. 3.0.2

The wurtzite lattice.

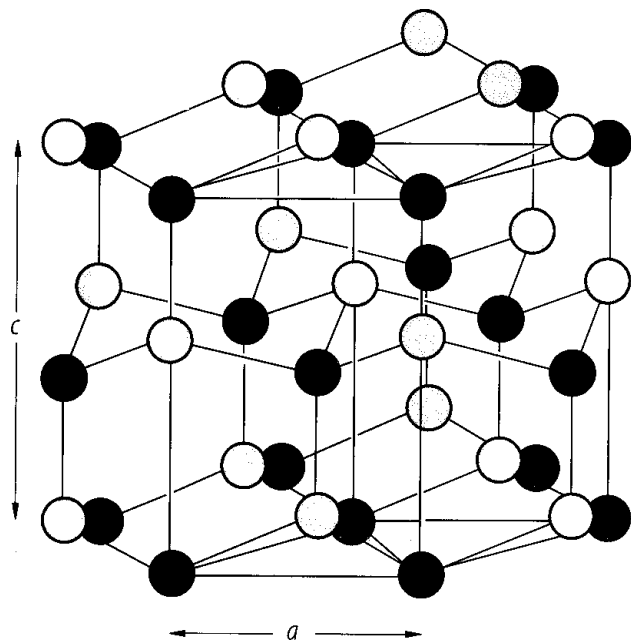


Fig. 3.0.3

The rocksalt lattice.

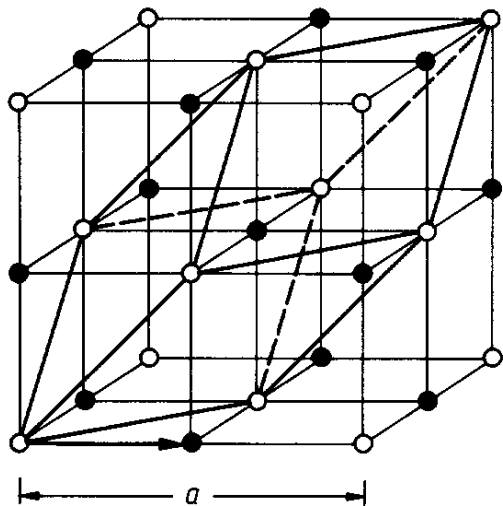


Fig. 3.0.4

The Brillouin zone for the zincblende and the rocksalt lattices.

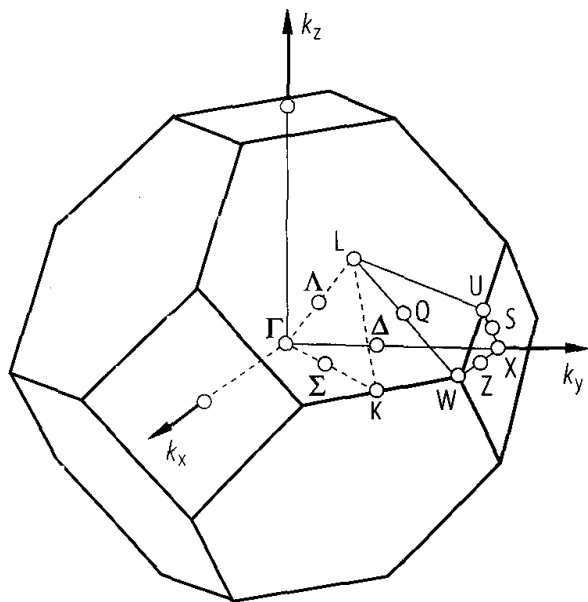


Fig. 3.0.5

The Brillouin zone of the wurtzite lattice.

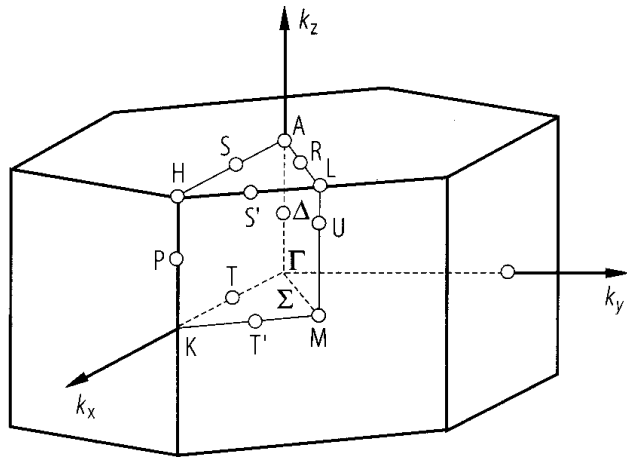


Fig. 3.0.6

Band structure of beryllium oxide.

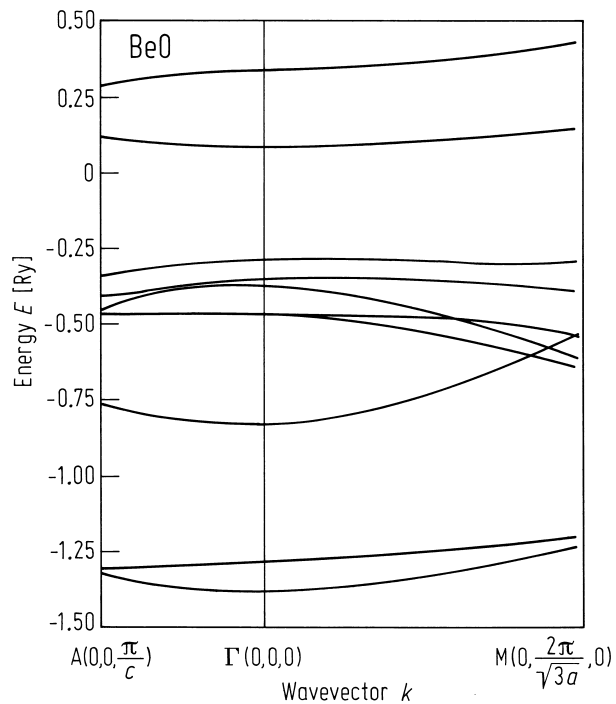


Fig. 3.0.7

Band structure of beryllium sulfide.

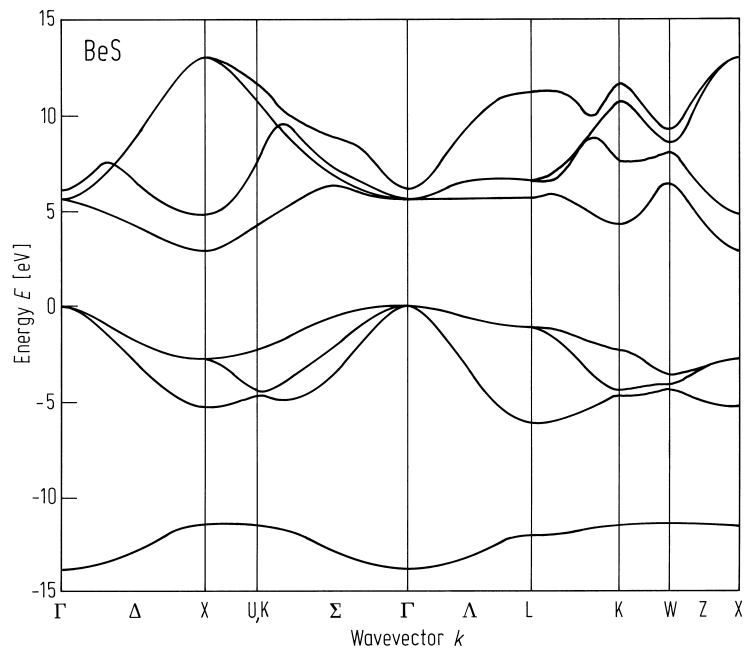
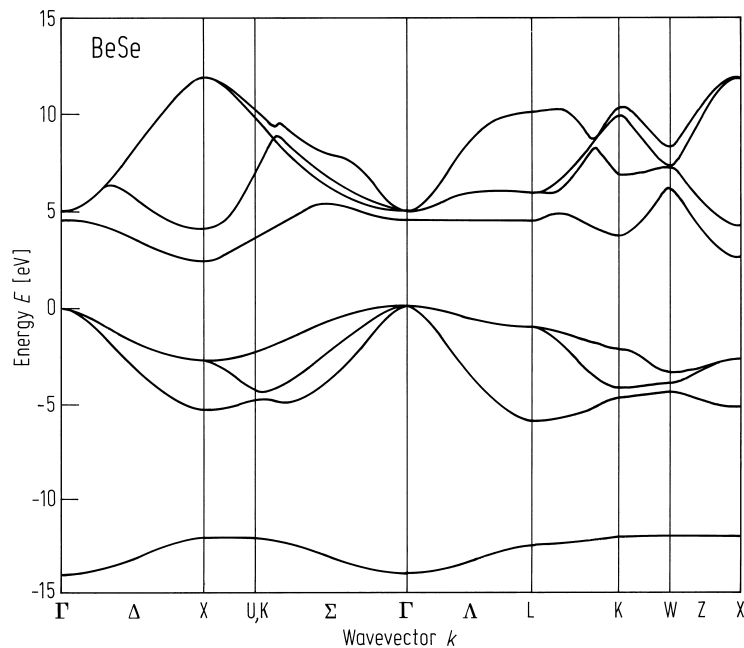
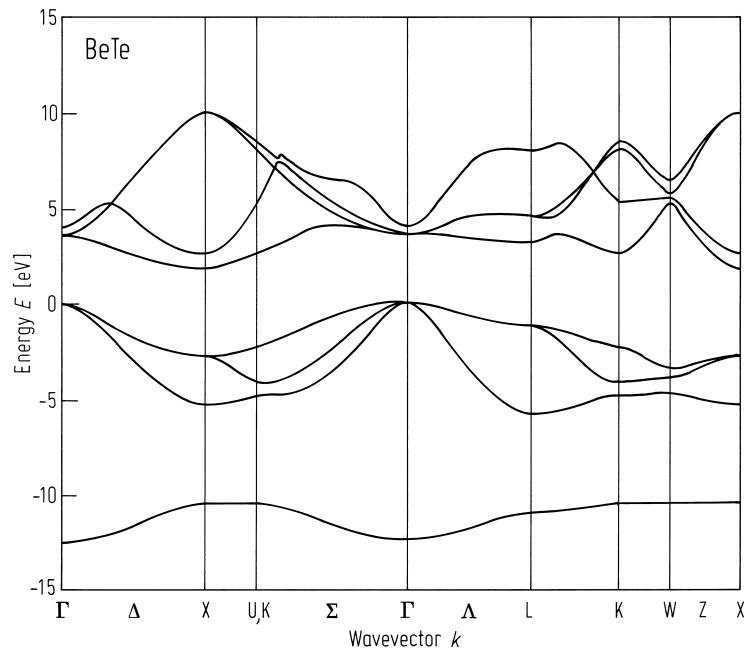


Fig. 3.0.8

Band structure of beryllium selenide.



Band structure of beryllium telluride.



Band structure of magnesium oxide.

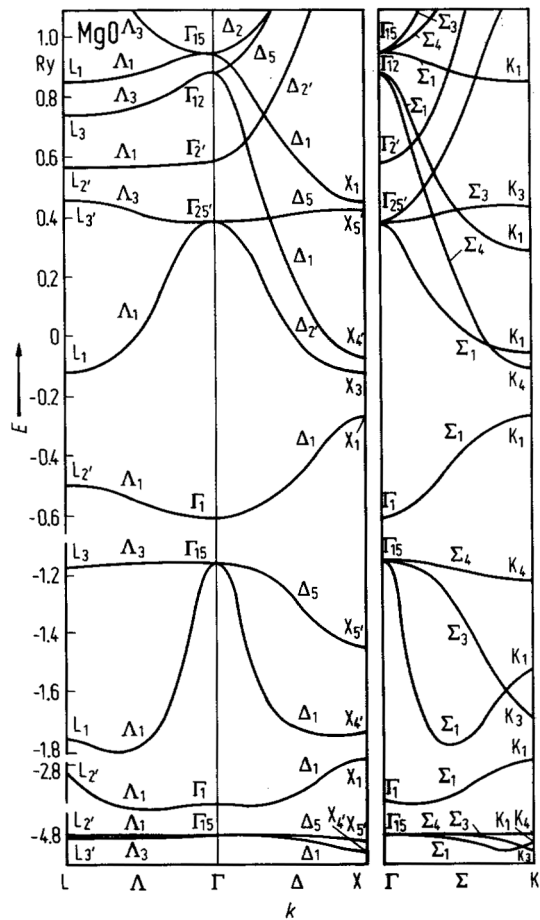


Fig. 3.0.11

Band structure of magnesium sulfide, (a) zincblende structure, (b) rocksalt structure.

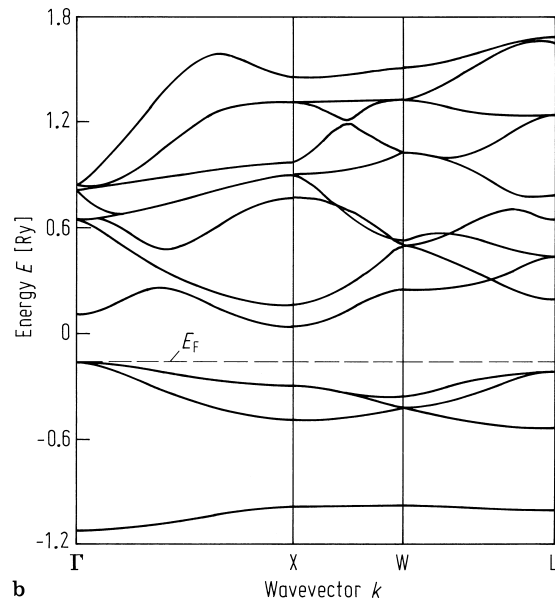
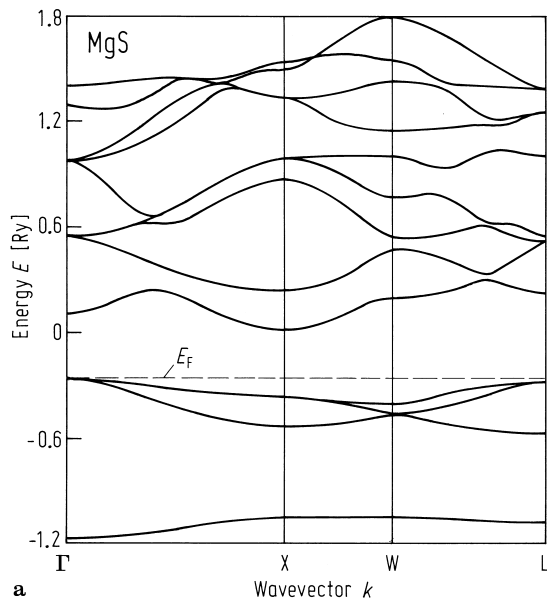


Fig. 3.0.12

Band structure of magnesium selenide, (a) zincblende structure, (b) rocksalt structure.

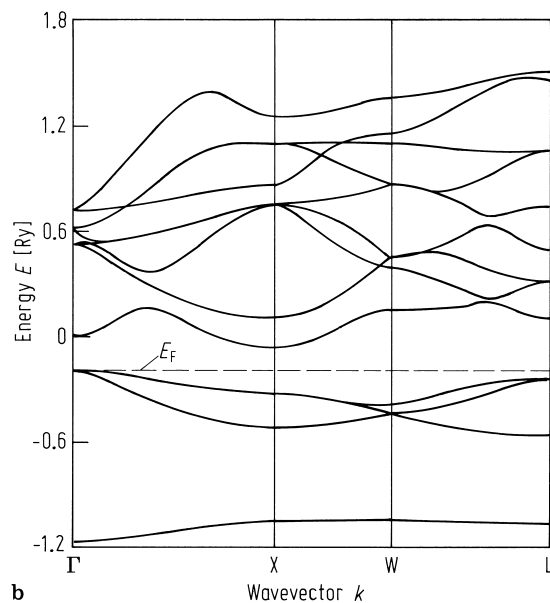
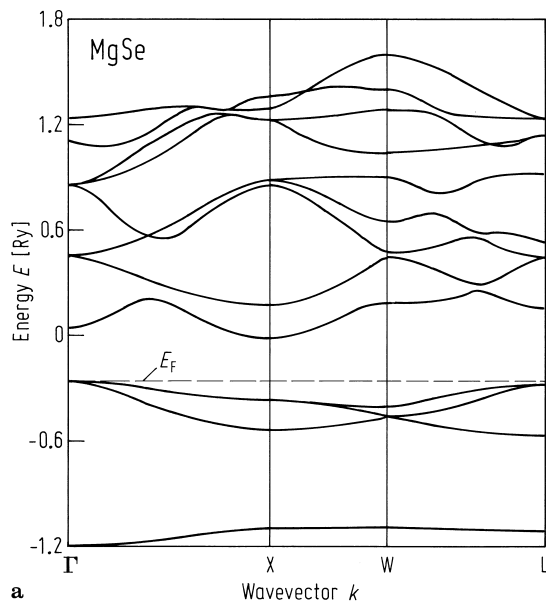
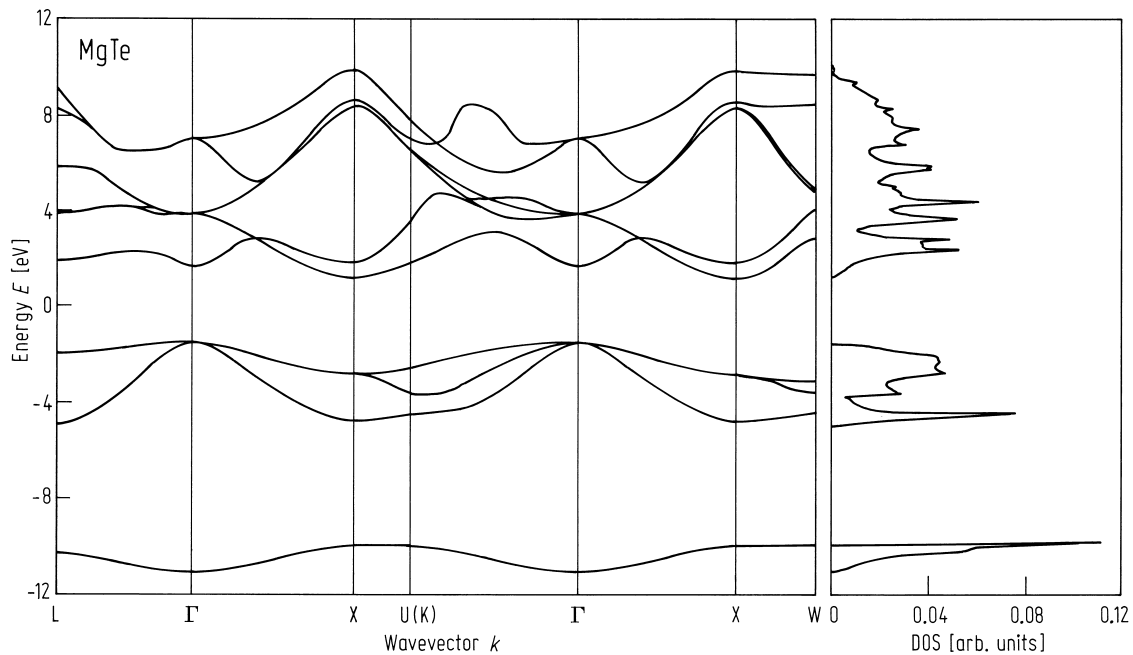
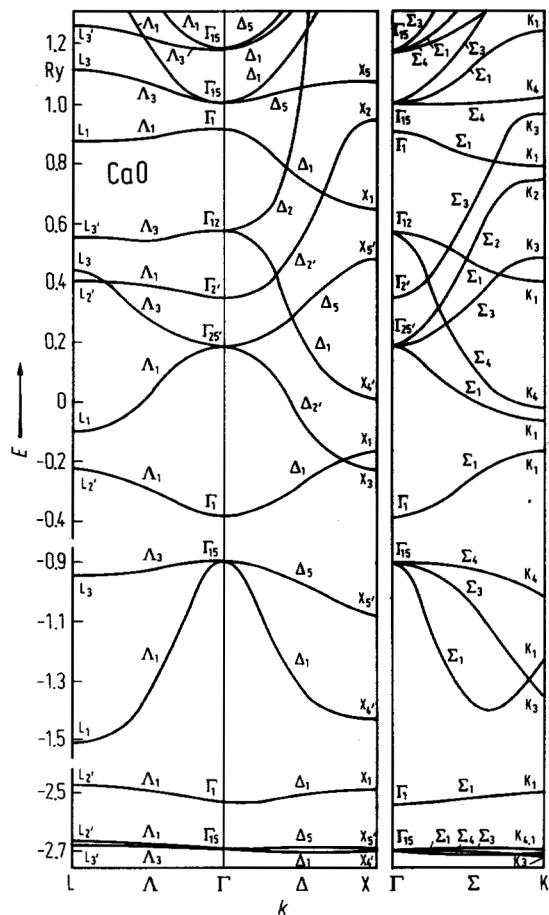


Fig. 3.0.13

Band structure of magnesium telluride.



Band structure of calcium oxide.



Band structure of zinc oxide.

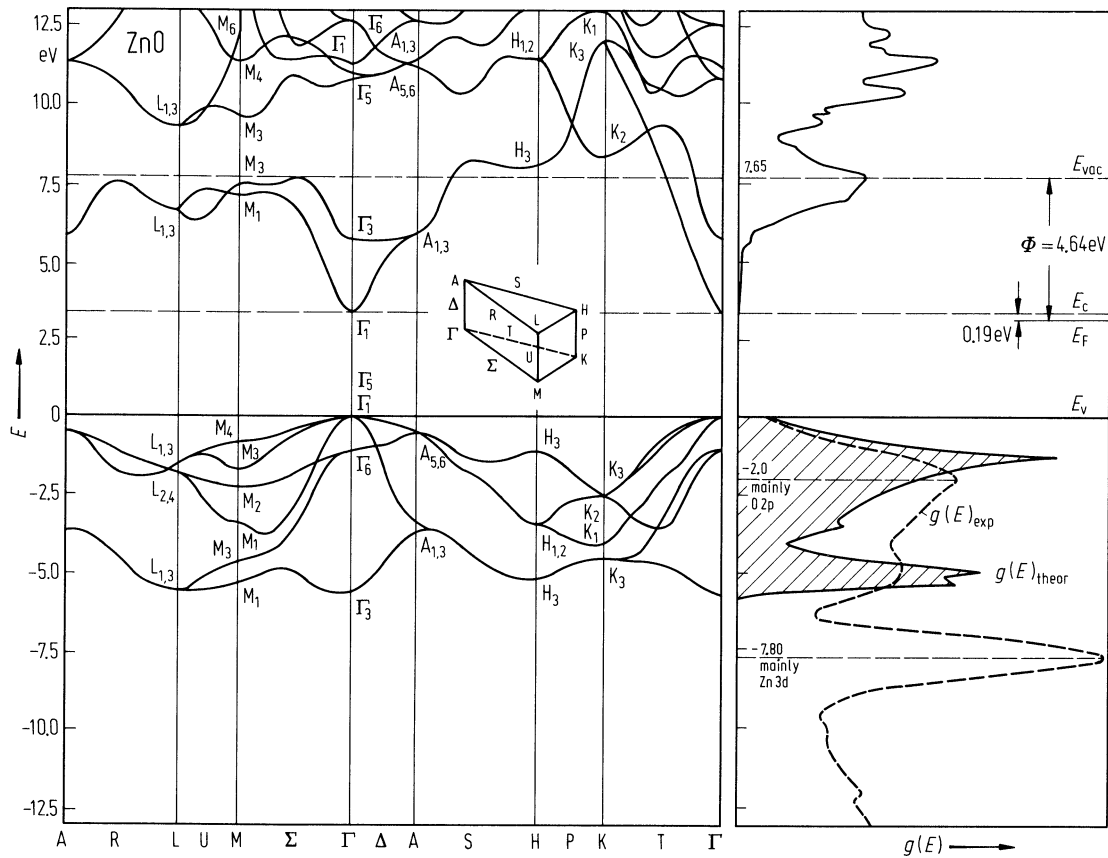


Fig. 3.0.16a,b

Band structure of cubic and hexagonal zinc sulfide.

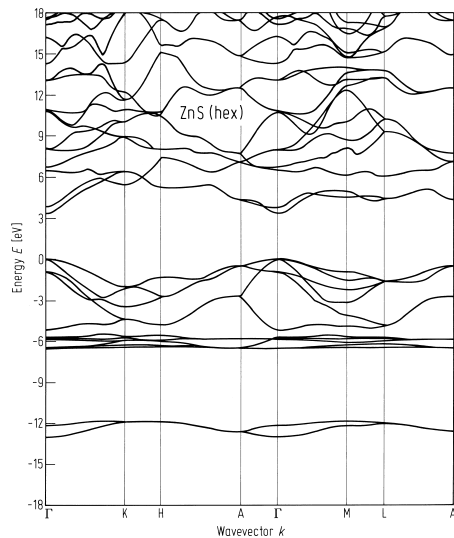
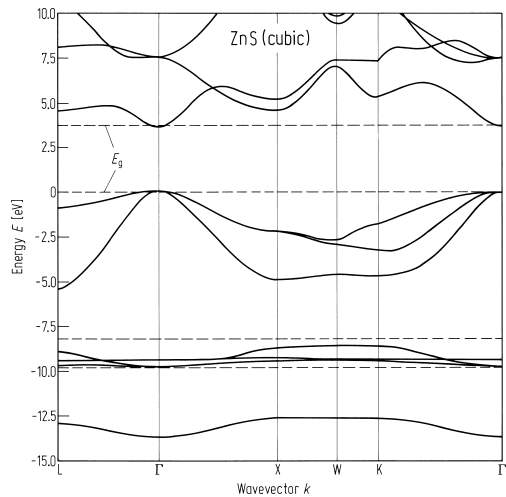
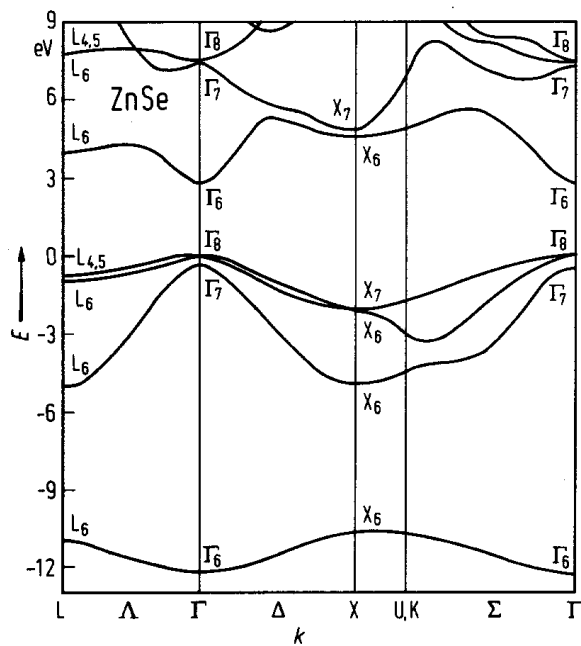


Fig. 3.0.17

Band structure of zinc selenide.



Band structure of zinc telluride.

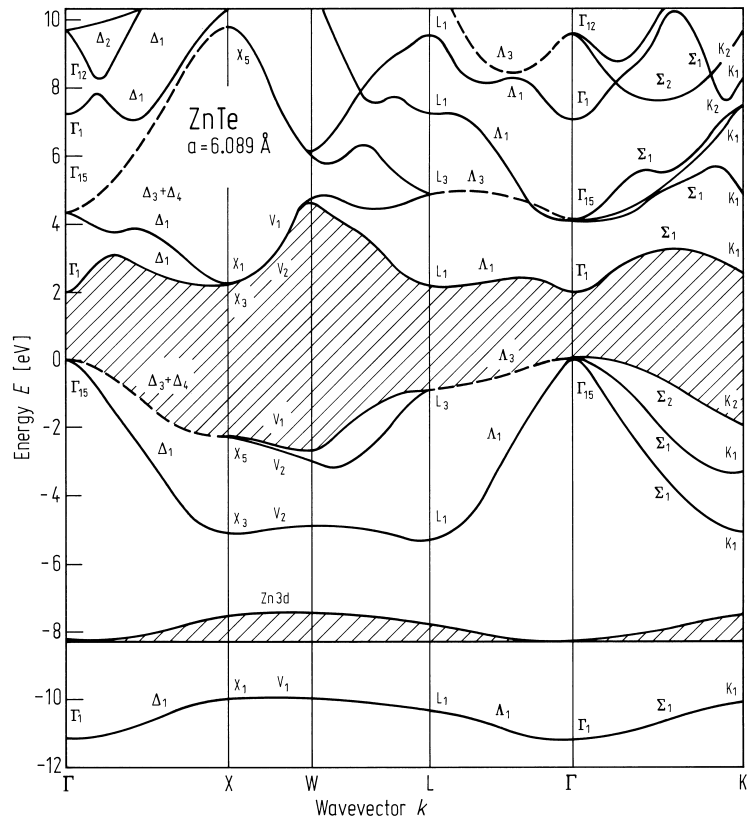


Fig. 3.0.19

Band structure of cadmium oxide.

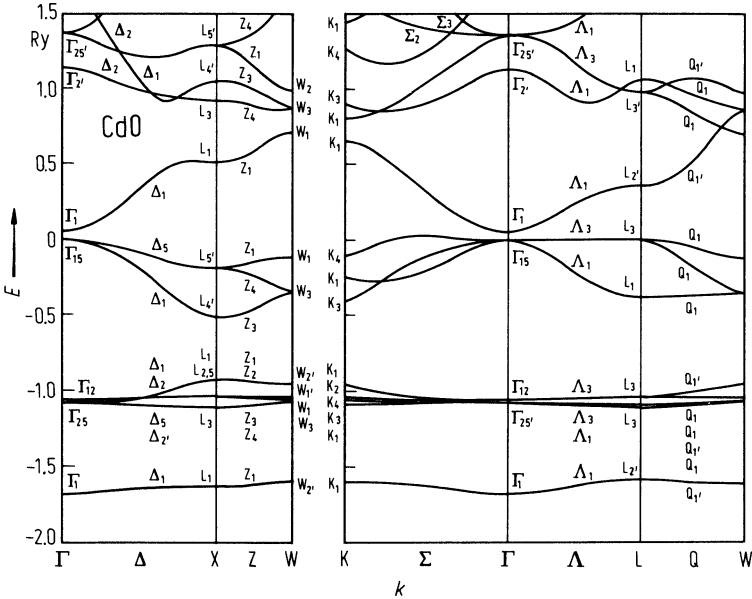


Fig. 3.0.20

Band structure of hexagonal cadmium sulfide.

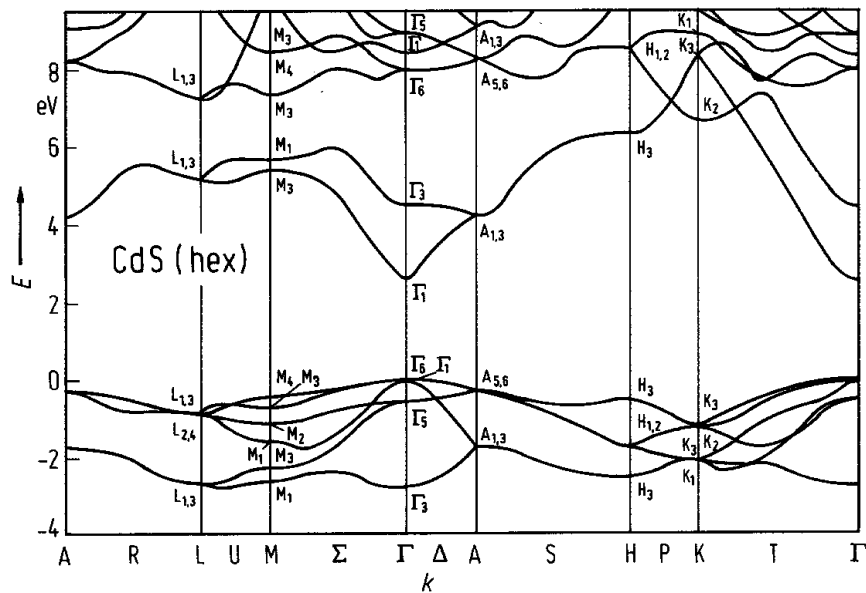


Fig. 3.0.21a,b

Band structure of hexagonal and cubic cadmium selenide

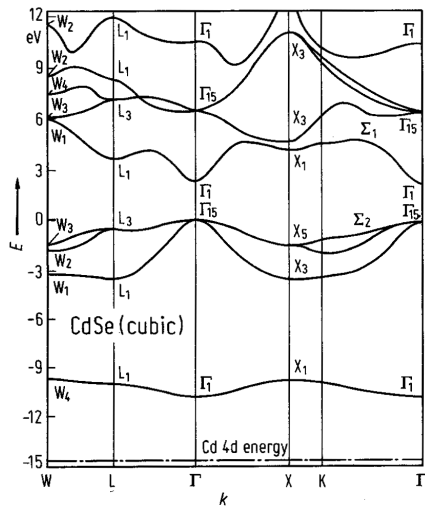
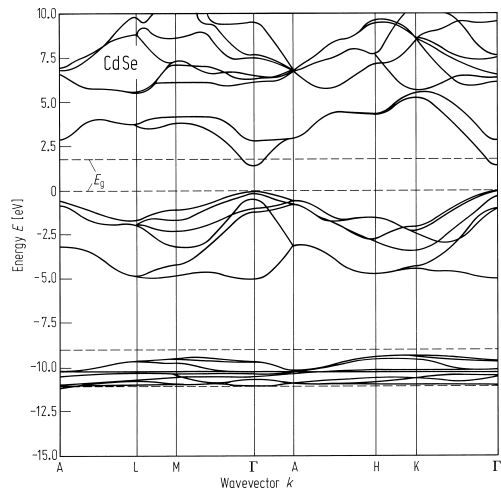


Fig. 3.0.22

Band structure of cadmium telluride.

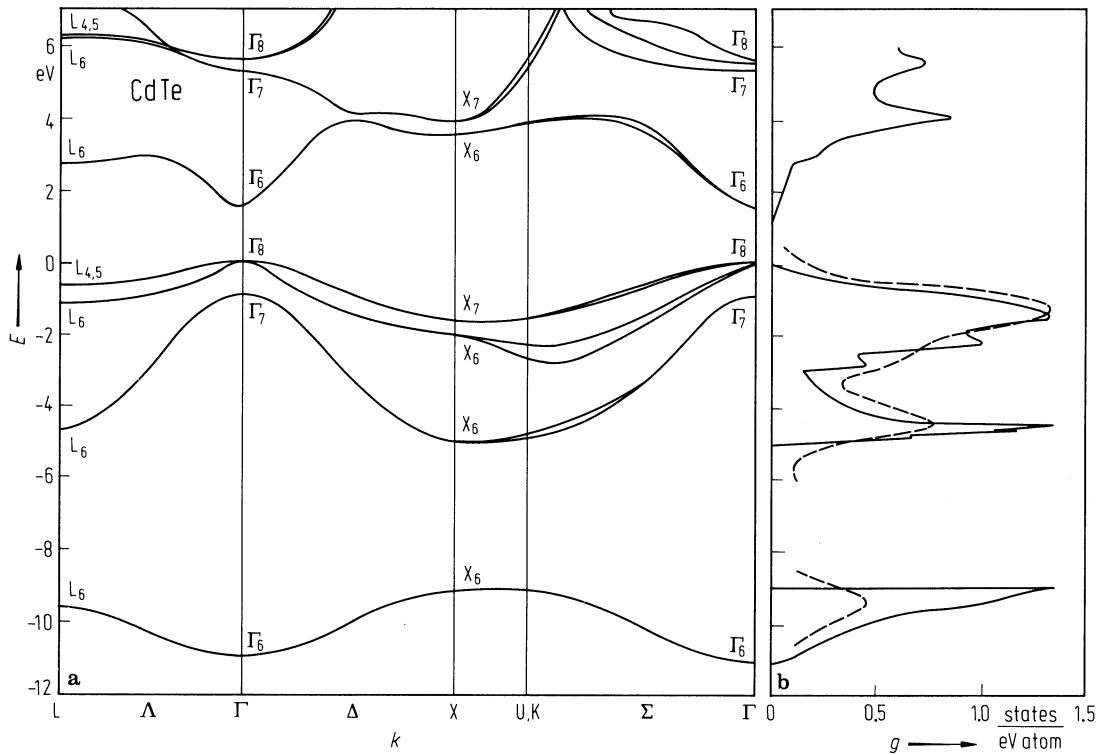


Fig. 3.0.23

Schematic band structure of the Hg – Cd – Se system near the Γ point.

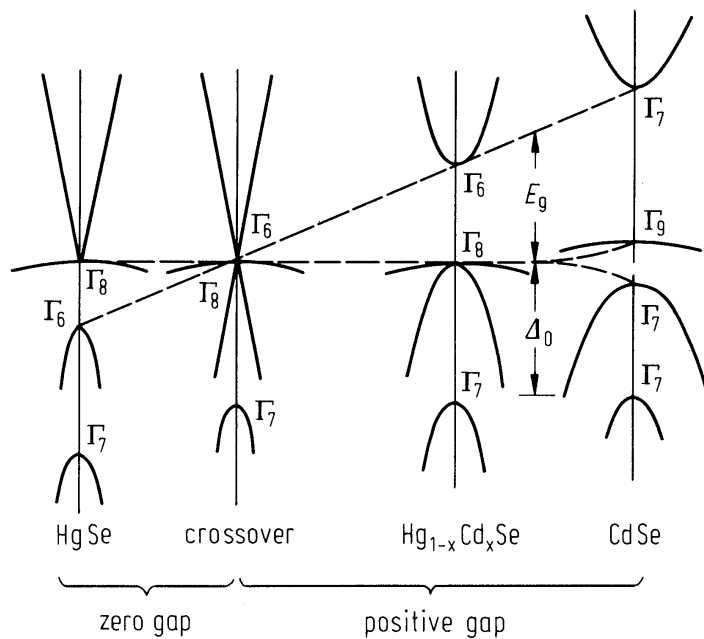
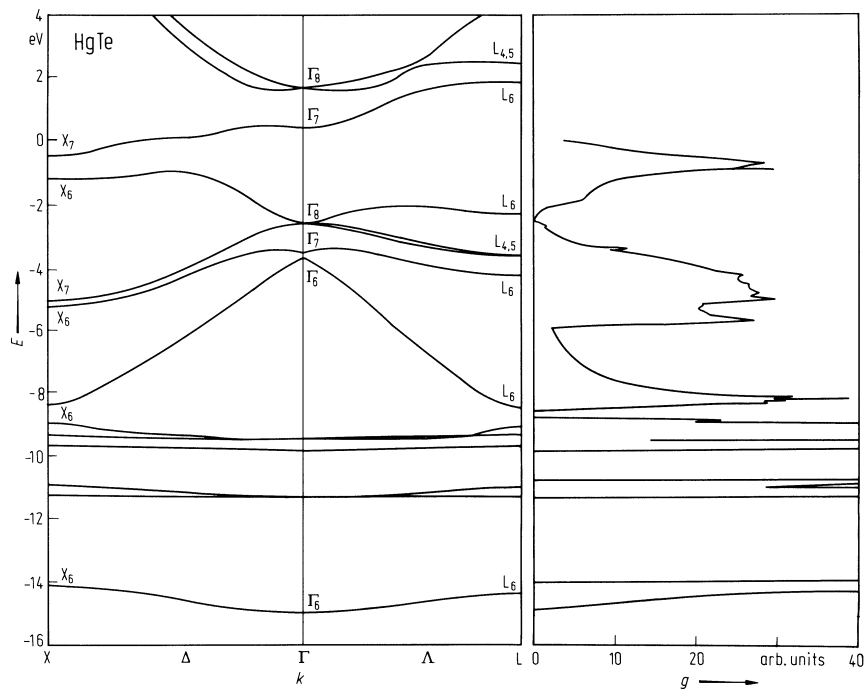


Fig. 3.0.24

Band structure of mercury telluride.



3.1 Beryllium oxide (BeO)

Crystal structure

The ground state of BeO is wurtzite (P₆₃mc-C_{6v}⁴, Fig. 3.0.2) , but the zincblende structure has also been observed. A transition with temperature from α-BeO (wurtzite) to β-BeO (polymorphous phase) has been detected by various techniques.

Electronic properties

energy gap

E_g	10.585 eV	excitonic, reflection	69R
-------	-----------	-----------------------	-----

band structure : see Fig. 3.0.6.

Lattice properties

lattice paramters

a	0.26979 nm	X-ray diffraction	83L
c	0.4380 nm		

linear thermal expansion coefficient

α	$9.7 \cdot 10^{-6} \text{ K}^{-1}$	$T = 100^\circ\text{C}$	80K
----------	------------------------------------	-------------------------	-----

density

d	3.01 g cm^{-3}	93S
-----	--------------------------	-----

melting temperature

T_m	2507°C	93C
-------	----------------------	-----

elastic constants and bulk modulus

c_{11}	460.6 GPa	RT	ultrasonic data	67C
c_{12}	126.5 GPa			
c_{13}	88.5 GPa			
c_{33}	491.6 GPa			
c_{44}	147.7 GPa			
B	224.4 GPa	249		

Debye temperature

Θ_D	1280 K	67C
------------	--------	-----

Transport properties

BeO, synonym beryllia, insulates electrically like a ceramic, conducts heat like a metal. The electrical resistivity is larger than $10^{16} \Omega \text{ cm}$ [93S].

Optical properties

BeO is transparent up to 9.4 eV (vacuum UV) and quite resistant to UV damage. Data for crystalline BeO are given below.

static dielectric constant

$\epsilon_{0\parallel}$	7.65	$T = 300 \text{ K}$	reflectance	68L
$\epsilon_{0\perp}$	6.94	$T = 300 \text{ K}$	reflectance	

refractive index

dispersion law $n = A + BL + CL^2 + D\lambda^2 + E\lambda^4$

reflectance, $T = 300$ K; λ in Å

62H

$L = 1/(\lambda^2 - 2.80 \cdot 10^6)$, $A = 1.699773$, $B = 745.1288 \text{ Å}^2$, $C = -4.331397 \cdot 10^{12} \text{ Å}^4$, $D = -8.194535 \cdot 10^{-12} \text{ Å}^{-2}$,
 $E = -1.659630 \cdot 10^{-20} \text{ Å}^{-4}$

References to 3.1

- 62H Herzberger, M., Salzberg, C.D.: J. Opt. Soc. Am. 52 (1962) 420.; Herzberger, M.: Opt. Acta 6 (1959) 197.
- 67C Cline, C.F., Dunegan, H.L., Henderson, G.W.: J. Appl. Phys. 38 (1967) 1944.
- 68L Loh, E.: Phys. Rev. 166 (1968) 673.
- 69R Roessler, D.M., Walker, W.C.: J. Phys. Chem. Solids 30 (1969) 157.
- 80K Kirk-Othmer, : Encyclopedia of Chemical Technology, 3rd edition, John Wiley Sons: New York 1978 to 1984.
- 83L Lazarev, V.B., Sobolev, V.V., Shaplygin, I.S.: Chemical and Physical Properties of Simple Metal Oxides, Moscow 1983.
- 90K Kuyabin, B.E., Lobach, V.A., Kruzhalov, A.V.: Sov. Phys. Solid State 32 (1990) 2138.
- 93C CRC Handbook of Chemistry and Physics, Lide, D.R. (ed.), CRC Press Inc. Boca Raton Fl.
- 93S Strem Catalog No 15, 1993-1994, Strem Chemicals, 7 Mullikan Way, Newburyport, MA 01950-4098.

Figures to 3.1

Fig. 3.0.2

The wurtzite lattice.

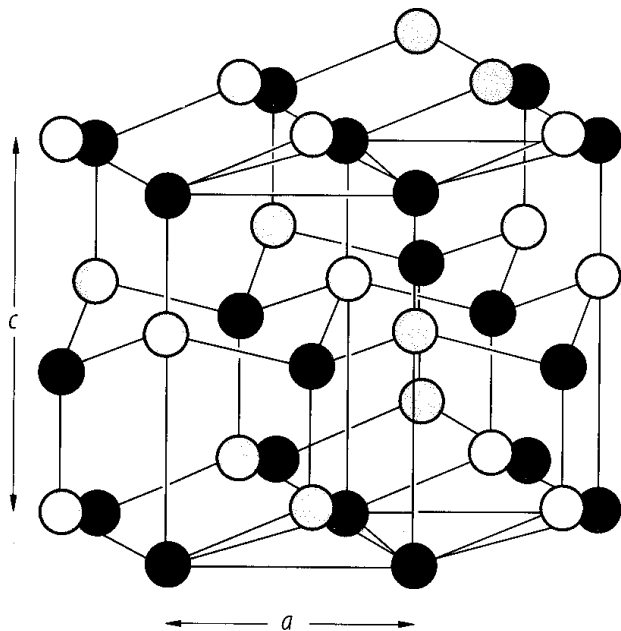


Fig. 3.0.5

The Brillouin zone of the wurtzite lattice.

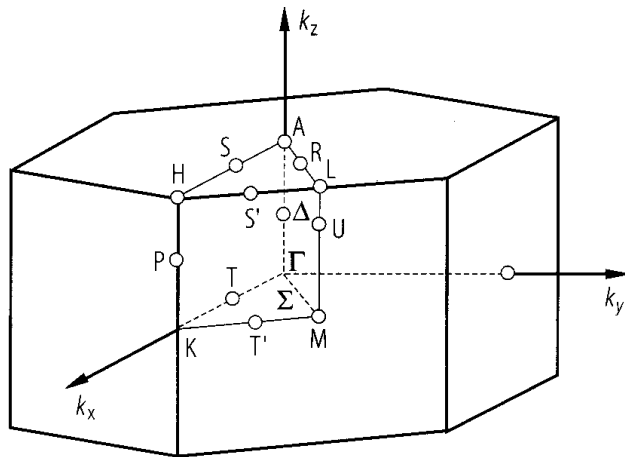
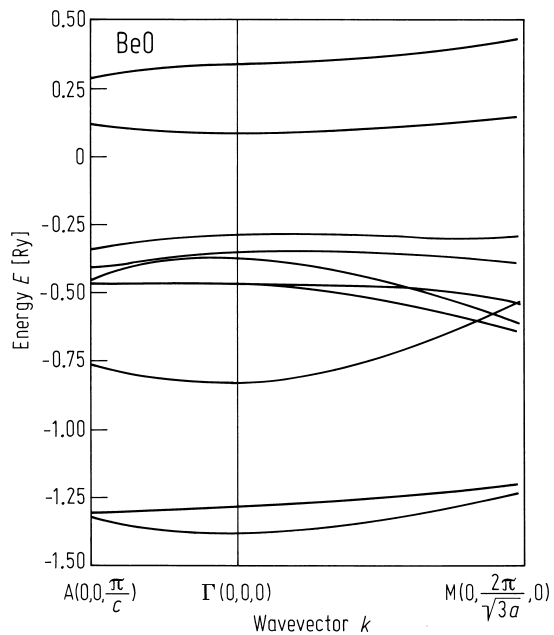


Fig. 3.0.6

BeO. Dispersion curves $E(k)$ along the high symmetry directions of the Brillouin zone of wurtzite BeO [90K].



3.2 Beryllium sulfide (BeS)

The stable BeS structure at normal pressure is the zincblende structure ($F\bar{4}3m - T_d^2$, Fig. 3.0.1) [72Y].

Physical properties

band structure

According to theory BeS is an indirect material with the highest valence band edge at Γ and the lowest conduction band edge at X (Fig. 3.0.7).

energy gap

$E_g(\Gamma-X)$	> 5.5 eV	absorption	72Y
-----------------	------------	------------	-----

lattice parameter

a	0.48630(5) nm	RT	XRD	72Y
-----	---------------	----	-----	-----

The electrical conductivity of polycrystalline BeS disks has been investigated in [93K, 95N] and has been found to be p-type. This has been attributed to Be vacancies or S interstitials.

density

d	2.36 g cm ⁻³	94C
-----	-------------------------	-----

References to 3.2

- | | |
|-----|---|
| 72Y | Yim, W.M., Dismukes, J.P., Stofko, E.J., Pfaff, R.J.: J. Phys. Chem. Solids 33 (1972) 501. |
| 93K | Kashahara, A., Ogawa, Y., Iwasaki, S., Nakamura, H.: Materials Transactions, JIM 34 (1993) 786. |
| 94C | CRC Handbook of Chemistry and Physics, Lide, D.R. (ed.),: CRC Press Inc. Boca Raton Fl. |
| 95N | Nakamura, H., Ogawa, Y., Kashahara, A., Iwasaki, S.: Materials Transactions JIM 36 (1995) 1263. |
| 97F | Friehlinghaus, D., Schroeder, K. Blügel, S. : Diplomarbeit 1997, Forschungszentrum Jülich. |

Figures to 3.2

Fig. 3.0.1

The zincblende lattice.

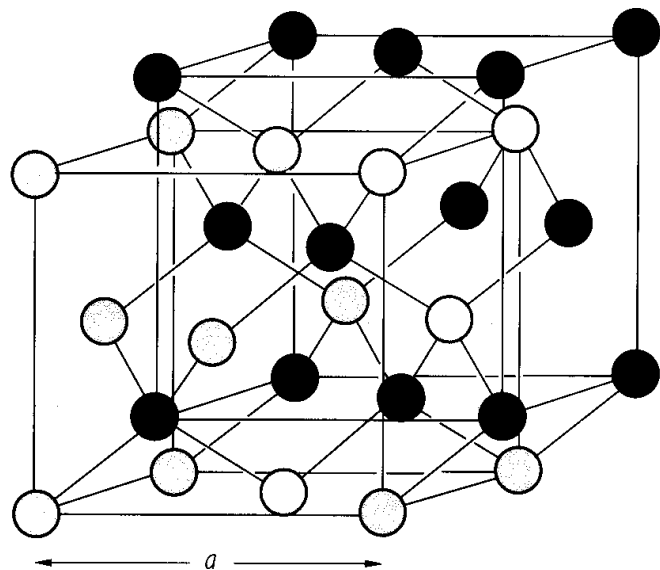
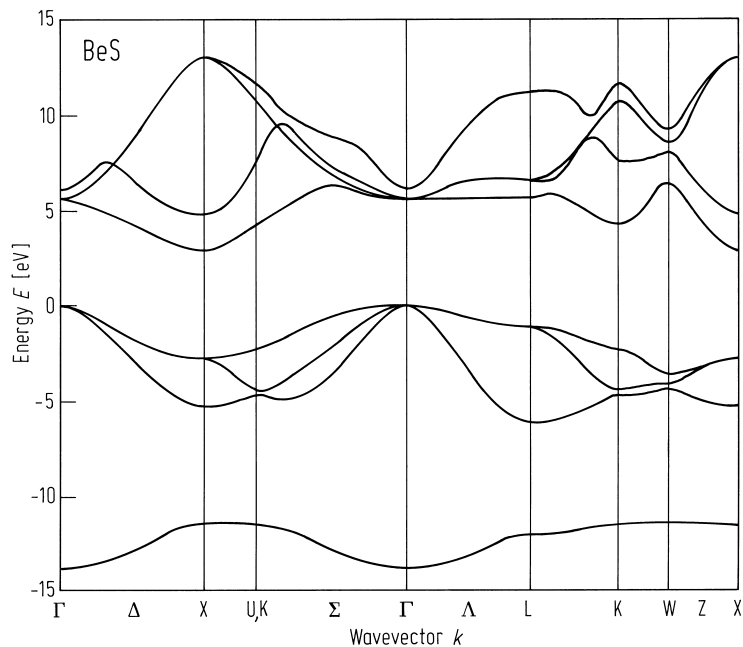


Fig. 3.2.1

BeS. Calculated band structure, obtained by first principles calculations based on the density functional theory in the local density approximation by use of a pseudopotential method with normconserving pseudopotentials [97F].



3.3 Beryllium selenide (BeSe)

The interest in BeSe is originating from the fact that ternary BeZnSe and BeMgZnSe alloys can be lattice matched to silicon substrates and can also be used as base material for blue-green emitting ZnSe based laser diodes grown on GaAs. The ternary alloy has a band gap of approximately 4 eV if lattice matched to silicon.

Physical properties

crystal structure

BeSe has the zincblende structure ($F\bar{4}3m - T_d^2$, Fig. 3.0.1).

According to theory BeSe is an indirect gap material with the highest valence band edge at Γ and the lowest conduction band edge at X. The experimentally determined band gap of BeSe is 5.6 eV at room temperature [98W].

band structure : Fig. 3.0.8.

lattice parameter

a	0.51520(23) nm	RT	epitaxial films, XRD	97G
-----	----------------	----	----------------------	-----

References to 3.3

- 97F Friehlinghaus, D.: Diplomarbeit 1997, Forschungszentrum Jülich.
- 97G Gall, R.: Diplomarbeit 1997, Universität Würzburg.
- 98W Wilmers, K., Wethkamp, T., Esser, N., Cobet, C., Richter, W., Wagner, V., Lugauer, H., Fischer, F., Gerhard, T., Keim, M., Cardona, M.: to be published in Phys. Rev. B (1998).

Figures to 3.3

Fig. 3.0.1

The zincblende lattice.

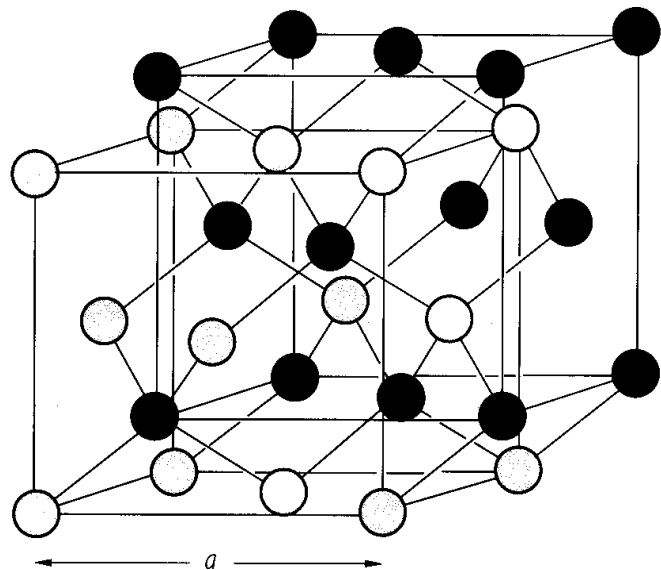
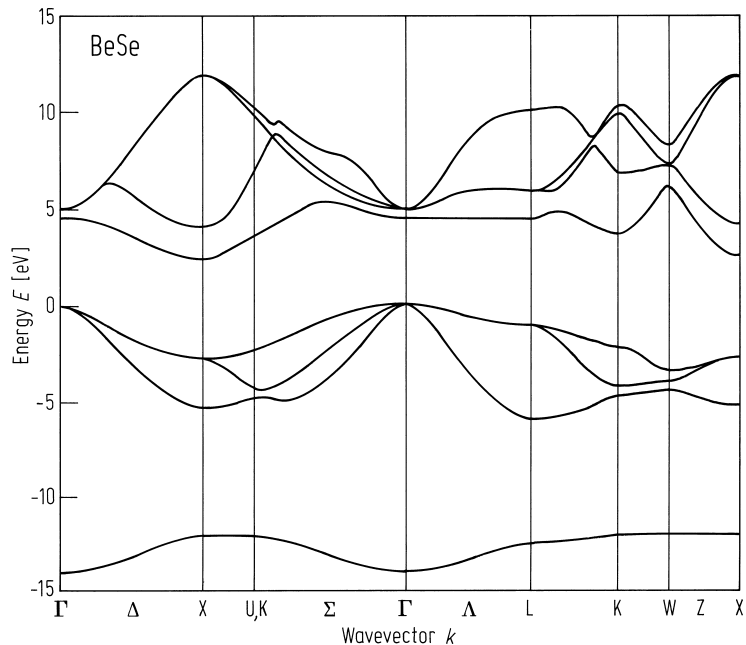


Fig. 3.0.8

BeSe. Band structure obtained by first principles calculations based on the density functional theory in the local density approximation by use of a pseudopotential method with normconserving pseudopotentials. [97F].



3.4 Beryllium telluride (BeTe)

Only very few reports on bulk BeTe are available in the literature. The interest in BeTe is originating from the close lattice match of this II-VI material to ZnSe and GaAs, and its usage in ZnSe based blue-green semiconductor laser diodes (e.g. for p-type contacts).

Crystal structure

The zincblende structure (Fig. 3.0.1) has been found to be the stable structure of BeTe at normal pressure and temperature.

Electronic and lattice properties

band structure : Fig. 3.0.9, Brillouin zone: Fig. 3.0.4.

energy gap

$E_{g,ind}$	2.8 eV	$T = 300\text{ K}$	optical reflection, ellipsometry	97W
$E_{g,dir}$	4.1 eV			

lattice parameters

a	0.56270(15) nm	$T = 300\text{ K}$	XRD, epitaxial films	97G
-----	----------------	--------------------	----------------------	-----

thermal expansion coefficient

α	$7.66(21) \cdot 10^{-6}\text{ K}^{-1}$	$T = 300\text{ K}$	XRD, epitaxial films	97G
----------	--	--------------------	----------------------	-----

Transport and optical properties

BeTe, like ZnTe, tends towards p-type conductivity. Using plasma assisted nitrogen doping during molecular beam epitaxy, very high p-type concentrations above 10^{20} cm^{-3} could be achieved [98W]. n-type doping of BeTe has not yet been reported. p-type BeTe thin films have been characterized by IR reflection, CV and van der Pauw measurements. Due to the high p-type doping levels, BeTe is used in efficient pseudomorphic p-contacts for ZnSe laser diodes.

far infrared properties

ϵ_{∞}	7	RT	infrared reflection	96B
$\bar{\nu}_{TO}$	461 cm^{-1}			
$\bar{\nu}_{LO}$	502 cm^{-1}			

References to 3.4

96B Becker, C., Küster, U., Kruse, R., Geurts, J., Lugauer, H., Fischer, F., Litz, Th., Waag, A., Landwehr, G.: Proc. Int. Conf. Physics of Semiconductors, Berlin 1996.

97F Frießlinghaus, D.: Diplomarbeit 1997, Forschungszentrum Jülich..

97G Gall, R.: Diplomarbeit 1997, Universität Würzburg.

97W Waag, A., Fischer, F., Lugauer, H.-J., Litz, Th., Gerhard, T., Nürnberger, J., Lunz, U., Zehnder, U., Ossau, W., Landwehr, G., Roos, B., Richter, H.: Mater. Sci. Eng. B 43 (1997) 65.

98W Waag, A., Fischer, F., Schüll, K., Baron, T., Lugauer, H.-J., Litz, Th., Zehnder, U., Gerhard, T., Landwehr, G.: Festkörperprobleme/Adv. Solid State Physics 37 (1998) 43.

Figures to 3.4

Fig. 3.0.1

The zincblende lattice.

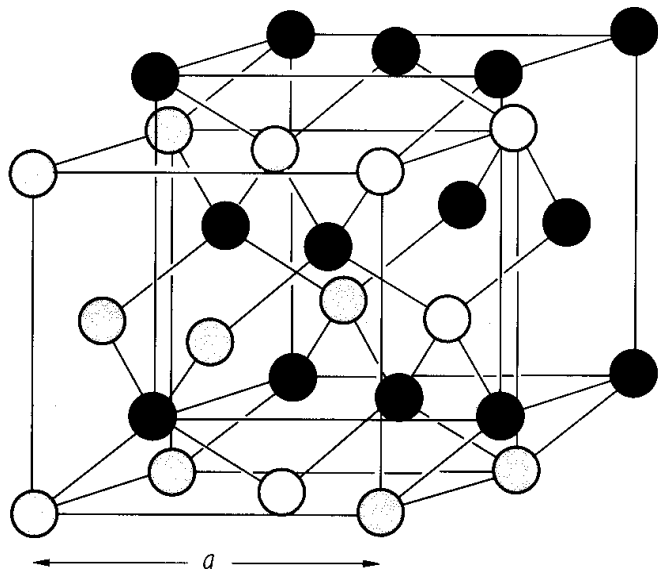


Fig. 3.0.4

The Brillouin zone for the zincblende and the rocksalt lattices.

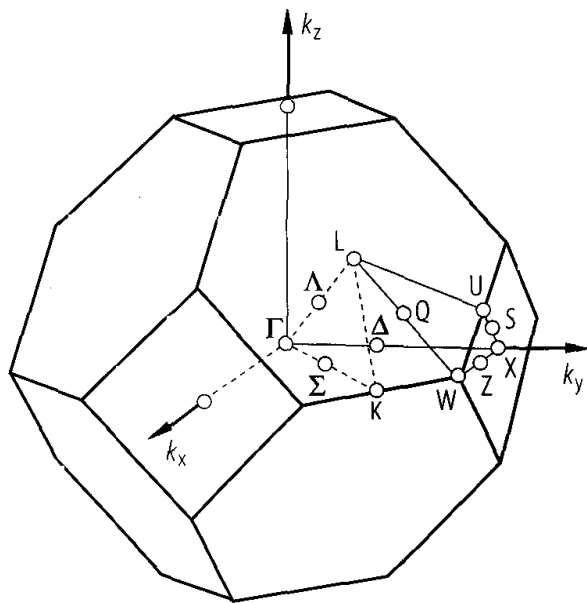
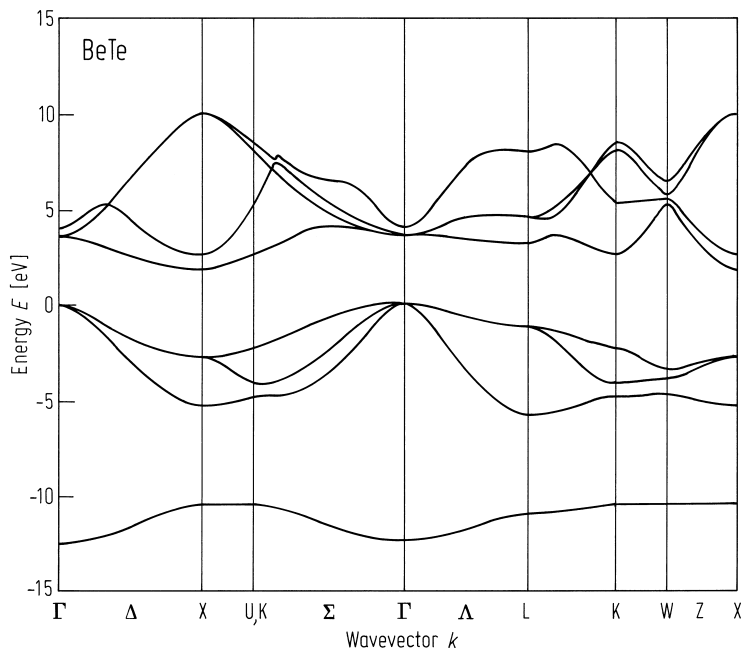


Fig. 3.0.9

BeTe. Band structure obtained by first principles calculations based on the density functional theory in the local density approximation by use of a pseudopotential method with normconserving pseudopotentials [97F].



3.5 Magnesium oxide (MgO)

Crystal structure

Under normal conditions, MgO crystallizes in the rocksalt (B1) structure (Fig. 3.0.3). This structure has been found to be stable at least up to 227 GPa [95D].

Electronic properties

band structure : Fig. 3.0.10, Brillouin zone: Fig. 3.0.4.

Disagreements exist about the position of the minimum of the lowest conduction band. [77D, 73W1 and 68F] place the minimum at Γ_1 and anticipate a direct gap, in [74P] the minimum is at X_3 indicating an indirect gap.

energy gap

$E_{\text{gx,dir}}$	7.672(10) eV	$T = 85 \text{ K}$	spin-orbit exciton states	73W3
$E_{\text{g,th}}$	7.9(7) eV	$T = 0 \text{ K}$	temperature dependence of microwave conductivity	77M

Lattice properties

lattice parameter

a	4.216 Å	$T = 298 \text{ K}$	X-ray diffraction measurements, powder samples	77H
-----	---------	---------------------	--	-----

linear thermal expansion coefficient

α	$9.84 \cdot 10^{-6} \text{ K}^{-1}$	$T = 283 \text{ K}$	measurement in a three-terminal capacitance cell, single crystal; temperature dependence: Fig. 3.5.1	73W2
----------	-------------------------------------	---------------------	--	------

phonon dispersion relations and phonon density of states

Fig. 3.5.2. For the Brillouin zone, see Fig. 3.0.4.

phonon frequencies

$\nu_{\text{TO}}(\Gamma)$	12.05 THz	$T = 300 \text{ K}$	determined from thin films by polarizrd specular reflectance	71B
$\nu_{\text{LO}}(\Gamma)$	21.52 THz	$T = 300 \text{ K}$		

second order elastic moduli

c_{11}	$29.71(6) \cdot 10^{11} \text{ dyn/cm}^2$	$T = 293 \text{ K}$	determined from single crystals by a resonance method, density $d = 3.578 \text{ g cm}^{-3}$	76S
c_{12}	$9.65(7) \cdot 10^{11} \text{ dyn/cm}^2$			
c_{44}	$15.57(2) \cdot 10^{11} \text{ dyn/cm}^2$			

third-order elastic moduli

c_{111}	$-489.5(150) \cdot 10^{11} \text{ dyn/cm}^2$	$T = 298 \text{ K}$	determined from the ultrasonic velocity as a function of uniaxial and hydrostatic pressure	65B
c_{112}	$-9.5(90) \cdot 10^{11} \text{ dyn/cm}^2$			
c_{123}	$-6.9(220) \cdot 10^{11} \text{ dyn/cm}^2$			
c_{144}	$11.3(40) \cdot 10^{11} \text{ dyn/cm}^2$			
c_{166}	$-65.9(20) \cdot 10^{11} \text{ dyn/cm}^2$			
c_{456}	$14.7(10) \cdot 10^{11} \text{ dyn/cm}^2$			

bulk modulus

B	160.3(3) GPa			95D
-----	--------------	--	--	-----

compressibility

κ	1.538 Mbar ⁻¹			85G
----------	--------------------------	--	--	-----

Debye temperature

$\Theta_D(0)$	948(4) K		calculated from elastic constants (see also [65A, 61W])	71M
---------------	----------	--	---	-----

density

d	3.576 g cm ⁻³	$T = 298$ K		75L
-----	--------------------------	-------------	--	-----

melting temperature

T_m	2827°C			87W
-------	--------	--	--	-----

boiling temperature

T_b	4070 K			75L
-------	--------	--	--	-----

Transport properties

Electrical transport measurements on alkaline earth oxides encounter several difficulties such as high resistance at low temperatures, strong influence of surface layers, high-temperature thermionic emission etc. The in parts contradictory results considerably depend on the sample purity and nature (pressed porous powders, sintered samples, polycrystals and single crystals) and the particular experimental conditions. As in several semiconducting oxides, conductivity and conduction type are also determined by the oxygen partial pressure of the ambient atmosphere (Fig. 3.5.3).

In high-purity MgO crystals "low" temperatures (< about 1600 K) favour ionic conduction, whereas above 2000 K electronic conduction is increasingly predominant. At low oxygen pressures (< 10⁻³ mbar) the conduction is n-type, at high pressures (> 10⁻¹ mbar) ionic and electronic hole conduction seem to be superimposed.

electrical conductivity : Fig. 3.5.3

thermoelectric power : Fig. 3.5.4.

mobility of charge carriers

μ_p	≈ 10 cm ² /Vs	$T = 350...400$ K	mean value estimated from analysis of post-bombardment conductivity	65P
---------	----------------------------------	-------------------	---	-----

thermal conductivity : Fig. 3.5.5.

Optical properties

dielectric constants

$\varepsilon(0)$	9.830	$T = 300$ K	capacitance measurement, single crystal	79W
$\varepsilon(\infty)$	2.944	$T = 300$ K	$\varepsilon(\infty) = n_\infty^2$, n_∞ from extrapolation of $n(\omega)$ to low frequencies ($h\nu \ll E_g$)	70B

For the real and imaginary parts of the dielectric constant see Fig. 3.5.6.

References to 3.5

- 36B Bouckaert, L. P., Smoluchowski, R., Wigner, E.: Phys. Rev. 50 (1936) 58.
65B Bogardus, E. H.: J. Appl. Phys. 36 (1965) 2504.
65P Pollard, J. H., Bowler, D. L., Pomerantz, M. A.: J. Phys. Chem. Solids 26 (1965) 1325.
66W White, G. K., Anderson, O. L.: J. Appl. Phys. 37 (1966) 430.
67R Roessler, D. M., Walker, W. C.: Phys. Rev. 159 (1967) 733.
68F Fong, C. Y., Saslow, W., Cohen, M. L.: Phys. Rev. 168 (1968) 992.
70B Boswarva, I. M.: Phys. Rev. B1 (1970) 1698.
70S Sangster, M. J. L., Peckham, C., Saunderson, D. H.: J. Phys. C. 3 (1970) 1026.
71B Bates, J. B., Brooker, M. H.: J. Phys. Chem. Solids 32 (1971) 2403.
71M Marklund, K., Mahmoud, S. A.: Physica Scripta 3 (1971) 75.
71O Osburn, C. M., Vest, R. W.: J. Am. Ceram. Soc. 54 (1971) 428.
73W1 Walch, P. F., Ellis, D. E.: Phys. Rev. B8 (1973) 5920.
73W2 White, G. K.: J. Phys. D: Appl. Phys. 6 (1973) 2070.
73W3 Whited, R. C., Flaten, C. J., Walker, W. C.: Solid State Commun. 13 (1973) 1903.
74A Afzal, F. A., Giutronich, J. E.: J. Phys. E.; Sci. Instr. 7 (1974) 579.
74K Kupperman, D. S., Weinstock, H., Chen, Y.: J. Low Temp. Phys. 14 (1974) 277.
74P Pantelides, S. T., Mickish, D. J., Kunz, A. B.: Phys. Rev. B10 (1974) 5203.
75L Landolt-Börnstein: Zahlenwerte und Funktionen aus Naturwissenschaften und Technik. N. S. Vol. III/7h1. Berlin 1975.
76S Sumino, Y., Ohno, I., Goto, T.: J. Phys. Earth 24 (1976) 263.
77D Daude, N., Jouanin, C., Gout, C.: Phys. Rev. B15 (1977) 2399.
77H Hirata, K., Moriya, K., Waseda, Y.: J. Mater. Sci. 12 (1977) 838.
77M Mochizuki, S., Sakurai, T.: Phys. Status Solidi. (a) 41 (1977) 411.
79K Kwang-Oh Park, Sivertsen, J. M.: J. Am. Ceram. Soc. 62 (1979) 218.
79W Wintersgill, M., Fontanella, J., Andeen, C., Schuele, D.: J. Appl. Phys. 50 (1979) 8259.
85G Goble, R. Y., Scott, S. D.: Can. J. Mineral. 23 (1985) 273.
87W Wriedt, H. A.: Bull. Alloy Phase Diagr. 8 (1987) 227.
94S Schütt, O., Pavone, P., Windl, W., Karch, K., Strauch, D.: Phys. Rev. B 50 (1994) 3746.
95D Duffy, T.S., Hemley, R.J., Ho-kwang Mao: Phys. Rev. Lett. 74 (1995) 1371.

Figures to 3.5

Fig. 3.0.3

The rocksalt lattice.

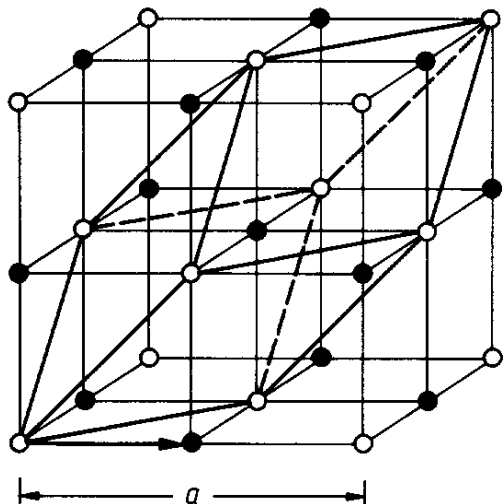


Fig. 3.0.4

The Brillouin zone for the zincblende and the rocksalt lattices.

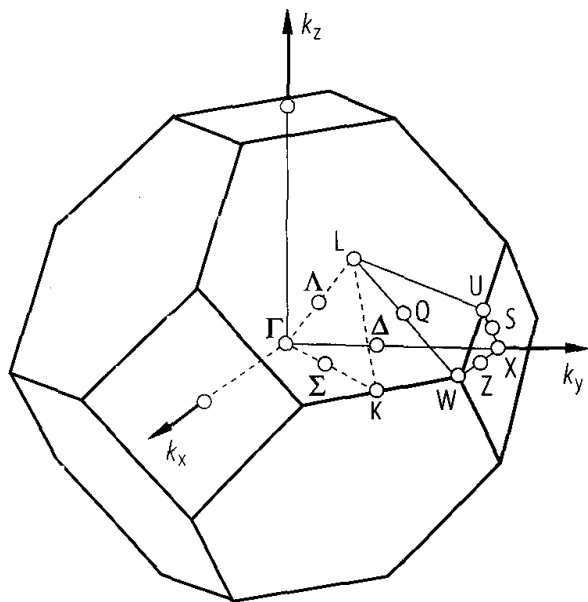


Fig. 3.0.10

MgO. Band Structure calculated by a combined tight-binding and pseudopotential method [77D]. Symmetry notations are those of [36B]. 1 Ry = 13.606 eV.

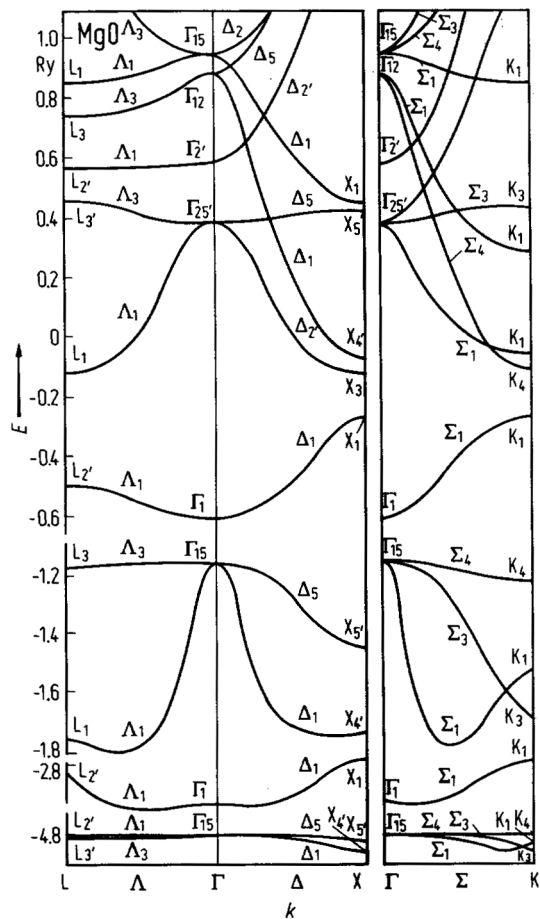


Fig. 3.5.1

MgO, BaO. Linear thermal expansion coefficient α vs. temperature. Open circles: [79K], full circles: [66W].

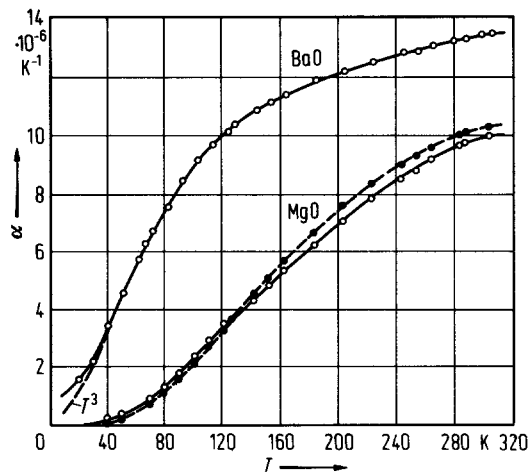


Fig. 3.5.2

MgO. Phonon dispersion curves (left panel) and density of states (right panel). Experimental data points [70S] and ab-initio calculations ([94S] solid lines).

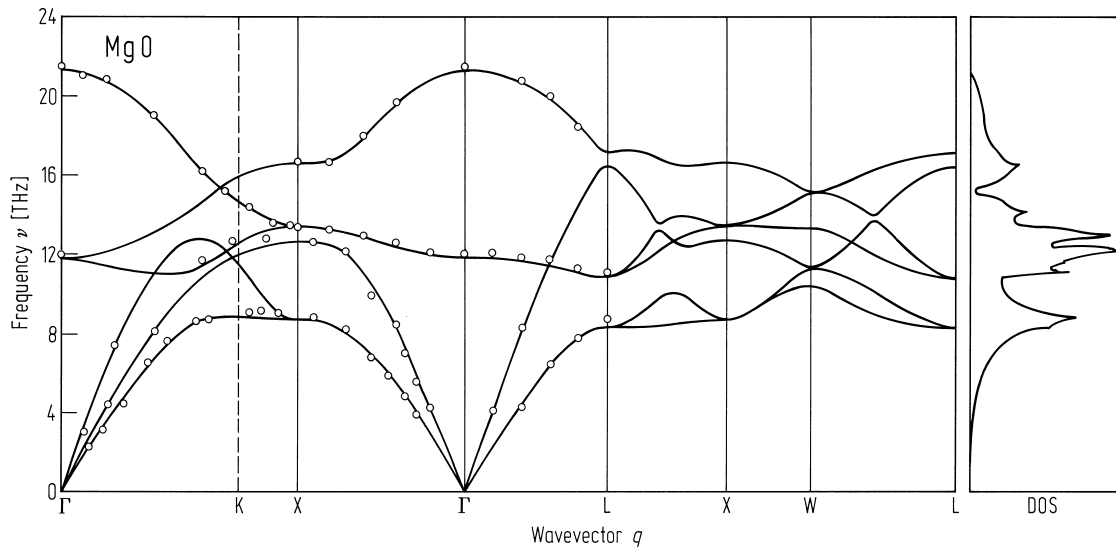


Fig. 3.5.3

MgO. Electrical conductivity σ of a high-purity single crystal at various temperatures vs. oxygen partial pressure p_{O_2} [710]. The numbers between the curves for 1673 K and 1773 K indicate the slopes of the adjacent straight lines.

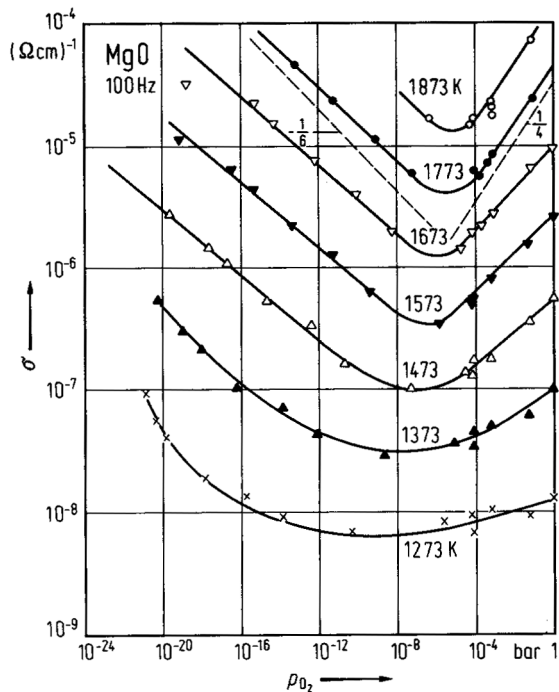


Fig. 3.5.4

MgO. Thermoelectric power S vs. temperature [74A]. Crystal contains an impurity concentration of 116 ppm. Ambient atmosphere free of oxygen.

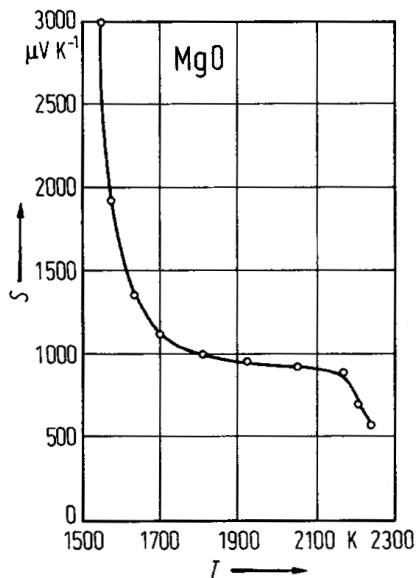


Fig. 3.5.5

MgO. Thermal conductivity κ vs. temperature [74K]. Curve a: high-purity crystal, b: after additive coloration in Mg vapor, c: after subsequent bleaching with uv light.

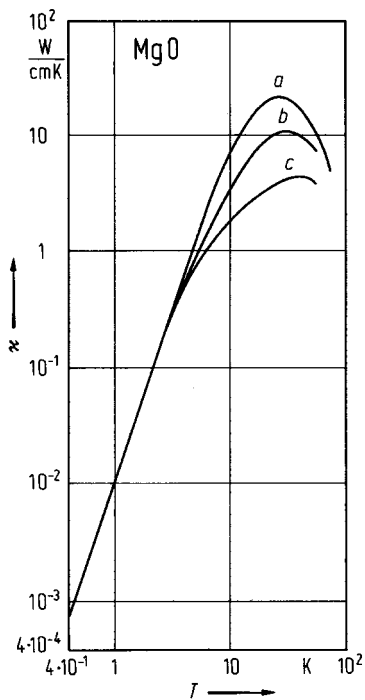
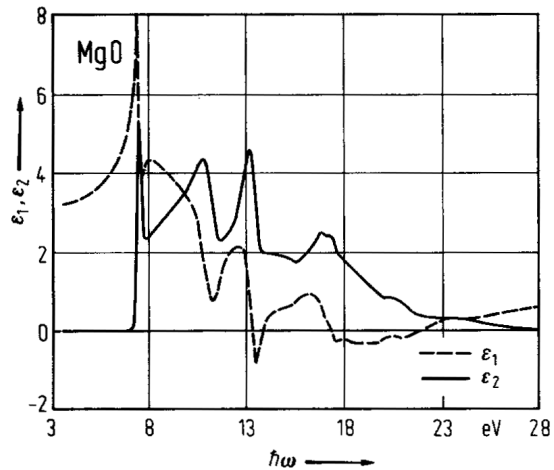


Fig. 3.5.6

MgO Real and imaginary part ϵ_1 and ϵ_2 of the dielectric constant vs photon energy at 300 K [67R].



3.6 Magnesium sulfide (MgS)

Crystal structure

MgS crystallizes in the rocksalt structure (B1, Fig. 3.0.3).

Electronic and lattice properties

band structure

The electronic structure and total energy of MgS has been studied using first principles self consistent local density calculations for different structures, finding a rocksalt structure as the stable structure for MgS [95L]. It has also been demonstrated experimentally that MgS crystallizes in the NaCl structure [93P].

Calculated band structure of the zincblende and rocksalt phase: Fig. 3.0.11 [96K].

energy gap

E_g	4.5 eV	$T = 77\text{ K}$,	extrapolation from $\text{Zn}_{1-x}\text{Mg}_x(\text{S,Se})$	92O
	4.87 eV	wurtzite	zincblende extrapolation from $\text{Zn}_{1-x}\text{Mg}_x\text{S}$	89C

lattice parameter

a	0.5203 nm	$T = 300\text{ K}$	XRD	63W
-----	-----------	--------------------	-----	-----

density

d	2.86 g cm^{-3}			93H
-----	-------------------------	--	--	-----

References to 3.6

63W Wyckoff, R.W.G.: Crystal Structures, Wiley: New York, 1963.
89C Chakrabarti, K., Mathur, V.K., Abbundi, R.J.: Phys. Rev. B 39 (1989) 10406.
92O Okuyama, H., Nakano, K., Miyajima, T., Akimoto, K.: J. Cryst. Growth 117 (1992) 139.
93H Hawleays Condensed Chemical Dictionary, 12th edition, Lewis, R.J.van Nostrand Reinhold, New York (1993).
93P Peiris, S.M., Powell, A.J., Heinz, D.L.: J. Phys. Chem. Solids 55 (1993) 413.
96K Kalpana, G., Palanivel, B., Thomas, R.M., Rajagopalan, M.: Physica B 222 (1996) 223.
95L Lee, S.G., Chang, K.J.: Phys. Rev. B 52 (1995) 1918.

Figures to 3.6

Fig. 3.0.3

The rocksalt lattice.

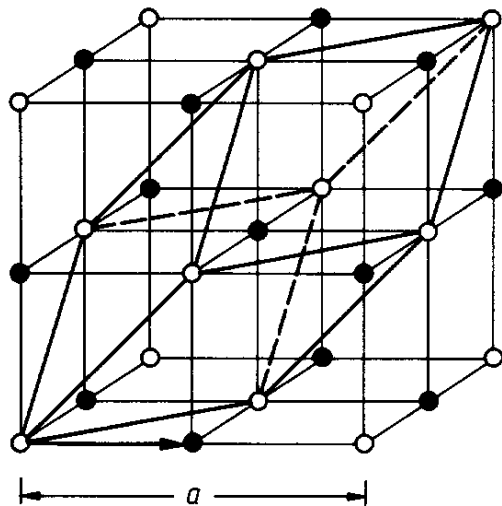
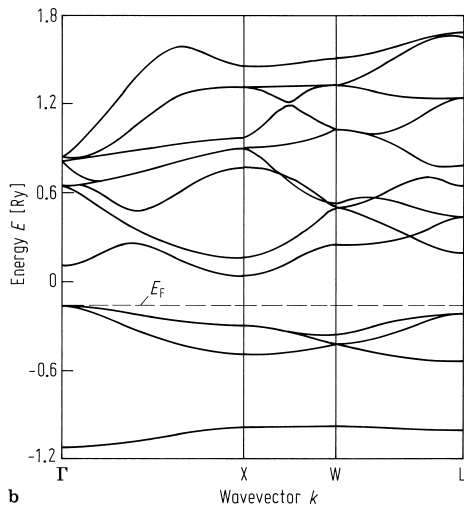
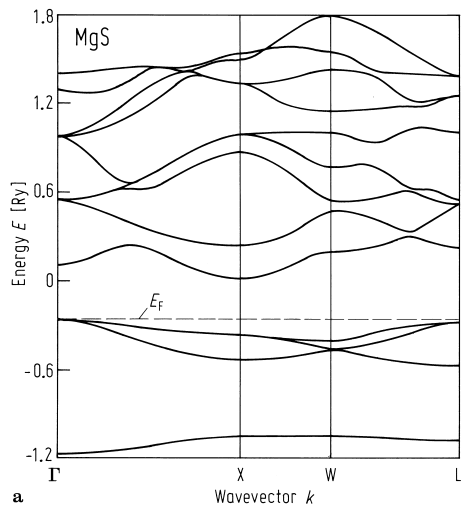


Fig. 3.0.11

MgS. Band structure of the zincblende B3 (a) and rocksalt B1 (b) structure, by using a tight binding muffin tin orbital method [96K].



3.7 Magnesium selenide (MgSe)

Crystal structure

MgSe crystallizes in the NaCl structure (B1, Fig. 3.0.3).

Electronic and lattice properties

band structure

The electronic structure and total energy of MgSe has been studied using first principles self consistent local density calculations for different structures, finding a NaCl structure as the stable structure [95L]. See Fig. 3.0.12.

energy gap

E_g	4.05 eV	$T = 300\text{ K}$	zincblende, extrapolation from $\text{Zn}_{1-x}\text{Mg}_x(\text{S,Se})$	96L
-------	---------	--------------------	--	-----

lattice parameter

a	0.5904 nm	300 K	XRD, zincblende	96L
	0.546 nm	300K	XRD, rocksalt	96J

dielectric constant

$\epsilon(\infty)$	3.8	RT	zincblende, Raman scattering	95H
--------------------	-----	----	------------------------------	-----

density

d	4.21 g cm ⁻³			89M
-----	-------------------------	--	--	-----

References to 3.7

89M The Merck Index, 11th Ed., Merck Co. Inc. Rahway N.Y. (1989).
95H Huang, D., Jin, C., Wang, D., Liu, X.: Appl. Phys. Lett. 67 (1995) 3611.
95L Lee, S.G., Chang, K.J.: Phys. Rev. B 52 (1995) 1918.
96J Jobst, B., Hommel, D., Lunz, U., Gerhard, T., Landwehr, G.: Appl. Phys. Lett. 69 (1996) 97.
96K Kalpana, G., Palanivel, B., Thomas, R.M., Rajagopalan, M.: Physica B 222 (1996) 223.
96L Litz, M., Watanabe, K., Korn, M., Ress, H., Lunz, U., Ossau, W., Waag, A., Landwehr, G., Walther, Th., Neubauer, B., Gerthsen, D., Schüssler, U.: J. Cryst. Growth 159 (1996) 54.

Figures to 3.7

Fig. 3.0.3

The rocksalt lattice.

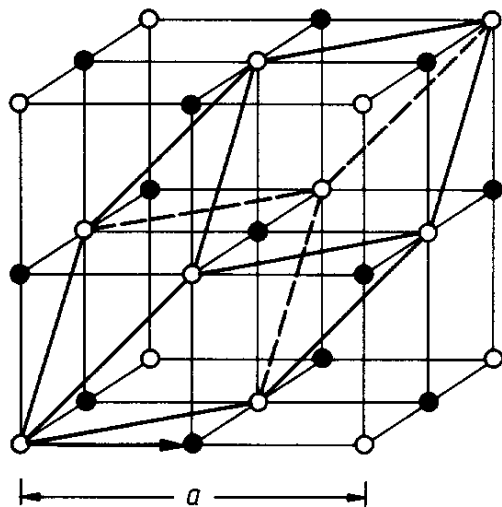
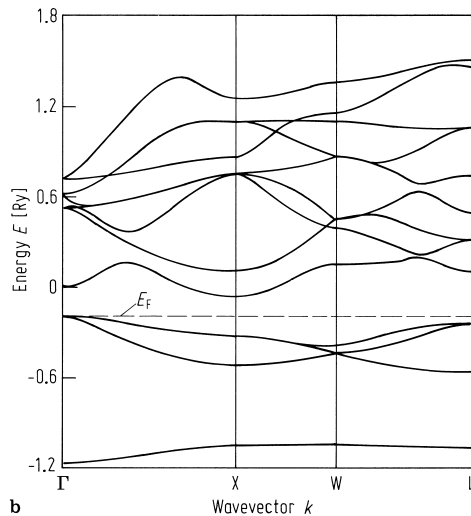
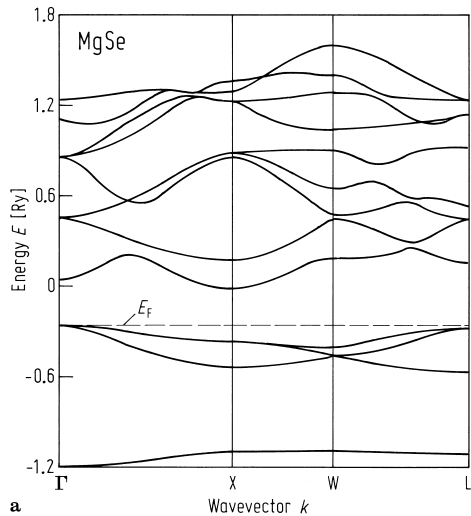


Fig. 3.0.12

MgSe. Band structure in the zincblende (a) and rocksalt (b) structure, by using a tight binding muffin tin orbital method [96K].



3.8 Magnesium telluride (MgTe)

Crystal structure

MgTe has been determined to have the wurtzite structure [71K, 51K, 71P] (Fig. 3.0.2).

Electronic and lattice properties

band structure

The band structure of zincblende MgTe has been calculated by [94F] (see Fig. 3.0.13).

energy gap

E_g	3.49 eV	RT	photoluminescence, epitaxial films, zincblende	96L
-------	---------	----	--	-----

lattice parameters

a	0.45303 nm			95C
c	0.74056 nm			

wavenumbers of phonons

$\bar{\nu}_{TO}$	235 cm ⁻¹	$T = 300\text{ K}$	Raman	96V
$\bar{\nu}_{LO}$	292 cm ⁻¹			

References to 3.8

51K Klemm, W., Wahl, K.: Anorg. Allgem. Chem. 266 (1951) 289.
71K Kuhn, A., Chevy, A., Naud, M.J.: J. Cryst. Growth 9 (1971) 263.
71P Parker, S.G., Reinberg, A.R., Pinnell, J.E., Holton, W.C.: J. Electrochem. Soc. 118 (1971) 979.
94F Freytag, B.: J. Phys: Condens. Matter 6 (1994) 9875.
95C van Camp, P.E., van Doren, V.E.: Int. J. Quant. Chem. 55 (1995) 339.
96L Litz, M.Th., Watanabe, K., Korn, M., Ress, H., Lunz, U., Ossau, W., Waag, A., Landwehr, G., Walter, Th., Neubauer, B., Gerthsen, D., Schüssler, U.: J. Cryst. Growth 159 (1996) 54.
96V Vogelgesang, R., Mayur, A.J., Dean Sciacca, M.E., Oh, M., Miotkowski, I., Ramdas, A.K., Rodriguez, S., Bauer, G.: J. Raman Spectroscopy 27 (1996) 239.

Figures to 3.8

Fig. 3.0.2

The wurtzite lattice.

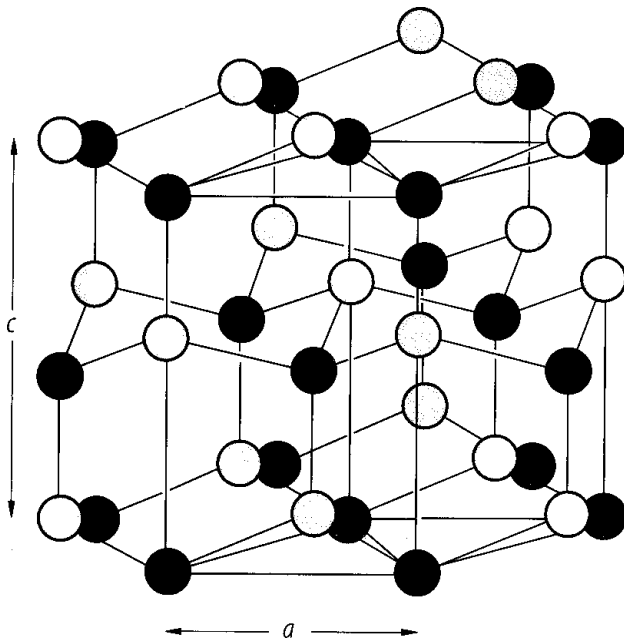
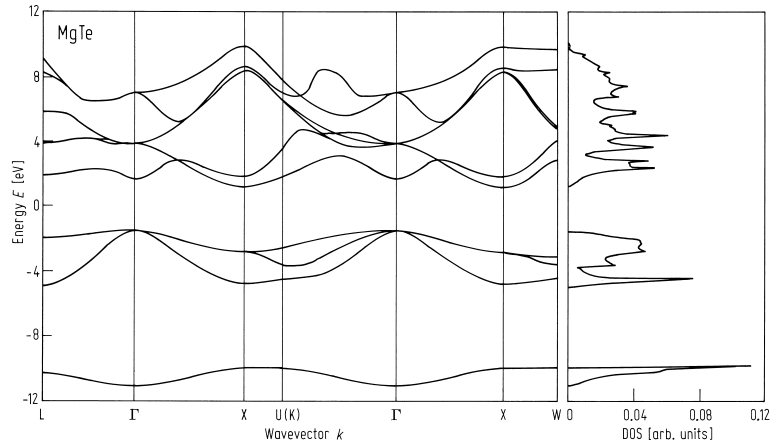


Fig. 3.0.13

MgTe. Band structure of zincblende MgTe according to [94F]. DOS in arbitrary units.



3.9 Calcium oxide (CaO)

Crystal structure

CaO crystallizes in the rocksalt structure (B1, Fig. 3.0.3).

Electronic properties

band structure : Fig. 3.0.14, Brillouin zone: Fig. 3.0.4.

Some controversy in the literature exists about the positions of the lowest conduction band minima. In [77D] the lowest minimum is the Γ_1 one and the minimum of the d states is at X_3 , below some s states but above Γ_1 . In [75S] the symmetry of the conduction band bottom is X_3 instead of Γ_1 , whereas in [72M] Γ_1 and X_3 are nearly degenerate.

energy gap

$E_{g,dir}$	6.931(6) eV	$T = 85$ K	spin-orbit exciton states	73W
$E_{g,th}$	7.8 eV	$T = 0$ K	estimated from the temperature	75K2

effective masses

m_n	$0.50 m_0$	$T = 700$ K	estimated by comparing measured and calculated Hall mobility	75K1
m_n^{**}	$0.68 m_0$	$T = 700...800$ K	polaron mass	75K1

Lattice properties

lattice parameter

a	4.8110(2) Å	$T = 297$ K	X-ray diffraction measurements, single crystal	68S
-----	-------------	-------------	--	-----

linear thermal expansion coefficient

α	$15.2 \cdot 10^{-6} \text{ K}^{-1}$	$T = 1100$...1600 K	mean value, X-ray diffraction, single crystal	71K1
----------	-------------------------------------	-------------------------	---	------

phonon dispersion relations and density of states : Fig. 3.9.1.

phonon frequencies

$\nu_{LO}(q/q_{max}=0.2)$	16.40(25) THz	$T = 293$ K	<100> direction, inelastic thermal neutron scattering (more extensive table in [71S1] and [71S2])	71S2
$\nu_{TO}(\Gamma)$	8.8(4) THz			
$\nu_{LO}(X)$	12.00(22) THz			
$\nu_{TO}(X)$	9.4(5) THz			
$\nu_{TA}(X)$	6.48(11) THz			

second order elastic moduli

c_{11}	221.89(60) GPa	$T = 298$ K	calculated from sound velocities, adiabatic condition	77C
c_{12}	57.81(66) GPa			
c_{44}	80.32 (10) GPa			

temperature dependence of elastic moduli

dc_{11}/dT	- 0.489 kbar/K	ultrasonic pulse echo technique	77C
dc_{12}/dT	- 0.052 kbar/K		
dc_{44}/dT	- 0.068 kbar/K		

bulk modulus				
B	114(9) GPa	RT	pulse-echo technique	72B
compressibility				
κ	3.32 Mbar ⁻¹			85G
Debye temperature (in K)				
$\Theta_D(0)$	605(2)		deduced from heat capacity measurements in the range 1.2 to 4.2 K; Θ_D values in the range 1.2 to 300K: see Fig. 3.9.2	69G
heat capacity				
C_p	14.700 J/mol K 42.210 J/mol K	$T = 100$ K $T = 300$ K		69G
density				
d	3.335 g cm ⁻³			75L
melting temperature				
T_m	2900 (−50, +300) K			87L
boiling temperature				
T_b	3123 K			75L

Transport properties

For general remarks see the comments on the transport properties of MgO. The charge carrier transport of CaO is discussed in various models, e.g. polaron band conduction [75K1, 75K2], hopping conduction through compensated semiconducting samples [66S], also with regard to a considerable contribution of ionic conductivity [62P]. From measurements of the oxygen pressure dependence of the conductivity in undoped CaO it is concluded that at low pressures ($< 10^{-2} \dots 10^{-4}$ mbar) n-type conduction, at higher pressures ($> 10^{-2} \dots 1$ mbar) p-type conduction exists [72F1, 53H]. In some cases this conclusion is confirmed by Hall and thermoelectric measurements [75K1, 72F2]. For intermediate pressures it is supposed that the lattice disorder (presumably of Schottky-type) gives rise to prevailing ionic conduction.

electrical conductivity: Figs. 3.9.3; **Hall mobility** : Fig. 3.9.4.

electron mobility

$\mu_{H,n}$	8 cm ² /Vs	$T = 700$ K, $p_{O_2} \leq 10^{-6}$ mbar	Hall mobility from measurements on single crystals; for temperature dependence $\mu_n \propto T^{-1.4}$, see Fig. 3.9.4	75K1
-------------	-----------------------	---	--	------

thermal conductivity

κ	0.3 W/cm K	$T = 300$ K	temperature dependence in the range 80...1100 K: Fig. 3.9.5	71K2
----------	------------	-------------	---	------

Optical properties

spectral dependence of optical constants in the range of interband transitions: Fig. 3.9.6.

dielectric constants

$\varepsilon(0)$	12.01 (10)	$T = 273$ K	capacitance measurement at 1 kHz and 10 kHz (data for $ (1/\varepsilon)d\varepsilon/dT _p$, $ (1/\varepsilon)d\varepsilon/dp _T$ and $ (1/\varepsilon)d\varepsilon/dT _p$, see <i>ibid.</i>	79B
$\varepsilon(\infty)$	3.27		compilation	81S

References to 3.9

- 36B Bouckaert, L. P., Smoluchowski, R., Wigner, E.: Phys. Rev. 50 (1936) 58.
- 53H Hauffe, K., Tränckler, G.: Z. Phys. 136 (1953) 166.
- 62P Pal'guev, S. F., Neuimin, A. D.: Sov. Phys. Solid State 4 (1962) 629.
- 66S Surplice, N. A.: Brit. J. Appl. Phys. 17 (1966) 175.
- 68S Smith, D. K., Leider, H. R.: J. Appl. Cryst. 1 (1968) 246.
- 69G Gmelin, E.: Z. Naturforsch. 24a (1969) 1794.
- 69W Whited, R. C., Walker, W. C.: Phys. Rev. 188 (1969) 1380.
- 71K1 Kamada, O., Takizawa, T., Sakurai, T.: Jpn. J. Appl. Phys. 10 (1971) 485.
- 71K2 Kovalev, N. N., Petrov, A. V., Sorokin, O. V.: Sov. Phys. Solid State 13 (1971) 233.
- 71S1 Saunderson, D. H., Peckham, G. E.: Int. Conf. Phonons, 1971 Rennes, M. A. Nusimovivi, (ed.), Paris 1971, p. 171.
- 71S2 Saunderson, D. H., Peckham, G. E.: J. Phys. C.; Solid State Phys. 4 (1971) 2009
- 72B Bartels, R. A., Vetter, V. H.: J. Phys. Chem. Solids 33 (1972) 1991.
- 72F1 Fischer, W. A., Janke, D., Zielinski, K.: Ber. Dt. Keram. Ges. 49 (1972) 362.
- 72F2 Fischer, W. A., Janke, D., Zielinski, K.: Ber. Dt. Keram. Ges. 49 (1972) 401.
- 72M Mattheiss, L. F.: Phys. Rev. B5 (1972) 290 and 306.
- 72V Vijayaraghavan, P. R., Marsongkohadi X., Iyengar, P. K.: in Proc. Symp. Neutron Inelastic Scattering IAEA: Vienna, 1972, p. 95.
- 73R Rieder, K. H., Weinstein, B. A., Cardona, M., Bilz, H.: Phys. Rev. B 8 (1973) 4780.
- 73W Whited, R. C., Flaten, C. J., Walker, W. C.: Solid State Commun. 13 (1973) 1903.
- 75K1 Kovalev, N. N., Krasin'kova, M. V.: Sov. Phys. Solid State 16 (1975) 1842.
- 75K2 Kovalev, N. N., Krasin'kova, M. V.: Sov. Phys. Solid State 16 (1975) 1960.
- 75L Landolt-Börnstein: Zahlenwerte und Funktionen aus Naturwissenschaften und Technik. N. S. Vol. III/17b1. Berlin 1975.
- 75S Seth, V., Chaney, R.: Phys. Rev. B12 (1975) 5923.
- 77C Chang, Z. P., Graham, E. K.: J. Phys. Chem. Solids 38 (1977) 1355.
- 77D Daude, N., Jouanin, C., Gout, C.: Phys. Rev. B15 (1977) 2399.
- 79B Bartels, R. A., Koo, J. C., Thomas, M. L.: Phys. Status Solidi (a) 52 (1979) K 213.
- 81S Sangster, M. L. J., Stoneham, A. M.: Philos. Mag. B 43 (1981) 597.
- 85G Goble, R. Y., Scott, S. D.: Can. J. Mineral. 23 (1985) 273.
- 87L Lamoreaux, R. H., Hildenbrand, D. L., Brewer, L.: J. Phys. Chem. Ref. Data 16 (1987) 419.
- 94S Schütt, O., Pavone, P., Windl. W., Karch, K., Strauch, D.: Phys. Rev. B 50 (1994) 3746.

Figures to 3.9

Fig. 3.0.3

The rocksalt lattice.

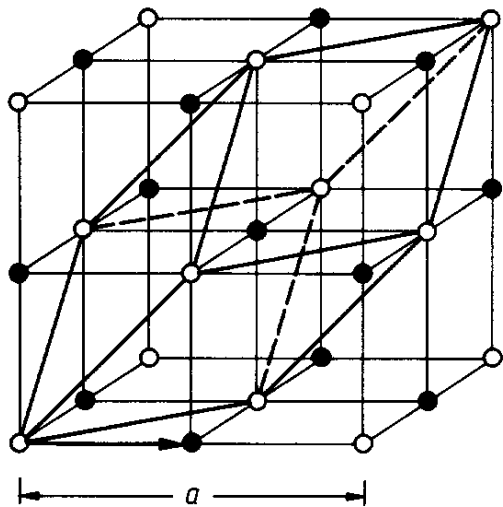


Fig. 3.0.4

The Brillouin zone for the zincblende and the rocksalt lattices.

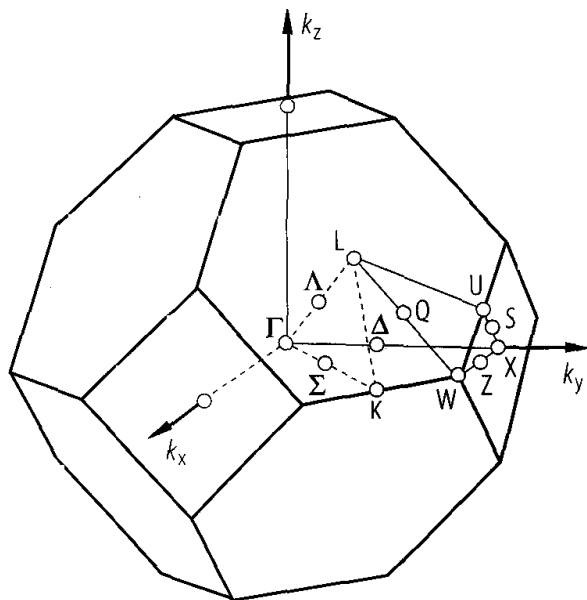


Fig. 3.0.14

CaO. Band structure calculated by a combined tight-binding and pseudopotential method [77D]. Symmetry notations are those of [36B].

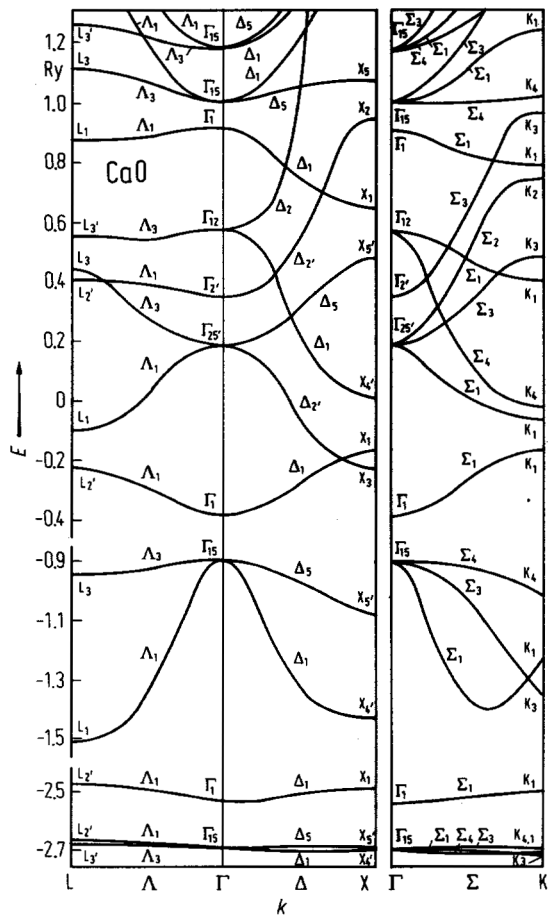


Fig. 3.9.1

CaO. Phonon dispersion curves (left panel) and density of states (right panel). Experimental neutron scattering data (open circles [71S2] and full circles [72V]), optical data (triangles [73R]) and ab-initio calculations ([94S] solid lines).

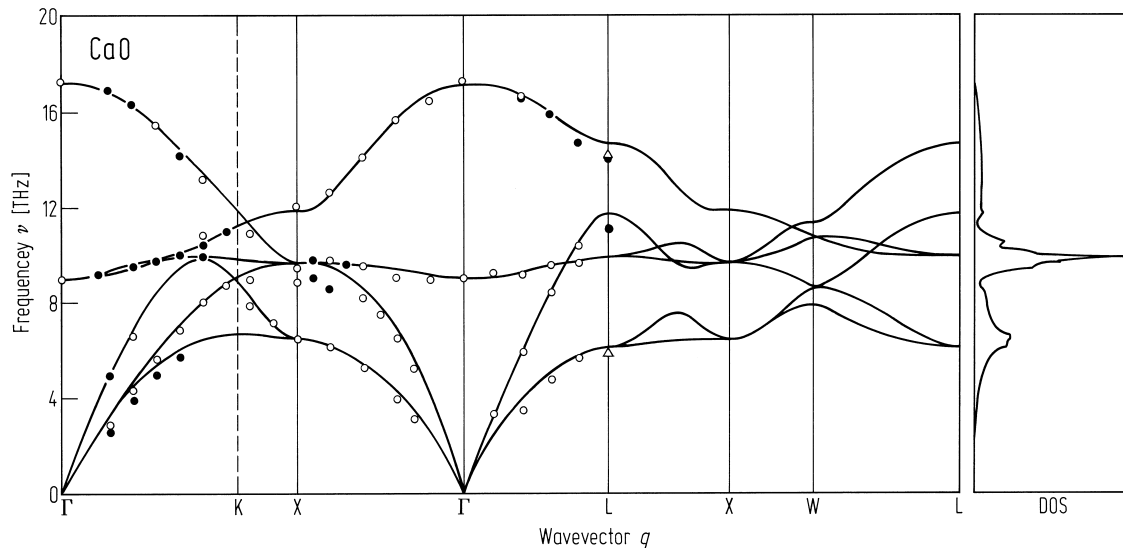


Fig. 3.9.2

CaO. Debye temperature Θ_D vs. temperature. Different symbols measured with different methods and from various authors. For details, see [69G].

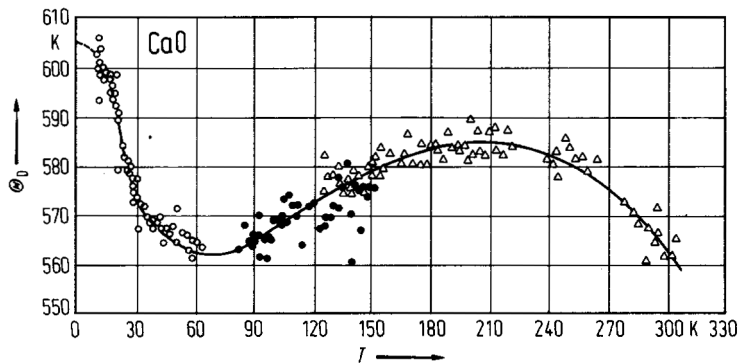


Fig. 3.9.3

CaO. Electrical conductivity σ (solid curves) and thermoelectric power S (dashed curves) of two single crystals vs. $1/T$ [75K2]. $p_{O_2} \geq 3 \cdot 10^{-5}$ mbar. n-type conduction at temperatures below the discontinuity.

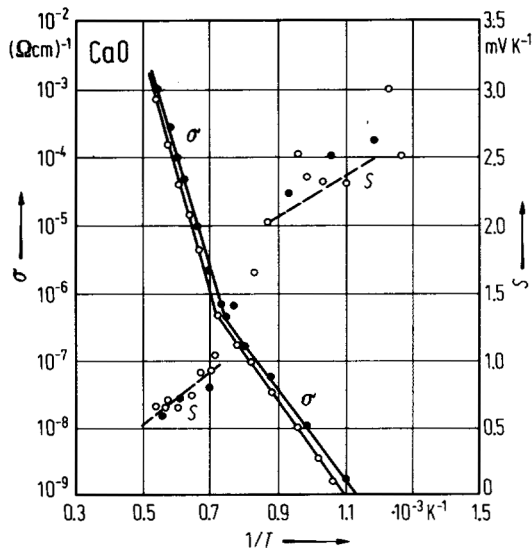


Fig. 3.9.4

BaO, SrO, CaO. Electron Hall mobility vs. temperature [75K1]. Different symbols correspond to different samples.

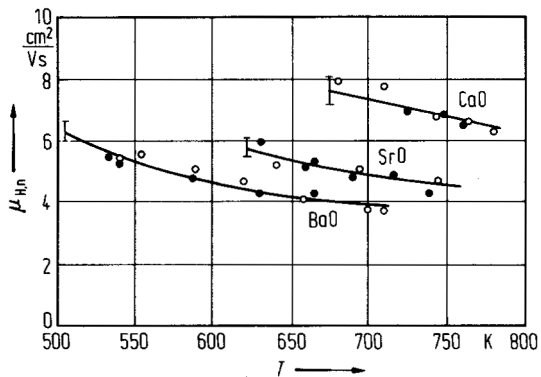


Fig. 3.9.5

MgO, CaO, SrO, BaO. Temperature dependence of the thermal conductivity κ of single crystals [71K1]. Dashed lines: $\kappa \propto T^{-1}$.

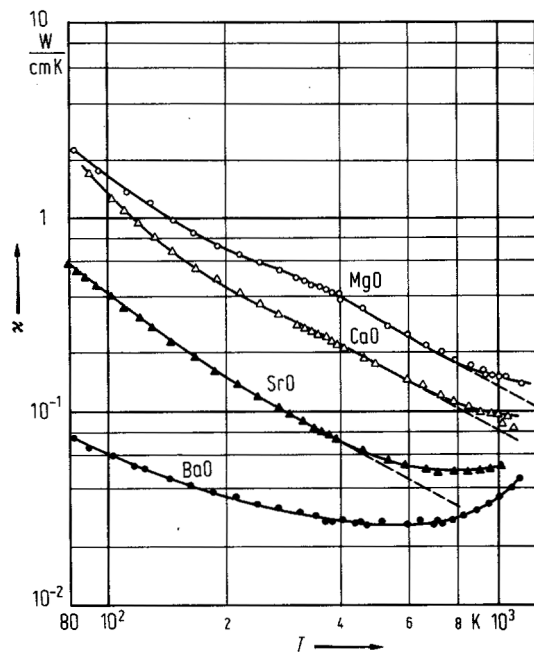
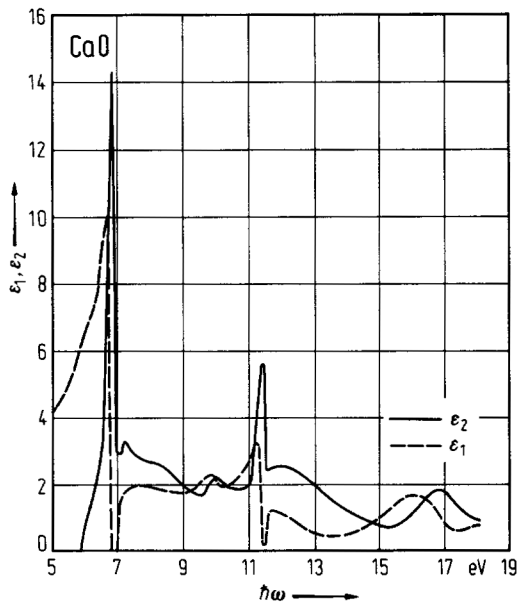


Fig. 3.9.6

CaO. Real and imaginary part ϵ_1 and ϵ_2 of the dielectric constant vs. photon energy [69W].



3.10 Strontium oxide (SrO)

Crystal structure

SrO crystallizes in the rocksalt structure (B1, Fig. 3.0.3).

Electronic properties

energy gap

$E_{g,opt}$	5.22eV	$T = 300\text{ K}$		
$E_{g,th}$	6.4 eV	$T = 0\text{ K}$	estimated from the temperature	75K2
$dE_{g,th}/dT$	$-1.7\cdot 10^{-3}$ eV K ⁻¹	$T = 1300...1900\text{ K}$	dependence of conductivity, mobility and thermoelectric power	

effective masses

m_n	$0.54\ m_0$	$T = 600...700\text{ K}$	estimated by comparing measured and calculated Hall mobility	75K2
-------	-------------	--------------------------	---	------

polaron mass

m_n^{**}	$0.77\ m_0$	$T = 600...700\text{ K}$	estimated by comparing measured and calculated Hall mobility	75K2
------------	-------------	--------------------------	---	------

Lattice properities

lattice parameter

a	5.159 Å		semiempirical calculation	91Z
-----	---------	--	---------------------------	-----

linear thermal expansion coefficient

α	$13.72\cdot 10^{-6}\text{ K}^{-1}$	$T = 293...593\text{ K}$	mean value, X-ray scattering (values up to 1500 K, see ibid.)	57B
----------	------------------------------------	--------------------------	--	-----

density

d	4.75 g cm^{-3}			75L
-----	-------------------------	--	--	-----

melting temperature

T_m	2930(30) K			87L
-------	------------	--	--	-----

boiling temperature

T_b	3300 K			78W
-------	--------	--	--	-----

phonon dispersion relations : Figs. 3.10.1.

phonon frequencies

$\nu_{TO}(\Gamma)$	7.02(10) THz	$T = 300\text{ K}$	inelastic thermal neutron scattering,	75R
$\nu_{LO}(\Gamma)$	14.47(15) THz			
$\nu_{TA}(L)$	3.33 (5) THz			
$\nu_{LA}(L)$	7.14(10) THz			
$\nu_{TO}(L)$	8.35(12) THz			
$\nu_{LO}(L)$	12.94(24) THz			

second order elastic moduli

c_{11}	175.47(37) GPa	$T = 298\text{ K}$	calculated from sound velocities,	77C
c_{12}	49.08 (35) GPa		adiabatic conditions	
c_{44}	55.87(13) GPa			

temperature dependence of elastic moduli

dc_{11}/dT	-0.471 kbar/K		ultrasonic pulse echo technique	77C
dc_{12}/dT	-0.031 kbar/K		(adiabatic conditions: $(dc^s/dp)_s$)	
dc_{44}/dT	-0.063 kbar/K			

bulk modulus

B	88(7) GPa	RT	pulse-echo technique	72B,72S
-----	-----------	----	----------------------	---------

Debye temperature

$\Theta_D(\infty)$	446(5) K		deduced from heat capacity measurements at very high temperatures Θ_D -values for 1.2 to 300 K: see Fig. 3.10.2	70G
--------------------	----------	--	---	-----

heat capacity

C_p	$0.53668 - 29.617 T^{-1} + 8.6937 \cdot 10^9 T^{-2} + \exp(-22400T^{-1}) \text{ J/g K}$		$T = 298...2650 \text{ K}$	84I
-------	---	--	----------------------------	-----

Transport properties

The charge carrier transport is discussed in various models, e.g. polaron band conduction [75K1, 75K2], hopping conduction through compensated semiconducting samples [66S], also in regard to a considerable contribution of ionic conductivity [62P, 68C]. In [75K1] it is supposed that the dominating scattering mechanism is optical mode scattering.

mobility of charge carriers

$\mu_{H,n}$	$5 \text{ cm}^2/\text{Vs}$	$T \approx 700 \text{ K},$ $p_{O_2} < 10^{-6} \text{ mbar}$	Hall mobility from measurements on single crystals; for temperature dependence ($\mu_n \propto T^{-1.4}$), see Fig. 3.10.3	75K1
-------------	----------------------------	--	--	------

thermal conductivity

κ	0.1 W/cm K	$T=300 \text{ K}$	temperature dependence in the range 80...1100 K: Fig. 3.10.4	71K
----------	----------------------	-------------------	--	-----

Optical properties

Spectral dependence of ϵ_2 : Figs. 3.10.5; refractive index: Fig. 3.10.6.

dielectric constants

$\epsilon(0)$	14.5(4)	$T = 273 \text{ K}$	capacitance measurement at 1 kHz and 10kHz	79B
$\epsilon(\infty)$	3.47 to 3.71	$T = 300 \text{ K}$	from refractive index in the spectral range 656.3 to 404.7 nm	66P

References to 3.10

- 35A Anderson, C. T.: J. Am. Chem. Soc. 57 (1935) 429.
57B Beals, R. J., Cook, R. L.: J. Am. Ceram. Soc. 40 (1957) 279.
62P Pal'guev, S. F., Neuimin, A. D.: Sov. Phys. Solid State 4 (1962) 629.
66P Pyncheon, G. E., Sieckmann, E. F.: Phys. Rev. 143 (1966) 595.
66S Surplice, N. A.: Brit. J. Appl. Phys. 17 (1966) 175.
68C Copeland, W. D., Swalin, R. A.: J. Phys. Chem. Solids 29 (1968) 313.
69G Gmelin, E.: Z. Naturforsch. 24a (1969) 1794.
70G Gmelin, E.: Z. Naturforsch. 25a (1970) 887.
71K Kovalev, N. N., Petrov, A. V., Sorokin, O. V.: Sov. Phys. Solid State 13 (1971) 233.
72B Bartels, R. A., Vetter, V. H.: J. Phys. Chem. Solids 33 (1972) 1991.
72G Galtier, M., Montaner, A., Vidal, G.: J. Phys. Chem. Solids 33 (1972) 2295.
72S Son, P. R., Bartels, R. A.: J. Phys. Chem. Solids 33 (1972) 819.
73R Rieder, K. H., Weinstein, B. A., Cardona, M., Bilz, H.: Phys. Rev. B 8 (1973) 4780.
74K Kearney, R. J., Cottini, M., Grilli, E., Baldini, G.: Phys. Status Solidi (b) 64 (1974) 49.
75K1 Kovalev, N. N., Krasin'kova, M. V.: Sov. Phys. Solid State 16 (1975) 1842.
75K2 Kovalev, N. N., Krasin'kova, M. V.: Sov. Phys. Solid State 16 (1975) 1960.
75L Landolt-Börnstein: Zahlenwerte und Funktionen aus Naturwissenschaften und Technik. N. S. Vol. III/7b1. Berlin 1975.
75R Rieder, K. H., Migoni, R., Renker, B.: Phys. Rev. B 12 (1975) 3374.
77C Chang, Z. P., Graham, E. K.: J. Phys. Chem. Solids 38 (1977) 1355.
78W CRC Handbook of Chemistry and Physics, R. C. Weast, ed., Cleveland 1978.
79B Bartels, R. A., Koo, J. C., Thomas, M. L.: Phys. Status Solidi (a) 52 (1979) K 213.
84I Irgashov, Kh., Tarasov, V., D., Chekhovskoi, V. Ya.: Russ. J. Phys. Chem. 58 (1984) 1124.
87L Lamoreaux, R. H., Hildenbrand, D. L., Brewer, L.: J. Phys. Chem. Ref. Data 16 (1987) 419.
91Z Zhang, H., Bukowinski, M. S. T.: Phys. Rev B 44 (1991) 2495.
94S Schütt, O., Pavone, P., Windl, W., Karch, K., Strauch, D.: Phys. Rev. B 50 (1994) 3746.

Figures to 3.10

Fig. 3.0.3

The rocksalt lattice.

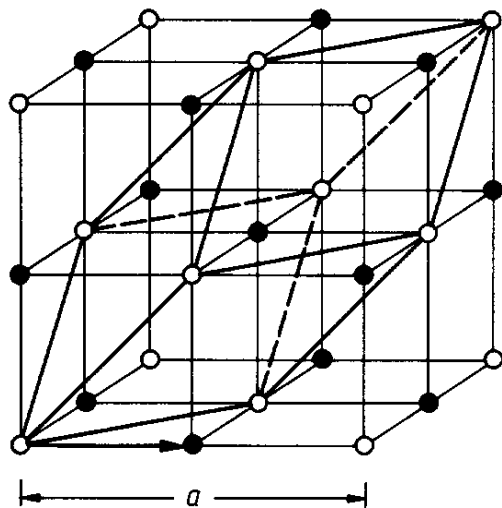


Fig. 3.10.1

SrO. Phonon dispersion curves and density of states [94S]. Experimental data points from neutron inelastic scattering (open circles [75R]), Raman scattering (triangles [73R]), and infrared reflectivity (solid circles [72G]) and ab-initio calculations ([94S] solid lines).

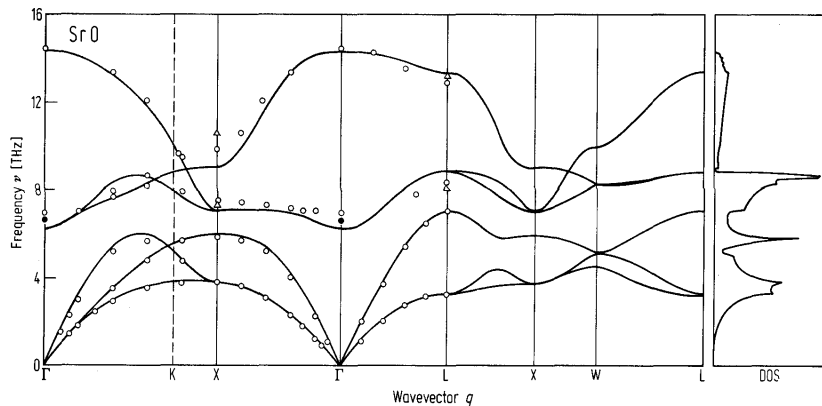


Fig. 3.10.2

SrO. Debye temperature Θ_D vs. temperature T . Open circles: [69G], full circles: [35A].

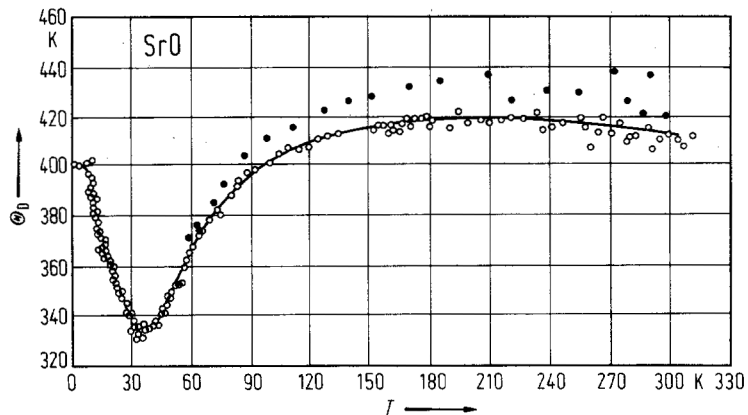


Fig. 3.10.3

BaO, SrO, CaO. Electron Hall mobility vs. temperature [75K1]. Different symbols correspond to different samples.

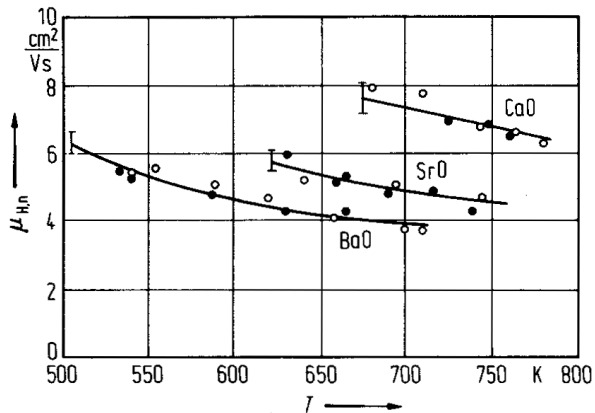


Fig. 3.10.4

MgO, CaO, SrO, BaO. Temperature dependence of the thermal conductivity κ of single crystals [71K]. Dashed lines: $\kappa \propto T^{-1}$.

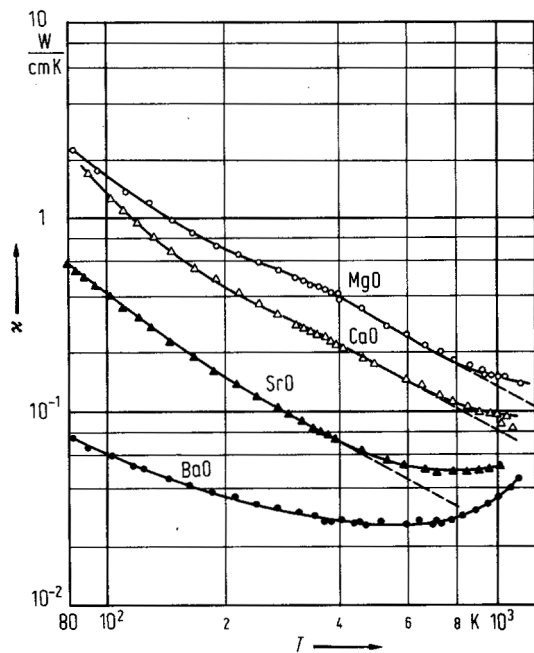


Fig. 3.10.5

SrO. Imaginary part ϵ_2 of the dielectric constant vs. photon energy at 5 K [74K].

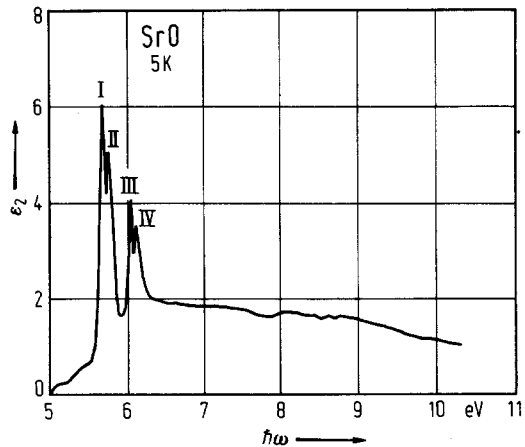
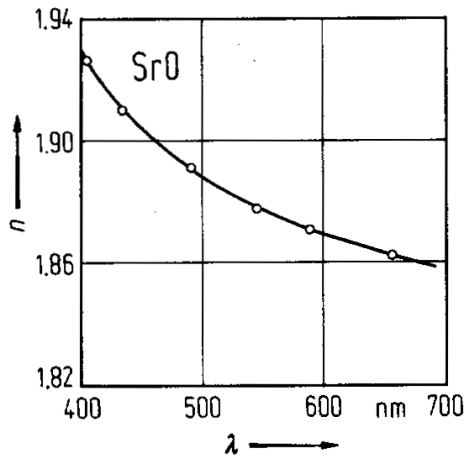


Fig. 3.10.6

SrO. Real refractive index n vs. wavelength λ [66P].



3.11 Barium oxide (BaO)

Crystal structure

BaO crystallizes in the rocksalt structure (B1, Fig. 3.0.3).

Electronic properties

With respect to the interpretation of the results the general remarks on the electronic structure of SrO hold for BaO, too. From the analysis of the optical spectra the following interband gap values are proposed [79R]: $E(\Gamma'_{8v}-\Gamma_{6c}^+)$: 4.286 eV; $E(X_{7v}-X_{7c}^+)$: 4.182 eV; $E(L_{3v}-L'_{2c})$: 3.89 eV.

energy gap

$E_{g,th}$	4.4 eV	$T = 0$ K	estimated from the temperature	75K2
$dE_{g,th}/dT$	$-1.0 \cdot 10^{-3}$ eV K ⁻¹	$T = 1100 \dots 2000$ K	dependence of conductivity, mobility and thermoelectric power	

effective masses

m_n	$0.59 m_0$	$T = 600$ K	estimated by comparing measured and calculated Hall mobility	75K1
-------	------------	-------------	--	------

polaron mass

m_n^{**}	$0.86 m_0$	$T = 500 \dots 700$ K	estimated by comparing measured and calculated Hall mobility	75K1
------------	------------	-----------------------	--	------

Lattice properties

lattice parameter

a	5.5363 (8) Å	$T = 300$ K	powder samples, quenched from 112°C at negligible oxygen pressure	73E
-----	--------------	-------------	---	-----

linear thermal expansion coefficient

α	12.8(9) $\cdot 10^{-6}$ K ⁻¹	$T = 200 \dots 400$ K	X-ray measurements, powder samples; for temperature dependence between 20 and 300 K, see Fig. 3.11.1	55Z
----------	---	-----------------------	--	-----

density

d	5.68 g cm ⁻³			75L
-----	-------------------------	--	--	-----

melting temperature

T_m	2290(30) K			87L
-------	------------	--	--	-----

boiling temperature

T_b	2270 K			75L
-------	--------	--	--	-----

phonon dispersion relations : Fig. 3.11.2. Brillouin zone: Fig. 3.0.4.

phonon frequencies

$\nu_{TO}(\Gamma)$	$4.32(6) \cdot 10^{12}$ s ⁻¹	$T = 300$ K	inelastic thermal neutron scattering, see Fig. 3.11.2	75C
$\nu_{LO}(\Gamma)$	$13.02(3) \cdot 10^{12}$ s ⁻¹			
$\nu_{TA}(L)$	$1.99(7) \cdot 10^{12}$ s ⁻¹			
$\nu_{LA}(L)$	$4.88 (27) \cdot 10^{12}$ s ⁻¹			
$\nu_{TO}(L)$	$6.58 (9) \cdot 10^{12}$ s ⁻¹			

second order elastic moduli

c_{11}	126.14(66) GPa	$T = 298\text{ K}$	calculated from sound velocities, adiabatic conditions	77C
c_{12}	50.03 (60) GPa			
c_{44}	33.68(30) GPa			

temperature dependence of second order elastic moduli

dc_{11}/dT	-0.538 kbar/K		ultrasonic pulse echo technique	77C
dc_{12}/dT	-0.090 kbar/K		(adiabatic conditions: $(dc^s/dp)_s$;	
dc_{44}/dT	-0.059 kbar/K		see [77C] also for isothermal conditions)	

bulk modulus

B	61(7) GPa	RT	pulse-echo technique	73V
-----	-----------	----	----------------------	-----

Debye temperature

$\Theta_D(\infty)$	370(4) K		deduced from heat-capacity measure- ments at very high temperatures temperature dependence: Fig. 3.11.5	70G
--------------------	----------	--	---	-----

heat capacity

C_p	$47.278\text{ J mol}^{-1}\text{K}^{-1}$		$T = 298.15\text{ K}$, see Fig. 3.11.4	89B
-------	---	--	---	-----

Transport properties

Electrical transport is mainly discussed in the picture of electronic conduction. The ionic contribution is small. In [75K1, 75K2] polaron conduction and predominant optical mode scattering is assumed.

electrical conductivity: Fig. 3.11.6

thermoelectric power : Fig. 3.11.7.

mobility of charge carriers

μ_n	$5\text{ cm}^2/\text{Vs}$	$T = 600\text{ K}$, $p_{\text{O}_2} < 10^{-6}\text{ mbar}$	Hall mobility from measurements on polycrystals; for temperature depen- dence ($\mu_n \propto T^{-1.4}$), see Fig. 3.11.8	75K1
---------	---------------------------	--	---	------

thermal conductivity

κ	0.03 W/cm K	$T = 300\text{ K}$	temperature dependence in the range 80...1100 K: Fig. 3.11.9	71K
----------	----------------------	--------------------	---	-----

Optical properties

Spectral dependence of ϵ_2 Fig. 3.11.10.

dielectric constant

$\epsilon(0)$	3.9034(5) to 4.1968(22)	$T = 296\text{ K}$	calculated from refractive index values in the spectral range 623.8...435.9 nm	75A
---------------	----------------------------	--------------------	---	-----

References to 3.11

- 35A Anderson, C. T.: J. Am. Chem. Soc. 57 (1935) 429.
55Z Zollweg, R. J.: Phys. Rev. 100 (1955) 671.
63S Surplice, N. A., Jones, R. P.: Brit. J. Appl. Phys. 14 (1963) 444.
66W White, G. K., Anderson, O. L.: J. Appl. Phys. 37 (1966) 430.
69G Gmelin, E.: Z. Naturforsch. 24a (1969) 1794.
70G Gmelin, E.: Z. Naturforsch. 25a (1970) 887.
71K Kovalev, N. N., Petrov, A. V., Sorokin, O. V.: Sov. Phys. Solid State 13 (1971) 233.
73E Elo, R. B., Murarka, S. P., Swalin, R. A.: J. Phys. Chem. Solids 34 (1973) 97.
73V Vetter, V. H., Bartels, R. A.: J. Phys. Chem. Solids 34 (1973) 1448.
74K Kearney, R. J., Cottini, M., Grilli, E., Baldini, G.: Phys. Status Solidi (b) 64 (1974) 49.
75A Anderson, C. J., Hensley, E. B.: J. Appl. Phys. 46 (1975) 443.
75C Chang, S. S., Tompson, C. W., Gürmen, E., Muhlestein, L. D.: J. Phys. Chem. Solids 36 (1975) 769.
75K1 Kovalev, N. N., Krasin'kova, M. V.: Sov. Phys. Solid State 16 (1975) 1842.
75K2 Kovalev, N. N., Krasin'kova, M. V.: Sov. Phys. Solid State 16 (1975) 1960.
75L Landolt-Börnstein: Zahlenwerte und Funktionen aus Naturwissenschaften und Technik. N. S. Vol. III/7b1. Berlin 1975.
77C Chang, Z. P., Graham, E. K.: J. Phys. Chem. Solids 38 (1977) 1355.
77K Kwang-Oh Park, Sivertsen, J. M.: J. Am. Ceram. Soc. 60 (1977) 537.
79K Kwang-Oh Park, Sivertsen, J. M.: J. Am. Ceram. Soc. 62 (1979) 218.
79R Rao, A. S., Kearney, R. J.: Phys. Status Solidi (b) 95 (1979) 243.
87L Lamoreaux, R. H., Hildenbrand, D. L., Brewer, L.: J. Phys. Chem. Ref. Data 16 (1987) 419.
89B Barin, I.: Thermochemical Data of Pure Substances, VCH, Weinheim, 1989.
94Z Zimmermann, E., Hack, K., Neuschütz, D.: Calphad: Comput. Coupling Phase Diagrams Thermochem. 19 (1994) 119.

Figures to 3.11

Fig. 3.0.3

The rocksalt lattice.

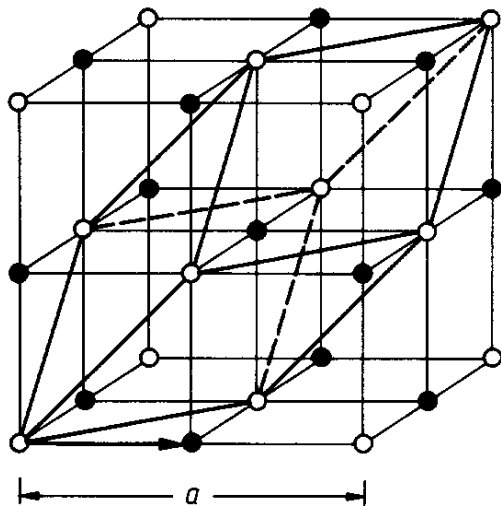


Fig. 3.0.4

The Brillouin zone for the zincblende and the rocksalt lattices.

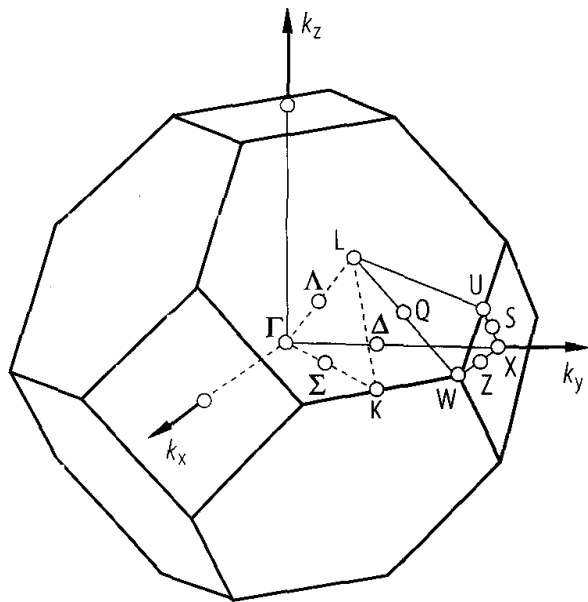


Fig. 3.11.1

MgO, BaO. Linear thermal expansion coefficient α vs. temperature. Open circles: [79K], full circles: [66W].

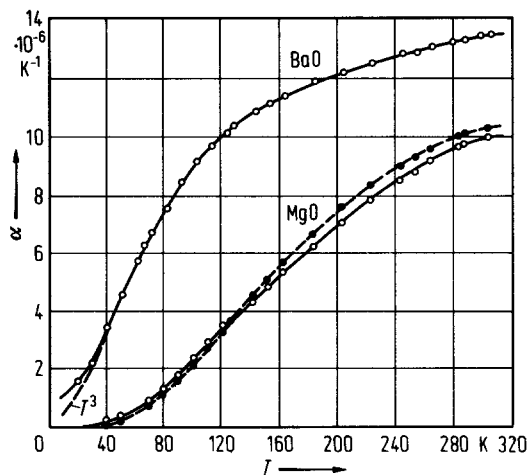


Fig. 3.11.2

BaO. Phonon dispersion curves. Open circles: transverse phonons; full circles: longitudinal phonons; solid and dashed lines: model calculations [75C].

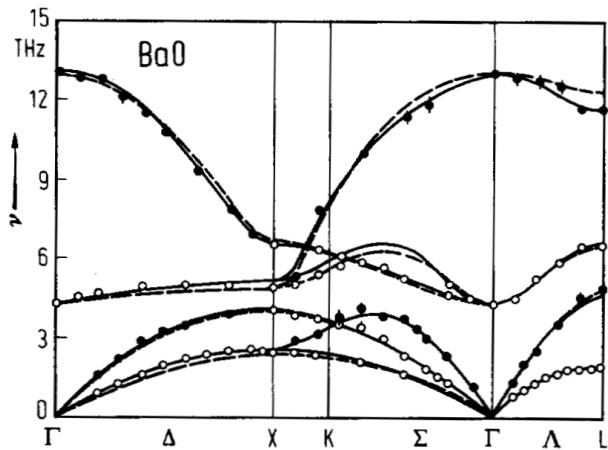


Fig. 3.11.3

BaO. Temperature dependence of elastic moduli c_{ik} . Sample annealed for 240 h at 1475 K and $p_{O_2} = 10^{-6}$ bar [77K].

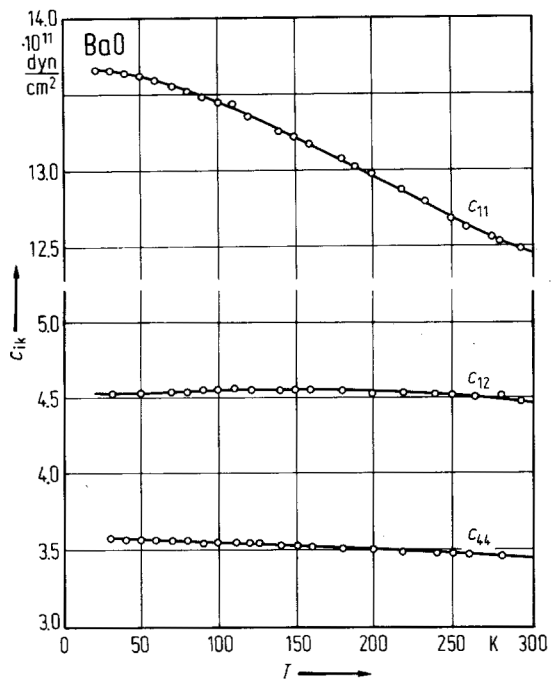


Fig. 3.11.4

BaO. Heat capacity, C_p , vs. T , symbols are experimental points from various authors. Fig. from [94Z].

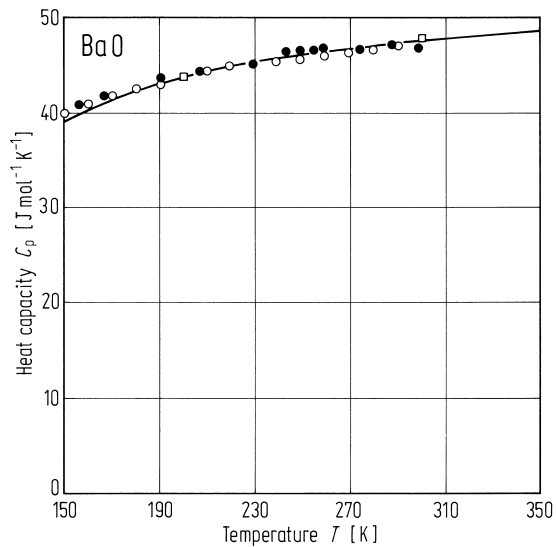


Fig. 3.11.5

BaO. Debye temperature Θ_D vs. temperature T . Open circles: [69G], full circles: [35A].

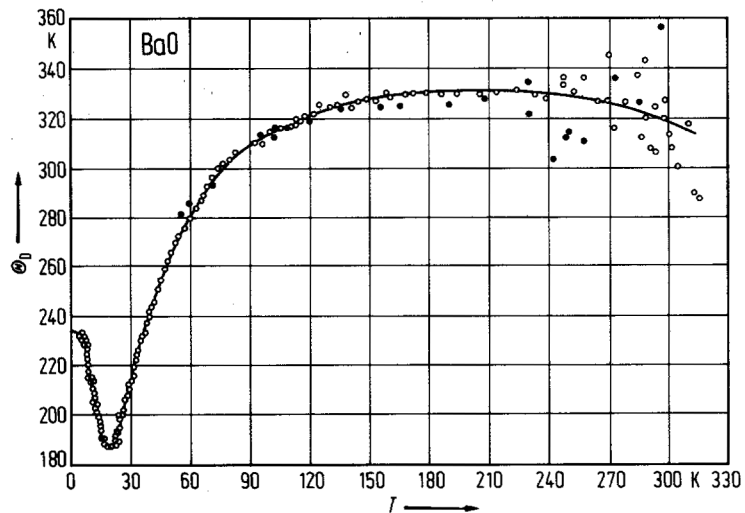


Fig. 3.11.6

BaO. Electrical conductivity σ (solid curves) and thermoelectric power S (dashed curves) of two crystals vs. $1/T$ [75K2]. $p_{O_2} \geq 3 \cdot 10^{-5}$ mbar. n-type conduction at temperatures below the discontinuity.

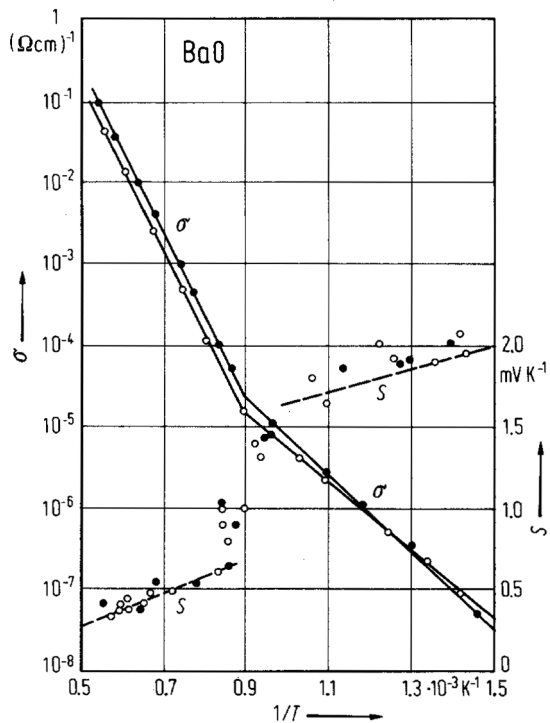


Fig. 3.11.7

BaO. Thermoelectric power S of two samples vs. reciprocal temperature [63S].

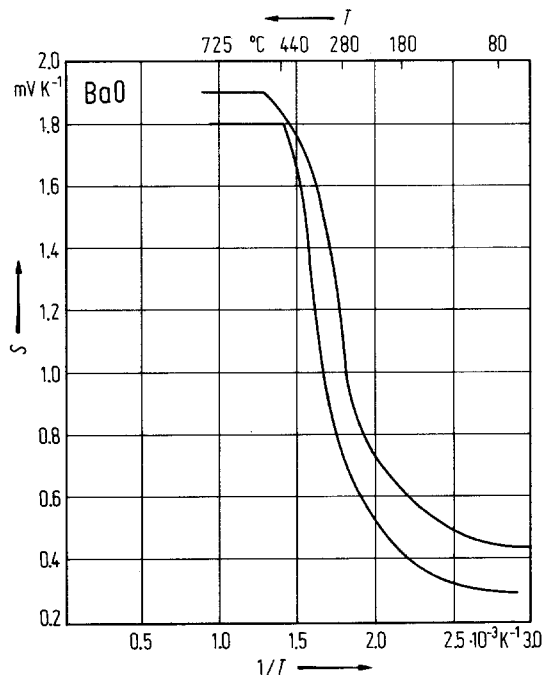


Fig. 3.11.8

BaO, SrO, CaO. Electron Hall mobility vs. temperature [75K1]. Different symbols correspond to different samples.

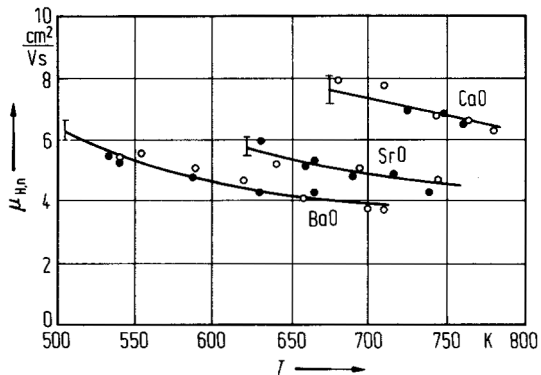


Fig. 3.11.9

MgO, CaO, SrO, BaO. Temperature dependence of the thermal conductivity κ of single crystals [71K]. Dashed lines: $\kappa \propto T^{-1}$.

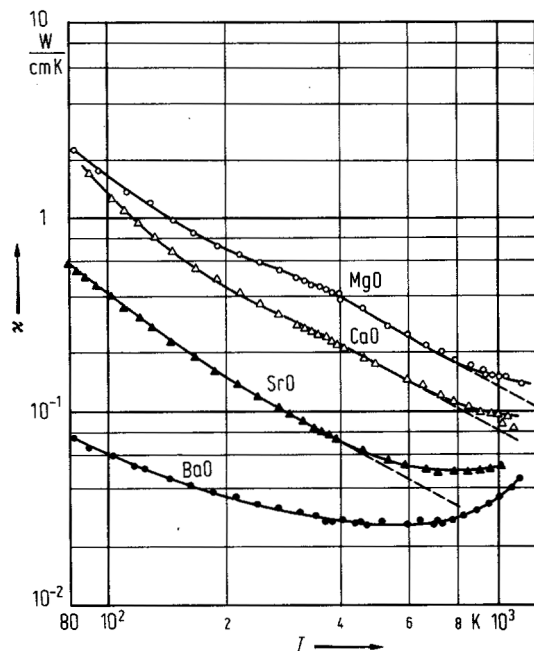
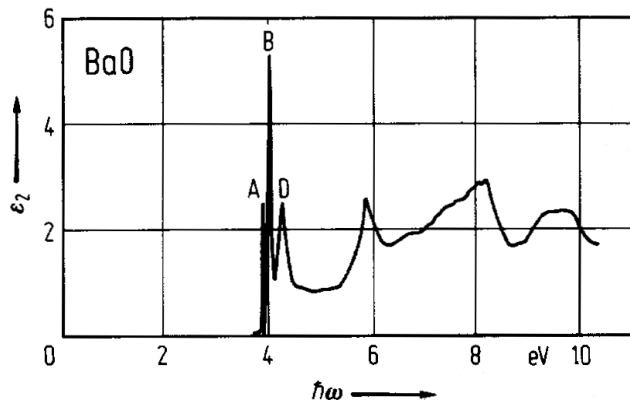


Fig. 3.11.10

BaO. Imaginary part ϵ_2 of the dielectric constant vs. photon energy at 5 K. For the discussion of the exciton peaks A–D, see [74K].



3.12 Zinc oxide (ZnO)

Crystal structure

Zinc oxide crystallizes in the wurtzite lattice (space group: $P6_3mc - C_{6v}^4$, Fig. 3.0.2).

Electronic properties

Band structure: Fig. 3.0.16, Brillouin zone: insert in Fig.3.0.16 and Fig. 3.0.5, density of states: Fig. 3.0.16.

The topmost valence band ($\Gamma_5 + \Gamma_1$) is split due to crystal field and spin-orbit coupling into three spin-degenerate states (Γ_7 , Γ_9 and Γ_7). Exciton states formed with holes in these valence band states are denoted A, B and C exciton, respectively. Due to the negative spin-orbit coupling (contribution from Zn 3d-states) the order of the two highest valence band states is reversed as compared with the other II–VI compounds with wurtzite structure. The conduction band edge originating from the 4s-states of Zn possesses Γ_7 -symmetry.

energies of symmetry points of the band structure (relative to the top of the valence band)

$E(\Gamma_{1v})$	– 17.08 eV	– 18.75 eV	results from ab-initio calculations handling the Zn3d electrons as core (first column) or as valence (second column) electrons:	93S
$E(\Gamma_{3v})$	– 16.24 eV	– 17.97 eV		
$E(\text{Zn}3d)$		– 5.17 eV		
$E(\Gamma_{3v})$	– 4.32 eV	– 4.03 eV		
$E(\Gamma_{6v})$	– 0.65 eV	– 0.85 eV		
$E(\Gamma_{1v})$	–	– 0.12 eV		
$E(\Gamma_{5v})$	– 0.11 eV	0.0 eV		
$E(\Gamma_{1c})$	2.13 eV	0.23 eV		
$E(\Gamma_{3c})$	6.64 eV	4.71 eV		
$E(M_{1v})$	– 16.31 eV	– 18.02 eV		
$E(M_{3v})$	– 16.05 eV	– 17.78 eV		
$E(\text{Zn}3d)$		– 4.99 eV		
$E(M_{1v})$	– 3.96 eV	– 3.76 eV		
$E(M_{3v})$	– 3.03 eV	– 3.75 eV		
$E(M_{1v})$	– 2.35 eV	– 2.95 eV		
$E(M_{2v})$	– 1.63 eV	– 2.42 eV		
$E(M_{3v})$	– 1.08 eV	– 1.35 eV		
$E(M_{4v})$	– 0.58 eV	– 0.93 eV		
$E(M_{1c})$	7.16 eV	5.34 eV		
$E(M_{3c})$	8.50 eV	6.55 eV		
$E(A_{1,3v})$	– 16.70 eV	– 18.37 eV		

energy gaps (distance A, B, C valence bands to conduction band)

E_g^A	3.4410(1) eV	$T = 6 \text{ K}$	two-photon absorption	95M
E_g^B	3.4434(1) eV			
E_g^C	3.4817(2) eV			

pressure dependence of energy gaps

dE_g^A/dp	24.7(1) eV GPa^{-1}	$T = 6 \text{ K}$	two-photon absorption	95M
dE_g^B/dp	25.3(1) eV GPa^{-1}	$T = 6 \text{ K}$		
dE_g^C/dp	26.8(2) eV GPa^{-1}	$T = 6 \text{ K}$		

exciton transition energies

$E_{\text{gx}}^{\text{A}}(\Gamma_5^{\text{para}})$	3.3756(1) eV	$T = 1.5 \text{ K}$	three-photon difference-frequency generation	93F
$E_{\text{gx}}^{\text{A}}(\Gamma_5^{\text{L}})$	3.3778(1) eV	1S excitons		
$E_{\text{gx}}^{\text{A}}(\Gamma_5^{\text{T}})$	3.3759(4) eV			
$E_{\text{gx}}^{\text{B}}(\Gamma_5^{\text{para}})$	3.3811(1) eV			
$E_{\text{gx}}^{\text{A}}(\Gamma_5^{\text{L}})$	3.4232 eV	$T = 1.5 \text{ K}$ 2S excitons	three-photon difference-frequency generation	93F
E_{gx}^{A}	3.4252(1) eV	$T = 6 \text{ K}$	two-photon absorption	95M
E_{gx}^{B}	3.4308(1) eV	2P excitons		
E_{gx}^{C}	3.4694(1) eV			

exciton binding energy

$E_{\text{b}}(\text{A})$	63.1 meV	$T = 6 \text{ K}$	two-photon absorption	95M
$E_{\text{b}}(\text{B})$	50.4 meV			
$E_{\text{b}}(\text{C})$	48.9 meV			

crystal-field splitting energy

Δ_{cf}	39.4(2) meV	$T = 6 \text{ K}$	two-photon absorption	95M
----------------------	-------------	-------------------	-----------------------	-----

spin-orbit splitting energy

Δ_{so}	− 3.5(2) meV	$T = 6 \text{ K}$	two-photon absorption	95M
----------------------	--------------	-------------------	-----------------------	-----

conduction electrons, effective masses

m_{n}	$0.275 m_0$	$n = 10^{17} \text{ cm}^{-3}$, $T = 6 \text{ K}$, $H = 80 \text{ kOe}$	cyclotron resonance, (direct) polaron mass	72B
----------------	-------------	--	--	-----

effective polaron mass of electrons

$m_{\text{n},\perp\text{c}}^{**}$	$0.3 m_0$	$T = 80 \text{ K}$	cyclotron resonance	96O
-----------------------------------	-----------	--------------------	---------------------	-----

holes, effective masses

$m_{\text{p}\parallel}(\text{A}) = m_{\text{p}\parallel}(\text{B})$	$0.59 m_0$	$T = 1.6 \text{ K}$	magnetoreflexion ($m_{\text{n}} = 0.28 m_0$), polaron mass	73H
$m_{\text{p}\perp}(\text{A}) = m_{\text{p}\perp}(\text{B})$	$0.59 m_0$			

g-values

$g_{\text{n},\parallel\text{c}} = g_{\text{n},\perp\text{c}}$	− 1.95		ESR, Zeeman effect for bound excitons	63M, 65R
---	--------	--	---------------------------------------	-------------

Lattice properties

lattice parameters

a	3.249(6) Å	X-ray diffraction	96K
c	5.2042(20) Å		
c/a	1.6018(7)Å		

temperature dependence of lattice parameters

Fig. 3.12.1 [70R]. From powder X-ray diffraction data taken between 4.2 K and 296 K:

$a [\text{\AA}] = 3.24835 - 1.0811 \cdot 10^{-5} T + 6.820 \cdot 10^{-8} \cdot T^2 - 6.109 \cdot 10^{-11} T^3 + 2.143 \cdot 10^{-14} T^4$	70R
---	-----

coefficients of thermal expansion (parallel and perpendicular to c -axis) (in 10^{-7} K^{-1})

$\alpha_{\parallel\text{c}}$	+ 29.2	$T = 399 \text{ K}$	interferometric and capacitance method; temperature dependence, see Fig. 3.12.2	69I
$\alpha_{\perp\text{c}}$	+ 47.5	$T = 300 \text{ K}$		

density

d	5.67526(19) g cm ⁻³	$T = 293$ K	hydrostatic weighing, material grown from the vapor phase	75H2
-----	--------------------------------	-------------	---	------

melting temperature

T_m	2242(5) K			87L
-------	-----------	--	--	-----

phonon dispersion curves : Fig. 3.12.3, Brillouin zone: Fig. 3.0.5.

According to the fact that there are 4 atoms per unit cell one can in general expect 12 phonon branches, 9 optical branches and 3 acoustic branches. Group theory predicts near the center of the Brillouin zone one A_1 branch, one doubly degenerate E_1 branch, two doubly degenerate E_2 branches and two B branches. The A_1 and E_1 branches are both Raman and infrared active, the E_2 branches are Raman active only, while the B branches are inactive. For the point group of ZnO and as result of the anisotropy of the force constants there are only 6 different frequencies observable, two only with Raman spectroscopy and four with Raman and ir spectroscopy.

wavenumbers of fundamental optical modes (bulk phonons)

$\bar{\nu}(E_2)$	101 cm ⁻¹	$T=300$ K	Raman spectroscopy	66D
$\bar{\nu}(E_2)$	437 cm ⁻¹			
$\bar{\nu}_{TO}(E_1)_{\perp c}$	407 cm ⁻¹			
$\bar{\nu}_{TO}(A_1)_{\parallel c}$	380 cm ⁻¹			
$\bar{\nu}_{LO}(E_1)_{\perp c}$	583 cm ⁻¹			
$\bar{\nu}_{LO}(A_1)_{\parallel c}$	574 cm ⁻¹			

second order elastic moduli

c_{11}	206(4) GPa		Brillouin scattering	95C
c_{13}	118(10) GPa		(ZnO film on Si substrate)	
c_{33}	211(4) GPa			
c_{44}	44.3(10) GPa			
c_{66}	44.0(10) GPa			

bulk modulus

B	183(7) GPa	RT	static pressure	96K
-----	------------	----	-----------------	-----

Debye temperature

Θ_D	440(25) K	$T=300$ K	calorimetric data	89R
------------	-----------	-----------	-------------------	-----

heat capacity

C_p [J mol ⁻¹ K ⁻¹]	$53.999 + 7.851 \cdot 10^{-4} T - 5.868 \cdot 10^5 T^{-2} - 127.50 T^{-1/2} + 1.9376 \cdot 10^{-6} T^2$			89R
	$T = 50 \dots 1800$ K (± 0.7 %)			adiabatic calorimetry

Transport properties

The electronic conductivity of pure stoichiometric ZnO ist still unknown. The concentration of foreign admixtures in undoped crystals is of the order of 10^{15} to 10^{16} cm⁻³. Since $E_{g,opt} = 3.2$ eV and impurity ionization energies are about 0.01 to 0.1 eV at temperatures below 900 K, impurity conduction is always observed. For temperatures above 900 K dissociation of the intrinsic material occurs. The conductivity depends on the surrounding atmosphere (O₂, Zn, Ar). Nevertheless it is possible to investigate the influence of intentional admixtures to the conductivity, the charge carrier concentration and mobility as a function of temperature and current direction.

Fig. 3.12.4 shows the conductivity for a crystal without intentional admixtures.

resistivity

Values of ρ given in literature depend strongly on special preparation conditions, see, e.g., [91I]. Therefore only a few exemplary data are indicated in the table. Most investigations have been conducted on thin films deposited with various techniques and always exhibiting considerable background impurity concentrations or being intentionally doped.

ρ	$10^8 \dots 10^9 \Omega \text{ cm}$	$T = 300 \text{ K}$	ultrapure bulk single crystals, hydrothermally grown under oxygen partial pressure	90S
	$5 \cdot 10^{-4} \Omega \text{ cm}$	$T = 300 \text{ K}$	ZnO:Ga at $n(\text{Ga}) = 3 \cdot 10^{20} \text{ cm}^{-3}$	95A
	$3 \cdot 10^{-3} \Omega \text{ cm}$		$n(\text{Ga}) = 1.3 \cdot 10^{20} \text{ cm}^{-3}$	
	$2 \cdot 10^{-2} \Omega \text{ cm}$		$n(\text{Ga}) = 3.3 \cdot 10^{18} \text{ cm}^{-3}$	
	$5 \cdot 10^{-4} \Omega \text{ cm}$	$T = 300 \text{ K}$	lowest value in ZnO:Al at $n(\text{Al}) = 3 \cdot 10^{20} \text{ cm}^{-3}$, Al-doped layers from plasma sputtering	98Y
	$10^{-2} \Omega \text{ cm}$	$T = 300 \text{ K}$	Al-doped layers from ionized deposition, with carrier concentration $1 \dots 4 \cdot 10^{20} \text{ cm}^{-3}$	89K

electron mobility

μ_n	$0.5 \dots 1 \text{ cm}^2 \text{V}^{-1} \text{s}^{-1}$	$T = 300 \text{ K}$	Al-doped layers from ionized deposition, with carrier concentration $1 \dots 4 \cdot 10^{20} \text{ cm}^{-3}$	89K
	$10 \dots 20 \text{ cm}^2 \text{V}^{-1} \text{s}^{-1}$	$T = 300 \text{ K}$	films grown by laser ablation, $n = 5 \cdot 10^{19} \dots 10^{20} \text{ cm}^{-3}$	97N
	up to $150 \text{ cm}^2 \text{V}^{-1} \text{s}^{-1}$	$T = 300 \text{ K}$	($E \perp c$), ZnO single crystals grown by a hydrothermal method	95V
	up to $167 \text{ cm}^2 \text{V}^{-1} \text{s}^{-1}$		($E \parallel c$)	

thermoelectric power (Seebeck coefficient): see Fig. 3.12.5.

thermal conductivity

κ_{av}	$0.54 \cdot 10^2 \text{ W K}^{-1} \text{ m}^{-1}$	$T = 300 \text{ K}$	steady-state longitudinal heat flow for temperature dependence see Fig. 3.12.6	72S
---------------	---	---------------------	--	-----

piezoelectrical strain and stress coefficients

There are three independent piezoelectrical strain constants d_{15} , d_{31} , and d_{33} ($d_{ij} = dP_i/dX_j$) and three independent piezoelectric stress moduli e_{15} , e_{31} , and e_{33} ($e_{ij} = dP_i/de_j$).

d_{15}	$-8.3 \cdot 10^{-12} \text{ As N}^{-1}$	RT	resonance – antiresonance	68C
d_{31}	$-5 \cdot 10^{-12} \text{ As N}^{-1}$			
d_{33}	$12.4 \cdot 10^{-12} \text{ As N}^{-1}$			
e_{15}	-0.353 As m^{-2}	RT		

Optical properties

The optical properties depend critically on the microstructure which in turn depends on the deposition technique. Common techniques are: reactive sputtering, dc and rc magnetron sputtering, spray pyrolysis, charged liquid cluster beam technique, pulsed laser deposition, and chemical vapor deposition.

refractive index

Fig. 3.12.7 shows the temperature dependence of the refractive index for selected wavelengths and different polarizations. Fig. 3.12.8 presents the spectral dependence of the complex refractive index in the energy range between 1.5 and 5.0 eV at room temperature.

		λ [nm]			
$n_{\omega,\perp c}$	2.239 (2.248)	405	$T = 293$ K	minimum of deviation, as grown crystal	54M
(value in	2.137 (2.151)	436		plane	
brackets: $n_{\omega,\parallel c}$)	2.097 (2.115)	460			
	2.064 (2.081)	492			
	2.059 (2.076)	497			
	2.025 (2.041)	546			
	2.011 (2.028)	578			
	2.009 (2.024)	589			
	2.001 (2.017)	610			
	1.984 (2.001)	671			

dielectric constants

Figs. 3.12.9 and 3.12.10 show the $\epsilon_1(E)$ and $\epsilon_2(E)$ spectrum for ZnO for both $E \parallel c$ and $E \perp c$ in the energy range between 1.5 and 5.0 eV at room temperature.

$\epsilon(0)_{\perp c}$	7.8		reflectivity via refractive index	67H
$\epsilon(0)_{\parallel c}$	8.75			
$\epsilon(\infty)_{\perp c}$	3.70			
$\epsilon(\infty)_{\parallel c}$	3.75			

electrooptical constants (Pockels constants)

Under the influence of electric fields the refractive index is changed due to the nonlinearity of the dielectric polarization (Pockels effect). As in the case of piezoelectric effects, corresponding to the hexagonal symmetry, there are three independent Pockels constants r_{31} , r_{33} , r_{51} (Voigt notation). Their value $r_{ij} = d(n_{ij}^{-2})/dE$ is dependent on the wavelength.

r_{51}	$-3.1 \cdot 10^{-10}$ cm V ⁻¹	$T = 295$ K,	electrotransmission	71M
$r_{13} - r_{33}$	$-1.4 \cdot 10^{-9}$ cm V ⁻¹	$\lambda \approx 400$ nm, constant stress, free crystal		

Impurities and defects

ionization energies of donors

H	0.05 eV 0.06.. .0.034 eV		Hall effect	57H 58H, 58R
In	0.024 eV			73M
Cu	0.190 eV		double doping	73M
Li	1.5 eV		Hall effect	60L
Zn	0.05 eV 0.043.. 0.045 eV			57H 75H1

ionization energies of shallow impurities

Zn interstitial	0.03...0.13 meV	T variable	conductivity activation energy study	92N
	0.02...0.20 meV	T variable	conductivity activation energy study	95N
	0.03 meV	$T = 300$ K	tunneling spectroscopy	91B
V_{Zn}	0.07 meV		cluster molecular orbital calculations	90S
Ni doped	0.055 meV	T variable	activation energy, thin films	97J
Cu doped	0.132 meV	T variable	activation energy, thin films	97J

ionization energies of deep impurities

O	0.59...0.66 eV	T variable	fit to temperature-dependent conductivity	86N
$\text{Cu}^{2+}/\text{Cu}^{+}+\text{h}$	3.25 eV	$T = 4.2$ K	PLE	87S
$\text{Co}^{2+}/\text{Co}^{3+}+\text{e}$	1.92 eV	$T = 300$ K	tunneling spectroscopy	91B
$\text{Mn}^{2+}/\text{Mn}^{3+}+\text{e}$	1.92 eV	$T = 300$ K	tunneling spectroscopy	91B
$\text{Fe}^{3+}(\text{d}^5)$	2.25(05) eV	$T = 2$ K	PL	92H
V_O	2.0 eV		cluster molecular orbital calculations	90S
	0.32 eV	$T = 300$ K	tunneling spectroscopy	91B

References to 3.12

- 35B Braekken, H., Jore, C.: Det Norske Videnshabers Skrifter NR8 (1935) 1 (cited in [70R]).
- 54M Mollwo, E.: Z. Angew. Phys. 6 (1954) 257.
- 57H Hutson, A. R.: Phys. Rev. 108 (1957) 222.
- 58H Heiland, G.: J. Phys. Chem. Solids 6 (1958) 155.
- 58R Rupprecht, H.: J. Phys. Chem. Solids 6 (1958) 144.
- 60L Lander, J. J.: J. Phys. Chem. Solids 15 (1960) 324.
- 63M Müller, K. A., Schneider, J.: Phys. Lett. 4 (1963) 288.
- 65R Reynolds, D. C., Litton, C. W., Collins, T. C.: Phys. Rev. 140 (1965) A 1726.
- 66D Damen, T. C., Porto, S. P. S., Tell, B.: Phys. Rev. 142 (1966) 570.
- 67H Heltemes, E. C., Swinney, H. L.: J. Appl. Phys. 38 (1967) 2387.
- 68C Crisler, D. F., Cupal, J. J., Moore, A. R.: Proc. IEEE 56 (1968) 225.
- 68P Park, Y. S., Schneider, J. R.: J. Appl. Phys. 39 (1968) 3049.
- 69I Ibach, H.: Phys. Status Solidi 33 (1969) 257.
- 70R Reeber, R. R., J. Appl. Phys. 41 (1970) 5063.
- 71M Madelung, O. W., Mollwo, E.: Z. Phys. 249 (1971) 12.
- 72B Button, K. J., Cohn, D. R., v. Ortenberg, M., Lax, B., Mollwo, E., Helbig, R.: Phys. Rev. Lett. 28 (1972) 1637.
- 72S Slack, G. A.: Phys. Rev. 6 (1972) 3791.
- 73B Bloom, S., Ortenburger, J.: Phys. Status Solidi (b) 58 (1973) 561.
- 73H Hümmer, K.: Phys. Status Solidi (b) 56 (1973) 249.
- 73M Mollwo, E., Müller, G., Wagner, P.: Solid State Commun. 13 (1973) 1283.
- 74H Helbig, R., Wagner, P.: J. Phys. Chem. Solids 35 (1974) 327.
- 74T Thoma, K., Dorner, B., Duesing, G., Wegener, W.: Solid State Commun. 15 (1974) 1111.
- 74W Wagner, P., Helbig, R.: J. Phys. Chem. Solids 35 (1974) 327.
- 75H1 Hagemark, K. J., Chacka, L. C.: J. Solid State Chem. 15 (1975) 261.
- 75H2 Hallwig, D., Mollwo, E.: Verhdlg. d. Deutsch. Phys. Gesellsch. 10 (1975) 350.
- 78W Wagner, P.: Dissertation Erlangen-Nürnberg, 1978.
- 80G Göpel, W., Bauer, R. S., Hansson, G.: Surf. Sci. 99 (1980) 138.
- 86N Nakagawa, M., Mitsudo, H.: Surf. Sci. 175 (1986) 157.
- 87L Lamoreaux, R. H., Hildenbrand, D. L., Brewer, L.: J. Phys. Chem. Ref. Data 16 (1987) 419.
- 87S Schulz, H.-J., Thiede, M.: Phys. Rev. B 35 (1987) 18.
- 89K Kuroyanagi, A.: J. Appl. Phys. 66 (1989) 5492.
- 89R Robie, R. A., Haselton, Jr., M. T., Hemingway, B. S.: J. Chem. Thermodyn. 21 (1989) 743.
- 90S Sakagami, N.: J. Cryst. Growth 99 (1990) 905.
- 91B Bonnell, D.A., Rohrer, G.S., French, R.H.: J. Vac. Sci. Technol. B 9 (1991) 551.
- 91I Igasaki, Y., Saito, H.: J. Appl. Phys. 70 (1991) 3613.
- 92H Heitz, R., Hoffmann, A., Broser, I.: Phys. Rev. B 45 (1992) 8977.
- 92N Natsume, Y., Sakata, H., Hirayama, T., Yanagida, H.: J. Appl. Phys. 72 (1992) 4203.
- 93F Fiebig, M., Fröhlich, D., Pahlke-Lerch, C.: Phys. Status Solidi (b) 177 (1993) 187.
- 93S Schröer, P., Krüger, P., Pollmann, J.: Phys. Rev. B 47 (1993) 6971.
- 95A Ataev, B.M., Bagamadova, A.M., Djabrailov, A.M., Mamedov, V.V., Rabadanov, R.A.: Thin Solid Films 260 (1995) 19.
- 95C Carlotti, G., Fioretto, D., Socino, G., Verona, E.: J. Phys. Condens. Matter 7 (1995) 9147.
- 95M Mang, A., Reimann, K., Rubenacke, S.: Solid State Commun. 94 (1995) 251.
- 95N Natsume, Y., Sakata, H., Hirayama, T.: Phys. Status Solidi (a) 148 (1995) 485.
- 95V Venger, E.F., Melnichuk, A.V., Melnichuk, L.Yu., Pasechnik, Yu.A.: Phys. Status Solidi (b) 188 (1995) 823.
- 96K Karzel, H., Potzel, W., Köfferlein, M., Schiessl, W., Steiner, M., Hiler, U., Kalvius, G. M., Mitchell, D. W., Das, T. P., Blaha, P., Schwarz, K., Pasternak, M. P.: Phys. Rev. B 53 (1996) 11425.
- 96O Oshikiri, M., Takehana, K., Asano, T., Kido, G.: Physica B 216 (1996) 351.
- 97J Jimenez-Gonzalez, A.E.: J. Solid State Chem. 128 (1997) 176.
- 97N Narasimhan, K.L., Pai, S.P., Palkar, V.R., Pinto, R.: Thin Solid Films 295 (1997) 104.
- 97Y Yoshikawa, H., Adachi, S.: Jpn. J. Appl. Phys. 36 (1997) 6237.
- 98Y Yamaki, Y., Yamaya, K., Araya, H., Nakanishi, H., Chichibu, S.: Proc. 2nd Int. Symp. Blue Laser and Light Emitting Diodes, Kisarazu, Chiba (Japan) 1998, Eds. Onabe, K., Hiramatsu, K., Itaya, K., Nakano, Y., Ohmsha Ltd. (Tokyo, Japan) 1998, p. 48.

Figures to 3.12

Fig. 3.0.2

The wurtzite lattice.

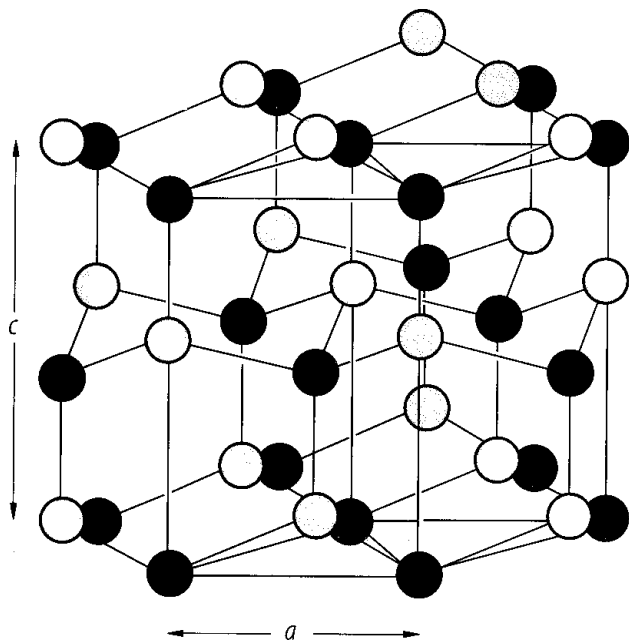
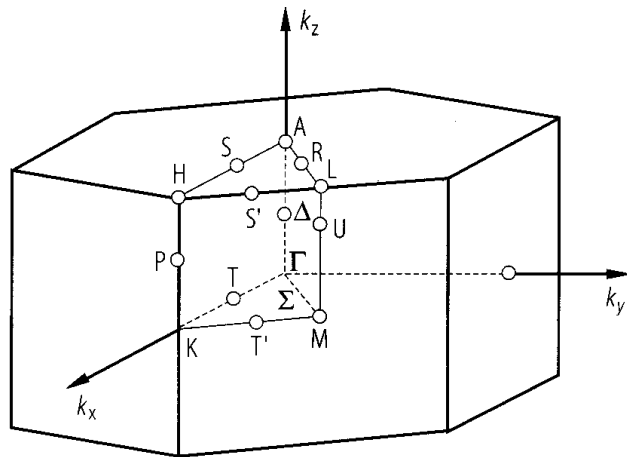


Fig. 3.0.5

The Brillouin zone of the wurtzite lattice.



ZnO. Band structure and calculated density of state. (solid line) of [73B] in comparison with a UPS spectrum (dashed line) [80G]. The experimental peak at -7.8eV indicates the energetic position of the Zn 3d states. Φ = work function.

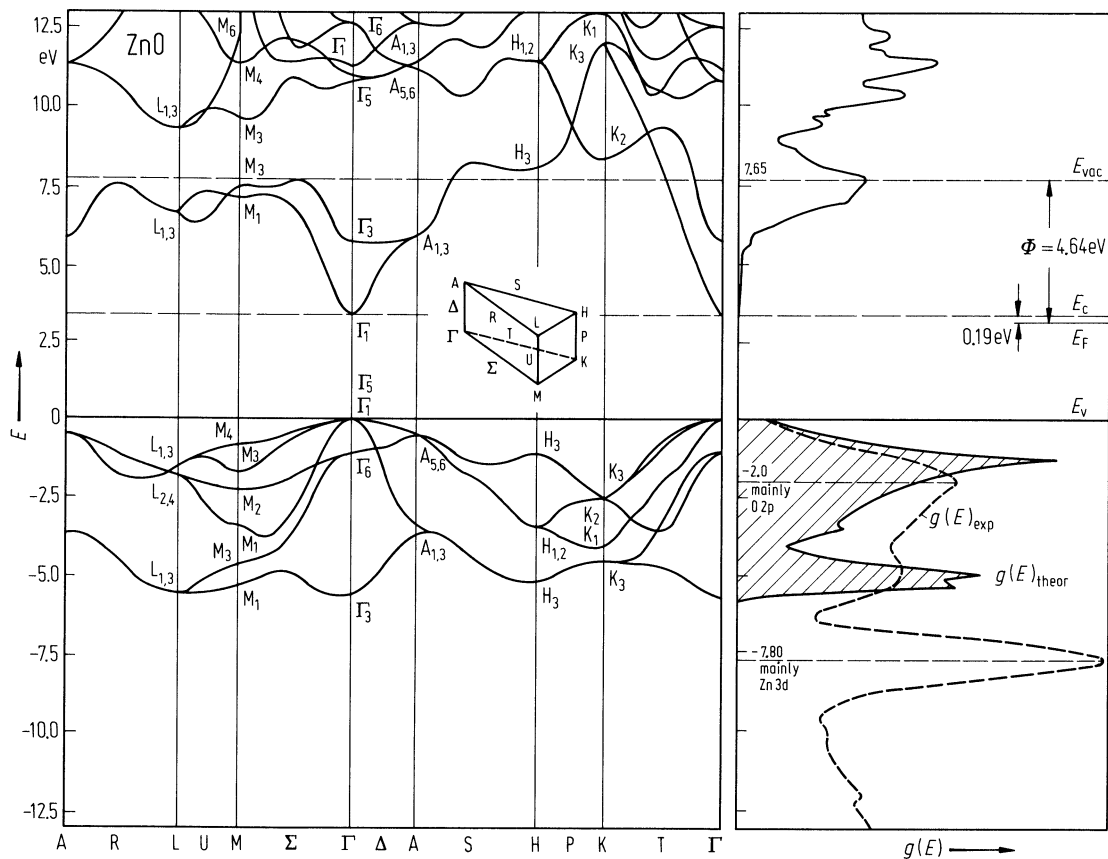


Fig. 3.12.1

ZnO. Temperature dependence of the lattice constants [70R]. Open circles, data from X-ray powder diffraction of [70R]; full circles, data of [35B]; full lines, fourth-order polynomial [70R].

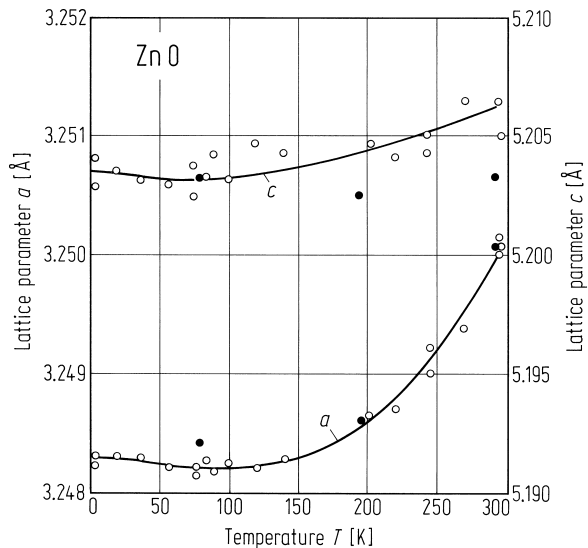


Fig. 3.12.2

ZnO. Coefficient of thermal expansion vs. temperature. Full lines: values fitted with two Einsteins terms with $\Theta_1 = 107$ K and $\Theta_2 = 590$ K [69I]. Open and full circles from capacitance and interferometric methods, respectively.

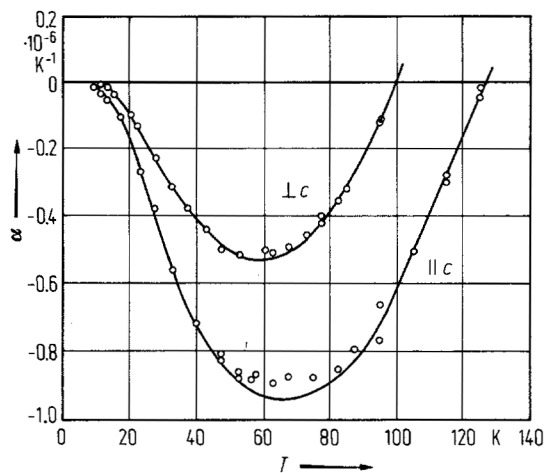
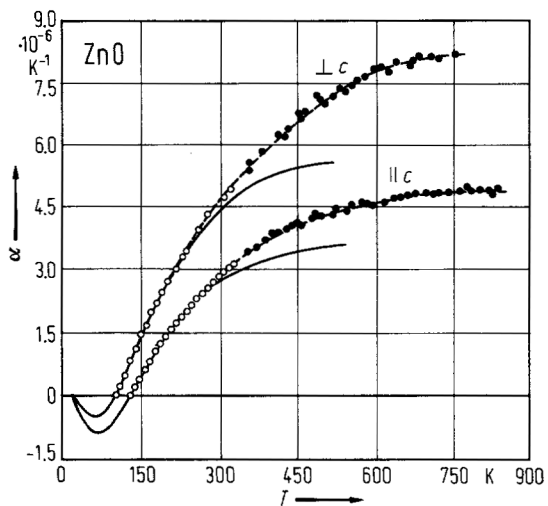


Fig. 3.12.3

ZnO. Phonon dispersion curves calculated and measured by inelastic neutron scattering. Open circles: predominantly longitudinal, full circles: predominantly transverse, as determined experimentally. Branches in different representations are drawn differently [74T].

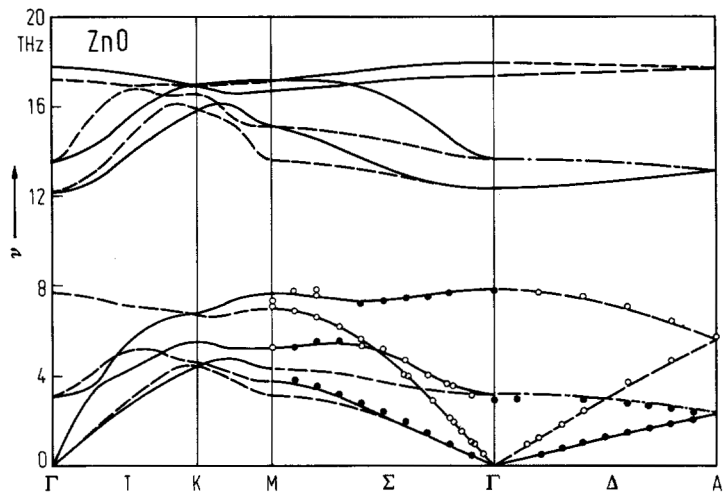


Fig. 3.12.4

ZnO. Electronic conductivity parallel and perpendicular to the c -axis vs. temperature. Crystals grown in Al_2O_3 ceramic without intentional admixtures [74H,74W].

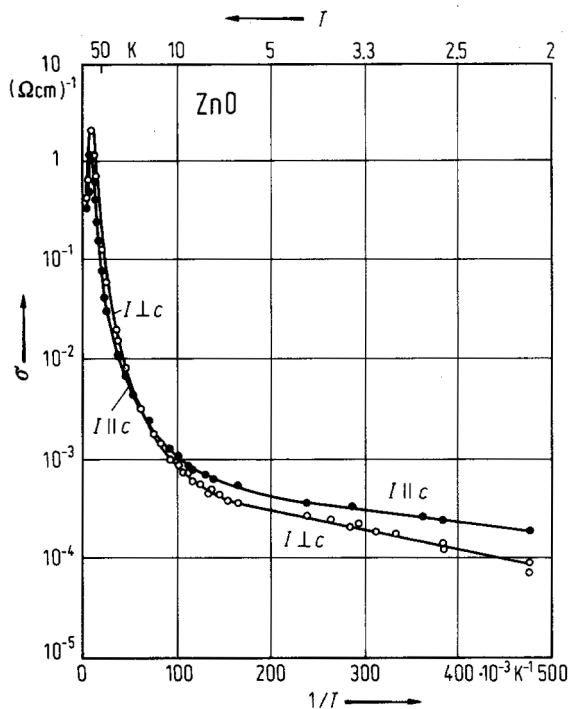


Fig. 3.12.5

ZnO. Electronic part of the thermoelectric power S^{el} and "phonon drag" part S^{ph} vs. temperature for temperature gradients parallel and perpendicular to the c -axis, $n = 1.6 \cdot 10^{16} \text{ cm}^{-3}$ [78W].

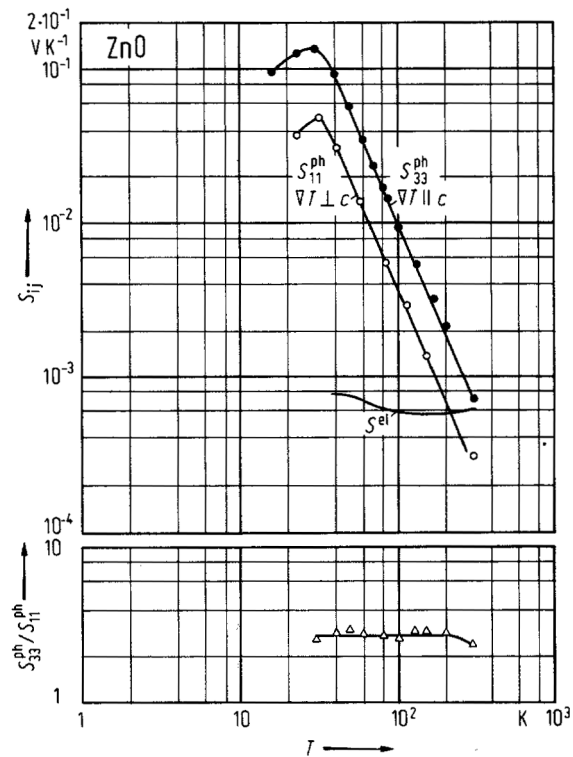


Fig. 3.12.6

ZnO. Thermal conductivity (lattice contribution) vs. temperature. Solid lines calculated [78W].

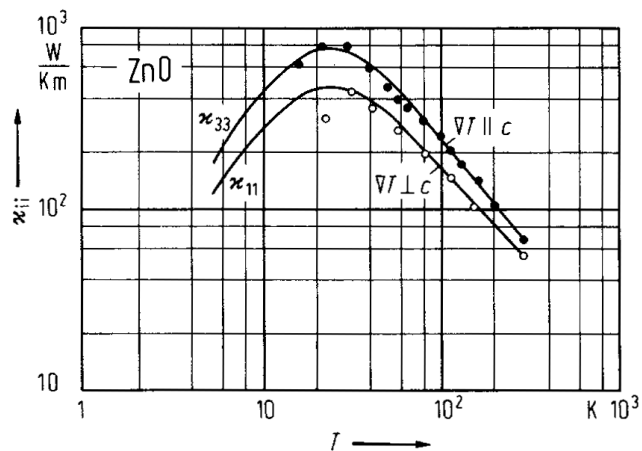


Fig. 3.12.7

ZnO. Refractive index vs. temperature for selected wavelengths. Open circles: $E \perp c$, full circles: $E \parallel c$ [68P].

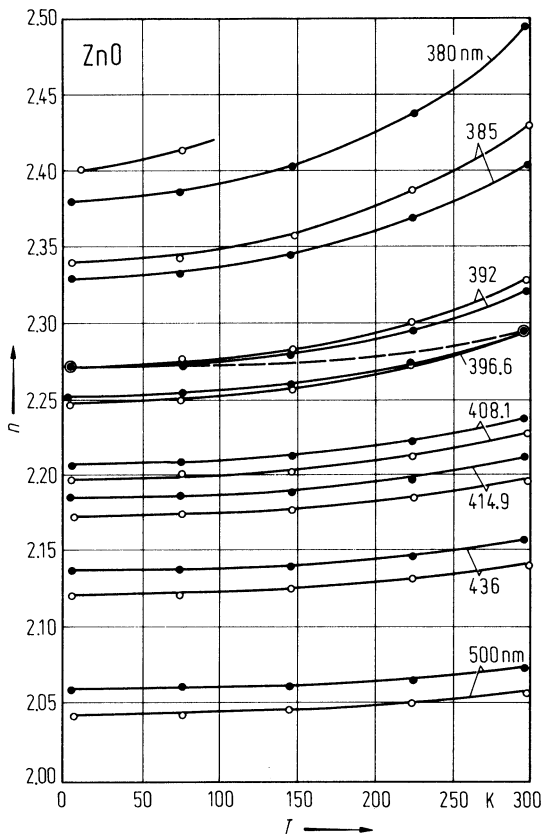


Fig. 3.12.8

ZnO. Numerically calculated spectral dependence of the complex refractive index, $n^* = n(E) + ik(E)$, for ZnO (solid lines). The circles represent experimental data at 300 K [97Y].

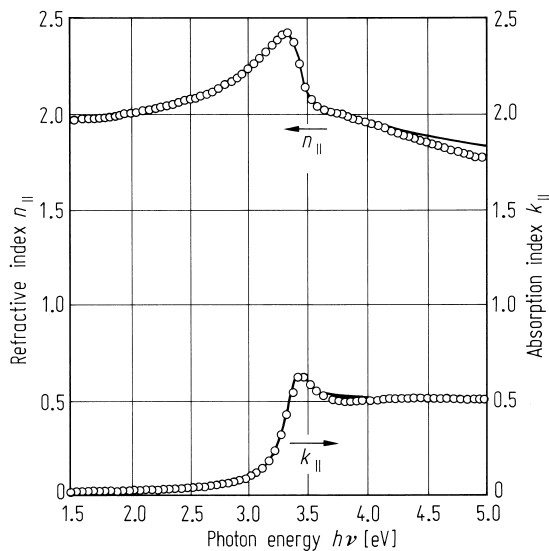
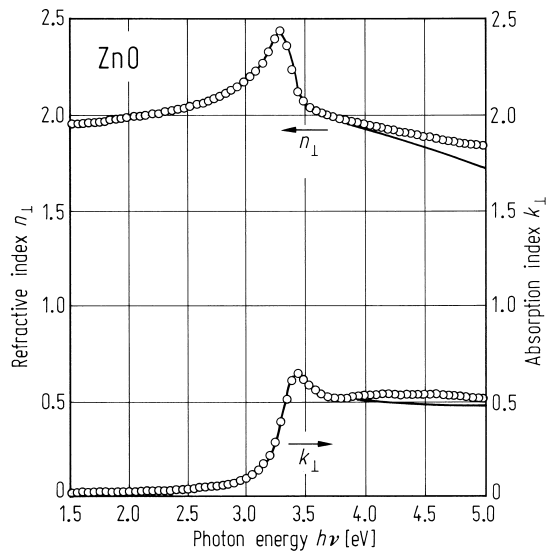


Fig. 3.12.9

ZnO. $\epsilon_1(E)$ spectrum measured by spectroscopic ellipsometry at room temperature (circles). The solid lines represent the best fitted results. Individual contributions of the various types of transitions to $\epsilon_1(E)$ are also shown by dashed lines [97Y].

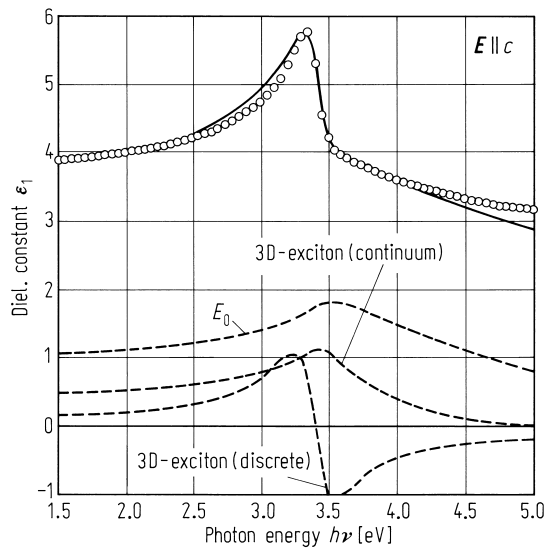
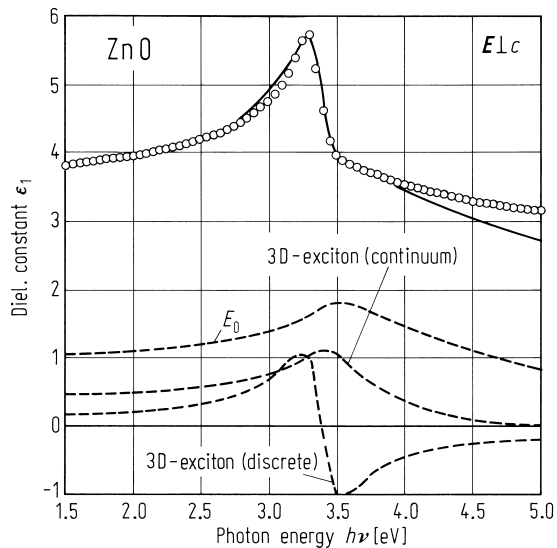
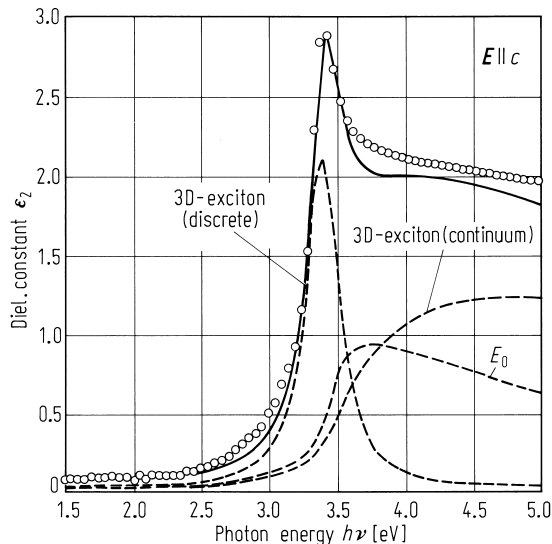
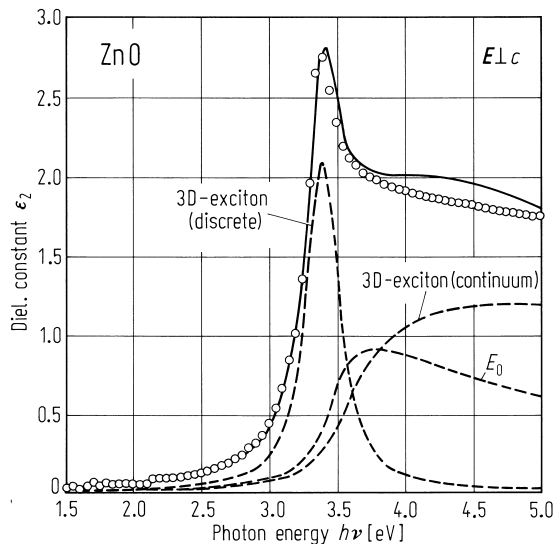


Fig. 3.12.10

ZnO. $\epsilon_2(E)$ spectrum measured by spectroscopic ellipsometry at room temperature (circles). The solid lines represent the best fitted results. Individual contributions of the various types of transitions to $\epsilon_2(E)$ are also shown by dashed lines [97Y].



3.13 Zinc sulfide (ZnS)

Crystal structure

ZnS bulk material exhibits at room temperature predominantly the cubic phase, often with hexagonal inclusions leading to polytypic material. Epitaxial ZnS has mostly been grown on GaAs and, thus, pseudomorphically assuming the cubic structure of the substrate material. In the following, all data refer to the cubic modification unless explicitly otherwise stated.

cubic modification: zincblende structure, space group $F\bar{4}3m - T_d^2$ (Fig. 3.0.1)

hexagonal modification: wurtzite structure, space group $P6_3mc - C_{6v}^4$ (Fig. 3.0.2)

Electronic properties, cubic modification

band structure : see Fig. 3.0.16a, Brillouin zone: Fig. 3.0.4.

Cubic ZnS is a direct-gap semiconductor with the smallest energy gap at the center of the Brillouin zone (Γ). Taking spin-orbit splitting into account the topmost valence band state Γ_{15v} splits into Γ_{8v} and Γ_{7v} ; further splitting into A, B, C levels is achieved by the crystal field.

energies of symmetry points of the band structure (relative to the top of the valence band $E(\Gamma_{15v})$)

Bands are denoted by their symmetry and ordered for ascending energy.

$E(\Gamma_{1v})$	- 13.51 eV			96C
$E(\Gamma_{15v,Zn3d})$	- 6.61 eV			
$E(\Gamma_{12v,Zn3d})$	- 5.98 eV			
$E(\Gamma_{1c})$	2.15 eV			
$E(\Gamma_{15c})$	6.49 eV			
$E(X_{1v})$	- 12.05 eV			
$E(X_{3v})$	- 4.87 eV			
$E(X_{5v})$	- 2.46 eV			
$E(X_{1c})$	3.18 eV			
$E(X_{3c})$	4.02 eV			
$E(L_{1v})$	- 12.43 eV			
$E(L_{1v})$	- 5.75 eV			
$E(L_{3v})$	- 0.96 eV			
$E(L_{1c})$	3.31 eV			

energy gap

$E_{g,dir}(\Gamma_{15v}-\Gamma_{1c})$	3.723(1) eV	$T = 300$ K	luminescence	97T
$E_{g,dir}(\Gamma_{8v}-\Gamma_{6c})$	3.78 eV	$T = 295$ K		
$(\Gamma_{7v}-\Gamma_{6c})$	3.76 eV	$T = 298$ K		65C

temperature dependence of energy gap : see Fig. 3.13.1.

pressure dependence of energy gap

Pressure shift has been described by the empirical fit $E_{1S}(p) = E_{1S}(0) + lp + qp^2$:

l [meV GPa ⁻¹]	63.5(7)	$T = 300$ K	E_0 gap, $E_0(p = 0) = 3.666$ eV, absorption	90V
q [meV GPa ⁻²]	- 1.31(5)		calculation	

exciton energies

$E_{\text{gx}}(\Gamma_5^{\text{T}}, 1\text{S})$	3.799...3.803 eV	$T = 2 \text{ K}$	reflectivity of ZnS/GaAs epilayers	94A
$\Delta_{\text{LT}} [\text{meV}]$	1.4...2.1 eV			
$E_{\text{gx}}(1\text{S})$	3.869...3.873 eV			
E_{gx}^{A}	3.698(1) eV	$T = 293 \text{ K}$	reflectivity	78S
E_{gx}^{B}	3.762(2) eV	$T = 293 \text{ K}$		
E_{gx}^{C}	3.762(2) eV			

exciton binding energy

$E_{\text{b}}(1\text{S})$	38(1) meV	$T = 10 \text{ K}$	absorption, heavy-hole exciton	97F
$E_{\text{b}}(2\text{S})$	10(2) meV			

critical point energies

$E_0 (= E_{\text{g}})$	3.75 eV	$T = 300 \text{ K}$	ellipsometry	93O
$E_0 + \Delta_0$	3.82 eV	$T = 300 \text{ K}$	ellipsometry	
$E_1 - G_1$	5.74 eV	$T = 300 \text{ K}$	G_1 : exciton binding energy, ellipsometry	
E_2	7.0 eV	$T = 300 \text{ K}$	ellipsometry	

spin-orbit splitting

$\Delta_0(\Gamma_{8\text{v}} - \Gamma_{7\text{v}})$	64 meV	$T = 293 \text{ K}$	reflectivity	78S
---	--------	---------------------	--------------	-----

g-factor of electrons and holes

g_{c}	1.8846	$T = 77 \text{ K}$	optically induced EPR	84B
g_{v}	0.93(1)	$T = 2 \text{ K}$	optically detected ESR of acceptors	83B

effective polaron mass of electrons

m_{n}^{**}	0.22 m_0		cyclotron resonance	94I
---------------------	------------	--	---------------------	-----

hole effective masses

$m_{\text{p,l}}$	0.23 m_0		calculated	81W
$m_{\text{p,h}}$	1.76 m_0			

Electronic properties, hexagonal modification

band structure: Fig. 3.0.16b, Brillouin zone: Fig. 3.0.5.

Hexagonal zinc sulfide is a direct semiconductor with the smallest energy gap at the center of the Brillouin zone (Γ). The topmost valence band ($\Gamma_5 + \Gamma_1$) is split due to crystal field and spin-orbit coupling into three spin-degenerate states (Γ_9 , Γ_7 , and Γ_7). Exciton states formed with holes in these valence band states are denoted A, B, and C excitons, respectively.

energies of symmetry points in the band structure (relative to the top of the valence band $E(\Gamma_{5v})$)

$E(\Gamma_{1v})$	- 13.65 eV	calculated values	94Z
$E(\Gamma_{3v})$	- 12.34 eV		
$E(\Gamma_{3v})$	- 5.35 eV		
$E(\Gamma_{6v})$	- 0.85 eV		
$E(\Gamma_{1v})$	- 0.09 eV		
$E(\Gamma_{1c})$	4.08 eV		
$E(\Gamma_{3c})$	5.06 eV		
$E(M_{1v})$	- 12.35 eV		
$E(M_{3v})$	- 11.88 eV		
$E(M_{1v})$	- 5.09 eV		
$E(M_{3v})$	- 4.31 eV		
$E(M_{1v})$	- 3.25 eV		
$E(M_{2v})$	- 2.12 eV		
$E(M_{3v})$	- 1.68 eV		
$E(M_{4v})$	- 0.84 eV		
$E(M_{1c})$	5.55 eV		
$E(M_{3c})$	6.32 eV		

energy gap

$E_{g,dir}(\Gamma_{5v}-\Gamma_{1c})$	3.91(25 eV)	$T = 1.8$ K	reflection	64W
	3.58(1) eV	$T = 300$ K	optical absorption	65C

temperature dependence of energy gap

dE_g/dT	- $3 \cdot 10^{-4}$ eV K ⁻¹		optical absorption	53P
-----------	--	--	--------------------	-----

exciton transition energies

E_{gx}^A	3.866 eV	$T = 77$ K, $E \perp c$	reflection	74K
E_{gx}^B	3.8945 eV			
E_{gx}^C	3.9834 eV	$T = 77$ K, $E \parallel c$		

higher interband transition energies

$E'_0(\Gamma_{5v}-\Gamma_{1c})$	5.65 eV	RT	reflection	64B2
$E_1(L_{3v}-L_{3c})$	9.6 eV	RT		
E_2	7.1...7.6 eV	RT	(E_2 corresponds to the transitions $X_{5v}-X_{1c}$; X_{3c} , in the cubic structure)	

crystal field splitting energy

Δ_{cf}	29(1) meV	$T = 1.8$ K	reflection	64W
---------------	-----------	-------------	------------	-----

spin-orbit splitting energy

Δ_0	92 meV	$T < 15$ K	reflection	66S
------------	--------	------------	------------	-----

g-factor of electrons and holes

g_c	2.3(2)	$T = 1.8$ K, $H \parallel c$	reflection, diamagnetic shift	64W
g_v	1.5	$H \parallel c$	magnetoabsorption	67M

effective electron mass

m_n	0.28(3) m_0	$H \parallel c, H \perp c$	magnetoabsorption	67M
-------	---------------	----------------------------	-------------------	-----

effective hole masses

$m_{p\parallel}$	$1.4\ m_0$		magnetoabsorption	67M
$m_{p\perp}$	$0.49(6)\ m_0$	$H \perp c$		

Lattice properties

lattice parameter (cubic zincblende modification)

a	$5.4053\ \text{\AA}$	RT	X-ray diffraction	85Y1
-----	----------------------	----	-------------------	------

lattice parameters (hexagonal wurtzite modification)

$a(2H)$	$3.820\ \text{\AA}$	$T = 299\ \text{K}$	X-ray diffraction	53S
$c(2H)$	$6.260\ \text{\AA}$	$T = 299\ \text{K}$		

for the temperature range from 0 to 300 K, see Fig. 3.13.2.

coefficient of linear thermal expansion : see Fig. 3.13.3.

phonon dispersion curves of cubic modification: Fig. 3.13.4; Brillouin zone: Fig. 3.0.4.

phonon wavenumbers, cubic modification

$\bar{\nu}_{\text{LO}}(\Gamma)$	$350\ \text{cm}^{-1}$	$T = 300\ \text{K}$	80K1
$\bar{\nu}_{\text{TO}}(\Gamma)$	$274\ \text{cm}^{-1}$		
$\bar{\nu}_{\text{LO}}(\text{X})$	$332(1)\ \text{cm}^{-1}$	$T = 300\ \text{K}$	80K1
$\bar{\nu}_{\text{TO}}(\text{X})$	$318(1)\ \text{cm}^{-1}$		
$\bar{\nu}_{\text{LA}}(\text{X})$	$212(1)\ \text{cm}^{-1}$		
$\bar{\nu}_{\text{TA}}(\text{X})$	$88(1)\ \text{cm}^{-1}$		
$\bar{\nu}_{\text{LO}}(\text{L})$	$334(1)\ \text{cm}^{-1}$		
$\bar{\nu}_{\text{TO}}(\text{L})$	$298(1)\ \text{cm}^{-1}$		
$\bar{\nu}_{\text{LA}}(\text{L})$	$192(1)\ \text{cm}^{-1}$		
$\bar{\nu}_{\text{TA}}(\text{L})$	$72(1)\ \text{cm}^{-1}$		

phonon wavenumbers, hexagonal modification

$\bar{\nu}_{\text{TA}}(\text{L}) - \text{E}_2$	$69.2\ \text{cm}^{-1}$	$T = 300\ \text{K}$	72S1
$\bar{\nu}_{\text{TO}}(\text{L}) - \text{E}_2$	$283\ \text{cm}^{-1}$		
$\bar{\nu}_{\text{TO}}-(\text{A}_1, \text{E}_1)$	$267\ \text{cm}^{-1}\ (\parallel c)$		
$\bar{\nu}_{\text{LO}}-(\text{A}_1, \text{E}_1)$	$347.8\ \text{cm}^{-1}\ (\perp c)$		

second order elastic moduli (cubic modification)

c_{11}	$10.32(5) \cdot 10^{10}\ \text{N m}^{-2}$	$T = 293\ \text{K}$	resonance method	63Z
c_{12}	$6.46\ (5) \cdot 10^{10}\ \text{N m}^{-2}$			
c_{44}^{E}	$4.62(4) \cdot 10^{10}\ \text{N m}^{-2}$			
c_{44}^{D}	$4.643 \cdot 10^{10}\ \text{N m}^{-2}$	$T = 298\ \text{K}$	resonance method	63B

temperature dependence of elastic moduli (zincblende structure): see Fig. 3.13.5.

second order elastic moduli (hexagonal modification)

c_{11}^E	$12.34(4) \cdot 10^{10} \text{ N m}^{-2}$	$T = 298 \text{ K}$	pulse method	73C
c_{12}^E	$5.85(4) \cdot 10^{10} \text{ N m}^{-2}$			
c_{13}^E	$4.55(1) \cdot 10^{10} \text{ N m}^{-2}$			
c_{33}^E	$13.96(3) \cdot 10^{10} \text{ N m}^{-2}$			
c_{44}^E	$2.885(1) \cdot 10^{10} \text{ N m}^{-2}$	$T = 298 \text{ K}$		
c_{66}^E	$3.245(1) \cdot 10^{10} \text{ N m}^{-2}$			
c_{11}^D	$13.03 \cdot 10^{10} \text{ N m}^{-2}$		resonance method	82D
c_{12}^D	$6.90 \cdot 10^{10} \text{ N m}^{-2}$			
c_{13}^D	$5.25 \cdot 10^{10} \text{ N m}^{-2}$			
c_{33}^D	$14.34 \cdot 10^{10} \text{ N m}^{-2}$			
c_{44}^D	$2.74 \cdot 10^{10} \text{ N m}^{-2}$			

bulk modulus (cubic modification)

B	$75.0(20) \text{ GPa}$	$p = p_{\text{tr}}, \text{ RT}$	X-ray diffraction	90V
-----	------------------------	---------------------------------	-------------------	-----

volume compressibility (cubic modification)

κ	0.763 Mbar^{-1}		wurtzite	85G
	0.767 Mbar^{-1}		zincblende	85G

Young's modulus

E	$9.65 \cdot 10^{10} \text{ N m}^{-2}$	RT	Irtran 2 (Kodak)	66B
-----	---------------------------------------	----	------------------	-----

Poisson's ratio (hexagonal modification)

ν	0.415			67C
-------	-------	--	--	-----

electromechanical coupling coefficients

cubic modification:

k_{14}	$7.95(2\%) \cdot 10^{-2}$	$T = 298 \text{ K}$	resonance method	63B
----------	---------------------------	---------------------	------------------	-----

hexagonal modification:

k_{31}	0.072	RT	resonance method	82D
k_{15}	0.084			
k_{33}	0.14			
k_h	$0.9 \cdot 10^{-2}$		(hydrostatic electromechanical coupling coefficient)	66K2

Debye temperature

cubic modification:

Θ_D	352 K	$T = 77 \text{ K}$	calculated from C_p	74R
------------	-------	--------------------	-----------------------	-----

hexagonal modification:

Θ_D	351 K	$T = 298 \text{ K}$	calculated from C_p	74R
------------	-------	---------------------	-----------------------	-----

For the temperature dependence of Θ_D in cubic ZnS (Irtran 2), see Fig. 3.13.6.**heat capacity** (polycrystalline ZnS)

C_p	$45.882 \text{ J mol}^{-1} \text{ K}^{-1}$ (wurtzite)	$T = 298.15 \text{ K}$		89B
	$45.358 \text{ J mol}^{-1} \text{ K}^{-1}$ (zincblende)	temperature dependence, see Fig. 3.13.7		

density

cubic modification:

d	4.088 g cm ⁻³	RT	78C
-----	--------------------------	----	-----

hexagonal modification:

d	4.087 g cm ⁻³	RT	78C
-----	--------------------------	----	-----

melting temperature

Under normal pressure ZnS sublimates before melting.

T_m	1991 K	88S
-------	--------	-----

Transport properties

(Photo)conductivity of ZnS strongly depends on growth conditions, dopants and doping characteristics etc.

electrical resistivity, cubic modification

Fig. 3.13.8 presents electron resistivity versus carrier concentration at 300 K.

ρ	1 Ω cm	$T = 300$ K	ZnS/GaAs, lowest value, substrate temperature 300 °C	85Y2
	$2 \cdot 10^{-3}$ Ω cm	$T = 300$ K	ZnS:I/GaAs, MOCVD	89K
	$4 \cdot 10^2$ Ω cm	$T = 300$ K	ZnS:Li/GaAs, $p = 7.5 \cdot 10^{15}$ cm ⁻³	90M

For the temperature dependence of the electrical conductivity (intrinsic conductivity), see Fig. 3.13.9.

carrier mobilities, cubic modification

Electron and hole mobilities are extremely dependent on sample structural quality, dopant's concentration, impurities compensation ratio, and details of the growth procedure. Therefore only a few values are listed which seem to represent upper limits obtained under the given conditions, respectively.

μ_n	230 cm ² /Vs	$T = 300$ K	calculation of mobility limit	90R
	3000 cm ² /Vs	$T = 77$ K		
	165 cm ² /Vs	$T = 300$ K,	drift mobility, values for different	64S
	79 cm ² /Vs	cubic,	samples	
	200...600 cm ² /Vs	$T = 300$ K	photo-Hall effect, values depending on irradiation	65N

For temperature dependence of electron mobility in the range 300...600 K, see Fig. 3.13.10.

μ_p	40 cm ² /Vs	$p = 6 \cdot 10^{18}$ cm ⁻³ RT	Hall effect, VPE material with N doping	89I
---------	------------------------	--	---	-----

thermal conductivity (cubic modification) (in W cm⁻¹ K⁻¹)

κ	3.6	$T = 30$ K	pulse method	72S2
	0.27	$T = 300$ K		

piezoelectric strain constant

cubic modification:

d_{14}	$3.117(3) \cdot 10^{-12}$ C/N	RT	synchro-ring method	80S
----------	-------------------------------	----	---------------------	-----

hexagonal modification:

d_{15}	$-4.37 \cdot 10^{-12}$ C/N	RT	resonance method	82D
d_{31}	$-2.14 \cdot 10^{-12}$ C/N			
d_{33}	$3.66 \cdot 10^{-12}$ C/N			

piezoelectric stress constants

cubic modification:

e_{14}	0.140(4) C/m ²	RT	synchro-ring method	80S
----------	---------------------------	----	---------------------	-----

hexagonal modification:

e_{15}	- 0.118 C/m ²	RT	resonance method	82D
e_{31}	- 0.238 C/m ²			
e_{33}	0.265 C/m ²			

Optical properties

absorption and refractive index (cubic modification)

Fig. 3.13.11 displays the spectral dependence of the absorption index and the refractive index of cubic ZnS at 300 K.

refractive index (hexagonal modification)

Fig. 3.13.12 displays the spectral dependence of the refractive index of hexagonal ZnS at 298 K.

dielectric function (cubic modification)

Fig. 3.13.13 gives the dielectric-function spectra of cubic ZnS within the spectral range from 1.2...5.6 eV.

dielectric constant (hexagonal modification)

ϵ_{11}^X	8.31	RT	resonance method	82D
ϵ_{33}^X	8.76			

temperature dependence of dielectric constant : see also Fig. 3.13.14.

electrooptical constants

cubic modification:

r_{41}	2.1·10 ⁻¹² m/V	$\lambda = 0.65 \mu\text{m}$	electrooptical measurement (retardation angle)	66K1
----------	---------------------------	------------------------------	--	------

hexagonal modification:

r_{13}	0.92·10 ⁻¹² m/V	$\lambda = 0.63 \mu\text{m}$		66K1
r_{33}	1.85·10 ⁻¹² m/V			

Impurities and defects

ionization energies of shallow donors

hydrogenic donor	0.03 eV	mean value	electrical transport measurements	67H
F	0.2/0.3 eV			67D
Al	0.0713(36) eV	T variable	donor, thermal ionization, electron emission in ESR	90G
Cl	0.25 eV	$T_p = 185$ K	thermoluminescence	58H
Sc	0.1844(149) eV	T variable	acceptor, thermal ionization, hole emission	90G
Ga	0.26 eV	ZnS:Cu,Ga	fractional-glow technique	66G
Sb	0.070 eV	$T = 4.2$ K	bulk, Sb-doped, derived from bound exciton and donor-band transition	91N
Br	0.26 eV	$T_p = 190$ K	thermoluminescence	58H
Cd	0.53 eV	$T_p = 285$ K	thermoluminescence	58H
In	0.50 eV	$T_p = 368$ K	thermoluminescence	58H
I	0.072(4) eV	ZnS:Cu,I $T = 5$ K	optical absorption	73B
	0.058(4) eV	ZnS:Cu,I	thermal depth from shallow-donor model applied to optical absorption	73B
unknown	0.0326(11) eV	T variable	acceptors, thermal ionization, hole emission in ESR	90G
	0.0342(5) eV			
	0.045 eV			
	0.066(5) eV			
	0.083(3) eV			
	0.1226(105) eV			

shallow acceptor ionization energies

Na	170 meV	$T = 4.2$ K	calculated from bound exciton	88K
Li	660 meV		optical methods	58H
unknown	100 meV	$T = 4.2$ K	bulk, Sb-doped, derived from bound exciton and band-acceptor transition	91N

References to 3.13

- 28C Clusius, K., Harteck, P.: Z. Phys. Chem. (Leipzig) 134 (1928) 243.
- 53P Piper, W. W.: Phys. Rev. 92 (1953) 23.
- 53S Swanson, H. E., Fuyat, R. K.: Natl. Bur. Stand. (U. S.) Circ. 539 (1953) 65.
- 58H Hoogenstraten, W.: Philips Res. Repts. 13 (1958) 515.
- 61B Birman, J. L., Samelson, H., Lempicki, A.: G. T. & E. Research and Development Journal 1 (1961) 1.
- 63B Bieniewski, T. M., Czyzak, S. J.: J. Opt. Soc. Am. 53 (1963) 496.
- 63Z Zarembovitch, A.: J. Phys. (Paris) 24 (1963) 1097.
- 64B1 Balkanski, M., Nusimovici, M., Le Toullec, R.: J. Phys. (Paris) 25 (1964) 305.
- 64B2 Balkanski, M., Pétroff, Y.: 7th Intern. Conf. on the Physics of Semiconductors. Paris 1964, Dunod, Paris, 1964, p. 245.
- 64S Spear, W. E., Le Comber, P. G.: Phys. Rev. Lett. 13 (1964) 434.
- 64W Wheeler, R. G., Miklosz, J. C.: 7th Intern. Conf. on the Physics of Semiconductors, Paris 1964, Dunod, Paris, 1964, p. 873.
- 65C Cardona, M., Harbeke, G.: Phys. Rev. A 137 (1965) 1467.
- 65N Narita, S., Nagasaka, K.: J. Phys. Soc. Jpn. 20 (1965) 1728.
- 66B Ballard, S. S., Browder, J. S.: Appl. Opt. 5 (1966) 1873.
- 66G Gobrecht, H., Hofmann, D.: J. Phys. Chem. Solids 27 (1966) 509.
- 66K1 Kaminow, I. P., Turner, E. H.: Proc. IEEE 54 (1966) 1374; Appl. Opt. 5 (1966) 1612.
- 66K2 Kobayakov, T. B.: Sov. Phys.-Crystallogr. (English Transl.) 11 (1966) 369.
- 66S Segall, B., Marple, D. T. F.: Physics and Chemistry of II-VI Compounds (M. Aven, J. S. Prener, eds.) North Holland Publ. Comp., Amsterdam, 1967, p. 319.
- 67C Cline, C. F., Dunegan, H. L., Henderson, G. W.: J. Appl. Phys. 38 (1967) 1944.
- 67D Devlin, S. S., in: Physics and Chemistry of II-VI Compounds (M-A. Aven, J. S. Prener. eds.) North-Holland Publ. Comp., Amsterdam, 1967 p. 604.
- 67H Halsted, R. E.: Physics and Chemistry of II-VI Compounds (M. Aven, J. S. Prener, eds.) North Holland Publishing Comp., Amsterdam 1967, p. 383.
- 67M Miklosz, J. C., Wheeler, R. G.: Phys. Rev. 153 (1967) 913.
- 67R Reeber, R. R., Powell, G. W.: J. Appl. Phys. 38 (1967) 1531.
- 68K Kobayakov, T. B., Pado, G. S.: Sov. Phys. Solid State (English Transl.) 9 (1968) 1707.
- 72S1 Schneider, J., Kirby, R. D.: Phys. Rev. B 6 (1972) 1290.
- 72S2 Slack, G. A.: Phys. Rev. B 6 (1972) 3791.
- 73B Baur, G., Wengert, R., Wittwer, V.: Phys. Status Solidi (a) 18 (1973) 337.
- 73C Chang, E., Barsch, G. R.: J. Phys. Chem. Solids 34 (1973) 1543.
- 73T Tsay, Y. F., Mitra, S. S., Vetelino, J. F.: J. Phys. Chem. Solids 34 (1973) 2167.
- 74K Kobayakov, I. B., Suslina, L. G., Fedorov, D. L.: Fiz. Tverd. Tela 16 (1974) 578; Sov. Phys. Solid State (English Transl.) 16 (1974) 374.
- 74R Reeber, R. R.: Phys. Status Solidi (a) 26 (1974) 253.
- 74V Vagelatos, N., Wehe, D., King, J. S.: J. Chem. Phys. 60 (1974) 3613.
- 75R Rode, D. L.: in "Semiconductors and Semimetals", Vol. 10, R. K. Willardson, A. C. Beer (eds.), Academic Press, New York 1975, p. 1.
- 77S Sheard, F. W., Smith, T. F., White, G. K., Birch, J. A.: Solid State Phys. 10 (1977) 645.
- 78C Cleveland Crystals, Inc., Cleveland, Ohio, Information sheet, August 1978.
- 78S Sobolev, V. V., Donetshkikh, V. J., Zagainov, E. F.: Sov. Phys. Semicond. (English Transl.) 12 (1978) 646.
- 80K1 Klein, C. A., Donadio, R. N.: J. Appl. Phys. 51 (1980) 797.
- 80K2 Kushwaha, M. S.: Phys. Status Solidi (b) 98 (1980) 623.
- 80S Sil'vestrova, I. M., Kobayakov, I. B., Shternberg, A. A.: Sov. Phys. Techn. Phys. (English Transl.) 25 (1980) 1433.
- 81T Talwar, D. N., Vandevyver, M., Kunc, K., Zigone, M.: Phys. Rev. B 24 (1981) 741.
- 81W Wang, C. S., Klein, B. M.: Phys. Rev. B 24 (1981) 3393.
- 82D Dan'kov, I. A., Kobayakov, I. B., Dabydov, S. Yu.: Fiz. Tverd. Tela 24 (1982) 3613; Sov. Phys. Solid State (English Transl.) 24 (1982) 2058.
- 83B Baranov, P. G., Bulanyi, M. F., Vetrov, V. A., Romanov, N. G.: Pis'ma Zh. Eksp. Teor. Fiz. 38 (1983) 517; JETP Lett. (English Transl.) 38 (1983) 623.
- 84B Backs, D., Hertrampf, A.: Phys. Status Solidi (b) 126 (1984) 343.
- 85G Goble, R. Y., Scott, S. D.: Can. J. Mineral. 23 (1985) 273.
- 85Y1 Yamanaka, T., Tokonami, M.: Acta Crystallogr. B 41 (1985) 298.
- 85Y2 Yoshikawa, A., Yamaga, S., Tanaka, K., Kasai, H.: J. Cryst. Growth 72 (1985) 13.

- 86K Kagayama, H.-M., Soma, T.: Phys. Status Solidi (b) 134 (1986) K 101.
- 87K Kagaya, H.-M., Soma, T.: Phys. Status Solidi (b) 142 (1987) 411
- 88K Kawakami, Y., Taguchi, T., Hiraki, A.: J. Cryst. Growth 89 (1988) 331.
- 88S Sharma, R.C., Chang, Y. A.: J. Cryst. Growth 88 (1988) 193.
- 89B Barin, I.: Thermochemical Data of Pure Substances, VCH, Weinheim, 1989.
- 89I Iida, S., Yatabe, T., Kinto, H.: Jpn. J. Appl. Phys. 28 (1989) L535.
- 89K Kawazu, Z., Kawakami, Y., Taguchi, T., Hiraki, A.: Mater. Sci. Forum 38-41 (1989) 555.
- 90G Godlewski, M., Zakrzewski, A.: J. Cryst. Growth 101 (1990) 517.
- 90M Mitsuishi, I., Shibatani, J., Kao, M.-H., Yamamoto, M., Yoshino, J., Kukimoto, H.: Jpn. J. Appl. Phys. 29 (1990) L733.
- 90R Ruda, H.E., Lai, B.: J. Appl. Phys. 68 (1990) 1714.
- 90V Ves, S., Schwarz, U., Christensen, N.E., Syassen, K., Cardona, M.: Phys. Rev. B 42 (1990) 9113.
- 91N Nagano, M., Kanie, H., Yoshida, I., Sano, M., Aoki, M.: Jpn. J. Appl. Phys. 30 (1991) 1915.
- 93O Ozaki, S., Adachi, S.: Jpn. J. Appl. Phys. 32 (1993) 5008.
- 93X Xu, Y.-N., Ching, W.Y.: Phys. Rev. B 48 (1993) 4335.
- 94A Abounadi, A., Di Blasio, M., Bouchara, D., Calas, J., Averous, M., Briot, O., Cloitre, T., Aulombard, R.L., Gil, B., Briot, N.: Phys. Rev. B 50 (1994) 11677.
- 94I Imanaka, Y., Miura, N.: Phys. Rev. B 50 (1994) 14065.
- 94Z Zakharov, O., Rubio, A., Blase, X., Cohen, M.L., Louie, S.G.: Phys. Rev. B 50 (1994) 10780.
- 96C Xiaojie Chen, Xinlei Hua, Jinsong Hu, Langlois, J.-M., Goddard, W.A., III: Phys. Rev. B 53 (1996) 1377.
- 96J Jeon, J.-B., Sirenko, Yu.M., Kim, K.W., Littlejohn, M.A., Strosio, M.A.: Solid State Commun. 99 (1996) 423.
- 96V Vogel, D., Krüger, P., Pollmann, J.: Phys. Rev. B 54 (1996) 5495
- 97F Fernandez, M., Prete, P., Lovergine, N., Mancini, A.M., Cingolani, R., Vasanelli, L., Perrone, M.R.: Phys. Rev. B 55 (1997) 7660.
- 97T Tran, T.K., Park, W., Tong, W., Kyi, M.M., Wagner, B.K., Summers, C.J.: J. Appl. Phys. 81 (1997) 2803.

Figures to 3.13

Fig. 3.0.1

The zincblende lattice.

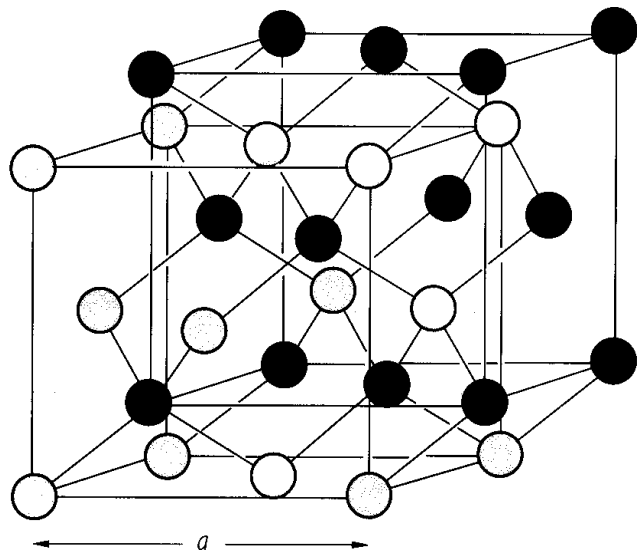


Fig. 3.0.2

The wurtzite lattice.

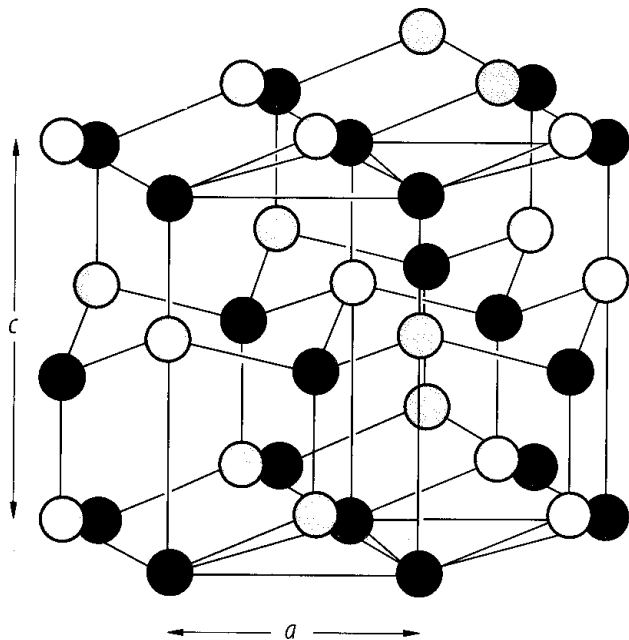


Fig. 3.0.4

The Brillouin zone for the zincblende and the rocksalt lattices.

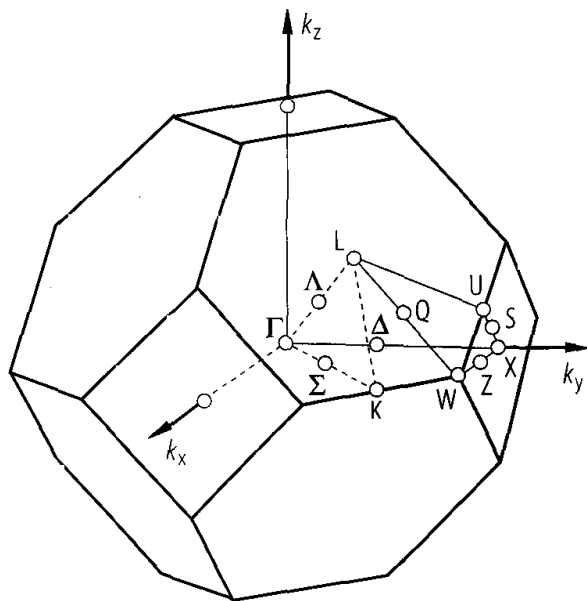


Fig. 3.0.5

The Brillouin zone of the wurtzite lattice.

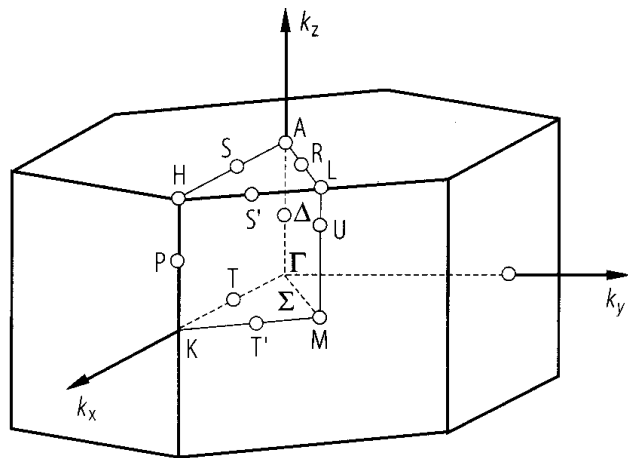


Fig. 3.0.17a

ZnS, cubic. Band structure for zinc-blende symmetry calculated by use of so-called self-interaction-corrected pseudopotentials in local-density approximation. Dashed lines: measured gap energies and d bands from various references [96V].

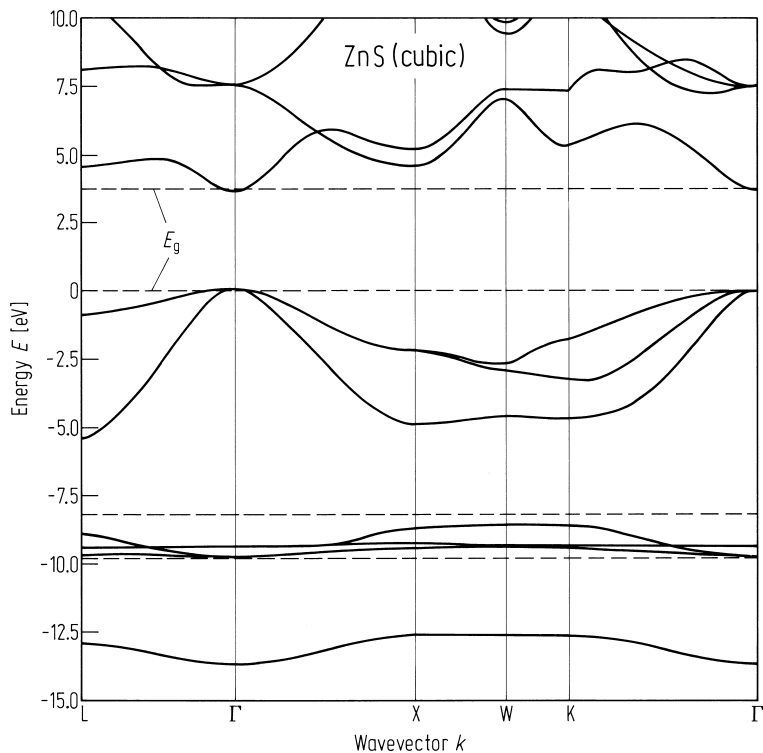


Fig. 3.0.17b

ZnS, hex. Band structure for wurtzite symmetry calculated in the local-density approximation [93X].

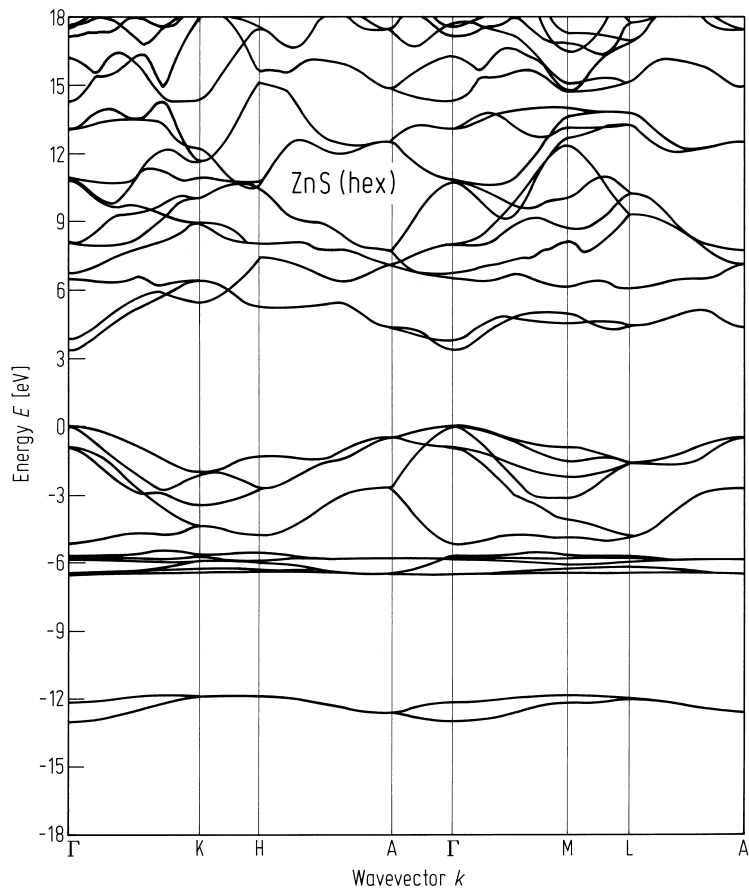


Fig. 3.13.1

ZnS, cubic. Direct energy gap ($\Gamma_{15v}-\Gamma_{1c}$) vs. temperature [73T]. Solid line: theoretical result. Circle: experimental data from [61B]. Triangle: experimental data from [65C].

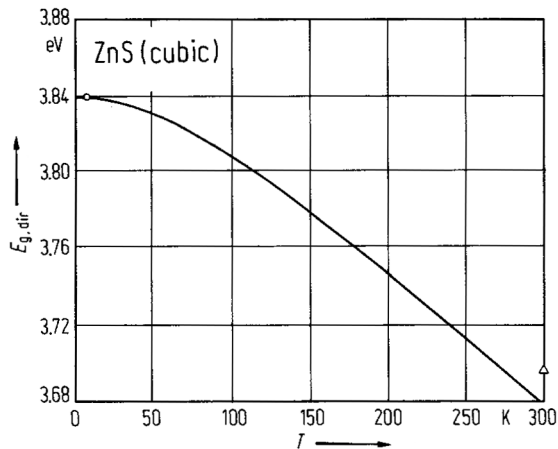


Fig. 3.13.2

ZnS, hex. (a) Lattice parameters a and c vs. temperature; (b) molar volume and c/a ratio vs. temperature [67R].

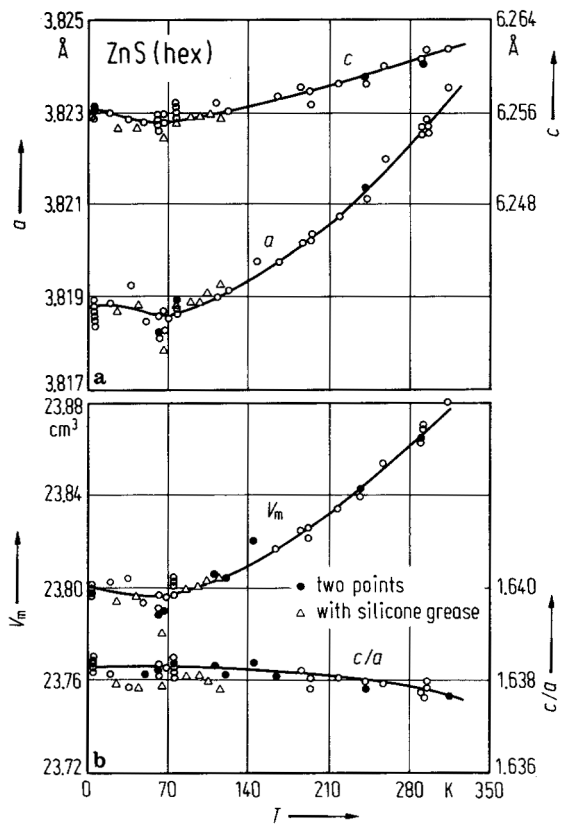


Fig. 3.13.3

ZnS. Linear thermal expansion coefficient α vs. T . Symbols: experimental points [87K].

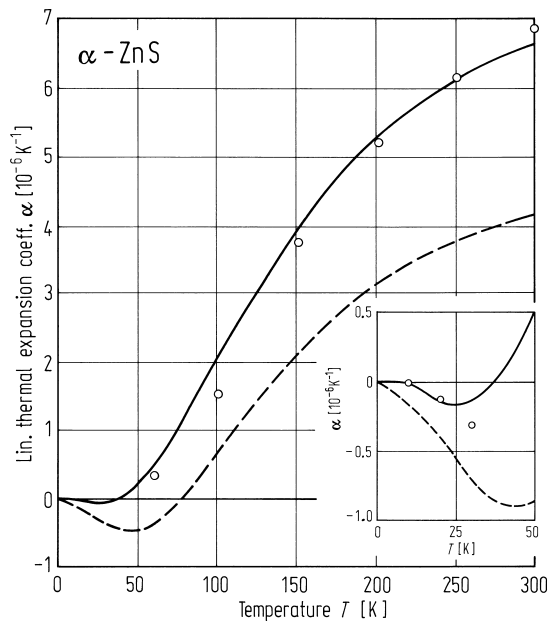


Fig. 3.13.4

ZnS, cubic. Phonon dispersion curves calculated from an 11-parameter rigid-ion model; dashed lines: normal pressure, solid lines: 150 kbar [81T]. Experimental points from inelastic neutron scattering [74V].

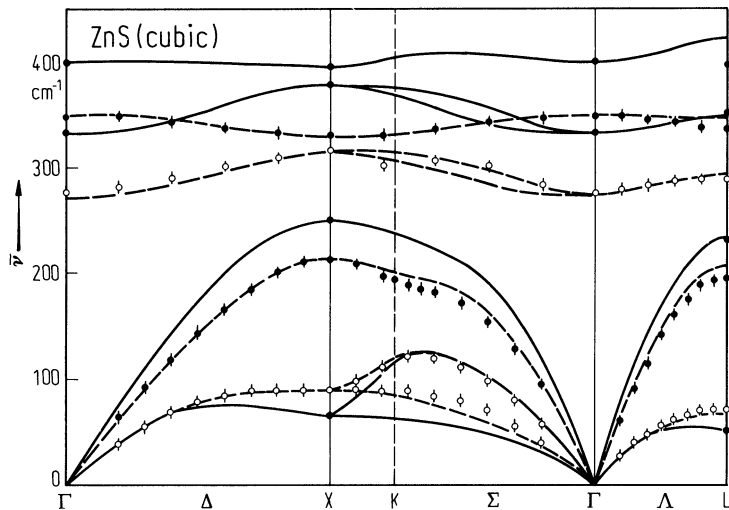


Fig. 3.13.5

ZnS, cubic. Second order elastic moduli c_{11} , c_{12} and c_{44} vs. temperature [63Z].

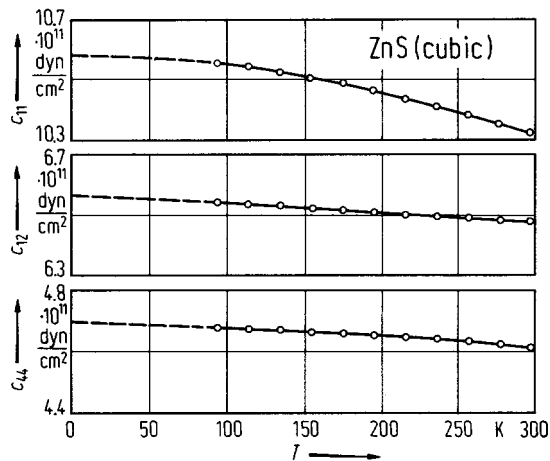


Fig. 3.13.6

ZnS. Debye temperature vs. temperature. (a) ZnS; polycrystalline (Kodak Irtran 2.95% cubic, 5% hexagonal) Debye temperature at $T = 0$ K calculated from elastic constants [77S]. (b) ZnS, cubic. Calculated using an eight-parameter bond-bending force model; experimental points are due to [28C, 80K2].

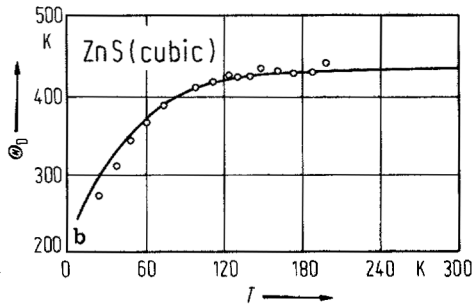
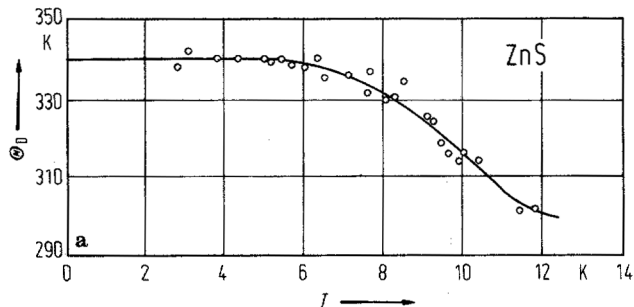


Fig. 3.13.7

ZnS. Heat capacity C_v . Solid line and dashed line calculated from first principles, symbols are experimental points [86K].

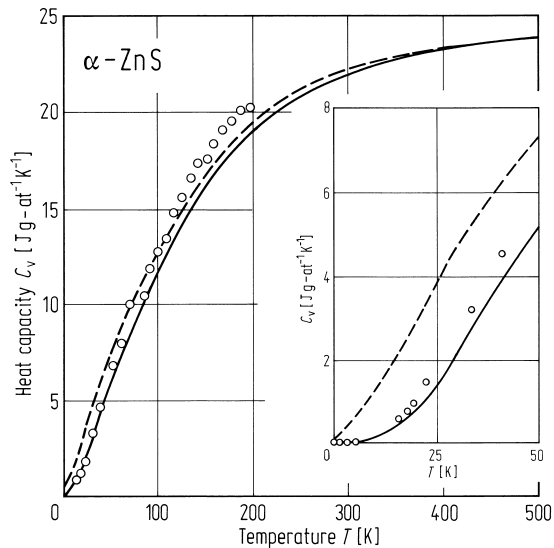


Fig. 3.13.8

ZnS. Total electron resistivity versus carrier concentration, for different impurity concentrations n_{imp} , at $T = 300$ K. Experimentally measured values are given, for references see [90R].

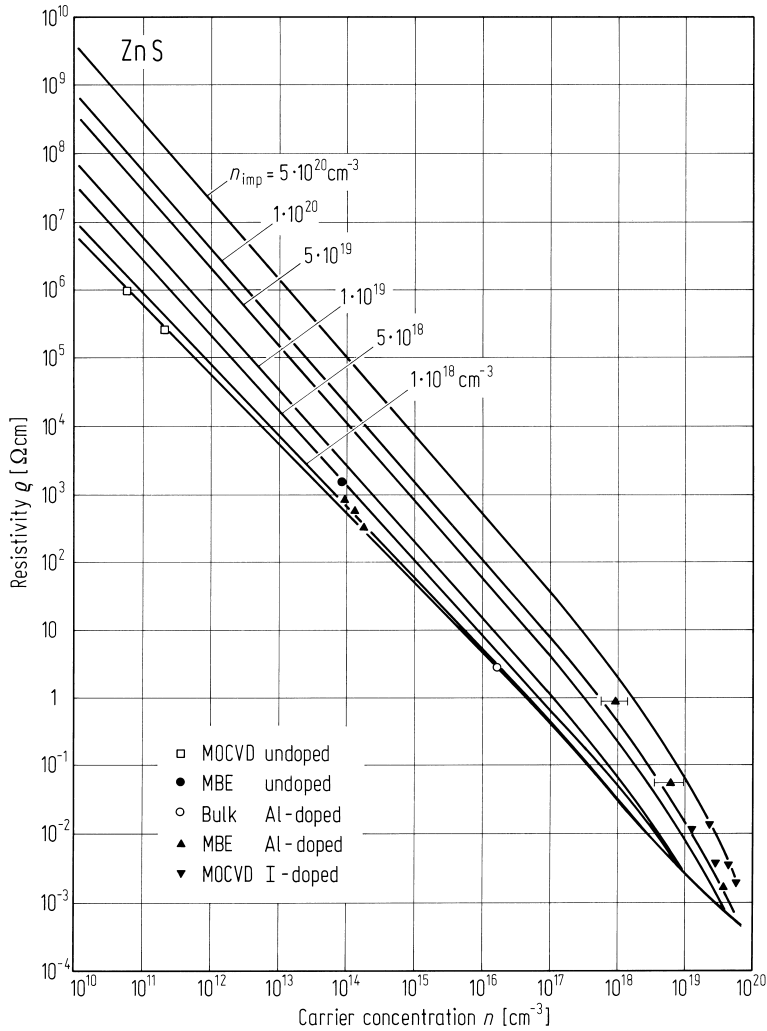


Fig. 3.13.9

ZnS, hex. Electrical conductivity vs. reciprocal temperature. The straight line can be represented by the function $A\exp(-E/2kT)$ with $E = 3.77(10)$ eV [53P].

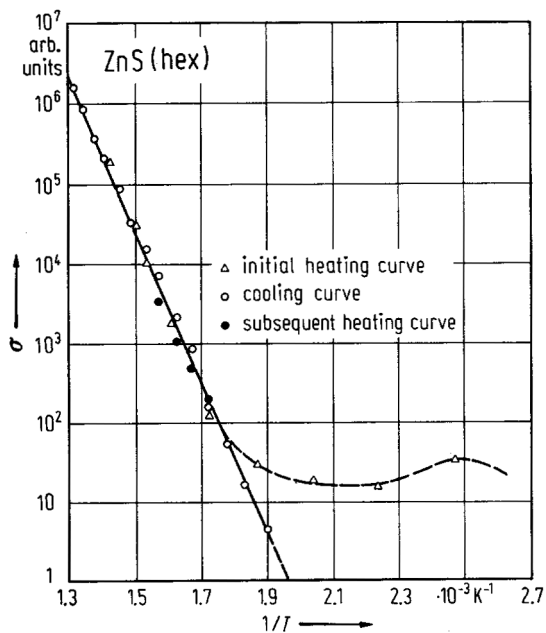


Fig. 3.13.10

ZnS, cubic. Electron mobility vs. temperature; experimental data from various sources are Hall mobilities, solid line: calculated drift mobility [75R].

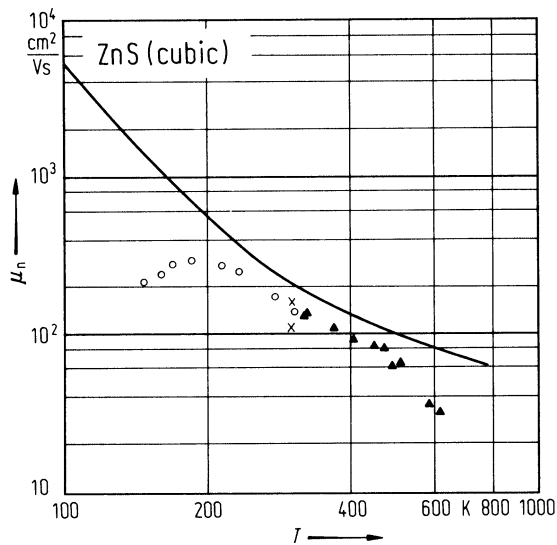


Fig. 3.13.11

ZnS, cubic. Numerically calculated spectral dependence of the complex refractive index, $n^* = n + ik$ (solid lines). The circles represent the measured data at $T = 300$ K [93O].

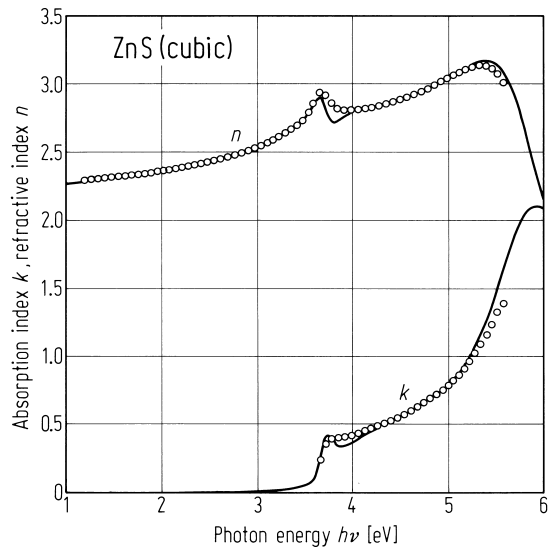


Fig. 3.13.12

ZnS, hex. Index of refraction vs. wavelength, n_o : ordinary ray, n_e : extraordinary ray [63B].

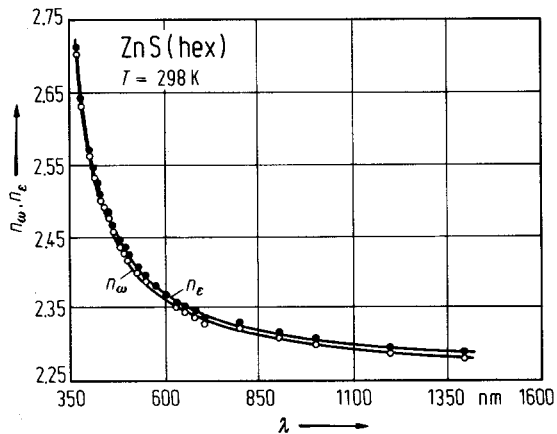


Fig. 3.13.13

ZnS, cubic. Dielectric-function spectra $\epsilon(E)$ measured by spectroscopic ellipsometry at 300 K after chemo-mechanical polishing of the sample (circles). The solid lines are calculated with the model dielectric function for interband critical points. The dashed lines represent the best-fitted standard critical-point line shapes [93O].

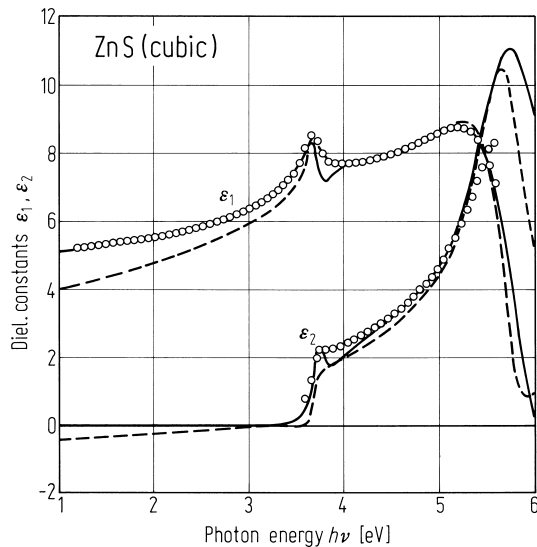
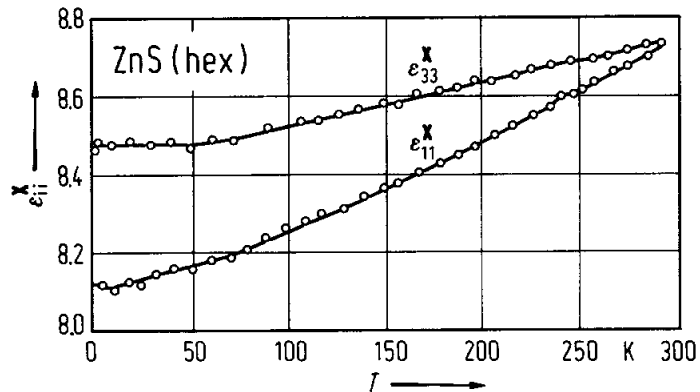


Fig. 3.13.14

ZnS, hex. Dielectric constant vs. temperature [68K]. At 300 K the dielectric constant of ZnS, hex. is isotropic.



3.14 Zinc selenide (ZnSe)

Crystal structure

Under ambient conditions, ZnSe crystallizes in the zincblende structure (space group $F\bar{4}3m - T_d^2$, Fig. 3.0.1).

Electronic properties

Band structure: Fig. 3.0.17, Brillouin zone: Fig. 3.0.4.

Zinc selenide is a direct gap semiconductor with the smallest energy gap at the center of the Brillouin zone (Γ). The topmost valence band (Γ_{15} , Fig. 3.0.18) is split due to spin-orbit coupling into a fourfold (Γ_8) and a twofold (Γ_7) state.

energies of symmetry points of the band structure (relative to the top of the valence band $E(\Gamma_{15v})$)

$E(\Gamma_{1v})$	– 13.49 eV	calculated	94Z
$E(\Gamma_{1c})$	2.84 eV		
$E(\Gamma_{15c})$	7.67 eV		
$E(X_{1v})$	– 12.07 eV		
$E(X_{3v})$	– 5.03 eV		
$E(X_{5v})$	– 2.08 eV		
$E(X_{1c})$	4.41 eV		
$E(X_{3c})$	5.01 eV		
$E(L_{1v})$	– 12.44 eV		
$E(L_{1v})$	– 5.23 eV		
$E(L_{3v})$	– 0.81 eV		
$E(L_{1c})$	4.14 eV		
$E(L_{3c})$	8.18 eV		

energy gap

$E_{g,dir}(\Gamma_{8v}-\Gamma_{6c})$	2.8222(1) eV	$T = 6$ K	two-photon spectroscopy	95M
--------------------------------------	--------------	-----------	-------------------------	-----

For temperature dependence of E_g , see Fig. 3.14.1.

exciton energies

Due to the large spin-orbit splitting (420...450 meV) only excitons with the hole in the topmost (Γ_8) valence band are observed. The ground state of this exciton is split according to the decomposition $\Gamma_{8v} \times \Gamma_{6c} = \Gamma_3 + \Gamma_4 + \Gamma_5$, only the Γ_5 exciton state is dipole allowed.

$E_{gx}(\Gamma_5^L, 1S)$	2.8036 eV	$T = 4$ K	reflectance	81L
$E_{gx}(\Gamma_5^T, 1S)$	2.8016 eV			
$E_{gx}(2S)$	2.8212 eV	$T = 2$ K	absorption spectroscopy	92A
$E_{gx}(2P)$	2.8175(1) eV	$T = 6$ K	two-photon spectroscopy	95M
$E_{gx}(3S)$	2.8247 eV	$T = 2$ K	extrapolated from magnetoabsorption	92A
$E_{gx}(3P)$	2.8203(1) eV	$T = 6$ K	two-photon spectroscopy	95M
$\Delta_{LT}(1S)$	0.0016 eV		absorption spectroscopy	96A
$\Delta(\Gamma_5^T-\Gamma_{3,4})$	– 0.0001(1) eV	$T = 10$ K	RBS	81S

exciton binding energy

$E_b(1S)$	20.8 meV	$T = 1.8$ K	absorption, strained layers	96N
$E_b(2P_{1/2})$	4.19 meV	$T = 1.6$ K	two-photon absorption	77S
$E_b(2P_{5/2}, \Gamma_7)$	4.80 meV			
$E_b(2P_{5/2}, \Gamma_8)$	5.15 meV			

critical points in reflectance at RT

location in zone	symmetry	trans. energy	method	
$\Gamma_{8v}-\Gamma_{6c} (E_0)$	M_0	2.68 eV	ellipsometry	94D
$\Gamma_{7v}-\Gamma_{6c} (E_0+\Delta_0)$	M_0	3.126(5) eV		
$L_{4,5v}-L_{6c} (E_1)$	M_1	4.750(5) eV		

spin-orbit splitting energies

$\Delta_0(\Gamma_{8v}-\Gamma_{7v})$	0.42 eV	$T = 295$ K	reflectivity	72E
$\Delta_1(L_{4,5v}-L_{6v})$	0.20 eV	$T = 300$ K	reflectivity, fitted value	

effective mass of electrons

m_n	0.160(2) m_0	$T = 4.2$ K	photoluminescence of donor complexes	80D
-------	----------------	-------------	--------------------------------------	-----

effective mass of holes

m_p	0.75 m_0	$T = 2.1...200$ K	fitting to calculation, phonon assisted direct exciton absorption	67H2
-------	------------	-------------------	---	------

g-factors

g_c	1.06(5)	$T = 4.2$ K	photoluminescence of donor complexes	80D
g_v	$-0.28(8)$		$E(m_i) = -2g_v\mu_B B$, magnetorefectance	79V

Lattice properties

lattice parameter

a	5.667(4) Å		X-ray diffraction	96K
-----	------------	--	-------------------	-----

coefficient of linear thermal expansion

α	$7.4 \cdot 10^{-6}$ K ⁻¹	$T = 300$ K	capacitance dilatometer, polycrystal	69B
temperature dependence: Fig. 3.14.2.				

density

d	5.266 g cm ⁻³		shock-wave experiment	82G
-----	--------------------------	--	-----------------------	-----

melting temperature

T_m	1799 K			88S
-------	--------	--	--	-----

phonon dispersion curves : Fig. 3.14.3. Brillouin zone: Fig. 3.0.4.

phonon energies

$h\nu_{\text{LO}}(\Gamma_1)$	30.99 meV		Raman	70L1
$h\nu_{\text{TO}}(\Gamma_{15})$	25.17 meV			
$h\nu_{\text{LA}}(\Gamma)$	19.8 meV		luminescence; doped with Cu and Fe	67H1
$h\nu_{\text{TA}}(\Gamma)$	8.0 meV			
$h\nu_{\text{LO}}(\text{X})$	27.64 meV		second order Raman spectra	72I
$h\nu_{\text{TO}}$	25.54 meV			
$h\nu_{\text{LA}}$	23.55 meV			
$h\nu_{\text{LO}}(\text{L})$	27.77 meV			
$h\nu_{\text{TO}}$	25.54 meV			
$h\nu(\text{W}_3)$	24.9 meV			
$h\nu(\text{W}_1)$	18.59 meV			
$h\nu(\text{W}'_2)$	11.53 meV			
$h\nu(\text{W}''_2)$	26.53 meV			
$h\nu(\text{W}'_4)$	14.26 meV			
$h\nu(\text{W}''_4)$	26.41 meV			

phonon frequencies

$\nu_{\text{LO}}(\Gamma)$	7.59 THz	$T = 300 \text{ K}$	neutron scattering	71H
$\nu_{\text{TO}}(\Gamma)$	6.39 THz	$T = 300 \text{ K}$	neutron scattering	71H

second order elastic moduli

c_{11}	90.3(19) GPa		Brillouin scattering	78W
c_{12}	53.6(23) GPa			
c_{44}	39.4(12) GPa			

temperature dependence of the second order elastic moduli

$(1/c_{11})dc_{11}/dT$	$-1.66 \cdot 10^{-4} \text{ K}^{-1}$	$T = 295 \text{ K}$	ultrasonic pulse method	70L2
$(1/c_{44})dc_{44}/dT$	$-1.07 \cdot 10^{-4} \text{ K}^{-1}$			
$(1/c_{12})dc_{12}/dT$	$-1.89 \cdot 10^{-4} \text{ K}^{-1}$			

compressibility

κ	0.595 Mbar ⁻¹			85G
----------	--------------------------	--	--	-----

Young's modulus

E	$7.24 \cdot 10^{11} \text{ dyn cm}^{-2}$			70M
-----	--	--	--	-----

shear modulus

G	$2.85 \cdot 10^{11} \text{ dyn cm}^{-2}$			70M
-----	--	--	--	-----

bulk modulus

B	62.4(7) GPa	$\text{RT}, p = 0$	ultrasonic pulse method	70L2
-----	-------------	--------------------	-------------------------	------

Debye temperature

Θ_{D}	339(2) K		temperature dependence, see Fig. 3.14.4	80C
---------------------	----------	--	---	-----

heat capacity

C_p	51.88 J mol ⁻¹ K ⁻¹	$T = 298.15 \text{ K}$	temperature dependence: see Fig. 3.14.5	89B
-------	---	------------------------	---	-----

Transport properties

(Photo)conductivity of ZnSe strongly depends on growth conditions, dopants and doping characteristics etc.

resistivity

Values of ρ given in literature depend strongly on special preparation conditions. Resistivity of not intentionally doped MBE layers is shown in Fig. 3.14.6.

undoped material

ρ	$10^5 \Omega \text{ cm}$	$T = 300 \text{ K}$	MOVPE film, van-der-Pauw technique	88O
	$17 \Omega \text{ cm}$	$T = 300 \text{ K}$	MOVPE films, van-der-Pauw technique	88M
	$4.16 \dots 30.1 \Omega \text{ cm}$	$T = 300 \text{ K}$	as-grown bulk, dipped in molten Zn	92C

carrier mobility

Electron and hole mobilities are extremely dependent on sample structural quality, dopant's concentration, impurities compensation ratio, and details of the growth procedure.

Fig. 3.14.7 shows typical data and an analysis with respect to phonon and defect scattering. See also Fig. 3.14.8 for the temperature dependence of the electron drift mobility and Fig. 3.14.9 for the temperature dependence of the hole mobility

μ_n	up to $400 \text{ cm}^2/\text{Vs}$	$T = 300 \text{ K}$	Ga-doped MOVPE film, $n \approx 10^{16} \text{ cm}^{-3}$	89S
μ_p	$110 \text{ cm}^2/\text{Vs}$	$T = 300 \text{ K}$	theoretical upper limit, zero compensation	86R

thermal conductivity

κ	$0.19 \text{ W K}^{-1} \text{ cm}^{-1}$	$T = 300 \text{ K}$	see also Fig. 3.14.10 for T -dependence	65S
----------	---	---------------------	---	-----

piezoelectric strain coefficient

d_{14}	$1.10(6) \text{ pC N}^{-1}$	$T = 300 \text{ K}$	piezoresonance	63B
----------	-----------------------------	---------------------	----------------	-----

piezoelectric stress coefficient

e_{14}	$0.049(4) \text{ C/m}^2$	$T = 300 \text{ K}$	piezoresonance	63B
----------	--------------------------	---------------------	----------------	-----

Optical properties

refractive index

Fig. 3.14.11 presents the energy dependence of the refractive index n and the absorption index k .

At $T = 298 \text{ K}$ polycrystalline values are smoothed by Herzberger dispersion equation

$$n = n_0 + b/(\lambda^2 - 0.028) + c/(\lambda^2 - 0.028)^2 + d\lambda^2 + e\lambda^4$$

n_0 : measured values; λ : wavelength in μm ; b : $5.1567472 \cdot 10^{-2}$; c : $2.4901923 \cdot 10^{-3}$; d : $-2.7245212 \cdot 10^{-8}$;
 e : $-9.8541275 \cdot 10^{-8}$ [70M]

dielectric constants

Fig. 3.14.12 shows the real and imaginary part of the dielectric function of bulk ZnSe between 1.5 eV and 6 eV at room temperature.

$\varepsilon(0)$	8.6	$T = 300 \text{ K}$	ellipsometry	91A
$\varepsilon(\infty)$	5.7			

Impurities and defects

ionization energies of shallow donors

$E_d(\text{Li}_\text{I})$	15(1) meV	$T = 4.2 \text{ K}$	PL, estimation from DAP band	92I
$E_d(\text{Na}_\text{I})$	16(1) meV			
$E_d(\text{Al})$	26.3 meV	$T = 4.2 \text{ K}$	resonant electronic Raman scattering	81B
$E_d(\text{Ga})$	27 meV			
$E_d(\text{In})$	28.1 meV			
$E_d(\text{F})$	29.3 meV			
$E_d(\text{Cl})$	26.1 meV			
$E_d(\text{I})$	30.4 meV			

shallow acceptor ionization energies

$E_a(\text{Li})$	118(2) meV	$T = 4.2 \text{ K}$	bound excitons and selective-pair PL	95Y
$E_a(\text{Na})$	98(2) meV			
$E_a(\text{K})$	94(2) meV			
$E_a(\text{N})$	112 meV	$T = 4.2 \text{ K}$	free-to-acceptor transition	93K
$E_a(\text{P})$	80...92 meV	$T = 4.2 \text{ K}$	PL	85Y
$E_a(\text{As})$	125 meV	$T = 77 \text{ K}$	As doped, photoconductivity	92H
$E_a(\text{Sb})$	69 meV	$T = 30 \text{ K}$	Sb doped, Haynes rule and free-to-bound as well as DAP band analysis	97T
$E_a(\text{Rb})$	89(2) meV	$T = 4.2 \text{ K}$	bound excitons and selective-pair PL	95Y
$E_a(\text{Cs})$	74(2) meV			
$E_a(\text{O})$	80 meV	$T = 4 \text{ K}$	PL	89A
$E_a(\text{V}_{\text{Zn}})$	218 meV	$T = 4 \text{ K}$	free-to-acceptor transition in doped ZnSe:N	95Z

References to 3.14

- 63B Berlincourt, D., Jaffe, H., Shiozawa, L. R.: Phys. Rev. 129 (1963) 1009.
- 65P Park, Y. S., Chan, F. L.: J. Appl. Phys. 36 (1965) 800.
- 65S Slack, G. A., in: Physics and Chemistry of II-VI Compounds, (M. Aven, J. S. Prener, eds.) 1967, p. 557.
- 67H1 Haanstra, J. J.: II-VI Semiconductor Compounds, (D. G. Thomas, ed.) W. A. Benjamin Inc. 1967, p. 207.
- 67H2 Hite, G. E., Marple, D. T. F., Aven, M., Segall, B.: Phys. Rev. 156 (1967) 850.
- 69B Browder, J. S., Ballard, S. S.: Appl. Opt. 8 (1969) 793.
- 70L1 LaCombe, J. L., Irwin, J. C.: Solid State Commun. 8 (1970) 1427.
- 70L2 Lee, B. H.: J. Appl. Phys. 41 (1970) 2984, 2988
- 70M Moses, A. J.: Hughes aircraft company, Culver City, California AD-704 555, 1970.
- 71H Hennion, B., Moussa, F., Pepy, G., Kunc, K.: Phys. Lett. A 36 (1971) 376.
- 72E Ebina, A., Yamamoto, M., Takahashi, T.: Phys. Rev. B 6 (1972) 3786.
- 72I Irwin, J. C., LaCombe, J.: Can. J. Phys. 50 (1972) 2596.
- 73F Freeout, J. L.: Phys. Rev. B 7 (1973) 3810.
- 73Y Yu, P. W., Park, Y. S.: Appl. Phys. Lett. 22 (1973) 345.
- 75S Smith, T. F., White, G. K.: J. Phys. C 8 (1975) 2031.
- 76C Chelikowsky, J. R., Cohen, M. L.: Phys. Rev. B 14 (1976) 556.
- 77S Sondergeld, M.: Phys. Status Solidi (b) 81 (1977) 253.
- 77T Touloukian, Y. S., Kirby, R. K., Taylor, R. E., Lee, T. Y. R.: Thermophysical Properties of Matter Vol. 13: Thermal Expansion, New York, Washington: IFI/Plenum (1977).
- 78W Wasa, K., Yamada, M., Hamaguchi, C.: Tech. Rep. Osaka University 28 (1978) 447.
- 79V Venghaus, H.: Phys. Rev. B 19 (1979) 3071.
- 80C Collins, J. G., White, G. K., Birch, J. A., Smith, T. F.: J. Phys. C 13 (1980) 1649.
- 80D Dean, P. J., Herbert, D. C., Lakee, A. M.: Proc. 15th Int. Conf. Physics of Semiconductors, Kyoto 1980, J. Phys. Soc. Jpn. 49 (1980) Suppl. A, 185.
- 80H Hagenberg, F.: Thesis, D 83; T. U. Berlin 1980.
- 80K Kushwaha, M. S., Kushwaha, S. S.: J. Phys. Chem. Solids 41 (1980) 489.
- 81B Blanconnier, P., Hogrel, J.F., Jean-Louis, A.M., Sermage, B.: J. Appl. Phys. 52 (1981) 6895
- 81L Lagois, J.: Phys. Rev. B 23 (1981) 5511.
- 81S Sermage, B., Fishman, G.: Phys. Rev. B 23 (1981) 5107.
- 81T Talwar, D. N., Vandevyver, M., Kunc, K., Zigone, M.: Phys. Rev. B 24 (1981) 741.
- 81W Wang, C. S., Klein, M. M.: Phys. Rev. B 24 (1981) 3293.
- 82G Gust, W. H.: J. Appl. Phys. 53 (1982) 4843.
- 85G Goble, R. Y., Scott, S. D.: Can. J. Mineral. 23 (1985) 273.
- 85Y Yao, T.: J. Cryst. Growth 72 (1985) 31.
- 86K Kagaya, H.-M., Soma, T.: Phys. Status Solidi (b) 134 (1986) K 101.
- 86R Ruda, H.E.: J. Appl. Phys. 59 (1986) 3516.
- 88M Morimoto, K., J. Appl. Phys. 64 (1988) 4951
- 88O Ohki, A., Shibata, N., Ando, K., Katsui, A.: J. Cryst. Growth 93 (1988) 692
- 88S Sharma, R.C., Chang, Y. A.: J. Cryst. Growth 88 (1988) 193.
- 89A Akimoto, K., Miyajima, T., Mori, Y.: Phys. Rev. B 39 (1989) 3138.
- 89B Barin, I.: Thermochemical Data of Pure Substances, VCH, Weinheim, 1989.
- 89S Skromme, B.J., Shibli, S.M., de Miguel, J.L., Tamargo, M.C.: J. Appl. Phys. 65 (1989) 3999.
- 90M Marshall, T., Gaines, J.: Appl. Phys. Lett. 56 (1990) 2669.
- 91A Adachi, S., Taguchi, T.: Phys. Rev B 43 (1991) 9569
- 92A Alev, G. N., Gavaleshko, N. P., Koshchug, O. S., Pleshko, V. I., Seisyan, R. P., Sushkevich, K. D.: Sov. Phys. Solid State 34 (1992) 1286
- 92C Cantwell, G., Harsch, W.C., Cotal, H.L., Markey, B.G., McKeever, S.W.S., Thomas, J.E.: J. Appl. Phys. 71 (1992) 2931.
- 92H Hingerl, K., Jantsch, W., Juza, Lang, M., Sitter, H., Lilja, J., Pessa, M., As, D.J., Rothmund, W.: J. Cryst. Growth 117 (1992) 341.
- 92I Isshiki, M., Park, K.S., Furukawa, Y., Uchida, W.: J. Cryst. Growth 112 (1992) 410.
- 93K Kawakami, Y., Ohnakado, T., Tsuka, M., Tokudera, S., Ito, Y., Fujita, Sz., Fujita, Sg.: J. Vac. Sci. Technol. B 11 (1993) 2057.
- 94D Dahmani, R., Salamanca-Riba, L., Nguyen, N.V., Chandler Horowitz, D., Jonker, B.T.: J. Appl. Phys. 76 (1994) 514

- 94Z Zakharov, O., Rubio, A., Blase, X., Cohen, M.L., Louie, S.G.: Phys. Rev. B 50 (1994) 10780.
- 95G Greene, R. G., Luo, H., Ruoff, H. L.: J. Phys. Chem. Solids 56 (1995) 521.
- 95M Mang, A., Reimann, K., Rübenacke, St.: Proc. 22nd Int. Conf. Phys. Semicond., Vancouver 1994, Lockwood, D.J (ed.), World Scientific (Singapore) 1995, p. 317.
- 95Y Yoshino, K., Matsushima, Y., Hiramatsu, M.: Jpn. J. Appl. Phys. 34 (1995) 61.
- 95Z Zhu, Z., Brownlie, G.D., Horsburgh, G., Thompson, P.J., Wang, S.Y., Prior, K.A., Cavenett, B.C.: Appl. Phys. Lett. 67 (1995) 2167.
- 96A Aliev, G.N., Seisyan, R.P., Coschug-Toates, O.: J. Cryst. Growth 159 (1996) 843.
- 96D Debernardi, A., Cardona, M.: Phys Rev. B 54 (1996) 11305.
- 96K Karzel, H., Potzel, W., Köfferlein, M., Schiessl, W., Steiner, M., Hiler, U., Kalvius, G. M., Mitchell, D. W., Das, T. P., Blaha, P., Schwarz, K., Pasternak, M. P.: Phys. Rev. B 53 (1996) 11425.
- 96N Neukirch, U., Weckendrup, D., Wundke, K., Gutowski, J., Hommel, D.: Phys. Status Solidi (b) 196 (1996) 473.
- 97T Takemura, M., Goto, H., Ido, T.: Jpn. J. Appl. Phys. 36 (1997) L540.

Figures to 3.14

Fig. 3.0.1

The zincblende lattice.

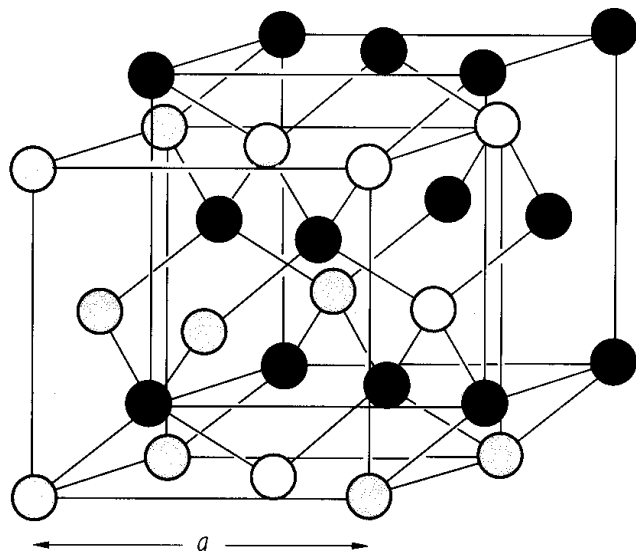


Fig. 3.0.4

The Brillouin zone for the zincblende and the rocksalt lattices.

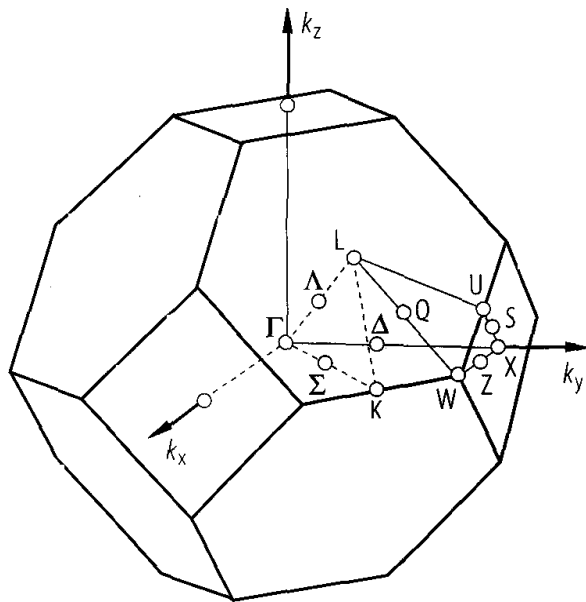


Fig. 3.0.18

ZnSe. Band structure along the principal symmetry directions [76C].

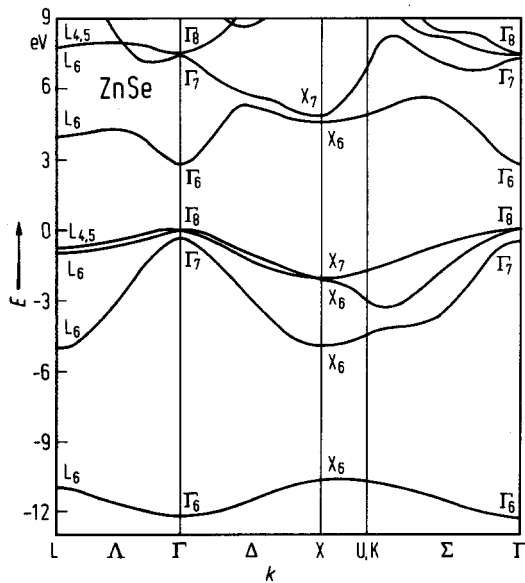


Fig. 3.14.1

ZnSe. Energy gap vs. temperature for an intrinsic crystal (full circles) and an iodine doped crystal (open circles). Values are smaller by an amount of about 0.05 eV than the values given by photoluminescence, because of the absorption tail which makes the curve raise [80H].

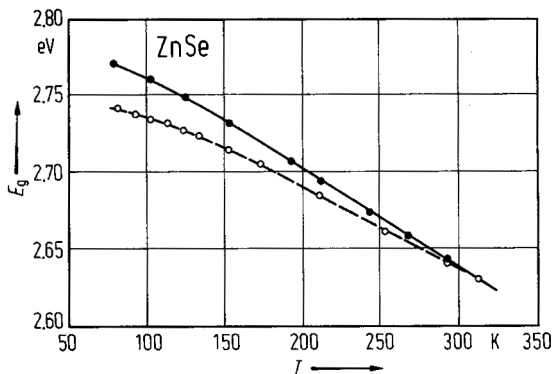


Fig. 3.14.2

ZnSe. Coefficient of linear thermal expansion. Experimental data points: solid circles from the compilation of [77T] and open circles from [75S]; theoretical curve from an ab-initio pseudopotential calculation [96D].

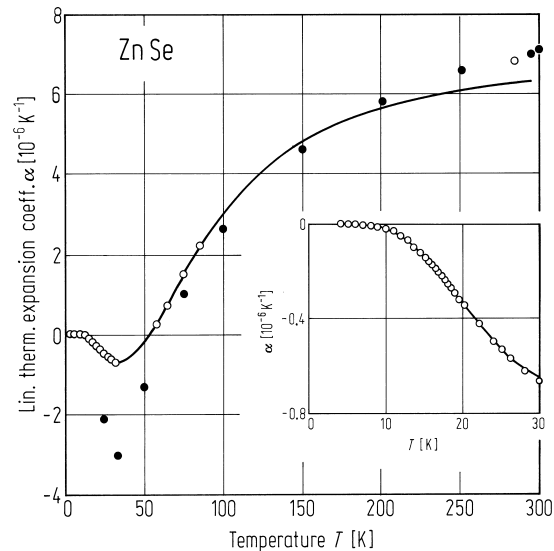


Fig. 3.14.3

ZnSe. Phonon dispersion curve: calculated curves from a bond-bending force-model in comparison with inelastic neutron scattering data [80K].

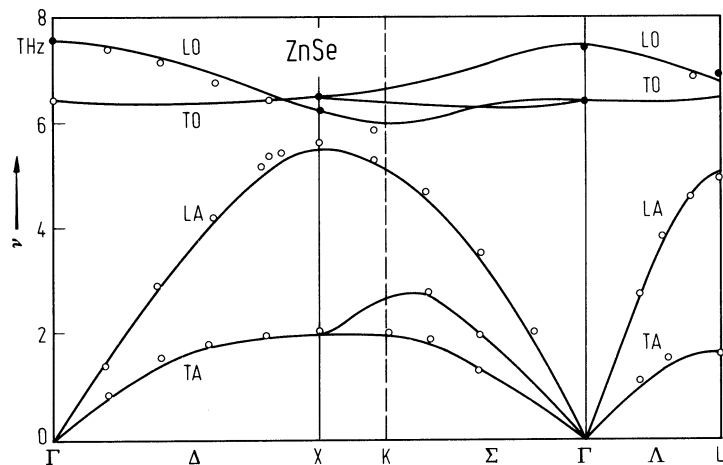


Fig. 3.14.4

ZnSe. Debye temperature vs. temperature; calculated curve at normal pressure (solid line) and at 40 kbar (dashed line) compared with experimental data from different sources [81T].

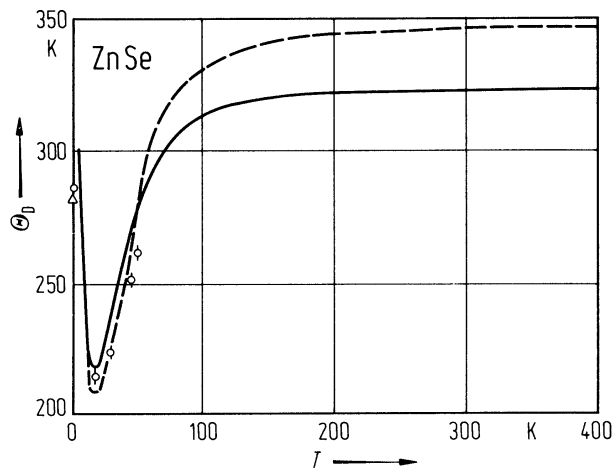


Fig. 3.14.5

ZnSe. Heat capacity at constant volume. Solid line and dashed line calculated from first principles, symbols experimental points [86K].

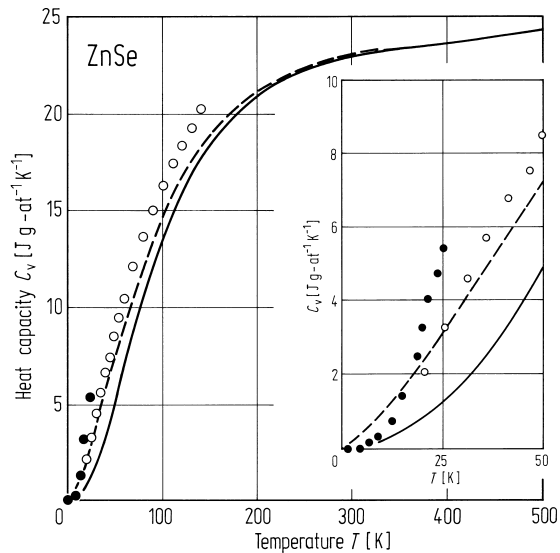


Fig. 3.14.6

ZnSe. (a) Resistivity versus $1/T$, (b) Hall electron mobility versus temperature for not intentionally doped MBE ZnSe layers demonstrating the common trend but slight quantitative differences for six samples [90M].

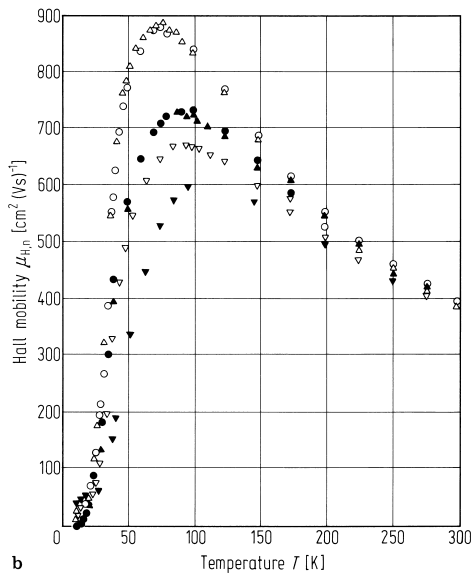
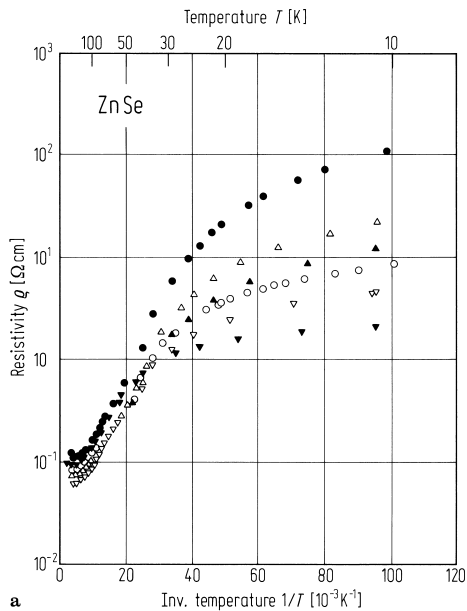


Fig. 3.14.7

ZnSe. Temperature dependence of electron (Hall) mobility in nominally undoped films grown at 280 °C. The open circles are experimental results, solid lines indicate calculated electron mobility under polar-optical phonon scattering (μ_{po}), charged-defect scattering ($\mu_I(1)$, $\mu_I(2)$), and resultant mobility ($\mu(1)$, $\mu(2)$) [85Y].

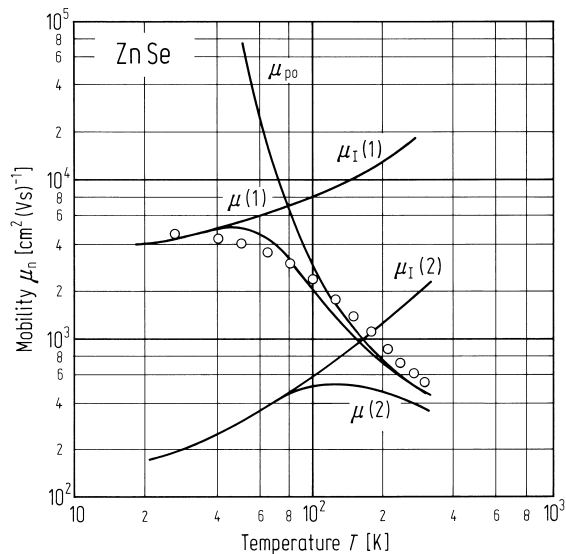


Fig. 3.14.8

ZnSe. Drift mobility of electrons vs. temperature. Open circles: Measured values, obtained by time of flight method [80H].

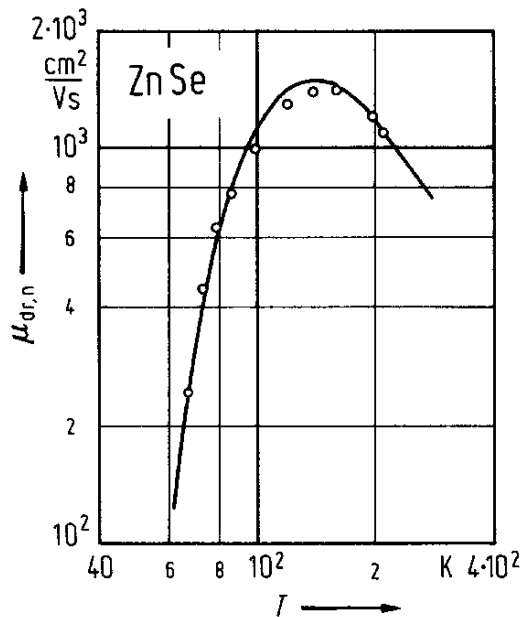


Fig. 3.14.9

ZnSe. Hole concentration and resistivity vs. inverse temperature. The solid line shows the fitted values with $E_a = 0.67$ eV, $n_a = 3.7 \cdot 10^{15} \text{ cm}^{-3}$, $n_d = 1.3 \cdot 10^{14} \text{ cm}^{-3}$, and $N_v/g = 7.2 \cdot 10^{14}$ (N_v : effective density of states in valence band, g : degeneracy) [73Y].

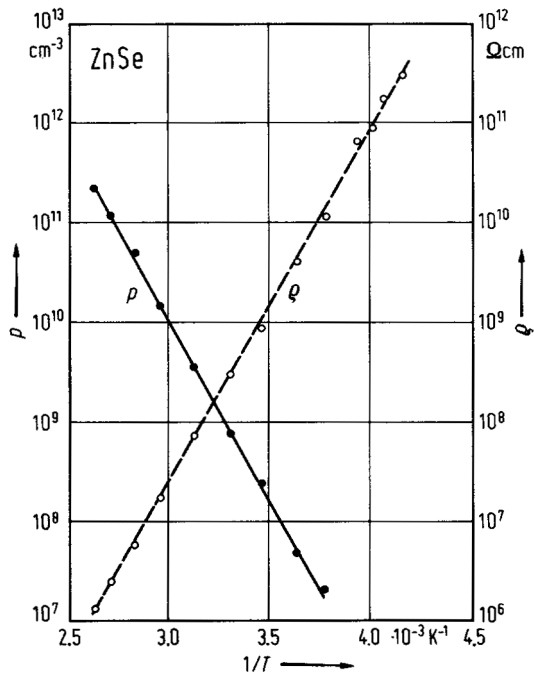


Fig. 3.14.10

ZnSe. Thermal conductivity vs. temperature [65S].

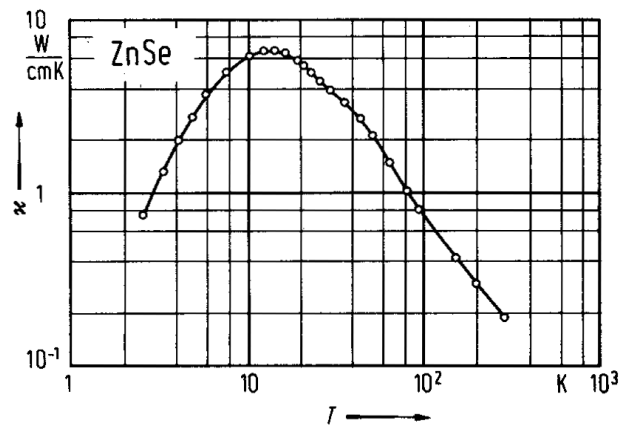


Fig. 3.14.11

ZnSe. Numerically calculated spectral dependence of the real refractive index n and the extinction coefficient k for ZnSe (solid lines). The solid (n) and open (k) circles are the experimental data [91A].

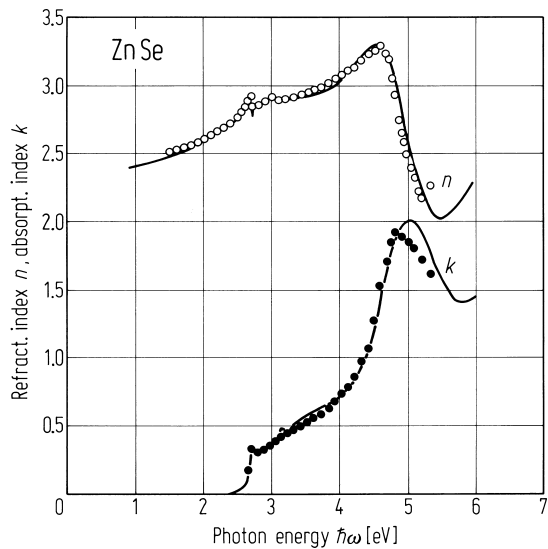
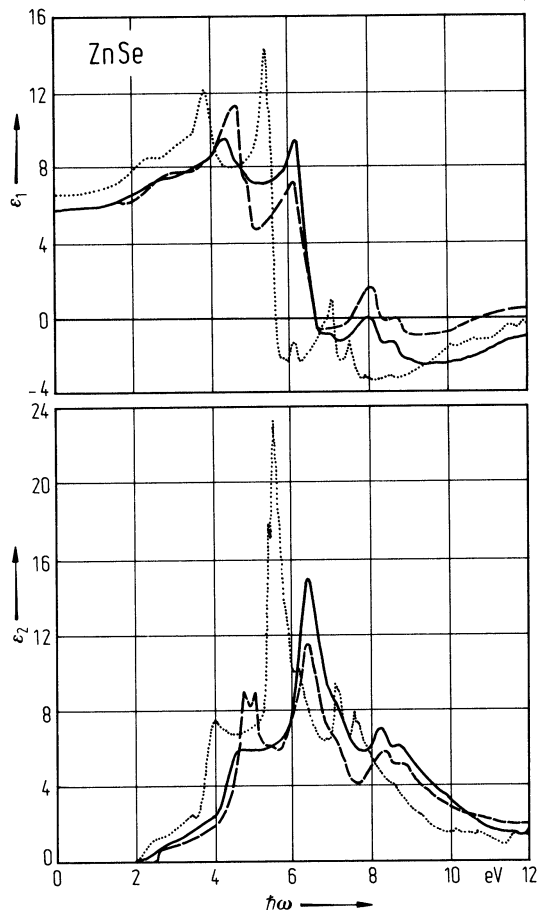


Fig. 3.14.12

ZnSe. Real and imaginary part of dielectric constant of cubic ZnSe, comparison of calculated spectra (interband contributions: dotted line, additional lifetime-broadening and self-energy corrections: solid line) from [81W] with experimental results (dashed line) from [73F].



3.15 Zinc telluride (ZnTe)

Crystal structure

Under normal conditions, ZnTe crystallizes in the zincblende structure(space group $F\bar{4}3m - T_d^2$, Fig. 3.0.1).

Electronic properties

band structure : Fig. 3.0.18, Brillouin zone, Fig. 3.0.4.

Zinc telluride is a direct gap semiconductor with the smallest energy gap at the center of the Brillouin zone (Γ). The topmost valence band (Γ_{15}) is split due to spin-orbit coupling into a fourfold (Γ_8) and a twofold (Γ_7) state.

energies of symmetry points of the band structure (relative to the top of the valence band $E(\Gamma_{15v})$)

$E(\Gamma_{1v})$	- 12.07 eV	see Fig. 3.0.19	94Z
$E(\Gamma_{1c})$	2.57 eV		
$E(\Gamma_{15c})$	5.91 eV		
$E(X_{1v})$	- 10.52 eV		
$E(X_{3v})$	- 5.27 eV		
$E(X_{5v})$	- 2.16 eV		
$E(X_{1c})$	3.47 eV		
$E(X_{3c})$	3.53 eV		
$E(L_{1v})$	- 10.95 eV		
$E(L_{1v})$	- 5.31 eV		
$E(L_{3v})$	- 0.88 eV		
$E(L_{1c})$	3.07 eV		
$E(L_{3c})$	6.52 eV		

energy gap

$E_{g,dir}(\Gamma_{8v}-\Gamma_{6c})$	2.3945 eV	$T < 2\text{ K}$	transmission spectroscopy	92A
	2.35 eV	$T = 300\text{ K}$	reflectivity	63C

temperature dependence of energy gap

d^2E_0/dT^2	- 1.832·10 ⁻³ meV/K ²	$0 < T < 47\text{ K}$	luminescence of epilayer	92Z
dE_g/dT	- 4.5·10 ⁻⁴ eV K ⁻¹	$T = 77...300\text{ K}$	absorption	61L

exciton energies

Due to the large spin-orbit splitting (0.9 eV) only excitons with the hole in the topmost (Γ_8) valence band are observed. The ground state of this exciton is split according to the decomposition $\Gamma_{8v} \times \Gamma_{6c} = \Gamma_3 + \Gamma_4 + \Gamma_5$, only the Γ_5 exciton state is dipole allowed.

$E_{gx}(\Gamma_5^T, 1S)$	2.3809 eV	$T = 1.6\text{ K}$	PL	92K
$\Delta_{LT}(1S)$	0.65(6) meV	T variable	T dependent absorption	94A
$E(2P_{3/2}, \Gamma_8)$	2.38892 eV	$T = 15\text{ K}$	two-photon absorption,	84F
$E(2P_{5/2}, \Gamma_8)$	2.38948 eV			
$E(2P_{5/2}, \Gamma_7)$	2.38980 eV			
$E(2P_{1/2}, \Gamma_6)$	2.39025 eV			

critical-point energies

$E_0 (=E_g)$	2.25 eV	$T = 300$ K	ellipsometry	97S
$E_1(\Lambda_{3v}-\Lambda_{1c})$	3.78 eV			
$E_1+\Delta_1$	4.34 eV			
$E_0 + \Delta_0$	3.20 eV			
$E_2(X_{5v}-X_{1c})$	5.23 eV			
	5.30 eV			

spin-orbit–splitting energy

$\Delta_0(\Gamma_{8v}-\Gamma_{7v})$	0.97 eV	$T = 80$ K	reflectivity	78S
-------------------------------------	---------	------------	--------------	-----

effective masses, conduction band

m_n	0.122(2) m_0	$T = 3.5$ K	cyclotron resonance	79C
m_n^{**}	0.124(2) m_0	$T = 1.5$ K	polaron mass, cyclotron resonance	94E

effective masses, valence band

m_p	0.6 m_0		estimated from hole mobility	63A
-------	-----------	--	------------------------------	-----

effective g-factors

$g_c [100]$	− 0.41(1)	$T = 1.8$ K	Zeeman spectroscopy of donor bound excitons	84R
$[111]$	− 0.40			
$[110]$	− 0.35(8)			

Lattice properties

lattice parameter

a	6.0882 Å	RT	X-ray diffraction	85Y
-----	----------	----	-------------------	-----

temperature dependence of lattice parameter

$a = 6.1015 + 5.157 \cdot 10^{-5}T + 8.2728 \cdot 10^{-9}T^2$ Å		T in °C , 0...450 °C		68H
---	--	------------------------	--	-----

linear thermal expansion coefficient

α	$830 \cdot 10^{-8}$ K ^{−1}	$T = 300$ K	experimental and theoretical for temperature dependence, see Fig. 3.15.1.	80S
----------	-------------------------------------	-------------	--	-----

phonon dispersion curves and phonon density of states

Fig. 3.15.2 shows a model fit to experimental data.

phonon frequencies

$\nu_{LO}(\Gamma)$	6.20(5) THz	RT	neutron scattering	74V
$\nu_{TO}(\Gamma)$	5.30(7) THz			
$\nu_{LO}(X)$	5.51(10) THz			
$\nu_{TO}(X)$	5.21(10) THz			
$\nu_{LA}(X)$	4.29(5) THz			
$\nu_{TA}(X)$	1.62(2) THz			
$\nu_{LO}(L)$	5.39(5) THz			
$\nu_{TO}(L)$	5.20(9) THz			
$\nu_{LA}(L)$	4.06(5) THz			
$\nu_{TA}(L)$	1.25(2) THz			

second order elastic moduli

c_{11}	72.2(2) GPa	RT	Brillouin scattering	77Y
c_{12}	40.9(6) GPa			
c_{44}	30.8(3) GPa			

temperature dependence of the second order elastic moduli

$(1/c_{11})dc_{11}/dT$	$-1.87 \cdot 10^{-4} \text{ K}^{-1}$	$T = 295 \text{ K}$	ultrasonic pulse method	70L1
$(1/c_{44})dc_{44}/dT$	$-2.03 \cdot 10^{-4} \text{ K}^{-1}$			
$(1/c_{12})dc_{12}/dT$	$-1.41 \cdot 10^{-4} \text{ K}^{-1}$			

third-order elastic moduli

c_{111}	-707 GPa		experimental	78P
c_{112}	-121 GPa			
c_{123}	-412 GPa			
c_{144}	183 GPa			
c_{166}	-217 GPa			
c_{456}	-229 GPa			

bulk modulus

B	52.8 GPa	$T = 4 \text{ K}$	experimental	80C
-----	----------	-------------------	--------------	-----

compressibility

κ	0.510 Mbar^{-1}			85G
----------	---------------------------	--	--	-----

heat capacity

C_p	$46.44 + 1.088 \cdot 10^{-2} T^{-2} \text{ J K}^{-1} \text{ mol}^{-1}$	$T = 298 \dots 1563 \text{ K}$, polycrystalline sample		92Y
-------	--	---	--	-----

Debye temperature

Θ_D	180(6) K	$T = 93 \dots 298 \text{ K}$	X-ray intensities from powders	72B
------------	----------	------------------------------	--------------------------------	-----

For temperature dependence, see Fig. 3.15.3

density

d	5.636 g/cm^3	$T = 298 \text{ K}$		63B
-----	------------------------	---------------------	--	-----

melting temperature

T_m	1563(8) K			97F
-------	-----------	--	--	-----

Transport properties

ZnTe is p-type due to deviation from stoichiometry when not intentionally doped, n-type doping is extremely difficult. Doping limits, e.g., with N as prominent acceptor material in devices, see [95B]. Transport properties of ZnTe strongly depend on growth conditions, dopants and doping characteristics etc.

resistivity

ρ	$5 \cdot 10^4 \text{ } \Omega \text{ cm}$	$T = 300 \text{ K}$	ZnTe:Ga crystals, Seebeck and Hall effect	88H
	$5 \cdot 10^6 \text{ } \Omega \text{ cm}$	$T = 77 \text{ K}$		

carrier mobilities

Electron and hole mobilities are extremely dependent on sample structural quality, dopant's concentration, impurities compensation ratio, and details of the growth procedure. Fig. 3.15.4 presents electron mobilities versus carrier concentration at 77 and 300 K.

μ_n	1500 cm ² /Vs	$T = 300$ K	calculation of mobility limit	91R
	330 cm ² /Vs	$T = 300$ K	for temperature dependence of the	64F
			electron and hole mobilities, see Fig. 3.15.5.	
μ_p	340 cm ² /Vs	$T = 300$ K	N doped, peak (Hall) mobility,	
			$p = 9 \cdot 10^{16}$ cm ⁻³	96G1

thermal conductivity

κ	0.18 W/Kcm	$T = 300$ K	see Fig. 3.15.6	63D
----------	------------	-------------	-----------------	-----

piezoelectric constants

d_{14}	$0.9 \cdot 10^{-12}$ C/N	$T = 298$ K		63B
e_{14}	0.028 C/m ²			

Optical properties

dielectric constants

$\varepsilon(0)$	10.3	RT	reflectivity	68R
$\varepsilon(\infty)$	7.28	$T = 300$ K	derived from refraction data	64M

Figs. 3.15.7 and 8 show the real and imaginary part ε_1 and ε_2 of the dielectric constant in the energy range 1.5...5.6 eV and 15...150 eV, respectively.

refractive index

Fig. 3.15.8 displays the real and imaginary part of the complex refractive index, n and k , in the energy range 0...5.6 eV and 15...150 eV, respectively.

photoelastic constants

p_{11}	0.144(7)	RT	Brillouin scattering,	77Y
p_{12}	0.094(5)		$\lambda = 632.8$ nm	
p_{44}	0.046(3)			

electrooptic coefficient

r_{41}	-4.71 pm V ⁻¹		calculated	97X
----------	----------------------------	--	------------	-----

Impurities and defects

ionization energies of shallow acceptors (E_a)

Li	61 meV	$T = 5...77$ K	photoluminescence	79M
Na	62.8 meV	$T = 4.2$ K	two-hole transitions in PL	85P
C	56 meV	$T = 10$ K	deduced from DAP luminescence	97L
N	53.6(7) meV	$T = 1.7$ K	free-to-bound transition	96G1
P	63.5 meV	$T = 4.2$ K	two-hole transitions in PL	85P
Na	62.8 meV	$T = 5...77$ K	photoluminescence	79M
As	79.0 meV	$T = 1.6$ K	two-hole transitions and selective pairs	80V
Ag	123 meV	$T = 4.2$ K	two-hole transitions in PL	85P
Cu	150 meV	$T = 4.2$ K	calculation from bound-exciton transitions	88A
Au	277 meV	$T = 1.6$ K	two-hole transitions and selective pairs	80V

ionization energies of shallow donors (E_d)

Ga	18.5(1) meV	$T = 2$ K	two-hole transitions in PL	92W
Al	19.5 meV	$T = 2$ K	selective PL, two-hole transitions	94W
Cl	20.1 meV	$T = 4.2$ K	two-electron transitions in PL	85P
I	17.9(1) meV	$T = 2$ K	two-hole transitions in PL	92W
Sc _{interstitial}	65 meV	$T = 4.5$ K	photogalvanic current spectra	89B

References to 3.15

- 54D De Launay, J.: J. Chem. Phys. 22 (1954) 1676.
- 59G Gul'yaev, P. V., Petrov, A. V.: Sov. Phys. Solid State 1 (1959) 330.
- 61L Loh, E., Newman, R.: J. Phys. Chem. Solids 21 (1961) 324.
- 63A Aven, M., Segall, B.: Phys. Rev. 130 (1963) 81.
- 63B Berlincourt, D., Jaffe, H., Shiozawa, L. R.: Phys. Rev. 129 (1963) 1009.
- 63C Cardona, M., Greenaway, D. L.: Phys. Rev. 131 (1963) 98.
- 63D Devlin, S. S. in: Physics and Chemistry of II-VI Compounds (M. Aven and J. S. Prener eds.) North-Holland Publishing Company - Amsterdam, 1963, p. 549.
- 64F Fisher, A. G., Carides, J. N., Dresner, J.: Solid State Commun. 2 (1964) 157.
- 64M Marple, D. T. F.: J. Appl. Phys. 35 (1964) 539.
- 68H Hadni, A., Claudel, J., Strimer, P.: Phys. Status Solidi 26 (1968) 241.
- 68R Riccius, H. D.: J. Appl. Phys. 39 (1968) 4381.
- 70L1 Lee, B. H.: J. Appl. Phys. 41 (1970) 2984.
- 70L2 Lee, B. H.: J. Appl. Phys. 41 (1970) 2988.
- 71S Smith, F. T. J.: Solid State Commun. 9 (1971) 957.
- 72B Blattner, R. J., Walford, L. K., Baldwin, T. O.: J. Appl. Phys. 43 (1972) 935.
- 74V Vagelatos, N., Wehe, D., King, J. S.: J. Chem. Phys. 60 (1974) 3613.
- 77Y Yamada, M., Yamamoto, K., Abe, K.: J. Phys. D 10 (1977) 1309.
- 78P Prasad, O., H.: PhD thesis, Osmania Universtiy, Hyderabad (1978), cited in [96S].
- 78S Sobolev, V. V., Donerskikh, V. I., Zagainov, E. F.: Fiz. Tekh. Poluprovodn. 12 (1978) 1089; Sov. Phys. Semicond. (English Transl.) 12 (1978) 646.
- 79C Clerjaud, B., Gelineau, A., Gallard, D., Saminadayar, K.: Phys. Rev. B 19 (1979) 2056.
- 79M Magnea, N., Beusahel, D., Pautrat, J. L., Pfister, J. C.: Phys. Status Solidi (b) 94 (1979) 627.
- 80C Collins, J. G., White, G. K., Birch, J. A., Smith, T. F.: J. Phys. C13 (1980) 1649.
- 80K Kushwaha, M. S., Kushwaha, S. S.: Can. J. Phys. 58 (1980) 351.
- 80S Soma, T.: Solid State Commun. 34 (1980) 927.
- 80V Venghaus, H., Dean, P.J.: Phys. Rev. B 21 (1980) 1596.
- 84F Fröhlich, D., Nöthe, A., Reimann, K.: Phys. Status Solidi (b) 125 (1984) 653.
- 84N Noguera, A., Wasim, S. M.: Solid State Commun. 50 (1984) 141.
- 84R Romestain, R., Dang, L. S., Nahmani, A.: J. Phys. (Paris) 45 (1984) 1175.
- 85G Goble, R. Y., Scott, S. D.: Can. J. Mineral. 23 (1985) 273.
- 85P Pautrat, J.L., Francou, J.M., Magnea, N., Molva, E., Saminadayar, K.: J. Cryst. Growth 72 (1985) 194.
- 85Y Yamanaka, T., Tokonami, M.: Acta Crystallogr. B 41 (1985) 298.
- 87B Bernard, J.E., Zunger, A.: Phys. Rev. B 36 (1987) 3199.
- 88A Andronik, I.K., Vavilov, V.S., Vu Zoan Mien, Mikhailash, P.G., Chukichev, M.V.: Sov. Phys. J. 8 (1988) 702 [Izvest. Vysshikh Ucheb. Zavedenii, Fizika 8 (1987) 68].
- 88H Hausmann, A., Roll, R.: Zeitschrift für Physik (Condensed Matter) B 72 (1988) 439.
- 89B Babii, P.I., Gamernik, R.V., Gnatenko, Yu.P., Krochuk, A.S.: Sov. Phys. Semicond. 23 (1989) 465 [Fiz. Tekh. Poluprovodn. 23 (1989) 739].
- 91R Ruda, H.E.: J. Phys. D 24 (1991) 1158.
- 91W Ward, L.: in Handbook Optical Constants Solids II, Ed. Palik, E. D., Academic Press (New York) 1991, p. 737.
- 92A Aliev, G.N., Gavaleshko, N.P., Koshchug, O.S., Pleshko, V.I., Seisyan, R.P., Sushkevich, K.D.: Sov. Phys. Solid State 34 (1992) 1286 [Fiz. Tverd. Tela 34 (1992) 2400].
- 92K Kudlek, G., Presser, N., Gutowski, J., Hingerl, K., Abramof, E., Sitter, H.: J. Cryst. Growth 117 (1992) 290.
- 92W Wagner, H.P., Leiderer, H.: Adv. Solid State Phys. 32 (1992) 221.
- 92Y Yu, T.-C., Brebrick, R. F.: J. Phase Equilibria 13 (1992) 476.
- 92Z Zhang, Y., Skromme, B.J., Turco-Sandroff, F.S.: Phys. Rev. B 46 (1992) 3872.
- 93B Bagot, D., Granger, R., Rolland, S.: Phys. Status Solidi (b) 177 (1993) 295.
- 93S Sato, K., Adachi, S.: J. Appl. Phys. 73 (1993) 926.
- 94A Aliev, G.N., Koshchug, O.S., Seisyan, R.P.: Phys. Solid State 36 (1994) 203.
- 94E Emanuelsson, P., Drechsler, M., Hofmann, D.M., Efros, A.L., Meyer, B.K., Clerjaud, B.: Solid State Commun. 90 (1994) 635.
- 94W Wolf, K., Naumov, A., Wagner, H.P., Gilg, F., Sahin, H., Stanzl, H., Gebhardt, W.: J. Lumin. 60-61 (1994) 544.
- 94Z Zakharov, O., Rubio, A., Blase, X., Cohen, M.L., Louie, S.G.: Phys. Rev. B 50 (1994) 10780.

- 95B Baron, T., Saminadayar, K., Magnea, N.: Appl. Phys. Lett. 67 (1995) 2972.
- 96G1 Grün, M., Haury, A., Cibert, J., Wasiela, A.: J. Appl. Phys. 79 (1996) 7386.
- 96G2 Guo, Q., Ikejira, M., Nishio, M., Ogawa, H.: Solid State Commun. 100 (1996) 813.
- 97F Feutelais, Y., Haloui, A., Legendre, B.: J. Phase Equilibria 18 (1997) 48.
- 97L Lovergine, N., Longo, M., Prete, P., Gerardi, C., Calcagnile, L., Cingolani, R., Mancini, A.M.: J. Appl. Phys. 81 (1997) 685.
- 97S Suzuki, K., Adachi, S.: J. Appl. Phys. 82 (1997) 1320.
- 97X Dongfeng Xue, Siyuan Zhang : J. Solid State Chemistry 128 (1997) 17.

Figures to 3.15

Fig. 3.0.1

The zincblende lattice.

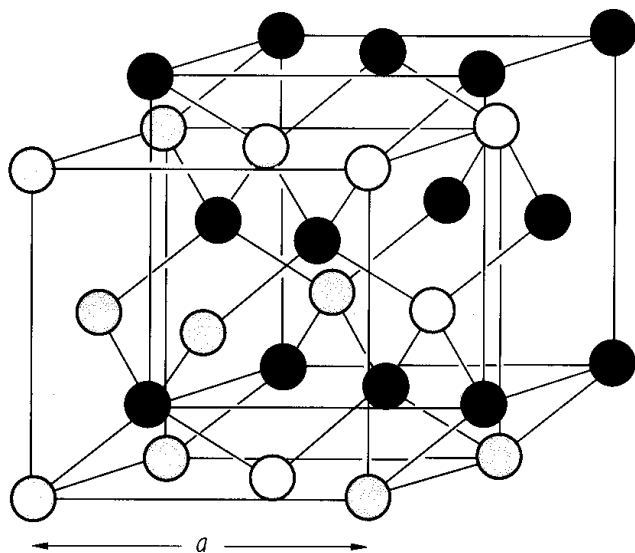


Fig. 3.0.4

The Brillouin zone for the zincblende and the rocksalt lattices.

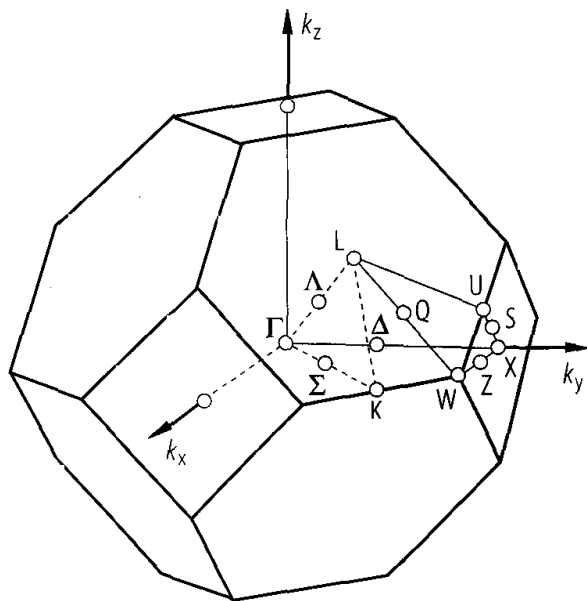


Fig. 3.0.19

ZnTe. Nonrelativistic self-consistent local-density band structure calculated with the Ceperly-Alder exchange correlation. Dashed lines show doubly degenerate bands. Shaded areas denote the fundamental band-gap region. The origin of the coordinate system is the anion site [87B].

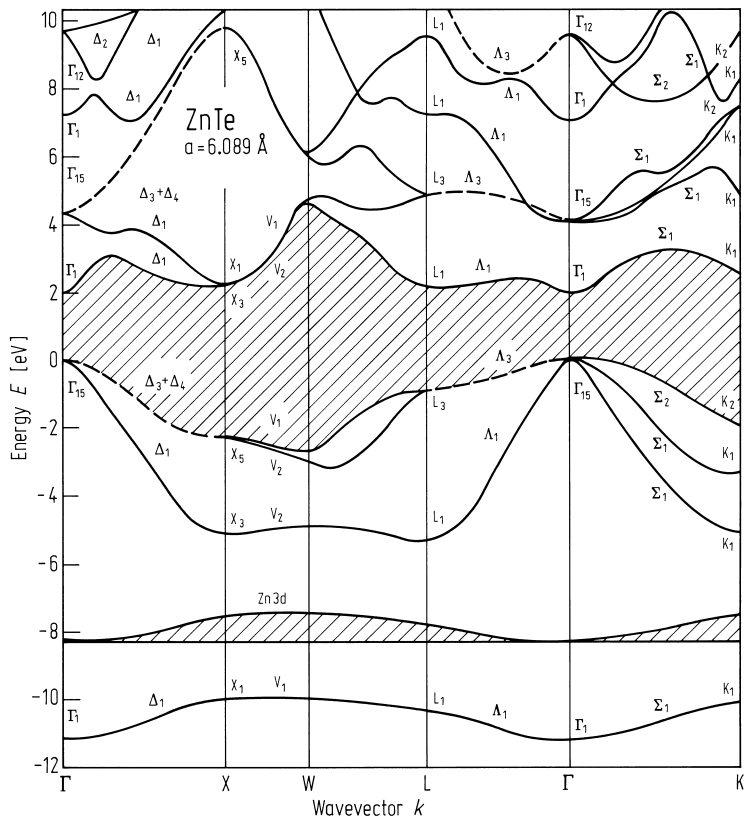


Fig. 3.15.1

ZnTe. Linear thermal expansion coefficient α vs. T . Solid line from semiempirical calculation, symbols and experimental points [93B].

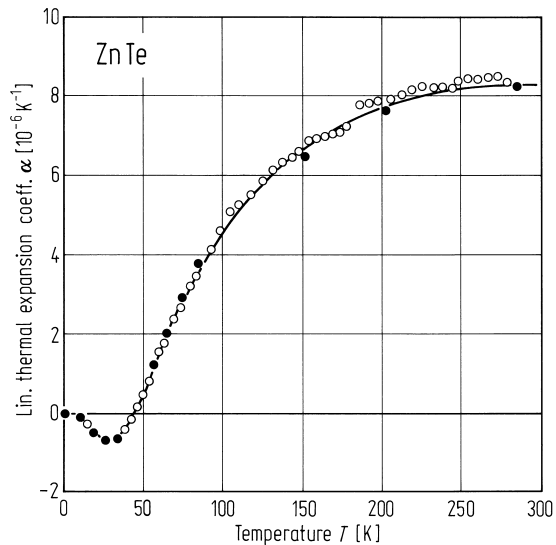


Fig. 3.15.2

ZnTe. Phonon dispersion curves and one-phonon density of states calculated from an 8-parameter bond bending force model in comparison with inelastic neutron scattering data (circles) [80K].

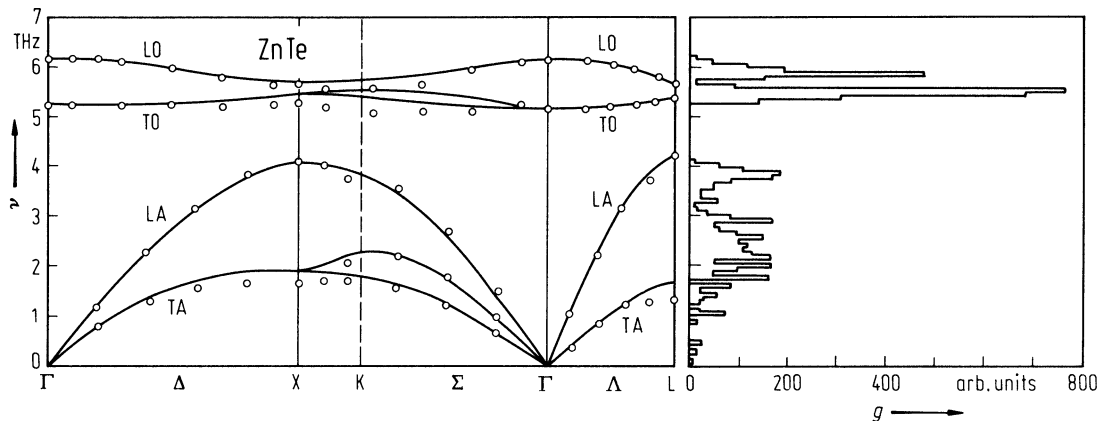


Fig. 3.15.3

ZnTe. Debye temperature vs. temperature. Experimental data (crosses [54D], circles [59G], triangles [65K]) are compared with calculated data of a valence shell model (broken line: nearly zero negative ionic charge, solid line: large positive ionic charge +2) [74V].

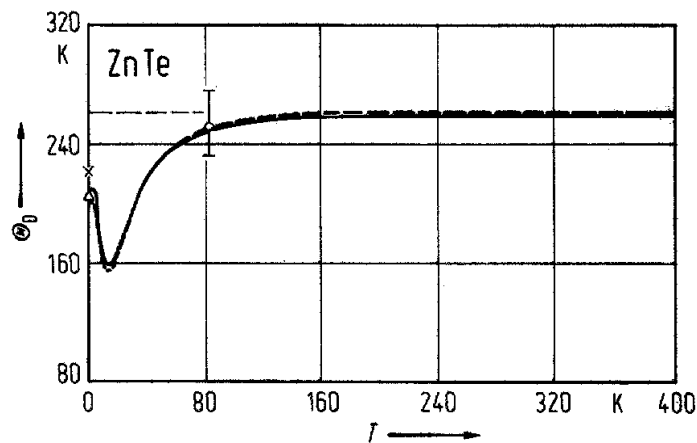


Fig. 3.15.4

ZnTe. Hall mobilities of electrons and holes in an doped sample vs. temperature [71S].

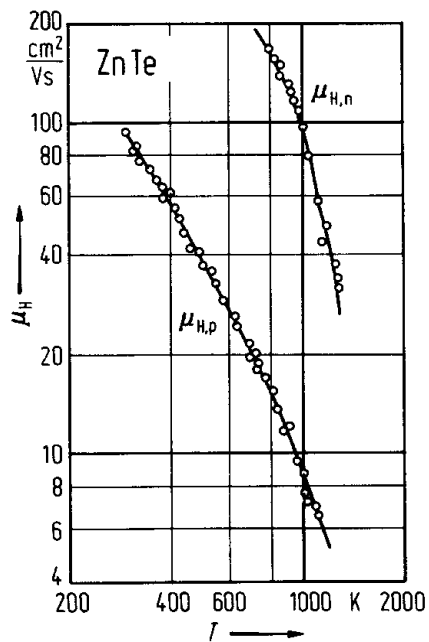


Fig. 3.15.5

α -ZnTe. Thermal conductivity κ vs T , symbols are experimental points [84N].

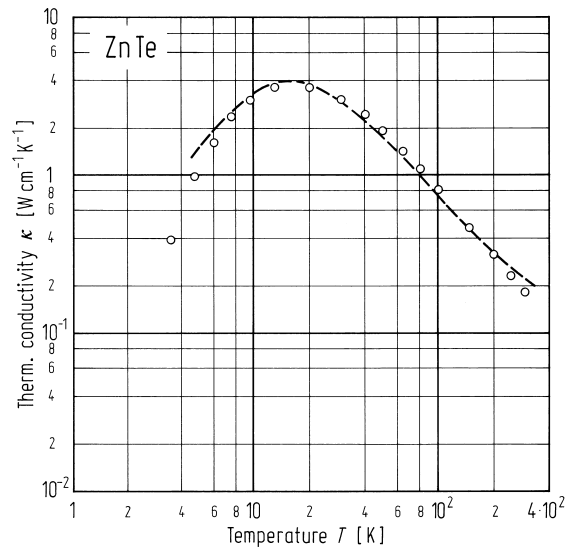


Fig. 3.15.6

ZnTe. Dielectric-function spectrum $\epsilon(\omega)$ measured by spectroscopic ellipsometry at RT (solid and open circles), the solid and dashed lines are calculated [93S]. The triangles are experimental data from [91W].

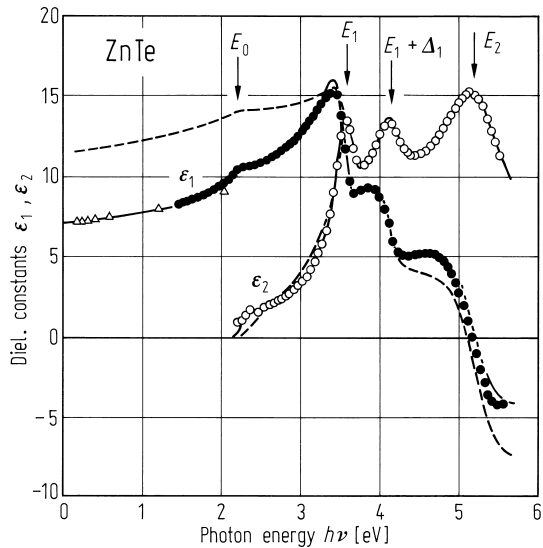


Fig. 3.15.7

ZnTe. Spectral dependence of the real and imaginary parts of the complex dielectric constant, ϵ_1 and ϵ_2 [96G2].

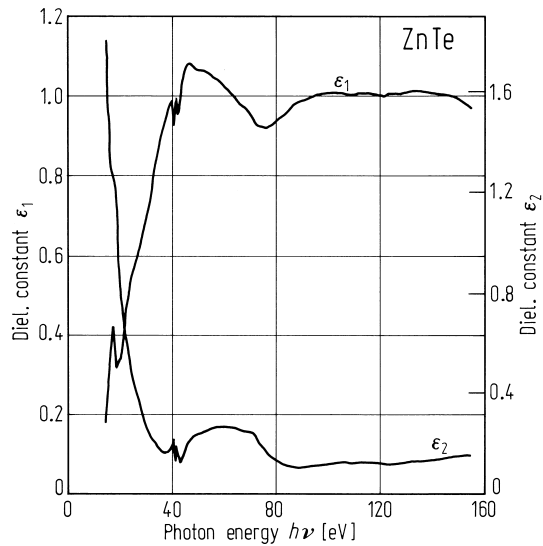
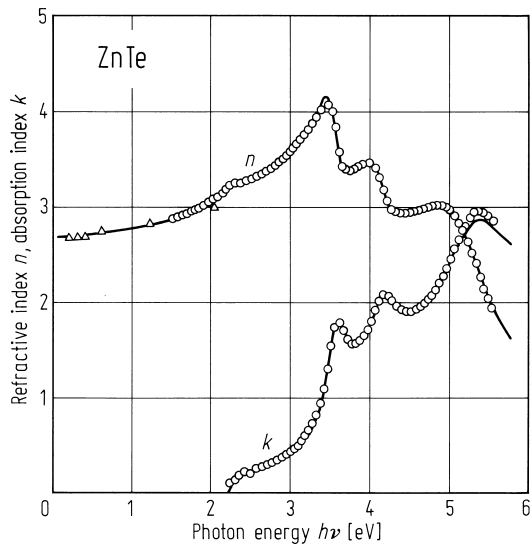


Fig. 3.15.8

ZnTe. Numerically calculated spectral dependence of the complex refractive index (n and k) (solid lines). The circles are measured ellipsometry data [93S]. The triangles are experimental data taken from [91W].



3.16 Cadmium oxide (CdO)

Crystal structure

Under normal conditions, CdO crystallizes in the rocksalt structure (space group: $Fm\bar{3}m - O_h^5$, Fig. 3.0.3).

Electronic properties

CdO is the only II–VI semiconductor which crystallizes in the rocksalt structure at standard pressure. Excess of Cd content gives rise to heavy n-type characteristics even of not intentionally doped samples.

band structure : Fig. 3.0.19, Brillouin zone: Fig. 3.0.4.

The lowest conduction band has its minimum at the point Γ_1 in the center of the Brillouin zone. Within the energy range of a few tenths of eV above its bottom the band is isotropic but highly nonparabolic. The nonparabolicity is revealed by the strong dependence of the optical electron mass on electron concentration [66F]. The lowest conduction band is separated from the higher bands by a small gap. The valence band consists of several branches with maxima at L_3 and Σ .

energies of symmetry points of the band structure (relative to the top of the valence band $E(\Gamma_{15v})$)

$E(\Gamma_{1v})$	– 22.9 eV	ab-initio calculation	83B
$E(\Gamma_{12v})$	– 14.4 eV	including correlation	
$E(\Gamma_{1c})$	0.8 eV		
$E(X'_{4v})$	– 7.1 eV		
$E(X'_{5v})$	– 2.6 eV		
$E(X_{1c})$	7.1 eV		
$E(L_{1v})$	– 5.1 eV		
$E(L_{3v})$	0.3 eV		
$E(L'_{2c})$	5.1 eV		
$E(K_{3v})$	– 5.7 eV		
$E(K_{1v})$	– 3.4 eV		
$E(K_{4v})$	– 1.5 eV		
$E(K_{1c})$	8.9 eV		

energy gaps

$E_{g,ind}^{(1)}(\Sigma_{3v}-\Gamma_{1c})$	1.09(5) eV	$T = 100$ K	thermoreflectance	76K
$E_{g,ind}^{(2)}(L_{3v}-\Gamma_{1c})$	0.84 eV			
$E_{g,dir}(\Gamma_{15v}-\Gamma_{1c})$	2.28 eV			

temperature dependence of energy gaps

$dE_{g,ind}^{(1)}/dT$	– 4.10(12)·10 ^{–4} eV K ^{–1}	$T = 78...173$ K	shift of the absorption edge	71K1
$dE_{g,dir}/dT$	– 4.2·10 ^{–4} eV K ^{–1}		shift of the absorption edge	72K

effective masses

m_n	0.33...0.46 m_0	$T = 81$ K	comparison of calculated and measured low temperature mobilities, $n = 0.38...6.34 \cdot 10^{19}$ cm ^{–3}	71K2
-------	-------------------	------------	--	------

dependence on electron concentration, Fig. 3.16.1.

g-factor of conduction electrons

g_c	1.806(5)	$T = 77$ K	ESR measurements	63M
-------	----------	------------	------------------	-----

Lattice properties

lattice parameter

a	4.689 Å			83B
-----	---------	--	--	-----

linear expansion coefficient

α	$14 \cdot 10^{-6} \text{ K}^{-1}$	$T = 300 \dots 770 \text{ K}$	dilatometer measurements	74V
----------	-----------------------------------	-------------------------------	--------------------------	-----

phonon frequencies

$\nu_{\text{TO}}(\Gamma)$	$7.85 \cdot 10^{12} \text{ s}^{-1}$	$T = 300 \text{ K}$	Kramers–Kronig analysis of infrared reflectivity	67F
$\nu_{\text{LO}}(\Gamma)$	$15.83 \cdot 10^{12} \text{ s}^{-1}$	$T = 300 \text{ K}$	calculated from ν_{TO} by means of the Lyddane-Sachs-Teller relation	67F
$\nu_{\text{LO}}(\text{L})$	$14.4 \cdot 10^{12} \text{ s}^{-1}$	$T = 2 \text{ K}$	Raman spectroscopy, tentative assignment	76S
$\nu_{\text{LO}}(\text{X})$	$15.6 \cdot 10^{12} \text{ s}^{-1}$	$T = 2 \text{ K}$	from comparison with corresponding spectra of alkaline-earth oxides with NaCl structure	
$\nu_{\text{TO}}(\text{X})$ (resp. $\nu_{\text{TO}}(\text{L})$)	$7.2 \cdot 10^{12} \text{ s}^{-1}$	$T = 2 \text{ K}$		

Debye temperature

Θ_{D}	255(6) K	$T = 300 \text{ K}$	calculated from X-ray diffractometer measurements	78S
---------------------	----------	---------------------	---	-----

melting temperature

T_{m}	$> 1500^{\circ}\text{C}$			87W
----------------	--------------------------	--	--	-----

heat capacity

C_{p}	$43.639 \text{ J mol}^{-1} \text{ K}^{-1}$		$T = 298.15 \text{ K}$ for temperature dependence up to 800 K, see Fig. 3.16.2	89B
----------------	--	--	---	-----

density

d	8.15 g cm^{-3}		X-ray crystal density method	75L
-----	--------------------------	--	------------------------------	-----

Transport properties

Due to a high degree of nonstoichiometry CdO generally is a highly degenerate n-type semiconductor. The conductivity is related to an excess of Cd in the lattice. Usually the electron concentration amounts to several 10^{19} cm^{-3} .

electrical resistivity

Values of ρ given in literature depend strongly on special preparation conditions. Large resistivities and carrier concentrations are due to strongly non-stoichiometric deposition.

ρ	$1.5 \cdot 10^{-3} \Omega \text{ cm}$	$T = 300 \text{ K}$	minimum value, substrate $T \approx 200^{\circ}\text{C}$, $n = 2 \cdot 10^{20} \text{ cm}^{-3}$, films grown on glass substrates by Cd evaporation in O glow discharge, $n = 10^{19} \dots 10^{20} \text{ cm}^{-3}$	98R
	$1.27 \dots 1.4 \cdot 10^{-3} \Omega \text{ cm}$	$T = 300 \text{ K}$	spray-pyrolytic films on glass substrates, $n = 2 \dots 3 \cdot 10^{20} \text{ cm}^{-3}$	94G1

electron mobility

Fig. 3.16.3 shows Hall mobility versus carrier concentration.

$\mu_{\text{H,n}}$	$180 \text{ cm}^2/\text{Vs}$	$T = 300 \text{ K}$	coldpressed CdO powder electrodes, $n = 1.1 \cdot 10^{19} \text{ cm}^{-3}$ $n = 1.8 \cdot 10^{19} \text{ cm}^{-3}$	90M
	$110 \text{ cm}^2/\text{Vs}$			

thermoelectric power

Fig. 3.16.4 shows thermoelectric power versus temperature.

Optical properties

refractive index

Fig. 3.16.5 shows the variation of the refractive index and the absorption index with wavelength.

n	1.95...2.65	$\lambda = 600 \text{ nm}$	deposited by spray pyrolysis	94G1
-----	-------------	----------------------------	------------------------------	------

dielectric constants

Fig. 3.16.6 shows the variation of the real and imaginary parts of the dielectric function with $(\hbar\omega)^{-2}$.

$\varepsilon(0)$	21.9	$T = 300 \text{ K}$	ir reflectivity, extrapolation to electron concentration $n = 0$	67F
------------------	------	---------------------	--	-----

$\varepsilon(\infty)$	2.1	$T = 300 \text{ K}$	transmittance, absorption	94G2
-----------------------	-----	---------------------	---------------------------	------

References to 3.16

- 62L Lamb, E. F., Tompkins, F. C.: Trans. Faraday Soc. 58 (1962) 1424.
- 63M Müller, K. A., Schneider, J.: Phys. Lett. 4 (1963) 288.
- 66F Finkenrath, H., Köhler, H., Lochmann, M.: Z. Angew. Phys. 21 (1966) 512.
- 67F Finkenrath, H., Uhle, N.: Solid State Commun. 5 (1967) 875.
- 68A Altwein, M., Finkenrath, H., Konak, C., Stuke, J., Zimmerer, G.: Phys. Status Solidi 29 (1968) 203.
- 71K1 Kocka, J., Konak, C.: Phys. Status Solidi (b) 43 (1971) 731.
- 71K2 Koffyberg, F. P.: Canad. J. Phys. 49 (1971) 435.
- 72K Köhler, H.: Solid State Commun. 11 (1972) 1687.
- 72M Mills, K. C.: High Temp.-High- Pressures 4 (1972) 371
- 74V Valeev, Kh. S., Kvaskov, V. H.: Inorg. Mater. 10 (1974) 1794.
- 75L Landolt-Börnstein: Zahlenwerte und Funktionen aus Naturwissenschaften und Technik. N. S. Vol. III/7b1, Berlin 1975.
- 76K Koffyberg, F. P.: Phys. Rev. B 13 (1976) 4470.
- 76S Schaack, G., Uhle, N.: Solid State Commun. 19 (1976) 315.
- 78S Subhadra. K. G.: Sirdeshmukh. D. B.: Pramana 10 (1978) 357.
- 83B Boettger, J. C., Kunz, A. B.: Phys. Rev. B 27 (1983) 1359.
- 87W Wriedt, H. A.: Bull. Alloy Phase Diagrams 8 (1987) 140.
- 89B Barin, I.: Thermochemical Data of Pure Substances, VCH, Weinheim, 1989.
- 90M Makuta, I.D., Poznyak, S.K., Kulak, A.I.: Solid State Commun. 76 (1990) 65.
- 94G1 Gurumurugan, K., Mangalaraj, D., Narayandass, S.K., Balasubramanian, C.: Phys. Status Solidi (a) 143 (1994) 85.
- 94G2 Gurumurugan, K., Mangalaraj, D., Narayandass, S.K.: Thin Solid Films 251 (1994) 7.
- 94V Varkey, A.J., Fort, A.F.: Thin Solid Films 239 (1994) 211.
- 98R Ramakrishna Reddy, K.T., Sravani, C., Miles, R.W.: J. Cryst. Growth 184/185 (1998) 1031.

Figures to 3.16

Fig. 3.0.3

The rocksalt lattice.

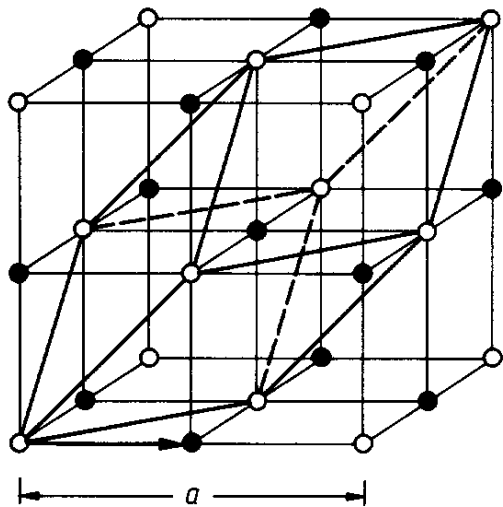


Fig. 3.0.4

The Brillouin zone for the zincblende and the rocksalt lattices.

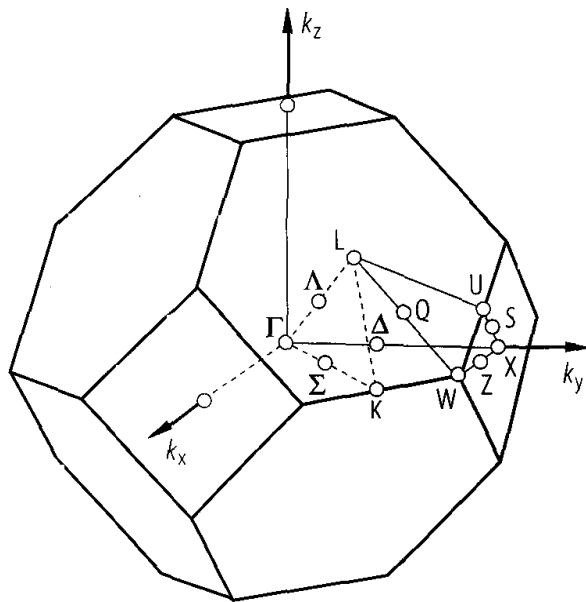


Fig. 3.0.20

CdO. Band structure from an ab-initio calculation [83B].

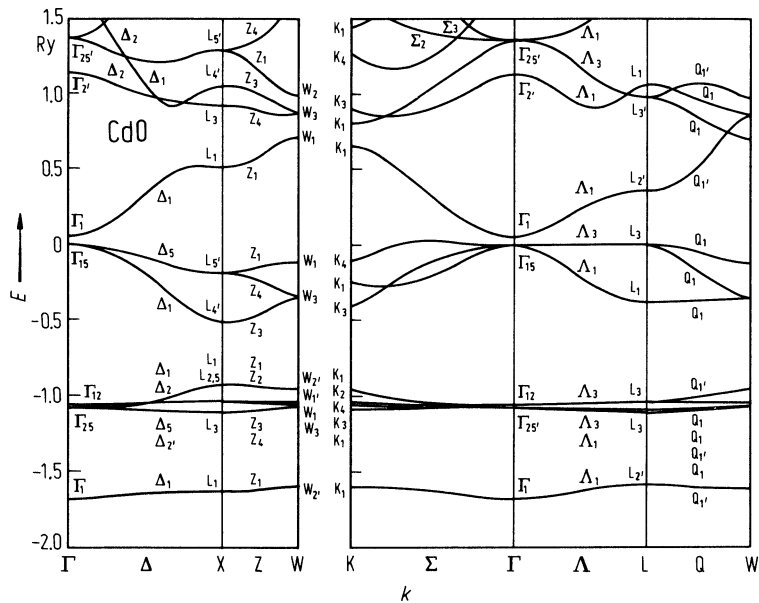


Fig. 3.16.1

CdO. Effective mass of electrons (related to the free electron mass m_0) vs. electron concentration [66F].

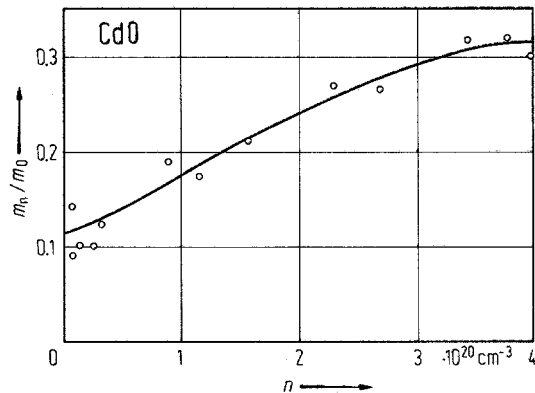


Fig. 3.16.2

CdO. Heat capacity C_p vs. temperature. Measurements of two authors [72M].

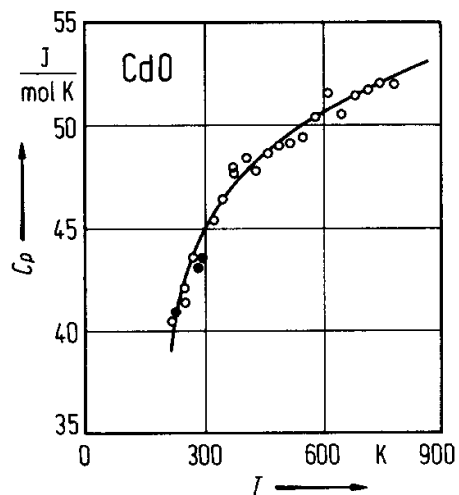


Fig. 3.16.3

CdO. Full drawn curves: measured temperature dependence of the Hall mobility μ_H . Dashed curves: calculated mobilities, (a) due to optical mode scattering, (b) due to ionized impurity scattering. Parameter: Electron concentration in units of 10^{18} cm^{-3} [71K2].

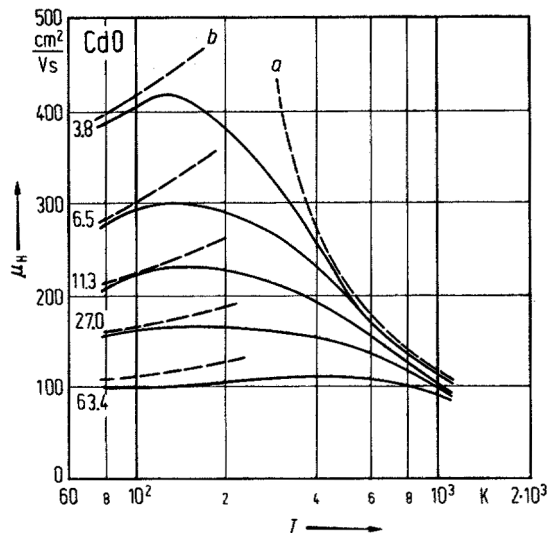


Fig. 3.16.4

CdO. Thermoelectric power S vs. temperature. Open circles and full circles for two different samples with $n \approx 2 \cdot 10^{20} \text{ cm}^{-3}$. Full drawn lines from calculation with fitted effective mass [62L].

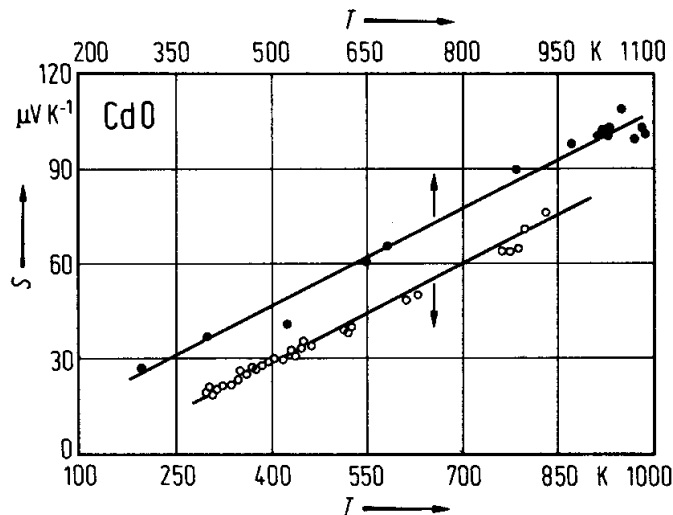


Fig. 3.16.5

CdO. Dispersion of the optical constants n and k of a film [94V].

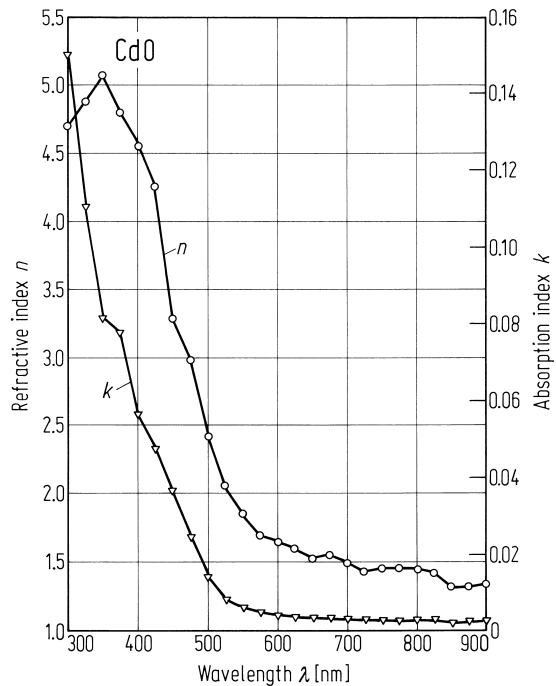
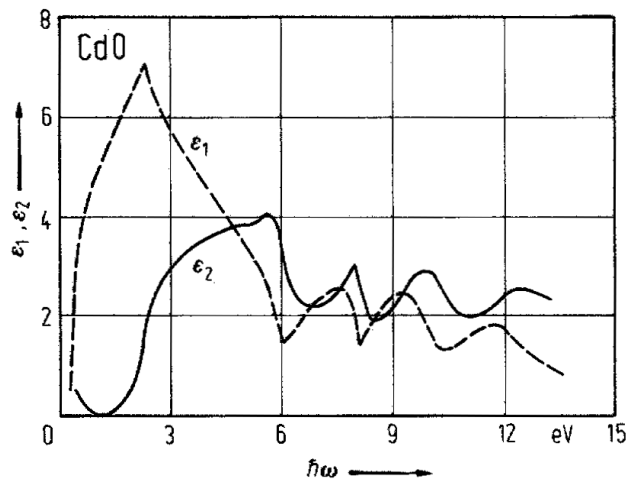


Fig. 3.16.6

CdO. Real (ϵ_1) and imaginary (ϵ_2) part of dielectric constant vs. photon energy at higher interband transitions [68A].



3.17 Cadmium sulfide (CdS)

Crystal structure

CdS crystallizes in different structures. The most common form is the hexagonal wurtzite structure (Fig. 3.0.2). The two other lattice forms are the face-centered zincblende-structure (Fig. 3.0.1) and the high-pressure NaCl phase (Fig. 3.0.3).

The cubic phase is less common and experiments in which powders or layers were converted to hexagonal CdS have led to the conclusion that cubic CdS is metastable in the temperature range 20°C...900°C [43R].

Electronic properties

If not otherwise stated all data in the documents on CdS refer to hexagonal CdS. A cubic modification is often observed in epitaxial layers. For hex. CdS, indices '⊥' and '||' at given quantities refer to orientation perpendicular and parallel to the *c* axis, respectively, unless explicitly otherwise stated.

band structure : Fig. 3.0.20, Brillouin zone: Fig. 3.0.5.

Cadmium sulfide is a direct gap semiconductor with the smallest energy gap at the center of the Brillouin zone (Γ). The topmost valence band (Γ₅ + Γ₁) is split due to crystal field and spin-orbit coupling into three spin-degenerate states (Γ₉, Γ₇ and Γ₇). Exciton states formed with holes in these valence band states are denoted A, B, and C exciton, respectively.

calculated energies of symmetry points of the band structure (relative to the top of the valence band *E*(Γ_{5v}))

<i>E</i> (Γ _{1v})	− 12.53 eV	see Fig. 3.0.21	94Z
<i>E</i> (Γ _{3v})	− 11.64 eV		
<i>E</i> (Γ _{3v})	− 4.32 eV		
<i>E</i> (Γ _{6v})	− 0.69 eV		
<i>E</i> (Γ _{1v})	− 0.06 eV		
<i>E</i> (Γ _{1c})	2.79 eV		
<i>E</i> (Γ _{3c})	4.54 eV		
<i>E</i> (M _{1v})	− 11.90 eV		
<i>E</i> (M _{3v})	− 11.32 eV		
<i>E</i> (M _{1v})	− 4.11 eV		
<i>E</i> (M _{3v})	− 3.50 eV		
<i>E</i> (M _{1v})	− 2.57 eV		
<i>E</i> (M _{2v})	− 1.72 eV		
<i>E</i> (M _{3v})	− 1.28 eV		
<i>E</i> (M _{4v})	− 0.68 eV		
<i>E</i> (M _{1c})	5.50 eV		
<i>E</i> (M _{3c})	5.55 eV		

energy band gaps of the three subbands

<i>E</i> _{g,dir} ^A (Γ _{9v} −Γ _{7c})	2.482 eV	<i>T</i> = 300 K	ellipsometry	95N
<i>E</i> _g ^B (Γ _{7v} −Γ _{7c})	2.496 eV			
<i>E</i> _g ^C (Γ _{7v} −Γ _{7c})	2.555 eV			

temperature dependence of the energy gaps : Fig. 3.17.1.

valence band splitting parameters

Spin-orbit and crystal-field splitting energies are deduced from band gap energies using the quasi-cubic model [67D]

$$\Delta E_{g1,2} = (1/2)(\Delta_{so} + \Delta_{cf}) \pm ((\Delta_{so} + \Delta_{cf})^2 - (8/3)\Delta_{so}\Delta_{cf})^{1/2}.$$

Δ _{so} (Γ)	0.0669 eV	<i>T</i> = 10 K	reflectivity	94T
Δ _{cf} (Γ)	0.0263 eV			

temperature coefficient of band gaps

$dE_g^{A,B,C}/dT$	$4.1 \cdot 10^{-4} \text{ eV K}^{-1}$	$T = 77 \dots 300 \text{ K}$	exciton reflectance	78S
-------------------	---------------------------------------	------------------------------	---------------------	-----

For temperature dependence of band gap, see Fig. 3.17.2.

conduction band, effective masses

From experiments the conduction band mass can be assumed to be nearly isotropic.

m_n	$0.25 m_0$	$T = 300 \text{ K}$	thermoelectric power	55K
	$0.2 \dots 0.16 m_0$	$T = 25 \dots 700 \text{ K}$	mobility analysis, OMS, PPS	60P

valence band, effective masses

$m_{p\perp}^A$	$0.7 (1) m_0$	$T = 1.6 \text{ K}$	exciton magneto-absorption	61H
$m_{p\parallel}^A$	$5 m_0$			

g-factors

$g_{c\perp}$	$1.78(5)$	$T = 1.6 \text{ K}$	exciton absorption	61H
$g_{c\parallel}$	$1.72(10)$			
$g_{v\parallel}^A$	$1.15(5)$	$T = 16 \text{ K}$	exciton absorption	61H
$g_{v\perp}^B$	0.8	$T = 1.8 \text{ K}$	line-shape analysis of excitonic polariton reflectivity	81B

exciton transition energies

$E_{gx}^A(\Gamma_5^T, 1S)$	2.5520 eV	$T = 1.3 \text{ K}$	light refraction at thin prisms	86B
$\Delta_{LT}^A(1S)$	2.2 meV			
$E_{gx}^B(\Gamma_5^T)$	2.5681 eV			
$\Delta_{LT}^B(\Gamma_5)$	1.4 meV			

effective masses

(M : exciton mass; μ : reduced mass, $m_{n,p}$: electron, hole mass)

M_{\perp}^A	$0.9 m_0$	TPRRS	80K
M_{\parallel}^A	$3.0 m_0$		
μ_{\perp}^A	$0.158(2) m_0$	two-photon spectroscopy	82S
$m_{n\perp}$	$0.210(3) m_0$		83S
$m_{p\perp}^A$	$0.64(2) m_0$		
$m_{p\perp}^B$	$0.64(17) m_0$		

Lattice properties

lattice parameters

a	4.1348 \AA	X-ray diffraction	63W2
c	6.7490 \AA		

The temperature dependence of the lattice constant a is represented in Fig. 3.17.3.

thermal expansion : Fig. 3.17.4.

As there are 4 atoms per unit cell in CdS with C_{6v}^4 symmetry one expects besides 3 acoustic branches 9 optical phonon branches. Group theory predicts as irreducible representations of the optical branches at the center of the Brillouin zone: one Γ_1 (nondegenerate), one Γ_5 (twofold degenerate), two Γ_6 (twofold degenerate), and two Γ_4 branches (nondegenerate). The Γ_1 and Γ_5 branches are both dipole and Raman active, the Γ_6 branches are Raman active, the Γ_4 branches are neither dipole nor Raman active.

phonon dispersion curves : Fig. 3.17.5.

phonon wavenumbers

$\bar{\nu}_{\text{LO}}(\Gamma_5, \perp c)$	307 cm ⁻¹	$T = 25 \text{ K}$	Raman spectroscopy	69A2
$\bar{\nu}_{\text{LO}_1}(\Gamma_1, \parallel c)$	305 cm ⁻¹			
$\bar{\nu}_{\text{TO}_1}(\Gamma_5, \perp c)$	242 cm ⁻¹			
$\bar{\nu}_{\text{TO}_1}(\Gamma_1, \parallel c)$	234 cm ⁻¹			
$\bar{\nu}_{\text{LO}_2}(\Gamma_6, \perp c)$	256 cm ⁻¹			
$\bar{\nu}_{\text{TO}_3}(\Gamma_6, \perp c)$	43 cm ⁻¹			

second order elastic moduli

c_{11}	90.7 GPa			60J
c_{13}	51.0 GPa			
c_{33}	93.8 GPa			
c_{44}	15.04 GPa			
c_{55}^{D}	16.30 GPa			

For temperature dependence of elastic moduli c_{11} , c_{33} , c_{44} : Fig. 3.17.6; c_{12} , c_{13} : Fig. 3.17.7.

temperature coefficients of the elastic moduli

$(1/s_{11})ds_{11}/dT$	$116 \cdot 10^{-6} \text{ K}^{-1}$	$T = 298 \text{ K}$	ultrasound resonance	63B
$(1/s_{12})ds_{12}/dT$	$87 \cdot 10^{-6} \text{ K}^{-1}$			
$(1/s_{44})ds_{44}/dT$	$96 \cdot 10^{-6} \text{ K}^{-1}$			
$(1/s_{33})ds_{33}/dT$	$-216 \cdot 10^{-6} \text{ K}^{-1}$			

electromechanical coupling factors

k_{31}	0.119	$T = 298 \text{ K}$	ultrasound resonance	63B
k_{33}	0.262			
k_{15}	0.188			
k_t	0.154			

volume compressibility

κ_v	$1.586 \cdot 10^{-7} \text{ bar}^{-1}$	$T = 300 \text{ K}$		70M
------------	--	---------------------	--	-----

Debye temperature

Θ_D	219.32 K		average elastic constants	67G
------------	----------	--	---------------------------	-----

For the T -dependence of Θ_D between 0 and 300 K, see Fig. 3.17.8.

heat capacity

C_p	$53.97 + 3.77 \cdot 10^{-3} T \text{ J mol}^{-1} \text{ K}^{-1}$	$T = 298 \dots 1678 \text{ K}$		79G
-------	--	--------------------------------	--	-----

density

d	4.82 g cm ⁻³	$T = 300 \text{ K}$		69A1
-----	-------------------------	---------------------	--	------

melting temperature

T_m	1405(10) °C			96S
	1750 K	$(p_{\text{min}} = 3.8 \text{ atm})$		63W1

Transport properties

Electrical transport in CdS is performed by electrons in the Γ_7 -conduction band and by holes in the Γ_9 -valence band. Because of compensating effects during the preparation of the samples and the ratio $\mu_n/\mu_p > 10$, CdS is normally n-type conducting; p-type conductivity is observed only in a few special cases.

The carrier concentration depends on impurity or defect content and on temperature. Furthermore the value can be changed markedly by irradiation (photoconductivity; CdS is known to be a model substance for a photo-conductor).

The temperature dependence of the conductivity and electron concentration (Hall effect data) is shown in Fig. 3.17.9.

Though pure intrinsic conductivity (σ_i) in CdS has not yet been observed (there is always an influence of defects for a semiconductor with a high band gap) some values of carrier concentrations and mobilities, determined at very high temperatures are almost intrinsic. For quantitative considerations, however, these values should be used with care.

nearly intrinsic conductivity

$\sigma_{i,n} = 2.81 \cdot 10^{-2} (\Omega\text{cm})^{-1}$ and $\sigma_{i,p} = 1.51 \cdot 10^{-2} (\Omega\text{cm})^{-1}$

thermal conductivity

$\kappa_L \qquad 0.20 \text{ W cm}^{-1} \text{ K}^{-1} \qquad T = 300 \text{ K} \qquad 64\text{H}$

See Fig. 3.17.10 for temperature dependence between 1.4 and 80K.

electron Hall mobility

Fig. 3.17.11 shows the temperature dependence of electron mobilities in ultrapure and less pure crystals.

$\mu_{H,n}$	$\geq 10000 \text{ cm}^2/\text{Vs}$	$T = 30 \dots 40 \text{ K}$	peak mobilities in ultrapure crystals	85B
	$160 \text{ cm}^2/\text{Vs}$	$T = 300 \text{ K}$	In-doped, $n=5 \cdot 10^{19} \text{ cm}^{-3}$	90B

hole mobility

μ_p	$15 \text{ cm}^2/\text{Vs}$	$T = 300 \text{ K}$	calculated from transient conductivity measurements at single highly resistive crystals	89W
---------	-----------------------------	---------------------	---	-----

Dependence of hole drift mobility on temperature: Fig. 3.17.12.

piezoelectric strain coefficients

d_{31}	$- 5.18(10) \cdot 10^{-12} \text{ C/N}$	$T = 298 \text{ K}$	ultrasound resonance	63B
d_{33}	$+ 10.32(21) \cdot 10^{-12} \text{ C/N}$			
d_{15}	$- 13.98(42) \cdot 10^{-12} \text{ C/N}$			

piezoelectric stress coefficients

e_{31}	$- 0.244 \text{ C/m}^2$	$T = 298 \text{ K}$	ultrasound resonance	63B
e_{33}	$+ 0.440 \text{ C/m}^2$			
e_{15}	$- 0.210 \text{ C/m}^2$			

Optical properties

refractive index and birefringence

$\Delta n (= n_{\parallel c} - n_{\perp c})$

Fig. 3.17.13 shows the complex refractive index in the spectral range from 2.24 to 2.44 eV. Fig. 3.17.14 shows the refractive index at 5 K in the fundamental absorption region for samples of different thickness [84B].

$n_{\perp c}$	$n_{\parallel c}$	$\Delta n [10^{-2}]$	$\lambda [\mu m]$	$T [K]$		
2.573	2.586		0.55	293	prism	69L
2.479	2.496		0.61			
2.417	2.434		0.69			
2.358	2.375		0.85			
2.296	2.312		1.50			
2.281		1.678	2	293	interference	69L
2.258		1.662	6			
2.187		1.408	14			
2.051			18			
1.880			24			

temperature dependence of the refractive index

		$T [^{\circ}C]$	$\lambda [\mu m]$		
$(1/n_{\perp})dn_{\perp}/dT$	$26.8 (3) \cdot 10^{-6} K^{-1}$	35...80	10.3	interference	77W
$(1/n_{\parallel})dn_{\parallel}/dT$	$27.8(2) \cdot 10^{-6} K^{-1}$				
$d(\Delta n)/dT$	$3.07(12) \cdot 10^{-6} K^{-1}$				

absorption coefficient

Fig. 3.17.15 shows the spectral dependence of the absorption coefficient and normal incidence reflectivity in the range from 1.2 to 5.7 eV.

dielectric constants

$\epsilon^{\perp}(0)$	8.28	$T = 300 K$	spectroscopic ellipsometry	95N
$\epsilon^{\perp}(\infty)$	5.23			
$\epsilon^{\parallel}(0)$	8.73			
$\epsilon^{\parallel}(\infty)$	5.29			

elastooptic constant

p_{44}	0.049	$T = 295 K,$ $\lambda = 633 nm$	Brillouin scattering	73W
----------	-------	------------------------------------	----------------------	-----

References to 3.17

- 55K Kröger, F. A., Vink, H. J., Volger, J.: Philips Res. Rep. 10 (1955) 39.
- 60D Devlin, S. S., Jost, J. M., Shiozawa, L. R.: Wadd Technical Report 60-11, 1960.
- 60J Jaffe, H., Berlincourt, D., Krueger, H., Shiozawa, L.: Proc. 14th Ann. Conf. Frequency Control (1960), unpublished, cited in [67C3].
- 60P Piper, W. W., Halsted, R. E.: Proc. 5th Int. Conf. Phys. Semicond., Prague, Academic Press, New York/London, 1961, 1046.
- 61H Hopfield, J. J., Thomas, D. G.: Phys. Rev. 122 (1961) 35.
- 63B Berlincourt D., Jaffe, H., Shiozawa, L. R.: Phys. Rev. 129 (1963) 1009.
- 63S Spear, W. E., Mort, J.: Proc. Phys. Soc. 81 (1963~) 30.
- 63W1 Woodbury, H. H.: J. Phys. Chem. Solids 24 (1963) 881.
- 63W2 Wyckoff, R. W. G.: Crystal Structures, John Wiley and Sons, New York, 1963, 108-112.
- 64H Holland, M. G.: Phys. Rev. 134 (1964) A 471.
- 67B Bergstresser, T. K., Cohen, M. L.: Phys. Rev. 164 (1967) 1069.
- 67G Gerlich, D.: J. Phys. Chem. Solids 28 (1967) 2575.
- 67N Nusimovici, M. A., Birman, J. L.: Proc. 7th Int. Conf. II-VI Semiconducting Compounds, Providence, R. I., USA, W. A. Benjamin Inc., New York, 1967, 1204.
- 69A1 Abrikosov, N. Kh., Bankina, V. F., Poretskaya, L. V., Shelimova, L. E., Skudnova, E. V.: in Semiconducting II-VI, IV-VI and V-VI Compounds, Plenum, New York, 1969, 27.
- 69A2 Arguello, C. A., Rousseau, D. L., Porto, S. P. S.: Phys. Rev. 181 (1969) 1351.
- 69L Lisitsa, M. P., Gudymenko, L. F., Malinko, V. N., Terekhova, S. F.: Phys. Status Solidi 31 (1969) 389.
- 69M Moore, G. E., Klein, M. V.: Phys. Rev. 179 (1969) 722. 85B Beene, J. L., Contwell, G.: J. Appl. Phys. 57 (1985) 1171.
- 70M Montavlo, R. A., Langer, D. W.: J. Appl. Phys. 41 (1970) 4101.
- 73W Wakita, K., Umeno, M., Tagaki, K., Miki, S.: J. Phys. Soc. Jpn. 35 (1973) 149.
- 76A Anedda, A., Fortin, E.: Phys. Status Solidi (a) 36 (1976) 385.
- 77W Weil, R., Neshmit, D.: J. Opt. Soc. Am. 67 (1977) 190.
- 78S Sobolev, V. V., Donetskina, V. J., Zagainov, E. F.: Sov. Phys. Semicond. (English Transl.) 12 (1978) 646.
- 79G Grytsiv, V. I., Tomashik, V. N., Tomashik, Z. F.: Inorg. Mater. 15 (1979) 30.
- 80K Kurtze, G., Maier, W., Kempf, K., Schmieder, G., Schrey, H., Klingshirn, C., Hönerlage, B., Rössler, U.: Proc. 15th Int. Conf. Physics of Semiconductors, Kyoto 1980; J. Phys. Soc. Jpn. 49 (1980), Suppl. A, 559.
- 80O Oskot-skii, V. S., Kobaykov, I. B., Solodukhin, A. V.: Fiz. Tverd. Tela 22 (1980) 1479; engl.: Sov. Phys. Solid State 22 (1980) 861.
- 81B Broser, I., Rosenzweig, M.: Solid State Commun. 36 (1980) 1027.
- 81H Hutson, A. R.: Phys. Rev. Lett. 46 (1981) 1159.
- 82S Seiler, D. G., Heiman, D., Feigenblatt, R., Aggarwal, R. L., Lax, B.: Phys. Rev. B 25 (1982) 7666.
- 83K Kobayashi, A., Sankey, O. F., Volz, S. M., Dow, J. D.: Phys. Rev. B 28 (1983) 935.
- 83S Seiler, D. G., Heiman, D., Wherrett, B. S.: Phys. Rev. B 27 (1983) 2355.
- 84B Bohnert, K., Fiodorra, F., Klingshirn, C.: Z. Phys. B 57 (1984) 263.
- 85B Beene, J. L., Contwell, G.: J. Appl. Phys. 57 (1985) 1171.
- 86B Baumert, R., Broser, I., Buschick, K.: IEEE J. Quantum Electron. QE-22 (1986) 1539.
- 89W Warman, J.M., de Haas, M.P., van Hövell tot Westeflier, S.W.F.M., Binsma, J.J.M., Kolar, Z.I.: J. Phys. Chem. 93 (1989) 5895.
- 90B Broser, I., Broser, R., Birkicht, E.: J. Cryst. Growth 101 (1990) 497.
- 92O Oberlé, J., Kippelen B., Daunois, A., Grun, J.-B.: Optics Commun. 90 (1992) 339.
- 94T Twardowski, A., Chern-Yu, K., Chen, F.R., Kuo, S.S., Ro, C.S., Chiu, K.C., Chou, W.C., Yang, S.L., Chuu, D.S., Chen, Y.F.: Phys. Status Solidi (b) 181 (1994) 439.
- 94Z Zakharov, O., Rubio, A., Blase, X., Cohen, M.L., Louie, S.G.: Phys. Rev. B 50 (1994) 10780.
- 95N Ninomiya, S., Adachi, S.: J. Appl. Phys. 78 (1995) 1183.
- 96S Sharma, R. C., Chang, Y. A.: J. Phase Equilibria 17 (1996) 425
- 97D Debernardi, A., Pyka, N. M., Göbel, A., Ruf, T., Lauck, R., Kramp, S., Cardona, M.: Solid State Commun. 103 (1997) 297.

Figures to 3.17

Fig. 3.0.1

The zincblende lattice.

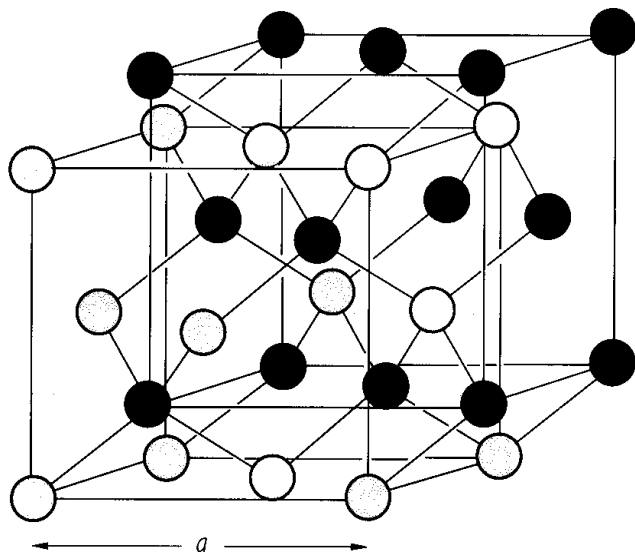


Fig. 3.0.2

The wurtzite lattice.

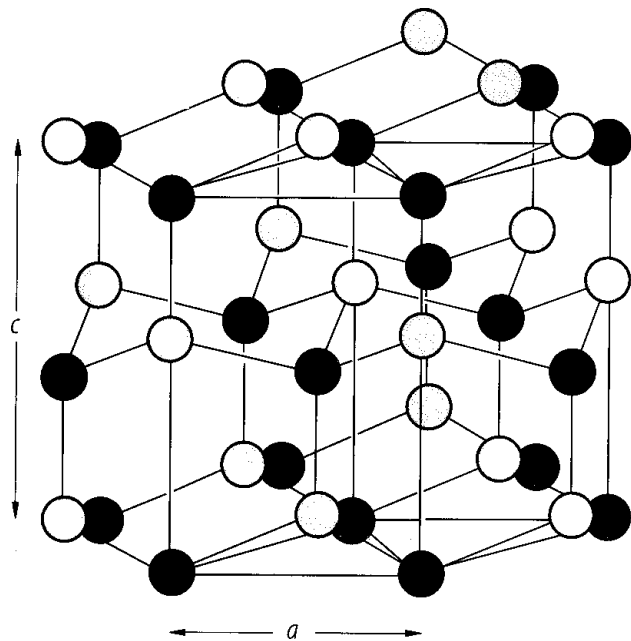


Fig. 3.0.3

The rocksalt lattice.

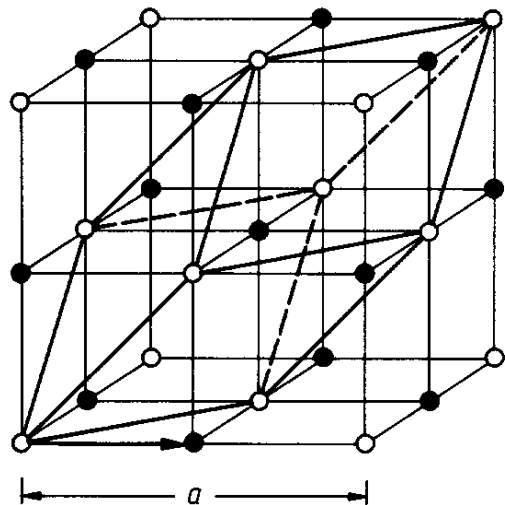


Fig. 3.0.5

The Brillouin zone of the wurtzite lattice.

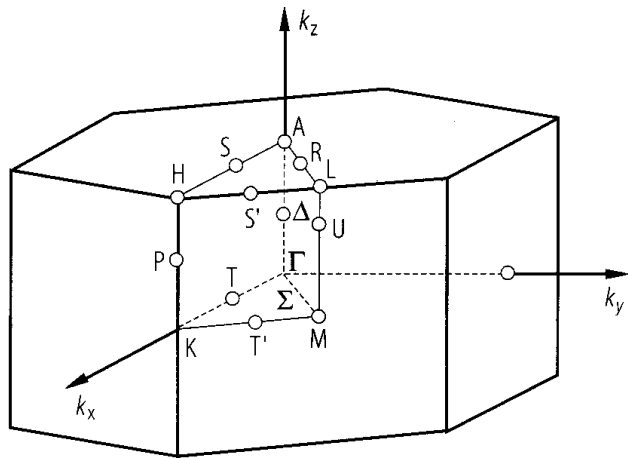


Fig. 3.0.21

CdS (hex). Band structure from an empirical tight binding model [83K] (solid line) compared with the pseudopotential band structure of [67B] (dashed line). Energy bands corresponding to the Cd 4d states and spin-orbit coupling are not considered in this calculation.

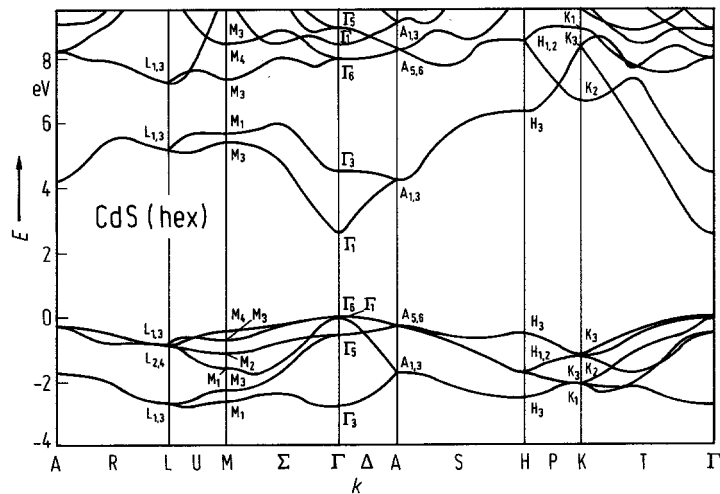


Fig. 3.17.1

CdS (hex). Energy of the A gap vs. temperature, experimental points from several authors [82S].

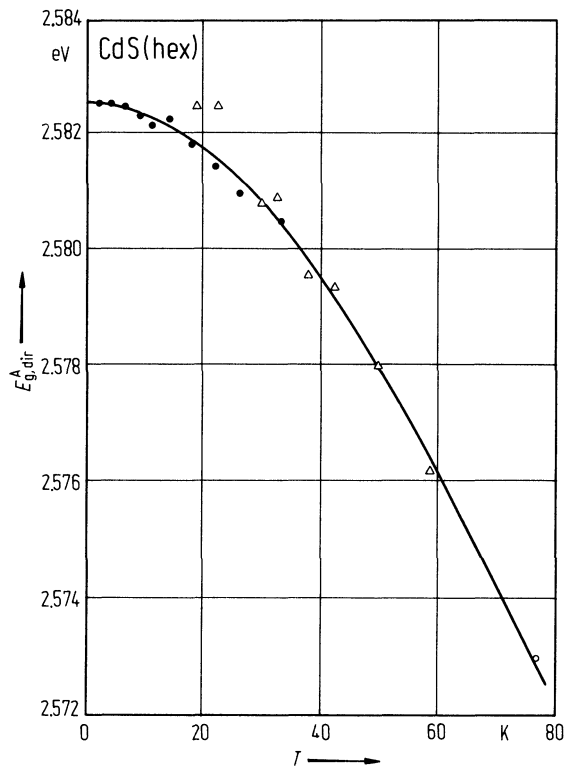


Fig. 3.17.2

CdS. Temperature vs. spectral position of the A and B excitons [76A].

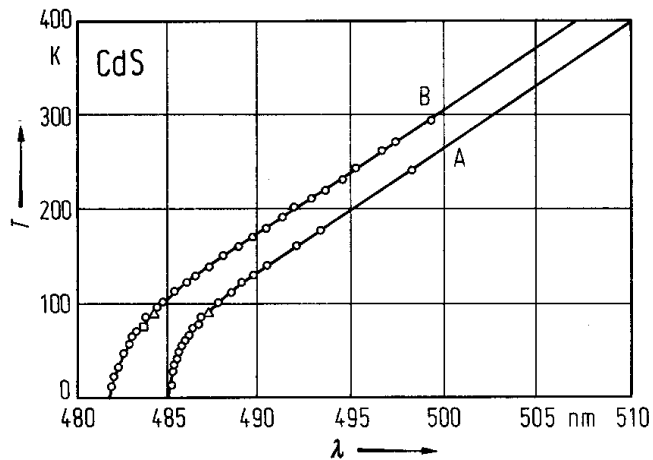


Fig. 3.17.3

CdS. Thermal expansion as measured by the change of lattice constant a with temperature [60D].

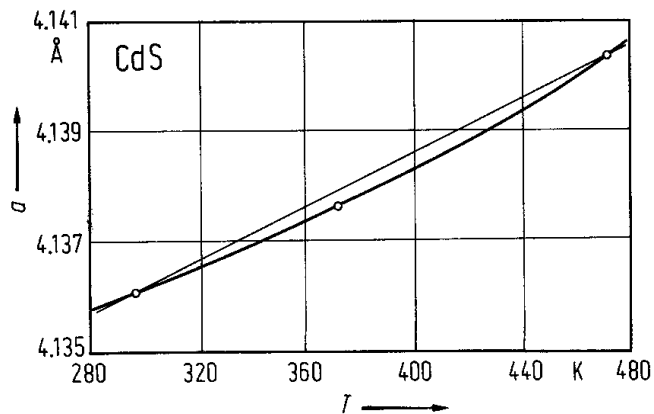


Fig. 3.17.4

CdS (hex.). Temperature dependence of the linear thermal expansion coefficients α_{\perp} (perpendicular to the c -axis, curve 1) and α_{\parallel} (parallel to the c -axis, curve 2) by dilatometer experiments [800].

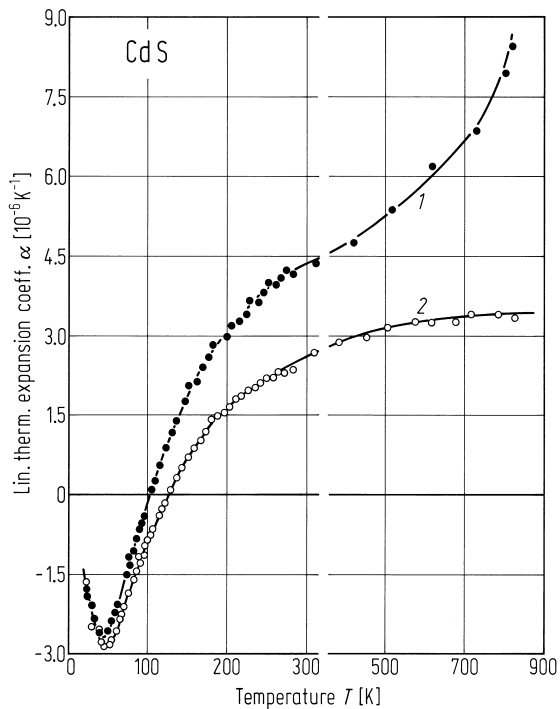


Fig. 3.17.5

CdS (hex.). Phonon dispersion curves [97D]. Data points from inelastic neutron scattering experiments and ab-initio calculations; the theoretical curves are scaled down from the ab-initio calculations by a factor of 0.95.

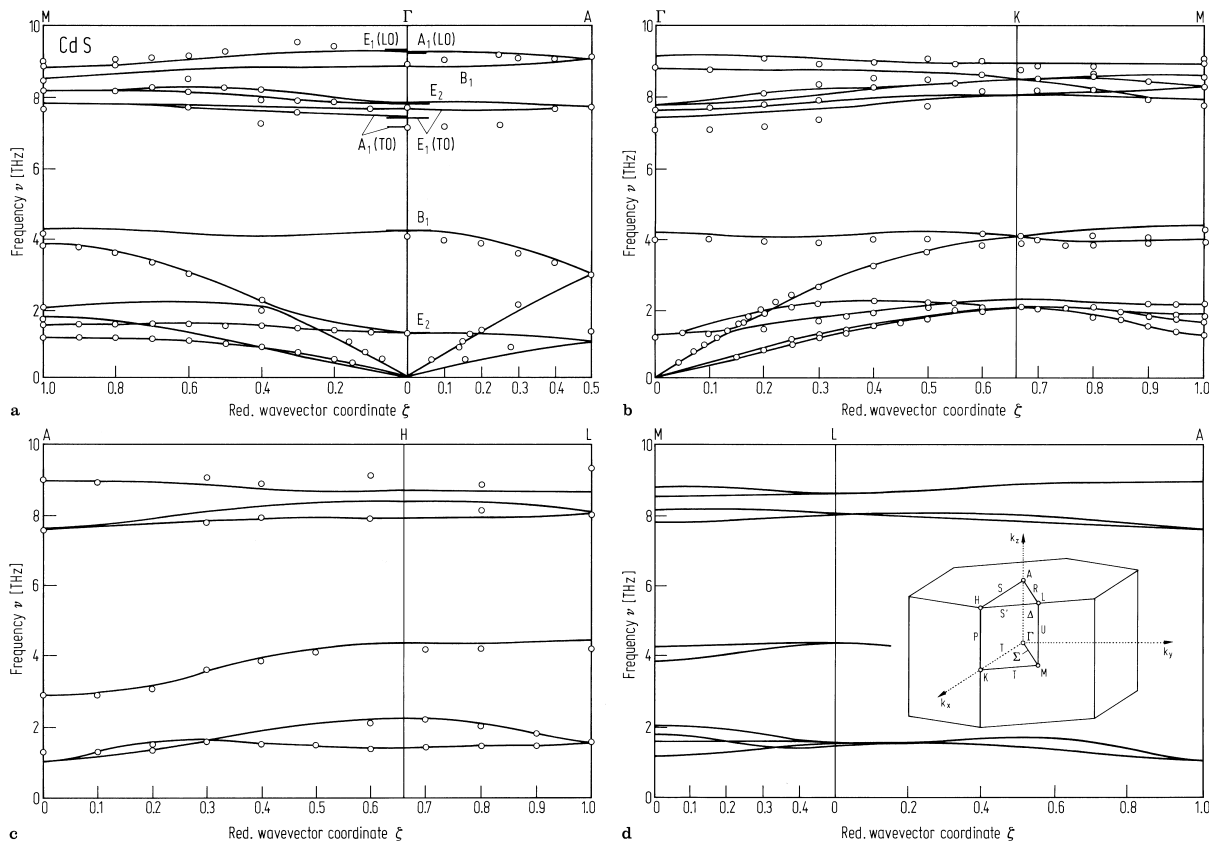


Fig. 3.17.6

CdS. The diagonal second order elastic moduli vs. temperature [67G].

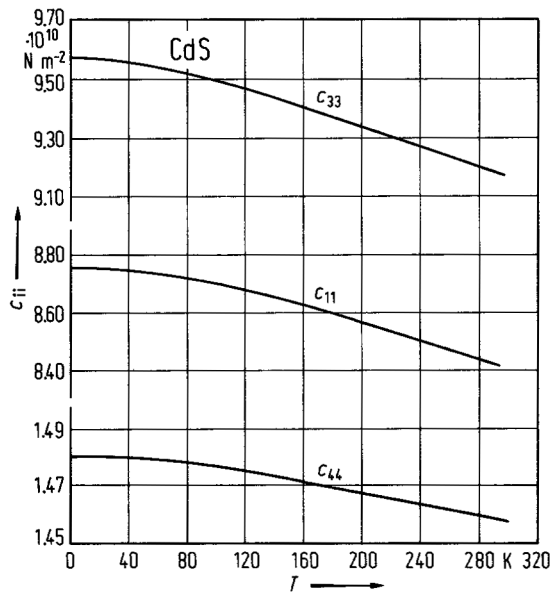


Fig. 3.17.7

CdS. The cross coupling elastic moduli vs. temperature [67G].

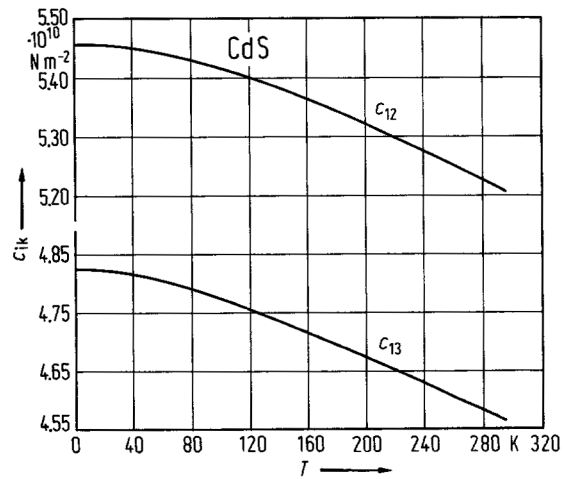


Fig. 3.17.8

CdS. Debye temperature vs. temperature. Computed value [67N].

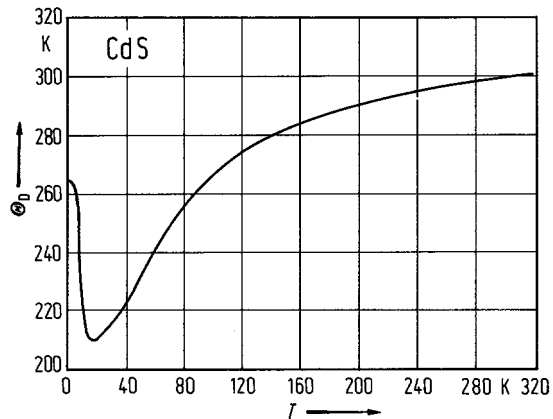


Fig. 3.17.9

CdS (hex). Electrical conductivity vs. reciprocal temperature for two bar samples oriented parallel and perpendicular to c -axis, and Hall-effect data for the same samples vs. reciprocal temperature [81H].

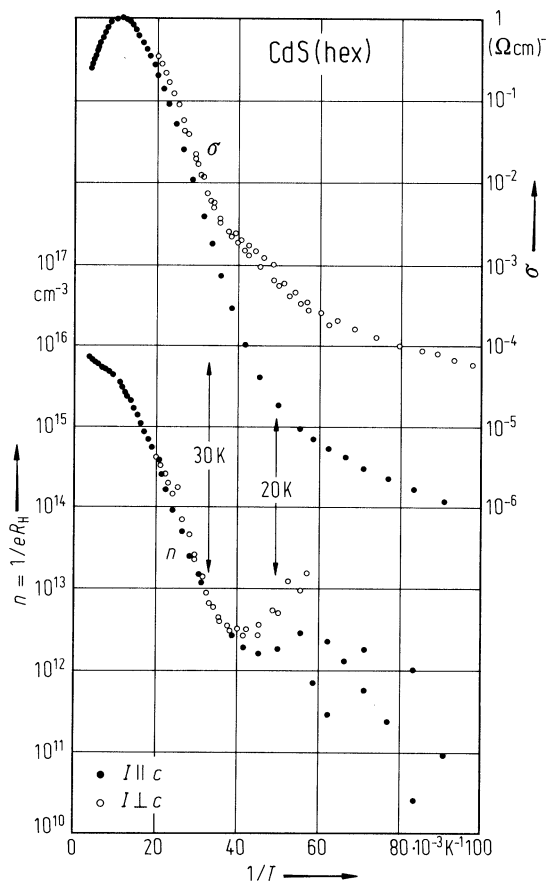


Fig. 3.17.10

CdS. Thermal conductivity vs. temperature for c -axis \parallel and \perp to the heat flow ΔT [69M].

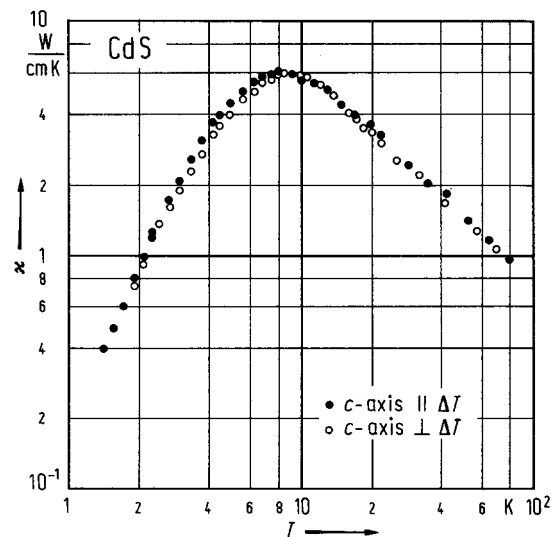


Fig. 3.17.11

CdS (hex). Temperature dependence of electron mobility in ultrapure (squares and triangles, $n_D, n_A, n_S \ll 10^{17} \text{ cm}^{-3}$, D donor, A acceptor, S sulphur vacancy) and less pure (crosses and circles) crystals showing the tendency towards lowering of peak mobility values and peak shift to higher temperatures [85B].

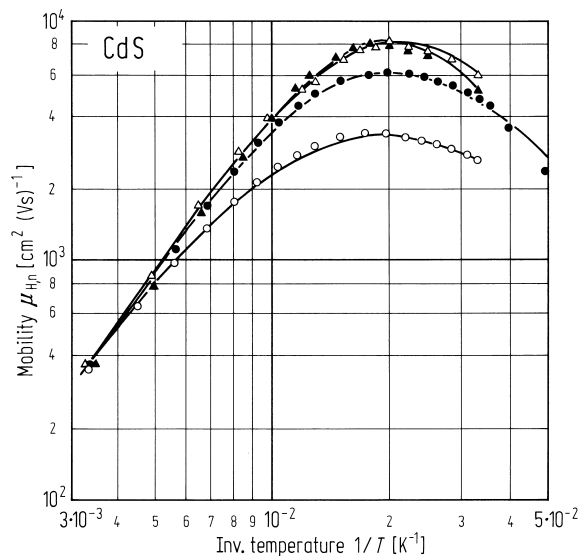


Fig. 3.17.12

CdS. Hole drift mobility vs. temperature for five different crystals, normalized to its room temperature value [63S].

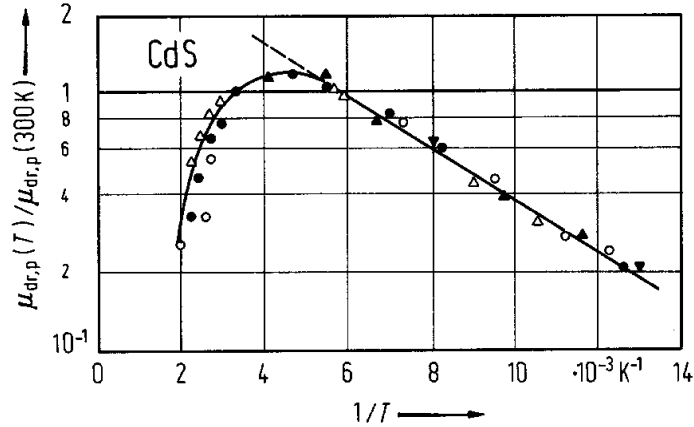


Fig. 3.17.13

CdS (hex). Dispersion of the refractive index. The symbols are experimental values and curves correspond to polynomial fits [92O].

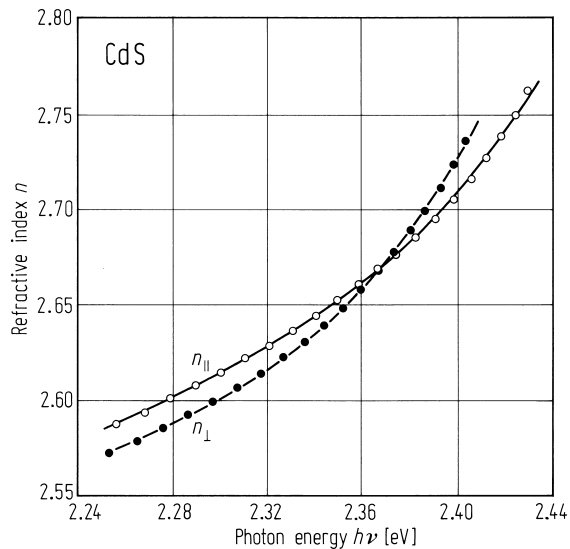


Fig. 3.17.14

CdS (hex). Index of refraction vs. photon energy for $E \perp c$ at 5 K from Fabry-Perot modes. Different symbols correspond to samples of various thicknesses [84B].

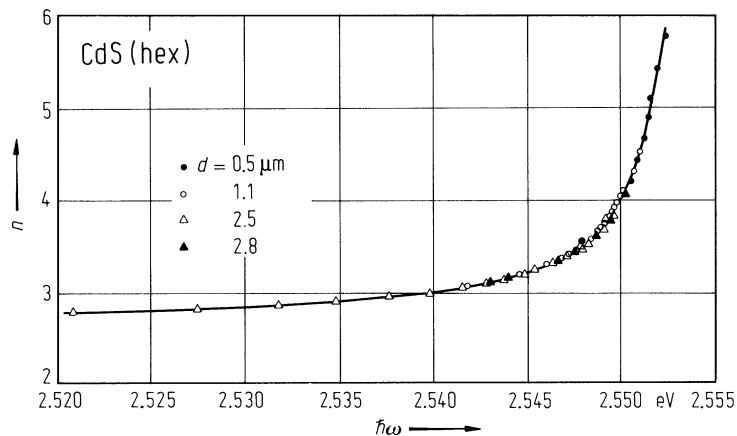
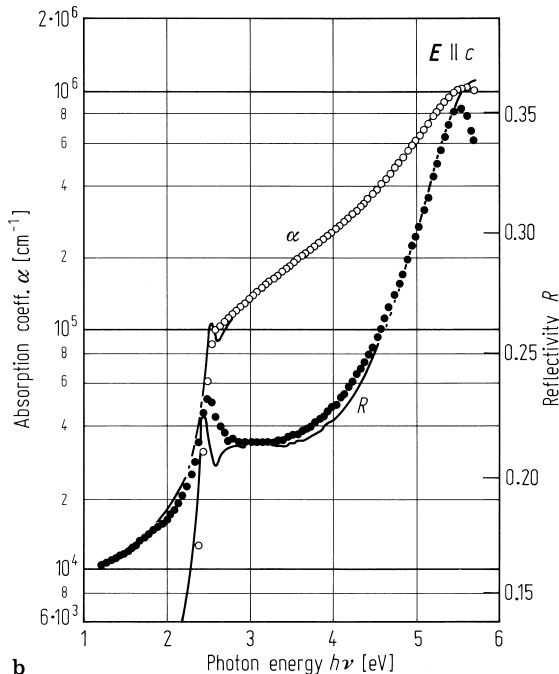
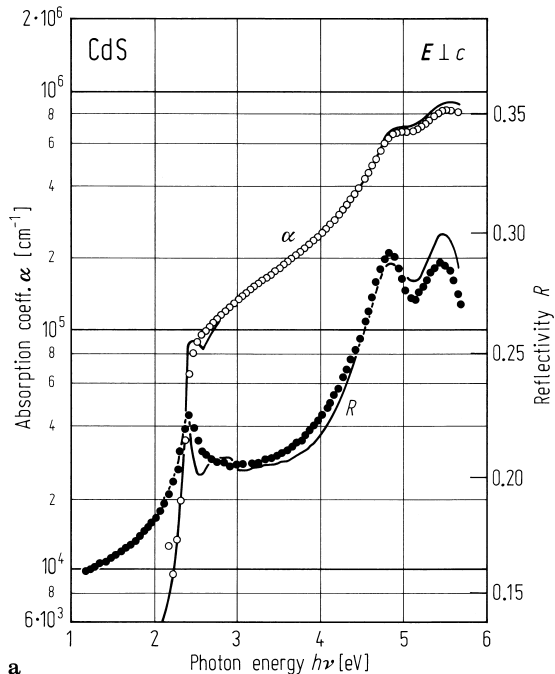


Fig. 3.17.15

CdS (hex). Numerically calculated spectral dependence of the absorption coefficient α and normal-incidence reflectivity R for $E \perp c$ (a) and $E \parallel c$ (b) (solid lines) at 300 K. The open and solid circles represent the experimental data, respectively [95N].



3.18 Cadmium selenide (CdSe)

Crystal structure

At ambient conditions, CdSe crystallizes in the zincblende structure. From ab-initio LAPW calculations, the energy of the zincblende structure is lower than that of the wurtzite structure by 1.4 meV/atom. Under increasing pressure, the wurtzite structure transforms to the rocksalt structure, the β-tin structure and yet unidentified structures, possibly orthorhombic or monoclinic.

cubic modification: zincblende, space group $F\bar{4}3m - T_d^2$ (Fig. 3.0.1)
hexagonal modification: wurtzite, space group $P6_3mc - C_{6v}^4$ (Fig. 3.0.2)

Electronic properties, hexagonal modification

band structure : Fig. 3.0.22a, Brillouin zone: Fig. 3.0.5.

The conduction band originates from the 5s states of cadmium. The minimum of energy is located at the center of the Brillouin zone (Γ-point), a second minimum about 1.7 eV higher is located at the A-point. The conduction band has for $k = 0$ Γ₇-symmetry with quantum number $J_z = \frac{1}{2}$.

The valence band results from the 4p states of selenium, having its maximum at the Γ-point, too, which leads to a direct band gap. As a result of crystal field and spin-orbit splitting the valence band at $k = 0$ is split into three sub-bands, conveniently named A, B and C.

energies of symmetry points in the band structure (relative to the top of the valence band)

$E(\Gamma_{1v})$	- 12.09 eV			95W1
$E(\Gamma_{3v})$	- 4.06 eV			
$E(\Gamma_{3c})$	3.12 eV			
$E(\Gamma_{6c})$	6.28 eV			
$E(M_{1v})$	- 3.88 eV			
$E(M_{3v})$	- 3.37 eV			
$E(M_{1v})$	- 2.51 eV			
$E(M_{2v})$	- 1.79 eV			
$E(M_{3v})$	- 1.35 eV			
$E(M_{4v})$	- 0.81 eV			
$E(M_{1c})$	4.17 eV			
$E(M_{3c})$	5.23 eV			

energy band gaps of the three subbands

$E_g^A(\Gamma_{9v}-\Gamma_{7c})$	1.732 eV	$T = 300$ K	ellipsometry	95N
$E_g^B(\Gamma_{7v}-\Gamma_{7c})$	1.761 eV			
$E_g^C(\Gamma_{7v}-\Gamma_{7c})$	2.161 eV			

valence band splitting parameters

Spin-orbit and crystal-field splitting energies are deduced from band gap energies using the quasi-cubic model [67D2]:

$$\Delta E_g^{1,2} = (1/2)(\Delta_{so} + \Delta_{cf}) \pm (1/2)((\Delta_{so} + \Delta_{cf})^2 - (8/3)\Delta_{so}\Delta_{cf})^{1/2}.$$

$\Delta_{so}(\Gamma)$	0.418 meV	$T = 4.2$ K	band gap transmission of mixed	62P
$\Delta_{cf}(\Gamma)$	0.039 meV		CdS _{1-x} Se _x crystals	

energy gap, temperature coefficients

dE_g/dT	$2.8 \cdot 10^{-4}$ eV K ⁻¹	$T = 0 \dots 250$ K	exciton absorption	79V
dE_g^A/dT	$3.63 \cdot 10^{-4}$ eV K ⁻¹	$T = 77 \dots 300$ K	exciton reflectance	78S
dE_g^B/dT	$3,53 \cdot 10^{-4}$ eV K ⁻¹			
dE_g^C/dT	$4.01 \cdot 10^{-4}$ eV K ⁻¹			

conduction band, effective masses

m_n	$0.112\ m_0$	$T = 20...300\ K$	cyclotron resonance	78M
-------	--------------	-------------------	---------------------	-----

valence band, effective masses

$m_{p\perp}^A$	$0.45(10)\ m_0$	$T = 1.8\ K$	exciton transmission	62W
$m_{p\parallel}^A$	$\geq 1\ m_0$			
$m_{p\perp}^B$	$0.9\ (2)\ m_0$			

g-factors

$g_{c\parallel}$	$0.6(1)$	$T = 1.8\ K$	exciton transmission	62W
$g_{c\perp}$	$0.51(5)$			
$g_{v\perp}^A$	0.0	$T = 1.6\ K$	bound exciton emission	70H
$g_{v\parallel}^A$	$1.41(5)$			

exciton energies

$E_{gx}^A(\Gamma_5^L, 1S)$	$1.8263\ eV$	$T = 1.6\ K$	magnetotransmission	84K
$\Delta_{LT}^A(1S)$	$0.00096\ eV$			
$E_{gx}^A(\Gamma_6, 1S)$	$1.82518\ eV$			
$E_{gx}^A(\Gamma_5^T, n=1)$	$1.735(2)\ eV$	$T = 293\ K$	reflectance	78S
$E_{gx}^B(\Gamma_5^T, n=1)$	$1.755(2)\ eV$	$T = 293\ K$		
$E_{gx}^C(\Gamma_5^T, n=1)$	$2.160(2)\ eV$	$T = 293\ K$		

Electronic properties, cubic modification

band structure : see Fig. 3.0.22b, Brillouin zone: Fig. 3.0.4.

calculated energies of symmetry points of the band structure (relative to the top of the valence band $E(\Gamma_{15v})$)

$E(\Gamma_{1v})$	$-12.76\ eV$		96C
$E(\Gamma_{15v}, Cd4d)$	$-7.93\ eV$		
$E(\Gamma_{12v}, Cd4d)$	$-7.43\ eV$		
$E(\Gamma_{1c})$	$0.45\ eV$		
$E(\Gamma_{15c})$	$5.80\ eV$		
$E(X_{1v})$	$-12.23\ eV$		
$E(X_{3v})$	$-4.28\ eV$		
$E(X_{5v})$	$-1.98\ eV$		
$E(X_{1c})$	$2.94\ eV$		
$E(X_{3c})$	$4.03\ eV$		
$E(L_{1v})$	$-12.36\ eV$		
$E(L_{1v})$	$-4.65\ eV$		
$E(L_{3v})$	$-0.80\ eV$		
$E(L_{1c})$	$2.24\ eV$		

energy gap

$E_{g,dir}(E_0)$	$1.74\ eV$	$T = 300\ K$	ellipsometry	95N
------------------	------------	--------------	--------------	-----

higher-interband transition energies (critical points in reflectance)

$E_0 + \Delta_0$	$2.05\ eV$	$T = 300\ K$	ellipsometry	94K
E_0'	$6.668\ eV$			
E_1	$4.314\ eV$			
$E_1 + \Delta_1$	$4.468\ eV$			
E_2	$6.069\ eV$			

spin-orbit splitting energy

Δ_0	470 meV	calculation	95W2
------------	---------	-------------	------

effective bare electron masses

m_n	$0.12 m_0$	calculation	94K
-------	------------	-------------	-----

effective bare hole masses

m_{hh}	2.14 m_0	[111] direction, calculation	94K
	0.9 m_0	[100] direction	
	1.7 m_0	[110] direction	
m_{lh}	0.16 m_0	[111] direction	
	0.18 m_0	[100] direction	
	0.16 m_0	[110] direction	
m_{so}	0.12 m_0	split-off band, calculation	94K

g-value of electrons

g	0.23	calculation	95W2
-----	------	-------------	------

exciton transition energy

$E_{gx}(1S)$	1.757(5) eV	extrapolated to $T = 0$ K, absorption	97G
--------------	-------------	---------------------------------------	-----

temperature dependence of exciton energy

Temperature shift of excitons has been described by Varshni's formula, $E_{1S}(T)=E_{1S}(0)-T^2\delta/(\Theta+T)$ [97G].

δ	$3.7(3) \cdot 10^{-4} \text{ eV K}^{-1}$	at $E_{1S}(0 \text{ K})=1.757(5) \text{ eV}$, absorption	97G
Θ	150(40) K		

Lattice properties**lattice parameters**

hexagonal modification:

The temperature dependence of the lattice constant a is represented in Fig. 3.18.1.

a	4.2999 Å	$T = 297 \text{ K}$	X-ray diffraction	76R
c	7.0109 Å			

zincblende modification:

a	6.077(5) Å	perp. to surface	energy-dispersive X-ray diffraction, MBE layer on GaAs(001)	89S
	6.078(1) Å	parallel to surface		

phonon dispersion curves : Fig. 3.18.2.**phonon wavenumbers**

$\bar{\nu}_{LO1}(\Gamma_1, c)$	210 cm^{-1}	$T = 300 \text{ K}$	I.R. spectroscopy	70B
$\bar{\nu}_{TO1}(\Gamma_5, \perp c)$	169 cm^{-1}	$T = 300 \text{ K}$	I.R. spectroscopy	70B
$\bar{\nu}_{LO2}(\Gamma_5, \perp c)$	212 cm^{-1}	$T = 300 \text{ K}$	I.R. spectroscopy	70B
$\bar{\nu}_{TO2}(\Gamma_1, c)$	166 cm^{-1}	$T = 300 \text{ K}$	I.R. spectroscopy	66G
$\bar{\nu}_{TA}(A_3)$	43.5 cm^{-1}	$T = 300 \text{ K}$	Zone edge phonon, Raman spectroscopy	77B

second order elastic moduli

c_{11}	74.6 GPa	RT	ultrasound measurements, 2 % error	93B
c_{12}	46.1 GPa			
c_{33}	81.7 GPa			
c_{44}	13.0 GPa			
c_{66}	14.3 GPa			

electromechanical coupling factor

k_{31}	0.0836(17)	$T = 298$ K	from ultrasound resonance	63B
k_{33}	0.194(8)			
k_{15}	0.1305(52)			
k_t	0.124(5)			

Debye temperature

Θ_D	181.7 K	$T = 0$ K		93B
------------	---------	-----------	--	-----

heat capacity

C_p [J mol ⁻¹ K ⁻¹]	$48.46 + 5.87 \cdot 10^{-3} T - 58154 \cdot T^{-2}$	monocryst., DSC, $\pm 2.5\%$, $T = 400 \dots 700$ K		89G
--	---	---	--	-----

density

d	5.81 g/cm ³	$T = 300$ K		69A
-----	------------------------	-------------	--	-----

melting temperature

T_m	1264(10)°C	assessed		96S
-------	------------	----------	--	-----

Transport properties

Electrical transport in CdSe is governed by electrons in the Γ_7 -conduction band and by holes in the Γ_9 -valence band. CdSe is mainly n-type conducting; this is due to compensating effects during the preparation of the samples and μ_n being about one order of magnitudes larger than μ_p . p-type conductivity is observed, however, in a few special cases [65I, 74B]. The carrier concentration depends on impurity or defect content and on temperature. Furthermore the value can be changed markedly by irradiation (photoconductivity).

intrinsic conductivity

Intrinsic conductivity (σ_i) in CdSe has been claimed to be observed in the temperature range 800...1500 K [60D, 68H]. Because of the possibility of thermal generation of lattice defects at such high temperatures the value should be used with care. There is a good coincidence, however, between band gap data determined by electrical and optical measurements.

nearly intrinsic conductivity

σ_i	$1 \cdot 10^{-3} (\Omega\text{cm})^{-1}$	$T = 800$ K		68H
	$1 (\Omega\text{cm})^{-1}$	$T = 1300$ K		

Using the mobilities given in [60D] or [70R] it follows by extrapolation for the

nearly intrinsic carrier concentration

$n \approx p$	$6 \cdot 10^{13} \text{ cm}^{-3}$	$T = 800$ K		
	$6 \cdot 10^{16} \text{ cm}^{-3}$	$T = 1300$ K		

photoconductivity

Photoconductivity in CdSe can be produced by all kinds of electromagnetic radiation (energy higher than the band gap) and also by high energetic particles (electrons, α -particles, etc). See also Fig. 3.18.3.

thermal conductivity

κ_L	0.09 Wcm ⁻¹ K ⁻¹	$T = 300$ K (lattice contribution)	70J
------------	--	------------------------------------	-----

electron mobility

μ_n	660 cm ² /Vs	$T = 300$ K	poly- and single-crystalline material	88R
	5000 cm ² /Vs	$T = 80$ K	dc Hall effect	67D1
	200 cm ² /Vs	$T = 800$ K		

Dependence on temperature: Fig. 3.18.4.

electron drift mobility

$\mu_{dr,n}$	720 cm ² /Vs	$T = 300$ K	time of flight measurement	72C
--------------	-------------------------	-------------	----------------------------	-----

hole Hall mobility

$\mu_{H,p}$	40 cm ² /Vs	$T = 300$ K	cubic CdSe/(100)GaAs, N-doped epitaxial films, free-hole concentration $1 \cdot 10^{17}$ cm ⁻³	94O
-------------	------------------------	-------------	---	-----

Seebeck coefficient

S	0.2 meV/K	$T = 300$ K		60D
	0.2 meV/K	$T = 300$ K	for $n = 10^{19}$ cm ⁻³	63D
	0.9 meV/K	$T = 300$ K	for $n = 10^{15}$ cm ⁻³	63D

Dependence on temperature: Fig. 3.18.5.

piezoelectric strain coefficients

d_{31}	- 3.92·10 ⁻¹² C/N	$T = 298$ K	from ultrasound resonance	63B
d_{33}	+ 7.84·10 ⁻¹² C/N	$T = 298$ K		63B
d_{15}	- 10.51·10 ⁻¹² C/N	$T = 298$ K		63B

piezoelectric stress coefficients

e_{31}	- 0.160 C/m ²	$T = 298$ K	from ultrasound resonance	63B
e_{33}	+ 0.347 C/m ²			
e_{15}	- 0.138 C/m ²			

Optical properties

refractive index and birefringence

Δn (= $n_{ c} - n_{\perp c}$)				
$n_{\perp c}$	$n_{ c}$	λ [μm],	T [K]	
2.608	2.626	0.85	293	prism
2.484	2.504	1.50		
	Δn [10 ⁻²]			
2.486	2.053	2	293	interference
2.445	2.114	6		
2.410	2.060	14		
2.376	1.351	20		
2.291	-	24		

Fig. 3.18.6 shows the complex refractive index for both hexagonal and cubic CdSe.

absorption coefficient

Fig. 3.18.7 shows the absorption coefficient, Fig. 3.18.8 the normal-incidence reflectivity, for both hexagonal and cubic CdSe.

dielectric constants

$\varepsilon^{\perp}(0)$	9.29	$T = 300 \text{ K}$	IR spectroscopy	66G
	9.15	$T = 100 \text{ K}$		
$\varepsilon^{\parallel}(0)$	10.16	$T = 300 \text{ K}$		
	9.29	$T = 100 \text{ K}$		
$\varepsilon^{\parallel}(\infty)$	6.30	$T = 300 \text{ K}$		
	6.30	$T = 100 \text{ K}$		
$\varepsilon^{\perp}(\infty)$	6.20	$T = 300 \text{ K}$		
	6.20	$T = 100 \text{ K}$		

Figs. 3.18.9 and 10 show the $\varepsilon_1(\omega)$ and $\varepsilon_2(\omega)$ spectra for hexagonal and cubic CdSe at 300 K, respectively.

References to 3.18

- 60D Devlin, S. S., Jost, J. M., Shiozawa, L. R.: Wadd Technical Report 60-11, 1960.
- 62P Pedrotti, F. L., Reynolds, D. C.: Phys. Rev. 127 (1962) 1584.
- 62W Wheeler, R. G., Dimmock, J. O.: Phys. Rev. 125 (1962) 1805.
- 63B Berlincourt, D., Jaffe, H., Shiozawa, L. R.: Phys. Rev. 129 (1963) 1009.
- 63D Dolega, U.: Z. Naturforsch. 15a (1963) 809.
- 65I Itakura, M., Toyoda, M.: Jpn. J. Appl. Phys. 4 (1965) 560.
- 66G Geick, R., Perry, C. H.: J. Appl. Phys. 37 (1966) 1994.
- 67D1 Devlin, S. S.: Physics and Chemistry of II-VI Compounds, M. Aven and J. S. Prener, eds., North Holland, Amsterdam, 1967, 549.
- 67D2 Dimmock, J. O.: Proc. 7th Int. Conf. II-VI Semiconducting Compounds, Providence, R. I., USA, W. A. Benjamin Inc., New York, 1967, 277.
- 68H Höschl, P., Kubalkowa, S.: Czech. J. Phys. 18 (1968) 13 897.
- 69A Abrikosov, N. K., Bankina, V. F., Poretskaya, L. V., Shelimova, L. E., Skudnova, E. V.: Semiconducting II-VI, IV-VI and V-VI Compounds, Plenum, New York, 1969, 27.
- 69L Lisitsa, M. P., Gudymenko, L. F., Malinko, V. N., Terekhova, S. F.: Phys. Status Solidi 31 (1969) 389.
- 69S Stukel, D. J., Euwema, R. N., Collins, T. C.: Phys. Rev. 179 (1969) 740.
- 70B Beserman, R., Balkanski, M.: Phys. Rev. B 1 (1970) 608.
- 70H Henry, C. H., Nassau, K., Shiever, J. W.: Phys. Rev. B 4 (1970) 2453.
- 70J Jacobs, P. L., Trey, R. K.: Proc. 9th Conf. on Thermal Conductivity, ed. H. R. Shanks, U. S. AEC, Oak Ridge, Tenn., 1970.
- 70L Lipskis, K., Sakalas, A., Viscakas, J.: Phys. Status Solidi (a) 2 (1970) 225.
- 70R Rode, D. L.: Phys. Rev. B 2 (1970) 4036.
- 72C Canali, C., Nava, F., Ottaviani, G., Paorici, C.: Sol. State Commun. 11 (1972) 105.
- 74B Baubinas, R., Januskevicius, Z., Sakalas, A., Viscakas, J.: Solid State Commun. 15 (1974) 1731.
- 76R Reeber, R. R.: J. Mat. Sci. 11 (1976) 590.
- 77B Beserman, R.: Solid State Commun. 23 (1977) 323.
- 78M Miura, N., Kido, G., Chikazumi, S.: Proc. 14th Int. Conf. Physics of Semiconductors, Edinburgh 1978, B. L. H. Wilson (ed.), p. 1109.
- 78S Sobolev, V. V., Donetskina, V. I., Zagainov, E. F.: Fiz. Tekh. Poluprovodn. 12 (1978) 1089; Sov. Phys. Semicond. 12 (1978) 646.
- 79V Voigt, J., Spiegelberg, F., Senoner, M.: Phys. Status Solidi (b) 91 (1979) 189.
- 84K Kochereshko, V. P., Röseler, J., Uraltsev, I. N., Henneberger, K.: Phys. Status Solidi (b) 124 (1984) 213.
- 85G Goble, R. Y., Scott, S. D.: Can. J. Mineral. 23 (1985) 273.
- 88R Roth, M., Burger, A.: Appl. Physics Lett. 52 (1988) 1234.
- 89B Barin, I.: Thermochemical Data of Pure Substances, VCH, Weinheim, 1989.
- 89G Glazov, V. W., Pashinkin, A. S., Malkova, A. S.: Russ. J. Phys. Chem. 63 (1989) 19.
- 89S Samarth, N., Luo, H., Furdyna, J. K., Qadri, S. B., Lee, Y. R., Ramdas, A. K., Otsuka, N.: Appl. Phys. Lett. 54 (1989) 2680.
- 93B Bonello, B., Fernandez, B.: J. Phys. Chem. Solids 54(1993) 209
- 93D Dal Corso, A., Baroni, S., Resta, R., deGironcoli, S.: Phys. Rev. B 47 (1993) 3588.
- 94K Kim, Y. D., Klein, M. V., Ren, S. F., Chang, Y. C., Luo, H., Samarth, N., Furdyna, J. K. Phys. Rev. B 49 (1994) 7262.
- 94O Ohtsuka, T., Kawamata, J., Ziqiang Zhu, Yao, T.: Appl. Phys. Lett. 65 (1994) 466.
- 95N Ninomiya, S., Adachi, S.: J. Appl. Phys. 78 (1995) 4681.
- 95W1 Wang, L.-W., Zunger, A.: Phys. Rev. B 51 (1995) 17398.
- 95W2 Willatzen, M., Cardona, M., Christensen, N.E.: Phys. Rev. B 51 (1995) 17992.
- 96C Xiaojie Chen, Xinlei Hua, Jinsong Hu, Langlois, J.-M., Goddard, W.A., III: Phys. Rev. B 53 (1996) 1377.
- 96M McMahon, M. I., Nelmes, R. J.: Phys. Status Solidi (b) 198 (1996) 389.
- 96S Sharma, R. C., Chang, Y. A.: J. Phase Equilibria 17 (1996) 140.
- 96V Vogel, D., Krüger, P., Pollmann, J.: Phys. Rev. B 54 (1996) 5495.
- 97G Gebhardt, W., Schötz, G., Bhargava, R. (ed.): Properties Wide Bandgap II-VI Semiconductors, EMIS Datareviews Series No. 17, INSPEC/IEE (London, U.K.) 1997, pp. 113.

Figures to 3.18

Fig. 3.0.1

The zincblende lattice.

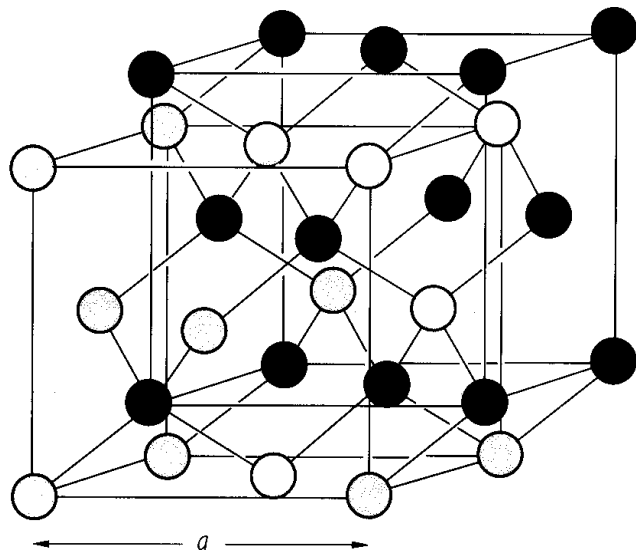


Fig. 3.0.2

The wurtzite lattice.

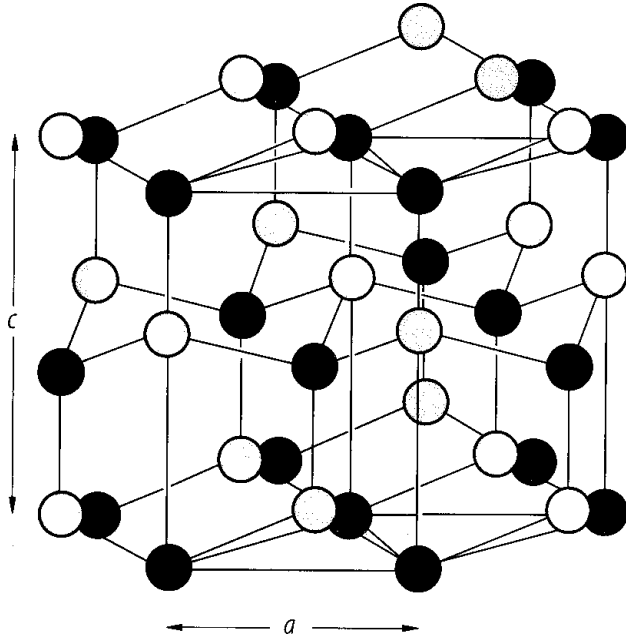


Fig. 3.0.4

The Brillouin zone for the zincblende and the rocksalt lattices.

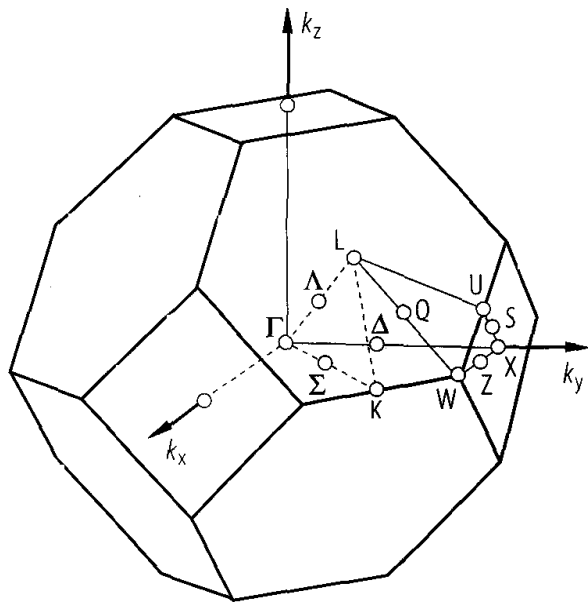


Fig. 3.0.5

The Brillouin zone of the wurtzite lattice.

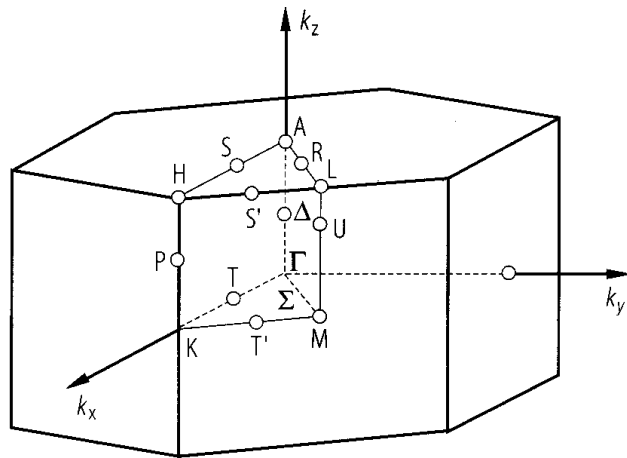


Fig. 3.0.22a

CdSe, hex. Band structure for wurtzite symmetry calculated by use of so-called self-interaction-corrected pseudopotentials in local-density approximation [96V]. Dashed lines: measured gap energies and d bands from various references.

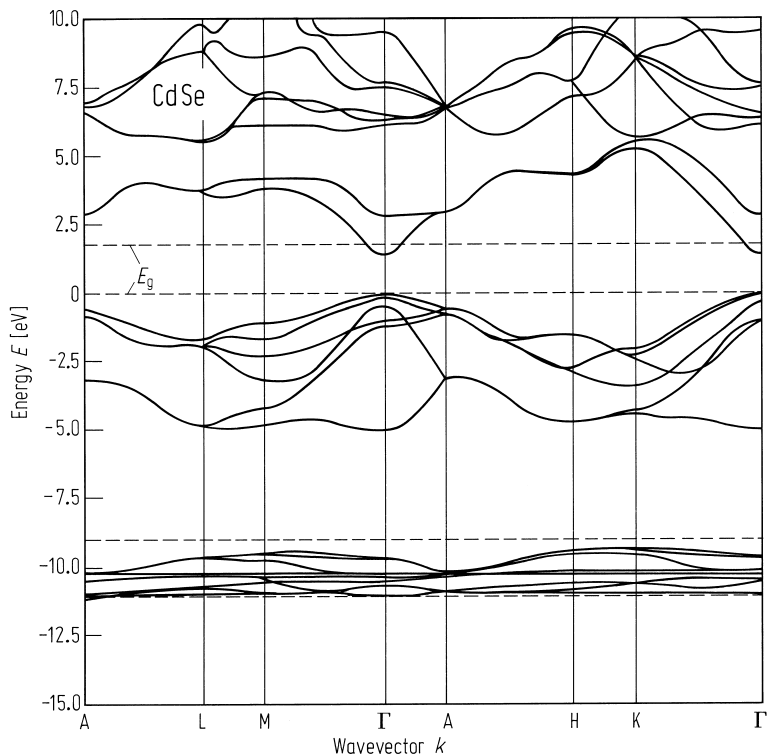


Fig. 3.0.22b

CdSe. Energy bands of cubic CdSe, calculated by the SC-OPW method [69S].

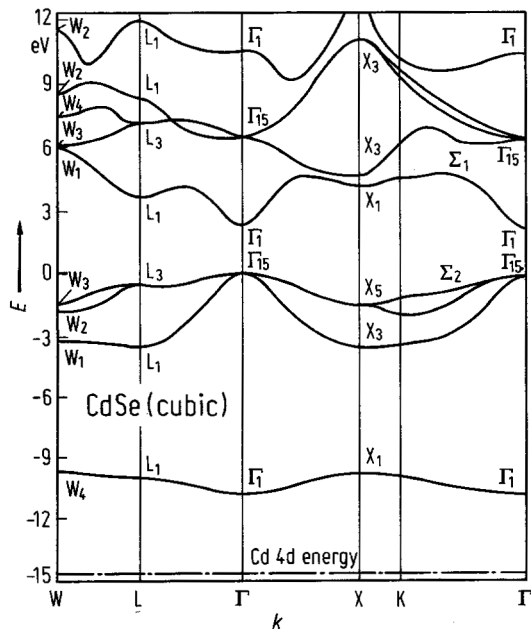


Fig. 3.18.1

CdSe. Lattice constant vs. temperature for hexagonal CdSe (thermal expansion) [60D].

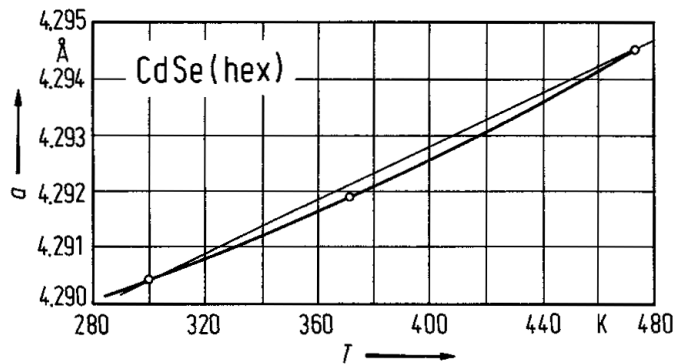


Fig. 3.18.2

CdSe. Phonon dispersion; theoretical curves from an ab-initio calculation [93D].

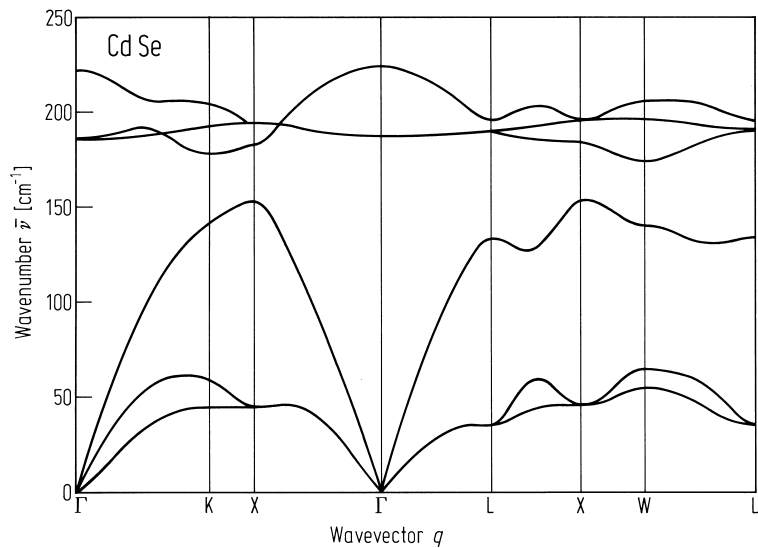


Fig. 3.18.3

CdSe. Hall mobility μ_H , carrier concentration n and photoconductivity σ^{ph} under constant illumination ($\lambda = 0.75 \mu\text{m}$) vs. temperature [70L].

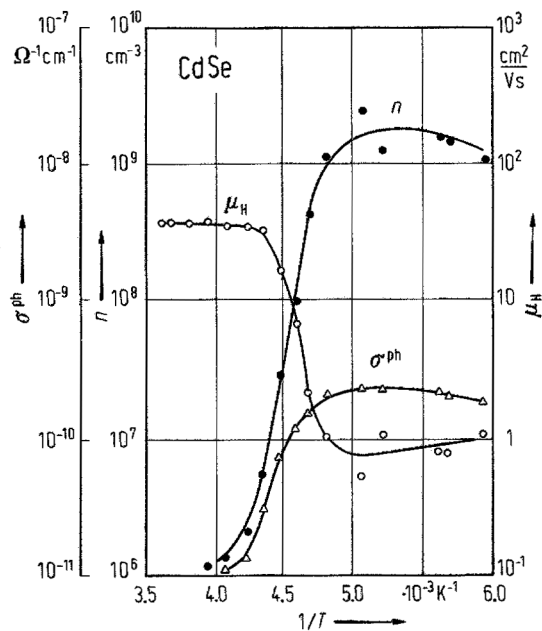


Fig. 3.18.4

CdSe. Electron Hall mobility vs. temperature for samples of different authors. Solid lines: Theoretical curve [70R].

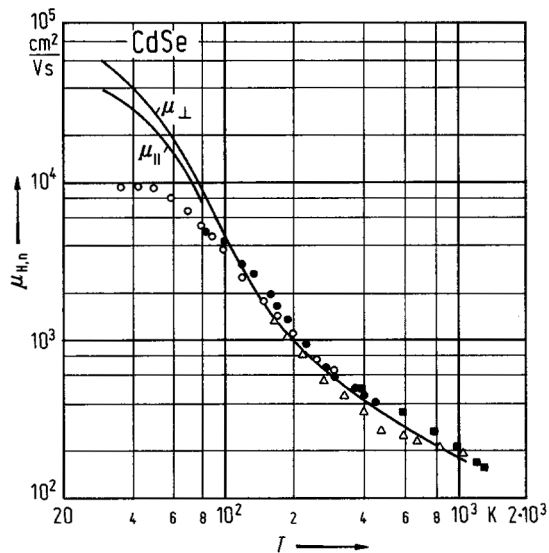


Fig. 3.18.5

CdSe. Thermoelectric power vs. temperature for a Ga doped sample [60D].

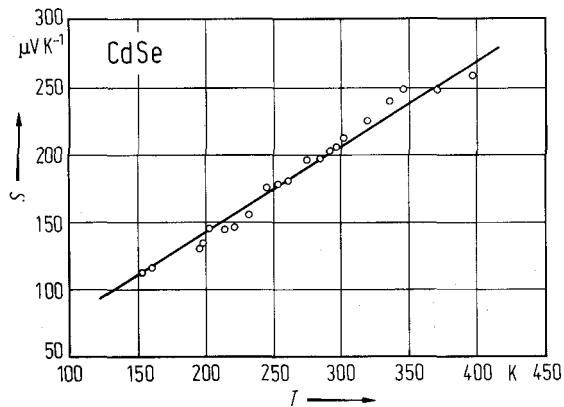


Fig. 3.18.6

CdSe, hex, cub. Numerically calculated complex refractive index, $n^*(E) = n(E) + ik(E)$, for both hexagonal and cubic material (solid lines). The solid circles represent the experimental data [95N].

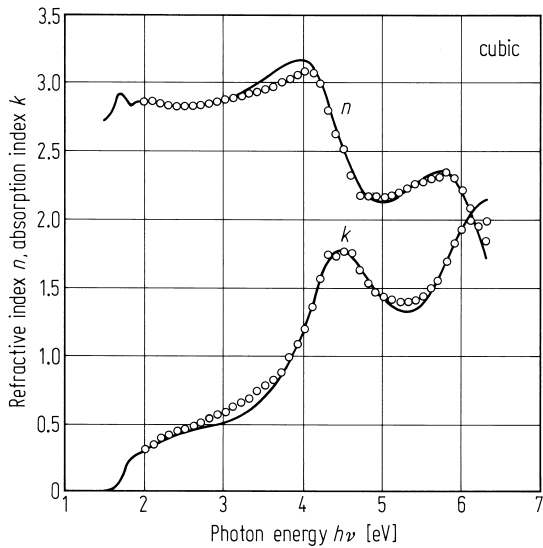
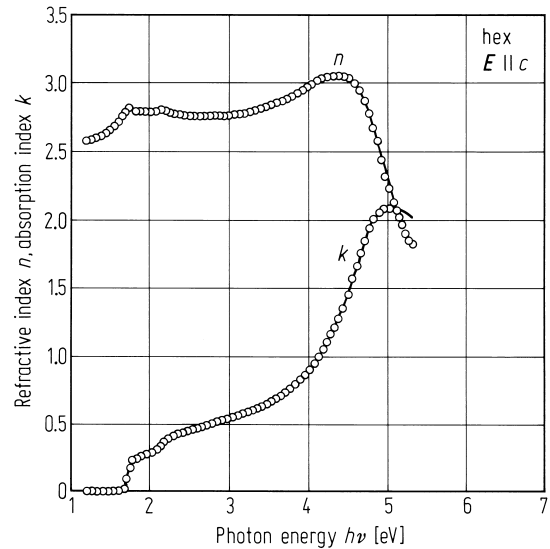
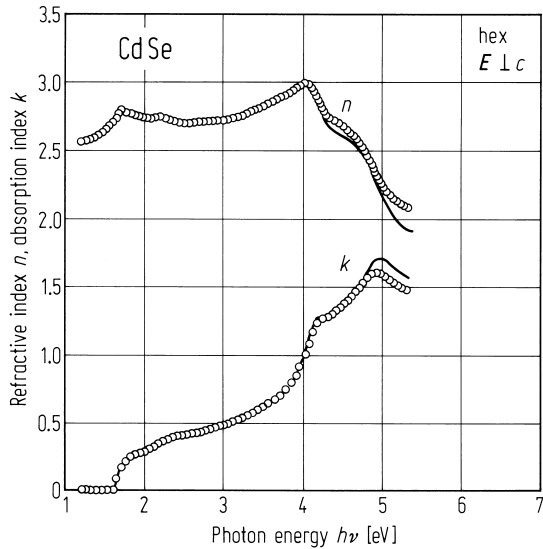


Fig. 3.18.7

CdSe, hex, cub. Numerically calculated absorption coefficient, α , for both hexagonal and cubic material (solid lines). The solid circles represent the experimental data [95N].

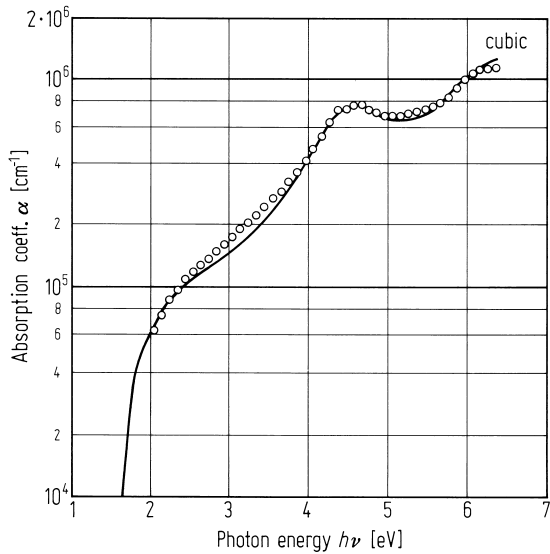
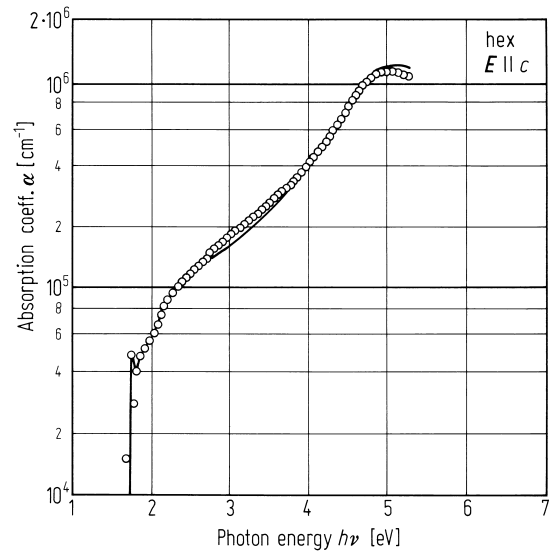
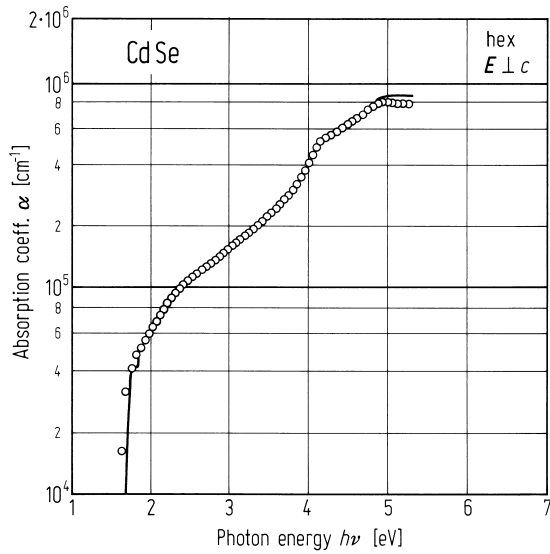


Fig. 3.18.8

CdSe, hex, cub. Numerically calculated reflection coefficient, R , for both hexagonal and cubic material (solid lines). The solid circles represent the experimental data [95N].

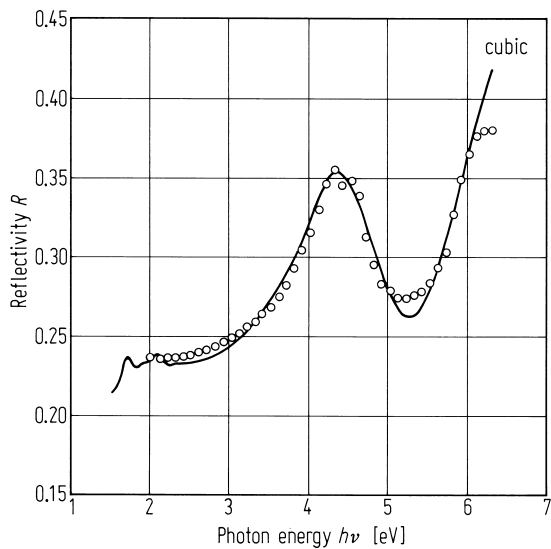
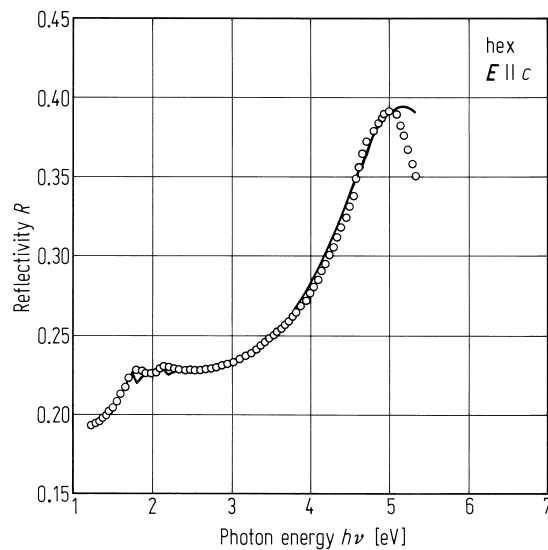
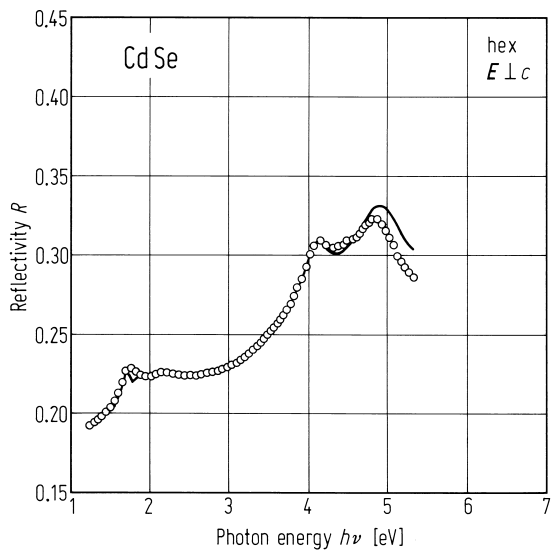


Fig. 3.18.9

CdSe, hex, cub. $\varepsilon_1(\omega)$ spectra for hexagonal and cubic CdSe at $T = 300$ K measured by spectroscopic ellipsometry (circles). The cubic data are taken from the literature [94K]. The solid curves show the best-fitted results [95N].

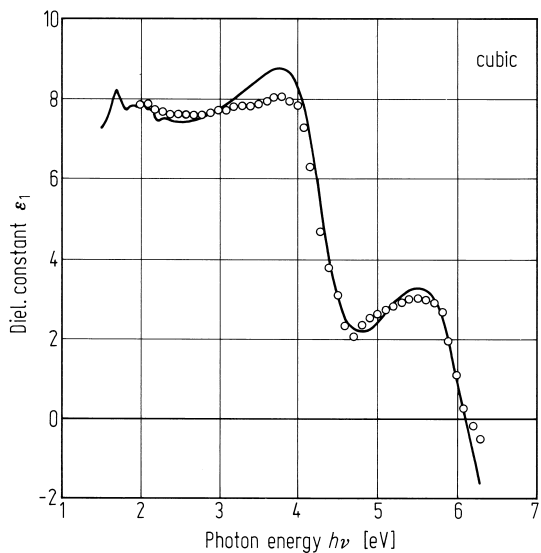
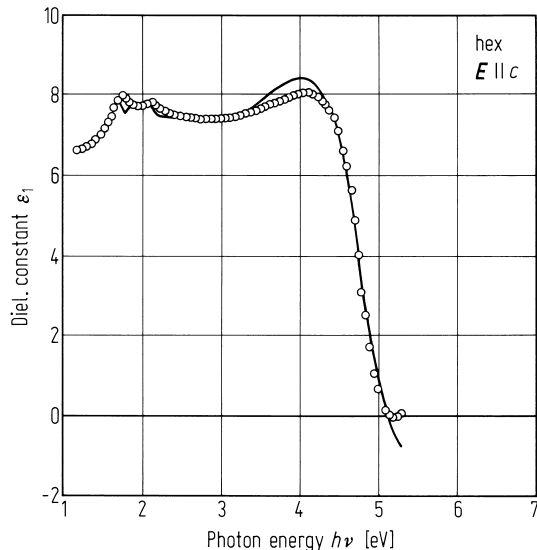
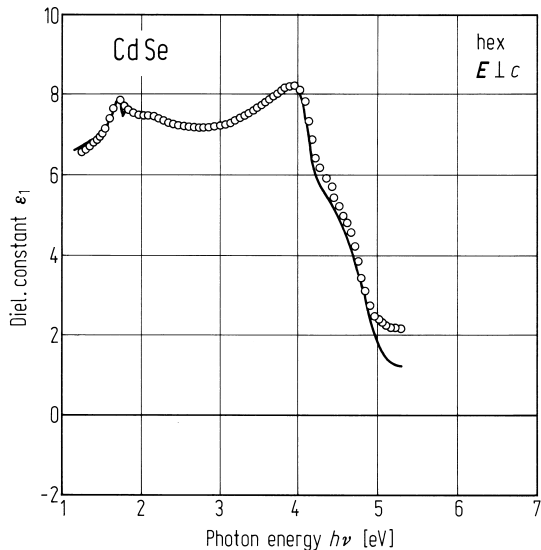
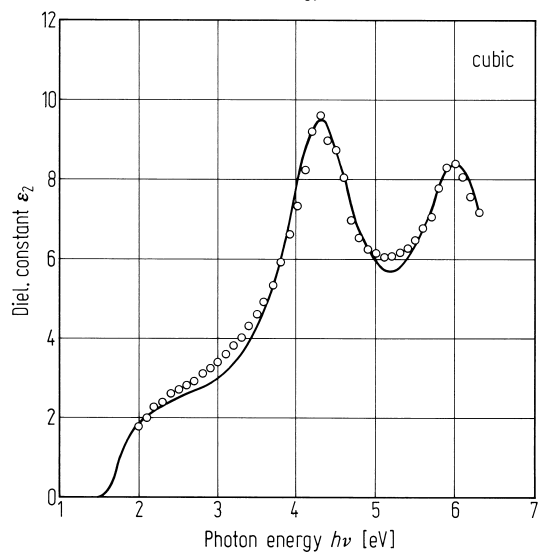
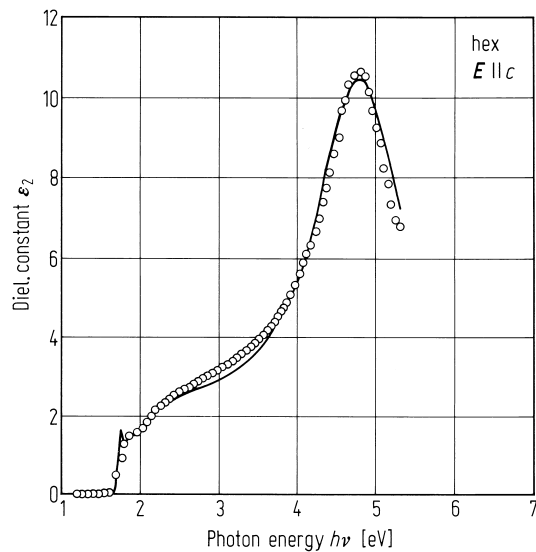
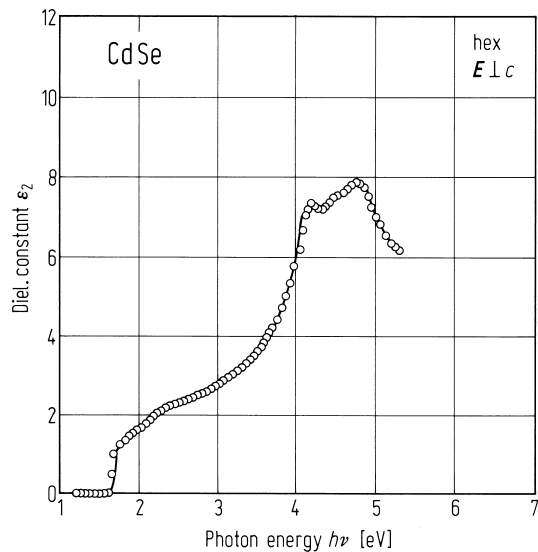


Fig. 3.18.10

CdSe, hex, cub. $\epsilon_2(\omega)$ spectra for hexagonal and cubic CdSe at 300 K measured by spectroscopic ellipsometry (solid circles). The cubic data are taken from the literature [94K]. The solid curves show the best-fitted results [95N]



3.19 Cadmium telluride (CdTe)

Crystal structure

Under normal conditions, CdTe crystallizes in the zincblende structure (space group $F\bar{4}3m - T_d^2$, Fig. 3.0.1).

Electronic properties

band structure : Fig. 3.0.23, Brillouin zone: Fig. 3.0.4.

Cadmium telluride is a direct gap semiconductor with the smallest energy gap at the center of the Brillouin zone (Γ). The topmost valence band is split due to spin-orbit coupling into a fourfold (Γ_8) and a twofold (Γ_7) state.

energies of symmetry points of the band structure (relative to the top of the valence band $E(\Gamma_{8v})$)

$E(\Gamma_{6v})$	– 11.07 eV		pseudopotential calculation	76C
$E(\Gamma_{7v})$	– 0.89 eV			
$E(\Gamma_{6c})$	1.59 eV			
$E(\Gamma_{7c})$	5.36 eV			
$E(\Gamma_{8c})$	5.61 eV			
$E(X_{6v})$	– 9.12 eV			
$E(X_{6v})$	– 5.05 eV			
$E(X_{6v})$	– 1.98 eV			
$E(X_{7v})$	– 1.60 eV			
$E(X_{6c})$	3.48 eV			
$E(X_{7c})$	3.95 eV			
$E(L_{6v})$	– 9.64 eV			
$E(L_{6v})$	– 4.73 eV			
$E(L_{6v})$	– 1.18 eV			
$E(L_{4,5v})$	– 0.65 eV			
$E(L_{6c})$	2.82 eV			
$E(L_{6c})$	6.18 eV			
$E(L_{4,5c})$	6.35 eV			

energy gap

$E_{g,dir}(\Gamma_{8v}-\Gamma_{6c})$	1.475 eV	RT	photoelectrochemical experiment	82L
$dE_{g,dir}/dT$	$-3 \cdot 10^{-4}$ eV/K	$T = 70 \dots 300$ K	piezoreflectance	73C

critical point energies

$E_g + \Delta_0(\Gamma_{7v}-\Gamma_{6c})$	2.4 eV	$T = 77, 300$ K	reflectance	63C
$E_1(\Lambda_{4,5v}-\Lambda_{6c})$	3.44 eV	$T = 77$ K		
$E_1 + \Delta_1(\Lambda_{6v}-\Lambda_{6c})$	4.01 eV	$T = 77$ K		
E'_0	5.20 eV	$T = 300$ K		
E_2	5.49 eV	$T = 77$ K		

spin-orbit splitting energy

$\Delta_0(\Gamma_{7v}-\Gamma_{8v})$	0.95(2) eV	$T = 300$ K	photoemission	91N
-------------------------------------	------------	-------------	---------------	-----

effective masses, conduction band

m_n [110]	0.096(3) m_0	$T = 1.5$ K	cyclotron resonance	80R
m_n [100]	0.094(4) m_0	$T = 1.8$ K	cyclotron resonance	82D
m_n [111]	0.095(4) m_0			

effective mass, valence band

$m_{p,l}$ [110]	0.12(2) m_0	$T = 1.5$ K	cyclotron resonance	80R
$m_{p,h}$ [110]	0.81(5) m_0			

g-factors of electrons

$ g_c $	1.652		Spin-Flip-Raman	95O
---------	-------	--	-----------------	-----

exciton energies

$E_{gx}(\Gamma_5^L, 1S)$	1.596375(5) eV	$T = 10$ K	RBS	83S,
$E_{gx}(\Gamma_5^T, 1S)$	1.595725(5) eV			84M
$E_{gx}(\Gamma_3 + \Gamma_4, 1S)$	1.595650(25) eV			
$E_{gx}(2S)$	1.6035 eV			80N
$\Delta_{LT}(1S)$	0.00065(5) eV	$T = 10$ K	RBS	83S

exciton binding energy

$E_b(1S)$	10.5 meV	$T = 1.64$ K	magnetoabsorption using $E_b = 4(E(2S) - E(1S))/3$	80N
-----------	----------	--------------	---	-----

Lattice properties**lattice parameter**

a	6.46 Å		X-ray diffraction	63M
-----	--------	--	-------------------	-----

linear thermal expansion coefficient

α [$10^{-6}K^{-1}$]	$= 4.932 \cdot 10^{-6} + 1.165 \cdot 10^{-9}T + 1.428 \cdot 10^{-12}T^2$ T in °C, 20...420 K, see also Fig. 3.19.1.			69B
------------------------------	---	--	--	-----

phonon dispersion curves : Figs. 3.19.2, Brillouin zone: Fig. 3.0.4.

phonon frequencies

$\nu_{LO}(\Gamma)$	5.08 (10) THz	$T = 300$ K	inelastic neutron scattering	74R
$\nu_{TO}(\Gamma)$	4.20(10) THz			
$\nu_{LO}(X)$	4.44(6) THz			
$\nu_{TA}(X)$	1.05(3) THz			
$\nu_{LO}(L)$	4.33 (6) THz			
$\nu_{TO}(L)$	4.33(7) THz			
$\nu_{LA}(L)$	3.25(8) THz			
$\nu_{TA}(L)$	0.88(3) THz			

second order elastic moduli

c_{11}	53.8 GPa	$T = 298$ K		73G
	56.2 GPa	$T = 77$ K		
c_{12}	37.4 GPa	$T = 298$ K		73G
	39.4 GPa	$T = 77$ K		
c_{44}	20.18 GPa	$T = 298$ K		73G
	20.61 GPa	$T = 77$ K		

For temperature dependence see Figs. 3.19.3 ... 5.

bulk modulus

B	42(2)		X-ray diffraction	85S
-----	-------	--	-------------------	-----

Debye temperature

Θ_D	140(3) K	X-ray, single crystal	75Z
$\Theta_D(0)$	158 K	low temperature data of $\Theta_D(T)$: Fig. 3.19.6	80J

heat capacity

C_p	$23.90_2 + 0.0057_6 T$	$\text{J K}^{-1} \text{mol}^{-1}$	$T = 300 \dots 533 \text{ K}$, polycrystalline sample see Fig. 3.19.7	91G
-------	------------------------	-----------------------------------	---	-----

density

d	5.87 g cm^{-3}	$T = 4 \text{ K}$		80C1
-----	--------------------------	-------------------	--	------

melting temperature

T_m	1366.6(70) K	mean of experimental values		95J
-------	--------------	-----------------------------	--	-----

Transport properties

CdTe bulk crystals can be doped n- and p-type conductive. High resistive ($\rho > 10^9 \Omega\text{cm}$) crystals can be obtained under various growth and doping conditions.

electrical conductivity, for temperature dependence in n-type CdTe, see Fig. 3.19.8.

electron mobility

Maximum electron Hall mobility of $110000 \text{ cm}^2/\text{Vs}$ was observed near 32 K [73T]. The low temperature mobility is governed by impurity scattering, whereas at elevated temperatures the mobility is limited by polar optical scattering, Fig. 3.19.9

hole mobility

$\mu_{H,p}$	$1200 \text{ cm}^2/\text{Vs}$	$T = 170 \text{ K}$	Hall effect	59N
	$60 \text{ cm}^2/\text{s}$	$T = 300 \text{ K}$	Hall effect	60Y

thermal conductivity

κ	$71 \pm 2.5\% \text{ mW/cm K}$	$T = 298 \text{ K}$	single crystal	94A
	10 W/cm K	$T = 8 \text{ K}$	theoretical maximum for a pure crystal, temperature dependence: Fig. 3.19.10	80J

Optical properties

The real and imaginary part of the dielectric function in the optical phonon region is shown in Fig. 3.19.11. Calculated optical constants (R , ϵ_1 , and ϵ_2) in the visible and near ultraviolet region together with an experimental reflectivity spectrum are presented in Fig. 3.19.12.

refractive index

n	2.70	$T = 300 \text{ K}$, $\lambda = 2.5 \mu\text{m}$	prism refraction	63M
-----	------	--	------------------	-----

dielectric constants

$\epsilon(\infty)$	7.1(1)	$T = 300 \text{ K}$		74R
$\epsilon(0)$	10.4	$T = 300 \text{ K}$		72B

References to 3.19

- 59N de Nobel, D.: Philips Res. Rep. 14 (1959) 361, 430.
60Y Yamada, S.: J. Phys. Soc. Jpn. 15 (1960) 1940.
63C Cardona, M., Greenaway, D. L.: Phys. Rev. 131 (1963) 98.
63M Marple, D. T. F.: Phys. Rev. 129 (1963) 2466.
63S Segall, B., Lorenz, M. R., Halsted, R. E.: Phys. Rev. 129 (1963) 2471.
69B Browder, J. S., Ballard, S. S.: Appl. Opt. 8 (1969) 793.
72B Baars, J., Sorger, F.: Solid State Commun. 10 (1972) 875.
73C Camassel, J., Auvergne, D., Mathieu, H., Triboulet, R., Varfainy, M.: Solid State Commun. 13 (1973) 63.
73G Greenough, R. D., Palmer, S. B.: J. Phys. D6 (1973) 587.
74R Row, J. M., Nicklow, R. M., Price, D. L., Zanio, K.: Phys. Rev. B 10 (1974) 671.
75B Birch, J. A.: J. Phys. CS (1975) 2043.
73T Triboulet, R., Marfaing, Y.: J. Electrochem. Soc. 120 (1973) 1260.
75Z Zubik, K., Valvova, V.: Czech. J. Phys. B 25 (1975) 1149.
76C Chelikowsky, J. R., Cohen, M. L.: Phys. Rev. B 14 (1976) 556.
78B Birch, J. R., Murray, D. K.: Infrared Physics 18 (1978) 283.
80C1 Collins, J. G., White, G. K., Birch, J. A., Smith, T. F.: J. Phys. C 13 (1980) 1649.
80C2 Czyzyk, M. T., Podgorny, M.: Phys. Status Solidi (b) 98 (1980) 507.
80J Jongler, J., Hetroit, C., Vuillermoz, P. L., Triboulet, J.: J. Appl. Phys. 51 (1980) 3171.
80K Kushwaha, M. S., Kushwaha, S. S.: Can. J. Phys. 58 (1980) 351.
80N Nawrocki, M., Twardowski, A.: Phys. Status Solidi (b) 97 (1980) K61.
80R Romestain, R., Weisbuch, C.: Phys. Rev. Lett. 45 (1980) 2067.
81M Mockizuki, K.: Jpn. J. Appl. Phys. 20 (1981) 671.
82D Dang, L. S., Neu, G., Romestain, R.: Solid State Commun. 44 (1982) 1187.
82L Lemasson, P.: Solid State Commun. 43 (1982) 627.
83S Sooryakumar, R., Cardona, M., Merle, J. C.: Solid State Commun. 48 (1983) 581.
84M Merle, J. C., Sooryakumar, R., Cardona, M.: Phys. Rev. B 30 (1984) 3261.
85S Strössner, K., Ves, S., Dieterich, W., Gebhardt, W., Cardona, M.: Solid State Commun. 56 (1985) 563.
86K Kagayama, H.-M., Soma, T.: Phys. Status Solidi (b) 134 (1986) K 101.
91G Gambino, M., Vassiliev, V., Bros, J. P.: J. Alloys Comp. 176 (1991) 13.
91N Niles, D. W., Hochst, H.: Phys. Rev. B 43 (1991) 1492.
93B Bagot, D., Granger, R., Rolland, S.: Phys. Status Solidi (b) 177 (1993) 295.
94A Alvarado, J. J., Zelaya-Angel, O., Sanchez-Sinencio, F., Torres-Delgado, G., Vargas, H., Gonzalez-Hernandez, J.: J. Appl. Phys. 76 (1994) 7217.
95J Jianrong, Y., Silk, N. J., Watson, A., Bryant, A. W., Argent, B. B.: Calphad: Comput. Coupling Phase Diagrams Thermochem. 19 (1995) 399.
95O Oestreich, M., Rühle, W. W.: Phys. Rev. Lett. 74 (1995) 2315.

Figures to 3.19

Fig. 3.0.1

The zincblende lattice.

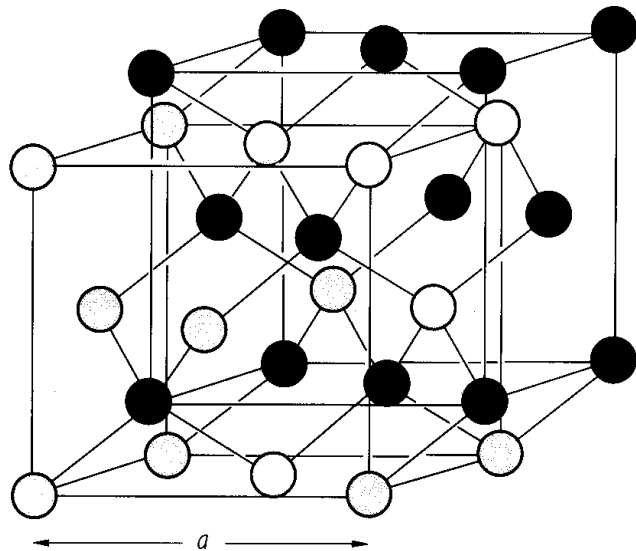


Fig. 3.0.4

The Brillouin zone for the zincblende and the rocksalt lattices.

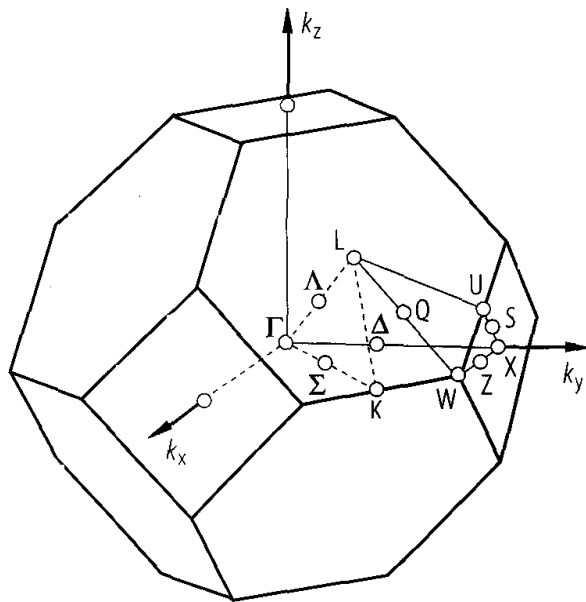


Fig. 3.0.23

CdTe. Band structure (a) and calculated electron density of states (solid curve) (in comparison with UPS experiments, dashed curve) (b) from a nonlocal pseudopotential calculation [76C].

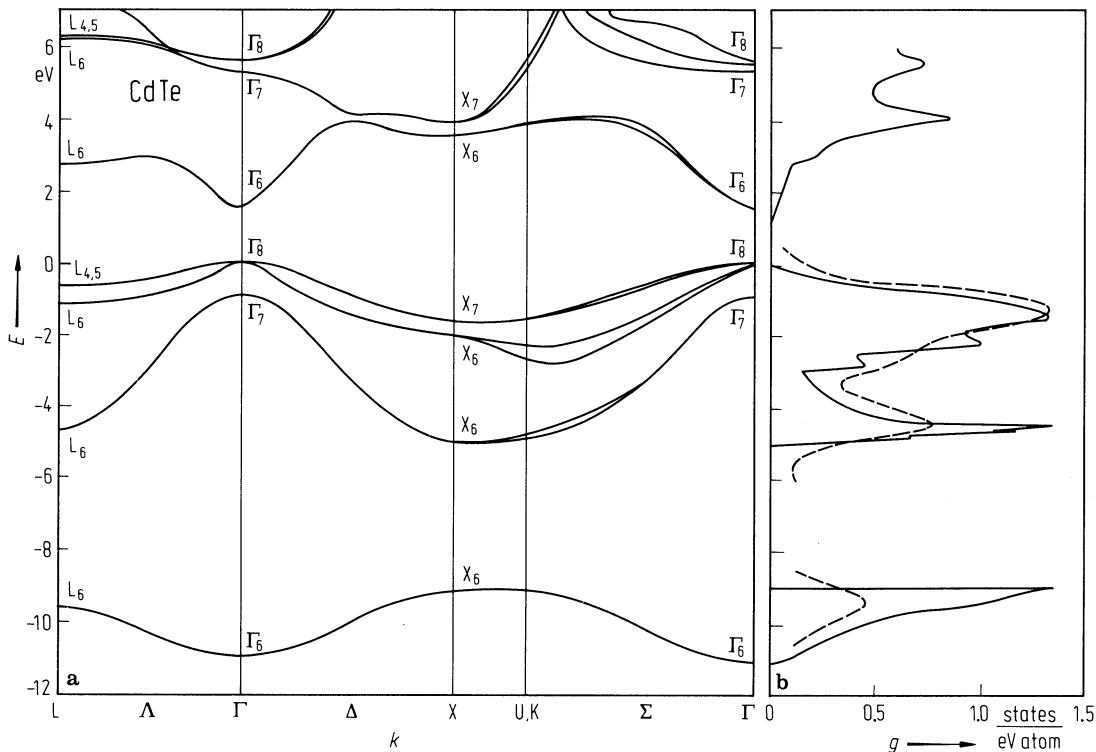


Fig. 3.19.1

CdTe. Linear thermal expansion coefficient α vs. T , solid line calculated from first principles, symbols experimental points [93B].

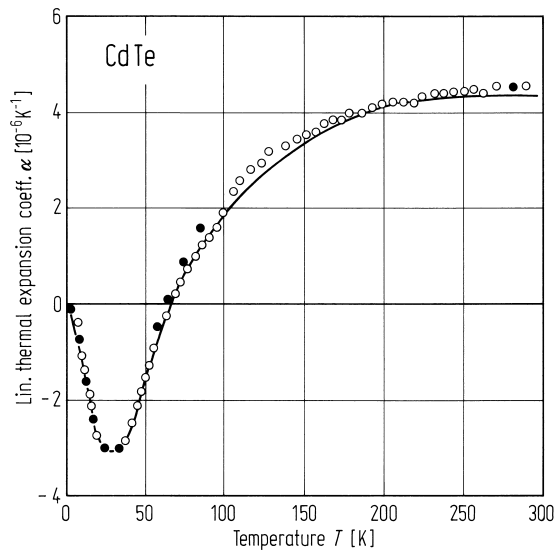


Fig. 3.19.2

CdTe. Phonon dispersion and one-phonon density of states calculated from an 8-parameter bond-bending force model in comparison with neutron scattering data [80K].

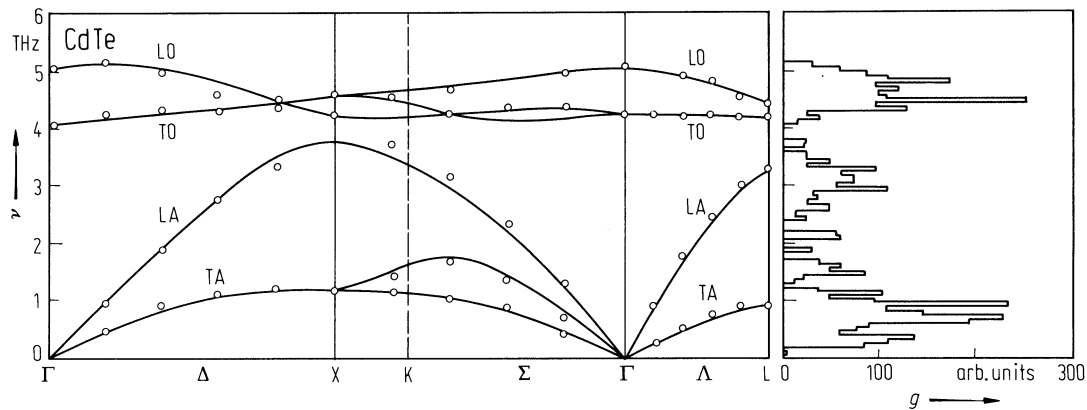


Fig. 3.19.3

CdTe. The elastic constant c_{44} as a function of temperature [73G]. Inset shows detail with T decreasing.

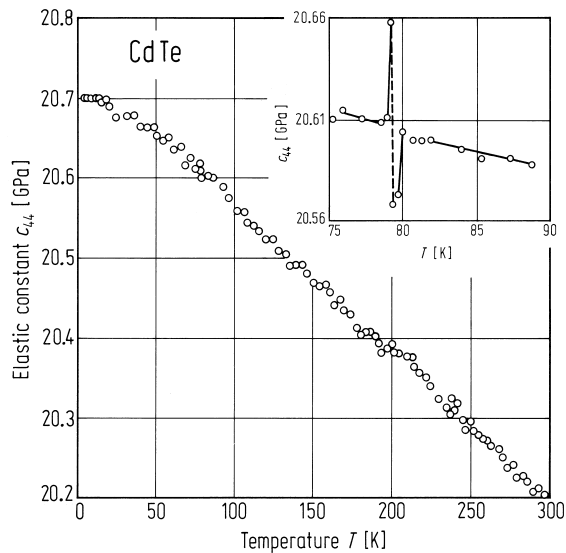


Fig. 3.19.4

CdTe. The elastic constant $(c_{11} + c_{12} + 2c_{44})/2$ as a function of temperature [73G].

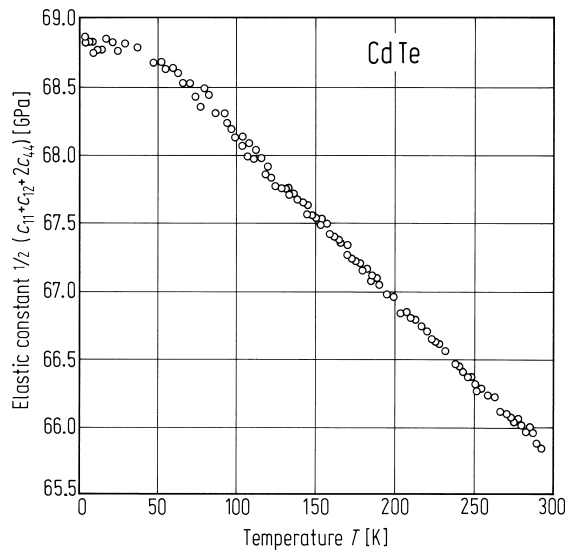


Fig. 3.19.5

CdTe. The elastic constant $c' = (c_{11} - c_{12})/2$ as a function of temperature [73G].

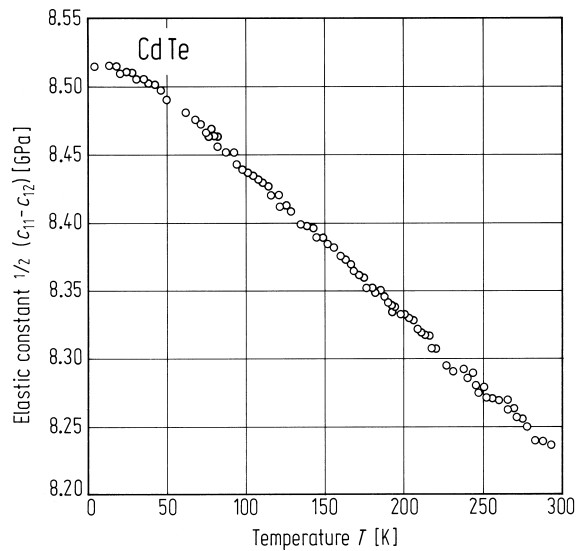


Fig. 3.19.6

CdTe. Debye temperature vs. temperature (full circles: calculated from elastic moduli, open circles: from experimental data of heat capacity) [75B].

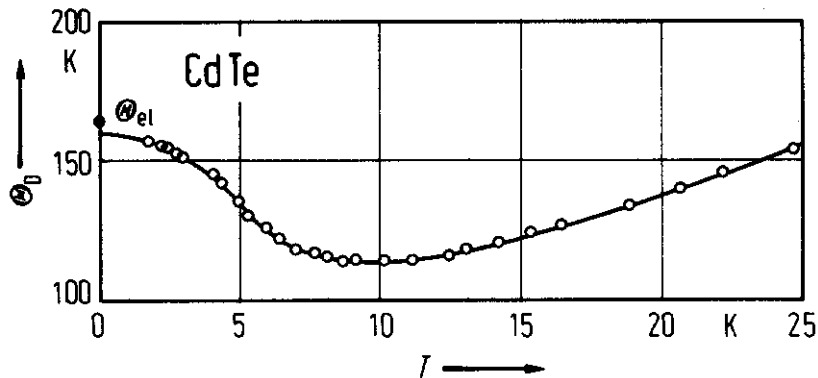


Fig. 3.19.7

CdTe. Heat capacity at constant volume, C_v , solid line and dashed line calculated from first principles and experimental points [86K].

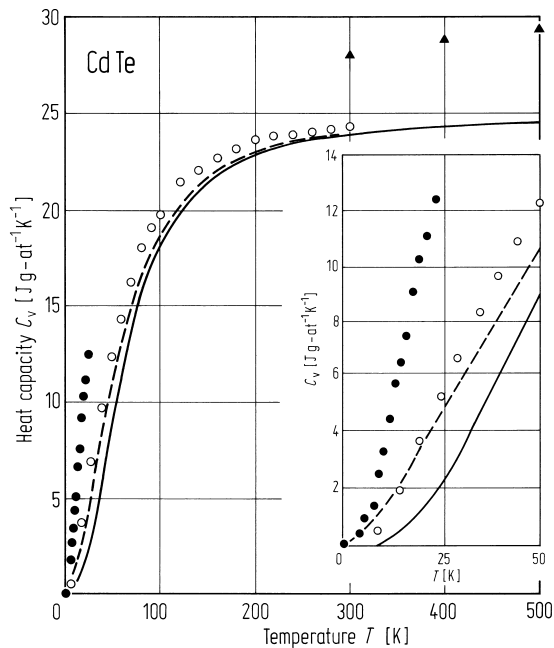


Fig. 3.19.8

CdTe. Electrical conductivity vs. inverse temperature for different n-type samples 1...3 [81M].

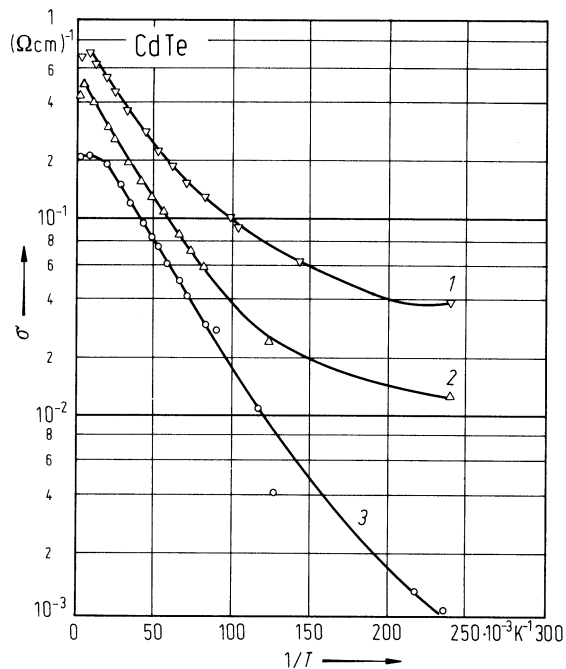


Fig. 3.19.9

CdTe. Experimental electron Hall mobility vs. temperature compared with theory (solid line) for polar optical scattering. Carrier concentration of the samples $n \approx 10^{15} \text{ cm}^{-3}$ at 300 K [63S].

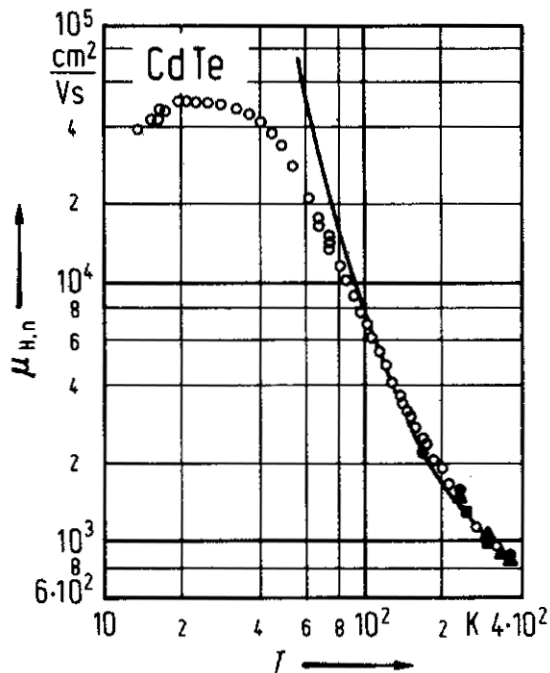


Fig. 3.19.10

CdTe. Thermal conductivity of different specimens vs. temperature. The results of two specimens 1 and 3 have been plotted reduced by a factor of 10. Point defect concentration of the samples 1: 3.42; 2: 3.99; 3: 3.42; 4: $2.66 \cdot 10^{18} \text{ cm}^{-3}$ [80J].

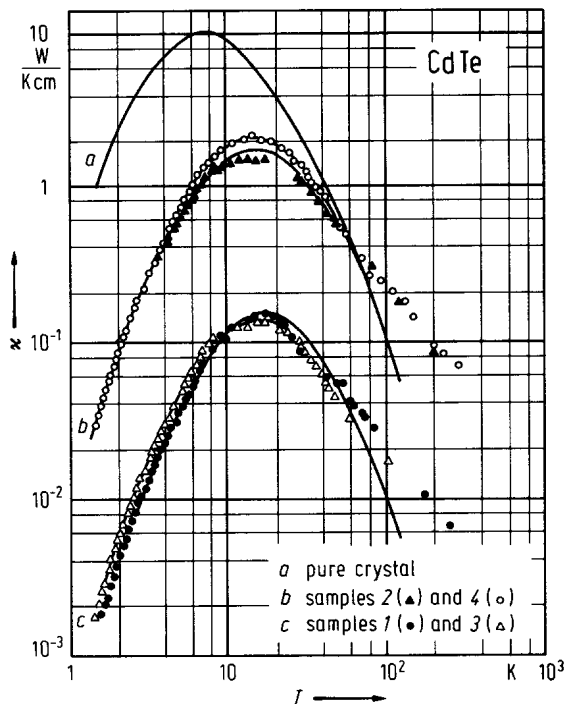


Fig. 3.19.11

CdTe. Real and imaginary part of permittivity vs. wavenumber at 290 K. Fit of experimental data (dots) with classical damped harmonic oscillator model (solid line). In the ϵ_1 -plot the dashed curve was calculated from the best fit to the ϵ_2 -data and vice versa [78B].

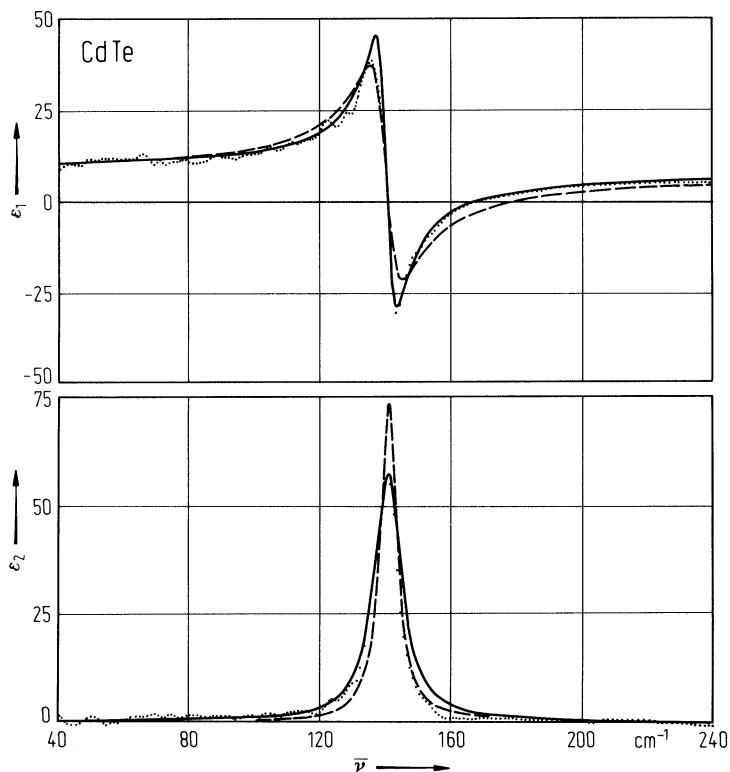
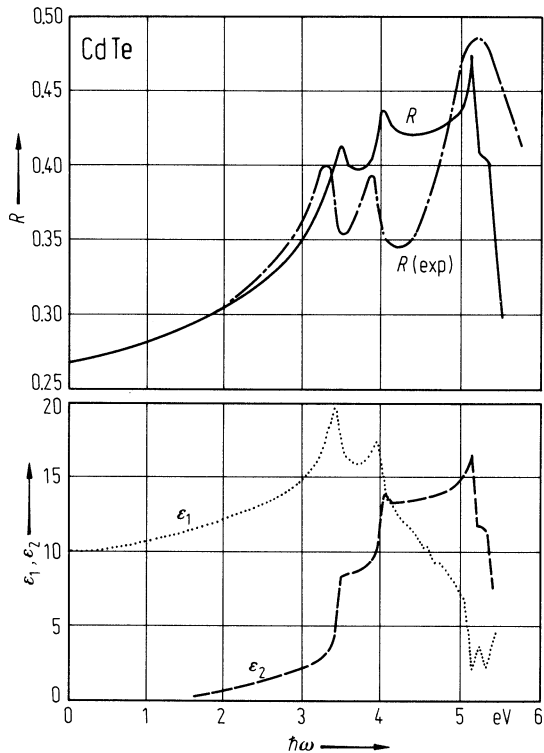


Fig. 3.19.12

CdTe. Optical spectra calculated from the band structure of [80C2]; dotted line: ϵ_1 , dashed line: ϵ_2 , solid line: R . For comparison the experimental reflectivity (dash-dotted line) is given.



3.20 Mercury oxide (HgO)

Physical properties

Only a few results are available:

From photoconductivity measurements an **energy gap** E_g of 2.19 eV [71S] and 2.80 eV [88H] was obtained.

Under atmospheric pressure mercury oxide has cinnabar structure or orthorhombic structure (D_{2h}^{16}).

lattice parameter

a	3.577 Å	$p = 0$	cinnabar phase, X-ray diffraction	58A
b	8.681 Å			
c	2.427 Å			
u	0.745			

density

d	11.080 g/cm ³	54A
-----	--------------------------	-----

The **refractive index** is reported to be $n = 2.5$ at $\lambda = 0.55 \mu\text{m}$ [39D].

References to 3.20

- 39D Dechene, G.: C. R. Acad. Sci. Inst. France 208 (1939) 95.
- 54A Aurivillius, K.: Acta Chem. Scand. 8 (1954) 523.
- 58A Aurivillius, K. L., Carlson, I.: Acta Chem. Scand. 12 (1958) 1297, cited in [93W].
- 71S Singh, V. H.: Indian J. Pure Appl. Phys. 9 (1971) 367, 368.
- 88H Hanafi, Z. M., Ismail, F.M.: Z. Phys. Chem. Neue Folge, 158 (1988) 81.

3.21 Mercury sulfide (HgS)

Crystal structure

HgS (cinnabar) exists in two poly-morphic modifications: the red α -HgS and the black β -HgS. Under atmospheric pressure the phase transition from α -HgS takes place near 340°C [73N, 62C]. The α -HgS modification, which is stable at room temperature and atmospheric pressure, is found e.g. in Almaden/Spain and San Luis Potosi/Mexico. Its space group is 32-D₃⁴.

β -HgS crystallizes in the cubic zinblende structure. group $\bar{4} 3m$ (T_d-symmetry) (Fig. 3.0.1) [70R].

a. Trigonal HgS (α -HgS)

Electronic properties

energy gap

E_g	2.03 eV	$T = 300\text{ K}$	absorption	91C
-------	---------	--------------------	------------	-----

effective mass of electrons : see Fig. 3.21.1.

Lattice properties

lattice parameters

a	4.14 Å	$p = 0$	X-ray diffraction	50A
b	9.49 Å			
c	2.292 Å			
u	0.720(3) Å			
v	0.480(10) Å			

coefficient of linear thermal expansion

$\alpha_{ }$	$1.88(8) \cdot 10^{-5}\text{ K}^{-1}$	$T = 20 \dots 200^\circ\text{C}$	parallel to c -axis	74O
α_{\perp}	$1.81(5) \cdot 10^{-5}\text{ K}^{-1}$		perpendicular to c -axis	

phonon wavenumbers

Optical phonon wavenumbers of the five E-modes of α -HgS from infrared reflectance and Raman measurements.

$E_1(\text{LO})$	356 cm^{-1}	infrared reflectance	73M
$E_1(\text{TO})$	347.6 cm^{-1}		
$E_2(\text{LO})$	296 cm^{-1}		
$E_2(\text{TO})$	284.2 cm^{-1}		
$E_3(\text{LO})$	156 cm^{-1}		
$E_3(\text{TO})$	115.5 cm^{-1}		
$E_4(\text{LO})$	98 cm^{-1}		
$E_4(\text{TO})$	92 cm^{-1}		
$E_5(\text{LO})$	50 cm^{-1}		
$E_5(\text{TO})$	42 cm^{-1}		

second order elastic moduli

c_{11}	$35.0(14) \cdot 10^9\text{ N/m}^2$	$T = 300\text{ K}$	73S
c_{33}	$48.6(5) \cdot 10^9\text{ N/m}^2$		
c_{66}	$13.0(5) \cdot 10^9\text{ N/m}^2$		

Transport properties

Data obtained from photo-Hall experiments for natural and synthetic crystals; only the highest observed mobilities are given in the following; carrier concentrations $n \approx 10^{10} \dots 10^{12} \text{ cm}^{-3}$ for natural crystals, $n \approx 10^{11} \dots 10^{12} \text{ cm}^{-3}$ for synthetic crystals

resistivity (parallel and perpendicular to the c -axis)

ρ_{\parallel}	6400 $\Omega \text{ cm}$	$T = 77 \text{ K}$	natural crystal	76B
	3450 $\Omega \text{ cm}$	$T = 300 \text{ K}$		
ρ_{\perp}	19900 $\Omega \text{ cm}$	$T = 77 \text{ K}$		
	11080 $\Omega \text{ cm}$	$T = 300 \text{ K}$		

mobility (maximum values parallel and perpendicular to c -axis)

μ_{\parallel}	157 cm^2/Vs	$T = 77 \text{ K}$	natural crystal	76B
	30 cm^2/Vs	$T = 300 \text{ K}$		
μ_{\perp}	49 cm^2/Vs	$T = 77 \text{ K}$		
	10 cm^2/Vs	$T = 300 \text{ K}$		

piezoelectric stress coefficient

e_{11}	0.315(16) C m^{-2}	piezoelectric resonant method	73S
----------	-----------------------------	-------------------------------	-----

Optical properties

refractive index

n_e	3.2560	$T = 298 \text{ K},$ $\lambda = 0.62 \mu\text{m}$	67B
n_0	2.9028		

The wavelength dependence of n_e and n_0 can be described for $\lambda = 0.62 \mu\text{m} \dots 11.0 \mu\text{m}$ by

$$n^2 = A + B/(1 - C/\lambda^2) + D/(1 - E/\lambda^2) \text{ [67B]}$$

with $A = 4.1506$, $B = 2.7896$, $C = 0.1328 \mu\text{m}^2$, $D = 1.1378$, $E = 705 \mu\text{m}^2$ for n_0 and $A = 4.0101$, $B = 4.3736$, $C = 0.1284 \mu\text{m}^2$, $D = 1.5604$, $E = 705 \mu\text{m}^2$ for n_e .

dielectric constants (parallel and perpendicular to the c -axis)

$\varepsilon_{\parallel}(0)$	21.5	$T = 80 \text{ K}$	synthetic crystal	73M
	23.5	$T = 300 \text{ K}$		
$\varepsilon_{\parallel}(\infty)$	7.4	$T = 80 \text{ K}$		
	7.9	$T = 300 \text{ K}$		
$\varepsilon_{\perp}(0)$	16.85	$T = 80 \text{ K}$		
	18.2	$T = 300 \text{ K}$		
$\varepsilon_{\perp}(\infty)$	5.38	$T = 80 \text{ K}$		
	6.25	$T = 300 \text{ K}$		

b. Zinblende HgS (β -HgS)

Electronic properties

β -HgS is a zero gap semiconductor (perfect semimetal) by virtue of a symmetry induced band degeneracy.

energy gap

E_g	0.54 eV	$T = 300 \text{ K}$	absorption measurement	70S
dE_g/dT	$7.7 \cdot 10^{-4} \text{ eV K}^{-1}$			

Lattice properties

lattice parameter

a	5.851 Å			67R
-----	---------	--	--	-----

coefficient of linear thermal expansion

α	$4.3(14) \cdot 10^{-6} \text{ K}^{-1}$	$T = 211...348^{\circ}\text{C}$		74O
----------	--	---------------------------------	--	-----

phonon dispersion curves : Fig. 3.21.2.

phonon wavenumbers

$(\nu/c)_{\text{TO}}$	$177.0(5) \text{ cm}^{-1}$	$T = 300 \text{ K}$	thin films	70R
$(\nu/c)_{\text{LO}}$	$224(1) \text{ cm}^{-1}$			

second order elastic moduli

c_{11}	$81.3 \cdot 10^9 \text{ N/m}^2$		calculated data	76K
c_{12}	$62.2 \cdot 10^9 \text{ N/m}^2$			
c_{44}	$26.4 \cdot 10^9 \text{ N/m}^2$			

compressibility

κ	0.230 Mbar^{-1}			85G
----------	---------------------------	--	--	-----

density

d	7.73 g cm^{-3}			55Z
-----	--------------------------	--	--	-----

Debye temperature

$\Theta_{\text{D}} (\alpha\text{-HgS})$	152 K	$T = 0 \text{ K}$	calorimetric	81K
$\Theta_{\text{D}} (\beta\text{-HgS})$	144 K	$T = 0 \text{ K}$	calorimetric	81K

heat capacity ($\alpha\text{-HgS}$)

$C_{\text{p}} [\text{J K}^{-1} \text{ mol}^{-1}]$	$45.61 + 15.48 \cdot 10^{-3} T$	$T = 298...1093 \text{ K}$		79G
---	---------------------------------	----------------------------	--	-----

melting temperature

T_{m}	1093 K			90K
----------------	--------	--	--	-----

density

d	7.75 g cm^{-3}	$\alpha\text{-HgS}$		85A
-----	--------------------------	---------------------	--	-----

Transport and optical properties

See Fig. 3.21.3 for temperature dependence of resistivity, electron mobility and electron concentration.

dielectric constants

$\varepsilon (0)$	18.2	$T = 300 \text{ K}$	calculated from optical phonon data	70R
$\varepsilon (\infty)$	11.36		and $\varepsilon (0)$	

References to 3.21

- 50A Aurivillius, K. L.: *Acta Chem. Scand.* 4 (1950) 1423, cited in [93W].
- 55Z Zhuse, V. P.: *Zh. Tekhn. Fiz. (USSR)* 25 (1955) 2079.
- 62C Curtis, O. L.: *J. Appl. Phys.* 33 (1962) 2461.
- 67B Bond, W. L., Boydand, G. D., Carter, H. L.: *J. Appl. Phys.* 38 (1967) 4090.
- 67R Roth, W. L.: in *Physics and Chemistry of II-VI Compounds* (M. Aven and J. S. Prener, eds.) North-Holland Publishing Company, Amsterdam, 1967.
- 70R Riccius, H. D., Siemsen, K. J.: *J. Chem. Phys.* 52 (1970) 4090.
- 70S Siemsen, K. J., Riccius, H. D.: *Phys. Status Solidi* 37 (1970) 445.
- 70Z Zallen, R., Lucovsky, G., Taylor, W., Pinczuk, A., Burstein, F.: *Phys. Rev. B* 1 (1970) 4058.
- 73M Marqueton, Y., Decamps, E. A.: *Phys. Status Solidi (b)* 60 (1973) 809.
- 73N Nusimovici, M. A., Meskaous, A.: *Phys. Status Solidi (b)* 58 (1973) 121.
- 73S Sapriel, J., Lancon, R.: *Proc. IEEE* 61 (1973) 678.
- 74O Ohmiya, T.: *J. Appl. Crystallogr.* 7 (1974) 396.
- 76B Butti, C., Raymond, A., Bombre, F.: *Phys. Status Solidi (a)* 36 (1976) 133.
- 76K Kumazaki, K.: *Phys. Status Solidi (a)* 33 (1976) 615.
- 79G Grytsiv, V. I., Tomashik, V. N., Tomashik, Z. F.: *Inorg. Mater.* 15 (1979) 30.
- 81K Khattak, G. D., Akbarzadeh, H., Keesom, P. H.: *Phys. Rev. B* 23 (1981) 2911.
- 85A Asadov, M. M.: *Inorg. Mater.* 21 (1985) 270.
- 85G Goble, R. Y., Scott, S. D.: *Can. J. Mineral.* 23 (1985) 273.
- 90K Kulakov, M. P.: *Inorg. Mater.* 26 (1990) 1947.
- 91C Choe Sung-Hyu, Yu Ki-Su, Kim Jae-Eun, Park Hae Yong, Kim Wha-Tek: *J. Mater. Res.* 6 (1991) 2677.
- 96S Szuskiewicz, W., Dybko, K., Dynowska, E., Gorecka, J., Witkowska, B., Hennion, B.: in *The Physics of Semiconductors*, Scheffler, M., Zimmermann, R., eds., World Scientific, Singapore 1996, p. 253 (Vol. 1).

Figures to 3.21

Fig. 3.0.1

The zincblende lattice.

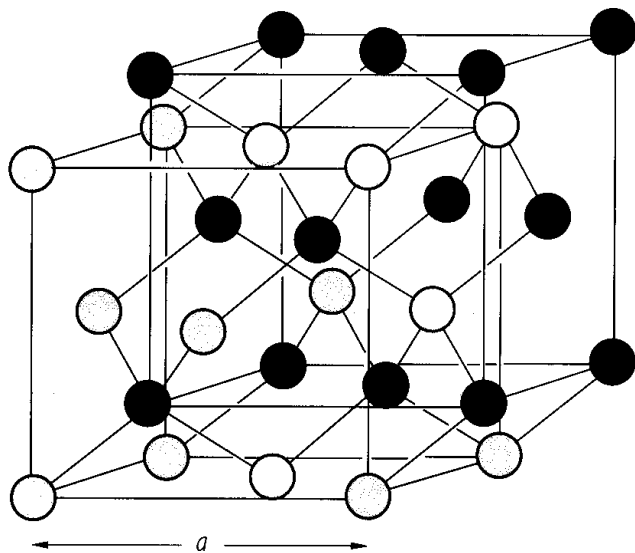


Fig. 3.21.1

α -HgS. Electron effective mass vs. carrier concentration from reflectivity measurements. Plasma reflection minima depending on carrier density were observed at the wavelength λ_{\min} [70S].

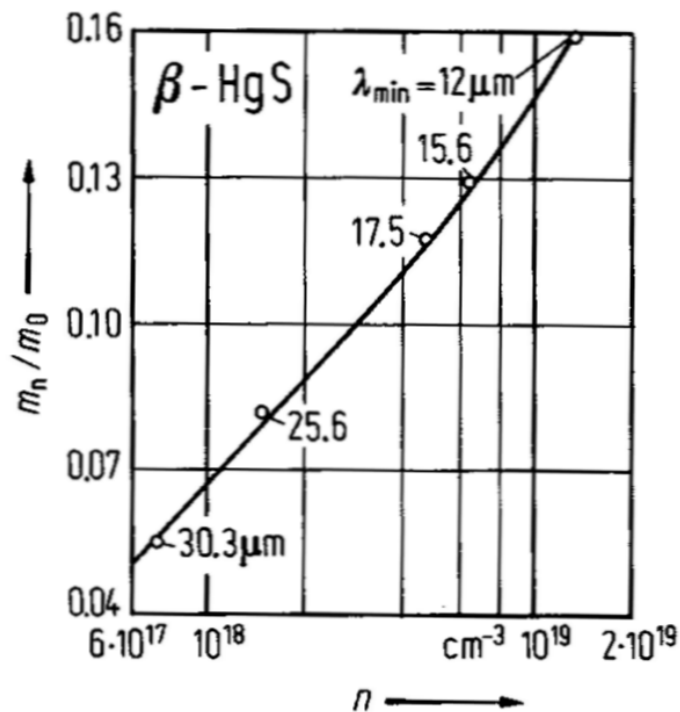


Fig. 3.21.2

β -HgS. Phonon dispersion curves [96S]. Experimental data points (at 10 K) from neutron scattering (open circles) and Raman scattering (solid circles) and rigid-ion model calculations (solid lines).

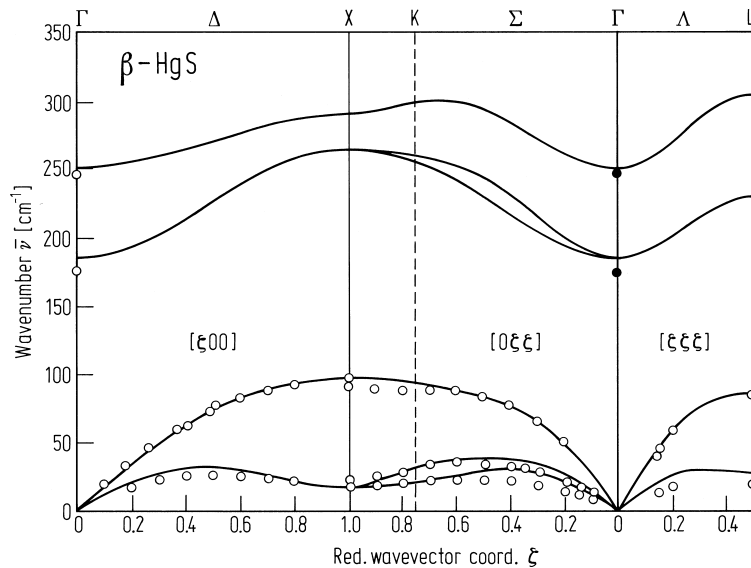
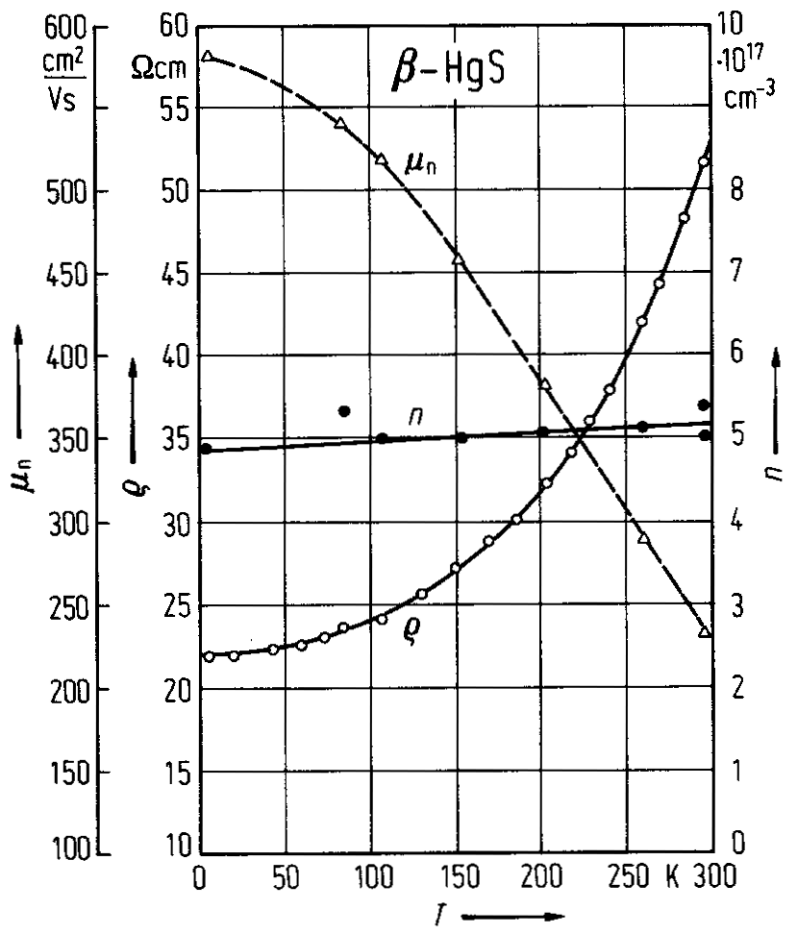


Fig. 3.21.3

β -HgS. Electrical resistivity ρ , electron mobility μ_n and electron concentration n vs. temperature of a 11.5 μm thick film [70Z].



3.22 Mercury selenide (HgSe)

Crystal structure

Under ambient conditions, HgSe crystallizes in the zincblende structure, space group $F\bar{4}3m - T_d^2$ (Fig. 3.0.1).

Electronic properties

band structure : (Brillouin zone, see Fig. 3.0.4)

Mercury selenide is a zero-gap material (semimetal), the lowest conduction band minimum and the top of the valence band are degenerate at the center of the Brillouin zone (Γ_8). Γ_8 is the fourfold component of the spin-orbit split valence band ($\Gamma_8 + \Gamma_7$). The Γ_6 level, which for most cubic semiconductors is the conduction band minimum with an energy larger than the Γ_8 state, is found below the Γ_8 state in HgSe ("negative energy gap", inverted band structure). For a schematic picture of the band structure around Γ , see Fig. 3.0.24.

energy gap

$E_g(\Gamma_{8v}-\Gamma_{6c})$	- 0.274 eV	$T = 4.2$ K	Shubnikov-de Haas effect of n-type HgSe	80G
	-0.061 eV	$T = 300$ K	for temperature dependence of E_g , see Fig. 3.22.1	74L

The temperature dependence of E_g from magnetoabsorption has been fitted with the relation (T in K)

$$E_g(T) = E(0) + \alpha T^2/(T+\beta), \text{ } 10 \text{ K} < T < 80 \text{ K}$$

80D

where $E(0) = - 0.2733$ eV, $\alpha = 1.02$ meV/K, $\beta = 16$ K

interband transitions

$E(\Gamma_{15v}-\Gamma_{15c})$	5.2 eV	$T = 12$ K	reflectivity	64S
$E(L_{3v}-L_{3c})$	8.3 eV			
$E(X_{5v}-X_{1c})$	5.7 eV			
$E(X_{5v}-X_{3c})$	6.6 eV			

spin-orbit splitting energies

$\Delta_0(\Gamma_{8v}-\Gamma_{7v})$	0.383(2) eV	$T = 4.2$ K	interband magnetoabsorption	82M
$\Delta_0(\Gamma_{15v})$	0.45 eV	$T = 12$ K	reflectivity	64S

effective masses

m_n	strongly dependent on electron concentration			62W
m_p	0.78 m_0			74L

Lattice properties

lattice parameter

a	5.997(5) Å	$p = 2.25$ GPa	angle-dispersive X-ray diffraction	96M
-----	------------	----------------	------------------------------------	-----

temperature dependence of lattice parameter

$$a \text{ [Å]} = 6.0854 + 28.61 \cdot 10^{-6} T + 4.93 \cdot 10^{-9} T^2 + 3.74 \cdot 10^{-12} T^3 \qquad T = 34...377^\circ\text{C}$$

70S

phonon dispersion curves

Fig. 3.22.2 (Brillouin zone, see Fig. 3.0.4)

phonon wavenumbers

$\bar{\nu}_{TO}$	130 cm^{-1}	RT	resonance Raman scattering	90K
$\bar{\nu}_{LO}$	174 cm^{-1}			

second order elastic moduli

c_{11}	62.2(1) GPa	$T = 292 \text{ K}$	ultrasound	82F
c_{12}	46.4 GPa			
c_{44}	22.7(1) GPa			

temperature dependence of the second order elastic moduli

See Fig. 3.22.3.

$(1/c_{11})dc_{11}/dT$	$-538 \cdot 10^{-6} \text{ K}^{-1}$		ultrasound	69L
$(1/c_{12})dc_{12}/dT$	$-640 \cdot 10^{-6} \text{ K}^{-1}$			
$(1/c_{44})dc_{44}/dT$	$-303 \cdot 10^{-6} \text{ K}^{-1}$			

bulk modulus

B	49.7 GPa	$T = 300 \text{ K}$		75K
-----	----------	---------------------	--	-----

compressibility

κ	0.230 Mbar^{-1}			85G
----------	---------------------------	--	--	-----

Debye temperature

Θ_D	142 K	$T = 0 \text{ K}$	calorimetric	81K
------------	-------	-------------------	--------------	-----

heat capacity

C_p	$45.56 + 14.10 \cdot 10^{-3} T \text{ J K}^{-1} \text{ mol}^{-1}$	$T = 298 \dots 1093 \text{ K}$		79G
-------	---	--------------------------------	--	-----

melting temperature

T_m	799°C		assessed	92S
-------	-------	--	----------	-----

density

d	8.11 g cm^{-3}			85A
-----	--------------------------	--	--	-----

Transport properties

All HgSe samples show n-type conductivity. As-grown crystals have carrier concentrations of about 10^{17} electrons/cm³.

For measurement of drift and Hall mobilities, see Fig. 3.22.4 and 5.

electron mobility

μ_n	$1.5 \cdot 10^4 \text{ cm}^2/\text{Vs}$	$T = 300 \text{ K}$	$5.9 \cdot 10^{17} \text{ cm}^{-3} \leq n \leq 200 \cdot 10^{17} \text{ cm}^{-3}$	75M
	$5.5 \cdot 10^4 \text{ cm}^2/\text{Vs}$	$T = 95 \text{ K}$	$4.2 \cdot 10^{17} \text{ cm}^{-3} \leq n \leq 200 \cdot 10^{17} \text{ cm}^{-3}$	

Optical properties

dielectric constants

$\varepsilon(0)$	25.6		reflectivity and Kramers–Kronig	75M
$\varepsilon(\infty)$	12...21		analysis from carrier concentration dependent fits on plasmon – LO phonon coupled mode data	

References to 3.22

- 62W Wright, G. H., Strauss, A. J., Harman, T. C.: Phys. Rev. 125 (1962) 1534.
64S Scouler, W. J., Wright, G. B.: Phys. Rev. 133 (1964) A 736.
69L Lehoczy, A., Nelson, D. A., Whitsett, C. R.: Ohys. Rev. 188 (1969) 1069.
70S Singh, H. P., Dayal, B.: Acta Crystallogr. A 26 (1970) 363.
74L Lehoczy, S. L., Broerman, J. G., Nelson, D. A., Whitsett, C. R.: Phys. Rev. B 9 (1974) 1598.
75K Kumazaki, K.: Phys. Status Solidi (a) 29 (1975) K 55.
75M Manabe, A., Mitsuishi, A.: Solid State Commun. 16 (1975) 743.
75R Rode, D. L.: in "Semiconductors and Semimetals", Vol. 10, R. K. Willardson, A. C. Beer (eds.), Academic Press, New York 1975, p. 1.
79G Gritsiv, V. I., Tomashik, V. N., Tomashik, Z. F.: Inorg. Mater. 15 (1979) 30.
79S Szuszkiewicz, W.: Phys. Status Solidi (b) 91 (1979) 361.
80D Dobrowolska, M., Dobrowolski, W., Mycielski, A.: Solid State Commun. 34 (1980) 441.
80G Galazka, R. R., Dobrowolski, W., Thullier, J. C.: Phys. Status Solidi (b) 98 (1980) 97.
81K Khattak, G. D., Akbarzadeh, H., Keesom, P. H.: Phys. Rev. B 23 (1981) 2911.
81W Whitsett, C. R., Broerman, J. G., Summers, C. J.: in "Semiconductors and Semimetals", Vol. 16, R. K. Willardson, A. C. Beer (eds.), Academic Press, New York 1981, p. 54.
82F Ford, P. J., Miller, A. J., Saunders, G. A., Yogurtçu, A. K., Furdyna, J. K., Jaczynski, M.: J. Phys. C 15 (1982) 657.
82K Kepa, H., Giebultowicz, T., Buras, H., Lebech, B., Clausen, K.: Phys. Scr. 25 (1982) 807.
82M Mycielski, A., Kossut, J., Dobrowolska, M., Dobrowolski, W.: J. Phys. C 15 (1982) 3293.
85A Asadov, M. M.: Inorg. Mater. 21 (1985) 270.
85G Goble, R. Y., Scott, S. D.: Can. J. Mineral. 23 (1985) 273.
90K Kumazaki, K.: Phys. Status Solidi (b) 160 (1990) K173.
92S Sharma, R. C., Chang, Y. A., Guminski, C.: J. Phase Equilibria 13 (1992) 663.
96M McMahon, M. I., Liu, H., Nelmes, R. J., Belmonte, S. A.: Phys. Rev. Lett. 77 (1996) 1781.
96S Szuszkiewicz, W., Dybko, K., Dynowka, E., Gorecka, J., Witkowska, B., Hennion, B.: in The Physics of Semiconductors, Scheffler, M., Zimmermann, R. (eds.), World Scientific, Singapore 1996, p. 253 (Vol. 1).

Figures to 3.22

Fig. 3.0.1

The zincblende lattice.

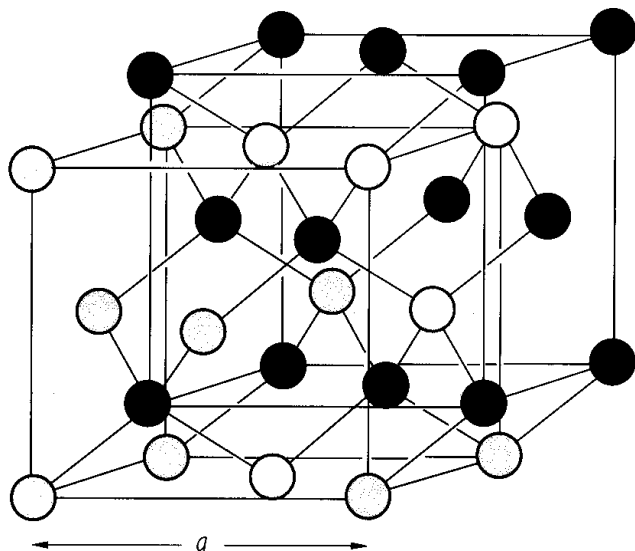


Fig. 3.0.4

The Brillouin zone for the zincblende and the rocksalt lattices.

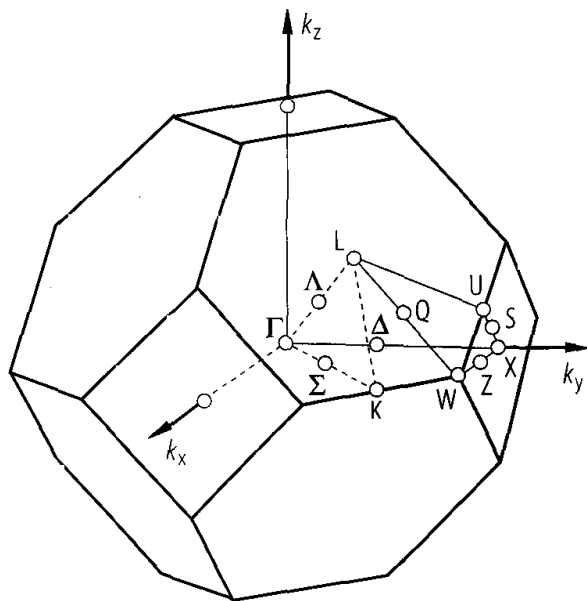


Fig. 3.0.24

HgSe. Schematic band structure of the Hg–Cd–Se system near the Γ point [81W].

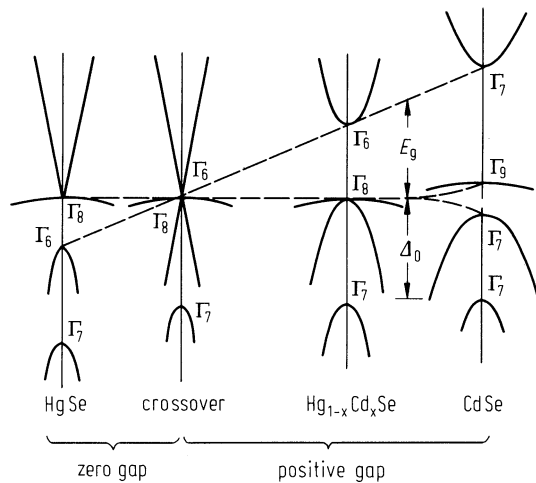


Fig. 3.22.1

HgSe. Energy gap vs. temperature [79S].

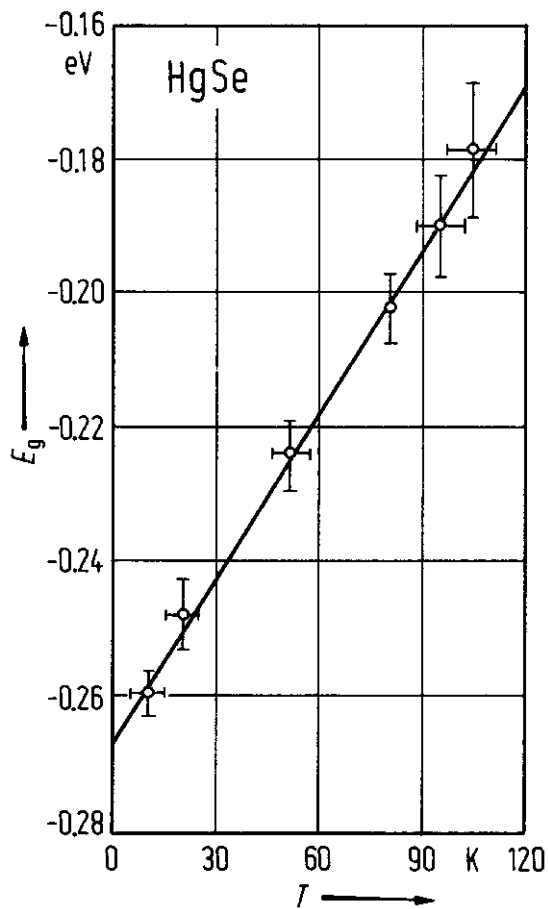


Fig. 3.22.2

HgSe. Phonon dispersion curves measured by neutron scattering at RT (open dots [82K]) and at 11 K (full dots [96S]) in comparison with calculations from a rigid-ion model (solid lines) [96S].

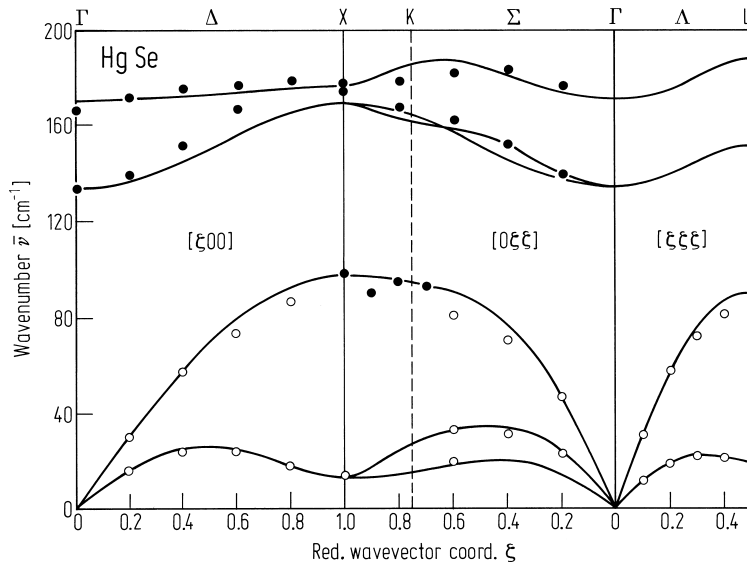


Fig. 3.22.3

HgSe. Second order elastic moduli as obtained from sound velocities as a function of temperature [69L].

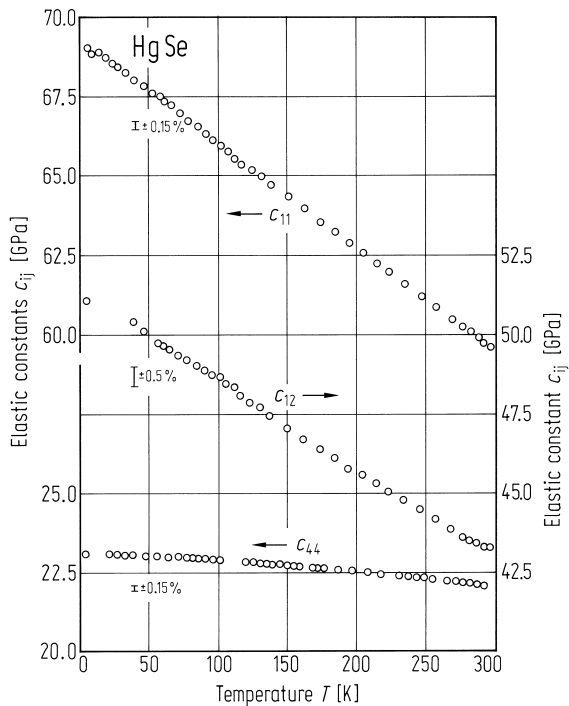


Fig. 3.22.4

HgSe. Electron drift mobility vs. electron concentration for two different temperatures; comparison between experimental data from various sources and theoretical results (solid curves) [75R].

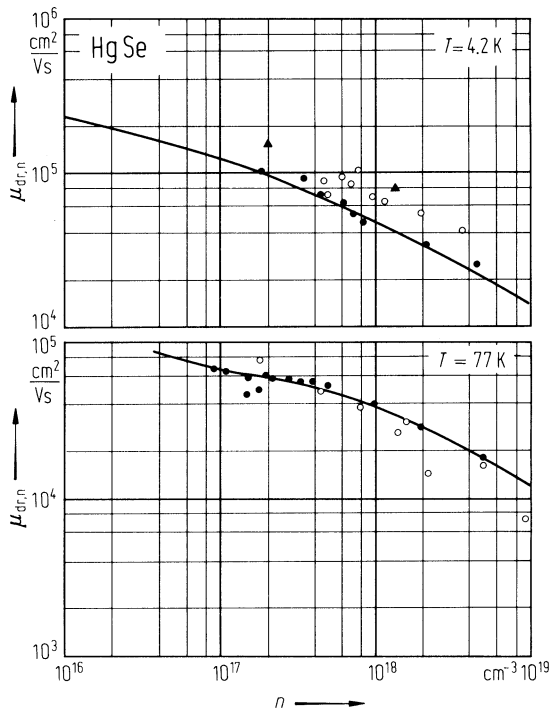
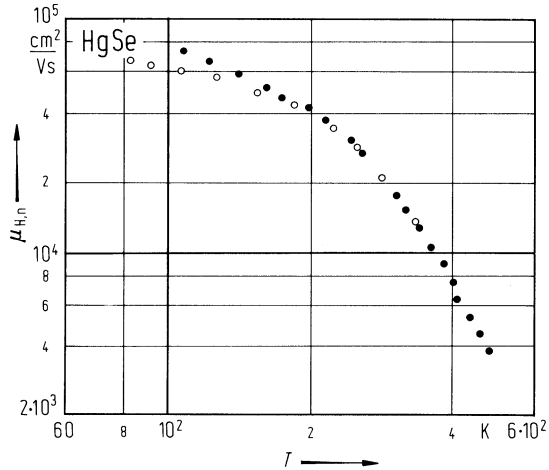


Fig. 3.22.5

HgSe. Hall mobility in the intrinsic range from different sources vs. temperature [75R].



3.23 Mercury telluride (HgTe)

Crystal structure

Under ambient conditions, HgTe crystallizes in the zincblende structure, space group $F\bar{4}3m - T_d^2$ (Fig. 3.0.1).

Electronic properties

band structure : Fig. 3.0.25, Brillouin zone: Fig. 3.0.4.

Mercury telluride is a zero-gap material (semimetal), the lowest conduction band minimum and the top of the valence band are degenerate at the center of the Brillouin zone (Γ_8). Γ_8 is the fourfold component of the spin-orbit split valence band ($\Gamma_8 + \Gamma_7$). The Γ_6 level, which for most cubic semiconductors is the conduction band minimum with an energy larger than the Γ_8 state, is found below the Γ_8 state in HgTe ("negative energy gap", inverted band structure).

energies of symmetry points of the band structure (relative to the top of the valence band)

$E(\Gamma_{6v})$	- 13.35 eV	empirical pseudopotential	82C
$E(\Gamma_{7v})$	- 1.065 eV	calculation	
$E(\Gamma_{6c})$	- 0.303 eV		
$E(\Gamma_{7c})$	4.8 eV		
$E(\Gamma_{8c})$	5.3 eV		
$E(X_{6v})$	- 5.70 eV		
$E(X_{6c})$	- 2.66 eV		
$E(X_{7v})$	- 2.33 eV		
$E(X_{6c})$	2.35 eV		
$E(X_{7c})$	3.2 eV		
$E(L_{6v})$	- 5.62 eV		
$E(L_{6c})$	- 1.36 eV		
$E(L_{4,5v})$	- 0.68 eV		
$E(L_{6c})$	1.28 eV		
$E(L_{6c})$	5.9 eV		
$E(L_{4,5c})$	6.18 eV		

energy gap

$E_g(\Gamma_{8v}-\Gamma_{6c})$	- 0.304 eV	$T = 0$ K	76K
		(extrapolated)	
	- 0.141(13) eV	$T = 300$ K	82H
		from various optical and magnetooptical data	

temperature dependence of energy gap

The experimental data of $E_g(T)$ for $T < 140$ K, see Fig. 3.23.1, have been fitted by an expression

$$E_g(T) = E_g(0) + \alpha T^2/(T+\beta)$$

with $E_g(0) = - 0.303$ eV, $\alpha = 7.2(2) \cdot 10^{-4}$ eV K⁻¹, $\beta = 30(10)$ K 77S

critical point energies

$E'_0(\Gamma_{8v}-\Gamma_{7c})$	4.14 eV	electroreflectance	73M
$E_1(L_{4,5v}-L_{6c})$	2.12 eV		
$E_1+\Delta_1(L_{6v}-L_{6c})$	2.87 eV		
$E_2(X_{7v}-X_{6c})$	4.71 eV		
$E_2+\delta(X_{6v}-X_{7c})$	5.6 eV		
$E(X_{7v}-X_{7c})$	5.43 eV	$T = 10$ K	reflectivity 72C
$E(\Gamma_{8v}-\Gamma_{8c})$	5.44 eV		

spin-orbit splitting energy

$$\Delta_0(\Gamma_{7v}-\Gamma_{8c}) \quad 1.08(2) \text{ eV} \quad T = 300 \text{ K}$$

effective masses

$m_n(\Gamma_8)$	$0.031(1) m_0$	$T = 4.4 \text{ K}$	interband magnetoabsorption	73G
$m_p(\Gamma_8) [100]$	$0.320 m_0$	$T = 4.2 \text{ K}$	interband magnetoreflexion	67G
$[110]$	$0.406 m_0$			
$[111]$	$0.445 m_0$			
$m_p(\Gamma_6)$	$0.3 m_0$	$T = 4...100 \text{ K}$	transport measurements	80D
	$0.028(1) m_0$	$T = 4.4 \text{ K}$	interband magnetoabsorption	73G

g-factor

$g_c(\Gamma_8)$	-22.5	$T = 4.2 \text{ K}$	local (non-local) approximation	79S
$g_v(\Gamma_8)$	4.2			
$g_v(\Gamma_6)$	$-41(4)$	$T = 4.4 \text{ K}$	magnetoabsorption	73G

Lattice properties**lattice parameter**

a	6.453 \AA	RT	energy-dispersive X-ray diffraction	83H
-----	---------------------	----	-------------------------------------	-----

coefficient of linear thermal expansion

α	$\approx 4.10^{-6} \text{ K}^{-1}$	$T = 77...300 \text{ K}$	see also Fig. 3.23.2	76D
----------	------------------------------------	--------------------------	----------------------	-----

phonon dispersion curves

Fig. 3.23.3 (Brillouin zone, see Fig. 3.0.4).

phonon energies and wavenumbers

$h\nu_{LO}(\Gamma)$	$14.86(16) \text{ meV}$	$T = 290 \text{ K}$	neutron scattering	82K
$h\nu_{TO}(\Gamma)$	$14.63(17) \text{ meV}$			
$h\nu_{LO}(X)$	$16.86(12) \text{ meV}$			
$h\nu_{TO}(X)$	$16.64(10) \text{ meV}$			
$h\nu_{LA}(X)$	$10.56 (7) \text{ meV}$			
$h\nu_{TA}(X)$	$1.97(2) \text{ meV}$			
$h\nu_{LO}(L)$	$18.07(24) \text{ meV}$			
$h\nu_{TO}(L)$	$15.86(18) \text{ meV}$			
$h\nu_{LA}(L)$	$9.97(6) \text{ meV}$			
$h\nu_{TA}(L)$	$2.28(2) \text{ meV}$			
$h\nu_{O1}(K)$	$16.86(12) \text{ meV}$			
$h\nu_{O2}(K)$	$16.64(10) \text{ meV}$			
$h\nu_{O3}(K)$	$16.62(11) \text{ meV}$			
$h\nu_{A1}(K)$	$11.00(10) \text{ meV}$			
$h\nu_{A2}(K)$	$1.79(5) \text{ meV}$			
$h\nu_{A3}(K)$	$1.88(2) \text{ meV}$			

second order elastic moduli

c_{11}	$5.87 \cdot 10^{10} \text{ N/m}^2$	$T = 77 \text{ K}$		71V
	$5.36 \cdot 10^{10} \text{ N/m}^2$	$T = 300 \text{ K}$		
c_{12}	$4.05 \cdot 10^{10} \text{ N/m}^2$	$T = 77 \text{ K}$		
	$3.66 \cdot 10^{10} \text{ N/m}^2$	$T = 300 \text{ K}$		

c_{44}	$2.23 \cdot 10^{10} \text{ N/m}^2$	$T = 77 \text{ K}$
	$2.110 \cdot 10^{10} \text{ N/m}^2$	$T = 300 \text{ K}$

For temperature dependence of c_{11} , c_{12} , and c_{44} , see Fig. 3.23.4.

bulk modulus

B	43(2) GPa	$T = 297 \text{ K}$	angle-dispersive X-ray diffraction	96B
-----	-----------	---------------------	------------------------------------	-----

Debye temperature

Θ_D	141.5 K		for dependence on temperature, see Fig. 3.23.5	75C
------------	---------	--	---	-----

melting temperature

T_m	943 K			90K
-------	-------	--	--	-----

density

d	8.21 g/cm ³			85A
-----	------------------------	--	--	-----

heat capacity

C_p	$52.09 + 9.08 \cdot 10^{-3} T \text{ J K}^{-1} \text{ mol}^{-1}$	$T = 298...943 \text{ K}$		92Y
-------	--	---------------------------	--	-----

Transport properties

The temperature dependence of **electrical conductivity** has been measured and compared with calculated curves assuming different scattering mechanisms, see Fig. 3.23.6.

electron mobility (maximum values)

μ_n	$35 \cdot 10^3 \text{ cm}^2/\text{Vs}$	$T = 300 \text{ K}$		67H
	$120 \cdot 10^3 \text{ cm}^2/\text{Vs}$	$T = 77 \text{ K}$		
	$800 \cdot 10^3 \text{ cm}^2/\text{Vs}$	$T = 4.2 \text{ K}$		73G

A calculation of the temperature dependent electron mobility and comparison with experimental data was performed by [81D], see Fig. 3.23.7.

hole mobility

The temperature dependence of hole mobilities from various sources is compared with calculations for different scattering processes in Fig. 3.23.8. For calculated temperature dependence of carrier concentrations with and without magnetic field, see Fig. 3.23.9.

thermal conductivity has been measured by [85N], Fig. 3.23.10.

Optical properties

Calculated optical spectra (ϵ_1 , ϵ_2 and R) are shown in Fig. 3.23.11.

dielectric constants

$\epsilon(0)$	21.0	$T = 77$ K	reflectance	72B
$\epsilon(\infty)$	15.2			

References to 3.23

- 67G Groves, S. H., Brown, R. N., Pidgeon, C. R.: Phys. Rev. 161 (1967) 779.
- 67H Harman, T. C.: Physics and Chemistry of II-VI Compounds (M. Aven and J. S. Prener, eds.), North-Holland Publishing Company, Amsterdam, 1967, p. 767.
- 71L Lakkad, S. C.: J. Appl. Phys. 42 (1971) 4277.
- 71V Vekilov, Yu. Kh., Rusakov, A. P.: Fiz. Tverd. Tela 13 (1971) 1157; engl.: Sov. Phys. Solid State 13 (1971) 956.
- 72B Baars, J., Sorger, F.: Solid State Commun. 10 (1972) 875.
- 72C Chadi, D. J., Walter, J. P., Cohen, M. L., Petroff, Y. Balkanski, M.: Phys. Rev. B 5 (1972) 3058.
- 73G Guldner, Y., Rigaux, C., Grynberg, M., Mycielski, A.: Phys. Rev. B 8 (1973) 3875.
- 73M Moritani, A., Taniguchi, K., Hamaguchi, C., Nakai, J.: J. Phys. Soc. Jpn 34 (1973) 79.
- 75C Cottam, R. I., Saunders, G. A.: J. Phys. Chem. Solids 36 (1975) 187.
- 76D Dornhaus, R., Nimtz, G.: Springer Tracts in Modern Physics, Vol. 78 (1976) 1-119.
- 76K Kim, R. S., Narita, S.: Phys. Status Solidi (b) 73 (1976) 741.
- 77S Szymanska, W.: Physics of Narrow Gap Semiconductors, Proc. III., Int. Conference, Warszawa, Sept. 1977 G. Rauluszkievicz, M. Gorska, and F. Kaczmarek, eds.) PWN-Polish-Scientific Publishers, Warszawa, 1978, p. 357.
- 79S Shinizu, K., Narita, S., Nisida, Y., Ivanow-Omskii, V. J.: Solid State Commun. 32 (1979) 327.
- 80C1 Collins, J. C., White, G. K., Birch, J. A., Smith, T. F.: J. Phys. C 13 (1980) 1649.
- 80C2 Czyzyk, M. T., Podgorny, M.: Phys. Status Solidi (b) 98 (1980) 507.
- 80D Dziuba, Z., Wrobel, J.: Phys. Status Solidi (b) 100 (1980) 379.
- 81D Dubowski, J. J., Dietl, T., Szymanska, W., Galazka, R. R.: J. Phys. Chem. Solids 42 (1981) 351.
- 82C Chen, A. B., Sher, A.: J. Vac. Sci. Technol. 21 (1982) 138.
- 82H Hansen, G. L., Schmit, J. L., Casselman, T. N.: J. Appl. Phys. 53 (1982) 7099.
- 82K Kepa, H., Giebultowicz, T., Buras, B., Lebech, H., Clausen, K.: Phys. Scr. 25 (1982) 807.
- 83H Huang, T., Ruoff, A. L.: Phys. Status Solidi (a) 77 (1983) K193.
- 85A Asadov, M. M.: Inorg. Mater. 21 (1985) 270.
- 85C Cade, N. A., Lee, P. M.: Solid State Commun. 56 (1985) 637.
- 85N Noguera, A., Wasim, S. M.: Phys. Rev. B 32 (1985) 8046.
- 90K Kulakov, M. P.: Inorg. Mater. 26 (1990) 1947.
- 92Y Yu, T.-C., Brebrick, R. F.: J. Phase Equilibria 13 (1992) 476.
- 93B Bagot, D., Granger, R., Rolland, S.: Phys. Status Solidi (b) 177 (1993) 295.
- 96B Besson, J. M., Grima, P., Gauthier, M., Itié, J. P., Mézouar, M., Häusermann, D., Hanfland, M.: Phys. Status Solidi (b) 198 (1996) 419.

Figures to 3.23

Fig. 3.0.1

The zincblende lattice.

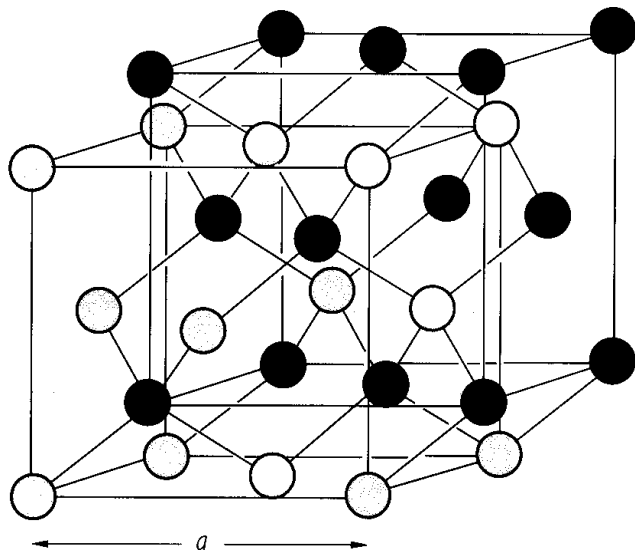


Fig. 3.0.4

The Brillouin zone for the zincblende and the rocksalt lattices.

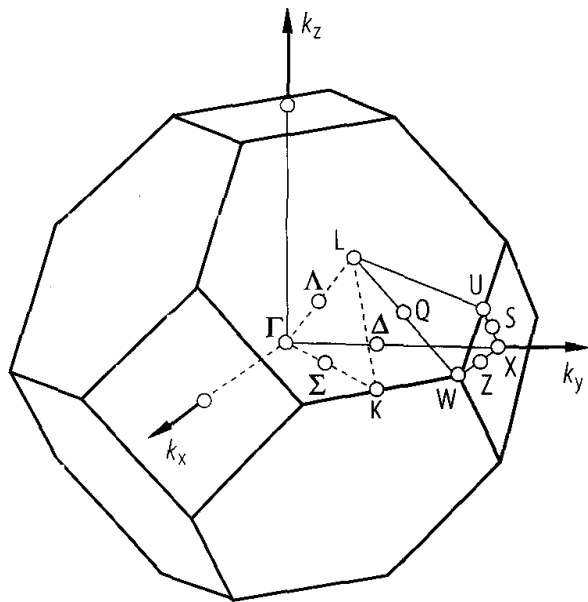


Fig. 3.0.25

HgTe. Band structure and density of states g calculated with the self-consistent LMTO local density approximation [85C].

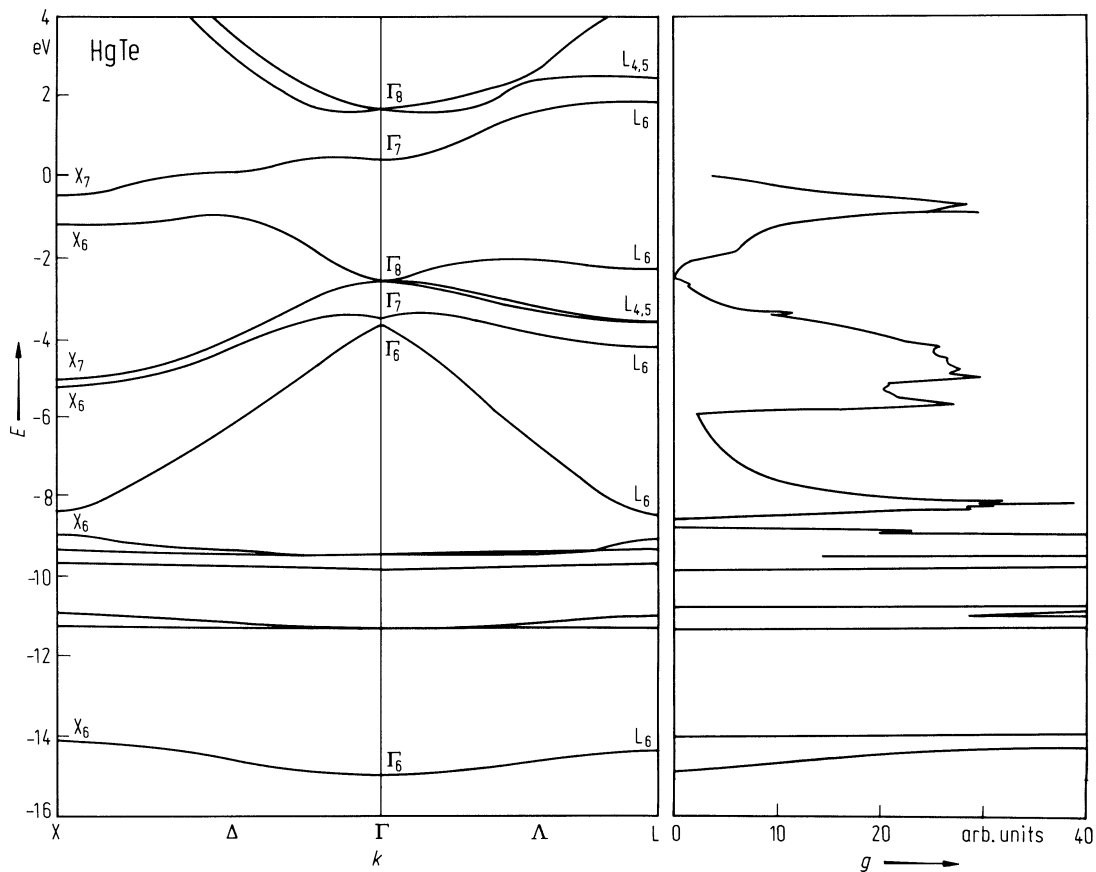


Fig. 3.23.1

HgTe. Negative energy gap E_g vs. temperature [77S]. bars: data from several authors.

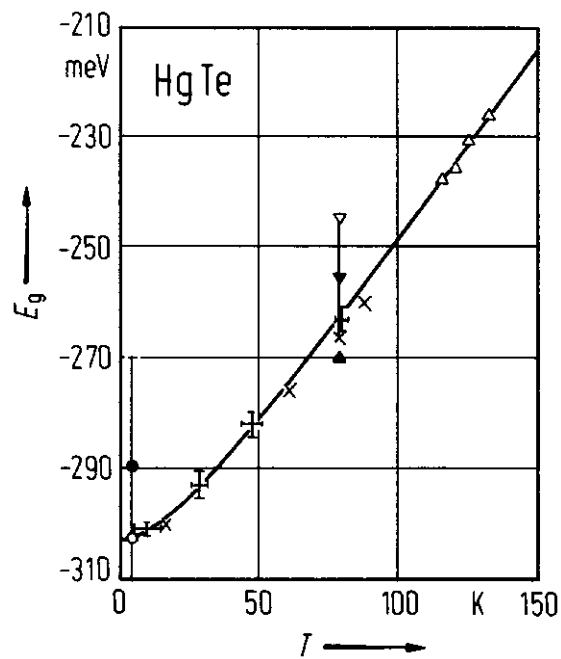


Fig. 3.23.2

HgTe. Linear thermal expansion coefficient α vs. T , symbols experimental points, full line calculated [93B].

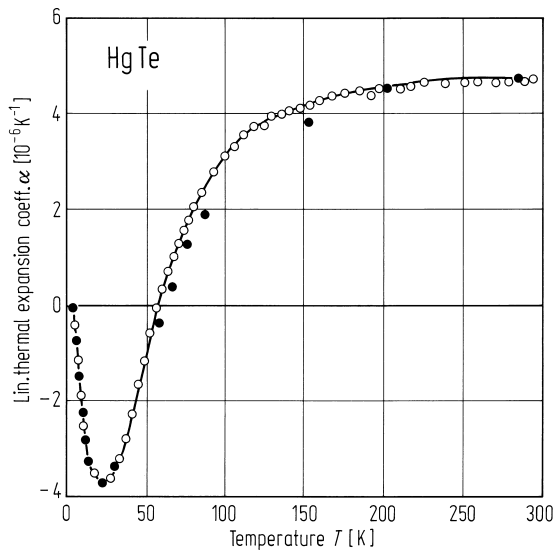


Fig. 3.23.3

HgTe. Phonon dispersion curves: neutron scattering data (symbols) and Raman data fitted by three different versions of the rigid ion model [82K].

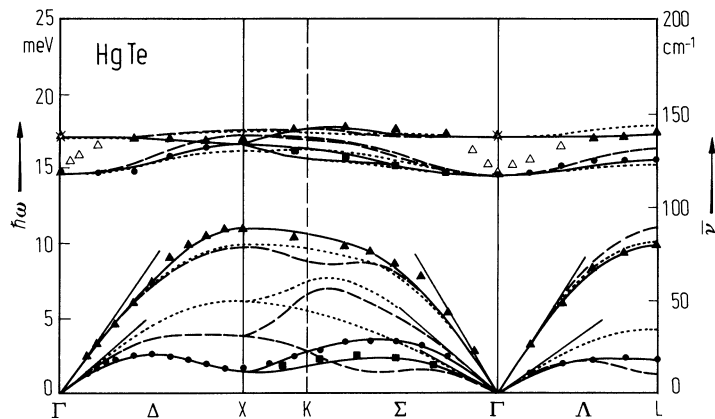


Fig. 3.23.4

HgTe. Second order elastic moduli (a) c_{11} , (b) c_{12} , and (c) c_{44} vs. temperature [75C]. The points are the experimental data and the crosses indicate the fit computed from the Lakkad [71L] model.

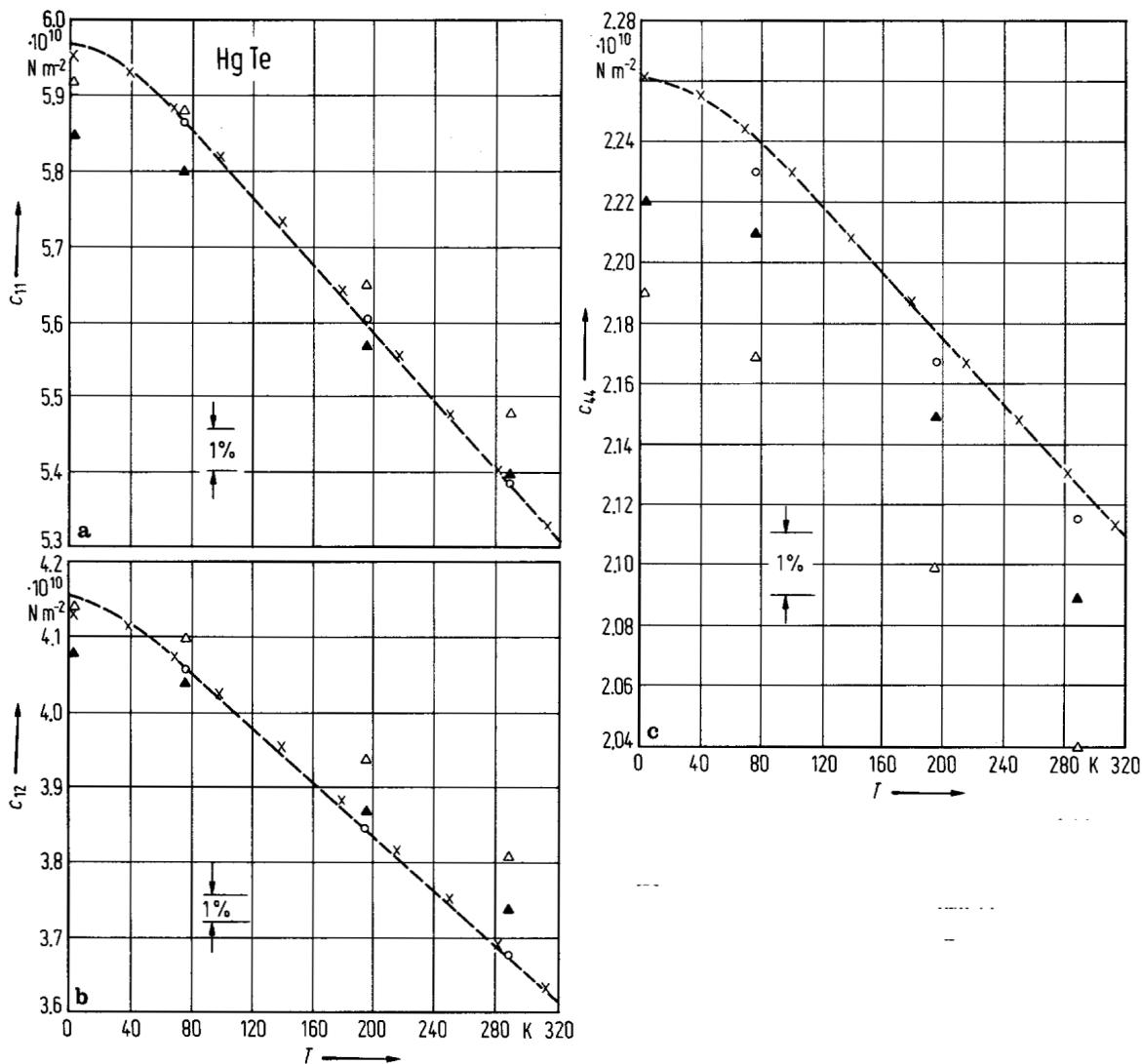


Fig. 3.23.5

HgTe. Debye temperature Θ_D vs. temperature. The values are calculated from individual measurements of heat capacity. The broken curves represent individual C_p/T^3 values fitted to a polynomial $a + bT^2 + cT^4$ by least squares and a value $\Theta_D(T=0) = 145.6$ K was obtained. A fit to a polynomial in T^2 obtained $\Theta_D(T=0) = 149.6$ K. The arrow denotes $\Theta_{D,\text{elastic}}(T=0) = 143$ K calculated from elastic data [80C1].

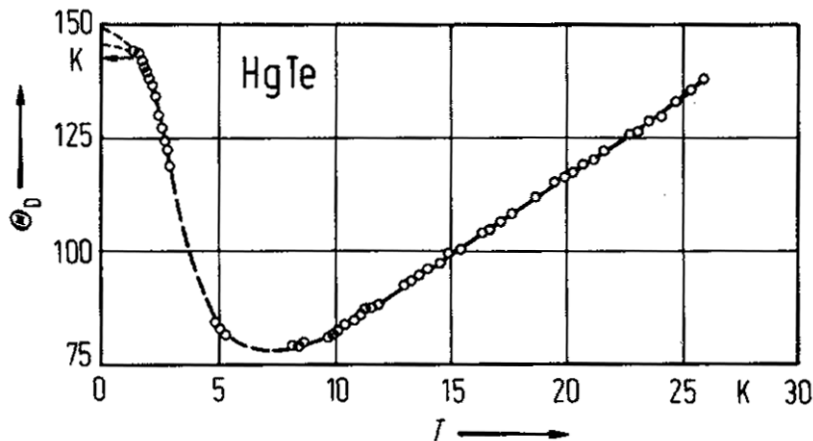


Fig. 3.23.6

HgTe. Electron conductivity vs. temperature. Experimental data (circles) in comparison with calculated curve assuming mixed scattering modes (solid line) and neglecting interband optical phonon scattering (broken line) [81D].

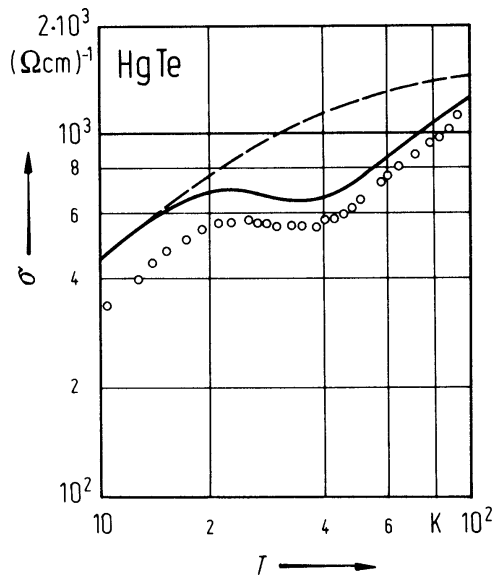


Fig. 3.23.7

HgTe. Electron mobility vs. temperature: calculated curves for piezoacoustic (PA), acoustic (AC), nonpolar (NPO), polar (PO), charged center (CC), and mixed scattering processes (solid line) in comparison with experimental data from various sources [81D].

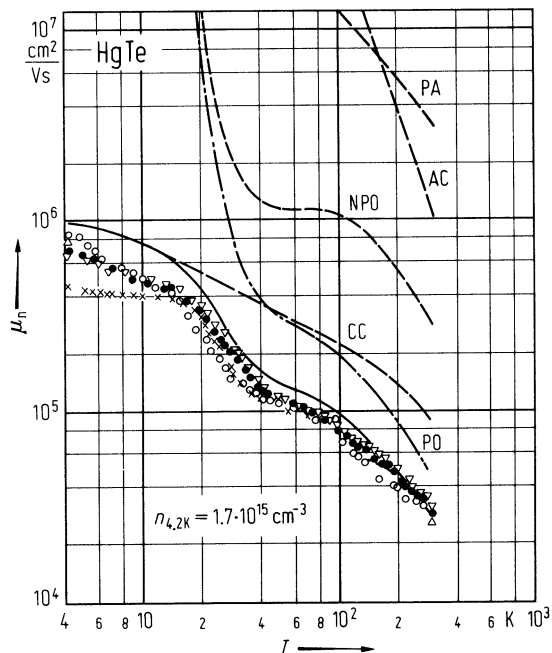


Fig. 3.23.8

HgTe. Hole mobility in the intrinsic range vs. temperature: theoretical estimates for acoustic (AC), nonpolar (NPO) and polar (PO) phonon scattering in comparison with experimental data from various sources [80D].

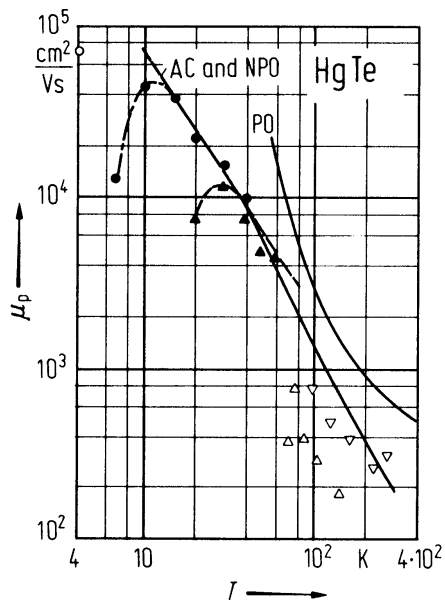


Fig. 3.23.9

HgTe. Intrinsic carrier concentration vs. temperature calculated for magnetic field of 20 kG (broken line) and without magnetic field (solid line) [80D].

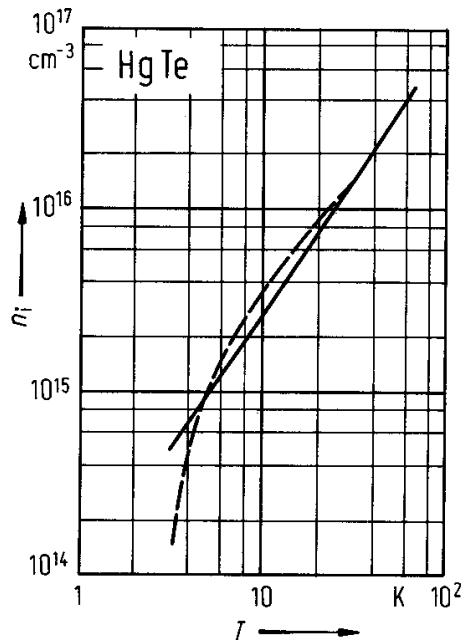


Fig. 3.23.10

HgTe. Thermal conductivity vs. temperature for three different samples solid lines represent theoretical fits [85N].

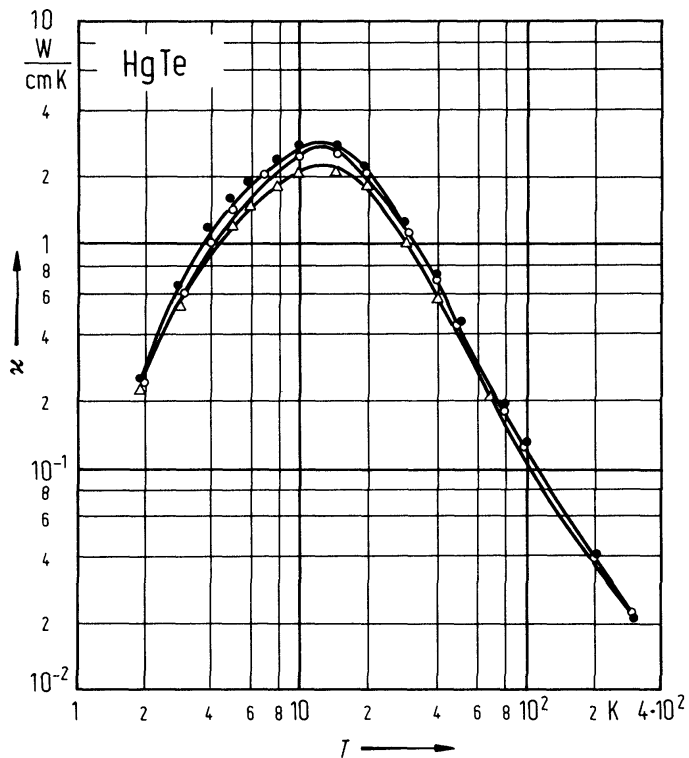
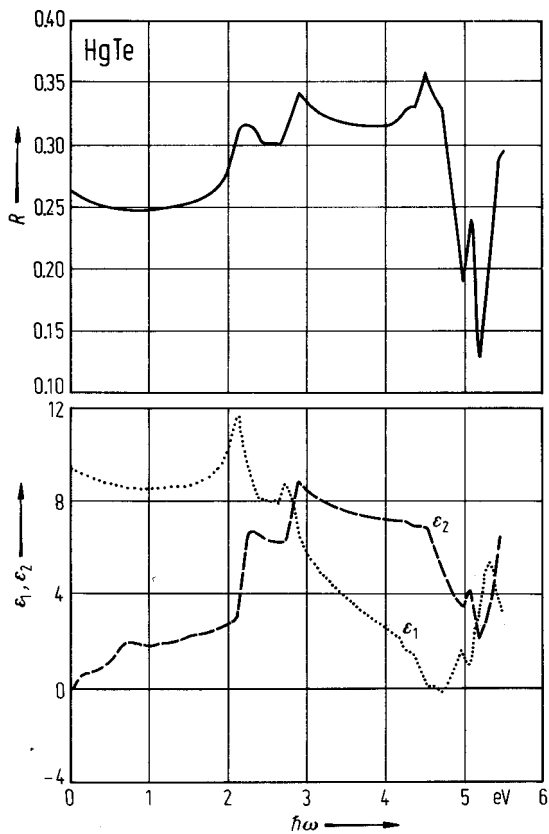


Fig. 3.23.11

HgTe. Optical spectra calculated from the band structure of [80C2]; dotted line: ϵ_1 , dashed line: ϵ_2 , solid line: R .



4 I-VII compounds

4.0 Crystal structure and electronic structure

4.0.1 Crystal structure

The *copper halogenides* CuF, CuCl, CuBr and CuI crystallize under normal conditions in the zincblende lattice.

The *silver halogenides* AgF, AgCl and AgBr crystallize under normal conditions in the rocksalt (NaCl) structure. AgI occurs in two modifications, the wurtzite and the zincblende lattice.

Figs. 4.0.1 ... 4.0.3 show the crystal structure and the Brillouin zones of these lattices.

For details of the structures, for high temperature and high pressure modifications, see the respective sections.

4.0.2 Electronic structure

The Brillouin zones of the zincblende and the rocksalt structures is the Brillouin zone of the face-centered lattice (Fig. 4.0.4); the Brillouin zone of the wurtzite structure the Brillouin zone of the hexagonal lattice (Fig. 4.0.5).

For the qualitative shape of energy bands in cubic and hexagonal structures see the remarks in section 2.0.2.

Special band structures

Figs. 4.0.6 ... 4.0.12 show the band structures of the semiconducting I-VII compounds. For an interpretation of these structures see the respective sections.

Figures to 4.0:

Fig. 4.0.1

The zincblende lattice.

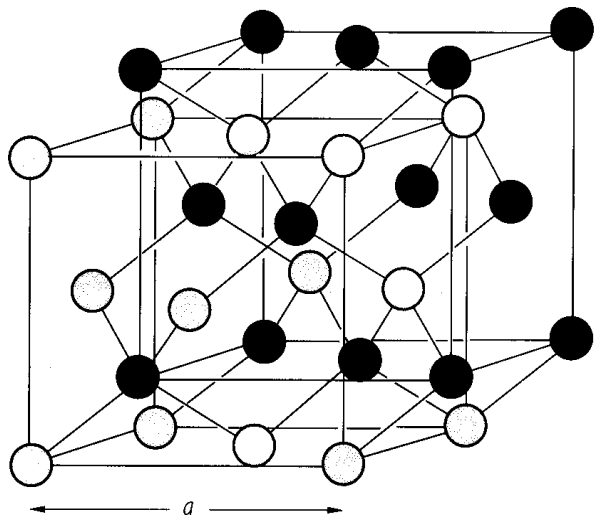


Fig. 4.0.2

The wurtzite lattice.

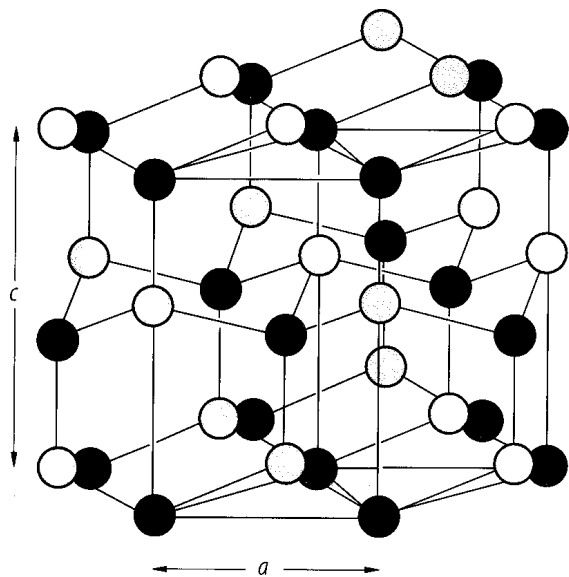


Fig. 4.0.3

The rocksalt lattice.

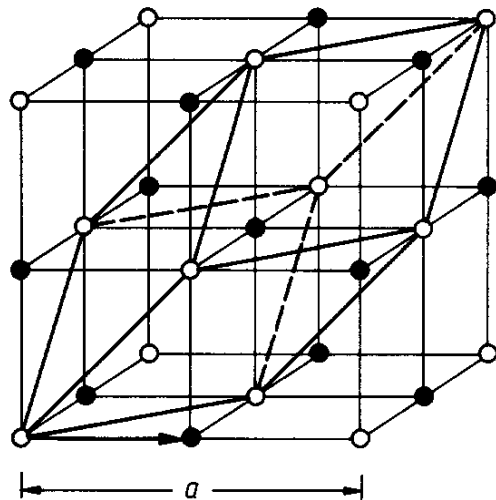


Fig. 4.0.4

The Brillouin zone for the zincblende and the rocksalt lattices.

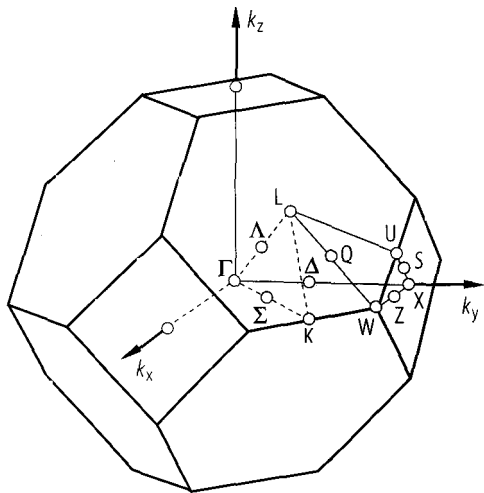


Fig. 4.0.5

The Brillouin zone of the wurtzite lattice.

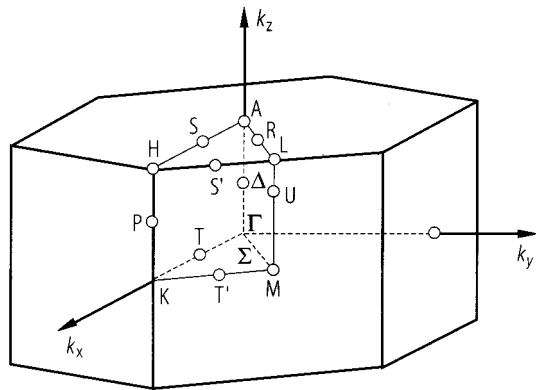


Fig. 4.0.6

Band structure of copper chloride.

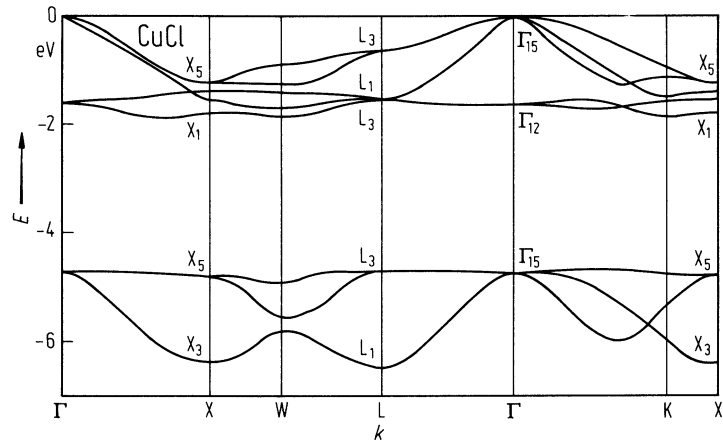


Fig. 4.0.7

Band structure of copper bromide.

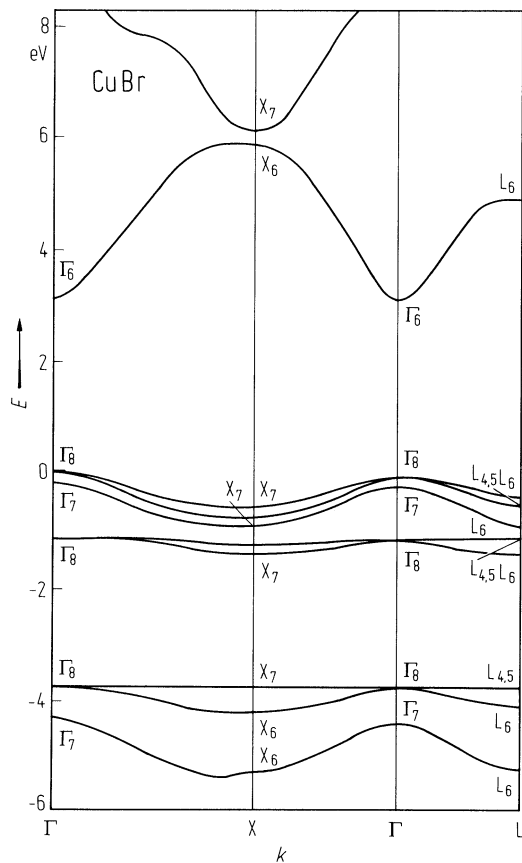


Fig. 4.0.8

Band structure of copper iodide.

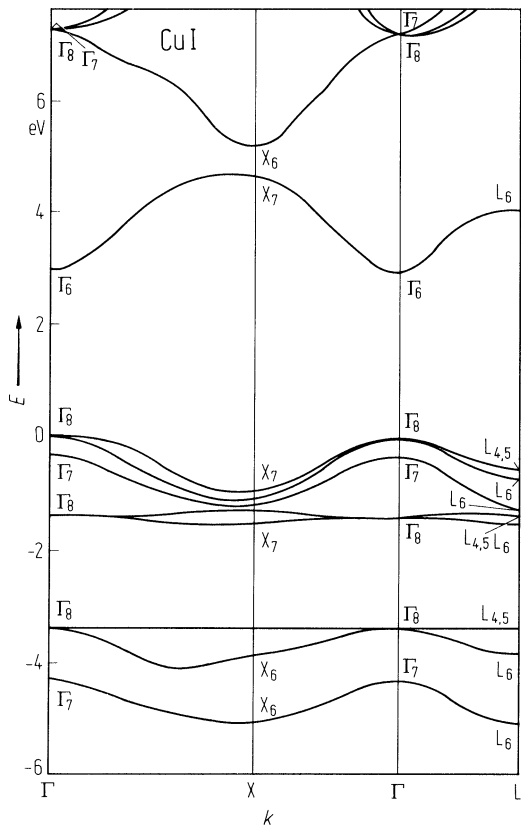


Fig. 4.0.9

Band structure of silver fluoride.

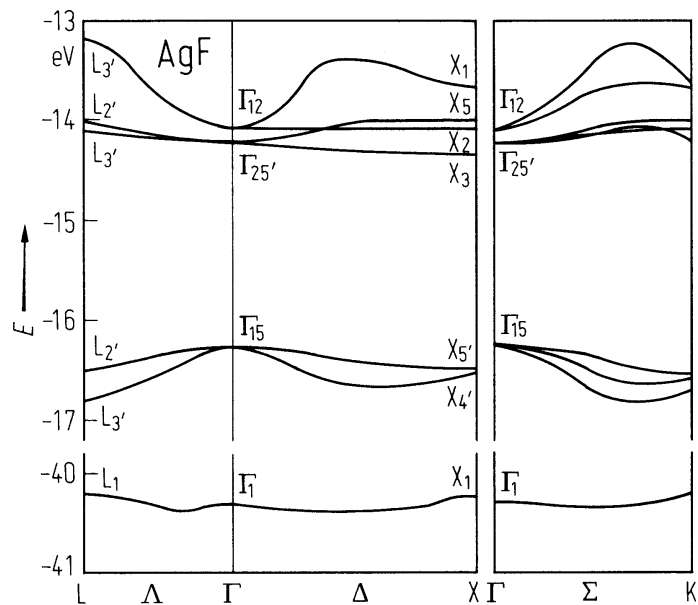


Fig. 4.0.10

Band structure of silver chloride.

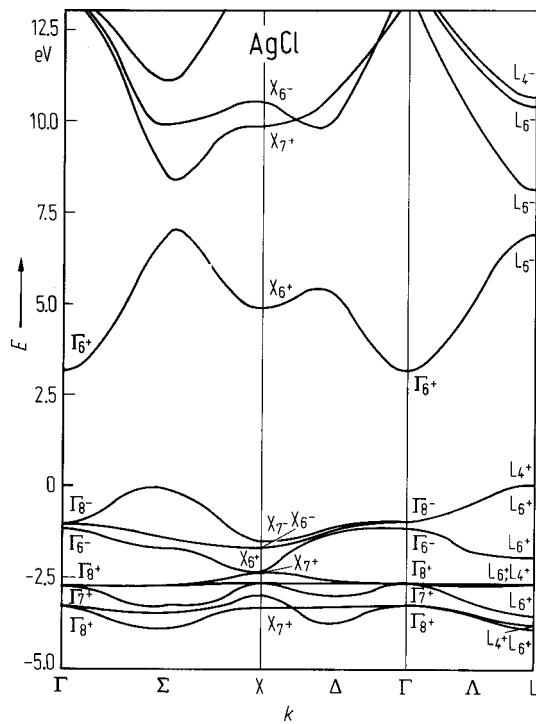


Fig. 4.0.11

Band structure of silver bromide.

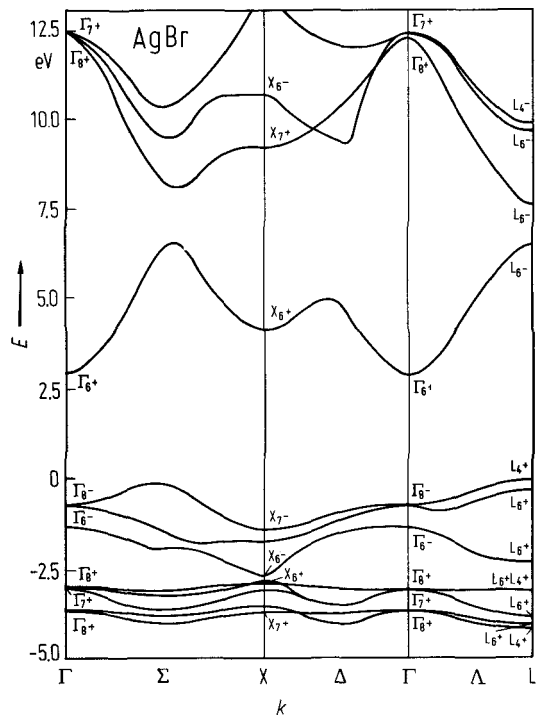
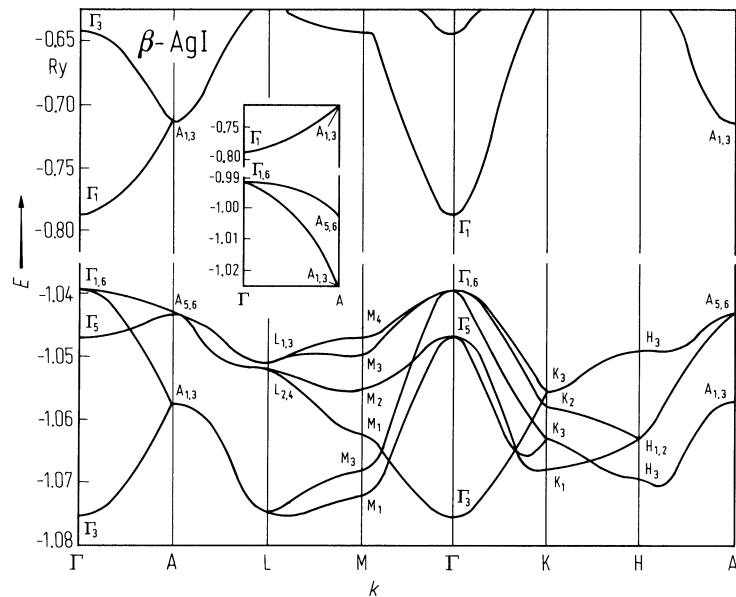


Fig. 4.0.12

Band structure of silver iodide.



4.1 Cuprous fluoride (CuF)

Crystal structure

γ -CuF crystallizes in the zincblende structure, $F\bar{4}3m - T_d^2$ (Fig. 4.0.1). CuF is chemically instable, nearly no data are available

Physical properties

phonon frequencies

$\nu_{TO}(\Gamma)$	13.59 THz	FP-LMTO calculation	89K
--------------------	-----------	---------------------	-----

second order elastic moduli

c_{11}	91.8 GPa	semiempirical TB calculation	94S
c_{12}	43.0 GPa		
c_{44}	35.8 GPa		

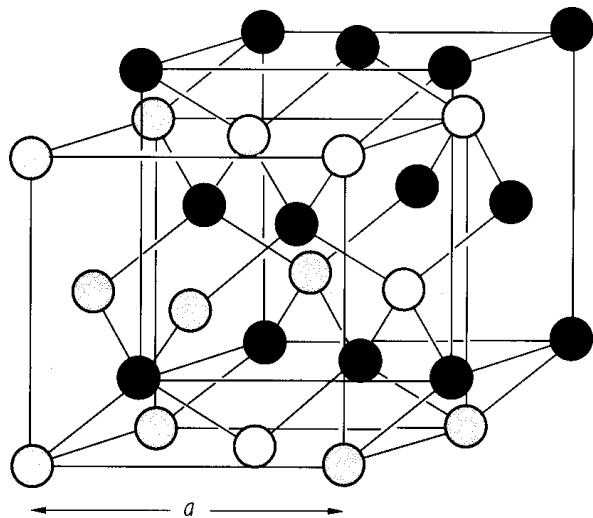
References to 4.1

- 89K Kremer, J. W., Weyrich, K. H.: Phys. Rev. B 40 (1989) 9900.
94S Shen, S. G.: J. Phys. Condens. Matter 6 (1994) 8733.

Figures to 4.1

Fig. 4.0.1

The zincblende lattice.



4.2 Cuprous chloride (γ -CuCl)

Crystal structure

γ -CuCl (zincblende structure, space group $T_d^2 - F\bar{4}3m$, Fig. 4.0.1) is stable at normal conditions.

A high temperature phase (β -CuCl, wurtzite, $P6_3mc-C_{6v}^4$, $a = 3.893 \text{ \AA}$, $c = 6.375 \text{ \AA}$ at 683 K has been detected by neutron scattering [88G].

Electronic properties

band structure : Figs. 4.0.6; Brillouin zone: Fig. 4.0.4.

CuCl is a direct gap semiconductor. The uppermost valence band maximum occurs at Γ . The triply degenerate Γ_{15} band is split by spin-orbit interaction into a doubly degenerate Γ_8 and a singlet Γ_7 state. Compared to the γ -modifications of CuBr, CuI and AgI, in CuCl the Γ_7 and Γ_8 valence band levels are inverted [63C, 65S], the Γ_7 state lying higher in energy in CuCl.

direct gap energy

$E_g(\Gamma_{7v}-\Gamma_{6c})$	3.3990(5) eV	$T = 2 \text{ K}$	from one- and two-photon absorption	95S
$E_g(\Gamma_{8v}-\Gamma_{6c})$	3.486(2) eV	$T = 6 \text{ K}$	from two-photon absorption	94R

higher direct gap energy

$E_{g,dir}(\Gamma_{12v}-\Gamma_{1c})$	5.19 eV	$T = 4.3 \text{ K}$	two-photon absorption from lower valence band	82F
---------------------------------------	---------	---------------------	---	-----

critical point energies of valence bands (relative to the Γ_{15} top of the valence band)

$E(\Gamma_{12v})$	-1.79 eV	$T = 4.3 \text{ K}$	two-photon absorption	82F
$E(X_{5v})$	-1.0(1) eV	$T = 80 \text{ K}$	angle-resolved uv photoemission	82W
$E(X_{3v}, X_{2v})$	-1.5(1) eV		valence band structure, see Fig. 4.0.6	
$E(X_{1v})$	-1.9(1) eV			
$E(X_{5v})$	-4.9(1) eV			
$E(X_{3v})$	-6.1(1) eV			
$E(L_{3v})$	-0.6(1) eV			

critical point energies of conduction bands (relative to the Γ_{15} top of the valence band)

$E(X_{1c})$	7.8 (2) eV	$T = 80 \text{ K}$	angle-resolved secondary electron emission	83G
$E(X_{3c})$	12.1 eV			
$E(L_{1c})$	8.1 eV			
$E(L_{1c})$	11.4 eV			

energies of transverse and longitudinal edge excitons

$Z_{1,2}$ and Z_3 originate from coupling of the lowest conduction band state Γ_6 to the uppermost valence band states $\Gamma_8(Z_{1,2})$ and $\Gamma_7(Z_3)$.

$E_{gx}(Z_3^T(1S))$	3.208 eV	$T = 6 \text{ K}$	from two-photon absorption	91F
$E_{gx}(Z_3^L(1S))$	3.2076(3) eV	$T = 6 \text{ K}$	from two-photon absorption	94R
$E_{gx}(Z_{1,2}^T(1S))$	3.2668 eV	$T = 6 \text{ K}$	from two-photon absorption	91F
$E_{gx}(Z_{1,2}^L(1S))$	3.2898 eV	$T = 6 \text{ K}$	from two-photon absorption	91F

energy of higher exciton state

$E_{\text{gx}}(\text{Z}_3(2\text{S}))$	3.366 eV	$T = 4.2 \text{ K}$	absorption (excitonic series not exactly hydrogen-like)	67R
$E_{\text{gx}}(\text{Z}_3(2\text{P}))$	3.3717(3) eV	$T = 2 \text{ K}$	from one- and two-photon absorption	95S
$E_{\text{gx}}(\text{Z}_3(2\text{S}))$	3.3664(3) eV			
$E_{\text{gx}}(\text{Z}_3(3\text{S}))$	3.3845(2) eV			
$E_{\text{gx}}(\text{Z}_3(4\text{S}))$	3.3909(2) eV			
$E_{\text{gx}}(\text{Z}_3(3\text{P}))$	3.3865(3) eV			

longitudinal-transverse exciton splitting energy

$\Delta E_{\text{ex}}^{\text{L-T}}(\text{Z}_{1,2})$	23.0 meV	$T = 6 \text{ K}$	from two-photon absorption	91F
$\Delta E_{\text{ex}}^{\text{L-T}}(\text{Z}_3)$	5.7 meV			

splitting of transverse exciton state and spin triplet state

$\Delta E_{\text{ex}}^{\text{T-t}}(\text{Z}_3)$	2.6 meV	$T = 1.8 \text{ K}$	luminescence/reflectivity under uniaxial stress	74S
	2.5 meV	$T = 4.2 \text{ K}$	magneto-reflectivity	71S1

spin orbit splitting of the valence band

Δ_{so}	- 40.4 meV	$T = 6 \text{ K}$	from different fits on the Z_3 - and $\text{Z}_{1,2}$ -exciton states	91F
----------------------	------------	-------------------	--	-----

exchange energy for T-exciton

$\Delta_{\text{T}} = \Delta_{\text{ex}} - \Delta_{\text{dip}}$	12.9 meV	$(T < 20 \text{ K})$	average from various experiments	77G
--	----------	----------------------	----------------------------------	-----

exchange energy for L-exciton

$\Delta_{\text{L}} = \Delta_{\text{ex}} + 2\Delta_{\text{dip}}$	32.6 meV	$(T < 30 \text{ K})$	average from various experiments	77G
---	----------	----------------------	----------------------------------	-----

electron-hole exchange energy

Δ	10(2) meV	$T = 100 \text{ K}$	uniaxial stress dependence of energies and relative intensities of $\text{Z}_{1,2}$ and Z_3 excitons	83B
----------	-----------	---------------------	---	-----

exciton radii **Z_3 -series**

$r(1\text{S})$	7.03 Å	$T = 4.2 \text{ K}$	analysis of exciton absorption series corrected for non-hydrogen-like energetic distances	71L
$r(2\text{S})$	35.5 Å			
$r(3\text{S})$	86 Å			
$r(1\text{S})$	4 Å	$T = 80 \text{ K}$	electroreflectivity	70M

exciton binding energy **Z_3 -series**

$E_{\text{b}}(1\text{S})$	190 meV	—	best value from various optical results	77G
	189 meV		analysis of exciton series, corrected for non-hydrogen-like energetic distances	71L
$E_{\text{b}}(2\text{S})$	119 meV			
$E_{\text{b}}(3\text{S})$	100 meV			

energy of biexciton state

$E_{\text{g,bi}}(\Gamma_1)$	6.372(1) eV	$T = 1.6 \text{ K}$	two-photon excitation	80M
-----------------------------	-------------	---------------------	-----------------------	-----

binding energy of biexciton

$E_{\text{b}}^{\text{biex}}$	32 meV	$T = 4.2 \text{ K}$	giant two-photon absorption	74G
------------------------------	--------	---------------------	-----------------------------	-----

effective masses

$m_n(\Gamma_{6c})$	$0.50(2) m_0$		analysis of luminescence	76H2
$m_p(\Gamma_{7v})$	$2.0(5) m_0$			

effective mass of transverse and longitudinal exciton states

$m_{ex}^T(Z_3)$	$2.5 m_0$	$T = 4.2 \text{ K}$	hyper-Raman scattering	80G
$m_{ex}^L(Z_3)$	$2.5 m_0$			

g-factors

$g_{eff}(Z_3)$	0.37	$T = 4.2 \text{ K}$	two-photon magnetoabsorption, value corresponds to $(1/2)(g(\Gamma_{6c})-g(\Gamma_{7v}))$	85F
$g_{eff}(Z_{1,2})$	$-0.3(1)$	$T = 4.2 \text{ K}$	magneto-reflectivity	71S1
$g(\Gamma_6)$	2.02	$T = 1.8 \text{ K}$	Faraday rotation	70K
$g(\Gamma_7)$	-1.38	$T = 1.8 \text{ K}$	Faraday rotation	70K
$g(\Gamma_8)$	0.28	—	band structure calculation	73K

Lattice and optical properties**lattice parameter**

a	$5.4202(2) \text{ \AA}$		neutron powder diffraction	94H2
-----	-------------------------	--	----------------------------	------

temperature dependence, see Fig. 4.2.1.

linear thermal expansion coefficient : Fig. 4.2.2.**volume thermal expansion coefficient**

β	$-2.34 \cdot 10^{-5} \text{ K}^{-1}$	$T = 40 \text{ K}$		76H1
	$0.24 \cdot 10^{-5} \text{ K}^{-1}$	$T = 100 \text{ K}$		
	$5.55 \cdot 10^{-5} \text{ K}^{-1}$	$T = 295 \text{ K}$		

phonon dispersion relations : Figs. 4.2.3**phonon density of states** : Fig. 4.2.4.**phonon frequencies**

$\nu_{TO}(\Gamma) \beta$	4.7 THz	$T = 5 \text{ K}$	inelastic neutron scattering	79H
γ	5.1 THz			
$\nu_{LO}(\Gamma) \beta$	4.83 THz	$T = 80 \text{ K}$		
γ	6.30 THz			
$\nu_{TA}(X_5)$	1.16(12) THz	$T = 4.2 \text{ K}$	inelastic neutron scattering	77P
$\nu_{LA}(X_3)$	3.69(20) THz		(more detailed table in [77P])	
$\nu_{TO}(X_5)$	6.5 THz			
$\nu_{LO}(X_1)$	7.00(12) THz			
$\nu_{TA}(L_3)$	1.00(12) THz			
$\nu_{LA}(L_1)$	3.40(14) THz			
$\nu_{TO}(L_3)$	5.70(10) THz			
$\nu_{LO}(L_1)$	7.34(16) THz			

second order elastic moduli

c_{11}	$0.47(5) \cdot 10^{12} \text{ dyn cm}^{-2}$	$T = 300 \text{ K}$	neutron scattering	77P
c_{12}	$0.362 \cdot 10^{12} \text{ dyn cm}^{-2}$			
c_{44}^E	$0.145(10) \cdot 10^{12} \text{ dyn cm}^{-2}$			
c_{44}^D	$0.16(2) \cdot 10^{12} \text{ dyn cm}^{-2}$			

isothermal compressibility

κ_T	$2.36 \cdot 10^{-12} \text{ cm}^2 \text{ dyn}^{-1}$	$T = 40 \text{ K}$	calculated from elastic constant	76H1
	$2.38 \cdot 10^{-12} \text{ cm}^2 \text{ dyn}^{-1}$	$T = 100 \text{ K}$	data	

bulk modulus

B	65.0 GPa		powder neutron diffraction	94H1
dB/dp	6.2		FP-LMTO calculation	89K

Debye temperature

Θ_D	187 K	$T = 4.5 \text{ K}$	from inelastic neutron scattering data (see Fig. 4.2.5 for temperature dependence)	77P
------------	-------	---------------------	---	-----

melting temperature

T_m	422°C		melting temperature of β -phase, $\gamma \rightarrow \beta$ phase transition at 407°C	72G
-------	-------	--	--	-----

density

d	4.136 g cm^{-3}		density of γ -phase	72G
-----	---------------------------	--	----------------------------	-----

heat capacity : Fig. 4.2.3.**dielectric constants**

$\varepsilon(0)$	7.9	$T = 293 \text{ K}$	unpublished infrared reflectivity (for temperature dependence, see Fig. 4.2.6)	72K
$d \ln \varepsilon(0)/dp$	$-3.5(2) \cdot 10^{-6} \text{ bar}^{-1}$			74H
$d \ln \varepsilon(0)/dT$	$1.02 \cdot 10^{-3} \text{ K}^{-1}$		$-200 < T < 20 \text{ °C}$	
$\varepsilon(\infty)$	2.19	$T = 293 \text{ K}$		74P

refractive index

n	2.1535(10)	$T = 300 \text{ K}$	at $\lambda[\mu\text{m}] = 0.4047$	82S
	2.1410(10)		0.4078	
	2.0720(10)		0.4358	
	2.0336(10)		0.4678	
	2.0234(10)		0.4800	
	2.0042 (10)		0.5086	
	1.9870(10)		0.5461	
	1.9760(10)		0.5791	
	1.9726(10)		0.5896	
	1.9584(10)		0.6438	
	1.9411(20)		0.7699	

prism refractometer method (Fig. 4.2.7)

piezoelectric stress coefficient

e_{14}	0.45 C m^{-2}	$T = 4.5 \text{ K}$	inelastic neutron scattering	77P
	$0.35 \cdot (1 + 1.21 \cdot 10^{-5} p - 2.4 \cdot 10^{-10} p^2) \text{ C m}^{-2}$		(p in bar)	74H
$d \ln e_{14}/dT$	$-0.90 \cdot 10^{-3} \text{ K}^{-1}$			
$d \ln e_{14}/d \ln V$	-4.8			

electrooptic constant

r_{14}^e	$-2.35(4) \cdot 10^{-12} \text{ mV}^{-1}$	$T = 300 \text{ K}$	constant strain coefficient at $0.633 \mu\text{m}$, heterodyne method	72K
------------	---	---------------------	---	-----

piezooptic constants

$\pi_{11} - \pi_{12}$	$-12.5 \cdot 10^{-12} \text{ m}^2 \text{ N}^{-1}$	$T = 300 \text{ K}$	at $\lambda = 0.5893 \text{ }\mu\text{m}$	71S2
π_{44}	$-6.4 \cdot 10^{-12} \text{ m}^2 \text{ N}^{-1}$			

second-order nonlinear dielectric susceptibility

d_{14}	$8.635 \cdot 10^{-12} \text{ mV}^{-1}$	$T = 295 \text{ K}$	from electrooptic constant at $0.633 \text{ }\mu\text{m}$	72K
----------	--	---------------------	---	-----

third-order nonlinear dielectric susceptibility

$\chi^{(3)}$	$3.0(9) \cdot 10^{-4} \text{ esu}$		extrapolated for vanishing excitation intensities	94H1
--------------	------------------------------------	--	--	------

electromechanical coupling constant

$(k_{15})^2$	$0.127 \cdot (1 + 3.26 \cdot 10^{-5} p - 3.1 \cdot 10^{-10} p^2)$	$(p \text{ in bar})$		74H
--------------	---	----------------------	--	-----

References to 4.2

- 63C Cardona, M.: Phys. Rev. 129 (1963) 69.
65S Shindo, K., Morita, A., Kamimura, H.: J. Phys. Soc. Jpn. 20 (1965) 2054.
67R Ringeissen, J., Nikitine, S.: J. Phys. (Paris) 28 (1967) C3-48.
70K Koda, T., Segawa, Y., Mitani, T.: Phys. Status Solidi 38 (1970) 821.
70M Mohler, F.: Phys. Status Solidi 38 (1970) 81.
71L Lewonczuk, S., Ringeissen, J., Nikitine, S.: J. Phys. (Paris) 32 (1971) 941.
71S1 Staude, W.: Phys. Status Solidi (b) 43 (1971) 367.
71S2 Schwab, C., Robino, P.: Opt. Commun. 4 (1971) 304.
72G Gray, D. E. (ed.): Am. Inst. of Physics Handbook, 3rd ed., section 9, McGraw Hill Book Comp. Inc., New York, Toronto, London 1972.
72K Kaminov, I. P., Turner, E. H.: Phys. Rev. B5 (1972) 1564.
73K Khan, M. A.: J. Phys. (Paris) 34 (1973) 597.
74G Gale, G. M., Mysyrowicz, A.: Phys. Rev. Lett. 32 (1974) 727.
74H Hanson, R. C., Helliwell, K., Schwab, C.: Phys. Rev. B 9 (1974) 2649.
74P Potts, J. F., Hanson, R. C., Walker, C. T., Schwab, C.: Phys. Rev. B9 (1974) 2711.
74S Suga, S., Koda, T.: Phys. Status Solidi (b) 66 (1974) 255.
76H1 Hochheimer, H. D., Shand, M. L., Potts, J. F., Hanson, R. C., Walker, C. T.: Phys. Rev. B14 (1976) 4630.
76H2 Hönerlage, B., Klingshirn, C. Grun, J. B.: Phys. Status Solidi (b) 78 (1976) 599.
77B Barron, T. H. K., Birch, J. A., White, O. K.: J. Phys. C: Solid State Phys. 10 (1977) 1617.
77G Goldmann, A.: Phys. Status Solidi (b) 81 (1977) 9.
77P Prevot, B., Hennion, B., Dorner, B.: J. Phys. C: Solid State Phys. 10 (1977) 3999.
79H Hennion, B., Prevot, B., Krauzman, M., Pick, R. M., Dorner, B.: J. Phys. C: Solid State Phys. 12 (1979) 1609.
80G Grun, J. B.: J. Phys. Soc. Jpn. 49 Suppl. A (1980,) 563.
80M Mita, T., Sôtome, K., Ueta, M.: J. Phys. Soc. Jpn. 48 (1980) 496.
81V Ves, S., Glötzel, D., Cardona, M., Overhof, H.: Phys. Rev. B 24 (1981) 3073.
82F Fröhlich, D., Volkenandt, H.: Solid State Commun. 43 (1982) 189
82S Schwab, C., Goltzené, A.: Progr. Cryst. Growth 5 (1982) 233.
82W Westphal, D., Goldmann, A.: J. Phys. C: Solid State Phys. 15 (1982) 6661.
83B Blacha, A., Ves, S., Cardona, M.: Phys. Rev. B 27 (1983) 6346.
83G Goldmann, A., Westphal, D.: J. Phys. C: Solid State Phys. 16 (1983) 1335.
85F Fröhlich, D., Hölscher, H., Mohler, E.: Proc. 17th Int. Conf. Phys. Semicond., Springer-Verlag, New York 1985, p. 1255.
88G Graneli, B., Dahlborg, U., Fischer, P.: Solid State Ionics 28/30 (1988) 284.
89K Kremer, J. W., Weyrich, K. H.: Phys. Rev. B 40 (1989) 9900.
91F Fröhlich, D., Kohler, P., Nieswand, W., Mohler, E.: Phys. Status Solidi (b) 167 (1991) 147.
94H1 Hasuo, M., Nagasawa, N., Itoh, T., Mysyrowicz, A.: J. Lumin. 60/61 (1994) 758.
94H2 Hull, S., Keen, D.: Phys. Rev. B 50 (1994) 5868.
94R Reimann, K., Rübenacke, St.: Phys. Rev. B49 (1994) 11021.
94W Wang, Cheng-Zhang, Yu, R., Krakauer, H.: Phys. Rev. Lett. 72 (1994) 368.
95S Saito, K., Hasuo, M., Hatano, T., Nagasawa, N.: Solid State Commun. 94 (1995) 33 .

Figures to 4.2

Fig. 4.0.1

The zincblende lattice.

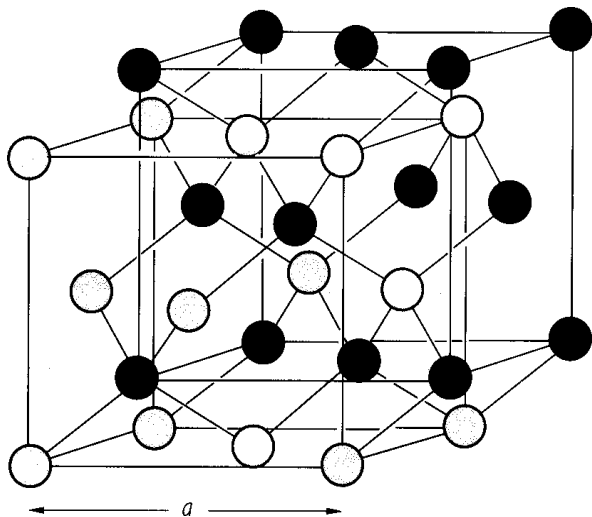
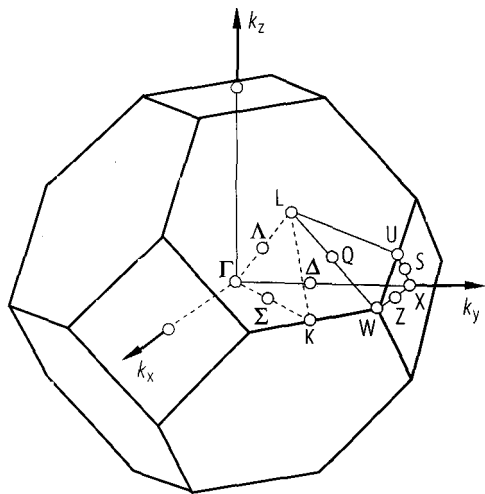


Fig. 4.0.4

The Brillouin zone for the zincblende and the rocksalt lattices.



CuCl. Semirelativistic valence band structure calculated from a self-consistent local-density potential with the LMTO-ASA (linear combination of muffin-tin-orbitals – atomic sphere approximation) method [81V]. $E = 0$ corresponds to uppermost valence band maximum.

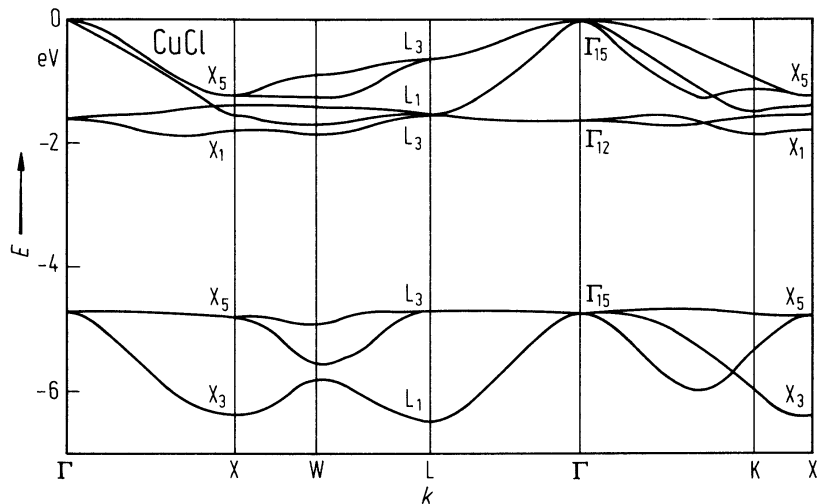


Fig. 4.2.1

CuCl. Lattice parameter vs. temperature showing strong negative thermal expansion between 0 K and 100 K [72P].

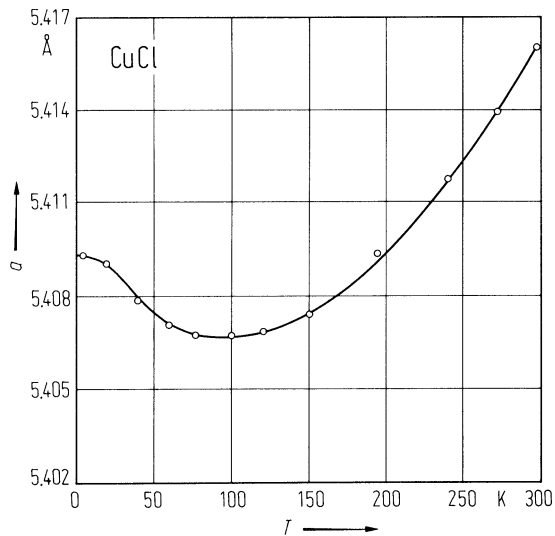
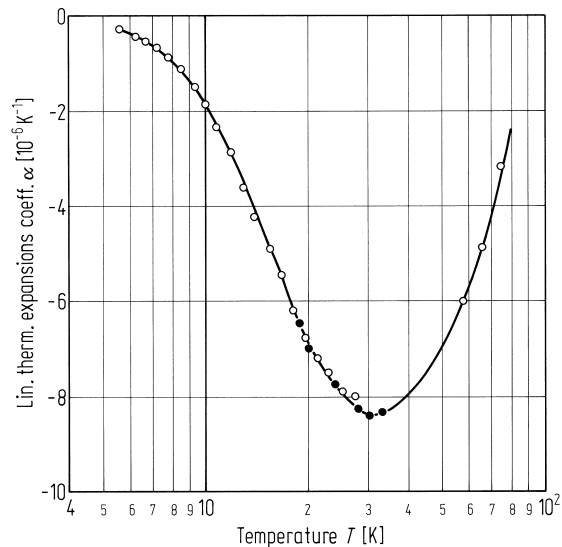
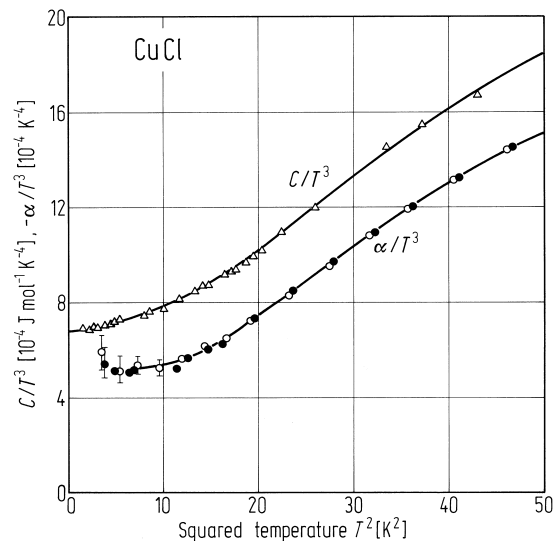


Fig. 4.2.2

CuCl. Left: Temperature dependence of the heat capacity; plotted is C/T^3 vs. T^2 . Right: Temperature dependence of the thermal expansion; plotted is α/T^3 vs. T^2 . Different symbols from different measurements. Right panel shows α vs. T [77B].



CuCl. Phonon dispersion. Experimental data points at 4.2 K (circles) [77P] and theoretical curves (squares and lines) from a full-potential LAPW calculation [94W].

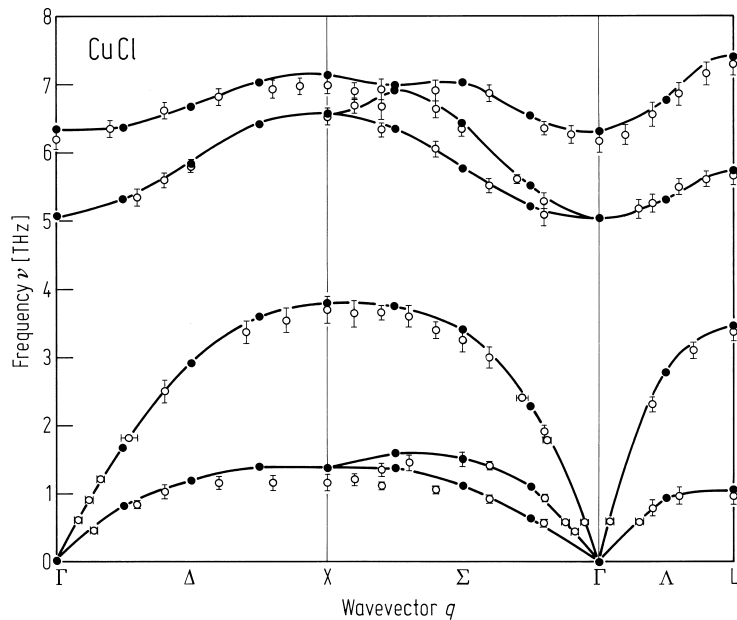


Fig. 4.2.4

CuCl. Phonon density of states derived from the neutron scattering data of Fig. 14 at 4.2 K. The individual contributions for Cu^+ (full line) and Cl^- (broken line) are illustrated showing that the acoustic modes mainly involve the motion of the heavier ion with small contribution from the lighter one, and vice versa for the optic modes [77P].

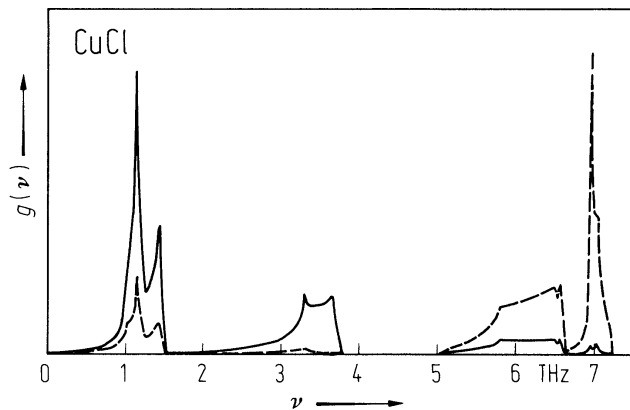


Fig. 4.2.5

CuCl. Temperature dependence of the Debye temperature. Full line computed from neutron scattering data [77P].

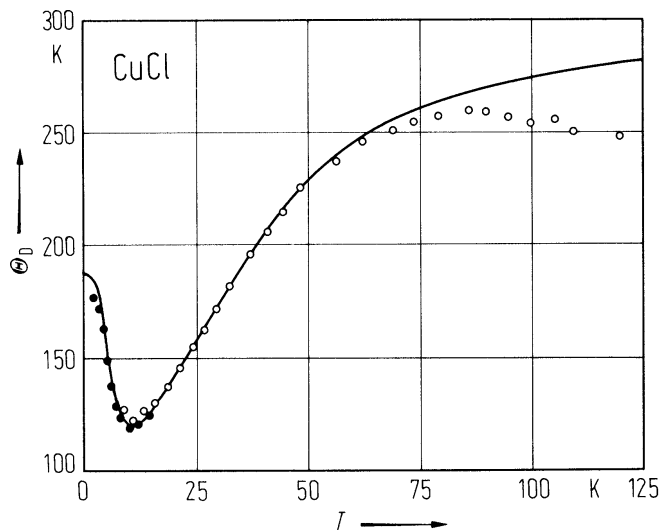


Fig. 4.2.6

CuCl. Low frequency dielectric constant $\epsilon(0)$ vs. temperature between 7 K and 295 K. The data are obtained using ultrasonic techniques (open circles) and Raman scattering data (full circles). $\epsilon(0)$ is normalized to the value 7.9 at 295 K [74P].

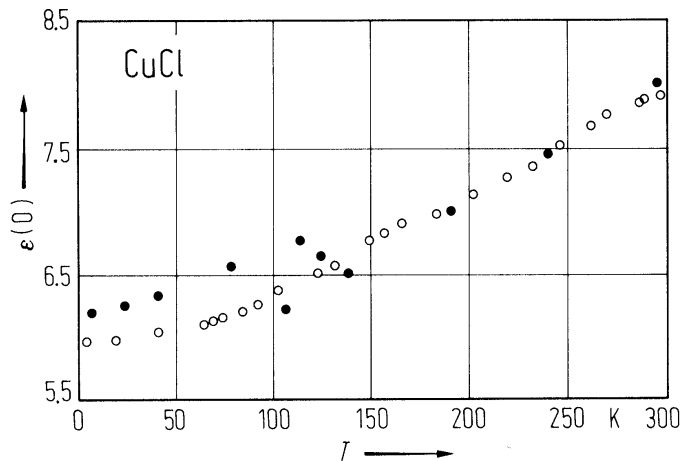
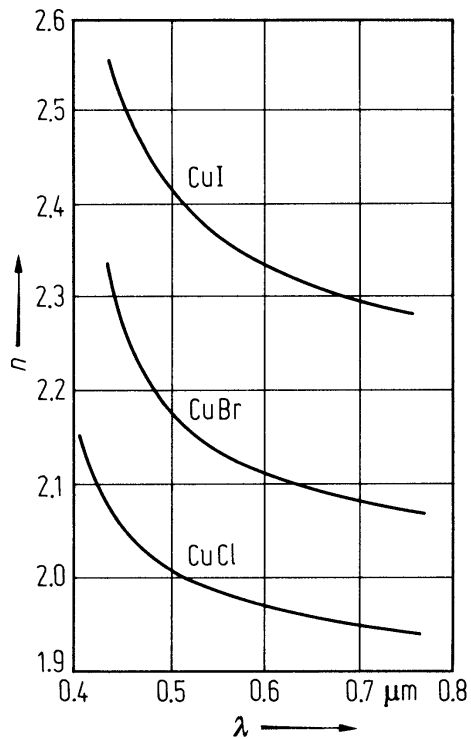


Fig. 4.2.7

CuCl, CuBr, CuI. Refractive index measured by the prism method as a function of wavelength in the visible at $T = 300$ K [82S].



4.3 Cuprous bromide (γ -CuBr)

Crystal structure

γ -CuBr crystallizes under normal conditions in the zincblende structure (space group $T_d^2 - \bar{F}43m$, Fig. 4.0.1).

high temperature phases

α -CuBr	cubic (Br-ions form b.c.c. lattice)	$a = 4.53 \text{ \AA}$	$T = 480^\circ\text{C}$	$469^\circ\text{C} < T < T_m (487^\circ\text{C})$, high ionic conductivity, lattice highly disordered	76F
	cubic, $Fm\bar{3}m$ (Br-ions form fcc lattice)	$a = 4.59(1) \text{ \AA}$	$T = 750 \text{ K}$	Bragg scattering	90Y
β -CuBr	wurtzite, $P6_3mc$ - C_{6v}^4	$a = 4.08(1) \text{ \AA}$ $c = 6.68(1) \text{ \AA}$ $a = 4.09(1) \text{ \AA}$ $c = 6.71(1) \text{ \AA}$ $a = 4.09(1) \text{ \AA}$ $c = 6.71(1) \text{ \AA}$	$T = 670 \text{ K}$ $T = 700 \text{ K}$ $T = 730 \text{ K}$	Bragg scattering	94N

Electronic properties

band structure : Fig. 4.0.7, Brillouin zone: Fig. 4.0.4.

The band structure is qualitatively similar to that of CuCl except the ordering of the uppermost spin-orbit split Γ_8 and Γ_7 valence band states. This leads to the $Z_{1,2}$ exciton transition being observed at lower energy than Z_3 .

direct gap energy

$E_g(\Gamma_{8v}-\Gamma_{6c})$	3.0726 eV	$T = 1.6 \text{ K}$	two-photon absorption	78M
	2.91 eV	$T = 300 \text{ K}$	absorption edge under hydrostatic pressure; value at zero pressure	81V

temperature coefficient of direct gap energy

$dE_{g,dir}/dT$	0.1 meV/K		temperature dependence of reflectivity	81L
-----------------	-----------	--	--	-----

pressure coefficient of direct gap energy

$dE_{g,dir}/dp$	10.0 meV/GPa	$T = 300 \text{ K}$	absorption	81V
-----------------	--------------	---------------------	------------	-----

critical point energies of valence bands (relative to the Γ_8 top of the valence band)

$E(\Gamma_6), E(L_6)$	- 15.4(3) eV		determined at RT by angle-resolved UV photoemission spectroscopy	93M
$E(L_6)$	- 5.6(3) eV			
$E(\Gamma_7)$	- 4.8(3) eV			
$E(L_6)$	- 4.7(3) eV			
$E(\Gamma_8), E(L_{4,5})$	- 4.2(2) eV			
$E(\Gamma_8), E(L_{4,5}), E(L_6)$	- 2.05(1) eV			
$E(L_6)$	- 1.4(3) eV			
$E(\Gamma_{7,8}), E(L_{4,5}), E(L_6)$	- 0.8(3) eV			

edge exciton transition energies

$E_{gx}(Z_{1,2}(1S))$	2.963 eV (Z_1) 2.972 eV (Z_2)	$T = 8 \text{ K}$	absorption	70K, 68T
$E_{gx}(Z_3(1S))$	3.119 eV	$T = 8 \text{ K}$	absorption	70K

transition energies to higher excited exciton states

$E_{\text{gx}}(\text{Z}_{1,2}(2\text{P}))$	3.0556 eV	$T=1.6\text{ K}$	two-photon absorption	78M
$E_{\text{gx}}(\text{Z}_{1,2}(3\text{P}))$	3.0650 eV			
$E_{\text{gx}}(\text{Z}_{1,2}(4\text{P}))$	3.0683 eV			

energies of transverse and longitudinal edge excitons

$E_{\text{gx}}(\text{Z}_{1,2}^{\text{T}}(1\text{S}))$	2.9644(2) eV	$T=4.2\text{ K}$	hyper-Raman scattering	80H
$E_{\text{gx}}(\text{Z}_{1,2}^{\text{L}}(1\text{S}))$	2.9774(2) eV	$T=6\text{ K}$	two-photon absorption	94R
$E_{\text{gx}}(\text{Z}_3^{\text{T}}(1\text{S}))$	3.116 eV	$T=4.2\text{ K}$	absorption	71L

energy of spin-triplet exciton states

$E_{\text{gx}}(\Gamma_3, \Gamma_4)$	2.9627(2) eV	$T=4.2\text{ K}$	hyper-Raman scattering	80H
-------------------------------------	--------------	------------------	------------------------	-----

longitudinal-transverse exciton splitting energy

$\Delta E_{\text{ex}}^{\text{L-T}}(\text{Z}_{1,2})$	12.7 meV	$T=1.6\text{ K}$	hyper-Raman scattering	80N
---	----------	------------------	------------------------	-----

splitting of transverse exciton state and spin triplet state

$\Delta E_{\text{ex}}^{\text{T-t}}(\text{Z}_{1,2})$	1.0 meV	$T=1.6\text{ K}$	hyper-Raman scattering	80N
---	---------	------------------	------------------------	-----

spin orbit splitting energy

Δ_0	150 meV	$T=100\text{ K}$	hydrostatic pressure dependence of thin film absorption	83B1
------------	---------	------------------	---	------

exchange energy for T-exciton

$\Delta_{\text{T}} = \Delta_{\text{ex}} - \Delta_{\text{dip}}$	8 meV	$T=8\text{ K}$	energy shift and intensity ratio of $\text{Z}_{1,2}$ and Z_3 exciton in $\text{CuBr}_x\text{Cl}_{1-x}$	70K
	10 meV	—	average from various exciton energy data ($\Delta_{\text{ex}} = 15\text{ meV}$, $\Delta_{\text{dip}} = 5\text{ meV}$)	77G

exchange energy for L-exciton

$\Delta_{\text{L}} = \Delta_{\text{ex}} + 2\Delta_{\text{dip}}$	25 meV	—	average from various exciton energy data ($\Delta_{\text{ex}} = 15\text{ meV}$, $\Delta_{\text{dip}} = 5\text{ meV}$)	77G
---	--------	---	--	-----

electron-hole exchange energy

Δ	2.7 (6) meV	$T=4.2\text{ K}$	hyper-Raman scattering	80H
	2.6(6) meV	$T=2\ldots 20\text{ K}$	resonant Brillouin scattering	81D
	5(2) meV	$T=100\text{ K}$	exciton absorption under uniaxial stress	83B2

exciton radii of $\text{Z}_{1,2}$ series

$r(1\text{S})$	12.5 Å	$T=4.2\text{ K}$	analysis of exciton absorption series corrected for non-hydrogen like energetic distances	71L
$r(2\text{S})$	52 Å			
$r(3\text{S})$	121 Å			

exciton binding energy of $Z_{1,2}$ -series

$E_b(1S)$	108 meV	—	best value from various optical results analysis of exciton series binding energies of 2S and 3S are doubtful due to complications by exciton-phonon interaction (see [78M])	77G
	109 meV	$T = 4.2$ K		71L
$E_b(2S)$	100 meV			
$E_b(3S)$	94 meV			
$E_b(2P_{1/2}(\Gamma_6))$	14.80 meV	$T = 1.6$ K	two-photon absorption	78M
$E_b(2P_{5/2}(\Gamma_7))$	15.88 meV			
$E_b(2P_{5/2}(\Gamma_8))$	17.35 meV			
$E_b(2P_{3/2}(\Gamma_8))$	19.55 meV			

effective masses

$m_n(\Gamma_{6c})$	$> 0.21 m_0$	$T = 1.6$ K	analysis of two-photon absorption considering anisotropy	78M
$m_p(\Gamma_{7v})$	$0.18 m_0$		tight-binding calculation	96F
$m_p(\Gamma_{8v})$	$4.19 m_0$	$T = 4.2$ K	tight-binding calculation	96F
	$23.2 m_0$		analysis of exciton spectra	71L
$m_{p,l}(\Gamma_{8v})$	$1.12 m_0$	$T = 2...20$ K	resonant Brillouin scattering, light hole masses for k along $[001]$, $[111]$, and $[110]$, respectively	81D
	$1.15 m_0$			
	$1.14 m_0$			
$m_{p,h}(\Gamma_{8v})$	$1.60 m_0$		heavy hole masses for k along $[001]$, $[111]$, and $[110]$, respectively.	
	$1.53 m_0$			
	$1.55 m_0$			

effective exciton mass

$m_{ex,l}(Z_{1,2})$	$0.86 m_0$	$T = 1.6$ K	two-photon excitation, light exciton mass for $k \parallel [111]$	80N
$m_{ex,h}(Z_{1,2})$	$2.6 m_0$	$T = 1.6$ K	heavy exciton mass for $k \parallel [111]$	
$m_{ex}(Z_{1,2}^L)$	$2.0 m_0$	$T = 2...20$ K	resonant Brillouin scattering, mass of longitudinal exciton for k along $[001]$, $[111]$, and $[110]$,	81D
	$2.08 m_0$			
	$2.06 m_0$			

g -factors

$g_{eff}(Z_{1,2})$	$0.22(5)$	$T = 4.5$ K	magneto-reflectivity and magneto- luminescence	76S
$g_{eff}(Z_3)$	$0.35(10)$	$T = 84$ K	Faraday rotation	71S2
$g(\Gamma_{6c})$	$1.84(10)$	$T = 1.6$ K	hyper-Raman scattering in magnetic field;	83M
κ	$-0.22(5)$		g -value of valence band ($k = 0$)	

Lattice properties

lattice parameter (γ -phase, zincblende structure)

a	$5.6773(2) \text{ \AA}$	$T = 35$ K	neutron powder diffraction	94A
	$5.6897(3) \text{ \AA}$	$T = 293$ K		
	$5.6991(3) \text{ \AA}$	$T = 383$ K		

For temperature dependence of the lattice parameter, see Fig. 4.3.1 [63W]

volume thermal expansion coefficient

β	$-0.54 \cdot 10^{-5} \text{ K}^{-1}$	$T = 40 \text{ K}$	determined from data quoted in [72P]	76H
	$1.92 \cdot 10^{-5} \text{ K}^{-1}$	$T = 100 \text{ K}$		
	$4.83 \cdot 10^{-5} \text{ K}^{-1}$	$T = 295 \text{ K}$		

phonon dispersion relations : Fig. 4.3.2, **phonon density of states** : Fig. 4.3.3.

phonon frequencies

$\nu_{\text{TO}}(\Gamma) \gamma$	$4.20 \cdot 10^{12} \text{ s}^{-1}$	$T = 2 \text{ K}$	polariton-Raman scattering	80V
β	$3.63 \cdot 10^{12} \text{ s}^{-1}$	$T = 80 \text{ K}$		
$\nu_{\text{LO}}(\Gamma) \gamma$	$5.07 \cdot 10^{12} \text{ s}^{-1}$	$T = 2 \text{ K}$		

second order elastic moduli

c_{11}	45.8(20) GPa	$T = 300 \text{ K}$	ultrasonic measurements	72H
c_{12}	35.4 GPa			
$(c_{11}-c_{12})/2$	5.2(2) GPa			
c_{44}^{E}	13.9(2) GPa			

isothermal compressibility

κ_{T}	$2.20 \cdot 10^{-12} \text{ cm}^2 \text{ dyn}^{-1}$	$T = 40 \text{ K}$	calculated from elastic constants	76H
---------------------	---	--------------------	-----------------------------------	-----

bulk modulus

B	36.6(8) GPa		neutron powder diffraction	94H
-----	-------------	--	----------------------------	-----

Debye temperature

Θ_{D}	161(2) K	$T = 0 \text{ K}$	determined from the C_{p} data temperature dependence: Fig. 4.3.4	78V
---------------------	----------	-------------------	---	-----

heat capacity

temperature dependence of heat capacity: Fig.4.3.5.

melting temperature

T_{m}	502°C		melting temperature of α -phase	93S
			$\gamma \rightarrow \beta$ phase transition at 386°C	76F
			$\beta \rightarrow \alpha$ phase transition at 469°C	

density

d	4.72 g cm^{-3}			72G
-----	--------------------------	--	--	-----

Transport and optical properties

ionic conductivity

α -CuBr presents an anion Br^- conductivity with a diffusion coefficient of $D = 10^{-7} \text{ cm}^2/\text{s}$ and a cation Cu^+ diffusion coefficient of $D = 3 \cdot 10^{-5} \text{ cm}^2/\text{s}$ [93J, 96T, 97M].

dielectric constants

$\varepsilon(0)$	6.4(6)	$T = 95 \text{ K}$	radio-frequency bridge	74T
$\varepsilon(\infty)$	4.062	$T = 295 \text{ K}$	prism refractometer method	74T

refractive index

n	2.3365(20)	$T = 300 \text{ K}$	at $\lambda[\mu\text{m}] = 0.4358$	82S
	2.2290(20)		0.4678	
	2.2072(20)		0.4800	
	2.1715(20)		0.5086	
	2.1411(20)		0.5461	
	2.1221(20)		0.5791	
	2.1174(20)		0.5896	
	2.0969(20)		0.6438	
	2.0695 (40)		0.7699	
prism refractometer method (see also Fig. 4.3.5)				

piezoelectric stress coefficient

e_{14}	0.222(15) C m^{-2}	$T = 77 \text{ K}/295 \text{ K}$	dynamic dilatometer method	74B
----------	-----------------------------	----------------------------------	----------------------------	-----

electrooptic constant

r_{14}^*	$-2.5 \cdot 10^{-12} \text{ mV}^{-1}$	$T = 295 \text{ K}$	at $\lambda = 0.633 \mu\text{m}$	
	$-3.0 \cdot 10^{-12} \text{ mV}^{-1}$		at $\lambda = 1.15 \mu\text{m}$ and $3.39 \mu\text{m}$	

piezooptic constants

$\pi_{11} - \pi_{12}$	$-10.9 \cdot 10^{-12} \text{ m}^2 \text{ N}^{-1}$	$T = 300 \text{ K}$	at $\lambda = 0.5893 \mu\text{m}$	71S1
π_{44}	$-5.8 \cdot 10^{-12} \text{ m}^2 \text{ N}^{-1}$			

second-order nonlinear dielectric susceptibility

d_{14}	$5.0 \cdot 10^{-12} \text{ mV}^{-1}$	$T = 90 \text{ K}$	from electrooptic constant	74T
			at $\lambda = 3.39 \mu\text{m}$	
	$5.0 \cdot 10^{-12} \text{ mV}^{-1}$		at $\lambda = 1.15 \mu\text{m}$	
	$2.8 \cdot 10^{-12} \text{ mV}^{-1}$		at $\lambda = 0.633 \mu\text{m}$	

References to 4.3

- 63W Wyckoff R. W. G.: "Crystal Structures" Vol. 1, John Wiley & Sons, New York 1963.
- 68T Takahashi, T., Goto, T.: J. Phys. Soc. Jpn. 25 (1968) 461.
- 70K Kato, Y., Yu, C. I., Goto, T.: J. Phys. Soc. Jpn. 28 (1970) 104.
- 71L Lewonczuk, S., Ringeissen, J., Nikitine, S.: J. Phys. (Paris) 32 (1971) 941.
- 71S1 Schwab, C., Robinc, P.: Opt. Commun. 4 (1971) 304.
- 71S2 Suga, S., Koda, T., Mitani, T.: Phys. Status Solidi (b) 48 (1971) 753.
- 72G Gray, D. E. (ed.): Am. Inst. of Physics Handbook, 3rd ed., section 9, McGraw Hill Book Comp. Inc., New York, Toronto, London 1972.
- 72H Hanson, R. C., Hallberg, J. R., Schwab, C.: Appl. Phys. Lett. 21 (1972) 490.
- 72P Plendl, J. N., Mansur, L. C.: Appl. Opt. 11 (1972) 1194.
- 73P Prevot, B., Carabatos, C., Schwab, C., Hennion, B., Moussa, F.: Solid State Commun. 13 (1973) 1725.
- 74B Boese, A., Mohler, F., Pitka, R.: J. Mater. Sci. 9 (1974) 1754.
- 74T Turner, F. M., Kaminov, I. P., Schwab, C.: Phys. Rev. B9 (1974) 2524.
- 76F Funke, K.: J. Solid State Chem. 11 (1976) 345.
- 76H Hochheimer, H. D., Shand, M. L., Potts, J. E., Hanson, R. C., Walker, C.T.: Phys. Rev. B14 (1976) 4630.
- 76S Suga, S., Cho, K., Bettini, M.: Phys. Rev. B13 (1976) 943.
- 77G Goldmann, A.: Phys. Status Solidi (b) 81 (1977) 9.
- 78M Mattausch, H. J., Uihlein, Ch.: Solid State Commun. 25 (1978) 447.
- 78V Vardeny, Z., Gilat, G., Moses, D.: Phys. Rev. B18 (1978) 4487.
- 80H Hönerlage, B., Rössler, U., Duy-Phach Vu, Bivas, A., Grun, J. B.: Phys. Rev. B 22 (1980) 797.
- 80N Nozue, Y., Ueta, M.: Solid State Commun. 36 (1980) 781.
- 80O Overhof, H.: Phys. Status Solidi (b) 97 (1980) 267.
- 80V Vardeny, Z., Brafman, O.: Phys. Rev. B21 (1980) 2585.
- 81D Duy-Phach Vu, Oka, Y., Cardona, M.: Phys. Rev. B 24 (1981) 765.
- 81L Lewonczuk, S., Gross, J. G., Ringeissen, J.: J. Phys. (Paris) Lett. 42 (1981) L-91.
- 81V Ves, S., Glötzel, D., Cardona, M., Overhof, H.: Phys. Rev. B 24 (1981) 3073.
- 82S Schwab, C., Goltzené, A.: Progr. Cryst. Growth 5 (1982) 233.
- 83B1 Blacha, A., Cardona, M., Christensen, N. E., Ves, S., Overhof, H.: Physica 117B & 118B (1983) 63.
- 83B2 Blacha, A., Ves, S., Cardona, M.: Phys. Rev. B 27 (1983) 6346. 71L Lewonczuk, S., Ringeissen, J., Nikitine, S.: J. Phys. (Paris) 32 (1971) 941.
- 83M Merle, J. C., Bivas, A., Wecker, C., Hönerlage, B.: Phys. Rev. B 27 (1983) 3709.
- 90Y Yude, Y., Boyson, H., Schulz, H.: Z. Kristallogr. 191 (1990) 79.
- 93J Johansson, J. X. M. Z., Sköld, K., Jorgensen, J.-E.: Solid State Ionics, Diffusion, & Reaction 59 (1993) 297.
- 93M Matzdorf, R., Skonieczny, J., Westhof, J., Engelhard, H., Goldmann, A.: J. Phys.: Condens. Matter 5 (1993) 3827.
- 93S Shirakawa, Y., Tamaki, S., Okazaki, H., Azuma, M.: J. Phys. Soc. Jpn. 62 (1993) 544.
- 94A Altorfer, F., Graneli, B., Fischer, P., Bühner, W.: J. Phys. Condens. Matter 6 (1994) 9949.
- 94H Hull, S., Keen, D.: Phys. Rev. B 50 (1994) 5868.
- 94N Nield, V. M., McGreevy, R. L., Keen, D. A., Hayes, W.: Physica B 202 (1994) 159.
- 94R Reimann, K., Rübenacke, St.: Phys. Rev. B 49 (1994) 1121.
- 96F Ferhat, M., Zaoui, A., Certier, M., Dufour, J.-P., Khelifa, B.: Mater. Sci. Eng. B 39 (1996) 95.
- 96T Tomoyose, T., Fukuchi, A., Aniya, M.: J. Phys. Soc. Jpn. 65 (1996) 3692.
- 97M McGreevy, R. L., Zheng-Johansson, J. X. M.: Solid State Ionics, Diff. & Reactions 95 (1997) 215.

Figures to 4.3

Fig. 4.0.1

The zincblende lattice.

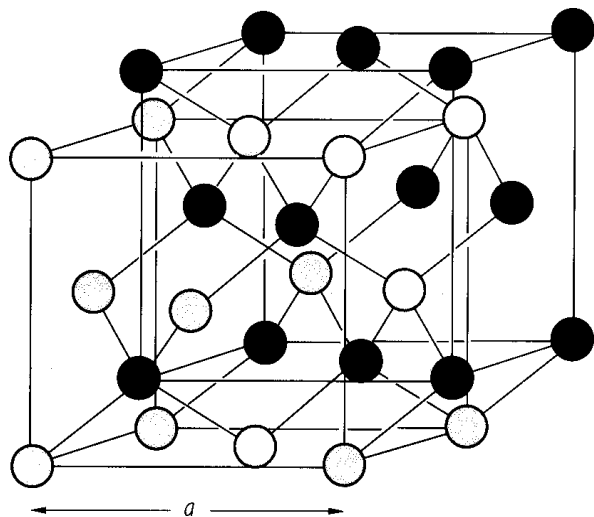


Fig. 4.0.4

The Brillouin zone for the zincblende and the rocksalt lattices.

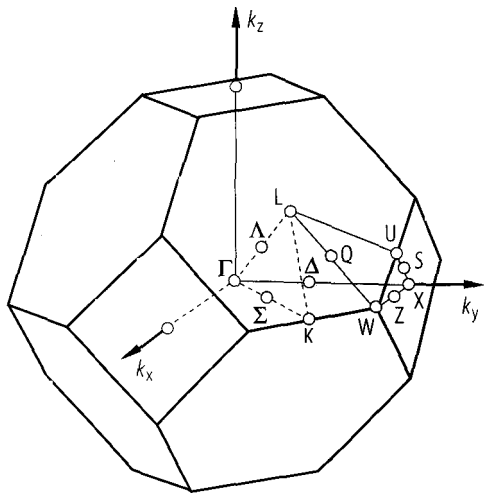


Fig. 4.0.7

CuBr. Electronic band structure calculated by means of the relativistic KKR method [80O].

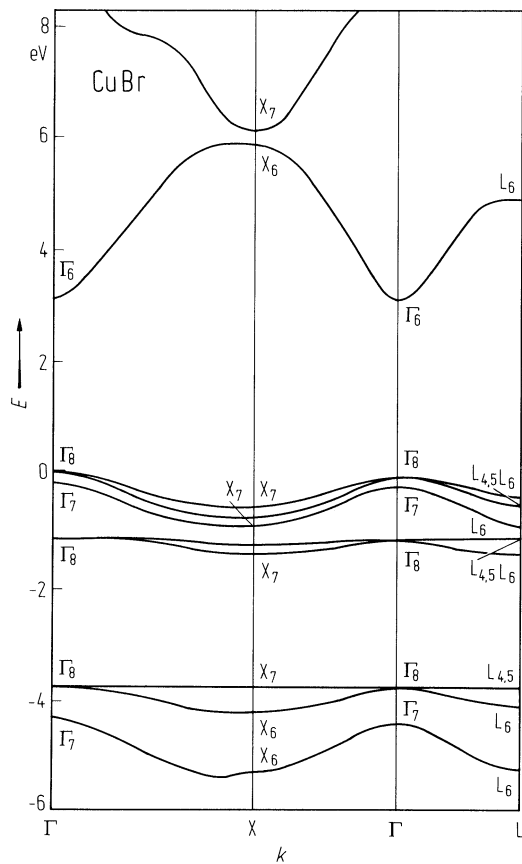


Fig. 4.3.1

CuBr. Temperature dependence of the lattice parameter showing negative thermal expansion at low temperatures [72P].

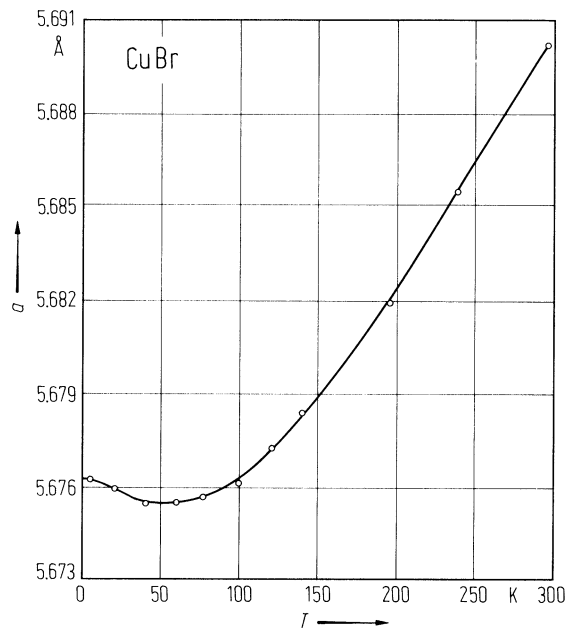


Fig. 4.3.2

CuBr. Phonon dispersion relations measured by inelastic neutron scattering at 77 K and 293 K, respectively. The full and dashed lines are shell-model fits with two-different sets of fitting parameters [76H].

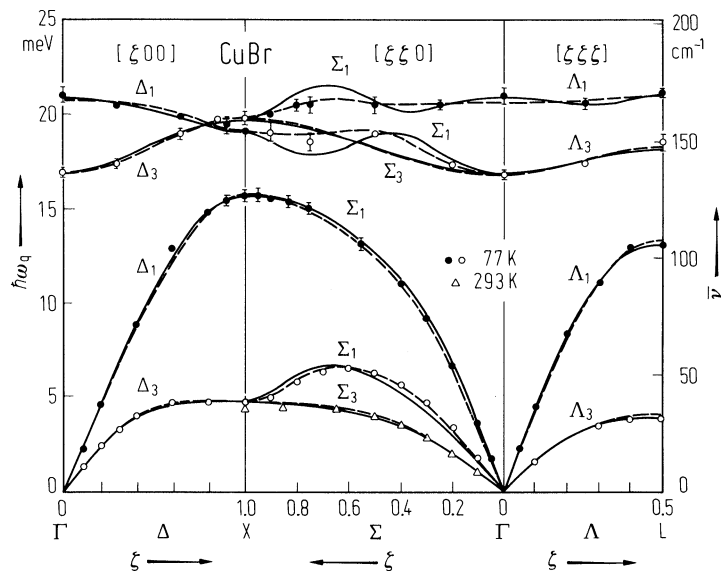


Fig. 4.3.3

CuBr. Phonon density of states derived from the neutron scattering data of Fig. 1 at 77 K. The full and dashed lines follow from two different shell-model fits of the dispersion relations [76H].

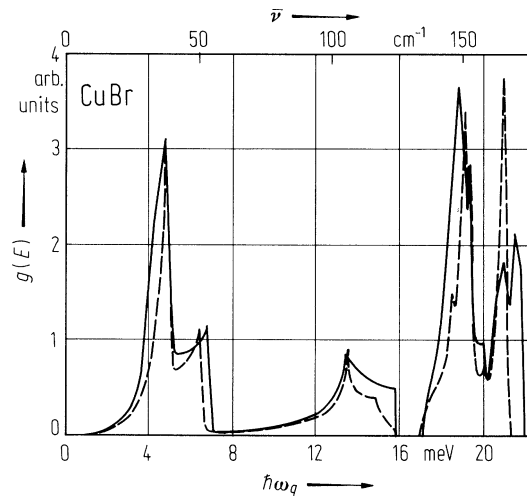


Fig. 4.3.4

CuBr. Temperature dependence of the Debye temperature. The theoretical data are computed from inelastic neutron scattering data of [73P] applying a 9 parameter shell model [78V].

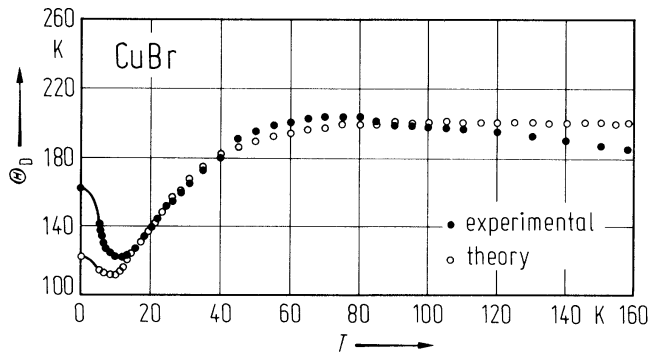


Fig. 4.3.5

CuBr. Heat capacity vs. temperature between 5 K and 160 K measured by the adiabatic calorimetric method (full circles). The open circles (theoretical) are obtained from inelastic neutron scattering data at room temperature of [73P]. Figure from [78V].

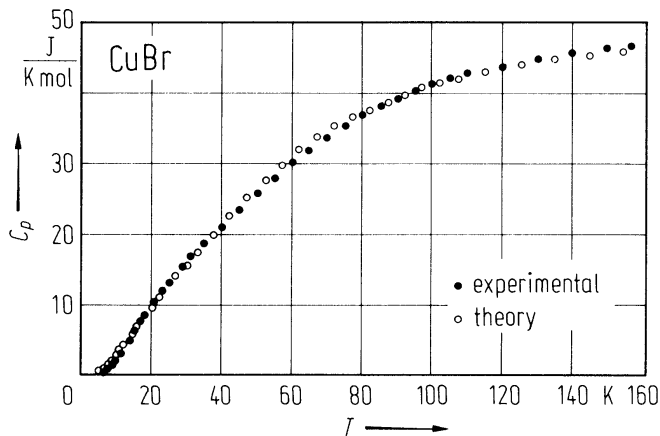
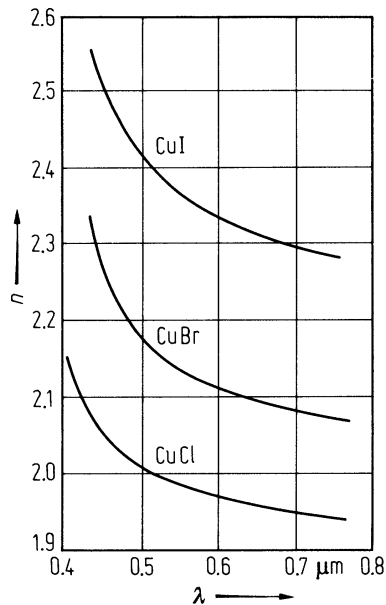


Fig. 4.3.6

CuCl, CuBr, CuI. Refractive index measured by the prism method as a function of wavelength in the visible at $T = 300\text{ K}$ [82S].



4.4 Cuprous iodide (γ -CuI)

Crystal structure

γ -CuI crystallizes at normal conditions in the zincblende structure (space group $T_d^2 - F\bar{4}3m$, Fig. 4.0.1).

high temperature phases

α -CuI	cubic (I-ions form f.c.c. lattice)	$a = 6.13 \text{ \AA}$	$T = 430^\circ\text{C}$	$408^\circ\text{C} < T < T_m (602^\circ\text{C})$, high ionic conductivity, lattice highly disordered	76F2
	cubic, $Fm\bar{3}m$ (I-ions form fcc lattice)	$a = 6.148(1) \text{ \AA}$	$T > 680 \text{ K}$	neutron scattering	90Y
Temperature dependence ($673 \text{ K} < T < T_m$) by neutron powder diffraction [95K]					
Melting temperature $T_m = 878 \text{ K}$					
β -CuI	wurtzite, $P6_3mc - C_{6v}^4$	$a = 4.289(9) \text{ \AA}$ $c = 7.189(5) \text{ \AA}$	$T < 680 \text{ K}$	neutron scattering	90Y
		$a = 4.30419(2) \text{ \AA}$ $c = 7.18510(5) \text{ \AA}$	$T = 655 \text{ K}$	neutron scattering	94K

Temperature dependence ($643 \text{ K} < T < 673 \text{ K}$) by neutron powder diffraction [95K]

Indications for different intermediate phases between 4 K and 800 K are reported in [93P, 95P] using monochromatic diffuse reflectance measurements.

Electronic properties

band structure : Band structure: Fig. 4.0.8, Brillouin zone: Fig. 4.0.4.

The band structure [80O] is qualitatively similar to CuBr with the Γ_8 valence band higher in energy than the Γ_7 . Compared to the calculations for CuCl and CuBr, in CuI the spin-orbit splittings are increased.

direct gap energy

$E_g(\Gamma_{8v} - \Gamma_{6c})$	3.118 eV	$T = 80 \text{ K}$	piezobirefringence	89G
	2.95 eV	$T = 300 \text{ K}$	absorption edge under hydrostatic pressure, value at zero pressure	81V

pressure coefficient of direct gap energy

$dE_{g,dir}/dp$	19.2 meV/GPa	$T = 300 \text{ K}$	absorption edge under hydrostatic pressure, value at zero pressure	81V
-----------------	--------------	---------------------	--	-----

edge exciton transition energies

$E_{gx}(Z_{1,2}(1S))$	3.06 eV	$T = 4.2 \text{ K}$	absorption	63C
$E_{gx}(Z_3(1S))$	3.70 eV			

longitudinal-transverse exciton splitting energy

$\Delta E_{ex}^{L-T}(Z_{1,2})$	6.1 meV	$T = 4.5 \text{ K}$	magneto-luminescence and -reflectance	80S
--------------------------------	---------	---------------------	---------------------------------------	-----

splitting of transverse exciton state and spin-triplet state

$\Delta E_{ex}^{T-t}(Z_{1,2})$	0.4 meV	$T = 4.5 \text{ K}$	magneto-luminescence and -reflectance	80S
--------------------------------	---------	---------------------	---------------------------------------	-----

transition energies to higher excited exciton states

$E_{\text{gx}}(\text{Z}_{1,2}(2\text{S}))$	3.106 eV	$T = 4.2 \text{ K}$	absorption	74B1
$E_{\text{gx}}(\text{Z}_{1,2}(2\text{P}))$	3.111 eV	$T = 4.2 \text{ K}$	two-photon absorption	
$E_{\text{gx}}(\text{Z}_{1,2}(3\text{P}))$	3.120 eV	$T = 4.2 \text{ K}$		

spin-orbit splitting energy

Δ_0	640 meV	$T = 100 \text{ K}$	hydrostatic pressure dependence of thin film absorption	83B
------------	---------	---------------------	--	-----

exciton radii of $\text{Z}_{1,2}$ -series

$r(1\text{S})$	16 Å	—	analysis of exciton absorption	70U
----------------	------	---	--------------------------------	-----

exciton binding energy of $\text{Z}_{1,2}$ -series

$E_{\text{b}}(1\text{S})$	58 meV	$T = 8 \text{ K}$	analysis of exciton and reflectivity data	68G
---------------------------	--------	-------------------	---	-----

electron-hole exchange energy

Δ	1.8(2) meV	$T = 100 \text{ K}$	exciton absorption under uniaxial stress	75A
----------	------------	---------------------	---	-----

effective masses

$m_{\text{n}}(\Gamma_{6\text{c}})$	0.30(1) m_0	—	analysis of luminescence	76H2
$m_{\text{p}}(\Gamma_{8\text{v}})$	2.4(3) m_0			

reduced effective exciton mass

$\mu_{\text{ex}}(\text{Z}_{1,2})$	0.27 m_0			73Y
-----------------------------------	------------	--	--	-----

g-factors

$g(\Gamma_{6\text{c}})$	0.68 (15)	$T = 4.5 \text{ K}$	magneto-reflectance, g-value of conduction band	80S
κ	-0.19		g-value of valence band ($k = 0$)	
$g_{\text{eff}}(\text{Z}_{1,2})$	0.35(5)	$T = 4.2 \text{ K}$	magnetic circular dichroism	73S

Lattice properties**lattice parameter**

a	6.05214(8) Å	$T = 303 \text{ K}$	powder neutron diffraction	95K
-----	--------------	---------------------	----------------------------	-----

volume thermal expansion coefficient

β	1.41·10 ⁻⁵ K ⁻¹	$T = 40 \text{ K}$	determined from data quoted in [72P]	76H1
	4.26·10 ⁻⁵ K ⁻¹	$T = 100 \text{ K}$		
	4.20·10 ⁻⁵ K ⁻¹	$T = 295 \text{ K}$		

phonon dispersion relations : Fig. 4.4.1 , **phonon density of states** : Fig. 4.4.2.

phonon frequencies

$\nu_{\text{TO}}(\Gamma)$	3.99·10 ¹² s ⁻¹	$T = 4.2 \text{ K}$	Raman scattering	76F1
	3.72·10 ¹² s ⁻¹	$T = 300 \text{ K}$	Raman scattering	74P
$\nu_{\text{LO}}(\Gamma)$	4.53·10 ¹² s ⁻¹	$T = 4.2 \text{ K}$	Raman scattering	76F1
	4.80·10 ¹² s ⁻¹	$T = 300 \text{ K}$	inelastic neutron scattering	72H

elastic moduli

c_{11}	45.1(20) GPa	$T = 300$ K	ultrasonic measurements	72H
c_{12}	30.7 GPa			
$(c_{11}-c_{12})/2$	07.2(2) GPa			
c_{44}^E	18.2(2) GPa			
c_{44}^D	18.5(2) GPa			

isothermal compressibility

κ_T	$2.48 \cdot 10^{-12}$ cm ² dyn ⁻¹	$T = 40$ K	calculated from elastic constant data	76H1
	$2.70 \cdot 10^{-12}$ cm ² dyn ⁻¹	$T = 295$ K		

bulk modulus

B	31(2) GPa		angle-dispersive X-ray diffraction	95H
-----	-----------	--	------------------------------------	-----

Debye temperature

Θ_D	168(1) K	$T = 0$ K	determined from the C_p data of Fig. 4.4.3	78V
------------	----------	-----------	--	-----

temperature dependence of heat capacity : Fig. 4.4.4**melting temperature**

T_m	595 °C		melting temperature of α -phase;	93S
			$\gamma \rightarrow \beta$ phase transition at 369°C,	76F1
			$\beta \rightarrow \alpha$ phase transition at 408°C	

density

d	5.667 g cm ⁻³			72G
-----	--------------------------	--	--	-----

Transport and optical properties**ionic conductivity**

α -CuI is a fast Cu ⁺ ion conductor with conductivity $\sigma > 0.1$ Ω^{-1} cm ⁻¹ for $T > 350^\circ\text{C}$.	93P
---	-----

dielectric constants

$\varepsilon(0)$	6.5	$T = 4$ K	quoted in [72H1]	72H1
$\varepsilon(\infty)$	4.58	$T = 300$ K	transmission/reflectivity measurements	74A

energy dependence of dielectric constant : Fig. 4.4.5**refractive index**

n	2.5621(20)	$T = 300$ K	at $\lambda[\mu\text{m}] = 0.4358$	82S
	2.4617(20)		0.4678	
	2.4485 (20)		0.4800	
	2.4110(20)		0.5086	
	2.3726(20)		0.5461	
	2.3475(20)		0.5791	
	2.3428(20)		0.5896	
	2.3156(20)		0.6438	
	2.2802(40)		0.7699	
			prism refractometer method (Fig. 4.4.6)	

piezoelectric stress coefficient

e_{14}	0.127(20) Cm ⁻²	$T = 77/295$ K	dynamic dilatometer method	74B2
----------	----------------------------	----------------	----------------------------	------

piezooptic constants

$\pi_{11} - \pi_{12}$	$-10.2 \cdot 10^{-12} \text{ m}^2 \text{ N}^{-1}$	$T = 300 \text{ K}$	at $\lambda = 0.5893 \text{ }\mu\text{m}$	71S
π_{44}	$-3.6 \cdot 10^{-12} \text{ m}^2 \text{ N}^{-1}$			

third-order nonlinear dielectric susceptibility

$\chi^{(3)}$	10^{-6} esu		biexciton resonant two-photon absorption	87K
--------------	-----------------------	--	--	-----

References to 4.4

- 63C Cardona, M.: Phys. Rev. 129 (1963) 69.
68G Goto, T., Takahashi, T.: J. Phys. Soc. Jpn. 24 (1968) 314.
70U Ueta, M.: Rev. Roum. Phys. 15 (1970) 369.
71S Schwab, C., Robinc, P.: Optics Commun. 4 (1971) 304.
72G Gray, D. E. (ed.): Am. Inst. of Physics Handbook, 3rd ed. section 9, McGraw Hill Book Comp. Inc., New York, Toronto, London 1972.
72H1 Hanson, R. C., Hallberg, J. R., Schwab, C.: Appl. Phys. Lett. 21 (1972) 490.
72H2 Hennion, B., Moussa, F., Prevot, B., Carabatos, C., Schwab, C.: Phys. Rev. Lett. 28 (1972) 964.
72P Plendl, J. N., Mansur, L. C.: Appl. Opt. 11 (1972) 1194.
73S Suga, S., Koda, T.: J. Phys. Soc. Jpn. 35 (1973) 944.
73Y Yu, C. T., Goto, T., Ueta, M.: J. Phys. Soc. Jpn. 34 (1973) 693.
74A Ageev, L. A., Miloslavskii, V. K., Maksimenko, T. I.: Opt. Spectrosc. (USSR) 36 (1974) 76.
74B1 Bivas, A., Marange, C.: J. Phys. (Paris) 35 (1974) C3-39.
74B2 Boese, A., Mohler, E., Pitka, R.: J. Mater. Sci. 9 (1974) 1754.
74P Prevot, B., Sieskind, M.: Phys. Status Solidi (b) 61 (1974) K121.
75A Ageev, L. A., Miloslavskii, V. K., Maksimenko, T. I.: Sov. Phys. Solid State 16 (1975) 1873.
76F1 Fukumoto, T., Nakashima, S., Tabuchi, K., Mitsuishi, A.: Phys. Status Solidi (b) 73 (1976) 341.
76F2 Funke, K.: Solid State Chem. 11 (1976) 345.
76H1 Hochheimer, H. D., Shand, M. L., Potts, J. F., Hanson, R. C., Walker, C. T.: Phys. Rev. B14 (1976) 4630.
76H2 Hönerlage, B., Klingshirn, C., Grun, J. B.: Phys. Status Solidi (b) 78 (1976) 599.
78V Vardeny, Z., Gilat, G., Moses, D.: Phys. Rev. B18 (1978) 4487.
80O Overhof, H.: Phys. Status Solidi (b) 97 (1980) 267.
80S Suga, S., Cho, K., Niji, Y., Merle, J. C., Sauder, T.: Phys. Rev. B 22 (1980) 4931.
81V Ves, S., Glötzel, D., Cardona, M., Overhof, H.: Phys. Rev. B24 (1981) 3073.
82S Schwab, C., Goltzené, A.: Progr. Cryst. Growth 5 (1982) 233.
83B Blacha, A., Cardona, M., Christensen, N. E., Ves, S., Overhof, H.: Physica 117B& 118B (1983) 63.
87K Kuwata, M.: J. Lumin. 38 (1987) 247.
89G Gogolin, O. V., Deiss, J. L., Tsitsichvili, E. G.: Il Nuovo Cimento D 11 (1989) 1525.
90Y Yude, Y., Boysen, H. Schulz, H.: Z. Kristallogr. 191 (1990) 79.
93P Pfitzner, A., Lutz, H. D.: Z. Kristallogr. 205 (1993) 165.
93S Shirakawa, Y., Tamaki, S., Okazaki, H., Azuma, M.: J. Phys. Soc. Jpn. 62 (1993) 544.
94K Keen, D. A., Hull, S.: J. Phys. Condens. Matter 6 (1994) 1637.
95H Hofmann, M., Hull, S., Keen, D. A.: Phys. Rev. B 51 (1995) 12022.
95K Keen, D. A., Hull, S.: J. Phys. Condens. Matter 7 (1995) 5793.
95P Paic, M.: Fizika A 4 (1995) 473.

Figures to 4.4

Fig. 4.0.1

The zincblende lattice.

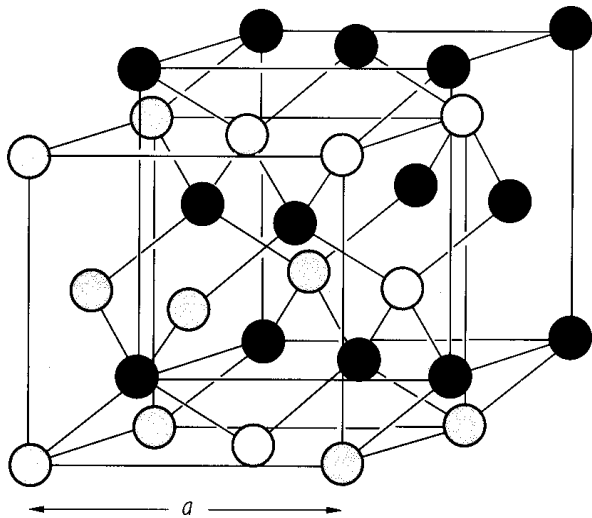
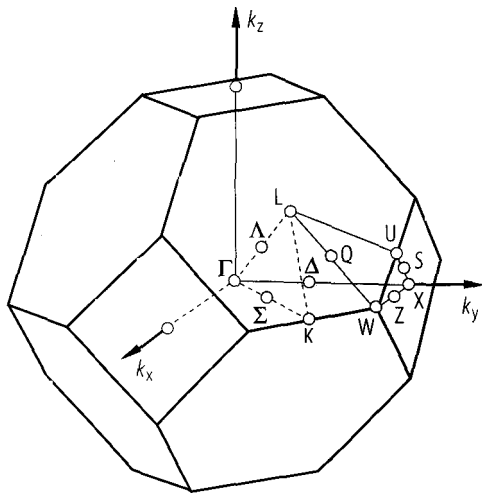


Fig. 4.0.4

The Brillouin zone for the zincblende and the rocksalt lattices.



CuI. Electronic band structure calculated by means of the relativistic KKR-method [800].

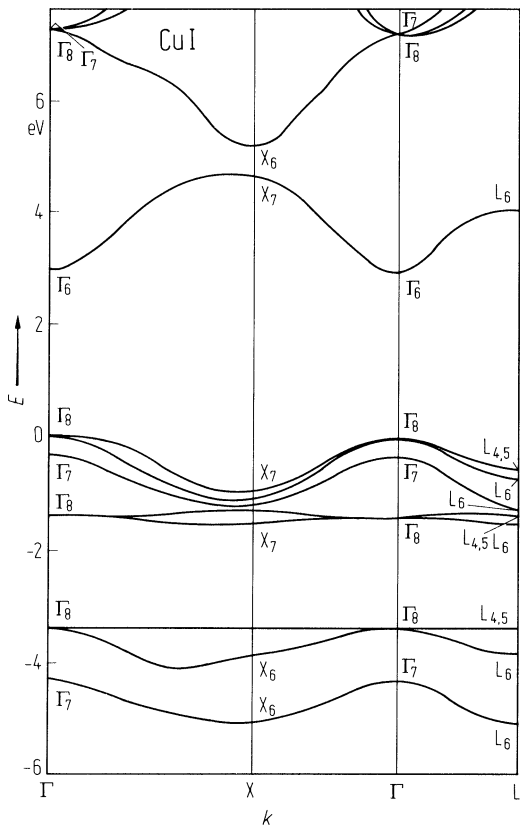


Fig. 4.4.1

CuI. Phonon dispersion relations measured by inelastic neutron scattering at room temperature. The full lines are obtained from a rigid ion model fit using 6 short-range parameters [72H2]. L, T: longitudinal and transverse polarizations.

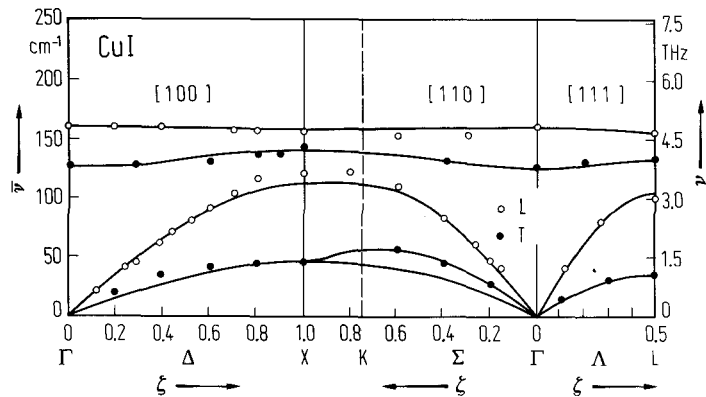


Fig. 4.4.2

CuI. Phonon density of states derived from the neutron scattering data of Fig. 5 at room temperature [72H2].

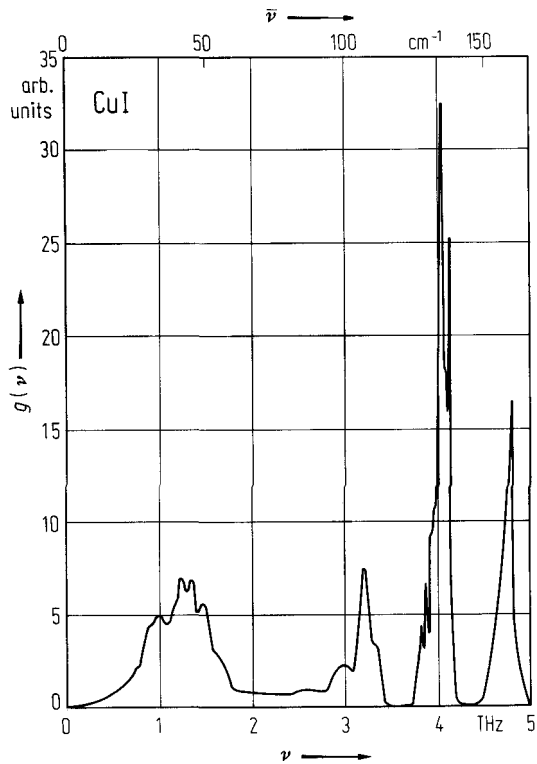


Fig. 4.4.3

CuI. Temperature dependence of the Debye temperature. The experimental data (full circles) are obtained from adiabatic calorimetric measurements of the heat capacity. The theoretical data (open circles) are computed from inelastic neutron scattering data of [72H2] applying a 9 parameter shell model [78V].

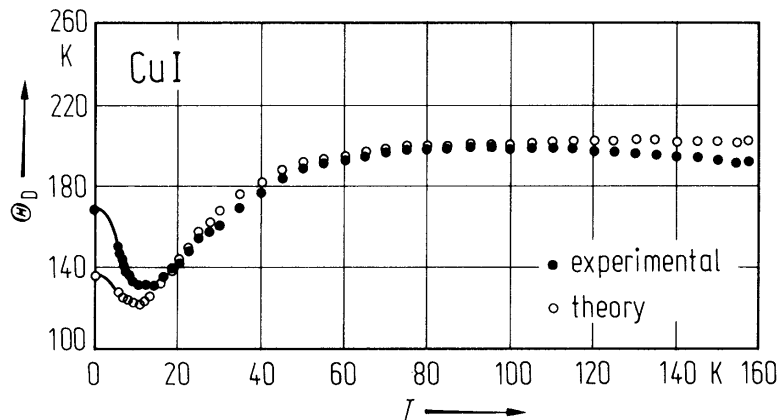


Fig. 4.4.4

CuI. Heat capacity vs. temperature between 5 K and 160 K measured by the adiabatic calorimetric method (experimental points). The open circles (theoretical) are obtained from inelastic neutron scattering data at room temperature [72H2]. Figure from [78V].

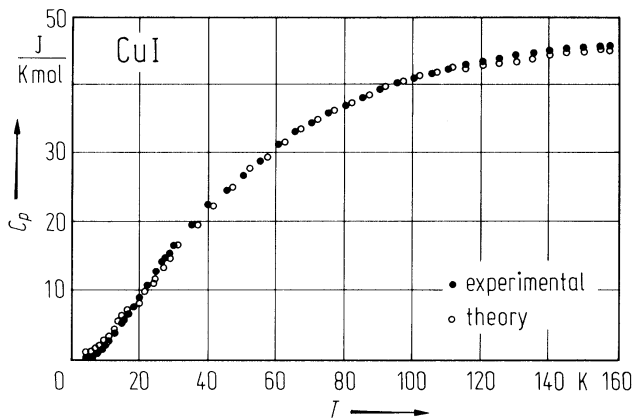


Fig. 4.4.5

CuI. Real (ϵ_1) and imaginary (ϵ_2) parts of the dielectric function vs. photon energy in the region of the $Z_{1,2}$ exciton at 4.2 K. Dashed line 2: suggested band-to-band transition. Dashed lines 1 and 3: exciton band assumed to be of symmetric and asymmetric line shape [74A].

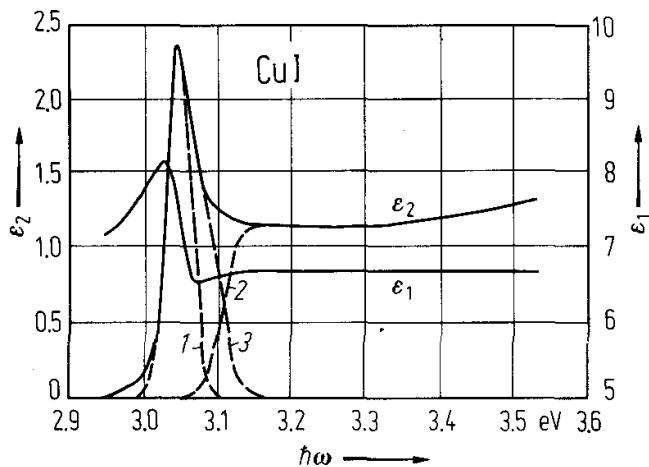
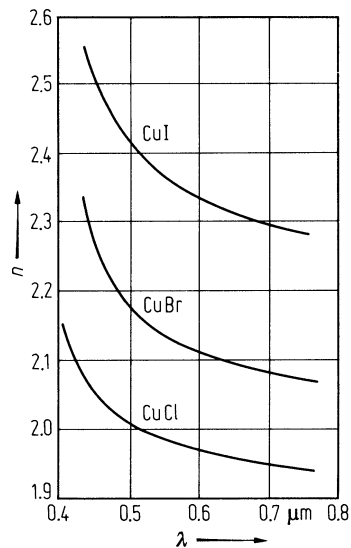


Fig. 4.4.6

CuCl, CuBr, CuI. Refractive index measured by the prism method as a function of wavelength in the visible at $T = 300\text{ K}$ [82S].



4.5 Silver monofluoride (AgF)

Crystal structure

AgF crystallized under normal conditions in the rocksalt structure (Fm3m – O_h⁵, Fig. 4.0.3)

Only crystalline thin films of AgF were prepared so far. The fact that it is hygroscopic and highly reactive, together with the existence of silver subfluoride (Ag₂F) and silver difluoride (AgF₂), have made it difficult to prepare samples suitable for spectroscopic examinations of all kinds [71M, 72B2]. Thus AgF remained largely unstudied up to now.

Electronic properties

band structure : Fig. 4.0.9, Brillouin zone: Fig. 4.0.4.

In contrast to AgCl and AgBr, the highest valence band is found to be largely formed from the Ag⁺ 4d-function and lies above the F⁻ 2p-valence band. The uppermost maximum is at L ([72B1] and Fig. 4.5.1) with subsidiary maxima at Σ and Δ. Selected electronic states have been computed, at points of high symmetry by means of the mixed basis method [72F]. The peculiar valence band ordering in AgF is thought to explain that direct and indirect exciton energies [71M] do not scale properly in going from AgBr to AgCl to AgF (for extensive discussions, see [72B1, 72F]).

The lowest conduction band minimum is suggested to be at Γ.

indirect exciton gap energy

$E_{\text{gx,ind}}(\text{L}_{3\text{v}}-\Gamma_{1\text{c}})$	2.8(3) eV	$T = 4.8 \text{ K}$	thin film absorption	71M
--	-----------	---------------------	----------------------	-----

direct exciton transition energy

$E_{\text{gx,dir}}$	4.63(2) eV	$T = 4.8 \text{ K}$	thin film absorption, line assigned to transition at Γ	71M
---------------------	------------	---------------------	--	-----

Lattice and optical properties

lattice parameter

a	4.936(1) Å	$T = 300 \text{ K}$	X-ray diffraction	71M
-----	------------	---------------------	-------------------	-----

phonon frequencies

$(\nu/c)_{\text{TO}}(\Gamma)$	$5.2 \cdot 10^{12} \text{ s}^{-1}$	$T = 143 \text{ K}$	infrared transmission	72B1
$(\nu/c)_{\text{LO}}(\Gamma)$	$9.66 \cdot 10^{12} \text{ s}^{-1}$	$T = 143 \text{ K}$		

Debye temperature

Θ_{D}	269 (16) K	$T = 0 \text{ K}$	average value	72B1
---------------------	------------	-------------------	---------------	------

melting temperature

T_{m}	708 K			72G
----------------	-------	--	--	-----

density

d	5.852 g cm ⁻³			72G
-----	--------------------------	--	--	-----

dielectric constants

$\varepsilon(0)$	10.6(7)	$T = 300 \text{ K}$	estimated from Lyddane-Sachs-Teller relation using $n = 1.73(2)$ from refraction index determined from ellipsometry	72B1
$\varepsilon(\infty)$	2.99	$T = 300 \text{ K}$		

refractive index

n	1.80(2)	$T = 300 \text{ K}$	from ellipsometry at 546.1 nm	72B1
-----	---------	---------------------	-------------------------------	------

References to 4.5

- 71M Marchetti, A. P., Bottger, G. L.: Phys. Rev. B3 (1971) 2604.
- 72B1 Birtcher, R. C., Deutsch, P. W., Wendelken, J. F., Kunz, A. B.: J. Phys. C: Solid State Phys. 5 (1972) 562.
- 72B2 Bottger, G. L., Geddes, A. L.: J. Chem. Phys. 56 (1972) 3735.
- 72F Fowler, W. B.: Phys. Status Solidi (b) 52 (1972) 591.
- 72G Am. Inst. of Physics Handbook (ed. D. F. Gray) McGraw Hill Book, 1972, 3rd ed., section 9.

Figures to 4.5

Fig. 4.0.3

The rocksalt lattice.

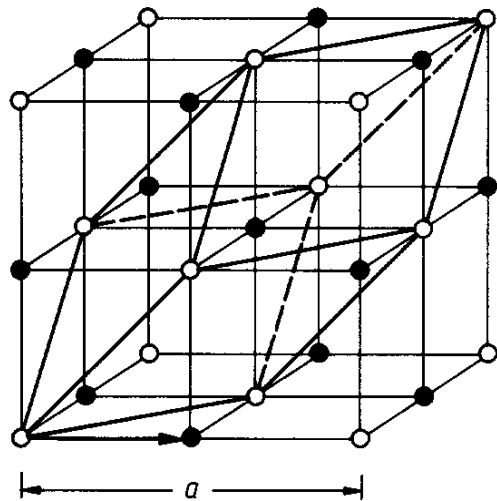


Fig. 4.0.4

The Brillouin zone for the zincblende and the rocksalt lattices.

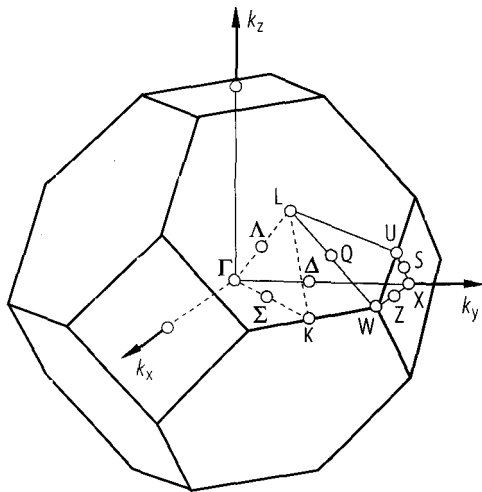
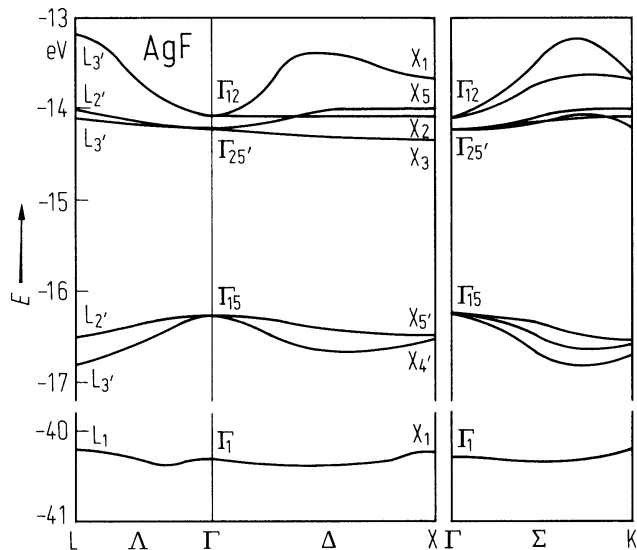


Fig. 4.0.9

AgF. Valence band structure calculated by means of the tight-binding method. Energy shown vs. reduced wavevector. Origin at Cl^- [72B1].



4.6 Silver chloride (AgCl)

Crystal structure

AgCl crystallized under normal conditions in the rocksalt structure ($Fm\bar{3}m - O_h^5$, Fig. 4.0.3) and retains this structure up to the melting temperature ($T_m = 728$ K). There is an indication of a phase transition at 7.1(3) GPa from the discontinuity of elastic properties under pressure [76V].

Electronic properties

band structure : Figs. 4.0.10, Brillouin zone: Fig. 4.0.4.

The complex valence band structure is due to mixing of the Ag^+ 4d- and Cl^- 3p-states placed within about 1 eV to each other. Due to inversion symmetry no mixing occurs at Γ ($k = 0$). There, the valence states are either mostly pure p of the halogen (Γ_{15}) or d of the metal (Γ_{12} , $\Gamma_{25'}$). Because of strong mixing for $k \neq 0$ uppermost maxima at L and Σ , nearly degenerate, are predicted in [65S, 76S1, 76W, 81O]. The valence band at Δ is found to be highest and nearly degenerate with the maximum at L and Σ . Inclusion of spin-orbit interaction (Fig. 1) splits Γ_{15} into Γ_8^- and Γ_6^- , and L_3 into L_4^+ , L_5^+ (degenerate) and L_6^+ (for different choice of origin: $L_3 \rightarrow L_3'$ and L_3' into L_4^- , L_5^- and L_6^-). The splittings estimated in [65B] are 0.13 eV (from spin-orbit splitting of atomic Cl) and 0.05 eV, respectively, while the KKR calculation of Fig. 4.0.10 gives 0.16 eV and 0.02 eV, respectively.

indirect exciton gap energy

$E_{gx,ind}(L_{3v}-\Gamma_{1c})$	3.248 eV	$T = 1.8$ K	absorption measurements	93S
----------------------------------	----------	-------------	-------------------------	-----

indirect exciton absorption threshold

$E_{gx,ind}^{thr} = E_{gx,ind} + h\nu_{TA}(L)$	3.2558 eV	$T = 1.8$ K	resonant light scattering	83N
--	-----------	-------------	---------------------------	-----

pressure and temperature coefficient:

$dE_{gx,ind}^{thr}/dp$	- 15 meV/GPa	$T = 1.5$ K	absorption edge under high hydrostatic pressure	85Y
------------------------	--------------	-------------	---	-----

$dE_{gx,ind}/dT$	- $8.7 \cdot 10^{-4}$ eV/K		temperature dependence of absorption edge	69B2
------------------	----------------------------	--	---	------

TO or LO assisted indirect exciton emission

$E_{x,ind}$	3.238 eV	$T = 2$ K	luminescence measurements	95K
-------------	----------	-----------	---------------------------	-----

exciton binding energy

$E_{b,ind}$	23(2) meV	$T = 4.2$ K	analysis of indirect absorption edge	68A1
-------------	-----------	-------------	--------------------------------------	------

electron-hole exchange interaction

Δ	0.7(1) meV	$T = 4.2$ K	high-field magnetoabsorption	78K
----------	------------	-------------	------------------------------	-----

g-factor

$g(\Gamma)$	1.878	$T = 1.2$ K	ENDOR stimulated echo on intrinsic, shallow trapped electron centers	95B
-------------	-------	-------------	--	-----

direct exciton gap energy

$E_{gx,dir}$	5.13(5) eV	$T = 4.2$ K	thin film transmission, spin-orbit splitting of 0.14(1) eV unresolved	71C
--------------	------------	-------------	---	-----

$dE_{gx,dir}/dp$	$6.12 \cdot 10^{-6}$ eV/bar	$T = 80$ K	hydrostatic pressure	69B2
	$4.9 \cdot 10^{-6}$ eV/bar	$T = 300$ K	hydrostatic pressure	68A2

direct band gap energy

$E_{g,dir}$	5.15(5) eV	$T = 4.2$ K	from thin film transmission assuming direct and indirect exciton binding energies to be equal	71C
-------------	------------	-------------	---	-----

effective polaron mass

$m_n^{**}(\Gamma)$	$0.431(40) m_0$	$T = 1.2 \text{ K}$	cold electron polaron mass, obtained from cyclotron resonance	71H
--------------------	-----------------	---------------------	---	-----

effective band mass

$m_n(\Gamma)$	$0.302(30) m_0$	$T = 1.2 \text{ K}$	derived from measured value of effective polaron mass	71H
---------------	-----------------	---------------------	---	-----

bound excitons**AgCl :I⁻** (bound exciton)**zero-phonon transition energy**

E_{zp}	3.2075 eV	$T = 2 \text{ K}$	absorption	69K
----------	-----------	-------------------	------------	-----

exciton localization and ionization energy

$E_{ex,loc}$	40.0(5) meV	$T = 2 \text{ K}$	$E_{gx,ind} - E_{zp}$ binding energy of exciton iodine	69K
--------------	-------------	-------------------	--	-----

$E_{ex,ion}$	34.46 meV	$T = 2 \text{ K}$	binding energy of electron to trapped hole	69K
--------------	-----------	-------------------	--	-----

AgCl :Br⁻ (bound exciton)**exciton localization energy**

$E_{ex,loc}$	34...40 meV	$T = 2 \text{ K}$		69K
--------------	-------------	-------------------	--	-----

exciton binding energy

$E_{ex,b}$	185 meV	$T = 2 \text{ K}$	equal to the binding energy of an exciton to the impurity	93S
------------	---------	-------------------	---	-----

biexciton binding energy

$E_{biex,b}$	333 meV	$T = 2 \text{ K}$	equal to the binding energy of a biexciton to the impurity	93S
--------------	---------	-------------------	--	-----

infrared absorption spectra, mode frequencies**AgCl :OH⁻**

ν	$104.06 \cdot 10^{12} \text{ s}^{-1}$	$T = 4.5 \text{ K}$	hydroxide stretching mode	71S
-------	---------------------------------------	---------------------	---------------------------	-----

AgCl :⁶Li⁺

ν	$6.85 \cdot 10^{12} \text{ s}^{-1}$	$T = 2 \text{ K}$	localized mode	73H, 75H
-------	-------------------------------------	-------------------	----------------	-------------

AgCl :⁷Li⁺

ν	$6.57 \cdot 10^{12} \text{ s}^{-1}$	$T = 2 \text{ K}$	localized mode	73H, 75H
-------	-------------------------------------	-------------------	----------------	-------------

transient infrared absorption spectra

Optical band-to-band excitation at liquid helium temperature produces transient absorption spectra in the far and near infrared. Their origin is assigned to transitions of localized electron centers.

transition energies of intrinsic electron center

E	33.5 meV	$T = 2 \text{ K}$	$1s \rightarrow 2p$ transition of electron-polaron bound to silver interstitial	69B1
	40.6 meV	$T = 2 \text{ K}$	$1s \rightarrow \infty$ transition	77S

transition energies of intrinsic hole center

E	1.18(3) eV	$T = 2$ K	agrees with static spectrum of the self-trapped hole in impurity doped AgCl	71K
-----	------------	-----------	---	-----

Lattice properties**lattice parameters** (NaCl structure)

a	5.46 Å		ab-initio pseudopotential calculation temperature dependence. Fig. 4.6.1	94K
-----	--------	--	--	-----

linear thermal expansion coefficient

α	$0.27 \cdot 10^{-4} \text{ K}^{-1}$	$T = 195$ K	from X-ray diffraction, Fig. 4.6.2	63N
----------	-------------------------------------	-------------	------------------------------------	-----

phonon dispersion relations : Fig. 4.5.3**phonon density of states** : Fig. 4.6.4.**phonon frequencies**

$\nu_{\text{TO}}(\Gamma)$	$3.63(3) \cdot 10^{12} \text{ s}^{-1}$	$T = 4$ K	ir transmission	72L1
	$3.15(6) \cdot 10^{12} \text{ s}^{-1}$	$T = 290$ K		
$\nu_{\text{LO}}(\Gamma)$	$5.88(9) \cdot 10^{12} \text{ s}^{-1}$	$T = 4$ K	ir reflectivity	72L1
	$5.79(9) \cdot 10^{12} \text{ s}^{-1}$	$T = 290$ K		
$(\nu/c)_{\text{TA}}(\text{L})$	$1.98(5) \cdot 10^{12} \text{ s}^{-1}$	$T = 1.8$ K	resonant Raman scattering	81N
$(\nu/c)_{\text{LA}}(\text{L})$	$3.12(5) \cdot 10^{12} \text{ s}^{-1}$	$T = 1.8$ K	resonant Raman scattering	81N

phonon wavenumbers

$\bar{\nu}_{\text{TO}}(\Gamma)$	118 cm^{-1}	$T = 4.2$ K	ir reflectivity	92M
$\bar{\nu}_{\text{LO}}(\Gamma)$	199 cm^{-1}	$T = 4.2$ K	ir reflectivity	92M

temperature dependence of TO wavenumber

$\bar{\nu}_{\text{TO}}(\Gamma)$	$121.0(1.0) \text{ cm}^{-1}$	$T = 2$ K	IR transmission	76L
	$117.5(1.0) \text{ cm}^{-1}$	$T = 90$ K		
	$112.5(2.0) \text{ cm}^{-1}$	$T = 200$ K		
	$105.0(2.0) \text{ cm}^{-1}$	$T = 290$ K		

second order elastic moduli

(in 10^{12} dyn/cm^2)		$T = 20 \dots 430^\circ\text{C}$				pulse-superposition technique		96H
	20°C	50°C	100°C	200°C	300°C	400°C	430°C	
c_{11}	0.596	0.578	0.548	0.489	0.429	0.357	0.330	
c_{12}	0.362	0.354	0.344	0.323	0.299	0.268	0.248	
c_{44}	0.0621	0.0615	0.0604	0.0582	0.0561	0.0536	0.0528	
c'_{11}	0.542	0.528	0.507	0.465	0.421	0.368	0.342	
c'	0.1180	0.1125	0.1030	0.0840	0.0655	0.0465	0.0410	

elastic compliances

s_{11}	$2.571 \cdot 10^{-12} \text{ cm}^2 \text{ dyn}^{-1}$	$T = 195$ K	calculated from elastic moduli	70L
s_{12}	$-0.933 \cdot 10^{-12} \text{ cm}^2 \text{ dyn}^{-1}$			
s_{44}	$15.32 \cdot 10^{-12} \text{ cm}^2 \text{ dyn}^{-1}$			

bulk modulus

B_S	$0.4733(19) \cdot 10^{12} \text{ dyn cm}^{-2}$	$T = 195 \text{ K}$	adiabatic bulk modulus from elastic moduli	70L
	$0.4403(18) \cdot 10^{12} \text{ dyn cm}^{-2}$	$T = 300 \text{ K}$		
B_T	$0.4590 \cdot 10^{12} \text{ dyn cm}^{-2}$	$T = 195 \text{ K}$	isothermal bulk modulus	70L
	$0.4174 \cdot 10^{12} \text{ dyn cm}^{-2}$	$T = 300 \text{ K}$		
B	$0.441 \cdot 10^{12} \text{ dyn cm}^{-2}$	$T = 290 \text{ K}$	pulse-superposition technique	96H
	$0.276 \cdot 10^{12} \text{ dyn cm}^{-2}$	$T = 703 \text{ K}$		

pressure dependence of bulk modulus

$B = 414.57 + 5.98 p$ (B and p in kbar)	dilatometer experiment	71V
--	------------------------	-----

compressibility

κ	$1.95 \cdot 10^{-12} \text{ cm}^2 \text{ dyn}^{-1}$	$T = 0 \text{ K}$	adiabatic compressibility calculated from elastic constants	67H
----------	---	-------------------	---	-----

Debye temperature

Θ_D	185 K	$T = 0 \text{ K}$	calculated from elastic constants data in the temperature range $2 \text{ K} \leq T \leq 20 \text{ K}$ shown in Fig. 4.6.5.	95Y
------------	-------	-------------------	---	-----

heat capacity

C_p	$4.70 \text{ J mol}^{-1} \text{ K}^{-1}$	$T = 15 \text{ K}$	calorimeter For temperature dependence, see Fig. 4.6.5.	33E
-------	--	--------------------	--	-----

melting temperature

T_m	728 K			72G
-------	-------	--	--	-----

density

d	$5.5667(2) \text{ g cm}^{-3}$	$T = 298 \text{ K}$	X-ray value	55B
-----	-------------------------------	---------------------	-------------	-----

Transport and optical properties

In AgCl the transport properties studied under optical band-to-band excitation are determined by the electrons in the conduction band at Γ . Due to strong interaction with the lattice, holes are efficiently self-trapped [68H, 71M], contributing only negligibly. The electron mobility above 40 K is determined by optical phonon scattering. At intermediate temperatures ($40 \text{ K} \geq T \geq 12 \text{ K}$) scattering from acoustic phonons occurs. Below 12 K, scattering from impurities determines the residual mobility resulting in sample dependent values [65M, 67M]

carrier mobility

$\mu_{H,n}$	$10^4 \dots 4 \cdot 10^4 \text{ cm}^2/\text{Vs}$	$T = 4.2 \text{ K}$	typical value of electron Hall mobility for low electric fields, limited by scattering from impurities, sample dependent For temperature dependence in the range $7 \text{ K} \leq T \leq 100 \text{ K}$, see [65M, 67M],	79K
-------------	--	---------------------	---	-----

thermal conductivity : see Fig. 4.6.6.

refractive index

n	2.09648 2.06385 2.04590	$T = 297 \text{ K}$	prism method, value at 500 nm value at 600 nm value at 700 nm	50T
-----	-------------------------------	---------------------	---	-----

For wavelength dependence of the refractive index, see Fig. 4.6.7, for the energy dependence of the optical constants in the range from 3.5 eV to 240 eV, see Fig. 4.6.8.

dielectric constants

$\varepsilon(0)$	9.55 (5)	$T = 2$ K	capacitance measurements in the frequency range 1...100 kHz; for temperature and pressure dependence, see [72L2]	72L2
	9.88 (5)	$T = 80$ K		
	10.02(5)	$T = 120$ K		
	10.57 (5)	$T = 190$ K		
	11.05(6)	$T = 255$ K		
$\varepsilon(\infty)$	3.97 (2)	$T = 2$ K	values quoted in [72L2]	72L2
	3.96(2)	$T = 80$ K		
	3.95(2)	$T = 120$ K		
	3.94(2)	$T = 190$ K		
	3.93 (2)	$T = 255$ K		

For energy dependence of the dielectric constant, see Fig. 4.6.9.

References to 4.6

- 31S Schröter, H.: Z. Phys. 67 (1931) 24.
- 33E Eastman, E. D., Milner, R. T.: J. Chem. Phys. 1 (1933) 444.
- 50T Tilton, L. W., Plyler, E. K., Stephens, R. E.: J. Opt. Soc. Am. 40 (1950) 540.
- 55B Berry, C.: Phys. Rev. 97 (1955) 676.
- 63N Nicklow, R. M., Young, R. A.: Phys. Rev. 129 (1963) 1936.
- 65B Bassani, F., Knox, R. S., Fowler, W. B.: Phys. Rev. 137 (1965) A1217.
- 65M Masumi, T., Ahrenkiel, R. K., Brown, F. C.: Phys. Status Solidi 11 (1965) 163.
- 65S Scop, P. M.: Phys. Rev. 139 (1965) A934.
- 67H Hidshaw, W., Lewis, J. T., Briscoe, C. V.: Phys. Rev. 163 (1967) 876.
- 67M Masumi, T.: Phys. Rev. 159 (1967) 761.
- 68A1 Ascarelli, G.: Phys. Lett. 26A (1968) 269.
- 68A2 Aust, R. B.: Phys. Rev. 170 (1968) 784.
- 68H Höhne, M., Stasiw, M.: Phys. Status Solidi 28 (1968) 247.
- 68W White III, J. J., Straley, J. W.: J. Opt. Soc. Am. 58 (1968) 759.
- 69B1 Brandt, R. C., Brown, F. C.: Phys. Rev. 181 (1969) 1241.
- 69B2 Brothers, A. D., Lynch, D. W.: Phys. Rev. 180 (1969) 911.
- 69K Kanzaki, H., Sakuragi, S.: J. Phys. Soc. Jpn. 27 (1969) 109.
- 70C Cheuk-Kin Chau, Klein, M. V.: Phys. Rev. B1 (1970) 2642.
- 70L Loje, K. F., Schuele, D. E.: J. Phys. Chem. Solids 31 (1970) 2051.
- 70V Vijayaraghavan, P. R., Nicklow, R. M., Smith, H. G., Wilkinson, M. K.: Phys. Rev. B1 (1970) 4819.
- 71C Carrera, N. J., Brown, F. C.: Phys. Rev. B4 (1971) 3651.
- 71H Hodby, J. W.: J. Phys. C: Solid State Phys. 4 (1971) L8.
- 71K Kanzaki, H., Sakuragi, S.: Solid State Commun. 9 (1971) 1667.
- 71M Marquardt, C. L., Williams, R. T., Kabler, M. N.: Solid State Commun. 9 (1971) 2285.
- 71S Sterk, F. J., Hanson, R. C.: Solid State Commun. 9 (1971) 1473.
- 71V Vaidya, S. N., Kennedy, G. C.: J. Phys. Chem. Solids 32 (1971) 951.
- 72G Am. Inst. of Physics Handbook (ed. D. E. Gray) McGraw Hill Book, 1972, 3rd ed., section 9.
- 72L1 Lowndes, R. P.: Phys. Rev. B 6 (1972) 1490.
- 72L2 Lowndes, R. P.: Phys. Rev. B6 (1972) 4667.
- 72P Plendl, J. N., Mansur, L. C.: Appl. Opt. 11 (1972) 1194.
- 73H Hattori, T., Ehara, K., Mitsuishi, A., Sakuragi, S., Kanzaki, H.: Solid State Commun. 12 (1973) 545.
74 (1995) 442.
- 75H Hattori, T., Ehara, K., Hamasaki, M., Mitsuishi, A.: Phys. Status Solidi (b) 70 (1975) 311.
- 76B Berg, W. T.: Phys. Rev. B13 (1976) 2641.
- 76L Lowndes, R. P., Rastogi, A.: Phys. Rev. B 14 (1976) 3598.
- 76S Smith, P. V.: J. Phys. Chem. Solids 37 (1976) 581.
- 76V Voronov, F. F., Grigor'ev, S. B.: Fiz. Tverd. Tela 18 (1976) 562; Sov. Phys. Solid State (English Transl.) 18 (1976) 325.
- 76W Shy-Yih Wang, J., Schlüter, M., Cohen, M. L.: Phys. Status Solidi (b) 77 (1976) 295.
- 77S Sakuragi, S., Kanzaki, H.: Phys. Rev. Lett. 38 (1977) 1302.
- 78K Kurita, S., Kobayashi, K.: J. Phys. Soc. Jpn. 44 (1978) 1583.
- 79K Komiyama, S., Masumi, T., Kajita, K.: Phys. Rev. B20 (1979) 5192.
- 81N Nakamura, K., Windscheil, J., von der Osten, W.: Solid State Commun. 39 (1981) 381 and J. Lumin. 24/25 (1981) 425.
- 81O Overhof, H.: private commun.
- 83N Nakamura, K., von der Osten, W.: J. Phys. C: Solid State Phys. 16 (1983) 6669.
- 85Y Yokoyama, T., Kobayashi, M.: J. Phys. Soc. Jpn. 54 (1985) 2329.
- 92M Mimotogi, S., Masumi, T.: J. Phys. Soc. Jpn. 61 (1992) 727.
- 93S Sonoike, S.: Jpn. J. Appl. Phys. 32 (1993) 3481.
- 94K Kirchhoff, F., Holender, J. M., Gillan, M. J.: Phys. Rev. B 49 (1994) 17420.
- 95B Bennebroek, M. T., Poluektov, O. G., Zakrzewski, A. J., Baranov, P. G., Schmidt, J.: Phys. Rev. Lett. 225.
- 95K Kobayashi, M., Matsushima, Y., Nishi, O., Mizuno, K., Matsui, A. H.: Proceedings SPIE 2362 (1995) 225.
- 95Y Yaminishi, T., Kanashiro, T., Michihiro, Y., Kishimoto, Y., Ohno, T.: J. Phys. Soc. Jpn. 64 (1995) 643.
- 96H Hughes, W. C., Cain, L. S.: Phys. Rev. B 53 (1996) 5174.

Figures to 4.6

Fig. 4.0.3

The rocksalt lattice.

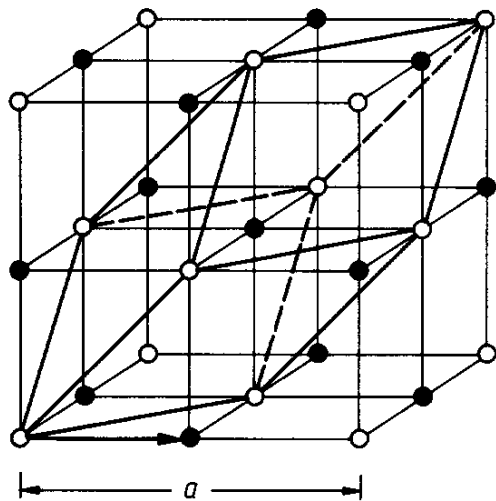
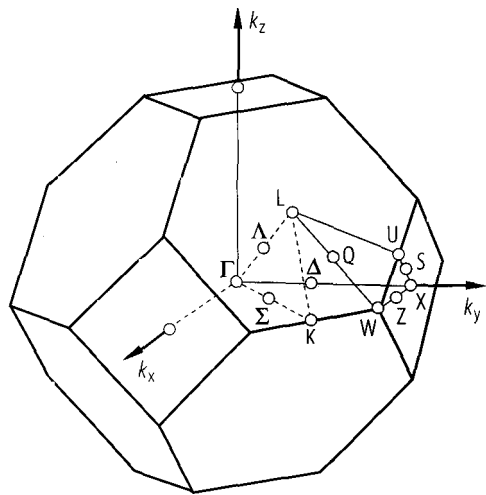


Fig. 4.0.4

The Brillouin zone for the zincblende and the rocksalt lattices.



AgCl. Electronic band structure calculated by means of the relativistic KKR method, spin-orbit splitting included. Energy vs. reduced wavevector. Origin at Ag^+ [81O].

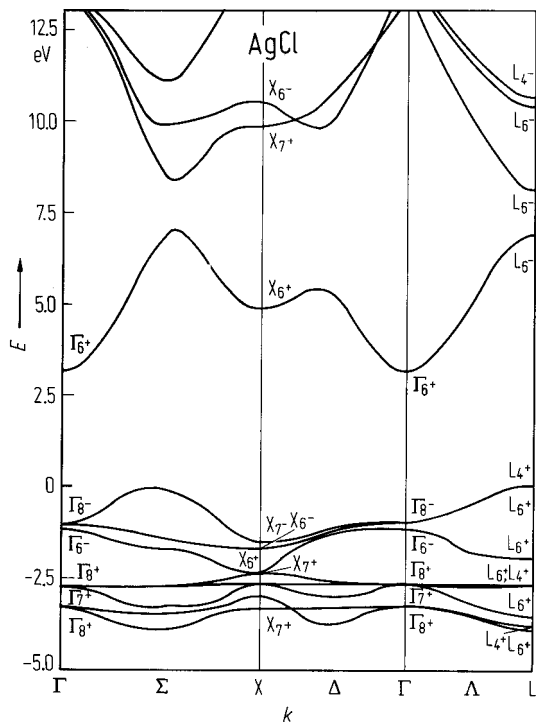


Fig. 4.6.1

AgCl. Lattice parameter vs. temperature [72P].

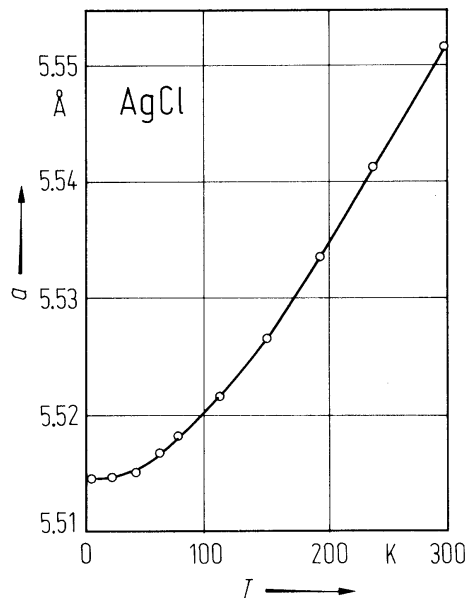


Fig. 4.6.2

AgCl. Linear thermal expansion coefficient vs. temperature between 120 K and 710 K measured by means of X-ray diffraction from single crystals (open circles). Comparison with earlier dilatometric data (full circles and triangles) show deviations below room temperature. Together with the theoretical curve (dashed line) these are discussed in [63N].

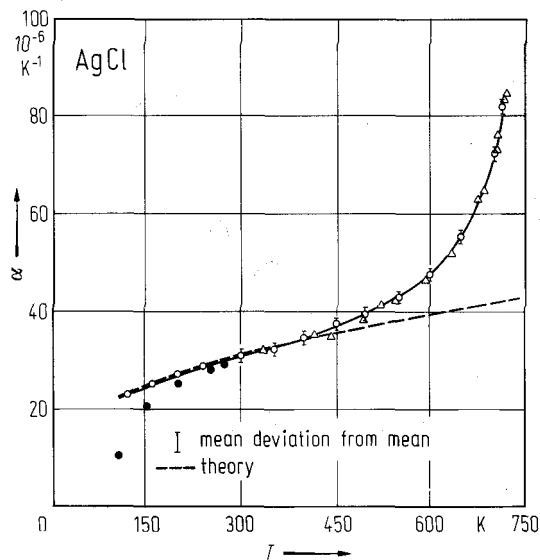


Fig. 4.6.3

AgCl. Phonon dispersion relations measured by inelastic neutron scattering at 78 K. Frequency shown vs. reduced wave vector coordinate along different directions in the Brillouin zone. The solid lines are the best least-squares fit of the experimental data on the basis of a 13-parameter shell model [70V].

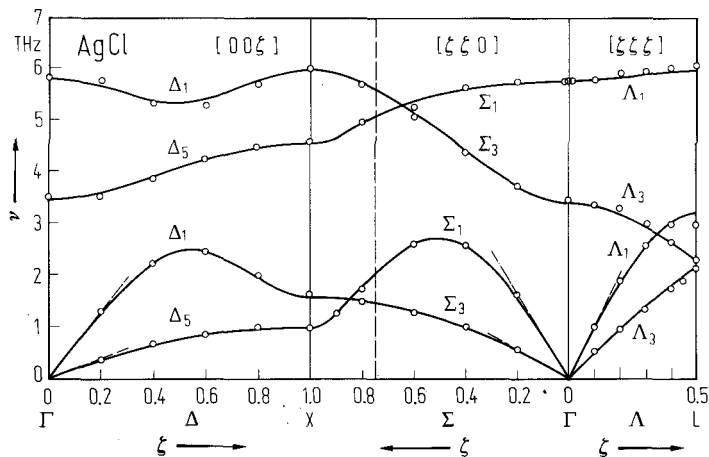


Fig. 4.6.4

AgCl. Phonon density of states vs. frequency calculated from the inelastic neutron scattering data at 78 K of Fig. 1 applying a 13-parameter shell model [70V].

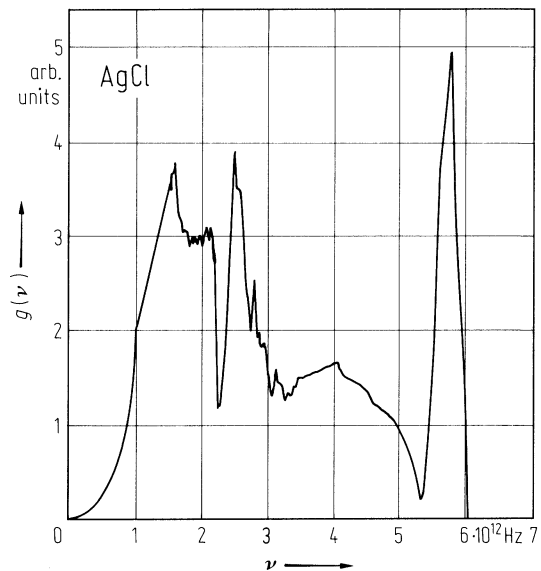


Fig. 4.6.5

AgCl. Upper part: Heat capacity vs. temperature squared between 2 K and 8.5 K measured by means of a calorimetric method. Experimental points are shown together with a fit below 7 K to the equation $C_v = aT^3 + bT^5 + cT^7 + \dots$ [76B]. The data join smoothly with those reported between 15 K and 292 K in [33E]. Lower part: Debye temperature vs temperature. Full line from inelastic neutron scattering data [70V]., dashed line and open circles from calorimetric measurements [76B, 33E], full circle from elastic constants [67H].

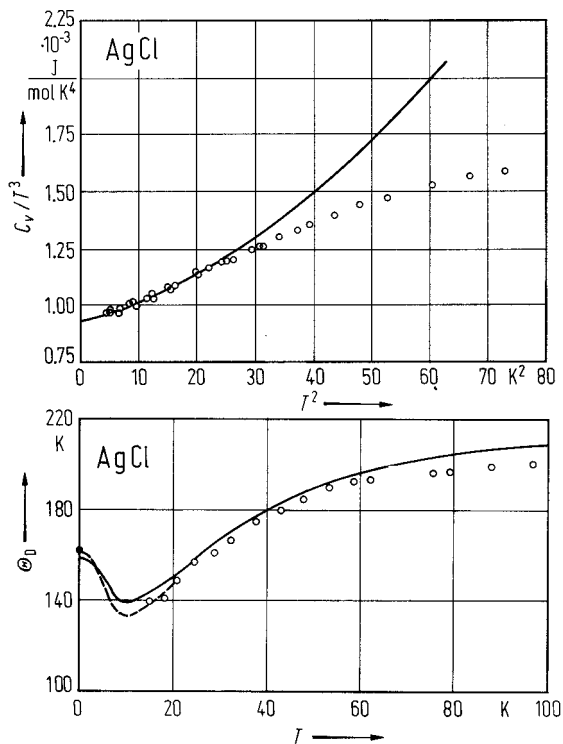


Fig. 4.5.6

AgCl, AgCl:Br⁻. Thermal conductivity vs. temperature at low temperatures for pure AgCl (curve A) and Br⁻-doped AgCl (curve B: 0.13 mol%, curve C: 1.7 mol%). The fit to the mixed crystal data is obtained employing a two-group-velocity model [70C].

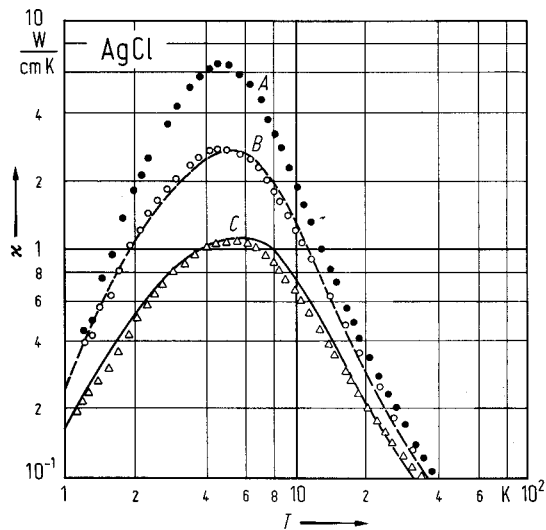


Fig. 4.6.7

AgCl. Refractive index vs wavelength in the extended range 578 nm to 20.6 μm at RT obtained with the prism method using minimum deviation [50T]. The data according to [31S] are shown by the full line.

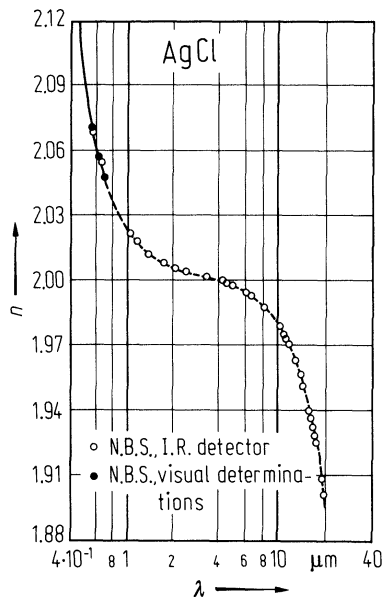


Fig. 4.6.8

AgCl. Optical constants n and k vs. photon energy over the extended range 3.5 eV to 240 eV at RT [71C]. The data in the range 6.7 eV to 30 eV are taken from [68W].

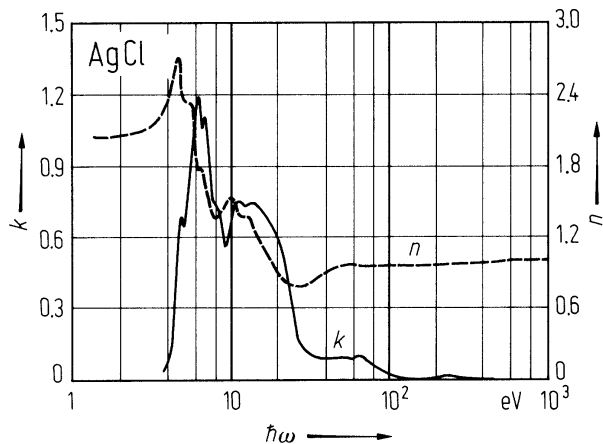
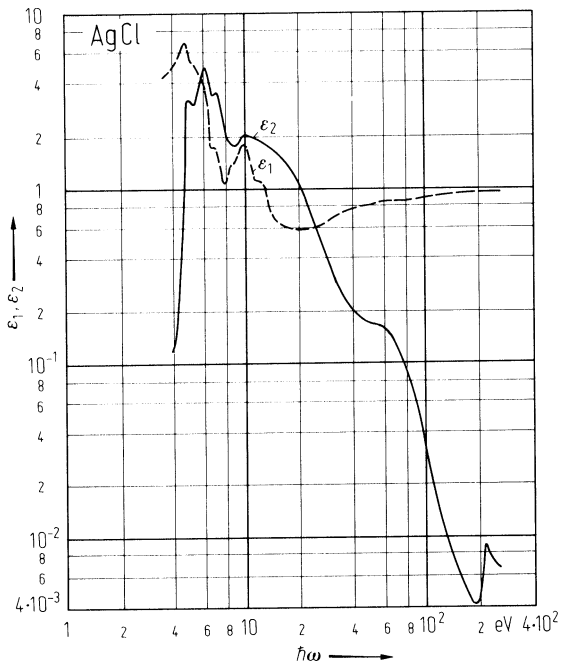


Fig. 4.6.9

AgCl. Real and imaginary parts of the dielectric constant vs. photon energy at RT over the energy range 3.5 eV to 240 eV calculated from the optical constants [71C].



4.7 Silver bromide (AgBr)

Crystal structure

Under ambient conditions, AgBr crystallizes in the rocksalt structure (NaCl-structure, space group $Fm\bar{3}m - O_h^5$, Fig. 4.0.3) and remains in this structure up to the melting temperature of $T_m = 701$ K.

Electronic properties

band structure : Fig. 4.0.11. Brillouin zone: Fig. 4.0.4.

The band structure is qualitatively similar to that of AgCl. Mixing at points away from $k = 0$ of the Br^- 4p-states with the Ag^+ 4d-states, lying slightly below, results in the uppermost valence band maximum at L and a maximum at X lower in energy.

indirect band gap energy

$E_{g,ind}(L_{3v}-\Gamma_{1c})$	2.7125(50) eV	$T = 1.8$ K	analysis of absorption edge	84S
---------------------------------	---------------	-------------	-----------------------------	-----

indirect exciton gap energy

$E_{gx,ind}$	2.6845 eV	$T = 1.8$ K	resonant light scattering and analysis of absorption edge	84S
--------------	-----------	-------------	--	-----

exciton binding energy

$E_{b,ind}$	28(5) meV	$T = 1.8$ K	analysis of absorption edge	84S
-------------	-----------	-------------	-----------------------------	-----

g-factor

g	1.4879(10)	$T = 10$ K	ESR on intrinsic, shallow trapped electron centers	89E
-----	------------	------------	---	-----

direct exciton gap energy

$E_{gx,dir}(\Gamma_{15v}-\Gamma_{1c})$	4.276(2) eV	$T = 4.2$ K	thin crystalline film transmission	71C
	3.96 eV	$T = 300$ K	reflectivity of crystalline samples	72W

direct band gap energy

$E_{g,dir}$	4.292(2) eV	$T = 4.2$ K	from thin film transmission, direct and indirect exciton binding energies assumed to be equal	71C
-------------	-------------	-------------	---	-----

effective polaron mass

$m_n^{**}(\Gamma)$	0.29(1) m_0	$T = 1.6$ K	electron polaron mass obtained from cyclotron resonance	89E
--------------------	---------------	-------------	--	-----

effective band mass

$m_{p }(L)$	1.25 m_0	$T = 1.7$ K	longitudinal hole mass	73T
$m_{p\perp}(L)$	0.52 m_0	$T = 1.7$ K	transverse hole mass	73T

Lattice properties

lattice parameter

a	5.77475(5) Å	$T = 298$ K	X-ray diffraction; for temperature dependence of the lattice parameter, see Fig. 4.7.1	55B
-----	--------------	-------------	--	-----

linear thermal expansion coefficient

α	$0.35 \cdot 10^{-4} K^{-1}$	$T = 295$ K		37S
	$5.0 \cdot 10^{-4} K^{-1}$	$T = 73$ K		

For temperature dependence in the range $4.2 \text{ K} \leq T \leq 290 \text{ K}$ see Fig. 4.7.2.

phonon dispersion relations : Fig. 4.7.3.

phonon frequencies

$(\nu/c)_{\text{TO}}(\Gamma)$	$2.66(5) \cdot 10^{12} \text{ s}^{-1}$	$T = 1.8 \text{ K}$	resonant Raman scattering	80W
	$2.27(7) \cdot 10^{12} \text{ s}^{-1}$	$T = 295 \text{ K}$	inelastic neutron scattering	75B
$(\nu/c)_{\text{LO}}(\Gamma)$	$4.16(5) \cdot 10^{12} \text{ s}^{-1}$	$T = 1.8 \text{ K}$	resonant Raman scattering	80W
	$4.14(9) \cdot 10^{12} \text{ s}^{-1}$	$T = 290 \text{ K}$	ir reflectivity	72L
$(\nu/c)_{\text{TA}}(\text{L})$	$1.62(5) \cdot 10^{12} \text{ s}^{-1}$	$T = 1.8 \text{ K}$	resonant Raman scattering	80W
$(\nu/c)_{\text{TO}}(\text{L})$	$2.01(2) \cdot 10^{12} \text{ s}^{-1}$			
$(\nu/c)_{\text{LA}}(\text{L})$	$2.86(5) \cdot 10^{12} \text{ s}^{-1}$			
$(\nu/c)_{\text{TA}}(\text{X})$	$0.94(5) \cdot 10^{12} \text{ s}^{-1}$			
$(\nu/c)_{\text{LA}}(\text{X})$	$1.40(5) \cdot 10^{12} \text{ s}^{-1}$			

second order elastic moduli

c_{11}	$0.6594(26) \cdot 10^{12} \text{ dyn cm}^{-2}$	$T = 0 \text{ K}$	extrapolated from 4.2 K,	69M
c_{12}	$0.3495(69) \cdot 10^{12} \text{ dyn cm}^{-2}$		ultrasonic technique	
c_{44}	$0.1003(4) \cdot 10^{12} \text{ dyn cm}^{-2}$			
c_{11}	$0.5317(21) \cdot 10^{12} \text{ dyn cm}^{-2}$	$T = 300 \text{ K}$		
c_{12}	$0.3303(66) \cdot 10^{12} \text{ dyn cm}^{-2}$			
c_{44}	$0.0794(3) \cdot 10^{12} \text{ dyn cm}^{-2}$			

For more detailed temperature dependence in the range $4.2 \text{ K} \leq T \leq 300 \text{ K}$, see Fig. 4.7.4.

bulk modulus

B_{S}	$0.4381(17) \cdot 10^{12} \text{ dyn cm}^{-2}$	$T = 195 \text{ K}$	adiabatic bulk modulus from elastic moduli, temperature dependence, see Fig. 4.7.5	70L
----------------	--	---------------------	---	-----

compressibility

κ	$2.47 \cdot 10^{-12} \text{ cm}^2 \text{ dyn}^{-1}$	$T = 300 \text{ K}$	adiabatic compressibility, calculated from elastic constants	70L
----------	---	---------------------	--	-----

Debye temperature

Θ_{D}	118 K...130 K	$T = 0 \text{ K}$	quoted from various sources (see Fig. 4.7.6 for temperature dependence of Θ_{D})	72B
---------------------	---------------	-------------------	---	-----

heat capacity

C_{p}	$51.79 \text{ J mol}^{-1} \text{ K}^{-1}$	$T = 289 \text{ K}$		
----------------	---	---------------------	--	--

For temperature dependence of heat capacity, see Fig. 4.7.7.

melting temperature

T_{m}	695 K		heat capacity measurements	68J
----------------	-------	--	----------------------------	-----

density

d	$6.4753(2) \text{ g cm}^{-3}$	$T = 298 \text{ K}$	X-ray value	55B
-----	-------------------------------	---------------------	-------------	-----

Transport properties

Both electrons in the conduction band at Γ and holes in the valence band at L, produced by optical band-to-band excitation of the samples, contribute to the transport properties. Contrary to AgCl, holes are not self-trapped in AgBr down to at least 1.7 K [73T, 74B].

carrier mobilities

$\mu_n(\Gamma)$	500...2000 cm ² /Vs	$T = 4.2$ K	magneto-resistance mobility for cubic micro-crystals of 0.5...1.3 μm cube size	82H
	60 cm ² /Vs	$T = 300$ K	drift mobility, LO-phonon scattering controlled	69A
$\mu_p(\text{L})$	$1.5 \cdot 10^5$ cm ² /Vs	$T = 1.7$ K	from linewidth of cyclotron resonance	73T
	2.0(5) cm ² /Vs	$T = 300$ K	Hall mobility	62H

For temperature dependence in the range $300 \text{ K} \leq T \leq 423 \text{ K}$, see Fig. 4.7.8.

Optical properties

Energy dependence of optical constants: Fig. 4.7.9, energy dependence of dielectric constant: Fig. 4.7.10.

dielectric constants

$\varepsilon(0)$	10.64(5)	$T = 2$ K	capacitance measurements 1...100 kHz	72L
	12.44	$T = 290$ K	capacitance measurements 5·10 ² ...2·10 ⁷ Hz	69L
$\varepsilon(\infty)$	4.68(2)	$T = 2$ K	values quoted in [72L], see also [69L]	72L
	4.62	$T = 290$ K	from refractive index data	69L

References to 4.7

- 37S Strelkow, P. G.: Phys. Z. Sowjetunion 12 (1937) 77.
- 55B Berry, C.: Phys. Rev. 97 (1955) 676.
- 62H Hanson, R. C.: J. Phys. Chem. 66 (1962) 2376.
- 68J Jost, W., Kubaschewski, P.: Z. Phys. Chem. 60 (1968) 69.
- 69A Ahrenkiel, R. K.: Phys. Rev. 180 (1969) 859.
- 69L Lowndes, R. P., Martin, D. H.: Proc. Roy. Soc. (London) A 308 (1969) 473.
- 69M Marklund, K., Vallin, J., Malimoud, S. A.: Uppsala University Institute of Physics, Report No. UIIP-645 (1969) .
- 70L Loje, K. F., Schuele, D. E.: J. Phys. Chem. Solids 31 (1970) 2051.
- 71C Carrera, N. J., Brown, F. C.: Phys. Rev. B4 (1971) 3651.
- 72B Bottger, G. L., Geddes, A. L.: J. Chem. Phys. 56 (1972) 3735.
- 72L Lowndes, R. P.: Phys. Rev. B6 (1972) 4667.
- 72P Plendl, J. N., Mansur, L. C.: Appl. Opt. 11 (1972) 1194.
- 72W White III, J. J.: J. Opt. Soc. Am. 62 (1972) 212.
- 73T Tamura, H., Masumi, T.: Solid State Commun. 12 (1973) 1183.
- 74B Baxter, I. E., Ascarelli, G.: Phys. Status Solidi (b) 62 (1974) 547.
- 75B Bühner, W.: Phys. Status Solidi (b) 68 (1975) 739.
- 76D Dorner, B., von der Osten, W., Bühner, W.: J. Phys. C: Solid State Phys. 9 (1976) 723.
- 80W Windscheif, J., von der Osten, W.: J. Phys. C: Solid State Phys. 13 (1980) 723.
- 81O Overhof H.: private commun.
- 82H Hirano, A., Masumi, T., Takada, S.: J. Appl. Phys. 53 (1982) 3093.
- 84S Sliwezuk, U., Stolz, H., von der Osten, W.: Phys. Status Solidi (b) 122 (1984) 203.
- 89E Eachus, R. S., Olm, M. T., Janes, R., Symons, M. C. R.: Phys. Status Solidi (b) 152 (1989) 583.

Figures to 4.7

Fig. 4.0.3

The rocksalt lattice.

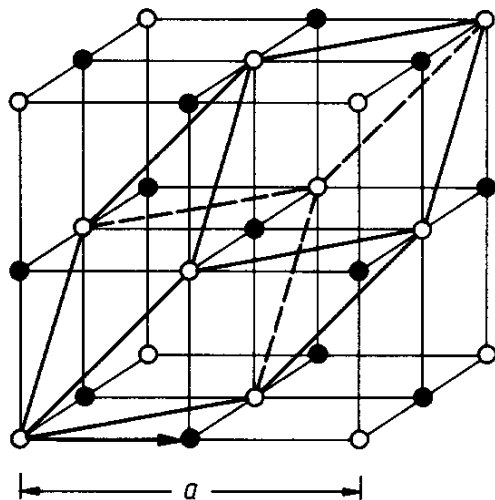


Fig. 4.0.4

The Brillouin zone for the zincblende and the rocksalt lattices.

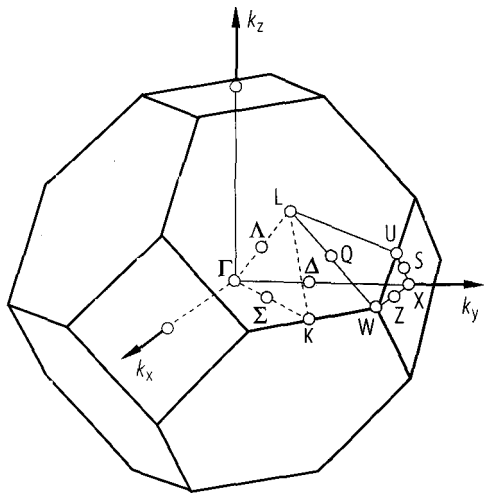


Fig. 4.0.11

AgBr. Electronic band structure calculated by means of the relativistic KKR method, spin-orbit splitting included. Energy plotted vs. reduced wave vector. Origin at Ag^+ [81O].

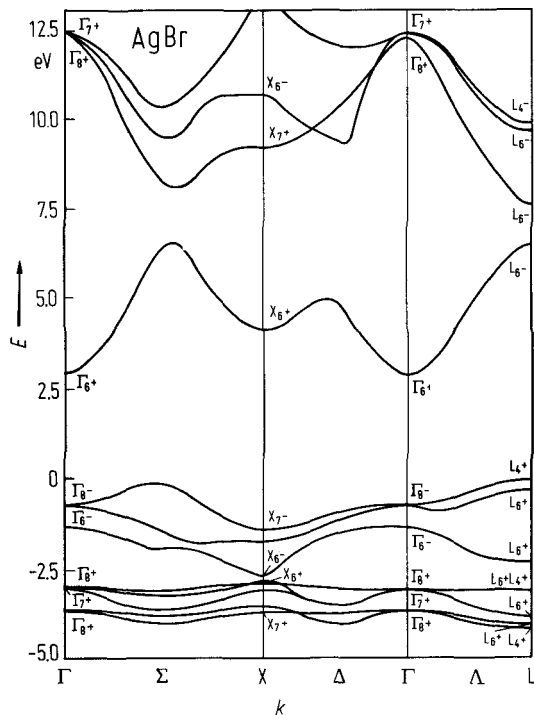


Fig. 4.7.1

AgBr. Lattice parameter vs. temperature [72P]. Note deviation in absolute value at 298 K from that quoted in [55B].

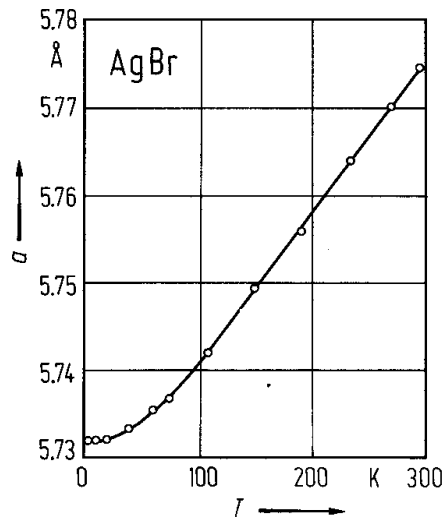


Fig. 4.7.2

AgBr. Linear thermal expansion coefficient vs. temperature between 4.2 K and 300 K obtained from lattice parameter determination by X-ray diffraction [69M]. Note deviation in absolute value at 295 K from that quoted in [37S].

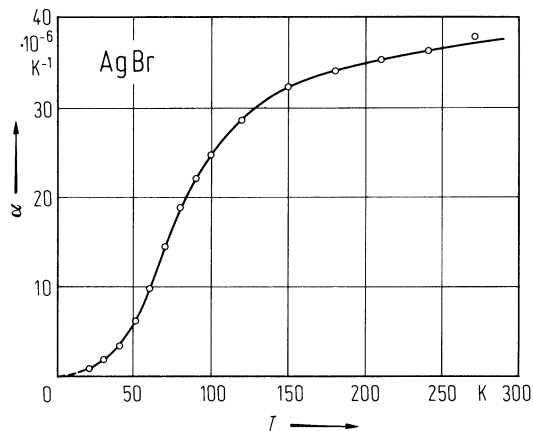


Fig. 4.7.3

AgBr. Phonon dispersion relations measured by inelastic neutron scattering at 85 K. Frequency shown vs. reduced wave vector coordinate along different directions in the Brillouin zone. The dashed lines are the best least-squares fit of the experimental data on the basis of a modified shell model [76D]. The initial slopes of the acoustic branches (full lines) are taken from the elastic constants of [70L]. open circles: longitudinal, full circles: transverse 1, triangles: transverse 2.

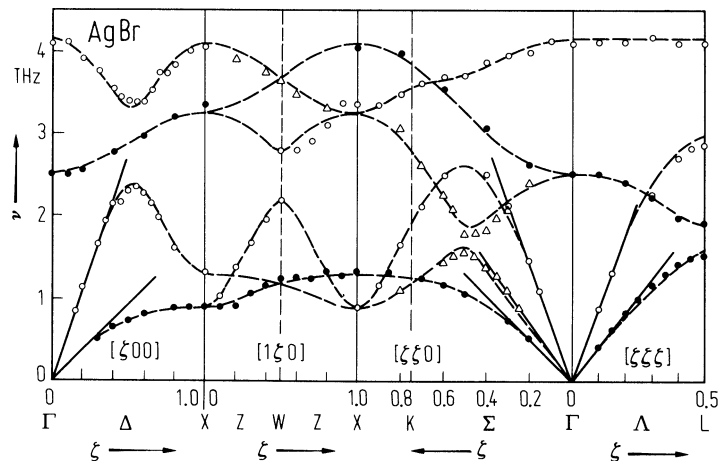


Fig. 4.7.4

AgBr. Elastic moduli vs. temperature as determined from ultrasonic measurements in the range 4.2 K to 300 K [69M].

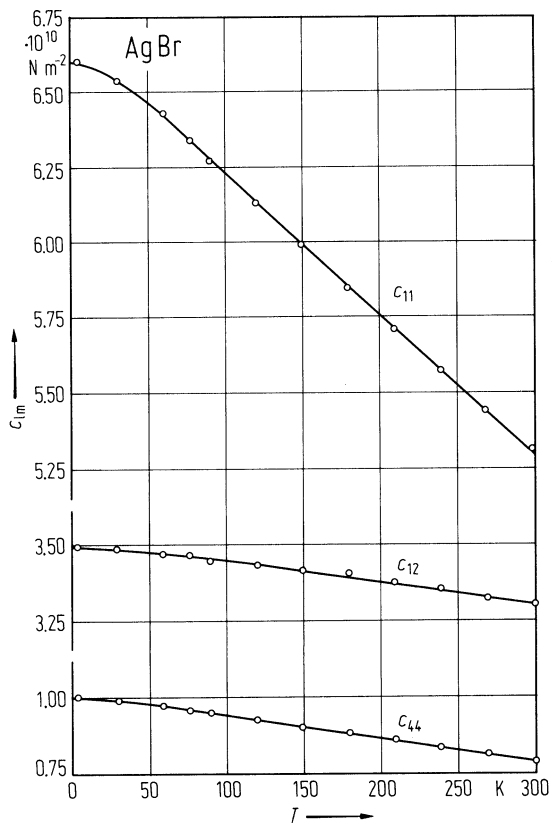


Fig. 4.7.5

AgBr. Adiabatic bulk modulus vs. temperature between 4.2 K and 300 K determined from elastic moduli [70L].

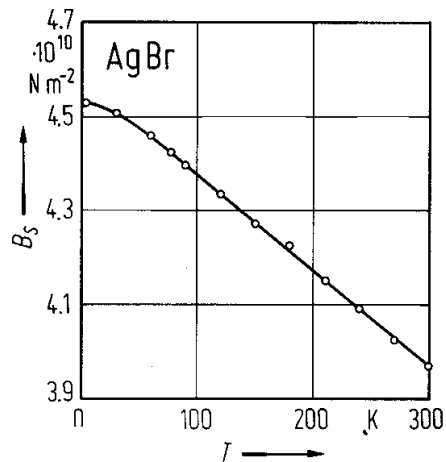


Fig. 4.7.6

AgBr. Temperature dependence of the Debye temperature computed from inelastic neutron scattering data applying a harmonic model. Full line: calculated from data at 80 K, dashed line: from data at 295 K [75B].

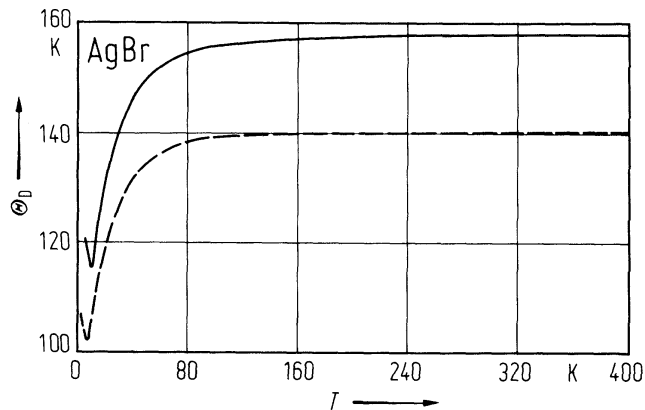


Fig. 4.7.7

AgBr. Heat capacity C_v vs. temperature calculated from the density of states. Note that extrapolation towards higher temperature is not precise because anharmonic softening of the dispersion relations with temperature is neglected [76D].

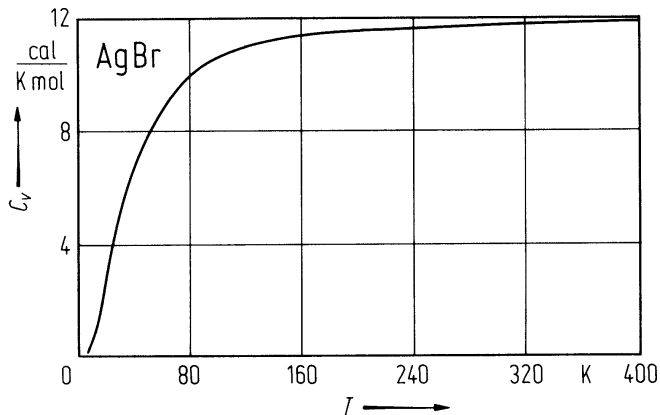


Fig. 4.7.8

AgBr. Hole Hall mobility vs. temperature between 300 K and 423 K from different samples [62H]. Lower temperature scale: T in K.

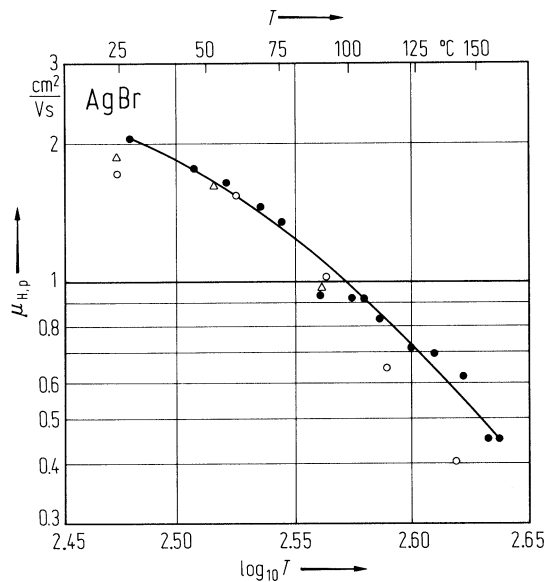


Fig. 4.7.9

AgBr. Optical constants n and k vs. photon energy in the range 3.5 eV to 7 eV at room, liquid-nitrogen and liquid-helium temperatures. The data are derived from thin film transmission measurements applying a Kramers-Kronig analysis. Spin-orbit split $\Gamma_{6v}^{-}, \Gamma_{8v}^{-} \rightarrow \Gamma_{1c}$ exciton transitions resolved [71C].

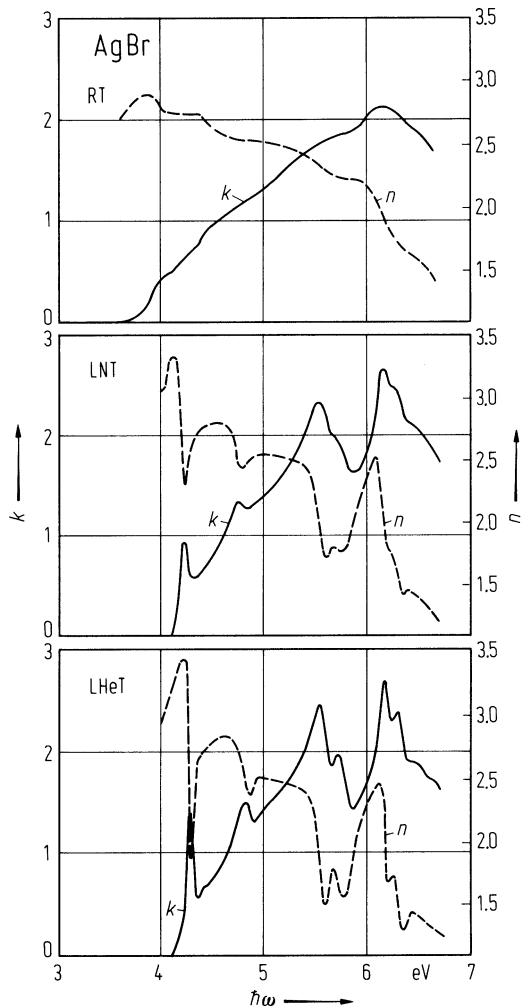
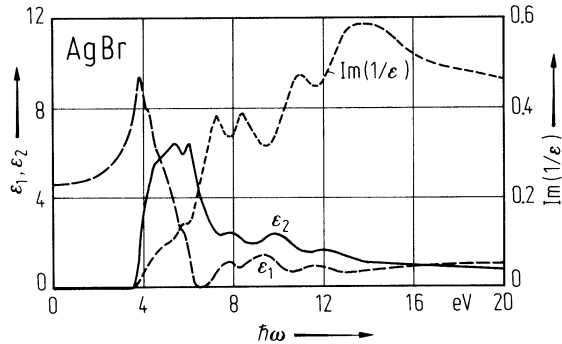


Fig. 4.7.10

AgBr. Real and imaginary parts of the dielectric constant and energy loss function vs. photon energy at room temperature in the range 0 to 20 eV obtained from the reflectivity spectrum by means of Kramers-Kronig analysis [72W].



4.8 Silver iodide (AgI)

Crystal structure

At room temperature and ambient pressure, a wurtzite phase (2H structure, β -AgI, AgI-II, Fig. 4.0.2) and a zincblende phase (γ -AgI, AgI-II', F43m, Fig. 4.0.1) can both exist. The wurtzite phase seems to be the stable phase below a temperature of 420 K, and the zincblende phase seems to be metastable, but has been found to be stable phase below a temperature of 413 K and a pressure of 588 MPa, the β -phase being found to be stable above 883 MPa [98P].

Electronic properties of wurtzite AgI (β -AgI)

The band structure is shown in Fig. 4.0.12, the Brillouin zone in Fig. 4.0.5.

The conduction band (including spin) has Γ_7 symmetry. The uppermost valence band (Γ_8) splits into Γ_9 and Γ_7 .

direct gap energies

$E_g(\Gamma_{9v}-\Gamma_{7c})$	3.0247(4) eV	$T = 1.6$ K	two-photon absorption, series limit of W_1 exciton	76D
$E_g(\Gamma_{7v}-\Gamma_{7c})$	3.064(3) eV	$T = 1.6$ K	two-photon absorption, series limit of W_2 exciton	76D

direct gap exciton energies

$E_{gxA}(\Gamma_{9v}-\Gamma_{7c})$	2.930 eV	$T = 90$ K	Faraday rotation	88M
$E_{gxB}(\Gamma_{7v}-\Gamma_{7c})$	2.983 eV	$T = 90$ K		

edge exciton transition energies

The W_1 -, W_2 - and W_3 -excitons are formed by electron-hole pair states of the Γ_7 conduction band and the Γ_9 , upper Γ_7 and lower Γ_7 valence bands, respectively. The W_1 - and W_2 -excitons are referred to as A and B excitons in the literature.

$E_{gx}(W_1(1S))$	2.95 eV	$T = 4.2$ K	absorption	63C
$E_{gx}(W_2(1S))$	2.99 eV			
$E_{gx}(W_3(1S))$	3.79 eV			

longitudinal–transverse splitting energies

$\Delta_{ex}^{L-T}(A, n=1)$	8(2) meV	$T = 1.5$ K	three-photon sum frequency	88F
$\Delta_{ex}^{L-T}(B, n=1)$	5(1) meV			
$\Delta_{ex}^{L-T}(A, n=2)$	0.8(4) meV			

spin-orbit splitting energy

Δ_0	840 meV	$T = 4.2$ K	energetic distance of W_1 and W_3 exciton in absorption	63C
------------	---------	-------------	---	-----

crystal field splitting energy

Δ_{cf}	36 meV	$T = 4.2$ K	energy difference of W_1 and W_2 excitons in absorption	63C
---------------	--------	-------------	---	-----

exciton binding energy

$E_b(W_1(1S))$	79(4) meV	$T = 4.5$ K	reflectivity/magnetic circular reflectivity	74B
----------------	-----------	-------------	---	-----

effective band mass

$m_n(\Gamma)$	0.23 m_0	$T = 90$ K	electron mass, derived from measured Faraday rotation	88M
---------------	------------	------------	---	-----

Electronic properties of zincblende AgI (γ -AgI)

band structure : Fig. 4.0.13. It compares with those for the γ -phases of the cuprous halides. For Brillouin zone, see Fig. 4.0.4.

direct gap energy

$E_{g,dir}(\Gamma_{8v}-\Gamma_{6c})$	2.82 eV	$T = 300$ K	absorption edge of γ -phase	81V
	2.91 eV	$T = 4$ K	absorption edge of γ -phase	63C

Lattice properties

lattice parameters

AgI-II, β -phase, wurtzite structure:

a	4.592(1) Å	$T = 297$ K		87Y
c	7.510(2) Å			
z	0.6274(5) Å			

AgI-II', γ -phase, zincblende structure:

a	6.499(2) Å	$p = 0.0001$ GPa	powder neutron diffraction	93K
-----	------------	------------------	----------------------------	-----

thermal expansion (AgI-II, β -phase): See Fig. 4.8.1.

phonon dispersion relations : see Fig. 4.8.2.

The striking features, compared to other wurtzite compounds, are the low energy of a TO mode in the zone center and the flat dispersion of all optic modes, resulting in two narrow energy bands for the upper six and the lower four modes.

phonon frequencies

$(\nu/c)_{TO}(A_1),$				
$(\nu/c)_{TO}(E_1)$	$3.18 \cdot 10^{12} \text{ s}^{-1}$	$T = 4/80$ K	Raman scattering	72B
$(\nu/c)_{LO}(A_1),$				
$(\nu/c)_{LO}(E_1)$	$3.72 \cdot 10^{12} \text{ s}^{-1}$	$T = 4/80$ K		
$(\nu/c)(\Gamma_4(E_2))$	$0.51 \cdot 10^{12} \text{ s}^{-1}$	$T = 80/293$ K		
$(\nu/c)(\Gamma_4(E_2))$	$3.36 \cdot 10^{12} \text{ s}^{-1}$	$T = 4/80$ K		

second order elastic moduli

γ -AgI:

c_{11}	27.7 GPa	bond-orbital calculation	94S
c_{12}	15.5 GPa		
c_{44}	9.5 GPa		

β -AgI:

c_{11}	$0.293(6) \cdot 10^{12} \text{ dyn cm}^{-2}$	$T = 298$ K	74F
c_{33}^D	$0.360(7) \cdot 10^{12} \text{ dyn cm}^{-2}$		
c_{33}^E	$0.354(10) \cdot 10^{12} \text{ dyn cm}^{-2}$		
c_{44}^E	$0.0373(8) \cdot 10^{12} \text{ dyn cm}^{-2}$		
c_{44}^D	$0.040(2) \cdot 10^{12} \text{ dyn cm}^{-2}$		
c_{66}	$0.0399(8) \cdot 10^{12} \text{ dyn cm}^{-2}$		
c_{12}	$0.213(7) \cdot 10^{12} \text{ dyn cm}^{-2}$		
c_{13}	$0.196(4) \cdot 10^{12} \text{ dyn cm}^{-2}$		

Debye temperature

Θ_D	114 K	$T = 10$ K	from ultrasonic measurements	74F
------------	-------	------------	------------------------------	-----

For temperature dependence of Θ_D from inelastic neutron scattering, see Fig. 4.8.3, temperature dependence of heat capacity: Fig. 4.8.4.

melting temperature

T_m	558°C		melting temperature of α -phase; $\beta \rightarrow \alpha$ phase transition 147°C	72G
-------	-------	--	---	-----

density

d	5.68 g cm ⁻³		density of β -AgI (density of γ -AgI: 6 g cm ⁻³)	72G
-----	-------------------------	--	---	-----

Transport and optical properties

ion mobilities

$\mu(\text{Ag}^+)$	$1.7 \cdot 10^{-3}$ cm ² /Vs	$470 \text{ K} < T < 770 \text{ K}$	Hall mobility of α -AgI	90L
--------------------	---	-------------------------------------	--------------------------------	-----

dielectric constants

$\varepsilon(0)$	7.0(3)	$T = 300$ K	low frequency capacity bridge	67B
$\varepsilon(\infty)$	4.91(3)	$T = 300$ K	–	72G

Spectral dependence of real and imaginary part of the dielectric constant of β -AgI: Fig. 4.8.5.

piezoelectric stress coefficient

e_{33}	0.20 C/m ²	$T = 298$ K	mechanical resonance	74F
e_{31}	– 0.078 C/m ²			
e_{15}	– 0.13(5) C/m ²		ultrasonic measurement	74F

References to 4.8

- 41P Pitzer, K. S.: J. Am. Chem. Soc. 63 (1941) 516.
- 63C Cardona, M.: Phys. Rev. 129 (1963) 69.
- 67B Bottger, G. L., Geddes, A. L.: J. Chem. Phys. 46 (1967) 3000.
- 72B Bottger, G. L., Damsgard, C. V.: J. Chem. Phys. 57 (1972) 1215.
- 72G Am. Inst. of Physics Handbook (ed. D. E. Gray), McGraw Hill Book, 1972, 3rd ed., section 9.
- 74B Bettini, M., Suga, S., Hanson, R.: Solid State Commun. 15 (1974) 1885.
- 74F Fjeldly, T.A., Hanson, R. C.: Phys. Rev. B 10 (1974) 3569.
- 76D Dinges, R., Fröhlich, D., Uihlein, Ch.: Phys. Status Solidi (b) 76 (1976) 613.
- 76S Smith, P. V.: J. Phys. Chem. Solids 37 (1976) 588.
- 77O Overhof, H.: J. Phys. Chem. Solids 38 (1977) 1214.
- 78B Bühner, W., Nicklow, R. M., Brüesch, P.: Phys. Rev. B17 (1978) 3362.
- 79B Bedikyan, L. D., Miloslavskii, V. K., Ageev, L. A.: Opt. Spectrosc. (USSR) 47 (1979) 403.
- 80H Harvey, G., Fletcher, N. H.: J. Phys. C: Solid State Phys. 13 (1980) 2969.
- 81V Ves, S., Glötzel, D., Cardona, M., Overhof, H.: Phys. Rev. B24 (1981) 3073.
- 87Y Yoshiasa, A., Koto, K., Kanamaru, F., Emura, S., Horiuchi, H.: Acta Crystallogr. B 43 (1987) 434.
- 88F Fröhlich, D., Köhler, P., Pahlke, Ch.: Europhys. Letters 7 (1988) 349.
- 88M Miloslavskii, V. K., Mussil, V. V., George, R.: Opt. Spektrosc. (USSR) 64 (1988) 131.
- 90L Liou, Y. J., Hudson, R. A., Wonnell, S. K., Slifkin, L.M.: Phys. Rev. B41 (1990) 10481.
- 93K Keen, D. A., Hull, S.: J. Phys. Condens. Matter 5 (1993) 23.
- 94S Shen, S. G.: J. Phys. Condens. Matter 6 (1994) 8733.
- 98P Patnaik, J. R. G., Sunandana, C. S.: J. Phys. Chem. Solids 59 (1998) 1059.

Figures to 4.8

Fig. 4.0.1

The zincblende lattice.

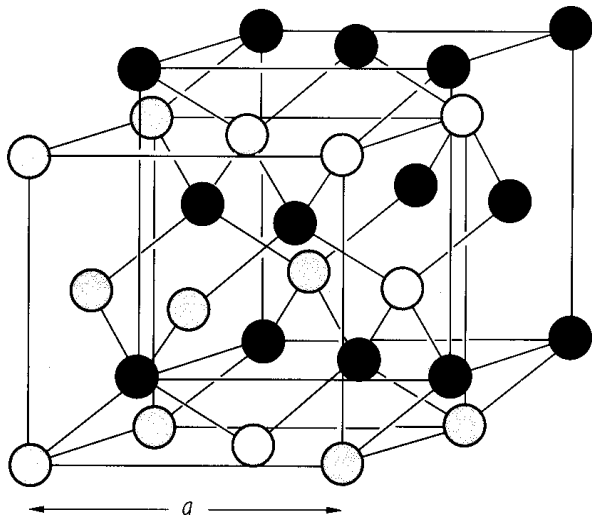


Fig. 4.0.2

The wurtzite lattice.

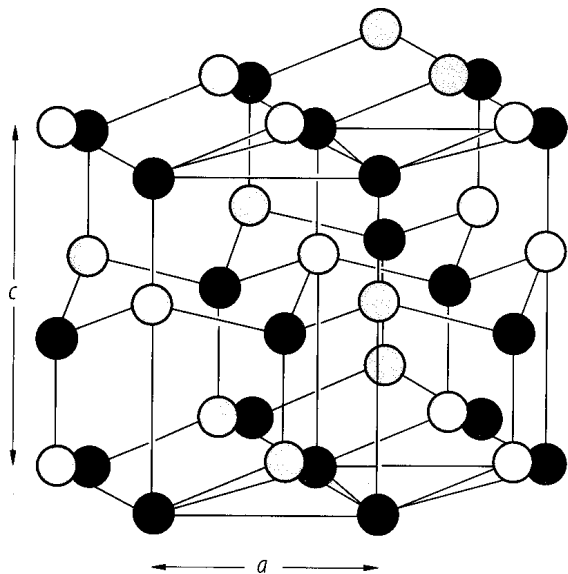


Fig. 4.0.4

The Brillouin zone for the zincblende and the rocksalt lattices.

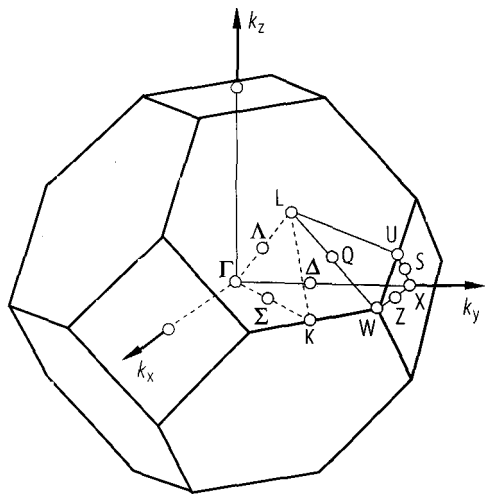
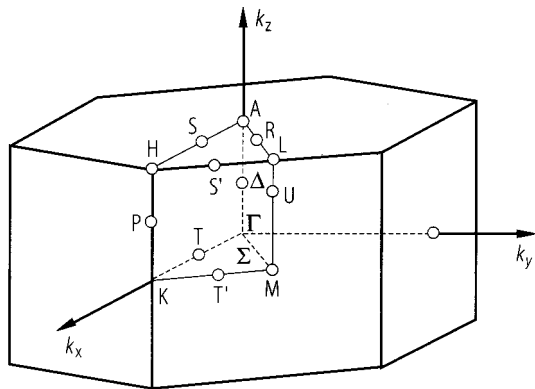
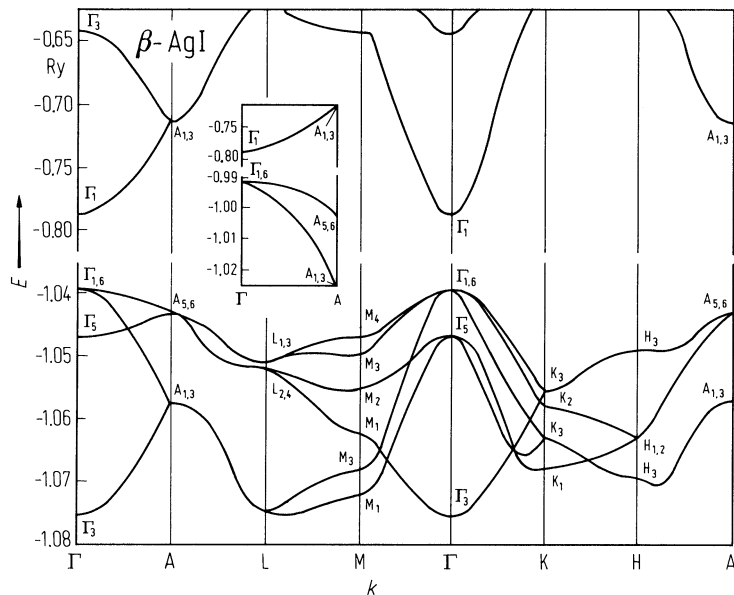


Fig. 4.0.5

The Brillouin zone of the wurtzite lattice.



β -AgI. Electronic band structure without spin calculated by means of the tight-binding approach, neglecting the silver 4d-electrons. Inclusion of spin-orbit interaction would split Γ_6 into Γ_9 and Γ_7 , while Γ_1 becomes Γ_7 . The inset represents the conduction and valence bands along Γ - A resulting from the consideration of the d-electrons. Note that Γ_5 and Γ_6 may be interchanged in the notation of some authors [76S]. 1 Ry = 13.6 eV.



γ -AgI. Electronic band structure calculated by means of the relativistic KKR method [770].

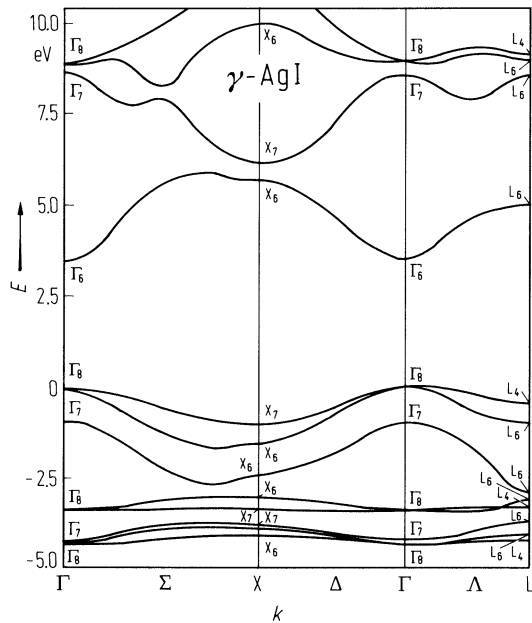


Fig. 4.8.1

β -AgI. Thermal expansion in c -direction vs. temperature obtained from dilatometric measurements [80H].

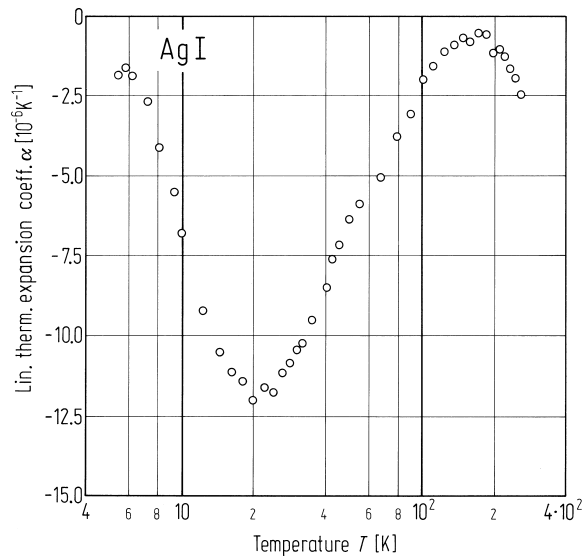


Fig. 4.8.2

β -AgI. Phonon dispersion relations measured by inelastic neutron scattering at 160 K. Dashed and solid lines are fits by a rigid-ion and valence-shell model, respectively [78B]. ξ : reduced wave vector coordinate. Polarization vector (experimental): full triangles: LA, full circles: TA ($\perp c$), full squares: TA ($\parallel c$), open triangles: LO, open circles: TO ($\perp c$), open squares: TO ($\parallel c$), diamonds: unknown.

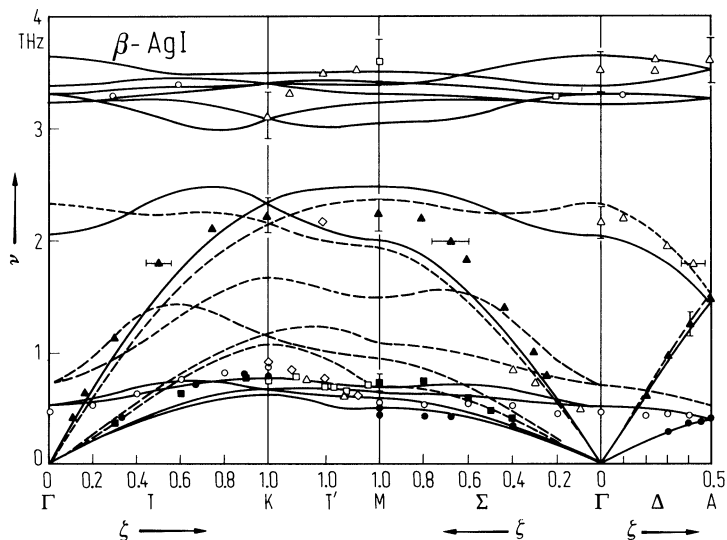


Fig. 4.8.3

β -AgI. Debye temperature vs. temperature computed from the heat capacity data of Fig. 2 (full line) [78B].

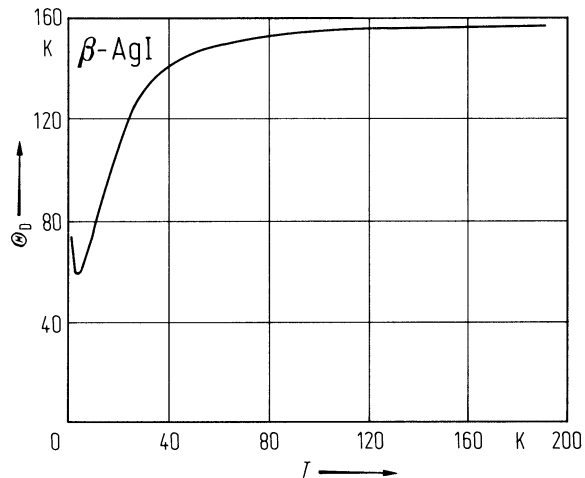


Fig. 4.8.4

β -AgI. Heat capacity vs. temperature for $T < 200$ K as obtained from the phonon density of states in harmonic approximation [78B]. The experimental points are taken from calorimetric measurements of [41P].

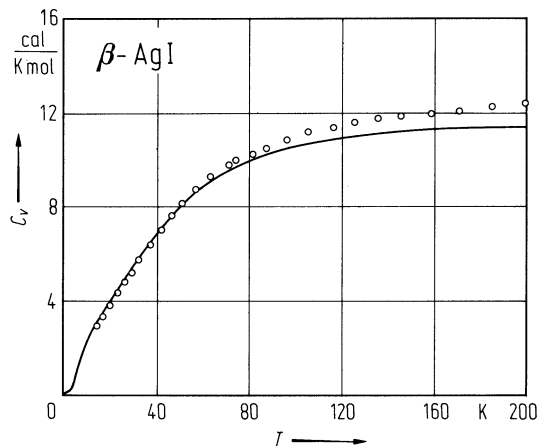
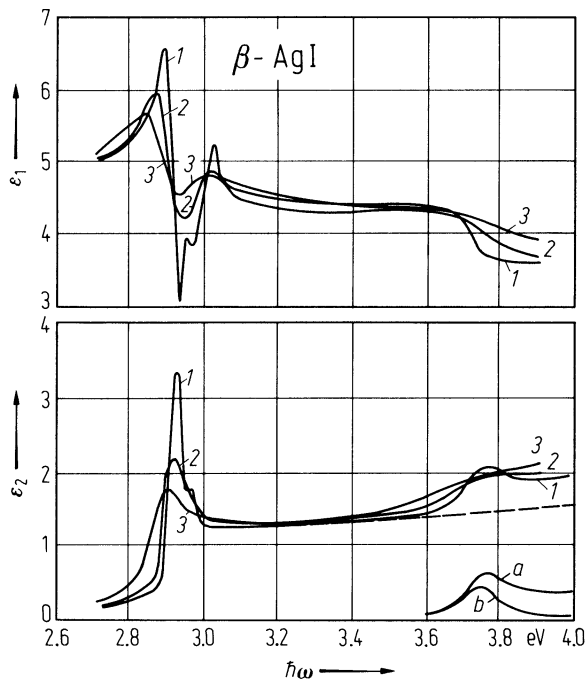


Fig. 4.8.5

β -AgI. Real (ϵ_1) and imaginary (ϵ_2) part of the dielectric constant vs. photon energy in the region of the W_1 , W_2 and W_3 exciton. The data are obtained from Kramers-Kronig analysis of the sample transmission between 0.22 μm and 1.2 μm . Curves 1, 2 and 3 correspond to measuring temperatures of 90 K, 293 K and 393 K, respectively. The inset shows contributions due to transitions from W_3 subband (a), and the W_3 exciton peak (b), respectively. Dashed line: background due to the low energy subbands [79B].



5 II₂-V₃ compounds

5.0 Crystal structures

The quasi-binary semiconducting III₂-VI₃ compounds presented in this chapter contain vacancies. They can be thought of as ternary structures if the vacancies are counted as zero valent atoms. It should however be noted that the trivalent element (Al, Ga, In) is generally overstoichiometric. Thus ordered-vacancy and disordered-vacancy compounds occur.

The structures occurring in these compounds are wurtzite type, zincblende type and spinel type. In In₂S₃ a layered structure is observed.

In particular the following structures occur:

α -Ga ₂ S ₃	ordered vacancies, wurtzite type
β -Ga ₂ S ₃	disordered vacancies, wurtzite type
γ -Ga ₂ S ₃	disordered vacancies, zincblende type
α -Ga ₂ Se ₃	disordered vacancies, zincblende type
β -Ga ₂ Se ₃	ordered vacancies, zincblende type
Ga ₂ Te ₃	disordered vacancies, zincblende type
α -In ₂ S ₃	disordered defect spinel
β -In ₂ S ₃	ordered defect spinel
γ -In ₂ S ₃	layered structure
α -In ₂ Te ₃	ordered vacancies, zincblende type
β -In ₂ Te ₃	disordered vacancies, zincblende type

Figs. 5.0.1...5.0.3 show as examples the lattices of α -Ga₂S₃ as an example for an ordered vacancies wurtzite type structure, of α -In₂Te₃ as an example for a ordered vacancies zincblende type structure and of β -In₂S₃ as an example for an ordered defect spinel structure.

For structural details as well as for the electronic structure see the respective sections.

Figures to 5.0

Fig. 5.0.1

Projection of the structure of α -Ga₂S₃ on the plane perpendicular to the c -axis.

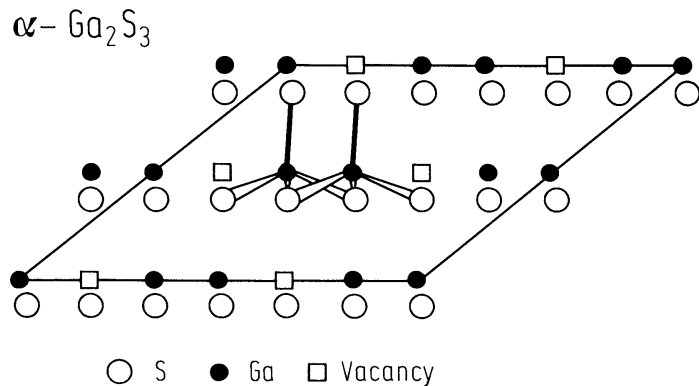


Fig. 5.0.2

Primitive unit cell of $\beta\text{-In}_2\text{S}_3$.

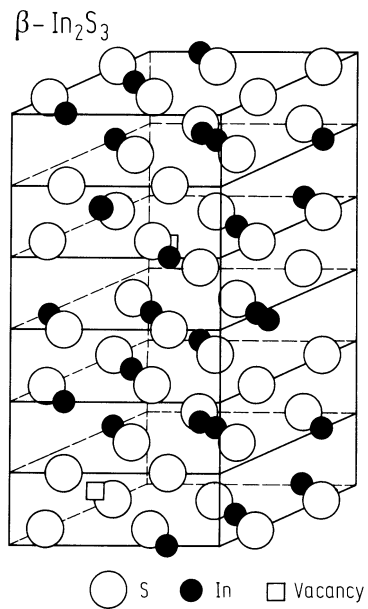
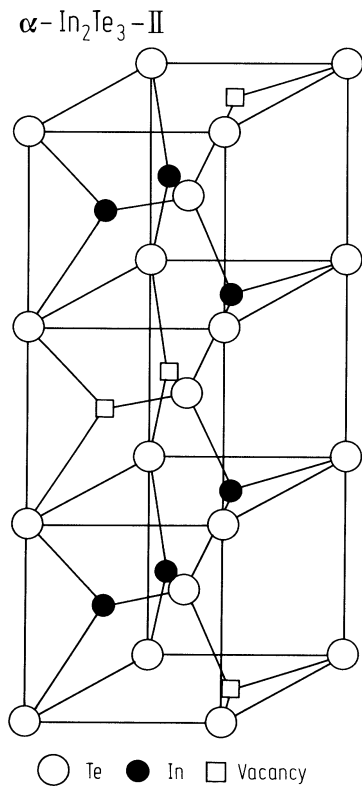


Fig. 5.0.3

Structure of $\alpha\text{-In}_2\text{Te}_3$.



5.1 Gallium sulfide (Ga₂S₃)

Crystal structure

Gallium sulfide occurs under normal conditions in three modifications:

α -Ga ₂ S ₃	ordered vacancies, wurtzite type: C _s ⁴ – Bb	$a = 11.094 \text{ \AA}$ $b = 9.578 \text{ \AA}$ $c = 6.395 \text{ \AA}$ $\gamma = 141^\circ 15'$	prepared by the reaction 3 H ₂ S + 2 Ga(OH) ₃ = Ga ₂ S ₃ + 6 H ₂ O at $T = 1020 \text{ K}$	76C
	disordered C ₆ ² – P6 ₁ or D ₆ ³ – P6 ₅			55H
β -Ga ₂ S ₃	disordered vacancies, wurtzite type: C _{6v} ⁴ – P6 ₃ mc	$a = 3.678(5) \text{ \AA}$ $c = 6.016(6) \text{ \AA}$	prepared as above at $T = 820 \text{ K}$; $d = 3.65 \text{ g cm}^{-3}$	49H
γ -Ga ₂ S ₃	disordered vacancies, zincblende type: T _d ² – F $\bar{4} 3m$	$a = 5.17 \text{ \AA}$	prepared as above at $T = 873 \text{ K}$; $d = 3.63 \text{ g cm}^{-3}$	49H1

Electronic properties

α -Ga₂S₃ :

energy gap

E_g	3.438 eV	$T = 1.6 \text{ K}$	transmission and reflectivity	77M1
-------	----------	---------------------	-------------------------------	------

other transition energies

E	3.388 eV	$T = 1.6 \text{ K}$	transmission and reflectivity	77M1
	3.424 eV	$T = 1.6 \text{ K}$	probably excitonic	
	3.387 eV	$T = 4.2 \text{ K}$	(no polarization dependence given)	
	3.423 eV	$T = 4.2 \text{ K}$		
	3.375 eV	$T = 77 \text{ K}$		
	3.410 eV	$T = 77 \text{ K}$		

β -Ga₂S₃ :

energy gap

E_g	2.48 eV	$T = 290 \text{ K}$	photoelectric effect	59G
-------	---------	---------------------	----------------------	-----

Lattice, transport and optical properties

lattice constants and density : see above under "crystal structure"

electrical conductivity, carrier concentration

Ga₂S₃:Fe (up to 1 mol%)

σ	$10^{-14} \Omega^{-1} \text{ cm}^{-1}$	$T = 300 \text{ K}$	temperature dependence is given in Fig. 5.1.1	89A
----------	--	---------------------	---	-----

n	$10^3 \dots 10^6 \text{ cm}^{-3}$			89A
-----	-----------------------------------	--	--	-----

β -Ga₂S₃ :

phonon frequency

ν_{TO}	$9.72 \cdot 10^{12} \text{ s}^{-1}$	RT	infrared reflectivity	77M2
	$10.44 \cdot 10^{12} \text{ s}^{-1}$		(no polarization dependence given)	

γ -Ga₂S₃ :

dielectric constants

$\varepsilon(0)$	7.5	RT	infrared reflectivity	73M
$\varepsilon(\infty)$	5.8			

phonon frequencies

ν_{TO}	$9.45 \cdot 10^{12} \text{ s}^{-1}$	RT	infrared reflectivity	73M
ν_{LO}	$10.8 \cdot 10^{12} \text{ s}^{-1}$			

melting temperature

T_{m}	1360 K	$p = 1.7 \cdot 10^{-2} \text{ bar}$		76C
----------------	--------	-------------------------------------	--	-----

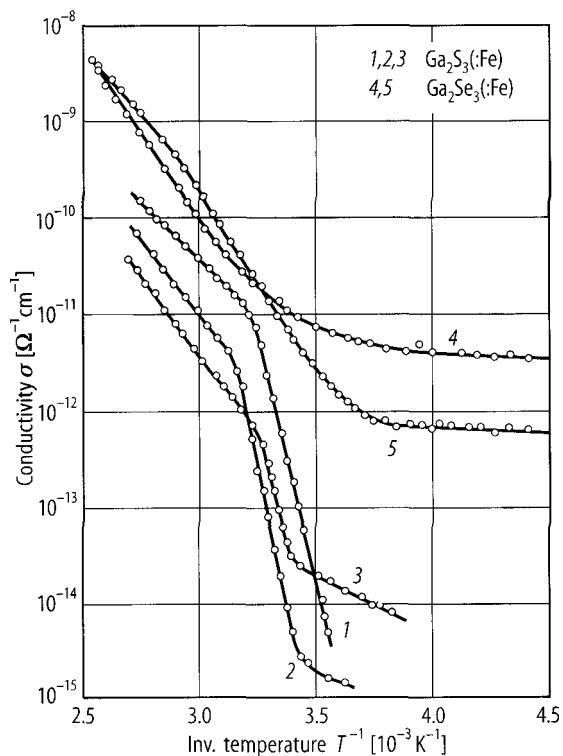
References to 5.1

- 49H Hahn, H., Klinger, W.: Z. Anorg. Chem. 259 (1949) 135.
55H Hahn, H., Frank, G.: Z. Anorg. Allg. Chem. 278 (1955) 333.
59G Gross, E. F., Navikov, B. V., Razbirin, B. S., Suslina, L. G.: Opt. i. Spektrosk. 6 (1959) 569.
73M Musaeva, L. G., Akhundov, G. A., Bakhyshev, A. E., Gasanli, N. M.: Phys. Status Solidi (b) 60 (1973) K1.
76C Collin, G., Flahaut, J., Guittard, M., Loireau-Lozach, A. M.: Mater. Res. Bull. 11 (1976) 285.
77M1 Mushinskii, V. P., Palaki, L. I., Chebotaru, V. V.: Phys. Status Solidi (b) 83 (1977) K149.
77M2 Musaeva, L. G., Khomutova, M. D., Gasanly, N. M.: Fiz. Tverd. Tela 19 (1977) 1766; Sov. Phys. Solid State (English Transl.) 19 (1977) 1030.
89A Askerov, I.M., Aslanov, G.K., Nasredinov, F.S., Tagiev, B.G.: Fiz. Tekh. Poluprovodn. 23 (1989) 1083; Sov. Phys. – Semicond. (Engl. Transl.) 23 (1989) 676.

Figures to 5.1

Fig. 5.1.1

Ga_2S_3 (:Fe), Ga_2Se_3 (:Fe). Temperature dependences of the electrical conductivity of 1) Ga_2S_3 , 2) $\text{Ga}_2\text{S}_3\text{:Fe}_{0.002}$, 3) $\text{Ga}_2\text{S}_3\text{:Fe}_{0.009}$, 4) Ga_2Se_3 , and 5) $\text{Ga}_2\text{Se}_3\text{:Fe}_{0.009}$ [89A].



5.2 Gallium selenide (Ga2Se3)

Crystal structure

Gallium selenide occurs under normal conditions in two modifications:

α -Ga ₂ Se ₃	disordered vacancies, zincblende type: T _d ² – F $\bar{4}$ 3m	$a = 5.418(1) \text{ \AA}$	$d = 4.92 \text{ g cm}^{-3}$	49H
β -Ga ₂ Se ₃	ordered vacancies, zincblende type: D _{4h} ²⁰ – I4 ₁ /acd	$a = 23.235 \text{ \AA}$ $c = 10.828 \text{ \AA}$	stable with excess Se $d = 4.91 \text{ g cm}^{-3}$	77K 80T

Electronic properties

energy gaps

single crystal:

$E_{g,dir}$	1.92 eV	RT	optical absorption	89K
E_g	1.793 eV	RT	evaluated from temperature dependent conductivity	95B
dE/dT	$5.0 \cdot 10^{-5} \text{ eV K}^{-1}$ $5.8 \cdot 10^{-4} \text{ eV K}^{-1}$	$T = 20...129 \text{ K}$ $T = 120...300 \text{ K}$		

thin film:

E_g	2.1 eV	RT	vacancy ordered phase optical absorption	92O
-------	--------	----	---	-----

amorphous:

E_g	1.75 eV	RT	optical absorption	93A
-------	---------	----	--------------------	-----

optical transition energies from reflection spectra

E_g	2.00 eV	$T = 300 \text{ K}$		72B
E_1	3.08 eV			
E_2	3.88 eV			
E_3	4.69 eV			
E	2.28 eV	$T = 77 \text{ K}$	electroabsorption, indirect transition	72A

effective masses

m_p	$1.14 \cdot 10^{-29} \text{ kg}$		Seebeck effect	95G
m_n	$8.52 \cdot 10^{-30} \text{ kg}$		Seebeck effect	95G

Lattice properties

lattice parameters and density : see above under "crystal structure".

phonon wavenumbers (Raman active)

$\bar{\nu}$	155 cm ⁻¹ 250 cm ⁻¹ 300 cm ⁻¹	A ₁ mode	thin films of vacancy-ordered Ga ₂ Se ₃	92Y
-------------	--	---------------------	---	-----

linear expansion coefficient

α	$10.2(64) \cdot 10^{-6} \text{ K}^{-1}$	β -Ga ₂ Se ₃		80T
----------	---	--	--	-----

melting temperature

T_m	1005(3) K			74S
-------	-----------	--	--	-----

Transport properties

carrier concentration, resistivity, mobility, thermoelectric power

p-type samples

p	$1.98 \cdot 10^7 \text{ cm}^{-3}$	$T = 398 \text{ K}$		95B
	10^{13} cm^{-3}		Fe-doped	89A
	$10^{12} \dots 10^{13} \text{ cm}^{-3}$		undoped thin films	86S
ρ	$1.15 \cdot 10^{11} \Omega \text{ cm}$	$T = 398 \text{ K}$		95B,
	$4.2 \cdot 10^7 \Omega \text{ cm}$	RT		89A
	$1 \cdot 10^{10} \Omega \text{ cm}$		Fe-doped	
	$1 \cdot 10^7 \dots 4.5 \cdot 10^{10} \Omega \text{ cm}$		Co-doped	
	$4.5(15) \cdot 10^{11} \Omega \text{ cm}$			94S
μ_p	$2274 \text{ cm}^2 \text{ V}^{-1} \text{ s}^{-1}$	$T = 255 \text{ K}$		95G
S	$35 \mu\text{V K}^{-1}$			

Hall coefficient

R_H	$3.16 \cdot 10^{11} \text{ cm}^3 \text{ C}^{-1}$	RT	undoped (no orientation given)	95B
-------	--	----	--------------------------------	-----

activation energy

E_A	0.32 eV		activation energy of conductivity	95B
-------	---------	--	-----------------------------------	-----

Optical properties

photoluminescence peaks

undoped samples

E	2.03 eV	$T = 4.2 \text{ K}$	ordered vacancies	94O
-----	---------	---------------------	-------------------	-----

References to 5.2

- 49H Hahn, H., Klinger, W.: Z. Anorg. Chem. 259 (1949) 135.
- 72A Askerov, I. M., Gadzhiev, V. A., Guseinova, E. S., Tagiev, B. G.: Phys. Status Solidi (b) 50 (1972) K113.
- 72B Bakhyshev, A. E., Musaeva, L. G., Akhundov, G. A.: Phys. Status Solidi (b) 54 (1972) K77.
- 77K Khan, M. Y.: J. Appl. Crystallogr. 10 (1977) 70.
- 80T Tonejc, A., Popovic, S., Grzeta-Plenkovic, B.: J. Appl. Crystallogr. 13 (1980) 24.
- 84S Sen, S., Bose, D.N.: Solid State Commun. 50 (1984) 39.
- 86S Sysoev, B.I., Bezryadin, N.N., Synorov, Yu.V., Agapov, B.L.: Phys. Status Solidi A 94 (1986) K129.
- 89A Askerov, I.M., Aslanov, G.K., Nasredinov, F.S., Tagiev, B.G.: Fiz. Tekh. Poluprovodn. 23 (1989) 1083; Sov. Phys. – Semicond. (Engl. Transl.) 23 (1989) 676.
- 89K Kwang-Ho, Park, Hyung-Gon, Kim, Wha-Tek, Kim, Chang-Dae, Kim, Hae-Mun, Jeong, Kie-Jin, Lee, Byong-Hyouk, Lee: Solid State Commun. 70 (1989) 971.
- 92O Okamoto, T., Kojima, N., Yamada, A., Konagai, M., Takahashi, K.: Jpn. J. Appl. Phys., Part 2 (Letters) 31 (1992) L143.
- 92Y Yamada, A., Kojima, N., Takahashi, K., Okamoto, T., Konagai, M.: Jpn. J. Appl. Phys., Part 2 (Letters) 31 (1992) L186.
- 93A Adachi, S., Ozaki, S.: Jpn. J. Appl. Phys. Part 1 (Regular Papers & Short Notes) 32 (1993) 4446.
- 94O Okamoto, T., Yamada, A., Konagai, M., Takahashi, K.: J. Cryst. Growth 138 (1994) 204.
- 94S Savchenko, K.V., Shchennikov, V.V.: Can. J. Phys. 72 (1994) 681.
- 95B Belal, A.E., Elshaikh, H.A., Ashraf, I.M.: Cryst. Res. Technol. 30 (1995) 135.
- 95G Gamal, G.A., Elshaikh, H.A.: Cryst. Res. Technol. 30 (1995) 867.

5.3 Gallium telluride (Ga2Te3)

Crystal structure

Ga2Te3	disordered vacancies, zincblende type: Td ² – F 4 3m	a = 5.874(5) Å 5.899 Å	d = 5.57 g cm ⁻³	49H 77B
	ordered vacancies, zincblende type: orthorhombic 8 × Ga2Te3/unit cell wurtzite like structure	a = 4.17 Å ≈ 2 ^{-1/2} a ₀ b = 23.60 Å ≈ 4a ₀ c = 12.52 Å ≈ 3·2 ^{-1/2} a ₀	doubtful (a ₀ : lattice constant of ZnS subcell)	63N 56H

Electronic properties

energy gap

single crystal:

E _{g,dir}	1.08 eV	RT	optical absorption	84S
E _{g,th}	1.55(3) eV	T = 293...1063 K	conductivity vs. temperature	56H
E _g	1.22 eV	T = 273 K	optical reflection	56H
	1.23(3) eV	T = 273 K	photoemission	55G
amorphous:				
E _g	1.2 eV	RT	ellipsometry	94O

Lattice properties

lattice parameters and density : see above under "crystal structure"

wavenumbers of IR active phonons

$\bar{\nu}$	37, 55, 91, 136, 175, 194, 210, 221, 242 cm ⁻¹	far-infrared transmission	94J
-------------	---	---------------------------	-----

wavenumbers of Raman active phonons

$\bar{\nu}$	16, 38, 55, 64, 86, 112, 134, 171, 220 cm ⁻¹	RT, Raman scattering spectra	94J
-------------	---	------------------------------	-----

linear expansion coefficient

α	8.3(3)·10 ⁻⁶ K ⁻¹	T = 300 K	61W
----------	---	-----------	-----

melting temperature

T _m	1063 K		80T
----------------	--------	--	-----

Transport properties

The transport is intrinsic even with up to 9 at% Cu or other elemental impurities including excess Ga [77S]. Even after irradiation the electrical conductivity is unchanged [73K].

carrier concentration, resistivity, mobility

n-type samples

n	4·10 ¹³ cm ⁻³	RT	94J
ρ	10 ⁵ ...10 ⁶ Ω cm		84S
	10 ⁴ ...10 ⁶ Ω cm		92W
μ_n	28 cm ² V ⁻¹ s ⁻¹	T = 310 K	84S
	0.31 cm ² V ⁻¹ s ⁻¹	RT	94J

conductivity

σ	10 ⁻⁶ ... 10 ⁻¹² Ω ⁻¹ cm ⁻¹	T = 77...300 K	94J
----------	--	----------------	-----

activation energies

E_A	0.78(2) eV	intrinsic conductivity	88N
	0.44 eV	intrinsic conductivity	84S
	0.18 eV	intrinsic conductivity	94J

Optical properties

dielectric constants

$\epsilon(0)$	10.95	from ESCA measurements	85S
$\epsilon(\infty)$	10.58		

References to 5.3

- 49H Hahn, H., Klinger, W.: Z. Anorg. Chem. 259 (1949) 135.
- 55G Gorgonova, N. A., Grigoreva, V. S., Konovalenko, B. M., Ryvkin, S. M.: Zh. Tekh. Fiz. 25 (1955) 1675.
- 56H Harbeke, G., Lautz, G.: Z. Naturforsch. 11a (1956) 1015.
- 61W Woolley, J. C., Pamplin, B. R.: J. Electrochem. Soc. 108 (1961) 874.
- 63N Newman, P. C., Cundall, J. A.: Nature (London) 200 (1963) 876.
- 73K Koshkin, V. M., Gal'chinetskii, L. P., Kulik, V. N., Minkiev, B. I., Ulmanis, U. A.: Solid State Commun. 13 (1973)1.
- 77B Burlaku, G. G., Markus, M. M., Tyrzin, V. G.: Izv. Akad. Nauk SSSR, Neorg. Mater. 13 (1977) 820.
- 77S Sheikh-Zananova, R. N., Ponomarev, V. F.: Izv. Akad. Nauk SSSR, Neorg. Mater. 13 (1977) 1308; Inorg. Mater. (USSR) (English Transl.) 13 (1977) 1056.
- 80T Tonejc, A., Popovic, S., Grzeta-Plenkovic, B.: J. Appl. Crystallogr. 13 (1980) 24.
- 84S Sen, S., Bose, D.N.: Solid State Commun. 50 (1984) 39.
- 85S Sen, S., Bose, D.N., Hegde, M.S.: Phys. Status Solidi B 129 (1985) K65.
- 88N Nasredinov, F.S., Masterov, V.F., Saidov, Ch.S., Seregin, P.P., Troitskaya, N.N., Tschirner, H.U.: Phys. Status Solidi A 107 (1988) 291.
- 92W Wuyts, K., Watte, J., Langouche, G., Silverans, R.E., Zegbe, G., Jumas, J.C.: J. Appl. Phys. 71 (1992) 744.
- 94J Julien, C., Ivanov, I., Ecrepont, C., Guittard, M.: Phys. Status Solidi A 145 (1994) 207.
- 94O Ozaki, S., Takada, K., Adachi, S.: Jpn. J. Appl. Phys. Part 1 (Regular Papers & Short Notes) 33 (1994) 6213.

5.4 Indium sulfide (In2S3)

Crystal structure

Indium sulfide occurs under normal conditions in three modifications:

α -In ₂ S ₃	disordered defect spinel type: O _h ⁷ – Fd3m tetrahedral sites full. octahedral sites: In and vacancies	$a = 5.36 \text{ \AA}$	stable at $T = 693...1023 \text{ K}$ stable at $T = 300 \text{ K}$ with excess In [70D]; may be badly crystallized β -In ₂ S ₃ [73S, 74A, 76K, 75E] $d = 4.63 \text{ g cm}^{-3}$; probably contains voids	49H 49H
β -In ₂ S ₃	ordered defect spinel type: D _{4h} ¹⁹ – I4 ₁ /amd octahedral sites full, tetrahedral 2/3	$a = 7.618(1) \text{ \AA}$ $c = 32.33(1) \text{ \AA}$	stable up to $T = 693 \text{ K}$, but see above; $d = 4.613 \text{ g cm}^{-3}$	70L, 76K
γ -In ₂ S ₃	layered structure (–S–In–S–In–S–...) S close packed, In octahedral, D _{3d} ³ – P $\bar{3}$ m1	$a = 3.8 \text{ \AA}$ $c = 9.04 \text{ \AA}$	stable above $T = 1023 \text{ K}$ annealing produces α or β phase [78B]; stable at $T = 300 \text{ K}$ with As or Sb; As, Sb in tetrahedral positions between layers [73D1, 76D] $d = 4.75(8) \text{ g cm}^{-3}$ with As, with As, $d = 4.80(8) \text{ g cm}^{-3}$ with Sb	70D 76D

Electronic properties

If not noted otherwise the data refer to n-type β -In₂S₃.

energy gaps

E_g	1.8(1) eV		transmission measurements	93D
thin film data:				
E_g	1.98 eV		optical band gap	91N
$E_{g,ind}$	2.20 eV	$T = 298\text{ K}$	optical band gap, tetragonal	86K
$E_{g,dir}$	2.3 eV		absorption measurements	94A
$dE_{g,dir}/dT$	$-7\cdot10^{-4}\text{ eV K}^{-1}$	$T = 77...360\text{ K}$		
$E_{g,th}$	2.30 eV		field emission deposited by spray pyrolysis	70L
$\gamma\text{-In}_2\text{S}_3\text{:As}$				
E_g	1.88 eV	$T = 300\text{ K}$	absorption	73D
$E_{g,th}$	1.38(15) eV		conductivity vs. T	
$\gamma\text{-In}_2\text{S}_3\text{:Sb}$				
E_g	1.44 eV	$T = 300\text{ K}$	absorption	73D
$E_{g,th}$	1.42(15) eV		conductivity vs. T	

structure in valence band (energy below E_F)

E	1.5 eV 3.9 eV 5.9 eV		X-ray photoemission	78I
-----	----------------------------	--	---------------------	-----

Lattice properties

lattice parameters and density : see above under "crystal structure".

thermal expansion : see Fig. 5.4.1

melting temperature

T_m	1363 K	75D1
-------	--------	------

Transport and optical properties

thermoelectric power

n-type samples

S	-100 mV K^{-1}	RT	93D
-----	-------------------------	----	-----

electrical resistivity: Fig. 5.4.2.

electrical conductivity

σ	$2.0\cdot 10^{-4}\text{ }\Omega^{-1}\text{cm}^{-1}$	91N
----------	---	-----

The temperature dependence of the electrical conductivity is given in Fig. 5.4.3 [88R].

resistivity in doped samples

$\gamma\text{-In}_2\text{S}_3\text{:As}$

ρ	$9(5)\cdot 10^7\text{ }\Omega^{-1}\text{ cm}^{-1}$	$T=300\text{ K}$	(no orientation dependence given)	73D2
--------	--	------------------	-----------------------------------	------

$\gamma\text{-In}_2\text{S}_3\text{:Sb}$

ρ	$3(2)\cdot 10^4\text{ }\Omega^{-1}\text{ cm}^{-1}$	$T=300\text{ K}$	73D2
--------	--	------------------	------

activation energies

E_A	0.26(2) eV	activation energy of conductivity	88G
	0.45 and 0.20 eV	Sn-doped samples	88R, 96M

dielectric constant

$\epsilon(0)$	13.5	$T=300\text{ K}$	63G
$\epsilon(\infty)$	6.5		

refractive index in doped samples

$\gamma\text{-In}_2\text{S}_3\text{:As}$

n	3.06(15)	$T=300\text{ K}$	73D2
-----	----------	------------------	------

$\gamma\text{-In}_2\text{S}_3\text{:Sb}$

n	2.84(15)	$T=300$	73D2
-----	----------	---------	------

References to 5.4

- 49H Hahn, H., Klinger, W.: Z. Anorg. Chem. 260 (1949) 97.
- 63G Gadick, G. F., Springford, M., Checinska, H.: Proc. Phys. Soc. 82 (1963) 16.
- 65R Rewald, W., Harbeke, G.: J. Phys. Chem. Solid 26 (1965) 1309.
- 70D Diehl, R., Nitsche, R., Ottermann, J.; Naturwissenschaften 51 (1970) 670.
- 70L Lutz, M. D., Häuseler, H.: Z. Naturforsch. 26a (1970) 323.
- 73D1 Diehl, R., Nitsche, R., Carpentier, C. D.: J. Appl. Crystallogr. 6 (1973) 497.
- 73D2 Diehl, R., Nitsche, R.: J. Cryst. Growth 29 (1973) 38.
- 73S Shafizade, R. B., Efendiev, E. G., Aliev, F. I.: Kristallografiya 18 (1973) 660; Sov. Phys. Crystallogr. (English Transl.) 18 (1973) 417.
- 74A Aliev, F. I., Efendiev, E. G., Shafizade, R. B.: Izv. Akad. Nauk Az. SSR, Ser. Fiz. Tekh. i. Mat. Nauk 4 (1974) 23.
- 75D Diehl, R., Nitsche, R.: J. Cryst. Growth 28 (1975) 306.
- 75E Efendiev, E. G., Aliev, F. I., Shafizade, R. B.: Izv. Akad. Nauk Az. SSR, Ser. Fiz. Tekh. i Mat. Nauk 1 (1975) 23.
- 76D Diehl, R., Carpentier, C. D., Nitsche, R.: Acta Crystallogr. B32 (1976) 1257.
- 76K Kundra, K. D., Ali, S. Z.: Phys. Status Solidi (a) 36 (1976) 517.
- 78B1 Bartzokas, D., Manolikas, C., Spyridelis, J.: Phys. Status Solidi (a) 47 (1978) 459.
- 78I Ihara, H., Abe, H., Endo, S., Irie, T.: Solid State Commun. 28 (1978) 563.
- 86K Kim, W.T., Kim, C.D.: J. Appl. Phys. 60 (1986) 2631.
- 88G George, J., Joseph, K.S., Pradeep, B., Palson, T.I.: Phys. Status Solidi A 106 (1988) 123.
- 88R Regel, A.R., Seregin, P.P., Nasredinov, F.S., Agzamov, A.A.: Fiz. Tekh. Poluprovodn. 22 (1988) 1144; Sov. Phys. – Semicond. (Engl. Transl.) 22 (1988) 724.
- 91N Nomura, R., Konishi, K., Matsuda, H.: Thin Solid Films 198 (1991) 339.
- 93D Dalas, E., Sakkopoulos, S., Vitoratos, E., Maroulis, G.: J. Mater. Sci. 28 (1993) 5456.
- 94A Asikainen, T., Ritala, M., Leskela, M.: Appl. Surf. Sci. 82-83 (1994) 122.
- 96M Morley, S., von der Emde, M., Zahn, D.R.T., Offermann, V., Ng, T.L., Maung, N., Wright, A.C., Fan, G.H., Poole, I.B., Williams, J.O.: J. Appl. Phys. 79 (1996) 3196.

Figures to 5.4

Fig. 5.4.1

β - In_2S_3 . Lattice parameters vs. temperature [76K].

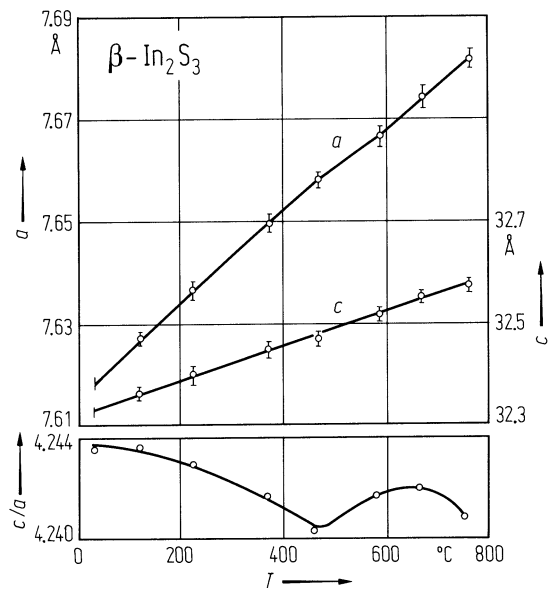


Fig. 5.4.2

β - In_2Se_3 . Resistivity vs reciprocal temperature for five undoped samples (1...5), one Cd-doped (6) and one P-doped sample (7) [65R]. Orientation not specified.

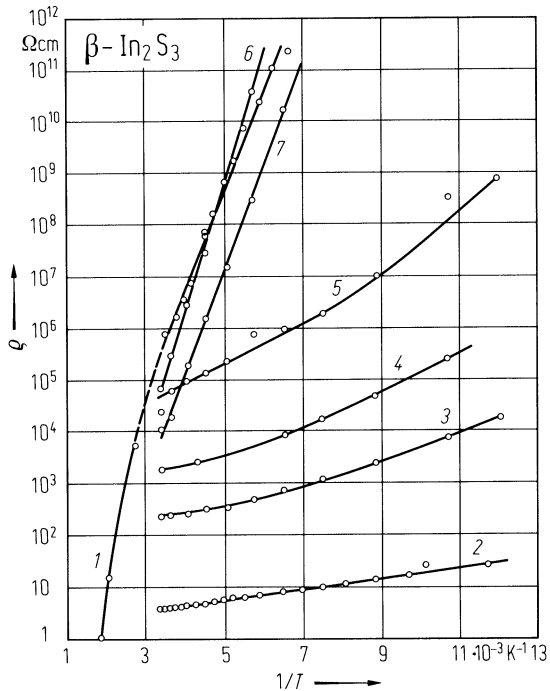
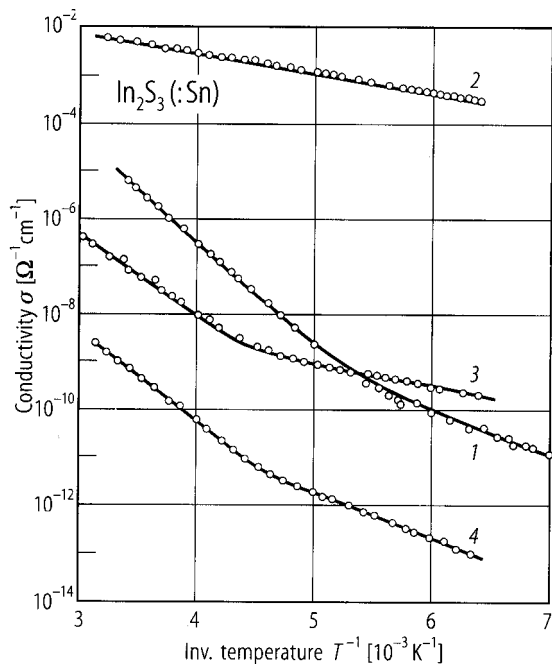


Fig. 5.4.3

β - In_2S_3 . The temperature dependence of the electrical conductivity of 1) In_2S_3 , 2) $\text{In}_2\text{S}_3 + 0.5$ at% Sn, 3) In_2S_3 after annealing in S-vapor, and 4) $\text{In}_2\text{S}_3 + 0.5$ at% Sn after annealing in S-vapor [88R].



5.5 Indium selenide (In2Se3)

Crystal structure

The literature on the structure of In2Se3 is confused and in some respects contradictory. Phases α, β, γ and δ were mentioned.

At normal conditions the phase α-In2Se3 is composed of layers, which are only weakly bound to each other. Each layer contains planes of Se and In in the sequence –Se–In–Se–In–Se– where the Se atoms in each plane build a triangular lattice with the lattice constant *a* = 4.025(25) Å at RT.

Another phase (β-In2Se3) is stable at higher temperatures, but can be supercooled to RT.

Electronic properties

band structure

The energy-band structure of crystalline In2Se3 (α-phase) was calculated by [89W] (see Fig. 5.5.1).

energy gap

<i>E_g</i>	1.3 eV		calculated	89W
	1.356 eV	RT	optical absorption, α-phase	90J
	1.812 eV	RT	optical absorption, γ-phase	
	1.308 eV	RT	optical absorption, β-phase (extrapolated from 523 K)	
<i>dE_g/dT</i>	7.5·10 ^{−4} eV K ^{−1}		optical absorption, α-phase	90J
	8.3·10 ^{−4} eV K ^{−1}		optical absorption, γ-phase	
thin film data				
<i>E_g</i>	1.5...1.6 eV		amorphous thin films	87W, 89W
<i>E_{g,ind}</i>	1.40 eV		polycrystalline, optical measurements	95M2
<i>E_{g,dir}</i>	1.16 eV	<i>T</i> = 300 K, <i>E</i> ⊥ <i>c</i>	β-phase, absorption	71M
<i>E_{g,th}</i>	1.41 eV	<i>E</i> ∥ <i>c</i>	β-phase, conductivity	71B

effective masses

<i>m_n</i>	0.035 <i>m</i> ₀	RT	from FIR reflectivity	88K
	0.24 <i>m</i> ₀		from resistivity and Hall measurements	91M

photoemission peak energies

(all energies relative to valence band maximum at 300 K)

<i>E</i>	1.326 eV	<i>T</i> = 4.2 K	annealed samples	88K
	1.319 eV	<i>T</i> = 4.2 K	quenched samples	88K

Lattice and optical properties

linear thermal expansion coefficient

<i>α</i>	12.4·10 ^{−6} K ^{−1}	<i>T</i> = 290...470 K	parallel to layer	75G
	11.5·10 ^{−6} K ^{−1}	(α-phase)	perpendicular to layer	

melting temperature

<i>T_m</i>	1163 K			76C
----------------------	--------	--	--	-----

phonon frequencies

<i>ν_{TO}</i>	2.723·10 ¹² s ^{−1}	RT, <i>E</i> ⊥ <i>c</i>	α-phase, infrared reflectivity	78K
	4.82·10 ¹² s ^{−1}			
	5.624·10 ¹² s ^{−1}			
<i>ν_{LO}</i>	2.835·10 ¹² s ^{−1}	RT, <i>E</i> ⊥ <i>c</i>	α-phase, infrared reflectivity,	78K
	5.286·10 ¹² s ^{−1}		Kramers-Kronig analysis	
	6.564·10 ¹² s ^{−1}			

dielectric constants

$\epsilon(0)$	16.68	$E \perp c$	infrared reflectivity	78K
$\epsilon(\infty)$	9.53	$E \perp c$		
$\epsilon(\infty)$	9.51	$E \perp c$	α -phase, from FIR	90J
	7.23	$E \perp c$	β -phase, from FIR	
	8.09	$E \perp c$	γ -phase, from FIR	

photoluminescence peaks

undoped samples

E	1.326 eV	$T = 4.2$ K	radiative recombination on intrinsic defects	86B
	1.523 eV	$T = 4.2$ K	radiative recombination of impurity bound excitons	

Transport properties

In the α -phase the electrical conductivity is metallic, although the optical gap is greater than 1 eV. This is interpreted as being due to shallow donors. The β -phase shows intrinsic semiconducting behavior. The σ vs. T curves show a large hysteresis due to the supercooling of the β -phase.

carrier concentration, resistivity, mobility, thermoelectric power

n-type samples

n	$3 \cdot 10^{16} \dots$	RT	annealed samples	88K
	$2 \cdot 10^{19} \text{ cm}^{-3}$			
ρ	$6.7 \text{ } \Omega \text{ cm}$	RT	single crystals	96J
μ_n	250...	RT	annealed samples	88K
	$490 \text{ cm}^2 \text{ V}^{-1} \text{ s}^{-1}$			

Fig. 5.5.2 shows the temperature dependence of electrical conductivity, Hall mobility and electron density of polycrystalline thin films [95M2].

The anisotropy of the electrical conductivity as a function of temperature is shown in Figs. 5.5.3 [91N].

electrical conductivity

σ	$2.7 \text{ } \Omega^{-1} \text{ cm}^{-1}$	RT, $E \perp c$	α -phase, undoped undoped	71B
	$0.8 \text{ } \Omega^{-1} \text{ cm}^{-1}$	RT, $E \parallel c$		
	$0.02 \dots 260 \text{ } \Omega^{-1} \text{ cm}^{-1}$			88K
	$2.1 \cdot 10^{-4} \dots$	RT	thin films	95M1
	$2.8 \cdot 10^{-1} \text{ } \Omega^{-1} \text{ cm}^{-1}$			
	$260 \text{ } \Omega^{-1} \text{ cm}^{-1}$	RT	single crystal	88F
anisotropy				
$\sigma_{\parallel} / \sigma_{\perp}$	$\approx 10^{-3}$	RT		88K
σ_{\parallel}	$0.799 \cdot 10^{-3} \text{ } \Omega^{-1} \text{ cm}^{-1}$	RT	parallel to cleavage plane	91N
σ_{\perp}	$4.138 \cdot 10^{-3} \text{ } \Omega^{-1} \text{ cm}^{-1}$	RT	perpendicular to cleavage plane	

mobility of charge carriers

μ_n	$10 \text{ cm}^2 \text{ V}^{-1} \text{ s}^{-1}$	$T = 300$ K	Hall effect	74R
---------	---	-------------	-------------	-----

activation energies

E_A	0.4 eV		activation energy of conductivity in amorphous thin film	87W,
				89W
	0.395 eV		amorphous thin film	95A
	$0.06 \dots 0.16$ eV		single crystal	96J

References to 5.5

- 71B Bidgin, D., Popovic, S., Celustka, B.: Phys. Status Solidi (a) 6 (1971) 295.
- 71M Mushinskii, V. P., Kobolev, V. I., Andronck, I. Ya.: Fiz. Tekh. Poluprovodn. 5 (1971) 1251; Sov. Phys. Semicond. (English Transl.) 5 (1971) 1104.
- 74R Romeo, N.: Phys. Status Solidi (a) 26 (1974) K187.
- 75G Gasanov, G. Sh., Mamedov, K. P., Suleimanov, Z. Y., Bagirov, S. B.: Izv. Akad. Nauk Az. SSR 4 (1975) 65.
- 76C Collin, G., Flahaut, J., Guittard, M., Loireau-Lozach, A. M.: Mater. Res. Bull. 11 (1976) 285.
- 78K Kambas, K., Spyridelis, J.: Mater. Res. Bull. 13 (1978) 653.
- 86B Balkanski, M., Julien, C., Chevy, A., Kambas, K.: Solid State Commun. 59 (1986) 423.
- 87W Watanabe, I., Sekiya, T.: J. Non-Cryst. Solids 97-98 (1987) 667.
- 88F Fotsing, J., Julien, C., Balkanski, M., Kambas, K.: Mater. Sci. Eng. B 1 (1988) 139.
- 88K Kambas, K., Fotsing, J., Hatzikraniotis, E., Julien, C.: Phys. Scr. 37 (1988) 397.
- 89W Watanabe, Y., Kaneko, S., Kawazoe, H., Yamane, M.: Phys. Rev. B 40 (1989) 3133.
- 90J Julien, C., Chevy, A., Siapkas, D.: Phys. Status Solidi A 118 (1990) 553.
- 91M Micocci, G., Tepore, A., Rella, R., Siciliano, P.: Phys. Status Solidi A 126 (1991) 437.
- 91N Nomura, R., Konishi, K., Matsuda, H.: Thin Solid Films 198 (1991) 339.
- 95A Afifi, M.A., Hegab, N.A., Bekheet, A.E.: Vacuum 46 (1995) 335.
- 95M1 Manno, D., Micocci, G., Rella, R., Siciliano, P., Tepore, A.: Vacuum 46 (1995) 997.
- 95M2 Micocci, G., Tepore, A., Rella, R., Siciliano, P.: Phys. Status Solidi A 148 (1995) 431.
- 96J Julien, C., Balkanski, M.: Mater. Sci. Eng. B38 (1996) 1.

Fig. 5.5.1

α - In_2Se_3 . Energy-band structure of crystalline In_2Se_3 in which all In-atoms are assumed to be tetrahedrally coordinated. Shaded area represents an energy-gap region. The first Brillouin zone is illustrated in the lower right portion. Energy scale on the vertical axes is taken to be normalized to Hartree-Fock atomic energies assumed in the calculation [89W].

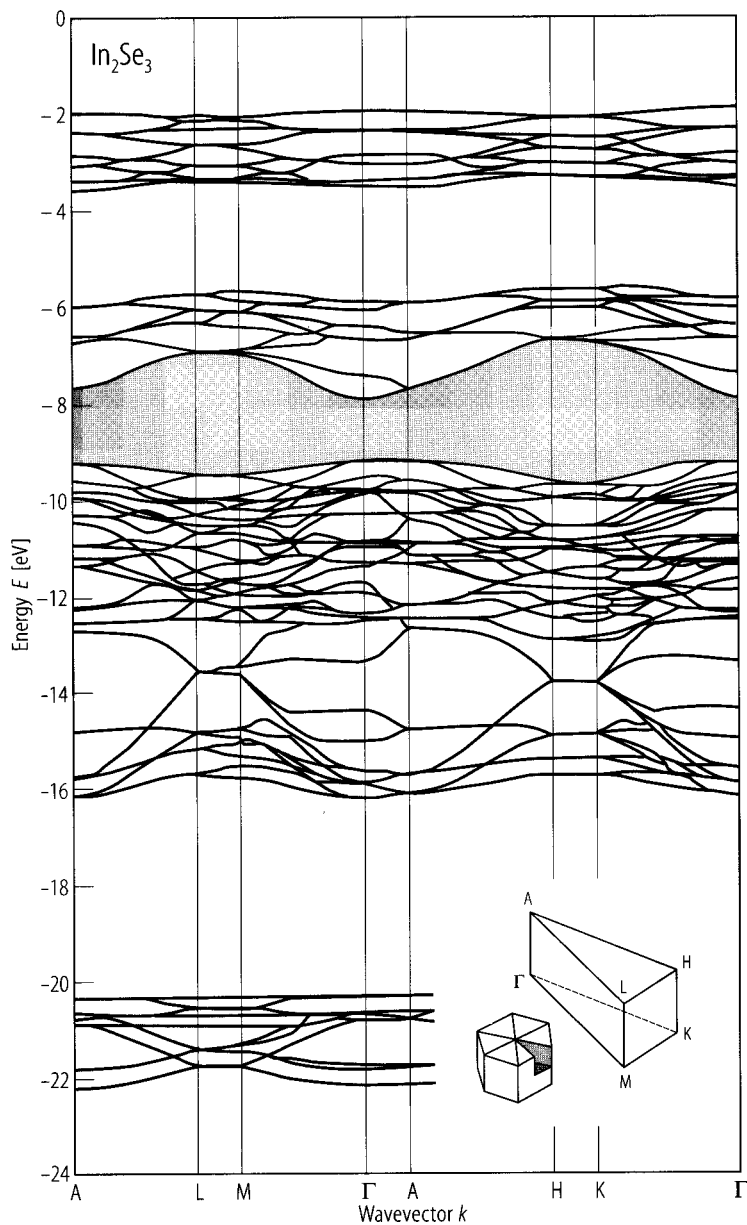


Fig. 5.5.2

In_2Se_3 . **(a)** Electrical conductivity σ , **(b)** Hall mobility $\mu_{H,n}$, **(c)** electron concentration n vs. $1/T$ of In_2Se_3 thin films for different annealing temperatures T_a : 1) as deposited, 2) 350 K, 3) 400 K, 4) 450 K, 5) 500 K, 6) 550 K, 7) 600 K [95M2].

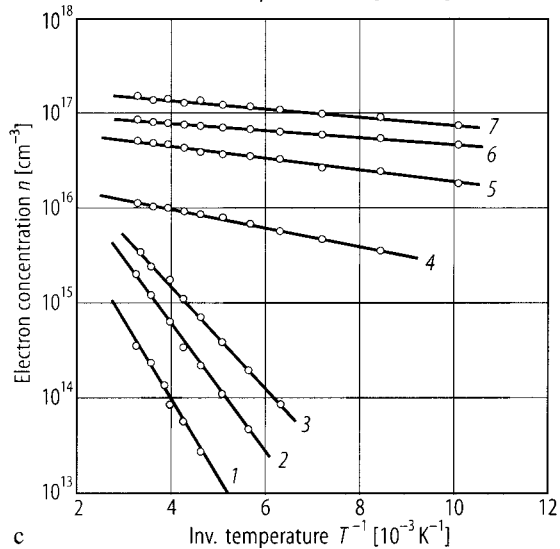
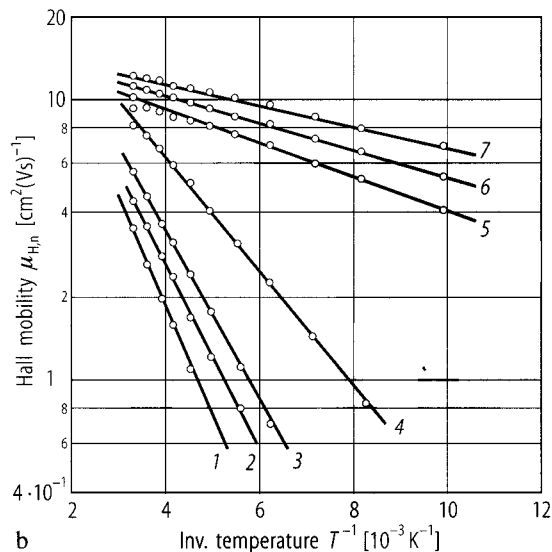
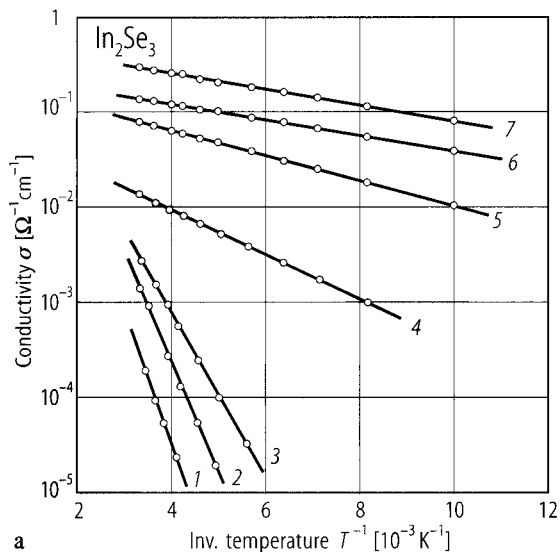
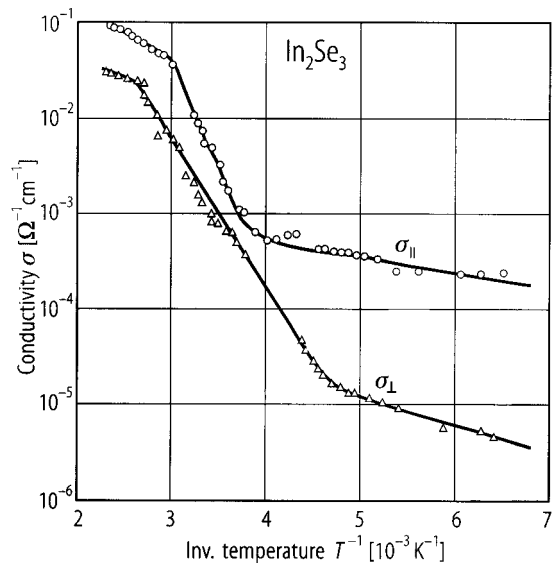


Fig. 5.5.3

α - In_2Se_3 . Plot of the electrical conductivity against $1/T$ for n-type In_2Se_3 parallel and perpendicular to the c -axis [91N].



5.6 Indium telluride (In₂Te₃)

Crystal structure

Indium telluride occurs under normal conditions in three modifications

α -In ₂ Te ₃	ordered vacancies, zincblende type: $T_d^2 - F\bar{4}3m$ $9 \times \text{In}_2\text{Te}_3/\text{unit cell}$	$a = 18.486(20) \text{ \AA}$	contains a Te atom with no first neighbors; probably mixture of 2 phases $d = 5.79 \text{ g cm}^{-3}$	54I, 60Z3, 71Z 60Z3
α -In ₂ Te ₃ -I	ordered vacancies, zincblende type, defect famatinite: $D_{2d}^{11} - I\bar{4}2m$	$a = 6.173(10) \text{ \AA}$ $c = 12.438(73) \text{ \AA}$	really In ₃ Te ₄ with less In; has been prepared as single crystal	75K, 57G
α -In ₂ Te ₃ -II	ordered vacancies, zincblende type: $C_{2v}^{20} - \text{Imm}2$, see Fig. 3	$(a_0 = 6.163 \text{ \AA})$ $a = 2^{-1/2}a_0$ $b = 3 \cdot 2^{-1/2}a_0$ $c = a_0$	not yet prepared as single crystal	59W, 75K, 78B
β -In ₂ Te ₃	disordered vacancies, zincblende type: $T_d^2 - F\bar{4}3m$	$a = 6.163 \text{ \AA}$	phase change: $T = 790...890\text{K}$, stable at lower temperature with excess In (almost always the case) $d = 5.73 \text{ g cm}^{-3}$	49H, 60Z1 60Z1

Electronic properties

energy gaps

E_g	1.0 eV	$T = 295 \text{ K}$	β -In ₂ Te ₃ ,absorption	72V
	1.026 eV	$T = 290 \text{ K}$	α -In ₂ Te ₃ , absorption	60P
dE_g/dT	$-5.6 \cdot 10^{-4} \text{ eV K}^{-1}$	$T = 82...295 \text{ K}$	β -In ₂ Te ₃ ,absorption	72V
	$-3.4 \cdot 10^{-4} \text{ eV K}^{-1}$	$T = 0...300 \text{ K}$	α -In ₂ Te ₃ ,Hall effect	60Z1

single crystal:

$E_{g,dir}$	1.09 eV	RT	photocurrent	93B
-------------	---------	----	--------------	-----

thin films

$E_{g,dir}$	1.05(3)...1.16 eV	RT	optical absorption	90R, 90Z1
-------------	-------------------	----	--------------------	-----------

temperature dependence, see Fig. 5.6.1.

effective masses

m_n	1.43 m_0		from thermopower	91N
m_n/ m_p	0.37			

Lattice and optical properties

lattice parameters and density : see above under "crystal structure"

sound velocity

v_1	$2.56 \cdot 10^5 \text{ cm s}^{-1}$	longitudinal	60Z2
-------	-------------------------------------	--------------	------

linear thermal expansion coefficient

α	$1.15(10) \cdot 10^{-4} \text{ K}^{-1}$	$T = 290...470 \text{ K}$	61W
----------	---	---------------------------	-----

melting temperature				
T_m	940 K			60Z2
refractive index				
n	3.4(3)	$\lambda = 2.2 \mu\text{m}$	$\alpha\text{-In}_2\text{Te}_3$	60Z1
dielectric constants				
$\varepsilon(0)$	12.3		from ESCA measurements	85S
	16		$\alpha\text{-In}_2\text{Te}_3$	60Z1
$\varepsilon(\infty)$	10.54		from ESCA measurements	

Transport properties

There is little difference between the properties of the two phases α and β .

carrier concentration, resistivity, mobility, thermoelectric power

p-type samples				
p	$3.16 \cdot 10^{10} \text{ cm}^{-3}$	RT	single crystal, Hall measurement	89H
ρ	$1.44 \cdot 10^5 \Omega \text{ cm}$	RT	single crystal	89H
μ_p	$210 \text{ cm}^2 \text{ V}^{-1} \text{ s}^{-1}$	$T = 350 \text{ K}$	single crystal	84S
	$1380 \text{ cm}^2 \text{ V}^{-1} \text{ s}^{-1}$	RT	single crystal	91N
S	$280 \mu\text{V K}^{-1}$	$T = 216 \text{ K}$	single crystal	91N
	$185 \mu\text{V K}^{-1}$	RT		

intrinsic electron concentration

n_i	$7.68 \cdot 10^{12} \text{ cm}^{-3}$	$T = 334 \text{ K}$	$\alpha\text{-In}_2\text{Te}_3$,	60Z1
	$4.1 \cdot 10^{13} \text{ cm}^{-3}$	$T = 417 \text{ K}$	T dependence of Hall constant	
	$1.6 \cdot 10^{15} \text{ cm}^{-3}$	$T = 556 \text{ K}$		

electrical conductivity

σ	$10^{-4} \dots 10^{-3} \Omega^{-1} \text{ cm}^{-1}$	$T = 300 \text{ K}$	recrystallized thin films	90Z2
----------	---	---------------------	---------------------------	------

electrical conductivity vs. T : Fig. 5.6.2

electrical resistivity

ρ	$1.8 \cdot 10^6 \Omega^{-1} \text{ cm}^{-1}$			75D
--------	--	--	--	-----

electron mobility

μ_n	$5 \dots 70 \text{ cm}^2/\text{Vs}$	$T = 0 \dots 300 \text{ K}$	Hall effect	60Z1
	$32 \text{ cm}^2/\text{Vs}$	RT	before quenching from 823 K (i.e. $\alpha\text{-In}_2\text{Te}_3$)	75D
	$28 \text{ cm}^2/\text{Vs}$	RT	after quenching from 823 K (i.e. $\beta\text{-In}_2\text{Te}_3$)	

activation energies

E_A	0.51 eV		activation energy of conductivity	88N
	0.16 eV	$T = 180 \dots 250 \text{ K}$	activation energy of conductivity	84S
	0.55 eV	$T = 250 \dots 450 \text{ K}$	activation energy of conductivity	
	0.01 eV	$T = 80 \dots 160 \text{ K}$	amorphous thin film	89Z
	0.03 eV	$T = 80 \dots 160 \text{ K}$	recrystallized thin film, $\beta\text{-In}_2\text{Te}_3$	
	0.47 eV	$T = 300 \dots 420 \text{ K}$	thin film	90Z1
	0.56 eV	$T = 420 \dots 540 \text{ K}$	thin film	

thermoelectric power (Seebeck coefficient)

S	$-400 \mu\text{V K}^{-1}$	$T = 714 \text{ K}$	$\alpha\text{-In}_2\text{Te}_3$	60Z1
	$-960 \mu\text{V K}^{-1}$	$T = 333 \text{ K}$		

thermal conductivity

κ	$11.22 \cdot 10^{-3} \text{ W cm}^{-1} \text{ K}^{-1}$	$T = 300 \text{ K}$	$\alpha\text{-In}_2\text{Te}_3$	60P,
	$6.95 \cdot 10^{-3} \text{ W cm}^{-1} \text{ K}^{-1}$	$T = 300 \text{ K}$	$\beta\text{-In}_2\text{Te}_3$	60Z2
	$7.87 \cdot 10^{-3} \text{ W cm}^{-1} \text{ K}^{-1}$	$T = 100 \text{ K}$	$\beta\text{-In}_2\text{Te}_3$	

References to 5.6

- 49H Hahn, H., Klinger, W.: Z. Anorg. Chem. 260 (1949) 97.
54I Inuzaka, H., Sugaike, S.: Proc. Jpn. Acad. 30 (1954) 383.
57G Gaines, R. V.: Am. Mineral. 42 (1957) 766.
59W Woolley, J. C., Pamplin, B. R., Holmes, P. T.: J. Less-Common Met. 1 (1959) 362.
60P Petrusovich, V. A., Sergeeva, V. M., Smirnov, I. A.: Fiz. Tverd. Tela 2 (1960) 2894; Sov. Phys. Solid State (English Transl.) 2 (1961) 2573.
60Z1 Zhuse, V. P., Sergeeva, V. M., Shelykh, A. I.: Fiz. Tverd. Tela 2 (1960) 2858; Sov. Phys. Solid State (English Transl.) 2 (1961) 2545.
60Z2 Zaslavskii, A. I., Sergeeva, V. M., Smirnov, I. A.: Fiz. Tverd. Tela 2 (1960) 2885; Sov. Phys. Solid State (English Transl.) 2 (1961) 2565.
60Z3 Zaslavskii, A. I., Sergeeva, V. M.: Fiz. Tverd. Tela 2 (1960) 2872; Sov. Phys. Solid State (English Transl.) 2 (1961) 2556.
61W Woolley, J. C., Pamplin, B. R.: J. Electrochem. Soc. 108 (1961) 874.
71Z Zaslavskii, A. I., Kartenko, N. F., Karachentseva, Z. A.: Fiz. Tverd. Tela 13 (1971) 1562; Sov. Phys. Solid State (English Transl.) 13 (1971) 2252.
72V Verkelis, I. Yu.: Fiz. Tverd. Tela 14 (1972) 1676; Sov. Phys. Solid State (English Transl.) 14 (1972) 1445.
75D Dmitriev, Y. N., Kulik, V. N., Gal'chinskii, L. P., Koshkin, V. M.: Fiz. Tverd. Tela 17 (1975) 3685; Sov. Phys. Solid State (English Transl.) 17 (1975) 2396.
75H Hughes, O. H., Nikolic, P. M., Doran, C. J., Vujatovic, S. S.: Phys. Status Solidi (b) 71 (1975) 105.
75K Karakostas, T., Economou, N. A.: Phys. Status Solidi (a) 31 (1975) 89.
78B Bleris, G. L., Karakostas, T., Economou, N. A., de Ridder, R.: Phys. Status Solidi (a) 50 (1978) 579.
84S Sen, S., Bose, D.N.: Solid State Commun. 50 (1984) 39.
85S Sen, S., Bose, D.N., Hegde, M.S.: Phys. Status Solidi B 129 (1985) K65.
88N Nasredinov, F.S., Masterov, V.F., Saidov, Ch.S., Seregin, P.P., Troitskaya, N.N., Tschirner, H.U.: Phys. Status Solidi A 107 (1988) 291.
89H Hussein, S.A., Nagat, A.T.: Phys. Status Solidi A 114 (1989) K205.
89Z Zahab, A.A., Abd-Lefdil, M., Cadene, M.: Phys. Status Solidi A 115 (1989) 491.
90R Rousina, R., Yousefi, G.H.: Mater. Lett. 9 (1990) 263.
90Z1 Zahab, A.A., Abd-Lefdil, M., Cadene, M.: Phys. Status Solidi A 117 (1990) K103.
90Z2 Zahab, A.A., Abd-Lefdil, M., Cadene, M.: Phys. Status Solidi A 117 (1990) K103.
91N Nagat, A.T., Nassary, M.M., El-Shaikh, H.A.: Semicond. Sci. Technol. 6 (1991) 979.
93B Belal, A.E., Hussein, S., Madkour, H., El Shaikh, H.: Indian J. Pure Appl. Phys. 31 (1993) 464.

Figures to 5.6

Fig. 5.6.1

α - In_2Te_3 . Energy gap vs. temperature [75H].

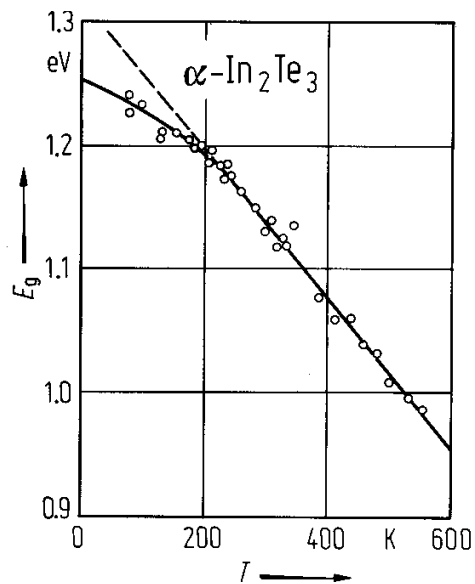
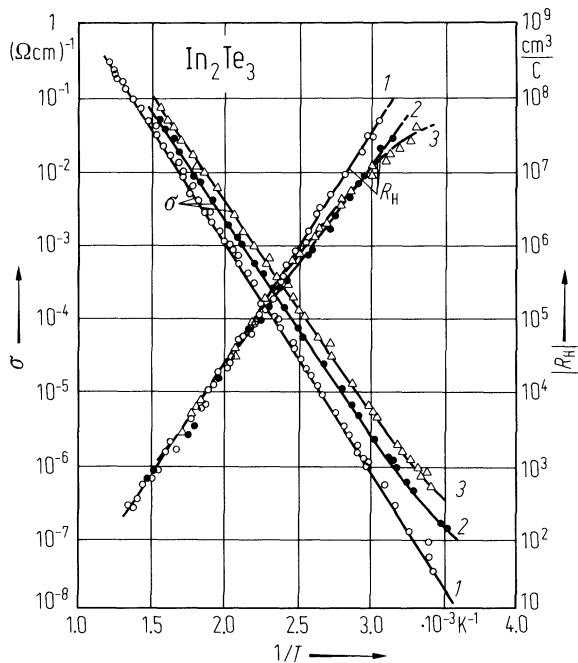


Fig. 5.6.2

In_2Te_3 . Electrical conductivity and Hall coefficient vs. reciprocal temperature. Degree of ordering decreases in the sequence 1, 2, 3, i.e. disorder can be quenched [60Z1].



6 I-III-VI₂ compounds

(included are I-Fe-VI₂ compounds)

6.0 Crystal structures and electronic structure

Nearly all semiconducting I-III-VI₂ compounds crystallize in the *chalcopyrite lattice* (Fig. 6.0.1). High-temperature phases show a disordered zincblende lattice, high-pressure phases a disordered rocksalt lattice.

Fig. 6.2 shows the Brillouin zone of fcc (zincblende) lattice and two Brillouin zones of chalcopyrite. Each point in the chalcopyrite Brillouin zone maps on to 4 different points of the zincblende zone. Thus the Γ point corresponds to Γ , X and two W points.

A useful starting point for a description of the electronic properties of compounds with chalcopyrite structure is the band structure of the zincblende parent compound represented in the smaller Brillouin zone of the ternary (see Fig. 6.0.2). These "folded back" curves can be labelled with the irreducible representations to which they correspond in both the chalcopyrite or zincblende space groups.

The tetragonal symmetry of the chalcopyrite lattice leads to a change in the band structure even at the center of the Brillouin zone Γ .

Non-degenerate band-edges at Γ ($\Gamma_1 \dots \Gamma_4$) are shaped according to $E(\mathbf{k}) = E(\Gamma) + (\hbar^2/2)(k_z^2/m_{\parallel} + (k_x^2 + k_y^2)/m_{\perp})$ with the z -axis parallel to the c -axis. Electrons are thus characterized by two effective masses: m_{\parallel} and m_{\perp} . From these two other effective masses are often defined: a density of states effective mass $m_{\text{ds}}^3 = m_{\perp}^2 m_{\parallel}$ and a conductivity effective mass $(1/m_c) = (1/3)(1/m_{\parallel} + 2/m_{\perp})$.

The Γ_5 -band is split at $k \neq 0$ into two bands:

$$E(\mathbf{k}) = E(\Gamma) + \hbar^2 k_z^2 / 2m(\Gamma) + (\hbar^2 / 2m)(a \pm (b^2 + c^2 \cos(4\varphi))^{1/2})(k_x^2 + k_y^2)$$

where φ is the angle between k_{\perp} and k_x in the $k_x k_y$ plane, with k_{\perp} the direction of \mathbf{k} perpendicular to the z -axis. Finally the Γ_6 - and Γ_7 -bands contain terms linear in k .

This simple picture is somewhat complicated by the effects of spin-orbit coupling which splits the Γ_5 state. This splitting is given by the formula: $E_{1,2} = -1/2(\Delta_{\text{so}} + \Delta_{\text{cf}}) \pm 1/2[(\Delta_{\text{so}} + \Delta_{\text{cf}})^2 - 8/3\Delta_{\text{so}}\Delta_{\text{cf}}]^{1/2}$, where Δ_{so} is the spin-orbit splitting in a cubic crystal field and Δ_{cf} is the crystal field splitting of the valence bands in the absence of spin-orbit coupling. The two solutions E_1 and E_2 give the separation of the two Γ_7 states from the Γ_6 . In chalcopyrite it is found that the crystal field splitting is negative, that is Γ_4 lies above Γ_5 and that this splitting is due almost entirely to the tetragonal compression. It compares very well with that expected from the corresponding zincblende compound under uniaxial pressure.

Fig. 6.0.3 ... 6.0.9 show the band structures of the most important semiconductors dealt with in this chapter.

Figures to 6.0

Fig. 6.0.1

The chalcopyrite lattice

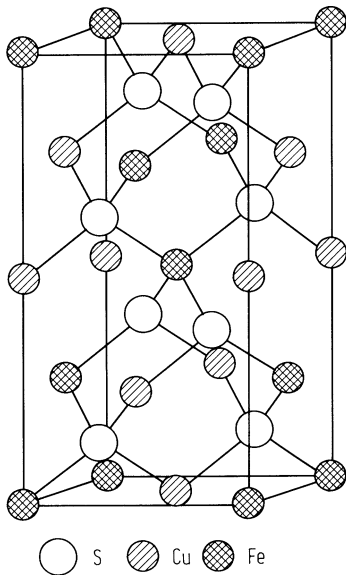


Fig. 6.0.2

Brillouin zone of the chalcopyrite lattice

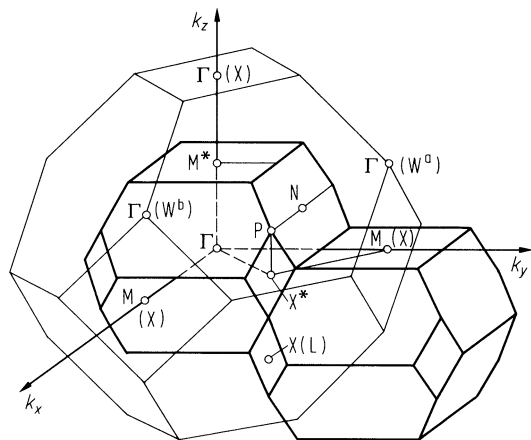


Fig. 6.0.3

Band structure of CuAlS_2 .

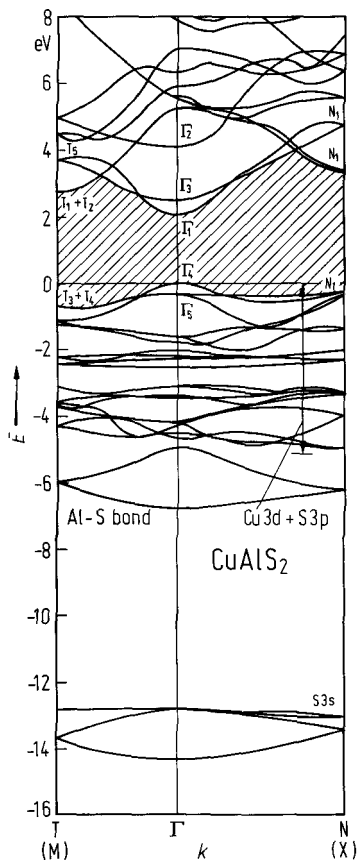


Fig. 6.0.4

Band structure of CuAlSe_2 .

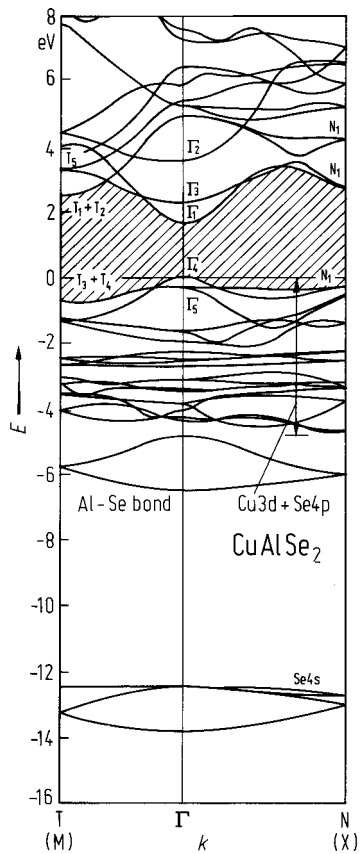


Fig. 6.0.5

Band structure of CuGaS_2 .

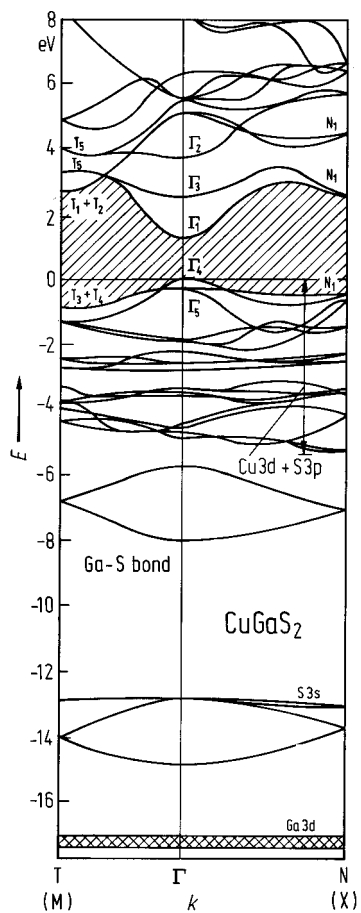


Fig. 6.0.6

Band structure of CuGaSe_2 .

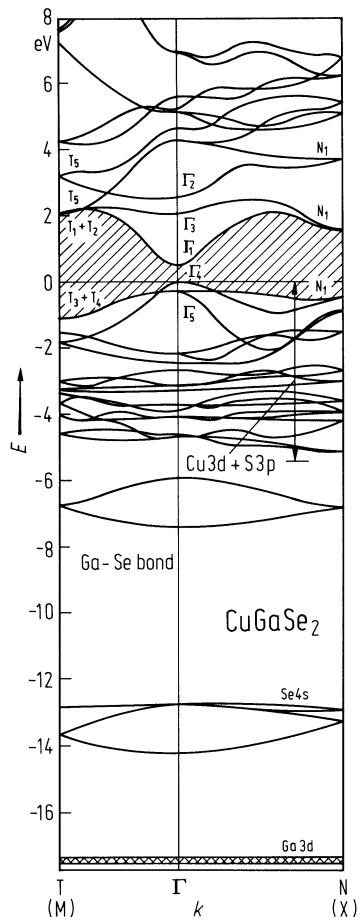


Fig. 6.0.7

Band structure of CuInS_2 .

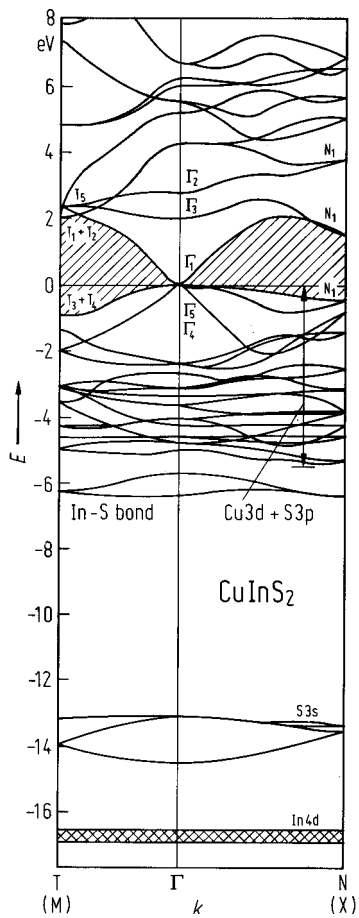


Fig. 6.0.8

Band structure of CuInSe_2 .

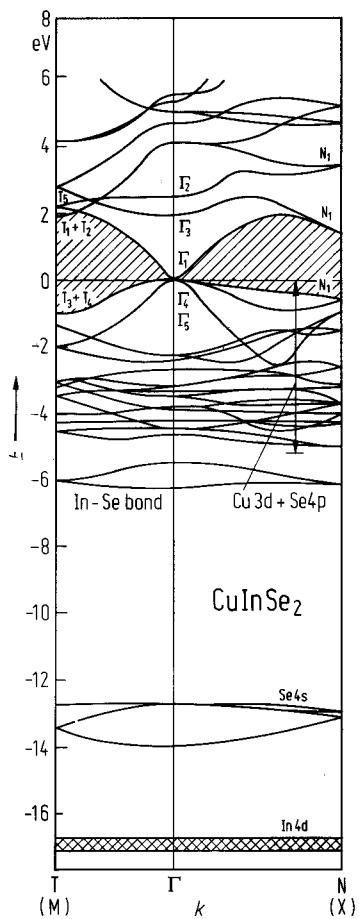
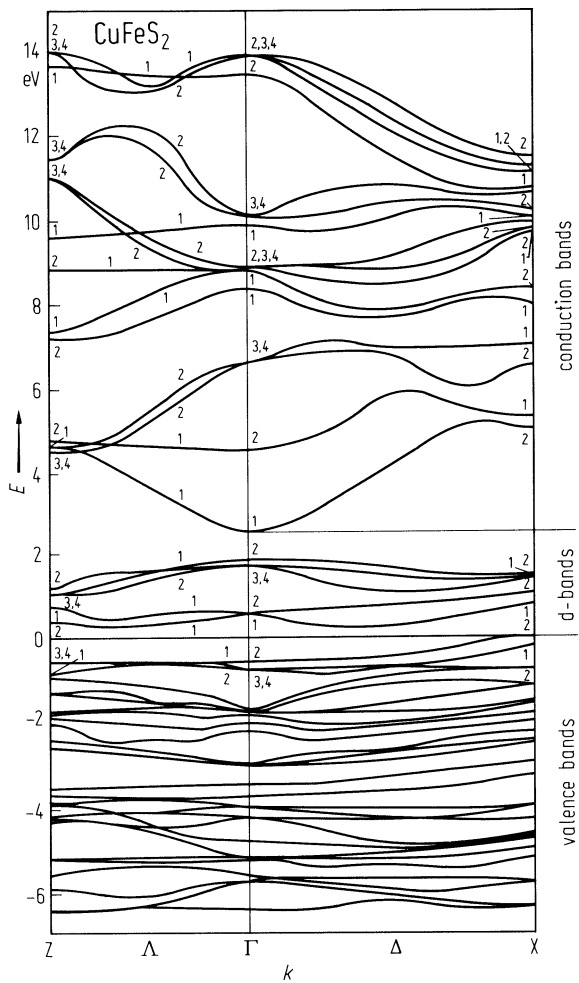


Fig. 6.0.9

Band structure of CuFeS_2 .



6.1 Copper aluminum sulfide (CuAlS2)

Crystal structure

CuAlS2 crystallizes in the chalcopyrite lattice (space group D2d12 – I4 2d, Fig. 6.0.1).

Electronic properties

band structure : see Fig. 6.0.3, Brillouin zone: Fig. 6.0.2.

energy gap

<i>E</i> _g	3.42 eV	<i>T</i> = 300K	transmission, <i>E</i> ⊥ <i>c</i>	85B
	3.34 eV	<i>T</i> = 300K	transmission, <i>E</i> ∥ <i>c</i>	85B
<i>dE</i> _g / <i>dT</i>	– 1.5...		from modulated phase-shift-	91S
	2.3·10 ^{–4} eV K ^{–1}		difference spectroscopy	

excitonic energy gap

<i>E</i> _{gx} (A)	3.54 eV	<i>T</i> = 78 K	absorption	73B
(B, C)	3.71 eV			

excitonic energy gap fine structure (from photoluminescence)

<i>E</i> _{gx}	3.475 eV	<i>T</i> = 10 K	bound exciton	92S
	3.500 eV		bound exciton	
	3.532 eV		bound exciton	
	3.540 eV		bound exciton	
	3.550 eV		free exciton	
	3.525 eV	<i>T</i> = 77 K	epitaxial layer on GaAs	95C

splitting energies (at Γ)

Δ _{cf}	– 0.13 eV	<i>T</i> = 300 K	electroreflectance	75S1
Δ _{so}	0 eV	<i>T</i> = 300 K		

Lattice properties

lattice parameters

<i>a</i>	5.32(1) Å	RT	75S2
<i>c</i>	10.430(15) Å		
<i>c/a</i>	1.960(1)		

density

<i>d</i>	3.45 g cm ^{–3}	RT	53H
----------	-------------------------	----	-----

bulk modulus

<i>B</i>	82.44 GPa	calculated from plasmon energy	96K
----------	-----------	--------------------------------	-----

melting temperature

<i>T</i> _m	1570 K		75S
-----------------------	--------	--	-----

wavenumbers of infrared and Raman active phonons

at RT		Symmetry			
		$\bar{1}4\bar{2}d$	$(F\bar{4}3m)$		
$\bar{\nu}_{LO}/\bar{\nu}_{TO}$	418/446 cm^{-1}	Γ_4	(Γ_{15})	all are Raman active; Γ_4, Γ_5 are IR active	75K
	497/444 cm^{-1}	Γ_5	(Γ_{15})		
	443 cm^{-1}	Γ_3	(W_2)		
	– /432 cm^{-1}	Γ_5	(W_4)		
	315 cm^{-1}	Γ_1	(W_1)		
	284/271 cm^{-1}	Γ_4	(W_2)		
	266/263 cm^{-1}	Γ_5	(X_5)		
	268 cm^{-1}	Γ_3	(X_3)		
	217/216 cm^{-1}	Γ_5	(W_3)		
	137/137 cm^{-1}	Γ_5	(W_4)		
	112/112 cm^{-1}	Γ_4	(W_2)		
	98 cm^{-1}	Γ_3	(W_2)		
	76/76 cm^{-1}	Γ_5	(X_5)		

Transport and optical properties

carrier concentration, resistivity, mobility

p-type samples					
p	5·10 ¹⁷ cm^{-3}			epitaxial layer, As-doped	92M
	3·10 ¹⁵ cm^{-3}				87D
ρ	1 $\Omega\text{ cm}$			epitaxial layer, As-doped	92M
	10 ⁴ ...10 ⁵ $\Omega\text{ cm}$	RT		single crystals, as grown	89A
	10 ³ $\Omega\text{ cm}$	RT		single crystals, annealed in S-atmosphere	87D
	< 3 $\text{cm}^2\text{ V}^{-1}\text{ s}^{-1}$	RT		single crystals	89A
μ_p					
n-type samples					
p	0.5...10 ² $\Omega\text{ cm}$	RT		single crystals, annealed in Cd-, Al-, and Zn-atmosphere	89A
μ_n	< 3 $\text{cm}^2\text{ V}^{-1}\text{ s}^{-1}$	RT		single crystals	89A

The temperature dependence of the electrical conductivity of CuAlS₂ crystals grown by CVT annealed under different conditions is given in Fig. 6.1.1 [89A].

activation energy

E_A	0.32 eV		activation energy of donors	89A
-------	---------	--	-----------------------------	-----

dielectric constants

$\epsilon(0)$	7.05	$E \parallel c$	from infrared reflection	95A
	8.14	$E \perp c$		
$\epsilon(\infty)$	4.8	$E \parallel c$	from infrared reflection	95A
	4.9	$E \perp c$		

References to 6.1

- 53H Hahn, H., Frank, G., Klingler, W., Meyer, A. D., Störger, G.: Z. Anorg. Allgem. Chem. 271 (1953) 153.
- 73B Bettini, M.: Solid State Commun. 13 (1973) 599.
- 75K Koschel, W. H., Bettini, M.: Phys. Status Solidi (b) 72 (1975) 729.
- 75S Shay, J. L., Wernick, J. H.: Ternary Chalcopyrite Semiconductors: Growth, Electronics, Properties and Applications. Pergamon, 1975.
- 85B Bodnar, I.V., Orlova, N.S.: Phys. Status Solidi A 91 (1985) 503.
- 87D Drabkin, I.A., Moizhes, B.Ya.: Fiz. Tekh. Poluprovodn. 21 (1987) 1715; Sov. Phys. – Semicond. (Engl. Transl.) 21 (1987) 1037.
- 89A Aksenov, I.A., Gulakov, I.R., Lipnitskii, V.I., Lukomskii, A.I., Makovetskaya, L.A.: Phys. Status Solidi A 115 (1989) K113.
- 91S Sato, K., Kudo, Y., Kijima, S., Samanta, L.K.: J. Cryst. Growth 115 (1991) 740.
- 92M Morita, Y., Narusawa, T.: Jpn. J. Appl. Phys., Part 2 (Letters), 31 (1992) 1396.
- 92S Shirakata, S., Aksenov, I., Sato, K., Isomura, S.: Jpn. J. Appl. Phys., Part 2 (Letters), 31 (1992) L1071.
- 95A Andriesh, A.M., Syrbu, N.N., Iovu, M.S., Tazlavan, V.E.: Phys. Status Solidi B 187 (1995) 83.
- 95C Chichibu, S., Nakanishi, H., Shirakata, S.: Appl. Phys. Lett. 66 (1995) 3513.
- 96K Kumar, V., Prasad, G.M., Chandra, D.: Cryst. Res. Technol. 31 (1996) 501.

Figures to 6.1

Fig. 6.0.1

The chalcopyrite lattice

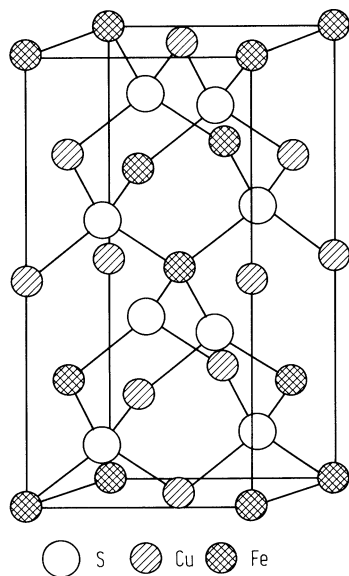
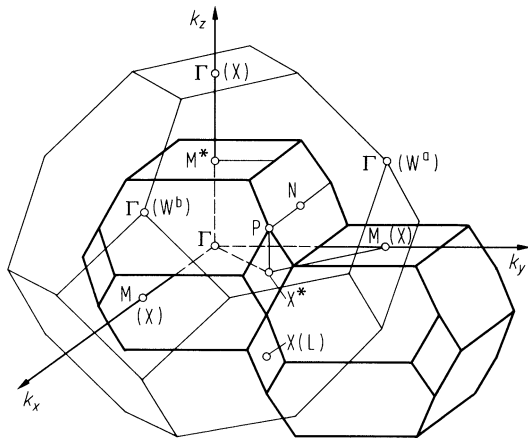


Fig. 6.0.2

Brillouin zone of the chalcopyrite lattice



Band structure of CuAlS₂.

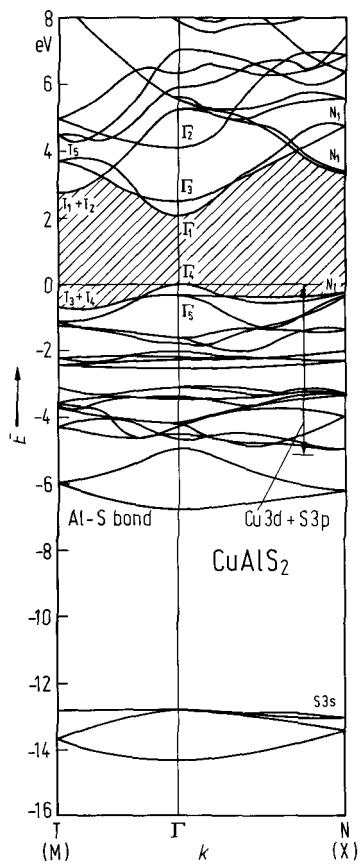
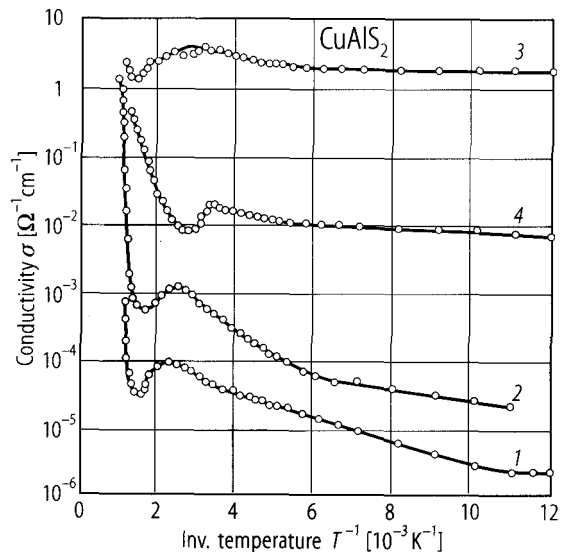


Fig. 6.1.1

CuAlS_2 . The electrical conductivity versus inverse temperature for single crystals, grown by the CVT method (1), and annealed in the presence of sulphur (2), zinc (3), and cadmium/aluminum (4) [89A].



6.2 Copper aluminum selenide (CuAlSe2)

Crystal structure

CuAlSe2 crystallizes in the chalcopyrite lattice (space group D2d¹² – I4[–]2d, Fig. 6.0.1).

Electronic properties

band structure : see Fig. 6.0.4, Brillouin zone: Fig. 6.0.2.

energy gap

<i>E</i> _{g,dir}	2.68 eV	RT	from optical absorption	93M
<i>E</i> _{g,dir} (A)	2.65 eV	<i>T</i> = 110 K	phase-shift-difference spectroscopy	77Y
(B)	2.88 eV			
(C)	3.02 eV			

excitonic energy gap

<i>E</i> _{gx}	2.739 eV		free exciton from photoreflectance	93C
<i>E</i> _{gx} (A)	2.77 eV	<i>T</i> = 20 K	phase-shift-difference spectroscopy	77Y
(B)	2.85 eV			
(C)	2.96 eV			

splitting energies (at Γ)

Δ_{cf}	– 0.17 eV		calculated	73B
	– 0.145 eV	<i>T</i> = 77 K	from photoreflectance, bulk material	93S
	– 0.18...0.19 eV	<i>T</i> = 77 K	from photoreflectance, thin film	93S
			film thickness: 0.26...0.3 μm	
Δ_{so}	– 0.16 eV		calculated	95W
	0.18 eV		calculated	
	0.18...0.19 eV	<i>T</i> = 77 K	from photoreflectance, bulk material	93S
	0.152		calculated	95W

Lattice properties

lattice parameters

<i>a</i>	5.61(1) Å	RT		75S2
<i>c</i>	10.92(6) Å			
<i>c/a</i>	1.95(1)			

density

<i>d</i>	4.69 g cm ^{–3}	RT		53H
----------	-------------------------	----	--	-----

melting temperature

<i>T</i> _m	1470 K			75S1
-----------------------	--------	--	--	------

Transport properties

carrier concentration, resistivity, mobility

p-type samples

<i>p</i>	3·10 ¹⁸ ...		Hall measurements, epilayers	93C
	1·10 ¹⁹ cm ^{–3}			
ρ	2.8·10 ² ...	RT	single crystal, undoped	91C
	7.1·10 ⁹ Ω cm			
μ_p	35 cm ² V ^{–1} s ^{–1}	RT	from Hall-measurements on single crystals	91C

n-type samples			
n	$4 \cdot 10^{18} \text{ cm}^{-3}$	epilayer	91M
ρ	$0.02 \text{ } \Omega \text{ cm}$	epilayer	91M
μ_n	$60 \text{ cm}^2 \text{ V}^{-1} \text{ s}^{-1}$	epilayer	91M

The temperature dependence of the Hall hole mobility is given in Fig. 6.2.1.

Optical properties

refractive indices

		$\lambda \text{ [}\mu\text{m]}$	
n_o	2.7797	0.50	75S
	2.5293	1.00	
	2.4969	1.50	
	2.4851	2.00	
	2.4795	2.50	
	2.4759	3.00	
	2.4733	3.50	
	2.4712	4.00	
	2.4685	4.50	
	2.4659	5.00	
n_e	2.7886	0.50	
	2.5179	1.00	
	2.4852	1.50	
	2.4734	2.00	
	2.4676	2.50	
	2.4638	3.00	
	2.4609	3.50	
	2.4586	4.00	
	2.4559	4.50	
	2.4533	5.00	
n	2.603	calculated from $\Delta\chi$	96R

Refractive index dispersion of ordinary and extraordinary beams for CuAlSe₂ is given in Fig. 6.2.2 [90B].

dielectric constants

$\varepsilon(0)$	8.28	$E \perp c$	from IR reflectivity	95A
	5.2	$E \parallel c$		
$\varepsilon(\infty)$	6.0	$E \perp c$	from IR reflectivity	95A
	6.67	$E \parallel c$		

References to 6.2

- 53H Hahn, H., Frank, G., Klingler, W., Meyer, A. D., Störger, G.: Z. Anorg. Allgem. Chem. 271 (1953) 153.
- 73B Bettini, M.: Solid State Commun. 13 (1973) 599.
- 75S1 Shay, J. L., Wernick, J. H.: Ternary Chalcopyrite Semiconductors: Growth, Electronics, Properties and Applications. Pergamon, 1975.
- 75S2 Suzuki, K., Kambara, T., Gondaira, K., Sato, K., Kondo, K., Teranishi, T.: J. Phys. Soc. Jpn. 39 (1975) 1310.
- 77Y Yamamoto, N., Horinka, H., Okada, K., Miyauchi, T.: Jpn. J. Appl. Phys. 16 (1977) 1817.
- 90B Bodnar, I.T., Bodnar, I.V.: Phys. Status Solidi A 121 (1990) K247.
- 91C Chichibu, S., Shishikura, M., Ino, J., Matsumoto, S.: J. Appl. Phys. 70 (1991) 1648.
- 91M Morita, Y., Narusawa, T.: Jpn. J. Appl. Phys., Part 2 (Letters), 30 (1991) L1238.
- 93C Chichibu, S., Matsumoto, S., Shirakata, S., Isomura, S.: J. Appl. Phys. 74 (1993) 6446.
- 93M Moon-Seog Jin, Suk-Ki Min, Han-Jo Lim, Hong-Lee Park, Wha-Tek Kim: Jpn. J. Appl. Phys., Supplement 32 (1993) 593.
- 93S Shirakata, S., Chichibu, S., Matsumoto, S., Isomura, S.: Jpn. J. Appl. Phys., Supplement 32 (1993) 494.
- 95A Abdelghany, A.: Appl. Phys. A 60 (1995) 77.
- 95W Wei, S., Zunger, A.: J. Appl. Phys. 78 (1995) 3846.
- 96R Reddy, R.R., Nazeer Ahammed, Y., Reddy, C.V.K., Buddhudu, S.: Cryst. Res. Technol. 31 (1996) 827.

Figures to 6.2

Fig. 6.0.1

The chalcopyrite lattice

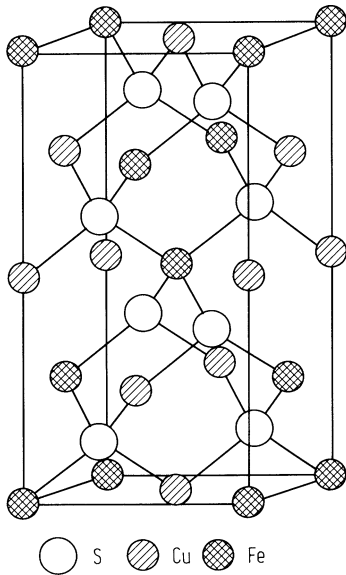


Fig. 6.0.2

Brillouin zone of the chalcopyrite lattice

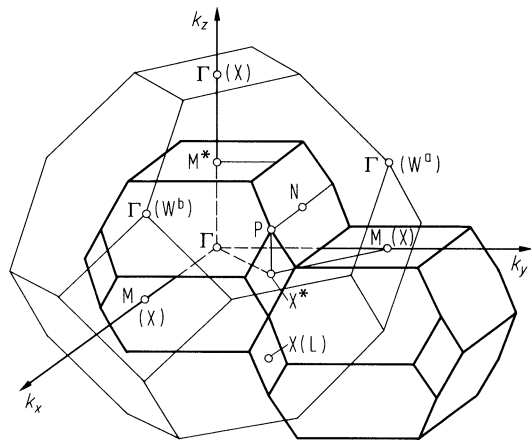


Fig. 6.0.4

Band structure of CuAlSe₂.

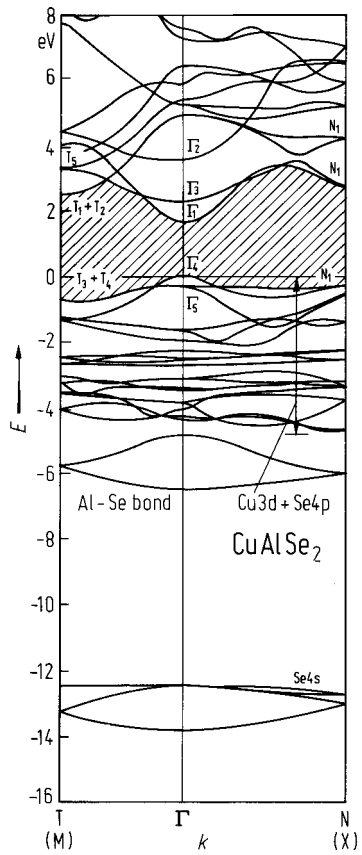


Fig. 6.2.1

CuAlSe_2 . Dependence of the Hall hole mobility on the temperature of a single crystal [91C].

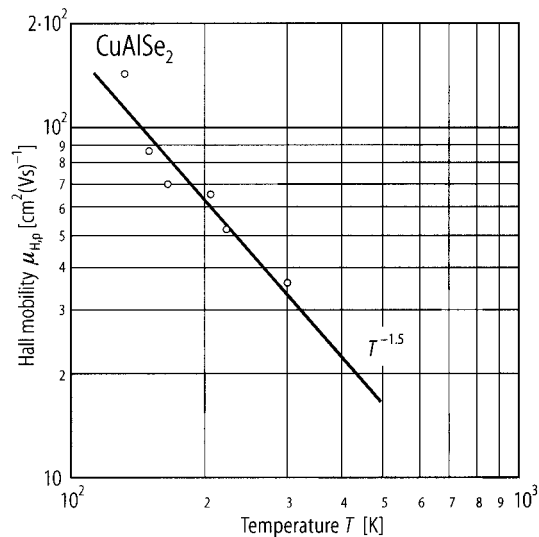
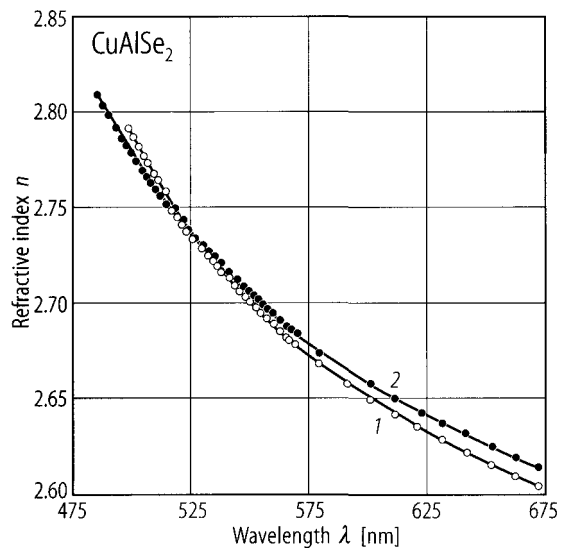


Fig. 6.2.2

CuAlSe₂. Refractive index dispersion of ordinary and extraordinary beams for a single crystal [90B].



6.3 Copper aluminum telluride (CuAlTe2)

Crystal structure

CuAlTe2 crystallizes in the chalcopyrite lattice (space group D2d¹² – I4[–]2d, Fig. 6.0.1).

Electronic properties

energy gap

$E_{g,dir}$ (A)	2.43 eV	$T = 300\text{ K}, E \parallel c$	electroreflectance	75S1
(B,C)	2.55 eV	$E \perp c$		
dE_g/dT (A)	$-2.2(2) \cdot 10^{-4}\text{ eV K}^{-1}$	$T = 80...300\text{ K}$	absorption	79H
dE_g/dp (A)	$3.4 \cdot 10^{-6}\text{ eV bar}^{-1}$	$T = 300\text{ K}$		76J

excitonic energy gap

E_{gx} (A)	2.467(2) eV	$T = 300\text{ K}$	cathodoluminescence	78S
(B,C)	2.596(1) eV		modulated phase difference	78H
Temperature coefficient of the exciton energy:			$-1.8 \cdot 10^{-4}\text{ eV K}^{-1}$	96I

splitting energies (at Γ)

valence band splitting

Δ_{cf}	-0.13 eV	$T = 77\text{ K}$	wavelength derivative reflectance	75T
Δ_{so}	-0.017 eV	$T = 77\text{ K}$	wavelength derivative reflectance	75T
			($\Delta_{so} \leq 0!$) (unresolved in other experiments [75S1, 75Y])	

effective masses

m_n	$0.13\ m_0$		phase-shift-difference	77Y
m_p	$0.69\ m_0$			

Lattice properties

lattice parameters

a	$5.96(1)\text{ \AA}$	RT		75S2
c	$11.77(3)\text{ \AA}$			
c/a	1.97			

density

d	5.47 g cm^{-3}	RT		53H
-----	-------------------------	----	--	-----

thermal expansion coefficient

$a\text{ [nm]} = 0.600818 + 3.26 \cdot 10^{-6}T + 6.09 \cdot 10^{-9}T^2 - 1.45 \cdot 10^{-12}T^3$	$(T\text{ in K})$	87O
$c\text{ [nm]} = 1.190740 + 4.24 \cdot 10^{-5}T + 3.33 \cdot 10^{-9}T^2 + 1.19 \cdot 10^{-12}T^3$		

Transport properties

resistivity

p-type samples				
ρ	$10^6\ \Omega\text{ cm}$	polycrystalline thin films		95E

The temperature dependence of the electrical conductivity for CuAlTe2 thin films in the range of 100...300 K is given in Fig. 6.3.1 [95E].

activation energies

E_A	0.25 eV	$T = 100...200\text{ K}$	activation energy of conductivity	95E
	0.96 eV	$T = 200...300\text{ K}$	of thin films	

Optical properties

refractive index

n	2.874	calculated from $\Delta\chi$	96R
-----	-------	------------------------------	-----

dielectric constants

$\epsilon_{0\parallel}$	10.8	calculated	95M
$\epsilon_{0\perp}$	11.0		
ϵ_0	10.9		
$\epsilon_{\infty\parallel}$	7.4		
$\epsilon_{\infty\perp}$	7.6		
ϵ_{∞}	7.5		

References to 6.3

- 53H Hahn, H., Frank, G., Klingler, W., Meyer, A. D., Störger, G.: Z. Anorg. Allgem. Chem. 271 (1953) 153.
- 75S1 Shay, J. L., Wernick, J. H.: Ternary Chalcopyrite Semiconductors: Growth, Electronics, Properties and Applications. Pergamon, 1975.
- 75S2 Suzuki, K., Kambara, T., Gondaira, K., Sato, K., Kondo, K., Teranishi, T.: J. Phys. Soc. Jpn. 39 (1975) 1310.
- 75T Tell, B., Bridenbaugh, P. M.: Phys. Rev. B 12 (1975) 3330.
- 75Y Yamamoto, N., Tohge, N., Miyauchi, T.: Jpn. J. Appl. Phys. 14 (1975) 192.
- 76J Jayaraman, A., Narayanamurti, V., Kasper, H. M., Chin, M. A., Maines, R. G.: Phys. Rev. B 14 (1976) 3516.
- 77Y Yamamoto, N., Horinka, H., Okada, K., Miyauchi, T.: Jpn. J. Appl. Phys. 16 (1977) 1817.
- 78H Horinaka, H., Yamamoto, N., Miyauchi, T.: Jpn. J. Appl. Phys. 17 (1978) 521.
- 78S Sermage, B.: Solid State Electron. 21 (1978) 1361.
- 79H Hörig, W., Neumann, H., Reccius, E., Weinert, H., Kühn, G., Schumann, B.: Phys. Status Solidi (a) 51 (1979) 57.
- 87O Orlova, N.S., Bodnar, I.V.: Cryst. Res. Technol. 22 (1987) 1409.
- 95E El Assali, K., Chahboun, N., Bekkay, T., Ameziane, E.L., Boustani, M., Khiara, A.: Solar Energy Mater. Solar Cells 39 (1995) 33.
- 95M Marquez, R., Rincon, C.: Phys. Status Solidi B 191 (1995) 115.
- 96I In-Hwan Choi, Yu, P.J.: J. Phys. Chem. Solids 57 (1996) 1695.
- 96R Reddy, R.R., Nazeer Ahammed, Y., Reddy, C.V.K., Buddhudu, S.: Cryst. Res. Technol. 31 (1996) 827.

Figures to 6.3

Fig. 6.0.1

The chalcopyrite lattice

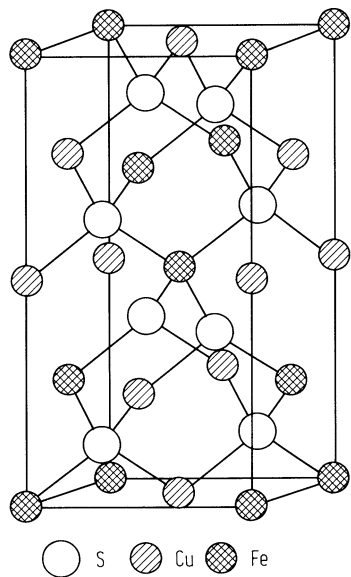
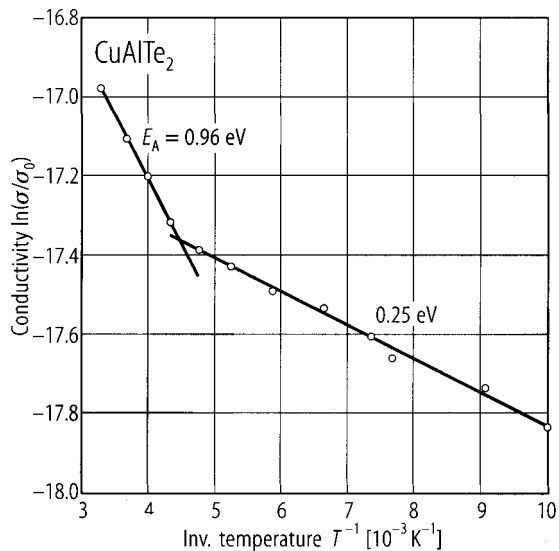


Fig. 6.3.1

CuAlTe_2 . Temperature dependence of the conductivity for thin films in the range of 100...300 K [95E]. $\sigma_0 = 1 \Omega^{-1}\text{cm}^{-1}$.



6.4 Copper gallium sulfide (CuGaS2)

Crystal structure

CuGaS2 crystallizes in the chalcopyrite lattice (space group D2d¹² – I4 2d, Fig. 6.0.1).

Electronic properties

band structure : see Fig. 6.0.5, Brillouin zone: Fig. 6.0.2.

energy gap

$E_{g,dir}$ (A)	2.43 eV	$T = 300\text{ K}, E \parallel c$	electroreflectance	75S1
(B,C)	2.55 eV	$E \perp c$		
dE_g/dT (A)	$-2.2(2) \cdot 10^{-4}\text{ eV K}^{-1}$	$T = 80...300\text{ K}$	absorption	79H

excitonic energy gap

E_{gx} (A)	2.467(2) eV	$T = 300\text{ K}$	cathodoluminescence	78S
(B,C)	2.596(1) eV		modulated phase difference	78H
E_{gx}	2.51 eV	$T = 5\text{ K}$	from optical absorption	96B

exciton emissions from photoluminescence

E	2.504 eV	$T = 4.2\text{ K}$	free-exciton emission	90S
	2.501 eV	$T = 4.2\text{ K}$	(D ⁰ /X) exciton complex	
	2.495 eV	$T = 4.2\text{ K}$	(A ⁰ /X) exciton complex	
	2.493 eV	$T = 4.2\text{ K}$	(A ⁰ /X) exciton complex	

valence band splitting energies (at Γ)

Δ_{cf}	0.129 eV	$T = 80\text{ K}$	from photocurrent excitation spectra	91S
Δ_{so}	< 7 meV			88S

Lattice properties

lattice parameters

a	5.35(2) Å	RT	75S2
c	10.46(2) Å		
c/a	1.960(2)		

density

d	4.38 g cm ⁻³	RT	77B
-----	-------------------------	----	-----

linear thermal expansion coefficient

α	$7.7 \cdot 10^{-6}\text{ K}^{-1}$	no temperature or orientation given	80B
----------	-----------------------------------	-------------------------------------	-----

Debye temperature

Θ_D	356 K	$T \rightarrow 0\text{ K}$	75A
------------	-------	----------------------------	-----

melting temperature

T_m	1550 K		76K
-------	--------	--	-----

wavenumber of infrared and Raman active phonons

($\bar{\nu}$ in cm^{-1} , $T=300\text{ K}$)

	[75K]	[80C]	Symmetry	
			$\bar{1}4\bar{2}d$	$(F\bar{4}3m)$
$\bar{\nu}_{\text{LO}}/\bar{\nu}_{\text{TO}}$	401/368	393/367	Γ_4	(Γ_{15})
	384/363	385/367	Γ_5	(Γ_{15})
	358	401	Γ_3	(W_2)
	352/332	347/332	Γ_5	(W_4)
	312	312	Γ_1	(W_1)
	281/267	288/286	Γ_4	(W_2)
	276/262	283/273	Γ_5	(X_5)
	203	238	Γ_3	(X_3)
	160/156	167/167	Γ_5	(W_3)
	—	147/147	Γ_5	(W_4)
	95/95	95/95	Γ_4	(W_2)
	97	116	Γ_3	(W_2)
	74/—	75/75	Γ_5	(X_5)

Transport properties

resistivity

p-type samples

ρ	$10^6 \dots 10^7\ \Omega\ \text{cm}$	single crystals, as grown	87O
--------	--------------------------------------	---------------------------	-----

activation energy

E_A	$0.05 \dots 0.056\ \text{eV}$	epilayers on GaAs, activation energy for conductivity	93M
-------	-------------------------------	--	-----

resistivity, carrier concentration and mobility

ρ	$1\ \Omega\ \text{cm}$	$T=300\ \text{K}$	p-type sample, annealed under maximum S-pressure; no anisotropy reported	75S1
p	$4 \cdot 10^{17}\ \text{cm}^{-3}$	$T=300\ \text{K}$		
μ_p	$15\ \text{cm}^2\ \text{V}^{-1}\ \text{s}^{-1}$	$T=300\ \text{K}$		

thermal conductivity

κ	$5.09\ \text{W}\ \text{m}^{-1}\ \text{K}^{-1}$	calculated	84M
----------	--	------------	-----

Optical properties

refractive index

The dispersion of the refractive index is given in Fig. 6.4.1 [90B].

coefficients in the formula: $n^2 = A + B/(1-C/\lambda^2) + D/(1-E/\lambda^2)$ 79B

<i>A</i>	3.9064	<i>T</i> = 290 K	ordinary index(O)
	4.3165		extraordinary index(E)
	4.0984	<i>T</i> = 390 K	O
	4.4834		E
<i>B</i>	2.3065	<i>T</i> = 290 K	O
	1.8692		F
	2.1419	<i>T</i> = 390 K	O
	1.7316		F
<i>C</i>	0.1149 μm ²	<i>T</i> = 290 K	O
	0.1364 μm ²		F
	0.1225 μm ²	<i>T</i> = 390 K	O
	0.1453 μm ²		F
<i>D</i>	1.5479	<i>T</i> = 290 K	O
	1.7575		F
	1.5955	<i>T</i> = 390 K	O
	1.7785		E
<i>E</i>	738.43 μm ²	<i>T</i> = 290 K	O+E
	738.43 μm ²	<i>T</i> = 390 K	O+E

λ [μm]			
<i>n</i> _o	2.7630	0.55	75S1
	2.5517	1.00	
	2.5051	2.00	
	2.4945	3.00	
	2.4884	4.00	
	2.4843	5.00	
	2.4774	6.00	
	2.4714	7.00	
	2.4639	8.00	
	2.4539	9.00	
	2.4429	10.00	
	2.4311	11.00	
	2.4171	12.00	
	2.3999	13.00	
<i>n</i> _e	2.7813	0.55	75S1
	2.5464	1.00	
	2.4991	2.00	
	2.4880	3.00	
	2.4816	4.00	
	2.4772	5.00	
	2.4694	6.00	
	2.4621	7.00	
	2.4539	8.00	
	2.4435	9.00	
	2.4311	10.00	
	2.4179	11.00	

linear electrooptic coefficient

λ [nm]			
<i>r</i> ₄₁	1.76·10 ⁻¹² m/V	633	RT
	1.9·10 ⁻¹² m/V	1150	
	1.1·10 ⁻¹² m/V	3390	
<i>r</i> ₆₃	1.35·10 ⁻¹² m/V	633	74T
	1.66·10 ⁻¹² m/V	1150	
	1.05·10 ⁻¹² m/V	3390	

dielectric constants

$\varepsilon(0)$	7.6	$T = 300 \text{ K}, E \parallel c$	75S1
	8.9	$E \perp c$	
$\varepsilon(\infty)$	6.1	$T = 300 \text{ K}, E \parallel c$	77S
	6.2	$E \perp c$	

References to 6.4

- 74T Turner, E. H., Buehler, F., Kasper, H.: Phys. Rev. B 9 (1974) 558.
- 75A Abrahams, S. C., Hsu, F. S. L.: J. Chem. Phys. 63 (1975) 1162.
- 75K Koschel, W. H., Bettini, M.: Phys. Status Solidi (b) 72 (1975) 729.
- 75S1 Shay, J. L., Wernick, J. H.: Ternary Chalcopyrite Semiconductors: Growth, Electronics, Properties and Applications. Pergamon, 1975.
- 75S2 Suzuki, K., Kambara, T., Gondaira, K., Sato, K., Kondo, K., Teranishi, T.: J. Phys. Soc. Jpn. 39 (1975) 1310.
- 76K Kokta, M., Carruthers, J. R., Crasso, M., Kasper, H. M., Tell, B.: J. Electron. Mater. 5 (1976) 69.
- 77B Bachmann, K. J., Hsu, F. S. L., Thiel, F. A., Kasper, H. M.: J. Electron. Mater. 6 (1977) 431.
- 77S Sermage, B., Voos, M.: Phys. Rev. B 15 (1977) 3935.
- 78H Horinaka, H., Yamamoto, N., Miyauchi, T.: Jpn. J. Appl. Phys. 17 (1978) 521.
- 78S Sermage, B.: Solid State Electron. 21 (1978) 1361.
- 79B Bhar, G. C., Ghosh, G.: J. Opt. Soc. Am. 69 (1979) 730.
- 79H Horig, W., Neumann, H., Reccius, E., Weinert, H., Kühn, G., Schumann, B.: Phys. Status Solidi (a) 51 (1979) 57.
- 80B Bhar, G. C., Ghosh, G. C.: Appl. Opt. 19 (1980) 1029.
- 80C Carlone, C., Olego, D., Jayaraman, A., Cardona, M.: Phys. Rev. B 22 (1980) 3877.
- 84M Makovetskaya, L.A., Belevich, N.N., Bodnar, I.V., Grutso, S.A., Yaroshevich, G.P.: Izv. Akad. Nauk SSSR, Neorg. Mater. 20 (1984) 382; Inorg. Mater. (Engl. Transl.) 20 (1984) 322.
- 87O Orlova, N.S., Bodnar, I.V.: Phys. Status Solidi A 101 (1987) 421.
- 88S Shirakata, S., Murakami, K., Isomura, S.: Jpn. J. Appl. Phys., Part 1, 27 (1988) 1780.
- 90B Bodnar, I.V., Bodnar, I.T.: Opt. Spektrosk. 68 (1990) 373; Opt. Spectrosc. (Engl. Transl.) 68 (1990) 218.
- 90S Shirakata, S., Saiki, K., Isomura, S.: J. Appl. Phys. 68 (1990) 291.
- 91S Susaki, M., Horinaka, H., Yamamoto, N.: Jpn. J. Appl. Phys., Part 1, 30 (1991) 2797.
- 93M Morohashi, M., Tsuboi, N., Terasako, T., Iida, S., Okamoto, S.: Jpn. J. Appl. Phys., Supplement, 32-3 (1993) 621.
- 96B Bellabarba, C., Gonzalez, J., Rincon, C.: Phys. Rev. B 53 (1996) 7792.

Figures to 6.4

Fig. 6.0.1

The chalcopyrite lattice

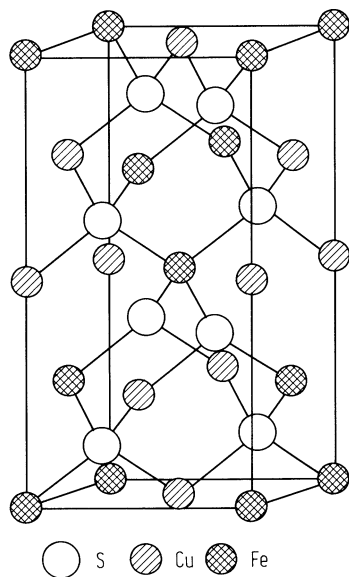


Fig. 6.0.2

Brillouin zone of the chalcopyrite lattice

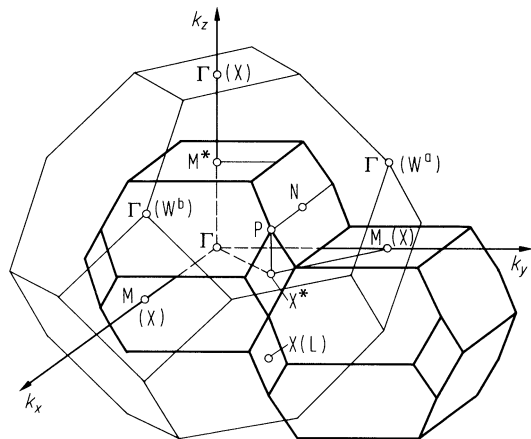


Fig. 6.0.5

Band structure of CuGaS_2 .

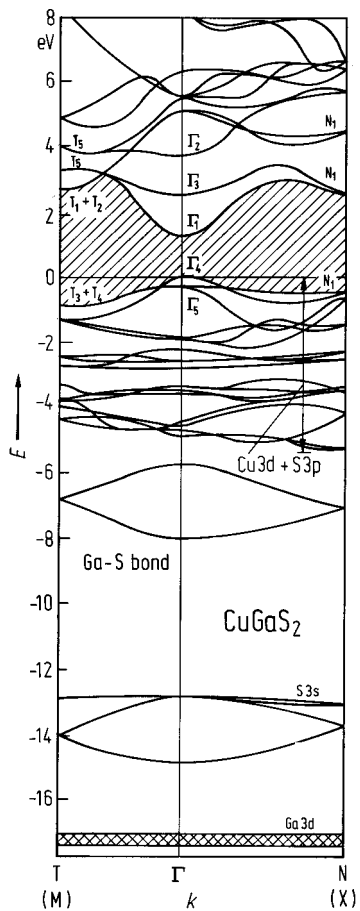
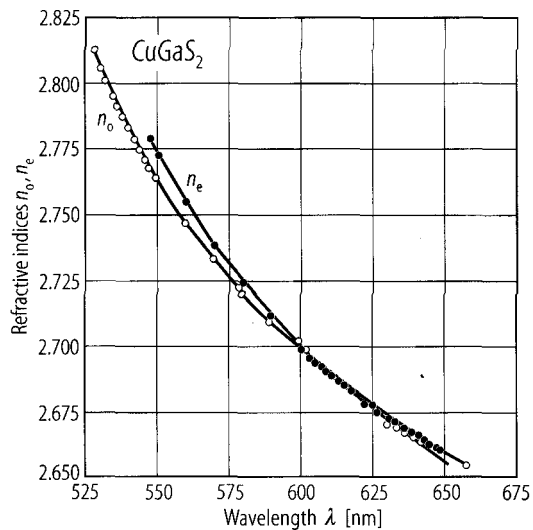


Fig. 6.4.1

CuGaS_2 . Values of the refractive indices of the ordinary and extraordinary rays as a function of wavelength for single crystals [90B]. T not given.



6.5 Copper gallium selenide (CuGaSe2)

Crystal structure

CuGaSe2 crystallizes in the chalcopyrite lattice (space group D2d¹² – I4[–]2d, Fig. 6.0.1).

Electronic properties

band structure : see Fig. 6.0.6, Brillouin zone: Fig. 6.0.2.

energy gap

$E_{g,dir}$ (A)	1.68 eV	$T = 300$ K	electroreflectance	75S1
(B)	1.75 eV			
(C)	1.96 eV			

Variation of the band gap with the temperature for CuGaSe2 is given in Fig. 6.5.1 [93B]

excitonic energy gap

E_{gx} (A)	1.695 eV	$T = 20$ K (n = 1)	phase-shift-difference spectroscopy	77T
--------------	----------	--------------------	-------------------------------------	-----

exciton binding energy

E_b (A)	16·10 ^{–3} eV			77Y
-----------	------------------------	--	--	-----

splitting energies (at Γ)

Δ_{cf}	– 0.139 eV	$T = 77$ K	from photoreflectance	94C
Δ_{so}	0.238 eV	$T = 77$ K	from photoreflectance	94C

Lattice properties

lattice parameters

a	5.61(1) Å		RT	75S2
c	11.00(2) Å			
c/a	1.960(4)			

density

d	5.57 g cm ^{–3}		RT	77B2
-----	-------------------------	--	----	------

linear thermal expansion coefficient

α	13.1(14)·10 ^{–6} K ^{–1} 5.2(7)·10 ^{–6} K ^{–1}	$T = 300...670$ K	a axis c axis	80B
----------	--	-------------------	----------------------	-----

Debye temperature

Θ_D	262.0(7) K	$T \rightarrow 0$ K		82B
------------	------------	---------------------	--	-----

melting temperature

T_m	1310...1340 K			75S1
-------	---------------	--	--	------

wavenumbers of IR active phonons (at RT)

		Symmetry			
		I4 [–] 2d	(F4 [–] 3m)		
$\bar{\nu}_{LO}/\bar{\nu}_{TO}$	278/254	Γ ₄	(Γ ₁₅)	infrared absorption	77B1
	276/250	Γ ₅	(Γ ₁₅)		
	196/178	Γ ₄	(W ₂)		
	190/170	Γ ₅	(W ₄)		

Transport properties

(p-type samples)

carrier concentration, resistivity, mobility, thermoelectric power

p-type samples

p	0.26...14·10 ⁻¹⁹ cm ⁻³	RT	thin films	95M
ρ	0.05...6 Ω cm		thin films	92L
μ_p	3.12... 21.4 cm ² V ⁻¹ s ⁻¹	RT	thin films	95M
S	0.084... 0.24 mV K ⁻¹	RT	thin films	95M

The temperature dependence of the resistivity in undoped and Sn-doped p-type CuGaSe₂ single crystals is shown in Fig. 6.5.2 [96S].

The temperature dependence of the Hall mobilities of undoped and Sn-doped CuGaSe₂ single crystals is shown in Fig. 6.5.3 [96S].

electrical conductivity

σ	1.3...86 Ω ⁻¹ cm ⁻¹	RT	thin films, four probe method	95M
----------	---	----	-------------------------------	-----

activation energy

E_A	0.240...0.270 eV	$T = 390...450$ K	activation energy of conductivity	94M
	0.080...0.090 eV	$T = 300...390$ K		

thermal conductivity

κ	0.129 W cm ⁻¹ K ⁻¹		calculated	95R
----------	--	--	------------	-----

Optical properties

refractive index

		λ [mm]	
n_o	2.9580	0.78	75S1
	2.8358	1.00	
	2.7430	2.00	
	2.7273	3.00	
	2.7211	4.00	
	2.7170	5.00	
	2.7133	6.00	
	2.7101	7.00	
	2.7060	8.00	
	2.7021	9.00	
	2.6974	10.00	
	2.6926	11.00	
	2.6872	12.00	
n_e	3.0093	0.78	75S1
	2.8513	1.00	
	2.7510	2.00	
	2.7344	3.00	
	2.7276	4.00	
	2.7232	5.00	
	2.7192	6.00	
	2.7158	7.00	
	2.7111	8.00	
	2.7065	9.00	
	2.7014	10.00	
	2.6981	11.00	
	2.6898	12.00	

References to 6.5

- 75S1 Shay, J. L., Wernick, J. H.: Ternary Chalcopyrite Semiconductors: Growth, Electronics, Properties and Applications. Pergamon, 1975.
- 75S2 Suzuki, K., Kambara, T., Gondaira, K., Sato, K., Kondo, K., Teranishi, T.: J. Phys. Soc. Jpn. 39 (1975) 1310.
- 77B1 Bodnar, I. V., Karoza, A. G., Smirnova, G. F.: Phys. Status Solidi (b) 84 (1977) K65.
- 77B2 Bachmann, K. J., Hsu, F. S. L., Thiel, F. A., Kasper, H. M.: J. Electron. Mater. 6 (1977) 431.
- 77T Teranishi, T., Sato, K., Saito, Y.: Inst. Phys. Conf; Ser. 35 (1977) 59.
- 77Y Yamamoto, N., Horinka, H., Okada, K., Miyauchi, T.: Jpn. J. Appl. Phys. 16 (1977) 1817.
- 80B Bhar, G. C., Ghosh, G. C.: Appl. Opt. 19 (1980) 1029.
- 82B Bohmhammel, K., Deus, P., Kühn, G., Möller, W.: Phys. Status Solidi (a) 71 (1982) 505.
- 92L Leon, M., Diaz, R., Rueda, F., Berghol, M.: Solar Energy Mater. Solar Cells 26 (1992) 295.
- 93B Bellabarba, C., Rincon, C.: Jpn. J. Appl. Phys., Supplement, 32 (1993) 599.
- 94C Chichibu, S., Harada, Y., Uchida, M., Wakiyama, T., Matsumoto, S., Shirakata, S., Isomura, S., Higuchi, H.: J. Appl. Phys. 76 (1994) 3009.
- 94M Miyake, H., Hata, M., Hamamura, Y., Sugiyama, K.: J. Cryst. Growth 144 (1994) 236.
- 95M Mansour, B.A., El-Hagary, M.A.: Thin Solid Films 256 (1995) 165.
- 96R Reddy, R.R., Nazeer Ahammed, Y., Reddy, C.V.K., Buddhudu, S.: Cryst. Res. Technol. 31 (1996) 827.
- 96S Susaki, M., Yamamoto, N., Prevot, B., Schwab, C.: Jpn. J. Appl. Phys., Part 1, 35 (1996) 1652.
- 97S Schoen, J. H., Alberts, V., Bucher, E.: J. Appl. Phys. 81 (1997) 2799.

Figures to 6.5

Fig. 6.0.1

The chalcopyrite lattice

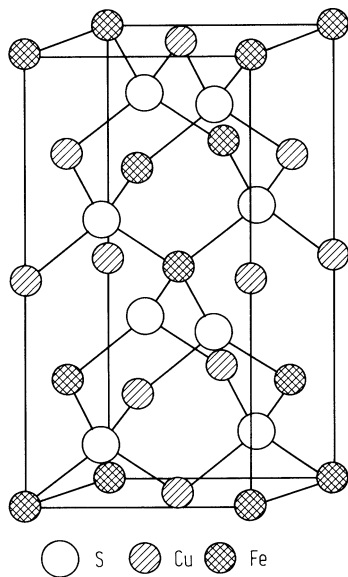


Fig. 6.0.2

Brillouin zone of the chalcopyrite lattice

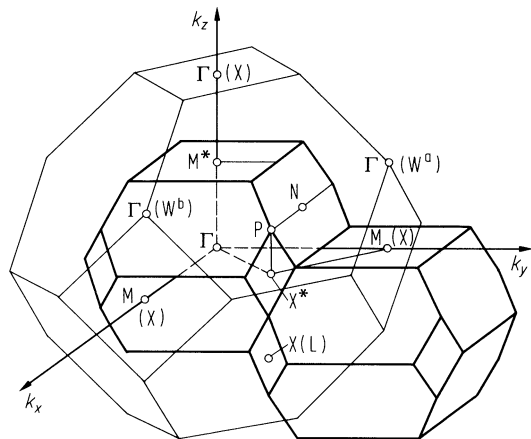


Fig. 6.0.6

Band structure of CuGaSe_2 .

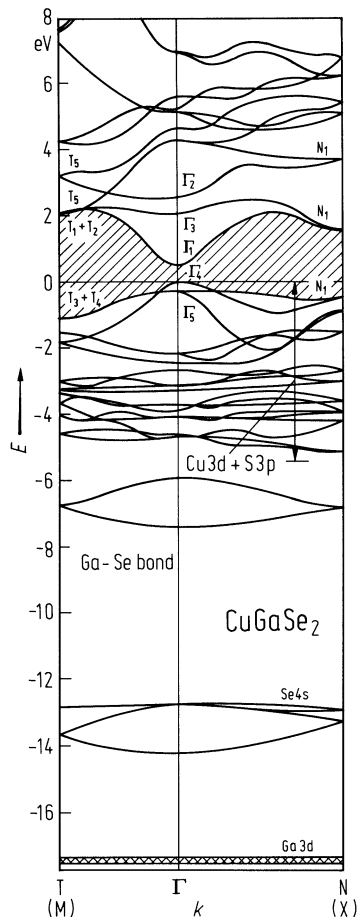


Fig. 6.5.1

CuGaSe₂. Variation of the band gap with the temperature [93B]. Solid line calculated.

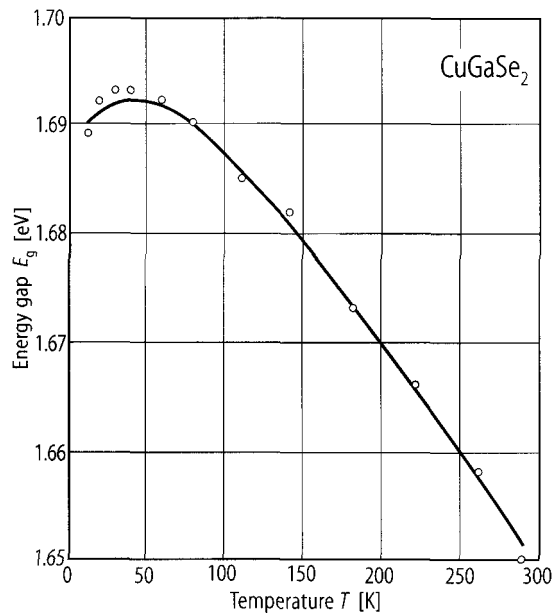


Fig. 6.5.2

CuGaSe₂. Resistivity versus temperature for various undoped (UD) and Sn-doped single crystals [96S].

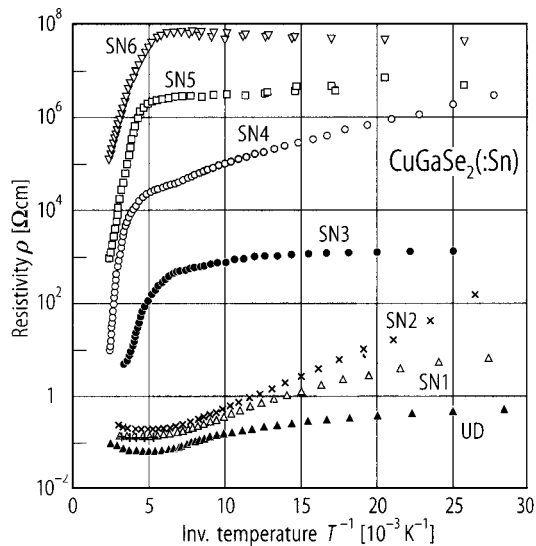
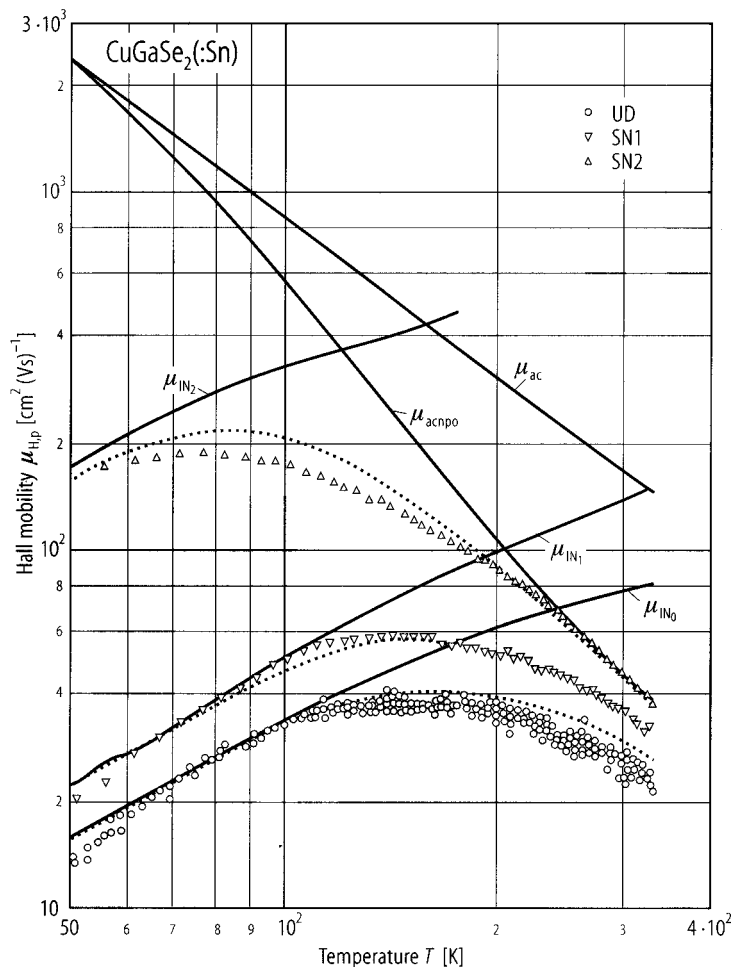


Fig. 6.5.3

CuGaSe₂. Temperature dependence of the Hall mobility of undoped (UD) and Sn-doped (SN1, SN2) single crystals. The values of the mobility are due to scattering at acoustic phonons μ_{ac} , nonpolar acoustic phonons μ_{acnp} , impurities (neutral and ionized) μ_{IN} , and the resulting fits are shown as solid lines [96S]. Dotted lines are not explained.



6.6 Copper gallium telluride (CuGaTe2)

Crystal structure

CuGaTe2 crystallizes in the chalcopyrite lattice (space group D2d¹² – I4̄ 2d, Fig. 6.0.1).

Electronic properties

energy gap

<i>E</i> _{g,dir}	1.23...1.26 eV		thin films, optical transmission	92L
(A)	1.227 eV	RT	transmission in polycrystalline,	79N
(B)	1.280 eV	RT	thin films	
(C)	1.97 eV	RT		

splitting energies (at Γ)

Δ _{cf}	– 0.08(4) eV	<i>T</i> = 300 K	transmission in "thin" polycrystalline	79N
Δ _{so}	0.71(4) eV	<i>T</i> = 300 K	films	

Lattice properties

lattice parameters

<i>a</i>	6.00(1) Å		RT	75S2
<i>c</i>	11.93(2) Å			
<i>c/a</i>	1.985(5)			

density

<i>d</i>	5.95 g cm ^{–3}		RT	77B
----------	-------------------------	--	----	-----

linear thermal expansion coefficient

α _c	6.6·10 ^{–6} K ^{–1}	RT	from XRD measurements	86B
α _{⊥c}	11.7·10 ^{–6} K ^{–1}	RT		

Debye temperature

Θ _D	226.2(8) K	<i>T</i> → 0 K		82B
----------------	------------	----------------	--	-----

melting temperature

<i>T</i> _m	1140 K			75S1
-----------------------	--------	--	--	------

phonon wavenumbers

ν̄	209.2(1) cm ^{–1}	<i>T</i> = 300 K	thin films	79N
	201.4(1) cm ^{–1}			
	166.4(5) cm ^{–1}			

Transport and optical properties

(p-type samples)

carrier concentration, mobility, conductivity and Seebeck coefficient

<i>p</i>	10 ¹⁸ cm ^{–3}			75S1
μ _p	50 cm ² V ^{–1} s ^{–1}			
σ	11 Ω ^{–1} cm ^{–1}			
<i>S</i>	2.7·10 ^{–1} VK ^{–1}			

activation energy

<i>E</i> _A	0.006...0.019 eV		activation energy of conductivity	87W
-----------------------	------------------	--	-----------------------------------	-----

thermal conductivity

The thermal conductivity as a function of temperature for p-type CuGaTe2 is shown in Fig. 6.6.1 [87W].

dielectric constants

$\epsilon(0)$	12.7	calculated	95M
$\epsilon(\infty)$	8.5	calculated	95M

refractive index

n	2.83(9)	$h\nu = 0.5$ eV	80H
-----	---------	-----------------	-----

References to 6.6

- 75S1 Shay, J. L., Wernick, J. H.: Ternary Chalcopyrite Semiconductors: Growth, Electronics, Properties and Applications. Pergamon, 1975.
- 75S2 Suzuki, K., Kambara, T., Gondaira, K., Sato, K., Kondo, K., Teranishi, T.: J. Phys. Soc. Jpn. 39 (1975) 1310.
- 77B Bachmann, K. J., Hsu, F. S. L., Thiel, F. A., Kasper, H. M.: J. Electron. Mater. 6 (1977) 431.
- 79N Neumann, H., Hörig, W., Reccius, E., Sobotta, H. . Schumann, B., Kühn, G.: Thin Solid Films 61 (1979) 13.
- 80H Hörig, W., Neumann, H., Savalev, V., Lagzdonis, J.: Phys. Lett. 78A (1980) 189.
- 82B Bohmhammel, K., Deus, P., Kühn, G., Möller, W.: Phys. Status Solidi (a) 71 (1982) 505.
- 86B Bodnar, I.V., Orlova, N.S.: Cryst. Res. Technol. 21 (1986) 1091.
- 87W Wasim, S.M., Noguera, A.: Solid State Commun. 64 (1987) 439.
- 92L Leon, M., Diaz, R., Rueda, F., Berghol, M.: Solar Energy Mater. Solar Cells 26 (1992) 295.
- 95M Marquez, R., Rincon, C.: Phys. Status Solidi B 191 (1995) 115.

Figures to 6.6

Fig. 6.0.1

The chalcopyrite lattice

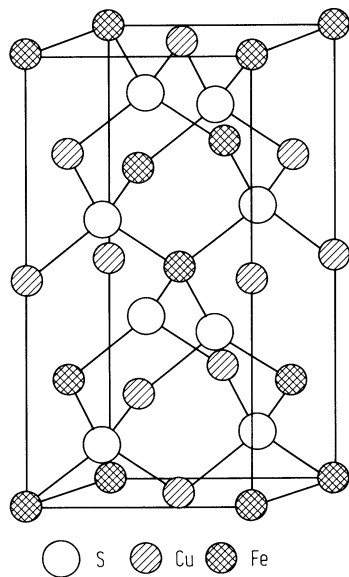
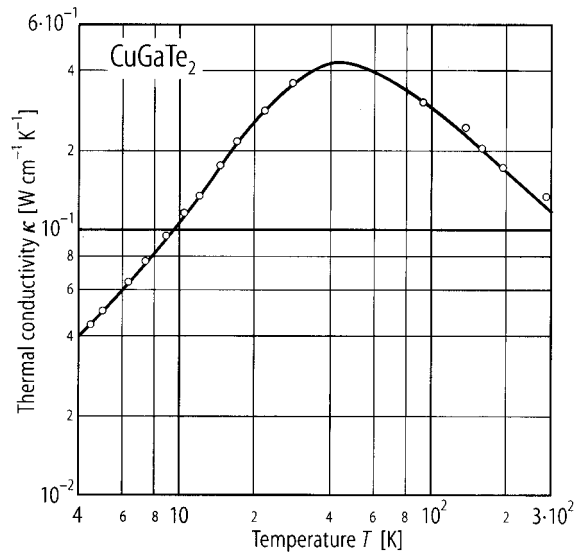


Fig. 6.6.1

CuGaTe_2 . Thermal conductivity as a function of temperature for p-type samples [87W].



6.7 Copper indium sulfide (roquesite, CuInS2)

Crystal structure

CuInS2 crystallizes in the chalcopyrite lattice (space group D2d¹² – I4[–]2d, Fig. 6.0.1).

Electronic properties

band structure : Fig. 6.0.7, Brillouin zone: Fig. 6.0.2.

energy gap

$E_{g,dir}$	1.53 eV		from electroreflectance	86H
	1.519 eV	RT	from EER, 10 ¹² phosphorus doped	
dE_g/dT	4.3·10 ^{–5} eV K ^{–1}	$T = <120$ K	single crystal	88H
	– 8.7·10 ^{–5} eV K ^{–1}	$T = >120$ K	single crystal	88H
$E_{g,dir}$ (A,B,C)	1.53 eV	$T = 300$ K	electroreflectance, bulk crystal	75S1

excitonic energy gap

E_{gx}	(A)	1.536 eV	$T = 2$ K	(n = 1) absorption	75S1
	(B)	1.554 eV		(n = 1)	

splitting energies (at Γ)

$\Delta_{cf}(\Gamma)$	> – 0.005 eV		75S1
$\Delta_{so}(\Gamma)$	– 0.02 eV		

effective masses

m_n	0.03 m_0		from electrolyte electroreflectance	87H
m_p	1.3 m_0		Hall effect	80H

Lattice properties

lattice parameters

a	5.52(1) Å	RT	75S2
c	11.08(6) Å		
c/a	2.00(1)		

density

d	4.74 g cm ^{–3}	RT	77B
-----	-------------------------	----	-----

Debye temperature

Θ_D	273 K	$T \rightarrow 0$ K	77B
------------	-------	---------------------	-----

melting temperature

T_m	1270...1320 K		75S1
-------	---------------	--	------

wavenumbers of infrared and Raman active phonons

		Symmetry			
		I $\bar{4}$ 2d	(F $\bar{4}$ 3m)		
$\bar{\nu}_{\text{LO}}/\bar{\nu}_{\text{TO}}$	352/323 cm^{-1}	Γ_4	(Γ_{15})	$T = 4.5 \text{ K}$, Γ_4 , Γ_5 are IR active, all are Raman active	75K
	339/321 cm^{-1}	Γ_5	(Γ_{15})		
	314/295 cm^{-1}	Γ_5	(W_4)		
	294 cm^{-1}	Γ_1	(W_1)		
	266/234 cm^{-1}	Γ_4	(W_2)		
	260/244 cm^{-1}	Γ_5	(X_5)		
	– /140 cm^{-1}	Γ_5	(W_3)		
	– /88 cm^{-1}	Γ_4	(W_2)		
	– /79 cm^{-1}	Γ_3	(W_2)		
	– /67 cm^{-1}	Γ_5	(X_5)		

Transport properties

resistivity, carrier concentration, mobility

p-type samples					
p	$3 \cdot 10^{17} \text{ cm}^{-3}$	RT	single crystals, sulfur-annealed		90H
ρ	$10 \dots 10^4 \Omega \text{ cm}$		thin films from reactive sputtering		95K
μ_p	$499 \text{ cm}^2 \text{ V}^{-1} \text{ s}^{-1}$		single crystal, p-doped		86L
n-type samples					
n	$10^{16} \dots 10^{17} \text{ cm}^{-3}$	RT	single crystals, as grown		90H
ρ	$1 \Omega \text{ cm}$	RT	single crystals, as grown		93H
	$10^3 \dots 10^4 \Omega \text{ cm}$		single crystals, Zn-doped (0.25 %)		90U
	$1 \dots 10 \Omega \text{ cm}$		single crystals, Zn-doped (0.5 %)		90U
	$0.1 \dots 1 \Omega \text{ cm}$		single crystals, Zn-doped (2.5 %)		90U
	$80 \Omega \text{ cm}$		In-rich thin films		95P
μ_n	$40 \text{ cm}^2 \text{ V}^{-1} \text{ s}^{-1}$	RT	single crystal, as grown		90H
	$20 \dots 50 \text{ cm}^2 \text{ V}^{-1} \text{ s}^{-1}$		polycrystalline tablets by sintering		90Y
	$165 \text{ cm}^2 \text{ V}^{-1} \text{ s}^{-1}$	RT	single crystal		93K

For temperature dependence of resistivity and mobilities, see Figs. 6.7.1...3.

Optical properties

refractive index

		$\lambda [\mu\text{m}]$	75S1
n_o	2.7907	0.90	
	2.7225	1.00	
	2.6020	2.00	
	2.5838	3.00	
	2.5760	4.00	
	2.5699	5.00	
	2.5645	6.00	
	2.5587	7.00	
	2.5522	8.00	
	2.5448	9.00	
	2.5366	10.00	
	2.5274	11.00	
	2.5166	12.00	
	2.5108	12.50	

n_e	2.7713	0.90	75S1
	2.7067	1.00	
	2.5918	2.00	
	2.5741	3.00	
	2.5663	4.00	
	2.5598	5.00	
	2.5539	6.00	
	2.5474	7.00	
	2.5401	8.00	
	2.5311	9.00	
	2.5225	10.00	
	2.5112	11.00	
	2.4987	12.00	

References to 6.7

- 75K Koschel, W. H., Bettini, M.: Phys. Status Solidi (b) 72 (1975) 729.
- 75S1 Shay, J. L., Wernick, J. H.: Ternary Chalcopyrite Semiconductors: Growth, Electronics, Properties and Applications. Pergamon, 1975.
- 75S2 Suzuki, K., Kambara, T., Gondaira, K., Sato, K., Kondo, K., Teranishi, T.: J. Phys. Soc. Jpn. 39 (1975) 1310.
- 76L Look, D. C., Manthuruthil, J. C.: J. Phys. Chem. Solids 37 (1976) 173.
- 77B Bachmann, K. J., Hsu, F. S. L., Thiel, F. A., Kasper, H. M.: J. Electron. Mater. 6 (1977) 431.
- 77M Mittleman, S. D., Singh, R.: Solid State Commun. 22 (1977) 659.
- 80H Hwang, H. L., Tu, C. C., Maa, J. S., Sun, C. Y.: Solar Energy Mater. 2 (1980) 433.
- 86H Hsu, T.M.: J. Appl. Phys. 59 (1986) 2538.
- 86L Lin, J.L., Lue, J.T., Yang, M.H., Hwang, H.L.: Appl. Phys. Lett. 48 (1986) 1057.
- 87H Haworth, L.I., Al-Saffar, I.S., Tomlinson, R.D.: Phys. Status Solidi A 99 (1987) 603.
- 88H Hsu, T.M., Lin, J.H.: Phys. Rev. B 37 (1988) 4106.
- 90H Hsu, T.M., Lee, J.S., Hwang, H.L.: J. Appl. Phys. 68 (1990) 283.
- 90U Ueng, H.Y., Hwang, H.L.: J. Phys. Chem. Solids 51 (1990) 11.
- 90Y Yamamoto, N., Ogiwara, J., Horinaka, H.: Jpn. J. Appl. Phys., Part 1, 29 (1990) 650.
- 93H Hsu, T.M.: Jpn. J. Appl. Phys., Supplement, 32 (1993) 537.
- 93K Koscielniak-Mucha, B., Opanowicz, A.: Phys. Status Solidi A 139 (1993) K73.
- 95K Kobayashi, S., Dan Yang Yu, Sarinanto, M.M., Kobayashi, Y., Kaneko, F., Kawakami, T.: Jpn. J. Appl. Phys., Part 2, 34 (1995) L513.
- 95P Park, G.C., Yoo, Y.T., Lee, J.: Synth. Met. 71 (1995) 1745.

Figures to 6.7

Fig. 6.0.1

The chalcopyrite lattice

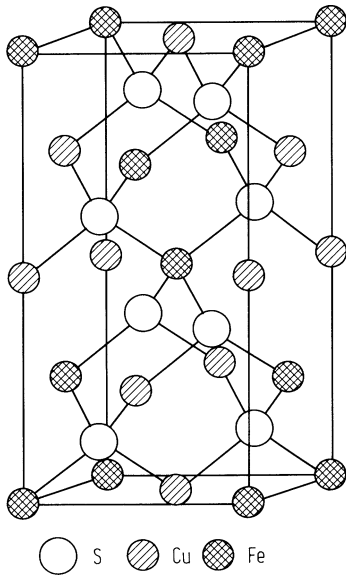


Fig. 6.0.2

Brillouin zone of the chalcopyrite lattice

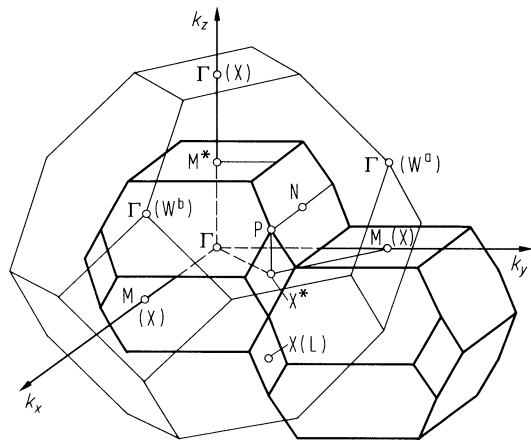


Fig. 6.0.7

Band structure of CuInS_2 .

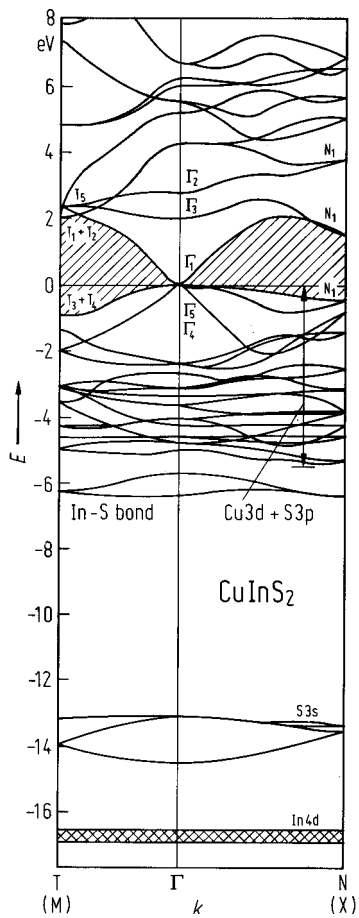
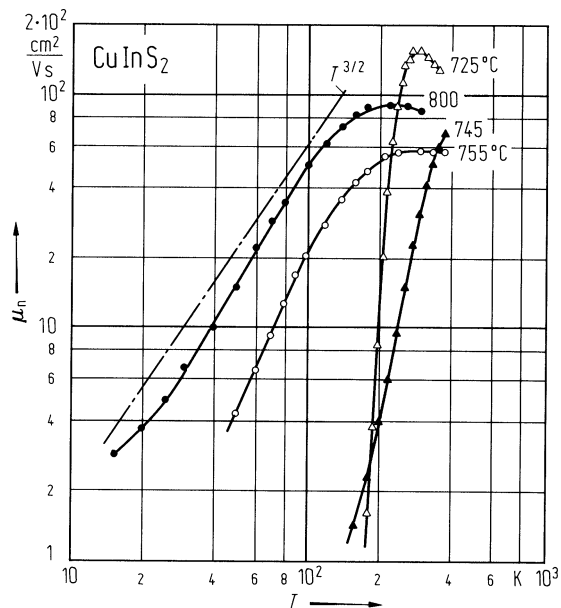


Fig. 6.7.1

CuInS₂. Electron mobility vs. temperature for various annealing temperatures (given as parameters) [76L].
Annealing atmosphere: In; single crystalline samples.



CuInS₂. Resistivity vs. reciprocal temperature for crystals annealed in Zn, Cd at $T = 920$ K, 1070 K [77M].

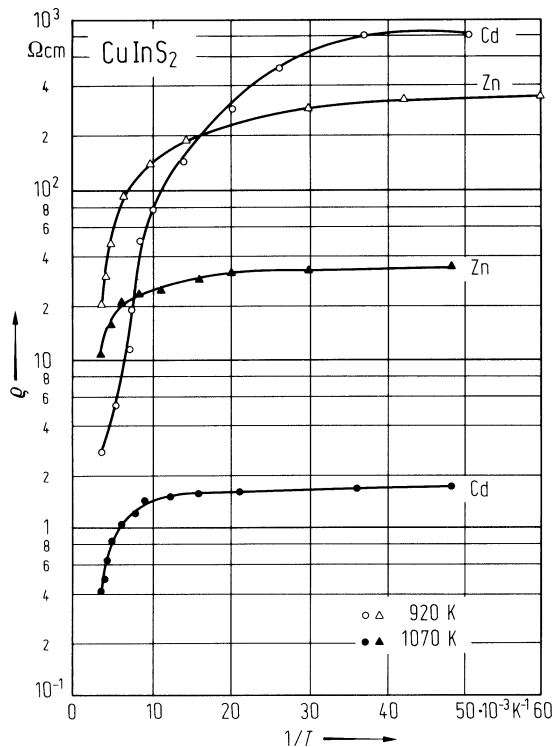
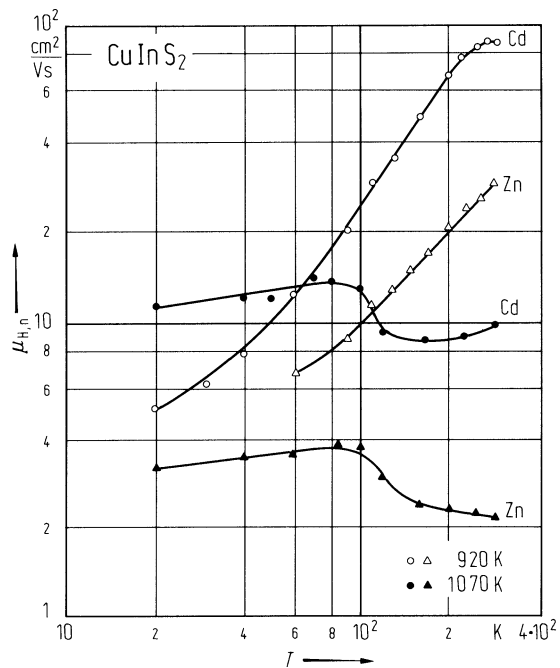


Fig. 6.7.3

CuInS₂. Electron Hall mobility vs. temperature [77M].



6.8 Copper indium selenide (roquesite, CuInSe2)

Crystal structure

CuInSe2 crystallizes in the chalcopyrite lattice (space group $D_{2d}^{12} - \bar{1}4\ 2d$, Fig. 6.0.1).

Electronic properties

band structure : Fig. 6.0.8, Brillouin zone: Fig. 6.0.2.

energy gap

$E_{g,dir}$	(1.010 ± 0.001) eV	RT, single crystal	absorption, lower E_g 's at RT are due to increased electron and ionized impurity concentration n and N_I respectively	86N
dE_g/dT	$-1.1 \cdot 10^{-4}$ eV K ⁻¹	$T = 100 \dots 300$ K		87N

excitonic energy gap

epitaxial films on GaAs (001) substrates

E_{X1}	1.0386 eV	$T = 2$ K	PL, free exciton, $n = 1$ [FE _{$n=1$}]	94N
----------	-----------	-----------	---	-----

splitting energies (at Γ)

Δ_{so}	0.8 eV		In 4d core state	87T
Δ_{cf}	+ 0.006 eV	$T = 77$ K	positive!	75S
Δ_{so}	0.23 eV	$T = 77$ K		

exciton binding energy

E_b	4.3 meV	$T = 2$ K	PL	97S
-------	---------	-----------	----	-----

effective masses

The Fermi surface of electrons is spherical and located at the center of the Brillouin zone [93A].

m_c^*	$0.082(2) m_0$		cyclotron mass value	93A
m_0^*	$0.077(2) m_0$		eff. mass at minimum of conduction band	
$m_n = m_p$	$0.087 m_0$	$T = 300$ K		92R

Lattice properties

lattice parameters

a	$5.78(1) \text{ \AA}$		RT	77H
c	$11.55(2) \text{ \AA}$			
c/a	2.00			

density

d	5.77 g cm^{-3}		RT	77B
-----	--------------------------	--	----	-----

coefficient of thermal expansion

X-ray studies on powder prepared from single crystals

$\alpha_{ }$	$7.90 \cdot 10^{-6} \text{ K}^{-1}$	RT	along c - axis	85B
α_{\perp}	$11.23 \cdot 10^{-6} \text{ K}^{-1}$	RT	along a - axis	

Debye temperature

Θ_D	243.7 K	$T \rightarrow 0$ K		90F
------------	---------	---------------------	--	-----

melting temperature

T_m	1260 K			75S
-------	--------	--	--	-----

compressibility				
κ	$2.3 \cdot 10^{-11} \text{ Pa}^{-1}$			87N

phonon dispersion

for measured acoustic and optical phonon dispersion relations in [001]-, [110]- and [100]-direction see Fig. 6.8.1a-c [93F].

wavenumbers of Raman active phonon

$\bar{\nu}$	174 cm^{-1}	A_1 mode	Raman on thin films	90Y
	76 cm^{-1}	B_1 mode		
$\bar{\nu}_{\text{LO}}/\bar{\nu}_{\text{TO}}$		$230/227 \text{ cm}^{-1}$	Γ_5 [W_{4u}]	92T
		229 cm^{-1}	Γ_3 [W_{2u}]	
		179 cm^{-1}	Γ_3 [X_3]	
	176 cm^{-1}	178 cm^{-1}	Γ_1 [W_1]	
	$77/77 \text{ cm}^{-1}$	$78/78 \text{ cm}^{-1}$	Γ_5 [W_{4l}]	
		67 cm^{-1}	Γ_3 [W_{2l}]	
	$60/58 \text{ cm}^{-1}$	$60/61 \text{ cm}^{-1}$	Γ_5 [X_{5l}]	

second order elastic moduli

c_{11}	$9.70 \cdot 10^{10} \text{ Nm}^{-1}$	$T = 300 \text{ K}$	inelastic neutron scattering	93F
c_{33}	$10.89 \cdot 10^{10} \text{ Nm}^{-1}$		on single crystal	
c_{44}	$3.62 \cdot 10^{10} \text{ Nm}^{-1}$			
c_{66}	$3.16 \cdot 10^{10} \text{ Nm}^{-1}$			
c_{12}	$5.97 \cdot 10^{10} \text{ Nm}^{-1}$			
c_{13}	$8.60 \cdot 10^{10} \text{ Nm}^{-1}$			

bulk modulus

B	$4.82 \cdot 10^{12} \text{ Pa}$	RT	dynamic pulse-echo overlap method	90F
-----	---------------------------------	----	-----------------------------------	-----

sound velocity

v_L	$3.77 \cdot 10^5 \text{ cm s}^{-1}$	RT	dynamic pulse echo overlap method	90F
v_T	$2.10 \cdot 10^5 \text{ cm s}^{-1}$	RT	dynamic pulse echo overlap method	90F

Transport properties

carrier concentration, resistivity, mobility, thermoelectric power

single crystals:

p-type

μ_n	$(6 \pm 3) \text{ cm}^2 \text{ V}^{-1} \text{ s}^{-1}$	RT	surface-acoustic-wave technique	93T
μ_p	$(3.1 \pm 0.15) \text{ cm}^2 \text{ V}^{-1} \text{ s}^{-1}$	RT		
p	$5 \cdot 10^{15} \text{ cm}^{-3}$	RT		

See also Figs. 6.8.2 and 6.8.3.

Optical properties

refractive index

n	2.05...2.72	$h\nu = 0.5 \dots 0.9 \text{ eV}$		91C
-----	-------------	-----------------------------------	--	-----

dielectric constants

$\varepsilon(0)$	15.2	$T = 300\text{K}, E \parallel c$	infrared	78R
	16.0	$E \perp c$		
$\varepsilon(\infty)$	8.5	$E \parallel c$	infrared	78R
	9.5	$E \perp c$		

References to 6.8

- 75S Shay, J. L., Wernick, J. H.: Ternary Chalcopyrite Semiconductors: Growth, Electronics, Properties and Applications. Pergamon, 1975.
- 77B Bachmann, K. J., Hsu, F. S. L., Thiel, F. A., Kasper, H. M.: J. Electron. Mater. 6 (1977) 431.
- 77H Haupt, H., Hess, K.: Inst. Phys. Conf. Ser.35 (1977) 5.
- 78N Neumann, H., Nguyen Van Nam, Höbler, H. J., Kühn, G.: Solid State Commun. 25 (1978) 899.
- 78R Riede, V., Sobotta, H., Neumann, H., Hoang Xuan Nguyen: Solid State Commun. 28 (1978) 449.
- 79I Irie, T., Endo, S., Kimura, S.: Jpn. J. Appl. Phys. 18 (1979) 1303.
- 85B Bodnar, I. V., Orlova, N. S.: Inorg. Mater. 21 (1985) 967.
- 86N Neumann, H., Tomlinson, R. D.: Solid States Commun. 57 (1986) 591.
- 87N Nakanishi, H., Endo, S., Irie, T., Chang, B. H.: Ternary Multinary Compd., Mater. Res. Soc. (1987) 99.
- 87T Takarabe, K., Irie, T.: Jpn. J. Appl. Phys. 26 (1987) 1828.
- 90F Fernández, B., Wasim, S. M.: Phys. Status Solidi A 122 (1990) 235.
- 90Y Yamanaka, S., Tanda, M., Horino, K., Ito, K., Yamada, A., Konagai, M., Takahashi, K.: IEEE PVSC 1 (1990) 132.
- 91C Chichibu, S., Shishikura, M., Ino, J., Matsumoto, S.: J. Appl. Phys. 70 (1991) 1648.
- 92R Rincon, C., Fernandez, B.: Phys. Status Solidi B 170 (1992) 531.
- 92T Tanino, H., Maeda, T., Fujikake, H., Nakanishi, H., Endo, S., Irie, T.: Phys. Rev. B 45 (1992) 13323.
- 93A Arushanov, E., Essaleh, L., Galibert, J., Leotin, J., Askenazy, S.: Physica B 184 (1993) 229.
- 93F Fouret, R., Hennion, B., Gonzales, J., Wasim, S. M.: Phys. Rev. B (Condensed Matter) 47 (1993) 8269.
- 93T Tabib-Azar, M., Moller, H. J., Shoemaker, N.: IEEE Transaction on Ultrasonics, Ferroelectrics and Frequency Control 40 (1993) 149.
- 94N Niki, S., Makita, Y., Yamada, A., Shibata, H., Fons, P. J., Obara, A.: 24th IEEE PVSC and First WCPEC 1 (1994) 132.
- 97S Schoen, J. H., Alberts, V., Bucher, E.: J. Appl. Phys. 81 (1997) 2799.

Figures to 6.8

Fig. 6.0.1

The chalcopyrite lattice

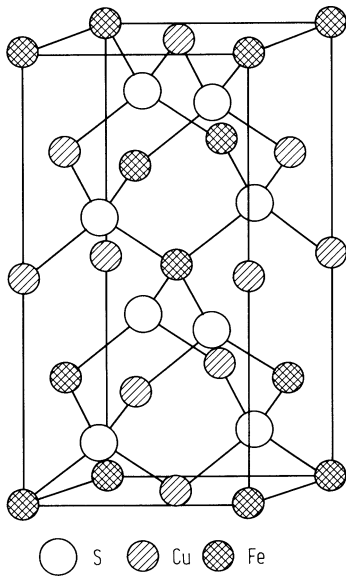


Fig. 6.0.2

Brillouin zone of the chalcopyrite lattice

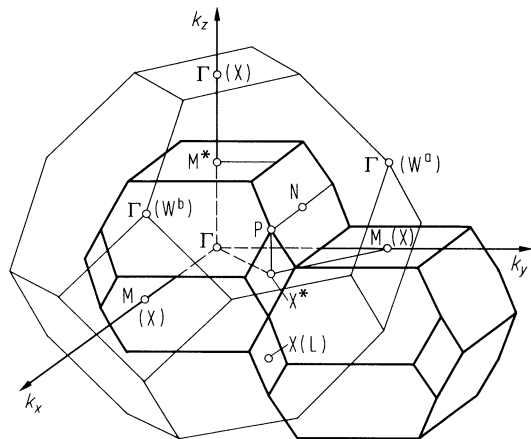


Fig. 6.0.8

Band structure of CuInSe_2 .

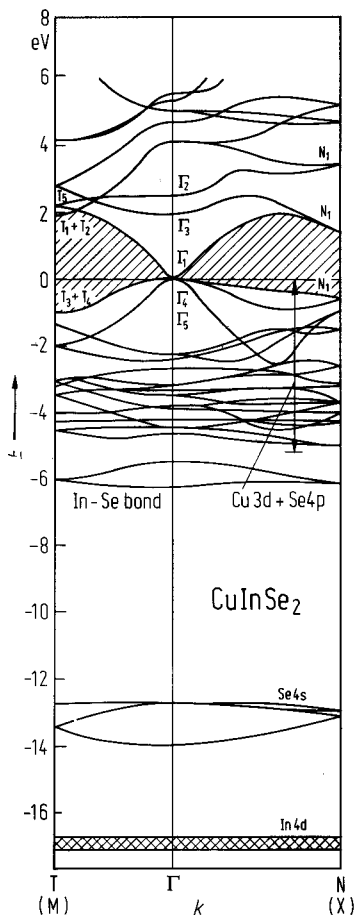


Fig. 6.8.1a

CuInSe₂. Phonon dispersion curves of TA[100] and LA[100] modes [93F].

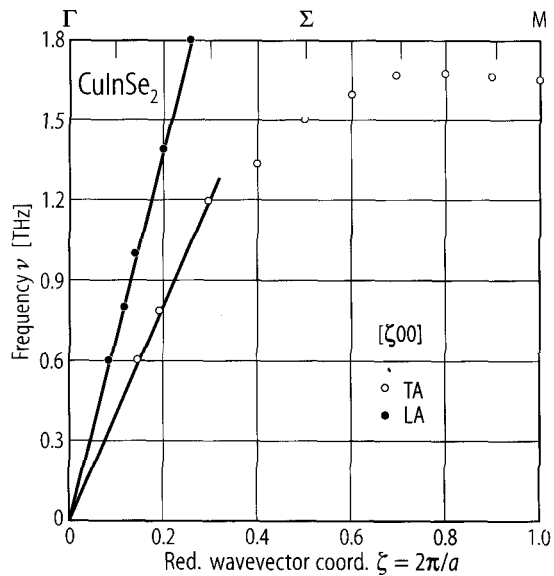


Fig. 6.8.1b

CuInSe₂. Phonon dispersion curves of LA[001], TA[001] and TO[001] modes [93F].

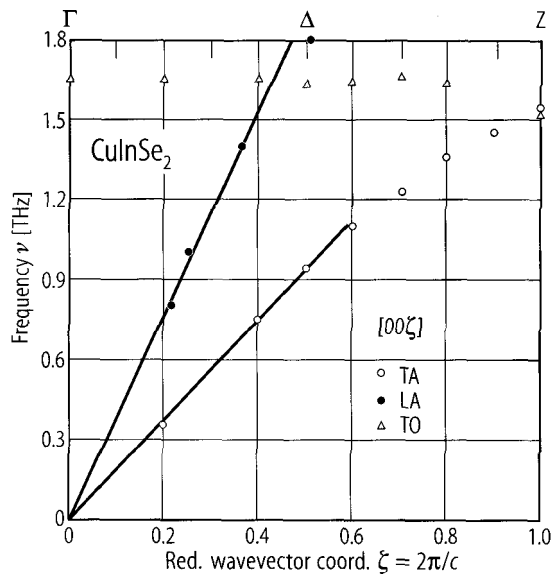


Fig. 6.8.1c

CuInSe_2 . Phonon dispersion curves of $\text{TA}_1[110]$, $\text{TA}_2[110]$, $\text{LA}[110]$ and $\text{TO}_2[110]$ modes [93F].

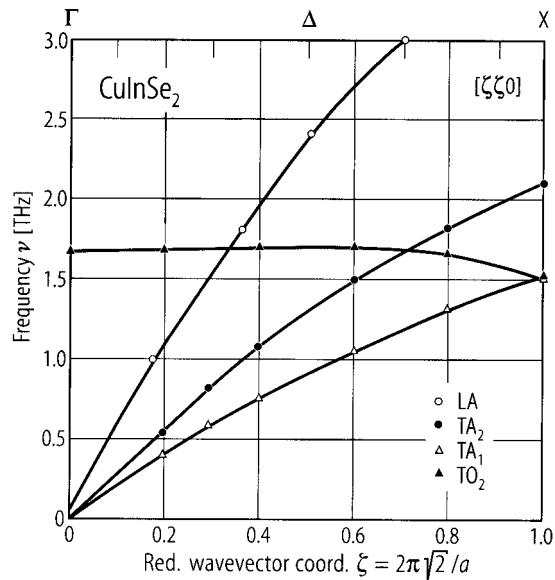


Fig. 6.8.2

CuInSe₂. Resistivity and Hall coefficient vs. reciprocal temperature for four p-type samples [79I].

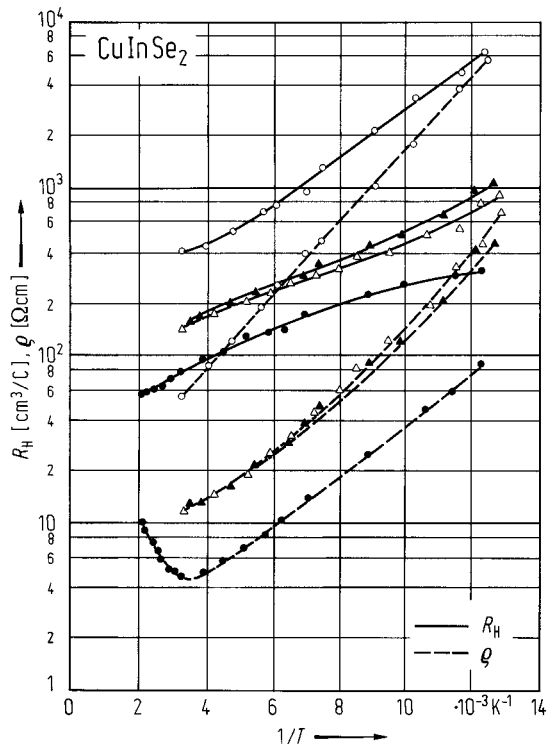
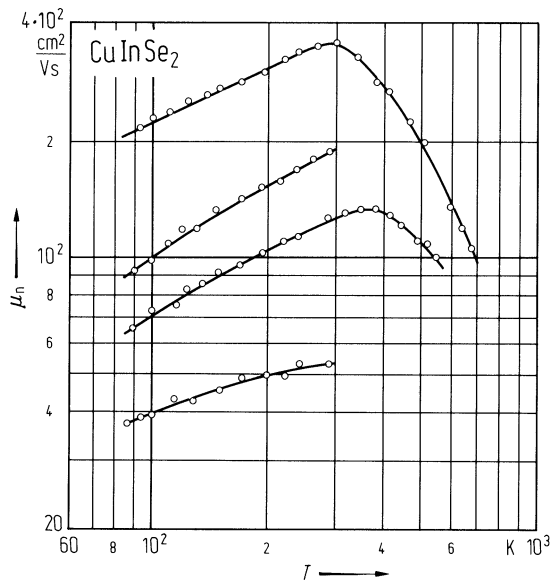


Fig. 6.8.3

CuInSe₂. Electron mobility vs. temperature for four n-type samples [78N].



6.9 Copper indium telluride (CuInTe2)

Crystal structure

CuInTe2 crystallizes in the chalcopyrite lattice (space group D2d¹² – I4̄2d, Fig. 6.0.1).

Electronic properties

energy gap

<i>E</i> _{g,dir}	0.983 eV	<i>T</i> = 370 K	from optical absorption	89M
---------------------------	----------	------------------	-------------------------	-----

spin orbit splitting energy (at Γ)

Δ _{so}	0.63 eV	<i>T</i> = 300 K	from intervalence-band absorption Fe-doped	87N
-----------------	---------	------------------	---	-----

Lattice properties

lattice parameters

<i>a</i>	6.17(1) Å	RT		75S2
<i>c</i>	12.34(2) Å			
<i>c/a</i>	2.00			

density

<i>d</i>	6.10 g cm ⁻³	RT		77B
----------	-------------------------	----	--	-----

Debye temperature

Θ _D	197.5 K	<i>T</i> → 0 K	from sound velocities	90F
	191.4 K			77B

melting temperature

<i>T</i> _m	1050 K			75S1
-----------------------	--------	--	--	------

wavenumbers of infrared active phonons (data in cm⁻¹, at RT)

ν̄	172,157,126,50 170,101,46	E modes (<i>E</i> ⊥ <i>c</i>) B ₂ modes(<i>E</i> ∥ <i>c</i>)	infrared reflectivity	81H
----	------------------------------	--	-----------------------	-----

Transport properties

carrier concentration, resistivity, mobility, thermoelectric power

p-type samples

<i>p</i>	3.69·10 ¹⁹ cm ⁻³	<i>T</i> = 300 K	single crystal, grown by PDF	87H
	1.87·10 ¹⁷ cm ⁻³	<i>T</i> = 300 K	single crystal, grown by Bridgman	
<i>ρ</i>	1.35·10 ⁻³ Ω cm	<i>T</i> = 300 K	single crystal, grown by PDF	
	6.60·10 ⁻¹ Ω cm	<i>T</i> = 300 K	single crystal, grown by Bridgman	
μ _p	125 cm ² V ⁻¹ s ⁻¹	<i>T</i> = 300 K	single crystal, grown by PDF	
	50.6 cm ² V ⁻¹ s ⁻¹	<i>T</i> = 300 K	single crystal, grown by Bridgman	

n-type samples

<i>n</i>	1.08·10 ¹⁷ cm ⁻³	<i>T</i> = 300 K	single crystal	88W
μ _n	189.2 cm ² V ⁻¹ s ⁻¹	<i>T</i> = 300 K	single crystal	88W

The temperature dependence of resistivity, hole concentration, and Hall mobility is shown in Fig. 6.9.1 [87H].

Optical properties

refractive index

<i>n</i>	3.05	<i>T</i> = 300 K	λ → ∞	78D
	2.71(9)	<i>T</i> = 300 K	hν = 0.5 eV, polycrystalline film	80H

dielectric constants

$\epsilon(0)$	10.5(8)	$T = 300 \text{ K}, E \perp c$	infrared reflectivity	80R
	12.9(8)	$E \parallel c$		
$\epsilon(\infty)$	8.7(5)	$T = 300 \text{ K}, E \perp c$		80R
	11.0(5)	$E \parallel c$		

References to 6.9

- 75S1 Shay, J. L., Wernick, J. H.: Ternary Chalcopyrite Semiconductors: Growth, Electronics, Properties and Applications. Pergamon, 1975.
- 75S2 Suzuki, K., Kambara, T., Gondaira, K., Sato, K., Kondo, K., Teranishi, T.: J. Phys. Soc. Jpn. 39 (1975) 1310.
- 77B Bachmann, K. J., Hsu, F. S. L., Thiel, F. A., Kasper, H. M.: J. Electron. Mater. 6 (1977) 431.
- 78D Davis, J. G., Bridenbaugh, P. M., Wagner, S.: J. Electron. Mater. 7 (1978) 39.
- 80H Hörig, W., Neumann, H., Savalev, V., Lagzdons, J.: Phys. Lett. 78A (1980) 189.
- 80R Riede, V., Neumann, H., Sobotta, H., Tomlinson, R. D., Elliott, F., Howarth, L.: Solid State Commun. 33 (1980) 557.
- 81H Holah, G. D., Schenk, A. A., Perkowitz, S.: Phys. Rev. B 23 (1981) 6288.
- 87H Haworth, L.I., Al-Saffar, I.S., Tomlinson, R.D.: Phys. Status Solidi A 99 (1987) 603.
- 87N Nakanishi, H., Endo, S., Irie, T., Chang, B. H.: Ternary Multinary Compd., Mater. Res. Soc. (1987) 99.
- 88W Wasim, S.M., Albornoz, J.G.: Phys. Status Solidi A 110 (1988) 575.
- 89M Mochizuki, K., Masumoto, K.: J. Cryst. Growth 98 (1989) 855.
- 90F Fernández, B., Wasim, S. M.: Phys. Status Solidi A 122 (1990) 235.

Figures to 6.9

Fig. 6.0.1

The chalcopyrite lattice

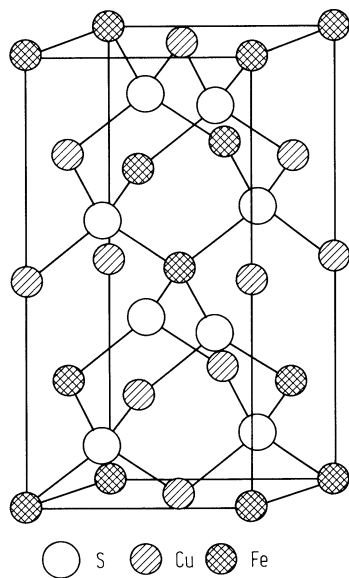
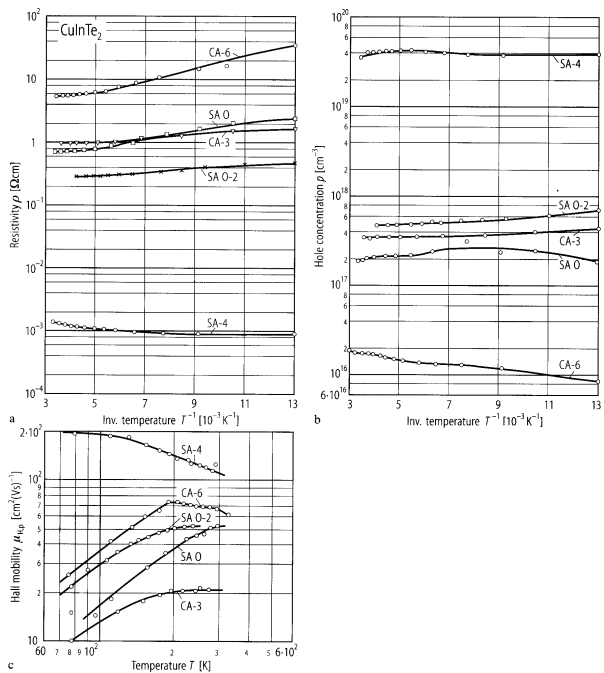


Fig. 6.9.1

CuInTe₂. Temperature dependence of (a) resistivity, (b) hole concentration, and (c) Hall mobility of various samples [87H].



6.10 Silver gallium sulfide (AgGaS2)

Crystal structure

AgGaS2 crystallizes in the chalcopyrite lattice (space group D2d¹² – I4[–]2d, Fig. 6.0.1).

Electronic properties

energy gap

$E_{g,dir}$	2.714 eV	$T = 5\text{ K}$	from reflectivity measurements	87A2
dE_g/dT	$1.0\cdot10^{-4}\text{ eV K}^{-1}$	$T < 80\text{ K}$	from reflectivity measurements	87A1
	$-2.2\cdot10^{-4}\text{ eV K}^{-1}$	$T > 110\text{ K}$		

The temperature variation of the AgGaS2 energy gap between 5 and 295 K is shown in Fig. 6.10.1 [87A1].

excitonic energy gap

E_{gx}	2.700 eV			86A
----------	----------	--	--	-----

exciton binding energy

E_b	0.0292 eV		from two-photon spectroscopy	95R
-------	-----------	--	------------------------------	-----

splitting energies (at Γ)

Δ_{cf}	-0.28 eV	$T = 77\text{ K}$		75S1
Δ_{so}	0	$T = 77\text{ K}$		

Lattice properties

lattice parameters

a	5.75(1) Å		RT	75S2
c	10.29(2) Å			
c/a	1.790(1)			

density

d	4.70 g cm ⁻³		RT	72A
-----	-------------------------	--	----	-----

Debye temperature

Θ_D	255 K	$T \rightarrow 0\text{ K}$		75A
------------	-------	----------------------------	--	-----

melting temperature

T_m	1264±3 K	at $p_{S_2} = 4.1\cdot10^5\text{ Pa}$		89M
	1220...1320 K			75S1

linear thermal expansion coefficient

The temperature dependence of the thermal expansion coefficients between 0 and 800 K is given in Fig. 6.10.2.

phonon dispersion : The calculated phonon spectrum and the density of states of AgGaS2 are shown in Fig. 6.10.3 [92T].

wavenumbers of infrared and Raman active phonons

(wavenumbers in cm^{-1} , $T = 300 \text{ K}$)

		Symmetry			
		$\bar{1}4\bar{2}d$	$(F\bar{4}3m)$		
$\bar{\nu}_{\text{LO}}/\bar{\nu}_{\text{TO}}$	392/368	Γ_5	(Γ_{15})	Γ_4, Γ_5 are IR active, all are Raman active	77L, 74H, 75L, 80C
	393/367	Γ_4	(Γ_{15})		74H, 75L, 80C
	340/321	Γ_5	(W_4)		74H, 75L, 77L
	334	Γ_3	(W_2)		75L, 75K
	224				74H
	295	Γ_1	(W_1)		74H, 75L, 80C
	240/213	Γ_4	(W_2)		74H, 75L
	215/213				80C
	230/223	Γ_5	(W_4)		74H, 75L
	190.5	Γ_3	(X_3)		75L
	160				74H
	161/157	Γ_5	(W_3)		77L, 74H, 75L, 80C
	95/95	Γ_5	(W_4)		
	65/65	Γ_4	(W_2)		74H, 75L, 80C
	54	Γ_3	(W_2)		
	36/36	Γ_5	(X_5)		77L, 75L, 80C

second order elastic moduli

c_{11}	$8.5 \cdot 10^{11} \text{ dyn/cm}^2$	calculated	92T2
c_{33}	$5.4 \cdot 10^{11} \text{ dyn/cm}^2$		
c_{44}	$3.6 \cdot 10^{11} \text{ dyn/cm}^2$		
c_{66}	$3.5 \cdot 10^{11} \text{ dyn/cm}^2$		
c_{12}	$4.3 \cdot 10^{11} \text{ dyn/cm}^2$		
c_{13}	$3.9 \cdot 10^{11} \text{ dyn/cm}^2$		

Transport properties

resistivity

ρ	$1.0 \cdot 10^6 \text{ } \Omega \text{ cm}$	yellow amorphous film	84V
	$1 \text{ } \Omega \text{ cm}$	black amorphous film	
	$3.0 \cdot 10^{10} \text{ } \Omega \text{ cm}$	polycrystalline film, as grown	
	$1.0 \cdot 10^{11} \text{ } \Omega \text{ cm}$	polycrystalline, annealed (500°C), vacuum	
	$5.0 \cdot 10^{13} \text{ } \Omega \text{ cm}$	polycrystalline, annealed (500°C), S-vapor	
	$1.0 \cdot 10^8 \text{ } \Omega \text{ cm}$	single crystal	

The temperature dependence of electrical conductivity for as-grown AgGaS_2 crystals with or without illumination is shown in Fig. 6.10.4.

activation energies

E_A	0.11 eV	shallow traps	93M
	0.03 eV	shallow traps	

thermal conductivity

κ_p	$0.014 \text{ W cm}^{-1} \text{ K}^{-1}$	\parallel optical axis	94B
κ_s	$0.015 \text{ W cm}^{-1} \text{ K}^{-1}$	\perp optical axis	94B

Optical properties

refractive index

coefficients in the formula $n^2 = A + B/(1 - C/\lambda^2) + D/(1 - E/\lambda^2)$.

	n_o	n_e
A	3.6280	4.0172
B	2.1686	1.5274
C	$0.1003 \cdot 10^{-12} \text{ m}^2$	$0.1310 \cdot 10^{-12} \text{ m}^2$
D	2.1753	2.1699
E	$950 \cdot 10^{-12} \text{ m}^2$	$950 \cdot 10^{-12} \text{ m}^2$
valid for $\lambda = (0.49 \dots 12.0) \mu\text{m}$		

76B

dielectric constants (at $T = 300 \text{ K}$)

$\epsilon(0)$	8.21	$E \parallel c$
	8.51	$E \perp c$
$\epsilon(\infty)$	5.50	$E \parallel c$
	5.90	$E \perp c$

75S1

References to 6.10

- 72A Adams, R., Russo, P., Arnofi, R., Wold, A.: Mater. Res. Bull. 7 (1972) 93.
- 74H Holah, G. D., Webb, J. S., Montgomery, H.: J. Phys. C: Solid State Phys. 7 (1974) 3875.
- 75A Abrahams, S. C., Hsu, F. S. L.: J. Chem. Phys. 63 (1975) 1162.
- 75K Koschel, W. H., Bettini, M.: Phys. Status Solidi (b) 72 (1975) 729.
- 75L Lockwood, D.J., Montgomery, H.: J. Phys. C.: solid State Phys. 8 (1975) 3241.
- 75S1 Shay, J. L., Wernick, J. H.: Ternary Chalcopyrite Semiconductors: Growth, Electronics, Properties and Applications. Pergamon, 1975.
- 75S2 Suzuki, K., Kambara, T., Gondaira, K., Sato, K., Kondo, K., Teranishi, T.: J. Phys. Soc. Jpn. 39 (1975) 1310.
- 76B Bhar, G. C.: Appl. Opt. 15 (1976) 305.
- 77L Lockwood, D. J.: Inst. Phys. Conf. Ser. 35 (1977) 97.
- 80C Carlone, C., Olego, D., Jayaraman, A., Cardona, M.: Phys. Rev. B 22 (1980) 3877.
- 84V Von Campe, H.: Thin Solid Films 111 (1984) 17.
- 85B Bodnar, I.V., Orlova, N.S.: Phys. Status Solidi A 91 (1985) 503.
- 86A Aicardi, J.P., Aguero, G.: Phys. Status Solidi A 95 (1986) 679.
- 87A1 Artus, L., Bertrand, Y.: Solid State Commun. 61 (1987) 733.
- 87A2 Artus, L., Bertrand, Y.: J. Phys. C 20 (1987) 1365.
- 89M Mochizuki, K., Masumoto, K.: J. Cryst. Growth 98 (1989) 855.
- 92T Tyuterev, V.G., Skachkov, S.I.: Nuovo Cimento D 14 (1992) 1091.
- 93M Moon-Seog Jin, Suk-Ki Min, Han-Jo Lim, Hong-Lee Park, Wha-Tek Kim: Jpn. J. Appl. Phys., Supplement 32 (1993) 593.
- 94B Beasley, J.D.: Appl. Opt. 33 (1994) 1000.
- 95R Reimann, K., Rübenacke, S., Steube, M.: Solid State Commun. 96 (1995) 279.

Figures to 6.10

Fig. 6.0.1

The chalcopyrite lattice

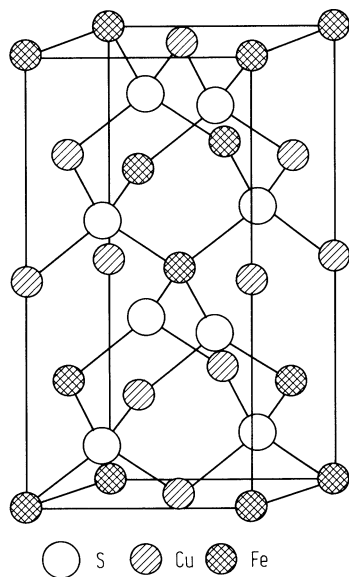


Fig. 6.10.1

AgGaS₂. Temperature variation of the energy gap between 5 and 295 K [87A].

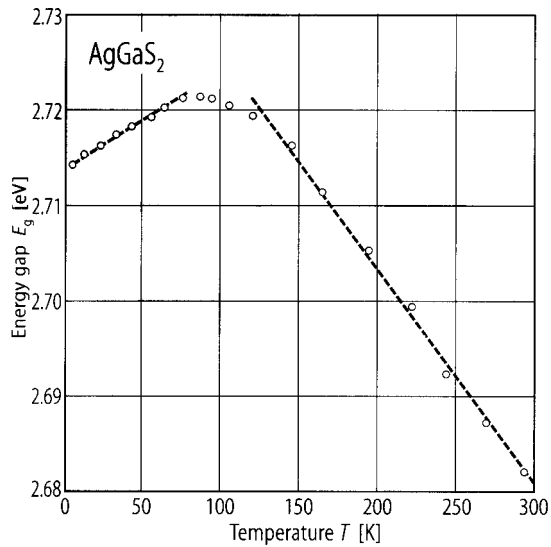


Fig. 6.10.2

AgGaS₂. Temperature dependence of the coefficients of thermal expansion α_{\perp} , α_{\parallel} , α_{BC} , $\alpha_K = \alpha_{\parallel} - \alpha_{\perp}$, α_{AC} , and α_x [85B]. α_{AC} : expansion coefficient along A – C bonds, α_{BC} : expansion coefficient along B – C bonds α_x : x = location of C atom relative to A and B atom.

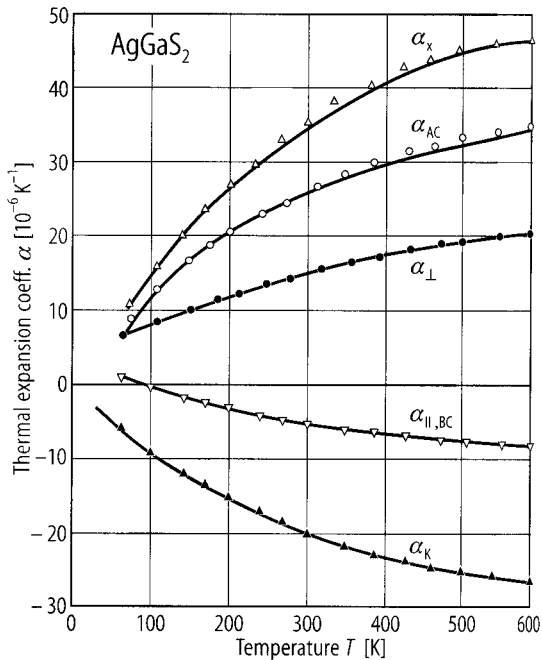


Fig. 6.10.3

AgGaS₂. The calculated phonon spectrum and the density of states. θ is the angle between the phonon wavevector and tetragonal axis [92T].

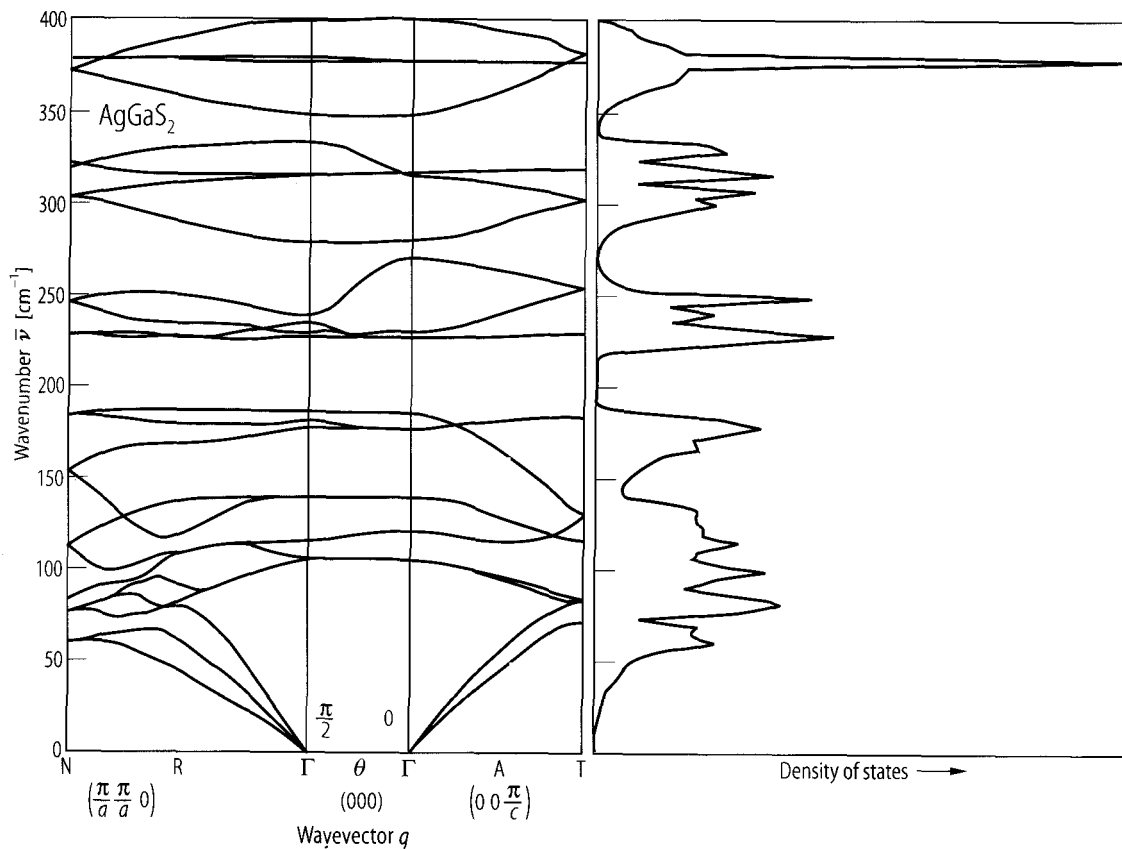
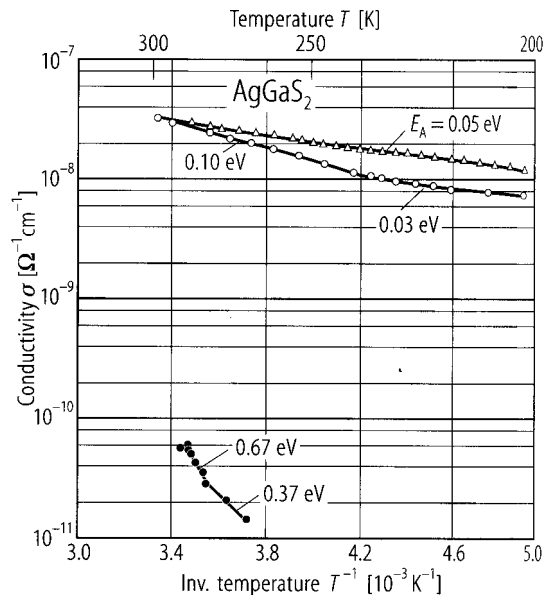


Fig. 6.10.4

AgGaS_2 . The temperature dependence of electrical conductivity for as-grown crystals with or without illumination by high pressure Hg lamp. Open circles and triangles show the conductivity of the samples grown from the charges with stoichiometric and with Ga_2S_3 excess compositions, respectively [93M].



6.11 Silver gallium selenide (AgGaSe2)

Crystal structure

AgGaSe2 crystallizes in the chalcopyrite lattice (space group $D_{2d}^{12} - \bar{1}4\,2d$, Fig. 6.0.1).

Electronic properties

energy gap

$E_{g,dir}$	1.814 eV	RT	from photoluminescence	96P
dE_g/dT	$1.8 \cdot 10^{-4}$ eV K ⁻¹	$T = 10 \dots 60$ K	pure single crystal	91S
	$-3.2 \cdot 10^{-4}$ eV K ⁻¹	$T = 95 \dots 300$ K	pure single crystal	91S

The temperature dependence of the band gap in AgGaSe2 is shown in Fig. 6.11.1 [86A].

splitting energies (at Γ)

Δ_{cf}	- 0.25 eV	$T = 303$ K	from photoconductivity	91M
Δ_{so}	0.30 eV	$T = 303$ K	from photoconductivity	91M

Lattice properties

lattice parameters

a	5.98(1) Å	RT		75S2
c	10.88(1) Å			
c/a	1.820(3)			

density

d	5.70 g cm ⁻³	RT		72A
-----	-------------------------	----	--	-----

coefficient of thermal expansion

α_{11}	- 6.4 · 10 ⁻⁶ K ⁻¹	$T = 298 \dots 423$ K		91E
	- 16.0 · 10 ⁻⁶ K ⁻¹	$T = 423 \dots 873$ K		
α_{33}	23.4 · 10 ⁻⁶ K ⁻¹	$T = 298 \dots 423$ K		
	18.0 · 10 ⁻⁶ K ⁻¹	$T = 423 \dots 873$ K		

melting temperature

T_m	1130 K			75S
-------	--------	--	--	-----

Calculated phonon dispersion curves for AgGaSe2 are shown in Fig. 6.11.2 [90A].

wavenumbers of infrared and Raman active phonons (wavenumbers in cm⁻¹, RT values)

		Symmetry			
		$\bar{1}4\,2d$	$(F\bar{4}\,3m)$		
$\bar{\nu}_{LO}/\bar{\nu}_{TO}$	274/248	Γ_5	(Γ_{15})	Γ_4, Γ_5 : IR active, all Raman active	77K
	162/158	Γ_5	(X_5)		77K
	80/76	$\Gamma_5 ?$			77K

second order elastic moduli

c_{11}	89.8 GPa			91E
c_{33}	58.0 GPa			
c_{44}	21.7 GPa			
c_{66}	13.3 GPa			
c_{12}	65.7 GPa			
c_{13}	45.1 GPa			

Transport properties

resistivity, electrical conductivity, Seebeck coefficient

ρ	$10^5 \, \Omega \, \text{cm}$	$T = 300 \, \text{K}$	different samples	75S1
σ	$8.8 \, \Omega^{-1} \, \text{cm}^{-1}$	$T = 300 \, \text{K}$		
S	$-7 \cdot 10^{-2} \, \text{V} \, \text{K}^{-1}$	$T = 300 \, \text{K}$		

electrical conductivity

σ	$< 10^{-8} \, \Omega^{-1} \, \text{cm}^{-1}$		single crystals, as-grown	96N
	$2 \cdot 10^{-1} \, \Omega^{-1} \, \text{cm}^{-1}$		single crystals, annealed (700°C)	96N
	$6 \cdot 10^{-6} \, \Omega^{-1} \, \text{cm}^{-1}$		single crystals, annealed in Se-vapor	96N

Temperature dependence of electrical conductivity: Fig. 6.11.3, variation of the electrical conductivity with inverse temperature for AgGaSe₂ thin films of different thicknesses: Fig. 6.11.4 [89M2].

activation energies

E_A	0.12 eV	$T = 303 \dots 450 \, \text{K}$	activation energy of conductivity	89M1
	0.86 eV	$T = 500 \dots 573 \, \text{K}$	activation energy of conductivity	

Optical properties

refractive index

coefficients in the formula: $n^2 = A + B/(1 - C/\lambda^2) + D/(1 - E/\lambda^2)$

	n_o	n_e	
A	4.6453	5.2912	76B
B	2.2057	1.3970	
C	$0.1379 \cdot 10^{-12} \, \text{m}^2$	$0.2845 \cdot 10^{-12} \, \text{m}^2$	
D	1.8377	1.9282	
E	$1.600 \cdot 10^{-12} \, \text{m}^2$	$1.600 \cdot 10^{-12} \, \text{m}^2$	

valid for $0.725 \, \mu\text{m} < \lambda < 13.5 \, \mu\text{m}$

dielectric constants

$\varepsilon(0)$	7.76	$T = 300 \, \text{K}, E \parallel c$	infrared	76M
	8.94	$E \perp c$		
$\varepsilon(\infty)$	6.11	$T = 300 \, \text{K}, E \parallel c$	infrared	76M
	6.18	$E \perp c$		

References to 6.11

- 72A Adams, R., Russo, P., Arnofi, R., Wold, A.: Mater. Res. Bull. 7 (1972) 93.
- 75S1 Shay, J. L., Wernick, J. H.: Ternary Chalcopyrite Semiconductors: Growth, Electronics, Properties and Applications. Pergamon, 1975.
- 75S2 Suzuki, K., Kambara, T., Gondaira, K., Sato, K., Kondo, K., Teranishi, T.: J. Phys. Soc. Jpn. 39 (1975) 1310.
- 76B Bhar, G. C.: Appl. Opt. 15 (1976) 305.
- 76M Miller, A., Holah, G. D., Dunnett, W. D., Iseler, G. W.: Phys. Status Solidi (b) 78 (1976) 569.
- 77K Kanellis, G., Kampas, K.: J. Phys. (Paris) 38 (1977) 833.
- 86A Artus, L., Bertrand, Y., Ance, C., Lopez-Soler, A.: Phys. Status Solidi B 138 (1986) 633.
- 89M1 Mal'sagov, A.U.: Izv. Akad. Nauk SSSR, Neorg. Mater. 25 (1989) 25; Inorg. Mater. (Engl. Transl.) 25 (1989) 17.
- 89M2 Mochizuki, K., Masumoto, K.: J. Cryst. Growth 98 (1989) 855.
- 90A Artus, L., Pujol, J., Pascual, J., Camassel, J.: Phys. Rev. B 41 (1990) 5727.
- 91E Eimerl, D., Marion, J., Graham, E.K., McKinstry, H.A., Haussühl, S.: IEEE J. Quantum Electron. 27 (1991) 142.
- 91M Murty, Y.S., Uthanna, S., Naidu, B.S., Reddy, P.J.: Solid State Commun. 79 (1991) 277.
- 91S Shukla, R., Khurana, P., Srivastava, K.K.: Philos. Mag. B 64 (1991) 389.
- 96N Nigge, K.-M., Baumgartner, F.P., Bucher, E.: Solar Energy Mater. Solar Cells 43 (1996) 335.
- 96P Petcu, M.C., Giles, N.C., Schunemann, P.G., Pollak, T.M.: Phys. Status Solidi B 198 (1996) 881.

Figures to 6.11

Fig. 6.0.1

The chalcopyrite lattice

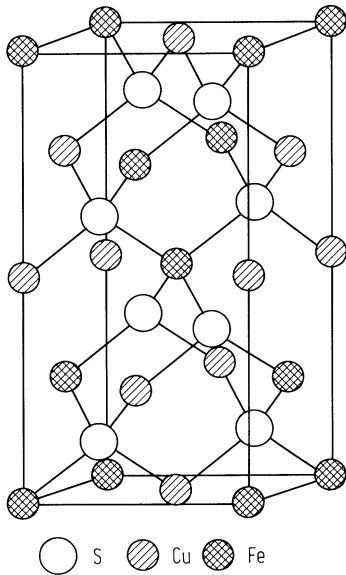


Fig. 6.11.1

AgGaSe₂. Temperature dependence of the band gap [86A]. AgInSe₂ for comparison.

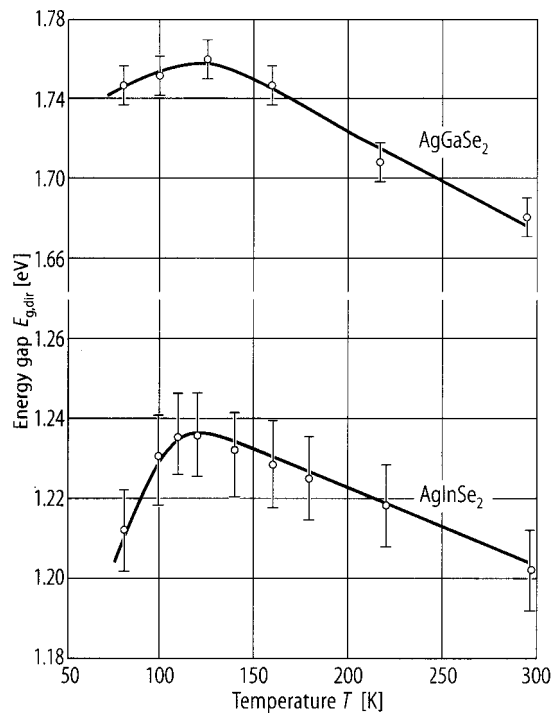


Fig. 6.11.2

AgGaSe₂ (a). Calculated phonon dispersion curves [90A]. Zn_{0.5}Cd_{0.5}Se (b) and ZnCdSe (c) for comparison.

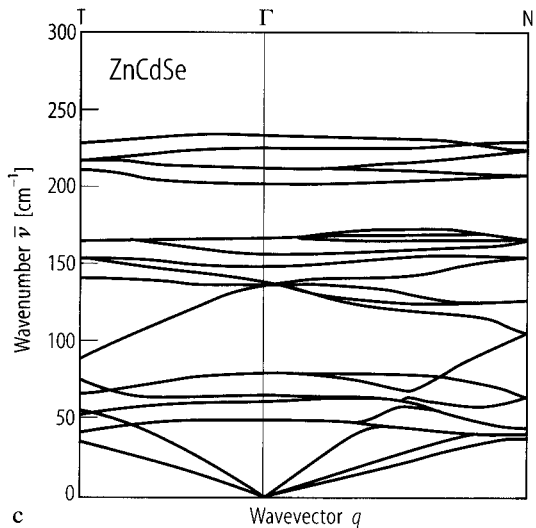
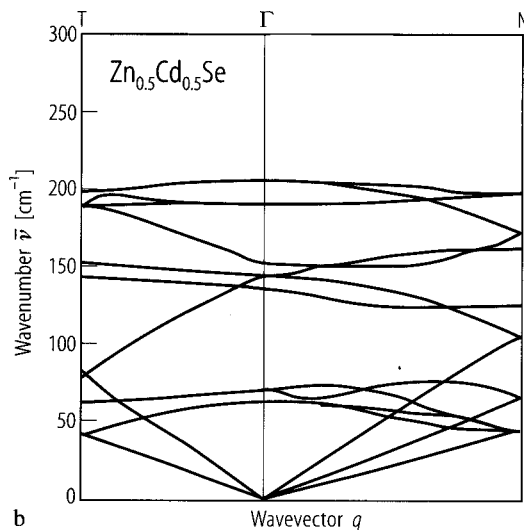
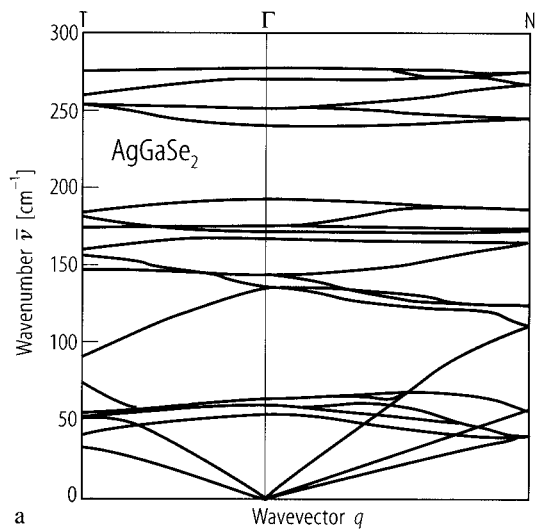


Fig. 6.11.3

AgGaSe₂. Electrical conductivity vs. reciprocal temperature for n-type sample [75S1].

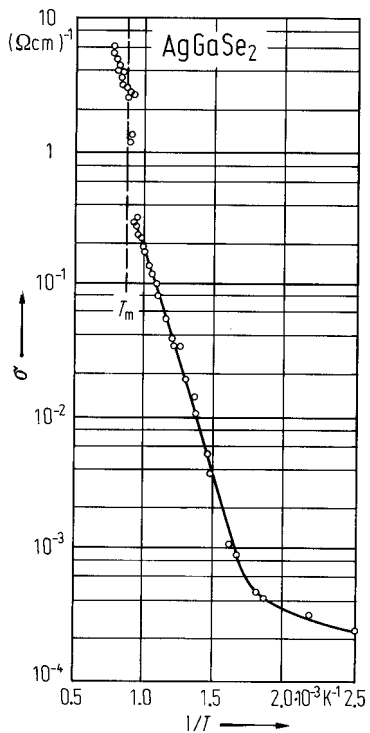
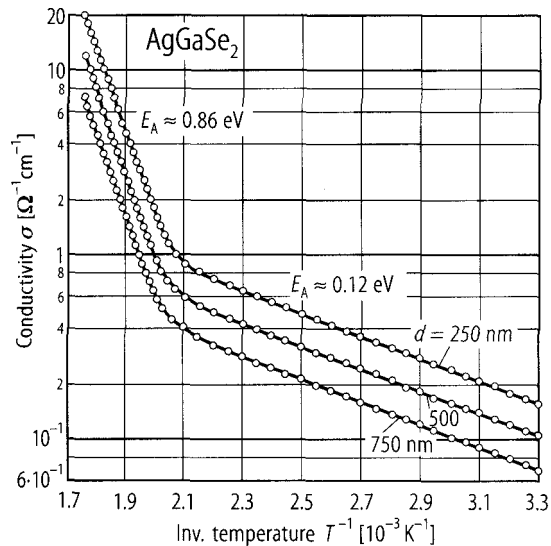


Fig. 6.11.4

AgGaSe₂. Variation of the electrical conductivity with inverse temperature for AgGaSe₂ thin films of different thicknesses [89M1]. Activation energies are indicated.



6.12 Silver gallium telluride (AgGaTe2)

Crystal structure

AgGaTe2 crystallizes in the chalcopyrite lattice (space group $D_{2d}^{12} - \bar{1}4\,2d$, Fig. 6.0.1).

Electronic properties

energy gap

$E_{g,dir}$	1.32 eV	$T = 300\text{ K}$	from optical transmission	89K
dE_g/dT	$3.6 \cdot 10^{-4}\text{ eV K}^{-1}$	$T = 80 \dots 350\text{ K}$		

Lattice properties

lattice parameters

a	6.29(1) Å	RT	75S2
c	11.95(1) Å		
c/a	1.90		

density

d	6.08 g cm^{-3}	RT	72A2
-----	-------------------------	----	------

Debye temperature

Θ_D	182.4 K	$T \rightarrow 0\text{ K}$	77B2
------------	---------	----------------------------	------

melting temperature

T_m	950 K		76K1
-------	-------	--	------

wavenumbers of infrared and Raman active phonons

$\bar{\nu}$	Raman	IR	RT	96J
		43 cm^{-1}		
	64 cm^{-1}	62 cm^{-1}		
	93 cm^{-1}			
	106 cm^{-1}			
		115 cm^{-1}		
	129 cm^{-1}			
	142 cm^{-1}	132 cm^{-1}		
	152 cm^{-1}			
	201 cm^{-1}	201 cm^{-1}		
		205 cm^{-1}		
	220 cm^{-1}			

Transport and optical properties

carrier concentration, resistivity, mobility (p-type samples)

p	$1 \dots 5 \cdot 10^{13}\text{ cm}^{-3}$	$T = 300\text{ K}$	single crystal	89K
ρ	$20 \dots 200\text{ }\Omega\text{ cm}$		thin films	89P
μ_p	$5 \dots 8\text{ cm}^2\text{ V}^{-1}\text{ s}^{-1}$	$T = 300\text{ K}$	single crystal	89K

dielectric constants

$\epsilon(0)$	14.5	$E \parallel c, T = 300\text{ K}$	77K
	15.0	$E \perp c$	
$\epsilon(\infty)$	11.0	$E \parallel c, T = 300\text{ K}$	
	11.86	$E \perp c$	

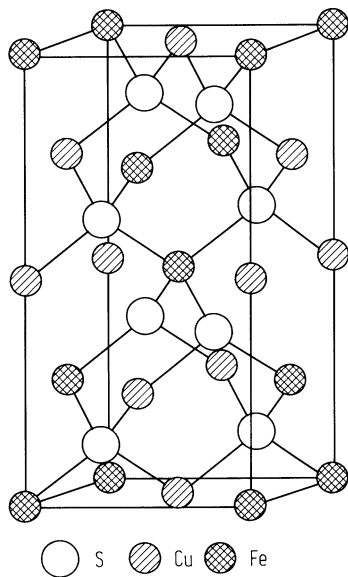
References to 6.12

- 72A2 Adams, R., Russo, P., Arnofi, R., Wold, A.: Mater. Res. Bull. 7 (1972) 93.
- 75S2 Suzuki, K., Kambara, T., Gondaira, K., Sato, K., Kondo, K., Teranishi, T.: J. Phys. Soc. Jpn. 39 (1975) 1310.
- 76K1 Kanellis, G., Kambas, C., Spyridelis, J.: Mater. Res. Bull. 11 (1976) 429.
- 77B2 von Bardeleben, H. J., Goltzené, A., Schwab, C.: Inst. Phys. Conf. Ser. 35 (1977) 43.
- 77K Kanellis, G., Kampas, K.: J. Phys. (Paris) 38 (1977) 833.
- 89K Kobayashi, S., Ohno, T., Kaneko, F., Maruyama, T., Tsuboi, N.: Jpn. J. Appl. Phys., Part 1, 28 (1989) 189.
- 89P Patel, S.M., Patil, M.C.: Mater. Lett. 7 (1989) 338.
- 96J Julien, C., Balkanski, M.: Mater. Sci. Eng. B38 (1996) 1.

Figures to 6.12

Fig. 6.0.1

The chalcopyrite lattice



6.13 Silver indium sulfide (AgInS2)

Crystal structure

AgInS2 crystallizes in the chalcopyrite lattice (space group D2d¹² – I4[–]2d, Fig. 6.0.1).

Electronic properties

energy gap

$E_{g,dir}$ (A)	1.87 eV	$T = 300$ K		74S
(B, C)	2.02 eV			

excitonic energy gap

E_{gx} (A)	1.880 eV	$T = 77$ K		74S
(B)	2.045 eV			

splitting energy (at Γ)

Δ_{cf}	– 0.165 eV	$T = 77$ K	electroreflectance	74S
---------------	------------	------------	--------------------	-----

Lattice properties

lattice parameters

a	5.82(1) Å	RT		75S2
c	11.17(2) Å			
c/a	1.92			

density

d	4.97 g cm ^{–3}	RT		53H
-----	-------------------------	----	--	-----

melting temperature

T_m	1150(10) K			74S
-------	------------	--	--	-----

coefficient of thermal expansion

α_{\perp}	8.33·10 ^{–6} K ^{–1}	\perp c -axis		87O
α_{\parallel}	– 6.90·10 ^{–6} K ^{–1}	\parallel c -axis		

The temperature dependence of the coefficients of thermal expansion in AgInS2 is shown in Fig. 6.13.1 [87O].

References to 6.13

53H Hahn, H., Frank, G., Klingler, W., Meyer, A. D., Störger, G.: Z. Anorg. Allgem. Chem. 271 (1953) 153.
74S Shay, J. L., Tell, B., Shiovone, L. M., Kasper, H. M., Thiel, F.: Phys. Rev. B 9 (1974) 1719.
75S Suzuki, K., Kambara, T., Gondaira, K., Sato, K., Kondo, K., Teranishi, T.: J. Phys. Soc. Jpn. 39 (1975) 1310.
87O Orlova, N.S., Bodnar, I.V.: Phys. Status Solidi A 101 (1987) 421.

Figures to 6.13

Fig. 6.0.1

The chalcopyrite lattice

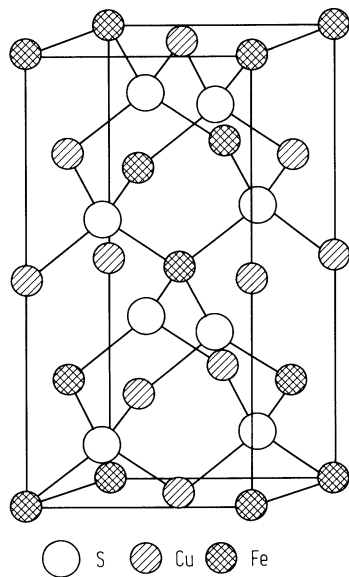
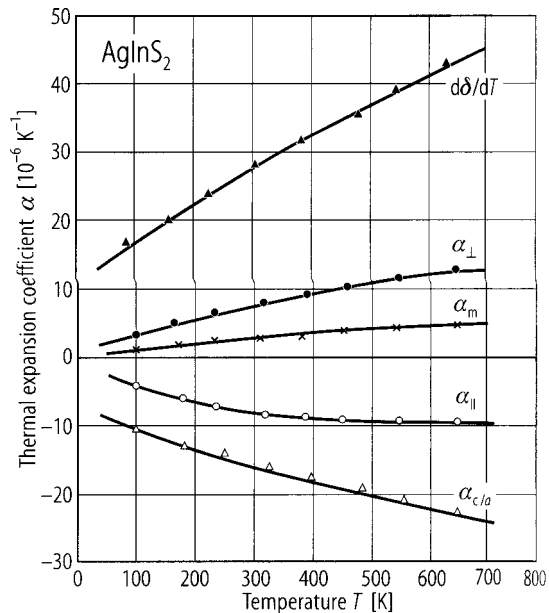


Fig. 6.13.1

AgInS₂. Temperature dependence of the coefficients of thermal expansion α_{\perp} ; α_{\parallel} ; α_m ; $\alpha_{c/a}$; $d\delta/dT$ [87O]. $\alpha_{\perp, \parallel}$: \perp , \parallel to c -axis; $\alpha_m = (\alpha_{\parallel} + 2\alpha_{\perp})/3$; $\delta = 2 - c/a$, tetragonal distortion; $\alpha_{c/a} = \alpha_{\parallel} - \alpha_{\perp}$.



6.14 Silver indium selenide (AgInSe2)

Crystal structure

AgInSe2 crystallizes in the chalcopyrite lattice (space group $D_{2d}^{12} - I\bar{4}2d$, Fig. 6.0.1).

Electronic properties

energy gap

$E_{g,dir}$ (A)	1.24 eV	$T = 300\text{ K}$	electroreflectance	75S1
(B)	1.33 eV			
(C)	1.60 eV			

excitonic energy gap

E_{gx} (A)	1.245 eV	$T = 2\text{ K}$	absorption, reflectivity, photoluminescence	75S1
--------------	----------	------------------	--	------

splitting energies

Δ_{cf}	- 0.12 eV	$T = 300\text{ K}$		75S1
Δ_{so}	0.30 eV			

Lattice properties

lattice parameters

a	6.095(15) Å	RT		75S2
c	11.69(3) Å			
c/a	1.92(1)			

density

d	5.82 g cm ⁻³	RT		72A2
-----	-------------------------	----	--	------

melting temperature

T_m	1055 K			74S
-------	--------	--	--	-----

linear thermal expansion coefficient

α_{\perp}	$8.48 \cdot 10^{-6}\text{ K}^{-1}$	$\perp c\text{-axis}$
α_{\parallel}	$-4.16 \cdot 10^{-6}\text{ K}^{-1}$	$\parallel c\text{-axis}$

The temperature dependence of the coefficients of thermal expansion in AgInSe2 is shown in Fig. 6.14.1 [87O].

wavenumbers of IR active phonons

		Symmetry	RT, infrared reflectivity	75K
$\bar{\nu}_{LO}/\bar{\nu}_{TO}$	235/217 cm ⁻¹	Γ_5		
	164/155 cm ⁻¹	Γ_4		
	161/148 cm ⁻¹	Γ_4		
	62/66 cm ⁻¹	Γ_5		
	43/43 cm ⁻¹	Γ_4		

Transport and optical properties

carrier concentration, resistivity, mobility, Seebeck coefficient

n-type samples

n	$8 \cdot 10^{15} \text{ cm}^{-3}$	thin films	96R	
ρ	$50 \dots 150 \text{ } \Omega \text{ cm}$	thin films	96R	
μ_n	$25 \text{ cm}^2 \text{ V}^{-1} \text{ s}^{-1}$	thin film	96R	
	$106 \text{ cm}^2 \text{ V}^{-1} \text{ s}^{-1}$	RT	thin films	87I
	$460 \text{ cm}^2 \text{ V}^{-1} \text{ s}^{-1}$	RT	single crystal	87I

activation energies for electrical conductivity

E_A	0.06 eV	in the solid state	95A
	0.37 eV	in the liquid state	

See also Figs. 6.14.2 and 6.14.3.

refractive indices

		$\lambda \text{ [}\mu\text{m]}$	
n_o	2.8265	1.05	75S1
	2.6761	2.00	
	2.6542	3.00	
	2.6463	4.00	
	2.6416	5.00	
	2.6381	6.00	
	2.6352	7.00	
	2.6318	8.00	
	2.6286	9.00	
	2.6251	10.00	
	2.6210	11.00	
	2.6167	12.00	
n_e	2.6838	2.00	
	2.6592	3.00	
	2.6504	4.00	
	2.6451	5.00	
	2.6414	6.00	
	2.6379	7.00	
	2.6343	8.00	
	2.6310	9.00	
	2.6274	10.00	
	2.6229	11.00	
	2.6183	12.00	

dielectric constant

$\varepsilon(0)$	10.73	$T = 300 \text{ K}, E \parallel c$	infrared reflectivity	78K
	11.94	$E \perp c$		
$\varepsilon(\infty)$	7.16	$T = 300 \text{ K}, E \parallel c$		
	7.20	$E \perp c$		

References to 6.14

- 72A Adams, R., Russo, P., Arnofi, R., Wold, A.: Mater. Res. Bull. 7 (1972) 93.
- 74S Shay, J. L., Tell, B., Shiavone, L. M., Kasper, H. M., Thiel, F.: Phys. Rev. B 9 (1974) 1719.
- 75K Kaufmann, U., Räuber, A., Schneider, J.: J. Phys. C: Solid State Phys. 8 (1975) L381.
- 75S1 Shay, J. L., Wernick, J. H.: Ternary Chalcopyrite Semiconductors: Growth, Electronics, Properties and Applications. Pergamon, 1975.
- 75S2 Suzuki, K., Kambara, T., Gondaira, K., Sato, K., Kondo, K., Teranishi, T.: J. Phys. Soc. Jpn. 39 (1975) 1310.
- 87I Isomura, S., Tomioka, S., Hayashi, H.: Ternary Multinary Compd., Mater. Res. Soc.(1987) 201.
- 87O Orlova, N.S., Bodnar, I.V.: Phys. Status Solidi A 101 (1987) 421.
- 95A Abdelghany, A.: Appl. Phys. A 60 (1995) 77.
- 96I In-Hwan Choi, Yu, P.J.: J. Phys. Chem. Solids 57 (1996) 1695.
- 96R Reddy, R.R., Nazeer Ahammed, Y., Reddy, C.V.K., Buddhudu, S.: Cryst. Res. Technol. 31 (1996) 827.

Figures to 6.14

Fig. 6.0.1

The chalcopyrite lattice

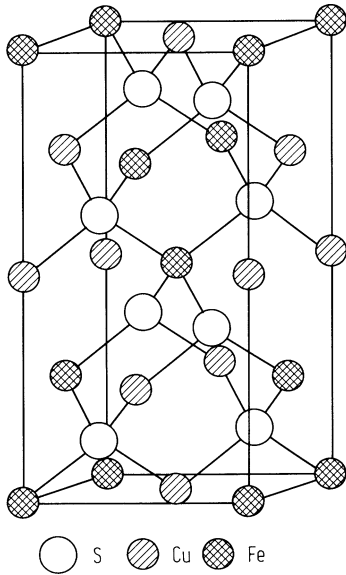


Fig. 6.14.1

AgInSe_2 . Temperature dependence of the coefficients of thermal expansion α_{\perp} ; α_{\parallel} ; α_m ; $\alpha_{c/a}$; $d\delta/dT$ [87O]. $\delta = 2 - c/a$, tetragonal distortion, α_{\perp} : \perp to c -axis, α_{\parallel} : \parallel to c -axis, $\alpha_{c/a} = \alpha_{\parallel} - \alpha$, $\alpha_m = (\alpha_{\parallel} + 2\alpha_{\perp})/3$.

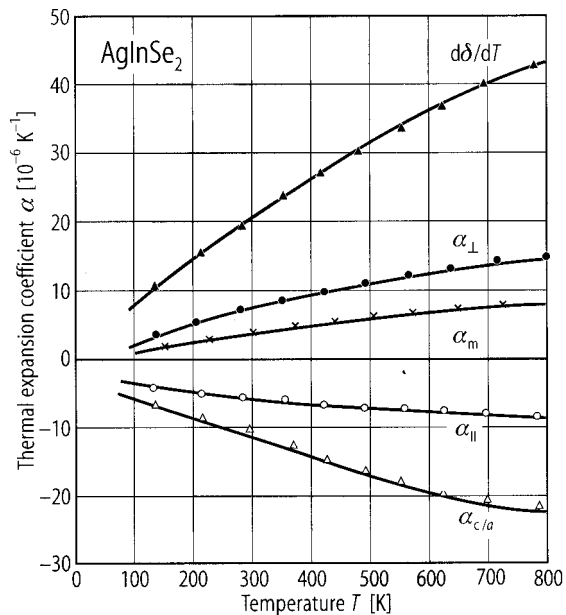


Fig. 6.14.2

AgInSe₂. Temperature dependence of the electrical properties of an n-type vacuum evaporated film [87I].

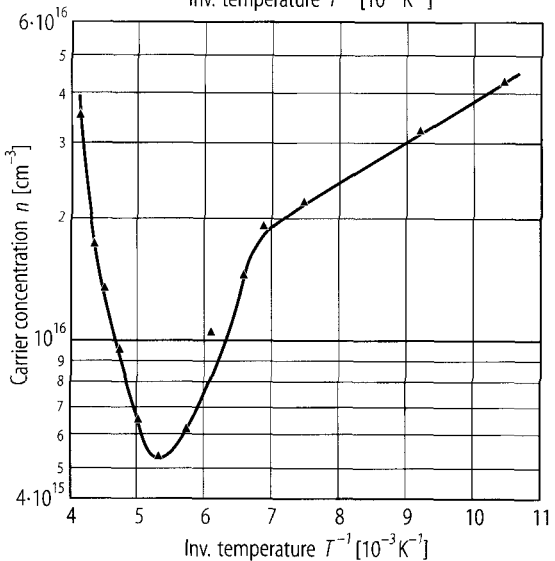
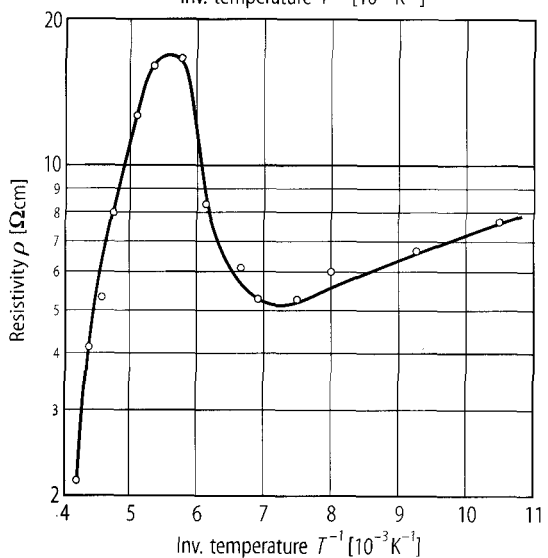
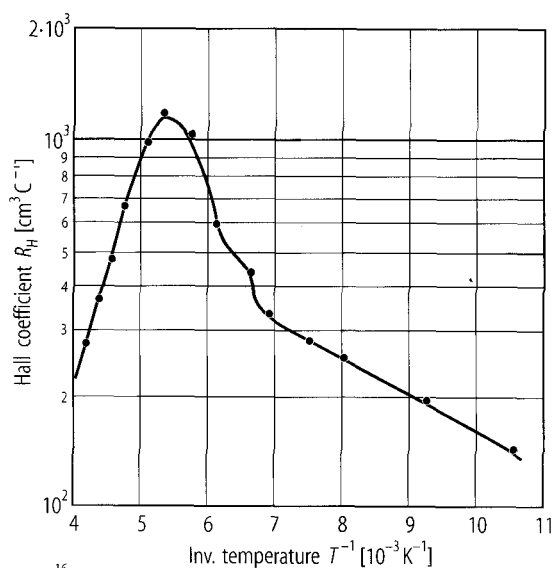
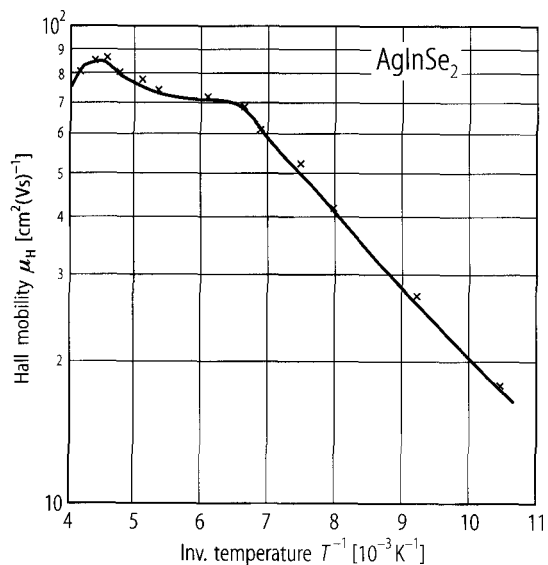
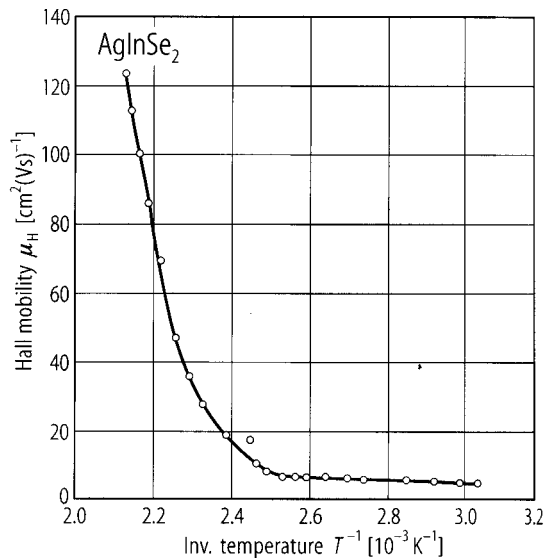


Fig. 6.14.3

AgInSe₂. Temperature dependence of the Hall mobility for a thin film deposited at 300 K [96I].



6.15 Silver indium telluride (AgInTe2)

Crystal structure

AgInTe2 crystallizes in the chalcopyrite lattice (space group D2d12 – I4 2d, Fig. 6.0.1).

Electronic properties

energy gap

Eg,dir 0.964 eV T = 300 K optical absorption, polycrystalline bulk 90Q

The variation of energy gap with temperature for AgInTe2 is given in Fig. 6.15.1 [90Q].

Lattice properties

lattice parameters

a 6.43(3) Å RT 75S
c 12.59(4) Å
c/a 1.96

density

d 6.05 g cm-3 RT 77B

linear thermal expansion coefficient

α⊥ 9.08·10-6 K-1 T = 300 K ⊥ c-axis
α|| - 2.00·10-6 K-1 || c-axis

The temperature dependence of the coefficients of thermal expansion in AgInTe2 is shown in Fig. 6.15.2 [87O].

Debye temperature

ΘD 155.9 K T → 0 K 77B

melting temperature

Tm 960(10) K 76K

wavenumbers of IR active phonons

νLO/νTO - /173 cm-1 Symmetry E ⊥ [111] infrared reflectivity at 300 K, 78K
181/168 cm-1 E || [111] unconventional polarization
181/166 cm-1 E ⊥ [111]
138/136 cm-1 E ⊥ [111]
136/131 cm-1 E || [111]
44/44 cm-1 E || [111]
43/42 cm-1 E ⊥ [111]

Transport and optical properties

electrical conductivity

σ 10-4... 10-5 Ω-1 cm-1 T = 290...331 K 91S

The temperature dependence of dc conductivity in bulk AgInTe2 is shown in Fig. 6.15.3 [93S].

activation energy

Ea 0.327 eV activation energy of conductivity 93S

dielectric constants

$\epsilon(0)$	7.68	$T = 300 \text{ K}, E \parallel [111]$	78K
	8.10	$E \perp [111]$	
$\epsilon(\infty)$	6.38	$T = 300 \text{ K}, E \parallel [111]$	
	6.48	$E \perp [111]$	

References to 6.15

- 75S Suzuki, K., Kambara, T., Gondaira, K., Sato, K., Kondo, K., Teranishi, T.: J. Phys. Soc. Jpn. 39 (1975) 1310.
- 76K Kanellis, G., Kambas, C., Spyridelis, J.: Mater. Res. Bull. 11 (1976) 429.
- 77B Bachmann, K. J., Hsu, F. S. L., Thiel, F. A., Kasper, H. M.: J. Electron. Mater. 6 (1977) 431.
- 78K Kanellis, G., Kampas, K.: Mater. Res. Bull. 13 (1978) 9.
- 87O Orlova, N.S., Bodnar, I.V.: Phys. Status Solidi A 101 (1987) 421.
- 90Q Quintero, M., Tovar, R., Bellabarba, C., Woolley, J.C.: Phys. Status Solidi B 162 (1990) 517.
- 91S Sato, K., Kudo, Y., Kijima, S., Samanta, L.K.: J. Cryst. Growth 115 (1991) 740.
- 93S Shukla, R.: Indian J. Pure Appl. Phys. 31 (1993) 894.

Figures to 6.15

Fig. 6.0.1

The chalcopyrite lattice

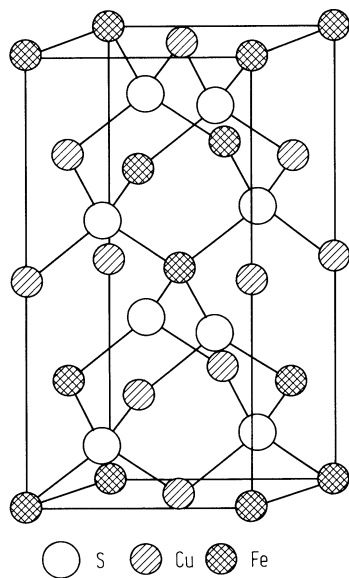


Fig. 6.15.1

AgInTe₂. Variation of energy gap with temperature. Circles: experimental data; continuous curve: fitted to the Manoogian-Leclerc equation [90Q].

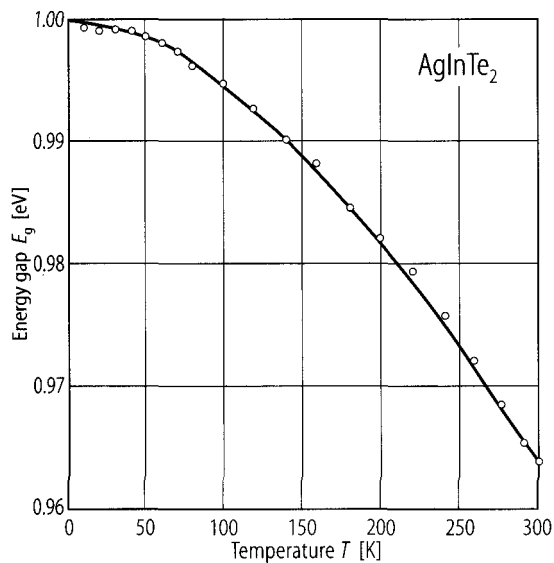


Fig. 6.15.2

AgInTe_2 . Temperature dependence of the coefficients of thermal expansion α_{\perp} ; α_{\parallel} ; α_m ; $\alpha_{c/a}$; $d\delta/dT$ [87O]. $\alpha_{\perp, \parallel}$: \perp, \parallel to the c -axis; $\alpha_m = (\alpha_{\parallel} - 2\alpha_{\perp})/3$; $\alpha_{c/a} = \alpha_{\parallel} - \alpha_{\perp}$; $\delta = 2 - c/a$, tetragonal distortion.

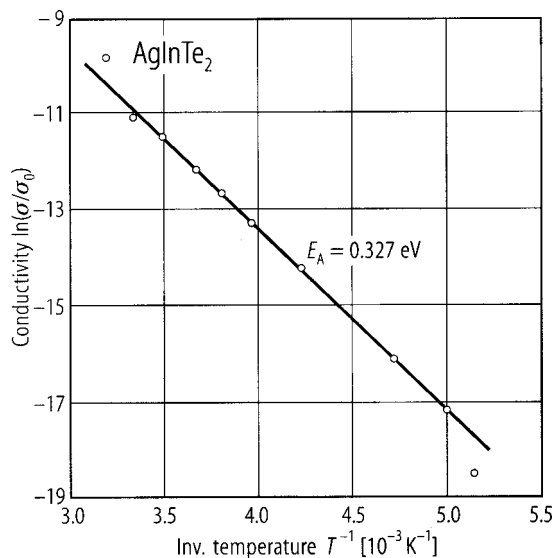
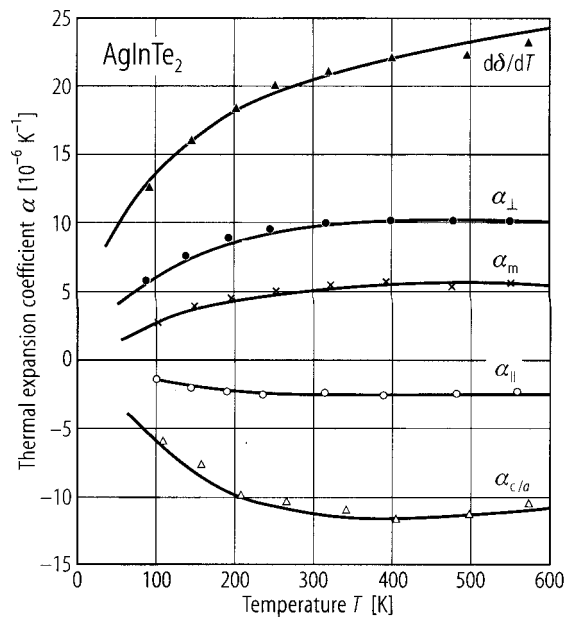


Fig. 6.15.3

AgInTe₂. Temperature dependence of dc conductivity in bulk AgInTe₂ [93S]. $\sigma_0 = 1 \Omega^{-1}\text{cm}^{-1}$.



6.16 Copper thallium sulfide (CuTlS₂)

CuTlS₂ crystallizes in the chalcopyrite lattice (space group $D_{2d}^{12} - I\bar{4}2d$, Fig. 6.0.1).

lattice parameters

a	5.58 Å	RT	75S
c	11.16 Å		
c/a	2.00		

density

d	6.13 g cm ⁻³	RT	79G
-----	-------------------------	----	-----

The energy gap is estimated to be $E_g = 1.39$ eV [83D].

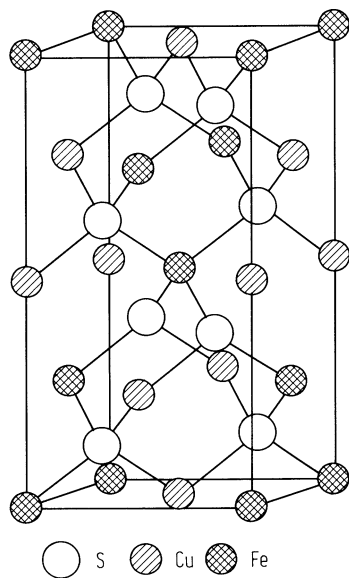
References to 6.16

- 75S Suzuki, K., Kambara, T., Gondaira, K., Sato, K., Kondo, K., Teranishi, T.: J. Phys. Soc. Jpn. 39 (1975) 1310.
- 79G Gardes, B., Brun, G., Raymond, A., Tedenac, J. C.: Mater. Res. Bull. 14 (1979) 943.

Figures to 6.16

Fig. 6.0.1

The chalcopyrite lattice



6.17 Copper thallium selenide (CuTlSe₂)

crystal structure

CuTlSe₂ crystallizes in the chalcopyrite lattice (space group $D_{2d}^{12} - \bar{4}2d$, Fig. 6.0.1).

lattice parameters

a	5.83 Å	RT	75S2
c	11.60 Å		
c/a	1.99 Å		

density

d	7.08 g cm ⁻³	RT	53H
-----	-------------------------	----	-----

melting temperature

T_m	680 K
-------	-------

electrical conductivity, Seebeck coefficient

σ	$6 \cdot 10^3 \Omega^{-1} \text{ cm}^{-1}$	$T = 300 \text{ K}$	no anisotropy	75S1
S	10^{-2} V K^{-1}	$T = 300 \text{ K}$		

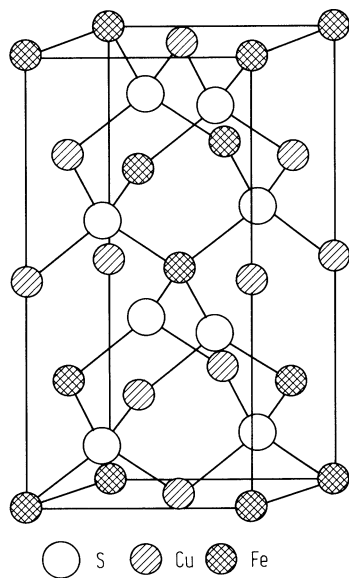
References to 6.17

- 53H Hahn, H., Frank, G., Klingler, W., Meyer, A. D., Störger, G.: Z. Anorg. Allgem. Chem. 271 (1953) 153.
75S1 Shay, J. L., Wernick, J. H.: Ternary Chalcopyrite Semiconductors: Growth, Electronics, Properties and Applications. Pergamon, 1975.
75S2 Suzuki, K., Kambara, T., Gondaira, K., Sato, K., Kondo, K., Teranishi, T.: J. Phys. Soc. Jpn. 39 (1975) 1310.

Figures to 6.17

Fig. 6.0.1

The chalcopyrite lattice



6.18 Copper thallium telluride (CuTlTe₂)

electrical conductivity, Seebeck coefficient, melting temperature

σ	$2.8 \cdot 10^3 \Omega^{-1} \text{ cm}^{-1}$	$T = 300 \text{ K}$	no anisotropy	75S
S	$8 \cdot 10^{-2} \text{ V K}^{-1}$	$T = 300 \text{ K}$		
T_m	650 K			

References to 6.18

- 75S Shay, J. L., Wernick, J. H.: Ternary Chalcopyrite Semiconductors: Growth, Electronics, Properties and Applications. Pergamon, 1975.

6.19 Silver thallium selenide (AgTlSe₂)

electrical conductivity, Seebeck coefficient, melting temperature

σ	$10^{-5} \Omega^{-1} \text{ cm}^{-1}$	$T = 300 \text{ K}$	no anisotropy	75S
S	0.8 V K^{-1}	300 K		
T_m	600 K			

References to 6.19

- 75S1 Shay, J. L., Wernick, J. H.: Ternary Chalcopyrite Semiconductors: Growth, Electronics, Properties and Applications. Pergamon, 1975.

6.20 Silver thallium telluride (AgTlTe₂)

electrical conductivity, Seebeck coefficient, melting temperature

σ	$4.1 \cdot 10^2 \Omega^{-1} \text{ cm}^{-1}$	$T = 300 \text{ K}$	no anisotropy	75S
S	$6 \cdot 10^{-2} \text{ V K}^{-1}$	$T = 300 \text{ K}$		

For transport properties of AgTlSe₂, see also [82A].

T_m	560 K
-------	-------

References to 6.20

- 75S Shay, J. L., Wernick, J. H.: Ternary Chalcopyrite Semiconductors: Growth, Electronics, Properties and Applications. Pergamon, 1975.

6.21 Copper iron sulfide, chalcopyrite (CuFeS2)

Electronic structure

band structure : see Fig. 6.0.9, Brillouin zone: Fig. 6.0.2.

energy gap

E_g	0.6 eV	absorption edge	72A
-------	--------	-----------------	-----

Lattice properties

lattice parameters

a	5.292 Å		72A
c	10.407 Å		

density

d	4.19 g cm ⁻³		74P
-----	-------------------------	--	-----

melting temperature

T_m	1120 K or 1150 K	contradictory reports	75S
-------	------------------	-----------------------	-----

wavenumbers of IR and Raman active phonons

			Symmetry			
			I 4 2d	(F 4 3m)		
$\bar{\nu}_{LO}/\bar{\nu}_{TO}$	385/360 cm ⁻¹	$T = 300$ K	Γ_4	(Γ_{15})	all modes IR and Raman active, except Γ_1	75K
	371/357 cm ⁻¹	$T = 300$ K	Γ_5	(Γ_{15})		
	330/322 cm ⁻¹	$T = 300$ K	Γ_5	(W_4)		
	296 cm ⁻¹	$T = 4.5$ K	Γ_1	(W_1)		
	272/262 cm ⁻¹	$T = 300$ K	Γ_4	(W_2)		
	267/263 cm ⁻¹	$T = 300$ K	Γ_5	(X_5)		
	- /179 cm ⁻¹	$T = 4.5$ K	Γ_5	(W_3)		
	- /105 cm ⁻¹	$T = 4.5$ K	Γ_5	(W_4)		
	- /90 cm ⁻¹	$T = 4.5$ K	Γ_4	(W_2)		
	- /72 cm ⁻¹	$T = 4.5$ K	Γ_5	(X_5)		

Transport properties

Hall mobility

μ_H	7 cm ² V ⁻¹ s ⁻¹	$i \perp c$	74P
---------	---	-------------	-----

carrier concentration, mobility, electrical conductivity

n-type samples

n	10 ¹⁶ ...10 ¹⁷ cm ⁻³	$T = 1.5$ K	from Hall measurements	93K
	10 ²¹ cm ⁻³		single crystal	87K
μ_n	~1 cm ² V ⁻¹ s ⁻¹	$T = 20$ -300 K	from Hall measurements	93K
	35 cm ² V ⁻¹ s ⁻¹		single crystal	87K

p-type sample

σ	100 Ω ⁻¹ cm ⁻¹	$T = 300$ K	(no anisotropy)	75S
μ_p	30 cm ² V ⁻¹ s ⁻¹	$T = 300$ K		

References to 6.21

- 72A Adams, R., Beaulieu, R., Vassiliadis, M., Wold, A.: Mater. Res. Bull. 7 (1972) 87.
- 74P Pitt, G. D., Vyas, M. K. R.: Solid State Commun. 15 (1974) 899.
- 75K Kaufmann, U., Räuber, A., Schneider, J.: J. Phys. C: Solid State Phys. 8 (1975) L381.
- 75S Shay, J. L., Wernick, J. H.: Ternary Chalcopyrite Semiconductors: Growth, Electronics, Properties and Applications. Pergamon, 1975.
- 78K Kanellis, G., Kampas, K.: Mater. Res. Bull. 13 (1978) 9.
- 93K Koscielniak-Mucha, B., Opanowicz, A.: Phys. Status Solidi A 139 (1993) K73.

Figures to 6.21

Fig. 6.0.2

Brillouin zone of the chalcopyrite lattice

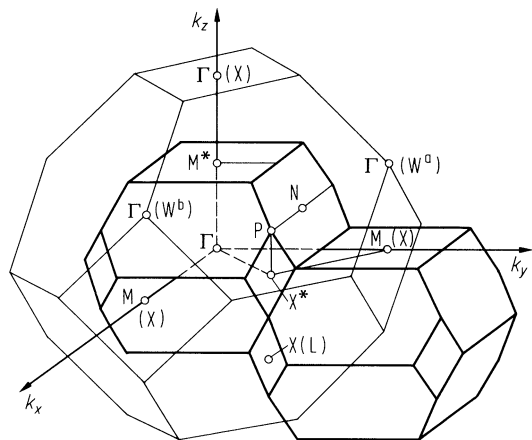
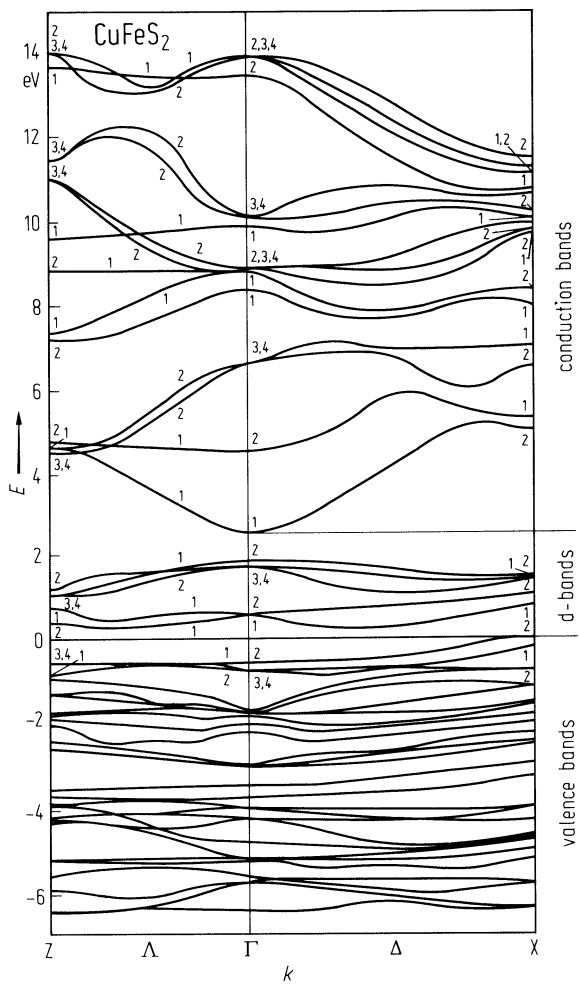


Fig. 6.0.9

Band structure of CuFeS_2 .



6.22 Copper iron selenide (CuFeSe₂)

electrical conductivity, mobility, melting temperature

σ	700 $\Omega^{-1} \text{ cm}^{-1}$	$T = 300 \text{ K}$	p-type	75S
μ_p	20 $\text{cm}^2 \text{ V}^{-1} \text{ s}^{-1}$	$T = 300 \text{ K}$	(no anisotropy)	
T_m	850 K			

References to 6.22

- 75S Shay, J. L., Wernick, J. H.: Ternary Chalcopyrite Semiconductors: Growth, Electronics, Properties and Applications. Pergamon, 1975.

6.23 Copper iron telluride (CuFeTe₂)

electrical conductivity, mobility, melting temperature

σ	$400 \Omega^{-1} \text{ cm}^{-1}$	$T = 300 \text{ K}$	p-type	75S
μ_p	$50 \text{ cm}^2 \text{ V}^{-1} \text{ s}^{-1}$	$T = 300 \text{ K}$	(no anisotropy)	
T_m	1015 K			

References to 6.23

- 75S Shay, J. L., Wernick, J. H.: Ternary Chalcopyrite Semiconductors: Growth, Electronics, Properties and Applications. Pergamon, 1975.

6.24 Silver iron selenide (AgFeSe₂)

electrical conductivity, mobility, melting temperature

σ	1500 $\Omega^{-1} \text{ cm}^{-1}$	$T = 300 \text{ K}$	n-type	75S
μ_n	250 $\text{cm}^2 \text{ V}^{-1} \text{ s}^{-1}$	$T = 300 \text{ K}$	(no anisotropy)	
T_m	1009 K			

References to 6.24

- 75S Shay, J. L., Wernick, J. H.: Ternary Chalcopyrite Semiconductors: Growth, Electronics, Properties and Applications. Pergamon, 1975.

6.25 Silver iron telluride (AgFeTe₂)

electrical conductivity, mobility, melting temperature

σ	$700 \Omega^{-1} \text{ cm}^{-1}$	$T = 300 \text{ K}$	n-type	75S
μ_n	$2000 \text{ cm}^2 \text{ V}^{-1} \text{ s}^{-1}$	$T = 300 \text{ K}$	(no anisotropy)	
T_m	953 K			

References to 6.25

- 75S Shay, J. L., Wernick, J. H.: Ternary Chalcopyrite Semiconductors: Growth, Electronics, Properties and Applications. Pergamon, 1975.

7 II-IV-V₂ compounds

7.0 Crystal structures and electronic structure

7.0.1 Crystal structure

Almost all semiconducting II-IV-V₂ compounds crystallize in the *chalcopyrite lattice* (Fig. 7.0.1).

7.0.2. Electronic structure

Fig. 7.0.2 shows the Brillouin zone of fcc (zincblende) and two Brillouin zones of chalcopyrite. Each point in the chalcopyrite Brillouin zone maps on to 4 different points of the zincblende zone. Thus the Γ point corresponds to Γ , X and two W points.

A useful starting point for a description of the electronic properties of compounds with chalcopyrite structure is the band structure of the zincblende parent compound represented in the smaller Brillouin zone of the ternary (see Fig. 7.0.2). These "folded back" curves can be labelled with the irreducible representations to which they correspond in both the chalcopyrite etc. or zincblende space groups.

The tetragonal symmetry of the chalcopyrite lattice leads to a change in the band structure even at the center of the Brillouin zone Γ .

Non-degenerate band-edges at Γ ($\Gamma_1 \dots \Gamma_4$) are shaped according to $E(\mathbf{k}) = E(\Gamma) + (\hbar^2/2)(k_z^2/m_{\parallel} + (k_x^2 + k_y^2)/m_{\perp})$ with the z-axis parallel to the c-axis. Electrons are thus characterized by two effective masses: m_{\parallel} and m_{\perp} . From these two other effective masses are often defined: a density of states effective mass $m_{\text{ds}}^3 = m_{\perp}^2 m_{\parallel}$ and a conductivity effective mass $(1/m_c) = (1/3)(1/m_{\parallel} + 2/m_{\perp})$.

The Γ_5 -band is split at $k \neq 0$ into two bands:

$$E(\mathbf{k}) = E(\Gamma) + \hbar^2 k_z^2 / 2m(\Gamma) + (\hbar^2 / 2m)(a \pm (b^2 + c^2 \cos(4\varphi))^{1/2})(k_x^2 + k_y^2)$$

where φ is the angle between k_{\perp} and k_x in the $k_x k_y$ plane, with k_{\perp} the direction of \mathbf{k} perpendicular to the z-axis. Finally the Γ_6 - and Γ_7 -bands contain terms linear in k .

This simple picture is somewhat complicated by the effects of spin-orbit coupling which splits the Γ_5 state. This splitting is given by the formula: $E_{1,2} = -1/2(\Delta_{\text{so}} + \Delta_{\text{cf}}) \pm 1/2[(\Delta_{\text{so}} + \Delta_{\text{cf}})^2 - 8/3\Delta_{\text{so}}\Delta_{\text{cf}}]^{1/2}$, where Δ_{so} is the spin-orbit splitting in a cubic crystal field and Δ_{cf} is the crystal field splitting of the valence bands in the absence of spin-orbit coupling. The two solutions E_1 and E_2 give the separation of the two Γ_7 states from the Γ_6 . In chalcopyrite it is found that the crystal field splitting is negative, that is Γ_4 lies above Γ_5 and that this splitting is due almost entirely to the tetragonal compression. It compares very well with that expected from the corresponding zincblende compound under uniaxial pressure.

Fig. 7.0.3 ... 7.0.12 show the band structures of the most important semiconductors dealt with in this chapter.

Figures to 7.0

Fig. 7.0.1

The chalcopyrite lattice

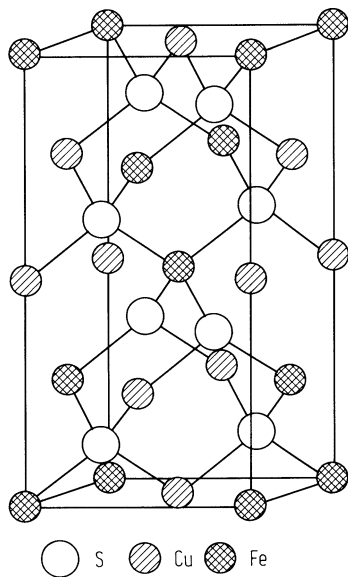


Fig. 7.0.2

Brillouin zone of the chalcopyrite lattice

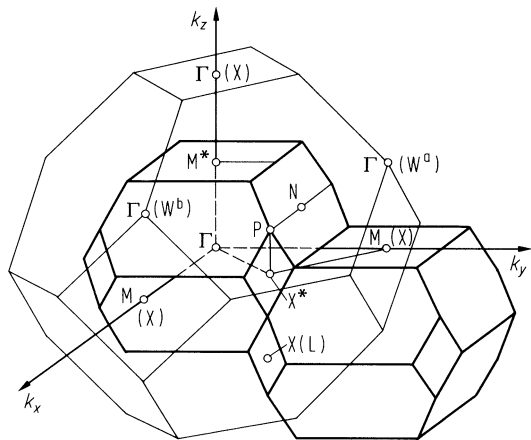


Fig. 7.0.3

Band structure of MgSiP_2 .

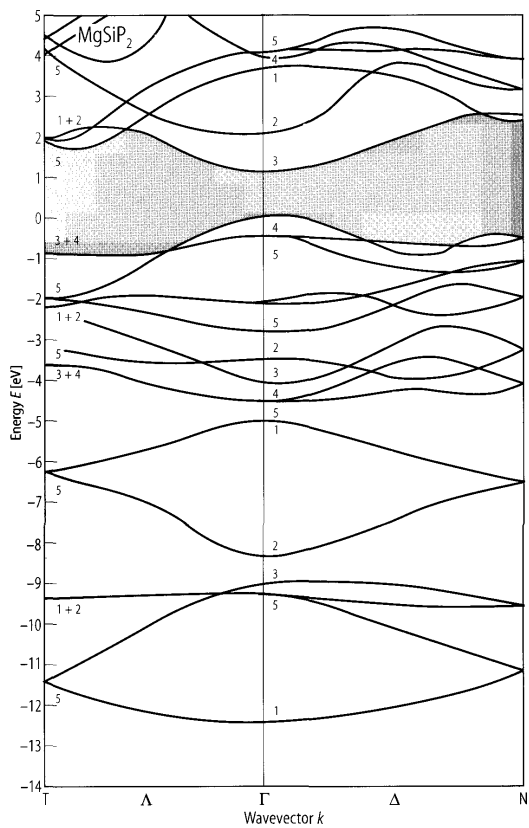


Fig. 7.0.4

Band structure of ZnSiP_2 .

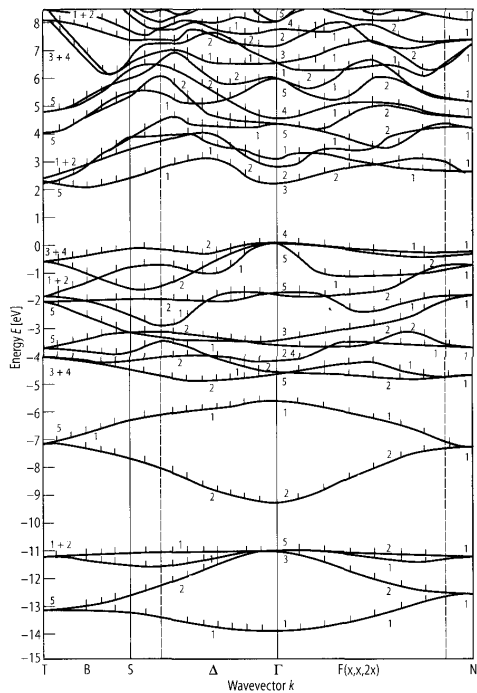
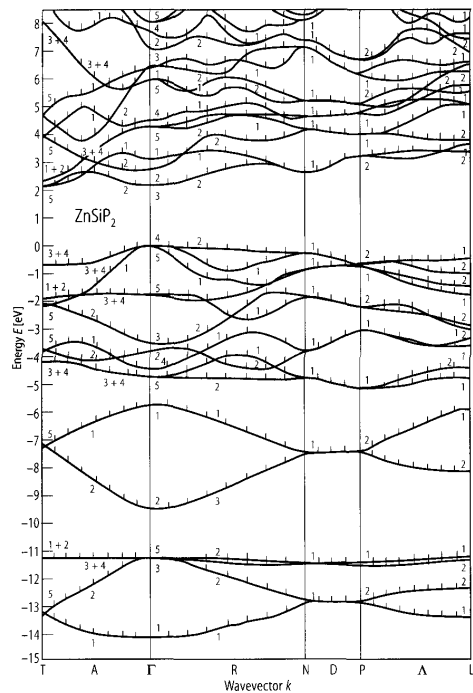


Fig. 7.0.5

Band structure of ZnSiAs_2 .

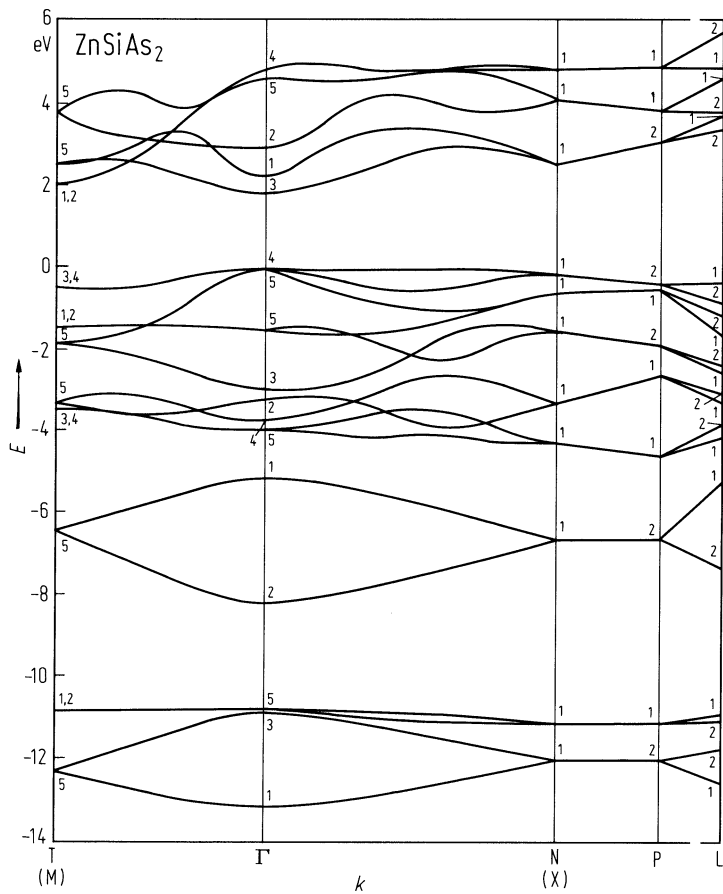


Fig. 7.0.6

Band structure of ZnGeP_2 .

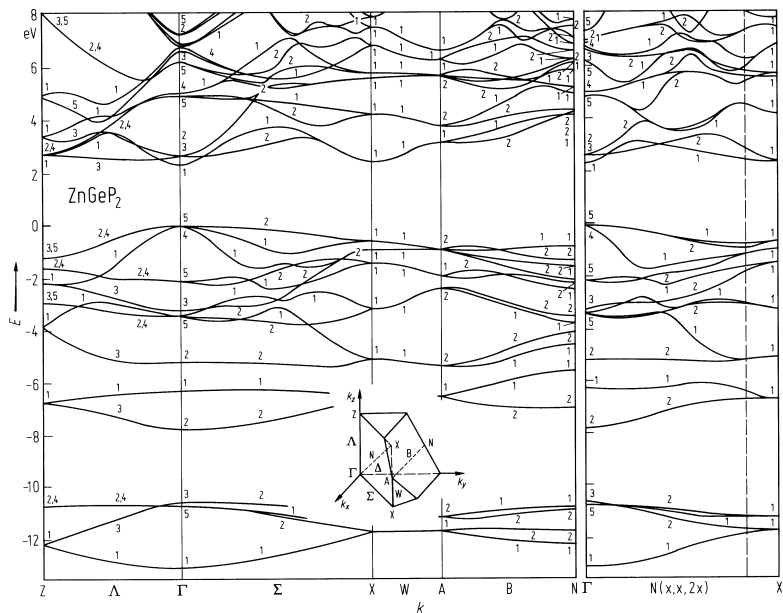


Fig. 7.0.7

Band structure of ZnSnSb_2 .

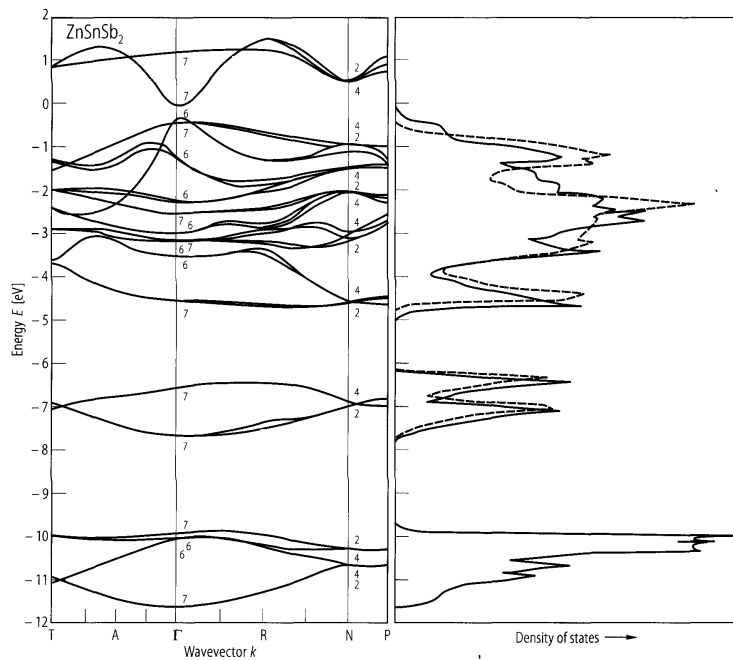


Fig. 7.0.8

Band structure of CdSiP_2 .

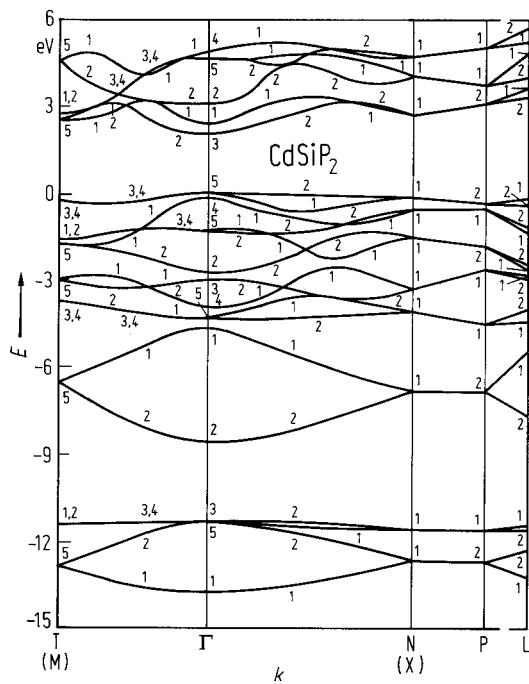


Fig. 7.0.9

Band structure of CdSiAs_2 .

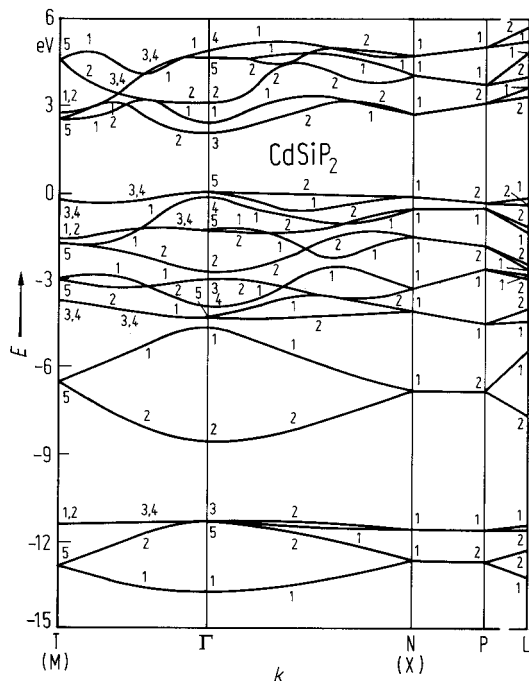


Fig. 7.0.10

Band structure of CdGeAs_2 .

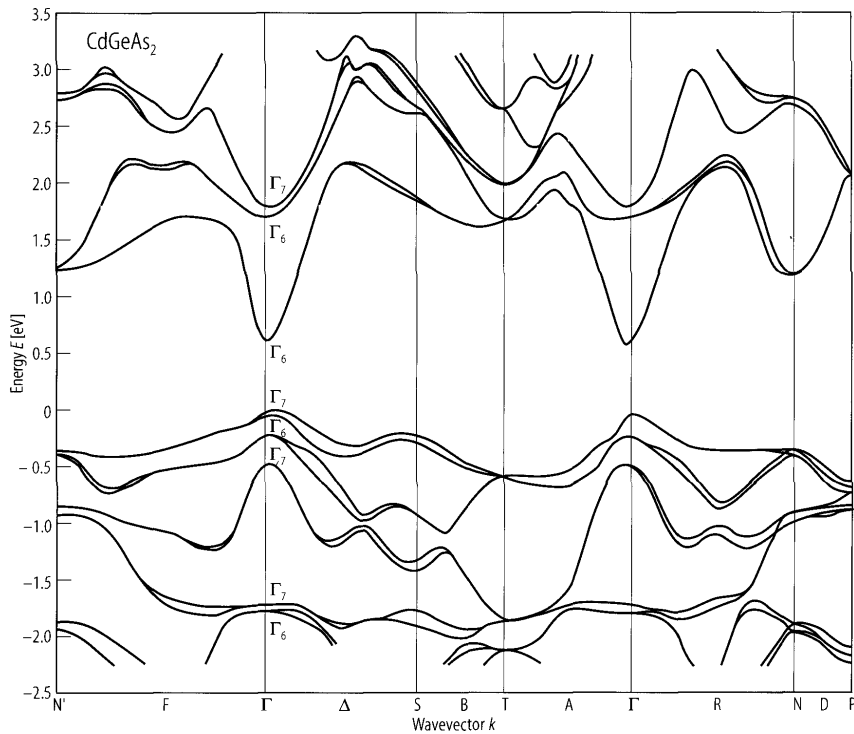


Fig. 7.0.11

Band structure of CdSnP_2 .

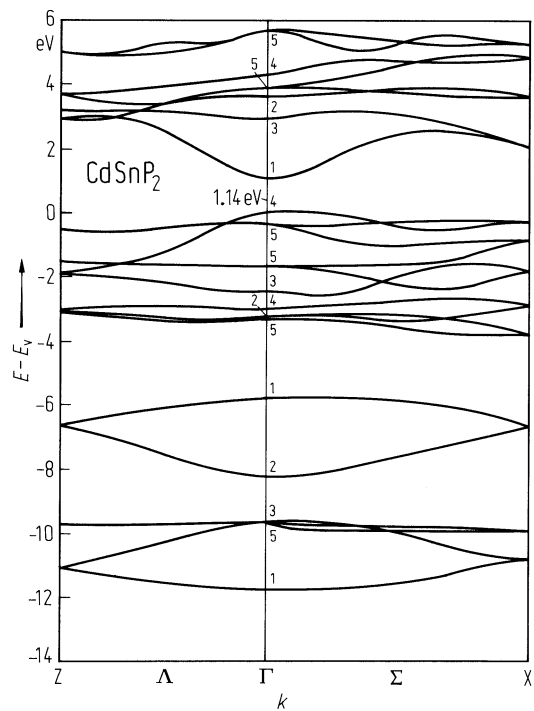
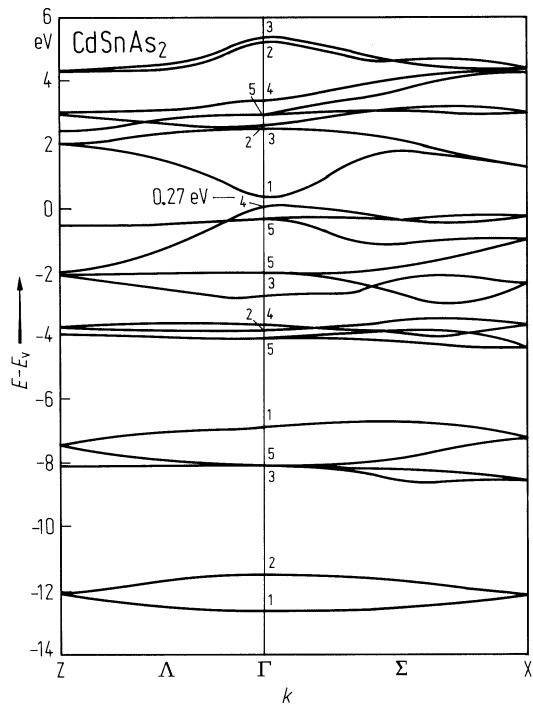


Fig. 7.0.12

Band structure of CdSnAs_2 .



7.1 Magnesium silicon phosphide (MgSiP₂)

Crystal structure

MgSiP₂ crystallizes in the chalcopyrite lattice (space group D_{2d}¹² – I $\bar{4}$ 2d, Fig. 7.0.1).

Electronic properties

band structure : Fig. 7.0.3, Brillouin zone: Fig. 7.0.2.

The band structure of MgSiP₂ was calculated by the use of the ab initio density-functional method [85M].

energy gaps

$E_{g,pseu}$	2.03 eV	$E \perp c$, RT	photoconductivity	78A
$E_{g,ind}$	2.26 eV	$E \perp c$	maybe pseudodirect	
	2.64 eV	$E \perp c$		
$E_{g,dir}$	2.82 eV	$E \parallel (\perp) c$	maybe pseudodirect	
	2.88 eV	$E \perp c$		
dE_g/dT	$-4.5 \cdot 10^{-4}$ eV K ⁻¹	$T = 77 \dots 300$ K	main feature of spectrum	

splitting energies

Δ_{cf}	- 0.08 eV	$T = 300$ K	experiment	78A
Δ_{so}	0.16 eV	$T = 300$ K		

Lattice and transport properties

lattice parameters

a	5.72(2) Å	RT		75S
c	10.12(25) Å			
c/a	1.766(3)Å			

electrical resistivity

ρ	$10^3 \dots 10^4$ Ω cm	$T = 300$ K	n-type sample (no anisotropy reported)	75T, 78A
	$10 \dots 10^2$ Ω cm	$T = 300$ K	In doped sample	78A

References to 7.1

75S Shay, T. L., Wernick, T. H.: "Ternary Chalcopyrite Semiconductors" Growth, Electronics, Properties and Applications. Pergamon, 1975.

75T Trykozko, R. T.: Mater. Res. Bull. 10 (1975) 489.

78A Averkieva, G. K., Mamedov, A., Prochukhan, V. D., Rud', Yu. V.: Fiz. Tekh. Poluprovodn. 12 (1987) 1732; Sov. Phys. Semicond. (English Transl.) 12 (1978) 1025.

85M Martins, J.L., Zunger, A.: Phys. Rev. B 32 (1985) 2689.

Figures to 7.1

Fig. 7.0.1

The chalcopyrite lattice

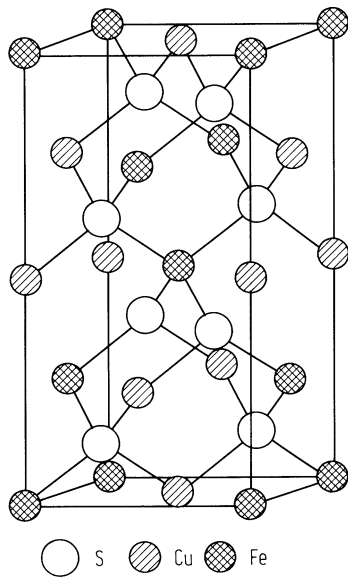


Fig. 7.0.2

Brillouin zone of the chalcopyrite lattice

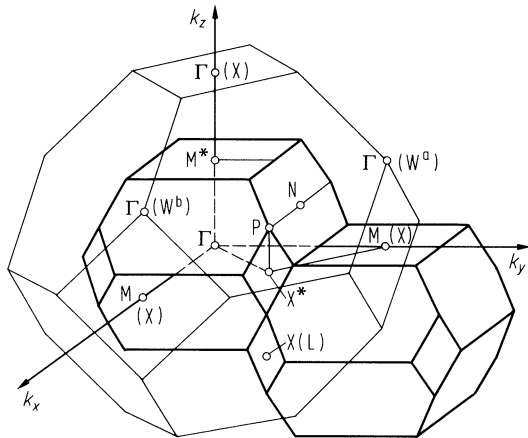
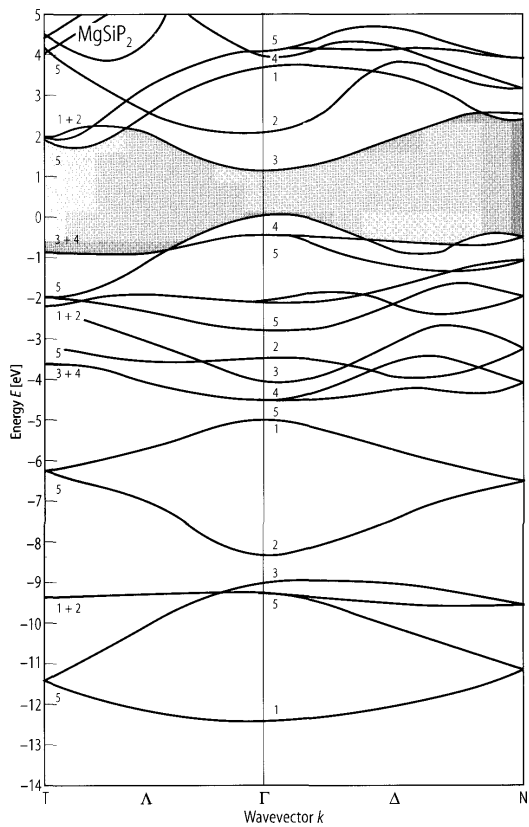


Fig. 7.0.3

Band structure of MgSiP_2 .



7.2 Zinc silicon phosphide (ZnSiP2)

Crystal structure

ZnSiP2 crystallizes in the chalcopyrite lattice (space group D2d12 – I4 2d, Fig. 5.0.1).

Electronic properties

band structure : Fig. 7.0.4, Brillouin zone: Fig. 7.0.2.

The energy band structure of ZnSiP2 calculated by the pseudopotential method [85Z].

energy gap

Eg,ind	2.00 eV	RT	from optical transmission	87H
Eg,dir	3.03 eV	T = 80 K; Γ4v(Γ15v) – Γ1c(Γ1c)	thermoreflection	75R
	3.16 eV	T = 80 K; Γ5v(Γ15v) – Γ1c(Γ1c)		
	2.96 eV	T = 300 K; Γ4v(Γ15v) – Γ1c(Γ1c)	electroreflectance	75S
	3.06 eV	T = 300 K; Γ5v(Γ15v) – Γ1c(Γ1c)		
dEg/dT	– 2.8(1)·10–4 eV K–1	T = 80...300 K	absorption	75H, 75S

splitting energies (at Γ)

Δcf	– 0.12 eV	T = 4.2 K	from optical absorption	86M
Δso	0.05 eV	T = 4.2 K		

exciton binding energy

Eb	0.022 eV	T = 124 K	absorption (E ⊥ c)	75H
----	----------	-----------	--------------------	-----

effective masses

mp	0.4(1) m0	T = 300 K	Hall effect	76P
mn	0.11(2) m0			

Lattice properties

lattice parameters

a	5.400(1) Å	RT		75S
c	10.438(3) Å			
c/a	1.933(1)			

density

d	3.35 g cm–3	RT		69B
---	-------------	----	--	-----

coefficients of thermal expansion

α	7.8·10–6 K–1 3.5·10–6 K–1	T = 300...1400 K	a axis c axis	79K, 75M
β	19.2·10–6 K–1	T = 300...1400 K	volume	

Debye temperature

Θ_D	445.2(23) K	$T \rightarrow 0$ K	from heat capacity	81B
------------	-------------	---------------------	--------------------	-----

melting temperature

T_m	1520...1640 K			75S
-------	---------------	--	--	-----

wavenumbers of Raman and infrared active phonons

		Symmetry			
		$\bar{1} \bar{4} 2d$	$(F \bar{4} 3m)$		
$\bar{\nu}_{LO}/\bar{\nu}_{TO}$	518/494 cm^{-1}	Γ_4	(Γ_{15})	RT, Raman and infrared spectra;	77H,
	518/494 cm^{-1}	Γ_5	(Γ_{15})	Γ_4, Γ_5 IR-active,	79G,
	466 cm^{-1}	Γ_3	(W_2)	all Raman active	75P
	464/461 cm^{-1}	Γ_5	(W_4)		
	359/343 cm^{-1}	Γ_4	(W_2)		
	337 cm^{-1}	Γ_1	(W_1)		
	335 cm^{-1}	Γ_3	(X_3)		
	327/321 cm^{-1}	Γ_5	(X_5)		
	264/246 cm^{-1}	Γ_5	(W_3)		
	187/185 cm^{-1}	Γ_5	(W_4)		
	145/145 cm^{-1}	Γ_4	(W_2)		
	102/102 cm^{-1}	Γ_5	(X_5)		

Transport properties

carrier concentration, electron mobility, activation energy, electrical resistivity

n-type samples				
n	10^{17} cm^{-3}	$T = 300$ K	conductivity	75S,
μ_n	$70...100 \text{ cm}^2 \text{ V}^{-1} \text{ s}^{-1}$	$T = 300$ K	Halleffect; see also Figs. 7.2.1, 7.2.2 for temperature dependence of σ, μ_n, R_H	65G, 76G
μ_{imp}	$0.02...0.35 \text{ cm}^2 \text{ V}^{-1} \text{ s}^{-1}$	$T = 300$ K	in impurity band	76S
E_A	$0.015...0.024 \text{ eV}$	$T = 77...1000$ K	activation energy of hopping	
ρ	$2.7 \cdot 10^5 ...$ $1.8 \cdot 10^6 \Omega \text{ cm}$	RT	single crystal	87H
p-type samples				
p	$6 \cdot 10^{13} ... 3 \cdot 10^{17} \text{ cm}^{-3}$	$T = 300$ K		78G
μ_p	$4...11 \text{ cm}^2 \text{ V}^{-1} \text{ s}^{-1}$	$T = 300$ K		

activation energies

E_A	0.62 eV	$T < 773$ K	activation energy of conductivity	92E
	0.26...0.33 eV		single crystal	87H

dielectric constants

$\epsilon(0)$	11.7(6)	$T = 300$ K; $E \perp c$	infrared reflectivity	75P
	11.15(10)	$E \parallel c$		
$\epsilon(\infty)$	9.26	$T = 300$ K; $E \perp c$	infrared reflectivity	
	9.68	$E \parallel c$		

refractive index

n	3.31	$T = 300$ K;		75B
		$\lambda = 600 \text{ nm}$		
	3.06	$\lambda = 900 \text{ nm}$		

References to 7.2

- 65G Goryunova, N. A., Kesamanly, F. P., Nasledov, D. N., Negreskul, V. V., Rud'Yu, V., Slobodchikov, S. V.: Fiz. Tverd. Tela 7 (1965) 1312; Sov. Phys. Solid State (English Transl.) 7 (1965) 1060.
- 69B Berger, L. T., Prochokhan, V. D.: "Ternary Diamond Like Semiconductors", New York, London: Consultants Bureau, 1969.
- 75B Bondriot, H., Foeller, B., Schneider, H. A.: Phys. Status Solidi (a) 30 (1975) K121.
- 75H Humphreys, R. G., Pamplin, B. R.: J. Phys. (Paris) 36 (1975) C3155.
- 75M Miller, A., Humphreys, R. G., Chapman, B.: J. Phys. (Paris) 36 (1975) C331.
- 75P Poplavnoi, A. S., Tyuterev, V. G.: Fiz. Tverd. Tela 17 (1975) 1055; Sov. Phys. Solid State (English Transl.) 17 (1975) 672.
- 75R Raudonis, A. V., Shileika, A. Yu.: Fiz. Tekh. Poluprovodn. 9 (1975) 1539; Sov. Phys. Semicond. (English Transl.) 9 (1975) 1014.
- 75S Shay, T. L., Wernick, T. H.: "Ternary Chalcopyrite Semiconductors" Growth, Electronics, Properties and Applications. Pergamon, 1975.
- 76G Grishchenko, G. A., Ljubchenko, A. V., Tychina, I. I., Ukr. Fiz. Zh. 21 (1976) 303.
- 76I Pasemann, L., Cordts, W., Heinrich, A., Monecke, J.: Phys. Status Solidi (b) 77 (1976) 527.
- 77H Humphreys, R. G.: Inst. Phys. Conf. Ser. 35 (1977) 105.
- 78G Grishchenko, G. A., Ljubchenko, A. V., Tychina, I. I.: Ukr. Fiz. Zh. 23 (1978) 958.
- 78Z Ziegler, F., Siegel, W., Kühnel, G.: Phys. Status Solidi (a) 49 (1978) K205.
- 79G Gorban, I. S., Gorynya, V. A., Lugovoi, V. I., Krasnolob, N. P., Salivon, G. I., Tychina, I. I.: Phys. Status Solidi (b) 93 (1979) 531.
- 79K Kozkina, I. I.: Vestn. Leningr. Univ. Fiz. Khim. 13 (1979) 83.
- 81B Bohmhammel, K., Deus, P., Schneider, H. A.: Phys. Status Solidi (a) 65 (1981) 563.
- 85Z Zakharov, N.A., Chaldyshev, V.A.: Fiz. Tekh. Poluprovodn. 19 (1985) 842; Sov. Phys. Semicond. (Engl. Transl.) 19 (1985) 518.
- 86M Madelon, R., Hurel, J., Paumier, E.: Phys. Status Solidi B 136 (1986) 679.
- 87H He-Sheng Shen, Guang-Qing Yao, Kershaw, R., Dwight, K., Wold, A.: J. Solid State Chem. 71 (1987) 176.
- 92E Endo, T., Sato, Y., Takizawa, H., Shimada, M.: J. Mater. Sci. Lett. 11 (1992) 567.

Figures to 7.2

Fig. 7.0.1

The chalcopyrite lattice

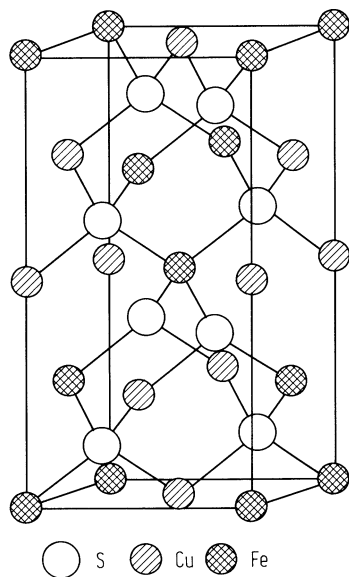


Fig. 7.0.2

Brillouin zone of the chalcopyrite lattice

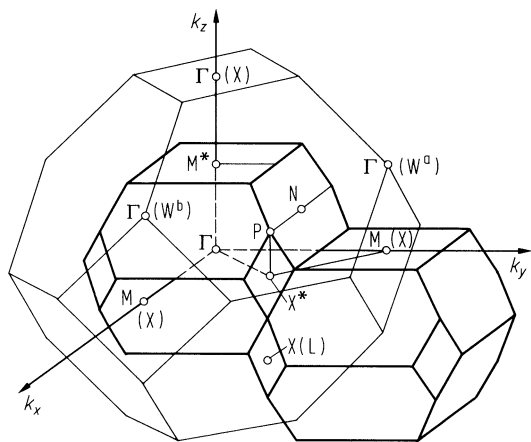


Fig. 7.0.4

Band structure of ZnSiP_2 .

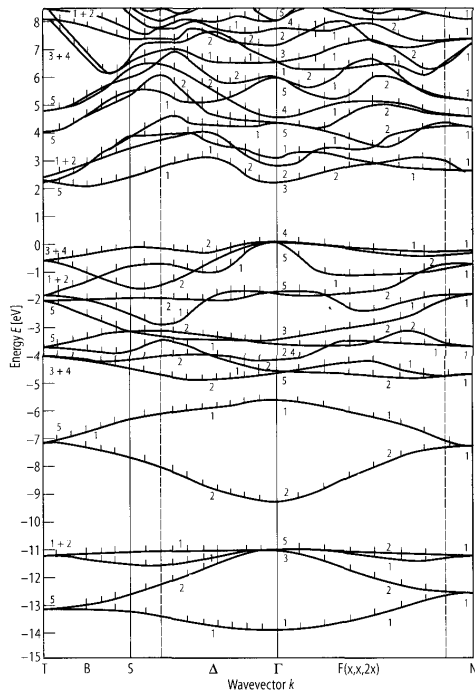
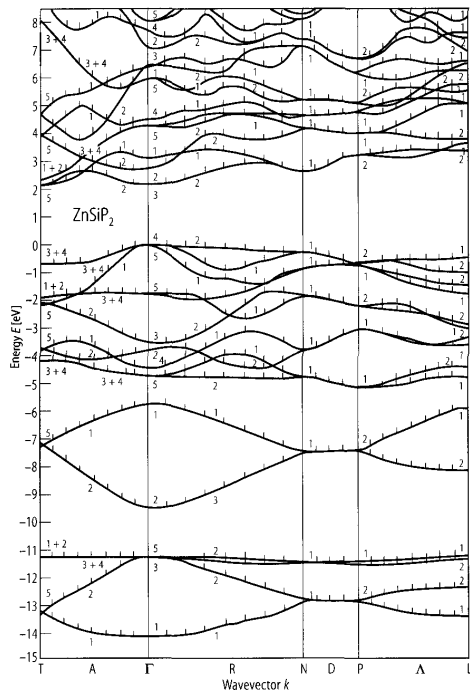


Fig. 7.2.1

ZnSiP₂. Conductivity and Hall coefficient of an n-type sample vs. (reciprocal) temperature [75S].

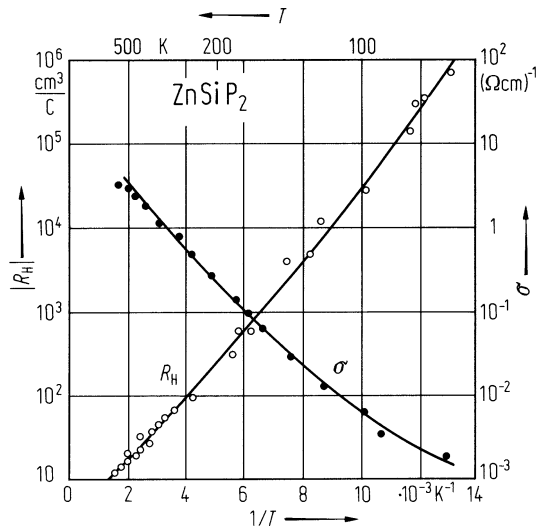
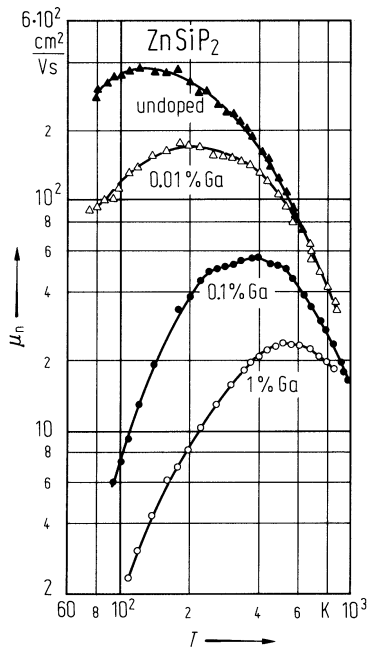


Fig. 7.2.2

ZnSiP₂. Electron mobility vs. temperature for an undoped and three Ga doped samples (n-type) [78Z].



7.3 Zinc silicon arsenide(ZnSiAs2)

Crystal structure

ZnSiAs2 crystallizes in the chalcopyrite lattice (space group D2d¹² – I 4 2d, Fig. 7.0.1).

Electronic properties

band structure : Fig. 7.0.5, Brillouin zone: Fig. 7.0.2.

energy gap

thin film data

$E_g(0)$	1.93 eV		from optical transmission	85N
dE_g/dT	$-5.5\cdot10^{-4}$ eV K ⁻¹	$T=223\dots323$ K	from optical transmission	85N
$E_{g,pseu}$	1.74 eV	$E\perp c, T=300$ K	photoconductivity	76R
	1.84 eV	$E\perp(\parallel) c$		
	1.93 eV	$E\parallel(\perp) c$		
	2.03 eV	$E\perp c$		
	2.09 eV	$E\perp c$		

splitting energies

Δ_{cf}	-0.13 eV	$T=300$ K	electroreflectance	71S,
Δ_{so}	0.286(6) eV			75T

effective masses

$m_{n\parallel}(\Gamma)$	0.92 m_0		from band gap calculations	84Z
$m_{n\perp}(\Gamma)$	0.28 m_0			
$m_{p\parallel}(\Gamma)$	0.13 m_0			
$m_{p\perp}(\Gamma)$	0.54 m_0			

Lattice properties

lattice parameters

a	5.606(5) Å		RT	75S
c	10.886(5) Å			
c/a	1.940(3)			

density

d	4.69 g cm ⁻³		RT	69B
-----	-------------------------	--	----	-----

thermal expansion coefficient

α_a	$7.6(3)\cdot10^{-6}$ K ⁻¹	$T=300$ K	a axis	88D
α_c	$3.3(2)\cdot10^{-6}$ K ⁻¹	$T=300$ K	c axis	

The temperature dependence of the principal linear thermal expansion coefficients is given in Fig. 7.3.1 [88D].

Debye temperature

Θ_D	346.6(12) K	$T\rightarrow 0$ K	from heat capacity	81B
------------	-------------	--------------------	--------------------	-----

melting temperature

T_m	1370 K			75S
-------	--------	--	--	-----

wavenumbers of Raman active phonons

		Symmetry	
		$\bar{1}\bar{4}2d$	
$\bar{\nu}_{LO}/\bar{\nu}_{TO}$	417/405 cm^{-1}	Γ_5	75M
	401/388 cm^{-1}	Γ_4	
	269/– cm^{-1}	Γ_4	
	262 cm^{-1}	Γ_3	
	236/– cm^{-1}	Γ_5	
	210/– cm^{-1}	Γ_5	
	203 cm^{-1}	Γ_1	
	162 cm^{-1}	Γ_1	
	133/– cm^{-1}	Γ_5	
	108 cm^{-1}	Γ_3	
	77/– cm^{-1}	Γ_5	

Transport properties

carrier concentration, electrical resistivity, hole mobility

p-type samples				
p	1.11·10 ¹⁴ ...	RT	single crystals, as grown	87C
	5.26·10 ¹⁶ cm^{-3}			
ρ	0.02...800 $\Omega\text{ cm}$		epitaxial layers by MOVPE	91A1
μ_p	1827 $\text{cm}^2\text{ V}^{-1}\text{ s}^{-1}$	RT	μ_p : drift mobility; single crystals, as grown	87C

see also Fig. 7.3.2

n-type(non-stoichiometric) sample (RT values)

n	10 ⁹ cm^{-3}			76R
μ_n	40 $\text{cm}^2\text{ V}^{-1}\text{ s}^{-1}$			

thermal conductivity

κ	0.14 $\text{W cm}^{-1}\text{ K}^{-1}$	T = 300 K		75S
----------	---------------------------------------	-----------	--	-----

Optical properties

energy dependence of reflection coefficient R , the dielectric constant ϵ_2 , and $-\text{Im } \epsilon^{-1}$: Fig. 7.3.3.

refractive index

Coefficients in the formula: $n^2 = A + B/(1 - C/\lambda^2) + D/(1 - E/\lambda^2)$ ($T = 300\text{ K}$) [76B1]:

	n_o	n_e
A	4.6066	4.9091
B	5.6912	5.5565
C	0.1437·10 ⁻¹² m^2	0.1578·10 ⁻¹² m^2
D	1.316	1.287
E	7·10 ⁻¹⁰ m^2	7·10 ⁻¹⁰ m^2

References to 7.3

- 69B Berger, L. T., Prochokhan, V. D.: "Ternary Diamond Like Semiconductors", New York, London: Consultants Bureau, 1969.
- 71S Shay, T. L., Buehler, F., Wernick, T. H.: Phys. Rev. B3 (1971) 2004.
- 75M Markov, Yu. F., Gromova, T. M., Rud', Yu. B., Tashtanova, M.: Fiz. Tverd. Tela 17 (1975) 1226; Sov. Phys. Solid State (English Transl.) 17 (1975) 796.
- 75S Shay, T. L., Wernick, T. H.: "Ternary Chalcopyrite Semiconductors" Growth, Electronics, Properties and Applications. Pergamon, 1975.
- 75T Trykozko, R. T.: Mater. Res. Bull. 10 (1975) 489.
- 76B Bhar, G. C.: Appl. Opt. 15 (1976) 305.
- 76R Rud', Yu. V., Ovezov, K.: Fiz. Tekh. Poluprovodn. 10 (1976) 951; Sov. Phys. Semicond. (English Transl.) 10 (1976) 561.
- 81B Bohmhammel, K., Deus, P., Schneider, H. A.: Phys. Status Solidi (a) 65 (1981) 563.
- 84Z Zakharov, N.A., Chaldyshev, V.A.: Fiz. Tekh. Poluprovodn. 18 (1984) 217; Sov. Phys. – Semicond. (Engl. Transl.) 18 (1984) 135.
- 85N Naseem, H.A., Burton, L.C., Andrews, J.E.: Thin Solid Films 129 (1985) 49.
- 87B Boudriot, H., Deus, K., Grundler, R., Schneider, H.A., Stockert, T.: Phys. Status Solidi B 143 (1987) K125.
- 87C Chippaux, D., Mercey, B., Deschanvres, A.: J. Phys. Chem. Solids 48 (1987) 447.
- 88D Deus, P., Voland, U., Neumann, H.: Phys. Status Solidi A 108 (1988) 225.
- 91A Achargui, N., Benachenhou, A., Foucaran, A., Bougnot, G., Coulon, P., Laurenti, J.P., Camassel, J.: J. Cryst. Growth 107 (1991) 410.

Figures to 7.3

Fig. 7.0.1

The chalcopyrite lattice

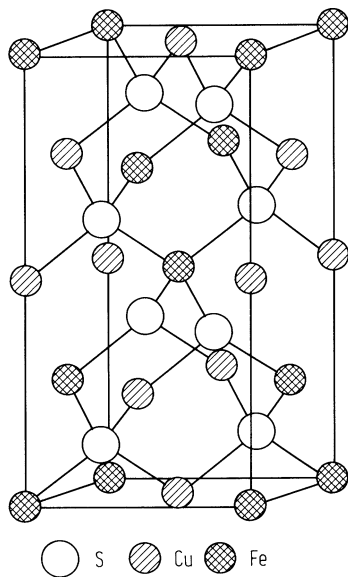


Fig. 7.0.2

Brillouin zone of the chalcopyrite lattice

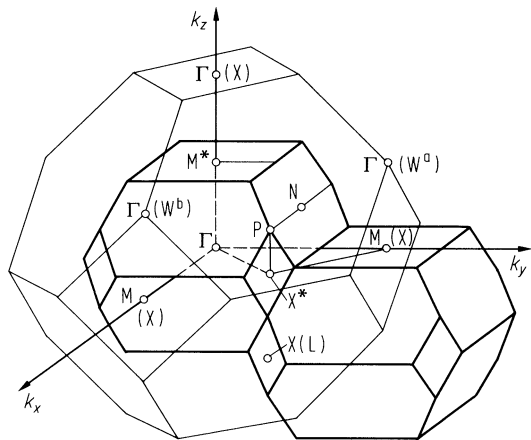


Fig. 7.0.5

Band structure of ZnSiAs₂.

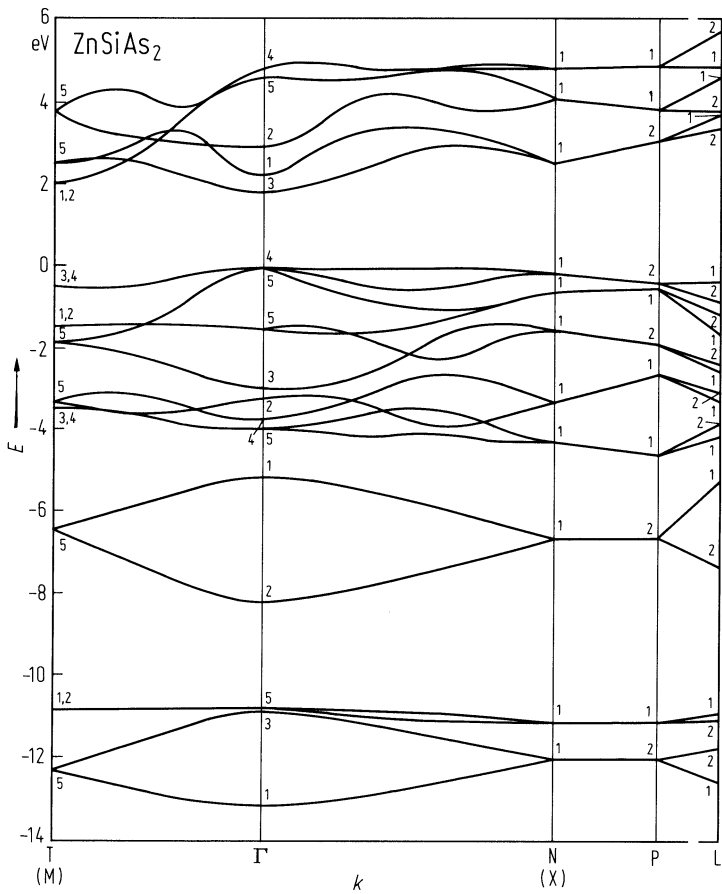


Fig. 7.3.1

ZnSiAs_2 . Temperature dependence of the principal linear thermal expansion coefficients α_a and α_c [88D].

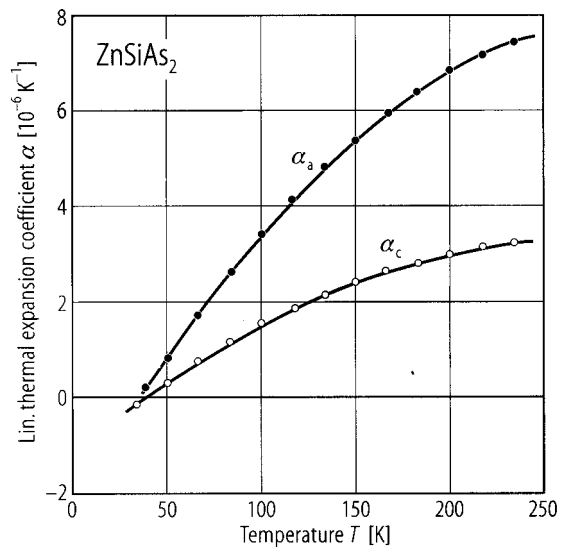


Fig. 7.3.2

ZnSiAs_2 . Resistivity, Hall coefficient and hole mobility vs. (reciprocal) temperature for a p-type sample [75S].

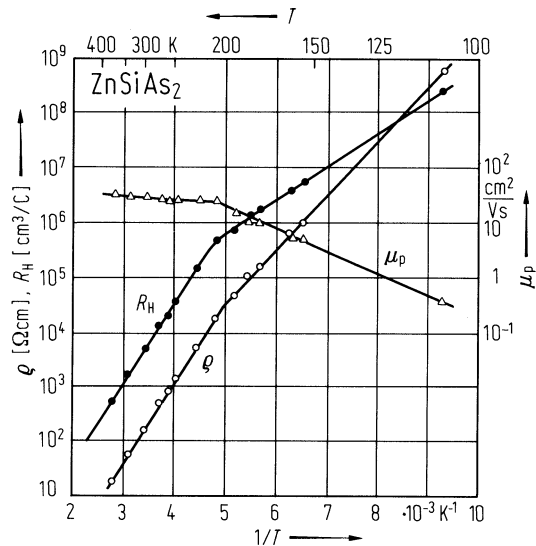
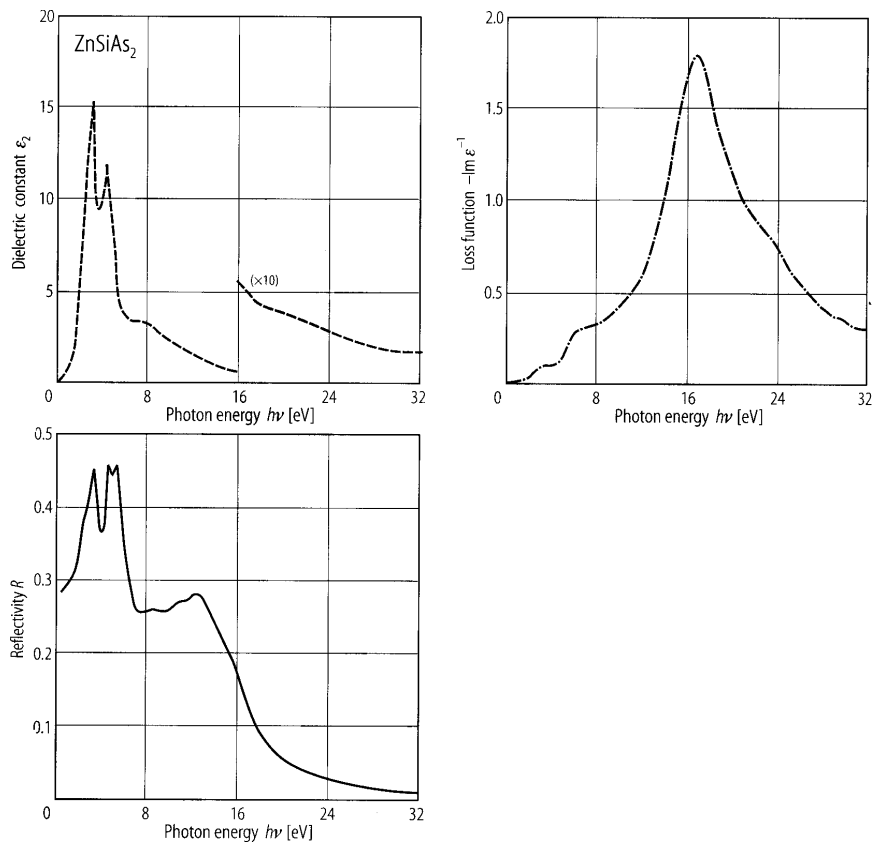


Fig. 7.3.3

ZnSiAs_2 . The energy dependence of reflection coefficient R , the dielectric constant ϵ_2 , and $-\text{Im } \epsilon^{-1}$ from transmission electron energy loss measurements [87B].



7.4 Zinc germanium nitride (ZnGeN₂)

Crystal structure

ZnGeN₂ has a wurtzite-like monoclinic structure [70M]

Electronic properties

energy gap

E_g	2.67 eV	$T = 300$ K	absorption (unpolarized)	74L
-------	---------	-------------	--------------------------	-----

Lattice and transport properties

lattice parameters

$a = c$	3.167 Å	RT	70M
b	5.194 Å		
β	118°53'		

carrier concentration, electrical resistivity, electron mobility

n	$10^{18} \dots 10^{19} \text{ cm}^{-3}$	$T = 300$ K	n-type sample	74L
ρ	$0.3 \dots 0.4 \text{ } \Omega \text{ cm}$	$T = 300$ K	(no anisotropy reported)	
μ_n	$0.5 \dots 5 \text{ cm}^2 \text{ V}^{-1} \text{ s}^{-1}$	$T = 100 \dots 300$ K		

References to 7.4

70M Maunaye, M., Lang, T.: Mater. Res. Bull. 5 (1970) 793.

74L Larson, W. L., Maruska, H. P., Stevenson, D. A.: J. Electrochem. Soc. 121 (1974) 1674.

7.5 Zinc germanium phosphide (ZnGeP2)

Crystal structure

ZnGeP2 crystallizes in the chalcopyrite lattice (space group $D_{2d}^{12} - \bar{1}4\,2d$, Fig. 7.0.1).

Electronic properties

band structure: Fig. 7.0.6, Brillouin zone: Fig. 7.0.2.

energy gaps and other band-band transitions

reflectivity ($T = 5\text{ K}$) 74V

$E_{g,pseu}$	2.14 eV	$\Gamma_{5v}-\Gamma_{3c}$ ($\Gamma_{15v}-X_{1c}$)	
$E_{g,dir}$	2.51 eV	$\Gamma_{4v}-\Gamma_{1c}$ ($\Gamma_{15v}-\Gamma_{1c}$)	
	2.63 eV	$\Gamma_{5v}-\Gamma_{1c}$ ($\Gamma_{15v}-\Gamma_{1c}$)	
	2.67 eV	$\Gamma_{5v}-\Gamma_{1c}$ ($\Gamma_{15v}-\Gamma_{1c}$)	
$E_{g,ind}$	1.80 eV	from optical transmission	87H

splitting energies

Δ_{cf}	- 0.08 eV	$T = 300\text{ K}$	electroreflectance	75S
Δ_{so}	0.09 eV			

effective masses

$m_{n,\perp}$	0.108 m_0	theory	75S
$m_{n,\parallel}$	0.105 m_0		
$m_{n,ds}$	0.11 m_0	(m_{ds} : density of states mass,	
$m_{n,c}$	0.11 m_0	m_c : conductivity mass)	
$m_{p1,\perp}$	(-1.8) m_0		
$m_{p1,\parallel}$	0.15 m_0		
$m_{p1,ds}$	0.79 m_0		

Lattice properties

lattice parameters

a	5.463(3) Å	RT	75S
c	10.74(3) Å		
c/a	1.965(5)		

density

d	4.04 g cm ⁻³	RT	58P
-----	-------------------------	----	-----

thermal expansion coefficient

α	1.8·10 ⁻⁶ K ⁻¹	$T = 300...1300\text{ K}$	a axis	75M
	5.0·10 ⁻⁶ K ⁻¹		c axis	
β	20·10 ⁻⁶ K ⁻¹	$T = 300...1300\text{ K}$	volume	

Debye temperature

Θ_D	428 K	$T \rightarrow 0\text{ K}$	75A
------------	-------	----------------------------	-----

melting temperature

T_m	1300(3) K		75S
-------	-----------	--	-----

wavenumbers of infrared and Raman active phonons

		Symmetry			
		$I\bar{4}2d$	$(F\bar{4}3m)$		
$\bar{\nu}_{LO}/\bar{\nu}_{TO}$	408/399 cm^{-1}	Γ_4	(Γ_{15})	$T = 78 \text{ K}, \Gamma_4, \Gamma_5$ IR active,	75B,
	404/387 cm^{-1}	Γ_5	(Γ_{15})	all Raman active	75G2,
	389 cm^{-1}	Γ_3	(W_2)		74B,
	376/369 cm^{-1}	Γ_5	(W_4)		75G1
	364 cm^{-1}	Γ_2	(X_1)	calculated [75B1]	
	359/344 cm^{-1}	Γ_4	(W_2)		
	331/329 cm^{-1}	Γ_5	(X_5)		
	328 cm^{-1}	Γ_1	(W_1)		
	247 cm^{-1}	Γ_3	(X_3)		
	204/202 cm^{-1}	Γ_5	(W_3)		
	142 cm^{-1}	Γ_5	(W_4)		
	120 cm^{-1}	Γ_3	(W_2)		
	96 cm^{-1}	Γ_5	(X_5)		

elastic moduli

c_{11}	$8.32 \cdot 10^{11} \text{ dyn cm}^{-2}$		calculated	96Z
c_{33}	$8.43 \cdot 10^{11} \text{ dyn cm}^{-2}$			
c_{44}	$3.50 \cdot 10^{11} \text{ dyn cm}^{-2}$			
c_{66}	$3.23 \cdot 10^{11} \text{ dyn cm}^{-2}$			
c_{12}	$4.47 \cdot 10^{11} \text{ dyn cm}^{-2}$			
c_{13}	$4.91 \cdot 10^{11} \text{ dyn cm}^{-2}$			

Transport properties

For temperature dependence of σ , R_H , μ , see also Fig. 7.5.1.

carrier concentration, electrical resistivity, hole mobility

p-type samples

p	10^{18} cm^{-3}	$T = 300 \text{ K}$	single crystal, after electron irradiation	84B
ρ	$2 \dots 5 \cdot 10^6 \Omega \text{ cm}$		single crystals	84B
μ_p	$20 \text{ cm}^2 \text{ V}^{-1} \text{ s}^{-1}$	$T = 300 \text{ K}$	single crystal, from LEC	93H

n-type samples

ρ	$10^6 \Omega \text{ cm}$		single crystal, from high pressure vapor transport	90X
--------	--------------------------	--	--	-----

activation energies

E_A	0.11 eV	$T < 220 \text{ K}$	activation energy of conductivity	87H
	0.58 eV	$T > 220 \text{ K}$		

thermal conductivity

$\kappa_{ c}$	$0.36 \text{ W cm}^{-1} \text{ K}^{-1}$	RT		94B
$\kappa_{\perp c}$	$0.35 \text{ W cm}^{-1} \text{ K}^{-1}$	RT		

Optical properties

refractive indices

coefficients in the formula $n^2 = A + B/(1 - C/\lambda^2) + D/(1 - E/\lambda^2)$

	<i>A</i>	<i>B</i>	<i>C</i> [10 ⁻¹² m ²]	<i>D</i>	<i>E</i> [10 ⁻¹² m ²]	<i>T</i> [K]	
<i>n</i> _o	4.6171	5.4709	0.1495	1.4912	662.55	670	80B
<i>n</i> _e	4.6791	5.6826	0.1567	1.4577	662.55		
<i>n</i> _o	4.5654	5.3382	0.1419	1.4913	662.55	470	
<i>n</i> _e	4.6732	5.4842	0.1499	1.4581	662.55		
<i>n</i> _o	4.5209	5.2917	0.1376	1.4911	662.55	370	
<i>n</i> _e	4.6559	5.4001	0.1460	1.4580	662.55		
<i>n</i> _o	4.4492	5.3338	0.1353	1.4736	662.55	320	79B
<i>n</i> _e	4.5717	5.4513	0.1435	1.4262	662.55		
<i>n</i> _o	4.4733	5.2658	0.1338	1.4909	662.55	270	
<i>n</i> _e	4.6332	5.3422	0.1426	1.4580	662.55		
<i>n</i> _o	4.3761	5.2540	0.1275	1.4903	662.55	170	80B
<i>n</i> _e	4.5801	5.2747	0.1368	1.4576	662.55		
<i>n</i> _o	4.2889	5.2688	0.1228	1.4898	662.55	90	
<i>n</i> _e	4.5285	5.2463	0.1326	1.4572	662.55		

References to 7.5

- 58P Pfister, H.: Acta Cryst. 11 (1958) 221.
74B Bettini, M., Miller, A.: Phys. Status Solidi (b) 66 (1974) 579.
74V Varea de Alvarez, C., Cohen, M. L., Kohn, S. F., Petroff, Y., Shen, YR.: Phys. Rev. B10 (1974) 5175.
75A Averkieva, G. K., Prochukhan, V. D., Rud', Yu. V., Tashtanova, M.: Izv. Akad. Nauk SSSR, Neorg. Mater. 11 (1975) 607.
75B Bettini, M.: Phys. Status Solidi (b) 69 (1975) 201.
75G1 Gorban', I. S., Gorynya, V. A., Lugovoi, V. I., Tychina, I. I.: Fiz. Tverd. Tela 17 (1975) 2631; Sov. Phys. Solid State (English Transl.) 17 (1976) 1749.
75G2 Grigor'eva, V. S., Markov, Yu. F., Rybakova, T. V.: Fiz. Tverd. Tela 17 (1975) 1993.
75M Miller, A., Humphreys, R. G., Chapman, B.: J. Phys. (Paris) 36 (1975) C331.
75S Shay, T. L., Wernick, T. H.: "Ternary Chalcopyrite Semiconductors" Growth, Electronics, Properties and Applications. Pergamon, 1975.
79B Bhar, G. C., Ghosh, G. C.: J. Opt. Soc. Am. 69 (1979) 730.
80B Bhar, G. C., Ghosh, G. C.: IEEE J. Quant Elec. 16 (1980) 838.
84B Boudriot, H., Grundler, R., Deus, K., Stockert, T., Schneider, H.A.: Phys. Status Solidi B 126 (1984) K149.
87B Boudriot, H., Deus, K., Grundler, R., Schneider, H.A., Stockert, T.: Phys. Status Solidi B 143 (1987) K125.
87H He-Sheng Shen, Guang-Qing Yao, Kershaw, R., Dwight, K., Wold, A.: J. Solid State Chem. 71 (1987) 176.
90X Xing, G.C., Bachmann, K.J., Posthill, J.B.: Appl. Phys. Lett. 56 (1990) 271.
93H Hobgood, H.M., Henningsen, T., Thomas, R.N., Hopkins, R.H., Ohmer, M.C., Mitchel, W.C., Fischer, D.W., Hegde, S.M., Hopkins, F.K.: J. Appl. Phys. 73 (1993) 4030.
94B Beasley, J.D.: Appl. Opt. 33 (1994) 1000.
96Z Zapol, P., Pandey, R., Ohmer, M., Gale, J.: J. Appl. Phys. 79 (1996) 671.

Figures to 7.5

Fig. 7.0.1

The chalcopyrite lattice

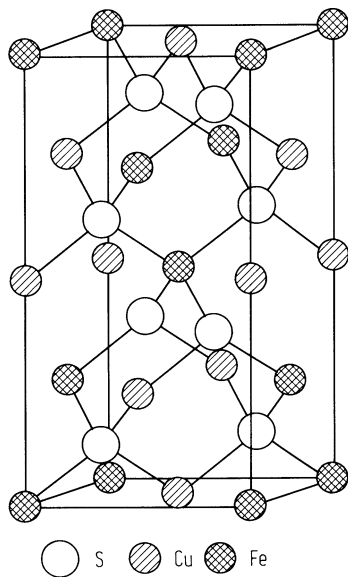


Fig. 7.0.2

Brillouin zone of the chalcopyrite lattice

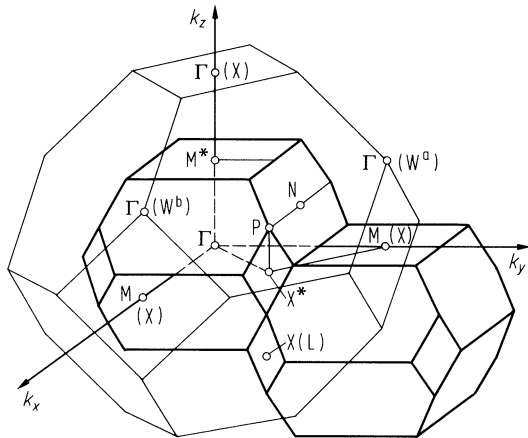


Fig. 7.0.6

Band structure of ZnGeP_2 .

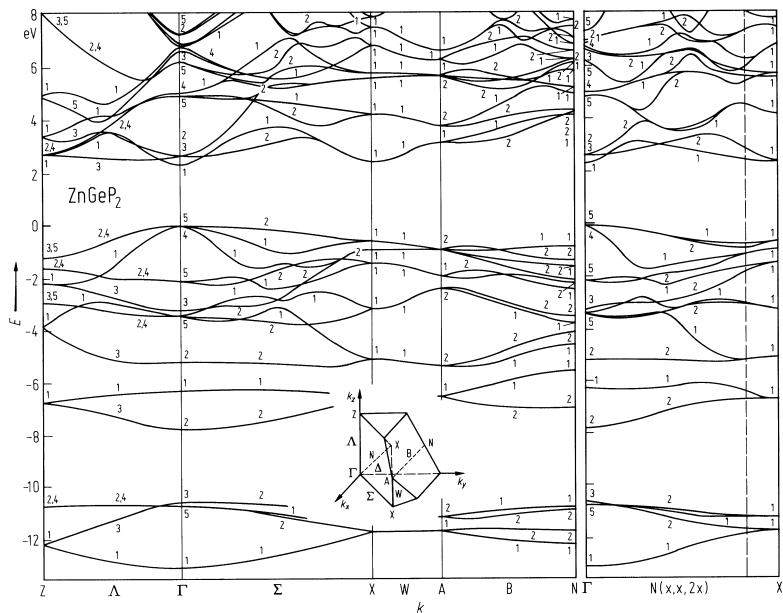
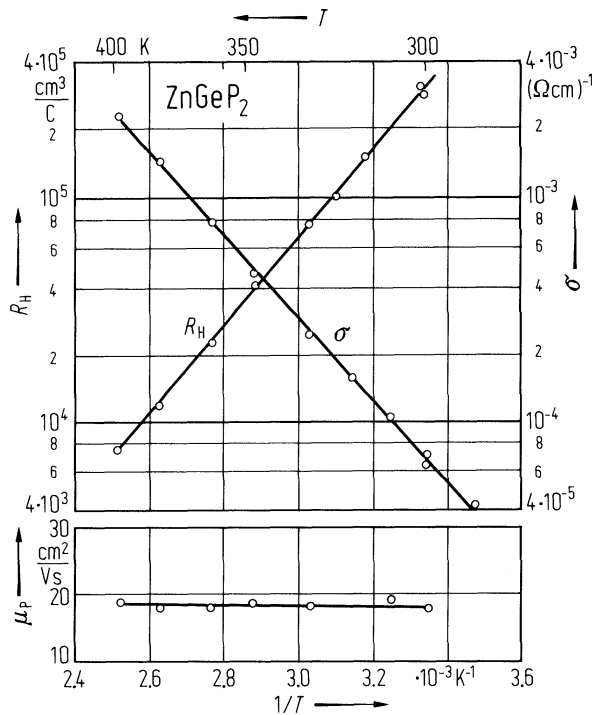


Fig. 7.5.1

ZnGeP₂. Conductivity, Hall coefficient and hole mobility vs. (reciprocal) temperature for a p-type sample with $p \approx 10^{13} \text{ cm}^{-3}$ [75S].



7.6 Zinc germanium arsenide (ZnGeAs₂)

Crystal structure

ZnGeAs₂ crystallizes in the chalcopyrite lattice (space group D_{2d}¹² – I $\bar{4}$ 2d, Fig. 7.0.1).

Electronic properties

energy gaps

thin film data

$E_{g,dir}$	1.15 eV		epilayer, optical transmission	89S
$E_{g,dir}$ (A)	1.15 eV	$T = 300$ K	electroreflectance	75S
(B)	1.19 eV			
(C)	1.48 eV			
$E_{g,th}$	1.16 eV	$T = 0$ K	conductivity	75A

splitting energies

Δ_{cf}	– 0.06 eV	$T = 300$ K		75S
Δ_{so}	0.31 eV			

effective masses

$m_{n,\perp}$	0.060 m_0		theoretical	75S
$m_{n,\parallel}$	0.058 m_0			
$m_{n,ds}$	0.059 m_0		(m_{ds} : density of states mass;	
$m_{n,c}$	0.059 m_0		m_c : conductivity mass)	
$m_{p1,\perp}$	0.82 m_0			
$m_{p1,\parallel}$	0.084 m_0			
$m_{p1,ds}$	0.38 m_0			

Lattice properties

lattice parameters

a	5.671(1) Å	RT		75S
c	11.153 Å			
c/a	1.966(1)			

density

d	5.26 g cm ^{–3}	RT		58P
-----	-------------------------	----	--	-----

melting temperature

T_m	1120...1145 K			75S
-------	---------------	--	--	-----

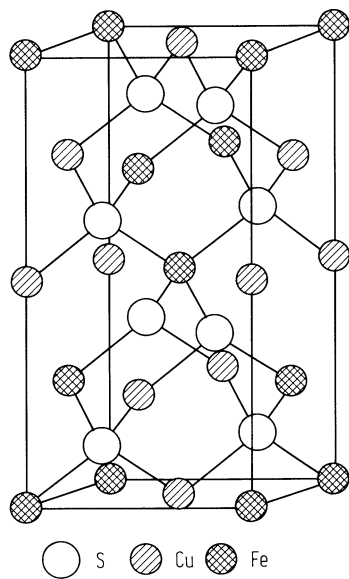
References to 7.6

58P Pfister, H.: Acta Cryst. 11 (1958) 221.
75A Averkieva, G. K., Prochukhan, V. D., Rud', Yu. V., Tashtanova, M.: Izv. Akad. Nauk SSSR, Neorg. Mater. 11 (1975) 607.
75S Shay, T. L., Wernick, T. H.: "Ternary Chalcopyrite Semiconductors" Growth, Electronics, Properties and Applications. Pergamon, 1975.
89S Sharma, S., Hong, K.S., Speyer, R.F.: J. Mater. Sci. Lett.8 (1989) 950.

Figures to 7.6

Fig. 7.0.1

The chalcopyrite lattice



7.7 Zinc tin phosphide (ZnSnP2)

Crystal structure

ZnSnP2 crystallizes in the chalcopyrite lattice (space group D2d12 – I4 2d, Fig. 7.0.1).

Electronic properties

energy gap

$E_{g,dir}$ (A,B)	1.66 eV	$T = 300$ K	electroreflectance	75S
(C)	1.75 eV			

splitting energies

Δ_{cf}	0	$T = 300$ K	($c/a = 2$)	75S
Δ_{so}	0.09 eV			

Lattice properties

lattice parameters

a	5.652(1) Å		RT	75S
c	11.305(3) Å			
c/a	2.000			

melting temperature

T_{perit}	1200 K		peritectic	75S
-------------	--------	--	------------	-----

wavenumbers of infrared active phonons

		Symmetry		
$\bar{\nu}_{LO}$	327...330 cm ⁻¹	Γ_4	$T = 300$ K	infrared reflectivity
	368 cm ⁻¹	Γ_5	$T = 300$ K	75S,
$\bar{\nu}$	322 cm ⁻¹	–	$T = 300$ K	75B
				disordered structure
				75S

Transport properties

carrier concentration, electrical resistivity, hole mobility

p-type samples

μ_p	35...47 cm ² V ⁻¹ s ⁻¹	$T = 300$ K	ZnSnP2, epilayer	89S
p	10 ¹⁶ ...10 ¹⁸ cm ⁻³			
ρ	5 Ω cm			

The temperature dependence of resistivity, mobility, Hall coefficient, and carrier concentration of ZnSnP2 are given in Figs. 7.7.1 and 7.7.2 [89S].

activation energies

E_A	0.046 eV		ZnSnP2, thin film	89S
	0.03...0.07 eV		ZnSnP2, single crystals	85A
	0.11 eV		activation energy of conductivity	75S

Optical properties

dielectric constants

$\epsilon(0)$	10.0	$T = 300$ K	chalcopyrite	75S
$\epsilon(\infty)$	8.08			
$\epsilon(0)$	10.8	$T = 300$ K	disordered zincblende	
$\epsilon(\infty)$	8.3			

References to 7.7

- 75B Bettini, M.: Phys. Status Solidi (b) 69 (1975) 201.
- 75S Shay, T. L., Wernick, T. H.: "Ternary Chalcopyrite Semiconductors" Growth, Electronics, Properties and Applications. Pergamon, 1975.
- 89S Sharma, S., Hong, K.S., Speyer, R.F.: J. Mater. Sci. Lett.8 (1989) 950.

Figures to 7.7

Fig. 7.0.1

The chalcopyrite lattice

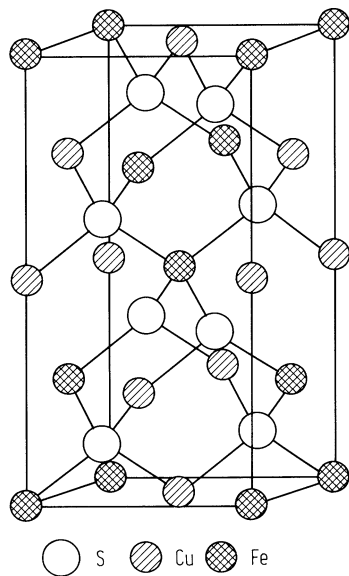


Fig. 7.7.1

ZnSnP₂. Resistivity and mobility as a function of temperature above room temperature [89S].

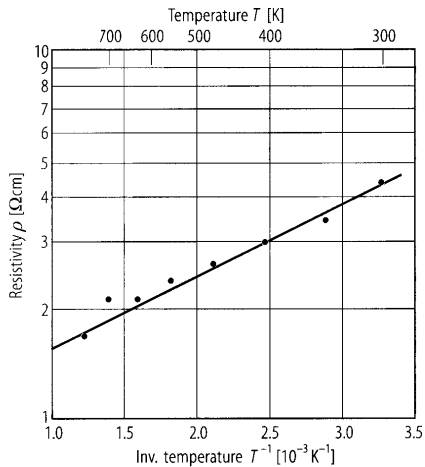
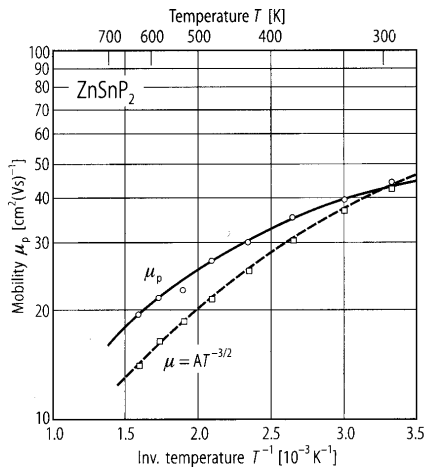
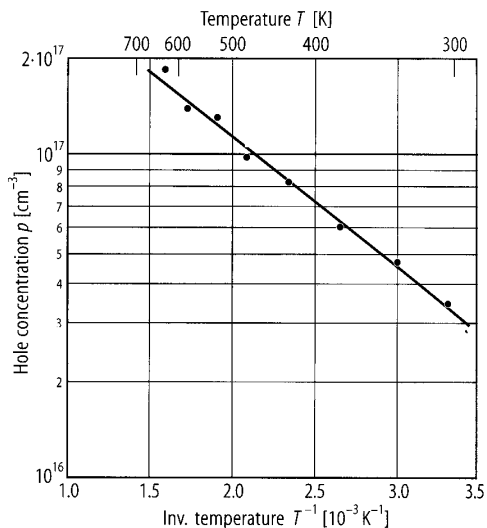
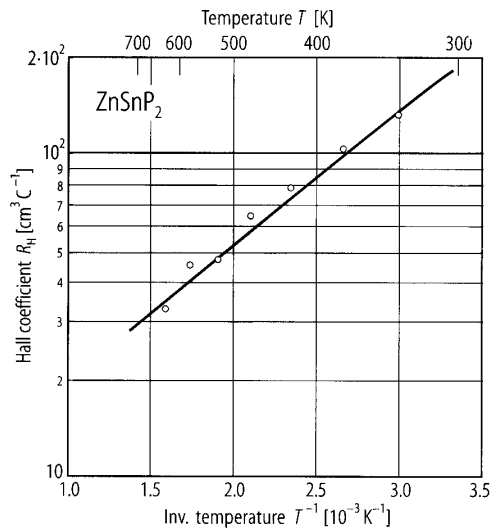


Fig. 7.7.2

ZnSnP_2 . Hall coefficient and carrier concentration as a function of temperature above room temperature [89S].



7.8 Zinc tin arsenide (ZnSnAs2)

Crystal structure

ZnSnAs2 crystallizes in the chalcopyrite lattice (space group D2d¹² – I4[–]2d, Fig. 7.0.1).

Electronic properties

energy gap

$E_{g,dir}$ (A,B)	0.745 eV	$T = 300$ K	electroreflectance	71K,
(C)	1.185 eV			75S
	0.63 eV	$T = 300$ K	epitaxial layers; absorption	78B
dE_g/dT	$2.7 \cdot 10^{-4}$ eV K ⁻¹			71S

splitting energies

Δ_{cf}	0 eV	$T = 300$ K	($c/a = 2$)	75S
Δ_{so}	0.34 eV			

effective masses

m_c	$0.048 m_0$		m_c : free charge carrier	90B
$m_p(V_1)$	$0.65 m_0$		effective mass	
$m_p(V_2)$	$0.065 m_0$			
$m_p(V_3)$	$0.16 m_0$			
m_p	$0.35 m_0$	$T = 5...200$ K	transport	80D

Lattice properties

lattice parameters

a	$5.8515(5)$ Å		RT	75S
c	$11.703(1)$ Å			
c/a	2.000			

density

d	5.53 g cm ⁻³		RT	69B
-----	---------------------------	--	----	-----

Debye temperature

Θ_D	$271.1(27)$ K	$T \rightarrow 0$ K		65A
------------	---------------	---------------------	--	-----

melting temperature

T_m	$1048(3)$ K			75B
-------	-------------	--	--	-----

Transport and optical properties

carrier concentration, electrical resistivity, hole mobility
p-type samples

p	$6.85 \cdot 10^{18}$ cm ⁻³	RT	ZnSnAs2, single crystal	95M
ρ	$7.05 \cdot 10^{-3}$ Ω cm			
μ_p	129 cm ² V ⁻¹ s ⁻¹			

dielectric constant

$\epsilon(0)$	15.6	$T = 300$ K		80D
---------------	------	-------------	--	-----

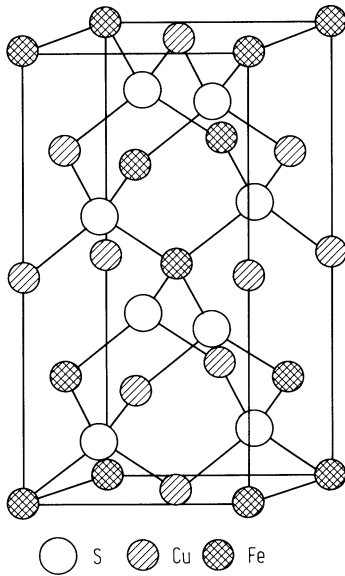
References to 7.8

- 65A Leroux-Hugon, P., Veyssie, J. J.: Phys. Status Solidi 8 (1965) 561.
- 69B Berger, L. T., Prochokhan, V. D.: "Ternary Diamond Like Semiconductors", New York, London: Consultants Bureau, 1969.
- 71K Kriviate, G. Z., Korneev, E. F., Shileika, A. Yu.: Fiz. Tekh. Poluprovodn. 13 (1971) 2242; Sov. Phys. Semicond. (English Transl.) 5 (1~72) 1961.
- 71S Shay, T. L., Buehler, F., Wernick, T. H.: Phys. Rev. B3 (1971) 2004.
- 75B Borshchevskii, A. S., Kotsyuruba, E. S.: Fiz. Tekh. Poluprovodn. 9 (1975) 2346; Sov. Phys. Semicond. (English Transl.) 9 (1976) 1513.
- 75S Shay, T. L., Wernick, T. H.: "Ternary Chalcopyrite Semiconductors" Growth, Electronics, Properties and Applications. Pergamon, 1975.
- 78B Bedair, S. M., Littlejohn, M. A.: J. Electrochem. Soc. 125 (1978) 952.
- 80D Duncan, W. M., Schreiner, A. F., Bedair, S. M., Littlejohn, M. A.: J. Lumin. 21 (1980) 137.
- 90B Brudnyi, V.N., Borisenko, S.I., Potapov, A.I.: Phys. Status Solidi A 118 (1990) 505.
- 95M Manimaran, M., Kalkura, S.N., Ramasamy, P.: J. Mater. Sci. Lett. 14 (1995) 1366.

Figures to 7.8

Fig. 7.0.1

The chalcopyrite lattice



7.9 Zinc tin antimonide (ZnSnSb2)

Crystal structure

ZnSnSb2 crystallizes in the chalcopyrite lattice (space group D2d¹² – I4[–]2d, Fig. 7.0.1).

Electronic properties

band structure : Fig. 7.0.7, Brillouin zone: Fig. 7.0.2.

The energy band structure of ZnSnSb2 was calculated by the pseudopotential method [89P].

energy gap

<i>E</i> _g	0.4 eV	<i>T</i> = 77 K	absorption	73B
	0.7 eV	<i>T</i> = 300 K	(unpolarized light)	

splitting energies

Δ _{cf}	0.03 eV	calculated	89P
Δ _{so}	0.87 eV		

effective masses

<i>m</i> _n	0.025 <i>m</i> ₀	<i>T</i> = 77 K, 300 K	73B
<i>m</i> _{p2}	0.031 <i>m</i> ₀		
<i>m</i> _{p3}	0.25 <i>m</i> ₀		

Lattice and transport properties

lattice parameters

<i>a</i>	6.273 Å	RT	75S
<i>c</i>	12.546 Å		
<i>c/a</i>	2.000		

hole concentration, hole mobility, Seebeck coefficient (at 300 K)

p-type sample

<i>p</i>	10 ²⁰ cm ^{–3}	75S
μ _p	70 cm ² V ^{–1} s ^{–1}	
<i>S</i>	36 μV K ^{–1} ?	

References to 7.9

73B Berger, L. I., Kradinova, L. V., Petrov, V. M., Prochukhan, V. D.: Izv. Akad. Nauk SSSR, Neorg. Mater. 9 (1973) 1258; Inorg. Mater. (USSR) (English Transl.) 9 (1973) 1118.

75S Shay, T. L., Wernick, T. H.: "Ternary Chalcopyrite Semiconductors" Growth, Electronics, Properties and Applications. Pergamon, 1975.

89P Polygalov, Y.I., Basalaev, Y.M., Zolotarev, M.L., Poplavnoi, A.S.: Fiz. Tekh. Poluprovodn. 23 (1989) 279; Sov. Phys. Semicond. (Engl. Transl.) 23 (1989) 173.

Figures to 7.9

Fig. 7.0.1

The chalcopyrite lattice

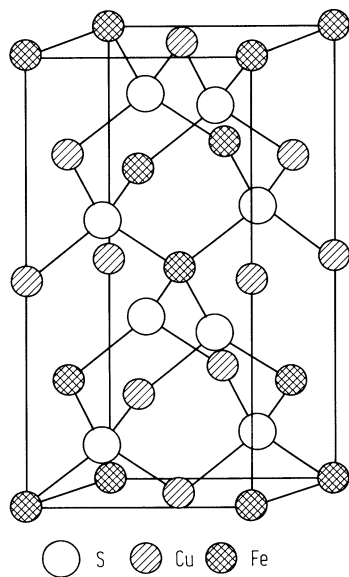


Fig. 7.0.2

Brillouin zone of the chalcopyrite lattice

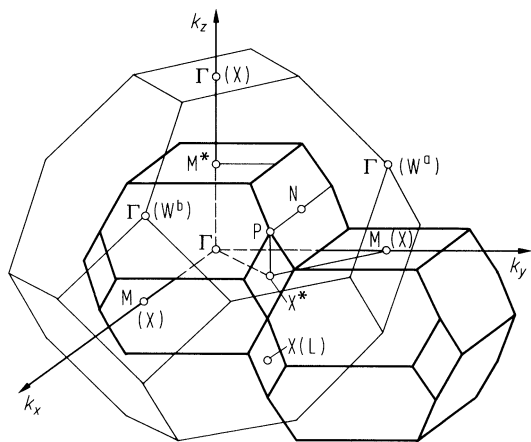
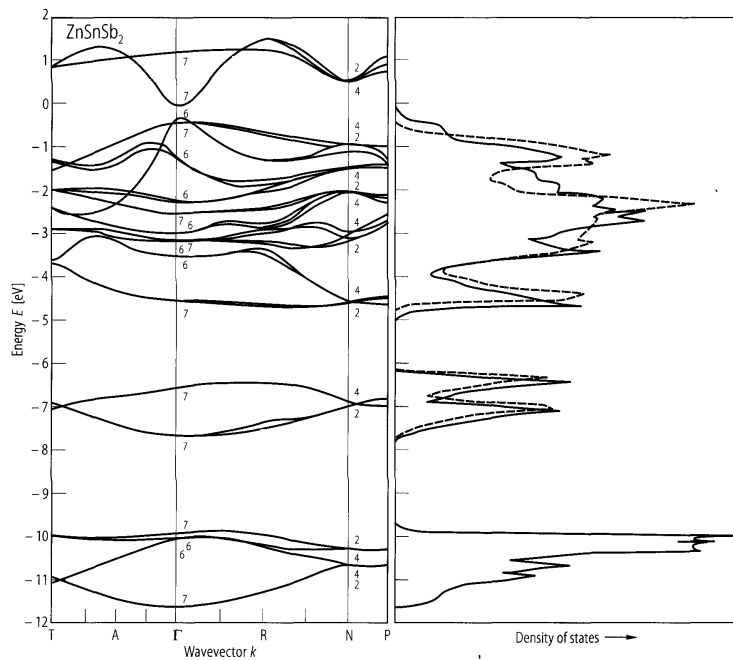


Fig. 7.0.7

Band structure of ZnSnSb_2 .



7.10 Cadmium silicon phosphide (CdSiP2)

Crystal structure

CdSiP2 crystallizes in the chalcopyrite lattice (space group $D_{2d}^{12} - I\bar{4} 2d$, Fig. 7.0.1).

Electronic properties

CdSiP2 is the only chalcopyrite material with a positive crystal field splitting(i.e. $E(\Gamma_5) > E(\Gamma_4)$). This is related to the large anionic displacement. The energy gap is generally said to be pseudodirect.

band structure : Fig. 7.0.8, Brillouin zone: Fig. 7.0.2.

energy gaps

$E_{g,pseu}$	2.2 eV	$T = 300\text{ K}$	absorption	70G, 79C
$E_{g,dir}$ (B)	2.71 eV	$T = 90\text{ K}$	thermoreflectance;	77A
(C)	2.75 eV		$\Gamma_{5v} (\Gamma_{15v}) - \Gamma_{1c} (\Gamma_{1c})$	
(A)	2.945 eV		$\Gamma_{4v} - \Gamma_{1c}$	
$dE_{g,dir}/dT$	$-3.5 \cdot 10^{-4} \text{ eV K}^{-1}$		refractive index	78A

excitonic energy gap

E_{gx}	2.085 eV	$n = 1;$ $T = 80\text{ K}$	absorption	80G
----------	----------	-------------------------------	------------	-----

splitting energies

Δ_{cf}	0.20 eV	$T = 90\text{ K}$	thermoabsorption	77A
Δ_{so}	0.07 eV			

effective masses

$m_{n }$	$1.068 m_0$			70G
$m_{n\perp}$	$0.124 m_0$			

Lattice properties

lattice parameters

a	$5.679(1) \text{ \AA}$	RT		75S
c	10.431 \AA			
c/a	$1.836(1)$			

density

d	3.97 g cm^{-3}	RT		69B
-----	--------------------------	------	--	-----

melting temperature

T_m	1390 K			75S
-------	-----------------	--	--	-----

wavenumbers of Raman active phonons

Symmetry	Wavenumber $\bar{\nu}$		
E	66 cm ⁻¹	RT	88S
B ₁	87 cm ⁻¹		
B ₂	109 cm ⁻¹		
E	158 cm ⁻¹		
E	263 cm ⁻¹		
E	286 cm ⁻¹		
B ₁	314 cm ⁻¹		
A ₁	323 cm ⁻¹		
E	453 cm ⁻¹		
B ₂ (TO)-E(TO)	485 cm ⁻¹		
B ₂ (LO)-E(LO)	508 cm ⁻¹		

Transport and optical properties

carrier concentration, electrical resistivity, electron mobilities

p-type samples

p	3·10 ¹² cm ⁻³	$T = 6$ K	single crystals, Cu-doped	89G
n	5·10 ¹⁴ cm ⁻³	$T = 300$ K	single crystals	89M
μ_n	80...100 cm ² V ⁻¹ s ⁻¹	$T = 300$ K	single crystal	89M

n-type samples (at 300 K)

n	10 ¹⁴ ...10 ¹⁵ cm ⁻³	(no anisotropy reported)	75S
μ_n	80...150 cm ² V ⁻¹ s ⁻¹		
ρ	≈ 10 ⁶ Ω cm		

refractive indices

n_o	3.414	$\lambda = 0.6328$ μm, $T = 300$ K	78I
n_e	3.379	$\lambda = 0.6328$ μm, $T = 300$ K	

References to 7.10

- 69B Berger, L. T., Prochokhan, V. D.: "Ternary Diamond Like Semiconductors", New York, London: Consultants Bureau, 1969.
- 70G Goryunova, N. A., Poplavnoi, A. S., Polygalov, Yu. I., Chaldyshev, V. A.: Phys. Status Solidi 39 (1970) 9.
- 75S Shay, T. L., Wernick, T. H.: "Ternary Chalcopyrite Semiconductors" Growth, Electronics, Properties and Applications. Pergamon, 1975.
- 77A Ambrazevicius, G. A., Babonas, G. A., Shileika, A. Yu.: Phys. Status Solidi (b) 82 (1977) K45.
- 78A Ambrazevicius, G. A., Babonas, G.: Litov. Fiz. Sb. 18 (1978) 765.
- 78I Iseler, G. W., Kildal, H., Menyuk, N.: J. Electron. Mater. 7 (1978) 737.
- 79C Cordts, W., Heinrich, A., Monecke, J.: Phys. Status Solidi (b) 96 (1979) 201.
- 80G Gorban, I. S., Krys'kov, Ts. A., Tennakun, M., Tychina, I. I., Chukichev, M. V.: Fiz. Tekh. Poluprovodn. 14 (1980) 975; Sov. Phys. Semicond. (English Transl.) 14 (1980) 577.
- 88S Shirakata, S.: Jpn. J. Appl. Phys., Part 1, 27 (1988) 2113.
- 89G Gorban, I.S., Korets, N.S., Kryskov, T.A., Chukichev, M.V.: Phys. Status Solidi A 115 (1989) 555.
- 89M Medvedkin, G.A., Rud, Y.V., Tairov, M.A.: Fiz. Tekh. Poluprovodn. 23 (1989) 1002; Sov. Phys. Semicond. (Engl. Transl.) 23 (1989) 625.

Figures to 7.10

Fig. 7.0.1

The chalcopyrite lattice

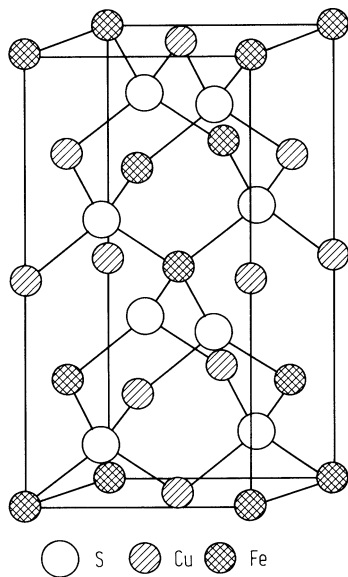


Fig. 7.0.2

Brillouin zone of the chalcopyrite lattice

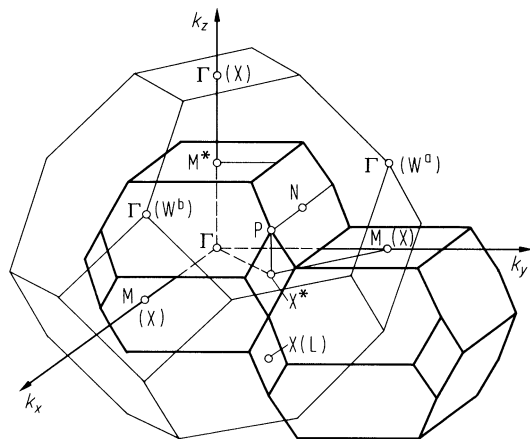
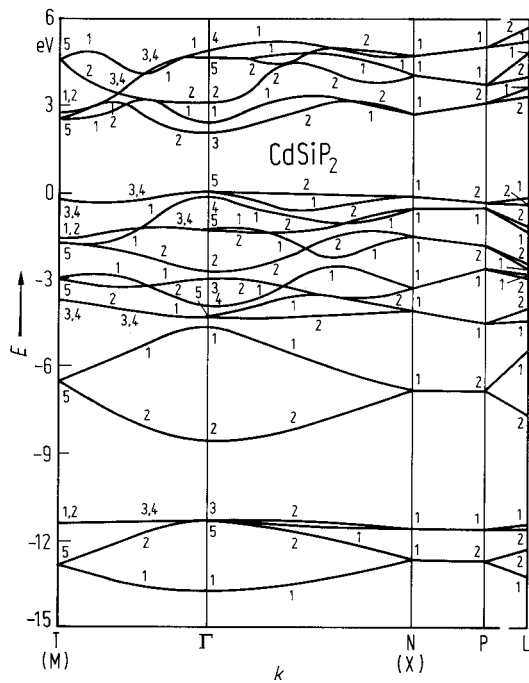


Fig. 7.0.8

Band structure of CdSiP_2 .



7.11 Cadmium silicon arsenide (CdSiAs₂)

Crystal structure

CdSiAs₂ crystallizes in the chalcopyrite lattice (space group D_{2d}¹² – I4̄ 2d, Fig. 7.0.1).

Electronic properties

band structure : Fig. 7.0.9, Brillouin zone: Fig. 7.0.2.

The energy band structure of CdSiAs₂ was calculated by the pseudopotential method including spin-orbit interaction [90B].

energy gap

$E_{g,dir}$ (A)	1.55 eV	$T = 300$ K	electroreflectance	75S,
(B)	1.74 eV			75T
(C)	1.99 eV			
	1.635 eV	$T = 1.7$ K	photoluminescence	75S,
				76M
dE_g/dT	$-2.3 \cdot 10^{-4}$ eV K ⁻¹		photoconductivity	76L

splitting energies (at Γ)

Δ_{cf}	-0.22 eV	$T = 300$ K	from optical absorption	89M
Δ_{so}	0.32 eV	$T = 300$ K	from optical absorption	89M

effective masses

$m_{n,\perp}$	$0.084 m_0$		calculated	75S
$m_{n,\parallel}$	$0.074 m_0$		(m_{ds} : density of states mass)	
$m_{n,ds}$	$0.080 m_0$			
$m_{p1,\perp}$	$(-3.6 m_0)$			
$m_{p1,\parallel}$	$0.090 m_0$			
$m_{p1,ds}$	$1.07 m_0$			

Lattice properties

lattice parameters

a	$5.885(1)$ Å	RT	75S
c	$10.881(1)$ Å		
c/a	1.849		

melting temperature

T_m	> 1120 K		75S
-------	------------	--	-----

Transport properties

carrier concentrations, electrical resistivity, hoel mobility

p-type samples

p	10^{16} cm ⁻³	$T = 300$ K	single crystals	86R
ρ	$10 \dots 100$ Ω cm	RT	single crystals	89C
μ_p	250 cm ² V ⁻¹ s ⁻¹	$T = 300$ K	single crystals	86R

n-type samples

n	10^{17} cm ⁻³	epilayer	89R
-----	----------------------------	----------	-----

The temperature dependence of resistance, free hole concentration, and Hall mobility is shown in Figs. 7.11.1, 7.11.2 [84A].

References to 7.11

- 75S Shay, T. L., Wernick, T. H.: "Ternary Chalcopyrite Semiconductors" Growth, Electronics, Properties and Applications. Pergamon, 1975.
- 75T Trykozko, R. T.: Mater. Res. Bull. 10 (1975) 489.
- 76L Lebedov, A. A., Ovezov, K., Prochukhan, V. D., Rud', Yu. V., Serginov, M.: Pis'ma Zh. Eksp. Teor. Fiz. 2 (1976) 385.
- 76M Mal'tseva, I. A., Prochukhan, V. D., Rud', Yu. V., Serginov, M.: Fiz. Tekh. Poluprovodn. 10 (1976) 1222; Sov. Phys. Semicond. (English Transl.) 10 (1976) 727.
- 84A Avirovic, M., Lux-Steiner, M., Elrod, U., Honigschmid, J., Bucher, E.: J. Cryst. Growth 67 (1984) 185.
- 86R Rud, Y.V., Serginov, M.: Izv. Akad. Nauk SSSR, Neorg. Mater. 22 (1986) 1208; Inorg. Mater. (Engl. Transl.) 22 (1986) 1056.
- 89C Cotting, T., von Känel, H., Leicht, G., Levy, F.: J. Electrochem. Soc. 136 (1989) 382.
- 89M Medvedkin, G.A., Rud, Y.V., Tairov, M.A.: Solid State Commun. 71 (1989) 307.
- 90B Basalae, Y.M., Zolotarev, M.L., Polygalov, Y.I., Poplavnoi, A.S.: Fiz. Tekh. Poluprovodn. 24 (1990) 916; Sov. Phys. Semicond. (Engl. Transl.) 24 (1990) 574.

Figures to 7.11

Fig. 7.0.1

The chalcopyrite lattice

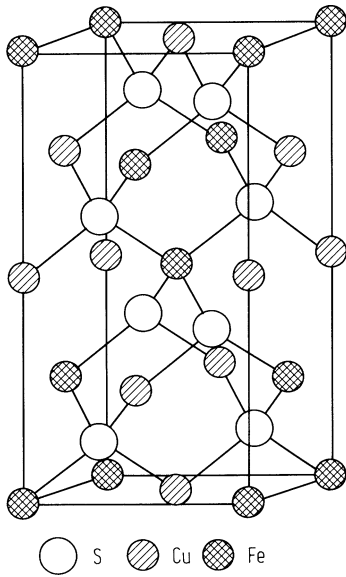


Fig. 7.0.2

Brillouin zone of the chalcopyrite lattice

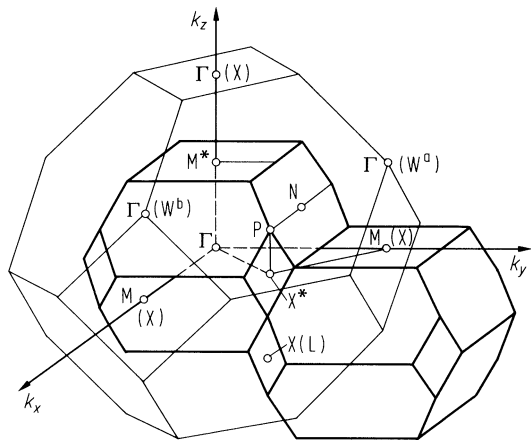


Fig. 7.0.9

Band structure of CdSiAs_2 .

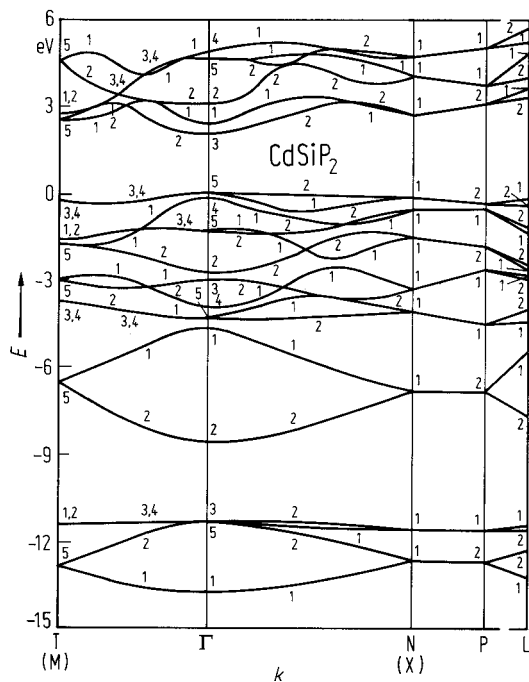


Fig. 7.11.1

CdSiAs_2 . Temperature dependence of the resistance of crystals grown by CVT [84A].

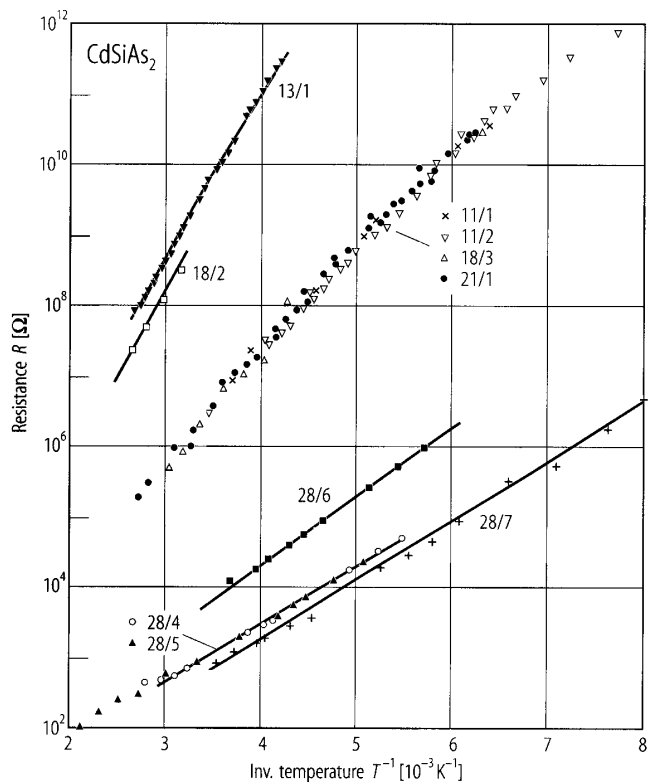
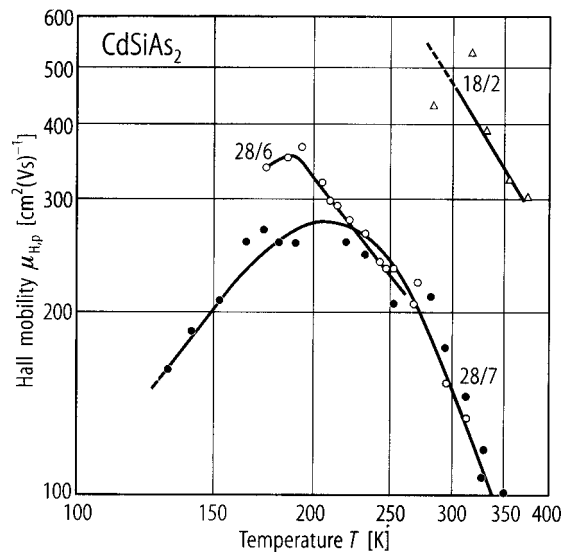


Fig. 7.11.2

CdSiAs_2 . Temperature dependence of the Hall mobility of crystals grown by CVT [84A].



7.12 Cadmium germanium phosphide (CdGeP₂)

Crystal structure

CdGeP₂ crystallizes in the chalcopyrite lattice (space group D_{2d}¹² – I $\bar{4}$ 2d, Fig. 7.0.1).

Electronic properties

energy gap				
E_g	1.73 eV	$T = 300$ K	from optical absorption	90M
dE_g/dT	$-3.8 \cdot 10^{-4}$ eV K ⁻¹	$T = 80 \dots 300$ K		90M

excitonic energy gap

E_{gx}	1.686 eV	$T = 300$ K, $E \parallel c$	photoconductivity	75B
	1.712 eV	$E \perp c$		

splitting energies

Δ_{cf}	-0.2 eV	$T = 300$ K	electroreflectance	75S
Δ_{so}	0.11 eV			

effective masses

$m_{n,\perp}$	$0.088 m_0$	calculated (m_{ds} : density of states mass)	75S
$m_{n,\parallel}$	$0.088 m_0$		
$m_{n,ds}$	$0.085 m_0$		
$m_{p1,\perp}$	$(-1.3 m_0)$		
$m_{p1,\parallel}$	$0.099 m_0$		
$m_{p1,ds}$	$0.56 m_0$		

Lattice properties

lattice parameters

a	$5.740(1)$ Å	RT	75S
c	$10.776(1)$ Å		
c/a	$1.878(1)$		

thermal expansion coefficient

α	$8.9 \cdot 10^{-6}$ K ⁻¹	$T = 300 \dots 1030$ K	a axis	75M
	$0.37 \cdot 10^{-6}$ K ⁻¹		c axis	
β	$1.8 \cdot 10^{-6}$ K ⁻¹	$T = 300 \dots 1030$ K	volume	

Debye temperature

Θ_D	340 K	$T \rightarrow 0$ K	75A
------------	---------	---------------------	-----

melting temperature

T_m	1073 K	75B
-------	----------	-----

wavenumbers of infrared and Raman active phonons
(in cm⁻¹), between parantheses the LO frequencies are noted

91A

	Experiment		Theory	
	IR (20 K)	Raman (77 K)	3 parameters	4 parameters
Γ_4	399 (409.5)	398 (407)	399	402
Γ_5	380.5 (400.5)	387 (400)	394	393
Γ_3	377	353	353	
Γ_5	356 (369)	358 (368)	356	355
			341	352
Γ_1		322	306	306
Γ_4	299.5 (317)	295 (314)	307	309
Γ_5	289 (297.5)	295 (296)	300	304
			278	268
Γ_3		228	188	177
Γ_5	181 (187)	184 (186)	184	183
Γ_5	118.5 (123)	123 (123)	107	114
Γ_4	91 (91)	91 (91)	95	98
Γ_3		88	90	98
Γ_5	63 (63)	64 (64)	83	64

Transport and optical properties

carrier concentrations, carrier mobilities, electrical resistivity

p-type samples

p	$(1\dots4)\cdot 10^{12}\text{ cm}^{-3}$	$T = 300\text{ K}$	single crystals, Cu-doped	88L1
ρ	$10^3\text{ }\Omega\text{ cm}$	$T = 300\text{ K}$	single crystals, Cu-doped	88L1
μ_p	$5\text{ cm}^2\text{ V}^{-1}\text{ s}^{-1}$	$T = 300\text{ K}$	single crystal, Ga-doped	88L2

n-type samples

n	10^{13} cm^{-3}	$T = 300\text{ K}$	single crystal	86L
ρ	$(1\dots3)\cdot 10^3\text{ }\Omega\text{ cm}$	$T = 300\text{ K}$	single crystals, In-doped	88L1
μ_n	$800\text{ cm}^2\text{ V}^{-1}\text{ s}^{-1}$	$T = 300\text{ K}$	single crystal	90M

thermal conductivity

κ	$0.11\text{ W cm}^{-1}\text{ K}^{-1}$	$T = 300\text{ K}$	75S
----------	---------------------------------------	--------------------	-----

refractive indices

coefficients in the formula $n^2 = A + B/(1 - C/\lambda^2) + D/(1 - E/\lambda^2)$

	A	B	$C\text{ [}10^{-12}\text{ m}^2\text{]}$	D	$E\text{ [}10^{-12}\text{ m}^2\text{]}$	$T\text{ [K]}$	
n_o	5.9677	4.2286	0.2021	1.6351	671.33	293	79B
n_e	6.1573	4.0970	0.2330	1.4925	671.33	293	
n_o	6.3737	3.9281	0.2069	1.6686	671.33	391	
n_e	6.9280	3.4442	0.2803	1.5515	617.33	391	

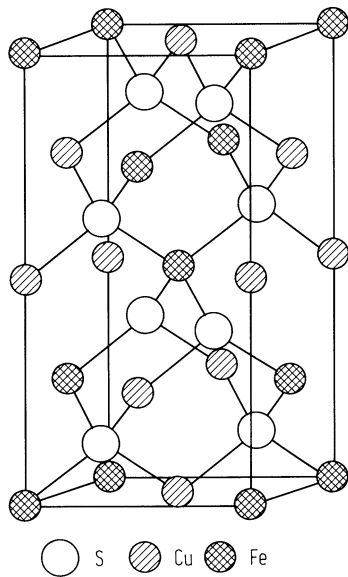
References to 7.12

- 75A Averkieva, G. K., Prochukhan, V. D., Rud', Yu. V., Tashtanova, M.: *Izv. Akad. Nauk SSSR, Neorg. Mater.* 11 (1975) 607.
- 75B Borshchevskii, A. S., Kotsyuruba, E. S.: *Fiz. Tekh. Poluprovodn.* 9 (1975) 2346; *Sov. Phys. Semicond. (English Transl.)* 9 (1976) 1513.
- 75M Miller, A., Humphreys, R. G., Chapman, B.: *J. Phys. (Paris)* 36 (1975) C331.
- 79B Bhar, G. C., Ghosh, G. C.: *J. Opt. Soc. Am.* 69 (1979) 730.
- 86L Lunev, A.V., Rud, Y.V., Tairov, M.A., Undalov, Y.K., Filippova, A.V.: *Zh. Prikl. Spektrosk.* 44 (1986) 247; *J. Appl. Spectrosc. (Engl. Transl.)* 44 (1986) 167.
- 88L1 Lunev, A.V., Rud, Y.V., Tairov, M.A., Undalov, Y.K.: *Zh. Tekh. Fiz.* 58 (1988) 1415; *Sov. Phys.-Techn. Phys. (Engl. Transl.)* 33 (1988) 843.
- 88L2 Lunev, A.V., Rud, Y.V., Tairov, M.A., Undalov, Y.K.: *Fiz. Tekh. Poluprovodn.* 22 (1988) 1115; *Sov. Phys. Semicond. (Engl. Transl.)* 22 (1988) 703.
- 90M Medvedkin, G.A., Rud, Y.V., Tairov, M.A.: *Fiz. Tekh. Poluprovodn.* 24 (1990) 1306; *Sov. Phys. Semicond. (Engl. Transl.)* 24 (1990) 821.
- 91A Artus, L., Pascual, J., Pujol, J., Camassel, J., Feigelson, R.S.: *Phys. Rev. B* 43 (1991) 2088.

Figures to 7.12

Fig. 7.0.1

The chalcopyrite lattice



7.13 Cadmium germanium arsenide (CdGeAs2)

Crystal structure

CdGeAs2 crystallizes in the chalcopyrite lattice (space group D2d¹² – I4[–]2d, Fig. 7.0.1).

Electronic properties

band structure : Fig. 7.0.10, Brillouin zone: Fig. 7.0.2.

The electronic energy band structure of CdGeAs2 calculated by the empirical pseudopotential method is given in Fig. 7.18 [91M].

energy gaps

$E_{g,dir}$ (A)	0.57 eV	$T = 300$ K	electroreflectance	75S
(B)	0.73 eV			
(C)	1.02 eV			
$E_{g,th}$	0.673 eV	$T = 0$ K	Hall effect	78I
$dE_{g,th}/dT$	$-3.5 \cdot 10^{-4}$ eV K ⁻¹	$T = 0...300$ K		

splitting energies

Δ_{cf}	- 0.21 eV	$T = 300$ K	electroreflectance	75S
Δ_{so}	0.33 eV			

effective masses

A calculation of the dependence of the effective masses of the electrons of the first-three magnetic sub-bands in CdGeAs2 on electron concentration in the presence of crossed electric and magnetic fields is given in Fig. 7.13.1 [88G].

m_n	0.26 m_0		Hall effect	78I
m_p	0.035 m_0			

Lattice properties

lattice parameters

a	5.943(1) Å		RT	75S
c	11.220(3) Å			
c/a	1.888(1)			

density

d	5.6 g cm ⁻³ (crystalline)		RT	69B
	5.35 g cm ⁻³ (amorphous)			

linear thermal expansion coefficient

α	1·10 ⁻⁶ K ⁻¹	$T = 370...570$ K	c axis	78I
	8...9·10 ⁻⁶ K ⁻¹		a axis	
			(large anisotropy)	

Debye temperature

Θ_D	240.9(14) K	$T \rightarrow 0$ K	from heat capacity	81B
	257(2) K	$T = 4.2$ K	from elastic moduli	82H

melting temperature

T_m	943 K			77S, 75B
-------	-------	--	--	-------------

phonon dispersion : Fig. 7.13.2.

wavenumbers of infrared active phonons

		Symmetry			
		I $\bar{4}$ 2d	(F $\bar{4}$ 3m)		
$\bar{\nu}_{\text{LO}}/\bar{\nu}_{\text{TO}}$	280/272 cm ⁻¹	Γ_5	(Γ_{15})	RT	77H
	278/270 cm ⁻¹	Γ_5	(Γ_{15})		
	258/255 cm ⁻¹	Γ_5	(W ₄)		
	210/203 cm ⁻¹	Γ_5	(W ₂)		
	206/200 cm ⁻¹	Γ_5	(X ₃)		
	101/159 cm ⁻¹	Γ_5	(W ₃)		
	98/95 cm ⁻¹	Γ_5	(W ₄)		

wavenumbers of Raman active phonons

		Symmetry		
$\bar{\nu}$	282 cm ⁻¹	Γ_4	calculated	92A
	280 cm ⁻¹	Γ_5		
	257 cm ⁻¹	Γ_5		
	254 cm ⁻¹	Γ_3		
	201 cm ⁻¹	Γ_2		
	205 cm ⁻¹	Γ_5		
	211 cm ⁻¹	Γ_4		
	182 cm ⁻¹	Γ_1		
	155 cm ⁻¹	Γ_5		
	162 cm ⁻¹	Γ_3		
	169 cm ⁻¹	Γ_2		
	80 cm ⁻¹	Γ_5		
	76 cm ⁻¹	Γ_4		
	75 cm ⁻¹	Γ_3		
	65 cm ⁻¹	Γ_5		

elastic moduli

		calculated	experimental	88A
c_{11}		6.8·10 ¹¹ dyn cm ⁻²	9.45·10 ¹¹ dyn cm ⁻²	
c_{33}		5.4·10 ¹¹ dyn cm ⁻²	8.34·10 ¹¹ dyn cm ⁻²	
c_{44}		1.3·10 ¹¹ dyn cm ⁻²	4.21·10 ¹¹ dyn cm ⁻²	
c_{66}		1.1·10 ¹¹ dyn cm ⁻²	4.08·10 ¹¹ dyn cm ⁻²	
c_{12}		5.2·10 ¹¹ dyn cm ⁻²	5.96·10 ¹¹ dyn cm ⁻²	
c_{13}		4.7·10 ¹¹ dyn cm ⁻²	5.97·10 ¹¹ dyn cm ⁻²	

Transport and optical properties

carrier concentrations and mobilities

p-type samples

p	(0.7...2)·10 ¹⁶ cm ⁻³	$T = 300$ K	78I, 76B2
μ_p	140...400 cm ² V ⁻¹ s ⁻¹	$T = 300$ K	

n-type samples (by vacuum anneal, or In, Al, Te doping) [76B2]

n	4·10 ¹⁶ ...10 ¹⁸ cm ⁻³	$T = 100$...500 K	78I
μ_n	1000...	$T = 100$...500 K	
	4000 cm ² V ⁻¹ s ⁻¹		

See also Figs. 7.13.3 and 7.13.4.

thermal conductivity

κ 0.42 W cm⁻¹ K⁻¹ $T = 300$ K 75S

refractive indices

coefficients in the formula $n^2 = A + B/(1 - C/\lambda^2) + D/(1 - E/\lambda^2)$

	A	B	C [10 ⁻¹² m ²]	D	E [10 ⁻¹² m ²]	T [K]	
n_o	10.1064	2.2988	1.0872	1.6247	1370	300	76B1
n_e	11.8018	1.2152	1.6971	1.6922	1370	300	

dielectric constants

$\epsilon(0)$	18.4±0.5	RT	crystalline	90K
$\epsilon(\infty)$	14.0±0.3	RT	crystalline	90K

References to 7.13

69B Berger, L. T., Prochokhan, V. D.: "Ternary Diamond Like Semiconductors", New York, London: Consultants Bureau, 1969.

75B Borshchevskii, A. S., Kotsyuruba, E. S.: Fiz. Tekh. Poluprovodn. 9 (1975) 2346; Sov. Phys. Semicond. (English Transl.) 9 (1976) 1513.

75S Shay, T. L., Wernick, T. H.: "Ternary Chalcopyrite Semiconductors" Growth, Electronics, Properties and Applications. Pergamon, 1975.

76B1 Bhar, G. C.: Appl. Opt. 15 (1976) 305.

76B2 Borshchevskii, A. S., Dagina, N. E., Lebedov, A. A., Ovezov, K., Polushina, I. K., Rud', Yu. V.: Fiz. Tekh. Poluprovodn. 10 (1976) 1571; Sov. Phys. Semicond. (English Transl.) 10 (1976) 934.

77H Holah, G. D., Miller, A., Dunnett, W. D., Iseler, G. W.: Solid State Commun. 23 (1977) 75.

77S Satow, T. Uemura, O., Watanabe, S.: Phys. Status Solidi (a) 44 (1977) 731.

78B Brudnyi, V. N., Krivov, M. A., Potapov, A. I., Polushina, I. K., Prochukhan, V. D., Rud', Yu. V.: Phys. Status Solidi (a) 49 (1978) 761.

78I Iseler, G. W., Kildal, H., Menyuk, N.: J. Electron. Mater. 7 (1978) 737.

81B Bohmhammel, K., Deus, P., Schneider, H. A.: Phys. Status Solidi (a) 65 (1981) 563.

82H Hailing, T., Saunders, G. A., Lambson, W. A., Feigelson, R. S.: J. Phys. C15 (1982) 1399.

88A Antropova, E.V., Kopytov, A.V., Poplavnoi, A.S.: Opt. Spektrosk. 64 (1988) 1285; Opt. Spectrosc. (Engl. Transl.) 64 (1988) 766.

88G Ghatak, K.P., Mondal, M.: Zeitschrift für Physik B 69 (1988) 471.

90B Baumgartner, F.P., Lux-Steiner, M., Bucher, E.: J. Electron. Mater. 19 (1990) 777.

90K Kug Sun Hong, Speyer, R.F., Condrate, R.A.: J. Phys. Chem. Solids 51 (1990) 969.

91M Madelon, R., Paumier, E., Hairie, A.: Phys. Status Solidi B 165 (1991) 435.

92A Artus, L., Pascual, J.: J. Phys.: Condensed Matter 4 (1992) 5835.

Figures to 7.13

Fig. 7.0.1

The chalcopyrite lattice

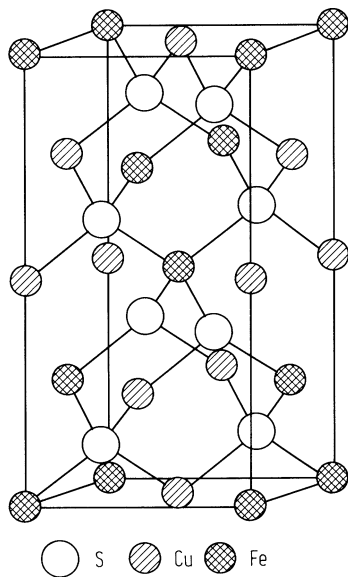


Fig. 7.0.2

Brillouin zone of the chalcopyrite lattice

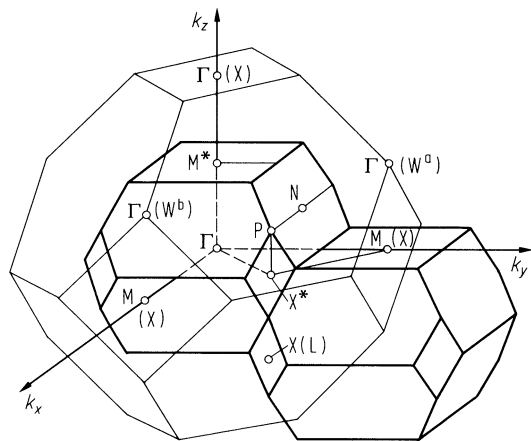


Fig. 7.0.10

Band structure of CdGeAs₂.

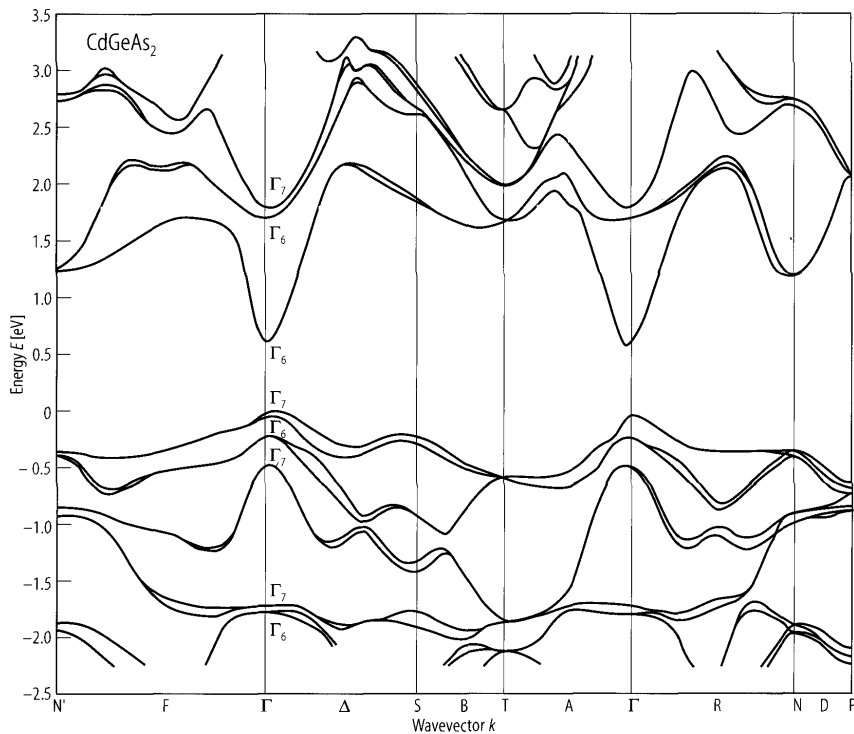


Fig. 7.13.1

CdGeAs_2 . Calculation of the dependence of the effective masses $m_z^*(E_F)$ of the electrons of the first-three magnetic sub-bands in CdGeAs_2 on electron concentration in the presence of crossed electric and magnetic fields. The dashed curve shows the same dependence when spin orbit splitting parameter $\Delta = 0.3$ eV and crystal field splitting parameter $\delta = 0$ [88G].

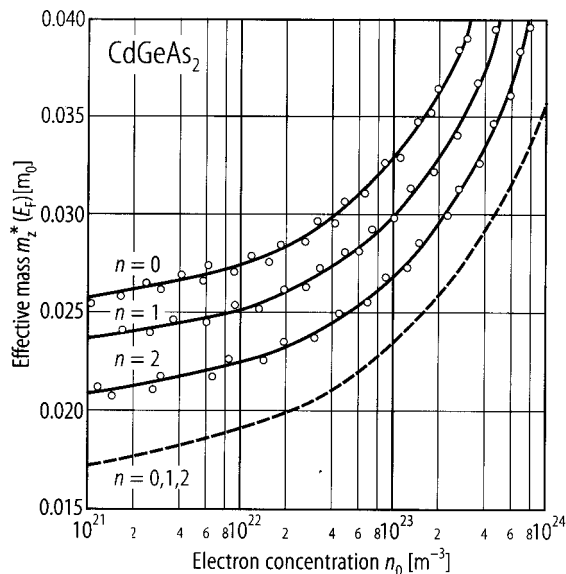


Fig. 7.13.2

CdGeAs_2 . Calculated phonon spectrum and one-phonon frequency distribution function [88A].

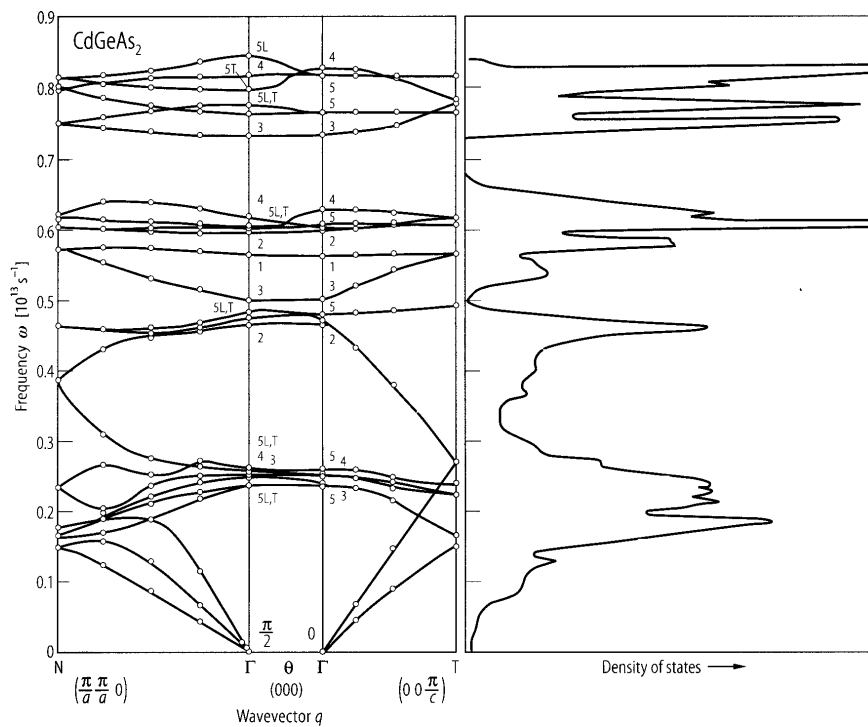


Fig. 7.13.3

CdGeAs_2 . Conductivity (circles) and Hall coefficient (triangles) vs. irradiation with 2 MeV electrons at $T = 300\text{ K}$ [78B]. (full symbols) initially n-type sample, (open symbols) initially p-type sample. Note the change of type at $\Phi = 3 \cdot 10^{17}\text{ electrons cm}^{-2}$ ($p \rightarrow n$).

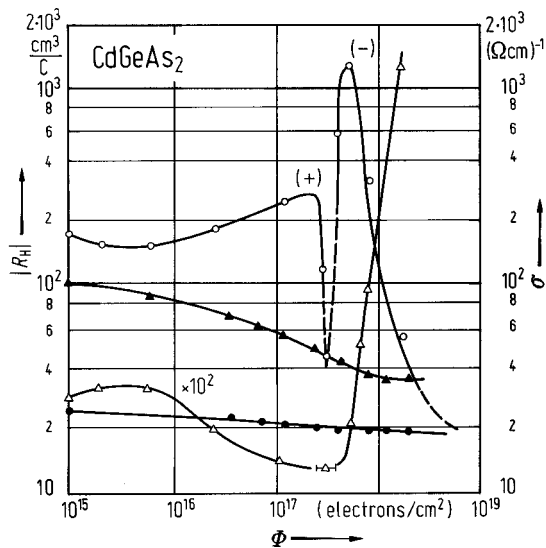
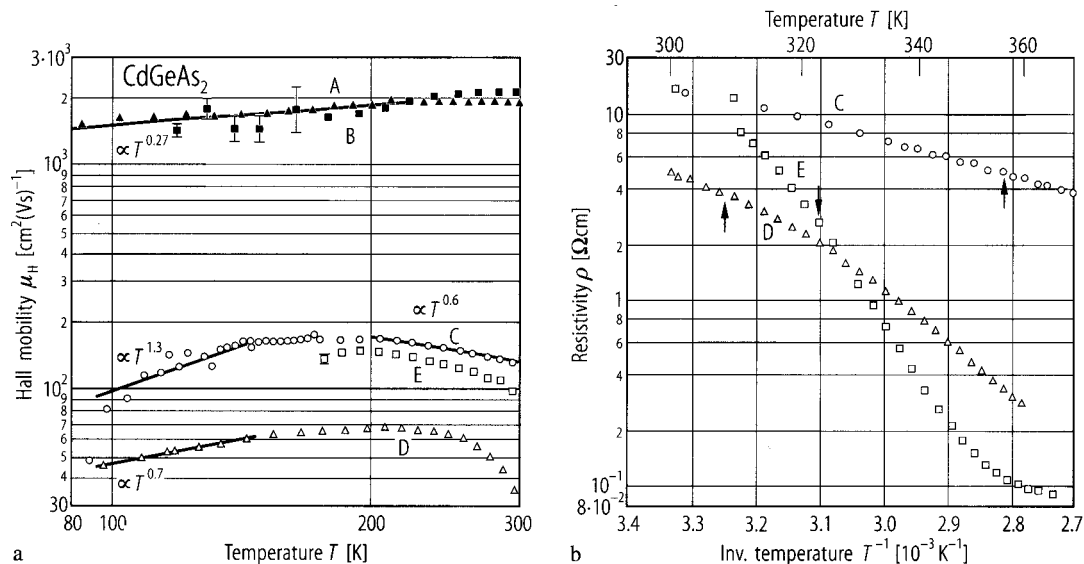


Fig. 7.13.4

CdGeAs_2 . (a) Variation of Hall mobility with T for as grown n -type sample (A) and (B), as grown p -type sample (C), and the vacuum heat treated samples (D) (500°C for 45 min) and (E) (500°C for 3 h). (b) Variation of resistivity with temperature for the samples of (a). Arrows indicate the temperatures at $R_H = 0$ [90B].



7.14 Cadmium tin phosphide (CdSnP₂)

Crystal structure

CdSnP₂ crystallizes in the chalcopyrite lattice (space group D_{2d}¹² – I $\bar{4}$ 2d, Fig. 7.0.1).

Electronic properties

band structure : see Fig. 7.0.11, Brillouin zone: Fig. 7.0.2.

energy gap

$E_{g,dir}$ (A)	1.17 eV	$T = 300$ K	electroreflectance	70S
(B)	1.25 eV			
(C)	1.33 eV			
dE_g/dT	$-2.8 \cdot 10^{-4}$ eV K ⁻¹			80Z, 78M

excitonic energy gap

E_{gx} (A)	1.2343 eV	$T = 1.7$ K	photoluminescence	75S
(B)	1.2353 eV			
(C)	1.2360 eV			

effective masses

$m_{n\perp}$	0.060 m_0	calculated	75S
$m_{n\parallel}$	0.056 m_0	calculated	75S
$m_{p1\perp}$	(−6.6 m_0)	calculated	75S
$m_{p1\parallel}$	0.69 m_0	calculated	75S

Lattice properties

lattice parameters

a	5.901(1) Å	RT	75S
c	11.514(4) Å		
c/a	1.951(1)		

melting temperature

T_m	840 K	75S
-------	-------	-----

wavenumbers of Raman active phonons (in cm⁻¹, at RT)

		Symmetry	
		I $\bar{4}$ 2d	
$\bar{\nu}_{LO}/\bar{\nu}_{TO}$	364/353	Γ_4	85I
	340/348	Γ_5	
	314/328	Γ_5	
	301	Γ_1	
	306/288	Γ_4	
	280/283	Γ_5	
	265	Γ_3	
	146/147	Γ_5	
	113	Γ_3	
	93/94	Γ_5	
	73/73	Γ_4	
	54/54	Γ_5	

wavenumbers of infrared active phonons

		Symmetry			
		$I\bar{4}2d$	$(F\bar{4}3m)$		
$\bar{\nu}_{LO}/\bar{\nu}_{TO}$	$353/-\text{cm}^{-1}$	Γ_4	(Γ_{15})	RT	78B
	$-/389\text{ cm}^{-1}$	Γ_5	(Γ_{15})		
	$327/318\text{ cm}^{-1}$	Γ_5	(W_4)		
	$-/295\text{ cm}^{-1}$	Γ_4	(W_2)		
	$285/279\text{ cm}^{-1}$	Γ_5	(X_5)		

Transport and optical properties

carrier concentrations, electron mobilities

p-type samples

p	10^{15} cm^{-3}	$T = 300\text{ K}$	single crystal	89M
-----	--------------------------	--------------------	----------------	-----

n-type samples

n	$8\cdot 10^{17}\text{ cm}^{-3}$	RT	single crystal	85F
μ_n	$1100\text{ cm}^2\text{ V}^{-1}\text{ s}^{-1}$	RT	single crystal	85F 76M

see also Fig. 7.14.1

absorption coefficient

α	$5.6\cdot 10^4\text{ cm}^{-1}$	$\lambda = 1050\text{ nm}$	single crystal	85F
----------	--------------------------------	----------------------------	----------------	-----

dielectric constants

$\epsilon(0)$	11.8	$T = 300\text{ K}$	infrared, unpolarized	75S
$\epsilon(\infty)$	10.0			

The dielectric constants $\epsilon_1(E)$ and $\epsilon_2(E)$ of CdSnP_2 derived from transmission electron energy loss spectra are shown in Fig. 7.14.2 [84B].

References to 7.14

- 70S Shay, T. L., Buehler, E., Wernick, T. H.: Phys. Rev. B2 (1970) 4104.
- 75S Shay, T. L., Wernick, T. H.: "Ternary Chalcopyrite Semiconductors" Growth, Electronics, Properties and Applications. Pergamon, 1975.
- 76M Medvedkin, G. A., Ovezov, K., Rud', Yu. V., Sokolova, V. I.: Fiz. Tekh. Poluprovodn. 10 (1976) 2081; Sov. Phys. Semicond. (English Transl.) 10 (1976) 1239.
- 76P Podol'skii, W. V., Karpovich, I. A., Zvonkov, B. N.: Fiz. Tekh. Poluprovodn. 10 (1976) 1004; Sov. Phys. Semicond. (English Transl.) 10 (1976) 594.
- 78B Brudnyi, V. N., Krivov, M. A., Potapov, A. I., Prochukhan, V. D., Rud', Yu. V.: Fiz. Tekh. Poluprovodn. 12 (1978) 1109; Sov. Phys. Semicond. (English Transl.) 12 (1978) 659.
- 78M Medvedkin, G. A., Rud', Yu. V., Valov, Yu. A., Sokolova, V. I.: Phys. Status Solidi (a) 45 (1978) K95.
- 80Z Ziegler, F., Siegel, W., Kühnel, G.: Phys. Status Solidi (a) 65 (1980) 625.
- 84B Boudriot, H., Grundler, R., Deus, K., Stockert, T., Schneider, H.A.: Phys. Status Solidi B 126 (1984) K149.
- 85F Folmer, J.C.W., Tuttle, J.R., Turner, J.A., Parkinson, B.A.: J. Electrochem. Soc. 132 (1985) 1608.
- 85I Irmer, G., Heinrich, A., Monecke, J.: Phys. Status Solidi B 132 (1985) 93.
- 89M Medvedkin, G.A., Rud', Y.V., Tairov, M.A.: Fiz. Tverd. Tela 31 (1989) 108; Sov. Phys. Solid State (Engl. Transl.) 31 (1989) 606.

Figures to 7.14

Fig. 7.0.1

The chalcopyrite lattice

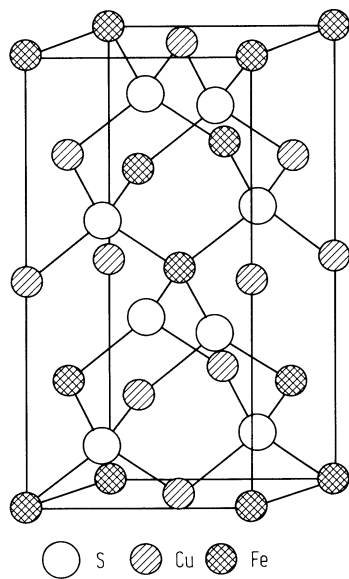


Fig. 7.0.2

Brillouin zone of the chalcopyrite lattice

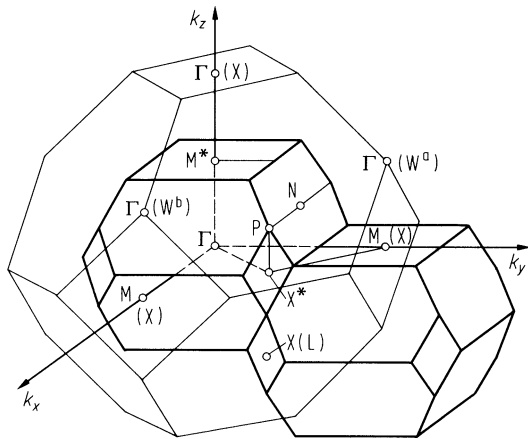


Fig. 7.0.10

Band structure of CdGeAs₂.

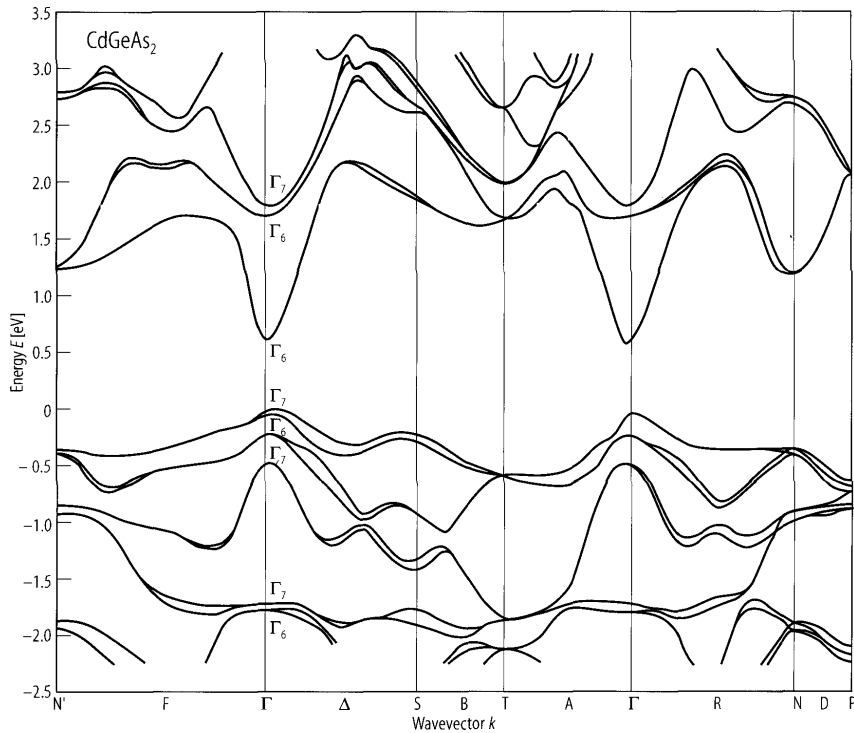


Fig. 7.14.1

CdSnP_2 . Electron concentration (curves 1, 4) and electron mobility (2, 3) vs. temperature in undoped (1, 2) and Cu doped (3, 4) samples [76P].

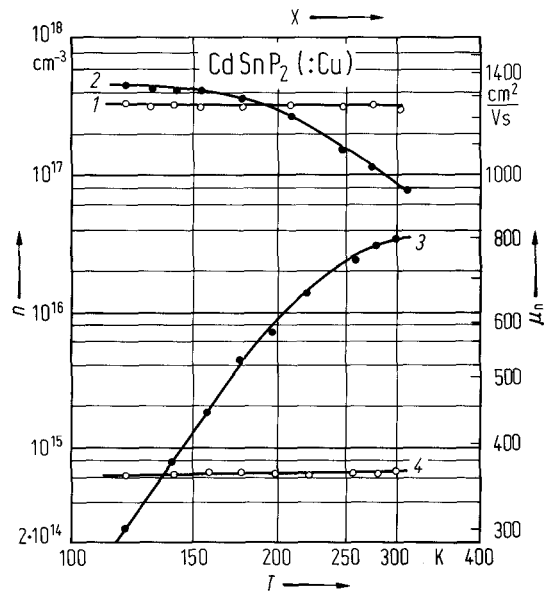
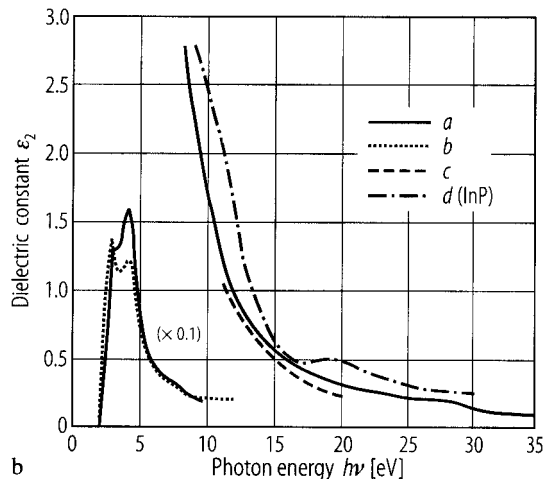
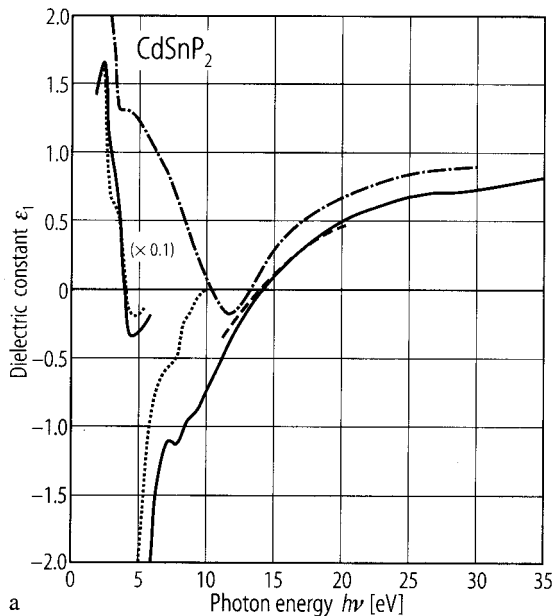


Fig. 7.14.2

CdSnP_2 . The dielectric function (a) ϵ_1 and (b) ϵ_2 derived from transmission electron energy loss spectra: (curve *a*) from TEL data; (b) from reflectivity measurements; (c) Drude model values. For comparison the values for InP (*d*) are shown [84B].



7.15 Cadmium tin arsenide (CdSnAs2)

Crystal structure

CdSnAs2 crystallizes in the chalcopyrite lattice (space group D2d¹² – I 4 2d, Fig. 7.0.1).

Electronic properties

band structure : see Fig. 7.0.12, Brillouin zone: Fig. 7.0.2.

energy gap

$E_{g,dir}$ (A)	0.26 eV	$T = 300\text{ K}$	electroreflectance	75S
(B)	0.30 eV			
(C)	0.79 eV			
dE_g/dT	$-2.2\cdot10^{-4}\text{ eVK}^{-1}$	$T = 0...300\text{ K}$	transport	75D
	$-2.3\cdot10^{-4}\text{ eV K}^{-1}$	$T = 300\text{ K}$	photoconductivity	81D

effective masses

$m_{n,\perp}$	$0.05\ m_0$		Faraday effect	78K,
$m_{n,\parallel}$	$0.048\ m_0$			75D
$m_{p1,\perp}$	$0.10\ m_0$		calculated	75D,
$m_{p1,\parallel}$	$0.018\ m_0$		calculated	80D1
$m_{p1,ds}$	$0.5\ m_0$		transport	

Lattice properties

lattice parameters

a	$6.089(5)\text{ \AA}$		RT	75S
c	$11.925(10)\text{ \AA}$			
c/a	$1.957(2)$			

density

d	5.71 g cm^{-3}		RT	75S
-----	-------------------------	--	----	-----

linear thermal expansion coefficient

α	$3.2\cdot10^{-6}\text{ K}^{-1}$	$T = 300\text{ K}$	a axis	80P
	$4.5\cdot10^{-6}\text{ K}^{-1}$		c axis	

Debye temperature

Θ_D	$234.4(53)\text{ K}$	$T \rightarrow 0\text{ K}$		65A
------------	----------------------	----------------------------	--	-----

melting temperature

T_m	$868(2)\text{ K}$			75S
-------	-------------------	--	--	-----

Transport and optical properties

carrier concentrations, electrical resistivity, carrier mobilities

n-type samples

n	$10^{18}...10^{19}\text{ cm}^{-3}$		single crystals	87N
μ_n	$6300\text{ cm}^2\text{ V}^{-1}\text{ s}^{-1}$		single crystals	87N

for T - and p -dependence, see also Fig. 7.15.1

n	10^{18} cm^{-3}	$T = 300\text{ K}$		76S,
ρ	$4.41\cdot10^{-4} \dots 1.35\cdot10^{-3}\text{ }\Omega\text{ cm}$	$T = 77...300\text{ K}$		75A1
μ_n	$1.1...1.5\cdot10^4\text{ cm}^2\text{ V}^{-1}\text{ s}^{-1}$	$T = 300\text{ K}$		75D

p-type samples (values for $T = 300$ K)

p	$1.9 \cdot 10^{17} \dots 1.8 \cdot 10^{19} \text{ cm}^{-3}$			75S, 75A2, 76D
σ	$35 \dots 116 \Omega^{-1} \text{ cm}^{-1}$			80D1,
μ_p	$42.6 \dots 36 \text{ cm}^2 \text{ V}^{-1} \text{ s}^{-1}$		heavy holes	80D2
	$546 \dots 510 \text{ cm}^2 \text{ V}^{-1} \text{ s}^{-1}$		light holes	

dielectric constant

$\varepsilon(0)$	12.1	$T = 300$ K	unpolarized	80P
------------------	------	-------------	-------------	-----

References to 7.15

- 65A Leroux-Hugon, P., Veyssie, J. J.: Phys. Status Solidi 8 (1965) 561.
- 75A1 Averkieva, G. K., Prochukhan, V. D., Rud', Yu. V., Tashtanova, M.: Izv. Akad. Nauk SSSR, Neorg. Mater. 11 (1975) 607.
- 75A2 Amirkhanov, Kh. I., Daunov, M. I., Magomedov, A. B., Magomedov, Ya. B., Emirov, S. N.: High Temp. - High Pressure 7 (1975) 690.
- 75D Daunov, M. I., Magdiev, B. N., Magomedov, A. B.: Fiz. Tekh. Poluprovodn. 9 (1975) 1747; Sov. Phys. Semicond. (English Transl.) 9 (1976) 1147.
- 75S Shay, T. L., Wernick, T. H.: "Ternary Chalcopyrite Semiconductors" Growth, Electronics, Properties and Applications. Pergamon, 1975.
- 76D Daunov, M. I., Magomedov, A. B.: Fiz. Tekh. Poluprovodn. to (1976) 641; Sov. Phys. Semicond. (English Transl.) 10 (1976) 383.
- 76S Siegel, W., Ziegler, F.: Exp. Tech. Phys. 24 (1976) 141.
- 78K Karavaev, G. F., Barisenko, S. I.: Izv. Vyssh. Uchebn. Zaved. Fiz. 6 (1978) 28.
- 80D1 Daunov, M. I., Magomedov, A. B.: Fiz. Tekh. Poluprovodn. 14 (1980) 341; Sov. Phys. Semicond. (English Transl.) 14 (1980) 199.
- 80D2 Daunov, M. I., Magomedov, A. B., Ramazanov, A. E.: Phys. Status Solidi (a) 60 (1980) 651.
- 80P Popov, A. S., Trifonova, E. P.: Phys. Status Solidi (a) 58 (1980) 679.
- 81D Dovletmuradov, Ch., Lebedev, A. A., Rud', Yu. V., Serginaov, M., Skoryukin, V. E.: Sov. Phys. Semicond. 15 (1981) 1369 (transl. from Fiz. Tekh. Poluprovodn. 15 (1981) 2357).
- 87N Nakashima, Y., Hamaguchi, C.: J Phys. Soc. Jpn. 56 (1987) 3248.

Figures to 7.15

Fig. 7.0.1

The chalcopyrite lattice

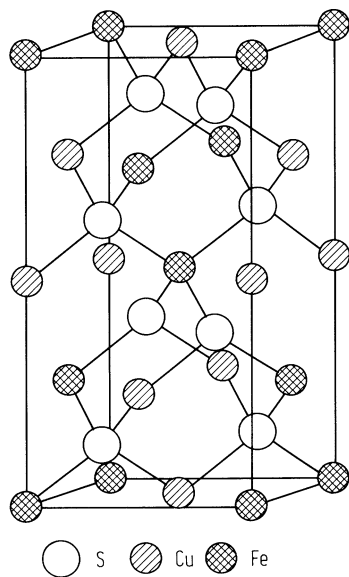


Fig. 7.0.2

Brillouin zone of the chalcopyrite lattice

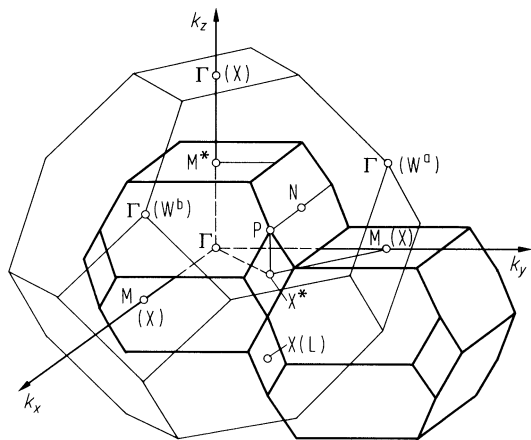


Fig. 7.0.12

Band structure of CdSnAs_2 .

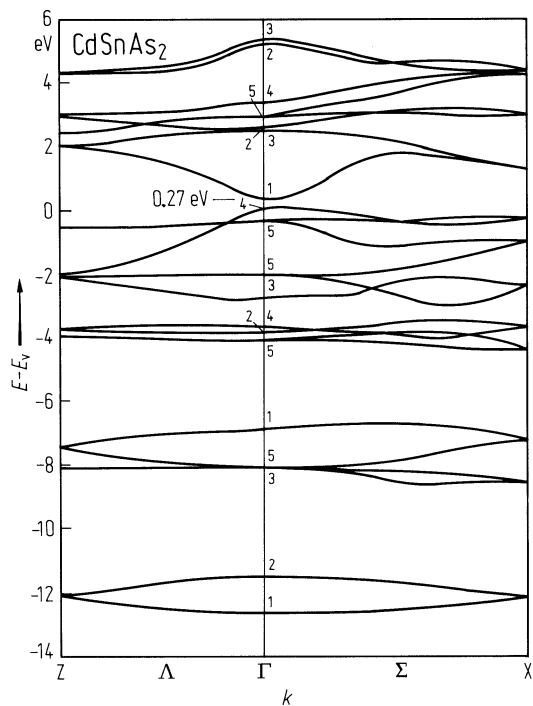
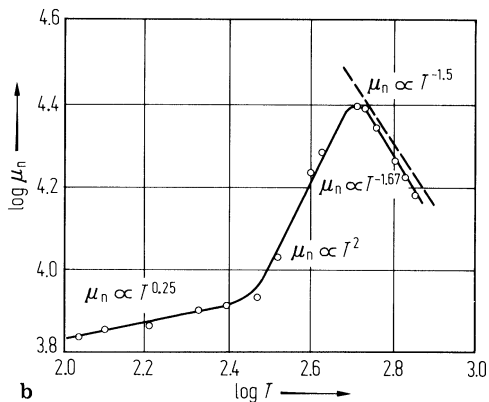
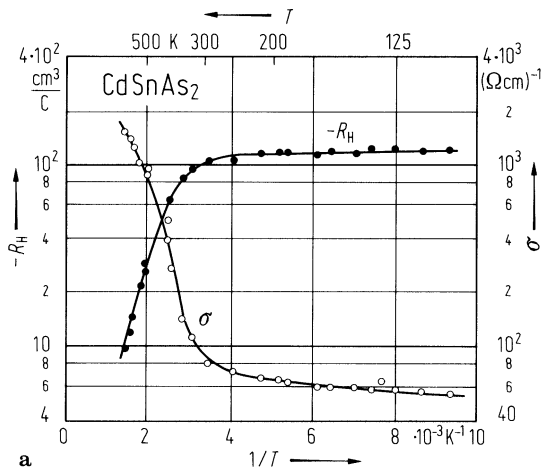


Fig. 7.15.1

CdSnAs_2 . (a) Conductivity and Hall coefficient vs. (reciprocal) temperature, (b) log electron mobility vs. $\log T$ for an n-type sample with $n = 6 \cdot 10^{16} \text{ cm}^{-3}$. T in K. μ in $\text{cm}^2 \text{ V}^{-1} \text{ s}^{-1}$ [75S].



8 I₂-IV-VI₃ compounds

8.0 Crystal structure

The I₂-IV-VI₃ compounds have received very little attention. Their structures are not known in detail. They generally adopt a disordered zincblende-like form with some tendency to superstructure formation, usually tetragonal, chalcopyrite like.

8.1 Copper germanium sulfide (Cu₂GeS₃)

Crystal structure, lattice properties

Cu ₂ GeS ₃	tetragonal	$a = 5.317 \text{ \AA}$ $c = 10.438 \text{ \AA}$	$T < 940 \text{ K}$ possible superstructure as below(monoclinic)	69B, 74K
	monoclinic; C _s ³ -Bm, C ₂ ³ -B2 or C _{2h} ³ -B2/m	$a = 7.464(5) \text{ \AA}$ $b = 22.38(1) \text{ \AA}$ $c = 10.640(1) \text{ \AA}$ $\gamma = 91^{\circ}52'$		74K
	cubic (disordered)	$a = 5.317 \text{ \AA}$	$T > 940 \text{ K}$	69B

linear thermal expansion coefficient

α	$7.2 \cdot 10^{-6} \text{ K}^{-1}$	$T = 300 \text{ K}$		64B
----------	------------------------------------	---------------------	--	-----

thermal conductivity

κ	$12 \cdot 10^{-3} \text{ W cm}^{-1} \text{ K}^{-1}$	$T = 300 \text{ K}$	with excess Ge	69B
	$7.7 \cdot 10^{-3} \text{ W cm}^{-1} \text{ K}^{-1}$	$T = 300 \text{ K}$		64B

Debye temperature

Θ_D	254 K	$T = 300 \text{ K}$		69B
------------	-------	---------------------	--	-----

heat capacity

c	$0.51 \text{ J g}^{-1} \text{ K}^{-1}$	$T = 300 \text{ K}$		69B
-----	--	---------------------	--	-----

melting temperature

T_m	1220(10) K		phase transition at 940 K	69B
-------	------------	--	---------------------------	-----

density

d	4.45 g cm^{-3}			74K 64K
-----	--------------------------	--	--	------------

wavenumbers of IR active phonons

$\bar{\nu}_{\text{LO}}/\bar{\nu}_{\text{TO}}$	427/421 cm ⁻¹	$E \parallel a_0$	infrared reflectivity	89N
	394/387 cm ⁻¹			
	351/343 cm ⁻¹			
	315/310 cm ⁻¹			
	296/294 cm ⁻¹			
	280/269 cm ⁻¹	$E \parallel b_0$		
	397/394 cm ⁻¹			
	353/334 cm ⁻¹			
	321/312 cm ⁻¹			
	272/252 cm ⁻¹			

Electronic and transport properties

energy gap

$E_{g,th}$	0.3 eV		transport	69B,
------------	--------	--	-----------	------

electrical conductivity, resistivity, carrier concentration, mobility

(at 300 K except where otherwise stated)

For temperature dependence of σ , ρ , see Figs. 8.1.1, 8.1.2.

p-type samples

σ	$17.3 \Omega^{-1} \text{ cm}^{-1}$	69B
p	$3 \cdot 10^{17} \text{ cm}^{-3}$	
μ_p	$360 \text{ cm}^2 \text{ V}^{-1} \text{ s}^{-1}$	

n-type samples

ρ	$3.2 \cdot 10^2 \Omega \text{ cm}$	74K
μ_n	$3 \text{ cm}^2 \text{ V}^{-1} \text{ s}^{-1}$	

References to 8.1

- 64K Kharakhonin, F. F., Petrov, V. M.: Fiz. Tverd. Tela 6 (1964) 2867.
- 69B Berger, L. I., Prochukhan, V. D.: Ternary Diamond-like Semiconductors. New York: Consultants Bureau, 1969.
- 70A Aliev, S. N., Magomedov, Ya. B., Shchegol'kova, Ya. B.: Teplofiz. Vys. Temp. 8 (1970) 672.
- 74K Khanafer, M., Gorochoy, O., Rivet, J.: Mater. Res. Bull. 9 (1974) 1543.
- 89N Neumann, H., Riede, V., Sharif, N., Sobotta, H., Omar, M.S.: J. Mater. Sci. Lett. 8 (1989) 1360.

Figures to 8.1

Fig. 8.1.1

Cu_2SnTe_3 (1), Cu_2GeTe_3 (2), Cu_2SnSe_3 (3), Cu_2GeSe_3 (4), Cu_2SnS_3 (5), Cu_2GeS_3 (6). Electrical conductivity vs reciprocal temperature (the perpendicular lines are melting temperatures) [70A]. (1, 2): metallic solid, semiconducting liquid, (3...6): intrinsic semiconductor.

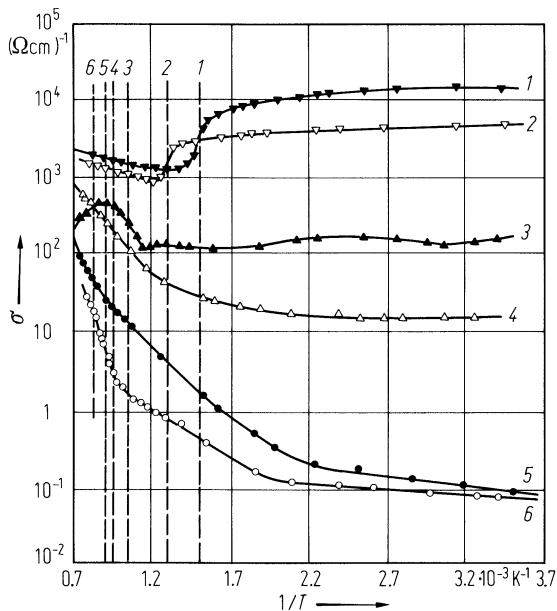
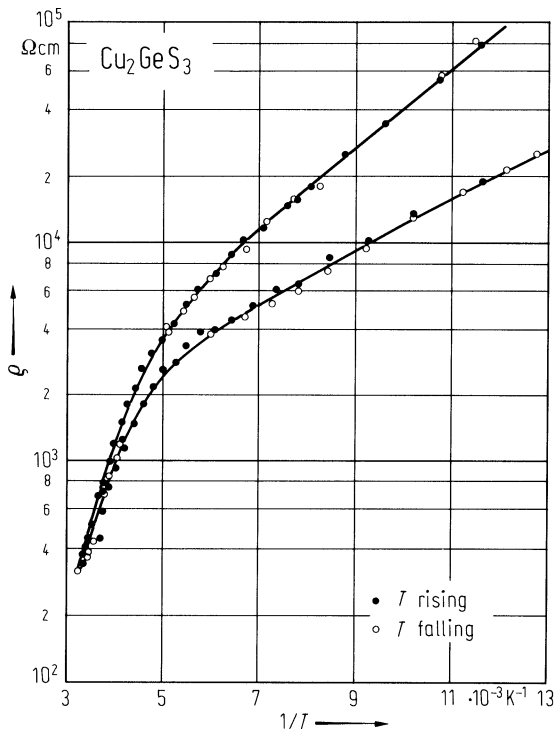


Fig. 8.1.2

Cu_2GeS_3 . Resistivity vs. reciprocal temperature [74K]. n-type sample.



8.2 Copper germanium selenide (Cu₂GeSe₃)

Crystal structure, lattice properties

Cu ₂ GeSe ₃	tetragonal	$a = 5.5913 \text{ \AA}$	$T = 303 \text{ K}$	69B, 70S
		$c = 10.977(2) \text{ \AA}$		
		$a = 5.6022(6) \text{ \AA}$	$T = 393 \text{ K}$	
		$c = 10.984(2) \text{ \AA}$		
		$a = 5.6103(6) \text{ \AA}$	$T = 473 \text{ K}$	
		$c = 10.987(3) \text{ \AA}$		
		$a = 5.6193(10) \text{ \AA}$	$T = 573 \text{ K}$	
	monoclinic	$c = 10.990(3) \text{ \AA}$		75S
		$a = 5.6193(10) \text{ \AA}$	$T = 673 \text{ K}$	
		$c = 10.994(5) \text{ \AA}$		
	cubic (disordered)	$a = 5.512 \text{ \AA}$	$T = 300 \text{ K}; \text{ Ge-deficient}$	75S
		$b = 5.598 \text{ \AA}$		
		$c = 5.486 \text{ \AA}$		
		$\beta = 98.7^\circ$		
		$a = 5.568 \text{ \AA}$	$T = 300 \text{ K}; \text{ Ge-excess}$	75S

linear thermal expansion coefficient

α	$8.4 \cdot 10^{-6} \text{ K}^{-1}$	$T = 300 \text{ K}$	64B
----------	------------------------------------	---------------------	-----

Debye temperature

Θ_D	168 K	$T = 300 \text{ K}$	69B
------------	-------	---------------------	-----

heat capacity

c	$0.34 \text{ J g}^{-1} \text{ K}^{-1}$	$T = 300 \text{ K}$	69B
-----	--	---------------------	-----

melting temperature

T_m	2050(10) K		69B
-------	------------	--	-----

density

d	5.57 g cm^{-3}		70S
-----	--------------------------	--	-----

Electronic and transport properties

energy gaps

E_g	0.94(5) eV	$T = 293 \text{ K}$	photoconductivity	64K
$E_{g,th}$	0.25 eV		transport, contradictory results	64K
	0.6(1) eV			
	1.1 eV			

electrical conductivity, hole concentration, hole mobility

p-type samples

σ	$50 \text{ \Omega}^{-1} \text{ cm}^{-1}$			62P
p	$6 \cdot 10^{20} \text{ cm}^{-3}$			
μ_p	$283 \text{ cm}^2 \text{ V}^{-1} \text{ s}^{-1}$		$\mu \propto T^{-3/2}$ after annealing [71E]	

see also Fig. 8.2.1.

thermal conductivity

κ	$2.4 \cdot 10^{-2} \text{ W cm}^{-1} \text{ K}^{-1}$	$T = 300 \text{ K}$	with excess Ge	69B
----------	--	---------------------	----------------	-----

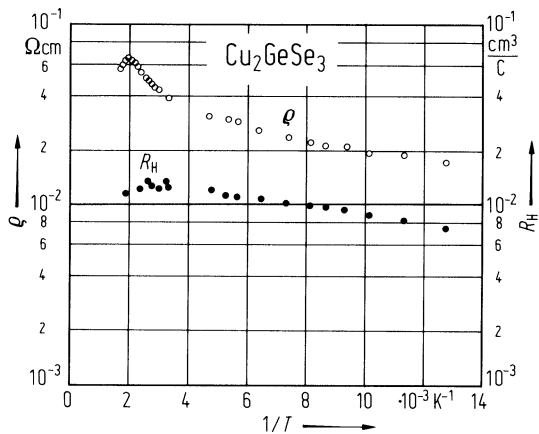
References to 8.2

- 62P Palatnik, L. S., Koshkin, V. M., Gal'chinetskii, L. P., Kolesnikov, V. I., Komnik, Yu. F.: Fiz. Tverd. Tela 4 (1962) 1430.
- 64B Berger, L. I., Balanevskaya, A. E.: Fiz. Tverd. Tela 6 (1964) 1311.
- 64K Kharakhorin, F. F., Petrov, V. M.: Fiz. Tverd. Tela 6 (1964) 2867.
- 69B Berger, L. I., Prochukhan, V. D.: Ternary Diamond-like Semiconductors. New York: Consultants Bureau, 1969.
- 70S Sharma, B. B.: Phys. Status Solidi (a) 2 (1970) K13.
- 71E Endo, S., Sudo, I., Irie, T.: Jpn. J. Appl. Phys. 10 (1971) 218.
- 75S Sharma, B. B., Ayyar, R., Singh, H.: Phys. Status Solidi (a) 29 (1975) K17.

Figures to 8.2

Fig. 8.2.1

Cu_2GeSe_3 . Resistivity and Hall coefficient vs. reciprocal temperature; as grown material, p-type ($p = 6 \cdot 10^{20} \text{ cm}^{-3}$) [71E].



8.3 Copper germanium telluride (Cu₂GeTe₃)

Crystal structure, lattice properties

Cu ₂ GeTe ₃	tetragonal	$a = 5.959 \text{ \AA}$ $c = 11.858 \text{ \AA}$	$T = 300 \text{ K}$; probably 2 phases	77S
-----------------------------------	------------	---	---	-----

melting temperature

T_m	800(50) K	69B
-------	-----------	-----

density

d	5.95 g cm ⁻³	69B
-----	-------------------------	-----

Transport properties

transport: metallic

electrical conductivity

σ	$1.4 \dots 3.9 \cdot 10^{-3} \Omega^{-1} \text{ cm}^{-1}$	$T = 300 \text{ K}$	62P, 69B
----------	---	---------------------	-------------

thermal conductivity

κ	$0.13 \text{ W cm}^{-1} \text{ K}^{-1}$	$T = 300 \text{ K}$	69B
----------	---	---------------------	-----

References to 8.3

- 62P Palatnik, L. S., Koshkin, V. M., Gal'chinetskii, L. P., Kolesnikov, V. I., Komnik, Yu. F.: Fiz. Tverd. Tela 4 (1962) 1430.
- 69B Berger, L. I., Prochukhan, V. D.: Ternary Diamond-like Semiconductors. New York: Consultants Bureau, 1969.
- 77S Sharma, B. B., Ayyar, R., Singh, H.: Phys. Status Solidi (a) 40 (1977) 691.

8.4 Copper tin sulfide (Cu₂SnS₃)

Crystal structure, lattice properties

Cu ₂ SnS ₃	cubic (disordered)	$a = 5.445 \text{ \AA}$	$T = 300 \text{ K}$; possible super-structure, see below (monoclinic)	69B
	monoclinic	$a = 23.10(1) \text{ \AA}$ $b = c = 6.25 \cdot 3n \text{ \AA}$ $\alpha = 101^\circ$	$T = 300 \text{ K}$	

linear thermal expansion coefficient

α	$7.8 \cdot 10^{-6} \text{ K}^{-1}$	$T = 300 \text{ K}$	64B
----------	------------------------------------	---------------------	-----

Debye temperature

Θ_D	168 K	$T = 300 \text{ K}$	69B
------------	-------	---------------------	-----

heat capacity

c	$0.34 \text{ J g}^{-1} \text{ K}^{-1}$	$T = 300 \text{ K}$	69B
-----	--	---------------------	-----

melting temperature

T_m	1120(10) K		69B
-------	------------	--	-----

density

d	5.02 g cm^{-3}		69B
-----	--------------------------	--	-----

Electronic and transport properties

energy gaps

E_g	0.91(1) eV	$T = 293 \text{ K}$	photoconductivity	64K
$E_{g,th}$	0.59 eV		transport	70A

electrical conductivity, carrier concentration, mobility

(at 300 K except where otherwise stated)

p-type samples

σ	$0.49 \text{ }\Omega^{-1} \text{ cm}^{-1}$	RT	62P
p	$6.1 \cdot 10^{17} \text{ cm}^{-3}$		
μ_p	$605 \text{ cm}^2 \text{ V}^{-1} \text{ s}^{-1}$		

n-type samples (monoclinic form)

ρ	$1.3 \dots 3.6 \cdot 10^{-2} \text{ }\Omega \text{ cm}$	for temperature dependence of ρ , see Fig. 8.4.1	74K
n	$1.2 \cdot 10^{20} \text{ cm}^{-3}$		
μ_n	$0.50 \text{ cm}^2 \text{ V}^{-1} \text{ s}^{-1}$		

thermal conductivity

κ	$2.8 \cdot 10^{-2} \text{ W cm}^{-1} \text{ K}^{-1}$	$T = 300 \text{ K}$	69B
----------	--	---------------------	-----

References to 8.4

62P Palatnik, L. S., Koshkin, V. M., Gal'chinetskii, L. P., Kolesnikov, V. I., Komnik, Yu. F.: Fiz. Tverd. Tela 4 (1962) 1430.

64B Berger, L. I., Balanetskaya, A. E.: Fiz. Tverd. Tela 6 (1964) 1311.

64K Kharakhorin, F. F., Petrov, V. M.: Fiz. Tverd. Tela 6 (1964) 2867.

69B Berger, L. I., Prochukhan, V. D.: Ternary Diamond-like Semiconductors. New York: Consultants Bureau, 1969.

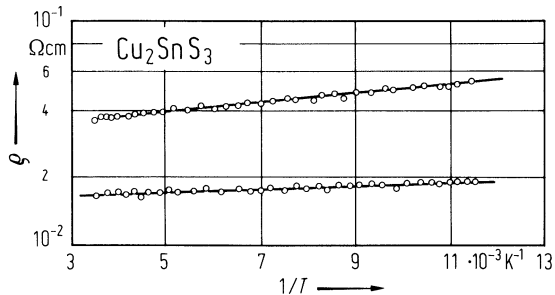
70A Aliev, S. N., Magomedov, Ya. B., Shchegol'kova, Ya. B.: Teplofiz. Vys. Temp. 8 (1970) 672.

74K Khanafer, M., Gorochoy, O., Rivet, J.: Mater. Res. Bull. 9 (1974) 1543.

Figures to 8.4

Fig. 8.4.1

Cu_2SnS_3 . Resistivity vs. reciprocal temperature for two n-type samples (monoclinic form) [74K].



8.5 Copper tin selenide (Cu₂SnSe₃)

Crystal structure, lattice properties

Cu ₂ SnSe ₃	cubic(disordered)	$a=5.6877(2)\text{ \AA}$	$T=300\text{ K}$	72S, 77S
-----------------------------------	-------------------	--------------------------	------------------	-------------

linear thermal expansion coefficient

α	$8.9\cdot10^{-6}\text{ K}^{-1}$	$T=300\text{ K}$		64B
	$20.4\cdot10^{-6}\text{ K}^{-1}$	$T=300\text{ K}$	(decreases at higher T)	72S

Debye temperature

Θ_D	148 K	$T=300\text{ K}$		69B
------------	-------	------------------	--	-----

heat capacity

c	$0.31\text{ J}^{-1}\text{ g}^{-1}\text{ K}^{-1}$	$T=300\text{ K}$		69B
-----	--	------------------	--	-----

melting temperature

T_m	970(5) K			69B
-------	----------	--	--	-----

density

d	5.94 g cm^{-3}			69N
-----	-------------------------	--	--	-----

Electronic and transport properties

energy gaps

E_g	0.96(5) eV	$T=293\text{ K}$	photoconductivity	64K
$E_{g,th}$	0.6...0.83 eV		transport	62P, 64K, 70A

electrical conductivity, carrier concentration, mobility

p-type samples, $T=300\text{ K}$

σ	$71...91\text{ }\Omega^{-1}\text{ cm}^{-1}$		for temperature dependence of σ , see Fig. 8.5.1	69B, 62P
p	$1.4\cdot10^{18}\text{ cm}^{-3}$			
μ_p	$870\text{ cm}^2\text{ V}^{-1}\text{ s}^{-1}$			

thermal conductivity

κ	$3.5\cdot10^{-2}\text{ W cm}^{-1}\text{ K}^{-1}$	$T=300\text{ K}$		69B
----------	--	------------------	--	-----

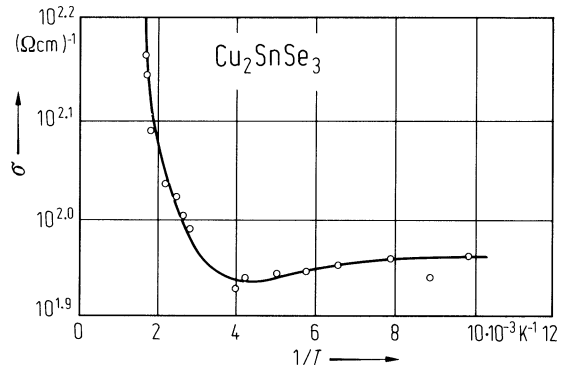
References to 8.5

62P Palatnik, L. S., Koshkin, V. M., Gal'chinetskii, L. P., Kolesnikov, V. I., Komnik, Yu. F.: Fiz. Tverd. Tela 4 (1962) 1430.
64B Berger, L. I., Balanevskaya, A. E.: Fiz. Tverd. Tela 6 (1964) 1311.
64K Kharakhorin, F. F., Petrov, V. M.: Fiz. Tverd. Tela 6 (1964) 2867.
69B Berger, L. I., Prochukhan, V. D.: Ternary Diamond-like Semiconductors. New York: Consultants Bureau, 1969.
69N Nakanishi, H., Endo, S., Irie, T.: Jpn. J. Appl. Phys. 8 (1969) 443.
70A Aliev, S. N., Magomedov, Ya. B., Shchegol'kova, Ya. B.: Teplofiz. Vys. Temp. 8 (1970) 672.
72S Sharma, B. B., Chavada, F. R.: Phys. Status Solidi (a) 14 (1972) 639.
77S Sharma, B. B., Ayyar, R., Singh, H.: Phys. Status Solidi (a) 40 (1977) 691.

Figures to 8.5

Fig. 8.5.1

Cu_2SnSe_3 . Electrical conductivity vs. reciprocal temperature [69B]. p-type sample. See also Fig. 1.



8.6 Copper tin telluride (Cu₂SnTe₃)

Crystal structure, lattice properties

Cu₂SnTe₃ cubic(disordered) $a = 6.094 \text{ \AA}$ $T = 300 \text{ K}$, probably 3 phases 77S

melting temperature

T_m 683 K 69B

density

d 6.51 g cm^{-3} 69B

Transport properties

electrical conductivity

p-type sample

σ $1.4 \cdot 10^4 \text{ } \Omega^{-1} \text{ cm}^{-1}$ $T = 300 \text{ K}$ for temperature dependence,
see Fig. 8.6.1 62P

thermal conductivity

κ $0.144 \text{ W cm}^{-1} \text{ K}^{-1}$ $T = 300 \text{ K}$ with excess Sn 69B
70 W cm⁻¹ K⁻¹ $T = 300 \text{ K}$ 70A

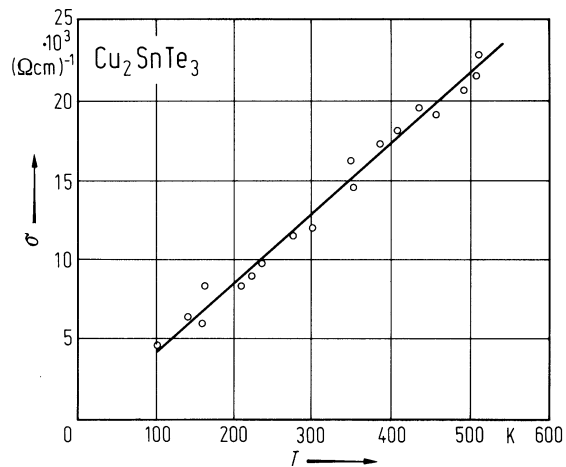
References to 8.6

62P Palatnik, L. S., Koshkin, V. M., Gal'chinetskii, L. P., Kolesnikov, V. I., Komnik, Yu. F.: Fiz. Tverd. Tela 4 (1962) 1430.
69B Berger, L. I., Prochukhan, V. D.: Ternary Diamond-like Semiconductors. New York: Consultants Bureau, 1969.
70A Aliev, S. N., Magomedov, Ya. B., Shchegol'kova, Ya. B.: Teplofiz. Vys. Temp. 8 (1970) 672.
77S Sharma, B. B., Ayyar, R., Singh, H.: Phys. Status Solidi (a) 40 (1977) 691.

Figures to 8.6

Fig. 8.6.1

Cu_2SnTe_3 . Electrical conductivity vs. temperature [69B].



8.7 Silver germanium selenide (Ag_2GeSe_3)

energy gaps

E_g	0.91(5) eV	$T = 77$ K	photoconductivity	64K
$E_{g,\text{th}}$	0.9(1) eV		transport	

electrical conductivity, carrier concentration, mobility

σ	$27 \Omega^{-1} \text{ cm}^{-1}$	$T = 300$ K		69B
p	$2 \cdot 10^{17} \text{ cm}^{-3}$			
μ_p	$850 \text{ cm}^2 \text{ V}^{-1} \text{ s}^{-1}$			

melting temperature

T_m	810 K			69B
-------	-------	--	--	-----

References to 8.7

- 64K Kharakhonin, F. F., Petrov, V. M.: Fiz. Tverd. Tela 6 (1964) 2867.
- 69B Berger, L. I., Prochukhan, V. D.: Ternary Diamond-like Semiconductors. New York: Consultants Bureau, 1969.

8.8 Silver germanium telluride (Ag_2GeTe_3)

energy gap

$E_{\text{g,th}}$	0.25 eV	transport	69B
-------------------	---------	-----------	-----

electrical conductivity, carrier concentration, mobility

(at 300 K)

σ	$92 \Omega^{-1} \text{ cm}^{-1}$		69B
----------	----------------------------------	--	-----

p	$8 \cdot 10^{17} \text{ cm}^{-3}$		
-----	-----------------------------------	--	--

μ_{p}	$720 \text{ cm}^2 \text{ V}^{-1} \text{ s}^{-1}$		69B
------------------	--	--	-----

melting temperature

T_{m}	600 K		69B
----------------	-------	--	-----

References to 8.8

69B Berger, L. I., Prochukhan, V. D.: Ternary Diamond-like Semiconductors. New York: Consultants Bureau, 1969.

8.9 Silver tin sulfide (Ag_2SnS_3)

energy gap

$E_{\text{g,th}}$ 0.5(1) eV transport 64K

electrical conductivity

see Fig. 8.9.1

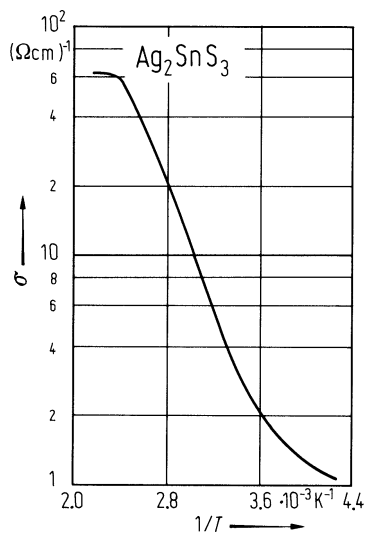
References to 8.9

64K Kharakhorin, F. F., Petrov, V. M.: Fiz. Tverd. Tela 6 (1964) 2867.

Figures to 8.9

Fig. 8.9.1

Ag_2SnS_3 . Electrical conductivity vs. reciprocal temperature [64K].



8.10 Silver tin selenide (Ag_2SnSe_3)

energy gaps

E_g	0.81(5) eV	$T = 293$ K	photoconductivity	64K
$E_{g,\text{th}}$	0.7(1) eV		transport	

electrical conductivity, carrier concentration, mobility (at 300 K)

σ	$146 \Omega^{-1} \text{cm}^{-1}$		69B
p	10^{18}cm^{-3}		
μ_p	$910 \text{cm}^2 \text{V}^{-1} \text{s}^{-1}$		

melting temperature

T_m	760 K	69B
-------	-------	-----

References to 8.10

- 64K Kharakhonin, F. F., Petrov, V. M.: Fiz. Tverd. Tela 6 (1964) 2867.
- 69B Berger, L. I., Prochukhan, V. D.: Ternary Diamond-like Semiconductors. New York: Consultants Bureau, 1969.

8.11 Silver tin telluride (Ag_2SnTe_3)

energy gap

$E_{\text{g,th}}$	0.08 eV	transport	69B
-------------------	---------	-----------	-----

electrical conductivity, carrier concentration, mobility (at 300 K)

σ	$48 \Omega^{-1} \text{ cm}^{-1}$		69B
p	$5 \cdot 10^{17} \text{ cm}^{-3}$		
μ_p	$600 \text{ cm}^2 \text{ V}^{-1} \text{ s}^{-1}$		

melting temperature

T_{m}	590 K		69B
----------------	-------	--	-----

References to 8.11

69B Berger, L. I., Prochukhan, V. D.: Ternary Diamond-like Semiconductors. New York: Consultants Bureau, 1969.

9 I₃-V-VI₄ compounds

9.0 Crystal structure

The I₃-V-VI₄ compounds have received very little attention from semiconductor physicists, in spite of the existence of three naturally occurring minerals, enargite, luzonite and famatinite, and the prediction of useful non-linear optical properties [77S].

Besides the usual disordered zincblende or wurtzite-like phases the I₃-V-VI₄ compounds adopt either the wurtzite-like enargite structure, space group C_{2v}^7 -Pmn2₁ (see Fig. 9.0.1) or the zincblende-like famatinite structure, space group D_{2d}^{11} - $I\bar{4}2m$ (see Fig. 9.0.2).

References to 9.0

77S Samanta, L. K., Bhar, G. C.: Phys. Status Solidi (a) 41 (1977) 331.

Figures to 9.0

Fig. 9.0.1

The enargite lattice

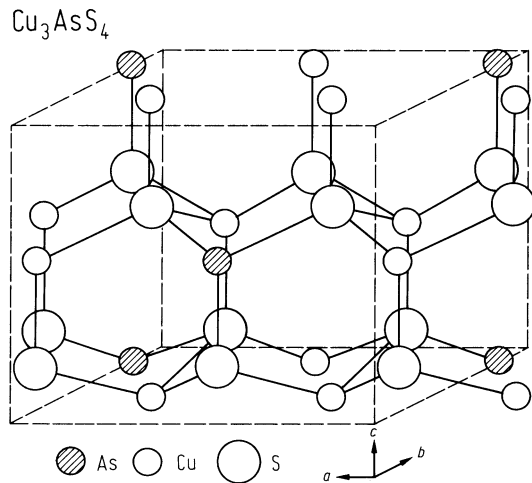
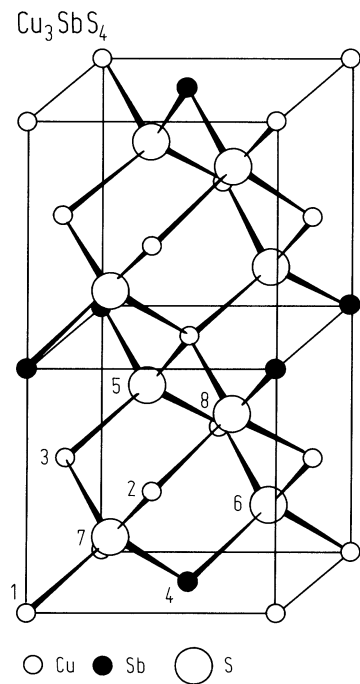


Fig. 9.0.2

The famatinite lattice



9.1 Copper thiophosphate (Cu₃PS₄)

crystal structure

enargite	$a = 7.296(2) \text{ \AA}$ $b = 6.319(2) \text{ \AA}$ $c = 6.072(2) \text{ \AA}$	$T = 300 \text{ K}$, phase transition $T = 370 \text{ K}$ (transport)	72G, 75H
----------	--	---	-------------

energy gap

$E_{g,th}$	2 eV	transport	75H
$E_{g,dir}$	2.35 eV	photoinsertion current quantum efficiency	87B

wavenumbers of infrared and Raman active phonons

$\bar{\nu}$	60 cm ⁻¹ 65 cm ⁻¹ 68 cm ⁻¹ 80 cm ⁻¹ 86 cm ⁻¹ 92 cm ⁻¹ 106 cm ⁻¹ 112 cm ⁻¹ 117 cm ⁻¹ 138 cm ⁻¹ 171 cm ⁻¹ 192 cm ⁻¹ 203 cm ⁻¹ 210 cm ⁻¹ 244 cm ⁻¹	external modes?	RT	78T
-------------	--	-----------------	----	-----

electrical conductivity, Seebeck coefficient

σ	$2.10^{-2} \dots$ $3 \cdot 10^{-4} \Omega^{-1} \text{ cm}^{-1}$	$T = 300 \text{ K}$	for temperature dependence see Fig. 9.1.1	75H
S	$8.5 \cdot 10^{-4} \text{ V K}^{-1}$	$T = 260 \text{ K}$		

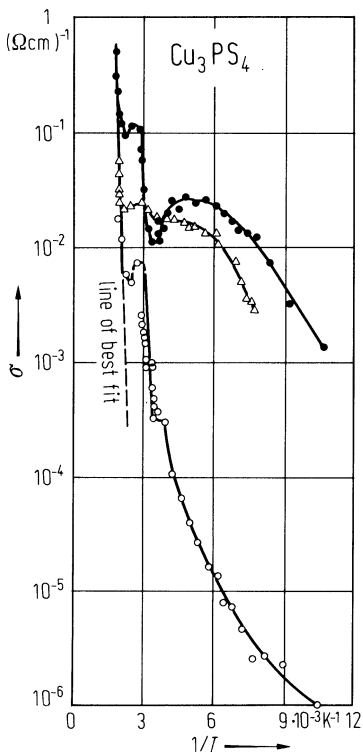
References to 9.1

72G Garin, J., Parthé, E.: Acta Crystallogr. B28 (1972) 3672.
75H Hindia, T. A., Valov, Yu. A.: Phys. Status Solidi (a) 30 (1975) K41.
78T Temperini, M. L. A., Sala, O., Bernstein, H. J.: Chem. Phys. Lett. 59 (1978) 10.
87B Betz, G., Fiechter, S., Tributsch, H.: J. Appl. Phys. 62 (1987) 4597.

Figures to 9.1

Fig. 9.1.1

Cu₃PS₄. Electrical conductivity vs. reciprocal temperature (several samples) [75H].



9.2 Copper thioarsenic, enargite, luzonite (Cu₃AsS₄)

Naturally occurring mineral, usually with considerable addition of Sb impurities.

crystal structure

Enargite: wurtzite-like structure, Luzonite: zincblende-like structure.

enargite	$a = 7.407(1) \text{ \AA}$ $b = 6.436(1) \text{ \AA}$ $c = 6.154(1) \text{ \AA}$	$T > 580 \text{ K}$	70A
famatinite	$a = 5.290 \text{ \AA}$ $c = 10.465 \text{ \AA}$	$T < 580 \text{ K}$	57G
usually called "luzonite"			

All data are for enargite.

linear thermal expansion coefficient

α	$3.2 \cdot 10^{-6} \text{ K}^{-1}$	$T = 300 \text{ K}$	69B
----------	------------------------------------	---------------------	-----

thermal conductivity

κ	$3.2 \cdot 10^{-2} \text{ W cm}^{-1} \text{ K}^{-1}$	$T = 300 \text{ K}$	69B
----------	--	---------------------	-----

melting temperature

T_m	931 K	phase transition at 580 K?	69T, 70A
-------	-------	----------------------------	-------------

energy gaps

E_g	1.24 eV	$T = 300 \text{ K}$	absorption	69B
$E_{g,th}$	0.8 eV		transport	

electrical conductivity, resistivity, carrier concentration, mobility (at 300 K)

n-type sample

σ	$200 \text{ } \Omega^{-1} \text{ cm}^{-1}$ $0.095 \text{ } \Omega^{-1} \text{ cm}^{-1}$	temperature dependence σ , Fig. 9.2.1		70A 69B
n	$7.8 \cdot 10^{19} \text{ cm}^{-3}$			
μ_n	$0.008 \text{ cm}^2 \text{ V}^{-1} \text{ s}^{-1}$			

p-type conduction is achieved by doping with Cl, I, Mn [69B].

p-type samples

p	10^{17} cm^{-3}	$T = 295 \text{ K}$	natural enargite, from Hall measurements	95P
ρ	$7 \text{ } \Omega \text{ cm}$			
μ_p	$9 \text{ cm}^2 \text{ V}^{-1} \text{ s}^{-1}$			

activation energy

E_A	0.11 eV	activation energy of conductivity	95P
-------	---------	-----------------------------------	-----

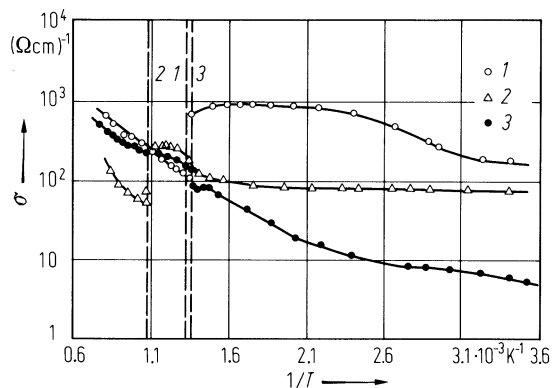
References to 9.2

- 57G Gaines, R. V.: Am. Mineralogist 42 (1957) 766.
 69B Berger, L. I., Prochukhan, V. D.: "Ternary Diamond-like Semiconductors". New York, London: Consultants Bureau 1969.
 69T Tanelli, G.: Rend. Accad. Lincei Sci. Fis. Mat. Nat. 46 (1969) 196.
 70A Adiwidjaja, G., Löhn, J.: Acta Crystallogr. B26 (1970) 2878.
 95P Pauporte, Th., Lincot, D.: Adv. Mater. Opt. Electron. 5 (1995) 289.

Figures to 9.2

Fig. 9.2.1

Cu_3AsSe_4 (1), Cu_3AsS_4 (2), Cu_3SbSe_4 (3). Electrical conductivity vs. reciprocal temperature (solid + liquid) (the perpendicular lines are melting temperatures) [70A].



9.3 Copper arsenic selenide (Cu₃AsSe₄)

crystal structure

Cu ₃ AsSe ₄	famatinite	$a = 5.570(3) \text{ \AA}$	$T < 713 \text{ K}$	69B
		$c = 10.957(5) \text{ \AA}$		
	disordered zincblende	$a = 5.5 \text{ \AA}$	$T > 713 \text{ K}, d = 7.02 \text{ g cm}^{-3} [67A]$	69B

linear thermal expansion coefficient

α	$9.5 \cdot 10^{-6} \text{ K}^{-1}$	$T = 300 \text{ K}$	69B
----------	------------------------------------	---------------------	-----

Debye temperature

Θ_D	169 K	$T = 300 \text{ K}$	69B
------------	-------	---------------------	-----

melting temperature

T_m	733 K	70A
-------	-------	-----

energy gaps

E_g	0.88 eV	$T = 300 \text{ K}$	absorption	69B
$E_{g,th}$	0.76 eV		transport	69B

electrical conductivity, Hall coefficient, carrier concentration, mobility

(at 300 K)

σ	$215 \text{ \Omega}^{-1} \text{ cm}^{-1}$	temperature dependence of σ , see Fig. 9.3.1	69B
R_H	$2.77 \text{ cm}^3 \text{ C}^{-1}$		
n	$2.7 \cdot 10^{18} \text{ cm}^{-3}$		
μ_n	$505 \text{ cm}^2 \text{ V}^{-1} \text{ s}^{-1}$		

thermal conductivity

κ	$1.9...2.7$	$T = 300 \text{ K}$	69A,
	$\cdot 10^{-2} \text{ W cm}^{-1} \text{ K}^{-1}$		69B

References to 9.3

69A Aliev, S. N., Gadzhiev, G. G., Magomedov, Ya. B.: Fiz. Tekh. Poluprovodn. 3 (1969) 1709; Sov. Phys. Semicond. (English Transl.) 3 (1970) 1437.

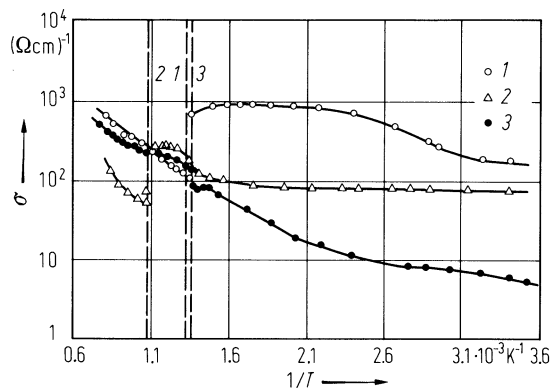
69B Berger, L. I., Prochukhan, V. D.: "Ternary Diamond-like Semiconductors". New York, London: Consultants Bureau 1969.

70A Adiwidjaja, G., Löhn, J.: Acta Crystallogr. B26 (1970) 2878.

Figures to 9.3

Fig. 9.3.1

Cu_3AsSe_4 (1), Cu_3AsS_4 (2), Cu_3SbSe_4 (3). Electrical conductivity vs. reciprocal temperature (solid + liquid) (the perpendicular lines are melting temperatures) [70A].



9.4 Copper antimony sulfide, famatinite (Cu_3SbS_4)

Naturally occurring mineral (from Sierra de Famatina, Argentina). Usually with considerable addition of As impurities. All data probably for tetragonal form.

crystal structure

Cu_3SbS_4	famatinite	$a = 5.385(1) \text{ \AA}$ $c = 10.754(2) \text{ \AA}$	$T = 300 \text{ K}$, $d = 4.635 \text{ g cm}^{-3}$ [57G]	72G
	cubic: $\text{O}_h^5\text{-Fm}3\text{m}$	$a = 10.74 \text{ \AA}$	thin films	69B
	disordered zincblende	$a = 5.28 \text{ \AA}$	high temperature, $d = 4.71 \text{ g cm}^{-3}$ [61A]	69B

energy gap

$E_{\text{g,th}}$	0.46 eV	transport	78A
-------------------	---------	-----------	-----

thermal conductivity

κ	$2.7 \cdot 10^{-2} \text{ W cm}^{-1} \text{ K}^{-1}$	$T = 300 \text{ K}$	78A
----------	--	---------------------	-----

melting temperature

T_{m}	830 K		69B
----------------	-------	--	-----

References to 9.4

- 57G Gaines, R. V.: Am. Mineralogist 42 (1957) 766.
61A Alieva, A. G., Pinsker, Z. G.: Kristallografiya 6 (1961) 204; Soviet Phys. Crystallogr. (English Transl.) 6 (1961) 161.
69B Berger, L. I., Prochukhan, V. D.: "Ternary Diamond-like Semiconductors". New York, London: Consultants Bureau 1969.
72G Garin, J., Parthé, E.: Acta Crystallogr. B28 (1972) 3672.
78A Amirkhanov, Kh. I., Gadzhiev, G. G., Magomedov, Ya. B.: Teplofiz. Vys. Temp. 16 (1978) 1232.

9.5 Copper antimony selenide (Cu₃SbSe₄)

crystal structure

Cu ₃ SbSe ₄	famatinite	$a = 5.645(1) \text{ \AA}$	$T < 688 \text{ K}$ [69A]	72G
		$c = 12.275(2) \text{ \AA}$		
	disordered zincblende	$a = 5.6$	$T > 688 \text{ K}$ [69A], $d = 5.94 \text{ g cm}^{-3}$ [67A]	69B

linear thermal expansion coefficient

α	$1.24 \cdot 10^{-5} \text{ K}^{-1}$	$T = 300 \text{ K}$		69B
----------	-------------------------------------	---------------------	--	-----

Debye temperature

Θ_D	131 K	$T = 300 \text{ K}$		69B
------------	-------	---------------------	--	-----

melting temperature

T_m	700 K		phase transition at 688 K	69A
-------	-------	--	---------------------------	-----

energy gap

E_g	0.31 eV	$T = 300 \text{ K}$	absorption	69B
	0.11 eV	$T = 300 \text{ K}$	transmission	69N
$E_{g,th}$	0.42 eV		transport	69B
	0.76 eV			76D
dE_g/dT	$1.27 \cdot 10^{-5} \text{ K}^{-1}$		cathodoluminescence	76D

effective mass

m_p	$0.73 m_0$	$T = 320 \text{ K}$	Seebeck effect	69N
-------	------------	---------------------	----------------	-----

hole concentration, mobility (at 300 K)

p-type samples (see Figs. 9.5.1...3 for temperature dependence of transport parameters)

p	$7 \cdot 10^{18} \text{ cm}^{-3}$		unannealed	76D
	$6 \dots 8 \cdot 10^{17} \text{ cm}^{-3}$		annealed	
μ_p	$60 \dots 40 \text{ cm}^2 \text{ V}^{-1} \text{ s}^{-1}$			

thermal conductivity

κ	1.46	$T = 300 \text{ K}$		69B
	$\cdot 10^{-2} \text{ W cm}^{-1} \text{ K}^{-1}$			

References to 9.5

- 67A Annamamedov, R., Berger, L. T., Petrov, V. M., Slobodchikov, S. V.: *Izv. Akad. Nauk SSSR, Neorg. Mater.* 3 (1967) 1370.
- 69A Aliev, S. N., Gadzhiev, G. G., Magomedov, Ya. B.: *Fiz. Tekh. Poluprovodn.* 3 (1969) 1709; *Sov. Phys. Semicond. (English Transl.)* 3 (1970) 1437.
- 69B Berger, L. I., Prochukhan, V. D.: "Ternary Diamond-like Semiconductors". New York, London: Consultants Bureau 1969.
- 69N Nakanishi, H., Endo, S., Irie, T.: *Jpn. J. Appl. Phys.* 8 (1969) 443.
- 70A Adiwidjaja, G., Löhn, J.: *Acta Crystallogr.* B26 (1970) 2878.
- 72G Garin, J., Parthé, E.: *Acta Crystallogr.* B28 (1972) 3672.
- 76D Dirochka, A. T., Ivanova, G. S., Kurbatov, L. N., Sinitsyn, E. V., Kharakhorin, F. F., Kholina, E. I.: *Izv. Akad. Nauk SSSR, Neorg. Mater.* 12 (1976) 339; *Inorg. Mater. (USSR) (English Transl.)* 12 (1976) 290.

Figures to 9.5

Fig. 9.5.1

Cu_3AsSe_4 (1), Cu_3AsS_4 (2), Cu_3SbSe_4 (3). Electrical conductivity vs. reciprocal temperature (solid + liquid) (the perpendicular lines are melting temperatures) [70A].

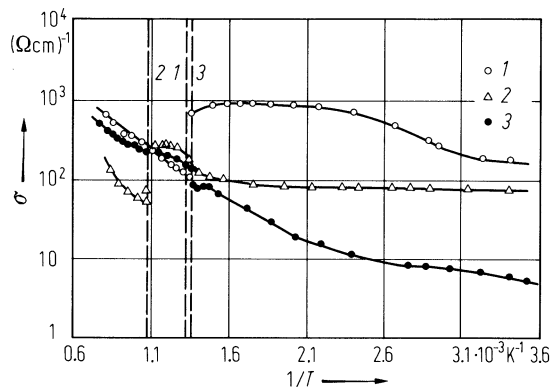


Fig. 9.5.2

Cu_3SbSe_4 . Resistivity, Hall coefficient vs. (reciprocal) temperature (various samples) [69N].

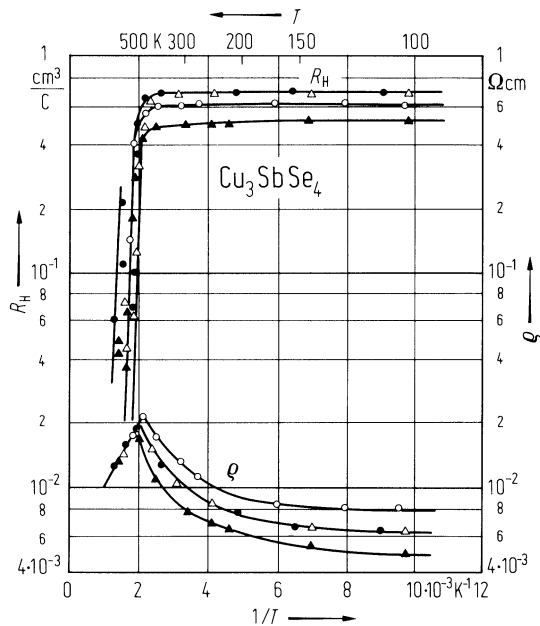
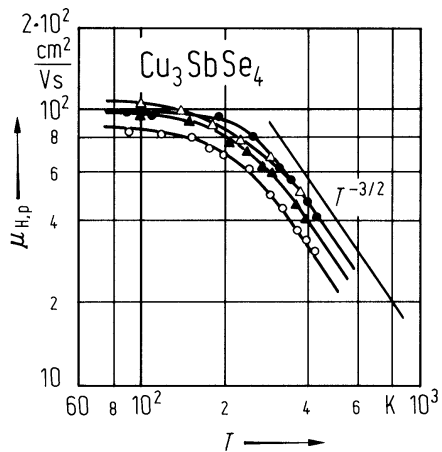


Fig. 9.5.3

Cu_3SbSe_4 . Hall mobility of holes vs. temperature (various samples) [69N].



9.6 Copper arsenic telluride (Cu_3AsTe_4)

electrical conductivity, Seebeck coefficient

temperature dependence: Fig. 9.6.1

thermal conductivity

κ	$5.9 \cdot 10^{-2} \text{ W cm}^{-1} \text{ K}^{-1}$	$T = 300 \text{ K}$	77G
----------	--	---------------------	-----

melting temperature

T_m	600 K	77G
-------	-------	-----

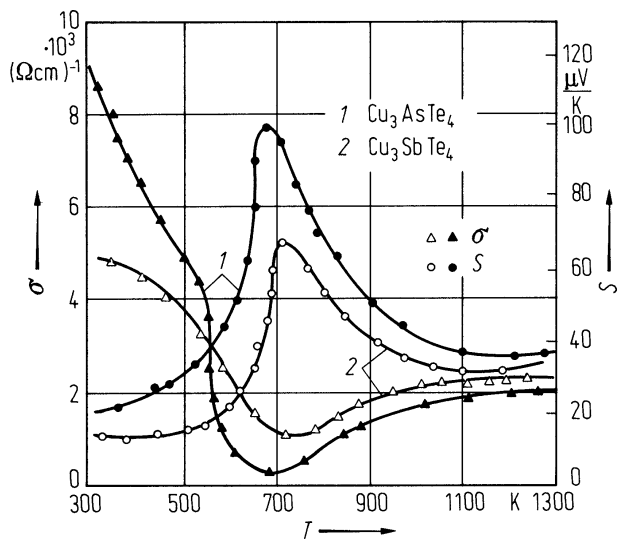
References to 9.6

77G Gadzhiev, G. G., Magdiev, B. N.: Teplofiz. Vys. Temp. 15 (1977) 425.

Figures to 9.6

Fig. 9.6.1

Cu_3AsTe_4 (1), Cu_3SbTe_4 (2). Electrical conductivity and thermoelectric power vs. temperature [77G].



9.7 Copper antimony telluride (Cu_3SbTe_4)

electrical conductivity, Seebeck coefficient

temperature dependence: Fig. 9.7.1

thermal conductivity

κ $5 \cdot 10^{-2} \text{ W cm}^{-1} \text{ K}^{-1}$ $T = 300 \text{ K}$ 77G

melting temperature

T_m 600 K 77G

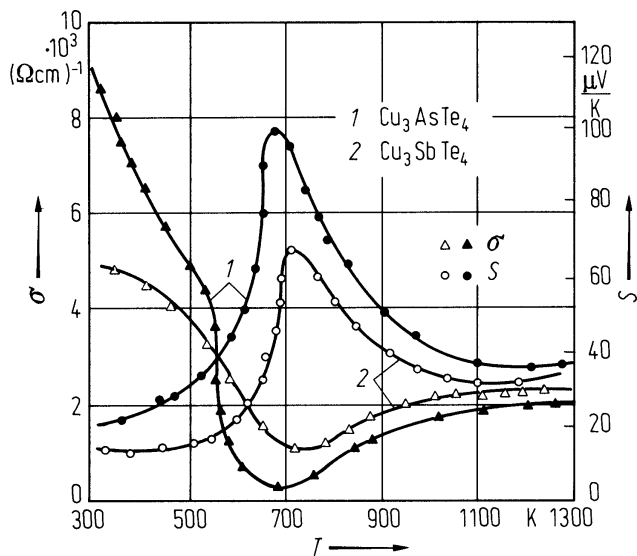
References to 9.7

77G Gadzhiev, G. G., Magdiev, B. N.: Teplofiz. Vys. Temp. 15 (1977) 425.

Figures to 9.7

Fig. 9.7.1

Cu_3AsTe_4 (1), Cu_3SbTe_4 (2). Electrical conductivity and thermoelectric power vs. temperature [77G].



10 II-III₂-VI₄ compounds

10.0 Crystal structure and electronic structure

The II-III₂-VI₄ compounds almost all have one of the two structures, defect stannite (space group $D_{2d}^{11}-I\bar{4}2m$, Fig. 10.0.1a) or defect chalcopyrite (space group $S_4^2-I\bar{4}$, Fig. 10.0.1b). Another structure occurring in this group ($CdIn_2S_4$) is the spinel structure (Fig. 10.2). For details see the respective sections.

Since chalcopyrite, defect stannite and defect chalcopyrite have the same Bravais lattice and similar space groups, they have many properties in common. For peculiarities and Brillouin zones see the discussion for chalcopyrite in section 6.0 or 7.0.

Figs. 10.0.3...5 show the band structures of $ZnIn_2S_4$, $CdIn_2S_4$ and $CdIn_2Se_4$.

References to 10.0

79A Aymerich, F., Meloni, F., Mula, G.: Solid State Commun. 29 (1979) 235.

Figures to 10.0

Fig. 10.0.1

Structure of (a) defect stannite and (b) defect chalcopyrite.

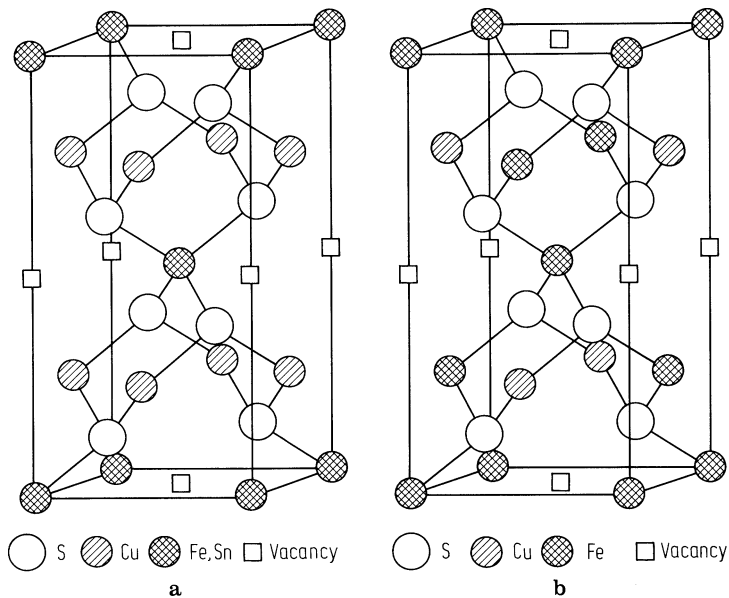
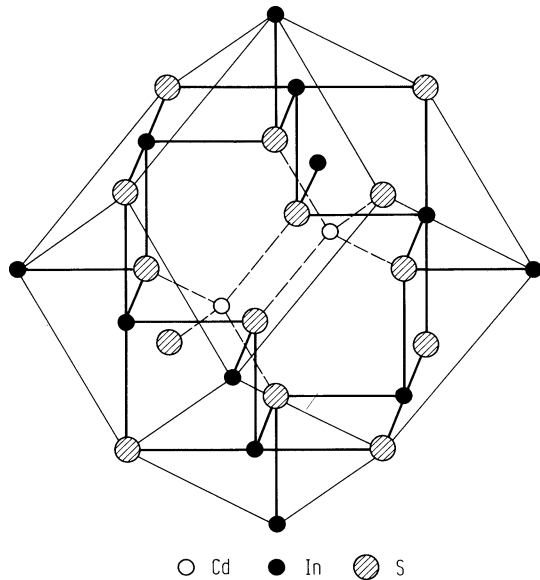


Fig. 10.0.2

Structure of spinel



ZnIn₂S₄. Band structure of α , β , and γ polytypes. Dashed lines: γ -phase, unfolded into BZ of β [79A]. $\Gamma-Z = k \parallel c$.

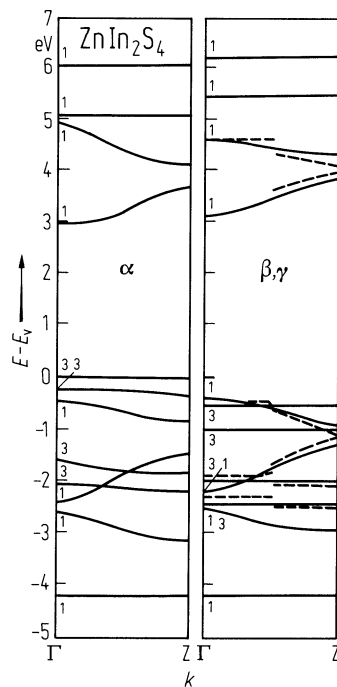


Fig. 10.0.4

Band structure of CdIn_2S_4

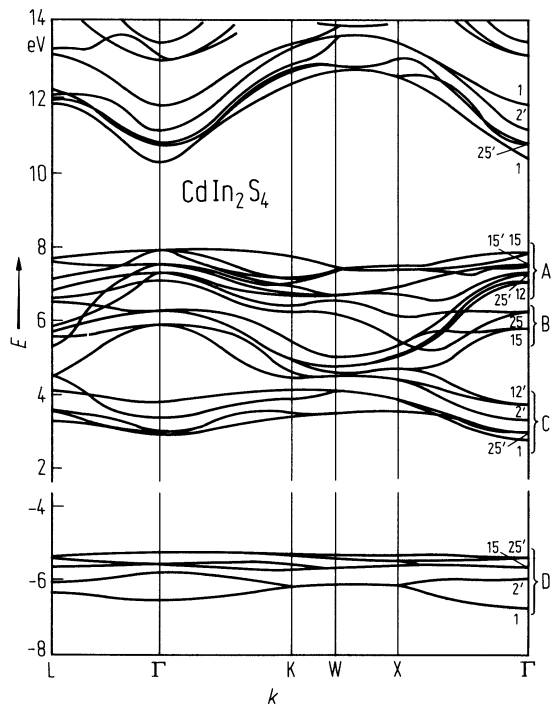
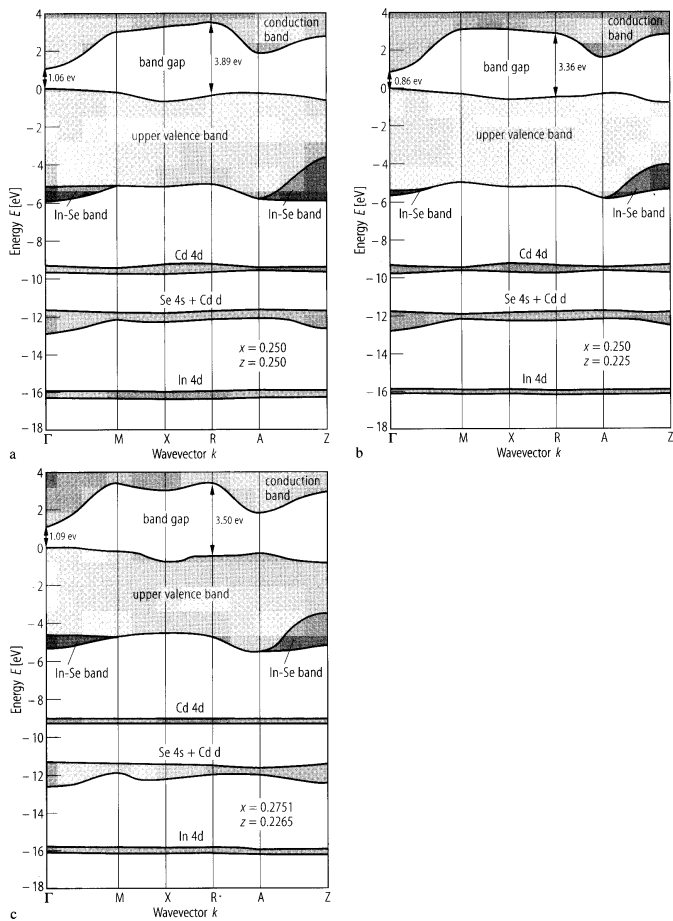


Fig. 10.0.5

Band structure of CdIn_2Se_4



10.1 Zinc aluminum sulfide (ZnAl_2S_4)

crystal structure

β' - ZnAl_2S_4 : wurtzite (space group $\text{C}_{6v}^4\text{-P6}_3\text{mc}$)

α - ZnAl_2S_4 : cubic (space group $\text{O}_h^7\text{-Fd3m}$)

lattice parameters, density

β' - ZnAl_2S_4 $a = 3.764 \text{ \AA}$, $c = 6.142 \text{ \AA}$, $d = 2.63 \text{ g cm}^{-3}$ 55H

α - ZnAl_2S_4 : $a = 9.988 \text{ \AA}$, $d = 3.30 \text{ g cm}^{-3}$ 55H

energy gap

$E_{g,\text{dir}}$ 3.7 eV RT optical absorption, wurtzite structure 95K

References to 10.1

55H Hahn, H., Frank, G., Klinger, W., Störger, A. D., Störger, G.: Z. Anorg. Allg. Chem. 279 (1955) 241.

95K Kai, T., Kaifuku, I., Aksenov, I., Sato, K.: Jpn. J. Appl. Phys., Part 1, 34 (1995) 4682.

10.2 Zinc gallium sulfide (ZnGa₂S₄)

Crystal structure

defect chalcopyrite ($S_4^2-I\bar{4}$) or defect stannite ($D_{2d}^{11}-I\bar{4}2m$)

Electronic properties

energy gap

$E_{\text{g,dir}}$	3.25 eV	$T = 298 \text{ K}$	optical absorption, pure crystals	93H,
--------------------	---------	---------------------	-----------------------------------	------

Lattice properties

lattice parameters

a	5.26 Å
	55H
c	10.4 Å
c/a	1.97
x	0.25
y	0.25
z	0.125

density

d 3.7 g cm⁻³ 55H

melting temperature

T_{m}	$> 1620 \text{ K}$	71C
----------------	--------------------	-----

wavenumbers of Raman active phonons

$\bar{\nu}$	Symmetry		
230 cm^{-1}	A	Raman spectroscopy	83L
320 cm^{-1}			
367 cm^{-1}			
108 cm^{-1}	E (TO)		
137 cm^{-1}			
260 cm^{-1}			
357 cm^{-1}			
371 cm^{-1}			
392 cm^{-1}	E (LO)		
170 cm^{-1}	B (TO)		
278 cm^{-1}			
380 cm^{-1}			
399 cm^{-1}	B (LO)		

heat capacity

smoothed values of the heat capacity (in J/mol K) [75M]

	ZnGa ₂ S ₄	ZnGa ₂ Se ₄	T [K]	ZnGa ₂ S ₄	ZnGa ₂ Se ₄	T [K]
C_p	2.92	4.98	13	100.5	128.4	120
	4.93	6.50	15	106.6	133.9	130
	8.78	12.97	20	113.0	138.5	140
	13.85	22.02	25	119.0	142.7	150
	21.38	29.82	30	124.2	146.9	160
	28.70	36.89	35	128.6	149.8	170
	35.06	43.93	40	133.0	153.0	180
	40.63	51.04	45	136.8	155.6	190
	45.40	57.32	50	139.0	157.7	200
	49.79	68.60	55	143.3	160.1	210
	53.97	69.87	60	145.3	161.0	220
	57.03	76.57	65	148.7	163.2	230
	62.55	82.05	70	151.7	164.1	240
	66.94	88.94	75	154.1	164.8	250
	69.96	94.34	80	156.3	165.5	260
	74.01	99.36	85	158.4	165.8	270
	77.95	104.3	90	160.5	166.4	280
	81.84	108.7	95	162.5	166.5	290
	85.69	113.0	100	164.6	166.6	300
	93.22	121.5	110			

Transport properties

electrical conductivity

The temperature dependence of electrical conductivity in ZnGa₂S₄ single crystals is shown in Fig. 10.2.1 [85V].

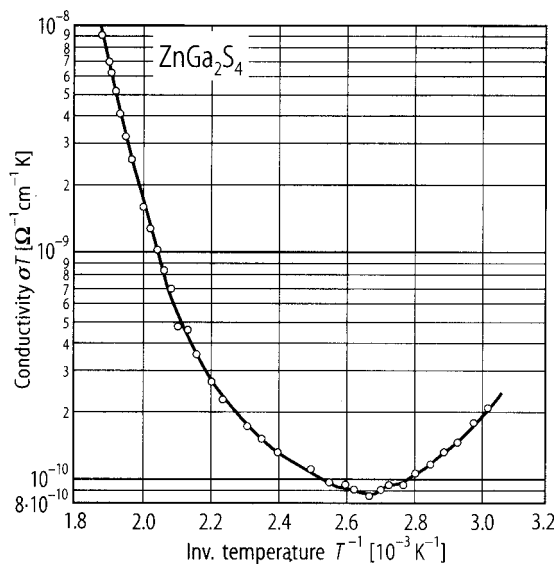
References to 10.2

- 55H Hahn, H., Frank, G., Klinger, W., Störger, A. D., Störger, G.: Z. Anorg. Allg. Chem. 279 (1955) 241.
71C Chedzey, H. A., Marshall, D. J., Parfitt, H. T., Robertson, D. S.: J. Phys. D: Appl. Phys. 4 (1971) 1320.
75M Mamedov, K. K., Kerimov, I. G., Veliev, R. K., Mekhtiev, M. I.: Izv. Akad. SSSR, Neorg. Mater. 11 (1975) 2062; Inorg. Mater. (USSR) (English Transl.) 11 (1975) 1767.
83L Lottici, P. P., Razzetti, C.: J. Phys. C16 (1983) 3449.
85V Veliev, R.K., Aldzhanov, M.A.: Phys. Status Solidi A 91 (1985) K23.
93H Hong-Lee Park, Hyung-Gon Kim, Hae-Mun Jeong, Chang-Dae Kim, Seung-Ho Cheon, Seung-Cheol Hyun, Wah-Tek Kim: Jpn. J. Appl. Phys., Supplement, 32-3 (1993) 473.

Figures to 10.2

Fig. 10.2.1

ZnGa_2S_4 . Temperature dependence of electrical conductivity in single crystals [85V].



10.3 Zinc gallium selenide (ZnGa2Se4)

Crystal structure

defect chalcopyrite (S4²⁻I4⁻) or defect stannite (D2d¹¹⁻I4⁻ 2m)

Electronic properties

energy gap

Eg,dir	2.18 eV	T = 298 K	from optical absorption	88W
Eg(T) = Eg(0) - aT ² /(T+b)				88Y
a	2.69·10 ⁻⁴ eV K ⁻¹			
b	- 460 K			

The temperature dependence of the optical energy gap for ZnGa2Se4:Cr²⁺ single crystals is shown in Fig. 10.3.1 [90W].

exciton binding energy

Eb	0.06 eV	T = 22 K	from optical absorption	88W
----	---------	----------	-------------------------	-----

Lattice properties

lattice parameters

a	5.48 Å			55H
c	10.9 Å			
c/a	2.00			
x	0.25			
y	0.25			
z	0.125			

density

d	5.13 g cm ⁻³			55H
---	-------------------------	--	--	-----

Debye temperature

ΘD	228 K	T → 0 K		89V
----	-------	---------	--	-----

heat capacity : see section 10.2.

Raman wavenumbers (at 300 K) [89T]

ν̄	285, 263, 250, 242, 235, 209, 193, 165, 145, 128, 109, 94, 84 cm ⁻¹
----	--

Transport properties

resistivity

ρ	2.5·10 ¹² Ω cm	pure single crystals	89Y
	4.1·10 ¹³ Ω cm	Co ²⁺ -doped single crystals	89Y

The temperature dependence of the electrical resistivity of ZnGa2Se4 is shown in Fig. 10.3.2 [89T].

References to 10.3

- 55H Hahn, H., Frank, G., Klinger, W., Störger, A. D., Störger, G.: Z. Anorg. Allg. Chem. 279 (1955) 241.
- 88W Wha-Tek Kim, Chang-Sub Chung, Yong-Geun Kim, Moon-Seog Jin, Hyung-Gon Kim: Phys. Rev. B 38 (1988) 2166.
- 88Y Yong-Geun Kim, Hyung-Gon Kim, Wah-Tek Kim: New Phys. (Korean Physical Society) 28 (1988) 756.
- 89T Tiginyanu, I.M., Ursaki, V.V., Fulga, V.N.: Fiz. Tekh. Poluprovodn. 23 (1989) 1725; Sov. Phys. Semicond. (Engl. Transl.) 23 (1989) 1069.
- 89V Veliev, R.K., Mamedov, K.K., Guseinov, G.G., Seidov, F.M.: Izv. Akad. Nauk SSSR, Neorg. Mater. 25 (1989) 1449 – Inorg. Mater. (Engl. Transl.) 25 (1989) 1226.
- 89Y Yong-Geun Kim, Hyung-Gon Kim, Wah-Tek Kim, Jin Sup Kim, Dong Sung Ma, Hong-Lee Park: Phys. Rev. B 39 (1989) 8747.
- 90W Wha-Tek Kim, Moon-Seog Jin, Seungcheor Hyeon, Yong-Geun Kim, Byong-Seo Park: Solid State Commun. 74 (1990) 123

Figures to 10.3

Fig. 10.3.1

ZnGa_2Se_4 . Temperature dependence of the optical energy gap for $\text{ZnGa}_2\text{Se}_4:\text{Cr}^{2+}$ (2 mol%) single crystals [90W].

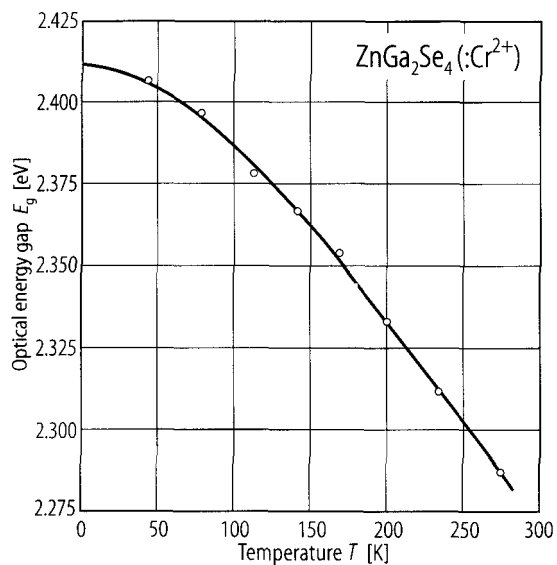
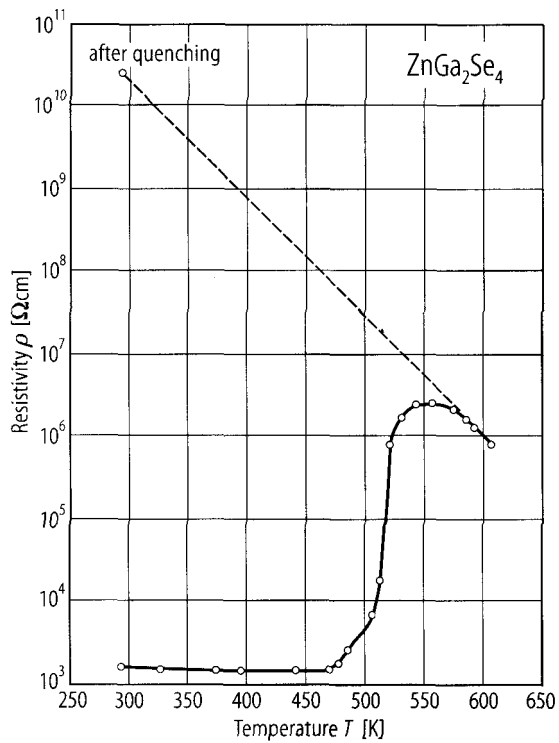


Fig. 10.3.2

ZnGa_2Se_4 . Temperature dependence of the electrical resistivity [89T].



10.4 Zinc thioindate (ZnIn2S4)

Crystal structure

ZnIn2S4 has a large number of polytypes. All polytypes however are comprised of hexagonal layers with *a* = 3.85(2) Å (the differences being in the packing of the layers) and *c* = *N*·3.086(3) Å where *N* = 4*Z* and *Z* = 1, 2, 3... is the number of formula units in the unit cell.

ZnIn2S4 (I): space group C3v¹–P3m1, lattice parameters (at 300 K): *a* = 3.85(2) Å, *c* = 12.34 Å [70D].

ZnIn2S4 (II) a: space group D3d³–P 3̄ m1, lattice parameters (at 300 K): *a* = 3.85(2) Å, *c* = 24.68(4) Å [71D].

ZnIn2S4 (II) b: space group C6v⁴–P63mc, lattice parameters (at 300 K): *a* = 3.85(2) Å, *c* = 24.68(4) Å [72D].

ZnIn2S4 (III) a: space group C3v⁵–R3m, lattice parameters (at 300 K): *a* = 3.85(2) Å, *c* = 37.02(4) Å [71D]

A very large number of polytypes for the layer structure type, including deviations from 1:2:4 stoichiometry, are known.

Electronic properties

All data are for the layered structure unless otherwise stated. Usually the polytype is ZnIn2S4 (III) a, but it is not always given.

band structure : see Fig. 10.0.3

energy gap

<i>E</i> _g	2.87(1) eV	<i>T</i> = 300 K; <i>E</i> ⊥ <i>c</i>	absorption	75R
<i>E</i> _{g,dir}	2.34 eV		Mn-doped ZnIn2S4 crystals	84V
	2.77 eV	RT	Zn3In2S6 polytype crystals	86A
	2.69 eV	RT	Zn2In2S5 polytype crystals	89K
<i>E</i> _g (⊥)	2.90 eV		from ellipsometry	84L
<i>E</i> _g ()	3.05 eV		from ellipsometry	84L

The temperature dependence of the energy gap in ZnIn2S4 is given in Fig. 10.4.1 [84A].

The temperature dependence of the energy gap in Zn2In2S5 is given in Fig. 10.4.2 [89K].

spinel modification

energy gap

<i>E</i> _g	2.4 eV	<i>T</i> = 80 K	photoluminescence and resonant Raman scattering	78U
-----------------------	--------	-----------------	---	-----

Lattice properties

frequencies of IR active phonons (in 10¹² s⁻¹, at 300 K)

ZnIn2S4 (III)

Infrared transmission [77H]

ν [10¹² s⁻¹] 20.55, 19.41, 16.23, 13.5, 11.52, 11.19, 10.83, 10.5, 10.17, 9.96, 9.66, 9.33, 8.97, 8.76, 8.19, 8.01, 7.8, 7.62, 6.99, 6.48, 5.76, 2.49, 1.23

ZnIn2S4 (spinel modification) [78U]

Infrared transmission [78U]

ν [10¹² s⁻¹] 6.75, 8.1, 9.3, 10.35

Raman wavenumbers for different polytypes

	ZnIn ₂ S ₄	Zn ₂ In ₂ S ₄	Zn ₃ In ₂ S ₆	RT	93R
$\bar{\nu}$ [cm ⁻¹]	246	251	252		
	173	185	185		
	100	171	160		
	74	123	71		
	39	74	63		
		63	57		
		57	27		
		38			
		31			
		22			
		16			

Transport and optical properties

electrical conductivity and Hall mobility : see Fig. 10.4.3

electrical resistivity, electron mobility

n-type samples

ρ	10 ¹⁰ Ω cm		single crystal	94Z
	0.8...10 Ω cm		single crystals, Mn-doped	84V
μ_n	40 cm ² V ⁻¹ s ⁻¹	RT	single crystals, Mn-doped	84V

activation energy

E_A	0.045 eV	$T = 100...300$ K	conductivity	76G
	0.02 eV	$T = 100...300$ K	Hall effect	

dielectric constant

$\epsilon(\infty)$	6.0	$T = 300$ K, $E \perp c$	infrared	76A
--------------------	-----	--------------------------	----------	-----

References to 10.4

- 70D Donika, F. G., Radautsan, S. I., Semiletov, S. A., Donika, T. V., Mustya, I. G., Zhitar, V. F.: Kristallografiya 15 (1970) 813; Sov. Phys. Crystallogr. (English Transl.) 15 (1971) 695.
- 71D Donika, F. G., Radautsan, S. I., Kiosse, G. A., Semiletov, S. A., Donika, T. V., Mustya, I. G.: Kristallografiya 16 (1971) 235; Sov. Phys. Crystallogr. (English Transl.) 16 (1971) 190.
- 72D Donika, F. G., Radautsan, S. I., Semiletov, S. A., Kiosse, G. A., Mustya, I. G.: Kristallografiya 17 (1972) 663; Sov. Phys. Crystallogr. (English Transl.) 17 (1972) 575.
- 75R Radautsan, S. I., Zhitar, V. F., Railyon, V. Ya.: Fiz. Tekh. Poluprovodn. 9 (1975) 2278; Sov. Phys. Semicond. (English Transl.) 9 (1975) 1476.
- 76A Arama, E. D., Vinogradov, E. A., Zhizhin, G. N., Zhitar, V. F., Mel'nik, N. N., Radautsan, S. I.: Dokl. Akad. Nauk SSSR 231 (1976) 1343.
- 76G Glidewell, C.: Inorg. Chim. Acta 19 (1976) L45.
- 77H Hermann, H.: Phys. Status Solidi (b) 82 (1977) 513.
- 78U Unger, W. K., Meuth, H., Irwin, J. C., Pink, H.: Phys. Status Solidi (a) 46 (1978) 81.
- 79A Aymerich, F., Meloni, F., Mula, G.: Solid State Commun. 29 (1979) 235.
- 84A Anagnostopoulos, A., Kambas, K., Ploss, B.: Phys. Status Solidi B 123 (1984) K155.
- 84L Logothetidis, S., Ves, S., Spyridelis, J.: Phys. Status Solidi B 122 (1984) 613.
- 84V Vigil, O., Calzadilla, O., Seuret, D., Vidal, J., Leccabue, F.: Solar Energy Mater. 10 (1984) 139.
- 86A Anagnostopoulos, A., Kambas, K., Spyridelis, J.: Mater. Res. Bull. 21 (1986) 407.
- 89K Kalomiro, J.A., Anagnostopoulos, A.N., Spyridelis, J.: Semicond. Sci. Technol. 4 (1989) 536.
- 93R Razzetti, C., Lottici, P.P., Bini, S., Curti, M.: Phys. Status Solidi B 177 (1993) 525.
- 94Z Zhitar, V.F., Machuga, A.I., Arama, E.D.: Fiz. Tekh. Poluprovodn. 28 (1994) 1668; Sov. Phys. Semicond. (Engl. Transl.) 28 (1994) 929.

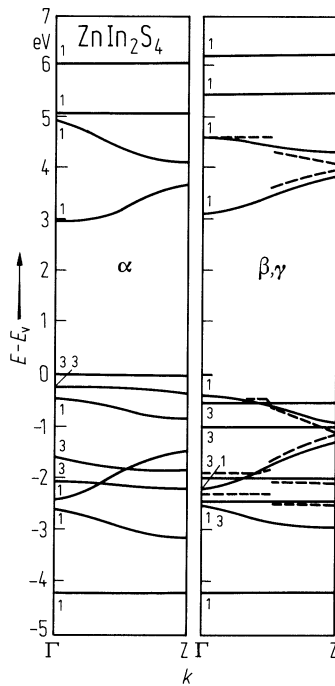


Fig. 10.4.1

ZnIn_2S_4 . The temperature dependence of the energy gap. The solid line represents the theoretical fit [84A].

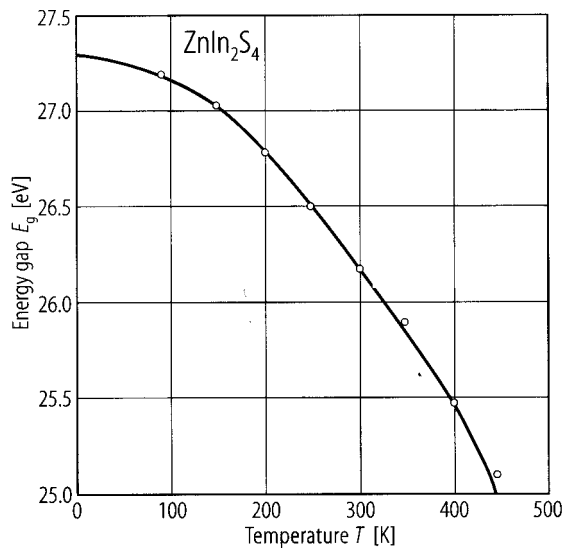


Fig. 10.4.2

$\text{Zn}_2\text{In}_2\text{S}_5$. The temperature dependence of the energy gap [89K].

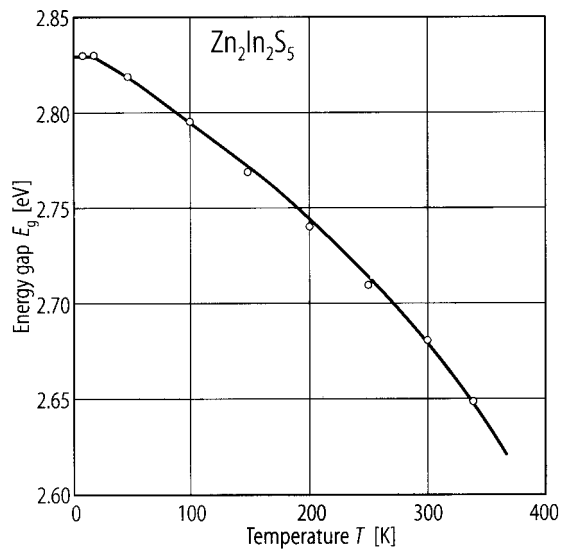
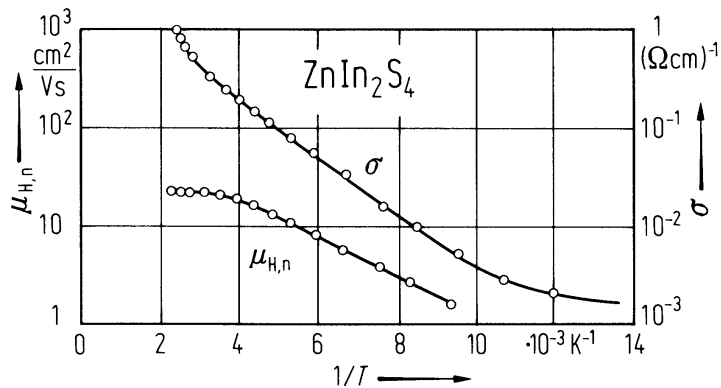


Fig. 10.4.3

ZnIn_2S_4 . Electrical conductivity and Hall mobility vs. reciprocal temperature [76G]. $E \perp c$; n-type sample.



10.5 Zinc indium selenide (ZnIn2Se4)

Crystal structure

defect chalcopyrite (S₄²⁻I $\bar{4}$)

Electronic properties

energy gap

$E_{g,dir}$	1.68 eV	$T = 300\text{ K}$	layered structure type, from transmission	90A
	2.0 eV	$T = 300\text{ K}$	photoconductivity	
dE_g/dT	$-3.1\cdot 10^{-9}\text{ eV K}^{-1}$	$T = 88\ldots 300\text{ K}$	photoconductivity(unpolarized)	74M

Lattice properties

lattice parameters

a	5.69 Å			55H
c	11.4 Å			
c/a	2.00			
x	0.26			
y	0.22			
z	0.13			

density

d	5.36 g cm ⁻³			55H
-----	-------------------------	--	--	-----

wavenumbers of infrared and Raman active phonons

		Proposed symmetry		
$\bar{\nu}_{LO}/\bar{\nu}_{TO}$	242/213 cm ⁻¹	E, B ₂	$T = 300\text{ K}$	93R
	203/196 cm ⁻¹	E, B ₂		
	165/164 cm ⁻¹	E		
	135 cm ⁻¹	A ₁		
	104/101 cm ⁻¹	B ₂		
	85/85 cm ⁻¹	E		
	68/67 cm ⁻¹	E		

Transport and optical properties

carrier concentration, resistivity, mobility

p-type samples

p	4·10 ¹³ ...	RT	thin films	92N
	5·10 ¹⁴ cm ⁻³			
ρ	2·10 ³ ...	RT	thin films	92N
	1.5·10 ⁴ Ω cm			
μ_p	15...25cm ² V ⁻¹ s ⁻¹	$T = 300\text{ K}$	thin films	92N

n-type samples

n	8·10 ²² cm ⁻³	$T = 300\text{ K}$	layered structure type	90A
ρ	0.1 Ω cm	$T = 300\text{ K}$	layered structure type	90A
μ_n	8·10 ⁻³ cm ² V ⁻¹ s ⁻¹	$T = 200\ldots 300\text{ K}$	layered structure type	90A

The temperature dependence of the hole mobility is shown in Fig. 10.5.1 [92N].

Hall coefficient

R_H	7.2·10 ⁻⁵ cm ³ C ⁻¹	$T = 200\ldots 300\text{ K}$	layered structure type	90A
-------	--	------------------------------	------------------------	-----

refractive index

The spectral behaviour of n and k for as deposited and annealed ZnIn_2Se_4 thin films is given in Fig. 10.5.2 [91S].

dielectric constants

$\epsilon(\infty)$	7.0	from IR reflectivity	89N
--------------------	-----	----------------------	-----

References to 10.5

- 55H Hahn, H., Frank, G., Klinger, W., Störger, A. D., Störger, G.: Z. Anorg. Allg. Chem. 279 (1955) 241.
- 74M Manca, P., Raga, F., Spiga, A.: Nuovo Cimento 19B (1974) 15.
- 89N Neumann, H., Kissinger, W., Lévy, F.: Cryst. Res. Technol. 24 (1989) K89.
- 90A Abdullayev, A.G., Kerimova, T.G., Kyazumov, M.G., Khidirov, A.S.: Thin Solid Films 190 (1990) 309.
- 91S Soliman, H.S., El-Nahass, M.M., Qusto, A.: J. Mater. Sci. 26 (1991) 1556.
- 92N Nowak, E., Neumann, H., Schumann, B., Steiner, B.: Phys. Status Solidi A 133 (1992) K13.
- 93R Razzetti, C., Lottici, P.P., Bini, S., Curti, M.: Phys. Status Solidi B 177 (1993) 525.

Figures to 10.5

Fig. 10.5.1

ZnIn₂Se₄. Temperature dependence of the hole mobility of *p*-type thin films [92N].

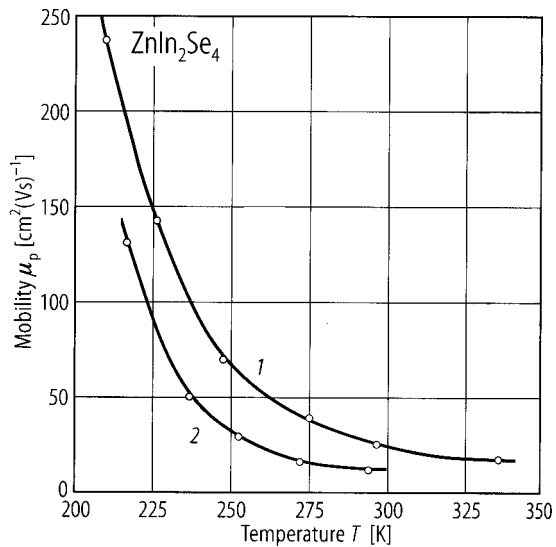
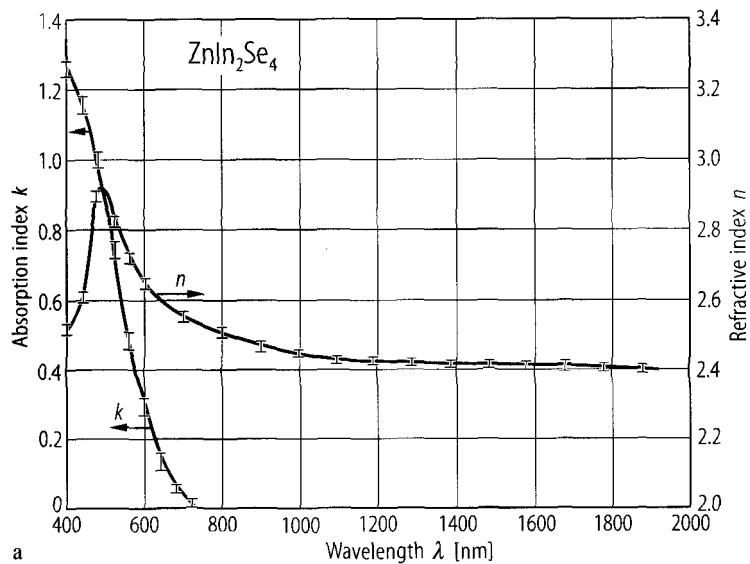
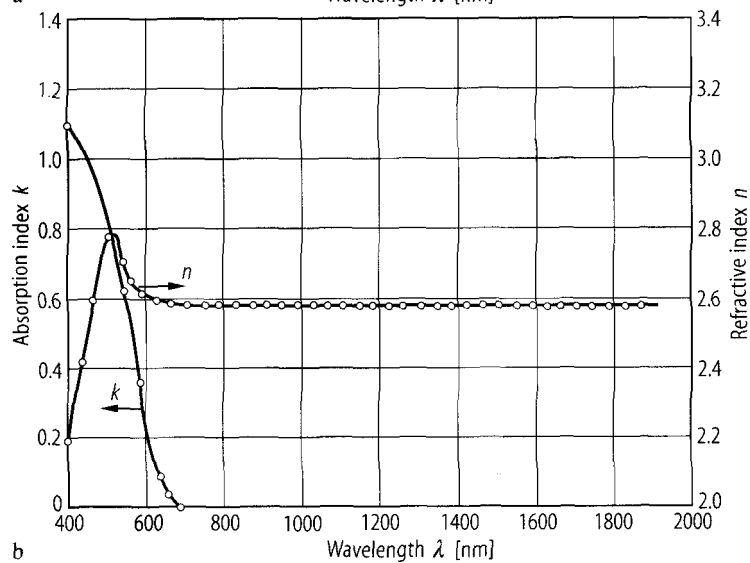


Fig. 10.5.2

ZnIn_2Se_4 . The spectral behaviour of n and k for as deposited (a) and annealed (b) thin films [91S].



a



b

10.6 Zinc indium telluride (ZnIn₂Te₄)

crystal structure

defect chalcopyrite (S₄²⁻I $\bar{4}$)

energy gaps

$E_{g,ind}$	1.35 eV	$T = 300\text{ K}$	unpolarized reflection	73M
$E_{g,dir}$	1.87 eV	$T = 300\text{ K}$		
dE_g/dT	$-6\cdot 10^{-4}\text{ eV K}^{-1}$			

lattice parameters

a	6.11 Å			55H
c	12.2 Å			
c/a	2.00			
x	0.25			
y	0.25			
z	0.125			

resistivity

ρ_d	$5.0(5)\cdot 10^6\text{ }\Omega\text{ cm}$	$T = 300\text{ K}$	n-type	74M
	$6\cdot 10^8\text{ }\Omega\text{ cm}$	$T = 300\text{ K}$	p-type	69B2
	$1.7\cdot 10^4\text{ }\Omega\text{ cm}$	$T = 300\text{ K}$	under illumination of $10^{14}\text{ photons/s at }\lambda = 0.58\text{ }\mu\text{m}$	69B1

References to 10.6

55H Hahn, H., Frank, G., Klinger, W., Störger, A. D., Störger, G.: Z. Anorg. Allg. Chem. 279 (1955) 241.
69B1 Berger, L. T., Prochukhan, V. D.: "Ternary Diamond-like Semiconductors". New York, London: Consultants Bureau, 1969.
69B2 Boltivets, N. S., Drobyazko, V. P., Mityurev, V. K.: Sov. Phys. Semicond. 2 (1969) 867.
73M Manca, P., Raga, F., Spiga, A.: Phys. Status Solidi (a) 16 (1973) K105.
74M Manca, P., Raga, F., Spiga, A.: Nuovo Cimento 19B (1974) 15.

10.7 Cadmium thiogallate (CdAl_2S_4)

crystal structure

defect chalcopyrite ($\text{S}_4^{2-}\text{I}\bar{4}$)

lattice parameters

a	5.55 Å	55H
c	10.3 Å	
c/a	1.82	
x	0.26	
y	0.25	
z	0.13	

density

d	3.04 g cm ⁻³	55H
-----	-------------------------	-----

energy gap

$E_{\text{g,dir}}$	3.398 eV	$T = 280 \text{ K}$	from optical absorption	97M
$E_{\text{g}}(0)$	4.33 eV		from optical absorption	92T

References to 10.7

- 55H Hahn, H., Frank, G., Klinger, W., Störger, A. D., Störger, G.: Z. Anorg. Allg. Chem. 279 (1955) 241.
92T Tiginyanu, I.M., Moldovian, N.A., Stoika, O.B.: Fiz. Tverd. Tela 34 (1992) 967; Sov. Phys. Solid State (Engl. Transl.) 34 (1992) 517.
97M Moon-Seog Jin, Wha-Tek Kim: Appl. Phys. Lett. 70 (1997) 484.

10.8 Cadmium thiogallate (CdGa2S4)

Crystal structure

defect chalcopyrite (S4²⁻I4⁻)

Electronic properties

energy gap

<i>E</i> _{g,dir}	3.16 eV	<i>T</i> = 300 K	from optical absorption	93L
---------------------------	---------	------------------	-------------------------	-----

There is some confusion about the nature of the energy gap. At room temperature absorption studies give a direct gap of 3.44 eV [69B] or 3.25 eV [77K] or an indirect gap of 3.05 eV [77R]. Reflectivity gives a first peak at 3.58 eV [77G, 72A, 73A] and photoconductivity at 3.35 eV [77K] or 3.65 eV [75R]. Absorption in thin films gives 3.50...3.63 eV [71K]. On the other hand the thermal gap is 2.92 eV [75R].

exciton binding energy

<i>E</i> _b	0.040 eV	<i>T</i> = 80 K	from cathodoluminescence spectrum	86G
-----------------------	----------	-----------------	-----------------------------------	-----

Lattice properties

lattice parameters

<i>a</i>	5.56 Å			55H
<i>c</i>	10.0 Å			
<i>c/a</i>	1.80			
<i>x</i>	0.27			
<i>y</i>	0.26			
<i>z</i>	0.14			

density

<i>d</i>	3.97 g cm ⁻³			55H
----------	-------------------------	--	--	-----

wavenumbers of infrared and Raman active phonons

The wavenumbers of infrared and Raman active phonons were calculated considering angular forces in the interatomic interactions in CdGa2S4 [94G]. A comparison with experimental observed modes is given below:

	Calculated	Observed	Mode	94G
$\bar{\nu}$	391 cm ⁻¹	393 cm ⁻¹	A	
	315 cm ⁻¹	312 cm ⁻¹		
	239 cm ⁻¹	219 cm ⁻¹		
	376 cm ⁻¹	372 cm ⁻¹	B	
	321 cm ⁻¹	323 cm ⁻¹		
	256 cm ⁻¹	254 cm ⁻¹		
	176 cm ⁻¹	162 cm ⁻¹		
	127 cm ⁻¹	142 cm ⁻¹		
	366 cm ⁻¹	362 cm ⁻¹	E	
	305 cm ⁻¹	324 cm ⁻¹		
	230 cm ⁻¹	240 cm ⁻¹		
	153 cm ⁻¹	135 cm ⁻¹		
91 cm ⁻¹	84 cm ⁻¹			

Transport properties

resistivity, mobility

n-type samples

ρ	$3\cdot 10^{11}\ \Omega\ \text{cm}$	single crystals, stoichiometric	85D	
	$7\cdot 10^{10}\ \Omega\ \text{cm}$	single crystals, 49.6 mol% Ga ₂ S ₃	85D	
	$4\cdot 10^{10}\ \Omega\ \text{cm}$	single crystals, 50.7 mol% Ga ₂ S ₃	85D	
ρ	$0.8\ldots 6\cdot 10^{13}\ \Omega\ \text{cm}$	$T = 293\text{K}$	n-type	75R
μ_n	$10(T/120)^{1.35}\ \text{cm}^2\ \text{V}^{-1}\ \text{s}^{-1}$	$T = 120\ldots 300\ \text{K}$	decreases in the presence of thermally stimulated current	76K

Optical properties

dielectric constants

$\varepsilon(0)$	9.6	$E \parallel c; T = 300\ \text{K}$	79K
	12.3	$E \perp c$	
$\varepsilon(\infty)$	6.2	$E \parallel c; T = 300\ \text{K}$	
	8.3	$E \perp c$	

refractive index

n_o	2.3	$\lambda = 500\ \text{nm}$	71K
-------	-----	----------------------------	-----

linear electrooptical coefficient

r_{13}	$0.37\cdot10^{-12}\ \text{m/V}$	$\lambda = 500\ \text{nm}$	71K
r_{63}	$3.5\cdot10^{-12}\ \text{m/V}$		

nonlinear dielectric susceptibility

d_{36}	$40.2\cdot10^{-12}\ \text{m/V}$	$\lambda = 1.064\ \mu\text{m}$	74L
----------	---------------------------------	--------------------------------	-----

References to 10.8

55H Hahn, H., Frank, G., Klinger, W., Störger, A. D., Störger, G.: Z. Anorg. Allg. Chem. 279 (1955) 241.

69B Berger, L. T., Prochukhan, V. D.: "Ternary Diamond-like Semiconductors". New York, London: Consultants Bureau, 1969.

71K Kaminow, J. P., Turner, E. H.: Handbook of Lasers, p. 447; Pressley, R. J. (ed.), Cleveland: Chemical Rubber Co. 1971.

72A Abdullaev, G. B., Guseinova, D. A., Kerimova, T. G., Nani, R. Kh.: Phys. Status Solidi (b) 54 (1972) K115.

73A Abdullaev, G. B., Guseinova, D. A., Kerimova, T. G., Nani, R. Kh.: Fiz. Tekh. Poluprovodn. 7 (1973) 840; Sov. Phys. Semicond. (English Transl.) 7 (1973) 575.

74L Levine, B. F., Bettea, C. G., Kasper, H. M.: IEEE J. Quant. Electron. 10 (1974) 904.

75R Radautsan, S. I., Zhitar, V. F., Railyon, V. Ya.: Fiz. Tekh. Poluprovodn. 9 (1975) 2278; Sov. Phys. Semicond. (English Transl.) 9 (1975) 1476.

76K Kivits, P.: J. Phys. C: Solid State 9 (1976) 605.

77G Guseinova, D. A., Kerimova, T. G., Nani, R. Kh.: Fiz. Tekh. Poluprovodn. 11 (1977) 1135; Sov. Phys. Semicond. (English Transl.) 11 (1977) 670.

77K Kshirsagar, S. T., Sinha, A. P. B.: J. Mater. Sci. 12 (1977) 1614.

77R Radautsan, S. I., Syrba, N. N., Nebola, I. I., Tyrziu, V. G., Bercha, D. M.: Fiz. Tekh. Poluprovodn. 11 (1977) 69; Sov. Phys. Semicond. (English Transl.) 11 (1977) 38.

79K Kerimova, T. G., Nani, R. Kh., Salaev, E. Yu., Shteinshraiber, V. Yu.: Fiz. Tverd. Tela 21 (1979) 2791; Sov. Phys. Solid State (English Transl.) 21 (1979) 1605.

85D Derid, Y.O., Georgobiana, A.N., Gruzintzev, A.N., Radautsan, S.I., Tiginyanu, I.M.: Cryst. Res. Technol. 20 (1985) 857.

86G Georgobiani, A.N., Gutan, V.B., Tiginyanu, I.M., Ursaki, V.V., Filina, T.F.: Phys. Status Solidi B 134 (1986) K47.

93L Luengo, J., Joshi, N.V.: J. Phys. Chem. Solids 54 (1993) 127.

94G Gallos, L.K., Anagnostopoulos, A.N., Argyrakos, P.: Phys. Rev. B 50 (1994) 14643.

10.9 Cadmium gallium selenide (CdGa2Se4)

Crystal structure

defect chalcopyrite (S₄²⁻I 4⁻)

Electronic properties

The size and nature of the electronic energy gap is disputed, ranging from an indirect gap of 1.97 eV [74R] to a direct gap of 2.57 eV [79B].

energy gap

$E_{g,dir}$	2.33 eV	$T = 290\text{ K}$	from optical absorption	87C
$E_g(T) = E_g(0) - aT^2/(T+b)$			com.	87C
$E_g(0)$	2.49 eV		pure single crystal	87C
	2.40 eV		Co-doped	
a	$1.57 \cdot 10^{-3}\text{ eV K}^{-1}$		pure single crystal	
	$6.58 \cdot 10^{-4}\text{ eV K}^{-1}$		Co-doped	
b	544 K		pure single crystal	
	53 K		Co-doped	

excitonic energy

E_{gx}	2.673 eV	$T = 90\text{ K}$	from wavelength modulated reflectance	84B
----------	----------	-------------------	---------------------------------------	-----

splitting energies

Δ_{so}	0.41 eV	$T = 300\text{ K}$		79B
Δ_{cf}	0.10 eV	$T = 300\text{ K}$		

Lattice properties

lattice parameters

a	5.73 Å			55H
c	10.7 Å			
c/a	1.87			
x	0.25			
y	0.26			
z	0.13			

density

d	6.28 g cm ⁻³			55H
-----	-------------------------	--	--	-----

linear thermal expansion coefficient

α	$4.9 \cdot 10^{-6}\text{ K}^{-1}$	$T = 300...873\text{ K}$	c axis	
	$14.0 \cdot 10^{-6}\text{ K}^{-1}$		a axis	

melting temperature

T_m	1250 K			78K
-------	--------	--	--	-----

wavenumbers of infrared and Raman active phonons

$\bar{\nu} [\text{cm}^{-1}]$	TO	LO	Symmetry		
	254...264	275...280	B	300 K, B, E are IR active, all are Raman active	79B,
	250...262	274...278	E		79K,
	241...250	242...249	E		79M,
	220...222	232...237	B		82B,
	194...196	198...202	B		
	188		A		
	176	178	B		
	174...178	180...183	E		
	141		A		
	124...125	127...128	B		
	105	105	E		
	76	76	B		
	68	70	E		
	53		E		
	47		E		

Transport and optical properties

resistivity, mobility

n-type samples

ρ	$3.0 \cdot 10^{10} \Omega \text{ cm}$		single crystal, pure d	87C
	$2.5 \cdot 10^{11} \Omega \text{ cm}$		single crystal, Co-doped	
μ_n	$40 \text{ cm}^2 \text{ V}^{-1} \text{ s}^{-1}$	RT		90H

The temperature dependence of the electron mobility and resistivity of CdGa_2Se_4 crystals are shown in Fig. 10.9.1 [90H].

dielectric constants

$\epsilon(0)$	9.7	$T = 300 \text{ K}(?)$; $E \perp c$	79K
	8.2	$E \parallel c$	
$\epsilon(\infty)$	6.7	$T = 300 \text{ K}(?)$; $E \perp c$	
	6.2	$E \parallel c$	

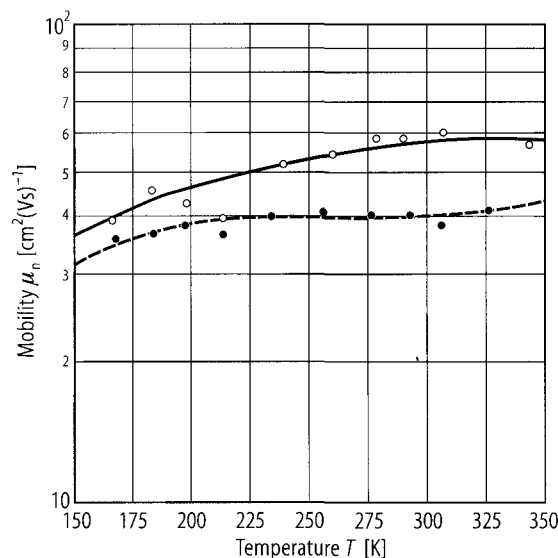
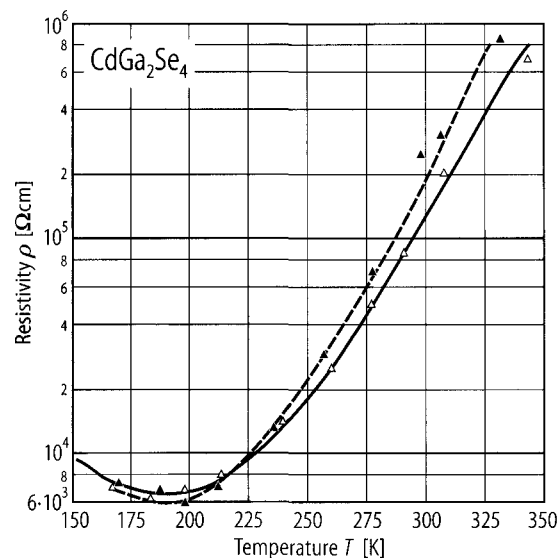
References to 10.9

- 55H Hahn, H., Frank, G., Klinger, W., Störger, A. D., Störger, G.: Z. Anorg. Allg. Chem. 279 (1955) 241.
- 78K Khuseinov, B., Mavlonov, Sh., Umarov, B. S.: Izv. Akad. Nauk SSSR, Neorg. Mater. 14 (1978) 863; Inorg. Mater. (USSR) (English Transl.) 14 (1978) 675.
- 79B Bacewicz, R., Lottici, P. P., Razzetti, C.: J. Phys. C: Solid State 12 (1979) 3603.
- 79K Kerimova, T. G., Nani, R. Kh., Salaev, E. Yu., Shteinshraiber, V. Yu.: Fiz. Tverd. Tela 21 (1979) 2791; Sov. Phys. Solid State (English Transl.) 21 (1979) 1605.
- 79M MacKinnon, A.: J. Phys. C 12 (1979) L655.
- 82B Razzetti, C., Lottici, P. P., Bacewicz, R.: J. Phys. C15 (1982) 5657.
- 84B Bacewicz, R.: Phys. Status Solidi B 122 (1984) K155.
- 87C Colocci, M., Fermi, F., Querzoli, R., Tarricone, L., Vinattieri, A.: Ternary Multinary Compd., Mater. Res. Soc. (1987) 271.
- 90H Horinaka, H., Uemura, A., Yamamoto, N.: J. Cryst. Growth 99 (1990) 785.

Figures to 10.9

Fig. 10.9.1

CdGa_2Se_4 . Temperature dependence of the electron mobility and resistivity of crystals measured under illumination of 2000 lx [90H]. Dashed line: $\text{CdSe} + \text{Ga}_2\text{Se}_3$.



10.10 Cadmium gallium telluride (CdGa₂Te₄)

Crystal structure

defect chalcopyrite ($S_4^{2-}\bar{I}\bar{4}$)

Electronic properties

energy gap

$E_{\text{g,dir}}$	1.5 eV	$T = 300$ K	unpolarized; reflectivity	77P
--------------------	--------	-------------	---------------------------	-----

Lattice properties

lattice parameters

a	6.08 Å	55H
c	11.7 Å	
c/a	1.93	
x	0.27	
y	0.26	
z	0.135	

density

<i>d</i>	5.63 g cm ⁻³	55H
----------	-------------------------	-----

wavenumbers of infrared active phonons

$\bar{\nu}_{\text{LO}}/\bar{\nu}_{\text{TO}}$	Polarization	Proposed assignment	93N
221/206 cm^{-1}	$E \perp c$	E ₁	
199/194 cm^{-1}		E ₂	
222/209 cm^{-1}	$E \parallel [111]$	B ₁	
199/197 cm^{-1}		E ₂	
188/183 cm^{-1}		B ₂	

References to 10.10

55H Hahn, H., Frank, G., Klinger, W., Störger, A. D., Störger, G.: Z. Anorg. Allg. Chem. 279 (1955) 241
77P Paulavichyus, A. B., Yasutis, V. V., Paukshte, Yu. A., Burneika, I. P.: Litov. Fiz. Sb. 17 (1977) 787.
93N Neumann, H., Moise, E., Schwer, H., Kramer, V.: Cryst. Res. Technol. 28 (1993) 635.

10.11 Cadmium thioindate (CdIn2S4)

Crystal structure

Spinel type, space group $T_d^2 - F\bar{4}3m$. There is some confusion regarding the exact type of spinel structure. Whether it is normal or inverse spinel, In on tetrahedral sites and Cd and In randomly distributed on the octahedral sites, or only partially inverted is in doubt [75S].

Electronic properties

band structure : see Fig. 10.0.4.

There is general agreement that the band gap is indirect and that the valence band maximum is not at Γ but probably along the Σ direction $[110]$ [77B]. The values of the indirect and direct gaps are however somewhat inconsistent.

energy gaps

$E_{g,ind}$	2.21 eV	$T = 300$ K	reflectivity	74F
	2.28 eV	$T = 300$ K	absorption	80N
$E_{g,dir}$	2.5 eV	$T = 300$ K	reflectivity	74F
	2.62 eV	$T = 300$ K	absorption	80N
$E_{g,th}$	2.2 eV		resistivity vs. T	76E

effective masses

m_n	$0.19 m_0$	$T = 70...500$ K	Hall effect and Seebeck effect	76E
m_{ds}	$0.3 m_0$		Seebeck effect	72A

Lattice properties

lattice parameter

a	10.797 Å	$T = 300$ K		55H
	10.818 Å			76G

density

d	4.93 g cm ⁻³			50H
	5.0 g cm ⁻³			70C

phonon wavenumbers

IR active phonons:

$\bar{\nu}$	307 cm ⁻¹	$T = 300$ K	T_{1u}	75S,
	215 cm ⁻¹			73Y
	171 cm ⁻¹			
	68 cm ⁻¹			
	293 cm ⁻¹	$T = 440$ K		
	206 cm ⁻¹			
	169 cm ⁻¹			
	67 cm ⁻¹			

Raman active phonons:

$\bar{\nu}$	366 cm ⁻¹	$T = 300$ K	A_{1g}	75S,
	312 cm ⁻¹		T_{2g}	73Y
	247 cm ⁻¹		T_{2g} (very weak)	
	185 cm ⁻¹		E_g	
	93 cm ⁻¹		T_{2g}	
	374 cm ⁻¹	$T = 76$ K	A_{1g}	
	316 cm ⁻¹		T_{2g}	
	192 cm ⁻¹		E_g	
	96 cm ⁻¹		T_{2g}	

second order elastic moduli

c_{11}	$12.15(10) \cdot 10^{10} \text{ N m}^{-2}$	$T = 300 \text{ K}$	Brillouin scattering	80Y
c_{12}	$2.46(46) \cdot 10^{10} \text{ N m}^{-2}$			
c_{44}	$2.57(5) \cdot 10^{10} \text{ N m}^{-2}$			

melting temperature

T_m	1378 K			70C
-------	--------	--	--	-----

Transport and optical properties

resistivity : Fig. 10.11.1

Nernst coefficient, Hall mobility : Fig. 10.11.2.

carrier concentration, mobility, electrical conductivity, resistivity

n-type samples

n	$1.3 \dots 1.6 \cdot 10^{19} \text{ cm}^{-3}$	$T = 125 \text{ K}$	stoichiometric samples	76E
	$2.7 \cdot 10^{13}$	$T = 125 \text{ K}$	samples with excess sulfur	76E
	$\dots 4.8 \cdot 10^{17} \text{ cm}^{-3}$			
μ_H	$320 \dots 400 \text{ cm}^2/\text{V s}$	$T = 125 \text{ K}$	stoichiometric samples	76E
	$25 \dots 100 \text{ cm}^2/\text{V s}$	$T = 125 \text{ K}$	samples with excess sulfur	76E
σ	$3.48 \cdot 10^{-2} \Omega^{-1} \text{ cm}^{-1}$	$T = 300 \text{ K}$		73A
ρ	$5 \cdot 10^7 \Omega \text{ cm}$	$T = 300 \text{ K}$	n-type	69B

refractive index

n	2.55	$\lambda = ?$		74F
-----	------	---------------	--	-----

elastooptic constants

p_{11}	0.027(5)	$T = 300 \text{ K}$	Brillouin scattering	80Y
p_{12}	0.093(9)			
p_{44}	-0.033(2)			

dielectric constants

$\epsilon(0)$	17		from effective charge	72A
$\epsilon(\infty)$	10		estimated from optical measurements; see also Fig. 10.11.3	

References to 10.11

50H Hahn, H., Klingler, W.: Z. Anorg. Allg. Chem. 263 (1950) 177.
55H Hahn, H., Frank, G., Klinger, W., Störger, A. D., Störger, G.: Z. Anorg. Allg. Chem. 279 (1955) 241.
69B Berger, L. T., Prochukhan, V. D.: "Ternary Diamond-like Semiconductors". New York, London: Consultants Bureau, 1969.
70C Czaja, W.: Phys. Kondens. Mater. 10 (1970) 299.
72A Abdullaev, G. B., Guseinova, D. A., Kerimova, T. G., Nani, R. Kh.: Phys. Status Solidi (b) 54 (1972) K115.
73A Abdullaev, G. B., Guseinova, D. A., Kerimova, T. G., Nani, R. Kh.: Fiz. Tekh. Poluprovodn. 7 (1973) 840; Sov. Phys. Semicond. (English Transl.) 7 (1973) 575.
73Y Yamamoto, K., Murakawa, T., Ohbayashi, Y., Hiroyasu, S., Abe, K.: J. Phys. Soc. Jpn. 35 (1973) 1258.
74F Fiejeta, H., Okada, Y.: Jpn. J. App. Phys. 13 (1974) 1823.
75S Shimizu, H., Ohbayashi, Y., Yamamoto, K., Abe, K.: J. Phys. Soc. Jpn. 38 (1975) 750.
76E Endo, S., Irie, T.: J. Phys. Chem. Solids 37 (1976) 201.
76G Glidewell, C.: Inorg. Chim. Acta 19 (1976) L45.
77B Baldereschi, A., Meloni, F., Aymerich, F., Mula, G.: Inst. Phys. Conf. Ser. 35 (1977) 193.
78G Grilli, E., Guzzi, M., Anedda, A., Raga, F., Serpi, A.: Solid State Commun. 27 (1978) 105.
80N Nakanishi, H.: Jpn. J. Appl. Phys. 19 (1980) 103.
80Y Yamada, M., Shirai, T., Yamamoto, K., Abe, K.: J. Phys. Soc. Jpn. 48 (1980) 874.

Figures to 10.11

Fig. 10.0.4

Band structure of CdIn_2S_4

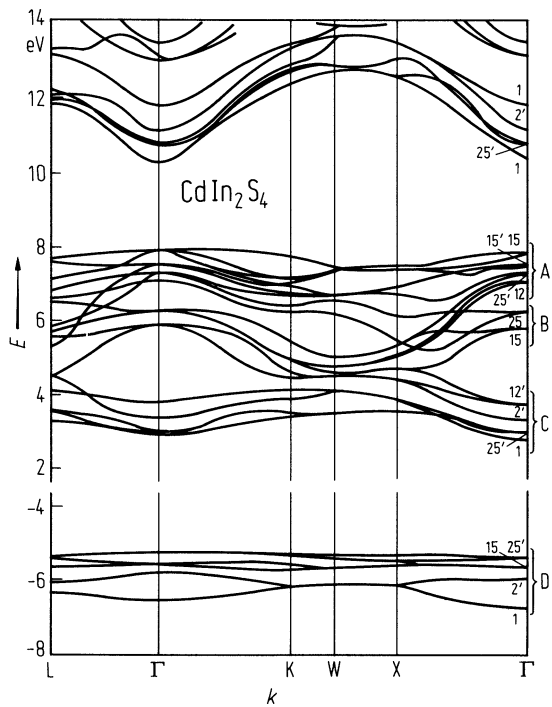


Fig. 10.11.1

CdIn_2S_4 . Resistivity vs. reciprocal temperature for various samples [76E].

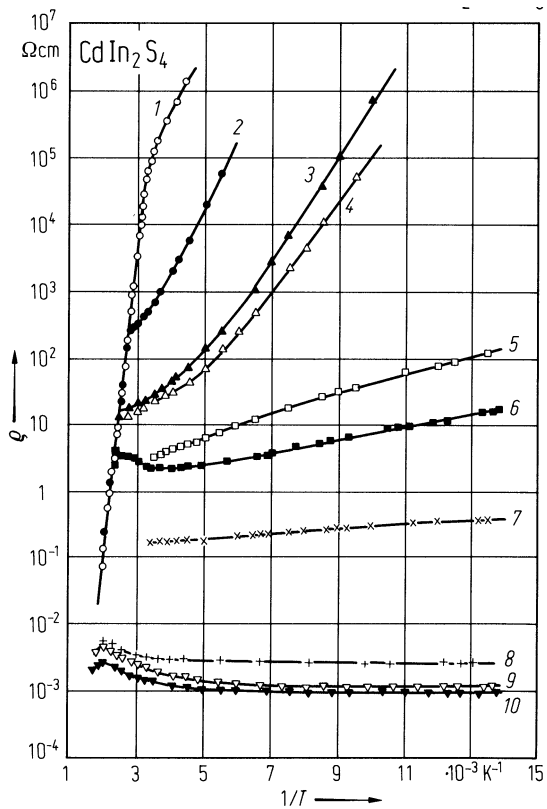


Fig. 10.11.2

CdIn_2S_4 . Nernst coefficient and Hall mobility vs. temperature for sample 8 of Fig. 1 [76E].

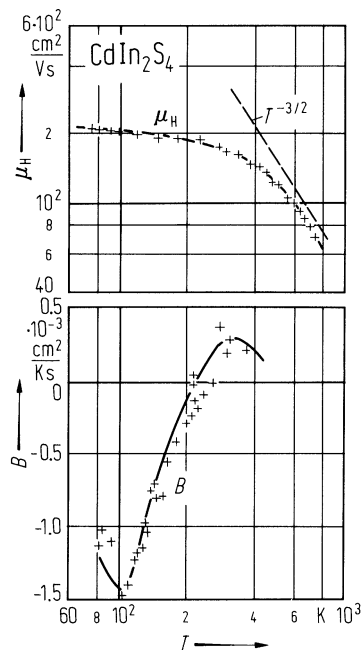
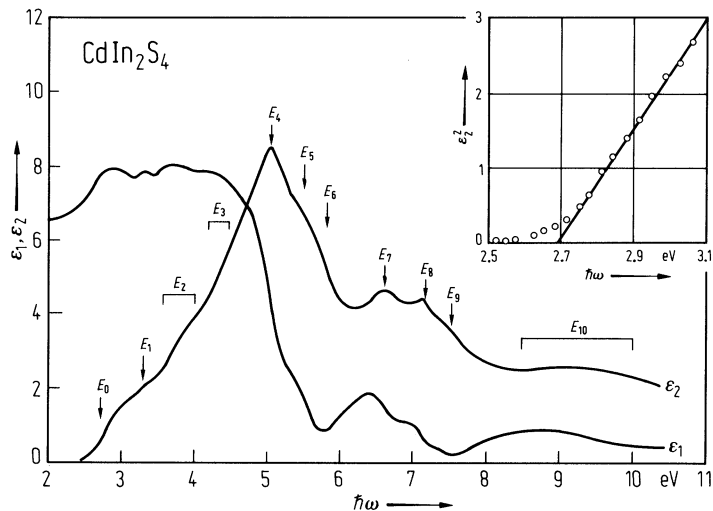


Fig. 10.11.3

CdIn_2S_4 . Real (ϵ_1) and imaginary (ϵ_2) part of dielectric constant vs. photon energy. Insert: ϵ_2^2 vs. photon energy. Critical points in ϵ_2 are designated by E_i [78G].



10.12 Cadmium indium selenide (CdIn2Se4)

Crystal structure

vac-CdIn2Se4 has an ordered vacancy structure which is unique to this compound.

α-phase: tetragonal (space group D2d1 – P 4 2m)This phase is sometimes referred to as pseudocubic since c = a although the space group is tetragonal.

β- and γ-phase: defect chalcopyrite (space group S42–I 4). Both phases differ in the c/a-ratio: β: c = 2a, γ: c = 4a.

Tetragonal phase (α-phase):

band structure : Fig. 10.0.5 [88B].

energy gap

Eg,dir	1.825 eV	RT	from electrolyte electroreflectance	84T
Eg,dir	1.67 eV	T = 293 K	from optical absorption, pure crystal	95S
Eg,ind	1.55 eV	T = 293 K	from optical absorption, pure crystal	95S
dEg,dir/dT	– 4.25·10–4 eV K–1	T = 150...300 K	from optical absorption	90G
dEg,ind/dT	– 4.37·10–4 eV K–1	T = 150...300 K		

The variation of the indirect and direct energy gap with temperature is shown in Fig. 10.12.1 [90G].

effective mass

mn	0.15(1) m0	T = 300 K	thermoelectric power	72K1
----	------------	-----------	----------------------	------

lattice parameters

a (= c)	5.81 Å	T = 300 K		55H, 79P, 80M
---------	--------	-----------	--	---------------

density

d	5.54 g cm–3			55H
---	-------------	--	--	-----

wavenumbers of infrared active phonons

		Symmetry		
νLO/νTO	238/213 cm–1	E modes (E ⊥ c)	RT, infrared reflectivity on single crystals	90N
	199/187 cm–1			
	239/214 cm–1	B2 modes(E ∥ c)		
	198/186 cm–1			

carrier concentration, resistivity, mobility, thermoelectric power

n-type samples

n	1015...1016 cm–3	T = 300 K	single crystals	85M
ρ	102...104 Ω cm	T = 300 K		
	105...106 Ω cm	T = 77 K		
μn	50 cm2 V–1s–1	T = 300 K		

Defect chalcopyrite phase (β-phase):

energy gaps

Eg,ind	1.30 eV	T = 300 K	absorption, unpolarized	72K2
Eg,dir	1.49 eV			

lattice parameters

a	5.81 Å	T = 300 K	β- and γ-phases	79P, 80M
---	--------	-----------	-----------------	----------

carrier concentration, Hall coefficient, resistivity (at 300 K, phase unclear)

n-type samples

n	10^{17} cm^{-3}	intrinsic	72K3
R_H	$-0.5 \text{ cm}^3 \text{ C}^{-1}$	not very T -dependent	72K1
ρ	$8 \cdot 10^5 \Omega \text{ cm}$		69B

p-type samples

S	$70 \mu\text{V K}^{-1}$		69B
-----	-------------------------	--	-----

References to 10.12

- 55H Hahn, H., Frank, G., Klinger, W., Störger, A. D., Störger, G.: Z. Anorg. Allg. Chem. 279 (1955) 241.
- 69B Berger, L. T., Prochukhan, V. D.: "Ternary Diamond-like Semiconductors". New York, London: Consultants Bureau, 1969.
- 72K1 Koval, L. S., Arushanov, E. K., Radautsan, S. I.: Phys. Status Solidi (a) 9 (1972) K73.
- 72K2 Koval, L. S., Markus, M. M., Radautsan, S. I.: Phys. Status Solidi (a) 9 (1972) K69.
- 72K3 Koval, L. S., Radautsan, S. I., Sobolev, V. V.: Izv. Akad. Nauk SSSR, Neorg. Mater 8 (1972) 2021; Inorg. Mater. (USSR) (English Transl.) 8 (1973) 1776.
- 79P Przedmojski, J., Patosz, B.: Phys. Status Solidi (a) 51 (1979) K1.
- 80M Manolikas, C., Bartzokas, D., van Tendebo, G., van Landuyt, T., Amelinckx, S.: Phys. Status Solidi (a) 59 (1980) 425.
- 84T Tomkiewicz, M., Siripala, W., Tenne, R.: J. Electrochem. Soc. 131 (1984) 736.
- 85M Mekhtiev, N.M., Guseinov, Z.Z., Salaev, E.Y.: Fiz. Tekh. Poluprovodn. 19 (1985) 1642; Sov. Phys. Semicond. (Engl. Transl.) 19 (1985) 1010.
- 88B Bernard, J.E., Zunger, A.: Phys. Rev. B 37 (1988) 6835.
- 90G Gariazzo, S., Serpi, A.: Phys. Rev. B 41 (1990) 7718.
- 90N Neumann, H., Kissinger, W., Lévy, F., Sobotta, H., Riede, V.: Cryst. Res. Technol. 25 (1990) 841.
- 95S Sung-Hyu Choe, Bok-Nam Park, Ki-Su Yu, Se-Jung Oh, Hong-Lee Park, Wha-Tek Kim: J. Phys. Chem. Solids 56 (1995) 89.

Figures to 10.12

Fig. 10.0.5

Band structure of CdIn_2Se_4

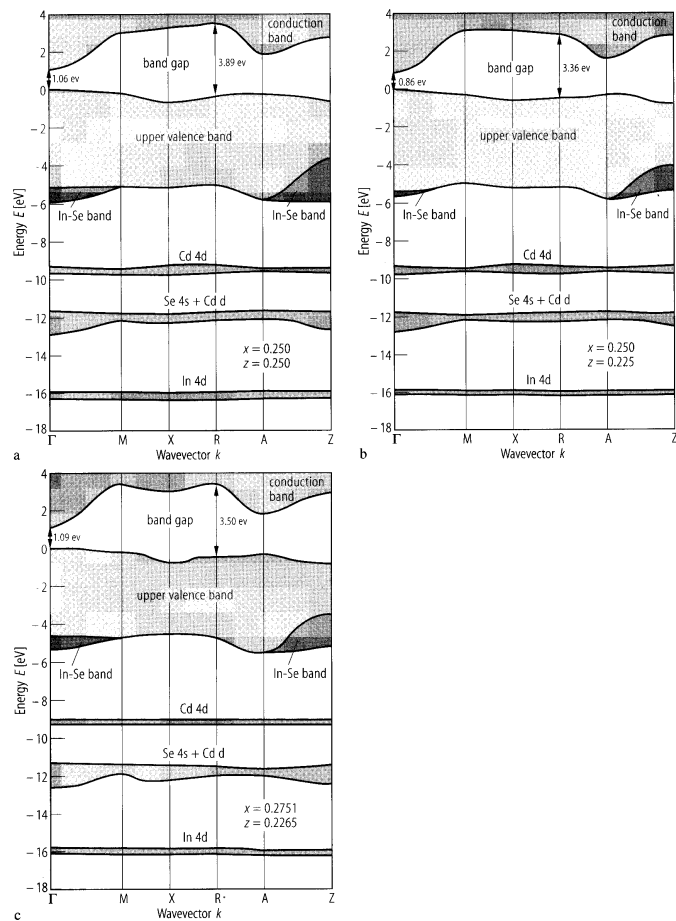
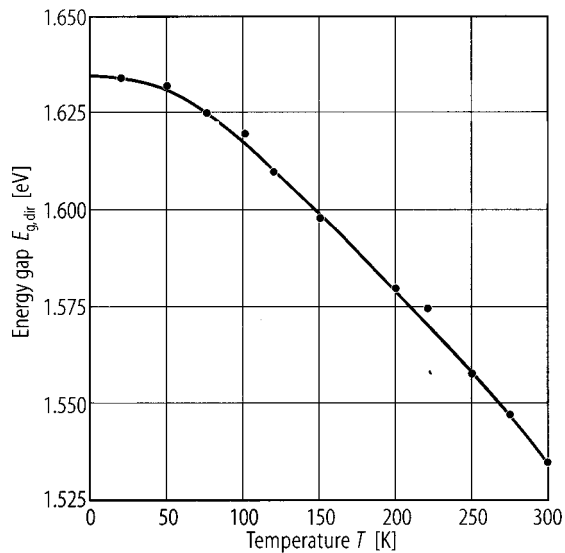
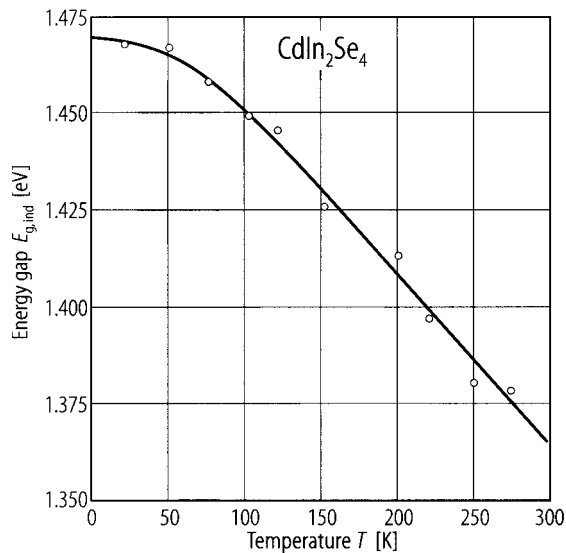


Fig. 10.12.1

CdIn_2Se_4 . Variation in the indirect energy gap $E_{g,\text{ind}}$ and direct energy gap $E_{g,\text{dir}}$ with temperature T . Full curve: Manoogian-Leclerc fit [90G].



10.13 Cadmium indium telluride (CdIn2Te4)

Crystal structure

defect chalcopyrite (S4²⁻I4⁻)

Electronic properties

energy gap

$E_{g,ind}$	1.15 eV	RT	from optical absorption	93C1
$E_{g,dir}$	1.25 eV	$T = 293\text{ K}$	absorption, unpolarized	72K
$E_g(T) = E_g(0) - aT^2/(T+b)$				93C1
$E_g(0)$	1.26 eV			
a	$5.7 \cdot 10^{-4}\text{ eV K}^{-1}$			
b	176 K			

The variation of the optical energy gap E_g with temperature T for CdIn2Te4 is given in Fig. 10.13.1 [96Q].

Lattice properties

lattice parameters

a	6.19 Å	55H
c	12.3 Å	
c/a	2.00	
x	0.26	
y	0.24	
z	0.13	

density

d	5.88 g cm ⁻³	55H
-----	-------------------------	-----

wavenumbers of infrared and Raman active phonons (in cm⁻¹, $T = 300\text{ K}$)

$\bar{\nu}_{LO}/\bar{\nu}_{TO}$	$\bar{\nu}$	Proposed symmetry	91R
Infrared	Raman		
190/187	187	E, B ₂	
183/169	—	E	
156/151	—	B ₂	
140/138	142	E	
- / -	124	A ₁	
- / -	100	A ₁	
76/ 75	—	B ₂	
65/64	63	E	
45/44	44	E	

Transport properties

carrier concentration, resistivity, mobility

p-type samples

p	10^{16} cm^{-3}	single crystal, Te-doped	87K
ρ	100...200 Ω cm	single crystal, Te-doped	87K

n-type samples

n	$2.5 \cdot 10^{11}\text{ cm}^{-3}$	RT	single crystals	93C1
ρ	$2.5 \cdot 10^6\text{ Ω cm}$	RT	single crystals	93C1
μ_n	$100\text{ cm}^2\text{ V}^{-1}\text{s}^{-1}$	RT	single crystals	93C1

Electrical conductivity, carrier concentration, and mobility vs inverse temperature for a CdIn_2Te_4 crystal are given in Fig. 10.13.2 [93C2].

activation energies

E_A	0.57 eV	$T > 350 \text{ K}$	activation energy of conductivity	93C2
	0.47 eV	$T < 350 \text{ K}$		

Optical properties

static dielectric constant

ϵ_r	11.0			91C
--------------	------	--	--	-----

electrooptic coefficient

r_{41}	3 pmV ⁻¹			94J
----------	---------------------	--	--	-----

References to 10.13

- 55H Hahn, H., Frank, G., Klinger, W., Störger, A. D., Störger, G.: Z. Anorg. Allg. Chem. 279 (1955) 241.
- 72K Koval, L. S., Arushanov, E. K., Radautsan, S. I.: Phys. Status Solidi (a) 9 (1972) K73.
- 87K Kianian, S., Eshragi, S.A., Stafsudd, O.M., Gentile, A.L.: J. Appl. Phys. 62 (1987) 1500.
- 91C Couturier, G., El Farji, A., Lestournelle, F., Launay, J.C.: J. Appl. Phys. 70 (1991) 4472.
- 91R Riede, V., Neumann, H., Kramer, V., Kittel, M.: Solid State Commun. 78 (1991) 211.
- 93C1 Couturier, G., Jean, B., Lambert, J.F., Joffre, P.: Mater. Sci. Eng.B 21 (1993) 333.
- 93C2 Couturier, G., Jean, B., Lambert, J.F., Launay, J.C., Joffre, P.: J. Appl. Phys. 73 (1993) 1813.
- 94J Jean, B., Couturier, G., Joffre, P.: J. Appl. Phys. 75 (1994) 3579.
- 96Q Quintero, M., Guerrero, E., Tovar, R., Morocoima, M., Grima, P., Cadenas, R.: J. Phys. Chem. Solids 57 (1996) 271.

Figures to 10.13

Fig. 10.13.1

CdIn_2Te_4 . Variation of the optical energy gap E_g with temperature T . Circles: experimental data; full curve: fitted to Manoogian-Leclerc equation [96Q].

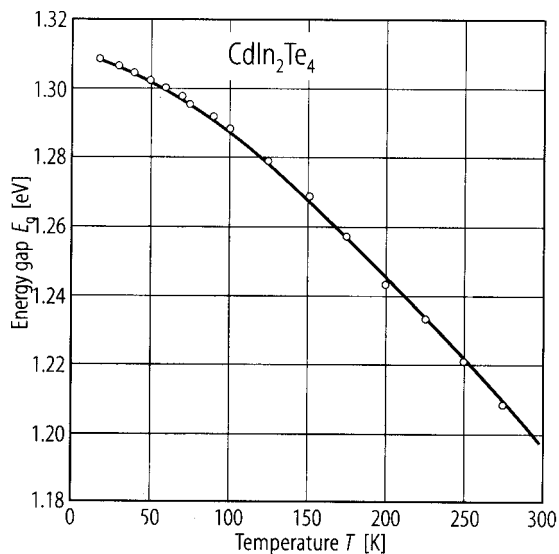
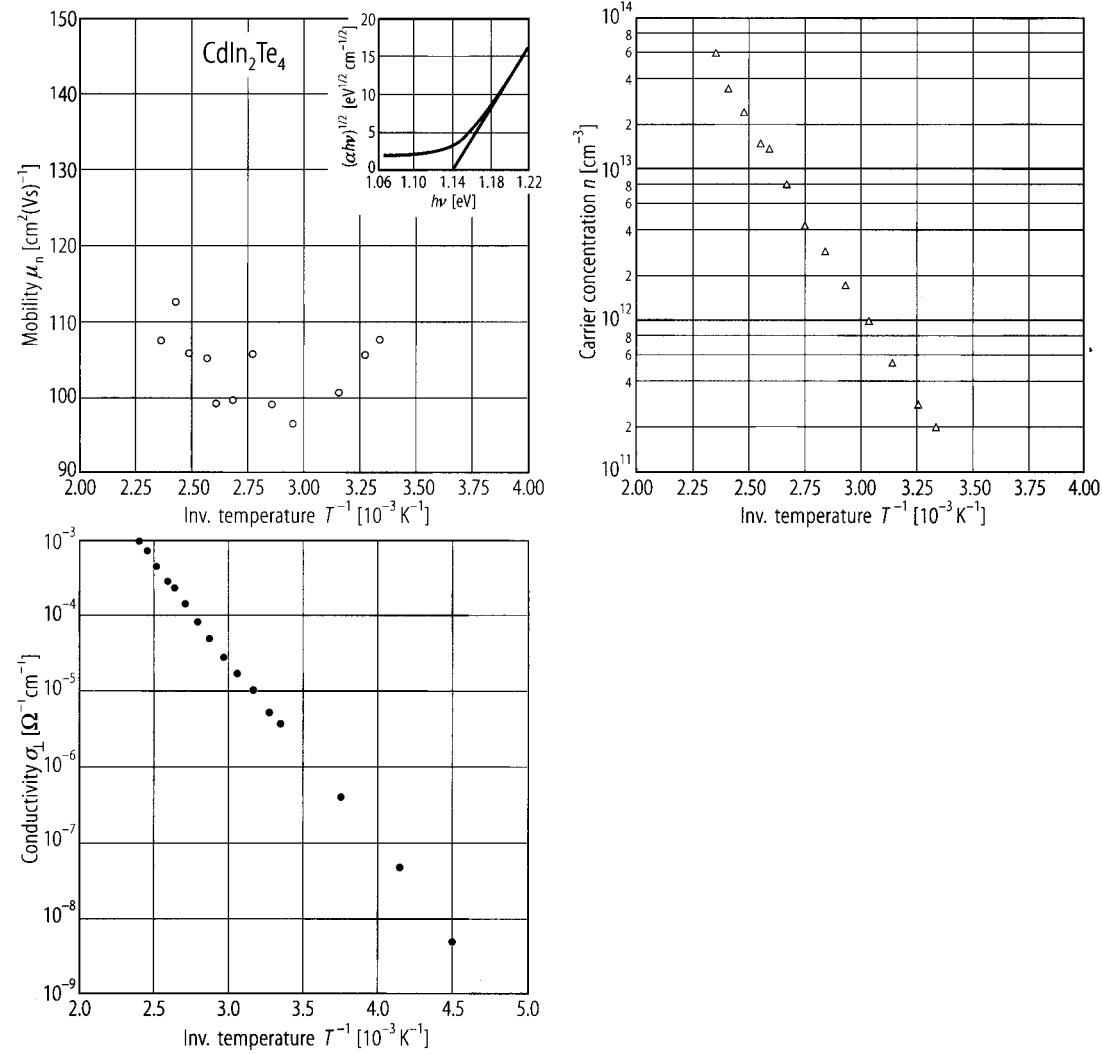


Fig. 10.13.2

CdIn_2Te_4 . Electrical conductivity, carrier concentration, and mobility vs inverse temperature for a crystal with the c axis perpendicular to the crystal plane [93C2].



10.14 Cadmium thallium selenide (CdTl₂Se₄)

crystal structure

hexagonal

lattice parameters

a	4.28 Å		76S
-----	--------	--	-----

c	6.67 Å		
-----	--------	--	--

energy gap

E_g	0.8 eV	calculated	76S
-------	--------	------------	-----

electrical conductivity

σ	$10^{-1} \dots 10^{-5} \Omega^{-1} \text{ cm}^{-1}$	$T = 77 \text{ K}$	no anisotropy	76S
----------	---	--------------------	---------------	-----

melting temperature

T_m	1200(50) K			76S
-------	------------	--	--	-----

References to 10.14

- 76S Sultanov, S., Mavlonov, Sh., Karimov, S., Kurbanov, Kh. M., Madazimov, A.: Izv. Akad. Nauk SSSR, Neorg. Mater 12 (1976) 115; Inorg. Mater. (USSR) (English Transl.) 12 (1976) 96.

10.15 Merury thiogallate (HgGa2S4)

crystal structure

defect chalcopyrite (S4²⁻I4⁻)

energy gaps

<i>E</i> _{g,ind}	2.79 eV	<i>T</i> = 300 K	these are alternative interpretations	61B
<i>E</i> _{g,dir}	2.84 eV	<i>T</i> = 300 K	of the same data	61B
	2.53 eV		(unpolarized optical measurements) calculated	79P

lattice parameters

<i>a</i>	5.49 Å			55H
<i>c</i>	10.2 Å			
<i>c/a</i>	1.86			
<i>x</i>	0.275			
<i>y</i>	0.265			
<i>z</i>	0.139			

density

<i>d</i>	4.95 g cm ⁻³			55H
----------	-------------------------	--	--	-----

electrical resistivity

<i>ρ</i> _d	10 ¹⁰ Ω cm	<i>T</i> = 300 K	dark resistivity	69B
<i>ρ</i> _i	7·10 ⁴ Ω cm	<i>T</i> = 300 K	under illumination of 10 ⁴ photons/s at 0.49 μm	69B

References to 10.15

55H Hahn, H., Frank, G., Klinger, W., Störger, A. D., Störger, G.: Z. Anorg. Allg. Chem. 279 (1955) 241.
61B Beun, J. A., Nitsche, R., Lichtensteiger, M.: Physica 27 (1961) 448.
69B Berger, L. T., Prochukhan, V. D.: "Ternary Diamond-like Semiconductors". New York, London: Consultants Bureau, 1969.
79P Przedmojski, J., Patosz, B.: Phys. Status Solidi (a) 51 (1979) K1.

10.16 Mercury gallium selenide (HgGa₂Se₄)

crystal structure

defect chalcopyrite (S₄²⁻I⁻4)

energy gap

$E_{g,dir}$	1.99 eV	$T = 293\text{ K}$	pure HgGa ₂ Se ₄ single crystals	91W
E_g	1.95 eV	$T = 300\text{ K}$	absorption, unpolarized	61B
dE_g/dT	$-(7...8) \cdot 10^{-4}\text{ eV K}^{-1}$	$T = 77...300\text{ K}$	photoconductivity	77L

splitting energies (at Γ)

Δ_{cf}	0.083 eV	$T = 10\text{ K}$	from reflectivity	86G2
Δ_{so}	0.059 eV	$T = 10\text{ K}$	from reflectivity	86G2

lattice parameters

a	5.70 Å			55H
c	10.7 Å			
c/a	1.88			
x	0.25			
y	0.25			
z	0.125			

density

d	6.10 g cm ⁻³			55H
-----	-------------------------	--	--	-----

electrical resistivity

ρ_d	$10^8...10^{10}\text{ }\Omega\text{ cm}$	$T = 300\text{ K}$	dark resistivty	69B
ρ_i	$2.7 \cdot 10^4\text{ }\Omega\text{ cm}$		under illumination of 10^4 photons/s at 0.62 μm	
ρ	$10^8...10^{10}\text{ }\Omega\text{ cm}$	$T = 300\text{ K}$	single crystals	86G1

References to 10.16

55H Hahn, H., Frank, G., Klinger, W., Störger, A. D., Störger, G.: Z. Anorg. Allg. Chem. 279 (1955) 241.
61B Beun, J. A., Nitsche, R., Lichtensteiger, M.: Physica 27 (1961) 448.
69B Berger, L. T., Prochukhan, V. D.: "Ternary Diamond-like Semiconductors". New York, London: Consultants Bureau, 1969.
77L Lebedov, A. A., Metlinskii, P. N., Rud, Yu. V., Tyrziu, V. G.: Fiz. Tekh. Poluprovodn. 11 (1977) 1038; Sov. Phys. Semicond. (English Transl.) 11 (1977) 615.
86G1 Georgobiani, A.N., Metlinskii, P.N., Radautsan, S.I., Tiginyanu, I.M., Ursaki, V.V.: Fiz. Tekh. Poluprovodn. 20 (1986) 1116; Sov. Phys. Semicond. (Engl. Transl.) 20 (1986) 702.
86G2 Georgobiani, A.N., Metlinskii, P.N., Radautsan, S.I., Tiginyanu, I.M., Ursaki, V.V.: Fiz. Tverd. Tela 28 (1986) 1179; Sov. Phys. Solid State (Engl. Transl.) 28 (1986) 659.
91W Wha-Tek Kim, Gi-Jun Cho, Chang-Sub Kim, Chang-Dae Kim: Phys. Rev. B 43 (1991) 14265.

10.17 Mercury indium telluride (HgIn₂Te₄)

Crystal structure

defect chalcopyrite (S₄²⁻I⁻4) and defect stannite (D_{2d}¹¹⁻I⁻4 2m)

Electronic properties

energy gap

<i>E</i> _{g,dir}	0.9 eV	<i>T</i> = 300 K, <i>E</i> ⊥ <i>c</i>	electroreflectance, absorption	77M
	0.94 eV	<i>T</i> = 300 K, <i>E</i> ∥ (⊥) <i>c</i>		
d <i>E</i> _g /d <i>T</i>	2.8·10 ⁻⁴ eV K ⁻¹	<i>T</i> = 4...300 K	electroreflectance	77M
<i>E</i> _{g,ind}	0.78 eV	RT	HgIn ₂ Te ₄ single crystal	88E

Lattice properties

lattice parameters (defect chalcopyrite)

<i>a</i>	6.17 Å	55H
<i>c</i>	12.3 Å	
<i>c/a</i>	2.00	
<i>x</i>	0.27	
<i>y</i>	0.23	
<i>z</i>	0.135	

lattice parameters (defect stannite)

<i>a</i>	6.17 Å	76M
<i>c</i>	12.3 Å	
<i>c/a</i>	2.00	

density (defect chalcopyrite)

<i>d</i>	6.34 g cm ⁻³	55H
----------	-------------------------	-----

wavenumbers of infrared and Raman active phonons (in cm⁻¹, at 300 K, *k* = 0)

		Symmetry		
$\bar{\nu}$	42	B ₂ (LO)	Raman active	76M
	50	B ₁	Raman active	
	61	B ₂ (LO)	Raman active	
	74	B ₂ (LO)	Raman active	
	100	A ₁	Raman active (very strong)	
	114	A ₂	calculated (inactive)	
	118 (122)	E (TO)	infrared (Raman) active	
	127	E (LO)	infrared (Raman) active	
	132	A ₁	Raman active	
	247	B ₂ (TO)	infrared active	
	153	B ₂ (LO)	infrared (Raman) active	
	155	B ₁	Raman active	
	160	E (TO)	infrared (Raman) active	
	169	E (LO)	infrared (Raman) active	
	180 (184)	B ₂ (TO)	infrared (Raman) active	
	184 (189)	B ₂ (LO)	infrared (Raman) active	
	181	E (TO)	Raman active	
	188	E (LO)	Raman active	

second order elastic moduli

c_{11}	$4.31 \cdot 10^{10} \text{ N m}^{-2}$	$T = 77 \text{ K}$	ultrasonic wave attenuation	76S
c_{12}	$2.54 \cdot 10^{10} \text{ N m}^{-2}$		For pressure dependence and further	
c_{13}	$2.18 \cdot 10^{10} \text{ N m}^{-2}$		elastic properties, see [82H].	
c_{33}	$4.47 \cdot 10^{10} \text{ N m}^{-2}$			
c_{44}	$2.14 \cdot 10^{10} \text{ N m}^{-2}$			
c_{66}	$2.41 \cdot 10^{10} \text{ N m}^{-2}$			

bulk modulus

B	$2.99 \cdot 10^{10} \text{ N m}^{-2}$	$T = 77 \text{ K}$		76S
-----	---------------------------------------	--------------------	--	-----

Transport and optical properties

carrier concentration, mobility

n	$3.5 \cdot 10^{15} \text{ cm}^{-3}$	$T = 300 \text{ K}$	n-type samples, no anisotropy	69B
μ_n	$200 \text{ cm}^2/\text{V s}$			

The temperature dependence of the resistivity, carrier density, and Hall mobility of HgIn₂Te₄ single crystals are given in Fig. 10.17.1 [88E].

dielectric constants

$\epsilon(0)$	9.64	$T = 300 \text{ K}; E \parallel c$	infrared reflectivity	76M
	11.06	$E \perp c$		
$\epsilon(\infty)$	8.53	$T = 300 \text{ K}; E \parallel c$		
	8.57	$E \perp c$		

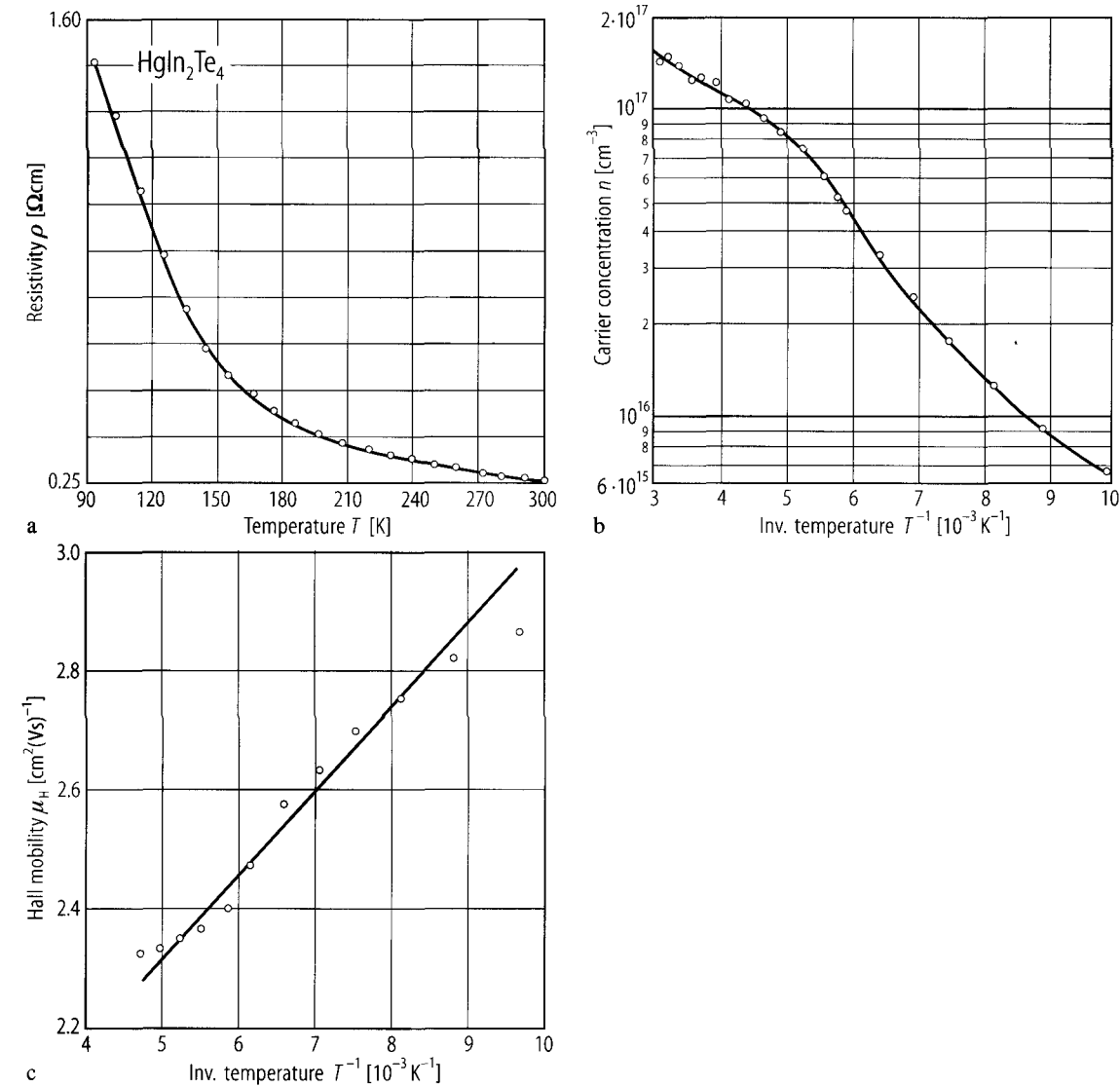
References to 10.17

55H Hahn, H., Frank, G., Klinger, W., Störger, A. D., Störger, G.: Z. Anorg. Allg. Chem. 279 (1955) 241.
69B Berger, L. T., Prochukhan, V. D.: "Ternary Diamond-like Semiconductors". New York, London: Consultants Bureau, 1969.
76M Miller, A., Lockwood, D. J., MacKinnon, A., Weaire, D.: J. Phys. C: Solid State 9 (1976) 2997.
76S Saunders, G. A., Seddon, T.: J. Phys. Chem. Solids 37 (1976) 873.
77M MacKinnon, A., Miller, A., Ross, G.: Inst. Phys. Conf. Ser. 35 (1977) 171.
82H Hailing, T., Saunders, G. A., Lambson, W. A.: Phys. Rev. B26 (1982) 5786.
88E Eshragi, S.A., Kianian, S., Ostrom, B., Stafsudd, O.M., Gentile, A.L.: Phys. Status Solidi A 105 (1988) 563.

Figures to 10.17

Fig. 10.17.1

HgIn₂Te₄. Temperature dependence of the resistivity (a), carrier density (b), and Hall mobility (c) of single crystals [88E].



10.18 HgIn_2Se_4 , $\text{Hg}_3\text{In}_2\text{Te}_6$, $\text{Hg}_5\text{In}_2\text{Te}_8$

energy gap

$E_{g,\text{dir}}$	0.74 eV	$T = 300 \text{ K}$	$\text{Hg}_3\text{In}_2\text{Te}_6$ single crystal	85G
	0.66 eV		$\text{Hg}_5\text{In}_2\text{Te}_8$ single crystal	91G
	1.16 eV	$T = 298 \text{ K}$	HgIn_2Se_4 single crystal	95M

carrier concentration, resistivity, mobility

n-type samples

n	$(0.5 \dots 2) \cdot 10^{13} \text{ cm}^{-3}$	$T = 300 \text{ K}$	$\text{Hg}_3\text{In}_2\text{Te}_6$ single crystals	85G
	$1.5 \cdot 10^{17} \text{ cm}^{-3}$	RT	HgIn_2Te_4 single crystals	88E
μ_n	$400 \text{ cm}^2 \text{ V}^{-1} \text{ s}^{-1}$	$T = 300 \text{ K}$	$\text{Hg}_3\text{In}_2\text{Te}_6$ single crystals	85G

References to 10.18

- 85G Grilli, E., Guzzi, M., Camerlenghi, E., Pio, F.: Phys. Status Solidi A 90 (1985) 691.
 88E Eshragi, S.A., Kianian, S., Ostrom, B., Stafssudd, O.M., Gentile, A.L.: Phys. Status Solidi A 105 (1988) 563.
 91G Grushka, G.G., Gavaleshko, N.P., Grushka, Z.M.: Fiz. Tekh. Poluprovodn. 25 (1991) 945; Sov. Phys. Semicond. (Engl. Transl.) 25 (1991) 570.
 95M Mak, V.T., Ibragim, A.M.: Pis'ma Zh. Tekhn. Fiz. 21 (1995) 65; Technical Phys. Lett. (Engl. Transl.) 21 (1995) 754.

10.19 Further II-III₂-VI₄ compounds with II = Mg, Ca

MgGa₂S₄

monoclinic structure

energy gap

$E_{g,dir}$	3.4 eV	$T = 300$ K	from photoluminescence	91M
-------------	--------	-------------	------------------------	-----

resistivity

ρ	$2 \cdot 10^{13} \Omega \text{ cm}$		single crystals	91M
--------	-------------------------------------	--	-----------------	-----

MgGa₂Se₄

energy gap

$E_{g,dir}$	2.20 eV	$T = 292$ K		88K
-------------	---------	-------------	--	-----

CaIn₂Se₄

melting temperature

T_m	1075 K		congruent melting temperature	87G
-------	--------	--	-------------------------------	-----

References to 10.19

- 87G Guliev, I.N., Rustamov, P.G., Yagubov, N.I.: Izv. Akad. Nauk SSSR, Neorg. Mater. 23 (1987) 1447; Inorg. Mater. (Engl.Transl.) 23 (1987) 1282.
- 88K Kim, H.-G., Kim, W.-T., Kim, Y.-G.: Phys. Rev. B 38 (1988) 9469.
- 91M Moldovian, N.A.: Izv. Akad. Nauk SSSR, Neorg. Mater.27 (1991) 2655; Inorg. Mater. (Engl.Transl.) 27 (1991) 2278.

11 Group III elements

11.0 Crystal structure and electronic structure of boron

11.0.1 Crystal structure

The different modifications of elementary boron and the related boron-rich borides exhibit complex structures, which are essentially composed of nearly regular B_{12} icosahedra and of structural elements consisting of fragments or condensed systems of icosahedra. These structure elements are bonded directly to one another or via single boron or foreign atoms thus forming rigid comparably open three-dimensional frameworks with a large variety of structures. In the open structures of all the icosahedral boron-rich solids there are voids of sufficient size to accommodate foreign atoms. This interstitial doping is very important to modify the semiconductor properties of these solids.

Only the rhombohedral phases of boron show semiconducting properties.

structure of α -rhombohedral boron:

α -rhombohedral boron is the low-temperature modification of elementary boron. It can be prepared at temperatures below about 1200°C only. At this temperature an irreversible transformation to β -rhombohedral boron takes place via three metastable phases [72R]. The structure may be considered as a slightly deformed cubic close packing of icosahedra. Space group: $R\bar{3}m$, 12 atoms per unit cell (Fig. 11.0.1)

structure of β -rhombohedral boron:

β -rhombohedral boron is the high-temperature, thermodynamically stable crystalline modification of elementary boron. Its unit cell (Fig. 11.0.2) consists of essentially 105 atoms (106.5 atoms, if some additional sites with very low occupation densities are taken into account). The structure formula $(B_{12})_4(B_{28})_2B$ exhibits four icosahedra, one of which is positioned at the vertex, three on the edge centers of the unit cell (both sites are crystallographically inequivalent) and two B_{28} units, which consist of three condensed icosahedra, each, arranged symmetrically to a centered single atom on the main diagonal of the unit cell, which diagonal is parallel to the crystallographic c -axis.

11.0.2 Electronic structure

Fig. 11.0.3 shows the band structure of α -B, Fig. 11.0.4 its Brillouin zone. An energy band scheme for β -B is shown in Fig. 11.0.5.

For details see the following section.

References to 11.0

- 72R Runow, P.: J. Mater. Sci. 7 (1972) 499.
93W Werheit, H., Laux, M., Kuhlmann, U.: Phys. Status Solidi (b) 176 (1993) 415.

Figures to 11.0

Fig. 11.0.1

B₁₂ icosahedra at the corners of the unit cell of α -rhombohedral boron viewed from above. Interatomic distances for the different types of bonds are indicated.

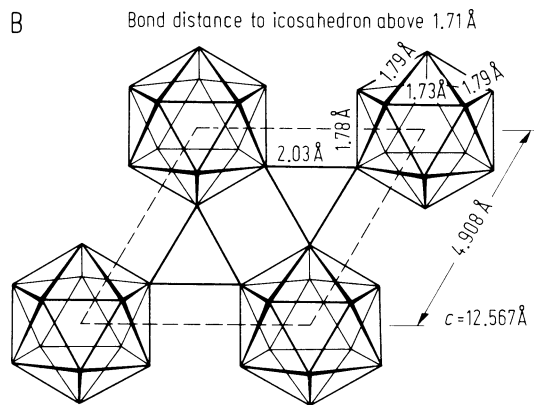


Fig. 11.0.2

Model of the unit cell of β -rhombohedral boron.

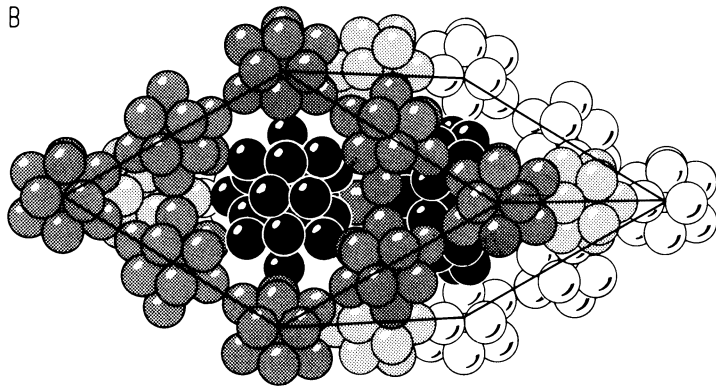


Fig. 11.0.3

Energy band structure along the $\Gamma - Z$ axis of α -boron.

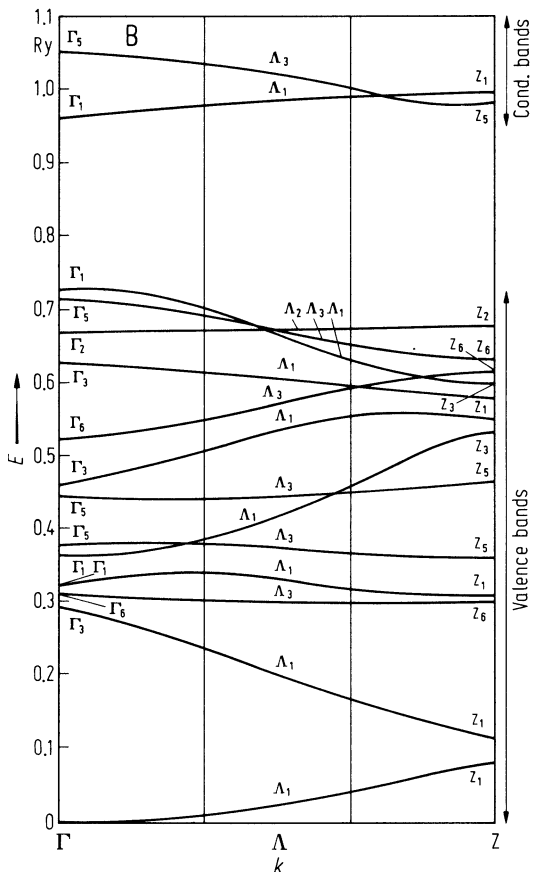


Fig. 11.0.4

Irreducible part of the Brillouin zone of α -boron.

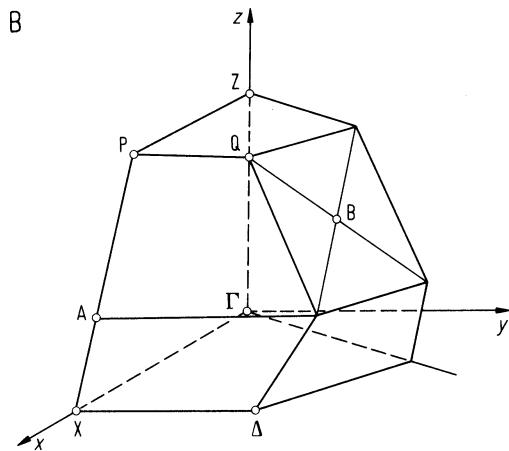
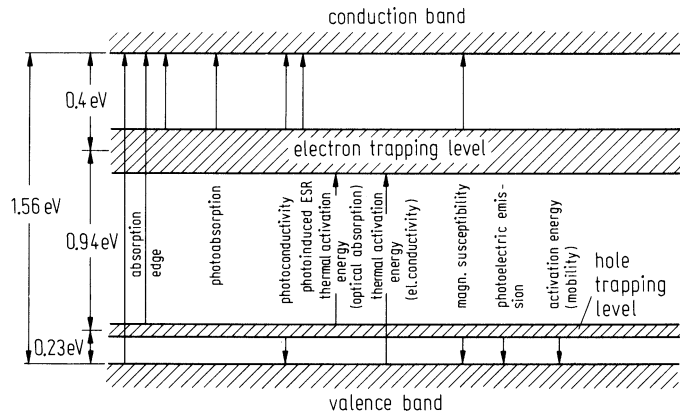


Fig. 11.0.5

β -rhombohedral boron. Energy band scheme. The vertical lines indicate the allowed optical transitions between different levels. Gap width 1.32(1) and 1.50(1) eV for $E \parallel c$ and 1.29(1) and 1.46(1) eV for $E \perp c$ respectively (values for extrapolation to $T = 0$ K) [93W].

Widely accepted band model for β -boron.



11.1. Boron: Physical properties

Electronic properties

general remarks

The boron-rich semiconductors with icosahedral structure elements are characterized by largely common features of electronic properties:

- a) The semiconducting icosahedral boron-rich solids are not in accordance with the general rule, which holds for crystals with simple periodic structures, that atoms with odd electron numbers are metallic in the condensed state.
- b) The band gaps of the boron-rich solids do not depend essentially on the crystal structure.
- c) In many cases of icosahedral boron-rich solids a split-off valence band about 0.19 eV above the valence band edge has been found.
- d) Icosahedral boron-rich solids are p-type semiconductors. Overcompensation to n-type demands donor densities of the order of 10^{20} cm^{-3} .
- e) The electronic transport is composed of band-type conduction and hopping side by side. Depending on temperature or chemical composition the share of both contributions varies.

As essential for the fundamental electronic properties of the icosahedral boron-rich solids the Jahn-Teller effect is assumed, by which the icosahedra are distorted and the electronic levels are split in consequence of the symmetry reduction. This splitting leads to a separation of occupied and unoccupied electronic levels of the isolated icosahedra, and in the solids to a largely unoccupied split-off valence band (see for example β -rhombohedral boron Fig. 11.0.5). Electronic transport is assumed to take place as a superposition of classical band-type conductivity in the valence band and hopping conductivity within the split-off valence band or by a kind of hopping-like transport in the main valence band due to holes, whose motion is strongly impeded by multiple trapping in occupied states of the split-off valence band.

α -rhombohedral boron

band structure : Fig. 11.0.3 (Brillouin zone: Fig. 11.0.4)

energy gap

E_g	0.73(2) eV	$T = 300 \text{ K}$	deep level to band (optical absorption)	90W
	1.49(2) eV		deep level to band or	
	1.63(2) eV		indirect allowed interband (optical absorption)	
	2.055(2) eV		indirect allowed interband (optical absorption)	91W

reduced effective mass

$2m_v/m_0$	0.029		absorption	91W
	0.034			90W

g-factor

g	2.0036	$T = 77 \text{ K}$	ESR	78S
	4.21			

β -rhombohedral boron

The actual energy band scheme of pure β -rhombohedral boron (Fig. 11.0.5) consists of the lower valence band, the split-off valence band (attributed to the Jahn-Teller effect), one conduction band and six equidistant intrinsic electron trapping levels (attributed to the interaction between electrons and specific intraicosahedral phonons).

energy gap

$E_{g,ind}$	1.32(1) eV	$T = 0$ K (extrapolated)	$E \parallel c$, opt. absorption, single crystal	93W
	1.29(1) eV		$E \perp c$	
	1.50 eV		$E \parallel c$	
	1.46 eV		$E \perp c$	

temperature dependence of the energy gap

empirical approximation by $E_g(T) = E_g(0) - \alpha T^2$ [69J, 70W1, 93W]

parameters of the empirically temperature dependence of the energy gap (Fig. 11.1.1)

α	$3.4(2) \cdot 10^{-7} \text{ K}^{-2} \text{ eV}$	$E \parallel c$	for gap 1.32 eV	93W
		$E \parallel c$	for gap 1.50 eV	
	$7.8(2) \cdot 10^{-7} \text{ K}^{-2} \text{ eV}$	$E \perp c$	for gap 1.29 eV	
		$E \perp c$	for gap 1.46 eV	

effective masses

m_n	$\approx 4.5 m_0$	from energy dependence of work function	77B
m_p	$\approx 1.8 m_0$		
m_n/m_p	≈ 2.5		

Lattice properties

α -rhombohedral boron

lattice parameters

rhombohedral description

a	5.057(3) Å	$T = 300$ K	precession and Weissenberg method	59D, 67H, 77N
α	58.06(5)°			

bulk modulus

B	224(15) GPa	$T = 300$ K	single crystal X-ray technique	93N
-----	-------------	-------------	--------------------------------	-----

optical phonons

Group theory gives: IR: 4 A_{2u} , 6 E_u ; Raman: 4 A_{1g} , 5 E_g [79B].

phonon wavenumbers, phonon cut-off

$\bar{\nu}$	300 cm^{-1}	$T = 300$ K	acoustic phonon cut-off	71S
	920 cm^{-1}		one-phonon cut-off	74G

IR-active one-phonon processes

$\bar{\nu}$	548 cm^{-1}	$T = 300$ K	powder absorption	74G
	705 cm^{-1}			
	806 cm^{-1}			
	920 cm^{-1}			
	1080 $\text{cm}^{-1}?$			
	1200 $\text{cm}^{-1}?$			

phonon dispersion curves: Fig. 11.1.2.

β-rhombohedral boron

lattice parameters

rhombohedral description

<i>a</i>	10.145(15) Å	<i>T</i> = 300 K	precession and Weissenberg method	63H,
<i>α</i>	65°17(8)'			67H

bulk modulus

<i>B</i>	185(7) GPa	<i>T</i> = 300K	neutron powder diffraction	93N
----------	------------	-----------------	----------------------------	-----

linear thermal expansion coefficient

<i>α</i> _{av}	6.47·10 ⁻⁶ K ⁻¹	<i>T</i> = 10...1028 K	average coefficient	97L
<i>α</i> _a	0.98·10 ⁻⁶ K ⁻¹		X-ray diffraction	
<i>α</i> _c	1.82·10 ⁻⁶ K ⁻¹			

optical phonons

ir modes: theor. 31 A_{2u}, 52 E_u, exp. 33 A_{2u} 30 E_u. Raman active modes: theor. 31 A_{1g}, 52 E_g, exp. 35 + 5 (uncertain).

phonon wavenumbers, phonon cut-off

<i>ν̄</i>	130 cm ⁻¹		acoustic phonon cut-off	71S
	1275 cm ⁻¹	<i>T</i> = 300 K	one-phonon cut-off	79B
	2200 cm ⁻¹	<i>T</i> = 300 K	two-phonon cut-off	72W

elastic constants

calculation for α-rhombohedral boron compared with experimental data for β-rhombohedral boron

(c _{ik} in GPa)	α-rhombohedral B				β-rhombohedral B	Exp.[74S]
	Theory [97S]				Theory [92L, 93L]	
	(I)	(II)	(III)			
	(ext.)	(+ int)				
<i>c</i> ₁₁	389.5	302.2	314.5	323.9	448.38	467
<i>c</i> ₃₃	455.1	309.4	327.4	333.7	588.90	473
<i>c</i> ₄₄	123.1	.0	.0	33.4		198
<i>c</i> ₁₂	129.8	137.1	130.1	122.4	110.42	241
<i>c</i> ₁₃	123.1	166.4	160.8	158.6	41.10	
<i>c</i> ₁₄	− 9.2	.0	.0	− 5.8		15.1
<i>c</i> ₁₅					24.49	

Young's modulus

<i>E</i>	up to 48.26·10 ¹⁰ Pa	<i>T</i> = 300 K	questionable if β-rhombohedral B	66H, 70B
----------	------------------------------------	------------------	----------------------------------	-------------

compressibility

<i>κ</i>	1.8·10 ⁻⁷ bar ⁻¹	<i>T</i> = 300 K	questionable if β-rhombohedral B the numerical values are based on	64N, 70B
----------	--	------------------	---	-------------

melting temperature

<i>T</i> _m	2365 K		DTA	73H
-----------------------	--------	--	-----	-----

Debye temperature

Θ_D	1305 K	$T = 400$ K	α -rhombohedral boron	86T
	1430 K	$T = 0$ K	derived	71S
	1540 K	$T = 4...20$ K	β -rhombohedral boron, from heat capacity	87C

heat capacity

C_p	10.21 J mol ⁻¹ K ⁻¹	$T = 298.15$ K	α -rhombohedral boron	86T
	2.879 J mol ⁻¹ K ⁻¹	$T = 300$ K	β -rhombohedral boron	60W

density

d	2.45...2.46 g cm ⁻³	$T = 296$ K	α -rhombohedral boron	60T
	2.326 g cm ⁻³	$T = 293$ K	β -rhombohedral boron, bulk	73H

Transport properties

α -rhombohedral boron

electrical conductivity

σ	10 ⁻³ ...3.10 ⁻² (Ωcm) ⁻¹	$T = 300$ K	extrinsic. see Fig. 11.1.3	60B, 79G
----------	--	-------------	----------------------------	-------------

mobility

μ	120 cm ² (Vs) ⁻¹	$T = 300$ K	Hall effect	81G
-------	--	-------------	-------------	-----

Temperature dependence of the hole mobility: $\mu_H \propto T^{-1.75}$ Fig. 11.1.4 [84G].

β -rhombohedral boron

The transport properties of β -rhombohedral boron have not been clarified definitely. They are mainly affected by levels of high concentration in the band gap.

dc conductivity

σ	10 ⁻⁷ ...10 ⁻⁶ (Ωcm) ⁻¹	$T = 300$ K	intrinsic	(for references, see Fig. 11.1.5)
	up to 20 (Ωcm) ⁻¹	$T = 300$ K	extrinsic	

carrier mobility

μ	10 ⁻⁵ ...3.10 ² cm ² /Vs	$T = 300$ K	obtained by different methods on samples of different origin and purity (see Fig. 11.1.6)
	10 ⁻¹ ...10 ⁻⁷ cm ² /Vs	$T = 77$ K	

thermal conductivity

κ	0.01 W cm ⁻¹ K ⁻¹		α -rhombohedral boron	79G
----------	---	--	------------------------------	-----

Optical properties

α -rhombohedral boron

optical spectra : absorption: Fig. 11.1.7.

dielectric constant

ϵ_0	6.5	$T = 300$ K	from electron energy-loss	97T
--------------	-----	-------------	---------------------------	-----

Dielectric function in the range of fundamental absorption derived from the electron energy loss spectrum in Fig. 11.1.8 [97T].

β -rhombohedral boron

optical spectra : optical constants of β -rhombohedral boron: Fig. 11.1.9.

dielectric constants

$\epsilon(0)$	10.6(2)	$T = 300$ K, static	polycrystalline sample	53L
$\epsilon(\infty)$	9.12(15)		$E \perp c$	70W4
	8.41(15)		$E \parallel c$	

References to 11.1

- 53L Lagrenaudi, J.: J. Chem. Phys. 50 (1953) 629.
- 59D Decker, B. F., Kasper, J. S.: Acta Crystallogr. 12 (1959) 503.
- 60B Becher, H. J.: Z. Anorg. Chem. 321 (1960) 317.
- 60H Horn, F. H., in: Boron, Vol. 1, Eds. Kohn, J. A., Nye, W. F., Gaule, O. K., New York: Plenum Press, 1960, p. 111.
- 60T Talley, C. P., Line Jr., L. E.: Nav. Res. Rev. 1960, 16 (April).
- 60W Wise, S. S., Margrave, J. L., Altman, R. L.: J. Phys. Chem. 64 (1960) 915.
- 63H Hoard, J. L., Hughes, R. E., Kennard, C. H. L., Sullenger, D. H., Weahlim, H. A., Sands, D. E.: J. Am. Chem. Soc. 85 (1963) 361.
- 64N Newkirk, A. E., Elemental Boron, in: Adams, R. M., Ed., Boron, Metallo-Boron Compounds and Boranes, Interscience Publishers, New York 1964, p. 301.
- 65B1 Borchert, W., Dietz, W., Herrmann, H.: Z. Angew. Phys. 19 (1965) 485.
- 65B2 Brungs, R. A., in: Boron, Vol. 2, Ed. O. K. Gaulé, New York: Plenum Press, 1965, p. 119.
- 65G1 Geist, D., Gläser, H. J.: J. Phys. Chem. Solids 26 (1965) 57.
- 65G2 Geist, D., in: Boron, Vol. 2, Ed. O. K. Gaulé, New York: Plenum Press, 1965, p. 203.
- 65H Horn, F. H., Taft, E. A., Oliver, D. W., in: Boron, Vol. 2, Ed. O. K. Gaulé, New York: Plenum Press, 1965, p. 231.
- 65J Jaumann, J., Schnell, J.: Z. Naturforsch. 20a (1965) 1639.
- 65N Neft, W., Seiler, K., in: Boron, Vol. 2, Ed. O. K. Gaulé, New York: Plenum Press, 1965, p. 143.
- 66H Herring, H. W., NASA Technical Note TND-3202 January 1966.
- 66S Sullenger, D. B., Kennard, Ch. L.: Sci. Am. 215 No. 7 (1966) 96.
- 67H Hoard, J. L., Hughes, R. E., in: General Introduction to Boron Chemistry, Ed. Muetterties E. L., New York: Wiley & Sons, 1966.
- 68D Dzhamagidze, Sh. Z., Mal'tsev, Yu. A., Shvangiradze, R. R.: Sov. Phys. Semicond. (English Transl.) 2 (1968) 320.
- 68G Golikova, O. A., Zhubanov, M. Zh., Klimashin, G. M.: Sov. Phys. Semicond. (English Transl.) 2 (1968) 451.
- 69J Jaumann, J., Werheit, H.: Phys. Status Solidi 33 (1969) 587.
- 70B Bower, J. O., in: Progress in Boron Chemistry, Ed. Brotherton and Steinberg, Pergamon Press 1970, p. 231.
- 70D Dietz, W., Herrmann, H., in: Boron, Vol. 3, Ed. Niemyski, T., Warsaw: Polish Scientific Publishers 1970, p. 195.
- 70G Golikova, O. A., Kiskachi, A. Yu., Khomidov, T.: Sov. Phys. Semicond. (English Transl.) 4 (1970) 683.
- 70W1 Werheit, H., in: Festkörperprobleme X, Ed. O. Madelung, Pergamon/Braunschweig: Vieweg 1970, p. 189.
- 70W2 Werheit, H., Leis, H. G.: Phys. Status Solidi 41 (1970) 247.
- 70W3 Werheit, H., Runow, P., Leis, H. G.: Phys. Status Solidi (a) 2 (1970) K 125.
- 70W4 Werheit, H., Hausen, A., Binnenbruck, H.: Phys. Status Solidi 42 (1970) K 57.
- 71S Slack, G. A., Oliver, D. W., Horn, F. H.: Phys. Rev. 114 (1971) 1714.
- 72R Runow, P.: J. Mater. Sci. 7 (1972) 499.
- 72W Werheit, H., Hansen, A., Binnenbruck, H.: Phys. Status Solidi (b) 51 (1972) 115.
- 73G1 Geist, D.: Z. Naturforsch. 28a (1973) 953.
- 73G2 Gewinner, O., Kubler, J., Koulmann, J. J., Jaéglé, A.: Phys. Status Solidi 59 (1973) 395.
- 73H Holcombe Jr., C. E., Smith, D. D., Lorc, J. D., Duerlesen, W. K., Carpenter, D. A.: High Temp. Sci. 5 (1973) 349.
- 73K Kubler, L., Gewinner, O., Koulmann, J. J., Jaéglé, A.: Phys. Status Solidi (b) 60 (1973) 117.
- 74A Adirovich, E. J., Abdullaev, Ja. S., Guljamov, K. V., Muminov, A., Sultanov, M.: in: Bor, poluchenie, structura i svojstva (Proc. 4th Int. Symp. Boron, Tbilisi, 1972) Izd. Mecniereba, Tbilisi (1974) p. 73.
- 74G Golikova, O. A., Drabkin, J. A., Zaitsev, V. K., Kazanin, M. M., Mirlin, D. N., Nelvson, IV., Tkalenko, E. N., Chomidov, T., in: Bor (see [74A]) p. 44.
- 74S Sil'vestrova, I.M., Beljaev, L.M., Niemyski, T., Pisarevskii, Yu.V.: in: Bor, Poluchenie, Structura i Svojstva (Proc. 4th Int. Symp. Boron, Tbilisi, 1972) Izd. Nauka, Moscow, 1974 p. 125.
- 76A Arsen'eva-Geil', A. N., Berezin, A. A., Melnikova, E. V.: Sov. Phys. Solid State (English Transl.) 17 (1976) 1624.
- 77B Berezin, A. A., Trunov, N. N.: Sov. Phys. Solid State (English Transl.) 19 (1977) 716.
- 77N Naslain, R., in: Boron and Refractory Borides, Ed. Matkovich, V. J., Berlin: Springer, 1977, p. 139.

- 78S Solov'ev, N. E., Makarov, V. S., Ugai, Ya. A.: *Izv. Akad. Nauk, Neorgan. Mater.* 14 (1978) 2252; *Inorg. Mater. USSR (English Transl.)* 14 (1979) 1762.
- 79B Binnenbruck, H., Werheit, H.: *Z. Naturforsch.* 34a (1979) 787.
- 79G Golikova, O. A., Solov'ev, N. E., Ugai, Ya. A., Feigel'man, V. A.: *Fiz. Tekh. Poluprovodn.* 13 (1979) 825; *Sov. Phys. Semicond. (English Transl.)* 13 (1979) 486.
- 79S Szadkowski, A.: *J. Less-Common Met.* 67 (1979) 551.
- 81G Golikova, O. A., Solov'ev, N. E., Ugai, Ya. A., Feigelman, V. A.: in: *Proc. 7th Int. Symp. Boron, Borides and Related Compounds*, Uppsala, Sweden, 1981 p. 362.
- 81P Perrot, F.: *Phys. Rev. B* 23 (1981) 2004.
- 81S Sidorin, K. K., Karin, M. G., Bobrikov, V. M., Shelich, A. I., Tsagareishvili, G. V., Gabuniya, D. L., Tavadze, G. F., Korsukova, M. M.: *J. Less-Common Met.* 82 (1981) 297; in: *Proc. 7th Int. Symp. Boron, Borides and Related Compounds*, Uppsala, Sweden, 1981 p. 297.
- 81W Werheit, H., de Groot, K., Malkemper, W., Lundström, T.: *J. Less-Common Met.* 82 (1981) 163; in: *Proc. 7th Int. Symp. Boron, Borides and Related Compounds*, Uppsala, Sweden, 1981 p. 163.
- 83G Golikova, O. A., Samatov, S.: *Phys. Status Solidi (a)* 77 (1983) 449.
- 84G Golikova, O. A.: *Phys. Status Solidi (a)* 86 (1984) K51.
- 86T Tsagareishvili, D. Sh., Tsagareishvili, G. V., Omiadze, I. S., Jobava, J. Sh., Naumov, V. N., Nogteva, V. V., Paukov, I. E.: in: *Proc. 8th Int. Symp. Boron, Borides, Carbides, Nitrides and Related Compounds*, Tbilisi, Oct. 8...12, 1984 (Special issue of *J. Less-Common Met.* Vol. 117, P. Rogl. ed., Elsevier: Lausanne, 1986 p. 143).
- 87C Cahill, D. G., Fischer, H. E., Warson, S. K., Pohl, R. O., Slack, G. A.: in: *Proc. 9th Int. Symp. Boron, Borides and Related Compounds*, University of Duisburg, Germany, Sept. 21...25, 1987., H. Werheit ed., University of Duisburg: Duisburg, 1987 p. 113.
- 87G Golikova, O. A.: *Phys. Status Solidi (a)* 101 (1987) 277.
- 90W Werheit, H.: in: *The Physics and Chemistry of Carbides, Nitrides and Borides*; NATO ASI Series E: Applied Sciences Vol. 185, R. Freer ed., Kluwer Academic Publishers: Dordrecht, 1990 p. 691.
- 91B Beckel, C. L., Yousaf, M., Fuka, M. Z., Raja, S. Y., Lu, N.: *Phys. Rev. B* 44 (1991) 2535.
- 91W Werheit, H., Kuhlmann, U., Solov'ev, N.E., Tsiskarishvili, G. P., Tsagareishvili, G.: in: *Boron-Rich Solids*, *Proc. 10th Int. Symp. Boron, Borides and Rel. Compounds*, Albuquerque, NM 1990 (AIP Conf. Proc. 231), D. Emin, T. L. Aselage, A. C. Switendick, B. Morosin, C. L. Beckel ed., American Institute of Physics: New York, 1991 p. 350.
- 92L Lee, Seongbok, Bylander, D. M., Kleinman, L.: *Phys. Rev. B* 45 (1992) 3245.
- 93L Lee, S., Bylander, D.M., Kleinman, L.: *Phys. Rev. B* 47 (1993) 10057.
- 93N Nelmes, R.J., Loveday, J.S., Allan, D.R., Besson, J.M., Hamel, G., Grima, P., Hull, S.: *Phys. Rev. B* 47 (1993) 7668.
- 93W Werheit, H., Laux, M., Kuhlmann, U.: *Phys. Status Solidi (b)* 176 (1993) 415.
- 96T Takeda, M., Kimura, K., Murayama, K.: *J. Non-Cryst. Solids* 198-200 (1996) 170; (*Proc. ICAS16* (1995) in Kobe (in press)).
- 97L Lundström, T., Lönnberg, B., Bauer, J.: (to be published in *J. Alloys Comp.*).
- 97S Shirai, K.: presented at the 12th ISBB'96, Baden, Austria, 1997
- 97T Terauchi, M., Kawamata, Y., Tanaka, M., Takeda, M., Kimura, K.: *J. Solid State Chem.* 133 (1997) 156.

Fig. 11.0.3

Energy band structure along the $\Gamma - Z$ axis of α -boron.

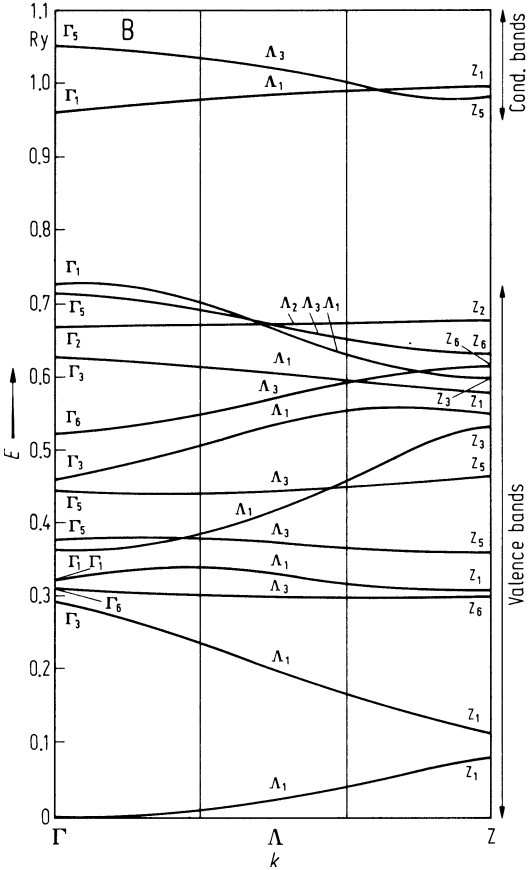


Fig. 11.0.4

Irreducible part of the Brillouin zone of α -boron.

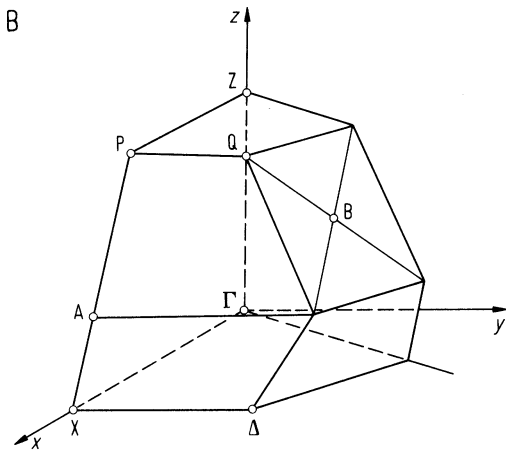


Fig. 11.0.5

β -rhombohedral boron. Energy band scheme. The vertical lines indicate the allowed optical transitions between different levels. Gap width 1.32(1) and 1.50(1) eV for $E \parallel c$ and 1.29(1) and 1.46(1) eV for $E \perp c$ respectively (values for extrapolation to $T = 0$ K) [93W].

Widely accepted band model for β -boron.

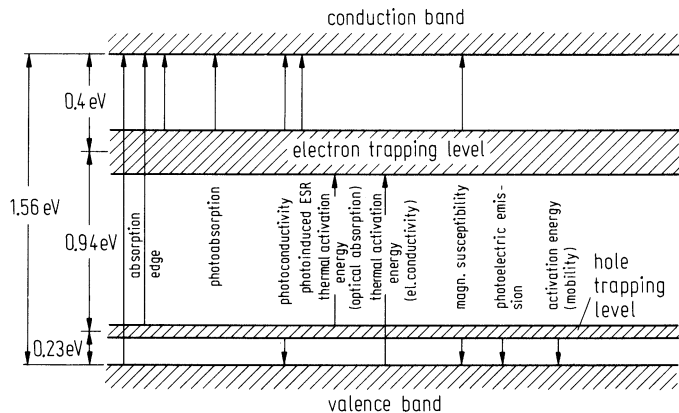


Fig. 11.1.1

β -rhombohedral boron. Temperature dependence of the experimentally determined band gaps and comparison with the adapted theory (see text). Fitting parameters for $E \parallel c$: $h\nu_q = 121.9$ meV and $\beta = 12$; for $E \perp c$: $h\nu = 94.1$ meV and $\beta = 14.5$ [93W].

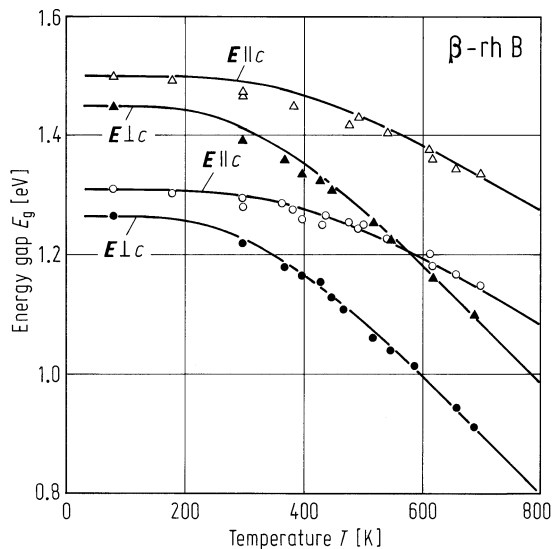


Fig. 11.1.2

α -rhombohedral boron. Calculated phonon dispersion curves obtained with phase difference in the c direction [91B].

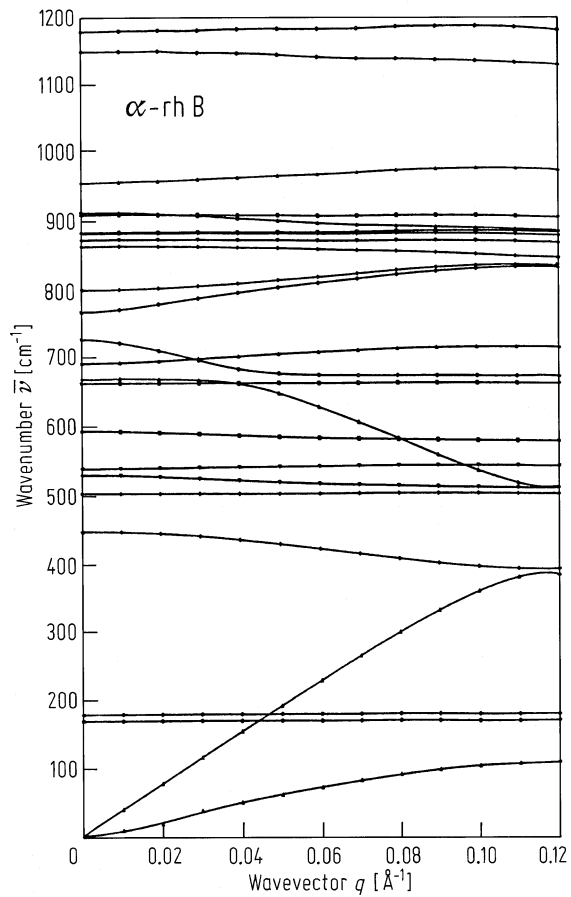


Fig. 11.1.3

α -rhombohedral B. Electrical conductivity vs. reciprocal temperature. Dashed line corresponds to an activation energy $E_A = 1$ eV [60H, 79G].

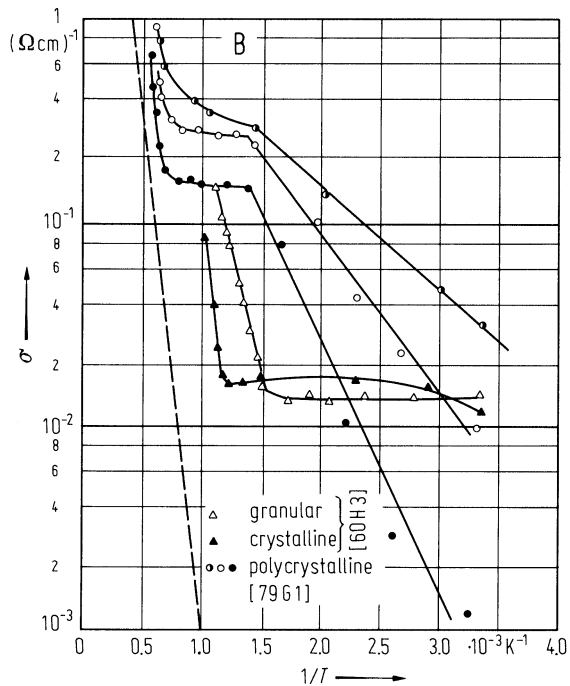


Fig. 11.1.4

α -rhombohedral boron. (a) Hall mobility (holes) vs. temperature [83G, 87G]. (b): log-log-plot of the Hall mobility. The fitted line corresponds to $\mu_{H,p} \propto T^{-1.75}$ [84G].

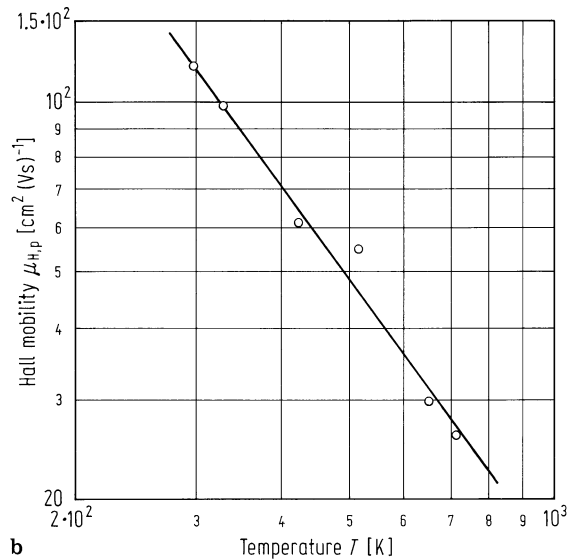
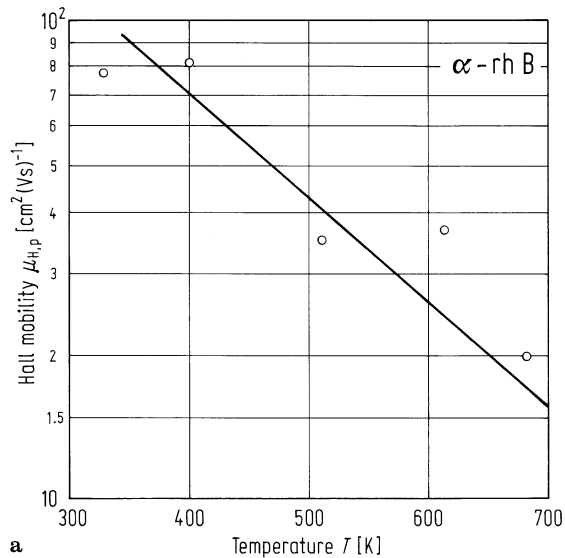


Fig. 11.1.5

β -rhombohedral B. Electrical conductivity vs. reciprocal temperature. Pure β -rhombohedral boron: 1, [70D, 64N, 65N, 65B1, 65B2, 65J, 68D, 70W2, 70G]; 2, [79S]. Doped β -rhombohedral boron: 3, [70W3] lapped surface; 4, [70W3] B₇O surface layer; 5, [65G1, 65G2] Mn-doped; 6, [65G1, 65G2] Fe-doped; 7, [65G1, 65G2] 3% C-doped; 8, [81W] FeB_{29.5}; 9, [68G] C-doped, $p = 3 \cdot 10^{20} \text{ cm}^{-3}$.

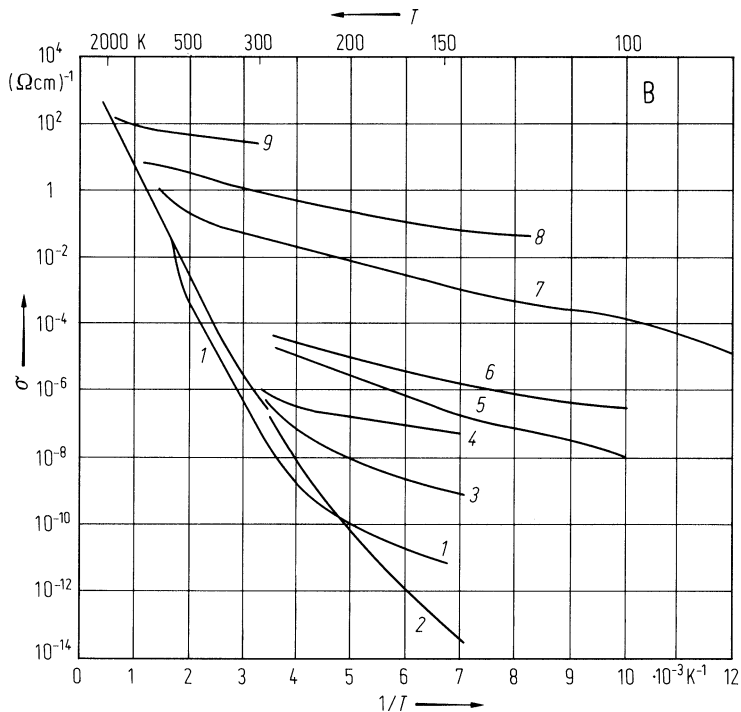


Fig. 11.1.6

β -rhombohedral boron. Drift mobility of holes vs. reciprocal temperature [96T].

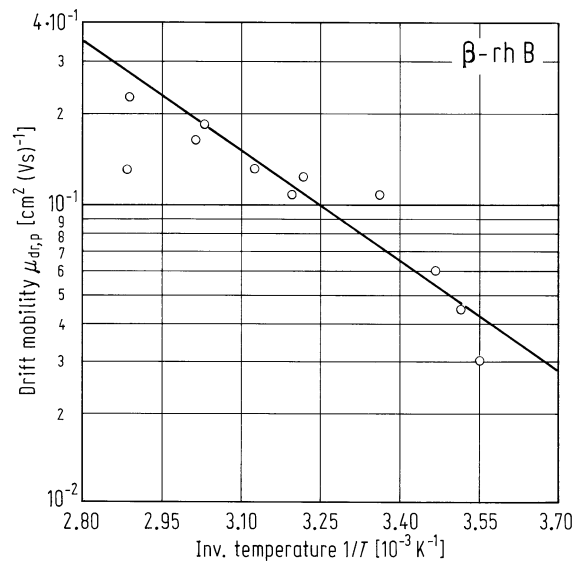


Fig. 11.1.7

α -rhombohedral B. Absorption coefficient vs. photon energy at the absorption edge [65H].

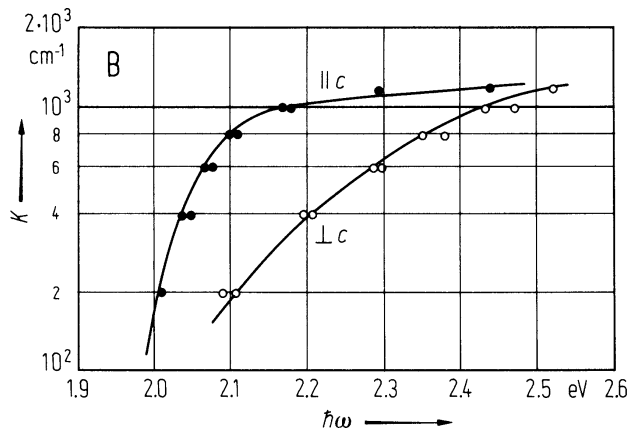


Fig. 11.1.8

α -rhombohedral boron. Real (ϵ_1 , full line) and imaginary part (ϵ_2 , broken line) of the dielectric function vs. photon energy [97T].

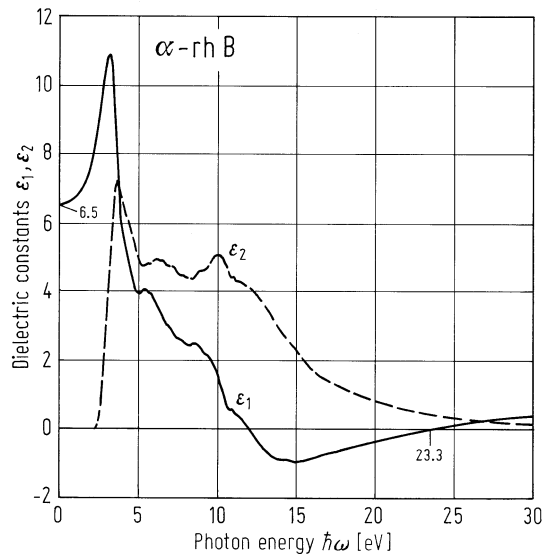
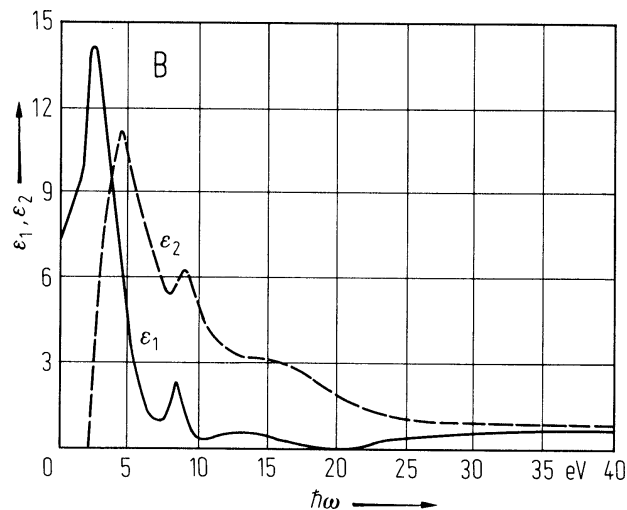


Fig. 11.1.9

β -rhombohedral B. Real and imaginary parts of the dielectric constant in the range of the fundamental absorption [81S].



12 Group V elements

12.0 Crystal structure and electronic structure

12.0.1 Crystal structure and Brillouin zones

Phosphorus:

Phosphorus shows a structural variety exceeded only by sulfur and possibly boron. The most common allotropes are: white, red and black phosphorus and some amorphous forms.

Black phosphorus is the most stable form of the allotropic modifications under standard conditions. It crystallizes in a layered structure with orthorhombic symmetry (Fig. 12.0.1, Brillouin zone: Fig. 12.0.2). The space group is $D_{2h}^{18}(=V_h^{18})$ –Bmab. The unit cell of black phosphorus contains eight atoms at the positions $\pm(0, v, u)$, $\pm(1/2, -v, u+1/2)$, $\pm(1/2, v+1/2, u)$ and $\pm(0, 1/2-v, u+1/2)$. Within the layers, each atom forms three covalent bonds essentially made of 3p orbitals. The layers are connected by weak van der Waals forces.

White phosphorus consists of tetrahedral P_4 molecules. The crystalline α (cubic) and β (hexagonal) modifications have not been fully characterized and are probably rotationally disordered plastic crystal phases.

Red phosphorus is not a single allotrope, but a term used to describe a variety of different forms, which are more or less red in color. The most common form of red phosphorus is amorphous red phosphorus, but powders of tetragonal, triclinic or cubic red phosphorus are also known.

Arsenic:

There are three crystalline modifications and some amorphous forms of arsenic under normal conditions.

Grey (α , ordinary) arsenic is the most stable form of arsenic under normal conditions. It is crystallized in a rhombohedral structure (A7-type; Fig. 12.0.3, Brillouin zone: Fig. 12.0.4). The space group is $R\bar{3}m - D_{3d}^5$.

Orthorhombic (ϵ , arsenolamprite) arsenic has a similar structure like black phosphorus [56K], but its structure can not be derived by a simple scaling of the bond length from black P [75S]. The unit cell contains eight atoms (Fig. 12.0.5) at the positions $\pm(0, u, v)$, $\pm(1/2, u+1/2, v)$, $\pm(1/2, u, v+1/2)$ and $\pm(0, u+1/2, 1/2-v)$. The structure consists of double layers separated by 5.50 Å.

Yellow arsenic shows a cubic symmetry and presumably consists of As_4 molecules. This allotrope is only metastable and decomposes easily to grey arsenic. Structural data are not available, since X-ray radiation destroys this modification.

Antimony:

Three allotropes of antimony under normal conditions are known: metallic, black and explosive antimony.

α -, (grey, ordinary) antimony is the most stable form of antimony under normal conditions. It crystallizes in a rhombohedral structure (A7 -type) like arsenic. The space group is $R\bar{3}m - D_{3d}^5$.

Black antimony is strong reactive on air and has an amorphous structure. Under vacuum, it transforms easily to crystalline metallic antimony during heating.

Explosive antimony is only metastable and transforms fiercely in metallic antimony during mechanical stress or heating. It was characterized to be amorphous by Kersten [32K]. According to Krebs et al. [55K] explosive antimony is probably not an allotropic form, but a mixed polymer.

Bismuth:

α -bismuth is the only stable form of bulk bismuth under normal conditions. It crystallizes in a rhombohedral A7-type structure, like arsenic and antimony. The space group is $R\bar{3}m - D_{3d}^5$. The primitive cell contains two atoms at the positions (u, u, u) and $-(u, u, u)$.

12.0.2 Electronic structure

Figs. 12.0.6...12.0.9 show the band structure of phosphorus, arsenic, antimony and bismuth.

References to 12.0

- 32K Kersten, H.: Physics 2 (1932) 276.
- 55K Krebs, H., Schultze-Gebhard, F., Thees, R.: Z. Anorg. Allg. Chem. 282 (1955) 177.
- 56K Krebs, H., Holz, W., Lippert, W., Worms, K. H.: Österr. Chem. Ztg. 57 (1956) 137.
- 75S Smith, P. M., Leadbetter, A. J., Apling, A. J.: Philos. Mag. B 31 (1975) 57.

Figures to 12.0

Fig. 12.0.1

Perspective view of the black phosphorus structure

black P

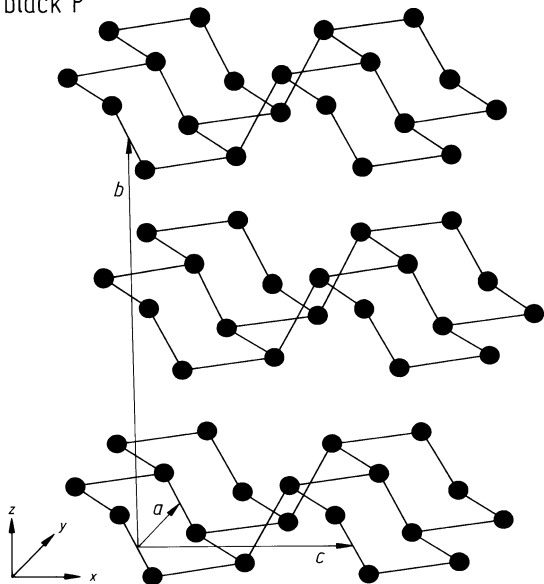


Fig. 12.0.2

Brillouin zone of black phosphorus

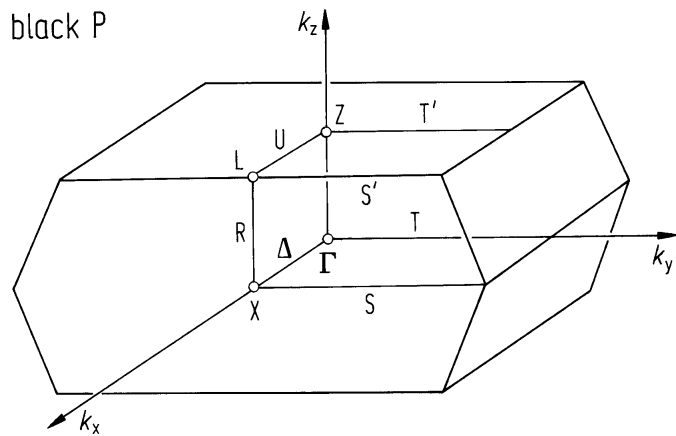


Fig. 12.0.3

Crystal structure of grey arsenic (a) and the cubic NaCl structure (b) from which it can be derived. The open and solid circles represent the two sublattices.

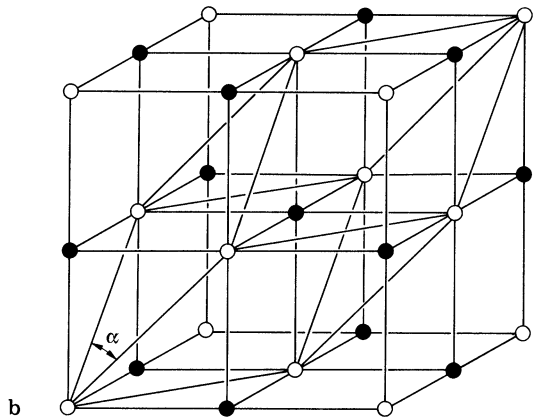
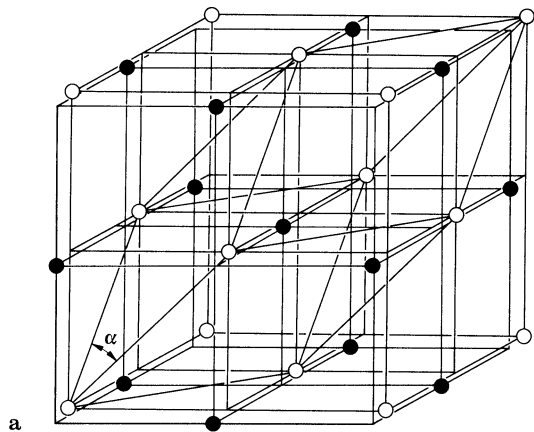


Fig. 12.0.4

Brillouin zone of grey arsenic showing points, lines and planes of symmetry.

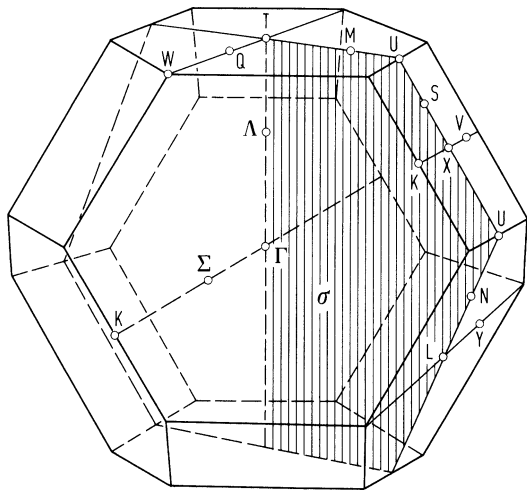


Fig. 12.0.5

The unit cell of orthorhombic arsenic.

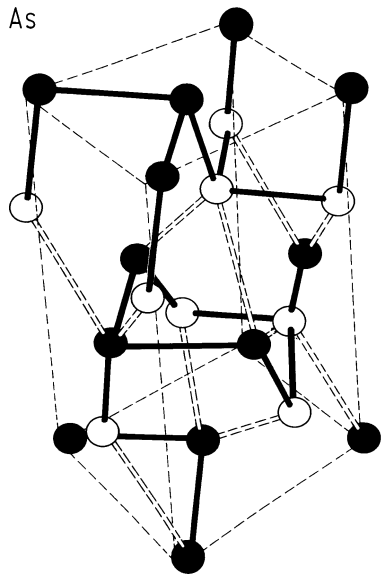


Fig. 12.0.6

Band structure and density of states of black phosphorus.

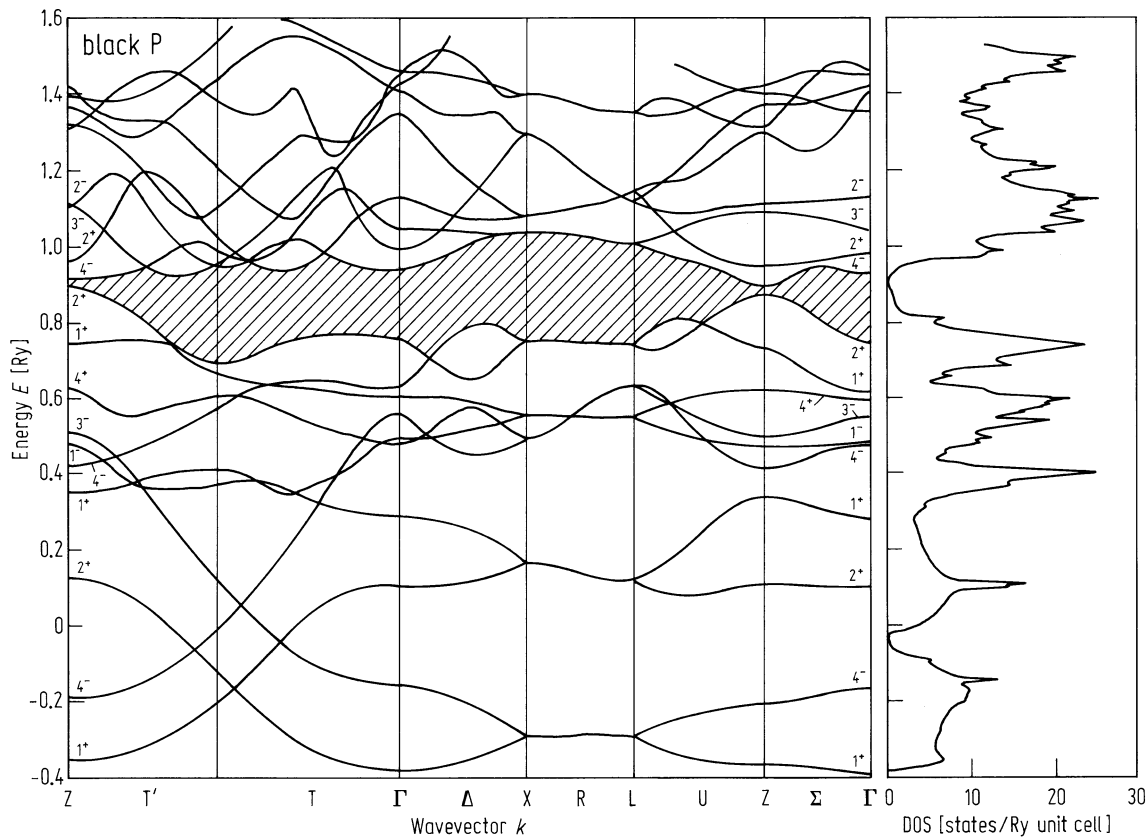


Fig. 12.0.7

Band structure of grey arsenic.

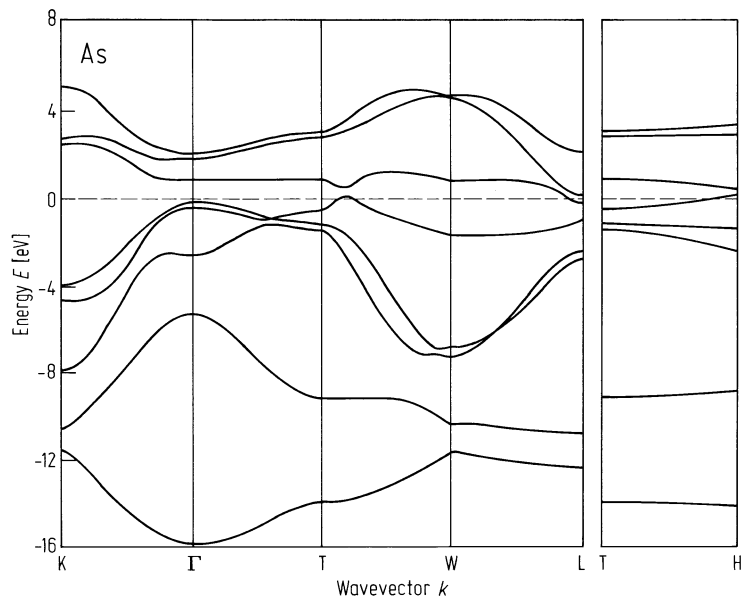
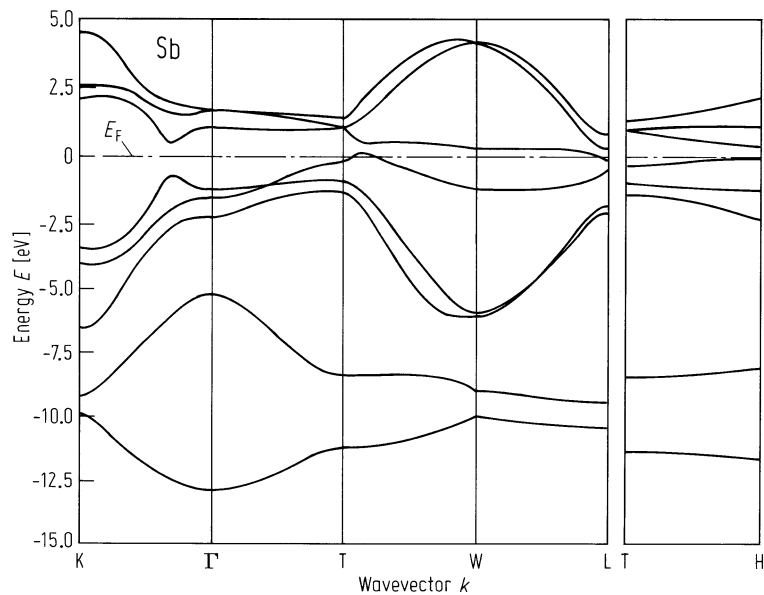
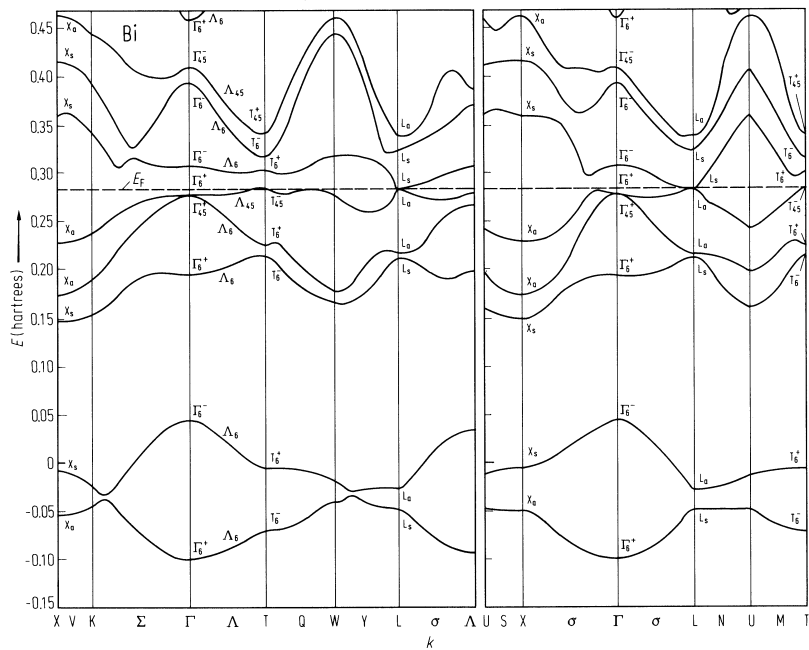


Fig. 12.0.8

Band structure of metallic antimony.



Band structure of bismuth.



12.1 Group V elements: Phosphorus

Crystal structure

see section 12.0.

Electronic properties

Black phosphorus is a narrow-gap semiconductor. A direct band gap of about 0.3 eV was found from experiments.

Red phosphorus is a semiconductor, too [52M]. But little is known about the electronic properties of red phosphorus. White phosphorus is an insulator with a band gap of about 3.7 eV.

Band structure of black phosphorus: Fig. 12.0.6, Brillouin zone: Fig. 12.0.2.

energy gap

E_g	0.3125 eV	$T = 300$ K	from photoconductivity of single crystalline black P prepared by bismuth flux method	91B
dE_g/dT	$1.75 \cdot 10^{-4}$ eV K ⁻¹	$(T > 160$ K)	from photoconductivity of single crystalline black P prepared by bismuth flux method; see also Fig. 12.1.1.	91B
	$2.33 \cdot 10^{-4}$ eV K ⁻¹	$(T < 160$ K)		

band-band exciton transitions and exciton binding energy

E_1	0.2764 eV	$T = 4.2$ K	absorption spectrum calculated by Kramers-Kronig transformation from reflection spectrum of single crystalline black P	86M
E_2	0.2823 eV			
E_b	$7.9 \cdot 10^{-3}$ eV	binding energy		

effective masses

m_{pa}	$0.625 m_0$	from cyclotron resonance measurements on single crystalline black P	90T
m_{pb}	$0.304 m_0$		
m_{pc}	$0.091 m_0$		
$m_{p \text{ av}}$	$0.258 m_0$		
m_{na}	$1.14 m_0$		
m_{nb}	$0.127 m_0$		
m_{nc}	$0.096 m_0$		
$m_{n \text{ av}}$	$0.24 m_0$		

Lattice properties

linear thermal expansion coefficient

α_1	$22 \cdot 10^{-6}$ K ⁻¹	for black P; $\alpha_{1,2,3}$: α in a, b, c direction, respectively.	53K
α_2	$39 \cdot 10^{-6}$ K ⁻¹		
α_3	$33 \cdot 10^{-6}$ K ⁻¹		

second order elastic moduli

c_{11}	$0.551 \cdot 10^2$ GPa	from v_{cc}	derived from ultrasound velocity measurements on black P at normal conditions for temperature dependence see Fig. 12.1.2	91K
c_{22}	$1.786 \cdot 10^2$ GPa	from v_{aa}		
c_{33}	$0.536 \cdot 10^2$ GPa	from v_{bb}		
c_{44}	$0.111 \cdot 10^2$ GPa	from v_{ba}		
c_{55}	$0.055 \cdot 10^2$ GPa	from v_{cb}		
c_{66}	$0.145 \cdot 10^2$ GPa	from v_{ca}		

bulk moduli

B_0	36(2) GPa	orthorhombic	from pressure dependence	83K
-------	-----------	--------------	--------------------------	-----

linear compressibility

κ_a	$1.8 \cdot 10^{-3} \text{ GPa}^{-1}$		calculated for black P using the force constant model	86K
κ_b	$14.8 \cdot 10^{-3} \text{ GPa}^{-1}$			

phonon dispersion curves : black P, see Fig. 12.1.3.				86K
---	--	--	--	-----

optical phonon frequencies (at the Γ -point)

$\bar{\nu}$	470 cm^{-1}	$\Gamma_1^+ (\text{A}_g^2)$	Raman active	calculated for black P using the force constant model; see also: [82K] and [83M]	86K
	360 cm^{-1}	$\Gamma_1^+ (\text{A}_g^1)$	Raman active		
	440 cm^{-1}	$\Gamma_2^+ (\text{B}_{2g}^1)$	Raman active		
	232 cm^{-1}	$\Gamma_2^+ (\text{B}_{2g}^2)$	Raman active		
	195 cm^{-1}	$\Gamma_3^+ (\text{B}_{1g})$	Raman active		
	441 cm^{-1}	$\Gamma_4^+ (\text{B}_{3g}^2)$	Raman active		
	470 cm^{-1}	$\Gamma_4^- (\text{B}_{3u})$	infrared active		
	213 cm^{-1}	$\Gamma_3^- (\text{B}_{1u})$	infrared active		
	412 cm^{-1}	$\Gamma_1^- (\text{A}_u)$	optically inactive		

Debye temperature

Θ_D			black P	86Y
------------	--	--	---------	-----

heat capacity

C_p	$\approx 22 \text{ J K}^{-1} \text{ mol}^{-1}$	$T = 300\text{K}$	black P; measured by an ac calorimetry apparatus	86Y
-------	--	-------------------	--	-----

density

d	2.70 g cm^{-3}		black P red P	35H
	2.34 g cm^{-3}			

melting temperature

T_m	590 K		red P	35H
	1300 K		black P	65S

Transport and optical properties

electrical resistivity

ρ	0.4 ... 2.3 $\Omega \text{ cm}$	$T = 300 \text{ K}$	single crystalline black P prepared under high pressure; for temperature dependence see Fig. 12.1.4	83A1
--------	---------------------------------	---------------------	--	------

Hall mobilities

$\mu_p (a\text{-axis})$	$\approx 5 \cdot 10^2 \text{ cm}^2 \text{ V}^{-1} \text{ s}^{-1}$	$T = 300 \text{ K}$	single crystalline p-type black P temperature dependence see Fig. 12.1.5, between $\approx 50 \text{ K}$ and $\approx 300 \text{ K}$ scattering on acoustic phonons is dominant	83A1
$\mu_p (b\text{-axis})$	$\approx 1.5 \cdot 10^2 \text{ cm}^2 \text{ V}^{-1} \text{ s}^{-1}$			
$\mu_p (c\text{-axis})$	$\approx 1.5 \cdot 10^3 \text{ cm}^2 \text{ V}^{-1} \text{ s}^{-1}$			

dielectric constants

ϵ_a	10.2	static	calculated; for frequency dependence, see Fig. 12.1.6	83A2
ϵ_b	8.3	static		
ϵ_c	12.5	static		

References to 12.1

- 35H Hultgren, R., Ginrich, N. S., Warren, D. E.: J. Chem. Phys. 3 (1935) 351.
- 52M Moss, T.S.: Photoconductivity in the Elements, Butterworths Scient. Publ.: London, 1952, p.141.
- 53K Keyes, R. W.: Phys. Rev. 92 (1953) 580.
- 65S Slack, G. A.: Phys. Rev. 139 (1965) A 507.
- 82K Kaneta, C., Katayama-Yoshida, H., Morita, A.: Solid State Commun. 44 (1982) 613.
- 83A1 Akahama, Y., Endo, S., Narita, S.: J. Phys. Soc. Jpn. 52 (1983) 2148.
- 83A2 Asahina, H., Maruyama, Y., Morita, A.: Physica B&C 117&118 (1983) 419.
- 83K Kikegawa, T., Iwasaki, H.: Acta Crystallogr. B39 (1983) 158.
- 83M Morita, A., Kaneta, C., Katayama-Yoshida, H.: Physica B&C 117-118 (1983) 517.
- 84A Asahina, H., Morita, A.: J. Phys. C 17 (1984) 1839.
- 86K Kaneta, C., Yoshida, H. K., Morita, S.: J. Phys. Soc. Jpn. 55 (1986) 1213.
- 86M Morita, A.: Appl. Phys. A39 (1986) 227.
- 86Y Yoshizawa, M., Shirotani, I., Fujimura, T.: J. Phys. Soc. Jpn. 55 (1986) 1196.
- 90T Takeyama, S., Miura, N., Akahama, Y., Endo, S.: J. Phys. Soc. Jpn. 59 (1990) 2400.
- 91B Baba, M., Nakamura, Y., Shibata, K., Morita, A.: Jpn. J. Appl. Phys. 2 30 (1991) L1178.
- 91K Kozuki, Y., Hanayama, Y., Kimura, M., Nishitake, T., Endo, S.: J. Phys. Soc. Jpn. 60 (1991) 1612.

Figures to 12.1

Fig. 12.0.2

Brillouin zone of black phosphorus

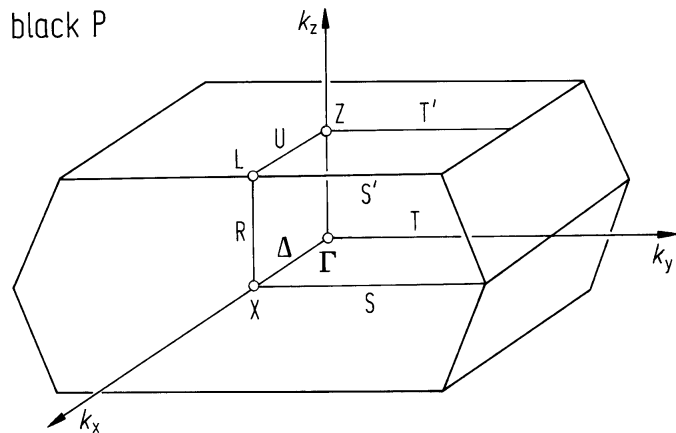


Fig. 12.0.6

Band structure and density of states of black phosphorus.

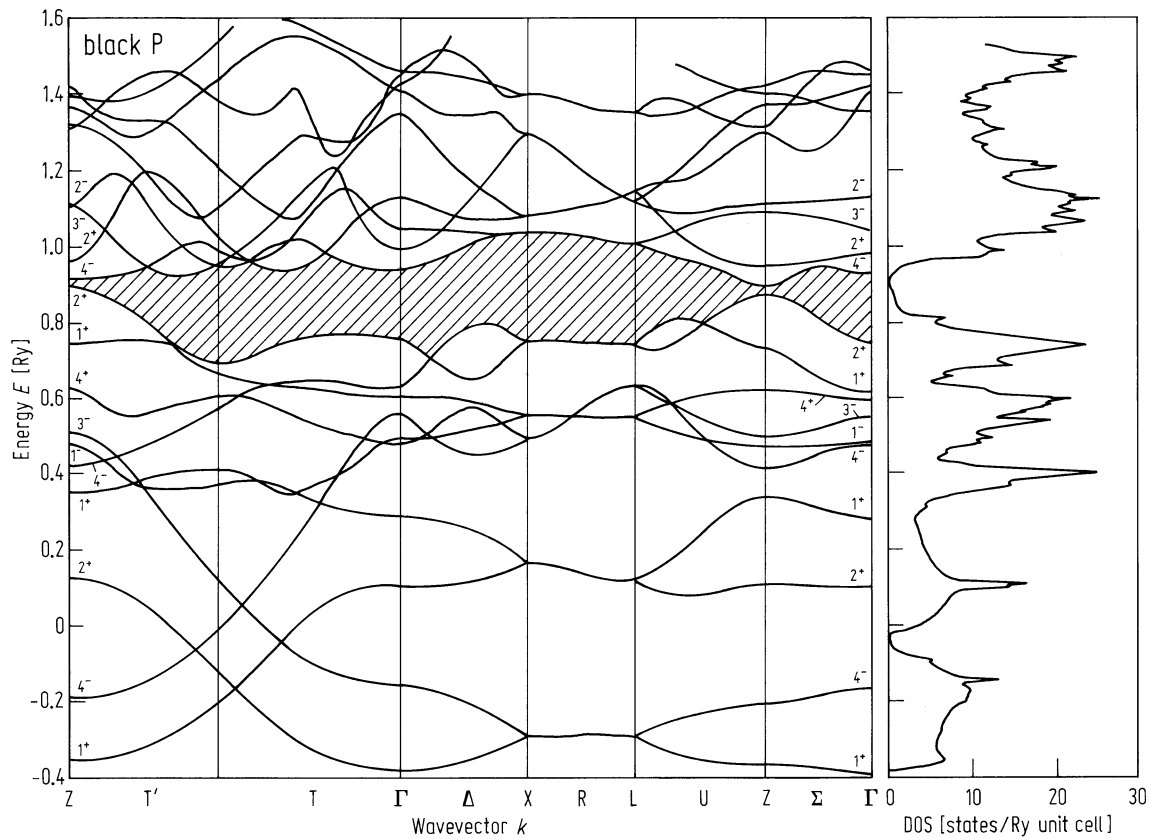


Fig. 12.1.1

P. Temperature dependence of the band-gap energy of black P determined by the temperature dependence of the photoconduction [91B].

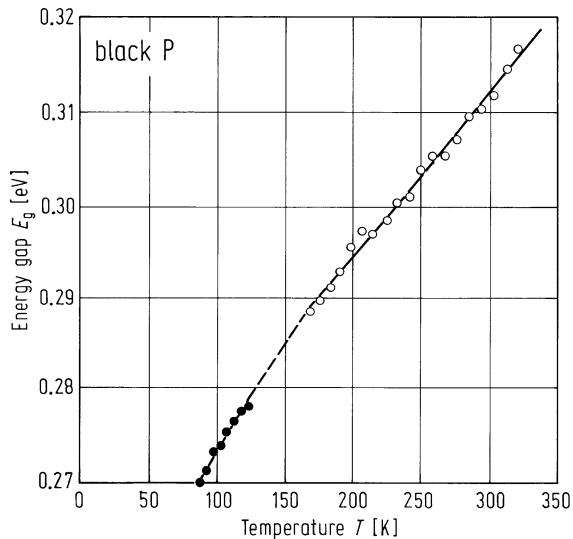


Fig. 12.1.2

P. Temperature dependence of second order elastic moduli of black P [86Y].

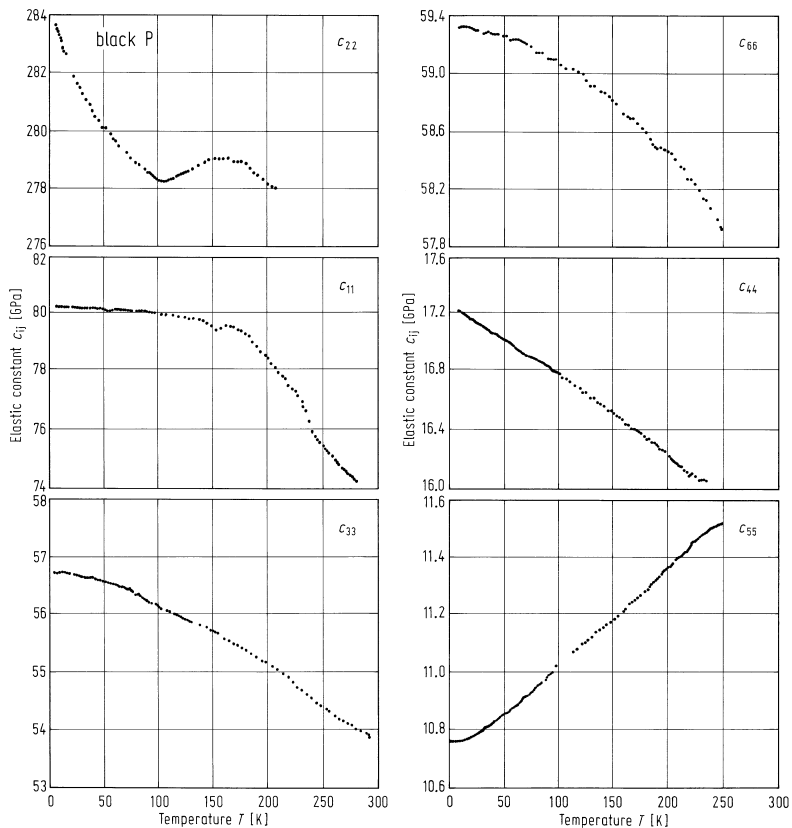


Fig. 12.1.3

P. Calculated phonon dispersion curves of black P using the valence force field model [86K].

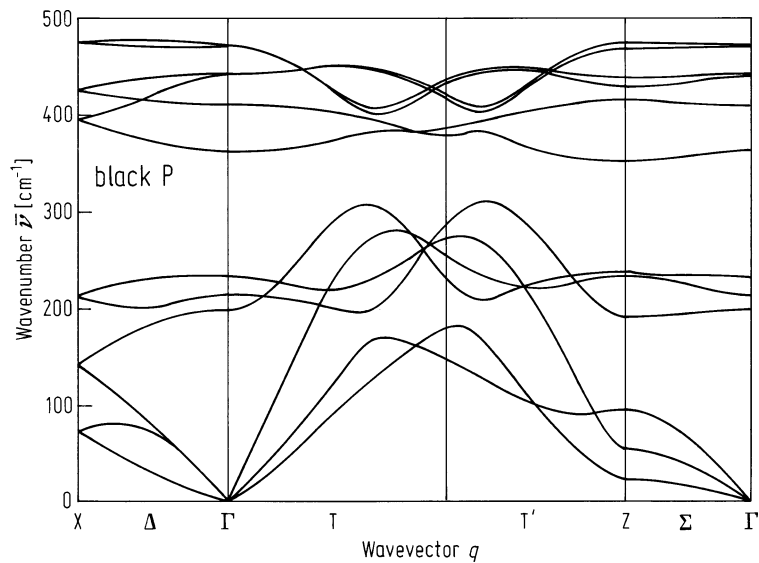


Fig. 12.1.4

P. Logarithmic resistivity curves against inverse temperature [83A1]. (a) Pure black P of p-type, prepared under high pressure. (b) Te-doped black P of n-type prepared under high pressure. The effective doping concentration is estimated to $2.2 \cdot 10^{16} \text{ cm}^{-3}$.

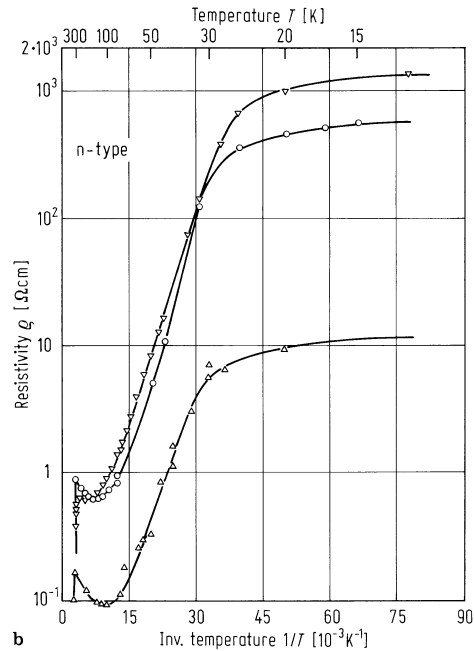
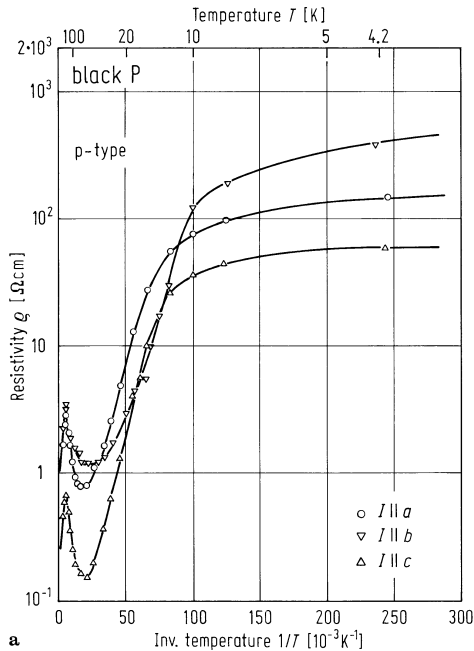


Fig. 12.1.5

P. Hall mobility of single crystalline black P [83A1], (a) p-type black P, (b) Te-doped n-type black P.

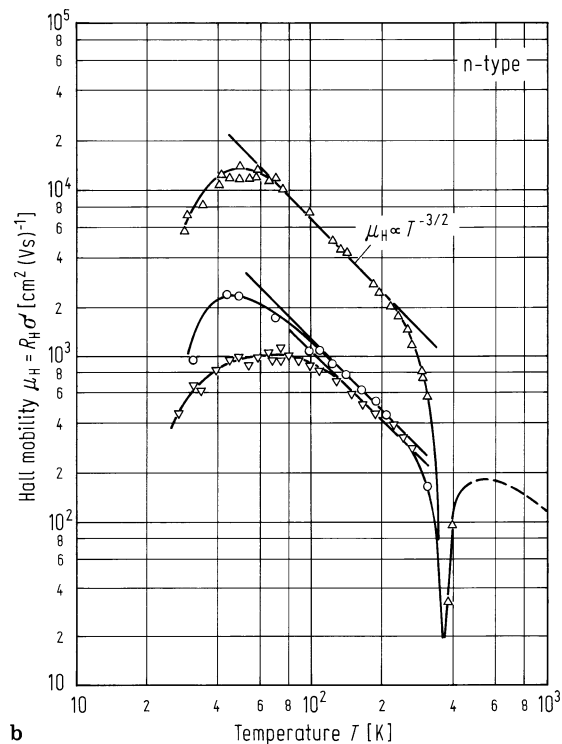
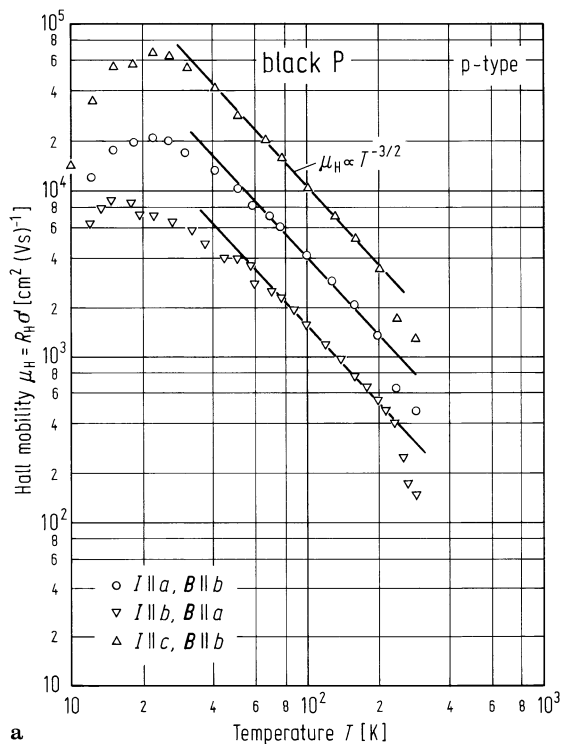
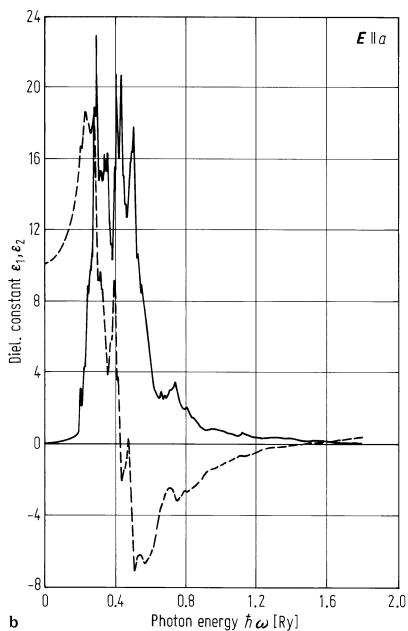
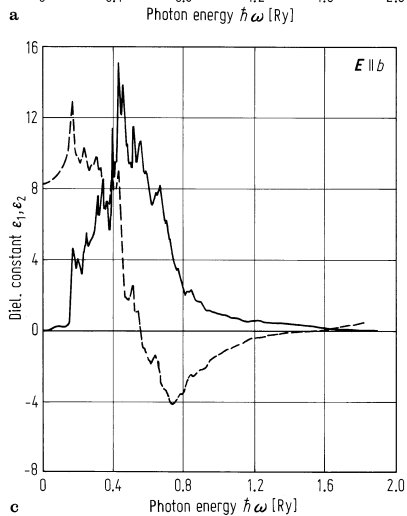
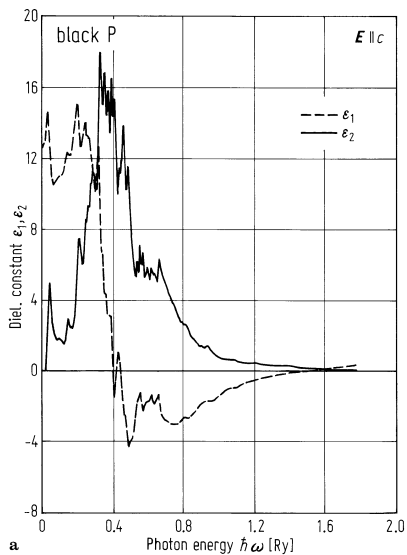


Fig. 12.1.6

P. Calculated dielectric function for black P (a) $E \parallel c$; (b) $E \parallel a$; (c) $E \parallel b$. Broken curves, $\text{real}(\epsilon)$; full curves, $\text{Im}(\epsilon)$ [84A].



12.2 Group V elements: Arsenic

Crystal structure

see section 12.0

Electronic properties

band structure of gray arsenic: Fig. 12.0.7, Brillouin zone: Fig. 12.0.4.

Gray arsenic is a semimetal and has the most metallic behavior of the group-V elements.

Amorphous arsenic is semiconducting with a band gap of about 1.2 ... 1.4 eV.

Little is known about the other allotropic forms of As. Orthorhombic As is a narrow- gap semiconductor with a band gap of about 0.3 eV [79G].

In the following data are given for rhombohedral As if not stated otherwise.

energy gap

$E_{g,dir}$ (near T on Q)	0.175 eV	from magnetoreflexion measurements at low temperatures (≤ 20 K)	67P
------------------------------	----------	--	-----

band overlap energy

E_0 (at H-L)	0.61 eV	first-principle calculation	90G
	0.43 eV	tight-binding calculation	93X
E_0 (L at T)	− 0.54 eV	band overlap energy from measurements of the Seebeck effect parallel and normal to C_3	70J

effective masses

m_{n1}	0.134 m_0	effective mass tensor components of electrons (at L) and α -holes (at T) at the Fermi level; from AKCR - measure- ments at $T = 1.15$ K. The tilt angles of electron and hole ellipsoids are -5.5° and -37.3° , respectively. The subscripts 1...3 refer to the crystallographic axes system with $X = C_2$, $Y = C_1$, and $Z = C_3$	71C
m_{n2}	1.252 m_0		
m_{n3}	0.141 m_0		
m_{n4}	1.644 m_0		
(= $ m_{n23} $)			
m_{p1}	0.146 m_0		
m_{p2}	0.104 m_0		
m_{p3}	0.166 m_0		
m_{p4}	0.153 m_0		
(= $ m_{p23} $)			

Lattice properties

lattice parameters

a	3.65 Å	X-ray powder diffraction of orthorhombic arsenic	75S	
b	4.47 Å			
c	11.00 Å			
a	4.1320 Å	$T = 299$ K	lattice parameters of the rhombohedral primitive cell; from X-ray diffraction measurements	69S
α	54.126°			
a	4.1063 Å	$T = 78$ K		
α	54.486°			

linear thermal expansion coefficient

$\alpha_{ }$	4100·10 ^{−8} K ^{−1}	$T = 283$ K	for temperature dependence, see Fig. 12.2.1 72W
α_{\perp}	122·10 ^{−8} K ^{−1}		

optical phonon frequencies (at the Γ point)

$\bar{\nu}$	195 cm^{-1}	E_g	Raman spectra at $T = 300 \text{ K}$	71Z
	257 cm^{-1}	A_{1g}	Results are confirmed by [90B]	

sound velocities

v_l	$4.79 \cdot 10^{-6} \text{ cm s}^{-1}$	$T = 300 \text{ K}$	propagation direction [100]	71P
v_{t1}	$2.99 \cdot 10^{-6} \text{ cm s}^{-1}$			
v_{t2}	$1.89 \cdot 10^{-6} \text{ cm s}^{-1}$			
v_l	$3.2 \cdot 10^{-6} \text{ cm s}^{-1}$		propagation direction [001]	
v_t	$2.05 \cdot 10^{-6} \text{ cm s}^{-1}$			

second order elastic moduli

c_{11}	$123.6 \cdot 10^{10} \text{ dyn cm}^{-2}$	$T = 300 \text{ K}$	from measurements of the ultrasonic	85G
c_{12}	$19.7 \cdot 10^{10} \text{ dyn cm}^{-2}$		wave velocity in crystalline As with	
c_{13}	$62.3 \cdot 10^{10} \text{ dyn cm}^{-2}$		$f = 10 \text{ MHz}$	
c_{14}	$-4.16 \cdot 10^{10} \text{ dyn cm}^{-2}$			
c_{33}	$59.1 \cdot 10^{10} \text{ dyn cm}^{-2}$			
c_{44}	$22.6 \cdot 10^{10} \text{ dyn cm}^{-2}$			

volume compressibility

κ_v	$17.2 \cdot 10^{-4} (\text{kbar})^{-1}$	$T = 300 \text{ K}$	for rhombohedral As	70P
------------	---	---------------------	---------------------	-----

bulk modulus

B	58 GPa		measured by X-ray investigation on rhombohedral As	90B
-----	--------	--	---	-----

Debye temperature

Θ_D	250 K	$T = 300 \text{ K}$	calculated from elastic constant data of rhombohedral As	70P
------------	-------	---------------------	---	-----

density

d	4.3 ... 5.2 g cm^{-3}		density of amorphous As	79G
	5.540 g cm^{-3}		density of orthorhombic As	79G
	2.07 g cm^{-3}		density of yellow As	79G
	6.2 ... 6.7 g cm^{-3}		density of fcc arsenic	79G
	4.770 g cm^{-3}		density of amorphous As	79H
	5.720 g cm^{-3}		density of rhombohedral (semimetallic) As	

melting temperature

T_m	1090 K		at atmospheric pressure	68S
-------	--------	--	-------------------------	-----

sublimation point

T_s	883 K			68S
-------	-------	--	--	-----

Transport and optical properties

Electronic transport occurs via band conduction. No hopping conduction has been observed.

intrinsic carrier concentration

n_i	$2.16 \cdot 10^{20} \text{ cm}^{-3}$	$T = 305 \text{ K}$	electron and hole (γ - and α -type) concen-	69J
-------	--------------------------------------	---------------------	--	-----

mobilities of charge carriers

μ_{n1}	460 cm ² V ⁻¹ s ⁻¹	$T = 305$ K	principal electron and hole mobilities	69J
μ_{n2}	40 cm ² V ⁻¹ s ⁻¹		calculated from galvanomagnetic measurements. The electron ellipsoid is	
μ_{n3}	550 cm ² V ⁻¹ s ⁻¹		tilted from the trigonal axis by an angle	
μ_{p1}	1210 cm ² V ⁻¹ s ⁻¹		of 82°, the hole pseudo-ellipsoid by an	
μ_{p2}	50 cm ² V ⁻¹ s ⁻¹		angle of 40° For temperature dependence	
μ_{p3}	680 cm ² V ⁻¹ s ⁻¹		of the mobility, see Fig. 12.2.2	

dielectric constant

ϵ_{33}	50			68R
-----------------	----	--	--	-----

Real (ϵ_1) and imaginary (ϵ_2) parts of the complex dielectric constant vs. photon energy, see Fig. 12.2.3.

thermal conductivity

κ_{11}	44 W m ⁻¹ K ⁻¹	$T = 300$ K	crystalline rhombohedral As; for temperature dependence in rhombohedral (semimetallic) As, see Fig. 12.2.4	77H
---------------	--------------------------------------	-------------	--	-----

References to 12.2

- 67P Priestley, M. G., Windmiller, L. R., Ketterson, J. B., Eckstein, Y.: Phys. Rev. 154 (1967) 671.
68R Riccius, H. D.: Proc. 9th Int. Conf. Phys. Semicond., Moscow 1968 (Nauka, Leningrad 1968) p. 185.
68S Handbook of the physico-chemical properties of the elements (ed. Samsonov, G. V.) IFI/Plenum, New York 1968, p. 128.
69J Jeavons, A. P., Saunders, G. A.: Phys. Roy. Soc. London A 310 (1969) 415.
69S Schiferl, D., Barrett, C. S.: J. Appl. Crystallogr. 2 (1969) 30.
70J Jeavons, A. P., Saunders, G. A.: Solid State Commun. 8 (1970) 995.
70P Pace, N. O., Saunders, G. A., Sümengen, Z.: J. Phys. Chem. Solids 31 (1970) 1467.
71C Cooper, O. S., Lawson, A. W.: Phys. Rev. B 4 (1971) 3261.
71P Pace, N. O., Saunders, G. A.: J. Phys. Chem. Solids 32 (1971) 1585.
71Z Zitter, R. N.: in: The Physics of Semimetals and Narrow Gap Semiconductors, , Carter, D. L.; Bate, R. T. ed., Pergamon Press: , 1971 p. 285.
72W White, O. K.: J. Phys. C 5 (1972) 2731.
74R Raisin, C., Leveque, G., Robin, J.: Solid State Commun. 14 (1974) 723.
75S Smith, P. M., Leadbetter, A. J., Apling, A. J.: Philos. Mag. B 31 (1975) 57.
77H Heremans, J., Issi, J.-P., Rashid, A. A. M., Saunders, G. A.: J. Phys. C 10 (1977) 4511.
79G Greaves, G. N., Elliott, S. R., Davis, E. A.: Adv. Phys. 28 (1979) 49.
79H Haemmerle, W. H., Golding, B.: Bull. Am. Phys. Soc. 24 (1979) 282 - BP3.
85G Grabov, V. M., Davydov, S. Yu., Mironov, Yu. P., Dzhumigo, A. M.: Sov. Phys.-Sol. St. 27 (1985) 1210.
90B Beister, H. J., Strössner, K., Syassen, K.: Phys. Rev. B 41 (1990) 5535.
90G Gonze, X., Michenaud, J.-P., Vigneron, J.-P.: Phys. Rev. B 41 (1990) 11827.
93X Xu, J. H., Wang, E. G., Ting, C. S., Su, W. P.: Phys. Rev. B 48 (1993) 17271.

Figures to 12.2

Fig. 12.0.4

Brillouin zone of grey arsenic showing points, lines and planes of symmetry.

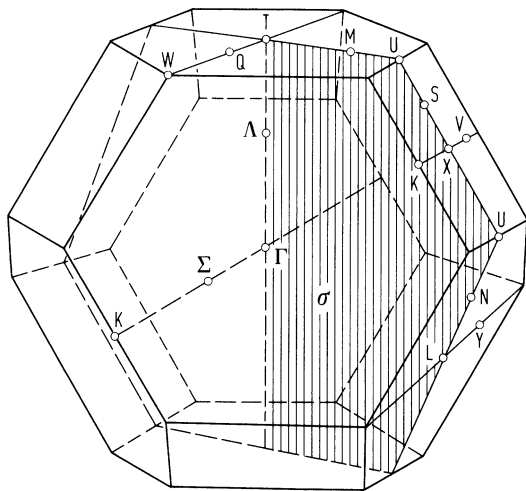


Fig. 12.0.7

Band structure of grey arsenic.

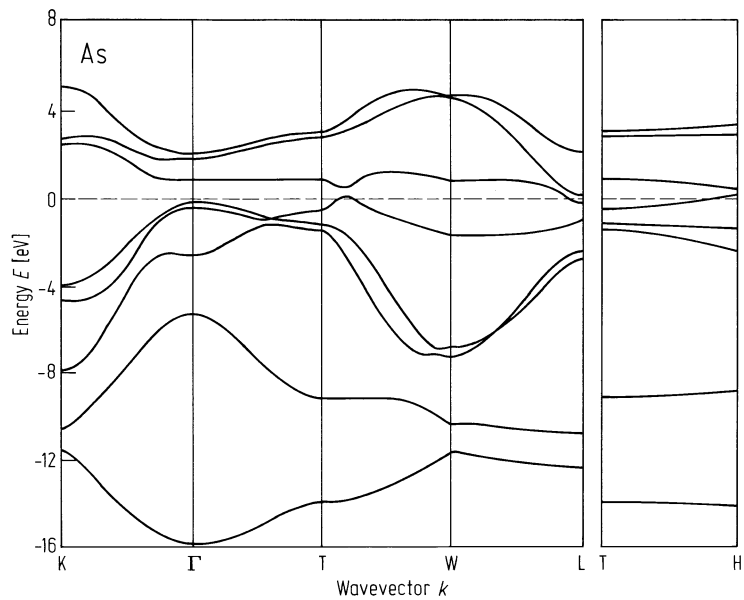


Fig. 12.2.1

As. a) Temperature dependence of the linear expansion coefficient α parallel to the trigonal axis (α_{\parallel} , triangles) and in a direction with $\Psi = 86^\circ$ from the trigonal axis (α'_{\perp} , circles). An enlarged sketch of the temperature range < 10 K is shown in b) [72W]. Note different scale for negative values of α_{\perp} in Fig. b).

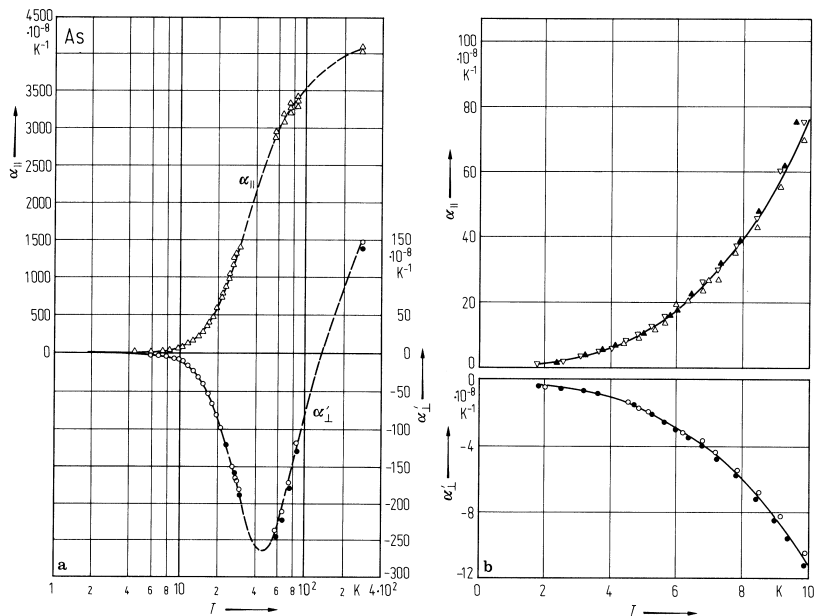


Fig. 12.2.2

As. Mobilities of electrons and holes vs. temperature. μ_{n1} , μ_{n3} and μ_{p3} show a slope -1.7 , μ_{p1} and μ_{p2} show a slope -1.5 and -2.0 . The values of μ_{n3} are scaled by a factor of 0.5 [69J].

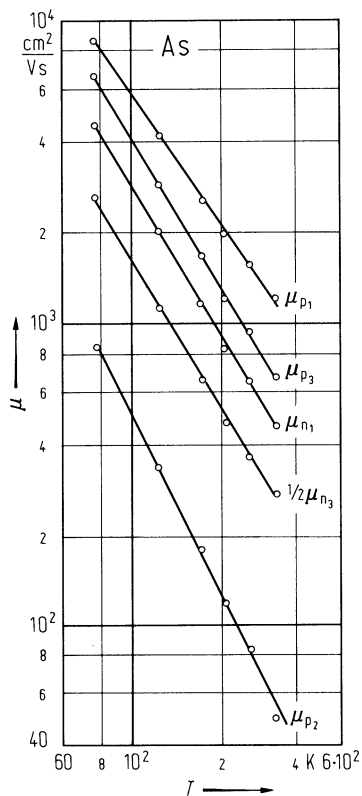


Fig. 12.2.3

As. Real (ϵ_1) and imaginary (ϵ_2) parts of the complex dielectric constant vs. photon energy calculated by Kramers-Kronig analysis of reflectivity data. To enlarge the energy range 8...25 eV the dielectric constant is multiplied by a factor of 10 [74R].

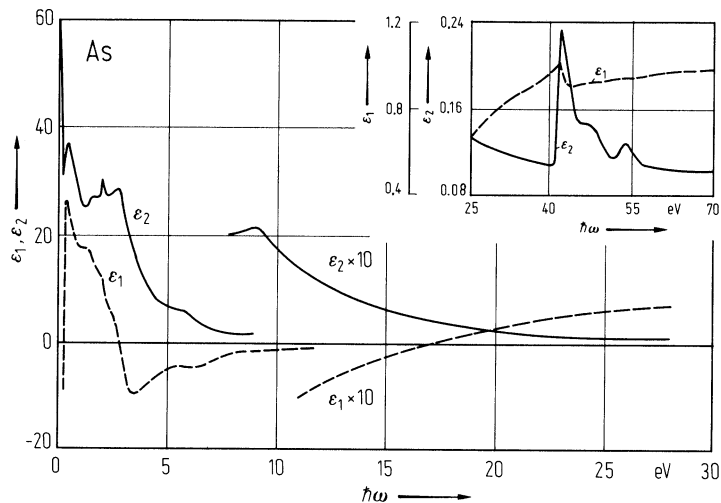
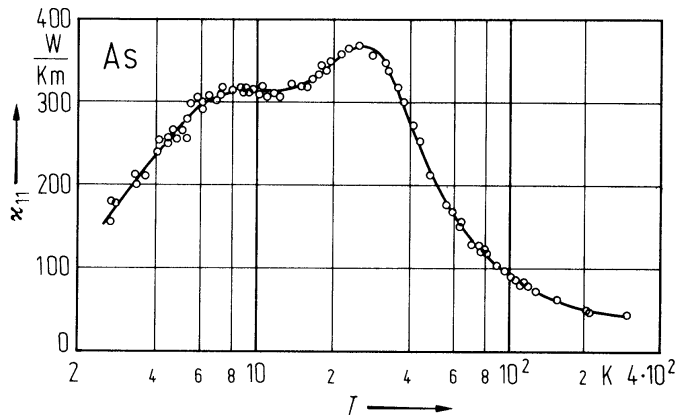


Fig. 12.2.4

As. Thermal conductivity κ_{11} of single crystal vs. temperature in the range 2...300 K [77H].



12.3 Group V elements: Antimony

Crystal structure

see section 12.0

Electronic properties

band structure : Fig. 12.0.8.

Gray antimony is a semimetal.

energy gap

$E_g(L)$	0.101 eV	direct energy band gap, obtained by magnetoreflexion studies	72H 65D
$E_g(T)$	0.149 eV	the position of the band gap at T is doubtful	72H

overlap energies

$E_0(at\ H_v-L_c)$	0.250 eV	pseudopotential calculation	66F
$E_0(L_{4c}-H_v)$	0.160 meV	band overlap between 77 K and 300 K from measurements of the thermoelectric power.	68S

effective masses

m_{n1}	0.068 m_0	effective mass tensor components of electrons and holes at the Fermi level; from cyclotron resonance measurements at $T = 1.5$ K. The tilt angles of the electron and hole ellipsoids are -4° and -36° , respectively. The subscripts 1...3 refer to the crystallographic axes system with $X = C_2$, $Y = C_1$, and $Z = C_3$	64D
m_{n2}	0.63 m_0		
m_{n3}	0.34 m_0		
m_{n4}	0.41 m_0		
(= m_{n23})			
m_{p1}	0.093 m_0		
m_{p2}	1.14 m_0		
m_{p3}	0.093 m_0		
m_{p4}	0.082 m_0		
(= m_{p23})			

Lattice properties

lattice parameters

a	4.3084 Å	$T = 298$ K	lattice parameters of the hexagonal unit cell from X-ray diffraction measurements; for temperature dependence, see Fig. 12.3.1	69S
c	11.2740 Å			

linear thermal expansion coefficient

$\alpha_{ }$	$1655 \cdot 10^{-8}\ K^{-1}$	$T = 283$ K	$\alpha_{ }$ and α_{\perp} are referred parallel and parallel and normal to the trigonal axis C_3	72W
α_{\perp}	$810 \cdot 10^{-8}\ K^{-1}$			

phonon dispersion relations : Fig. 12.3.2.

phonon wavenumbers

$\bar{\nu}(A_{1g})$	154.6 cm^{-1}	$T = 0$ K	frequencies of the Raman-active $A_{1g}(LO)$ - and $E_g(TO)$ phonons.	77H
$\bar{\nu}(E_g)$	116 cm^{-1}			

sound velocities

v_l	$3.891 \cdot 10^5 \text{ cm s}^{-1}$	$[100], T = 300 \text{ K}$	for more directions, see [66B]	66B
v_{t1}	$2.930 \cdot 10^5 \text{ cm s}^{-1}$	$[100]$		
v_{t2}	$1.508 \cdot 10^5 \text{ cm s}^{-1}$	$[100]$		
v_l	$2.591 \cdot 10^5 \text{ cm s}^{-1}$	$[001]$		
v_t	$2.423 \cdot 10^5 \text{ cm s}^{-1}$	$[001]$		

second order elastic constants

c_{11}	$101.3 \cdot 10^{10} \text{ dyn cm}^{-2}$	$T = 300 \text{ K}$	from measurements of ultrasonic wave	66B
c_{13}	$29.2 \cdot 10^{10} \text{ dyn cm}^{-2}$		velocities	
c_{33}	$45.0 \cdot 10^{10} \text{ dyn cm}^{-2}$			
c_{44}	$39.3 \cdot 10^{10} \text{ dyn cm}^{-2}$			
c_{14}	$20.9 \cdot 10^{10} \text{ dyn cm}^{-2}$			
c_{66}	$33.4 \cdot 10^{10} \text{ dyn cm}^{-2}$			
c_{12}	$34.5 \cdot 10^{10} \text{ dyn cm}^{-2}$			

linear compressibility

$\kappa_{ }$	$1.78 \cdot 10^{-6} \text{ bar}^{-1}$	$T = 300 \text{ K}$		72W
κ_{\perp}	$0.36 \cdot 10^{-6} \text{ bar}^{-1}$			

bulk modulus

B	62.46 GPa		calculated for simple cubic Sb	88S
	72.13 GPa		calculated for bcc Sb	

Debye temperature

Θ_D	209.6 K	$T < 2 \text{ K}$	from heat capacity measurements in the temperature range 0.4...2 K	68B
------------	---------	-------------------	--	-----

heat capacity

C_p	$0.0508 \text{ cal g}^{-1} \text{ K}^{-1}$	$T = 270...370 \text{ K}$	measured on polycrystalline Sb for temperature dependence, see Fig. 12.3.3	60K
-------	--	---------------------------	---	-----

density

d	6.69 g cm^{-3}	$T = 300 \text{ K}$		72W
-----	--------------------------	---------------------	--	-----

melting temperature

T_m	903 K		at atmospheric pressure	68S
-------	-------	--	-------------------------	-----

Transport properties

Since ordinary antimony is a semimetal, the charge carriers are electrons from the conduction band and holes from the valence band. Due to the rhombohedral symmetry of the crystal, antimony has two resistivities ρ_{11} and ρ_{33} . The transport process in antimony can be described by a two-band multivalley model [67Ö], [68S]. The small effective mass of the charge carriers results in a high carrier mobility.

mobilities of charge carriers

μ_{p1}	$2.75 \cdot 10^3 \text{ cm}^2/\text{Vs}$	$p = 0$	from Hall effect and magnetic resistivity	83K
μ_{p2}	$0.25 \cdot 10^3 \text{ cm}^2/\text{Vs}$		measurements on metallic Sb, calculated	
μ_{p3}	$3.24 \cdot 10^3 \text{ cm}^2/\text{Vs}$		with the assumption of a tilt angle of	
μ_{n1}	$3.20 \cdot 10^3 \text{ cm}^2/\text{Vs}$		$\theta_n = 6^\circ$; θ_p was estimated to $\theta_p = 24^\circ$;	
μ_{n2}	$0.01 \cdot 10^3 \text{ cm}^2/\text{Vs}$		unfortunately the authors give no	
μ_{n3}	$1.23 \cdot 10^3 \text{ cm}^2/\text{Vs}$		information about sample temperature	

Temperature dependence, see Fig. 12.3.4.

thermal conductivity

κ	$13 \text{ W m}^{-1} \text{ K}^{-1}$	$T = 300 \text{ K}$	whole thermal conductivity of Sb film	90V1
			with thickness $d = 230 \text{ nm}$	
κ_L	$5 \text{ W m}^{-1} \text{ K}^{-1}$		lattice contribution to thermal conductivity	
κ_e	$8 \text{ W m}^{-1} \text{ K}^{-1}$		charge carrier contribution to the thermal	

Optical properties

Spectral dependence of optical constants: Fig. 12.3.5.

dielectric constant

ϵ_{33}	80	$T = 4.2 \text{ K}$	from infrared absorption measurements	63N
			conductivity	

References to 12.3

- 60K Klemm, W., Spitzer, H., Nierman, H.: Angew. Chem. 72 (1960) 985.
63N Nanney, C.: Phys. Rev. 129 (1963) 109.
64C Cardona, M., Greenaway, D. L.: Phys. Rev. 133 (1964) A 1685.
64D Datars, W. R., Van der Koy, J.: IBM J. Res. Dev. 8 (1964) 247.
65D Dresselhaus, M. S., Mavroides, J. G.: Phys. Rev. Lett. 14 (1965) 259.
66B de Bretteville, A., Cohen, E. R., Balloto, A. D., Greenberg, I. N., Epstein, S.: Phys. Rev. 148 (1966) 575.
66F Falicov, L. M., Lin, P. J.: Phys. Rev. 141 (1966) 562.
67C Culbert, H. V.: Phys. Rev. 157 (1967) 560.
67M Mc Collum, D. C., Taylor, W. A.: Phys. Rev. 156 (1967) 782.
67Ö Öktö, Ö., Saunders, G. A.: Proc. Phys. Soc. 91 (1967) 156.
68B Blewer, R. S., Zebouni, N. H., Grenier, C. G.: Phys. Rev. 174 (1968) 700.
68S Saunders, G. A., Öktü, Ö.: J. Phys. Ch. S. 29 (1968) 327.
69S Schiferl, D., Barrett, C. S.: J. Appl. Crystallogr. 2 (1969) 30.
70C Colian, H. K., Krusius, M., Pickett, G. R.: Phys. Rev. B 1 (1970) 2888.
71S Sobolev, V. V., Donetskikh, V. I.: Sov. Phys. JETP 32 (1971) 1.
72H Huntley, D. A., Apps, M. J.: J. Phys. F 2 (1972) L17.
72W White, O. K.: J. Phys. C 5 (1972) 2731.
75A Aspnes, D. E.: Phys. Rev. B 12 (1975) 4008.
77H Höhne, J., Wenning, U., Schulz, H., Hüfner, S.: Z. Phys. B 27 (1977) 297.
78F Fischer, P., Sosnowska, I., Szymanski, M.: J. Phys. C 11 (1978) 1043.
83K Kechin, V. V., Likhter, A. I.: Phys. Status Solidi (b) 117 (1983) K13.
88S Sasaki, T., Shindo, K., Niizeki, K.: Solid State Commun. 67 (1988) 569.
89S Strümpfer, R., Lüth, H.: Thin Solid Films 177 (1989) 287.
90V1 Völklein, F., Kessler, E.: Phys. Status Solidi (b) 158 (1990) 521.
90V2 Völklein, F.: Thin Solid Films 191 (1990) 1.

Figures to 12.3

Fig. 12.0.8

Band structure of metallic antimony.

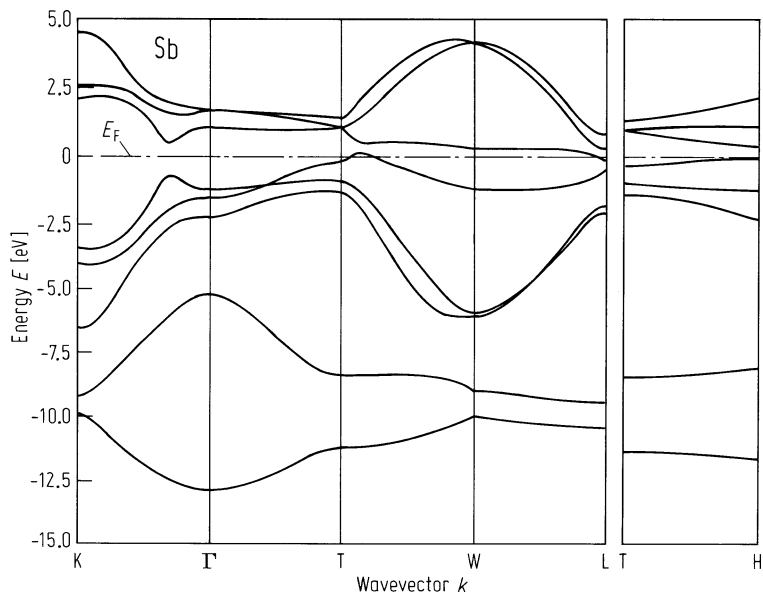


Fig. 12.3.1

Sb, As, Bi. Temperature dependence of the hexagonal lattice constants of Sb, As, Bi. The ratio c/a at $T = 5$ K is equal to 2.6100 for Sb, 2.7805 for As, and 2.6049 for Bi. The experimental data were obtained from neutron diffraction [78F]. Full symbols are from X-ray diffraction [69S]. Dashed lines indicate T_m .

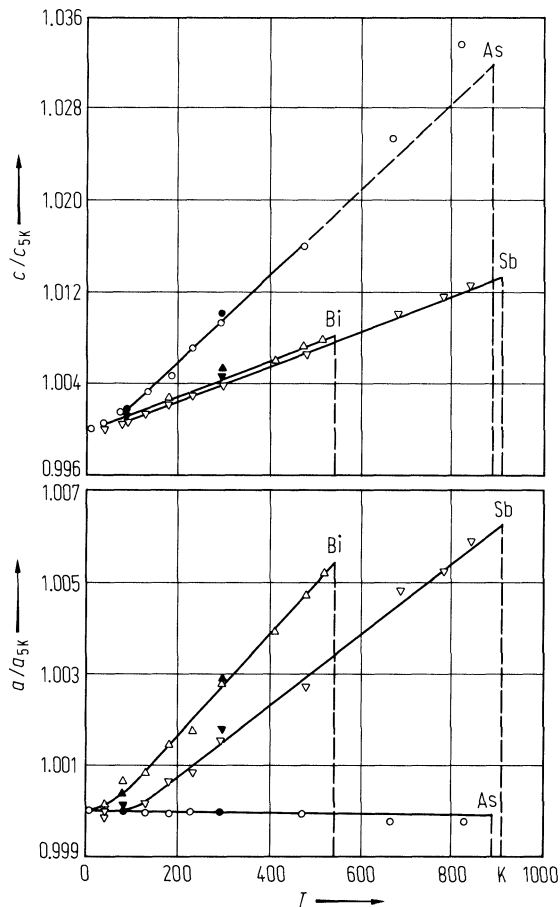


Fig. 12.3.2

Sb. Phonon dispersion relation (frequency vs. reduced wave vector coordinate) at $T = 295$ K; (a): $\langle 111 \rangle$ -direction (along ΓT), (b): $\langle 100 \rangle$ -direction (along ΓL), (c): $\langle 110 \rangle$ -direction (along ΓX). The experimental points were obtained by inelastic neutron scattering with normal modes polarized in the (101)-mirror plane. The smooth curves have been calculated from the 9th-neighbour Born-von Karman model. The straight solid lines through the origin indicate calculated sound velocities, the straight dashed line in the ΓL -direction indicates the sound velocity for the acoustic modes polarized normal to the mirror-plane [71S].

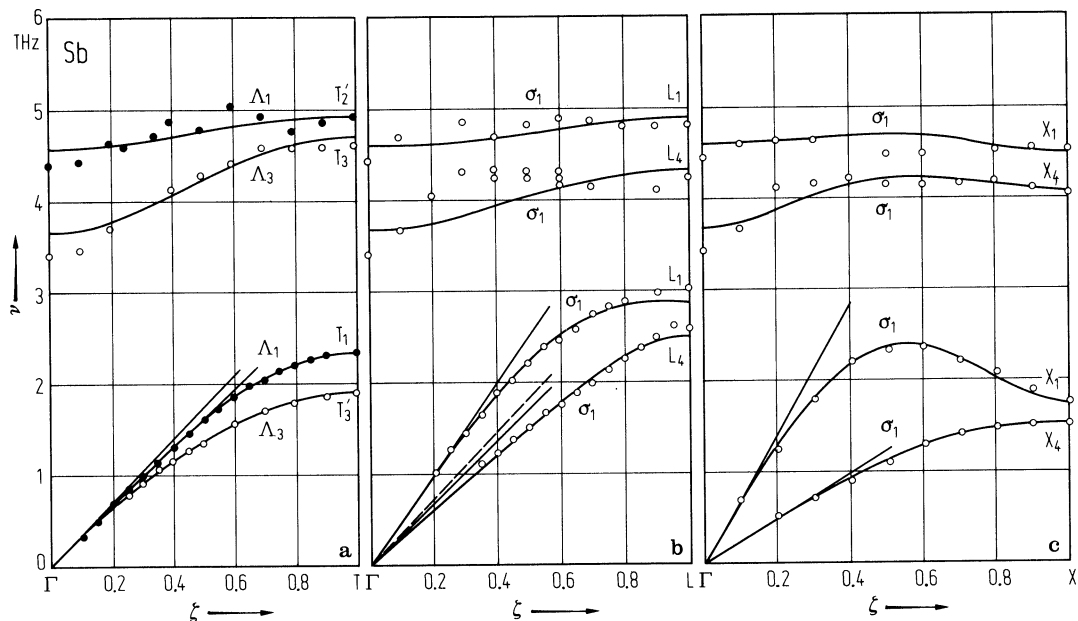


Fig. 12.3.3

Sb. Total heat capacity C_p vs. temperature. The experimental points can be fitted (solid line) by the following relation: $C_p = 8.5 T + 1120 T^3 + 0.0064 T^{-2} [\text{mJ mol}^{-1} \text{ K}^{-1}] [70\text{C}]$. Full circles from [67C] and [67M].

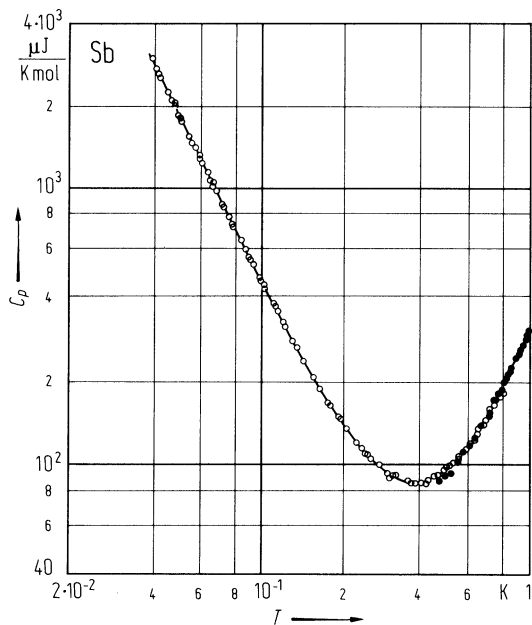


Fig. 12.3.4

Sb. Electron mobility μ_n and hole mobility μ_p in polycrystalline Sb thin films as function of the temperature and film thickness [90V2].

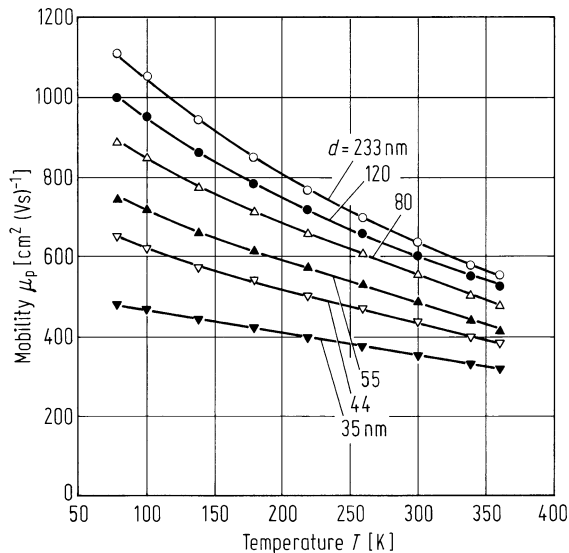
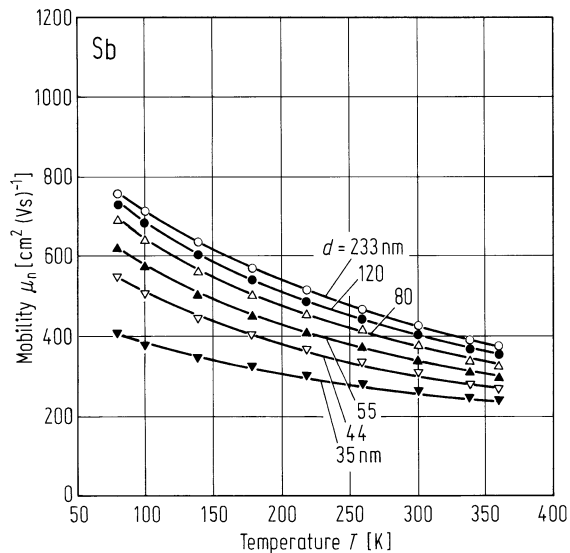
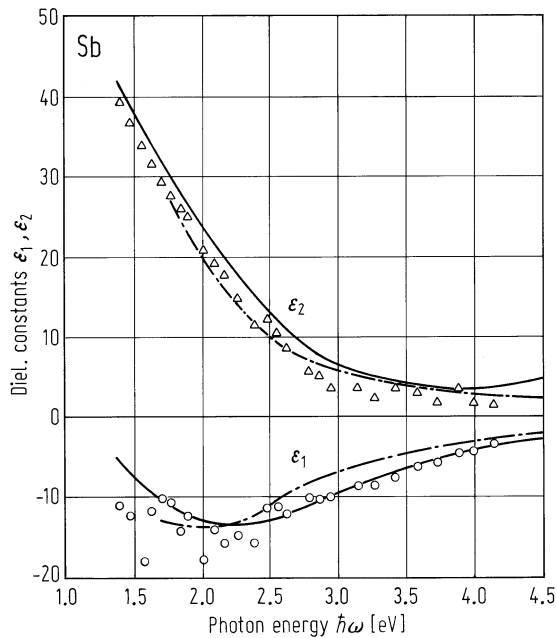


Fig. 12.3.5

Sb. Dielectric functions ϵ_1 and ϵ_2 of polycrystalline antimony vs. photon energy: single points are ellipsometric measurements from [89S], dashed lines are ellipsometric measurements from [75A] and solid lines are calculated by Kramers - Kronig analysis of reflectivity spectra from [64C]. The figure was adapted from [89S].



12.4 Group V elements: Bismuth (Bi)

Crystal structure

see section 12.0

Electronic properties

band structure: Fig. 12.0.9.

energy gap (pseudogap)

$E_{g,dir}$	0.0136 eV		from magnetoreflexion measurements	74V
$(L_{a,v}(3) - L_{s,c}(3))$			(see also Fig. 12.4.1)	
$E_{g,dir}$	0.25 eV	$T = 0$ K	hole band-gap at the T-point; fit parameter	69I
$(T_{45v}^-(1) - T_{6c}^+(3))$			in Alvén-wave transmission experiments	

overlap energy

$E_0(T_v-L_c)$	0.044 eV		calculated by deformation theory	66F
----------------	----------	--	----------------------------------	-----

effective masses

m_{n1}	0.00113 m_0	S	effective mass tensor components of elec- trons (at L) and holes (at T) at the band edge; from SdH-oscillation and Alvén wave transmission measurements of [64S] (S) and [69I] (I), respectively. The tilt angle of the electron ellipsoid equals -6° . The subscripts 1...3 refer to the crystallographic axes system with $X = C_2, Y = C_1$, and $Z = C_3$	64S, 69I
	0.00139 m_0	I		
m_{n2}	0.26 m_0	S		
	0.291 m_0	I		
m_{n3}	0.00443 m_0	S		
	0.0071 m_0	I		
m_{n4}	$-0.0195 m_0$	S		
$(= m_{n23})$	$\pm 0.0359 m_0$	I		
m_{p1}	0.059 m_0	I		
m_{p2}	0.059 m_0	I		
m_{p3}	0.634 m_0	I		

Lattice properties

lattice parameters

a	4.7458 Å	$T = 298$ K	lattice parameters of the rhombohedral primitive cell	69S
α	57.23°			

linear thermal expansion coefficient

$\alpha_{ }$	$11.85 \cdot 10^{-8} \text{ K}^{-1}$	$T = 4$ K	see also Fig. 12.4.2.
α_{\perp}	$1.70 \cdot 10^{-8} \text{ K}^{-1}$	$T = 4$ K	

phonon dispersion relations : see Fig.12.4.3.

Since there are two atoms per unit cell there will be one acoustic and one optical branch in the phonon spectrum each with one longitudinal and two degenerate transverse modes. For zone-center phonons with $k = 0$ the three optical lattice modes of type A_{1g} and E_g are all Raman active and infrared inactive with the two modes degenerated.

phonon wavenumbers

$\bar{\nu}_{\text{TO}}(\Gamma)$	74 cm ⁻¹	$T = 75 \text{ K}$	from inelastic neutron scattering at 300 K	64Y
$\bar{\nu}_{\text{LO}}(\Gamma)$	100 cm ⁻¹		and 75 K. At room temperature, the	
$\bar{\nu}_{\text{TA}}(\text{T})$	38.7 cm ⁻¹		frequencies are about 1.5 percent lower	
$\bar{\nu}_{\text{LA}}(\text{T})$	59.4 cm ⁻¹			
$\bar{\nu}_{\text{TO}}(\text{T})$	101 cm ⁻¹			
$\bar{\nu}_{\text{LO}}(\text{T})$	108 cm ⁻¹			

sound velocities

(from ultrasonic wave measurements at 1.6 K [68W] and 300 K [60E])

v_{LA}	$2.540 \cdot 10^5 \text{ cm s}^{-1}$	$T = 300 \text{ K}$	[100]-direction	68W
$v_{\text{TA,I}}$	$0.850 \cdot 10^5 \text{ cm s}^{-1}$	$T = 300 \text{ K}$	[100]-direction, lower branch	
$v_{\text{TA,II}}$	$1.550 \cdot 10^5 \text{ cm s}^{-1}$	$T = 300 \text{ K}$	[100]-direction, upper branch	
v_{LA}	$2.571 \cdot 10^5 \text{ cm s}^{-1}$	$T = 300 \text{ K}$	[010]-direction	
$v_{\text{TA,I}}$	$1.022 \cdot 10^5 \text{ cm s}^{-1}$	$T = 300 \text{ K}$	[010]-direction, lower branch	
$v_{\text{TA,II}}$	$1.407 \cdot 10^5 \text{ cm s}^{-1}$	$T = 300 \text{ K}$	[010]-direction, upper branch	
v_{LA}	$1.972 \cdot 10^5 \text{ cm s}^{-1}$	$T = 300 \text{ K}$	[001]-direction	
v_{TA}	$1.074 \cdot 10^5 \text{ cm s}^{-1}$	$T = 300 \text{ K}$	[001]-direction	

second order elastic moduli

c_{11}	63.37 GPa	$T = 300 \text{ K}$	from measurements of the ultrasonic	85G
c_{12}	24.49 GPa		wave velocity in rhombohedral Bi with	
c_{13}	24.84 GPa		$f = 10 \text{ MHz}$	
c_{14}	7.21 GPa			
c_{33}	38.37 GPa			
c_{44}	11.57 GPa			

linear compressibility

κ	1.82 Mbar ⁻¹	$\parallel C_3$		72W
	0.62 Mbar ⁻¹	$\perp C_3$		

Young's modulus

E	$2.12 \cdot 10^{11} \text{ dyn cm}^{-2}$	$\parallel C_3$	evaluated from ultrasonic attenuation	75G
	$3.10 \cdot 10^{11} \text{ dyn cm}^{-2}$	$\perp C_3$	measurements at $T = 299 \text{ K}$	

bulk modulus

B_S	$0.326 \cdot 10^{-3} \text{ Mbar}$			72W
-------	------------------------------------	--	--	-----

Debye temperature

Θ_D	86.5 K	$\parallel C_3$	evaluated from ultrasonic attenuation	75G
	104.8 K	$\perp C_3$	measurements at $T = 299 \text{ K}$ with	
			longitudinal and transverse modes	

heat capacity

C_p	0.101 J mol ⁻¹ K ⁻¹	$T = 4 \text{ K}$	evaluated from measurements of the linear	72W
	21.4 J mol ⁻¹ K ⁻¹	$T = 75 \text{ K}$	thermal expansion coefficients in a	
	25.9 J mol ⁻¹ K ⁻¹	$T = 283 \text{ K}$	temperature range 2...283 K.	

density			
d	9.8 g cm^{-3}	$T = 300 \text{ K}$	72W

melting temperature			
T_m	544.5 K	at atmospheric pressure	68S

Transport properties

According to the energy band structure of bismuth the charge carriers are mainly holes from the T-point and electrons from L-points of the Brillouin zone. But thermally activated L-holes have an essential influence on the transport properties of bismuth, too [86M], [81M], [79H].

mobilities of charge carriers

μ_{n1}	$1.2 \cdot 10^4 \text{ cm}^2/\text{Vs}$	$T = 293 \text{ K}$	2.7 μm thick Bi film; calculated from galvanomagnetic properties under the assumption $n = p = n_i$	83D
μ_{n2}	$0.04 \cdot 10^4 \text{ cm}^2/\text{Vs}$			
μ_{p1}	$0.26 \cdot 10^4 \text{ cm}^2/\text{Vs}$			
μ_{n1}	$2.8 \cdot 10^4 \text{ cm}^2/\text{Vs}$	$T = 200 \text{ K}$		
μ_{n2}	$0.062 \cdot 10^4 \text{ cm}^2/\text{Vs}$			
μ_{p1}	$0.42 \cdot 10^4 \text{ cm}^2/\text{Vs}$			
μ_{n1}	$5.3 \cdot 10^4 \text{ cm}^2/\text{Vs}$	$T = 100 \text{ K}$		
μ_{n2}	$0.11 \cdot 10^4 \text{ cm}^2/\text{Vs}$			
μ_{p1}	$0.24 \cdot 10^4 \text{ cm}^2/\text{Vs}$			

piezoresistance coefficients

π_{11}	$3.58 \cdot 10^{-9} \text{ } \Omega \text{ cm bar}^{-1}$	$T = 77 \text{ K}$	least-square-fit data from measurements of stress induced changes of the electric field	66B
π_{33}	$6.60 \cdot 10^{-9} \text{ } \Omega \text{ cm bar}^{-1}$			
π_{44}	$2.79 \cdot 10^{-9} \text{ } \Omega \text{ cm bar}^{-1}$			
π_{13}	$7.76 \cdot 10^{-9} \text{ } \Omega \text{ cm bar}^{-1}$			
π_{31}	$-2.10 \cdot 10^{-9} \text{ } \Omega \text{ cm bar}^{-1}$			
π_{14}	$-15.79 \cdot 10^{-9} \text{ } \Omega \text{ cm bar}^{-1}$			

thermal conductivity

κ_{tot}	$5.20 \text{ W m}^{-1} \text{ K}^{-1}$	$T = 295 \text{ K}$	total thermal conductivity of Bi film of 350 nm thickness lattice contribution total carrier contribution	86V
κ_L	$1.90 \text{ W m}^{-1} \text{ K}^{-1}$			
κ_c	$3.30 \text{ W m}^{-1} \text{ K}^{-1}$			

for temperature dependence, see Fig. 12.4.4.

Optical properties

dielectric constants

$\epsilon_{xx}(0)$	105	$T = 300 \text{ K}$	from IR-reflectivity measurements	76G
$\epsilon_{yy}(0)$	105			
$\epsilon_{zz}(0)$	84			

For spectral dependence of the dielectric constant, see Fig. 12.4.5.

refractive index, extinction coefficient

n	1.7	$\bar{\nu} = 10^4 \text{ cm}^{-1}$	from absorption measurements at 2.5 K with polycrystalline samples with $n = 5 \cdot 10^{17} \text{ cm}^{-3}$.	65P
k	3.3			
n	2.6	$\bar{\nu} = 10^3 \text{ cm}^{-1}$		
k	4.0			

References to 12.4

- 39E Erfling, H. D.: Ann. Phys. Leipzig 34 (1939) 136.
- 60C Cave, E. F., Holroyd, L. V.: J. Appl. Phys. 31 (1960) 1357.
- 60E Eckstein, Y., Lawson, A. W., Reneker, D. H.: J. Appl. Phys. 31 (1960) 1534.
- 64S Smith, G. E., Baraff, O. A., Rowell, J. M.: Phys. Rev. 135 (1964) A 1118.
- 64Y Yarnell, J. L., Warren, J. L., Wenzel, R. G., Koenig, S. H.: IBM J. Res. Dev. 8 (1964) 234.
- 65L Lenham, A. P., Treherne, D. M., Metcalfe, R. J.: J. Opt. Soc. Am. 55 (1965) 1072.
- 65P Potapov, F. V.: Sov. Phys. JETP 20 (1965) 307.
- 66B Bate, R. T., Drobish, W. E., Einspruch, N. O.: Phys. Rev. 149 (1966) 485.
- 66F Falkovskii, L. A., Razina, G. S.: Sov. Phys. JETP 22 (1966) 187.
- 68S Handbook of the physico-chemical properties of the elements (ed. Samsonov, G. V.) IFI/Plenum, New York 1968, p. 128.
- 68W Waither, K.: Phys. Rev. 174 (1968) 782.
- 69B Bunton, G. V., Weintroub, S.: J. Phys. C 2 (1969) 116.
- 69I Isaacson, R. T., Williams, G. A.: Phys. Rev. 185 (1969) 682.
- 69S Schiferl, D., Barrett, C. S.: J. Appl. Crystallogr. 2 (1969) 30.
- 70M Macfarlane, R. E.: Proc. Conf. Phys. Semimetals and Narrow-gap Semiconductors, Dallas 1970 (Carter, D. L. and Bate, R. T., eds., Pergamon Press, Oxford, 1971) p. 289.
- 70W Wang, P. Y., Jam, A. L.: Phys. Rev. B2 (1970) 2978.
- 72W White, O. K.: J. Phys. C 5 (1972) 2731.
- 74U Uher, C., Goldsmid, H. J.: Phys. Status Solidi (b) 65 (1974) 765.
- 74V Verdun, H. R., Drew, H. D.: Phys. Rev. Lett. 33 (1974) 1608.
- 75G Gopinathan, K. K., Padmini, A. R. K. L.: Solid State. Commun. 16 (1975) 817.
- 79H Heremans, J., Hansen, O.P.: J. Phys. C 12 (1979) 3483.
- 81M Mikhail, I.F.I., Hansen, O.P.: J. Phys. C 14 (1981) L27.
- 82V Vasek, P., Svoboda, P., Streda, P.: Czech. J. Phys. B32 (1982) 791.
- 83D de Kuijper, A.H., Bisschop, J.: Thin Solid Films 110 (1983) 99.
- 85G Grabov, V. M., Davydov, S. Yu., Mironov, Yu. P., Dzhumigo, A. M.: Sov. Phys.-Sol. St. 27 (1985) 1210.
- 86M Mikhail, I.F.I.: Phys. Status Solidi (b) 136 (1986) 643.
- 86V Völklein, F., Kessler, E.: Thin Solid Films 142 (1986) 169.

Figures to 12.4

Fig. 12.0.9

Band structure of bismuth.

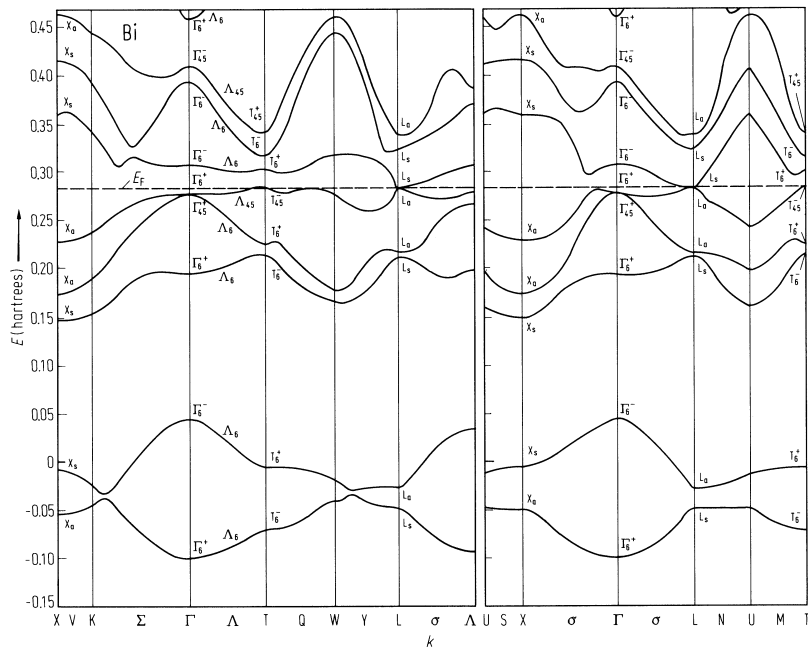


Fig. 12.4.1

Bi. Energy gap at the L point vs. temperature Data were obtained from magnetotransmission experiments The curve can be fitted by the following relation: $E_g = (13.6 + 2.1 \cdot 10^{-3} T + 2.5 \cdot 10^{-4} T^2)$ [meV] [74V].

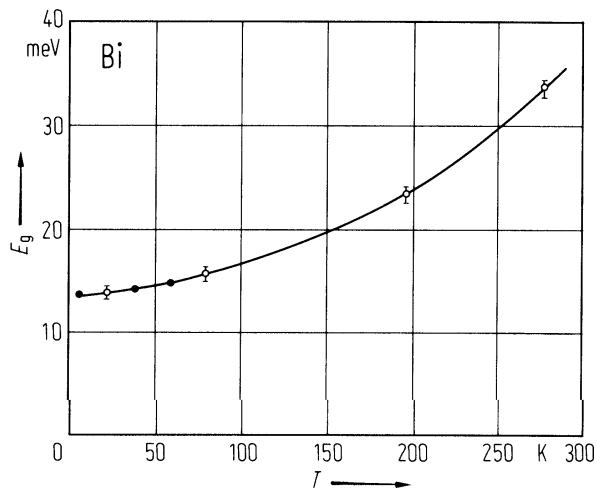


Fig. 12.4.2

Bi. Temperature dependence of the linear expansion coefficients α_{\parallel} and α_{\perp} below room temperature [72W]. Open symbols are measurements from [72W]. Full circles are from [60C], the dashed curves were obtained from [69B] and the step curve from [39E], Fig. from [72W].

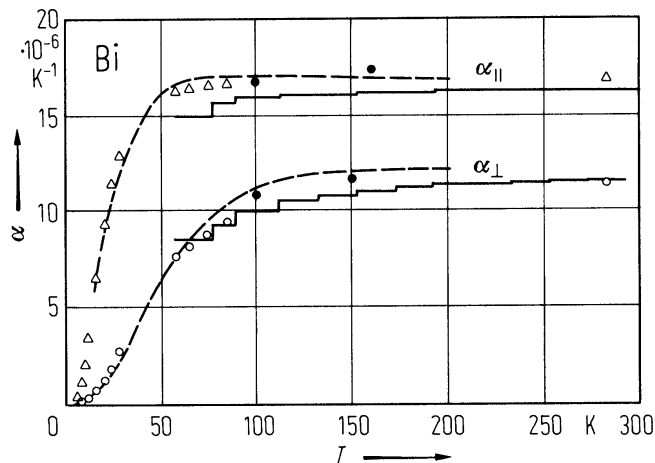


Fig. 12.4.3

Bi. Phonon dispersion curves (angular frequency vs. reduced wave vector) at 75 K. The initial slopes of the acoustic modes were computed from the elastic constants of [60E]. The smooth curves are drawn for convenience and have no theoretical significance. The data points were obtained by neutron inelastic scattering [70M].

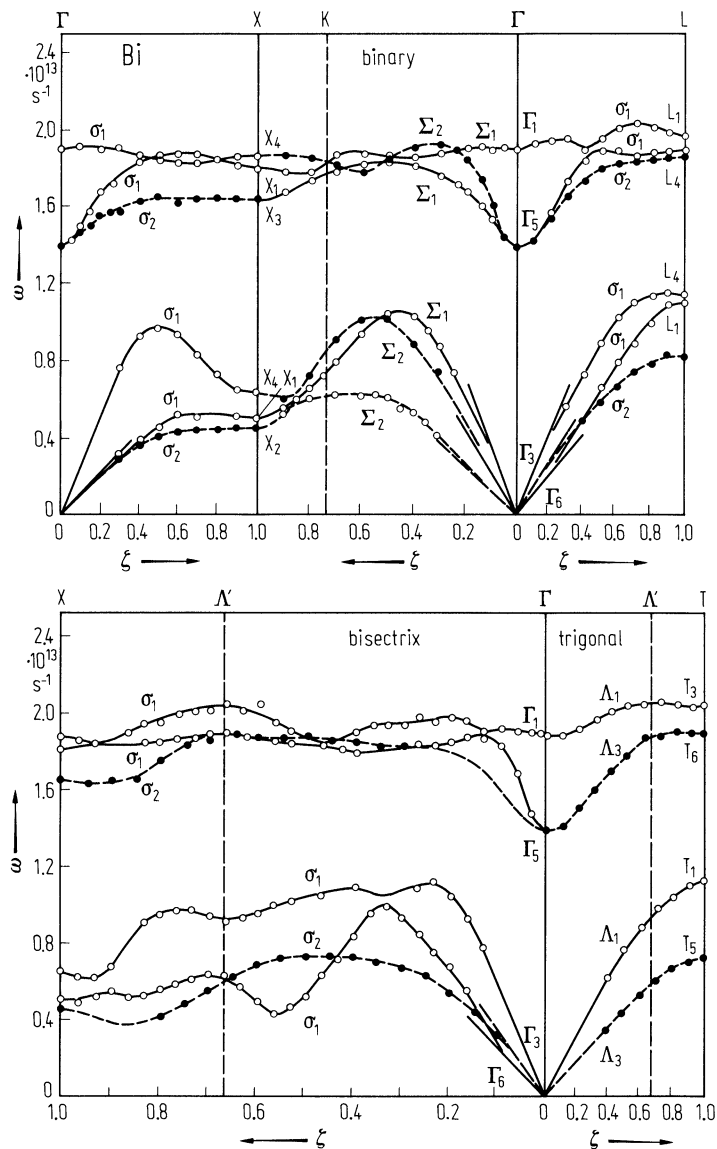


Fig. 12.4.4

Bi. Temperature dependence of the total thermal conductivity of single crystalline Bi. The measured direction deviates about 38° from the trigonal axis. The circles are measured, the triangles are calculated [82V]. (See also [74U]).

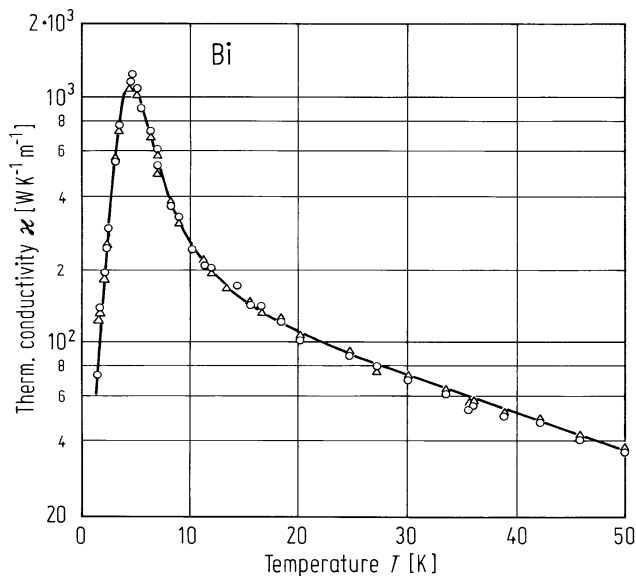
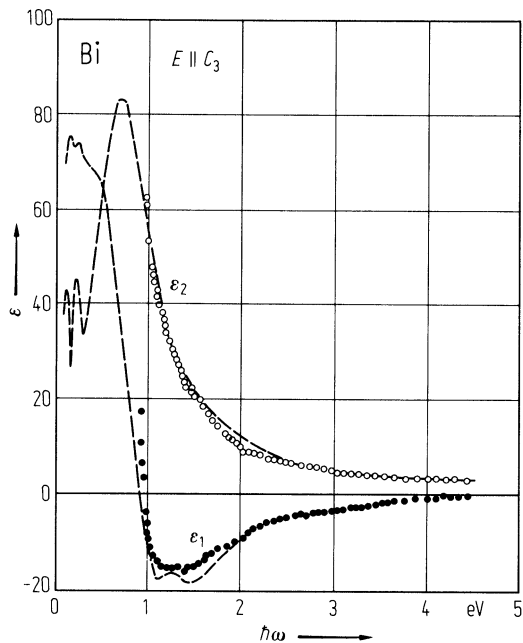


Fig. 12.4.5

Bi. Real- and imaginary parts of the dielectric constant vs. photon energy at 300 K [70W]. The experimental data were obtained from ellipsometry and piezorefectance measurements. The dashed curves represent data from [65L].



13 Group VI elements

13.0. Crystal structure and electronic structure

13.0.1 Crystal structure

Sulfur

Nearly 50 allotropes of sulfur are known, based on different tightly bound molecular subunits with relatively weak intermolecular bonds. The molecules are mostly puckered rings with 6, 7, 8, 9, 10, 12, 18 or 20 members. Bond length and bond angles as well as the shortest intermolecular contacts show little variation among the different modifications.

α -S consists of crown like shaped S_8 molecules. 16 molecules belong to the orthorhombic cell, 4 molecules to the primitive cell. The centers of the molecules are located at $(0\ 0\ 0, 0\ 1/2\ 1/2, 1/2\ 0\ 1/2, 1/2\ 1/2\ 0)$, $\pm(1/8\ 1/8\ z)$, $(1/8\ 1/8\ z+1/4)$ on twofold axes parallel to c . The plane of the molecules is either parallel to the (110) or to the (110) planes which leads to stacking of the molecules in two sets of almost perpendicular columns (Fig. 13.0.1).

The space group is $Fddd$ (D_{2h}^{24}); the local symmetry of the molecular sites is C_2 , the symmetry of the molecule is approximately $\bar{8}\ 2m$ (D_{4d}).

Selenium

Selenium crystallizes in at least six allotropes of trigonal, monoclinic, orthorhombic or rhombohedral structure. The only modification stable under ambient conditions is the trigonal form. In the following only data for this modification are presented.

Trigonal Se is isomorphic with Te with a lattice which consists of helical chains arranged in a hexagonal array (Fig. 13.0.2, Brillouin zone: Fig. 13.0.3). The structure can be considered as a distorted cubic primitive lattice.

space group: $P3_121$ (D_3^4) or $P3_221$ (D_3^6) for right handed or left handed helices. The Bravais lattice is hexagonal.

Tellurium

At normal conditions Te crystallizes in a trigonal chain structure (A8) isomorphously with Se. Whereas for Se the intrachain bonds are much stronger than the interchain ones, this difference is smaller for Te: tellurium is more isotropic.

13.0.2 Electronic structure

Figs. 13.0.4 ... 13.0.6 show the band structure of selenium and tellurium.

Figures to 13.0

Fig. 13.0.1

Projection of the orthorhombic sulfur structure along the b-axis (left) and the c-axis (right).

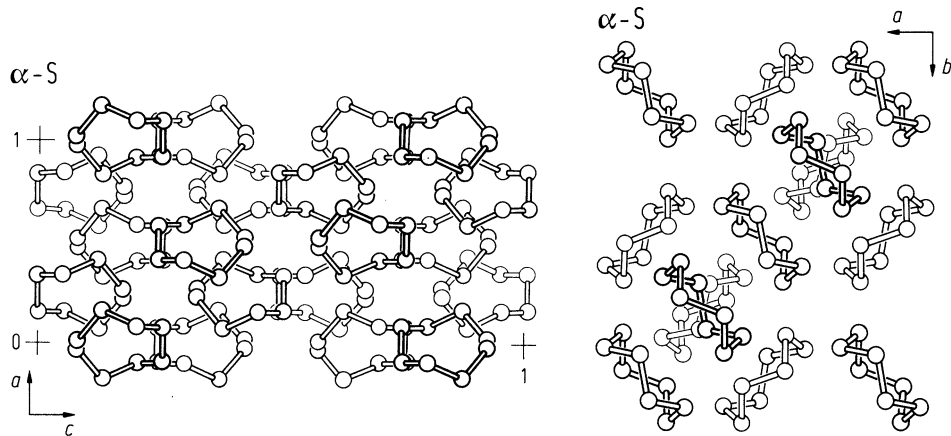


Fig. 13.0.2

Lattice (a) and configuration of the chains (b) of trigonal Se and Te

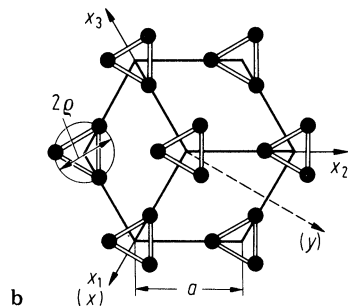
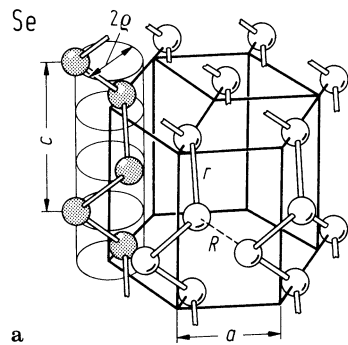


Fig. 13.0.3

Brillouin zone of trigonal Se and Te

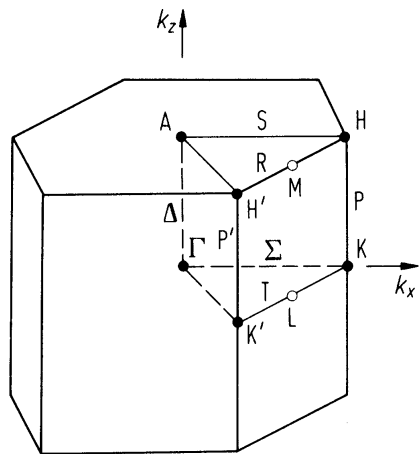


Fig. 13.0.4

Band structure of selenium.

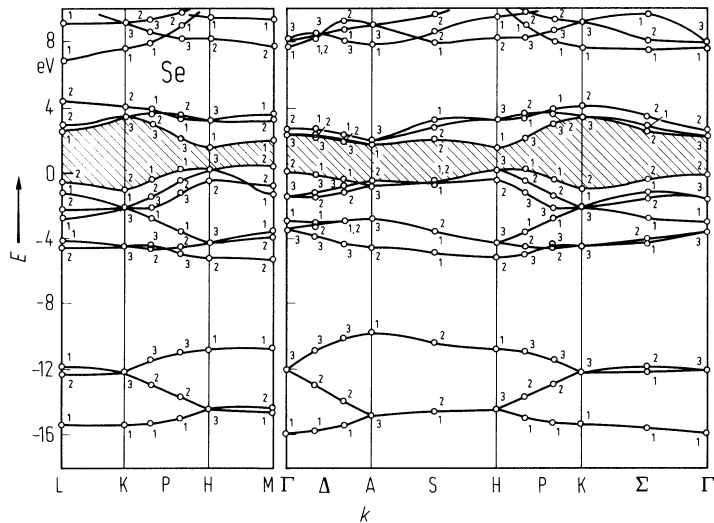


Fig. 13.0.5

Band structure and density of states of tellurium.

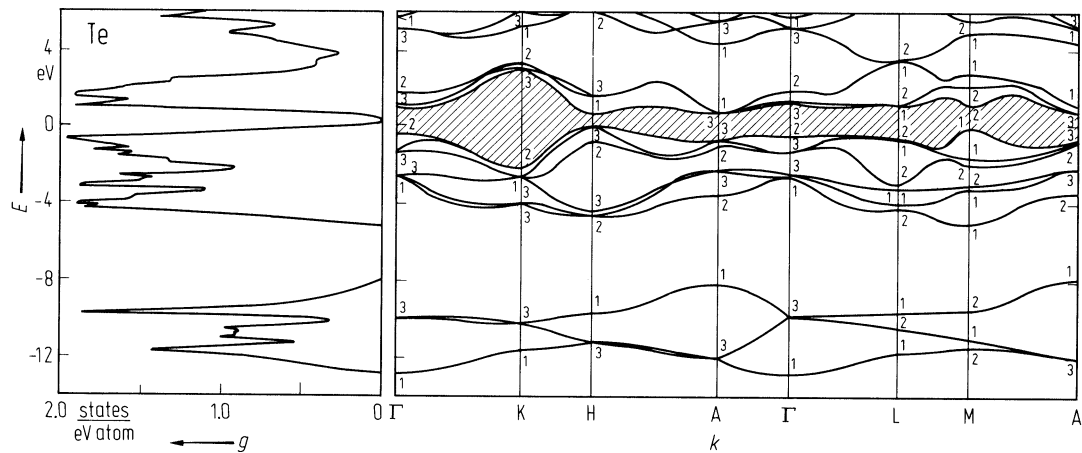
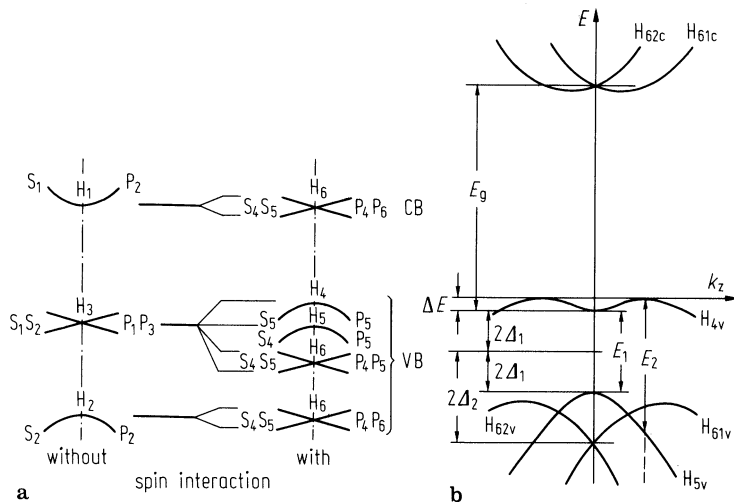


Fig. 13.0.6

Te. Splitting of the bands near the energy gap at H due to spin interaction. a) schematic, b) definitions of parameters.



13.1 Sulfur (S)

Crystal structure

see section 13.0.

Physical properties have been studied almost exclusively on orthorhombic α -S which, consisting of S₈ molecules, is the most stable modification under ambient conditions

Electronic properties

energy gap

$E_{g,ind}$	2.84 eV	$T = 280$ K	extrapolated absorption edge	87A
$dE_{g,ind}/dT$	$-2 \cdot 10^{-3}$ eV K ⁻¹		shift of absorption edge	86A

Lattice properties

lattice parameters

a [Å]	b [Å]	c [Å]	T [K]	Ref.
10.4633	12.8786	24.4784	298	77C

melting temperature or dissociation temperature

T_m	421 K	S ₁₂ orthorhombic	78S
	397 K	S ₂₀ orthorhombic	73D

phonon properties, general, orthorhombic α -modification

Infrared and Raman spectra of the crystal are not much different from the spectra of the S₈ molecule. According to the D_{4d} symmetry of the molecule 11 fundamentals are predicted.

phonon dispersion: Fig. 13.1.1

zone center phonon wavenumbers (orthorhombic sulfur (S₁₂))

internal modes

$\bar{\nu}(A_{2u}, E_u)$	465 cm ⁻¹	$T = 295$ K	IR-data	74S2
$\bar{\nu}(E_u)$	425 cm ⁻¹			
$\bar{\nu}(A_{2u})$	265 cm ⁻¹			
$\bar{\nu}(E_u)$	250 cm ⁻¹			
$\bar{\nu}(E_u)$	165 cm ⁻¹			
$\bar{\nu}(A_{2u})$	72 cm ⁻¹			
$\bar{\nu}(E_u)$	62 cm ⁻¹			

second order elastic moduli

c_{11}	$1.422 \cdot 10^5$ bar	$T = 293$ K	light scattering on ultrasonic waves	69H
c_{22}	$1.268 \cdot 10^5$ bar		(15 MHz)	
c_{33}	$1.83 \cdot 10^5$ bar			
c_{12}	$0.299 \cdot 10^5$ bar			
c_{13}	$0.314 \cdot 10^5$ bar			
c_{23}	$0.795 \cdot 10^5$ bar			
c_{44}	$0.827 \cdot 10^5$ bar			
c_{55}	$0.428 \cdot 10^5$ bar			
c_{66}	$0.437 \cdot 10^5$ bar			

volume compressibility				
κ_V	10^{-5} bar^{-1}			58B

thermal expansion coefficients				
α_a	$6.7 \cdot 10^{-5} \text{ K}^{-1}$	$T = 291 \text{ K}$		1887S
α_b	$7.8 \cdot 10^{-5} \text{ K}^{-1}$	$T = 291 \text{ K}$		1887S
α_c	$2.0 \cdot 10^{-5} \text{ K}^{-1}$	$T = 291 \text{ K}$		1887S

Debye temperature				
$\Theta_D(0)$	250 K		α -S	64G

heat capacity				
C_p	$22.60 \text{ J mol}^{-1} \text{ K}^{-1}$	$T = 298.15 \text{ K}$	α -S, calorimetry	37E

density				
d	2.069 g cm^{-3}	$T = 295 \text{ K}$	α -S, flotation method	74S1

Transport properties

The conductivity of sulfur is extremely small. Carrier mobilities are very different for electrons and holes. At low temperatures the hole mobility is trap controlled but at higher temperatures a lattice mobility in the range 5...10 cm²/V s is observed pointing to transport in narrow bands. The mobility of the electrons is much smaller, below 10⁻³ cm²/V s, and is activated.

electrical conductivity				
σ	$11 \cdot 10^{-17} (\Omega \text{cm})^{-1}$	$T = 295 \text{ K}$	natural crystal	1890M
	$75 \cdot 10^{-17} (\Omega \text{cm})^{-1}$	$T = 350 \text{ K}$	natural crystal	1890M
	$0.005 \cdot 10^{-17} (\Omega \text{cm})^{-1}$	$T = 300 \text{ K}$	crystal grown from CS ₂ solution	27N

hole mobility				
μ_p	$6.5 \cdot 10^{-4} \text{ cm}^2/\text{Vs}$	$T = 300 \text{ K}$	drift experiment, see also Fig. 13.1.2	67G

electron mobility				
μ_n	$6.2 \cdot 10^{-4} \text{ cm}^2/\text{Vs}$	$T = 294 \text{ K}$	drift experiment see also Fig. 13.1.3	66G

activation energy of electron mobility				
E_A	0.167 eV	$T = 300 \text{ K}$	drift experiment	66G

polaron binding energy (electron)				
$E_{b,pol}$	0.48 eV		analysis of electron drift experiments	66G

polaron band width				
W	0.1 eV		calculated from electron drift mobility	66G
	0.06 eV	[001]		70N
	0.04 eV	[100]		70N
	0.055 eV	[010]		70N

Optical properties

optical spectra

Absorption constant vs. photon energy: Fig. 13.1.4.

dielectric constant

$\epsilon(0), (\parallel a)$	3.59	$T = 300 \text{ K}$	electrical resonance circuit ($\lambda \approx 75 \text{ cm}$)	03S
$\epsilon(0), (\parallel b)$	3.83	$T = 300 \text{ K}$		03S
$\epsilon(0), (\parallel c)$	4.62	$T = 300 \text{ K}$	see also Fig. 13.1.5	

refractive index

n_a	2.0120	$T = 293 \text{ K}, \lambda = 467 \text{ nm}$	11S
	2.0938		
	2.3380		

References to 13.1

- 1887S Schrauff, A. Z.: Z. Kristallogr. 12 (1887) 321.
1890M Monkmann, J.: Proc. Roy. Soc. (London) 46 (1890) 136.
03S Schmidt, W.: Ann. Phys. u. Chem. IV 11 (1903) 114.
11S Schmidt, E.: Thesis, Rostock 1911/12.
27N Neumann, H.: Z. Phys. 45 (1927) 717.
36R Rathenau, G.: Physica 3 (1936) 42.
37E Eastmann, E. D., Garwork, W. C.: J. Am. Chem. Soc. 59 (1937) 1264.
58B Bridgeman, P. W.: The physics of high pressure; Bell London 1958.
64G Gscheidner, K.: Solid State Phys. 16 (1964) 370.
66G Gibbons, D. J., Spear, W. E.: J. Phys. Chem. Solids 27 (1966) 1917.
66S Spear, W. E., Adams, A. R.: J. Phys. Chem. Solids 27 (1966) 281.
67G Gill, W. D., Street, G. B., MacDonald, R. E.: J. Phys. Chem. Solids 28 (1967) 1517.
69H Haussühl, S.: Z. Naturforsch. 24a (1969) 865.
70N Nitzki, V., Stössel, W.: Phys. Status Solidi (b) 39 (1970) 309.
73D Debaerdemaeker, T., Hellner, E., Kutoglu, A., Schmidt, M., Wilhelm, E.: Naturwissenschaften 60 (1973) 300.
74S1 Schmidt, M., Wilhelm, E., Debaerdemaeker, T., Hellner, E., Kutoglu, A.: Z. Anorg. Allgem. Chem. 405 (1974) 153.
74S2 Steudel, R., Rebsch, M.: J. Mol. Spectrosc. 51 (1974) 189.
75L Luty, T., Pawley, G. S.: Phys. Status Solidi (b) 69 (1975) 551.
75R Rinaldo, R. P., Pawley, G. S.: J. Phys. C5 (1975) 599.
76E Emerald, R. L., Drews, R. E., Zallen, R.: Phys. Rev. B 14 (1976) 808.
77C Coppens, P., Yang, Y. W., Blessing, R. H., Cooper, W. F., Larsen, F. K.: J. Amer. Chem. Soc. 99 (1977) 760.
78S Steudel, R., Mäusle, H.-J.: Z. Naturforsch. 33a (1978) 951.
86A Abass, A. K., Ahmad, N. H.: J. Phys. Chem. Solids 47 (1986) 143.
87A Abass, A. K.: Phys. Status Solidi (a) 103 (1987) 281.

Figures to 13.1

Fig. 13.1.1

S (α -S). Phonon energies vs. reduced wave-vector coordinate for the lowest phonon branches [75L]. Experimental points are obtained by neutron scattering [75R]; solid lines calculated.

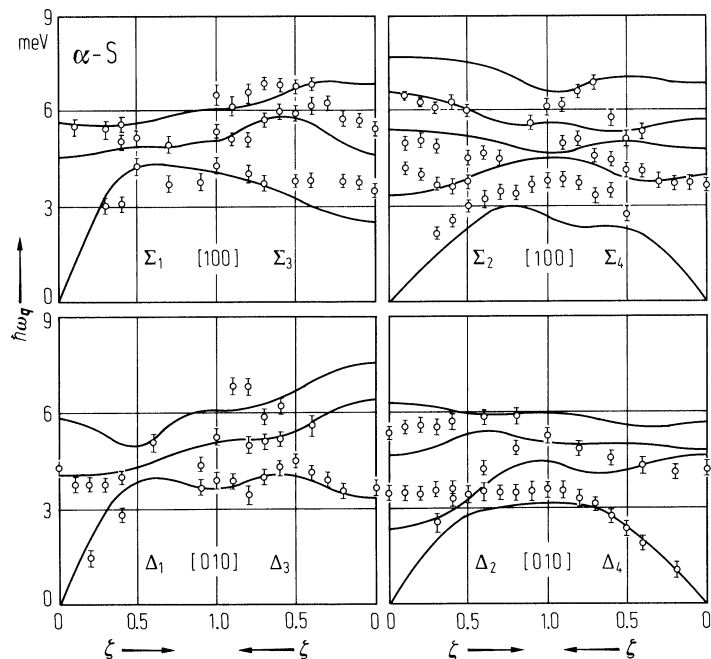


Fig. 13.1.2

S (α -S). Hole drift mobility $\mu_{dr,p}$ vs. reciprocal temperature [67G].

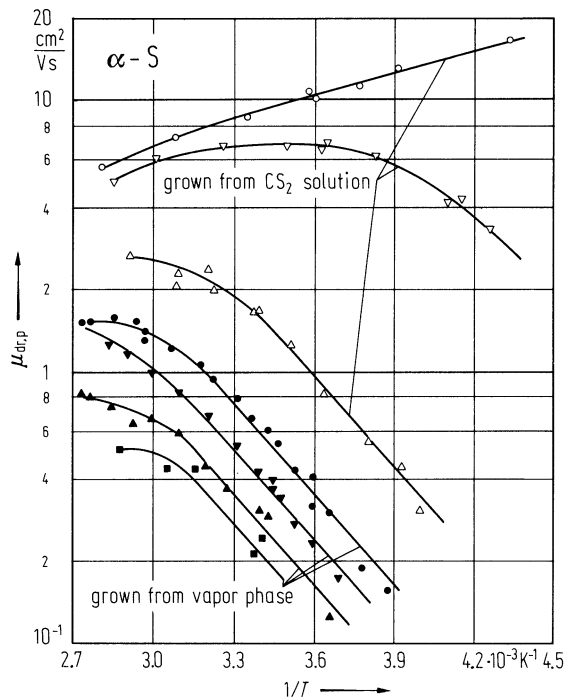


Fig. 13.1.3

S (α -S). Electron drift mobility $\mu_{dr,n}$ vs. reciprocal temperature of various samples grown from CS₂ solution. The insert indicates the drift direction and the hole mobility μ_p (cm² V⁻¹ s⁻¹) at 300 K of the respective sample [66G].

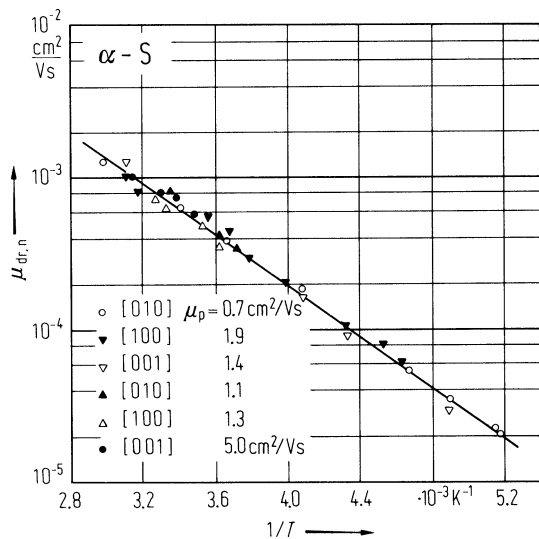


Fig. 13.1.4

S (α -S). Absorption constant K vs. photon energy at room temperature obtained from samples of different thickness d . The marks (x) correspond to data from [36R]. [66S].

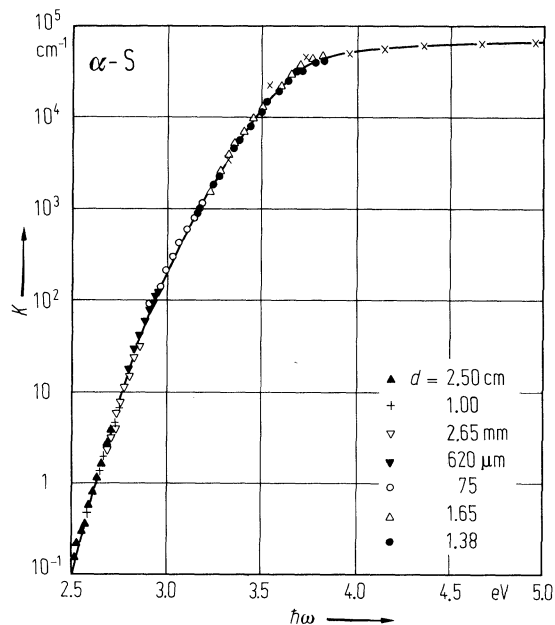
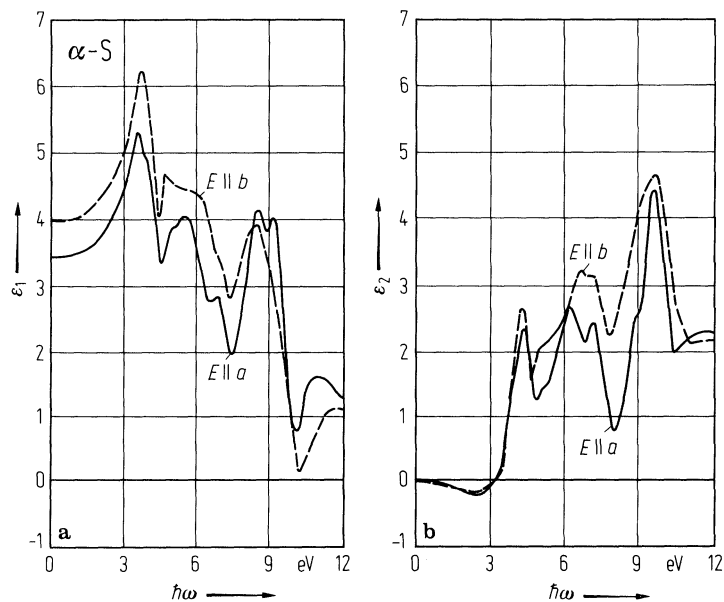


Fig. 13.1.5

S (α -S). a) Real part ϵ_1 and b) imaginary part ϵ_2 of the dielectric constant vs. photon energy for two polarizations of light [76E].



13.2 Selenium (Se)

Crystal structure

see section 13.0.

Electronic properties

band structure of trigonal selenium : Fig. 13.0.4, Brillouin zone: Fig. 13.0.3.

The band structure of trigonal selenium is characterized by distinct groups of band triplets corresponding to different types of chemical bonds in the crystal. Little hybridization of 4s and 4p states occurs [74S, 75J, 82I, 95C].

The lowest band triplet ($-16 \text{ eV} < E < -10 \text{ eV}$) originates from the 4s states. The large band width results from the considerable overlap between 4s states of nearest neighbors along the chain.

The upper valence bands ($-6 \text{ eV} < E < 0$) originate from the 4p states, the lower triplet corresponding to the bonding states of the two covalent bonds within the chain.

The upper triplet ($-2 \text{ eV} < E < 0$) are the so called lone pair p-states. They do not participate in intrachain bonding but contribute to four weak interchain bonds.

The first narrow conduction band triplet corresponds to the antibonding states of the covalent intrachain p-bonds. The wide higher conduction bands are derived from 5s and 4d states.

indirect energy gap

$E_{g,\text{ind}}(\text{R}_{3,4\text{v}}-\text{H}_{6\text{c}})$	1.8525 eV	$T = 1.4 \text{ K}, E \parallel c, \perp c$	excitonic photoluminescence	79M
$dE_{g,\text{ind}}/dT$	$1.7 \cdot 10^{-1} \text{ eV K}^{-1}$	$30 \text{ K} < T < 80 \text{ K}$	electroabsorption, non-linear shift, see Fig. 13.2.1	72L

direct energy gaps

$E_{g,\text{dir}}(\text{H}_{5\text{v}}-\text{H}_{6\text{c}})$	1.948 eV	$T = 5 \text{ K}, E \perp c$	excitonic electroreflectance	71W
$(\text{H}_{4\text{v}}-\text{H}_{6\text{c}})$	1.990 eV	$T = 5 \text{ K}, E \perp c$	electroreflectance	71W
$(\text{H}_{5\text{v}}-\text{H}_{6\text{c}})$	1.95 eV	$T = 300 \text{ K}, E \perp c$	excitonic reflectance peak	67H
$(\text{H}_{4\text{v}}-\text{H}_{6\text{c}})$	1.98 eV	$T = 300 \text{ K}, E \perp c$	reflectance peak, interpreted as band gap	67H
$dE_{g,\text{dir}}/dT$	$2.7 \cdot 10^{-4} \text{ eV K}^{-1}$	$30 \text{ K} < T < 80 \text{ K}$	electroreflectance, non-linear shift, see Fig. 13.2.1	71W

interband transitions of higher energy

$\text{H}_{6\text{v}}-\text{H}_{6\text{c}}$ transition:

E	2.11 eV	$T = 300 \text{ K}, E \parallel c, \perp c$	reflectance peak	67H
dE/dT	$3.8 \cdot 10^{-4} \text{ eV K}^{-1}$	$30 \text{ K} < T < 80 \text{ K}$	electroreflectance, non-linear shift	71W

$\text{A}_{6\text{v}}-\text{A}_{6\text{c}}$ transition:

E	3.109 eV	$T = 5 \text{ K}, E \parallel c$	electroreflectance	71W
dE/dT	$-4.5 \cdot 10^{-4} \text{ eV K}^{-1}$	$T > 80 \text{ K}$	electroreflectance	71W

$\text{A}_{4,5\text{v}}-\text{A}_{6\text{c}}$ transition:

E	3.347 eV	$T = 5 \text{ K}, E \perp c$	electroreflectance	71W
dE/dT	$-3.3 \cdot 10^{-4} \text{ eV K}^{-1}$	$T > 80 \text{ K}$	electroreflectance	71W

effective mass

m_{ds}	$1.4 m_0$	density of states mass, estimated from thermoelectric power with an isotropic single valence band maximum	71B
m_{\perp}/m_{\parallel}	3...4	exciton mass ratio at the direct gap, estimated from electroreflectance	71W
$m_{p\perp}/m_{p\parallel}$	3.5	ratio of valence band mass estimated from magnetoconductivity	67M1

Lattice properties

The lattice properties reflect the highly anisotropic bonds and the competition between two short intra-chain and four much longer interchain bonds.

lattice parameters

$a = 4.374 \text{ \AA}$, $c = 4.951 \text{ \AA}$ at 300 K 74H

thermal expansion coefficients

$\alpha_{\perp c}$	$6.98 \cdot 10^{-5} \text{ K}^{-1}$	$T = 300 \text{ K}$	dilatometric measurements	78G
$\alpha_{\parallel c}$	$-1.34 \cdot 10^{-5} \text{ K}^{-1}$	$T = 300 \text{ K}$	for temperature dependence, see Fig. 13.2.2	

phonon dispersion curves : Fig. 13.2.3, Brillouin zone: Fig. 13.0.3.

Corresponding to three atoms in the unit cell there are nine phonon branches with a spectral distribution which reflects the different bonds in the lattice. The upper triplet of optical branches is related to the strong covalent intrachain bonds. The weaker interchain bonds contribute to the lower triplet of optical phonons.

phonon wavenumbers

$(\nu/c)(A_2, \Gamma_2)$	100 cm^{-1}	$T = 300 \text{ K}$, $E \parallel c$	IR reflectivity	67L
$(\nu/c)(E_1, \Gamma_3)$	144 cm^{-1}	$T = 300 \text{ K}$, $E \perp c$	IR reflectivity	67L
$(\nu/c)(E_2, \Gamma_3)$	225 cm^{-1}	$T = 300 \text{ K}$, $E \perp c$	IR reflectivity	67L
$(\nu/c)(A_1, \Gamma_1)$	238.5 cm^{-1}		Raman spectroscopy	73R

sound velocities

v_l	$2.106 \cdot 10^3 \text{ m s}^{-1}$	$v \parallel a$	ultrasonic data, $T = 298 \text{ K}$	79R
v_{st} (slow transverse)	$0.809 \cdot 10^3 \text{ m s}^{-1}$	$v \parallel a$		
v_{ft} (fast transverse)	$2.13 \cdot 10^3 \text{ m s}^{-1}$	$v \parallel a$		
v_{ql} (quasi-longitudinal)	$2.314 \cdot 10^3 \text{ m s}^{-1}$	$v \perp a, \perp c$		
v_{qt} (quasi-transverse)	$1.609 \cdot 10^3 \text{ m s}^{-1}$	$v \perp a, \perp c$		
v_t	$1.302 \cdot 10^3 \text{ m s}^{-1}$	$v \perp a, \perp c$		
v_l	$4.173 \cdot 10^3 \text{ m s}^{-1}$	$v \parallel c$		
v_t	$1.953 \cdot 10^3 \text{ m s}^{-1}$	$v \parallel c$		
v_{ql} (quasi-longitudinal)	$3.639 \cdot 10^3 \text{ m s}^{-1}$	propagation v in $Y-Z$ plane,		
v_{qt} (quasi-transverse)	$1.606 \cdot 10^3 \text{ m s}^{-1}$	46°40' inclination with respect to the c -axis		
v_t	$1.064 \cdot 10^3 \text{ m s}^{-1}$			

second order elastic moduli

c_{11}	$1.98 \cdot 10^5$ bar	$T = 298$ K	calculated from ultrasonic data	79R
c_{66}	$0.66 \cdot 10^5$ bar			
c_{33}	$8.36 \cdot 10^5$ bar			
c_{44}	$1.83 \cdot 10^5$ bar			
c_{13}	$2.02 \cdot 10^5$ bar			
$ c_{14} $	$0.69 \cdot 10^5$ bar			

compression moduli

$B_a = -a \, dp/da$	$2.66 \cdot 10^5$ bar	$T = 300$ K	X-ray studies	77K
$B_c = -c \, dp/dc$	$-12.55 \cdot 10^5$ bar	$T = 300$ K	X-ray studies	77K

bulk modulus

B	$1.49 \cdot 10^5$ bar		X-ray studies	77K
-----	-----------------------	--	---------------	-----

Debye temperature

Θ_D	152.5 K	$T = 300$ K	from low temperature heat capacity	69L
------------	---------	-------------	------------------------------------	-----

heat capacity

C_p	$24.53 \, \text{J K}^{-1} \text{mol}^{-1}$	$T = 298.16$ K	polycrystalline samples	70M
-------	--	----------------	-------------------------	-----

For temperature dependence of C_v and C_p see Fig. 13.2.4.

density

d	$4.69 \, \text{g cm}^{-3}$		X-ray density, rhombohedral Se	80M
	$4.67 \, \text{g cm}^{-3}$		X-ray density, orthorhombic Se	81N
	$4.819 \, \text{g cm}^{-3}$	$T = 298$ K		68N

melting temperature

T_m	493 K		polycrystalline material containing iodine	93S
-------	-------	--	--	-----

Transport properties

The electrical conductivity of trigonal Se is extrinsic and p-type due to shallow acceptors which are completely ionized at $T = 77$ K. Despite a temperature independent carrier concentration the conductivity is activated. The main scattering mechanism is due to acoustical phonons. Impurities have little influence on single crystals but alter the conductivity of polycrystalline samples.

electrical conductivity

σ	$10^{-6} \dots 10^{-5} \, \Omega^{-1} \text{cm}^{-1}$	$T = 300$ K	at RT increasing with deformation of the crystals	64S
----------	---	-------------	---	-----

extrinsic carrier concentration

p	$10^{13} \dots 10^{15} \text{cm}^{-3}$	$100 \text{ K} < T < 400 \text{ K}$	thermoelectric power measurements, depending on crystal quality	65S 51P
	10^{14}cm^{-3}		Hall effect measurements	69H

carrier mobilities

see Fig. 2

μ_H	$0.12 \text{ cm}^2/\text{V s}$	$T = 300$ K	Hall mobility, activated	69H
$\mu_{p,\parallel c}$	$26 \text{ cm}^2/\text{V s}$	$T = 300$ K	acoustoelectric current saturation, see Fig. 13.2.5	67M2
$(\mu_p \parallel \mu_{p\perp})^{1/2}$	$80 \text{ cm}^2/\text{V s}$	$T = 300$ K	magnetoresistance, assuming inhomogeneous carrier concentration	74C

thermal conductivity

$\kappa_{\perp c}$	$2.43 \cdot 10^{-2}$ W cm ⁻¹ K ⁻¹	$T = 300$ K	for temperature dependence, see Fig. 13.2.6 66A	
$\kappa_{\parallel c}$	$4.50 \cdot 10^{-2}$ W cm ⁻¹ K ⁻¹	$T = 300$ K		70T

piezoelectric strain coefficients

d_{11}	$6.5 \cdot 10^{-11}$ mV ⁻¹	$T = 300$ K	piezoeffect measurements	57G
d_{14}	$2.54 \cdot 10^{-11}$ mV ⁻¹	$\nu < 12$ MHz	variation of impedance near mechanical resonance	73K

piezoelectric stress coefficients

e_{11}	0.32 As m ⁻²	$T = 300$ K	single crystal	79R
$ e_{14} $	0.10 As m ⁻²			

Optical properties

Real part ϵ_1 and the imaginary part ϵ_2 of the dielectric constant, Fig. 13.2.7.

dielectric constants

$\epsilon(0)$	7.43	$T = 300$ K, $E \perp c$	oscillator fit of ir spectra	74D
$\epsilon(0)$	12.24	$T = 300$ K, $E \parallel c$		
$\epsilon(\infty)$	6.97	$T = 300$ K, $E \perp c$		
$\epsilon(\infty)$	11.62	$T = 300$ K, $E \parallel c$		

refractive index

		T [K], λ [μ m]		
$n_{\parallel c}$	3.608(8)	300, 1.06	minimum deflection of light passing a selenium prism.	69G
	3.573(8)	1.15		
	3.46(1)	3.39		
	3.41(1)	10.6		
$n_{\perp c}$	2.790(8)	300, 1.06		
	2.737(8)	1.15		
	2.65(1)	3.39		
	2.64(1)	10.6		

See also Fig. 13.2.8.

infrared nonlinear dielectric susceptibilities

		λ [μ m]		
d_{11}	$184(84) \cdot 10^{-11}$ mV ⁻¹	28	second harmonic generation	73S
			possibly an electronic resonance	
	$16(4) \cdot 10^{-11}$ mV ⁻¹	10.6	second harmonic generation	67J
	$9.7(25) \cdot 10^{-11}$ mV ⁻¹	10.6	second harmonic generation	71D
	$8 \cdot 10^{-11}$ mV ⁻¹	10.6	second harmonic generation	66P
	$0.41 \cdot 10^{-11}$ mV ⁻¹	1.15	second harmonic generation	68T
	$0.5 \cdot 10^{-11}$ mV ⁻¹	1.15	light beam modulation by Pockels effect	69A

References to 13.2

- 40S Straumanis, M. E.: Z. Kristallogr. A 102 (1940) 432.
- 51P Plessner, K. W.: Proc. Phys. Soc. London Sect. B 64 (1951) 671.
- 57G Gobrecht, H., Hamisch, H., Tausend, A.: Z. Phys. 148 (1957) 209.
- 64S Stuke, J.: Phys. Status Solidi 6 (1964) 441.
- 65S Stuke, J., Wendt, K.: Phys. Status Solidi 8 (1965) 533.
- 66A Abdullaev, G. B., Mekhtieva, S. I., Abdinov, D. S., Aliev, G. M., Alieva, S. G.: Phys. Status Solidi 13 (1966) 315.
- 66P Patel, C. K. N.: Phys. Rev. Lett. 16 (1966) 613.
- 67A Adams, A. R., Baumann, F., Stuke, J.: Phys. Status Solidi 23 (1967) K99.
- 67H Henrion, W.: Phys. Status Solidi 20 (1967) K 145.
- 67J Jerphagnon, J. J., Batifol, E., Sourbe, M.: C. R. Acad. Sci. (Paris) Ser. B265 (1967) 400.
- 67L Lucovsky, G., Keezer, R. C., Burstein, E.: Solid State Commun. 5 (1967) 439.
- 67M1 Mell, H., Stuke, J.: Phys. Status Solidi 24 (1967) 183.
- 67M2 Mort, J.: Phys. Rev. Lett. 18 (1967) 540.
- 67T Tutihasi, S., Chen, I.: Phys. Rev. 158 (1967) 623.
- 68K Kirby, R. K., Rothrock, B. D.: J. Am. Ceram. Soc. 51 (1968) 535.
- 68L Leiga, A. G.: J. Opt. Soc. Am. 58 (1968) 880.
- 68N Niserson, L. A., Glazov, V. M.: Izv. Akad. Nauk SSSR, Neorgan. Mater. 4 (1968) 1849.
- 68T Turner, E. H., Kaminov, I. P., Kolb, E. D.: IEEE J. Quantum Electron. QE 4 (1968) 234.
- 69A Adams, J. E., Haas, W., in: The physics of Selenium and Tellurium, ed. W. C. Cooper, Pergamon Press, New York 1969, p. 293.
- 69G Gampel, L., Johnson, F. M.: J. Opt. Soc. Am. 59 (1969) 72.
- 69H Haussühl, S.: Z. Naturforsch. 24a (1969) 865.
- 69L Lasjaunias, J. C.: C. R. Acad. Sci. (Paris) Ser. B 269 (1969) 763.
- 70M Moynihan, C. T., Schnaus, U. E.: Mater. Sci. Eng. 6 (1970) 277.
- 70T Touloukian, Y. S., Ho, C. Y.: Thermophysical Properties of Matter, TPCR Data Series Vol. 1, Thermal Conduction, Metallic Elements and Alloys, Plenum Data Corp., New York, 1970, p. 324.
- 71D Day, G. W.: Appl. Phys. Lett. 18 (1971) 347.
- 71W Weiser, G., Stuke, J.: Phys. Status Solidi (b) 45 (1971) 691.
- 72L Lingelbach, W., Stuke, J., Weiser, G., Treusch, J.: Phys. Rev. B 5 (1972) 243.
- 73R Richter, W., Renucci, J. B., Cardona, M.: Phys. Status Solidi (b) 56 (1973) 223
- 73S Sherman, G. M., Coleman, P. D.: J. Appl. Phys. 44 (1973) 238.
- 74C Chang, K. T., Champness, C. H.: Phys. Status Solidi (a) 21 (1974) 309.
- 74D Danielewicz, E. J., Coleman, P. D.: Appl. Opt. 13 (1974) 1164.
- 74H Hamilton, W., Lassier, B., Kay, M.: J. Phys. Chem. Solids 35 (1974) 1089.
- 74S Stuke, J., in: Selenium, ed. R. A. Zingaro, W. C. Cooper, Van Nostrand Reinhold Comp., New York, Cincinnati, Toronto, London, Melbourne 1974, p. 174.
- 75G Große, R., Swoboda, H., Tausend, A.: J. Phys. C5 (1975) L 445.
- 75J Joannopoulos, J. D., Kastner, M.: Solid State Commun. 17 (1975) 221.
- 75L Lingelbach, W., Weiser, G.: Phys. Status Solidi (b) 70 (1975) 461.
- 75T Teuchert, W. D., Geick, R., Landwehr, G., Wendel, M., Weber, W.: J. Phys. C5 (1975) 3725.
- 77K Keller, R., Holzapfel, W. B., Schulz, H.: Phys. Rev. B16 (1977) 4404.
- 78G Große, R., Krause, P., Meissner, M., Tausend, A.: J. Phys. C11 (1978) 45.
- 69G Grosse, P.: Die Festkörpereigenschaften von Tellur, in: Springer Tracts in Modern Physics, Vol. 48, ed. by G. Höhler, Springer, Berlin-Heidelberg-New York 1969.
- 79M Moreth, B.: Phys. Rev. Lett. 42 (1979) 264; Thesis, University of Dortmund 1979.
- 79R Royer, D., Dieulesaint, E.: J. Appl. Phys. 50 (1979) 4042.
- 80H Hansen, F. Y., McMurray, M. L.: J. Chem. Phys. 72 (1980) 5550.
- 80M Miyamoto, Y.: Jpn. J. Appl. Phys. 19 (1980) 1813.
- 81N Nagata, K., Tashiro, H., Miyamoto, Y.: Jpn. J. Appl. Phys. 20 (1981) 2265.
- 82I Isomäki, H. M., v. Boehm, J.: Solid State Commun. 41 (1982) 765.
- 93S Bernède, J. C., Safoula, G., Godoy, A., Bernède, J. C., Alimi, K., Touriri, S.: Phys. Status Solidi (a) 135 (1993) K63.
- 95C Clark, S. J., Ackland, G. J., Akbarzadeh, H.: J. Phys. Chem. Solids 56 (1995) 329.

Figures to 13.2

Fig. 13.0.3

Brillouin zone of trigonal Se and Te

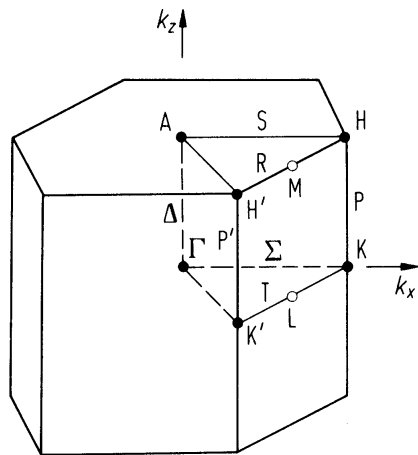


Fig. 13.0.4

Band structure of selenium.

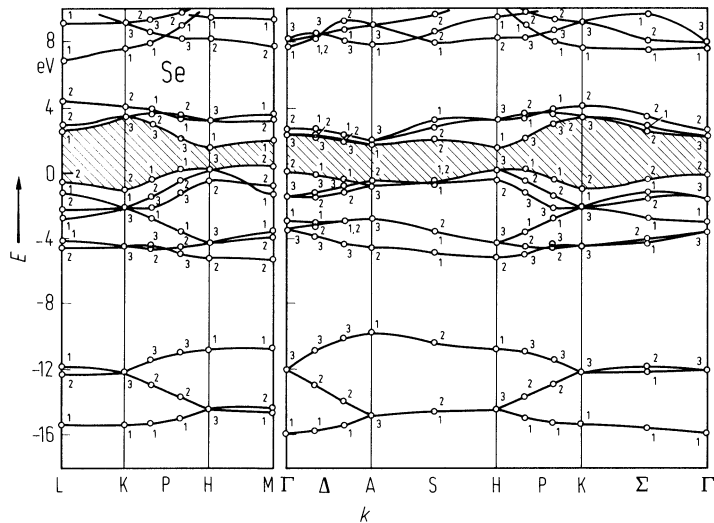


Fig. 13.2.1

Se (trigonal). Indirect [75L] and direct energy gap vs. temperature [71W]. Slope of ascending part is indicated.

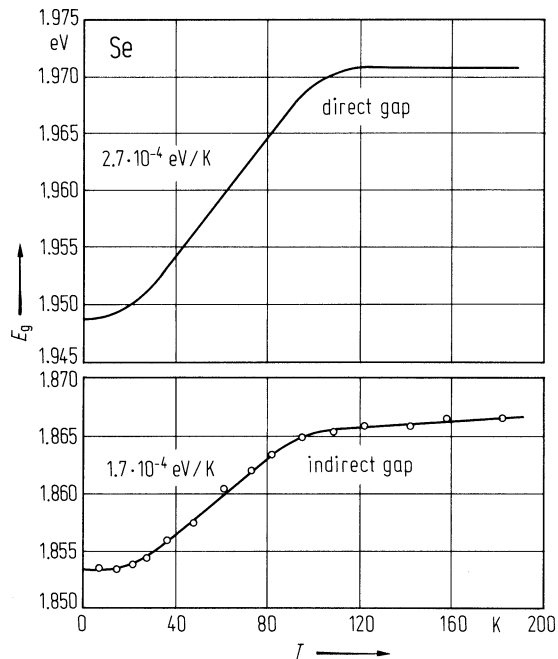


Fig. 13.2.2

Se (trigonal). Thermal expansion coefficient α parallel and perpendicular to the c -axis vs. temperature. Data points: full triangles [40S], full circles [64S], open triangles [75G], open circles [68K], polycrystalline sample, curves [78G]. [78G].

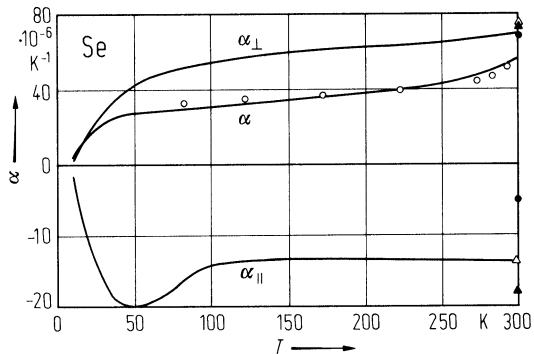


Fig. 13.2.3

Se (trigonal). Phonon dispersion relation calculated on the basis of short range potential field model [80H]. Experimental points from [75T].

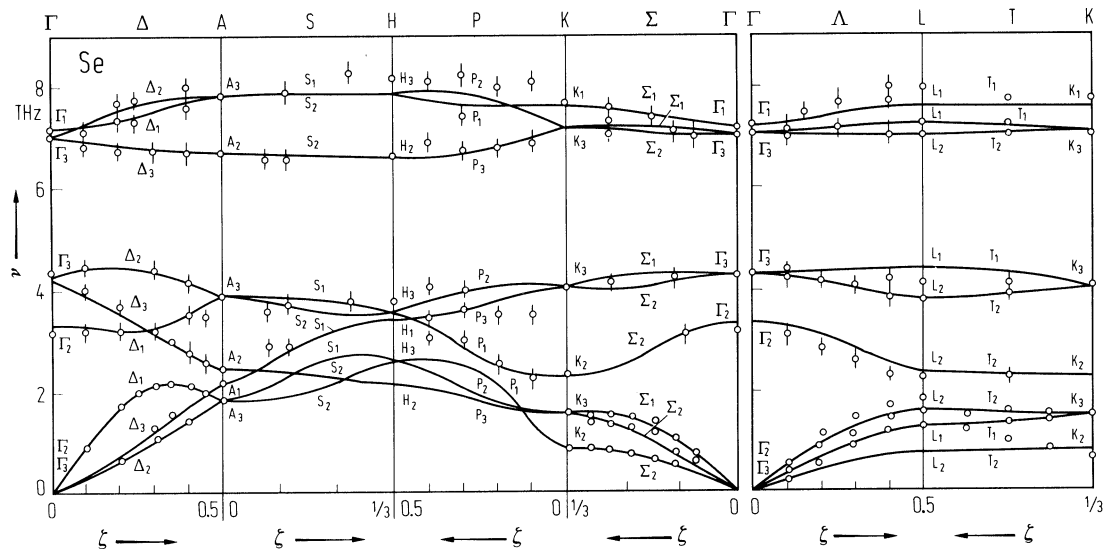


Fig. 13.2.4

Se (trigonal). Heat capacity C_v vs. temperature. Data points: [78G]. [79G].

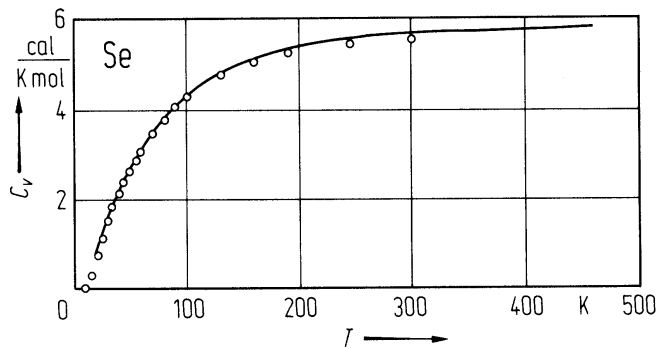


Fig. 13.2.5

Se (trigonal). Drift mobility of holes $\mu_{\text{dr,p}}$ vs. reciprocal temperature. The dashed curves represent a variation of μ_{p} with $T^{-3/2}$ [67M1].

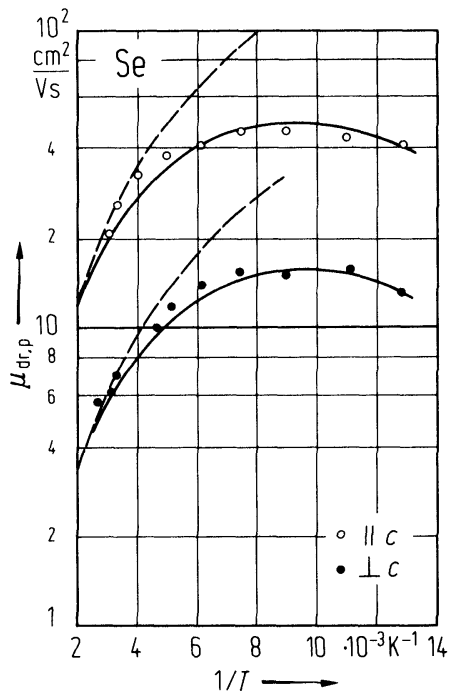


Fig. 13.2.6

Se (trigonal). Thermal conductivity κ parallel and perpendicular to the c -axis vs. temperature. *A*: single crystal grown from the vapor phase; *B*, *C*, *D*: single crystal grown from the melt; dashed curve: polycrystalline sample [67A].

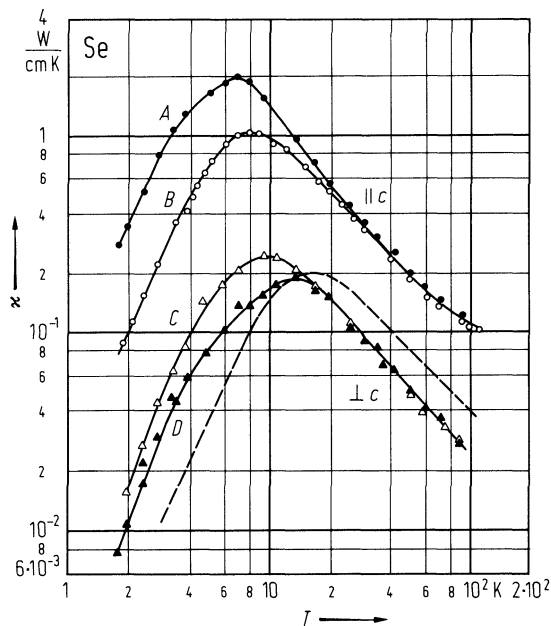


Fig. 13.2.7

Se (trigonal). The real part ϵ_1 and the imaginary part ϵ_2 of the dielectric constant for polarization of light $E \parallel c$ and $E \perp c$, composed of the results of [67T] and [68L]. [74S].

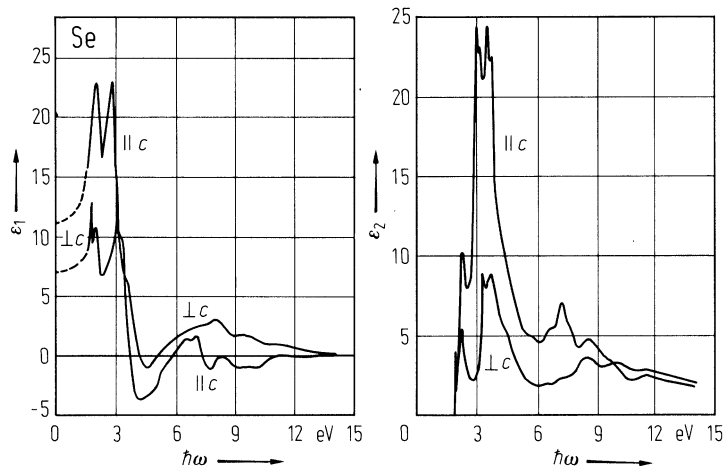
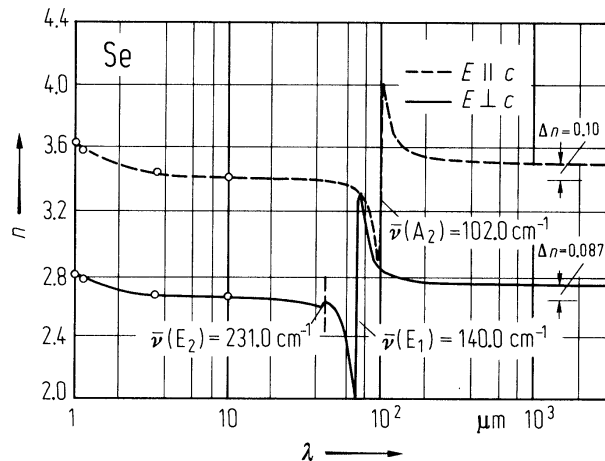


Fig. 13.2.8

Se (trigonal). Refractive index n vs. photon wavelength for polarization of light $E \parallel c$ (dashed curve) and $E \perp c$ (solid curve). Open circles are from [69G] ($\Delta n = n(0) - n(\infty)$). [74D].



13.3 Tellurium (Te)

Crystal structure

see section 13.0

Electronic properties

band structure : see Fig. 13.0.5, Brillouin zone: Fig. 13.0.3.

The band structure of Te shows a system of four band-triplets: a lowest triplet of s-character, and about 4 eV higher two overlapping triplets of p-character. These three triplets build up the occupied valence bands. The fourth triplet (p-character) is the lowest conduction band.

The valence-conduction band gap is a direct one, situated at points H, the corners of the Brillouin zone. Near H the bands are known in more detail. Due to the low symmetry of the point H the Kramers-degeneracy of the bands is lifted, when spin-effects are taken into account: the twofold degenerate H₃-band splits into H₄ + H₅ + H₆ (Fig. 13.0.6), which at most are degenerate at point H.

energy gap

E_g	0.335 eV	$T = 4.2$ K	interband-magnetoabsorption	68G
-------	----------	-------------	-----------------------------	-----

dependence of E_g on temperature and pressure

dE_g/dT	$+1.8 \cdot 10^{-4}$ eV K ⁻¹	$T = 4.2$ K	see also Fig. 13.3.1	68G
-----------	---	-------------	----------------------	-----

effective masses

$m_{p\perp}$	$0.114 m_0$	$T = 10$ K;	Faraday rotation due to free carriers	77R
$m_{p\parallel}$	$0.109 m_0$	$T = 4.2$ K	cyclotronresonance absorption	71P
$m_{n\perp}$	$0.060 m_0$	$T = 10$ K	Faraday rotation due to free carriers	74L
$m_{n\parallel}$	$0.050 m_0$	$T = 10$ K		

Transverse and longitudinal transport mass of holes vs. hole concentration, see Fig. 13.3.2.

anisotropy and nonparabolicity parameters of valence bands and conduction bands near the gap

valence band

$k \cdot p$ -calculation based on a coupling of the four highest valence bands H_{4v}, H_{5v}, H_{61v}, H_{62v}.

$$E_{H_{4v}/H_{5v}} = Ak_{\perp}^2 + Bk_z^2 + \beta k_{\perp}^4 + \beta' k_{\perp}^2 k_z^2 - 2|\Delta_1| \pm ((2|\Delta_1| + \eta k_{\perp}^2 + \xi k_{\perp}^4 + \xi' k_{\perp}^2 k_z^2)^2 + S^2 k_z^2)^{1/2}$$

Ref.	[70K]	[71N]	[70W]	[72B]	
A	-2.57	-2.67	-2.12	-3.26	$\cdot 10^{-15}$ eV cm ²
B	-4.09	-3.94	-4.20	-3.63	$\cdot 10^{-15}$ eV cm ²
β	1.1	6.0	3.0	6.0	$\cdot 10^{-29}$ eV cm ⁴
β'	0	0	2	4	$\cdot 10^{-29}$ eV cm ⁴
$2 \Delta_1 $	6.315	6.315	6.315	6.315	$\cdot 10^{-2}$ eV
η	-1.18	-1.31	-2.12	0	$\cdot 10^{-15}$ eV cm ²
ξ	4	7	0	0	$\cdot 10^{-30}$ eV cm ⁴
ξ'	0	0	0	0	eV cm ⁴
$ S $	2.62	2.57	2.49	2.48	$\cdot 10^{-8}$ eV cm

conduction band

k-*p*-calculation based on a coupling of the two lowest conduction bands H_{61c}, H_{62c}. Leads to *k*-linear terms also in the conduction bands.

$$E_{H_{61c}/H_{62c}} = ak_{\perp}^2 + bk_z^2 + E_g \pm (M^2k_{\perp}^2 + N^2k_z^2)^{1/2}$$

Ref.	[73S]	[77B]	
<i>a</i>	3.65	4.2	·10 ⁻¹⁵ eV cm ²
<i>b</i>	5.47	6.7	·10 ⁻¹⁵ eV cm ²
<i>M</i>	2.125	3.6	·10 ⁻⁹ eV cm
<i>N</i>	7.12	5.8	·10 ⁻⁹ eV cm
<i>E</i> _g	0.337	0.336	eV

Lattice properties

phonon dispersion relations : Fig. 13.3.3.

There are three atoms in the unit cell of Te. Consequently Te has – like trigonal Se – three acoustical and six optical phonon branches. The optical modes at *q* = 0 are: two double degenerate Γ₃(E) being infrared – (*E*⊥*c*) and Raman active, one Γ₂ (A₂) infrared – (*E*||*c*) active only and one Γ₁ (A₁) Raman active only.

phonon frequencies

<i>ν</i> (A ₁)	3.609·10 ¹² Hz	<i>T</i> = 295 K	Raman data	71P
<i>ν</i> _{TO} (A ₂)	2.593·10 ¹² Hz	<i>T</i> = 300 K	IR data	69G
<i>ν</i> _{LO} (A ₂)	2.818·10 ¹² Hz	<i>T</i> = 300 K	Raman data	72R
<i>ν</i> _{TO} (E')	2.764·10 ¹² Hz	<i>T</i> = 300 K	Raman data	71P
<i>ν</i> _{LO} (E')	3.087·10 ¹² Hz	<i>T</i> = 300 K	Raman data	72R
<i>ν</i> _{TO} (E'')	4.218·10 ¹² Hz	<i>T</i> = 295 K	Raman data	71P
<i>ν</i> _{LO} (E'')	4.257·10 ¹² Hz	<i>T</i> = 300 K	IR data	69G

sound velocities

<i>v</i> _l (<i>z</i>)	3.36·10 ⁵ cm s ⁻¹	<i>T</i> = 300 K	<i>q</i> [001]: longitudinal	75F
<i>v</i> _t (<i>z</i>)	2.26·10 ⁵ cm s ⁻¹		<i>q</i> [001]: transverse	
<i>v</i> _l (<i>x</i>)	2.30·10 ⁵ cm s ⁻¹		<i>q</i> [100]: longitudinal	
<i>v</i> _{ft} (<i>x</i>)	2.42·10 ⁵ cm s ⁻¹		<i>q</i> [100]: fast transverse	
<i>v</i> _{st} (<i>x</i>)	0.98·10 ⁵ cm s ⁻¹		<i>q</i> [100]: slow transverse	
<i>v</i> _{ql} (<i>y</i>)	2.66·10 ⁵ cm s ⁻¹		<i>q</i> [010]: quasi longitudinal	
<i>v</i> _{qt} (<i>y</i>)	1.79·10 ⁵ cm s ⁻¹		<i>q</i> [010]: quasi transverse	
<i>v</i> _t (<i>y</i>)	1.42·10 ⁵ cm s ⁻¹		<i>q</i> [010]: transverse	

second order elastic moduli

<i>c</i> ₁₁	3.30·10 ¹¹ dyn cm ⁻²	<i>T</i> = 300 K	calculated from sound velocities measured	75F
<i>c</i> ₁₂	0.86·10 ¹¹ dyn cm ⁻²	<i>T</i> = 300 K	by the pulse echo method	64M
<i>c</i> ₁₃	2.31·10 ¹¹ dyn cm ⁻²	<i>T</i> = 300 K		75F
<i>c</i> ₁₄	1.19·10 ¹¹ dyn cm ⁻²			
<i>c</i> ₃₃	7.05·10 ¹¹ dyn cm ⁻²			
<i>c</i> ₄₄	3.19·10 ¹¹ dyn cm ⁻²			
<i>c</i> ₆₆	1.25·10 ¹¹ dyn cm ⁻²			

volume compressibility

κ _v	0.52·10 ⁻¹¹ cm ² dyn ⁻¹	X-ray analysis under hydrostatic pressure	25B
----------------	--	---	-----

thermal expansion

$(1/a)da/dT = \alpha_{\perp}$	$2.97 \cdot 10^{-5} \text{ K}^{-1}$	$T = 300 \text{ K}$	70I
$(1/c)dc/dT = \alpha_{\parallel}$	$-0.229 \cdot 10^{-5} \text{ K}^{-1}$	$T = 300 \text{ K}$	70I

For other temperatures (2...500 K), see Fig. 13.3.4.

heat capacity

C_p	$24.380 \text{ J mol}^{-1} \text{ K}^{-1}$	$T = 300 \text{ K}$	67D
-------	--	---------------------	-----

density

d	6.24 g cm^{-3}	67D
-----	--------------------------	-----

melting temperature

T_m	723 K	67D
-------	-----------------	-----

Transport properties

Undoped tellurium crystals show intrinsic conductivity for $T > 200 \text{ K}$. Extrinsic conductivity is of p-type, n-type crystals are not known. For a systematic doping group V-elements are used, they act as shallow acceptors.

The mobility is governed by acoustic and polar optical phonon scattering. At low temperatures the transport properties strongly depend on the defects in the samples. In high-quality crystals the important scattering process is scattering on ionized impurities.

intrinsic transport properties (at 293 K)

$\sigma_{i,11}$	$1.56 \text{ } \Omega^{-1} \text{ cm}^{-1}$	69G
$\sigma_{i,33}$	$3.04 \text{ } \Omega^{-1} \text{ cm}^{-1}$	
$R_{H,i1} = R_{H,i3}$	$408 \text{ cm}^3 \text{ C}^{-1}$	low field limit
n_i	$5.6 \cdot 10^{15} \text{ cm}^{-3}$	conductivity and Hall coefficient
$\mu_{n,\parallel c}$	$2380 \text{ cm}^2/\text{V s}$	comparison of conductivity and Hall
$\mu_{n,\perp c}$	$1150 \text{ cm}^2/\text{V s}$	coefficient of extrinsic and intrinsic
$\mu_{p,\parallel c}$	$1260 \text{ cm}^2/\text{V s}$	samples
$\mu_{p,\perp c}$	$650 \text{ cm}^2/\text{V s}$	
$E_{g,th}$	0.33 (2) eV	average activation energy of $n_i(T)$, $T = 250 \dots 600 \text{ K}$

Intrinsic transport properties between 250 K and 650 K: Figs. 13.3.5 and 13.3.6.

extrinsic transport properties

Examples of large mobilities as observed in high quality crystals:

$\mu_{p\parallel}$	$8.5 \cdot 10^3 \text{ cm}^2/\text{Vs}$	$T = 77 \text{ K},$	conductivity and Hall coefficient	73H
		$p = 1.8 \cdot 10^{14} \text{ cm}^{-3}$		
	$8.5 \cdot 10^4 \text{ cm}^2/\text{Vs}$	$T = 2 \dots 5 \text{ K},$	conductivity and Hall coefficient	73B
		$p = 1.5 \cdot 10^{14} \text{ cm}^{-3}$		

Dependence of the hole mobility on concentration and temperature: Fig. 13.3.7.

piezoresistance coefficients

The piezoresistance depends strongly on the concentration of impurities and on temperature in the range of intrinsic or mixed conductivity.

		T [K], p [10^{15} cm^{-3}]		
$\pi_{11} = \pi_{22}$	$-0.8 \cdot 10^{-10} \text{ cm}^2 \text{ dyn}^{-1}$	200,	2	68H
π_{33}	$0.5 \cdot 10^{-10} \text{ cm}^2 \text{ dyn}^{-1}$	200,	9	
$\pi_{12} = \pi_{21}$	$-0.3 \cdot 10^{-10} \text{ cm}^2 \text{ dyn}^{-1}$	200,	2	
$\pi_{13} = \pi_{23}$	$+0.4 \cdot 10^{-10} \text{ cm}^2 \text{ dyn}^{-1}$	200,	9	
$\pi_{31} = \pi_{32}$	$-0.6 \cdot 10^{-10} \text{ cm}^2 \text{ dyn}^{-1}$	200,	2	
$\pi_{15} = -\pi_{25} = \pi_{46}$	$-0.3 \cdot 10^{-10} \text{ cm}^2 \text{ dyn}^{-1}$	200,	2	
$\pi_{51} = -\pi_{52} = \pi_{64}$	$< 0.1 \cdot 10^{-10} \text{ cm}^2 \text{ dyn}^{-1}$	200,	2	
$\pi_{55} = \pi_{66}$	$-0.2 \cdot 10^{-10} \text{ cm}^2 \text{ dyn}^{-1}$	200,	2	

thermoelectric power

(see also Fig. 13.3.8)

$S_{11} \approx S_{33}$	$-1.0 \cdot 10^{-4} \text{ V K}^{-1}$	$T = 293 \text{ K},$	intrinsic conducting sample	69G
	$+3.4 \cdot 10^{-4} \text{ V K}^{-1}$	$T = 293 \text{ K}, p = 4.8 \cdot 10^{17} \text{ cm}^{-3}$		

thermal conductivity

κ_{33}	$2.27 \cdot 10^{-2}$	$T = 300 \text{ K}$	59D
		$\text{W cm}^{-1} \text{ K}^{-1}$	

For lower temperatures, see Fig. 13.3.9, for higher temperatures, see [59D].

piezoelectric strain coefficients

d_{11}	$0.55 \cdot 10^{-8} \text{ V}^{-1} \text{ cm}$	$T = 300 \text{ K}$	piezoelectric Hall effect method	69G
d_{14}	$\pm 0.5 \cdot 10^{-8} \text{ V}^{-1} \text{ cm}$		positive sign for space group D_3^6 , negative sign for D_3^4	69G

Optical properties

optical constants in the visible spectral range

($h\nu = 1.5 \dots 3 \text{ eV}$, (ν/c) = 11000...25000 cm^{-1}). See also Fig. 13.3.10. 69T

(ν/c) 10^4 cm^{-1}	n_{\perp}	k_{\perp}	n_{\parallel}	k_{\parallel}	(ν/c) 10^4 cm^{-1}	n_{\perp}	k_{\perp}	n_{\parallel}	k_{\parallel}
1.144	5.59	0.659	7.14	2.56	1.744	5.26	3.52	5.47	5.16
1.181	5.68	0.760	6.95	2.80	1.782	5.01	3.57	4.91	5.20
1.219	5.78	0.895	6.81	2.86	1.819	4.81	3.63	4.65	5.21
1.256	5.84	1.06	6.73	2.89	1.856	4.62	3.69	4.39	5.20
1.294	5.86	1.17	6.74	2.93	1.894	4.43	3.76	4.20	5.16
1.332	5.87	1.26	6.78	3.03	1.931	4.25	3.78	3.99	5.08
1.369	5.95	1.36	6.80	3.18	1.969	4.07	3.77	3.81	5.01
1.407	6.04	1.52	6.86	3.47	2.006	3.91	3.77	3.63	4.93
1.444	6.09	1.72	6.85	3.65	2.044	3.76	3.76	3.46	4.85
1.482	6.12	2.02	6.77	3.86	2.100	3.55	3.72	3.21	4.71
1.519	6.11	2.25	6.58	4.10	2.175	3.27	3.66	2.98	4.52
1.557	6.07	2.45	6.40	4.36	2.250	3.01	3.57	2.76	4.39
1.594	5.97	2.70	6.21	4.60	2.325	2.77	3.47	2.54	4.27
1.632	5.82	2.94	6.00	4.77	2.400	2.56	3.39	2.35	4.15
1.669	5.67	3.16	5.76	4.92	2.475	2.37	3.29	2.22	3.96
1.707	5.49	3.37	5.45	5.06					

dielectric constants

$\epsilon_{11}(0)$	30	$T = 5 \text{ K}, 80 \text{ K},$	from harmonic oscillator analysis of IR	77R
$\epsilon_{33}(0)$	43	$T = 300 \text{ K}$	reflectivity and multiple reflection	
$\epsilon_{11}(\infty)$	23		interference effects	
$\epsilon_{33}(\infty)$	36			

References to 13.3

- 25B Bridgeman, P. W.: Proc. Am. Acad. Arts Sci. 60 (1925) 303.
- 59D Devyatkova, E. D., Noizhes, B. Y., Smirnov, I. A., Sov. Phys. Solid State (English Transl.) 1 (1959) 555.
- 63P Parfenev, R. V., Pogarskii, A. M., Farbshtein, I. I.: Sov. Phys. Solid State (English Transl.) 4 (1963) 2630.
- 64M Malgrange, J. L., Quentin, G., Thuillier, J. M.: Phys. Status Solidi 4 (1964) 139.
- 67A Adams, A. R., Baumann, F., Stuke, J.: Phys. Status Solidi 23 (1967) K99.
- 67D D'Ans-Lax: "Taschenbuch für Chemiker und Physiker", Vol. 1, ed.: Lax, E. and Synowietz, C., Springer Verlag, Berlin-Heidelberg-New York (1967), p. 102.
- 68G Grosse, P., Winzer, K.: Phys. Status Solidi 26 (1968) 139.
- 69G Grosse, P.: Die Festkörpereigenschaften von Tellur, in: Springer Tracts in Modern Physics, Vol. 48, ed. by G. Höhler, Springer, Berlin-Heidelberg-New York 1969.
- 69T Tutihasi, S., Roberts, G. G., Keezer, R. C., Drews, R. E.: Phys. Rev. 177 (1969) 1143.
- 70I Ibach, H., Ruin, R.: Phys. Status Solidi 41 (1970) 719.
- 70K Kamimura, M., Nakao, K., Doi, T., in: Proceedings of the X. International Conference on the Physics of Semiconductors, ed. by P. Keller, J. C. Hensel, F. Stern, U. S. Atomic Energy Commission, Oak Ridge 1970, p. 342.
- 70W Weiler, M. H.: Solid State Commun. 8 (1970) 1017.
- 71N Nakao, K., Doi, T., Kamimura, M.: J. Phys. Soc. Jpn. 30 (1971) 1400.
- 71P Pine, A. S., Dresselhaus, G.: Phys. Rev. B4 (1971) 356.
- 71B Beyer, W., Mell, H., Stuke, J.: Phys. Status Solidi (b) 45 (1971) 153.
- 72B Bammes, P., Klucker, R., Koch, E. E., Tuomi, T.: Phys. Status Solidi (b) 49 (1972) 561.
- 72R Richter, W.: J. Phys. Chem. Solids 33 (1972) 2123.
- 73B Bauer, G., Kahlert, H., von Klitzing, K., Landwehr, G.: Phys. Status Solidi (b) 59 (1973) 479.
- 73H Hoerstel, W., Kusnick, D., Spitzer, M.: Phys. Status Solidi (b) 60 (1973) 213.
- 73S Shinno, H., Yoshizaki, R., Tanaka, S., Doi, T., Kamimura, H.: J. Phys. Soc. Jpn. 35 (1973) 525.
- 74L Lutz, M., Stolze, H., Grosse, P.: Phys. Status Solidi (b) 62 (1974) 665.
- 75F Fjeldly, T. A., Richter, W.: Phys. Status Solidi (b) 72 (1975) 555.
- 77B Blinowski, J., Rebmann, G., Rigaux, G., Mycielski, J.: J. Phys. (Paris) 38 (1977) 1139.
- 77R Rautenberg, M.: Dissertation RWTH Aachen 1977.
- 79R Richter, W., in: The Physics of Selenium and Tellurium, ed. by E. Gerlach and P. Grosse, Springer Series in Solid-State Sciences Vol. 13, Springer, Berlin-Heidelberg-New York 1979, p. 36.

Figures to 13.3

Fig. 13.03

Brillouin zone of trigonal Se and Te

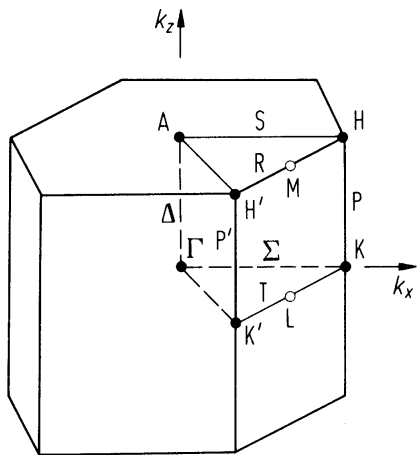
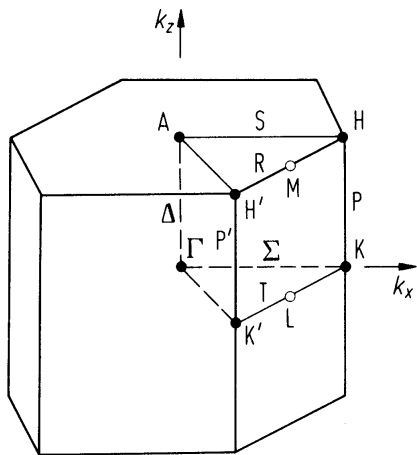


Fig. 13.0.5

Band structure and density of states of tellurium.

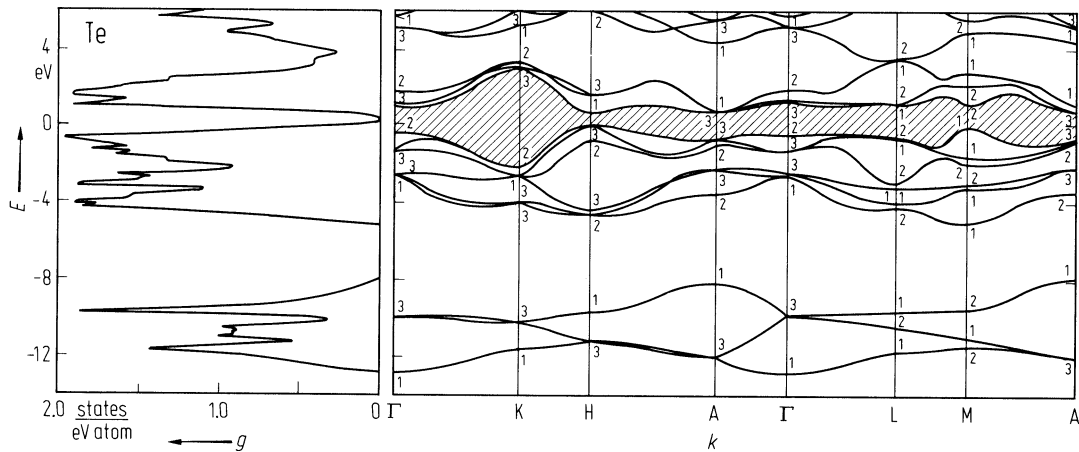


Fig. 13.0.6

Te. Splitting of the bands near the energy gap at H due to spin interaction. a) schematic [69G], b) definitions of parameters.

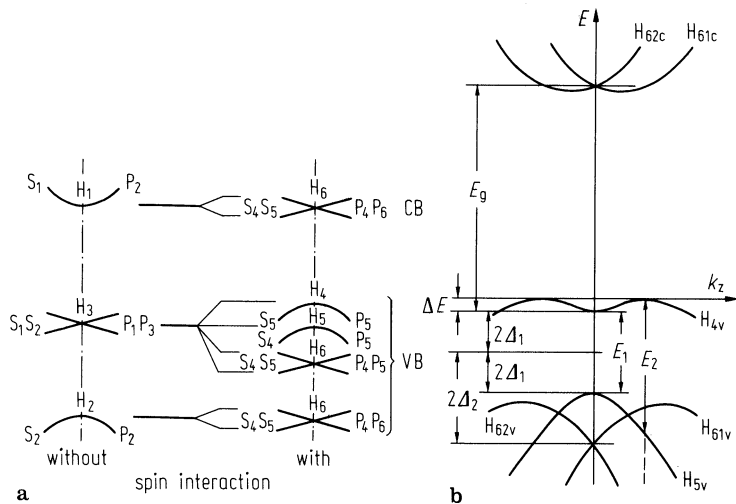


Fig. 13.3.1

Te. E_g vs. T . Dashed line: average activation energy of n_i [69G].

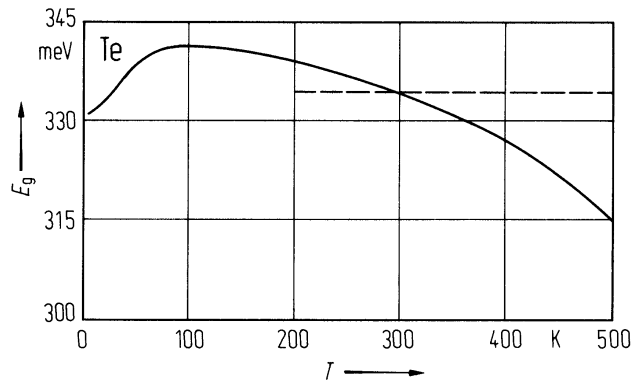


Fig. 13.3.2

Te. Transverse (a) and longitudinal (b) transport mass of holes vs. hole concentration. Determined from the susceptibility of free carriers in the submillimeter range [77R].

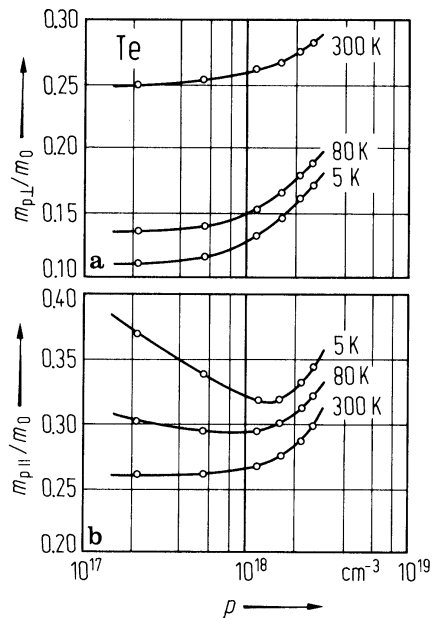


Fig. 13.3.3

Te. Phonon dispersion curves [79R]. Dashed lines: theory.

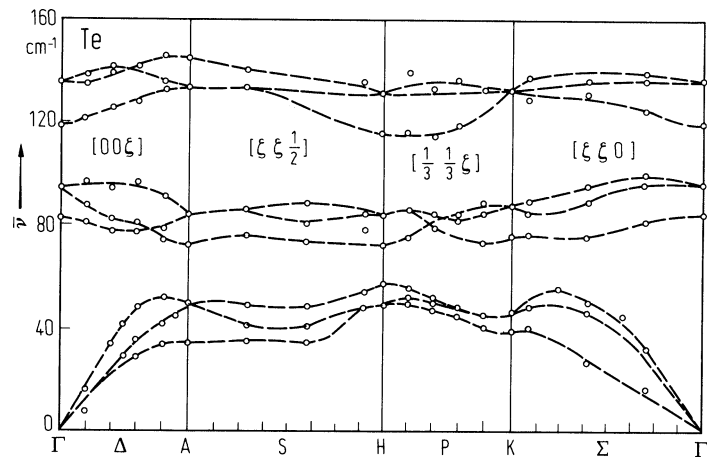


Fig. 13.3.4

Te. Linear thermal expansion coefficient vs. temperature [70I].

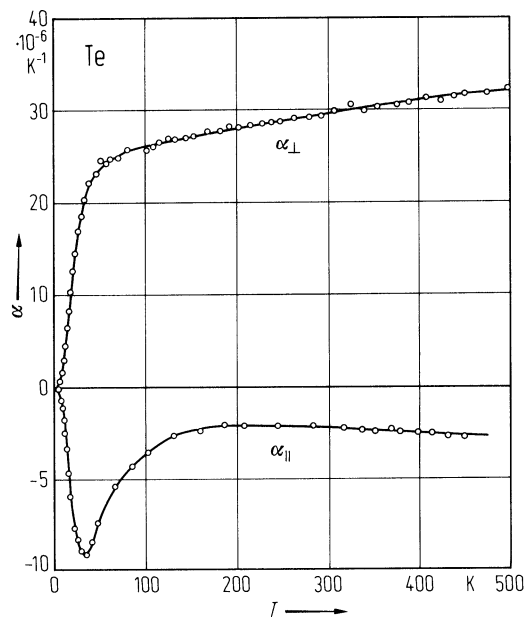


Fig. 13.3.5

Te. Intrinsic conductivity vs. temperature [69G].

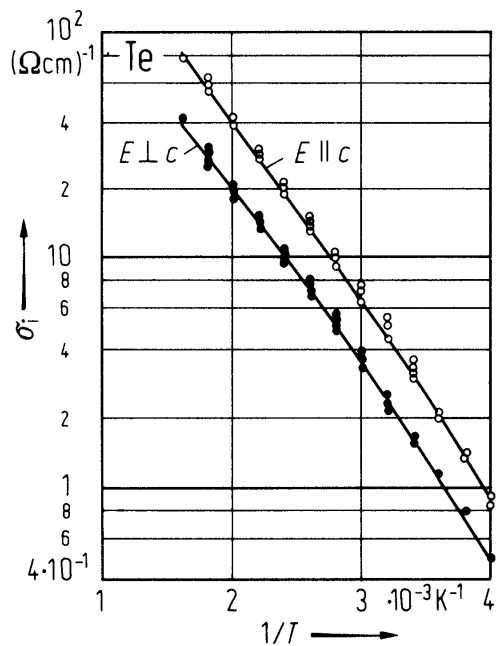


Fig. 13.3.6

Te. Intrinsic mobility and mobility ratio vs. temperature ($b_{\parallel} \approx b_{\perp}$) [69G].

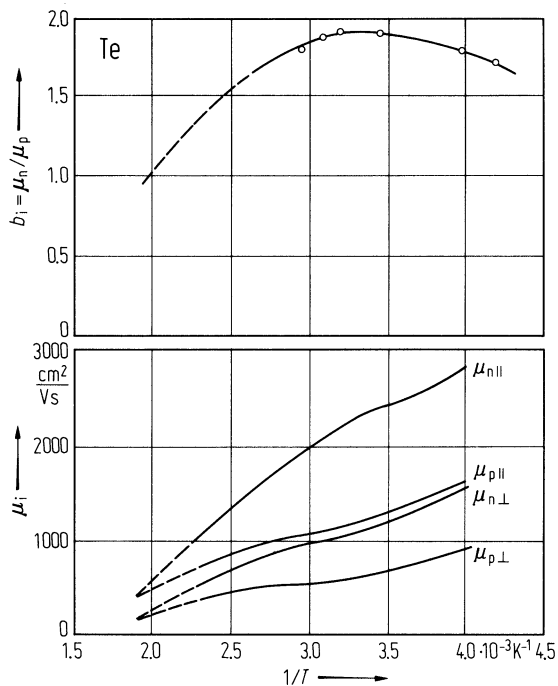


Fig. 13.3.7

Te. Hole mobility vs. temperature [63P]. Parameter: hole concentration (in cm^{-3}); curve 1: $p = 5.9 \cdot 10^{13}$, 2: $2.2 \cdot 10^{14}$, 3: $2.4 \cdot 10^{15}$, 4: $8.6 \cdot 10^{15}$, 5: $8.4 \cdot 10^{16}$, 6: $4.6 \cdot 10^{18}$.

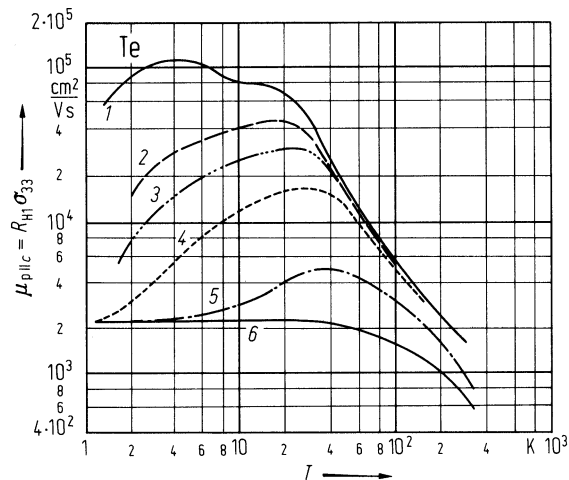


Fig. 13.3.8

Te. Thermoelectric power vs. temperature for various acceptor concentrations. Nr. 1...7: $n_a = 6.1 \cdot 10^{14}$; $4.0 \cdot 10^{16}$; $4.8 \cdot 10^{17}$; $6.9 \cdot 10^{17}$; $2.2 \cdot 10^{18}$; $2.5 \cdot 10^{18}$; $5.0 \cdot 10^{18} \text{ cm}^{-3}$ [69G].

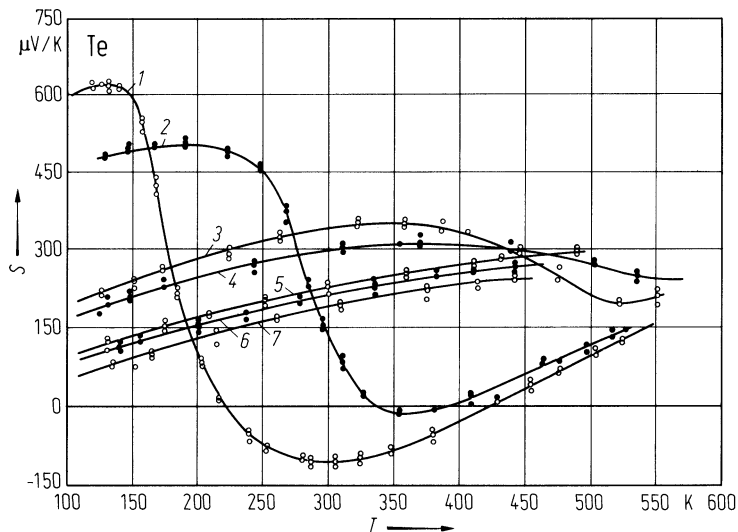


Fig. 13.3.9

Te. Thermal conductivity vs. temperature [67A].

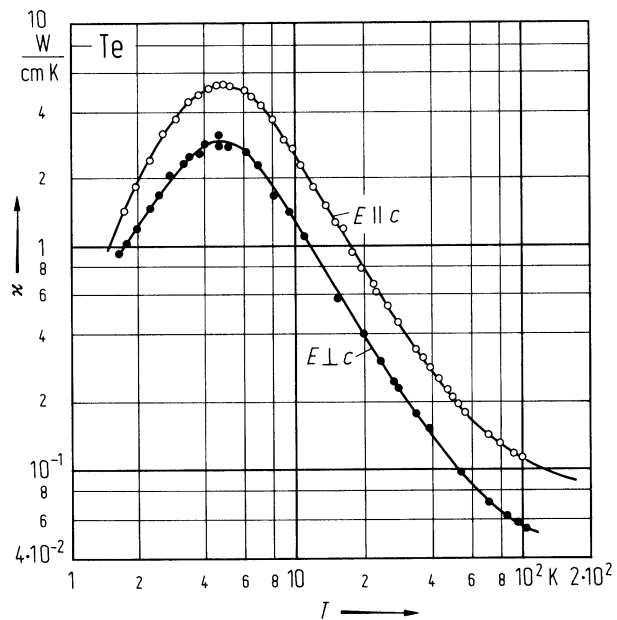
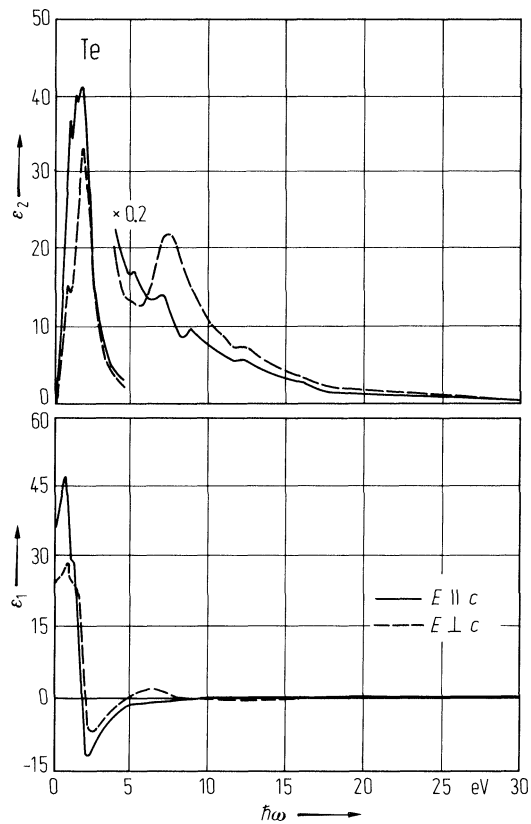


Fig. 13.3.10

Te. Real and imaginary part of dielectric constant vs. photon energy at 300 K [72B].



14 IA_x–IB_y compounds

14.0. Crystal structure and electronic structure of IA_x–IB_y compounds

Among the alkali-noble metals (Cu,Ag,Au) intermetallic alloys stable compounds with stoichiometric composition 1:1 have been observed for the Au systems and for LiAg. For CsAu strong experimental evidence for semiconducting behavior exists, whereas for RbAu the experimental situation is less clear.

CsAu and RbAu crystallize in the cesium chloride structure (Fig. 14.0.1, space group: O_h^1 (Pm3m), Brillouin zone: Fig. 14.0.2). Both the alkali atoms and the gold atoms form simple cubic sublattices, with lattice parameter a .

Figs. 14.0.3 and 14.0.4 show the band structure of CsAu and RbAu, respectively.

References to 14.0

78O Overhof, H., Knecht, J., Fischer, R., Hensel, F.: J. Phys. F 8 (1978) 1607.

Figures to 14.0

Fig. 14.0.1

Cesium chloride structure.

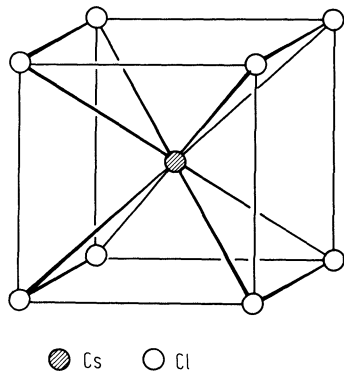
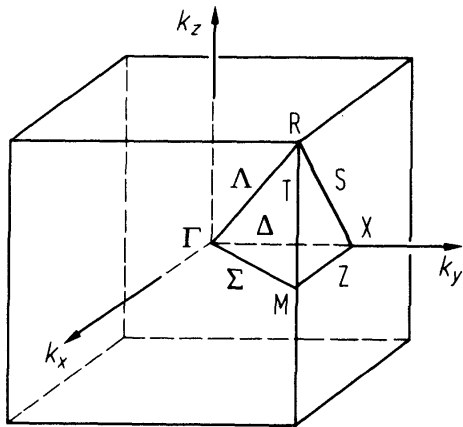
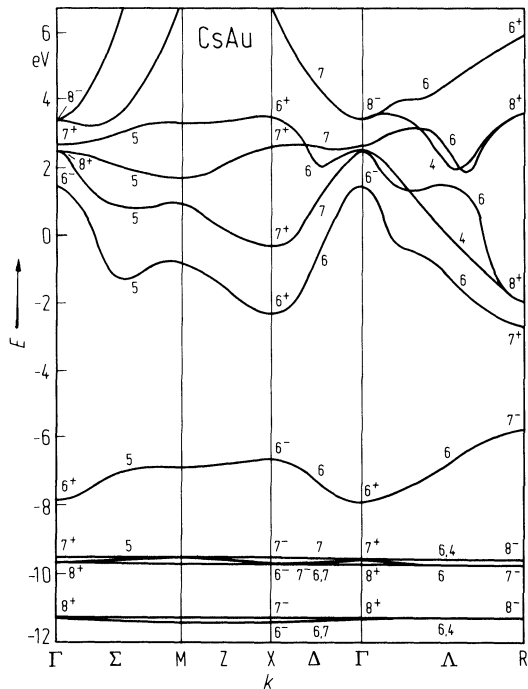


Fig. 14.0.2

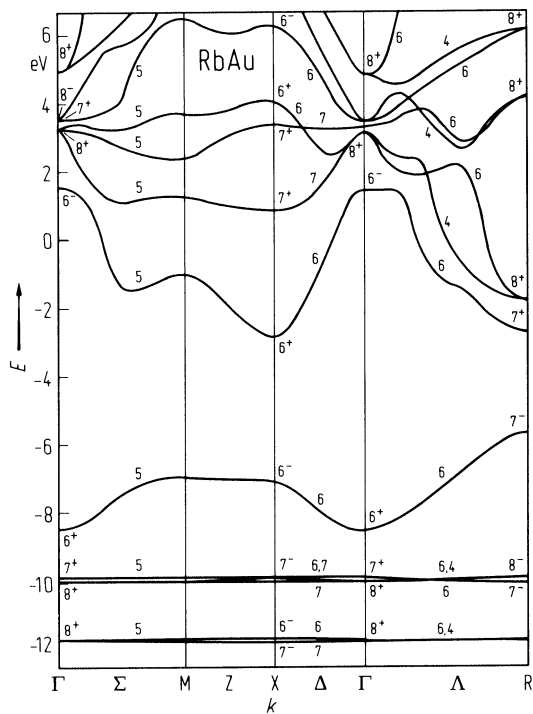
CsAu. Brillouin zone for the simple cubic lattice.



CsAu. Energy band structure according to a full relativistic KKR calculation with an ionic ansatz potential [78O].



RbAu. Band structure calculated with a full relativistic KKR method and an ionic ansatz potential [78O].



14.1 CsAu

Crystal structure

see section 14.0.

Electronic properties

band structure: Fig. 14.0.3 [78O], Brillouin zone: Fig. 14.0.2.

The conduction bands are essentially free electron like and the lowest set has minima at the X and R points of the Brillouin zone.

The uppermost valence band consists of a filled s-like band with a width smaller by a factor of 2.5 than a free electron band. Due to the large Au–Au interatomic distance the lower lying d-bands show very little dispersion and appear essentially as core-like states with a spin orbit splitting between Au 5d_{5/2} and Au 5d_{3/2} of 1.5 eV. The same is true for the p-bands of Cs.

energy gap

E_g	2.5 eV	$T = 300$ K	optical absorption edge	79M
dE_g/dT	$-4 \cdot 10^{-4}$ eV K ⁻¹	$T = 300$ K	shift of absorption	

Lattice properties

lattice parameter

a	4.258(1) Å			93Z
-----	------------	--	--	-----

density

d	7.065 g cm ⁻³	$T = 300$ K	determined from structure data	59S
-----	--------------------------	-------------	--------------------------------	-----

melting temperature

T_m	590°C		thermal analysis	61K
-------	-------	--	------------------	-----

Transport properties

resistivity : Fig. 14.1.1

Hall coefficient and mobility : Figs. 14.1.2, 14.1.3.

No success in growing good crystals of pure CsAu has been reported so far. Consequently the existing transport data refer to extrinsic carriers.

mobility of charge carriers

μ_n	35 cm ² /V s	$T = 300$ K	Hall mobility	63W
μ_p	210 cm ² /V s	$T = 300$ K	Hall mobility	67H

References to 14.1

- 59S Spicer, W. E., Sommer, A. H., White, J. G.: Phys. Rev. 115 (1959) 57.
61K Kienast, G., Verma, J.: Z. Anorg. Allg. Chem. 310 (1961) 143
63W Wooten, F., Condas, G. A.: Phys. Rev. 131 (1963) 657.
67H Hall, R. F., Wright, H. C.: Brit. J. Appl. Phys. 18 (1967) 33.
78O Overhof, H., Knecht, J., Fischer, R., Hensel, F.: J. Phys. F 8 (1978) 1607.
79M Münster, P., Freyland, W.: Phil. Mag. B 39 (1979) 93.
93Z Zachwieja, U.: Z. Anorg. Allg. Chem. 619 (1993) 1095.

Figures to 14.1

Fig. 14.0.2

CsAu. Brillouin zone for the simple cubic lattice.

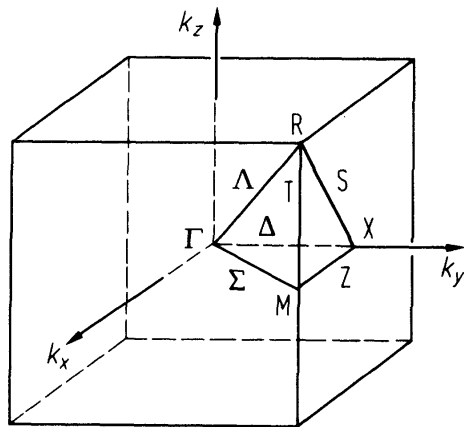


Fig. 14.0.3

CsAu. Energy band structure according to a full relativistic KKR calculation with an ionic ansatz potential [78O].

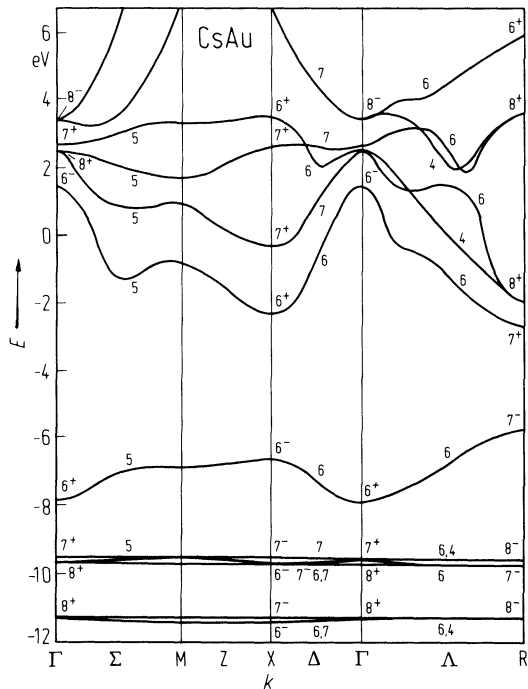


Fig. 14.1.1

CsAu. Resistivity vs. temperature measured on three different films of 1300 Å thickness [63W].

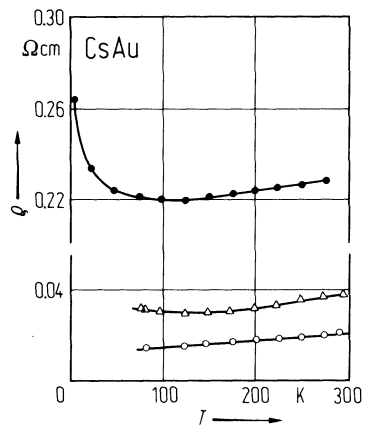


Fig. 14.1.2

CsAu. Hall mobility of electrons vs. temperature for the same samples as in Fig. 1 [63W].

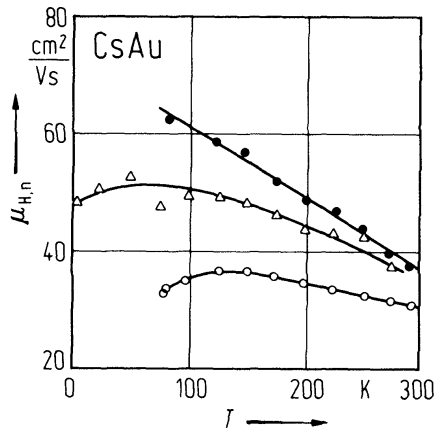
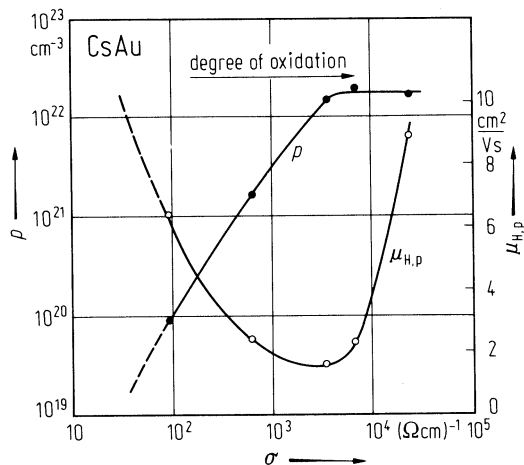


Fig. 14.1.3

CsAu. Hall mobility of holes (right scale) and hole concentration (left scale) vs. conductivity for films of 2700 Å thickness for different degrees of oxidation, increasing to the right [67H].



14.2 RbAu

crystal structure : section 14.0.

band structure: Fig. 14.0.4, Brillouin zone: Fig. 14.0.2.

According to the KKR calculation the band structure is very similar to that of CsAu [78O].

energy gap

The optical gap is about 2.5 eV at room temperature and about 2.2 eV at 480°C [84N].

lattice parameter

a	4.098(1) Å	93Z
-----	------------	-----

melting temperature

T_m	498°C	thermal analysis	61K
-------	-------	------------------	-----

No detailed transport measurements are reported to date. The visual appearance of RbAu is nonmetallic, brown.

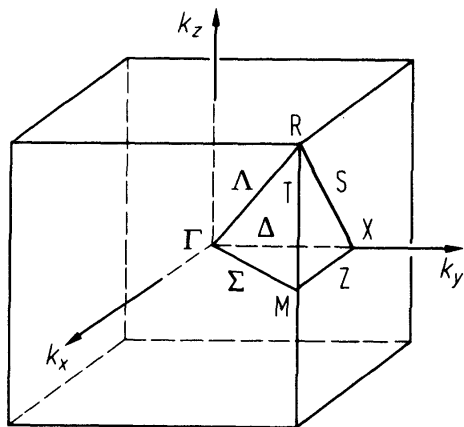
References to 14.2

- | | |
|-----|---|
| 61K | Kienast, G., Verma, J.: Z. Anorg. Allg. Chem. 310 (1961) 143 |
| 78O | Overhof, H., Knecht, J., Fischer, R., Hensel, F.: J. Phys. F 8 (1978) 1607. |
| 84N | Nicoloso, N., Freyland, W.: Ber. Bunsenges. Phys. Chem. 88 (1985) 953. |
| 93Z | Zachwieja, U.: Z. Anorg. Allg. Chem. 619 (1993) 1095. |

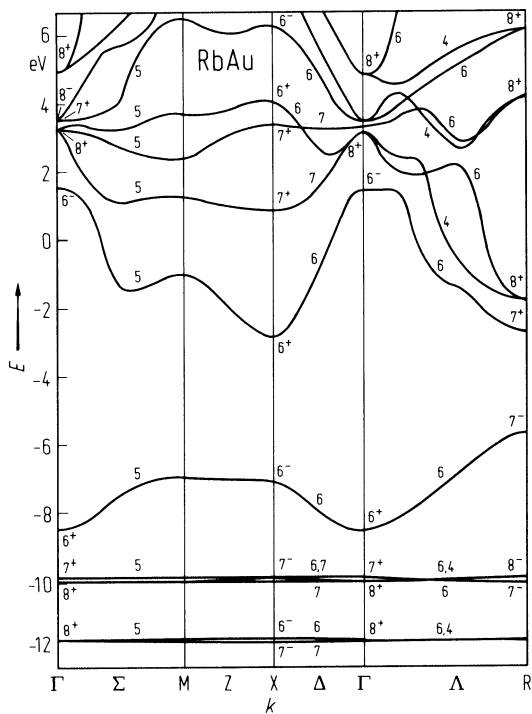
Figures to 14.2

Fig. 14.0.2

CsAu. Brillouin zone for the simple cubic lattice.



RbAu. Band structure calculated with a full relativistic KKR method and an ionic ansatz potential [78O].



15 I_x - V_y compounds

15.0 Crystal structure and electronic structure

15.0.1 Crystal structure of I-V compounds

The compounds NaSb and KSb crystallize in the monoclinic LiAs-structure (Fig. 15.0.1). The Sb-atoms form singly bonded infinite spiral chains parallel to the b -axis.

The compounds RbSb and CsSb crystallize in an orthorhombic lattice (Fig. 15.0.2) isotypic with the NaP structure [79S]. The main features of this structure are again infinite Sb-chains parallel to the b -axis. The space group is D_2^4 ($P2_12_12_1$).

15.0.2 Crystal structure of I_3 -V compounds

Most of the I_3 -V compounds are known to exist both in a hexagonal and a cubic modification. For Na_3Sb and Na_3Bi only the hexagonal form has been observed, whereas for Li_3Bi , Cs_3Bi , and Cs_3Sb only the cubic modification has been reported.

The hexagonal structure of the I_3 -V compounds ($I = Li, Na, K, Rb$; $V = Bi, Sb$ with exception of Li_3Bi) is isotypic with the Na_3As structure (Fig. 15.0.3). The space group is D_{6h}^4 ($P6_3/mmc$). The cubic modifications of β - Li_3Sb , K_3Sb , Rb_3Sb , Li_3Bi , K_3Bi , Rb_3Bi and Cs_3Bi are isotypic with the BiF_3 structure (Fig. 15.0.4).

For the heavy alkali metal-V compounds Rb_3Sb and Cs_3Bi a different assignment has been proposed [65W], which is isotypic with the structure of the Cs_3Sb compound. According to [61G, 57J] this one most probably crystallizes in the NaTl structure (Fig. 15.0.5).

15.0.3 Electronic structure

Figs. 15.0.6...11 show the Brillouin zone and band structures of several I_x - V_y compounds.

References to 15.0

- 57J Jack, K. H., Wachtel, M. M.: Proc. Roy. Soc. (London) Ser. A239 (1957) 46.
- 61G Gnutzmann, G., Dorn, F. W., Klemm, W.: Z. Anorg. Ang. Chem. 309 (1961) 210.
- 65W Wyckoff, R. W. G.: Crystal Structures, Vol. 1 and 2, 2nd. Ed., Interscience Publishers, New York 1965.
- 68O Ossmann, G. W., McGrath, J. W.: J. Chem. Phys. 49 (1968) 783.
- 74M Mostovskii, A. A., Chaldyshev, V. A., Karavaev, C. F., Klimin, A. I., Ponomarenko, I. N.: Izv. Akad. Nauk SSSR, Ser. Fiz. 38 (1974) 195; Bull. Acad. Sc. USSR, Phys. Ser. (English Transl.) 38 (1974) 10.
- 76M Mostovskii, A. A., Chaldyshev, V. A., Kiselev, V. P., Klimin, A. I.: Izv. Akad. Nauk SSSR, Ser. Fiz. 40 (1976) 2490; Bull. Acad. Sc. USSR, Phys. Ser. (English Transl.) 40 (1976) 36.
- 79S Schnering von, H. G., Hönle, W., Krogull, G.: Z. Naturforsch. 34b (1979) 1678.

Figures to 15.0

Fig. 15.0.1

NaSb. Left part: the monoclinic structure of NaSb projected along its b axis, origin in lower left; fractional y -parameters ($\cdot 100$) are inscribed in each atom. Right part a packing drawing of the NaSb arrangement seen along its b axis; atoms have their metallic radii, the smaller antimony atoms being line-shaded [65W].

NaSb

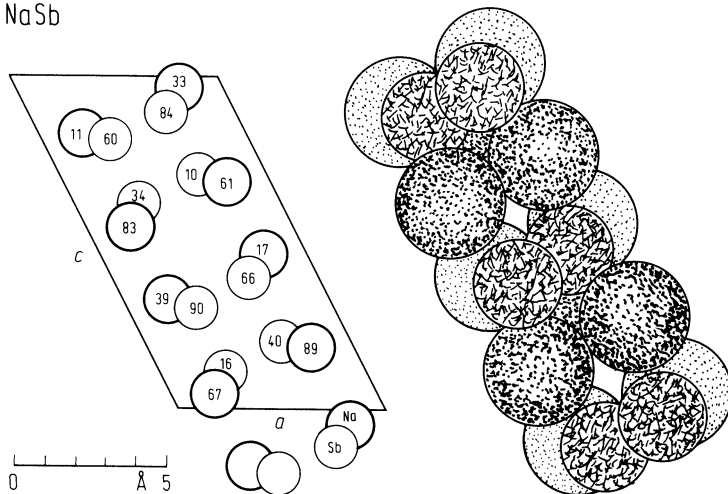
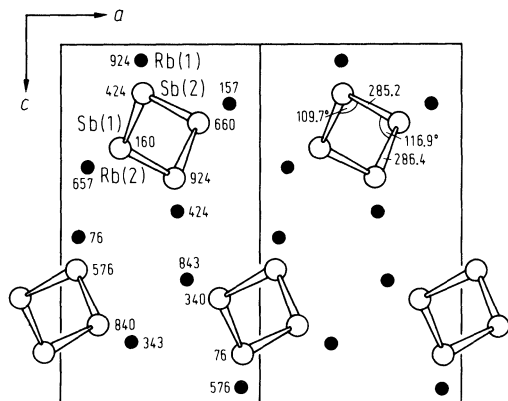


Fig. 15.0.2

The orthorhombic structure of RbSb (left) and CsSb (right) projected along the b axis; the projection of the Sb helices is indicated by open circles; each drawing contains the y -parameters ($\cdot 1000$) in the left part and the Sb–Sb bond lengths (in pm) and -angles in the right part [79S].

RbSb



CsSb

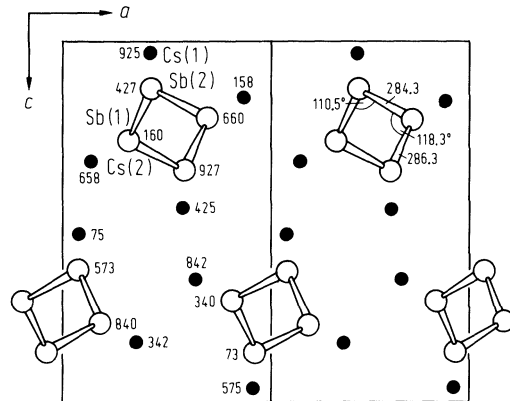


Fig. 15.0.3

The Na_3As structure presented by a projection of the hexagonal unit cell (As atoms are line-shaded) [65W, 68O]. Numbers within the circles in the lower part give the fractional distances in terms of cell axes of atoms above the plane of projection.

Na_3As

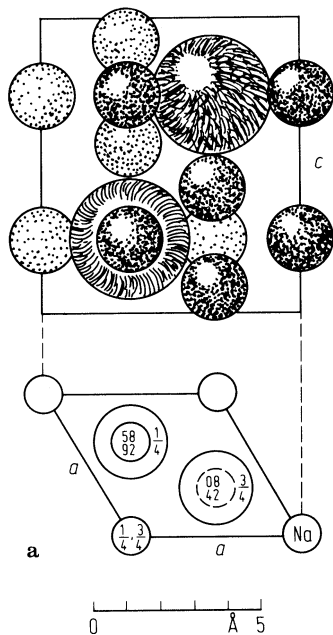


Fig. 15.0.4

The BiF_3 structure; left part: projection on a cube face, the small circles are bismuth atoms, numbers in circles correspond to height of atoms above the plane of projection in terms of cell axes; right part: a packing drawing of half the atoms of BiF_3 in the unit cube [65W].

BiF_3

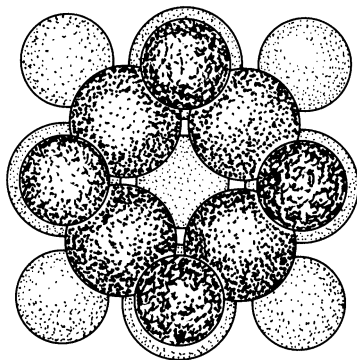
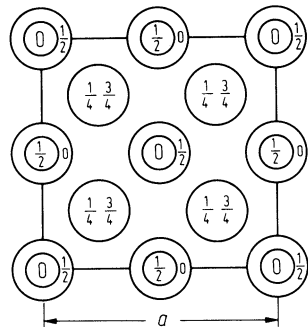


Fig. 15.0.5

The NaTl-structure; both kinds of atoms form a diamond lattice shifted relative to each other by $(1/2, 1/2, 1/2)$.

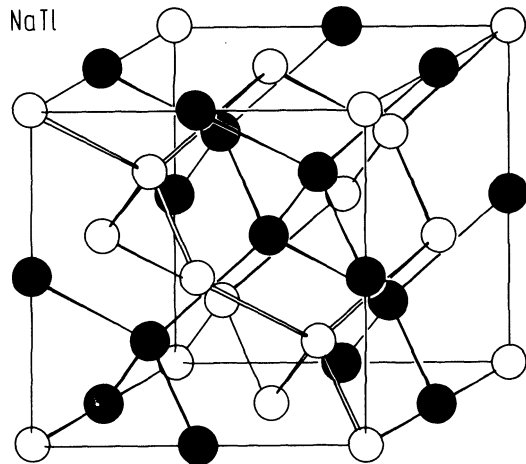


Fig. 15.0.6

K_3Sb . Brillouin zone of cubic K_3Sb .

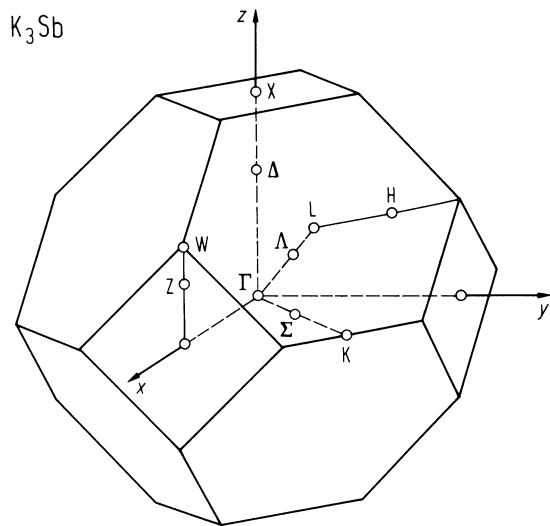


Fig. 15.0.7

K_3Sb . Band structure calculated by an empirical pseudo-potential method. Energy spectrum of a) cubic and b) hexagonal K_3Sb without allowance for spin-orbit interaction [76M].

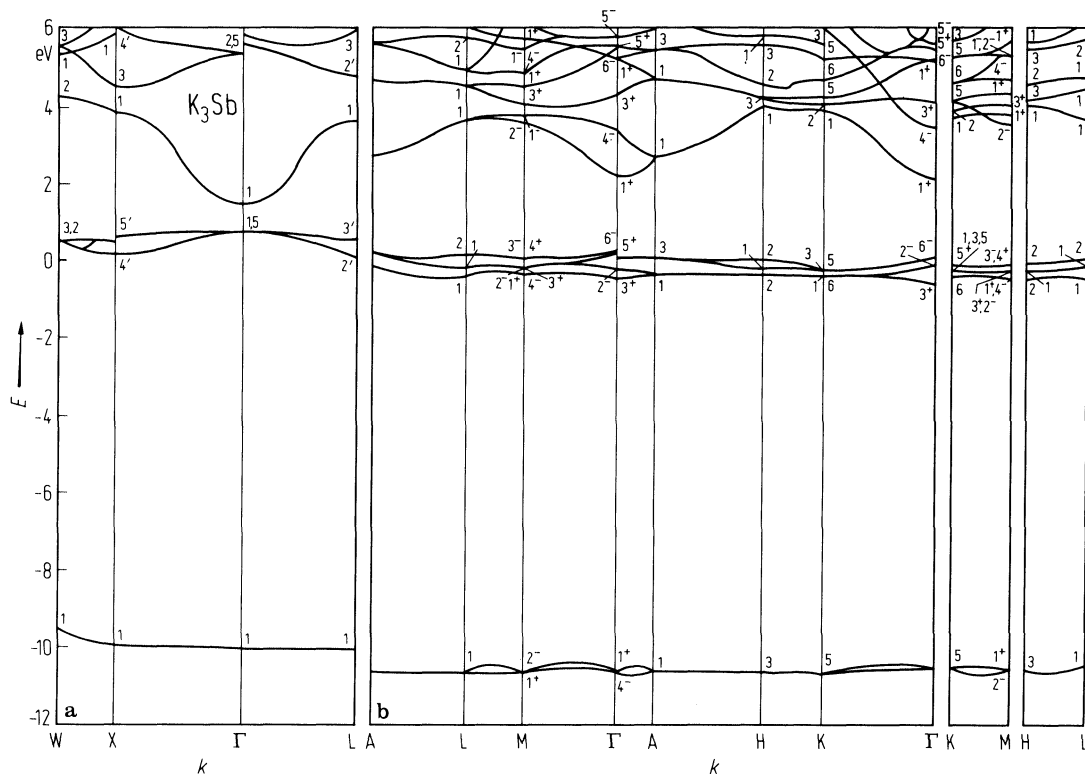


Fig. 15.0.8

Rb_3Sb . Band structure of cubic Rb_3Sb calculated by an empirical pseudo-potential method [74M].

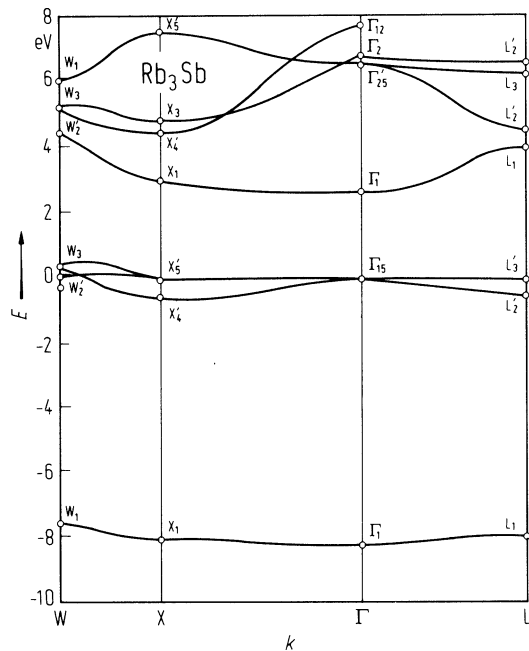


Fig. 15.0.9

Cs_3Sb . Band structure calculated by an empirical pseudo-potential method [74M].

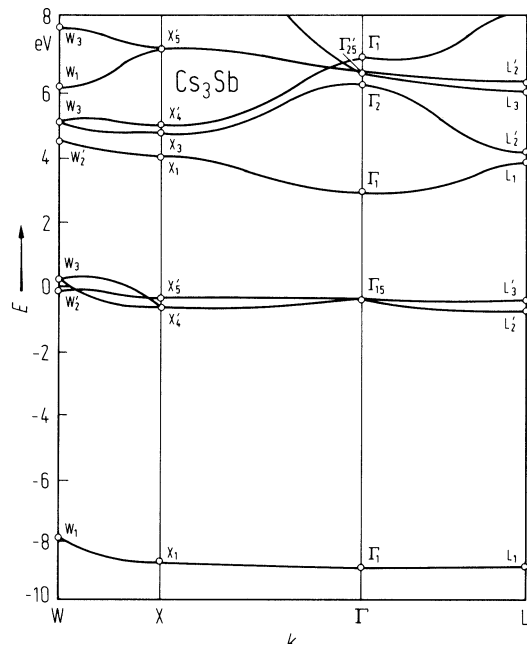


Fig. 15.0.10

Na_2KSb . Band structure calculated by an empirical pseudopotential method [74M].

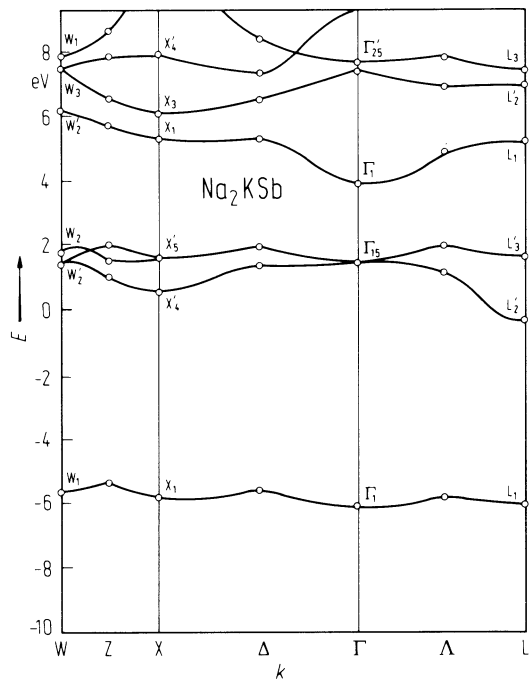
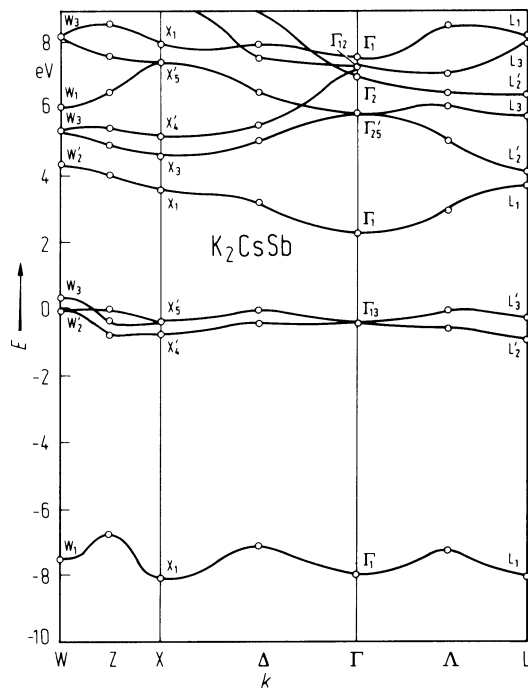


Fig. 15.0.11

K_2CsSb . Band structure calculated by an empirical pseudopotential method [74M].



15.1 I-V compounds (NaSb, KSb, RbSb, CsSb)

Semiconducting behavior of NaSb, KSb and CsSb has been observed by measurements of the electrical conductivity on thin evaporated films. From the temperature dependence of conductivity the following activation energies have been determined: $E_A = 0.82$ eV [60U] for NaSb, 0.88 eV [53S] for KSb, and 0.61 eV [60M] to 0.63 eV [60K] for CsSb.

lattice parameters

NaSb	$a = 6.80 \text{ \AA}$	$b = 6.34 \text{ \AA}$	$c = 12.48 \text{ \AA}$	$\beta = 117.6^\circ$	59C
KSb	7.18 \AA	6.97 \AA	13.40 \AA	115.1°	61B
RbSb	7.315 \AA	7.197 \AA	12.815 \AA		79S
CsSb	7.575 \AA	7.345 \AA	13.273 \AA		79S

melting temperature T_m

NaSb	465°C	60U
KSb	610°C	65E
RbSb	610°C	65E
CsSb	586°C	65E

References to 15.1

- 53S Suhrmann, K., Kangro, Cl.: Naturwissenschaften 49 (1953) 137.
- 59C Cromer, D. T.: Acta Crystallogr. 12 (1959) 41.
- 60K Kunze, C.: Ann. Physik 6 (1960) 89.
- 60M Miyake, K.: J. Appl. Phys. 31 (1960) 76.
- 60U Ugai, Ya. A., Vigutova, T. N.: Fiz. Tverd. Tela 1 (1959) 1786; Sov. Phys. Solid State (English Transl.) 1 (1960) 1635.
- 61B Busmaun, B., Lohmeyer, S.: Z. Anorg. Allg. Chem. 312 (1961) 53.
- 65E Elliot, R. P.: Constitution of Binary Alloys, First Supplement, McGraw Hill, New York 1965.
- 79S Schnering von, H. G., Hönle, W., Krogull, G.: Z. Naturforsch. 34b (1979) 1678.

15.2. I₃-V compounds

15.2.1 Lattice parameters and melting temperatures

lattice parameters (hexagonal modification)

α -Li ₃ Sb	$a = 4.710 \text{ \AA}$	$c = 8.326 \text{ \AA}$	65W
Na ₃ Sb	5.355 \AA	9.496 \AA	65W
K ₃ Sb	6.025 \AA	10.693 \AA	65W, 75D
Rb ₃ Sb	6.29 \AA	11.17 \AA	60Z
Na ₃ Bi	5.448 \AA	9.655 \AA	65W
K ₃ Bi	6.178 \AA	10.933 \AA	65W
Rb ₃ Bi	6.42 \AA	11.46 \AA	60Z

lattice parameters (cubic modification)

β -Li ₃ Sb	$a = 6.572 \text{ \AA}$	65W
K ₃ Sb	8.493 \AA	66S
Rb ₃ Sb	8.84 \AA	61C, 75D
Li ₃ Bi	6.721 \AA	65W
K ₃ Bi	8.805 \AA	65S
Rb ₃ Bi	8.98 \AA	61G
Cs ₃ Bi	9.31 \AA	61G

lattice parameter (Cs₃Sb structure)

Cs ₃ Sb	$a = 9.128 \text{ \AA}$	65W
Rb ₃ Sb	8.84 \AA	65W
Cs ₃ Bi	9.305 \AA	65W

melting temperature T_m

Li ₃ Sb	1150...1300°C	58H
Li ₃ Bi	1145°C	58H
Na ₃ Sb	859°C	69S
K ₃ Sb	812°C	65E
Cs ₃ Sb	725°C	65E
Rb ₃ Sb	733°C	65E
Rb ₃ Bi	642°C	65E
Cs ₃ Bi	635°C	65E

15.2.2 Li₃Sb, Li₃Bi

Measurements of the electrical conductivity (Figs. 15.2.1, 15.2.2) have been performed on thin evaporated films [66G, 67G]. These results show a strong dependence on small amounts of Na and K impurities which may enter the film during sample preparation [68S].

From the temperature dependence of conductivity the following values of the activation energies of the intrinsic compounds have been obtained: $E_A \approx 1.0 \text{ eV}$ [66G] for Li₃Sb, 0.7 eV [67G] for Li₃Bi.

At elevated temperatures a relatively high partial ionic conductivity of Li ions is reported [77W]: $\approx 10^{-3} \text{ } \Omega^{-1} \text{ cm}^{-1}$ at 360°C for Li₃Sb, $\approx 10^{-1} \text{ } \Omega^{-1} \text{ cm}^{-1}$ at 380°C for Li₃Bi.

5.2.3 Na3Sb

band structure

The band structure of hexagonal Na3Sb has been calculated by an empirical pseudopotential method on the basis of effective atomic potentials of the Heine-Abarenkov type [74M, 76M]. The calculated width of the lower conduction band is of order 2 eV, the bottom being at point Γ of the Brillouin zone. The calculated direct gap energy is $E_g(\Gamma_{2v}^- - \Gamma_{1c}^+) = 1.15$ eV [76M]. The valence band consists of two narrow subbands, below 1 eV wide, and separated by a significant energy gap.

energy gap

E_g	1.1 eV	$T = 300$ K		58S
-------	--------	-------------	--	-----

Measurements of the **thermoelectric power** indicate n-type conduction [59I, 68S].

refractive index and absorption index : see Fig. 15.2.3.

5.2.4 K3Sb

band structure

see Fig. 15.0.7, Brillouin zone: Fig. 15.0.6 (cubic K3Sb).

For both cubic and hexagonal K3Sb the band structure has been calculated by an empirical pseudopotential method on the basis of model potentials of the Heine-Abarenkov type [74M, 76M]. The nonlocal nature of the potassium potential and the effect of spin-orbit interaction of antimony have been taken into account [76M].

The lowest set of conduction bands has minima at the Γ -point of the Brillouin zone. In the cubic structure the lowest conduction band is separated by a forbidden energy band from the higher conduction bands. A direct energy gap is calculated of $E_g(\Gamma_{15v} - \Gamma_{1c}) = 1.44$ eV for cubic K3Sb, and $E_g(\Gamma_{6v}^- - \Gamma_{1c}^+) = 2.06$ eV for hexagonal K3Sb[76M].

The valence band consists of two subbands which show relatively weak dispersion and which are separated by a significant energy gap. The effect of spin-orbit interaction of order 1 eV mainly leads to a splitting of the upper valence band and the higher conduction bands, see Fig. 15.0.7.

energy gap

E_g	1.1 eV	$T = 300$ K,	spectral response of photo-	58S
		hexagonal	conductivity	
	1.4 eV	cubic	optical absorption	68S

electrical conductivity: Fig. 15.2.4.

Measurements of absolute thermoelectric power and of doping dependence of conductivity indicate n-type conduction for hexagonal K3Sb, whereas cubic K3Sb should be a p-type conductor [68S].

From the temperature dependence of conductivity the activation energy of the intrinsic compound is given as $E_A = 0.75$ eV [78G] to 0.79 eV [53S], yet without specification of the structure of the samples in these experiments.

Extinction coefficient k and index of refraction n : Fig. 15.2.5.

15.2.5 Rb3Sb

band structure

The energy spectrum of Fig. 15.0.8 has been calculated for an ordered cubic structure with the symmetry of O_h^5 ; spin-orbit interaction, however, has not been taken into account [74M].

energy gap

E_g	1.0 eV	$T = 300$ K	spectral response of photo-	68S
			conductivity	

optical absorption spectrum: Fig. 15.2.6.

Both n- and p-type transport behavior may occur depending on structure [68S]. From conductivity measurements on thin films in the temperature range from -162°C to $+60^{\circ}\text{C}$ an activation energy of about 0.4 eV is reported [56H].

15.2.6 Cs_3Sb

band structure: Fig. 15.0.9.

The energy spectrum of Fig. 15.0.9 has been calculated for an ordered cubic structure with the symmetry of O_h^5 without including spin-orbit interaction. The top of the valence band is expected at the W_3 level.

energy gap

E_g	1.6 eV	$T = 300 \text{ K}$	56W, 58S, 68S
-------	--------	---------------------	---------------

electrical conductivity : Fig. 15.2.7.

From the reported results the activation energy of conductivity varies from less than 0.4 eV at lower temperatures up to 1.2 eV around 300 K.

hole mobility

μ_p	$10 \text{ cm}^2/\text{Vs}$	$T = 300 \text{ K}$	Hall mobility	54S
---------	-----------------------------	---------------------	---------------	-----

15.2.7 Rb_3Bi , Cs_3Bi

Only a few papers have been published on the electronic properties of these compounds. Indication for semi-conductivity of both Rb_3Bi and Cs_3Bi has been obtained by measurements of the temperature dependence of the electrical conductivity which yield an activation energy of 0.04 to 0.4 eV for both compounds [56H].

energy gap (Cs_3Bi)

E_g	$\leq 0.7 \text{ eV}$	$T = 300 \text{ K}$	estimated from optical absorption	61S
-------	-----------------------	---------------------	-----------------------------------	-----

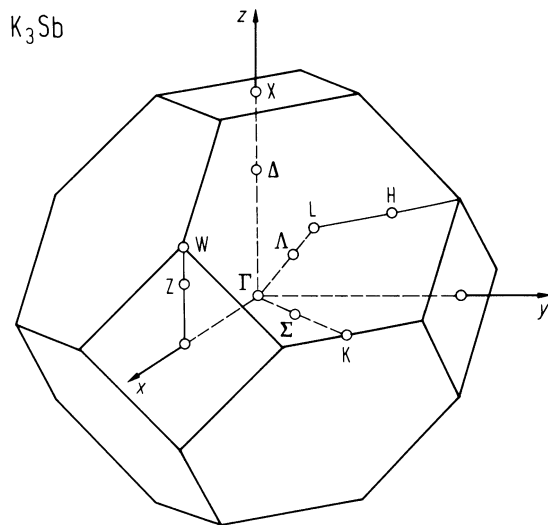
References to 15.2

- 53S Suhrmann, K., Kangro, Cl.: *Naturwissenschaften* 49 (1953) 137.
- 54S Sakata, T.: *J. Phys. Soc. Jpn.* 9 (1954) 1030.
- 56H Harper, W. J., Choyke, W. J.: *J. Appl. Phys.* 27 (1956) 1358.
- 56W Wallis, G.: *Ann. Physik* 17 (1956) 401.
- 58S Spicer, W. E.: *Phys. Rev.* 112 (1958) 114.
- 59I Imamura, S.: *J. Phys. Soc. Jpn.* 14 (1959) 1491.
- 60Z Zhuravlev, N. N., Smirnov, V. A., Mingazin, T. A.: *Kristallografiya* 5 (1960) 134; *Sov. Phys. Crystallogr. (English Transl.)* 5 (1960) 124.
- 61C Chikawa, J., Imamura, S., Tanaka, K., Shimoji, M.: *J. Phys. Soc. Jpn.* 16 (1961) 1175.
- 61G Gnatzmann, G., Dorn, F. W., Klemm, W.: *Z. Anorg. Ang. Chem.* 309 (1961) 210.
- 61S Sommer, A. H., Spicer, W. E.: *J. Appl. Phys.* 32 (1961) 1036.
- 65S Suchet, J. P.: *Chemical Physics of Semiconductors*, D. van Nostrand Comp., London 1965.
- 65W Wyckoff, R. W. G.: *Crystal Structures*, Vol. 1 and 2, 2nd. Ed., Interscience Publishers, New York 1965.
- 66G Gobrecht, R.: *Phys. Status Solidi* 13 (1966) 429.
- 66S Sommer, A. H., McCarroll, W. H.: *J. Appl. Phys.* 37 (1966) 174.
- 67G Gobrecht, R.: *Ann. Physik* 20 (1967) 262.
- 68S Sommer, A. H.: *Photoemissive Materials*, John Wiley, New York 1968.
- 73E Ebina, A., Takahashi, T.: *Phys. Rev. B* 7 (1973) 4712.
- 74M Mostovskii, A. A., Chaldyshev, V. A., Karavaev, C. F., Klimin, A. I., Ponomarenko, I. N.: *Izv. Akad. Nauk SSSR, Ser. Fiz.* 38 (1974) 195; *Bull. Acad. Sc. USSR, Phys. Ser. (English Transl.)* 38 (1974) 10.
- 75D Dowman, A. A., Jones, F. H., Beck, A. H.: *J. Phys. D* 8 (1975) 69.
- 76M Mostovskii, A. A., Chaldyshev, V. A., Kiselev, V. P., Klimin, A. I.: *Izv. Akad. Nauk SSSR, Ser. Fiz.* 40 (1976) 2490; *Bull. Acad. Sc. USSR, Phys. Ser. (English Transl.)* 40 (1976) 36.
- 77W Wepper, W., Huggins, R. A.: *J. Solid State Chem.* 22 (1977) 297.
- 78G Ghosh, C., Varma, B. P.: *J. Appl. Phys.* 49 (1978) 4549.

Figures to 15.2

Fig. 15.0.6

K_3Sb . Brillouin zone of cubic K_3Sb .



K₃Sb. Band structure calculated by an empirical pseudo-potential method. Energy spectrum of a) cubic and b) hexagonal K₃Sb without allowance for spin-orbit interaction [76M].

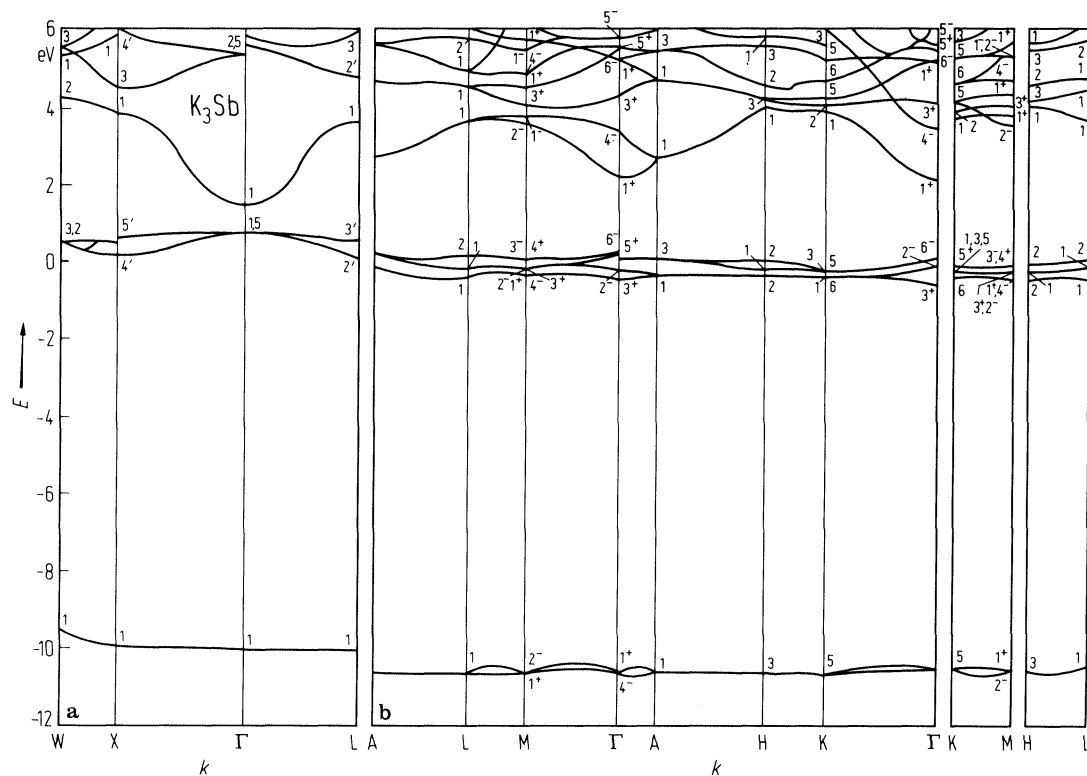


Fig. 15.0.8

Rb_3Sb . Band structure of cubic Rb_3Sb calculated by an empirical pseudo-potential method [74M].

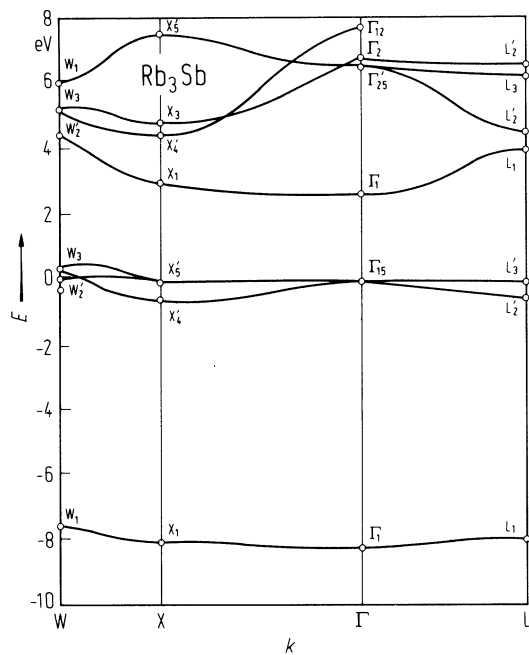


Fig. 15.0.9

Cs_3Sb . Band structure calculated by an empirical pseudo-potential method [74M].

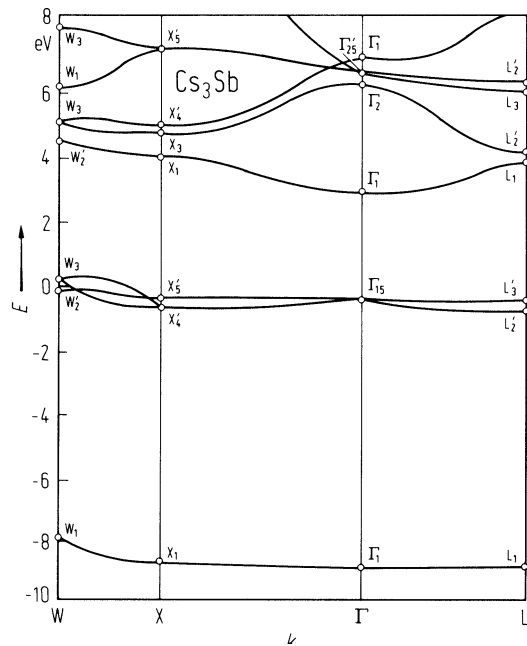


Fig. 15.2.1

Li_3Sb . Reciprocal electrical resistance $1/R$ vs. temperature: 1, sample with Na impurities; 2, pure Li_3Sb [66G].

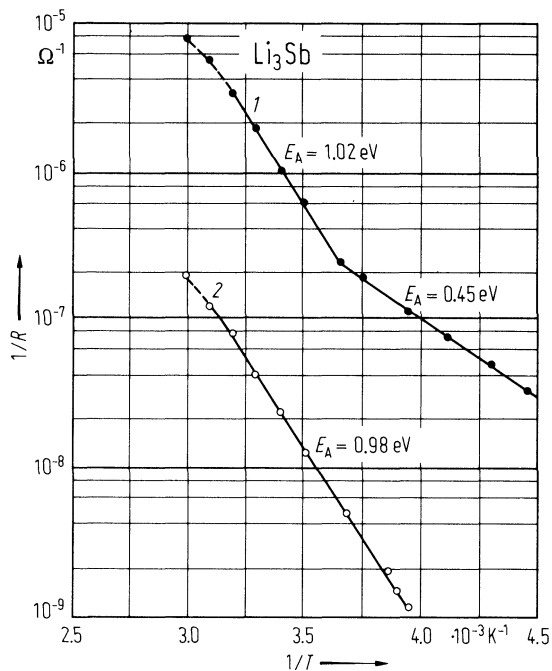


Fig. 15.2.2

Li_3Bi . Reciprocal electrical resistance $1/R$ vs. temperature: 1, sample with Na impurities; 2, without Na impurities [67G].

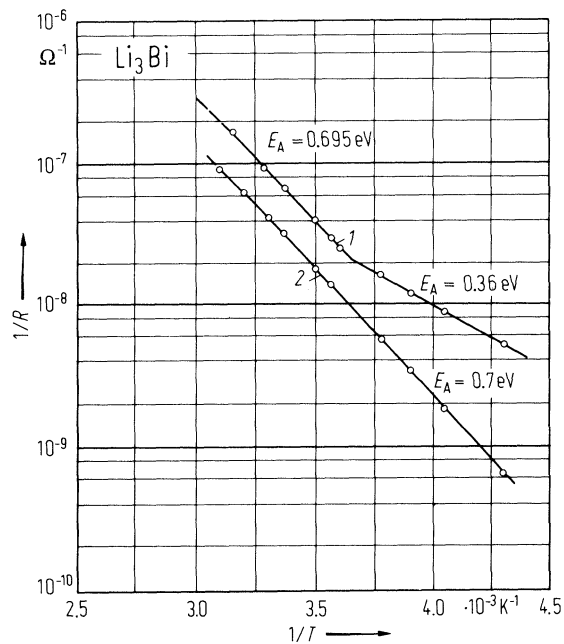


Fig. 15.2.3

Na_3Sb and Na_2KSb . Index of refraction n and extinction coefficient k vs. photon energy at 300 K [73E].

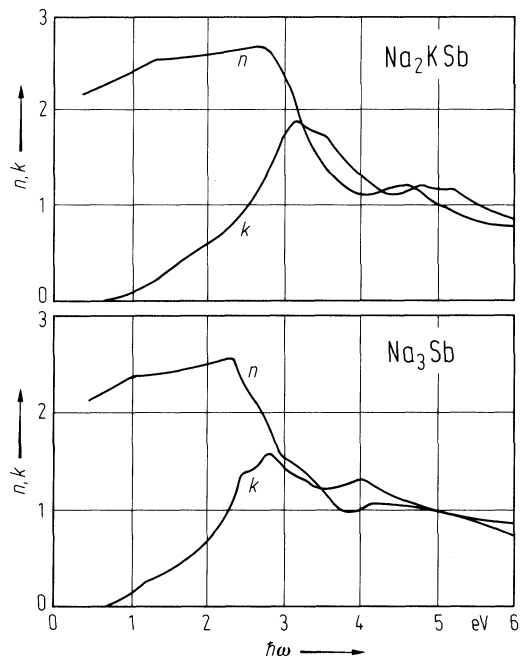


Fig. 15.2.4

Na_2KSb , $\text{Na}_2\text{KSb}(\text{Cs})$, K_2CsSb and K_3Sb . Electrical conductivity vs. temperature; conductivity values are not absolute as the curves are displaced vertically for sake of convenience. Activation energies are indicated [78G].

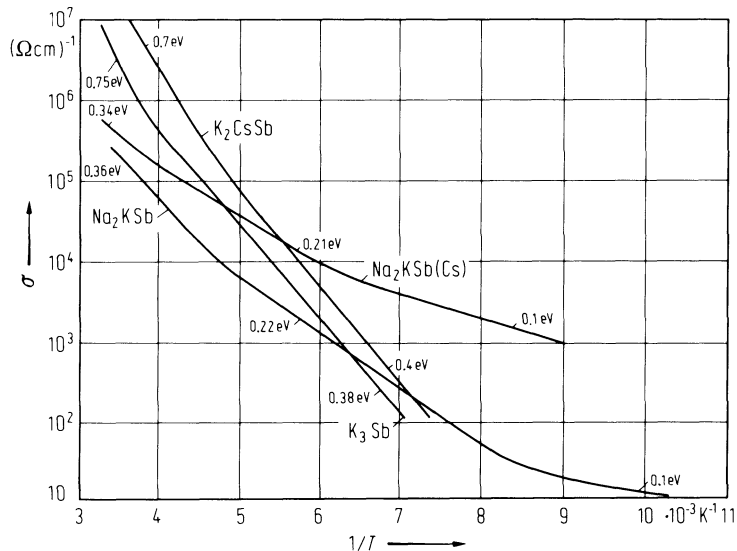


Fig. 15.2.5

K_3Sb . Extinction coefficient k and index of refraction n vs. photon energy at 300 K of a) cubic and b) hexagonal K_3Sb [73E].

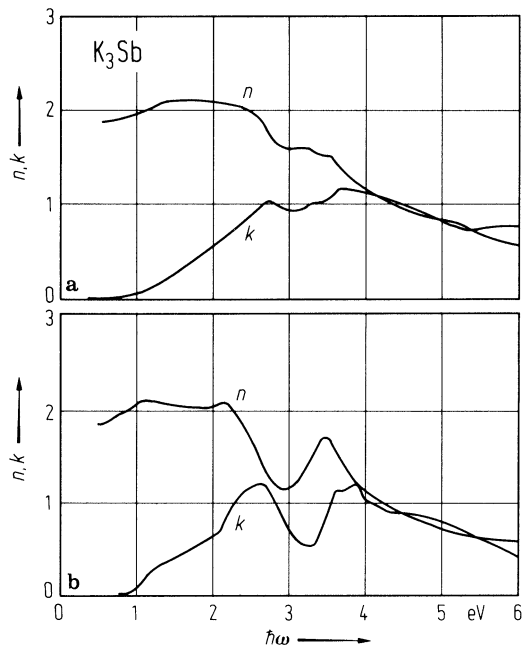


Fig. 15.2.6

Rb₃Sb. Optical absorption (arb. units) vs. photon energy at 300 K [68S].

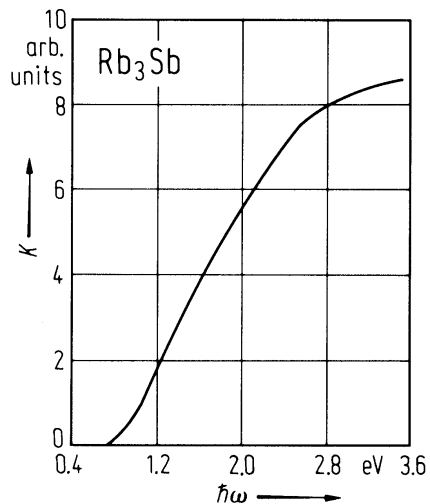
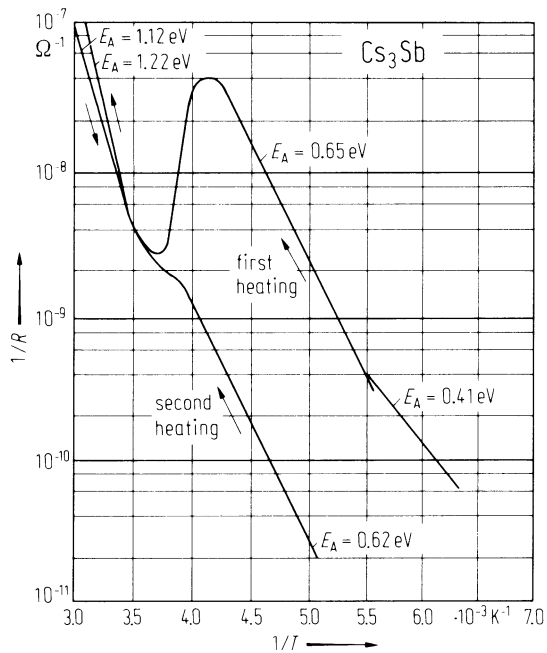


Fig. 15.2.7

Cs_3Sb . Reciprocal resistance vs. reciprocal temperature [56W].



15.3 I₂-I-V compounds

Among the bialkali-antimony compounds detailed structure determinations have been reported for Na₂KSb and K₂CsSb which are isostructural to the BiF₃ type.

15.3.1 Na₂KSb

band structure: 15.0.10.

energy gap

E_g	1.0 eV	$T = 300$ K	spectral response of photoconductivity and optical absorption	58S
-------	--------	-------------	---	-----

electrical conductivity: Fig. 15.3.14

mobility of charge carriers

μ_p	2.6...4.8 cm ² /Vs	$T = 300$ K	Hall mobility	70H
---------	-------------------------------	-------------	---------------	-----

extrinsic carrier concentration

n	5...10·10 ¹⁷ cm ⁻³	$T = 300$ K	from conductivity and Hall coefficient	70H
-----	--	-------------	--	-----

optical properties

Imaginary part of dielectric constant: Fig. 15.3.2. Extinction coefficient k and index of refraction n : Fig. 15.3.3.

15.3.2 K₂CsSb

band structure: Fig. 15.0.11.

energy gap

E_g	1.0 eV		spectral response of photoconductivity and optical absorption	67N
-------	--------	--	---	-----

According to [68S] p-type conduction is suggested. An extremely high resistance in comparison to all other alkali antimonides has been observed for K₂CsSb at room temperature [68S].

15.3.3 Na₂RbSb, Na₂CsSb, K₂RbSb, Rb₂CsSb

According to [76D] the following energy gaps E_g and electron affinities χ are reported:

Na ₂ RbSb:	$E_g = 1.0$ eV and $\chi = 0.8$ eV
Na ₂ CsSb:	$E_g = 0.8$ eV and $\chi = 0.7$ eV
K ₂ RbSb:	$E_g = 1.2$ eV and $\chi = 0.8$ eV
Rb ₂ CsSb:	$E_g = 1.5$ eV and $\chi = 0.2$ eV.

A detailed experimental determination of the stoichiometry of the investigated compounds has not been reported in [76D].

References to 15.3

- 58S Spicer, W. E.: Phys. Rev. 112 (1958) 114.
- 67N Nathan, R., Mee, C. H. B.: Int. J. Electron. 23 (1967) 349.
- 68S Sommer, A. H.: Photoemissive Materials, John Wiley, New York 1968.
- 70H Hofmann, H. H., Deutscher, K., Scharmann, A.: Z. Phys. 236 (1970) 298.
- 73E Ebina, A., Takahashi, T.: Phys. Rev. B 7 (1973) 4712.
- 74M Mostovskii, A. A., Chaldyshev, V. A., Karavaev, C. F., Klimin, A. I., Ponomarenko, I. N.: Izv. Akad. Nauk SSSR, Ser. Fiz. 38 (1974) 195; Bull. Acad. Sci. USSR, Phys. Ser. (English Transl.) 38 (1974) 10.
- 76D Denisov, V. P., Klimin, A. I.: Izv. Akad. Nauk SSSR, Ser. Fiz. 40 (1976) 2502; Bull. Acad. Sci. USSR, Phys. Ser. (English Transl.) 40 (1976) 46.
- 78G Ghosh, C., Varma, B. P.: J. Appl. Phys. 49 (1978) 4549.

Figures to 15.3

Fig. 15.0.10

Na₂KSb. Band structure calculated by an empirical pseudopotential method [74M].

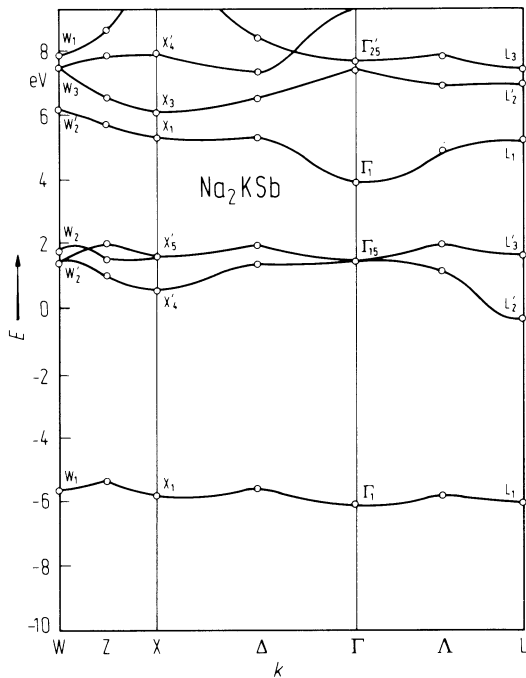


Fig. 15.0.11

K_2CsSb . Band structure calculated by an empirical pseudopotential method [74M].

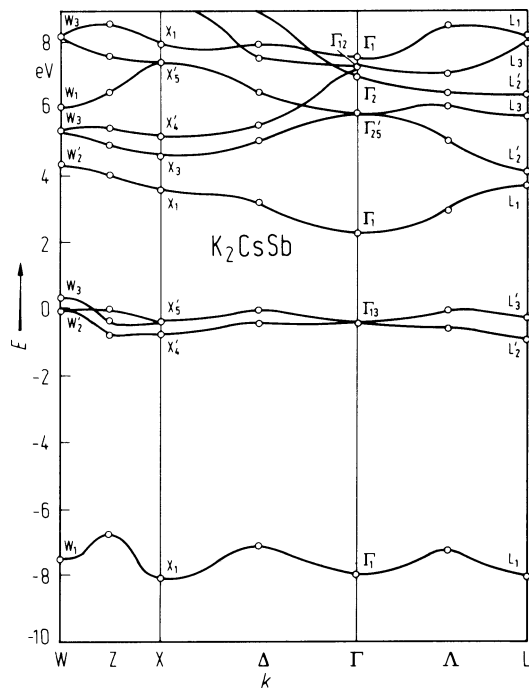


Fig. 15.3.1

Na_2KSb , $\text{Na}_2\text{KSb}(\text{Cs})$, K_2CsSb and K_3Sb . Electrical conductivity vs. temperature; conductivity values are not absolute as the curves are displaced vertically for sake of convenience. Activation energies are indicated [78G].

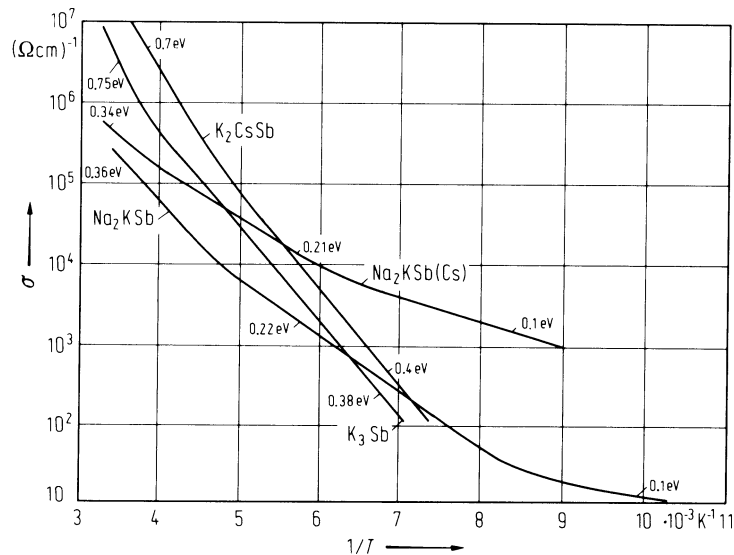


Fig. 15.3.2

Na_3Sb and Na_2KSb . Imaginary part of dielectric constant vs. photon energy at 300 K [73E].

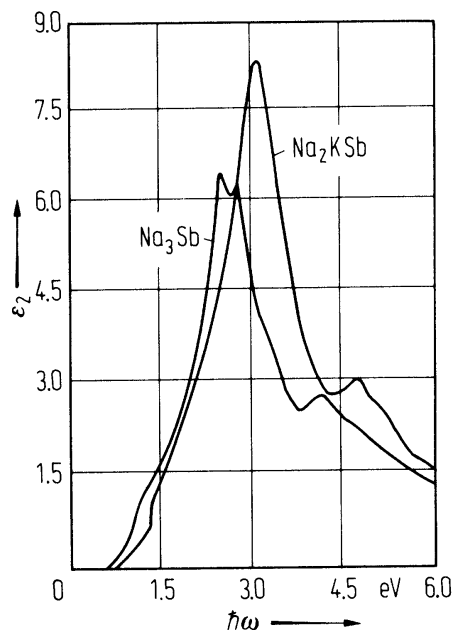
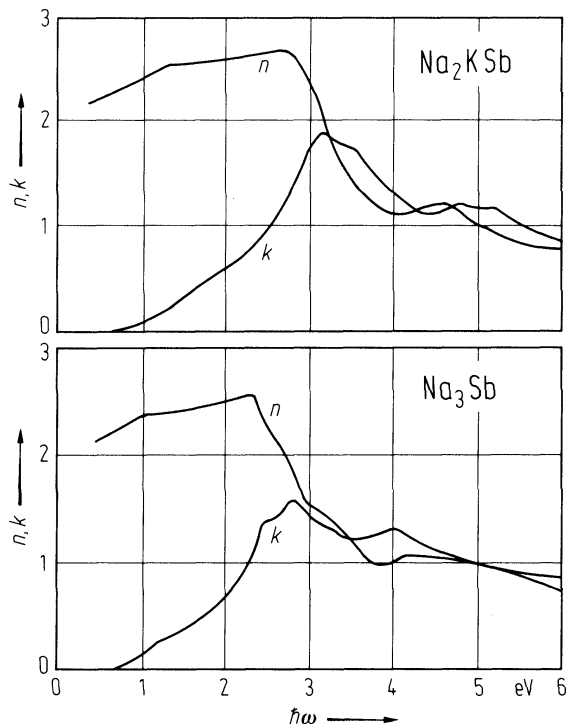


Fig. 15.3.3

Na_3Sb and Na_2KSb . Index of refraction n and extinction coefficient k vs. photon energy at 300 K [73E].



16 I_x-VI_y compounds

16.0 Crystal structure and electronic structure

Among the I_x-VI_y compounds the oxides, sulfides, selenides and tellurides of copper and silver are of interest in semiconductor physics.

16.0.1 Copper compounds

The structure of **CuO**, the natural tenorite mineral, is monoclinic; the tetramolecular cell has following parameters:

a [Å]	b [Å]	c [Å]	β [°]	
4.6927(4)	3.4283(4)	5.1370(6)	99.546(9)	91A

The space group C_{2h}⁶-C2/c has been ascribed to the structure of the tenorite. Each copper is coordinated to four coplanar oxygens at the corners of a parallelogram. The oxygen is coordinated to four coppers at the corners of a distorted tetrahedron. The six nearest oxygens to each copper complete a strongly distorted octahedron. The CuO₄ parallelograms form ribbons along [110] direction and alternating in [010] direction. Each ribbon is linked to adjacent chains of other groups by sharing corners (Fig. 16.0.1).

Cu₂O has a cubic structure, the cuprite (natural Cu₂O mineral) type, of space group T_h²-Pn3 [65W] or O_h⁴-Pn3m [72P] with following unit cell parameters: $a = 4.27$ Å at $p \approx 0$ GPa [82W2]. Copper has two O neighbors, and the site symmetry is D_{3d}. Oxygen has four Cu neighbors, and the site symmetry is T_d. The lattice can be considered as two ice-type structures linked by Cu-Cu bonds (Fig. 16.0.2). Band structure of Cu₂O: Fig. 16.0.5.

Cu₂S occurs in several stoichiometric and nonstoichiometric (Cu_{2-x}S) modifications:

Orthorhombic chalcocite (= low temperature chalcocite or γ -Cu₂S): space group: C_{2v}¹⁵-Ab2m. The unit cell contains 96 Cu₂S formula units. Lattice parameters $a = 11.885$ Å, $b = 27.325$ Å, $c = 13.496$ Å [87G]

Hexagonal chalcocite : β -Cu₂S is stable between 103.5°C and 435°C. The structure is hexagonal with the S atoms arranged in a nearly perfect close-packing and the Cu atoms distributed in the interstices in an almost fluid-like way [87G]. Space group: D_{6h}⁴-P6₃/mmc. The unit cell contains 4 Cu₂S molecules. The lattice parameters are: $a = 4.005$ Å and $c = 6.806$ Å according to [85P].

Digenite : The region of the copper sulfide system where the mineral digenite occurs, $1.74 < x < 1.95$, exhibits an intricate manifold of phases. There are only two discrete equilibrium forms of digenite, corresponding to compositions $x = 1.89$ and $x = 1.84$. A sequence of superlattice ordering transitions is reported in digenite-type crystals [86G]. *Low temperature digenite* is observed for $T < 80^\circ\text{C}$ and $1.765 < x < 1.79$; space group is O_h⁷-Fd3m. The cubic unit cell with an edge of $a = 27.71$ Å corresponds to a superstructure of an elementary cubic cell with $a' = 5.54$ Å edge length. That phase seems to be unstable when pure and needs to be stabilized by Fe in the natural mineral digenite [74G]. *High temperature digenite* is observed for $T > 80^\circ\text{C}$ and has the space group O_h⁵ - Fm3m. The unit cell corresponds to an edge length of $a = 5.57$ Å ($\approx a'$ of digenite LT). Cu atoms are distributed statistically; the range of existence is $1.73 < x < 1.84$, somewhat broader than for LT digenite [74G].

Djurleite corresponds to $1.935 < x < 1.955$. The orthorhombic (or pseudo-orthorhombic) cell contains 128 Cu₂S formula units and parameters are: $a = 26.92$ Å, $b = 15.71$ Å, $c = 13.56$ Å [74G].

Djurleite (Cu_{1.938}S) was also found to be monoclinic with space group P2₁/n and the following unit cell parameters: $a = 26.90$ Å, $b = 15.75$ Å, $c = 13.57$ Å, $\beta = 90^\circ 13'$ [82S]. The monoclinic cell contains also 248 Cu and 128 S.

Cu₂Se has been classified in the cubic system with space group O_h⁵-Fm3m in which four selenium ions occupy the 4(a) sites. Seven copper ions are statistically distributed over the 32(f)_I sites of this space group and the remaining copper ion is distributed over the 32(f)_{II} sites [89S, 93S]. An $\alpha - \beta$ phase transition occurs at $T = 408$ K.

Cu₂Te undergoes four polymorphic transitions at 180°C, 305°C and 460...555°C. For the room temperature form a hexagonal structure has been suggested with cell parameters $a = 4.17$ Å, $c = 21.71$ Å [94E].

16.0.2 Silver compounds

The properties of the *silver oxides* are comparable to those of the copper oxides, at least for the monovalent compounds. Several oxides are known, Ag_2O and AgO , but also Ag_2O_3 or Ag_7O_{11} and Ag_4O_3 .

AgO : Monoclinic AgO has the following unit cell parameters: $a = 5.85 \text{ \AA}$, $b = 3.47 \text{ \AA}$, $c = 5.49 \text{ \AA}$, $\beta = 107.5^\circ$, and a space group $\text{C}_{2h}^5\text{-P2}_1/\text{c}$. This structure consists of a deformed face centered cubic metal atom arrangement with equal proportions of linearly coordinated Ag (I) and approximately square planar coordinated Ag (III) atoms, see Fig. 16.0.3 [86Y]. Tetragonal AgO has the following unit cell parameters: $a = 6.833(3) \text{ \AA}$, $c = 9.122(4) \text{ \AA}$, and a space group $\text{I4}_1/\text{a}$ [83H]. Tetragonal silver oxide shows structural features similar to those of monoclinic AgO. Its metal atom arrangement forms a distorted face-centered cubic substructure which contains two non equivalent Ag sites in equal proportion.

Ag₂O has the cuprite cubic structure, whose space group is $\text{T}_h^2\text{-Pn}3$, with $a = 4.72 \text{ \AA}$ at 26°C or space group $\text{O}_h^4\text{-Pn}3\text{m}$ with $a = 4.736 \text{ \AA}$ at room temperature [82W].

The *silver sulfides, selenides and tellurides* crystallize in several modifications:

$\alpha\text{-Ag}_2\text{S}$. The natural mineral acanthite is monoclinic with a tetramolecular unit with: $a = 4.23 \text{ \AA}$, $b = 6.91 \text{ \AA}$, $c = 7.87 \text{ \AA}$, $\beta = 99^\circ 35'$. Space group: $\text{C}_{2h}^5\text{-P2}_1/\text{n}$ [35R, 57F, 73G]:

Tetragonal Ag₂S has been observed in a narrow temperature range, between the α and β phases, at 170°C to 180°C . The tetragonal cell has $a = b = 6.90 \text{ \AA}$, $c = 4.77 \text{ \AA}$.

$\beta\text{-Ag}_2\text{S}$ the natural mineral argentite is stable for $T > 180^\circ\text{C}$, and corresponds again to a bcc sulfur lattice with $a = 4.88 \text{ \AA}$, but Ag ions are distributed statistically.

$\gamma\text{-Ag}_2\text{S}$, the high-temperature phase with a fcc sulfur lattice is also cubic with $a = 6.209 \text{ \AA}$ at 600°C .

$\alpha\text{-Ag}_2\text{Se}$. The structural data are contradictory. The anionic lattice has been described as nearly fcc. An earlier determination yields a tetragonal face-centered cell, with $a = b = 7.06 \text{ \AA}$, $c = 4.98 \text{ \AA}$ [59J]. Other authors consider an orthorhombic cell (space group $\text{D}_2^4\text{-P2}_12_12_1$), with $a = 4.333 \text{ \AA}$, $b = 7.062 \text{ \AA}$ and $c = 7.764 \text{ \AA}$ [73G].

$\beta\text{-Ag}_2\text{Se}$. The high temperature phase has the structure of the Cu_2O -type, with a bcc anionic lattice, and $a = 4.99 \text{ \AA}$ at 170°C . The cations are distributed on the 4e, h and g sites [59J]. The space group then is $\text{O}_h^9\text{-Im}3\text{m}$.

$\alpha\text{-Ag}_2\text{Te}$. $\alpha\text{-Ag}_2\text{Te}$ has been described as rhombic or monoclinic but with a space group $\text{C}_{2h}^5\text{-P2}_1/\text{c}$. It has also been described as monoclinic with the space group $\text{P2}_1/\text{n}$ with the following parameters: $a = 8.15 \text{ \AA}$, $b = 4.47 \text{ \AA}$, $c = 8.09 \text{ \AA}$, $\beta = 112^\circ 40'$ [87M].

$\beta\text{-Ag}_2\text{Te}$. $\beta\text{-Ag}_2\text{Te}$ has an fcc Te lattice, and the Ag ions are distributed statistically. It was reported to be fcc, with lattice spacing $a = 6.572 \text{ \AA}$ at 250°C or with an average fcc structure and $a \approx 6.6 \text{ \AA}$ [87M]. See Fig. 16.0.4.

$\gamma\text{-Ag}_2\text{Te}$. $\gamma\text{-Ag}_2\text{Te}$ has a bcc Te lattice, the Ag ions are distributed statistically and $a = 5.29 \text{ \AA}$ [61F].

16.0.3 Electronic structure

Only one band structure calculation on $\text{I}_x\text{-VI}_y$ compounds has been published. Fig. 16.0.5 shows the band structure of Cu_2O .

References to 16.0

- 35R Rahlfs, P.: Z. Phys. Chem. Abt. B31 (1935) 157.
57F Frueh, A. J.: Acta Crystallog. 10 (1957) 764.
59J Junod, P.: Helv. Phys. Acta 32 (1959) 567 and 601.
61F Frueh, A. J.: Am. Mineral. 46 (1961) 654.
65W Wyckoff, R. W. G.: Crystal Structures, Vol. 1, 2nd Edition, J. Wiley, New York 1965.
72P Povarennykh, A. S.: Crystal Chem. Classification of Minerals, Vol. 1, Plenum Press, New York 1972.
73G Gmelin's Handbuch der anorganischen Chemie, Verlag Chemie GmbH Weinheim. Bergstrasse, 5nd Edition. Silber, Teil B3, 1973.
74G Guastavino, F.: These d'Etat Montpellier 1974.
80K Kleinman, L., Mednick, K.: Phys. Rev. B 21 (1980) 1549.
82S Sands, T. D., Washburn, J., Gronsky, R.: Phys. Status Solidi (a) 72 (1982) 551.
82W Werner, A., Hochheimer, H. D.: Phys. Rev. B25 (1982) 5929.
83H Hahn, T. (ed.), International Tables for Crystallography A, Reidel, Dordrecht, 1983.
85P Pakeva, S., Germanova, K.: J. Phys. D: Appl. Phys. 18 (1985) 1371.
86G Gray, J. N., Clarke, R.: Phys. Rev. B 33 (1986) 2056.
86Y Yvon, K., Bezing, A., Tissot, P., Fischer, P.: J. Solid State Chem. 65 (1986) 225.
87G Gronvold, F., Westrum, E. F. Jr.: J. Chem. Thermodyn. 19 (1987) 1183.
87M Manolikas, C.: J. Solid State Chem. 66 (1987) 1.
89S Sakuma, T., Sugiyama, K., Matsubara, E., Waseda, Y.: Mater. Trans. JIM 30 (1989) 365.
91A Asbrink, S., Waskowska, A.: J. Phys. Condens. Matter 3 (1991) 8173.
92G Gmelin, E.: Indian J. Pure Appl. Phys. 30 (1992) 596.
93S Sakuma, T., Suzuki, F., Saitoh, S., Sugiyama, K., Matsubara, E., Waseda, Y.: J. Phys. Soc. Jpn. 62 (1993) 3513.
94E El-Bahrawi, M. S., Khodier, S., Kishk, S. S., Nagib, N. N.: Appl. Phys. A 58 (1994) 601.

Figures to 16.0

Fig. 16.0.1

CuO. Tenorite structure. Perspective view showing 4 unit cells. Spheres represent oxygen, ellipsoids are coppers. The numbers refer to different copper ions [92G].

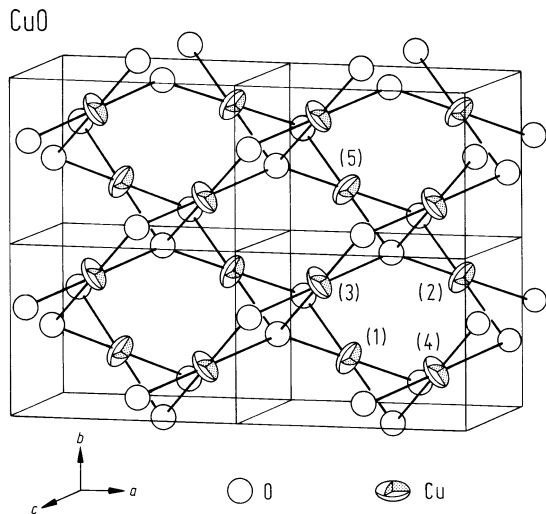


Fig. 16.0.2

Cu_2O . Cuprite structure. a) origin on an O site; b) origin on a Cu site.

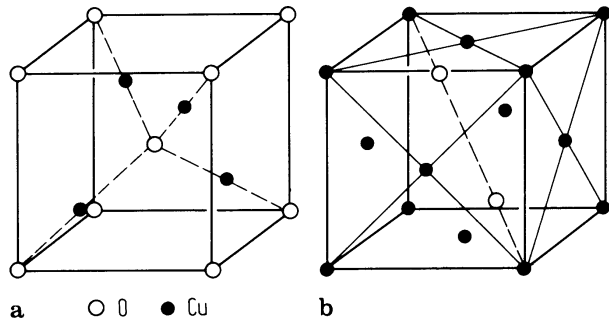


Fig. 16.0.3

AgO. Structure segment of monoclinic AgO (a) viewed approximately down the twofold axis, compared to that in tetragonal AgO (b) viewed approximately perpendicular to the fourfold axis [86Y]. Unit cells indicated by solid lines. Heavy full lines: metal-oxygen bonds. Open arrows indicate directions of third-nearest metal neighbors which differ in both structures.

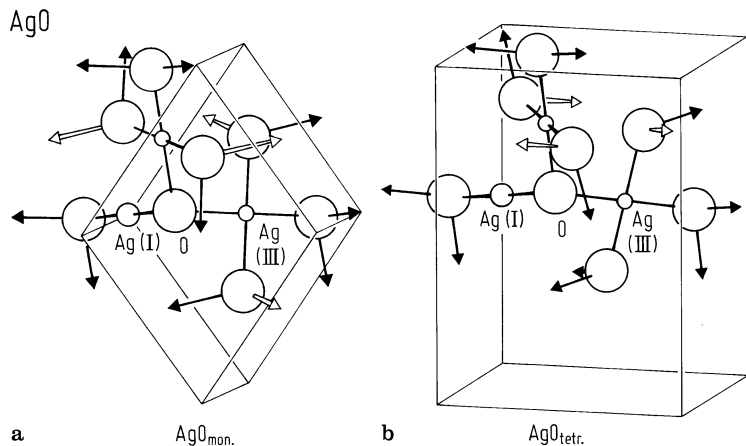


Fig. 16.0.4

Ag_2Te . Structural model for $\beta\text{-Ag}_2\text{Te}$ [87M].

Ag_2Te

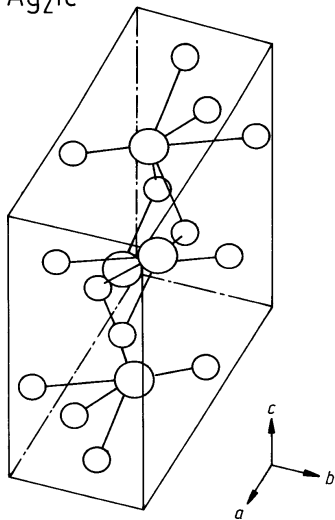
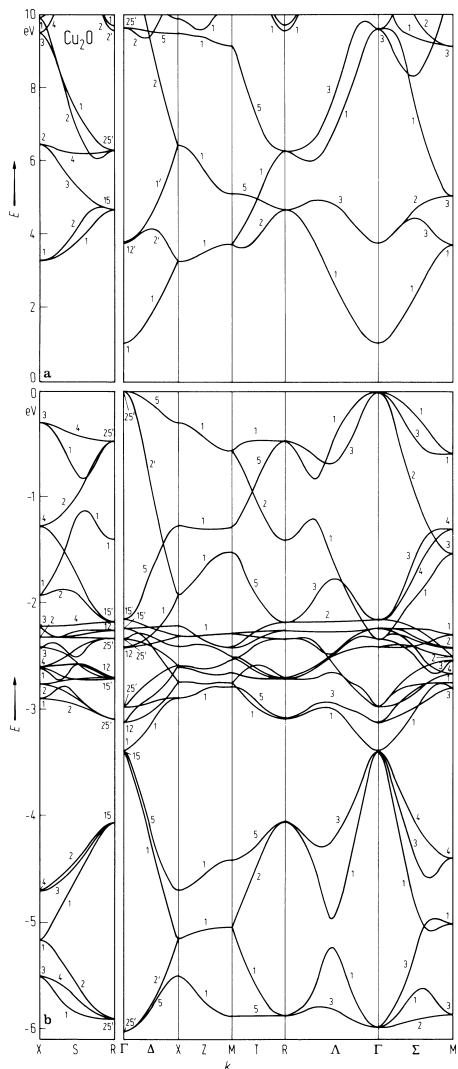


Fig. 16.0.5

Cu_2O . a) Conduction energy bands of Cu_2O (in eV), b) valence energy bands of Cu_2O (in eV) [80K].



16.1 Cupric oxide (CuO)

Crystal structure

For structure and lattice parameters see section 16.0.

Electronic properties

No calculated band structure.

energy gap

$E_{g,ind}$	1.4(3) eV	ultraviolet photoemission spectroscopy	88G
E_g	1...1.7 eV	from various sources	92G

Lattice properties

For structure and lattice parameters see section 16.0 above.

coefficient of linear thermal expansion

α	$\approx 0 \text{ K}^{-1}$	$T = 213...230 \text{ K}$	see Fig. 16.1.1	92G
----------	----------------------------	---------------------------	-----------------	-----

density (mineral tenorite)

d	6.569 g cm^{-3}	$T = 293 \text{ K}$		58G
-----	---------------------------	---------------------	--	-----

melting temperature

T_m	$\approx 1630 \text{ K}$			92G
-------	--------------------------	--	--	-----

phonon dispersion relations

Phonon dispersion curves of CuO have been measured in different axes by inelastic neutron scattering and fitted by a 22 rigid ion model (Fig. 16.1.1) [90R]. The zone center modes decompose according to factor group [89C]: $\Gamma = 4A_u + 5B_u + A_g + 2B_g$. The three acoustic modes are represented by $A_u + 2B_u$, the six $3A_u + 3B_u$ modes are infrared active and the three $A_g + 2B_g$ modes are Raman active.

phonon wavenumbers

A_g	296 cm^{-1}	$T = 300 \text{ K}$	RS	90H
B_{1g}	344 cm^{-1}			
B_{2g}	629 cm^{-1}			
A_{1u}	161 cm^{-1}	$T = 300 \text{ K}$	IR Reflection	90K
A_{2u}	321 cm^{-1}			
A_{3u}	478 cm^{-1}			
B_{1u}	147 cm^{-1}			
B_{2u}	530 cm^{-1}			
B_{3u}	590 cm^{-1}			

sound velocity

Velocities of sound v_L as deduced from the slopes of the acoustic branches (Fig. 16.1.2) with mainly longitudinal character [90R].

$v_L [100]$	$6.4 \cdot 10^5 \text{ cm s}^{-1}$	$T = 296 \text{ K}$	inelastic neutron scattering	90R
$v_L [010]$	$4.1 \cdot 10^5 \text{ cm s}^{-1}$	$T = 296 \text{ K}$		
$v_L [001]$	$7.8 \cdot 10^5 \text{ cm s}^{-1}$	$T = 296 \text{ K}$		
$v_L [101]$	$5.4 \cdot 10^5 \text{ cm s}^{-1}$	$T = 296 \text{ K}$		
	$9.1 \cdot 10^5 \text{ cm s}^{-1}$	$T = 296 \text{ K}$		
$v_L [111]$	$6.8 \cdot 10^5 \text{ cm s}^{-1}$	$T = 296 \text{ K}$		

heat capacity

No singularity between 10 K and 300 K. Above 300 K C_p displays an unusual behaviour in many respects, more details in [92G].

C_p	39.13 J mol ⁻¹ K ⁻¹	$T = 250$ K	high resolution calorimetry	89L
-------	---	-------------	-----------------------------	-----

Debye temperature

Θ_D	391 (10) K	$T = 0$ K	from $C_p(T)$	92G
------------	------------	-----------	---------------	-----

Transport properties

From the empirical prediction expectation, CuO should be an n-type semiconductor. However, almost all reported semiconducting CuO is of the p-type [92S]. Above 650°C, CuO is nearly stoichiometric and exhibits intrinsic conduction [92G].

resistivity

ρ	$\approx 180 \Omega \text{ cm}$	$T = 123\ldots 400$ K	sputtered films	96P
--------	---------------------------------	-----------------------	-----------------	-----

thermal activation energy of the electrical conductivity

E_A	0.13...0.6 eV	$T \approx 298$ K		92G
-------	---------------	-------------------	--	-----

thermoelectric power

S	180...250 $\mu\text{V K}^{-1}$			78H
-----	--------------------------------	--	--	-----

The temperature dependence of the Seebeck coefficient (thermoelectric power) for pure and Li- or Al-doped CuO has been measured [92S].

Optical properties

Reflectance and transmittance (Fig. 16.1.3). Absorption coefficient (Fig. 16.1.4).

Magnetic properties

Below the Néel temperature T_N (230 K) CuO is an antiferromagnet whose magnetic moments are oriented along the b axis of a monoclinic cell. At $T = T_L \cong 213$ K a first-order phase transition from the low-temperature collinear 3D-AFM phase into an intermediate noncollinear incommensurate 3D-AFM phase, which exists in a narrow temperature range $T_L \leq T \leq T_N \cong 230$ K (the Néel temperature), is observed, and at temperatures $T > T_N$ it transforms into a high temperature, low dimensional quantum antiferromagnetic phase [96S].

References to 16.1

- 58G Gmelins Handbook der organischen Chemie. Verlag Chemie GmbH Weinheim, Bergstrasse. Kupfer, Teil B1, 1958.
- 78H Hanscombe, P.: Thin Solid Films 51 (1978) L25.
- 88G Ghijsen, J., Tjeng, L. H., van Elp, J., Eskes, H., Westerink, J., Sawatzky, G. A., Czyzyk, M. T.: Phys. Rev. B 38 (1988) 11322.
- 89L Loram, J.W., Mirza, K.A., Joyce, C.P., Osborne, A.J.: Europhys. Lett. 8 (1989) 263.
- 90H Hagemann, H., Bill, H., Sadowski, W., Walker, E., François, M.: Solid State Commun. 73 No 6 (1990) 447.
- 90K Kliche, G., Popovic, Z. V.: Phys. Rev. B 42 (1990) 10060.
- 90R Reichardt, W., Gompf, F., Aïn, M., Wanklyn, B. M.: Z. Phys. B: Condens. Matter 81 (1990) 19.
- 92G Gmelin, E.: Indian J. Pure Appl. Phys. 30 (1992) 596.
- 95M Marabelli, F., Parravicini, G.B., Salghetti-Drioli, F.: Phys. Rev. B52 (1995) 1433.
- 96P Parreta, A., Jayaraj, M. K., Di Nocera, A., Loreti, S., Quercia, L., Agati, A.: Phys. Status Solidi (a) 155 (1996) 399.
- 96S Sukhorukov, Yu. P., Loshkareva, N. N., Samokhvalov, A. A., Naumov, S. V., Moskvina, A. S., Ochinnikov, A.S.: JETP Lett. 63 (1996) 267.

Figures to 16.1

Fig. 16.1.1

CuO. Thermal expansion as function of temperature for the [110] direction [92G].

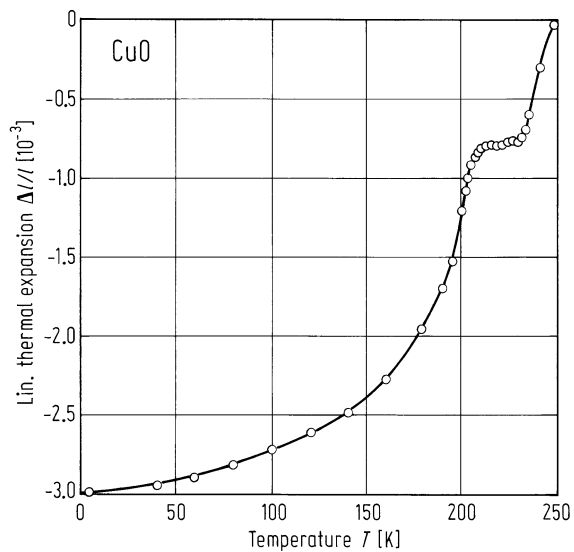


Fig. 16.1.2

CuO. Phonon dispersion curves at 296 K [90R]. Open circles (full circles, triangles) represent phonons measured in longitudinal (transverse) configuration. The solid curves were calculated with a rigid ion model. The branches are labelled according to their representation.

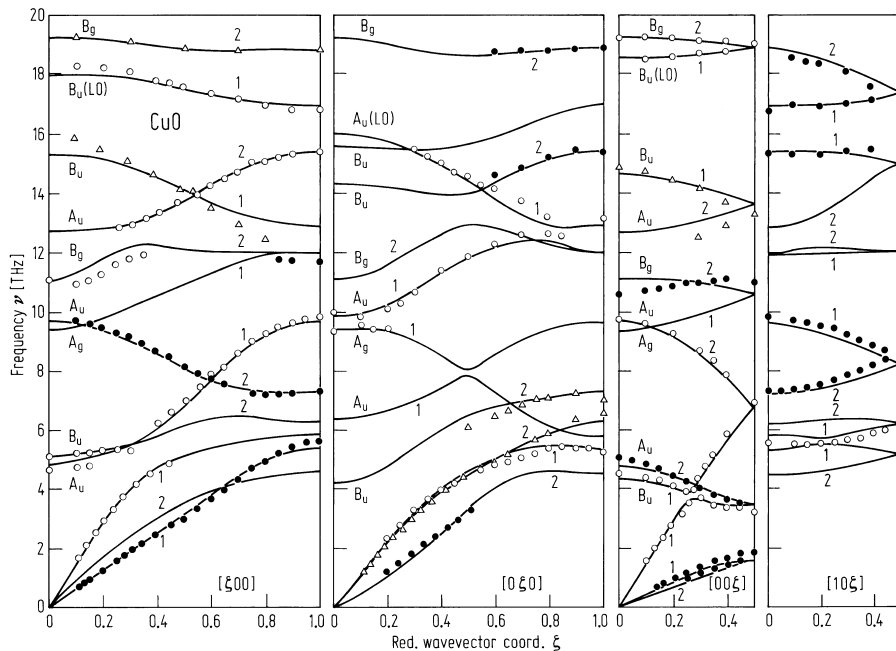


Fig. 16.1.3

CuO. Reflectance and transmittance at room temperature of two samples S1 and S2, $\approx 200\ \mu\text{m}$ and $\approx 60\ \mu\text{m}$ thick, respectively. The line is the bulk reflectivity measured on a polished surface of a thick monocrystal [95M].

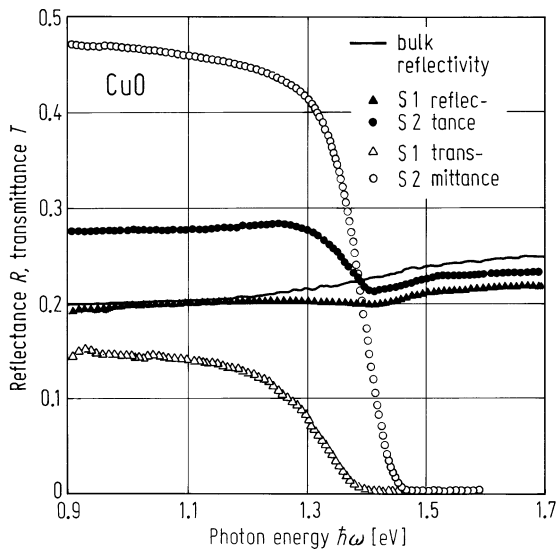
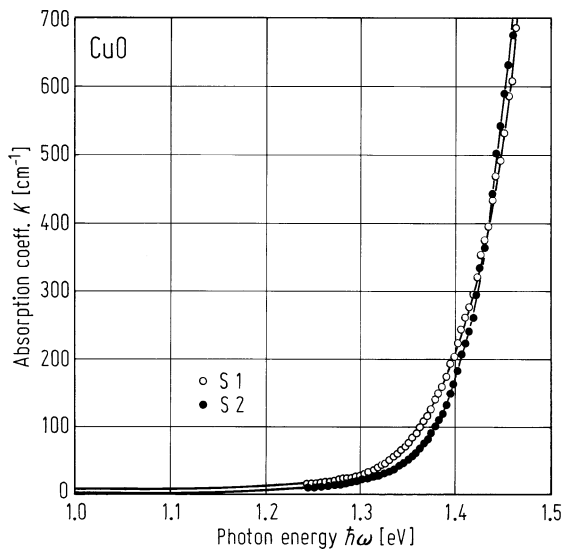


Fig. 16.1.4

CuO. Absorption coefficient obtained for two samples S1 and S2 (for notation see Fig. 2 [95M]). The different fractions of light lost for diffusion and nonparallelism of the surface are given by $(1-c_1)$ and $(1-c_2)$, respectively, where $c_1 = 0.6$, $c_2 = 0.69$ for S1 and $c_1 = 0.9$, $c_2 = 0.93$ for S2.



16.2 Cuprous oxide (Cu₂O)

Crystal structure

For structure and lattice parameters see section 16.0.

Cu₂O is one of the first known semiconductors. Its structure is responsible for its peculiar excitonic spectrum. Cu₂O is metastable at room temperature.

Electronic properties

band structure : Fig. 16.0.5.

energy gap

$E_{g,dir}$ ($\Gamma_{7v}^{+}-\Gamma_{6c}^{+}$)	2.17 eV	$T = 4.2$ K	optical absorption: limit of the "yellow" excitonic series	61N
--	---------	-------------	--	-----

interband transitions of higher energy

$E(\Gamma_{8v}^{+}-\Gamma_{6c}^{+})$	2.304 eV	$T = 4.2$ K	optical absorption: limit of the "green" excitonic series	61G
$E(\Gamma_{7v}^{+}-\Gamma_{8c}^{+})$	2.624 eV	$T = 4.2$ K	optical absorption: limit of the "blue" excitonic series	66D
$E(\Gamma_{8v}^{+}-\Gamma_{8c}^{-})$	2.755 eV	$T = 4.2$ K	optical absorption: limit of the "violet" excitonic series	66D

effective masses

m_{n,ω_c}	0.99 m_0		cyclotron resonance at 137 GHz	76H
m_{p,ω_c}	0.58 m_0	$T = 1.7$ K	cyclotron resonance at	76H

$m_{n,\omega_c} = 0.99 m_0$ and $m_{p,\omega_c} = 0.58 m_0$ are ascribed to the polaron masses in the upper valence band and the lowest conduction band (band masses of 0.56 m_0 and 0.93 m_0 [76H]).

excitons

Three exciton series have been extensively studied.

"Yellow" series

E_g	2.1725eV	$T = 4.2$ K		61N
R	0.9743 eV	$T = 4.2$ K		

"Green" series

E_g	2.3042 eV	$T = 4.2$ K	optical absorption	61G
R	0.1497 eV	42 K		

"Blue" series

E_g	2.6243 eV	$T = 4.2$ K	optical absorption	66D
R	0.5578 eV	$T = 4.2$ K		

Lattice properties

linear thermal expansion coefficient

α	23·10 ⁻⁸ K ⁻¹	$T = 283$ K		78W
	-2.93·10 ⁻⁸ K ⁻¹	$T = 80$ K	(minimal value of α)	

phonon dispersion relation

 : Fig. 16.2.1

3 acoustic and 15 optical branches. The zone center phonons are classified as $\Gamma = 3\Gamma_{15} + \Gamma_{25} + \Gamma'_{12} + \Gamma'_{25} + \Gamma'_2$. In a perfect lattice Γ'_{25} is Raman active and only two optical Γ_{15} phonons are IR active.

phonon frequencies

$\nu(\Gamma_{25})$	$2.61 \cdot 10^{12} \text{ s}^{-1}$	$T = 293 \text{ K}$	inelastic neutron scattering	76B
$\nu(\Gamma'_{12})$	$3.15 \cdot 10^{12} \text{ s}^{-1}$	$T = 293 \text{ K}$	inelastic neutron scattering	76B
$\nu_{\text{TO}}(\Gamma_{15})$	$4.386 \cdot 10^{12} \text{ s}^{-1}$	$T = 300 \text{ K}$	IR absorption and Raman scattering	73D
$\nu_{\text{LO}}(\Gamma_{15})$	$4.48 \cdot 10^{12} \text{ s}^{-1}$	$T = 300 \text{ K}$	IR absorption and Raman scattering	73D
$\nu_{\text{TO,LO}}(\Gamma_{15})$	$5.28 \cdot 10^{12} \text{ s}^{-1}$	$T = 300 \text{ K}$	IR absorption	63O
$\nu(\Gamma'_2)$	$10.40 \cdot 10^{12} \text{ s}^{-1}$	$T = 293 \text{ K}$	inelastic neutron scattering	76B
$\nu(\Gamma'_{25})$	$15.44 \cdot 10^{12} \text{ s}^{-1}$	$T < 300 \text{ K}$	RS; compilation	75P1
$\nu_{\text{TO}}(\Gamma_{15})$	$19.04 \cdot 10^{12} \text{ s}^{-1}$	$T < 300 \text{ K}$	RS; compilation	75P1
$\nu_{\text{LO}}(\Gamma_{15})$	$19.94 \cdot 10^{12} \text{ s}^{-1}$	$T < 300 \text{ K}$	RS; compilation	75P1

compressional wave velocity

v_{L}	$4.5405 \cdot 10^5 \text{ cm s}^{-1}$	$T = 298 \text{ K}$	ultrasonic interferometry	74M
dv_{L}/dp	$6.43 \cdot 10^{-1} \text{ cm s}^{-1} \text{ bar}^{-1}$	$T = 298 \text{ K}$	ultrasonic interferometry	74M

shear wave velocity

v_{T}	$1.3025 \cdot 10^5 \text{ cm s}^{-1}$	$T = 298 \text{ K}$	ultrasonic interferometry	74M
dv_{T}/dp	$-4.23 \cdot 10^{-1} \text{ cm s}^{-1} \text{ bar}^{-1}$	$T = 298 \text{ K}$	ultrasonic interferometry	74M

second order elastic moduli

c_{11}	$12.61 \cdot 10^{11} \text{ dyn cm}^{-2}$	$T = 293 \text{ K}$	inelastic neutron scattering	76B
	$11.65 \cdot 10^{11} \text{ dyn cm}^{-2}$		pulse echo	70H
c_{12}	$10.86 \cdot 10^{11} \text{ dyn cm}^{-2}$	$T = 293 \text{ K}$	inelastic neutron scattering	76B
	$10.53 \cdot 10^{11} \text{ dyn cm}^{-2}$		pulse echo	70H
c_{44}	$1.36 \cdot 10^{11} \text{ dyn cm}^{-2}$	$T = 293 \text{ K}$	inelastic neutron scattering	76B
	$1.21 \cdot 10^{11} \text{ dyn cm}^{-2}$		pulse echo	70H
$c_{11} - c_{12}$	$1.75 \cdot 10^{11} \text{ dyn cm}^{-2}$	$T = 293 \text{ K}$	inelastic neutron scattering	76B

Young's modulus

E	$3.012 \cdot 10^{10} \text{ Nm}^{-2}$	$T = 298 \text{ K}$	ultrasonic interferometry	74M
dE/dp	-1.88	$T = 298 \text{ K}$	ultrasonic interferometry	74M

shear modulus

G	$1.035 \cdot 10^{10} \text{ Nm}^{-2}$	$T = 298 \text{ K}$	ultrasonic interferometry	74M
dG/dp	-0.67	$T = 298 \text{ K}$	ultrasonic interferometry	74M

isothermal compressibility

κ	$8.93 \cdot 10^{-11} \text{ m}^2 \text{ N}^{-1}$	$T = 298 \text{ K}$	ultrasonic interferometry	74M
----------	--	---------------------	---------------------------	-----

Debye temperature

Θ_{D}	188 K	$T = 298 \text{ K}$	ultrasonic interferometry	74M
---------------------	-------	---------------------	---------------------------	-----

density

d	$5.749...6.14 \text{ g cm}^{-3}$		variation due to the presence of voids in most synthetic materials	58G
-----	----------------------------------	--	--	-----

melting temperature

T_{m}	1508 K		(at 0.6 Torr)	58G
----------------	--------	--	---------------	-----

Transport and optical properties

Cu₂O is usually p-type. No n-type material could be prepared. As grown material has high resistivity ($\rho > 10^6 \Omega \text{ cm}$). ρ depends strongly on annealing or photoexcitation. The temperature dependence of electrical conductivity is plotted in Fig. 16.2.2

resistivity (lowest bulk resistivity)

ρ	35 $\Omega \text{ cm}$	$T = 300 \text{ K}$	undoped	79T
--------	------------------------	---------------------	---------	-----

thermal activation energy of the electrical conductivity

E_A	0.20...0.38 eV	$T = 298 \text{ K}$	oxygen saturated sample	82W
	0.48...0.70 eV	$T = 298 \text{ K}$	sample annealed at 1050°C	82W

mobility

μ	70 $\text{cm}^2 \text{ V}^{-1} \text{ s}^{-1}$	$T = 298 \text{ K}$	oxygen saturated sample	82W
-------	--	---------------------	-------------------------	-----

See also Fig. 16.2.3

dielectric constants

$\epsilon(0)$	7.11	$T = 300 \text{ K}$	optical transmission and reflection	63O
$\epsilon(\infty)$	6.46	$T = 300 \text{ K}$	optical transmission and reflection	63O

References to 16.2

- 58G Gmelins Handbook der organischen Chemie. Verlag Chemie GmbH Weinheim, Bergstrasse. Kupfer, Teil B1, 1958.
- 61G Grun, J. B., Sieskind, M., Nikitine, S.: J. Phys. Radium 22 (1961) 176.
- 61N Nikitine, S., Grun, J. B., Sieskind, M.: J. Phys. Chem. Solids 17 (1961) 292.
- 63O O'Keeffe, M.: J. Chem. Phys. 39 (1963) 1789.
- 66D Daunois, A., Deiss, J. L., Meyer, B.: J. Phys. (Paris) 27 (1966) 142.
- 70H Hallberg, J., Hanson, R. C.: Phys. Status Solidi (b) 42 (1970) 305.
- 73D Dawson, P., Hargreave, M. M., Wilkinson, G. R.: J. Phys. Chem. Solids 34 (1973) 2201.
- 74M Manghnani, M. H., Brower, W. S., Parker, H. S.: Phys. Status Solidi (a) 25 (1974) 69.
- 75P1 Petroff, Y., Yu, P. Y., Shen, Y. R.: Phys. Rev. B 12 (1975) 2488.
- 75P2 Pollack, O. P., Trivich, D.: J. Appl. Phys. 46 (1975) 163.
- 76B Beg, M. M., Shapiro, S. M.: Phys. Rev. B 13 (1976) 1728.
- 76H Hodby, J. W., Jenkins, T. E., Schwab, C., Tamura, H., Trivich, D.: J. Phys. C 9 (1976) 1429.
- 78W White, G. K.: J. Phys. C 11 (1978) 2171.
- 79T Tapiero, M., Nogu  t, C., Zielinger, J. P., Schwab, C., Pierrat, D.: Rev. Phys. Appl. 14 (1979) 231.
- 80K Kleinman, L., Mednick, K.: Phys. Rev. B 21 (1980) 1549.
- 81M Maluenda, J., Farhi, R., Petot-Ervas, G.: J. Phys. Chem. Solids 42 No10 (1981) 911.
- 82W Wang, G. J., Weichman, F. L.: Can. J. Phys. 60 (1982) 1648.

Figures to 16.2

Fig. 16.0.5

Cu_2O . a) Conduction energy bands of Cu_2O (in eV), b) valence energy bands of Cu_2O (in eV) [80K].

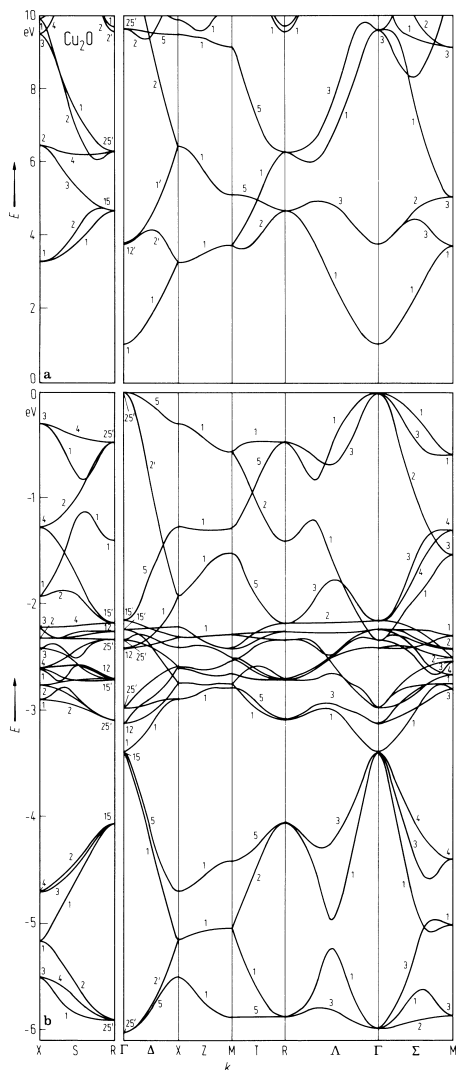


Fig. 16.2.1

Cu_2O . Phonon dispersion relations measured in Cu_2O by inelastic neutron scattering. The measurements are compared with the rigid-ion model (heavy lines) in $[\xi 00]$, $[\xi \xi 0]$, and $[\xi \xi \xi]$ directions. The thin lines are a guide to the eye [76B].

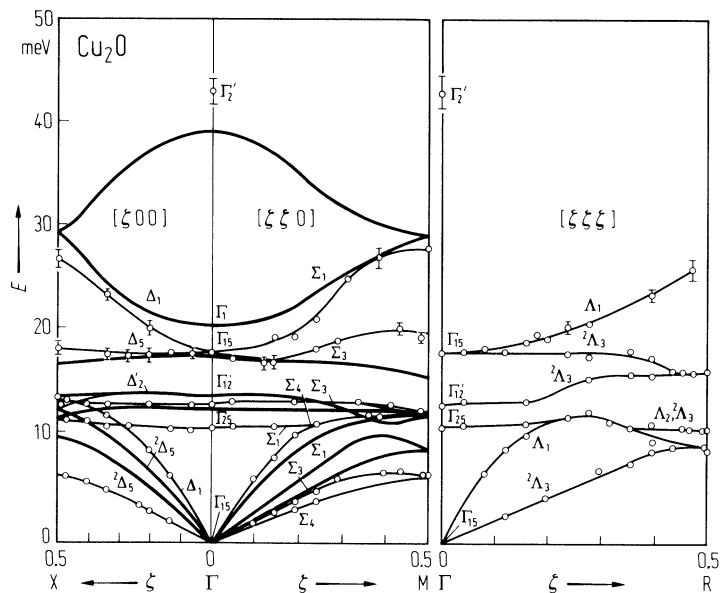


Fig. 16.2.2

Cu_2O . Electrical conductivity vs. temperature [81M]. The results were obtained for two samples by measuring the conductivity of the same specimen by increasing or decreasing the temperature and by varying the oxygen partial pressure at the same temperature.

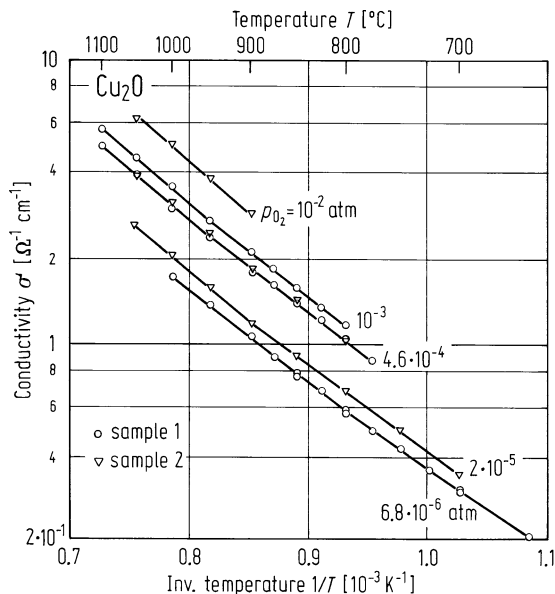
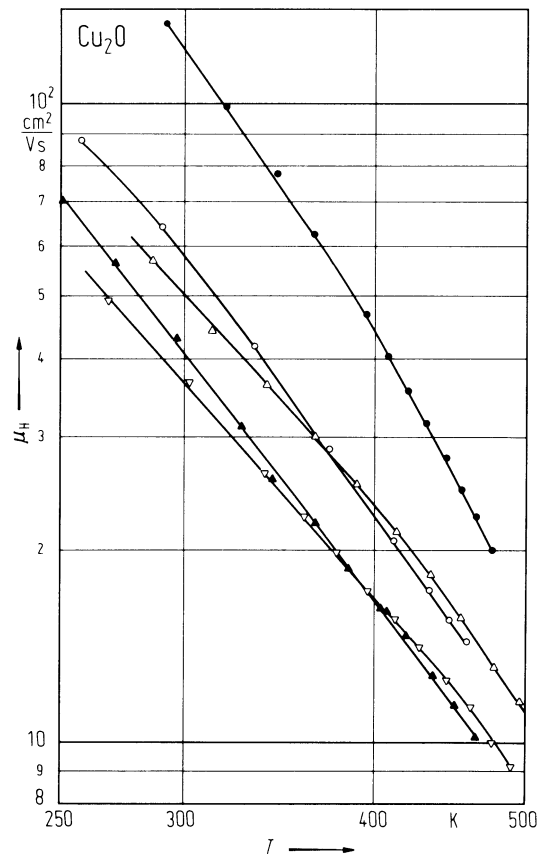


Fig. 16.2.3

Cu₂O. Temperature variation of the mobility for 5 samples [75P2].



16.3 Copper sulfides (Cu₂S, Cu_{2-x}S)

Crystal structure

For structure and lattice parameters see section 16.0.

Electronic properties

energy gaps

β-Cu₂S (chalcocite) has an indirect gap, with the conduction band minimum at the Γ point, but the valence band edge at a non-zero value of the electron wavevector. The valence band originates from sulfur 3p wave-function, the conduction band is expected to be essentially of Cu 4s type.

$E_{g,ind}$	1.21 eV	$T = 300$ K	optical reflexion and absorption	65M
$E_{g,dir}$	1.7 eV	$T = 300$ K	optical absorption and reflection	69R
E_g	1.183 eV	$T = 120$ K	tetragonal phase (photoconductivity)	85P
	1.0 eV	$T = 300$ K	orthorhombic Cu ₂ S (from different sources)	

Djurleite has a direct gap:

$E_{g,dir}$	1.3 eV	$T = 300$ K	optical absorption	73M
-------------	--------	-------------	--------------------	-----

effective masses

Effective masses do not vary drastically from Cu₂S to Cu_{1.8}S [74G].

m_p	(1.65...1.82) m_0	$T < 300$ K	(β-Cu ₂ S). from thermoelectric power	74G
	1.8 m_0	$T = 300$ K	(digenite LT). from plasma frequency	74G

Lattice properties

isothermal compressibility

κ	$\approx 40 \cdot 10^{-12}$ m ² N ⁻¹	$T = 300$ K	γ-Cu ₂ S	87G
----------	--	-------------	---------------------	-----

linear thermal expansion coefficient

α	208·10 ⁻⁶ K ⁻¹	$T = 283...373$ K	γ-Cu ₂ S	87G
	$\approx 80 \cdot 10^{-6}$ K ⁻¹	$T = 393...598$ K	β-Cu ₂ S	

heat capacity

molar heat capacity: Fig. 16.3.1

density

d	5.8 g cm ⁻³	β-Cu ₂ S	74G
	5.6 g cm ⁻³	digenite LT	74G
	(5.63...5.747) g cm ⁻³	djurleite	74G

melting temperature

T_m	1100°C	depends strongly on stoichiometry	74G
-------	--------	-----------------------------------	-----

Transport and optical properties

As grown Cu_{2-x}S are p-type degenerate semiconductors. Conductivity depends strongly on non-stoichiometry (Fig. 16.3.2). For Cu₂S, jumps of conductivity occur at the phase transition temperatures, but there is a marked hysteresis at low temperatures (Fig. 16.3.3).

Cu₂S:Cd is semi-insulating (Fig. 16.3.4) [74G].

resistivity

ρ 0.06...0.4 Ω cm $T = 300$ K 74G

mobility of holes

μ_p 3.02...4.75 cm²V⁻¹s⁻¹ $T = 300$ K 74G

see also Fig. 16.3.5.

carrier concentration

p (3.5...0.33)·10¹⁹ cm⁻³ $T = 300$ K 74G

thermoelectric power

S (267...327) μ V K⁻¹ $T = 300$ K 74G

Digenite also has a high carrier concentration. As may be expected resistivity is much lower than for Cu₂S.

Optical constants from R and T : Fig 16.3.6.

References to 16.3

- 65M Marshall, R., Mitra, S. S.: J. Appl. Phys. 36 (1965) 3882.
- 69R Ramoin, M., Sorbier, J. P., Bretzner, J. F., Martinuzzi, S.: C. R. Acad. Sci. Ser. B 268 (1969) 1097.
- 73M Mulder, B. J.: Phys. Status Solidi (a) 15 (1973) 409 and (a) 18 (1973) 633.
- 73O Okamoto, K., Kawai, S.: Jpn. J. Appl. Phys. 12 (1973) 1130.
- 74G Guastavino, F.: These d'Etat Montpellier 1974.
- 85P Pakeva, S., Germanova, K.: J. Phys. D: Appl. Phys. 18 (1985) 1371.
- 87G Gronvold, F., Westrum, E. F. Jr.: J. Chem. Thermodyn. 19 (1987) 1183.

Figures to 16.3

Fig. 16.3.1

Cu₂S. Molar heat capacity. Different symbols and lines are from various authors. The deviation between the values of the different authors are shown in the center of the figure. Figure from [87G].

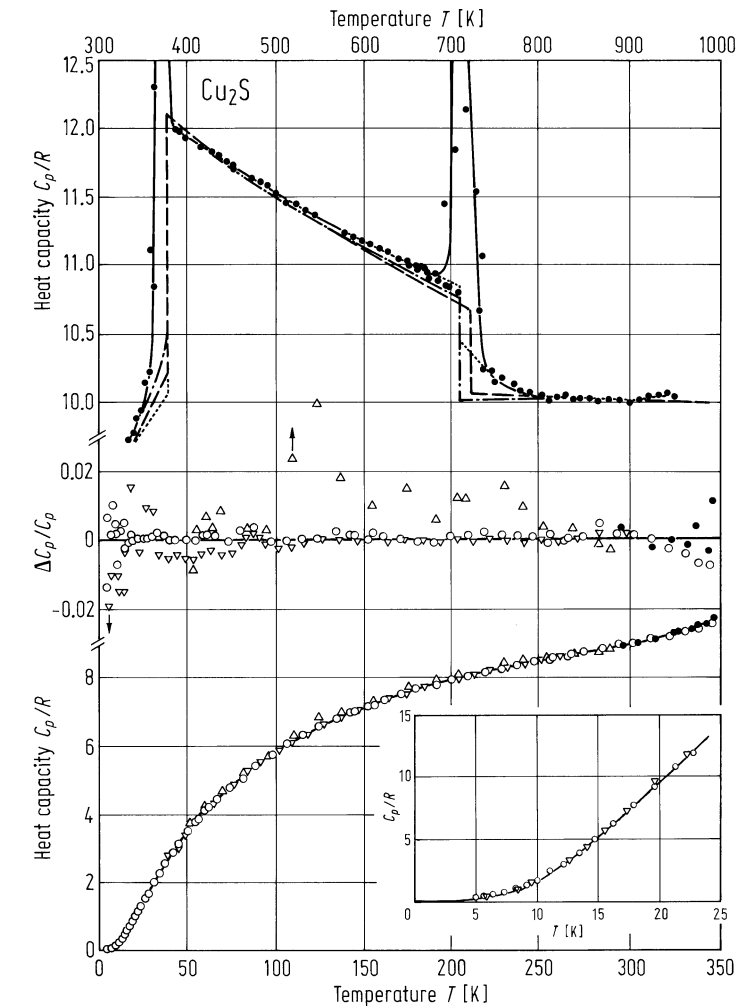


Fig. 16.3.2

Cu_2S . Electrical conductivity vs. deviation from stoichiometry for Cu_{2-x}S [73O].

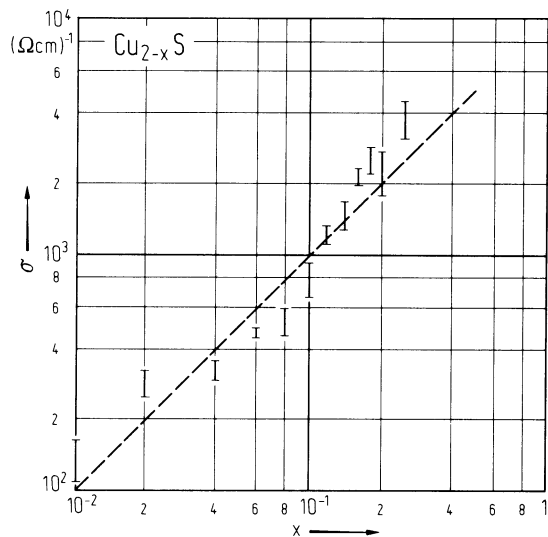


Fig. 16.3.3

Cu_2S . Electrical conductivity vs. temperature for several non-stoichiometric copper sulfides [73O].

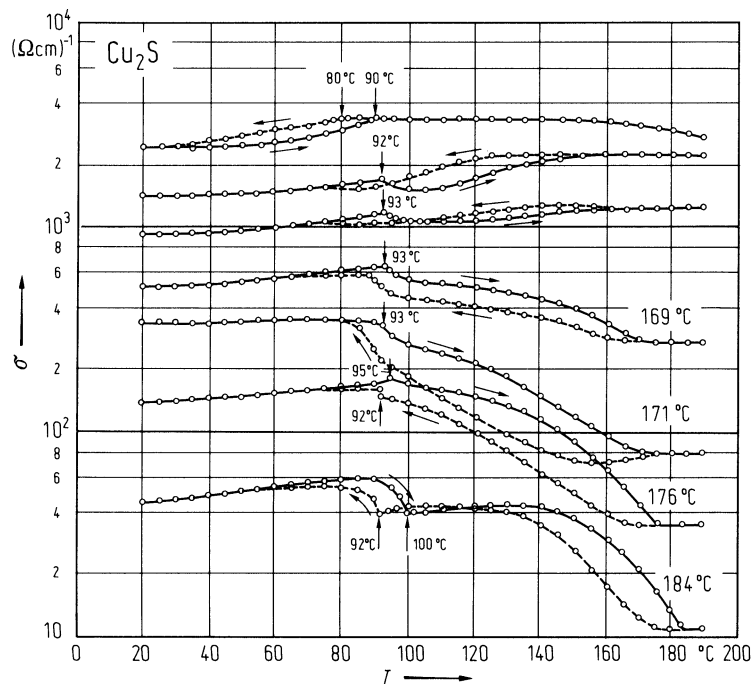


Fig. 16.3.4

Cu_2S . Resistivity ρ and Hall coefficient R_H vs. reciprocal temperature for $\beta\text{-Cu}_2\text{S}$ [74G].

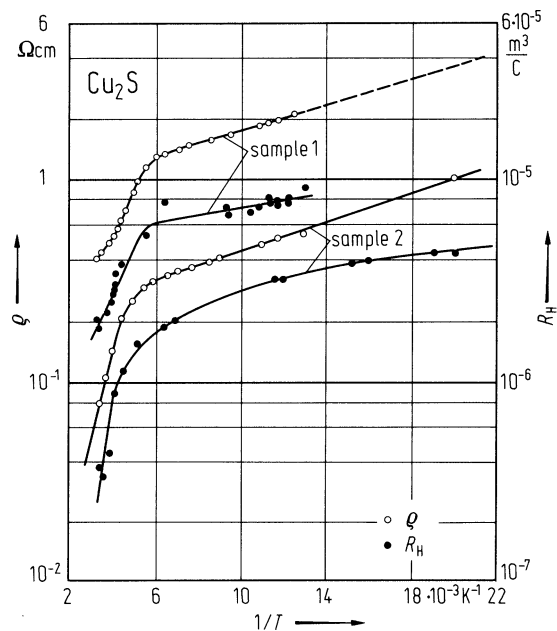


Fig. 16.3.5

Cu₂S. Hole mobility in digenite vs. carrier concentration p [74G].

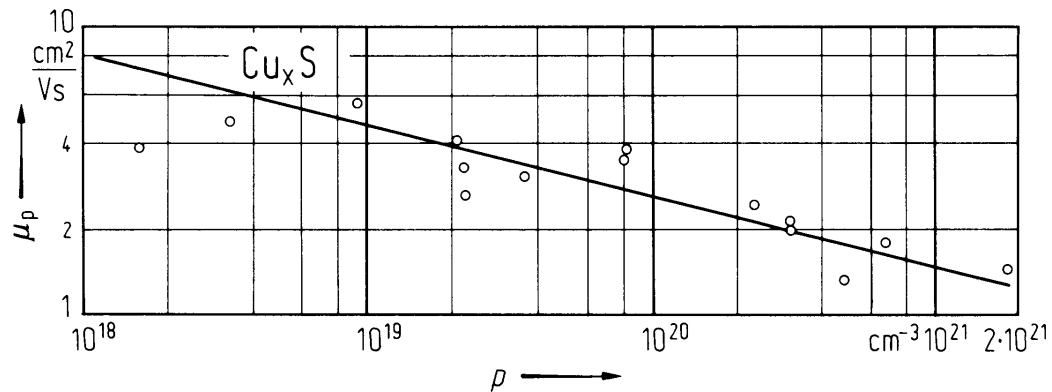
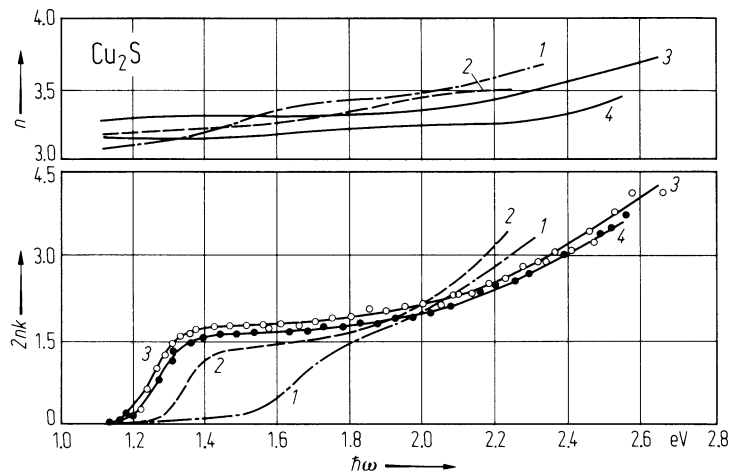


Fig. 16.3.6

Cu_2S . Refractive index (n) and imaginary part of the complex dielectric constant ($2nk$; k dimensionless) vs. photon energy of platelets of chalcocite with different orientation of the crystal axis [73M].



16.4 Copper selenides (Cu₂Se, Cu_{2-x}Se)

Crystal structure

For structure and lattice parameters see section 16.0.

Electronic properties

Cu_{2-x}Se is a p-type extrinsic semiconductor with a forbidden energy gap of 1.1...1.29 eV [87P] and an anomalously high cation conductivity in the α-phase [84Y].

energy gap

E_g	1.20 eV (1.0...1.1) eV	$T \approx 298$ K	Cu _{1.9} Se (berzelianite) thin film compilation in [78V]	87P
-------	---------------------------	-------------------	---	-----

effective masses

m_p	0.5 m_0	$T = 300$ K	Fig. 16.4.1	78V
-------	-----------	-------------	-------------	-----

For the density of states mass see 16.4.2.

Lattice properties

heat capacity

C_p	73.4 J mol ⁻¹ K ⁻¹ 84 J mol ⁻¹ K ⁻¹	$T = 193$ K...393 K $T = 403$ K...773 K	calorimetry	73K
-------	--	--	-------------	-----

density

d	7.1 g cm ⁻³ 7.0 g cm ⁻³ 6.8 g cm ⁻³ 6.6 g cm ⁻³	crookesite berzelianite umagite athabascaite	72P 72P 72P 72P
-----	--	---	--------------------------

Transport and optical properties

Electrical conductivity (Fig. 16.4.3). Hall mobility (Fig. 16.4.4).The following data are for nearly stoichiometric Cu₂Se.

resistivity

ρ	0.1...2·10 ⁻² Ω cm	$T = 300$ K	(Cu _{2-x} Se thin films). Van der Pauw method	87P
--------	-------------------------------	-------------	---	-----

carrier concentration

p	1.9·10 ²⁰ cm ⁻³	$T = 300$ K		78V
-----	---------------------------------------	-------------	--	-----

optical properties : the reflection spectra show a plasma resonance in the near IR (Fig. 16.4.5).

dielectric constant

$\epsilon(\infty)$	11.0...11.6	$T = 300$ K		73G
--------------------	-------------	-------------	--	-----

References to 16.4

72P Povarennykh, A. S.: Crystal Chem. Classification of Minerals, Vol. 1, Plenum Press, New York 1972.
73G Gorbachev, V. V., Putilin, I. M.: Phys. Status Solidi (a) 16 (1973) 553.
73K Kubaschewski, P., Nölting, J.: Ber. Bunsenges. Phys. Chem. 77 (1973) 74.
78V Voskanyan, A. A., Inglizyan, P. N., Lalykin, S. P., Plyutto, I. A., Shevchenko, Ya. M.: Fiz. Tekh. Poluprovodn. 12 (1978) 2096.
87P Padam, G. K.: Thin Solid Films 150 (1987) L89.

Figures to 16.4

Fig. 16.4.1

Cu₂Se. Effective hole mass vs. carrier concentration [73G].

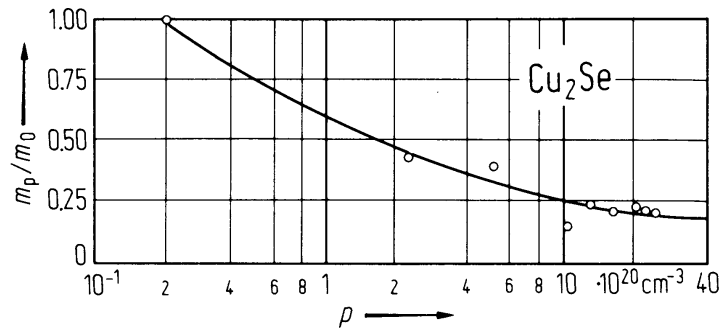


Fig. 16.4.2

Cu_2Se . Density of states effective mass m_{ds} vs. temperature [78V]. Note logarithmic scales.

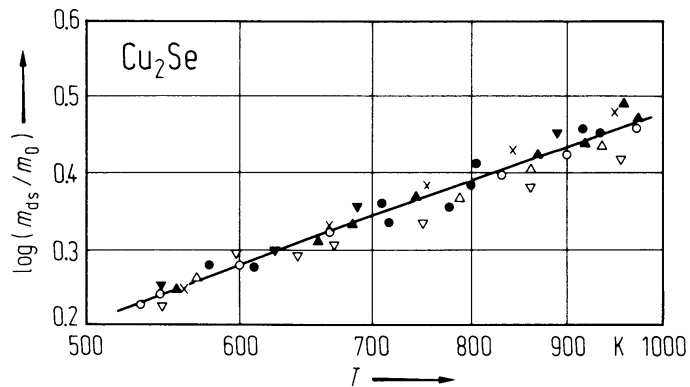


Fig. 16.4.3

Cu_2Se . Temperature dependence of the electronic conductivity for several samples [78V]. From sample 1...9 Se excess increases, and also the carrier density (from $1.9 \dots 24.5 \cdot 10^{20} \text{ cm}^{-3}$). Note logarithmic temperature scale.

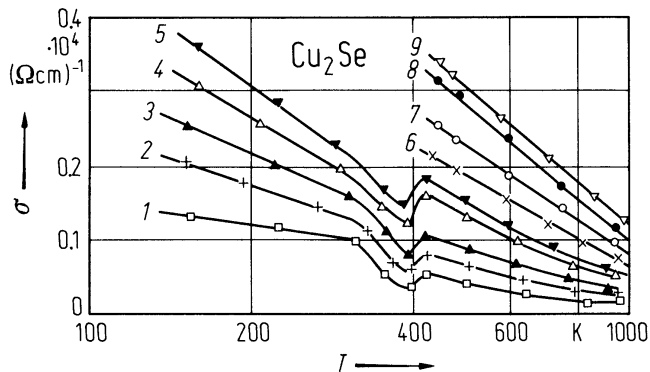


Fig. 16.4.4

Cu_2Se . Temperature dependence of the Hall mobility for different samples [78V]..

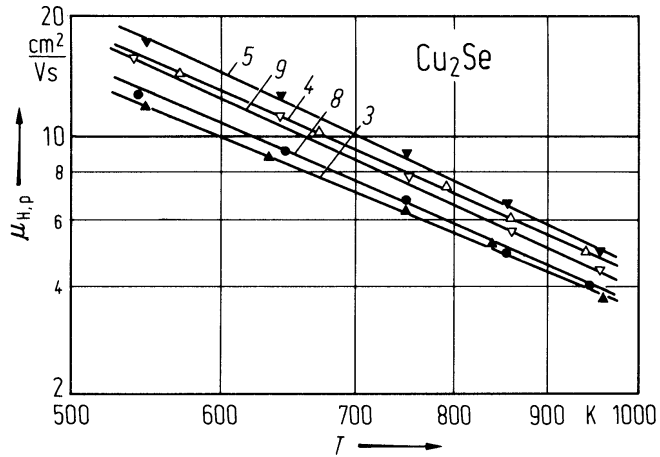
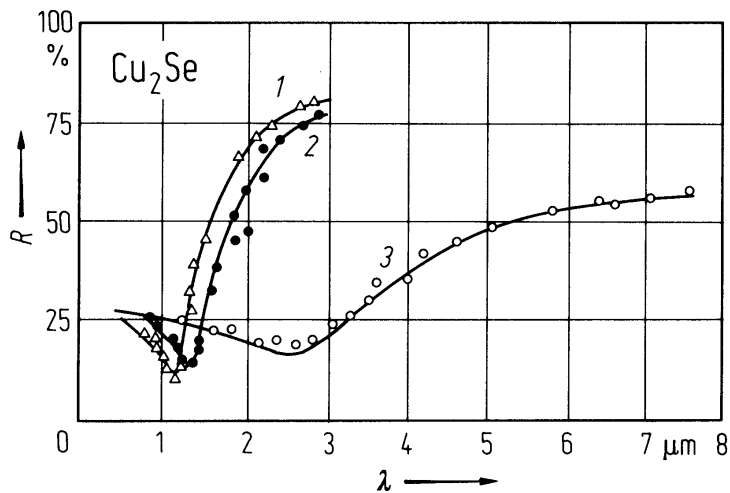


Fig. 16.4.5

Cu_2Se . Experimental and calculated (solid line) values of the reflectivity vs. wavelength for different carrier concentrations: 1, $p = 2.04 \cdot 10^{21} \text{ cm}^{-3}$; 2, $p = 1.04 \cdot 10^{21} \text{ cm}^{-3}$; 3, $p = 0.51 \cdot 10^{21} \text{ cm}^{-3}$ [73G].



16.5 Copper tellurides (Cu₂Te, Cu_{2-x}Te)

Crystal structure

For structure and lattice parameters see section 16.0.

Electronic properties

energy gaps

Both direct and indirect energy gap exist in Cu₂Te. $E_{g,dir}$ strongly depends on the value of x in Cu_{2-x}Te while $E_{g,ind}$ decreases slightly as x increases. Proposed band structure of Cu_{2-x}Te in [94M].

$E_{g,dir}$	0.8 eV	Cu _{1.9} Te thin film (transmission)	83D
$E_{g,ind}$	0.50 eV	transport properties	73G

hole effective mass

m_p	0.39 m_0	$T = 300$ K	from thermoelectric coefficient	94M
-------	------------	-------------	---------------------------------	-----

Lattice properties

heat capacity

C_p	77 J mol ⁻¹ K ⁻¹	$T = 333$ K
-------	--	-------------

density

d	7.3 g cm ⁻³	weissite	72P
	7.5 g cm ⁻³	rickardite	72P

Transport and optical properties

Cu₂Te is a highly degenerate p-type semiconductor. Carrier concentrations are extremely high (10²⁰...10²¹cm⁻³ at RT) and temperature independent [94M]. It has a high conductivity which increases at high temperatures and presents discontinuities at 250K, or at 280 K and 640 K. Electrical conductivity, thermoelectric power and Hall coefficient as function of temperature ranging from 90 K to 480 K for Cu_{2-x}Te (0 ≤ x ≤ 0.25) thin films are plotted in Fig. 16.5.1.

carrier concentration

p	0.35·10 ²⁰ cm ⁻³	$T = 300$ K	86M
-----	--	-------------	-----

Seebeck coefficient (thermoelectric power)

S	10 μV K ⁻¹	$T = 300$ K	Cu ₂ Te thin film	94M
	≈ 370 μV K ⁻¹	$T = 300$ K	Cu ₂ Te single crystal	85S

Hall coefficient

R_H	22.32·10 ³ cm ³ C ⁻¹	Cu ₂ Te thin film	94M
-------	---	------------------------------	-----

The absorption coefficient varies like $K = A (h\nu - E_g)^p$ with $p \approx 2.1$ (A is a constant and E_g the energy gap), suggesting an indirect gap (Fig. 16.5.2).

References to 16.5

72P Povarennykh, A. S.: Crystal Chem. Classification of Minerals, Vol. 1, Plenum Press, New York 1972.
73G Glazov, V. M., Burkhanov, A. S.: Fiz. Tech. Poluprovodn. 7 (1973) 1401.
83D Dawar, A. L., Kumar, A., Kumar, P., Mathur, P. C.: J. Less Common Met. 91 (1983) 83.
85S Sorokin, G. P., Idrichen, G.Z., Sorokina, Z.M.: Inorg. Mater 21 (1985) 912.
86M Mansour, B., Mukhtar, F., Barakati, G. G.: Phys. Status Solidi (a) 95 (1986) 703.
94E El-Bahrawi, M. S., Khodier, S., Kishk, S. S., Nagib, N. N.: Appl. Phys. A 58 (1994) 601.
94M Mansour, B. A., Farag, B. S., Khodier, S. A.: Thin Solid Films 247 (1994) 112.

Figures to 16.5

Fig. 16.5.1

Cu₂Te. Temperature dependence of (a) electrical conductivity σ , (b) thermoelectric power S and (c) Hall coefficient R_H [94M].

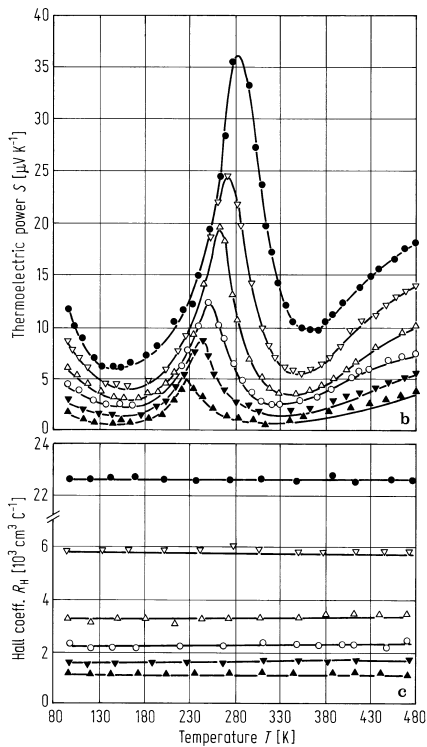
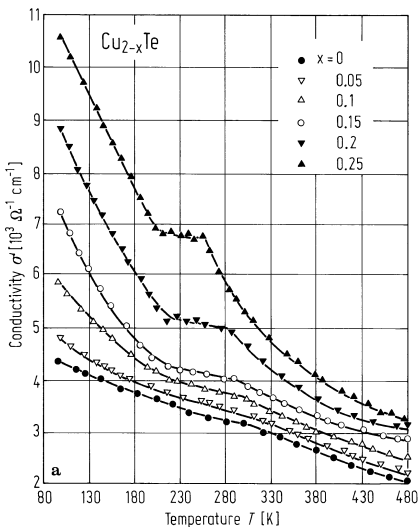
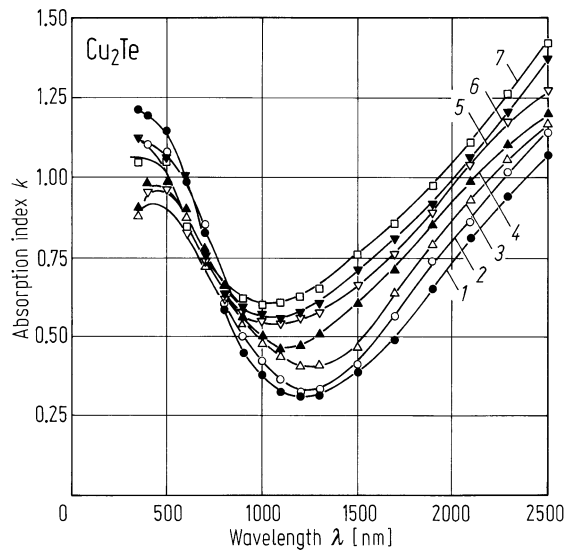


Fig. 16.5.2

Cu₂Te. Absorption index of cuprous telluride films of various thicknesses vs. wavelength [94E].



16.6 Silver oxides (Ag_xO_y)

Crystal structure

For structure and lattice parameters see section 16.0.

AgO

physical properties

AgO is an n-type semiconductor. After exposition to oxygen plasma, thin films contain about 12% O excess. At high pressures, it becomes a degenerate semiconductor [51N].

Resistivity: about (1...5)·10⁶ Ω cm on 250 Å films [75F].

density

d 7.44 g cm⁻³ 75F

Ag₂O

energy gap, effective masses, Ag₂O

The band structure is expected to be similar to Cu₂O; the exciton spectrum has been studied extensively and it yields the gap value.

energy gap

<i>E_{g,dir}</i>	1.571 eV	<i>T</i> = 4 K	exciton absorption	77A
	1.2 eV	<i>T</i> = 293 K	photoconductivity	64F
	1.4 eV	<i>T</i> = 223 K		
	1.6 eV	<i>T</i> = 143 K		
<i>dE_g/dT</i>	2·10 ⁻³ eV K ⁻¹	<i>T</i> = 140...300 K		

effective masses

<i>m_n</i>	0.7 <i>m</i> ₀	<i>T</i> = 4.2 K	(from <i>m_p/m_n</i> and <i>m_p</i> ⁻¹ + <i>m_n</i> ⁻¹ obtained with exciton spectra)	72K
<i>m_p</i>	1.9 <i>m</i> ₀	<i>T</i> = 4.2 K		

density

d 6.9 g cm⁻³ 75F

melting temperature

T_m 1088 K 71G

phonon frequencies

<i>ν</i>	2.55·10 ¹² s ⁻¹	<i>T</i> = 293 K	IR absorption	64M
	2.62·10 ¹² s ⁻¹	<i>T</i> = 100 K		
	2.76·10 ¹² s ⁻¹	<i>T</i> = 4.2 K		

heat capacity : see Fig. 16.6.1 [62G]

resistivity : see Fig. 16.6.2 [64F]

References to 16.6

- 51N Neidind, A. B., Kazarnovskii, I. A.: Dokl. Akad. Nauk SSSR 78 (1951) 713.
- 62G Gerkin, RE., Pitzer, K. S.: J. Amer. Chem. Soc. 84 (1962) 2662.
- 64F Fortin, E., Weichman, F. L.: Phys. Status Solidi 5 (1964) 515.
- 64M Mc Devitt, N. T., Davidson, A. D.: J. O. S. A. 55 (1965) 209.
- 71G Gmelins Handbuch der Anorganischen Chemie. Verlag Chemie GmbH Weinheim, Bergstrasse. Silber, Teil B1, 1971.
- 72K Kreingol'd, F. I., Kulinkin, B. S.: Fiz. Tekh. Poluprovodn. 6 (1972) 2380.
- 75F Farhat, E., Donnadieu, A., Robin, J.: Thin Solid Films 30 (1975) 83.
- 77A Agekyan, V. T.: Phys. Status Solidi (a) 43 (1977) 11.

Figures to 16.6

Fig.16.6.1

Ag_2O . Heat capacity of macrocrystalline silver oxide vs. temperature [62G].

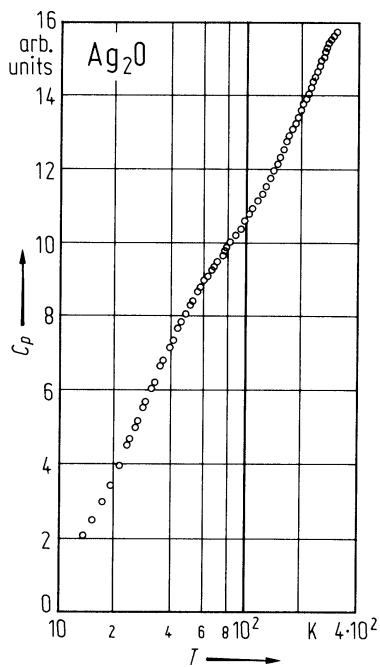
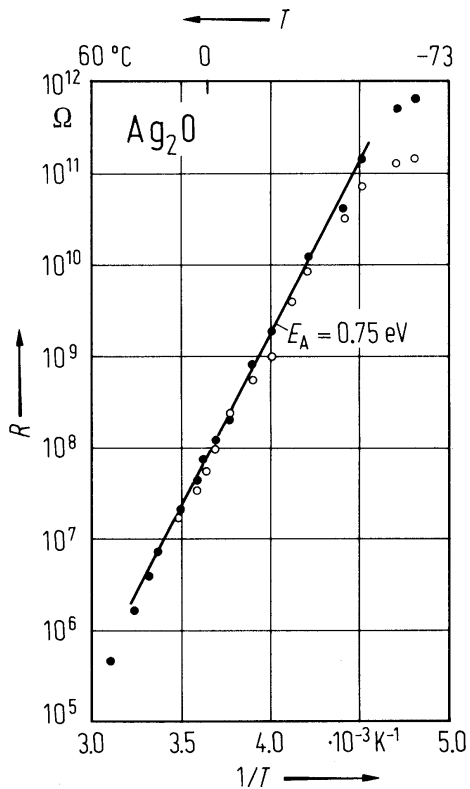


Fig. 16.6.2

Ag_2O . Resistance of a Ag_2O film vs. temperature [64F].



16.7 Silver sulfide (Ag2S)

Crystal structure

For structure and lattice parameters see section 16.0.

Electronic properties

energy gaps, effective masses, α-modification

energy gaps

$E_{g,ind}$	0.85 eV	$T = 300\text{ K}$	photoconductivity	77J
$E_{g,dir}$	1.0 eV	$T = 300\text{ K}$	photoconductivity	77J
dE_g/dT	$-1.2\cdot10^{-3}\text{ eV K}^{-1}$	$T = 300\dots580\text{ K}$	shift of optical absorption edge (Fig. 16.7.1)	77J

effective masses

m_n	$4.65\ m_0$	$T = 365\text{ K}$	electrical conductivity, Hall effect	59J
m_p	$7.59\ m_0$	$T = 365\text{ K}$	and thermoelectric power	59J

energy gap, effective masses, β-modification

energy gap

E_g	0.3eV		transport measurements	77J
dE_g/dT	$-3\cdot10^{-4}\text{ eV K}^{-1}$		optical absorption shift	77J

effective masses

m_n	$0.23\ m_0$		from electrochemical measurements	67R
m_p	$0.23\ m_0$			67R

Lattice properties

α-modification

linear thermal expansion coefficient

α	$2.0\cdot10^{-5}\text{ K}^{-1}$			85O
----------	---------------------------------	--	--	-----

phonon frequencies

ν	$2.1\cdot10^{12}\text{ s}^{-1}$	$T = 4.2\text{ K}$	IR reflectivity	73B
	$2.7\cdot10^{12}\text{ s}^{-1}$			
	$4.2\cdot10^{12}\text{ s}^{-1}$			
	$6.9\cdot10^{12}\text{ s}^{-1}$			
	$8.1\cdot10^{12}\text{ s}^{-1}$			

compressibility

κ	$2.9\cdot10^{-12}\text{ cm}^2\text{ dyn}^{-1}$	$T \approx 273\text{ K}$		85O
----------	--	--------------------------	--	-----

heat capacity (in cal mol⁻¹ K⁻¹)

C_p	76.15	$T = 298.16\text{ K}$		62W
-------	-------	-----------------------	--	-----

Debye temperature

Θ_D	70 K		from $C_p(T)$	62W
------------	------	--	---------------	-----

density

d	7.234 g cm^{-3}	$T = 300\text{ K}$	(temperature dependence: Fig. 16.7.2)	73G
-----	--------------------------	--------------------	---------------------------------------	-----

melting temperature

T_m	838°C		85O
	825°C	from phase diagram	73G

Transport properties

α -modification

In the low temperature phase, the influence of stoichiometry on the respective magnitude of ionic and electronic conductivity is important [59J]. α -Ag₂S is n-type. Donor level at 0.11 eV below the conduction band. Mobility of charge carriers (Fig. 16.7.3).

carrier mobilities

μ_n	63.5 cm ² /V s	$T = 365$ K	conductivity and Hall effect	59J
μ_p	18.7 cm ² /V s	$T = 365$ K	conductivity and Hall effect	59J

intrinsic carrier concentration

n_i	$3.7 \cdot 10^{15}$ cm ⁻³	$T = 365$ K	conductivity and Hall effect	59J
	$1.1 \cdot 10^{16}$ cm ⁻³	$T = 400$ K		
	$6 \cdot 10^{16}$ cm ⁻³	$T = 431$ K		

electrical conductivity : Fig. 16.7.4 [77J].

β - and γ -modification

The crystallographic phase transition is correlated to a large increase of the electrical conductivity σ (by a factor of $10^2 \dots 10^3$) (Fig. 16.7.5). Most samples show a negative $d\sigma/dT$ (metallic character) (Fig. 16.7.6) [77J].

thermoelectric power: Fig. 16.7.7.

electron mobility

μ_n	160 cm ² /V s	$T = 500$ K	59J
---------	--------------------------	-------------	-----

intrinsic carrier concentration

n_i	$2.7 \cdot 10^{19}$ cm ⁻³	$T = 473$ K	73B
	$4 \cdot 10^{19}$ cm ⁻³	$T = 500$ K	59J

References to 16.7

- 59J Junod, P.: Helv. Phys. Acta 32 (1959) 567 and 601.
62W Walsh, P. N., Art, E. W., White, D.: J. Phys. Chem. 66 (1962) 1546.
67R Rickert, H.: Festkörperprobleme 6 (1967) 85.
73B Brüesch, P., Wulschleger, J.: Solid State Commun. 13 (1973) 9.
73G Gmelin's Handbuch der anorganischen Chemie, Verlag Chemie GmbH Weinheim. Bergstrasse, 5nd Edition. Silber, Teil B3, 1973.
77J Junod, P., Hediger, H., Kilchör, B., Wulschleger, J.: Philos. Mag. 36 (1977) 941.
85O Okazaki, H., Takano, A.: Z. Naturforsch. 40a (1985) 986.

Figures to 16.7

Fig. 16.7.1

Ag_2S . Energy gap vs. temperature. In the α -phase, $dE_g/dT = -1.2 \cdot 10^{-3}$ eV/K. In the β -phase the value of dE_g/dT is smaller ($dE_g/dT = -3 \cdot 10^{-4}$ eV/K) [77J].

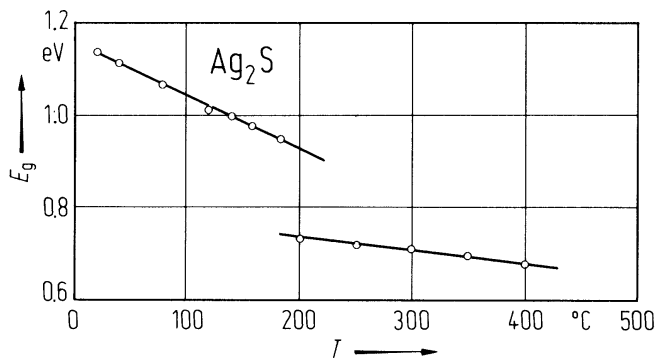


Fig. 16.7.2

Ag_2S . Density vs. temperature [73G1].

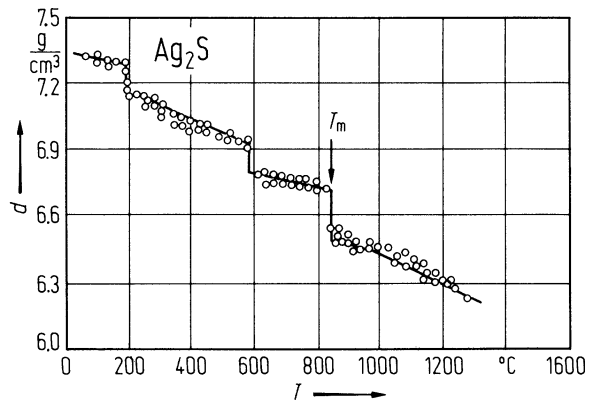


Fig. 16.7.3

Ag_2S . Hall mobility vs. temperature, for α - and β - Ag_2S [59J]. Note logarithmic scales.

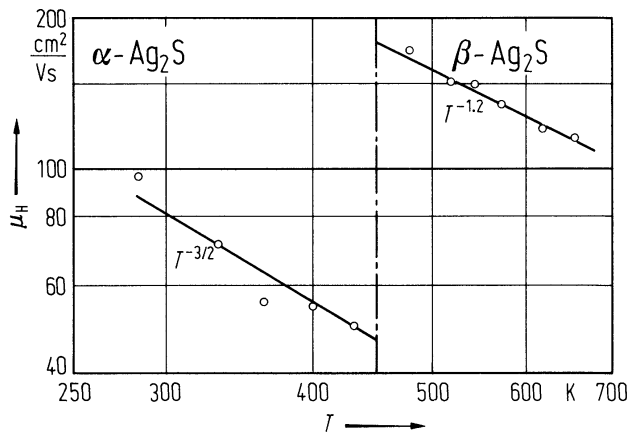


Fig. 16.7.4

Ag_2S . Electrical conductivity vs. reciprocal temperature. The different points (open circles, filled circles, etc.) correspond to nominally pure and stoichiometric samples measured without electrochemical control of the Ag/S ratio. In the β -phase ($T > T_{\alpha,\beta}$) both the absolute value and the slope of the conductivity are well determined. In the α -phase ($T < T_{\alpha,\beta}$) the influence of the thermal history of the different samples is clearly demonstrated [77J].

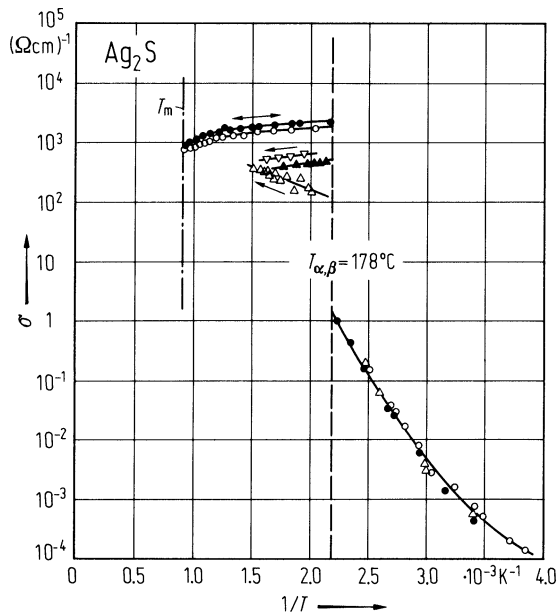


Fig. 16.7.5

Ag_2S . Temperature dependence of the resistivities of Ag_2S in different states. Thirteen samples of nominally pure and stoichiometric Ag_2S have been measured between $T_{\alpha,\beta} = 451 \text{ K}$ and about 1350 K , the arrows corresponding to the direction of the temperature variation. The phase change at about 870 K has only a small influence whereas the values measured in the liquid phase are essentially determined by the thermal history of the sample. The conductivities of all samples in the solid phase are equal and reproducible (curve 1...13) if, after melting, the temperatures are not decreased to values lower than $T_{\alpha,\beta}$ [77J].

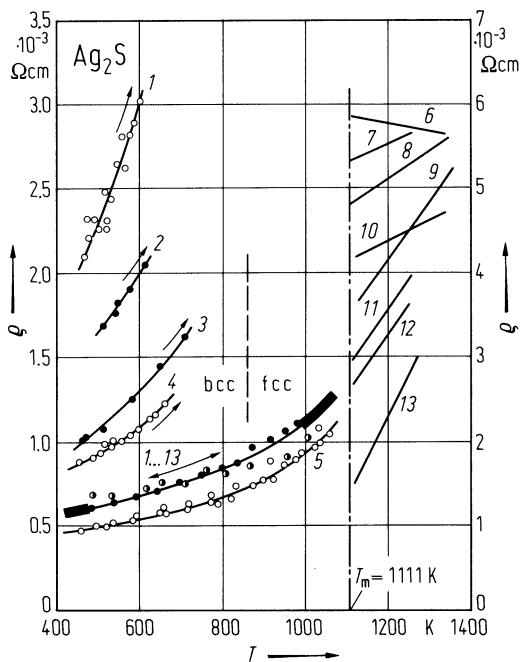


Fig. 16.7.6

Ag_2S . Electrical conductivity vs. reciprocal temperature. The different points (open circles, filled circles, etc.) correspond to nominally pure and stoichiometric samples measured without electrochemical control of the Ag/S ratio. In the β -phase ($T > T_{\alpha,\beta}$) both the absolute value and the slope of the conductivity are well determined. In the α -phase ($T < T_{\alpha,\beta}$) the influence of the thermal history of the different samples is clearly demonstrated [77J].

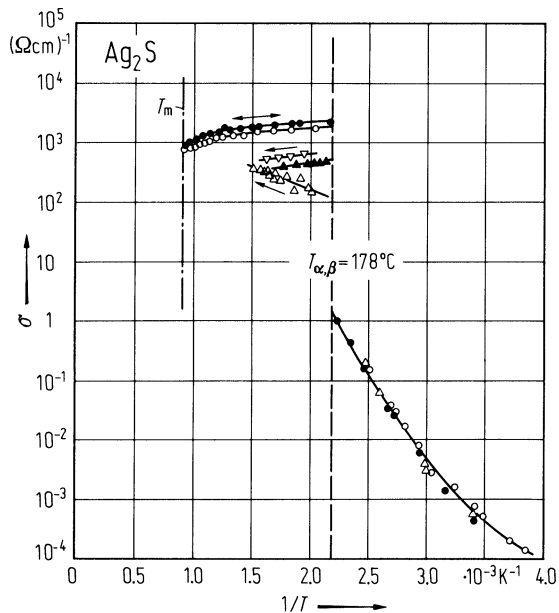
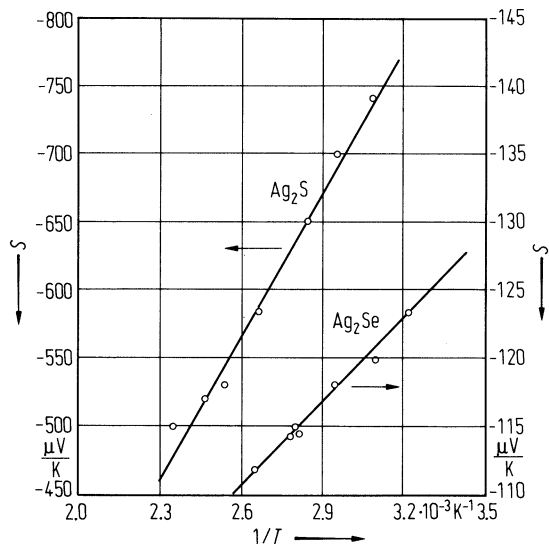


Fig. 16.7.7

Ag_2S , Ag_2Se . Thermoelectric power vs. reciprocal temperature [59J].



16.8 Silver selenide (Ag₂Se)

Crystal structure

For structure and lattice parameters see section 16.0.

Electronic properties

energy gap, effective masses

Ag₂Se is an n-type degenerate semiconductor of high (nearly 10¹⁹ cm⁻³) carrier concentration, irregularly high carrier mobility and with a degree of ionic conduction [80A].

energy gap

E_g	0.15 eV	$T = 293$ K	optical absorption	77J
-------	---------	-------------	--------------------	-----

effective masses

m_n	0.32 m_0	$T < T_{\alpha,\beta}$	transport data	59J
m_p	0.54 m_0	$T < T_{\alpha,\beta}$		59J

Lattice properties

linear thermal expansion coefficient

α	35.4·10 ⁻⁶ K ⁻¹		α -Ag ₂ Se	73G
	18.1·10 ⁻⁶ K ⁻¹		β -Ag ₂ Se	

Debye temperature

Θ_D	190 K	$T = 80$ K ...160 K	calorimetry	59G
------------	-------	------------------------	-------------	-----

density

d	8.25 g cm ⁻³	$T = 300$ K	temperature dependence: Fig. 16.38.1	59J
-----	-------------------------	-------------	--------------------------------------	-----

melting temperature

T_m	1153...1170 K			77J
-------	---------------	--	--	-----

Transport properties

electrical conductivity : Fig. 16.8.2 [59J, 77J]

carrier mobilities

μ_n	1990 cm ² /V s	$T = 349$ K	conductivity and Hall data	59J
μ_p	523 cm ² /V s	$T = 349$ K		

intrinsic carrier concentration

n_i	3.2·10 ¹⁸ cm ⁻³	$T = 349$ K	conductivity and Hall data	59J
-------	---------------------------------------	-------------	----------------------------	-----

References to 16.8

- 59G Gul'yaev, P. V., Petrov, A. V.: Fiz. Tverd. Tela 1 (1959) 368; Sov. Phys. Solid State (English Transl.) 1 (1959) 330.
- 59J Junod, P.: Helv. Phys. Acta 32 (1959) 567 and 601.
- 73G Gmelin's Handbuch der anorganischen Chemie, Verlag Chemie GmbH Weinheim. Bergstrasse, 5nd Edition. Silber, Teil B3, 1973.
- 77J Junod, P., Hediger, H., Kilchör, B., Wullschlegel, J.: Philos. Mag. 36 (1977) 941.
- 80A Abdullayev, A. G., Aliyev, V. K., Fufayeva, T. G., Skugareva, L. I: Thin Solid Fims 73 (1980) L7.

Figures to 16.8

Fig. 16.8.1

Ag_2Se . Density vs. temperature [73G1].

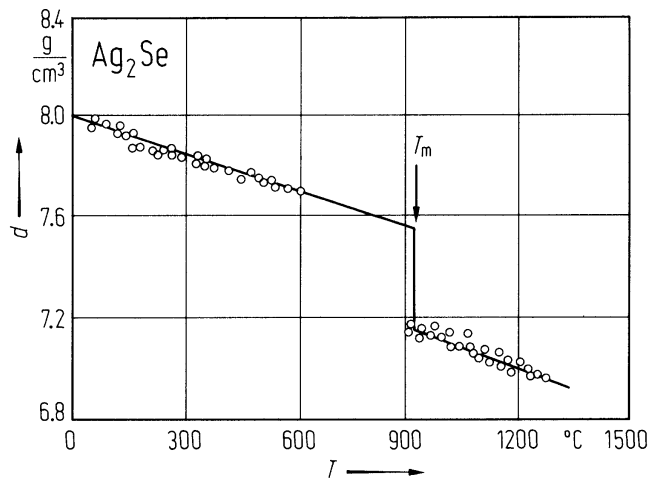
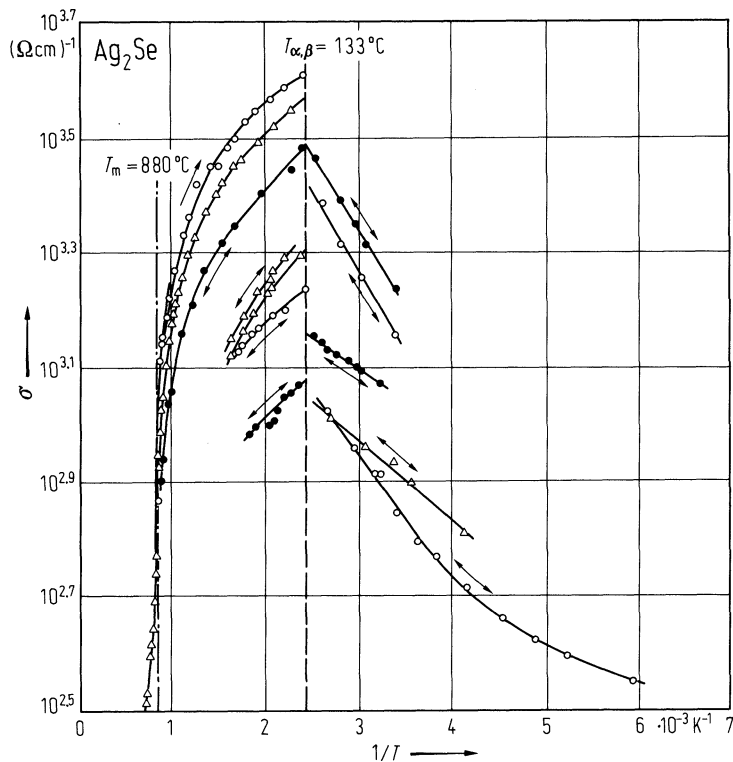


Fig. 16.8.2

Ag_2Se . Electrical conductivity vs. reciprocal temperature. For $T < T_{\alpha,\beta} = 133^\circ\text{C}$ all the measured samples demonstrate semiconducting properties. For $T > T_{\alpha,\beta}$ the coefficient $d\sigma/dT$ is always < 0 . The different curves, corresponding all to nominally pure and stoichiometric samples, demonstrate the influence of thermal history on the electrical conductivity of Ag_2Se [77J].



16.9 Silver telluride (Ag₂Te)

Crystal structure

For structure and lattice parameters see section 16.0.

Physical properties (α-Ag₂Te)

energy gap

$E_g \approx 0.67 \text{ eV}$ optical absorption edge 55A

electron effective masses

$m_n 0.026...0.034 m_0$ $T = 63...83.4 \text{ K}$ Hall effect and thermoelectric power 61W

Hall effect : see Fig. 16.9.1 [73G1].

thermoelectric power : see Fig. 16.9.2 [61W].

Ag₂Te remains a strongly degenerate semiconductor at low temperatures.

electrical conductivity : see Fig. 16.9.3 [61W, 73G1]

activation energy of electrical conductivity

$E_A 0.13 \text{ eV}$ conductivity 73G1

mobility of carriers

(Fig. 16.9.4)

$\mu_n (1...2) \cdot 10^3 \text{ cm}^2/\text{V s}$ $T = 300 \text{ K}$ Hall effect 73G1

$\mu_{n,max} 9 \cdot 10^3 \text{ cm}^2/\text{V s}$ $T = 180 \text{ K}$ (maximum of $\mu(T)$) 67D

density

$d 8.08...8.41 \text{ g cm}^{-3}$ $T = 300 \text{ K}$ (Fig. 16.9.5) 73G1

Physical properties (β- and γ-Ag₂Te)

energy gap

$E_g 0.20 \text{ eV}$ $T = 500...650 \text{ K}$ Hall effect 68N

effective masses

$m_n 0.077 m_0$ $T = 438 \text{ K}$ Hall effect and thermoelectric power 59M

$m_p 1.5 m_0$ $T = 438 \text{ K}$

mobility of carriers

$\mu_n 1440 \text{ cm}^2/\text{V s}$ $T = 438 \text{ K}$ Hall effect 73G1

$\mu_p 18 \text{ cm}^2/\text{V s}$ $T = 438 \text{ K}$ Hall effect 58M

melting temperature

$T_m 955^\circ\text{C}$ from phase diagram 58H

References to 16.9

- 55A Appel, J.: Z. Naturforsch. 10a (1955) 530.
- 58H Hansen, M.: Constitution of Binary Alloys, 2nd Edition, Mc Graw Hill, New York 1958.
- 58M Miyatani, S.: J. Phys. Soc. Jpn. 13 (1958) 341 and Miyatani, S., Yokota, I.: J. Phys. Soc. Jpn. 14 (1959) 750.
- 59M Miyatani, S., Yakota, I.: J. Phys. Soc. Jpn. 14 (1959) 750.
- 61W Wood, C., Harrap, C., Kane, W. M.: Phys. Rev. 121 (1961) 978.
- 67D Dalven, R., Gill, R.: J. Appl. Phys. 38 (1967) 753.
- 68N Nguyen Van Dong, Pham Ngutung: Phys. Status Solidi 30 (1968) 557.
- 73G1 Gmelin's Handbuch der anorganischen Chemie, Verlag Chemie GmbH Weinheim. Bergstrasse, 5nd Edition. Silber, Teil B3, 1973.
- 73G2 Gorbachev, V. V., Putilin, I. M.: Phys. Status Solidi (a) 16 (1973) 553.

Figures to 16.9

Fig. 16.9.1

Ag_2Te . Hall coefficient vs. reciprocal temperature, for the low temperature range and various samples [73G2].

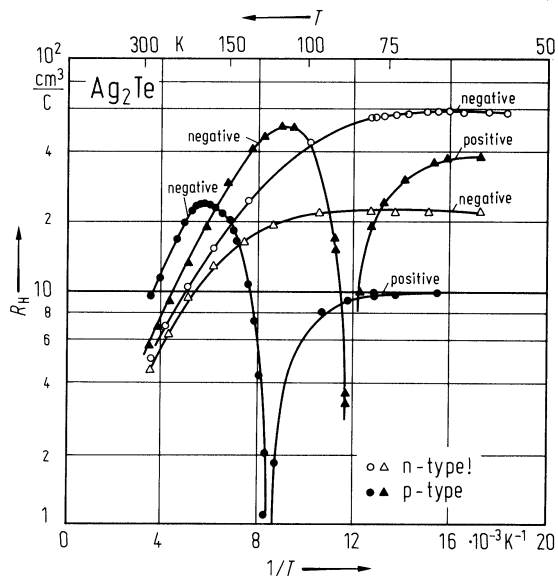


Fig. 16.9.2

Ag_2Te . Thermoelectric power for two n- and two p-type Ag_2Te samples vs. reciprocal temperature [61W].

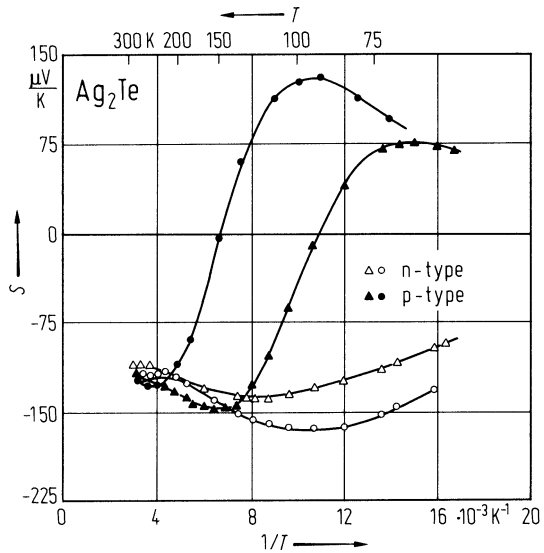


Fig. 16.9.3

Ag_2Te . Resistivity vs. reciprocal temperature for two n- and p-type Ag_2Te samples [61W].

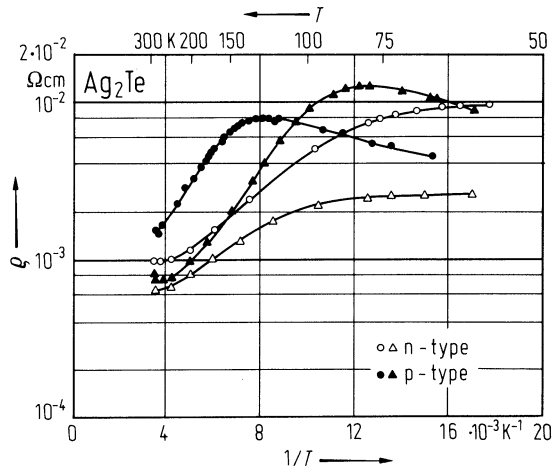


Fig. 16.9.4

Ag_2Te . Mobility μ_n for different compositions (concentration of Te in at%) vs. temperature [73G2].

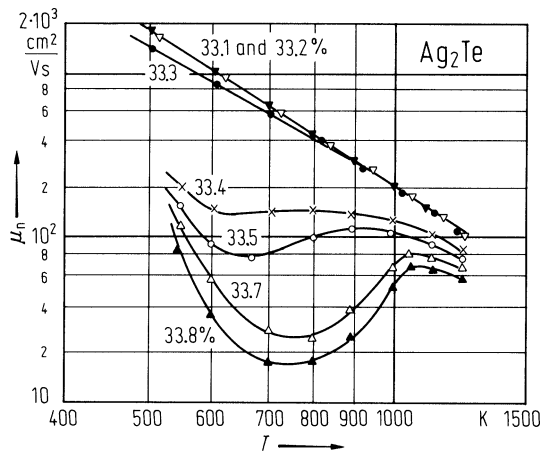
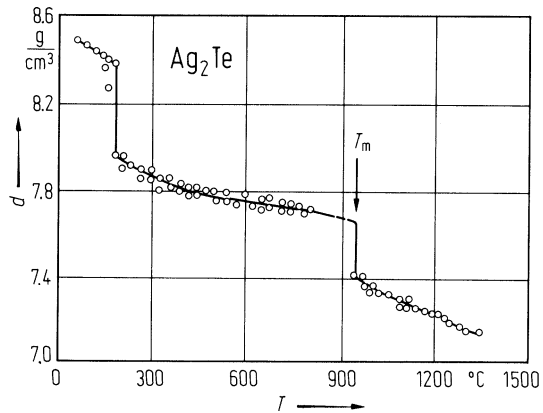


Fig. 16.0.5

Ag_2Te . Density vs. temperature [73G1].



17 II_x-IV_y compounds

17.0 Crystal structure and electronic properties

The most important semiconductors of this group are the silicide, germanide, stannide and plumbide of magnesium.

Mg₂Si crystallizes in the antifluorite structure (Fig. 17.0.1a). The X atoms form an fcc sublattice with lattice constant a , and the Mg atoms form a simple cubic sublattice with lattice constant $a/2$. X atoms are situated in the center of cubes built by the Mg atoms whereas Mg atoms are tetrahedrally coordinated by X atoms. The lattice can be thought of as a zincblende lattice where the cations at $(a/2)(1,1,1)$ are replaced by two Mg-atoms at $(a/2)(1,1,1)$ and $(3a/2)(1,1,1)$, respectively. Thus the antifluorite lattice has inversion symmetry in contrast to the zincblende lattice. The primitive cell (Fig. 17.0.1b) contains three atoms (one formula unit) with eight valence electrons.

The *space group* is O_h^5 (Fm3m). The *Bravais lattice* is the face centered cubic lattice (fcc).

The *Brillouin zone* is shown in Fig. 17.0.2. *Band structures* of the four Mg₂-IV compounds are shown in Figs. 17.0.3...17.0.6.

Besides the Mg₂-IV compounds some Ca₂-IV compounds and some Ba,Sr-IV₂ compounds are known as semiconductors. See section 17.5 and 17.6 for details.

References to 17.0

- 70A Aymerich, F., Mula, G.: Phys. Status Solidi (b) 42 (1970) 697.
- 70V Van Dyke, J. P., Hermann, F.: Phys. Rev. B2 (1970) 1644.

Figures to 17.0

Fig. 17.0.1

The antifluorite lattice of the Mg_2X -compounds. a) Face centered sublattice of the X-atoms (lattice constant a) and simple cubic sublattice of the Mg-atoms (lattice constant $a/2$); b) primitive cell.

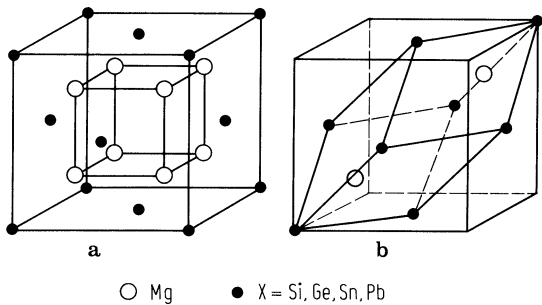


Fig. 17.0.2

Mg_2X -compounds. Brillouin zone (fcc Bravais lattice).

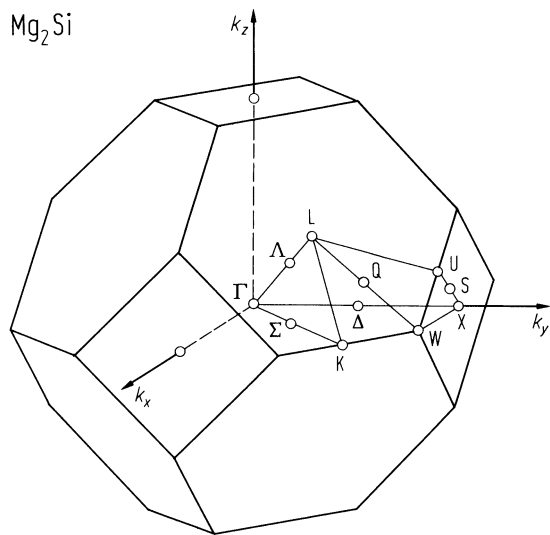


Fig. 17.0.3

Mg_2Si . Band structure calculated by a non-relativistic pseudopotential method [70A].

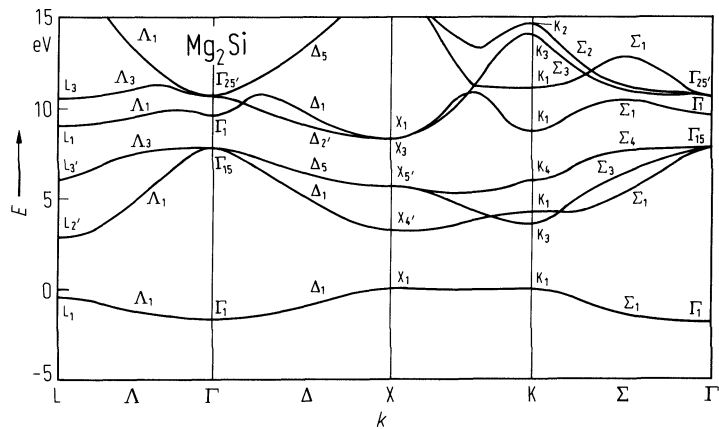


Fig. 17.0.4

Mg₂Ge. Band structure calculated by a non-relativistic pseudopotential method [70A].

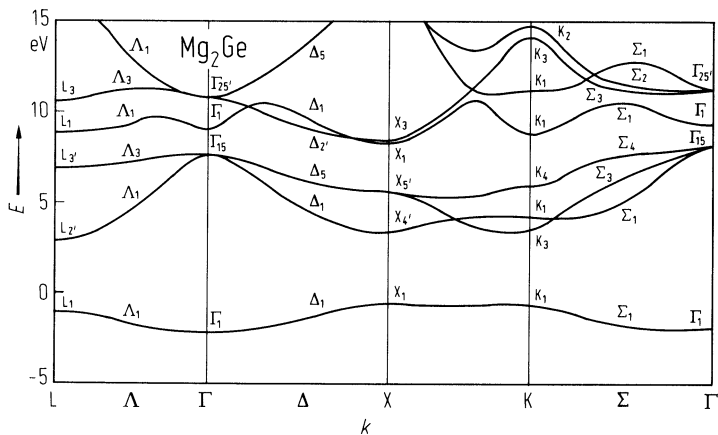


Fig. 17.0.5

Mg₂Sn. Band structure calculated by a non-relativistic pseudopotential method [70A].

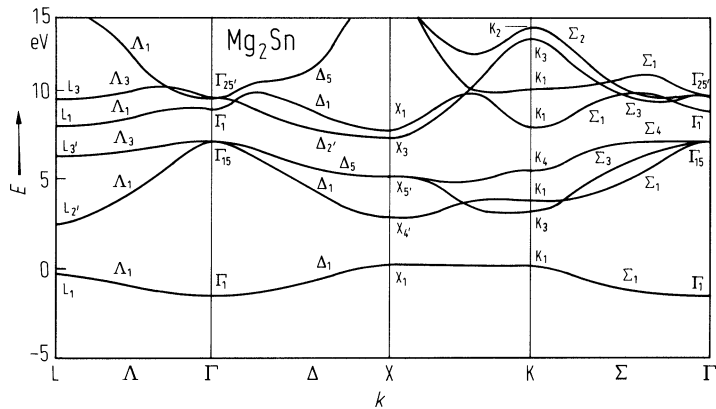
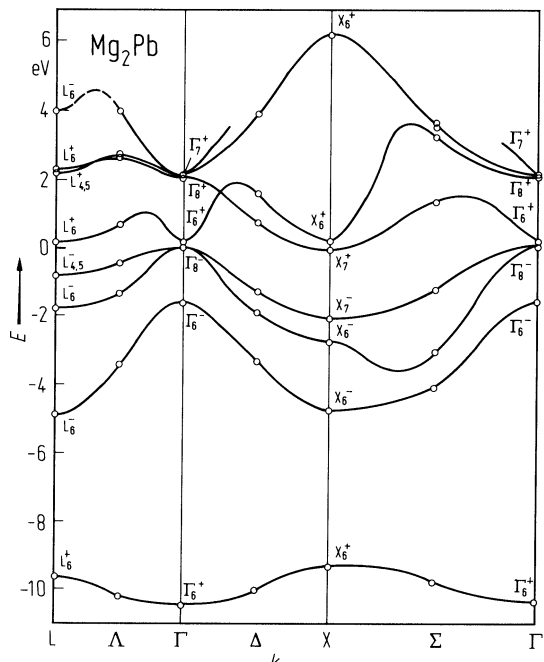


Fig. 17.0.6

Mg_2Pb . Energy band structure calculated with a relativistic OPW method [70V].



17.1 Magnesium silicide (Mg₂Si)

Crystal structure

see section 17.0.

Electronic properties

band structure : see Fig. 17.0.3, Brillouin zone: Fig. 17.0.2.

The lowest set of conduction bands has its minima at (or near to) the points X on the surface of the Brillouin zone. Surfaces of constant energy are prolate ellipsoids of revolution around the extrema. A second set of conduction bands follows at X at a slightly higher energy.

The valence band consists of an upper set of three bands with six electrons per primitive cell and a lower s-like band with two electrons per primitive cell. The top of the valence band shows a "germanium-like" degeneracy of a heavy hole band and a light hole band at Γ . A third valence band maximum is split off by spin-orbit interaction.

energy gaps

$E_{g,ind}(\Gamma_{15v}-X_{3c})$	0.77 eV	$T = 0$ K	temperature dependence of conductivity and Hall coefficient	55W
$E_{g,dir}(\Gamma_{15v}-\Gamma_{1c})$	2.27 eV	$T = 300$ K	electroreflectance	68V
$dE_{g,ind}/dT$	$-5 \cdot 10^{-4}$ eV K ⁻¹	$T = 90 \dots 370$ K	shift of absorption edge	61K

intra conduction band transition energy

$E(X_{1c}-X_{3c})$	0.40 eV		absorption band	66L
--------------------	---------	--	-----------------	-----

intra valence band transition energies

Δ_0 (at Γ_{15v})	0.03 eV		absorption band (spin-orbit splitting at Γ)	66L
Δ_1 (at $L_{3'v}$)	0.02 eV		Raman spectrum (spin-orbit splitting at L)	76O

effective masses

m_n	$0.46 m_0$		Hall effect	58M
m_p	$0.87 m_0$		Hall effect	58M

Lattice properties

lattice parameter

a	6.338 Å			67E
-----	---------	--	--	-----

volume expansion coefficient

β	$3.44 \cdot 10^{-5}$ K ⁻¹	$T = 300$ K		75D
$d\beta/dT$	$14.0 \cdot 10^{-9}$ K ⁻²			75D

compressibility

κ	$1.81 \cdot 10^{-12}$ cm ² /dyn	$T = 300$ K	from elastic constants	67G
----------	--	-------------	------------------------	-----

phonon dispersion relations

Fig. 17.1.1, Brillouin zone: Fig. 17.0.2.

Being three atoms in the unit cell of Mg₂Si there are one acoustic and two optical branches in the phonon spectrum. At $q = 0$ one of the optical branches is triply degenerate and Raman active (symmetry: $\Gamma_{25'}$, F_{2g}-phonon). The other (infrared active) branch of symmetry Γ_{15} (F_{1u}-phonon) is split by the macroscopic Coulomb field into a doubly degenerate TO mode and a LO mode.

phonon frequencies

$\nu_{\text{TO}}(\Gamma_{15})$	$8.0 \cdot 10^{12} \text{ s}^{-1}$	$T = 300 \text{ K}$	infrared reflectivity	63M
$\nu_{\text{LO}}(\Gamma_{15})$	$9.8 \cdot 10^{12} \text{ s}^{-1}$			
	$10.56 \cdot 10^{12} \text{ s}^{-1}$	$T = 77 \text{ K}$	Raman spectroscopy	71A
$\nu(\Gamma_{25'})$	$7.75 \cdot 10^{12} \text{ s}^{-1}$	$T = 300 \text{ K}$		
	$7.86 \cdot 10^{12} \text{ s}^{-1}$	$T = 77 \text{ K}$		

sound velocities

ν_{LA}	$7.68 \cdot 10^5 \text{ cm s}^{-1}$	$T = 300 \text{ K}$	[110]-direction	65W
$\nu_{\text{TA,I}}$	$4.83 \cdot 10^5 \text{ cm s}^{-1}$		[110]-direction, lower branch	
$\nu_{\text{TA,II}}$	$4.97 \cdot 10^5 \text{ cm s}^{-1}$		[110]-direction, upper branch	
ν_{LA}	$7.65 \cdot 10^5 \text{ cm s}^{-1}$		[111]-direction	
ν_{TA}	$4.95 \cdot 10^5 \text{ cm s}^{-1}$		[111]-direction	

second order elastic moduli

c_{11}	$12.1(2) \cdot 10^{11} \text{ dyn cm}^{-2}$	$T = 300 \text{ K}$	calculated from sound velocities	65W
c_{12}	$2.2(2) \cdot 10^{11} \text{ dyn cm}^{-2}$		(for temperature dependence, see Fig. 17.1.2)	
c_{44}	$4.64(5) \cdot 10^{11} \text{ dyn cm}^{-2}$			

Debye temperature

Θ_{D}	417 K	$T = 300 \text{ K}$
---------------------	-------	---------------------

lattice heat capacity

C_{v}	$0.001 \text{ J mol}^{-1} \text{ K}^{-1}$	$T = 5 \text{ K}$	from heat capacity measurements	67G
	$0.013 \text{ J mol}^{-1} \text{ K}^{-1}$	$T = 10 \text{ K}$		
	$8.82 \text{ J mol}^{-1} \text{ K}^{-1}$	$T = 50 \text{ K}$		
	$33.81 \text{ J mol}^{-1} \text{ K}^{-1}$	$T = 100 \text{ K}$		
	$67.87 \text{ J mol}^{-1} \text{ K}^{-1}$	$T = 300 \text{ K}$		

density

d	1.88 g cm^{-3}			55W
-----	--------------------------	--	--	-----

melting temperature

T_{m}	1102°C			53B
----------------	--------	--	--	-----

Transport properties

Electrical transport occurs via band conduction. No polaron effects or hopping conduction have been observed. The dominating scattering mechanisms are optical mode and impurity scattering.

electrical conductivity, Hall effect : Fig. 17.1.3.

mobility of charge carriers

μ_{n}	$550 \text{ cm}^2/\text{V s}$	$T = 300 \text{ K}$	Hall mobility, for temperature dependence, see Fig. 17.1.4	62H
μ_{p}	$70 \text{ cm}^2/\text{V s}$			

intrinsic carrier concentration

n_{i}	$1 \cdot 10^{14} \text{ cm}^{-3}$	$T = 300 \text{ K}$	from conductivity and Hall coefficient	55W
----------------	-----------------------------------	---------------------	--	-----

thermal conductivity : see Fig. 17.1.5

Optical properties

Spectral dependence of optical constants: Fig. 17.1.6.

dielectric constants

$\varepsilon(0)$	20	from infrared reflectivity	63M
$\varepsilon(\infty)$	13.3	from infrared reflectivity	63M

References to 17.1

- 53B Busch, G., Winkler, U.: *Helv. Phys. Acta* 26 (1953) 578.
55W Winkler, U.: *Helv. Phys. Acta* 28 (1955) 633.
58M Morris, R. G., Redin, R. D., Danielson, G. C.: *Phys. Rev.* 109 (1958) 1909.
61K Koenig, P., Lynch, D. W., Danielson, G. C.: *J. Phys. Chem. Solids* 20 (1961) 122.
62H Helier, M. W., Danielson, G. C.: *J. Phys. Chem. Solids* 23 (1962) 601.
63M McWilliams, D., Lynch, D. W.: *Phys. Rev.* 130 (1963) 2248.
65W Whitten, W. B., Chung, P. L., Danielson, G. C.: *J. Phys. Chem. Solids* 26 (1965) 49.
66L Loit, L. A., Lynch, D. W.: *Phys. Rev.* 141 (1966) 681.
67E Eldridge, J. M., Miller, E., Komarek, K. L.: *Trans. Met. Soc. AIME* 239 (1967) 775.
67G Gerstein, B. C., Jelinek, F. J., Habenschuss, M., Shickell, W. D., Mullay, J. R., Chung, P. L.: *J. Chem. Phys.* 47 (1967) 2109.
68V Väsques, F., Forman, R. A., Cardona, M.: *Phys. Rev.* 176 (1968) 905.
69S Scouler, W. S.: *Phys. Rev.* 178 (1969) 1353.
70A Aymerich, F., Mula, G.: *Phys. Status Solidi (b)* 42 (1970) 697.
71A Anastassakis, E., Burstein, E.: *Solid State Commun.* 9 (1971) 1525.
72L Li, P. W., Lee, S. N., Danielson, G. C.: *Phys. Rev. B* 6 (1972) 442.
75D Dutchak, Ya. I., Yarmolyuk, V. P., Fedyshin, Yu. I.: *Izv. Akad. Nauk, Neorg. Mater.* 11 (1975) 1227; *Inorg. Mater. (USSR) (English Transl.)* 11 (1975) 1047.
76O Onari, S., Cardona, M.: *Phys. Rev. B* 14 (1976) 3520.

Figures to 17.1

Fig. 17.0.2

Mg_2X -compounds. Brillouin zone (fcc Bravais lattice).

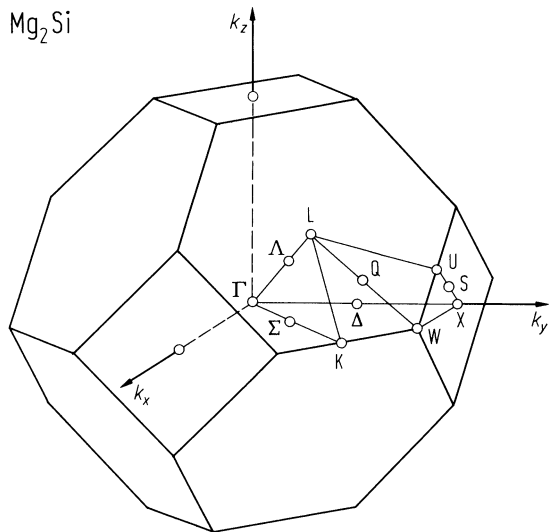


Fig. 17.0.3

Mg_2Si . Band structure calculated by a non-relativistic pseudopotential method [70A].

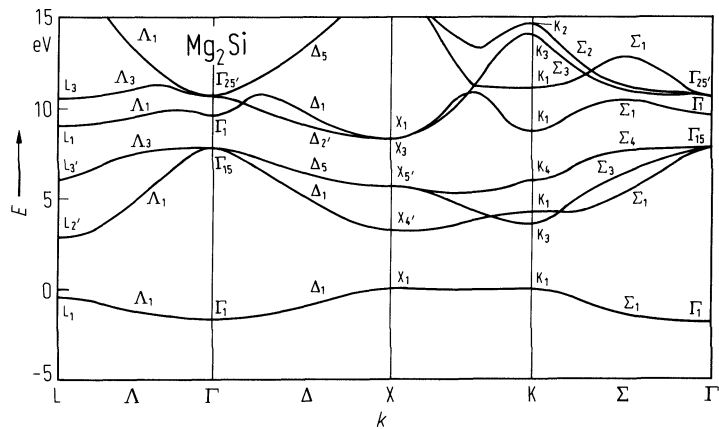


Fig. 17.1.1

Mg_2Si . Phonon dispersion relations for the principal symmetry directions in the Brillouin zone [65W].

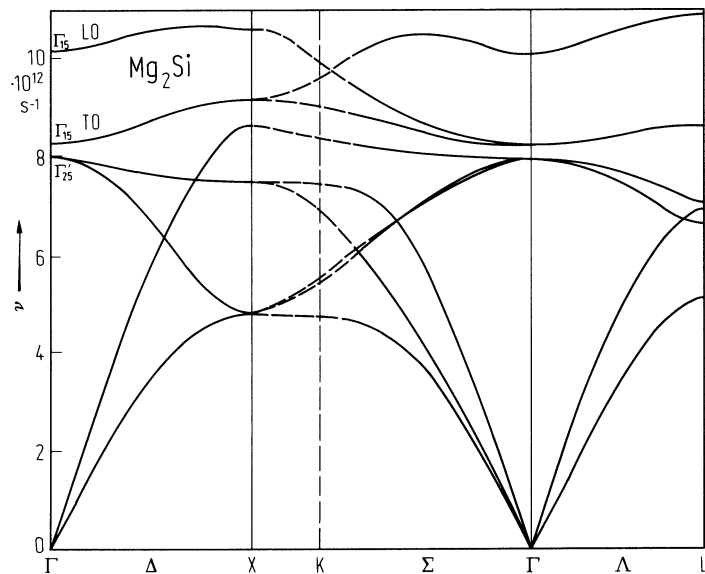


Fig. 17.1.2

Mg_2Si . Elastic moduli c_{ik} vs. temperature calculated from sound velocity data [65W]. Solid lines: least square fits.

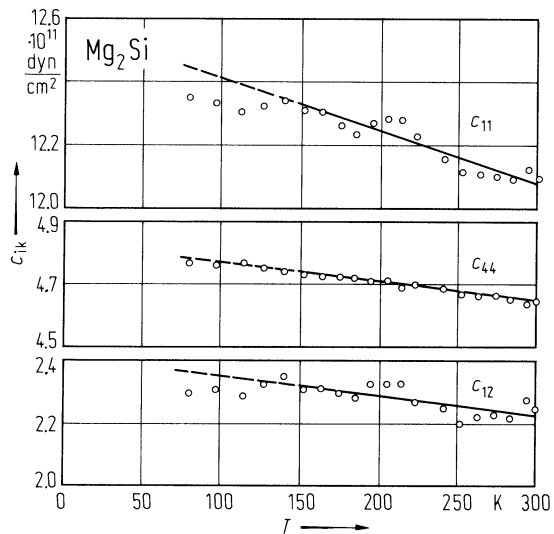


Fig. 17.1.3

Mg_2Si . Electrical conductivity vs. temperature for three n-type samples in the range of mixed conduction [55W]. 1, $\text{Mg}_2\text{Si} + 2\text{‰ Mg}$; 2, Mg_2Si ; 3, $\text{Mg}_2\text{Si} + 2\text{‰ Si}$.

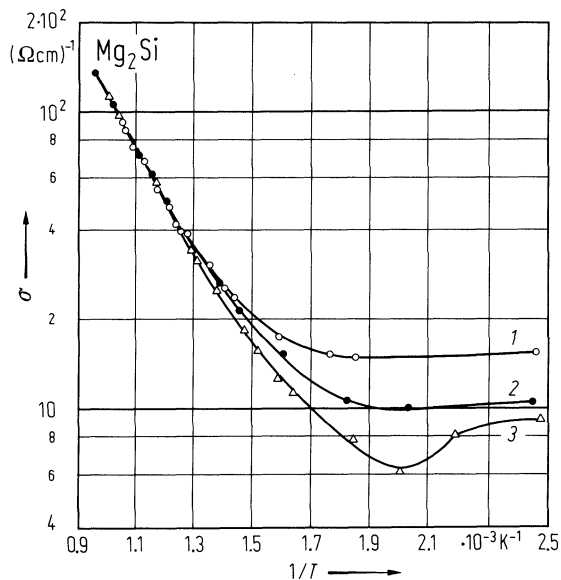


Fig. 17.1.4

Mg_2Si . Hall mobility vs. temperature [62H].

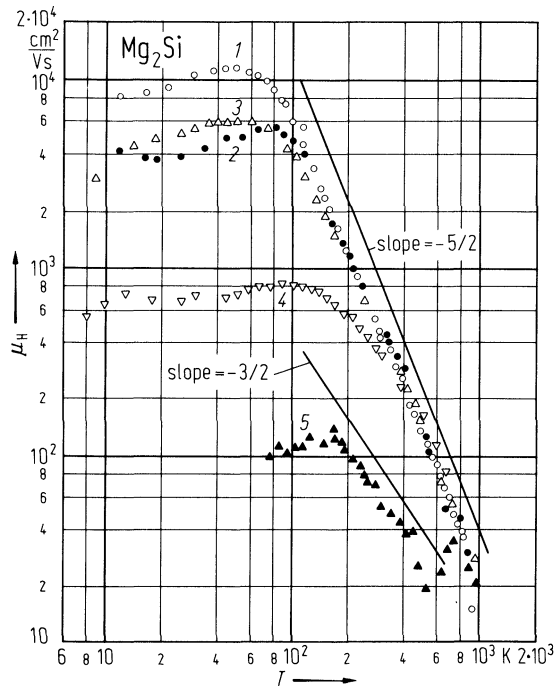


Fig. 17.1.5

Mg_2X -compounds. Thermal conductivity vs. temperature for Mg_2Si , Mg_2Ge and Mg_2Sn [72M].

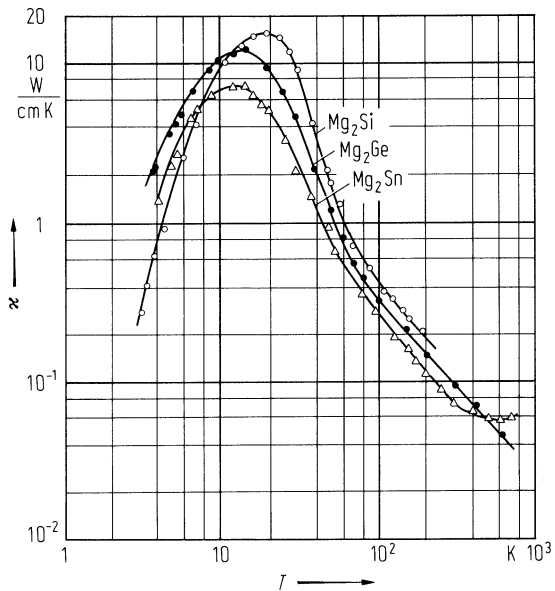
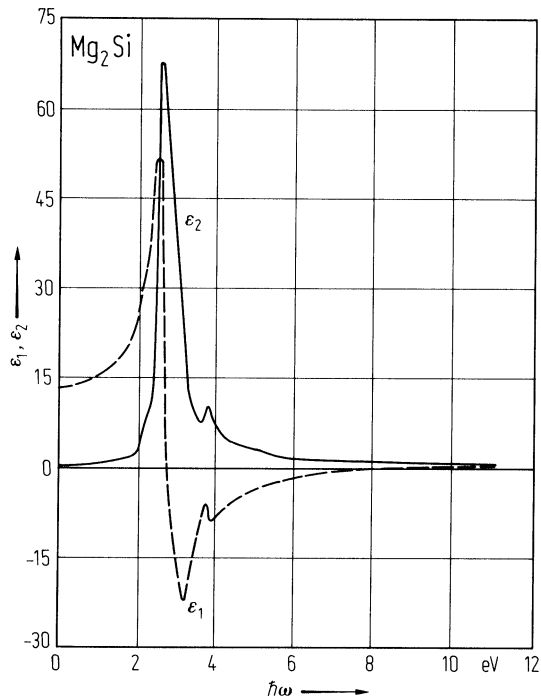


Fig. 17.1.6

Mg_2Si . Real and imaginary parts of the dielectric constant ϵ_1 and ϵ_2 vs. photon energy [69S].



17.2 Magnesium germanide (Mg₂Ge)

Crystal structure

see section 17.0.

Electronic properties

band structure: Fig. 17.0.4, Brillouin zone: Fig. 17.0.2.

For general aspects of the band structure, see the remarks on the band structure of Mg₂Si.

energy gap

$E_{g,ind}(\Gamma_{15v}-X_{1c})$	0.74 eV	$T = 0$ K	temperature dependence of conductivity and Hall coefficient	55W
	0.548 eV	$T = 300$ K	shape of absorption edge	64M
$E_{g,dir}(\Gamma_{15v}-\Gamma_{1c})$	1.64 eV	$T = 300$ K	electroreflection	68V
$dE_{g,ind}/dT$	$-2 \cdot 10^{-4}$ eV K ⁻¹		surface barrier photoresponse	64M
$dE_{g,dir}/dT$	$-3.5 \cdot 10^{-4}$ eV K ⁻¹		surface barrier photoresponse	64M

intra conduction band transition

$E(X_{3c}-X_{1c})$	0.58 eV		absorption band	66L
--------------------	---------	--	-----------------	-----

intra valence band transitions

Δ_0 (at Γ_{15v})	0.20 eV		absorption band	66L
Δ_1 (at $L_{3'v}$)	0.13 eV	$T = 300$ K	(spin-orbit splitting at Γ) electroreflection	68V

effective masses

m_n	$0.18 m_0$		conductivity and Hall coefficient	58R
m_p	$0.31 m_0$			

Lattice properties

lattice parameter

a	6.393 Å			67E
-----	---------	--	--	-----

volume expansion coefficient

β	$7.33 \cdot 10^{-6}$ K ⁻¹		from elastic constants.	66G
---------	--------------------------------------	--	-------------------------	-----

Linear expansion coefficient α and the fractional change in length $\Delta l/l$ vs. temperature, Fig. 17.2.1.

compressibility

κ	$1.83 \cdot 10^{-12}$ cm ² dyn ⁻¹	$T = 300$ K	from elastic constants	66G
----------	---	-------------	------------------------	-----

phonon dispersion relations : Fig. 17.2.2, Brillouin zone: Fig. 17.0.2.

phonon frequencies

$\nu_{TO}(\Gamma_{15})$	$6.2 \cdot 10^{12}$ s ⁻¹	$T = 300$ K	infrared reflectivity	63M
$\nu_{LO}(\Gamma_{15})$	$7.1 \cdot 10^{12}$ s ⁻¹	$T = 300$ K	infrared reflectivity	63M
$\nu(\Gamma_{25'})$	$7.64 \cdot 10^{12}$ s ⁻¹	$T = 300$ K	Raman spectroscopy	71A2
$E_{ph,ind}$	0.025 eV	$T = 0$ K	phonon participating in the indirect band-band transition $\Gamma_{15} - X_3$	66L

sound velocities

v_{LA}	$6.3 \cdot 10^5 \text{ cm s}^{-1}$	$T = 300 \text{ K}$	[100]-direction, temperature	65C
v_{TA}	$3.8 \cdot 10^5 \text{ cm s}^{-1}$		independent in the range 50...300 K	
v_{LA}	$6.2 \cdot 10^5 \text{ cm s}^{-1}$		[111]-direction	
v_{TA}	$3.8 \cdot 10^5 \text{ cm s}^{-1}$			

second order elastic moduli

c_{11}	$11.79(15) \cdot 10^{11} \text{ dyn cm}^{-2}$	$T = 300 \text{ K}$	calculated from sound velocities	65C
c_{12}	$2.30(50) \cdot 10^{11} \text{ dyn cm}^{-2}$		(for temperature dependence, see Fig. 17.2.3)	
c_{44}	$4.65 (10) \cdot 10^{11} \text{ dyn cm}^{-2}$			

Debye temperature

Θ_D	363.0 K	$T = 300 \text{ K}$		66G
------------	---------	---------------------	--	-----

lattice heat capacity

C_v	$0.007 \text{ J mol}^{-1} \text{ K}^{-1}$	$T = 5 \text{ K}$	from heat capacity measurements	66G
	$0.051 \text{ J mol}^{-1} \text{ K}^{-1}$	$T = 10 \text{ K}$		
	$13.85 \text{ J mol}^{-1} \text{ K}^{-1}$	$T = 50 \text{ K}$		
	$40.89 \text{ J mol}^{-1} \text{ K}^{-1}$	$T = 100 \text{ K}$		
	$69.62 \text{ J mol}^{-1} \text{ K}^{-1}$	$T = 300 \text{ K}$		

density

d	3.09 g cm^{-3}			55W
-----	--------------------------	--	--	-----

melting temperature

T_m	1115°C			53B
-------	--------	--	--	-----

Transport properties

Electrical transport occurs via band conduction. No polaron effects or hopping conduction have been observed.
Conductivity, Hall effect: Fig. 17.2.4.

mobility of charge carriers

μ_n	$310 \text{ cm}^2/\text{V s}$	$T = 300 \text{ K}$	Hall mobility, temperature dependence	72L
	$2200 \text{ cm}^2/\text{V s}$	$T = 77 \text{ K}$	in the intrinsic range: $T^{-1.5}$, see Fig. 17.2.5	
μ_p	$106 \text{ cm}^2/\text{V s}$	$T = 300 \text{ K}$	Hall mobility, temperature dependence:	55W
	$1180 \text{ cm}^2/\text{V s}$	$T = 77 \text{ K},$ $p = 6.4 \cdot 10^{16} \text{ cm}^{-3}$	Hall mobility, compensated material	74S

intrinsic carrier concentration

n_i	$2 \cdot 10^{14} \text{ cm}^{-3}$	$T = 300 \text{ K}$	from conductivity and Hall coefficient	55W
-------	-----------------------------------	---------------------	--	-----

thermal conductivity : see Fig. 17.2.6

Optical properties

Spectral dependence of infrared reflectivity: Fig. 17.2.7, of index of refraction and extinction coefficient: Fig. 17.2.8, of the dielectric function: Fig. 17.2.9.

dielectric constants

$\epsilon(0)$	21.7		Raman spectroscopy	71A1
$\epsilon(\infty)$	13.9			

References to 17.2

- 53B Busch, G., Winkler, U.: *Helv. Phys. Acta* 26 (1953) 578.
- 55W Winkler, U.: *Helv. Phys. Acta* 28 (1955) 633.
- 58R Redin, R. D., Morris, R. G., Danielson, G. C.: *Phys. Rev.* 109 (1958) 1916.
- 63M McWilliams, D., Lynch, D. W.: *Phys. Rev.* 130 (1963) 2248.
- 64M Mead, C. A.: *J. Appl. Phys.* 35 (1964) 2460.
- 65C Chung, P. H., Whitten, W. B., Danielson, G. C.: *J. Phys. Chem. Solids* 26 (1965) 1753.
- 66G Gerstein, B. C., Chung, P. L., Danielson, G. C.: *J. Phys. Chem. Solids* 27 (1966) 1161.
- 66L Loit, L. A., Lynch, D. W.: *Phys. Rev.* 141 (1966) 681.
- 67E Eldridge, J. M., Miller, E., Komarek, K. L.: *Trans. Met. Soc. AIME* 239 (1967) 775.
- 68V Vásques, F., Forman, R. A., Cardona, M.: *Phys. Rev.* 176 (1968) 905.
- 69S Scouler, W. S.: *Phys. Rev.* 178 (1969) 1353.
- 70A Aymerich, F., Mula, G.: *Phys. Status Solidi (b)* 42 (1970) 697.
- 71A1 Anastassakis, E., Burstein, E.: *Solid State Commun.* 9 (1971) 1525.
- 71A2 Anastassakis, E., Perry, C. H.: *Solid State Commun.* 9 (1971) 407.
- 72L Li, P. W., Lee, S. N., Danielson, G. C.: *Phys. Rev. B* 6 (1972) 442.
- 72M Martin, J. J.: *J. Phys. Chem. Solids* 33 (1972) 1139.
- 74S Shanks, H. R.: *J. Cryst. Growth* 23 (1974) 190.

Figures to 17.2

Fig. 17.0.2

Mg_2X -compounds. Brillouin zone (fcc Bravais lattice).

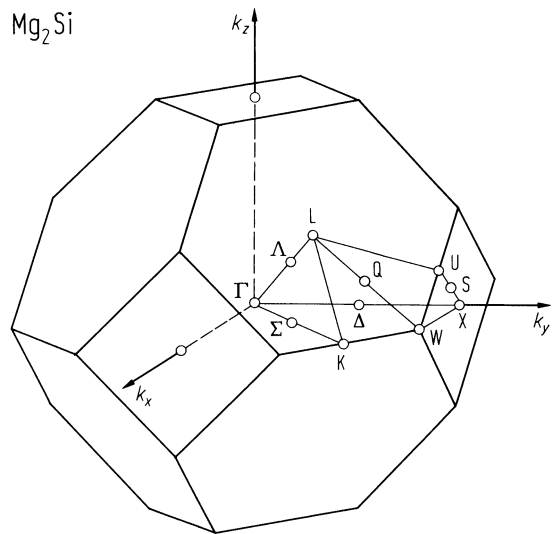


Fig. 17.0.4

Mg₂Ge. Band structure calculated by a non-relativistic pseudopotential method [70A].

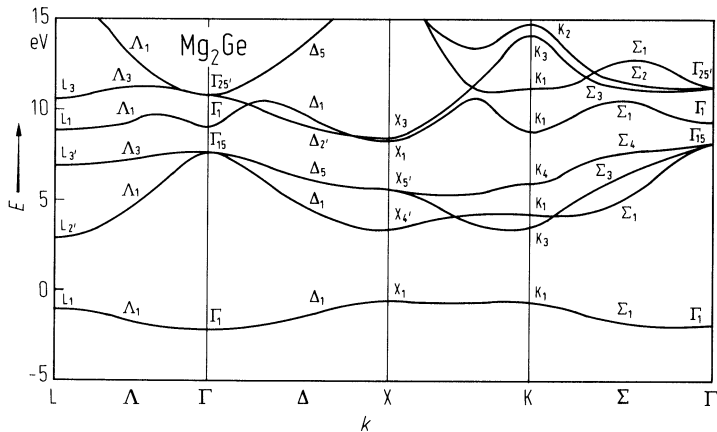


Fig. 17.2.1

Mg_2Ge . Linear expansion coefficient α and the fractional change in length $\Delta l/l$ vs. temperature, determined by a resistance strain-gauge method [65C].

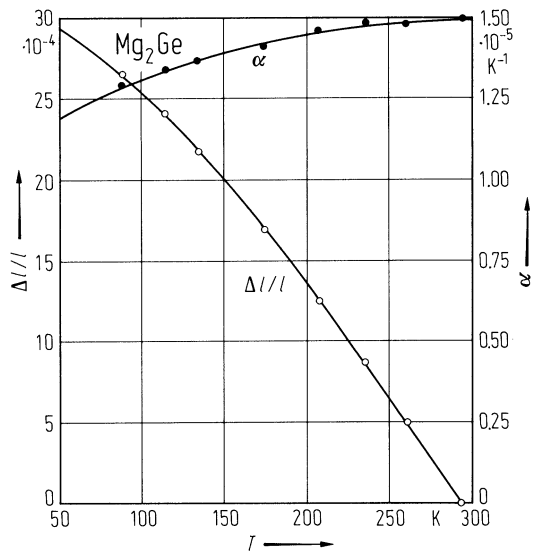


Fig. 17.2.2

Mg_2Ge . Phonon dispersion relations for three symmetry directions calculated by two different shell models using experimentally determined parameters. In model I the short range second neighbor interactions are assumed to be central. In model II the short range forces between Mg atoms are assumed to be zero [65C]. Error in figure: Mg_2Se should read Mg_2Ge !

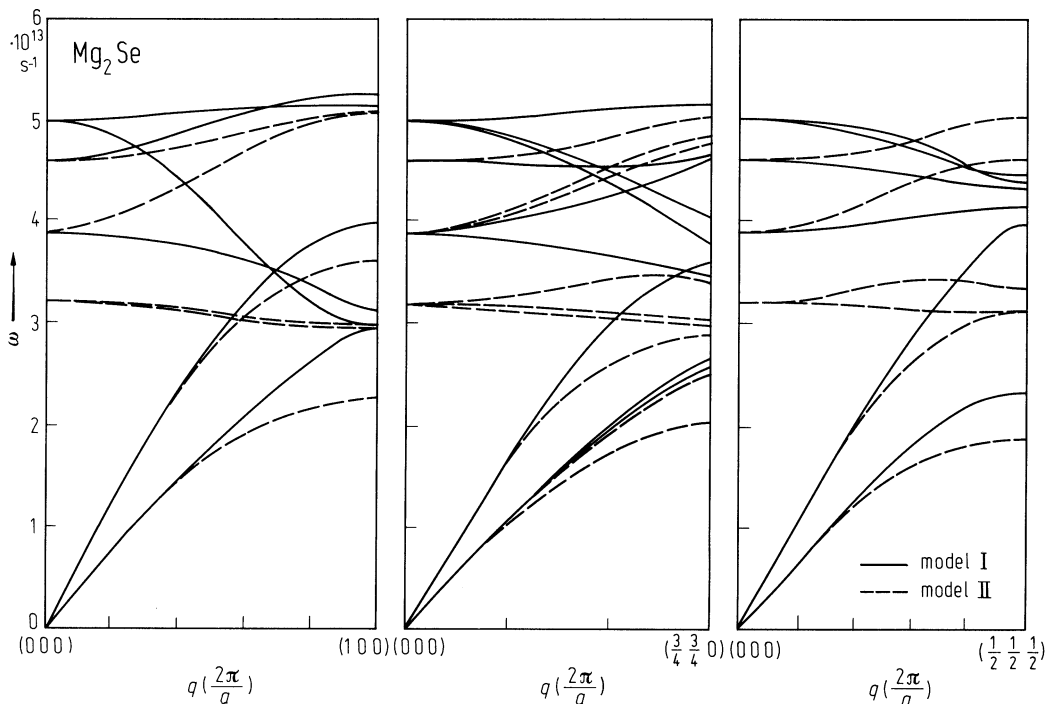


Fig. 17.2.3

Mg_2Ge . Second order elastic moduli c_{ik} vs. temperature [65C].

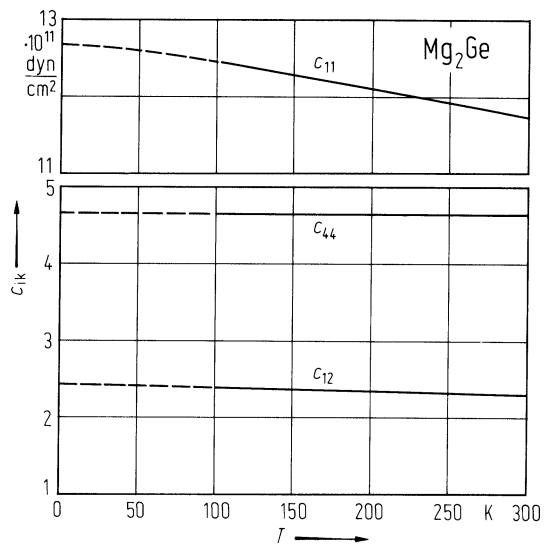


Fig. 17.2.4

Mg₂Ge. Electrical resistivity vs. temperature of three n-type and two p-type samples [58R].

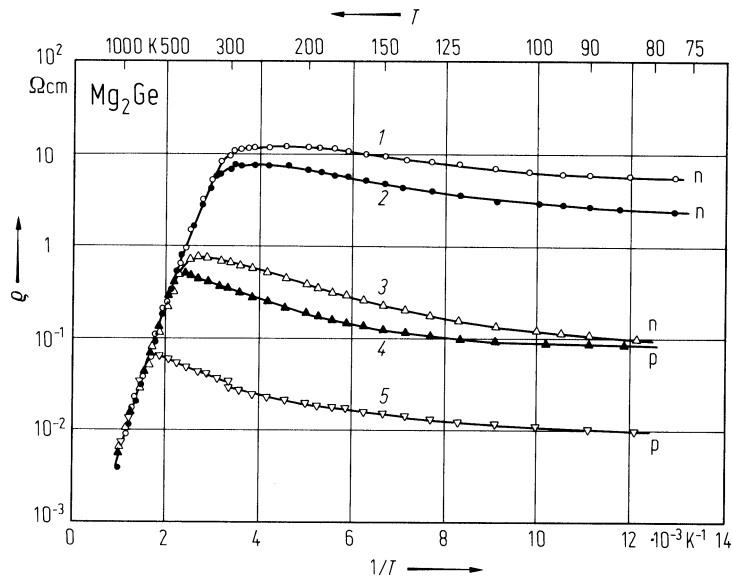


Fig. 17.2.5

Mg₂Ge. Hall mobility vs. temperature [72L].

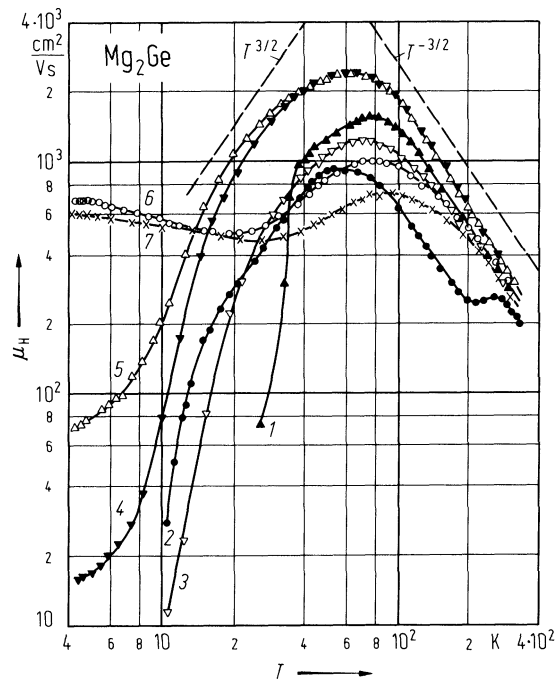


Fig. 17.2.6

Mg₂X-compounds. Thermal conductivity vs. temperature for Mg₂Si, Mg₂Ge and Mg₂Sn [72M].

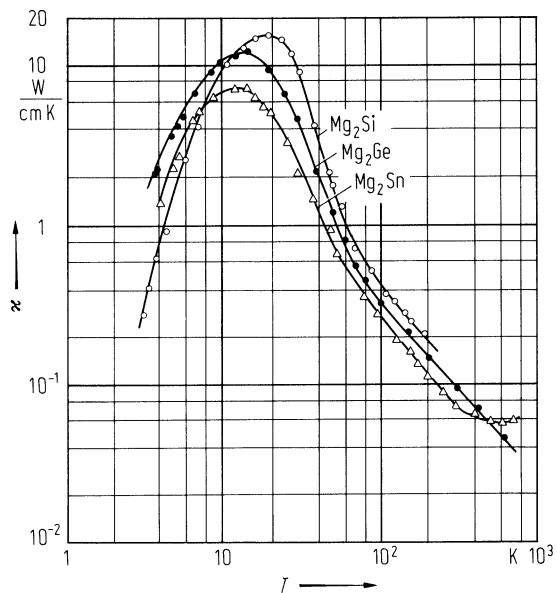


Fig. 17.2.7

Mg_2Ge . Infrared reflectivity vs. wavelength for an n-type sample with $n = 2.75 \cdot 10^{16} \text{ cm}^{-3}$ (solid line). Dashed line: theoretical fit for a one-resonance model [63M].

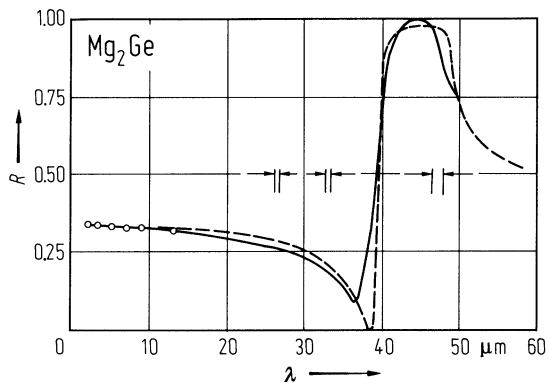


Fig. 17.2.8

Mg₂Ge. Index of refraction n and extinction coefficient k vs. photon energy [69S].

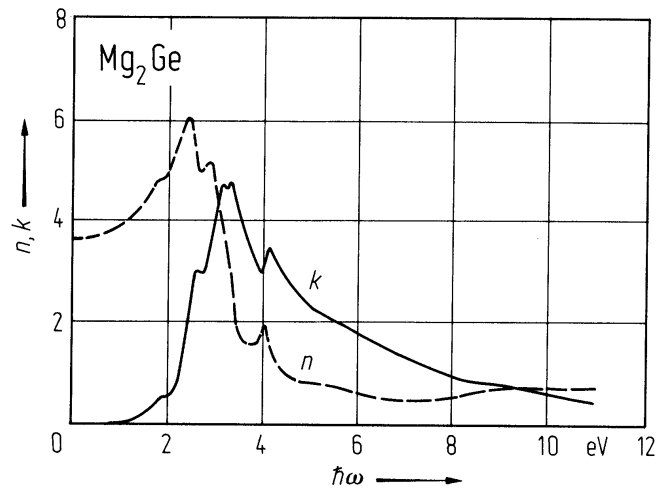
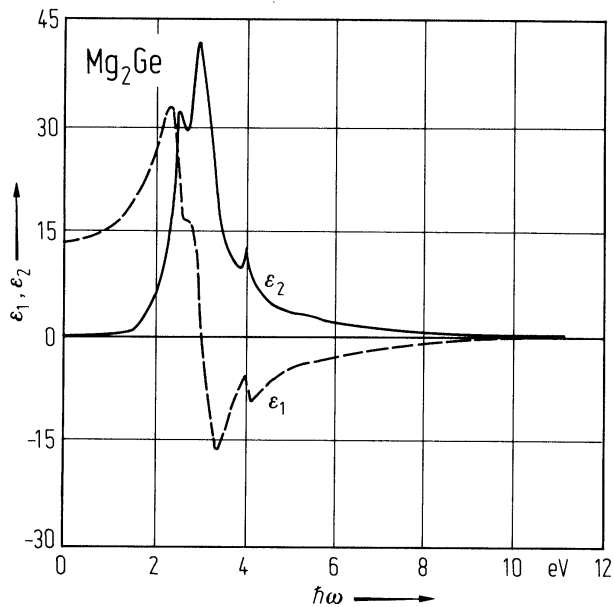


Fig. 17.2.9

Mg₂Ge. Real and imaginary parts ϵ_1 and ϵ_2 of the dielectric constant vs. photon energy [69S].



17.3 Magnesium stannide (Mg₂Sn)

Crystal structure

see section 17.0.

Electronic properties

band structure: Fig. 17.0.5, Brillouin zone: Fig. 17.0.2.

For general aspects of the band structure, see the remarks on the band structure of Mg₂Si. According to the variation of the indirect gap in solid solutions with Mg₂Sn the symmetry of the lowest and the second-lowest conduction band is interchanged compared with Mg₂Si and Mg₂Ge.

energy gap

$E_{g,\text{ind}}(\Gamma_{15v}-X_{3c})$	0.30 eV	$T = 15 \text{ K}$	extrapolation of straight-line part	64L
	0.23 eV	$T = 300 \text{ K}$	of absorption coefficient to zero	
$E_{g,\text{dir}}(\Gamma_{15v}-\Gamma_{1c})$	(1.2 eV)		(calculated from band structure)	70A
$dE_{g,\text{ind}}/dT$	$-1.7 \cdot 10^{-4} \text{ eV K}^{-1}$		shift of absorption edge	64L

intra conduction band transitions

$E_{c2} - E_{c1}$	0.125 eV	$T = 300 \text{ K}$	pressure dependence of conductivity	72T
$(X_{1c}-X_{3c})$				

intra valence band transitions

Δ_0 (at Γ_{15v})	0.48 eV	$T = 300 \text{ K}$	electroreflection	68V
			(spin-orbit splitting at Γ)	
Δ_1 (at $L_{3'v}$)	0.27 eV	$T = 77 \text{ K}$	Raman spectroscopy	76O
Δ_2 ($X_{5'v}$)	0.14 eV	$T = 77 \text{ K}$	Raman spectroscopy	76O

effective masses

m_n	$1.2 m_0$		density of states mass, from	64L
			conductivity measurements	
m_p	$0.10 m_0$		free carrier absorption	64L

Lattice properties

lattice parameter

a	6.762 Å			67E
-----	---------	--	--	-----

volume expansion coefficient

β	$2.97 \cdot 10^{-5} \text{ K}^{-1}$	$T = 300 \text{ K}$		67J
---------	-------------------------------------	---------------------	--	-----

compressibility

κ	$2.83 \cdot 10^{-12} \text{ cm}^2 \text{ dyn}^{-1}$	$T = 300 \text{ K}$	from elastic constants	67J
----------	---	---------------------	------------------------	-----

Debye temperature

Θ_D	240.0 K	$T = 300 \text{ K}$		67J
------------	---------	---------------------	--	-----

lattice heat capacity

C_v	0.0191 J mol ⁻¹ K ⁻¹	$T = 5$ K	from heat capacity measurements	67J
	0.241 J mol ⁻¹ K ⁻¹	$T = 10$ K		
	20.55 J mol ⁻¹ K ⁻¹	$T = 50$ K		
	47.12 J mol ⁻¹ K ⁻¹	$T = 100$ K		
	72.50 J mol ⁻¹ K ⁻¹	$T = 300$ K		

density

d	3.59 g cm ⁻³			55W
-----	-------------------------	--	--	-----

melting temperature

T_m	778°C			53B
-------	-------	--	--	-----

phonon dispersion relations : Fig.17.3.1, Brillouin zone: Fig. 17.0.2.

phonon frequencies

$\nu_{\text{TO}}(\Gamma_{15})$	$5.56 \cdot 10^{12}$ s ⁻¹	$T = 300$ K	inelastic thermal neutron scattering	70K
$\nu_{\text{LO}}(\Gamma_{15})$	$6.96 \cdot 10^{12}$ s ⁻¹	$T = 100 \dots 300$ K		66G1
$\nu(\Gamma_{25'})$	$6.67 \cdot 10^{12}$ s ⁻¹	$T = 300$ K	thermal neutron scattering	70K
$\nu_{\text{TA}}(\text{X}_{5'})$	$2.21 \cdot 10^{12}$ s ⁻¹			
$\nu_{\text{LA}}(\text{X}_{4'})$	$3.68 \cdot 10^{12}$ s ⁻¹			
$\nu_{\text{TO,I}}(\text{X}_{2'})$	$4.47 \cdot 10^{12}$ s ⁻¹			
$\nu_{\text{LO,I}}(\text{X}_5)$	$4.58 \cdot 10^{12}$ s ⁻¹			
$\nu_{\text{TO,II}}(\text{X}_{5'})$	$6.79 \cdot 10^{12}$ s ⁻¹			
$\nu_{\text{LO,II}}(\text{X}_1)$	$9.07 \cdot 10^{12}$ s ⁻¹			
$\nu_{\text{TA}}(\text{L}_{3'})$	$1.60 \cdot 10^{12}$ s ⁻¹			
$\nu_{\text{LA}}(\text{L}_{2'})$	$3.43 \cdot 10^{12}$ s ⁻¹			
$\nu_{\text{TO,I}}(\text{L}_3)$	$5.97 \cdot 10^{12}$ s ⁻¹			
$\nu_{\text{LO,I}}(\text{L}_1)$	$6.00 \cdot 10^{12}$ s ⁻¹			
$\nu_{\text{TO,II}}(\text{L}_{3'})$	$5.91 \cdot 10^{12}$ s ⁻¹			
$\nu_{\text{LO,II}}(\text{L}_1)$	$7.60 \cdot 10^{12}$ s ⁻¹			
$E_{\text{ph,ind}}$	0.008 eV		phonon participating in the indirect band-band transition $\Gamma_{15v} - \text{X}_{3c}$	64L

sound velocities

v_{LA}	$4.8 \cdot 10^5$ cm s ⁻¹	$T = 300$ K	[100]-direction, almost temperature independent in the range 50...300 K, [110]-direction [111]-direction	67D
v_{TA}	$3.3 \cdot 10^5$ cm s ⁻¹			
v_{TA}	$2.9 \cdot 10^5$ cm s ⁻¹			
v_{LA}	$5.0 \cdot 10^5$ cm s ⁻¹			
v_{TA}	$3.0 \cdot 10^5$ cm s ⁻¹			

second order elastic moduli

c_{11}	$8.24(33) \cdot 10^{11}$ dyn cm ⁻²	$T = 300$ K	calculated from sound velocities (for temperature dependence, see Fig. 17.3.2)	67D
c_{12}	$2.08(23) \cdot 10^{11}$ dyn cm ⁻²			
c_{44}	$3.66(7) \cdot 10^{11}$ dyn cm ⁻²			

Transport properties

Electrical transport occurs via band conduction. No polaron effects or hopping conduction have been observed. Conductivity and galvanomagnetic effects: Figs. 17.3.3, 17.3.4.

mobility of charge carriers

μ_n	210 cm ² /V s	$T = 300$ K	Hall mobility, temperature dependence: $T^{-2.5}$ (see also Fig 17.3.4)	55W
μ_p	250 cm ² /V s	$T = 300$ K	Hall mobility, temperature dependence in the intrinsic range $T^{-2.5}$, in the mixed conduction range $T^{-1.5}$, see Fig. 17.3.5	66G1

intrinsic carrier concentration

n_i	$3 \cdot 10^{17}$ cm ⁻³	$T = 300$ K	conductivity and Hall coefficient	55W
-------	------------------------------------	-------------	-----------------------------------	-----

thermal conductivity : see Fig. 17.3.6

Optical properties

Absorption edge: Fig. 17.3.7, spectral dependence of optical constants: Figs. 17.3.8, 17.3.9.

dielectric constants

$\epsilon(0)$	23.75		infrared reflectivity	64K
$\epsilon(\infty)$	15.5			64K
	17		infrared reflectivity	63M

References to 17.3

- 53B Busch, G., Winkler, U.: *Helv. Phys. Acta* 26 (1953) 578.
- 55W Winkler, U.: *Helv. Phys. Acta* 28 (1955) 633.
- 63M McWilliams, D., Lynch, D. W.: *Phys. Rev.* 130 (1963) 2248.
- 64K Kahan, A., Lipson, H. G., Loewenstein, E. V.: *Proc. Int. Conf. Phys. Semiconductors, Paris 1964* (Dunod Cie., Paris 1964) p. 1067.
- 64L Lipson, H. G., Kahan, A.: *Phys. Rev. A* 133 (1964) 800.
- 64U Umeda, J.: *J. Phys. Soc. Jpn.* 19 (1964) 2052.
- 66G1 Geick, R., Habel, W. J., Perry, C. H.: *Phys. Rev.* 148 (1966) 824.
- 66G2 Gerstein, B. C., Chung, P. L., Danielson, G. C.: *J. Phys. Chem. Solids* 27 (1966) 1161.
- 67D Davis, L. C., Whitten, W. B., Danielson, G. C.: *J. Phys. Chem. Solids* 28 (1967) 439.
- 67E Eldridge, J. M., Miller, E., Komarek, K. L.: *Trans. Met. Soc. AIME* 239 (1967) 775.
- 68C Crossmann, L. D., Danielson, G. C.: *Phys. Rev.* 171 (1968) 867.
- 68V Vásques, F., Forman, R. A., Cardona, M.: *Phys. Rev.* 176 (1968) 905.
- 69S Scouler, W. S.: *Phys. Rev.* 178 (1969) 1353.
- 70A Aymerich, F., Mula, G.: *Phys. Status Solidi* (b) 42 (1970) 697.
- 70K Kearney, R. J., Worlton, T. G., Schmunk, R. E.: *J. Phys. Chem. Solids* 31 (1970) 1085.
- 72M Martin, J. J.: *J. Phys. Chem. Solids* 33 (1972) 1139.
- 72T Thrasher, P. H., Kearney, R. J.: *Phys. Status Solidi* (b) 53 (1972) 623.
- 76O Onari, S., Cardona, M.: *Phys. Rev. B* 14 (1976) 3520.

Figures to 17.3

Fig. 17.0.2

Mg₂X-compounds. Brillouin zone (fcc Bravais lattice).

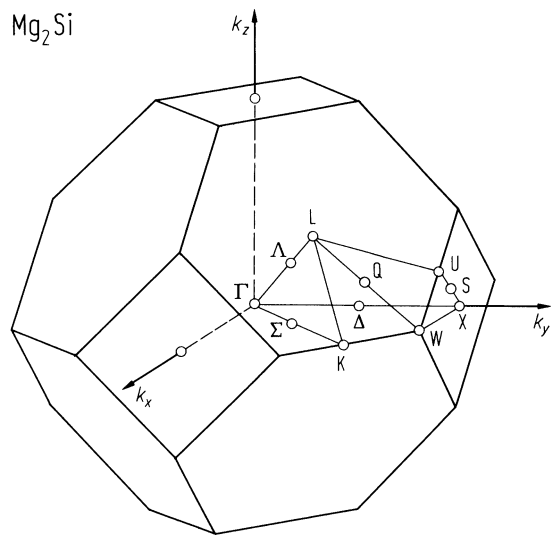


Fig. 17.0.5

Mg_2Sn . Band structure calculated by a non-relativistic pseudopotential method [70A].

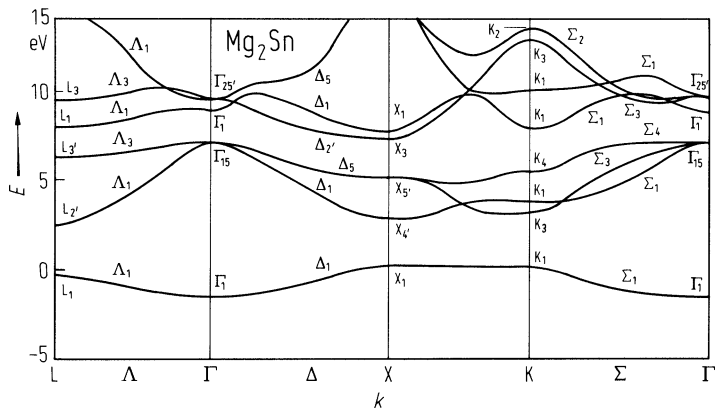


Fig. 17.3.1

Mg_2Sn . Phonon dispersion relations for three symmetry directions. Experimental points obtained by inelastic thermal neutron scattering. Open circles and full circles indicate branches having transverse and longitudinal polarizations, respectively, for the Δ and Λ branches whereas the X branches do not have symmetry determined polarizations. The curves are the result of a ten parameter shell model which was a least square fit to the data [70K].

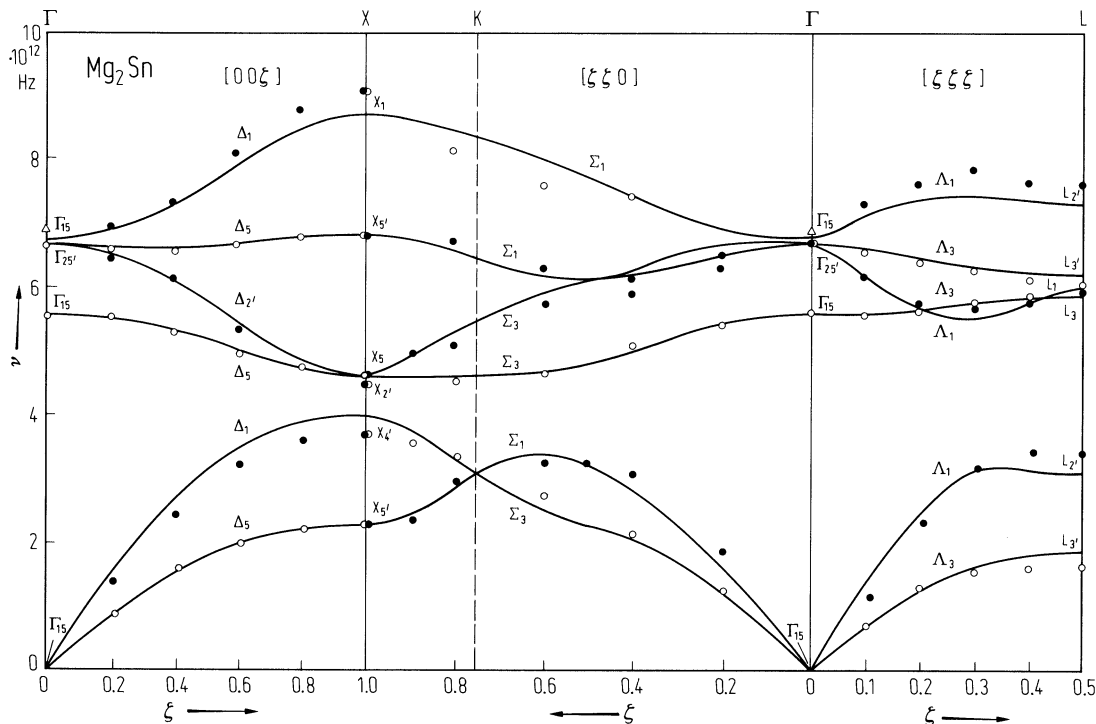


Fig. 17.3.2

Mg₂Sn. Second order elastic moduli c_{ik} vs. temperature calculated from the sound velocity data of Fig. 1 [67D].

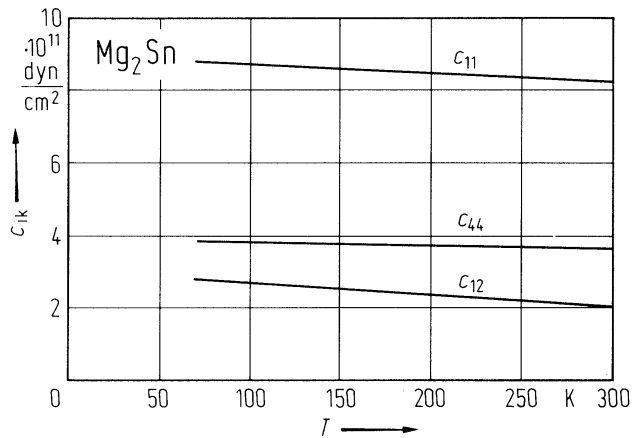


Fig. 17.3.3

Mg_2Sn . Resistivity vs. temperature for six n-type samples with electron concentrations between $3 \cdot 10^{16} \text{ cm}^{-3}$ and $6 \cdot 10^{16} \text{ cm}^{-3}$ in the range of mixed conduction [68C].

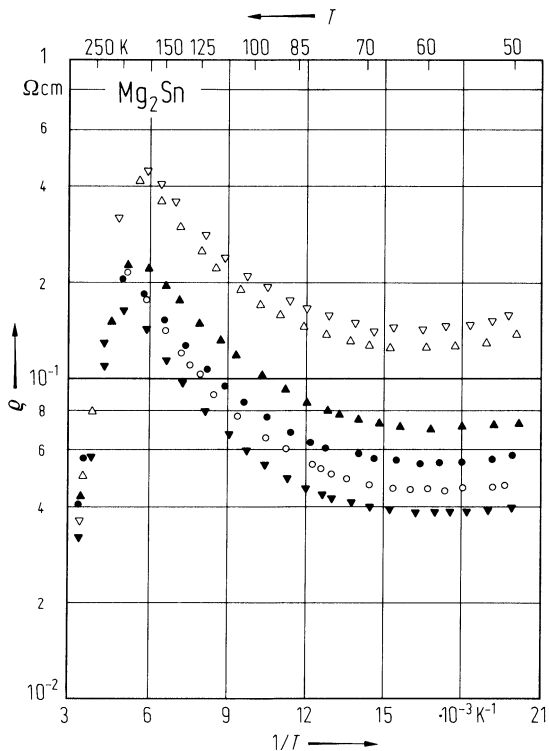


Fig. 17.3.4

Mg_2Sn . Hall mobility vs. temperature [64U].

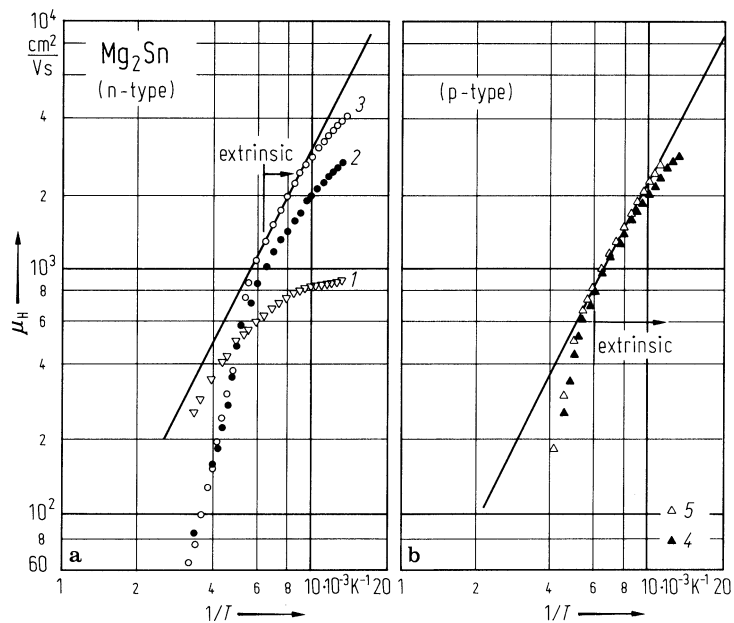


Fig. 17.3.5

Mg_2Sn . Hole Hall mobility vs. temperature determined from the free carrier contribution to the reflectivity (circles) and from electrical measurements (solid line) [66G2].

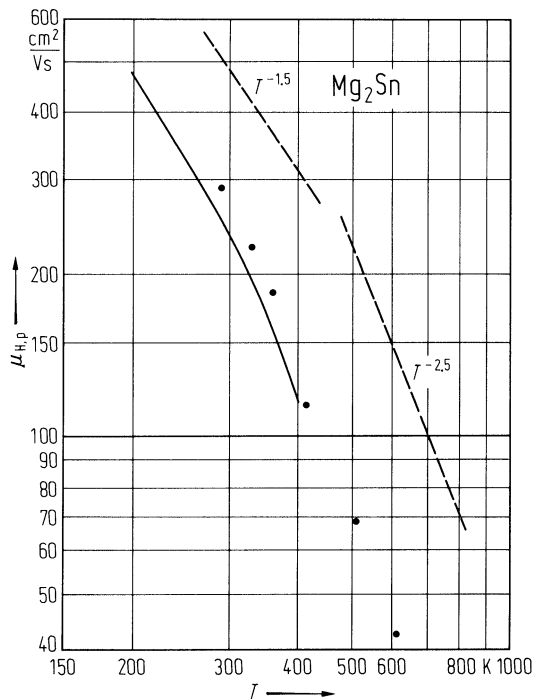


Fig. 17.3.6

Mg_2X -compounds. Thermal conductivity vs. temperature for Mg_2Si , Mg_2Ge and Mg_2Sn [72M].

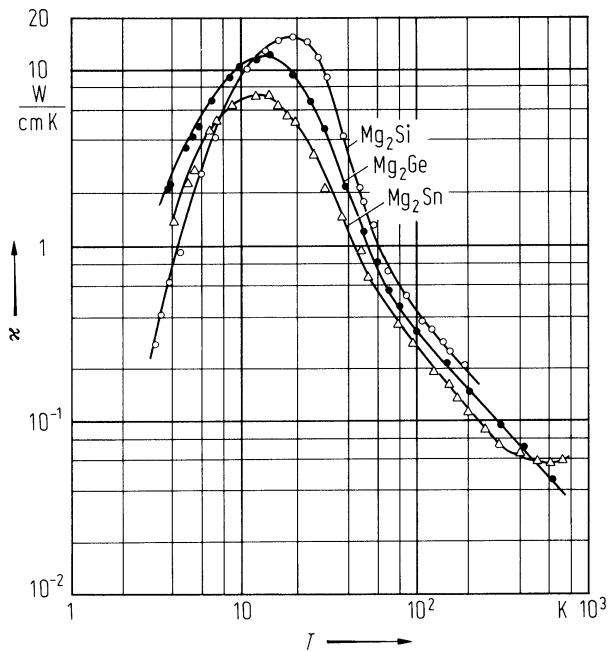


Fig. 17.3.7

Mg_2Sn . Absorption coefficient of an n-type sample ($n_d = 8.3 \cdot 10^{16} \text{ cm}^{-3}$) vs. photon energy at different temperatures after subtraction of free carrier absorption. The peak at about 0.17 eV originates from intra conduction band transitions at X [64L].

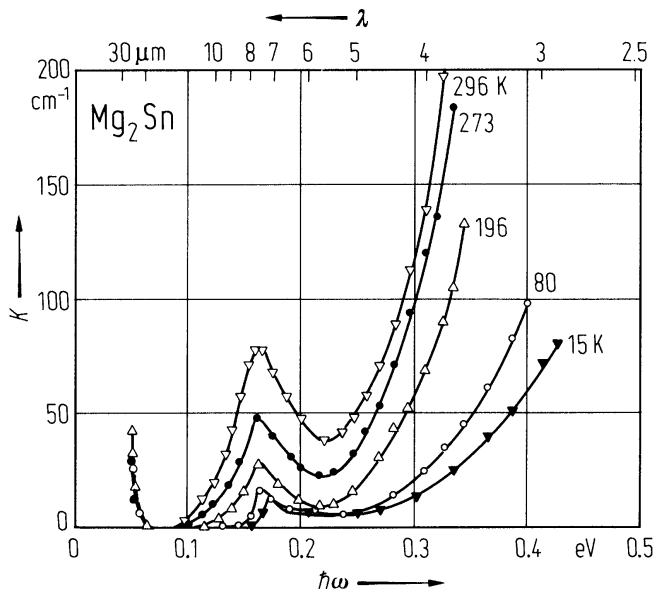


Fig. 17.3.8

Mg₂Sn. Real and imaginary parts of the dielectric constant ϵ_1 and ϵ_2 vs. photon energy [69S].

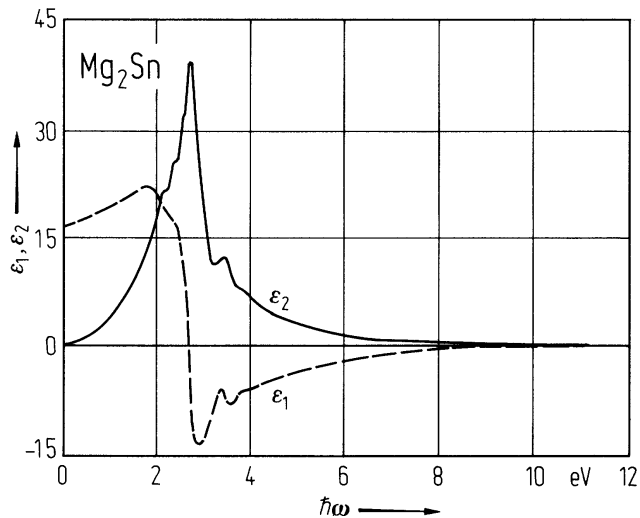
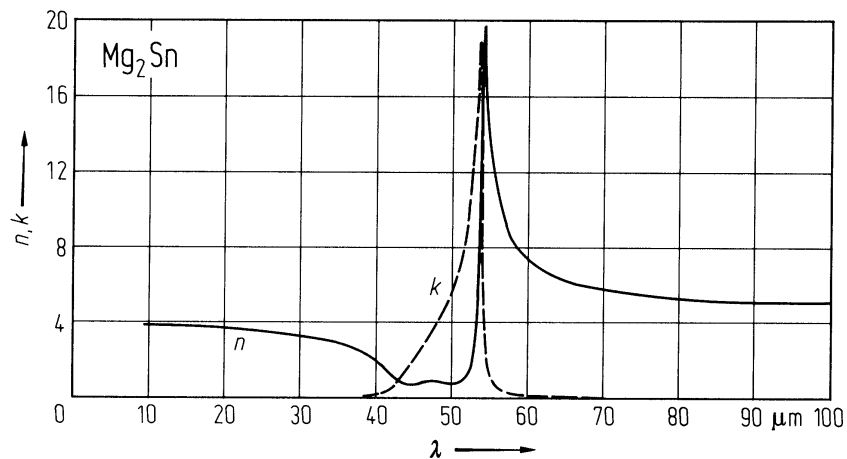


Fig. 17.3.9

Mg_2Sn . Index of refraction n and extinction coefficient k vs. wavelength in the wavelength region of Fig. [64K].



17.4 Magnesium plumbide (Mg2Pb)

Crystal structure

see section 17.0.

Electronic properties

band structure: Fig. 17.0.6, Brillouin zone: Fig. 17.0.2.

Mg2Pb is a semi-metal. Conduction band and valence band slightly overlap. In spite of this overlapping the general aspects of the band structure are similar to the other Mg2X-compounds. Thus, the valence band consists of two bands degenerated at Γ (symmetry Γ8-) and a split-off band (symmetry Γ7+). The heavy hole valence band is warped whereas the light hole band is almost spherical. The minima of the conduction band (overlapping with the Γ8-bands) are situated at X.

energy gap

$E_{g,ind}$	- 0.15 (5) eV	estimate based on effective mass and carrier concentration data	70V
-------------	---------------	---	-----

anisotropy parameter of heavy hole valence band

A	- 15.3	magnetoresistance	71S2
B	12.1		
C	11.0		

effective masses

$m_{p,h}$	0.35(2) m_0	[1 0 0]-direction, Shubnikov-de Haas effect	70V
	0.45 (6) m_0		
	0.45 (6) m_0		
$m_{p,l}$	0.04 m_0	[1 1 1]-direction	71S2

Lattice properties

lattice parameter

a	6.860 Å		71A2
-----	---------	--	------

volume expansion coefficient

β	3.0·10-5 K-1	$T = 300$ K	extrapolated from Mg2Si, -Ge, -Sn	71S1
---------	--------------	-------------	-----------------------------------	------

compressibility

κ	2.59·10-12 cm2 dyn-1	$T = 300$ K	from elastic constants	71S1
----------	----------------------	-------------	------------------------	------

Debye temperature

Θ_D	244.0 K	$T = 300$ K		71S1
------------	---------	-------------	--	------

lattice heat capacity

C_v	0.0723 J mol-1 K-1	$T = 5$ K	from heat capacity measurements	71S1
	0.9496 J mol-1 K-1	$T = 10$ K		
	25.647 J mol-1 K-1	$T = 50$ K		
	49.715 J mol-1 K-1	$T = 100$ K		
	72.431 J mol-1 K-1	$T = 300$ K		

density

d	5.54 g cm^{-3}			55W
-----	--------------------------	--	--	-----

melting temperature

T_m	555°C			53B
-------	---------------------	--	--	-----

phonon frequencies

$\nu_{\text{LO}}(\Gamma_{15})$	$5.79 \cdot 10^{12} \text{ s}^{-1}$	$T = 77 \text{ K}$	Raman spectroscopy	71A1
$\nu(\Gamma_{25'})$	$6.42 \cdot 10^{12} \text{ s}^{-1}$	$T = 300 \text{ K}$	Raman spectroscopy	71A2

Transport properties

(see also Fig. 17.3.1)

mobilities of charge carriers

μ_n	$1.2 \cdot 10^4 \text{ cm}^2/\text{V s}$	$T = 4.2 \text{ K}$	magnetoresistance	71S2
$\mu_{p,h}$	$1.4 \cdot 10^4 \text{ cm}^2/\text{V s}$			
$\mu_{p,l}$	$8.3 \cdot 10^4 \text{ cm}^2/\text{V s}$			

carrier concentrations

n	$3.5 \cdot 10^{19} \text{ cm}^{-3}$	$T = 4.2 \text{ K}$	magnetoresistance	71S2
p_h	$3.6 \cdot 10^{19} \text{ cm}^{-3}$			
p_l	$5.4 \cdot 10^{17} \text{ cm}^{-3}$			

References to 17.4

53B Busch, G., Winkler, U.: *Helv. Phys. Acta* 26 (1953) 578.
55W Winkler, U.: *Helv. Phys. Acta* 28 (1955) 633.
62B Busch, G., Moldanova, M.: *Helv. Phys. Acta* 35 (1962) 500.
70V Van Dyke, J. P., Hermann, F.: *Phys. Rev. B* 2 (1970) 1644.
71A1 Anastassakis, E., Burstein, E.: *Solid State Commun.* 9 (1971) 1525.
71A2 Anastassakis, E., Perry, C. H.: *Phys. Rev. B* 4 (1971) 1251.
71S1 Schwartz, R. G., Shanks, H., Gerstein, B. C.: *J. Solid State Chem.* 3 (1971) 533.
71S2 Stringer, G. A., Higgins, R. J.: *Phys. Rev. B* 3 (1971) 506.

Figures to 17.4

Fig. 17.0.2

Mg_2X -compounds. Brillouin zone (fcc Bravais lattice).

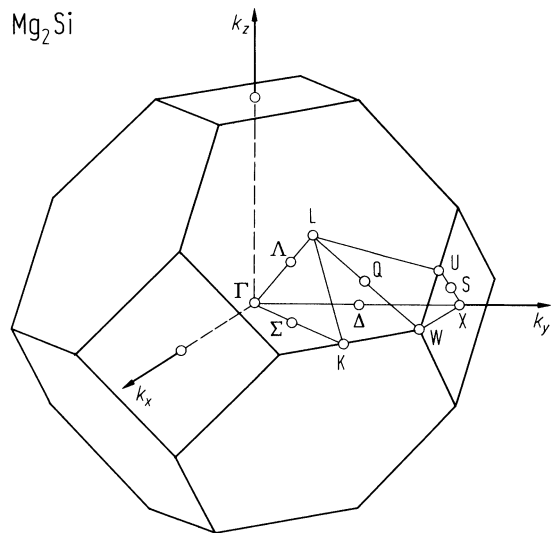


Fig. 17.0.6

Mg_2Pb . Energy band structure calculated with a relativistic OPW method [70V].

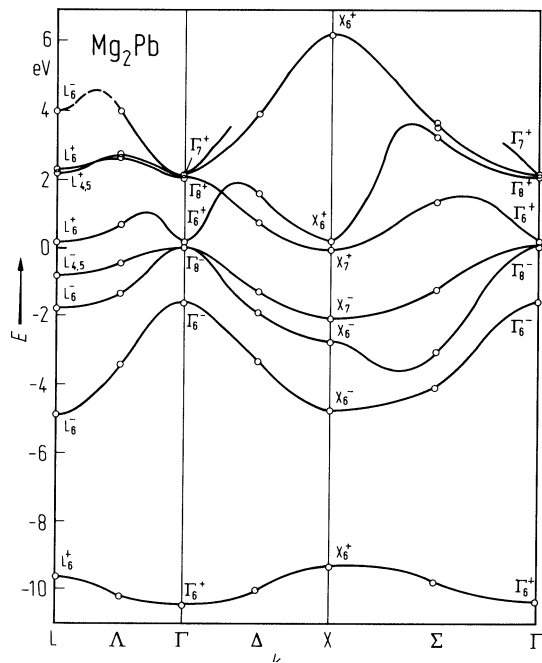
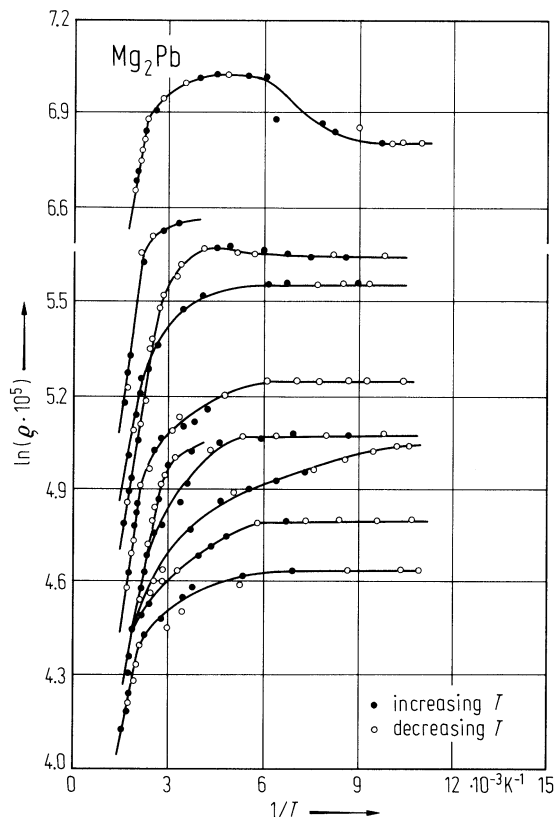


Fig. 17.3.1

Mg_2Pb . Electrical resistivity vs. temperature for several p-type samples [62B]. ρ in Ω cm.



17.5 Ca₂Si, Ca₂Sn, Ca₂Pb

The calcium compounds Ca₂Si, Ca₂Sn, Ca₂Pb crystallize in an orthorhombic (anti-PbCl₂) structure (Pnam) with

	<i>a</i> [Å]	<i>b</i> [Å]	<i>c</i> [Å]	Ref.
Ca ₂ Si	7.667	9.002	4.799	55E
Ca ₂ Sn	7.975	9.562	5.044	60E
Ca ₂ Pb	8.072	9.467	5.100	60E

According to [54B] the compounds Ca₂Si, Ca₂Sn and Ca₂Pb are semiconductors with energy gaps of 1.9 eV, 0.9 eV and 0.46 eV, respectively.

References to 17.5

- 54B Busch, G., Junod, P., Katz, U., Winkler, U.: Helv. Phys. Acta 27 (1954) 193.
55E Eckerlin, P., Wölfel, E.: Z. Anorg. Allg. Chem. 280 (1955) 321.
60E Eckerlin, P.: Z. Anorg. Allg. Chem. 307 (1960) 145.

17.6 BaSi₂, BaGe₂, SrGe₂

From several known II-IV₂-compounds BaSi₂, BaGe₂ and SrGe₂ are described as semiconductors [68B, 70J]. They crystallize in an orthorhombic structure with eight formula units in the elementary cell. The anion sublattice consists of isolated Ge- or Si-tetrahedra in a similar arrangement as the P₄-tetrahedra in white phosphorus. The space group is D_{2h}¹⁶ (Pnma) [68B, 70J]. The lattice constants are

	a [Å]	b [Å]	c [Å]	Ref.
BaSi ₂	8.92	6.75	11.57	68B
BaGe ₂	9.09	6.83	11.65	70J
SrGe ₂	8.74	6.65	11.25	70J

The paper on the structure of these compounds ([74E]) contains only the remark that the room temperature resistivity of the samples were 7 Ω cm, 7 Ω cm and 2 Ω cm and the energy gaps 1.3 eV, 1.0 eV and 0.9 eV, respectively.

References to 17.6

- 68B Betz, A., Schäfer, H., Weiss, A., Wulf, R.: Z. Naturforsch. 23b (1968) 878.
70J Janzon, K. H., Schäfer, H., Weiss, A.: Z. Anorg. Chem. 372 (1970) 87.
74E Evers, J., Weiss, A.: Mater. Res. Bull. 9 (1974) 549.

18 II_x-V_y compounds

18.0 Crystal structure and electronic structure

18.0.1 II₃-V₂ compounds

II₃-V₂ phosphides

α -Zn₃P₂ and Cd₃P₂ are isomorphous (space group P4₂/nmc–D_{4h}¹⁵). The crystal structure can be regarded as a Na₂O lattice (or anti-CaF₂ lattice) in which one quarter of the metal sites are vacant. These vacancies lead to a distortion from the ideal cubic symmetry and to a bigger unit cell. The structure consists of alternate layers of Zn/Cd and P atoms, stacked perpendicular to the [001] direction and separated by a distance of about one-eighth of the *c*-value.

The band structures of α -Zn₃P₂ and α -Cd₃P₂ are shown in Figs. 18.0.1 and 18.0.2, the Brillouin zone in the inset of Fig. 18.0.2.

II₃-V₂ arsenides

α -Mg₃As₂ is the low temperature modification of Mg₃As₂ with anti-Mn₂O₃ structure (D₃⁵ type). The cubic face centered unit cell contains 16 molecules in one formula unit [33Z].

The crystal structure of arsenides Me₃As₂ (Me = Zn, Cd) differs from that for phosphides Me₃P₂ only in the arrangement of the zinc vacancy site (space group I4₁cd–C_{4v}¹²). As a result of this difference, the unit cell of Me₃P₂ is smaller than that of Me₃As₂. In arsenides each unit cell contains sixteen layers of atoms instead of the eight layers that occurred for Me₃P₂. In tetragonal structure of both modifications, α -Zn₃As₂ (Fig. 18.0.3), and α' -Zn₃As₂ (Fig. 18.0.4), arsenic atoms are slightly displaced from the ideal positions of close packing.

The Brillouin zone for Zn₃As₂ and Cd₃As₂ is shown in Fig. 18.0.5, the band structure of Cd₃As₂ in Fig. 18.0.6.

18.0.2 II-V₂ compounds

II-V₂ phosphides

In the tetragonal unit cell of ZnP₂ (or CdP₂) all atoms are tetrahedrally coordinated and each Zn atom is bonded to P atoms, whereas each P atom is bonded to 2 Zn and 2 P atoms. The main fragments of structure of all higher Zn and Cd phosphides are spiral phosphorus chains similar to the chains in crystalline P, Fig. 18.0.7. P chains are oriented along certain crystallographic directions: for the tetragonal α -ZnP₂ and β -CdP₂ the directions are [010] and [100]; for the orthorhombic α -CdP₂, it is [010]. In β -ZnP₂, all the atoms are tetrahedrally coordinated. Orthorhombic α -CdP₂ almost exactly follows β -CdP₂ in its structure.

Brillouin zone: Fig. 18.0.8. *Band structure* of ZnP₂ and CdP₂: Fig. 18.0.9.

II-V₂ arsenides

The two non-equivalent Zn sites and four non-equivalent As sites in ZnAs₂ are each coordinated tetrahedrally: the Zn sites to four As and the As sites to two Zn and two As. The As atoms are arranged in semi-spiral chains parallel to the *c*-axis Fig. 18.0.10. In CdAs₂ both cadmium and arsenic atoms are tetrahedrally coordinated.

18.0.3 II-V₄ compounds

CdP₄, MgP₄

In CdP₄ are the Cd atoms octahedrally coordinated, while the P atoms have a tetrahedral distorted coordination. In the structure of CdP₄ [56K] there are two crystallographically distinct sites for the P atoms, the anion-anion coordination being 2 for P(1) and 3 for P(2). The P(1) and P(2) atoms are bonded together and form spiral chains which are linked together in a three-dimensional array by P(2[–])–P(2) bonds, Fig. 18.0.11. The P chains are oriented in [010] direction, Fig. 18.0.7 [80A].

The crystal structure of MgP₄ is covalent and iso-structural with CdP₄ [56K].

18.0.4 II-V compounds

The crystal structure of ZnSb can be treated as strongly deformed sphalerite. All atoms are tetrahedrally coordinated with one atom of the same kind and three ones of the other kind. ZnAs (and CdAs) are isostructural with ZnSb (and CdSb), Fig. 18.0.12.

For further $\text{II}_x\text{-V}_y$ compounds see sections 18.14 and 18.15.

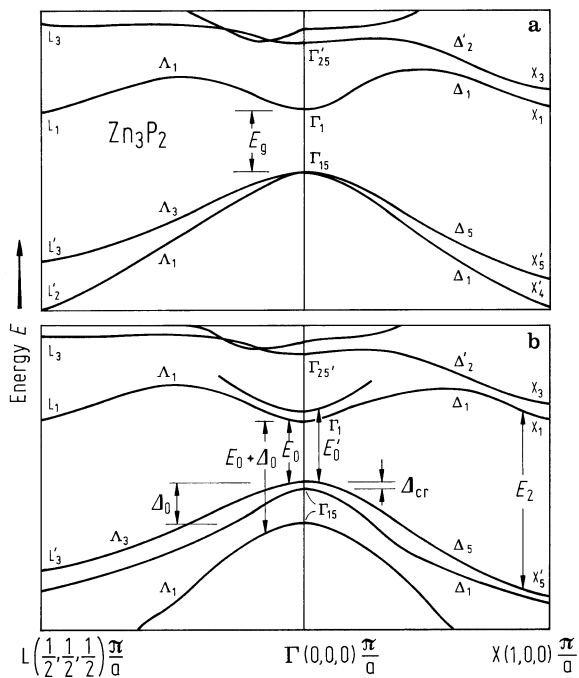
References to 18.0

- 33Z Zintl, F., Husemann, F.: Z. Phys. Chem. B 21 (1933) 138.
- 56K von Krebs, H., Müller, K. H., Zürn, G.: Z. Anorg. Allg. Chem. 285 (1956) 25.
- 64P Pearson, W. B.: Acta Crystallogr. 17 (1964) 1.
- 71S Sobolev, V. V., Syrbu, N. N.: Phys. Status Solidi (b) 43 (1971) 73.
- 74F Fleett, M.: Acta Crystallogr. B 30 (1974) 122.
- 75C Clavaguera, M. T.: J. Phys. Chem. Solids 36 (1975) 1205.
- 76P Pietraszko, A., Lukaszewicz, K.: Bull. Acad. Pol. Sci., Ser. Sci. Chim. 24 (1976) 459.
- 77B Blom, F. A. P., Burg, J. W.: J. Phys. Chem. Solids 38 (1977) 19.
- 79B Becla, P., Gumieny, Z., Misiewicz, J.: Opt. Appl. 9 (1979) 143.
- 79P Pawlikowski, J. M., Misiewicz, J., Sujak-Cyruł, B., Wróbel, J.: Phys. Status Solidi (b) 92 (1979) K123.
- 80A Alejnikova, K. B., Arsenov, A. V., Kavetsky, V. S., Lukin, A. N.: Proc. Intern. Symp. on "Physics and Chemistry of II-V Comp." Mogilany, Poland 1980, ed. M. Gelten, L. Zdanowicz, Eindhoven Univ., Netherlands, p. 43.
- 91N Nayak, A., Rao, D.R., Banerjee, H.D.: Solid State Commun. 78 (1991) 149.

Figures to 18.0

Fig. 18.0.1

Zn_3P_2 . Energy band structure near the Γ point (not in scale). (a) Lin-Chung pseudopotential calculation (without spin-orbit and crystal field interaction). (b) experimental results [91N].



Cd₃P₂. Energy bands calculated by the pseudopotential method. The dashed lines show the approximate structure deduced from symmetry properties and compatibility relations for the space group D_{4h}¹⁵. The inset shows the Brillouin zone for the primitive tetragonal lattice of Cd₃P₂ with indicated representation domain. [79P].

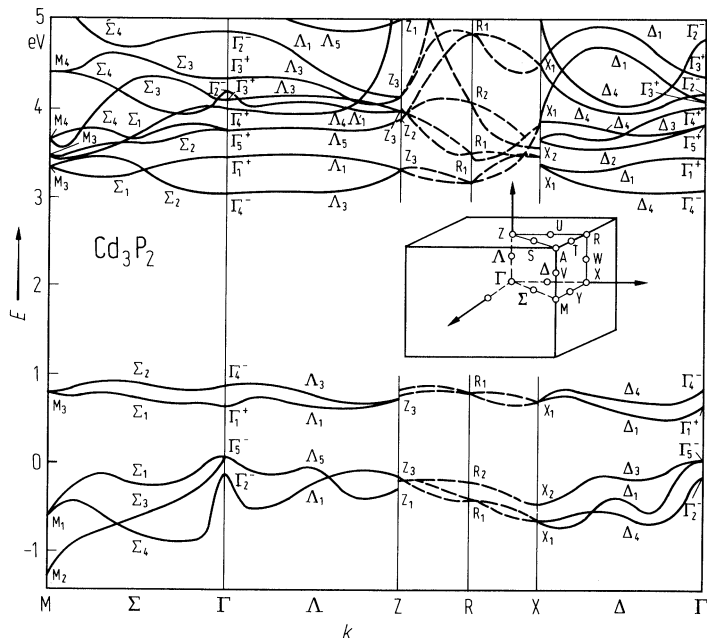


Fig. 18.0.3

Zn_3As_2 . (a) Crystal structure of $\alpha\text{-Zn}_3\text{As}_2$. (b) The xy projections of the layers of the small fluorite unit cell in the crystal structure of $\alpha\text{-Zn}_3\text{As}_2$. Crosses: void centers of vacant tetrahedra of the As atoms [76P].

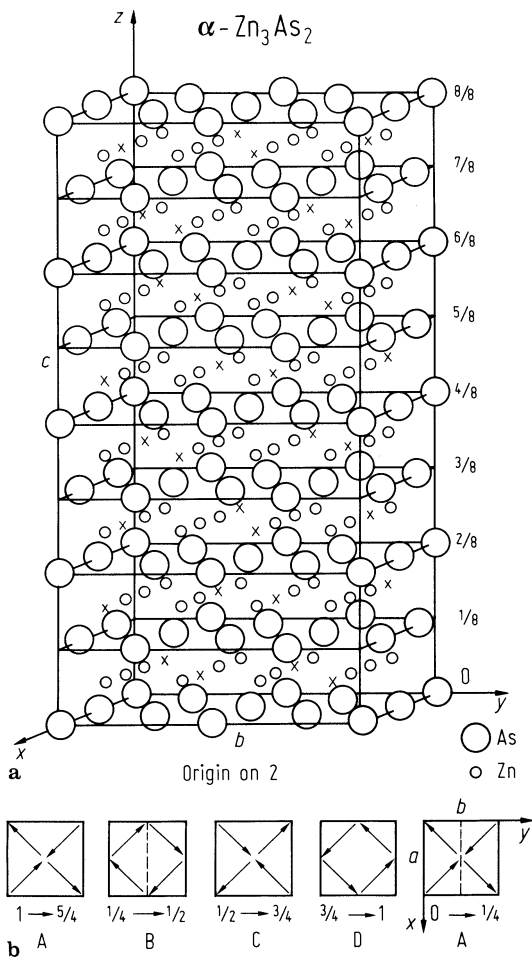
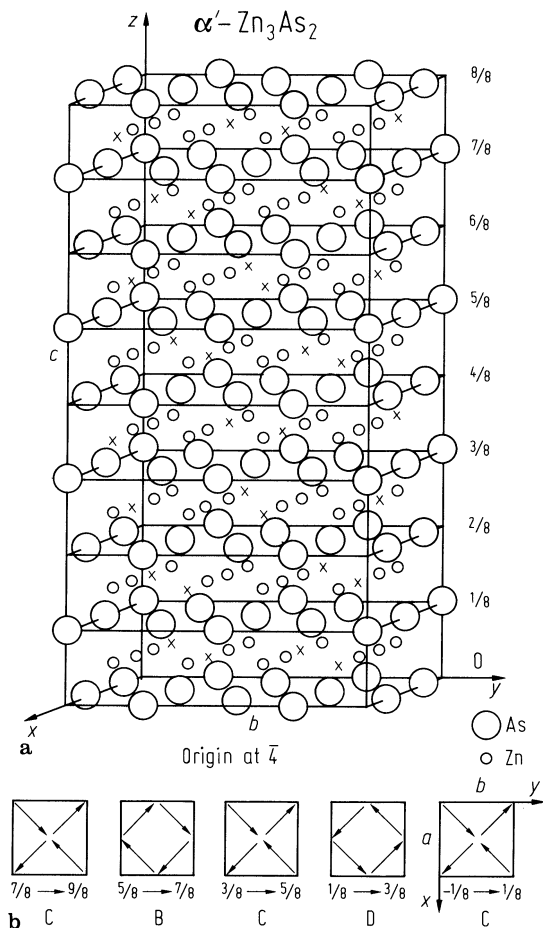


Fig. 18.0.4

Zn_3As_2 . (a) Crystal structure of α' - Zn_3As_2 . For comparison with the α -structure the origin has been shifted to $\bar{4}$; (b) The xy -projections of the layers of the small fluorite unit cell in the crystal structure of α' - Zn_3As_2 . Crosses: void centers of vacant tetrahedra of the As atoms [76P].



Cd₃As₂. Brillouin zone (a) for the body-centered tetragonal structure C_{4v}^{12} ($c > 2^{1/2}a$) showing symmetry points and axes, (b) for the fluorite (CaF₂) structure [75C].



Fig. 18.0.6

Cd_3As_2 . $E(k)$ relation for the four level energy bands model. The wave vector k (in 10^6 cm^{-1}) is directed a) 0° , b) 5° , c) 90° from the tetragonal c -axis [77B]; see also [79B]. Energies are labelled with respect to E_c .

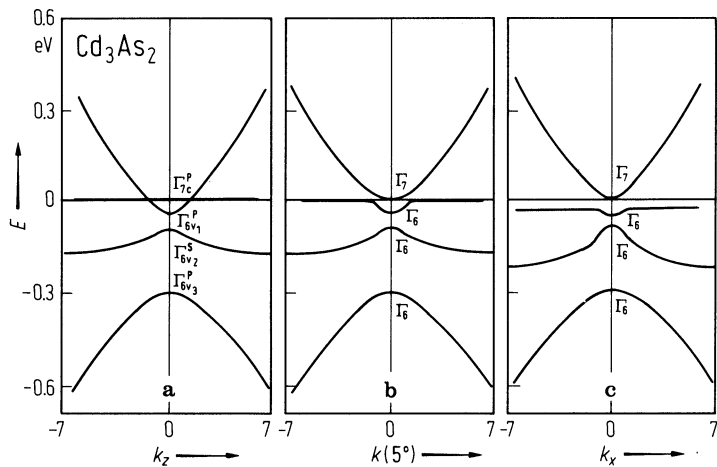


Fig. 18.0.7

(a) CdP_4 , (b) $\alpha\text{-ZnP}_2$ and $\beta\text{-CdP}_2$, (c) $\beta\text{-ZnP}_2$ and $\alpha\text{-CdP}_2$, (d) Cd_7P_{10} . Crystal structure and spiral phosphorus chains in higher Zn and Cd phosphides of the II-V group [80A].

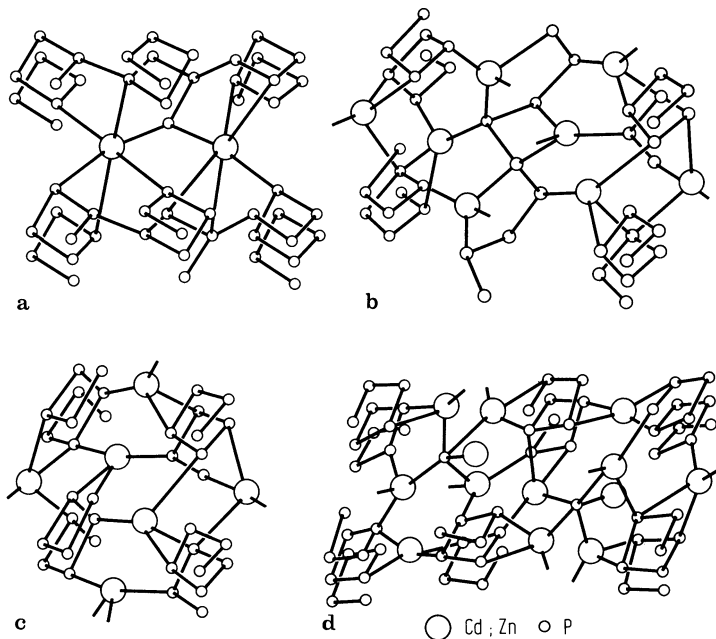


Fig. 18.0.8

α -ZnP₂, β -CdP₂. Brillouin zone [71S].

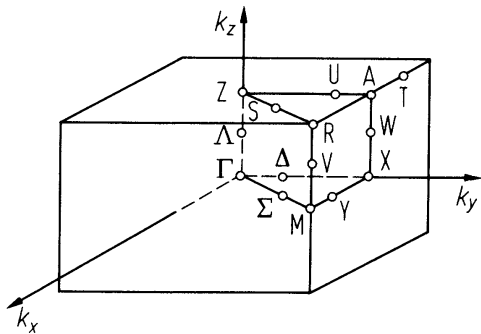
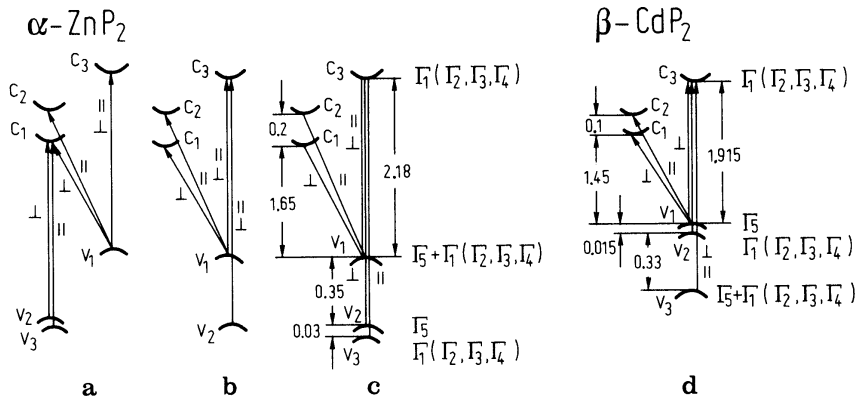


Fig. 18.0.9

α -ZnP₂, β -CdP₂. Different versions of the electronic band structure in the vicinity of the interband gap (main optical transitions) of α -ZnP₂ (a, b, c) and β -CdP₂ (d) on the basis of photoconductivity and reflectivity data. Energy values for 293 K [71S].

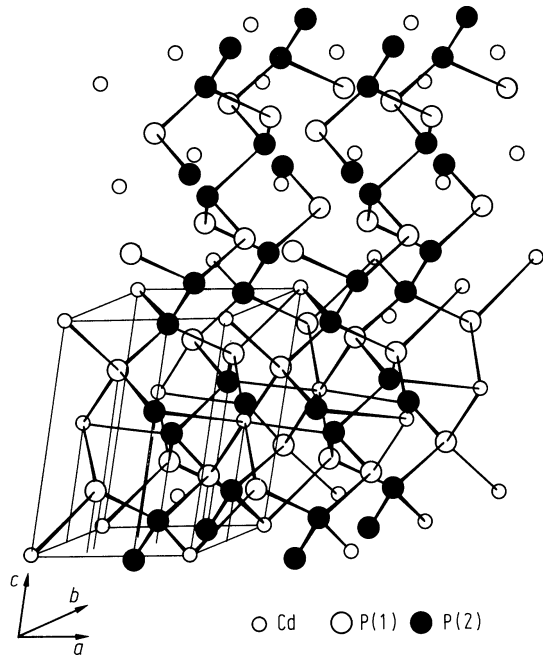


ZnAs₂. (a) Crystal structure of monoclinic ZnAs₂; (b) Zn and As environments in ZnAs₂ [74F].



Fig. 18.0.11

CdP_4 . The monoclinic structure. Bonds between all atoms are shown in the lower part and the anion subarrays are emphasized in the upper part of the diagram [64P] or [56K].



18.1 Magnesium arsenide (Mg₃As₂)

crystal structure

see section 18.0.

energy gap

E_g	2.2 eV	$T = 0$ K	extrapolated from resistivity and Hall data	68P
dE_g/dT	$-9 \cdot 10^{-4}$ eV K ⁻¹			

lattice parameter

a	12.33 Å			33Z
-----	---------	--	--	-----

melting temperature

T_m	1073 K			58A
-------	--------	--	--	-----

resistivity

ρ	10^5 Ω cm	$T = 500$ K	n-type conduction; for temperature dependence, see Fig. 18.1.1	68P
--------	-------------	-------------	--	-----

Hall coefficient

R_H	106 cm ³ C ⁻¹	$T = 500$ K		68P
-------	---------------------------------------	-------------	--	-----

mobility

$\mu_{H,n}$	$10 \dots 20$ cm ² /V s	$T = 500$ K		68P
-------------	------------------------------------	-------------	--	-----

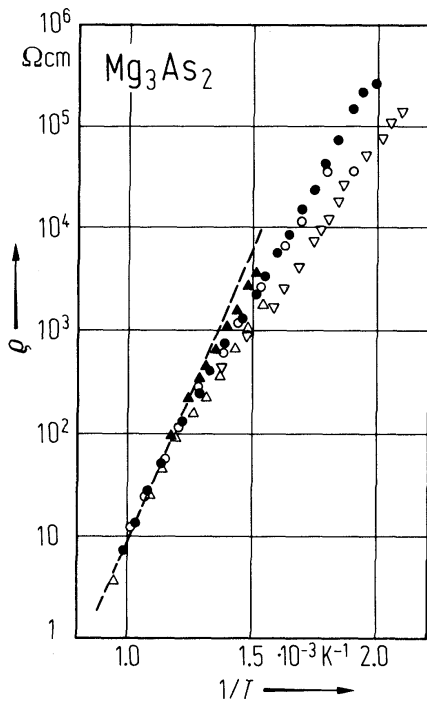
References to 18.1

33Z	Zintl, F., Husemann, F.: Z. Phys. Chem. B 21 (1933) 138.
58A	Arija, S. M., Morozova, M. P., Chuan Tsi-Tao, Voll, F.: Zh. Obshch. Khim. 27 (1958) 293.
68P	Pigon, K.: Helv. Phys. Acta 41 (1968) 1104.

Figures to 18.1

Fig. 18.1.1

Mg_3As_2 . Resistivity of polycrystalline samples vs. reciprocal temperature [68P].



18.2 Zinc phosphide (Zn₃P₂)

Crystal structure

see section 18.0

Electronic properties

band structure : Fig. 18.0.1, Brillouin zone: Fig. 18.0.2 (next section).

According to theoretical calculations for the hypothetical anti-fluorite structure (CaF₂, [71L]) the lowest valence band in Zn₃P, (as well as in Cd₃P,) is a phosphorus s-like level. The second band is a Zn (Cd) s-like band. The third and fourth bands are s-like about Zn (Cd) and p-like about the P-atoms. The conduction band minima and valence band maxima occur exactly at the center of the Brillouin zone.

energy gap

$E_{g,ind}(\Gamma)$	1.35 eV	$T = 300$ K	absorption	80Z
$E_{g,dir}$	1.42 eV		$(\Gamma_{15v}^0(\Gamma_{7v})-\Gamma_{1c}(\Gamma_{6c}))$	

spin-orbit splitting of the valence band

$\Delta_{so}(\Gamma)$	0.11 eV		calculated by the pseudopotential method	78D
	0.16 eV	$T = 300$ K	derivative spectra of thin film	91N

crystal field splitting energy

$\Delta_{cr}(\Gamma)$	0.02 eV	$T = 300$ K	derivative spectra	91N
-----------------------	---------	-------------	--------------------	-----

Lattice properties

lattice parameters

a	8.09(2) Å		for α -Zn ₃ P ₂	35S
c	11.45(3) Å			
a	5.82 Å	$T = 1153$ K	for β -Zn ₃ P ₂	77D

coefficient of linear thermal expansion

α	$8.33 \cdot 10^{-6} \text{ K}^{-1}$	$T = 300$ K	dilatometric method, α -Zn ₃ P ₂	77D
	$13.7 \cdot 10^{-6} \text{ K}^{-1}$	$T > 1140$ K	β -Zn ₃ P ₂	72Z

sound velocities

v_{LA}	$5.1809(119) \cdot 10^5 \text{ cm s}^{-1}$	RT	propagation of ultrasonic wave	76O
v_{TA}	$2.5017(57) \cdot 10^5 \text{ cm s}^{-1}$			

Young's modulus

E	$9.8 \cdot 10^6 \text{ N cm}^{-2}$	$T = 300$ K	from ultrasonic wave propagation	77D
-----	------------------------------------	-------------	----------------------------------	-----

shear modulus

G	$3.7 \cdot 10^6 \text{ N cm}^{-2}$	$T = 300$ K	from ultrasonic wave propagation	77D
-----	------------------------------------	-------------	----------------------------------	-----

Poisson's constant

ν	0.35(1)	$T = 300$ K	from ultrasonic wave propagation	76O
-------	---------	-------------	----------------------------------	-----

compressibility

κ	$0.9 \cdot 10^{-7} \text{ cm}^2 \text{ N}^{-1}$	$T = 300$ K	adiabatic	77D
----------	---	-------------	-----------	-----

Debye temperature

Θ_D	320 K	$T = 300$ K	from elastic constants	77D
------------	-------	-------------	------------------------	-----

heat capacity

C_p	47.10 J mol ⁻¹ K ⁻¹	$T = 55$ K	calorimetric method in the temperature range 55...300 K	77D
	120.2 J mol ⁻¹ K ⁻¹	$T = 300$ K		
C_v	47.06 J mol ⁻¹ K ⁻¹	$T = 55$ K		
	119.3 J mol ⁻¹ K ⁻¹	$T = 300$ K		

density

d	4.485 g cm ⁻³	$T = 300$ K	pycnometric method	77D
	4.59 g cm ⁻³	$T = 300$ K	X-ray measurement	77P

melting temperature

T_m	1466 K		under $p_{\text{tot}} \approx 7$ bar	75A
-------	--------	--	--------------------------------------	-----

Transport properties

(all data for p-type samples, see Fig. 18.2.1)

intrinsic carrier concentration

p_i	$3.56 \cdot 10^{14}$ cm ⁻³	$T = 300$ K	from Hall measurements	75S
-------	---------------------------------------	-------------	------------------------	-----

resistivity

ρ	$10 \dots 10^5$ Ω cm	$T = 300$ K		75S
--------	-----------------------------	-------------	--	-----

hole mobility

μ_p	$10 \dots 20$ cm ² /V s	$T = 300$ K	Hall mobility	53L,
	50 cm ² /V s	$T = 77$ K	temperature dependence proportional $T^{-3/2}$	77C, 80Z

Optical properties

refractive index

n	3.2...3.4	$T = 300$ K	infrared region 1...2.5 μm	79F, 80Z
	3.4...4	$T = 300$ K	visible region 0.5...1 μm	77C, 80Z

Spectral dependence: see Fig. 18.2.2.

dielectric constant

$\epsilon(0)$	11	$f = 1.9 \cdot 10^9$ s ⁻¹	resonance method Kramers-Kronig analysis of reflectivity spectra, see Fig. 18.2.3	77Z
---------------	----	--------------------------------------	---	-----

References to 18.2

- 35S Stackelberg, M. V., Paulus, R.: Z. Phys. Chem. Abt. B 28 (1935) 427.
- 53L Lagrenaudie, J.: J. Chim. Phys. 50 (1953) 545.
- 72Z Zdanowicz, W., Krolicki, F., Pleniewicz, P.: Acta Phys. Polon. A 41 (1972) 27.
- 75A Antiukov, A. M., Smolarenko, F. M.: Izv. Akad. Nauk BSSR, Ser. Khim., 5 (1975) 100.
- 75S Shevchenko, V. Ya., Babarina, L. P., Kozlov, S. E., Lazarev, V. B.: Neorgan. Mater. 11 (1975) 1719.
- 76O Opuska, L., Opuski, A.: Phys. Status Solidi (a) 35 (1976) K183.
- 77C Catalano, A., Dalal, V., Fagen, E. A., Hall, R. B., Masi, J. V., Meakin, J. D., Warfield, G., Barnett, A. M.: Proc. Inter. Photovoltaic Solar Energy Conf., Luxemburg 1977, D. Reidel Dordrecht, 1977, p. 644.
- 77D Demidenko, A. F., Danilenko, G. N., Danilenko, V. E., Lazarev, V. B., Shevchenko, V. Ya., Marenkin, S. F., Kozlov, S. F.: Neorgan. Mater. 13 (1977) 214.
- 77P Pistorius, C. W. F. T., Clark, J. B., Coetzer, J., Kruger, G. J., Kunze, O. A.: High Temp.-High Pressure 9 (1977) 471.
- 77Z Zynbina, G. A., Toropcev, V. P., Shehukin, O. S.: Neorgan. Mater. 13 (1977) 355.
- 78D Dowgialio-Pleniewicz, B., Pieniewicz, P.: Phys. Status Solidi (b) 87 (1978) 309.
- 79F Fagen, E. A.: J. Appl. Phys. 50 (1979) 6505.
- 80Z Zdanowicz, L., Zdanowicz, W., Petelenz, D., Kloc, K.: Acta Phys. Polon. A 57 (1980) 159.
- 88M Misiewicz, J., Wrobel, J.M., Clayman, B.P.: Solid State Commun. 66 (1988) 747.
- 91N Nayak, A., Rao, D.R., Banerjee, H.D.: Solid State Commun. 78 (1991) 149.

Figures to 18.2

Fig. 18.0.1

Zn_3P_2 . Energy band structure near the Γ point (not in scale). (a) Lin-Chung pseudopotential calculation (without spin-orbit and crystal field interaction). (b) experimental results [91N].

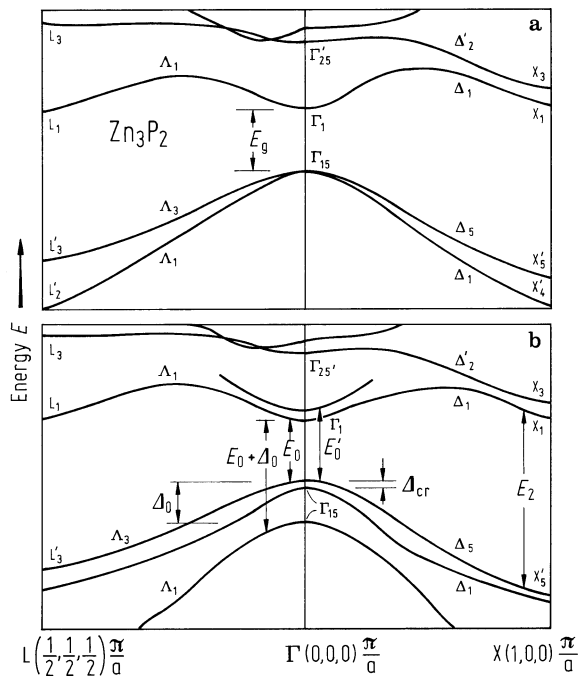


Fig. 18.2.1

Zn_3P_2 . Resistivity, Hall coefficient and Hall mobility vs. reciprocal temperature [75S].

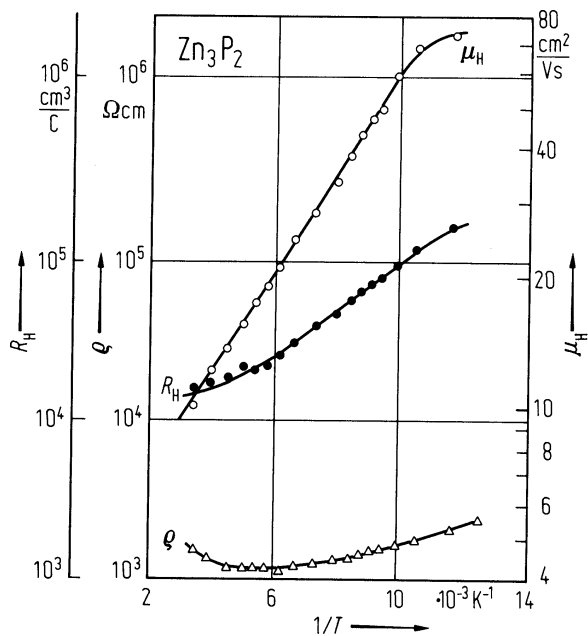


Fig. 18.2.2

Zn_3P_2 . Refractive index n and extinction coefficient k of polycrystalline thin films of different thicknesses vs. wavelength [79F].

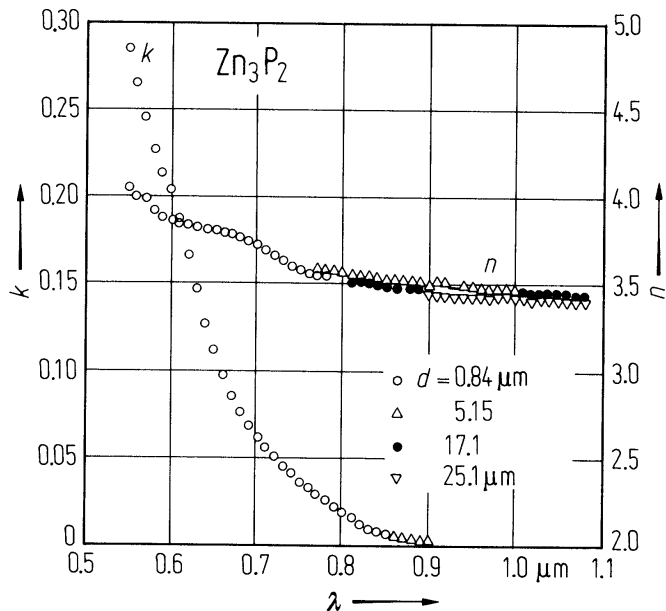
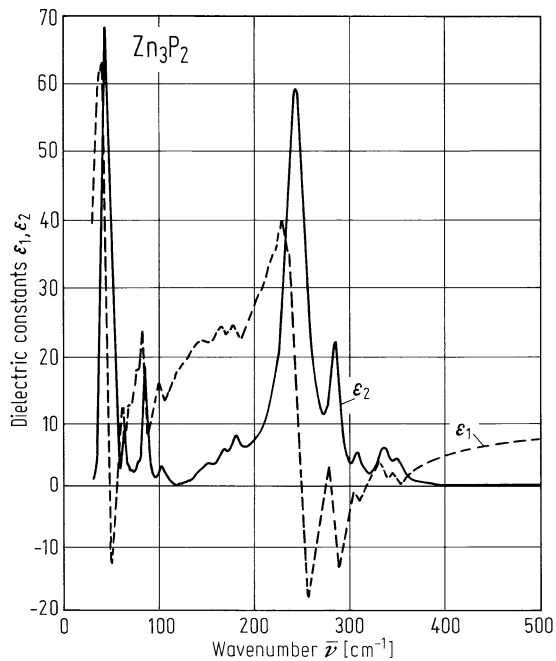


Fig. 18.2.3

Zn_3P_2 . Real and imaginary parts of the dielectric constant calculated by means of Kramers-Kronig analysis of reflectivity spectra at 295 K [88M].



18.3 Zinc arsenide (Zn₃As₂)

Crystal structure

see section 18.0

Electronic properties

energy gap

$E_{g,dir}$	0.86 eV	$T = 0$ K	extrapolated from temperature dependence of Hall coefficient and resistivity	75P
dE_g/dT	0.99...1.0 eV	$T = 300$ K	thermoreflectance and absorption	79P
	$-4.55 \cdot 10^{-4}$ eV K ⁻¹	$T = 5...80$ K	optical measurements	79P

For the temperature dependence of E_g , see also Fig. 18.3.1.

spin-orbit splitting energy, valence band

$\Delta_{so}(\Gamma)$	0.33 eV		calculated by the pseudopotential method	78D
	0.35 eV		thermoreflectance	75A

crystal field splitting energy

$\Delta_{cr}(\Gamma)$	0.07 eV		calculated	78D
-----------------------	---------	--	------------	-----

effective masses

m_p	0.65 m_0	$T = 600...800$ K	for Cu-doped samples	61P
m_n	1.70 m_0	$T = 600...800$ K	for Cu-doped samples	

Lattice properties

lattice parameters

a	11.7786 Å	$T = 300$ K	α -Zn ₃ As ₂	76P
c	23.6432 Å			
a	11.789 Å	$T = 457$ K	α' -Zn ₃ As ₂	76P
c	23.635 Å			
a	5.959 Å	$T = 1053$ K	β -Zn ₃ As ₂	68W

coefficient of linear thermal expansion

α	$10.4 \cdot 10^{-6}$ K ⁻¹	$T = 300$ K	α -Zn ₃ As ₂	77D
----------	--------------------------------------	-------------	---	-----

Debye temperature

Θ_D	124 K	$T = 300$ K		77D
------------	-------	-------------	--	-----

heat capacity

C_p	21.66 J mol ⁻¹ K ⁻¹	$T = 50$ K	calorimetric method	87G
	72.59 J mol ⁻¹ K ⁻¹	$T = 300$ K		
C_v	26.14 J mol ⁻¹ K ⁻¹	$T = 55$ K	calorimetric method	87G
	72.52 J mol ⁻¹ K ⁻¹	$T = 300$ K		

density

d	5.609 g cm ⁻³	$T = 300$ K	α -Zn ₃ As ₂ , X-ray measurements	76P
	5.601 g cm ⁻³	$T = 463$ K	α' -Zn ₃ As ₂	
	5.578 g cm ⁻³	$T = 300$ K	β -Zn ₃ As ₂ , pycnometric measurement	35S

melting temperature

T_{m}	1288 K			79G
----------------	--------	--	--	-----

sound velocities

v_{LA}	$4.080 \cdot 10^5 \text{ cm s}^{-1}$	RT	velocity of ultrasonic wave	77D
v_{TA}	$1.980 \cdot 10^5 \text{ cm s}^{-1}$		propagation	

compressibility

κ	$1.7 \cdot 10^{-7} \text{ cm}^2 \text{ N}^{-1}$	$T = 300 \text{ K}$	adiabatic	77D
----------	---	---------------------	-----------	-----

Transport properties

(all data for p-type samples)

hole concentration

p	$7.3 \cdot 10^{17} \text{ cm}^{-3}$	$T = 300 \text{ K}$	extrinsic range	61P
-----	-------------------------------------	---------------------	-----------------	-----

resistivity

ρ	$10 \dots 25 \text{ } \Omega \text{ cm}$	$T = 300 \text{ K}$		58S
--------	--	---------------------	--	-----

hole mobility

μ_{p}	$160 \text{ cm}^2/\text{V s}$	$T = 77 \text{ K}$	resistivity, $n_{\text{a}} = 4.8 \cdot 10^{17} \text{ cm}^{-3}$, see Fig. 18.3.2	77S
------------------	-------------------------------	--------------------	--	-----

thermal conductivity

κ	$2.2 \cdot 10^{-2} \text{ W cm}^{-1} \text{ K}^{-1}$		66U1	
----------	--	--	------	--

Optical properties

refractive index

n	3.85	$T = 300 \text{ K}$, $\lambda = 2 \dots 12 \text{ } \mu\text{m}$	for thin films	77Z
-----	------	--	----------------	-----

dielectric constant

$\varepsilon(0)$	$10 \dots 11.8$		resonance method, $f = 1.9 \cdot 10^9 \text{ s}^{-1}$	66U, 77Z
------------------	-----------------	--	---	-------------

References to 18.3

- 35S Stackelberg, M. V., Paulus, R.: Z. Phys. Chem. Abt. B 28 (1935) 427.
- 58S Silvey, G. A.: J. Appl. Phys. 29 (1958) 226.
- 61P Pigoti, K.: Bull. Acad. Pol. Sci., Ser. Sci. Chim. 9 (1961) 751.
- 66U Ugai, Ya. A., Gukov, O. Ya., Ozerov, L. A.: Neorgan. Mater. 1 (1966) 87.
- 68W Weglowski, S., Lukaszewicz, K.: Bull. Acad. Pol. Sci., Ser. Sci. Chim. 16 (1968) 177.
- 75A Arushanov, E. K., Lukianova, L. N., Markus, M. M., Nateprov, A. N., Chuiko, G. P., in: "Physics and Chemistry of Semiconductor Compounds", ed. Shtiintsa, Kishinev 1975, p. 18 (in Russian).
- 75P Pawlikowski, J. M., Becla, P.: Acta Phys. Polon. A 47 (1975) 721.
- 76P Pietraszko, A., Lukaszewicz, K.: Bull. Acad. Pol. Sci., Ser. Sci. Chim. 24 (1976) 459.
- 77D Demidenko, A. F., Danilenko, G. N., Danilenko, V. E., Lazarev, V. B., Shevchenko, V. Ya., Marenkin, S. F., Kozlow, S. F.: Neorgan. Mater. 13 (1977) 214.
- 77S Shevchenko, V. Ya., Marenkin, S. F., Ponomarev, V. F.: Neorgan. Mater. 13 (1977) 1898.
- 77Z Zynbina, G. A., Toropcev, V. P., Shehukin, O. S.: Neorgan. Mater. 13 (1977) 355.
- 78D Dowgialio-Plenkiewicz, B., Pienkiewicz, P.: Phys. Status Solidi (b) 87 (1978) 309.
- 79B Becla, P., Gumienny, Z., Misiewicz, J.: Opt. Appl. 9 (1979) 143.
- 79G Glazov, V. M., Kasymova, M., Regel, A. P.: Fiz. Tekh. Poluprovodn. 13 (1979) 2049.
- 79P Pawlikowski, J. M., Misiewicz, J., Sujak-Cyruł, B., Wróbel, J.: Phys. Status Solidi (b) 92 (1979) K123.
- 87G Guskov, V.N., Greenberg, J.H., Lazarev, V.B., Kotliar, A.A.: Neorg. Mater. 23 (1987) 1418.

Figures to 18.3

Fig. 18.3.1

Zn_3As_2 . Energy gap vs. temperature in the range 80...300 K [79B].

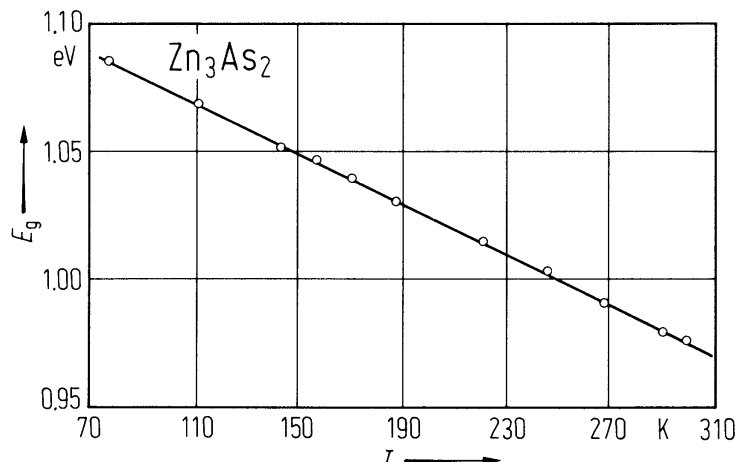
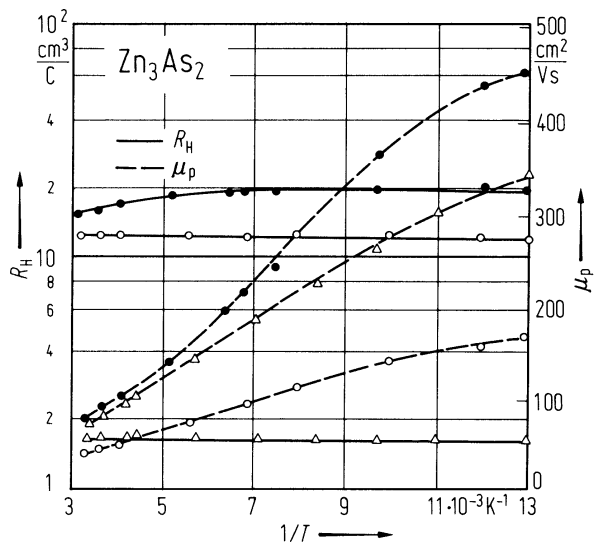


Fig. 18.3.2

Zn_3As_2 . Hall coefficient and hole mobility vs. reciprocal temperature; open circles: undoped, triangles: Cl doped, full circles: Te doped [77S].



18.4 Cadmium phosphide (Cd₃P₂)

Crystal structure

see section 18.0

Electronic properties

band structure and Brillouin zone : Fig.18.0.2.

The extrema of the conduction and valence bands occur at the Γ -point. The valence band consists of three subbands due to the influence of a tetragonal crystal field and spin-orbit interaction. The distance between the two conduction band edges which occur at the Γ -point is about 0.1 eV. The lower s-like conduction band is practically spherical but non-parabolic.

energy gap

E_g	0.50 eV	$T = 300$ K	absorption and photoconduction	64H
dE_g/dT	$-3 \cdot 10^{-4}$ eV K ⁻¹		absorption, photoconduction	72R

spin-orbit splitting energy, valence band

$\Delta_{so}(\Gamma)$	0.1 eV	$T = 4.2$ K	experimental from SdH oscillations	85C
-----------------------	--------	-------------	------------------------------------	-----

crystal field splitting energy

$\Delta_{cf}(\Gamma)$	0.034(17) eV	$T = 4.2$ K, $B = 19$ T	SdH oscillations	85C
-----------------------	--------------	-------------------------	------------------	-----

electron effective mass

cyclotron effective mass, calculated from temperature dependence of Shubnikov-de Haas oscillations

m_n	0.049(1) m_0	$T = 1.6...4.2$ K, $B \perp c$	$n = 1.1 \cdot 10^{17}$ cm ⁻³	80A
	0.045(3) m_0	$B \parallel c$		
$m_{ds,n}$	0.0487 m_0	$T = 4.2$ K	$n = 1.1 \cdot 10^{17}$ cm ⁻³	76R
	0.0517 m_0		$n = 2.9 \cdot 10^{17}$ cm ⁻³	
	0.055...0.075 m_0	$T = 90$ K	$n = 0.44...4.8 \cdot 10^{18}$ cm ⁻³	73R
	0.047(5) m_0	$T = 90$ K	$n = 1.3 \cdot 10^{18}$ cm ⁻³	78J
	0.045 (5) m_0	$T = 300$ K		80C, 78G

For dependence of m_n on electron concentration at 90 K calculated from absorption measurements and other empirical data, see Fig. 18.4.1.

electron effective mass at the bottom of the conduction band

m_n	0.050(5) m_0	$T = 310$ K		74R1
-------	----------------	-------------	--	------

hole effective mass

$m_{p,h}$	0.5(1) m_0	$T = 90...300$ K	absorption	78G
$m_{p,l}$	0.13 m_0		theory	78J

Lattice properties

lattice parameters

a	8.746(20) Å			75S
c	12.28(3) Å			

coefficient of linear thermal expansion

α	$9.63 \cdot 10^{-6}$ K ⁻¹	$T = 300$ K	dilatometric measurement	77D
----------	--------------------------------------	-------------	--------------------------	-----

Debye temperature

Θ_D	270 K	$T = 300$ K	from elastic constants	77D
$\Theta_{D,\max}$	322 K	$T = 200$ K		

heat capacity

C_p	$121.6 \text{ J mol}^{-1} \text{ K}^{-1}$	$T = 300$ K	calorimetric method	77D
C_v	$120.4 \text{ J mol}^{-1} \text{ K}^{-1}$	$T = 300$ K		

density

d	5.64 g cm^{-3}	$T = 300$ K	X-ray measurements	35S
-----	--------------------------	-------------	--------------------	-----

melting temperature

T_m	1012(2) K			35S
-------	-----------	--	--	-----

sound velocities

v_{LA}	$4.1501(95) \cdot 10^5 \text{ cm s}^{-1}$	$T = 300$ K		76O
v_{TA}	$2.0021(48) \cdot 10^5 \text{ cm s}^{-1}$	$T = 300$ K		

Young's modulus

E	$6.054 \cdot 10^6 \text{ N cm}^{-2}$	$T = 300$ K	ultrasonic wave propagation	76O
-----	--------------------------------------	-------------	-----------------------------	-----

shear modulus

G	$2.246(4) \cdot 10^6 \text{ N cm}^{-2}$	$T = 300$ K		76O
-----	---	-------------	--	-----

Poisson's ratio

ν	0.35(1)	$T = 300$ K		76O
-------	---------	-------------	--	-----

compressibility

κ	$1.6 \cdot 10^{-6} \text{ cm}^2 \text{ N}^{-1}$	$T = 300$ K		77D
----------	---	-------------	--	-----

Transport properties

(data on n-type samples)

electron concentration

n	$0.2...7 \cdot 10^{18} \text{ cm}^{-3}$	$T = 300$ K	Hall effect	65Z
-----	---	-------------	-------------	-----

resistivity

ρ	$9...25 \cdot 10^{-3} \Omega \text{ cm}$	$T = 300$ K		65Z
--------	--	-------------	--	-----

electron mobility

$\mu_{H,n}$	$0.15...0.4 \cdot 10^4 \text{ cm}^2/\text{V s}$	$T = 300$ K	in extrinsic range: $\mu \propto T^{-1}$	65Z, 64H
-------------	---	-------------	--	-------------

thermal conductivity (electronic part)

κ_{el}	$0.35...0.37 \text{ W m}^{-1} \text{ K}^{-1}$	$T = 110$ K	from Righi-Leduc effect	77B
---------------	---	-------------	-------------------------	-----

Optical properties

dielectric constant

$\epsilon(0)$	37	$T = 300$ K	calculated from empirical values	78R
$\epsilon(\infty)$	14...17	$T = 300$ K	calculated from empirical values	78R

References to 18.4

- 35S Stackelberg, M. V., Paulus, R.: Z. Phys. Chem. Abt. B 28 (1935) 427.
- 64H Haacke, G., Castellion, G. A.: J. Appl. Phys. 35 (1964) 2484.
- 65Z Zdanowicz, W., Wojakowski, A.: Phys. Status Solidi 10 (1965) K93.
- 72R Radoff, P. L., Bishop, S. G.: Phys. Rev. B 5 (1972) 442.
- 73R Radautsan, S. J., Arushanov, E. K., Nateprov, A. N., Marushyak, L. S.: Phys. Status Solidi (a) 19 (1973) K71.
- 74R1 Radautsan, S. J., Arushanov, E. K., Nateprov, A. N., Oleinik, D. A.: Phys. Status Solidi (a) 25 (1974) K57.
- 74R2 Radautsan, S. J., Arushanov, E. K., Nateprov, A. N.: Phys. Status Solidi (a) 23 (1974) K59.
- 75S Shevchenko, V. Ya., Babarina, L. P., Kozlov, S. E., Lazarev, V. B.: Neorgan. Mater. 11 (1975) 1719.
- 76O Opuska, L., Opuski, A.: Phys. Status Solidi (a) 35 (1976) K183.
- 76R Radautsan, S. J., Arushanov, E. K., Nateprov, A. N., Chuiko, G. P.: Arsenid i fosfid kadmiya, Kishiney, ed. Shtiintsa 1973.
- 77B Blom, F. A. P., Burg, J. W.: J. Phys. Chem. Solids 38 (1977) 19.
- 77D Demidenko, A. F., Danilenko, G. N., Danilenko, V. E., Lazarev, V. B., Shevchenko, V. Ya., Marenkin, S. F., Kozlov, S. F.: Neorgan. Mater. 13 (1977) 214.
- 78G Gelten, M. J., Lieshout, A. van Es, C. M., Blom, F. A. P.: J. Phys. C 11 (1978) 227.
- 78J Jay-Gerin, J. P., Aubin, M. J., Caron, L. G.: Phys. Rev. B 18 (1978) 5675.
- 78R Radautsan, S. J., Arushanov, E. K., Lashkul, A. V., Naterpov, A. N.: Fiz. Tekh. Poluprovodn. 12 (1978) 1864.
- 79P Pawlikowski, J. M., Misiewicz, J., Sujak-Cyruł, B., Wróbel, J.: Phys. Status Solidi (b) 92 (1979) K123.
- 80A Arushanov, F. K., Lashkul, A. V., Mashovets, D. V., Nateprov, A. N., Radautsan, S. I., Sologub, V. V.: Proc. Intern. Symp. on "Physics and Chemistry of II-V Compounds", Mogilany, Poland 1980, eds. M. Gelten, L. Zdanowicz, Eindhoven Univ., Netherlands, p. 153; see also the same authors in: Phys. Status Solidi (b) 102 (1980) K 121.
- 80C Chuiko, G. P.: Fiz. Tekh. Poluprovodn. 14 (1980) 629.
- 85C Cisowski, J., Portal, J.C., Broto, J.M., Arushanov, E.K., Kloc, K., Burian, A.: Acta Phys. Polon. A 67 (1985) 475.

Figures to 18.4

Fig. 18.0.2

Cd_3P_2 . Energy bands calculated by the pseudopotential method. The dashed lines show the approximate structure deduced from symmetry properties and compatibility relations for the space group D_{4h}^{15} . The inset shows the Brillouin zone for the primitive tetragonal lattice of Cd_3P_2 with indicated representation domain.

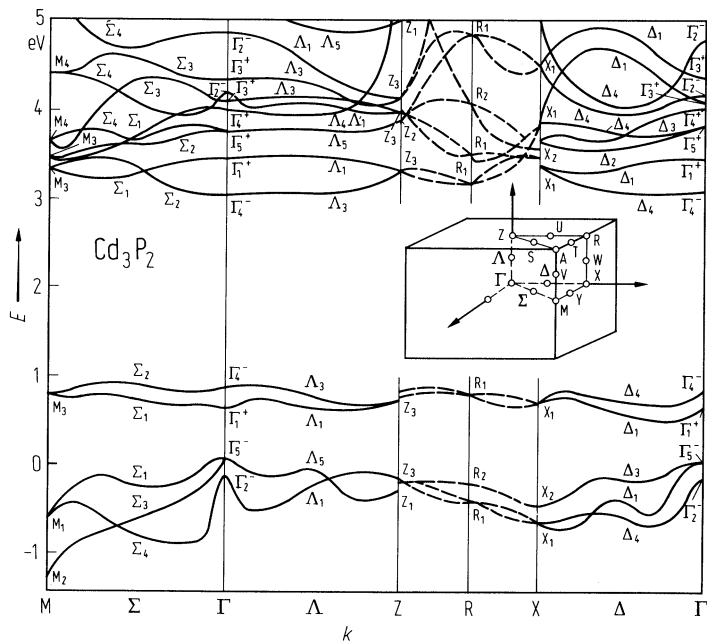
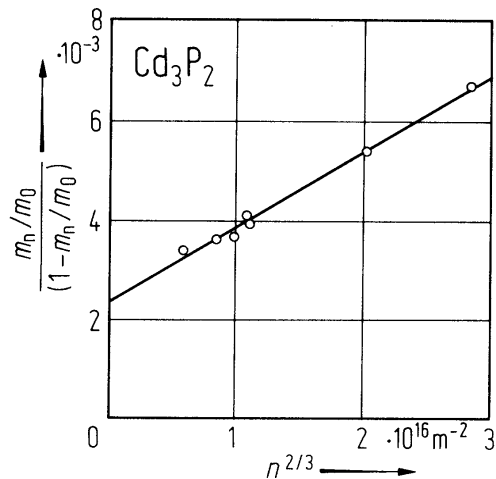


Fig. 18.4.1

Cd_3P_2 . Variation of the low-temperature electronic effective mass at the Fermi level with electron concentration at 90 K [74R2].



18.5 Cadmium arsenide (Cd₃As₂)

Crystal structure

see section 18.0

Electronic properties

band structure: Fig. 18.0.6, Brillouin zone: Fig. 18.0.5

According to [77B3] the value of E_g and the positive value of Δ_{cr} , indicate that Cd₃As₂ has an inverted anisotropic band structure with positive crystal splitting (resembling HgTe under tensile stress).

energy gap

E_g	– 0.19 eV	$T = 300$ K	indirect gap between the heavy hole band and the lowest conduction band	77A1, 77Z
	– 0.11 eV	$T = 110$ K	empirical data, assuming three band approximation of Kane's model	79D, 77A2
dE_g/dT	– $3.3 \cdot 10^{-4}$ eV K ^{–1}		Hall effect measurements on single crystals	77B1, 79B

spin-orbit splitting energy

$\Delta_{so}(\Gamma)$	0.21...0.31 eV	$T = 300$ K	calculated and experimental (thermoreflectance)	77A2
-----------------------	----------------	-------------	---	------

crystal field splitting energy

$\Delta_{cr}(\Gamma)$	0.07eV		calculated	78D
-----------------------	--------	--	------------	-----

effective mass of electrons

m_n	0.035...0.076 m_0	$T = 300$ K	electrical and thermomagnetic measurements	60Z
-------	---------------------	-------------	--	-----

effective mass, heavy holes

$m_{p,h}$	0.12 m_0			77A2
-----------	------------	--	--	------

Lattice properties

lattice parameters

α -Cd ₃ As ₂				
a	12.6461 Å	$T = 300$ K	Temperature dependence in the range 300 K...493 K: Fig. 18.5.1	73P
c	25.4378 Å			
α' -Cd ₃ As ₂				
a	12.6848 Å	$T = 503$ K	Temperature dependence in the range 503 K...729 K: Fig. 18.5.1	73P
c	25.4887 Å			
α'' -Cd ₃ As ₂				
a	9.0364 Å	$T = 750$ K	Temperature dependence in the range 749 K...791 K: Fig. 18.5.1	73P
c	12.6606 Å			
β -Cd ₃ As ₂				
a	6.4033 Å		$a = a_0 = b_0 = c_0$	73P

coefficient of linear thermal expansion

data from X-ray measurements				
α_{11}	$12.2 \cdot 10^{-6} \text{ K}^{-1}$	$T = 296 \dots 398 \text{ K}$	$\alpha\text{-Cd}_3\text{As}_2$ (α_{11} : a -direction, α_{33} : c -direction)	73P
α_{33}	$12.4 \cdot 10^{-6} \text{ K}^{-1}$			

Debye temperature

Θ_D	93 K	$T = 300 \text{ K}$	from heat capacity	77D
------------	------	---------------------	--------------------	-----

heat capacity

C_p	$125.5 \text{ J mol}^{-1} \text{ K}^{-1}$	$T = 300 \text{ K}$	calorimetric method	77D
-------	---	---------------------	---------------------	-----

density

d	6.18 g cm^{-3}	$T = 473 \text{ K}$		68G
-----	--------------------------	---------------------	--	-----

melting temperature

T_m	994 K			35S
-------	-------	--	--	-----

sound velocities

v_{LA}	$3.552 \cdot 10^5 \text{ cm s}^{-1}$	$T = 300 \text{ K}$	velocity of ultrasonic wave	76O
v_{TA}	$1.600 \cdot 10^5 \text{ cm s}^{-1}$	$T = 300 \text{ K}$	velocity of ultrasonic wave	76O

Young's modulus

E	$4.364 \cdot 10^6 \text{ N cm}^{-2}$	$T = 300 \text{ K}$		76O
-----	--------------------------------------	---------------------	--	-----

shear modulus

G	$1.59 \cdot 10^6 \text{ N cm}^{-2}$	$T = 300 \text{ K}$		76O
-----	-------------------------------------	---------------------	--	-----

Poisson's ratio

ν	0.37	$T = 300 \text{ K}$		76O
-------	------	---------------------	--	-----

Transport properties

electron concentration

n	$0.06 \dots 12 \cdot 10^{18} \text{ cm}^{-3}$	$T = 300 \text{ K}$	poly- and single crystals	79B
-----	---	---------------------	---------------------------	-----

electrical resistivity

σ	$0.23 \dots 6.4 \cdot 10^{-4} \Omega \text{ cm}$	$T = 77 \dots 300 \text{ K}$	poly- and single crystals For temperature dependence, see Fig. 18.5.2	60Z
----------	--	------------------------------	---	-----

Hall mobility of electrons

$\mu_{H,n}$	$9.8 \text{ cm}^2/\text{V s}$	$T = 80 \text{ K}$	Temperature dependence in the range 4.2...300 K: Fig. 18.5.3 single crystals, $n = 5 \cdot 10^{17} \text{ cm}^{-3}$	73R,
	$10.1 \text{ cm}^2/\text{V s}$	$T = 4.2 \text{ K}$		69R
	$2.6 \text{ cm}^2/\text{V s}$	$T = 300 \text{ K}$		77B2

thermal conductivity

κ	$0.0245 \text{ W cm}^{-1} \text{ K}^{-1}$	$T = 300 \text{ K}$	polycrystal, see Fig. 18.5.4	69A
	$0.15 \text{ W cm}^{-1} \text{ K}^{-1}$	$T = 4.2 \text{ K}$		

Optical properties

refractive index

n	5.5...6	$T = 90 \dots 300 \text{ K}$ $\lambda = 6 \dots 14 \mu\text{m}$	interferometric data for thin films	77Z, 74Z, 72R
-----	---------	--	--	---------------------

dielectric constants

$\epsilon(0)$	36	calculated for $n = 2 \cdot 10^{18} \text{ cm}^{-3}$	77J
$\epsilon(\infty)$	16	absorption and reflection	80G

References to 18.5

- 35S Stackelberg, M. V., Paulus, R.: Z. Phys. Chem. Abt. B 28 (1935) 427.
- 60Z Zdanowicz, W.: Proc. Intern. Conf. Semicond. Phys., Prague 1960; Publ. House of Czech. Acad. Sci., Prague 1961, p. 1095.
- 68G Glazov, V. M., Kasymova, M.: Dokl. Akad. Nauk SSSR 183 (1968) 141.
- 68T Trzebiatowski, W., Krdlicki, F., Zdanowicz, W.: Bull. Acad. Pol. Sci., Ser. Sci. Chim. 16 (1968) 343.
- 69A Armitage, D., Goldsmid, H. J.: J. Phys. C 2 (1969) 2138.
- 69R Rosenman, I.: J. Phys. Chem. Solids 30 (1969) 1385.
- 72R Radoff, P. L., Bishop, S. G.: Phys. Rev. B 5 (1972) 442.
- 73P Pietraszko, A., Lukaszewicz, K.: Phys. Status Solidi (a) 18 (1973) 723.
- 73R Radautsan, S. J., Arushanov, E. K., Chuiko, G. P.: Phys. Status Solidi (a) 20 (1973) 221.
- 74Z Zivitz, M., Stevenson, J. R.: Phys. Rev. B 10 (1974) 161.
- 75C Clavaguera, M. T.: J. Phys. Chem. Solids 36 (1975) 1205.
- 76O Opuska, L., Opuski, A.: Phys. Status Solidi (a) 35 (1976) K183.
- 76R Radautsan, S. J., Arushanov, E. K., Nateprov, A. N., Chuiko, G. P.: Arsenid i fosfid kadmiya, Kishiney, ed. Shtiintsa 1973.
- 77A1 Aubin, M. J., Jay-Gerin, J. P., Caron, L. G.: Phys. Rev. B15 (1977) 3872.
- 77A2 Aubin, M. J., Jay-Gerin, J. P., Caron, L. G.: Solid State Commun. 21 (1977) 659.
- 77B1 Blom, F. A. P., Burg, J. W.: J. Phys. Chem. Solids 38 (1977) 19.
- 77B2 Blom, F. A. P., Gelten, M. J.: Proc. 3rd Inter. Conf. Physics of Narrow-gap Semicond., PWN Warsaw 1977, p. 257.
- 77B3 Bodnar, J.: Proc. 3rd Inter. Conf. Physics of Narrow-gap Semicond., PWN Warsaw 1977.
- 77D Demidenko, A. F., Danilenko, G. N., Danilenko, V. E., Lazarev, V. B., Shevchenko, V. Ya., Marenkin, S. F., Kozlov, S. F.: Neorgan. Mater. 13 (1977) 214.
- 77J Jay-Gerin, J. P., Aubin, M. J., Caron, L. G.: Solid State Commun. 21 (1977) 771.
- 77Z Zdanowicz, L., Kwiecien, T.: Vacuum 27 (1977) 409.
- 78D Dowgiallo-Plenkiewicz, B., Plenkiewicz, P.: Phys. Status Solidi (b) 87 (1978) 309.
- 78L Lazarev, V. B., Shevchenko, V. Ya., Greenberg, Ya. G., Sobolev, V. V.: "Semiconducting Compounds of II-V Group", ed. Nauka Moscow 1978.
- 79B Becla, P., Gumienny, Z., Misiewicz, J.: Opt. Appl. 9 (1979) 143.
- 79D Dowgiallo-Plenkiewicz, B., Plenkiewicz, P.: Mater. Sci. 5 (1979) 51.
- 80G Gelten, M. J., Van Es, C. M., Blom, F. A. P., Jongeneelen, J. W. F.: Solid State Commun. 33 (1980) 833.
- 86B Bartkowski, K., Rafalowicz, J., Zdanowicz, W.: Int. J. Thermophys. 7 (1986) 765.

Figures to 18.5

Fig. 18.0.5

Cd_3As_2 . Brillouin zone (a) for the body-centered tetragonal structure C_{4v}^{12} ($c > 2^{1/2}a$) showing symmetry points and axes, (b) for the fluorite (CaF_2) structure [75C].

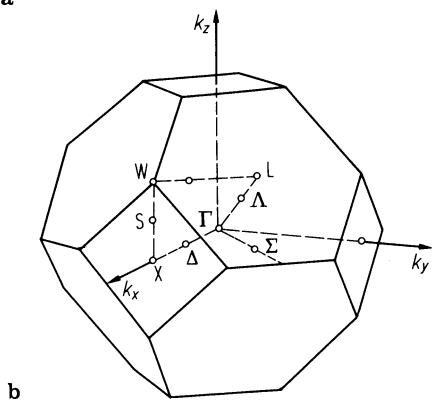
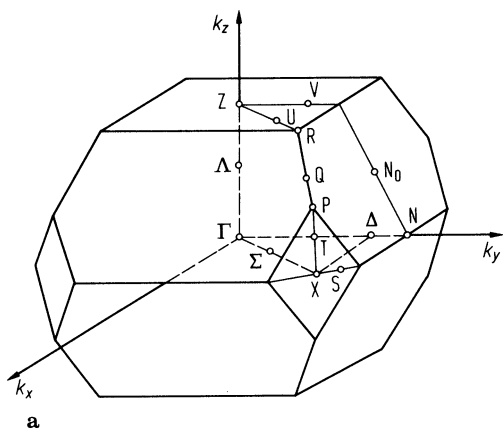


Fig. 18.0.6

Cd_3As_2 . $E(k)$ relation for the four level energy bands model. The wave vector k (in 10^6 cm^{-1}) is directed a) 0° , b) 5° , c) 90° from the tetragonal c -axis [77B1]; see also [79B]. Energies are labelled with respect to E_c .

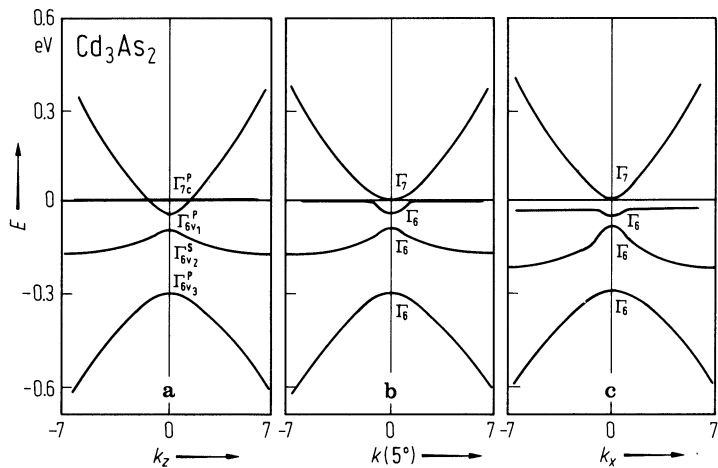


Fig. 18.5.1

Cd_3As_2 and Zn_3As_2 . Lattice parameters reduced to the prototypic unit cell (A) and linear expansion Δl (B) from dilatometric measurements vs. temperature of heating; [73P] and [68T].

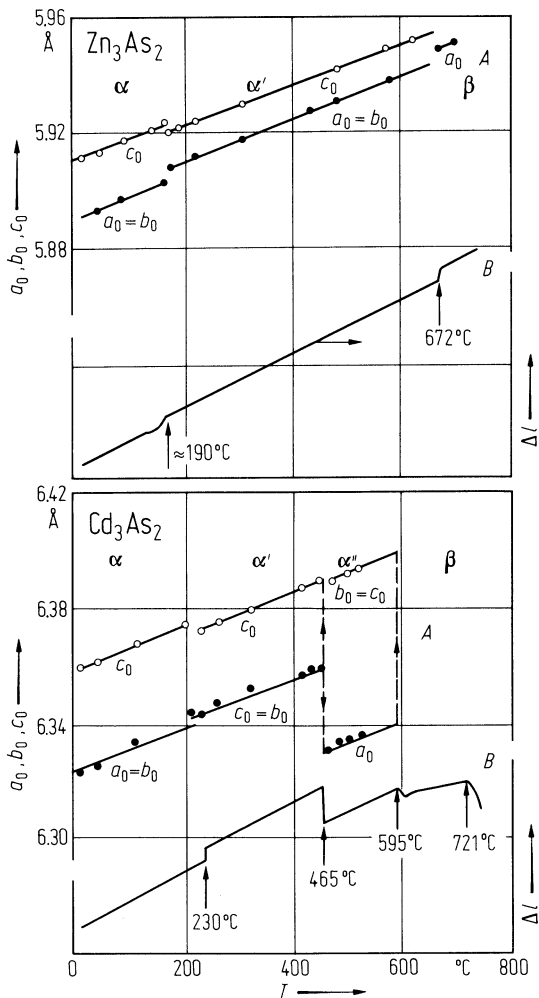


Fig. 18.5.2

Cd_3As_2 . Resistivity vs. reciprocal temperature for various samples in the range 500...77 K [76R].

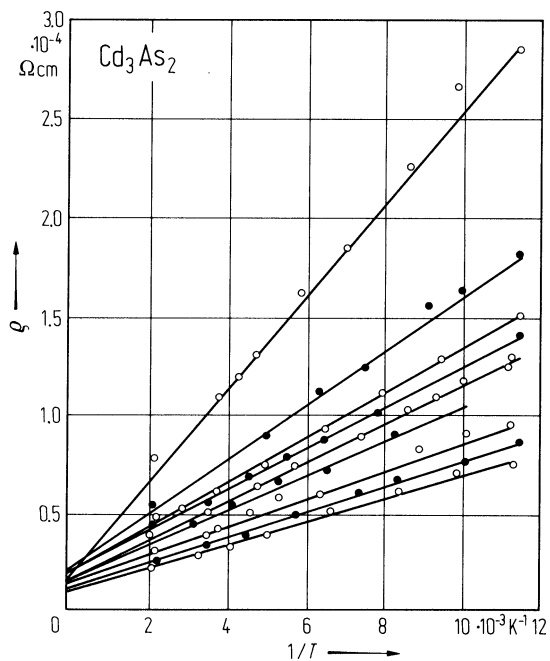


Fig. 18.5.3

Cd_3As_2 . Electron Hall mobility vs. temperature for various samples in the range $T = 4.2 \dots 300$ K. Electron concentration n (in 10^{18} cm^{-3}): curve 1: 1.05, 2: 1.33, 3: 3.20, 4: 1.92, 5: 9.60, 6: 2.5 [78L].

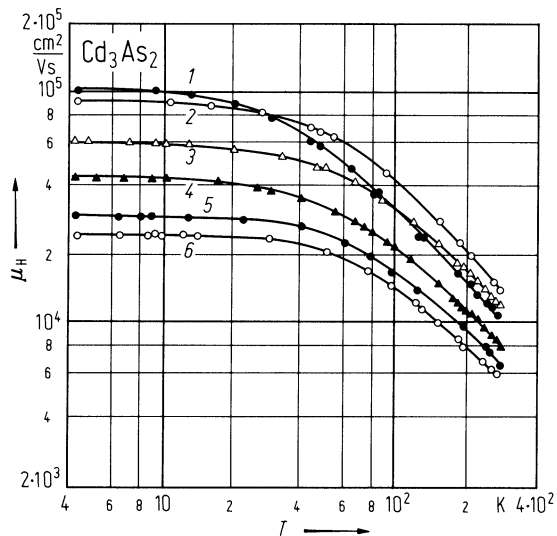
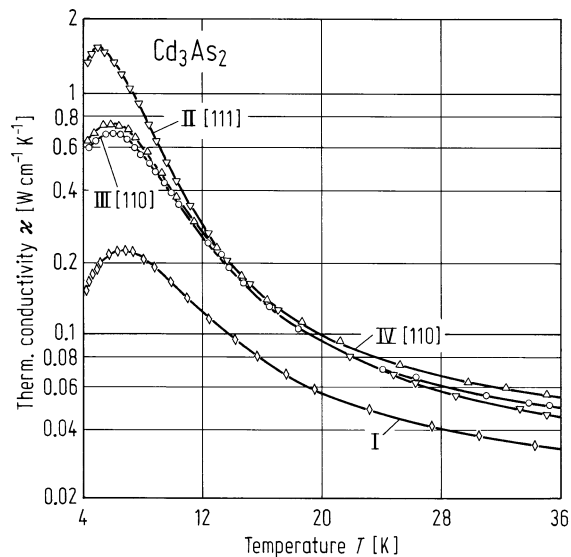


Fig. 18.4

Cd_3As_2 . The temperature dependence of the thermal conductivity κ , for single crystal (in 3 directions) and polycrystalline Cd_3As_2 . I - polycrystalline sample; II, III, and IV - single crystal samples [86B].



18.6 Zinc phosphide (ZnP2)

Crystal structure

see section 18.0

α-modification :

Electronic properties

band structure

The valence and conduction bands are composed of three subbands (Fig. 18.0.9a...c) [71S2]. The valence subbands v1, v2, v3 and the c3 conduction subband are situated at the Γ point, while the c1 and c2 conduction subbands are away from the center of the Brillouin zone (Fig. 18.0.8) [71S2]. For more details, see [71S1] and [71S2].

energy gaps

$E_{g,ind}$	1.65 eV	$E \perp c, T = 293\text{ K}$	absorption edge	71S1
	1.85 eV	$E \parallel c, T = 293$		
$dE_{g,ind}/dT$	$-2.3 \cdot 10^{-4}\text{ eV K}^{-1}$	$T = 77...293\text{ K}$		71S1
$E_{g,dir}$	2.18 eV	$E \parallel c, T = 293\text{ K}$		71S1
		$E \perp c$		
$dE_{g,dir}/dT$	$-5.5 \cdot 10^{-4}\text{ eV K}^{-1}$	$T = 77...293\text{ K}$		71S1

exciton levels

E_{gx}	2.210(2) eV	$T = 4.2\text{ K}$	photoluminescence	70R
	2.195 eV		formation of free exciton with emission of a phonon	

Lattice properties

lattice parameters

a	5.08(1) Å			63H,
c	18.59 (5) Å			65W

coefficient of linear thermal expansion

α	$3.8 \cdot 10^{-6}\text{ K}^{-1}$	$T = 300\text{ K}$	dilatometric method	77S
----------	-----------------------------------	--------------------	---------------------	-----

heat capacity

C_p	$65.56\text{ J mol}^{-1}\text{ K}^{-1}$	$T = 298\text{ K}$	measurement performed on vacuum adiabatic calorimeter in the range 360...390 K	80S
-------	---	--------------------	--	-----

density

d	3.536 g cm^{-3}	X-ray measurement		63H
-----	--------------------------	-------------------	--	-----

melting temperature

T_m	1258(1) K			70R
-------	-----------	--	--	-----

sound velocity

v_{LA}	$5.950 \cdot 10^5\text{ cm s}^{-1}$	$T = 376...380\text{ K}$	calculated from dilatometric measurement	80K
----------	-------------------------------------	--------------------------	--	-----

optical activity of lattice vibrations

The factor group D4 yields 72 atomic vibrations and 69 optical branches. Their reduced representation is $\Gamma_{vib} = 9A_1 + 8A_2 + 9B_1 + 17E$. The reduced representation of the Raman active vibrations is $\Gamma^R_{vib} = 9A_1 + 9B_1 + 9B_2 + 17E$. That of their active vibrations is $\Gamma^{ir}_{vib} = 8A_2 + 17E$.

Transport properties

(measurements only on p-type samples)

electrical conductivity

σ	$3.3 \cdot 10^{-8} \Omega^{-1} \text{ cm}^{-1}$	$T = 300 \text{ K}$		78G
----------	---	---------------------	--	-----

hole concentration

p	$1.2 \cdot 10^{10} \text{ cm}^{-3}$	$T = 300 \text{ K}$	Hall effect	78G
-----	-------------------------------------	---------------------	-------------	-----

hole mobility

$\mu_{\text{H,p}}$	$1.8 \cdot 10^3 \text{ cm}^2/\text{V s}$	$T = 300 \text{ K}$	for more details, see [78G]	78G
--------------------	--	---------------------	-----------------------------	-----

β -modification :

Electronic properties

band structure

The valence band is composed of four subbands $v_1 \dots v_4$, whereas the conduction band consists of three subbands $c_1 \dots c_3$. One version of the band structure is shown in Fig. 18.6.1 [72S].

energy gap

E_g	1.42 eV	$T = 0 \text{ K}$	extrapolated from Hall and resistivity data	75Z
-------	---------	-------------------	---	-----

effective mass of electrons

m_{na}	$0.7(1) m_0$	$T = 1.5 \text{ K}$	$B = 6 \text{ T}$	96E
m_{nb}	$1.1(2) m_0$			
m_{nc}	$0.18(4) m_0$			

effective mass of holes

m_{pa}	$1.1(2) m_0$	$T = 1.5 \text{ K}$	$B = 6 \text{ T}$	96E
m_{pb}	$1.4(3) m_0$			
m_{pc}	$0.20(4) m_0$			

Lattice properties

lattice parameters

a	$8.85(2) \text{ \AA}$			63H
b	$7.29(2) \text{ \AA}$			
c	$7.56(2) \text{ \AA}$			
β	$102.30(2)^\circ$			

coefficient of linear thermal expansion

α	$2.6 \cdot 10^{-6} \text{ K}^{-1}$	dilatometric measurement	77S
----------	------------------------------------	--------------------------	-----

heat capacity

C_p	$73.3 + 14 \cdot 10^{-3} T$ [J mol ⁻¹ K ⁻¹]	calorimetric method, temperature range 300...1000 K	75S
-------	---	---	-----

density

d	3.47 g cm^{-3} 3.55 g cm^{-3}	pycnometric method calculated from X-ray data	63H
-----	--	--	-----

melting temperature

T_m	1265(1) K	70R
-------	-----------	-----

Transport and optical properties

(mostly p-type crystals)

carrier concentrations

p	$8 \cdot 10^{14} \dots 6.5 \cdot 10^{15} \text{ cm}^{-3}$	$T = 300 \text{ K}$	Hall effect, Fig. 18.6.2	78G
n	$2 \cdot 10^{15} \text{ cm}^{-3}$		(sample doped with Ga)	78G

electrical resistivity

ρ	$3 \text{ } \Omega \text{ cm}$	$T = 300 \text{ K}$	78G
	$100 \text{ } \Omega \text{ cm}$	$T = 300 \dots 700 \text{ K}$	75Z

electron mobility

μ_{H}	1...3.5 cm ² /V s	$T = 300 \text{ K}$		75Z
μ_{n}	0.81 cm ² /V s	$T = 300 \text{ K}$	Ga-doped sample	78G

dielectric constants

ε_a	9.1(3)	$T = 1.5 \text{ K}$	$B = 6 \text{ T}$	96E,
ε_b	11.1(3)			88T
ε_c	9.3(3)			

References to 18.6

- 63H Hegyi, I. J., Loebner, E. E., Poor, Jr., E. W., White, J. G.: J. Phys. Chem. Solids 24 (1963) 333.
65W White, J. G.: Acta Crystallogr. 18 (1965) 217.
70R Rubenstein, M., Dean, P. J.: J. Appl. Phys. 41 (1970) 1777.
71S1 Sobolev, V. V., Syrbu, N. N.: Phys. Status Solidi (b) 43 (1971) K87.
71S2 Sobolev, V. V., Syrbu, N. N.: Phys. Status Solidi (b) 43 (1971) 73.
72S Sobolev, V. V., Syrbu, N. N.: Phys. Status Solidi (b) 51 (1972) 863.
75S Sirota, N. N., Antyukhov, A. M., Smolarenko, E. M.: Dokl. Akad. Nauk BSSR 19 (1975) 1092.
75Z Zdanowicz, W., Wilczak, B., Zdanowicz, L., Sysoev, B. Y., Bityutskaya, L. A., Synorov, V. F.: Acta Phys. Polon. A 48 (1975) 27.
77S Sirota, N. N., Antiukhov, A. M., Smolarenko, E. M.: Neorgan. Mater. 13 (1977) 358.
78G Gorban, I. S., Grishchenko, G. A., Sakalas, A. P., Sodeika, A. S., Tichina, I. I., Tkachenko, A. K.: Phys. Status Solidi (a) 48 (1978) 329.
80K Käräjämäki, F., Laiho, R., Levola, T., Sheleg, A. U.: Semicond. Insulat. 5 (1980) 153.
80S Sheleg, A. U., Smolarenko, F. M., Tekhanovich, P. P., Povlovskaya, B. E., Trukhan, V. M.: Neorgan. Mater. 16 (1980) 347.
88T Taguchi, S., Goto, T., Takeda, M., Kido, G.: J. Phys. Soc. Jpn. 57 (1988) 3256.
96E Engbring, J., Fröhlich, D., Schepe, R., Spitzer, S., Arimoto, O., Nakamura, K.: Phys. Status Solidi (b) 196 (1996) 461.

Figures to 18.6

Fig. 18.0.8

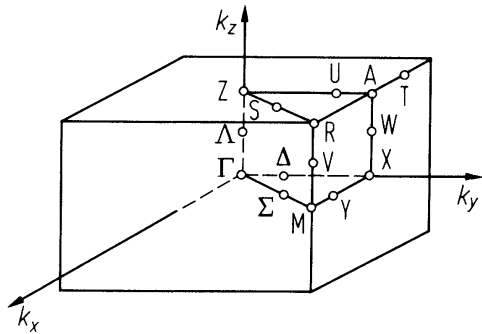
 α -ZnP₂, β -CdP₂. Brillouin zone [71S2].

Fig. 18.0.9

α -ZnP₂, β -CdP₂. Different versions of the electronic band structure in the vicinity of the interband gap (main optical transitions) of α -ZnP₂ (a, b, c) and β -CdP₂ (d) on the basis of photoconductivity and reflectivity data. Energy values for 293 K [71S2].

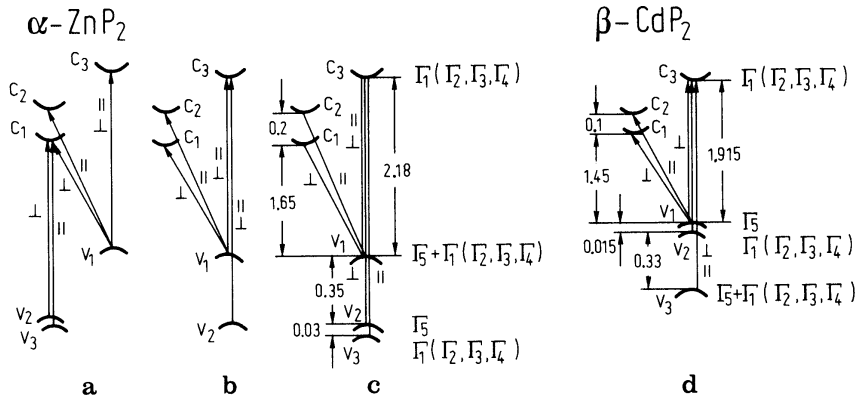


Fig. 18.6.1

β -ZnP₂ (a), α -ZnP₂ (b). Electronic band model with main optical transitions obtained from photoconductivity, reflectivity and edge absorption spectra at $T = 293$ K. For the energy values (in eV) compare the tables [72S].

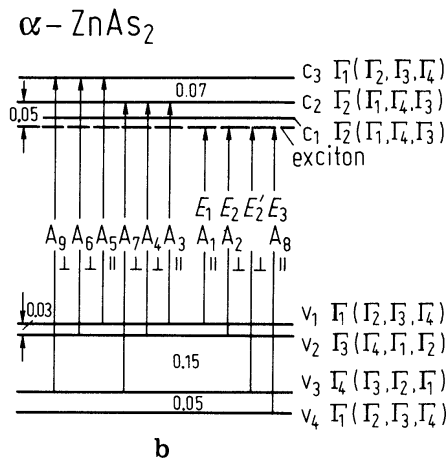
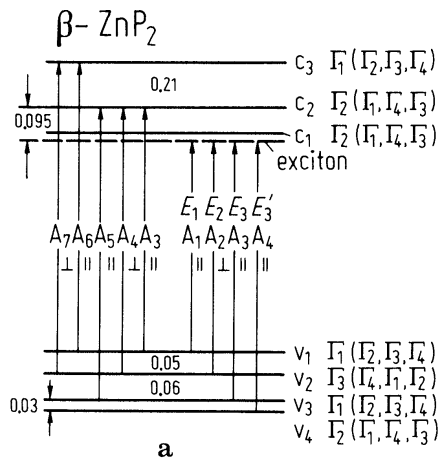
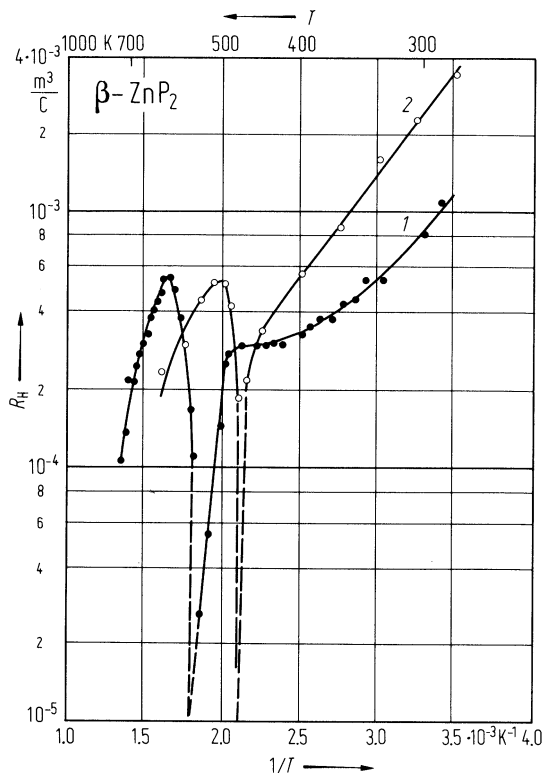


Fig. 18.6.2

β -ZnP₂. Temperature dependence of Hall coefficient; 1, for the crystals obtained from vapor phase; 2, for the crystal obtained from liquid phase [75Z].



18.7 Zinc arsenide (ZnAs2)

Crystal structure

see section 18.0

Electronic properties

band scheme: Fig. 18.7.1.

energy gap

$E_{g,dir}$	0.973 eV	$T = 293\text{ K}, E \perp c$	from transmission spectra, $E_{g,dir} = E_{gx,dir} + E_{b,dir}$	97M
dE_g/dT	$-3.1(2) \cdot 10^{-4}\text{ eV K}^{-1}$	$E \parallel c$	absorption in the range 77...293 K	72S
	$-4.6(2) \cdot 10^{-4}\text{ eV K}^{-1}$	$E \perp c$		

excitonic band gaps

$E_{gx,ind}$	0.875 eV	$T = 293\text{ K}, E \parallel c$	from absorption spectra	97M
$E_{gx,dir}$	0.939 eV	$T = 293\text{ K}, E \parallel c$	from photoconductivity and short-circuit photocurrent spectra	97M

exciton binding energy

$E_{b,dir}$	17.5 meV	$T = 5...100\text{ K}, E \perp c$	from transmission spectra (forbidden series of free exciton, $n = 1, 2, 3$)	97M, 96M 97M
-------------	----------	-----------------------------------	--	--------------------

crystal field splitting energy

Δ_{cr}	17 meV	$T = 293\text{ K}$	from absorption, photoconductivity and short-circuit photocurrent spectra	97M
	7 meV	$T = 77\text{ K}$		

Lattice properties

lattice parameters

a	9.21(3) Å			79L
b	7.64(3) Å			
c	7.985(3) Å			
β	102°28'			

coefficient of linear thermal expansion

α	$8.2 \cdot 10^{-6}\text{ K}^{-1}$	$T = 300\text{ K}$	dilatometric method	68G
----------	-----------------------------------	--------------------	---------------------	-----

compressibility

κ	$10.6 \cdot 10^{-7}\text{ cm}^2\text{ N}^{-1}$	$T = 300\text{ K}$	from sound velocity	77D
----------	--	--------------------	---------------------	-----

Debye temperature

Θ_D	234 K	$T = 300\text{ K}$		77D
------------	-------	--------------------	--	-----

heat capacity

C_p	$72.60\text{ J mol}^{-1}\text{ K}^{-1}$	$T = 300\text{ K}$		77D
C_v	$72.52\text{ J mol}^{-1}\text{ K}^{-1}$	$T = 300\text{ K}$		

density

d	5 g cm ⁻³	$T = 300\text{ K}$	X-ray data For temperature dependence of d , see Fig. 18.7.2	59L
-----	----------------------	--------------------	--	-----

melting temperature

T_m	1041(1) K	$p(\text{As}) = 3.3 \text{ atm}$		59L
-------	-----------	----------------------------------	--	-----

Transport properties

Undoped ZnAs₂ samples are characterized by large anisotropy Hall coefficient, resistivity and Seebeck coefficient.

carrier concentrations

p	$2 \cdot 10^{14} \text{ cm}^{-3}$	$T = 300 \text{ K}$	undoped sample	66U
n	$8 \cdot 10^{16} \text{ cm}^{-3}$	$T = 300 \text{ K}$	Se and Te doped sample	

resistivity

ρ	$10 \dots 10^5 \Omega \text{ cm}$	$T = 300 \text{ K}$	large anisotropy, depending on crystallographic direction	77C
--------	-----------------------------------	---------------------	---	-----

mobility

μ_p	$50 \dots 100 \text{ cm}^2/\text{V s}$	$T = 300 \text{ K}$	undoped and non-oriented samples	61T, 77C, 66U
μ_n	$240 \dots 500 \text{ cm}^2/\text{V s}$	$T = 300 \text{ K}$	Se and Te doped samples, temperature dependence $\propto T^{-1.35}$ in the intrinsic range	66U

thermal conductivity

$\kappa [\text{W m}^{-1} \text{ K}^{-1}]$	$2.44 \cdot 10^3/T+B$	$T = 70 \dots 300 \text{ K}$	$B = 19 \text{ K}$ for [100] direction $B = -57.8 \text{ K}$ for [010] direction $B = -29.7 \text{ K}$ for [001] direction	92N
---	-----------------------	------------------------------	--	-----

Optical properties

index of refraction

n	3.38	$T = 300 \text{ K}$	absorption measurements with unpolarized light on non oriented samples	61T
-----	------	---------------------	--	-----

dielectric constant

$\varepsilon(0)$	14.5 (3)	$T = 300 \text{ K}$	resonance method at $f = 1.9 \cdot 10^9 \text{ s}^{-1}$	66U
	15.5 (5)		in b -direction	
	15.0 (5)		in c -direction in a -direction	

References to 18.7

- 59L Lyons, V. J.: J. Phys. Chem. 63 (1959) 1142.
- 61T Turner, W. J., Fishler, A. S., Reese, W. E.: Phys. Rev. 121 (1961) 759.
- 66U Ugai, Ya. A., Zyubina, T. A.: Neorgan. Mater. 2 (1966) 9.
- 68G Glazov, V. M., Kasymova, M.: Dokl. Akad. Nauk SSSR 183 (1968) 141.
- 72S Sobolev, V. V., Syrbu, N. N.: Phys. Status Solidi (b) 51 (1972) 863.
- 77C Clemen, C., Müller, A., Munz, P., Hönigschmid, Y., Bucher, F.: Europ. Photovoltaic Conf. Luxemburg 1977, p. 638.
- 77D Danilenko, G. N., Danilenko, V. E., Karapetyant, M. H., Lazarev, V. B., Marenkin, S. F., Shevchenko, V. Ya.: Neorgan. Mater. 13 (1977) 1736.
- 79L Lazarev, V. B., Marenkin, S. F., Maksimova, S. I., Guseinov, B., Shevchenko, V. Ya.: Neorgan. Mater. 15 (1979) 749.
- 92N Nadtochii, Y.G., Pischikov, D.I., Burtsev, Y.N. Zakharov, S.V., Marenkin, S.F., Lazarev, V.B.: Neorg. Mater. 28 (1992) 293.
- 97M Morozova, V. A., Semenenja, T. V., Marenkin, S. F., Forsh, E. A., Koshelev, O. G.: Neorg. Mater. 33 (1997) 920.

Figures to 18.7

Fig. 18.7.1

β -ZnP₂ (a), α -ZnAs₂ (b). Electronic band model with main optical transitions obtained from photoconductivity, reflectivity and edge absorption spectra at $T=293$ K. For the energy values (in eV) compare the tables [72S].

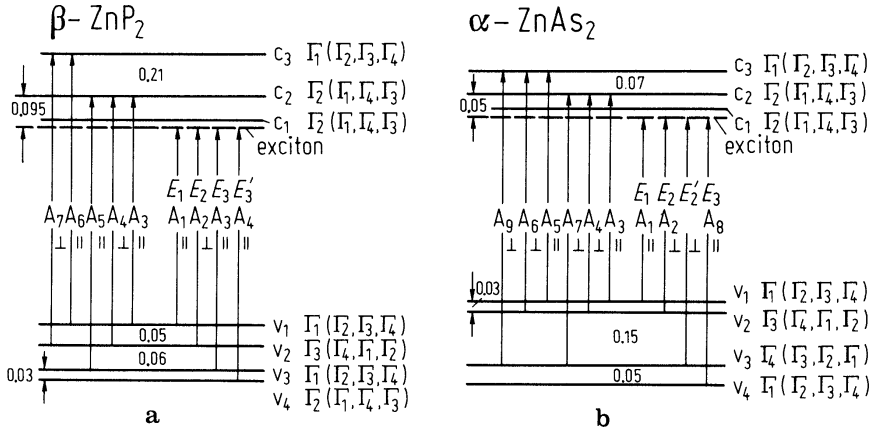
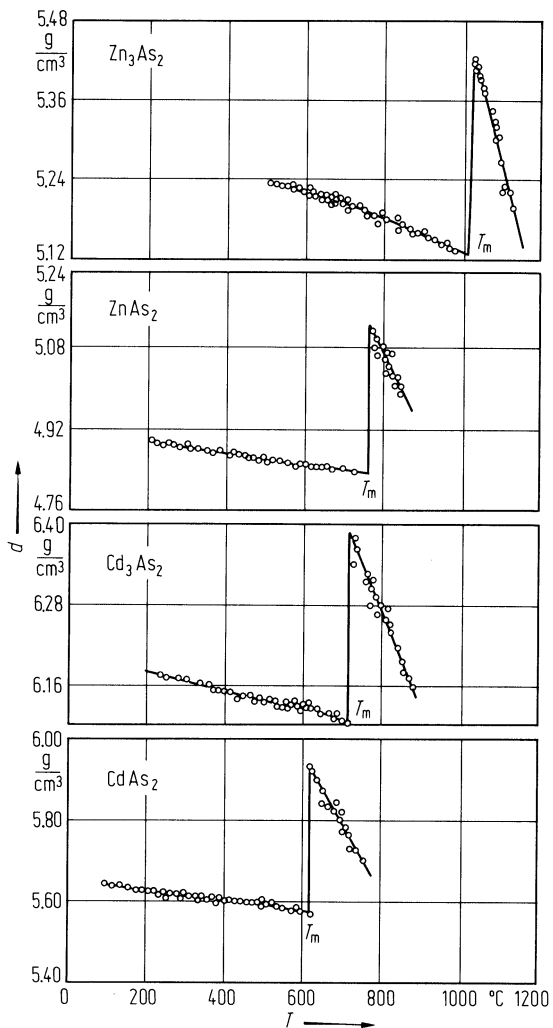


Fig. 18.7.2

ZnAs_2 , CdAs_2 , Cd_3As_2 , Zn_3As_2 . Density vs. temperature in solid and liquid phases [68G].



18.8 Cadmium phosphide (CdP₂)

Crystal structure

see section 18.0

Electronic properties

The data are for the β -modification, if not stated otherwise.

band structure

The energy band structure, based on photoconductivity measurements [71S1, 71S2, 71S3] and on wavelength modulated photoresponse measurements, is similar to the band structure of α -ZnP₂. The valence and conduction bands are composed of three subbands. All valence subbands and the c_3 -conduction band are situated at Γ , whereas the c_1 and c_2 -subbands are away from the center of the Brillouin zone [71S1, 71S2].

energy gap

$E_{g,ind}$	1.55 eV	$E \perp c, T = 293 \text{ K}$	absorption edge	71S1
	1.65 eV	$E \parallel c, T = 293 \text{ K}$		
$E_{g,dir}$	2.02(2) eV	$T = 293 \text{ K}$	absorption edge for non-oriented crystal and non-polarized light	65Z
	1.92 eV	$E \perp c, T = 293 \text{ K}$	absorption edge	71S1
$dE_{g,ind}/dT$	$-4.2 \cdot 10^{-4} \text{ eV K}^{-1}$	$E \perp c$		71S1
	$-3.7 \cdot 10^{-4} \text{ eV K}^{-1}$	$E \parallel c$		

exciton transition energy

E_{gx}	2.135 eV	$T = 63 \text{ K}$	cathodoluminescence, with $E_g = 2.151 \text{ eV}$ an exciton binding energy of 16(3) meV has been obtained	72V
----------	----------	--------------------	---	-----

Lattice properties

lattice parameters

α -CdP ₂				
a	9.90 Å			70O
b	5.408 Å			
c	5.471 Å			
β -CdP ₂				
a	5.29 Å			69H
c	19.74 Å			

coefficient of linear thermal expansion

α	$4.46 \cdot 10^{-6} \text{ K}^{-1}$	$T = 300 \text{ K}$	dilatometric method for temperature dependence in the range 300...580 K, see Fig. 18.8.1	77S
----------	-------------------------------------	---------------------	--	-----

sound velocity

v_{LA}	$5.130 \cdot 10^5 \text{ cm s}^{-1}$	$T = 373 \text{ K}$	from dilatometric and X-ray measurements	80S2
----------	--------------------------------------	---------------------	---	------

second order elastic moduli

$c_{33}, c_{44}, c' = 1/2(c_{11} + c_{12} + 2c_{66}), c'' = 1/2(c_{11} - c_{12})$ in the range $T = 78...260 \text{ K}$, see Fig. 18.8.2 [89S].

heat capacity

C_p	6848 J mol ⁻¹ K ⁻¹	$T = 298 \text{ K}$		80S2
-------	--	---------------------	--	------

density

d	4.19 g cm ⁻³	X-ray measurements	35S
-----	-------------------------	--------------------	-----

melting temperature

T_m	1057 K		77B
-------	--------	--	-----

References to 18.8

- 35S Stackelberg, M. V., Paulus, R.: Z. Phys. Chem. Abt. B 28 (1935) 427.
- 65Z Zdanowicz, W., Wojakowski, A.: Phys. Status Solidi 10 (1965) K93.
- 69H Horn, J.: Bull. Acad. Pol. Sci., Ser. Sci. Chim. 17 (1969) 69.
- 70O Olofsson, O., Sullman, J.: Acta Crystallogr. B26 (1970) 1883.
- 71S1 Sobolev, V. V., Syrбу, N. N.: Phys. Status Solidi (b) 43 (1971) K87.
- 71S2 Sobolev, V. V., Syrбу, N. N.: Phys. Status Solidi (b) 43 (1971) 73.
- 71S3 Sobolev, V. V., Syrбу, N. N., Zyubina, T. A., Ugai, Ya. A.: Fiz. Tekh. Poluprovodn. 5 (1971) 327.
- 72V Vavilov, V. S., Koval, V. S., Negrei, V. D., Potykevich, I. V., Potykievich, Yu. V., Chukichev, M. V.: Fiz. Tekh. Poluprovodn. 6 (1972) 281; Sov. Phys. Semicond. (English Transl.) 6 (1972) 241.
- 77B Blom, F. A. P., Gelten, M. J.: Proc. 3rd Inter. Conf. Physics of Narrow-gap Semicond., PWN Warsaw 1977, p. 257.
- 77S Sirota, N. N., Antiukhov, A. M., Smolarenko, E. M.: Neorgan. Mater. 13 (1977) 358.
- 80S1 Sheleg, A. U., Novikov, V. P.: Proc. Intern. Symp. on "Physics and Chemistry of II-V Compounds", Mogilany, Poland 1980, eds. M. Gelten, L. Zdanowicz, Eindhoven Univ., Netherlands, p. 255.
- 80S2 Sheleg, A. U., Smolarenko, F. M., Tekhanovich, P. P., Povlovskaya, B. E., Trukhan, V. M.: Neorgan. Mater. 16 (1980) 347.
- 89S Soshnikov, L.E., Sheleg, A.U.: Phys. Status Solidi (a) 111 (1989) 485.

Figures to 18.8

Fig. 18.8.1

β -CdP₂. Lattice parameters and relative change in length vs. temperature. X-ray and dilatometric measurements [80S1].

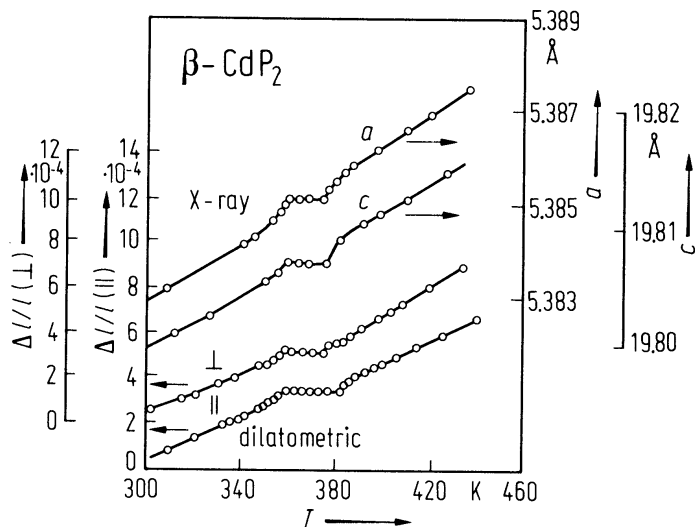
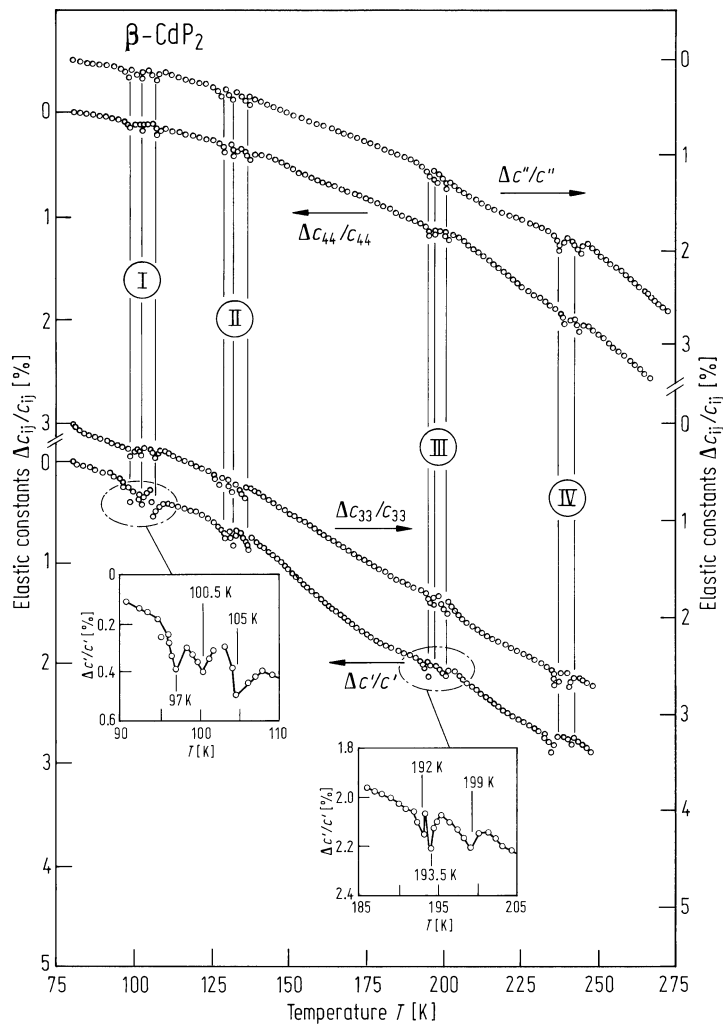


Fig. 18.8.2

CdP_2 . Variation with temperature of the elastic constants c_{33} , c_{44} , $c' = 1/2(c_{11} + c_{12} + 2c_{66})$, $c'' = 1/2(c_{11} - c_{12})$ for $\beta\text{-CdP}_2$. Temperature ranges with anomalous behaviour of the elastic constants are denoted as I to IV [89S].



18.9 Cadmium arsenide (CdAs₂)

Crystal structure

see section 18.0

Electronic properties

The surfaces of constant energy are simple ellipsoids of revolution directed along the fourfold symmetry *c*-axis of the tetragonal crystal [60S, 61F].

energy gap

E_g	1.00 eV	$T = 297\text{ K}, E \parallel c$	absorption edge	61T
	1.04 eV	$T = 297\text{ K}, E \perp c$		
$E_{g,\text{ind}}$	0.995 eV	$T = 293\text{ K}, E \parallel c$	from absorption, photoconductivity and short-circuit photocurrent spectra,	96M1, 96M2
	1.000 eV	$T = 293\text{ K}, E \perp c$		
$dE_{g,\text{ind}}/dT$	$-5.6 \cdot 10^{-4}\text{ eV K}^{-1}$	$E \parallel c, E \perp c$	from absorption spectra in the range $T = 77 \dots 293\text{ K}$	96M1

exciton binding energy

$E_{b,\text{ind}}$	14.5 meV	$E \parallel c, E \perp c$	from absorption and short-circuit photocurrent spectra in the range $T = 77 \dots 120\text{ K}$	96M2
--------------------	----------	----------------------------	---	------

crystal field splitting energy

Δ_{cr}	4...5 meV	$T = 77 \dots 293\text{ K}$	from absorption and photoconductivity spectra	96M1, 96M2
----------------------	-----------	-----------------------------	---	------------

effective masses

$m_{n\perp}$	0.58 (4) m_0	$T = 1.5\text{ K},$ in <i>c</i> -direction	cyclotron resonance (20...35 kMc s ⁻¹)	60S
$m_{n\parallel}$	0.150(30) m_0			
$m_{p\perp}$	0.346 (25) m_0			
$m_{p\parallel}$	0.094 (30) m_0			

Lattice properties

lattice parameters

<i>a</i>	7.954 (3) Å			70C
<i>c</i>	4.678(2) Å			

coefficient of linear thermal expansion

α	$6.8 \cdot 10^{-6}\text{ K}^{-1}$	$T = 300\text{ K}$	dilatometric method	68G
----------	-----------------------------------	--------------------	---------------------	-----

compressibility

κ	$2.4 \cdot 10^{-7}\text{ cm}^2\text{ N}^{-1}$	$T = 300\text{ K}$	from sound velocity	77D
----------	---	--------------------	---------------------	-----

Debye temperature

Θ_D	84 K	$T = 300\text{ K}$		79G
------------	------	--------------------	--	-----

heat capacity

C_p	74.75 J mol ⁻¹ K ⁻¹	$T = 300\text{ K}$		77D
C_v	74.46 J mol ⁻¹ K ⁻¹	$T = 300\text{ K}$		

density

<i>d</i>	5.88 g cm ⁻³	$T = 300\text{ K}$	X-ray data temperature dependence in the range 373...1000 K, see Fig. 18.9.1	68H
----------	-------------------------	--------------------	---	-----

melting temperature			
T_m	894 K	at 1 atm of As	68G

Transport properties

(all data for n-type samples)

CdAs₂ samples are characterized by large anisotropy, resistivity and Seebeck coefficient; see [89M], [92M].

electron concentration

n	$7.5 \cdot 10^{14} \text{ cm}^{-3}$	$T = 297 \text{ K}$	Hall effect	61T,
	$7 \cdot 10^{16} \text{ cm}^{-3}$	$T = 4.2 \text{ K}$	from Hall effect	88Z

resistivity

ρ	$7..80 \text{ } \Omega \text{ cm}$	$T = 297 \text{ K}$		61T
	$10^2...10^5 \text{ } \Omega \text{ cm}$	$T = 4.2 \text{ K}$		89Z

electron mobility

μ_n	$100 \text{ cm}^2/\text{V s}$	$T = 297 \text{ K}$	in <i>a</i> -direction	61T
	$400 \text{ cm}^2/\text{V s}$		in <i>c</i> -direction	

thermal conductivity

κ	$0.096 \text{ W cm}^{-1} \text{ K}^{-1}$			65U
----------	--	--	--	-----

Optical properties

optical spectra

Spectral dependence of the dielectric function: Fig. 18.9.2.

dielectric constants

$\epsilon(0)$	17.4	$T = 300 \text{ K}, E \parallel c$	best oscillator fit	72G
	15.4	$E \perp c$		
$\epsilon(\infty)$	13.8	$E \parallel c$		
	11.5	$E \perp c$		

References to 18.9

60S Stevenson, M. J.: Proc. Int. Conf. Semicond. Phys., Prague 1960; Publ. House of Czech. Acad. Sci., Prague 1961, p. 1083.

61F Fischler, A. S.: Phys. Rev., 122 (1961) 425.

61T Turner, W. J., Fishler, A. S., Reese, W. E.: Phys. Rev. 121 (1961) 759.

65U Ugai, Ya. A., Iguatiev, N. A., Marshakova, T. A., Aleynikova, K. B.: Neorgan. Mater. 1 (1965) 1323.

68G Glazov, V. M., Kasymova, M.: Dokl. Akad. Nauk SSSR 183 (1968) 141.

68H Horn, J., Lukaszewicz, K.: Roczn. Chem. 42 (1968) 993.

70C Cervinka, L., Hruby, A.: Acta Crystallogr. B26 (1970) 457.

72G Gregora, I., Petzelt, J.: Phys. Status Solidi (b) 49 (1972) 271.

77D1 Danilenko, G. N., Danilenko, V. E., Karapetyant, M. H., Lazarev, V. B., Marenkin, S. F., Shevchenko, V. Ya.: Neorgan. Mater. 13 (1977) 1736.

79G Glazov, V. M., Kasymova, M., Regel, A. P.: Fiz. Tekh. Poluprovodn. 13 (1979) 2049.

88Z Zdanowicz, E., Portal, J.C., Wojciechowski, W., Sokotowski, V.A.: Acta Phys. Polon. A 73 (1988) 385.

89M Misiewicz, J.: J. Phys. Chem. Solids 50 (1989) 1013.

89Z Zdanowicz, E., Biskupski, G., Dubois, H., Onbraham.: Acta Phys. Polon. A 75 (1989) 347.

92M Marenkin, S.F., Raukman, A.M. Lazarev, V.B: Neorg. Mater. 28 (1992) 1813.

96M1 Morozova, V.A., Semeninja, T.V., Marenkin, S.F., Koshelev, O.G, Raukman, A.M., Loseva, S.M.: Neorg. Mater. 32 (1996) 17.

96M2 Morozova, V.A., Semeninja, T.V, Marenkin, S.F., Koshelev, O.G., Raukman, A.M., Loseva, S.M.: Neorg. Mater. 32 (1996) 1329.

Figures to 18.9

Fig. 18.9.1

ZnAs_2 , CdAs_2 , Cd_3As_2 , Zn_3As_2 . Density vs. temperature in solid and liquid phases [68G].

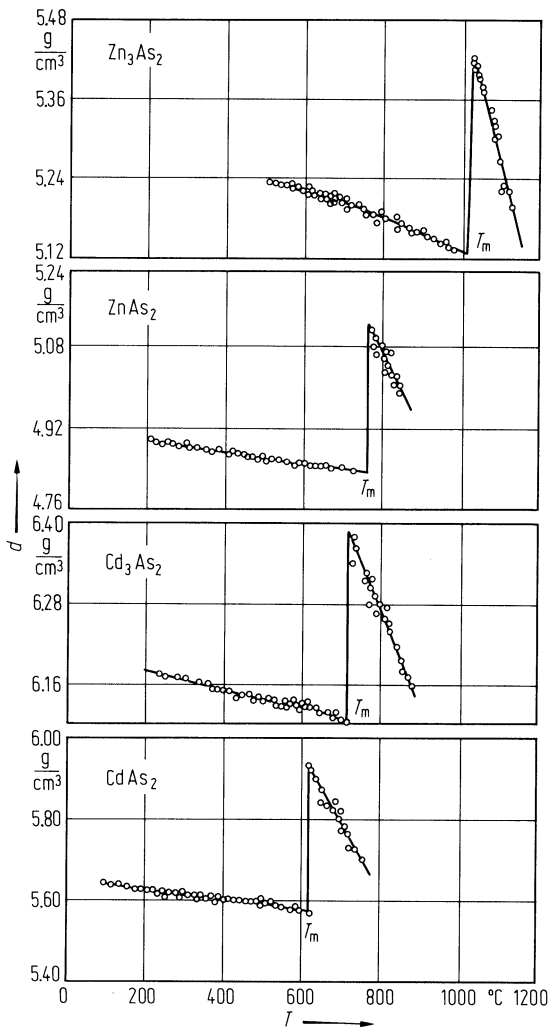
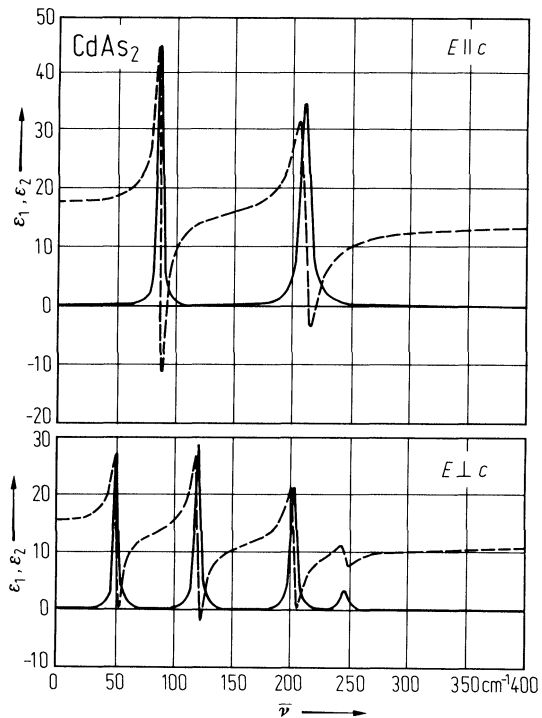


Fig. 18.9.2

CdAs_2 . Real (ϵ_1 , dashed lines) and imaginary (ϵ_2 , solid lines) parts of the best-fit dielectric function vs. wavenumber [72G].



18.10 Cadmium tetraphosphide (CdP₄)

Crystal structure

see section 18.0

Electronic properties

energy gap

E_g	0.90 eV	$T = 293 \text{ K}, E \parallel c$	absorption edge	73M
	0.99 eV	$T = 293 \text{ K}, E \perp c$		
	1.15 eV	$T = 0 \text{ K}$	extrapolated from resistivity and Hall measurements	66Z
dE_g/dT	$-3.7 \cdot 10^{-4} \text{ eV K}^{-1}$	$E \parallel c$	absorption edge in the range 77...300 K	73M
	$-2.7 \cdot 10^{-4} \text{ eV K}^{-1}$	$E \perp c$		

crystal field splitting energy

Δ_{cr}	0.09 eV	$T = 293 \text{ K}$		73M
---------------	---------	---------------------	--	-----

Lattice properties

lattice parameters

a	5.27 Å			56K
b	5.19 Å			
c	7.66 Å			
β	80°32'			

density

d	2.04 g cm ⁻³		X-ray measurement	56K
-----	-------------------------	--	-------------------	-----

Transport properties

(p-type samples)

hole concentration

p	$2 \cdot 10^{16} \text{ cm}^{-3}$	$T = 300 \text{ K}$	Hall effect	66Z
-----	-----------------------------------	---------------------	-------------	-----

resistivity

ρ	3.5...5.5 Ω cm	$T = 300 \text{ K}$	temperature dependence in the range 100...600 K, Fig. 18.10.1	66K, 66Z
--------	----------------	---------------------	---	-------------

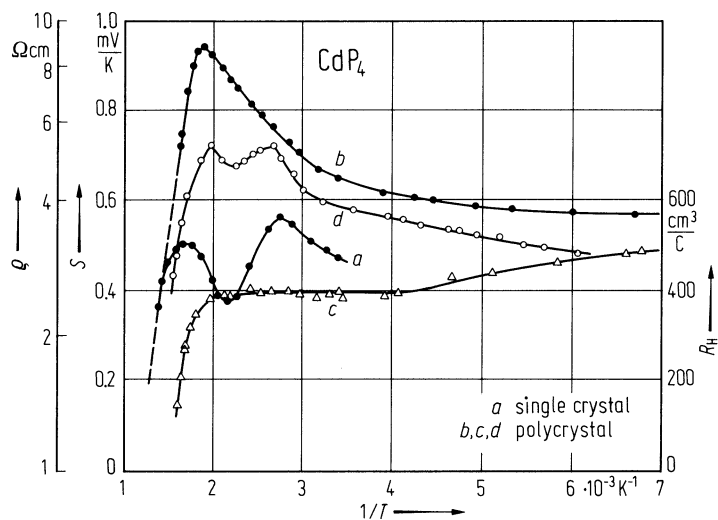
References to 18.10

- 56K von Krebs, H., Müller, K. H., Zürn, G.: Z. Anorg. Allg. Chem. 285 (1956) 25.
66K Kovaleva, I. S., Dimitriev, A. V., Zhizheyko, U. A.: Neorgan. Mater. 2 (1966) 403.
66Z Zdanowicz, W., Wojakowski, A.: Phys. Status Solidi 16 (1966) K129.
73M Malinowskij, V. T., Syrbu, N. N.: Poluprovodn. pribory i materialy, Izd. Shtiintza, Kishinev 1973, p. 10.

Figures to 18.10

Fig. 18.10.1

CdP_4 . Temperature dependence of the resistivity (*a*, *b*), Hall coefficient (*c*) and thermoelectric power (*d*) [66Z].



18.11 Zinc antimonide (ZnSb)

Crystal structure

see section 18.0

Electronic properties

band structure: according to pseudopotential calculations [73Y] the maxima of the valence band are located at $k = (0.8\pi/a, 0, 0)$ (heavy hole band, Σ_4 symmetry). A light hole band with Σ_1 symmetry and extrema at $k = (0.5\pi/a, 0, 0)$ occurs below the Σ_4 band. Also below the Σ_4 band two heavy hole bands with Δ_2 and Δ_1 symmetry exist. Conduction band minima of Σ_1 symmetry are located at $k = (0.5\pi/a, 0, 0)$ and of Λ_1 symmetry at $k = (0, 0, 0.8\pi/a)$.

energy gaps

$E_{g,ind}$	0.5 eV	$T = 300$ K	absorption edge, measurements for three polarizations	69K
$E_{g,dir}$	1.11 eV	$T = 4.2$ K, $E \parallel a$		
	1.09 eV	$E \parallel b$		
	1.05 eV	$E \parallel c$		

Fermi surface

only slightly cigar shaped energy ellipsoid of revolution along a -direction, measured by cyclotron resonance [60S].

effective mass of current carriers on Fermi surface

m_{\perp}	$0.146(10) m_0$	$T = 4.2$ K	cyclotron resonance	60S
m_{\parallel}	$0.175(10) m_0$			

effective mass of holes

$m_{p,h}$	$0.35...0.54 m_0$			61F
-----------	-------------------	--	--	-----

Lattice properties

lattice parameters

a	6.218 \AA			35O
b	7.741 \AA			
c	8.115 \AA			

melting temperature

T_m	819 K		ZnSb melts incongruently	48A
-------	-------	--	--------------------------	-----

density

d	6.36 g cm^{-3}			48A
-----	--------------------------	--	--	-----

Debye temperature

Θ_D	225 K	$T = 80$ K		59G
------------	-------	------------	--	-----

Transport properties

(all data for p-type samples)

hole concentration

p	10^{16} cm^{-3}		temperature dependence and anisotropy of Hall coefficient, see Fig. 18.11.1b	64M
-----	---------------------------	--	---	-----

resistivity

temperature dependence and anisotropy, see Fig. 18.11.1a

hole mobility (anisotropic)

μ_c	800 cm ² /V s	$T = 100$ K	c -direction, $\mu \propto T^{-1/2}$	64M
μ_a	200 cm ² /V s		a -direction	
			Temperature dependence and anisotropy, see Fig. 18.11.2	

thermal conductivity

κ	0.013 W cm ⁻¹ K ⁻¹	$T = 300$ K		59T
----------	--	-------------	--	-----

Optical properties

refractive index

n	4.7	$T = 300$ K,	b -direction	69K
	5	$\lambda = 2$ μ m	c -direction	
	5.4		a -direction	

References to 18.11

35O Olander, A.: Z. Kristallogr. 91 (1935) 243.
48A Almin, K. E.: Acta Chem. Scand. 2 (1948) 400.
59G Guntlev, P. V., Petrov, A. V.: Fiz. Tekh. Poluprovodn. 1 (1959) 368.
59T Toman, K.: J. Phys. Chem. Solids 11 (1959) 342.
60S Stevenson, M. J.: Proc. Int. Conf. Semicond. Phys., Prague 1960; Publ. House of Czech. Acad. Sci., Prague 1961, p. 1083.
61F Fischler, A. S.: Phys. Rev., 122 (1961) 425.
64M Masumoto, K., Komiya, H.: J. Jpn. Inst. Metals 28 (1964) 273.
64N Naake, M. J., Belcher, S. C.: J. Appl. Phys. 35 (1964) 3064.
69K Komiya, N., Masumoto, K., Fan, N. J.: Phys. Rev. A 133 (1969) 1679.
73Y Yamada, Y.: J. Phys. Soc. Jpn. 35 (1973) 1600.

Figures to 18.11

Fig. 18.11.1

ZnSb. p-type. Temperature dependence of resistivity (a) and Hall coefficient (b) tensor components [64M].

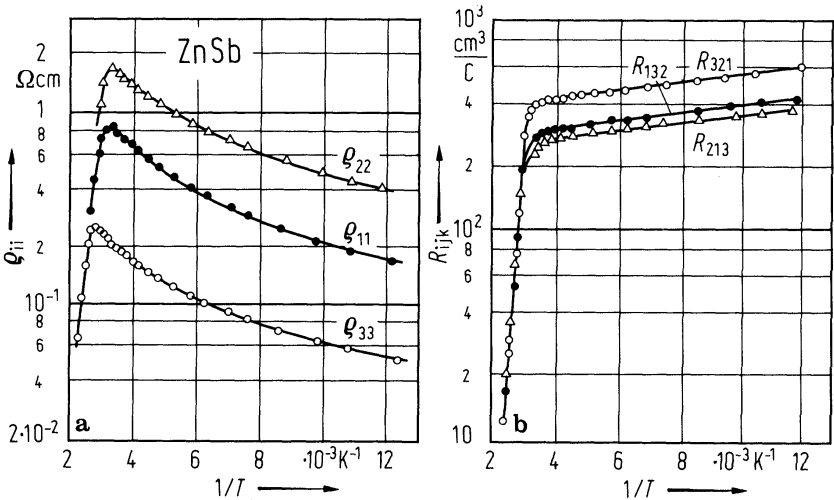
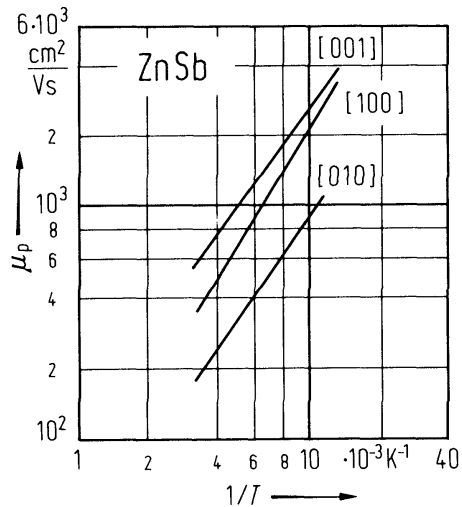


Fig. 18.11.2

ZnSb. p-type. Hole mobility vs. reciprocal temperature for three principal directions [64N].



18.12 Cadmium antimonide (CdSb)

Crystal structure

see section 18.0

Electronic properties

band structure: According to pseudopotential calculations [73Y] the top of the valence band is localized at $k = (0.8\pi/a, 0, 0)$ having Σ_4 symmetry. A light holes band is situated with its maxima at $k = (0.5\pi/a, 0, 0)$ about 0.12 eV below the Σ_4 band. Heavy hole bands with Δ_2 and Δ_1 symmetries have extrema 0.3 eV below the Σ_4 band. The theoretical valence band width is 10.2 eV The minima of the conduction band are located at $k = (0.5\pi/a, 0, 0)$ (Σ_1 symmetry) and $k = (0, 0, 0.8\pi/a)$ (Λ_1 symmetry). The next bands begin about 0.8 eV above these minima. The theoretical value of the indirect forbidden gap is 0.49 eV ($\Sigma_{4v} - \Sigma_{1c}$ transitions), that of the direct gap at Γ ($\Gamma_{4v} - \Gamma_{1c}$) is 1.63 eV.

energy gap

$E_{g,ind}$	0.485 eV	$T = 295\text{ K}, E \parallel a$		70B
	0.472 eV	$E \parallel b$		
	0.459 eV	$E \parallel c$		
dE_g/dT	$-5.4 \cdot 10^{-4}\text{ eV K}^{-1}$			61T
$E_{g,dir}$	0.70...0.75 eV	$T = 300\text{ K}$	absorption edge	64Z

electron effective mass

m_n	0.6...0.7 m_0	$T = 100...450\text{ K}$	thermoelectric power	62A, 61T
-------	-----------------	--------------------------	----------------------	-------------

hole effective mass

m_p	0.02...0.48 m_0	$T = 300\text{ K}$	ir reflectivity, within plasma resonance range, $p = 1.3 \cdot 10^{18}\text{ cm}^{-3}$... $2 \cdot 10^{19}\text{ cm}^{-3}$	69Z
-------	-------------------	--------------------	---	-----

Lattice properties

lattice parameters

a	6.471 Å			48A
b	8.253 Å			
c	8.526 Å			

Debye temperature

Θ_D	180 K	$T = 80\text{ K}$		63S
------------	-------	-------------------	--	-----

density

d	6.98 g cm ⁻³	$T = 300\text{ K}$	calculated	54F
-----	-------------------------	--------------------	------------	-----

melting temperature

T_m	729 K		CdSb melts congruently	54F
-------	-------	--	------------------------	-----

Transport properties

Electrical transport is realized via band conduction. Neither polaron effects nor hopping conduction have been observed.

resistivity, Hall coefficient : see Fig. 18.12.1.

carrier mobility

μ_p	300...700 cm ² /V s	$T = 300\text{ K}$	Hall mobility (anisotropic)	61G
μ_n	100...660 cm ² /V s	$T = 300\text{ K}$		

thermal conductivity

κ	$10^{-2} \text{ W cm}^{-1} \text{ K}^{-1}$	$T = 300 \text{ K}$	77L
----------	--	---------------------	-----

Optical properties

refractive index

n	4.5	$T = 300 \text{ K},$	c -direction	64Z,
	4.58	$\lambda = 3.1 \mu\text{m}$	b -direction	60T
	4.78		a -direction	

dielectric constant

$\epsilon(0)$	16.4	60T
---------------	------	-----

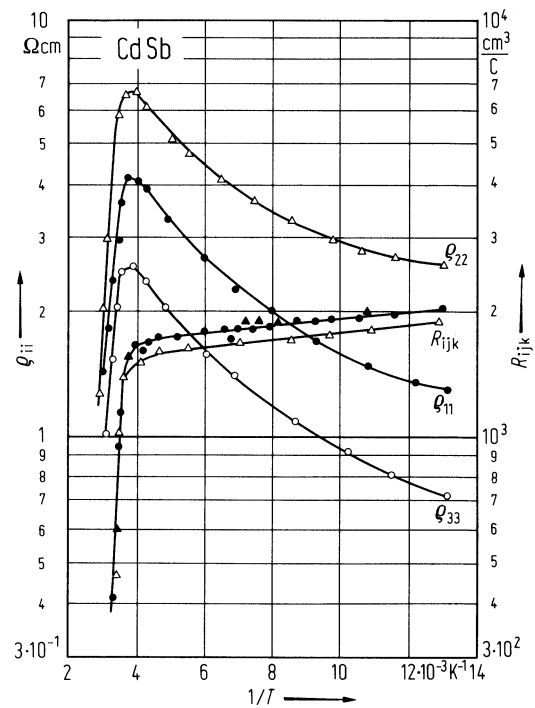
References to 18.12

- 48A Almin, K. E.: Acta Chem. Scand. 2 (1948) 400.
54F Fisher, H. J., Phillips, A.: J. Metals 6 (1954) 1060.
60T Turner, W. J., Fischler, A. S., Reese, W. E.: Proc. Int. Conf. Semicond. Phys., Prague 1960; Publ. House of Czech. Acad. Sci., Prague 1961, p. 1080.
61G Giriat, W., Migula, Z., Sicovski, A.: Acta Phys. Polon. 20 (1961) 919.
61T Turner, W. J., Fishler, A. S., Reese, W. E.: Phys. Rev. 121 (1961) 759.
62A Andronik, L. K., Kot, M. V., Shcherban, A. D.: Trudy Kishinev. Gos. Univ. 1 (1962) 37.
63S Shmalevski, V. Ya., Mikolaychuk, A. G.: Fiz. Metal. Metalloved. 16 (1963) 136.
64Z Zavetova, M.: Czech. J. Phys. B 14 (1964) 615.
66K Kawasaki, T., Tanaka, T.: J. Phys. Soc. Jpn. 21 (1966) 2475.
69Z Zavetova, M., Vorlicek, V.: Czech. J. Phys. B 19 (1969) 677.
70B Bercha, D. M., Boerts, A. N., Gertovich, T. S., Rarenko, I. M., Tovstyuk, K. D.: Fiz. Tverd. Tela 12 (1970) 2397.
73Y Yamada, Y.: J. Phys. Soc. Jpn. 35 (1973) 1600.
77L Lovert, D. R.: Semimetals and Narrow-Bandgap Semicond., ed. Pion Limited, London 1977, p. 218.

Figures to 18.12

Fig. 18.12.1

CdSb, p-type. Temperature dependence of resistivity and Hall coefficient tensors components along principal crystallographic axes [66K].



18.13 Zinc antimonide (Zn₄Sb₃)

Crystal structure and lattice parameters

Zn₄Sb₃ is known in several modifications. It is metastable at room temperature [78L].

lattice parameters

<i>a</i>	7.981 Å	α -Zn ₄ Sb ₃	72K
<i>b</i>	7.495 Å		
<i>c</i>	10.72 Å		
<i>a</i>	10.74 Å	β -Zn ₄ Sb ₃	65B
<i>b</i>	12.20 Å		
<i>c</i>	8.20 Å		
β	100.0(5) ^o	γ -Zn ₄ Sb ₃	71I
<i>a</i>	12.231 Å		
<i>c</i>	12.417 Å		

Physical parameters

β -Zn₄Sb₃:

energy gap

E_g	1.0 eV	$T = 0$ K	extrapolated from Hall data	78L
-------	--------	-----------	-----------------------------	-----

hole effective mass

m_p	0.12 m_0	$p \approx 9 \cdot 10^{17} \text{ cm}^{-3}$		78L
-------	------------	---	--	-----

hole concentration

p	$8.6 \cdot 10^{17} \dots$ $1 \cdot 10^{19} \text{ cm}^{-3}$	$T = 300$ K	Hall effect	78L
-----	--	-------------	-------------	-----

resistivity

ρ	$7.3 \cdot 10^{-3} \Omega \text{ cm}$	$T = 300$ K	temperature dependence: Fig. 18.13.1	63U
--------	---------------------------------------	-------------	--------------------------------------	-----

hole mobility

$\mu_{H,p}$	998 $\text{cm}^2/\text{V s}$	$T = 300$ K	$p \approx 9 \cdot 10^{17} \text{ cm}^{-3}$	63U,
-------------	------------------------------	-------------	---	------

melting temperature

T_m	836 K	Zn ₄ Sb ₃ melts incongruently		58H
-------	-------	---	--	-----

density

d	6.81 g cm^{-3}	$T = 300$ K	pycnometric method	69U
-----	-------------------------	-------------	--------------------	-----

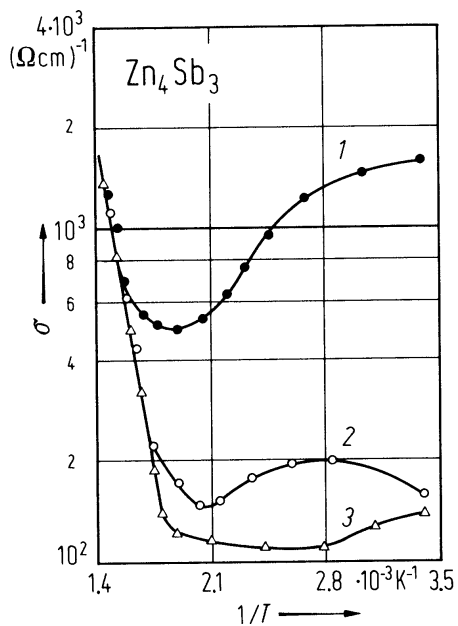
References to 18.13

- 58H Hansen, M., Anderko, K.: Constitution of Binary Alloys, McGraw-Hill, N. Y. 1958.
63U Ugai, Ya. A., Averbakh, E. M., Gukova, Yu. Ya., Lavrov, V. V.: Dokl. Akad. Nauk SSSR 149 (1963) 1387.
65B Bokii, G. B., Kievtsova, R. F.: Zh. Strukt. Khim. 6 (1965) 866.
71I Ignatiev, N. A., Ugai, Ya. A., Alejnikova, K. B., Rabotkina, N. S.: Zh. Strukt. Khim. 12 (1971) 729.
72K Kostur, T. A.: Kand. Dis. Chernovitskii Gos. Univ., 1972.
78L Lazarev, V. B., Shevchenko, V. Ya., Greenberg, Ya. G., Sobolev, V. V.: "Semiconducting Compounds of II–V Group", ed. Nauka Moscow 1978.

Figures to 18.13

Fig. 18.13.1

Zn_4Sb_3 . Electrical conductivity vs. temperature: 1, sample fast cooled; 2, slow cooled; 3, obtained by zone recrystallization [63U].



18.14 Cadmium antimonide (Cd₄Sb₃)

Lattice parameters and density

Cd₄Sb₃ is metastable at room temperature similarly to Zn₄Sb₃, it exists in several modifications.

lattice parameters

<i>a</i>	13.07 Å	α-Cd ₄ Sb ₃	78L,
<i>c</i>	22.45 Å		67M
<i>a</i>	8.152 Å	β-Cd ₄ Sb ₃	78L,
<i>b</i>	8.165 Å		72K,
<i>c</i>	11.960 Å		71I
<i>a</i>	13.07 Å	γ-Cd ₄ Sb ₃	73A,
<i>c</i>	13.07 Å		71I

density

<i>d</i>	6.87 g cm ⁻³	<i>T</i> = 300 K	pycnometric method of single crystal samples	96K
----------	-------------------------	------------------	--	-----

melting temperature

<i>T</i> _m	703 K		melts incongruently	67U
-----------------------	-------	--	---------------------	-----

Electronic and transport parameters

β-Cd₄Sb₃:

energy gap

<i>E</i> _g	1.2...1.6 eV		electrical measurements	78L
-----------------------	--------------	--	-------------------------	-----

hole concentration

<i>p</i>	3·10 ¹⁸ ...3·10 ¹⁹ cm ⁻³	<i>T</i> = 300 K		78L
----------	---	------------------	--	-----

resistivity

<i>ρ</i>	1·10 ⁻² Ω cm	<i>T</i> = 300 K		65U, 62U
----------	-------------------------	------------------	--	-------------

hole mobility

<i>μ</i> _{H,p}	110 cm ² /V s	<i>T</i> = 300 K	<i>p</i> = 3·10 ¹⁸ cm ⁻³ , Fig. 18.14.1	65U
-------------------------	--------------------------	------------------	---	-----

thermal conductivity

<i>κ</i>	1.37·10 ⁻² W cm ⁻¹ K ⁻¹	<i>T</i> = 300 K		65U
----------	--	------------------	--	-----

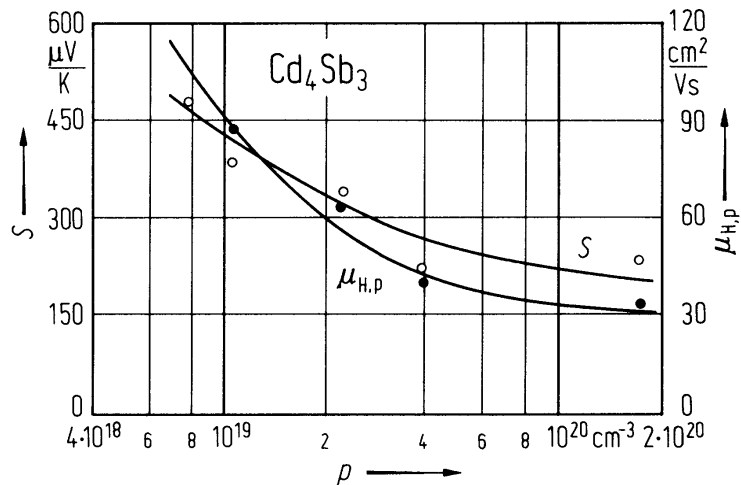
References to 18.14

- 62U Ugai, Ya. A., Averbakh, F. M., Marshakova, T. A., Matveyev, O. V.: Fiz. Tverd. Tda 4 (1962) 615.
65U Ugai, Ya. A., Iguatiev, N. A., Marshakova, T. A., Aleynikova, K. B.: Neorgan. Mater. 1 (1965) 1323.
67M Marshakova, T. A.: Kand. Dis. Voronezhski Gos. Univ. 1967.
67U Ugai, Ya. A., Marshakova, T. A., Alejnikova, K. B., Demina, N. P.: Neorgan. Mater. 3 (1967) 1360.
71I Ignatiev, N. A., Ugai, Ya. A., Alejnikova, K. B., Rabotkina, N. S.: Zh. Strukt. Khim. 12 (1971) 729.
72K Kostur, T. A.: Kand. Dis. Chernovitskii Gos. Univ., 1972.
73A Alejnikova, K. B.: Kand. Dis. Voronezhski Gos. Univ., 1973.
78L Lazarev, V. B., Shevchenko, V. Ya., Greenberg, Ya. G., Sobolev, V. V.: "Semiconducting Compounds of II-V Group", ed. Nauka Moscow 1978.
96K Kirii, V.G., Kirii, A.V., Marenkin, S.F., Marenkin, D.S.: Zh. Neorg. Khim. 11 (1996) 1693.

Figures to 18.14

Fig. 18.14.1

Cd_4Sb_3 . Hall mobility and thermoelectric power vs. hole concentration [78L].



18.15 Cd₇P₁₀

Space group: Fdd2; the orthorhombic cell contains 8 molecules [79Z].

lattice parameters

<i>a</i>	23.0(1) Å		79Z
<i>b</i>	27.50(15) Å		
<i>c</i>	4.62(3) Å		

density

<i>d</i>	5.01 g cm ⁻³	X-ray measurements	79Z
----------	-------------------------	--------------------	-----

melting temperature

<i>T</i> _m	1019 K	Cd ₇ P ₁₀ melts incongruently	68B
-----------------------	--------	---	-----

some semiconductor parameters

<i>E</i> _{g,dir}	1.73 eV	<i>T</i> = 300 K	absorption edge	80A
<i>dE</i> _g / <i>dT</i>	− 4.5·10 ^{−4} eV K ^{−1}	<i>T</i> = 80...300 K		
<i>S</i>	1000 μV K ^{−1}	<i>T</i> = 300 K		80A

At 300 K Cd₇P₁₀ is a p-type semiconductor; in [68B] Cd₇P₁₀ is presented as Cd₂P₃.

References to 18.15

- 68B Berak, J., Pruchnik, Z.: Roczn. Chem. 42 (1968) 1403.
79Z Zavalkhin, F. I., Alejnikova, K. B., Rahotkina, N. S., Arsenov, A. V.: Zh. Strukt. Chim. 20 (1979) 146.
80A Alejnikova, K. B., Arsenov, A. V., Kavetsky, V. S., Lukin, A. N.: Proc. Intern. Symp. on "Physics and Chemistry of II-V Comp." Mogilany, Poland 1980, ed. M. Gelten, L. Zdanowicz, Eindhoven Univ., Netherlands, p. 43.

18.16 Cd₆P₇

Space group: $P\bar{4}3m$, the cubic unit cell contains 12 formula units [80A]

lattice constant

<i>a</i>	10.567(1) Å	80A, 68B
----------	-------------	-------------

energy gap

<i>E_{g,dir}</i>	0.85 eV	<i>T</i> = 300 K	absorption edge	80A
<i>dE_g/dT</i>	− 2.7·10 ^{−4} eV K ^{−1}	<i>T</i> = 80...300 K		

resistivity

<i>ρ</i>	0.8 Ω cm	<i>T</i> = 300 K	van der Pauw method	80A
----------	----------	------------------	---------------------	-----

electron concentration

<i>n</i>	1.5·10 ¹⁷ cm ^{−3}	<i>T</i> = 300 K		80A
----------	---------------------------------------	------------------	--	-----

electron mobility

<i>μ_n</i>	4200 cm ² /V s	<i>T</i> = 300 K		80A
----------------------	---------------------------	------------------	--	-----

melting temperature

<i>T_m</i>	1016 K			68B
----------------------	--------	--	--	-----

density

<i>d</i>	5.39 g cm ^{−3}	X-ray measurements	80A
	5.37 g cm ^{−3}	pycnometric method	

References to 18.16

68B Berak, J., Pruchnik, Z.: Roczn. Chem. 42 (1968) 1403.
80A Alejnikova, K. B., Arsenov, A. V., Kavetsky, V. S., Lukin, A. N.: Proc. Intern. Symp. on "Physics and Chemistry of II-V Comp." Mogilany, Poland 1980, ed. M. Gelten, L. Zdanowicz, Eindhoven Univ., Netherlands, p. 43.

19 II-VII₂ compounds

19.0 Crystal structure and electronic structure of group II-dihalides

A considerable number of group II-dihalides crystallize in layer structures. The metal ions are mostly octahedrally surrounded by the halide ions. All halide ions are close packed. The layers are held together by van der Waals forces.

Two types of stacking are possible: 1. CdI₂ type (hexagonal), space group D_{3d}³, 2. CdCl₂ type (rhombohedral), space group D_{3d}⁵.

CdI₂ structure (Fig. 19.0.1 [63W])

The basic structure is hexagonal, contains one molecule per cell and is called 2H according to the Ramsdell notation. The crystal can be viewed as a hexagonal close-packing of iodine ions with the cadmium ions nested between alternate layers of iodine. The cadmium ions are at the centres of octahedra which are joined together in sheets perpendicular to the threefold crystal axis by having iodine atoms in common. The sheets are stacked one above another.

Brillouin zone: Fig. 19.0.2, *band structure* of CdI₂: Fig. 19.0.3.

CdCl₂ structure (Fig. 19.0.4 [63W])

The structure differs from the CdI₂ structure in having its anions in a cubic rather than a hexagonal close-packing. Its unit cell is a rhombohedron containing a single molecule.

From the Cd dihalides, CdCl₂, CdBr₂ and CdI₂ are known as semiconductors. CdCl₂ and CdBr₂ crystallize in the hexagonal CdCl₂ structure, CdI₂ in the CdI₂ structure.

From the Hg dihalides, HgCl₂, HgBr₂ and HgI₂ are known as semiconductors. HgCl₂ crystallizes in the orthorhombic structure, space group V_h¹⁶ (D_{2h}¹⁶). HgBr₂ and the β (yellow) phase of HgI₂ crystallize in the orthorhombic structure of space group C_{2v}¹². This is a layer-like structure resembling the CdI₂ and CdCl₂ structures.

The α (red) phase of HgI₂ is tetragonal; *Brillouin zone:* Fig. 19.0.5, *band structure* of HgI₂: Fig. 19.0.6.

References to 19.0

- 63W Wykoff, R. W. G.: Crystal Structures, Vol. 1, Interscience Publishers, New York, 1963.
76Y Yee, J. H., Sherohman, J. W., Armantrout, G. A.: IEEE Trans. Nucl. Sci. NS-23 (1976) 117.
77M McCanny, J. V., Williams, R. H., Murray, R. B., Kemeny, P. C.: J. Phys. C 10 (1977) 4255.

Figures to 19.0

Fig. 19.0.1

Crystal structure of CdI_2 , space group D_{3d}^3 [63W].

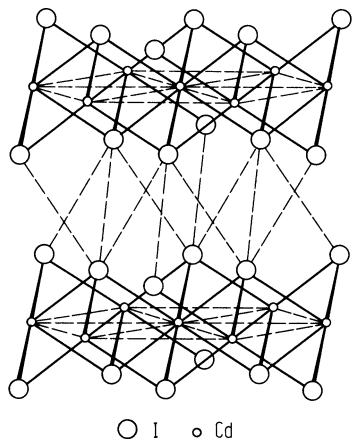
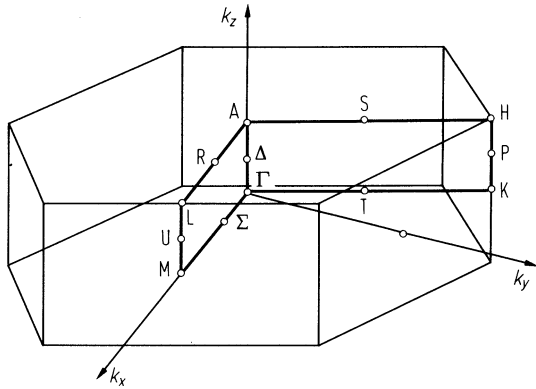


Fig. 19.0.2

Brillouin zone of the hexagonal structure.



CdI₂. Modified semiempirical tight binding band structure. Single-group notation [77M].

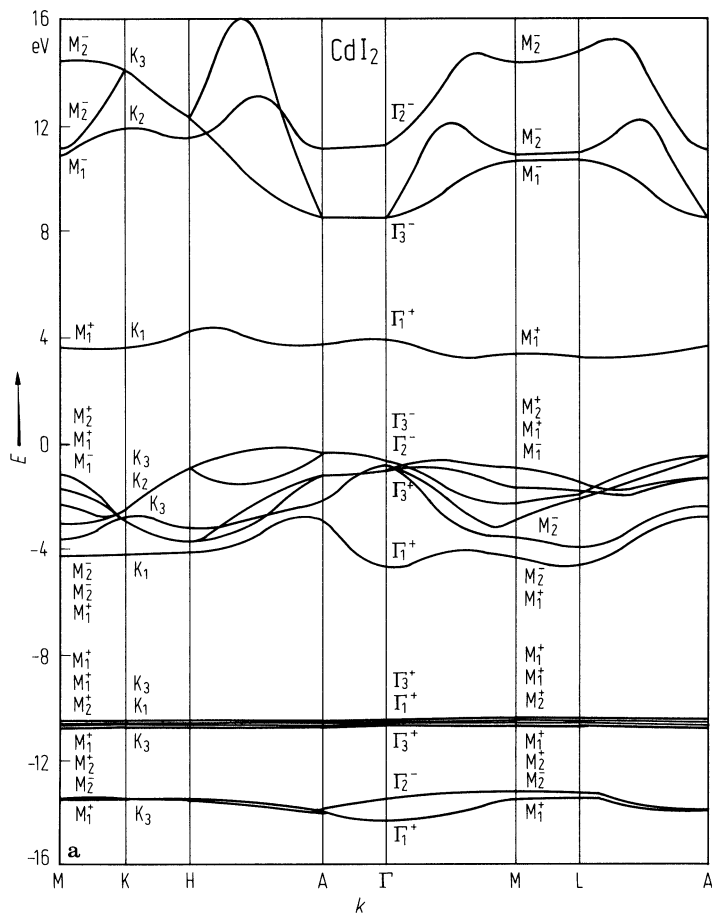


Fig. 19.0.4

Unit rhombohedron of the CdCl_2 structure, space group D_{3d}^5 [63W].

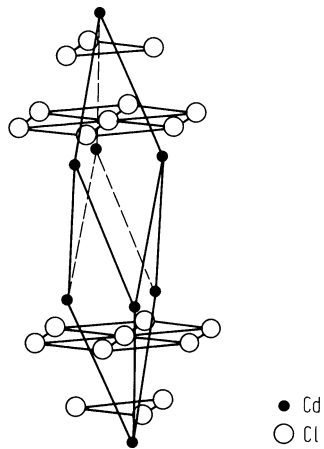


Fig. 19.0.5

HgI_2 . Brillouin zone of the tetragonal lattice [76Y].

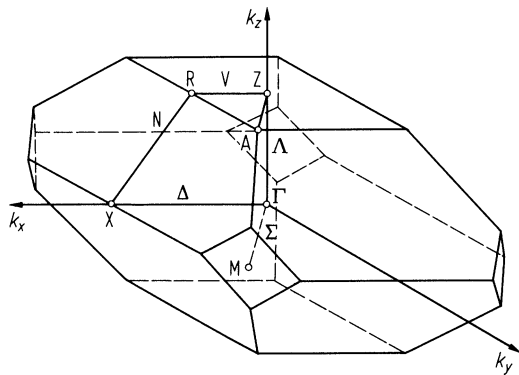
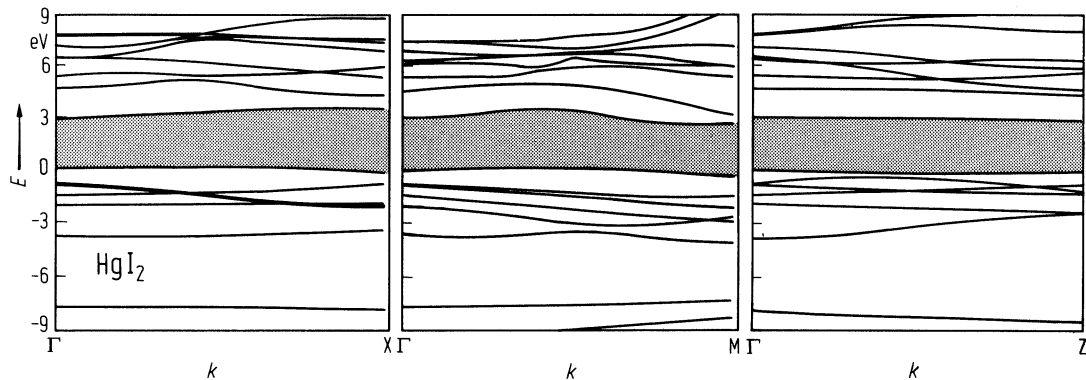


Fig. 19.0.6

α -HgI₂. Pseudopotential band structure for three symmetry directions [76Y].



19.1 Cadmium dichloride (CdCl_2)

crystal structure

see section 19.0.

interband transition energy

$E(X)$	$> 5.9 \text{ eV}$	$T = 4.2 \text{ K}, E \perp c$	reflectance	77K
--------	--------------------	--------------------------------	-------------	-----

lattice parameters

a	6.23 \AA	rhombohedral unit cell	63W
β	$36^\circ 2'$		
a'	3.854 \AA	hexagonal unit cell	63W
c'	17.457 \AA		

density

d	4.047 g/cm^3	$T = 298 \text{ K}$	75W
-----	------------------------	---------------------	-----

melting temperature

T_m	841 K	75W
-------	-----------------	-----

dielectric function : real part ϵ_1 and imaginary part ϵ_2 : Fig. 19.1.1.

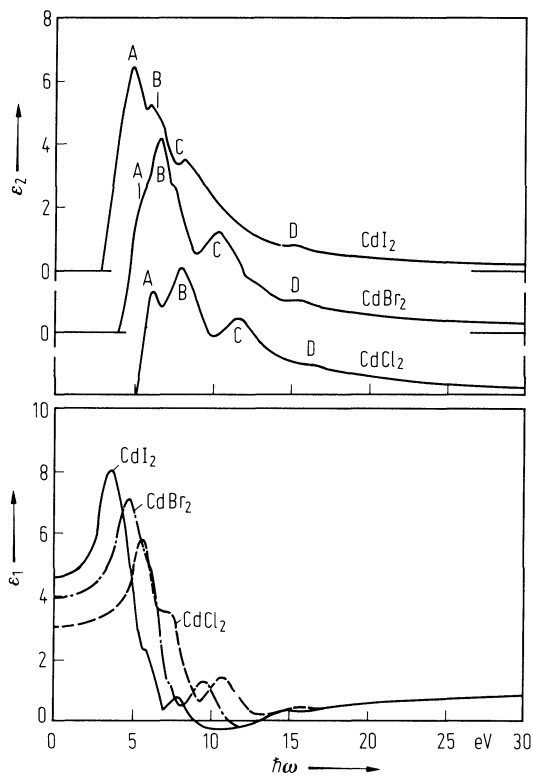
References to 19.1

- | | |
|-----|--|
| 63W | Wykoff, R. W. G.: Crystal Structures, Vol. 1, Interscience Publishers, New York, 1963. |
| 75W | Weast, R. C. ed.: Handbook of Chemistry and Physics, CRC Press, Cleveland, 1975. |
| 81B | Bringans, R. D., Liang, W. Y.: J. Phys. C. 14 (1981) 1065. |

Figures to 19.1

Fig. 19.1.1

CdCl_2 , CdBr_2 , CdI_2 . Real part ϵ_1 and imaginary part ϵ_2 of the dielectric function vs. photon energy [81B].



19.2 Cadmium dibromide (CdBr₂)

crystal structure

see section 19.0.

interband transition energy

$E(X)$	> 4.9 eV	$T = 4.2$ K, $E \perp c$	reflectance	77K
--------	------------	--------------------------	-------------	-----

lattice parameters

a	6.63 Å	rhombohedral unit cell	63W
β	34°42'		
a'	3.95 Å	hexagonal unit cell	63W
c'	18.67 Å		

density

d	5.192 g/cm ³	$T = 298$ K	75W
-----	-------------------------	-------------	-----

melting temperature

T_m	840 K	75W
-------	-------	-----

dielectric function

real part ϵ_1 and imaginary part ϵ_2 : Fig. 19.2.1.

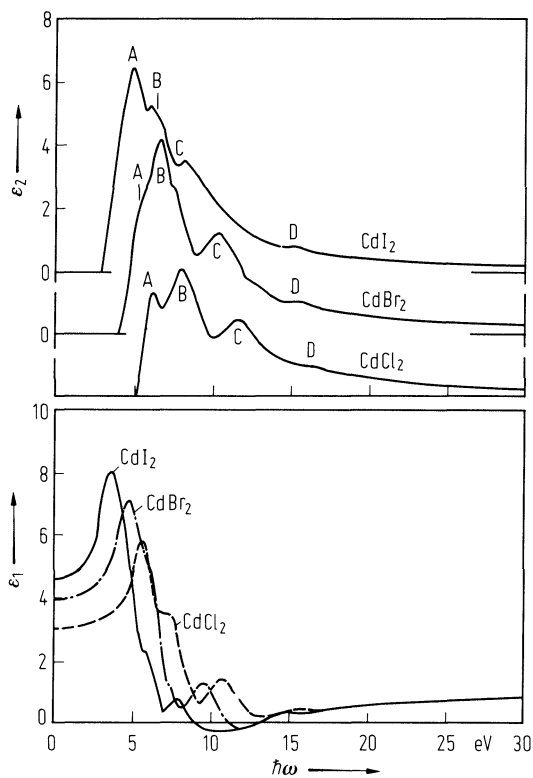
References to 19.2

- | | |
|-----|--|
| 63W | Wykoff, R. W. G.: Crystal Structures, Vol. 1, Interscience Publishers, New York, 1963. |
| 75W | Weast, R. C. ed.: Handbook of Chemistry and Physics, CRC Press, Cleveland, 1975. |
| 77K | Kondo, S., Matsumoto, H.: Solid State Commun. 24 (1977) 695. |
| 81B | Bringans, R. D., Liang, W. Y.: J. Phys. C. 14 (1981) 1065. |

Figures to 19.2

Fig. 19.2.1

CdCl_2 , CdBr_2 , CdI_2 . Real part ϵ_1 and imaginary part ϵ_2 of the dielectric function vs. photon energy [81B].



19.3 Cadmium diiodide (CdI₂)

Electronic properties

band structure

Fig. 19.0.3. Brillouin zone: Fig. 19.0.2.

energy gap

$E_{\text{g,ind}}(\Gamma_{2v^-}-L_{1c^+})$ 3.4729 eV $T = 2 \text{ K}, E \perp c$ transmission 75T

$dE_{\text{g,ind}}/dT$ $-1.2 \cdot 10^{-4} \text{ eV K}^{-1}$ $T = 80 \dots 300 \text{ K}$ transmission 65G

spin-orbit splitting energy

$\Delta_{\text{so}}(\text{Cd}4d_{5/2} - 4d_{3/2})$ 0.58 eV 77M

Lattice properties

lattice parameters (for various polytypes)

$a(2\text{H})$	4.24 Å	$T = 295 \text{ K}$	63W
$c(2\text{H})$	6.835 Å		
$a(4\text{H})$	4.24 Å		
$c(4\text{H})$	13.671 Å		
$a(6\text{H})$	4.24 Å		
$c(6\text{H})$	20.505 Å		
$a(8\text{H})$	4.24 Å		
$c(8\text{H})$	27.34 Å		
$a(10\text{H})$	4.24 Å		
$c(10\text{H})$	34.17 Å		
$a(12\text{H})$	4.24 Å		
$c(12\text{H})$	41.01 Å		

further polypes are known, in total more than 200.

coefficient of linear thermal expansion

α_{\parallel}	$3.72 \cdot 10^{-5} \text{ K}^{-1}$	$T = 270 \text{ K}$	dilatometric technique	66K
α_{\perp}	$2.48 \cdot 10^{-5} \text{ K}^{-1}$		For T -dependence, see Fig. 19.3.1	

density

d 5.670 g/cm³ $T = 298 \text{ K}$ 75W

melting temperature

T_{m} 660 K 75W

phonon wavenumbers (ir active modes)

$\bar{\nu}_{\text{TO}}(E_u)$	79 cm ⁻¹	$T = 300 \text{ K}, E \perp c$	infrared reflectance	77L
$\bar{\nu}_{\text{LO}}(E_u)$	132 cm ⁻¹			
$\bar{\nu}_{\text{TO}}(A_{2u})$	136 cm ⁻¹	$T = 300 \text{ K}, E \parallel c$		
$\bar{\nu}_{\text{LO}}(A_{2u})$	152 cm ⁻¹			

sound velocity

v_{\perp}/v_{\parallel} 1.38 $T = 295 \text{ K}$ Brillouin scattering 75S

second order elastic moduli (in 10^{10} dyn/cm²)

c_{11}	43.1(9)	$T = 295$ K	Brillouin scattering	75S
c_{33}	22.5(5)			
c_{44}	5.5 (3)			
c_{12}	20.4(10)			
c_{13}	8.9(5)			
c_{14}	≈ 0			

Optical properties

refractive index

n	1.83	$T = 295$ K, $\lambda = 0.5350$ μm , $E \perp c$	interferometric technique, Fig. 19.3.2	70B
	1.80	$T = 295$ K $\lambda = 0.5461$ μm , $E \perp c$		

dielectric constants

$\epsilon(0)_{\perp}$	12.9	$T = 300$ K	infrared reflectance	77L
$\epsilon(0)_{\parallel}$	5.9			
$\epsilon(\infty)_{\perp}$	4.6			
$\epsilon(\infty)_{\parallel}$	4.3			

dielectric function

real part ϵ_1 and imaginary part ϵ_2 : Fig. 19.3.3.

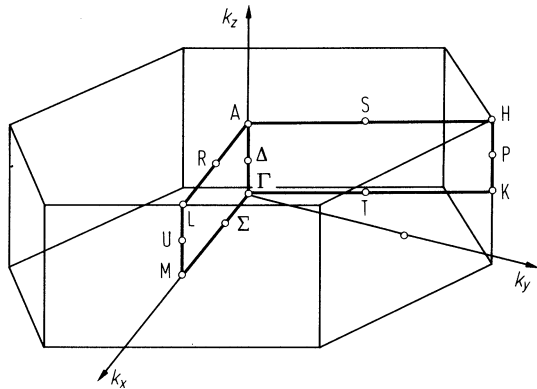
References to 19.3

63W Wykoff, R. W. G.: Crystal Structures, Vol. 1, Interscience Publishers, New York, 1963.
65G Greenaway, D. L., Nitsche, R.: J. Phys. Chem. Solids 26 (1965) 1445.
66K Kovalevskaya, Yu. A., Strelkov, P. G.: Sov. Phys. Solid State (English Transl.) 8 (1966) 1044; Fiz. Tverd. Tela 8 (1966) 1302.
70B Barakat, N., El-Dessouky, T.: Optica Acta 17 (1970) 791.
75S Sandercock, J. R.: Festkörperprobleme XV (1975) 765.
75T Takemura, Y., Komatsu, T., Kaifu, Y.: Phys. Status. Solidi (b) 72 (1975) K 87.
75W Weast, R. C. ed.: Handbook of Chemistry and Physics, CRC Press, Cleveland, 1975.
77L Lucovsky, G., White, R. M.: Nuovo Cimento 38B (1977) 290.
77M McCanny, J. V., Williams, R. H., Murray, R. B., Kemeny, P. C.: J. Phys. C 10 (1977) 4255.
81B Bringans, R. D., Liang, W. Y.: J. Phys. C. 14 (1981) 1065.

Figures to 19.3

Fig. 19.0.2

Brillouin zone of the hexagonal structure.



CdI₂. Modified semiempirical tight binding band structure. Single-group notation [77M].

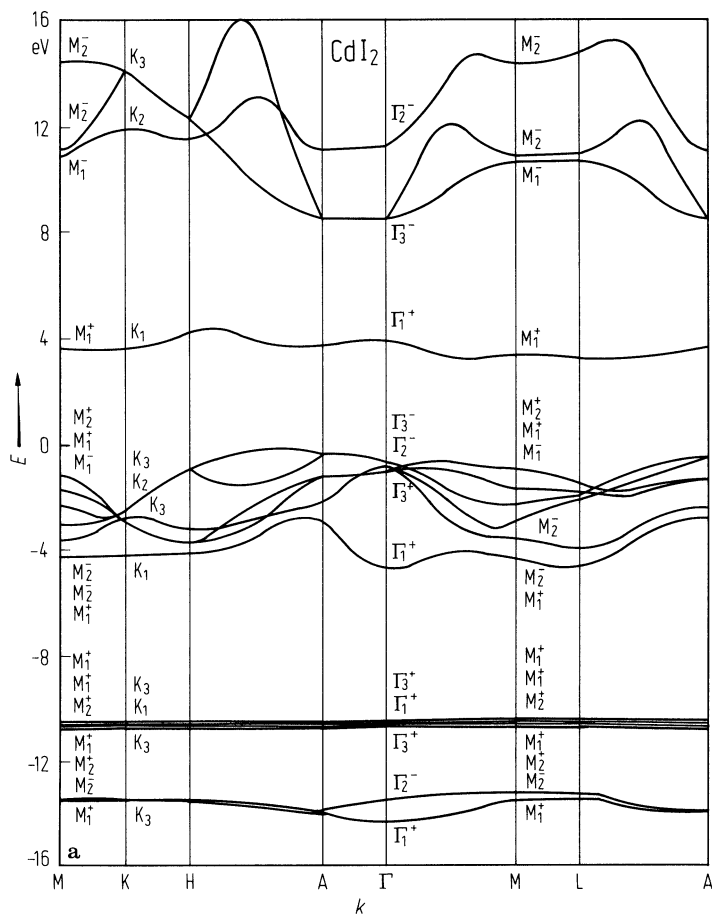


Fig. 19.3.1

CdI_2 . Thermal expansion coefficient vs. temperature perpendicular to the c -axis (1) and parallel to the c -axis (2) [66K].

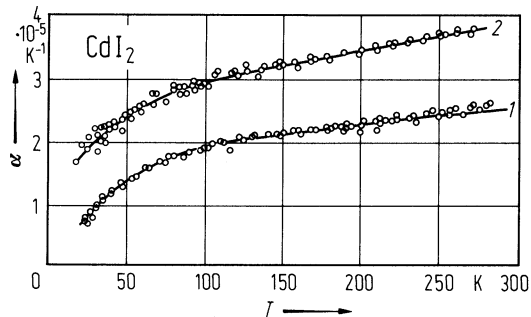


Fig. 19.3.2

CdI_2 . Refractive index n for $E \perp c$ vs. wavelength [70B].

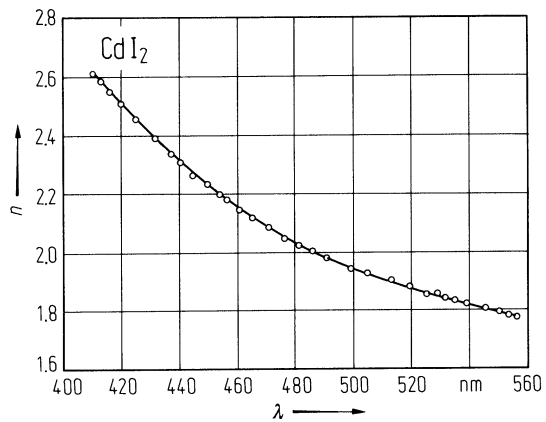
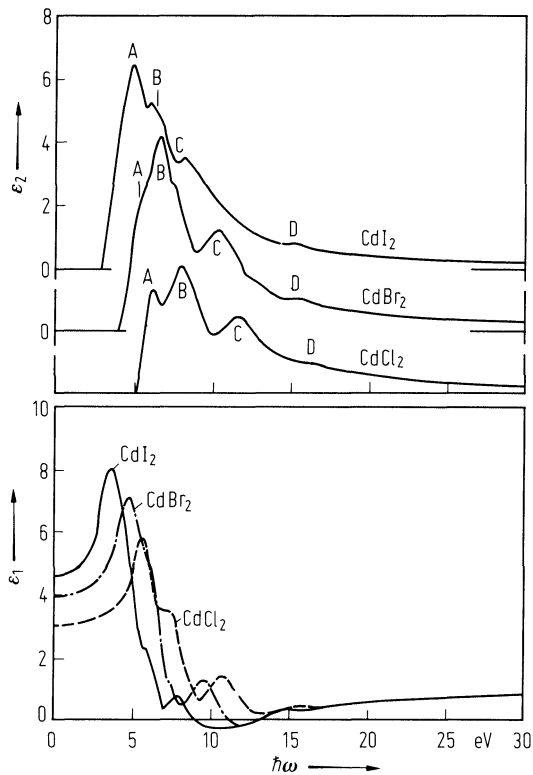


Fig. 19.3.3

CdCl_2 , CdBr_2 , CdI_2 . Real part ϵ_1 and imaginary part ϵ_2 of the dielectric function vs. photon energy [81B].



19.4 Mercury diiodide (HgI₂)

Electronic properties

All values given are for the (red) α -phase if not otherwise noted)

band structure : Fig. 19.0.6. Brillouin zone: Fig. 19.0.5.

The conduction band is s-like, the energy gap is indirect and occurs along the $\Gamma - M$ direction.

energy gap

$E_{g,dir}(\Gamma_{7v}^- - \Gamma_{6c}^+)$	2.397(1) eV	$T = 2 \text{ K}, E \perp c$	analysis of wavelength modulated reflectance	77A
	2.140(5) eV	$T = 300 \text{ K}$	electroabsorption	71C
dE_g/dT	$-6.5 \cdot 10^{-4} \text{ eV/K}$	$T = 50 \dots 400 \text{ K}$	transmission, reflectance, Fig. 19.4.1	74H

exciton binding energy

E_b	166(10) meV	$T = 2 \text{ K}, E \perp c$	analysis of WMR including ground state correction	77A
at $E_g(\Gamma_{7v}^- - \Gamma_{6c}^+)$				

spin-orbit splitting energy

$\Delta_{so}(\Gamma_{7v}^- - \Gamma_{6v}^-(2))$	1.012 eV	$T = 4.2 \text{ K}$	reflectance	75A
	0.99 eV	$T = 78 \text{ K}$	photoluminescence	75A

crystal field splitting energy

$\Delta_{cf}(\Gamma_{7v}^- - \Gamma_{6v}^-(1))$	0.199 eV	$T = 4.2 \text{ K}$	reflectance	72K
	0.19 eV	$T = 78 \text{ K}$	photoluminescence	75A

polaron masses

$m_{n\perp}^{**}$	0.37(2) m_0	$T = 1.6 \text{ K}$	cyclotron resonance	78B
$m_{p\perp}^{**}$	1.03(10) m_0			
$m_{n\parallel}^{**}$	0.31(3) m_0		cyclotron resonance and mobility	
$m_{p\parallel}^{**}$	2.06(51) m_0			

Lattice properties

lattice parameters

a	4.357 Å	$T = 300 \text{ K}$	tetragonal D_{4h}^{15} structure,	63W
c	12.36 Å		2 molecules per unit cell	

thermal expansion

$(1/c)dc/dT$	$6 \cdot 10^{-5} \text{ K}^{-1}$			76M
--------------	----------------------------------	--	--	-----

density

d	6.36 g/cm ³	$T = 300 \text{ K}$		75W
-----	------------------------	---------------------	--	-----

melting temperature

T_m	532 K			75W
-------	-------	--	--	-----

phonon dispersion relations : Fig. 19.4.2

78P

phonon wavenumbers

Raman active modes:

$\bar{\nu}(\text{E}_\text{g}^3)$	17.4 cm ⁻¹	$T = 300 \text{ K}$	Raman scattering	77H
$\bar{\nu}(\text{B}_{1\text{g}}^2)$	29.8 cm ⁻¹	$T = 300 \text{ K}$	Raman scattering	77H
$\bar{\nu}(\text{E}_\text{g}^2)$	115 cm ⁻¹	$T = 300 \text{ K}$	Raman scattering	77H
$\bar{\nu}(\text{B}_{1\text{g}}^1)$	142 cm ⁻¹	$T = 300 \text{ K}$	Raman scattering	77H

infrared active modes:

$\bar{\nu}(\text{E}_\text{u}^2)$	116 cm ⁻¹			
$\bar{\nu}(\text{A}_{2\text{u}}^1)$	125 cm ⁻¹	$T = 300 \text{ K}$	infrared transmission	77H

sound velocities

$v_{\perp\perp}$	$2.23(8) \cdot 10^5 \text{ cm s}^{-1}$	$T = 300 \text{ K}$	inelastic neutron scattering	78P
$v_{\text{t}\perp}$	$0.74(3) \cdot 10^5 \text{ cm s}^{-1}$			
$v_{\parallel\parallel}$	$1.55(5) \cdot 10^5 \text{ cm s}^{-1}$			
$v_{\text{t}\parallel}$	$1.07(2) \cdot 10^5 \text{ cm s}^{-1}$			

second order elastic moduli

c_{11}	$3.303(13) \cdot 10^{11} \text{ dyn cm}^{-2}$		ultrasound propagation	75H
c_{33}	$1.634(6) \cdot 10^{11} \text{ dyn cm}^{-2}$			
c_{44}	$0.723(5) \cdot 10^{11} \text{ dyn cm}^{-2}$			
c_{66}	$0.231(2) \cdot 10^{11} \text{ dyn cm}^{-2}$			
c_{12}	$0.559(8) \cdot 10^{11} \text{ dyn cm}^{-2}$			
c_{13}	$1.168(17) \cdot 10^{11} \text{ dyn cm}^{-2}$			

Transport properties

drift mobilities

$\mu_{\text{dr},\text{n}}^{\parallel}$	100 cm ² /V s	$T = 300 \text{ K}, E \parallel c$	for T -dependence, see Fig. 19.4.3	76M
$\mu_{\text{dr},\text{n}}^{\perp}$	65 cm ² /V s	$T = 300 \text{ K}, E \perp c$	for T -dependence, see Fig. 19.4.3	
$\mu_{\text{dr},\text{p}}^{\parallel}$	6(1) cm ² /V s	$T = 300 \text{ K}, E \parallel c$	time-of-flight method, for T -dependence, see Fig. 19.4.3	

drift velocity

$v_{\text{dr},\text{n}}$		$T = 300 \text{ K},$ $E \leq 2 \cdot 10^5 \text{ V/cm}$	for field dependence, see Fig. 19.4.4	74M
--------------------------	--	--	--	-----

Optical properties

refractive index

n_{\perp}	2.39(1)	$T = 300 \text{ K},$ long-wavelength limit, $n_{\perp} = \epsilon(\infty)_{\perp}^{1/2}$	extrapolated from infrared transmission	77A
-------------	---------	--	--	-----

for spectral dependence of n_{\perp} , see Fig. 19.4.5 60S

dielectric constants

$\varepsilon(0)_{\perp}$	25.9	$(\nu/c) \leq 30 \text{ cm}^{-1}$, $T = 4...300 \text{ K}$	ir reflectance and transmission	75B
$\varepsilon(0)_{\parallel}$	8.5			
$\varepsilon(\infty)_{\perp}$	5.15	$(\nu/c) \geq 200 \text{ cm}^{-1}$	ir reflectance and transmission	75B
	5.71(5)		ir transmission	77A
$\varepsilon(\infty)_{\parallel}$	6.8		ir reflectance and transmission	75B
	4.97(5)		ir transmission	77A
real part				
ε_1	8.30	$\lambda = 0.5461 \text{ }\mu\text{m}$	ellipsometry	75P
imaginary part				
ε_2	1.2	$\lambda = 0.5461 \text{ }\mu\text{m}$	ellipsometry	75P
for spectral dependence of ε_1 and ε_2 in the range 2...10 eV, see Fig. 19.4.6				81A

References to 19.4

- 60S Sieskind, M.: Rev. Opt. Theor. Instrum. 39 (1960) 239.
- 63W Wykoff, R. W. G.: Crystal Structures, Vol. 1, Interscience Publishers, New York, 1963.
- 71C Chester, M., Colemann, C. C.: J. Phys. Chem. Solids 32 (1970) 223.
- 72K Kanzaki, K., Imai, I.: J. Phys. Soc. Jpn. 32 (1972) 1003.
- 74H Harbeke, G., Tosatti, E.: Proc. 12th Int. Conf. Phys. Semicond., Stuttgart 1974, p. 626.
- 74M Martin, G. M., Bach, P., Guétin, P.: Appl. Phys. Lett. 25 (1974) 286.
- 75A Akopyan, I., Novikov, B., Permogorov, S., Selkin, A., Travnikov, V.: Phys. Status Solidi. (b) 70 (1975) 353.
- 75B Burkhard, H., Clasen, R., Stubb, I.: Verh. Dtsch. Phys. Ges. (VI) 10 (1975) 391.
- 75H Haussuehl, S., Scholz, H.: Krist. Tech. 10 (1975) 1175.
- 75P Ponpon, I. P., Stuck, R., Siffert, P., Meyer, B., Schwab, C.: IEEE Trans. Nucl. Sci. NS-22 (1975) 182.
- 75W Weast, R. C. ed.: Handbook of Chemistry and Physics, CRC Press, Cleveland, 1975.
- 76M Minder, R., Ottaviani, G., Canali, C.: J. Phys. Chem. Solids 37 (1976) 417.
- 76Y Yee, J. H., Sherohman, J. W., Armantrout, G. A.: IEEE Trans. Nucl. Sci. NS-23 (1976) 117.
- 77A Anedda, A., Raga, F., Grilli, F., Guzzi, M.: Nuovo Cimento 38B (1977) 439.
- 77H Hummel, B., Burkhard, H., Faymonville, R., Grosse, P., Richter, W.: Verh. Dt. Phys. Ges. (VI) (1977) 75.
- 78B Bloch, P. D., Hodby, J. W., Schwab, C., Stacey, D. W.: J. Phys. C. 11 (1978) 2579.
- 78P Prevot, B., Schwab, C., Dorner, B.: Phys. Status Solidi (b) 88 (1978) 327.
- 81A Anedda, A., Grilli, E., Guzzi, M., Raga, F., Serpi, A.: Solid State Commun. 39 (1981) 1121.

Figures to 19.4

Fig. 19.0.5

HgI₂. Brillouin zone of the tetragonal lattice [76Y].

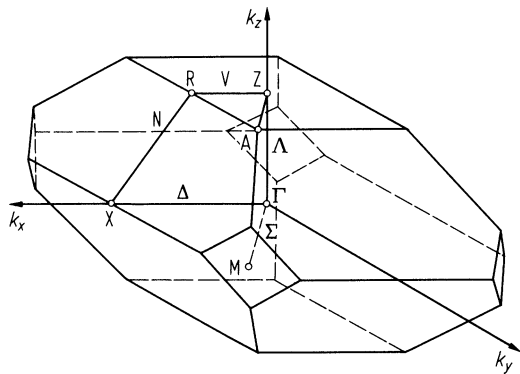


Fig. 19.0.6

HgI₂. Pseudopotential band structure for three symmetry directions [76Y].

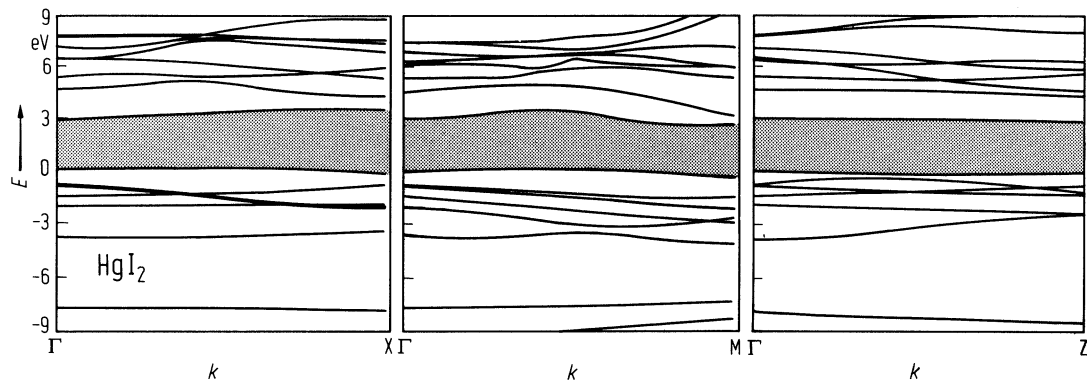


Fig. 19.4.1

HgI_2 . Energy gap vs. temperature. From transmission (full circles) and reflectance (open circles) measurements [74H].

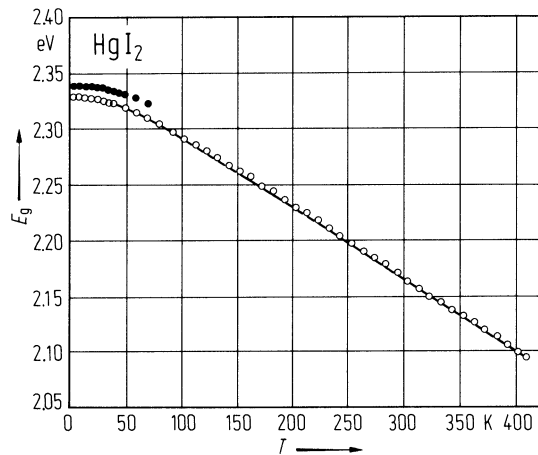


Fig. 19.4.2

HgI_2 . Low-energy phonon dispersion curves at RT. Lines are guides to the eye [78P]. Full (empty) symbols stand for acoustic (optic) vibrations either in transverse (squares) or longitudinal (circles) geometries, with polarization within the layer plane. Triangles refer to modes with polarization parallel to the principal axis.

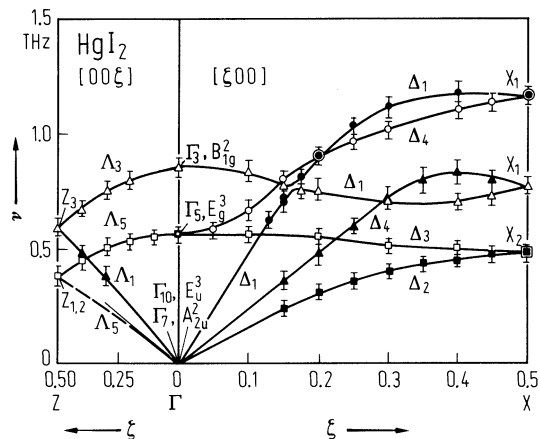


Fig. 19.4.3

HgI₂ Electron drift mobility vs. temperature. Open circles: $E \perp c$; other symbols: $E \parallel c$ [76M]. Different full symbols according to different sample thicknesses.

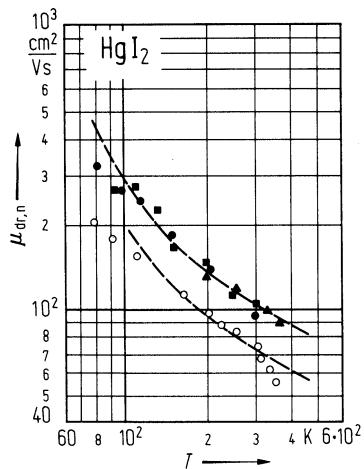


Fig. 19.4.4

HgI₂. Hole drift mobility vs. temperature, $E \parallel c$ [75P].

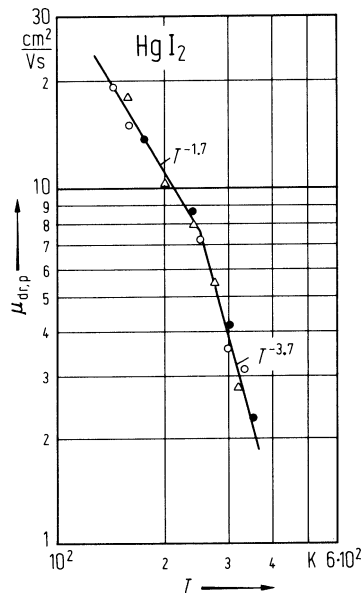


Fig. 19.4.5

HgI₂. Refractive index for $E \perp c$ vs. wavelength [60S].

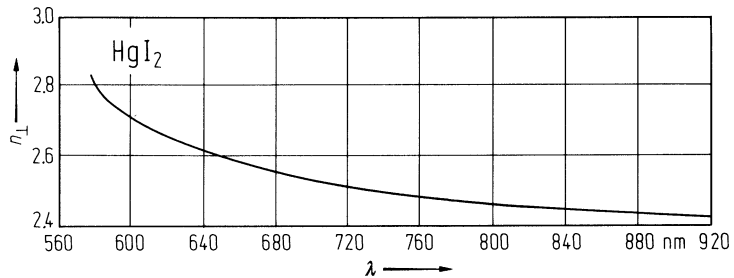
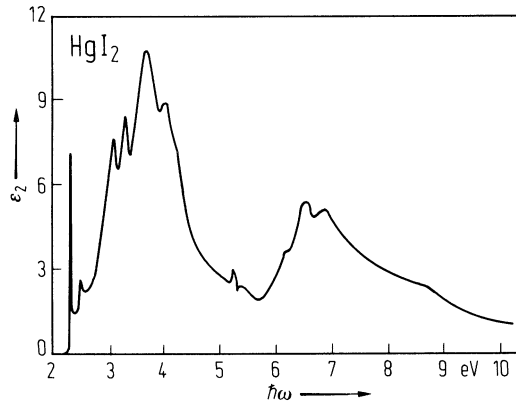


Fig. 19.4.6

HgI₂. Imaginary part of the dielectric constant vs. photon energy [81A].



20 III_x–VI_y compounds

(including III-III-VI₂ compounds; for III₂-VI₃ compounds see chapter 5)

20.0 Crystal structure and electronic structure

20.0.1 III-VI compounds

Most of the III-VI compounds crystallize in layer-type structures. The bonding is strongly covalent within the layers and much weaker between them. In the binary compounds, the cations prefer the tetrahedral coordination. Cation pairs in the crystal saturate the bonding and are responsible for the semiconducting behavior, unless a fraction of the cation are monovalent in corresponding crystallographic sites. Polytypism and stacking faults are frequent but have minor influence on several properties.

The GaSe type structure (*GaS*, *GaSe*, *InSe*) is described in terms of stacking of hexagonal layers of D_{3h} symmetry (Fig. 20.0.1) [61B]. Four basic polytypes are known (Fig. 20.0.2) [74H]:

	polytype:	space group:
β-GaSe	2H	D _{6h} ⁴ – P6 ₃ /mmc
ε-GaSe	2H	D _{3h} ¹ – P $\bar{6}$ m2
γ-GaSe	3R	C _{3v} ⁵ – R3m
δ-GaSe	4H	C _{6v} ⁴ – P6 ₃ mc

The *Brillouin zone* of the β-polytypes is shown in Fig. 20.0.3. The band structures of GaS, GaSe and InSe are shown in Figs. 20.0.4...6, respectively.

The *rhombohedral phase 3R-GaS* is obtained if overstoichiometric in sulfur ($x \geq 0.52$) [87P].

The GaSe type structure of *InSe* is stable at 300K up to $p = 10.3$ GPa where InSe undergoes a non-reversible phase transition to the NaCl type structure with metallic character [91S].

The monoclinic *GaTe* type structure is a distorted form of the GaSe structure with essentially the same coordination [65H], (Fig. 20.0.7). Space group: C_{2h}³ – B2/m.

The orthorhombic structure of *InS* is not layered and contains eight atoms per unit cell [66H], (Fig. 20.0.8). Space group: D_{2h}¹² – Pmnn.

InTe crystallizes normally in a tetragonal form.

In the tetragonal structure of the TlSe type (*TlS*, *TlSe*, *InTe*) one finds two crystallographically different sites for monovalent and trivalent cations, respectively [76M1] with fourteen chemical formula units per elementary cell, [78M2], (see Fig. 20.0.9) . Space groups: TlSe: D_{4h}¹⁸ – I4/mcm, TlTe: D_{4h}¹⁸ – I4/mcm.

The *band structure* of TlSe is shown in Fig. 20.0.10.

20.0.2 Further III_x–VI_y compounds

Besides the monochalcogenides AB and the sesquichalcogenides A₂B₃, only few phases of the polychalcogenides A_xB_y of group III elements have been studied up to the present time. The existence of the monoclinic phases In₆S₇ and Tl₅Te₃ has been established. For a long time, an incorrect composition has been assigned for the following phases:

In₄Se₃ instead of In₂Se

In₄S₅ and In₅S₆ instead of In₆S₇

In₅Se₆ instead of In₆Se₇

In₂Te, In₉Te₇ and In₃Te₂ instead of In₄Te₃

Tl₂Se corresponds to Tl₅Se₃ because of anomalous large homogeneity range

Tl₂Te instead of Tl₅Te₃.

The quoted compounds are summarized in the following table

x/y	Ga _x S _y	In _x S _y	Tl _x S _y	Ga _x Se _y	In _x Se _y	Tl _x Se _y	Ga _x Te _y	In _x Te _y	Tl _x Te _y
2/1	Ga ₂ S		Tl ₂ S ₅	Ga ₂ Se		Tl ₂ Se			Tl ₂ Te
5/3						Tl ₅ Se ₃			Tl ₅ Te ₃
4/3			Tl ₄ S ₃		In ₄ Se ₃			In ₄ Te ₃	
5/4		In ₅ S ₄							
5/6					In ₅ Se ₆				
6/7		In ₆ S ₇			In ₆ Se ₇				
4/5	Ga ₄ S ₅								
3/4		In ₃ S ₄					Ga ₃ Te ₄	In ₃ Te ₄	
5/7					In ₅ Se ₇				
3/5									
1/2			TlS ₂						
2/5			Tl ₂ S ₅				Ga ₂ Te ₅	In ₂ Te ₅	
1/3							GaTe ₃		

Data on such compounds are given in sections 20.10...18.

20.0.3 III-III-VI₂ compounds

Most of the ternary chalcogenides of the TlInSe₂ family are related with the TlSe-type structure (space group, D_{4h}¹⁸ – I4/mcm) (see Fig. 20.0.11). The structure is layered and polytypism has been demonstrated in the case of TlInS₂ with at least two well-established polymorphs α and β. In this structure, the coordination number of the monovalent thallium cation is eight. Gallium or indium are included as trivalent cations with tetrahedral coordination and dominant covalent bonding [73M]. In the case of the TlGaSe₂-type structure, the staggering of the layers of Ga₄Se₁₀-tetrahedra and the distribution of the Tl^I-ions in between are illustrated in Fig. 20.0.12, [78M].

Data on such compounds are given in sections 20.19...24.

Figs. 20.0.13 and 20.0.14 show the *band structures* of TlGaTe₂ and TlInSe₂, respectively.

References to 20.0

- 48W Wyckoff, R. W. G.: Crystal Structures, Vol. 1, Wiley, N. Y., 1948, p. 133.
- 61B Basinski, Z. S., Dove, D. B., Mooser, E.: *Helv. Phys. Acta* 34 (1961) 373.
- 65H Hulliger, F., Mooser, E.: *Progr. Solid State Chem.* 2 (1965) 330.
- 66H Hogg, J. H. C., Duffin, W. J.: *Phys. Status Solidi* 18 (1966) 755.
- 67G Guseinov, G. D., Ramazanzade, A. M., Kerimova, EM., Ismailov, M. Z.: *Phys. Status Solidi* 22 (1967) K117.
- 73M Mooser, F., Schlüter, M.: *Nuovo Cimento* B18 (1973) 164.
- 74H Hoff, R. M., Irwin, J. C.: *Phys. Rev. B* 10 (1974) 3464.
- 76M Man, L. I., Imamov, R. M., Semiletov, S. A.: *Kristallografiya* 21 (1976) 628; *Sov. Phys. Crystallogr.* (English Transl.) 21 (1976) 355.
- 76S Schlüter, M., Camassel, J., Kohn, S., Voitchovsky, J. P., Shen, Y. R., Cohen, M. L.: *Phys. Rev. B* 13 (1976) 3534.
- 78D Depeursinge, Y., Doni, E., Girlanda, R., Baldereschi, A., Maschke, K.: *Solid State Commun.* 27 (1978) 1449.
- 78M1 Mamedov, K. K., Aldzhanov, M. A., Kerimov, I. G., Mekbtiev, M. I.: *Fiz. Tverd. Tela* 20 (1978) 42; *Sov. Phys. Solid State* (English Transl.) 20 (1978) 22.
- 78M2 Morigaki, K., Dawson, P., Cavenett, B. C.: *Solid State Commun.* 28 (1978) 829.
- 78M3 Müller, D., Hahn, H.: *Z. Anorg. Allg. Chem.* 438 (1978) 258.
- 81A1 Abutalybov, G. I., Aliev, A. A., Nizametdinova, M. A., Oridzhev, G. S., Nani, R. Kh.: *Fiz. Tekh. Poluprovodn.* 15 (1981) 851; *Sov. Phys. Semicond.* (English Transl.) 15 (1981) 486.
- 81D Depeursinge, Y.: *Nuovo Cimento B* 64 (1981) 111.
- 84A Allakhverdiev, K. R., Babaev, S. S., Bakhyshev, N. A., Mamedov, T. G., Salaev, E. Yu.: *Fiz. Tekh. Poluprovodn.* 18 (1984) 1307; *Sov. Phys. Semicond.* (English Transl.) 18 (1984) 817.
- 85G Gashimzade, F. M., Guliev, D.: *Phys. Status Solidi (b)* 131 (1985) 201.
- 87P Pardo, M. P., Flahaut, J.: *Mater. Res. Bull.* 22 (1987) 323.
- 91S Schwarz, U., Goni, A. R., Syassen, K., Cantarero, A., Chevy, A.: *High Pressure Res.* 8 (1991) 396.

Figures to 20.0

Fig. 20.0.1

GaSe. The four-fold layer met in GaS, GaSe and InSe; cations: small shaded circles; anions: large open circles [61B].

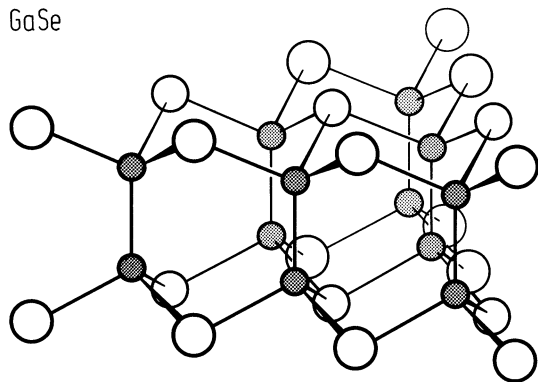


Fig. 20.0.2

GaSe. Layer structures with cation pairs and tetrahedral cation coordination; (110) sections through the hexagonal cells. a) ϵ -GaSe; b) γ -GaSe; c) β -GaSe; d) δ -GaSe [74H].

GaSe

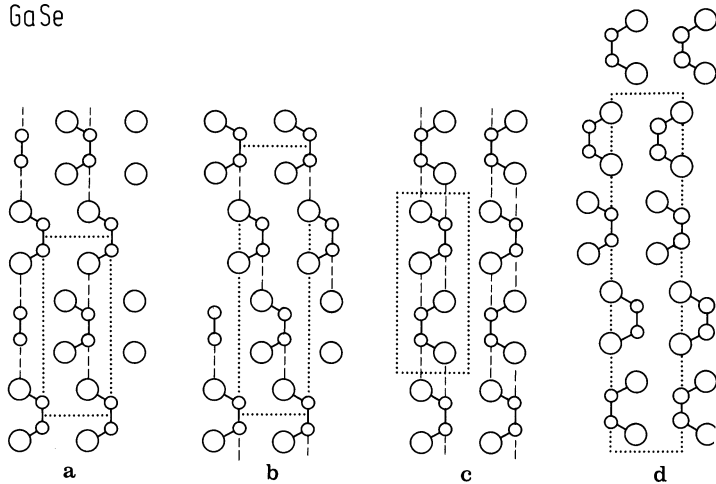


Fig. 20.0.3

Brillouin zone for the hexagonal lattice. g_1, g_2, g_3 : reciprocal basis vectors; $g_1 \parallel k_x, g_3 \parallel k_z$.

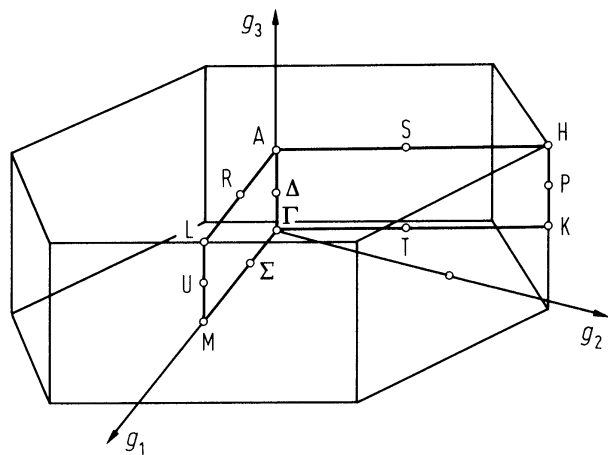
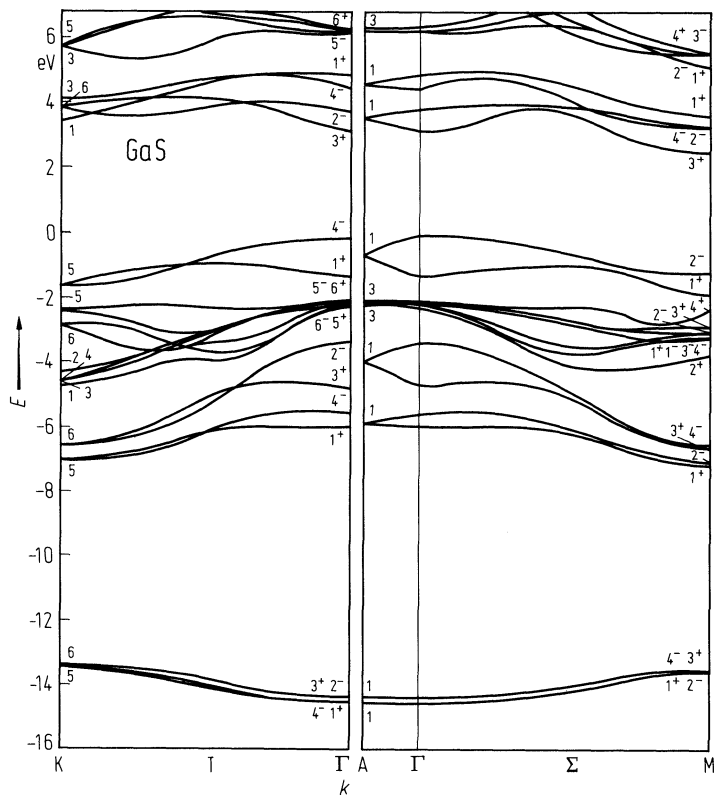
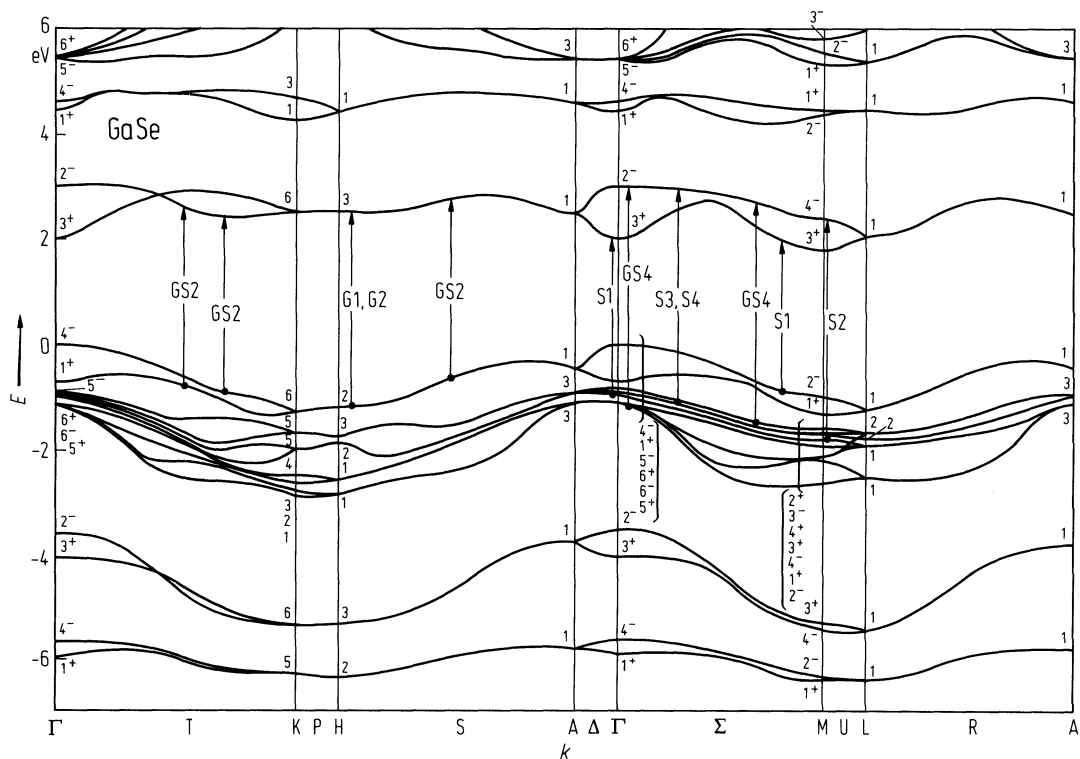


Fig. 20.0.4

GaS. Empirical pseudopotential band structure for the β -polytype [81D].



GaSe. Empirical pseudopotential band structure for the β -polytype. Optical transitions contributing to the observed structures in the reflectivity spectrum are indicated [76S].



InSe. Empirical pseudopotential band structure for the ϵ -polytype [78D].

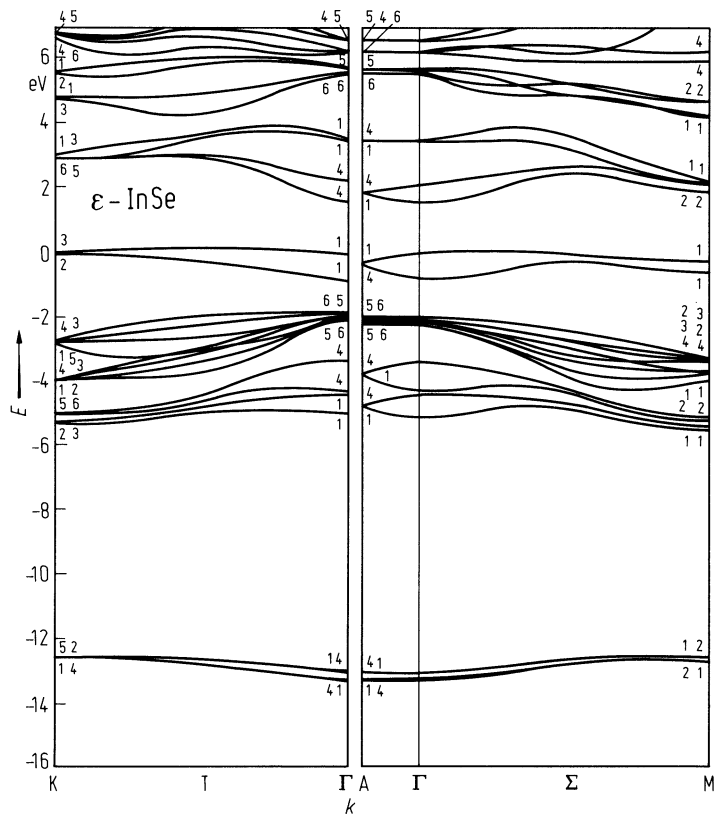


Fig. 20.0.7

GaTe. The monoclinic structure of GaTe; Ga: small circles; Te: large circles [65H].

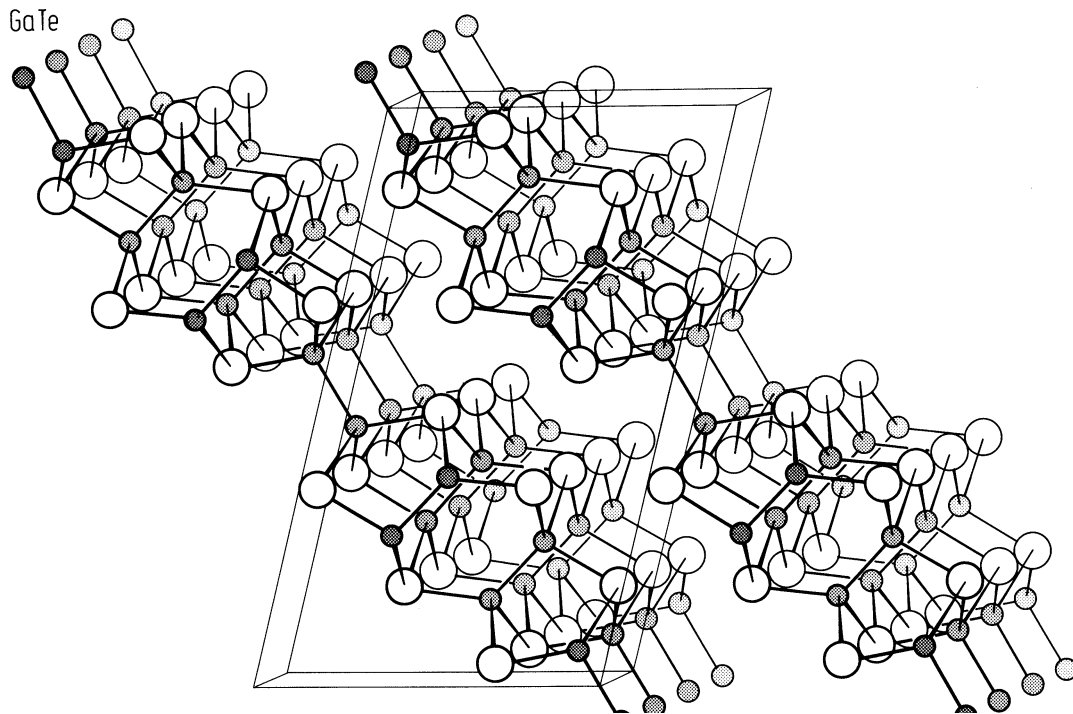


Fig. 20.0.8

InS. The orthorhombic structure of β -InS; In: small shaded circles; S: large open circles [66H].

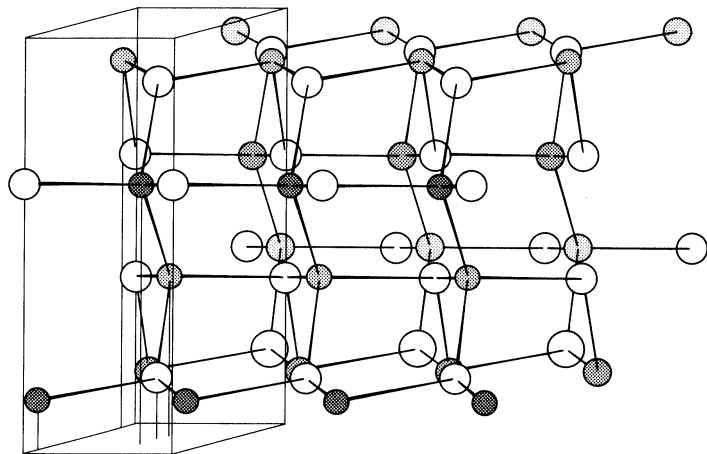
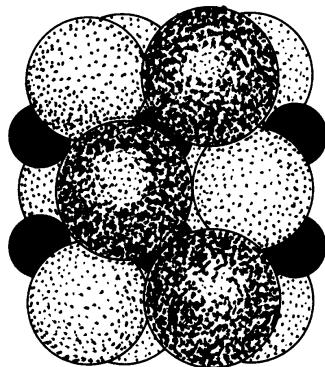
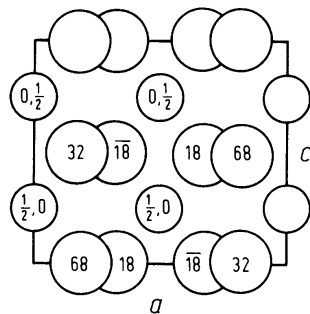


Fig. 20.0.9

TlSe. The tetragonal structure of TlSe projected along the b -axis. Small circles: Tl; large circles: Se [48W]. Integer numbers in circles refer to fractional y coordinates.

TlSe



5 Å

Fig. 20.0.10

TlSe. Empirical pseudopotential band structure [81A].

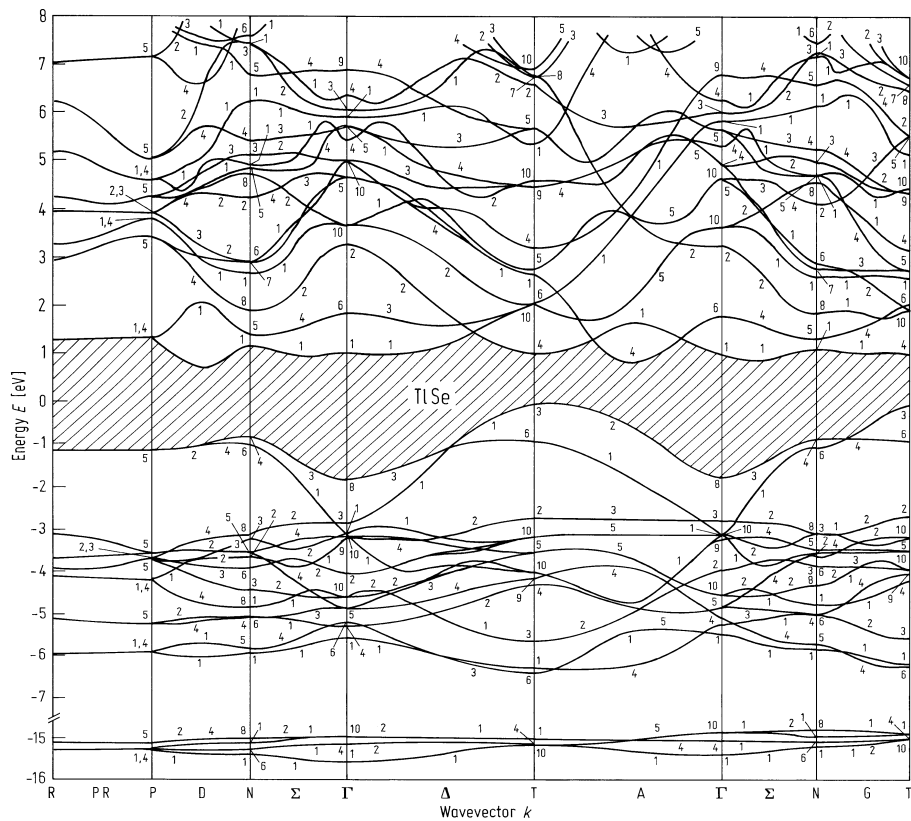


Fig. 20.0.11

TlInSe_2 . Crystal structure [67G].

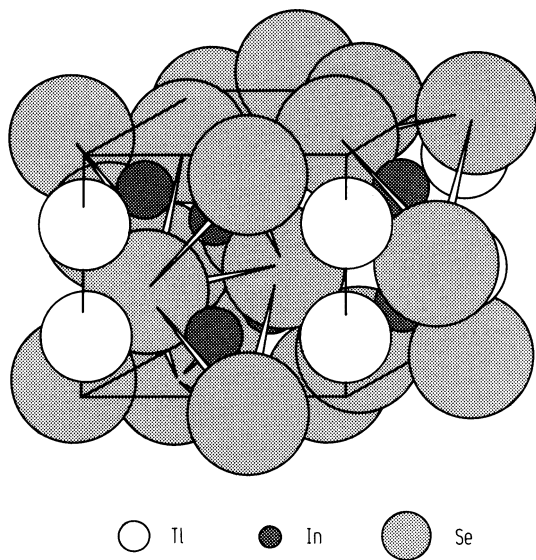


Fig. 20.0.12

TlGaSe_2 . Layered crystal structure of TlGaSe_2 . The position of the Tl^{I} ions is shown between the stacking of the anion layers built of $\text{Ga}_4\text{Se}_{10}$ polyhedra [78M3].

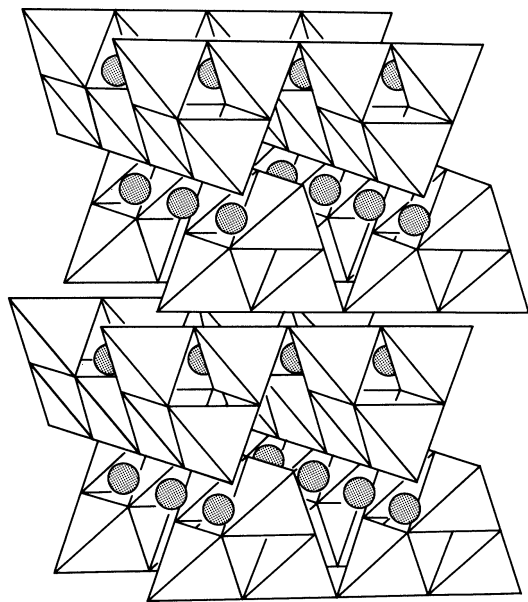


Fig. 20.0.13

TlGaTe_2 . Calculated band structure, typical of compounds with TlSe type structure [85G].

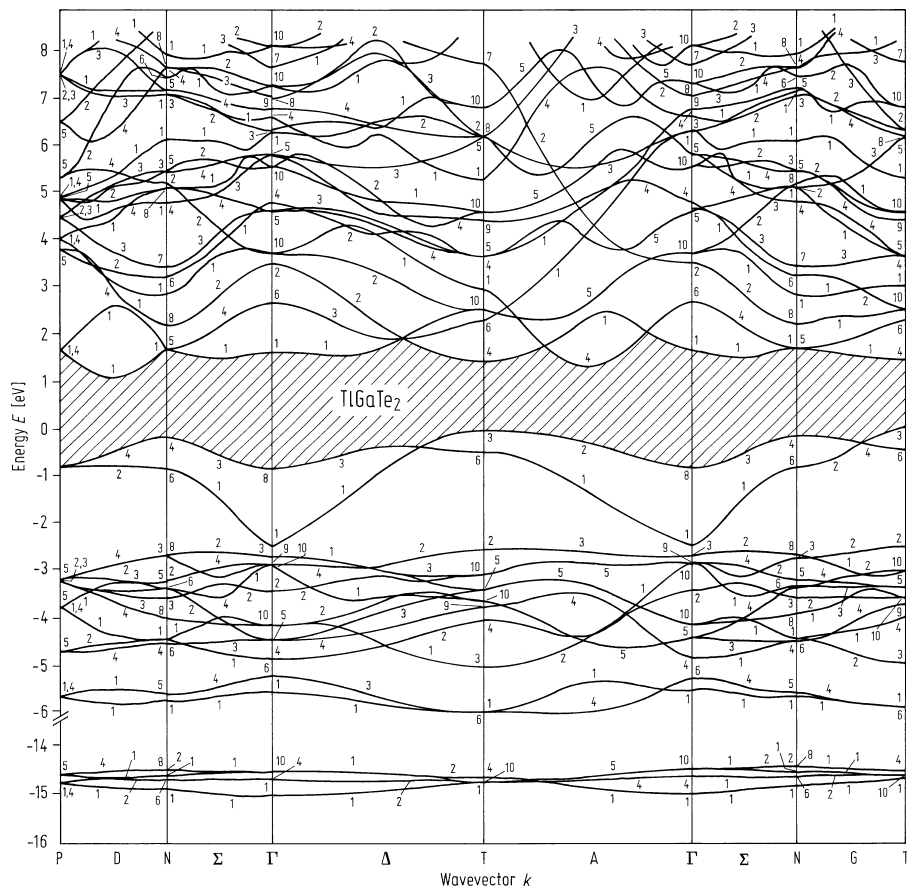
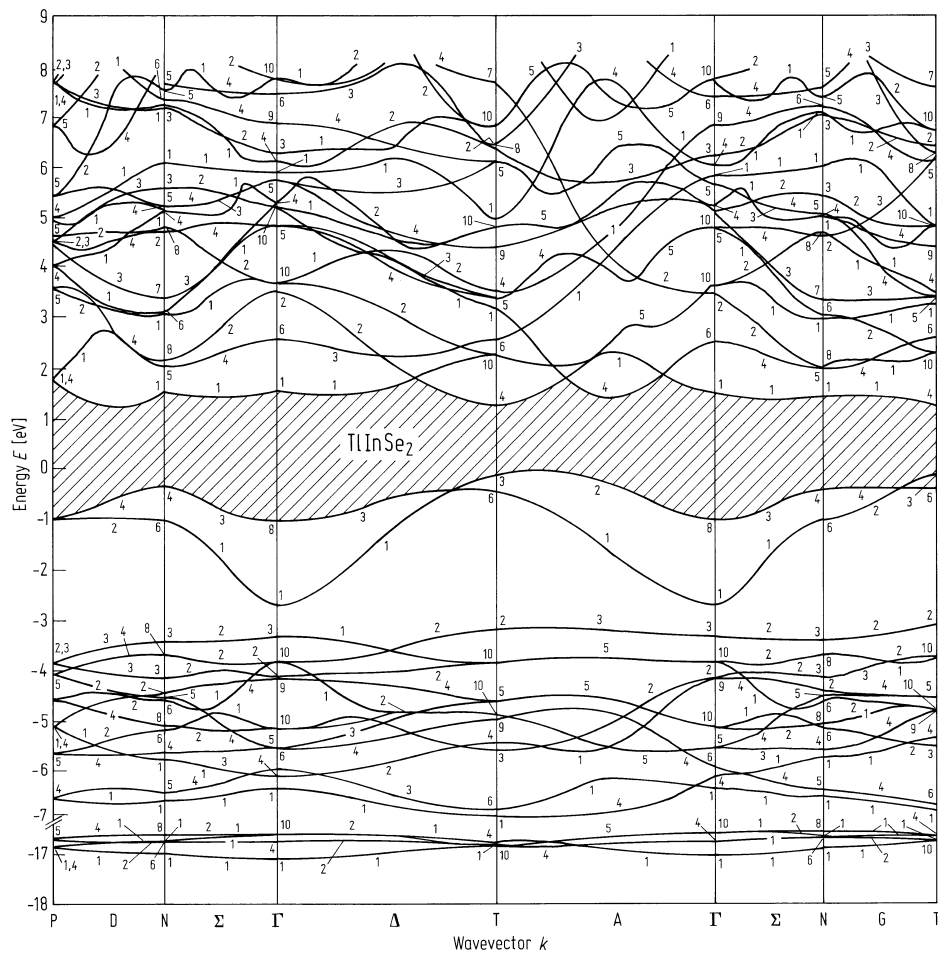


Fig. 20.0.14

TlInSe₂. Empirical pseudopotential band structure [84A].



20.1 Gallium sulfide (GaS)

Crystal structure

see section 20.0.

Electronic properties

The best known polytype is β-GaS.

band structure

see Fig. 20.0.4; Brillouin zone, Fig. 20.0.3.

GaS is an indirect gap semiconductor. The electronic band structure is very similar to that of GaSe. The valence band maximum is at the Γ-point The conduction band is characterized by 6 equivalent minima at the M point.

direct gap

$E_{g,dir}(\Gamma_{4v}^{-}-\Gamma_{3c}^{+})$ 3.050(2) eV $T = 77$ K optical absorption 69A

direct exciton transition energy

$E_{gx,dir}(\Gamma_{4v}^{-}-\Gamma_{3c}^{+})$ 3.029 eV $T = 4.2$ K optical absorption in GaS_xSe_{1-x} 80S

binding energy of direct exciton

E_b 37 meV $T = 77$ K electroabsorption 77G

indirect exciton transition energy

$E_{gx,ind}$ 2.576(1) eV $T = 77$ K wavelength modulated absorption 75K

For temperature dependence of indirect exciton transition energy, see Fig. 20.1.1.

electron effective mass

m_n $5 m_0$ $T = 300$ K, $\perp c$ temperature dependence of the 71K
 $n = 10^{21}$ cm⁻³ Hall mobility

Lattice properties

lattice parameters

a 3.587 Å $T = 300$ K, β-GaSe type 76K
 c 15.492 Å single crystal

a 3.605 Å $T = 300$ K γ-type GaSe, overstoichiometric in S 87P
 c 23.43 Å

linear thermal expansion coefficients

$\alpha_{||}$ $8.25 \cdot 10^{-6}$ K⁻¹ $T = 300$ K, $|| c$ 80R
 α_{\perp} $9.0 \cdot 10^{-6}$ K⁻¹ $\perp c$

Debye temperature

Θ_D 263 K $T = 4...10$ K heat capacity measurements 78M

For dependence on temperature, see Fig. 20.1.2.

heat capacity

C_p 46.2 J mol⁻¹ K⁻¹ $T = 300$ K 72M

temperature dependence of C_p

A 41.35 J mol⁻¹ K⁻¹ 298 K $\leq T \leq 1000$ K A, B are parameters in empirical 74M
 B $1.57 \cdot 10^{-3}$ J mol⁻¹ K⁻¹ relation $C_p = A + BT$ 77M

density

d	3.86 g cm^{-3}	RT		69R
-----	--------------------------	----	--	-----

melting temperature

T_m	1233 K		congruent melting	74M
-------	--------	--	-------------------	-----

For phonon dispersion measured by neutron inelastic scattering of acoustic phonons, see Fig. 20.1.3.

wavenumbers of lattice vibration modes at Γ

$$(\Gamma = 2A_{1g} + 2A_{2u} + 2B_{1u} + 2B_{2g} + 2E_{1g} + 2E_{1u} + 2E_{2g} + 2E_{2u})$$

$\bar{\nu}(E_{2g}^2)$	22.0 cm^{-1}	$T = 295 \text{ K}$	Raman active	79K
$\bar{\nu}(E_{1g}^2)$	74.8 cm^{-1}		Raman active	
$\bar{\nu}(A_{1g}^1)$	187.9 cm^{-1}		Raman active	
$\bar{\nu}(E_{1g}^2)$	291.2 cm^{-1}		Raman active	
$\bar{\nu}(E_{2g}^1)$	295.0 cm^{-1}		Raman active	
$\bar{\nu}(E_{1u})$	296 cm^{-1}	$E \perp c$	transverse optic	
$\bar{\nu}(E_{1u})$	319 cm^{-1}	$E \parallel c$	transverse optic	80R
$\bar{\nu}(E_{1u})$	337 cm^{-1}	$E \parallel c$	longitudinal optic	80R
$\bar{\nu}(E_{1u})$	359 cm^{-1}	$E \perp c$	longitudinal optic	79K

second order elastic moduli

c_{44}	$0.996(15) \cdot 10^{11} \text{ dyn cm}^{-2}$	$T = 300 \text{ K},$	ultrasonic measurements	83G
c_{13}	$1.25(52) \cdot 10^{11} \text{ dyn cm}^{-2}$	$p \leq 3 \text{ kbar}$		
c_{12}	$3.47(10) \cdot 10^{11} \text{ dyn cm}^{-2}$			
c_{33}	$3.85(4) \cdot 10^{11} \text{ dyn cm}^{-2}$			
c_{11}	$12.33(7) \cdot 10^{11} \text{ dyn cm}^{-2}$			

isothermal compressibility

κ_{\parallel}	$0.30 \cdot 10^{-12} \text{ cm}^2 \text{ dyn}^{-1}$	$\perp c, T = 300 \text{ K}$		80R
κ_{\perp}	$0.37 \cdot 10^{-12} \text{ cm}^2 \text{ dyn}^{-1}$	$\parallel c$		80R

Transport properties**dark conductivity**

σ_{\parallel}	$4 \cdot 10^{-13} \Omega^{-1} \text{ cm}^{-1}$	$T = 400 \text{ K}$	vapor grown crystal	71P
σ_{\perp}	$8 \cdot 10^{-10} \Omega^{-1} \text{ cm}^{-1}$		dependence on temperature: see Fig. 20.1.4	

thermal conductivity (lattice contribution)

κ_L	$0.010 \text{ W cm}^{-1} \text{ K}^{-1}$	$T = 300 \text{ K}, \parallel c$		70S
	$0.098 \text{ W cm}^{-1} \text{ K}^{-1}$	$\perp c$		

electron mobility

$\mu_{H,n}$	$12 \text{ cm}^2/\text{V s}$	$T = 300 \text{ K}$	p-type GaS, $i \perp c, B \parallel c$; Hall mobility of illuminated crystal	69K
-------------	------------------------------	---------------------	--	-----

For dependence on temperature, see Fig. 20.1.5.

hole mobility

$\mu_{H,p}$	$16 \text{ cm}^2/\text{V s}$	$T = 300 \text{ K}$	n-type GaS, $i \perp c, B \parallel c$; Hall mobility of illuminated crystal	69K
-------------	------------------------------	---------------------	--	-----

Optical properties

ordinary refractive index

A	$4.251 \cdot 10^{-4} \mu\text{m}^6$	$T = 300 \text{ K}, E \perp c,$	prism and fringe measurements;	76M
B	$3.283 \cdot 10^{-3} \mu\text{m}^4$	$0.386 \leq \lambda$	A, B, C and D are parameters	
C	$2.789 \cdot 10^{-2} \mu\text{m}^2$	$\leq 0.990 \mu\text{m}$	in empirical relation	
D	2.555		$n_{\perp} = A/\lambda^6 + B/\lambda^4 + C/\lambda^2 + D$	

A	$2.303 \cdot 10^{-2} \mu\text{m}^6$	$T = 300 \text{ K}, E \parallel c,$	prism and fringe measurements;	76M
B	$-0.2091 \mu\text{m}^4$	$0.427 \leq \lambda$	A, B, C and D are parameters in	
C	$0.5666 \mu\text{m}^2$	$\leq 0.480 \mu\text{m}$	empirical relation	
D	2.021		$n_{\parallel} = A/\lambda^6 + B/\lambda^4 + C/\lambda^2 + D$	

dielectric constants

real part (for spectral dependence at 300 K, see Fig. 20.1.6)

$\varepsilon(\infty)$	5.3	$E \parallel c$	infrared reflectivity	80R
$\varepsilon(0)$	5.9	$E \parallel c$		
$\varepsilon(\infty)$	6.7	$E \perp c$		
$\varepsilon(0)$	10.0	$E \perp c$		

imaginary part: for spectral dependence at 300 K, see Fig. 20.1.6.

References to 20.1

- 68A Andriyashik, M. V., Yusakhnovskii, M., Timofeev, V. B., Yakimova, A. S.: Phys. Status Solidi 28 (1968) 277.
- 69K Kipperman, A. H. M., Vermij, C. J.: Nuovo Cimento B 63 (1969) 29.
- 69R Rustamov, P. G., Melikova, Z. D., Nasirov, Ya. N., Alidzhanov, M. A.: Izv. Akad. Nauk SSSR, Neorg. Mater. 5 (1969) 881; Bull. Acad. Sci. USSR, Inorg. Mater. (English Transl.) 5 (1969) 750.
- 70S Spitzer, D. P.: J. Phys. Chem. Solids 31 (1970) 19.
- 71K Kipperman, A. H. M.: Solid State Commun. 9 (1971) 1825.
- 71P Pati, S. G., Tredgold, R. H.: J. Phys. C4 (1971) 3199.
- 72M Mamedov, K. K., Kerimov, I. C., Mekhtiev, M. I., Masimov, E. A.: Izv. Akad. Nauk. SSSR, Neorg. Mater. 8 (1972) 2096; Bull. Acad. Sci. USSR, Inorg. Mater. (English Transl.) 8 (1972) 1843.
- 74M Mills, K. C.: Thermodynamic Data for Inorganic Sulphides, Selenides and Tellurides, Butterworth, London, 1974.
- 75K Karaman, M. I., Mushinskii, V. P.: Fiz. Tekh. Poluprovodn. 9 (1975) 1415; Sov. Phys. Semicond. (English Transl.) 9 (1975) 934.
- 76K Kuhn, A., Chevy, A.: Acta Crystallogr. B 32 (1976) 983.
- 76M Man, L. I., Imamov, R. M., Semiletov, S. A.: Kristallografia 21 (1976) 628; Sov. Phys. Crystallogr. (English Transl.) 21 (1976) 355.
- 77D Depeursinge, C.: Thesis, Lausanne 1977, unpublished.
- 77G Guseinov, G. D., Abdullayeva, S. G., Aksianov, I. G., Gajiyev, V. A.: Mater. Res. Bull. 12 (1977) 207.
- 77M Mamedov, K. K., Mdzhanov, I. G., Kerimov, I. G., Mekhtiev, M. I.: Fiz. Tverd. Tela 19 (1977) 1471; Sov. Phys. Sol. State (English Transl.) 19 (1977) 857.
- 77P Powell, B. M., Jandl, S., Brebner, J. L., Levy, F.: J. Phys. C 10 (1977) 3039.
- 78M Mamedov, K. K., Aldzhanov, M. A., Kerimov, I. G., Mekbtiev, M. I.: Fiz. Tverd. Tela 20 (1978) 42; Sov. Phys. Solid State (English Transl.) 20 (1978) 22.
- 79K Kuroda, N., Nishina, Y.: Phys. Rev. B 19 (1979) 1312.
- 79P Piacentini, M., Olson, C. G., Baizarotti, A., Girlanda, R., Grasso, V., Doni, F.: Nuovo Cimento B54 (1979) 248.
- 80R Riede, V., Neumann, H., Hoang Xuan Nguyen, Sobotta, H., Levy, F.: Physica 100 B (1980) 355.
- 80S Serizawa, H., Sasaki, Y., Nishina, Y.: J. Phys. Soc. Jpn. 48 (1980) 490.
- 81D Depeursinge, Y.: Nuovo Cimento B 64 (1981) 111.
- 83G Gatulle, M., Fischer, M., Chevy, A.: Phys. Status Solidi (b) 119 (1983) 327.
- 87P Pardo, M. P., Flahaut, J.: Mater. Res. Bull. 22 (1987) 323.

Figures to 20.1

Fig. 20.0.3

Brillouin zone for the hexagonal lattice. g_1, g_2, g_3 : reciprocal basis vectors; $g_1 \parallel k_x, g_3 \parallel k_z$.

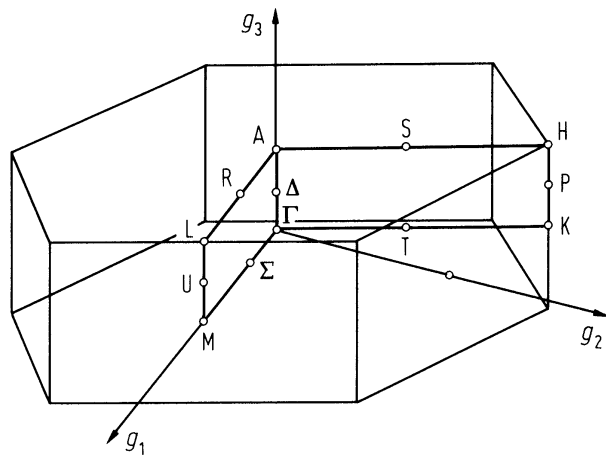


Fig. 20.0.4

GaS. Empirical pseudopotential band structure for the β -polytype [81D].

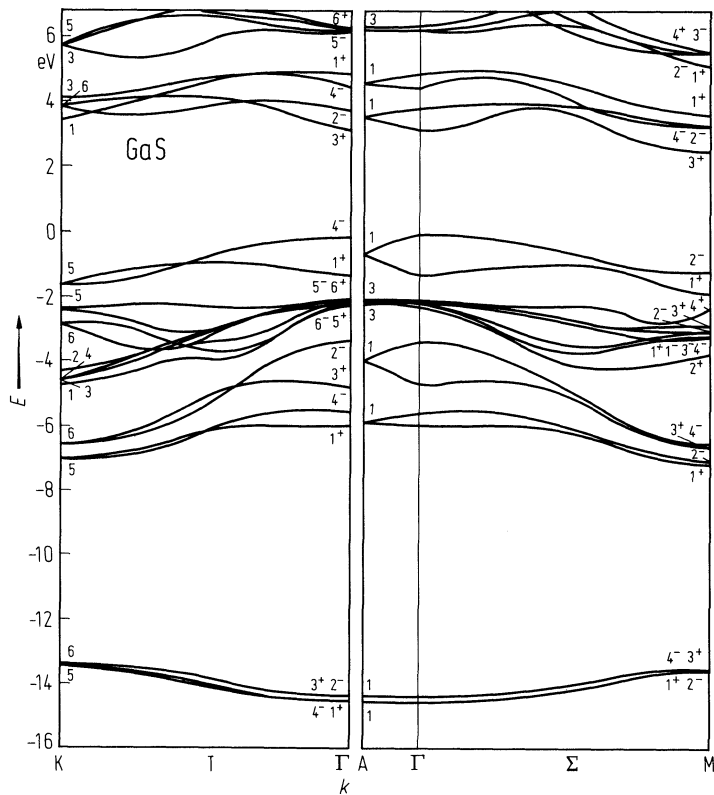


Fig. 20.1.1

GaS. Energetic position of indirect exciton ground state transition vs. temperature [77D].

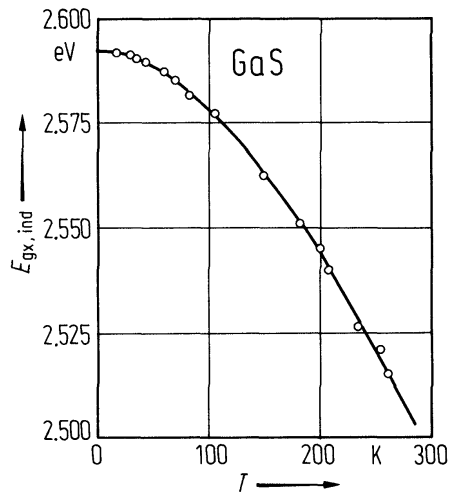


Fig. 20.1.2

GaS, GaSe, GaTe. Debye temperature vs. temperature [78M].

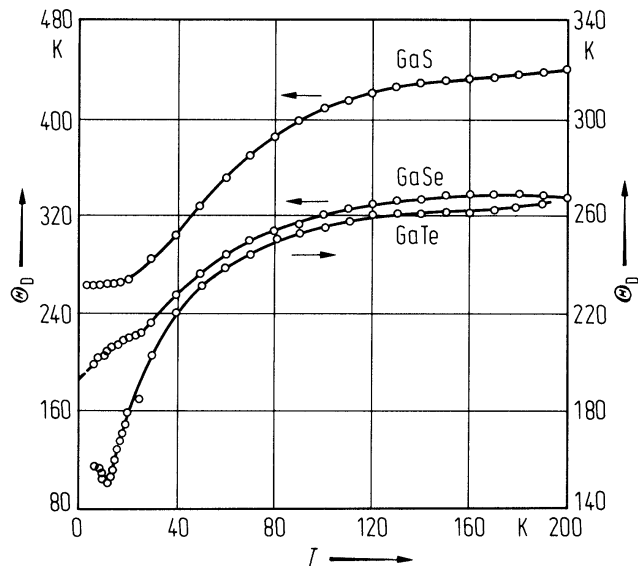


Fig. 20.1.3

GaS. Frequency of the phonon dispersion curves vs. reduced wave vector coordinate. The symbols represent experimental results for the longitudinal modes (open circles), transverse modes polarized along c (full circles) and transverse modes polarized in the basal plane (triangles) [77P].

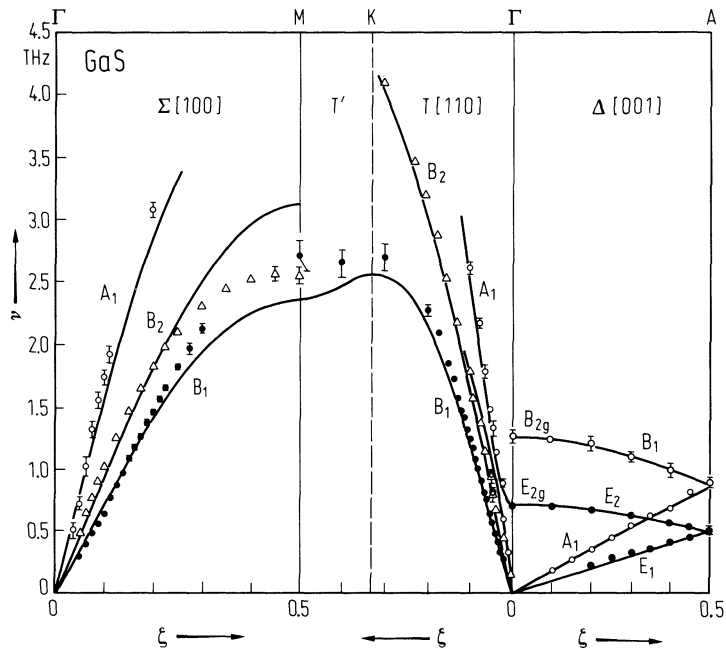


Fig. 20.1.4

GaS, GaSe. Electrical conductivity vs. inverse temperature; n-type GaS (full circles), n-type GaSe (open circles) [71K]. Measurements on platelike crystals in the direction of layers.

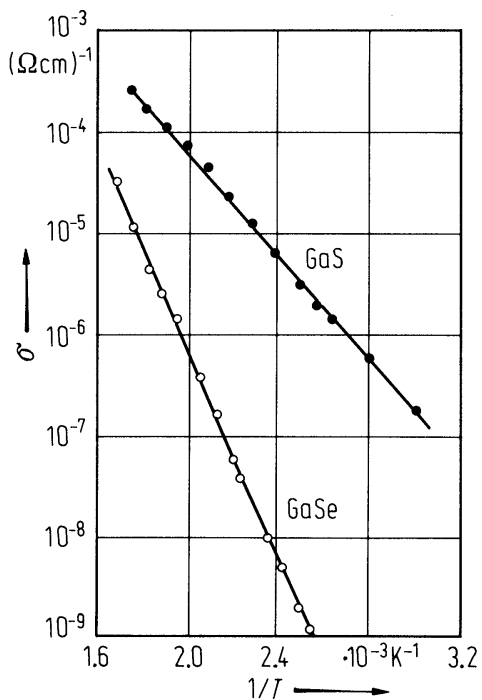


Fig. 20.1.5

GaS. Hall mobility vs. temperature of illuminated GaS platelets ($I \perp$ layers, $B \perp$ layers): iodine transported crystals, n-type (full triangles), sublimated crystal, n-type (full circles), sublimated crystal, p-type (open symbols) [69K].

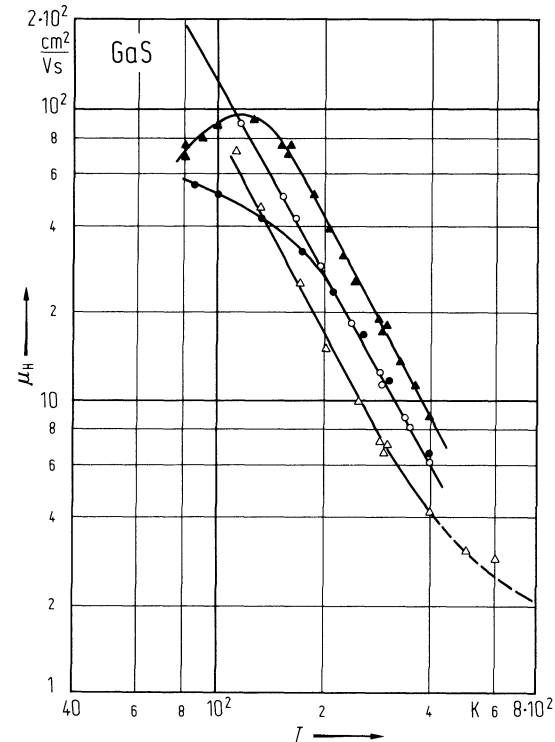
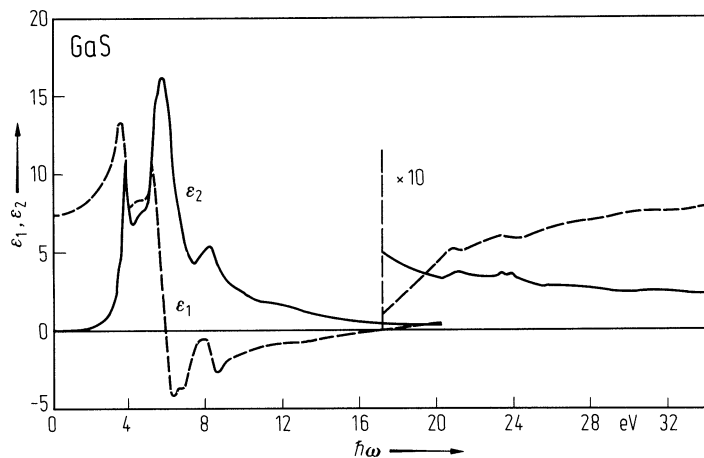


Fig. 20.1.6

GaS. Real and imaginary part of the dielectric constant vs. photon energy at 300 K. The optical functions were obtained from Kramers-Kronig transformation of the reflectivity spectrum, which was measured at an angle of incidence of 10° [79P].



20.2 Gallium selenide (GaSe)

Crystal structure

see section 20.0.

The most commonly occurring form of GaSe is a mixture of ϵ and γ polytypes. These modifications mix easily into each other because of the low stacking fault energy [81B].

Electronic properties

band structure : Fig. 20.0.5, (hexagonal) Brillouin zone: Fig. 20.0.3.

The valence band maximum is at the Γ point. The conduction band is characterized by six equivalent minima at the M point. The conduction band edge at Γ is nearly degenerate with the minima at the M point.

direct energy gap

$E_{g,\text{dir}}(\Gamma_{4v}^- - \Gamma_{3c}^+)$	2.1275(10) eV	$T = 4.2$ K	photoluminescence, optical absorption	74V
	2.021 eV	$T = 300$ K	composition dependence of optical absorption in $\text{GaSe}_x\text{Te}_{1-x}$	79C

temperature coefficient of direct energy gap

$dE_{g,\text{dir}}/dT$	$-4.14 \cdot 10^{-4}$ eV K $^{-1}$	$280 \text{ K} < T < 340 \text{ K}$	optical absorption	71G
------------------------	------------------------------------	-------------------------------------	--------------------	-----

See also temperature coefficient of direct exciton gap and Fig. 20.2.1.

direct exciton gap

$E_{g,\text{dir}}(1S, \Gamma_6)$	2.10980(5) eV	$T = 1.7$ K	optical absorption and reflection	73M
	2.026 eV	$T = 300$ K	ϵ , γ -polytype optical absorption, δ -polytype	75L

temperature coefficient of direct exciton gap

$dE_{g,\text{dir}}/dT$	$-4.14 \cdot 10^{-4}$ eV K $^{-1}$	$280 \text{ K} < T < 340 \text{ K}$	optical absorption	71G
------------------------	------------------------------------	-------------------------------------	--------------------	-----

binding energy of direct exciton

$E_b(1S, \Gamma_6)$	19.7 meV	$T = 1.7$ K	optical absorption, ϵ , γ -polytype and β -polytype, band edge calculated by assuming n^{-2} -excitonic series	73M
---------------------	----------	-------------	--	-----

indirect energy gap

$E_{g,\text{ind}}(\Gamma_{4v}^- - M_{3c}^+)$	2.103(3) eV	$T = 4.2$ K	photoluminescence	74V
--	-------------	-------------	-------------------	-----

g-factor of free electrons

$g_{c\parallel}$	1.13(1)	$T = 2$ K	optically detected magnetic resonance	78M2
$g_{c\perp}$	1.2	$T = 2$ K	magneto-optical absorption	73B

g-factor of free holes

$g_{v\parallel}$	1.72(2)	$T = 2$ K	optically detected magnetic resonance	78M2
------------------	---------	-----------	---------------------------------------	------

conduction band, effective masses

$m_{n\perp}$	$0.5 m_0$		time-of-flight and magneto-Stark effect measurements	74O
$m_{n\parallel}$	$1.6 m_0$			

valence band, effective masses

$m_{p\perp}$	$0.8\ m_0$	time-of-flight and magneto-Stark effect measurements	74O
$m_{p\parallel}$	$0.2\ m_0$		

Lattice properties

lattice parameters

a	$3.755\ \text{\AA}$	$T = 300\ \text{K}$	β -GaSe	61J
c	$15.94\ \text{\AA}$			
a	$3.755\ \text{\AA}$	$T = 300\ \text{K}$	ε -GaSe	76H
c	$15.95\ \text{\AA}$			
a	$3.755\ \text{\AA}$	$T = 300\ \text{K}$	γ -GaSe	76T
c	$23.92\ \text{\AA}$			
a	$3.755\ \text{\AA}$	$T = 300\ \text{K}$	δ -GaSe	75K
c	$31.99\ \text{\AA}$			

linear thermal expansion coefficient

for dependence on the temperature in the range $0\ \text{K} < T < 400\ \text{K}$, see Fig. 20.2.2.

Debye temperature

Θ_D	189 K	$T \rightarrow 0$	calorimetric measurements	78M1
------------	-------	-------------------	---------------------------	------

heat capacity

A	$44.66\ \text{J mol}^{-1}\ \text{K}^{-1}$	$298\ \text{K} < T < 1200\ \text{K}$	A, B are parameters of empirical relation $A + BT^{-3}$.	67M
B	$1 \cdot 10^{-5}\ \text{J mol}^{-1}\ \text{K}^2$			

density

d	$5.03\ \text{g cm}^{-3}$	$T = 298\ \text{K}$		34K
-----	--------------------------	---------------------	--	-----

melting temperature

T_m	938°C			77L2
-------	---------------------	--	--	------

phonon properties

The vibrational spectra strongly depend on the polytypic modification of the crystal [79K].

Phonon dispersion relations, see Fig. 20.2.3.

sound velocity

v_t	$1.185 \cdot 10^5\ \text{cm s}^{-1}$	$T = 298\ \text{K}, \parallel c$	transverse, pulse technique at 1.67 MHz	67K
v_l	$2.482 \cdot 10^5\ \text{cm s}^{-1}$	$\parallel c$	longitudinal	
v_t	$2.641 \cdot 10^5\ \text{cm s}^{-1}$	$\perp c$	transverse	
v_l	$4.515 \cdot 10^5\ \text{cm s}^{-1}$	$\perp c$	longitudinal	

second order elastic moduli

c_{55}	$0.70 \cdot 10^{11}\ \text{dyn cm}^{-2}$	$T = 295\ \text{K}$	ultrasonic measurements, $\nu = 1.67\ \text{MHz}$	67K
c_{33}	$3.07 \cdot 10^{11}\ \text{dyn cm}^{-2}$			
c_{12}	$3.24 \cdot 10^{11}\ \text{dyn cm}^{-2}$			
c_{66}	$3.5 \cdot 10^{11}\ \text{dyn cm}^{-2}$			
c_{11}	$10.24 \cdot 10^{11}\ \text{dyn cm}^{-2}$			

isothermal compressibility

κ_\perp	$0.5 \cdot 10^{-12}\ \text{cm}^2\ \text{dyn}^{-1}$	$T = 300\ \text{K}, \perp c$	82P
κ_\parallel	$2.49 \cdot 10^{-12}\ \text{cm}^2\ \text{dyn}^{-1}$	$T = 300\ \text{K}, \parallel c$	

Transport properties

The structural anisotropy is responsible for a preferentially effective scattering of the charge carriers by optical phonons polarized perpendicular to the layers [67F]. The measured electrical conductivity is usually intrinsic and its value depends on the elaboration of the sample.

electrical conductivity

Results at room temperature scatter immensely. The value of the resistivity ρ can vary between $20 \text{ } \Omega \text{ cm}$ [71T] and $10^7 \text{ } \Omega \text{ cm}$ [67F] depending on the purity of the material and on the preparation technique. In n-type compensated GaSe:Sn, the resistivity reaches the value of $1.8 \cdot 10^9 \text{ } \Omega \text{ cm}$ at room temperature [67F].

For a typical temperature dependence, see Fig. 20.2.4.

thermal conductivity

κ_L	$0.021 \text{ W cm}^{-1} \text{ K}^{-1}$	$T = 300 \text{ K}, \parallel c$		70S
	$0.16 \text{ W cm}^{-1} \text{ K}^{-1}$	$\perp c$		

For dependence on the temperature $600 \text{ K} < T < 1400 \text{ K}$, see Fig. 20.2.5.

hole mobility

$\mu_{\text{dr,p}}$	$60 \text{ cm}^2/\text{V s}$	$T = 300 \text{ K}$	$E \perp c$, drift mobility	76M1
	$210 \text{ cm}^2/\text{V s}$	$T = 300 \text{ K}$	$E \parallel c$, drift mobility, time-of-flight technique	

For dependence on temperature, see Fig. 20.2.6.

electron mobility

$\mu_{\text{dr,n}}$	$80 \text{ cm}^2/\text{V s}$	$T = 300 \text{ K}$	$E \parallel c$, drift mobility	76M2
	$300 \text{ cm}^2/\text{V s}$	$T = 300 \text{ K}$	$E \perp c$, drift mobility, time-of-flight technique	76M2

For dependence on temperature: see Fig. 20.26.

Optical properties

ordinary refractive index

A	$1.939 \cdot 10^{-3} \text{ } \mu\text{m}^6$	$T = 300 \text{ K}, E \perp c$,	prism and fringe measurements;	76M1
B	$-7.246 \cdot 10^{-3} \text{ } \mu\text{m}^4$	$0.408 < \lambda$	A, B, C and D are parameters	
C	$9.466 \cdot 10^{-2} \text{ } \mu\text{m}^2$	$< 0.620 \text{ } \mu\text{m}$	in empirical relation	
D	2.689		$n_{\perp} = A/\lambda^6 + B/\lambda^4 + C/\lambda^2 + D$ see also Fig. 20.2.7	
A	$-1.245 \cdot 10^{-2} \text{ } \mu\text{m}^6$	$T = 300 \text{ K}, E \parallel c$	prism and fringe measurements	76M1
B	$0.1697 \text{ } \mu\text{m}^4$	$0.425 < \lambda$	A, B, C and D are parameters in	
C	$-0.6926 \text{ } \mu\text{m}^2$	$< 0.600 \text{ } \mu\text{m}$	empirical relation	
D	3.562		$n_{\parallel} = A/\lambda^6 + B/\lambda^4 + C/\lambda^2 + D$ see also Fig. 20.2.7	

real part of the dielectric constant

(for spectral dependence, see Fig. 20.24)

$\varepsilon(\infty)$	5.76	$E \parallel c, T = 295 \text{ K}$	infrared reflectivity	77L1
$\varepsilon(0)$	6.18	$E \parallel c$		
$\varepsilon(\infty)$	7.44	$E \perp c$		
$\varepsilon(0)$	10.6	$E \perp c$		

imaginary part of the dielectric constant : for spectral dependence, see Fig. 20.2.8.

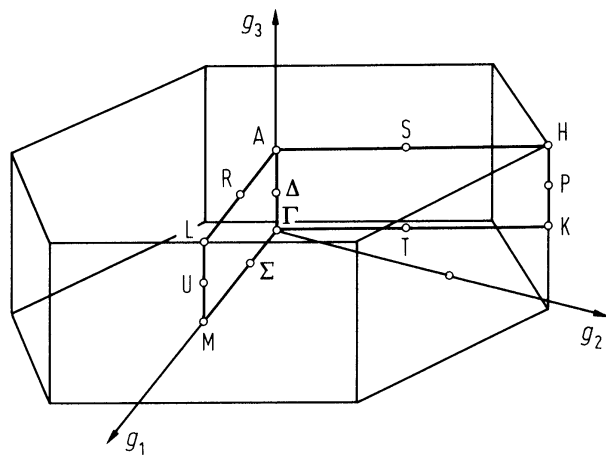
References to 20.2

- 34K Klemm W., v. Vogel, H. U.: Z. Anorg. Allg. Chem. 219 (1934) 45.
- 61J Jellinek, F., Hahn, H.: Z. Naturforsch. 16b (1961) 713.
- 67F Fivaz, R., Mooser, E.: Phys. Rev. 163 (1967) 743.
- 67K Khalilov, K. H. M., Rzaev, K. I.: Sov. Phys. Crystallogr. (English Transl.) 11 (1967) 786.
- 67M Mamedov, K. N., Kerimov, I. G., Kostryukov, V. N., Mekhtiev, H. M.: Fiz. Tech. Poluprovodn. 1 (1967) 441; Sov. Phys. Semicond. (English Transl.) 1 (1967) 363.
- 70S Spitzer, D. P.: J. Phys. Chem. Solids 31 (1970) 19.
- 71G Gandolfo, M., Gratton, E., Somma, F., Vecchia, P.: Phys. Status Solidi (b) 48 (1971) 729.
- 71T Tatsuyama, C., Hamaguchi, C., Tomita, H., Nakai, J.: Jpn. J. Appl. Phys. 10 (1971) 1698.
- 72A Aliev, N. G., Kerimov, I. G., Kurbanov, M. M., Mamedov, T. A.: Fiz. Tverd. Tela 14 (1972) 1522; Sov. Phys. Solid State (English Transl.) 14 (1972) 1304.
- 72F Fedorov, V. I., Machuev, V. I.: Fiz. Tekh. Poluprovodn. 6 (1972) 173; Sov. Phys. Semicond. (English Transl.) 6 (1972) 142.
- 73M Mooser, F., Schlüter, M.: Nuovo Cimento B18 (1973) 164.
- 74O Ottaviani, O., Canali, C., Nava, F., Schmid, Ph., Mooser, F., Minder, R., Zschokke, I.: Solid State Commun. 14 (1974) 933.
- 74V Voitchovsky, J. P., Mercier, A.: Nuovo Cimento B22 (1974) 273.
- 75K Kuhn, A., Chevalier, R., Rimsky, A.: Acta Crystallogr. B31 (1975) 2841.
- 75L Le Toullec, R., Balkanski, M., Besson, J. M.: Phys. Lett. A55 (1975) 245.
- 76F Fivaz, R. C., Schmid, Ph. E.: Physics and Chemistry of Materials with Layered Structures, Vol. 4 Optical and Electrical Properties, P. A. Lee Ed., D. Reidel Publ. Comp. 1976, p. 343384.
- 76H Hulliger, F.: Structural Chemistry of Layer Type Phases in Physics and Chemistry of Materials with Layered Structures. Vol. 5, F. Levy Ed., D. Reidel Publ. Comp. 1976.
- 76J Jandl, S., Brebner, J. L., Powell, B. M.: Phys. Rev. B 13 (1976) 686.
- 76M1 McMath, T. A., Irwin, J. C.: Phys. Status Solidi (a) 38 (1976) 731.
- 76M2 Minder, R., Ottaviani, G., Canali, C.: J. Phys. Chem. Solids 37 (1976) 417.
- 76S Schlüter, M., Camassel, J., Kohn, S., Voitchovsky, J. P., Shen, Y. R., Cohen, M. L.: Phys. Rev. B 13 (1976) 3534.
- 76T Terhell, J. C. J. M., Van der Vleuten, W. C.: Mater. Res. Bull. 11 (1976) 101; Mater. Res. Bull. 19 (1975) 577.
- 77L1 Le Toullec, R., Picciolo, N., Mejatty, M. S., Balkanski, M.: Nuovo Cimento B38 (1977) 159.
- 77L2 Leveque, G., Bertrand, Y., Robin, J.: J. Phys. C 10 (1977) 343.
- 78M1 Mamedov, K. K., Aldzhanov, M. A., Kerimov, I. G., Mekhtiev, M. I.: Fiz. Tverd. Tela 20 (1978) 42; Sov. Phys. Solid State (English Transl.) 20 (1978) 22.
- 78M2 Morigaki, K., Dawson, P., Cavenett, B. C.: Solid State Commun. 28 (1978) 829.
- 79C Camassel, J., Merle, P., Mathieu, H., Gouskov, A.: Phys. Rev. B19 (1979) 1060.
- 79K Kuroda, N., Nishina, Y.: Phys. Rev. B 19 (1979) 1312.
- 79P1 Piacentini, M., Doni, E., Girlanda, R., Grasso, V., Balzarotti, A.: Nuovo Cimento B 54 (1 979) 269.
- 81B Bastov, T. J., Campbell, I. D., Whitfield, H. J.: Solid State Comm. 39 (1981) 307.
- 82P Polian, A., Grimsditch, M., Fischer, M., Gatlulle, M.: J. Phys. Letters 43 (1982) L405.

Figures to 20.0

Fig. 20.0.3

Brillouin zone for the hexagonal lattice. g_1, g_2, g_3 : reciprocal basis vectors; $g_1 \parallel k_x, g_3 \parallel k_z$.



GaSe. Empirical pseudopotential band structure for the β -polytype. Optical transitions contributing to the observed structures in the reflectivity spectrum are indicated [76S].

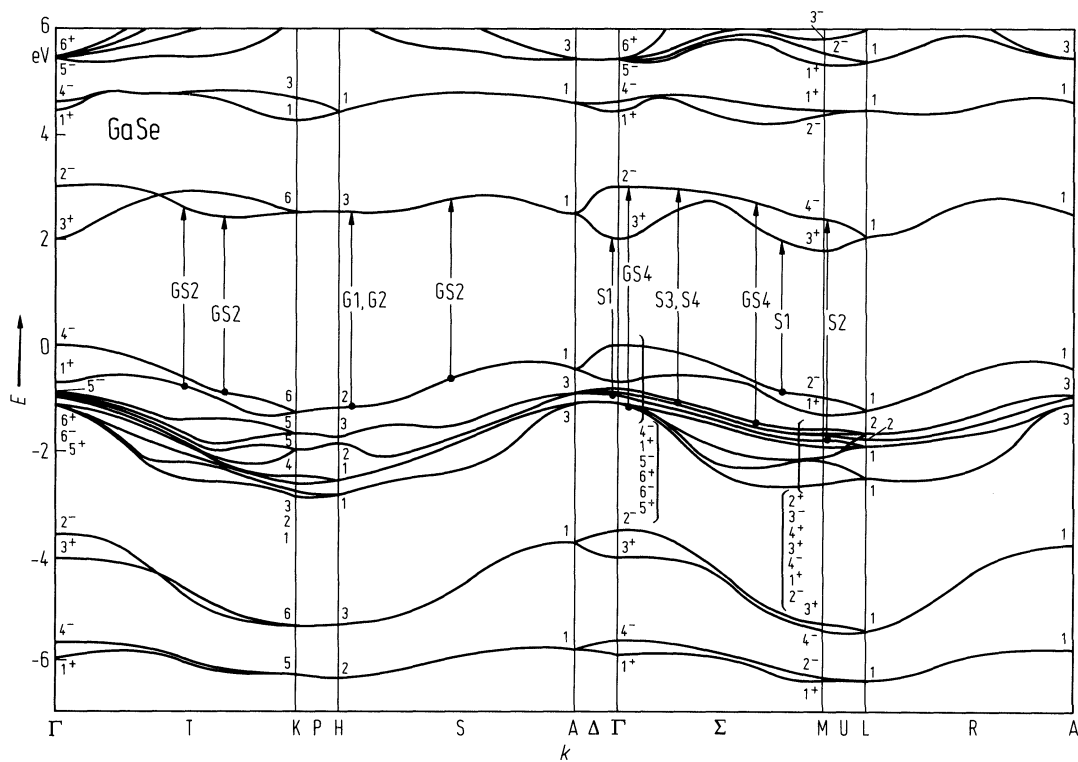


Fig. 20.2.1

GaSe. Energetic position of the ground state ($n = 1$ open circles) and of the first excited state ($n = 2$, full circles) of the free exciton vs. temperature [74V].

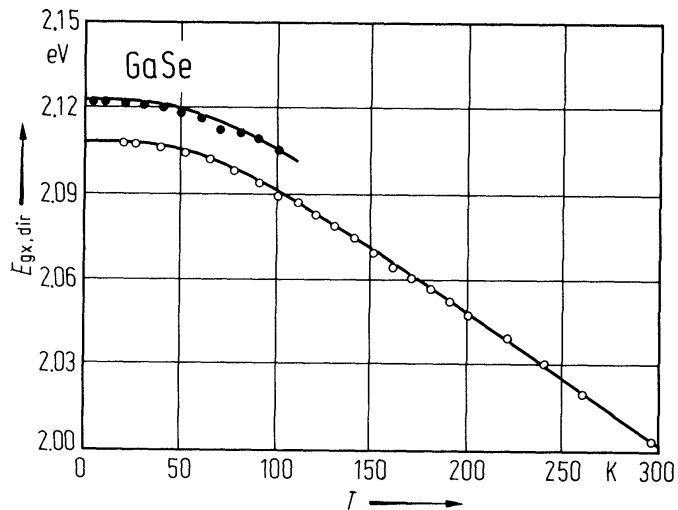


Fig. 20.2.2

GaSe. Coefficients of linear thermal expansion vs. temperature, 1, α_{\parallel} measured parallel with the c -axis; 2, α_{\perp} measured parallel with the layers [72A].

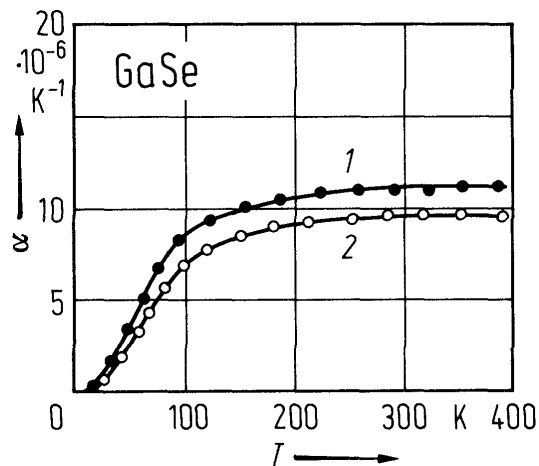


Fig. 20.2.3

GaSe. Phonon frequency vs. reduced wave vector coordinate in the Δ and Σ directions. Solid circles, Δ_1 , Σ_1 ; open circles Δ_3 , Σ_3 ; [76J].

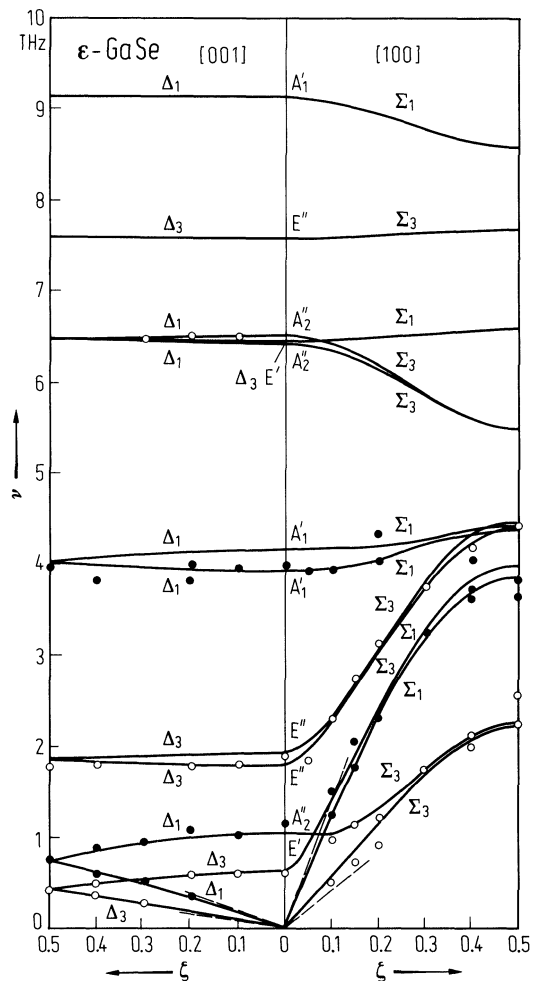


Fig. 20.2.4

GaSe. Electrical resistivity vs. inverse temperature. ρ_{\parallel} is the resistivity parallel with the c -axis (open circles); ρ_{\perp} is the resistivity parallel with the layers (full circles) [71T].

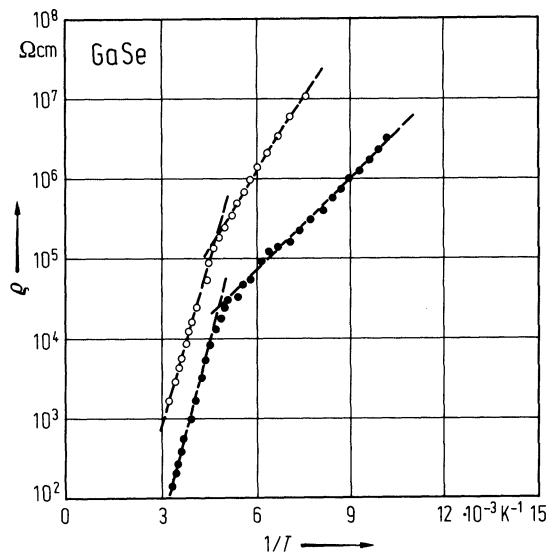


Fig. 20.2.5

GaSe, InSe. Thermal conductivity vs. temperature. Full circles: GaSe; other symbols: InSe [72F].

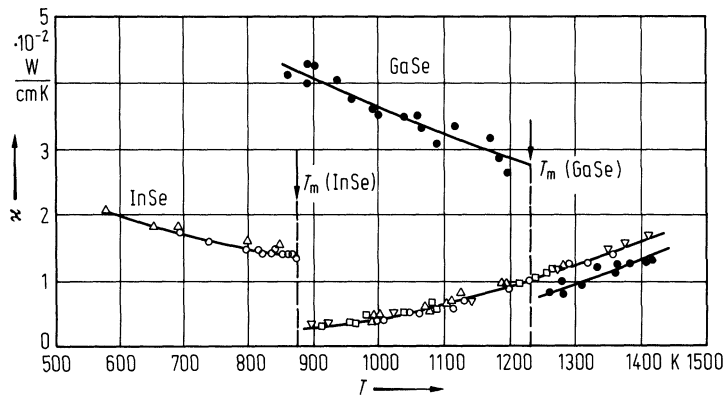


Fig. 20.2.6

GaSe. Mobilities vs. temperature. $\mu_{p\perp}$, $\mu_{n\perp}$: Hall mobilities of holes and electrons parallel with the layers; $\mu_{p\parallel}$, $\mu_{n\parallel}$: drift mobilities of holes and electrons parallel with the c -axis [76F].

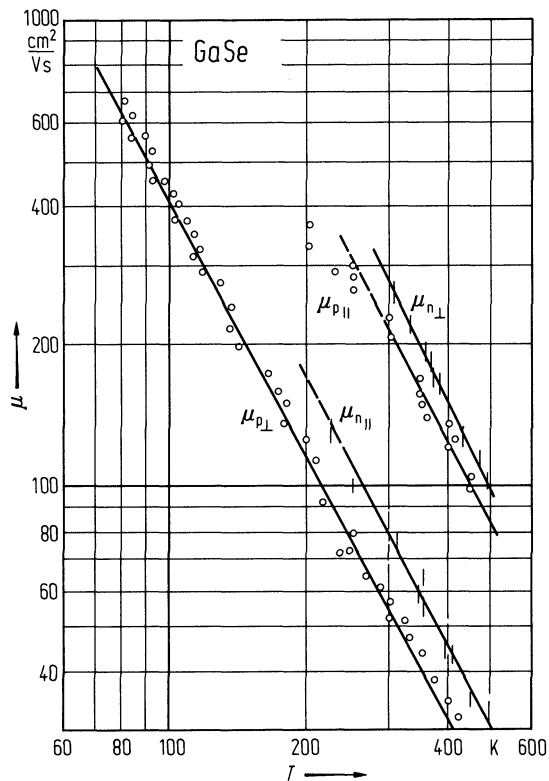


Fig. 20.2.7

GaSe. Refractive index for $E \perp c$ (n_{\perp}) and $E \parallel c$ (n_{\parallel}) at room temperature vs. photon energy [77L1].

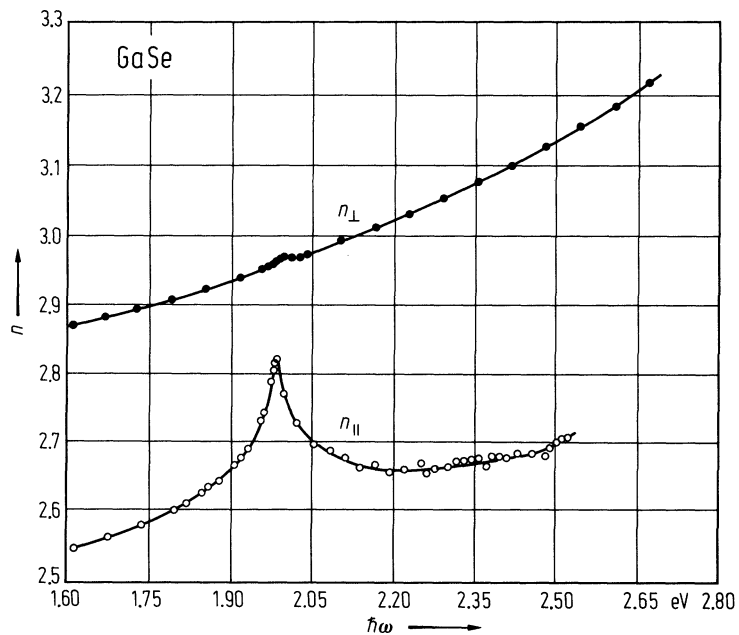
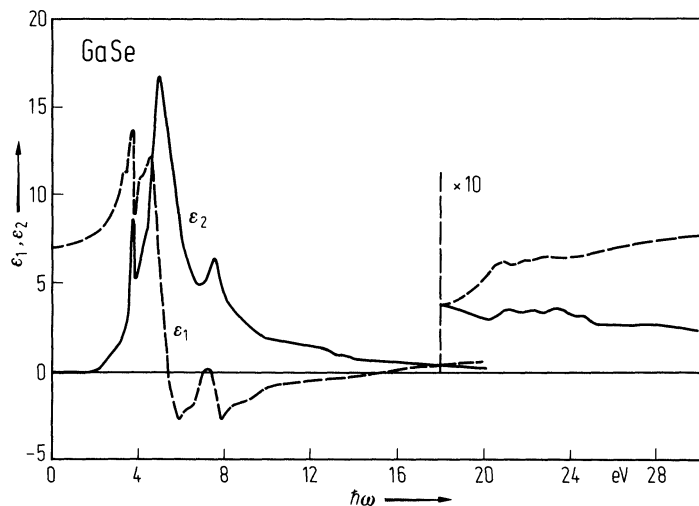


Fig. 20.2.8

GaSe. Real and imaginary parts of the dielectric constant vs. photon energy at RT. The optical functions were obtained from Kramers-Kronig transformation of the reflectivity spectrum, which was measured at an angle of incidence of 10° [79P].



20.3 Gallium telluride (GaTe)

Crystal structure

see section 20.0.

Electronic properties

The electronic band structure of GaTe is not known. It has been established experimentally that GaTe is a direct semiconductor with an energy gap of about 1.7 eV at room temperature. The layer character of GaTe is less pronounced than in the case of GaS and GaSe.

direct energy gap

$E_{g,dir}$	1.799 eV	$T = 1.6$ K	optical absorption	79C
	1.694 eV	$T = 295$ K	wavelength and thermomodulated reflectivity	77G
$dE_{g,dir}/dT$	$-5.0 \cdot 10^{-4}$ eV K ⁻¹	$T > 100$ K	optical absorption see Fig. 20.3.1	79K

direct exciton transition energy

$E_{gx,dir}(1S)$	1.780(2) eV	$T = 1.6$ K	optical absorption	79C
	1.667 eV	$T = 300$ K	optical absorption	79C

temperature coefficient of direct exciton gap

$dE_{gx,dir}/dT$	$-4.19 \cdot 10^{-4}$ eV K ⁻¹	$280\text{ K} < T < 340\text{ K}$	optical absorption	71G
------------------	--	-----------------------------------	--------------------	-----

exciton binding energy

$E_b(1S)$	25 meV	$T = 284$ K	optical transmission	70T
-----------	--------	-------------	----------------------	-----

valence band, effective masses

$m_{p\perp}$	$1.0\ m_0$		temperature dependence of the drift mobility	78G
$m_{p\parallel}$	$0.2\ m_0$			

Lattice properties

lattice parameters

a	17.44 Å	$T = 300$ K	monoclinic single crystal	79J
b	10.456 Å			
c	4.077 Å			
γ	104.4°			

linear thermal expansion coefficients

α_{\parallel}	$7.85 \cdot 10^{-6}$ K ⁻¹	$T = 295$ K, $\parallel c$		76M
α_{\perp}	$13.22 \cdot 10^{-6}$ K ⁻¹			

Debye temperature

Θ_D	158 K	$T < 9$ K		78M
------------	-------	-----------	--	-----

heat capacity

A	53.989 J mol ⁻¹ K ⁻¹	$298\text{ K} < T < 2000\text{ K}$	A, B, C are parameters in the empirical relation $A + BT + CT^{-2}$	68U
B	6.2810^{-5} J mol ⁻¹ K ⁻²			
C	$8.29 \cdot 10^4$ J mol ⁻¹ K			

density

d	5.44 g cm ⁻³	$T = 298$ K		34K
-----	-------------------------	-------------	--	-----

melting temperature

T_m	824°C		congruent melting	79A
-------	-------	--	-------------------	-----

sound velocity

v	$3.4 \cdot 10^5 \text{ cm s}^{-1}$	$T = 298 \text{ K}$	$v = 1.67 \text{ MHz}$	70B
-----	------------------------------------	---------------------	------------------------	-----

isothermal compressibility

κ_{av}	$1.428 \cdot 10^{-12} \text{ cm}^2 \text{ dyn}^{-1}$	$T = 295 \text{ K}$		73K
---------------	--	---------------------	--	-----

Transport properties

electrical conductivity

σ	$4 \cdot 10^2 \text{ } \Omega^{-1} \text{ cm}^{-1}$	$T = 298 \text{ K}$	within the layers?	70B
----------	---	---------------------	--------------------	-----

For dependence on temperature, see Fig. 20.3.2.

thermal conductivity

κ	$0.014 \text{ W cm}^{-1} \text{ K}^{-1}$	$T = 300 \text{ K}, \parallel c$		70S
	$0.087 \text{ W cm}^{-1} \text{ K}^{-1}$	$\perp c$		

hole mobility

$\mu_{H,p}$	$25 \dots 40 \text{ cm}^2/\text{Vs}$	$T = 300 \text{ K}$	Hall effect within the layers ($\perp c$ -axis)	96P
-------------	--------------------------------------	---------------------	--	-----

For dependence on temperature, see Fig. 20.3.3.

electron mobility : for dependence on temperature, see Fig. 20.3.4.

Optical properties

refractive index

n	2.7	$T = 300 \text{ K},$ $\lambda = 10 \text{ } \mu\text{m}$	multiple interference technique	70T
-----	-----	---	---------------------------------	-----

For spectral dependence, see Fig. 20.3.5.

dielectric constants, real part

(for spectral dependence, see Fig. 20.34)

$\varepsilon(\infty)$	6.97	$E \perp c$	reflection or transmission spectra	77B
$\varepsilon(\infty)$	7.29	$E \parallel c$		
$\varepsilon(0)$	9.66	$E \perp c$		
$\varepsilon(0)$	10.58	$E \parallel c$		

dielectric constant, imaginary part: for spectral dependence, see Fig. 20.3.6.

References to 20.3

- 34K Klemm W., v. Vogel, H. U.: Z. Anorg. Allg. Chem. 219 (1934) 45.
- 59F Fielding, P., Fischer, G., Mooser, E.: J. Phys. Chem. Solids 8 (1959) 434.
- 62F Fischer, G., Brebner, J. L.: J. Phys. Chem. Solids 23 (1962) 1363.
- 68U Uy, O. M., Muenow, D. W., Ficalora, F. J., Margrave, J. L.: Trans. Faraday Soc. 64 (1968) 2998.
- 70B Bhan, S., Schubert, K.: J. Less Common Met. 20 (1970) 229.
- 70S Spitzer, D. P.: J. Phys. Chem. Solids 31 (1970) 19.
- 70T Tatsuyama, C., Watanabe, Y., Hamaguchi, C.: J. Phys. Soc. Jpn. 29 (1970) 150.
- 71G Gandolfo, M., Gratton, E., Somma, F., Vecchia, P.: Phys. Status Solidi (b) 48 (1971) 729.
- 73K Kerimov, I. G., Aliev, N. G., Kurbanov, M. M.: Fiz. Tekh. Poluprovodn. 7 (1973) 2366; Sov. Phys. Semicond. (English Transl.) 7 (1974) 1575.
- 76M Mills, K. C.: High Temp. - High Pressure 8 (1976) 225.
- 77B Belenkii, G. L., Alieva, L. N., Nani, R. K.H., Salaev, E. Yu., Shteinshraiber, V. Ya.: Fiz. Tverd. Tela 19 (1977) 282; Sov. Phys. Solid State (English Transl.) 19 (1977) 162.
- 77G Giorgianni, U., Mondio, G., Perillo, P., Saitta, G., Vermigho, G.: J. Phys. (Paris) 38 (1977) 1293.
- 77L Leveque, G., Bertrand, Y., Robin, J.: J. Phys. C 10 (1977) 343.
- 78G Gouskov, L., Gouskov, A.: Solid State Comm. 28 (1978) 99.
- 78M Mamedov, K. K., Aldzhanov, M. A., Kerimov, I. G., Mekbtiev, M. I.: Fiz. Tverd. Tela 20 (1978) 42; Sov. Phys. Solid State (English Transl.) 20 (1978) 22.
- 79A Alapini, F., Flahaut, J., Guittard, M., Jaulmes, S., Julien-Pouzol, M.: J. Solid State Chem. 28 (1979) 309.
- 79C Camassel, J., Merle, P., Mathieu, H., Gouskov, A.: Phys. Rev. B19 (1979) 1060.
- 79J Julien-Pouzol, M., Jaulmes, S., Guittard, M., Alapini, F.: Acta Crystallogr. B 35 (1979) 2848.
- 79K Kuroda, N., Nishina, Y.: Phys. Rev. B 19 (1979) 1312.
- 96P Pal, S., Bose, D. N.: Solid State Commun. 97 (1996) 725.

Figures to 20.3

Fig. 20.3.1

GaTe. Energetic position of direct exciton ground state and of absorption band E_3 vs. temperature [79K].

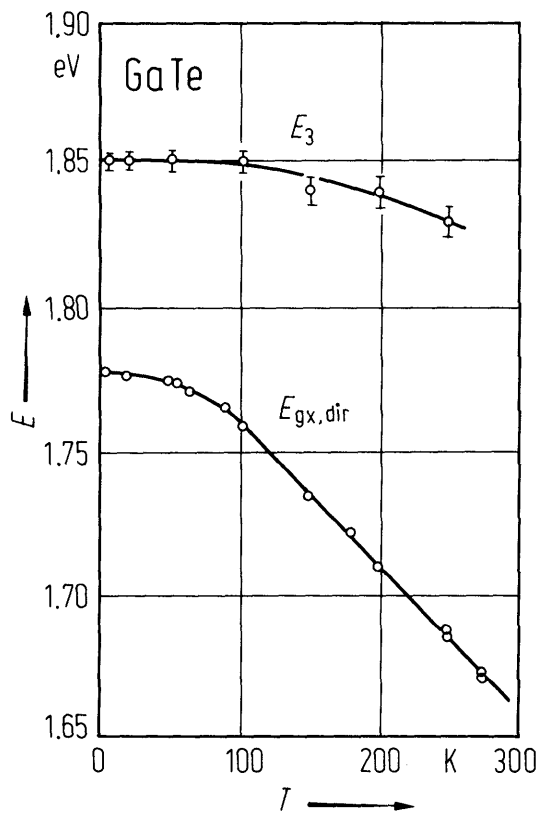


Fig. 20.3.2

GaTe. Electrical resistivity vs. inverse temperature. Full circles: resistivity parallel with the c -axis; other samples: resistivity along the layers [62F].

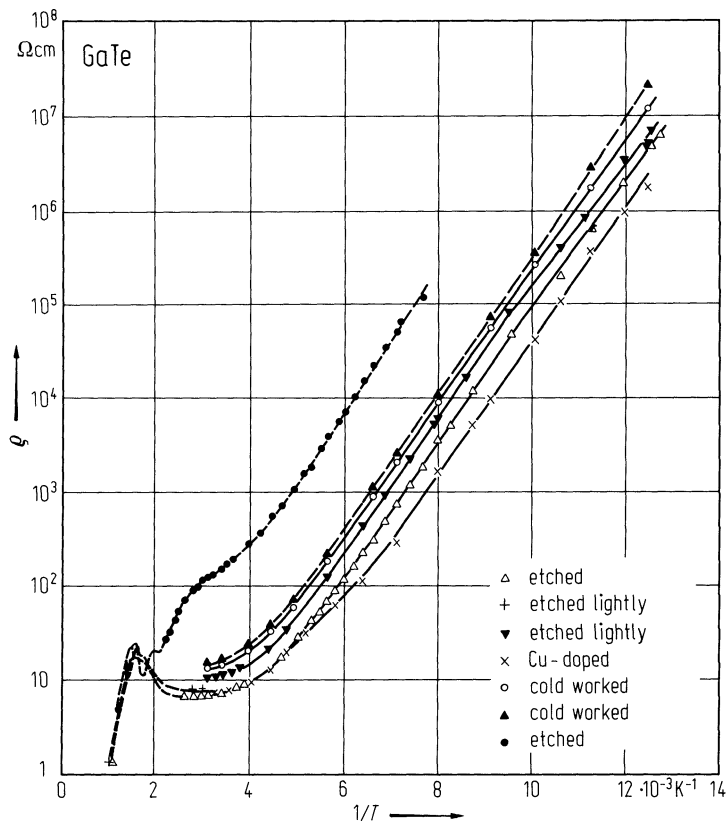


Fig. 20.3.3

GaTe. Hall mobility vs. temperature for various samples of p-type GaTe. $\mu_{p\perp}$: hole mobility along the layers; $\mu_{p\parallel}$: hole mobility perpendicular to the layers [78G].

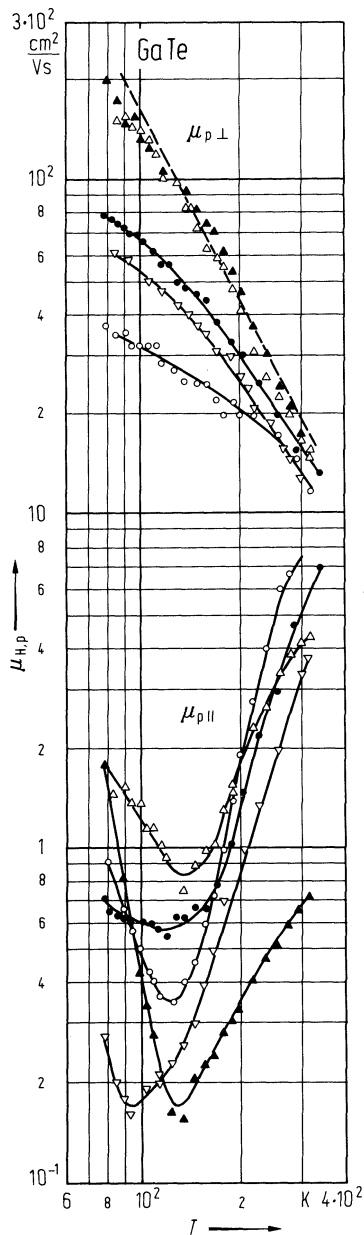


Fig. 20.3.4

GaTe. Electron mobility vs. temperature [59F]. Polycrystals with large single crystalline regions; $I \parallel$ layers.

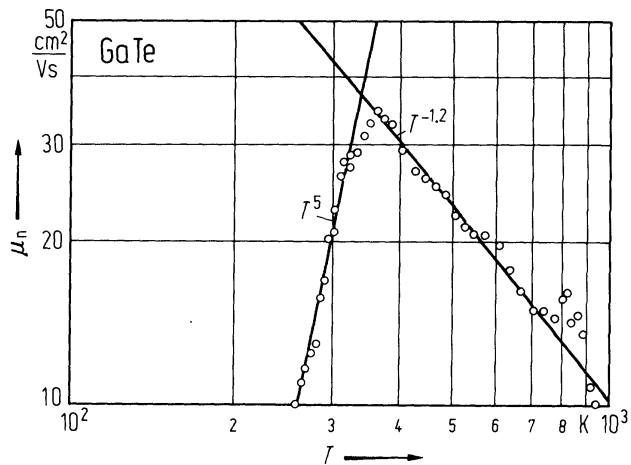


Fig. 20.3.5

GaTe. Refractive index and real part of dielectric constant at $T = 300$ K vs. photon energy [70T]. Illumination at normal incidence to the layers.

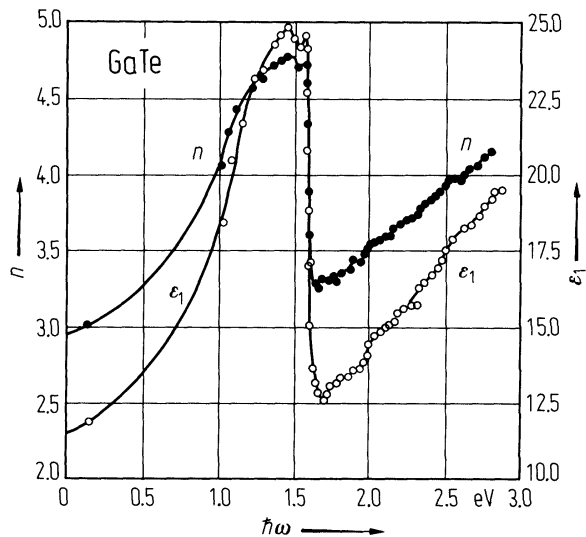
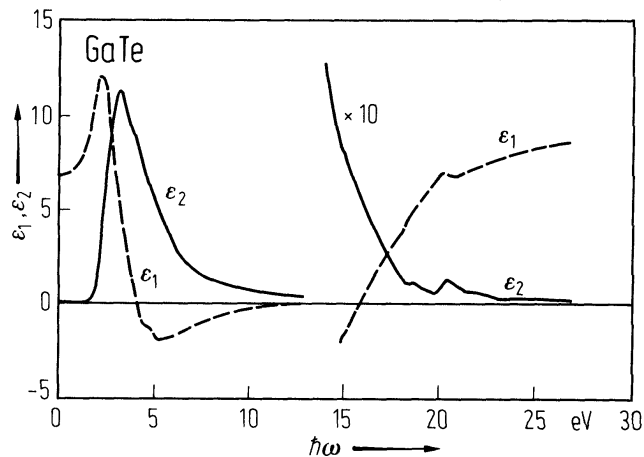


Fig. 20.3.6

GaTe. Real and imaginary parts of the dielectric constant vs. photon energy. $T=300$ K, unpolarized light, light incidence normal to the layers [77L].



20.4 Indium sulfide (InS)

Crystal structure

see section 20.0.

Electronic properties

InS is an indirect semiconductor with a band gap of about 1.9 eV at room temperature. The available experimental information is rather limited.

indirect energy gap

$E_{g,ind}$	1.896 (10) eV	$T = 300\text{ K}$	after linear extrapolation of absorption coefficient	77N
$dE_{g,ind}/dT$	$-7.9 \cdot 10^{-4}\text{ eV K}^{-1}$	$150\text{ K} < T < 330\text{ K}$	optical absorption,	77N

direct energy gap

$E_{g,dir}$	2.45 eV	$T = 290\text{ K}$		74N
-------------	---------	--------------------	--	-----

direct exciton gap

$E_{gx,dir}$	2.56 eV	$T = 4.2\text{ K}$	optical absorption (unpolarized radiation $\perp c$)	74N
--------------	---------	--------------------	---	-----

conduction band, effective mass

m_n	$0.4\ m_0$		Schottky-barrier, thermoionic emission	79T
-------	------------	--	--	-----

Lattice properties

lattice parameters

a	3.944 Å	$T = 295\text{ K}$	powder data, orthorhombic system	54S, 66D
b	4.447 Å			
c	10.648 Å			

linear thermal expansion coefficient :

for dependence on temperature for polycrystalline and single crystalline samples, see Fig. 20.4.1.

heat capacity

C_p	$47.80\text{ J mol}^{-1}\text{ K}^{-1}$	$T = 300\text{ K}$	calorimetric measurements	68C
-------	---	--------------------	---------------------------	-----

density

d	5.18 g cm^{-3}	$T = 298\text{ K}$		34K
-----	-------------------------	--------------------	--	-----

isothermal compressibility

κ_{\perp}	$4.060 \cdot 10^{-12}\text{ cm}^2\text{ dyn}^{-1}$	$T = 280\text{ K}$	$\perp c$	73A
κ_{\parallel}	$6.07 \cdot 10^{-12}\text{ cm}^2\text{ dyn}^{-1}$		$\parallel c$	

Transport properties

electrical conductivity : for dependence on temperature of the electrical resistivity, see Fig. 20.4.2.

electron mobility

$\mu_{H,n}$	$50\text{ cm}^2/\text{V s}$	$T = 300\text{ K}, i \perp c$	n-type	77N
-------------	-----------------------------	-------------------------------	--------	-----

Optical properties

dielectric constant, real part

$\varepsilon(\infty)$	15.2	$T = 295 \text{ K}$	IR reflectivity	79G
-----------------------	------	---------------------	-----------------	-----

References to 20.4

- 34K Klemm W., v. Vogel, H. U.: Z. Anorg. Allg. Chem. 219 (1934) 45.
- 54S Schubert, K., Dörre, E., Günzel E.: Naturwiss. 41 (1954) 448.
- 66D Duffin, W. J., Hogg, J. H. C.: Acta Crystallogr. 20 (1966) 566.
- 69C Cruceana, F., Sladaru, St.: J. Mater. Sci. 4 (1969) 410.
- 73A Alicy, N. C., Kerimov, I. C., Kurbanov, M. M.: Fiz. Tverd. Tela 14 (1972) 3707; Sov. Phys. Solid State (English Transl.) 14 (1973) 3106.
- 74N Nishino, T., Takakura, H., Hamakawa, Y.: Jpn. J. Appl. Phys. 13 (1974) 1921.
- 77N Nishino, T., Hamakawa, Y.: Jpn. J. Appl. Phys. 16 (1977) 1291.
- 79G Gasanly, N. M., Gakhramanov, N. F., Dzhabadov, B. M., Tagirov, V. I., Vinogradov, E. A.: Phys. Status Solidi (b) 95 (1979) K89.
- 79T Takanabe, K., Nishino, T., Hamakawa, Y.: Jpn. J. Appl. Phys. 18 (1979) 107.

Figures to 20.4

Fig. 20.4.1

InS. Linear thermal expansion coefficient vs. temperature. 1, α_{\parallel} parallel with the c -axis; 2, α_{\perp} along the layers; 3, polycrystalline sample [73A].

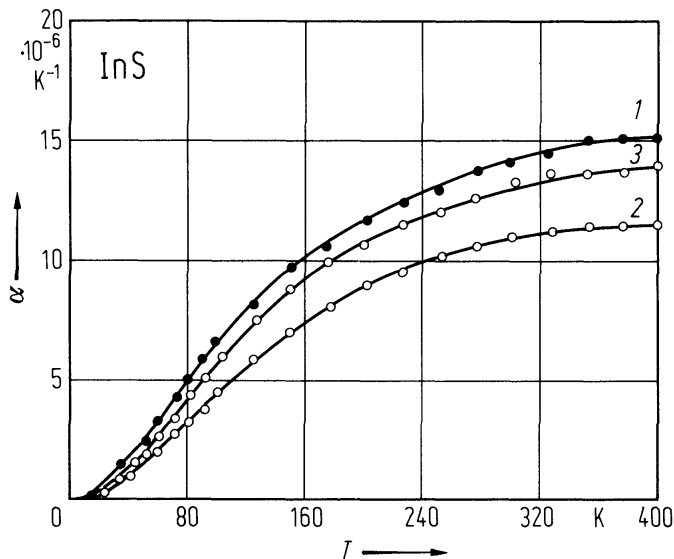
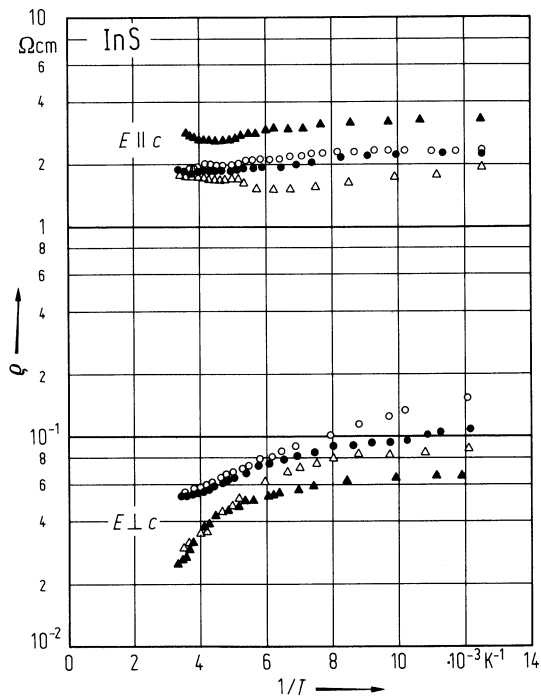


Fig. 20.4.2

InS. Resistivity vs. inverse temperature for several crystals grown from the melt. $E \parallel c$, resistivity parallel with the c -axis; $E \perp c$, resistivity perpendicular to the c -axis [77N].



20.5 Indium selenide (InSe)

Crystal structure

see section 20.0.

Electronic properties

band structure, Fig. 20.0.6, (hexagonal) Brillouin zone: Fig. 20.0.3.

The band structure of InSe is very similar to that of GaSe, however, the dispersion of the energy bands in the $k_z = 0$ plane as well as parallel to the k_z -axis is smaller than for GaSe. InSe is an indirect semiconductor. The position of the band extrema within the Brillouin zone is somewhat uncertain.

indirect energy gap

$E_{g,ind}$	1.305 eV	$T = 5$ K	X transition (?) stimulated emission spectra	92A
	1.172 eV	$T = 300$ K	photoconductivity	77S

temperature coefficient of indirect energy gap

$dE_{g,ind}/dT$	$-4.2 \cdot 10^{-4}$ eV K $^{-1}$	$85 \text{ K} < T < 250 \text{ K}$	cathodoluminescence	76E
-----------------	-----------------------------------	------------------------------------	---------------------	-----

indirect exciton transition energy

$E_{gx,ind}$	1.269(1) eV	$T = 77$ K, $E \parallel c$	optical absorption	76B
--------------	-------------	-----------------------------	--------------------	-----

binding energy of indirect exciton

E_b	76 meV		optical absorption, two-dimensional ($n+1/2$) $^{-2}$ Rydberg series assumed for indirect exciton, γ -polytype	79I
	20 (4) meV		as above, β -polytype	76B

binding energy of direct exciton ground state

E_b	14.4 meV	$T = 4.5$ K	optical absorption spectra	93G
-------	----------	-------------	----------------------------	-----

direct energy gap

$E_{g,dir}(\Gamma_{4v}^- - \Gamma_{3c}^+)$	1.3525 eV	$T = 1.6$ K	optical absorption	78C
	1.2635 eV	$T = 293$ K		

temperature coefficient of direct energy gap

$dE_{g,dir}/dT$	$-3.7 \cdot 10^{-4}$ eV K $^{-1}$	$100 \text{ K} < T < 300 \text{ K}$	optical absorption see Fig. 20.5.1	78C
a	1352.5 meV	$0 < T < 300 \text{ K}$	optical absorption	78C
b	65 meV		a, b, c are parameters in empirical relation	
c	162 K		$E_{g,dir} = a - b/(\exp(c/T) - 1)$	

direct exciton transition energy

$E_{gx,dir}(1S)$	1.3383 eV	$T = 1.6$ K	optical absorption	78C
	1.257 eV	$T = 300$ K	optical absorption, β -polytype	68A

temperature coefficient of direct exciton gap

$dE_{gx,dir}/dT$	$-3.6 \cdot 10^{-4}$ eV K $^{-1}$	$100 \text{ K} < T < 300 \text{ K}$	optical absorption	78C
------------------	-----------------------------------	-------------------------------------	--------------------	-----

binding energy of direct exciton ground state

$E_b(1S)$	13.7(15) meV	$T = 4.2$ K	modulated magneto-optical absorption	78M
-----------	--------------	-------------	--------------------------------------	-----

conduction band, effective masses

m_n	0.143 m_0	$T = 300$ K, $\parallel c$	resonance Raman scattering	80K2
	0.156 m_0	$\perp c$		

valence band, effective masses

m_p	0.50 m_0	$T = 300$ K, $\perp c$	resonance Raman scattering	80K2
	1.54 m_0	$\parallel c$		

Lattice properties**lattice parameters**

a	4.002 Å	$T = 300$ K	γ -type, 3R (single crystal data)	80R
c	24.946 Å			
a	4.005 Å		β -type 2H (polycrystal data)	79P
c	16.640 Å			
a	4.04 Å		β -type 2H (thin film)	58S
c	16.90 Å			
a	4.00 Å		ϵ -type 2H (vapor grown single crystal)	81C
c	16.70 Å			

linear thermal expansion coefficient

dependence on the temperature and anisotropy, see Fig. 20.5.2.

Debye temperature

Θ_D	190 K	$T = 295$ K	elastic wave velocity	77I
------------	-------	-------------	-----------------------	-----

heat capacity

C_p	50.31 J mol ⁻¹ K ⁻¹	$T = 55...298$ K	calorimetric measurements	67M
-------	---	------------------	---------------------------	-----

density

d	5.55 g cm ⁻³	$T = 295^\circ\text{C}$		34K
-----	-------------------------	-------------------------	--	-----

melting temperature

T_m	933 K			74M
-------	-------	--	--	-----

second order elastic moduli

c_{44}	1.17(10)·10 ¹¹ dyn cm ⁻²	$T = 295$ K	ultrasonic measurements	83G
c_{12}	2.70(9)·10 ¹¹ dyn cm ⁻²			
c_{13}	3.0(2)·10 ¹¹ dyn cm ⁻²			
c_{33}	3.60(3)·10 ¹¹ dyn cm ⁻²			
c_{11}	7.30(5)·10 ¹¹ dyn cm ⁻²			

isothermal compressibility

κ_\perp	7.33·10 ⁻¹³ cm ² dyn ⁻¹	$T = 320$ K, $\perp c$		73A
κ_\parallel	10.00·10 ⁻¹³ cm ² dyn ⁻¹	$T = 320$ K, $\parallel c$		

Transport properties

electrical conductivity

For dependence on temperature, see Fig. 20.5.3.

σ_{\perp}	$2.2 \cdot 10^{-5} \Omega^{-1} \text{ cm}^{-1}$	$T = 298 \text{ K}$	dark conductivity Te – Au contacts	76I
------------------	---	---------------------	---------------------------------------	-----

thermal conductivity

κ	$37 \text{ W cm}^{-1} \text{ K}^{-1}$	$\parallel c$		70S
	$120 \text{ W cm}^{-1} \text{ K}^{-1}$	$\perp c$		

electron mobility

$\mu_{n\perp}$	$230 \text{ cm}^2/\text{Vs}$	$T = 295 \text{ K}$	Bridgman grown crystal ($n = 8.6 \cdot 10^{15} \text{ cm}^{-3}$)	92J
μ'_n	$1.3 \cdot 10^6 \text{ cm}^2 \text{ K}^{1.6}/\text{Vs}$	$220 \text{ K} < T < 300 \text{ K}$	μ'_n is a parameter in the empirical relation $\mu_n = \mu'_n T^{-1.6} (I \perp c, B \parallel c)$	81S

hole mobility

μ'_p	$1.4 \cdot 10^7 \text{ cm}^2 \text{ K}^{2.3}/\text{Vs}$	$220 \text{ K} < T < 300 \text{ K}$	μ'_p is a parameter in the empirical relation $\mu_p = \mu'_p T^{-2.3} (I \perp c, B \parallel c)$	81S
----------	---	-------------------------------------	---	-----

Optical properties

ordinary refractive index

n_{\perp}	2.97	$T = 300 \text{ K},$ $h\nu = 1.8 \text{ eV},$ $E \perp c$	interference fringes	80K1
-------------	------	---	----------------------	------

For spectral dependence, see Fig. 20.5.4.

dielectric constants, real part

(for spectral dependence, see Fig. 20.4.5).

$\varepsilon(\infty)$	4.9	$E \parallel c, T = 295 \text{ K}$	IR reflectivity	79A1, 79A2
$\varepsilon(0)$	5.4	$E \parallel c$		
$\varepsilon(\infty)$	6.2	$E \perp c$		
$\varepsilon(0)$	8.6	$E \perp c$		

dielectric function, imaginary part : for spectral dependence, see Fig. 20.4.5.

References to 20.5

- 34K Klemm W., v. Vogel, H. U.: Z. Anorg. Allg. Chem. 219 (1934) 45.
- 54D Damon, R. W., Redington, R. W.: Phys. Rev. 96 (1954) 1498.
- 58S Semiletov, S. A.: Kristallografia 3 (1958) ; Sov. Phys. Crystallogr. (English Transl.) 3 (1958) 292.
- 67M Mamedov, K. K., Kerimov, I. G., Kostryukov, U. N., Guseinov, G. D.: Zh. Fiz. Khim. 41 (1967) 1300.
- 68A Andriyashik, M. V., Yusakhnovskii, M., Timofeev, V. B., Yakimova, A. S.: Phys. Status Solidi 28 (1968) 277.
- 70S Spitzer, D. P.: J. Phys. Chem. Solids 31 (1970) 19.
- 73A Alicy, N. C., Kerimov, I. C., Kurbanov, M. M.: Fiz. Tverd. Tela 14 (1972) 3707; Sov. Phys. Solid State (English Transl.) 14 (1973) 3106.
- 74M Mills, K. C.: Thermodynamic Data for Inorganic Sulphides, Selenides and Tellurides, Butterworth, London, 1974.
- 76B Bakumenko, V. L., Kovalyuk, Z. D., Kurbatov, L. N., Chishko, V. F.: Fiz. Tekh. Poluprovodn. 10 (1976) 1045; Sov. Phys. Semicond. (English Transl.) 10 (1976) 621.
- 76E Egorov, V. V., Kurbatov, L. N., Soroko-Novitskii, N. V.: Fiz. Tekh. Poluprovodn. 10 (1976) 703; Sov. Phys. Semicond. (English Transl.) 10 (1976) 418.
- 76I Imai, K., Abe, Y.: J. Electrochem. Soc. Jpn. 123 (1976) 576.
- 77G Grasso, V., Perillo, P.: Solid State Commun. 21 (1977) 323.
- 77I Iskender-Zade, Z. A., Faradzhev, V. D., Agaev, A. I.: Fiz. Tverd. Tela 19 (1977) 851; Sov. Phys. Solid State (English Transl.) 19 (1977) 492.
- 77S Segura, A., Besson, J. M., Chevy, A., Martin, M. S.: Nuovo Cimento B 38 (1977) 345.
- C1 Camassel, J., Merle, P., Mathieu, H.: Phys. Rev. B 17 (1978) 4718.
- 78D Depeursinge, Y., Doni, E., Girlanda, R., Baldereschi, A., Maschke, K.: Solid State Commun. 27 (1978) 1449.
- 78M Merle, J. C., Bartiroma, R., Borsella, E., Piacentini, M., Savoia, A.: Solid State Commun. 28 (1978) 251.
- 79A1 Alieva, L. N., Belenkii, G. L., Reshina, I. I., Salaev, E. Yu., Shteinshraiber, V. Ya.: Fiz. Tverd. Tela 21 (1979) 155; Sov. Phys. Solid State (English Transl.) 21 (1979) 90.
- 79A2 Allakhverdiev, K. R., Babaev, S. S., Salaev, E. Yu., Tagyev, M. M.: Phys. Status Solidi (b) 96 (1979) 177.
- 79I Ikari, T., Koga, Y.: J. Phys. Soc. Jpn. 47 (1979) 1017.
- 79P Popovic, S., Tonejc, A., Grzeta-Plenkovic, B., Celusta, B., Trojko, R.: J. Appl. Crystallogr. 12 (1979) 416.
- 80K1 Kuroda, N., Munataka, I., Nishina, Y.: Solid State Commun. 33 (1980) 687.
- 80K2 Kuroda, N., Nishina, Y.: Solid State Commun. 34 (1980) 481.
- 80R Rigault, J., Rimsky, A., Kuhn, A.: Acta Crystallogr. B 36 (1980) 916.
- 81C Chevy, A.: J. Cryst. Growth 51 (1981) 157.
- 81S Shigetomi, S., Ikari, T., Koga, Y., Shigetomi, S.: Jpn. J. Appl. Phys. 20 (1981) L343.
- 83G Gatulle, M., Fischer, M., Chevy, A.: Phys. Status Solidi (b) 119 (1983) 327.
- 92A Abdullaev, G. B., Godzhaev, I. O., Kakhramanov, N. B., Suleimanov, R. A.: Fiz. Tverd. Tela 34 (1992) 75; Sov. Phys. Solid State (English Transl.) 34 (1992) 39.
- 92J Julien, C., Eddrief, M., Balkanski, M., Chevy, M.: Phys. Rev. B46 (1992) 2435.
- 93G Gnadenko, Yu. P., Zhirko, Yu. I.: Phys. Status Solidi (b) 180 (1993) 147.

Figures to 20.5

Fig. 20.0.3

Brillouin zone for the hexagonal lattice. g_1, g_2, g_3 : reciprocal basis vectors; $g_1 \parallel k_x, g_3 \parallel k_z$.

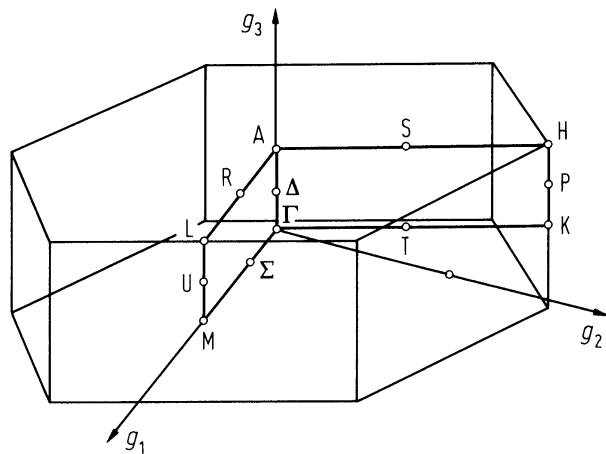


Fig. 20.0.6

InSe. Empirical pseudopotential band structure for the ϵ -polytype [78D].

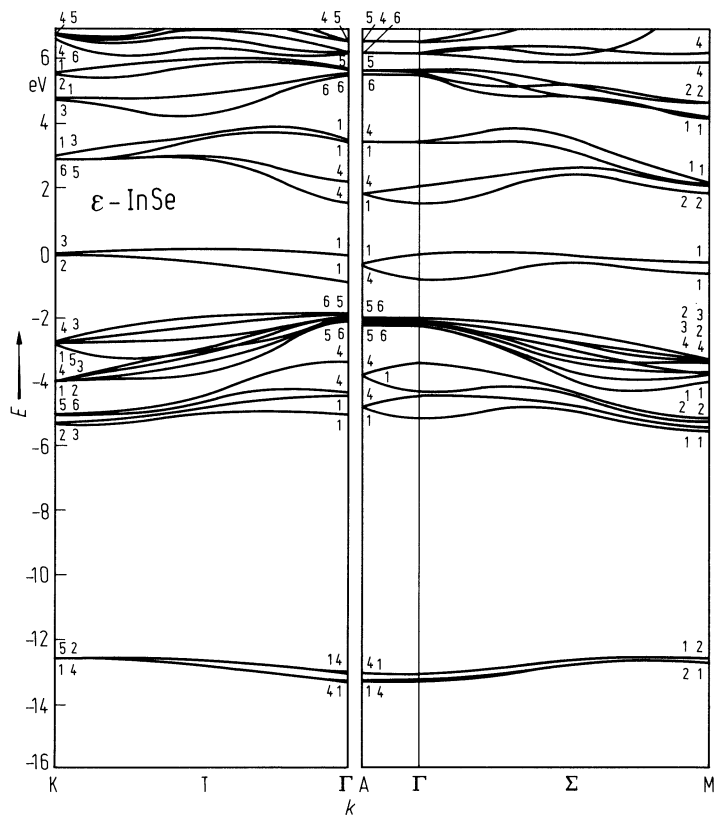


Fig. 20.5.1

InSe. Energetic position of the direct exciton ground state ($n = 1$), of the first excited state ($n = 2$), and of the direct band edge $E_{g,dir}$ vs. temperature [78C].

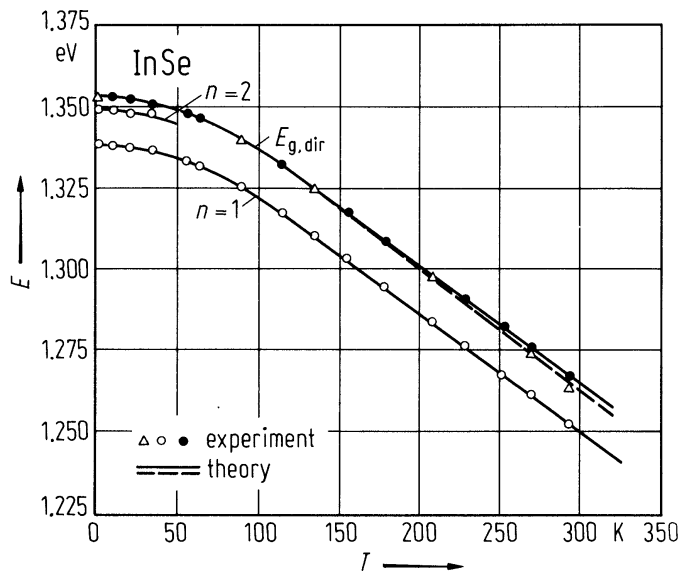


Fig. 20.5.2

InSe, InTe. Linear thermal expansion coefficient vs. temperature. InSe: 1, parallel with the c -axis; 2, perpendicular to the c -axis; InTe(tetr.): 3, parallel with the c -axis; 4, perpendicular to the c -axis [73A].

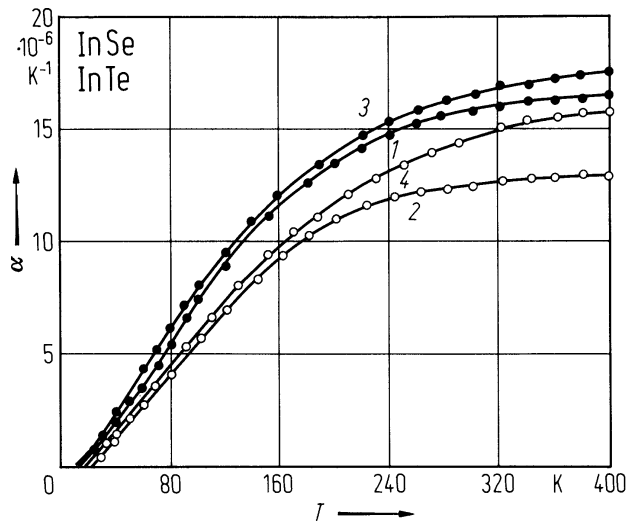


Fig. 20.5.3

InSe. Electrical conductivity vs. inverse temperature. Circles: conductivity perpendicular to the c -axis (different samples); triangles: conductivity parallel with the c -axis. Activation energy is indicated [54D].

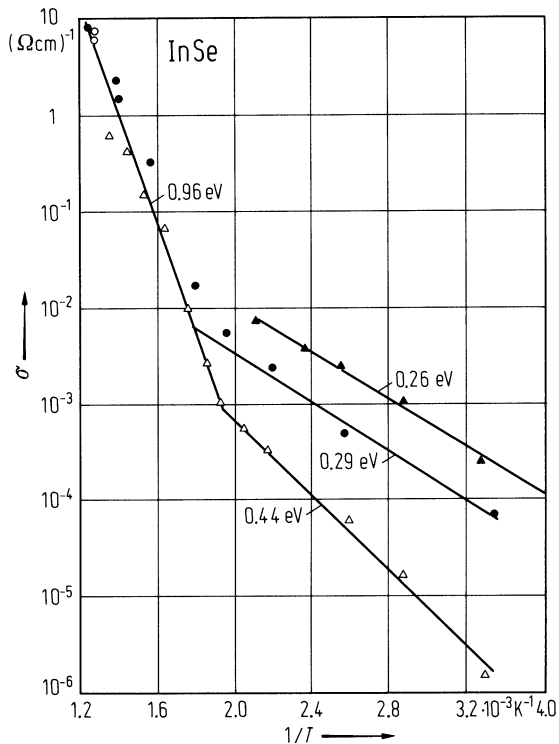


Fig. 20.5.4

InSe. Real (n), imaginary (k) part of the refractive index and effective number of electrons (N_{eff}) involved in the optical transitions for $E \perp c$ vs. photon energy [77G].

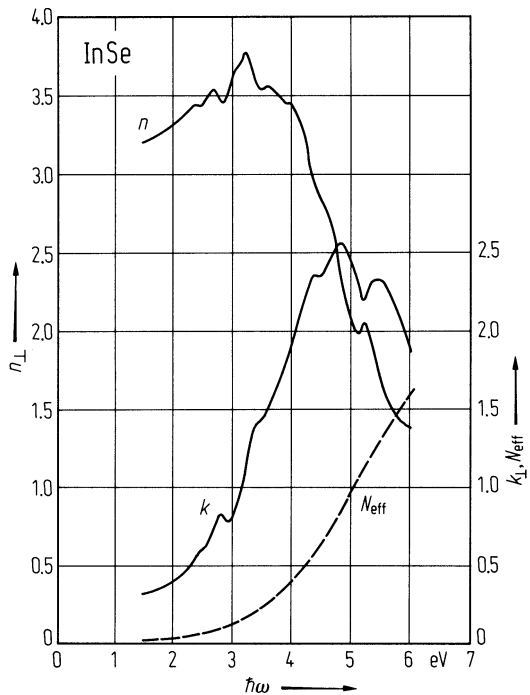
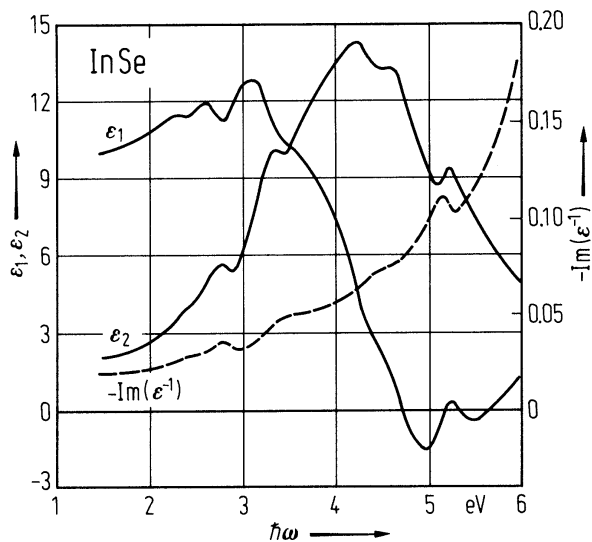


Fig. 20.5.5

InSe. Real (ϵ_1), imaginary (ϵ_2) parts of the dielectric constant for $E \perp c$ and energy loss function $-\text{Im}(\epsilon^{-1})$ vs photon energy [77G].



20.6 Indium telluride (InTe)

Crystal structure

see section 20.0.

Electronic properties

In the TlSe-type structure (space group D_{4h}^{18}) InTe is a semiconductor.

direct energy gap

$E_{g,dir}$	1.160(2) eV	$T = 300\text{K}$	optical absorption	96P
-------------	-------------	-------------------	--------------------	-----

conduction band, effective mass

m_n	$0.09\ m_0$		density of states mass	70G
-------	-------------	--	------------------------	-----

valence band, effective masses

$m_{p }$	$0.125\ m_0$	$\parallel\ c\text{-axis}$	thermoelectric power vs. temperature,	96P,
$m_{p\perp}$	$0.765\ m_0$	$\perp\ c\text{-axis}$	infrared reflectivity	81R
m_p	$0.26\ m_0$		density of states mass	70G

Lattice properties

lattice parameters

a	$8.454\ \text{\AA}$	$T = 300\ \text{K}$	TlSe-type structure, needle-like	76H
c	$7.152\ \text{\AA}$		crystals	

linear thermal expansion coefficient

α	$1.99\cdot 10^{-5}\ \text{K}^{-1}$	$297 \leq T \leq 505\ \text{K}$	$\parallel\ a\text{-axis}$, tetragonal InTe	85C
	$1.9\cdot 10^{-5}\ \text{K}^{-1}$		$\parallel\ c\text{-axis}$	

For dependence on temperature for tetragonal InTe, in the range 13...400 K, perpendicular and parallel to the c -axis, see Fig. 20.6.1.

heat capacity

C_p	$48.22\ \text{J mol}^{-1}\ \text{K}^{-1}$	$T = 300\ \text{K}$	calorimetric measurements	72M
-------	---	---------------------	---------------------------	-----

density

d	$6.29\ \text{g cm}^{-3}$	$T = 294\ \text{K}$		34K
-----	--------------------------	---------------------	--	-----

melting temperature

T_m	$965\ \text{K}$			74M
-------	-----------------	--	--	-----

wavenumbers of lattice vibration modes at Γ

($\Gamma = A_{1g} + 2A_{2g} + B_{1g} + 2B_{2g} + 3E_g + B_{1u} + 3A_{2u} + 4E_u$)

$\bar{\nu}(E_g)$	$46\ \text{cm}^{-1}$	$T = 295\ \text{K}$	Raman active	80N
$\bar{\nu}(B_{1g})$	$86\ \text{cm}^{-1}$		Raman active	
$\bar{\nu}(E_u)$	$100\ \text{cm}^{-1}$	$T = 295\ \text{K}$	transverse optic, $E \perp c$	81R
$\bar{\nu}(A_{2u})$	$117\ \text{cm}^{-1}$		transverse optic, $E \parallel c$	
$\bar{\nu}(A_{1g})$	$126\ \text{cm}^{-1}$		Raman active	80N
$\bar{\nu}(E_g)$	$139\ \text{cm}^{-1}$		Raman active	
$\bar{\nu}(A_{2u})$	$142\ \text{cm}^{-1}$		transverse optic, $E \parallel c$	81R

isothermal compressibility

κ_{\perp}	$1.214 \cdot 10^{-12} \text{ cm}^2 \text{ dyn}^{-1}$	$T = 320 \text{ K}, \perp c$	73A
κ_{\parallel}	$1.357 \cdot 10^{-12} \text{ cm}^2 \text{ dyn}^{-1}$	$T = 320 \text{ K}, \parallel c$	

bulk modulus

B	465(5) kbar	$p = 0$	tetragonal structure	85C
-----	-------------	---------	----------------------	-----

Transport properties

electrical conductivity

σ	$60 \Omega^{-1} \text{ cm}^{-1}$	$T = 293 \text{ K}$	polycrystal	76D
	$2.5 \dots 4 \cdot 10^{-2} \Omega^{-1} \text{ cm}^{-1}$	$T = 298 \text{ K}$	evaporated thin films	

For dependence on temperature, see Fig. 20.6.2

thermal conductivity

κ	$0.018 \text{ W cm}^{-1} \text{ K}^{-1}$	$T = 300 \text{ K}, \parallel c$		70G
----------	--	----------------------------------	--	-----

hole mobility

μ_p	$150 \text{ cm}^2/\text{V s}$	$T = 300 \text{ K}$		70G
$\mu_{H,p\parallel}$	$50 \dots 60 \text{ cm}^2 \text{ V}^{-1} \text{ s}^{-1}$	$T = 300 \text{ K}$	Bridgman grown crystal,	91P
$\mu_{H,p\perp}$	$10 \dots 15 \text{ cm}^2 \text{ V}^{-1} \text{ s}^{-1}$		$(p = (2.1 \dots 3.1) \cdot 10^{18} \text{ cm}^{-3})$	

Optical properties

dielectric constant

$\varepsilon(\infty)$	14.0	$E \perp c$	IR reflectivity	81R
	14.7	$E \parallel c$		
ε_{\perp}	11.5		$E \perp c$, Al Schottky barrier at 1 MHz	96P
ε_{\parallel}	12.8		$E \parallel c$	

References to 20.6

- 34K Klemm W., v. Vogel, H. U.: Z. Anorg. Allg. Chem. 219 (1934) 45.
57S Sugaike, S.: Mineral. J. 2 (1957) 63.
70G Guseinov, G. D., Abduliayev, G. B., Bidzinova, S. M., Seidov, F. M., Ismailov, M. Z., Pashayev, A. M.: Phys. Lett. A 33 (1970) 421.
72M Mamedov, K. K., Kerimov, I. C., Mekhtiev, M. I., Masimov, E. A.: Izv. Akad. Nauk. SSSR, Neorg. Mater. 8 (1972) 2096; Bull. Acad. Sci. USSR, Inorg. Mater. (English Transl.) 8 (1972) 1843.
73A Alicy, N. C., Kerimov, I. C., Kurbanov, M. M.: Fiz. Tverd. Tela 14 (1972) 3707; Sov. Phys. Solid State (English Transl.) 14 (1973) 3106.
74M Mills, K. C.: Thermodynamic Data for Inorganic Sulphides, Selenides and Tellurides, Butterworth, London, 1974.
76D Dovletov, K., Erniyazov, Kh., Malkova, A. S.: Izv. Akad. Nauk SSSR, Neorg. Mater. 12 (1976) 1964; Bull. Acad. Sci. USSR, Inorg. Mater. (English Transl.) 12 (1976) 1613.
76H Hogg, J. H. C., Sutherland, H. H.: Acta Crystallogr. B32 (1976) 2689.
80N Nizametdinova, M. A.: Phys. Status Solidi (b) 97 (1980) K9.
81R Riede, V., Neumann, H., Sobotta, H., Levy, F.: Solid State Commun. 38 (1981) 71.
85C Chattopadhyay, T., Santandrea, R. P., von Schnering, H. G.: J. Phys. Chem. Solids 46 (1985) 351.
91P Pal, S., Bose, D. N., Asokan, S., Gopal, E. S. R.: Solid State Comm. 80 (1981) 753.
96P Pal, S., Bose, D. N.: Solid State Commun. 97 (1996) 725.

Figures to 20.6

Fig. 20.6.1

InSe, InTe. Linear thermal expansion coefficient vs. temperature. InSe: 1, parallel with the c -axis; 2, perpendicular to the c -axis; InTe(tetr.): 3, parallel with the c -axis; 4, perpendicular to the c -axis [73A].

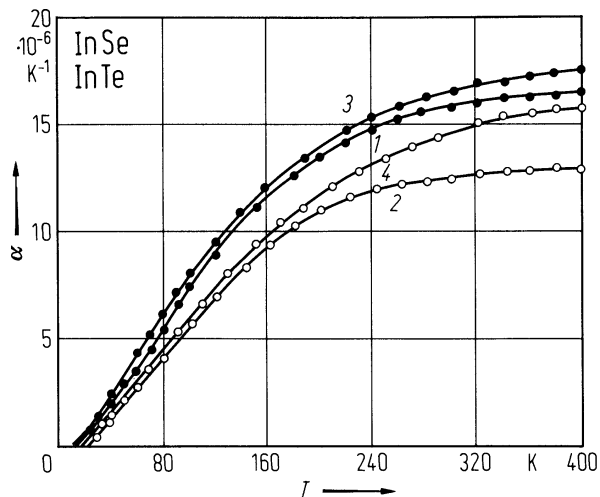
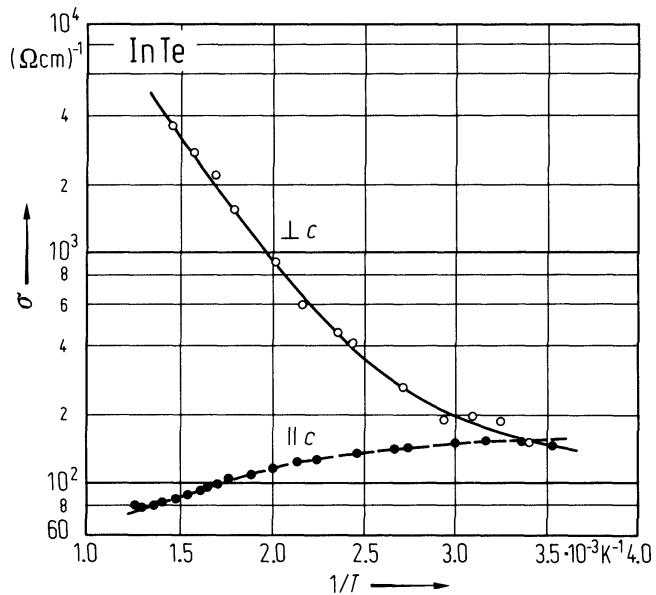


Fig. 20.6.2

InTe. Electrical conductivity vs. inverse temperature [57S].



20.7 Thallium sulfide (TlS)

Crystal structure

see section 20.0.

Electronic properties

indirect energy gap

$E_{g,\text{ind}}$	1.36 eV	$T = 300 \text{ K}, E \perp c$	optical absorption	71I
	1.37 eV	$T = 300 \text{ K}, E \parallel c$		

direct energy gap

$E_{g,\text{dir}}$	1.50 eV	$E \perp c$	optical absorption	71I
	1.57 eV	$E \parallel c$		

conduction band, effective mass

m_n	$0.07 m_0$	density of states mass	70G
-------	------------	------------------------	-----

valence band, effective mass

m_p	$0.11 m_0$	density of states mass	70G
-------	------------	------------------------	-----

Lattice properties

lattice parameters

a	7.787 \AA	$T = 295 \text{ K}$	TlSe type	78C
c	6.807 \AA			

density

d	7.60 g cm^{-3}	$T = 300 \text{ K}$	picnometric measurement	70G
-----	--------------------------	---------------------	-------------------------	-----

Debye temperature

Θ_D	106 K	$T = 0 \text{ K}$		84A
------------	-----------------	-------------------	--	-----

heat capacity

C_p	$209.9 \text{ J kg}^{-1} \text{ K}^{-1}$	$T = 298.15 \text{ K}$		84A
-------	--	------------------------	--	-----

Transport properties

electrical conductivity

for dependence on temperature of the electrical resistivity $\rho = 1/\sigma$, see Fig. 20.7.1.

hole mobility

μ_p	$20 \text{ cm}^2/\text{V s}$	$T = 300 \text{ K}$		70G
---------	------------------------------	---------------------	--	-----

mobility ratio

b	0.4	$T = 300 \text{ K}$		70G
-----	-------	---------------------	--	-----

thermal conductivity

κ	$0.032 \text{ W cm}^{-1} \text{ K}^{-1}$	$T = 300 \text{ K}, \perp c$		70G
----------	--	------------------------------	--	-----

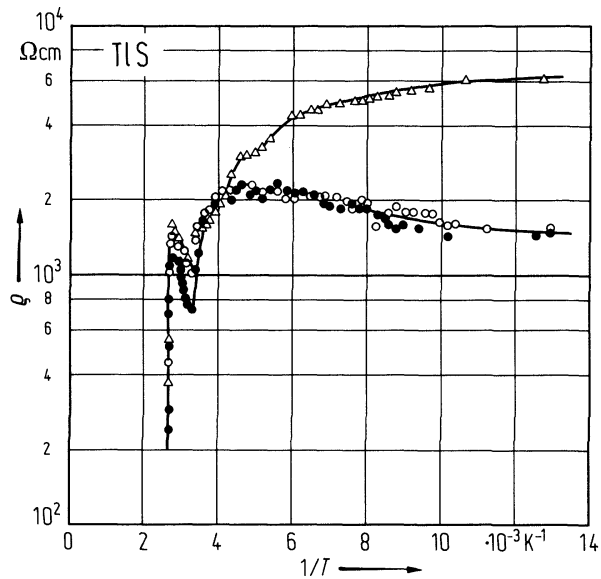
References to 20.7

- 70G Guseinov, G. D., Abduliayev, G. B., Bidzinova, S. M., Seidov, F. M., Ismailov, M. Z., Pashayev, A. M.: Phys. Lett. A 33 (1970) 421.
- 71I Itoga, R. S., Kannewurf, C. R.: J. Phys. Chem. Solids 32 (1971) 1099.
- 78C Cervinka, L., Hruby, A.: J. Non-Cryst. Solids 30 (1978) 191.
- 84A Abdullaeva, S. G., Abdullaev, A. M., Mamedov, K. K., Mamedov, N. T.: Fiz. Tverd. Tela 26 (1984) 618; Sov. Phys. Solid State (English Transl.) 26 (1984) 375.

Figures to 20.7

Fig. 20.7.1

TlS. Electrical resistivity vs. inverse temperature (various samples) [711]. Single crystals, $I \parallel c$.



20.8 Thallium selenide (TlSe)

Crystal structure

see section 20.0.

Electronic properties

band structure : Fig. 20.0.10.

indirect energy gap

$E_{\text{g,ind}}(\text{T}_3\text{-D}_1)$	0.73 eV	$T = 300$ K	$E \perp, \parallel c$, optical absorption	83V
---	---------	-------------	---	-----

direct energy gap

$E_{\text{g,dir}}(T_3\text{-}T_4)$	1.095 eV	$T = 300$ K	$E \perp, \parallel c$, optical absorption	83V
------------------------------------	----------	-------------	---	-----

direct excitonic gap

$E_{\text{g,dir}}$	0.745(10) eV	$T = 300$ K	indirect band gap of 0.74...0.77 eV
--------------------	--------------	-------------	-------------------------------------

temperature coefficient of direct excitonic gap

$dE_{\text{gX,dir}}/dT$	$-2.1 \cdot 10^{-4} \text{ eV K}^{-1}$	$90 \text{ K} < T < 300 \text{ K}$	optical absorption	75A
-------------------------	--	------------------------------------	--------------------	-----

conduction band, effective mass

m_{n}	$0.27\ m_0$	$\parallel c\text{-axis}$	81G
	$0.35\ m_0$	$\perp c\text{-axis}$	

valence band, effective mass

m_p	$0.32\ m_0$	$\perp\ c\text{-axis}$	81G
	$4.4\ m_0$	$\parallel\ c\text{-axis}$	

Lattice properties

lattice parameters

c	7.00 Å	$T = 300$ K	tetragonal	76M
a	8.02 Å			

linear thermal expansion coefficients

α_{\parallel}	$0.96 \cdot 10^{-5} \text{ K}^{-1}$	$T = 297 \text{ K}, \parallel c,$	72S
α_{\perp}	$3.16 \cdot 10^{-5} \text{ K}^{-1}$	along the layers	

volume thermal expansion coefficient

β	$7.28 \cdot 10^{-5} \text{ K}^{-1}$	$T = 288 \dots 388 \text{ K}$	72S
---------	-------------------------------------	-------------------------------	-----

Debye temperature

Θ_{H} -dependence on temperature in the range 60...135 K, see Fig. 20.8.1.

heat capacity

C_p	$50.23 \text{ J K}^{-1} \text{ mol}^{-1}$	$T = 298 \text{ K}$	For dependence on temperature, see Fig. 20.8.1	67M
-------	---	---------------------	--	-----

density

d	8.15 g cm ⁻³	$T = 25^{\circ}\text{C}$	picnometric	72G
-----	-------------------------	--------------------------	-------------	-----

melting temperature

$$T_m \quad 623 \text{ K} \quad 72 \text{ G}$$

phonon dispersion and wavenumbers

For phonon vibration modes at low energy, dispersion curves measured by neutron inelastic scattering, see Fig. 20.8.2.

second order elastic moduli

c_{12}	$0.3 \cdot 10^{11} \text{ dyn cm}^{-2}$	$T = 297 \text{ K}$	static measurement	72S
c_{66}	$1.2 \cdot 10^{11} \text{ dyn cm}^{-2}$			
c_{13}	$1.7 \cdot 10^{11} \text{ dyn cm}^{-2}$			
c_{44}	$3.2 \cdot 10^{11} \text{ dyn cm}^{-2}$			
c_{33}	$4.2 \cdot 10^{11} \text{ dyn cm}^{-2}$			
c_{11}	$4.5 \cdot 10^{11} \text{ dyn cm}^{-2}$			

isothermal compressibility

κ	$4.5 \cdot 10^{-12} \text{ cm}^2 \text{ dyn}^{-1}$	$T = 297 \text{ K}$		72S
----------	--	---------------------	--	-----

Young's moduli

E	$1.7 \cdot 10^2 \text{ kbar}$	$E \perp c$	81G
	$3.0 \cdot 10^2 \text{ kbar}$	$E \parallel c$	

Transport properties

electrical conductivity

For dependence on temperature of the electrical resistivity, see Fig. 20.8.3.

σ	$2 \dots 4 \cdot 10^3 \Omega^{-1} \text{ cm}^{-1}$	$T = 295 \text{ K}$	dark conductivity of p-type evaporated thin films (Ag, Au ohmic contacts)	69M
----------	--	---------------------	--	-----

thermal conductivity

κ_{\perp}	$0.012 \text{ W cm}^{-1} \text{ K}^{-1}$	$\perp c$	70G
κ_{\parallel}	$0.021 \text{ W cm}^{-1} \text{ K}^{-1}$	$\parallel c$	

hole mobility

μ_p	$40 \text{ cm}^2/\text{V s}$	$T = 295 \text{ K}$	$I \perp c, B \perp c$	70G
μ_H	$15 \dots 150 \text{ cm}^2/\text{V s}$	$T = 295 \text{ K}$		71I

Optical properties

dielectric constants, real part

$\varepsilon(\infty)$	12	$T = 295 \text{ K}$	$E \parallel c, E \perp c$	77N
$\varepsilon(0)$	15.03	$T = 295 \text{ K}$	$E \perp c$, IR reflectivity	78A
$\varepsilon(0)$	20.25		$E \perp c$, submillimeter wave spectroscopy	

References to 20.8

- 67M Mamedov, K. K., Kerimov, I. G., Kostryukov, U. N., Guseinov, G. D.: Zh. Fiz. Khim. 41 (1967) 1300.
- 69M Mangalam, M. J., Rao, K. N., Rangarajan, N., Siddiqi, M. I. A., Suryanarayana, C. V.: Jpn. J. Appl. Phys. 8 (1969) 1258.
- 70G Guseinov, G. D., Abduliayev, G. B., Bidzinova, S. M., Seidov, F. M., Ismailov, M. Z., Pashayev, A. M.: Phys. Lett. A 33 (1970) 421.
- 71I Itoga, R. S., Kannewurf, C. R.: J. Phys. Chem. Solids 32 (1971) 1099.
- 72G Guseinov, G. D., Abdullayev, G. B., Cojayev, E. M., Rzayeva, La. A., Agayev, G. A.: Mater. Res. Bull. 7 (1972) 1497.
- 72S Shin, K., Hashimoto, K.: Technol. Repts. Kyushi Univ. 45 (1972) 820.
- 75A Abutalybov, G. I., Belle, Mr.: Fiz. Tekh. Poluprovodn. 9 (1975) 1330; Sov. Phys. Semicond. (English Transl.) 9 (1975) 878.
- 76M Man, L. I., Imamov, R. M., Semiletov, S. A.: Kristallografia 21 (1976) 628; Sov. Phys. Crystallogr. (English Transl.) 21 (1976) 355.
- 77N Nizametdinova, MA., Guseinov, Dzh. A., Shteinshraiber, V. Ya.: Fiz. Tverd. Tela 19 (1977) 2011; Sov. Phys. Solid State (English Transl.) 19 (1977) 1177.
- 78A Akhmedov, A. M., Bakhyshev, A. F., Lebedev, A. A., Yakobson, M. A.: Fiz. Tekh. Poluprovodn. 12 (1978) 520; Sov. Phys. Semicond. (English Transl.) 12 (1978) 299.
- 81A1 Abutalybov, G. I., Aliev, A. A., Nizametdinova, M. A., Orudzhev, G. S., Nani, R. Kh.: Fiz. Tekh. Poluprovodn. 15 (1981) 851; Sov. Phys. Semicond. (English Transl.) 15 (1981) 486.
- 81A2 Aliev, A. M., Nizametdinova, M. A., Steinschreiber, V. Ya.: Phys. Status Solidi (b) 107 (1981) K181.
- 81G Gashimzade, F. M., Orudzhev, G. S.: Fiz. Tekh. Poluprovodn. 15 (1981) 1311; Sov. Phys. Semicond. (English Transl.) 15 (1981) 757.
- 83V Valyukonis, G. R., Nizametdinova, M. A., Shileika, A. Yu.: Fiz. Tekh. Poluprovodn. 17 (1983) 946; Sov. Phys. Semicond. (English Transl.) 17 (1983) 595.

Figures to 20.8

Fig. 20.0.10

TlSe. Empirical pseudopotential band structure [81A1].

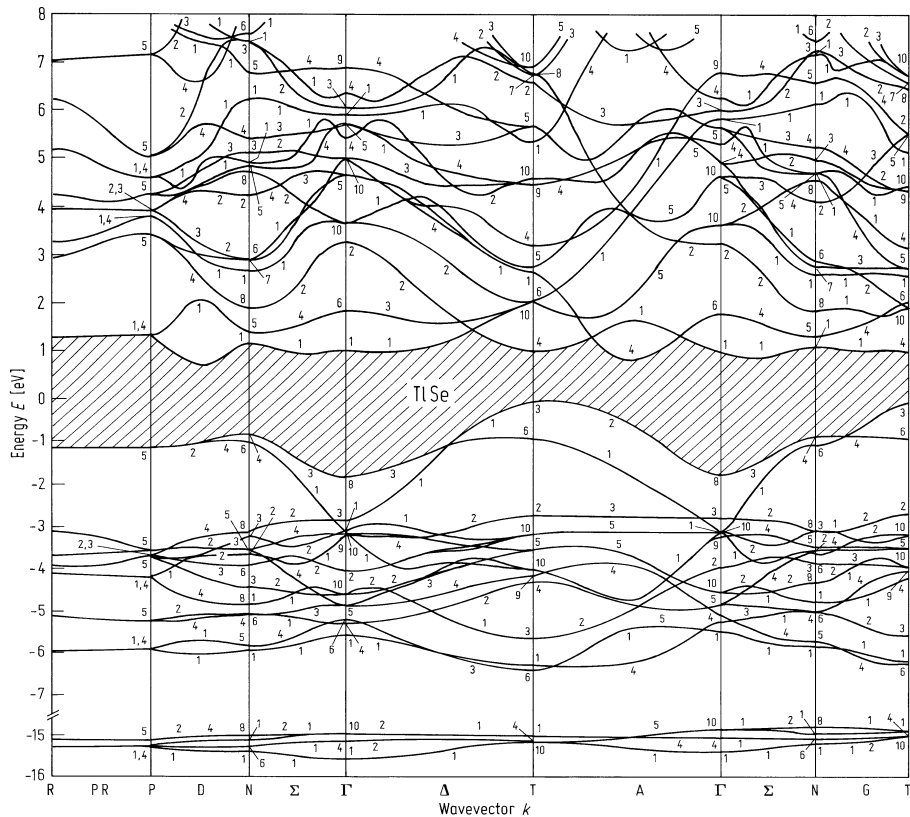


Fig. 20.8.1

TlSe. Heat capacity and Debye temperature vs. temperature [81A2]. Open and full circles: C_p from other literature.

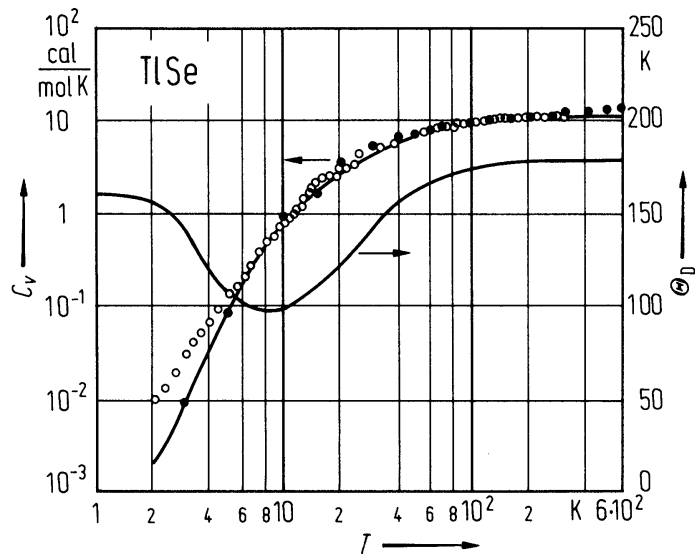


Fig. 20.8.2

TlSe. Frequency of the phonon dispersion curves vs. reduced wave vector coordinate. The symbols represent experimental results of neutron inelastic scattering; the solid lines are calculated; the dashed lines join experimental points [84V].

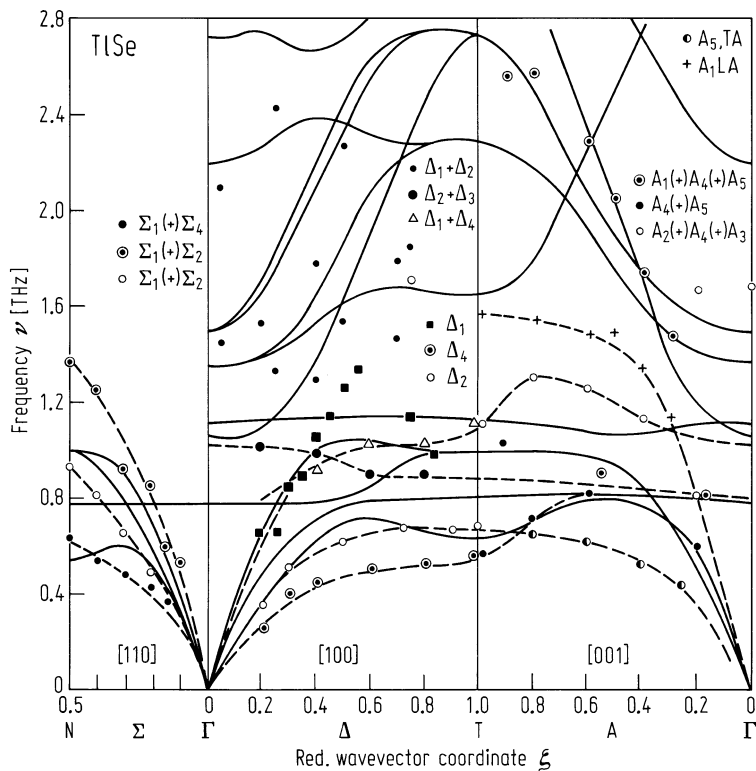
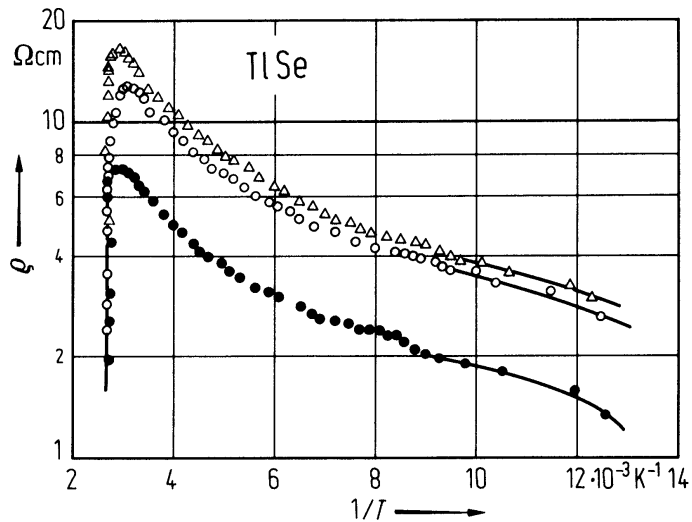


Fig. 20.8.3

TlSe. Electrical resistivity vs. inverse temperature (various samples) [71I]. Single crystal, $I \parallel c$.



20.9 Thallium telluride (TlTe)

Crystal structure

see section 20.0.

Electronic properties

conduction band, effective mass

m_n	$0.03\ m_0$	density of states mass	70G
-------	-------------	------------------------	-----

valence band, effective mass

m_p	$0.5\ m_0$	density of states mass	70G
-------	------------	------------------------	-----

Lattice properties

lattice parameters

a	$12.954\ \text{\AA}$	$T = 300\ \text{K}$	Weissenberg diagram	69B
c	$6.178\ \text{\AA}$			

density

d	$8.40\ \text{g cm}^{-3}$	$T = 298\ \text{K}$	picnometric measurement	70G
-----	--------------------------	---------------------	-------------------------	-----

heat capacity

C_p	$159.8\ \text{J kg}^{-1}\ \text{K}^{-1}$	$T = 298.15\ \text{K}$		75I
-------	--	------------------------	--	-----

Transport properties

electrical conductivity

σ	$1...2\ \Omega^{-1}\ \text{cm}^{-1}$	$T = 300\ \text{K}$	crystal obtained by normal-freezing	66F
	$5\cdot 10^3\ \Omega^{-1}\ \text{cm}^{-1}$	$T = 100\ \text{K}$	p-type, single crystal, obtained from	69C
	$1.6\cdot 10^3\ \Omega^{-1}\ \text{cm}^{-1}$	$T = 400\ \text{K}$	Te-rich melt.	

temperature dependence: Fig. 20.9.1.

thermal conductivity

$\kappa_{ }$	$0.024\ \text{W cm}^{-1}\ \text{K}^{-1}$	$ \ c$		70G
---------------	--	---------	--	-----

hole mobility

μ_p	$60\ \text{cm}^2/\text{V s}$	$T = 300\ \text{K}$		70G
	$1120\ \text{cm}^2/\text{V s}$	$T = 4.2\ \text{K}$	Hall mobility	72J

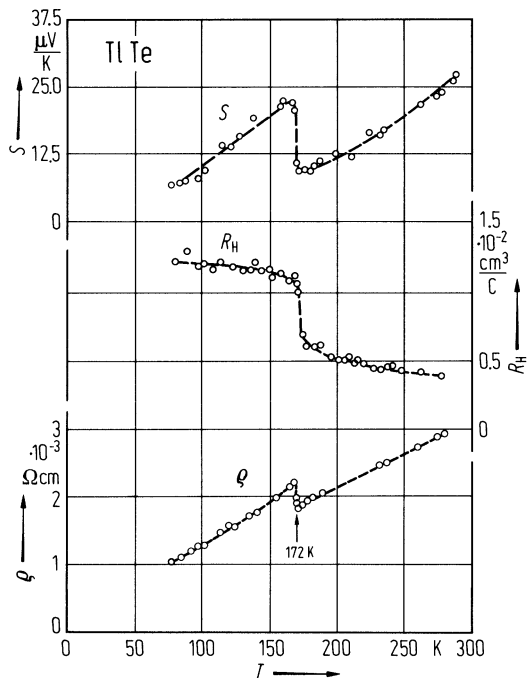
References to 20.9

66F	Flicker, P., Grass, F.: Z. Metallkunde 57 (1966) 641.
69B	Burkhardt, K., Schubert, K.: J. Less Common Metals 18 (1969) 426.
69C	Cruceana, F., Sladaru, St.: J. Mater. Sci. 4 (1969) 410.
70G	Guseinov, G. D., Abduliayev, G. B., Bidzinova, S. M., Seidov, F. M., Ismailov, M. Z., Pashayev, A. M.: Phys. Lett. A 33 (1970) 421.
72J	Jensen, J. D., Burke, J. R., Ernst, D. W., Allgaier, R. S.: Phys. Rev. B 6 (1972) 319.
75I	Ikari, T., Hashimoto, K.: Phys. Status Solidi (a) 31 (1975) K115.

Figures to 20.9

Fig. 20.9.1

TlTe. Electrical resistivity, Hall coefficient and Seebeck coefficient vs. temperature (polycrystalline ingot) [75I].



20.10 In₆S₇

direct energy gap

$E_{g,dir}$	0.890 eV	$T = 300$ K	photoconductivity spectra	80G
-------------	----------	-------------	---------------------------	-----

indirect energy gap

$E_{g,ind}$	0.7 eV	$T = 300$ K	optical absorption	78T
-------------	--------	-------------	--------------------	-----

temperature coefficient of indirect energy gap

$dE_{g,ind}/dT$	$-2.8 \cdot 10^{-4}$ eV K ⁻¹		optical absorption	78T
-----------------	---	--	--------------------	-----

lattice parameters

a	9.090 Å	$T = 300$ K	space group C ₂ ² – P2 ₁ (formerly	67H
b	3.887 Å		P2 ₁ /m)	
c	17.705 Å			
β	108.20°			

density

d	5.08 g cm ⁻³		X-ray, calculated	67H
-----	-------------------------	--	-------------------	-----

References to 20.10

- | | |
|-----|--|
| 67H | Hogg, J. H. C., Duffin, W. J.: Acta Crystallogr. 23 (1967) 111. |
| 78T | Tagirov, V. I., Ismailov, I. M., Khusein, A. Kh.: Fiz. Tekh. Poluprovodn. 12 (1978) 2027; Sov. Phys. Semicond. (English Transl.) 12 (1978) 1205. |
| 80G | Gavaleshko, N. P., Kitsa, M. S., Savchuk, A. I., Simchuk, R. N.: Fiz. Tekh. Poluprovodn. 14 (1980) 1390; Sov. Phys. Semicond. (English Transl.) 14 (1980) 822. |

20.11 In₄Se₃

direct energy gap

$E_{\text{g,dir}}$	0.64 eV	$E \parallel c$, forbidden	optical absorption (formerly quoted for In ₂ Se)	67B
	0.65 eV	$E \parallel a$, forbidden		

lattice parameters

a	15.297(1) Å	$T = 297$ K	space group	73H
b	12.308(1) Å		D _{2h} ¹² – Pnnm	
c	4.081(1) Å			

linear thermal expansion coefficient

α_{\parallel}	$2.1 \cdot 10^{-6}$ K ⁻¹	$T = 300$ K	along the layers (formerly reported for In ₂ Se)	74L
----------------------	-------------------------------------	-------------	---	-----

Debye temperature

Θ_{D}	73.7 K	RT	from the temperature dependence of the thermal conductivity between 2 and 30 K.	78A
---------------------	--------	----	---	-----

density

d	6.02 g cm ⁻³	RT	X-ray, calculated	73H1
-----	-------------------------	----	-------------------	------

electrical conductivity

σ	10^{-1} Ω ⁻¹ cm ⁻¹	$T = 300$ K	average conductivity	78S
----------	--	-------------	----------------------	-----

For dependence on temperature, see Fig. 20.11.1.

thermal conductivity

for dependence on temperature, see Fig. 20.11.2

References to 20.11

67B Bercha, D. M., Borets, AN., Stakhira, I. M., Towstyuk, K. D.: Phys. Status Solidi 21 (1967) 769.
73H Hogg, J. H. C., Sutherland, H. H., Williams, D. J.: Acta Crystallogr. B 29 (1973) 1590.
74L Logvinenko, A. A., Spitkovskii, I. M., Stakhira, I. M.: Fiz. Tverd. Tela 16 (1974) 2743; Sov. Phys. Solid State (English Transl.) 16 (1975) 1774.
78A Anders, F. F., Volchok, I. V., Sukharevskii, B. Ya.: Fiz. Nizk. Temp. 4 (1978) 1202; Sov. J. Low. Temp. Phys. (English Transl.) 4 (1978) 566.
78S Savchin, V. P., Stakhira, I. M.: Fiz. Tekh. Poluprovodn. 12 (1978) 2137; Sov. Phys. Semicond. (English Transl.) 12 (1978) 1273.

Figures to 20.11

Fig. 20.11.1

In_4Se_3 . Electrical conductivity (a) and Hall coefficient (b) vs. inverse temperature for three orientations. 1, σ_{aa} ; 2, σ_{bb} ; 3, σ_{cc} ; 4, $R_{H,abc}$; 5, $R_{H,bca}$; 6, $R_{H,cba}$ ($R_{H,ijk} = I \parallel i, B \parallel j, U_H \parallel k$) [78S].

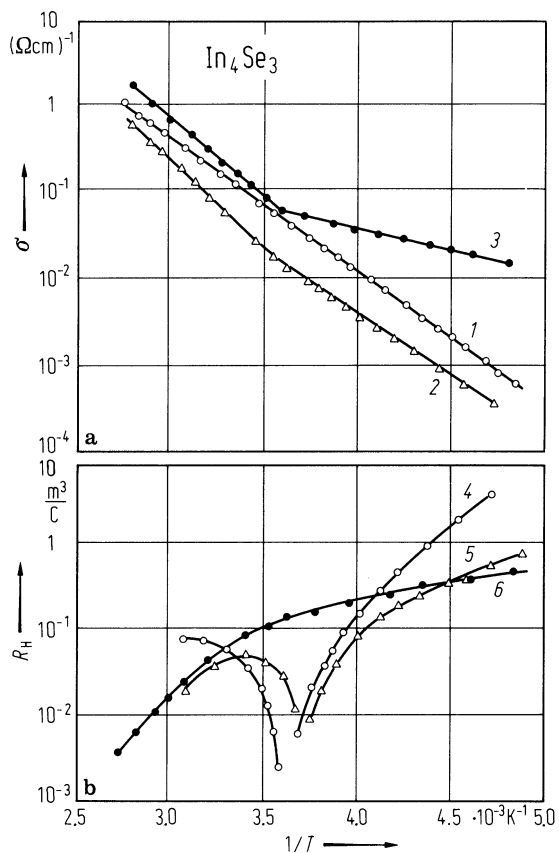
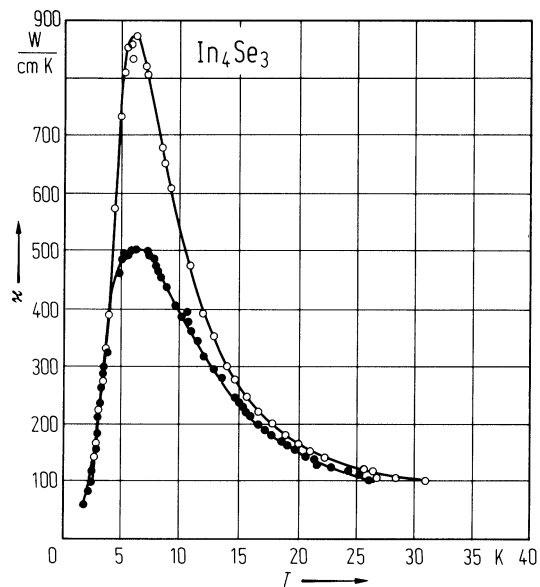


Fig. 20.11.2

In_4Se_3 . Thermal conductivity vs. temperature (data from two samples, measurements probably along the natural cleavage plane) [78A].



20.12 In₆Se₇

direct band gap

$E_{g,dir}$	0.64 eV	$T = 300\text{ K}$	$E \parallel b$, optical absorption	78K
	0.86 eV		$E \parallel c$	

indirect band gap

$E_{g,ind}$	0.34 eV	$T = 300\text{ K}$	$E \parallel c$, optical absorption	78K
-------------	---------	--------------------	--------------------------------------	-----

temperature coefficient of the absorption edge

dE_g/dT	$3 \cdot 10^{-4}\text{ eV K}^{-1}$	$T = 90 \dots 300\text{ K}$	$E \parallel b, E \parallel c$	78K
-----------	------------------------------------	-----------------------------	--------------------------------	-----

conduction band, effective mass

m_n	$0.45\ m_0$		electrical measurements, $\parallel c$	77K
-------	-------------	--	--	-----

valence band, effective mass

m_p	$0.27\ m_0$		electrical measurement	77K
-------	-------------	--	------------------------	-----

lattice parameters

a	9.430 \AA	$T = 300\text{ K}$	space group $C_2^2 - P2_1$	71H
b	4.063 \AA			
c	18.378 \AA			
β	109.34°			

density

d	6.10 g cm^{-3}	$T = 295\text{ K}$	toluene displacement method	71H
	6.21 g cm^{-3}	$T = 295\text{ K}$	X-ray, calculated	71H

melting temperature

T_m	933 K			89N
-------	----------------	--	--	-----

electrical conductivity

for dependence of the resistivity $\rho = 1/\sigma$ on temperature, see Fig. 20.12.1

hole mobility

$\mu_{H,p}$	$240\text{ cm}^2\text{V}^{-1}\text{s}^{-1}$	$T = 300\text{ K}$		89N
-------------	---	--------------------	--	-----

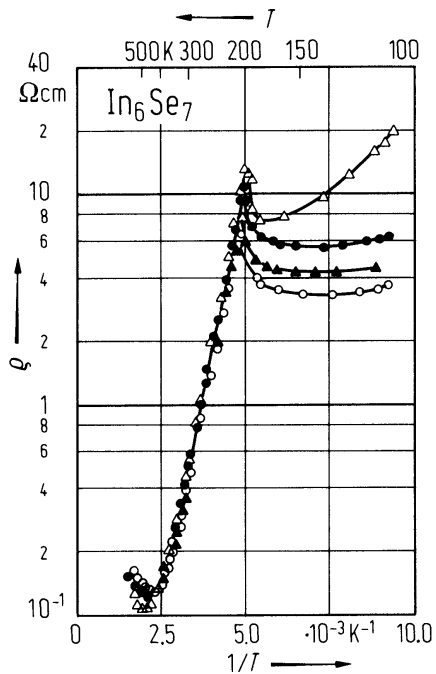
References to 20.12

71H	Hogg, J. H. C.: Acta Crystallogr. B 27 (1971) 1630.
73M	Mori, S.: J. Phys. Soc. Jpn. 35 (1973) 310.
77K	Kitsa, M. S., Gavaleshko, N. P.: Izv. Akad. Nauk SSSR, Neorg. Mater. 13 (1977) 2110; Bull. Acad. Sci. USSR, Inorg. Mater. (English Transl.) 13 (1977) 1687.
78K	Kitsa, M. S., Gavaleshko, N. P., Simchuk, RN., Savchuk, A. I.: Izv. Akad. Nauk SSSR, Neorg. Mater. 14 (1978) 955; Bull. Acad. Sci. USSR, Inorg. Mater. (English Transl.) 14 (1978) 749.
89N	Nagat, A. T.: Cryst. Res. Technol. 24 (1989) K65.

Figures to 20.12

Fig. 20.12.1

In_6Se_7 . Electrical resistivity vs. inverse temperature (data from various samples) [73M]. Uppermost curve (triangles): $I \perp (001)$, other curves: $I \parallel b$.



20.13 In₆₀Se₄₀

direct energy gap

$E_{\text{g,dir}}$	0.8 eV	$T = 300 \text{ K}$	amorphous film	96M
--------------------	--------	---------------------	----------------	-----

electrical conductivity

σ	$1 \text{ } \Omega^{-1} \text{ cm}^{-1}$	$T = 300 \text{ K}$	n-type	96M
----------	--	---------------------	--------	-----

activation energy for the electrical conductivity

E_{A}	0.3 eV	$T = 300 \text{ K}$		96M
----------------	--------	---------------------	--	-----

References to 20.13

96M Marsillac, S., Bernède, J. C., Conan, A.: J. Mater. Sci. 31 (1996) 581.

20.14 In₅₀Se₅₀

direct energy gap

$E_{g,dir}$	1.1 eV	$T = 300$ K	amorphous thin film	96M
-------------	--------	-------------	---------------------	-----

electrical conductivity

σ	$3 \cdot 10^{-3} \Omega^{-1} \text{ cm}^{-1}$	$T = 300$ K	p-type	96M
----------	---	-------------	--------	-----

activation energy for the electrical conductivity

E_A	0.5 eV	$T = 300$ K		96M
-------	--------	-------------	--	-----

References to 20.14

96M Marsillac, S., Bernède, J. C., Conan, A.: J. Mater. Sci. 31 (1996) 581.

20.15 In₄₀ Se₆₀

direct energy gap

$E_{g,dir}$	1.4 eV	$T = 300$ K	amorphous thin film	96M
-------------	--------	-------------	---------------------	-----

electrical conductivity

σ	$1 \cdot 10^{-3} \Omega^{-1} \text{cm}^{-1}$	$T = 300$ K	p-type	96M
----------	--	-------------	--------	-----

activation energy for the electrical conductivity

E_A	0.6 eV	$T = 300$ K		96M
-------	--------	-------------	--	-----

References to 20.15

96M Marsillac, S., Bernède, J. C., Conan, A.: J. Mater. Sci. 31 (1996) 581.

20.16 In₅Se₆

monoclinic crystal

energy gap

E_g	0.31 eV	73M
-------	---------	-----

lattice parameters

a	1.765 Å	RT	monoclinic, P2/m	92J
b	0.409 Å			
c	0.945 Å			
β	101.0°			

dielectric constant, real part

$\varepsilon(\infty)$	9.37	92J
$\varepsilon(0)$	18.23	

References to 20.16

73M Mori, S.: J. Phys. Soc. Jpn. 35 (1973) 310.

92J Julien, C., Eddrief, M., Balkanski, M., Chevy, M.: Phys. Rev. B46 (1992) 2435.

20.17 In₄Te₃

direct energy gap

$E_{g,dir}$	0.48 eV	$T = 295\text{ K}$	$E \parallel [001]$	74G
-------------	---------	--------------------	---------------------	-----

temperature coefficients of direct energy gap

$dE_{g,dir}/dT$	$-4.2 \cdot 10^{-4}\text{ eV K}^{-1}$	$122\text{ K} < T < 295\text{ K}$	$E \parallel [001]$	74G
-----------------	---------------------------------------	-----------------------------------	---------------------	-----

lattice parameters

a	15.630(3) Å	$T = 300\text{ K}$	space group D _{2h} ¹² – Pnnm	73H
b	12.756(3) Å			
c	4.441(2) Å			

The correct formula for In₂Te and In₉Te₇ likely is In₄Te₃

density

d	6.32 g cm ⁻³	$T = 300\text{ K}$	X-ray, calculated	73H
-----	-------------------------	--------------------	-------------------	-----

References to 20.17

- 73H Hogg, J. H. C., Sutherland, H. H.: Acta Crystallogr. B 29 (1973) 2483.
74G Gertovich, T. S., Rarenko, I. M., Tovstyuk, K. D.: Izv. Akad. Nauk SSSR, Neorg. Mater. 10 (1974) 925;
Bull. Acad. Sci. USSR, Inorg. Mater. (English Transl.) 10 (1974) 792.

20.18 Ti_5Te_3

lattice parameters

a	8.929 Å	$T = 300 \text{ K}$	Cr ₅ B ₃ -type, space group D _{4h} ¹⁸ – I4/mcm	70B
c	12.620 Å			

electrical conductivity

σ	$0.367 \cdot 10^4 \Omega^{-1} \text{ cm}^{-1}$	$T = 400 \text{ K}$	metallic conductivity see also Fig. 20.18.1	69C
	$1.32 \cdot 10^4 \Omega^{-1} \text{ cm}^{-1}$	$T = 100 \text{ K}$		

hole mobility

μ_p	72 cm ² /V s	$T = 4.2 \text{ K}$	polycrystalline sample	68J
	2 cm ² /V s	$T = 300 \text{ K}$		

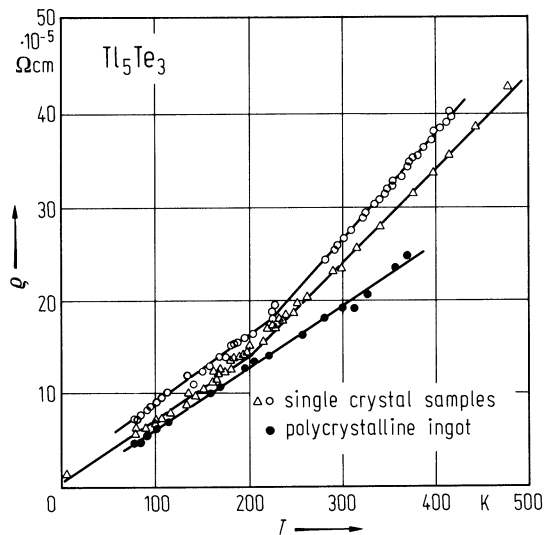
References to 20.18

- 68J Juodakis, A., Kannewurf, C. R.: J. Appl. Phys. 39 (1968) 3003.
69C Cruceana, F., Sladaru, St.: J. Mater. Sci. 4 (1969) 410.
70B Bhan, S., Schubert, K.: J. Less Common Met. 20 (1970) 229.

Figures to 20.18

Fig. 20.18.1

Tl_5Te_3 . Electrical resistivity vs. temperature [68J].



20.19 TlGaS₂

Crystal structure

see section 20.0

Electronic properties

The electronic band structure of TlGaS₂ is not known. Experimentally it is found that TlGaS₂ is an indirect semiconductor. The gap width is 2.46 eV at room temperature. Optical transitions near the band edge are polarized $E \perp c$ [78B].

indirect energy gap

$E_{g,ind}$	2.46 eV	$T = 293$ K	spectral dependence of absorption coefficient.	79B
$dE_{g,ind}/dT$	$-3.5 \cdot 10^{-4}$ eV K ⁻¹	$77\text{ K} < T < 300\text{ K}$	optical absorption	79B

direct energy gap

$E_{g,dir}$	2.544 eV	$T = 293$ K	optical absorption, analysis of spectral dependence of absorption coefficient	78B
$dE_{g,dir}/dT$	$-1 \cdot 10^{-4}$ eV K ⁻¹	$77\text{ K} < T < 300\text{ K}$	optical absorption	79B

direct exciton gap

$E_{gx,dir}$	2.62 eV	$T = 110$ K	optical absorption	79B
--------------	---------	-------------	--------------------	-----

Lattice properties

lattice parameters

a	7.26 Å	$T = 295$ K	monoclinic, space group	75I2
b	7.26 Å		$C_{2h}^2 - P2_1/m$	
c	59.60 Å = 4·14.9 Å			
β	91°11'			

density

d	5.56 g cm ⁻³	$T = 298$ K		74M
	4.22 g cm ⁻³			67G

melting temperature

T_m	905°C		congruent melting	72G
	883°C			67G

Debye temperature

temperature dependence, $5 < T < 50$ K, see Fig. 20.19.1

heat capacity

temperature dependence, $5 < T < 300$ K, see Fig. 20.19.1

Transport properties

electrical conductivity

σ	$10^{-11} \dots 10^{-12}$ Ω ⁻¹ cm ⁻¹	$T = 298$ K	along the layers?	72K
	10^{-5} Ω ⁻¹ cm ⁻¹	$T = 800$ K	σ along the layers	67G

thermal conductivity

κ_{\parallel}	$0.039 \text{ W cm}^{-1} \text{ K}^{-1}$	$T = 300 \text{ K}, \parallel c$	70G
κ_{\perp}	$0.16 \text{ W cm}^{-1} \text{ K}^{-1}$	$\perp c$	

Optical properties

dielectric constant, real part

$\varepsilon(0)$	26	capacitance measurement	72K
	31	thin evaporated film	78D

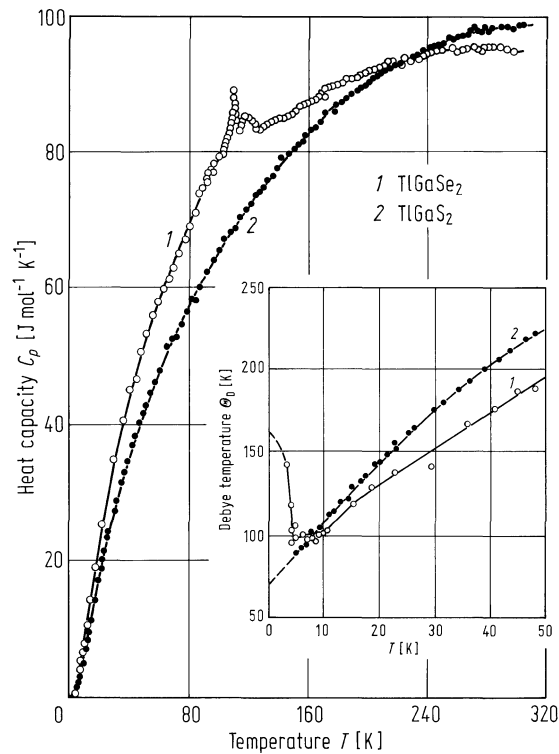
References to 20.19

- 67G Guseinov, G. D., Ramazanzade, A. M., Kerimova, EM., Ismailov, M. Z.: Phys. Status Solidi 22 (1967) K117.
- 70G Guseinov, G. D., Abduliayev, G. B., Bidzinova, S. M., Seidov, F. M., Ismailov, M. Z., Pashayev, A. M.: Phys. Lett. A 33 (1970) 421.
- 72G Guseinov, G. D., Abdullayev, G. B., Cojayev, E. M., Rzayeva, La. A., Agayev, G. A.: Mater. Res. Bull. 7 (1972) 1497.
- 72K Karpovich, I. A., Chervova, A. A., Demidova, L. I., Leonov, E. I., Orlov, V. M.: Izv. Akad. Nauk. SSSR, Neorg. Mater. 8 (1972) 70; Bull. Acad. Sci. USSR, Inorg. Mater (English Transl.) 8 (1972) 58.
- 74M Müller, D., Poltmann, F. E., Hahn, H.: Z. Naturforsch. 29b (1974) 117.
- 75I1 Ikari, T., Hashimoto, K.: Phys. Status Solidi (a) 31 (1975) K115.
- 78B Bakhyshov, A. F., Lebedev, A. A., Khalafov, Z. D., Yakobson, M. A.: Fiz. Tekh. Poluprovodn. 12 (1978) 555; Sov. Phys. Semicond. (English Transl.) 12 (1978) 320.
- 78D Demidova, L. I., Chervova, A. A., Karaseva, L. A., Shilova, M. V.: Vyssh. Ucherb. Zav. Fiz. 3 (1978) 134; Sov. Phys. J. (English Transl.) 3 (1978) 386.
- 79B Bakhyshov, A. E., Boules, S., Faradzhov, F. E., Mamedov, M. Sh., Tagirov, V. I.: Phys. Status Solidi (b) 95 (1979) K121.
- 84A Abdullaeva, S. G., Abdullaev, A. M., Mamedov, K. K., Mamedov, N. T.: Fiz. Tverd. Tela 26 (1984) 618; Sov. Phys. Solid State (English Transl.) 26 (1984) 375.

Figures to 20.19

Fig. 20.19.1

TlGaS₂, TlGaSe₂. Heat capacity and Debye temperature (insert) vs. temperature for (1) TlGaSe₂ and(2) TlGaS₂ [84A].



20.20 TlGaSe2

Crystal structure

see section 20.0

Electronic properties

TlGaSe2 is an indirect semiconductor with a gap of 2.03 eV at room temperature.

indirect energy gap

$E_{g,ind}$	2.03 eV	$T = 300\text{ K}$	optical absorption ($E \parallel$ cleavage plane)	79B
-------------	---------	--------------------	--	-----

indirect exciton transition energy

$E_{gx,ind}$	2.054 eV	$T = 6\text{ K}$	differential absorption ($E \parallel$ layer plane)	81A
--------------	----------	------------------	--	-----

direct energy gap

$E_{g,dir}$	2.23 eV	$T = 300\text{ K}$	optical absorption, analysis of spectral dependence of absorption coefficient	79B
-------------	---------	--------------------	---	-----

direct exciton transition energy

$E_{gx,dir}(1S)$	2.128 eV	$T = 6\text{ K}$	optical absorption, polarization $E \parallel \sigma, E \perp c$	81A
------------------	----------	------------------	--	-----

temperature coefficient of indirect energy gap

$dE_{g,ind}/dT$	$-1.8 \cdot 10^{-4}\text{ eV K}^{-1}$	$77\text{ K} < T < 300\text{ K}$	optical absorption	79B
-----------------	---------------------------------------	----------------------------------	--------------------	-----

temperature coefficient of direct energy gap

$dE_{g,dir}/dT$	$-1.23 \cdot 10^{-4}\text{ eV K}^{-1}$	$T < 100\text{ K}$		85A
-----------------	--	--------------------	--	-----

exciton binding energy

E_b	43 meV	$T = 6\text{ K}$	optical absorption, n = 1, 2 direct excitons observed, $1/n^2$ -Rydberg series assumed	81A
-------	--------	------------------	--	-----

conduction band, effective mass

m_n	$0.37\ m_0$		density of states mass	70G
-------	-------------	--	------------------------	-----

valence band, effective mass

m_p	$0.68\ m_0$		density of states mass	70G
-------	-------------	--	------------------------	-----

Lattice properties

lattice parameters

a	10.772 \AA	$T = 300\text{ K}$	monoclinic, space group $C_s^4 - Cc$	78M
b	10.771 \AA			
c	15.636 \AA			
β	100.6°			

density

d	6.19 g cm^{-3}		experimental	70G,
-----	-------------------------	--	--------------	------

melting temperature

T_m	780°C			75I1
	820°C		incongruent melting	67G

Debye temperature

Θ_D	97 K	$T < 10$ K	heat capacity	87A
temperature dependence ($5 < T < 50$ K), see Fig. 20.20.1				

heat capacity

temperature dependence ($5 < T < 50$ K), see Fig. 20.20.1

Transport properties

electrical conductivity

σ	$10^{-6} \dots 10^{-10} \Omega^{-1} \text{ cm}^{-1}$	$T = 298$ K	p-type; for dependence on temperature, see Fig. 20.20.2; σ along the layers?	72K
----------	--	-------------	---	-----

electron mobility

μ_n	$26 \text{ cm}^2/\text{V s}$	$T = 300$ K		70G
---------	------------------------------	-------------	--	-----

hole mobility

μ_p	$65 \text{ cm}^2/\text{V s}$	$T = 300$ K	For temperature dependence, see Fig. 20.20.3	70G
---------	------------------------------	-------------	--	-----

thermal conductivity

κ_{\perp}	$0.025 \text{ W cm}^{-1} \text{ K}^{-1}$	$T = 300$ K, $\perp c$		70G
κ_{\parallel}	$0.059 \text{ W cm}^{-1} \text{ K}^{-1}$	$\parallel c$		

Optical properties

dielectric constants, real part

$\varepsilon(\infty)$	13.2	$T = 295$ K	IR reflectivity ($E \perp c$)	76A
$\varepsilon(0)$	20.4			

For temperature dependence as a function of orientation, Fig. 20.20.4

References to 20.20

- 67G Guseinov, G. D., Ramazanzade, A. M., Kerimova, EM., Ismailov, M. Z.: Phys. Status Solidi 22 (1967) K117.
- 70G Guseinov, G. D., Abduliayev, G. B., Bidzinova, S. M., Seidov, F. M., Ismailov, M. Z., Pashayev, A. M.: Phys. Lett. A 33 (1970) 421.
- 72K Karpovich, I. A., Chervova, A. A., Demidova, L. I., Leonov, E. I., Orlov, V. M.: Izv. Akad. Nauk. SSSR, Neorg. Mater. 8 (1972) 70; Bull. Acad. Sci. USSR, Inorg. Mater (English Transl.) 8 (1972) 58.
- 75B Bakhyshov, A. D., Musaeva, L. G., Lebedev, A. A., Yakobson, M. A.: Fiz. Tekh. Poluprovodn. 9 (1975) 1548; Sov. Phys. Semicond. (English Transl.) 9 (1975) 1021.
- 75I Ikari, T., Hashimoto, K.: Phys. Status Solidi (a) 31 (1975) K115.
- 76A Abdullaev, G. B., Allekhverdiev, K. R., Nant, R. Kh., Salaev, E. Yu., Sardarly, R. M.: Phys. Status Solidi (a) 34 (1976) K115.
- 78M Müller, D., Hahn, H.: Z. Anorg. Allg. Chem. 438 (1978) 258.
- 79B Bakhyshov, A. E., Boules, S., Faradzov, F. E., Mamedov, M. Sh., Tagirov, V. I.: Phys. Status Solidi (b) 95 (1979) K121.
- 81A Abdullaeva, S. G., Belenkii, G. L., Godzhaev, M. O., Mamedov, N. T.: Phys. Status Solidi (b) 103 (1981) K61.
- 84A1 Abdullaeva, S. G., Abdullaev, A. M., Mamedov, K. K., Mamedov, N. T.: Fiz. Tverd. Tela 26 (1984) 618; Sov. Phys. Solid State (English Transl.) 26 (1984) 375.
- 84A2 Aliev, R. A., Allakhverdiev, K.R., Baranov, A. I., Ivanov, N. R., Sardarly, R. M.: Fiz. Tverd. Tela 26 (1984) 1271; Sov. Phys. Solid State (English Transl.) 26 (1984) 775.
- 85A Abdullaev, N. A., Allakhverdiev, K. R., Belenkii, G. L., Mamedov, T. G., Suleimanov, R. A., Sharifov, Ya. N.: Solid State Commun. 53 (1985) 601.
- 87A Aldzhanov, M. A., Guseinov, N. G., Mamedov, Z. N.: Phys. Status Solidi (a) 100 (1987) K145.

Figures to 20.20

Fig. 20.20.1

TlGaS₂, TlGaSe₂. Heat capacity and Debye temperature (insert) vs. temperature for (1) TlGaSe₂ and(2) TlGaS₂ [84A1].

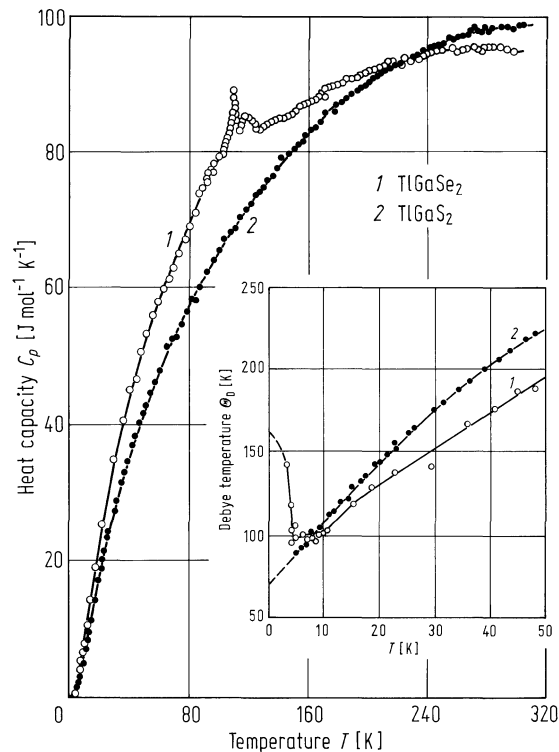


Fig. 20.20.2

TiGaSe₂. Electrical conductivity vs. inverse temperature. 1, $\rho_{300\text{K}} = 10^{10} \Omega\text{cm}$; 2, $10^9 \Omega\text{cm}$; 3, $10^8 \Omega\text{cm}$ [75B].

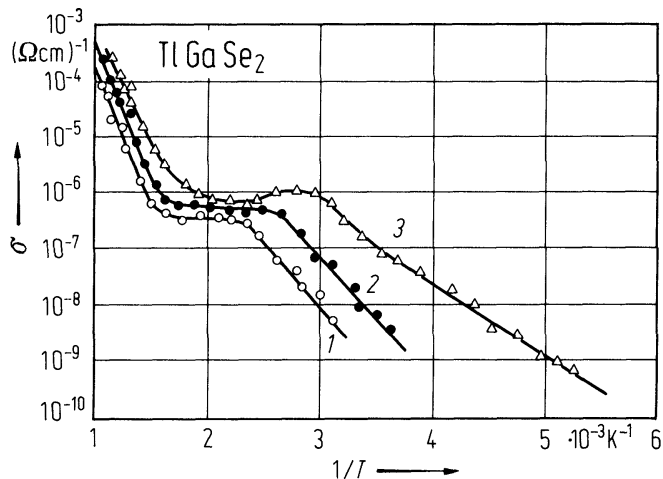


Fig. 20.20.3

TlGaSe₂. Hole mobility vs. temperature [67G] in cm² V⁻¹ s⁻¹, T in K, $I \parallel$ layer, $B \perp$ cleavage plane.

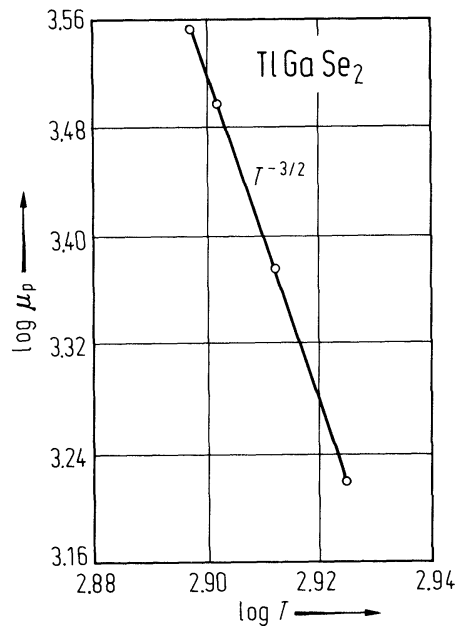
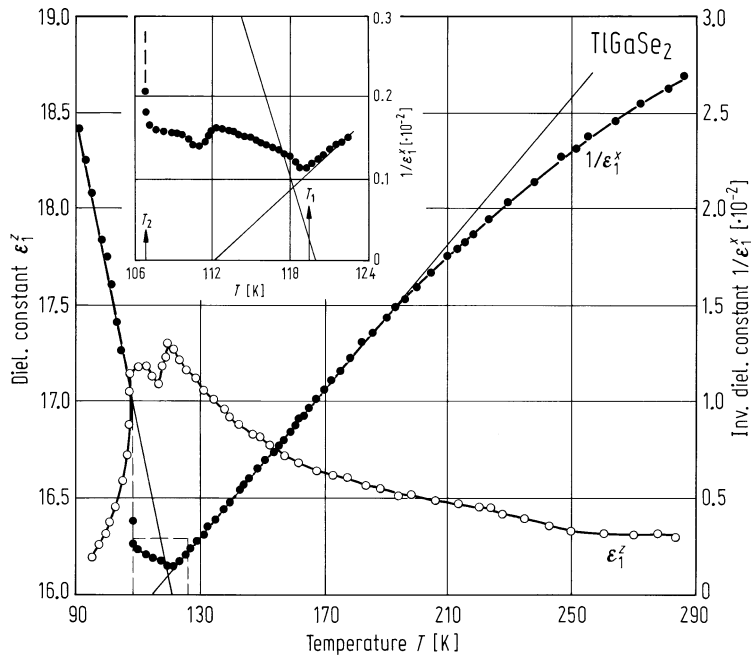


Fig. 20.20.4

TlGaSe₂. Dielectric constant vs. temperature; real part along the pseudo tetragonal axis (open circles) and perpendicular to the axis (full circle) [84A2].



20.21 TlGaTe2

Crystal structure

see section 20.0

Electronic properties

Band structure, see Fig. 20.0.13

energy gap

$E_{g,th}$	1.2 eV	$T = 0\text{ K}$	conductivity	67G
dE_g/dT	$-2.10 \cdot 10^{-4}\text{ eV K}^{-1}$			70G

conduction band, effective mass

m_n	$0.12\ m_0$		density of states mass	70G
-------	-------------	--	------------------------	-----

valence band, effective mass

m_p	$0.23\ m_0$		density of states mass	70G
-------	-------------	--	------------------------	-----

Lattice properties

lattice parameters

a	8.429 Å	$T = 300\text{ K}$	Weissenberg diagram, TlSe-type,	73M
c	6.865 Å		tetragonal space group	
			$D_{4h}^{18} - I4/mcm$	

density

d	7.32 g cm ⁻³	$T = 298\text{ K}$	picnometric measurement	70G
	7.05 g cm ⁻³	$T = 298\text{ K}$	picnometric measurement	73M
	7.36 g cm ⁻³		calculated	70G
	7.164 g cm ⁻³		calculated	73M

melting temperature

T_m	773(5)°C		incongruent melting	67G
-------	----------	--	---------------------	-----

Debye temperature

Θ_D	105 K	$T < 8\text{ K}$	see also Fig. 20.21.1	85A
	210 K	$T \rightarrow \infty$		

heat capacity

A	$-10.4\text{ J mol}^{-1}\text{K}^{-1}$	$10 < T < 32\text{ K}$	A, B are parameters of empirical relation	85A
B	$1.63\text{ J mol}^{-1}\text{K}^{-2}$		$C_v = A + BT$	
			see also Fig. 20.21.1	

Transport properties

electrical conductivity :

σ	$3.2 \cdot 10^{-4}\ \Omega^{-1}\text{ cm}^{-1}$	$T = 325\text{ K}$		67G
----------	---	--------------------	--	-----

electron mobility

μ_n	66 cm ² /V s	$T = 300\text{ K}$		70G
---------	-------------------------	--------------------	--	-----

hole mobility

μ_p	96 cm ² /V s	$T = 300$ K	70G
---------	-------------------------	-------------	-----

thermal conductivity

κ_{\parallel}	0.069 W cm ⁻¹ K ⁻¹	$\parallel c$	70G
κ_{\perp}	0.44 W cm ⁻¹ K ⁻¹	$\perp c$	

Optical properties

dielectric constants

$\epsilon(\infty)$	14.8	$E \perp c$	80G
	13.1	$E \parallel c$	

References to 20.21

- 67G Guseinov, G. D., Ramazanzade, A. M., Kerimova, EM., Ismailov, M. Z.: Phys. Status Solidi 22 (1967) K117.
- 70G Guseinov, G. D., Abduliayev, G. B., Bidzinova, S. M., Seidov, F. M., Ismailov, M. Z., Pashayev, A. M.: Phys. Lett. A 33 (1970) 421.
- 73M Müller, D., Eulenberger, G., Hahn, H.: Z. Anorg. Allg. Chem. 398 (1973) 207.
- 80G Gasanly, N. M., Goncharov, A. F., Dshavadov, B. M., Melnik, N. N., Tagirov, V. I., Vinogradov, E. A.: Phys. Status Solidi (b) 97 (1980) 367.
- 85A Aldzhanov, M. A., Mamedov, K. K., Abdurragimov, A. A.: Phys. Status Solidi (b) 131 (1985) K35.
- 85G Gashimzade, F. M., Guliev, D.: Phys. Status Solidi (b) 131 (1985) 201.

Figures to 20.21

Fig. 20.0.13

TlGaTe_2 . Calculated band structure, typical of compounds with TlSe type structure [85G].

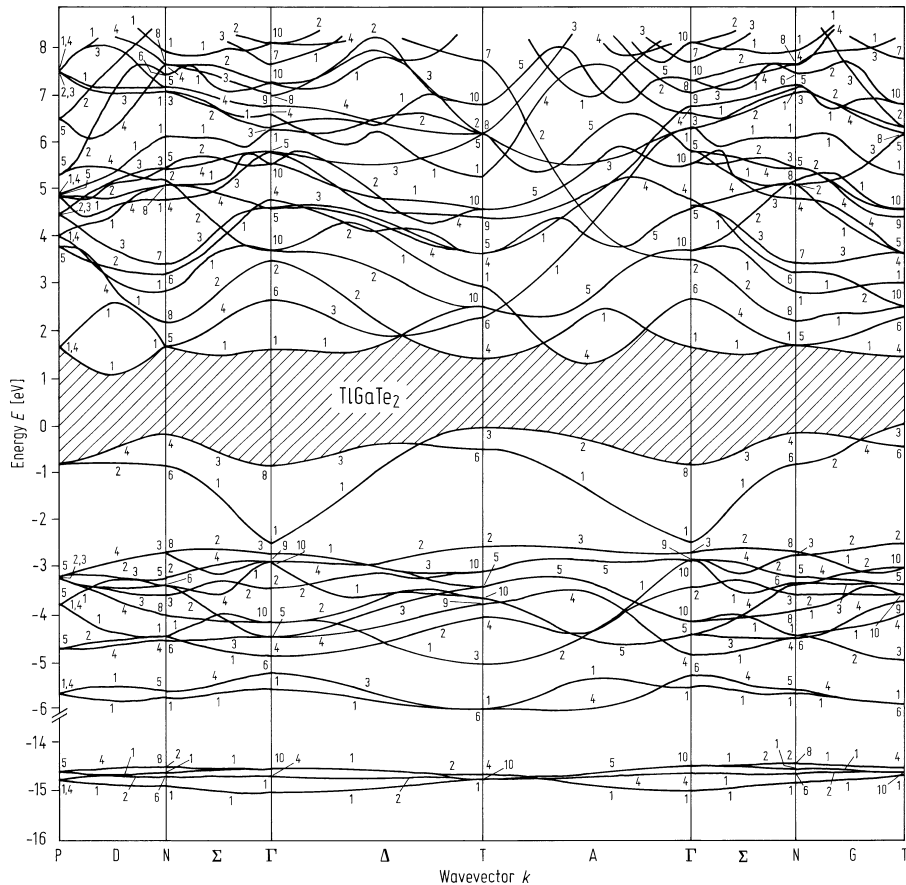
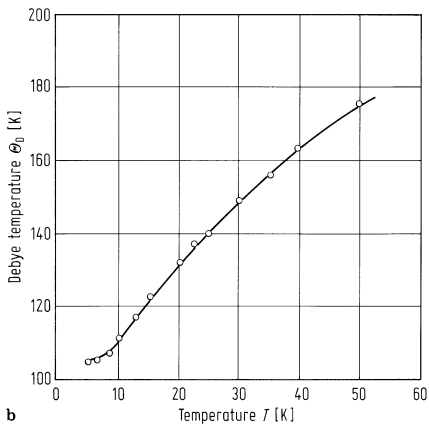
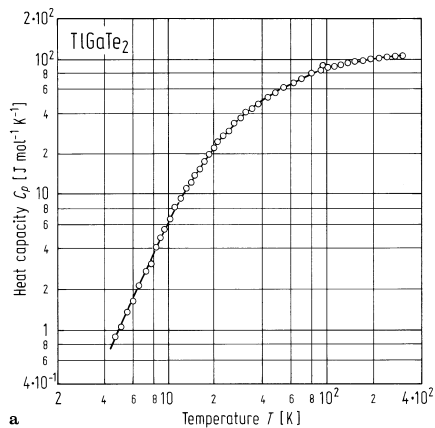


Fig. 20.21.1

TlGaTe₂. Heat capacity (a), Debye temperature (b) vs. temperature [85A].



20.22 TlInS2

Crystal structure

see section 20.0

Electronic properties

TlInS2 is an indirect semiconductor with a gap width of about 2.2 eV. The electronic band structure of TlInS2 is not known.

indirect energy gap

$E_{g,ind}$	2.2 eV		temperature dependence of electrical conductivity, α -structure see Fig. 20.22.1 for temperature dependence	69G
-------------	--------	--	---	-----

$dE_{g,ind}/dT$	$-1\cdot 10^{-3}$ eV K ⁻¹	$77\text{ K} < T < 293\text{ K}$	optical absorption, α -structure ($E \perp c$)	78A
-----------------	--------------------------------------	----------------------------------	---	-----

direct exciton gap

$E_{gx,dir}$	2.516 eV	$T = 4.2\text{ K}$	optical absorption, monoclinic structure ($E \perp c$)	78A
	2.393 eV	$T = 293\text{ K}$	electroabsorption ($E \perp c$)	77G
$dE_{gx,dir}/dT$	$-6.5\cdot 10^{-4}$ eV K ⁻¹	$77\text{ K} < T < 300\text{ K}$	electroabsorption	77G

binding energy of direct exciton

E_b	33 meV		absorption spectra	82B
-------	--------	--	--------------------	-----

conduction band, effective mass

m_n	$0.34\ m_0$		α - and β -type, density of states mass	70G
-------	-------------	--	--	-----

valence band, effective mass

m_p	$0.784\ m_0$		α - and β -type, density of states mass	70G
-------	--------------	--	--	-----

Lattice properties

lattice parameters

a	7.67 Å	$T = 295\text{ K}$	TlInS2 (α) , hexagonal, space group $C_{6v}^2 - P6mm$ or $D_{2h}^6 - P6/mcc$	75I
c	14.98 Å			

linear thermal expansion coefficient

for dependence on the temperature ($30 < T < 250\text{ K}$) see Fig. 20.22.2

density

d	4.95 g cm ⁻³		α -TlInS2, picnometric	69G
	5.64 g cm ⁻³		β -TlInS2, picnometric	

melting temperatures

T_m	870 K		α -TlInS2	70G
	1030 K		β -TlInS2	75I

Transport properties

electrical conductivity

σ	$10^{-12} \Omega^{-1} \text{ cm}^{-1}$	$T = 298 \text{ K}$	probably β -TlInS ₂ (transparent material) , along the layers?	72K
----------	--	---------------------	---	-----

α -TlInS₂: for dependence on temperature, see Fig. 20.22.3 ($300 \text{ K} < T < 900 \text{ K}$) and [69G].

electron mobility

μ_n	$68 \text{ cm}^2/\text{V s}$	$T = 300 \text{ K}$	α - and β -type	70G
---------	------------------------------	---------------------	------------------------------	-----

hole mobility

μ_p	$170 \text{ cm}^2/\text{V s}$	$T = 300 \text{ K}$	α - and β -type	70G
---------	-------------------------------	---------------------	------------------------------	-----

For dependence on temperature in the range $300 \text{ K} < T < 900 \text{ K}$, see Fig. 20.22.4.

thermal conductivity

κ_{\perp}	$0.02 \text{ W cm}^{-1} \text{ K}^{-1}$	$T = 300 \text{ K}, \perp c$	α -type	70G
κ_{\perp}	$0.044 \text{ W cm}^{-1} \text{ K}^{-1}$	$\perp c$	β -type	70G
κ_{\parallel}	$0.069 \text{ W cm}^{-1} \text{ K}^{-1}$	$\parallel c$	β -type	70G

Optical properties

refractive index : Fig. 20.22.5.

dielectric constant, real part

$\epsilon(0)$	26	capacitance measurement, probably β -type, perpendicular to the layers?	72K
---------------	----	---	-----

For real and imaginary parts vs. temperature, see Fig. 20.22.6.

References to 20.22

- 69G Guseinov, G. D., Mooser, E., Kerimova, E. M., Gamidov, R. S., Alekseev, I. V., Jsmailov, M. Z.: Phys. Status Solidi 34(1969) 33.
- 70G Guseinov, G. D., Abduliayev, G. B., Bidzinova, S. M., Seidov, F. M., Ismailov, M. Z., Pashayev, A. M.: Phys. Lett. A 33 (1970) 421.
- 72K Karpovich, I. A., Chervova, A. A., Demidova, L. I., Leonov, E. I., Orlov, V. M.: Izv. Akad. Nauk. SSSR, Neorg. Mater. 8 (1972) 70; Bull. Acad. Sci. USSR, Inorg. Mater (English Transl.) 8 (1972) 58.
- 75I Isaacs, T. J., Hopkins, R. H.: J. Cryst. Growth 29 (1975) 121.
- 77G Guseinov, G. D., Abdullayeva, S. G., Aksianov, I. G., Gajiyev, V. A.: Mater. Res. Bull. 12 (1977) 207.
- 78A Akhmedov, A. M., Bakhyshov, A. F., Lebedev, A. A., Yakobson, M. A.: Fiz. Tekh. Poluprovodn. 12 (1978) 520; Sov. Phys. Semicond. (English Transl.) 12 (1978) 299.
- 80A Allakhverdiev, K. R., Ouliev, R. I., Kulevskii, L. A., Savelev, A. D., Savelev, E. Yu., Smirnov, V. V.: Phys. Status Solidi (a) 60 (1 980) 309.
- 82B Bakirov, M. Ya., Zeinalov, N. M., Abdullaeva, S. G., Gajiyev, V. A., Gojayev, E. M.: Solid State Commun. 44 (1982) 205.
- 84A1 Aliev, R. A., Allakhverdiev, K.R., Baranov, A. I., Ivanov, N. R., Sardarly, R. M.: Fiz. Tverd. Tela 26 (1984) 1271; Sov. Phys. Solid State (English Transl.) 26 (1984) 775.
- 84A2 Allakhverdiev, K. R., Babaev, S. S., Bakhyshov, N. A., Mamedov, T. G., Salaev, E. Yu.: Fiz. Tekh. Poluprovodn. 18 (1984) 1307; Sov. Phys. Semicond. (English Transl.) 18 (1984) 817.
- 85A Abdullaev, N. A., Allakhverdiev, K. R., Belenkii, G. L., Mamedov, T. G., Suleimanov, R. A., Sharifov, Ya. N.: Solid State Commun. 53 (1985) 601.

Figures to 20.22

Fig. 20.22.1

TlInS₂. Electronic energy vs. temperature, of the exciton absorption maximum $E_{\text{gx,dir}}$ and the band gap energy $E_{\text{g,ind}}$ [84A2].

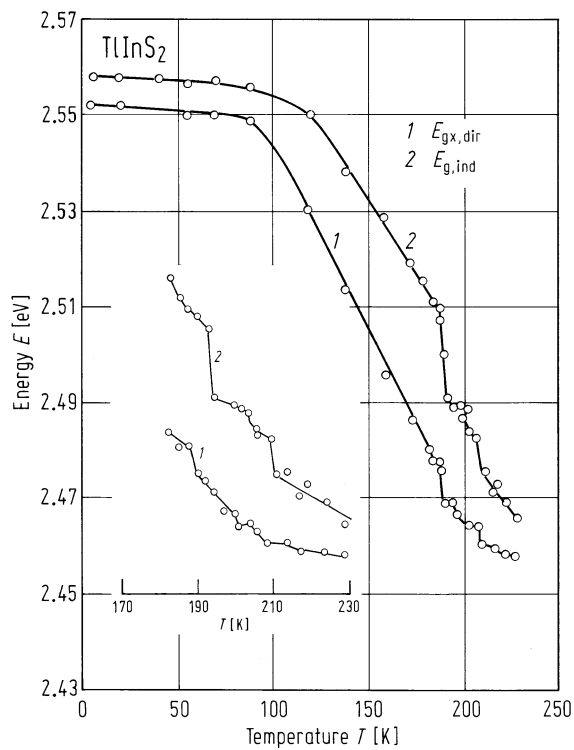


Fig. 20.22.2

TlInS₂. Linear thermal expansion coefficient vs. temperature for the two directions perpendicular and parallel to the layers; anomaly at the phase transition at $T = 200$ K [85A].

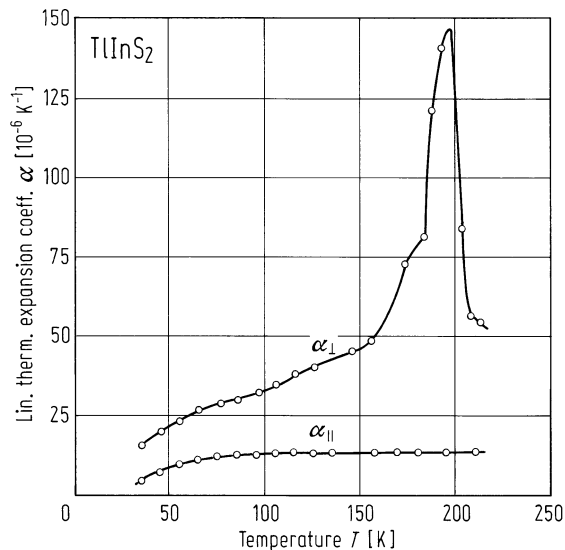


Fig. 20.22.3

TlInS₂. a) Electric conductivity vs. inverse temperature, b) Hall coefficient vs. inverse temperature (α -type) [69G]. $I \parallel (110)$, $B \perp (110)$.

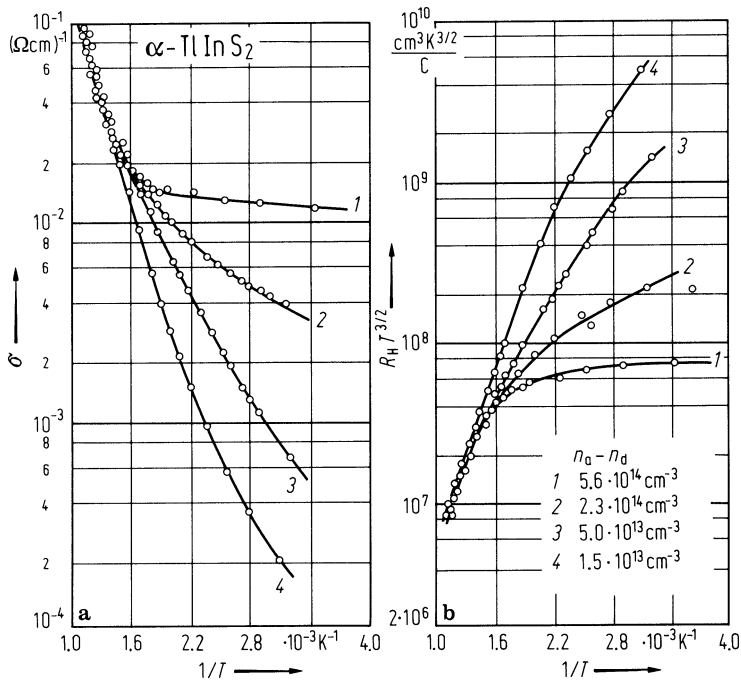


Fig. 20.22.4

TlInS₂. Hole mobility vs. temperature (α -type) [69G]. $I \parallel (110)$, $B \perp (110)$.

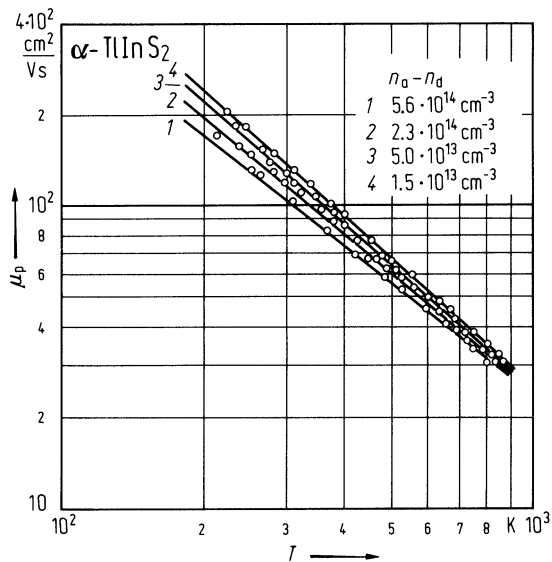


Fig. 20.22.5

TlInS₂. Ordinary (n_{\perp}) and extraordinary (n_{\parallel}) index of refraction vs. wavelength [80A].

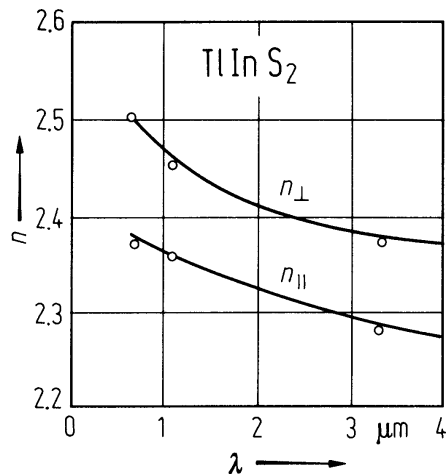
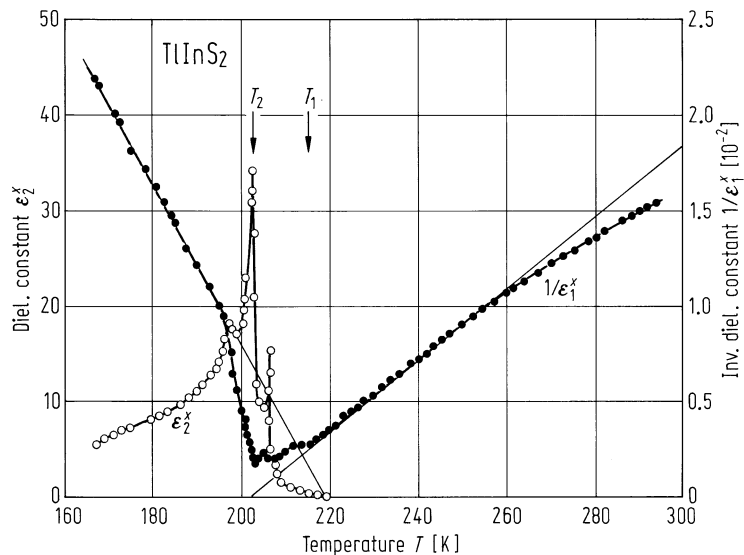


Fig. 20.22.6

TlInS₂. Dielectric constant, imaginary part (open circles) and inverse real part (full circles) vs. temperature; structural transition at $T_2 = 202$ K and $T_1 = 216$ K [84A1].



20.23 TlInSe2

Crystal structure

see section 20.0

Electronic properties

TlInSe2 is an indirect semiconductor with a gap width of about 1.1 eV. The electronic band structure of TlInSe2 is not known.

band structure : see Fig. 20.0.14

indirect energy gap

$E_{g,ind} (T_3-D_1)$	1.190(2) eV	$T = 290\text{ K}$	$E \parallel c$, allowed, optical absorption edge	82A
	1.228(2) eV		$E \perp c$	

direct energy gap

$E_{g,dir} (T_3-T_4)$	1.257 eV	$T = 290\text{ K}$	$E \parallel c$, forbidden	82A
	1.285 eV		$E \perp c$	

temperature coefficients of energy gaps

$dE_{g,ind} / dT$	$0.9 \cdot 10^{-4} \text{ eV K}^{-1}$		$E \parallel c$	82A
$dE_{g,dir} / dT$	$1.4 \cdot 10^{-4} \text{ eV K}^{-1}$		$E \parallel c$	
$dE_{g,ind} / dT$	$1.6 \cdot 10^{-4} \text{ eV K}^{-1}$		$E \perp c$	
$dE_{g,dir} / dT$	$2.3 \cdot 10^{-4} \text{ eV K}^{-1}$		$E \perp c$	

conduction band, effective mass

m_n	$0.31\ m_0$	density of states mass		69G
-------	-------------	------------------------	--	-----

valence band, effective mass

m_p	$0.65\ m_0$	density of states mass		69G
-------	-------------	------------------------	--	-----

Lattice properties

lattice parameters

a	$8.075\ \text{\AA}$	$T = 295\text{ K}$	TlSe-type, tetragonal, space group	73M
c	$6.847\ \text{\AA}$		$D_{4h}^{18} - I4/mcm$	

density

d	6.90 g cm^{-3}	$T = 298\text{ K}$	picnometric	72G
-----	-------------------------	--------------------	-------------	-----

melting temperature

T_m	808°C		congruent melting	72G
-------	---------------------	--	-------------------	-----

Transport properties

electrical conductivity

for dependence on temperature, see Figs. 20.23.1, 20.23.2; for piezoresistance measurements, see [77G].

electron mobility

μ_n	$225\text{ cm}^2/\text{V s}$	$T = 300\text{ K}$		70G
---------	------------------------------	--------------------	--	-----

hole mobility

m_p	450 cm ² /V s	$T = 300$ K	for dependence on temperature in the range $300\text{ K} < T \leq 900\text{ K}$, see Fig. 20.23.3	70G
-------	--------------------------	-------------	--	-----

thermal conductivity

κ_{\parallel}	0.031 W cm ⁻¹ K ⁻¹	$T = 300$ K	$\parallel c$	70G
κ_{\perp}	0.074 W cm ⁻¹ K ⁻¹		$\perp c$	

Optical properties

dielectric constants

$\varepsilon(\infty)$	10.2	$E \perp c$	oscillator fit to reflectivity	80G
	8.0	$E \parallel c$		

References to 20.23

- 69G Guseinov, G. D., Mooser, E., Kerimova, E. M., Gamidov, R. S., Alekseev, I. V., Jsmailov, M. Z.: Phys. Status Solidi 34(1969) 33.
- 70G Guseinov, G. D., Abduliyayev, G. B., Bidzinova, S. M., Seidov, F. M., Ismailov, M. Z., Pashayev, A. M.: Phys. Lett. A 33 (1970) 421.
- 72G Guseinov, G. D., Abdullayev, G. B., Cojayev, E. M., Rzayeva, La. A., Agayev, G. A.: Mater. Res. Bull. 7 (1972) 1497.
- 73M Müller, D., Eulenberger, G., Hahn, H.: Z. Anorg. Allg. Chem. 398 (1973) 207.
- 77G Giorgianni, U., Mondio, G., Perillo, P., Saitta, G., Vermigho, G.: J. Phys. (Paris) 38 (1977) 1293.
- 78B Bakhyshev, A. F., Lebedev, A. A., Khalafov, Z. D., Yakobson, M. A.: Fiz. Tekh. Poluprovodn. 12 (1978) 555; Sov. Phys. Semicond. (English Transl.) 12 (1978) 320.
- 80G Gavaleshko, N. P., Kitsa, M. S., Savchuk, A. I., Simchuk, R. N.: Fiz. Tekh. Poluprovodn. 14 (1980) 1390; Sov. Phys. Semicond. (English Transl.) 14 (1980) 822.
- 82A Allakhverdiev, K. R., Mamedov, T. G., Salaev, E. Yu., Effendieva, I. K.: Phys. Status Solidi (b) 113 (1982) K43.
- 84A Allakhverdiev, K. R., Babaev, S. S., Bakhyshev, N. A., Mamedov, T. G., Salaev, E. Yu.: Fiz. Tekh. Poluprovodn. 18 (1984) 1307; Sov. Phys. Semicond. (English Transl.) 18 (1984) 817.

Fig. 20.0.14

TlInSe₂. Empirical pseudopotential band structure [84A].

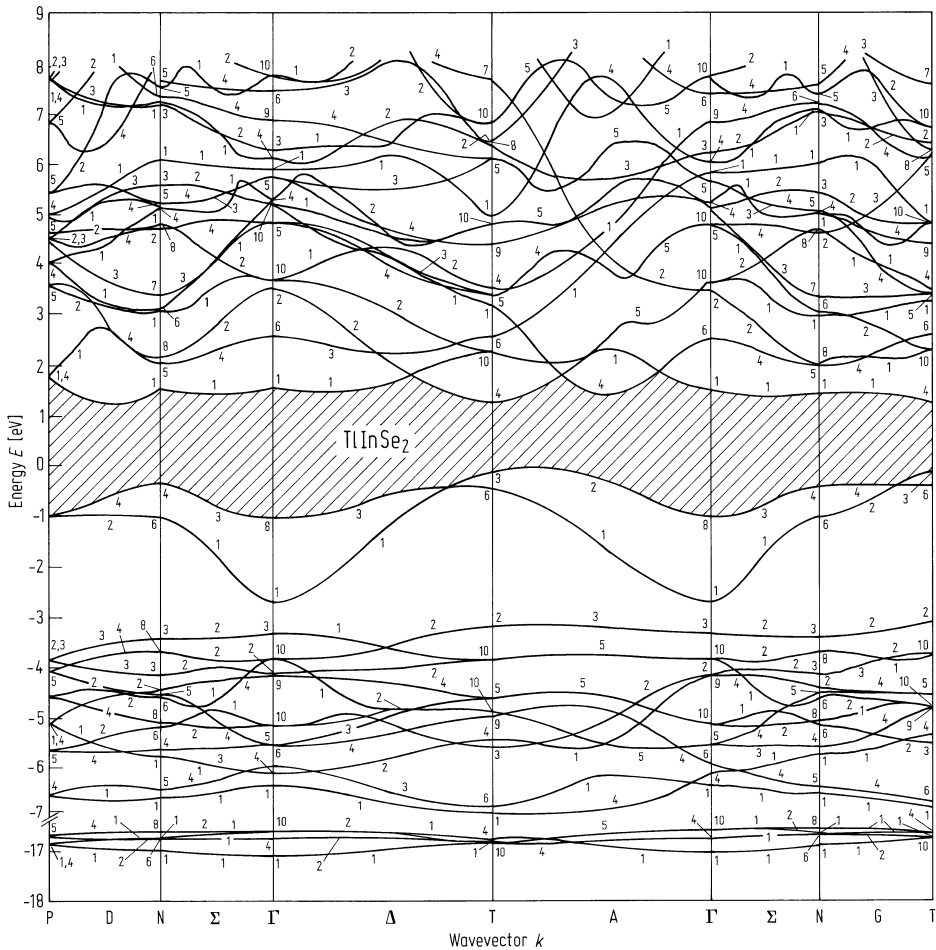


Fig. 20.23.1

TlInSe₂. Electrical conductivity vs. inverse temperature (a), Hall coefficient vs. inverse temperature (b) [69G]. $I \parallel (110)$, $B \perp (110)$.

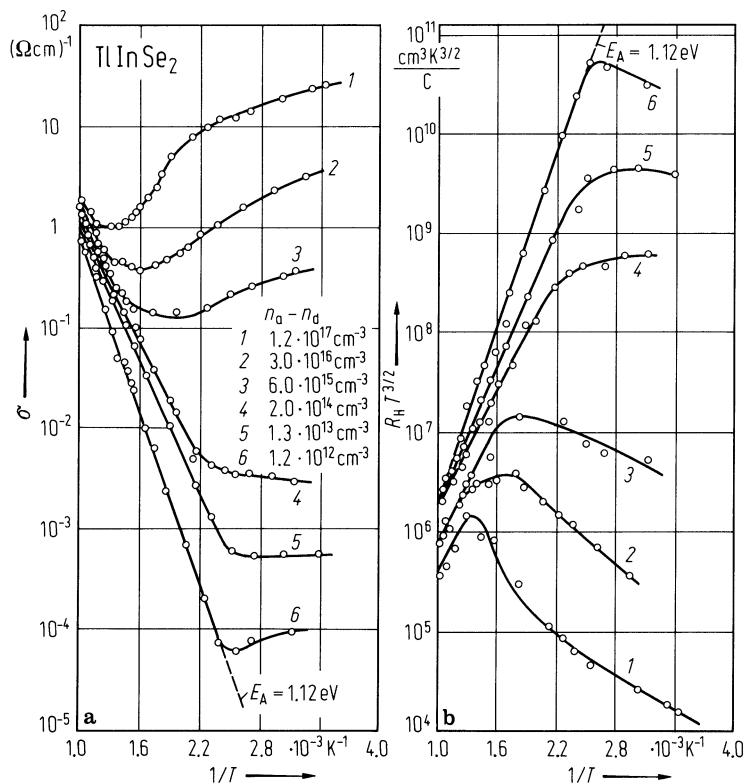


Fig. 20.23.2

TlInSe₂. Electrical conductivity of single crystals vs. temperature, $i \parallel c$ (1), $i \perp c$ (2) [78B].

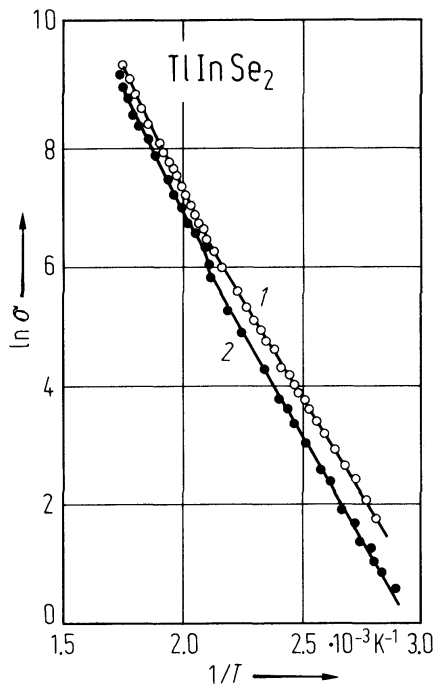
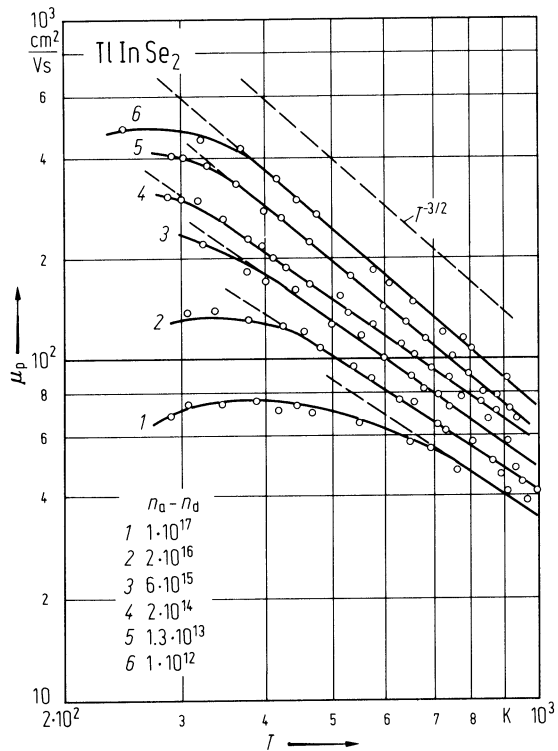


Fig. 20.23.3

TlInSe₂. Hole mobility vs. temperature [69G].



20.24 TlInTe2

Crystal structure

see section 20.0

Electronic properties

band structure similar to TlInSe2.

energy gap

$E_{g,ind}$	0.963 eV	$T = 290\text{ K}$	$E \perp c$, optical absorption	85A2
	0.976 eV		$E \parallel c$	
dE_g/dT	$-0.75 \cdot 10^{-4}\text{ eV K}^{-1}$	$30 < T < 300\text{ K}$	optical absorption	84A1

conduction band, effective mass

m_n	$0.08\ m_0$		density of states mass	69G
-------	-------------	--	------------------------	-----

valence band, effective mass

m_p	$0.31\ m_0$		density of states mass	69G
-------	-------------	--	------------------------	-----

Lattice properties

lattice parameters

a	8.494 \AA	$T = 295\text{ K}$	TlSe-type, tetragonal, space group, $D_{4h}^{18} - I4/mcm$	73M
c	7.181 \AA			

linear thermal expansion coefficient

α	$1.1 \cdot 10^{-5}\text{ K}^{-1}$	$T = 300\text{ K}$	polycrystalline sample	84A2
----------	-----------------------------------	--------------------	------------------------	------

density

d	7.26 g cm^{-3}		calculated (X-ray)	69G
-----	-------------------------	--	--------------------	-----

melting temperature

T_m	$772(5)^{\circ}\text{C}$			67G
-------	--------------------------	--	--	-----

Debye temperature

Θ_D	134 K	$T \rightarrow 0\text{ K}$	specific heat	85A1
------------	----------------	----------------------------	---------------	------

heat capacity

for heat capacity vs. temperature, see Fig. 20.24.1 ($5 < T < 300\text{ K}$).

Transport properties

electrical conductivity : for dependence on temperature, see Fig. 20.24.2.

electron mobility

μ_n	$420\text{ cm}^2/\text{V s}$	$T = 300\text{ K}$		70G
---------	------------------------------	--------------------	--	-----

hole mobility

m_p	$600\text{ cm}^2/\text{V s}$	$T = 300\text{ K}$	for dependence on temperature, see Fig. 20.24.3	70G
-------	------------------------------	--------------------	--	-----

thermal conductivity

κ_{\perp}	$0.018\text{ W cm}^{-1}\text{ K}^{-1}$	$T = 300\text{ K}$	$\perp c$	70G
κ_{\parallel}	$0.024\text{ W cm}^{-1}\text{ K}^{-1}$		$\parallel c$	

Optical properties

dielectric constants

$\varepsilon(\infty)$	14.2	$E \perp c$	oscillator fit to reflectivity data	80G
	11.6	$E \parallel c$		

References to 20.24

- 67G Guseinov, G. D., Ramazanzade, A. M., Kerimova, EM., Ismailov, M. Z.: Phys. Status Solidi 22 (1967) K117.
- 69G Guseinov, G. D., Mooser, E., Kerimova, E. M., Gamidov, R. S., Alekseev, I. V., Jsmailov, M. Z.: Phys. Status Solidi 34(1969) 33.
- 70G Guseinov, G. D., Abduliayev, G. B., Bidzinova, S. M., Seidov, F. M., Ismailov, M. Z., Pashayev, A. M.: Phys. Lett. A 33 (1970) 421.
- 73M Müller, D., Eulenberger, G., Hahn, H.: Z. Anorg. Allg. Chem. 398 (1973) 207.
- 80G Gasanly, N. M., Goncharov, A. F., Dshavadov, B. M., Melnik, N. N., Tagirov, V. I., Vinogradov, E. A.: Phys. Status Solidi (b) 97 (1980) 367.
- 84A1 Abdullaeva, S. G., Abdullaev, A. M., Mamedov, K. K., Mamedov, N. T.: Fiz. Tverd. Tela 26 (1984) 618; Sov. Phys. Solid State (English Transl.) 26 (1984) 375.
- 84A2 Aliev, R. A., Allakhverdiev, K.R., Baranov, A. I., Ivanov, N. R., Sardarly, R. M.: Fiz. Tverd. Tela 26 (1984) 1271; Sov. Phys. Solid State (English Transl.) 26 (1984) 775.
- 85A1 Aldzhanov, M. A., Mamedov, K. K.: Fiz. Tverd. Tela 27 (1985) 3114; Sov. Phys. Solid State (English Transl.) 27 (1985) 1871.
- 85A2 Aldzhanov, M. A., Mamedov, K. K., Abdurragimov, A. A.: Phys. Status Solidi (b) 131 (1985) K35.

Figures to 20.24

Fig. 20.24.1

TlInTe₂. Heat capacity vs. temperature [85A1].

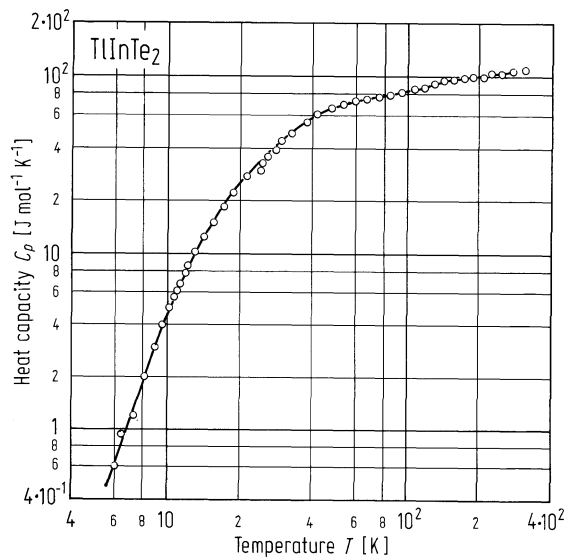


Fig. 20.24.2

TlInTe₂. Electrical conductivity vs. inverse temperature (a), Hall coefficient vs. inverse temperature (b) [69G]. Single crystals; 4, 5 measurements, parallel (||) and perpendicular (⊥) to the cleavage plane, polycrystalline specimen 6.

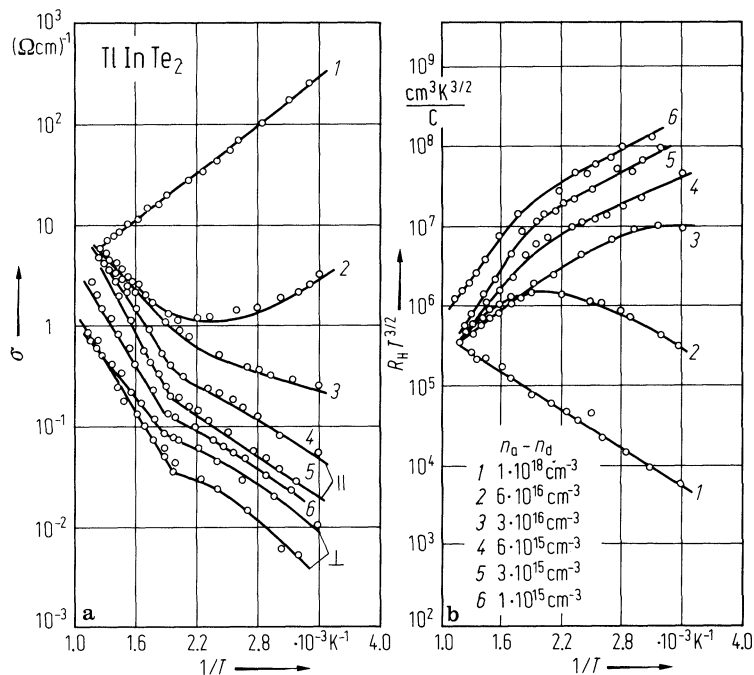
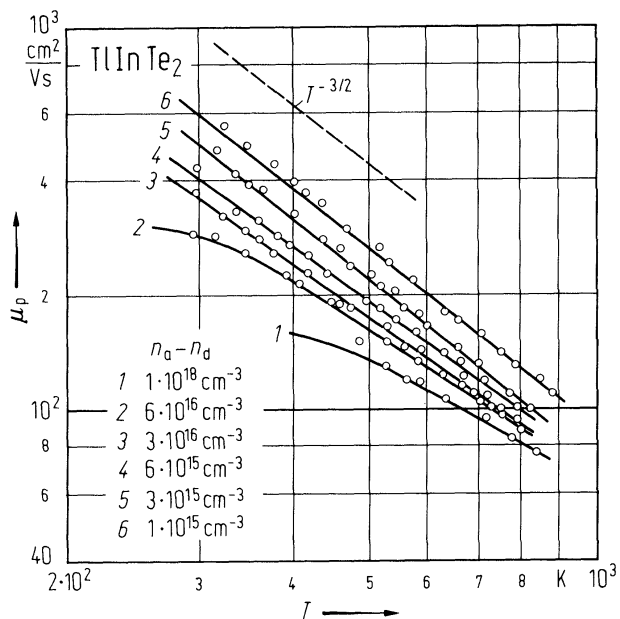


Fig. 20.24.3

TlInTe₂. Hole mobility vs. temperature [69G].



21 III-VII compounds

21.0 Crystal structure and electronic structure

Thallous halides are distinctly different from the well-known semiconducting compounds of the type $A_N B_{VIII-N}$ and also from the alkali halides through the filled cationic 6s-shell, which exceeds the rare gas configuration. These cationic s-electrons are the reason for many peculiar properties of these compounds as e.g. highly ionic bond and extremely high ionic polarizability combined with a "semiconductor-like" energy gap (about 3 eV) and high electronic polarizability, strong electron-phonon coupling combined with Wannier-type excitons, which are due to intracationic transitions.

Depending on external conditions at least TlCl, TlBr, and TlI may be found in the CsCl-, the NaCl- and the TlI-lattice, the latter being the only known representative of the orthorhombic space-group D_{2h}^{17} (Cmcm) (Fig. 21.0.1).

crystal structure of Tl-compounds

TlF	(I)	tetragonal	space group:	$I4/mmm - D_{4h}^{17}$
	(II)	orthorhombic		$Fmmm - D_{2h}^{23}$
TlCl	(I)	CsCl-type		$Pm3m - O_h^1$
	(II)	orthorhombic		$Cmcm - D_{2h}^{17}$
	(III)	NaCl-type		$Fm3m - O_h^5$
TlBr	(I)	CsCl-type		$Pm3m - O_h^1$
	(II)	orthorhombic		$Cmcm - D_{2h}^{17}$
	(III)	NaCl-type		$Fm3m - O_h^5$
TlI	(I)	CsCl-type		$Pm3m - O_h^1$
	(II)	orthorhombic		$Cmcm - D_{2h}^{17}$
	(III)	NaCl-type		$Fm3m - O_h^5$

Brillouin zones :

CsCl-type compounds: Fig. 21.0.2, orthorhombic compounds: Fig. 21.0.3, NaCl-type: Fig. 21.0.4.

energy bands

TlCl(I): Fig. 21.0.5, TlBr(I): Fig. 21.0.6, TlI(I,II,III): Fig. 21.0.7a,b,c.

References to 21.0

- 71O Overhof, H., Treusch, J.: Solid State Commun. 9 (1971) 53.
75H Heidrich, K., Staude, W., Treusch, J., Overhof, H.: Solid State Commun. 16 (1975) 1043.
75V Van Dyke, S. P., Samara, G. A.: Phys. Rev. B 11 (1975) 4935.

Figures to 21.0

Fig. 21.0.1

Enlarged unit cells for (a) NaCl-type, (b) orthorhombic, (c) CsCl-type compounds.

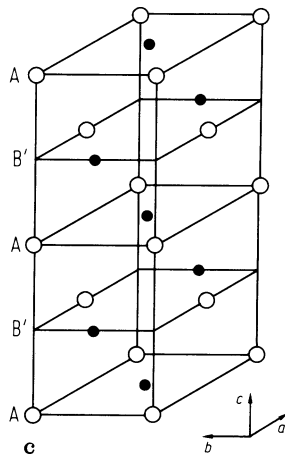
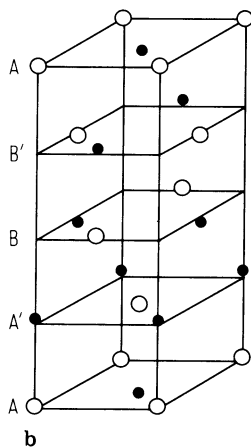
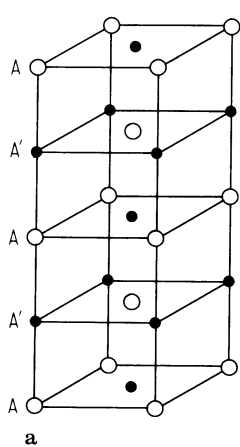


Fig. 21.0.2

Brillouin zone for the CsCl lattice.

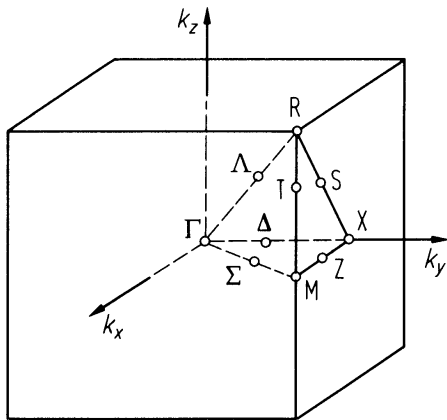


Fig. 21.0.3

Brillouin zone for the orthorhombic lattice.

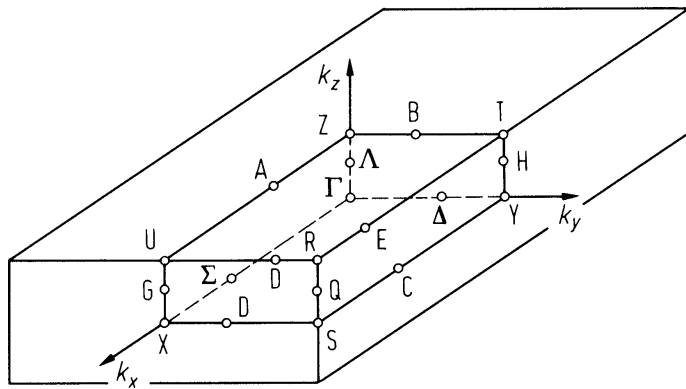


Fig. 21.0.4

Brillouin zone for the NaCl lattice.

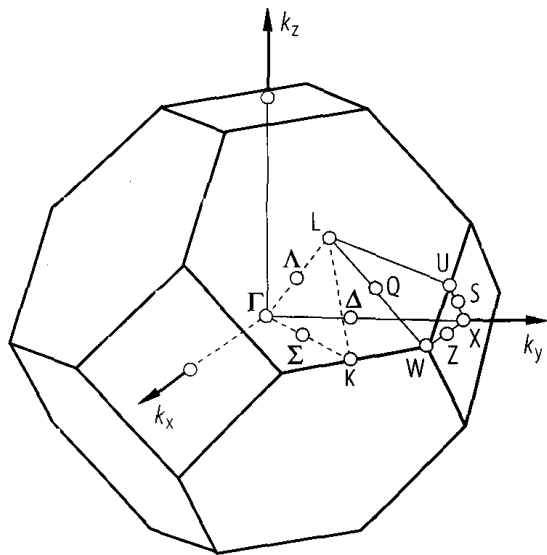


Fig. 21.0.5

TlCl(I). Band structure of sc-TlCl calculated with relativistic KKR-method [71O].

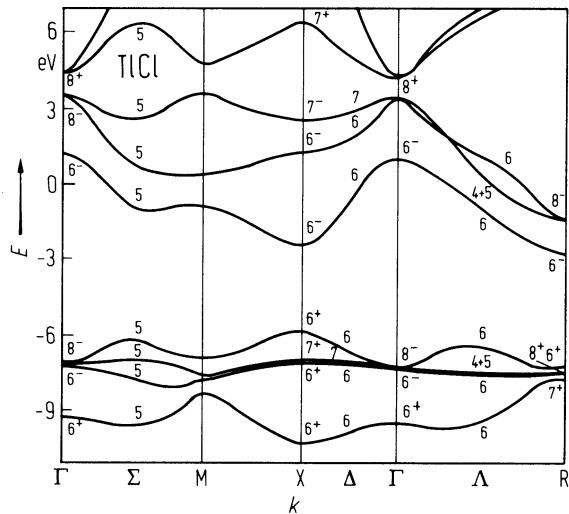


Fig. 21.0.6

TlBr(I). Band structure of sc-TlBr calculated with relativistic KKR-method [71O].

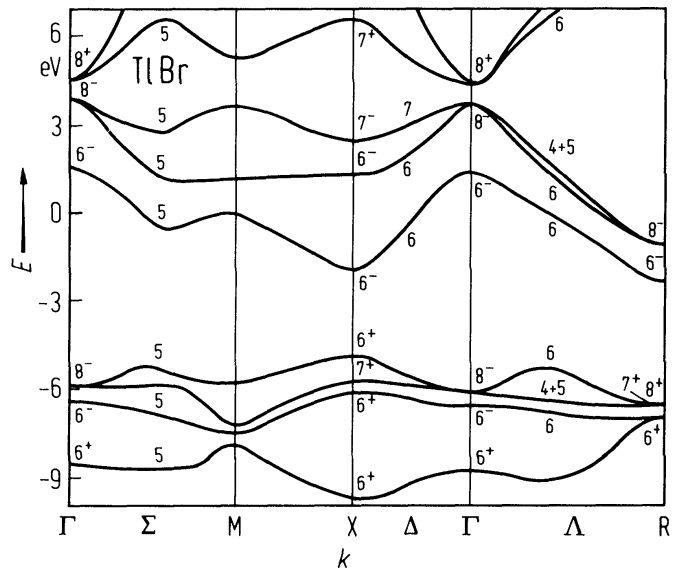


Fig. 21.0.7a

TlI(I). Band structure of sc-TlI calculated with relativistic KKR-method [75H].

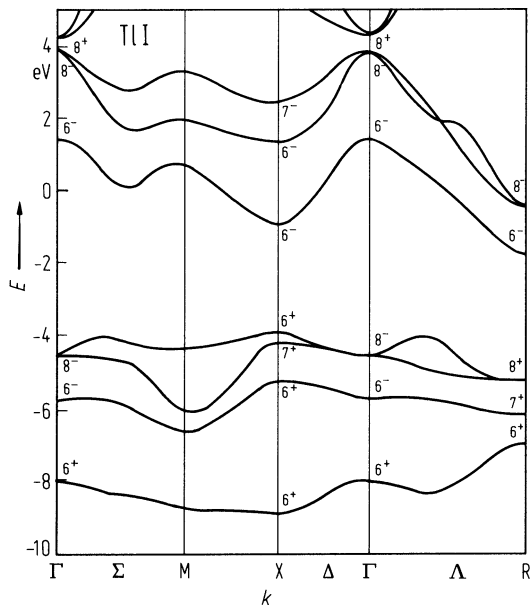


Fig. 21.0.7b

TlI(II). Band structure of orthorhombic TlI calculated with the OPW-method neglecting spin-orbit interaction [75V].

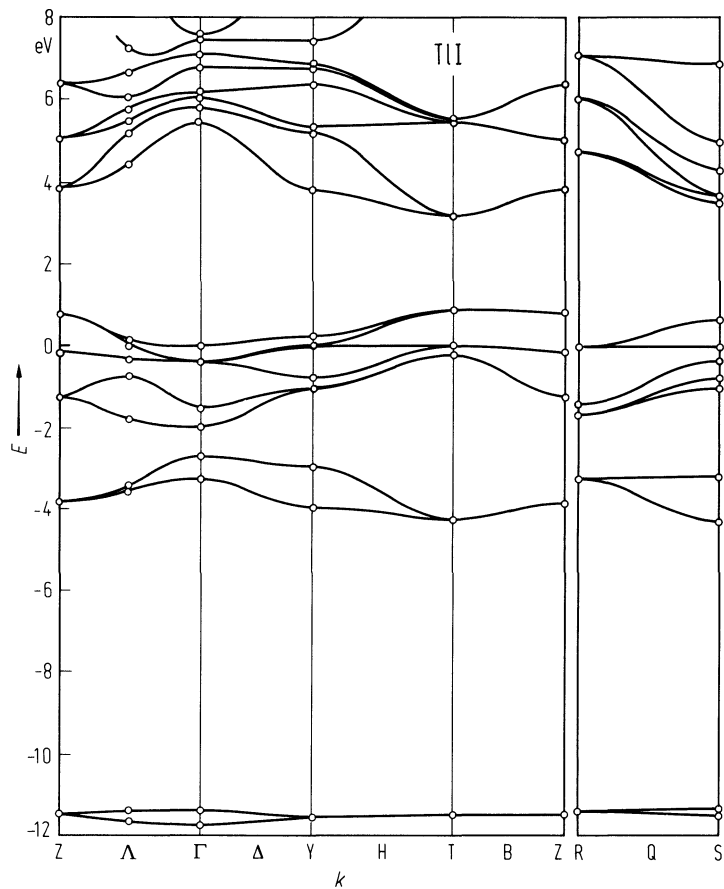
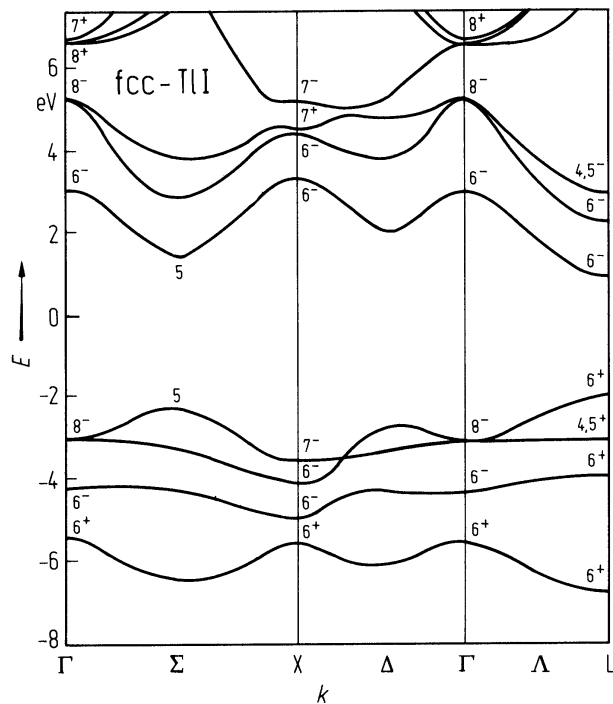


Fig. 21.0.7c

TII(III). Band structure for fcc-TII calculated with relativistic KKR-method [75H].



21.1 Thallium fluoride (TlF)

Physical properties

lattice parameters

TlF (I)				
<i>a</i>	3.771 Å	<i>T</i> = 410 K	X-ray scattering on powdered samples	68P
<i>c</i>	6.115 Å			

TlF (II)				
<i>a</i>	5.190 Å	<i>T</i> = 300 K	X-ray scattering	69B
<i>b</i>	5.506 Å			
<i>c</i>	6.092 Å			

phonon frequencies (TlF (II) -phase)

<i>ν</i> ₁	2.56·10 ¹² s ⁻¹		infrared spectroscopy	69R
<i>ν</i> ₂	3.90·10 ¹² s ⁻¹			
<i>ν</i> ₃	5.44·10 ¹² s ⁻¹			
<i>ν</i> ₄	14.2·10 ¹² s ⁻¹			

dielectric constant (TlF (II) -phase)

<i>ε</i> (0)	17.3	<i>T</i> = 0 K	the high temperature value is	71R
	19.7	<i>T</i> = 300 K	measured at a frequency of 10 ⁶ s ⁻¹	

melting temperature

<i>T</i> _m	595.4 K		normal pressure melting temperature	65C
-----------------------	---------	--	-------------------------------------	-----

References to 21.1

65C Cubicciotti, D., Eding, H.: J. Chem. Eng. Data 10 (1965) 343.
68P Pistorius, C. W. F. T., Clark, J. B.: Phys. Rev. 173 (1968) 692.
69B Bachrach, R. Z.: Solid State Commun. 7 (1969) 1023.
69R Ruoff, A., Weidlein, J.: Z. Anorg. Allg. Chem. 370 (1969) 113.
71R Rao, K. V., Smakula, A.: Mater. Res. Bull. 6 (1971) 1047.

21.2 Thallium chloride (TlCl)

Electronic properties (TlCl (I)-phase)

band structure : Fig. 21.0.5, Brillouin zone: Fig. 21.0.2.

The upper valence band consists of a mixture of Tl-6s-type and Cl-3p-type bands with eight electrons per unit cell. In addition there is a lower Cl-3s-type valence band with two electrons per unit cell. The top of the valence band is situated at point X of the BZ and has X_1^+ (X_6^+) -symmetry. The lowest set of conduction bands is Tl-6p-type with an absolute minimum at the R-point and a closely neighbored minimum at the X-point with symmetry X_4^- (X_6^-).

energy gaps and related parameters

$E_{\text{gx,ind}}$ ($X_{6v}^+ - R_{6c}^-$)	3.225(1) eV	$T = 4.2$ K	optical absorption, line shape fitting to an indirect forbidden exciton	74N
$E_{\text{b,ind}}$	0.023(3) eV	$T = 4.2$ K	binding energy of indirect exciton	79F
$E_{\text{gx,dir}}$ ($X_{6v}^+ - X_{6c}^-$)	3.4008 eV	$T = 4$ K	low and high energy component of the intervalley split direct exciton.	78F
$E_{\text{b,dir}}$	0.0113 eV	$T = 4.2$ K	binding energy of the high energy component of the intervalley split exciton, from magnetoabsorption	71K
$dE_{\text{g,dir}}/dT$	$+ 4.6 \cdot 10^{-4}$ eV K ⁻¹	$T = 4...300$ K	average value from one- and two-photon absorption, see Fig. 21.2.1	70B, 72F

effective masses (polaron masses)

$m_n^{**}(\text{R})$	0.55(3) m_0		cyclotron resonance assigned to bottom of conduction band at R	72H
$m_n^{**}(\text{X})$	0.7 m_0		magnetoreflexion measurements at the direct exciton series	79N
$m_{\text{p}\parallel}^{**}(\text{X})$	0.58(3) m_0		cyclotron resonance values assigned to top of the valence band at X	72H
$m_{\text{p}\perp}^{**}(\text{X})$	0.98(4) m_0			72H

Lattice properties

lattice parameters

<i>TlCl (I)</i>				
<i>a</i>	3.84145(12) Å	<i>T</i> = 293 K	electron interference	64W
<i>TlCl (II)</i>				
<i>a</i>	4.74(3) Å	<i>T</i> = 300 K	electron diffraction on thin layers evaporated onto NaCl, KBr, KI	63U
<i>b</i>	4.27(3) Å	(evaporation		
<i>c</i>	12.4 Å	at 200...240 K)		
<i>TlCl (III)</i>				
<i>a</i>	6.30(2) Å	<i>T</i> = 300 K	electron diffraction on thin layers evaporated onto KBr	51S

Debye temperature

Θ_D	141.1 K	$T = 0$ K	calculated from the elastic constants at 0 K	75G
	393.5 K	$T = 290$ K		

density				
d	7.01829 g cm ⁻³	$T = 300$ K	from X-ray scattering experiments	55S

melting temperature

T_m	704.0 K		normal pressure melting temperature;	65C
-------	---------	--	--------------------------------------	-----

phonon dispersion relations for TlCl (I) : Fig. 21.2.2.

The lattice properties of TlCl (I) are similar to the simple cubic TlBr.

phonon frequencies

$\bar{\nu}_{\text{TO}}(\Gamma)$	$1.89 \cdot 10^{12}$ s ⁻¹	$T = 300$ K	infrared absorption and reflection	61J
$\bar{\nu}_{\text{LO}}(\Gamma)$	$5.19 \cdot 10^{12}$ s ⁻¹	$T = 290$ K		72L
$\bar{\nu}(\text{M})$	$0.31 \cdot 10^{12}$ s ⁻¹	$T = 4.2$ K	optical absorption at the forbidden indirect exciton	79F

sound velocities

v_{LA}	$2.392 \cdot 10^5$ cm s ⁻¹	$T = 300$ K	[100]-direction	72K
v_{TA}	$1.057 \cdot 10^5$ cm s ⁻¹		[100]-direction	
v_{LA}	$2.252 \cdot 10^5$ cm s ⁻¹		[110]-direction	
$v_{\text{TA,I}}$	$1.057 \cdot 10^5$ cm s ⁻¹		[110]-direction, lower branch	
$v_{\text{TA,II}}$	$1.328 \cdot 10^5$ cm s ⁻¹		[110]-direction, upper branch	
v_{LA}	$2.203 \cdot 10^5$ cm s ⁻¹		[111]-direction	
v_{TA}	$1.245 \cdot 10^5$ cm s ⁻¹		[111]-direction	

second order elastic moduli

c_{11}	$4.015 \cdot 10^{11}$ dyn cm ⁻²	$T = 300$ K	ultra sound velocity measurements	72K
	$4.066 \cdot 10^{11}$ dyn cm ⁻²		([75G] contains also data from 150...	75G
c_{44}	$0.7843 \cdot 10^{11}$ dyn cm ⁻²		300 K)	72K
	$0.77 \cdot 10^{11}$ dyn cm ⁻²			75G
c_{12}	$1.537 \cdot 10^{11}$ dyn cm ⁻²		(for temperature dependence,	72K
	$1.587 \cdot 10^{11}$ dyn cm ⁻²		see Fig. 21.2.3)	75G

Transport properties (TlCl(I)-phase)

Unlike usual ionic crystals, TlCl has rather large photoconductivity even at low temperatures in the fundamental absorption region. Both, electrons and holes are mobile. The dominating scattering mechanisms are: coupling to the polar optical phonon, deformation potential coupling and scattering at isoelectronic impurities.

mobilities of charge carriers

μ_n	20.0 cm ² /V s	$T = 298$ K	from drift mobility measurements	67K
			between 90 and 330 K.	
			For temperature dependence, see Fig. 21.2.4	
	$5 \cdot 10^3$ cm ² /V s	$T = 4.2$ K	from cyclotron resonance	69T
μ_p	$6.5 \cdot 10^3$ cm ² /V s	$T = 19.6$ K	for temperature dependence,	68M
			see Fig. 21.2.5	

dielectric constants

$\epsilon(0)$	37.2	$T = 2$ K	low frequency ($10^3 \dots 10^6$ s ⁻¹)	72L
	32.7	$T = 293$ K	capacity measurements	

$\epsilon(0)$ shows a Curie-Weiss behaviour with $\Theta_{\text{pe}} = -2100$ K [72L]. (Θ_{pe} = paraelectric Curie temperature).

$\epsilon(\infty)$	5.00	$T = 2$ K	from refractive index data	69L
	4.76	$T = 290$ K		

References to 21.2

- 51S Schulz, L. G.: Acta Crystallogr. 4 (1951) 487.
- 55S Smakula, A., Kalnajs, J.: Phys. Rev. 99 (1955) 1737, 1744, 1747.
- 61J Jones, G. O., Martin, D. H., Mawer, P. A., Perry, C. H.: Proc. Roy. Soc. (London) Ser. A216 (1961) 10.
- 63U Ungelenk, J.: Phys. Kondensierten Materie 1 (1963) 152.
- 64W Witt, W.: Z. Naturforsch. 19a (1964) 1363.
- 65C Cubicciotti, D., Eding, H.: J. Chem. Eng. Data 10 (1965) 343.
- 67K Kobayashi, K., Kawai, T., Kanada, M.: J. Phys. Soc. Jpn. 23 (1967) 305.
- 68M Makita, Y., Kobayashi, K., Kanada, M., Kawai, T.: J. Phys. Soc. Jpn. 25 (1968) 816.
- 69L Lowndes, R. P., Martin, D. R.: Proc. Roy. Soc. (London) Ser. A398 (1969) 473.
- 69T Tamura, H., Masumi, T., Kobayashi, K.: Proc. 3rd Int. Conf. on Photoconductivity 1969 (Pergamon Press, Oxford 1971) p. 183.
- 70B Bachrach, R. Z., Brown, F. C.: Phys. Rev. B1 (1970) 818.
- 71K Kawai, T., Kobayashi, K., Kurita, M., Makita, Y.: J. Phys. Soc. Jpn. 30 (1971) 1101.
- 71O Overhof, H., Treusch, J.: Solid State Commun. 9 (1971) 53.
- 72F Fröhlich, D., Treusch, J., Kottler, W.: Phys. Rev. Lett. 29 (1972) 1603.
- 72H Hodby, J. W., Jenkin, G. T., Kobayashi, K., Tamura, H.: Solid State Commun. 10 (1972) 1017.
- 72K Kodama, M., Saito, S., Minomura, S.: J. Phys. Soc. Jpn. 33 (1972) 1361.
- 72L Lowndes, R. P.: Phys. Rev. B6 (1972) 1490.
- 74N Nakahara, J., Kobayashi, K., Fujii, A.: J. Phys. Soc. Jpn. 37 (1974) 1312.
- 75G Gluyas, M., Hunter, R., James, B. W.: J. Phys. C8 (1975) 271.
- 78F Fujita, M., Ohno, N., Nakamura, K.: J. Phys. Soc. Jpn. 44 (1978) 1861.
- 79F Fujii, A., Nakahara, S., Kobayashi, K., Fujii, Y.: J. Phys. Soc. Jpn. 46 (1979) 1218.
- 79N Nakahara, S.: Solid State Commun. 29 (1979) 115.

Figures to 21.2

Fig. 21.0.2

Brillouin zone for the CsCl lattice.

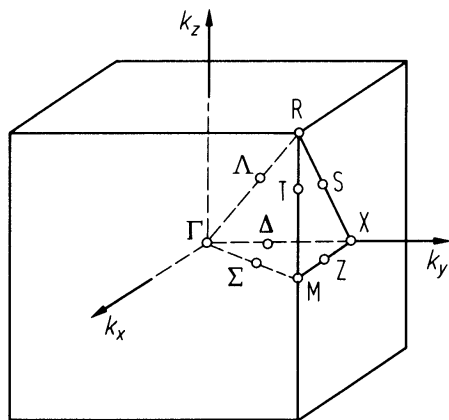


Fig. 21.0.5

TlCl(I). Band structure of sc-TlCl calculated with relativistic KKR-method [710].

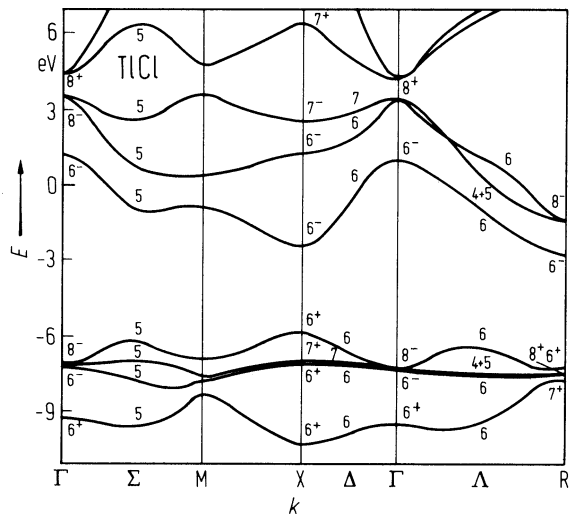


Fig. 21.2.1

TlCl(I). Energy gap vs. temperature. Full circles: one-photon absorption [70B], open circles: two-photon absorption [72F].

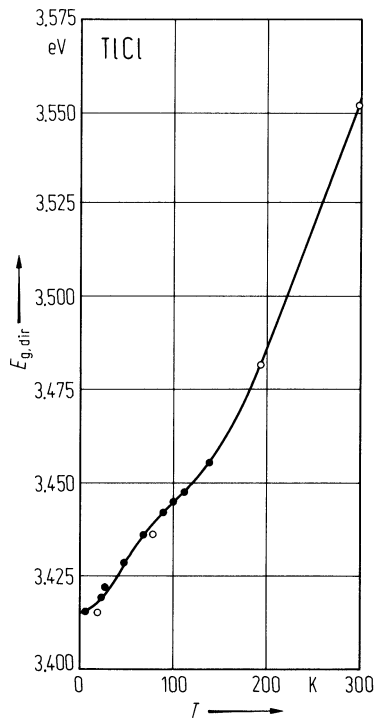


Fig. 21.2.2

TlBr(I). Phonon frequencies vs. wave vector along $[110]$ from neutron scattering (circles) and infrared data (triangles) [72L].

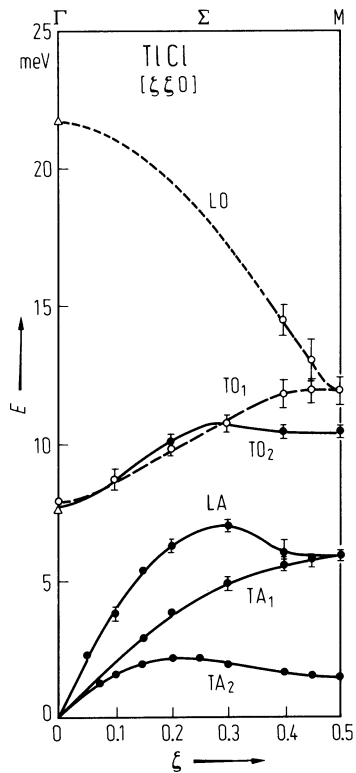


Fig. 21.2.3

TlCl(I). Second order elastic moduli vs. temperature from measurements of ultrasonic wave transit times [75G].

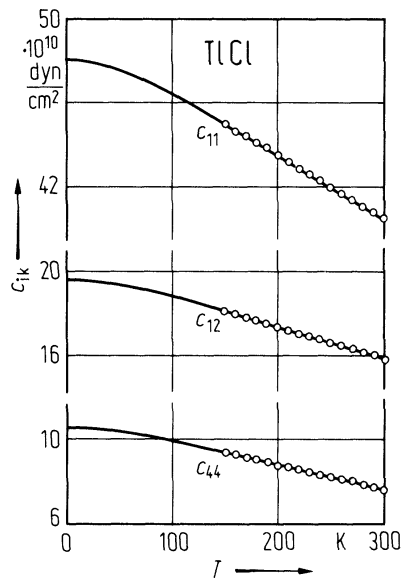


Fig. 21.2.4

TlCl(I). Drift mobilities of electrons vs. inverse temperature. Full line represents microscopic mobility for pure crystals. (1) $n_t = 8.4 \cdot 10^{14} \text{ cm}^{-3}$, (2) $n_t = 1.2 \cdot 10^{16} \text{ cm}^{-3}$ (3) $n_t = 3.3 \cdot 10^{16} \text{ cm}^{-3}$ [67K]. n_t : number of traps.

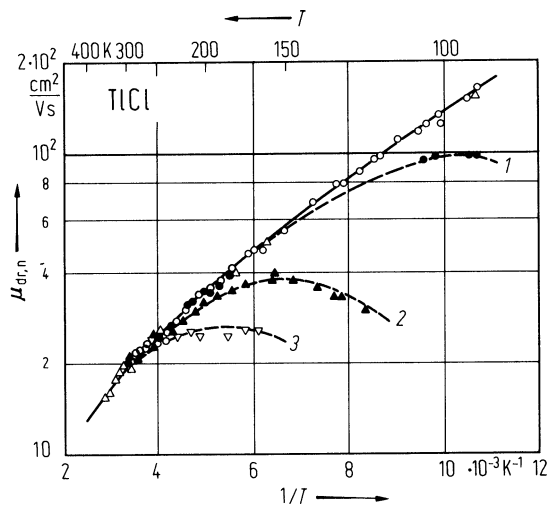
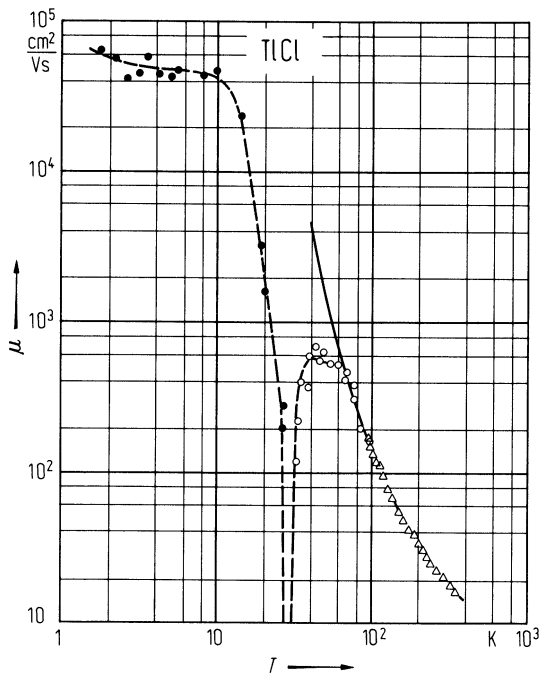


Fig. 21.2.5

TlCl(I). Hall mobility of photocarriers vs. temperature. Full circles: positive carrier sign, open circles: negative carrier sign, triangles: drift mobilities [68M].



21.3 Thallium bromide (TlBr)

Electronic properties (TlBr(I)-phase)

band structure : Fig. 21.0.6, Brillouin zone: Fig. 21.0.2.

The general shape of bands is the same as in simple cubic TlCl, the main difference being the larger spin-orbit splitting of the 4p-type bromine valence levels.

energy gaps and related parameters

$E_{\text{gx,ind}}(\text{X}_{6\text{v}}^+-\text{R}_{6\text{c}}^-)$	2.650 eV	$T = 2 \text{ K}$	optical absorption, line shape fitting for an indirect forbidden exciton	74N
$E_{\text{b,ind}}$	0.023 eV			74N
$E_{\text{gx,dir}}(\text{X}_{6\text{v}}^+-\text{X}_{6\text{c}}^-)$	3.009 eV 3.0104 eV	$T = 4 \text{ K}$	low and high energy component of the intervalley split direct exciton.	78F
$E_{\text{b,dir}}$	0.0091(11) eV	$T = 4.2 \text{ K}$	binding energy of the high energy component of the exciton	80N
$dE_{\text{g,dir}}/dT$	$3.3 \cdot 10^{-4} \text{ eV K}^{-1}$	$T = 4 \dots 200 \text{ K}$	average value from one- and two-photon absorption, see Fig. 21.3.1	70G, 70B, 72F

effective masses (polaron masses)

$m_{\text{n}}^{**}(\text{R})$	0.525(30) m_0		cyclotron resonance	72H
$m_{\text{n}}^{**}(\text{X})$	0.45...0.51 m_0		magnetoabsorption and reflexion on the direct exciton series	80N
$m_{\text{p}\parallel}^{**}(\text{X})$	0.55(3) m_0		cyclotron resonance	72H
$m_{\text{p}\perp}^{**}(\text{X})$	0.74(3) m_0			

Lattice properties

lattice parameters

<i>TlBr (I)</i>				
<i>a</i>	3.98588 Å	<i>T</i> = 300 K	X-ray scattering	55S
<i>TlBr (II)</i>				
<i>a</i>	4.96(3) Å	<i>T</i> = 300 K	electron diffraction on thin layers evaporated onto NaCl, KCl, KI	63U
<i>b</i>	4.39(3) Å	(evaporation		
<i>c</i>	12.5 Å	at 200...240 K)		
<i>TlBr (III)</i>				
<i>a</i>	6.58 Å	<i>T</i> = 300 K	electron diffraction on thin layers evaporated onto LiF, NaCl, and KBr	51S

volume expansion coefficient (TlBr(I)-phase)

β	$1.479 \cdot 10^{-4} \text{ K}^{-1}$	$T = 260 \text{ K}$	for temperature dependence of linear expansion coefficient, see Fig. 21.3.2	67M, 72R
---------	--------------------------------------	---------------------	---	-------------

Debye temperature

Θ_{D}	290(20) K	$T = 290 \text{ K}$	see also Fig. 21.3.3	67C
---------------------	-----------	---------------------	----------------------	-----

density

d	7.45292 g cm ⁻³	$T = 300 \text{ K}$	X-ray scattering	55S
-----	----------------------------	---------------------	------------------	-----

melting temperature

T_m	733.2 K	normal pressure melting temperature,	65C
-------	---------	--------------------------------------	-----

phonon dispersion relations for TlBr (I) : Fig. 21.3.4.

The lattice properties are similar to the simple cubic TlCl. Due to the high polarizability of the cationic s-shell the static dielectric constant is unusually large. As a consequence the longitudinal-transverse splitting of the optical phonon branch is in the range of pure ionic material, although the value of the electronic dielectric constant is semiconductor-like.

phonon frequencies (TlBr (I))

$\nu_{TO}(\Gamma)$	$1.39 \cdot 10^{-12} \text{ s}^{-1}$	$T = 100 \text{ K}$	inelastic neutron scattering	67C
$\nu_{LO}(\Gamma)$	$3.37 \cdot 10^{-12} \text{ s}^{-1}$			
$\nu(X)$	$0.68 \cdot 10^{-12} \text{ s}^{-1}$			
$\nu(M)$	$0.54 \cdot 10^{-12} \text{ s}^{-1}$			
$\nu(R)$	$1.32 \cdot 10^{-12} \text{ s}^{-1}$			

second order elastic moduli

c_{11}	$3.76 \cdot 10^{11} \text{ dyn cm}^{-2}$	$T = 298 \text{ K}$	ultrasonic velocity measurements	67M
c_{44}	$0.757 \cdot 10^{11} \text{ dyn cm}^{-2}$	$T = 298 \text{ K}$	for temperature dependence	
c_{12}	$1.458 \cdot 10^{11} \text{ dyn cm}^{-2}$	$T = 298 \text{ K}$	(4.2...700 K) , see Fig. 21.3.5	

Transport properties (TlBr(I)-phase)

Transport properties and scattering mechanisms of carriers are similar to those of TlCl.

mobility of charge carriers

μ_n	$15000 \text{ cm}^2/\text{V s}$	$T = 7.3 \text{ K}$	photoexcited Hall mobility	72M
	$30 \text{ cm}^2/\text{V s}$	$T = 298 \text{ K}$	between 1.8 and 100 K; between 90 and 330 K; for temperature dependence, see Fig. 21.3.6	
μ_p	$35000 \text{ cm}^2/\text{V s}$	$T = 1.8 \text{ K}$		71K
	$4 \text{ cm}^2/\text{V s}$	$T = 298 \text{ K}$	drift mobility, see Fig. 21.3.6	

Optical properties

dielectric constants (TlBr(I)-phase)

$\epsilon(0)$	30.6	$T = 293 \text{ K}$	capacity measurements; for temperature dependence, see Fig. 21.3.7	68S
---------------	------	---------------------	---	-----

$\epsilon(0)$ shows a Curie-Weiss behavior with $\Theta_{pe} = -1600 \text{ K}$ [72L] (Θ_{pe} : paraelectric Curie temperature).

$\epsilon(\infty)$	5.64	$T = 2 \text{ K}$	from refractive index data	69L
	5.34	$T = 290 \text{ K}$		

References to 21.3

- 51S Schulz, L. G.: Acta Crystallogr. 4 (1951) 487.
- 55S Smakula, A., Kalnajs, J.: Phys. Rev. 99 (1955) 1737, 1744, 1747.
- 63U Ungelenk, J.: Phys. Kondensierten Materie 1 (1963) 152.
- 65C Cubicciotti, D., Eding, H.: J. Chem. Eng. Data 10 (1965) 343.
- 67C Cowley, E. R., Okazaki, A.: Proc. Roy Soc. (London) Ser. A300 (1967) 45.
- 67M Morse, G. E., Lawson, A. W.: J. Phys. Chem. Solids 28 (1967) 939.
- 68S Samara, G. A.: Phys. Rev. 165 (1968) 959.
- 69L Lowndes, R. P., Martin, D. R.: Proc. Roy Soc. (London) Ser. A398 (1969) 473.
- 70B Bachrach, R. Z., Brown, F. C.: Phys. Rev. B1 (1970) 818.
- 70G Grant, A. J., Liang, W. Y., Yoffe, A. D.: Phil. Mag. 22 (1970) 1129.
- 71B Brade, R. N., Yates, B.: J. Phys. C4 (1971) 417.
- 71K Kawai, T., Kobayashi, K., Kurita, M., Makita, Y.: J. Phys. Soc. Jpn. 30 (1971) 1101.
- 71O Overhof, H., Treusch, J.: Solid State Commun. 9 (1971) 53.
- 72F Fröhlich, D., Treusch, J., Kottler, W.: Phys. Rev. Lett. 29 (1972) 1603.
- 72H Hodby, J. W., Jenkin, G. T., Kobayashi, K., Tamura, H.: Solid State Commun. 10 (1972) 1017.
- 72M Makita, Y., Kobayashi, K.: J. Phys. Soc. Jpn. 32 (1972) 1262.
- 72R Redmond, A. D., Yates, B.: J. Phys. C5 (1972) 1589.
- 74N Nakahara, J., Kobayashi, K., Fujii, A.: J. Phys. Soc. Jpn. 37 (1974) 1312.
- 78F Fujita, M., Ohno, N., Nakamura, K.: J. Phys. Soc. Jpn. 44 (1978) 1861.
- 80N Nakahara, S., Fujii, A.: J. Phys. Soc. Jpn. 48 (1980) 1184.

Figures to 21.3

Fig. 21.0.2

Brillouin zone for the CsCl lattice.

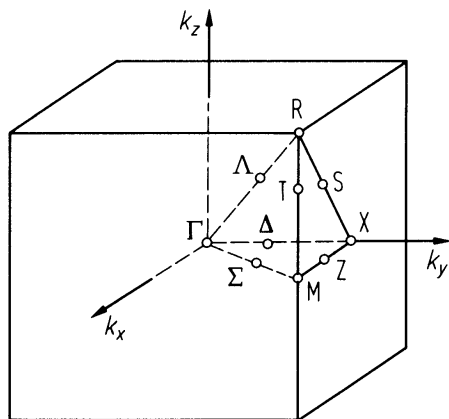


Fig. 21.0.6

TlBr(I). Band structure of sc-TlBr calculated with relativistic KKR-method [71O].

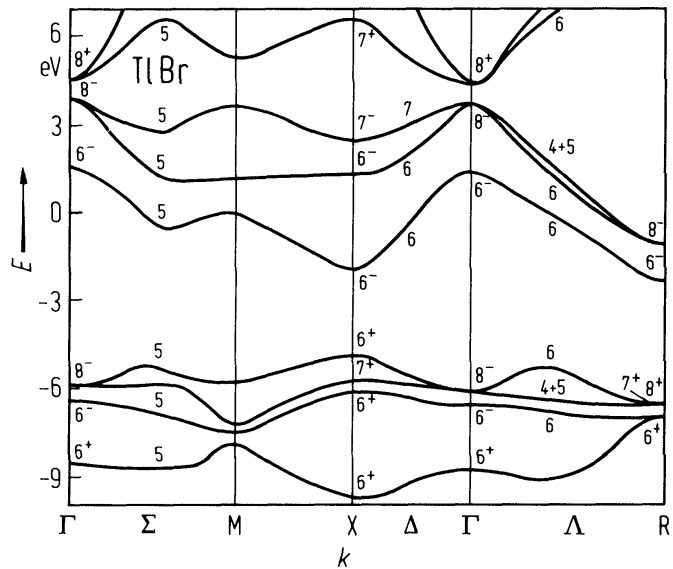


Fig. 21.3.1

TlBr(I). Energy gap vs. temperature. Full circles: [71B], triangles: [70G], one-photon absorption; open circles: [72F], two-photon absorption.

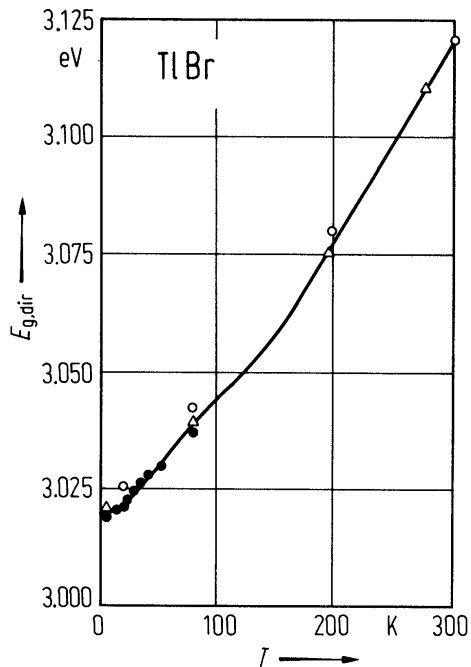


Fig. 21.3.2

TlBr(I). Linear thermal expansion coefficient vs. temperature from various authors [72R].

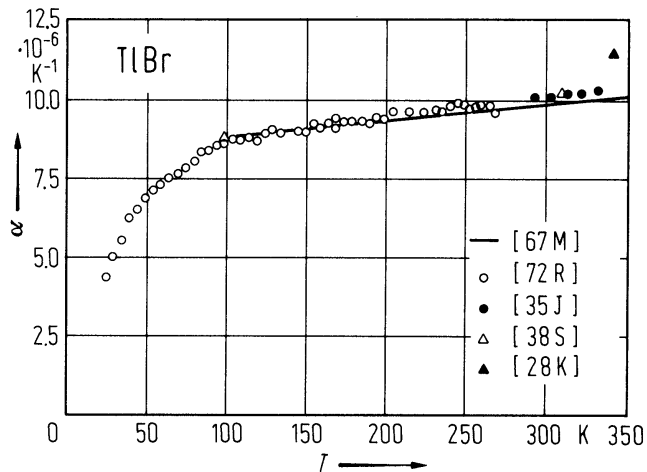


Fig. 21.3.3

TlBr(I). Debye temperature vs. temperature. Inset shows details below 20 K. Circles: heat capacity measurements [71B], full line: calculated [67C], dashed line: interpolated, triangle: calculated from low temperature elasticity measurements.

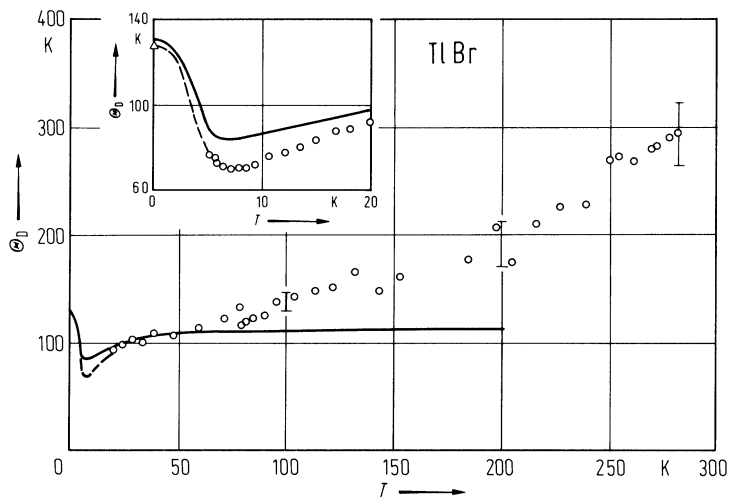


Fig. 21.3.4

TlBr(I). Phonon frequencies vs. wave vector along $[110]$ and $[111]$ -directions measured with neutron scattering at 100 K. Full circles: transverse modes, open circles: longitudinal modes, crosses: L and T modes almost degenerate.

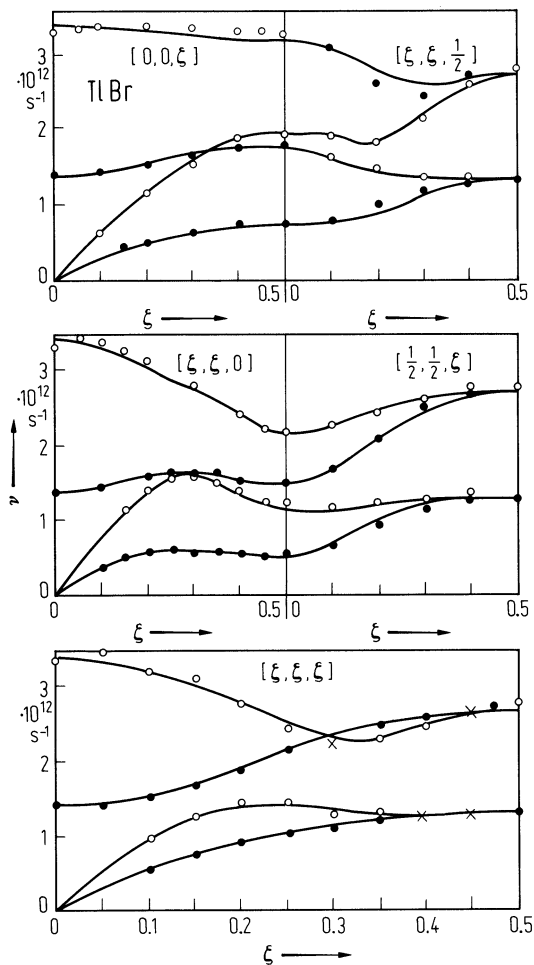


Fig. 21.3.5

TlBr(I). Second order elastic moduli vs. temperature from ultrasonic velocity measurements using a pulse-echo technique [67M]. c_{12} is calculated from c_{11} and c_{44} .

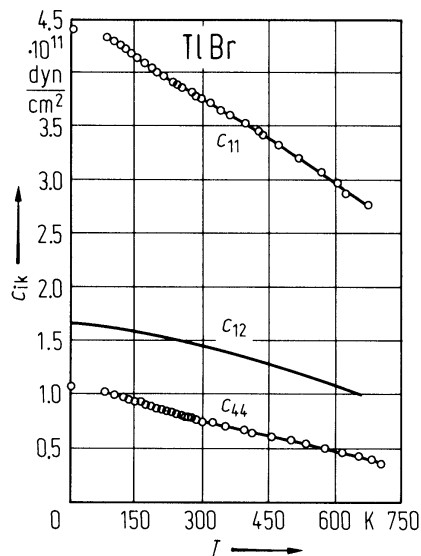


Fig. 21.3.6

TlBr(I). Electron and hole drift mobilities vs. inverse temperature [71K]. Debye temperature is indicated by an arrow.

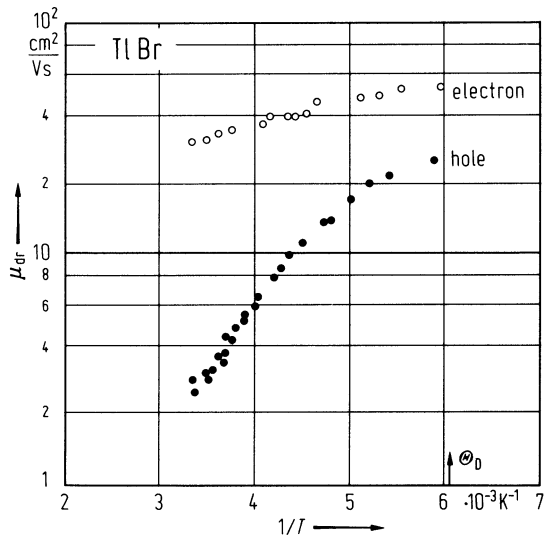
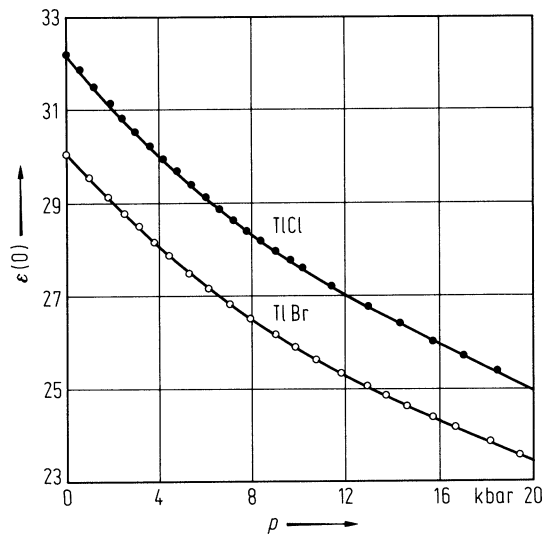


Fig. 21.3.7

TlCl(I), TlBr(I). Static dielectric constants for sc crystals vs. pressure at 295 K and a frequency of 10^4 s^{-1} [68S].



21.4 Thallium iodide

Electronic properties (Tl(I)-phase)

band structure : Fig. 21.0.7a, Brillouin zone: Fig. 2.10.2.

The band structure is analogous to those of TlCl and TlBr. Quantitative changes in the valence band are due to large spin-orbit splitting of the I-5p-levels.

energy gaps and related parameters

$E_{g,ind}(X_{6v}^{+}-R_{6c}^{-})$	2.1 eV	$T = 77$ K	optical absorption on thin layers evaporated onto CsI.	75H
$E_{gx,dir}$	2.7778 eV	$T = 4$ K	optical absorption on thin layers	77F
$E_{b,dir}$	0.011(1) eV	$T = 4$ K		77F

Electronic properties (Tl(II)-phase)

band structure : Fig. 21.0.7b, Brillouin zone: Fig. 21.0.3.

The upper valence band consists of I-5p and Tl-6s type bands with 16 electrons per unit cell. In addition there is a lower I-6s type valence band with 4 electrons per unit cell. The top of the valence band occurs at the T-point of the BZ [75V].

The conduction band is Tl-6p type with two closely neighbored minima at Z and T.

energy gaps and related parameters

$E_{gx,dir}$	2.867 eV	$T = 4.7$ K	optical absorption on strain reduced films	69B
$E_{g,dir}$	2.8 eV	$T = 80$ K	optical absorption on thin films	70G
$dE_{g,dir}/dT$	< 0 eV/K	$T = 4.7$ K	optical absorption on strain reduced films	69B

Electronic properties (Tl(III)-phase)

band structure : Fig. 21.0.7c, Brillouin zone: Fig. 21.0.4.

energy gaps

$E_{gx,dir}$	2.92 eV	$T = 77$ K	optical absorption on thin layers evaporated onto RbI	75H
$E_{g,dir}(L_{6v}^{+}-L_{6c}^{-})$	3 eV		(an exciton binding energy of 50...100 meV is estimated)	

Lattice properties

lattice parameters

<i>TlI (I)</i>				
a	4.205(7) Å	$T = 290$ K	X-ray scattering on layers evaporated onto amorphous substrate	61B
	4.2099(3) Å	$T = 293$ K	X-ray scattering, extrapolation from bulk measurements at temperatures between 440...570 K	67S

temperature dependence, Fig. 21.4.1

<i>TlI (II)</i>				
a	4.59 Å	$T = 290$ K	electron diffraction on thin evaporated layers (Note different nomenclature as compared to [67S])	63U
b	5.25 Å			
c	12.93 Å			

temperature dependence, Fig. 21.4.2

TII (III)

<i>a</i>	6.96...6.99 Å	<i>T</i> = 300 K	X-ray diffraction on thin layers evaporated on heated substrates. <i>a</i> depends on substrate	60K
----------	---------------	------------------	--	-----

density (TII(II))

<i>d</i>	7.088 g cm ⁻³	<i>T</i> = 280 K		67S
----------	--------------------------	------------------	--	-----

melting temperature

<i>T_m</i>	715.2 K		normal pressure melting temperature	65C
----------------------	---------	--	-------------------------------------	-----

phonon frequencies

$\nu_{\text{TO}}(\Gamma)$	$1.62 \cdot 10^{12} \text{ s}^{-1}$	<i>T</i> = 4.2 K	infrared absorption and reflection	61J
$\nu_{\text{LO}}(\Gamma)$	$2.9(5) \cdot 10^{12} \text{ s}^{-1}$		estimated from the Lyddane-Sachs-Teller relation	69B

Optical properties

dielectric constants

TII (I)

$\epsilon(0)$	29.6	<i>T</i> = 300 K	extrapolated to room temperature and normal pressure	68S
---------------	------	------------------	--	-----

TII (III)

$\epsilon(0)$	20.0	<i>T</i> = 0 K		68S
	21.2	<i>T</i> = 300 K	For temperature dependence, see Fig. 21.4.3	71R
$\epsilon(\infty)$	5.8...6.8			69B

References to 21.4

- 60K Kahn, I. H.: Proc. Phys. Soc. 76 (1960) 507.
- 61B Blackmann, M., Khan, I. H.: Proc. Phys. Soc. 77 (1961) 471.
- 61J Jones, G. O., Martin, D. H., Mawer, P. A., Perry, C. H.: Proc. Roy. Soc. (London) Ser. A216 (1961) 10.
- 63U Ungelenk, J.: Phys. Kondensierten Materie 1 (1963) 152.
- 65C Cubicciotti, D., Eding, H.: J. Chem. Eng. Data 10 (1965) 343.
- 67S Samare, G. A., Walters, L., Northrop, D.: J. Phys. Chem. Solids 28 (1967) 1875.
- 68S Samara, G. A.: Phys. Rev. 165 (1968) 959.
- 69B Bachrach, R. Z.: Solid State Commun. 7 (1969) 1023.
- 70G Grant, A. J., Liang, W. Y., Yoffe, A. D.: Phil. Mag. 22 (1970) 1129.
- 71R Rao, K. V., Smakula, A.: Mater. Res. Bull. 6 (1971) 1047.
- 75H Heidrich, K., Staude, W., Treusch, J., Overhof, H.: Solid State Commun. 16 (1975) 1043.
- 75V Van Dyke, S. P., Samara, G. A.: Phys. Rev. B 11 (1975) 4935.
- 77F Fuji, A., Takiyama, K., Nakahara, S., Kobayashi, K.: J. Phys. Soc. Jpn. 42 (1977) 525.

Figures to 21.4

Fig. 21.0.2

Brillouin zone for the CsCl lattice.

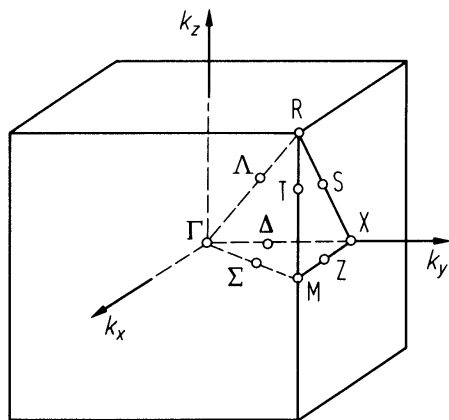


Fig. 21.0.3

Brillouin zone for the orthorhombic lattice.

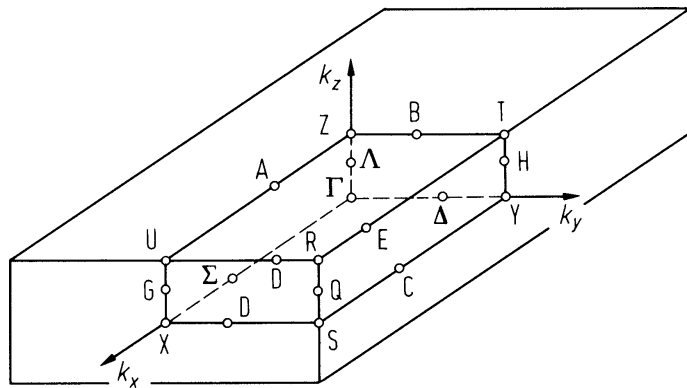


Fig. 21.0.4

Brillouin zone for the NaCl lattice.

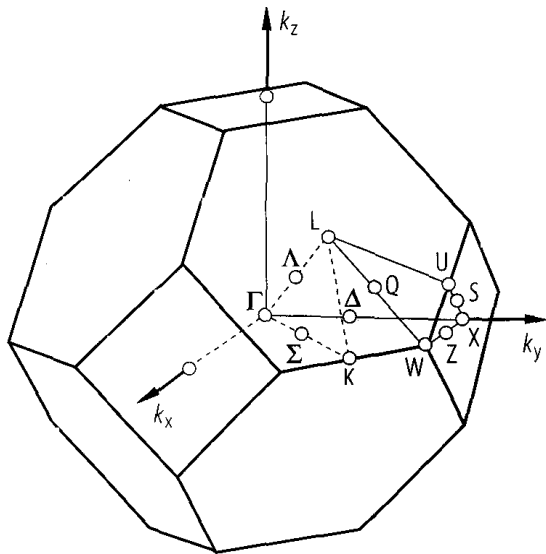


Fig. 21.0.7a

TlI(I). Band structure of sc-TlI calculated with relativistic KKR-method [75H].

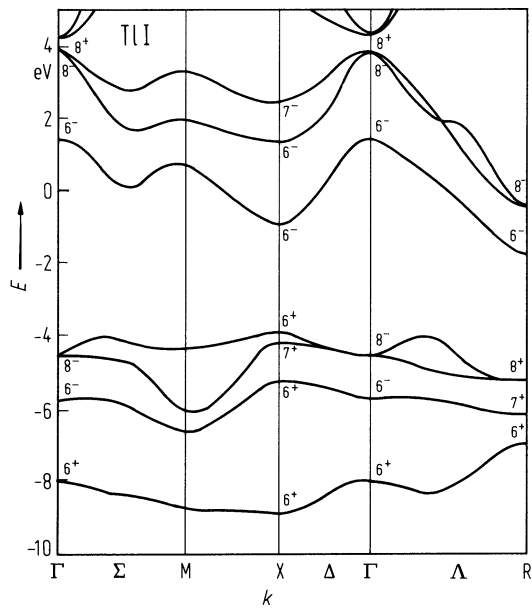


Fig. 21.0.7b

TlI(II). Band structure of orthorhombic TlI calculated with the OPW-method neglecting spin-orbit interaction [75V].

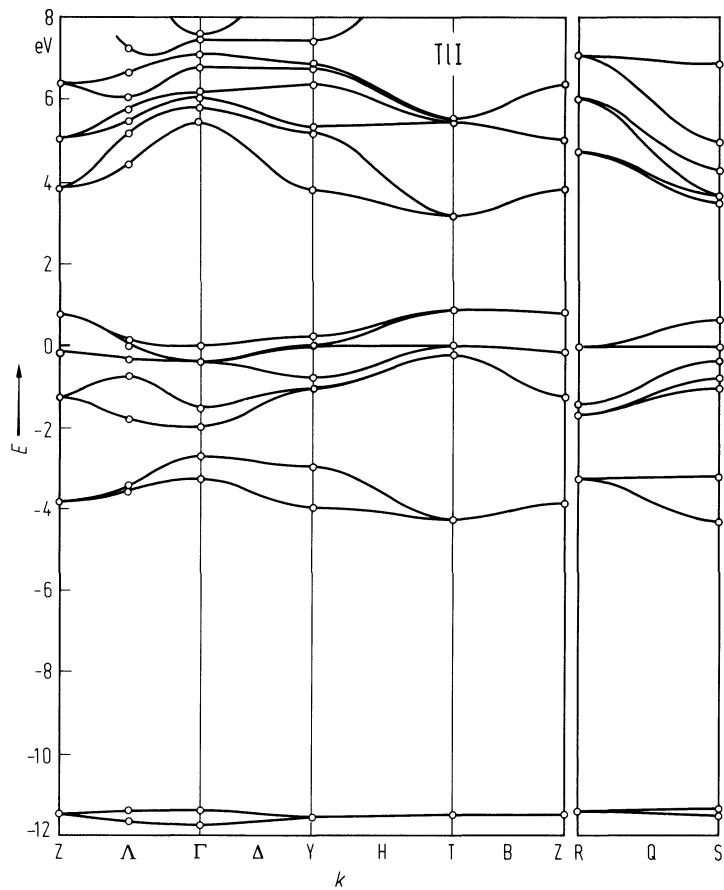


Fig. 21.0.7c

TlI(III). Band structure for fcc-TlI calculated with relativistic KKR-method [75H].

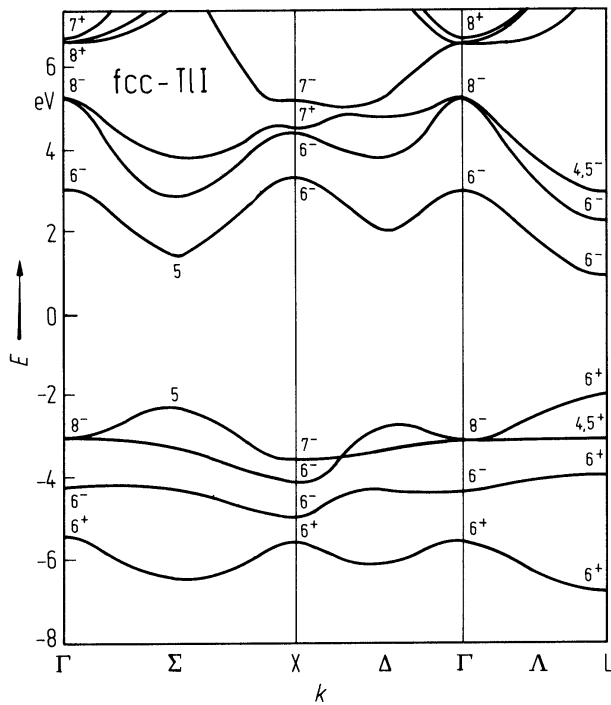


Fig. 21.4.1

TlI(I). Lattice parameter vs. temperature at 1 bar [67S].

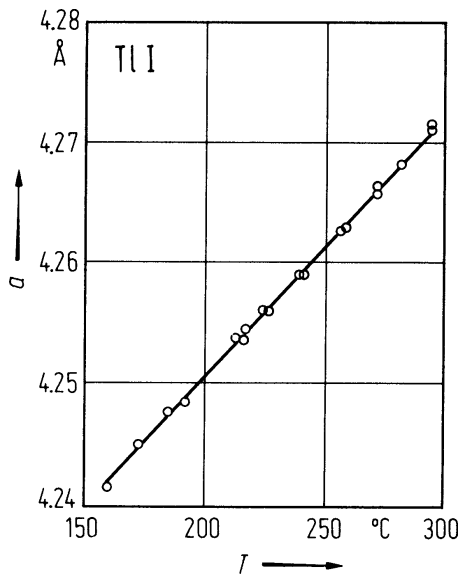


Fig. 21.4.2

TlI(II). Lattice parameters of orthorhombic TlI vs. temperature at 1 bar [67S].

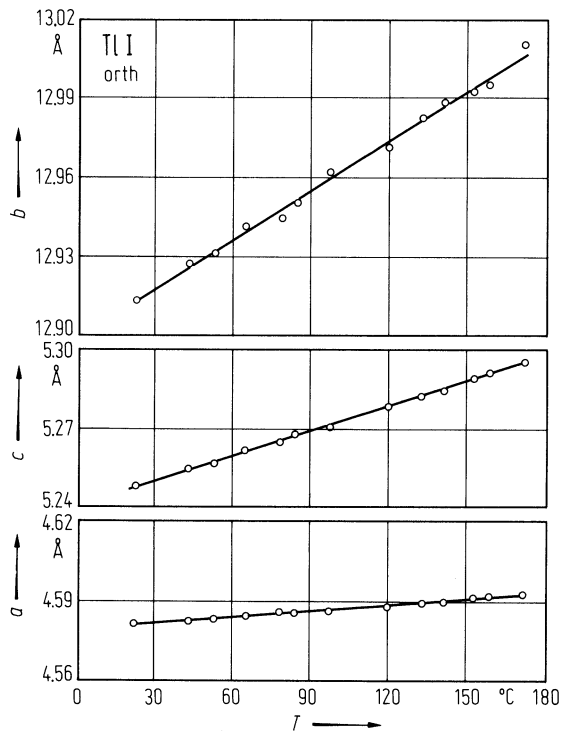
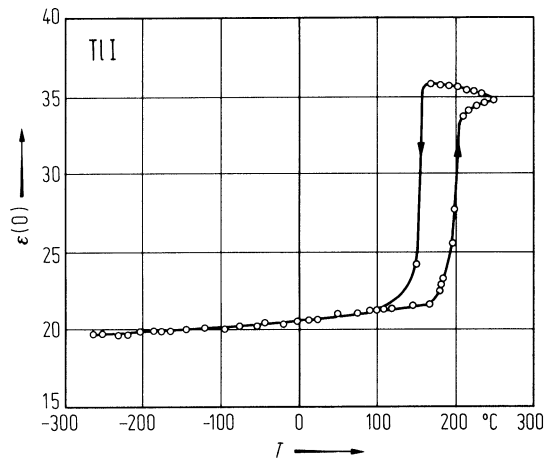


Fig. 21.4.3

TlI(II). Static dielectric constant vs. temperature at a frequency of $3 \cdot 10^8 \text{ s}^{-1}$. The observed hysteresis around 190°C is due to the orthorhombic-cubic phase transition [71R].



22 IV-V compounds

22.0 Crystal structure and lattice parameters

22.0.1 SiP, GeP, SiAs, GeAs

Compounds of the type IV-V mostly crystallize in a monoclinic structure (space group $C_{2h}^3 - C2/m$). The lattice consists of distorted octahedra of the group V atoms perpendicular to the (010) plane (parallel to the $(\bar{2}01)$ plane). The octahedra share edges and each octahedron contains two group IV atoms. Each group IV atom is bound tetrahedrally to three group V atoms and one group IV atom, whereas each group V atom has three group IV atoms as closest neighbors. The unit cell of the lattice contains 12 formula units [65W].

lattice parameters of the monoclinic phases [67W]

	a [Å]	b [Å]	c [Å]	β [deg]
SiAs	15.98	3.668	9.53	106.0
GeP	15.44	3.638	9.19	101.1
GeAs	15.59	3.792	9.49	101.3

Silicon phosphide SiP crystallizes in an orthorhombic structure [79U] with $a = 20.85$ Å, $b = 13.96$ Å, $c = 3.54$ Å.

22.0.2 SiP₂, SiAs₂, GeAs₂

The IV-V₂ compounds SiP₂, SiAs₂ and GeAs₂ crystallize in an orthorhombic lattice (space group $D_{2h}^9 - Pbam$). Each group IV atom is tetrahedrally surrounded by four group V neighbors. Each IV-V₄ tetrahedron shares three corners with adjacent tetrahedra. The fourth corners are connected in pairs by V-V bonds [62B].

SiP₂ and SiAs₂ have been also prepared in the pyrite structure [67W]. Here the Si atoms form a three-dimensional network of octahedra, each of which containing a pair of P- or As-atoms.

lattice parameters in the orthorhombic modification [67W]

	a [Å]	b [Å]	c [Å]	
SiP ₂	13.97	10.08	3.436	According to [67S] the unit cell of SiP ₂ is twice as long; in the b -direction is also reported: $a = 13.64$ Å, $b = 20.06$ Å, $c = 3.51$ Å.
SiAs ₂	14.53	10.37	3.636	
GeAs ₂	14.76	10.16	3.728	

lattice parameters in the pyrite modification [68D]

	a [Å]	da/dT [Å K ⁻¹]
SiP ₂	5.7045(3)	9.4·10 ⁻⁶ (298...1173 K)
SiAs ₂	6.0232(3)	

References to 22.0

- 62B Bryden, S. H.: Acta Crystallogr. 15 (1962) 167.
- 65W Wadsten, T.: Acta Chem. Scand. 19 (1965) 1232.
- 67S Spring-Thorpe, A. S.: Mater. Res. Bull. 4 (1967) 125.
- 67W Wadsten, T.: Acta Chem. Scand. 21 (1967) 593, 1374.
- 68D Donahue, P. C., Siemons, W. J., Gillson, J. L.: J. Phys. Chem. Solids 29 (1968) 807.
- 79U Ugai Ya. A., Demidenko, A. F., Koshchenko, V. I., Yachmenov, V. E., Sokolev, L. I., Goncharov, E. G.: Izv. Akad. Nauk SSSR, Neorg. Mater. 15 (1979) 731; Inorg. Mat. (USSR) (English Transl.) 15 (1979) 578.

22.1 SiP, GeP

Crystal structure and lattice parameters

see section 22.0.

Physical properties

Only few information exists about the semiconducting properties of these compounds. [79U] reports optical energy gaps of 2 eV for SiP and of 0.95 eV for GeP. Densities determined by hydrostatic weighing are $d = 4.150(5)$ g cm⁻³ for GeP and 2.37 g cm⁻³ for SiP. In this paper the temperature dependence of the heat capacity C_p is tabulated and used for the determination of the Debye temperature and several thermodynamic functions.

References to 22.1

- 79U Ugai Ya. A., Demidenko, A. F., Koshchenko, V. I., Yachmenov, V. E., Sokolev, L. I., Goncharov, E. G.: Izv. Akad. Nauk SSSR, Neorg. Mater. 15 (1979) 731; Inorg. Mat. (USSR) (English Transl.) 15 (1979) 578.

22.2 SiAs

Crystal structure and lattice parameters

see section 22.0.

Electronic properties

energy gaps

$E_{g,ind}$	1.45(3) eV	$T = 300\text{ K}, E \perp b$	transmission measurements	70M
$E_{g,dir}$	1.57(1) eV	$T = 300\text{ K}, E \perp b$	(allowed transition)	
	1.48(1) eV	$T = 300\text{ K}, E \parallel b$	(forbidden transition)	
$E_{g,th}$	2.03 eV	$T = 0\text{ K}, I \parallel b$	temperature dependence of resistivity	71C

Transport parameters

ρ	28 $\Omega\text{ cm}$	cleaved single	p-type sample; $I \parallel$ cleavage plane,	80S
R_H	480 $\text{cm}^3\text{ C}^{-1}$	crystal, RT	$B \perp$ cleavage plane	
p	$1.3 \cdot 10^{16}\text{ cm}^{-3}$			
S	820 $\mu\text{V K}^{-1}$			
μ_H	24 $\text{cm}^2/\text{V s}$			
$m_{p,ds}$	0.8 m_0			

Further transport data (Hall coefficient, resistivity): see Figs. 22.2.1, 22.2.2.

Lattice and optical properties

dielectric constant

$\epsilon(\infty)$	9.6(6)	illumination at normal incidence to cleavage plane	73K
--------------------	--------	---	-----

melting temperature

T_m	1083 $^{\circ}\text{C}$		65W
-------	-------------------------	--	-----

For optical data: see Figs. 22.2.3...5.

References to 22.2

65W Wadsten, T.: Acta Chem. Scand. 19 (1965) 1232.
70M Miller, L. C. F., Kannenwurf, C. R.: J. Phys. Chem. Solids 31 (1970) 849.
71C Chu, T. L., Kunioka, A., Kelm, R. W.: Solid State Electron. 14 (1971) 1259.
73K Kunioka, A., Ho, K. K., Sakai, Y.: J. Appl. Phys. 44 (1973) 1895.
80S Sudo, I.: Jpn. J. Appl. Phys. 19 (1980) 755.

Figures to 22.2

Fig. 22.2.1

SiAs. Reciprocal of the product of Hall coefficient (measured with current flowing along the b -axis) and electron charge e as a function of temperature. $1/R_{\text{H}}e$ is not identical with the carrier concentration since SiAs is highly anisotropic. Activation energies E_{A} are also indicated [71C].

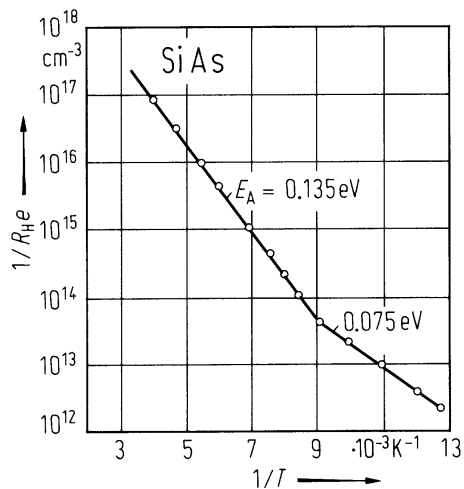


Fig. 22.2.2

SiAs. Ratio of the Hall coefficient and resistivity vs. temperature. R_H/ρ is not identical with the carrier mobility since SiAs is highly anisotropic [71C].

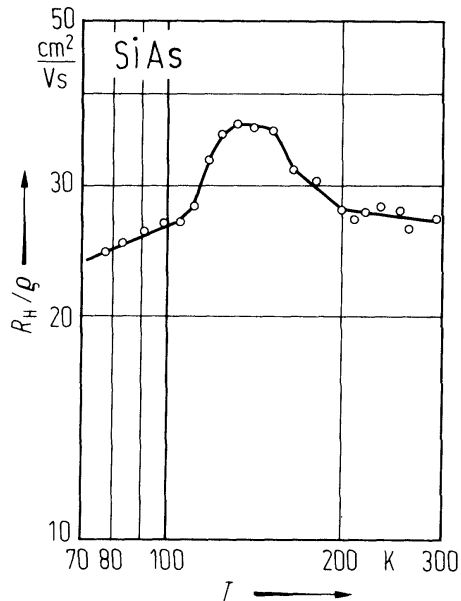


Fig. 22.2.3

SiAs, Absorption coefficient vs. wavelength on the high transmission side of the fundamental edge for two typical samples and both polarization directions of the electric field relative to the b -axis. The insert figure continue: the absorption behavior for unpolarized radiation to longer wavelengths [70M].

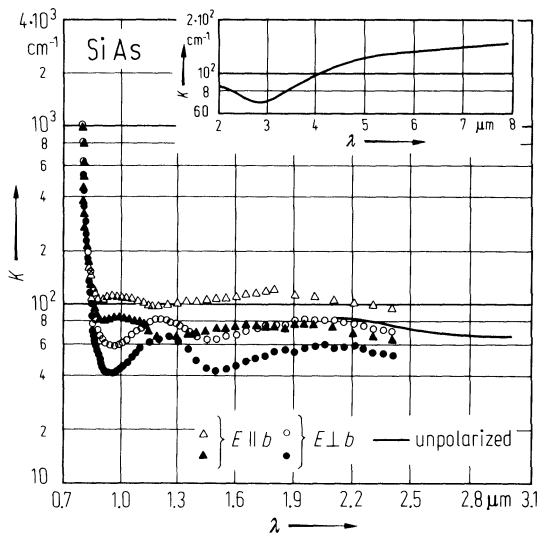


Fig. 22.2.4

SiAs. Real and imaginary parts of the dielectric constant (ϵ_1 and ϵ_2 , respectively) from the visible to the infrared region [73K].

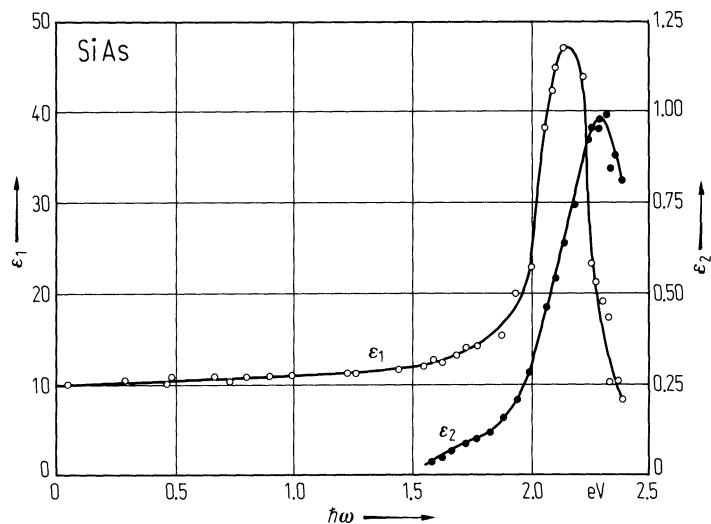
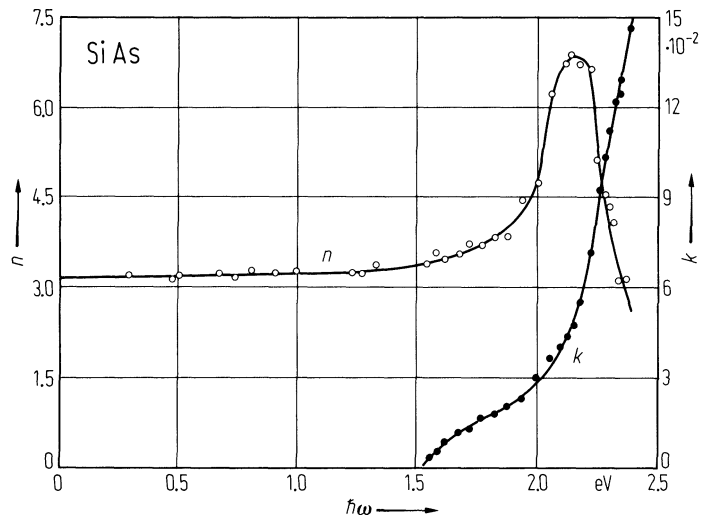


Fig. 22.2.5

SiAs. Refractive index n and extinction coefficient k as calculated from the data of Fig. 2 [73K].



22.3 GeAs

Crystal structure and lattice parameters

see section 22.0.

Physical properties

$E_{\text{g,ind}}$	0.65(1) eV	$T = 300 \text{ K}, E \parallel b$	transmission measurements (forbidden transition)	71R
$E_{\text{g,dir}}$	1.65(2) eV	$T = 300 \text{ K}, E \parallel b$	(forbidden transition)	
	1.01(1) eV	$T = 300 \text{ K}, E \perp c$	(forbidden transition)	
T_{m}	737°C			

For temperature dependence of electrical conductivity, see Fig. 22.3.1.

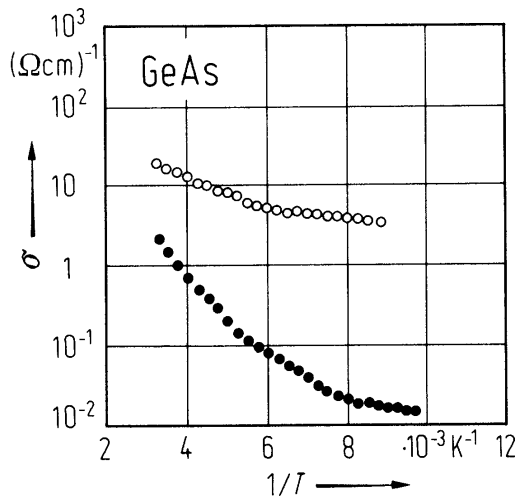
References to 22.3

71R Rau, S. W., Kannenwurf, C. R.: Phys. Rev. B3 (1971) 2581.

Figures to 22.3

Fig. 22.3.1

GeAs. Electrical conductivity vs. temperature for two samples. Current flow parallel to the b -axis [71R].



22.4 SiP₂, SiAs₂

Crystal structure and lattice parameters

see section 22.0.

Physical properties

Only data on the pyrite type modification have been reported [68D, 67M]. From galvanomagnetic measurements (Fig. 22.4.1) it can be deduced that both substances are semimetals with a nearly filled Brillouin zone, electrons as well as holes contributing to the electrical properties. De Haas-van Alphen measurements show a most spherical Fermi surface with a group of four ellipsoidal sheets prolate along the trigonal axes.

Measurements at RT on a p-type sample of SiP₂ gave a resistivity of $10^7 \Omega \text{ cm}$ parallel to (001) and $10^{11} \Omega \text{ cm}$ perpendicular to (001), an activation energy for the resistivity of $E_A \approx 0.9 \text{ eV}$, a low mobility ($< 1 \text{ cm}^2/\text{V s}$). The optical energy gap is reported to be 1.89 eV , the density is $2.7(2) \text{ g cm}^{-3}$ (exp.) and 2.54 g cm^{-3} (calc.). [67S]

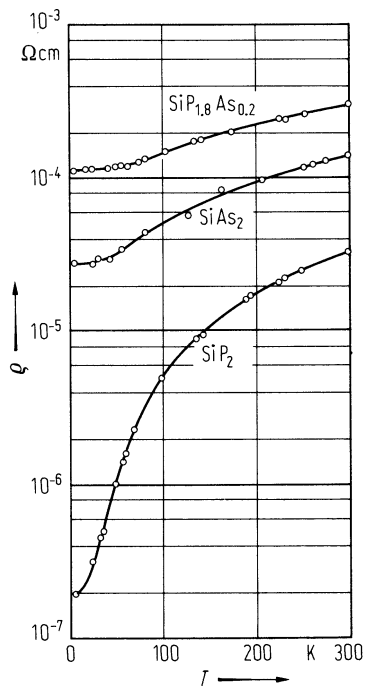
References to 22.4

- 67M Marcus, S. M.: Phys. Lett. A25 (1967) 468.
- 67S Spring-Thorpe, A. S.: Mater. Res. Bull. 4 (1967) 125.
- 68D Donahue, P. C., Siemons, W. J., Gillson, J. L.: J. Phys. Chem. Solids 29 (1968) 807.

Figures to 22.4

Fig. 22.4.1

Resistivity vs. temperature for SiP, SiAs and SiP_{1.8}As_{0.2} samples [68D].



22.5 GeAs₂

Crystal structure and lattice parameters

see section 22.0.

Physical properties

energy gaps

$E_{\text{g,ind}}$	1.06(1) eV	$T = 300 \text{ K}, E \parallel c$	absorption measurements (allowed transition)	71R
$E_{\text{g,dir}}$	1.10(1) eV	$T = 300 \text{ K}, E \parallel b$	(forbidden transition)	
	1.77(3) eV	$E \parallel c$		

mobility

μ_{p}	60 cm ² /V s	$T = 300 \text{ K}$	conductivity and Hall effect of a sample with $p = 5 \cdot 10^{17} \text{ cm}^{-3}$, $I \parallel b, B \perp b$ (see Fig. 22.5.1)	71R
------------------	-------------------------	---------------------	--	-----

melting temperature

T_{m}	732°C			71R
----------------	-------	--	--	-----

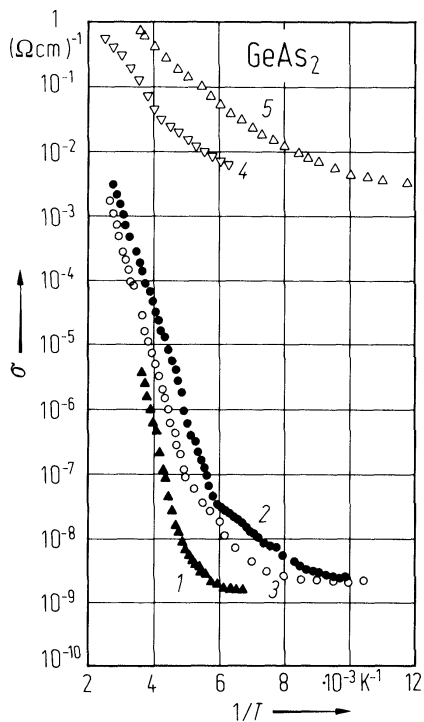
References to 22.5

71R Rau, S. W., Kannenwurf, C. R.: Phys. Rev. B3 (1971) 2581.

Figures to 22.5

Fig. 22.5.1

GeAs_2 . Electrical conductivity vs. temperature for five samples. Samples 1...3 were cut from the same crystal but differently orientated to the current flow ($I \parallel a$ -axis (1), $I \parallel b$ -axis (2), $I \parallel c$ -axis (3)). For samples 4 and 5 I was parallel to the c -axis [71R].



23 IV_x-VI_y compounds

23.0 Crystal structure and electronic structure

23.0.1 IV-VI compounds: GeS, GeSe, SnS, SnSe

The sulfides and selenides of germanium and tin have structures which can be described as quasi-tetragonal distortions of the rocksalt structure. The distortion reduces the six half bonds acting in the rocksalt structure to three single bonds in the orthorhombic GeS-type structure [76L], Fig. 23.0.1. There are some similarities to the structure of black phosphorus. The unit cell contains four molecules. *Space group*: D_{2h}^{16} .

Brillouin zone: Fig. 23.0.2, *band structures* of GeS, SnS and SnSe: Figs. 23.0.3...5.

23.0.2 IV-VI compounds: GeTe, SnTe

The structure of the monotellurides of germanium and tin is rocksalt like (space group: $Fm\bar{3}m - O_h^5$) with slight deformations due to phase transitions. The high temperature β -phase shows the perfect NaCl-structure (see Fig. 23.0.6a), stable above 670 K and 100 K for GeTe and SnTe, respectively. Below T_{tr} a distortion along the cubic $[111]$ axes takes place, forming the As-like rhombohedral α -phase. (*Space group*: $R\bar{3}m - C_{3v}^5$) (see Fig. 23.0.6b).

Brillouin zone: Fig. 23.0.7, *band structures* of GeTe and SnTe: Figs. 23.0.8, 23.0.9a,b.

23.0.3 IV-VI compounds: PbO, PbS, PbSe, PbTe

PbO exists in two polymorphic forms: the tetragonal (red) modification stable up to about 550°C and the orthorhombic (yellow) modification above that temperature [50B, 61W, 67S] (the high temperature form, however, can exist even at room temperature). *Space group*: tetragonal: $P4/nmm - D_{4h}^7$, orthorhombic: $Pbma - D_{2h}^{11}$.

PbS, PbSe and PbTe crystallize in the cubic rocksalt structure. At high pressures (at RT) the compounds undergo a polymorphic transition in which the NaCl-type structure changes to an orthorhombic structure (space group: $Pnma - D_{2h}^{16}$).

PbTe is at low temperatures near a structural phase transition from the NaCl to the rhombohedral structure (C_{3v}), the transition temperature, however, is negative. Extrapolated transition temperatures were found between -10 K and -150 K depending on the quality of the crystal [83N].

Brillouin zone: Fig. 23.70., *band structures* of PbS, PbSe and PbTe: Figs. 23.0.10...12.

23.0.4 IV-VI₂ compounds: GeO₂, SnO₂, PbO₂, GeS₂, GeSe₂, SnS₂, SnSe₂

GeO₂, SnO₂, PbO₂: These compounds crystallize in the rutile structure (Fig. 23.0.13). *Space group*: $D_{4h}^{14} - P4_2/nmm$. GeO₂ exists at room temperature also in the trigonal quartz structure. *Space group*: $D_3^4 - P3_121$.

Brillouin zone of the rutile structure: Fig. 23.0.14, *band structures* of SnO₂: Fig. 23.0.15.

GeS₂, GeSe₂:

(1) *monoclinic structure*, 16 molecules per unit cell. *Space group*: $C_{2h}^5 - P2_1/c$.

(2) *orthorhombic structure*, 24 molecules per unit cell, Fig. 23.0.16. *Space group*: $D_{2h}^{13} - Pmmn$.

SnS₂, SnSe₂: SnS₂ and SnSe₂ crystallize in the CdI₂ structure (Fig. 23.0.17). The Sn-atom has six octahedral neighbors. The normal stacking sequence is X-M-XX-M-X, but other stacking types are known. *Space group*: D_{3d}^3 .

Brillouin zone: Fig. 23.0.18, *band structures* of SnS₂ and SnSe₂: Figs. 23.0.19 and 23.0.20.

23.0.5 IV₂-VI₃ compounds: Si₂Te₃, Sn₂S₃, PbSnS₃, SnGeS₃, PbGeS₃

Si₂Te₃: The present model for Si₂Te₃ is that 3/4 of the Si atoms occupy tetrahedral interstices between alternate Te layers while the remaining 1/4 occupy octahedral interstices between the remaining Te layers. In this case the Si-Te distance for octahedral Te is 2.84 Å [76L] (Fig. 23.0.21a). The unit cell contains 4 molecules. Space group: C_{3v}⁴ – P31c. It is also possible to interpret the X-ray data with all Si-atoms located in tetrahedral interstices (Fig. 23.0.21b).

Sn₂S₃, PbSnS₃, SnGeS₃, PbGeS₃: The Me^{II}Sn^{IV}S₃ compounds have an orthorhombic crystal symmetry [67M]. The structure can be characterized by double SnS₆-octahedron chains parallel to the crystallographic *c*-axis, Fig. 23.0.22. The unit cell contains four molecules. *Space group*: D_{2h}¹⁶ – Pnam.

References to 23.0

- 50B Byström, A.: Dissertation, University of Stockholm 1950.
- 61W White, W. B., Dachille, F., Roy, R. S.: Am. Ceram. Soc. 44 (1961) 170.
- 67M Mootz, D., Puhi, H.: Acta Crystallogr. 23 (1967) 471.
- 67S Strömquist, R., Dickens, B.: J. Phys. Chem. Solids 28 (1967) 823.
- 68H Hermann, F., Kortum, R. L., Ortenburger, I., van Dyke, J. P.: J. Phys. (Paris) Suppl. 29 (1968) C462.
- 69T Tung, Y., Cohen, L. M.: Phys. Rev. 180 (1969) 823.
- 71T Tsang, Y. W., Cohen, M. L.: Phys. Rev. B 3 (1971) 1254.
- 72P Pearson, W. B.: The Crystal Chemistry and Physics of Metals and Alloys; Wiley & Sons 1972.
- 72S Snykers, M., Delavignette, P., Amelinckx, S.: Mater. Res. Bull. 7 (1972) 831.
- 73K Kohn, S. E., Yu, P. Y., Petroff, Y., Shen, Y. R., Tsang, Y., Cohen, M. L.: Phys. Rev. B8 (1973) 1477.
- 73W Williams, K. H., Murray, K. B., Govan, D. W., Thomas, J. W., Evans, E. L.: J. Phys. C6 (1973) 3631.
- 75G Gregora, I., Stetter, W.: Phys. Status Solidi (b) 71 (1975) K187.
- 75M Martinez, G., Schlüter, M., Cohen, M. L.: Phys. Rev. B11 (1975) 651 and 660.
- 76L Levy, F.: Structural Chemistry of Layer-Type Phases; Reidel Publishing Comp. 1976.
- 77G Grandke, T., Ley, L.: Phys. Rev. B 16 (1977) 832.
- 77M Margaritondo, G., Rowe, J. E., Schlüter, M., Kasper, H.: Solid State Commun. 22 (1977) 753.
- 78C Car, R., Ciucci, G., Quartapelle, L.: Phys. Status Solidi (b) 86 (1978) 471.
- 78P Powell, M. J., Marseglia, E. A., Liang, WY.: J. Phys. C11 (1978) 895.
- 79M Melvin, J. S., Hendry, D. C.: J. Phys. C 12 (1979) 3003.
- 79R Robertson, J.: J. Phys. C 12 (1979) 4753.
- 80P Parke, A. W., Srivastava, G. P.: Phys. Status Solidi (b) 101 (1980) K31.
- 83N Nimtz, G., Schlicht, B.: Springer Tracts in Modern Physics, Vol. 98, 1, Berlin, Heidelberg, New York, Tokyo: Springer-Verlag 1983.

Figures to 23.0

Fig. 23.0.1

Pictorial view of the GeS structure [72P].

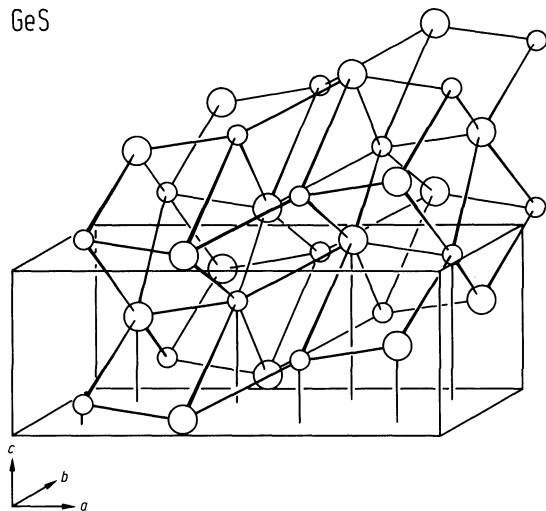


Fig. 23.0.2

GeS. Brillouin zone for a simple orthorhombic Bravais lattice, e.g. GeS [77G].

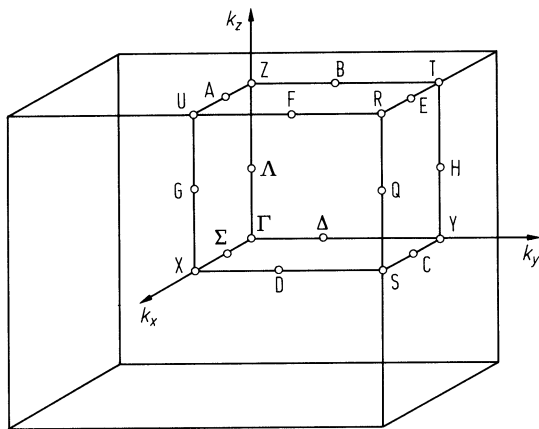


Fig. 23.0.3

GeS. Band structure calculated along the main symmetry lines by means of an empirical pseudopotential method [77G]. (a) and (b) show different directions within the Brillouin zone.

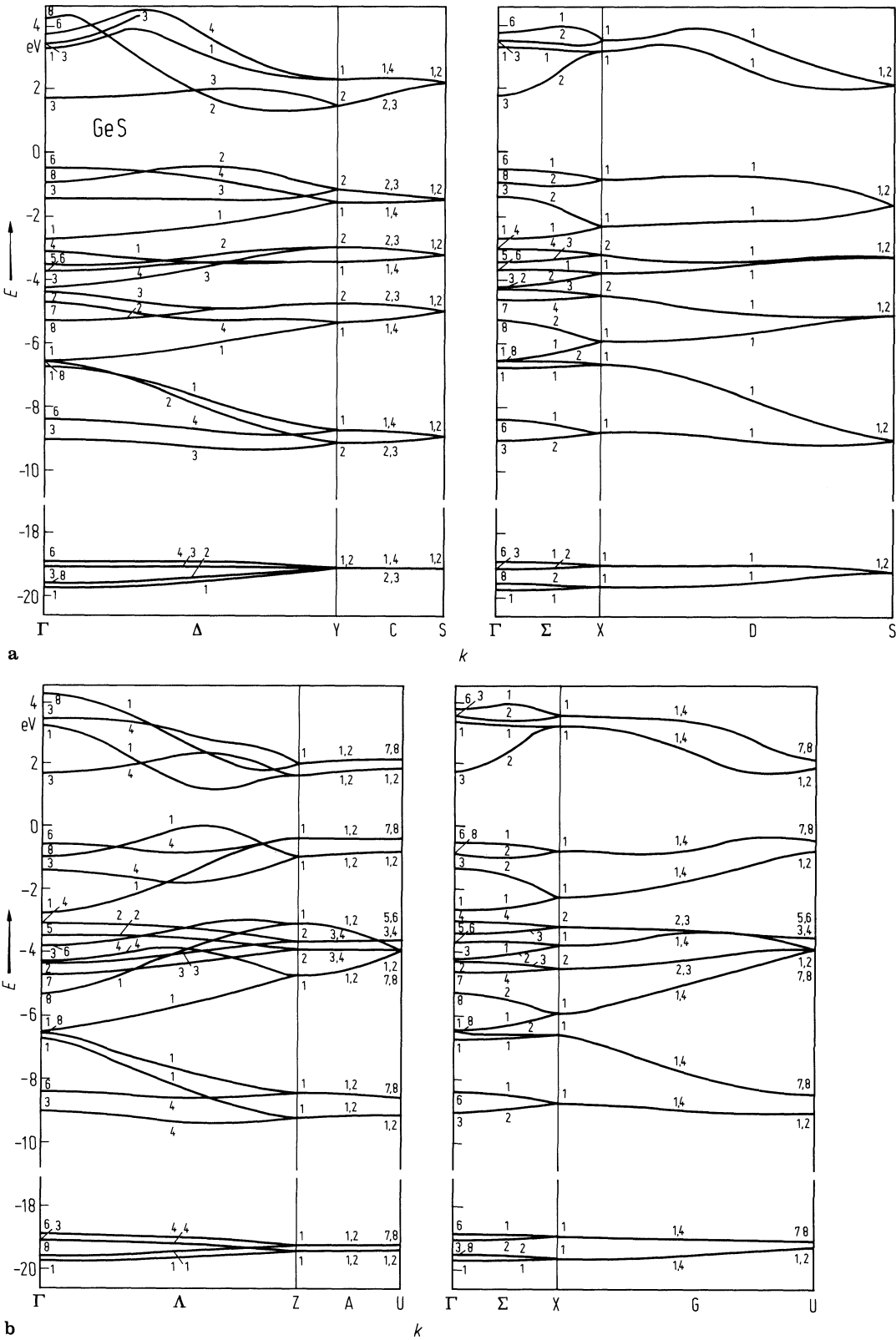


Fig. 23.0.4

SnS. Structure of the valence bands calculated along the main symmetry lines by the empirical pseudopotential method [80P].

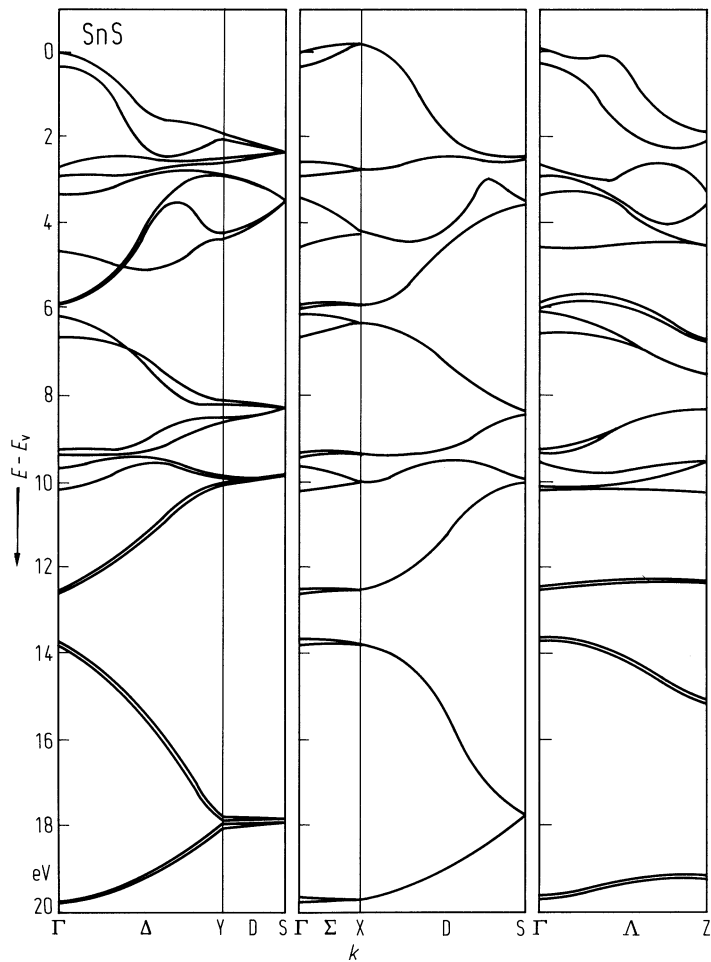


Fig. 23.0.5

SnSe. Pseudopotential band structure calculated along the high symmetry lines [78C]. 1 Ry = 13.6 eV.

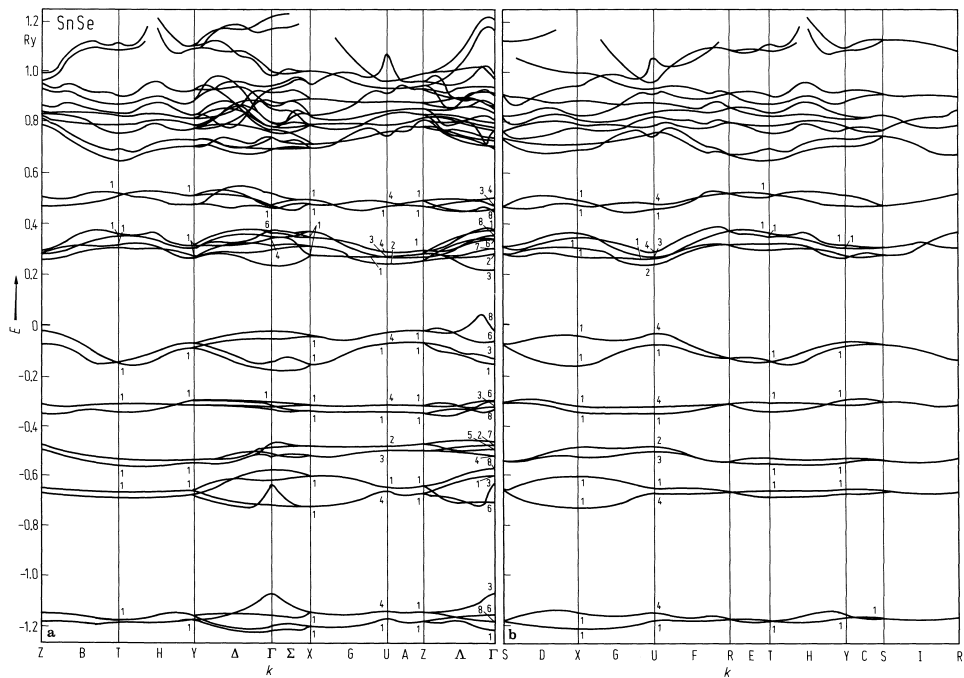


Fig. 23.0.6

GeTe, SnTe. (a) Elementary cell of the NaCl-like structure. (b) The rhombohedral unit cell of the NaCl-type lattice. A distortion along $[111]$ direction combined with a sublattice shift causes the rhombohedral As-like B13 phase of GeTe and SnTe, redrawn after [72S].

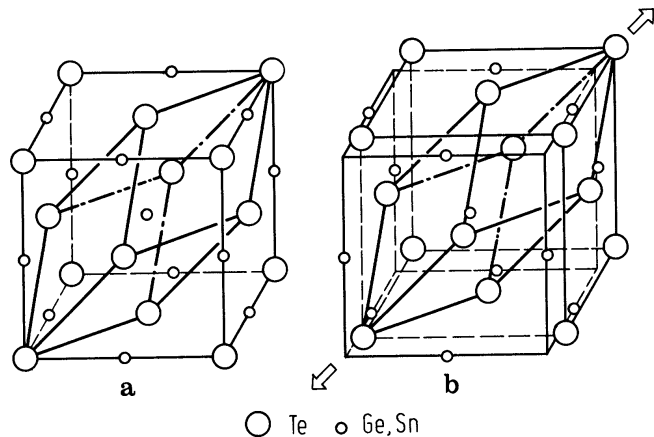


Fig. 23.0.7

GeTe. Brillouin zone of the fcc lattice of the NaCl structure.

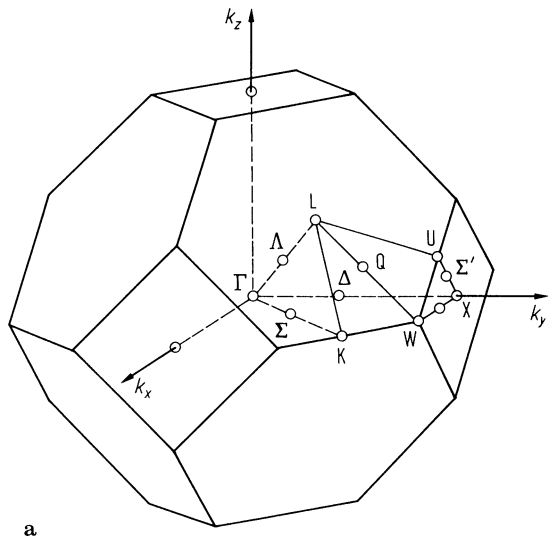


Fig. 23.0.8

GeTe. Electronic energy band structure [69T].

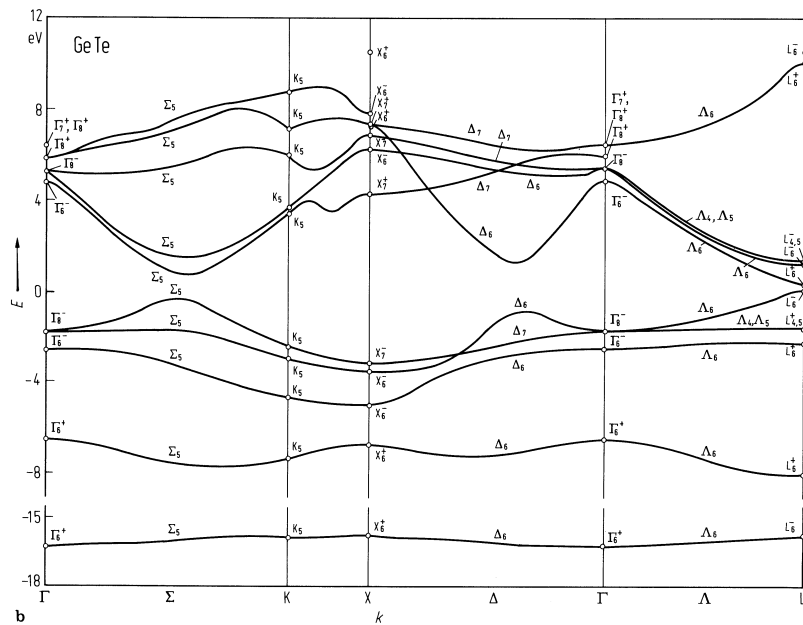


Fig. 23.0.9a

α -SnTe. Energy vs. relative wavevector Δk near L for zero temperature, calculated with the empirical pseudopotential method (EPM). Fermi levels corresponding to different hole concentrations p are indicated [71T]. The calculation was done for the α -phase. The phase transition has not been taken into account.

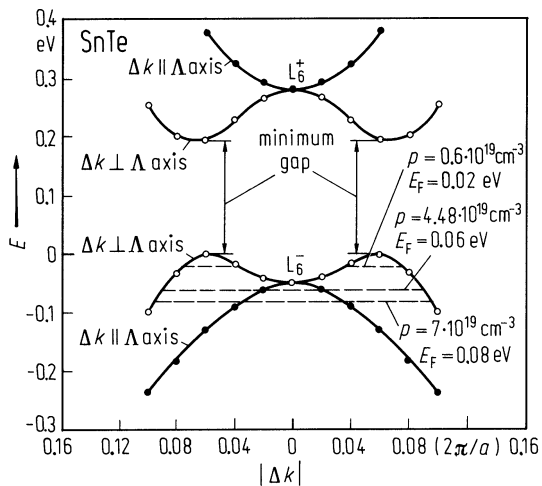


Fig. 23.0.9b

β -SnTe. Band structure obtained by a self-consistent relativistic calculation [79M]. 1 Ry = 13.6 eV.

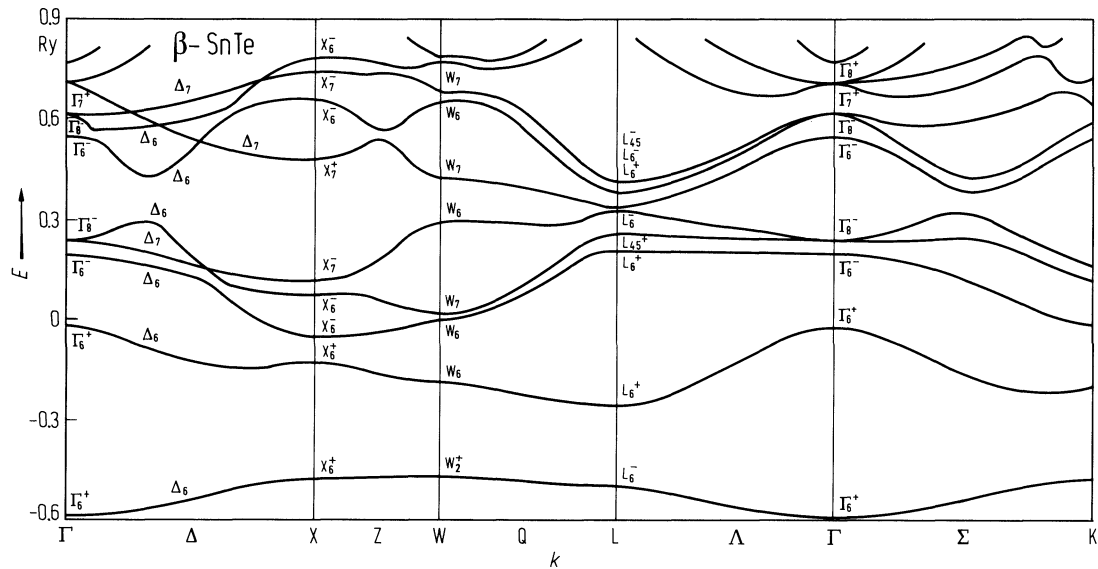


Fig. 23.0.10

PbS. Band structure calculated by the empirical pseudopotential method [73K].

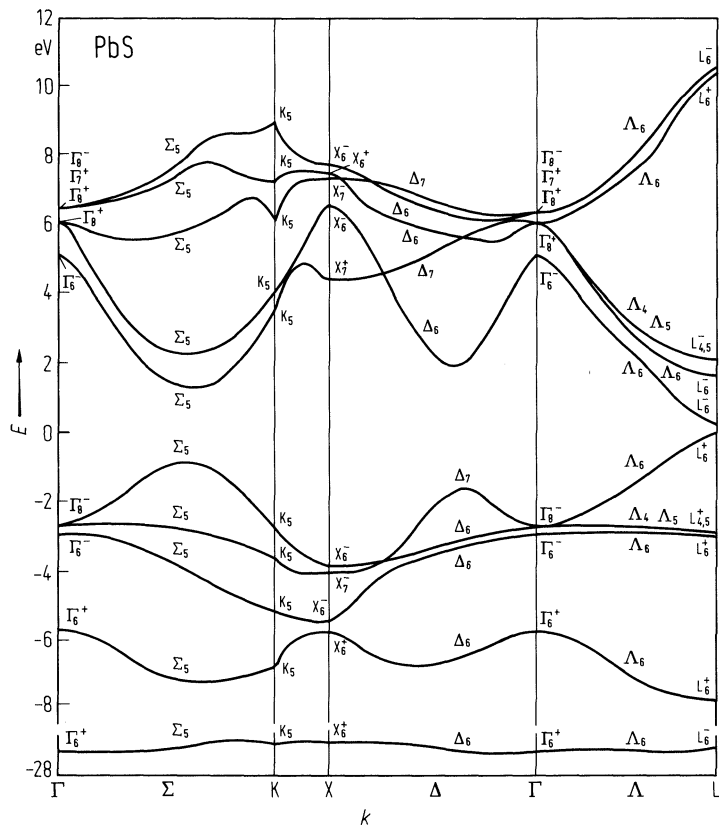


Fig. 23.0.11

PbSe. Band structure and density of states from an empirical pseudopotential method calculation [75M].

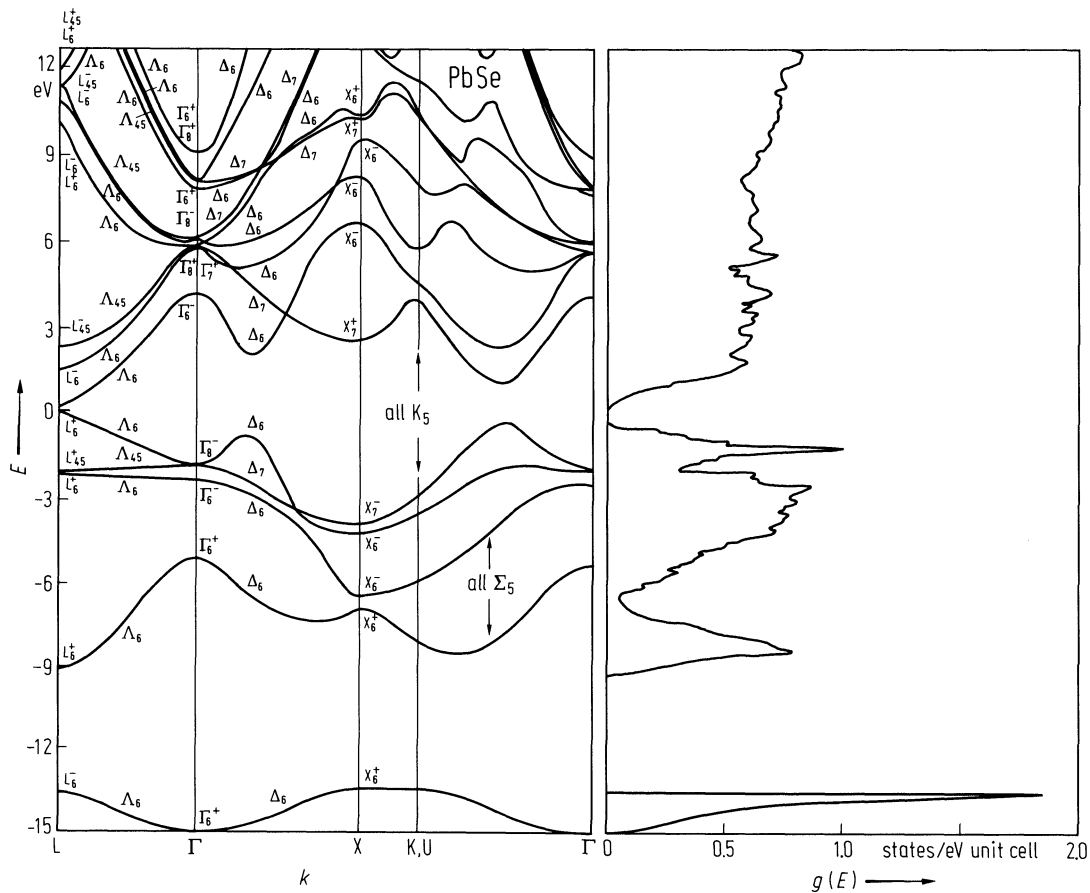


Fig. 23.0.12

PbTe. (a) Band structure and density of states from an empirical pseudopotential method calculation [75M]. (b) Theoretical values of energy levels at the L-point calculated by different models [83N]: a) APW-method [65C], b) OPW-method [68H], c) KKR-method [70O], d) nonlocal EP-method [75M].

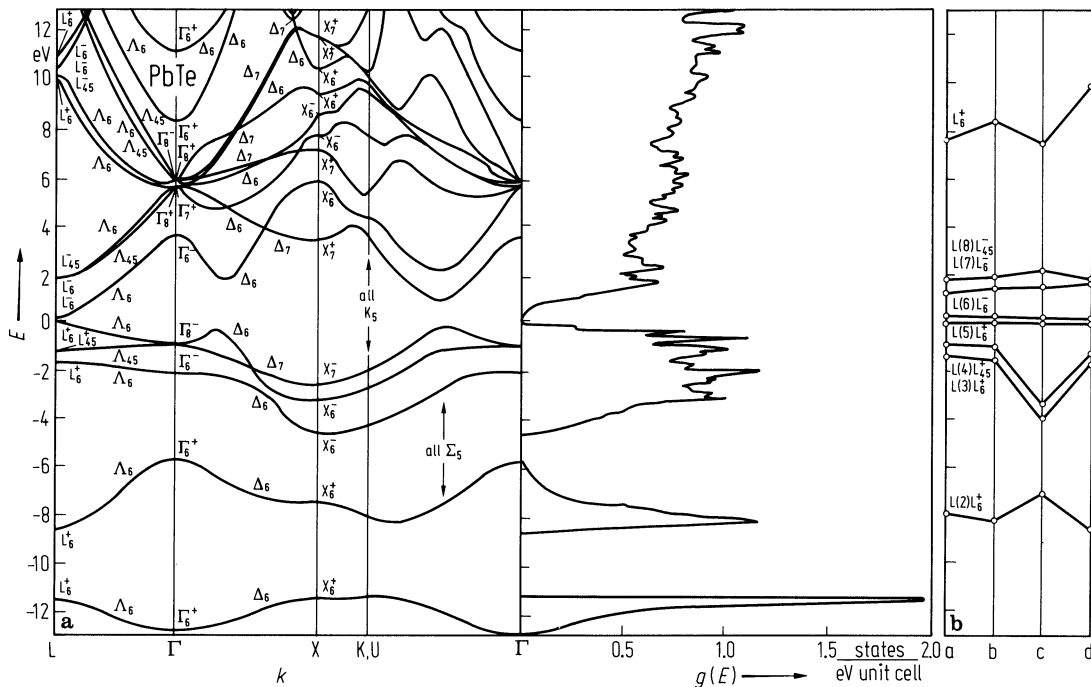


Fig. 23.0.13

Rutile structure for the group IV dioxides. Small circles: metal atoms, large circles: oxygen atoms.

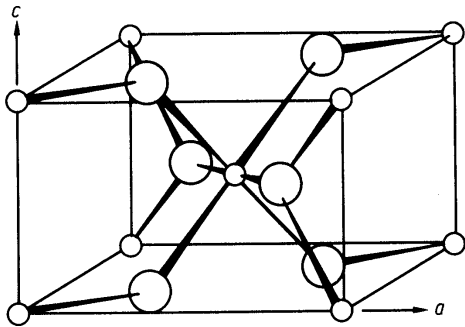
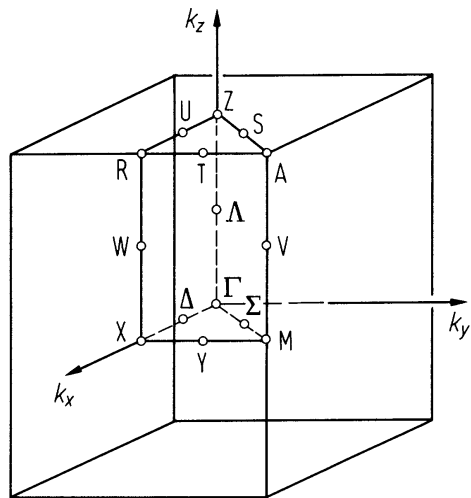


Fig. 23.0.14

SnO_2 . Brillouin zone for the rutile structure.



SnO₂. Calculated band structure (Sn–O and O–O interactions are included in the calculation) [79R].

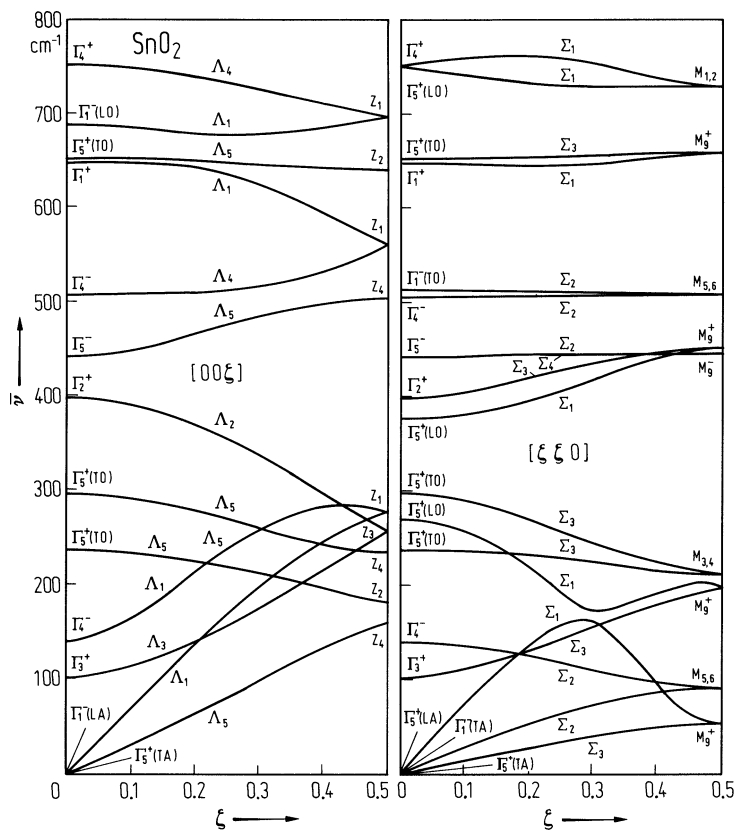


Fig. 23.0.16

Diagram of the structure of GeS_2 and GeSe_2 [72P].

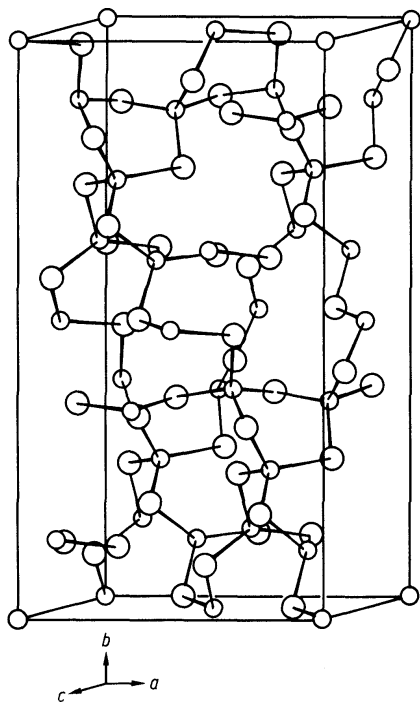


Fig. 23.0.17

Crystal structure of SnS_2 and SnSe_2 , (a) general form of layer structure, (b) $(11\bar{2}0)$ -section, (c) octahedral coordination in the layer, (d) packing of atoms in SnSe_2 [75G].

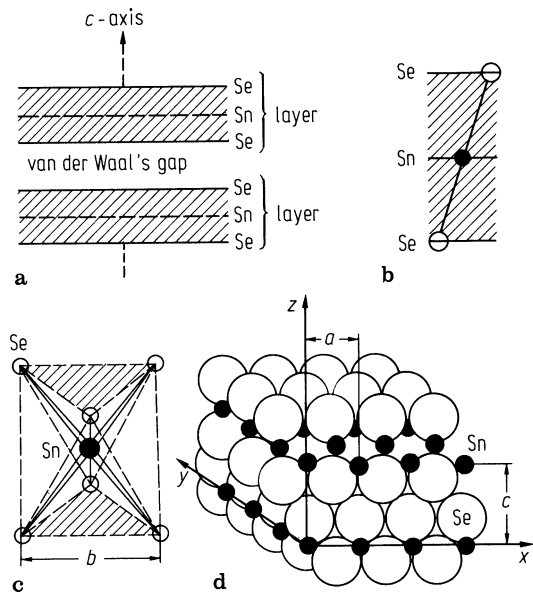


Fig. 23.0.18

SnS_2 . Brillouin zone of the SnS_2 structure.

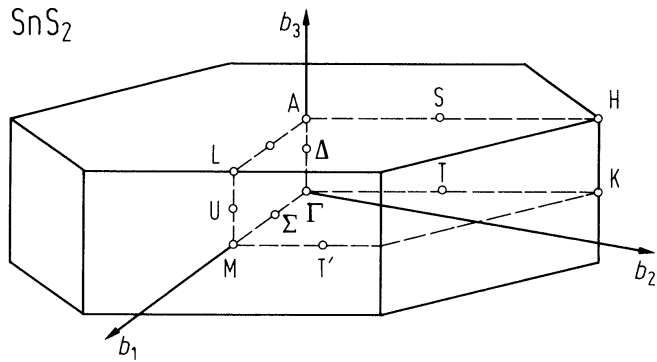
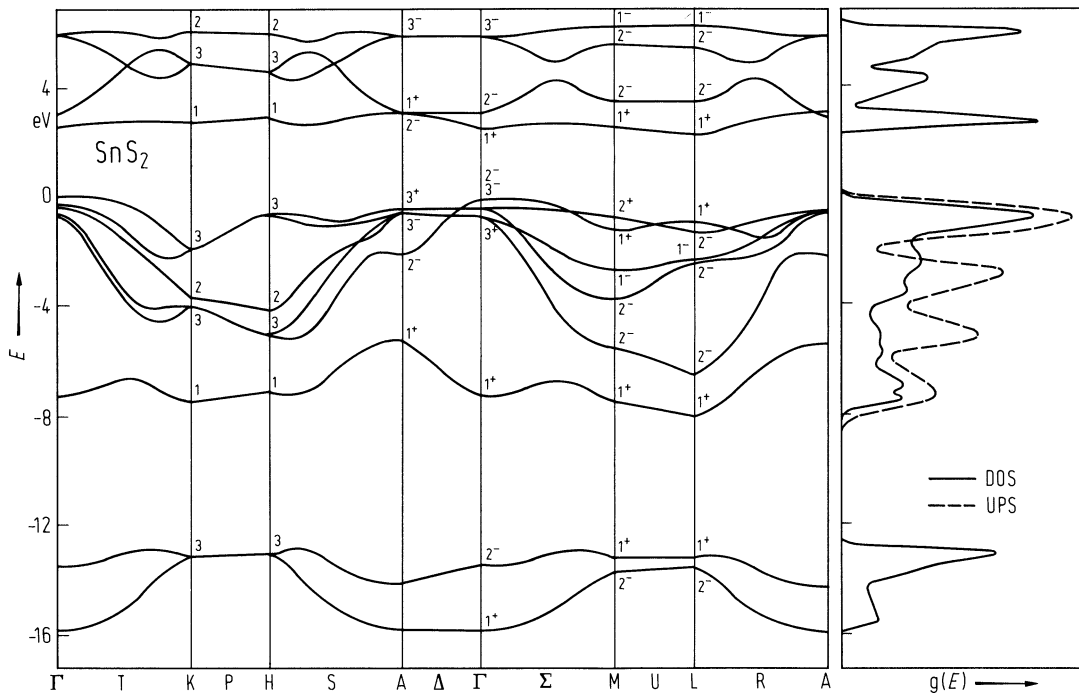


Fig. 23.0.19a

SnS₂. Tight binding band structure calculation and density of states (DOS) compared to UPS measurements given by [77M, 79R] for 2H polytype.



SnS₂. Calculated band structure for 4H-SnS₂ [78P].

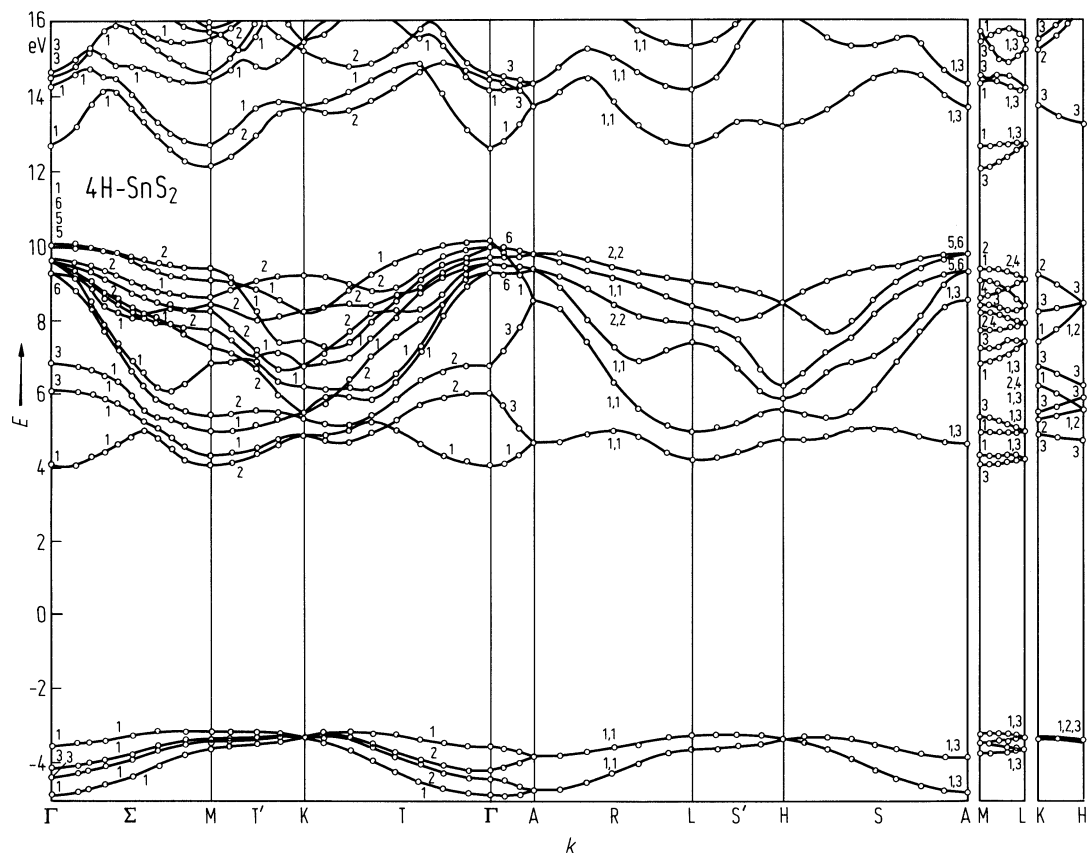


Fig. 23.0.20

SnSe₂. Tight binding band structure calculation and density of states (DOS) compared to XPS measurements given by [73W, 79R].

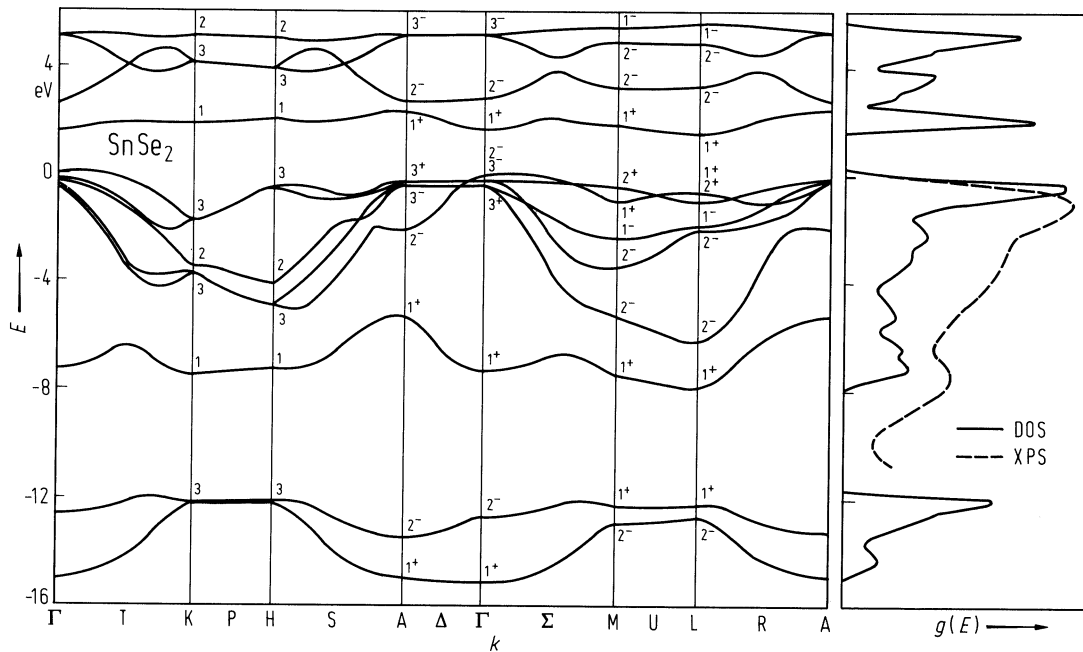
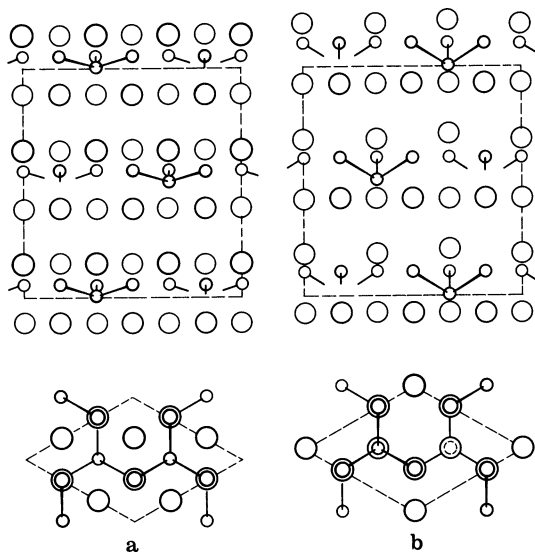
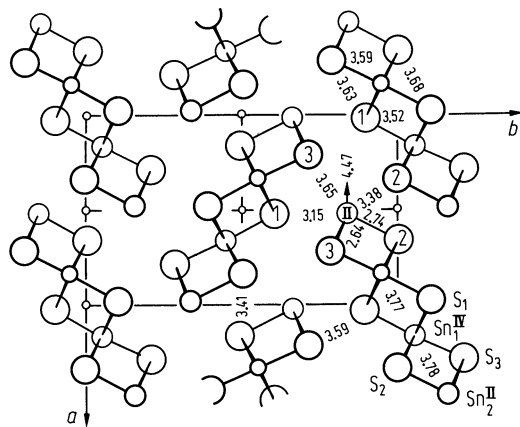


Fig. 23.0.21

(101) sections and projections along [001] of the two models proposed for Si_2Te_3 . a) One quarter of the Si atoms in octahedral interstices; b) all Si atoms in tetrahedral interstices, small circles: Si-atoms [76L].



Structure of Sn_2S_3 . The bold circles represent atoms with $z = 3/4$ and the light circles atoms with $z = 1/4$ [67M]. Distances in Å.



23.1 Germanium sulfide (GeS)

Crystal structure

see section 23.0.

Electronic properties

band structure, see Fig. 23.0.3, Brillouin zone: Fig. 23.0.2.

energy gap

$E_{g,dir}(\Lambda_{1v}-\Lambda_{1c})$	1.65eV	$T = 300\text{ K}, E \parallel a$	absorption	77E
dE_g/dT	$-8.1 \cdot 10^{-4}\text{ eV K}^{-1}$	$T = 105...300\text{ K}, E \parallel a$	absorption at different temperatures	80H
	$-5.8 \cdot 10^{-4}\text{ eV K}^{-1}$	$T = 115...300\text{ K}, E \parallel b$		

valence band, effective mass

m_p	$0.5\ m_0$	$T = 295\text{ K}$	$I - T$ characteristic, $E = 5.1 \cdot 10^7\text{ V/cm}$	76V
$m_{p\parallel}/m_{p\perp}$	<15		estimation from photoconductivity measurements	80W, 79W

Lattice properties

lattice parameters

a	10.44 Å	RT		76L
b	3.65 Å			
c	4.3 Å			

heat capacity

C_p	$47.4\text{ J mol}^{-1}\text{ K}^{-1}$	$T = 300\text{ K}$		74M
-------	--	--------------------	--	-----

density

d	4.01 g cm^{-3}	$T = 300\text{ K}$		69O
-----	-------------------------	--------------------	--	-----

melting temperature

T_m	938 K	$p = 1\text{ kbar}$		74M
-------	-------	---------------------	--	-----

phonon dispersion curves : Fig. 23.1.1, Brillouin zone: Fig. 23.0.2.

There are seven infrared active and twelve Raman active phonons. The Raman and infrared modes are split due to the interlayer interactions.

phonon frequencies

$\nu_{TO}(B_{1u})$	$3.52 \cdot 10^{12}\text{ s}^{-1}$	$E \parallel a, T = 300\text{ K}$	IR-reflectivity	76W
$\nu_{LO}(B_{1u})$	$3.70 \cdot 10^{12}\text{ s}^{-1}$			
$\nu_{TO}(B_{1u})$	$7.70 \cdot 10^{12}\text{ s}^{-1}$			
$\nu_{LO}(B_{1u})$	$9.74 \cdot 10^{12}\text{ s}^{-1}$			
$\nu_{TO}(B_{2u})$	$6.02 \cdot 10^{12}\text{ s}^{-1}$	$E \parallel b, T = 300\text{ K}$		
$\nu_{LO}(B_{2u})$	$8.93 \cdot 10^{12}\text{ s}^{-1}$			
$\nu_{TO}(B_{3u})$	$3.15 \cdot 10^{12}\text{ s}^{-1}$			
$\nu_{LO}(B_{3u})$	$3.2 \cdot 10^{12}\text{ s}^{-1}$			
$\nu_{TO}(B_{3u})$	$7.10 \cdot 10^{12}\text{ s}^{-1}$			
$\nu_{LO}(B_{3u})$	$8.25 \cdot 10^{12}\text{ s}^{-1}$			
$\nu_{TO}(B_{3u})$	$8.39 \cdot 10^{12}\text{ s}^{-1}$			
$\nu_{LO}(B_{3u})$	$9.59 \cdot 10^{12}\text{ s}^{-1}$			

phonon frequencies (continued)

$\nu_1(\text{A}_{1\text{g}})$	$1.43 \cdot 10^{12} \text{ s}^{-1}$	$T = 300 \text{ K}$	Raman shift	76W,
$\nu_2(\text{A}_{1\text{g}})$	$3.31 \cdot 10^{12} \text{ s}^{-1}$			75G
$\nu_3(\text{A}_{1\text{g}})$	$7.11 \cdot 10^{12} \text{ s}^{-1}$			
$\nu_4(\text{A}_{1\text{g}})$	$8.04 \cdot 10^{12} \text{ s}^{-1}$			
$\nu_1(\text{B}_{2\text{g}})$	$2.27 \cdot 10^{12} \text{ s}^{-1}$			
$\nu_2(\text{B}_{2\text{g}})$	$3.4 \cdot 10^{12} \text{ s}^{-1}$			
$\nu_3(\text{B}_{2\text{g}})$	$3.94 \cdot 10^{12} \text{ s}^{-1}$			
$\nu_4(\text{B}_{2\text{g}})$	$7.23 \cdot 10^{12} \text{ s}^{-1}$			
$\nu_1(\text{B}_{3\text{g}})$	$1.64 \cdot 10^{12} \text{ s}^{-1}$			
$\nu_2(\text{B}_{3\text{g}})$	$6.33 \cdot 10^{12} \text{ s}^{-1}$			
$\nu_1(\text{B}_{1\text{g}})$	$2.87 \cdot 10^{12} \text{ s}^{-1}$			
$\nu_2(\text{B}_{1\text{g}})$	$6.42 \cdot 10^{12} \text{ s}^{-1}$			

Transport properties

GeS is a high resistivity material of p-type conduction [69A].

For temperature dependence of the conductivity, see Fig. 23.1.2; for temperature dependence of the mobility, see Fig. 23.1.3.

mobility

μ_{p}	$90 \text{ cm}^2/\text{V s}$	$T = 300 \text{ K}$	photoconductivity measurements on thin GeS films (p-type)	76S
------------------	------------------------------	---------------------	--	-----

thermal conductivity : see Fig. 23.1.4.

Optical properties

optical spectra : refractive index: Fig. 23.1.5; dielectric constant: Fig. 23.1.6.

dielectric constants

$\epsilon(0)$	25.1	$E \parallel a, T = 300 \text{ K}$	from Kramers-Kronig analysis of infrared data	76W
	29.5	$E \parallel b$		
	30.0	$E \parallel c$		
$\epsilon(\infty)$	14.8	$E \parallel a$		
	12.0	$E \parallel b$		
	10.0	$E \parallel c$		

References to 23.1

- 69A Abrikosov, N. Kb., Bankina, V. F., Posetskaya, L. V., Shelimova, L. B., Skudnova, E. V.: Semiconducting II-VI, IV-VI and V-VI compounds, New York: Plenum Press 1969, p. 65135.
- 69O Okhotin, A. S., Kresovnikov, A. N., Aivazov, A. A., Pushkarskii, A. S.: Phys. Status Solidi 31 (1969) 485.
- 71D Dalven, R.: Phys. Rev. B3 (1971) 1953.
- 74M Mills, K. C.: Thermodynamic Data for Inorganic Sulphides, Selenides and Tellurides, London: Butterworths 1974.
- 75G Gregora, I., Stetter, W.: Phys. Status Solidi (b) 71 (1975) K187.
- 76G Gregora, I., Velicky, B., Zavetova, M.: J. Phys. Chem. Solids 37 (1976) 785.
- 76L Levy, F.: Structural Chemistry of Layer-Type Phases; Reidel Publishing Comp. 1976.
- 76S Smith, T. F., Birch, J. A., Collings, J. G.: J. Phys. C 9 (1976) 4375.
- 76V Vodenicharov, C., Stanchev, A.: Thin Solid Films 37 (1976) 157.
- 76W Wiley, J. D., Buckel, W. J., Schmidt, R. L.: Phys. Rev. B 13 (1976) 2489.
- 77E Bymard, R., Otto, A.: Phys. Rev. B 16 (1977) 1616.
- 77F Frey, A.: Dissertation TH Stuttgart 1977.
- 77G Grandke, T., Ley, L.: Phys. Rev. B 16 (1977) 832.
- 79W Wiley, J. D., Pennington, S.: Phys. Status Solidi 96 (1979) K43.
- 80H Haritonides, J., Lambros, A.: J. Phys. Chem. Solids 41 (1980) 659.
- 80W Wiley, J. D., Thomas, D., Schoenherr, B., Breitschwerdt, A.: J. Phys. Chem. Solids 41 (1980) 801.

Figures to 23.1

Fig. 23.0.2

GeS. Brillouin zone for a simple orthorhombic Bravais lattice, e.g. GeS [77G].

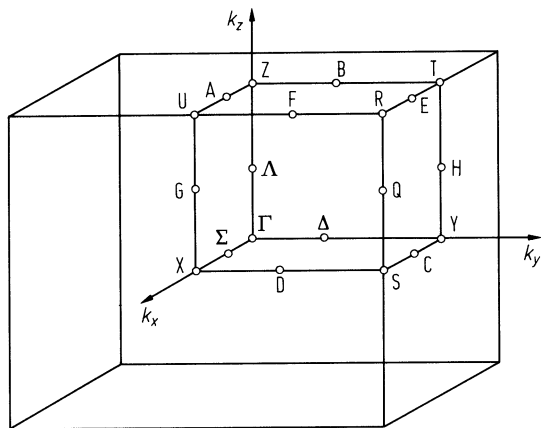
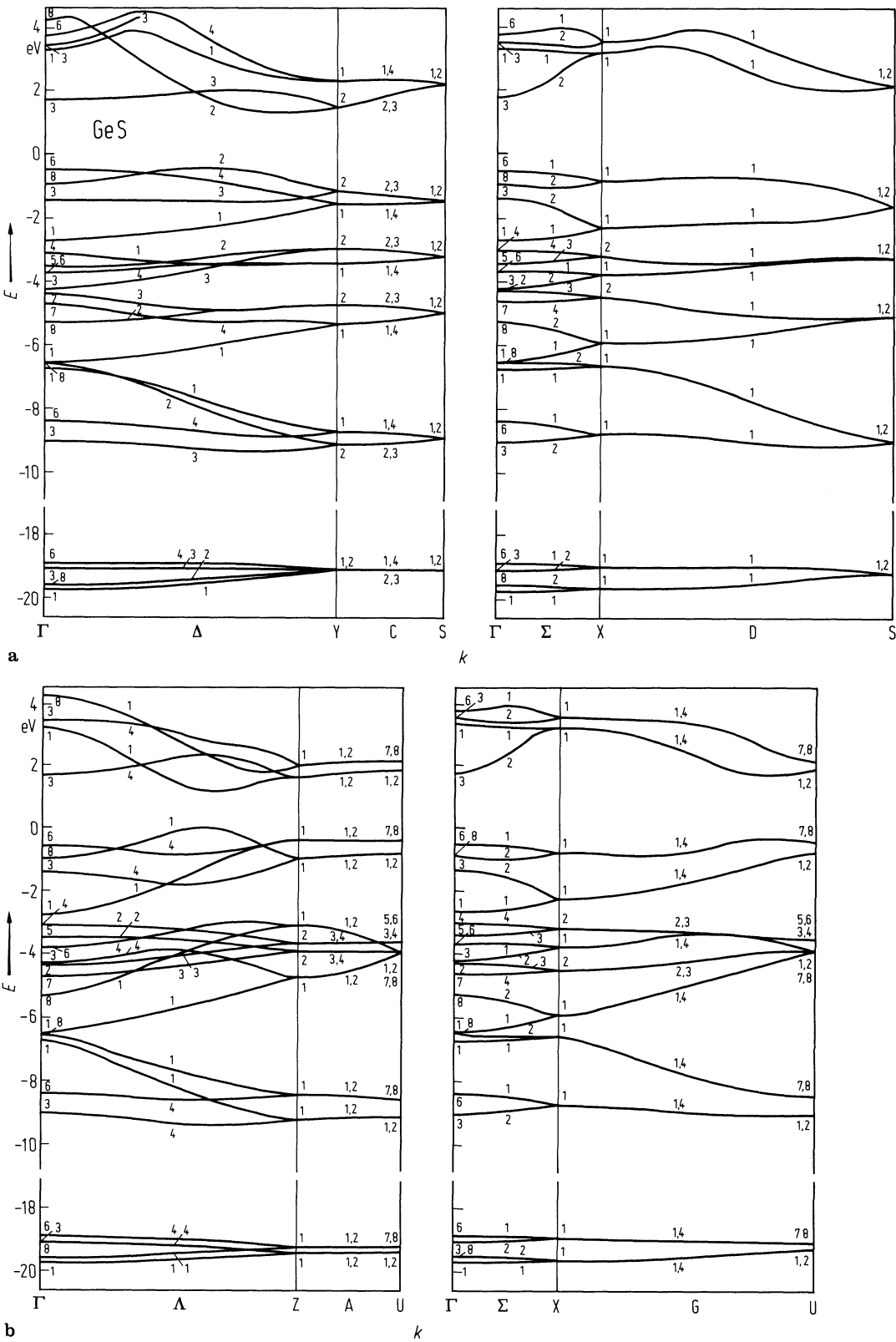


Fig. 23.0.3

GeS. Band structure calculated along the main symmetry lines by means of an empirical pseudopotential method [77G]. (a) and (b) show different directions within the Brillouin zone.



GeS. Phonon dispersion curves (frequency vs. reduced wave vector coordinate) [77F]. The neutron scattering results are represented by circles and triangles, the optical measurements by squares and the calculations by solid lines.

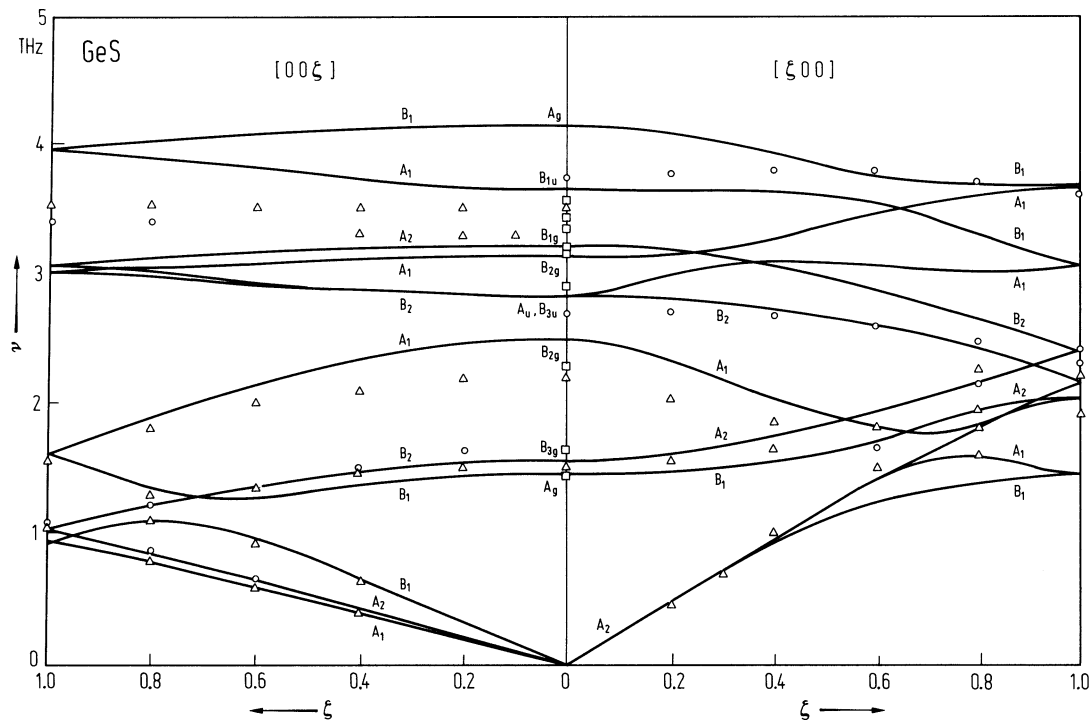


Fig. 23.1.2

GeS. Electrical conductivity vs. reciprocal temperature of p-type needle-shaped single crystals in the range 200...400 K [71D].

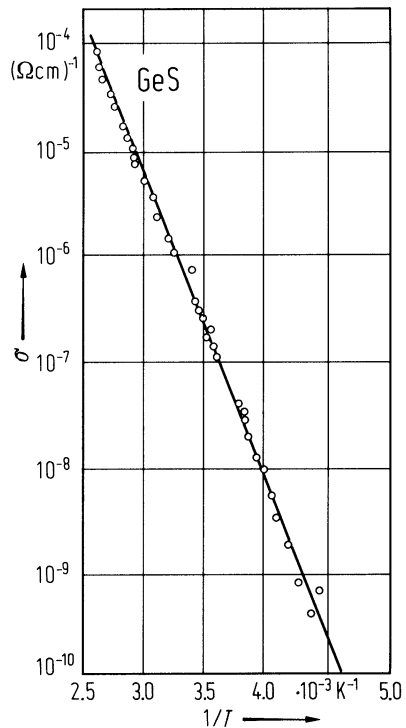


Fig. 23.1.3

GeS. Mobility vs. temperature (T in K) for a film of thickness $d = 730$ nm in the range 300...400 K [76S].

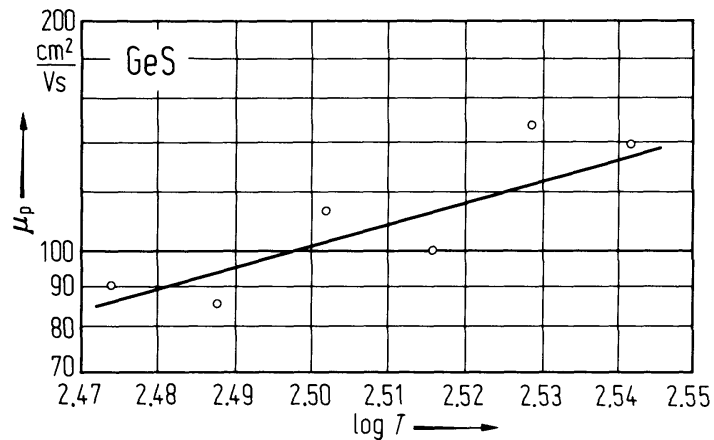


Fig. 23.1.4

GeS, GeSe. Thermal conductivity of single crystals vs. temperature [69O]. (The crystals were not orientated due to their small size.).

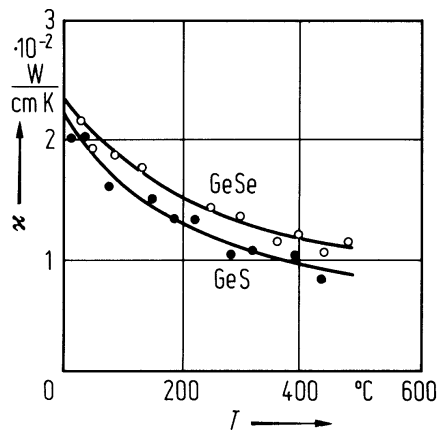


Fig. 23.1.5

GeS. Refractive index vs. photon energy. Open and full circles indicate prism and interference measurements, respectively. The solid curve is a three-parameter fit to the electronic part of dispersion [76G].

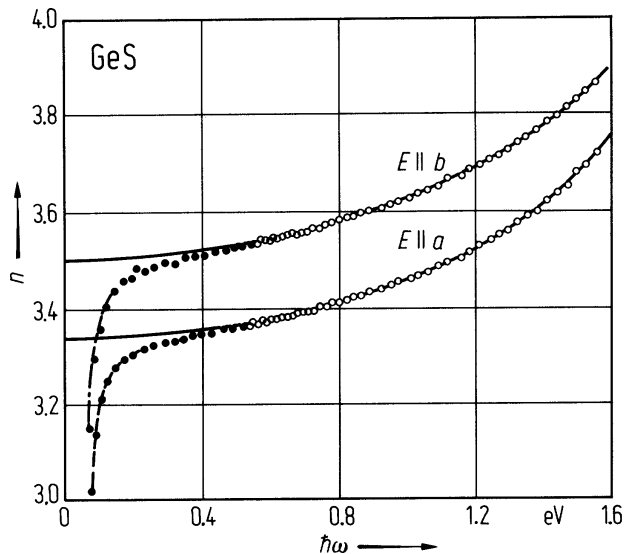
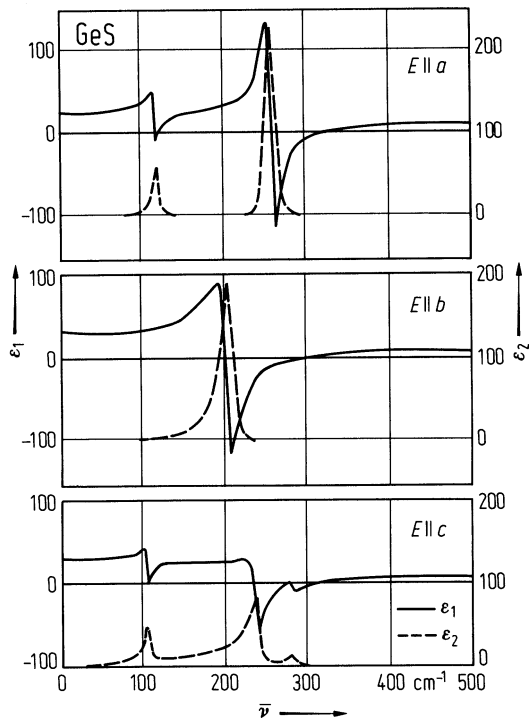


Fig. 23.1.6

GeS. The real (solid line) and imaginary part of the complex dielectric function obtained from Kramers-Kronig analysis of IR reflectivity spectra [76W].



23.2 Germanium selenide (GeSe)

Crystal structure

see section 23.0.

Electronic properties

energy gap

$E_{\text{g,ind}}$	1.075 eV	$T = 300 \text{ K}, E \parallel a$	absorption measurement,	79E
	1.080 eV	$T = 300 \text{ K}, E \parallel b$	indirect transition	
$dE_{\text{g,ind}}/dT$	$-0.86 \cdot 10^{-3} \text{ eV K}^{-1}$	$T = 100 \dots 300 \text{ K}, E \parallel a$		76V
	$-0.5 \cdot 10^{-3} \text{ eV K}^{-1}$	$T = 100 \dots 300 \text{ K}, E \parallel b$		

Lattice properties

lattice parameters

a	10.82 Å	RT		63W
b	3.85 Å			
c	4.4 Å			

heat capacity

C_p	49.9 J mol ⁻¹ K ⁻¹	$T = 300 \text{ K}$		74M
-------	--	---------------------	--	-----

density

d	5.52 g cm ⁻³	$T = 300 \text{ K}$		67D
-----	-------------------------	---------------------	--	-----

melting temperature

T_m	948 K			74M
-------	-------	--	--	-----

phonon dispersion relations : Fig. 23.2.1

phonon frequencies

$\nu_{\text{TO}}(\text{B}_{1\text{u}})$	$5.56 \cdot 10^{12} \text{ s}^{-1}$	$T = 300 \text{ K}$	infrared active phonons	76C
$\nu_{\text{LO}}(\text{B}_{1\text{u}})$	$6.69 \cdot 10^{12} \text{ s}^{-1}$			
$\nu_{\text{TO}}(\text{B}_{1\text{u}})$	$5.23 \cdot 10^{12} \text{ s}^{-1}$			
$\nu_{\text{LO}}(\text{B}_{1\text{u}})$	$5.32 \cdot 10^{12} \text{ s}^{-1}$			
$\nu_{\text{TO}}(\text{B}_{1\text{u}})$	$2.63 \cdot 10^{12} \text{ s}^{-1}$			
$\nu_{\text{LO}}(\text{B}_{1\text{u}})$	$2.72 \cdot 10^{12} \text{ s}^{-1}$			
$\nu_{\text{TO}}(\text{B}_{3\text{u}})$	$5.92 \cdot 10^{12} \text{ s}^{-1}$			
$\nu_{\text{LO}}(\text{B}_{3\text{u}})$	$6.51 \cdot 10^{12} \text{ s}^{-1}$			
$\nu_{\text{TO}}(\text{B}_{3\text{u}})$	$5.14 \cdot 10^{12} \text{ s}^{-1}$			
$\nu_{\text{LO}}(\text{B}_{3\text{u}})$	$5.8 \cdot 10^{12} \text{ s}^{-1}$			
$\nu_{\text{TO}}(\text{B}_{3\text{u}})$	$2.48 \cdot 10^{12} \text{ s}^{-1}$			
$\nu_{\text{LO}}(\text{B}_{3\text{u}})$	$2.57 \cdot 10^{12} \text{ s}^{-1}$			
$\nu_{\text{TO}}(\text{B}_{2\text{u}})$	$4.48 \cdot 10^{12} \text{ s}^{-1}$			
$\nu_{\text{LO}}(\text{B}_{2\text{u}})$	$6.27 \cdot 10^{12} \text{ s}^{-1}$			
$\nu_1(\text{A}_{1\text{g}})$	$5.62 \cdot 10^{12} \text{ s}^{-1}$	$T = 300 \text{ K}$	Raman shift	76C
$\nu_2(\text{A}_{1\text{g}})$	$5.2 \cdot 10^{12} \text{ s}^{-1}$			
$\nu_3(\text{A}_{1\text{g}})$	$2.48 \cdot 10^{12} \text{ s}^{-1}$			
$\nu_4(\text{A}_{1\text{g}})$	$1.16 \cdot 10^{12} \text{ s}^{-1}$			
$\nu_1(\text{B}_{1\text{g}})$	$4.9 \cdot 10^{12} \text{ s}^{-1}$			
$\nu_2(\text{B}_{1\text{g}})$	$2.3 \cdot 10^{12} \text{ s}^{-1}$			

phonon frequencies (continued)

$\nu_1(\text{B}_{2\text{g}})$	$6.72 \cdot 10^{12} \text{ s}^{-1}$
$\nu_2(\text{B}_{2\text{g}})$	$5.32 \cdot 10^{12} \text{ s}^{-1}$
$\nu_3(\text{B}_{2\text{g}})$	$3.04 \cdot 10^{12} \text{ s}^{-1}$
$\nu_4(\text{B}_{2\text{g}})$	$1.46 \cdot 10^{12} \text{ s}^{-1}$
$\nu_1(\text{B}_{3\text{g}})$	$4.51 \cdot 10^{12} \text{ s}^{-1}$
$\nu_2(\text{B}_{3\text{g}})$	$1.16 \cdot 10^{12} \text{ s}^{-1}$

Transport properties

GeSe shows p-type semiconducting properties. The carrier concentration and the temperature of the mobility depends on the stoichiometry of the composition of Ge and Se and on the heat treatment of growth of the crystal [60A2].

For $\rho(T)$, $R_{\text{H}}(T)$, $\mu_{\text{H}}(T)$, see Fig. 23.2.2.

Optical properties

reflectivity : Fig. 23.2.3.

dielectric constants

$\epsilon(0)$	21.9	$E \parallel a, T = 300 \text{ K}$	obtained from Kramers-Kronig transformation of IR spectra	76C
	30.4	$E \parallel b$		
	25.8	$E \parallel c$		
$\epsilon(\infty)$	18.7	$E \parallel a$	see also Fig. 23.2.3	
	21.9	$E \parallel b$		
	14.4	$E \parallel c$		

References to 23.2

60A1 Albers, W., Haas, C., Van Der Maesen, F.: J. Phys. Chem. Solids 15 (1960) 306.
60A2 Asanabe, S., Okazaki, A.: J. Phys. Soc. Jpn. 15 (1960) 989.
63W Wyckoff, R. W. G.: Crystal Structures, Vol. 1, Second Edition, Wiley & Sons 1963.
67D D'Ans-Lax: Taschenbuch f. Chemiker u. Physiker, Vol. 1, Berlin, Heidelberg, New York: Springer 1967.
74M Mills, K. C.: Thermodynamic Data for Inorganic Sulphides, Selenides and Tellurides, London: Butterworths 1974.
76C Chandrasekhar, H. R., Zwick, U.: Solid State Commun. 18 (1976) 1509.
76V Vlachos, S. V., Lambros, A. P., Thanailakis, A., Economou, N. A.: Phys. Status Solidi (b) 76 (1976) 727.
77E Bymard, R., Otto, A.: Phys. Rev. B 16 (1977) 1616.
77F Frey, A.: Dissertation TH Stuttgart 1977.
79E El-Korashy, A. M.: Inst. Phys. Conf . Ser. 43 (1979) chapter 23.

Figures to 23.2

Fig. 23.2.1

GeSe. Calculated phonon dispersion relations [77F].

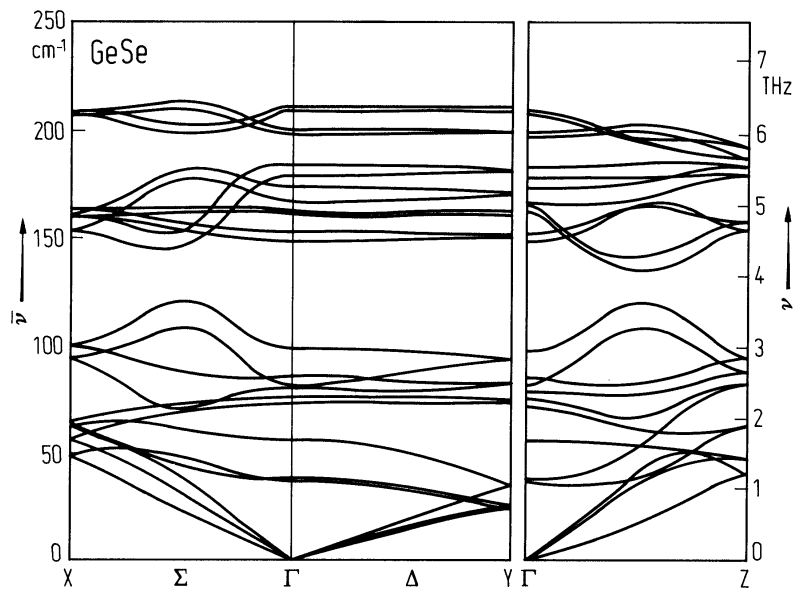


Fig. 23.2.2

GeSe. Resistivity (a), Hall coefficient (b) and Hall mobility (c) perpendicular to the c -axis vs. reciprocal temperature for different single crystals (p-type) with stoichiometric compositions [60A1].

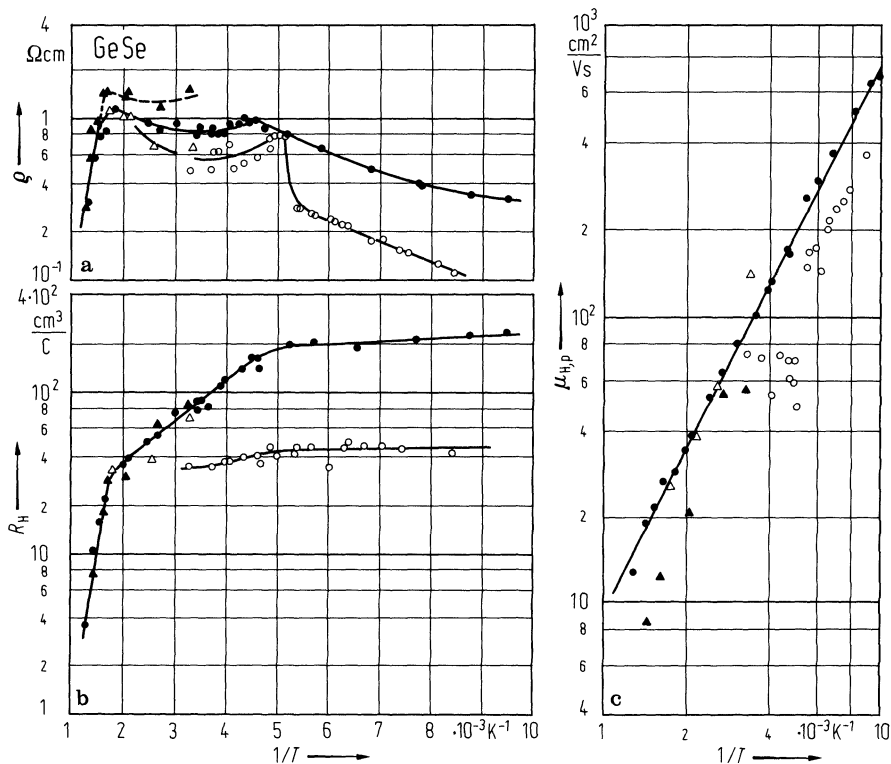


Fig. 23.2.3

GeSe. Room temperature reflectivity vs. wavenumber for three principal polarizations. The arrows at the right-hand side indicate the final value of reflectivity measured at 4000 cm^{-1} [76C].

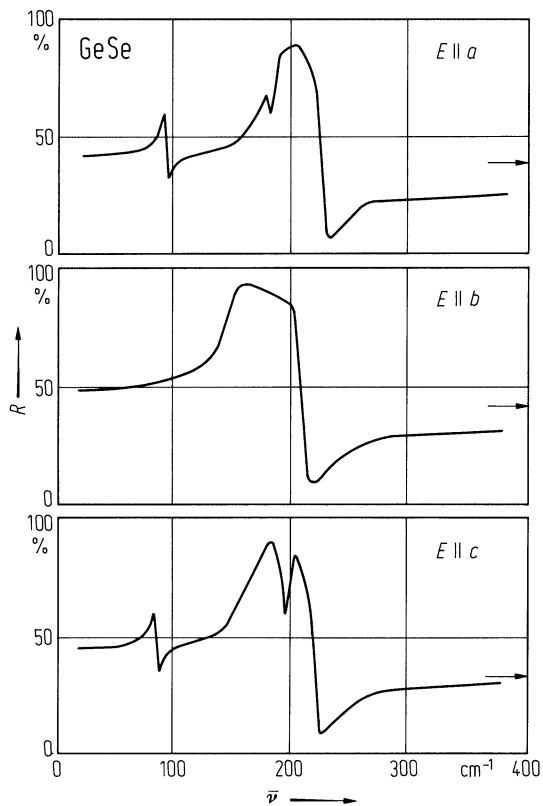
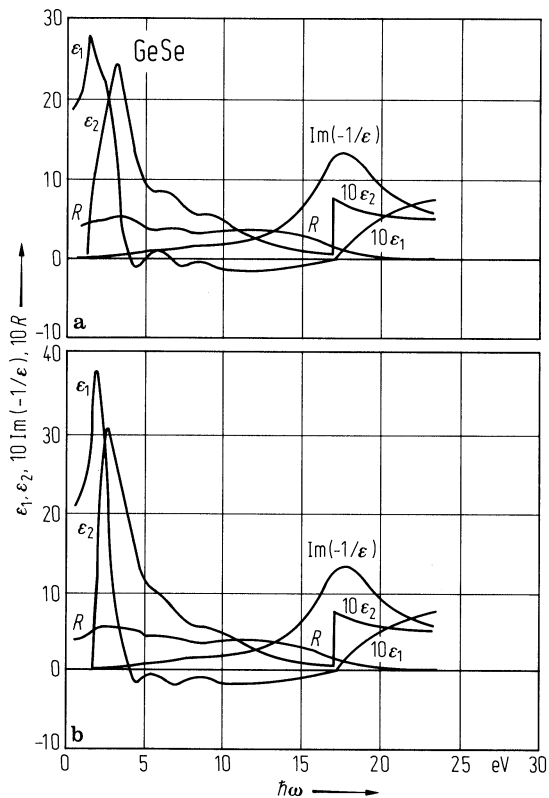


Fig. 23.2.4

GeSe. Real and imaginary part of dielectric function and energy loss function $\text{Im}(-1/\epsilon)$ vs. photon energy determined from Kramers-Kronig analysis of reflectivity spectra [77E]. a) $E \parallel a$, b) $E \parallel b$. Reflectivity R is also shown.



23.3 Germanium telluride (GeTe)

Crystal structure

see section 23.0.

Electronic properties

band structure : Fig. 23.0.8, Brillouin zone: Fig. 23.0.7.

energy gaps

$E_g(L_{6v}^- - L_{6c}^+)$	0.1...0.2 eV	$p = 5.7 \cdot 10^{20} \text{ cm}^{-3}$, $T = 300 \text{ K}$	tunnel diode characteristic	70B
$E_{g,\text{opt}}$	0.73...0.95 eV	$T = 300 \text{ K}$, α -phase	reflectivity, shifted to higher energies due to Burstein shift, both heavy and light holes are responsible.	69B
$dE_{g,\text{opt}}/dT$	$-4.2 \cdot 10^{-4} \text{ eV K}^{-1}$	$T = 77...300 \text{ K}$	temperature dependence of reflectivity (optical gap)	69B

effective masses

$m_{p,l}$	$1.15 m_0$	α -phase	electrical transport data	69L,
$m_{p,h}$	$5 m_0$			77K1
$m_{n,h}$	$0.48...0.78 m_0$	α -phase	calculated, heavy electron band	73L

Lattice properties

As-like phase (α -phase)

lattice parameters

The $\text{Ge}_{1-x}\text{Te}_x$ lattice parameters are varying with composition x

a	$5.984(1) \text{ \AA}$	$\text{Ge}_{0.497}\text{Te}_{0.503}$	(Ge-saturated)	72H
α	$88^\circ 10' \pm 0.1'$			
a	$5.966(1) \text{ \AA}$	$\text{Ge}_{0.488}\text{Te}_{0.512}$	(Te-saturated)	
α	$88^\circ 10' \pm 0.5'$			

NaCl-like phase (β -phase)

lattice parameter

(at T_{tr})

a	$6.0121(2) \text{ \AA}$	$T = 396^\circ\text{C}$	X-ray	67Z
-----	-------------------------	-------------------------	-------	-----

heat capacity

C_p	$(11.5 + 3.0 \cdot 10^{-3} T)$ $\text{cal K}^{-1} \text{ mol}^{-1}$	$T = 298...998 \text{ K}$		74M
-------	--	---------------------------	--	-----

density

d	$6.193(5) \text{ g cm}^{-3}$	$T = 25^\circ\text{C}$	$\text{Ge}_{0.497}\text{Te}_{0.503}$; α -phase	65S
-----	------------------------------	------------------------	--	-----

melting temperature

The maximum melting temperature of $\text{Ge}_{1-x}\text{Te}_x$ occurs at $724(1)^\circ\text{C}$ and 49.84 at% Te [66B, 74M]. The Te-rich solidus increases in Te content with decreasing temperature down to 500°C , where it is 51.32 at% Te. The stoichiometric solid is in equilibrium with a 52 at% Te liquid and lies within the homogeneity range down to at least 600°C [66B].

phonon wavenumbers

$\bar{\nu}(\text{A}_{1g})$	140 cm^{-1}	α -phase	Raman shift ($T_{tr} = 625 \text{ K}$)	70S
$\bar{\nu}_{\text{TO,LO}}(\text{E}_g)$	98 cm^{-1}			

Transport properties

As grown from the melt $\text{Ge}_{1-x}\text{Te}_x$ is always found to have high hole conductivity, the carrier density varying between $3 \cdot 10^{20} \text{ cm}^{-3}$ and $13 \cdot 10^{20} \text{ cm}^{-3}$ with varying stoichiometry [64K]: excess Te increases, excess Ge decreases the number of holes. The composition at which the defects in the lattice change from being due to excess Ge to being due to excess Te occurs at $x = 0.5037$ [69L].

resistivity

ρ	$\approx 2 \cdot 10^{-4} \Omega \text{ cm}$	$T = 300 \text{ K},$ α -phase	for temperature dependence of the resistivity of α -GeTe, see Fig. 23.3.1	70B
--------	---	---	---	-----

mobility

μ	$15 \dots 120 \text{ cm}^2/\text{V s}$	$T = 300 \text{ K},$ α -phase		70B
-------	--	---	--	-----

Optical properties

optical spectra

real and imaginary part of the dielectric function: Fig.23.3.2.

refractive index

n	5.5	$\lambda = 1.5 \mu\text{m}$	GeTe film	69B
-----	-----	-----------------------------	-----------	-----

absorption index

k	0.5	$\lambda = 1.5 \mu\text{m},$ $T = 300 \text{ K}$		69B
-----	-----	---	--	-----

dielectric constant

$\epsilon(\infty)$	36	$T = 295 \text{ K},$	Kramers-Kronig analysis	69B
	37.5	$T = 295 \text{ K},$	reflectivity of bulk material	68T

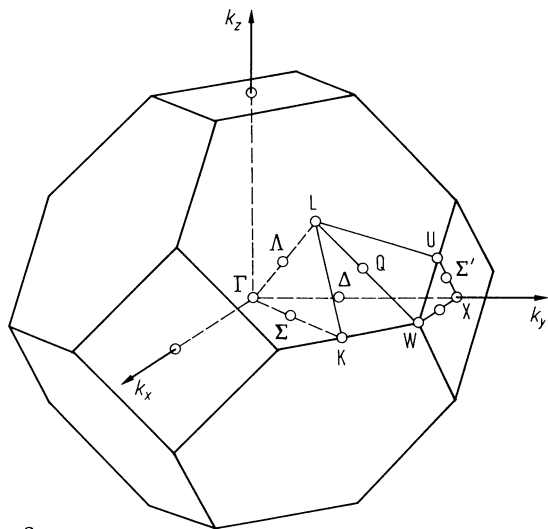
References to 23.3

- 64K Kolomoets, N., Lev, B., Sysoeva, L.: Sov. Phys. Solid State 6 (1964) 551.
65S Shelimova, L. E., Abrikosov, N. Kh., Zhdanova, V. V.: Russ. J. Inorg. Chem. 10 (1965) 650.
66B Brebrick, R. F.: J. Phys. Chem. Solids 27 (1966) 1495.
67Z Zhukova, T. B., Zaslavskii, A.: Sov. Phys. Crystallogr. 12 (1967) 28.
68T Tsu, R., Howard, W. E., Esaki, L.: Phys. Rev. 172 (1968) 779.
69B Bahl, S. K., Chopra, K. L.: J. Appl. Phys. 40 (1969) 4940.
69L Lewis, J. E.: Phys. Status Solidi 35 (1969) 737.
69T Tung, Y., Cohen, L. M.: Phys. Rev. 180 (1969) 823.
70B Bahl, S. K., Chopra, K. L.: J. Appl. Phys. 41 (1970) 2196.
70S Steigmeier, E. F., Harbecke, G.: Solid State Commun. 8 (1970) 1275.
72H Hohnke, D. K., Holloway, H., Kaiser, S.: J. Phys. Chem. Solids 33 (1972) 2053.
73S Strauss, A. J., Harman, T. C.: J. Electron. Mater. 2 (1973) 71.
74M Mills, K. C.: Thermodynamic Data for Inorganic Sulphides, Selenides and Tellurides, London: Butterworths 1974.
77K1 Kopinets, I. F.: Poluprovodn. Tekh. Mikroelektron. 25 (1977) 3.
77K2 Korzhuev, M. A., Shelimova, L. E., Abrikosov, N. Kh.: Sov. Phys. Semicond. 11 (1977) 171.

Figures to 23.3

Fig. 23.0.7

GeTe. Brillouin zone of the fcc lattice of the NaCl structure.



GeTe. Electronic energy band structure [69T].

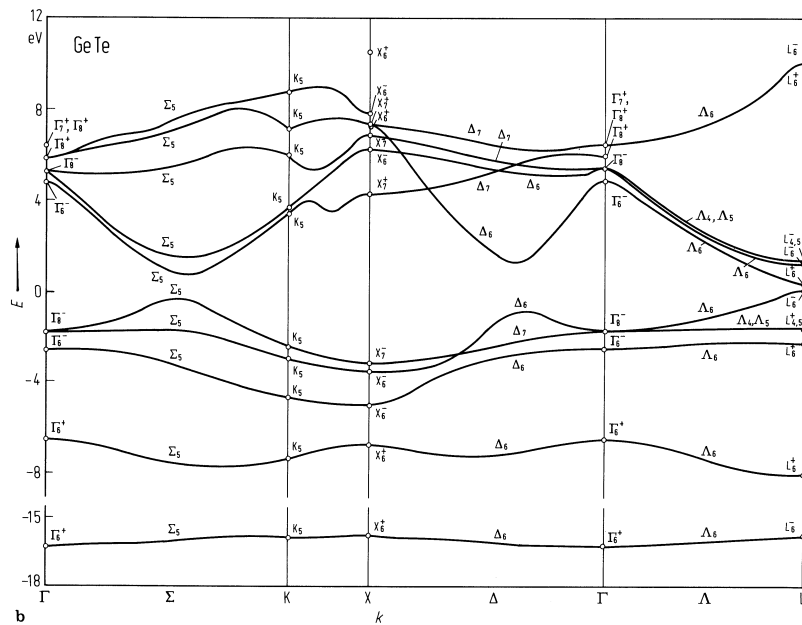


Fig. 23.3.1

α -GeTe. Electrical resistivity vs. temperature of a single crystal with 50.36 at% Te ($T_{tr}(\alpha \rightarrow \beta) = 668$ K). Full circles: heating of ρ_{33} (\parallel to the trigonal axis); open circles: cooling of ρ_{33} (\parallel to the trigonal axis); full triangles: heating of ρ_{11} (\perp to the trigonal axis), open triangles: cooling of ρ_{11} (\perp to the trigonal axis) [77K2].

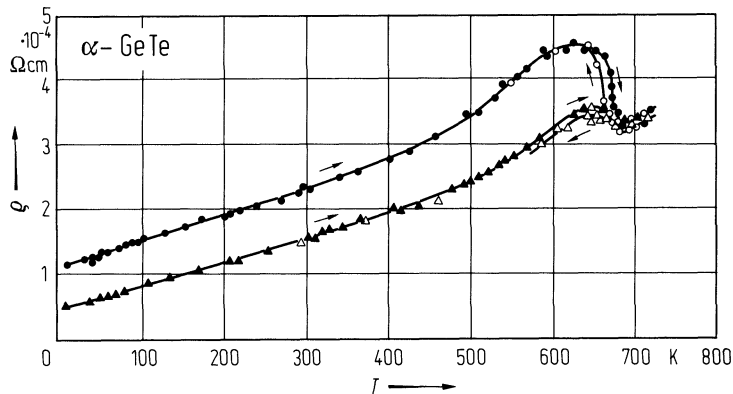
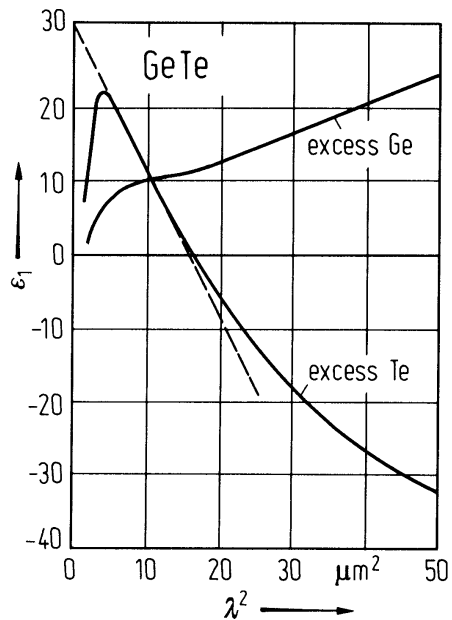


Fig. 23.3.2

GeTe. Real part of the dielectric function vs. squared wavelength obtained from reflectance by Kramers-Kronig analysis [73L]. Excess Ge α -phase, excess Te γ -phase.



23.4 Tin sulfide (SnS)

Crystal structure

see section 23.0.

Electronic properties

band structure : Fig. 23.0.4, Brillouin zone: Fig. 23.0.2.

energy gap

$E_{g,ind}$	1.42 eV	$T = 300\text{ K}, E \parallel a$	absorption measurement	74L
	1.095 eV	$T = 300\text{ K}, E \parallel b$		60A2
$dE_{g,ind}/dT$	$-4.05 \cdot 10^{-4}\text{ eV K}^{-1}$	$T = 100...300\text{ K}, E \parallel a$		74L
	$-4.37 \cdot 10^{-4}\text{ eV K}^{-1}$	$T = 100...300\text{ K}, E \parallel b$		

effective masses

$m_p(\parallel a)$	$0.2\ m_0$	$T = 300\text{ K}$	determined from free carrier reflectivity	61A
$m_p(\parallel b)$	$0.2\ m_0$			
$m_p(\parallel c)$	$1\ m_0$			
$m_{ds,p}$	$0.95\ m_0$	$T = 300\text{ K}$	from thermoelectric power measurements	60A1
$m_{ds,n}$	$0.45\ m_0$		calculated from $m_{ds,p}$ (knowing the density of states of electrons and holes)	65R

Lattice properties

lattice parameters

a	11.20 \AA		RT	63W
b	3.99 \AA			
c	4.34 \AA			

linear thermal expansion coefficient

α	$2.8 \cdot 10^{-7}\text{ K}^{-1}$	$T = 300\text{ K}$	from interference measurements	74L
----------	-----------------------------------	--------------------	--------------------------------	-----

Debye temperature

Θ_D	270 K	$T = 80\text{ K}$		69A
------------	----------------	-------------------	--	-----

heat capacity

C_p	$45\text{ J mol}^{-1}\text{ K}^{-1}$	$T = 300\text{ K}$		74M
	$29.3\text{ Jmol}^{-1}\text{ K}^{-1}$	$T = 80\text{ K}$		69A

density

d	5.08 g cm^{-3}	$T = 300\text{ K}$		69A
-----	-------------------------	--------------------	--	-----

melting temperature

T_m	1153 K			74M
-------	-----------------	--	--	-----

phonon frequencies

$\nu_{TO}(B_{1u})$	$6.64 \cdot 10^{12}\text{ s}^{-1}$	$T = 300\text{ K}$	IR reflectivity measurements	77F,
$\nu_{LO}(B_{1u})$	$8.28 \cdot 10^{12}\text{ s}^{-1}$			77C
$\nu_{TO}(B_{1u})$	$5.32 \cdot 10^{12}\text{ s}^{-1}$			
$\nu_{LO}(B_{1u})$	$6.43 \cdot 10^{12}\text{ s}^{-1}$			
$\nu_{TO}(B_{1u})$	$2.96 \cdot 10^{12}\text{ s}^{-1}$			
$\nu_{LO}(B_{1u})$	$3.2 \cdot 10^{12}\text{ s}^{-1}$			

phonon frequencies (continued)

$\nu_{\text{TO}}(\text{B}_{3\text{u}})$	$6.58 \cdot 10^{12} \text{ s}^{-1}$		
$\nu_{\text{LO}}(\text{B}_{3\text{u}})$	$8.64 \cdot 10^{12} \text{ s}^{-1}$		
$\nu_{\text{TO}}(\text{B}_{3\text{u}})$	$5.62 \cdot 10^{12} \text{ s}^{-1}$		
$\nu_{\text{LO}}(\text{B}_{3\text{u}})$	$5.77 \cdot 10^{12} \text{ s}^{-1}$		
$\nu_{\text{TO}}(\text{B}_{3\text{u}})$	$2.06 \cdot 10^{12} \text{ s}^{-1}$		
$\nu_{\text{LO}}(\text{B}_{3\text{u}})$	$2.12 \cdot 10^{12} \text{ s}^{-1}$		
$\nu_{\text{TO}}(\text{B}_{2\text{u}})$	$4.34 \cdot 10^{12} \text{ s}^{-1}$		
$\nu_{\text{LO}}(\text{B}_{2\text{u}})$	$7.92 \cdot 10^{12} \text{ s}^{-1}$		
$\nu(\text{A}_{1\text{g}})$	$6.52 \cdot 10^{12} \text{ s}^{-1}$	Raman shift	77C
$\nu(\text{A}_{1\text{g}})$	$5.74 \cdot 10^{12} \text{ s}^{-1}$		
$\nu(\text{A}_{1\text{g}})$	$2.84 \cdot 10^{12} \text{ s}^{-1}$		
$\nu(\text{A}_{1\text{g}})$	$1.2 \cdot 10^{12} \text{ s}^{-1}$		
$\nu(\text{B}_{1\text{g}})$	$6.22 \cdot 10^{12} \text{ s}^{-1}$		
$\nu(\text{B}_{1\text{g}})$	$2.09 \cdot 10^{12} \text{ s}^{-1}$		
$\nu(\text{B}_{2\text{g}})$	$8.67 \cdot 10^{12} \text{ s}^{-1}$		
$\nu(\text{B}_{2\text{g}})$	$2.54 \cdot 10^{12} \text{ s}^{-1}$		
$\nu(\text{B}_{2\text{g}})$	$2.09 \cdot 10^{12} \text{ s}^{-1}$		
$\nu(\text{B}_{3\text{g}})$	$4.9 \cdot 10^{12} \text{ s}^{-1}$		
$\nu(\text{B}_{3\text{g}})$	$1.41 \cdot 10^{12} \text{ s}^{-1}$		

Transport properties

Pure SnS crystals show p-type conduction with carrier concentrations of $1...3 \cdot 10^{18} \text{ cm}^{-3}$ [61A]. The conductivity is caused by an excess of sulfur.

Temperature dependence of mobility: Fig. 23.4.1; temperature dependence of conductivity: Fig. 23.4.2.

hole mobility

$\mu_{\text{p}}(\perp c)$	$\approx 90 \text{ cm}^2/\text{V s}$	$T = 300 \text{ K},$ $p \approx 10^{18} \text{ cm}^{-3}$	Hall mobility	61A
---------------------------	--------------------------------------	---	---------------	-----

Optical properties

optical spectra

refractive index: Fig. 23.4.3; dielectric function: Fig. 23.4.4.

dielectric constants

$\epsilon(0)$	32(4)	$E \parallel a, T = 300 \text{ K}$	from Kramers-Kronig transformation	77C
	48(5)	$E \parallel b$	of IR data	
	32(4)	$E \parallel c$		
$\epsilon(\infty)$	14(2)	$E \parallel a$		
	16(2)	$E \parallel b$		
	16(2)	$E \parallel c$	for comparison, see also [76C]	

References to 23.4

- 58Y Yabumoto, T.: J. Phys. Soc. Jpn. 13 (1958) 972.
- 60A1 Albers, W., Haas, C., Van Der Maesen, F.: J. Phys. Chem. Solids 15 (1960) 306.
- 60A2 Asanabe, S., Okazaki, A.: J. Phys. Soc. Jpn. 15 (1960) 989.
- 61A Albers, W., Haas, C., Vink, H. J., Wasscher, J. D.: J. Appl. Phys. 32 (1961) 2220.
- 63W Wyckoff, R. W. G.: Crystal Structures, Vol. 1, Second Edition, Wiley & Sons 1963.
- 65R Rau, H.: J. Phys. Chem. Solids 27 (1966) 761.
- 69A Abrikosov, N. Kb., Bankina, V. F., Posetskaya, L. V., Shelimova, L. B., Skudnova, E. V.:
Semiconducting II-VI, IV-VI and V-VI compounds, New York: Plenum Press 1969, p. 65135.
- 74L Lambros, A. P., Gerleas, D., Economou, N. A.: J. Phys. Chem. Solids 35 (1974) 537.
- 74M Mills, K. C.: Thermodynamic Data for Inorganic Sulphides, Selenides and Tellurides, London:
Butterworths 1974.
- 76C Chamberlain, J. M., Nikolic, P., Merdan, M., Mihajiovic, P.: J. Phys. C 9 (1976) L637.
- 77C Chandrasekhar, H., Humphreys, R. G., Zwick, U., Cardona, M.: Phys. Rev. B 15 (1977) 2177.
- 77E Bymard, R., Otto, A.: Phys. Rev. B 16 (1977) 1616.
- 77F Frey, A.: Dissertation TH Stuttgart 1977.
- 80P Parke, A. W., Srivastava, G. P.: Phys. Status Solidi (b) 101 (1980) K31.

Figures to 23.4

Fig. 23.0.2

GeS. Brillouin zone for a simple orthorhombic Bravais lattice, e.g. GeS [77G].

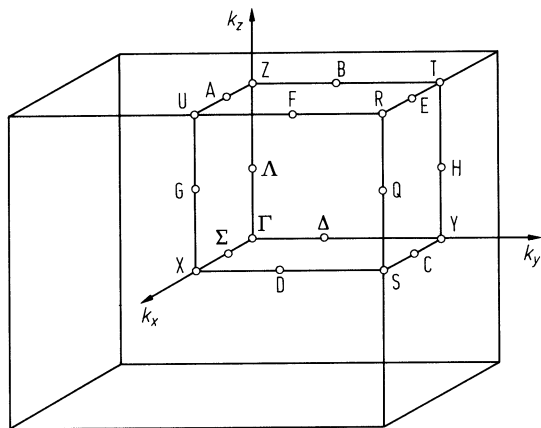


Fig. 23.0.4

SnS. Structure of the valence bands calculated along the main symmetry lines by the empirical pseudopotential method [80P].

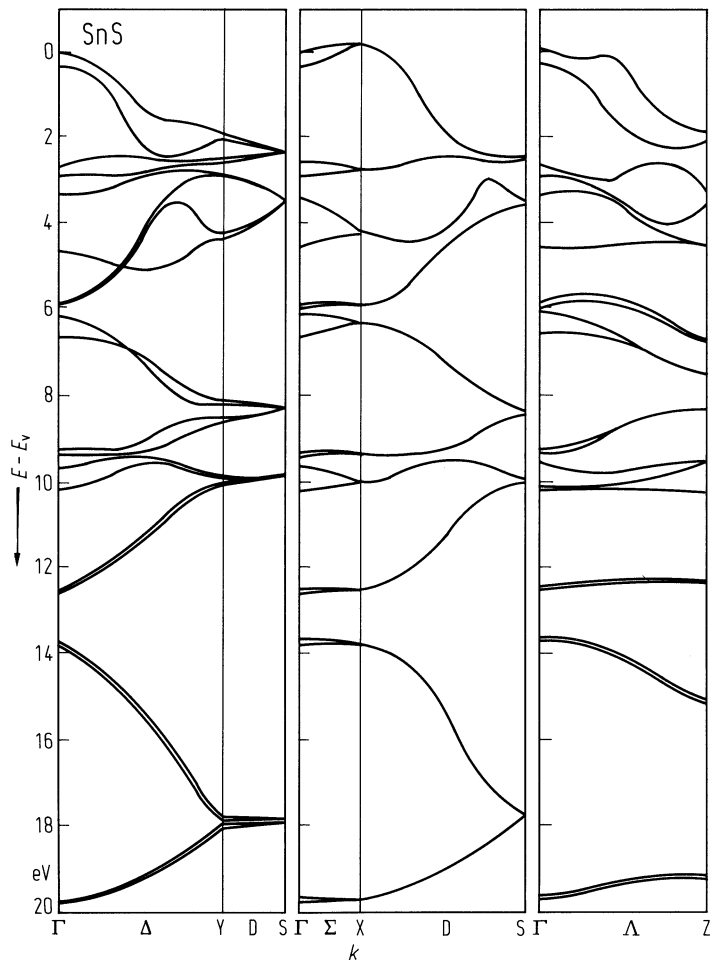


Fig. 23.4.1

SnS. Hall mobility of holes perpendicular to the c -axis $(\mu_a \cdot \mu_b)^{1/2}$ vs. temperature [61A].

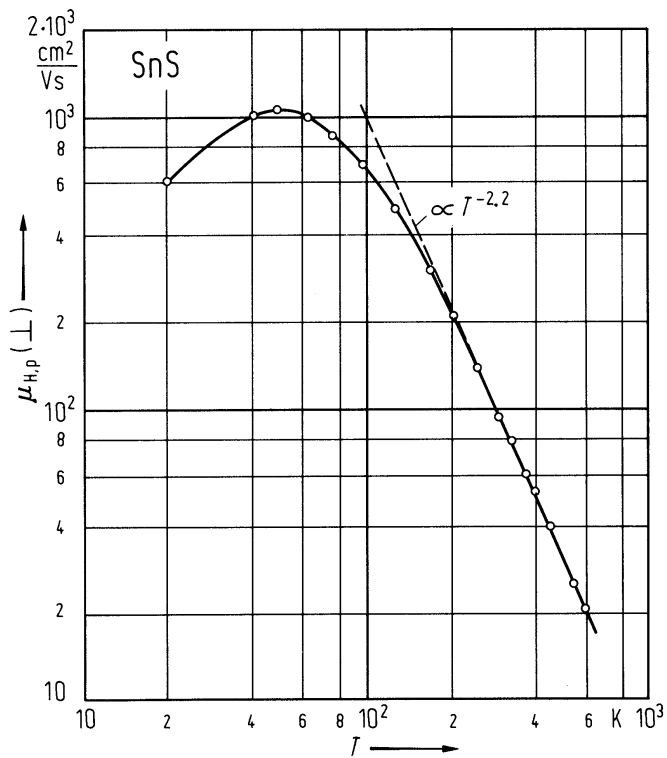


Fig. 23.4.2

SnS. Electrical conductivity of single crystals vs. reciprocal temperature [58Y].

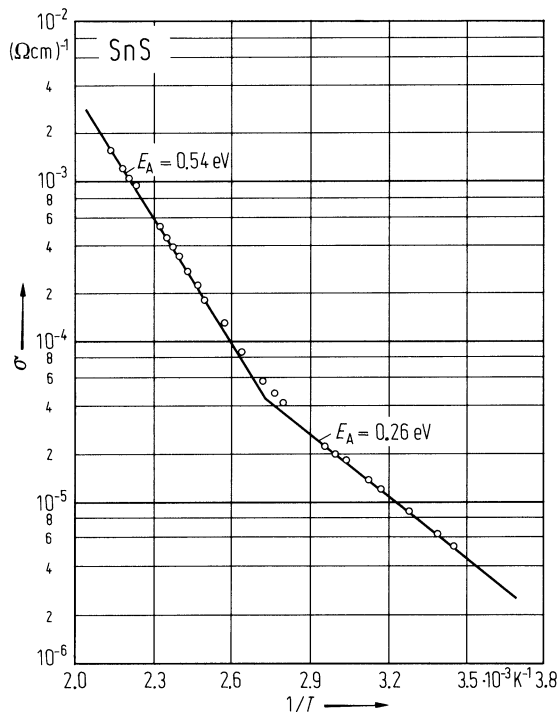


Fig. 23.4.3

SnS. Refractive index at 300 K vs. wavelength with $E \parallel a$ and $E \parallel b$ [74L].

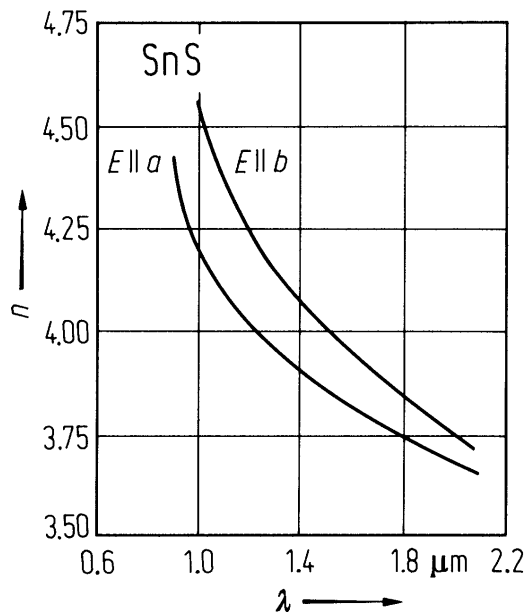
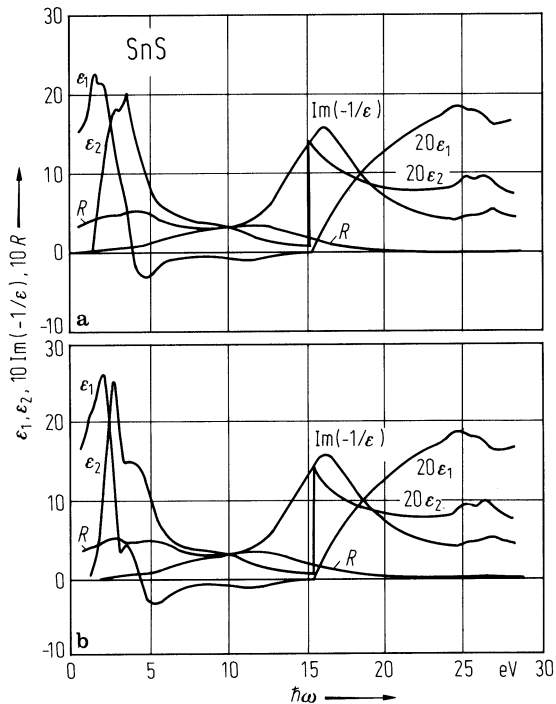


Fig. 23.4.4

SnS. Real and imaginary parts of the dielectric function and energy loss function $\text{Im}(-1/\epsilon)$ vs. photon energy $[77\text{E}]$. (a) $E \parallel a$, (b) $E \parallel b$.



23.5 Tin selenide (SnSe)

Crystal structure

see section 23.0.

Electronic properties

band structure : Fig. 23.0.5; Brillouin zone: Fig. 23.0.2.

energy gap

$E_{g,ind}$	0.9 eV	$T = 300\text{ K}$	from absorption	62A
-------------	--------	--------------------	-----------------	-----

effective mass

$m_p(\perp c)$	0.15 m_0		optical measurement	69A
	0.5 m_0		from thermoelectric power	59A

Lattice properties

lattice parameters

a	11.57 Å			
b	4.19 Å			
c	4.46 Å			
			RT	76L

Debye temperature

Θ_D	210 K	$T = 80\text{ K}$		69A
------------	-------	-------------------	--	-----

heat capacity

C_p	5.05 J mol ⁻¹ K ⁻¹	$T = 300\text{ K}$		74M
-------	--	--------------------	--	-----

melting temperature

T_m	1153 K			74M
-------	--------	--	--	-----

phonon frequencies

$\nu_{TO}(B_{1u})$	4.49·10 ¹² s ⁻¹	$T = 300\text{ K}$	IR reflectivity	77C
$\nu_{LO}(B_{1u})$	5.38·10 ¹² s ⁻¹			
$\nu_{TO}(B_{1u})$	3.68·10 ¹² s ⁻¹			
$\nu_{LO}(B_{1u})$	4.46·10 ¹² s ⁻¹			
$\nu_{TO}(B_{1u})$	2.39·10 ¹² s ⁻¹			
$\nu_{LO}(B_{1u})$	2.54·10 ¹² s ⁻¹			
$\nu_{TO}(B_{3u})$	4.25·10 ¹² s ⁻¹			
$\nu_{LO}(B_{3u})$	5.71·10 ¹² s ⁻¹			
$\nu_{TO}(B_{3u})$	3.89·10 ¹² s ⁻¹			
$\nu_{LO}(B_{3u})$	4.22·10 ¹² s ⁻¹			
$\nu_{TO}(B_{3u})$	1.67·10 ¹² s ⁻¹			
$\nu_{LO}(B_{3u})$	1.7·10 ¹² s ⁻¹			
$\nu_{TO}(B_{2u})$	2.87·10 ¹² s ⁻¹			
$\nu_{LO}(B_{2u})$	5.14·10 ¹² s ⁻¹			

phonon frequencies (continued)

$\nu(A_g)$	$4.51 \cdot 10^{12} \text{ s}^{-1}$	$T = 300 \text{ K}$	Raman shift	77C
$\nu(A_g)$	$3.89 \cdot 10^{12} \text{ s}^{-1}$			
$\nu(A_g)$	$2.12 \cdot 10^{12} \text{ s}^{-1}$			
$\nu(A_g)$	$0.987 \cdot 10^{12} \text{ s}^{-1}$			
$\nu(B_{1g})$	$3.98 \cdot 10^{12} \text{ s}^{-1}$			
$\nu(B_{1g})$	$1.7 \cdot 10^{12} \text{ s}^{-1}$			
$\nu(B_{2g})$	$5.05 \cdot 10^{12} \text{ s}^{-1}$		calculated	77F
$\nu(B_{2g})$	$4.1 \cdot 10^{12} \text{ s}^{-1}$		Raman shift	77C
$\nu(B_{2g})$	$1.67 \cdot 10^{12} \text{ s}^{-1}$			
$\nu(B_{2g})$	$1.20 \cdot 10^{12} \text{ s}^{-1}$			
$\nu(B_{3g})$	$3.23 \cdot 10^{12} \text{ s}^{-1}$			
$\nu(B_{3g})$	$1.11 \cdot 10^{12} \text{ s}^{-1}$			

Transport properties

Temperature dependence of Hall coefficient and resistivity of n-type SnSe: Fig. 23.5.1; temperature dependence of mobility and carrier concentration: Fig. 23.5.2.

carrier concentration

p	$3 \cdot 10^{15} \dots 2 \cdot 10^{18} \text{ cm}^{-3}$			77M
-----	---	--	--	-----

mobility

$\mu_p(\perp c)$	$\leq 7 \cdot 10^3 \text{ cm}^2/\text{V s}$	$T = 77 \text{ K},$ $p = 3.3 \cdot 10^{16} \text{ cm}^{-3}$	Hall mobility in pure single crystals	77M
------------------	---	--	---------------------------------------	-----

Optical properties

optical spectra : dielectric function: Fig. 23.5.3.

dielectric constants

$\varepsilon(0)$	45(5)	$E \parallel a, T = 300 \text{ K}$	from Kramers-Kronig analysis of	77C
	62(6)	$E \parallel b$	infrared reflectivity	
	42(5)	$E \parallel c$		
$\varepsilon(\infty)$	13(2)	$E \parallel a$		
	17(2)	$E \parallel b$		
	16(2)	$E \parallel c$		

References to 23.5

- 59A Asanabe, S.: J. Phys. Soc. Jpn. 14 (1959) 281.
- 61U Umeda, J.: J. Phys. Soc. Jpn. 16 (1961) 124.
- 62A Albers, W., Haas, O., Ober, H., Schodder, G. R., Wasscher, J. D.: J. Phys. Chem. Solids 23 (1962) 215.
- 69A Abrikosov, N. Kb., Bankina, V. F., Posetskaya, L. V., Shelimova, L. B., Skudnova, E. V.: Semiconducting II-VI, IV-VI and V-VI compounds, New York: Plenum Press 1969, p. 65135.
- 74M Mills, K. C.: Thermodynamic Data for Inorganic Sulphides, Selenides and Tellurides, London: Butterworths 1974.
- 76L Levy, F.: Structural Chemistry of Layer-Type Phases; Reidel Publishing Comp. 1976.
- 77C Chandrasekhar, H., Humphreys, R. G., Zwick, U., Cardona, M.: Phys. Rev. B 15 (1977) 2177.
- 77F Frey, A.: Dissertation TH Stuttgart 1977.
- 77G Grandke, T., Ley, L.: Phys. Rev. B 16 (1977) 832.
- 77M Maier, H., Daniel, D. R.: J. Electron. Mater. 6 (1977) 693.
- 78C Car, R., Ciucci, G., Quartapelle, L.: Phys. Status Solidi (b) 86 (1978) 471.

Fig. 23.0.5

SnSe. Pseudopotential band structure calculated along the high symmetry lines [78C]. 1 Ry = 13.6 eV.

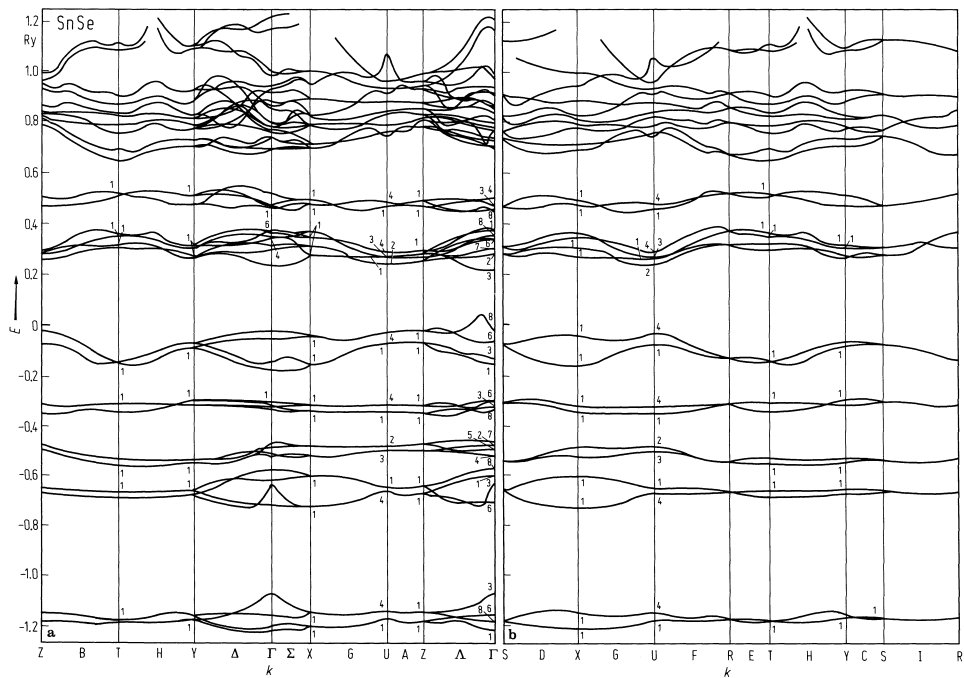


Fig. 23.5.1

SnSe. Hall coefficient and resistivity of Sb doped n-type single crystals vs. reciprocal temperature. The effect of annealing and quenching on the crystals is a decreasing and increasing of the carrier concentration [61U].

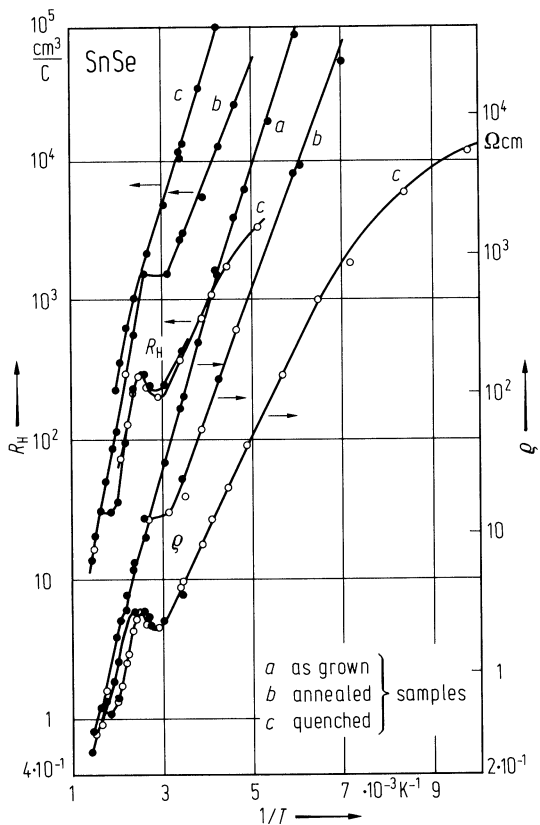


Fig. 23.5.2

SnSe. Hall mobility $\mu_{H,p} \parallel (001)$ and hole concentration p vs. temperature [77M]. (a) low hole concentration; (b) high hole concentration.

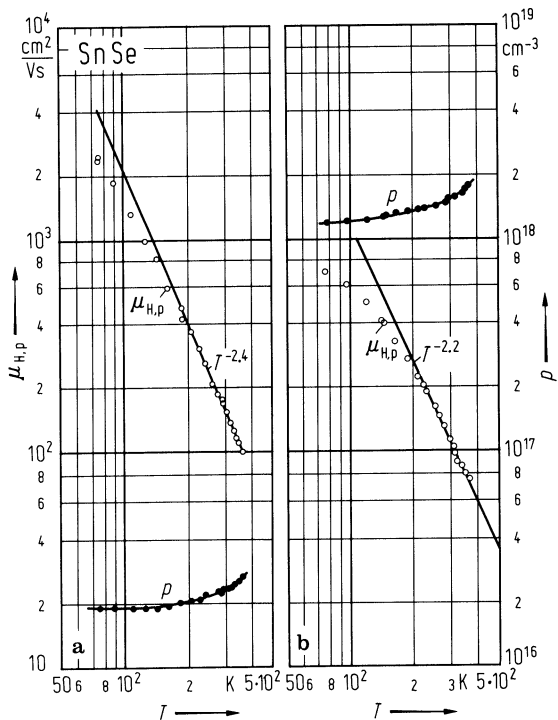
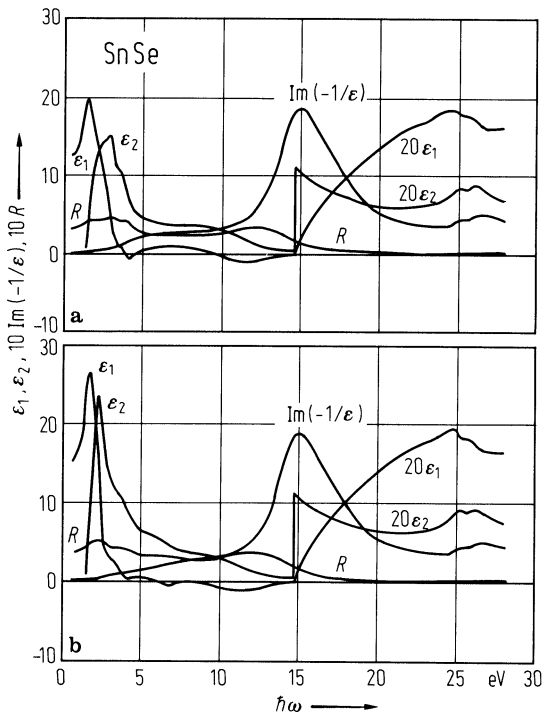


Fig. 23.5.3

SnSe. Real and imaginary part of the dielectric function and the energy loss function $\text{Im}(-1/\epsilon)$ vs. photon energy [77F]. (a) $E \parallel a$, (b) $E \parallel b$. Reflectivity R is also shown.



23.6 Tin telluride (SnTe)

Crystal structure

see section 23.0.

Electronic properties

All data for β -phase if not otherwise stated.

band structure: Fig. 23.0.9a, Brillouin zone: Fig. 23.0.7.

Principal structures are equal to those of PbTe. The main conduction and valence band edges occur at or near the centers of the hexagonal faces (L points of the fcc Brillouin zone, the valence band top with L_6^- , the conduction band edge with L_6^+ symmetry [76K]). The constant-energy surfaces near the main valence-band maxima have a highly prolate $\langle 111 \rangle$ -orientated form (de Haas-van Alphen measurements, [65B, 66B2, 72S]) and have probably a saddle point. Band structure near L: Fig. 23.0.9b.

energy gaps

E_g	0.36 eV	$T = 12 \text{ K}, 77 \text{ K},$ $p = 3.6 \cdot 10^{19} \text{ cm}^{-3}$ (α -phase)	optical absorption measurement	69B
$E_{g,\text{opt}}$	0.6 eV	$T = 300 \text{ K},$ $p \approx 4 \cdot 10^{20} \text{ cm}^{-3}$ (β -phase)	optical gap; shifted to higher energy due to Burstein shift; extrapolation to lower carrier concentration gives an optical gap $E_g = 0.19 \text{ eV}$ at RT.	74O

valence band, effective masses

m_p	$0.066 m_0$	$T = 300 \text{ K},$ $p = 3.6 \cdot 10^{19} \text{ cm}^{-3}$	free carrier absorption measurements, susceptibility effective masses	69B
-------	-------------	---	--	-----

Lattice properties

As-like phase (α -phase)

The α -phase is only existent if the carrier concentration (due to off-stoichiometry) is less than $p = 1.5 \cdot 10^{20} \text{ cm}^{-3}$ [76S1].

lattice parameters

a	6.325 \AA	$T = 5 \text{ K}$	76L
α	89.895°		

NaCl-like phase (β -phase)

lattice parameter

a	6.3268 \AA	$T = 300 \text{ K}$	71B
-----	----------------------	---------------------	-----

linear thermal expansion coefficient

α	$21.3 \cdot 10^{-6} \text{ K}^{-1}$	$p \approx 1 \cdot 10^{20} \text{ cm}^{-3},$ $T = 80 \dots 300 \text{ K}$	not stated if α - or β -phase	70B
----------	-------------------------------------	--	--	-----

Temperature dependence of the linear thermal expansion coefficient: Fig. 23.6.1.

Debye temperature : Fig. 23.6.2.

heat capacity : Fig. 23.6.3.

density

d	6.445(10) g cm ⁻³	$T = 25^\circ\text{C}$	determined by weighing for $2 \cdot 10^{20} \text{ cm}^{-3} < p_{300\text{K}}$ $< 18.4 \cdot 10^{20} \text{ cm}^{-3}$	63B
-----	------------------------------	------------------------	---	-----

phonon dispersion relations : Fig. 23.6.4.

The primitive unit cell of SnTe contains one Sn and one Te atom, so that there are in the NaCl-like phase a threefold degenerate optical IR-active and an acoustical mode. Below T_{tr} in the rhombohedral phase the inversion symmetry is broken and phonons arise in $[111]$ direction as well as twofold degenerate in the (100) plane, which are now Raman active.

phonon frequencies

$\nu_{\text{TO}}(000)$	0.78(5) THz	$T = 100 \text{ K},$	inelastic neutron scattering	69C
$\nu_{\text{LO}}(000)$	4.17(8) THz	β -phase		

sound velocities

ν_{LA}	$3.171 \cdot 10^5 \text{ cm s}^{-1}$	$[110]$ direction	ultrasonic measurements at 300 K, true carrier density	76S1
ν_{TA1}	$1.220 \cdot 10^5 \text{ cm s}^{-1}$	$[110]$ direction polarized in $[001]$	$p = 4.5 \cdot 10^{20} \text{ cm}^{-3}$ (β -phase)	
ν_{TA2}	$2.869 \cdot 10^5 \text{ cm s}^{-1}$	$[110]$ direction polarized in $[1\bar{1}0]$		

second order elastic moduli

$(1/2)(c_{11}-c_{12})$	$5.358 \cdot 10^{11} \text{ dyn cm}^{-2}$	$T = 300 \text{ K},$ $p = 4.5 \cdot 10^{20} \text{ cm}^{-3}$	ultrasonic measurements, (β -phase)	76S1
c_{44}	$0.969 \cdot 10^{11} \text{ dyn cm}^{-2}$		c_{44} is markedly affected by hole concentration, in contrast to	
c_{11}	$10.93 \cdot 10^{11} \text{ dyn cm}^{-2}$			
c_{12}	$0.21 \cdot 10^{11} \text{ dyn cm}^{-2}$		$(1/2)(c_{11}-c_{12})$	
$(c_{11}+2c_{12})/3$	$3.78 \cdot 10^{11} \text{ dyn cm}^{-2}$		for temperature dependence, see Fig. 23.6.5	

Transport properties

Temperature dependence of electrical conductivity for different carrier concentrations: Fig. 23.6.6.

mobility

μ_p	840 cm ² /V s	$T = 300 \text{ K}, \beta$ -phase	from fit of optical absorption data,	69B
	2000 cm ² /V s	$T = 77 \text{ K}, \alpha$ -phase	$p = 3.6 \cdot 10^{19} \text{ cm}^{-3}$	
	2800 cm ² /V s	$T = 12 \text{ K}, \alpha$ -phase		

temperature dependence of Hall mobility for different carrier concentrations: Fig. 23.6.7.

Optical properties

optical spectra

reflectivity spectrum, Fig. 23.6.8; dielectric function, Fig. 23.6.9.

dielectric constant

$\epsilon(0)$	1200(200)	LST-relation applied on TO-frequency	66P
---------------	-----------	---	-----

References to 23.6

- 62S Sagar, A., Miller, R. C.: Proc. Int. Conf. Phys. Semicond. Exeter July 1962, ed. A. C. Stickland (1962) 653.
- 63B Brebrick, R. F.: J. Phys. Chem. Solids 24 (1963) 27.
- 64C Cardona, M., Geenway, D.: Phys. Rev. 133 (1964) 1685.
- 65B Burke, J. R., Allgaier, R. S., Houston Jr., B. B., Babiskin, J., Siebenmann, P. G.: Phys. Rev. Lett. 14 (1965) 360.
- 66B Burke, J. R., Houston, B., Savage, H. T.: J. Phys. Soc. Jpn. 21, Suppl. (1966) 384.
- 66N Novikova, S. I., Shelimova, L. E.: Sov. Phys. Solid State 7 (1966) 2052.
- 66P Pawley, G. S., Cochran, W., Cowley, R. A., Dolling, G.: Phys. Rev. Lett. 17 (1966) 753.
- 69B Beattie, A. G.: J. Appl. Phys. 40 (1969) 4814.
- 69C Cowley, E. R., Darby, J. K., Pawley, G. S.: J. Phys. C 2 (1969) 1916.
- 70B Belson, H. S., Houston, B.: J. Appl. Phys. 41 (1970) 423.
- 71B Brebrick, R. F.: J. Phys. Chem. Solids 32 (1971) 551.
- 71T Tsang, Y. W., Cohen, M. L.: Phys. Rev. B 3 (1971) 1254.
- 72A Allgaier, R. S., Houston, B.: Phys. Rev. B 5 (1972) 2186.
- 72K1 Kästner, P.: Phys. Status Solidi (b) 53 (1972) 753.
- 72K2 Korn, D. M., Braunstein, R.: Phys. Rev. B 5 (1972) 4837.
- 72S Savage, H. T., Houston, B., Burke Jr., J. R.: Phys. Rev. B 6 (1972) 2292.
- 74O Ota, Y., in: Rabii, Phys. of IV-VI-Comp. and Alloys; London: Gordon and Breach Science Publishers, 1974, 113.
- 76K Kemeny, P. C., Cardona, M.: J. Phys. C 9 (1976) 1361.
- 76L Levy, F.: Structural Chemistry of Layer-Type Phases; Reidel Publishing Comp. 1976.
- 76S1 Seddon, T., Gupta, S. C., Saunders, G. A.: Solid State Commun 20 (1976) 69.
- 76S2 Smith, T. F., Birch, J. A., Collings, J. G.: J. Phys. C 9 (1976) 4375.
- 77H Hatta, I., Kobayashi, K. L. I.: Solid State Commun. 22 (1977) 775.
- 79M Melvin, J. S., Hendry, D. C.: J. Phys. C 12 (1979) 3003.

Figures to 23.6

Fig. 23.0.7

GeTe. Brillouin zone of the fcc lattice of the NaCl structure.

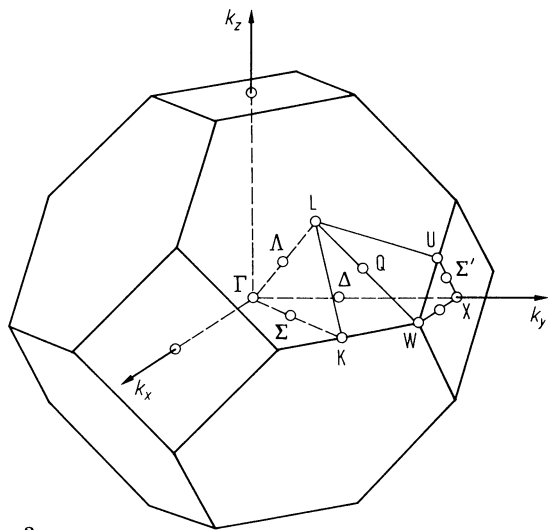
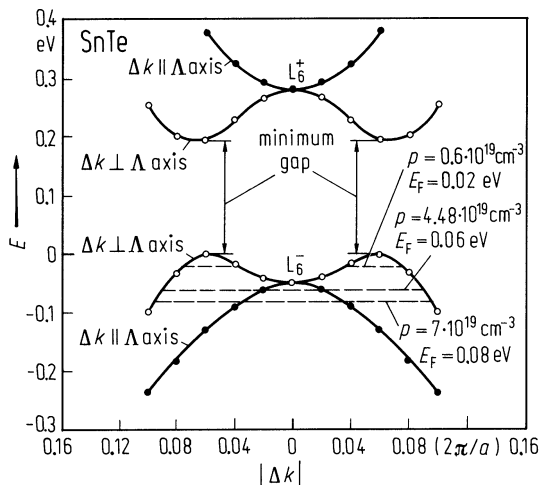


Fig. 23.0.9a

α -SnTe. Energy vs. relative wavevector Δk near L for zero temperature, calculated with the empirical pseudopotential method (EPM). Fermi levels corresponding to different hole concentrations p are indicated [71T]. The calculation was done for the α -phase. The phase transition has not been taken into account.



β -SnTe. Band structure obtained by a self-consistent relativistic calculation [79M]. 1 Ry = 13.6 eV.

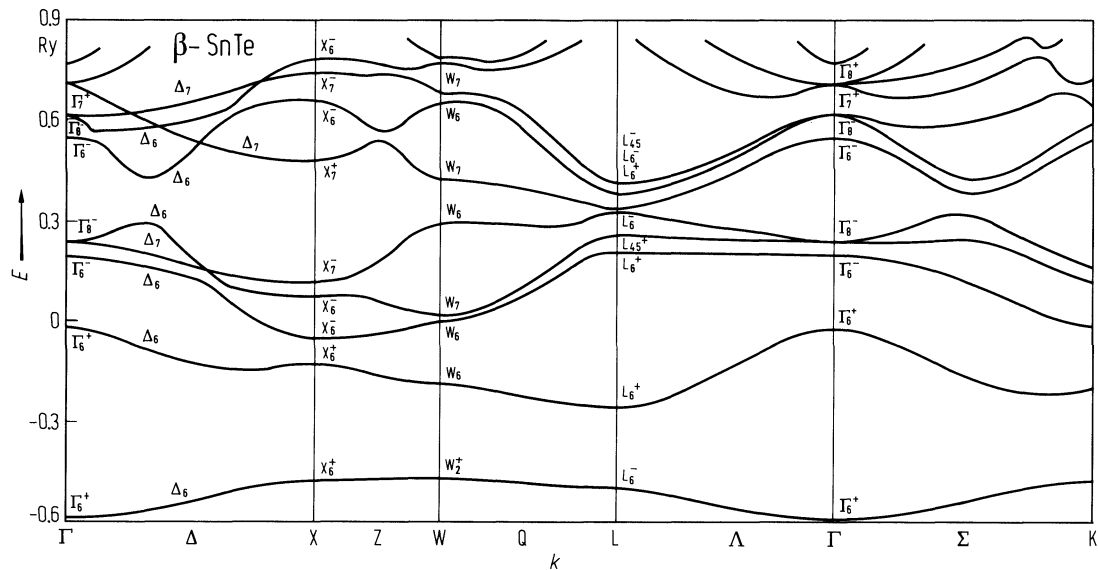


Fig. 23.6.1

SnTe. Linear thermal expansion coefficient vs. temperature for a sample with $p \approx 8 \cdot 10^{20} \text{ cm}^{-3}$. The full circles are data taken from [66N], [76S2]. No evidence for a phase transition was found.

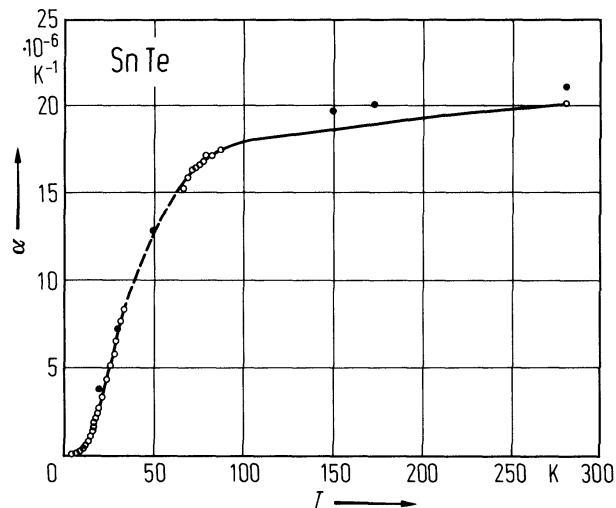


Fig. 23.6.2

SnTe. Debye temperature Θ_D vs. temperature derived from the variation of the lattice heat capacity ($p = 8 \cdot 10^{20} \text{ cm}^{-3}$). Shaded area represents the absolute limits on the zero temperature limit $\Theta_D(0)$. Dashed curve: [69C]. [76S2]. No phase transition observed.

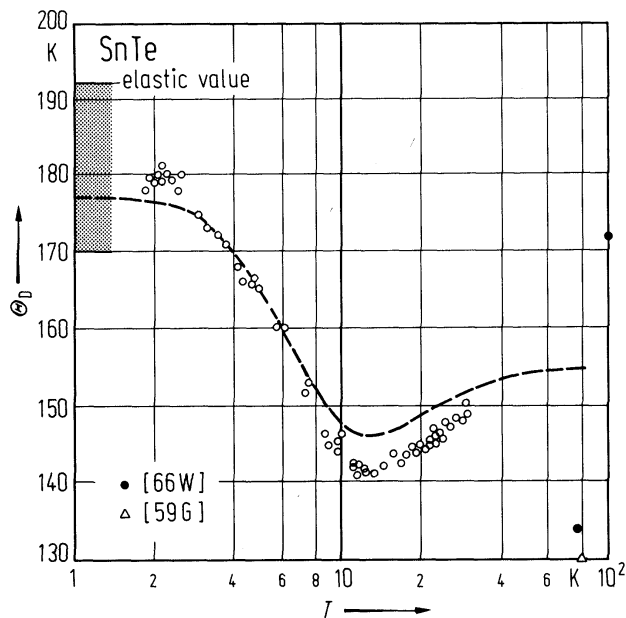


Fig. 23.6.3

SnTe. Heat capacity vs. temperature. The kink in the curve is attributed to the cubic–rhombohedral phase transition ($p^* = 1.8 \cdot 10^{20} \text{ cm}^{-3}$) [77H].

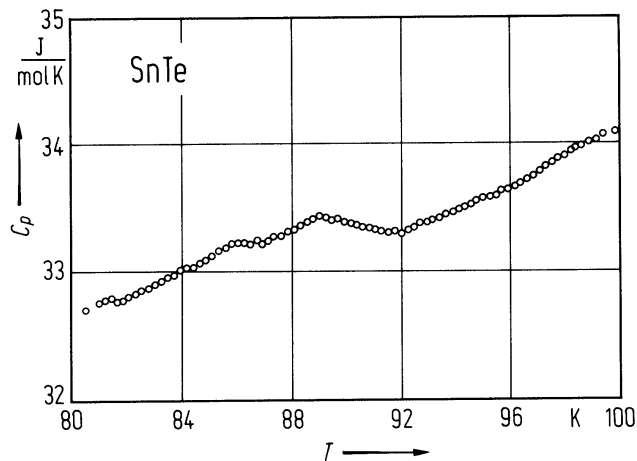


Fig. 23.6.4

SnTe. Frequency vs. reduced wave vector coordinate ζ at 100 K. Measurements of inelastic neutron scattering of modes polarized in the $(1\bar{1}0)$ plane ($p = 5 \cdot 10^{20} \text{ cm}^{-3}$), Open circles: longitudinal; full circles: transverse; solid line: non-ionic model; broken line: ionic model with ionic charge = 1.34 e [69C]. No transition to α -phase reported.

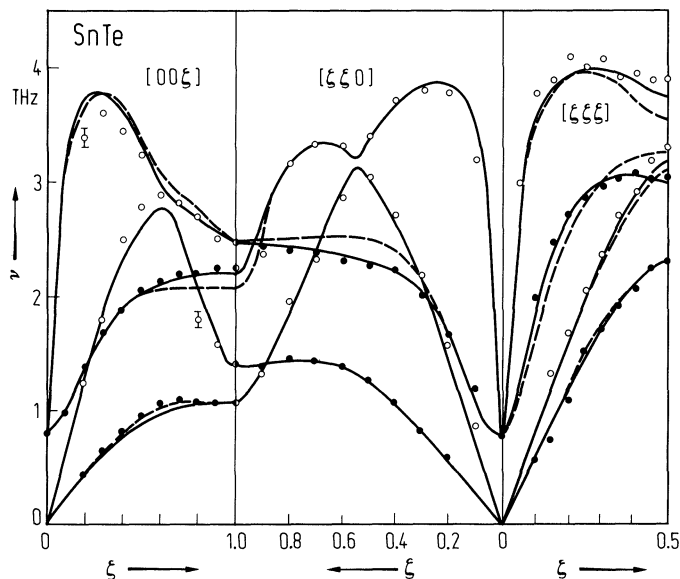


Fig. 23.6.5

SnTe. Elastic moduli vs. temperature for a sample with $p^* = 6 \cdot 10^{20} \text{ cm}^{-3}$ [69B]. (No phase transition reported.)

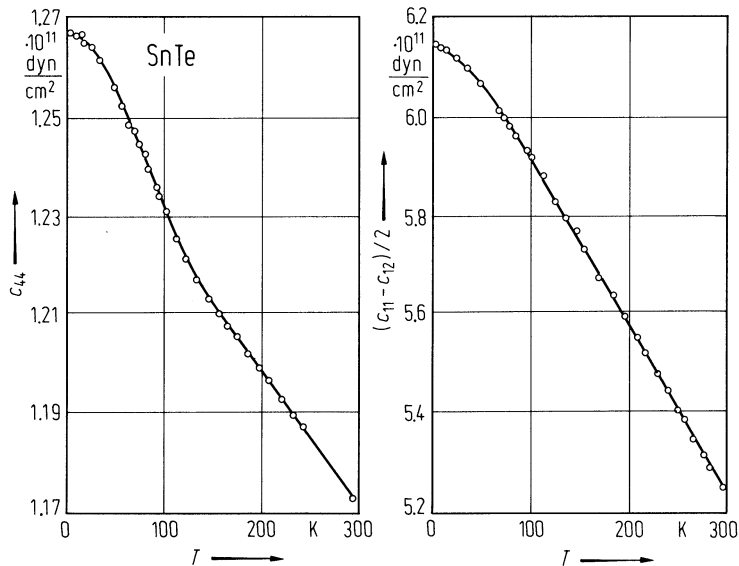
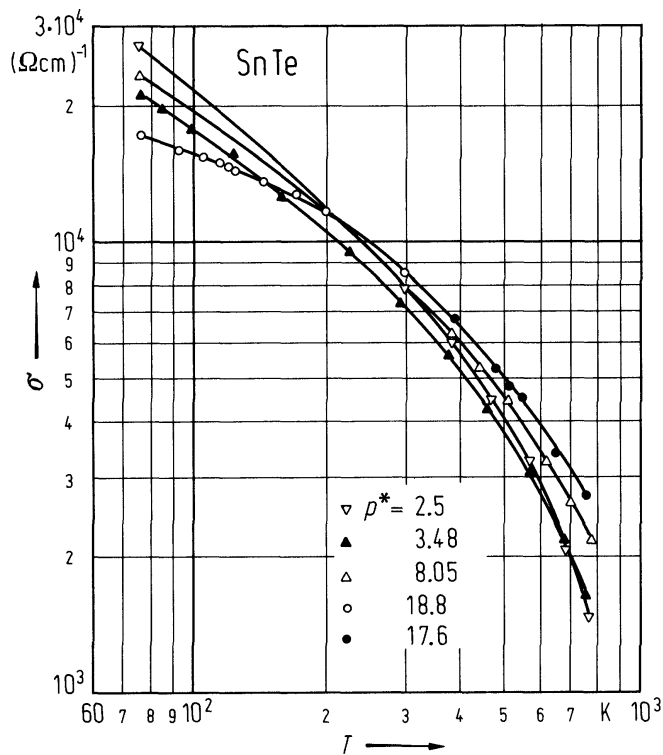


Fig. 23.6.6

SnTe. Electrical conductivity vs. temperature. Carrier concentration p^* ($= 1/R_H(77K)e$) in 10^{20} cm^{-3} [62S].



SnTe. Hall mobility vs. temperature for different carrier concentrations. *A*: $p^* = 1.4 \cdot 10^{20} \text{ cm}^{-3}$, *B*: $p^* = 7.73 \cdot 10^{20} \text{ cm}^{-3}$, *C*: $p^* = 1.74 \cdot 10^{20} \text{ cm}^{-3}$ with $p^* = 1/R_H(4.2\text{K})e$ and $\mu = R_H(4.2\text{K}) \cdot \sigma(T) [72\text{A}]$.

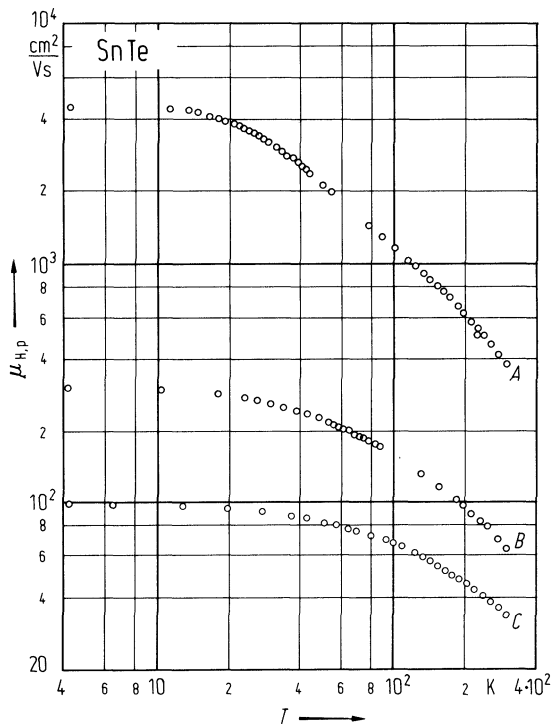


Fig. 23.6.8

SnTe. Reflectivity vs. photon energy at room temperature ($p^* = 8 \cdot 10^{20} \text{ cm}^{-3}$). The peaks are labelled according to [64C], [72K2].

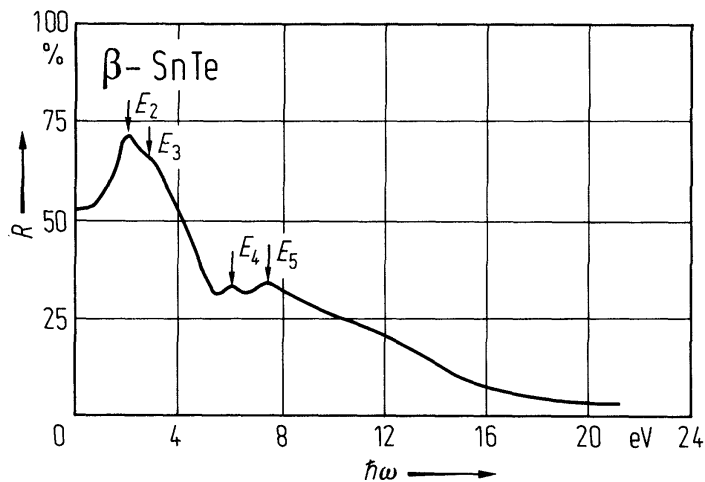
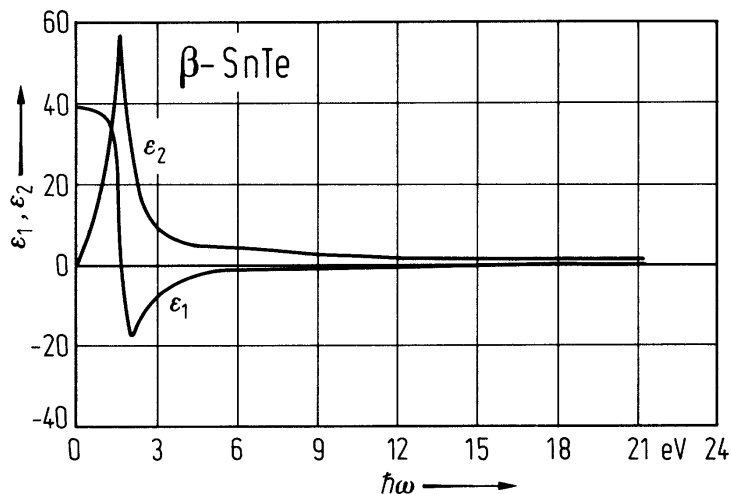


Fig. 23.6.9

SnTe. Real and imaginary parts of the dielectric function vs. photon energy from Kramers-Kronig analysis of reflectivity data of a polycrystalline sample with $p^* = 8 \cdot 10^{20} \text{ cm}^{-3}$ at 300K [72K1].



23.7 Lead monoxide (PbO)

Crystal structure

see section 23.0.

Electronic properties

Both the tetragonal (red) and the orthorhombic (yellow) forms of PbO are wide gap semiconductors. The energy gaps of both modifications are assumed to be indirect.

indirect energy gaps

tetragonal modification

$E_{g,ind}$	2.07 eV	$T = 290\text{ K}$	reflectivity, polycrystals	63I
dE_g/dT	$1.0(1)\cdot 10^{-4}\text{ eV/K}$	$T = 290...573\text{ K}$	reflectivity, polycrystals	63I

orthorhombic modification

$E_{g,ind}$	2.78 eV	$T = 290\text{ K}$	reflectivity, polycrystals	63I
dE_g/dT	$1.15(10)\cdot 10^{-3}\text{ eV/K}$	$T = 290...573\text{ K}$	reflectivity, polycrystals	63I

direct energy gaps

tetragonal modification

$E_{g,dir}$	2.75 eV	$T = 300\text{ K}$	absorption, single crystals, unpolarized light along c axis	68K1
-------------	---------	--------------------	--	------

orthorhombic modification

$E_{g,dir}$	3.36 eV	$T = 300\text{ K}$	reflectivity, transmission on films	68K2
-------------	---------	--------------------	-------------------------------------	------

Lattice properties

lattice parameters

tetragonal modification

a	3.97 Å	$T = 300\text{ K}$		61K
c	5.02 Å			67S

orthorhombic modification (at 300 K, normal pressure)

a	5.489 Å			61K
b	4.755 Å			61K
c	5.891 Å			61K

density

d	9.53 g/cm ³	$T = 300\text{ K}$	tetragonal modification	67H
	8.0 g/cm ³	$T = 300\text{ K},$ normal pressure	orthorhombic modification	67H

melting temperature

T_m	890°C			61L
-------	-------	--	--	-----

phonon frequencies

tetragonal modification

$\nu_1(\text{TO?})$	6.0...6.3 THz	$T = 77\text{ K}$	luminescence	79K
$\nu_2(\text{TO?})$	13.8...14.3 THz	$T = 77\text{ K}$	luminescence	79K

Transport properties

For data of electron Hall mobility vs. temperature, see Fig. 23.7.1

Optical properties

Orthorhombic modification: for dielectric constant, see Fig. 23.7.2.

refractive index

n	2.74	$\lambda = 600 \text{ nm},$	thin film, tetragonal modification	62C
		$T = 300 \text{ K}$		
	2.81	$\lambda = 521 \text{ nm},$		
		$T = 300 \text{ K}$		

References to 23.7

- 61K Kay, M. I.: Acta Crystallogr. 14 (1961) 80.
- 61L Lappe, F.: J. Phys. Chem. Solids 29 (1961) 173.
- 62C Chapham, P. B.: J. Sci. Instrum. 39 (1962) 596.
- 63I Izvozchikov, V. A.: Sov. Phys. Solid State 4 (1963) 2014.
- 67H Handbook of Chemistry and Physics, Weast, R. C. (ed.) , 48th edition, The Chemical Rubber Co. 1967.
- 67S Strömquist, R., Dickens, B.: J. Phys. Chem. Solids 28 (1967) 823.
- 68K1 Keezer, R. C., Bowman, D. L., Becker, J. H.: J. Appl. Phys. 39 (1968) 2062.
- 68K2 Kramarenko, N. L., Miloslavskii, V. K., Naboikin, Yu. V.: Opt. Spectrosc. USSR 24 (1968) 251.
- 79H Harris, E. P., Hauge, P. S., Kircher, C. J.: Appl. Phys. Lett. 34 (1979) 680.
- 79K Korneichuk, V. A., Nedzvetskii, D. S., Chistyakova, N. Ya., Sheinkman, M. K.: Sov. Phys. Solid State 21 (1979) 1436.

Fig. 23.7.1

PbO. Temperature dependence of the Hall mobility ($\mu_H \parallel a$) of five tetragonal single crystals [68K2].

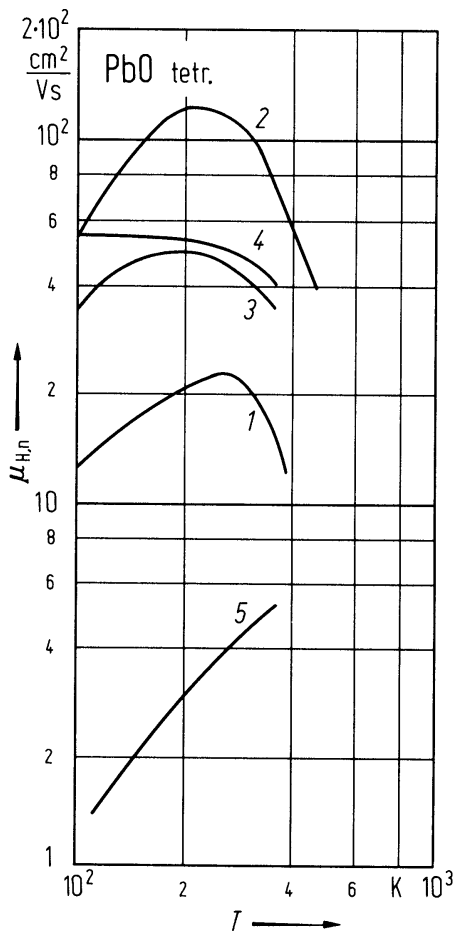
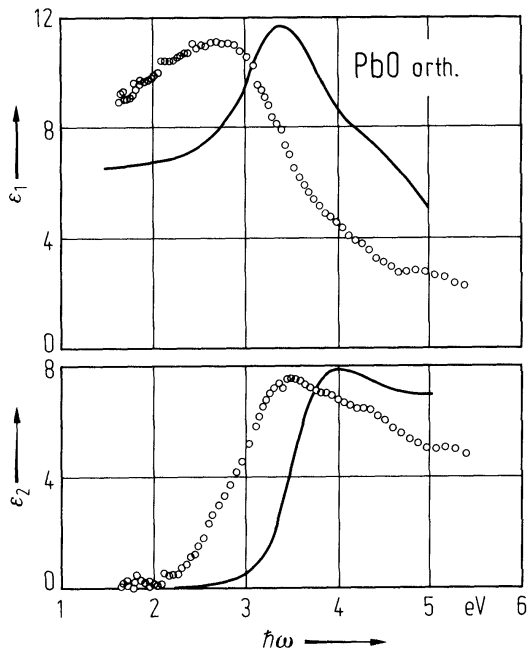


Fig. 23.7.2

PbO. Real (ϵ_1) and imaginary (ϵ_2) parts of the dielectric constant of orthorhombic crystals vs. photon energy (RT, normal pressure) determined from spectroscopic ellipsometry [79H]. Solid curves are data from reflection and transmission measurements on films [68K2].



23.8 Lead sulfide (PbS)

Crystal structure

see section 23.0.

Electronic properties

PbS is a narrow gap semiconductor with extrema of conduction and valence bands at the L point of the Brillouin zone.

band structure : Fig. 23.0.10, Brillouin zone: Fig. 23.0.7.

energy gap

$E_{g,dir}(L_{6v}^{+}-L_{6c}^{-})$	0.286 eV	$T = 4.2\text{ K}$	magnetoabsorption,	64M
	0.42 eV	$T = 300\text{ K}$	reflectivity and transmittance, films	65S
$dE_{g,dir}/dT$	+ 0.52 meV/ K	$T = 100...400\text{ K}$	from various experiments	83N

effective masses

The surfaces of constant energy for both electrons and holes are prolate spheroids of revolution. The major axis of the spheroid is a [1 1 1] direction and its center is at the L point as shown in Fig. 23.8.1.

$m_{\perp,n}$	0.080(10) m_0	$T = 4\text{ K}$	Shubnikov-de Haas effect (SdH)	64C
$m_{\parallel,n}$	0.105(15) m_0	$T = 4\text{ K}$		
$m_{\perp,p}$	0.075(100) m_0	$T = 4\text{ K}$	SdH	64C
$m_{\parallel,p}$	0.105(15) m_0	$T = 4\text{ K}$		

Lattice properties

lattice parameters

a	5.936 Å	$T = 300\text{ K}$		74H
-----	---------	--------------------	--	-----

linear thermal expansion coefficient

α	$72 \cdot 10^{-6}\text{ K}^{-1}$	$T = 300\text{ K}$	for temperature dependence, see Fig. 23.8.2	79R
----------	----------------------------------	--------------------	--	-----

Debye temperature

Θ_D	145(7) K	$T = 300\text{ K}$	from X-ray Bragg reflection data	78S
	229 K	$T = 300\text{ K}$	from elastic constants	60J

heat capacity

C_p	11.4 cal/mol K	$T = 200\text{ K}$	for temperature dependence,	54P
C_v	11.2 cal/mol K	$T = 200\text{ K}$	see Fig. 23.8.3	

density

d	7.597 g cm^{-3}	$T = 300\text{ K}$		74H
-----	--------------------------	--------------------	--	-----

melting temperature

T_m	1110°C			73S
-------	--------	--	--	-----

phonon dispersion curves : Fig. 23.8.4

phonon frequencies

$\nu_{\text{LO}}(\Gamma)$	6.14 THz	$T = 296 \text{ K}$	inelastic neutron scattering	67E
$\nu_{\text{TO}}(\Gamma)$	1.96 THz			
$\nu_{\text{LO}}(\text{X})$	2.78 THz		computed from various	73D
$\nu_{\text{TO}}(\text{X})$	2.66 THz		experimental data	
$\nu_{\text{LA}}(\text{X})$	1.64 THz			
$\nu_{\text{TA}}(\text{X})$	1.2 THz			
$\nu_{\text{LO}}(\text{L})$	7.13 THz			
$\nu_{\text{TO}}(\text{L})$	5.83 THz			
$\nu_{\text{LA}}(\text{L})$	3.05 THz			
$\nu_{\text{TA}}(\text{L})$	1.47 THz			

second order elastic moduli

c_{11}	$12.4(6) \cdot 10^6 \text{ N cm}^{-2}$	$T = 300 \text{ K}$		58H
c_{12}	$3.3 (3) \cdot 10^6 \text{ N cm}^{-2}$			
c_{44}	$2.3(2) \cdot 10^6 \text{ N cm}^{-2}$			

bulk moduli

B_{S}	$5.2876 \cdot 10^6 \text{ N cm}^{-2}$	$T = 295 \text{ K}$	atmospheric pressure,	76P
B_{T}	$4.9855 \cdot 10^6 \text{ N cm}^{-2}$	$T = 295 \text{ K}$	bulk single crystal	

Transport properties

Hall mobility

μ_{n}	$700 \text{ cm}^2/\text{V s}$	$T = 300 \text{ K}$	synthetic (single) crystal	65Z
	$13500 \text{ cm}^2/\text{V s}$	$T = 77 \text{ K}$	$n = 2 \cdot 10^{18} \text{ cm}^{-3}$ for temperature dependence of Hall mobility, see Fig. 23.8.5	

Optical properties

optical spectra : reflectivity: Fig. 23.8.6a; real and imaginary parts of the dielectric constant: Fig. 23.8.6b.

dielectric constants

$\varepsilon(0)$	169	$T = 300 \text{ K}$		73D
$\varepsilon(\infty)$	17.2	$T = 300 \text{ K}$		73D

References to 23.8

- 54P Parkinson, D. H., Quarrington, J. E.: Proc. Phys. Soc. 67 (1954) 569.
- 58H Huntington, H. B.: Solid State Phys. 7 (1958) 213.
- 60J Joshi, S. K., Mitra, S. S.: Proc. Phys. Soc. 76 (1960) 295.
- 63N Novikova, S. I., Abrikosov, N. Kh.: Sov. Phys. Solid State 5 (1963) 1397.
- 64C Cuff K. F., Ellet, M. K., Kulgin, C. D., Williams, L. R.: Proc. Int. Conf. Phys. Semicond. Paris 1964, 677.
- 64M Mitchell, D. L., Palik, E. D., Zemel, J. N.: Proc. 7th Int. Conf. Phys. Semicond. 1964, 325.
- 65S Schoolar, R. B., Dixon, J. R.: Phys. Rev. A137 (1965) 667.
- 65Z Zemel, J. N., Jensen, J. D., Schoolar, R. B.: Phys. Rev. A140 (1965) 330.
- 67E Elcombe, M. M.: Proc. R. Soc. London, Ser. A300 (1967) 210.
- 71T Thompson, T. E., Aron, P. R., Chandrasekhar, B. S., Langenberg, D. N.: Phys. Rev. B4 (1971) 518.
- 73D Dalven, R.: in "Solid State Physics", Ehrenreich, H., Seitz, F., Turnbull, D. (eds.) New York: Academic Press, 1973, Vol. 28, p. 179.
- 73K Kohn, S. E., Yu, P. Y., Petroff, Y., Shen, Y. R., Tsang, Y., Cohen, M. L.: Phys. Rev. B8 (1973) 1477.
- 73S Strauss, A. J., Harman, T. C.: J. Electron. Mater. 2 (1973) 71.
- 74H Harman, T. C., Meingailis, I.: Appl. Solid State Sci. 4 (1974) 1.
- 76P Peresada, G. I., Ponyatovskii, E. G., Sokolovskaya, Zh. D.: Phys. Status Solidi (a) 35 (1976) K177.
- 78S Subhadra, K. G., Sirdeshmukh, D. B.: Pramana 10 (1978) 357.
- 79R Robertson, J.: J. Phys. C 12 (1979) 4753.
- 83N Nimtz, G., Schlicht, B.: Springer Tracts in Modern Physics, Vol. 98, 1, Berlin, Heidelberg, New York, Tokyo: Springer-Verlag 1983.

Figures to 23.8

Fig. 23.0.7

GeTe. Brillouin zone of the fcc lattice of the NaCl structure.

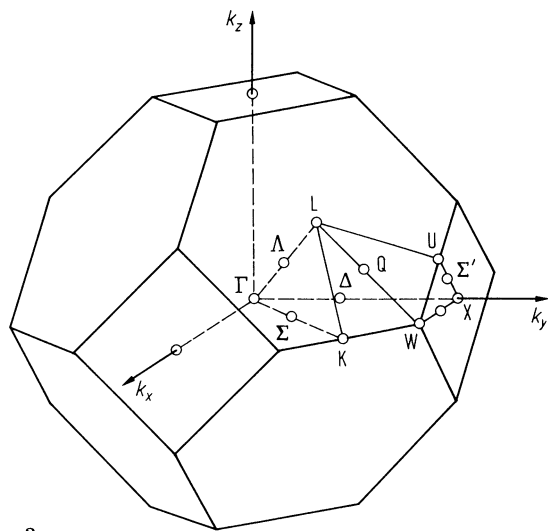


Fig. 23.0.10

PbS. Band structure calculated by the empirical pseudopotential method [73K].

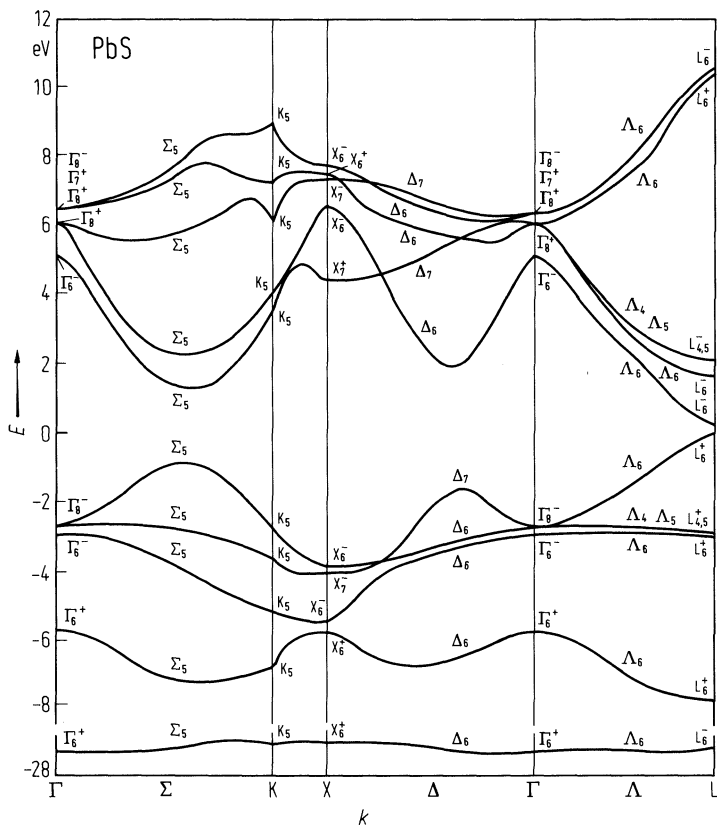


Fig. 23.8.1

PbS. Brillouin zone showing the eight $[111]$ -directed hemi-spheroidal surfaces of constant energy which contain the carriers (either electrons or holes) [71T].

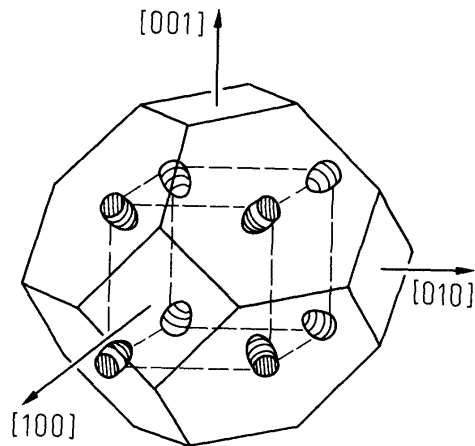


Fig. 23.8.2

PbS. Linear thermal expansion coefficient vs. temperature [63N].

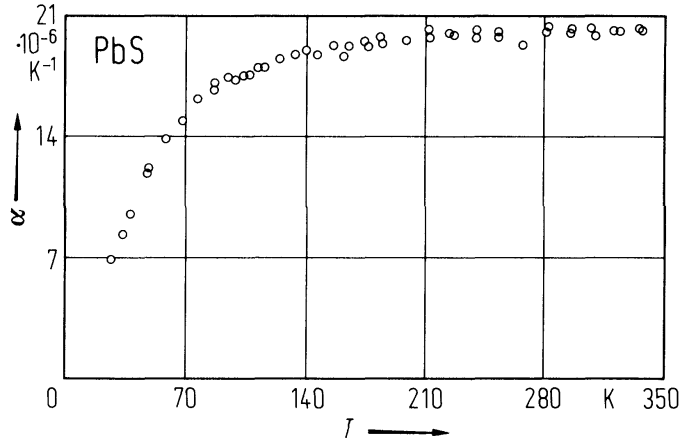


Fig. 23.8.3

PbS. Molar heat capacity C_p vs. temperature [54P]. Different symbols represent data from various authors.

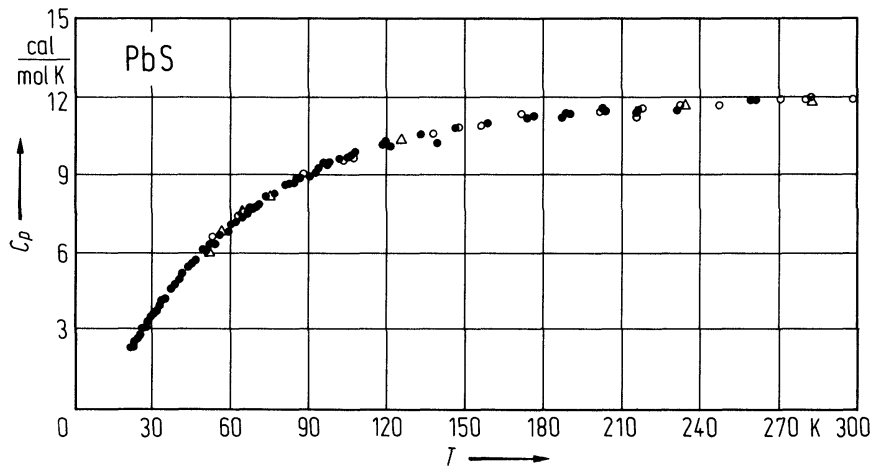


Fig. 23.8.4

PbS. Dispersion curves at 296 K. The full and open circles are experimental data from inelastic neutron scattering and correspond to transverse and longitudinal modes respectively. The solid line represents computed data from a model in which core-shell forces have been included in the nearest neighbor interaction [67E].

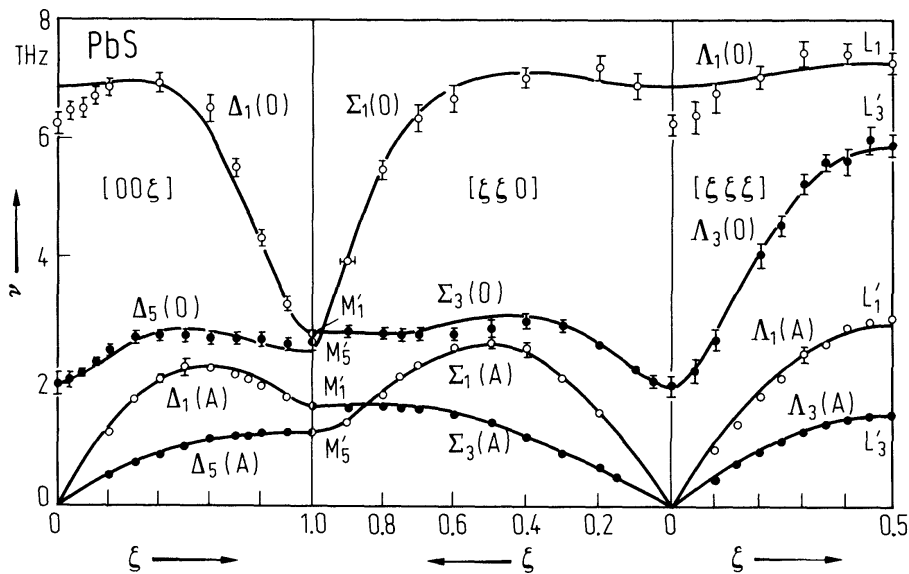


Fig. 23.8.5

PbS. Hall mobility vs. (reciprocal) temperature of epitaxial films, the Hall coefficients of which are shown in Fig. 3. The solid line represents typical bulk material data [65Z].

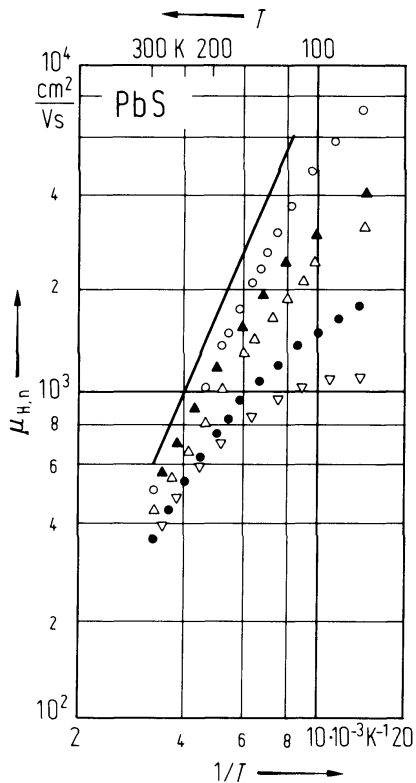
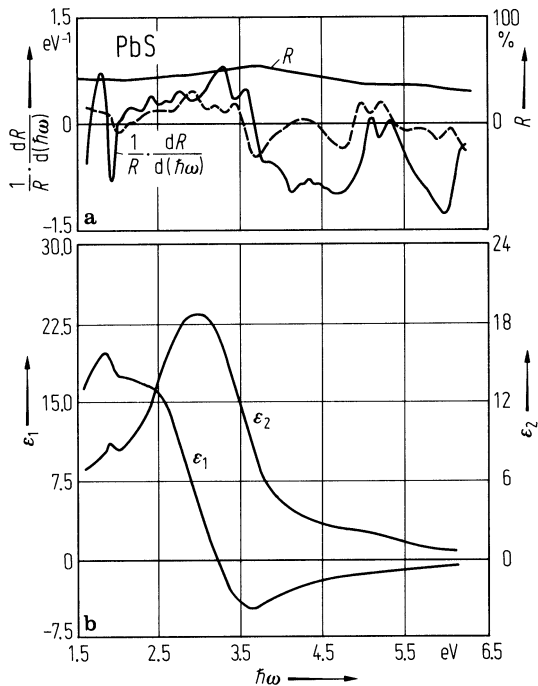


Fig. 23.8.6

PbS. (a) Reflectivity and derivative reflectivity vs. photon energy at 5 K. The dashed curve is the theoretical $(1/R)dR/d(h\nu)$ spectra from empirical pseudopotential method calculations of the band structure. Bulk single crystals. (b) ϵ_1 and ϵ_2 calculated by Kramers-Kronig analysis of the $(1/R)dR/d(h\nu)$ spectrum of Fig. a [73K].



23.9 Lead selenide (PbSe)

Crystal structure

see section 23.0.

Electronic properties

band structure

PbSe is a narrow gap semiconductor with extrema of conduction and valence bands at the L point of the Brillouin zone.

band structure : Fig. 23.0.11, Brillouin zone: Fig. 23.0.7.

energy gap

$E_{g,dir}(L_{6v}^{+}-L_{6c}^{-})$	0.145eV	$T = 4\text{ K}$	laser emission, single crystal films	74H
	0.278 eV	$T = 300\text{ K}$		70S
$dE_{g,dir}/dT$	+ 0.51 meV/ K	$T = 100...400\text{ K}$	from various experiments	83N
See also Fig. 23.9.1				

effective masses

The surfaces of constant energy for both electrons and holes are prolate spheroids of revolution. The major axis of the spheroid is a [1 1 1] direction and its center is at the L point.

$m_{\perp,n}$	$0.040\ m_0$	$T = 4\text{ K}$	SdH	64C
$m_{\parallel,n}$	$0.070\ m_0$	$T = 4\text{ K}$		
$m_{\perp,p}$	$0.034\ m_0$	$T = 4\text{ K}$	SdH	64C
$m_{\parallel,p}$	$0.068\ m_0$	$T = 4\text{ K}$		

electron-polaron effective mass

m_n^{**}	$1.04\ m_0$	$T = 77\text{ K}$	calculated from experimental data	71D
------------	-------------	-------------------	-----------------------------------	-----

density of states mass

$m_{ds,n}$	$0.12\ m_0$	$T = 4\text{ K}$	for dependence on carrier concentration, see Fig. 23.9.2	74H
------------	-------------	------------------	--	-----

band edge g-factors

$g_{c\parallel}$	27(7)	$T = 4\text{ K}$	SdH	64C
$g_{c\perp}$	17.6	$T = 1.5\text{ K}$	$n = 6\cdot10^{17}\text{ cm}^{-3}$, magnetoacoustic quantum oscillations	72K, 74B
$g_{v\parallel}$	32(7)	$T = 4\text{ K}$	SdH	64C
$g_{v\perp}$	17.1	$T = 1.4\text{ K}$	$p = 1.2\cdot10^{18}\text{ cm}^{-3}$, magnetoacoustic quantum oscillations	72K, 74B

Lattice properties

lattice parameter

a	6.124 \AA	$T = 299\text{ K}$	NaCl-structure	69D
-----	--------------------	--------------------	----------------	-----

linear thermal expansion coefficient

α	$1.940\cdot10^{-5}\text{ K}^{-1}$	$T = 300\text{ K}$	polycrystalline samples;	64N
	$1.737\cdot10^{-5}\text{ K}^{-1}$	$T = 100\text{ K}$	for temperature dependence of α ,	
	$0.765\cdot10^{-5}\text{ K}^{-1}$	$T = 30\text{ K}$	see Fig. 23.9.3	

Debye temperature

Θ_D	156(2) K	$T = 0$ K	from ultrasonic measurements	71L
	144 K	$T = 25$ K	from calorimetric measurements	54P

density

d	8.26 g cm ⁻³	$T = 300$ K		71L
-----	-------------------------	-------------	--	-----

melting temperature

T_m	1082°C			74H
-------	--------	--	--	-----

phonon frequencies

$\nu_{LO}(\Gamma)$	3.99 THz	$T = 4.2$ K	tunnel spectroscopy	61H
$\nu_{TO}(\Gamma)$	1.32 THz	$T = 1.4$ K	transmission	64B

sound velocities

v_T	1415 ms ⁻¹	$T = 300$ K	along [100]	63C
v_L	3860 ms ⁻¹	$T = 300$ K	along [100]	
v_T	1690 ms ⁻¹	$T = 300$ K	along [011]	

second order elastic moduli

c_{11}	12.37(5)·10 ⁶ N cm ⁻²	$T = 298.2$ K	single crystals	71L
c_{12}	1.93(4)·10 ⁶ N cm ⁻²	$T = 298.2$ K		
c_{44}	1.591(5)·10 ⁶ N cm ⁻²	$T = 298.2$ K		
$(c_{11}+2c_{12})/3$	5.41·10 ⁶ N cm ⁻²	$T = 298.2$ K		
$(c_{11}-c_{12})/2$	5.22·10 ⁶ N cm ⁻²	$T = 298.2$ K		

Transport properties

Hall mobilities

The carrier mobility is limited by defect scattering at low temperatures, at elevated temperatures the polar optical phonon scattering becomes dominating.

μ_n	1 cm ² /V s	$T = 300$ K	$n = 7 \cdot 10^{17}$ cm ⁻³ , epitaxial films	65Z
	26 cm ² /V s	$T = 77$ K	$n = 6.5 \cdot 10^{17}$ cm ⁻³ , bulk single	73M
	200 cm ² /V s	$T = 4$ K	crystals	
μ_p	27 cm ² /V s	$T = 77$ K	$p = 10^{18}$ cm ⁻³ , bulk single crystals	73M
	230 cm ² /V s	$T = 4$ K		

for temperature dependence of Hall mobility, see Fig. 23.9.4.

Optical properties

refractive index : for temperature dependence, see Fig. 23.9.5.

dielectric constants

$\epsilon(0)$	210	$T = 300$ K	calculated using Lyddane-Sachs-Teller relation	73K
$\epsilon(\infty)$	23.9	$T = 300$ K	reflectivity, epitaxial films	65Z

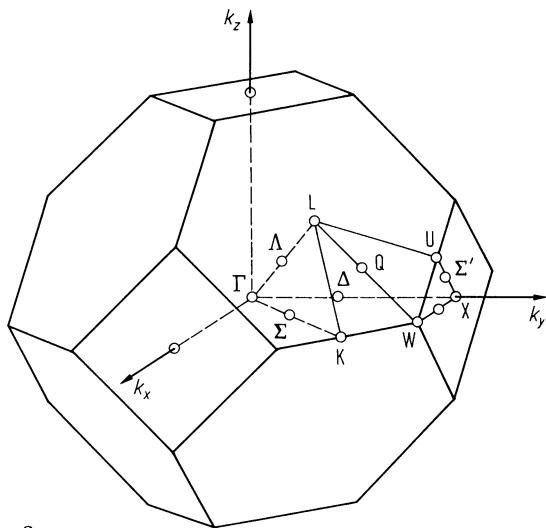
References to 23.9

- 54P Parkinson, D. H., Quarrington, J. E.: Proc. Phys. Soc. 67 (1954) 569.
- 61H Hall, R. N., Racette, J. H.: J. Appl. Phys. 32 (1961) 2078.
- 63C Chudinov, A. A.: Sov. Phys. Crystallogr. 8 (1963) 374.
- 64B Burstein, F., Wheeler, R., Zemel, Z.: Proc. 7th Int. Conf. Phys. Semicond. 1964, 1065.
- 64C Cuff K. F., Ellet, M. K., Kulgin, C. D., Williams, L. R.: Proc. Int. Conf. Phys. Semicond. Paris 1964, 677.
- 64M Mitchell, D. L., Palik, E. D., Zemel, J. N.: Proc. 7th Int. Conf. Phys. Semicond. 1964, 325.
- 64N Novikova, S. I., Abrikosov, N. Kh.: Sov. Phys. Solid State 5 (1964) 1397.
- 65Z Zemel, J. N., Jensen, J. D., Schoolar, R. B.: Phys. Rev. A140 (1965) 330.
- 68D Dubrovskaya, I. N., Efimova, B. A., Nensberg, E. D.: Fiz. Tekh. Poluprov. 2 (1968) 530.
- 69D Dalven, K.: Infrared Phys. 9 (1969) 141.
- 70S Schlichting, U.: Dissertation Technische Universität Berlin 1970.
- 70V Vinogradova, M. N., Gunko, T. S., Ukhanov, Yu. I., Tselishcheva, N. S., Shershneva, L. M.: Fiz. Tekh. Poluprov. 2 (1970) 1968.
- 71D Dalven, R.: Phys. Rev. B3 (1971) 1953.
- 71L Lippmann, G., Kästner, P., Wanninger, W.: Phys. Status Solidi (a) 6 (1971) K 159.
- 72K Kästner, P.: Phys. Status Solidi (b) 53 (1972) 753.
- 73K Kohn, S. E., Yu, P. Y., Petroff, Y., Shen, Y. R., Tsang, Y., Cohen, M. L.: Phys. Rev. B8 (1973) 1477.
- 73M Martinez, G.: Phys. Rev. B8 (1973) 4686.
- 73S Schlichting, U., Gobrecht, K. H.: J. Phys. Chem. Solids 34 (1973) 753.
- 74B Bangert, E., Kästner, P.: Phys. Status Solidi (b) 61 (1974) 503.
- 74H Harman, T. C., Meingailis, I.: Appl. Solid State Sci. 4 (1974)1.
- 74Z Zawadaski, W.: Adv. Phys. 23 (1974) 435.
- 75M Martinez, G., Schlüter, M., Cohen, M. L.: Phys. Rev. B11 (1975) 651 and 660.
- 79G Grisar, K.: in [79P].
- 79P Preier, H.: Appl. Phys. 20 (1979) 189.
- 83N Nimtz, G., Schlicht, B.: Springer Tracts in Modern Physics, Vol. 98, 1, Berlin, Heidelberg, New York, Tokyo: Springer-Verlag 1983.

Figures to 23.9

Fig. 23.0.7

GeTe. Brillouin zone of the fcc lattice of the NaCl structure.



PbSe. Band structure and density of states from an empirical pseudopotential method calculation [75M].

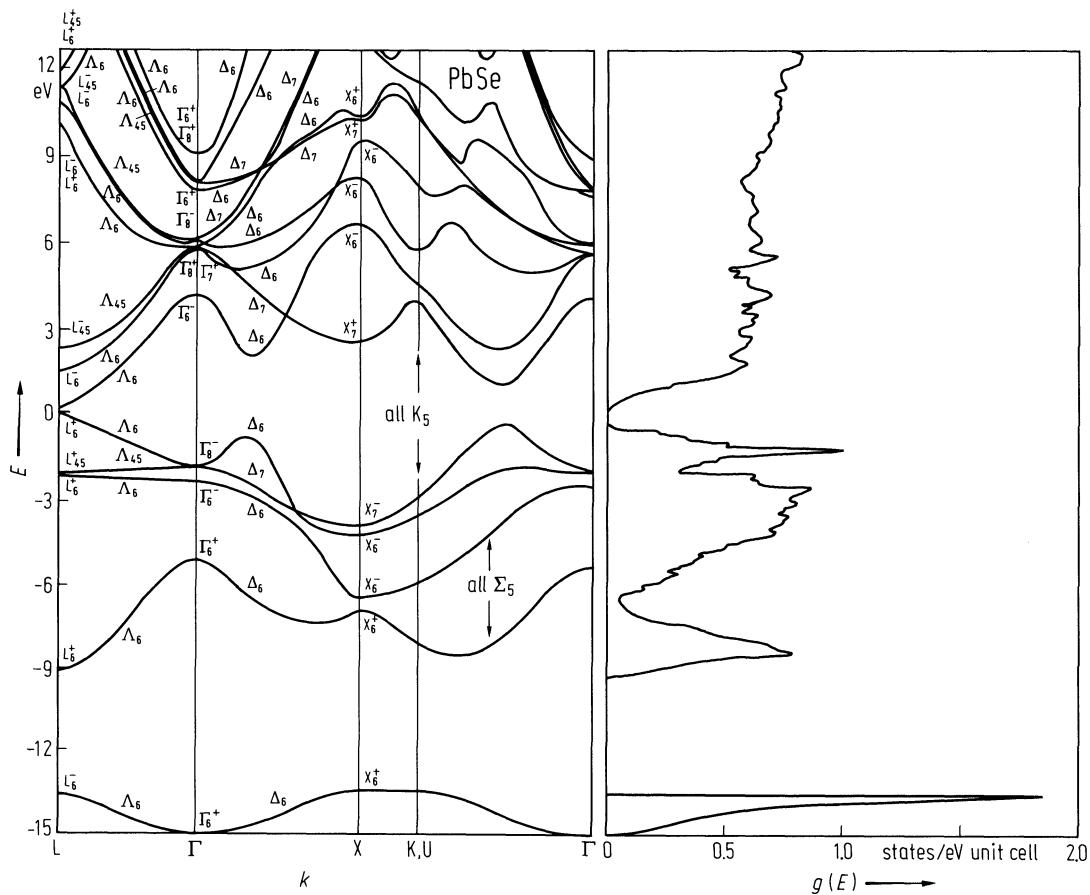


Fig. 23.9.1

PbSe. Energy gap vs. temperature [83N]. The solid line represents an empirical relation [79G]. Experimental data from : [64M, 65B, 65Z].

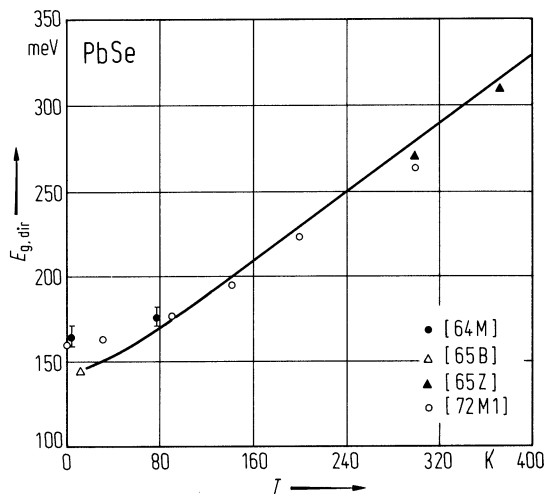


Fig. 23.9.2

PbSe. Density of states mass at lower temperatures vs. electron concentration. The straight line is calculated [74Z]. Experimental data: open triangle: (Shubnikov-de Hans data) [64C]; cross: (interband magnetoabsorption) [64M]; open circles: (thermomagnetic data) [68D]; full circles: (reflectance) [70V]; full triangles: [74Z].

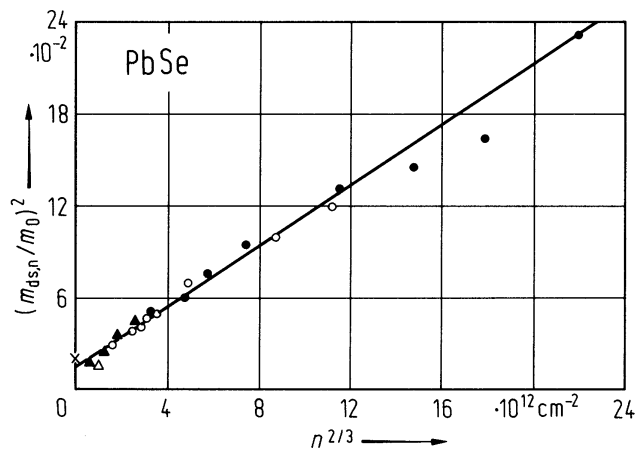


Fig. 23.9.3

PbSe. Linear thermal expansion coefficient vs. temperature [64N].

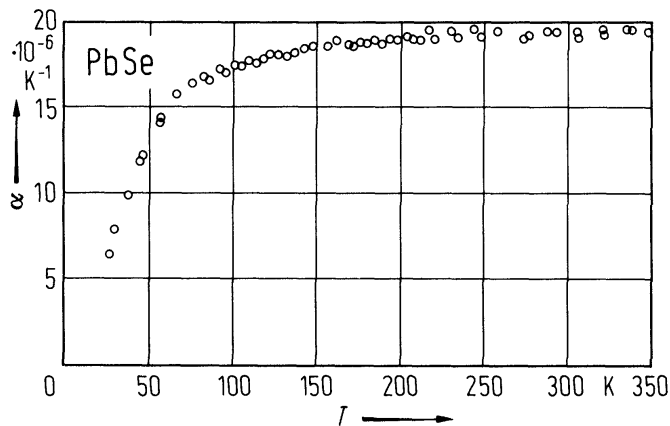


Fig. 23.9.4

PbSe. Hall mobility vs. temperature for low carrier concentrations [73S].

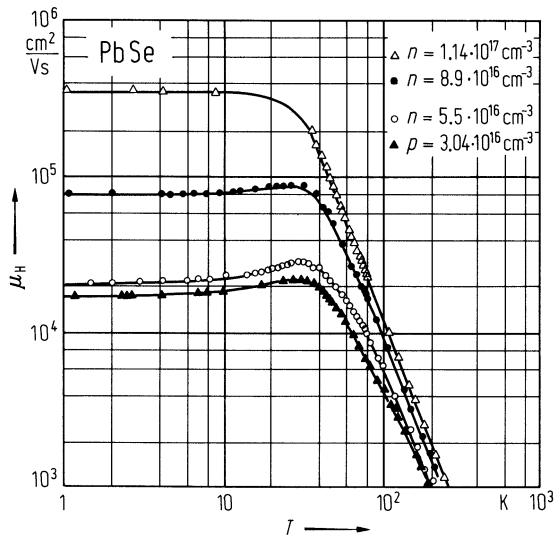
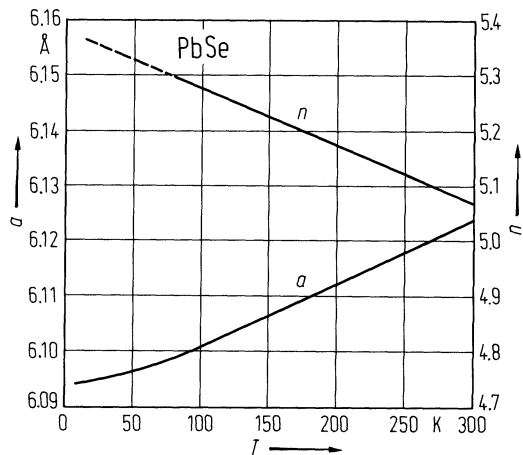


Fig. 23.9.5

PbSe. Refractive index n (maximum at fundamental absorption edge) and lattice constant a vs. temperature [79P]. Single crystal films.



23.10 Lead telluride (PbTe)

Crystal structure

see section 23.0.

Electronic properties

PbTe is a narrow gap semiconductor with extrema of conduction and valence bands at the L point of the Brillouin zone. Various experiments gave evidence of a second valence band extremum presumably located near the maximum of the Σ-line of the Brillouin zone. At elevated temperatures this extremum becomes the valence band edge.

band structure : Fig. 23.0.12, Brillouin zone: Fig. 23.0.7.

energy gaps

$E_{g,dir}(L_{6v}^{+}-L_{6c}^{-})$	311 meV	$T = 300\text{ K}$	magnetooptics, single crystal films	79P
$E_{g,ind}(\Sigma_{5v}-L_{6c}^{-})$	360 meV	$T > 420\text{ K}$	magnetotransport and warm hole conductivity	77S
$E_{g,dir}(T)$	$171.5+((12.8)^2+0.19(T+20)^2)^{1/2}\text{ meV}$	$T = 0...300\text{ K}$	magnetooptics, single crystal films	79G
$dE_{g,ind}/dT$	≈ 0	$T = 0...600\text{ K}$	magnetotransport and warm hole conductivity	77S

effective masses, conduction band

The surfaces of constant energy for both electrons and holes are prolate spheroids of revolution. The major axis of the spheroid is a [1 1 1] direction and its center is at the L point.

$m_{\perp,n}$	$0.024(3)\ m_0$	$T = 4\text{ K}$	SdH	64C
$m_{\parallel,n}$	$0.24(5)\ m_0$			
$m_{\perp,p}$	$0.022(3)\ m_0$			
$m_{\parallel,p}$	$0.31(5)\ m_0$			

g-factors of electrons and holes

$g_{c\parallel}$	60.0(10)	$T = 4.2\text{ K}$	magnetoplasma reflection, $n = 2\cdot 10^{17}\text{ cm}^{-3}$	80I
$g_{c\perp}$	17.5(10)	$T = 4.2\text{ K}$	magnetoplasma reflection, $n = 2\cdot 10^{17}\text{ cm}^{-3}$	80I
$g_{v\parallel}$	58.3(10)	$T = 4.2\text{ K}$	FIR spin resonance, $p = 4\cdot 10^{16}\text{ cm}^{-3}$	79S
$g_{v\perp}$	18.8(15)	$T = 4.2\text{ K}$	FIR spin resonance, $p = 4\cdot 10^{16}\text{ cm}^{-3}$	79S

Lattice properties

lattice parameter

a	6.462 Å	$T = 300\text{ K}$	NaCl structure	69D
-----	---------	--------------------	----------------	-----

linear thermal expansion coefficient

α	$1.97\cdot 10^{-5}\text{ K}^{-1}$	$T = 77...300\text{ K}$	for temperature dependence, see Fig. 23.10.1	63N
----------	-----------------------------------	-------------------------	---	-----

Debye temperature

Θ_D	136 K	$T = 100\text{ K}$	from heat capacity	54P
------------	-------	--------------------	--------------------	-----

heat capacity

C_p	11.9 cal mol ⁻¹ K ⁻¹	$T = 200$ K	for temperature dependence, see Fig. 23.10.2	54P
C_v	11.7 cal mol ⁻¹ K ⁻¹	$T = 200$ K		

density

d	8.242 g cm ⁻³	$T = 300$ K	74H
	8.219 g cm ⁻³	$T = 300$ K	81M

melting temperature

T_m	924°C		70S, 74H
-------	-------	--	-------------

phonon dispersion curves : see Fig. 23.10.3.

phonon frequencies

$\nu_{\text{TO}}(\Gamma)$	0.965 THz	$T = 300$ K	far-IR index matching	76T
ν_{LO}	3.42 THz	$T = 293$ K		66C

sound velocities

v_T	$1.260 \cdot 10^5$ cm s ⁻¹	$T = 300$ K	along [100]	62C
v_L	$3.590 \cdot 10^5$ cm s ⁻¹	$T = 300$ K	along [100]	
v_T	$1.610 \cdot 10^5$ cm s ⁻¹	$T = 300$ K	along [011]	

second-order elastic moduli

c_{11}	$10.53(2) \cdot 10^6$ N cm ⁻²	$T = 300$ K		81M
c_{12}	$0.70(2) \cdot 10^6$ N cm ⁻²	$T = 300$ K		
c_{44}	$1.322(1) \cdot 10^6$ N cm ⁻²	$T = 300$ K		

third-order elastic moduli

c_{111}	$-18.5(6) \cdot 10^7$ N cm ⁻²	$T = 300$ K	single crystal, $p = 3 \cdot 10^{18}$ cm ⁻³	81M
c_{112}	$0.35(1) \cdot 10^7$ N cm ⁻²			
c_{123}	$-0.97(2) \cdot 10^7$ N cm ⁻²			
c_{144}	$0.44(2) \cdot 10^7$ N cm ⁻²			
c_{166}	$-0.98(5) \cdot 10^7$ N cm ⁻²			
c_{456}	$0.120(1) \cdot 10^7$ N cm ⁻²			

bulk moduli

B_S	$3.976 \cdot 10^6$ N cm ⁻²	$T = 300$ K	single crystal, $p = 3 \cdot 10^{18}$ cm ⁻³	81M
B_T	$3.839 \cdot 10^6$ N cm ⁻²	$T = 300$ K		

Transport properties

intrinsic carrier concentration : for temperature dependence: see Fig. 23.10.4.

Hall mobilities

The carrier mobility is limited by defect scattering at low temperatures, at elevated temperatures the polar optical phonon scattering becomes dominating; for a review on carrier scattering in PbTe. see [71R, 83N].

For temperature dependence of mobility, see Fig. 8.10.10.5.

$\mu_{H,n}$	1730 cm ² /V s	$T = 300$ K	bulk material	58A
	800000 cm ² /V s	$T = 4.2$ K	bulk material	58A
$\mu_{H,p}$	780 cm ² /V s	$T = 300$ K	bulk material	58A
	256000 cm ² /V s	$T = 4.2$ K	bulk material	58A

thermal conductivity

κ	190 cm s g cal ⁻¹	$n = 3.4 \cdot 10^{18}$ cm ⁻³ $T = 300$ K		75A
----------	------------------------------	---	--	-----

Optical properties

optical spectra : real and imaginary parts of the dielectric constant: Fig. 23.10.6.

dielectric constants

$\epsilon(0)$	414	$T = 300$ K	derived from IR-index matching	76T
$\epsilon(\infty)$	33	$T = 300$ K	(thickness: 6.9 μ m), n (77 K) = $8.2 \cdot 10^{16}$ cm ⁻³	

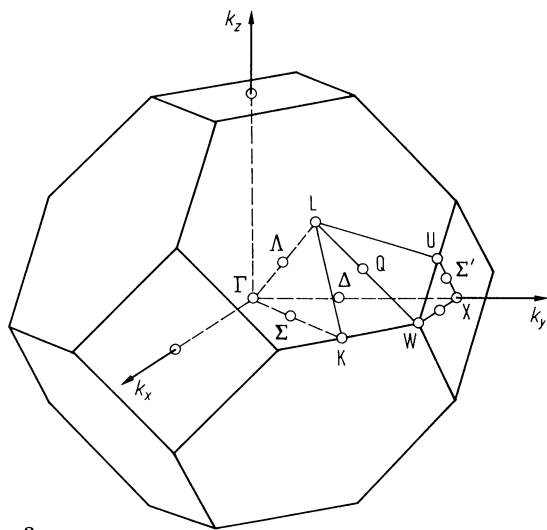
References to 23.10

- 54P Parkinson, D. H., Quarrington, J. E.: Proc. Phys. Soc. 67 (1954) 569.
- 58A Allgaier, R. S., Scanlon, W. W.: Phys. Rev. 111 (1958) 1029.
- 62C Chudinov, A. A.: Sov. Phys. Solid State 4 (1962) 553.
- 63N Novikova, S. I., Abrikosov, N. Kh.: Sov. Phys. Solid State 5 (1963) 1397.
- 64C Cuff K. F., Ellet, M. K., Kulgin, C. D., Williams, L. R.: Proc. Int. Conf. Phys. Semicond. Paris 1964, 677.
- 65C Conklin, J. B., Johnson, L. E., Pratt, G. W.: Phys. Rev. A 137 (1965) 1282.
- 66C Cochran, W., Cowley, R. A., Dolling, G., Elcombe, M. M.: Proc. Roy. Soc. A293 (1966) 433.
- 68H Hermann, F., Kortum, R. L., Ortenburger, I., van Dyke, J. P.: J. Phys. (Paris) Suppl. 29 (1968) C462.
- 69D Dalven, K.: Infrared Phys. 9 (1969) 141.
- 70O Overhof, H., Rössler, U.: Phys. Status Solidi 37 (1970) 691.
- 70S Steininger, J.: J. Appl. Phys. 41 (1970) 2713.
- 71R Ravich, Yu. I., Efimova, B. A., Tamarchenko, V. I.: Phys. Status Solidi (b) 43 (1971) 11 and 453.
- 73K Kohn, S. E., Yu, P. Y., Petroff, Y., Shen, Y. R., Tsang, Y., Cohen, M. L.: Phys. Rev. B8 (1973) 1477.
- 74H Harman, T. C., Meingailis, I.: Appl. Solid State Sci. 4 (1974) 1.
- 75A Alekseeva, G. T., Efimova, B. A., Logachev, Yu. A.: Sov. Phys. Semicond. 9 (1975) 83
- 75M Martinez, G., Schlüter, M., Cohen, M. L.: Phys. Rev. B11 (1975) 651 and 660.
- 76T Tenant, W. E.: Solid State Commun. 20 (1976) 613.
- 77S Sitter, H., Lischka, K., Heinrich, H.: Phys. Rev. B16 (1977) 680.
- 78S Schlicht, B., Dornhaus, K., Nimtz, G., Haas, L. D., Jakobus, T.: Solid State Electron. 21 (1978) 1481.
- 79A Acharya, S., Srivastava, N.: Phys. Status Solidi (b) 56 (1979) K1.
- 79P Preier, H.: Appl. Phys. 20 (1979) 189.
- 79S Schaber, H., Doezeza, K. E.: Solid State Commun. 31 (1979) 197.
- 80I Ichiguchi, T., Nishikawa, S., Murase, K.: Solid State Commun. 34 (1980) 309.
- 81M Miller, A. J., Saunders, G. A., Yogurtcu, Y. K.: J. Phys. C14 (1981) 1569.
- 83N Nimtz, G., Schlicht, B.: Springer Tracts in Modern Physics, Vol. 98, 1, Berlin, Heidelberg, New York, Tokyo: Springer-Verlag 1983.

Figures to 23.10

Fig. 23.0.7

GeTe. Brillouin zone of the fcc lattice of the NaCl structure.



PbTe. (a) Band structure and density of states from an empirical pseudopotential method calculation [75M]. (b) Theoretical values of energy levels at the L-point calculated by different models [83N]: a) APW-method [65C], b) OPW-method [68H], c) KKR-method [70O], d) nonlocal EP-method [75M].

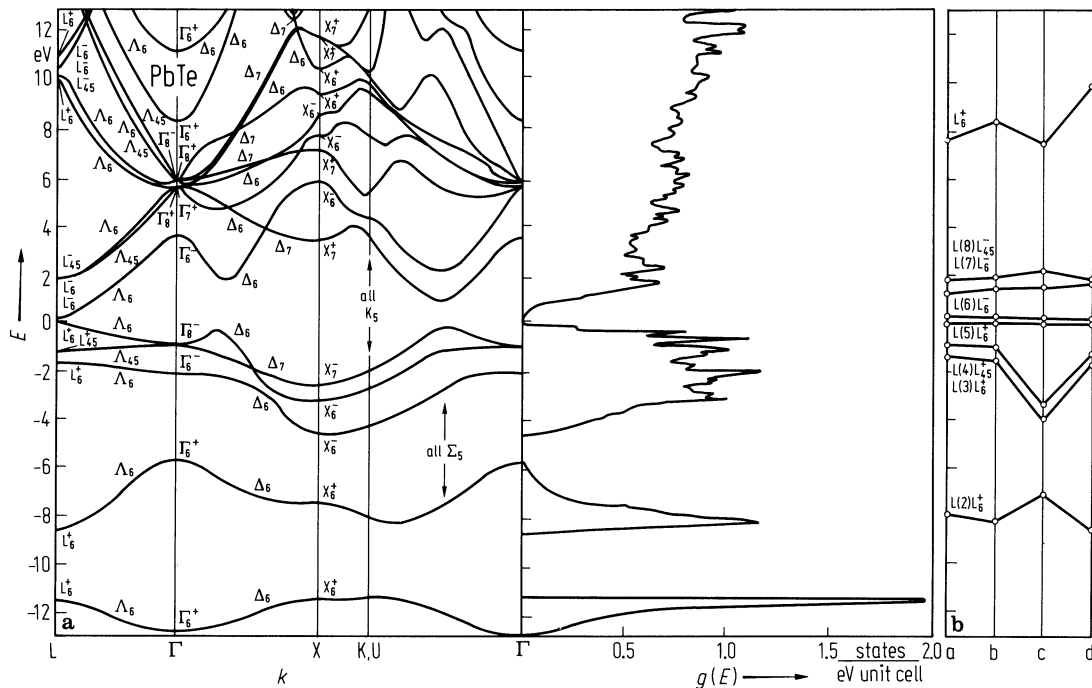


Fig. 23.10.1

PbTe. Linear thermal expansion coefficient vs. temperature [63N].

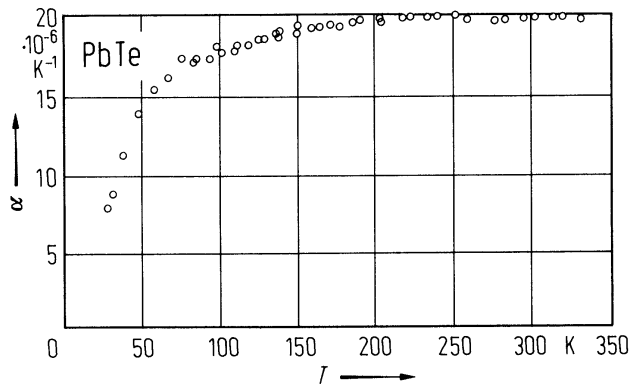


Fig. 23.10.2

PbTe. Heat capacity vs. temperature [54P].

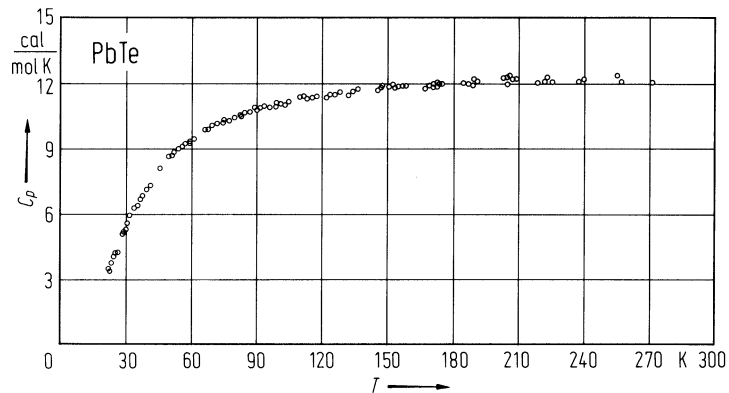


Fig. 23.10.3

PbTe. Dispersion relations at 296 K (frequency vs. reduced wave vector coordinate). Full and open circles are experimental data from inelastic neutron scattering corresponding to transverse and longitudinal modes, respectively. Solid lines: model calculations including core-shell forces [66C].

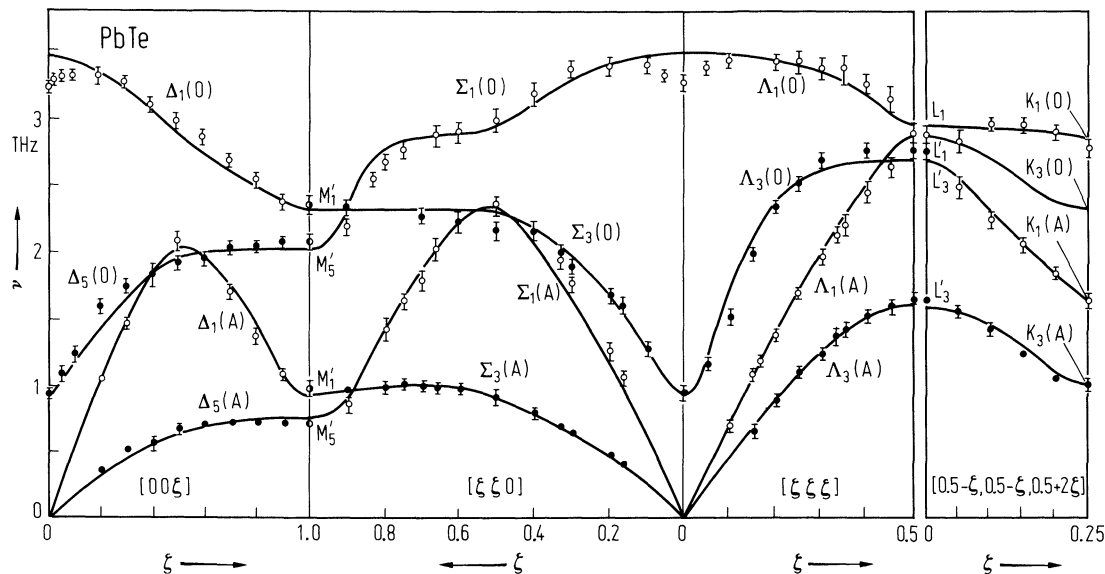


Fig. 23.10.4

PbTe. Intrinsic carrier concentration vs. temperature calculated using multiband model with band parameters from [79A] and $E_g(T)$ -relation from [79P] in [83N].

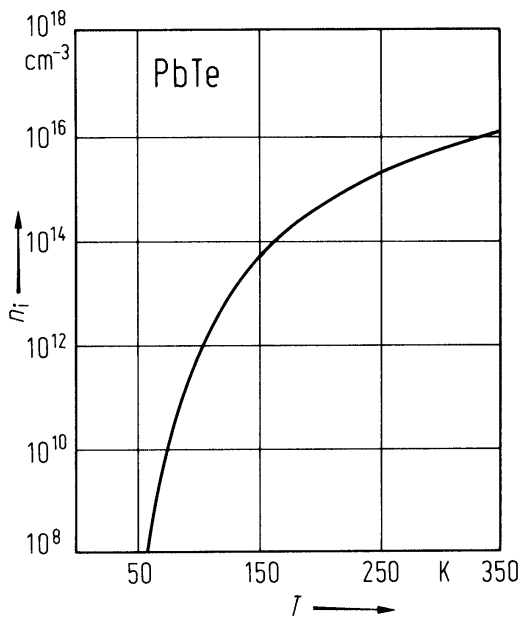


Fig. 23.10.5

PbTe. Hall mobility as a function of temperature for two single crystal films (same samples as in Fig. 2) [78S].

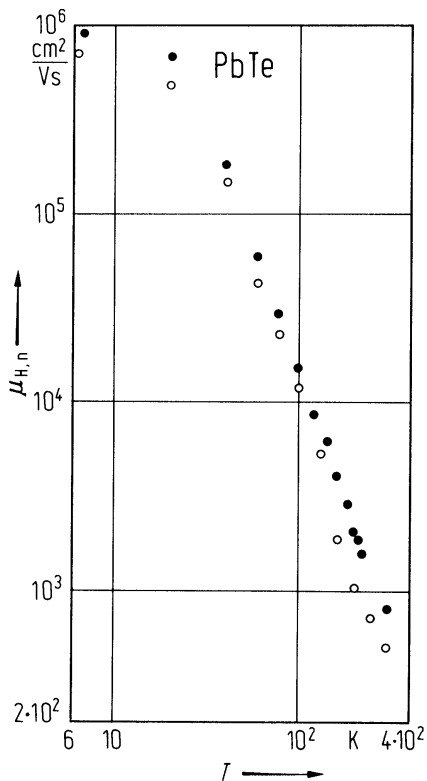
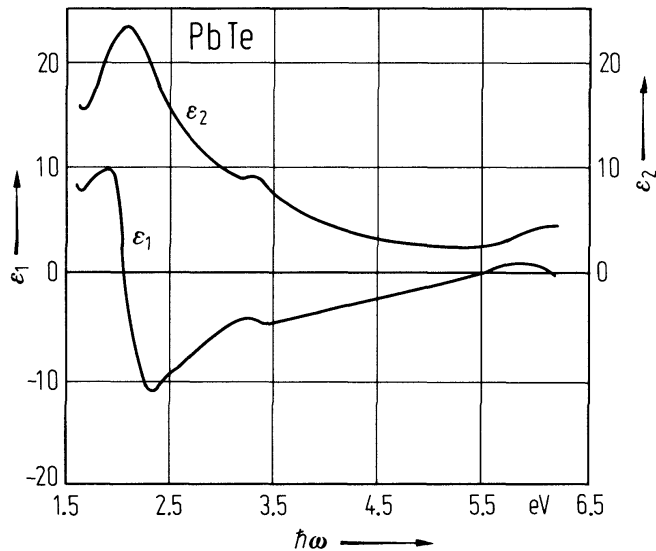


Fig. 23.10.6

PbTe. ϵ_1 and ϵ_2 vs. photon energy at 5 K calculated by Kramers-Kronig analysis of the $(1/R)dR/d(h\nu)$ spectra [73K].



23.11 Germanium dioxide (GeO₂)

Crystal structure

see section 23.0.

Electronic properties

(All data for tetragonal GeO₂ (rutile structure))

The band structure of GeO₂ is similar to that of SnO₂ but there exists some disagreement about the symmetry of fundamental absorption edge.

energy gaps

$E_{g,dir}$	5.35 eV	$T = 300\text{ K}, E \perp c$	absorption measurement, $\Gamma_{5v}^{+}-\Gamma_{1c}^{+}$ direct transition	71A
	6 eV	$T = 300\text{ K}, E \parallel c$	absorption measurement, direct transition	71A

Lattice properties

lattice parameters

a	4.395 Å			63W
c	2.859 Å			
u	0.307			

heat capacity

C_p	52.09 J mol ⁻¹ K ⁻¹	$T = 300\text{ K}$		67D
-------	---	--------------------	--	-----

density

d	6.24 g cm ⁻³			67D
-----	-------------------------	--	--	-----

melting temperature

T_m	1086°C			67D
-------	--------	--	--	-----

phonon frequencies

$\nu_{TO}(A_{2u})$	1.56·10 ¹³ s ⁻¹	$T = 300\text{ K}, E \parallel c$	IR reflectivity	71K
$\nu_{LO}(A_{2u})$	2.44·10 ¹³ s ⁻¹			
$\nu_{TO}(E_u)$	1.0·10 ¹³ s ⁻¹	$T = 300\text{ K}, E \perp c$		
$\nu_{LO}(E_u)$	1.45·10 ¹³ s ⁻¹			
$\nu_{TO}(E_u)$	1.95·10 ¹³ s ⁻¹			
$\nu_{LO}(E_u)$	2.03·10 ¹³ s ⁻¹			
$\nu_{TO}(E_u)$	2.12·10 ¹³ s ⁻¹			
$\nu_{LO}(E_u)$	2.55·10 ¹³ s ⁻¹			
$\nu(E_g)$	2.03·10 ¹³ s ⁻¹		Raman shift	70S
$\nu(A_{1g})$	2.1·10 ¹³ s ⁻¹			
$\nu(B_{2g})$	2.6·10 ¹³ s ⁻¹			

second order elastic moduli

c_{11}	$3.37 \cdot 10^{12} \text{ dyn cm}^{-2}$	75S
c_{33}	$599 \cdot 10^{12} \text{ dyn cm}^{-2}$	
c_{44}	$1.62 \cdot 10^{12} \text{ dyn cm}^{-2}$	
c_{66}	$2.58 \cdot 10^{12} \text{ dyn cm}^{-2}$	
c_{12}	$1.88 \cdot 10^{12} \text{ dyn cm}^{-2}$	
c_{13}	$1.87 \cdot 10^{12} \text{ dyn cm}^{-2}$	

bulk and torsional moduli

B	$2.59 \cdot 10^{12} \text{ dyn cm}^{-2}$	75S
G	$1.51 \cdot 10^{12} \text{ dyn cm}^{-2}$	

Transport properties

electrical conductivity : For temperature dependence, see Fig. 23.11.1.

Optical properties

refractive index

n	1.99	$E \parallel c, \lambda = 599 \text{ nm}$	67D
	2.05	$E \perp c$	

dielectric constants

$\epsilon(0)$	12.2	$E \parallel c, T = 300 \text{ K}$	71K
	14.5	$E \perp c$	
$\epsilon(\infty)$	4.1	$E \parallel c, T = 300 \text{ K}$	71K
	4.6	$E \perp c$	

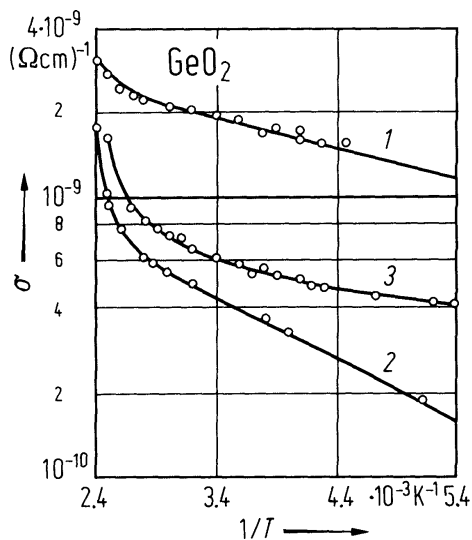
References to 23.11

63W Wyckoff, K. W. G.: Crystal Structures, Vol. 1, Second Edition Wiley & Sons 1963.
67D D'Ans-Lax: Taschenbuch für Chemiker und Physiker, Vol. 1, 3. Auflage, Berlin-Heidelberg-New York: Springer 1967.
70S Schlichting, U.: Dissertation Technische Universität Berlin 1970.
71A Arlinghaus, F. J., Albers, Jr., W. A.: J. Phys. Chem. Solids 32 (1971) 1455.
71K Kahan, A., Goodrum, J. W., Singh, K. S., Mitra, S. S.: J. Appl. Phys. 42 (1971) 4444.
75S Striefler, M. E., Barsch, G. K.: Phys. Status Solidi (b) 67 (1975) 143.
80K Kahn, M. N., Kahn, M. T., Hogarth, C. A.: Phys. Status Solidi (a) 61 (1980) 251.

Figures to 23.11

Fig. 23.11.1

GeO_2 . Electrical conductivity vs. reciprocal temperature for 1, Al- GeO_2 -Cu film, thickness 262 Å, 2, Ag- GeO_2 -Cu film, thickness 1200 Å; 3, Ag- GeO_2 -Ag film, thickness 262 Å. Ag, Al and Cu are used as electrodes [80K].



23.12 Germanium disulfide (GeS₂)

Crystal structure

see section 23.0.

Electronic properties

(All data for orthorhombic GeS₂)

energy gap

E_g	3.425 eV	$T = 300$ K	direct forbidden transition	79N1
-------	----------	-------------	-----------------------------	------

Lattice properties

lattice parameters

a	11.66 Å	63W
b	22.34 Å	
c	6.86 Å	

heat capacity

C_p	65.6 J mol ⁻¹ K ⁻¹	$T = 300$ K	74M
-------	--	-------------	-----

melting temperature

T_m	1113 K	74M
-------	--------	-----

IR phonon frequencies (in 10¹² s⁻¹)

$E \parallel a, T = 300$ K	from transmission measurements	79N1
----------------------------	--------------------------------	------

ν	1.46, 1.61, 1.82, 1.97, 2.33, 2.54, 3.06, 3.5, 3.8, 4.51, 4.75, 5.17, 5.47, 5.92, 6.13, 6.58, 7.09, 7.3, 8.16, 9.06, 10, 10.3, 11, 11.3
-------	---

$E \parallel a, T = 300$ K	from reflection measurements	79N2
----------------------------	------------------------------	------

ν	2.99, 4.49, 5.32, 10.9, 11.4, 12.3, 12.9, 13.2
-------	--

$E \parallel b, T = 300$ K	from transmission measurements	79N1
----------------------------	--------------------------------	------

ν	1.67, 2.03, 2.51, 2.69, 3.14, 3.44, 3.74, 4.31, 4.9, 5.11, 5.47, 6.64, 7.09, 7.3, 7.74, 8.1, 9.12, 9.99, 10.3, 11.1, 11.5, 11.7, 11.8
-------	---

$E \parallel b, T = 300$ K	from reflection measurements	79N2
----------------------------	------------------------------	------

ν	4.25, 4.54, 4.9, 5.47
-------	-----------------------

Optical properties

dielectric constants

$\epsilon(0)$	12	$T = 300$ K, $E \perp c$	spectral dependence of ϵ_1 and ϵ_2 :	79N1
$\epsilon(\infty)$	6.8	$T = 300$ K, $E \perp c$	Fig. 23.12.1	

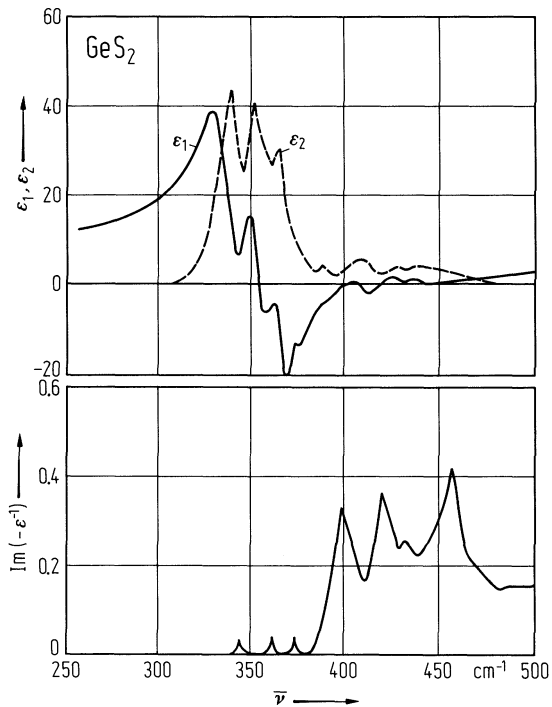
References to 23.12

- | | |
|------|--|
| 63W | Wyckoff, K. W. G.: Crystal Structures, Vol. 1, Second Edition Wiley & Sons 1963. |
| 74M | Mooser, E., Schüter, I. Ch., Schlüter, M.: J. Phys. Chem. Solids 35 (1974) 1269. |
| 79N1 | Nikolic, P. M.: Tehnicka Fizika 20 (1979) 37. |
| 79N2 | Nikolic, P. M., Popovic, Z. V.: J. Phys. C 12 (1979) 1151. |

Figures to 23.12

Fig. 23.12.1

GeS_2 . Real (ϵ_1) and imaginary (ϵ_2) parts of the complex dielectric function and the imaginary part of $-1/\epsilon$ vs. wavenumber obtained from Kramers-Kronig analysis of the reflectivity spectrum [79N1].



23.13 Germanium diselenide (GeSe2)

Crystal structure

see section 23.0.

Electronic properties

Only very little is known about the electronic properties. According to [70B] the absorption edge for band-to-band transition obeys Urbach's rule.

energy gap

E_g	2.485 eV	$T = 300\text{ K}$	direct transition, unpolarized	68G
-------	----------	--------------------	--------------------------------	-----

Lattice properties

lattice parameters

a	12.22 Å	62C
b	23.036 Å	
c	6.953 Å	

heat capacity

C_p	71.1 J mol ⁻¹ K ⁻¹	$T = 300\text{ K}$	74M
-------	--	--------------------	-----

melting temperature

T_m	1013 K	74M
-------	--------	-----

IR phonon frequencies (in 10¹² s⁻¹)

$E \parallel a, T = 300\text{ K}$	from reflectivity measurements	78P1
-----------------------------------	--------------------------------	------

ν_{TO}	2.63, 3.08, 7.83, 8.04, 8.4, 8.88, 9.06
ν_{LO}	2.68, 3.14, 8.13, 8.28, 8.7, 8.91, 9.09

$E \parallel b, T = 300\text{ K}$	
ν_{TO}	2.45, 2.87, 3.68, 7.8, 8.75, 9.09
ν_{LO}	2.48, 2.93, 3.72, 8.61, 8.91, 9.15

$E \parallel c, T = 300\text{ K}$	
ν_{TO}	9.63, 9.9
ν_{LO}	9.69, 10.2

Transport properties

resistivity : for temperature dependence, see Fig. 23.13.1.

Optical properties

optical spectra : refractive index: Fig. 23.13.2; dielectric function: Fig. 23.13.3.

dielectric constants

$\epsilon(0)$	9.5	$E \parallel a$	78P1
	11.5	$E \parallel b$	
	11.8	$E \parallel c$	
	7	$E \parallel a$	
	8	$E \parallel b$	
	11	$E \parallel c$	
$\epsilon(\infty)$			

References to 23.13

- 61A Albers, W., Haas, C., Vink, H. J., Wasscher, J. D.: J. Appl. Phys. 32 (1961) 2220.
- 62C Ch'ün-Hua, L., Pashinkin, A. S., Novoselova, A. V.: Russ. J. Inorg. Chem. 7 (1962) 1117.
- 68G Gavaleshko, N. P., Kurik, M. V., Savchuk, A. I.: Sov. Phys. Semicond. 1 (1968) 920.
- 70B Bahl, S. K., Chopra, K. L.: J. Appl. Phys. 41 (1970) 2196.
- 74M Mooser, E., Schüter, I. Ch., Schlüter, M.: J. Phys. Chem. Solids 35 (1974) 1269.
- 78P1 Popovic, Z. V., Nikolic, P. M.: Solid State Commun 27 (1978) 561.
- 78P2 Powell, M. J., Marseglia, E. A., Liang, WY.: J. Phys. C11 (1978) 895.

Figures to 23.13

Fig. 23.13.1

GeSe₂. Resistivity vs. inverse temperature for two single crystals [61A].

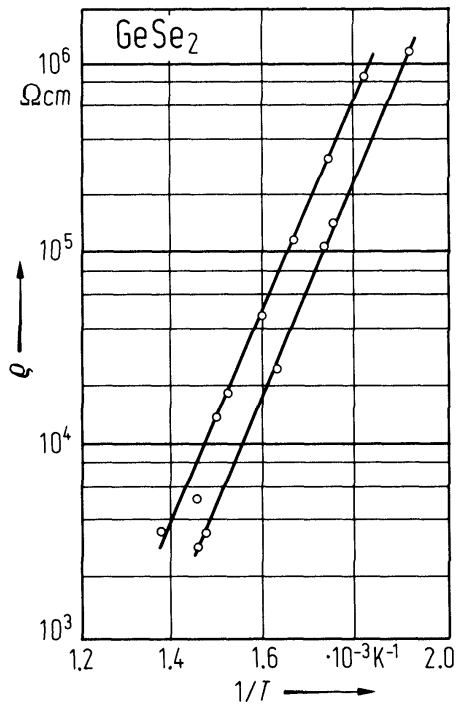


Fig. 23.13.2

GeSe₂. Real (n) and imaginary (k) parts of the complex index of refraction obtained by Kramers-Kronig analysis of the reflectivity spectra [78P2]. Fig. (a): $E \parallel a$; (b): $E \parallel b$; (c): $E \parallel c$.

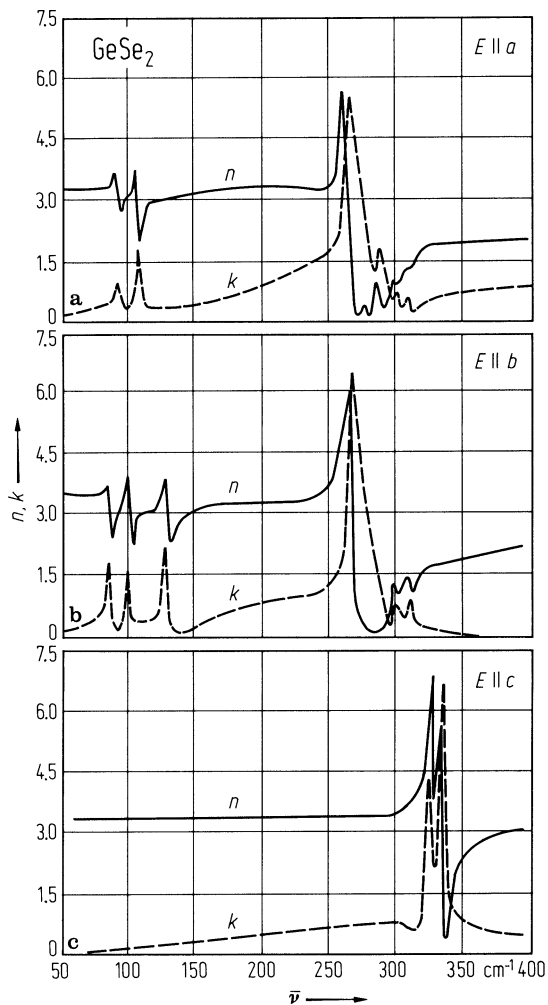
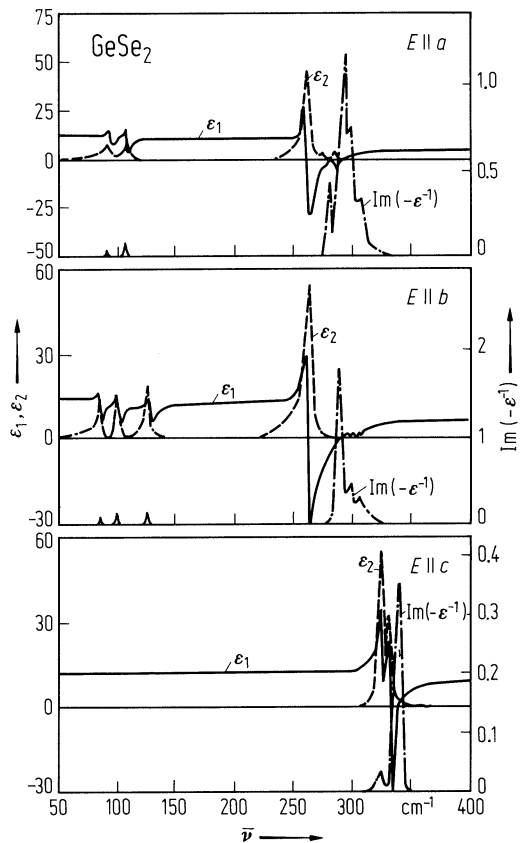


Fig. 23.13.3

GeSe₂. Real (ϵ_1) and imaginary (ϵ_2) parts of the complex dielectric function and the imaginary part of $-1/\epsilon$, vs. wavenumber, obtained using Kramers-Kronig analysis of the reflectivity spectra for all three polarization directions [78P2].



23.14 Tin dioxide (SnO₂)

Crystal structure

see section 23.0.

Electronic properties

band structure: Fig. 23.0.15; Brillouin zone: Fig. 23.0.14.

The lowest conduction band has its minimum at the Γ point in the Brillouin zone and is an 90% tin s-like state. It is very similar to that for a free electron in spite of the overall ionic character of SnO₂ [79R, 75J]. The upper valence band consists of a set of three bands (2^+ , 3^+ and 5^+). The valence band maximum is a Γ_3^+ state.

energy gap

$E_{\text{gx,dir}}(\Gamma_{3v}^+ - \Gamma_{1c}^+)$	3.596 eV	$T = 4 \text{ K}, E \perp c$	exciton absorption, forbidden transition	66S
	3.99 eV	$T = 4 \text{ K}, E \parallel c$		
$dE_{\text{gx,dir}}/dT$	$1.2 \cdot 10^{-3} \text{ eV K}^{-1}$	$T = 300 \dots 1300 \text{ K},$ $E \perp c, E \parallel c$		66S

excitonic binding energy

E_b	0.13 eV		absorption	77A
-------	---------	--	------------	-----

conduction band, effective masses

m_{\perp}	$0.299 m_0$	$T = 19 \dots 42 \text{ K}$	cyclotron resonance measurements	71B
m_{\parallel}	$0.234 m_0$			
$m_{\text{ds,n}}$	$0.275 m_0$		calculated from m_{\perp} and m_{\parallel}	71B

Lattice properties

lattice parameters

a	4.737 Å			63W
c	3.186 Å			
u	0.307			

thermal expansion coefficients

$\alpha_{\perp c}$	$4.0 \cdot 10^{-6} \text{ K}^{-1}$	$T = 93 \dots 700 \text{ K}$	from temperature dependence of	73P
$\alpha_{\parallel c}$	$3.7 \cdot 10^{-6} \text{ K}^{-1}$		lattice constants	
β	$11.7 \cdot 10^{-6} \text{ K}^{-1}$		volume expansion coefficient	

Debye temperature

Θ_D	570 K		calculated from elastic constants	80T
------------	-------	--	-----------------------------------	-----

heat capacity

C_p	$52.59 \text{ J mol}^{-1} \text{ K}^{-1}$	$T = 300 \text{ K}$		67D
-------	---	---------------------	--	-----

density

d	6.994 g cm^{-3}	$T = 300 \text{ K}$	pycnometric density	80T
	7.02 g cm^{-3}	$T = 300 \text{ K}$	X-ray density	67D

melting temperature

T_m	$> 1930^\circ\text{C}$			67D
-------	------------------------	--	--	-----

phonon dispersion relations : Fig. 23.14.1; Brillouin zone: Fig. 23.0.14.

The unit cell contains 6 atoms. Therefore 18 phonons exist of which 3 are acoustical and 15 optical modes. The inversion symmetry of the rutile structure leads to four infrared active phonons ($3\Gamma_5^+$, $1\Gamma_1^-$) and four Raman active phonons (Γ_3^+ , Γ_5^- , Γ_1^+ , Γ_4^+).

phonon frequencies

$\nu_{\text{TO}}(\Gamma_5^+)$	$7.29 \cdot 10^{12} \text{ s}^{-1}$	$T = 100 \text{ K}, E \perp c$	IR reflectivity	71K
$\nu_{\text{LO}}(\Gamma_5^+)$	$8.25 \cdot 10^{12} \text{ s}^{-1}$			
$\nu_{\text{TO}}(\Gamma_5^+)$	$8.76 \cdot 10^{12} \text{ s}^{-1}$			
$\nu_{\text{LO}}(\Gamma_5^+)$	$10.9 \cdot 10^{12} \text{ s}^{-1}$			
$\nu_{\text{TO}}(\Gamma_5^+)$	$18.4 \cdot 10^{12} \text{ s}^{-1}$			
$\nu_{\text{LO}}(\Gamma_5^+)$	$23 \cdot 10^{12} \text{ s}^{-1}$			
$\nu_{\text{TO}}(\Gamma_1^-)$	$14.2 \cdot 10^{12} \text{ s}^{-1}$			
$\nu_{\text{LO}}(\Gamma_1^-)$	$21 \cdot 10^{12} \text{ s}^{-1}$	$T = 100 \text{ K}, E \parallel c$		
$\nu(\Gamma_3^+)$	$3.68 \cdot 10^{12} \text{ s}^{-1}$	$T = 300 \text{ K}$	Raman spectra	73P
$\nu(\Gamma_5^-)$	$14.2 \cdot 10^{12} \text{ s}^{-1}$	$T = 100 \text{ K}$		71K
$\nu(\Gamma_1^+)$	$19 \cdot 10^{12} \text{ s}^{-1}$			
$\nu(\Gamma_4^+)$	$23.3 \cdot 10^{12} \text{ s}^{-1}$			

second order elastic moduli

c_{11}	$2.61 \cdot 10^{12} \text{ dyn cm}^{-2}$		measurement of transit time of	75C,
c_{33}	$4.5 \cdot 10^{12} \text{ dyn cm}^{-2}$		ultrasonic waves	75S,
c_{44}	$1.03 \cdot 10^{12} \text{ dyn cm}^{-2}$			80S
c_{66}	$2.08 \cdot 10^{12} \text{ dyn cm}^{-2}$			
c_{12}	$1.78 \cdot 10^{12} \text{ dyn cm}^{-2}$			
c_{13}	$1.56 \cdot 10^{12} \text{ dyn cm}^{-2}$			

bulk and torsional moduli

B	$2.13 \cdot 10^{12} \text{ dyn cm}^{-2}$			75C
G	$1.02 \cdot 10^{12} \text{ dyn cm}^{-2}$			

compressibility

$\kappa_{\perp c}$	$1.3 \cdot 10^{-13} \text{ cm}^2 \text{ dyn}^{-1}$	$T = 296 \text{ K}$	pressure dependence of lattice	73P
$\kappa_{\parallel c}$	$1.9 \cdot 10^{-13} \text{ cm}^2 \text{ dyn}^{-1}$		constants	
κ_v	$4.5 \cdot 10^{-13} \text{ cm}^2 \text{ dyn}^{-1}$		volume compressibility	

Transport properties

Electrical transport occurs via band conduction. Only n-type material is known. The free carrier concentration changes with oxygen deficiency. A review of electrical properties is given in [76J].

For temperature dependence of mobility, carrier concentration and conductivity, see Fig. 23.76.

electrical conductivity

$\sigma_{\perp c} / \sigma_{\parallel c}$	1	$T = 77 \text{ K}$	for σ , see also Fig. 23.14.2	71F
	1.2	$T = 300 \text{ K}$		

electron mobility

μ_n	150 cm ² /V s	$T = 300$ K	$n = 2.2 \cdot 10^{18}$ cm ⁻³
	240 cm ² /V s	$T = 300$ K	$n = 8.6 \cdot 10^{16}$ cm ⁻³
	260 cm ² /V s	$T = 300$ K	$n = 8.5 \cdot 10^{15}$ cm ⁻³

thermal conductivity

$\kappa_{ c}$	0.98 W cm ⁻¹ K ⁻¹	$T = 300$ K	static measurement according to	80T
$\kappa_{\perp c}$	0.55 W cm ⁻¹ K ⁻¹	$T = 300$ K	Fourier law	

Optical properties

dielectric constants

$\epsilon(0)$	13.5	$E \perp c, T = 300$ K,	from IR reflectivity	68S
	9.58	$E \parallel c$		

References to 23.14

63W Wyckoff, K. W. G.: Crystal Structures, Vol. 1, Second Edition Wiley & Sons 1963.
66S Summitt, H. K., Borrelli, N. F.: J. Appl. Phys. 37 (1966) 2200.
67D D'Ans-Lax: Taschenbuch f. Chemiker u. Physiker, Vol. 1, Berlin, Heidelberg, New York: Springer 1967.
68S Summitt, K.: J. Appl. Phys. 39 (1968) 3762.
71B Button, K. J., Fonstad, C. G., Dreybrodt, W.: Phys. Rev. B4 (1971) 4539.
71F Fonstad, C. G., Rediker, K. H.: J. Appl. Phys. 42 (1971) 2911.
71K Katiyar, R. S., Dawson, P., Hargreave, M., Wilkinson, G. K.: J. Phys. C4 (1971) 2421.
73P Peercy, P. S., Morosin, D.: Phys. Rev. B7 (1973) 2779.
75C Chang, E., Graham, E. K.: J. Geophys. Res. 80 (1975) 2595.
75J Jaquemin, J. L., Bordure, O. J. Phys. Chem. Solids 36 (1975) 1081.
75S Striefler, M. E., Barsch, G. K.: Phys. Status Solidi (b) 67 (1975) 143.
76J Jarzebski, Z. M., Marton, J. P.: J. Electrochem. Soc. 123 (1976) 299C.
77A Agekyan, V. T.: Phys. Status Solidi 43 (1977) 11.
79R Robertson, J.: J. Phys. C 12 (1979) 4753.
80S Shanker, J., Jam, V. K.: Phys. Status Solidi (a) 59 (1980) 355.
80T Tuerkes, P., Pluntke, Ch., Helbig, K.: J. Phys. C 13 (1980) 4941.

Figures to 23.14

Fig. 23.0.14

SnO_2 . Brillouin zone for the rutile structure.

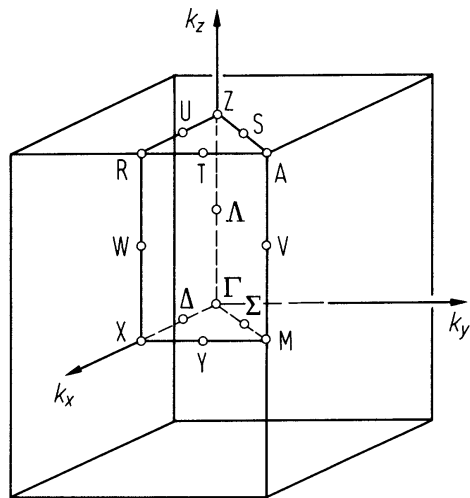


Fig. 23.0.15

SnO₂. Calculated band structure (Sn–O and O–O interactions are included in the calculation) [79R].

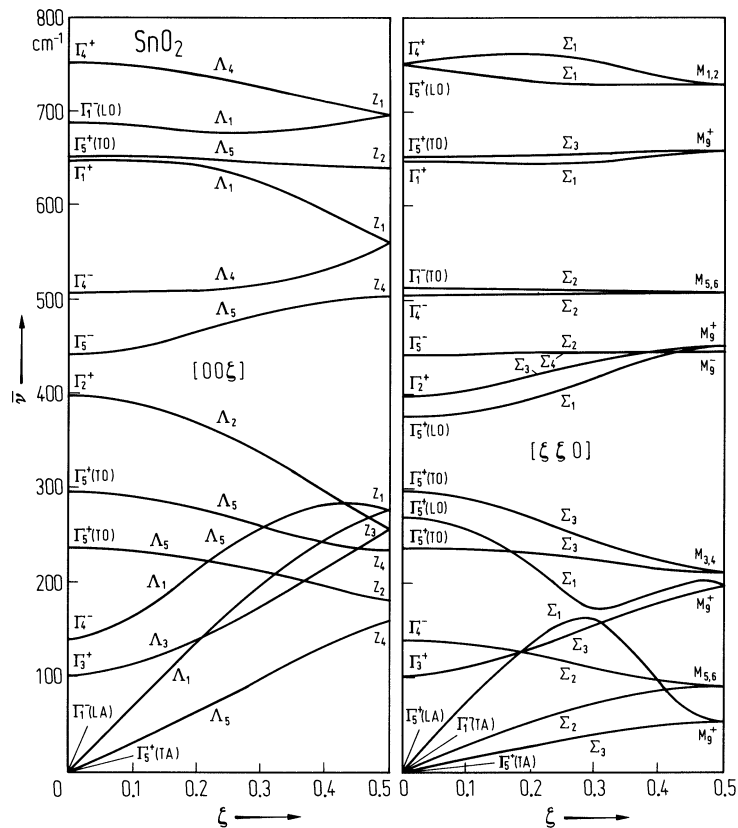


Fig. 23.14.1

SnO₂. Calculated phonon dispersion curves (wavenumber vs. reduced wave vector coordinate) [71K2].

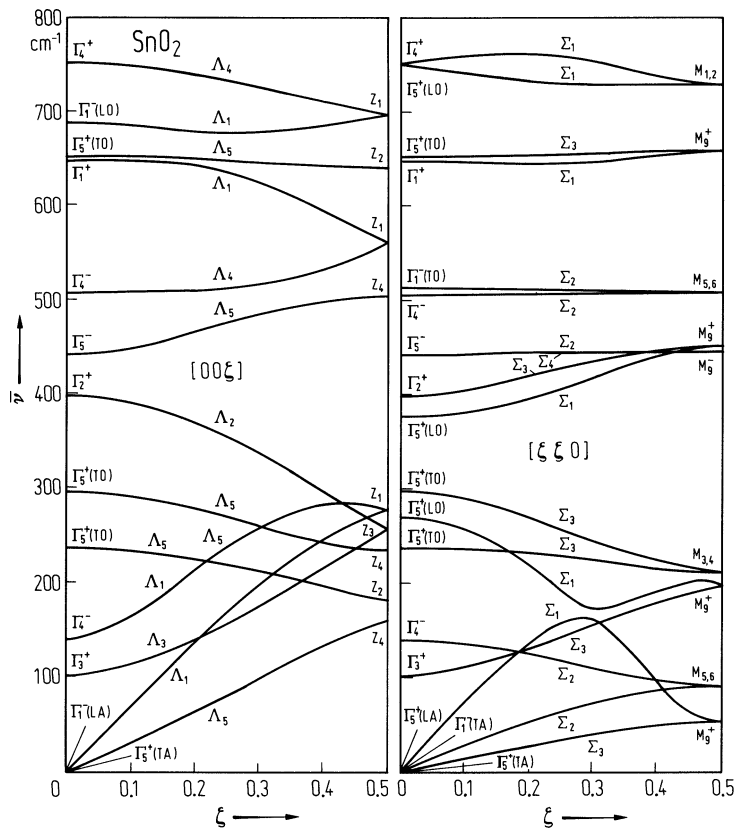
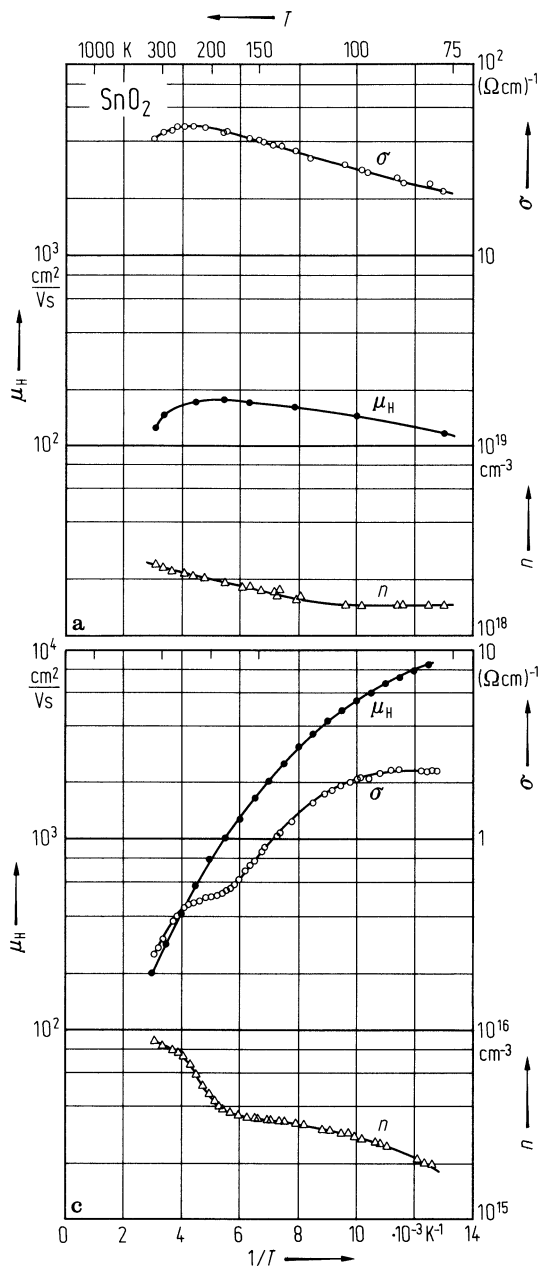


Fig. 23.14.2

SnO₂. Carrier concentration, Hall mobility and conductivity vs. (reciprocal) temperature between 80 and 325 K [71F]. (a) high concentration sample; (b) low concentration sample; (c) lowest concentration sample studied.



23.15 Tin disulfide (SnS2)

Crystal structure

see section 23.0.

Electronic properties

All data refer to the 2H polytype if not otherwise stated.

band structure

Band structures of 2H and 4H-SnS2: Fig. 23.0.16a,b; Brillouin zone: Fig. 23.0.14.

energy gaps ($E \perp c$ for all measurements)

$E_{g,ind}$	2.07(2) eV	$T = 300$ K	(forbidden transition)	66D
$E_{g,dir}$	2.88(2) eV	$T = 300$ K	(forbidden transition)	66D
$E_{g,th}$	2.18 eV	2H-SnS2	temperature dependence of intrinsic	79A
	1.89 eV	4H-SnS2	conductivity	
	1.59 eV	6H-SnS2		
	1.15 eV	24R-SnS2		
	0.92 eV	24H-SnS2		

temperature dependence of indirect energy gap

$dE_{g,ind}/dT$	$-8.6 \cdot 10^{-4}$ eV K ⁻¹	$T = 77...300$ K, $E \perp c$	65G
-----------------	---	----------------------------------	-----

Lattice properties

phonon dispersion curves : Fig. 23.15.1.

The basis of CdI2 structure crystals SnS2 and SnSe2 (2H polytype) consists of three atoms which lead to nine vibrational modes. The irreducible representation at the zone center is $\Gamma = A_{1g} + 2A_{2u} + E_g + 2E_u$. The acoustic modes are $A_{2u} + E_u$, the two Raman active modes $A_{1g} + E_g$ and the two IR-active modes $A_{2u} + E_u$ [76L, 77L].

phonon frequencies

$\nu(A_{1g})$	$9.49 \cdot 10^{12}$ s ⁻¹	$T = 77$ K	2H-SnS2, from Raman spectrum	77S
$\nu(E_g)$	$6.22 \cdot 10^{12}$ s ⁻¹	$T = 77$ K		
$\nu(A_1 + E)$	$9.48 \cdot 10^{12}$ s ⁻¹	$T = 77$ K	4H-SnS2, from Raman spectrum	77S
$\nu(E)$	$6.46 \cdot 10^{12}$ s ⁻¹	$T = 77$ K		
$\nu(E)$	$6.17 \cdot 10^{12}$ s ⁻¹	$T = 77$ K		
$\nu(E)$	$5.62 \cdot 10^{12}$ s ⁻¹	$T = 77$ K		
$\nu(E)$	$0.837 \cdot 10^{12}$ s ⁻¹	$T = 77$ K		

heat capacity

C_p	70.06 J mol ⁻¹ K ⁻¹	$T = 298$ K	74M
	17.3 J mol ⁻¹ K ⁻¹	$T = 53$ K	77M

density

d	4.47 g cm ⁻³	$T = 300$ K	pycnometric density	77M
	4.5 g cm ⁻³	$T = 300$ K	X-ray-density	

melting temperature

T_m	1038 K		74M
-------	--------	--	-----

Transport properties

SnS₂ is an n-type semiconductor with carrier concentrations of about 10¹⁷...10¹⁸ cm⁻³. The mobility of carriers perpendicular to the *c*-axis shows normal lattice scattering ($\mu_n \propto T^{-1.9}$), while parallel to the *c*-axis the mobility is associated with a hopping mechanism which shows exponential temperature dependence and an activation energy of $E_A = 0.18$ eV [70G].

resistivity

ρ	1.11 Ω cm	$T = 300$ K, $E \perp c$	$n = 2 \cdot 10^{17}$ cm ⁻³ , from free carrier reflectivity	76L
--------	------------------	--------------------------	---	-----

mobility

μ_n	51.5 cm ² /V s	$T = 300$ K, $E \perp c$	Hall mobility, $n = 2 \cdot 10^{17}$ cm ⁻³	76L
---------	---------------------------	--------------------------	---	-----

temperature dependence of electrical conductivity and mobility : Figs. 23.15.2...4

Optical properties

optical spectra : dielectric function: Figs. 23.15.5, 23.15.6.

refractive index

n_o	2.85	$T = 300$ K,		69L
$n_o - n_e$	0.69	$\lambda = 0.69$ μ m	birefringence	

dielectric constants

$\epsilon(0)$	17.7	$T = 300$ K, $E \perp c$	from Kramers Kronig analysis of	76L
	6.19	$T = 300$ K, $E \parallel c$	IR-spectra and oscillator fit including	
$\epsilon(\infty)$	7.57	$T = 300$ K, $E \perp c$	the free carrier contributions	
	5.65	$T = 300$ K, $E \parallel c$		

References to 23.15

65G Greenaway, D. L., Nitsche, K.: J. Phys. Chem. Solids 26 (1965) 1145.
66D Domingo, G., Itoga, K. S., Kannewurf, C. K.: Phys. Rev. 143 (1966) 536.
69L Lee, P. A., Said, G., Davis, R., Lim, T. H.: J. Phys. Chem. Solids 30 (1969) 2719.
70G Gowers, J. P., Lee, P. A.: Solid State Commun. 8 (1970) 1447.
72P Pearson, W. B.: The Crystal Chemistry and Physics of Metals and Alloys; Wiley & Sons 1972.
73S Schlichting, U., Gobrecht, K. H.: J. Phys. Chem. Solids 34 (1973) 753.
74M Mills, K. C.: Thermodynamic Data for Inorganic Sulphides, Selenides and Tellurides, London: Butterworths 1974.
76L Lucovsky, G., Mikkelsen jr., J. C., Liang, W. Y., White, R. M.: Phys. Rev. B 14 (1976) 1663.
77L Lucovsky, G., White, K. M.: Nuovo Cimento 38B (1977) 290.
77S Smith, A. J., Meek, P. E., Liang, W. Y.: J. Phys. C 10 (1977) 1321.
79A Acharya, S., Srivastava, N.: Phys. Status Solidi (b) 56 (1979) K1.
79B Bertrand, Y., Leveque, G.: J. Phys. C 12 (1979) 2907.

Figures to 23.15

Fig. 23.0.14

SnO_2 . Brillouin zone for the rutile structure.

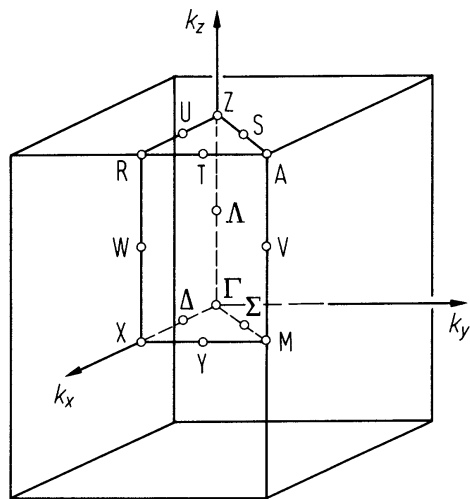


Fig. 23.0.16

Diagram of the structure of GeS_2 and GeSe_2 [72P].

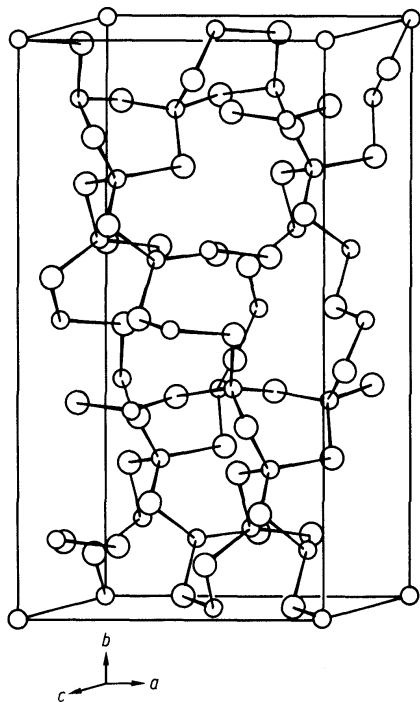


Fig. 23.15.1

SnS_2 . Phonon dispersion curves along the principal symmetry directions of the Brillouin zone of 2H-SnS_2 calculated by using a dynamical model. The experimental zone-center mode frequencies are indicated [77S].

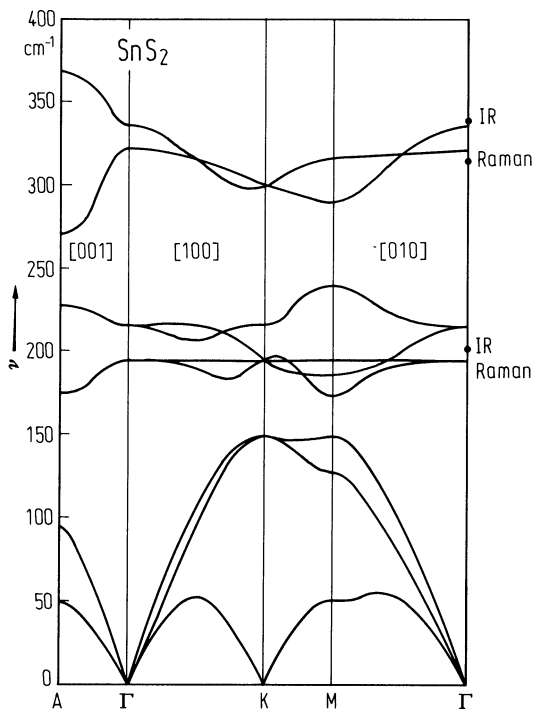


Fig. 23.15.2

SnS_2 . Conductance vs. reciprocal temperature (thickness $d = 90\ \mu\text{m}$; surface $A = 3.2\ \text{mm}^2$; $\sigma = \sigma_0 \cdot \exp(-E_A/kT)$ showing three distinct regions for $\sigma \parallel c$) [73S].

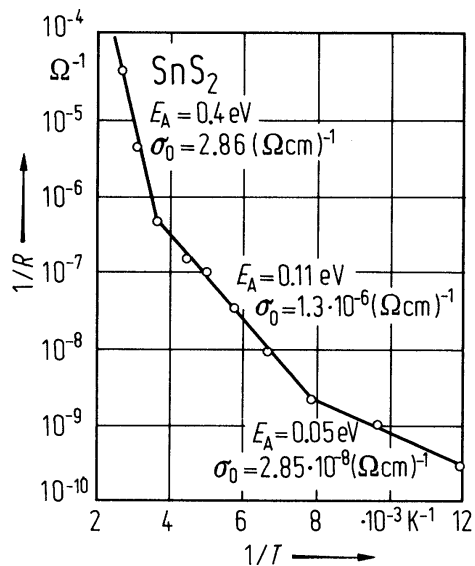


Fig. 23.15.3

SnS₂. Electron Hall mobility ($I \perp c$) vs. temperature [70G].

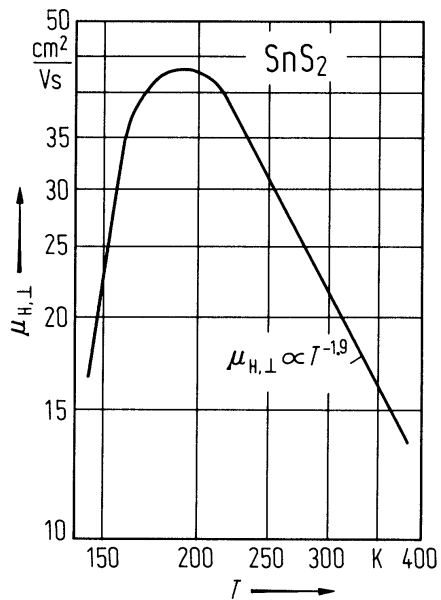


Fig. 23.15.4

SnS₂. Electron Hall mobility ($I \parallel c$) vs. reciprocal temperature [70G].

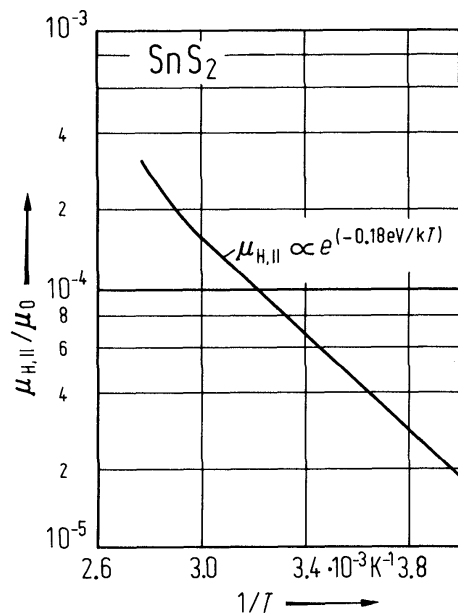


Fig. 23.15.5

SnS_2 . Dielectric functions ϵ_2 and $-\text{Im}(1/\epsilon)$ vs. wavenumber as calculated from oscillator parameters. The dashed line ϵ_2 functions and the solid line energy-loss functions are computed using only the first order phonon terms. The second set of energy-loss curves (---) is calculated including the contribution of the damped plasmon as well [76L].

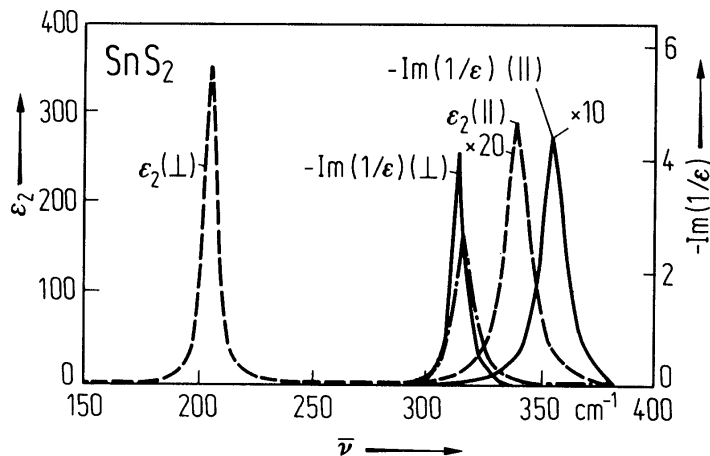
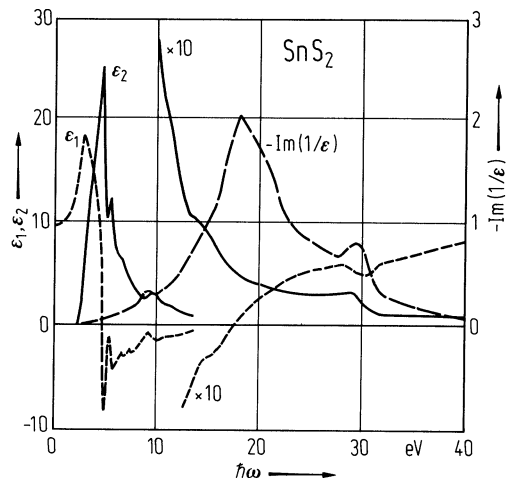


Fig. 23.15.6

SnS_2 . Dielectric functions (ϵ_1 , ϵ_2) and energy-loss function vs. photon energy obtained by Kramers-Kronig analysis of reflectivity spectra ($E \perp c$) [79B].



23.16 Tin diselenide (SnSe2)

Crystal structure

see section 23.0.

All data refer to the 2H-polytype if not stated otherwise.

Electronic properties

band structure : Fig. 23.0.17, Brillouin zone. Fig. 23.0.14.

energy gaps (polarization $E \perp c$)

$E_{g,ind}$	0.97 eV	$T = 300\text{ K}$	(forbidden transition)	66D
$E_{g,dir}$	1.62 eV	$T = 300\text{ K}$	(forbidden transition)	66D
$E_{g,th}$	1 eV		temperature dependence of intrinsic conductivity	61A

conduction band, effective mass

m_{ds}	$2.9\ m_0$	$T = 290\text{ K}$	$n \approx 1.2 \cdot 10^{20}\text{ cm}^{-3}$, calculated from Hall measurements	72L
----------	------------	--------------------	---	-----

Lattice properties

density

d	6.01 g cm^{-3}	$T = 300\text{ K}$		77M
-----	-------------------------	--------------------	--	-----

melting temperature

T_m	948 K			74M
-------	-------	--	--	-----

phonon dispersion : Fig. 23.16.1.

phonon frequencies

$\nu_{TO}(A_{2u})$	$7.20 \cdot 10^{12}\text{ s}^{-1}$	$T = 300\text{ K}, E \parallel c$	from IR-reflectivity, 2H-SnSe2	76L
$\nu_{LO}(A_{2u})$	$7.4 \cdot 10^{12}\text{ s}^{-1}$	$T = 300\text{ K}, E \parallel c$		
$\nu_{TO}(E_u)$	$4.30 \cdot 10^{12}\text{ s}^{-1}$	$T = 300\text{ K}, E \perp c$		
$\nu_{LO}(E_u)$	$6.1 \cdot 10^{12}\text{ s}^{-1}$	$T = 300\text{ K}, E \perp c$		
$\nu(A_{1g})$	$5.51 \cdot 10^{12}\text{ s}^{-1}$	$T = 300\text{ K}$	2H-SnSe2, from Raman spectrum	77S
$\nu(E_g)$	$3.25 \cdot 10^{12}\text{ s}^{-1}$	$T = 300\text{ K}$		

second order elastic moduli

c_{11}	$10.32(18) \cdot 10^{11}\text{ dyn cm}^{-2}$	determined from acoustic phonon dispersion	77B
c_{33}	$2.76(13) \cdot 10^{11}\text{ dyn cm}^{-2}$		
c_{44}	$1.35(6) \cdot 10^{11}\text{ dyn cm}^{-2}$		

Transport properties

SnSe2 is an n-type semiconductor with carrier concentrations typically from $10^{17} \dots 10^{18}\text{ cm}^{-3}$ [76G]. p-type conductivity is also reported [61B].

electrical resistivity

ρ	0.28 $\Omega\text{ cm}$	$T = 300\text{ K}, E \parallel c$	$n = 7.9 \cdot 10^{17}\text{ cm}^{-3}$, from free carrier reflectivity	76L
	0.27 $\Omega\text{ cm}$	$T = 300\text{ K}, E \perp c$	$n = 7.9 \cdot 10^{17}\text{ cm}^{-3}$, dc measurements	76L

For temperature dependence, see Fig. 23.16.2.

hole mobility

μ_n	29.3 cm ² /V s	$T = 300 \text{ K}, E \perp c$	Hall mobility, $n = 1.5 \cdot 10^{18} \text{ cm}^{-3}$ For temperature, see Fig. 23.16.3	76L
---------	---------------------------	--------------------------------	---	-----

thermal conductivity

$\kappa_{\perp}/\kappa_{\parallel}$	≈ 6	$T = 250 \text{ K}$	see also Fig. 23.16.4	61B
-------------------------------------	-------------	---------------------	-----------------------	-----

Optical properties

refractive indices

n_o	3.26	$T = 290 \text{ K},$ $\lambda = 1 \mu\text{m}$	for spectral dependence of refractive index	69E
n_e	2.88	$T = 290 \text{ K},$ $\lambda = 1 \mu\text{m}$		

dielectric constants

$\varepsilon(0)$	21.47 9.97	$T = 300 \text{ K}, E \perp c$ $E \parallel c$	from Kramers-Kronig analysis of IR spectra and oscillator fit including free carrier contributions, see also [76K]	76L
$\varepsilon(\infty)$	10.7 9.42	$T = 300 \text{ K}, E \perp c$ $E \parallel c$	For spectral dependence of dielectric function, see Fig. 23.16.5.	

References to 23.16

- 61A Asanabe, S.: J. Phys. Soc. Jpn. 16 (1961) 1789.
61B Busch, G., Fröhlich, C., Hulliger, F., Steigmeier, E.: Helv. Phys. Acta 34 (1961) 359.
66D Domingo, G., Itoga, K. S., Kannewurf, C. K.: Phys. Rev. 143 (1966) 536.
69E Evans, B. L., Hazelwood, K. A.: J. Phys. D 2 (1969) 1507.
72L Likhter, A. I., Pel, E. G., Prysyazhnyuk, S. I.: Phys. Status Solidi (a) 14 (1972) 265.
74M Mills, K. C.: Thermodynamic Data for Inorganic Sulphides, Selenides and Tellurides, London: Butterworths 1974.
75G Gregora, I., Stetter, W.: Phys. Status Solidi (b) 71 (1975) K187.
76G Garg, A. K., Agnihotri, O. P., Jam, A. K., Iyagi, K. C.: J. Appl. Phys. 47 (1976) 997.
76K Koehler, H., Becker, C. K.: Phys. Status Solidi (b) 76 (1976) K15.
762 Lucovsky, G., Mikkelsen jr., J. C., Liang, W. Y., White, R. M.: Phys. Rev. B 14 (1976) 1663.
77B Brebner, J. L., Jandi, S., Powell, B. M.: Nuovo Cimento 38B (1977) 263.
77M Margaritondo, G., Rowe, J. E., Schlüter, M., Kasper, H.: Solid State Commun. 22 (1977) 753.
77S Smith, A. J., Meek, P. E., Liang, W. Y.: J. Phys. C 10 (1977) 1321.

Figures to 23.16

Fig. 23.0.14

SnO_2 . Brillouin zone for the rutile structure.

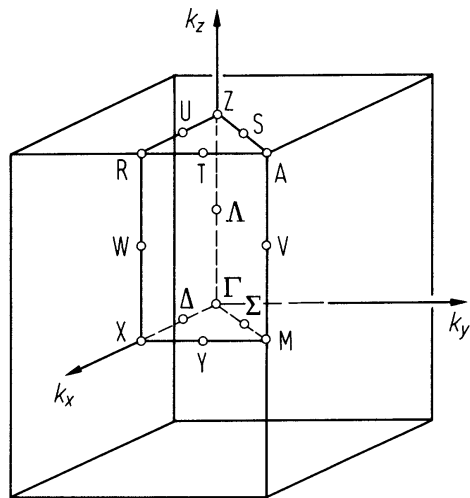


Fig. 23.0.17

Crystal structure of SnS_2 and SnSe_2 , (a) general form of layer structure, (b) $(11\bar{2}0)$ -section, (c) octahedral coordination in the layer, (d) packing of atoms in SnSe_2 [75G].

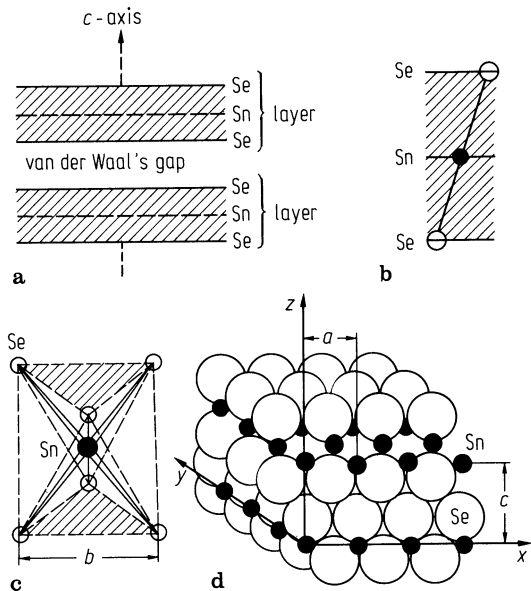


Fig. 23.16.1

SnSe_2 . Phonon dispersion curves (frequency vs. reduced wave vector coordinate) measured along the Σ and Γ directions. In the geometry used only one of the mainly transverse modes was observable [77B]. A', B: acoustic phonon branches in Σ and Γ direction, respectively.

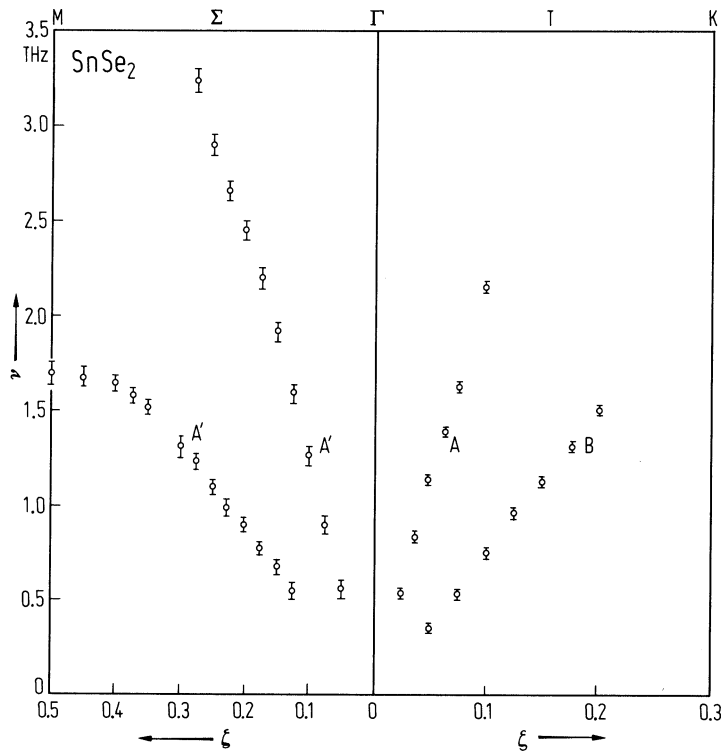


Fig. 23.16.2

SnSe₂. Resistivity ρ_{\perp} (conductivity σ_{\perp}) vs. reciprocal temperature. $n = 1.57 \cdot 10^{18} \text{ cm}^{-3}$ at 290 K [69E].

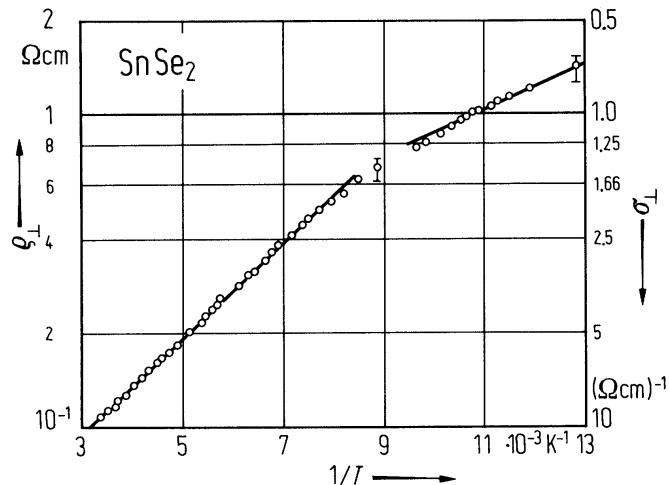


Fig. 23.16.3

SnSe_2 . Electron Hall mobility in the basal plane vs. temperature. From 290...500 K $\mu \propto T^{-3/2}$ [72L].

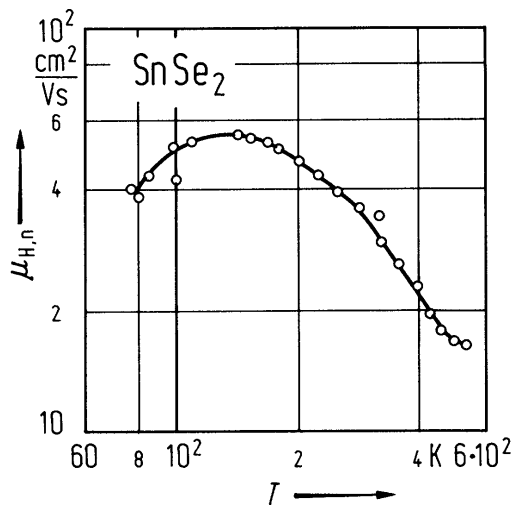


Fig. 23.16.4

SnSe_2 . Temperature dependence of thermal conductivity [61B].

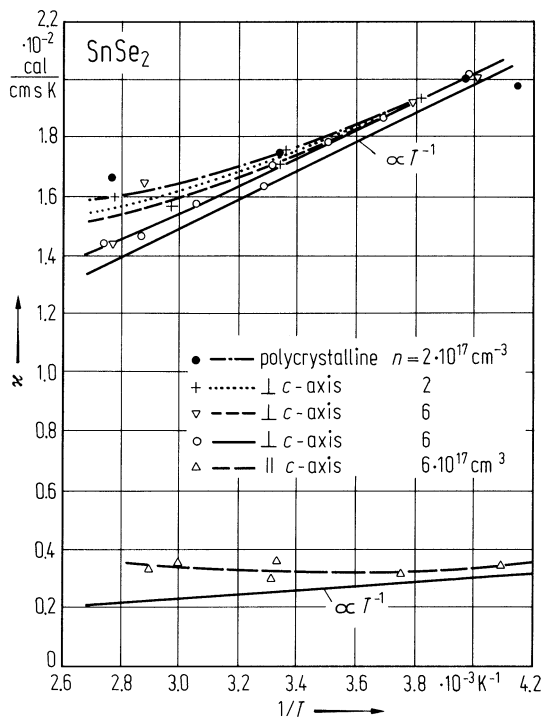
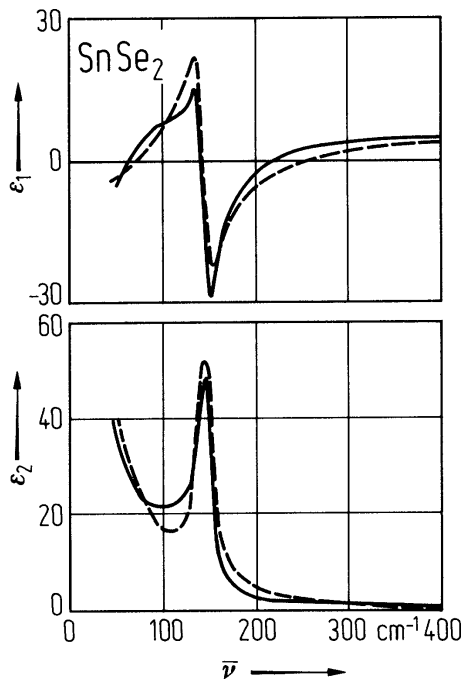


Fig. 23.16.5

SnSe_2 . Real (ϵ_1) and imaginary (ϵ_2) part of the dielectric function vs. wavenumber ($E \perp c$) obtained from Kramers-Kronig analysis of the reflectivity curve (solid curves) and by numerical calculations (dashed curves) on the basis of a classical oscillator taking into consideration the influence of free carriers [76K].



23.17 Si₂Te₃

Crystal structure

see section 23.0.

Electronic properties

Most knowledge of the electronic properties of Si₂Te₃ comes from optical measurement. Due to the rapid decomposition of the surface of Si₂Te₃ to SiO₂ and Te in the presence of water vapour [78B] the results of optical and electrical measurements depend on preparation and handling of the samples.

energy gaps

$E_{g,ind}$	1.82 eV	$T = 300\text{ K}$	indirect forbidden	66R
	1.89 eV	$T = 300\text{ K}$	indirect allowed	
$E_{g,dir}$	2.18 eV	$T = 300\text{ K}$	direct forbidden, from absorption measurement	66R
$dE_{g,dir}/dT$	$-1.22 \cdot 10^{-3}\text{ eV K}^{-1}$		from absorption	73L

effective masses

$\mu_{ c}$	$2.7\ m_0$		reduced mass of electrons and holes from Franz-Keldysh effect	76B
$m_{n,p}(c)$	$5.4\ m_0$		calculated from the reduced mass of electrons and holes	

heat capacity

C_p	$1.25 \cdot 10^2\text{ J mol}^{-1}\text{ K}^{-1}$	$T = 300\text{ K}$		74M
-------	---	--------------------	--	-----

density

d	4.5 g cm^{-3}	$T = 300\text{ K}$	pycnometric density	66B
-----	------------------------	--------------------	---------------------	-----

melting temperature

T_m	1165 K			66B
-------	--------	--	--	-----

Transport properties

Si₂Te₃ is a p-type semiconductor with a strong anisotropy of the electrical conductivity due to the hexagonal layer structure. The analysis of the photocurrent indicates a trap level at 0.45 eV below the conduction band and a broad distribution of recombination centers at 0.9 eV [77Z].

carrier concentration

p	$3 \cdot 10^6\text{ cm}^{-3}$	$T = 300\text{ K}$		77Z
-----	-------------------------------	--------------------	--	-----

hole mobility

$\mu_p(c)$	$2 \cdot 10^{-3}\text{ cm}^2/\text{V s}$	$T = 283\text{ K}$		77Z
--------------	--	--------------------	--	-----

electrical conductivity : for temperature dependence, see Fig. 23.17.1

Seebeck coefficient and resistivity as a function of temperature: Fig. 23.17.2.

thermal conductivity

κ	$4...5 \cdot 10^{-3}\text{ W K}^{-1}\text{ cm}^{-1}$	$T = 300\text{ K}$		66B
----------	--	--------------------	--	-----

Optical properties

Spectral dependence of refractive index and extinction coefficient: Fig. 23.17.3.

References to 23.17

- 66B Bailey, L. G.: J. Phys. Chem. Solids 27 (1966) 1593.
- 66R Rau, J. W., Kannewurf, C. R.: J. Phys. Chem. Solids 27 (1966) 1097.
- 73L Lambros, A. P., Economou, N. A.: Phys. Status Solidi (b) 57 (1973) 793.
- 73P Petersen, K. E., Birkholz, U., Adler, D.: Phys. Rev. B 8 (1973) 1453.
- 74M Mills, K. C.: Thermodynamic Data for Inorganic Sulphides, Selenides and Tellurides, London: Butterworths 1974.
- 76B Brückel, B., Birkholz, U., Ziegler, K.: Phys. Status Solidi (b) 78 (1976) K23.
- 77Z Ziegler, K., Birkholz, U.: Phys. Status Solidi (a) 39 (1977) 467.
- 78B Bauer, H. P., Birkholz, U.: Phys. Status Solidi (a) 49 (1978) 127.

Figures to 23.17

Fig. 23.17.1

Si_2Te_3 . Electrical conductivity vs. reciprocal temperature of single crystals. Open circles: parallel to c -axis, full circles: normal to c -axis [77Z]. Activation energies E_A are indicated.

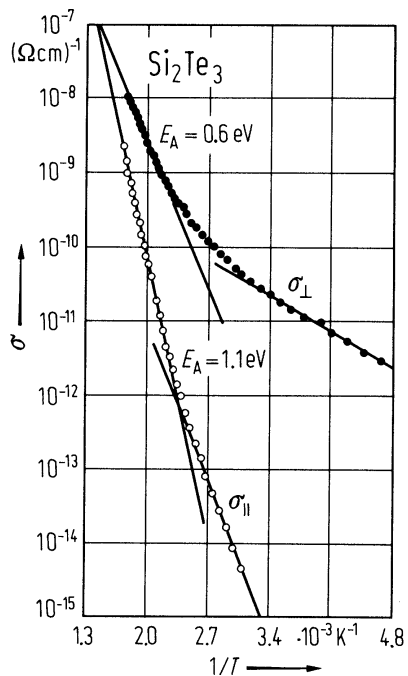


Fig. 23.17.2

Si_2Te_3 . Seebeck coefficient and electrical resistivity vs. temperature for undoped, pressed and sintered Si_2Te_3 [66B].

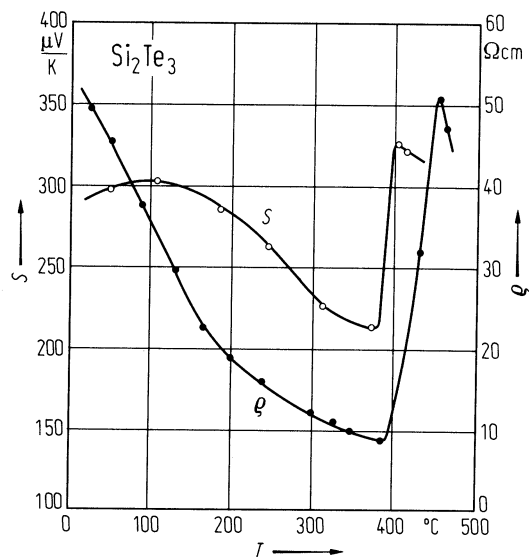
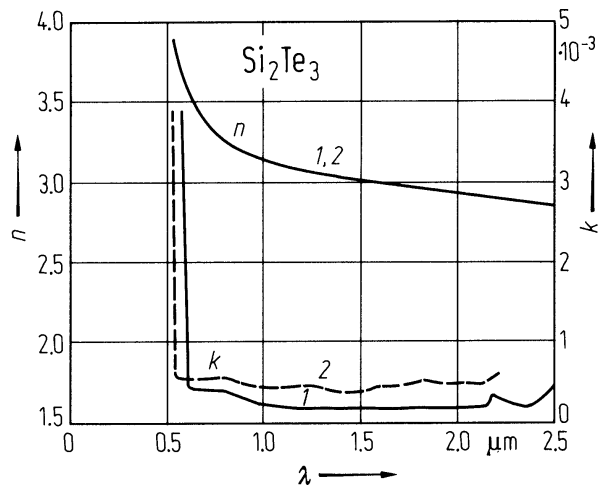


Fig. 23.17.3

Si_2Te_3 . Optical constants n and k vs. wavelength at 300 K (curve 1, full line) and 100 K (curve 2, dashed line) [73P, 77Z].



23.18 Sn_2S_3 , PbSnS_3 , SnGeS_3 , PbGeS_3

Only little work is reported about the semiconducting ternary compounds $\text{Me}^{\text{II}}\text{Me}^{\text{IV}}\text{S}_3$ with $\text{Me}^{\text{II}} = \text{Sn}, \text{Pb}$ and $\text{Me}^{\text{IV}} = \text{Ge}, \text{Sn}$. Their electronic energy gaps are determined between 0.8 and 2.5 eV [75A].

energy gaps

Sn_2S_3				
E_g	0.95 eV	$T = 300 \text{ K}$	absorption measurement	75A
PbSnS_3				
E_g	0.9 eV	$T = 0 \text{ K}$	from temperature dependence of conductivity between 160...300 K	75A
SnGeS_3				
E_g	2.23 eV	$T = 300 \text{ K}$	absorption measurement	75A
PbGeS_3				
E_g	2.4 eV	$T = 300 \text{ K}$	absorption measurement	75A

References to 23.18

75A v. Alpen, U., Fenner, J., Gmelin, E.: Mater. Res. Bull. 10 (1975) 175.

24 IV-VII₂ compounds

24.0 Crystal structure and electronic structure

PbF_2 (α -phase), $PbCl_2$ and $PbBr_2$ crystallize in an orthorhombic structure (space group: V_{2h}^{16}). This structure can be thought of as a considerably distorted close-packing of halogen atoms with the lead atoms accommodated in the same plane with them. PbF_2 also occurs in a cubic fluorite structure (β -phase, space group: O_h^5).

PbI_2 crystallizes in the hexagonal CdI_2 structure. *Band structure*: Fig. 24.0.1.

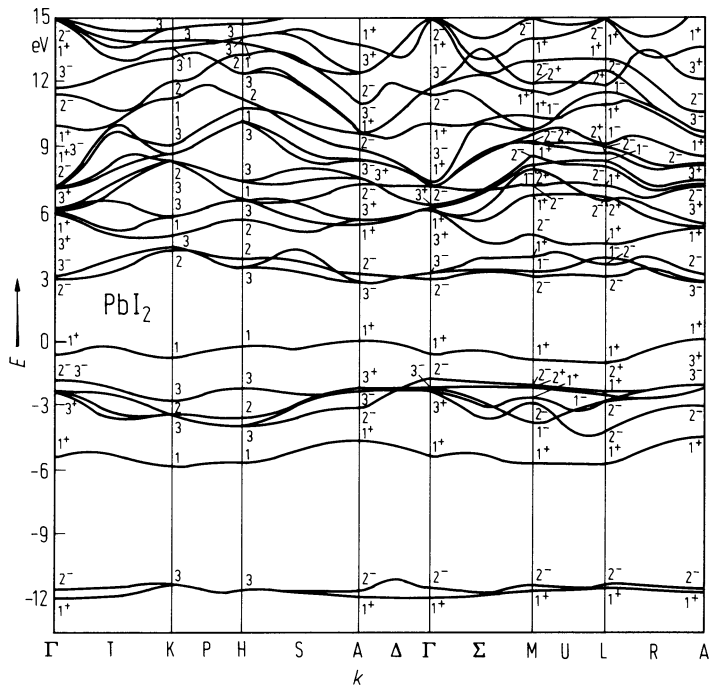
References to 24.0

74S Schlüter, I. Ch., Schlüter, M.: Phys. Rev. B 68 (1974) 1652.

Figures to 24.0

Fig. 24.0.1

PbI_2 . Three-dimensional empirical pseudopotential method band structure; single group notation [74S].



24.1 Lead difluoride (PbF2)

Electronic properties

If not stated otherwise all data refer to the cubic β-PbF2.

excitonic energy gap (cationic, Pb 6s–6p transition)

E_{gx}	5.68 eV	$T = 4.2 \text{ K}$	reflectance, doublet structure	73P
dE_{gx}/dT	$-1.2(2) \cdot 10^{-4} \text{ eV K}^{-1}$	$T = 123 \dots 273 \text{ K}$	transmission	76B

Lattice properties

If not stated otherwise all data refer to the cubic β-PbF2.

lattice parameters

a	7.63574 Å	$T = 291 \text{ K}$	α-PbF2 (orthorhombic V_{2h}^{16} phase, 4 molecules per unit cell)	63W
b	6.42689 Å			
c	3.89098 Å			
a	5.92732 Å	$T = 291 \text{ K}$	β-PbF2 (cubic fluorite O_h^5 phase)	63W
a	5.940 Å	$T = 295 \text{ K}$		66S

coefficient of linear thermal expansion

α	$0.41 \cdot 10^{-8} \text{ K}^{-1}$	$T = 4 \text{ K}$	Fig. 24.1.1	80W
	$2.87 \cdot 10^{-5} \text{ K}^{-1}$	$T = 283 \text{ K}$		

Debye temperature

Θ_D	230 K	$T = 10 \text{ K}$	thermal expansion calorimetry	80W 78L
	225.3 K	$T = 295 \text{ K}$		

heat capacity

C_p	69(7) J K ⁻¹ mol ⁻¹	$T = 400 \dots 640 \text{ K}$	differential scanning calorimetry	79R
-------	---	-------------------------------	-----------------------------------	-----

density

d	8.48 g cm ⁻³		α-PbF2	66S
	7.659 g cm ⁻³		β-PbF2	

melting temperature

T_m	855°C			75W
-------	-------	--	--	-----

phonon dispersion relations : Fig. 24.1.2

phonon wavenumbers

$\bar{\nu}_{\text{TO}}$	102 cm ⁻¹	RT	infrared reflectance	65A
$\bar{\nu}_{\text{LO}}$	337 cm ⁻¹			

Raman wavenumber

$\bar{\nu}_{\text{R}}$	253 cm ⁻¹	$T = 4 \text{ K}$	Raman scattering	77H
------------------------	----------------------	-------------------	------------------	-----

second order elastic moduli

c_{11}	$9.34 \cdot 10^{11} \text{ dyn cm}^{-2}$	RT	from elastic compliances, see below See also [78D]	70H
c_{12}	$4.40 \cdot 10^{11} \text{ dyn cm}^{-2}$			
c_{44}	$2.10 \cdot 10^{11} \text{ dyn cm}^{-2}$			

elastic compliances

s_{11}	$1.534(7) \cdot 10^{-12} \text{ cm}^2 \text{ dyn}^{-1}$	RT	oscillator resonance technique	70H
s_{12}	$-0.49(1) \cdot 10^{-12} \text{ cm}^2 \text{ dyn}^{-1}$			
s_{44}	$4.756(1) \cdot 10^{-12} \text{ cm}^2 \text{ dyn}^{-1}$			

compressibility

κ	$1.53 \cdot 10^{-3} \text{ kbar}^{-1}$	$T = 16.3 \text{ K}$	dielectric measurements	76S
	$1.65 \cdot 10^{-3} \text{ kbar}^{-1}$	$T = 295.0 \text{ K}$		

bulk modulus

B_S	63 GPa	$T = 295 \text{ K}$	from thermal expansion	80W
-------	--------	---------------------	------------------------	-----

Optical properties

If not stated otherwise all data refer to the cubic β -PbF₂.

refractive index

n	1.75450(4)	$T = 291.7 \text{ K},$ $\lambda = 0.7065 \text{ }\mu\text{m}$	prism method	55J
-----	------------	--	--------------	-----

reflectance : Fig. 24.1.3 (77 K, 4...30 eV) , Fig. 24.1.4 (295 K, 10...150 μm)

dielectric constants

$\epsilon(\infty)$	3.120	$T = 295 \text{ K}$		66S
$\epsilon(0)$	27.4	$T = 295 \text{ K}$	infrared reflectance	65A

spectral dependence of real and imaginary parts of the dielectric constants at 295 K: Fig. 24.1.5.

References to 24.1

55J Jones, D. A.: Proc. Phys. Soc. (London) B68 (1955) 165.
63W Wykoff, R. W. G.: Crystal Structures, Vol. 1, New York: Interscience Publishers, 1963.
65A Axe, J. D., Gaglianella, J. W., Scardefield, J. E.: Phys. Rev. A 139 (1965) 1211.
66S Schmidt, E. D. D., Vedam, K.: J. Phys. Chem. Solids 27 (1966) 1563.
70H Hart, S.: J. Phys. D 3 (1970) 430.
73P Plekhanov, V.: Phys. Status Solidi (b) 57 (1973) K 55.
75W Weast, R. C. (ed.): Handbook of Chemistry and Physics, CRC Press, Cleveland 1975.
76B Brothers, A. D., Pajor, J. T.: Phys. Rev. B 14 (1976) 4570.
76S Samara, G. A.: Phys. Rev. B 13 (1976) 4529.
77B Beaumont, J. H., Bourdillon, A. J., Bordas, J.: J. Phys. C 10 (1977) 761.
77H Hayes, W., Rushworth, A. J., Ryan, J. F., Elliott, R. J., Kleppmann, W. G.: J. Phys. C 10 (1977) L111
.78D Dickens, M. H., Hutchings, M. T.: J. Phys. C 11 (1978) 461.
78L Lawless, W. N.: Phys. Rev. B 17 (1978) 1458.
79R Rimai, D. S., Sladek, R. J.: Solid State Commun. 31 (1979) 473.
80W White, G. K.: J. Phys. C 13 (1980) 4905.

Figures to 24.1

Fig. 24.1.1

PbF₂. Coefficient of linear thermal expansion over T^3 vs. T^2 for two samples [80W].

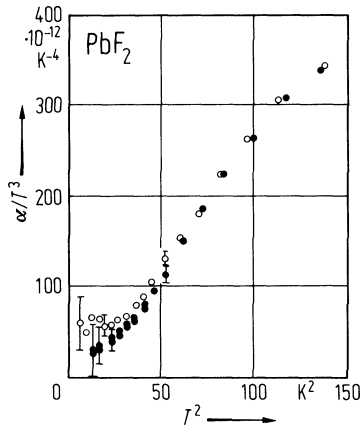


Fig. 24.1.2

PbF_2 . Phonon dispersion relations in the $[001]$, $[110]$, and $[111]$ directions at 10 K. The solid and broken lines are calculated from best fits to two models. Open (full) circles are predominantly longitudinal (transverse) modes, triangles represent points which were not included in the fitting procedure [78D].

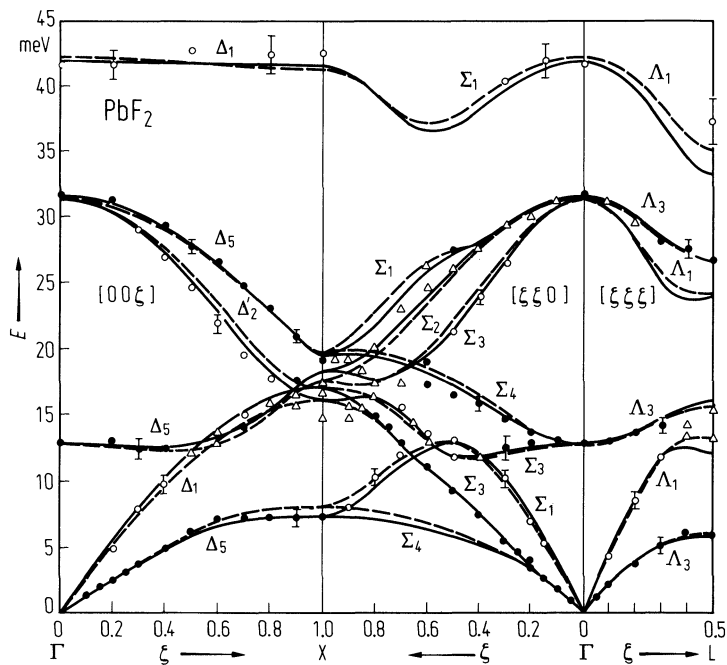


Fig. 24.1.3

PbF₂. Reflectance vs. photon energy at 77 K [77B].

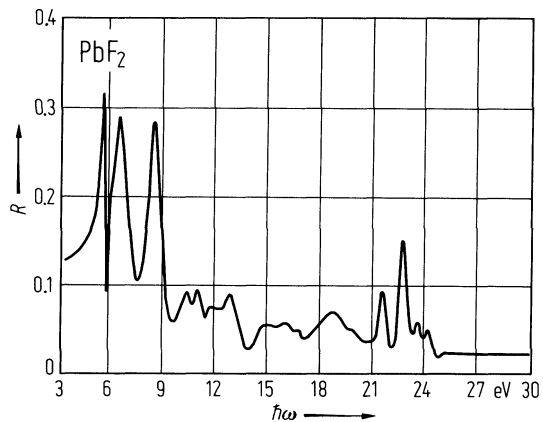


Fig. 24.1.4

PbF_2 . Reflectance vs. wavelength. The solid line is a fit to a harmonic oscillator function [65A].

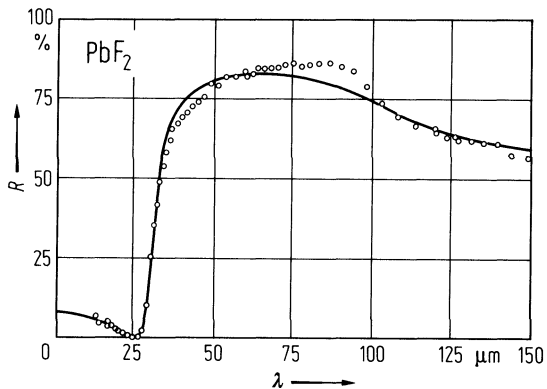
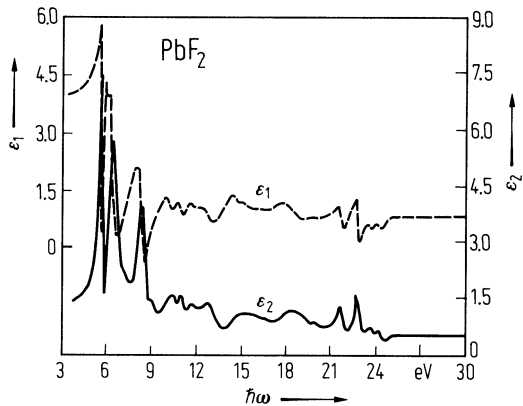


Fig. 24.1.5

PbF_2 . Real part (broken line) and imaginary part (solid line) of the dielectric constant vs. photon energy [77B].



24.2 Lead dichloride (PbCl₂)

Electronic properties

energy gap

E_g	4.863(5) eV	calculated from data below	72L
-------	-------------	----------------------------	-----

excitonic energy gaps (cationic, Pb 6s – 6p transition)

$E_{gx}(A_{1g}-B_{1u})$	4.690(5) eV	$T = 78\text{ K}, E \parallel a$	reflectance	75P
$E_{gx}(A_{1g}-B_{2u})$	4.710(5) eV	$E \parallel b$		
$E_{gx}(A_{1g}-B_{3u})$	4.650(5) eV	$E \parallel c$		

temperature dependence of excitonic energy gap

dE_{gx}/dT	$-3.6(4) \cdot 10^{-4}\text{ eV K}^{-1}$	$T = 123...273\text{ K}$	transmission	76B
--------------	--	--------------------------	--------------	-----

reduced exciton mass

μ_{ex}	$0.33\ m_0$	$T = 5\text{ K}$	transmission	72L
------------	-------------	------------------	--------------	-----

exciton binding energy

E_b	0.170(5) eV	$T = 5\text{ K}$	transmission and Kramers-Kronig analysis	72L
-------	-------------	------------------	--	-----

exciton Bohr radius

r_{ex}	8.05 Å			72L
----------	--------	--	--	-----

Lattice properties

lattice parameters

a	9.030 Å	$T = 291\text{ K}$	orthorhombic V_{2h}^{16} structure,	63W
b	7.608 Å		4 molecules per unit cell	
c	4.525 Å			

density

d	5.85 g cm ⁻³			75W
-----	-------------------------	--	--	-----

melting temperature

T_m	501°C			75W
-------	-------	--	--	-----

Optical properties

optical spectra : reflectance: Fig. 24.2.1.

dielectric constants : real and imaginary parts: Fig. 24.2.2.

References to 24.2

- 63W Wykoff, R. W. G.: Crystal Structures, Vol. 1, New York: Interscience Publishers, 1963.
72L Liidya, G. G., Plekhanov, V. G.: Opt. Spectrosc. 32 (1972) 43.
73P Plekhanov, V.: Phys. Status Solidi (b) 57 (1973) K 55.
75P Plekhanov, V. G.: Phys. Status Solidi (b) 68 (1975) K 35.
75W Weast, R. C. (ed.): Handbook of Chemistry and Physics, CRC Press, Cleveland 1975.
76B Brothers, A. D., Pajor, J. T.: Phys. Rev. B 14 (1976) 4570.

Figures to 24.2

Fig. 24.2.1

PbCl_2 . Reflectance vs. photon energy at 77 K [75P].

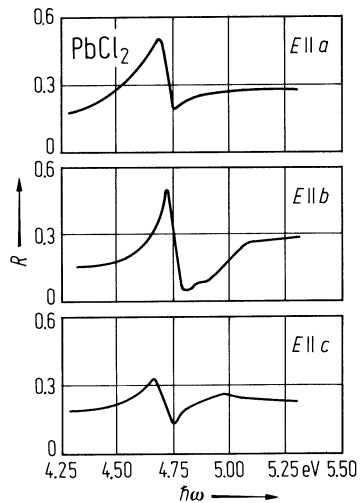
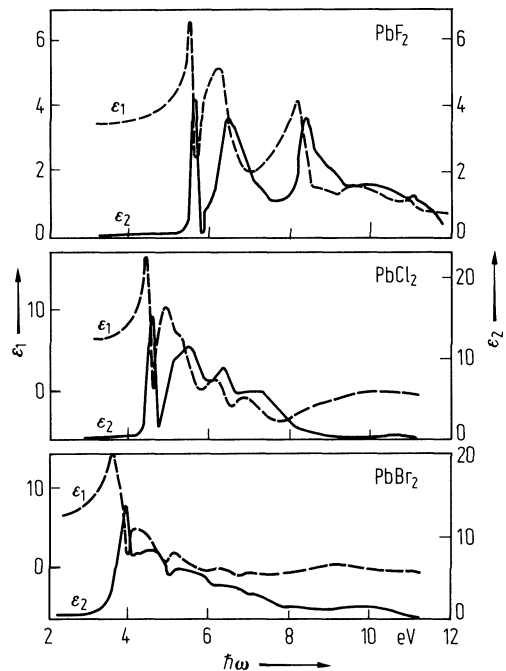


Fig. 24.2.2

PbCl_2 , PbBr_2 , PbF_2 . Real and imaginary parts of the dielectric constant vs. photon energy at 78 K [73P].



24.3 Lead dibromide (PbBr2)

Electronic properties

excitonic energy gaps (cationic Pb 6s – 6p transition)

$E_{\text{gx}}(\text{A}_{1\text{g}}\text{--B}_{1\text{u}})$	3.955(4) eV	$E \parallel a, T = 77 \text{ K}$	reflectance	75P
$E_{\text{gx}}(\text{A}_{1\text{g}}\text{--B}_{2\text{u}})$	3.975(4) eV	$E \parallel b$		
$E_{\text{gx}}(\text{A}_{1\text{g}}\text{--B}_{3\text{u}})$	3.935(4) eV	$E \parallel c$		

temperature dependence of excitonic energy gap

dE_{gx}/dT	$-3.9(3) \cdot 10^{-4} \text{ eV K}^{-1}$	$T = 123 \dots 273 \text{ K}$	transmission	76B
---------------------	---	-------------------------------	--------------	-----

exciton Bohr radius

r_{ex}	7.15 Å		transmission	71K
-----------------	--------	--	--------------	-----

reduced exciton mass

μ_{ex}	0.59 m_0	$T = 295 \text{ K}$	exciton spectra	71K
-------------------	------------	---------------------	-----------------	-----

Lattice properties

lattice parameters

a	9.466 Å	$T = 291 \text{ K}$	orthorhombic $V_{2\text{h}}^{16}$ structure,	63W
b	8.068 Å		4 molecules per unit cell	
c	4.767 Å			

density

d	6.66 g cm ⁻³			75W
-----	-------------------------	--	--	-----

melting temperature

T_{m}	373°C			75W
----------------	-------	--	--	-----

Optical properties

optical spectra : reflectance: Fig. 24.3.1.

dielectric constants : real and imaginary parts: Fig. 24.3.2.

References to 24.3

63W Wykoff, R. W. G.: Crystal Structures, Vol. 1, New York: Interscience Publishers, 1963.
71K Kramarenko, N. K., Miloslavskii, V. K.: Phys. Status Solidi (b) 48 (1971) K 177.
73P Plekhanov, V.: Phys. Status Solidi (b) 57 (1973) K 55.
75P Plekhanov, V. G.: Phys. Status Solidi (b) 68 (1975) K 35.
75W Weast, R. C. (ed.): Handbook of Chemistry and Physics, CRC Press, Cleveland 1975.
76B Brothers, A. D., Pajor, J. T.: Phys. Rev. B 14 (1976) 4570.

Figures to 24.3

Fig. 24.3.1

PbBr_2 . Reflectance vs. photon energy at 77 K [75P].

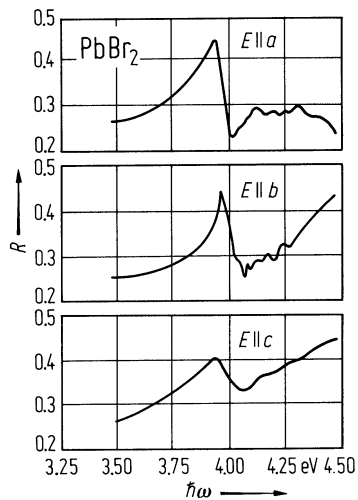
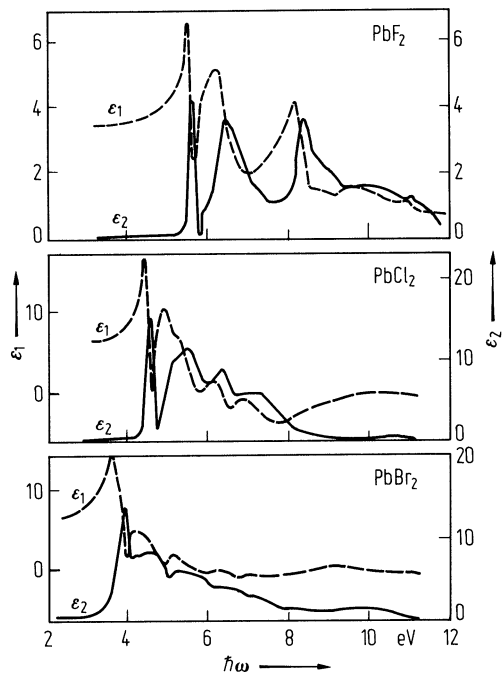


Fig. 24.3.2

PbCl_2 , PbBr_2 , PbF_2 . Real and imaginary parts of the dielectric constant vs. photon energy at 78 K [73P].



24.4 Lead diiodide (PbI₂)

Electronic properties

(All values for the 2H type if not otherwise noted)

band structure

2H modification: Fig. 24.0.1.

energy gaps

2H modification:

$E_{\text{g,dir}}(\text{A}_{4\text{v}}^{+}-\text{A}_{4\text{c}}^{-})$ (or $\text{A}_{4\text{g}}-\text{A}_{4\text{u}}$)	2.552(5) eV	$T = 4. \text{ K}, E \perp c$	reflectance and Kramers-Kronig analysis	69G
--	-------------	-------------------------------	---	-----

4H modification:

$E_{\text{g,dir}}(\Gamma_{8\text{v}}(1) - \Gamma_{8\text{c}}(2))$	2.562(5) eV	$T = 4.2 \text{ K}, E \perp c$	reflectance and Kramers-Kronig analysis	69G
---	-------------	--------------------------------	---	-----

band edge exciton transition energies

2H modification:

$E(1\text{s}) (= E_{\text{gx}})$	2.495 eV	$T = 4.2 \text{ K}, E \perp c$	reflectance and Kramers-Kronig analysis	69G
$E(2\text{s})$	2.518 eV			
$E(3\text{s})$	2.536 eV			

4H modification:

$E(1\text{s})$	2.505 eV	$T = 4.2 \text{ K}, E \perp c$	reflectance and Kramers-Kronig analysis	64N, 69G
$E(2\text{s})$	2.529 eV			
$E(3\text{s})$	2.550 eV			

spin-orbit splitting in the conduction band

$\Delta(\text{A}_{4^{-}}-\text{A}_{5,6^{-}})$	0.81 eV	$T = 4.2 \text{ K}$	reflectance	75H
---	---------	---------------------	-------------	-----

effective masses

m_{n}^{\parallel}	1.25 m_0	$T = 300 \text{ K}, \parallel c$ $\perp c$	drift mobility	76M
m_{n}^{\perp}	0.25 m_0			
m_{p}^{\parallel}	1.1 m_0	$T = 300 \text{ K}, \parallel c$ $\perp c$	drift mobility	
m_{p}^{\perp}	1.1 m_0			

Lattice properties

lattice parameters (for the various polytypes)

a (2H)	4.557 Å	$T = 295$ K	63W
c (2H)	6.979 Å		
a (4H)	4.557 Å	$T = 295$ K	
c (4H)	13.958 Å		
c (6H)	20.937 Å		
c (6R)	20.937 Å		
c (12R)	41.874 Å		

thermal expansion

$(1/a)da/dT$	4.0(1)·10 ⁻⁵ K ⁻¹	$T = 250...400 \text{ K}$	2H polytype, see Fig. 24.4.1.	79S
$(1/c)dc/dT$	3.6(1)·10 ⁻⁵ K ⁻¹			

density

d	6.16 g cm^{-3}		75W
-----	--------------------------	--	-----

melting temperature

T_m	402°C		75M
-------	---------------------	--	-----

phonon dispersion relations : Fig. 24.4.2.

phonon wavenumbers

ir active modes, 2H modification

$(\nu/c)(E_{u,TO})$	51.7 cm^{-1}	$T = 4.2 \text{ K}, E \perp c$	infrared reflectance	76L
$(\nu/c)(E_{u,LO})$	108 cm^{-1}	$T = 4.2 \text{ K}, E \perp c$		
$(\nu/c)(A_{2u,TO})$	96 cm^{-1}	$T = 4.2 \text{ K}, E \parallel c$		77L
$(\nu/c)(A_{2u,LO})$	121 cm^{-1}	$T = 4.2 \text{ K}, E \parallel c$		77L

Raman active modes, 2 H modification

$(\nu/c)(E_g)$	$79.0(5) \text{ cm}^{-1}$	$T = 77 \text{ K}$		76G
$(\nu/c)(A_{1g})$	$98.0(5) \text{ cm}^{-1}$	$T = 77 \text{ K}$		76G
$2(\nu/c)(E_u)$	106 cm^{-1}	$T = 400 \text{ K}$		79S
$(\nu/c)(A_{2u})$	113 cm^{-1}			
$2(\nu/c)(E_g)$	$165(5) \text{ cm}^{-1}$			
$4(\nu/c)(E_u)$	$205(5) \text{ cm}^{-1}$			
$2(\nu/c)(A_{2u})$	$220(5) \text{ cm}^{-1}$			

sound velocities

$v_{T^{\perp}[001]}$	$1.00(2) \cdot 10^5 \text{ cm s}^{-1}$	$T = 295 \text{ K}$	Brillouin scattering	75S
$v_{L^{\perp}[001]}$	$1.80(2) \cdot 10^5 \text{ cm s}^{-1}$	$T = 295 \text{ K}$	Brillouin scattering	75S
	$1.54(8) \cdot 10^5 \text{ cm s}^{-1}$		inelastic neutron scattering	76D
$v_{T[110]}$	$1.10(8) \cdot 10^5 \text{ cm s}^{-1}$		polarized out of plane	76D
$v_{L[110]}$	$1.81(10) \cdot 10^5 \text{ cm s}^{-1}$			
$v_{T[100]}$	$1.07(6) \cdot 10^5 \text{ cm s}^{-1}$		polarized out of plane	
	$0.94(4) \cdot 10^5 \text{ cm s}^{-1}$			
$v_{L[100]}$	$1.86(10) \cdot 10^5 \text{ cm s}^{-1}$			

second order elastic moduli

c_{11}	$27.7(5) \cdot 10^{10} \text{ dyn cm}^{-2}$	$T = 295 \text{ K}$	Brillouin scattering	75S
c_{33}	$20.2(4) \cdot 10^{10} \text{ dyn cm}^{-2}$			75S
c_{44}	$6.2(2) \cdot 10^{10} \text{ dyn cm}^{-2}$			75S
c_{12}	$9.6(9) \cdot 10^{10} \text{ dyn cm}^{-2}$			75S
c_{13}	$11.3(6) \cdot 10^{10} \text{ dyn cm}^{-2}$			75S
c_{14}	$3.0(2) \cdot 10^{10} \text{ dyn cm}^{-2}$			75S

Transport properties**carrier mobilities**

$\mu_{n\perp}$	$1300 \dots 4600 \text{ cm}^2/\text{V s}$	$T = 3.3 \text{ K}$	transverse magnetoconductivity and Hall effect, Fig. 24.4.3	78B
$\mu_{p\perp}$	$2600 \dots 3000 \text{ cm}^2/\text{V s}$			

Optical properties

optical spectra : reflectance: Fig. 24.4.4.

dielectric constants

$\epsilon(0)_{\perp}$	26.4	$T = 300 \text{ K}$	infrared reflectance	76L
$\epsilon(0)_{\parallel}$	9.3			77L
$\epsilon(\infty)_{\perp}$	6.25	$T = 300 \text{ K}$	infrared reflectance	67D
$\epsilon(\infty)_{\parallel}$	5.9			77L

for spectral dependence of real and imaginary parts of the dielectric constant from reflectance and Kramers-Kronig analysis, see Fig. 24.4.5.

References to 24.4

- 63W Wykoff, R. W. G.: Crystal Structures, Vol. 1, New York: Interscience Publishers, 1963.
- 64N Nikitine, S., Schmitt-Burckel, J., Biellmann, J., Ringeisen, J.: J. Phys. Chem. Solids 35 (1964) 951.
- 67D Dugan, A. E., Henisch, H. K.: J. Phys. Chem. Solids 28 (1967) 971.
- 69G Gähwiller, Ch., Harbeke, G.: Phys. Rev. 185 (1969) 1141.
- 72S Sirdesmukh, D. B., Deshpande, V. T.: Current Sci. 41 (1972) 210.
- 74S Schlüter, I. Ch., Schlüter, M.: Phys. Rev. B 68 (1974) 1652.
- 75H Harbeke, G., Tosatti, E.: RCA Rev. 36 (1975) 40.
- 75M Mussil, V. V., Miloslavskii, V. K., Karmazin, V. V.: Fiz. Tverd. Tela 17 (1975) 859; Sov. Phys. Solid State (English Transl.) 17 (1975) 545.
- 75S Sandercock, J. R.: Festkörperprobleme XV (1975) 183.
- 75W Weast, R. C. (ed.): Handbook of Chemistry and Physics, CRC Press, Cleveland 1975.
- 76D Dorner, B., Ghosh, R. E., Harbeke, G.: Phys. Status Solidi (b) 73 (1976).
- 76G Grisel, A., Schmid, Ph.: Phys. Status Solidi (b) 73 (1976) 587.
- 76L Lucovsky, G., White, R. M., Liang, W. Y., Zallen, R., Schmid, Ph.: Solid State Commun. 18 (1976) 811.
- 76M Minder, R., Ottaviani, G., Canali, C.: J. Phys. Chem. Solids 37 (1976) 417.
- 77B Beaumont, J. H., Bourdillon, A. J., Bordas, J.: J. Phys. C 10 (1977) 761.
- 77L Lucovsky, G., White, R. M.: Nuovo Cimento, Soc. Ital. Fis. B 38 (1977) 290.
- 78B Bloch, P. D., Hodby, J. W., Jenkins, T. E., Stacey, D. W., Lang, G., Levy, F., Schwab, C.: J. Phys. C 11 (1978) 4997.
- 79S Sears, W. M., Klein, M. L., Morrison, J. A.: Phys. Rev. B 19 (1979) 2305.

Figures to 24.4

Fig. 24.0.1

PbI_2 . Three-dimensional empirical pseudopotential method band structure; single group notation [74S].

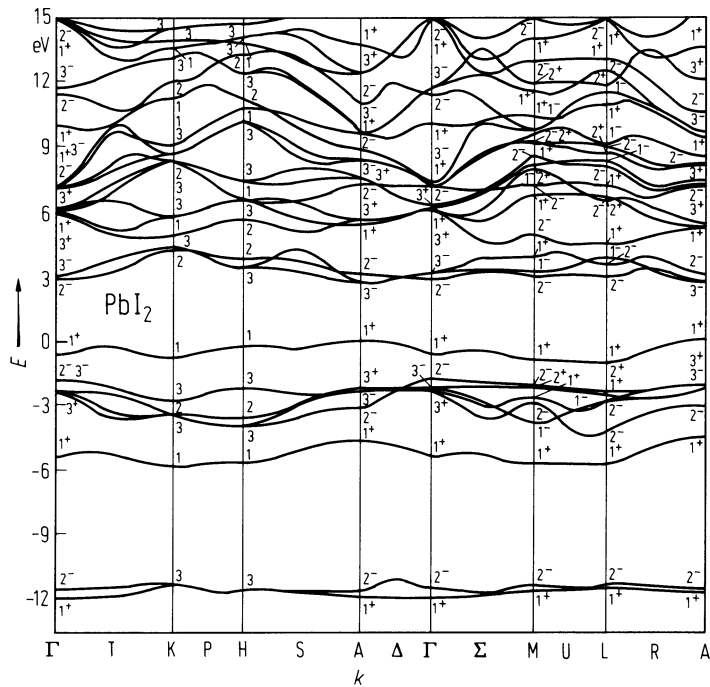


Fig. 24.4.1

PbI_2 . Lattice parameters vs. temperature; open circles: [79S]; data shifted to fit full circles [72S].

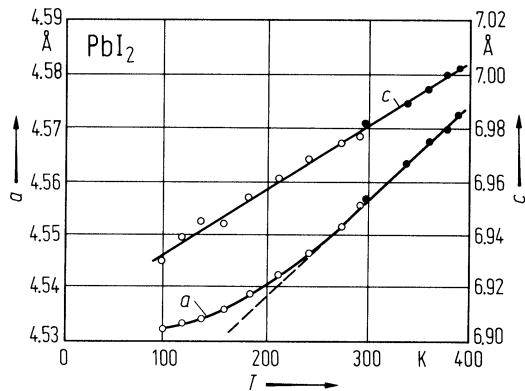


Fig. 24.4.2

PbI_2 . Phonon dispersion relations [76D]. Open circles: measured in longitudinal geometry, full circles: in transverse geometry in the hexagonal plane, triangles: in transverse geometry parallel to z .

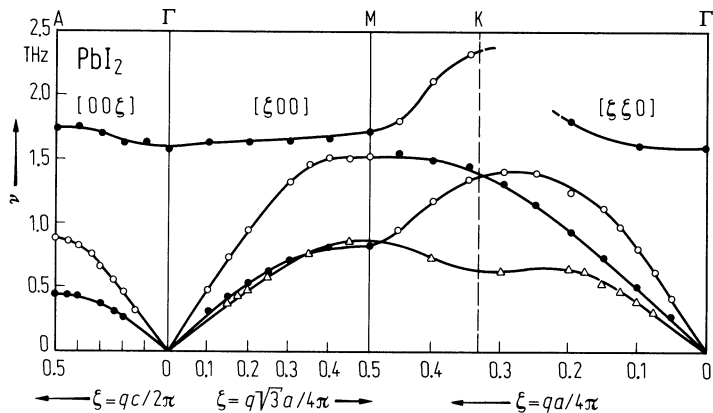


Fig. 24.4.3

PbI₂. Electron mobility in two 2H-samples vs. temperature (μ_M : magnetoconductivity mobility, μ_H : Hall mobility, μ_{dr} : drift mobility) [78B].

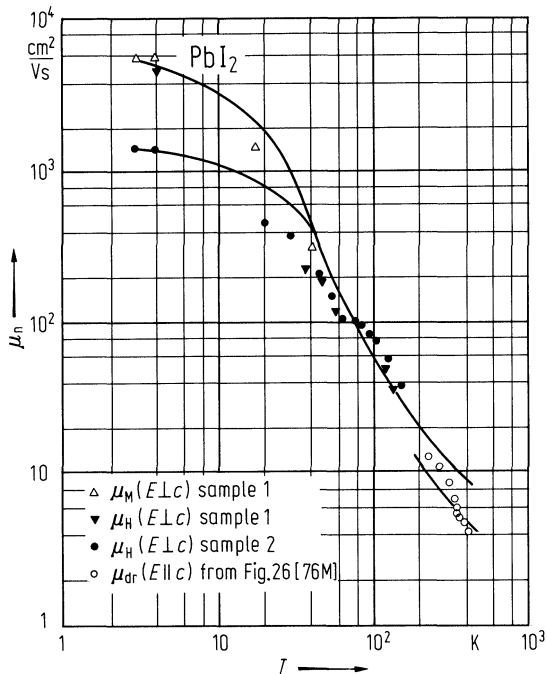


Fig. 24.4.4

PbI_2 . Reflectance (a) and absorption coefficient (b) derived from reflectance by Kramers-Kronig analysis vs. photon energy at 4.5 K (solid line) and 77 K (dashed line) [69G].

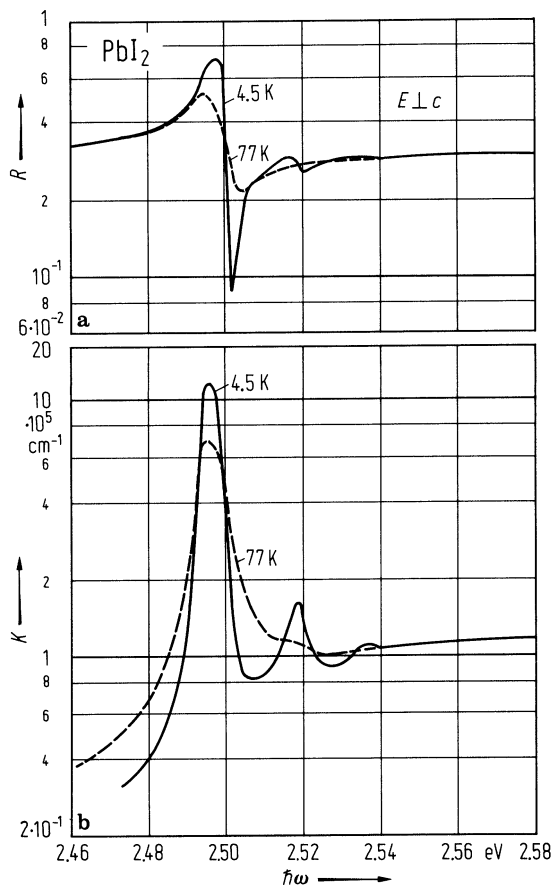
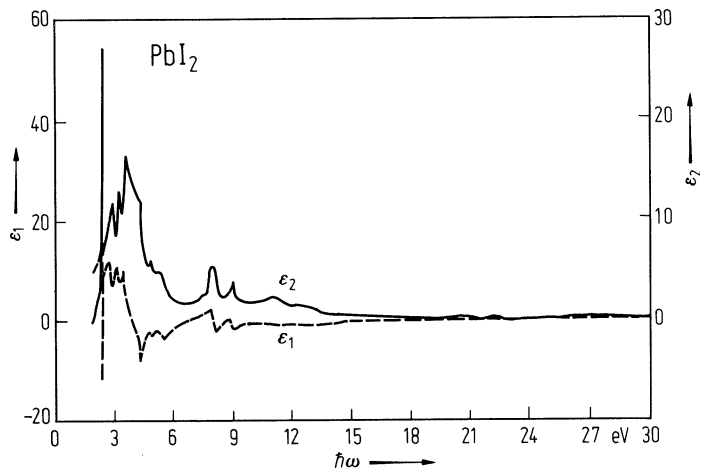


Fig. 24.4.5

PbI₂. Real (dashed line) and imaginary (solid line) parts of the dielectric constant vs. photon energy at 77 K [77B].



25 V_X-VI_Y compounds

25.0 Crystal structure and electronic structure

25.0.1 V₂VI₃ compounds

As₂O₃ : There exists a low temperature form (cubic arsenolite) and monoclinic high-temperature forms (claudetite I and claudetite II):

cubic arsenolite : Molecular structure; 16 molecules/unit cell; space group $O_h^7 - Fd3m$ [64W]. The As₄O₆ molecules themselves consist of an octahedron of oxygen atoms containing a tetrahedron of arsenic atoms; the arsenic atoms occupy four of the octahedral faces (Fig. 25.0.1).

claudetite I, claudetite II : The mineral claudetite is built up of two continuous spiral layers in the form of the letter S (Fig. 25.0.2). They account for the excellent cleavage observed in the [010] direction. The interatomic distances are the same as in arsenolite [62B]. As₂O₃ claudetite I: Monoclinic, space group $C_{2h}^5 - P2_1/n$, $Z = 4$ [76H]. As₂O₃ claudetite II: Structure: monoclinic as claudetite I, but less compressed layers.

As₂S₃, As₂Se₃ : Orpiment structure, monoclinic, space group $C_{2h}^5 - P2_1/n$, $Z = 4$. Each As atom is covalently bound to three S atoms in a triangular pyramidal unit. Each S atom is shared by two As atoms. The van der Waals bonds between layers are weak and the crystals cleave in a plane containing the *a* and *c* axis (Fig. 25.0.3).

Band structure of As₂Se₃: Fig. 25.0.4.

As₂Te₃ : Space group $C_{2h}^3 - C2/m$, 4 molecules/unit cell (Fig.25.0.5).

Sb₂S₃, Sb₂Se₃, Bi₂S₃ : The compounds are nearly isomorphous. The lattice is orthorhombic. There are four molecules per unit cell, i.e. 20 atoms in the positions $\pm (u, v, 1/4; 1/2-u, v+1/2, 1/4)$.

The structure of Sb₂S₃ consists of two infinite ribbons (Sb₄S₆)_n along the *c* axis, which are weakly bound in the *b* direction, the shortest interatomic distances between the ribbons in *b* direction are about 1.5 times larger than those in the ribbon. This leads to easy cleavage in the (010) -plane (Fig.25.0.6).

Band structure of Sb₂S₃: Fig. 25.0.7.

Sb₂Te₃, Bi₂Se₃, Bi₂Te₃ : Tetradymite group: the name tetradymite denotes to the mineral Bi₂Te₂S which has essentially the same crystal structure as the compounds Bi₂Te₃, Bi₂Se₃, Sb₂Te₃. Tetradymite (Bi₂Te₂S) structure: trigonal, space group $D_{3d}^5 - R(-3)m$, $Z = 1(3)$ [76H].

Brillouin zone: Fig. 25.0.8, *band structure* of Bi₂Te₃: Fig. 25.0.9.

Bi₂O₃ : Bi₂O₃ exists in several polymorphic forms at RT, the most important being monoclinic α - and tetragonal β -Bi₂O₃ (γ -Bi₂O₃ only exists in an impurity-stabilized form).

α -Bi₂O₃: The structure is built up of equidistant layers parallel to the *yz*-plane. Every second layer consists of Bi atoms. Monoclinic, space group $C_{2h}^5 - P2_1/c$, 4 molecules/unit cell.

β -Bi₂O₃ [72A]: Tetragonal, space group $D_{2d}^4 - P(-4)2_1c$, 4 molecules/unit cell. The bismuth atoms are arranged in a fcc subcell with $a \approx 5.5$ Å. The coordination around bismuth is four-fold, and the coordination polyhedron can be described by a distorted trigonal bipyramid where one of the basal corners is occupied by the inert electron pair (Fig. 25.0.10).

25.0.2 Realgar (As₄S₄)

Molecule crystal, space group $C_{2h}^5 - P2_1/n$, 4 molecules/unit cell. The As₄S₄ molecule is described in the cradle model: four sulfur and four arsenic atoms, covalently bound, form a square and a tetrahedron, respectively. The sulfur square cuts through the arsenic tetrahedron in the middle [72M], Fig. 25.0.11. Two modifications α and β are reported and confirmed [72B, 79S].

References to 25.0

- 62B Becker, K. A., Plieth, K., Stranski, I. N.: Progress in Inorganic Chemistry 4, ed. by F. A. Cotton, J. Wiley, New York, 1962, 1...72.
- 63C Carron, G. J.: Acta Crystallogr. 16 (1963) 338.
- 64W Wyckoff, R. W. G.: Crystal Structures 2, J. Wiley and Sons, New York, 1964.
- 68B Borghese, F., Donato, F.: Nuovo Cimento 53B (1968) 283.
- 70C Caywood, L. P., Jr., Miller, G. R.: Phys. Rev. B 2 (1970) 3209.
- 71K Khasabov, A. G., Nikiforov, I. Ya.: Sov. Phys. Crystallogr. 16 (1971) 28.
- 72A Aurivilius, B., Malmros, G.: Transactions of the Royal Institute of Techn. Stockholm, Sweden Nr. 291 (1972) 545.
- 72B Bastow, T. J., Whitfield, H. J.: Solid State Commun. 11 (1972) 1015.
- 72M Mullen, D. J. E., Nowacki, W.: Z. Kristallogr. 136 (1972) 48.
- 73C Cornet, J., Rossier, D.: J. Non-Cryst. Solids 12 (1973) 85.
- 73P Petzelt, J., Grigas, J.: Ferroelectrics 5 (1973) 59.
- 75W Wells, A. F.: Structural Anorganic Chemistry 4th Ed., Clarendon Press, Oxford, 1975.
- 76H Hulliger, F.: Structural Chemistry of Layer-Type Phases, D. Reidel Publishing Company, Dordrecht, Holland, 1976.
- 78A Althaus, H. L., Weiser, G., Nagel, S.: Phys. Status Solidi (b) 87 (1978) 117.
- 79S Slade, M. L., Zallen, R.: Solid State Commun. 30 (1979) 357.
- 79W Weiser, G. in: Proc. Int. Conf. Phys. Selenium and Tellurium, Königstein, 1979; E. Gerlach and P. Grosse, eds.; Springer-Verlag Berlin, Heidelberg, New York, 1979.

Figures to 25.0

Fig. 25.0.1

As_4O_6 -molecule; full circles As, open circles O [75W].

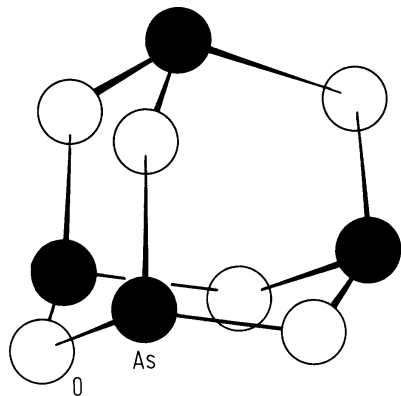


Fig. 25.0.2

The layer-type modification of As_2O_3 . Above: claudetite I; As atoms dotted. Below: claudetite II; right: projection along $[010]$ perpendicular to the layers, left: one layer projected onto the (a, b) -plane [76H].

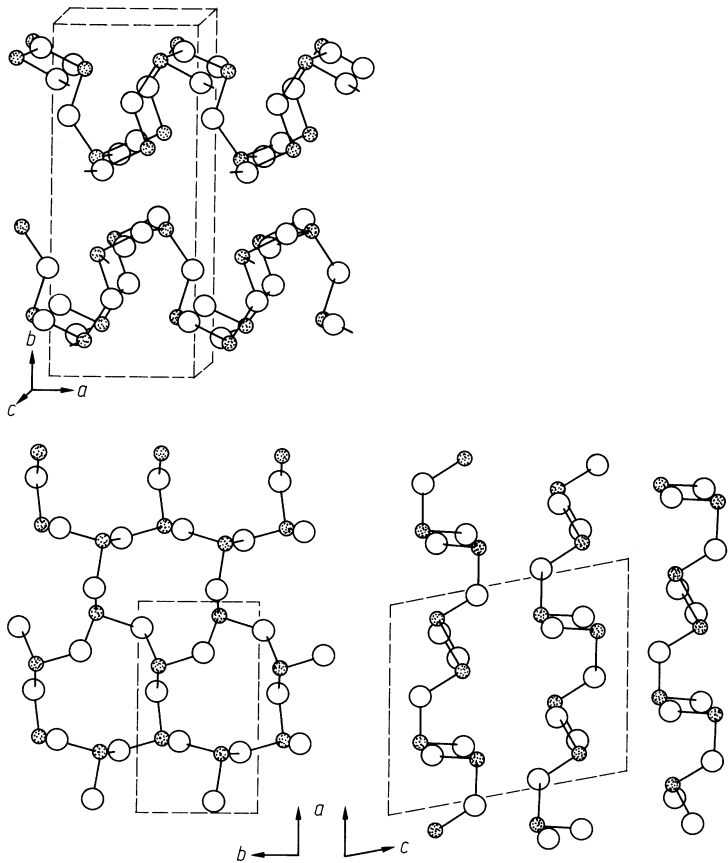


Fig. 25.0.3

Two projections of the structure of orpiment As_2S_3 . Arsenic atoms dotted. The structure is isomorphous to As_2Se_3 [76H].

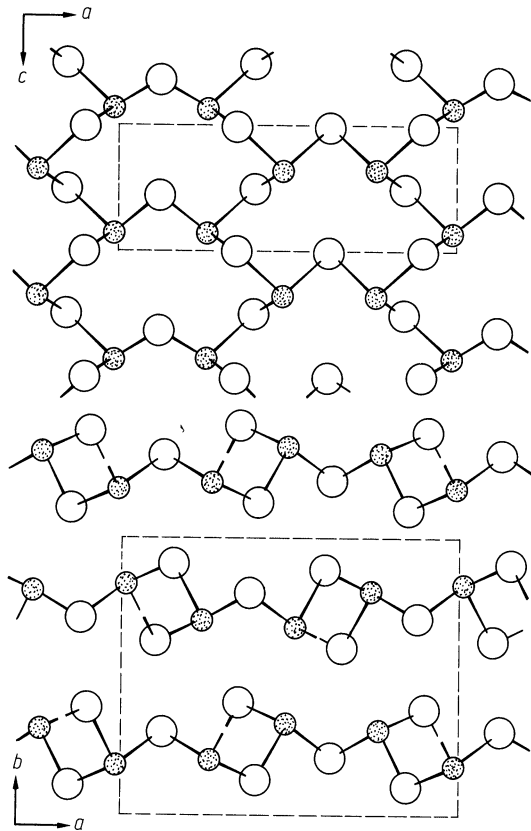


Fig. 25.0.4

As₂Se₃. Band structure calculated by LCAO method. Σ - and A-axes $\parallel a$, Λ -, G- and H-axes $\parallel c$, Δ - and B-axes $\parallel b$, the stacking axis of the layers [78A, 79W].

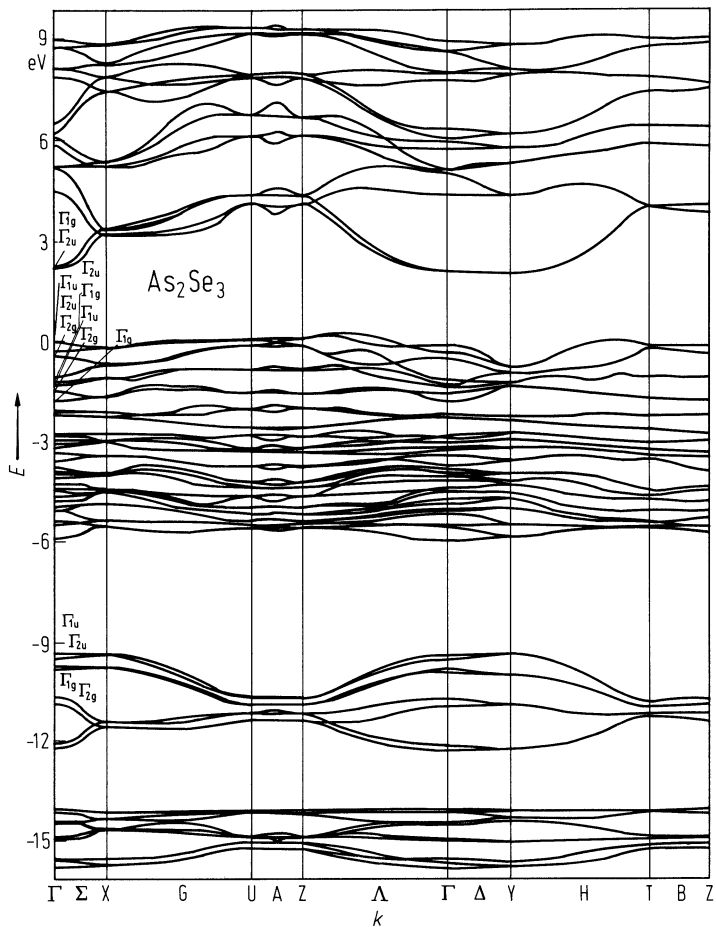


Fig. 25.0.5

Schematic representation of the monoclinic structure of As_2Te_3 . Crystallographic data from [63C] were used. Crystalline As_2Te_3 is composed of complex chains parallel to the binary axis of the monoclinic cell. A portion of an individual chain is shown on the figure. All tellurium atoms are threefold-coordinated, whereas arsenic atoms are either tetrahedrally (T-sites) or octahedrally (O-sites) coordinated [73C].

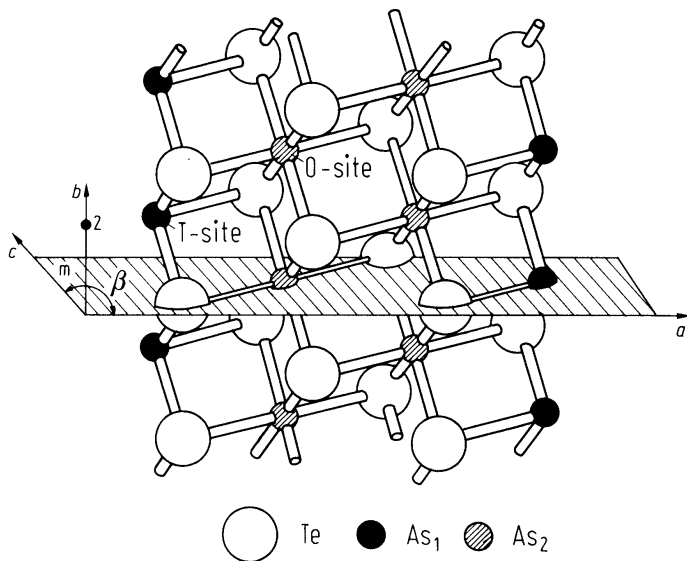


Fig. 25.0.6

Sb_2S_3 -type structure; projection of one ribbon in the (010) plane along the $[0(-1)0]$ direction [73P].

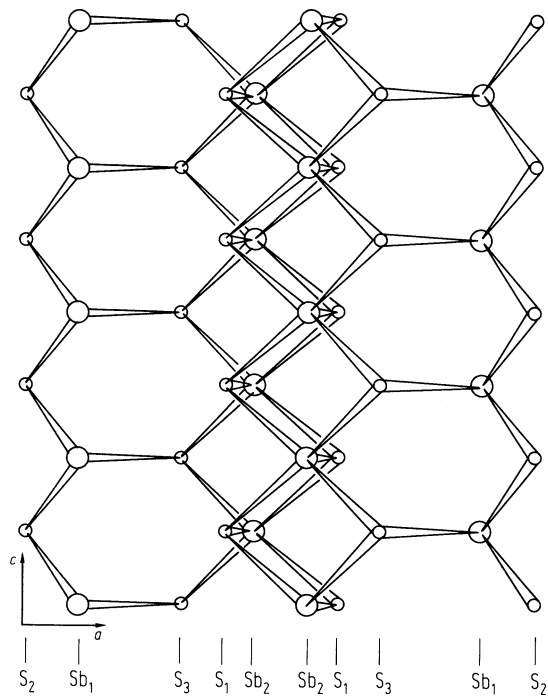


Fig. 25.0.7

Sb_2S_3 . Band structure along the Δ -axis. The solid lines correspond to the Δ_1 representation and the dashed lines correspond to Δ_2 [71K]. 1 Ry = 13.6 eV.

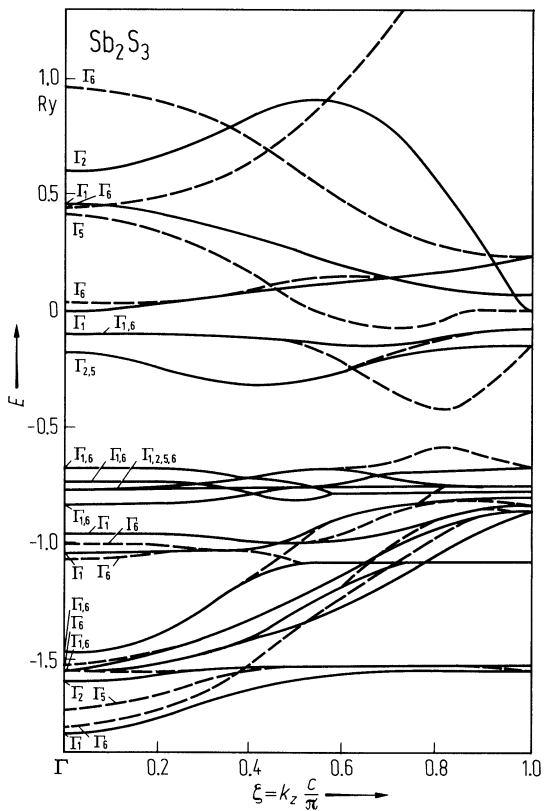
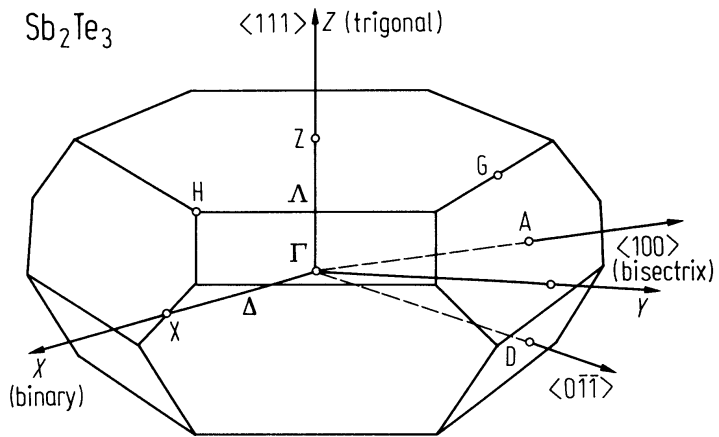


Fig. 25.0.8

Sb_2Te_3 . Brillouin zone [70C].



Bi₂Te₃. Empirical pseudopotential band structure with the inclusion of spin-orbit coupling [68B]. 1 Ry = 13.6 eV.

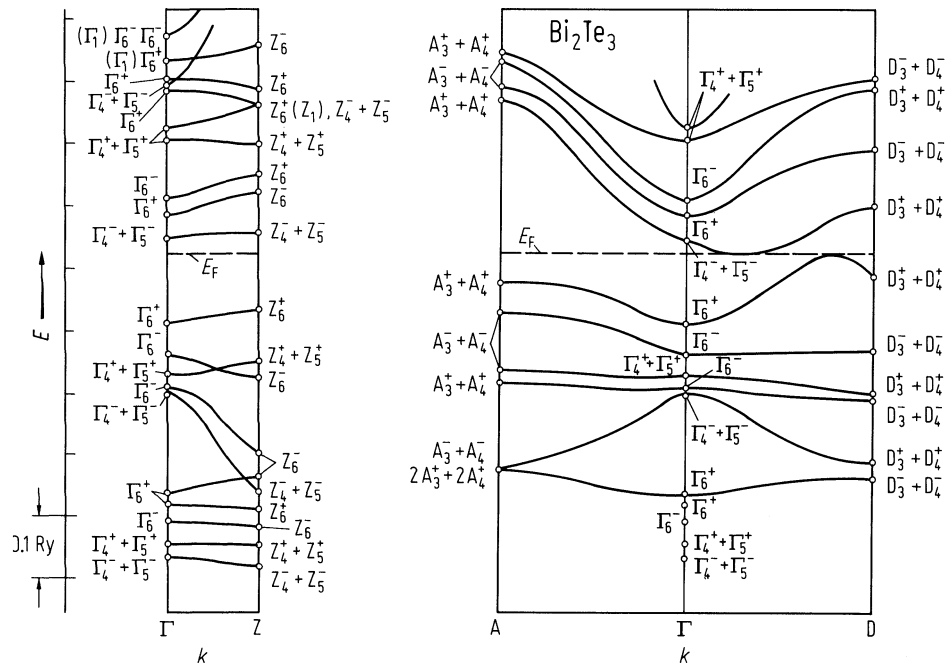


Fig. 25.0.10

Picture of a BiO_4 polyhedron showing the trigonal bipyramid (e: inert electron pair); angle $\text{O}_1\text{--Bi--O}_2$: 115° ; angle $\text{O}_3\text{--Bi--O}_4$: 172° . Bi–O bond lengths: $1.96\text{\AA}\dots 2.45\text{\AA}$ [72A].

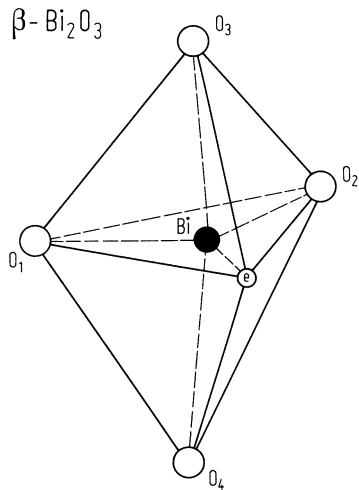
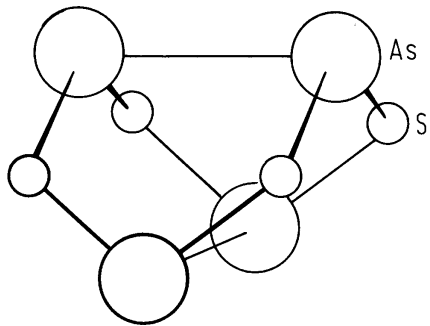


Fig. 25.0.11

The "cradle-type" As_4S_4 molecule [75W].



25.1 Arsenic oxide (As₂O₃)

Physical properties

Only some optical properties have been investigated.

peak energy of valence states (binding energy)

$E_v - E$	3.1, 5.3, 7.6, 13.4, 23.0 eV	(arsenolite) , from photoemission	77K
-----------	------------------------------	-----------------------------------	-----

refractive index

n	1.755	at $\lambda = 589.3$ nm	(arsenolite)	67D
-----	-------	-------------------------	--------------	-----

lattice parameters

arsenolite: $a = 11.0745$ Å (at 300 K); $u = 0.885$, $v = 0.235$

claudetite I: $a = 5.25$ Å, $b = 12.90$ Å, $c = 4.53$ Å, $\beta = 93.9^\circ$

claudeteie II: $a = 7.390$ Å, $b = 4.645$ Å, $c = 9.115$ Å, $\beta = 78.3^\circ$

heat capacity

C_p	(35.04 + 203.48 $\cdot 10^{-3} T)$ J mol ⁻¹ K ⁻¹	$T = 273$ K...548 K	(arsenolite and claudetite)	73B
-------	---	---------------------	-----------------------------	-----

density

d	3.89 g/cm ³	$T = 300$ K	(arsenolite)	62B
	4.23 g/cm ³	$T = 300$ K	(claudetite I)	
	4.02 g/cm ³	$T = 300$ K	(claudetite II)	

melting temperature

T_m	551 K	under pressure	(arsenolite)	73B
	585 K	under pressure	(claudetite)	62B

References to 25.1

- 62B Becker, K. A., Plieth, K., Stranski, I. N.: Progress in Inorganic Chemistry 4, ed. by F. A. Cotten, J. Wiley, New York, 1962, 1...72.
- 67D D'Ans-Lax: Taschenbuch flir Chemiker und Physiker I, Berlin, Heidelberg, New York: Springer, 1967.
- 73B Barin, I., Knacke, O.: Thermochemical properties of inorganic substances, Berlin, Heidelberg, New York: Springer, 1973.
- 77K Kosakov, A., Neumann, H., Leonhardt, G.: Phys. Lett. 62A (1977) 95.

25.2 Arsenic sulfide (As2S3)

Electronic properties

The electronic band structures of the isomorphous compounds As2S3 and As2Se3 are very similar. The energy band structure of As2S3 can be roughly derived from that of As2Se3 by rigidly separating valence and conduction band by an additional 0.7 eV [76Z]. The direct gap occurs at the Γ-point.

energy gaps

$E_{g,dir}$	2.6 eV	$T = 300\text{ K}, E \parallel c;$	optical gap	76Z
		$E \parallel a$		
$E_{g,th}$	2.78 eV	extrapolated to $T = 0\text{ K}$	thermal gap	
$dE_{g,dir}/dT$	$-7 \cdot 10^{-4}\text{ eV K}^{-1}$	$T = 290...77\text{ K}$	from optical absorption	67E
	$-1.6 \cdot 10^{-3}\text{ eV K}^{-1}$	$T = 400...300\text{ K}$	from optical absorption with unpolarized light; below 200 K no temperature dependence	74Z

Lattice properties

lattice parameters

a	11.475 Å			76H
b	9.577 Å,			
c	4.256 Å			
β	90°41'			

heat capacity

C_p	$(105.72 + 3.65 \cdot 10^{-2}T)\text{ J K}^{-1}\text{ mol}^{-1}$	$T = 298...585\text{ K}$		74M
-------	--	--------------------------	--	-----

melting temperature

T_m	585 K			74M
-------	-------	--	--	-----

Transport properties

mobility, resistivity

$\mu_{dr,n}$	1 cm ² /V s	$T = 207...465\text{ K}$	electron drift mobility independent of temperature, transient photo- conductivity techniques; for hole mobility, see Fig. 25.2.1	60K, 77S
		$\mu \parallel b$		
ρ_{\perp}	$3 \cdot 10^{15}\text{ }\Omega\text{ cm}$		dark resistivity perpendicular to the layers	74B

Optical properties

Reflectivity survey spectrum, Fig. 25.2.2, refractive index, Fig. 25.2.3.

dielectric constants

$\epsilon(\infty)$	8.8	$E \parallel a$	deduced from reflectivity and capacitance measurements of different authors	76Z
	7.0	$E \parallel b$		
	5.7	$E \parallel c$		
$\epsilon(0)$	12.1	$E \parallel a$		
	10.7	$E \parallel b$		
	5.9	$E \parallel c$		

References to 25.2

- 60K Kepler, R. G.: Phys. Rev. 119 (1960) 1226.
- 67E Evans, B. L., Young, P. A.: Proc. Roy. Soc. A 297 (1967) 230.
- 74B Blossey, D. F., Zallen, R.: Phys. Rev. B 9 (1974) 4306.
- 74M Mills, K. C.: Thermodynamic Data for Inorganic Sulphides, Selenides and Tellurides, Butterworth, London, 1974.
- 74Z Zarkis, J. R., Fritzsche, H.: Phys. Status Solidi (b) 64 (1974) 123.
- 76H Hulliger, F.: Structural Chemistry of Layer-Type Phases, D. Reidel Publishing Company, Dordrecht, Holland, 1976.
- 76Z Zallen, R., Blossey, D. F.: Opt Prop., electr. struct. and photocond. of arsenic chalc. layer cryst.; D. Reidel Publishing Company, Dordrecht, Holland, 1976.
- 77S Schein, L. B.: Phys. Rev. B 15 (1977) 1024.

Figures to 25.2

Fig. 25.2.1

As_2S_3 . Semilogarithmic plot of mobility vs. T^{-1} showing that the hole mobility is activated and the magnitude of the mobility varies among samples [77S]. $\mu = \mu_0 e^{-E_A/kT}$, $\mu \parallel b$ (perpendicular to layers).

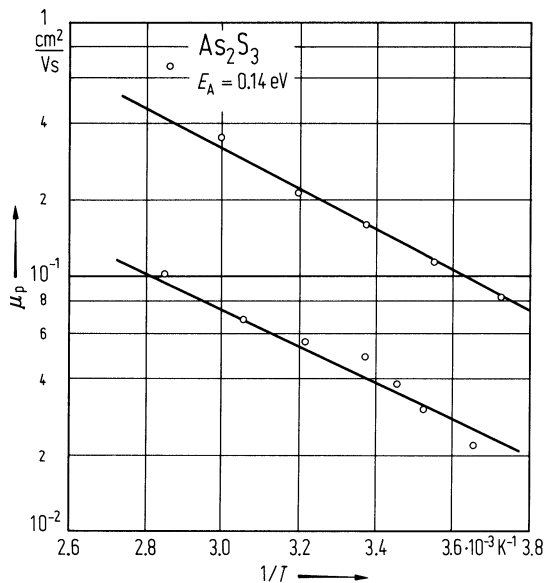


Fig. 25.2.2

As_2S_3 . Survey spectrum showing an overview of the optical properties of crystalline As_2S_3 from the far infrared to the far ultraviolet. The reflectivity for the in-plane polarization $E \parallel c$ has been composed over a four-decade range of photon energies [76Z]. $\hbar\nu_p$: plasma energy, E_g : energy gap.

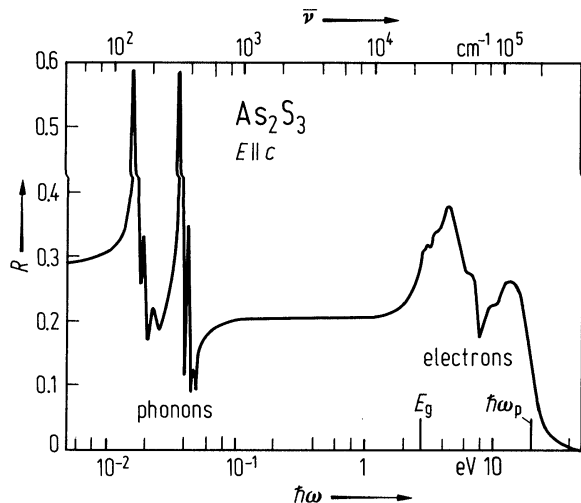
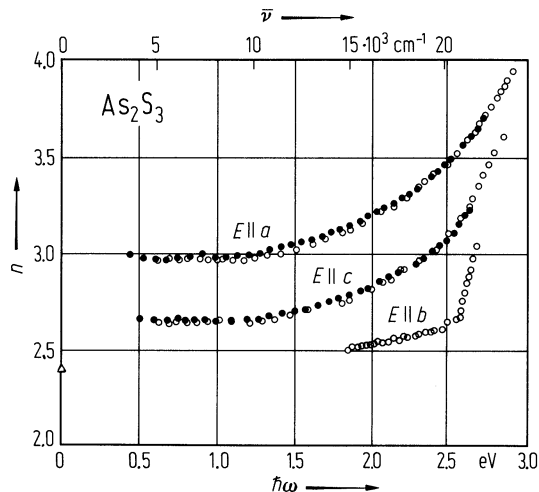


Fig. 25.2.3

As_2S_3 . Refractive indices vs. photon energy in the transparent regime for the principal optical polarizations. The open circles shown for all three polarizations are from [67E], full circles are room temperature results for the two in-plane polarizations, and the open triangle near the zero-frequency axis is from a capacitance measurement for the plane normal polarization [76Z].



25.3 Arsenic selenide (As2Se3)

Electronic properties

band structure : Fig. 25.0.4.

The energy band structures of the isomorphous compounds As2S3 and As2Se3 are very similar. The energy band structure of As2S3 can be roughly derived from that of As2Se3 by rigidly separating valence and conduction band by an additional 0.7 eV [76Z]. The direct gap occurs at the Γ-point.

energy gaps

$E_{g,dir}$	2.15 eV	$T = 10\text{ K}, E \parallel a; E \parallel c$	(optical) direct gap at Γ ; from reflectivity (further indirect transitions at a threshold of 2.0 eV)	78A
$E_{g,th}$	1.85 eV 2.01 eV	$T = 300\text{ K}$ extrapolated to $T = 0\text{ K}$	thermal gap	76Z 76Z
$dE_{g,dir}/dT$	$-7.9 \cdot 10^{-4}\text{ eV K}^{-1}$	$T = 80...274\text{ K}$	from optical absorption with unpolarized light	70G

spin-orbit splitting energies

$\Delta(\Gamma)$	15 meV	in conduction band	80A
$\Delta(\Gamma)$	40 meV	in both valence bands	80A

Lattice parameters

lattice parameters and atomic positions [76H]: all atoms in 4(e): $\pm (x, y, z; 1/2-x, y+1/2, 1/2-z)$

$a = 12.053\text{ \AA}, b = 9.890\text{ \AA}, c = 4.277\text{ \AA}, \beta = 90^{\circ}28'$

	x	y	z
As ₁	0.1483	0.1977	0.2637
As ₂	0.8512	0.3180	0.4847
Se ₁	-0.0699	0.1143	0.3987
Se ₂	0.3720	0.4092	0.3539
Se ₃	0.3468	0.3037	0.1153

heat capacity

C_p	$(95.88 + 8.58 \cdot 10^{-2}T)\text{ J K}^{-1}\text{ mol}^{-1}$	$T = 298\text{ K}...650\text{ K}$	74M
-------	---	-----------------------------------	-----

melting temperature

T_m	650 K	74M
-------	-------	-----

Transport properties

resistivity

ρ	$10^{12}\text{ }\Omega\text{ cm}$	$T = 300\text{ K}, \parallel b$	perpendicular to the layers	71A
--------	-----------------------------------	---------------------------------	-----------------------------	-----

mobility

$\mu_{dr,n}$	$20...80\text{ cm}^2/\text{V s}$	$T = 300\text{ K}, \parallel b$	time-of-flight technique	77M
--------------	----------------------------------	---------------------------------	--------------------------	-----

temperature dependence of conductivity and mobility: Figs. 25.3.1, 25.3.2.

Optical properties

Optical constants, absorption, dielectric function: Figs. 25.3.3...5.

dielectric constants

$\varepsilon(0)$	12.4	$E \parallel c$	from oscillator fit to reflectivity	71Z
$\varepsilon(\infty)$	8.8	$E \parallel c$		
$\varepsilon(0)$	13.9	$E \parallel a$		
$\varepsilon(\infty)$	10.5	$E \parallel a$		

References to 25.3

- 70G Grant, A. J., Yoffe, A. D.: Solid State Commun. 8 (1970) 1919.
- 71A Adler, D.: Amorphous semiconductors, CRC Press, Cleveland, Ohio, USA, 1971.
- 71Z Zallen, R., Slade, M. L., Ward, A. T.: Phys. Rev. B 3 (1971) 4257.
- 74M Mills, K. C.: Thermodynamic Data for Inorganic Sulphides, Selenides and Tellurides, Butterworth, London, 1974.
- 76B Bordas, J.: Some aspects of modul. spectr. in layer materials; D. Reidel Publishing Company, Dordrecht, Holland, 1976.
- 76H Hulliger, F.: Structural Chemistry of Layer-Type Phases, D. Reidel Publishing Company, Dordrecht, Holland, 1976.
- 76Z Zallen, R., Blossey, D. F.: Opt Prop., electr. struct. and photocond. of arsenic chalc. layer cryst.; D. Reidel Publishing Company, Dordrecht, Holland, 1976.
- 77M Marshall, J. M.: J. Phys. C 10 (1977) 1283.
- 78A Althaus, H. L., Weiser, G., Nagel, S.: Phys. Status Solidi (b) 87 (1978) 117.
- 79W Weiser, G. in: Proc. Int. Conf. Phys. Selenium and Tellurium, Königstein, 1979; E. Gerlach and P. Grosse, eds.; Springer-Verlag Berlin, Heidelberg, New York, 1979.
- 80A Althaus, H. L., Weiser, G.: Phys. Status Solidi (b) 99 (1980) 537.

Figures to 25.3

Fig. 25.0.4

As₂Se₃. Band structure calculated by LCAO method. Σ - and A-axes $\parallel a$, Λ -, G- and H-axes $\parallel c$, Δ - and B-axes $\parallel b$, the stacking axis of the layers [78A, 79W].

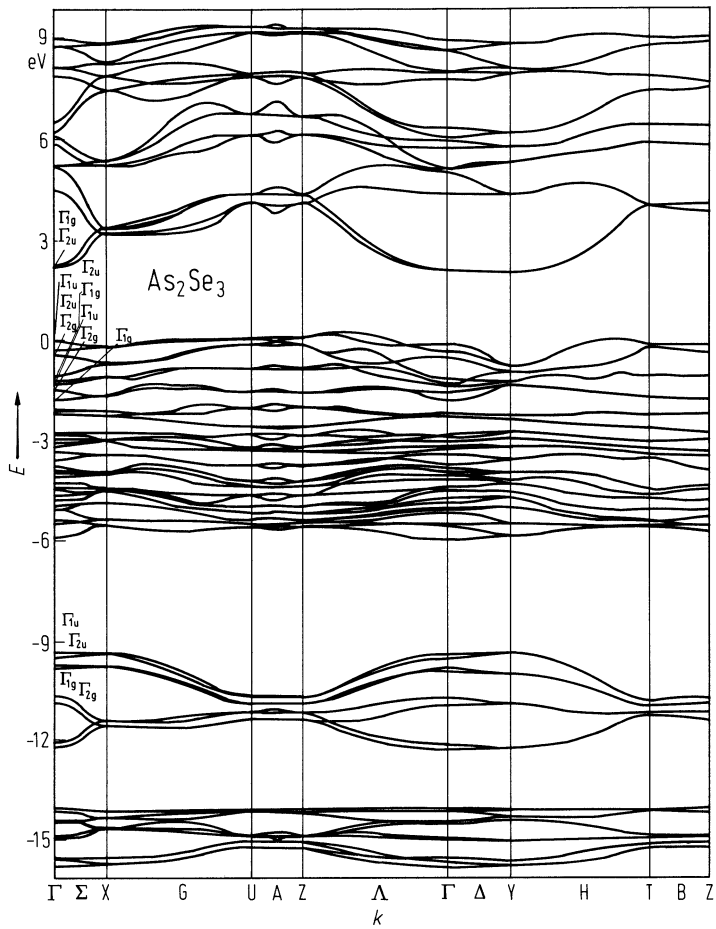


Fig. 25.3.1

As_2Se_3 . Typical data for the temperature dependence of the low-field electrical conductivity ($\sigma \parallel b$) [77M].

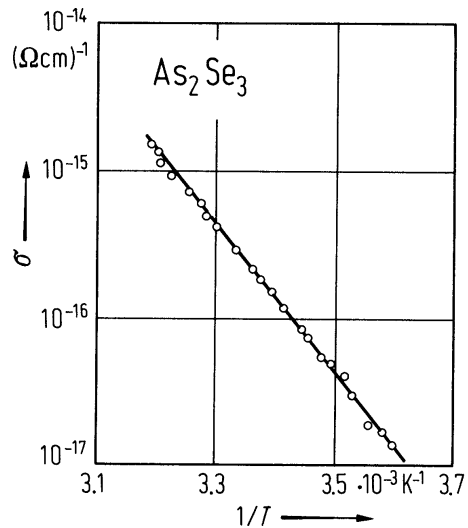


Fig. 25.3.2

As_2Se_3 . Temperature dependence of the electron drift mobility ($\mu \parallel b$) in various crystals at low applied electric fields [77M].

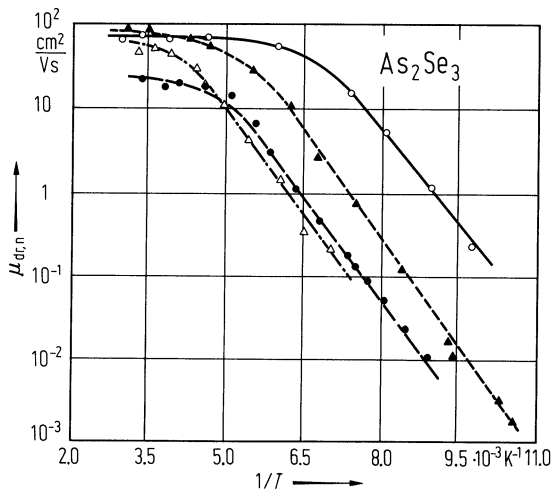


Fig. 25.3.3

As_2Se_3 . Optical constants vs. wavenumber [71Z].

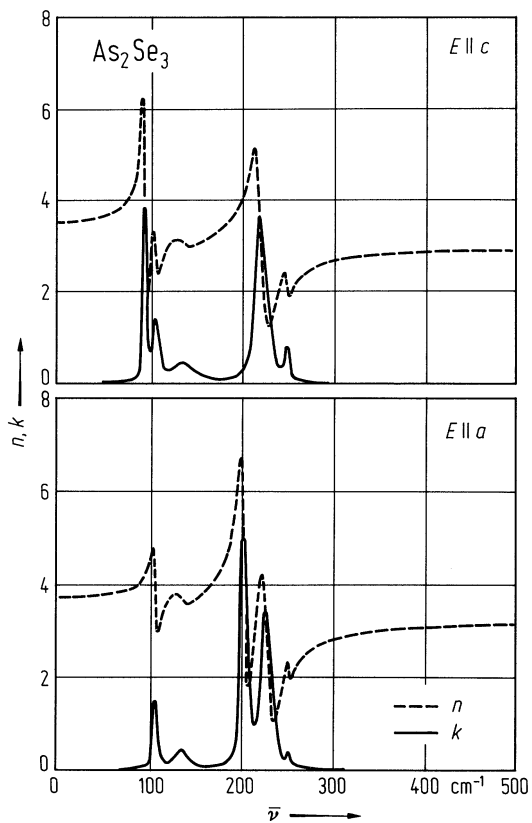


Fig. 25.3.4

As_2Se_3 . Absorption coefficient vs. photon energy at 10 K for $E \perp c$ (full line) and $E \parallel c$ (dashed line) [76B].

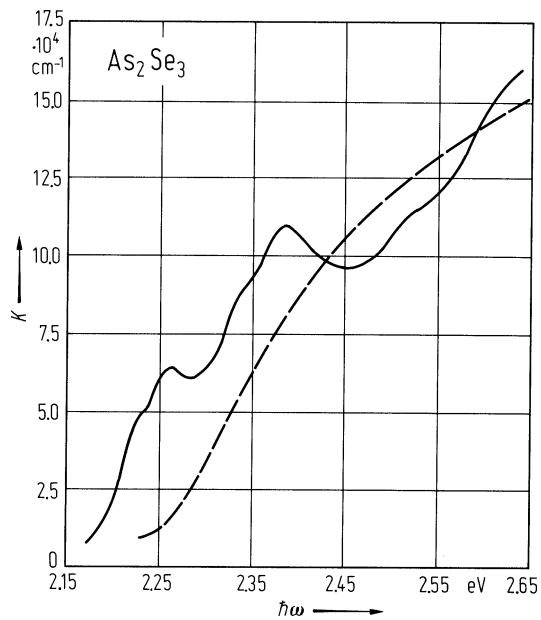
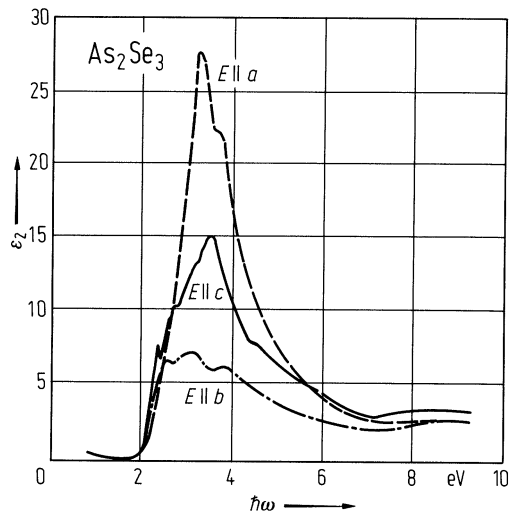


Fig. 25.3.5

As_2Se_3 . Imaginary part of the dielectric function vs. photon energy [78A].



25.4 Arsenic telluride (As₂Te₃)

lattice properties

$a = 14.339 \text{ \AA}, b = 4.006 \text{ \AA}, c = 9.873 \text{ \AA}, \beta = 95.0^\circ [76H]$			
T_m	648 K		74M
C_p	$(135.28 + 4.44 \cdot 10^{-2} T - 1.86 \cdot 10^6 T^{-2})$ $\text{J K}^{-1} \text{ mol}^{-1}$	$T = 298 \dots 648 \text{ K}$	74M

electronic and transport properties

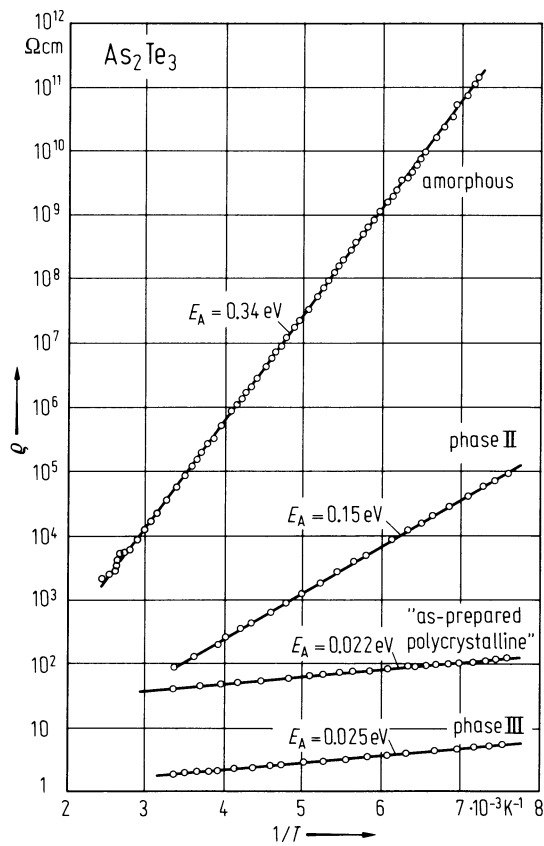
E_g	0.9 eV	$T = 510 \dots 570 \text{ K}$	from electrical conductivity, polycrystalline, monoclinic As ₂ Te ₃	77P
m_n	0.36 m_0		thermoelectric power	57H
m_p	0.50 m_0			
electrical resistivity: Fig. 25.4.1.				
μ_n	170 cm ² /V s		monoclinic; polycrystalline samples $n = 1.8 \cdot 10^{18} \text{ cm}^{-3}$	69A
μ_p	80 cm ² /V s		monoclinic; polycrystalline samples $p = 4 \cdot 10^{19} \text{ cm}^{-3}$	69A
κ	0.025 W cm ⁻¹ K ⁻¹		thermal conductivity; monoclinic; polycrystalline sample	69A

References to 25.4

57H Harman, T. C., Paris, B., Miller, S. E., Goering, H. L.: J. Phys. Chem. Solids 2 (1957) 181.
69A Abrikosov, N. Kh., Bankina, V. F., Poretskaya, L. V., Shelimova, L. E., Skudnova, E. V.:
Semiconducting II-VI, IV-VI and V-VI-compounds; Plenum Press, N. Y., 1969.
74M Mills, K. C.: Thermodynamic Data for Inorganic Sulphides, Selenides and Tellurides, Butterworth,
London, 1974.
76H Hulliger, F.: Structural Chemistry of Layer-Type Phases, D. Reidel Publishing Company, Dordrecht,
Holland, 1976.
77P Platakis, N. S.: J. Non-Cryst. Solids 24 (1977) 365.

Fig. 25.4.1

As_2Te_3 . Electrical resistivity of As_2Te_3 vs. $1/T$ in the temperature range 135...400 K [77P]. Activation energies are indicated.



25.5 Antimony sulfide (Sb2S3)

Electronic properties

Sb2S3 is a weakly polar semiconducting ferroelectric which exhibits phase transitions associated with small structural changes in the coordination sphere of the Sb atoms. Moreover it is a good photoconductor.

band structure : Fig. 25.0.7.

energy gap

$E_{g,dir}$	1.88 eV	$T = 300\text{ K}, E \parallel a$	from reflectivity (optical gap)	69S2
$dE_{g,dir}/dT$	$-9 \cdot 10^{-4}\text{ eV/K}$	$T < 311\text{ K}$	values depend on stoichiometry of the samples, see Fig. 25.5.1	77G

Lattice properties

lattice parameters

a	11.299 Å			64W
b	11.310 Å			
c	3.8389 Å			

sound velocity

v_{\parallel}	$2.71 \cdot 10^5 (\pm 5\%) \text{ cm s}^{-1}$	sound velocity along the c -axis	72G
v_{\perp}	$1.6 \cdot 10^5 (\pm 5\%) \text{ cm s}^{-1}$	sound velocity perpendicular to the c -axis	

Debye temperature

Θ_D	310 K	$T = 80\text{ K}$	59G
------------	-------	-------------------	-----

heat capacity

C_p	$(101.91 + 6.06 \cdot 10^{-2} T) \text{ J mol}^{-1} \text{ K}^{-1}$	$T = 298 \dots 823\text{ K}$	74M
-------	---	------------------------------	-----

density

d	4.60 g cm^{-3}		74M
-----	--------------------------	--	-----

melting temperature

T_m	823 K		74M
-------	-------	--	-----

Transport properties

dc conductivity

$\sigma_{\parallel c}$	$3.3 \cdot 10^{-8} \Omega^{-1} \text{ cm}^{-1}$	$T = 300\text{ K}$	55I
$\sigma_{\perp c}$	$2 \cdot 10^{-9} \Omega^{-1} \text{ cm}^{-1}$		

temperature dependence of electrical conductivity : Fig. 25.5.2.

Optical properties

Reflectivity spectrum: Fig. 25.5.3.

refractive index

n	2.7...2.75	$\bar{\nu} = (2.5 \dots 7.5) \text{ cm}^{-1}, E \perp c$	62S
-----	------------	--	-----

dielectric constants

$\epsilon(0)_{\parallel}$	100...260	$T = 320 \text{ K}, E \parallel c$	at 10^3 Hz	68G
	180	$T = 300 \text{ K}, E \parallel c$	at 10^3 Hz	72G
$\epsilon(0)_{\perp}$	22	$T = 320 \text{ K}, E \perp c$	from reflectivity data	73P
	15	$T = 300 \text{ K}, E \perp c$	at 10^3 Hz	72G
$\epsilon(\infty)_{\parallel}$	9.5	$T = 320 \text{ K}, E \parallel c$		73P
$\epsilon(\infty)_{\perp}$	7.2	$T = 320 \text{ K}, E \perp c$		

For dielectric constant, see also Fig. 25.5.4.

References to 25.5

- 55I Ibuke, S., Yochimatsu, S.: J. Phys. Soc. Jpn. 10 (1955) 549.
- 59G Gul'tyaev, P. V., Petrov, A. V.: Sov. Phys.-Solid State 1 (1959) 330.
- 62S Skubenko, A. F., Lapshii, S. V.: Sov. Phys.-Solid State 4 (1962) 327.
- 64W Wyckoff, R. W. G.: Crystal Structures 2, J. Wiley and Sons, New York, 1964.
- 68G Grigas, I. P., Karpus, A. S.: Sov. Phys.-Solid State 9 (1968) 2265.
- 69S1 Shoemaker, G. E., Rayne, J. A., Ure Jr., R. W.: Phys. Rev. 185 (1969) 1046.
- 69S2 Shutov, S. D., Sobolev, V. V., Popov, Y. V., Shestatskii, S. N.: Phys. Status Solidi 31 (1969) K23.
- 71K Khasabov, A. G., Nikiforov, I. Ya.: Sov. Phys.Crystallogr. 16 (1971) 28.
- 72G Grigas, I. P., Kunigelis, V. F., Orlyukas, A. S., Samulionis, V. I.: Sov. Phys.Solid State 14 (1972) 796.
- 73P Petzelt, J., Grigas, J.: Ferroelectrics 5 (1973) 59.
- 74M Mills, K. C.: Thermodynamic Data for Inorganic Sulphides, Selenides and Tellurides, Butterworth, London, 1974.
- 77G G umann, A., Orliukas, A., Bohac, P.: Helv. Phys. Acta 59 (1977) 773.
- 78R Roy, B., Chakraborty, B. R., Bhattacharya, R., Dutta, A. K.: Solid State Commun. 25 (1978) 937.
- 79G Ghosh, C., Varma, B. P.: Solid State Commun. 31 (1979) 683.

Figures to 25.5

Fig. 25.0.7

Sb_2S_3 . Band structure along the Δ -axis. The solid lines correspond to the Δ_1 representation and the dashed lines correspond to Δ_2 [71K]. 1 Ry = 13.6 eV.

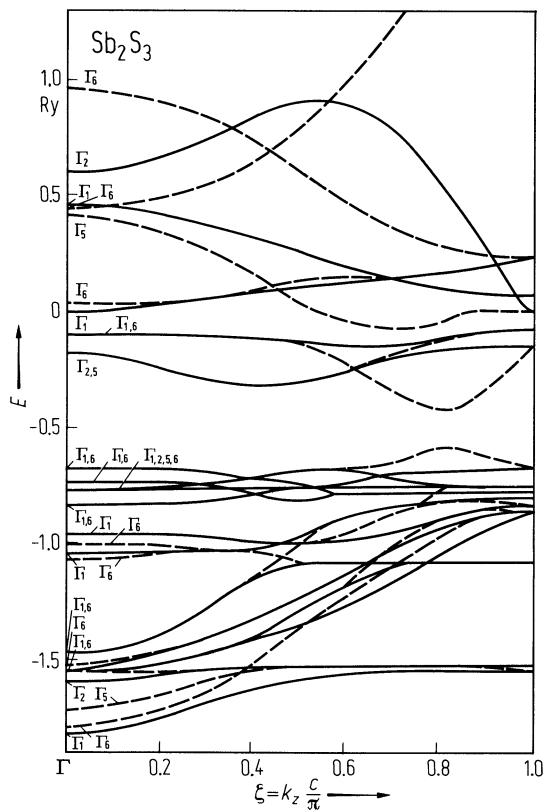


Fig. 25.5.1

Sb_2S_3 . Energy gap vs. temperature for different samples. 1: $\text{Sb}_{1.96}\text{S}_{3.04}$; 2: $\text{Sb}_{2.01}\text{S}_{2.99}$; 3: $\text{Sb}_{1.98}\text{S}_{3.02}$; 4: $\text{Sb}_{1.91}\text{S}_{3.09}$; 5: $\text{Sb}_{1.97}\text{S}_{3.03}$ [77G].

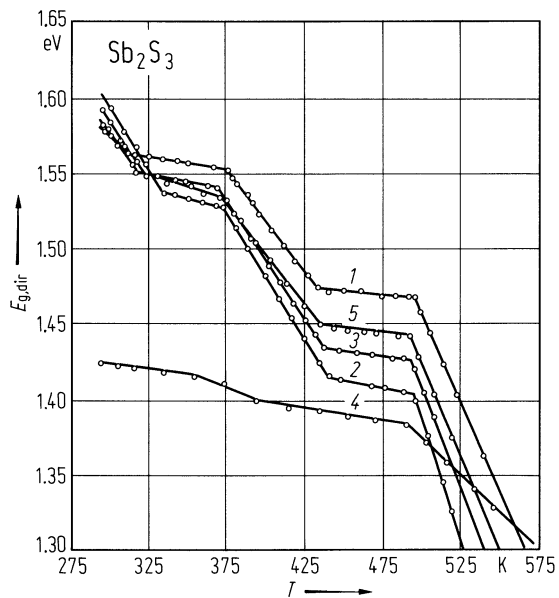


Fig. 25.5.2

Sb_2S_3 . Electrical conductivity vs. reciprocal temperature along a -, b - and c -axes [78R].

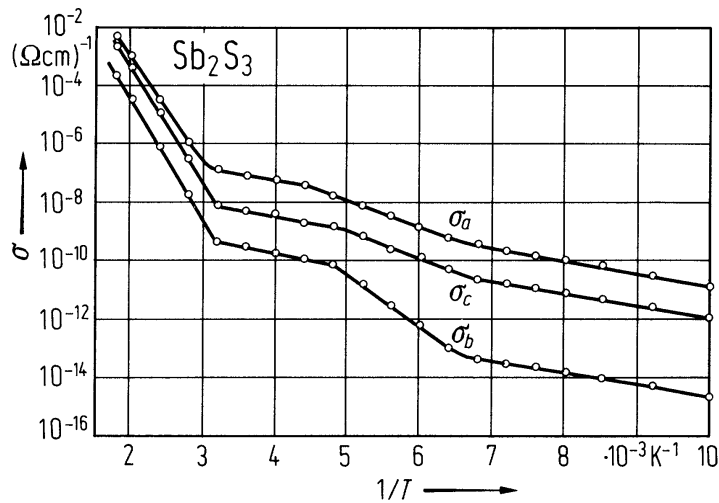


Fig. 25.5.3

Sb_2S_3 . Reflectivity vs. photon energy at 295 K and 90 K. The scale corresponds to curves for $E \parallel c$ and $E \parallel b$ at 295 K. Other curves are shifted to the bottom: $E \parallel a$ (295 K) by 3%, $E \parallel c$ (90 K) by 9%, $E \parallel a$ (90 K) by 10%, $E \parallel b$ (90 K) by 7% [69S1].

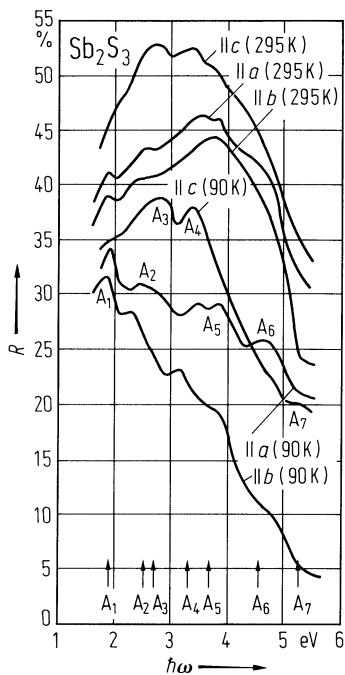
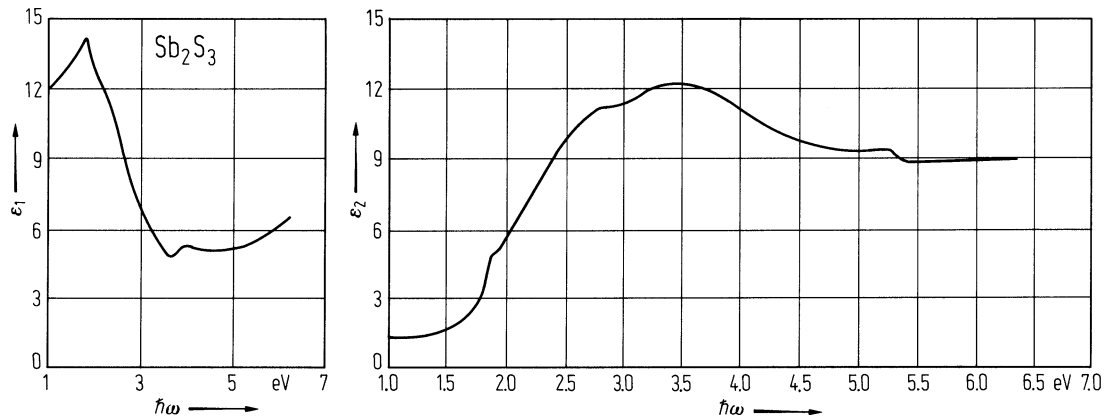


Fig. 25.5.4

Sb_2S_3 . Real and imaginary part of the dielectric constant vs. photon energy for a polycrystalline sample [79G].



25.6 Antimony selenide (Sb₂Se₃)

Electronic properties

Due to the complicated primitive cell little data on the band structure is available.

energy gaps

$E_{g,ind}$	1.11(2) eV	$T = 293\text{ K}; E \parallel a, c$	transmission measurement; indirect gap	78K
	1.11 eV	$T = 293\text{ K}, E \parallel c$	spectral dependence of	78K
	1.13 eV	$E \perp c$	photoconductivity	
$E_{g,dir}$	1 eV	$T = 300\text{ K}, E \perp b$	transmission and reflectivity measurements; direct gap	70P
$E_{g,th}$	1.08...1.32 eV	extrapolated to $T = 0\text{ K}$	differs from sample to sample due to different pinning of the Fermi level in the energy gap	74G
$dE_{g,ind}/dT$	$-5.5 \cdot 10^{-4}\text{ eV K}^{-1}$	$80\text{ K} < T < 293\text{ K};$ $E \parallel a, c$	temperature dependence of optical properties	78K

Lattice properties

lattice parameters

a	11.62 Å			64W
b	11.77 Å			
c	3.962 Å			

Debye temperature

Θ_D	240 K	$T = 80\text{ K}$		69A
------------	-------	-------------------	--	-----

heat capacity

C_p	$(123.93 + 1.026$ $\cdot 10^{-2}T)\text{ J mol}^{-1}\text{ K}^{-1}$	$T = 290...888\text{ K}$		79S
-------	--	--------------------------	--	-----

melting temperature

T_m	885 K			69A
-------	-------	--	--	-----

Transport properties

electrical conductivity

σ	$\approx 10^{-7}\text{ }\Omega^{-1}\text{ cm}^{-1}$	$T = 285\text{ K}$	hole conductivity; depends strongly on growth conditions	63K
$\sigma_{ c}$	$4.6 \cdot 10^2\text{ }\Omega^{-1}\text{ cm}^{-1}$	$T = 300\text{ K}$	highly degenerate p-type sample	72A
$\sigma_{ }/\sigma_{\perp}$	2.2	$T = 300\text{ K}$	electrical conductivity parallel and perpendicular to cleavage planes (see however [74G], [80C])	78K

carrier mobilities

μ_n	15 cm ² /V s	$T = 300\text{ K}$	mobilities parallel to cleavage planes	69A
μ_p	42 cm ² /V s			

Optical properties

FIR-reflectivity spectra, absorption coefficient: Figs. 25.6.1 25.6.2.

dielectric constants

$\epsilon(\infty)_{\parallel}$	15.1	$E \parallel c, T = 90, 300 \text{ K}$	73P
$\epsilon(\infty)_{\perp}$	14.5	$E \perp c, T = 90 \text{ K}$	
	13.7	$T = 300 \text{ K}$	
$\epsilon(0)_{\parallel}$	128	$E \parallel c, T = 90 \text{ K}$	from FIR reflectivity
	133	$T = 300 \text{ K}$	73P

See also Fig. 25.6.3.

References to 25.6

- 63K Kuznetsov, V. G., Palkina, K. K., Dmitriev, A. V.: Russ. J. Inorg. Chem. 8 (1963) 1116.
64W Wyckoff, R. W. G.: Crystal Structures 2, J. Wiley and Sons, New York, 1964.
69A Abrikosov, N. Kh., Bankina, V. F., Poretskaya, L. V., Shelimova, L. E., Skudnova, E. V.: Semiconducting II-VI, IV-VI and V-VI-compounds; Plenum Press, N. Y., 1969.
70P Procarione, W., Wood, C.: Phys. Status Solidi 42 (1970) 871.
72A Addis, F. W., Olsen, L. C.: Bull. Am. Phys. Soc. 17 (1972) 304.
73P Petzelt, J., Grigas, J.: Ferroelectrics 5 (1973) 59.
74G Gilbert, L. R., van Pelt, B., Wood, C.: J. Phys. Chem. Solids 35 (1974) 1629.
78K Kosek, F., Tulka, J., Stourac, L.: Czech. J. Phys. B 28 (1978) 325.
79S Sullivan, C. L., Prusaczik, J. E., Miller, R. A., Carlson, K. D.: High Temp. Sci. 11 (1979) 95.

Figures to 25.6

Fig. 25.6.1

Sb_2Se_3 . Far infrared reflectivity vs. wavenumber; dashed line: 90 K, solid line: 300 K [73P].

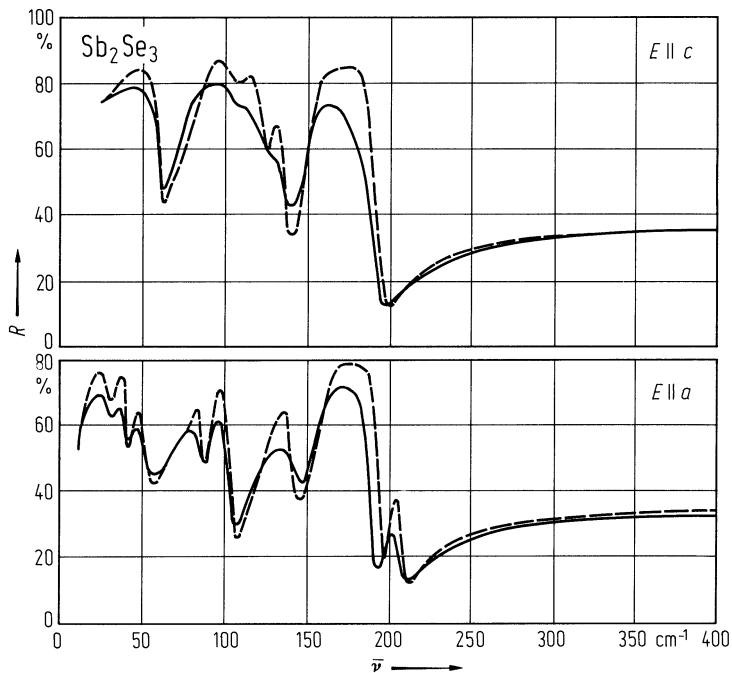


Fig. 25.6.2

Sb_2Se_3 . Absorption coefficient vs. photon energy at 293 K and 80 K [78K]; see also [74G].

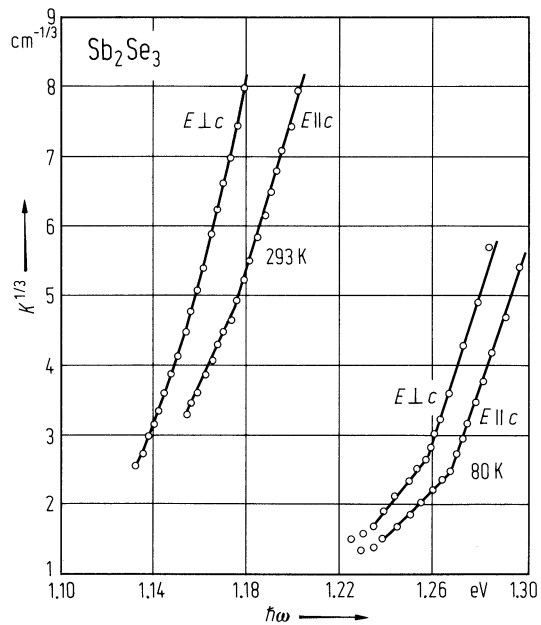
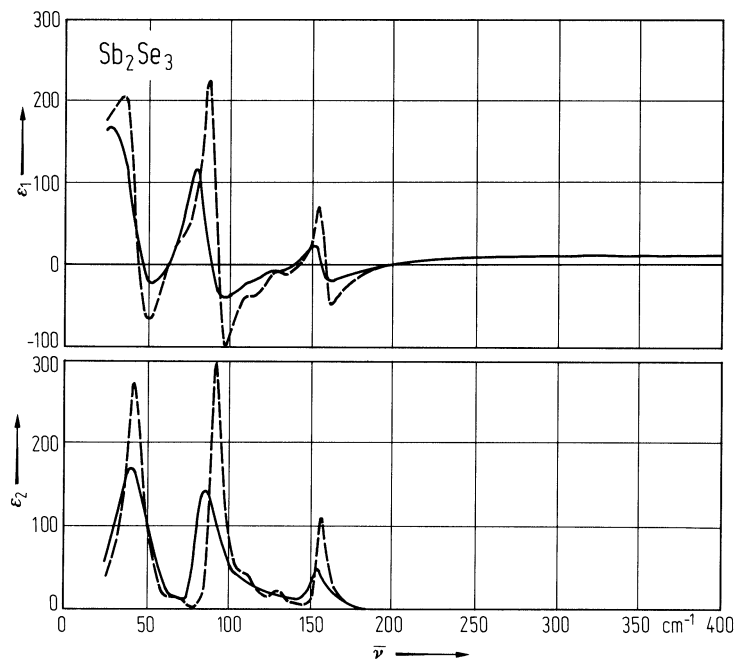


Fig. 25.6.3

Sb_2Se_3 . Real and imaginary part of the dielectric function vs. wavenumber, ($E \parallel c$, dashed line: 90 K, solid line: 300 K) determined from Kramers-Kronig-analysis [73P].



25.7 Antimony telluride (Sb₂Te₃)

Electronic properties

band structure

Two valence bands are discussed [73M, 65R, 68S]. Lower band: For the surfaces of constant energy two models are discussed: Either 12 prolate ellipsoids around the extrema, 4 in each binary-trigonal plane [73M] or 6 ellipsoids, 2 in each mirror plane [67S]. Upper band: Multi-valley structure indicated by Shubnikov-de Haas oscillations [73M].

energy gap

E_g	0.28 eV	$T = 299\text{ K}, E \perp c$	absorption edge	62S
-------	---------	-------------------------------	-----------------	-----

gap between two valence band edges

ΔE	0.23 eV	$T = 300\text{ K}$	electrical conductivity and thermo-electrical power ($\sigma, S \parallel$ cleavage plane).	65R
------------	---------	--------------------	--	-----

effective masses, lower valence band

m_1	0.034 m_0	$T = 1.8\text{ K}$ $B \parallel$ trigonal axis	Shubnikov-de Haas oscillations (12 valley model); $m_{1,2,3}$: masses along the principal axes of the ellipsoids	73M
m_2	0.34 m_0			
m_3	0.54 m_0			
m_{ds}	0.97 m_0			
$m_{\omega c}$	0.14 m_0			

effective masses, upper valence band

m_1	0.084 m_0	$T = 300\text{ K}$	weak field Hall measurements (6 valley model, acoustic phonons); $m_{1,2,3}$: masses along the principal axes of the ellipsoids; tilt angle 52.4° between bisectrix axis and ellipsoid	88S
m_2	1.24 m_0			
m_3	0.127 m_0			
m_{ds}	0.781 m_0			

Lattice properties

lattice parameters

a_{hex}	4.25 Å			64W
c_{hex}	30.35 Å			
a_{rh}	10.426 Å			
α	23.52°			

linear coefficient of thermal expansion

$\alpha_{\perp c}$	2.2·10 ⁻⁵ K ⁻¹	$T = 300...400\text{ K}$	X-ray measurement	81K
$\alpha_{\parallel c}$	2.7·10 ⁻⁵ K ⁻¹			

density

d	6.505 g cm ⁻³		X-ray density	74A
-----	--------------------------	--	---------------	-----

melting temperature

T_m	894 K			69A
-------	-------	--	--	-----

Debye temperature

Θ_D	160 K	$T = 80\text{ K}$	heat capacity measurement with a Nernst calorimeter	71Z
------------	-------	-------------------	---	-----

heat capacity

C_p	$128.8 \text{ J mol}^{-1} \text{ K}^{-1}$	$T = 298 \text{ K}$		71Z
-------	---	---------------------	--	-----

phonon dispersion curves : Fig. 25.7.1; Brillouin zone: Fig. 25.0.8.

phonon frequencies

$\nu(\text{A}_{1g}^{\text{I}})$	2.07 THz	$T = 300 \text{ K}$	Raman scattering (not IR-active)	77R
$\nu(\text{A}_{1g}^{\text{II}})$	5.07 THz			77R
$\nu(\text{E}_g^{\text{I}})$	1.29 THz			82R
$\nu(\text{E}_g^{\text{II}})$	3.36 THz			77R

Transport properties

hole mobility

μ_p	$3020 \text{ cm}^2/\text{V s}$	$E \perp c, T = 290 \text{ K}$	Hall effect, $p = 1.1 \cdot 10^{19} \text{ cm}^{-3}$; on thin film sample grown on s.i. GaAs by metalorganic chemical vapor deposition	
μ_{pl}/μ_{pu}	0.0093		mobility ratio of holes in lower/upper valence band	95K
μ_p	$270 \text{ cm}^2/\text{V s}$	$E \perp c, T = 300 \text{ K}$	conductivity, Hall effect	57B

carrier concentration

p_l/p_u	391		ratio of carrier concentration in lower/ upper valence band	95K
p	$15 \cdot 10^{19} \text{ cm}^{-3}$	$T = 294 \text{ K}$	optical and galvanomagnetic measurements	72H

electrical conductivity : Fig. 25.7.2.

thermal conductivity

$\kappa_{\perp c}$	$28...48 \cdot 10^{-3} \text{ W cm}^{-1} \text{ K}^{-1}$	$T = 300 \text{ K}$	depends on carrier concentration	73S
	$40...73 \cdot 10^{-3} \text{ W cm}^{-1} \text{ K}^{-1}$	$T = 100 \text{ K}$		

Optical properties

reflectivity, refractive index: Fig. 25.7.3.

dielectric constants

$\epsilon(0)_{\perp}$	168	$T = 80 \text{ K}$	IR reflectivity fit	75D
$\epsilon(0)_{\parallel}$	36.5	$T = 80 \text{ K}$		
$\epsilon(\infty)_{\perp}$	51	$T = 300 \text{ K}$		73U
$\epsilon(\infty)_{\parallel}$	32.5	$T = 300 \text{ K}$		

See also Fig. 25.7.3.

References to 25.7

- 57B Black, J., Conwell, E. M., Seigle, L., Spencer, C. W.: J. Phys. Chem. Solids 2 (1957) 240.
62S Sehr, R., Testardi, L. R.: J. Phys. Chem. Solids 23 (1962) 1219.
64W Wyckoff, R. W. G.: Crystal Structures 2, J. Wiley and Sons, New York, 1964.
65R Rönnlund, B., Beckmann, O., Levy, H.: J. Phys. Chem. Solids 26 (1965) 1281.
67S Schwartz, H., Björck, G., Beckmann, O.: Solid State Commun. 5 (1967) 905.
68S Sobolev, V. V., Shutov, S. D., Popov, Yu. V., Shestatskii, S. N.: Phys. Status Solidi 30 (1968) 349.
69A Abrikosov, N. Kh., Bankina, V. F., Poretskaya, L. V., Shelimova, L. E., Skudnova, E. V.:
Semiconducting II-VI, IV-VI and V-VI-compounds; Plenum Press, N. Y., 1969.
70C Caywood, L. P., Jr., Miller, G. R.: Phys. Rev. B 2 (1970) 3209.
71Z Zallen, R., Slade, M. L., Ward, A. T.: Phys. Rev. B 3 (1971) 4257.
72H Horák, J., Tichy, L., Vasko, A., Frumar, M.: Phys. Status Solidi (a) 14 (1972) 289.
73M von Middendorff, A., Dietrich, K., Landwehr, G.: Solid State Commun. 13 (1973) 443.
73S Süssmann, H.: Wiss. Z. Uni. Halle 12 (1973) 65.
73U Unkelbach, K. H.: Dissertation, RWTH Aachen, 1973.
74A Anderson, Th. L., Krause, H. Brigitte: Acta Crystallogr. B 30 (1974) 1307.
75D Drope, R.: Dissertation, RWTH Aachen, 1975.
76G Grosse, P., Burkhard, H., Wagner, V., Dörner, B.: ILL-experimental report 04-01-044, Grenoble, 1976.
77R Richter, W., Köhler, H., Becker, C. R.: Phys. Status Solidi (b) 84 (1977) 619.
78E Eichler, W., Simon, G.: Phys. Status Solidi (b) 86 (1978) K85.
80R Rabe, J.: Diploma Thesis, RWTH Aachen, 1980.
81K Krost, A.: Dissertation, RWTH Aachen, 1981.
82R Richter, W., Krost, A., Nowak, U., Anastassakis E.: Z. Phys. B 49 (1982) 191.
88S Stordeur, M., Stölzer, M., Sobotta, H., Riede, V.: Phys. Status Solidi (b) 150 (1988) 165.
95K Kulbachinskii, V.A., Dashevskii, Z.M., Inoue, M., Sasaki, M., Negishi, H., Gao, W.X., Losták, P.,
Horák, J., de Visser, A.: Phys. Rev. B 52 (1995) 10915.

Figures to 25.7

Fig. 25.0.8

Sb_2Te_3 . Brillouin zone [70C].

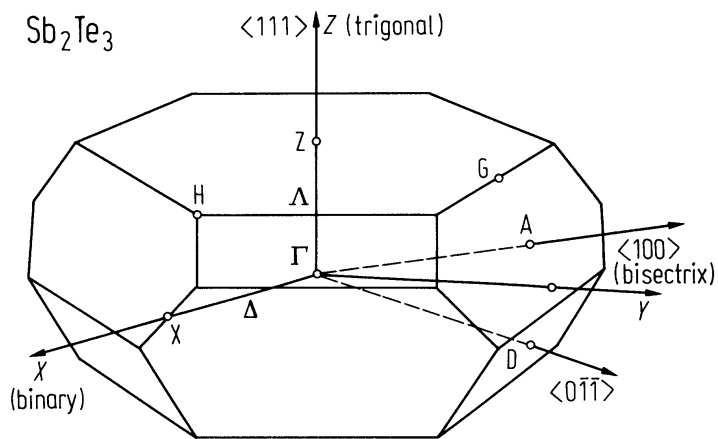


Fig. 25.7.1

Sb_2Te_3 . Phonon dispersion curves [76G]. The experimental points are fitted by a model based on 3 central forces, 3 angle forces and interlayer forces (dashed lines) [75D]. Solid lines: sound velocity measurements; open circles: neutron scattering; full circles: IR data; triangles: Raman data.

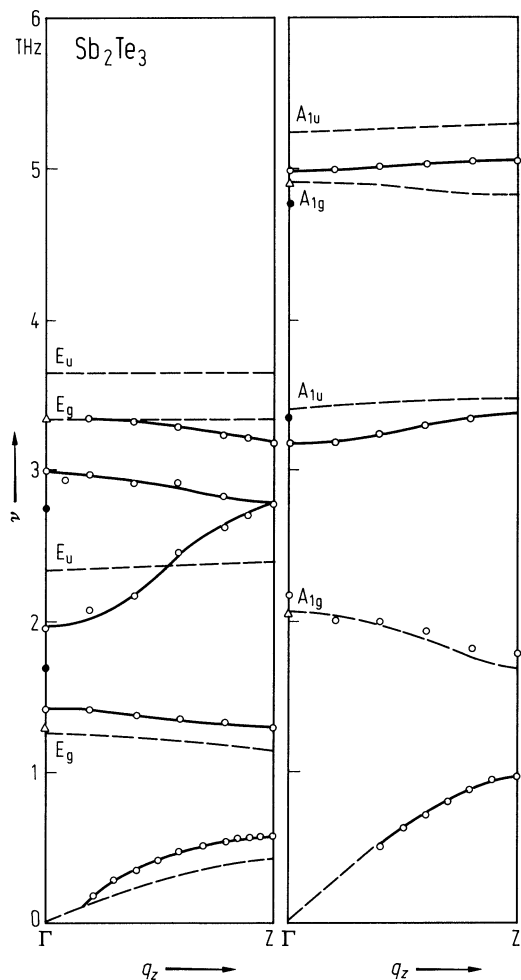


Fig. 25.7.2

Sb_2Te_3 . Electrical resistivity coefficients ρ_{33} ($i \parallel c$), ρ_{11} ($i \perp c$) vs. temperature [78E].

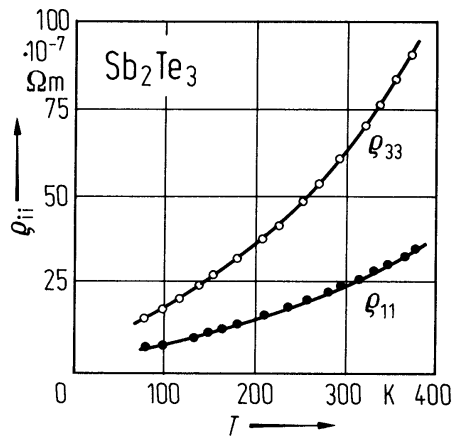


Fig. 25.7.3

Sb_2Te_3 . Reflectivity, real and imaginary part of the refractive index calculated by a Kramers-Kronig analysis of reflectivity data of [68S] and [82R] vs. photon energy at 300 K. The electrical field vector is perpendicular to the trigonal axis [82R].

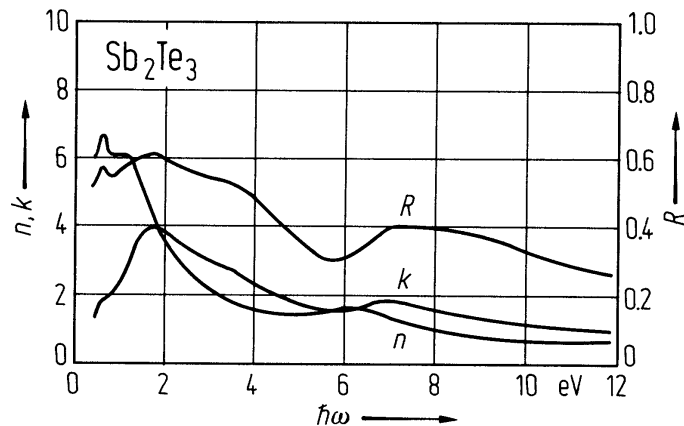
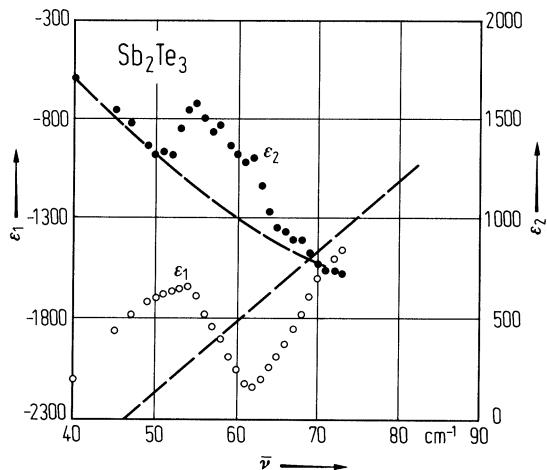


Fig. 25.7.4

Sb_2Te_3 . Real and imaginary part of the dielectric function vs. wavenumber in the phonon region. $E \perp c$; the dashed lines are the contributions from the free carriers [80R].



25.8 Bismuth oxide (Bi₂O₃)

Electronic properties

energy gaps

E_g	2.85 eV	$T = 300$ K	orthorhombic phase, optical gap	78D2
	2.6 eV	$T = 300$ K	tetragonal phase, optical gap	
$E_{g,th}$	1.6 eV	$T = 0$ K	polycrystalline thin films, independent of structural phase	78D1
dE_g/dT	$9 \cdot 10^{-4}$ eV K ⁻¹	$T = 77 \dots 300$ K	optical gap, tetragonal phases	78D2

Lattice properties

lattice parameters

a	5.848 Å	α -Bi ₂ O ₃	70M
b	8.166 Å		
c	7.510 Å		
β	113.0°		
a	7.743 Å	β -Bi ₂ O ₃	
c	5.631 Å		

Transport properties

Bi₂O₃ exhibits n- and p-type conductivity depending on heat treatment and oxygen pressure [49M], [64Z].

temperature dependence of electrical conductivity: Fig. 25.8.1.

thermal conductivity : see Fig. 25.8.2

heat capacity

C_p	$(103.58 + 33.49 \cdot 10^{-3} T)$ J mol ⁻¹ K ⁻¹	$T = 298$ K...800 K	73B
-------	--	---------------------	-----

density

d	8.929 g cm ⁻³	α -Bi ₂ O ₃	67D
-----	--------------------------	--	-----

melting temperature

T_m	1090 K		73B
-------	--------	--	-----

References to 25.8

- 49M Mansfield, R.: Proc. Phys. Soc. (London) B 62 (1949) 476.
 64Z Zolyan, T. S., Regel, A. R.: Sov. Phys.-Solid State 5 (1964) 1762.
 67D D'Ans-Lax: Taschenbuch für Chemiker und Physiker I, Berlin, Heidelberg, New York: Springer, 1967.
 70M Malmros, G.: Acta Chem. Scand. 24 (1970) 384.
 73B Barin, I., Knacke, O.: Thermochemical properties of inorganic substances, Berlin, Heidelberg, New York: Springer, 1973.
 78D1 Dolocan, V.: Phys. Status Solidi (a) 45 (1978) KISS.
 78D2 Dolocan, V.: Appl. Phys. 16 (1978) 405.
 78F Fedorov, V. I., Davydov, I. Ya.: High Temp. 16 (1978) 654.

Figures to 25.8

Fig. 25.8.1

Bi_2O_3 . Temperature dependence of electrical conductivity (polycrystalline samples): circles: data from [64Z]; triangles: data from [78F] (ac measurements); dashed curve: data from [78F] (dc measurements). T_{tr} indicates a structural phase transition from $\alpha\text{-Bi}_2\text{O}_3$ to $\beta\text{-Bi}_2\text{O}_3$; T_{m} is the melting temperature [78F].

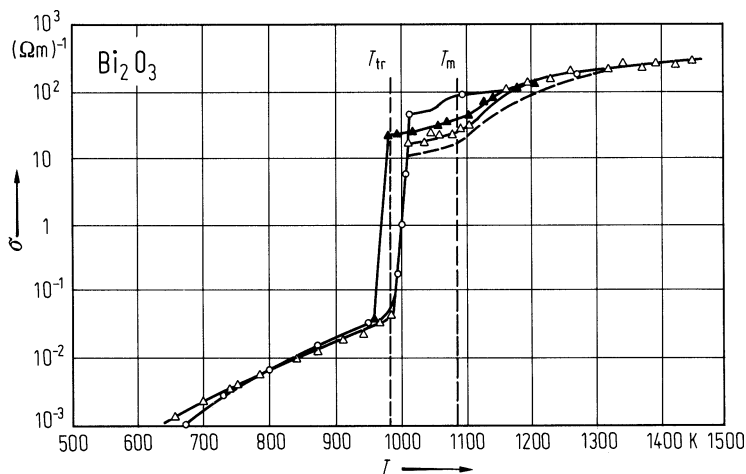
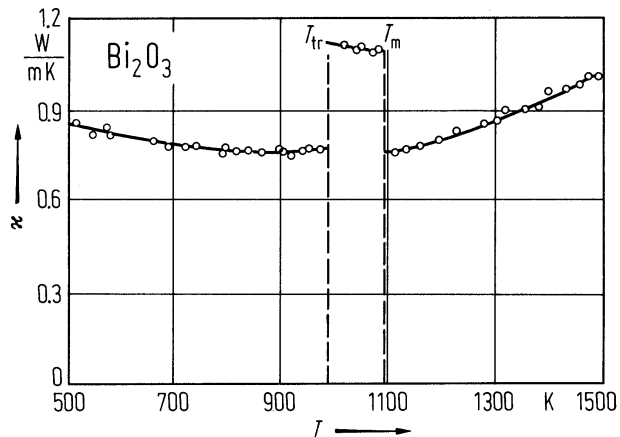


Fig. 25.8.2

Bi_2O_3 . Temperature dependence of thermal conductivity (polycrystalline sample). T_{tr} indicates a structural phase transition, T_{m} is the melting temperature [78F].



25.9 Bismuth sulfide (Bi₂S₃)

Physical properties

energy gaps

E_g	1.3 eV	$T = 300 \text{ K}, E \perp b$	absorption edge (optical gap)	61G
	1.45 eV	$T = 77 \text{ K}, E \perp b$		
dE_g/dT	$-8 \cdot 10^{-4} \text{ eV K}^{-1}$	$T = 77 \dots 300 \text{ K}$		61G
$E_{g,th}$	1.0 eV	$T = 0 \text{ K}$	temperature dependence of conductivity	69A

lattice parameters

a	11.150 Å			64W
b	11.300 Å			
c	3.981 Å			

electron concentration

n	$3 \cdot 10^{18} \text{ cm}^{-3}$	$T = 300 \text{ K}$		69A
-----	-----------------------------------	---------------------	--	-----

electron mobility

μ_n	$200 \text{ cm}^2/\text{V s}$	$T = 300 \text{ K}$	μ in cleavage plane	69A
---------	-------------------------------	---------------------	-------------------------	-----

electrical conductivity

σ	$10^{-6} \dots 10^{-7} \Omega^{-1} \text{ cm}^{-1}$	$T = 300 \text{ K}$	σ in cleavage plane	69A
	$10 \Omega^{-1} \text{ cm}^{-1}$		samples with excess bismuth	

refractive indices

n_α	1.315	$\lambda = 589.3 \text{ nm}$		67D
n_β	1.900			
n_γ	1.670			

dielectric constants

$\epsilon(0)_\parallel$	120	$T = 300 \text{ K}$	at 1 kHz	69Y
$\epsilon(0)_\perp$	38	$T = 300 \text{ K}, E \perp c$	from reflectivity	73P
$\epsilon(\infty)_\parallel$	13	$T = 300 \text{ K}, E \parallel c$		
$\epsilon(\infty)_\perp$	9	$T = 300, 90 \text{ K}, E \perp c$		

References to 25.9

- 61G Gildart, L., Kline, J. M., Mattox, D. M.: J. Phys. Chem. Solids 18 (1961) 286.
64W Wyckoff, R. W. G.: Crystal Structures 2, J. Wiley and Sons, New York, 1964.
67D D'Ans-Lax: Taschenbuch für Chemiker und Physiker I, Berlin, Heidelberg, New York: Springer, 1967.
69A Abrikosov, N. Kh., Bankina, V. F., Poretskaya, L. V., Shelimova, L. E., Skudnova, E. V.: Semiconducting II-VI, IV-VI and V-VI-compounds; Plenum Press, N. Y., 1969.
69Y Yuodvirshis, A. V., Kedavichus, V. V., Pipinis, P. A.: Sov. Phys.Solid State 11 (1969) 1158.
73P Petzelt, J., Grigas, J.: Ferroelectrics 5 (1973) 59.

25.10 Bismuth selenide (Bi2Se3)

Electronic properties

band structure

No energy band calculations are performed. From Shubnikov-de Haas and Hall effect data a single valley structure is deduced for the conduction band. A second conduction band with an energy gap of 160 meV is postulated. The Fermi surface is approximately an ellipsoid around the *k*-axis with a weak trigonal warping. Only little is known about the valence band [75K2].

energy gaps

<i>E</i> _{g,dir}	160 (±10%) meV	<i>T</i> = 77 K, <i>E</i> ⊥ <i>c</i>	deduced from reflectivity measurements; direct optical gap corrected for Burstein shift	74K2, 65G
<i>E</i> _{g,th}	160(10) meV			75K2
d <i>E</i> _{g,dir} /d <i>T</i>	− 2·10 ^{−4} eV K ^{−1}	<i>T</i> = 77...300 K		57B, 74K2

effective masses

<i>m</i> _{ωc}	0.124 <i>m</i> ₀	<i>B</i> ∥ <i>c</i>	temperature dependence of Shubnikov-de Haas amplitudes, independent of band edge effective mass (extrapolated to <i>n</i> = 0)	73K
<i>m</i> _p	0.125 <i>m</i> ₀ ±10%	<i>E</i> ⊥ <i>c</i>		74K2
<i>m</i> _{n⊥}	0.02 <i>m</i> ₀		band edge effective mass (extrapolated to <i>n</i> = 0)	69G
<i>m</i> _{ωp⊥}	0.186 <i>m</i> ₀		from plasma edge analysis <i>n</i> = 3·10 ¹⁹ cm ^{−3} ... <i>n</i> = 8·10 ¹⁷ cm ^{−3}	69G

g-factor

<i>g</i> _c	32(3)	<i>B</i> ∥ <i>c</i>	Shubnikov-de Haas measurements at 1.6...4.2K	75K1
	23(3)	<i>B</i> ⊥ <i>c</i>		

Lattice properties

lattice parameters

<i>a</i> _{hex}	4.138 Å			64W
<i>c</i> _{hex}	28.64 Å			
<i>a</i> _{rh}	9.841 Å			
α	24.27°			

phonon dispersion curves : Fig. 25.10.1.

Debye temperature

Θ _D (0)	182(3) K	(Θ _D (<i>T</i>): Fig. 25.10.2)	69S
--------------------	----------	---	-----

heat capacity (in J K⁻¹ mol⁻¹)

C_p	124.3	$T = 298$ K	for temperature dependence, see Fig. 25.10.3	74M
C_v	(118.61 + 19.26·10 ⁻³ T)	$T = 298...995$ K		
	0.708	$T = 10$ K		74M
	4.049	$T = 20$ K		
	7.566	$T = 30$ K		
	10.802	$T = 40$ K		
	13.523	$T = 50$ K		
	15.701	$T = 60$ K		
	17.375	$T = 70$ K		
	18.715	$T = 80$ K		
	19.762	$T = 90$ K		

density

d	7.68 g cm ⁻³	X-ray density	60W
-----	-------------------------	---------------	-----

melting temperature

T_m	979 K		69A
-------	-------	--	-----

Transport properties

electrical resistivity : Figs. 25.10.4, 25.10.5.

electrical conductivity

$\sigma_{\perp}/\sigma_{\parallel}$	3.05...3.51		92S
	4.4		69G

carrier mobility ($\mu \perp c$)

$\mu_{H,n}$	690 cm ² /Vs	$T = 300$ K	$n = 1.8 \cdot 10^{19}$ cm ⁻³ (300 K)	74H
$\mu_{H,p}$	42 cm ² /Vs	$T = 300$ K	$p = 1.5 \cdot 10^{19}$ cm ⁻³	72W
μ_{dr}	175 cm ² /Vs	$T = 300$ K	for temperature dependence see Figs. 25.10.6, 25.10.7	

thermal conductivity

κ	0.025 W cm ⁻¹ K ⁻¹	$T = 300$ K, $\kappa \perp c$		69A
	0.0134 W cm ⁻¹ K ⁻¹	$T = 300$ K, $\kappa \perp c$	lattice contribution	63J

Optical properties

Reflectivity, dielectric function: Figs. 25.10.8, 25.10.9.

dielectric constants

$\epsilon(0)_{\perp}$	113	deduced from oscillator fit to IR reflectivity	77R
$\epsilon(\infty)_{\perp}$	29	plasma edge fit with a Drude model	77R, 79T
$\epsilon(\infty)_{\parallel}$	16.5...18.4	plasma edge fit, depending on impurities	92S

References to 25.10

- 57B Black, J., Conwell, E. M., Seigle, L., Spencer, C. W.: J. Phys. Chem. Solids 2 (1957) 240.
- 60W Wiese, J. R., Muldower, L.: J. Phys. Chem. Solids 15 (1960) 13.
- 63J Joffe, A. V., Kuznetsov, V. G., Palkina, K. K.: Russ. J. Inorg. Chem. 8 (1963) 1113.
- 64W Wyckoff, R. W. G.: Crystal Structures 2, J. Wiley and Sons, New York, 1964.
- 65G Greenaway, D. L., Harbeke, G.: J. Phys. Chem. Solids 26 (1965) 1585.
- 69A Abrikosov, N. Kh., Bankina, V. F., Poretskaya, L. V., Shelimova, L. E., Skudnova, E. V.: Semiconducting II-VI, IV-VI and V-VI-compounds; Plenum Press, N. Y., 1969.
- 69G Gobrecht, H., Seeck, S.: Z. Phys. 222 (1969) 93.
- 69S Shoemaker, G. E., Rayne, J. A., Ure Jr., R. W.: Phys. Rev. 185 (1969) 1046.
- 72W Woollam, J. A., Beale, H., Spain, I. L.: Phys. Lett. 41A (1972) 319.
- 73K Köhler, H.: Phys. Status Solidi (b) 58 (1973) 91.
- 74H Hyde, G. R., Beale, H. A., Spain, I. L.: J. Phys. Chem. Solids 35 (1974) 1719.
- 74K1 Köhler, H., Becker, C. R.: Phys. Status Solidi (b) 61 (1974) 533.
- 74K2 Köhler, H., Hartmann, J.: Phys. Status Solidi (b) 63 (1974) 171.
- 74M Mills, K. C.: Thermodynamic Data for Inorganic Sulphides, Selenides and Tellurides, Butterworth, London, 1974.
- 75D Drope, R.: Dissertation, RWTH Aachen, 1975.
- 75K1 Köhler, H., Wüchner, F.: Phys. Status Solidi (b) 67 (1975) 665.
- 75K2 Köhler, H., Fabricius, A.: Phys. Status Solidi (b) 71 (1975) 487.
- 77R Richter, W., Köhler, H., Becker, C. R.: Phys. Status Solidi (b) 84 (1977) 619.
- 79T Tichy, L., Horák, J.: Phys. Rev. B 19 (1979) 1126.
- 92S Stordeur, M., Ketavong, K.K., Priemuth, A., Sobotta, H., Riede, V.: Phys. Status Solidi (b) 169 (1992) 505.

Figures to 25.10

Fig. 25.10.1

Bi_2Se_3 . Calculated phonon dispersion curves based on a model with 3 central forces, 3 angle forces and interlayer forces. The same model was used to fit the experimental data for Sb_2Te_3 [75D]. Full circles: Experimental Raman data; open circles: experimental IR data.

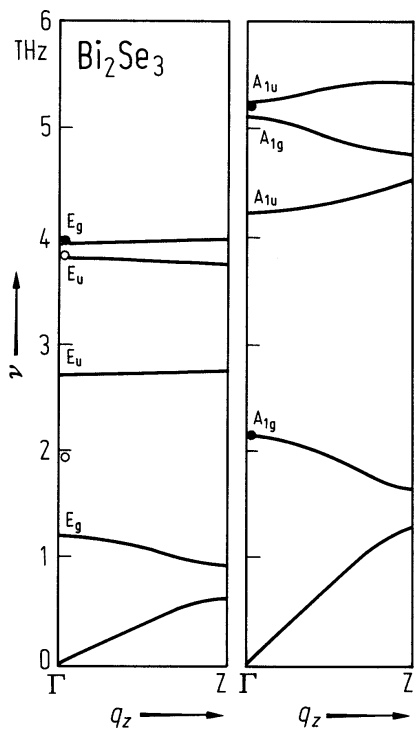


Fig. 25.10.2

Bi_2Se_3 . Temperature variation of Θ_D ; the insert shows the behavior near absolute zero [69S].

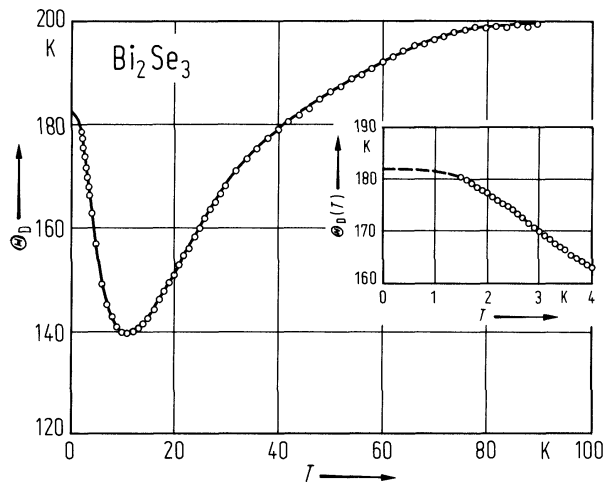


Fig. 25.10.3

Bi_2Se_3 . Plot of C_p/T vs. T^2 [69S].

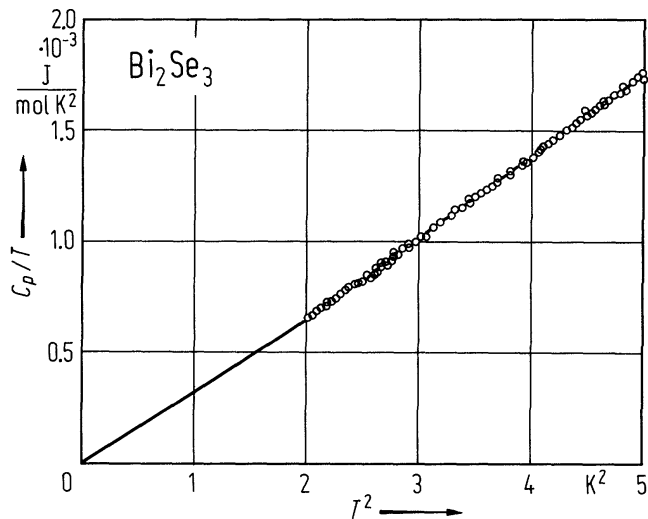


Fig. 25.10.4

Bi_2Se_3 . Resistivity vs. temperature of 4 p-type samples [75K2].

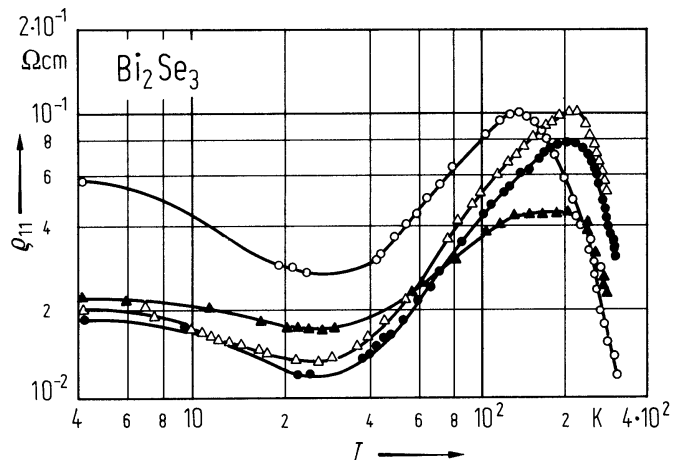


Fig. 25.10.5

Bi_2Se_3 . Resistivity vs. temperature of 4 n-type samples [75K2].

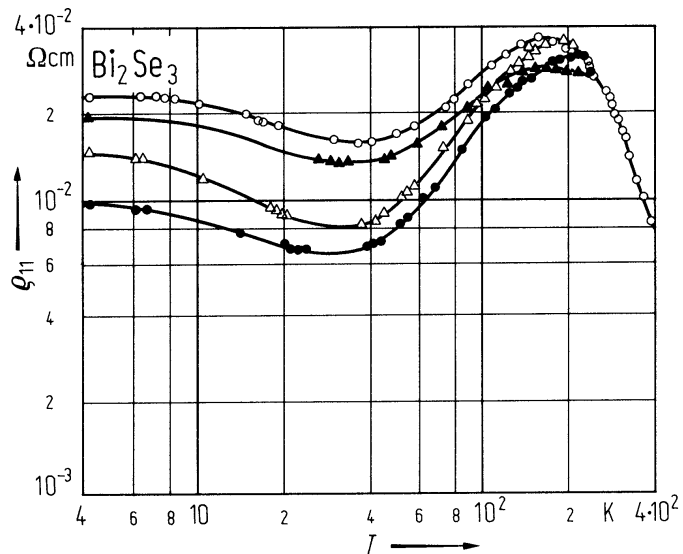


Fig. 25.10.6

Bi_2Se_3 . Hall mobilities of 4 n-type samples: full triangles: $n = 5.4 \cdot 10^{17} \text{ cm}^{-3}$; open triangles: $n = 8.7 \cdot 10^{16} \text{ cm}^{-3}$; open circles: $n = 1.6 \cdot 10^{17} \text{ cm}^{-3}$; full circles: $n = 1.2 \cdot 10^{17} \text{ cm}^{-3}$ vs. temperature [75K2].

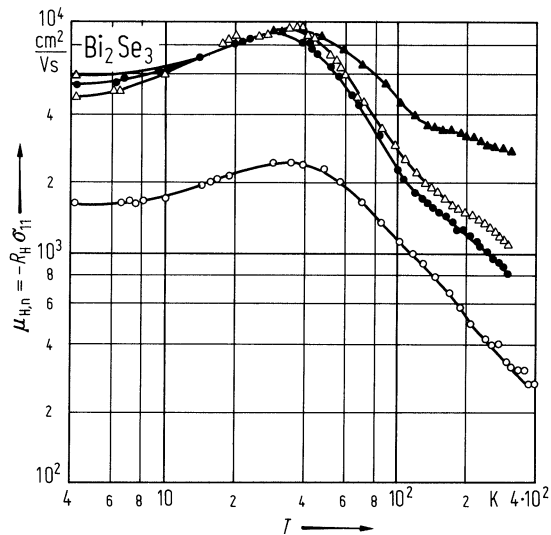


Fig. 25.10.7

Bi_2Se_3 . Hall mobilities of 4 p-type samples: open triangles: $p = 6.7 \cdot 10^{17} \text{ cm}^{-3}$; full triangles: $p = 7.2 \cdot 10^{16} \text{ cm}^{-3}$; open circles: $p = 6.9 \cdot 10^{16} \text{ cm}^{-3}$ full circles: $p = 5.4 \cdot 10^{17} \text{ cm}^{-3}$ vs. temperature [75K2].

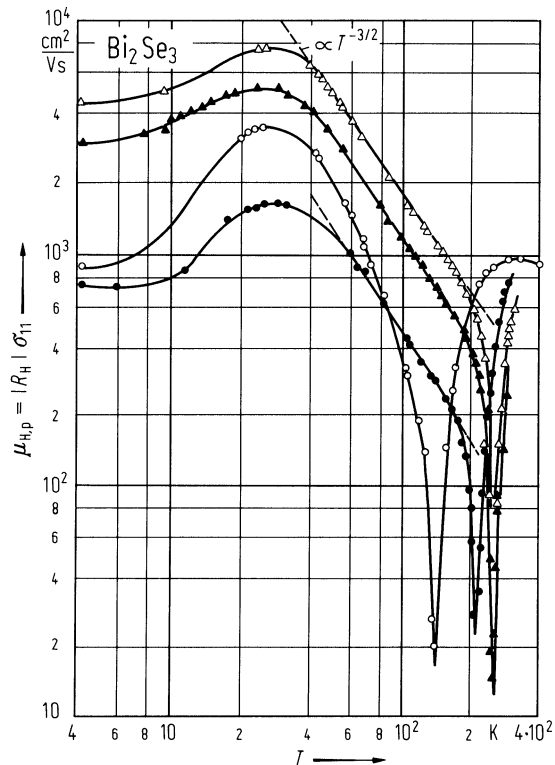


Fig. 25.10.8

Bi_2Se_3 . Reflectivity vs. wavenumber in the phonon region, $E \perp c$, 300 K [74K1].

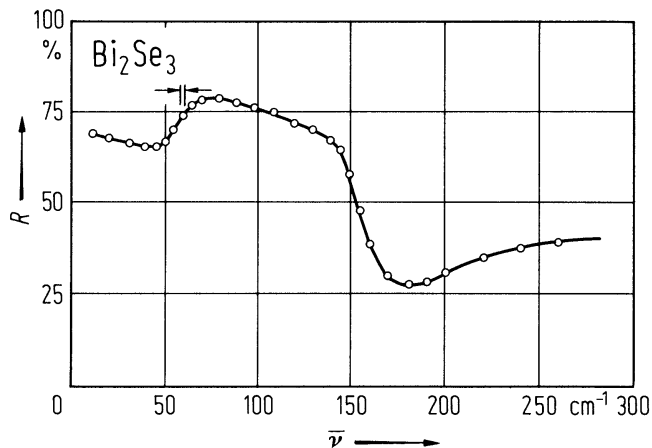
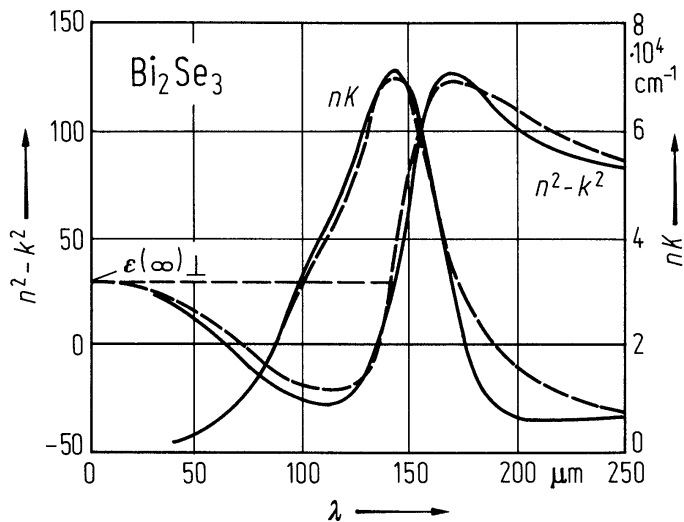


Fig. 25.10.9

Bi_2Se_3 . Real and imaginary part of the dielectric constant vs. wavelength from Kramers-Kronig analysis of reflectivity data (solid lines), $E \perp c$; theoretical fit using a Drude-Lorentz model with two oscillators (dashed lines) [74K1].



25.11 Bismuth telluride (Bi_2Te_3)

Electronic properties

band structure : Fig. 25.0.9 [68B], Brillouin zone: Fig. 25.0.8.

The band structure calculations [68B, 71T] predict a six-valley structure for both the highest valence and the lowest conduction band occurring along the direction M – D.

A quasirelativistic band structure calculation was performed, a six-valley model for both the conduction and valence band is deduced. According to the calculation, Bi_2Te_3 has an indirect energy gap with $E_{\text{g,ind}} = 0.149 \text{ eV}$ [85O].

energy gaps

$E_{\text{g,ind}}$	0.13 eV	$E \perp c, T = 293 \text{ K}$	absorption edge (indirect transitions)	62S
	0.14 eV		absorption edge (Moss' criterion)	
$E_{\text{g,th}}$	0.16 eV		temperature dependence of resistivity	57H
	0.15 eV			62S
$dE_{\text{g,ind}}/dT$	$-1.5 \cdot 10^{-4} \text{ eV K}^{-1}$	$T = 85 \text{ K} \dots 300 \text{ K}$	absorption edge (Moss' criterion)	62S

gap between two valence band edges

ΔE	0.0205 eV	$B \parallel c$	Shubnikov-de Haas oscillations	76K1
------------	-----------	-----------------	--------------------------------	------

gap between two conduction band edges

ΔE	0.03 eV		Hall effect	69S
------------	---------	--	-------------	-----

effective masses

$m_{\omega_{\text{p}\perp}}$	$0.109 m_0$	$T = 300 \text{ K}$	effective plasma frequency	88S
$m_{\omega_{\text{p}\parallel}}$	$0.279 m_0$		(p-type Bi_2Te_3)	
$m_{\text{ds,p}}$	$0.690 m_0$		total density of states mass at the band edge from weak field Hall measurements (six-valley model, acoustic phonon scattering)	
m_{p1}	$0.064 m_0$		first valence band edge principal mass parameters (weak field Hall measurements); tilt angle: 39.6° between bisectrix axis and ellipsoid	
m_{p2}	$0.730 m_0$			
m_{p3}	$0.196 m_0$			

g-factor ellipsoid

$g_{1\text{c}}$	24	$T = 1.6 \dots 4.2 \text{ K},$ B up to 15 T	spin-splitting of Shubnikov-de Haas oscillations (band edge principal values); tilt angle $31.50 \pm 10\%$ between bisectrix axis and g-ellipsoid	76K2
$g_{2\text{c}}$	41.2			
$g_{3\text{c}}$	≈ 2			

Lattice properties

lattice parameters

a_{hex}	4.383 Å			64W
c_{hex}	30.487 Å			
a_{rh}	10.473 Å			
α	24.17°			

linear thermal expansion coefficients

α_{\perp}	$14.4(4) \cdot 10^{-6} \text{ K}^{-1}$	$T = 300 \text{ K}$	X-ray measurements, dependence on carrier concentration	74B
α_{\parallel}	$21.3(4) \cdot 10^{-6} \text{ K}^{-1}$	$T = 300 \text{ K}$		

Debye temperature

$\Theta_D(0)$	$164.9(2) \text{ K}$	$\Theta_D(T)$: Fig. 25.11.1	69S
---------------	----------------------	------------------------------	-----

heat capacity

C_p	$(108.06 + 5.53 \cdot 10^{-2} T) \text{ J K}^{-1} \text{ mol}^{-1}$	$T = 293 \dots 850 \text{ K}$	74M
-------	---	-------------------------------	-----

density

d	7.86 g cm^{-3}	63D
-----	--------------------------	-----

melting temperature

T_m	858 K	63D
-------	-----------------	-----

phonon dispersion curves : Fig. 5.12.11.2

second order elastic moduli

c_{11}	$6.847 \cdot 10^{11} \text{ dyn cm}^{-2}$	$T = 280 \text{ K}$	the moduli are believed accurate to 0.25 % except c_{13} , which was determined to 0.5%	72J
c_{66}	$2.335 \cdot 10^{11} \text{ dyn cm}^{-2}$			
c_{33}	$4.768 \cdot 10^{11} \text{ dyn cm}^{-2}$			
c_{44}	$2.738 \cdot 10^{11} \text{ dyn cm}^{-2}$			
c_{13}	$2.704 \cdot 10^{11} \text{ dyn cm}^{-2}$			
c_{14}	$1.325 \cdot 10^{11} \text{ dyn cm}^{-2}$			

sound velocities

v_{11}	$2.95 \cdot 10^5 \text{ cm s}^{-1}$	$T = 280 \text{ K}$	calculated from elastic moduli	72J
v_{66}	$1.72 \cdot 10^5 \text{ cm s}^{-1}$			
v_{33}	$2.46 \cdot 10^5 \text{ cm s}^{-1}$			
v_{44}	$1.87 \cdot 10^5 \text{ cm s}^{-1}$			
v_{13}	$1.85 \cdot 10^5 \text{ cm s}^{-1}$			
v_{14}	$1.30 \cdot 10^5 \text{ cm s}^{-1}$			

Transport properties

electrical resistivity

ρ_{33}	$3.785 \cdot 10^{-5} \Omega \text{ m}$	$T = 293 \text{ K}$	75S
ρ_{11}	$1.403 \cdot 10^{-5} \Omega \text{ m}$	$T = 293 \text{ K}$	

mobility

μ_H	$2.7 \cdot 10^3 \text{ cm}^2/\text{V s}$	$T = 77 \text{ K}, \mu \perp c$	$p = 16 \cdot 10^{18} \text{ cm}^{-3}$	66C
	$5.1 \cdot 10^3 \text{ cm}^2/\text{V s}$		$p = 8.33 \cdot 10^{18} \text{ cm}^{-3}$	
	$18 \cdot 10^3 \text{ cm}^2/\text{V s}$		$n = 1.02 \cdot 10^{18} \text{ cm}^{-3}$	
	$7 \cdot 10^3 \text{ cm}^2/\text{V s}$		$n = 8.33 \cdot 10^{18} \text{ cm}^{-3}$	
	$4.7 \cdot 10^3 \text{ cm}^2/\text{V s}$		$n = 16 \cdot 10^{18} \text{ cm}^{-3}$	
	$3.8 \cdot 10^3 \text{ cm}^2/\text{V s}$		$n = 25 \cdot 10^{18} \text{ cm}^{-3}$	
	$2.7 \cdot 10^3 \text{ cm}^2/\text{V s}$		$n = 33.8 \cdot 10^{18} \text{ cm}^{-3}$	

Electrical conductivity and Hall mobility vs. T , Figs. 25.11.3, 25.11.4.

Optical properties

optical constants : Fig. 25.11.5.

dielectric constants

$\epsilon(0)_{\perp}$	290	$T = 15 \text{ K}$	deduced from oscillator fit to IR reflectivity	77R
$\epsilon(\infty)_{\perp}$	85	$T = 300 \text{ K}$	fit to the plasma edge by a Drude	77R
	85	$T = 15 \text{ K}$	model	60A
$\epsilon(0)_{\parallel}$	75	$T = 15 \text{ K}$	see $\epsilon(0)_{\perp}$	77R
$\epsilon(\infty)_{\parallel}$	50	$T = 300 \text{ K}$	see $\epsilon(\infty)_{\perp}$	77R
	50	$T = 15 \text{ K}$		64G

thermal conductivity

κ_{11}/κ_{33}	1.25...1.5	$T = 100...300 \text{ K}$		89K
---------------------------	------------	---------------------------	--	-----

for temperature dependence see Fig. 25.11.6

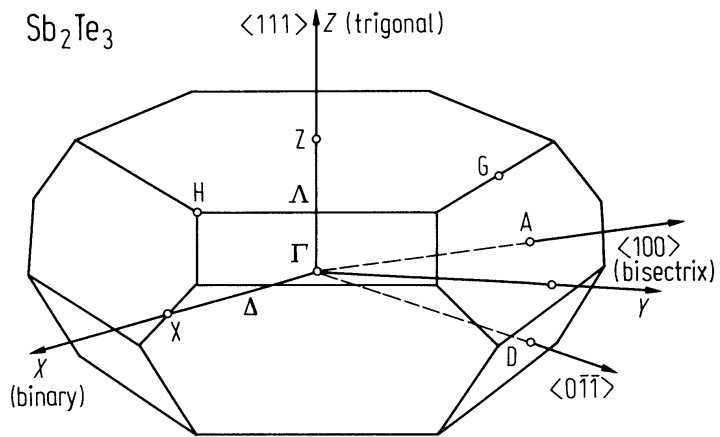
References to 25.11

- 57H Harman, T. C., Paris, B., Miller, S. E., Goering, H. L.: J. Phys. Chem. Solids 2 (1957) 181.
- 60A Austin, I. G.: Proc. Phys. Soc. 76 (1960) 169.
- 62S Sehr, R., Testardi, L. R.: J. Phys. Chem. Solids 23 (1962) 1219.
- 63D Drabble, J. R. in: Progress in Semiconductors, A. F. Gibson and R. E. Burgess, eds., John Wiley & Sons, Inc., New York, 1963, Vol. 7.
- 64G Groth, R., Schnabel, P.: J. Phys. Chem. Solids 25 (1964) 1261.
- 64W Wyckoff, R. W. G.: Crystal Structures 2, J. Wiley and Sons, New York, 1964.
- 65G Greenaway, D. L., Harbeke, G.: J. Phys. Chem. Solids 26 (1965) 1585.
- 65S Sälzer, O., Nieke, H.: Ann. Phys. (Leipzig) 7. Folge, 15 (1965) 192.
- 66C Champness, C. H., Kipling, A. L.: Can. J. Phys. 44 (1966) 769.
- 68B Borghese, F., Donato, F.: Nuovo Cimento 53B (1968) 283.
- 69S Shoemaker, G. E., Rayne, J. A., Ure Jr., R. W.: Phys. Rev. 185 (1969) 1046.
- 70C Caywood, L. P., Jr., Miller, G. R.: Phys. Rev. B 2 (1970) 3209.
- 70S Smirnov, I. A., Shadrachev, Kutasov, V. A.: Sov. Phys. Solid State 11 (1970) 2681.
- 71T Toge, R., Miller, G. R. in: Phys. Semimetals and Narrow gap semiconductors, D. L. Carter, R. T. Bate, eds., Pergamon Press, Oxford, 1971.
- 72J Jenkins, J. O., Rayne, J. A., Ure, jr., R. W.: Phys. Rev. B5 (1972) 3171.
- 74B Barnes, J. O., Rayne, J. A., Ure Jr, R. W.: Phys. Lett. 46A (1974) 317.
- 74M Mills, K. C.: Thermodynamic Data for Inorganic Sulphides, Selenides and Tellurides, Butterworth, London, 1974.
- 75S Stordeur, M., Kühnberger, W.: Phys. Status Solidi (b) 69 (1975) 377.
- 76K1 Köhler, H.: Phys. Status Solidi (b) 74 (1976) 591.
- 76K2 Köhler, H.: Phys. Status Solidi (b) 75 (1976) 127.
- 77R Richter, W., Köhler, H., Becker, C. R.: Phys. Status Solidi (b) 84 (1977) 619.
- 78W Wagner, V., Dolling, G., Powell, B. M., Landwehr, G.: Phys. Status Solidi (b) 85 (1978) 311.
- 85O Oleshko, E. V., Korolyshin, V. N.: Sov. Phys. Solid State 27 (1985) 1723.
- 88S Stordeur, M., Stölzer, M., Sobotta, H., Riede, V.: Phys. Status Solidi (b) 150 (1988) 165.
- 89K Kaibe, H., Tanaka, Y., Sakata, M., Nishida, I.: J. Phys. Chem. Solids 50 (1989) 945.

Figures to 25.11

Fig. 25.0.8

Sb_2Te_3 . Brillouin zone [70C].



Bi₂Te₃. Empirical pseudopotential band structure with the inclusion of spin-orbit coupling [68B]. 1 Ry = 13.6 eV.

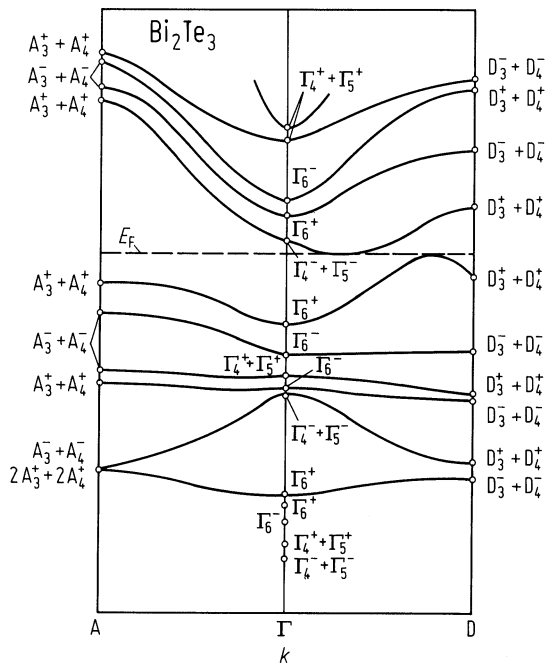


Fig. 25.11.1

Bi_2Te_3 . Temperature variation of the Debye temperature. The inset shows the behavior near absolute zero and the corresponding value of $\Theta_D(0)$ obtained from elastic data [69S].

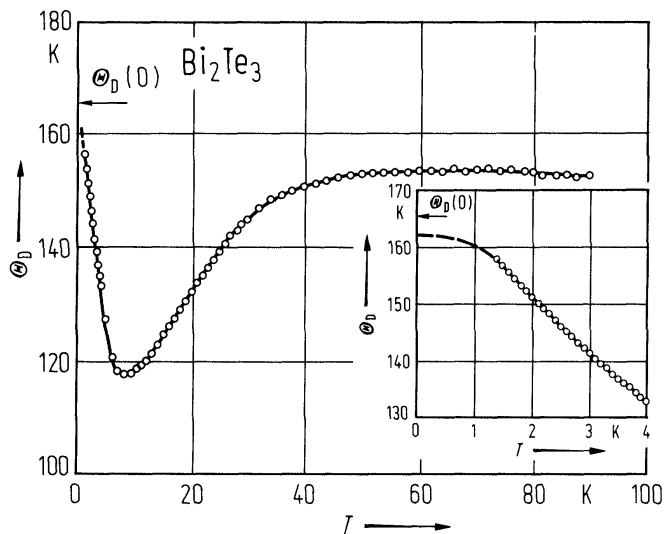


Fig. 25.11.2

Bi_2Te_3 . Frequencies of longitudinal (Λ_1) and transverse (Λ_3) vibration modes propagating along the trigonal axis vs. reduced wave vector coordinate; $T = 77$ K. The curves are fits, based on a model with nearest neighbor and next nearest neighbor forces [78W]. Ra: Raman modes, FIR: far infrared modes.

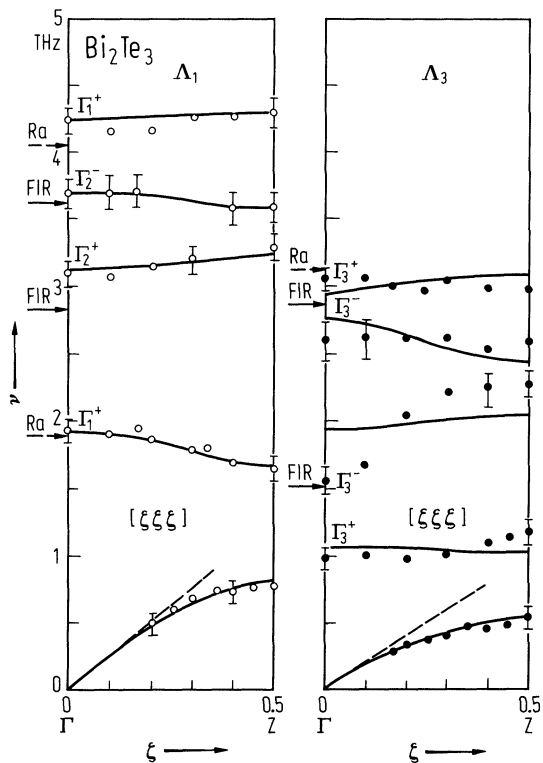


Fig. 25.11.3

Bi_2Te_3 . Electrical conductivity vs. reciprocal temperature for two p-type and five n-type bismuth telluride samples ($\sigma \perp c$) [66C].

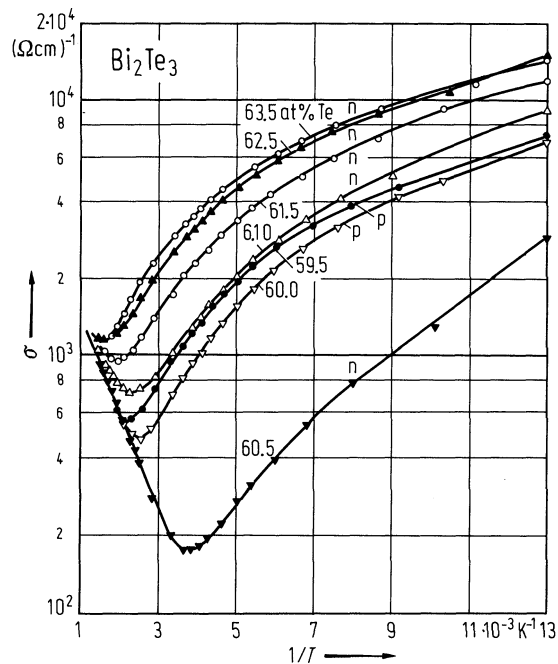


Fig. 25.11.4

Bi_2Te_3 . Hall mobility ($\mu_H \perp c$) vs. temperature for two p-type (dashed lines) and five n-type (solid lines) bismuth telluride samples. The experimental points have been removed for clarity [66C].

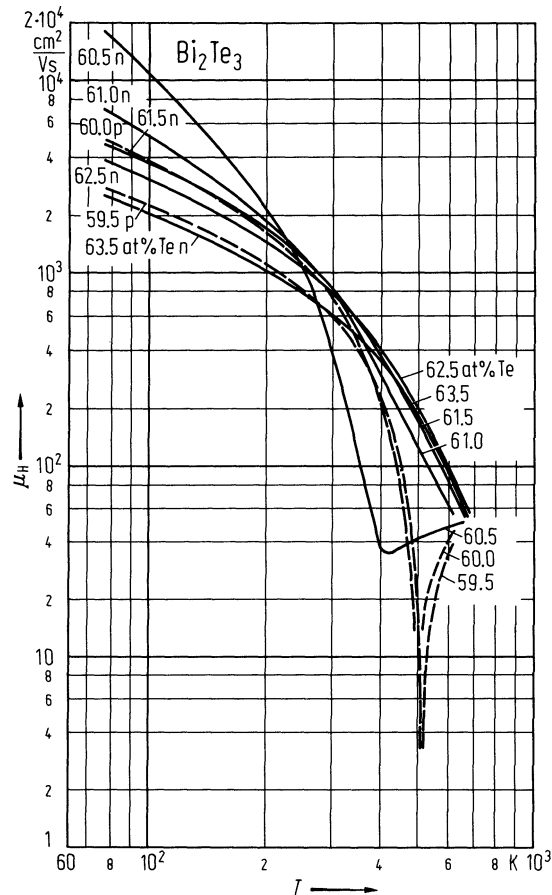


Fig. 25.11.5

Bi_2Te_3 . Optical constants n and k and energy loss function $-\text{Im}(1/\epsilon)$ vs. photon energy from Kramers-Kronig analysis, $E \perp c$ [65G].

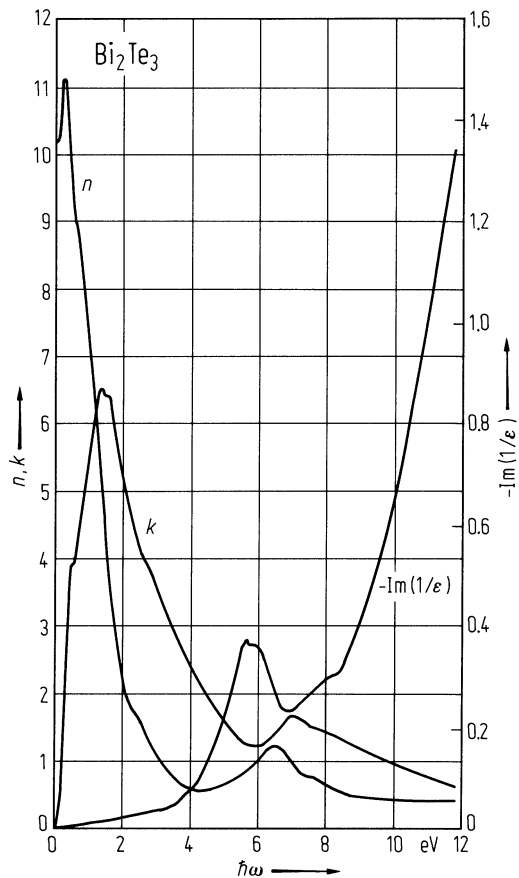
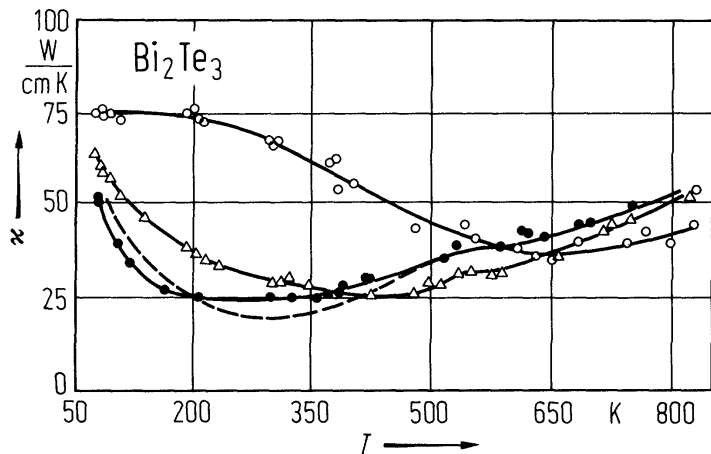


Fig. 25.11.6

Bi_2Te_3 . Thermal conductivity ($\kappa \perp c$) vs. temperature for undoped (dashed line) and different doped Bi_2Te_3 samples. Open circles: very high doped n-type sample [70S]; see also [65S].



25.12 Realgar (As₄S₄)

Physical properties

energy gap

E_g	2.40(5) eV	photoconductivity measurements	66S
-------	------------	--------------------------------	-----

coefficient of volume thermal expansion

β	$\approx 0.8 \cdot 10^{-4} \text{ K}^{-1}$		78Z
---------	--	--	-----

lattice parameters

a	9.325 Å		72M
b	13.571 Å		
c	6.587 Å		
β	106°23'		

volume compressibility

κ_v	$0.6 \cdot 10^{-2} \text{ kbar}^{-1}$		78Z
------------	---------------------------------------	--	-----

drift mobilities

$\mu_{\text{dr,p}}$	12 cm ² /V s	$T = 300 \text{ K}$	$\perp (010)$, hole mobility	66S
$\mu_{\text{dr,n}}$	0.02 cm ² /V s	$T = 300 \text{ K}$	$\perp (010)$, electron mobility	66S

refractive indices in different directions

n_α	2.538	$\lambda = 589.3 \text{ nm}$	67D
n_β	2.700		
n_γ	2.704		

heat capacity

C_p	$(82.98 + 3.74 \cdot 10^{-2} T) \text{ J K}^{-1} \text{ mol}^{-1}$	$T = 298 \dots 2000 \text{ K}$	74M
-------	--	--------------------------------	-----

density

d	3.506 g cm ⁻³		67D
-----	--------------------------	--	-----

melting temperature

T_m	580 K		74M
-------	-------	--	-----

References to 25.12

- 66S Street, G. B., Gill, W. D.: Phys. Status Solidi 18 (1966) 601.
67D D'Ans-Lax: Taschenbuch flir Chemiker und Physiker I, Berlin, Heidelberg, New York: Springer, 1967.
72M Mullen, D. J. E., Nowacki, W.: Z. Kristallogr. 136 (1972) 48.
74M Mills, K. C.: Thermodynamic Data for Inorganic Sulphides, Selenides and Tellurides, Butterworth, London, 1974.
78Z Zallen, R., Slade, M. L.: Phys. Rev. 18 (1978) 5775.

26 V-VII₃ compounds

26.0 Crystal structure and electronic structure of AsI₃, SbI₃, BiI₃

AsI₃, SbI₃ and BiI₃ form layer lattices with octahedral coordination (Fig. 26.0.1a) similar to the CdI₂-lattice. In AsI₃ and SbI₃ crystals the metal atom is shifted out of the center forming rippled layers (Fig. 26.0.1b) with molecular character. On the contrary, the Bi atom sits in the center of the octahedron leading to completely cross-linked layers. The rhombohedral elementary cell consists of two molecules (Fig. 26.0.1c).

Space group: AsI₃: $C_{3i}^2 - R\bar{3}m$ [80E], BiI₃: $D_{3d}^5 - R\bar{3}m$ [95R], SbI₃: $P2_1/c$ [84P].

Band structure of BiI₃: Fig. 26.0.2.

References to 26.0

- 76S Schlüter, S., Cohen, M. L., Kohn, S. F., Fong, C. Y.: Phys. Status Solidi (b) 78 (1976) 737.
- 80E Enjalbert, R., Galy, J.: Acta Crystallogr. B36 (1980) 914-916.
- 84P Pohl, S., Saak, W.: Z. Kristallogr. 169 (1984) 177-184.
- 95R Ruck, M.: Z. Kristallogr. 210 (1995) 650-655.

Figures to 26.0

Fig. 26.0.1a

AsI_3 , SbI_3 , BiI_3 . Metal-iodine octahedron.

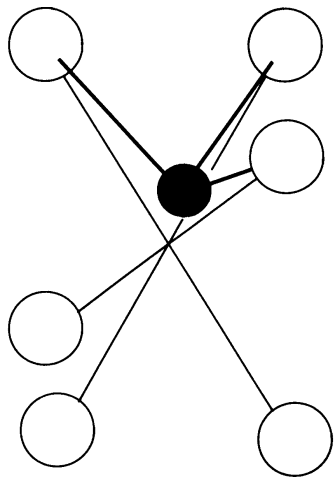


Fig. 26.0.1b

AsI_3 , SbI_3 . Schematic drawing of the layer lattice with rippled layers of the metal atoms.

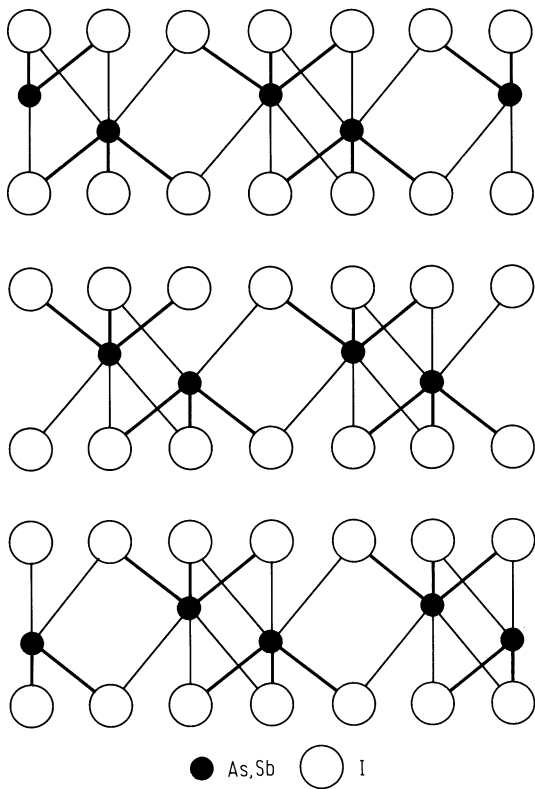
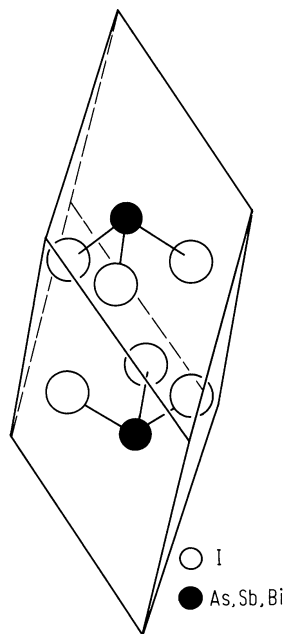
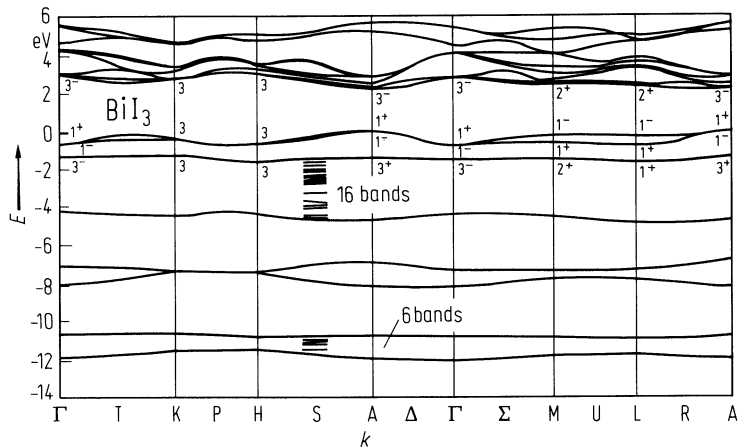


Fig. 26.0.1c

AsI_3 , SbI_3 , BiI_3 . Rhombohedral elementary cell with two molecules.



BiI₃. Band structure (without spin-orbit effects). For clarity, only the outermost bands are plotted [76S].



26.1 Arsenic triiodide (AsI3)

Electronic properties

AsI3 is a direct gap material.

energy gap

$E_{g,dir}$	2.47eV	$T = 90\text{ K}$	transmission vapor grown crystals, sublimed layers	67T
$dE_{g,dir}/dT$	$-8.2\cdot 10^{-4}\text{ eV K}^{-1}$	$T = 90...420\text{ K}$		

Lattice properties

thermal expansion

α_{av}	$9\cdot 10^{-5}\text{ K}^{-1}$	$T = 0...78\text{ K}$	α_{av} : average expansion coefficient	32B
	$17\cdot 10^{-5}\text{ K}^{-1}$	$T = 78...194\text{ K}$		

density

d	4.688 g cm^{-3}	$T = 25^{\circ}\text{C}$		32B
-----	--------------------------	--------------------------	--	-----

melting temperature

T_m	141°C		vapor grown crystals	77G
-------	-----------------------	--	----------------------	-----

lattice dynamics

The lattice modes A_g and E_g are Raman active, A_u and E_u IR active.

optical phonon wavenumbers (in cm^{-1})

mode type	AsI3-crystal infrared [91A]	AsI3-powder infrared [91A]	Raman species [88A]	Raman frequency [88A]
n_3	197	200	E_g	206.5
n_1	151	200	A_g	180
n_4	-	102.5	E_g	83.5
n_2	79	79	A_g	76.5
L_{xy}	64.5	65	E_g	64
T_z			A_g	61
L_z	50	49	A_g	43
T_{xy}			E_g	37.5

Optical properties, photoconductivity

As AsI_3 crystals are not very stable in air only very little is known about the optical properties of the fundamental electronic absorption edge [74C].

optical spectra : Figs. 26.1.1, 26.1.2.

dielectric constants

$\epsilon(0)$	7.9(8)	$E \perp c, T = 300\text{ K}$	microwave method	73V
	4.7(3)	$E \parallel c, T = 300\text{ K}$		
$\epsilon(\infty)$	4.8	$E \perp c, T = 300\text{ K}$	reflectivity	74C
	3.9	$E \parallel c, T = 300\text{ K}$		

References to 26.1

- 32B Biltz, W., Sapper, A.: Z. Anorg. Chem. 203 (1932) 277.
- 67T Turjanica, I. D., Chepur, D. V.: Ukr. Fiz. Zh. 12 (1967) 500.
- 73V Vits, P.: Diplomarbeit, RWTH Aachen 1973
- 74C Clasen, R.: Thesis, RWTH Aachen 1974.
- 77G Gasinets, S. M., Shpyrko, G. M., Golovei, M. I. . Mel'nichenko. T. N.: J. Inorg. Mater. (English Transl.) 13 (1977) 748.
- 88A Anderson, A., Campbell, J. A., Syme, R. W. G. : J. Raman Spectrosc. 19 (1988) 379-382.
- 91A Anderson, A., Campbell, J. A. : Phys. Status Solidi (b) 163 (1991) 527-531.

Figures to 26.1

Fig. 26.1.1

AsI_3 , SbI_3 , BiI_3 . Far-infrared reflectivity spectra (solid line) and oscillator fit (dashed line) of single crystals at 80 K, $E \perp c$ (reflectivity vs. wavenumber) [74C].

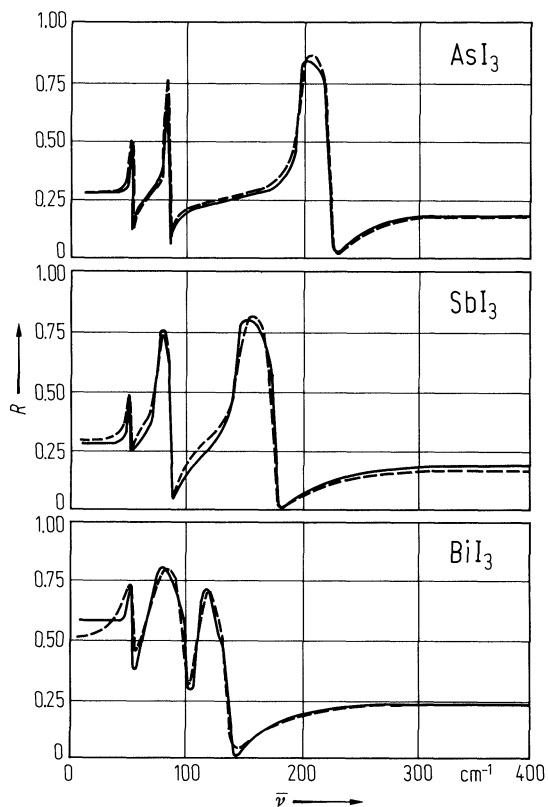
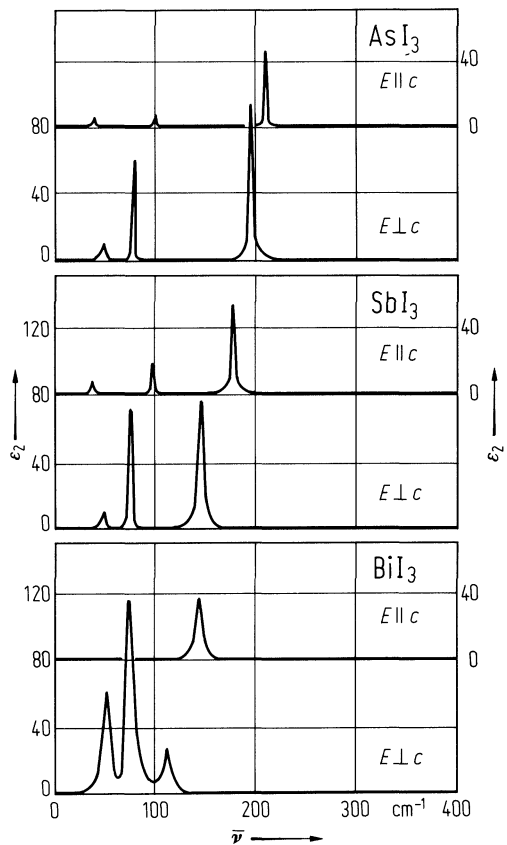


Fig. 26.1.2

AsI_3 , SbI_3 , BiI_3 . Imaginary part of dielectric constant vs. wavenumber, from reflectivity measurements [74C].



26.2 Antimony triiodide (SbI3)

Electronic properties

SbI3 is a direct gap material.

energy gap

$E_{g,dir}$	2.41 eV	$T = 90\text{ K}$	transmission, vapor grown crystals and sublimed layers	67T
$dE_{g,dir}/dT$	$-9\cdot 10^{-4}\text{ eV K}^{-1}$ $+7.3(32)\cdot 10^{-4}\text{ eV K}^{-1}$	$T = 90\ldots 420\text{ K}$ $T = 90\ldots 270\text{ K}$	evaporated layers on quartz substrates, exciton peak	77B

reduced effective masses

μ	$0.0024\ m_0$ $0.0056\ m_0$	$c \perp H$ $c \parallel H$	magnetoabsorption	75K
-------	--------------------------------	--------------------------------	-------------------	-----

Lattice properties

density

d	4.848 g cm^{-3}	$T = 24^{\circ}\text{C}$		1877C
-----	--------------------------	--------------------------	--	-------

melting temperature

T_m	170°C		vapor grown crystals	77G
-------	-----------------------	--	----------------------	-----

optical phonon wavenumbers (in cm^{-1})

mode type	AsI3-crystal infrared [91A]	AsI3-powder infrared [91A]	Raman species [88A]	Raman frequency [88A]
n_3	188	184	E_g	158
n_1	151	152	A_g	132.5
n_4	107	97.5	E_g	81
n_2	79	79	A_g	67
L_{xy}	64	64	E_g	62
T_z			A_g	47.5
L_z	50	49.5	A_g	40
T_{xy}			E_g	35.5

elastic constants

measured by Brillouin scattering at room temperature (in 10^6 N/cm^2) [85K]

$c_{11} = 1.5$	$c_{12} = -0.50$	$c_{13} = 0.40$	$ c_{14} = 0.10$
$ c_{25} = 0.25$	$c_{33} = 0.93$	$c_{44} = 0.47$	

Transport properties

resistivity

dependence on temperature: Fig. 26.2.1.

ρ_{\perp}	$4.25\cdot 10^9\ \Omega\text{ cm}$	$T = 300\text{ K}$	single crystals, very pure Sb and I	67B
----------------	------------------------------------	--------------------	-------------------------------------	-----

activation energy of intrinsic resistivity

E_A	$0.96\ldots 1.16(5)\text{ eV}$ $0.20(5)\text{ eV}$	solid phase liquid phase	part A – C, Fig. 26.5	61F
-------	---	-----------------------------	-----------------------	-----

Optical properties

optical spectra : Figs. 26.2.2, 26.2.3.

dielectric constants

$\varepsilon(0)$	16.0(23)	$E \perp c, T = 300 \text{ K}$	microwave method	73V
	8.9(11)	$E \parallel c, T = 300 \text{ K}$		
$\varepsilon(\infty)$	5.3	$E \perp c, T = 300 \text{ K}$	reflectivity	74C
	4.4	$E \parallel c, T = 300 \text{ K}$		

References to 26.2

- 1877C Cooke, J. P.: Proc. Am. Acad. Arts Sci. 13 (1877/78) 77.
61F Fischer, G.: Helv. Phys. Acta 34 (1961) 827.
67B Belotskii, D. P., Antipov, I. N., Krylyuk, N. V.: Ukr. Khim. Zh. 33 (1967) 14.
67T Turjanica, I. D., Chepur, D. V.: Ukr. Fiz. Zh. 12 (1967) 500.
73V Vits, P.: Diplomarbeit, RWTH Aachen 1973
74C Clasen, R.: Thesis, RWTH Aachen 1974.
75K Kolosyuk, V. N., Vashchenko, V. I., Berezdetskii, T. I.: Opt. Spectrosc. (USSR) 39 (1975) 335.
77B Brothers, A. D., Wieliczka, D. M.: Phys. Status Solidi (b) 80 (1977) 201.
77G Gasinets, S. M., Shpyrko, G. M., Golovei, M. I., Mel'nichenko, T. N.: J. Inorg. Mater. (English Transl.) 13 (1977) 748.
85K Kato, E., Komatsu, T., Kaifu, Y.: J. Phys. Soc. Jpn. 54 (1985) 3597-3604.
88A Anderson, A., Campbell, J. A., Syme, R. W. G.: J. Raman Spectrosc. 19 (1988) 379-382.
91A Anderson, A., Campbell, J. A.: Phys. Status Solidi (b) 163 (1991) 527-531.

Figures to 26.2

Fig. 26.2.1

SbI_3 , BiI_3 . Resistivity (ρ_{\perp}) vs. (reciprocal) temperature [61F]. SbI_3 : ABC intrinsic resistivity, BC change of mobility of charge carriers, CD melting temperature, DE liquid phase. BiI_3 : AB impurity range, BC intrinsic resistivity, CD premelting or decomposition phenomena, DE melting temperature, EF liquid phase.

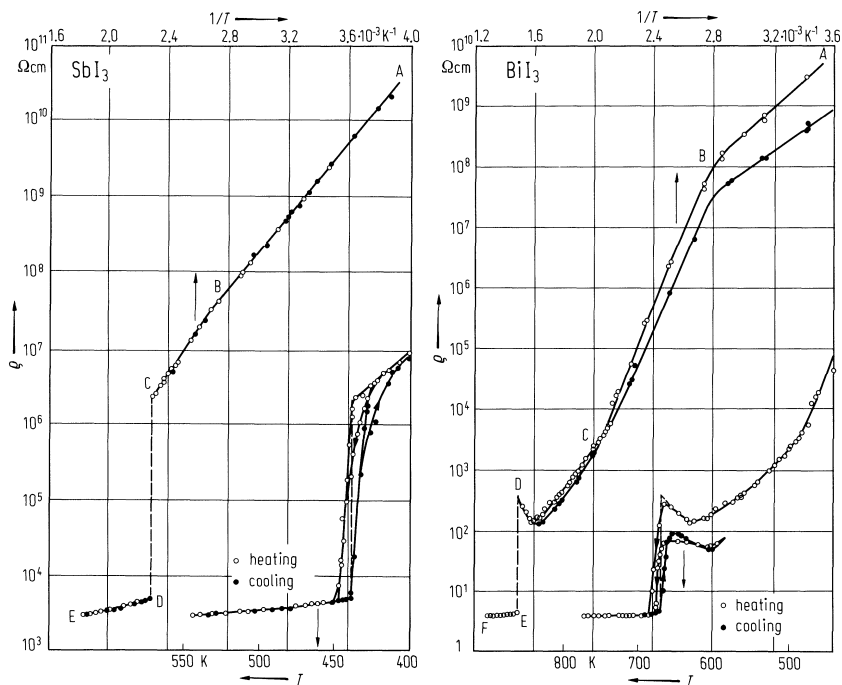


Fig. 26.2.2

AsI_3 , SbI_3 , BiI_3 . Far-infrared reflectivity spectra (solid line) and oscillator fit (dashed line) of single crystals at 80 K, $E \perp c$ (reflectivity vs. wavenumber) [74C].

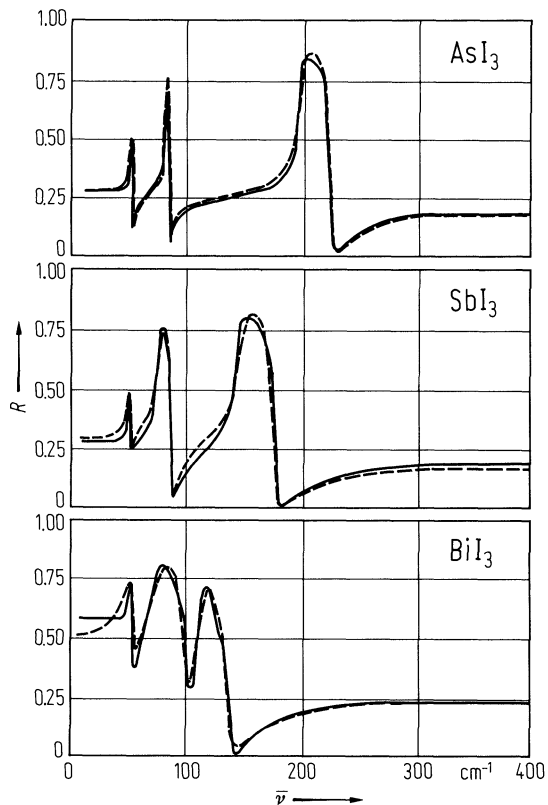
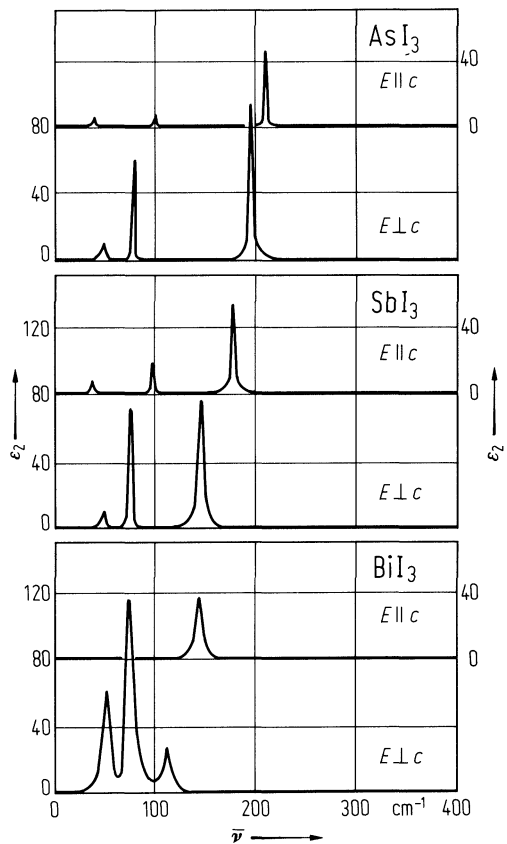


Fig. 26.2.3

AsI_3 , SbI_3 , BiI_3 . Imaginary part of dielectric constant vs. wavenumber, from reflectivity measurements [74C].



26.3 Bismuth triiodide (BiI3)

Electronic properties

band structure: Fig. 26.0.2.

BiI3 is a direct gap material. In BiI3 the fundamental gap appears at point A. A lot of excitonic states can be observed.

energy gaps

$E_{g,dir}$	1.78 eV	$T = 300\text{ K}$	transmission, solution grown layer	89C
	2.011 eV	$T = 2\text{ K}$	photocalorimetric, single crystal	89A
$dE_{g,dir}/dT$	$-3.5\cdot 10^{-4}\text{ eV K}^{-1}$	$T = 90\ldots 420\text{ K}$	crystals and sublimed layers	

reduced effective masses

μ	$0.0014\ m_0$	$c \perp H$	indirect transition,	75K
	$0.0024\ m_0$	$c \parallel H$	magnetoabsorption	

Lattice properties

density

d	5.64 g cm^{-3}	single crystals	68B
-----	-------------------------	-----------------	-----

melting temperature

T_m	400°C		77G
	406°C	probes made by synthesis from the elements	65C

boiling point

T_b	542°C	extrapolated	59C
-------	-----------------------	--------------	-----

optical phonon wavenumbers (in cm^{-1})

	$T = 300\text{ K [74C]}$	$T = 80\text{ K [74C]}$	$T = 4.2\text{ K [74P]}$
$\bar{\nu}_{TO}(n'_i,E_u)$	107.7	109.9	
E_g	115.4	114.6	111
A_u	140.6	140.7	
A_g		93.3	94
$\bar{\nu}_{TO}(n''_i,E_u)$	70.0	72.4	
E_g	23.8	22.4	
A_u	50	52	
A_g		58.1	56
$\bar{\nu}_{TO}(T',E_g)$	54	54.1	
A_g		75(?)	
$\bar{\nu}_{TO}(R',E_u)$	50.0	48.9	
E_g	35	35.3	
A_g			

$\bar{\nu}_{LO}(n''_i)$	151 cm^{-1}	$T = 300\text{ K}$	transmission oblique incidence	74C
-------------------------	----------------------	--------------------	--------------------------------	-----

elastic constants

measured by Brillouin scattering at 83 K (in 10^6 N/cm^2)

$c_{11} = 2.9$	$c_{12} = 0.50$	$c_{13} = 0.90$	$ c_{14} = 0.20$
$ c_{25} = 0$	$c_{33} = 2.6$	$c_{44} = 0.70$	

85K

Transport properties

resistivity

ρ_{\perp}	$8 \cdot 10^7 \Omega \text{ cm}$	$T = 293 \text{ K}$		67B
	$2 \cdot 10^9 \Omega \text{ cm}$	$T = 300 \text{ K}$	photoconductivity (dark current)	63E

dependence on temperature: Fig. 26.3.1.

activation energy of intrinsic resistivity

E_A	2.52(10) eV	solid phase	part B–C in Fig. 26.3.1	61F
-------	-------------	-------------	-------------------------	-----

Optical properties

optical spectra : Figs. 26.3.2...4.

dielectric constants

$\varepsilon(0)$	54(25)	$E \perp c, T = 300 \text{ K}$	microwave method	73V
	8.6(10)	$E \parallel c, T = 300 \text{ K}$		
$\varepsilon(\infty)$	7.1	$E \perp c, T = 300 \text{ K}$	reflectivity	74C
	6.4	$E \parallel c, T = 300 \text{ K}$		

third order susceptibility

$\chi^{(3)}$	10^{-2} e.s.u.			88A
--------------	--------------------------	--	--	-----

References to 26.3

- 59C Cubicciotti, D., Keneshea, F. J.: J. Phys. Chem. 63 (1959) 295.
61F Fischer, G.: Helv. Phys. Acta 34 (1961) 827.
63E Evans, B. L.: Proc. Roy. Soc. (London) Ser. A 276 (1963) 136.
65C Cubicciotti, D., Eding, H.: J. Phys. Chem. 69 (1965) 3621.
67B Belotskii, D. P., Antipov, I. N., Krylyuk, N. V.: Ukr. Khim. Zh. 33 (1967) 14.
68B Belotskii, D. P., Timofeev, V. B., Antipov, I. N., Vashchenko, V. I., Bespal'chenko, V. A.: Russ. J. Phys. Chem. 42 (1968) 740.
73V Vits, P.: Diplomarbeit, RWTH Aachen 1973
74C Clasen, R.: Thesis, RWTH Aachen 1974.
74P Petroff, Y., Yu, P. Y., Shen, Y. R.: Phys. Status Solidi (b) 61 (1974) 419.
75K Kolosyuk, V. N., Vashchenko, V. I., Berezdet'skii, T. I.: Opt. Spectrosc. (USSR) 39 (1975) 335.
76S Schlüter, S., Cohen, M. L., Kohn, S. F., Fong, C. Y.: Phys. Status Solidi (b) 78 (1976) 737.
77G Gasinets, S. M., Shpyrko, G. M., Golovei, M. I., Mel'nichenko, T. N.: J. Inorg. Mater. (English Transl.) 13 (1977) 748.
77K Kaifu, Y., Komatsu, T., Aikami, T.: Nuovo Cimento B 38 (1977) 449.
85K Kato, E., Komatsu, T., Kaifu, Y.: J. Phys. Soc. Jpn. 54 (1985) 3597-3604.
88A Anderson, A., Campbell, J. A., Syme, R. W. G.: J. Raman Spectrosc. 19 (1988) 379-382.
89A Akai, I., Karasawa, T., Kaifu, Y.: J. Phys. Soc. Jpn. 58 (1989) 718-725.
89C Chaudhuri, T. K., Patra, A. B., Basu, P. K., Saraswat, R. S., Acharya, H. N.: Mater. Lett. 8 (1989) 361-363.

Figures to 26.3

Fig. 26.0.2

BiI₃. Band structure (without spin-orbit effects). For clarity, only the outermost bands are plotted [76S].

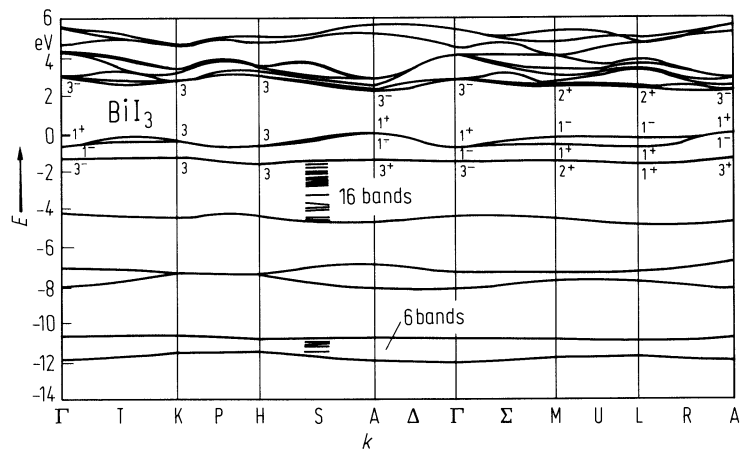


Fig. 26.3.1

SbI_3 , BiI_3 . Resistivity (ρ_{\perp}) vs. (reciprocal) temperature [61F]. SbI_3 : ABC intrinsic resistivity, BC change of mobility of charge carriers, CD melting temperature, DE liquid phase. BiI_3 : AB impurity range, BC intrinsic resistivity, CD premelting or decomposition phenomena, DE melting temperature, EF liquid phase.

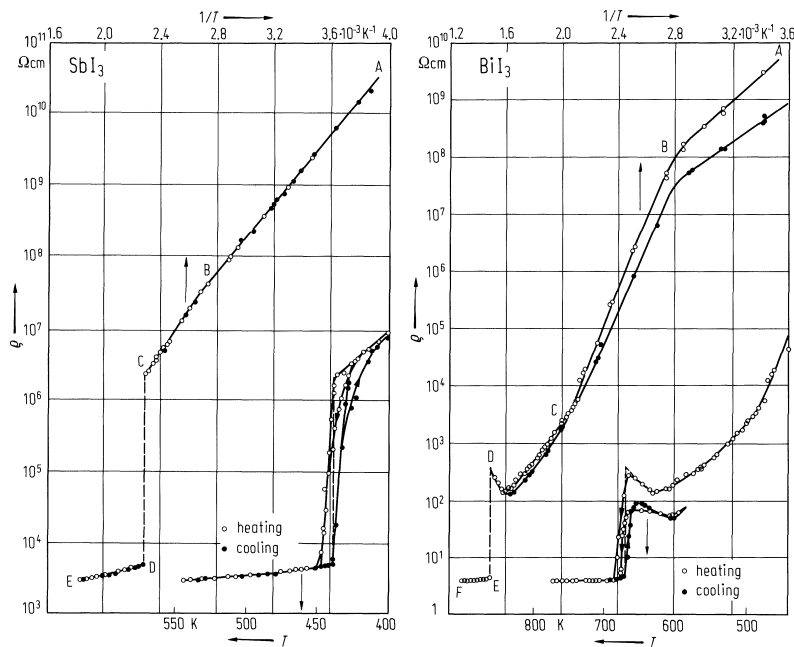


Fig. 26.3.2

AsI_3 , SbI_3 , BiI_3 . Far-infrared reflectivity spectra (solid line) and oscillator fit (dashed line) of single crystals at 80 K, $E \perp c$ (reflectivity vs. wavenumber) [74C].

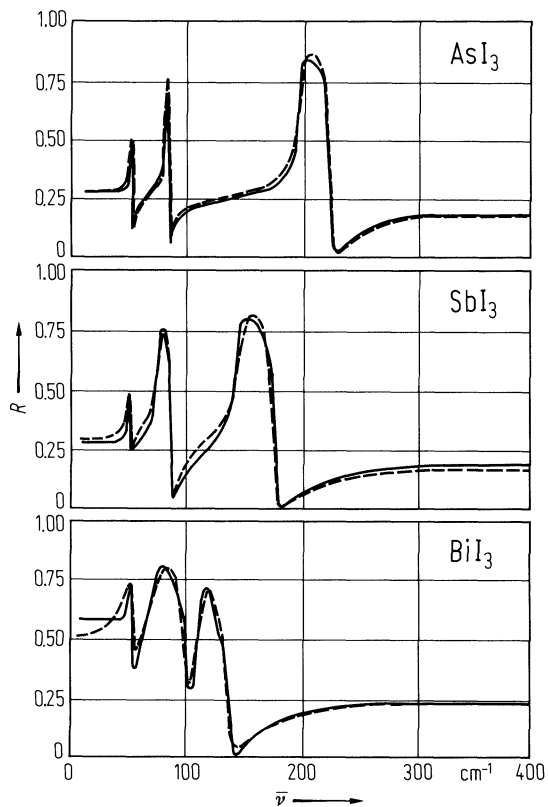


Fig. 26.3.3

AsI_3 , SbI_3 , BiI_3 . Imaginary part of dielectric constant vs. wavenumber, from reflectivity measurements [74C].

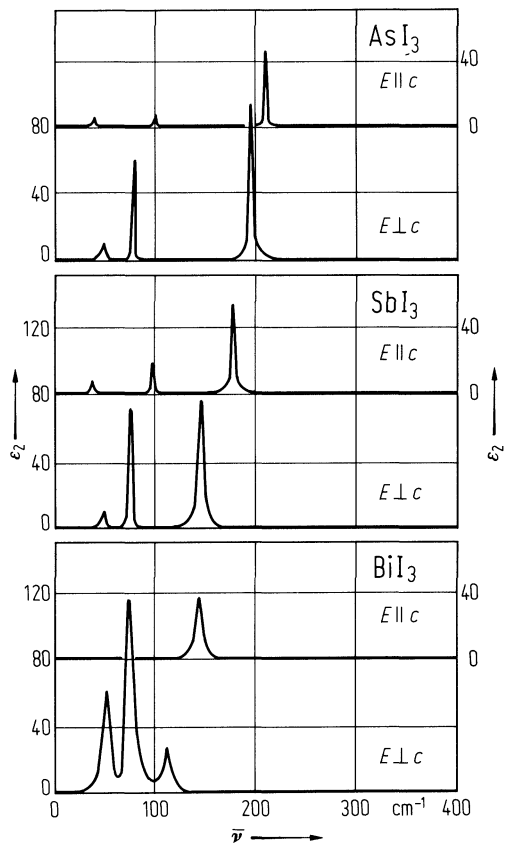
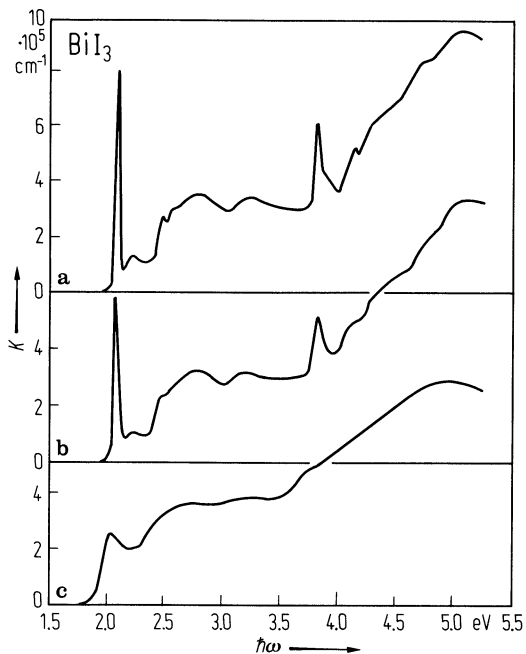


Fig. 26.3.4

BiI_3 . Absorption coefficient vs. photon energy of single crystals calculated by Kramers-Kronig analysis a) 6 K, b) 77 K, c) 286 K; $E \perp c$ [77K].



27 I_x-IV_y-VI_z compounds

27.0 Crystal structure of I_x-IV_y-VI_z compounds

The *I₈-IV-VI₆* compounds are isoelectronic analogues to the II₃-V₂ compounds. They exhibit a pronounced low-temperature polymorphism with a fcc high-temperature phase (γ -phase, space group O²-P4₂32) and six low-temperature phases: α , α' , α'' , β , β' , β'' . From these α'' is cubic (space group T³-I23 or T⁵-I2₁3). The structure of the other phases is not clear, β' and β'' may be cubic or monoclinic with $a \approx b \approx c$, $\beta \approx 90^\circ$.

Ag₈GeS₆ and Ag₈SnS₆ are known as the minerals argyrodite and canfieldite, respectively. The following structure data are known (Ag-compounds: [68G, 81K], Cu compounds: [65H, 74K, 82A])

Substance	Temperature of phase transformation [°C]	Lattice parameters(in Å)		
		at 25°C	of γ -phase at	T [°C]
Ag ₈ SiS ₆	234 ($\alpha'' \rightarrow \gamma$)	21.00	10.63	250
Ag ₈ GeS ₆	223 ($\alpha'' \rightarrow \gamma$)	21.19	10.70	240
Ag ₈ SnS ₆	172 ($\alpha'' \rightarrow \gamma$)	21.43	10.85	200
Ag ₈ SiSe ₆	10 ($\alpha' \rightarrow \beta''$)	10.87	10.97	150
	40 ($\beta'' \rightarrow \gamma$)			
Ag ₈ GeSe ₆	-4 ($\alpha' \rightarrow \beta'$)	10.95	10.99	65
	48 ($\beta' \rightarrow \gamma$)			
Ag ₈ SnSe ₆	83 ($\beta' \rightarrow \gamma$)	11.07	11.12	200
Ag ₈ SiTe ₆	-78 ($\alpha \rightarrow \beta$)		11.515	20
	-10 ($\beta \rightarrow \gamma$)			
Ag ₈ GeTe ₆	-52 ($\alpha \rightarrow \beta$)		11.570	20
	-29 ($\beta \rightarrow \gamma$)			
Cu ₈ SiS ₆			9.76	20
Cu ₈ GeS ₆	55 ($\beta' \rightarrow \gamma$)	9.90	9.909(5)	60
Cu ₈ SiSe ₆			10.17	20
Cu ₈ GeSe ₆	56			

For structural data of other I_x-IV_y-VI_z compounds see sections 27.9 and 27.10.

References to 27.0

65H Hahn, H., Schulze, H., Sechser, L.: *Naturwissenschaften* 52 (1965) 451.
68G Gorochof, O.: *Bull. Soc. Chim. France* 6 (1968) 2263.
74K Khanafer, M., Gorochof, O., Rivet, J.: *Mater. Res. Bull.* 9 (1974) 1543.
81K Katty, A., Gorochof, O., Letoffe, J. M.: *J. Solid State Chem.* 38 (1981) 259.
82A Aliev, M. J., Arasly, D. G., Dzhabrailov, T. G.: *Sov. Phys. Solid State* 24 (1982) 150 (transl. from *Fiz. Tverd. Tela* 24 (1982) 268).

27.1 Ag8GeS6 (argyrodite)

Crystal structure

see section 27.0.

Physical properties

energy gap

E_g	1.39 eV	$T = 293\text{ K}$	"red edge" of photoconductivity spectrum	72O
dE_g/dT	$-8.5\cdot 10^{-4}\text{ eV K}^{-1}$	α "-phase	temperature shift of absorption edge	77K

phonon energies

$h\nu_i$	93 meV	$T = 330\text{ K}$	infrared absorption bands (phonon transitions)	75B
	96 meV			
	98 meV			

electrical conductivity

σ	$10^{-3}\text{ }\Omega^{-1}\text{ cm}^{-1}$	$T = 280\text{ K}$		76P
----------	---	--------------------	--	-----

thermal conductivity

κ	$3\cdot 10^{-3}\text{ W cm}^{-1}\text{ K}^{-1}$			76P
----------	---	--	--	-----

melting point

T_m	955°C			68G
-------	-------	--	--	-----

density

d_{calc}	6.30 g cm^{-3}			65H
d_{exp}	6.21 g cm^{-3}	$T = 298\text{ K}$		68G

References to 27.1

65H Hahn, H., Schulze, H., Sechser, L.: Naturwissenschaften 52 (1965) 451.
68G Gorochov, O.: Bull. Soc. Chim. France 6 (1968) 2263.
72O Osipishin, I. S., Butsko, N. I., Gasii, H. I., Zhezhnich, I. D.: Sov. Phys. Semicond. 6 (1972) 974 (transl. from Fiz. Tekh. Poluprovodn. 6 (1972) 1121).
75B Bendorius R., Irzikevicius A., Kinduris, A. . Tsvetkova, E. V.: Phys. Status Solidi (a) 28 (1975) K125.
76P Petrov, A. V., Orlov, V. M., Zaitsev, V. K., Feigel'man: Sov. Phys. Solid State 17 (1976) 2407 (transl. from Fiz. Tverd. Tela 17 (1975) 3703).
77K Kinduris, A., Shileika, A.: 3rd Int. Conf. on Ternary Compounds, Edinburgh 1977, The Institute of Physics, London 1977, p. 67.

27.2 Ag₈SnS₆ (canfieldite)

Crystal structure

see section 27.0.

Physical properties

energy gap

E_g	1.28 eV	$T = 295\text{ K}$	fundamental absorption edge	76K, 77K
dE_g/dT	$-5\cdot 10^{-4}\text{ eV K}^{-1}$	γ -phase		76K, 77K

electrical conductivity

σ	$10^{-3}\text{ }\Omega^{-1}\text{ cm}^{-1}$	$T = 280\text{ K}$		76P
----------	---	--------------------	--	-----

thermal conductivity

κ	$3.2\cdot 10^{-3}\text{ W cm}^{-1}\text{ K}^{-1}$		76P
----------	---	--	-----

melting point

T_m	839°C		68G
-------	-------	--	-----

density

d_{calc}	6.31 g cm^{-3}		65H
d_{exp}	6.28 g cm^{-3}	$T = 298\text{ K}$	68G

References to 27.2

65H Hahn, H., Schulze, H., Sechser, L.: *Naturwissenschaften* 52 (1965) 451.
68G Gorochof, O.: *Bull. Soc. Chim. France* 6 (1968) 2263.
76K Kinduris, A. S., Bendorius, R. A., Senulene, D. B.: *Sov. Phys. Semicond.* 10 (1976) 916 (transl. from. *Fiz. Tekh. Poluprovodn.* 10 (1976) 1544).
77K Kinduris, A., Shileika, A.: 3rd Int. Conf. on Ternary Compounds, Edinburgh 1977, The Institute of Physics, London 1977, p. 67.

27.3 Ag₈SiSe₆

Crystal structure

see section 27.0.

Physical properties

energy gap

E_g	0.97 eV	$T = 295\text{ K}$	absorption edge	76B, 77K
-------	---------	--------------------	-----------------	-------------

phonon energy

$h\nu_i$	70 meV	$T = 330\text{ K}$	infrared absorption bands	75B
	80 meV			
	104 meV			

melting point

T_m	930°C			68G
-------	-------	--	--	-----

density

d_{calc}	7.06 g cm ⁻³			68G
d_{exp}	6.95 g cm ⁻³	$T = 298\text{ K}$		68G

References to 27.3

68G Gorochov, O.: Bull. Soc. Chim. France 6 (1968) 2263.
75B Bendorius R., Irzikevicius A., Kinduris, A. . Tsvetkova, E. V.: Phys. Status Solidi (a) 28 (1975) K125.
76B Bendorius, R. A., Kinduris, A. S., Tsvetkova, E. V., Shileika, A. Yu.: Inorg. Mater. (USSR) 12 (1976) 1437; (transl. from Izv. Akad. Nauk SSSR, Neorg. Mater. 12 (1976) 1745).
77K Kinduris, A., Shileika, A.: 3rd Int. Conf. on Ternary Compounds, Edinburgh 1977, The Institute of Physics, London 1977, p. 67.

27.4 Ag8GeSe6

Crystal structure

see section 27.0.

Physical properties

energy gap

E_g	0.84...0.88 eV	$T = 300\text{ K}$	conductivity, photoconductivity,	76B,
dE_g/dT	$-5 \cdot 10^{-4}\text{ eV K}^{-1}$		temperature shift of absorption edge	76K

phonon energies

$h\nu_i$	55 meV	$T = 330\text{ K}$	infrared absorption bands	75B
	62 meV			
	71 meV			

electrical conductivity : Fig. 27.4.1

melting point

T_m	902°C			68G
-------	-------	--	--	-----

density

d_{calc}	7.13 g cm ⁻³			68G
d_{exp}	7.07 g cm ⁻³	$T = 298\text{ K}$		68G

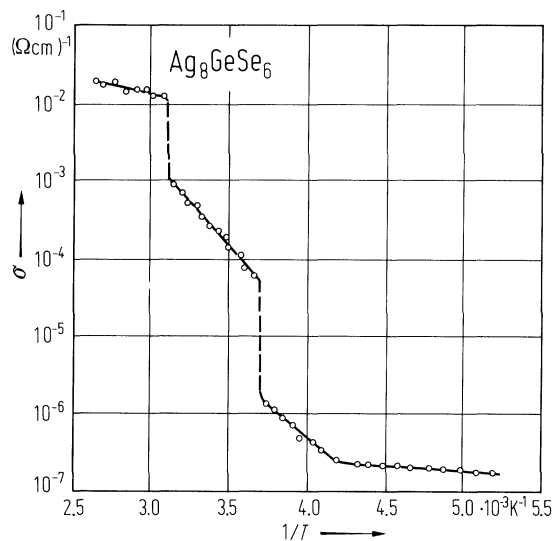
References to 27.4

68G Gorochov, O.: Bull. Soc. Chim. France 6 (1968) 2263.
75B Bendorius R., Irzikevicius A., Kinduris, A. . Tsvetkova, E. V.: Phys. Status Solidi (a) 28 (1975) K125.
76B Bendorius, R. A., Kinduris, A. S., Tsvetkova, E. V., Shileika, A. Yu.: Inorg. Mater. (USSR) 12 (1976) 1437; (transl. from Izv. Akad. Nauk SSSR, Neorg. Mater. 12 (1976) 1745).
76K Kinduris, A. S., Bendorius, R. A., Senulene, D. B.: Sov. Phys. Semicond. 10 (1976) 916 (transl. from. Fiz. Tekh. Poluprovodn. 10 (1976) 1544).
77O Osipishin, I. S.: Sov. Phys. Semicond. 11 (1977) 102 (transl. from Fiz. Tekh. Poluprovodn. 11 (1977) 181).

Figures to 27.4

Fig. 27.4.1

Ag_8GeSe_6 . Temperature dependence of the conductivity showing steps in the conductivity [77O].



27.5 Ag₈SnSe₆

Crystal structure

see section 27.0.

Physical properties

energy gap

E_g	0.83 eV	$T = 295$ K	absorption edge	76B
dE_g/dT	$-5 \cdot 10^{-4}$ eV K ⁻¹	γ -phase	temperature shift of absorption edge	76K, 77K

photon energy

$h\nu_i$	53 meV	$T = 330$ K	infrared absorption band	75B
	57 meV			
	63 meV			

electrical conductivity

σ	$2 \cdot 10^{-2} \dots 70$ Ω^{-1} cm ⁻¹	$T = 280$ K	data on several samples (temperature dependence of conductivity, Fig. 27.5.1)	76P
----------	---	-------------	---	-----

Seebeck coefficient

S	$-160 \dots -730$ μ V K ⁻¹			76P
-----	---	--	--	-----

thermal conductivity

κ	$(3.1 \dots 3.5) \cdot 10^{-3}$ W cm ⁻¹ K ⁻¹			76P
----------	---	--	--	-----

peritectic temperature

T_{perit}	735°C		temperature of peritectic decomposition	68G
--------------------	-------	--	--	-----

density

d_{calc}	7.12 g cm ⁻³			68G
d_{exp}	7.01 g cm ⁻³	$T = 298$ K		68G

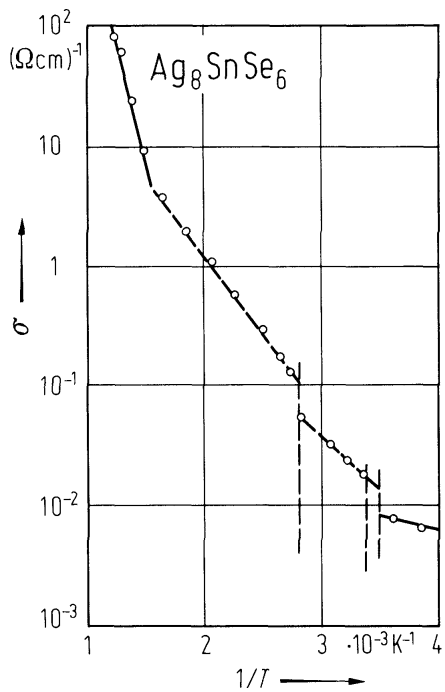
References to 27.5

- 68G Gorochoy, O.: Bull. Soc. Chim. France 6 (1968) 2263.
75B Bendorius R., Irzikevicius A., Kinduris, A. . Tsvetkova, E. V.: Phys. Status Solidi (a) 28 (1975) K125.
76B Bendorius, R. A., Kinduris, A. S., Tsvetkova, E. V., Shileika, A. Yu.: Inorg. Mater. (USSR) 12 (1976) 1437; (transl. from Izv. Akad. Nauk SSSR, Neorg. Mater. 12 (1976) 1745).
76K Kinduris, A. S., Bendorius, R. A., Senulene, D. B.: Sov. Phys. Semicond. 10 (1976) 916 (transl. from. Fiz. Tekh. Poluprovodn. 10 (1976) 1544).
76P Petrov, A. V., Orlov, V. M., Zaitsev, V. K., Feigel'man: Sov. Phys. Solid State 17 (1976) 2407 (transl. from Fiz. Tverd. Tela 17 (1975) 3703).
77K Kinduris, A., Shileika, A.: 3rd Int. Conf. on Ternary Compounds, Edinburgh 1977, The Institute of Physics, London 1977, p. 67.

Figures to 27.5

Fig. 27.5.1

Ag_8SnSe_6 . Electrical conductivity vs. reciprocal temperature [76P].



27.6 Ag₈GeTe₆

Crystal structure

see section 27.0.

Physical properties

energy gap

E_g	0.47 eV	$T = 295$ K	absorption edge	77K
dE_g/dT	$< 1 \cdot 10^{-4}$ eV K ⁻¹		temperature shift of absorption edge	77K

density

d_{calc}	7.31(7) g cm ⁻³			81K
d_{exp}	7.22 g cm ⁻³	$T = 298$ K		81K

References to 27.6

- 77K Kinduris, A., Shileika, A.: 3rd Int. Conf. on Ternary Compounds, Edinburgh 1977, The Institute of Physics, London 1977, p. 67.
- 81K Katty, A., Gorochoy, O., Letoffe, J. M.: J. Solid State Chem. 38 (1981) 259.

27.7 Cu₈GeS₆

Crystal structure

see section 27.0.

Physical properties

energy gap

E_g	0.10 eV	β' -phase	74K
	0.04 eV	γ -phase	

electrical resistivity : Fig. 27.7.1

melting point

T_m	980(3)°C	74K
-------	----------	-----

density

d_{calc}	5.28 g cm ⁻³	74K
d_{exp}	5.97 g cm ⁻³	$T = 298 \text{ K}$ 74K

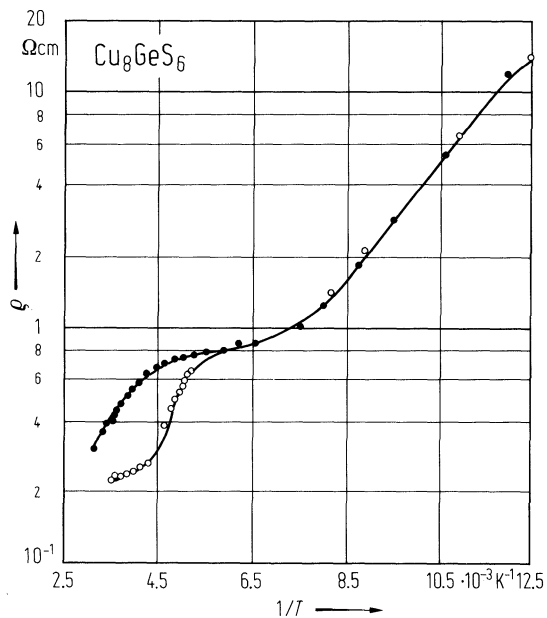
References to 27.7

74K Khanafer, M., Gorochoy, O., Rivet, J.: Mater. Res. Bull. 9 (1974) 1543.

Figures to 27.7

Fig. 27.7.1

Cu_8GeS_6 . Resistivity of two samples vs. reciprocal temperature [74K].



27.8 Cu₈GeSe₆

Crystal structure

see section 27.0.

Physical properties

density

d_{calc}	6.27 g cm ⁻³	65H
d_{exp}	5.97 g cm ⁻³	65H

electrical and thermal conductivity : Fig. 27.8.1.

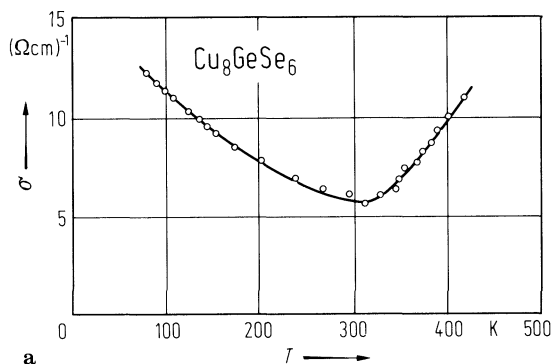
References to 27.8

- 65H Hahn, H., Schulze, H., Sechser, L.: Naturwissenschaften 52 (1965) 451.
82A Aliev, M. J., Arasly, D. G., Dzhabrailov, T. G.: Sov. Phys. Solid State 24 (1982) 150 (transl. from Fiz. Tverd. Tela 24 (1982) 268).

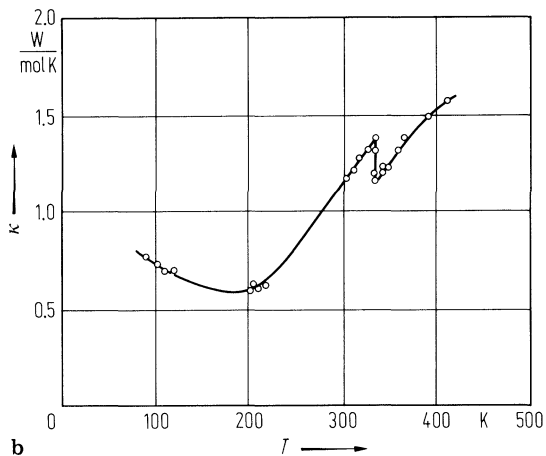
Figures to 27.8

Fig. 27.8.1

Cu_8GeSe_6 . Electrical conductivity (a) and thermal conductivity (b) vs. (reciprocal) temperature [82A]. Unit of thermal conductivity κ as given in the original paper.



a



b

27.9 Cu₄Ge₃S₅, Cu₄Ge₃Se₅ and Cu₄Sn₃Se₅

The compounds Cu₄Ge₃S₅, Cu₄Ge₃Se₅ and Cu₄Sn₃Se₅ (melting points $T_m = 675(3)^\circ\text{C}$, 615°C and 600°C , respectively) are proven as semiconductors in [77D]. Hall mobilities are in the range of 10 to 300 cm²/Vs.

Crystal structure

Cu₄Ge₃S has a tetragonal lattice with $a = 5.30 \text{ \AA}$ and $c = 10.48 \text{ \AA}$ at RT, Cu₄Ge₃Se₅ has a fcc lattice with $a = 5.53 \text{ \AA}$ at RT [77D]. The structure of Cu₄Sn₃Se₅ is not known.

References to 27.9

- 77D Dovletov, K., Tashliev, K., Rozyeva, K. A., Ashirov, A., Anikin, A. V.: Inorg. Mater. (USSR) 13 (1977) 889 (transl. from Izv. Akad. Nauk SSSR, Neorg. Mater. 13 (1977) 1092).

27.10 Cu₄SnS₄

Cu₄SnS₄ has an orthorhombic lattice with $a = 13.70(1) \text{ \AA}$, $b = 7.750(5) \text{ \AA}$, $c = 6.454(5) \text{ \AA}$ at room temperature. At $T = -41^\circ\text{C}$ a phase transition occurs without a change of the lattice parameters [74K].

Physical properties

energy gap

E_g	0.03 eV	high-temperature phase	74K
	0.11 eV	low-temperature phase	

electrical conductivity : Fig. 27.10.1

hole mobility

μ_p	3 cm ² /Vs	$T = 300 \text{ K}$	74K
---------	-----------------------	---------------------	-----

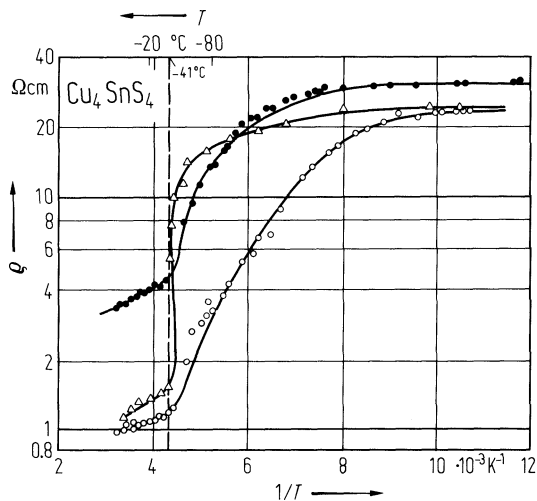
References to 27.10

74K Khanafer, M., Gorochoy, O., Rivet, J.: Mater. Res. Bull. 9 (1974) 1543.

Figures to 27.10

Fig. 27.10.1

Cu_4SnS_4 . Resistivity of three samples vs. (reciprocal) temperature [74K].



28 I_X-V_Y-VI_Z compounds

28.0 Crystal structure and electronic structure

28.0.1 I–V–VI₂ compounds (I = Ag, V = Sb, Bi, VI = S, Se, Te)

All AgSbX₂ and AgBiX₂ compounds with X = S, Se, Te crystallize (at least in their high-temperature modification) in the face centered cubic NaCl structure with I- and V-atoms distributed statistically between the close-packed layers of VI-atoms [59G].

lattice parameters

Substance	<i>a</i> [Å]	<i>T</i> [°C]		Ref.
AgSbS ₂	5.6514(5)	> 403		77B
AgSbSe ₂	5.786(3)	25		59G
AgSbTe ₂	6.078(3)	25		59G
AgBiS ₂	5.648(3)	25	The 25°-values for AgBiS ₂ (Se ₂ ,Te ₂) are data for the high temperature phases. For the room-temperature phases see below	59G
	5.682(3)	200		59G
	5.693(3)	243		59G
AgBiSe ₂	5.832(3)	25		59G
	5.887(3)	300		59G
AgBiTe ₂	6.155(3)	25		59G

Below 380°C AgSbS₂ crystallizes in a monoclinic α-phase (space group: C_{2h}³-A2/m or Aa) with *a* = 13.2269(13) Å, *b* = 4.4112(5) Å, *c* = 12.8798(11) Å, β = 98.48(1)° [77B].

lattice parameters (room-temperature phase)

	<i>a</i> [Å]	<i>c</i> [Å]	<i>d</i> _x [g cm ⁻³]	Ref.
AgBiS ₂	4.07(2)	19.06(5)	6.94	59G
AgBiSe ₂	4.18(2)	19.67(5)	7.94	59G
AgBiTe ₂	4.37(2)	20.76(5)	8.30	59G

28.0.2 I₃-V-VI₃ compounds: Ag₃AsS₃, Ag₃SbS₃

Ag₃AsS₃ and Ag₃SbS₃ crystallize in a non-centrosymmetric uniaxial structure (space group C_{6v}³-R3c).

lattice parameters (in hexagonal description, RT values)

Substance	<i>a</i> [Å]	<i>c</i> [Å]	Ref.
Ag ₃ AsS ₃	10.80	8.69	73D
Ag ₃ SbS ₃	11.058	8.698	73G

band structure of Ag₃AsS₃: Fig. 28.0.1, Brillouin zone: Fig. 28.0.2.

References to 28.0

- 59G Geller, S., Wernick, J. H.: Acta Crystallogr. 12 (1959) 46.
73D Dovgii, Ya. O., Korolyshin, V. N., Moroz, E. T.: Sov. Phys. Dokl. 17 (1973) 1070 (transl. from Dokl. Akad. Nauk SSSR 207 (1972) 71).
77B Bohac, P., Orliukas, A., Gäumann, A., Girgis, K.: Helv. Phys. Acta 50 (1977) 853.

Figures to 28.0

Fig. 28.0.1

Ag_3AsS_3 . Band structure along two principal axes in the Brillouin zone estimated by group theoretical considerations and the experimental results of Figs. 3 and 4 [73D].

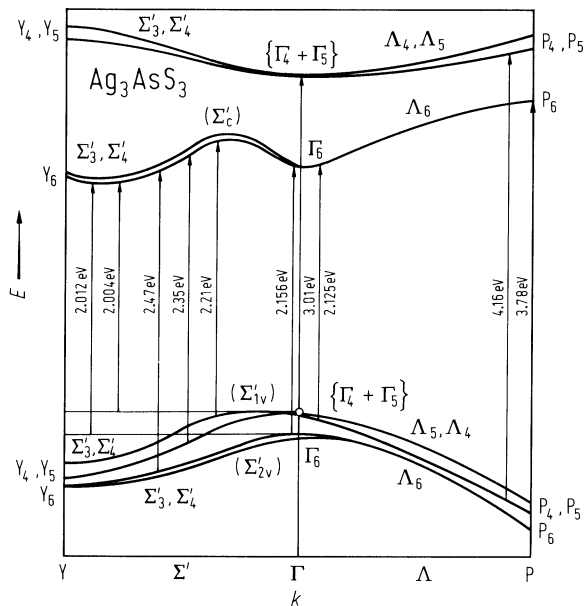
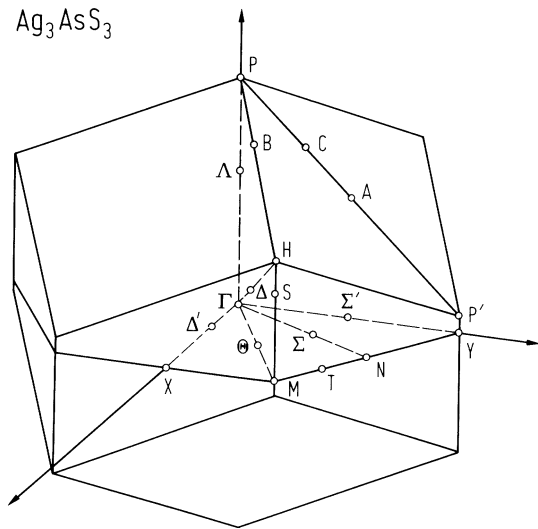


Fig. 28.0.2

Ag_3AsS_3 . Brillouin zone of the proustite structure [73D].



28.1 AgAsS₂

Physical properties

energy gap

$E_{g,ind}$	2.084 eV	$T = 295$ K	indirect absorption edge,	74G
		polarization \perp crystal axis		
	2.108 eV	polarization \parallel crystal axis		
$E_{g,dir}$	2.14 eV	$T = 293$ K	maximum in the spectral distribution of photoconductivity	75G

electrical resistivity

ρ	$9 \cdot 10^9 \Omega \text{ cm}$	$T = 293$ K		75G
--------	----------------------------------	-------------	--	-----

melting point

T_m	419°C			75G
-------	-------	--	--	-----

References to 28.1

- 74G Golovach, I. I., Slivka, V. Yu., Dovgoshei, N. I., Syrbu, N. N., Bogdanova, A. V., Golovei, M. I.: Sov. Phys. Semicond. 9 (1974) 834 (transl. from Fiz. Tekh. Poluprovodn. 9 (1974) 1260).
- 75G Golovach, I. I., Dovgoshei, N. I., Slivka, V. Yu., Suslikov, L. M., Golovei, M. I., Bogdanova, A. V.: Inorg. Mater. 11 (1975) 820 (transl. from Izv. Akad. Nauk SSSR, Neorg. Mater. 11 (1975) 956).

28.2 AgAsSe₂

Physical properties

energy gap

E_g	0.8...1.0 eV	58W
-------	--------------	-----

melting point

T_m	390°C	58W
-------	-------	-----

References to 28.2

58W Wernick, J. H., Geller, S., Benson, K. E.: J. Phys. Chem. Solids 4 (1958) 154.

28.3 AgAsTe₂

Physical properties

energy gap

E_g 0.8...1.0 eV

58W

melting point

T_m 325°C

58W

References to 28.3

58W Wernick, J. H., Geller, S., Benson, K. E.: J. Phys. Chem. Solids 4 (1958) 154.

28.4 AgSbS₂

Crystal structure

see section 28.0.

Physical properties

energy gap

E_g	1.73 eV	$T = 300$ K	optical energy gap, Fig. 28.4.1	77B
dE_g/dT	$-1.96 \cdot 10^{-3}$ eV/K	$T < 653$ K		77B
	$-1.58 \cdot 10^{-4}$ eV/K	$T = 653 \dots 676$ K		
	$-4.95 \cdot 10^{-4}$ eV/K	$T > 676$ K		

activation energy

$E_A(\sigma)$	0.89 eV	$T < 476$ K	activation energy of conductivity;	79V
	1.64 eV	$T > 476$ K	the electrical conductivity increases exponentially with rising temperature, see Fig. 28.4.2	

hole mobility

$\mu_{H,p}$	0.24 cm ² /Vs	$T = 300$ K		79V
-------------	--------------------------	-------------	--	-----

melting point

T_m	512(2)°C			77B
-------	----------	--	--	-----

density

d_{calc}	5.42 g cm ⁻³		X-ray density; for temperature dependence of experimental density	59G
------------	-------------------------	--	--	-----

References to 28.4

59G Geller, S., Wernick, J. H.: Acta Crystallogr. 12 (1959) 46.
77B Bohac, P., Orliukas, A., Gäumann, A., Girgis, K.: Helv. Phys. Acta 50 (1977) 853.
79V Valynkenas, V. I., Orlyukas, A. S., Sakals, A. P., Mikolaitis, V. A.: Sov. Phys. Solid State 21 (1979) 1499 (transl. from Fiz. Tverd. Tela 21 (1979) 2449).

Figures to 28.4

Fig. 28.4.1

AgSbS_2 . Energy gap vs. temperature [77B].

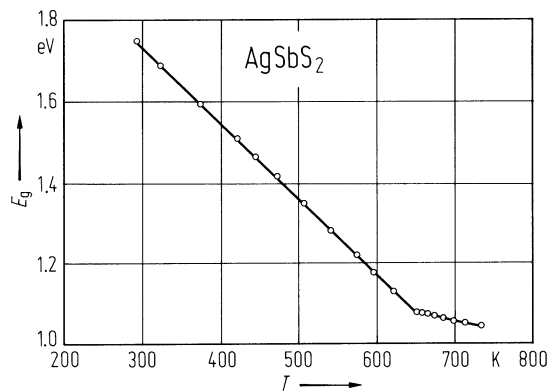
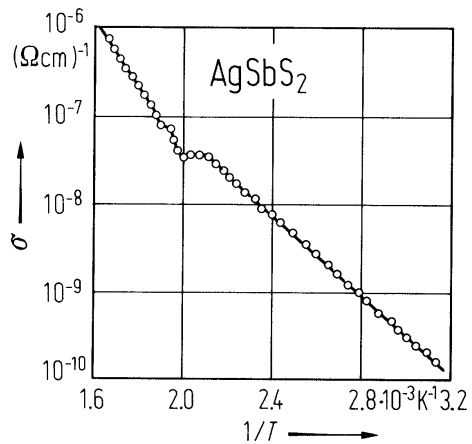


Fig. 28.4.2

AgSbS₂. Electrical conductivity vs reciprocal temperature [79V].



28.5 AgSbSe₂

Crystal structure

see section 28.0.

Physical properties

energy gap

$E_{g,th}$	0.58...0.62 eV	from conductivity	68A
------------	----------------	-------------------	-----

hole mobility

μ_p	1500 cm ² /Vs		68A
---------	--------------------------	--	-----

For temperature dependence of transport parameters, see Fig. 28.5.1

thermal conductivity

κ	1.1·10 ⁻³ cal/K cm s	practically independent of temperature	62P
----------	---------------------------------	--	-----

Debye temperature

Θ_D	175 K		62P
------------	-------	--	-----

linear thermal expansion coefficient

α	23·10 ⁻⁶ K ⁻¹	$T = 295...675$ K	62P
----------	-------------------------------------	-------------------	-----

melting point

T_m	636°C		62P
-------	-------	--	-----

density

d_{calc}	6.60 g cm ⁻³		59G
------------	-------------------------	--	-----

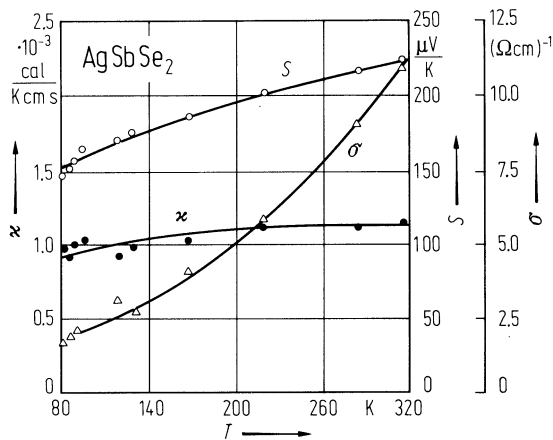
References to 28.5

59G	Geller, S., Wernick, J. H.: Acta Crystallogr. 12 (1959) 46.
62P	Petrov, A. V., Shtrum, E. L.: Sov. Phys. Solid State 4 (1962) 1061 (transl. from Fiz. Tverd. Tela 4 (1962) 1442).
68A	Abdullaev, G. B., Mal'sagov, A. U., Glazov, V. M.: Inorg. Mater. 4 (1968) 1082 (transl. from Izv. Akad. Nauk SSSR, Neorg. Mater. 4 (1968) 1233).

Figures to 28.5

Fig. 28.5.1

AgSbSe_2 . Temperature dependence of thermal conductivity, electrical conductivity, and Seebeck coefficient of a sample slowly cooled from the melting point to room temperature [62P].



28.6 AgSbTe₂

Crystal structure

see section 28.0.

Physical properties

electrical conductivity

σ	$160\ \Omega^{-1}\ \text{cm}^{-1}$	$T = 300\ \text{K}$	58Z
----------	------------------------------------	---------------------	-----

hole mobility

μ_p	$75\ \text{cm}^2/\text{Vs}$	$T = 300\ \text{K}$	58Z
---------	-----------------------------	---------------------	-----

thermal conductivity

κ	$1.7 \cdot 10^{-3}\ \text{cal/K cm s}$	$T = 80 \dots 400\ \text{K}$	60H
----------	--	------------------------------	-----

linear thermal expansion coefficient

α	$23 \cdot 10^{-6}\ \text{K}^{-1}$	$T = 295 \dots 375\ \text{K}$	58Z
----------	-----------------------------------	-------------------------------	-----

melting point

T_m	561°C		68K
-------	---------------------	--	-----

density

d_{calc}	$7.12\ \text{g cm}^{-3}$		59G
-------------------	--------------------------	--	-----

References to 28.6

58Z	Zhuse, V. P., Sergeeva, V. M., Shtrum, E. L.: Sov. Phys. Tech. Phys. 3 (1958) 1925 (transl. from Zh. Tekhn. Fiz. 28 (1958) 2093).
59G	Geller, S., Wernick, J. H.: Acta Crystallogr. 12 (1959) 46.
60H	Haake, G., Poganski, S.: Proc. Int. . Phys. Semicond., Prague 1960, Publ. House of the Acad. Sci., Prague 1960, p. 999.
68K	Krestovnikov, A. N., Mal'sagov, A. U., Glazov, V. M.: Inorg. Mater. 4 (1968) 119 (transl. from Izv. Akad. Nauk SSSR, Neorg. Mater. 4 (1968) 144).

28.7 AgBiS₂

Crystal structure

see section 28.0.

Physical properties

energy gap

E_g	0.9 eV	from reflectivity measurements	75G
-------	--------	--------------------------------	-----

electrical conductivity

σ	$4 \cdot 10^3 \Omega^{-1} \text{ cm}^{-1}$	$T = 293 \text{ K}$	75G
----------	--	---------------------	-----

melting point

T_m	810°C		75G
-------	-------	--	-----

density

d_{calc}	7.02 g cm ⁻³	$T = 300 \text{ K}$	59G
	6.90 g cm ⁻³	$T = 473 \text{ K}$	
	6.86 g cm ⁻³	$T = 516 \text{ K}$	

References to 28.7

- 59G Geller, S., Wernick, J. H.: Acta Crystallogr. 12 (1959) 46.
75G Golovach, I. I., Dovgoshei, N. I., Slivka, V. Yu., Suslikov, L. M., Golovei, M. I., Bogdanova, A. V.: Inorg. Mater. 11 (1975) 820 (transl. from Izv. Akad. Nauk SSSR, Neorg. Mater. 11 (1975) 956).

28.8 AgBiSe₂

Crystal structure

see section 28.0.

Physical properties

electrical conductivity

σ	$180 \Omega^{-1} \text{ cm}^{-1}$	$T = 293 \text{ K}$	58Z
----------	-----------------------------------	---------------------	-----

melting point

T_m	762°C		58Z
-------	---------------------	--	-----

density

d_{calc}	7.95 g cm^{-3}	$T = 300 \text{ K}$	59G
	7.72 g cm^{-3}	$T = 573 \text{ K}$	

References to 28.8

- 58Z Zhuse, V. P., Sergeeva, V. M., Shtrum, E. L.: Sov. Phys. Tech. Phys. 3 (1958) 1925 (transl. from Zh. Tekhn. Fiz. 28 (1958) 2093).
- 59G Geller, S., Wernick, J. H.: Acta Crystallogr. 12 (1959) 46.

28.9 AgBiTe2

Crystal structure

see section 28.0.

Physical properties

energy gap

E_g	0.075 eV	high-temperature phase	estimate from Hall coefficient of quenched sample	62P
	0.16 eV	room-temperature phase	estimate from Hall coefficient of annealed sample	

electrical conductivity

σ	1300 $\Omega^{-1} \text{ cm}^{-1}$	$T = 293\text{K}$	cf. Fig. 28.9.1	58Z
----------	------------------------------------	-------------------	-----------------	-----

thermal conductivity

κ	1.4...1.8·10 ⁻³ cal/K cm s			58Z
----------	--	--	--	-----

linear thermal expansion coefficient

α	20·10 ⁻⁶ K ⁻¹	$T > 120^\circ\text{C}$	indication of a phase transition between the intermediate and the room-temperature phase	58Z
	25·10 ⁻⁶ K ⁻¹	$T < 120^\circ\text{C}$		

melting point

T_m	520°C		NaCl (high-temperature) phase	58Z
-------	-------	--	-------------------------------	-----

density

d_{calc}	8.14 g cm ⁻³			59G
-------------------	-------------------------	--	--	-----

References to 28.9

58Z Zhuse, V. P., Sergeeva, V. M., Shtrum, E. L.: Sov. Phys. Tech. Phys. 3 (1958) 1925 (transl. from Zh. Tekhn. Fiz. 28 (1958) 2093).

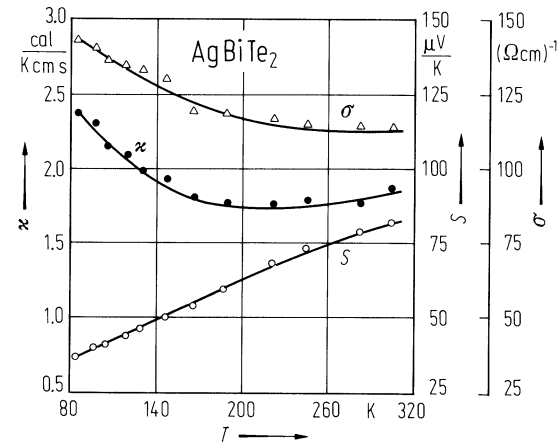
59G Geller, S., Wernick, J. H.: Acta Crystallogr. 12 (1959) 46.

62P Petrov, A. V., Shtrum, E. L.: Sov. Phys. Solid State 4 (1962) 1061 (transl. from Fiz. Tverd. Tela 4 (1962) 1442).

Figures to 28.9

Fig. 28.9.1

AgBiTe₂. Temperature dependence of electrical conductivity, thermal conductivity and Seebeck coefficient of a quenched sample [62P].



28.10 CuSbSe₂

CuSbSe₂ crystallizes in the orthorhombic lattice (D_{2h}¹⁶-Pnma) (lattice parameters at RT: $a = 6.40$ Å, $b = 3.95$ Å, $c = 15.33$ Å) [64I].

Physical properties

energy gap

$E_{g,th}$	0.83 eV	68A
------------	---------	-----

electrical conductivity

σ	$4 \Omega^{-1} \text{ cm}^{-1}$	58Z
----------	---------------------------------	-----

hole mobility

μ_p	$5 \text{ cm}^2/\text{Vs}$	58Z
---------	----------------------------	-----

melting point

T_m	480°C	68A
-------	-------	-----

References to 28.10

- | | |
|-----|--|
| 58Z | Zhuse, V. P., Sergeeva, V. M., Shtrum, E. L.: Sov. Phys. Tech. Phys. 3 (1958) 1925 (transl. from Zh. Tekhn. Fiz. 28 (1958) 2093). |
| 68A | Abdullaev, G. B., Mal'sagov, A. U., Glazov, V. M.: Inorg. Mater. 4 (1968) 1082 (transl. from Izv. Akad. Nauk SSSR, Neorg. Mater. 4 (1968) 1233). |

28.11 CuSbTe₂

Crystal structure

CuSbTe₂ possesses a Bi₂Te₃-like hexagonal structure with $a = 4.22 \text{ \AA}$, $c = 29.9 \text{ \AA}$ (at RT) [58Z].

Physical properties

electrical conductivity

σ	$3000 \text{ } \Omega^{-1} \text{ cm}^{-1}$	58Z
----------	---	-----

thermal conductivity

κ	$3.2 \cdot 10^{-3} \text{ cal/K cm s}$	62P
----------	--	-----

linear thermal expansion coefficient

α	$20.5 \cdot 10^{-6} \text{ K}^{-1}$	$T = 20 \dots 300^\circ\text{C}$	62P
----------	-------------------------------------	----------------------------------	-----

Debye temperature

Θ_D	175K	62P
------------	------	-----

melting point

T_m	530°C	62P
-------	-------	-----

References to 28.11

- | | |
|-----|---|
| 58Z | Zhuse, V. P., Sergeeva, V. M., Shtrum, E. L.: Sov. Phys. Tech. Phys. 3 (1958) 1925 (transl. from Zh. Tekhn. Fiz. 28 (1958) 2093). |
| 62P | Petrov, A. V., Shtrum, E. L.: Sov. Phys. Solid State 4 (1962) 1061 (transl. from Fiz. Tverd. Tela 4 (1962) 1442). |

28.12 CuBiSe₂

Crystal structure

CuBiSe₂ is reported to crystallize in the fcc structure with $a = 5.69 \text{ \AA}$ [58Z].

Physical properties

electrical conductivity

σ	$1200 \text{ } \Omega^{-1} \text{ cm}^{-1}$	58Z
----------	---	-----

linear thermal expansion coefficient

α	$20.8 \cdot 10^{-6} \text{ K}^{-1}$	$T < 260^\circ\text{C}$	polymorphic transition	58Z
	$25 \cdot 10^{-6} \text{ K}^{-1}$	$T > 260^\circ\text{C}$		

melting point

T_m	585°C	58Z
-------	---------------------	-----

References to 28.12

58Z Zhuse, V. P., Sergeeva, V. M., Shtrum, E. L.: Sov. Phys. Tech. Phys. 3 (1958) 1925 (transl. from Zh. Tekhn. Fiz. 28 (1958) 2093).

28.13 CuBiTe₂

Crystal structure

CuBiTe₂ possesses a Bi₂Te₃-like hexagonal structure with $a = 4.35 \text{ \AA}$, $c = 30.1 \text{ \AA}$ (at RT) [58Z].

Physical properties

electrical conductivity

σ	$2000 \text{ } \Omega^{-1} \text{ cm}^{-1}$	58Z
----------	---	-----

linear thermal expansion coefficient

α	$23 \cdot 10^{-6} \text{ K}^{-1}$	$T = 20 \dots 400^\circ\text{C}$	58Z
----------	-----------------------------------	----------------------------------	-----

melting point

T_m	520°C	58Z
-------	---------------------	-----

References to 28.13

58Z Zhuse, V. P., Sergeeva, V. M., Shtrum, E. L.: Sov. Phys. Tech. Phys. 3 (1958) 1925 (transl. from Zh. Tekhn. Fiz. 28 (1958) 2093).

28.14 Ag₃AsS₃

Crystal structure

see section 28.0.

Ag₃AsS₃ (proustite) and Ag₃SbS₃ (pyrargite) are important for non-linear optical applications (especially optical mixing [67H]). Both semiconductors are transparent over a wide spectral range. They are pyro- and piezoelectric. By its non-centrosymmetric uniaxial structure they have a large refractive index and a large birefringence [69B].

Physical properties

band structure

see Fig. 28.0.1, Brillouin zone; Fig. 28.0.2.

energy gaps

$E_{g,ind}$	2.012 eV	$T = 300\text{ K}, E \parallel c$	71D
	2.004 eV	$E \perp c$	
$E_{g,dir}$	2.156 eV	$E \parallel c$	
	2.125 eV	$E \perp c$	
dE_g/dT	$-3.48 \cdot 10^{-4}\text{ eV/K}$	$T = 77 \dots 300\text{ K}$	71D 69D

electrical conductivity

σ_{el}	$0.53 \cdot 10^{-5}\text{ }\Omega^{-1}\text{ cm}^{-1}$	$T = 300\text{ K}, \parallel c\text{ axis}$	electronic conductivity, measured with ac (10 kHz)	74B
	$1.22 \cdot 10^{-5}\text{ }\Omega^{-1}\text{ cm}^{-1}$	$\perp c\text{ axis}$	temperature dependence of electronic conductivity	69B, 69D

dielectric constants

$\epsilon(0)$	21.4	$T = 295\text{ K}, E \parallel c$	very high apparent dielectric constants are observed at low frequencies (≈ 1000) due to space charge effects involving ionic conduction and electrode processes	75R
	44.5	$E \perp c$		
$\epsilon(\infty)$	6.3	$E \parallel c$		75R
	7.45	$E \perp c$		

melting point

T_m	480°C			57W
-------	-------	--	--	-----

References to 28.14

57W Wernick, J. H., Benson, K. E.: J. Phys. Chem. Solids 3 (1957) 157.
67H Hulme, K. F., Jones, O., Davies, P. H., Hobden, M. V.: Appl. Phys. Lett. 10 (1967) 133.
69B Bardsley, W., Davies, P. H., Hobden, M. V., Hulme, K. F., Jones, O., Pomeroy, W., Warner, J.: Optoelectronics 1 (1969) 29.
69D Davis, P. H., Elliott, C. T., Hulme, K. F.: Brit. J. Appl. Phys. Ser. 2, 2 (1969) 165.
71D Dovgii, Ya. O., Butsko, N. I., Korolyshin, V. N., Moroz, E. T.: Sov. Phys. Solid State 13 (1971) 995 (transl. from Fiz. Tverd. Tela 13 (1971) 1202).
73D Dovgii, Ya. O., Korolyshin, V. N., Moroz, E. T.: Sov. Phys. Dokl. 17 (1973) 1070 (transl. from Dokl. Akad. Nauk SSSR 207 (1972) 71).
74B Butsko, N. I., Pidorya, M. M., Krushel'nitskaya, T. D.: Sov. Phys. Crystallogr. 18 (1974) 540 (transl. from Kristallografiya 18 (1973) 855).
75R Riccius, H. D., Carey, P. R., Siimann, O.: Phys. Status Solidi (b) 72 (1975) K99.

Figures to 28.14

Fig. 28.0.1

Ag_3AsS_3 . Band structure along two principal axes in the Brillouin zone estimated by group theoretical considerations and the experimental results of Figs. 3 and 4 [73D].

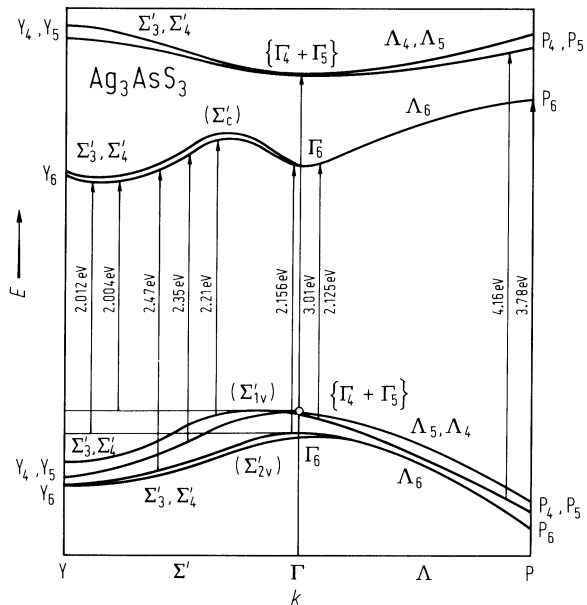
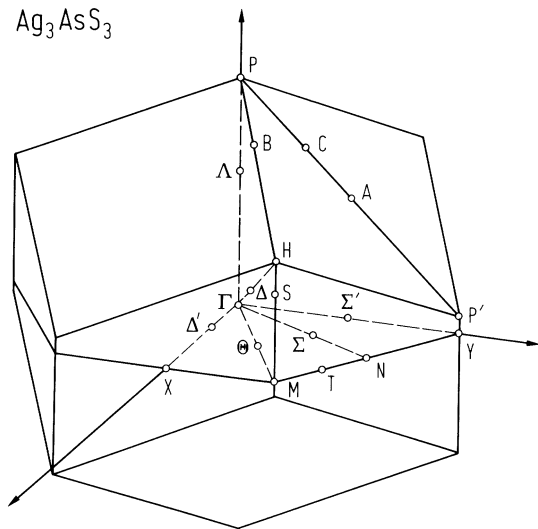


Fig. 28.0.2

Ag_3AsS_3 . Brillouin zone of the proustite structure [73D].



28.15 Ag₃SbS₃

Crystal structure

see section 28.0. See also the remarks in section 28.14.

Physical properties

energy gap

$E_{g,th}$	1.77 eV		from conductivity	75G
E_g	1.93 eV	$T = 300\text{ K}$	absorption edge	73G

electrical conductivity

σ	$0.3 \cdot 10^{-4} \Omega^{-1} \text{ cm}^{-1}$ $0.6 \cdot 10^{-4} \Omega^{-1} \text{ cm}^{-1}$	$T = 300\text{ K}$, $\parallel c$ axis $\perp c$ axis	measured with ac (10 KHz); temperature dependence of conductivity and carrier activation energies, see Fig. 28.15.1 and [75G]	74B
----------	--	---	--	-----

dielectric constant

$\varepsilon(0)$	27	$T = 300\text{ K}$		73G
------------------	----	--------------------	--	-----

melting point

T_m	473(3)°C			73G
-------	----------	--	--	-----

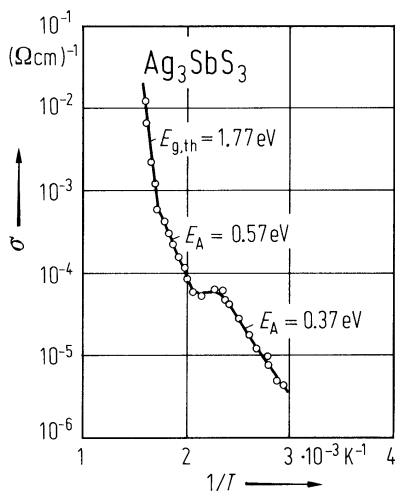
References to 28.15

- 73G Golovei, M. I., Gurjan, M. I., Olekseyuk, I. D., Rez, I. S., Voroshilov, Yu. V., Roman, I. Y.: Krist. Tech. 8 (1973) 453.
- 74B Butsko, N. I., Pidorya, M. M., Krushel'nitskaya, T. D.: Sov. Phys. Crystallogr. 18 (1974) 540 (transl. from Kristallografiya 18 (1973) 855).
- 75G Golovach, I. I., Dovgoshei, N. I., Slivka, V. Yu., Suslikov, L. M., Golovei, M. I., Bogdanova, A. V.: Inorg. Mater. 11 (1975) 820 (transl. from Izv. Akad. Nauk SSSR, Neorg. Mater. 11 (1975) 956).

Figures to 28.15

Fig. 28.15.1

Ag_3SbS_3 . Electrical conductivity vs. reciprocal temperature for a single crystal showing activation energies of $E_A = 0.37 \text{ eV}$ and 0.57 eV and $E_{g,\text{th}} = 1.77 \text{ eV}$ [75G].



29 II_x-III_y-VI_z compounds

29.0 Crystal structure of II-III-VI₂ compounds

Crystal structure

The II-III-VI₂ compounds crystallize in a trigonal (α) modification and a tetragonal (β) modification. The lattice of the α -phase consists of a hexagonal close-packed arrangement of VI-atoms with II-atoms and III-atoms located in layers in the octahedral sites. The space group is $D_{3d}^3-P\bar{3}m1$ or C_{3v}^1-P3m1 [67G]. The exact structure of the β -phase is not yet known. There are eight molecules in the unit cell. A tentative determination of the space group yielded $D_{4h}^{17}-I4/mmm$ [66G].

lattice parameters

	Substance	a [Å]	c [Å]	Ref.
Trigonal phase:	CdInS ₂	3.603	6.825	69G1
	CdTlS ₂	3.645	6.825	67G
	CdTlSe ₂	3.723	7.073	69G2
	CdTITe ₂	3.890	7.220	69G2
Tetragonal phase:	CdInS ₂	11.586	6.522	69G1
	CdInSe ₂	12.152	7.14	69G1
	CdInTe ₂	12.612	7.434	69G1
	CdTlS ₂	11.784	6.668	69G1
	CdTlSe ₂	12.174	7.212	69G1
	CdTITe ₂	12.669	7.528	69G1
	ZnInTe ₂	12.18	6.09	69G1
	HgTlS ₂	12.20(5)	6.60(2)	66G

References to 29.0

- 66G Guseinov, G. D., Ismailov, M. Z., Talybov, A. G.: Phys. Status Solidi 18 (1966) 929.
67G Guseinov, G. D., Ismailov, M. Z., Guseinov, G. G.: Mater. Res. Bull. 2 (1967) 765.
69G1 Guseinov, G. D., Abdullaev, G. B., Kerimova, F. M., Gamidov, R. S., Guseinov, G. G.: Mater. Res. Bull. 4 (1969) 807.
69G2 Guseinov, G. D., Guseinov, G. G., Ismailov, M. Z., Godzhaev, E. M.: Inorg. Mater. 5 (1969) 27 (transl. from Izv. Akad. Nauk SSSR, Neorg. Mater. 5 (1969) 33).

29.1 CdInS₂

Crystal structure

see section 29.0.

Physical properties

β -CdInS₂ [69G]

energy gap

$$\begin{array}{ll} E_{\text{g,th}} & 1.70\ldots 1.74 \text{ eV} \\ dE_{\text{g}}/dT & -1.43 \cdot 10^{-4} \text{ eV K}^{-1} \end{array}$$

temperature dependence of conductivity
and Hall coefficient

effective masses

$$\begin{array}{ll} m_{\text{n}} & 0.172 m_0 \\ m_{\text{p}} & 0.44 m_0 \end{array}$$

analysis of transport measurements

density

$$\begin{array}{ll} d_{\text{calc}} & 4.421 \text{ g cm}^{-3} \\ d_{\text{exp}} & 4.420 \text{ g cm}^{-3} \end{array}$$

For electrical conductivity, Hall coefficient and Hall mobilities above room temperature, see Fig. 29.1.1.

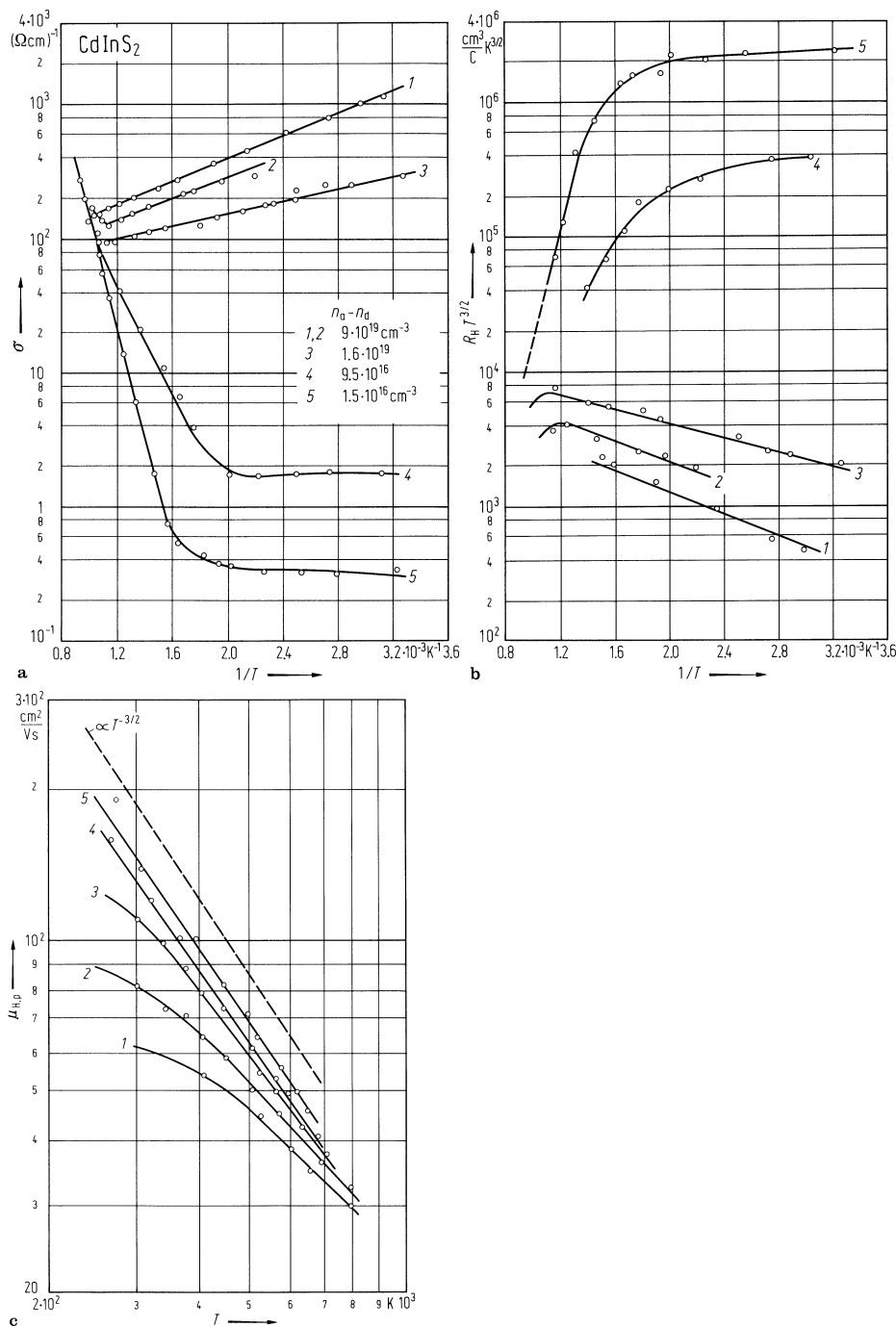
References to 29.1

69G Guseinov, G. D., Abdullaev, G. B., Kerimova, F. M., Gamidov, R. S., Guseinov, G. G.: Mater. Res. Bull. 4 (1969) 807.

Figures to 29.1

Fig. 29.1.1

β -CdInS₂(Se₂,Te₂). Temperature dependence of the conductivity σ (a), the Hall coefficient R_H (b) and the Hall mobility $\mu_{H,p}$ (c) of samples with impurity concentrations of 6 to $7 \cdot 10^{16} \text{ cm}^{-3}$ [69G].



29.2 CdInSe₂

Crystal structure

see section 29.0.

Physical properties

β -CdInSe₂ [69G]

energy gap

$$E_{g,th} \quad 1.40 \dots 1.42 \text{ eV}$$

$$dE_g/dT \quad 1.03 \cdot 10^{-4} \text{ eV K}^{-1}$$

temperature dependence of conductivity,

Hall effect, thermoelectric power (Fig. 29.2.1)

effective masses

$$m_p \quad 0.23 m_0$$

density

$$d_{calc} \quad 4.97 \text{ g cm}^{-3}$$

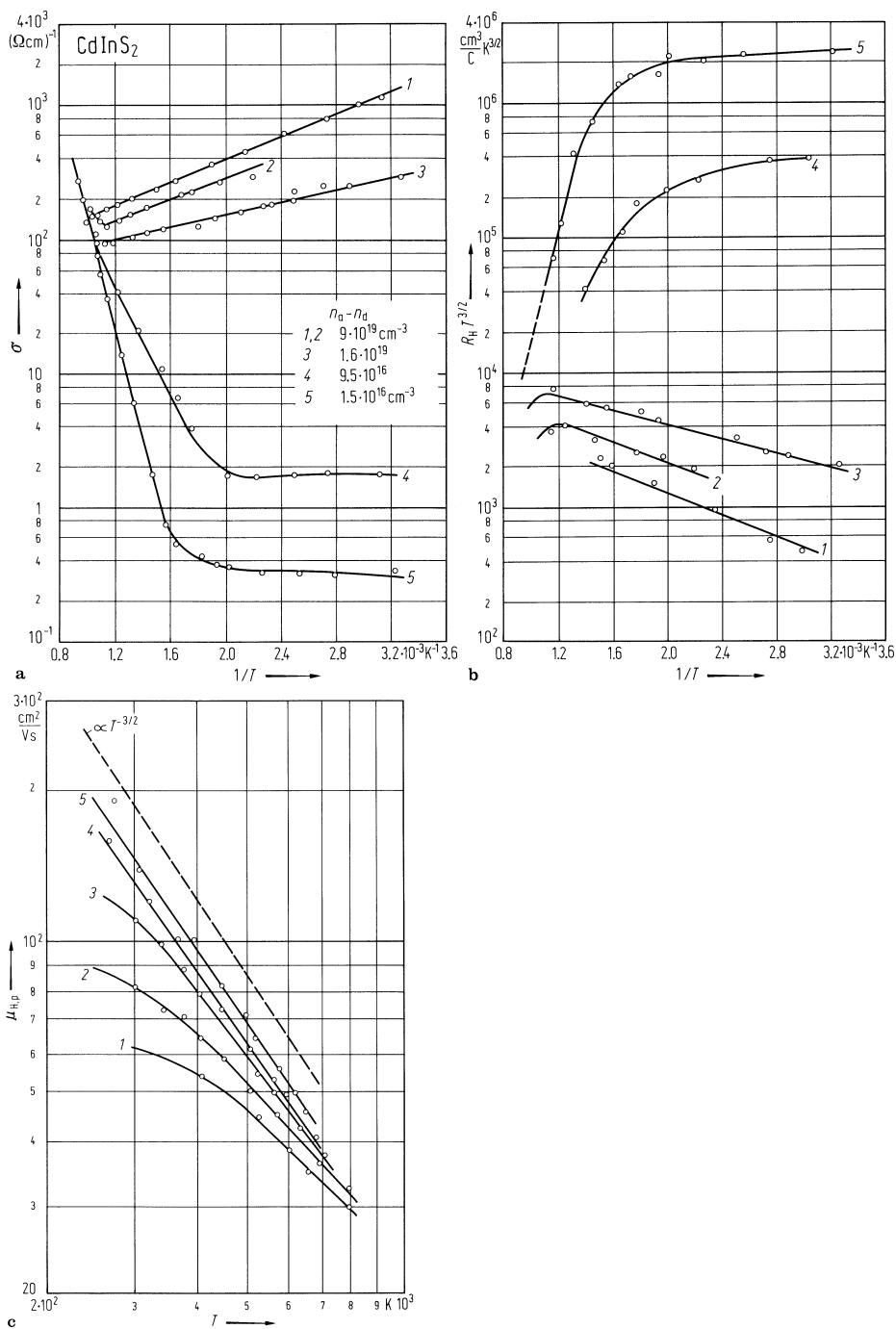
$$d_{exp} \quad 4.970 \text{ g cm}^{-3}$$

References to 29.2

- 69G Guseinov, G. D., Abdullaev, G. B., Kerimova, F. M., Gamidov, R. S., Guseinov, G. G.: Mater. Res. Bull. 4 (1969) 807.

Fig. 29.2.1

β -CdInS₂(Se₂,Te₂). Temperature dependence of the conductivity σ (a), the Hall coefficient R_H (b) and the Hall mobility $\mu_{H,p}$ (c) of samples with impurity concentrations of 6 to $7 \cdot 10^{16} \text{ cm}^{-3}$ [69G].



29.3 CdInTe₂

Crystal structure

see section 29.0.

Physical properties

β -CdInTe₂ [69G]

energy gap

$$\begin{array}{ll} E_{g,\text{th}} & 1.10 \dots 1.12 \text{ eV} \\ dE_g/dT & -2.54 \cdot 10^{-4} \text{ eV K}^{-1} \end{array}$$

temperature dependence of conductivity
and Hall coefficient (Fig. 29.3.1)

effective masses

$$\begin{array}{ll} m_n & 0.08 m_0 \\ m_p & 0.18 m_0 \end{array}$$

density

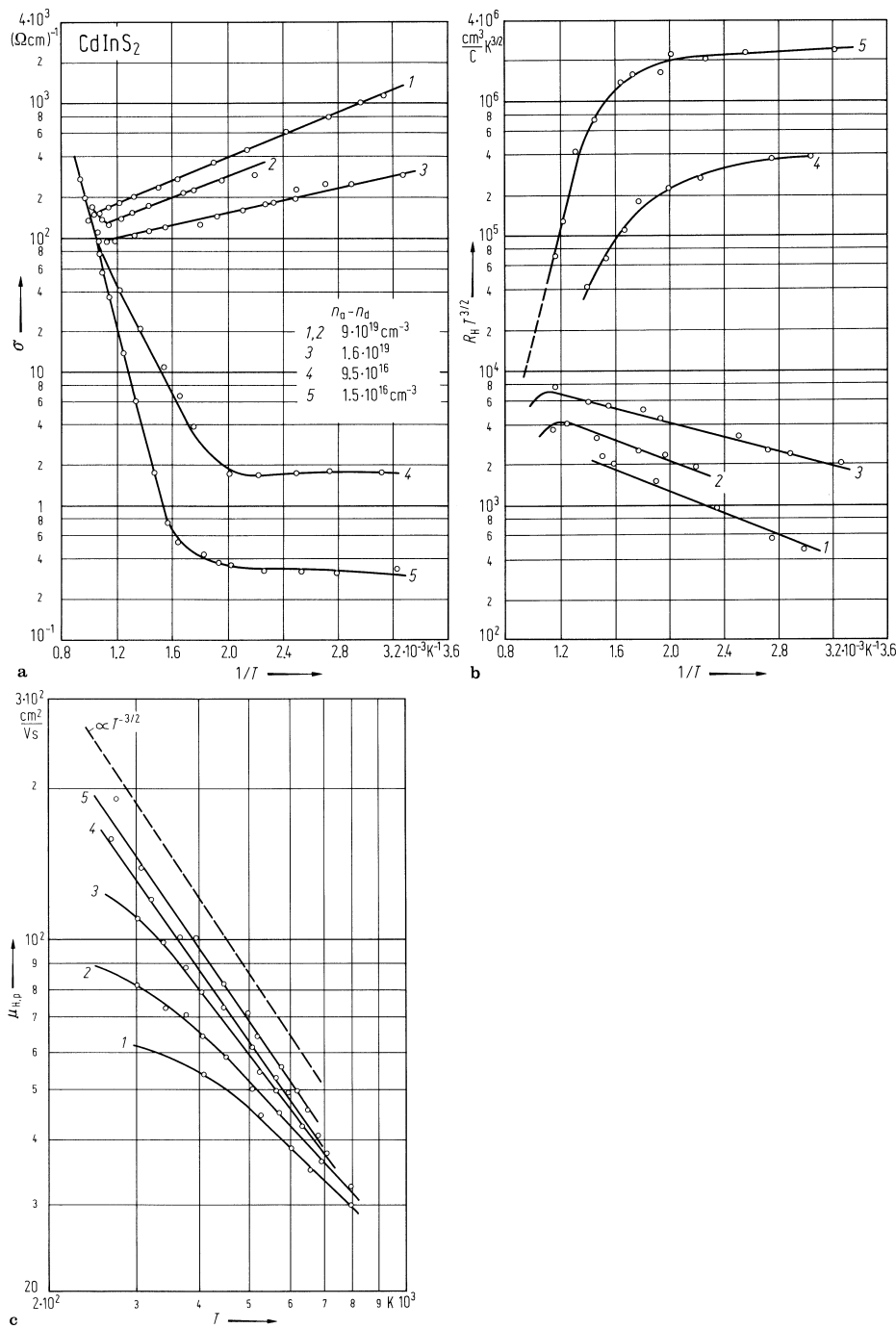
$$\begin{array}{ll} d_{\text{calc}} & 5.41 \text{ g cm}^{-3} \\ d_{\text{exp}} & 5.550 \text{ g cm}^{-3} \end{array}$$

References to 29.3

- 69G Guseinov, G. D., Abdullaev, G. B., Kerimova, F. M., Gamidov, R. S., Guseinov, G. G.: Mater. Res. Bull. 4 (1969) 807.

Fig. 29.3.1

β -CdInS₂(Se₂,Te₂). Temperature dependence of the conductivity σ (a), the Hall coefficient R_H (b) and the Hall mobility $\mu_{H,p}$ (c) of samples with impurity concentrations of 6 to $7 \cdot 10^{16} \text{ cm}^{-3}$ [69G].



29.4 CdTlS₂

Crystal structure

see section 29.0.

Physical properties

α -CdTlS₂

energy gap

E_g	1.46 eV	$T = 0$ K	temperature dependence	67G,
	1.52 eV		of conductivity (Fig. 29.4.1)	69G2
	1.56 eV	$T = 300$ K	of Hall coefficient (Fig. 29.4.1)	
dE_g/dT	$-1.3 \cdot 10^{-4}$ eV K ⁻¹		spectral dependence of photoconductivity	67G,
				69G2

effective masses

m_p	$0.6 m_0$		analysis of transport measurements	69G2
m_n	$0.19 m_0$			

hole mobility

μ_p	4200 cm ² /Vs	$T = 300$ K	Hall mobility of a polycrystalline sample.	69G2
---------	--------------------------	-------------	--	------

For temperature dependence of electrical conductivity, Hall coefficient and Hall mobility see Fig. 29.4.1.

melting point

T_m	600°C			69G2
-------	-------	--	--	------

intrinsic concentration

n_i	$1.08 \cdot 10^{19}$ cm ⁻³	$T = 730$ K		69G2
-------	---------------------------------------	-------------	--	------

density

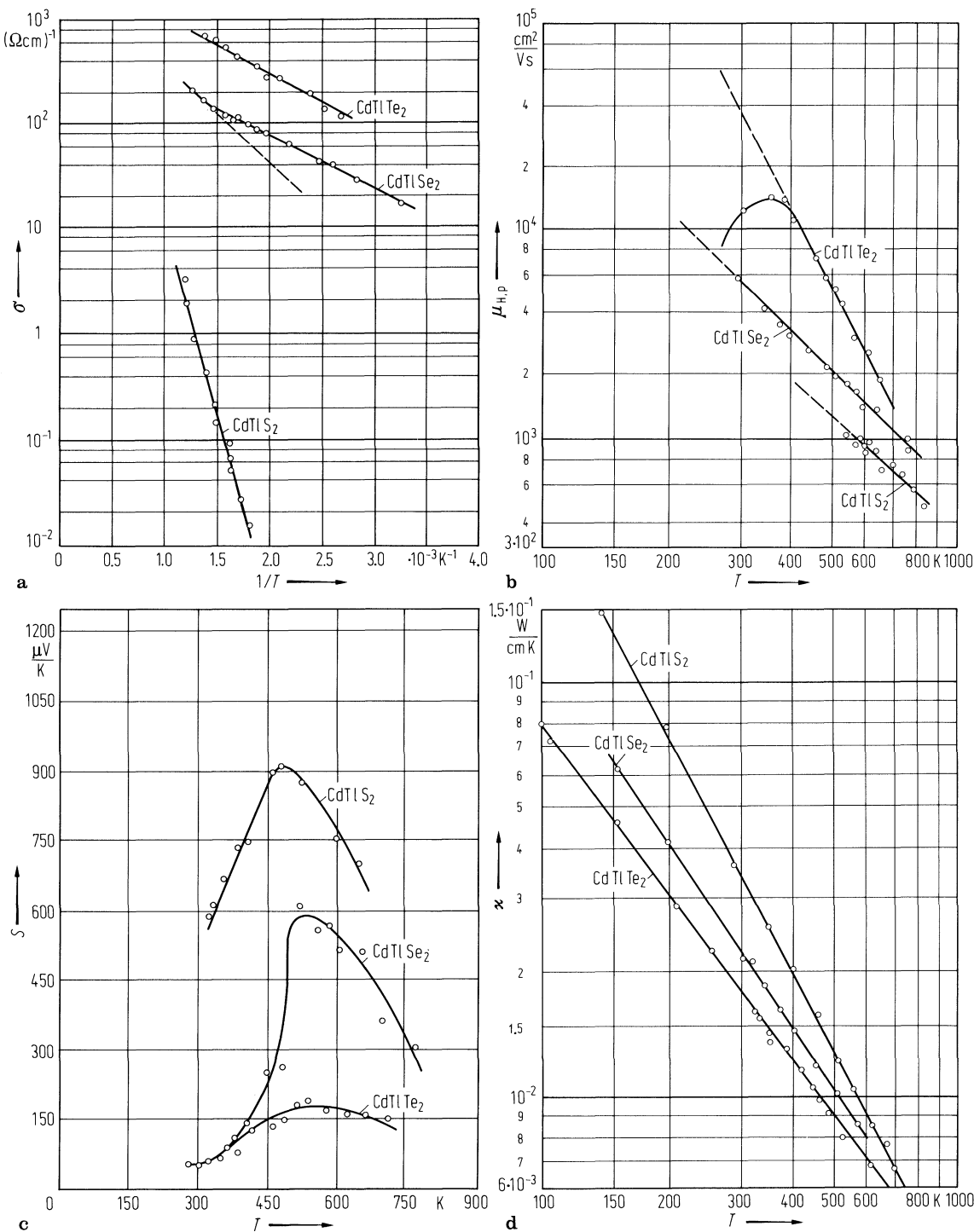
d_{calc}	5.06 g cm ⁻³			69G1
d_{exp}	5.05 g cm ⁻³			69G1

References to 29.4

67G Guseinov, G. D., Ismailov, M. Z., Guseinov, G. G.: Mater. Res. Bull. 2 (1967) 765.
69G1 Guseinov, G. D., Abdullaev, G. B., Kerimova, F. M., Gamidov, R. S., Guseinov, G. G.: Mater. Res. Bull. 4 (1969) 807.
69G2 Guseinov, G. D., Guseinov, G. G., Ismailov, M. Z., Godzhaev, E. M.: Inorg. Mater. 5 (1969) 27 (transl. from Izv. Akad. Nauk SSSR, Neorg. Mater. 5 (1969) 33).

Fig. 29.4.1

α -CdTiS₂(Se₂,Te₂) Temperature dependence of the electrical conductivity σ (a), the Hall mobility $\mu_{H,p}$ (b), the thermoelectric power S (c) and the thermal conductivity κ (d) of p-type samples [69G].



29.5 CdTeSe₂

Crystal structure

see section 29.0.

Physical properties

α -CdTeSe₂

energy gap

$E_{g,th}$	0.40 eV	conductivity, Hall effect	69G2
dE_g/dT	$-4.1 \cdot 10^{-4}$ eV K ⁻¹		69G2

effective masses

m_n	$0.11 m_0$	analysis of transport measurements	69G2
m_p	$0.65 m_0$		

density

d_{calc}	5.91 g cm^{-3}		69G1
d_{exp}	5.89 g cm^{-3}		69G1

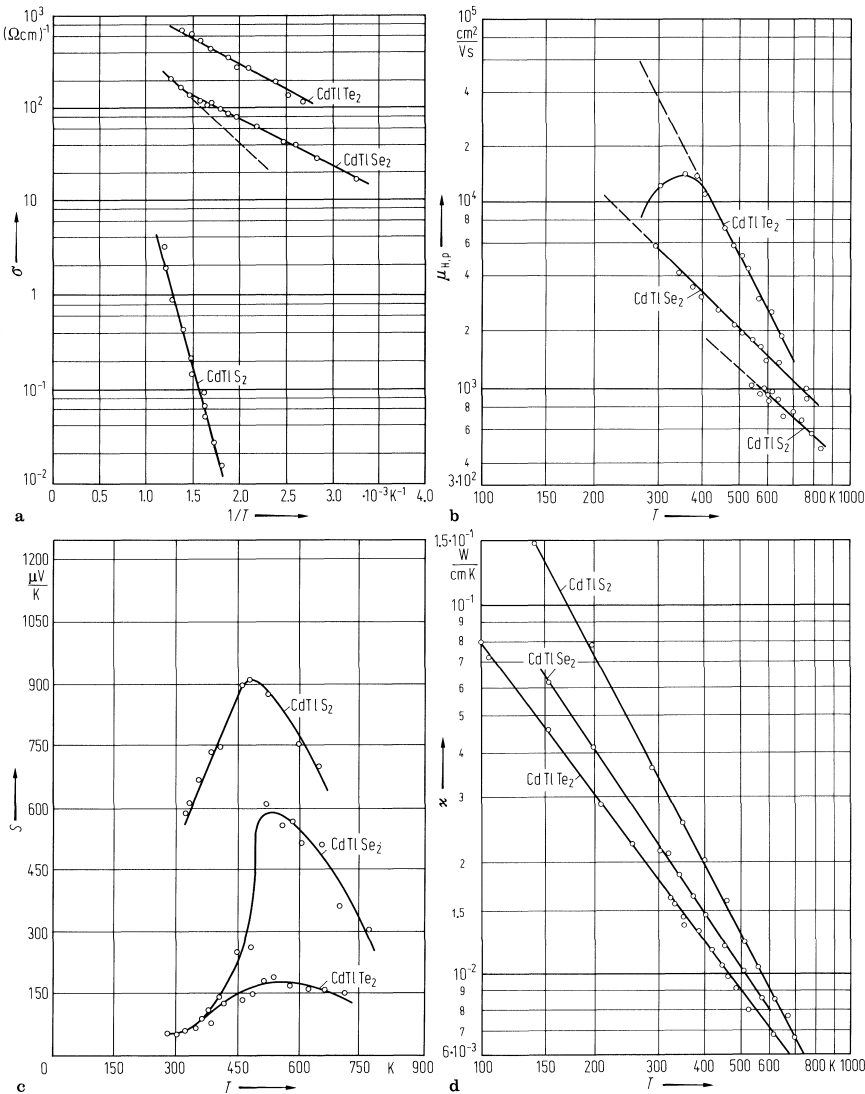
Measurement of transport coefficients and of the Hall mobility, see Fig. 29.5.1.

References to 29.5

- 69G1 Guseinov, G. D., Abdullaev, G. B., Kerimova, F. M., Gamidov, R. S., Guseinov, G. G.: Mater. Res. Bull. 4 (1969) 807.
- 69G2 Guseinov, G. D., Guseinov, G. G., Ismailov, M. Z., Godzhaev, E. M.: Inorg. Mater. 5 (1969) 27 (transl. from Izv. Akad. Nauk SSSR, Neorg. Mater. 5 (1969) 33).

Fig. 29.5.1

α -CdTiS₂(Se₂,Te₂) Temperature dependence of the electrical conductivity σ (a), the Hall mobility $\mu_{H,p}$ (b), the thermoelectric power S (c) and the thermal conductivity κ (d) of p-type samples [69G2].



29.6 CdTlTe₂

Crystal structure

see section 29.0.

Physical properties

α -CdTlTe₂

energy gap

$E_{g,th}$	0.18 eV	conductivity, Hall effect	69G2
------------	---------	---------------------------	------

density

d_{calc}	6.28 g cm ⁻³		69G1
------------	-------------------------	--	------

d_{exp}	6.40 g cm ⁻³		69G1
-----------	-------------------------	--	------

Measurements of transport coefficients and of Hall mobility, see Fig. 29.6.1.

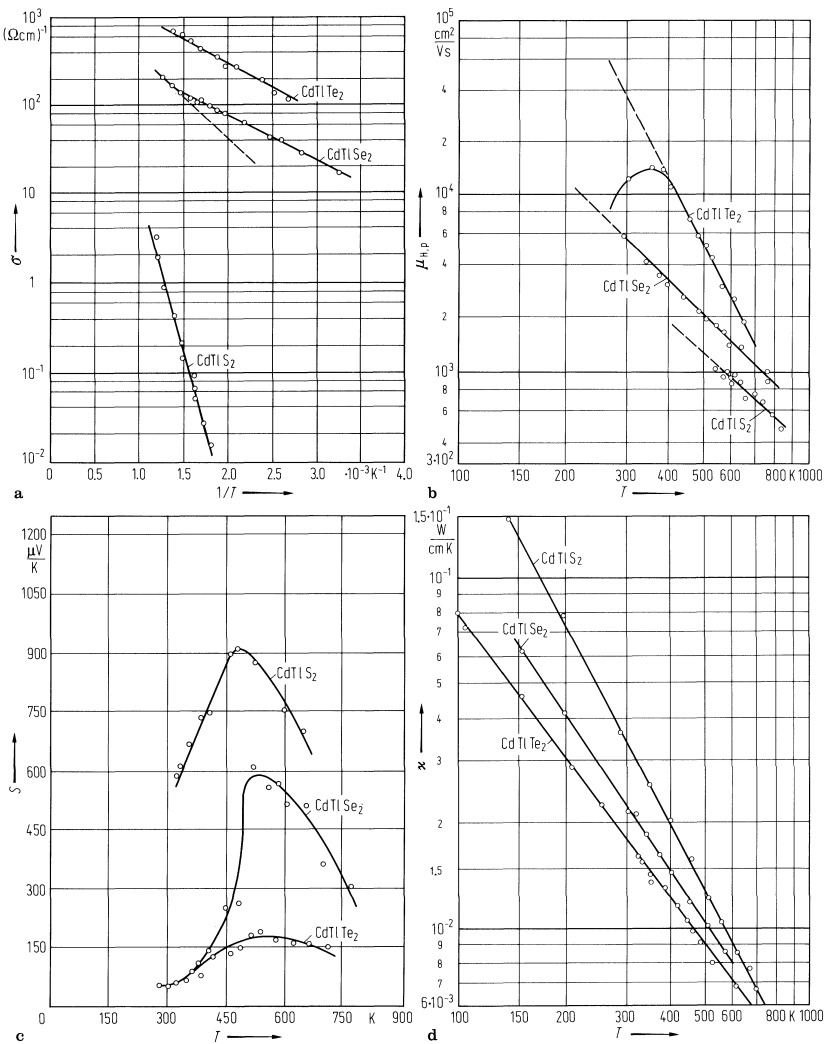
References to 29.6

- 69G1 Guseinov, G. D., Abdullaev, G. B., Kerimova, F. M., Gamidov, R. S., Guseinov, G. G.: Mater. Res. Bull. 4 (1969) 807.
- 69G2 Guseinov, G. D., Guseinov, G. G., Ismailov, M. Z., Godzhaev, E. M.: Inorg. Mater. 5 (1969) 27 (transl. from Izv. Akad. Nauk SSSR, Neorg. Mater. 5 (1969) 33).

Figures to 29.6

Fig. 29.6.1

α -CdTiS₂(Se₂,Te₂) Temperature dependence of the electrical conductivity σ (a), the Hall mobility $\mu_{H,p}$ (b), the thermoelectric power S (c) and the thermal conductivity κ (d) of p-type samples [69G2].



29.7 HgTlS₂

Crystal structure

see section 29.0.

Physical properties

energy gap

E_g	1.28 eV	$T = 300 \text{ K}$	conductivity (Fig. 29.7.1)	66G
	1.25 eV		maximum in the spectral distribution of photoconductivity	68G
dE_g/dT	$-2.46 \cdot 10^{-4} \text{ eV K}^{-1}$		shift of absorption edge	68G

density

d_{calc}	6.34 g cm^{-3}			68G
-------------------	--------------------------	--	--	-----

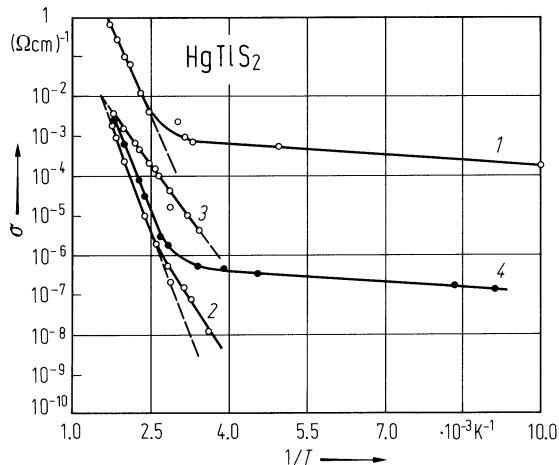
References to 29.7

- 68G Guseinov, G. D., Ismailov, M. Z., Talybov, A. G.; Inorg. Mater. 4 (1968) 440 (transl. from Izv. Akad. Nauk SSSR, Neorg. Mater. 4 (1968) 514).

Figures to 29.7

Fig. 29.7.1

HgTlS₂. Electrical conductivity vs. reciprocal temperature for four different samples (1, 2 single crystals, 3 polycrystalline, 4 polycrystalline with partially oriented crystals) [68G].



30 III_x-V_y-VI_z compounds

30.0 Crystal structure of III-V-VI₂ compounds

The III-V-VI₂ compounds can be considered as analogues to the IV-VI compounds.

TlSbTe₂ and the three Bi compounds *TlBiS₂(Se₂,Te₂)* crystallize in a rhombohedral structure (space group D_{3d}⁵-R $\bar{3}$ m). The lattice parameters are given for TlSbTe₂ and TlBiTe₂ as $a = 8.177(10)$ Å, $\alpha = 31^\circ 25'(15)'$ and $a = 8.137(10)$ Å, $\alpha = 32^\circ 18'(15)'$, respectively, [61H]. For TlBiS₂ the lattice parameters are given in hexagonal description as $a = 4.15(3)$ Å, $c = 10.91(4)$ Å [74B] and for TlBiSe₂ as $a = 4.24$ Å, $c = 22.33$ Å [63M].

TlAsS₂ crystallizes in a monoclinic structure (C_{2h}⁵-P2₁/c) with $a = 6.11$ Å, $b = 11.33$ Å, $c = 12.27$ Å, $\beta = 104.2^\circ$ [59Z].

TlSbS₂ crystallizes in a disordered NaCl-structure (O_h⁵-Fm3m, lattice parameter $a = 5.87...5.94$ Å [59S]) like many of the I-V-VI₂ compounds.

TlSbSe₂ has an orthorhombic structure with $a = 4.20$ Å, $b = 9.0$ Å, $c = 24.0$ Å according to [75B]

These compounds – as well as many other III_x-V_y-VI_z compounds with semiconducting properties – occur as ternary phases in the phase diagrams of the pseudo-binary systems (III_xV_y)-(III_u-VI_v) and (III_x-VI_y)-(V_uVI_v).

References to 30.0

- 59S Semiletov, S. A., Man, L. I.: Sov. Phys. Crystallogr. 4 (1959) 383 (transl. from Kristallografiya 4 (1959) 414).
- 59Z Zemann, A., Zemann, J.: Acta Crystallogr. 12 (1959) 1002.
- 61H Hockins, E. F., White, J. G.: Acta Crystallogr. 14 (1961) 328.
- 74B Brandt, N. B., Gitsu, D. V., Popovich, N. S., Sidorov, V. I., Chudinov, S. M.: Sov. Phys. Semicond. 8 (1974) 390 (transl. from Fiz. Tekh. Poluprovodn. 8 (1974) 609).
- 75B Botgros, I. V., Zbigli, K. R., Stanchu, A. V., Stepanov, G. I., Cheban, A. G., Chumak, G. D.: Inorg. Mater. 11 (1975) 1675 (transl. from Izv. Akad. Nauk SSSR, Neorg. Mater. 11 (1975) 1953).

30.1 TlAsS₂

Crystal structure

see section 30.0.

Physical properties

energy gap

E_g	1.3 eV	$T = 300$ K	77B
-------	--------	-------------	-----

melting point

T_m	260°C		77B
-------	-------	--	-----

density

d	5.53 g cm ⁻³		59Z
-----	-------------------------	--	-----

References to 30.1

- 59Z Zemann, A., Zemann, J.: Acta Crystallogr. 12 (1959) 1002.
- 77B Baidakov, L. A., Funtikov, V. A.: Inorg. Mater. 13 (1977) 749 (transl. from Izv. Akad. Nauk SSSR, Neorg. Mater. 13 (1977) 914).

30.2 TlSbS₂

Crystal structure

see section 30.0.

Physical properties

energy gap

$E_{g,th}$	1.42 eV		temperature dependence of conductivity	69D
$E_{g,ind}$	1.556 eV	$T = 300\text{ K}$	reflectivity (allowed indirect transition)	70S
$E_{g,dir}$	1.69 eV	$T = 300\text{ K}$	reflectivity (allowed direct transition)	70B

phonon energies

$h\nu_{LA}$	33.2 meV	$T = 300\text{ K}$	analysis of reflectivity spectra	75S
$h\nu_{TA}$	9.3 meV			
$h\nu_{LO}$	35.6 meV			
$h\nu_{TO}$	38.8 meV			

dielectric constants

$\epsilon(\infty)$	10.732	$T = 300\text{ K}$	from dispersion of $n_\infty = \epsilon(\infty)^{1/2}$	70S
$\epsilon(0)$	11.891	$T = 300\text{ K}$		75S

electrical resisitivity

ρ	$10^9\ \Omega\text{ cm}$	$T = 293\text{ K}$		74Z
--------	--------------------------	--------------------	--	-----

melting point

T_m	484(2)°C			74B
-------	----------	--	--	-----

density

d_{calc}	6.40...6.18 g cm ⁻³			59S
------------	--------------------------------	--	--	-----

References to 30.2

59S Semiletov, S. A., Man, L. I.: Sov. Phys. Crystallogr. 4 (1959) 383 (transl. from Kristallografiya 4 (1959) 414).

69D Dembovskii, S. A., Lisovskii, L. G., Bunin, V. M., Kanishcheva, A. S.: Inorg. Mater. 5 (1969) 1724 (transl. from Izv. Akad. Nauk SSSR, Inorg. Mater 5 (1968) 2023).

70B Botgros, I. V., Stepanov, G. I., Chinik, B. S., Stratan, G. I., Kantser, Ch. T.: Sov. Phys. Solid State 12 (1970) 495 (transl. from Fiz. Tverd. Tela 12 (1970) 643).

70S Stepanov, G. I., Botgros, I. V., Chinik, H. S., Dontsoi, P. I.: Sov. Phys. Solid State 12 (1970) 1423 (transl. from Fiz. Tverd. Tela 12 (1970) 1797).

74B Brandt, N. B., Gitsu, D. V., Popovich, N. S., Sidorov, V. I., Chudinov, S. M.: Sov. Phys. Semicond. 8 (1974) 390 (transl. from Fiz. Tekh. Poluprovodn. 8 (1974) 609).

74Z Zhitar', V. F., Popovich, N. S., Gitsu, D. V., Radautsan, S. I.: Sov. Phys. Semicond. 8 (1974) 644 (transl. from Fiz. Tekh. Poluprovodn. 8 (1974) 996).

75S Stepanov, G. I., Botgros, I. V., Chinik, H. S., Kogalnichanu, N. F., Cheban, A. G.: Sov. Phys. Solid State 17 (1975) 97 (transl. from Fiz. Tverd. Tela 17 (1975) 166).

30.3 TlBiS₂

Crystal structure

see section 30.0.

Physical properties

energy gap

E_g	0.40 eV	69D
-------	---------	-----

melting point

T_m	740°C	69D
-------	-------	-----

References to 30.3

69D Dembovskii, S. A., Lisovskii, L. G., Bunin, V. M., Kanishcheva, A. S.: Inorg. Mater. 5 (1969) 1724 (transl. from Izv. Akad. Nauk SSSR, Inorg. Mater 5 (1968) 2023).

30.4 TlBiSe₂

Crystal structure

see section 30.0.

Physical properties

energy gap

E_g	0.28 eV	69D
-------	---------	-----

melting point

T_m	720°C	69D
-------	-------	-----

References to 30.4

69D Dembovskii, S. A., Lisovskii, L. G., Bunin, V. M., Kanishcheva, A. S.: Inorg. Mater. 5 (1969) 1724 (transl. from Izv. Akad. Nauk SSSR, Inorg. Mater 5 (1968) 2023).

30.5 TlBiTe₂

Highly degenerate semiconductor [72J] with Hall mobilities of electrons of 64 cm²/Vs at 300 K and 128 cm²/Vs at 4.2K, $n = 5 \cdot 10^{19}$ cm⁻³, $T_m = 535^\circ\text{C}$, $d_{\text{exp}} = 8.06$ g cm⁻³ [61H]. For conductivity and Hall coefficient, see Fig. 30.5.1, see also [81V].

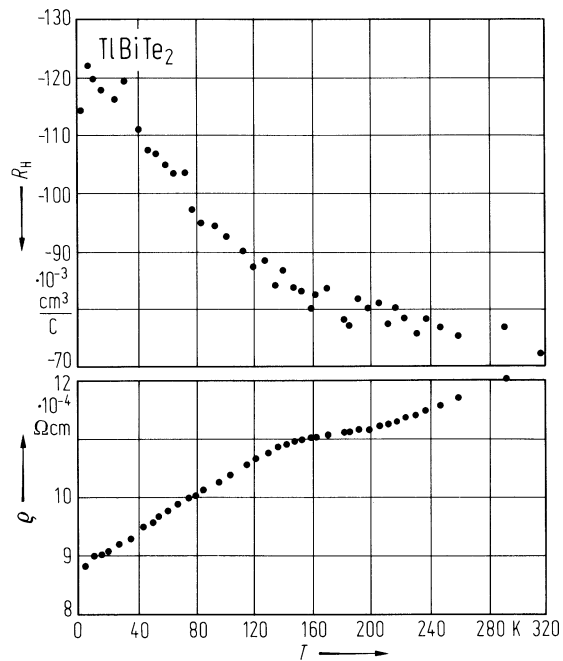
References to 30.5

- 61H Hockins, E. F., White, J. G.: Acta Crystallogr. 14 (1961) 328.
- 72J Jensen, J. D., Burke, J. R., Ernst, D. W., Allgaier, R. S.: Phys. Rev. B 6 (1972) 319.
- 81V Valassiades, O., Polychroniadis, E. K., Stoemenos, J., Economou, N. A.: Phys. Status Solidi (a) 65 (1981) 215.

Figures to 30.5

Fig. 30.5.1

TlBiTe₂. Temperature dependence of the conductivity and the Hall coefficient [72J].



30.6 Ga₆Sb₅Te

Crystal structure

see section 30.0.

Physical properties [66K]

energy gap

E_g	0.65 eV	$T = 300$ K	conductivity, see Fig. 30.2
	0.80 eV	$T = 0$ K	

electrical resistivity

ρ	3.8 Ω cm	$p = 2 \cdot 10^{17}$ cm ⁻³
--------	-----------------	--

hole mobility

μ_p	9.5 cm ² /Vs	$T = 300$ K
---------	-------------------------	-------------

thermal conductivity

κ_L	$7.0 \cdot 10^{-2}$ W/cm K
------------	----------------------------

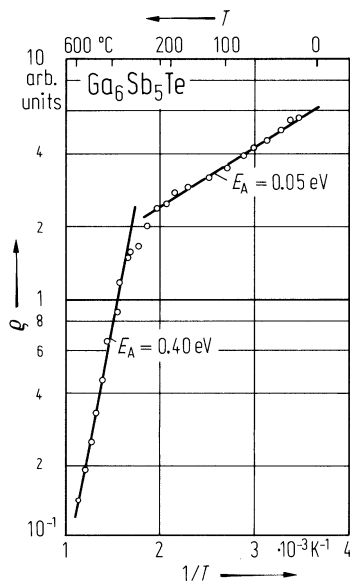
References to 30.6

66K Kurata, K., Hirai, T.: Solid State Electron. 9 (1966) 633.

Figures to 30.6

Fig. 30.6.1

$\text{Ga}_6\text{Sb}_5\text{Te}$. Resistivity vs. (reciprocal) temperature [66K]. Activation energies are indicated.



30.7 In₆Sb₅Te

Crystal structure

see section 30.0.

Physical properties [66K]

electrical resistivity

$$\rho \quad 0.7 \cdot 10^{-3} \, \Omega \, \text{cm} \quad n = 8 \cdot 10^{18} \, \text{cm}^{-3}$$

electron mobility

$$\mu_n \quad 1200 \, \text{cm}^2/\text{Vs} \quad T = 300 \, \text{K}$$

thermal conductivity

$$\kappa_L \quad 3.1 \cdot 10^{-2} \, \text{W/cm K}$$

References to 30.7

66K Kurata, K., Hirai, T.: Solid State Electron. 9 (1966) 633.

30.8 In₇SbTe₆

Crystal structure

see section 30.0.

Physical properties [66K]

electrical resistivity

$$\rho \quad 2.5 \cdot 10^{-3} \, \Omega \, \text{cm} \quad p = 5 \cdot 10^{18} \, \text{cm}^{-3}$$

hole mobility

$$\mu_p \quad 440 \, \text{cm}^2/\text{Vs} \quad T = 300 \, \text{K}$$

thermal conductivity

$$\kappa_L \quad 3.6 \cdot 10^{-2} \, \text{W/cm K}$$

References to 30.8

66K Kurata, K., Hirai, T.: Solid State Electron. 9 (1966) 633.

31 IV_x-V_y-VI_z compounds

31.0 Crystal structure of IV_x-V_y-VI_z compounds

31.0.1 Bi₁₂SiO₂₀, Bi₁₂GeO₂₀

These materials crystallizes in a cubic structure with space group $T_3 - I23$ [67B1, 67B2]. The lattice constants are $a = 10.10433(5)$ Å at 296 K for Bi₁₂SiO₂₀ and $a = 10.1455(8)$ Å at 298 K for Bi₁₂GeO₂₀. The positions of the atoms in the unit cell are very complicated (see e.g. [82B]).

31.0.2 Further IV_x-V_y-VI_z compounds

See sections 31.3 and 31.4.

References to 31.0

- 67B1 Ballman, A. A.: J. Crystal Growth 1 (1967) 37.
- 67B2 Bernstein, J. L.: J. Crystal Growth 1 (1967) 45.
- 82B Babonas, G. A., Zhogova, E. A., Zaretskii, Yu. G., Kurbatov, G. A., Ukhanov, Yu. I., Shmartsev, Yu. V.: Sov. Phys. Solid State 24 (1982) 921 (transl. from Fiz. Tverd. Tela 24 (1982) 1612).

31.1 Bi12SiO20

Crystal structure

see section 31.0.

The material is an optically active [66L, 70F], electro-optic [66L] photoconductor. Bi12SiO20 shows photoelastic behavior, too [78K].

Physical properties

energy gap

E_g	3.25 eV	$T = 300\text{ K}$	from measurements of photo-current excitation	73H
-------	---------	--------------------	---	-----

effective mass

m_n	$14\ m_0$		photocarrier kinetic response	74L
-------	-----------	--	-------------------------------	-----

electron mobility

$\mu_{dr,n}$	$0.029(3)\text{ cm}^2/\text{Vs}$	$T = 80\text{ K}$	drift mobility from transit time measurements, for temperature dependence, see Fig. 31.1.1	73H
--------------	----------------------------------	-------------------	--	-----

electrical resistivity

ρ	$5\cdot 10^{13}\ \Omega\text{ cm}$ $> 10^4\ \Omega\text{ cm}$	p-type		74Z 73H
--------	--	--------	--	------------

dielectric constant

$\epsilon(0)$	56			74Z
---------------	----	--	--	-----

phonon modes

data from *reflectivity* [79W] (in cm^{-1})

TO-modes:	89, 99, 107, 115, 136, 175, 195, 208, 237, 288, 314, 353, 462, 531, 579, 609
LO-modes:	91, 101, 112, 118, 168, 185, 196, 212, 257,289, 351, 374, 506, 557, 591, 615

data from *Raman spectra* [72V] (in cm^{-1})

TO-modes:	98.8, 114.4, 209.0, 238.0, 827.4
LO-modes:	53.5, 100.7, 112.4,167.0, 180.7,185.0, 213.0, 841.0
LO+TO-modes:	44.4, 50.6, 58.0, 89.2, 105.7, 135.5, 352.0, 509.1

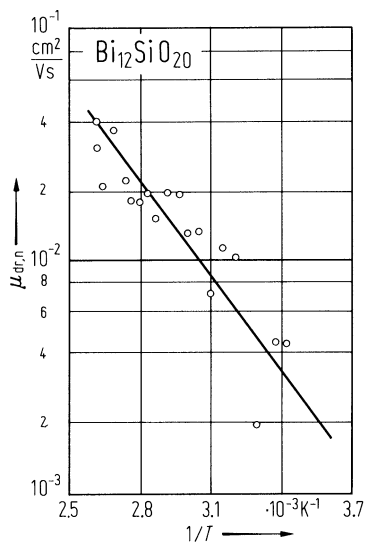
References to 31.1

66L Lenzo, P. V., Spencer, E. G., Ballman, A. A.: Appl. Opt. 5 (1966) 1688.
70F Feldmann, A., Brower, W. S., Horowitz, D.: Appl. Phys. Lett. 16 (1970) 201.
72V Venugopalan, S., Ramdas, A. K.: Phys. Rev. B 5 (1972) 4065.
73H Hou, S. L., Lauer, R. B., Aldrich, R. E.: J. Appl. Phys. 44 (1973) 2652.
74L Lauer, R. B.: J. Appl. Phys. 45 (1974) 1794.
74Z Zhukova, T. B., Kutasov, V. A., Parfen'eva, L. S., Smirnov, I. A.: Inorg. Mater. 10 (1974) 1903 (transl. from Izv. Akad. Nauk SSSR, Neorg. Mater. 10 (1974) 2221).
78K Kleszczewski, Z.: Arch. Acoust. 3 (1978) 175.
79W Wojdowski, W., Lukasiewicz, T., Nazarewicz, W., Zmija, J.: Phys. Status Solidi (b) 94 (1979) 649.
80K Kostyuk, B. Kh., Kudzin, A. Yu., Sokolyanskii, G. Kh.: Sov. Phys. Solid State 22 (1980) 1429 (transl. from Fiz. Tverd. Tela 22 (1980) 2454).

Figures to 31.1

Fig. 31.1.1

$\text{Bi}_{12}\text{SiO}_{20}$. Drift mobility of carriers vs. reciprocal temperature in a field of $2.3 \cdot 10^4$ V/cm [80K].



31.2 Bi12GeO20

Crystal structure

see section 31.0.

Physical properties

energy gap

Eg 3.25 eV photoconductivity 71L

electron mobility

μdr,n 4.51·10-3 cm2/Vs effective drift mobility in transit time measurements 71L

electrical resistivity

ρ 8·1010 Ω cm p-type 67L, 71A

dielectric constant

ε(0) 40 71A

density

dcalc 9.222(2) g cm-3 67A

phonon modes

data from reflectivity [79W] (in cm-1)

TO-modes: 97, 105, 123, 130, 177, 190, 205, 232, 271, 303, 356,459, 526, 571, 600, 682
LO-modes: 100, 114, 129, 154, 179, 193, 209, 254, 281, 355, 372, 497, 555, 578, 612, 894

data from Raman spectra [72V] (in cm-1)

TO-modes: 207.0
LO-modes: 48.1, 54.6, 111.2, 153.0, 178.5, 194.4, 208.5, 691.8
LO+TO-modes: 44.6, 52.4, 57.5, 99.0, 105.8, 124.0, 131.2, 305.0, 338.0, 357.5,488.3, 678.6

References to 31.2

67A Abrahams, S. C., Jamieson, P. H., Bernstein, J. L.: J. Chem. Phys. 47 (1967) 4034.
67L Lenzo, P. V., Spencer, E. G., Ballman, A. A.: Phys. Rev. Lett. 19 (1967) 641.
71A Aldrich, R. E., Hou, S. L., Harvill, M. L.: J. Appl. Phys. 42 (1971) 493.
71L Lenzo, P. V.: J. Appl. Phys. 43 (1971) 1107.
72V Venugopalan, S., Ramdas, A. K.: Phys. Rev. B 5 (1972) 4065.
79W Wojdowski, W., Lukasiewicz, T., Nazarewicz, W., Zmija, J.: Phys. Status Solidi (b) 94 (1979) 649.

31.3 PbSb₂S₄, GeSb₂Te₄, GeBi₂Te₄, SnBi₂Te₄

PbSb₂S₄ (zinkenite) crystallizes in the F5₆ orthorhombic lattice with $a = 12.29 \text{ \AA}$, $b = 13.6 \text{ \AA}$, $c = 8.66 \text{ \AA}$ [74D1]. From photoconductivity spectra values of 1.13 eV ($T = 300 \text{ K}$) and 1.38 eV ($T = 77 \text{ K}$) for the energy gap have been deduced. The electrical conductivity at RT of an n-type sample was $\sigma = 1.45 \cdot 10^{-7} \text{ } \Omega^{-1} \text{ cm}^{-1}$ [74D1, 74D2].

GeSb₂Te₄ crystallizes in the hexagonal D_{3d}⁵-R $\bar{3}$ m lattice with $a = 4.21 \text{ \AA}$ and $c = 40.6 \text{ \AA}$. The samples studied [72F] were strongly degenerate n-type with $\sigma_{\perp} = 4.3 \cdot 10^3 \text{ } \Omega^{-1} \text{ cm}^{-1}$ at RT. The electron Hall mobility at 300 K was 30 cm²/Vs (for the temperature dependence, see Fig. 31.3.1). From reflectivity measurements near the plasma edge a dielectric constant of 39 and a conductivity effective mass of 0.55 m_0 were calculated.

GeBi₂Te₄ has the same structure as GeSb₂Te₄ with $a = 4.28 \text{ \AA}$, $c = 39.2 \text{ \AA}$. The optical energy gap is reported to be $E_g = 0.23 \text{ eV}$ at RT. Experimental data on transport parameters can be explained with a two-conduction-band model with $m_{n1} = 0.24 m_0$, $m_{n2} = 0.88 m_0$ and $E_{c2} - E_{c1} = 0.13(6) \text{ eV}$ [79T].

SnBi₂Te₄ has the same structure as GeSb₂Te₄. Some preliminary results are reported in [74Z].

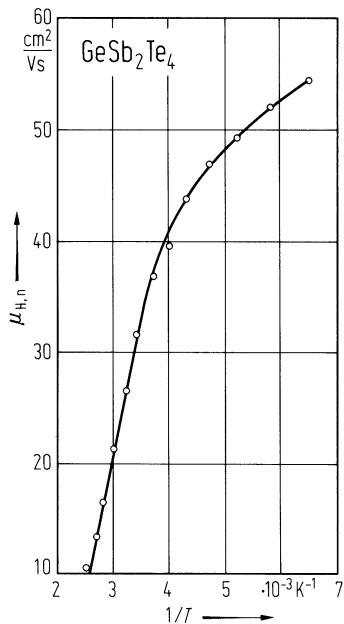
References to 31.3

- 72F Frumar, M., Tichy, L., Horak, J., Klikorka, J.: Mater Res. Bull. 7 (1972) 1075.
- 74D1 Dmytriv, A. Yu., Koval'skii, P. N., Makarenko, V. V.: Sov. Phys. Semicond. 7 (1974) 1097 (transl. from Fiz. Tekh. Poluprovodn. 7 (1974) 1641).
- 74D2 Dmytriv, A. Yu., Koval'skii, P. N., Makarenko, V. V.: Sov. Phys. Semicond. 7 (1974) 1493 (transl. from Fiz. Tekh. Poluprovodn. 7 (1974) 2241).
- 74Z Zhukova, T. B., Kutasov, V. A., Parfen'eva, L. S., Smirnov, I. A.: Inorg. Mater. 10 (1974) 1903 (transl. from Izv. Akad. Nauk SSSR, Neorg. Mater. 10 (1974) 2221).
- 79T Tichy, L., Frumar, M., Klikorka, J.: Phys. Status Solidi (a) 56 (1979) 323.

Figures to 31.3

Fig. 31.3.1

GeSb₂Te₄. Hall mobility of an n-type sample vs. reciprocal temperature [72F].



31.4 GeBi₄Te₇, GeSb₄Te₇, PbBi₄Te₇

These compounds crystallize in a layer structure with space group $D_{3d}^3-P\bar{3}m1$. The lattice parameters are

Substance	a [Å]	c [Å]	Ref.
GeSb ₄ Te ₇	4.21	23.65	74F
GeBi ₄ Te ₇	4.36	24.11	76K
PbBi ₄ Te ₇	4.42	23.6	71F

For **SnBi₄Te₇** only a few preliminary results have been reported in [74Z].

GeSb₄Te₇ [74F]: The samples studied were strongly degenerate p-type with $\sigma_{\perp} = 3.42 \cdot 10^3 \Omega^{-1} \text{ cm}^{-1}$ and $\sigma_{\parallel} = 1.032 \cdot 10^3 \Omega^{-1} \text{ cm}^{-1}$ at room temperature. The transport measurements could be described using a six-valley model for the valence band. Analysis of transport and optical measurements yielded a Hall mobility at RT of 39 cm^2/Vs , a dielectric constant of $\epsilon(0) = 39$ and a conductivity effective mass of $0.46 m_0$.

GeBi₄Te₇ [76K]: The samples studied were strongly degenerate n-type with $\sigma_{\perp} = 1.907 \cdot 10^3 \Omega^{-1} \text{ cm}^{-1}$ and $\sigma_{\parallel} = 1.017 \cdot 10^3 \Omega^{-1} \text{ cm}^{-1}$ at room temperature. The transport measurements could be described using a simple three-valley model for the conduction band. Analysis of reflectivity measurements yielded a dielectric constant $\epsilon(0) = 35$ and a conductivity effective mass of $0.27 m_0$.

PbBi₄Te₇ [71F]: The samples studied were strongly degenerate n-type with $\sigma_{\perp} \approx 10^3 \Omega^{-1} \text{ cm}^{-1}$. The Hall mobility μ_{\perp} was of the order of 15 cm^2/Vs at room temperature (Fig. 31.4.1). From the reflectivity near the plasma edge a dielectric constant of $\epsilon(0) = 44$ and an effective carrier mass of $0.29 m_0$ were calculated.

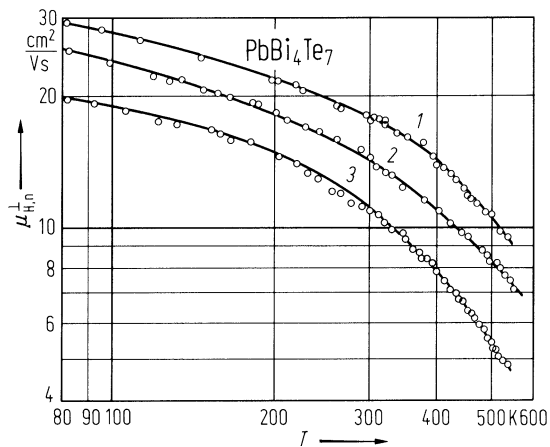
References to 31.4

- 71F Frumar, M., Horak, J.: Phys. Status Solidi (a) 6 (1971) K133.
74F Frumar, M., Tichy, L., Matyas, M., Zelizko, J.: Phys. Status Solidi (a) 22 (1974) 535.
76K Klikorka, J., Fumar, M., Tichy, L., Panek, L., Ticha, H.: J. Phys. Chem. Solids 37 (1976) 477.

Figures to 31.4

Fig. 31.4.1

PbBi_4Te_7 . Electron mobility vs. temperature in three samples with 1: $\sigma_{\perp} = 1.1 \cdot 10^3 \Omega^{-1} \text{ cm}^{-1}$, 2: $\sigma_{\perp} = 1.3 \cdot 10^3 \Omega^{-1} \text{ cm}^{-1}$, 3: $\sigma_{\perp} = 2.0 \cdot 10^3 \Omega^{-1} \text{ cm}^{-1}$, respectively [71F].



32 V-VI-VII compounds

32.0 Crystal structure and electronic structure

Crystal structure

V-VI-VII compounds occur as ternary compounds in the pseudobinary phase diagrams of the (V-VII₃)-(V₂-VI₃) system. Several lattice structures exist:

(a) Most V-VI-VII semiconductors crystallize in a structure of space group symmetry D_{2h}^{16} -Pnam. The unit cell contains four formula units. The atoms are arranged in chains along the *c* axis (Fig. 32.0.1).

lattice parameters and densities

Substance	<i>a</i> [Å]	<i>b</i> [Å]	<i>c</i> [Å]	<i>d_x</i> [g cm ⁻³]	Ref.
SbSI	8.52	10.13	4.10	5.33	67K
SbSBr	8.20	9.70	3.95	4.94	50D1
SbSeI	8.65	10.38	4.12	5.88	50D2
SbSeBr	8.30	10.20	3.95	5.57	50D2
SbTeI	9.18	10.8	4.23	5.96	51D
BiSCl	7.70	9.87	4.02	6.04	50D1
BiSBr	8.02	9.70	4.01	6.83	50D1
BiSI	8.46	10.15	4.14	6.87	50D1
BiSeCl	12.37	18.10	4.08	7.05	50D2
BiSeBr	8.18	10.47	4.11	6.94	50D2
BiSeI	8.71	10.54	4.19	7.16	50D2

(b) The BiO-halogen compounds crystallize in a structure of space group symmetry D_{4h}^7 -P4/nmm. Sheets of oxygen alternate with sheets of bismuth. Double layers of halogen atoms lie between the metal and oxygen sheets [68B]. Two formula units are contained in the unit cell of this laminar tetragonal structure.

Substance	<i>a</i> [Å]	<i>c</i> [Å]	lattice stable below
BiOCl	3.883	7.347	575°C
BiOBr	3.915	8.076	560°C
BiOI	3.984	9.128	300°C

(c) BiTeBr and BiTeI crystallize in a hexagonal layered structure of space group symmetry D_{3d}^3 - $\bar{P}3m1$.

Substance	<i>a</i> [Å]	<i>c</i> [Å]	Ref.	<i>d_x</i> [g cm ⁻³]	Ref.
BiTeBr	4.23(1)	6.48(1)	68H	6.90	51D
BiTeI	4.30(1)	6.80(1)		7.01	

Electronic structure

Figs. 32.0.2...4 show the band structures of (paraelectric and ferroelectric) SbSI and its Brillouin zone.

References to 32.0

- 50D1 Dönges, E.: Z. Anorg. Allg. Chem. 263 (1950) 112.
- 50D2 Dönges, E.: Z. Anorg. Allg. Chem. 263 (1950) 280.
- 51D Dönges, E.: Z. Anorg. Allg. Chem. 265 (1951) 56.
- 67K Kikuchi, A., Oka, Y., Sawaguchi, E.: J. Phys. Soc. Jpn. 23 (1967) 337.
- 73N Nako, K., Balkanski, M.: Phys. Rev. B8 (1973) 5759.

Figures to 32.0

Fig. 32.0.1

SbSI. Crystal structure of the paraelectric phase as an example for the $D_{2h}16$ –Pnam lattice [67K]

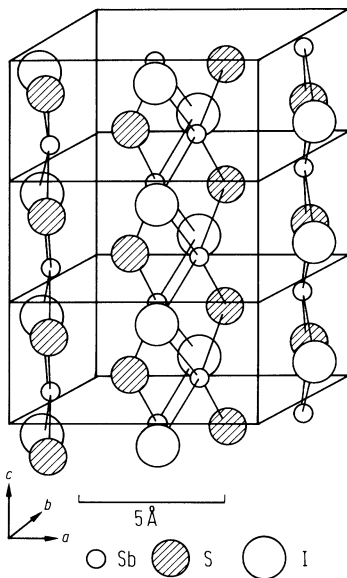


Fig. 32.0.2

SbSI. Band structure of the paraelectric phase calculated with the pseudopotential method using the atomic positions at 35°C as parameters [73N].

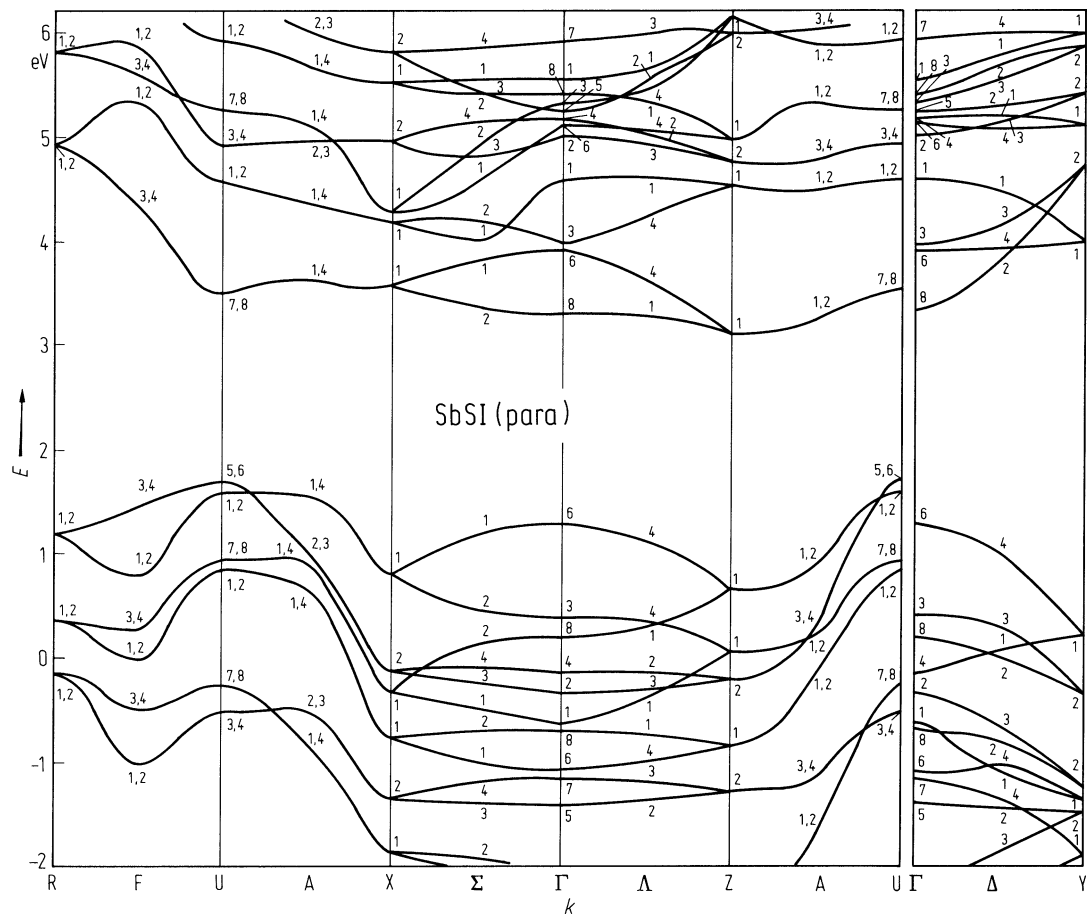
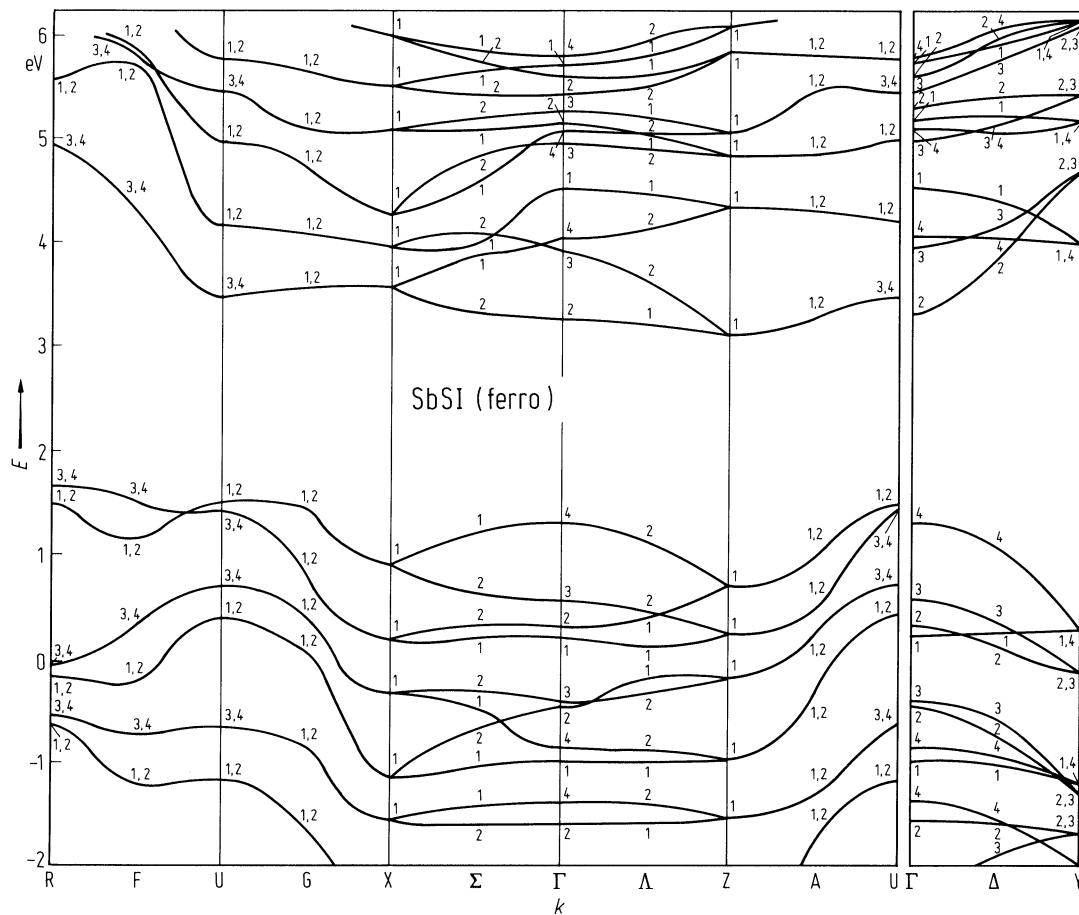
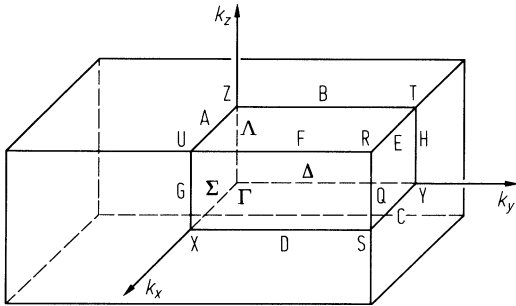


Fig. 32.0.3

SbSI. Band structure of the ferroelectric phase calculated with the pseudopotential method using the atomic positions at 5°C as parameters [73N].



SbSI. Brillouin zone of the paraelectric and ferroelectric phases [73N].



32.1 AsSBr

Physical properties

energy gap

E_g	2.5 eV	temperature dependence of conductivity (Fig. 32.1.1)	65A
-------	--------	--	-----

electrical resistivity

ρ	$> 10^{12} \Omega \text{ cm}$		65A
--------	-------------------------------	--	-----

electron mobility

$\mu_{H,n}$	$< 10^{-1} \text{ cm}^2/\text{Vs}$		65A
-------------	------------------------------------	--	-----

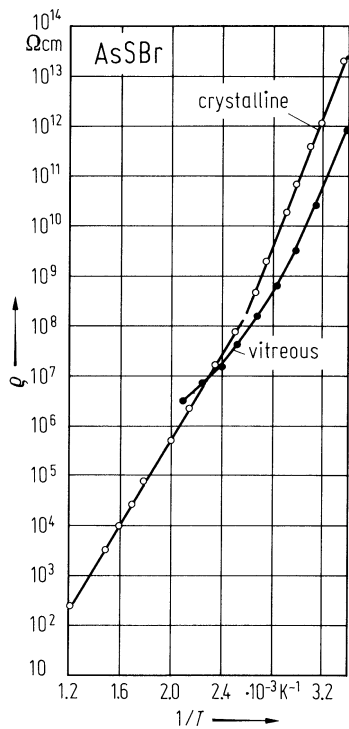
References to 32.1

65A Antonini, J. F., Brun, R.: Nuovo Cimento 35 (1965) 956.

Figures to 32.1

Fig. 32.1.1

AsSBr. Resistivity vs. reciprocal temperature for a crystalline and a vitreous sample [65A].



32.2 SbSI

SbSI is by far the most interesting and most investigated V-VI-VII compound being a photoconductor and having a paraelectric – ferroelectric phase transition near room temperature [62F].

Crystal structure

see section 32.0.

Physical properties

band structure: Fig. 32.0.2 (paraelectric phase), Fig. 32.0.3 (ferroelectric phase), Brillouin zone: Fig. 32.0.4.

The calculated band structures show an indirect gap in both phases: Z_{1c} – $U_{5,6v}$ in the paraelectric phase, Z_{1c} – $R_{3,4v}$ in the ferroelectric phase. The lowest direct transition occurs at U: $U_{7,8c}$ – $U_{5,6v}$ for $E \parallel c$, $U_{7,8c}$ – $U_{1,2v}$ for $E \perp c$ (paraelectric phase), $U_{3,4c}$ – $U_{3,4v}$ for $E \parallel c$, $U_{3,4c}$ – $U_{1,2v}$ for $E \perp c$ (ferroelectric phase). In contrast to [73N] the band structure presented in [74F] shows a direct gap at Γ

energy gap

$E_{g,dir}$	1.88 eV	$E \parallel c, T = 25^{\circ}C$	absorption edge	63H
	1.95 eV	$E \perp c$		

temperature dependence of energy gap

dE_g/dT	$-2.2(2) \cdot 10^{-3} \text{ eV/K}$	$T < \Theta_C$	absorption	63H
-----------	--------------------------------------	----------------	------------	-----

melting point

T_m	$\approx 400^{\circ}C$			64M
-------	------------------------	--	--	-----

phonon dispersion relations : Fig. 32.2.1, Brillouin zone: Fig. 32.0.4.

The vibrational spectrum of SbSI is very complicated. The unit cell of the lattice contains 4 formula units. Thus there are 3 acoustic and 33 optical branches. The optical activity of the optical modes in this description is

paraelectric phase:	infrared active:	2 A_u -modes($E \parallel c$),	4 B_u -modes ($E \perp c$)
	Raman active:	6 A_g -modes,	3 B_g -modes
ferroelectric phase:	infrared active:	8A-modes ($E \parallel c$),	7 B-modes ($E \perp c$)
	these modes are also Raman active.		

wavenumbers of infrared active modes ($k \approx 0$)

$\bar{\nu}_T$	9 cm^{-1}	$T = 298 \text{ K}, E \parallel c$	designation according to	71A
$\bar{\nu}_L$	111 cm^{-1}	(paraelectric phase)	simplified C_{2h}^2 lattice	
$\bar{\nu}_T$	179(10) cm^{-1}			
$\bar{\nu}_L$	261(10) cm^{-1}			
$\bar{\nu}_T$	78 cm^{-1}			
$\bar{\nu}_L$	82 cm^{-1}			
$\bar{\nu}_T$	120 cm^{-1}			
$\bar{\nu}_L$	124 cm^{-1}			
$\bar{\nu}_T$	270 cm^{-1}			
$\bar{\nu}_L$	276 cm^{-1}			
$\bar{\nu}_T$	327 cm^{-1}			
$\bar{\nu}_L$	332 cm^{-1}			

wavenumbers of infrared active modes ($k \approx 0$) (continued)

$\bar{\nu}_T$	16 cm ⁻¹	$T = 275$ K, $E \parallel c$	designation according to	71A
$\bar{\nu}_T$	60 cm ⁻¹	(ferroelectric phase)	simplified C ₂ ² lattice	
$\bar{\nu}_L$	100 cm ⁻¹			
$\bar{\nu}_T$	108 cm ⁻¹			
$\bar{\nu}_L$	115 cm ⁻¹			
$\bar{\nu}_T$	138 cm ⁻¹			
$\bar{\nu}_L$	140 cm ⁻¹			
$\bar{\nu}_T$	178(10) cm ⁻¹			
$\bar{\nu}_L$	217(10) cm ⁻¹			
$\bar{\nu}_T$	247 cm ⁻¹			

wavenumbers of Raman active modes

$\bar{\nu}(A_g)$	51 cm ⁻¹	$T = 299$ K	A _g -symmetry in simplified C _{2h} ²	71A
	66 cm ⁻¹	(paraelectric	lattice	
	107 cm ⁻¹	phase)		
	137 cm ⁻¹			
	149 cm ⁻¹			
	329 cm ⁻¹			
$\bar{\nu}(B_g)$	37 cm ⁻¹		B _g -symmetry in simplified C _{2h} ²	71A
	212 cm ⁻¹		lattice	
	239 cm ⁻¹			
	soft mode	$T = 250$ K		72T
		(ferroelectric		
		phase)		

second order elastic moduli

c_{11}	3.09(9)·10 ⁸ N cm ⁻²	paraelectric	70S
c_{22}	3.27(4)·10 ⁸ N cm ⁻²	phase,	
c_{33}	4.95(6)·10 ⁸ N cm ⁻²	$T = 22^\circ\text{C}$	
c_{44}	2.21(3)·10 ⁸ N cm ⁻²		
c_{55}	0.92(3)·10 ⁸ N cm ⁻²		
c_{66}	0.60(2)·10 ⁸ N cm ⁻²		
c_{12}	0.96(9)·10 ⁸ N cm ⁻²		
c_{13}	0.93(30)·10 ⁸ N cm ⁻²		
c_{23}	1.58(12)·10 ⁸ N cm ⁻²		
c_{11}	3.06(9)·10 ⁸ N cm ⁻²	ferroelectric	70S
c_{22}	3.14(4)·10 ⁸ N cm ⁻²	phase,	
c_{33}	5.18(6)·10 ⁸ N cm ⁻²	$T \approx 12^\circ\text{C}$	
c_{44}	2.24(3)·10 ⁸ N cm ⁻²		
c_{55}	0.99(3)·10 ⁸ N cm ⁻²		
c_{66}	0.59(2)·10 ⁸ N cm ⁻²		
c_{12}	0.85(9)·10 ⁸ N cm ⁻²		
c_{13}	0.97(30)·10 ⁸ N cm ⁻²		
c_{23}	1.44(12)·10 ⁸ N cm ⁻²		

electrical resistivity

ρ	$10^8 \dots 10^9 \Omega \text{ cm}$	along c axis	68C
--------	-------------------------------------	----------------	-----

electron mobility

$\mu_{H,n}$	$50 \dots 100 \text{ cm}^2/\text{Vs}$	mobility of photoexcited carriers measured with the photo Hall effect in a Li doped sample	67A
-------------	---------------------------------------	--	-----

refractive index (at $\lambda = 633 \text{ nm}$)

n_a	2.87	paraelectric	70S
n_b	3.63	phase,	
n_c	4.55	$T = 22^\circ\text{C}$	
n_a	2.87	ferroelectric	
n_b	3.57	phase,	
n_c	4.44	$T \approx 12^\circ\text{C}$	

dielectric constant

$\epsilon_{\parallel c}$	$6.2 \cdot 10^4$	at Θ_C , $f = 1 \text{ kHz}$	64M
--------------------------	------------------	--	-----

Electrical conduction in SbSI is dominated by contact phenomena due to the presence of strong field regions near the contacts [73A] and space charge limited currents.

References to 32.2

- 62F Fatuzzo, E., Harbeke, G., Merz, W. J., Nitsche, R. . Roetschi, R., Ruppel, W.: Phys. Rev. 127 (1962) 2036.
- 63H Harbeke, G.: J. Phys. Chem. Solids 24 (1963) 957.
- 64M Mori, T., Tamura, H.: J. Phys. Soc. Jpn 19 (1964) 1247.
- 67A Alekseeva, V. G., Landsberg, E. G.: Sov. Phys. Solid State 8 (1967) 2518 (transl. from Fiz. Tverd. Tela 8 (1966) 3138).
- 68C Chepur, D. V., Bercha, D. M., Turyanitsa, I. D., Slivka, V. Yu.: Phys. Status Solidi 30 (1968) 461.
- 70S Sandcock, J. R.: Opt. Commun. 3 (1970) 73.
- 71A Agrawal, D. K., Perry, C. H.: Phys. Rev. B4 (1971) 1893.
- 72T Teng, M. K., Balkanski, M., Massot, M.: Phys. Rev. B5 (1972) 1031.
- 73A Artobolevskaya, E. S., Chenskii, E. V., Gvozdover, R. S., Petrov, V. I.: Sov. Phys. Solid State 14 (1973) 1935 (transl. from Fiz. Tverd. Tela 14 (1972) 2236).
- 73N Nako, K., Balkanski, M.: Phys. Rev. B8 (1973) 5759.
- 74F Fong, C. Y., Petroff, Y., Kohn, S., Shen, Y. R.: Solid State Commun. 14 (1974) 681.
- 77P Pierrefeu, A., Steigmeier, E. F., Dorner, B.: Phys. Status Solidi (b) 80 (1977) 167.

Figures to 32.2

Fig. 32.0.2

SbSI. Band structure of the paraelectric phase calculated with the pseudopotential method using the atomic positions at 35°C as parameters [73N].

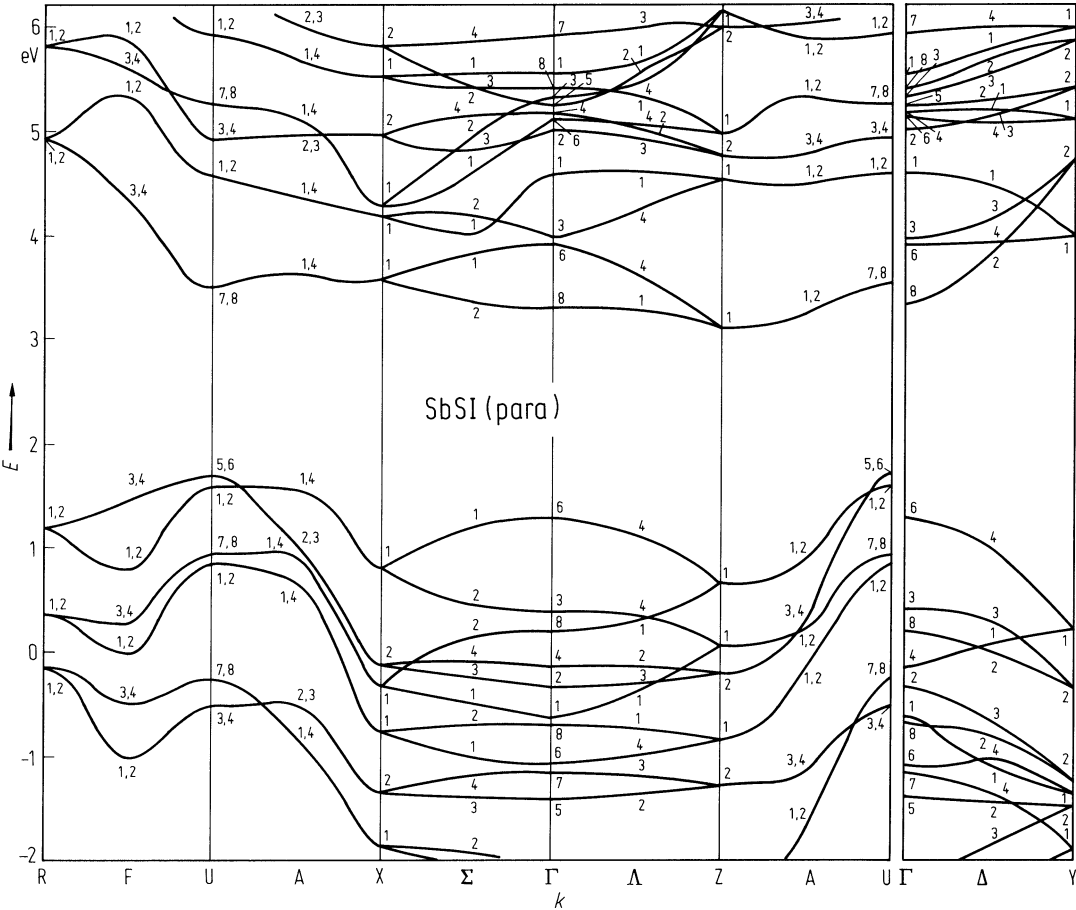


Fig. 32.0.3

SbSI. Band structure of the ferroelectric phase calculated with the pseudopotential method using the atomic positions at 5°C as parameters [73N].

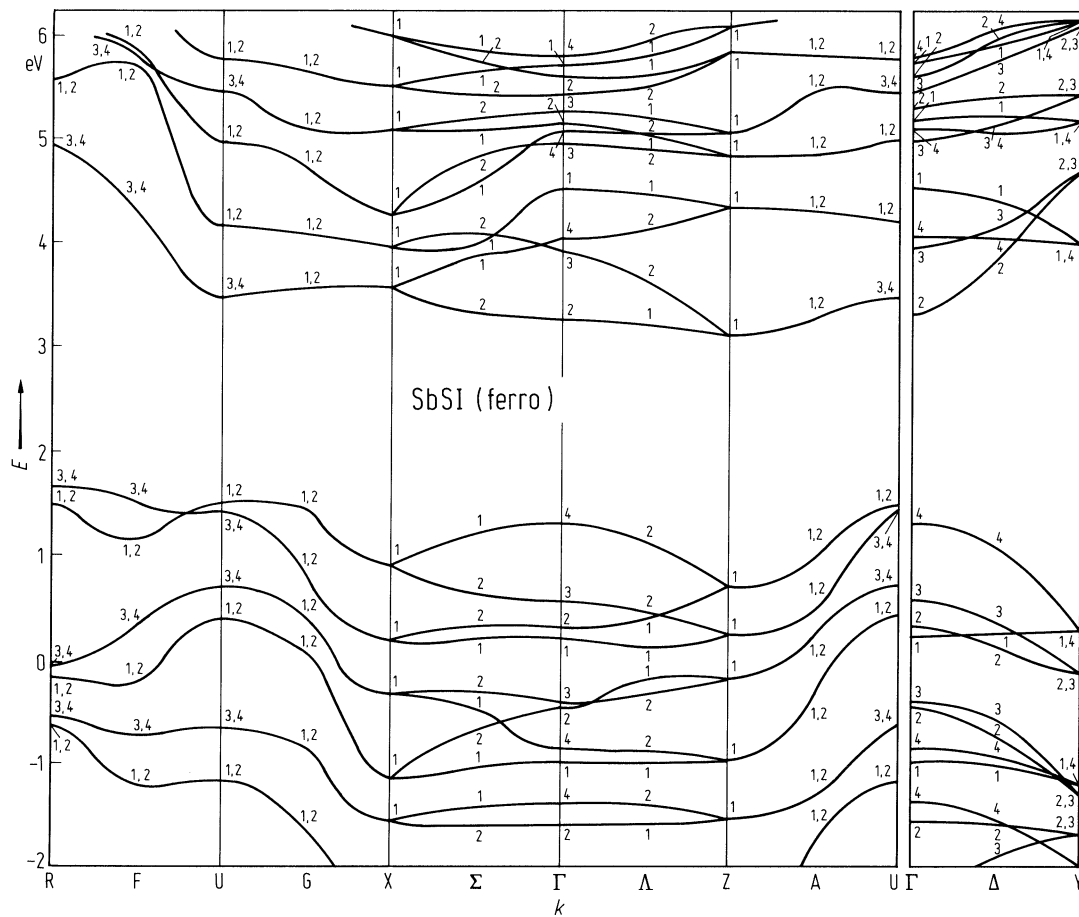


Fig. 32.0.4

SbSI. Brillouin zone of the paraelectric and ferroelectric phases [73N].

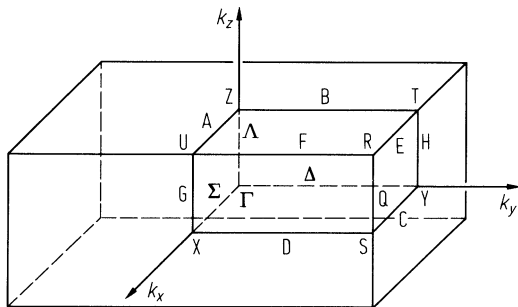
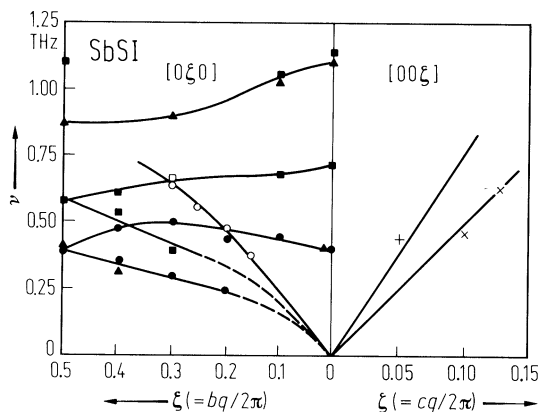


Fig. 32.2.1

SbSI. Phonon dispersion curves along the cubic axes of the Brillouin zone (Fig. 32.5). Open symbols: longitudinal modes, closed symbols: transverse polarized modes. Cubes: ferroelectric phase, triangles: paraelectric phase, + and \times : 10.3 and 23,3°C, respectively [77P].



32.3 SbSBr

Crystal structure

see section 32.0.

Physical properties

energy gap

E_g	2.26 eV	$E \perp c$, RT	68C
	2.20 eV	$E \parallel c$	
dE_g/dT	$-8 \cdot 10^{-4}$ eV/K	$T = 20^\circ\text{C}$	68C

electrical resistivity

ρ	$10^6 \Omega \text{ cm}$	along c axis	68C
--------	--------------------------	----------------	-----

refractive index

n_a	2.64	$\lambda = 570 \text{ nm}$	refractive index along crystal	68C
n_b	3.13		axes	
n_c	4.01			

References to 32.3

68C Chepur, D. V., Bercha, D. M., Turyanitsa, I. D., Slivka, V. Yu.: Phys. Status Solidi 30 (1968) 461.

32.4 SbSeBr

Crystal structure

see section 32.0.

Physical properties

energy gap

E_g	1.92 eV	$E \perp c$	68C
	1.88 eV	$E \parallel c$	
dE_g/dT	$-7.2 \cdot 10^{-4}$ eV/K		68C

References to 32.4

68C Chepur, D. V., Bercha, D. M., Turyanitsa, I. D., Slivka, V. Yu.: Phys. Status Solidi 30 (1968) 461.

32.5 SbSeI

Crystal structure

see section 32.0.

Physical properties

energy gap

E_g	1.68 eV	$E \perp c$	68C
-------	---------	-------------	-----

	1.66 eV	$E \parallel c$	
dE_g/dT	$-8 \cdot 10^{-4}$ eV/K		68C

electrical resistivity

$\rho_{\parallel c}$	$10^7 \Omega \text{ cm}$		68C
----------------------	--------------------------	--	-----

References to 32.5

68C Chepur, D. V., Bercha, D. M., Turyanitsa, I. D., Slivka, V. Yu.: Phys. Status Solidi 30 (1968) 461.

32.6 SbTeI

Crystal structure

see section 32.0.

Physical properties

energy gap

E_g	1.28 eV	$E \perp c$	68C
	1.25 eV	$E \parallel c$	

electrical resistivity

$\rho_{\parallel c}$	$10^4 \Omega \text{ cm}$	68C
----------------------	--------------------------	-----

References to 32.6

68C Chepur, D. V., Bercha, D. M., Turyanitsa, I. D., Slivka, V. Yu.: Phys. Status Solidi 30 (1968) 461.

32.7 BiOCl

Crystal structure

see section 32.0.

Physical properties

energy gap

$E_{g,ind}$	3.455 eV	RT	optical absorption	72S
$E_{g,dir}$	3.50 eV	RT	optical absorption	72S
dE_g/dT	$-6.3 \cdot 10^{-4}$ eV/K	$T = 90 \dots 600$ K		72S

phonon energy

$h\nu_{TO}(\Gamma)$	35.3 meV 65.4 meV (16.6 meV)	infrared bands	73P
---------------------	------------------------------------	----------------	-----

References to 32.7

- 72S Shtilikha, M. V., Chepur, D. V.: Sov. Phys. Semicond. 6 (1972) 389 (transl. from Fiz. Tekh. Poluprovodn. 6 (1972) 451).
- 73P Puga, G. D., Borets, A. N., Bercha, D. M., Shtilikha, M. V.: Sov. Phys. Solid State 14 (1973) 1830 (transl. from Fiz. Tverd. Tela 14 (1972) 2125).

32.8 BiOBr

Crystal structure

see section 32.0.

Physical properties

energy gap

$E_{g,ind}$	2.924 eV	$T = 293$ K	absorption	72S
$E_{g,dir}$	3.00 eV		absorption	72S
dE_g/dT	$-7.4 \cdot 10^{-4}$ eV/K	$T = 90 \dots 600$ K		72S

phonon energy

$h\nu_{TO}(\Gamma)$	32.8 meV		infrared bands	73P
	64.4 meV			
	(14.6 meV)			

References to 32.8

- 72S Shtilikha, M. V., Chepur, D. V.: Sov. Phys. Semicond. 6 (1972) 389 (transl. from Fiz. Tekh. Poluprovodn. 6 (1972) 451).
- 73P Puga, G. D., Borets, A. N., Bercha, D. M., Shtilikha, M. V.: Sov. Phys. Solid State 14 (1973) 1830 (transl. from Fiz. Tverd. Tela 14 (1972) 2125).

32.9 BiOI

Crystal structure

see section 32.0.

Physical properties

energy gap

$E_{g,ind}$	1.890 eV	RT	absorption edge	72S
$E_{g,dir}$	1.94 eV	RT	absorption edge	72S
dE_g/dT	$-8.1\cdot10^{-4}$ eV/K	$T=90...600$ K		72S
	$-5.6\cdot10^{-4}$ eV/K	$T<300$ K	phase transition at 300 K?	73B
	$-8.2\cdot10^{-4}$ eV/K	$T>300$ K		

phonon energies

$h\nu_{TO}(\Gamma)$	60.4 meV		infrared bands	73P
	30.8 meV			
	12.8 meV			
	70.6 meV			

References to 32.9

72S Shtilikha, M. V., Chepur, D. V.: Sov. Phys. Semicond. 6 (1972) 389 (transl. from Fiz. Tekh. Poluprovodn. 6 (1972) 451).

73P Puga, G. D., Borets, A. N., Bercha, D. M., Shtilikha, M. V.: Sov. Phys. Solid State 14 (1973) 1830 (transl. from Fiz. Tverd. Tela 14 (1972) 2125).

32.10 BiSCl

Crystal structure

see section 32.0.

Physical properties

energy gap

E_g	1.93 eV	$E \perp c$	68C
	1.89 eV	$E \parallel c$	

electrical resistivity

ρ	$10^3 \dots 10^4 \Omega \text{ cm}$	see also [60N, 64N]	68C
--------	-------------------------------------	---------------------	-----

References to 32.10

68C Chepur, D. V., Bercha, D. M., Turyanitsa, I. D., Slivka, V. Yu.: Phys. Status Solidi 30 (1968) 461.

32.11 BiSBr

Crystal structure

see section 32.0.

Physical properties

energy gap

E_g	1.97 eV	$E \perp c$	68C,
	1.95 eV	$E \parallel c$	68H
dE_g/dT	$-7.6 \cdot 10^{-4}$ eV/K		68C

electrical resistivity

ρ	$10^3 \dots 10^4 \Omega \text{ cm}$	along c axis, n-type sample	68C
--------	-------------------------------------	----------------------------------	-----

References to 32.11

- 68C Chepur, D. V., Bercha, D. M., Turyanitsa, I. D., Slivka, V. Yu.: Phys. Status Solidi 30 (1968) 461.
68H Horak, J., Rodot, H.: C. R. Acad. Sci. Paris 267 (1968) 1427.

32.12 BiSI

Crystal structure

see section 32.0.

Physical properties

energy gap

E_g	1.58 eV	$E \perp c$	68C
	1.56 eV	$E \parallel c$	
dE_g/dT	$-7 \cdot 10^{-4}$ eV/K		68C

electrical resistivity

ρ	$10^7 \Omega \text{ cm}$		68C
--------	--------------------------	--	-----

References to 32.12

68C Chepur, D. V., Bercha, D. M., Turyanitsa, I. D., Slivka, V. Yu.: Phys. Status Solidi 30 (1968) 461.

32.13 BiSeBr

Crystal structure

see section 32.0.

Physical properties

energy gap

E_g	1.54 eV	$E \perp c$	68H
	1.50 eV	$E \parallel c$	

References to 32.13

68H Horak, J., Rodot, H.: C. R. Acad. Sci. Paris 267 (1968) 1427.

32.14 BiSeI

Crystal structure

see section 32.0.

Physical properties

energy gap

E_g	1.32 eV	$E \perp c$	68C
	1.3 eV	$E \parallel c$	
dE_g/dT	$-6.5 \cdot 10^{-4}$ eV/K		68C

electrical resistivity

ρ	$10^2 \dots 10^3 \Omega \text{ cm}$	along c axis	68C
--------	-------------------------------------	----------------	-----

References to 32.14

68C Chepur, D. V., Bercha, D. M., Turyanitsa, I. D., Slivka, V. Yu.: Phys. Status Solidi 30 (1968) 461.

32.15 BiTeBr

Crystal structure

see section 32.0.

Physical properties

energy gap

E_g	0.55 eV	$E \parallel c$		68C
$E_{g,ind}$	0.472 eV	$T = 295$ K	absorption edge	73B
$E_{g,dir}$	0.501 eV	$T = 295$ K	absorption edge	73B
$dE_{g,ind}/dT$	$-1.85 \cdot 10^{-4}$ eV/K	$T > 100$ K		73B
$dE_{g,dir}/dT$	$-2.93 \cdot 10^{-4}$ eV/K	$T > 100$ K		73B

phonon energies

$h\nu$	14 meV		phonons participating in indirect	73B
	29 meV		transitions	
	44 meV			

electrical conductivity : Fig. 32.15.1

density

d_{exp}	6.65 g cm^{-3}			51D
-----------	--------------------------	--	--	-----

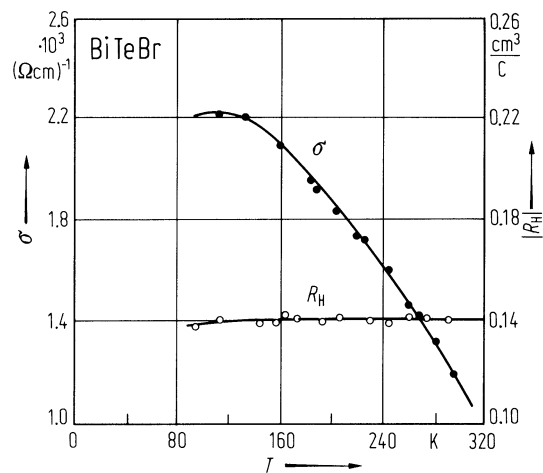
References to 32.15

51D Dönges, E.: Z. Anorg. Allg. Chem. 265 (1951) 56.
68C Chepur, D. V., Bercha, D. M., Turyanitsa, I. D., Slivka, V. Yu.: Phys. Status Solidi 30 (1968) 461.
73B Berezhnoi, A. A., Mamedov, A. M.: Sov. Phys. Solid State 15 (1973) 1023 (transl. from Fiz. Tverd. Tela 15 (1973) 1525).
80M Matyas, M., Horak, J., Klubickova, B.: Phys. Status Solidi (a) 61 (1980) 419.

Figures to 32.15

Fig. 32.15.1

BiTeBr. Electrical conductivity ($\sigma \parallel c$) and Hall coefficient ($B \perp c$) vs. temperature for an n-type single crystal [80M].



32.16 BiTeI

Crystal structure

see section 32.0.

Physical properties

energy gap

E_g	0.39 eV	$T = 295\text{ K}$	absorption, reflection	70H
$E_{g,ind}$	0.448 eV	$T = 295\text{ K}$	position of the indirect absorption	68C
	0.479 eV	$T = 5\text{ K}$	edge (gap including energy of the participating phonon)	

Hall mobility

μ_H^\perp	280...445 cm ² /Vs	degenerate sample, RT	conductivity, Hall effect (see also Figs. 32.16.1, 32.16.2)	68H
---------------	-------------------------------	-----------------------	---	-----

effective mass

m_n	0.20...0.25 m_0	$n = 3.5...7.6 \cdot 10^{19}\text{ cm}^{-3}$		70H
-------	-------------------	--	--	-----

dielectric constants

$\epsilon(0)$	14.5(15)		absorption of free carriers	70H
$\epsilon(\infty)$	19(2)	$E \perp c$		80L

density

d_{exp}	6.91 g cm ⁻³			51D
-----------	-------------------------	--	--	-----

References to 32.16

51D Dönges, E.: Z. Anorg. Allg. Chem. 265 (1951) 56.
68C Chepur, D. V., Bercha, D. M., Turyanitsa, I. D., Slivka, V. Yu.: Phys. Status Solidi 30 (1968) 461.
68H Horak, J., Rodot, H.: C. R. Acad. Sci. Paris 267 (1968) 1427.
70H Horak, J.: J. Phys. (Paris) 31 (1970) 121.
78D Nguyen Tat Dich, Lostak, P., Horak, J.: Czech. J. Phys. B28 (1978) 1297.
80L Lostak, P., Horak, J., Vasko, A., Nguyen Tat Dich: Phys. Status Solidi (a) 59 (1980) 311.

Figures to 32.16

Fig. 32.16.1

BiTeI. Electrical conductivity ($\sigma \perp c$) and Hall coefficient ($B \parallel c$) vs. temperature for three samples [78D].

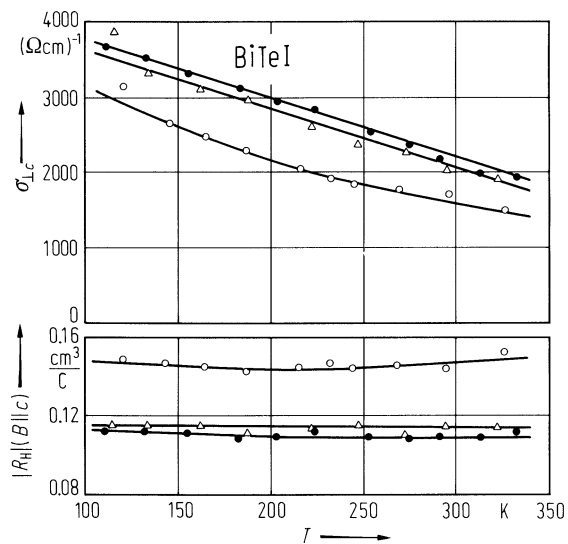
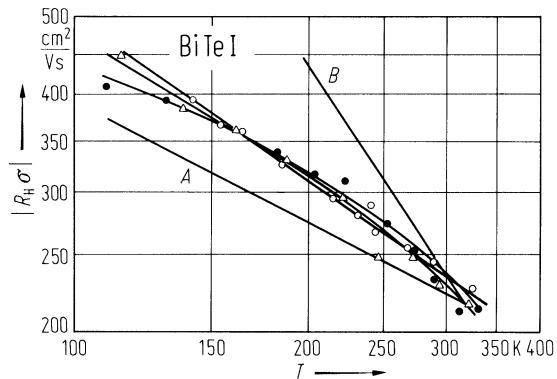


Fig. 32.16.2

BiTeI. Hall mobility $\mu_H = |\sigma R_H|$. Theoretical curves *A* for optical phonon scattering, *B* for acoustic phonon scattering [78D].



33 Other ternary compounds

33.1 Cu₃In₅Se₉

Physical properties

[80T1, 80T2]

energy gap

E_g	1.10 eV	$T = 300$ K	photoconductivity maximum
	1.18 eV	$T = 77$ K	
	0.96 eV	$T = 0$ K	extrapolated from conductivity, Fig. 33.1.1

hole mobility: Fig. 33.1.2

lattice parameters

a	8.47 Å
c	17.41 Å

melting point

T_m	1025°C
-------	--------

density

d	5.568 g cm ⁻³
-----	--------------------------

References to 33.1

- 80T1 Tagirov, V. I., Gakhramanov, A. G., Guseinov, A. G., Aliev, F. M., Guseinov, G. G.: Sov. Phys. Crystallogr. 25 (1980) 237 (transl. from Kristallografiya 25 (1980) 411).
- 80T2 Tagirov, V. I., Gakhramanov, A. G., Guseinov, A. G., Aliev, F. M.: Sov. Phys. Semicond. 14 (1980) 831 (transl. from Fiz. Tekh. Poluprovodn. 14 (1980) 1403).

Figures to 33.1

Fig. 33.1.1

$\text{Cu}_3\text{In}_5\text{Se}_9$. Electrical conductivity and Hall coefficient vs. reciprocal temperature [80T1].

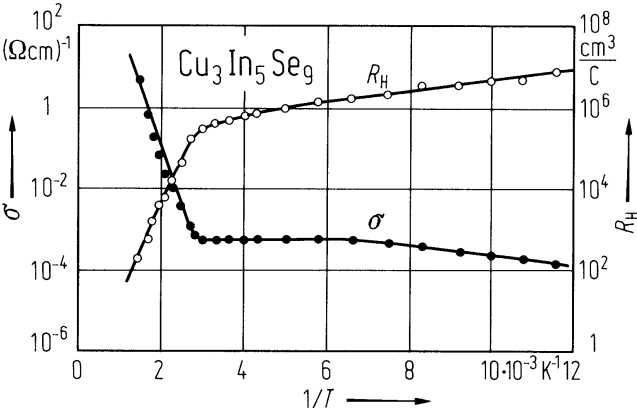
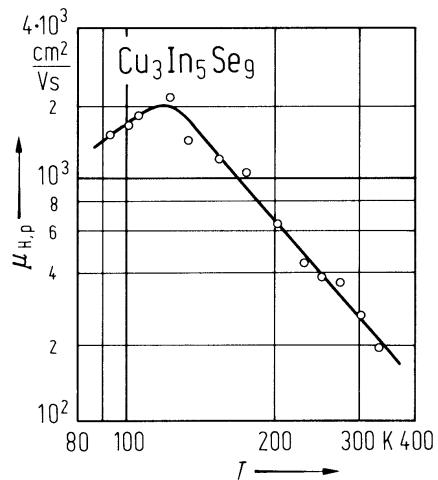


Fig. 33.1.2

$\text{Cu}_3\text{In}_5\text{Se}_9$. Hall mobility of holes vs. temperature [80T2].



33.2 Cu₃Ga₅Se₉

Physical properties

[80T1, 80T2]

energy gap

E_g 1.74 eV $T = 300$ K reflectivity

lattice parameters

a 8.01 Å
 c 16.46 Å

melting point

T_m 1100°C

density

d 5.330 g cm⁻³

References to 33.2

- 80T1 Tagirov, V. I., Gakhramanov, A. G., Guseinov, A. G., Aliev, F. M., Guseinov, G. G.: Sov. Phys. Crystallogr. 25 (1980) 237 (transl. from Kristallografiya 25 (1980) 411).
- 80T2 Tagirov, V. I., Gakhramanov, A. G., Guseinov, A. G., Aliev, F. M.: Sov. Phys. Semicond. 14 (1980) 831 (transl. from Fiz. Tekh. Poluprovodn. 14 (1980) 1403).

33.3 Ag₃In₅Se₉

Physical properties

[80T1, 80T2]

energy gap

E_g 1.22 eV $T = 300$ K photoconductivity

melting point

T_m 825°C

density

d 5.668 g cm⁻³

References to 33.3

- 80T1 Tagirov, V. I., Gakhramanov, A. G., Guseinov, A. G., Aliev, F. M., Guseinov, G. G.: Sov. Phys. Crystallogr. 25 (1980) 237 (transl. from Kristallografiya 25 (1980) 411).
- 80T2 Tagirov, V. I., Gakhramanov, A. G., Guseinov, A. G., Aliev, F. M.: Sov. Phys. Semicond. 14 (1980) 831 (transl. from Fiz. Tekh. Poluprovodn. 14 (1980) 1403).

33.4 Ag₃Ga₅Se₉

Physical properties

[80T1, 80T2]

energy gap

E_g 1.92 eV $T = 300$ K reflectivity

melting point

T_m 884°C

density

d 6.720 g cm⁻³

References to 33.4

- 80T1 Tagirov, V. I., Gakhramanov, A. G., Guseinov, A. G., Aliev, F. M., Guseinov, G. G.: Sov. Phys. Crystallogr. 25 (1980) 237 (transl. from Kristallografiya 25 (1980) 411).
- 80T2 Tagirov, V. I., Gakhramanov, A. G., Guseinov, A. G., Aliev, F. M.: Sov. Phys. Semicond. 14 (1980) 831 (transl. from Fiz. Tekh. Poluprovodn. 14 (1980) 1403).

33.5 Cu₂Ga₄Te₇

Physical properties

[73C]

energy gap

$E_{g,th}$	1.08 eV	$T = 300\text{ K}$	conductivity, Fig. 33.5.1 absorption
E_g	1.04 eV		

hole mobility

$\mu_{H,p}$	120 cm ² /Vs	$T = 300\text{ K},$ $p = 10^{18}\text{ cm}^{-3}$	see Fig. 33.5.2
-------------	-------------------------	---	-----------------

lattice parameter

a	5.93 Å
-----	--------

melting point

T_m	874°C
-------	-------

density

d	5.93 g cm ⁻³	X-ray experimental
	5.84 g cm ⁻³	

References to 33.5

73C Congiu, A., Garbato, L., Manca, P.: Mater. Res. Bull. 8 (1973) 293.

Figures to 33.5

Fig. 33.5.1

$\text{Cu}_2\text{Ga}_4\text{Te}_7$. Electrical conductivity vs. (reciprocal) temperature [73C].

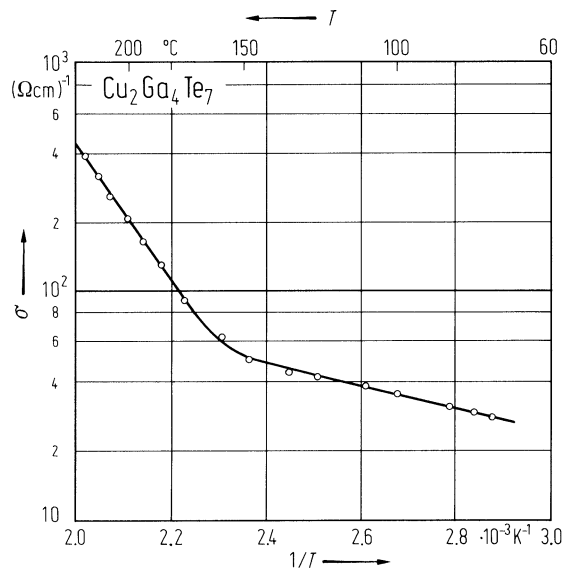
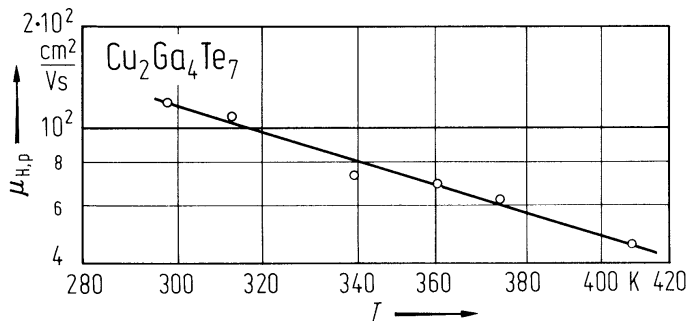


Fig. 33.5.2

$\text{Cu}_2\text{Ga}_4\text{Te}_7$. Hall mobility of holes vs. (reciprocal) temperature [73C].



33.6 Cu₂In₄Te₇

Physical properties

I₂-III₄-VI₇ compound (sphalerite structure). [72C]

energy gap

$E_{\text{g,th}}$ 1.10 eV conductivity, Fig. 33.6.1

hole mobility

$\mu_{\text{H,p}}$ 0.27 cm²/Vs $p = 7.3 \cdot 10^{15}$ cm⁻³,
 $T = 300$ K see Fig. 33.6.2

lattice parameter

a 6.16 Å

melting point

T_{m} 795(5)°C

density

d 6.02 g cm⁻³ X-ray
5.93 g cm⁻³ experimental

References to 33.6

72C Congiu, A., Garbato, L., Manca, P., Serici, S.: J. Electrochem. Soc. 119 (1972) 280.

Figures to 33.6

Fig. 33.6.1

$\text{Cu}_2\text{In}_4\text{Te}_7$. Electrical conductivity of two samples vs. (reciprocal) temperature [72C].

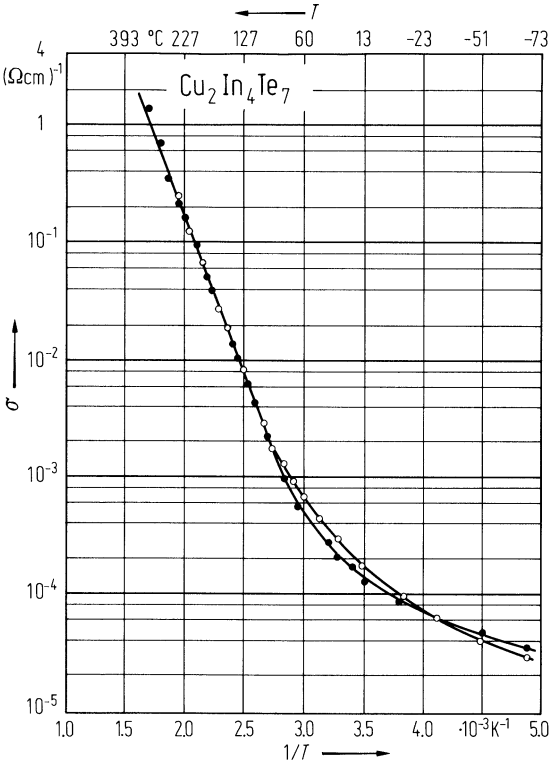
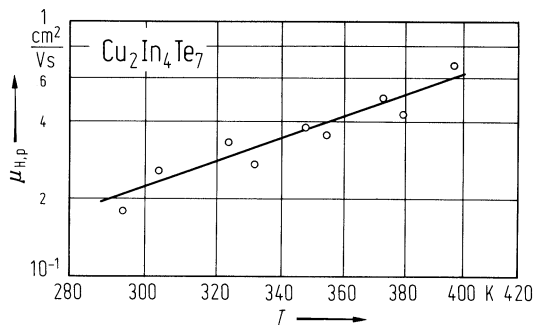


Fig. 33.6.2

$\text{Cu}_2\text{In}_4\text{Te}_7$. Hall mobility of holes vs. temperature [72C].



33.7 CuIn₃Te₅

Physical properties

I-III₃-VI₅ compounds (sphalerite structure) [71C]

energy gap

$E_{\text{g,th}}$ 1.20 eV conductivity, Fig. 33.7.1

hole mobility

$\mu_{\text{H,p}}$ 0.1 cm²/Vs $p = 3 \cdot 10^{15}$ cm⁻³,
 $T = 300$ K

lattice parameter

a 6.16 Å

melting point

T_{m} 772(5)°C

density

d 5.94 g cm⁻³ experimental

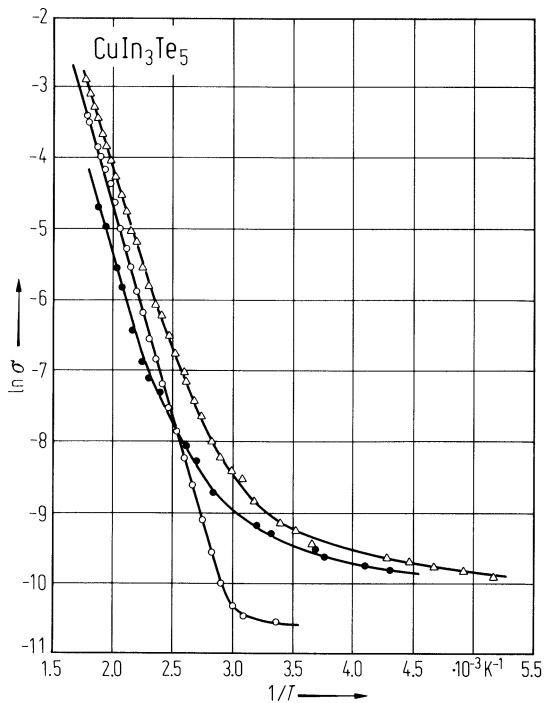
References to 33.7

71C Congiu, A., Garbato, L., Serci, S.: Phys. Status Solidi (a) 5 (1971) K15.

Figures to 33.7

Fig. 33.7.1

CuIn_3Te_5 . Electrical conductivity of three samples vs. reciprocal temperature [71C], σ in $\Omega^{-1} \text{ cm}^{-1}$.



33.8 AgIn₃Te₅

Physical properties

I-III₃-VI₅ compound (sphalerite structure).

energy gap, lattice parameter

$E_g = 1.1(1)$ eV, $a = 6.2476$ Å has been reported in [64O].

References to 33.8

64O O'Kane, D. F., Mason, D. R.: J. Electrochem. Soc. 114 (1964) 546.

33.9 AgIn₅S₈

Physical properties

I-III₅-VI₈ compound (spinel type) [77P]

energy gap

E_g	1.7 eV	$T = 300\text{ K}$	optical gap, direct transition
-------	--------	--------------------	--------------------------------

electron mobility

$\mu_{H,n}$	4 cm ² /Vs	$n = 1.4$ $\cdot 10^{18}\text{ cm}^{-3}$, $T = 300\text{ K}$	Fig. 33.9.1
-------------	-----------------------	---	-------------

lattice parameter

a	10.822 Å
-----	----------

melting point

T_m	1075(10)°C
-------	------------

density

d	4.85 g cm ⁻³	experimental
-----	-------------------------	--------------

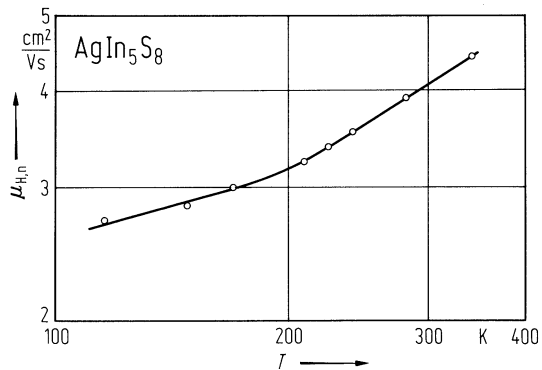
References to 33.9

77P Paorici, C., Zanotti. L., Romeo, N., Sberveglieri, C., Tarricone, L.: Mater. Res. Bull. 12 (1977) 1207.

Figures to 33.9

Fig. 33.9.1

AgIn_5S_8 . Electron Hall mobility of a single crystal vs. temperature [77P].



33.10 AgIn₉Te₁₄

AgIn₉Te₁₄ is cited as semiconductor with $E_{g,th} \approx 1.50$ eV, $\mu_{H,n} = 40$ cm²/Vs at 600 K [67C], see Figs. 33.10.1, 33.10.2.

References to 33.10

67C Chiang, P. W., O'Kane, D. F., Mason, D. R.: J. Electrochem. Soc. 114 (1967) 759.

Figures to 33.10

Fig. 33.10.1

$\text{AgIn}_9\text{Te}_{14}$. Electrical conductivity vs. reciprocal temperature [67C]. The two curves at lower temperatures correspond to the first and second heating cycle.

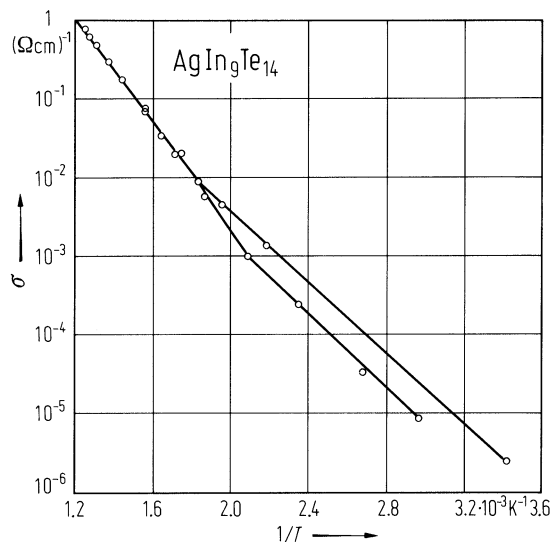
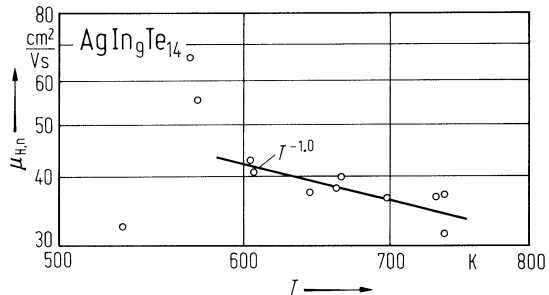


Fig. 33.10.2

AgIn₉Te₁₄. Carrier mobility vs. temperature [67C].



33.11 Cd₂SnO₄

This compound has been prepared as crystalline powder or (amorphous) thin film only [77L, 77S, 72N]. An optical gap of $E_g = 2.06$ eV and a carrier mobility of $\mu_H = 35$ cm²/Vs have been reported. Space group: D_{2h}⁹-Pbam, $a = 5.5674(5)$ Å, $b = 9.8871(9)$ Å, $c = 3.1923(4)$ Å.

References to 33.11

- 72N Nozik, A. J.: Phys. Rev. B6 (1972) 453.
- 77L Lloyd, P.: Thin Solid Films 41 (1977) 113.
- 77S Shannon, R. D., Gillson, J. L., Bouchard, R. J.: J. Phys. Chem. Solids 38 (1977) 877.

33.12 CdSnO₃

According to [77S] CdSnO₃ is a semiconductor with $E_g = 0.3$ eV. Structure: ilmenite(C_{3i}^2 - $R\bar{3}$), $a = 5.4530(5)$ Å, $c = 14.960(3)$ Å.

References to 33.12

77S Shannon, R. D., Gillson, J. L., Bouchard, R. J.: J. Phys. Chem. Solids 38 (1977) 877.

33.13 Li_3CuO_3

N-type semiconductor with $E_g = 0.88$ eV [75M]

References to 33.13

75M Migeon, H. N., Courtois, A., Zanne, M., Gleitzer, Ch., Aubry, J.: Rev. Chim. Miner. 12 (1975) 203.

33.14 Hg₃PS₃, Hg₃PS₄

Semiconductors with E_g around 2 eV [68O]

References to 33.14

- 68O Olekseyuk, I. D., Golovei, I. D.: Inorg. Mater. 4 (1968) 1462 (transl. from Izv. Akad. Nauk SSSR Neorg. Mater. 4 (1968) 1676).

34 Boron compounds

34.0 General remarks

The boron compounds and especially the borides show a wide variety of structures and compositions which include single atoms, connected pairs, multiple chains, planar networks and polyhedral groupings which are preferably based on octahedra, icosahedra or even more complex polyhedral structures. This variety is the consequence of the peculiar electronic structure of boron characterized by an unpaired electron in the $2s^2 2p^1$ configuration of the outer electron shell of the isolated boron atom, and leading to the various combinations of $s^2 p$, sp , sp^2 and sp^3 electron configurations by the electron interchange between boron atoms or by the interaction with electrons of other atoms.

Among the more than hundred compounds investigated the most important group comprises the compounds of boron with group VB elements: BN, BP, and BAs. These compounds are explicitly described in chapter 2. In the following we present such compounds of boron with elements of other groups of the Periodic System for which reliable data are available. All these compounds have very complicated structures consisting of B_{12} icosahedra. The compound YB_{66} for instance has a unit cell with 104 icosahedra i.e. 1248 atoms.

34.1 Boron-hydrogen alloys

34.1.1 BH_x

energy gap

E_g	1.10(5) eV	$T = 300\text{K}$	9 at % H	80B
	1.15(5) eV		11 at% H	
	1.7(1) eV		24 at% H	
80B	Bagley, B. G., Aspnes, D. E., Adams, A. C., Benenson, R. E., J. Non-Cryst. Solids 35-36 Pt. 1 (1980) 441.			

34.2 Binary boron-lithium compounds

34.2.1 Li₃B₁₄

Structure: tetragonal, 112 boron atoms and 24 Li atoms per unit cell. Space group: $I\bar{4}2d$ [88M].

energy gap

E_g	1.4...1.6 eV	$T = 600...900$ K	from electrical conductivity	84M2, 84M1, 88M, 90B
-------	--------------	-------------------	------------------------------	-------------------------

84M1 Mair, G.: Thesis, University of Stuttgart, Germany, 1984.

84M2 Mair, G., Neper, R., von Schnering, H.G.: Annual Rep. Max-Planck-Institut FKF I (1984) 30.

88M Mair, G., Nesper, R., von Schnering, H.G.: J. Solid State Chem. 75 (1988) 30.

90B Bullett, D.W.: in: The Physics and Chemistry of Carbides, Nitrides and Borides; NATO ASI Series E: Applied Sciences Vol. 185, R. Freer ed., Kluwer Academic Publishers: Dordrecht, 1990, p. 555.

34.2.2 LiB₆

energy gap

E_g	1.4...1.6 eV	$T = 600...900$ K	from electrical conductivity	84M2, 84M1, 88M, 90B
-------	--------------	-------------------	------------------------------	-------------------------

84M1 Mair, G.: Thesis, University of Stuttgart, Germany, 1984.

84M2 Mair, G., Neper, R., von Schnering, H.G.: Annual Rep. Max-Planck-Institut FKF I (1984) 30.

88M Mair, G., Nesper, R., von Schnering, H.G.: J. Solid State Chem. 75 (1988) 30.

90B Bullett, D.W.: in: The Physics and Chemistry of Carbides, Nitrides and Borides; NATO ASI Series E: Applied Sciences Vol. 185, R. Freer ed., Kluwer Academic Publishers: Dordrecht, 1990, p. 555.

34.2.3 Li₆B₁₉

energy gap

E_g	1.4...1.6 eV	600...900 K	from electrical conductivity	84M2, 84M1, 88M, 90B
-------	--------------	-------------	------------------------------	-------------------------

84M1 Mair, G.: Thesis, University of Stuttgart, Germany, 1984.

84M2 Mair, G., Neper, R., von Schnering, H.G.: Annual Rep. Max-Planck-Institut FKF I (1984) 30.

88M Mair, G., Nesper, R., von Schnering, H.G.: J. Solid State Chem. 75 (1988) 30.

90B Bullett, D.W.: in: The Physics and Chemistry of Carbides, Nitrides and Borides; NATO ASI Series E: Applied Sciences Vol. 185, R. Freer ed., Kluwer Academic Publishers: Dordrecht, 1990, p. 555.

34.3 Ternary boron-lithium compounds

34.3.1 LiAlB₁₄

The boron framework contains four B₁₂ icosahedra and eight isolated B atoms in the unit cell. The icosahedra are centered at 0,0,0; 1/2,1/2,0; 0,0,1/2; 1/2,1/2,1/2 being oriented with one of their mirror planes parallel to the (100) plane. There are two kinds of intericosahedral B – B bonds. One of them is parallel to the *c*-axis and the other one parallel to the (110) planes thus leading to infinite chains of B₁₂ icosahedra. All icosahedra are crystallographically equivalent, the isolated B atoms as well. Six apical atoms of an icosahedron are linked to those of neighboring icosahedra, the remaining six are linked via the isolated B atoms. The Li and Al atoms are accommodated in the large holes between the icosahedra.

lattice : orthorhombic; space group: D_{2h}²⁸ – Imam [81H].

energy gap

$E_{g,ind}$	1.82 eV	$T = 300\text{ K}$	single crystals (orientation not defined); optical absorption	81W
81W	Will, G., Kirfel, A., Josten, B., Fröhlich, T.: J. Less-Common Met. 82 (1981) 255 (Proc. 7th Int. Symp. Boron, Borides and Relectrical Compounds, Uppsala, Sweden, 1981).			

34.3.2 LiBC

Completely intercalated heterographite. Space group: P6₃/mmc

energy gap

E_g	4.2 eV	calculated (INDO procedure)	95W
	2.5 eV	calculated (LMTO method)	
95W	Wörle, M., Nesper, R., Mair, G., Schwarz, M., v. Schneering, H.G.: Z. Anorg. Allg. Chem. 621 (1995) 1153.		

34.4 Boron-sodium compounds

34.4.1 NaB₆

There is some controversy, whether NaB₆ cristallizes in the CaB₆ structure or not.

Based on the CaB₆ structure the calculated band structure is basically similar in topology to that of CaB₆. But because of the lower number of electrons introduced by the monovalent metal the position of the Fermi level is expected at – 9.1 eV, i.e. within the valence band [76P]. This contrasts with the high electrical resistance which indicates semiconducting behavior.

resistivity

ρ	$10^6 \Omega \text{ cm}$	$T = 300 \text{ K}$	sintered sample	77N
77B	Berezin, A. A., Golikova, O. A., Zaitsev, V. R., Kazanin, M. M., Orlov, V. M., Tkalenko, E. N., in: Boron and Refractory Borides, (Matkovich V. 1., ed.) Springer: Berlin, Heidelberg, New York 1977, p. 52.			
77N	Naslain, R., Etourneau, J., Hagenmuller, P.: see [77B], p. 262.			

34.4.2 NaB₁₅

The elementary cell contains four formula groups. The structure can be described as a stacking of rather compact planes of quasi-spherical icosahedral clusters of boron atoms with a packing diameter of about 5.1 Å. Otherwise it can be described as an alignment of icosahedron chains parallel to the *c*-axis, which are centered at (*x* = 0; *y* = 0) and (*x* = 1/2; *y* = 1/2). Two types of isolated boron atoms are present in the structure. The covalent skeleton formed by the boron atoms has two types of interstitial sites, one of them formed by 16, the other one by 12 boron atoms.

lattice : orthorhombic; space group: D_{2h}²⁸ – Imam.

energy gap

E_g	0.32 eV	$T > 300 \text{ K}$	electrical conductivity	77N
-------	---------	---------------------	-------------------------	-----

electrical conductivity

σ	$4 \cdot 10^{-4} \Omega^{-1} \text{ cm}^{-1}$	$T = 300 \text{ K}$	polycrystalline sample, sintered at 650°C, pressure 50 kbar	77N
77B	Berezin, A. A., Golikova, O. A., Zaitsev, V. R., Kazanin, M. M., Orlov, V. M., Tkalenko, E. N., in: Boron and Refractory Borides, (Matkovich V. 1., ed.) Springer: Berlin, Heidelberg, New York 1977, p. 52.			
77N	Naslain, R., Etourneau, J., Hagenmuller, P.: see [77B], p. 262.			

34.5 Boron-potassium compounds

34.5.1 KB₆

KB₆ is isostructural with CaB₆

lattice : cubic; space group: O_h¹ – Pm3m.

electronic structure

The calculated band structure is basically similar in topology to that of CaB₆ with the empty d orbitals of potassium forming a narrow set of bands in the accessible conduction region. The band gap (at X) is reduced by the d-orbital participation. The Fermi level (at – 8.1 eV) is very close to the lower edge of the energy gap; only a few holes are left vacant [76P, 77P].

energy gap

E_g	0.29 eV	$T \geq 300$ K	electrical conductivity	77N
-------	---------	----------------	-------------------------	-----

electrical conductivity

σ	$10^{-4} \Omega^{-1} \text{ cm}^{-1}$	$T = 300$ K	For temperature dependence	77N
----------	---------------------------------------	-------------	----------------------------	-----

activation energy

E_A	0.008 eV	$T < 120$ K	electrical conductivity	77N
-------	----------	-------------	-------------------------	-----

76P Perkins, P. G., Sweeney, A. V. J.: J. Less-Common Met. 47 (1976) 165.

77N Naslain, R., Etourneau, J., Hagenmuller, P.: see [77B], p. 262.

77B Berezin, A. A., Golikova, O. A., Zaitsev, V. R., Kazanin, M. M., Orlov, V. M., Tkalenko, E. N., in: Boron and Refractory Borides, (Matkovich V. I., ed.) Springer: Berlin, Heidelberg, New York 1977, p. 52.

77P Perkins, P. G.: see [77B], p. 31.

34.6 Beryllium-aluminum-boron compounds

34.6.1 $\text{Al}_{\sim(1\pm x)}\text{Be}_{\sim(1\pm y)}\text{B}_{22}$

There are numerous compounds of the approximate chemical compositions $\text{Al}_{\sim(1\pm x)}\text{Be}_{\sim(1\pm y)}\text{B}_{22}$ ($x+y \sim 2$) with $\alpha\text{-AlB}_{12}$ type structure.

The crystal structure is strongly related to that of $\alpha\text{-AlB}_{12}$, but the metal distribution is different. The beryllium atoms are accommodated in the two types of truncated tetrahedral holes which are vacant in $\alpha\text{-AlB}_{12}$ [79H].

space group : $D_4^4 - P4_12_12$ or $D_4^8 - P4_32_12$.

energy gaps

E_g	2.12 eV	$T = 300 \text{ K}$	optical absorption	79G
	2.1 eV	$T \geq 800 \text{ K}$	electrical conductivity	

activation energies

E_A	0.7 eV	$T = 300 \dots 500 \text{ K}$	electrical conductivity	79G
	0.55 eV	$T = 200 \dots 300 \text{ K}$		

79G Golikova, O. A., Kazanin, M. M., Orlov, V. M., Tkalenko, E. N., Fedorov, M. I.: J. Less-Common Met. 67 (1979) 363.

79H Higashi, I.: J. Less-Common Met. 67 (1979) 7.

34.7 Boron-aluminum-magnesium compounds

34.7.1 MgAlB₁₄

The structure can be considered as being constituted of distorted, closest-packed layers of quasi-spherical icosahedra stacked directly one above the other in the *c*-direction [65M, 70M, 77M1, 77M2]. Another description is based on chains of B₁₂ icosahedra running in the *c*-direction. In a chain, the icosahedra are orientated in such a way that one of their mirror planes is parallel to the bc-plane, one of their pseudo fivefold axes being alternately inclined 7.88° to the *c*-axis [76N]. The chains are linked either by direct inter-icosahedral B – B bonds or by bridges involving isolated B atoms. The metal atoms partially occupy interstitial holes in the boron network.

space group : D_{2h}²⁸ – Imam.

energy gaps

<i>E_g</i>	0.27 eV		<i>E_F</i> – <i>E_V</i>	87G
			estimated from electrical conductivity, pure material	
	0.47 eV		estimated from electrical conductivity, Ni-doped material	83G
	0.16(1) eV	<i>T</i> = 300 K	optical absorption, deep level to band	93W
	0.63(1) eV		optical absorption, deep level to band	
	0.99(3) eV		indirect allowed interband with phonon emission	
	1.51(1) eV		indirect allowed interband with phonon emission	

electrical conductivity (polycrystalline samples)

<i>σ</i>	2·10 ⁻¹ Ω ⁻¹ cm ⁻¹	<i>T</i> = 300 K	pure MgAlB ₁₄	79B
	5·10 ⁻² Ω ⁻¹ cm ⁻¹		Ni-alloyed	

- 79B Bairamashvili, I. A., Kekelidze, L. I., Golikova, O. A., Orlov, V. M.: J. Less-Common Met. 67 (1979) 461.
- 83G Golikova, O.A., Samatov, S.: Phys. Status Solidi (a) 77 (1983) 449.
- 87G Golikova, O.A., Kazanin, M.M.: Phys. Status Solidi (a) 103 (1987) K41.
- 93W Werheit, H., Kuhlmann, U., Krach, G., Higashi, I., Lundström, T., Yu, Y.: J. Alloys Compounds 202 (1993) 269.

34.7.2 Al_{1.44} Mg_{0.65}B₂₂

β-tetragonal boron structure or orthorhombic γ-AlB₁₂ type. Space group: P2₁2₁2₁ (γ-AlB₁₂ type)

energy gap (in eV)

<i>E_g</i>	0.315(6)	<i>T</i> = 293 K		94W
	0.567(5)			
	0.709(8)			
	0.873(6)			
	1.625(6)			
	1.779(6)			
	1.864(6)			
	1.919(6)			
	1.973(6)			

- 94W Werheit, H., Krach, G., Kuhlmann, U., Higashi, I., Gurin, V.N., Korsukova, M.M.: Proc. 11th Int. Symp. Boron, Borides and Relectrical Compounds, Tsukuba, Japan, August 22 - 26, 1993, Jpn. J. Appl. Phys. Series 10 (1994), p. 96.

34.8 Boron-alkaline earth compounds

The CaB_6 -type lattice structure, the same for all alkaline earth hexaborides, is characterized by a three-dimensional skeleton of B_6 octahedra, whose interstices are occupied by metal atoms.

space group: $\text{O}_h^1 - \text{Pm}3\text{m}$.

34.8.1 CaB_6

energy gap

E_g	2.11 eV		calculated	77P
	0.4 eV	$T > 820 \text{ K}$	electrical resistance	63J
	0.2 eV	$T > 500 \text{ K}$	electrical conductivity	70P

resistivity

ρ	0.1 $\Omega \text{ cm}$	$T = 300 \text{ K}$	polycrystal	63J
	0.43 $\Omega \text{ cm}$	$T = 300 \text{ K}$		70P

63J Johnson, R. W., Daane, H. H.: J. Chem. Phys. 38 (1963) 425.

70E Economy, J., Matkovich, V.I.: Boron 3, T. Niemyski, ed., PWN Warsaw, 1970, 159.

70P Paderno, Yu. B., Goryachev, Yu. M., Garf, E. S.: see [70E] p. 175.

77B1 Berezin, A. A., Golikova, O. A., Zaitsev, V. R., Kazanin, M. M., Orlov, V. M., Tkalenko, E. N., in: Boron and Refractory Borides, (Matkovich V. I., ed.) Springer: Berlin, Heidelberg, New York 1977, p. 52.

77P Perkins, P. G.: see [77B], p. 31.

34.8.2 SrB_6

energy gap

E_g	3.68 eV		calculated	77P
	0.38 eV	$T > 1250 \text{ K}$	electrical resistance	63J
	0.45 eV	$T > 700 \text{ K}$		60E

resistivity

ρ	0.216 $\Omega \text{ cm}$	$T = 300 \text{ K}$	singlecrystal	63J
--------	---------------------------	---------------------	---------------	-----

60B Binder, I., La Placa, S., Post, B.; Boron I, J.A. Kohn, W.F. Nye, G.K. Gaulé, eds., Plenum Press, New York, 1960, 86.

60E Eubank, W. R., Pruitt, L. E., Thurnaner, H.: see [60B], p. 116.

63J Johnson, R. W., Daane, H. H.: J. Chem. Phys. 38 (1963) 425.

77B Berezin, A. A., Golikova, O. A., Zaitsev, V. R., Kazanin, M. M., Orlov, V. M., Tkalenko, E. N., in: Boron and Refractory Borides, (Matkovich V. I., ed.) Springer: Berlin, Heidelberg, New York 1977, p. 52.

77P Perkins, P. G.: see [77B], p. 31.

34.8.3 BaB_6

energy gap

E_g	2.64 eV		calculated	77P
	0.15 eV	$T > 300 \text{ K}$	electrical conductivity	70P

resistivity

ρ	0.07 $\Omega \text{ cm}$	$T = 300 \text{ K}$		70P
--------	--------------------------	---------------------	--	-----

70E Economy, J., Matkovich, V.I.: Boron 3, T. Niemyski, ed., PWN Warsaw, 1970, 159.

70P Paderno, Yu. B., Goryachev, Yu. M., Garf, E. S.: see [70E] p. 175.

77B Berezin, A. A., Golikova, O. A., Zaitsev, V. R., Kazanin, M. M., Orlov, V. M., Tkalenko, E. N., in: Boron and Refractory Borides, (Matkovich V. I., ed.) Springer: Berlin, Heidelberg, New York 1977, p. 52.

77P Perkins, P. G.: see [77B], p. 31.

94H Higashi, I., Kobayashi, M., Bobayashi, K., Lundström, T., Tergenius, L.-E., Ito, T.: Proc. 11th Int. Symp. Boron, Borides and Relectrical Compounds, Tsukuba, Japan, August 22 - 26, 1993, Jpn. J. Appl. Phys. Series 10 (1994), p. 7.

34.9.3 β-AlB₁₂

This compound is sometimes identified with Al₃C₂B₄₈.

lattice : orthorhombic.

energy gaps

E_g	2.5 eV	$T=300\text{ K}$	optical absorption	74G
$E_{g,th}$	2.5 eV	$T\geq 700\text{ K}$	electrical conductivity	76G, 79G

electrical conductivity

σ	$5\cdot 10^{-9}\text{ }\Omega^{-1}\text{ cm}^{-1}$	$T=300\text{ K}$	polycrystal;	76G
74G	Golikova, O. A., Zaitsev, V. K., Orlov, V. M., Petrov, A. V., Stilbans, L. S., Tkalenko, E. N.: Phys. Status Solidi (a) 21 (1974) 405.			
76G	Golikova, O. A., Kazanin, M. M., Lutsenko, E. L., Orlov, V. M., Tkalenko, E. N., Zaitsev, V. K.: Proc. 13th Int. Conf. Phys. Semiconductivity, Rome (Ed. Fumi F. G.) Tipografia Marves, Rome, 1976, p. 497.			
79G	Golikova, O. A.: Phys. Status Solidi (a) 51 (1979) 11.			

34.9.4 γ-AlB₁₂

energy gap of Si-doped γ-AlB₁₂ (Al_{1.0}Si_{0.7}B_{15.6})

E_g	0.36 eV	$T=300\text{ K}$	deep level	88W
	0.56 eV		deep level	
	0.69 eV		deep level	
	0.78 eV		deep level	
	0.91 eV		deep level	
	1.00 eV		indirect allowed or non-direct	
	1.71 eV		indirect allowed or non-direct	

activation energy

E_A	0.22 eV	$T=100...375\text{ K}$	electrical conductivity	91P
-------	---------	------------------------	-------------------------	-----

electrical conductivity

σ	$2.5\cdot 10^{-4}\text{ }\Omega^{-1}\text{ cm}^{-1}$	$T=293\text{ K}$		91P
----------	--	------------------	--	-----

88W	Werheit, H., Kuhlmann, U., Tanaka, T.: (unpublished results).			
91P	Prikhna, T.A., Kisly, P.S.: in: Boron-Rich Solids, Proc. 10th Int. Symp. Boron, Borides and Relectrical Compounds, Albuquerque, NM 1990 (AIP Conf. Proc. 231), D. Emin, T.L. Aselage, A.C. Switendick, B. Morosin, C.L. Beckel ed., American Institute of Physics: New York, 1991, p. 590.			

34.10 Boron-yttrium compounds

34.10.1 YB₆₆

Structure: cubic. Space group: Fm3c [69R, 97H].

energy gap (in eV)

E_g	2.73	$T = 180...280$ K	sum of opt. and therm. excitation energy	97S
	0.8	$T > 500$ K	estimated from electrical conductivity	77S
	1.0		derived from electrical conductivity	87G

electrical conductivity

σ	$3 \cdot 10^{-2} \Omega^{-1} \text{cm}^{-1}$	$T = 300$ K		86G
	$4 \cdot 10^{-6} \Omega^{-1} \text{cm}^{-1}$	$T = 300$ K		87W2
	$1.5 \cdot 10^{-4} \Omega^{-1} \text{cm}^{-1}$	$T = 300$ K		94G1

Hall mobility

μ_H	$5 \cdot 10^{-2}...2 \text{ cm}^2 \text{V}^{-1} \text{s}^{-1}$	$T = 300$ K		91W
---------	--	-------------	--	-----

77S Slack, G. A., Oliver, D. W., Brower, G. D., Young, J. D.: J. Phys. Chem. Solids 38 (1977) 45.

86G Golikova, O.A., Tadzhiev, A.: J. Non-Cryst. Solids 87 (1986) 64.

87W2 Werheit, H., Haupt, H., Kuhlmann, U., Siejak, V., Tanaka, T.: in: Proc. 9th Int. Symp. Boron, Borides and Relectrical Compounds, University of Duisburg, Germany, Sept. 21 - 25, 1987, H. Werheit ed., University of Duisburg: Duisburg, 1987, p. 383.

91W Werheit, H., Kuhlmann, U., Tanaka, T.: in: Boron-Rich Solids, Proc. 10th Int. Symp. Boron, Borides and Relectrical Compounds, Albuquerque, NM 1990 (AIP Conf. Proc. 231), D. Emin, T.L. Aselage, A.C. Switendick, B. Morosin, C.L. Beckel ed., American Institute of Physics: New York, 1991, p. 125.

94G1 Golikova, O.A., Domashevskaya, E.P., Kazanin, M.M., Terekhov, V.A.: Proc. 11th Int. Symp. Boron, Borides and Relectrical Compounds, Tsukuba, Japan, August 22 - 26, 1993, Jpn. J. Appl. Phys. Series 10 (1994), p. 56.

97S Sakairi, Y., Takeda, M., Kimura, K., Tanaka, T.: J. Solid State Chem. 133 (1997) 195 (Proc. 12th Int. Symp. Boron, Borides and Relectrical Compounds, Baden, Austria, 1996).

34.11 Lanthanide hexaborides

34.11.1 LaB₆

cP7-CaB₆ type structure. Space group: Pm $\bar{3}$ m

energy gap

E_g ~ 2 eV $T = 300$ K optical absorption 80G

resistivity

ρ $1.3 \cdot 10^{-5} \Omega \text{ cm}$ $T = 300$ K 91S

80G Gurin, V.N., Korsukova, M.M., Karin, M.G., Sidorin, K.K., Smirnov, I.A., Shelikh, A.I.: Sov. Phys. Solid State 22 (1980) 418.

91S Sidorov, V.A., Stepanov, N.N., Ziok, O.B., Chvostanzev, L.G., Smirnov, N.A., Korsukova, M.M.: Fiz. Tverd. Tela 33 (1991) 1271(in Russian).

34.11.2 CeB₆

energy gap

E_g 45 meV $T = 13 \dots 53$ K electron-tunneling 98A

98A Ambler, B., Fisk, Z., Sarrao, J.L., v. Molnar, S., Meisel, M.W., Sharifi, F.: Phys. Rev. B 57 (1998) 8747.

34.11.3 SmB₆

energy gap

E_g 5 meV electrical conductivity 77E

E_d 3 meV $T = 3 \dots 20$ K donor level; dynamanical conductivity 99G

dc electrical conductivity

σ $5.3 \cdot 10^3 \Omega^{-1} \text{ cm}^{-1}$ $T = 300$ K 84K

electron mobility

μ $2.79 \cdot 10^{-4} \text{ cm}^2 \text{ V}^{-1} \text{ s}^{-1}$ $T = 300$ K estimated 79A
 $0.85 \text{ cm}^2 \text{ V}^{-1} \text{ s}^{-1}$ $T = 293$ K $\rho = 6.0 \cdot 10^{-4} \Omega \text{ cm}$

77B Berezin, A. A., Golikova, O. A., Zaitsev, V. R., Kazanin, M. M., Orlov, V. M., Tkalenko, E. N., in: Boron and Refractory Borides, (Matkovich V. 1., ed.) Springer: Berlin, Heidelberg, New York 1977, p. 52.

77E Etourneau, J., Mercuno, J. P., Hagenmuler, P.: see [77B84K Konovalova, E.S., Paderno, Yu.B., Perepeliza, N.I., Dudnik, E.M., Yanosh, Sh., Flachbart, K., Reiffers, M.: Fiz. Tverd. Tela 26 (1984) 2138 (in Russian).

79A Allen, J. W., Batlogg, B., Wachter, P.: Phys. Rev. 20B (1979) 4807.

84K Konovalova, E.S., Paderno, Yu.B., Perepeliza, N.I., Dudnik, E.M., Yanosh, Sh., Flachbart, K., Reiffers, M.: Fiz. Tverd. Tela 26 (1984) 2138 (in Russian).

99G Gorshunov, B., Sluchanko, N., Volkov, A., Dressel, M., Knebel, G., Loidl, A., Kunii, S.: Phys. Rev. B 59 (1999) 1808.

34.11.4 EuB₆

electronic properties

EuB₆ is a magnetic semiconductor. It has been assumed that the Eu²⁺:4f⁷ level is located in the band gap. Eu vacancies would introduce holes in the 4f⁷ configuration.

The semiconducting behavior in the paramagnetic region changes to semimetallic behavior at the ferromagnetic ordering temperature $T_C = 13.7$ K [81T, 80G1].

energy gap

E_g	~1 eV	$T = 300$ K	derived from optical absorption	80G2
-------	-------	-------------	---------------------------------	------

energy gaps (or activation energy for conduction)

E_g	0.38 eV		electrical conductivity	69F
	0.30 eV		electrical conductivity	73G, 77E

resistivity

ρ	$6.16 \cdot 10^{-4} \Omega \text{ cm}$	$T = 300$ K		80G1
	$1 \cdot 10^{-2} \Omega \text{ cm}$	$T = 300$ K		77E, 74M
	$2 \Omega \text{ cm}$	$T = 300$ K	possibly carbon-doped	69P, 75S

electron mobility

μ_n	$2560 \text{ cm}^2/\text{V s}$	$T = 4.2$ K	electrical conductivity and	80G1
	$300 \text{ cm}^2/\text{V s}$	$T = 100 \dots 150$ K	Hall effect	
	$100 \text{ cm}^2/\text{V s}$	$T = 290$ K		

- 69F Fisk, Z., Matthias, B.T., Corenzwit, E.: Proc. Nat. Acad. Sci. 64 (1969) 1151.
 69P Paderno, Yu.B., Novikov, V.I., Garf, E.S.: Poroshk. Metall. 11 (1969) 70 (in Russian).
 73G Gust, W.H., Holt, A.C., Roye, E.B.: J. Appl. Phys. 44 (1973) 550.
 74M Mercurio, J.P., Etourneau, J., Naslain, R., Hagenmuller, P., Goodenough, J.B.: J. Solid State Chem. 9 (1974) 7.
 75S Samsonov, G.V., Serebryakova, T.I., Neronov, V.A.: in: Boridy, Moskva Atomizdat, 1975.
 77B Berezin, A. A., Golikova, O. A., Zaitsev, V. R., Kazanin, M. M., Orlov, V. M., Tkalenko, E. N., in: Boron and Refractory Borides, (Matkovich V. 1., ed.) Springer: Berlin, Heidelberg, New York 1977, p. 52.
 77E Etourneau, J., Mercuno, J. P., Hagenmuller, P.: see [77B], p. 115.
 80G1 Guy, C.N., v. Molnar, S., Etourneau, J., Fisk, Z.: Solid State Commun. 33 (1980) 1055.
 80G2 Gurin, V.N., Korsukova, M.M., Karin, M.G., Sidorin, K.K., Smirnov, I.A., Shelikh, A.I.: Sov. Phys. Solid State 22 (1980) 418.
 81T Tsagareishvili, G.V., Baimarashvili, I.A., Oganezov, K.A., Tabudsidze, M.L., Tsagareishvili, O.A.: J. Less-Common Met. 82 (1981) 131.

34.11.5 YbB₆

Structure: cubic. Space group: Pm3m

energy gaps (or activation energy for conduction)

E_g	0.14 eV	electrical conductivity	77E, 73G1
	0.081 eV		80L

effective mass of electrons

m_n	$0.47 m_0$	$T = 300 \text{ K}$	estimated from plasma frequency in analogy to EuB_6	99W
-------	------------	---------------------	---	-----

electrical conductivity

σ	$40 \Omega^{-1} \text{ cm}^{-1}$	$T = 300 \text{ K}$		73G1, 77E
	$30 \Omega^{-1} \text{ cm}^{-1}$			73M

73G1 Goodenough, J. B., Mercurlo, J. P., Etourneau, I., Naslain, R., Hagenmuller, P.: C. R. Acad. Sci. (Paris) 277 (1973) 1239.

73M Mercurio, J. P., Etourneau, J., Naslain, R., Hagenmuller, P.: Mater. Res. Bull. 8 (1973) 837.

77B Berezin, A. A., Golikova, O. A., Zaitsev, V. R., Kazanin, M. M., Orlov, V. M., Tkalenko, E. N., in: Boron and Refractory Borides, (Matkovich V. I., ed.) Springer: Berlin, Heidelberg, New York 1977, p. 52.

77E Etourneau, J., Mercuro, J. P., Hagenmuller, P.: see [77B], p. 115.

80L Lannin, J.S., Messier, R.: Phys. Rev. Lett. 45 (1980) 1119.

99W Werheit, H., Au, T., Schmechel, R., Paderno, Yu.B., Konovalova, E.S.: J. Solid State Chem. (2000) (Proc. 13th Int. Symp. Boron, Borides and Relectrical Compounds, Dinard, France, Sept. 1999).

34.12 Lanthanide hexaborides of the type LaB₆₆

34.12.1 SmB₆₆

energy gaps and activation energy

E_g	0.80 eV	electrical conductivity	81G
	0.63 eV	Seebeck coefficient	86G
E_A	0.15 eV	distance between mobility edge and E_F	86G

electrical conductivity

σ	$1 \cdot 10^{-2} \Omega^{-1} \text{cm}^{-1}$	$T = 300 \text{ K}$	87G
----------	--	---------------------	-----

carrier concentration, Hall mobility

p	$4 \cdot 10^{15} \text{ cm}^{-3}$	$T = 300 \text{ K}$	86G
$\mu_{H,p}$	$15 \text{ cm}^2/\text{V s}$		

81G Golikova, O.A., Tadzhiiev, A.: J. Less-Common Met. 82 (1981) 169. (Proc. 7th Int. Symp. Boron, Borides and Relectrical Compounds, Uppsala, Sweden, 1981).

86G Golikova, O.A., Tadzhiiev, A.: J. Non-Cryst. Solids 87 (1986) 64.

87G Golikova, O.A., Kazanin, M.M.: Phys. Status Solidi (a) 103 (1987) K41.

34.12.2 GdB₆₆

energy gaps and activation energy

E_g	0.87 eV	electrical conductivity	86G
	0.68 eV	Seebeck coefficient	87G
E_A	0.2 eV		87G

electrical conductivity

σ	$2 \cdot 10^{-3} \Omega^{-1} \text{ cm}^{-1}$	$T = 300 \text{ K}$	87G
	$1 \cdot 10^{-3} \dots 7 \cdot 10^{-2} \Omega^{-1} \text{ cm}^{-1}$	$T = 300 \text{ K}$	86G
		GdB _x (x = 72 ... 80)	91G

carrier concentration, Seebeck coefficient, and Hall mobility

(at $T = 300 \text{ K}$)

p	$1.5 \cdot 10^{15} \text{ cm}^{-3}$	derived from Hall effect	81G
S	$+ 390 \mu\text{V K}^{-1}$		
$\mu_{H,p}$	$15 \text{ cm}^2/\text{V s}$		

81G Golikova, O.A., Tadzhiiev, A.: J. Less-Common Met. 82 (1981) 169. (Proc. 7th Int. Symp. Boron, Borides and Relectrical Compounds, Uppsala, Sweden, 1981).

86G Golikova, O.A., Tadzhiiev, A.: J. Non-Cryst. Solids 87 (1986) 64.

87G Golikova, O.A., Kazanin, M.M.: Phys. Status Solidi (a) 103 (1987) K41.

91G Golikova, O.A., Amanzhanov, N., Tadzhiiev, A.: in: Boron-Rich Solids, Proc. 10th Int. Symp. Boron, Borides and Relectrical Compounds, Albuquerque, NM 1990 (AIP Conf. Proc. 231), D. Emin, T.L. Aselage, A.C. Switendick, B. Morosin, C.L. Beckel ed., American Institute of Physics: New York, 1991, p. 121.

34.12.3 DyB₆₆

energy gap

E_g	0.72 eV	electrical conductivity	87G
-------	---------	-------------------------	-----

electrical conductivity

σ	$7 \cdot 10^{-3} \Omega^{-1} \text{cm}^{-1}$	$T = 300 \text{ K}$	87G
	$3.2 \cdot 10^{-5} \Omega^{-1} \text{cm}^{-1}$	$T = 300 \text{ K}$	91W

Hall mobility

μ_H	$10 \text{ cm}^2 \text{V}^{-1} \text{s}^{-1}$		86G, 87G
---------	---	--	-------------

86G Golikova, O.A., Tadzhiev, A.: J. Non-Cryst. Solids 87 (1986) 64.
87G Golikova, O.A., Kazanin, M.M.: Phys. Status Solidi (a) 103 (1987) K41.
91W Werheit, H., Kuhlmann, U., Tanaka, T.: in: Boron-Rich Solids, Proc. 10th Int. Symp. Boron, Borides and Relectrical Compounds, Albuquerque, NM 1990 (AIP Conf. Proc. 231), D. Emin, T.L. Aselage, A.C. Switendick, B. Morosin, C.L. Beckel ed., American Institute of Physics: New York, 1991, p. 125.

34.12.4 YbB₆₆

energy gap

E_g	1.27 eV	electrical conductivity	87G
	1.10 eV	Seebeck coefficient	86G
E_A	0.10 eV	distance between mobility edge and E_F	

electrical conductivity

σ	$6 \cdot 10^{-3} \Omega^{-1} \text{cm}^{-1}$	$T = 300 \text{ K}$	87G
----------	--	---------------------	-----

carrier concentration

p	$1 \cdot 10^{16} \text{ cm}^{-3}$	$T = 300 \text{ K}$	86G
-----	-----------------------------------	---------------------	-----

Hall mobility

μ_H	$5 \text{ cm}^2 \text{V}^{-1} \text{s}^{-1}$	$T = 300 \text{ K}$	86G
---------	--	---------------------	-----

86G Golikova, O.A., Tadzhiev, A.: J. Non-Cryst. Solids 87 (1986) 64.
87G Golikova, O.A., Kazanin, M.M.: Phys. Status Solidi (a) 103 (1987) K41.

34.13 MgAlB₁₄ type orthorhombic borides with lanthanides

Structure: orthorhombic MgAlB₁₄ type. Space group: Imma or Ima2

34.13.1 ErAlB₁₄

energy gaps

E_g	0.33(3) eV	$T = 300$ K	deep level to band (probably due to Er)	93W
	0.97(1) eV		indirect allowed interband	
	1.30(1) eV		indirect allowed interband	

electrical conductivity

σ	$3 \cdot 10^{-1} \Omega^{-1} \text{cm}^{-1}$	$T = 300$ K	94W2
----------	--	-------------	------

93W Werheit, H., Kuhlmann, U., Krach, G., Higashi, I., Lundström, T., Yu, Y.: J. Alloys Compounds 202 (1993) 269.

94W2 Werheit, H., Krach, G., Kuhlmann, U., Higashi, I., Lundström, T., Yu, Y.: Proc. 11th Int. Symp. Boron, Borides and Relectrical Compounds, Tsukuba, Japan, August 22 - 26, 1993, Jpn. J. Appl. Phys. Series 10 (1994), p. 98.

34.14 Boron compounds with group IV elements

34.14.1 Boron carbide (BC)

Boron carbide has a large homogeneity range extending from B_{4.3}C to B_{~11}C.

Structure: rhombohedral. Space group: D_{3d}⁵ – R $\bar{3}$ m;

band structure calculations

Band structure calculations yield insulating/semiconducting character for B₁₂C₃ (structure formula B₁₁C(CBC)) and metallic character for B₁₃C₂ (structure formula B₁₂(CBC)).

energy gaps

E_g	0.18 eV	$T = 300\text{ K}$	transition energies obtained	92W
	0.47 eV		from optical absorption	
	0.77 eV			
	0.92 eV			
	1.20 eV			
	2.01 eV			
	2.17 eV			
	2.97 eV			
	3.16 eV			
	3.41 eV			
	3.58 eV			
	3.94 eV			
	4.13 eV			
	4.67 eV			
	4.85 eV			
	5.81 eV			
	6.00 eV			

$E_{g,ind}$	0.48 eV	$T = 300K$	optical absorption	71W
-------------	---------	------------	--------------------	-----

transport properties

In agreement with the energy band structure calculations, for boron carbide an energy band structure is assumed with flat bands and accordingly high effective masses ($m^* \approx 5...10\ m_0$) and low mobilities of the delocalized carriers ($\mu \approx 30...330\text{ cm}^2\text{V}^{-1}\text{s}^{-1}$). The main contribution to the charge transport comes from localized carriers (polarons?) with low mobilities ($\mu \approx 3\text{ cm}^2\text{V}^{-1}\text{s}^{-1}$) hopping between certain localized states in the band gap.

electrical conductivity

σ	$2.5 \cdot 10^{-4}\ \Omega^{-1}\text{cm}^{-1}$	$T = 77\text{ K}$	single crystal, nearly B _{4.3} C	87W
	$11\ \Omega^{-1}\text{cm}^{-1}$	$T = 295\text{ K}$	$\sim 10\text{ at. \% C}$	93S
	$22\ \Omega^{-1}\text{cm}^{-1}$		$\sim 13.2\text{ at. \% C}$	
	$12\ \Omega^{-1}\text{cm}^{-1}$		$\sim 15.5\text{ at. \% C}$	
	$5\ \Omega^{-1}\text{cm}^{-1}$		$\sim 18\text{ at. \% C}$	
	$3\ \Omega^{-1}\text{cm}^{-1}$		$\sim 18.6\text{ at. \% C}$	
	$3.5\ \Omega^{-1}\text{cm}^{-1}$		$\sim 20\text{ at. \% C}$	

hole mobility

$\mu_{H,p}$	$37\text{ cm}^2\text{V}^{-1}\text{s}^{-1}$	$T = 77\text{ K}$	Hall effect, single crystal, B _{~4.3} C (ESK boron carbide)	87W
-------------	--	-------------------	---	-----

71W Werheit, H., Binnenbruck, H., Hausen, A.: Phys. Status Solidi (b) 47 (1971) 153.
87W Werheit, H., Franz, R., Schneider, D., Wolf, M., Brann, G.: in: Proc. 9th Int. Symp. Boron, Borides and Relectrical Compounds, University of Duisburg, Germany, Sept. 21 - 25, 1987, H. Werheit ed., University of Duisburg: Duisburg, 1987, p. 381.
92W Werheit, H., Laux, M., Kuhlmann, U., Telle, R.: Phys. Status Solidi (b) 172 (1992) K81.
93S Samara, G.A., Tardy, H.L., Venturini, E.L., Aselage, T.L., Emin, D.: Phys. Rev. B 48 (1993) 1468.

34.15 Boron-silicon compounds

34.15.1 SiB₁₄

The crystalline structure has been suggested to be isotypic with β -rhombohedral boron. It is based on a nearly cubic closest-packed arrangement of B₈₄ units. Additionally a (B₇Si₃)–Si–(B₇Si₃) group is expected to be arranged along the trigonal axis of the rhombohedral cell (i.e. the crystallographic *c*-axis) [70M, 77M2].

electrical conductivity

σ	$6 \cdot 10^{-6} \Omega^{-1} \text{ cm}^{-1}$	$T = 300 \text{ K}$	78D, 78P1, 78P2, 79P
----------	---	---------------------	----------------------

resistivity

ρ	$60 \dots 7.6 \cdot 10^4 \Omega \text{ cm}$	$T = 300 \text{ K}$	76A
--------	---	---------------------	-----

mobility

$\mu_{\text{H,p}}$	$< 1 \text{ cm}^2/\text{V s}$	$T = 300 \text{ K}$	Hall mobility	76A
--------------------	-------------------------------	---------------------	---------------	-----

70M Matkovich, V. I., Economy, J.: Acta Crystallogr. B 26 (1970) 616.

76A Armas, B., Combescure, C., Dusseau, J. M., Lepetre, I. P., Robert, J. L., Pistoulet, B.: J. Less-Common Met. 47 (1976) 135.

77B Berezin, A. A., Golikova, O. A., Zaitsev, V. R., Kazanin, M. M., Orlov, V. M., Tkalenko, E. N., in: Boron and Refractory Borides, (Matkovich V. I., ed.) Springer: Berlin, Heidelberg, New York 1977, p. 52.

77M2 Matkovich, V. I., Economy, J.: see [77B], p. 96.

78D Dusseau, J. M., Ensueque, L., Im-Sareoun, Lepetre, T. P.: Phys. Status Solidi (a) 47 (1978) K 11.

78P1 Pistoulet, B., Robert, J. L., Dusseau, J. M., Ensueque, L.: J. Non-Cryst. Solids 29 (1978) 29.

78P2 Pistoulet, B., Robert, J. L., Dusseau, J. M.: see [78P1], p. 1009.

79P Pistoulet, B., Robert, J. L., Dusseau, J. M., Roche, F., Girard, P., Ensueque, L.: J. Less-Common Met. 67 (1979) 131.

34.16 Boron-zirconium compounds

34.16.1 ZrB₂

resistivity

ρ	30 n Ω m	86I
--------	-----------------	-----

carrier mobility

μ_{H}	$6.66 \cdot 10^{-2} \text{ m}^2 \text{V}^{-1} \text{ s}^{-1}$	86I
------------------	---	-----

86I Ishizawa, Y., Tanaka, T.: in: Inst. Phys. Conf. Ser. No. 75: Chapter I, Adam Hilger: 1986, p. 29.

34.17 Boron-nitrogen compounds

34.17.1 B₃₆N₂₄

energy gap

E_g	1.9 eV	calculated	94K
94K	Kawai, J., Muramatsu, Y., Kobayashi, M., Higashi, I., Adachi, H.: Proc. 11th Int. Symp. Boron, Borides and Relectrical Compounds, Tsukuba, Japan, August 22 - 26, 1993, Jpn. J. Appl. Phys. Series 10 (1994), p. 72.		

34.18 Boron-phosphorus compounds

34.18.1 B₆P (B₁₂P₂); B₁₃P₂

α-rhombohedral boron structure group. Space group: D_{3d}⁵ – R $\bar{3}$ m.

Boron phosphide as a new refractory semiconductor [88K].

energy gap

<i>E_g</i>	3.46 eV	<i>T</i> = 300 K	indirect-allowed	97W
	2.75(1) eV	<i>T</i> = 300 K	indirect-allowed (Si-doped B ₁₂ P ₂)	97W
	1.187(5) eV		deep level to parabolic band	
<i>E_{g,ind}</i>	3.3 eV	<i>T</i> = 300 K,	optical absorption	65B,
		<i>E</i> ⊥ <i>c</i>		67B

activation energy of the electrical conductivity

<i>E_A</i>	0.85 eV	<i>T</i> ^{–1/4} temperature dependence, Si-doped wafer	99K
----------------------	---------	--	-----

electrical conductivity

σ	10 ^{–3} ...10 ^{–1} Ω ^{–1} cm ^{–1}	<i>T</i> = 300 K	films obtained by different methods of preparation	92K, 94K, 97K
---	---	------------------	---	---------------------

Hall mobiliy

μ _H	2.9...31.7 cm ² V ^{–1} s ^{–1}	<i>T</i> = 300 K	Si-doped wafer	99K
----------------	--	------------------	----------------	-----

65B Burmeister, R. A. Jr., Greene, P. E.: Bull. Am. Phys. Soc. Ser. 1110 (1965) 1184.
67B Burmeister, R. A. Jr., Greene, P. E.: Trans. MS. AIME 239 (1967) 408.
88K Kumashiro, Y.: New Mater. New Processes 4 (1988) 1.
92K Kumashiro, Y., Yokoyama, T., Nakamura, J., Matsuda, K., Yoshida, H., Takahashi, J.: in: Mater. Res. Soc. Symp. Proc. Vol. 242, Mater. Res. Soc. 1992, p. 629.
94K Kumashiro, Y., Yokoyama, T., Nakamura, J., Takahashi, J.: Proc. 11th Int. Symp. Boron, Borides and Relectrical Compounds, Tsukuba, Japan, August 22 - 26, 1993, Jpn. J. Appl. Phys. Series 10 (1994), p. 168.
97K Kumashiro, Y., Yokoyama, T., Sato, A., Ando, Y.: J. Solid State Chem. 133 (1997) 314 (Proc. 12th Int. Symp. Boron, Borides and Relectrical Compounds, Baden, Austria, 1996).
97W Werheit, H., Kuhlmann U., Shirai, K., Kumashiro, Y.: J. Solid State Chem. 133 (1997) 140 (Proc. 12th Int. Symp. Boron, Borides and Relectrical Compounds, Baden, Austria, 1996).
99K Kumashiro, Y., Yokoyama, T., Ando, Y.: J. Solid State Chem. (2000) (Proc. 13th Int. Symp. Boron, Borides and Relectrical Compounds, Dinard, France, Sept. 1999).

34.19 Boron-arsenic compounds

34.19.1 B₆As (B₁₂As₂); B₁₃As₂

α -rhombohedral boron structure group. Space group: $D_{3d}^5 - R \bar{3} m$.

energy gap

E_g	3.47 eV	$T = 300$ K	optical (from plot $\alpha^{1/2}$ vs. E)	83S
	2.78 eV		Z \rightarrow A(calculated)	95L
	4.81 eV		Γ (calculated)	
	4.21 eV		X (calculated)	
	3.07 eV		Z (calculated)	
	2.97 eV		A (calculated)	
	4.21 eV		D (calculated)	

83S Slack, G.A., McNelly, T.F., Taft, E.A.: J. Phys. Chem. Solids 44 (1983) 1009.

95L Li, Dong, Ching, W.Y.: Phys. Rev . B 52 (1995) 17073.

35 Binary transition metal compounds

35.1 Compounds with elements of the IVth group

35.1.1 Mn₁₁Si₁₉, Mn₂₆Si₄₅

energy gaps

$E_{g,th}$ 0.8 eV $T = 0$ K 69N

effective masses

m_n $> 10^3 m_0$ $T = 300$ K 69N

m_p $10 m_0$ $T = 300$ K 69N

hole mobility

μ_p $230 \text{ cm}^2/\text{V s}$ $T = 300$ K Hall mobility 69I

$\mu_{p||}$ $1.7 \text{ cm}^2/\text{V s}$ $T = 300$ K 74A

$\mu_{p\perp}$ $7.9 \text{ cm}^2/\text{V s}$ $T = 300$ K 74A

electrical conductivity

σ $160 \Omega^{-1} \text{ cm}^{-1}$ along [001], RT extrinsic region 69I

$800 \Omega^{-1} \text{ cm}^{-1}$ along [100] 69I

69I Ivanova, L. D., Abrikosoy, N. Kh., Elagina, E. I., Khvostikova, V. D.: Izv. Akad. Nauk SSSR, Neorg. Mater. 5 (1969) 1933 (translation: Inorg. Mater. 5 (1969) 1645).

69N Nikitin, F. N., Tarasov, V. I., Andreev, A. A., Shumilova, L. N.: Fz. Tverd. Tela 11 (1969) 3389 (translation: Sov. Phys. Solid State 11 (1969/70) 2757).

74A Abrikosov, N. Kh., Ivanova, L. D.: Izv. Akad. Nauk SSSR, Neorg. Mater. 10 (1974) 1016 (translation: Inorg. Mater. 10 (1974) 873).

35.1.2 Mn₁₅Si₂₆

energy gap

E_g 0.702 eV $T = 0$ K from $\log p \propto E_g/2kT$ measured 81K

along [001] and along [100]

0.70 eV $T = 900...1200$ K from $\log(R_H T^{3/2}) \propto E_g/2kT$ 81K

effective masses

m_p $11 m_0$ along [100] from thermoelectric power near 600 K 81K

$15 m_0$ along [001]

hole mobility

μ_p $1.2 T^{-3/2}$ along [100], Hall mobility; temperature dependence 81K

cm^2/Vs $T > 200$ K shows that acoustic phonon scattering is dominant

81K Kawasumi, I., Sakata, M., Nishida, I., Masumoto, K.: J. Mater. Sci. 16 (1981) 355.

35.1.3 CrSi₂

crystal structure

hexagonal, space group D₄⁶-P6₂22

energy gap

$E_{g,th}$	0.16 eV	from $\log \rho \propto E_g/2kT$, $T = 300...550$ K	56A
	0.29...0.32 eV	from $\log \rho$ vs. T^{-1}	78N

effective masses

(\parallel : along c ; \perp : within the (a_1, a_2) -plane)

m_n	$\approx 7 m_0$	density of states mass	64S
m_p	$\approx 5 m_0$	density of states mass	64S
$m_{p\parallel}$	$5 m_0$		72N
$m_{p\perp}$	$3 m_0$		72N

resistivity

ρ	$\approx 10 \cdot 10^{-4} \Omega \text{ cm}$	RT	highly degenerate p-type region	64S, 72N, 78N
--------	--	----	---------------------------------	---------------------

carrier mobilities

μ_n	$0.27 \text{ cm}^2/\text{V s}$	RT	73N
μ_p	$8 \text{ cm}^2/\text{V s}$	RT	73N

- 56A Abrikosov, N. Kh., Bankina, V. F.: Dokl. Akad. Nauk SSSR 108 (1956) 627.
 64S Shinoda, D., Asanabe, S., Sasaki, Y.: J. Phys. Soc. Jpn. 19 (1964) 269.
 72N Nishida, I.: J. Mater. Sci. 7 (1972) 1119.
 73N Nikitin, F. N., Tarasov, V. I., Zaitsev, V. K.: Fiz. Tverd. Tela 15 (1973) 1254 (translation: Sov. Phys. Solid State 15 (1973) 846).
 78N Nishida, I., Sakata, T.: J. Phys. Chem. Solids 39 (1978) 499.

35.1.4 ReSi₂, Re_{1-x}M_xSi₂

energy gap

$E_{g,th}$	0.21...0.22 eV	$T = 0$ K	from $\rho(T)$ in the range 500...1200 K	83S
	0.195 eV	RT	from optical reflectivity	83S

resistivity

ρ	0.003...0.01 $\Omega \text{ cm}$	RT	four-probe ac method, polycrystalline sample	83S
--------	----------------------------------	----	---	-----

- 83S Siegrist, T., Hulliger, F., Travaglini, G.: J. Less-Common Met. 92 (1983) 119.

35.1.5 Ru₂Si₃

space group D_{2h}¹⁴ – Pbcn, $Z = 8$.

energy gap

$E_{g,th}$	0.7 eV	from resistivity measurement	80S
------------	--------	------------------------------	-----

- 80S Susz, C. P., Muller, J., Yvon, K., Parthé, F.: J. Less-Common Met. 71 (1980) P1.

35.1.6 Ru₂Ge₃

space group D_{2h}¹⁴ – Pbcn, Z = 8.

energy gap

$E_{g,th}$	0.52 eV		from $\rho \propto \exp(E_g/2kT)$, $T = 550...700$ K, polycrystalline bar	80S
80S	Susz, C. P., Muller, J., Yvon, K., Parthé, F.: J. Less-Common Met. 71 (1980) P1.			

35.1.7 FeSi₂

energy gaps

$E_{g,th}$	0.88 eV	$T = 0$ K	from $\log \rho \propto E_g/2kT$ in the intrinsic range	64W
------------	---------	-----------	--	-----

mobilities of charge carriers

μ_n	0.26 cm ² /V s	$T = 300$ K	assuming small polarons in n-type FeSi ₂	68B
			(activation energy of the mobility 0.06 eV)	
μ_p	2...4 cm ² /V s	$T = 300$ K	$\mu_p \propto T^{1/2}$ in the extrinsic range	68B

64W	Ware, R. M., Mc Neill, D. J.: Proc. IEE 111 (1964) 178.			
68B	Birkholz, U., Schelm, J.: Phys. Status Solidi 27 (1968) 413.			

35.1.8 OsSi₂

energy gaps

$E_{g,th}$	> 0.26 eV		from $\log \rho \propto E_g/2kT$; $T = 400...700$ K, sintered sample	82H
82H	Hulliger, F.: unpublished.			

35.2 Compounds with elements of the Vth group

35.2.1 MnP₄

monoclinic modification (8L – MnP₄)

energy gap

E_g	0.28 eV	given as $E_A = 0.14$ eV, from $\log \rho \propto E_A/kT$	65J
-------	---------	--	-----

resistivity

ρ	30 Ω cm	RT	four-probe technique, crystals prepared at 1500...1700 K and 30...35 kbar, unknown orientation	65J
--------	----------------	----	--	-----

triclinic 6-layer modification (6L – MnP₄)

energy gap

E_g	0.54 eV	given as $E_A = 0.27$ eV, from $\log \rho \propto E_A/kT$ between 300 and 420 K, crystals from tin flux	80J
-------	---------	--	-----

triclinic 2-layer modification (2L – MnP₄)

energy gap

E_g	> 0.08 eV	intrinsic conductivity range not reached at 420 K, crystals prepared by a transport reaction with iodine	80J
-------	-----------	--	-----

65J Johnston, W. D., Miller, R. C., Damon, D. H.: J. Less-Common Met. 8 (1965) 272.

80J Jericho, M. H., Simpson, A. H., Frindt, R. F.: Phys. Rev. B22 (1980) 4907.

35.2.2 FeP₂

energy gap

$E_{g,th}$	0.37 eV	from $\log \rho \propto E_g/2kT$, $T = 400...550$ K, single crystal	71B
------------	---------	--	-----

mobility of charge carriers :

below 60 K	$\mu_H \propto T^{0.8}$		71B
above 300 K	$\mu_H \propto T^{-2...-2.5}$		

71B Boda, G., Stenström, B., Sagredo, V., Beckman, O., Carlsson, B., Rundqvist, S.: Phys. Scripta 4 (1971) 132.

35.2.3 FeAs₂

energy gap

$E_{g,th}$	0.22 eV	from $\log \rho \propto E_g/2kT$ intrinsic above 170 K	72F
------------	---------	---	-----

resistivity

ρ	0.002 Ω cm	natural crystal	65J
--------	-------------------	-----------------	-----

65J Johnston, W. D., Miller, R. C., Damon, D. H.: J. Less-Common Met. 8 (1965) 272.

72F Fan, A. K. L., Rosenthal, G. H., McKinzie, H. L., Wold, A.: J. Solid State Chem. 5 (1972) 136.

35.2.4 FeSb₂

energy gap

$E_{g,th}$	$\approx 7\text{ eV}$		polycrystalline, $T = 550\ldots 800\text{ K}$	60D
60D	Dudkin, L. D., Vaidanich, V. I.: Fiz. Tverd. Tela 2 (1960) 1526; translation: Sov. Phys. Solid State 2 (1960) 1384.			

35.2.5 RuP₂

energy gap

E_g	$\approx 1\text{ eV}$	RT	from diffuse reflectance of sintered samples	63H
resistivity				
ρ	$0.09\ldots 0.26\text{ }\Omega\text{ cm}$	RT	crystals with 0.85 wt% Sn For temperature dependence in the range 77...300 K	77K
63H	Hulliger, F.: Nature (London) 198 (1963) 1081.			
77K	Kaner, R., Castro, C. A., Gruska, R. P., Wold, A.: Mat. Res. Bull. 12 (1977) 1143.			

35.2.6 RuPAs

energy gap

E_g	$\approx 0.8\text{ eV}$	RT	from diffuse reflectance of sintered powder	63H
63H	Hulliger, F.: Nature (London) 198 (1963) 1081.			

35.2.7 RuAs₂

energy gap

E_g	$\approx 0.8\text{ eV}$	$T = 295\text{ K}$	from diffuse reflectance of powder	63H
63H	Hulliger, F.: Nature (London) 198 (1963) 1081.			

35.2.8 RuSb₂

energy gap

$E_{g,th}$	$> 0.3\text{ eV}$		from $\log \rho \propto E_g/2kT$ above 450 K, sintered sample	63H
63H	Hulliger, F.: Nature (London) 198 (1963) 1081.			

35.2.9 OsP₂

energy gap

E_g	$\approx 1.2\text{ eV}$	RT	from diffuse reflectance of sintered samples	63H
63H	Hulliger, F.: Nature (London) 198 (1963) 1081.			

35.2.10 OsAs₂

energy gap

E_g ≈ 0.9 eV RT from diffuse reflectance 63H

63H Hulliger, F.: Nature (London) 198 (1963) 1081.

35.2.11 OsSb₂

energy gap

$E_{g,th}$ > 0.3 eV from $\log \rho \propto E_g/2kT$ above 600 K; sintered material 63H

resistivity

ρ 150 Ω cm RT sintered sample 63H

63H Hulliger, F.: Nature (London) 198 (1963) 1081.

35.2.12 CoP₂

energy gap

$E_{g,th}$ > 0.02 eV from $\rho(T)$ below room temperature 72D

72D Donohue, P. C.: Mat. Res. Bull. 7 (1972) 943.

35.2.13 CoAs₂

energy gap

$E_{g,th}$ ≈ 0.15 eV from $\log \rho \propto E_g/2kT$, sintered sample 59H

59H Hulliger, F.: Helv. Phys. Acta 32 (1959) 615.

35.2.14 CoSb₂

energy gap

$E_{g,th}$ 0.2 eV (?) polycrystal from $\log \rho \propto E_g/2kT$, $T = 550 \dots 800$ K, measured across the arsenopyrite \rightarrow marcasite transition 56D

56D Dudkin, L. D., Abrikosov, N. Kh.: Zhur. Neorg. Khim. 1 (1956) 2096.

35.2.15 RhP₂

energy gap

E_g ≈ 1 eV RT from diffuse reflectance of powder samples 63H

63H Hulliger, F.: Nature (London) 198 (1963) 1081.

35.2.16 RhAs₂

energy gap

E_g	1.15 eV	RT	from diffuse reflectance of powder samples	63H
-------	---------	----	--	-----

63H Hulliger, F.: Nature (London) 198 (1963) 1081.

35.2.17 RhAsSb

energy gap

$E_{g,th}$	$\approx 0.4\text{eV}$		from $\log \rho \propto E_g/2kT$, $T = 300\dots500\text{ K}$; sintered sample	63H
------------	------------------------	--	---	-----

63H Hulliger, F.: Nature (London) 198 (1963) 1081.

35.2.18 IrP₂

energy gap

E_g	$\approx 1\text{ eV}$	$T = 295\text{ K}$	from diffuse reflectance, powder sample	63H
-------	-----------------------	--------------------	---	-----

63H Hulliger, F.: Nature (London) 198 (1963) 1081.

35.2.19 IrAs₂

energy gap

E_g	1 eV	RT	from diffuse reflectance of powder samples	63H
-------	------	----	--	-----

63H Hulliger, F.: Nature (London) 198 (1963) 1081.

35.2.20 IrAsSb

energy gap

$E_{g,th}$	$\approx 0.4\text{ eV}$		from $\log \rho \propto E_g/2kT$ up to 800 K	63H
------------	-------------------------	--	--	-----

resistivity

ρ	$\approx 20\ \Omega\text{ cm}$	RT	sintered sample	63H
--------	--------------------------------	----	-----------------	-----

63H Hulliger, F.: Nature (London) 198 (1963) 1081.

35.2.21 NiP₂

energy gap

E_g	0.73 eV	RT	from optical absorption (0.5...3.5 eV), single crystal	78O
-------	---------	----	---	-----

activation energy of resistivity

E_A	0.002 eV		from $\log \rho \propto E_A/kT$, $T = 35...100$ K, single crystal	78O
-------	----------	--	---	-----

resistivity

ρ	0.39 Ω cm	RT	van der Pauw method	
78O	Odile, J. P., Soled, S., Castro, C. A., Wold, A.: Inorg. Chem. 17 (1978) 283.			

35.2.22 NiAs₂ (β -NiAs₂) (rammelsbergite, marcasite type)

energy gap

$E_{g,th}$	0.05 eV		from $\log \rho \propto E_g/2kT$, $T = 400...500$ K, sintered sample	59H
------------	---------	--	--	-----

59H Hulliger, F.: Helv. Phys. Acta 32 (1959) 615.

35.2.23 PdP₂

energy gap

$E_{g,th}$	0.6...0.7 eV		from $\log \rho \propto E_g/2kT$, sintered sample	63H
------------	--------------	--	--	-----

63H Hulliger, F.: Nature (London) 198 (1963) 1081.

35.2.24 PdPAs

energy gap

$E_{g,th}$	0.45 eV		from $\log \rho \propto E_g/2kT$ above 550 K, sintered sample	63H
------------	---------	--	--	-----

63H Hulliger, F.: Nature (London) 198 (1963) 1081.

35.2.25 PtP₂

energy gap

$E_{g,th}$	> 0.6 eV		from $\log \rho \propto E_g/2kT$ above 600 K, sintered sample	63H
------------	----------	--	--	-----

63H Hulliger, F.: Nature (London) 198 (1963) 1081.

35.2.26 PtPAs

energy gap

$E_{g,th}$	≥ 0.4 eV		from $\log \rho \propto E_g/2kT$, sintered sample	63H
------------	---------------	--	--	-----

63H Hulliger, F.: Nature (London) 198 (1963) 1081.

35.2.27 PtAs₂

energy gap

$E_{g,th}$	0.5 eV	from $\log \rho \propto E_g/2kT$, sintered sample	63H
	0.8 eV	from $\log \rho \propto E_g/2kT$	65J
		$T = 700 \dots 1000$ K, sintered sample	
	0.17 eV	from $\log \rho \propto E_g/2kT$, $T = 300 \dots 500$ K	66B

63H Hulliger, F.: Nature (London) 198 (1963) 1081.

65J Johnston, W. D., Miller, R. C., Damon, D. H.: J. Less-Common Met. 8 (1965) 272.

66B Bennett, S. L., Heyding, R. D.: Can. J. Chem. 44 (1966) 3017.

35.2.28 PtSb₂

energy gaps

$E_{g,th}$	≥ 0.05 eV		from $\log \rho \propto E_g/2kT$	63H
			polycrystalline sample	
$E_{g,ind}$	≈ 0.10 eV		indirect gap from optical	65D,
			absorption	68R
$E_{g,dir}$	> 0.4 eV	$T = 4$ K	from the energy dependence of the	72D
			cyclotron mass	
			$m_{\omega c}(E) = m_{\omega c}(0)/(1+(2E/E_{g,dir}))$;	
			$m_{\omega c}$ changes by less than 5%	
			when E increases by 0.11 eV	

effective masses

$m_{n\parallel}$	0.53...0.66 m_0	low T ...high T	calculated from theoretical band	65E
			model based on experimental data	
			from [65D]	
$m_{n\perp}$	0.37...0.49 m_0	low T ...high T		
$m_{p\parallel}$	0.52...0.55 m_0	low T ...high T	based on theoretical band model	65E
			and data from [65D]	
	0.35 m_0	$T = 77$ K	using the theoretical model of [65E]	73A
			with $m_{\parallel}/m_{\perp} = 0.77$	
	0.66 m_0	$T = 310$ K		
$m_{p\perp}$	0.60...0.82 m_0	low T ...high T		65E
	0.45 m_0	$T = 77$ K		73A
	0.85 m_0	$T = 310$ K		

electrical resistivity

ρ	0.001 Ω cm	$T = 250$ K		68R
--------	-------------------	-------------	--	-----

mobility of charge carriers (in cm²/V s)

μ_n	420	$T = 300$ K	from $\rho(T)$ and $R_H(T)$ in the mixed-	68R
μ_p	830	$T = 300$ K	$\mu_n = 4.15 \cdot 10^6 T^{-3/2} \exp(12.6 \text{ K}/T)$	68R

63H Hulliger, F.: Nature (London) 198 (1963) 1081.

65D Damon, D. H., Miller, R. C., Sagar, A.: Phys. Rev. A 138 (1965) 636.

65E Emtage, P. R.: Phys. Rev. A 138 (1965) 246.

68R Reynolds, R. A., Brau, M. J., Chapman, R. A.: J. Phys. Chem. Solids 29 (1968) 755.

72D Damon, D. H., Miller, R. C., Emtage, P. R.: Phys. Rev. B5 (1972) 2175.

73A Abdullaev, A. A., Angelova, L. A., Kuznetsov, V. K., Ormont, A. B., Pashintsev, Yu. I.: Phys. Status Solidi (a) 18 (1973) 459.

35.2.29 FeP₄

energy gap

E_A	0.0014 eV	$T = 4...70$ K	from $\log \rho \propto E_A/kT$	80G
-------	-----------	----------------	---------------------------------	-----

resistivity

ρ	$3 \cdot 10^4 \Omega \text{ cm}$	RT		78S
--------	----------------------------------	----	--	-----

78S Sugitani, M., Kimomura, N., Koizumi, M., Kume, S.: J. Solid State Chem. 26 (1978) 195.

80G Grandjean, F., Gerard, A., Krieger, U., Heiden, C., Braun, D. J., Jeitschko, W.: Solid State Commun. 33 (1980) 261.

35.2.30 RuP₄ (r)

(CdP₄-type modification)

energy gap

E_g	0.38 eV		given as $E_A = 0.19$ eV, from $\log \rho \propto E_A/kT$, $T = 300...500$ K	82F
-------	---------	--	--	-----

electrical resistivity

ρ	$800 \Omega \text{ cm}$	RT	pressed pellets of microcrystalline	82F
--------	-------------------------	----	-------------------------------------	-----

82F Flörke, U., Jeitschko, W.: J. Less-Common Met. 86 (1982) 247.

35.2.31 RuP₄ (h)

energy gap

E_g	0.64 eV		given as $E_A = 0.32$ eV, from $\log \rho \propto E_A/kT$, $T = 400...550$ K	82F
-------	---------	--	--	-----

82F Flörke, U., Jeitschko, W.: J. Less-Common Met. 86 (1982) 247.

35.2.32 OsP₄ (r)

(CdP₄-type modification)

energy gap

E_g	0.40 eV		given as $E_A = 0.20$ eV, from $\log \rho \propto E_A/kT$, $T = 300...500$ K	82F
-------	---------	--	--	-----

electrical resistivity

ρ	$\approx 500 \Omega \text{ cm}$	RT	pressed powder from tin flux;	82F
--------	---------------------------------	----	-------------------------------	-----

82F Flörke, U., Jeitschko, W.: J. Less-Common Met. 86 (1982) 247.

35.2.33 OsP₄ (h)

energy gap

E_g 0.60 eV

given as $E_A = 0.30$ eV, from
 $\log \rho \propto E_A/kT$, $T = 40 \dots 500$ K

82F

electrical resistivity

ρ $\approx 40 \cdot 10^4 \Omega \text{ cm}$ $T = 400$ K

pressed powder from tin flux;

82F

82F Flörke, U., Jeitschko, W.: J. Less-Common Met. 86 (1982) 247.

35.3 Chalcogenides

S: structure (space group), CG: crystal growth (the numbers in parentheses correspond to T_1 and T_2 , the temperatures (in °C) of the hot and cold end of the crystal growth tube, respectively), C: colour.

35.3.1 $\text{Ti}_{1+x}\text{S}_2$

$(0 \leq x \leq 0.1)$

Data from [63H, 65G, 67G, 68C, 69L, 72T, 75C, 75T1, 75T2, 75W2, 77F, 78B, 83H]

(at 1000°C: $0.04 \leq x \leq 0.1$, at 500°C: $0.03 \leq x \leq 0.1$, at 600°C: $0 \leq x \leq 0.1$)

lattice parameters

a	3.407 Å	$x \approx 0$	S: $C6, D_{3d}^3 - P\bar{3}m1$
c	5.695 Å		CG: halogen transport (900/800)

density

d	3.22 g cm ⁻³	C: brassy
-----	-------------------------	-----------

resistivity

ρ_{\perp}	$5 \cdot 10^{-3} \Omega \text{ cm}$	n-type, synthetic single crystal	$d\rho/dp < 0$
$\rho_a = \rho_0 + \rho_1 T^2 = 1.95 \cdot 10^{-4} \Omega \text{ cm}$ $+ (2.0 \cdot 10^{-8}/k^2 T^2) [\Omega \text{ cm}]$			$\rho_1 \propto n^{-5/3}$, where n = carrier concentration; shows electron- electron scattering is dominant

Hall mobility

$\mu_{H\perp}$	9.7 cm ² /V s	$dR_H/dp = 0$
----------------	--------------------------	---------------

electron concentration

n	$9 \cdot 10^{20} \text{ cm}^{-3}$
-----	-----------------------------------

effective electron mass

m_n	$1.5 m_0$
-------	-----------

energy gap

E_g	0.7 eV	optical gap
	0.7 eV	indirect gap, calculated

linear thermal expansion coefficient

α_a	$0.96 \cdot 10^{-5} \text{ K}^{-1}$
α_c	$1.94 \cdot 10^{-5} \text{ K}^{-1}$

63H Hulliger, F.: Nature (London) 200 (1963) 1064.
65G Greenaway, D. L., Nitsche, R.: J. Phys. Chem. Solids 26 (1965) 1445.
67G Gilles, P. W.: Applications of fundamental Thermodynamics to Metallurgical processes, Fitterer, G. R. (ed.), New York: Gordon and Breach, Science Publishers Inc. 1967, p. 281.
68C Conroy, L. E., Park, K. C.: Inorg. Chem. 7 (1968) 459.
69L Lee, P. A., Said, G., Davis, R., Lim, T. H.: J. Phys. Chem. Solids 30 (1969) 2719.
72T Thompson, A. H., Pisharody, K. R., Koehler Jr., R. F.: Phys. Rev. Lett. 29 (1972) 163.
75C Cianelli, R. R., Scanlon, J. C., Thompson, A. H.: Mater. Res. Bull. 10 (1975) 1379.
75T1 Thompson, A. H.: Phys. Rev. Lett. 35 (1975) 1786.

- 75T2 Thompson, A. H., Gamble, F. R., Symon, C. R.: Mater. Res. Bull. 10 (1975) 915.
 77F Friend, R. H., Jerome, D., Liang, W. Y., Mikkelsen, J. C., Yoffe, A. D.: J. Phys. C 10 (1977) L705.
 78B Bullett, D. W.: J. Phys. C 11 (1978) 4501.
 83H Handbook of Chemistry and Physics, 64th ed. (ed.: R. C. Weast), CRC Press. Inc. 1983.

35.3.2 TiS_{3-x}

(0 ≤ x ≤ ?)

Data from [61G, 63H, 75F]

lattice parameters

<i>a</i>	4.955 Å	S: ZrSe ₃ -type, C _{2h} ² – P2 ₁ /m
<i>b</i>	3.401 Å	CG: sublimed from polycrystalline
<i>c</i>	S.775 Å	mass with excess sulfur at 610°C
<i>β</i>	97.32°	C: graphite

resistivity

<i>ρ_b</i>	4.0 Ω cm	n-type, synthetic single crystal
----------------------	----------	--

energy gap

<i>E_g</i>	0.9 eV	n-type, synthetic single crystal	optical gap
----------------------	--------	--	-------------

- 61G Grimmeiss, H. G., Rabenau, A., Hahn, H., Ness, P.: Z. Elektrochem. 65 (1961) 776.
 63H Hulliger, F.: Nature (London) 200 (1963) 1064.
 75F Furuseth, S., Brattas, L., Kjekshus, A.: Acta Chem. Scand. 29A (1975) 623.

35.3.3 Ti_{1+x}Se₂

(0 ≤ x ≤ 0.018)

Data from [76D, 77F, 78B, 78Z]

lattice parameters

<i>a</i>	3.537 Å	S: C6, D _{3d} ³ – P $\bar{3}$ m1
<i>c</i>	6.00 Å	second-order phase transition at <i>T</i> _{tr} = 200 K, <i>T</i> < <i>T</i> _{tr} : transverse atomic displacements with <i>q</i> = (1/2, 0, 1/2)
		CG: halogen transport (900/≤800) C: metallic

resistivity

<i>ρ_⊥</i>	1.32·10 ⁻³ Ω cm	p-type,	d <i>ρ</i> /d <i>p</i> < 0
<i>ρ_∥</i>	3·10 ⁻³ Ω cm	synthetic single crystal	

Hall coefficient

$R_H (B c)$	$3.25 \cdot 10^{-2} \text{ cm}^3/\text{C}$	p-type synthetic single crystal	$dR_H/dp < 0$
--------------	--	---------------------------------------	---------------

hole concentration

p	10^{20} cm^{-3}
-----	---------------------------

energy gap

E_g	$\approx 0.0 \text{ eV}$	optical gap (semimetal)
	0.0 eV	calculated

76D DiSalvo, F. J., Moncton, D. E., Waszczak, J. V.: Phys. Rev. B14 (1976) 4321.
77F Friend, R. H., Jerome, D., Liang, W. Y., Mikkelsen, J. C., Yoffe, A. D.: J. Phys. C 10 (1977) L705.
78B Bullett, D. W.: J. Phys. C 11 (1978) 4501.
78Z Zunger, A., Freeman, A. J.: Phys. Rev. B17 (1978) 1839.

35.3.4 Zr₂S₃

Data from [58M1, 58M2]

lattice parameters

a	10.253 \AA	S: defective B1, random Zr vacancies C: black
-----	----------------------	---

esistivity

ρ	$0.08 \text{ } \Omega \text{ cm}$	n-type, polycrystalline sample
--------	-----------------------------------	-----------------------------------

58M1 McTaggart, F. K., Wadsley, A. D.: Aust. J. Chem. 11 (1958) 445.
58M2 McTaggart, F. K.: Aust. J. Chem. 11 (1958) 471.

35.3.5 ZrS₂

Data from [65G, 68C, 69L, 78B, 83H]

lattice parameters

a	3.66 \AA	S: C6, $D_{3d}^3 - P\bar{3}m1$
c	5.85 \AA	CG: halogen transport (900/800)

density

d	3.87 g cm^{-3}	C: violet metallic
-----	--------------------------	--------------------

resistivity

ρ_{\perp}	$0.76 \text{ } \Omega \text{ cm}$	n-type, synthetic single crystal
----------------	-----------------------------------	-------------------------------------

Hall mobility, electron concentration

$\mu_{H\perp}$	$4.3 \text{ cm}^2/\text{V s}$	n-type, synthetic
n	$1.1 \cdot 10^{18} \text{ cm}^{-3}$	single crystal

energy gap

E_g	1.7 eV	optical gap, $dE_g/dT = -4.2 \cdot 10^{-4} \text{ eV K}^{-1}$
	1.7 eV	indirect gap, calculated
65G	Greenaway, D. L., Nitsche, R.: J. Phys. Chem. Solids 26 (1965) 1445.	
68C	Conroy, L. E., Park, K. C.: Inorg. Chem. 7 (1968) 459.	
69L	Lee, P. A., Said, G., Davis, R., Lim, T. H.: J. Phys. Chem. Solids 30 (1969) 2719.	
78B	Bullett, D. W.: J. Phys. C 11 (1978) 4501.	
83H	Handbook of Chemistry and Physics, 64th ed. (ed.: R. C. Weast), CRC Press. Inc. 1983.	

35.3.6 ZrS_{3-x}

($0 \leq x \leq 0.05$)

Data from [61G, 63H, 73S, 75F]

lattice parameters

a	5.123 Å	S: ZrSe ₃ -type, $C_{2h}^2 - P2_1/m$
b	3.627 Å	CG: halogen transport
c	8.986 Å	(750...900/550....600)
β	97.15°	C: dark orange

resistivity

ρ_b	$10^4 \Omega \text{ cm}$	n-type, synthetic single crystal
----------	--------------------------	-------------------------------------

energy gap

E_g	2.8 eV	optical gap
61G	Grimmeiss, H. G., Rabenau, A., Hahn, H., Ness, P.: Z. Elektrochem. 65 (1961) 776.	
63H	Hulliger, F.: Nature (London) 200 (1963) 1064.	
73S	Schairer, W., Shafer, M. W.: Phys. Status. Solidi (a) 17 (1973) 181.	
75F	Furuseth, S., Brattas, L., Kjekshus, A.: Acta Chem. Scand. 29A (1975) 623.	

35.3.7 Zr₂Se₃

Data from [58M1, 58M2]

lattice parameters

a	3.757 Å	S: hexagonal
c	18.63 Å	C: (black)

resistivity

ρ	$7 \cdot 10^{-3} \Omega \text{ cm}$	n-type, polycrystalline sample
--------	-------------------------------------	-----------------------------------

58M1	McTaggart, F. K., Wadsley, A. D.: Aust. J. Chem. 11 (1958) 445.	
58M2	McTaggart, F. K.: Aust. J. Chem. 11 (1958) 471.	

35.3.8 Zr_{1+x}Se₂

(0.05 ≤ x ≤ 0.08)

Data from [58M, 65G, 69L, 73B, 78B]

lattice parameters

<i>a</i>	3.76 Å	S: C6, D _{3d} ³ – P $\bar{3}$ m1
<i>c</i>	6.15 Å	CG: halogen transport (900/800) C: metallic grey

resistivity

ρ	0.1 Ω cm	n-type, poly-
--------	----------	---------------

energy gap

<i>E_g</i>	0.87 eV	Zr _{1.05} Se ₂	optical gap
	1.2 eV	ZrSe ₂	optical gap
	1.0 eV		indirect gap, calculated

- 58M McTaggart, F. K.: Aust. J. Chem. 11 (1958) 471.
65G Greenaway, D. L., Nitsche, R.: J. Phys. Chem. Solids 26 (1965) 1445.
69L Lee, P. A., Said, G., Davis, R., Lim, T. H.: J. Phys. Chem. Solids 30 (1969) 2719.
73B Brattas, L., Kjekshus, A.: Acta Chem. Scand. 27 (1973) 1290.
78B Bullett, D. W.: J. Phys. C 11 (1978) 4501.

35.3.9 ZrSe₃

Data from [61G, 65K, 75F, 79B]

lattice parameters

<i>a</i>	5.411 Å	S: ZrSe ₃ type, C _{2h} ² – P2 ₁ /m
<i>b</i>	3.749 Å	CG: from crystalline mass
<i>c</i>	9.444 Å	C: dark grey
β	97.45°	

resistivity

ρ_b	10 ³ Ω cm	n-type, synthetic single crystal
----------	----------------------	-------------------------------------

energy gap

<i>E_g</i>	1.25 eV	optical gap
	1.6 eV	direct gap, calculated
	1.5 eV	indirect gap, calculated

- 61G Grimmeiss, H. G., Rabenau, A., Hahn, H., Ness, P.: Z. Elektrochem. 65 (1961) 776.
65K Kronert, V. W., Plieth, K.: Z. Anorg. Allg. Chem. 336 (1965) 207.
75F Furuseth, S., Brattas, L., Kjekshus, A.: Acta Chem. Scand. 29A (1975) 623.
79B Bullett, D. W.: J. Phys. C 12 (1979) 277.

35.3.10 Hf₂S₃

Data from [58M1, 58M2]

lattice parameters

<i>a</i>	3.635 Å	S: hexagonal, cation vacancies randomly distributed on alternate (111) planes of B8 structure C: light yellow-brown
<i>c</i>	5.89 Å	

resistivity

ρ	150 Ω cm	n-type, polycrystalline sample
--------	----------	-----------------------------------

Seebeck coefficient

<i>S</i>	− 200 μV K ^{−1}
----------	--------------------------

58M1 McTaggart, F. K., Wadsley, A. D.: Aust. J. Chem. 11 (1958) 445.
58M2 McTaggart, F. K.: Aust. J. Chem. 11 (1958) 471.

35.3.11 HfS₂

Data from [65G, 68S2, 70W, 78B]

lattice parameters

<i>a</i>	3.622 Å	S: C ₆ , D _{3d} ³ – P $\bar{3}$ m1 CG: halogen transport (900/800) C: dark-red metallic
<i>c</i>	5.88 Å	

resistivity

ρ_{\perp}	3.3·10 ⁷ ...10 ⁸ Ω cm	n-type, synthetic single crystal
----------------	--	--

energy gap

<i>E_g</i>	1.96 eV	optical gap, <i>dE_g/dT</i> = − 4.3·10 ^{−4} eV/K indirect gap, calculated
	1.9 eV	
<i>E_{g,th}</i>	2.1 eV	
		<i>T</i> > 500 K

58M1 McTaggart, F. K., Wadsley, A. D.: Aust. J. Chem. 11 (1958) 445.
58M2 McTaggart, F. K.: Aust. J. Chem. 11 (1958) 471.
70W Wieting, T. J.: J. Phys. Chem. Solids 31 (1970) 2148.
78B Bullett, D. W.: J. Phys. C 11 (1978) 4501.

35.3.12 HfS₃

Data from [61G, 63H, 71L, 73S, 75F]

lattice parameters

<i>a</i>	5.09 Å	S: ZrSe ₃ type, C _{2h} ² – P2 ₁ /m
<i>b</i>	3.59 Å	CG: halogen transport
<i>c</i>	8.96 Å	(750...900/550...600)
<i>β</i>	98.4°	C: ochre

resistivity

<i>ρ_b</i>	10 ² Ω cm	synthetic single crystal
----------------------	----------------------	--------------------------

energy gap

<i>E_g</i>	3.1 eV	optical gap
----------------------	--------	-------------

61G Grimmeiss, H. G., Rabenau, A., Hahn, H., Ness, P.: Z. Elektrochem. 65 (1961) 776.
63H Haraldsen, H., Kjekshus, A., Rost, E., Steffensen, A.: Acta Chem. Scand. 17 (1963) 1283.
71L Landolt-Börnstein (New Series), ed.: K. H. Hellwege, Vol. III/6, Springer Verlag: Berlin, Heidelberg, New York 1971.
73S Schairer, W., Shafer, M. W.: Phys. Status. Solidi (a) 17 (1973) 181.
75F Furuseth, S., Brattas, L., Kjekshus, A.: Acta Chem. Scand. 29A (1975) 623.

35.3.13 HfSe₂

Data from [65G, 73B, 78B]

lattice parameters

<i>a</i>	3.733 Å	S: C6, D _{3d} ³ – P $\bar{3}$ m1
<i>c</i>	6.146 Å	CG: halogen transport (900/800)
		C: dark-red metallic

energy gap

<i>E_g</i>	1.05 eV	synthetic	<i>dE_g/dT</i> = – 6.8·10 ^{–4} eV/K
		single crystal	(<i>E_g</i> : optical gap)
	1.1 eV		indirect gap, calculated

65G Greenaway, D. L., Nitsche, R.: J. Phys. Chem. Solids 26 (1965) 1445.
73B Brattas, L., Kjekshus, A.: Acta Chem. Scand. 27 (1973) 1290.
78B Bullett, D. W.: J. Phys. C 11 (1978) 4501.

35.3.14 1T-TaS₂

lattice parameters

Data from [71C, 71T, 72C, 73M, 74G, 74W, 75S, 75W1, 75W2, 76W, 77D, 77T, 77W, 77Y, 79I, 80J, 80S, 83H]

a	3.365 Å	(modified by formation of charge density waves)	S: C6, D _{3d} ³ – P $\bar{3}$ m1. First-order
c	5.853 Å		semiconductor-semiconductor
			transition at $T_d = 150...200$ K
			first-order semiconductor-metal
			transition at $T_d' = 325...350$ K
			$dT_d'/dp = -3.48$ K/kbar,
			$dT_d(\uparrow)/dp = -5.65$ K/kbar,
			$dT_d(\downarrow)/dp$ is non-linear, curve
			fitted to $182(1-(p/5.7))^{1/2}$,
			p in kbar. \uparrow and \downarrow correspond
			to heating and cooling, respectively

resistivity

ρ_a	$10^{-3} \Omega \text{ cm}$	n-type	CG: halogen transport (920/820)
		synthetic single	
		crystal	C: golden yellow

Hall coefficient, electron concentration

$R_H (B \parallel c)$	$-10^{-3} \text{ cm}^3/\text{C}$
n	10^{22} cm^{-3}

energy gap

E_g	2.3 eV	calculated
$E_{g,\text{th}}$	$2 \cdot 10^{-4} \text{ eV}$	$5 \text{ K} < T < 140 \text{ K}$
	$4 \cdot 10^{-2} \text{ eV}$	$250 \text{ K} < T < 340 \text{ K}$

- 71C Chu, C. W., Huang, S., Hambourger, P. D., Thompson, A. H.: Phys. Lett 36A (1971) 93.
71T Thompson, A. H., Gamble, F. R., Revelli, J. F.: Solid State Commun. 9 (1971) 981.
72C Cemic, L., Neuhaus, A.: High Temp.- High Pressures 4 (1972) 97.
73M Mori, N., Mitsui, T., Yomo, S.: Solid State Commun. 13 (1973) 1083.
74G Grant, A. J., Griffiths, T. M., Pitt, G. D., Yoffe, A. D.: J. Phys. C 7 (1974) L249.
74W Williams, P. M., Parry, G. S., Scruby, C. B.: Philos. Mag. 29 (1974) 695.
75S Scruby, C. B., Williams, P. M., Parry, G. S.: Philos. Mag. 31 (1975) 255.
75W1 Wertheim, G. K., Di Salvo, F. J., Chiang, S.: Phys. Lett. A54 (1975) 304.
75W2 Wilson, J. A., Di Salvo, F. J., Mahajan, S.: Adv. Phys. 24 (1975) 117.
76W Williams, P. M. in "Crystallography and Crystal Chemistry of Materials with Layered Structures", F. Levy (ed.) Dordrecht: Reidel, 1976, 51.
77D DiSalvo, F. J., Graebner, J. E.: Solid State Commun. 23 (1977) 825.
77T Tani, T., Osada, T., Tanaka, S.: Solid State Commun. 22 (1977) 269.
77W Woolley, A. M., Wexler, G.: J. Phys. C 10 (1977) 2601.
77Y Yamada, Y., Takatera, H.: Solid State Commun. 21 (1977) 41.
79I Inada, R., Onuki, Y., Tanuma, S.: Phys. Lett. 69A (1979) 453.
80J Jericho, M. H., Simpson, A. H., Frindt, R. F.: Phys. Rev. B22 (1980) 4907.
80S Sezermann, O., Simpson, A. M., Jericho, M. H.: Solid State Commun. 36 (1980) 737.
83H Haza, T., Abe, Y., Okwamoto, Y.: Phys. Rev. Lett. 51 (1983) 678.

35.3.15 TaS₃

Data from [63A, 64B, 77S, 78T, 79I]

lattice parameters

<i>a</i>	36.804 Å	$T < 210 \dots 218$ K	S: orthorhombic, $D_2^5 - C222_1$
<i>b</i>	15.173 Å		semiconductor-metal transition
<i>c</i>	3.340 Å		at 210...218 K due to Peierls instability (Ta – Ta dimers in chains for $T < T_{tr}$)
			$dT_{tr}/dp = -1.3$ K/kbar
			CG: from elements at 700 °C in vacuum and slow cooling

resistivity

ρ_c	$3 \cdot 10^{-4} \Omega \text{ cm}$	p-type, synthetic single crystal
----------	-------------------------------------	----------------------------------

energy gap

$E_{g,th}$	0.3 eV	$120 < T < 200$ K	$dE_{g,th}/dp = -8$ K/kbar
------------	--------	-------------------	----------------------------

- 63A Aslanov, L. A., Simanov, Yu. P., Novoselova, A. V., Ukrainski, Yu. M.: Russ. J. Inorg. Chem. 8 (1963) 1381.
- 64B Bjerkelund, E., Kjekshus, A.: Z. Anorg. Allg. Chem. 328 (1964) 235.
- 77S Sambongi, T., Tsutsumi, K., Shiozaki, Y., Yamamoto, M., Yamaya, K., Abe, Y.: Solid State Commun. 22 (1977) 729.
- 78T Tsutsumi, K., Sambongi, T., Kagoshima, S., Ishiguro, T.: J. Phys. Soc. Jpn. 44 (1978) 1735.
- 79I Inada, R., Onuki, Y., Tanuma, S.: Phys. Lett. 69A (1979) 453.

35.3.16 CrS

Data from [57J, 60K, 69P, 76V, 77J, 77M, 83H]

lattice parameters, density

<i>a</i>	3.826 Å	structure: monoclinic, C2/c (hexagonal, space group $D_{3h}^4 - C\bar{6}2c$ with $a = 2 \cdot 3^{1/2} a_0 = 12$ Å and $c = 2c_0 = 11.74$ Å. where a_0, c_0 are the lattice parameters of undistorted B8 cell, also used for low temperature, semiconducting phase [77L]).
<i>b</i>	5.913 Å	
<i>c</i>	6.089 Å	
β	101°36'	
<i>d</i>	4.85 g cm ⁻³	

resistivity

ρ	0.1...1 Ω cm	p-type, polycrystalline sample for CrS _x and $x \leq 1.12$	Semiconductor-metal transition at 550 K, $dT_{tr}/dp = -15$ K/kbar. Transition at 24 kbar (at RT) to metallic phase. Antiferromagnetic, $T_N = 450$ K, $p_A = 3.5 \mu_B/\text{Cr atom}$ at 80 K, moments directed along <i>c</i> axis.
--------	--------------	---	--

- 57J Jellinek, F.: Acta Crystallogr. 10 (1957) 620.
- 60K Kuz'min, R. N., Zhuravlev, N. N., Losievskaya, S. A.: Kristallografiya 4 (1960) 218; translation: Sov. Phys. Cryst. 4 (1960) 202.

69P	Popma, T. J. A., Van Bruggen, C. F.: J. Inorg. Nucl. Chem. 31 (1969) 73.
76V	Vaidya, S. N., Karunakaran, C., Joshi, D. K., Karkhanavala, M. D.: Proc. Nucl Phys. Solid State Phys. Symp. 19C (1976) 44.
77J	Joshi, D. K., Karunakaran, C., Vaidya, S. N., Karkhanavala, M. D.: Mater. Res. Bull. 12 (1977) 1111.
77M	Makovetskii, G. I., Ryzhkovskii, V. M., Shakhlevich, G. M.: Phys. Status. Solidi (a) 1977) K127.
83H	Haza, T., Abe, Y., Okwamoto, Y.: Phys. Rev. Lett. 51 (1983) 678.

35.3.17 Cr₂S₃

Data from [57J, 69S, 70V, 73B, 76B, 83H]

lattice parameters, density

<i>a</i>	5.939 Å	structure: trigonal, $C_{3i}^2 - R\bar{3}$, n- or p-type depending on preparation; ferrimagnetic, $T < T_C = 120$ K with three magnetic sub- lattices, Curie-Weiss para- magnetism, $T > 300$ K, $\Theta_p = -585(3)$ K; $C_A = 2.12(1)$ cm ³ K/g-atom
<i>c</i>	16.65 Å	
<i>d</i>	3.77 g cm ⁻³	

resistivity, Hall mobility, electron concentration

ρ	$2.6 \cdot 10^3 \Omega \text{ cm}$	n-type, poly- crystal
μ_H	$4 \text{ cm}^2/\text{V s}$	
<i>n</i>	$8 \cdot 10^{18} \text{ cm}^{-3}$	grown by halogen transport

energy gap

$E_{g,\text{th}}$	1.1 eV	$T \approx 275$ K
-------------------	--------	-------------------

resistivity

ρ	$7 \cdot 10^3 \Omega \text{ cm}$	p-type, single
--------	----------------------------------	----------------

energy gap

$E_{g,\text{th}}$	0.1 eV
-------------------	--------

57J	Jellinek, F.: Acta Crystallogr. 10 (1957) 620.
69S	Sleight, A. W., Bither, T. A.: Inorg. Chem. 8 (1969) 566.
70V	Van Bruggen, C. F., Vellinga, M. H., Haas, C.: J. Solid State Chem. 2 (1970) 303.
73B	Babot, D., Chevreton, M.: J. Solid State Chem. 8 (1973) 166.
76B	Babot, D., Peix, G., Chevreton, M.: J. Phys. (Paris) Colloq. 4 (1976) 111.
83H	Haza, T., Abe, Y., Okwamoto, Y.: Phys. Rev. Lett. 51 (1983) 678.

35.3.18 Cr_{2+x}Se₃ (x = 0.04)

Data from [73B, 73Y]

lattice parameters

<i>a</i>	6.28 Å	structure: trigonal, $P\bar{3}1c$ for Cr ₂ Se ₃ , antiferromagnetic with $T_N = 43$ K and $p_{\text{eff}} = 3.84 \mu_B$
<i>c</i>	11.64 Å	

resistivity

ρ	0.32 Ω cm	polycrystal
--------	------------------	-------------

energy gap

$E_{g,th}$	0.148 eV	$T > 310$ K
	0.05 eV	$T < 310$ K

73B Babot, D., Chevreton, M.: J. Solid State Chem. 8 (1973) 166.

73Y Yuzuri, M.: J. Phys. Soc. Jpn. 35 (1973) 1252.

35.3.19 Cr₃Se₄

Data from [71L, 73B, 73Y]

lattice parameters

a	6.299 Å	structure: monoclinic, $C_{2h}^3 - I2/m$, antiferromagnetic with $T_N = 82$ K and $p_{eff} = 4.49 \mu_B$
b	3.607 Å	
c	11.731 Å	
β	91°52'	

resistivity

ρ	0.2 Ω cm	polycrystal
--------	-----------------	-------------

energy gap

$E_{g,th}$	0.14 eV
------------	---------

71L Landolt-Börnstein (New Series), ed.: K. H. Hellwege, Vol. III/6, Springer Verlag: Berlin, Heidelberg, New York 1971.

73B Babot, D., Chevreton, M.: J. Solid State Chem. 8 (1973) 166.

73Y Yuzuri, M.: J. Phys. Soc. Jpn. 35 (1973) 1252.

35.3.20 Cr_{1-x}Te

($0 \leq x \leq 0.25$)

Data from [60H, 66S, 76G, 78L]

lattice parameters, resistivity, Seebeck coefficient, energy gap

a	3.93 Å	S: B8, $D_{6h}^4 - P6_3/mmc$, ferromagnetic, $T_C = 343$ K, $p_A = 2.39 \mu_B/\text{Cr atom at } 0 \text{ K}$. T_C depends on x . $dT_C/dp = -6 \text{ K/kbar}$, $p > 28 \text{ kbar}$ no ferromagnetism observed CG: Bridgman method at 1280°C	
c	6.15 Å		
ρ	$10^{-3} \Omega$ cm		n-type, poly-
S	$-24 \mu\text{V K}^{-1}$		crystalline
$E_{g,th}$	0.02 eV		sample

60H Hirone, T., Chiba, S.: J. Phys. Soc. Jpn. 15 (1960) 1991.

66S Suchet, J., Druille, R., Loners, J.: Inorg. Mater. (USSR) (English Transl.) 2 (1966) 679.

76G Grazhdankina, N. P., Bersenev, Yu. S.: High Temp.- High Pressures 8 (1976) 613.

78L Lambert-Andron, B., Urazhdankina, N. P., Vettier, C.: J. Phys. (Paris) Lett. 39 (1978) 43.

35.3.21 2H-MoS₂

Data from [60J, 69C, 69W, 72A, 76N, 77E, 78B, 78E]

lattice parameters, resistivity, electron concentration

a	3.16 Å		S: hexagonal, $D_{4h}^6 - P6_3/mmc$
c	12.29 Å		CG: from polycrystalline mass at 1015°C
			C: black
ρ_{\perp}	33 Ω cm	n-type,	$d\sigma_{\perp}/dp = 0.065 \Omega^{-1} \text{ cm}^{-1}/\text{kbar}$,
n	$6 \cdot 10^{15} \text{ cm}^{-3}$	synthetic	$p < 10 \text{ kbar}$,
		single	$d\sigma_{\perp}/dp = 0.03 \Omega^{-1} \text{ cm}^{-1}/\text{kbar}$,
		crystal	$12 \leq p \leq 30 \text{ kbar}$,
			$\sigma_{\perp}/\sigma_{\parallel} \approx 200$.
			($\rho_{\perp} = 0.27 \Omega \text{ cm}$ [70W])

energy gap

E_g	1.971 eV	$T = 77 \text{ K}$	optical gap,
			$dE_g/dp = -3.8 \text{ meV/kbar}$
	0.7 eV		($= -2.5 \text{ meV/kbar}$ for a natural crystal)
	1.4 eV		indirect gap, calculated
			direct gap, calculated
$E_{g,\text{th}}$	0.47 eV	$T < 300 \text{ K}$	
	1.27 eV	$T > 790 \text{ K}$	

- 60J Jellinek, F., Brauer, G., Müller, H.: Nature (London) 185 (1960) 376.
69C Connell, G. A. N., Wilson, J. A., Yoffe, A. D.: J. Phys. Chem. Solids 30 (1969) 287.
69W Wilson, J. A., Yoffe, A. D.: Adv. Phys. 18 (1969) 193.
72A AlHilli, A. A., Evans, B. L.: J. Cryst. Growth 15 (1972) 93.
76N Neville, R. A., Evans, B. L.: Phys. Status. Solidi (b) 73 (1976) 597.
77E El-Mahalawy, S. H., Evans, B. L.: Phys. Status. Solidi (b) 79 (1977) 713.
78B Bullett, D. W.: J. Phys. C 11 (1978) 4501.
78E El-Mahalawy, S. H., Evans, B. L.: Phys. Status Solidi (b) 86 (1978) 151.

35.3.22 3R-MoS₂

Data from [67F, 69C, 70W, 72A]

lattice parameters, resistivity, energy gap

a	3.17 Å		S: trigonal, $C_{3v}^5 - R3m$
c	18.38 Å		CG: halogen transport (947/890)
ρ_{\perp}	0.3 Ω cm	synthetic	$\sigma_{\perp}/\sigma_{\parallel} \approx 200$
E_g	1.9 eV	single	optical gap,
$E_{g,\text{th}}$	0.25 eV	crystal	$dE_g/dp = -2.5 \text{ meV/kbar}$ for a natural crystal

- 67F Fivaz, R., Mooser, E.: Phys. Rev. 163 (1967) 743.
69C Connell, G. A. N., Wilson, J. A., Yoffe, A. D.: J. Phys. Chem. Solids 30 (1969) 287.
70W Wieting, T. J.: J. Phys. Chem. Solids 31 (1970) 2148.
72A AlHilli, A. A., Evans, B. L.: J. Cryst. Growth 15 (1972) 93.

35.3.23 MoS₂

Data from [75G] (data for non-specified types)

resistivity, Hall mobility, electron concentration

ρ_{\perp}	18 Ω cm	n-type,
$\mu_{H\perp}$	57 cm ² /V s	natural
n	$6 \cdot 10^{15}$ cm ⁻³	crystal

energy gap

E_g	1.9 eV	optical gap
$E_{g,th}$	1.6 eV	

resistivity, Hall mobility, hole concentration

ρ_{\perp}	2.0 Ω cm	p-type,
$\mu_{H\perp}$	20 cm ² /V s	synthetic
p	$1.6 \cdot 10^{17}$ cm ⁻³	single crystal

65G Greenaway, D. L., Nitsche, R.: J. Phys. Chem. Solids 26 (1965) 1445.

35.3.24 2H-MoSe₂

Data from [62B, 69W, 71E, 72A, 72B, 75G, 77E]

lattice parameters

a	3.288 Å	S: hexagonal, D _{6h} ⁴ – P6 ₃ /mmc (3R-MoSe ₂ also exists with $a = 3.292$ Å, $c = 19.392$ Å) CG: from polycrystalline mass at 1000°C C: black
c	12.92 Å	

resistivity, Seebeck coefficient, electron concentration

ρ_{\perp}	$\approx 1 \dots 5$ Ω cm	n-type,	$\sigma_{\perp}/\sigma_{\parallel} \approx 200$
S_{\perp}	-900 μ V K ⁻¹	synthetic	
n	$0.35 \dots 1.6 \cdot 10^{17}$ cm ⁻³	single crystal	

energy gap

E_g	1.6 eV	optical gap,
	1.6 eV	$dE_g/dp = 1.2$ meV/kbar
$E_{g,th}$	0.28 eV	direct gap, calculated
	0.95 eV	$T < 300$ K
		$T > 760$ K

62B Brixner, L. H.: J. Inorg. Nucl. Chem. 24 (1962) 257.

69W Wilson, J. A., Yoffe, A. D.: Adv. Phys. 18 (1969) 193.

71E Evans, B. L., Hazelwood, R. A.: Phys. Status. Solidi (a) 4 (1971) 181.

72A AlHilli, A. A., Evans, B. L.: J. Cryst. Growth 15 (1972) 93.

72B Bromley, R. A., Murray, R. B., Yoffe, A. D.: J. Phys. CS (1972) 759.

75G Grant, A. J., Griffiths, T. M., Pitt, G. D., Yoffe, A. D.: J. Phys. C 8 (1975) L17.

77E El-Mahalawy, S. H., Evans, B. L.: Phys. Status. Solidi (b) 79 (1977) 713.

35.3.25 2H-MoTe_{2-x}

(0.01 ≤ x ≤ 0.1)

Data from [66B, 70V, 70W, 72A, 72B, 72D, 75G, 79C]

lattice parameters

<i>a</i>	3.519 Å	hexagonal	S: semiconductor-metal transition at T_{tr} , where $T_{tr} = 820^{\circ}\text{C}$ for Te-rich MoTe _{2-x} and $T_{tr} = 880^{\circ}\text{C}$ for Mo-rich MoTe _{2-x} . $T < T_{tr}$: hexagonal, $D_{6h}^4 - P6_3/mmc$ $T > T_{tr}$: monoclinic, $C_{2h}^2 - P2_1/m$ CG: halogen transport (900/700); high-temperature form halogen transport (1000/900) and water quenched
<i>c</i>	13.964 Å	modification	
<i>a</i>	6.33 Å	monoclinic	
<i>b</i>	3.469 Å	modification	
<i>c</i>	13.86 Å		
β	93°55'		

resistivity, Seebeck coefficient, Hall coefficient, electron concentration

ρ_{\perp}	0.5...8.5 Ω cm	n-type,
S_{\perp}	- 422 μV K ⁻¹	synthetic
$R_H (B \parallel c)$	- 24.17 cm ³ /C	single
<i>n</i>	2.6·10 ¹⁷ cm ⁻³	crystal

energy gap

E_g	1.1 eV	optical gap direct energy gap, calculated
	1.2 eV	
$E_{g,th}$	1.08 eV	

66B	Brown, B. E.: Acta Crystallogr. 20 (1966) 268.
70V	Van Bruggen, C. F., Vellinga, M. H., Haas, C.: J. Solid State Chem. 2 (1970) 303.
70W	Wieting, T. J.: J. Phys. Chem. Solids 31 (1970) 2148.
72A	AlHilli, A. A., Evans, B. L.: J. Cryst. Growth 15 (1972) 93.
72B	Bromley, R. A., Murray, R. B., Yoffe, A. D.: J. Phys. CS (1972) 759.
72D	Davey, B., Evans, H. L.: Phys. Status. Solidi (a) 13 (1972) 483.
75G	Grant, A. J., Griffiths, T. M., Pitt, G. D., Yoffe, A. D.: J. Phys. C 8 (1975) L17.
79C	Conan, A., Delaunay, D., Bonnet, A., Moustafa, A. G., Spiesser, M.: Phys. Status. Solidi (b) 94 (1979) 279.

35.3.26 3R-WS₂

Data from [64W, 70W, 72B]

lattice parameters

<i>a</i>	3.162 Å	S: trigonal, $C_{3v}^5 - R3m$ (hexagonal $P6_3/mmc$ also exists with $a = 3.155$ Å, $c = 12.35$ Å) CG: (i) Na ₂ CO ₃ flux at 900°C, (ii) halogen transport
<i>c</i>	18.50 Å	

resistivity

ρ_{\perp}	0.04 Ω cm	synthetic
	0.1 Ω cm	single crystal
		natural crystal

energy gap

E_g	2.1 eV	direct gap, calculated
	2.07 eV	optical gap
64W	Ware, R. M., Mc Neill, D. J.: Proc. IEE 111 (1964) 178.	
70W	Wieting, T. J.: J. Phys. Chem. Solids 31 (1970) 2148.	
72B	Bromley, R. A., Murray, R. B., Yoffe, A. D.: J. Phys. CS (1972) 759.	

35.3.27 2H-WSe₂

Data from [62B, 67F, 69W, 72A, 72B, 72D, 77E, 78E, 79A]

lattice parameters

a	3.282 Å	S: hexagonal, $D_{6h}^4 - P6_3/mmc$
c	12.937 Å	CG: (i) from polycrystalline mass, (ii) halogen transport (800/720) C: black

resistivity, Seebeck coefficient, hole concentration

ρ_{\perp}	0.167 Ω cm	p-type,	$\sigma_{\perp}/\sigma_{\parallel} \approx 200$ ($\rho_{\perp} = 1.3$ Ω cm [70W])
S_{\parallel}	990 μ V K ⁻¹	synthetic	
p	$2.35 \cdot 10^{17}$ cm ⁻³	single crystal	

energy gap

E_g	1.78 eV	optical gap
	1.73 eV	direct gap, calculated
$E_{g,th}$	0.17 eV	$T < 300$ K
	1.33 eV	$T > 890$ K

effective hole mass

m_p	0.01 m_0	optical effective hole mass
-------	------------	-----------------------------

Hall mobility, Hall coefficient

$\mu_{H\perp}$	100 cm ² /V s	n-type
$R_{H\perp}$	- 80 cm ³ /C	

electron concentration

n	$1.25 \cdot 10^{16}$ cm ⁻³
-----	---------------------------------------

62B	Brixner, L. H.: J. Inorg. Nucl. Chem. 24 (1962) 257.	
67F	Fivaz, R., Mooser, E.: Phys. Rev. 163 (1967) 743.	
69W	Wilson, J. A., Yoffe, A. D.: Adv. Phys. 18 (1969) 193.	
72A	AlHilli, A. A., Evans, B. L.: J. Cryst. Growth 15 (1972) 93.	
72B	Bromley, R. A., Murray, R. B., Yoffe, A. D.: J. Phys. CS (1972) 759.	
72D	Davey, B., Evans, H. L.: Phys. Status. Solidi (a) 13 (1972) 483.	
77E	El-Mahalawy, S. H., Evans, B. L.: Phys. Status. Solidi (b) 79 (1977) 713.	
78E	El-Mahalawy, S. H., Evans, B. L.: Phys. Status Solidi (b) 86 (1978) 151.	
79A	Anedda, A., Fortin, E., Raga, F.: Can. J. Phys. 57 (1979) 368.	

35.3.28 WTe₂

Data from [66B, 66K, 72A]

lattice parameters

a	6.282 Å	S: orthorhombic, $C_{2v}^7 - Pnm2_1$ CG: halogen transport (900/700)
b	3.496 Å	
c	14.07 Å	

resistivity, Seebeck coefficient, Hall coefficient

ρ_{\perp}	$0.75 \cdot 10^{-3} \Omega \text{ cm}$	n-type,	p-type $T \leq 60 \text{ K}$,
S_{\parallel}	$-30 \mu\text{V K}^{-1}$	synthetic	n-type $60 \text{ K} < T \leq 600 \text{ K}$
$R_{H\perp}$	$-5 \cdot 10^{-2} \text{ cm}^3/\text{C}$	single crystal	

ρ	$1.5 \cdot 10^{-3} \Omega \text{ cm}$	poly-	p-type $T \leq 60 \text{ K}$,
S	$-10 \mu\text{V K}^{-1}$	crystalline	n-type $60 \text{ K} < T \leq 400 \text{ K}$
R_H	$2 \cdot 10^{-2} \text{ cm}^3 \text{ C}^{-1}$	sample	p-type $400 \text{ K} < T \leq 600 \text{ K}$

66B	Brown, B. E.: Acta Crystallogr. 20 (1966) 268.		
66K	Kabashima, S.: J. Phys. Soc. Jpn. 21 (1966) 945.		
72A	AlHilli, A. A., Evans, B. L.: J. Cryst. Growth 15 (1972) 93.		

35.3.29 α -MnS

Data from [56C, 67H, 67S, 70M, 70R, 70W, 71L, 78H]

lattice parameters

a	5.223 Å	$T > T_N$	S: cubic B1, $O_h^5 - Fm3m$; $T < T_N$: trigonal distortion; anti-ferromagnetic, $T_N = 130 \text{ K}$, $p_{\text{eff}} = 5.6 \mu\text{B}$, $\Theta_p = -465 \text{ K}$. Ferromagnetic (111) sheets coupled antiparallel; spins in ferromagnetic (111) planes CG: (i) in silica gel between 4°C and 41°C, (ii) halogen transport (1050/550) C: green
a	5.198 Å	$T < T_N$	
β	90.099°		

resistivity, Seebeck coefficient

ρ	$10^3 \Omega \text{ cm}$	p-type,
S	$850 \mu\text{V K}^{-1}$	synthetic single crystal

Hall mobility

μ_H	$10 \text{ cm}^2/\text{V s}$	$T = 625 \text{ K}$
---------	------------------------------	---------------------

Hall coefficient

R_H	$10^2 \text{ cm}^3/\text{C}$
-------	------------------------------

energy gap

E_g	2.8 eV		optical gap
	3.2 eV		direct gap, calculated
$E_{g,th}$	0.62 eV	$T < 435$ K	
	3.0 eV	$T > 590$ K	
56C	Corliss, L. M., Elliott, N., Hastings, J. M.: Phys. Rev. 104 (1956) 924.		
67H	Huffman, D. R., Wild, R. L.: Phys. Rev. 156 (1967) 989.		
67S	Schwartz, A., Tauber, A., Shappirino, J. R.: Mater. Res. Bull. 2 (1967) 375.		
70M	Morosin, B.: Phys. Rev. B1 (1970) 236.		
70R	Rustamov, A. G., Kerimov, I. G., Valiev, L. M., Babaev, S. Kh.: Inorg. Mater. 6 (1970) 1176.		
70W	Wieting, T. J.: J. Phys. Chem. Solids 31 (1970) 2148.		
71L	Landolt-Börnstein (New Series), ed.: K. H. Hellwege, Vol. III/6, Springer Verlag: Berlin, Heidelberg, New York 1971.		
78H	Heikens, H. H., Van Bruggen, C. F., Haas, C.: J. Phys. Chem. Solids 39 (1978) 833.		

35.3.30 β -MnS

Data from [56C, 71L]

lattice parameters

a	5.606 Å	structure: cubic, B3, $T_d^2 - F\bar{4}3m$, antiferromagnetic, $T_N = 160$ K, $p_{eff} = 5.82 \mu_B$, $\Theta_p = -982$ K, fcc ordering of 3rd kind; spins along c axis of tetragonal magnetic cell
56C	Corliss, L. M., Elliott, N., Hastings, J. M.: Phys. Rev. 104 (1956) 924.	
71L	Landolt-Börnstein (New Series), ed.: K. H. Hellwege, Vol. III/6, Springer Verlag: Berlin, Heidelberg, New York 1971.	

35.3.31 γ -MnS

Data from [56C, 67S, 71L]

lattice parameters

a	3.99 Å	S: hexagonal, B4, $C_{6v}^4 - P6_3mc$, antiferromagnetic, $T_N = 100$ K, $p_{\text{eff}} = 6.1 \mu_B$, $\Theta_p = -932$ K. Pairs of ferromagnetic (011) sheets of orthorhombic cell coupled antiparallel ($a_{\text{orth}} = 3^{1/2}a_{\text{hex}}$, $b_{\text{orth}} = 2a_{\text{hex}}$, $c_{\text{orth}} = c_{\text{hex}}$), spins along ortho-[011] CG: in silica gel between 4°C and 41°C C: pink	
c	6.47 Å		
56C	Corliss, L. M., Elliott, N., Hastings, J. M.: Phys. Rev. 104 (1956) 924.		
67S	Schwartz, A., Tauber, A., Shappirino, J. R.: Mater. Res. Bull. 2 (1967) 375.		
71L	Landolt-Börnstein (New Series), ed.: K. H. Hellwege, Vol. III/6, Springer Verlag: Berlin, Heidelberg, New York 1971.		

35.3.32 α -MnSe

Data from [68C, 70R, 71D, 71L, 72C, 78I]

lattice parameter, resistivity, Seebeck coefficient

a	5.464 Å		S: cubic, B1, $O_h^5 - Fm\bar{3}m$;
ρ	$10^4 \Omega \text{ cm}$	p-type,	B8 above $p = 90 \text{ kbar}$, anti-
S	$60 \mu\text{V K}^{-1}$	synthetic	ferromagnetic, $T_N(\uparrow) = 248 \text{ K}$,
		single	$T_N(\downarrow) = 197 \text{ K}$, $p_{\text{eff}} = 5.88 \mu_B$,
		crystal	$\Theta_p = -373 \text{ K}$. Ferromagnetic
			(111) sheets coupled anti-
			parallel; spins in (111) planes.
			β -form ($a = 5.82 \text{ Å}$, space
			group $T_d^2 - F\bar{4}3m$) and γ -form
			($a = 4.12 \text{ Å}$, $c = 6.72 \text{ Å}$,
			space group $C_{6v}^4 - P6_3mc$)
			are unstable
			CG: chemical transport
			(1000/600)

energy gap

E_g	2.5 eV		optical gap
$E_{g,\text{th}}$	0.48 eV	$283 \leq T \leq 197 \text{ K}$	
		(cooling)	

- 68C Carpay, F. M. A.: Philips Res. Rep., Suppl. 10 (1968)1.
70R Rustamov, A. G., Kerimov, I. G., Valiev, L. M., Babaev, S. Kh.: Inorg. Mater. 6 (1970) 1176.
71D Decker, D. L., Wild, R. L.: Phys. Rev. B4 (1971) 3425.
71L Landolt-Börnstein (New Series), ed.: K. H. Hellwege, Vol. III/6, Springer Verlag: Berlin, Heidelberg, New York 1971.
72C Cemic, L., Neuhaus, A.: High Temp.- High Pressures 4 (1972) 97.
78I Ito, T., Ito, K., Oka, M.: Jpn. J. Appl. Phys. 17 (1978) 371.

35.3.33 MnTe

Data from [54P, 56U, 61B, 61J, 64W1, 64W2, 72M, 77A]

lattice parameters

a	4.144 Å	B8 modifi-	S: B8, $D_{6h}^4 - P6_3/mmc$, above
c	6.703 Å	cation	1040°C B1 mod. ($O_h^5 - Fm\bar{3}m$),
			antiferromagnetic, $T_N = 310 \text{ K}$,
			$\Theta_p = -584 \text{ K}$, $p_{\text{eff}} = 5.91 \mu_B$
a	6.03 Å	B1 modifi-	CG: Bridgman-Stockbarger from
		cation	Te-rich melt

resistivity

ρ	$10^{-3} \Omega \text{ cm}$	$T = 200 \text{ K}$,	electron-spin scattering
		p-type,	$\tau_{\text{em}}(T_N) = 10^{-5} \text{ s}$; relaxation of
		poly-	magnon system $\tau_m(T_N) = 4 \cdot 10^{-12} \text{ s}$;
		crystalline	large magnon drag for $T > 200 \text{ K}$;
		sample	$T_N = 310 \text{ K}$

Seebeck coefficient

S $50 \mu\text{V K}^{-1}$ $T = 200 \text{ K}$

hole concentration

p $5 \cdot 10^{19} \text{ cm}^{-3}$ $T < T_N$

carrier mobility

μ_H $50 \text{ cm}^2/\text{V s}$ mobility excluding magnetic contributions ($m_p = 0.5 m_0$)

μ_{dr} $6 \text{ cm}^2/\text{V s}$

μ_{opt} $115 \text{ cm}^2/\text{V s}$ optical mobility

energy gap

E_g 1.3 eV optical gap

54P Palmer, W.: J. Appl. Phys. 25 (1954) 12 S.
56U Uchida, E., Kondoh, H., Fukuoka, N.: J. Phys. Soc. Jpn. 11 (1956) 27.
61B Banewicz, J. J., Heidelberg, R. F., Luxem, A. H.: J. Phys. Chem. 65 (1961) 615.
61J Johnston, W. D., Sestrich, D. E.: J. Inorg. Nucl. Chem. 19 (1961) 229
64W1 Wasscher, J. D., Seuter, A. M. J. H., Haas, C.: Proc. Int. Conf. Phys. Semiconductors (1964) 1269.
64W2 Wasscher, J. D., Haas, C.: Phys. Lett. 8 (1964) 302.
72M Mateika, D.: J. Cryst. Growth 13/14 (1972) 698.
77A Allen, J. W., Lucovsky, G., Mikkelsen Jr., J. C.: Solid State Commun. 24 (1977) 367.

35.3.34 MnTe₂

Data from [65J, 68L, 71L, 74A, 77O]

lattice parameters, resistivity, Seebeck coefficient, Hall coefficient

a 6.943 \AA structure: pyrite, C2, $T_h^6 - \text{Pa}3$,
antiferromagnetic, $T_N = 87.2 \text{ K}$,
 $p_{\text{eff}} = 5.84 \mu_B$, $\Theta_p = -472 \text{ K}$

ρ $0.1 \Omega \text{ cm}$ p-type, poly-
 S $300 \mu\text{V K}^{-1}$ crystalline
 R_H $40 \text{ cm}^3/\text{C}$ sample

65J Johnston, W. D., Miller, R. C., Damon, D. H.: J. Less-Common Met. 8 (1965) 272.
68L Lin, M. S., Hacker Jr., H.: Solid State Commun. 6 (1968) 687.
71L Landolt-Börnstein (New Series), ed.: K. H. Hellwege, Vol. III/6, Springer Verlag: Berlin, Heidelberg, New York 1971.
74A Avdeev, B. V., Krashenin, Yu. P.: Sov. Phys. Solid State 15 (1974) 2028.
77O Okada, O., Miyadai, T.: J. Phys. Soc. Jpn. 43 (1977) L343.

35.3.35 TcS₂

Data from [71W]

lattice parameters

<i>a</i>	6.415 Å	S: triclinic, primitive (unspecified) CG: halogen transport (1150/1080)
<i>b</i>	6.375 Å	
<i>c</i>	6.659 Å	
<i>α</i>	103.61°	
<i>β</i>	62.97°	
<i>γ</i>	118.96°	

density

<i>d</i>	5.066 g cm ⁻³	calculated
----------	--------------------------	------------

energy gap

<i>E_g</i>	1.0 eV	synthetic single crystal	optical gap
----------------------	--------	-----------------------------	-------------

71W Wildervanck, J. C., Jellinek, F.: J. Less-Common Met 24 (1971) 73.

35.3.36 TcSe₂

Data from [71W]

energy gap

<i>E_g</i>	0.88 eV	synthetic single crystal	S: triclinic CG: halogen transport (1080/1000) optical gap
----------------------	---------	-----------------------------	--

71W Wildervanck, J. C., Jellinek, F.: J. Less-Common Met 24 (1971) 73.

35.3.37 ReS₂

Data from [71W, 83H]

lattice parameters

<i>a</i>	6.455 Å	S; triclinic, C ₁ ¹ – P $\bar{1}$. CG: halogen transport (1150/1080)
<i>b</i>	6.362 Å	
<i>c</i>	6.401 Å	
<i>α</i>	105.04°	
<i>β</i>	91.6°	
<i>γ</i>	118.97°	

density

<i>d</i>	7.506 g cm ⁻³ 7.613 g cm ⁻³	experimental calculated
----------	--	----------------------------

resistivity

<i>ρ_⊥</i>	10 ³ Ω cm	synthetic single crystal
----------------------	----------------------	-----------------------------

energy gap

E_g	1.33 eV		optical gap
$E_{g,th}$	0.4 eV	$T = 160...570$ K	
	1.0 eV	$T = 570...920$ K	

71W Wildervanck, J. C., Jellinek, F.: J. Less-Common Met 24 (1971) 73.

83H Haza, T., Abe, Y., Okwamoto, Y.: Phys. Rev. Lett. 51 (1983) 678.

35.3.38 ReSe₂

Data from [65A, 71W]

lattice parameters

a	6.727 Å	S: triclinic, $C_1^1 - P\bar{1}$
b	6.606 Å	CG: halogen transport (1080/1000)
c	6.72 Å	
α	118.93°	
β	91.82°	
γ	104.93°	

density

d	9.219 g cm ⁻³	calculated
	9.237 g cm ⁻³	experimental

energy gap

E_g	1.15 eV	synthetic single crystal	optical gap
-------	---------	-----------------------------	-------------

65A Alcock, N. W., Kjekshus, A.: Acta Chem. Scand. 19 (1965) 79.

71W Wildervanck, J. C., Jellinek, F.: J. Less-Common Met 24 (1971) 73.

35.3.39 Fe_{1-x}S

(0 < x < 0.055)

Data from [56K1, 56K2, 57H, 58M3, 60A, 61F, 61M, 64B, 64K, 65B, 68M, 70D, 71N, 73T, 74A, 76C, 76H, 76M, 78W]

lattice parameters

a	5.964 Å	$x \approx 0$,	S: hexagonal, $D_{3h}^4 - P\bar{6}2c$,
c	11.744 Å	$T = 300$ K < T_α	$T < T_\alpha = 413$ K ($x \approx 0$)
			orthorhombic, B31,
			$D_{2h}^{16} - Pmcn$, $T_\alpha < T < T_s$
			hexagonal. B8, $D_{6h}^4 - P6_3mmc$,
			$T > T_s$
			CG: Bridgman method
			C: golden yellow

resistivity, Seebeck coefficient

ρ_{\perp}	$10^{-1} \Omega \text{ cm}$, $x = 0.006$	p-type, antiferromagnetic, $T_N = 600 \text{ K}$,
S_{\perp}	$15 \text{ cm}^2/\text{V s}$, $x = 0.025$	synthetic $p_{\text{eff}} = 5.5 \mu_B$, $\Theta_p = -1160 \text{ K}$.
S_{\parallel}	$50 \mu\text{V K}^{-1}$, $x = 0.025$	single Spin-flip transition at $T_s = 420 \text{ K}$.
	$260 \mu\text{V K}^{-1}$, $x = 0.006$	crystal $dT_N/dp = 3.2 \text{ K/kbar}$

Hall coefficient, carrier mobility, hole concentration

R_H	$0.7 \cdot 10^{-4} \text{ cm}^3/\text{C}$	$R_{H\parallel} = R_{H\perp}$
p	$8.5 \cdot 10^{22} \text{ cm}^{-3}$	
$\mu_{H\parallel}$	$2.8 \cdot 10^{-4} \text{ cm}^2/\text{V s}$	
	$0.21 \text{ cm}^2/\text{V s}$	$T = 150^\circ\text{C}$
$\mu_{H\perp}$	$0.16 \text{ cm}^2/\text{V s}$	
$\mu_{p\perp}$	$0.16 \text{ cm}^2/\text{V s}$	from Seebeck and resistivity data

56K1 Kamigaichi, T., Hihara, T., Tazaki, H., Hirahara, E.: J. Phys. Soc. Jpn. 11 (1956) 606.
56K2 Kamigaichi, T., Hihara, T., Tazaki, H., Hirahara, E.: J. Phys. Soc. Jpn. 11 (1956) 1123.
57H Hihara, T., Murakami, M., Hirahara, E.: J. Phys. Soc. Jpn. 12 (1957) 743.
58M Murakami, M., Hirahara, E.: J. Phys. Soc. Jpn. 13 (1958) 1407.
60A Andresen, A. F.: Acta Chem. Scand. 14 (1960) 919.
61F Fujime, S., Murakami, M., Hirahara, E.: J. Phys. Soc. Jpn. 16 (1961) 183.
61M Murakami, M.: J. Phys. Soc. Jpn. 16 (1961) 187.
64B1 Bertaut, E. F.: Bull. Soc. Sci. Bretagne 39 (1964) 67.
64K Kullerud, G.: Fortschr. Mineral. 41 (1964) 235.
65B Bertaut, E. F., Burlet, P., Chappert, J.: Solid State Commun. 3 (1965) 335.
68M Masayuki, U.: Z. Anorg. Allg. Chem. 361 (1968) 94.
70D DeMedicis, R.: Rev. Chim. Miner. 7 (1970) 723.
71N Nakazawa, H., Morimoto, N.: Mater. Res. Bull. 6 (1971) 345.
73T Takahashi, T.: Solid State Commun. 13 (1973) 1335.
74A Anzai, S., Ozawa, K.: Phys. Status. Solidi (a) 24 (1974) K31.
76C Coey, J. M. D., Roux-Buisson, H., Brusetti, R.: J. Phys. (Paris) Colloq. 4 (1976) 1.
76H Horwood, J. L., Townsend, M. G., Webster, A. H.: J. Solid State Chem. 17 (1976) 35.
76M Moldenhauer, W., Brückner, W.: Phys. Status. Solidi (a) 34 (1976) 565.
78W Wintenberger, M., Buevoz, J. L.: Solid State Commun. 27 (1978) 511.

35.3.40 FeS₂ (pyrite)

Data from [54M, 68B1, 68B2, 76S, 79S, 83H]

lattice parameters

a	5.418 \AA	S: pyrite, C2, $T_h^6 - \text{Pa}3$
-----	---------------------	-------------------------------------

density

d	5.0 g cm^{-3}	CG: chemical transport (715/655)
-----	-------------------------	----------------------------------

resistivity, Seebeck coefficient, Hall mobility, Hall coefficient, energy gap

ρ	$1.74 \Omega \text{ cm}$	n-type
S	$-500 \mu\text{V K}^{-1}$	synthetic single
μ_H	$230 \text{ cm}^2/\text{V s}$	crystal
R_H	$-400 \text{ cm}^3/\text{C}$	
$E_{g,\text{th}}$	0.02 eV	$T < 60 \text{ K}$
	0.4 eV	$T = 298 \text{ K}$
	0.92 eV	$T = 500 \text{ K}$

resistivity, Hall mobility, Hall coefficient, electron concentration, energy gap

ρ	0.06 Ω cm	n-type
μ_H	100 cm ² /V s	natural
R_H	– 6.5 cm ³ /C	crystal
n	1.1·10 ¹⁸ cm ^{–3}	
E_g	0.95 eV	optical gap

resistivity, Hall mobility, Hall coefficient, hole concentration, energy gap

ρ	2.2 Ω cm	p-type
μ_H	1.3 cm ² /V s	natural
R_H	2.8 cm ³ /C	crystal
p	2.6·10 ¹⁸ cm ^{–3}	
$E_g(T)$	$E_g(0) + aT + bT^2$	$T < 425$ K
		with $E_g(0) = 0.835$ eV, $a = 4 \cdot 10^{-5}$ eV/K $b = -7.4 \cdot 10^{-7}$ eV/K ²

54M Marinace, J. C.: Phys. Rev. 96 (1954) 593.

68B1 Bertaut, E. F., Cohen, J., Lambert-Andron, H., Mollard, P.: J. Phys. (Paris) 29 (1968) 813.

68B2 Bither, T. A., Bouchard, R. J., Cloud, W. H., Donohue, P. C., Siemons, W. J.: Inorg. Chem. 7 (1968) 2208.

76S Schlegel, A., Wachter, P.: J. Phys. C 9 (1976) 3363.

79S Seehra, M. S., Seehra, S. S.: Phys. Rev. B19 (1979) 6620.

83H Handbook of Chemistry and Physics, 64th ed. (ed.: R. C. Weast), CRC Press. Inc. 1983.

35.3.41 Fe_{1-x}Se

Data from [56H, 66S, 71L, 73A1, 73A2]

lattice parameters

a	3.548 Å	$x = 0$	structure: hexagonal, B8, D _{6h} ⁴ – P6 ₃ /mmc.
c	5.733 Å		Metal-semiconductor transition at 350 K. Ferrimagnetic, $T_C = 445$ K

resistivity, Seebeck coefficient

ρ	10 ³ Ω cm	p-type, poly-
S	10 μ V K ^{–1}	crystalline sample

energy gap

$E_{g,th}$	0.14 eV	$T > 350$ K
------------	---------	-------------

56H Hirone, T., Chiba, S.: J. Phys. Soc. Jpn. 11 (1956) 666.

66S Serre, J., Druille, R.: Compt. Rend. Ser. B 262 (1966) 639.

71L Landolt-Börnstein (New Series), ed.: K. H. Hellwege, Vol. III/6, Springer Verlag: Berlin, Heidelberg, New York 1971.

73A1 Abdullaev, G. B., Akhmedov, N. R., Yalilov, N. Z., Abdinov, D. Sh.: Phys. Status Solidi (a) 20 (1973) K29.

73A2 Akhmedov, N. R., Dzhalilov, N. Z., Abdinov, D. Sh.: Inorg. Mater. 9 (1973) 1271.

35.3.42 FeSe_{2-x}

(0 ≤ x ≤ 0.05)

Data from [68B, 71L]

lattice parameters

a 5.786 Å S: pyrite, C2, T_h⁶ – Pa3

resistivity, Seebeck coefficient, energy gap

ρ	$2 \cdot 10^{-2} \Omega \text{ cm}$	n-type	CG: under 65 kbar pressure at
<i>S</i>	$-28 \mu\text{V K}^{-1}$	synthetic	1200°C
$E_{\text{g,th}}$	0.2 eV	single crystal	C: silvery

68B Bertaut, E. F., Cohen, J., Lambert-Andron, H., Mollard, P.: J. Phys. (Paris) 29 (1968) 813.

71L Landolt-Börnstein (New Series), ed.: K. H. Hellwege, Vol. III/6, Springer Verlag: Berlin, Heidelberg, New York 1971.

35.3.43 FeSe₂

Data from [58F, 61D, 71L]

lattice parameters

a 4.789 Å structure: marcasite, C18, D_{2h}¹² – Pnnm
b 5.768 Å
3.575 Å

resistivity, Seebeck coefficient, energy gap

ρ	1.0 Ω cm	p-type, poly-crystalline sample	n-type for $T > 300 \text{ K}$
<i>S</i>	62 μV K ⁻¹		
$E_{\text{g,th}}$	0.3(1) eV		

58F Fischer, G.: Can. J. Phys. 36 (1958) 1435.

61D Dudkin, L. D., Vaidanich, V. I.: Sov. Phys. Solid State 2 (1961) 1384.

71L Landolt-Börnstein (New Series), ed.: K. H. Hellwege, Vol. III/6, Springer Verlag: Berlin, Heidelberg, New York 1971.

35.3.44 FeTe₂ (marcasite)

Data from [61D, 70B1, 70B2, 71L]

lattice parameters

a 5.265 Å S: marcasite, C18, D_{2h}¹²-Pnnm
b 6.268 Å CG: halogen transport
c 3.874 Å

resistivity, Seebeck coefficient

ρ	$1.5 \cdot 10^{-2} \Omega \text{ cm}$	p-type, poly-crystalline sample
<i>S</i>	64 μV K ⁻¹	

energy gap

$E_{g,th}$ 0.92 eV $T > 600$ K

61D Dudkin, L. D., Vaidanich, V. I.: Sov. Phys. Solid State 2 (1961) 1384.

70B1 Brostigen, G., Kjekshus, A.: Acta Chem. Scand. 24 (1970) 1925.

70B2 Brostigen, G., Kjekshus, A.: Acta Chem. Scand. 24 (1970) 2993.

71L Landolt-Börnstein (New Series), ed.: K. H. Hellwege, Vol. III/6, Springer Verlag: Berlin, Heidelberg, New York 1971.

35.3.45 RuS₂

Data from [63H, 71L]

lattice parameters

a 5.609 Å structure: pyrite, C2, $T_h^6 - Pa3$

energy gap

E_g 1.8 eV optical gap
diamagnetic

63H Hulliger, F.: Nature (London) 200 (1963) 1064.

71L Landolt-Börnstein (New Series), ed.: K. H. Hellwege, Vol. III/6, Springer Verlag: Berlin, Heidelberg, New York 1971.

35.3.46 RuSe₂

Data from [63H3, 71L]

lattice parameters

a 5.934 Å structure: pyrite, C2, $T_h^6 - Pa3$

Seebeck coefficient, energy gap

S $-120 \mu V K^{-1}$ n-type, poly- diamagnetic
 E_g 1.0 eV crystalline sample optical gap
 $E_{g,th}$ > 0.6 eV

63H Hulliger, F.: Nature (London) 200 (1963) 1064.

71L Landolt-Börnstein (New Series), ed.: K. H. Hellwege, Vol. III/6, Springer Verlag: Berlin, Heidelberg, New York 1971.

35.3.47 RuTe₂

Data from [73H3, 71L]

lattice parameters

a 6.39 Å structure: pyrite, C2, $T_h^6 - Pa3$
 a 5.271 Å $T = 77$ K marcasite, C18, $D_{2h}^{12} - Pnnm$,
 b 6.387 Å
 c 4.038 Å

Seebeck coefficient, energy gap

S	$-200 \mu\text{V K}^{-1}$	n-type, poly-	diamagnetic
$E_{\text{g,th}}$	0.25 eV	crystalline	
		sample	

63H Hulliger, F.: Nature (London) 200 (1963) 1064.

71L Landolt-Börnstein (New Series), ed.: K. H. Hellwege, Vol. III/6, Springer Verlag: Berlin, Heidelberg, New York 1971.

35.3.48 OsS₂

Data from [63H, 71L, 83H]

lattice parameter

a	5.619 Å	structure: pyrite, C2, T _h ⁶ – Pa3
-----	---------	--

density

d	9.47 g cm ⁻³	diamagnetic
-----	-------------------------	-------------

energy gap

E_{g}	2.0 eV	polycrystalline	optical gap
		sample	

63H Hulliger, F.: Nature (London) 200 (1963) 1064.

71L Landolt-Börnstein (New Series), ed.: K. H. Hellwege, Vol. III/6, Springer Verlag: Berlin, Heidelberg, New York 1971.

83H Handbook of Chemistry and Physics, 64th ed. (ed.: R. C. Weast), CRC Press. Inc. 1983.

35.3.49 OsTe₂

Data from [63H1, 71L]

lattice parameters

a	6.397 Å		structure: pyrite, C2, T _h ⁶ – Pa3
a	5.2804 Å	$T = 77 \text{ K}$	marcasite, C18, D _{2h} ¹² – Pnnm,
b	6.4018 Å		
c	4.0481 Å		

Seebeck coefficient, energy gap

S	$-100 \mu\text{V K}^{-1}$	n-type, poly-	diamagnetic
$E_{\text{g,th}}$	> 0.2 eV	crystalline sample	

71L Landolt-Börnstein (New Series), ed.: K. H. Hellwege, Vol. III/6, Springer Verlag: Berlin, Heidelberg, New York 1971.

83H Handbook of Chemistry and Physics, 64th ed. (ed.: R. C. Weast), CRC Press. Inc. 1983.

35.3.50 Rh_{2/3}S₂

Data from [64H, 71L]

lattice parameters

a 5.58 Å structure: defect pyrite, C2, T_h⁶ – Pa3

Seebeck coefficient, energy gap

S – 400 μV K^{–1} n-type, poly-
 E_g > 1.5 eV crystalline sample optical gap

64H Hulliger, F.: Nature (London) 204 (1964) 644.

71L Landolt-Börnstein (New Series), ed.: K. H. Hellwege, Vol. III/6, Springer Verlag: Berlin, Heidelberg, New York 1971.

35.3.51 Rh₂S₃

Data from [64H, 67P, 83H]

lattice parameters

a 8.462 Å structure: orthorhombic, D_{2h}¹⁴ – Pbcn
 b 5.985 Å
 c 6.138 Å

density

d 6.40 g cm^{–3}

Seebeck coefficient, energy gap

S – 300 μV K^{–1} n-type, poly-
 $E_{g,th}$ 0.8 eV crystalline sample

64H Hulliger, F.: Nature (London) 204 (1964) 644.

69P Popma, T. J. A., Van Bruggen, C. F.: J. Inorg. Nucl. Chem. 31 (1969) 73.

83H Handbook of Chemistry and Physics, 64th ed. (ed.: R. C. Weast), CRC Press. Inc. 1983.

35.3.52 RhS_{≈3}

Data from [64H]

lattice parameters

a 5.58 Å structure: C2 (trigonal distortion)
 α > 90°

Seebeck coefficient, energy gap

S – 400 μV K^{–1} n-type, poly- diamagnetic
 E_g > 1.5 eV crystalline sample optical gap

64H Hulliger, F.: Nature (London) 204 (1964) 644.

35.3.53 Rh₂Se₂(Se₂)

Data from [64H]

lattice parameters

<i>a</i>	20.91 Å	structure: IrSe ₂ structure, D _{2h} ¹⁶ – Pnam (C2 at high <i>T</i> , metallic) diamagnetic
<i>b</i>	5.95 Å	
<i>c</i>	3.709 Å	

Seebeck coefficient, energy gap

<i>S</i>	– 80 μV K ^{–1}	n-type, poly-crystalline sample	optical gap
<i>E_g</i>	0.6 eV		

64H Hulliger, F.: Nature (London) 204 (1964) 644.

35.3.54 RhSe_{≈3}

Data from [37B, 64H]

lattice parameters

<i>a</i>	5.962 Å	structure: C2 (trigonal distortion)
<i>α</i>	90°44'	

Seebeck coefficient, energy gap

<i>S</i>	– 30 μV K ^{–1}	n-type, poly-crystalline sample	optical gap
<i>E_g</i>	0.7 eV		

37B Biltz, W.: Z. Anorg. Allg. Chem. 233 (1937) 282.

64H Hulliger, F.: Nature (London) 204 (1964) 644.

35.3.55 Ir₂S₂(S₂)

Data from [64H, 83H]

lattice parameters

<i>a</i>	19.78 Å	structure: D _{2h} ¹⁶ -Pnam diamagnetic
<i>b</i>	5.624 Å	
<i>c</i>	3.565 Å	

density

<i>d</i>	8.43 g cm ^{–3}
----------	-------------------------

Seebeck coefficient, energy gap

<i>S</i>	250 μV K ^{–1}	p-type, poly-crystalline sample	optical gap
<i>E_g</i>	0.9 eV		

64H Hulliger, F.: Nature (London) 204 (1964) 644.

83H Handbook of Chemistry and Physics, 64th ed. (ed.: R. C. Weast), CRC Press. Inc. 1983.

35.3.56 IrS_{≈3}

Data from [37B1, 37B2, 64H]

lattice parameters

a	5.5 Å	structure: C2 (trigonal distortion)
α	> 90°	

energy gap

E_g	2.0 eV	polycrystal	optical gap
-------	--------	-------------	-------------

37B1 Biltz, W.: Z. Anorg. Allg. Chem. 233 (1937) 282.

37B2 Biltz, W., Laar, J., Ehrlich, P., Meisel, K.: Z. Anorg. Allg. Chem. 233 (1937) 257.

64H Hulliger, F.: Nature (London) 204 (1964) 644.

35.3.57 Ir₂Se₂(Se₂)

Data from [58B, 64H]

lattice parameters

a	20.94 Å	structure: orthorhombic, D _{2h} ¹⁶ – Pnam
b	5.93 Å	
c	3.74 Å	diamagnetic

Seebeck coefficient, energy gap

S	300 μV K ⁻¹	p-type, polycrystalline sample	optical gap
E_g	1.0 eV		

58B Barricelli, L. B.: Acta Crystallogr. 11 (1958) 75.

64H Hulliger, F.: Nature (London) 204 (1964) 644.

35.3.58 Ir_{2/3}Se₂

Data from [37B, 64H]

lattice parameters

a	5.96 Å	structure: C2 (trigonal distortion)
α	> 90°	

Seebeck coefficient, energy gap

S	– 150 μV K ⁻¹	n-type, polycrystalline sample
$E_{g,th}$	≥ 0.45 eV	

37B Biltz, W.: Z. Anorg. Allg. Chem. 233 (1937) 282.

64H Hulliger, F.: Nature (London) 204 (1964) 644.

35.3.59 Ni_{1-x}S

(0 ≤ x ≤ 0.06)

Data from [59L, 62K, 63S, 64K, 65H, 67S, 68S1, 68S2, 70O1, 70O2, 71H, 71T, 72K, 73K, 74B, 74C, 74M, 76B, 76C]

lattice parameters

a, c	$x = 0$, quenched from $T > 620$ K;	S: B8, $D_{6h}^4 - P6_3/mmc$ CG: halogen transport (720/650) slowly cooled to 550°C and quenched C: golden yellow
--------	--	---

resistivity, Seebeck coefficient

	$10^{-4} \Omega \text{ cm}$	n-type synthetic single crystal
S_{\perp}	$-3 \mu\text{V K}^{-1}$	

Hall mobility, Hall coefficient, carrier concentrations

$\mu_{H\perp}$	$1...5 \text{ cm}^2/\text{V s}$	Semiconductor-metal transition at
$R_{H\perp}$	$-10^{-4} \text{ cm}^3/\text{C}$	$T_{tr} = 265$ K, accompanied by
n	$4 \cdot 10^{22} \text{ cm}^{-3}$	antiferromagnetic-paramagnetic
p	$2 \cdot 10^{20} \text{ cm}^{-3}$	transition. T_{tr} depends on x and
$\mu_{H\perp}$	$1...5 \text{ cm}^2/\text{V s}$	p , it disappears for $x > 0.035$
		and $p > 20$ kbar.
		Latent heat = 282 cal/mol

- 59L Laffitte, M.: Bull. Soc. Chim. Fr. 1959, 1211.
62K Kullerud, G., Yund, R. A.: J. Petrol. 3 (1962) 126.
63S Sparks, J. T., Komoto, T.: J. Appl. Phys. 34 (1963) 1191.
64K Kullerud, G.: Fortschr. Mineral. 41 (1964) 235.
65H Hulliger, F.: J. Phys. Chem. Solids 26 (1965) 639.
67S Schwartz, A., Tauber, A., Shappirino, J. R.: Mater. Res. Bull. 2 (1967) 375.
68S1 Sparks, J. T., Komoto, T.: Rev. Mod. Phys. 40 (1968) 752.
68S2 Sparks, J. T., Komoto, T.: J. Appl. Phys. 39 (1968) 715.
70O1 Ohtani, T., Kosuge, K., Kachi, S.: J. Phys. Soc. Jpn. 28 (1970) 1588.
70O2 Ohtani, T., Kosuge, K., Kachi, S.: J. Phys. Soc. Jpn. 29 (1970) 521.
71H Horwood, J. L., Ripley, L. G., Townsend, M. G., Trembley, R. J.: J. Appl. Phys. 42 (1971) 1476.
71T Thompson, A. H., Gamble, F. R., Revelli, J. F.: Solid State Commun. 9 (1971) 981.
72K Koehler Jr., R. F., Feigelson, R. S., Swarts, H. W., White, R. L.: J. Appl. Phys. 43 (1972) 3127.
73K Koehler Jr., R. F., White, R. L.: J. Appl. Phys. 44 (1973) 1682.
74B Barker Jr., A. S., Rемаika, J. P.: Phys. Rev. B10 (1974) 987.
74C Coey, J. M. D., Brusetti, R., Kallel, A., Schweizer, J., Fuess, H.: Phys. Rev. Lett. 32 (1974) 1257.
74M Mattheiss, L. F.: Phys. Rev. B10 (1974) 995.
76B Babot, D., Peix, G., Chevreton, M.: J. Phys. (Paris) Colloq. 4 (1976) 111.
76C Coey, J. M. D., Roux-Buisson, H., Brusetti, R.: J. Phys. (Paris) Colloq. 4 (1976) 1.

35.3.60 NiS₂

Data from [68B1, 68B2, 70H, 71L, 71W, 72G, 72K, 73G, 73M]

lattice parameters

a 5.69 Å S: pyrite, C2, T_h⁶ – Pa3

resistivity, Seebeck coefficient, energy gap

ρ	1 Ω cm	p-type	CG: halogen transport (740/710)
S	311 μV K ⁻¹	synthetic single crystal	C: shiny black

E_g	0.27 eV		optical gap
$E_{g,th}$	0.64 eV	$T > 380$ K	Semiconductor-metal transition
	0.14 eV	$T = 140...380$ K	for $p > 30$ kbar at RT.
	0.009 eV	$T < 140$ K	$dT_{tr}/dp = 6(1)$ K/kbar
dE_g/dT	– 0.4 meV/K		E_g : optical gap
dE_A/dp	– 4.3(3) meV/kbar		(= (1/2)($dE_{g,th}/dp$))

68B1 Bither, T. A., Bouchard, R. J., Cloud, W. H., Donohue, P. C., Siemons, W. J.: Inorg. Chem. 7 (1968) 2208.

68B2 Bouchard, R. J.: J. Cryst. Growth 2 (1968) 40.

70H Hastings, J. M., Corliss, L. M.: IBM J. Res. Dev. 14 (1970) 227.

71L Landolt-Börnstein (New Series), ed.: K. H. Hellwege, Vol. III/6, Springer Verlag: Berlin, Heidelberg, New York 1971.

71W Wildervanck, J. C., Jellinek, F.: J. Less-Common Met 24 (1971) 73.

72G Gautier, F., Krill, G., Lapierre, M. F., Robert, C.: Solid State Commun. 11 (1972) 1201.

72K Koehler Jr., R. F., Feigelson, R. S., Swarts, H. W., White, R. L.: J. Appl. Phys. 43 (1972) 3127.

73G Gautier, F., Krill, G., Lapierre, M. F., Robert, C.: J. Phys. C 6 (1973), L320.

73M Mori, N., Mitsui, T., Yomo, S.: Solid State Commun. 13 (1973) 1083.

35.3.61 PdS

Data from [57G, 65H, 83H]

lattice parameters

a 6.429 Å structure: tetragonal, B34, C_{4h}² – P4₂/m

c 6.608 Å

density

d 6.6 g cm⁻³

Seebeck coefficient, energy gap

S	– 250 μV K ⁻¹	n-type, poly-	diamagnetic
$E_{g,th}$	0.5 eV	crystalline sample	

57G Gronvold, F., Rost, E.: Acta Crystallogr. 10 (1957) 329.

65H Hulliger, F.: J. Phys. Chem. Solids 26 (1965) 639.

83H Handbook of Chemistry and Physics, 64th ed. (ed.: R. C. Weast), CRC Press. Inc. 1983.

35.3.62 PdS₂

Data from [56G, 57G, 65H, 83H]

lattice parameters

<i>a</i>	5.46 Å	structure: orthorhombic, D _{2h} ¹⁵ – Pbca
<i>b</i>	5.54 Å	
<i>c</i>	7.53 Å	

density

<i>d</i>	4.7...4.8 g cm ⁻³
----------	------------------------------

resistivity, Seebeck coefficient, energy gap

ρ	100 Ω cm	n-type, poly-	diamagnetic
<i>S</i>	– 240 μV K ⁻¹	crystalline	
<i>E_{g,th}</i>	0.7...0.8 eV	sample	

56G Gronvold, F., Rost, E.: Acta Chem. Scand. 10 (1956) 1620.

57G Gronvold, F., Rost, E.: Acta Crystallogr. 10 (1957) 329.

65H Hulliger, F.: J. Phys. Chem. Solids 26 (1965) 639.

83H Handbook of Chemistry and Physics, 64th ed. (ed.: R. C. Weast), CRC Press. Inc. 1983.

35.3.63 PdSe

Data from [65H, 71L]

lattice parameters

<i>a</i>	6.73 Å	structure: B34, C _{4h} ² – P4 ₂ /m
<i>c</i>	6.91 Å	

Seebeck coefficient, energy gap

<i>S</i>	– 120 μV K ⁻¹	n-type, poly-
<i>E_{g,th}</i>	0.2 eV	crystalline sample

65H Hulliger, F.: J. Phys. Chem. Solids 26 (1965) 639.

71L Landolt-Börnstein (New Series), ed.: K. H. Hellwege, Vol. III/6, Springer Verlag: Berlin, Heidelberg, New York 1971.

35.3.64 PdSe₂

Data from [57G, 65H]

lattice parameters

<i>a</i>	5.74 Å	structure: orthorhombic, D _{2h} ¹⁵ – Pbca
<i>b</i>	5.87 Å	
<i>c</i>	7.69 Å	

resistivity, Seebeck coefficient, energy gap

ρ	1 Ω cm	p-type, poly-	diamagnetic
<i>S</i>	500 μV K ⁻¹	crystalline	
<i>E_{g,th}</i>	0.4 eV	sample	

57G Gronvold, F., Rost, E.: Acta Crystallogr. 10 (1957) 329.

65H Hulliger, F.: J. Phys. Chem. Solids 26 (1965) 639.

35.3.65 PtS

Data from [65H, 79C, 83H]

lattice parameters, density

<i>a</i>	3.469 Å	substance: tetragonal, B17, P4 ₂ /mmc
<i>c</i>	6.109 Å	
<i>d</i>	10.04 g cm ⁻³	
<i>a</i>	6.409 Å	B34, C _{4h} ² – P4 ₂ /m, <i>p</i> = 30 kbar
<i>c</i>	6.596 Å	

resistivity, Seebeck coefficient, energy gap

ρ	102 Ω cm	p-type, poly-crystalline sample	tetragonal phase
<i>S</i>	50 μV K ⁻¹		diamagnetic
<i>E_g</i>	0.8 eV		optical gap
<i>E_{g,th}</i>	0.64 eV		
ρ	10 Ω cm	polycrystalline sample	B34 high-pressure phase
<i>E_{g,th}</i>	0.38 eV		

65H Hulliger, F.: J. Phys. Chem. Solids 26 (1965) 639.
79C Collins, R., Kaner, R., Russo, P., Wold, A., Avignant, D.: Inorg. Chem. 18 (1979) 727.
83H Handbook of Chemistry and Physics, 64th ed. (ed.: R. C. Weast), CRC Press. Inc. 1983.

35.3.66 Pt_{0.97}S₂

Data from [74F, 77M]

lattice parameters

<i>a</i>	3.542 Å	S: trigonal, D _{3d} ³ – P $\bar{3}$ m1 CG: halogen transport with traces of phosphorus (800/740)
<i>c</i>	5.043 Å	

resistivity, Seebeck coefficient

ρ_{\perp}	2·10 ⁻² Ω cm	p- or n-type, synthetic single crystal	diamagnetic
<i>S</i> _⊥	500 μV K ⁻¹		

energy gap

<i>E_g</i>	0.95 eV	optical gap; indirect gap for both <i>E</i> _⊥ and <i>E</i> between d states of Pt with VB (max) at M (or L) and CB (min) at Γ.
d <i>E_g</i> /d <i>T</i>	– 3.7(2)·10 ⁻⁴ eV/K	
<i>E_{g,th}</i>	0.4 eV	

74F Finley, A., Schleich, D., Ackerman, J., Soled, S., Wold, A.: Mater. Res. Bull. 9 (1974) 1655.
77M Mankai, C., Martinez, G., Gorochoy, O.: Phys. Rev. 16B (1977) 4666.

35.3.67 PtSe₂

Data from [65H]

lattice parameters

a 3.724 Å

c 5.062 Å

substance: trigonal, C₆, D_{3d}³ – P $\bar{3}$ m1

Seebeck coefficient, energy gap

S 40 μV K⁻¹

$E_{g,th}$ 0.1 eV

p-type, poly-crystalline sample

65H Hulliger, F.: J. Phys. Chem. Solids 26 (1965) 639.

36 Binary rare earth compounds

Substances:

36.1 LaH_x

crystal structure	cubic (O _h ⁵ – Fm3m)		
energy gap			
E_g	0.1 eV	$T < 210$ K	80B
80B	Barnes, R. G., Beaudry, B. J., Creel, R. B., Torgeson, D. R., de Groot, D. G.: Solid State Commun. 36 (1980) 105.		

36.2 LaD_x

crystal structure	cubic (O _h ⁵ – Fm3m)			79M
semiconductor:	$2.89 \leq x \leq 3$	$T < 210$ K		80B
energy gap				
E_g	0.1 eV	$T < 210$ K, $x = 3$		80B
79M	Müller, H., Knappe, P., Greis, O.: Z. Phys. Chem. 114 (1979) 45.			
80B	Barnes, R. G., Beaudry, B. J., Creel, R. B., Torgeson, D. R., de Groot, D. G.: Solid State Commun. 36 (1980) 105.			

36.3 CeH_x

crystal structure	cubic (O _h ⁵ – Fm3m)			72L1
electrical conductivity				
σ	$\approx 10 \Omega^{-1} \text{ cm}^{-1}$	$x = 2.81$, n-type		69L
activation energy for electrical conductivity				
E_A	0.104 eV	$x = 2.81$, $T = 200$ K		72L2
69L	Libowitz, G. G., Pack, J. G.: J. Chem. Phys. 50 (1969) 3557.			
72L1	Libowitz, G. G.: Ber. Bunsenges. Phys. Chem. 8 (1972) 837.			
72L2	Libowitz, G. G., Pack, J. G., Binnie, W. P.: Phys. Rev. B 6 (1972) 4540.			

36.4 EuH₂

crystal structure		orthorhombic (D _{2h} ¹⁶ – Pnma)		75H
<i>E</i> _g	1.85 eV	optical absorption		93V
<i>ρ</i>	484 μΩcm	<i>T</i> = 260 K		
75H	Haschke, J. M., Clark, M. R.: High Temp. Sci. 7 (1975) 152.			
93V	Vajda, P., Daou J.N.: "The rare-earth hydrogen systems" in: Metal-Hydrogen Systems, Vol. 1, Aladjem, A., Lewis, F.A. (eds.), Weinheim: VCH, ch. 3a (1993).			

36.5 YP

energy gap

E_g	$\approx 0.45\text{ eV}$	82G
82G	Gusatinskii, A.N., Alperovich, G.I., Soldatov, A.V.: Phys. Stat. Sol. (b) 112 (1982) 599.	

36.6 LaP

energy gap

E_g	$\approx 0.25\text{ eV}$	Fig. 1 (X-ray spectroscopy)	82G
82G	Gusatinskii, A.N., Alperovich, G.I., Soldatov, A.V.: Phys. Stat. Sol. (b) 112 (1982) 599.		

36.7 SmP

energy gap

E_g	$\approx 0.38\text{ eV}$	82G
82G	Gusatinskii, A.N., Alperovich, G.I., Soldatov, A.V.: Phys. Stat. Sol. (b) 112 (1982) 599.	

36.8 ErP

energy gap

E_g	$\approx 0.75\text{ eV}$	X-ray spectroscopy	82G
82G	Gusatinskii, A.N., Alperovich, G.I., Soldatov, A.V.: Phys. Stat. Sol. (b) 112 (1982) 599.		

36.9 LuP

energy gap

E_g	$\approx 0.5\text{ eV}$	Fig. 1 (X-ray spectroscopy)	82G
82G	Gusatinskii, A.N., Alperovich, G.I., Soldatov, A.V.: Phys. Stat. Sol. (b) 112 (1982) 599.		

36.10 SmS

crystal structure

cubic ($O_h^5 - Fm3m$)

energy gap

E_g	$\approx 0.4\text{ eV}$	4f-cond. band	X-ray spectroscopy	82G
	3.4 eV	val.-cond. band		

electrical conductivity

σ	$10^2 \dots 10^3\ \Omega^{-1}\text{ cm}^{-1}$	70J
	$20 \dots 30\ \Omega^{-1}\text{ cm}^{-1}$	78S

electron mobility

μ_n	$20 \dots 25\text{ cm}^2/\text{V s}$	78S
---------	--------------------------------------	-----

70J	Jayaraman, A., Narayanamurti, V., Bucher, E., Maines, R. G.: Phys. Rev. Lett. 25 (1970) 1430.		
78S	Smirnov, I. A., Oskotskii, V. S.: Sov. Phys. Usp. 21 (2) (1978) 117.		
82G	Gusatinskii, A.N., Alperovich, G.I., Soldatov, A.V.: Phys. Stat. Sol. (b) 112 (1982) 599.		

36.11 SmSe

crystal structure		cubic (O _h ⁵ – Fm3m)	
energy gap			
E_g	0.46(2) eV	4f–5d transition	70J
	1.4(2) eV	4p ⁶ –5d, 6s trans.	74D
electrical conductivity			
σ	3·10 ^{–4} Ω ^{–1} cm ^{–1}		70J
70J	Jayaraman, A., Narayanamurti, V., Bucher, E., Maines, R. G.: Phys. Rev. Lett. 25 (1970) 1430.		
74D	Dumas, J., Schlenker, C.: Phys. Status Solidi (a) 22 (1974) 89.		

36.12 SmTe

crystal structure		cubic (O _h ⁵ – Fm3m)	
energy gap			
E_g	0.63 eV	4f–5d transition	70J
electrical conductivity			
σ	≈ 10 ^{–3} Ω ^{–1} cm ^{–1}		70J
70J	Jayaraman, A., Narayanamurti, V., Bucher, E., Maines, R. G.: Phys. Rev. Lett. 25 (1970) 1430.		

36.13 EuO

crystal structure		cubic (O _h ⁵ – Fm3m)	
energy gap			
E_g	4.1 eV	2p ⁶ – 5d, 6s transition	73E
	3.9 eV	2p ⁶ – 5d, 6s transition	75M
	1.12 eV	4f – 5d transition	72W,
electrical conductivity, electron concentration, electron mobility, activation energy for electrical conductivity			
σ	1.6...4.5·10 ³ Ω ^{–1} cm ^{–1}	$T = 4$ K	nonactivated 73S
n	3.4...7.5·10 ¹⁹ cm ^{–3}	$T = 4$ K	metallic phase
μ_n	290...370 cm ² /V s	$T = 4$ K	
σ	50...1.4·10 ^{–5} Ω ^{–1} cm ^{–1}		73S
E_A	0.3 eV		
effective electron mass			
m_n	0.42 m_0		81P
72W	Wachter, P.: CRC Crit. Rev. Solid State Sci. 3/12 (1972) 189.		
73E	Eastman, D. E.: Phys. Rev. B 8 (1973) 6027.		
73S	Shapira, Y., Foner, S., Peed, T. B.: Phys. Rev. B 8 (1973) 2299.		
75M	Mariot, J. M., Karnatak, R. C.: Solid State Commun. 16 (1975) 611.		
81P	Patil, C. G., Krishnamurthy, B. S.: Phys. Status Solidi (b) 105 (1981) 391.		

36.14 EuS

crystal structure		cubic	(O _h ⁵ – Fm3m)	
energy gap				
E _g	≈1.5 eV	4f-cond. band	X-ray spectroscopy	82G
	3.4 eV	val.-cond. band	(K, L _{2,3} -emission, K-absorption)	
electrical conductivity				
σ	≈ 10 ⁻⁹ Ω ⁻¹ cm ⁻¹			71B
	6...60 Ω ⁻¹ cm ⁻¹			72S
	60...700 Ω ⁻¹ cm ⁻¹	T = 4 K		
electron mobility				
μ _n	30 cm ² /V s			72S
71B	Bayer, E., Zinn, W.: Z. Angew. Phys. 32 (1971) 83.			
72S	Sadovskaya, O. A., Stepanov, E. P., Khrapov, V. V., Yarembash, E. I.: Inorg. Mater. (USSR) 8 (1972) 708.			
82G	Gusatinskii, A.N., Alperovich, G.I., Soldatov, A.V.: Phys. Stat. Sol. (b) 112 (1982) 599.			

36.15 EuSe

crystal structure		cubic (O _h ⁵ – Fm3m)		
energy gap				
<i>E_g</i> (4f – 5d)	1.80 eV		optical spectroscopy	72W
electrical conductivity				
σ	≈ 10 ⁻¹ Ω ⁻¹ cm ⁻¹	<i>T</i> = 76 K		78H
	10 ⁻⁷ Ω ⁻¹ cm ⁻¹		high resistivity sample	
	1...10 Ω ⁻¹ cm ⁻¹	n-type		81Y
Hall mobility				
μ_H	0.5 cm ² V ⁻¹ s ⁻¹	<i>B</i> = 5 T, <i>T</i> = 76 K		78H
72W	Wachter, P.: CRC Crit. Rev. Solid State Sci. 3/12 (1972) 189.			
78H	Heleskivi, J., Mäenpää, M.: Phys. Ser. 18 (1978) 441.			
81Y	Yamada, K., Heleskivi, J., Salin, A.: Solid State Commun. 37 (1981) 957.			

36.16 EuTe

crystal structure		cubic ($O_h^5 - Fm3m$)	
energy gap			
$E_g(4f - 5d)$	2.0 eV	optical spectroscopy	71G
electrical conductivity			
σ	$10^{-8} \Omega^{-1} \text{ cm}^{-1}$	high resistivity sample	71G
	$40...250 \Omega^{-1} \text{ cm}^{-1}$		72S
	$0.13...4 \Omega^{-1} \text{ cm}^{-1}$		$T = 4 \text{ K}$
electron mobility			
μ_n	$33...58 \text{ cm}^2/\text{V s}$		72S
71G	Günterodt, G., Wachter, B., Imboden, D. M.: Phys. Kondens. Mater. 12 (1971) 292.		
72S	Sadovskaya, O. A., Stepanov, E. P., Khrapov, V. V., Yarembash, E. I.: Inorg. Mater. (USSR) 8 (1972) 708.		

36.17 TmTe

crystal structure		cubic (O _h ⁵ – Fm3m)	
energy gap			
E _g	0.35 eV	optical determination absorption	75S
	0.22eV		71B
activation energy for electrical conductivity			
E _A	0.2 eV		75B
resistivity			
ρ	0.77 Ω cm	nonstoichiometric Tm _{0.94} Te	83O
71B	Bayer, E., Zinn, W.: Z. Angew. Phys. 32 (1971) 83.		
75B	Bucher, E., Andres, K., di Salvo, F. J., Maita, J. P., Gossard, A. C., Cooper, A. S., Hull jr., G. W.: Phys. Rev. B 11 (1975) 500.		
75S	Suryanarayanan, R., Güntherodt, G., Freeouf, J. L., Holtzberg, F.: Phys. Rev. B12 (1975) 421 5.		
83O	Ott, H. R., Hulliger, F.: Z. Phys. B Condens. Matter 49 (1983) 323.		

36.18 YbS

crystal structure		cubic (O _h ⁵ – Fm3m)		
energy gap				
E _g	≈0.4 eV	4f-cond. band	X-ray spectroscopy	82G
	3.2 eV	val.-cond. band	(K, L _{2,3} -emission, K-absorption)	
	0.98 eV		optical spectroscopy	71B
	1.1 eV			74N
	1.325(5) eV	4f → conduction band transition		80G
E	1.8 eV	4f ¹⁴ (1S ₀) → 4f ¹³ (² F _{7/2})5d transition;		80G
	2.8 eV	4f ¹⁴ (1S ₀) → 4f ¹³ (² F _{5/2})5d transition		

activation energy for electrical conductivity

E_A	0.3...0.4 eV	p-type	80G
-------	--------------	--------	-----

71B Bayer, E., Zinn, W.: Z. Angew. Phys. 32 (1971) 83.
74N Narayanamurti, V., Jayaraman, A., Bucher, E.: Phys. Rev. B 9 (1974) 2521.
80G Glurdzhidze, L. N., Kekhainov, T. D., Uzirishvili, D. G., Bzhalava, T. L., Sanadze, V. V.: Sov. Phys. Solid State 22 (3) (1980) 388.
82G Gusatinskii, A.N., Alperovich, G.I., Soldatov, A.V.: Phys. Stat. Sol. (b) 112 (1982) 599.

36.19 YbSe

crystal structure		cubic ($O_h^5 - Fm3m$)	
energy gap			
E_g	1.5 eV		74N
resistivity			
ρ	100 Ω cm		64R
64R	Reid, F. J., Matson, L. K., Miller, J. F., Himes, R. C.: J. Phys. Chem. Solids 25 (1964) 969.		
74N	Narayanamurti, V., Jayaraman, A., Bucher, E.: Phys. Rev. B 9 (1974) 2521.		

36.20 YbTe

crystal structure		cubic (O _h ⁵ – Fm3m)		
energy gap				
E _g	1.8 eV			74N
resistivity				
ρ	10 ⁴ ...10 ⁶ Ω cm			60B 64R

60B Brixner, L. H.: J. Inorg. Nucl. Chem. 15 (1960) 199.
64R Reid, F. J., Matson, L. K., Miller, J. F., Himes, R. C.: J. Phys. Chem. Solids 25 (1964) 969.
74N Narayanamurti, V., Jayaraman, A., Bucher, E.: Phys. Rev. B 9 (1974) 2521.

36.21 Sm_3S_4

crystal structure cubic (Th₃P₄-type, T_d⁶ – I $\bar{4}$ 3d)

electrical conductivity

σ 1.8 Ω^{-1} cm⁻¹

activation energy

E_A	0.132 eV	$T > 125$ K	from electrical conductivity	76B1,
	0.142 eV	$T < 125$ K	from electrical conductivity	76B2
	0.13 eV		from electrical conductivity	76E
	0.1...0.2eV			77V
	≈ 0.1 eV			77V

76B1 Batlogg, B., Kaldis, E., Schlegel, A., v. Schulthiess, G., Wachter, P.: Solid State Commun. 19 (1976) 673.

76B2 Batlogg, B., Kaldis, E., Wachter, P.: J. Magn. Magn. Mater. 3 (1976) 96.

76E Escorne, M., Ghazali, A., Leroux-Hugon, P., Smirnov, I. A.: Phys. Lett. 56A (1976) 475.

77V Vitins, J., Wachter, P.: Physica 89 B (1977) 234.

36.22 Eu₃S₄

crystal structure cubic (Th₃P₄-type, T_d⁶ – I $\bar{4}$ 3d)

energy gap

E_g	1.7 eV	optical absorption edge	76V
-------	--------	-------------------------	-----

activation energy

E_A	0.22 (1) eV		from conductivity	67B
	0.32(1) eV	$T < 186$ K	from conductivity	83P
	0.160(5) eV	$T > 186$ K		
	0.21(1) eV	$T < 175$ K	from conductivity; endothermic DTA	70H
	0.163(4) eV	$T > 175$ K	transition at 170 K	

67B Berkooz, O., Malamud, M., Shtrikman, S.: Solid State Commun. 6 (1967) 185.

70H Henderson, J. R. Muramoto, M., Gruber, J. B., Menzel, R.: J. Chem. Phys. 52 (1970) 2311.

76V Vitins, J., Wachter, P.: Phys. Lett. 58A (1976) 275.

83B Balabanova, L.A., Zhuze, V.P., Ostroumova, E.G., Shul'man, S.G.: Sov. Phys. Solid State 25(6) (1983) 971.

36.23 La₂O₃

structure : hexagonal

activation energy for electrical conductivity

E_A	2.40 eV	$T = 700...1200$ K,	val.-cond. band	88L
-------	---------	---------------------	-----------------	-----

electrical conductivity

σ	$2.40 \cdot 10^3 \Omega^{-1} \text{m}^{-1}$	p-type
----------	---	--------

mobility

μ_p	$0.628 \text{ cm}^2 \text{V}^{-1} \text{s}^{-1}$	$T = 900$ K
---------	--	-------------

μ_n	$0.602 \text{ cm}^2 \text{V}^{-1} \text{s}^{-1}$	$T = 900$ K
---------	--	-------------

88L Lal, H.B., Kanchan Gaur: J. Mater. Sci. 23 (1988) 919.

36.24 Nd₂O₃

structure : hexagonal

activation energy for electrical conductivity

E_A 2.36 eV $T = 700...1200\text{ K,}$ 88L
4f³-cond. band

electrical conductivity

σ $3.16 \cdot 10^3\text{ }\Omega^{-1}\text{m}^{-1}$ n-type

mobility

μ_n $0.188\text{ cm}^2\text{V}^{-1}\text{s}^{-1}$ $T = 900\text{ K}$

88L Lal, H.B., Kanchan Gaur: J. Mater. Sci. 23 (1988) 919.

36.25 Sm₂O₃

structure : monoclinic

activation energy for electrical conductivity

E_A 2.12 eV $T = 800...1200\text{ K,}$ 88L
val. band-4f⁶

electrical conductivity

σ $2.68 \cdot 10^2\text{ }\Omega^{-1}\text{m}^{-1}$ p-type

mobility

μ_p $0.084\text{ cm}^2\text{V}^{-1}\text{s}^{-1}$ $T = 900\text{ K}$

88L Lal, H.B., Kanchan Gaur: J. Mater. Sci. 23 (1988) 919.

36.26 Eu₂O₃

structure : cubic

activation energy for electrical conductivity

E_A 1.84 eV $T = 800...1200\text{ K,}$ 88L
val. band-4f⁷

electrical conductivity

σ $4.63 \cdot 10^1\text{ }\Omega^{-1}\text{m}^{-1}$ p-type

mobility

μ_p $0.327\text{ cm}^2\text{V}^{-1}\text{s}^{-1}$ $T = 900\text{ K}$

88L Lal, H.B., Kanchan Gaur: J. Mater. Sci. 23 (1988) 919.

36.27 Tb₂O₃

structure : monoclinic

activation energy for electrical conductivity

E_A 2.24 eV $T = 750...900\text{ K}$, 88L
4f⁸-cond. band

electrical conductivity

σ $3.08 \cdot 10^7\ \Omega^{-1}\text{m}^{-1}$ n-type

mobility

μ_n $2.10\text{ cm}^2\text{V}^{-1}\text{s}^{-1}$ $T = 900\text{ K}$

88L Lal, H.B., Kanchan Gaur: J. Mater. Sci. 23 (1988) 919.

36.28 Dy₂O₃

structure : cubic

activation energy for electrical conductivity

E_A 2.82 eV $T = 800...1200\text{ K}$, 88L
val.-cond. band

electrical conductivity

σ $4.13 \cdot 10^1\ \Omega^{-1}\text{m}^{-1}$ p-type

mobility

μ_p $0.011\text{ cm}^2\text{V}^{-1}\text{s}^{-1}$ $T = 900\text{ K}$

μ_n $0.010\text{ cm}^2\text{V}^{-1}\text{s}^{-1}$ $T = 900\text{ K}$

88L Lal, H.B., Kanchan Gaur: J. Mater. Sci. 23 (1988) 919.

36.29 Ho₂O₃

structure : cubic

activation energy for electrical conductivity

E_A 2.74 eV $T = 800...1200\text{ K}$, 88L
val.-cond. band

electrical conductivity

σ $5.13 \cdot 10^2\ \Omega^{-1}\text{m}^{-1}$ p-type

mobility

μ_p $0.133\text{ cm}^2\text{V}^{-1}\text{s}^{-1}$ $T = 900\text{ K}$

μ_n $0.128\text{ cm}^2\text{V}^{-1}\text{s}^{-1}$ $T = 900\text{ K}$

88L Lal, H.B., Kanchan Gaur: J. Mater. Sci. 23 (1988) 919.

36.30 Er₂O₃

structure : cubic

activation energy for electrical conductivity

E_A	3.04 eV	$T = 800...1200\text{ K},$ val.-cond. band	88L
-------	---------	---	-----

electrical conductivity

σ	$1.66 \cdot 10^3\ \Omega^{-1}\text{m}^{-1}$	p-type
----------	---	--------

mobility

μ_p	$0.449\text{ cm}^2\text{V}^{-1}\text{s}^{-1}$	$T = 900\text{ K}$
---------	---	--------------------

μ_n	$0.420\text{ cm}^2\text{V}^{-1}\text{s}^{-1}$	$T = 900\text{ K}$
---------	---	--------------------

88L	Lal, H.B., Kanchan Gaur: J. Mater. Sci. 23 (1988) 919.
-----	--

36.31 Tm₂O₃

structure : cubic

activation energy for electrical conductivity

E_A	2.84 eV	$T = 800...1200\text{ K},$ val. band-4f ¹³	88L
-------	---------	--	-----

electrical conductivity

σ	$2.96 \cdot 10^2\ \Omega^{-1}\text{m}^{-1}$	p-type
----------	---	--------

mobility

μ_p	$0.426\text{ cm}^2\text{V}^{-1}\text{s}^{-1}$	$T = 900\text{ K}$
---------	---	--------------------

88L	Lal, H.B., Kanchan Gaur: J. Mater. Sci. 23 (1988) 919.
-----	--

36.32 Yb₂O₃

structure : cubic

activation energy for electrical conductivity

E_A	2.66 eV	$T = 800...1200\text{ K},$ val. band-4f ¹⁴	88L
-------	---------	--	-----

electrical conductivity

σ	$2.36 \cdot 10^2\ \Omega^{-1}\text{m}^{-1}$	p-type
----------	---	--------

mobility

μ_p	$0.321\text{ cm}^2\text{V}^{-1}\text{s}^{-1}$	$T = 900\text{ K}$
---------	---	--------------------

88L	Lal, H.B., Kanchan Gaur: J. Mater. Sci. 23 (1988) 919.
-----	--

36.33 β -La₂S₃

crystal structure tetragonal ($D_{4h}^{20} - I4_1/acd$)

energy gap

E_g	2.58 eV	direct	optical determination	80L
	2.6 eV	direct	fundamental absorption edge	81S
	1.38 eV		indirect or impurity tail	80L

electrical resistivity

ρ	$2 \cdot 10^{12} \dots 4 \cdot 10^{14} \Omega \text{ cm}$			82A
--------	---	--	--	-----

80L Leiss, M.: J. Phys. C 13 (1980) 151.

81S Scharmer, E. G., Leiß, M., Huber, G.: J. Lumin. 24/25 (1981) 751.

82A Astalleva, L. V., Skornyakov, G. P., Kamarzin, A. A., Malovitskii, Y. N.: Sov. Phys. Solid State 24 (1982) 367.

36.34 γ -La₂S₃

crystal structure cubic (Th_3P_4 -defect structure, $T_d^6 - \bar{I}4\bar{3}d$)

energy gap

E_g	$2.76 \pm 0.1 \text{ eV}$		optical energy gap	85Z
	$2.8 \pm 0.25 \text{ eV}$		thermodynamic	85Z
	1.9 eV		X-ray spectra	83S
	2.9 eV		optical gap	80K
	2.4 eV	$T = 148 \text{ K}$	optical gap	82B, 81B
	2.8(1) eV		optical gap	79Z

79Z Zhuze, V. P., Kamarzin, A. A., Karin, M. G., Sidorin, K. K., Shelykh, A. I.: Sov. Phys. Solid State 21 (1979) 1968.

80K Kaminskii, A. A., Sarkisov, C. E., Chan Niok, Denisenko, G. A., Kamarzin, A. A., Sokolov, V. V., Klypin, V. V., Maloviikii, Yu. N.: Izv. Akad. Nauk SSSR, Neorg. Mater. 16 (1980) 1333.

81B Bludau, W., Wichelhaus, W.: J. Appl. Phys. 52 (1981) 2750.

82B Batirov, T. M., Verkhovskaya, K. A., Kamarzin, A. A., Malovitskii, Y. N., Lisoivan, V. I., Fridkin, V. M.: Sov. Phys. Solid State 24 (1982) 746.

83S Soldatov, A. V., Gusatinskii, A. N., Karin, M. G., Sidorin, K. K., Sadovskaya, O. A.: Inorg. Mater. 19 (1983) 951-954.

85Z Zhuze, V. P., Karin, M. G., Sidorin, K. K., Sokolov, V. V., Shelykh, A. I.: Sov. Phys. Solid State 27(12) (1985) 2205.

36.35 β -La₁₀S₁₄O

crystal structure tetragonal ($D_{4h}^{20} - I4_1/acd$)

energy gap

E_g	2.69(7) eV		optical determination	81B
-------	------------	--	-----------------------	-----

81B Batirov, T. M., Fridkin, V. M., Kamarzin, A. A., Malovitskii, Y. I., Verkhovskaya, K. A.: Phys. Status Solidi (a) 65 (1981) K163.

36.36 La₂Te₃

crystal structure		cubic (Th ₃ P ₄ -defect structure, T _d ⁶ – I $\bar{4}$ 3d)	
electrical conductivity			
σ	$10^{-4} \Omega^{-1} \text{ cm}^{-1}$	n-type	65R
activation energy for electrical conductivity			
E_A	0.43 eV		65R
65R	Ramsey, T. H., Steinfink, H., Weiss, E. J.: J. Appl. Phys. 36 (1965) 548.		

36.37 γ -Ce₂S₃

crystal structure		cubic (Th ₃ P ₄ -defect structure, T _d ⁶ – I $\bar{4}$ 3d)	
energy gap			
E_g	2.06 eV	optical energy gap	64K
electrical conductivity			
σ	$10^{-10} \Omega^{-1} \text{ cm}^{-1}$		71A
activation energy			
E_A	2.23 eV	from electrical conductivity	67M
64K	Kurnick, S.W., Meyer, C.: J. Phys. Solids 25 (1964) 115.		
67M	Marchenko, V. I., Samsonov, G. V.: Chem. Bond in Semicond. and Solids (ed. N. N. Sirota) New York: Consultants Bureau 1967.		
71A	Atoji, M.: J. Chem. Phys. 54 (1971) 3226.		

36.38 γ -Nd₂S₃

crystal structure		cubic (Th ₃ P ₄ -defect structure, T _d ⁶ – I $\bar{4}$ 3d)	
energy gap			
E_g	$2.50 \pm 0.1 \text{ eV}$	optical gap	85Z
activation energy			
E_A	2.7...3.8 meV	electrical measurement	77T
electrical conductivity			
σ	$10^{-10} \Omega^{-1} \text{ cm}^{-1}$	n-type	70H
	$10^2 \Omega^{-1} \text{ cm}^{-1}$	S-excess	70H
	$1...2 \cdot 10^{-3} \Omega^{-1} \text{ cm}^{-1}$		74T
70H	Henderson, J. R. Muramoto, M., Gruber, J. B., Menzel, R.: J. Chem. Phys. 52 (1970) 2311.		
74T	Taher, S. M. A., Gruber, J. B., Olsen, L. C.: J. Chem. Phys. 69 (1974) 2050.		
77T	Taher, M. A., Gruber, J. B.: Phys. Rev. B 16 (1977) 1624.		
85Z	Zhuze, V.P., Karin, M.G., Sidorin, K.K., Sokolov, V.V., Shelykh, A.I.: Sov. Phys. Solid State 27(12) (1985) 2205.		

36.39 γ -Sm₂S₃

crystal structure		cubic (Th ₃ P ₄ -defect structure, T _d ⁶ – I $\bar{4}$ 3d)		
energy gap				
E_g	2.6 ± 0.1 eV	optical gap		85Z
electrical conductivity				
σ	< 10 ⁻⁹ Ω ⁻¹ cm ⁻¹	near stoichiometric samples	reflectivity	83B
83B	Balabanova, L.A., Zhuze, V.P., Ostroumova, E.G., Shul'man, S.G.: Sov. Phys. Solid State 25(6) (1983) 971.			
85Z	Zhuze, V.P., Karin, M.G., Sidorin, K.K., Sokolov, V.V., Shelykh, A.I.: Sov. Phys. Solid State 27(12) (1985) 2205.			

36.40 γ -Gd₂S₃

crystal structure		cubic (Th ₃ P ₄ -defect structure, T _d ⁶ — I $\bar{4}$ 3d)		
energy gap				
E _g	3.4 eV	optical gap		82B
	1.4 eV		X-ray spectra	83S
electrical conductivity				
σ	250 Ω ⁻¹ cm ⁻¹	n-type		74T
	10 ⁻⁸ Ω ⁻¹ cm ⁻¹			82B
activation energy for electrical conductivity				
E _A	1.6...1.9 meV			77T
74T	Taher, S. M. A., Gruber, J. B., Olsen, L. C.: J. Chem. Phys. 69 (1974) 2050.			
77T	Taher, M. A., Gruber, J. B.: Phys. Rev. B 16 (1977) 1624.			
82B	Batirov, T. M., Verkhovskaya, K. A., Kamarzin, A. A., Malovitskii, Y. N., Lisoivan, V. I., Fridkin, V. M.: Sov. Phys. Solid State 24 (1982) 746.			
83S	Soldatov, A.V., Gusatinskii, A.N., Karin, M.G., Sidorin, K.K., Sadovskaya, O.A.: Inorg. Mater. 19 (1983) 951-954.			

36.41 γ -Dy₂S₃

crystal structure

cubic (Th₃P₄-defect structure, $T_d^6 - \bar{1}43d$)

energy gap

E_g 3 eV optical absorption edge 70H

activation energy

E_A 1.5 meV electrical measurement 77T

electrical conductivity

σ 250 $\Omega^{-1} \text{ cm}^{-1}$ n-type see also Fig. 6 67H
10⁻¹⁰ $\Omega^{-1} \text{ cm}^{-1}$ 70H,
82B

67H Henderson, J. R., Muramoto, M., Loh, E.: J. Chem. Phys. 47 (1967) 3347.

70H Henderson, J. R. Muramoto, M., Gruber, J. B., Menzel, R.: J. Chem. Phys. 52 (1970) 2311.

77T Taher, M. A., Gruber, J. B.: Phys. Rev. B 16 (1977) 1624.

82B Batirov, T. M., Verkhovskaya, K. A., Kamarzin, A. A., Malovitskii, Y. N., Lisoivan, V. I., Fridkin, V. M.: Sov. Phys. Solid State 24 (1982) 746.

36.42 δ -Ho₂S₃

crystal structure

monoclinic ($C_{2h}^2 - P2_1/m$)

electrical conductivity

σ 0.14·10⁻⁶ $\Omega^{-1} \text{ cm}^{-1}$ 68S

activation energy for electrical conductivity

E_A 0.5 eV 68S

68S Sleight, A. W., Prewitt, C. T.: Inorg. Chem. 7 (1968) 2282.

36.43 γ -Ho₂O₃

energy gap

E_g 0.7 eV X-ray spectra 83S

83S Soldatov, A.V., Gusatinskii, A.N., Karin, M.G., Sidorin, K.K., Sadovskaya, O.A.: Inorg. Mater. 19 (1983) 951-954.

36.44 γ -Yb₂S₃

energy gap

E_g 0.5 eV X-ray spectra 83S

83S Soldatov, A.V., Gusatinskii, A.N., Karin, M.G., Sidorin, K.K., Sadovskaya, O.A.: Inorg. Mater. 19 (1983) 951-954.

36.45 ϵ -Yb₂S₃

crystal structure rhombohedral (Al₂O₃-structure, $D_{3d}^6 - R\bar{3}c$)

electrical conductivity

σ $3 \cdot 10^{-5} \Omega^{-1} \text{ cm}^{-1}$ 68S

activation energy for electrical conductivity

E_A 0.29 eV 68S

68S Sleight, A. W., Prewitt, C. T.: Inorg. Chem. 7 (1968) 2282.

36.46 Gd₂Cl₃

structure : monoclinic, C2/m

energy gap

E_g 0.85 eV 85K

85K Kremer, R.K.: Thesis (Darmstadt, Germany) 1985.

36.47 Tb₂Cl₃

energy gap

E_g 1.1 eV 85K

85K Kremer, R.K.: Thesis (Darmstadt, Germany) 1985.

37 Ternary transition metal compounds

37.1 Pnigochalcogenides

37.1.1 FePS

energy gap

$E_{g,th}$	0.25 eV		from $\log \rho \propto E_g/2kT$ above 500 K; sintered sample	59H
------------	---------	--	--	-----

59H Hulliger, F.: *Helv. Phys. Acta* 32 (1959) 615.

37.1.2 FeAsS

energy gap

$E_{g,th}$	0.3...0.5 eV		from $\log \rho \propto E_g/2kT$ measured on minerals and sintered samples	59H
------------	--------------	--	---	-----

59H Hulliger, F.: *Helv. Phys. Acta* 32 (1959) 615.

37.1.3 FeAsSe

energy gap

$E_{g,th}$	0.6 eV		from $\log \rho \propto E_g/2kT$, $T = 600...900$ K; sintered sample	59H
------------	--------	--	--	-----

59H Hulliger, F.: *Helv. Phys. Acta* 32 (1959) 615.

37.1.4 RuPS

energy gap

E_g	> 1.4 eV	RT	from diffuse reflectance	63H
-------	----------	----	--------------------------	-----

63H Hulliger, F.: *Nature (London)* 201 (1963) 381.

37.1.5 RuAsS

energy gap

E_g	≈ 1.2 eV	RT	from diffuse reflectance	63H
-------	------------------	----	--------------------------	-----

63H Hulliger, F.: *Nature (London)* 201 (1963) 381.

37.1.6 RuSbTe

energy gap

$E_{g,th}$	0.5 eV		from $\log \rho \propto E_g/2kT$ above 500 K	63H
------------	--------	--	--	-----

63H Hulliger, F.: *Nature (London)* 201 (1963) 381.

37.1.7 OsPS

energy gap

E_g	> 1.4 eV	RT	from diffuse reflectance	63H
-------	----------	----	--------------------------	-----

63H Hulliger, F.: *Nature (London)* 201 (1963) 381.

37.1.8 OsAsS

energy gap

E_g	1.3 eV	RT	from diffuse reflectance	63H
-------	--------	----	--------------------------	-----

63H Hulliger, F.: *Nature (London)* 201 (1963) 381.

37.1.9 OsSbS

energy gap

$E_{g,th}$ 1.2 eV from $\log \rho \propto E_g/2kT$, above 700 K 63H
63H Hulliger, F.: Nature (London) 201 (1963) 381.

37.1.10 OsPSe

energy gap

E_g ≈ 1.4 eV RT from diffuse reflectance 63H
63H Hulliger, F.: Nature (London) 201 (1963) 381.

37.1.11 OsSbSe

energy gap

E_g < 0.05 eV (?) RT 60 μm thick samples were 66B
66B Banus, M. D., Lavine, M. C.: Mat. Res. Bull. 1 (1966) 3.

resistivity

ρ 0.12 Ω cm RT sample No.9, prepared in a 66B
66B Banus, M. D., Lavine, M. C.: Mat. Res. Bull. 1 (1966) 3.

37.1.12 OsSbTe

energy gap

E_g < 0.05 eV (?) RT 60 μm thick samples were 66B
completely opaque in the wavelength
range 0.5 to 25 μm

resistivity

ρ $82.2 \cdot 10^{-3}$ Ω cm RT sintered sample 66B
66B Banus, M. D., Lavine, M. C.: Mat. Res. Bull. 1 (1966) 3.

37.1.13 CoAsS

energy gap for $x = 0.04$ ($\text{CoAs}_{0.96}\text{S}_{1.04}$)

$E_{g,th}$ 0.18 eV from $\log \rho \propto E_g/2kT$ 76A
semiconductor \rightarrow metal transition at $x \approx 0.06$ ($\text{CoAs}_{0.94}\text{S}_{1.06}$)

76A Adachi, K., Togawa, E., Kimura, F.: J. Phys. (Paris) 37 (1976) C429.

37.1.14 CoSbS

(pararammelsbergite-type modification)

energy gap

$E_{g,th}$ 0.5 eV from $\log \rho \propto E_g/2kT$ above 600 K 59H
space group $D_{2h}^{15} - \text{Pbca}$
59H Hulliger, F.: Helv. Phys. Acta 32 (1959) 615.

37.1.15 CoAsSe

energy gap

$E_{g,th}$	0.2 eV		from $\log \rho \propto E_g/2kT$ up to 670K (refers possibly to the marcasite-type modification)	59H
------------	--------	--	--	-----

space group $D_{2h}^{15} - Pbca$

59H Hulliger, F.: Helv. Phys. Acta 32 (1959) 615.

37.1.16 PdPS

energy gap

E_g	1.4 eV		given as $E_A = 0.7$ eV, from $\log \rho \propto E_A/kT$, $T = 300...450$ K, on single crystals	71B
-------	--------	--	--	-----

resistivity

ρ	$90 \cdot 10^6 \Omega \text{ cm}$	$T = 298 \text{ K}$	from four-probe resistivity measurements on single crystals	71B
--------	-----------------------------------	---------------------	--	-----

71B Bither, T. A., Donohue, P. C., Young, S.: J. Solid State Chem. 3 (1971) 300.

37.1.17 PdPSe

activation energy

E_A	0.15 eV		from $\log \rho \propto E_A/kT$, $T = 300...400$ K on single crystals ($E_g > 0.3$ eV ?)	71B
-------	---------	--	---	-----

resistivity

ρ	$30 \Omega \text{ cm}$	$T = 300 \text{ K}$	from four-probe resistivity measurements on single crystals	71B
--------	------------------------	---------------------	--	-----

71B Bither, T. A., Donohue, P. C., Young, S.: J. Solid State Chem. 3 (1971) 300.

37.2 Spinels and related compounds

37.2.1 MnGa₂S₄

crystal structure: monoclinic, space group C_{2h}⁶– C2/c (low temperature α-phase) [81R].

energy gap

$E_{g,th}$	1.2 eV	from conductivity (600 K < T < 750 K)	77R
------------	--------	--	-----

electrical conductivity

σ	$3.98 \cdot 10^{-4} \Omega^{-1} \text{ cm}^{-1}$	polycrystalline material	77R
----------	--	--------------------------	-----

77R Rustamov, P. G., Guseinova, M. A., Alidzhanov, M. A., Safarov, M. G.: Inorg. Mater. (USSR) 12 (1976) 1218.

37.2.2 MnSb₂S₄

energy gap

$E_{g,th}$	1 eV	from conductivity (600 K < T < 750 K)	77R
------------	------	--	-----

electrical conductivity

σ	$2.51 \cdot 10^{-4} \Omega^{-1} \text{ cm}^{-1}$	polycrystalline material	77R
----------	--	--------------------------	-----

77R Rustamov, P. G., Guseinova, M. A., Alidzhanov, M. A., Safarov, M. G.: Inorg. Mater. (USSR) 12 (1976) 1218.

37.2.3 Fe(FeRh)S₄

This compound is a ferrimagnetic p-type semiconductor [73H].

energy gap

$E_{g,th}$	0.05 eV	from conductivity	73H
------------	---------	-------------------	-----

resistivity

ρ	$2.2 \cdot 10^{-3} \Omega \text{ cm}$	RT	73H
	$1.7 \cdot 10^{-2} \Omega \text{ cm}$	$T = 80 \text{ K}$	

73H Harada, S.: Mater. Res. Bull. 8 (1973) 1361.

37.2.4 CdCr₂S₄

crystal structure : spinel, space group O_h⁷-Fd3m.

energy gap

E_g	1.57 eV	optical measurements	66H
	2.48 eV	photoconductivity ($\lambda = 520 \text{ nm}$, single crystal)	72L

Most samples show n-type conductivity.

activation energy of conductivity

E_A	0.15 eV	$T = 120...140 \text{ K}$	77G
	0.17...0.35 eV	$T = 200 \text{ K}$	

66H Holt, S. L., Bouchard, R. J., Wold, A.: J. Phys. Chem. Solids 27 (1966) 755.

72L Larsen, P. K., Wittekoek, S.: Phys. Rev. Lett. 29 (1972) 1597.

77G Golik, L. L., Elinson, M. I., Kun'kova, Z. E., Novikov, L. N., Grigorovich, S. M., Ukrainskii, Yu. M.: Sov. Microelectron. 6 (1977) 152.

37.2.5 FeCr₂S₄

crystal structure: spinel (Fig. 1), space group O_h⁷-Fd3m.

carrier concentration

<i>p</i>	1·10 ¹⁹ cm ⁻³	<i>T</i> = 77 K	p-type conduction according to sign of Hall and Seebeck coefficient	78W
	2·10 ¹⁹ cm ⁻³	<i>T</i> = 200 K		

hole mobility

μ_p	0.2 cm ² /Vs	<i>T</i> = 77 K		78W
	0.3 cm ² /Vs	<i>T</i> = 200 K		

activation energy for electrical conductivity

<i>E_A</i>	0.02 eV	<i>T</i> > <i>T_C</i>		72G, 68G 77E
	0.22 eV	"for higher temperatures"		

68G Goldstein, L., Gibart, P.: C. R. Acad. Sci. Ser. B 269 (1968) 471.
72G Goldstein, L., Gibart, P.: AIP Conf. Proc. 5 (1972) 883.
77E Eivazov, E. A., Rustamov, A. G., Ibragimov, B. B.: Inorg. Mater. 13 (1977) 354.
78W Watanabe, T., Nakada, I.: Jpn. J. Appl. Phys. 17 (1978) 1745.

37.2.6 CoCr₂S₄

crystal structure

spinel, space group O_h⁷-Fd3m.

transport properties

p-type conduction found in [65B].

65B Baltzer, P. K., Lehmann, H. W., Robbins, M.: Phys. Rev. Lett. 15 (1965) 493.

37.2.7 HgCr₂S₄

crystal structure : spinel, space group O_h⁷-Fd3m.

energy gap

<i>E_g</i>	1.42 eV		70H
----------------------	---------	--	-----

activation energy of conductivity

<i>E_A</i>	0.36 eV	<i>T</i> = 20...100 °C	75O
	1.2 eV	<i>T</i> = 100...400 °C	
	2.0 eV	<i>T</i> = 400...600 °C	

70H Harbeke, G., Lehmann, H. W.: Solid State Commun. 8 (1970) 1281.
75O Okónska-Kozłowska, I., Konopka, D., Jelonek, M., Heimann, J., Pietkiewicz, J., Chelkowski, A.: J. Solid State Chem. 14 (1975) 349.

37.2.8 BaCr₂S₄

crystal structure : hexagonal with nine formula units in the unit cell [71O].

energy gap

<i>E_g</i>	1.0...1.5 eV	optical absorption edge	71O
----------------------	--------------	-------------------------	-----

71O Ombo, W. P. F. A. M., Bommerson, J. C., Heikens, H. H., Risselada, H., Vellinga M. B., Van Bruggen, C. F., Haas, C., Jellinek, F.: Phys. Status Solidi (a) 5 (1971) 349.

37.2.9 CdCr₂Se₄

crystal structure

spinel, space group O_h⁷–Fd3m.

Ferromagnetic semiconductor.

energy gap

E_g	1.7 eV	71A
	1.2 eV	70S
	1.32 eV	70A

transport properties

CdCr₂Se₄ can be p-type or n-type depending on the method of preparation [67L]. Substitution of monovalent elements such as Ag for Cd render the material p-type, while trivalent elements such as In replacing Cd render the material n-type [68W1, 68W2].

67L Lehmann, H. W.: Phys. Rev. 163 (1967) 488.
68W1 Wen, C. P., Hershenov, B., von Philipsborn, H., Pinch, H.: IEEE Trans. Magn. 4 (1968) 702.
68W2 Wen, C. P., Hershenov, B., von Philipsborn, H., Pinch, H.: Appl. Phys. Lett. 13 (1968) 188.
70A Amith, A., Friedman, L.: Phys. Rev. B2 (1970) 434.
70S Shepherd, I. W.: Solid State Commun. 8 (1970) 1835.
71A Ahrenkiel, R. K., Moser, F., Lyu, S.: J. Appl. Phys. 42 (1971) 1452.

37.2.10 CuCr₂S_{4-x}Se_x

(acc. to [79K])

electrical resistivity

ρ	0.04 Ω cm	$x = 0.5$	$T =$	semiconducting behavior for $x = 1$
	0.04 Ω cm	$x = 1.0$	300 K	and $x = 1.5$ (see also Figs. 1, 2)
	0.01 Ω cm	$x = 1.5$		

carrier concentration

p	$6 \cdot 10^{20} \text{ cm}^{-3}$	$x = 1.0$	$T =$
	$6 \cdot 10^{20} \text{ cm}^{-3}$	$x = 1.5$	100 K

mobility

μ_p	0.15 cm^2/Vs	$x = 1.0$	$T =$
	0.70 cm^2/Vs	$x = 1.5$	100 K

activation energy

E_A	1.5 meV	$x = 1.0$	$T = 77 \text{ K}$
	50 meV		$T = 200 \text{ K}$
	7.1 meV	$x = 1.5$	$T = 77 \text{ K}$
	66 meV		$T = 200 \text{ K}$

79K Koroleva, L. I., Shalimova, M. A.: Sov. Phys. Solid State 21 (1979) 266.

37.2.11 HgCr₂Se₄

crystal structure

spinel, space group O_h⁷-Fd3m.

Ferromagnetic semiconductor.

energy gap

E_g	0.44 eV	$T = 78\text{ K}$	optical measurements	71L
	0.84 eV	$T = 300\text{ K}$		

resistivity

ρ	1.2 $\Omega\text{ cm}$	$T = 300\text{ K}$		71L
	310 $\Omega\text{ cm}$	$T = 77\text{ K}$		

Hall mobility

μ_H	300...1200 cm^2/Vs	$T = 4.2\text{ K}$		78G
---------	------------------------------------	--------------------	--	-----

effective masses

m^*	0.3 m_0	p-type	from Hall effect at RT	81S
	0.35 m_0	n-type		

71L Lee, T. H., Coburn, T., Gluck, R.: Solid State Commun. 9 (1971) 1821.
78G Goldstein, L., Gibart, P., Selmi, A.: J. Appl. Phys. 49 (1978) 1474.
81S Samokhalov, A. A., Gizhevskii, D. A., Loshkareva, N. N., Arbuzova, T. I., Simonova, M. I., Chebotaev, N. M.: Sov. Phys. Solid State 23 (1981) 2016.

37.2.12 ZnCr₂Se₄

crystal structure

spinel, space group O_h⁷-Fd3m.

energy gap

E_g	1.285 eV	optical measurement	66B2
-------	----------	---------------------	------

resistivity in $\Omega\text{ cm}$ at 300 K, room-temperature values of the **Hall coefficient** (in cm^3/C), **carrier concentration** (in cm^{-3}), **Hall mobility** (in cm^2/Vs).

ρ	40	no doping, no annealing treatment	74W
R_H	130		
n	$4.8 \cdot 10^{16}$		
μ_H	3		
ρ	28	same crystal as above, annealing treatment	
R_H	200		
n	$3.1 \cdot 10^{16}$	Se 60 mg, 600°C for 22 h	
μ_H	7		

66B2 Busch, G., Magyar, B., Wachter, P.: Phys. Lett. 23 (1966) 438.
74W Watanabe, T.: J. Phys. Soc. Jpn. 37 (1974) 140.

37.3 Further chalcogenides

37.3.1 Mn_xNbS₂

crystal structure

Sandwiches of hexagonally packed planes of metal between planes of chalcogen.

energy gap

E_g	0.85 eV	Mn _{0.3} NbS ₂	from photoemission	77F
-------	---------	------------------------------------	--------------------	-----

Hall coefficients, carrier concentration, resistivity, mobility

R_H	$9.7 \cdot 10^{-4} \text{ cm}^3 \text{ C}^{-1}$	Mn _{0.3} NbS ₂	orientation not specified	77F
n	$6.5 \cdot 10^{21} \text{ cm}^{-3}$			
ρ	$1.5 \cdot 10^{-4} \Omega \text{ cm}$			
μ	$6.3 \text{ cm}^2 \text{ V}^{-1} \text{ s}^{-1}$			

77F Friend, R. H., Deal, A. R., Yoffe, A. D.: Philos. Mag. 35 (1977) 1269.

37.3.2 Me_xNbS₂ (Me = Fe,Co,Ni)

crystal structure

Sandwiches of hexagonally packed planes of metal between planes of chalcogen.

energy gap

E_g	1.05 eV	Fe _{0.3} NbS ₂	(E_g = d-band width)	77F
	0.90 eV	Co _{0.3} NbS ₂	from photoemission	
	0.85 eV	Ni _{0.3} NbS ₂		

Hall coefficient, carrier concentration, resistivity, mobility

R_H	$1.4 \cdot 10^{-3} \text{ cm}^3 \text{ C}^{-1}$	Fe _{0.3} NbS ₂	orientation not specified	77F
n	$4.5 \cdot 10^{21} \text{ cm}^{-3}$			
ρ	$3.2 \cdot 10^{-4} \Omega \text{ cm}$			
μ	$4.4 \text{ cm}^2 \text{ V}^{-1} \text{ s}^{-1}$			
R_H	$1.7 \cdot 10^{-3} \text{ cm}^3 \text{ C}^{-1}$	Co _{0.3} NbS ₂		
n	$3.8 \cdot 10^{21} \text{ cm}^{-3}$			
ρ	$3.5 \cdot 10^{-4} \Omega \text{ cm}$			
μ	$5.1 \text{ cm}^2 \text{ V}^{-1} \text{ s}^{-1}$			
R_H	$9.4 \cdot 10^{-4} \text{ cm}^3 \text{ C}^{-1}$	Ni _{0.3} NbS ₂		
n	$6.6 \cdot 10^{21} \text{ cm}^{-3}$			
ρ	$2.2 \cdot 10^{-4} \Omega \text{ cm}$			
μ	$4.3 \text{ cm}^2 \text{ V}^{-1} \text{ s}^{-1}$			

77F Friend, R. H., Deal, A. R., Yoffe, A. D.: Philos. Mag. 35 (1977) 1269.

37.3.3 Ti_3VS_4

crystal structure

cubic, space group $T_d^3-\bar{1}4\ 3m$

energy gap

E_g 1.76 eV photoconductivity 74S

74S Shilova, M. V., Karpovich, I. A.: Inorg. Mater. 10 (1974) 475.

37.3.4 Cu_3VS_4

crystal structure

cubic [79P], space group $T_d^1-P\bar{4}\ 3m$ [78A]

Cu_3VS_4 is a semiconducting material with a small number of mobile ions ($n = 10^{17} \dots 10^{20} \text{ cm}^{-3}$)

electrical conductivity

σ $10^{-3} \dots 10 \ \Omega^{-1} \text{ cm}^{-1}$ 78A

Hall mobility

μ_H $4 \text{ cm}^2 \text{ V}^{-1} \text{ s}^{-1}$ 78A

78A Arribart, H., Sapoval, D., Gorochoy, O., Le Nagard, N.: Solid State Commun. 26 (1978) 435.

79P Petritis, D., Martinez, G.: Inst. Phys. Conf. Ser. 43 (1979) 677.

38 Ternary rare earth compounds

For a large number of rare earth compounds data on energy gaps or activation energies for conductivity are published. We list here only crystal structure, energy gaps resp. activation energies and transport data for those compounds where at least E_g or E_A data are available.

Substances

38.1 NdTiO₃

cubic (O _h ¹ -Pm3m)	76G
orthorhombic (D _{2h} ¹⁶ -Pbnm)	78B
E_A 0.06 eV	78B
σ 6.7 $\Omega^{-1} \text{ cm}^{-1}$ p-type	78B
76G Ganguly, P., Parkash, O., Rao, C. N. R.: Phys. Status Solidi (a) 36 (1976) 669.	
78B Bazuev, G. V., Shveikin, G. P.: Izv. Akad. Nauk SSSR, Neorg. Mater. 14 (1978) 267.	

38.2 SmTiO₃

orthorhombic (D _{2h} ¹⁶ -Pbnm)	69M
E_A 0.15 eV	78B
σ 0.24 $\Omega^{-1} \text{ cm}^{-1}$ p-type	78B
69M McCarthy, G. J., White, W. B., Roy, R.: Mater. Res. Bull. 4 (1969) 251.	
78B Bazuev, G. V., Shveikin, G. P.: Izv. Akad. Nauk SSSR, Neorg. Mater. 14 (1978) 267.	

38.3 GdTiO₃

orthorhombic (D _{2h} ¹⁶ -Pbnm)	69M
E_A 0.19 eV	78B
σ 3.6 $10^{-2} \Omega^{-1} \text{ cm}^{-1}$ p-type	78B
69M McCarthy, G. J., White, W. B., Roy, R.: Mater. Res. Bull. 4 (1969) 251.	
78B Bazuev, G. V., Shveikin, G. P.: Izv. Akad. Nauk SSSR, Neorg. Mater. 14 (1978) 267.	

38.4 TbTiO₃

orthorhombic (D _{2h} ¹⁶ -Pbnm)	69M
E_A 0.2 eV	78B
σ 9.1·10 ⁻³ $\Omega^{-1} \text{ cm}^{-1}$ p-type polycrystalline sample	78B
69M McCarthy, G. J., White, W. B., Roy, R.: Mater. Res. Bull. 4 (1969) 251.	
78B Bazuev, G. V., Shveikin, G. P.: Izv. Akad. Nauk SSSR, Neorg. Mater. 14 (1978) 267.	

38.5 HoTiO₃

orthorhombic (D _{2h} ¹⁶ -Pbnm)			69M
E _A	0.2 eV		78B
σ	1.1·10 ⁻² Ω ⁻¹ cm ⁻¹	p-type	78B
69M	McCarthy, G. J., White, W. B., Roy, R.: Mater. Res. Bull. 4 (1969) 251.		
78B	Bazuev, G. V., Shveikin, G. P.: Izv. Akad. Nauk SSSR, Neorg. Mater. 14 (1978) 267.		

38.6 ErTiO₃

orthorhombic (D _{2h} ¹⁶ -Pbnm)			69M
E _A	0.24 eV		78B
σ	7.1·10 ⁻³ Ω ⁻¹ cm ⁻¹	p-type	78B
69M	McCarthy, G. J., White, W. B., Roy, R.: Mater. Res. Bull. 4 (1969) 251.		
78B	Bazuev, G. V., Shveikin, G. P.: Izv. Akad. Nauk SSSR, Neorg. Mater. 14 (1978) 267.		

38.7 YbTiO₃

orthorhombic (D _{2h} ¹⁶ -Pbnm)			69M
E _A	0.24 eV		78B
σ	8.3·10 ⁻³ Ω ⁻¹ cm ⁻¹	p-type	78B
	≈ 10 ⁻¹ Ω ⁻¹ cm ⁻¹	polycrystalline sample;	76G
69M	McCarthy, G. J., White, W. B., Roy, R.: Mater. Res. Bull. 4 (1969) 251.		
76G	Ganguly, P., Parkash, O., Rao, C. N. R.: Phys. Status Solidi (a) 36 (1976) 669.		
78B	Bazuev, G. V., Shveikin, G. P.: Izv. Akad. Nauk SSSR, Neorg. Mater. 14 (1978) 267.		

38.8 CeVO₃

tetragonal			74M
E _A	0.041 eV	T = 120...170 K	76S
	0.054 eV	T = 170...300 K	
74M	McCarthy, G. J., Sipe, C. A., McIlvried: Mater. Res. Bull. 9 (1974) 1279.		
76S	Sakai, T., Adachi, G., Shiokawa, J.: Mater. Res. Bull. 11 (1976) 1295.		

38.9 PrVO₃

orthorhombic (D _{2h} ¹⁶ -Pbnm)			74M
E _A	0.065 eV	T = 100...180 K	76S
	0.103 eV	T = 180...300 K	
74M	McCarthy, G. J., Sipe, C. A., McIlvried: Mater. Res. Bull. 9 (1974) 1279.		
76S	Sakai, T., Adachi, G., Shiokawa, J.: Mater. Res. Bull. 11 (1976) 1295.		

38.10 NdVO₃

orthorhombic (D _{2h} ¹⁶ -Pbnm)			74M
E_A	0.16 eV		76G
	0.060 eV	$T = 100...130$ K	76S
	≈ 0 eV	$T = 130...300$ K	
74M	McCarthy, G. J., Sipe, C. A., McIlvried: Mater. Res. Bull. 9 (1974) 1279.		
76G	Ganguly, P., Parkash, O., Rao, C. N. R.: Phys. Status Solidi (a) 36 (1976) 669.		
76S	Sakai, T., Adachi, G., Shiokawa, J.: Mater. Res. Bull. 11 (1976) 1295.		

38.11 SmVO₃

orthorhombic (D _{2h} ¹⁶ -Pbnm)			74M
E_A	0.106 eV	$T = 100...175$ K	76S
	0.130 eV	$T = 175...300$ K	
74M	McCarthy, G. J., Sipe, C. A., McIlvried: Mater. Res. Bull. 9 (1974) 1279.		
76S	Sakai, T., Adachi, G., Shiokawa, J.: Mater. Res. Bull. 11 (1976) 1295.		

38.12 EuVO₃

orthorhombic (D _{2h} ¹⁶ -Pbnm)			74M
E_A	0.099 eV	$T = 110...175$ K	76S
	0.132 eV	$T = 175...300$ K	
	0.18 eV		76G
74M	McCarthy, G. J., Sipe, C. A., McIlvried: Mater. Res. Bull. 9 (1974) 1279.		
76G	Ganguly, P., Parkash, O., Rao, C. N. R.: Phys. Status Solidi (a) 36 (1976) 669.		
76S	Sakai, T., Adachi, G., Shiokawa, J.: Mater. Res. Bull. 11 (1976) 1295.		

38.13 GdVO₃

orthorhombic (D _{2h} ¹⁶ -Pbnm)			74M
E_A	0.100 eV	$T = 100...165$ K	76S
	0.141 eV	$T = 165...300$ K	
	0.20 eV		76G
	0.96 eV	$T > 520$ K	75P
	0.23 eV	$T < 520$ K	
σ	$10^{-6} \Omega^{-1} \text{ cm}^{-1}$	p-type	75P
74M	McCarthy, G. J., Sipe, C. A., McIlvried: Mater. Res. Bull. 9 (1974) 1279.		
75P	Palanisamy, T., Gopalakrishnan, J., Sastri, M. V. C.: Z. Anorg. Allgem. Chem. 415 (1975) 275.		
76G	Ganguly, P., Parkash, O., Rao, C. N. R.: Phys. Status Solidi (a) 36 (1976) 669.		
76S	Sakai, T., Adachi, G., Shiokawa, J.: Mater. Res. Bull. 11 (1976) 1295.		

38.14 TbVO₃

orthorhombic (D _{2h} ¹⁶ -Pbnm)			74M
<i>E_A</i>	0.101 eV	<i>T</i> = 105...185 K	76S
	0.116 eV	<i>T</i> = 185...300 K	
74M	McCarthy, G. J., Sipe, C. A., McIlvried: Mater. Res. Bull. 9 (1974) 1279.		
76S	Sakai, T., Adachi, G., Shiokawa, J.: Mater. Res. Bull. 11 (1976) 1295.		

38.15 DyVO₃

orthorhombic (D _{2h} ¹⁶ -Pbnm)			74M
<i>E_A</i>	0.095 eV	<i>T</i> = 100...190 K	76S
	0.125 eV	<i>T</i> = 190...300 K	
74M	McCarthy, G. J., Sipe, C. A., McIlvried: Mater. Res. Bull. 9 (1974) 1279.		
76S	Sakai, T., Adachi, G., Shiokawa, J.: Mater. Res. Bull. 11 (1976) 1295.		

38.16 HoVO₃

orthorhombic (D _{2h} ¹⁶ -Pbnrn)			74M
<i>E_A</i>	0.102 eV	<i>T</i> = 120...180 K	76S
	0.128 eV	<i>T</i> = 180...300 K	
74M	McCarthy, G. J., Sipe, C. A., McIlvried: Mater. Res. Bull. 9 (1974) 1279.		
76S	Sakai, T., Adachi, G., Shiokawa, J.: Mater. Res. Bull. 11 (1976) 1295.		

38.17 ErVO₃

orthorhombic (D _{2h} ¹⁶ -Pbnm)			74M
<i>E_A</i>	0.121 eV	<i>T</i> = 125...190 K	76S
	0.173 eV	<i>T</i> = 190...300 K	
74M	McCarthy, G. J., Sipe, C. A., McIlvried: Mater. Res. Bull. 9 (1974) 1279.		
76S	Sakai, T., Adachi, G., Shiokawa, J.: Mater. Res. Bull. 11 (1976) 1295.		

38.18 TmVO₃

orthorhombic (D _{2h} ¹⁶ -Pbnm)			74M
<i>E_A</i>	0.122 eV	<i>T</i> = 130...185 K	76S
	0.166 eV	<i>T</i> = 185...300 K	
74M	McCarthy, G. J., Sipe, C. A., McIlvried: Mater. Res. Bull. 9 (1974) 1279.		
76S	Sakai, T., Adachi, G., Shiokawa, J.: Mater. Res. Bull. 11 (1976) 1295.		

38.19 YbVO₃

orthorhombic (D _{2h} ¹⁶ -Pbnm)			74M
E_A	0.125 eV	$T = 100...190$ K	76S
	0.169 eV	$T = 190...300$ K	
	0.17 eV		76G
74M	McCarthy, G. J., Sipe, C. A., McIlvried: Mater. Res. Bull. 9 (1974) 1279.		
76G	Ganguly, P., Parkash, O., Rao, C. N. R.: Phys. Status Solidi (a) 36 (1976) 669.		
76S	Sakai, T., Adachi, G., Shiokawa, J.: Mater. Res. Bull. 11 (1976) 1295.		

38.20 LuVO₃

orthorhombic (D _{2h} ¹⁶ -Pbam)			74M
E_A	0.127 eV	$T = 120...185$ K	76S
	0.171 eV	$T = 185...300$ K	
74M	McCarthy, G. J., Sipe, C. A., McIlvried: Mater. Res. Bull. 9 (1974) 1279.		
76S	Sakai, T., Adachi, G., Shiokawa, J.: Mater. Res. Bull. 11 (1976) 1295.		

38.21 LaCrO₃

orthorhombic (D _{2h} ¹⁶ -Pbnm)			57G
rhombohedral for $T > 540$ K			73T
E_A	0.6 eV	$T = 300...800$ K	67R
	0.55 eV	$T = 300...800$ K	69M
	0.22 eV	$T = 300...800$ K	71S
	0.18 eV	$T = 77...300$ K	77W
	0.25 eV	$T < 350$ K	80T
	0.28 eV	$T = 350...685$ K	
	0.22 eV	$T = 685...1000$ K	
σ	$10^{-2} \Omega^{-1} \text{ cm}^{-1}$	p-type	77W
p	$5 \cdot 10^{19} \text{ cm}^{-3}$		77W
μ_p	$5.2 \cdot 10^{-4} \text{ cm}^2 \text{ V}^{-1} \text{ s}^{-1}$		77W
	$5 \cdot 10^{-3} \text{ cm}^2 \text{ V}^{-1} \text{ s}^{-1}$		69M
E_g	4.7 eV		70S,
			71S
57G	Geller, S.: Acta Crystallogr. 10 (1957) 243.		
67R	Ruiz, J. S., Anthony, A. M., Foex, M. M.: C. R. Acad. Sc. Paris 264 (1967) 1271.		
69M	McCarthy, G. J., White, W. B., Roy, R.: Mater. Res. Bull. 4 (1969) 251.		
70S	Subba Rao, G. V., Ferraro, J. R., Rao, C. N. R.: J. Appl. Spectrosc. 24 (1970) 436.		
71S	Subba Rao, G. V., Wanklyn, B. M., Rao, C. N. R.: J. Phys. Chem. Solids 32 (1971) 345.		
73T	Terao, N.: C. R. Acad. Sci. (Paris) Ser. C 276 (1973) 5.		
77W	Webb, J. B., Sayer, M., Mansingh, A.: Can. J. Phys. 55 (1977) 1725.		

38.22 NdCrO₃

orthorhombic (D _{2h} ¹⁶ -Pbnm)			63Q
E_A	0.29 eV	$T = 300 \dots 625$ K	80T
	0.22 eV	$T = 625 \dots 1000$ K	
63Q	Quezel-Ambrunaz, S., Mareschal, M.: Bull. Soc. Fr. Mineral. Crystallogr. 36 (1963) 204.		
80T	Tripathi, A. K., Lal, H. B.: Mater. Res. Bull. 15 (1980) 233.		

38.23 SmCrO₃

orthorhombic (D _{2h} ¹⁶ -Pbnm)			63Q
	0.20 eV	$T = 625 \dots 1000$ K	
E_A	0.36 eV	$T = 300 \dots 625$ K	80T
63Q	Quezel-Ambrunaz, S., Mareschal, M.: Bull. Soc. Fr. Mineral. Crystallogr. 36 (1963) 204.		
80T	Tripathi, A. K., Lal, H. B.: Mater. Res. Bull. 15 (1980) 233.		

38.24 DyCrO₃

orthorhombic (D _{2h} ¹⁶ -Pbnm)				63Q
E _A	0.27 eV			71S
σ	3.1·10 ⁻⁴ Ω ⁻¹ cm ⁻¹	T = 20°C, p-type	pressed polycrystalline pellets	712
	3.6·10 ⁻³ Ω ⁻¹ cm ⁻¹	T = 500°C, p-type		
	6.6·10 ⁻³ Ω ⁻¹ cm ⁻¹	T = 700°C, p-type		
63Q	Quezel-Ambrunaz, S., Mareschal, M.: Bull. Soc. Fr. Mineral. Crystallogr. 36 (1963) 204.			
71S	Subba Rao, G. V., Wanklyn, B. M., Rao, C. N. R.: J. Phys. Chem. Solids 32 (1971) 345.			

38.25 HoCrO₃

orthorhombic (D _{2h} ¹⁶ -Pbnm)				63Q
E _A	0.33 eV			71S
σ	9·10 ⁻⁵ Ω ⁻¹ cm ⁻¹	T = 200°C,	p-type pressed polycrystalline pellets;	71S
	1.41·10 ⁻³ Ω ⁻¹ cm ⁻¹	T = 500°C, p-type		
	3.1·10 ⁻³ Ω ⁻¹ cm ⁻¹	T = 700°C, p-type		
63Q	Quezel-Ambrunaz, S., Mareschal, M.: Bull. Soc. Fr. Mineral. Crystallogr. 36 (1963) 204.			
71S	Subba Rao, G. V., Wanklyn, B. M., Rao, C. N. R.: J. Phys. Chem. Solids 32 (1971) 345.			

38.26 YbCrO₃

orthorhombic (D _{2h} ¹⁶ -Pbnm)				63Q
E _A	0.37 eV			71S
σ	3·10 ⁻⁵ Ω ⁻¹ cm ⁻¹	T = 200°C, p-type	pressed polycrystalline pellets	71S
	9.2·10 ⁻⁴ Ω ⁻¹ cm ⁻¹	T = 500°C, p-type		
	1.62·10 ⁻³ Ω ⁻¹ cm ⁻¹	T = 700°C, p-type		
63Q	Quezel-Ambrunaz, S., Mareschal, M.: Bull. Soc. Fr. Mineral. Crystallogr. 36 (1963) 204.			
71S	Subba Rao, G. V., Wanklyn, B. M., Rao, C. N. R.: J. Phys. Chem. Solids 32 (1971) 345.			

38.27 LaMn_{0.75}Mo_{0.25}O₃

orthorhombic

E_A 0.3 eV

σ $5 \cdot 10^{-5} \Omega^{-1} \text{ cm}^{-1}$ $T = 50^\circ\text{C}$ pressed polycrystalline pellet

80S Subramanian, M. A., Torardi, C. C., Johnson, D. C., Pannetier, J., Sleight, A. W.: J. Solid State Chem. 72 (1988) 24.

38.28 HoMnO₃

hexagonal (C_{6v}^3 -P6₃cm)

70P

orthorhombic (D_{2h}^{16} -Pbnm) (high pressure phase)

66W

E_A 0.57 eV

71S

σ $1 \cdot 10^{-5} \Omega^{-1} \text{ cm}^{-1}$ $T = 200^\circ\text{C}$, p-type pressed polycrystalline pellet;
 $5.6 \cdot 10^{-4} \Omega^{-1} \text{ cm}^{-1}$ $T = 500^\circ\text{C}$, p-type
 $1.5 \cdot 10^{-3} \Omega^{-1} \text{ cm}^{-1}$ $T = 700^\circ\text{C}$, p-type

71S

66W Waintal, A., Capponi, J. J., Bertaut, E. F.: Solid State Commun. 4 (1966) 125.

70P Pauthenet, R., Veyret, C.: J. Phys. (Paris) 31 (1979) 65.

71S Subba Rao, G. V., Wanklyn, B. M., Rao, C. N. R.: J. Phys. Chem. Solids 32 (1971) 345.

38.29 YbMnO₃

hexagonal (C_{6v}^3 -P6₃cm)

63Y

orthorhombic (high-pressure phase)

67W

E_A 0.73 eV

71S

σ $3.1 \cdot 10^{-4} \Omega^{-1} \text{ cm}^{-1}$ $T = 500^\circ\text{C}$, p-type pressed polycrystalline pellet
 $2.9 \cdot 10^{-3} \Omega^{-1} \text{ cm}^{-1}$ $T = 700^\circ\text{C}$, p-type

71S

63Y Yakel, H. L., Koebler, W. C., Bertaut, E. F., Forrat, E. F.: Acta Crystallogr. 16 (1 963) 957.

67W Waintal, A., Chenavas, J.: Mater. Res. Bull 2 (1967) 819.

71S Subba Rao, G. V., Wanklyn, B. M., Rao, C. N. R.: J. Phys. Chem. Solids 32 (1971) 345.

38.30 LaFeO₃

orthorhombic (D_{2h}^{16} -Pbnm)

56G

rhombohedral above 980°C

59D

E_A 0.39 eV $T < 470^\circ\text{C}$

71S

0.22 eV $T > 470^\circ\text{C}$

σ $2.5 \cdot 10^{-3} \Omega^{-1} \text{ cm}^{-1}$ $T = 500^\circ\text{C}$, p-type pressed polycrystalline pellet
 $4.4 \cdot 10^{-3} \Omega^{-1} \text{ cm}^{-1}$ $T = 700^\circ\text{C}$, p-type

71S

56G Geller, S., Wood, E. A.: Acta Crystallogr. 9 (1956) 563.

59D Dalziel, J. A. W.: J. Chem. Soc. London 1959, 1993.

71S Subba Rao, G. V., Wanklyn, B. M., Rao, C. N. R.: J. Phys. Chem. Solids 32 (1971) 345.

38.31 LaFe_{0.75}Mo_{0.25}O₃

orthorhombic

E_A 0.14 eV

σ $3.2 \cdot 10^{-3} \Omega^{-1} \text{ cm}^{-1}$ $T = 50^\circ\text{C}$, pressed polycrystalline pellets

80S Subramanian, M. A., Torardi, C. C., Johnson, D. C., Pannetier, J., Sleight, A. W.: J. Solid State Chem. 72 (1988) 24.

38.32 PrFe_{0.75}Mo_{0.25}O₃

orthorhombic

E_A 0.15 eV

σ $3.1 \cdot 10^{-3} \Omega^{-1} \text{ cm}^{-1}$ $T = 50^\circ\text{C}$, pressed polycrystalline pellet, n-type

80S Subramanian, M. A., Torardi, C. C., Johnson, D. C., Pannetier, J., Sleight, A. W.: J. Solid State Chem. 72 (1988) 24.

38.33 NdFe_{0.75}Mo_{0.25}O₃

orthorhombic

E_A 0.19 eV

σ $2.6 \cdot 10^{-3} \Omega^{-1} \text{ cm}^{-1}$ $T = 50^\circ\text{C}$, pressed polycrystalline pellet, n-type

80S Subramanian, M. A., Torardi, C. C., Johnson, D. C., Pannetier, J., Sleight, A. W.: J. Solid State Chem. 72 (1988) 24.

38.34 SmFe_{0.75}Mo_{0.25}O₃

orthorhombic

E_A 0.2 eV

σ $3 \cdot 10^{-3} \Omega^{-1} \text{ cm}^{-1}$ $T = 50^\circ\text{C}$, pressed polycrystalline pellet
n-type

80S Subramanian, M. A., Torardi, C. C., Johnson, D. C., Pannetier, J., Sleight, A. W.: J. Solid State Chem. 72 (1988) 24.

38.35 EuFe_{0.75}Mo_{0.25}O₃

orthorhombic

E_A 0.2 eV

σ $2 \cdot 10^{-3} \Omega^{-1} \text{ cm}^{-1}$ $T = 50^\circ\text{C}$, pressed polycrystalline pellet, n-type

80S Subramanian, M. A., Torardi, C. C., Johnson, D. C., Pannetier, J., Sleight, A. W.: J. Solid State Chem. 72 (1988) 24.

38.36 GdFeO₃

orthorhombic (D_{2h}¹⁶-Pbnm)

70M

E_A	0.89 eV	$T < 385^\circ\text{C}$	p-type semiconductor;	71S
	1.10 eV	$T > 385^\circ\text{C}$		

70M Marezio, M., Remeika, J. P., Dernier, P. D.: Acta Crystallogr. B 26 (1970) 2008.

71S Subba Rao, G. V., Wanklyn, B. M., Rao, C. N. R.: J. Phys. Chem. Solids 32 (1971) 345.

38.37 GdFe_{0.75}Mo_{0.25}O₃

orthorhombic

E_A 0.23 eV

σ $1.8 \cdot 10^{-3} \Omega^{-1} \text{cm}^{-1}$ $T = 50^\circ\text{C}$ pressed polycrystalline pellet; n-type

80S Subramanian, M. A., Torardi, C. C., Johnson, D. C., Pannetier, J., Sleight, A. W.: J. Solid State Chem. 72 (1988) 24.

38.38 TbFe_{0.75}Mo_{0.25}O₃

orthorhombic

E_A 0.23 eV

σ $9.1 \cdot 10^{-4} \Omega^{-1} \text{cm}^{-1}$ $T = 50^\circ\text{C}$, pressed polycrystalline pellet
n-type

80S Subramanian, M. A., Torardi, C. C., Johnson, D. C., Pannetier, J., Sleight, A. W.: J. Solid State Chem. 72 (1988) 24.

38.39 DyFe_{0.75}Mo_{0.25}O₃

orthorhombic

E_A 0.26 eV

σ $5.9 \cdot 10^{-4} \Omega^{-1} \text{cm}^{-1}$ $T = 50^\circ\text{C}$, pressed polycrystalline pellet
n-type

80S Subramanian, M. A., Torardi, C. C., Johnson, D. C., Pannetier, J., Sleight, A. W.: J. Solid State Chem. 72 (1988) 24.

38.40 HoFeO₃

orthorhombic (D_{2h}¹⁶-Pbnm)

E_A	1.10 eV	$T < 367^\circ\text{C}$	71S
	0.31 eV	$T > 367^\circ\text{C}$	

σ $8.4 \cdot 10^{-4} \Omega^{-1} \text{cm}^{-1}$ $T = 500^\circ\text{C}$, p-type pressed polycrystalline pellets 71S
 $2.2 \cdot 10^{-3} \Omega^{-1} \text{cm}^{-1}$ $T = 700^\circ\text{C}$, p-type

71S Subba Rao, G. V., Wanklyn, B. M., Rao, C. N. R.: J. Phys. Chem. Solids 32 (1971) 345.

38.41 HoFe_{0.75}Mo_{0.25}O₃

orthorhombic

E_A 0.3 eV

σ $1.4 \cdot 10^{-4} \Omega^{-1} \text{ cm}^{-1}$ $T = 50^\circ\text{C}$, pressed polycrystalline pellet
n-type

80S Subramanian, M. A., Torardi, C. C., Johnson, D. C., Pannetier, J., Sleight, A. W.: J. Solid State Chem. 72 (1988) 24.

38.42 ErFe_{0.75}Mo_{0.25}O₃

orthorhombic

E_A 0.3 eV

σ $1.4 \cdot 10^{-4} \Omega^{-1} \text{ cm}^{-1}$ $T = 50^\circ\text{C}$, pressed polycrystalline pellet
n-type

80S Subramanian, M. A., Torardi, C. C., Johnson, D. C., Pannetier, J., Sleight, A. W.: J. Solid State Chem. 72 (1988) 24.

38.43 TmFe_{0.75}Mo_{0.25}O₃

orthorhombic

E_A 0.32 eV

σ $5.3 \cdot 10^{-5} \Omega^{-1} \text{ cm}^{-1}$ $T = 50^\circ\text{C}$, pressed polycrystalline pellet
n-type

80S Subramanian, M. A., Torardi, C. C., Johnson, D. C., Pannetier, J., Sleight, A. W.: J. Solid State Chem. 72 (1988) 24.

38.44 YbFeO₃

orthorhombic (D_{2h}¹⁶-Pbnm)

65E

E_A 1.05 eV $T > 700^\circ\text{C}$

71S2

σ $1 \cdot 10^{-5} \Omega^{-1} \text{ cm}^{-1}$ $T = 500^\circ\text{C}$, p-type pressed polycrystalline pellet
 $9.3 \cdot 10^{-4} \Omega^{-1} \text{ cm}^{-1}$ $T = 700^\circ\text{C}$, p-type

71S2

65E Eibschütz, M.: Acta Crystallogr. 19 (1965) 337.

71S2 Subba Rao, G. V., Wanklyn, B. M., Rao, C. N. R.: J. Phys. Chem. Solids 32 (1971) 345.

38.45 YbFe_{0.75}Mo_{0.25}O₃

orthorhombic

E_A 0.37 eV

σ $4.8 \cdot 10^{-5} \Omega^{-1} \text{ cm}^{-1}$ $T = 50^\circ\text{C}$, pressed polycrystalline pellet
n-type

80S Subramanian, M. A., Torardi, C. C., Johnson, D. C., Pannetier, J., Sleight, A. W.: J. Solid State Chem. 72 (1988) 24.

38.46 LuFe_{0.75}Mo_{0.25}O₃

orthorhombic

$$E_A \quad 0.36 \text{ eV}$$

$$\sigma \quad 4 \cdot 10^{-5} \Omega^{-1} \text{ cm}^{-1} \quad T = 50^\circ\text{C}, \quad \text{pressed polycrystalline pellet}$$

n-type

80S Subramanian, M. A., Torardi, C. C., Johnson, D. C., Pannetier, J., Sleight, A. W.: J. Solid State Chem. 72 (1988) 24.

38.47 LaCo_{0.75}Mo_{0.25}O₃

orthorhombic

$$E_A \quad 0.22 \text{ eV}$$

$$\sigma \quad 8.3 \cdot 10^{-4} \Omega^{-1} \text{ cm}^{-1} \quad T = 50^\circ\text{C}, \quad \text{pressed polycrystalline pellet}$$

n-type

80S Subramanian, M. A., Torardi, C. C., Johnson, D. C., Pannetier, J., Sleight, A. W.: J. Solid State Chem. 72 (1988) 24.

38.48 LaCo_{0.75}W_{0.25}O₃

orthorhombic

lattice parameters

$$a \quad 5.586 \text{ \AA}$$

$$b \quad 5.628 \text{ \AA}$$

$$c \quad 7.983 \text{ \AA}$$

$$E_A \quad 0.33 \text{ eV}$$

$$\sigma \quad 1.2 \cdot 10^{-4} \Omega^{-1} \text{ cm}^{-1} \quad T = 50^\circ\text{C}, \quad \text{pressed polycrystalline pellet}$$

n-type

80S Subramanian, M. A., Torardi, C. C., Johnson, D. C., Pannetier, J., Sleight, A. W.: J. Solid State Chem. 72 (1988) 24.

38.49 LaNi_{0.75}Mo_{0.25}O₃

cubic (O_h⁵-Fm3m)

$$E_A \quad 0.11 \text{ eV}$$

$$\sigma \quad 0.63 \Omega^{-1} \text{ cm}^{-1} \quad T = 50^\circ\text{C},$$

p-type

80S Subramanian, M. A., Torardi, C. C., Johnson, D. C., Pannetier, J., Sleight, A. W.: J. Solid State Chem. 72 (1988) 24.

38.50 LaNi_{0.75}W_{0.25}O₃

cubic (O_h⁵-Fm3m)

E_A	0.23 eV		
σ	$2.5 \cdot 10^{-5} \Omega^{-1} \text{ cm}^{-1}$	$T = 50^\circ\text{C}$, p-type	
80S	Subramanian, M. A., Torardi, C. C., Johnson, D. C., Pannetier, J., Sleight, A. W.: J. Solid State Chem. 72 (1988) 24.		

38.51 La₂(WO₄)₃

monoclinic (C _{2h} ⁶ -A2/a)				65N
σ	1.23·10 ² Ω ⁻¹ m ⁻¹	p-type		88L
E _A	2.40 eV	T = 1050 ... 1200 K,		88L
		val. - cond. band		
	2.24 eV	T = 600...950 K,		79D
		n-type		
	2.40 eV	T = 1050...1200 K,		
		p-type		
μ _n	1.15...0.81 cm ² V ⁻¹ s ⁻¹	T = 600...950 K	polycrystalline pellet	79D
65N	Nassau, K., Levinstein, H. J., Loiacono, G. M.: J. Phys. Chem. Solids 26 (1965) 1805.			
79D	Dar, N., Lal, H. B.: Mater. Res. Bull. 14 (1979) 1263.			
88L	Lal, H. B., Kanchan Gaur, : J. Mater. Sci. 23 (1988) 919.			

38.52 Ce₂(WO₄)₃

monoclinic (C _{2h} ⁶ -A2/a)				65N
σ	5.20·10 ¹ Ω ⁻¹ m ⁻¹	n-type		88L
E_A	1.9 eV	$T = 600...800$ K,		79D
	1.90 eV	$T = 600 \dots 800$ K,		88L
		4f ¹ - cond. band		
μ_n	1.30 cm ² V ⁻¹ s ⁻¹	$T = 900$ K		88L
μ_n	1.3...1.05 cm ² V ⁻¹ s ⁻¹	$T = 600...800$ K	polycrystalline pellet	79D
65N	Nassau, K., Levinstein, H. J., Loiacono, G. M.: J. Phys. Chem. Solids 26 (1965) 1805.			
79D	Dar, N., Lal, H. B.: Mater. Res. Bull. 14 (1979) 1263.			
88L	Lal, H. B., Kanchan Gaur, : J. Mater. Sci. 23 (1988) 919.			

38.53 Pr₂(WO₄)₃

monoclinic (C _{2h} ⁶ -A2/a)			65N
σ	$1.30 \cdot 10^1 \Omega^{-1} \text{m}^{-1}$	n-type	88L
	$1.06 \cdot 10^2 \Omega^{-1} \text{m}^{-1}$	p-type	88L
E_A	2.48 eV	$T = 1000 \dots 1200 \text{ K}$, val. - cond. band	88L
	2.12 eV	$T = 600 \dots 950 \text{ K}$, 4f ² - cond. band	88L
	2.12 eV	$T = 600 \dots 950 \text{ K}$, n-type	79D
	2.48 eV	$T = 1000 \dots 1200 \text{ K}$, p-type	
μ_n	$0.32 \dots 0.23 \text{ cm}^2 \text{ V}^{-1} \text{ s}^{-1}$	$T = 600 \dots 950 \text{ K}$ polycrystalline sample	79D
μ_n	$0.25 \text{ cm}^2 \text{ V}^{-1} \text{ s}^{-1}$	$T = 900 \text{ K}$	88L
65N	Nassau, K., Levinstein, H. J., Loiacono, G. M.: J. Phys. Chem. Solids 26 (1965) 1805.		
79D	Dar, N., Lal, H. B.: Mater. Res. Bull. 14 (1979) 1263.		
88L	Lal, H. B., Kanchan Gaur, : J. Mater. Sci. 23 (1988) 919.		

38.54 Nd₂(WO₄)₃

monoclinic (C _{2h} ⁶ -A2/a)			65N
σ	$2.60 \cdot 10^3 \Omega^{-1} \text{m}^{-1}$	p-type	88L
E_A	2.50 eV	$T = 600 \dots 1000^\circ \text{C}$, p-type	79D
	2.60 eV	$T = 1050 \dots 1200^\circ \text{C}$, p-type	
	2.50 eV	$T = 1000 \dots 1200 \text{ K}$, val.-cond. band	88L
μ_n	$0.89 \dots 0.42 \text{ cm}^2 \text{ V}^{-1} \text{ s}^{-1}$	$T = 600 \dots 1000^\circ \text{C}$ polycrystalline pellet	79D
	$0.99 \dots 0.82 \text{ cm}^2 \text{ V}^{-1} \text{ s}^{-1}$	$T = 1050 \dots 1200^\circ \text{C}$	
	$0.60 \text{ cm}^2 \text{ V}^{-1} \text{ s}^{-1}$	$T = 900 \text{ K}$	88L
μ_p	$1.13 \dots 0.53 \text{ cm}^2 \text{ V}^{-1} \text{ s}^{-1}$	$T = 600 \dots 1000^\circ \text{C}$	79D
	$1.29 \dots 1.06 \text{ cm}^2 \text{ V}^{-1} \text{ s}^{-1}$	$T = 1050 \dots 1200^\circ \text{C}$	
	$0.86 \text{ cm}^2 \text{ V}^{-1} \text{ s}^{-1}$	$T = 900 \text{ K}$	88L
65N	Nassau, K., Levinstein, H. J., Loiacono, G. M.: J. Phys. Chem. Solids 26 (1965) 1805.		
79D	Dar, N., Lal, H. B.: Mater. Res. Bull. 14 (1979) 1263.		
88L	Lal, H. B., Kanchan Gaur, : J. Mater. Sci. 23 (1988) 919.		

38.55 Sm₂(WO₄)₃

monoclinic (C _{2h} ⁶ -A2/a)			65N
σ	$6.50 \cdot 10^1 \Omega^{-1} \text{m}^{-1}$	p-type	88L
E_A	2.00 eV	$T = 600 \dots 1200 \text{ K}$,	88L
		val. band - 4f ⁶	
	2 eV	$T = 600 \dots 1200 \text{ K}$	79D
		p-type	
μ_p	$1.59 \dots 0.95 \text{ cm}^2 \text{V}^{-1} \text{s}^{-1}$	$T = 600 \dots 1200 \text{ K}$ polycrystalline pellet	79D
65N	Nassau, K., Levinstein, H. J., Loiacono, G. M.: J. Phys. Chem. Solids 26 (1965) 1805.		
79D	Dar, N., Lal, H. B.: Mater. Res. Bull. 14 (1979) 1263.		
88L	Lal, H. B., Kanchan Gaur, : J. Mater. Sci. 23 (1988) 919.		

38.56 EuWO₄

scheelite-type (C _{4h} ⁶)			71M
E_g	3.1 eV	from conductivity	74L
E_A	0.08 eV	$T = 680 \text{ K}$	74L
	0.3 eV	$T = 725 \text{ K}$	
σ	$10^{-8} \Omega^{-1} \text{cm}^{-1}$	$T < 500 \text{ K}$, $\perp c$	74L
μ_{pol}	$10^{-2} \text{ cm}^2 \text{V}^{-1} \text{s}^{-1}$		74L
m^{**}	$100 m_0$	$T > 725 \text{ K}$	74L
71M	McCarthy, G. J.: Mater. Res. Bull. 6 (1971) 31.		
74L	Lal, H. B., Dar, N., Kumar, A.: J. Phys. C 7 (1974) 4335.		

38.57 Eu₂(WO₄)₃

monoclinic (C _{2h} ⁶ -A2/a)			65N
σ	$2.35 \cdot 10^2 \Omega^{-1} \text{m}^{-1}$	p-type	88L
E_A	1.84 eV	$T = 600 \dots 800 \text{ K}$,	88L
		val. band - 4f ⁷	
	1.84 eV	$T = 600 \dots 790 \text{ K}$,	79D
		p-type	
	2.40 eV	$T = 900 \dots 1200 \text{ K}$,	
		p-type	
μ_p	$5.70 \dots 4.64 \text{ cm}^2 \text{V}^{-1} \text{s}^{-1}$	$T = 600 \dots 790 \text{ K}$ polycrystalline sample	79D
	$5.02 \text{ cm}^2 \text{V}^{-1} \text{s}^{-1}$	$T = 900 \text{ K}$	88L
m^{**}	$418.4 m_0$		76L
65N	Nassau, K., Levinstein, H. J., Loiacono, G. M.: J. Phys. Chem. Solids 26 (1965) 1805.		
76L	Lal, H. B., Dar, N., Lundgren, L.: J. Phys. Soc. Jpn. 41 (1976) 1216.		
79D	Dar, N., Lal, H. B.: Mater. Res. Bull. 14 (1979) 1263.		
88L	Lal, H. B., Kanchan Gaur, : J. Mater. Sci. 23 (1988) 919.		

38.58 Cu3ErS3

trigonal (P3̄)

Eg 1.62 eV

81R Rustamov, , P. G., Aliev, O. M.: Akad. Nauk SSSR, Izd. ELM, Baku 1981 (russian).

38.59 Cu3TmS3

trigonal (P3̄)

Eg 1.60 eV

81R Rustamov, , P. G., Aliev, O. M.: Akad. Nauk SSSR, Izd. ELM, Baku 1981 (russian).

38.60 Gd2CuO4

tetragonal (K2NiF4-type) 74G, 61F

EA	0.90 eV	T = 100...287°C	74G
	0.40 eV	T = 287...582	
	0.80 eV	T = 582...900°C	

61F Foex, M.: Bull. Soc. Chim. France 1961, 109.
74G George, A. M., Gopalakrishnan, I. K., Karkhanavala, M. D.: Mater. Res. Bull. 9 (1974) 721.

38.61 Gd2(WO4)3

orthorhombic (F2/d) 65N

μn	0.14...0.05 cm² V⁻¹ s⁻¹	79D
μp	0.46...0.16 cm² V⁻¹ s⁻¹	79D

65N Nassau, K., Levinstein, H. J., Loiacono, G. M.: J. Phys. Chem. Solids 26 (1965) 1805.
79D Dar, N., Lal, H. B.: Mater. Res. Bull. 14 (1979) 1263.

38.62 Tb2(WO4)3

[81V]

EA	1.15 eV	T < 1010 K	activation energies for conductivity
	1.85 eV	T > 1010 K	
σ0	8.15·10⁻² Ω⁻¹cm⁻¹	T < 1010 K	pre-exponential factors for conductivity
	2.44·10² Ω⁻¹cm⁻¹	T > 1010 K	

81V Verma, B.K., Lal, H.B.: Mater. Res. Bull. 16 (1981) 1579-1591.

38.63 Dy2(WO4)3

EA	0.87 eV	T < 940 K	activation energies for conductivity
	1.60 eV	T > 940 K	
σ0	9.27·10⁻³ Ω⁻¹cm⁻¹	T < 940 K	pre-exponential factors for conductivity
	7.13·10¹ Ω⁻¹cm⁻¹	T > 940 K	

81V Verma, B.K., Lal, H.B.: Mater. Res. Bull. 16 (1981) 1579-1591.

38.64 Ho₂(WO₄)₃

E_A	1.35 eV	$T < 1000$ K	activation energies for conductivity
	2.00 eV	$T > 1000$ K	
σ_0	$2.02 \cdot 10^{-1} \Omega^{-1} \text{cm}^{-1}$	$T < 1000$ K	pre-exponential factors for conductivity
	$3.28 \cdot 10^2 \Omega^{-1} \text{cm}^{-1}$	$T > 1000$ K	
81V	Verma, B.K., Lal, H.B.: Mater. Res. Bull. 16 (1981) 1579-1591.		

38.65 Er₂(WO₄)₃

E_A	1.20 eV	$T < 1025$ K	activation energies for conductivity
	2.00 eV	$T > 1025$ K	
conductivity			
σ_0	$2.00 \cdot 10^{-1} \Omega^{-1} \text{cm}^{-1}$	$T < 1025$ K	pre-exponential factors for conductivity
	$1.64 \cdot 10^3 \Omega^{-1} \text{cm}^{-1}$	$T > 1025$ K	
81V	Verma, B.K., Lal, H.B.: Mater. Res. Bull. 16 (1981) 1579-1591.		

38.66 Tm₂(WO₄)₃

E_A	1.25 eV	$T < 900$ K	activation energies for conductivity
	1.55 eV	$T > 900$ K	
conductivity			
σ_0	$2.02 \cdot 10^{-1} \Omega^{-1} \text{cm}^{-1}$	$T < 900$ K	pre-exponential factors for conductivity
	$1.06 \cdot 10^1 \Omega^{-1} \text{cm}^{-1}$	$T > 900$ K	
81V	Verma, B.K., Lal, H.B.: Mater. Res. Bull. 16 (1981) 1579-1591.		

38.67 Yb₂(WO₄)₃

E_A	1.30 eV	$T < 970$ K	activation energies for conductivity
	1.90 eV	$T > 970$ K	
σ_0	$4.28 \cdot 10^{-1} \Omega^{-1} \text{cm}^{-1}$	$T < 970$ K	pre-exponential factors for conductivity
	$5.17 \cdot 10^2 \Omega^{-1} \text{cm}^{-1}$	$T > 970$ K	
81V	Verma, B.K., Lal, H.B.: Mater. Res. Bull. 16 (1981) 1579-1591.		

38.68 Gd₂(MoO₄)₃

E_A	3.40 eV	$T = 900 \dots 1200$ K,	$\sigma = \sigma_0 \cdot \exp(-E_A/2kT)$;	88L
		val. - cond. band		
σ	$5.05 \cdot 10^2 \Omega^{-1} \text{m}^{-1}$	n-type		
μ	$0.011 \text{ cm}^2 \text{V}^{-1} \text{s}^{-1}$	$T = 900$ K	$\mu \approx \mu_n \approx \mu_p$	
σ_0	$5.05 \cdot 10^2 \Omega^{-1} \text{m}^{-1}$	$T > 900$ K		87P
	$1.67 \cdot 10^{-2} \Omega^{-1} \text{m}^{-1}$	$770 \text{ K} < T < 900 \text{ K}$		
	$8.35 \cdot 10^{-4} \Omega^{-1} \text{m}^{-1}$	$T < 770 \text{ K}$		
E_A	1.70 eV	$T > 900$ K	$\sigma = \sigma_0 \cdot \exp(-E_A/kT)$	87P
	0.90 eV	$770 \text{ K} < T < 900 \text{ K}$		
	0.68 eV	$T < 770 \text{ K}$		
μ_n	$1.08 \cdot 10^{-6} \text{ m}^2 \text{V}^{-1} \text{s}^{-1}$	$T = 1100$ K		
87P	Pratap, V., Gaur, K., Lal, H. B.: Mater. Res. Bull. 22 (1987) 1381-1393.			
88L	Lal, H. B., Kanchan Gaur, : J. Mater. Sci. 23 (1988) 919.			

38.69 Tb₂(MoO₄)₃

E_A	3.40 eV	$T = 910 \dots 1200$ K, $\sigma = \sigma_0 \cdot \exp(-E_A/2kT)$	88L
		val. - cond. band	
σ	$5.05 \cdot 10^2 \Omega^{-1}m^{-1}$	n-type	
μ	$0.011 \text{ cm}^2V^{-1}s^{-1}$	$T = 900$ K	$\mu \approx \mu_n \approx \mu_p$
σ_0	$5.05 \cdot 10^2 \Omega^{-1}m^{-1}$	$T > 910$ K	pre-exponential factor
	$5.45 \cdot 10^{-4} \Omega^{-1}m^{-1}$	$770 \text{ K} < T < 910 \text{ K}$	
	$2.16 \cdot 10^{-3} \Omega^{-1}m^{-1}$	$T < 770$ K	
E_A	1.70 eV	$T > 910$ K	$\sigma = \sigma_0 \cdot \exp(-E_A/kT)$
	0.63 eV	$770 \text{ K} < T < 910 \text{ K}$	
	0.70 eV	$T < 770$ K	
E_g	3.40 eV		
μ_n	$1.08 \cdot 10^{-6} \text{ m}^2V^{-1}s^{-1}$	$T = 1100$ K	
87P	Pratap, V., Gaur, K., Lal, H. B.: Mater. Res. Bull. 22 (1987) 1381-1393.		
88L	Lal, H. B., Kanchan Gaur, : J. Mater. Sci. 23 (1988) 919.		

38.70 Dy₂(MoO₄)₃

E_A	3.50 eV	$T = 920 \dots 1200$ K, $\sigma = \sigma_0 \cdot \exp(-E_A/2kT)$	88L
		val. - cond. band	
σ	$8.10 \cdot 10^4 \Omega^{-1}m^{-1}$	n-type	
μ	$0.237 \text{ cm}^2V^{-1}s^{-1}$	$T = 900$ K	$\mu \approx \mu_n \approx \mu_p$
σ_0	$8.10 \cdot 10^4 \Omega^{-1}m^{-1}$	$T > 920$ K	87P
	$3.94 \cdot 10^{-1} \Omega^{-1}m^{-1}$	$705 \text{ K} < T < 920 \text{ K}$	
	$3.71 \cdot 10^{-2} \Omega^{-1}m^{-1}$	$T < 705$ K	
E_A	1.75 eV	$T > 920$ K	$\sigma = \sigma_0 \cdot \exp(-E_A/kT)$
	0.84 eV	$705 \text{ K} < T < 900 \text{ K}$	
	0.76 eV	$T < 705$ K	
E_g	3.50 eV		
μ_n	$2.37 \cdot 10^{-5} \text{ m}^2V^{-1}s^{-1}$	$T = 1100$ K	
87P	Pratap, V., Gaur, K., Lal, H. B.: Mater. Res. Bull. 22 (1987) 1381-1393.		
88L	Lal, H. B., Kanchan Gaur, : J. Mater. Sci. 23 (1988) 919.		

38.71 Ho₂(MoO₄)₃

E_A	3.60 eV	$T = 830 \dots 1200$ K, $\sigma = \sigma_0 \cdot \exp(-E_A/2kT)$	88L
		val. - cond. band	
σ	$3.04 \cdot 10^4 \Omega^{-1}m^{-1}$	n-type	
μ	$0.187 \text{ cm}^2V^{-1}s^{-1}$	$T = 900$ K	$\mu \approx \mu_n \approx \mu_p$
σ_0	$3.04 \cdot 10^4 \Omega^{-1}m^{-1}$	$T > 830$ K	87P
	$6.48 \cdot 10^{-3} \Omega^{-1}m^{-1}$	$715 \text{ K} > T > 630 \text{ K}$	
E_A	1.80 eV	$T > 830$ K	$\sigma = \sigma_0 \cdot \exp(-E_A/kT)$
	0.72 eV	$715 \text{ K} > T > 630 \text{ K}$	
E_g	3.60 eV		
μ_n	$1.87 \cdot 10^{-5} \text{ m}^2V^{-1}s^{-1}$	$T = 1100$ K	
87P	Pratap, V., Gaur, K., Lal, H. B.: Mater. Res. Bull. 22 (1987) 1381-1393.		
88L	Lal, H. B., Kanchan Gaur, : J. Mater. Sci. 23 (1988) 919.		

38.72 Er₂(MoO₄)₃

E_A	3.74 eV	$T = 1000 \dots 1200 \text{ K}$, $\sigma = \sigma_0 \cdot \exp(-E_A/2kT)$ val. - cond. band	88L
σ	$4.96 \cdot 10^6 \Omega^{-1}\text{m}^{-1}$	n-type	
μ	$2.37 \text{ cm}^2\text{V}^{-1}\text{s}^{-1}$	$T = 900 \text{ K}$	$\mu \approx \mu_n \approx \mu_p$
σ_0	$4.96 \cdot 10^6 \Omega^{-1}\text{m}^{-1}$	$T > 1000 \text{ K}$	87P
	$7.31 \cdot 10^1 \Omega^{-1}\text{m}^{-1}$	$770 \text{ K} > T > 520 \text{ K}$	
E_A	1.87 eV	$T > 1000 \text{ K}$	$\sigma = \sigma_0 \cdot \exp(-E_A/kT)$
	1.00 eV	$770 \text{ K} > T > 520 \text{ K}$	87P
E_g	3.74 eV		
μ_n	$2.37 \cdot 10^{-3} \text{ m}^2\text{V}^{-1}\text{s}^{-1}$	$T = 1100 \text{ K}$	
87P	Pratap, V., Gaur, K., Lal, H. B.: Mater. Res. Bull. 22 (1987) 1381-1393.		
88L	Lal, H. B., Kanchan Gaur, : J. Mater. Sci. 23 (1988) 919.		

38.73 Tm₂(MoO₄)₃

E_A	3.84 eV	$T = 1000 \dots 1200 \text{ K}$, $\sigma = \sigma_0 \cdot \exp(-E_A/2kT)$ val. - cond. band	88L
σ	$1.85 \cdot 10^6 \Omega^{-1}\text{m}^{-1}$	n-type	
μ	$1.93 \text{ cm}^2\text{V}^{-1}\text{s}^{-1}$	$T = 900 \text{ K}$	$\mu \approx \mu_n \approx \mu_p$
σ_0	$1.85 \cdot 10^6 \Omega^{-1}\text{m}^{-1}$	$T > 1000 \text{ K}$	87P
	$1.78 \cdot 10^1 \Omega^{-1}\text{m}^{-1}$	$T < 800 \text{ K}$	
E_A	1.92 eV	$T > 1000 \text{ K}$	$\sigma = \sigma_0 \cdot \exp(-E_A/kT)$
	1.16 eV	$T < 800 \text{ K}$	87P
E_g	3.84 eV		
μ_n	$1.93 \cdot 10^{-3} \text{ m}^2\text{V}^{-1}\text{s}^{-1}$	$T = 1100 \text{ K}$	
87P	Pratap, V., Gaur, K., Lal, H. B.: Mater. Res. Bull. 22 (1987) 1381-1393.		
88L	Lal, H. B., Kanchan Gaur, : J. Mater. Sci. 23 (1988) 919.		

38.74 Yb₂(MoO₄)₃

E_A	4.00 eV	$T = 1000 \dots 1200 \text{ K}$, $\sigma = \sigma_0 \cdot \exp(-E_A/2kT)$ val. - cond. band	88L
σ	$8.92 \cdot 10^6 \Omega^{-1}\text{m}^{-1}$	n-type	
μ	$9.31 \text{ cm}^2\text{V}^{-1}\text{s}^{-1}$	$T = 900 \text{ K}$	$\mu \approx \mu_n \approx \mu_p$
σ_0	$8.92 \cdot 10^6 \Omega^{-1}\text{m}^{-1}$	$T > 1000 \text{ K}$	87P
	$4.28 \cdot 10^6 \Omega^{-1}\text{m}^{-1}$	$800 \text{ K} < T < 1000 \text{ K}$	
	$2.34 \cdot 10^1 \Omega^{-1}\text{m}^{-1}$	$T < 800 \text{ K}$	
E_A	2.00 eV	$T > 1000 \text{ K}$	$\sigma = \sigma_0 \cdot \exp(-E_A/kT)$
	1.60 eV	$800 \text{ K} < T < 1000 \text{ K}$	87P
	1.14 eV	$T < 800 \text{ K}$	
E_g	4.00 eV		
μ_n	$9.31 \cdot 10^{-3} \text{ m}^2\text{V}^{-1}\text{s}^{-1}$	$T = 1100 \text{ K}$	
87P	Pratap, V., Gaur, K., Lal, H. B.: Mater. Res. Bull. 22 (1987) 1381-1393.		
88L	Lal, H. B., Kanchan Gaur, : J. Mater. Sci. 23 (1988) 919.		

38.75 La₂Te₃O₉

E_g 4.0 ± 0.05 eV
 4.37 ± 0.05 eV water content: 6 H₂O (moles)

82V Voloshina, A. L., Ivanchenko, L.A., Obolonchik, V.A., Lugovskaya, E.S.: Soviet Powder Metallurgy and Metal Ceramics 21 (1982) 728-731.

38.76 Sm₂Mo₂O₇

cubic (Fd3m)

ρ $6 \cdot 10^{-2} \Omega$ cm powder data
 E_A 0.01 eV activation energy from resistivity vs. T

80S Subramanian, M. A., Subba Rao, G. V.: J. Solid State Chem. 31 (1980) 329.

38.77 Eu₂Mo₂O₇

cubic (Fd3m)

ρ $5 \cdot 10^{-2} \Omega$ cm powder data
 E_A 0.01 eV activation energy from resistivity vs. T

87G Greedan, J. E., Sato, M., Ali, N., Datars, W. R.: J. Solid State Chem. 68 (1987) 300.

38.78 Gd₂Mo₂O₇

cubic (Fd3m)

ρ $5 \cdot 10^{-2} \Omega$ cm powder data
 E_A 0.01 eV activation energy from resistivity vs. T

87G Greedan, J. E., Sato, M., Ali, N., Datars, W. R.: J. Solid State Chem. 68 (1987) 300.

38.79 Dy₂Mo₂O₇

cubic (Fd3m)

ρ $3 \cdot 10^{-2} \Omega$ cm powder data
 E_A 0.02 eV activation energy from resistivity vs. T

87G Greedan, J. E., Sato, M., Ali, N., Datars, W. R.: J. Solid State Chem. 68 (1987) 300.

38.80 Er₂Mo₂O₇

cubic (Fd3m)

ρ $2 \cdot 10^{-2} \Omega$ cm powder data
 E_A 0.05 eV activation energy from resistivity vs. T

87G Greedan, J. E., Sato, M., Ali, N., Datars, W. R.: J. Solid State Chem. 68 (1987) 300.

38.81 Pr₂Te₃O₉

E _g	4.14 ± 0.05 eV	
	4.34 ± 0.05 eV	water content:
		5.8 H ₂ O (moles)
82V	Voloshina, A. L., Ivanchenko, L.A., Obolonchik, V.A., Lugovskaya, E.S.: Soviet Powder Metallurgy and Metal Ceramics 21 (1982) 728-731.	

38.82 Nd₂Te₃O₉

E _g	4.10 ± 0.05 eV	
	4.35 ± 0.05 eV	water content:
		5.3 H ₂ O (moles)
82V	Voloshina, A. L., Ivanchenko, L.A., Obolonchik, V.A., Lugovskaya, E.S.: Soviet Powder Metallurgy and Metal Ceramics 21 (1982) 728-731.	

38.83 Sm₂Te₃O₉

E _g	4.3 ± 0.05 eV	
	4.3 ± 0.05 eV	water content:
		4.8 H ₂ O (moles)
82V	Voloshina, A. L., Ivanchenko, L.A., Obolonchik, V.A., Lugovskaya, E.S.: Soviet Powder Metallurgy and Metal Ceramics 21 (1982) 728-731.	

38.84 Eu₂Te₃O₉

E _g	4.0 ± 0.05 eV	
	4.2 ± 0.05 eV	water content:
		3.8 H ₂ O (moles)
82V	Voloshina, A. L., Ivanchenko, L.A., Obolonchik, V.A., Lugovskaya, E.S.: Soviet Powder Metallurgy and Metal Ceramics 21 (1982) 728-731.	

38.85 Gd₂Te₃O₉

E _g	4.05 ± 0.05 eV	
	4.3 ± 0.05 eV	water content:
		4.9 H ₂ O (moles)
82V	Voloshina, A. L., Ivanchenko, L.A., Obolonchik, V.A., Lugovskaya, E.S.: Soviet Powder Metallurgy and Metal Ceramics 21 (1982) 728-731.	

38.86 Tb₂Te₃O₉

E _g	4.0 ± 0.05 eV	
	4.2 ± 0.05 eV	water content:
		4.6 H ₂ O (moles)
82V	Voloshina, A. L., Ivanchenko, L.A., Obolonchik, V.A., Lugovskaya, E.S.: Soviet Powder Metallurgy and Metal Ceramics 21 (1982) 728-731.	

38.87 Dy₂Te₃O₉

E _g	3.93 ± 0.05 eV	
	4.35 ± 0.05 eV	water content:
		5.1 H ₂ O (moles)
82V	Voloshina, A. L., Ivanchenko, L.A., Obolonchik, V.A., Lugovskaya, E.S.: Soviet Powder Metallurgy and Metal Ceramics 21 (1982) 728-731.	

38.88 Ho₂Te₃O₉

E _g	4.15 ± 0.05 eV	
	4.3 ± 0.05 eV	water content:
		5.3 H ₂ O (moles)
82V	Voloshina, A. L., Ivanchenko, L.A., Obolonchik, V.A., Lugovskaya, E.S.: Soviet Powder Metallurgy and Metal Ceramics 21 (1982) 728-731.	

38.89 Er₂Te₃O₉

E _g	3.8 ± 0.05 eV	
	4.2 ± 0.05 eV	water content:
		5.0 H ₂ O (moles)
82V	Voloshina, A. L., Ivanchenko, L.A., Obolonchik, V.A., Lugovskaya, E.S.: Soviet Powder Metallurgy and Metal Ceramics 21 (1982) 728-731.	

38.90 Tm₂Te₃O₉

E _g	3.8 ± 0.05 eV	
	4.4 ± 0.05 eV	water content:
		4.8 H ₂ O (moles)
82V	Voloshina, A. L., Ivanchenko, L.A., Obolonchik, V.A., Lugovskaya, E.S.: Soviet Powder Metallurgy and Metal Ceramics 21 (1982) 728-731.	

38.91 Yb₂Te₃O₉

E _g	3.8 ± 0.05 eV	
	4.4 ± 0.05 eV	water content:
		5.4 H ₂ O (moles)
82V	Voloshina, A. L., Ivanchenko, L.A., Obolonchik, V.A., Lugovskaya, E.S.: Soviet Powder Metallurgy and Metal Ceramics 21 (1982) 728-731.	

38.92 Lu₂Te₃O₉

E _g	3.92 ± 0.05 eV	
	4.4 ± 0.05 eV	water content:
		4.9 H ₂ O (moles)
82V	Voloshina, A. L., Ivanchenko, L.A., Obolonchik, V.A., Lugovskaya, E.S.: Soviet Powder Metallurgy and Metal Ceramics 21 (1982) 728-731.	

38.93 La₂Mo₃O₉

tetragonal

ρ	92.12 Ω cm	n-type	semiconductor - metal: $\approx 250^\circ\text{C}$
E_A	0.20 eV		

95S Shi, F., Meng, J., Ren, Yu.: Mater. Res. Bull. 30 (10) (1995) 1285-1291.

38.94 Ce₂Mo₃O₉

tetragonal

ρ	52.17 Ω cm	n-type	semiconductor - metal: $\approx 250^\circ\text{C}$
E_A	0.19 eV		activation energy

95S Shi, F., Meng, J., Ren, Yu.: Mater. Res. Bull. 30 (10) (1995) 1285-1291.

38.95 Pr₂Mo₃O₉

tetragonal

ρ	50.98 Ω cm	n-type	semiconductor - metal: $\approx 250^\circ\text{C}$
E_A	0.17 eV		activation energy

95S Shi, F., Meng, J., Ren, Yu.: Mater. Res. Bull. 30 (10) (1995) 1285-1291.

38.96 Nd₂Mo₃O₉

tetragonal

ρ	38.9748 Ω cm	n-type	semiconductor - metal: $\approx 250^\circ\text{C}$
E_A	0.16 eV		activation energy

95S Shi, F., Meng, J., Ren, Yu.: Mater. Res. Bull. 30 (10) (1995) 1285-1291.

38.97 Sm₂Mo₃O₉

tetragonal

ρ	23.92 Ω cm	n-type	semiconductor - metal: $\approx 250^\circ\text{C}$
E_A	0.12 eV		activation energy

95S Shi, F., Meng, J., Ren, Yu.: Mater. Res. Bull. 30 (10) (1995) 1285-1291.

38.98 Gd₂Mo₃O₉

tetragonal

ρ	7.61 Ω cm	n-type	semiconductor - metal: $\approx 250^\circ\text{C}$
E_A	0.11 eV		activation energy

95S Shi, F., Meng, J., Ren, Yu.: Mater. Res. Bull. 30 (10) (1995) 1285-1291.

38.99 Dy₂Mo₃O₉

tetragonal

ρ	7.51 Ω cm	n-type	semiconductor - metal: $\approx 250^\circ\text{C}$
E_A	0.11 eV		activation energy

95S Shi, F., Meng, J., Ren, Yu.: Mater. Res. Bull. 30 (10) (1995) 1285-1291.

38.100 TbCrS₃

σ	$8.71 \cdot 10^{-6} \Omega^{-1} \text{cm}^{-1}$	n-type
E_g	1.04 eV	

81R Rustamov, , P. G., Aliev, O. M.: Akad. Nauk SSSR, Izd. ELM, Baku 1981 (russian).

38.101 HoCrS₃

σ	$1.29 \cdot 10^{-6} \Omega^{-1} \text{cm}^{-1}$	n-type
E_g	1.06 eV	

81R Rustamov, , P. G., Aliev, O. M.: Akad. Nauk SSSR, Izd. ELM, Baku 1981 (russian).

38.102 ErCrS₃

σ	$4.9 \cdot 10^{-6} \Omega^{-1} \text{cm}^{-1}$	n-type
E_g	1.08 eV	

81R Rustamov, , P. G., Aliev, O. M.: Akad. Nauk SSSR, Izd. ELM, Baku 1981 (russian).

38.103 TmCrS₃

σ	$6.5 \cdot 10^{-6} \Omega^{-1} \text{cm}^{-1}$	n-type
E_g	1.03 eV	

81R Rustamov, , P. G., Aliev, O. M.: Akad. Nauk SSSR, Izd. ELM, Baku 1981 (russian).

38.104 YbCrS₃

σ	$5.14 \cdot 10^{-6} \Omega^{-1} \text{cm}^{-1}$	n-type
E_g	1.10 eV	

81R Rustamov, , P. G., Aliev, O. M.: Akad. Nauk SSSR, Izd. ELM, Baku 1981 (russian).

38.105 LuCrS₃

σ	$2.2 \cdot 10^{-6} \Omega^{-1} \text{cm}^{-1}$	n-type
E_g	1.12 eV	

81R Rustamov, , P. G., Aliev, O. M.: Akad. Nauk SSSR, Izd. ELM, Baku 1981 (russian).

38.106 YCrS₃

σ	$7.8 \cdot 10^{-6} \Omega^{-1} \text{cm}^{-1}$	n-type
E_g	1.13 eV	

81R Rustamov, , P. G., Aliev, O. M.: Akad. Nauk SSSR, Izd. ELM, Baku 1981 (russian).

38.107 GdCrSe₃

orthorhombic

$$\begin{array}{lll} \sigma & 8.8 \cdot 10^{-4} \, \Omega^{-1} \, \text{cm}^{-1} & \text{p-type} \\ E_g & 0.83 \, \text{eV} & \end{array}$$

81R Rustamov, , P. G., Aliev, O. M.: Akad. Nauk SSSR, Izd. ELM, Baku 1981 (russian).

38.108 TbCrSe₃

$$\begin{array}{lll} \sigma & 2.9 \cdot 10^{-2} \, \Omega^{-1} \, \text{cm}^{-1} & \text{p-type} \\ E_g & 0.43 \, \text{eV} & \end{array}$$

81R Rustamov, , P. G., Aliev, O. M.: Akad. Nauk SSSR, Izd. ELM, Baku 1981 (russian).

38.109 DyCrSe₃

$$\begin{array}{lll} \sigma & 1 \cdot 10^{-3} \, \Omega^{-1} \, \text{cm}^{-1} & \text{p-type} \\ E_g & 0.50 \, \text{eV} & \end{array}$$

81R Rustamov, , P. G., Aliev, O. M.: Akad. Nauk SSSR, Izd. ELM, Baku 1981 (russian).

38.110 HoCrSe₃

$$\begin{array}{lll} \sigma & 1 \cdot 10^{-5} \, \Omega^{-1} \, \text{cm}^{-1} & \text{p-type} \\ E_g & 0.78 \, \text{eV} & \end{array}$$

81R Rustamov, , P. G., Aliev, O. M.: Akad. Nauk SSSR, Izd. ELM, Baku 1981 (russian).

38.111 ErCrSe₃

$$\begin{array}{lll} \sigma & 4.9 \cdot 10^{-2} \, \Omega^{-1} \, \text{cm}^{-1} & \text{p-type} \\ E_g & 0.38 \, \text{eV} & \end{array}$$

81R Rustamov, , P. G., Aliev, O. M.: Akad. Nauk SSSR, Izd. ELM, Baku 1981 (russian).

38.112 TmCrSe₃

$$\begin{array}{lll} \sigma & 1.9 \cdot 10^{-3} \, \Omega^{-1} \, \text{cm}^{-1} & \text{p-type} \\ E_g & 0.32 \, \text{eV} & \end{array}$$

81R Rustamov, , P. G., Aliev, O. M.: Akad. Nauk SSSR, Izd. ELM, Baku 1981 (russian).

81R Rustamov, , P. G., Aliev, O. M.: Akad. Nauk SSSR, Izd. ELM, Baku 1981 (russian).

38.113 YbCrSe₃

$$\begin{array}{lll} \sigma & 4.8 \cdot 10^{-6} \, \Omega^{-1} \, \text{cm}^{-1} & \text{p-type} \\ E_g & 0.80 \, \text{eV} & \end{array}$$

81R Rustamov, , P. G., Aliev, O. M.: Akad. Nauk SSSR, Izd. ELM, Baku 1981 (russian).

38.114 LuCrSe₃

σ	$2.0 \cdot 10^{-2} \Omega^{-1} \text{ cm}^{-1}$	p-type
E_g	0.28 eV	

81R Rustamov, , P. G., Aliev, O. M.: Akad. Nauk SSSR, Izd. ELM, Baku 1981 (russian).

38.115 Pr₂CrS₄

monoclinic

σ	$1.2 \Omega^{-1} \text{ cm}^{-1}$	$T = 300 \text{ K}$
	$325 \Omega^{-1} \text{ cm}^{-1}$	$T = 700 \text{ K}$
E_g	0.33 eV	

81R Rustamov, , P. G., Aliev, O. M.: Akad. Nauk SSSR, Izd. ELM, Baku 1981 (russian).

38.116 Nd₂CrS₄

σ	$13.23 \Omega^{-1} \text{ cm}^{-1}$	$T = 300 \text{ K}$
	$24.54 \Omega^{-1} \text{ cm}^{-1}$	$T = 700 \text{ K}$
E_g	0.33 eV	

81R Rustamov, , P. G., Aliev, O. M.: Akad. Nauk SSSR, Izd. ELM, Baku 1981 (russian).

38.117 Sm₂CrS₄

σ	$30.55 \Omega^{-1} \text{ cm}^{-1}$	$T = 300 \text{ K}$
	$20.81 \Omega^{-1} \text{ cm}^{-1}$	$T = 700 \text{ K}$
E_g	0.20 eV	

81R Rustamov, , P. G., Aliev, O. M.: Akad. Nauk SSSR, Izd. ELM, Baku 1981 (russian).

38.118 Pr₂CrSe₄

monoclinic

σ	$19.8 \Omega^{-1} \text{ cm}^{-1}$	$T = 300 \text{ K}$	
	$30.79 \Omega^{-1} \text{ cm}^{-1}$	$T = 700 \text{ K}$	n-type
E_g	0.21 eV		

81R Rustamov, , P. G., Aliev, O. M.: Akad. Nauk SSSR, Izd. ELM, Baku 1981 (russian).

38.119 Nd₂CrSe₄

σ	$28.22 \Omega^{-1} \text{ cm}^{-1}$	$T = 300 \text{ K}$	
	$38.12164 \Omega^{-1} \text{ cm}^{-1}$	$T = 700 \text{ K}$	n-type
E_g	0.29 eV		

81R Rustamov, , P. G., Aliev, O. M.: Akad. Nauk SSSR, Izd. ELM, Baku 1981 (russian).

38.120 Sm₂CrSe₄

σ	$51.47 \Omega^{-1} \text{ cm}^{-1}$	$T = 300 \text{ K}$	
	$29.39 \Omega^{-1} \text{ cm}^{-1}$	$T = 700 \text{ K}$	n-type
E_g	0.28 eV		

81R Rustamov, , P. G., Aliev, O. M.: Akad. Nauk SSSR, Izd. ELM, Baku 1981 (russian).

38.121 Gd₂CrSe₄

σ	51.00 $\Omega^{-1} \text{ cm}^{-1}$	$T = 300 \text{ K}$	n-type
	2.30 $\Omega^{-1} \text{ cm}^{-1}$	$T = 700 \text{ K}$	
E_g	0.27 eV		

81R Rustamov, , P. G., Aliev, O. M.: Akad. Nauk SSSR, Izd. ELM, Baku 1981 (russian).

38.122 Tb₂CrSe₄

σ	13.3 $\Omega^{-1} \text{ cm}^{-1}$	$T = 300 \text{ K}$	n-type
	6.09 $\Omega^{-1} \text{ cm}^{-1}$	$T = 700 \text{ K}$	
E_g	0.25 eV		

81R Rustamov, , P. G., Aliev, O. M.: Akad. Nauk SSSR, Izd. ELM, Baku 1981 (russian).

38.123 Dy₂CrSe₄

σ	11.38 $\Omega^{-1} \text{ cm}^{-1}$	$T = 300 \text{ K}$	n-type
	8.56 $\Omega^{-1} \text{ cm}^{-1}$	$T = 700 \text{ K}$	
E_g	0.25 eV		

81R Rustamov, , P. G., Aliev, O. M.: Akad. Nauk SSSR, Izd. ELM, Baku 1981 (russian).

38.124 Yb₂CrSe₄

σ	3.36 $\Omega^{-1} \text{ cm}^{-1}$	$T = 300 \text{ K}$	n-type
	8.48 $\Omega^{-1} \text{ cm}^{-1}$	$T = 700 \text{ K}$	
E_g	0.23 eV		

81R Rustamov, , P. G., Aliev, O. M.: Akad. Nauk SSSR, Izd. ELM, Baku 1981 (russian).

38.125 Y₂CrSe₄

monoclinic

σ	24.7 $\Omega^{-1} \text{ cm}^{-1}$	$T = 300 \text{ K}$	n-type
	11.04 $\Omega^{-1} \text{ cm}^{-1}$	$T = 700 \text{ K}$	
E_g	0.23 eV		

81R Rustamov, , P. G., Aliev, O. M.: Akad. Nauk SSSR, Izd. ELM, Baku 1981 (russian).

38.126 EuCr₂Te₄

σ	186.2 $\Omega^{-1} \text{ cm}^{-1}$	
E_g	0.11 eV	

81R Rustamov, , P. G., Aliev, O. M.: Akad. Nauk SSSR, Izd. ELM, Baku 1981 (russian).

38.127 YbCr₂S₄

σ	1.4 $\Omega^{-1} \text{ cm}^{-1}$	
E_g	0.34 eV	

81R Rustamov, , P. G., Aliev, O. M.: Akad. Nauk SSSR, Izd. ELM, Baku 1981 (russian).

38.128 YbCr₂Se₄

σ 3.6 $\Omega^{-1} \text{ cm}^{-1}$
 E_g 0.25 eV

81R Rustamov, , P. G., Aliev, O. M.: Akad. Nauk SSSR, Izd. ELM, Baku 1981 (russian).

38.129 Tb₂(W_{2/3}V_{4/3})O₇

cubic (O_h⁷-Fd3m)

E_A 0.21 eV

σ 4.8·10⁻⁴ $\Omega^{-1} \text{ cm}^{-1}$ p-type polycrystalline sample

79S Subramanian, M. A., Aravamudan, G., Subba Rao, G. V.: Mater. Res. Bull. 14 (1979) 1457.

38.130 Dy₂(W_{2/3}V_{4/3})O₇

cubic (O_h⁷-Fd3m)

E_A 0.20 eV

σ 5.3·10⁻⁴ $\Omega^{-1} \text{ cm}^{-1}$ p-type polycrystalline sample

79S Subramanian, M. A., Aravamudan, G., Subba Rao, G. V.: Mater. Res. Bull. 14 (1979) 1457.

38.131 Ho₂(W_{2/3}V_{4/3})O₇

cubic (O_h⁷-Fd3m)

E_A 0.23 eV

σ 3.4·10⁻⁴ $\Omega^{-1} \text{ cm}^{-1}$ p-type polycrystalline sample

79S Subramanian, M. A., Aravamudan, G., Subba Rao, G. V.: Mater. Res. Bull. 14 (1979) 1457.

38.132 Er₂(W_{2/3}V_{4/3})O₇

cubic (O_h⁷-Fd3m)

E_A 0.24 eV

σ 3.6·10⁻⁴ $\Omega^{-1} \text{ cm}^{-1}$ p-type polycrystalline sample

79S Subramanian, M. A., Aravamudan, G., Subba Rao, G. V.: Mater. Res. Bull. 14 (1979) 1457.

38.133 Tm₂V₂O₇

[79S]

cubic (O_h⁷-Fd3m)

E_A 0.042 eV $T = 90...273 \text{ K}$
0.44 eV $T = 273...350 \text{ K}$

σ 1.09·10⁻³ $\Omega^{-1} \text{ cm}^{-1}$ n-type polycrystalline sample;

79S Subramanian, M. A., Aravamudan, G., Subba Rao, G. V.: Mater. Res. Bull. 14 (1979) 1457.

38.134 Tm₂V_{4/3}W_{2/3}O₇

cubic (O_h⁷-Fd3m)

E_A	0.24 eV		
σ	$3.4 \cdot 10^{-4} \Omega^{-1} \text{ cm}^{-1}$	p-type	polycrystalline sample
79S	Subramanian, M. A., Aravamudan, G., Subba Rao, G. V.: Mater. Res. Bull. 14 (1979) 1457.		

38.135 Yb₂V₂O₇

[77S]

E_A	0.047 eV	$T = 90 \dots 273 \text{ K}$	polycrystalline sample;
	0.44 eV	$T = 273 \dots 350 \text{ K}$	temperature dependence of
77S	Shinike, T., Adachi, G., Shiokawa, J.: Mater. Res. Bull. 12 (1977) 1149.		

38.136 Yb₂V_{4/3}W_{2/3}O₇

cubic (O_h⁷-Fd3m)

E_A	0.24 eV		
σ	$2.3 \cdot 10^{-4} \Omega^{-1} \text{ cm}^{-1}$		p-type polycrystalline sample;
79S	Subramanian, M. A., Aravamudan, G., Subba Rao, G. V.: Mater. Res. Bull. 14 (1979) 1457.		

38.137 Lu₂V₂O₇

cubic (O_h⁷-Fd3m)

E_A	0.043 eV	$T = 90 \dots 273 \text{ K}$	
	0.42 eV	$T = 273 \dots 350 \text{ K}$	
σ	$6.37 \cdot 10^{-4} \Omega^{-1} \text{ cm}^{-1}$	n-type	polycrystalline sample;
77S	Shinike, T., Adachi, G., Shiokawa, J.: Mater. Res. Bull. 12 (1977) 1149.		

38.138 La₂Pb₂O₇

cubic (Fd3m)

ρ	1010 $\Omega \text{ cm}$	powder data	
E_A	0.5 eV		activation energy from resistivity vs. T
69S	Sleight, A. W.: Inorg. Chem. 8 (1969) 1807.		

38.139 Gd₂Ti₂O₇

cubic (Fd3m)

ρ	$3.7 \cdot 10^3 \Omega \text{ cm}$	powder data	
E_A	0.25 eV		activation energy from resistivity vs. T
	0.25 eV		activation energy from resistivity vs. T
	0.25 eV		activation energy from resistivity vs. T
71S	Sleight, A. W., Gillson, J. L.: Mater. Res. Bull. 6 (1971) 781.		

38.140 Dy₂Mn₂O₇

cubic (Fd3m)

ρ	$1 \cdot 10^6 \Omega \text{ cm}$	powder data	
E_A	0.37 eV		activation energy from resistivity vs. T

80S Subramanian, M. A., Torardi, C. C., Johnson, D. C., Pannetier, J., Sleight, A. W.: J. Solid State Chem. 72 (1988) 24.

38.141 Ho₂Mn₂O₇

cubic (Fd3m)

ρ	$8 \cdot 10^7 \Omega \text{ cm}$	powder data	
E_A	0.45 eV		activation energy from resistivity vs. T

80S Subramanian, M. A., Torardi, C. C., Johnson, D. C., Pannetier, J., Sleight, A. W.: J. Solid State Chem. 72 (1988) 24.

38.142 Er₂Mn₂O₇

cubic (Fd3m)

ρ	$3 \cdot 10^7 \Omega \text{ cm}$	powder data	
E_A	0.47 eV		activation energy from resistivity vs. T

80S Subramanian, M. A., Torardi, C. C., Johnson, D. C., Pannetier, J., Sleight, A. W.: J. Solid State Chem. 72 (1988) 24.

38.143 Tm₂Mn₂O₇

cubic (Fd3m)

ρ	$2 \cdot 10^7 \Omega \text{ cm}$	powder data	
E_A	0.48 eV		activation energy from resistivity vs. T

80S Subramanian, M. A., Torardi, C. C., Johnson, D. C., Pannetier, J., Sleight, A. W.: J. Solid State Chem. 72 (1988) 24.

38.144 Lu₂Mn₂O₇

cubic (Fd3m)

ρ	$2 \cdot 10^8 \Omega \text{ cm}$	powder data	
E_A	0.51 eV		activation energy from resistivity vs. T

80S Subramanian, M. A., Torardi, C. C., Johnson, D. C., Pannetier, J., Sleight, A. W.: J. Solid State Chem. 72 (1988) 24.

38.145 Y₂Mn₂O₇

cubic (Fd3m)

ρ	$3 \cdot 10^6 \Omega \text{ cm}$	powder data	
E_A	0.38 eV		activation energy from resistivity vs. T

80S Subramanian, M. A., Torardi, C. C., Johnson, D. C., Pannetier, J., Sleight, A. W.: J. Solid State Chem. 72 (1988) 24.

38.146 Pr₂Ru₂O₇

cubic (Fd3m)

ρ 1.0 Ω cm powder data

E_A 0.2 eV activation energy from resistivity vs. T

71S Sleight, A. W., Gillson, J. L.: Mater. Res. Bull. 6 (1971) 781.

38.147 Nd₂Ru₂O₇

cubic (Fd3m)

ρ 1.6 Ω cm single crystal data

E_A 0.11 eV activation energy from resistivity vs. T

93S Subramanian, M. A., Sleight, A. W.: in: Handbook on the Physics and Chemistry of Rare Earths, Vol. 16, eds. K. A. Gschneidner Jr and L. Eyring, Elsevier Science (1993), p. 225.

38.148 Eu₂Ru₂O₇

cubic (Fd3m)

ρ 1.2 Ω cm single crystal data

E_A 0.3 eV activation energy from resistivity vs. T

71S Sleight, A. W., Gillson, J. L.: Mater. Res. Bull. 6 (1971) 781.

38.149 Gd₂Ru₂O₇

cubic (Fd3m)

ρ 0.2 Ω cm single crystal data

E_A 0.1 eV activation energy from resistivity vs. T

71S Sleight, A. W., Gillson, J. L.: Mater. Res. Bull. 6 (1971) 781.

38.150 Yb₂Ru₂O₇

cubic (Fd3m)

ρ 1 Ω cm single crystal data

E_A 0.12 eV activation energy from resistivity vs. T

71S Sleight, A. W., Gillson, J. L.: Mater. Res. Bull. 6 (1971) 781.

38.151 Y₂Ru₂O₇

cubic (Fd3m)

ρ 10 Ω cm powder data

E_A 0.3 eV activation energy from resistivity vs. T

71S Sleight, A. W., Gillson, J. L.: Mater. Res. Bull. 6 (1971) 781.

38.152 Nd₂Ir₂O₇

cubic (Fd3m)

ρ $28 \cdot 10^{-2} \Omega \text{ cm}$ single crystal data

E_A 0.08 eV activation energy from resistivity vs. T

71S Sleight, A. W., Gillson, J. L.: Mater. Res. Bull. 6 (1971) 781.

38.153 Sm₂Ir₂O₇

cubic (Fd3m)

ρ $3.5 \cdot 10^{-2} \Omega \text{ cm}$ single crystal data

E_A 0.08 eV activation energy from resistivity vs. T

71S Sleight, A. W., Gillson, J. L.: Mater. Res. Bull. 6 (1971) 781.

38.154 Eu₂Ir₂O₇

cubic (Fd3m)

ρ $7.0 \cdot 10^{-2} \Omega \text{ cm}$ single crystal data

E_A 0.09 eV activation energy from resistivity vs. T

71S Sleight, A. W., Gillson, J. L.: Mater. Res. Bull. 6 (1971) 781.

38.155 Dy₂Ir₂O₇

cubic (Fd3m)

ρ $2.0 \cdot 10^{-1} \Omega \text{ cm}$ single crystal data

E_A 0.07 eV activation energy from resistivity vs. T

71S Sleight, A. W., Gillson, J. L.: Mater. Res. Bull. 6 (1971) 781.

38.156 Y₂Ir₂O₇

cubic (Fd3m)

ρ 30 $\Omega \text{ cm}$ powder data

E_A 0.17 eV activation energy from resistivity vs. T

71S Sleight, A. W., Gillson, J. L.: Mater. Res. Bull. 6 (1971) 781.

38.157 Gd₂Os₂O₇

cubic (Fd3m)

ρ $1 \cdot 10^{-2} \Omega \text{ cm}$ powder data

E_A 0.01 eV activation energy from resistivity vs. T

73S Shaplygin, I. S., Lazarev, V. B.: Mater. Res. Bull. 8 (1973) 761.

78L Lazarev, V. B., Shaplygin, I. S.: Mater. Res. Bull. 13 (1978) 229; Russ. J. Inorg. Chem. 13 (1978) 163.

38.158 Nd₂Pt₂O₇

cubic (Fd3m)

ρ $2 \cdot 10^{-1} \Omega \text{ cm}$ single crystal data

E_A 0.14 eV activation energy from resistivity vs. T

73S Shaplygin, I. S., Lazarev, V. B.: Mater. Res. Bull. 8 (1973) 761.

78L Lazarev, V. B., Shaplygin, I. S.: Mater. Res. Bull. 13 (1978) 229; Russ. J. Inorg. Chem. 13 (1978) 163.

38.159 Gd₂Pt₂O₇

cubic (Fd3m)

ρ $7 \cdot 10^{-2} \Omega \text{ cm}$ single crystal data

E_A 0.3 eV activation energy from resistivity vs. T

73S Shaplygin, I. S., Lazarev, V. B.: Mater. Res. Bull. 8 (1973) 761.

78L Lazarev, V. B., Shaplygin, I. S.: Mater. Res. Bull. 13 (1978) 229; Russ. J. Inorg. Chem. 13 (1978) 163.

38.160 LaSbSe₃

orthorhombic, Sb₂S₃ type

E_g 1.25 eV

σ $4.4 \cdot 10^{-6} \Omega^{-1} \text{ cm}^{-1}$

81R Rustamov, , P. G., Aliev, O. M.: Akad. Nauk SSSR, Izd. ELM, Baku 1981 (russian).

38.161 CeSbSe₃

E_g 1.20 eV

σ $4 \cdot 10^{-6} \Omega^{-1} \text{ cm}^{-1}$

81R Rustamov, , P. G., Aliev, O. M.: Akad. Nauk SSSR, Izd. ELM, Baku 1981 (russian).

38.162 PrSbSe₃

E_g 1.40 eV

σ $4 \cdot 10^{-7} \Omega^{-1} \text{ cm}^{-1}$

81R Rustamov, , P. G., Aliev, O. M.: Akad. Nauk SSSR, Izd. ELM, Baku 1981 (russian).

38.163 NdSbSe₃

E_g 1.56 eV

σ $8.6 \cdot 10^{-8} \Omega^{-1} \text{ cm}^{-1}$

81R Rustamov, , P. G., Aliev, O. M.: Akad. Nauk SSSR, Izd. ELM, Baku 1981 (russian).

38.164 SmSbSe₃

E_g 1.63 eV

σ $9.7 \cdot 10^{-5} \Omega^{-1} \text{ cm}^{-1}$

81R Rustamov, , P. G., Aliev, O. M.: Akad. Nauk SSSR, Izd. ELM, Baku 1981 (russian).

38.165 GdSbSe₃

$$\begin{array}{ll} E_g & 1.22 \text{ eV} \\ \sigma & 5.67 \cdot 10^{-8} \Omega^{-1} \text{ cm}^{-1} \end{array}$$

81R Rustamov, , P. G., Aliev, O. M.: Akad. Nauk SSSR, Izd. ELM, Baku 1981 (russian).

38.166 SmBiTe₃

space group: D_{3d}⁵-R $\overline{3}$ m

$$E_g \quad 0.18 \text{ eV} \dots 0.23 \text{ eV} \quad \text{only range given}$$

79R Rustamov, P.G., Sadygov, F.M., Melikova, Z.D., Alidzhanov, M.A., Ali-Zade, M.Z.: Inorg. Mater. 15 (1979) 607-608.

38.167 TbBiTe₃

space group: D_{3d}⁵-R $\overline{3}$ m

$$E_g \quad 0.18 \text{ eV} \dots 0.23 \text{ eV} \quad \text{only range given}$$

79R Rustamov, P.G., Sadygov, F.M., Melikova, Z.D., Alidzhanov, M.A., Ali-Zade, M.Z.: Inorg. Mater. 15 (1979) 607-608.

38.168 HoBiTe₃

space group: D_{3d}⁵-R $\overline{3}$ m

$$E_g \quad 0.18 \text{ eV} \dots 0.23 \text{ eV} \quad \text{only range given}$$

79R Rustamov, P.G., Sadygov, F.M., Melikova, Z.D., Alidzhanov, M.A., Ali-Zade, M.Z.: Inorg. Mater. 15 (1979) 607-608.

38.169 TmBiTe₃

space group: D_{3d}⁵-R $\overline{3}$ m

$$E_g \quad 0.18 \text{ eV} \dots 0.23 \text{ eV} \quad \text{only range given}$$

79R Rustamov, P.G., Sadygov, F.M., Melikova, Z.D., Alidzhanov, M.A., Ali-Zade, M.Z.: Inorg. Mater. 15 (1979) 607-608.

38.170 LuBiTe₃

space group: D_{3d}⁵-R $\overline{3}$ m

$$E_g \quad 0.18 \text{ eV} \dots 0.23 \text{ eV} \quad \text{only range given}$$

79R Rustamov, P.G., Sadygov, F.M., Melikova, Z.D., Alidzhanov, M.A., Ali-Zade, M.Z.: Inorg. Mater. 15 (1979) 607-608.

38.171 YBiTe₃

space group: D_{3d}⁵-R $\bar{3}$ m

E_g 0.18 eV ... 0.23 eV only range given

78R Rustamov, P., Sadygov, F., Melikova, Z., Safarov, M.: Zh. Neorg. Khim. 23 (1978) 849.

79R Rustamov, P.G., Sadygov, F.M., Melikova, Z.D., Alidzhanov, M.A., Ali-Zade, M.Z.: Inorg. Mater. 15 (1979) 607-608.

38.172 EuSb₂S₄

orthorhombic (Pbam)

E_g 1.2 eV

σ $5 \cdot 10^{-4} \Omega^{-1} \text{ cm}^{-1}$

81R Rustamov, , P. G., Aliev, O. M.: Akad. Nauk SSSR, Izd. ELM, Baku 1981 (russian).

38.173 EuSb₂Se₄

orthorhombic (Pbam)

E_g 0.83 eV

σ $2.6 \cdot 10^{-4} \Omega^{-1} \text{ cm}^{-1}$

81R Rustamov, , P. G., Aliev, O. M.: Akad. Nauk SSSR, Izd. ELM, Baku 1981 (russian).

38.174 EuSb₂Te₄

Th₃P₄ type

E_g 0.76 eV

σ $0.9 \Omega^{-1} \text{ cm}^{-1}$

μ $1000 \text{ cm}^2 \text{ V}^{-1} \text{ s}^{-1}$

81R Rustamov, , P. G., Aliev, O. M.: Akad. Nauk SSSR, Izd. ELM, Baku 1981 (russian).

38.175 EuBi₂Te₄

Th₃P₄ type

E_g 0.7 eV

σ $210 \Omega^{-1} \text{ cm}^{-1}$

μ $6500 \text{ cm}^2 \text{ V}^{-1} \text{ s}^{-1}$

81R Rustamov, , P. G., Aliev, O. M.: Akad. Nauk SSSR, Izd. ELM, Baku 1981 (russian).

38.176 Cu₃SmS₃

monoclinic

E_g 1.81 eV from conductivity

81R Rustamov, , P. G., Aliev, O. M.: Akad. Nauk SSSR, Izd. ELM, Baku 1981 (russian).

38.177 Cu₃GdS₃

monoclinic

E_g 1.62 eV from conductivity

81R Rustamov, , P. G., Aliev, O. M.: Akad. Nauk SSSR, Izd. ELM, Baku 1981 (russian).

38.178 Cu₃TbS₃

trigonal ($P\bar{3}$)

E_g 1.62 eV from conductivity

81R Rustamov, , P. G., Aliev, O. M.: Akad. Nauk SSSR, Izd. ELM, Baku 1981 (russian).

38.179 Cu₃DyS₃

trigonal ($P\bar{3}$)

E_g 1.60 eV from conductivity

81R Rustamov, , P. G., Aliev, O. M.: Akad. Nauk SSSR, Izd. ELM, Baku 1981 (russian).

38.180 Cu₃YS₃

trigonal ($P\bar{3}$)

E_g 1.78 eV from conductivity

81R Rustamov, , P. G., Aliev, O. M.: Akad. Nauk SSSR, Izd. ELM, Baku 1981 (russian).

38.181 Cu₃HoS₃

trigonal ($P\bar{3}$)

E_g 1.65 eV from conductivity

81R Rustamov, , P. G., Aliev, O. M.: Akad. Nauk SSSR, Izd. ELM, Baku 1981 (russian).

38.182 Cu₃LuS₃

E_g 1.50 eV from conductivity

81R Rustamov, , P. G., Aliev, O. M.: Akad. Nauk SSSR, Izd. ELM, Baku 1981 (russian).

38.183 Cu₃ScS₃

trigonal ($P\bar{3}$)

E_g 1.86 eV from conductivity

81R Rustamov, , P. G., Aliev, O. M.: Akad. Nauk SSSR, Izd. ELM, Baku 1981 (russian).

38.184 Cu₃SmSe₃

monoclinic(C_{2h}⁴-P2/b)

E_g 0.15 eV from conductivity

81R Rustamov, , P. G., Aliev, O. M.: Akad. Nauk SSSR, Izd. ELM, Baku 1981 (russian).

38.185 Cu₃GdSe₃

trigonal (P $\bar{3}$)

E_g 0.14 eV from conductivity

81R Rustamov, , P. G., Aliev, O. M.: Akad. Nauk SSSR, Izd. ELM, Baku 1981 (russian).

38.186 Cu₃TbSe₃

trigonal (P $\bar{3}$)

E_g 0.16 eV from conductivity

81R Rustamov, , P. G., Aliev, O. M.: Akad. Nauk SSSR, Izd. ELM, Baku 1981 (russian).

38.187 Cu₃DySe₃

trigonal (P $\bar{3}$)

E_g 0.20 eV from conductivity

81R Rustamov, , P. G., Aliev, O. M.: Akad. Nauk SSSR, Izd. ELM, Baku 1981 (russian).

38.188 Cu₃YSe₃

trigonal (P $\bar{3}$)

E_g 0.88 eV from conductivity

81R Rustamov, , P. G., Aliev, O. M.: Akad. Nauk SSSR, Izd. ELM, Baku 1981 (russian).

38.189 Cu₃HoSe₃

trigonal (P $\bar{3}$)

E_g 0.16 eV from conductivity

81R Rustamov, , P. G., Aliev, O. M.: Akad. Nauk SSSR, Izd. ELM, Baku 1981 (russian).

38.190 Cu₃YbSe₃

trigonal (P $\bar{3}$)

E_g 0.20 eV from conductivity

81R Rustamov, , P. G., Aliev, O. M.: Akad. Nauk SSSR, Izd. ELM, Baku 1981 (russian).

38.191 Cu₃ScSe₃

trigonal (P $\bar{3}$)

E_g 0.30 eV from conductivity

81R Rustamov, , P. G., Aliev, O. M.: Akad. Nauk SSSR, Izd. ELM, Baku 1981 (russian).

38.192 Cu₃SmTe₃

trigonal (P $\bar{3}$).

E_g 0.23 eV from conductivity

n 1.73·10²⁰ cm⁻³

R_H 0.036 cm³ C⁻¹

81R Rustamov, , P. G., Aliev, O. M.: Akad. Nauk SSSR, Izd. ELM, Baku 1981 (russian).

38.193 Cu₃TbTe₃

trigonal (P $\bar{3}$)

E_g 0.46 eV from conductivity

n 2·10²⁰ cm⁻³

R_H 0.052 cm³ C⁻¹

81R Rustamov, , P. G., Aliev, O. M.: Akad. Nauk SSSR, Izd. ELM, Baku 1981 (russian).

38.194 Cu₃DyTe₃

trigonal (P $\bar{3}$)

E_g 0.34 eV from conductivity

n 1.5·10¹⁹ cm⁻³

R_H 0.095 cm³ C⁻¹

81R Rustamov, , P. G., Aliev, O. M.: Akad. Nauk SSSR, Izd. ELM, Baku 1981 (russian).

38.195 Cu₃YTe₃

trigonal (P $\bar{3}$)

E_g 0.72 eV from conductivity

n 2.3·10²⁰ cm⁻³

R_H 0.027 cm³ C⁻¹

81R Rustamov, , P. G., Aliev, O. M.: Akad. Nauk SSSR, Izd. ELM, Baku 1981 (russian).

38.196 Cu₃HoTe₃

trigonal ($P\bar{3}$)

E_g	0.26 eV	from conductivity
n	$1.6 \cdot 10^{18} \text{ cm}^{-3}$	
R_H	$0.560 \text{ cm}^3 \text{ C}^{-1}$	

81R Rustamov, , P. G., Aliev, O. M.: Akad. Nauk SSSR, Izd. ELM, Baku 1981 (russian).

38.197 Cu₃ErTe₃

trigonal ($P\bar{3}$)

E_g	0.24 eV	from conductivity
n	$2.4 \cdot 10^{20} \text{ cm}^{-3}$	
R_H	$0.049 \text{ cm}^3 \text{ C}^{-1}$	

81R Rustamov, , P. G., Aliev, O. M.: Akad. Nauk SSSR, Izd. ELM, Baku 1981 (russian).

38.198 Cu₃TmTe₃

trigonal ($P\bar{3}$)

E_g	0.14 eV	from conductivity
n	$2.8 \cdot 10^{20} \text{ cm}^{-3}$	
R_H	$0.087 \text{ cm}^3 \text{ C}^{-1}$	

81R Rustamov, , P. G., Aliev, O. M.: Akad. Nauk SSSR, Izd. ELM, Baku 1981 (russian).

38.199 Cu₅HoS₄

hexagonal

E_g	0.53 eV	from conductivity
n	$2.3 \cdot 10^{20} \text{ cm}^{-3}$	
R_H	$0.027 \text{ cm}^3 \text{ C}^{-1}$	

76R Rustamov, P. G., Aliev, G. M., Guseinov, G. G., Alidzhanov, M. A., Agaev, A. B.: Izv. Akad. Nauk SSSR, Neorg. Mater. 12 (1976) 1192.

38.200 Cu₅LuS₄

hexagonal

E_g	0.50 eV	from conductivity
n	$1.3 \cdot 10^{16} \text{ cm}^{-3}$	
R_H	$4.796 \text{ cm}^3 \text{ C}^{-1}$	

σ $1.24 \cdot 10^{-2} \Omega^{-1} \text{ cm}^{-1}$

76R Rustamov, P. G., Aliev, G. M., Guseinov, G. G., Alidzhanov, M. A., Agaev, A. B.: Izv. Akad. Nauk SSSR, Neorg. Mater. 12 (1976) 1192.

38.201 Cu₅GdSe₄

hexagonal

E_g	0.64 eV	from conductivity
n	$10.6 \cdot 10^{19} \text{ cm}^{-3}$	
R_H	$0.059 \text{ cm}^3 \text{ C}^{-1}$	
σ	$3 \cdot 10^{-2} \Omega^{-1} \text{ cm}^{-1}$	

76R Rustamov, P. G., Aliev, G. M., Guseinov, G. G., Alidzhanov, M. A., Agaev, A. B.: Izv. Akad. Nauk SSSR, Neorg. Mater. 12 (1976) 1192.

38.202 Cu₅TbSe₄

hexagonal

E_g	1.04 eV	from conductivity
n	$1.77 \cdot 10^{19} \text{ cm}^{-3}$	
	$0.353 \text{ cm}^3 \text{ C}^{-1}$	
σ	$\approx 1 \cdot 10^{-3} \Omega^{-1} \text{ cm}^{-1}$	

76R Rustamov, P. G., Aliev, G. M., Guseinov, G. G., Alidzhanov, M. A., Agaev, A. B.: Izv. Akad. Nauk SSSR, Neorg. Mater. 12 (1976) 1192.

38.203 Cu₅YbSe₄

hexagonal

E_g	0.80 eV	from conductivity
n	$11.6 \cdot 10^{19} \text{ cm}^{-3}$	
R_H	$0.054 \text{ cm}^3 \text{ C}^{-1}$	
σ	$\approx 8 \cdot 10^{-2} \Omega^{-1} \text{ cm}^{-1}$	

76R Rustamov, P. G., Aliev, G. M., Guseinov, G. G., Alidzhanov, M. A., Agaev, A. B.: Izv. Akad. Nauk SSSR, Neorg. Mater. 12 (1976) 1192.

38.204 Cu₅LuSe₄

hexagonal

E_g	1.00 eV	from conductivity
n	$8.7 \cdot 10^{19} \text{ cm}^{-3}$	
R_H	$0.072 \text{ cm}^3 \text{ C}^{-1}$	
σ	$\approx 1 \cdot 10^{-3} \Omega^{-1} \text{ cm}^{-1}$	

76R Rustamov, P. G., Aliev, G. M., Guseinov, G. G., Alidzhanov, M. A., Agaev, A. B.: Izv. Akad. Nauk SSSR, Neorg. Mater. 12 (1976) 1192.

38.205 GdBrH₂

R $\bar{3}$ m

E_g	2.66 eV
-------	---------

85K Kremer, R. K.: Thesis, Darmstadt, Germany, 1985.

38.206 TbBrD₂

R $\bar{3}$ m

E_g 2.66 eV

90K Kremer, R. K., Bauhofer, W., Mattausch, HJ., Brill, W., Simon, A.: Solid State Commun. 73 (1990) 281.

38.207 ZnTm₂S₄

orthorhombic (Er₂MnS₄-type)

E_g 3.6 eV from optical absorption

73Y Yim, W. M., Fan, A. K., Stolko, E. J.: J. Electrochem. Soc. 120 (1973) 441.

38.208 ZnYb₂S₄

orthorhombic (Er₂MnS₄-type)

E_g 2.5 eV from optical absorption

73Y Yim, W. M., Fan, A. K., Stolko, E. J.: J. Electrochem. Soc. 120 (1973) 441.

38.209 ZnLu₂S₄

orthorhombic (Er₂MnS₄-type)

E_g 3.7 eV from optical absorption

73Y Yim, W. M., Fan, A. K., Stolko, E. J.: J. Electrochem. Soc. 120 (1973) 441.

38.210 ZnSc₂S₄

spinel

E_g 2.1 eV from optical absorption;

73Y Yim, W. M., Fan, A. K., Stolko, E. J.: J. Electrochem. Soc. 120 (1973) 441.

38.211 CdLa₂S₄

Th₃P₄-type

E_g 1.30 eV

2.6 eV from optical absorption

σ $1.6 \cdot 10^{-4} \Omega^{-1} \text{ cm}^{-1}$ n-type

73Y Yim, W. M., Fan, A. K., Stolko, E. J.: J. Electrochem. Soc. 120 (1973) 441.

89A Agaev, A. B., Rustamov, P. G., Aliev, O. M., Azadaliev, R. A.: Inorg. Mater. 25 (1989) 250-254.

38.212 CdCe₂S₄

Th₃P₄-type

σ $1.8 \cdot 10^{-4} \Omega^{-1} \text{ cm}^{-1}$ n-type

E_g 1.35 eV

89A Agaev, A. B., Rustamov, P. G., Aliev, O. M., Azadaliev, R. A.: Inorg. Mater. 25 (1989) 250-254.

38.213 CdPr₂S₄

trigonal

Th₃P₄-type

E_g 1.43 eV

2.1 eV

from optical absorption

σ $3.2 \cdot 10^{-5} \Omega^{-1} \text{ cm}^{-1}$ n-type

73Y Yim, W. M., Fan, A. K., Stolko, E. J.: J. Electrochem. Soc. 120 (1973) 441.

89A Agaev, A. B., Rustamov, P. G., Aliev, O. M., Azadaliev, R. A.: Inorg. Mater. 25 (1989) 250-254.

38.214 CdNd₂S₄

Th₃P₄-type

E_g 1.48 eV

73Y Yim, W. M., Fan, A. K., Stolko, E. J.: J. Electrochem. Soc. 120 (1973) 441.

38.215 CdSm₂S₄

Th₃P₄-type

σ $6.3 \cdot 10^{-6} \Omega^{-1} \text{ cm}^{-1}$ n-type

E_g 1.30 eV

89A Agaev, A. B., Rustamov, P. G., Aliev, O. M., Azadaliev, R. A.: Inorg. Mater. 25 (1989) 250-254.

38.216 CdGd₂S₄

Th₃P₄-type

σ $3.5 \cdot 10^{-5} \Omega^{-1} \text{ cm}^{-1}$ n-type

E_g 1.15 eV

89A Agaev, A. B., Rustamov, P. G., Aliev, O. M., Azadaliev, R. A.: Inorg. Mater. 25 (1989) 250-254.

38.217 CdTb₂S₄

Th₃P₄-type

σ $1.6 \cdot 10^{-5} \Omega^{-1} \text{ cm}^{-1}$ n-type

E_g 1.18 eV

73Y Yim, W. M., Fan, A. K., Stolko, E. J.: J. Electrochem. Soc. 120 (1973) 441.

89A Agaev, A. B., Rustamov, P. G., Aliev, O. M., Azadaliev, R. A.: Inorg. Mater. 25 (1989) 250-254.

38.218 CdDy₂S₄

spinel-type

E_g 2.5 eV from optical absorption

1.20 eV

σ $2.55 \cdot 10^{-7} \Omega^{-1} \text{ cm}^{-1}$ n-type

73Y Yim, W. M., Fan, A. K., Stolko, E. J.: J. Electrochem. Soc. 120 (1973) 441.

89A Agaev, A. B., Rustamov, P. G., Aliev, O. M., Azadaliev, R. A.: Inorg. Mater. 25 (1989) 250-254.

38.219 CdEr₂S₄

spinel-type

E_g 1.8 eV from optical absorption

1.30 eV

σ $3.6 \cdot 10^{-7} \Omega^{-1} \text{ cm}^{-1}$ n-type

73Y Yim, W. M., Fan, A. K., Stolko, E. J.: J. Electrochem. Soc. 120 (1973) 441.

89A Agaev, A. B., Rustamov, P. G., Aliev, O. M., Azadaliev, R. A.: Inorg. Mater. 25 (1989) 250-254.

38.220 CdTm₂S₄

spinel-type

σ n-type

E_g 2.4 eV from optical absorption

73Y Yim, W. M., Fan, A. K., Stolko, E. J.: J. Electrochem. Soc. 120 (1973) 441.

89A Agaev, A. B., Rustamov, P. G., Aliev, O. M., Azadaliev, R. A.: Inorg. Mater. 25 (1989) 250-254.

38.221 CdYb₂S₄

spinel-type

lattice parameters

a 11.0684 Å

11.04 Å

E_g 1.38 eV

$\approx 2.5 \text{ eV}$

from optical absorption

further parameters

T_m 1890 K

d 5.79 g cm⁻³ exp.

5.81 g cm⁻³ calc.

σ $1.6 \cdot 10^{-6} \Omega^{-1} \text{ cm}^{-1}$ n-type

S 70 μV K⁻¹

73Y Yim, W. M., Fan, A. K., Stolko, E. J.: J. Electrochem. Soc. 120 (1973) 441.

89A Agaev, A. B., Rustamov, P. G., Aliev, O. M., Azadaliev, R. A.: Inorg. Mater. 25 (1989) 250-254.

38.222 CdSc₂S₄

spinel

E_g 2.3 eV from optical absorption

73Y Yim, W. M., Fan, A. K., Stolko, E. J.: J. Electrochem. Soc. 120 (1973) 441.

38.223 LaGaSe₃

E_g 2.1 eV

$\sigma \approx 10^{-6} \Omega^{-1} \text{ cm}^{-1}$

81R Rustamov, , P. G., Aliev, O. M.: Akad. Nauk SSSR, Izd. ELM, Baku 1981 (russian).

38.224 CeGaSe₃

E_g 2.2 eV

$\sigma \approx 10^{-6} \Omega^{-1} \text{ cm}^{-1}$

81R Rustamov, , P. G., Aliev, O. M.: Akad. Nauk SSSR, Izd. ELM, Baku 1981 (russian).

38.225 PrGaSe₃

E_g 2.14 eV

$\sigma \approx 10^{-6} \Omega^{-1} \text{ cm}^{-1}$

81R Rustamov, , P. G., Aliev, O. M.: Akad. Nauk SSSR, Izd. ELM, Baku 1981 (russian).

38.226 NdGaSe₃

E_g 2.16 eV

$\sigma \approx 10^{-6} \Omega^{-1} \text{ cm}^{-1}$

81R Rustamov, , P. G., Aliev, O. M.: Akad. Nauk SSSR, Izd. ELM, Baku 1981 (russian).

38.227 SmGaSe₃

E_g 2.0 eV

$\sigma \approx 10^{-6} \Omega^{-1} \text{ cm}^{-1}$

81R Rustamov, , P. G., Aliev, O. M.: Akad. Nauk SSSR, Izd. ELM, Baku 1981 (russian).

38.228 EuGa₂S₄

orthorhombic, PbGa₂Se₄ type

E_g 1.70 eV

$\sigma 3.2 \cdot 10^{-6} \Omega^{-1} \text{ cm}^{-1}$ p-type

80A Aliev, O.M.: Inorg. Mater. 16 (1980) 1027-31; Izv. Akad. Nauk SSSR, Ser. Neorg. Mater. 16 (1980) 1514.

38.229 EuGa₂Se₄

orthorhombic, PbGa₂Se₄ type

$$E_g \quad 1.56 \text{ eV}$$

$$\sigma \quad 3.2 \cdot 10^{-5} \Omega^{-1} \text{ cm}^{-1} \quad \text{p-type}$$

80A Aliev, O.M.: Inorg. Mater. 16 (1980) 1027-31; Izv. Akad. Nauk SSSR, Ser. Neorg. Mater. 16 (1980) 1514.

38.230 EuGa₂Te₄

orthorhombic, PbGa₂Se₄ type

$$E_g \quad 1.43 \text{ eV}$$

$$\sigma \quad 1 \cdot 10^{-5} \Omega^{-1} \text{ cm}^{-1} \quad \text{p-type}$$

80A Aliev, O.M.: Inorg. Mater. 16 (1980) 1027-31; Izv. Akad. Nauk SSSR, Ser. Neorg. Mater. 16 (1980) 1514.

38.231 EuIn₂S₄

orthorhombic, PbGa₂Se₄ type

$$E_g \quad 1.50 \text{ eV}$$

80A Aliev, O.M.: Inorg. Mater. 16 (1980) 1027-31; Izv. Akad. Nauk SSSR, Ser. Neorg. Mater. 16 (1980) 1514.

38.232 EuIn₂Se₄

orthorhombic, PbGa₂Se₄ type

$$E_g \quad 1.31 \text{ eV}$$

$$\sigma \quad 3 \cdot 10^{-5} \Omega^{-1} \text{ cm}^{-1} \quad \text{p-type}$$

80A Aliev, O.M.: Inorg. Mater. 16 (1980) 1027-31; Izv. Akad. Nauk SSSR, Ser. Neorg. Mater. 16 (1980) 1514.

38.233 EuIn₂Te₄

orthorhombic, PbGa₂Se₄ type

$$E_g \quad 1.22 \text{ eV}$$

$$\sigma \quad 2 \cdot 10^{-5} \Omega^{-1} \text{ cm}^{-1} \quad \text{p-type}$$

80A Aliev, O.M.: Inorg. Mater. 16 (1980) 1027-31; Izv. Akad. Nauk SSSR, Ser. Neorg. Mater. 16 (1980) 1514.

38.234 LaIn₃S₆

orthorhombic, space group: Pbam

$$E_g \quad 1.03 \text{ eV}$$

$$\sigma \quad 2.0 \cdot 10^{-5} \Omega^{-1} \text{ cm}^{-1}$$

80A Aliev, O.M.: Inorg. Mater. 16 (1980) 1027-31; Izv. Akad. Nauk SSSR, Ser. Neorg. Mater. 16 (1980) 1514.

38.235 CeIn₃S₆

orthorhombic, space group: Pbam

$$E_g \quad 1.11 \text{ eV}$$

$$\sigma \quad 1.77 \cdot 10^{-5} \Omega^{-1} \text{ cm}^{-1}$$

80A Aliev, O.M.: Inorg. Mater. 16 (1980) 1027-31; Izv. Akad. Nauk SSSR, Ser. Neorg. Mater. 16 (1980) 1514.

38.236 PrIn₃S₆

orthorhombic, space group: Pbam

$$E_g \quad 1.14 \text{ eV}$$

$$\sigma \quad 1.71 \cdot 10^{-5} \Omega^{-1} \text{ cm}^{-1}$$

80A Aliev, O.M.: Inorg. Mater. 16 (1980) 1027-31; Izv. Akad. Nauk SSSR, Ser. Neorg. Mater. 16 (1980) 1514.

38.237 NdIn₃S₆

orthorhombic, space group: Pbam

$$E_g \quad 1.15 \text{ eV}$$

$$\sigma \quad 1.55 \cdot 10^{-5} \Omega^{-1} \text{ cm}^{-1}$$

80A Aliev, O.M.: Inorg. Mater. 16 (1980) 1027-31; Izv. Akad. Nauk SSSR, Ser. Neorg. Mater. 16 (1980) 1514.

38.238 SmIn₃S₆

orthorhombic, space group: Pbam

$$E_g \quad 1.18 \text{ eV}$$

$$\sigma \quad 2.27 \cdot 10^{-5} \Omega^{-1} \text{ cm}^{-1}$$

80A Aliev, O.M.: Inorg. Mater. 16 (1980) 1027-31; Izv. Akad. Nauk SSSR, Ser. Neorg. Mater. 16 (1980) 1514.

38.239 GdIn₃S₆

orthorhombic, space group: Pbam

$$\begin{array}{ll} E_g & 1.13 \text{ eV} \\ \sigma & 1.5 \cdot 10^{-5} \Omega^{-1} \text{ cm}^{-1} \end{array}$$

80A Aliev, O.M.: Inorg. Mater. 16 (1980) 1027-31; Izv. Akad. Nauk SSSR, Ser. Neorg. Mater. 16 (1980) 1514.

38.240 TbIn₃S₆

orthorhombic, space group: Pbam

$$\begin{array}{ll} E_g & 1.20 \text{ eV} \\ \sigma & 9.0 \cdot 10^{-6} \Omega^{-1} \text{ cm}^{-1} \end{array}$$

80A Aliev, O.M.: Inorg. Mater. 16 (1980) 1027-31; Izv. Akad. Nauk SSSR, Ser. Neorg. Mater. 16 (1980) 1514.

38.241 DyIn₃S₆

orthorhombic, space group: Pbam

$$\begin{array}{ll} E_g & 1.22 \text{ eV} \\ \sigma & 7.3 \cdot 10^{-6} \Omega^{-1} \text{ cm}^{-1} \end{array}$$

38.242 YIn₃S₆

orthorhombic, space group: Pbam

$$\begin{array}{ll} E_g & 1.16 \text{ eV} \\ \sigma & 4.6 \cdot 10^{-5} \Omega^{-1} \text{ cm}^{-1} \end{array}$$

80A Aliev, O.M.: Inorg. Mater. 16 (1980) 1027-31; Izv. Akad. Nauk SSSR, Ser. Neorg. Mater. 16 (1980) 1514.

38.243 HoIn₃S₆

orthorhombic, space group: Pbam

$$\begin{array}{ll} E_g & 1.23 \text{ eV} \\ \sigma & 6.2 \cdot 10^{-6} \Omega^{-1} \text{ cm}^{-1} \end{array}$$

80A Aliev, O.M.: Inorg. Mater. 16 (1980) 1027-31; Izv. Akad. Nauk SSSR, Ser. Neorg. Mater. 16 (1980) 1514.

38.244 ErIn₃S₆

orthorhombic, space group: Pbam

$$\begin{array}{ll} E_g & 1.28 \text{ eV} \\ \sigma & 5.17 \cdot 10^{-6} \Omega^{-1} \text{ cm}^{-1} \end{array}$$

80A Aliev, O.M.: Inorg. Mater. 16 (1980) 1027-31; Izv. Akad. Nauk SSSR, Ser. Neorg. Mater. 16 (1980) 1514.

38.245 LaTiS₂

E_g 1.67 eV

87G Godzhaev, E. M., Nagiev, A. B., Bairamov, D. D., Dzhafarova, S.Z., Godzhaeva, F.M.: Inorg. Mater. 23 (1989) 453-454.

38.246 CeTiS₂

E_g 1.53 eV

87G Godzhaev, E. M., Nagiev, A. B., Bairamov, D. D., Dzhafarova, S.Z., Godzhaeva, F.M.: Inorg. Mater. 23 (1989) 453-454.

38.247 PrTiS₂

E_g 1.53 eV

87G Godzhaev, E. M., Nagiev, A. B., Bairamov, D. D., Dzhafarova, S.Z., Godzhaeva, F.M.: Inorg. Mater. 23 (1989) 453-454.

38.248 NdTiS₂

E_g 1.63 eV

87G Godzhaev, E. M., Nagiev, A. B., Bairamov, D. D., Dzhafarova, S.Z., Godzhaeva, F.M.: Inorg. Mater. 23 (1989) 453-454.

38.249 LaTiSe₂

E_g 1.33 eV

87G Godzhaev, E. M., Nagiev, A. B., Bairamov, D. D., Dzhafarova, S.Z., Godzhaeva, F.M.: Inorg. Mater. 23 (1989) 453-454.

38.250 CeTiSe₂

E_g 1.26 eV

87G Godzhaev, E. M., Nagiev, A. B., Bairamov, D. D., Dzhafarova, S.Z., Godzhaeva, F.M.: Inorg. Mater. 23 (1989) 453-454.

38.251 PrTiSe₂

α -NaFeO₂ type (rhombohedral, lattice parameters given for hexagonal axes)

E_g 1.19 eV

74K Kabré, S., Julien-Pouzol, M., Guittard, M.: Bull. Soc. Chim. France 9/10 (1974) 1881.

87G Godzhaev, E. M., Nagiev, A. B., Bairamov, D. D., Dzhafarova, S.Z., Godzhaeva, F.M.: Inorg. Mater. 23 (1989) 453-454.

38.252 NdTiSe₂

α -NaFeO₂ type (rhombohedral, lattice parameters given for hexagonal axes)

E_g 1.26 eV

74K Kabré, S., Julien-Pouzol, M., Guittard, M.: Bull. Soc. Chim. France 9/10 (1974) 1881.

87G Godzhaev, E. M., Nagiev, A. B., Bairamov, D. D., Dzhafarova, S.Z., Godzhaeva, F.M.: Inorg. Mater. 23 (1989) 453-454.

38.253 EuTiSe₂

E_g 0.42 eV

87G Godzhaev, E. M., Nagiev, A. B., Bairamov, D. D., Dzhafarova, S.Z., Godzhaeva, F.M.: Inorg. Mater. 23 (1989) 453-454.

38.254 LaTiTe₂

E_g 1.23 eV

87G Godzhaev, E. M., Nagiev, A. B., Bairamov, D. D., Dzhafarova, S.Z., Godzhaeva, F.M.: Inorg. Mater. 23 (1989) 453-454.

38.255 CeTiTe₂

E_g 0.95 eV

87G Godzhaev, E. M., Nagiev, A. B., Bairamov, D. D., Dzhafarova, S.Z., Godzhaeva, F.M.: Inorg. Mater. 23 (1989) 453-454.

38.256 PrTiTe₂

α -NaFeO₂ type (rhombohedral, lattice parameters given for hexagonal axes)

E_g 0.79 eV

72K Kabré, S., Julien-Pouzol, M., Guittard, M.: C. R. Acad. Sci. (Paris) Ser. C 275 (1972) 1367.

87G Godzhaev, E. M., Nagiev, A. B., Bairamov, D. D., Dzhafarova, S.Z., Godzhaeva, F.M.: Inorg. Mater. 23 (1989) 453-454.

38.257 NdTiTe₂

α -NaFeO₂ type (rhombohedral, lattice parameters given for hexagonal axes)

E_g 0.79 eV

72K Kabré, S., Julien-Pouzol, M., Guittard, M.: C. R. Acad. Sci. (Paris) Ser. C 275 (1972) 1367.

87G Godzhaev, E. M., Nagiev, A. B., Bairamov, D. D., Dzhafarova, S.Z., Godzhaeva, F.M.: Inorg. Mater. 23 (1989) 453-454.

38.258 La₂GeSe₅

E_g 1.7 eV optical gap

78M Murguzow, M. I.: Fiz. Tekh. Poluprovoda. 12 (1978) 1823; Sov. Phys. Semicond. (English Transl.) 12 (1978) 1080.

38.259 La₂SnSe₅

E_g 1.65 eV optical gap

78M Murguzow, M. I.: Fiz. Tekh. Poluprovoda. 12 (1978) 1823; Sov. Phys. Semicond. (English Transl.) 12 (1978) 1080.

38.260 Ce₂GeSe₅

E_g 1.55 eV optical gap

78M Murguzow, M. I.: Fiz. Tekh. Poluprovoda. 12 (1978) 1823; Sov. Phys. Semicond. (English Transl.) 12 (1978) 1080.

38.261 Ce₂SnSe₅

E_g 1.52 eV optical gap

78M Murguzow, M. I.: Fiz. Tekh. Poluprovoda. 12 (1978) 1823; Sov. Phys. Semicond. (English Transl.) 12 (1978) 1080.

38.262 Pr₂GeSe₅

E_g 1.85 eV optical gap

78M Murguzow, M. I.: Fiz. Tekh. Poluprovoda. 12 (1978) 1823; Sov. Phys. Semicond. (English Transl.) 12 (1978) 1080.

38.263 Pr₂SnSe₅

E_g 1.65 eV optical gap

78M Murguzow, M. I.: Fiz. Tekh. Poluprovoda. 12 (1978) 1823; Sov. Phys. Semicond. (English Transl.) 12 (1978) 1080.

38.264 Nd₂GeSe₅

E_g 1.90 eV optical gap

78M Murguzow, M. I.: Fiz. Tekh. Poluprovoda. 12 (1978) 1823; Sov. Phys. Semicond. (English Transl.) 12 (1978) 1080.

38.265 Nd₂SnSe₅

E_g	1.70 eV	optical gap
78M	Murguzow, M. I.: Fiz. Tekh. Poluprovoda. 12 (1978) 1823; Sov. Phys. Semicond. (English Transl.) 12 (1978) 1080.	

38.266 Sm₂GeSe₅

E_g	2.00 eV	optical gap
78M	Murguzow, M. I.: Fiz. Tekh. Poluprovoda. 12 (1978) 1823; Sov. Phys. Semicond. (English Transl.) 12 (1978) 1080.	

38.267 Sm₂SnSe₅

E_g	1.88 eV	optical gap
78M	Murguzow, M. I.: Fiz. Tekh. Poluprovoda. 12 (1978) 1823; Sov. Phys. Semicond. (English Transl.) 12 (1978) 1080.	

38.268 Gd₂GeSe₅

E_g	1.90 eV	optical gap
78M	Murguzow, M. I.: Fiz. Tekh. Poluprovoda. 12 (1978) 1823; Sov. Phys. Semicond. (English Transl.) 12 (1978) 1080.	

38.269 Gd₂SnSe₅

E_g	1.70 eV	optical gap
78M	Murguzow, M. I.: Fiz. Tekh. Poluprovoda. 12 (1978) 1823; Sov. Phys. Semicond. (English Transl.) 12 (1978) 1080.	

33.15 Cd₄(P,As)₂(Cl,Br,I)₃

Cubic semiconductors, E_g about 1.8...2.3 eV [63S]

References to 33.15

63S Suchov, L., Stemple, N. R.: J. Electrochem. Soc. 110 (1963) 766.